

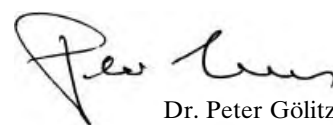
EDITORIAL

And Hückel Was Correct After All—A Withdrawal and an Apology

In the second April issue (No. 8, pp. 1429–1431) this year we published a communication from J. B. Lambert et al. in which an astonishingly stable salt of the pentamethylcyclopentadienyl cation was reported. Following the Hückel rule this antiaromatic cation should, in fact, be highly unstable, and for decades attempts at its preparation and definite characterization have failed—however, perhaps this time the counterion, tetrakis(pentafluorophenyl)borate, had worked wonders. In any case, after two rounds of refereeing by three experts the communication was accepted, and, following publication (April 15) naturally caused quite a stir. Unfortunately, it must now be said that the experimental results were incorrectly interpreted, which was quickly discovered. On April 22, G. Bertrand and co-workers submitted a manuscript in which they showed that the species generated by Lambert et al. was, in fact, a pentamethylcyclopentenyl cation. To keep damage to a minimum we published this manuscript as fast as possible (on May 7) on the *Angewandte Chemie* homepage, fol-

lowing refereeing by those experts who had evaluated the Lambert et al. communication, and after giving J. B. Lambert the opportunity to comment, which resulted in his co-authorship. The edited version of this manuscript can be found in this issue (p. 2275 ff), together with a short theoretical treatment by T. Müller (p. 2276 ff), as well as a “statement” from J. B. Lambert (p. 2279).

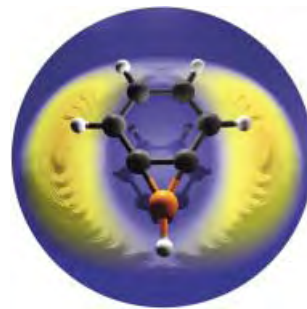
As the Editor I regret that we did not examine the original manuscript more critically, and that its publication has resulted in unnecessary work to reproduce the results experimentally and theoretically.



Dr. Peter Göllitz

COVER PICTURE

The cover picture shows benzoborirene, the product of the crossed-molecular-beam reaction between benzene molecules and boron atoms, displayed above the three-dimensional plot of the angular- and translational-energy-dependent flux of the benzoborirene molecules in the center-of-mass system. As the reaction conditions preclude secondary collisions, the intermediate initially formed from the reactive collision decays by ejection of a hydrogen atom. The structure of the benzoborirene depicted is based on a DFT computation, which, combined with results of highly accurate coupled-cluster calculations has been used to assign the reaction product by comparing experimental and theoretical reaction energies. Details are described by R. I. Kaiser and H. F. Bettinger on p. 2350 ff.

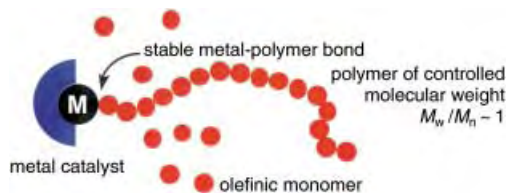


REVIEW

Contents

Polyolefins are ubiquitous materials in everyday life:

Although these polymers are traditionally synthesized by heterogeneous transition-metal catalysts, recent advances in single-site catalysts have given birth to a wide array of new materials of precise stereochemistry (see picture). Although olefin-polymerization techniques are superior to their ionic and radical counterparts regarding stereochemical control, they have been inferior in the category of living polymerization. Recent advances in alkene-polymerization catalysts are rapidly eliminating this deficit.



Angew. Chem. **2002**, *114*, 2340–2361

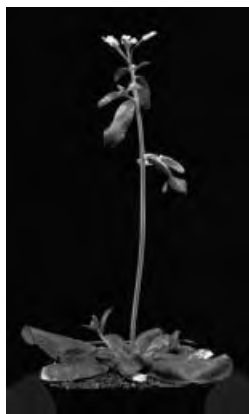
G. W. Coates,* P. D. Hustad,
S. Reinartz 2236–2257

Catalysts for the Living Insertion
Polymerization of Alkenes: Access to
New Polyolefin Architectures Using
Ziegler–Natta Chemistry

Keywords: alkenes • block copolymers •
homogeneous catalysis • living
polymerization • Ziegler–Natta catalysis

MINIREVIEW

The manipulation of iron uptake in plants is close to being realized. Proteins participating in iron transport have been identified and characterized in the model plant *Arabidopsis thaliana*. From this result it will be possible to engineer crop plants that take up more iron for nutritional improvement or plants that clean up toxic minerals from contaminated environments.



Angew. Chem. **2002**, *114*, 2363–2368

D. Staiger* 2259–2264

Chemical Strategies for Iron Acquisition
in Plants

Keywords: chelates • iron • reduction •
siderophores • transport proteins

HIGHLIGHTS

Improved protecting-group strategies are used in two successful methods for the synthesis of oligoribonucleotides. The effective production of these compounds is of growing importance in the context of RNA interference, a phenomenon that is exploited for investigations into protein function.

R. Micura* 2265–2269

Small Interfering RNAs and Their
Chemical Synthesis

Keywords: gene silencing • nucleic acids •
oligonucleotides • protecting groups •
RNA

Angew. Chem. **2002**, *114*, 2369–2373

The structures of AuH and AuI are already known, now the long-sought-after molecules AuH₃ (= (H₂)AuH) and AuH₅ (= H₃Au(H₂)) have been detected by matrix isolation spectroscopy. Based on new calculations, the global minimum for AuI₃, a missing member of the gold halides, has been elucidated to be that of an L-shaped moiety (C_s symmetry; charge transfer from the I₂ unit to the AuI).

Angew. Chem. **2002**, *114*, 2373–2375

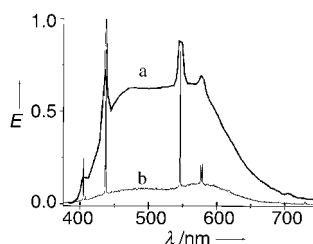
M.-J. Crawford,*
T. M. Klapötke* 2269–2271

Hydrides and Iodides of Gold

Keywords: ab initio calculations • gold • halogens • hydrides • matrix isolation

CORRESPONDENCE

Stray light is a possible source of interference in the electroluminescence spectrum of ITO/NPB/(mdppy)BF/LiF/Al reported by Wang and co-workers (see picture, trace a). Chou et al. observed that four major peaks that correspond to mercury overlap with the reported peaks (trace b).



P.-T. Chou,* C.-C. Cheng, C.-S. Chiou,
G.-R. Wu 2273

Comment on the Communication “Highly Efficient White Organic Electroluminescence from a Double-Layer Device Based on a Boron Hydroxyphenylpyridine Complex” by Wang et al.

Y. Liu, J. Guo, H. Zhang,
Y. Wang* 2274

Reply

Keywords: boron • electroluminescence • luminescence • stray light • thin films

Angew. Chem. **2002**, *114*, 2377

Angew. Chem. **2002**, *114*, 2378

VIPs

The following communications are “Very Important Papers” in the opinion of two referees. They will be published shortly (those marked with a diamond will be published in the next issue). Short summaries of these articles can be found on the *Angewandte Chemie* homepage at the address <http://www.angewandte.org>

Catalytic Activity and Poisoning of Specific Sites on Supported Metal Nanoparticles

S. Schauermaun, J. Hoffmann, V. Johánek, J. Hartmann, J. Libuda,* H.-J. Freund ◆

Understanding Zeolite Catalysis: Inverse Shape Selectivity Revised

M. Schenk, S. Calero, T. L. M. Maesen, L. L. van Benthem, M. G. Verbeek, B. Smit* ◆

Highly Selective Transport of Organic Compounds by Using Supported Liquid Membranes Based on Ionic Liquids

L. C. Branco, J. G. Crespo, C. A. M. Afonso*

Atom-Transfer Tandem Radical Cyclization Reactions Promoted by Lewis Acids

D. Yang,* S. Gu, H.-W. Zhao, N.-Y. Zhu

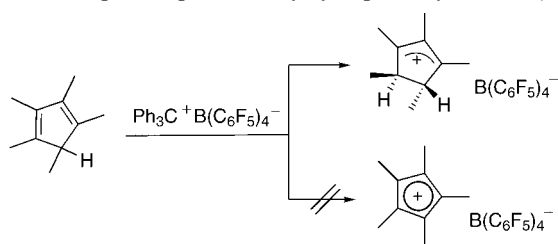
Metallabenzene and Valence Isomers: Synthesis and Characterization of a Platinabenzene

V. Jacob, T. J. R. Weakley, M. M. Haley*

Electronic and Steric Effects on Catalysts for CO₂/Epoxide Polymerization: Extremely Subtle Modifications Resulting in Superior Activities

D. R. Moore, M. Cheng, E. B. Lobkovsky, G. W. Coates*

Not $C_5Me_5^+$ (I): $C_5Me_5^+$ remains triplet! The reaction of triphenylmethyl tetrakis(pentafluorophenyl)borate with pentamethylcyclopentadiene does not lead to a stable antiaromatic singlet pentamethylcyclopentadiene cation, but to the unexpected pentamethylcyclopentenyl cation (see scheme).



Angew. Chem. **2002**, *114*, 2379–2380

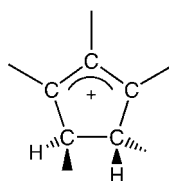
M. Otto, D. Scheschkewitz, T. Kato,
M. M. Midland, J. B. Lambert,
G. Bertrand* 2275–2276

The Stable Pentamethylcyclopentadienyl
Cation Remains Unknown

Keywords: antiaromaticity •
carbocations • cyclopentadienyl cation •
cyclopentenyl cation • structure
elucidation



Not $C_5Me_5^+$ (II): The search for the elusive singlet cyclopentadienyl cation must continue. Quantum-mechanical calculations of both structure and NMR chemical shifts suggest that the recently reported X-ray structure is that of a cyclopentenyl cation (see picture).



Angew. Chem. **2002**, *114*, 2380–2382

T. Müller* 2276–2278

Comment on the X-Ray Structure of
Pentamethylcyclopentadienyl Cation

Keywords: antiaromaticity •
carbocations • cyclopentadienyl cation •
cyclopentenyl cation • density functional
calculations • structure elucidation

Not $C_5Me_5^+$ (III): Because of the evidence presented in the above Correspondence the authors are retracting the conclusions of their publication “The Stable Pentamethylcyclopentadienyl Cation” which were entirely those of the main author and imply no reflection on the part of his co-workers (whose experimental and theoretical work is valid).

Angew. Chem. **2002**, *114*, 2383–2383

J. B. Lambert* 2279–2279

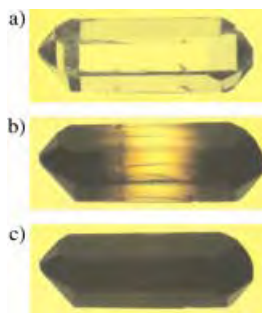
Statement

Keywords: antiaromaticity • aromaticity •
carbocations • cyclopentadienyl cation •
cyclopentenyl cation • structure
elucidation

COMMUNICATIONS

Efficient guest exchange: The organic zeolite analogue $TPP \cdot x(THF)$ ($x = 0.35–0.65$) takes up I_2 quickly when exposed to iodine vapor. The previously colorless crystals (a) color at the ends (b), and after 1–2 days the iodine has permeated all the way through the crystal (c). The conductivity values of the $TPP \cdot y(I_2)$ crystals are of the same order as those of elemental I_2 . TPP = tris(*o*-phenylenedioxy)cyclotriphosphazene.

Angew. Chem. **2002**, *114*, 2385–2388

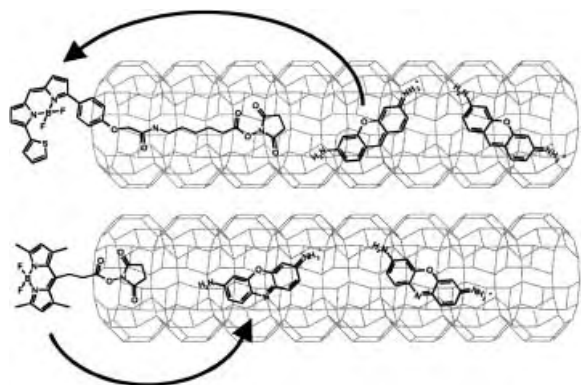


T. Hertzsch, F. Budde, E. Weber,
J. Hulliger* 2281–2284

Supramolecular-Wire Confinement of I_2
Molecules in Channels of the Organic
Zeolite Tris(*o*-phenylenedioxy)cyclo-
triphosphazene

Keywords: conducting materials •
iodine • phosphazenes • zeolite
analogues

Stopcock fluorophores at the ends of zeolite L channels can trap electronic excitation energy from pyronine⁺ molecules inside the crystal (see scheme, top). The reverse process, that is, the injection of electronic excitation energy through such stopcocks (bottom), was achieved with oxonine⁺ molecules inside the zeolite channels.



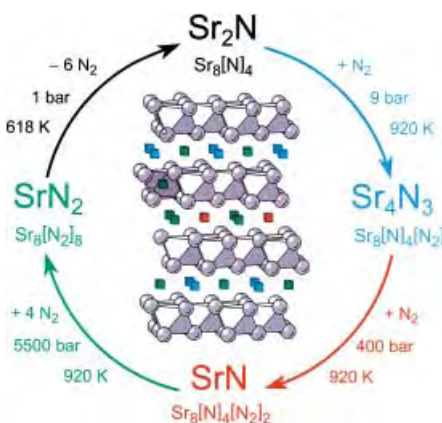
Angew. Chem. **2002**, *114*, 2389–2392

H. Maas, G. Calzaferri* 2284–2288

Trapping Energy from and Injecting Energy into Dye–Zeolite Nanoantennae

Keywords: donor–acceptor systems • dyes/pigments • fluorescence • supramolecular chemistry • zeolites

The reaction of molecular nitrogen with the layered subnitride Sr₂N leads to intercalation and formation of single-phase Sr₂N[N₂]_{0.25} (≡ Sr₄N₃; see scheme) under mild conditions (*T* = 650 °C, *p*_{N₂} = 9 bar). N₂ is reduced to the diazenide stage [N₂^{2−}], while half of the strontium is oxidized to Sr²⁺. The intercalation is reversible.



Angew. Chem. **2002**, *114*, 2392–2394

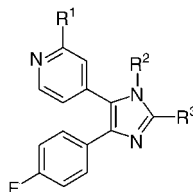
Y. Prots, G. Auffermann, M. Tovar, R. Kniep* 2288–2290

Sr₄N₃: A Hitherto Missing Member in the Nitrogen Pressure Reaction Series
Sr₂N → Sr₄N₃ → SrN → SrN₂

Keywords: diazenides • intercalation • nitrides • pressure synthesis • subvalent compounds



Regioselective synthetic approaches to tetrasubstituted imidazoles (see picture) are reported. These highly substituted heterocycles are potent inhibitors of cytokine release and therefore interesting candidates for anti-inflammatory drugs.



Angew. Chem. **2002**, *114*, 2408–2411

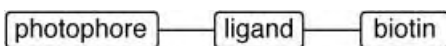
S. Laufer,* G. Wagner, D. Kotschenreuther 2290–2293

Ones, Thiones, and *N*-Oxides: An Exercise in Imidazole Chemistry

Keywords: drug design • inhibitors • medicinal chemistry • nitrogen heterocycles • synthetic methods



Two generally applicable reagents for photoaffinity probes have been developed. They contain an *m*-nitrophenyl ether function with a trifluoromethyldiazirine side chain (photophore group), as well as a biotin tag for the identification of labeled proteins or peptides and either a free hydroxy or a squaramide group for the attachment of any suitably functionalized ligand which directs the reagent to the binding site of the target molecule (see picture).



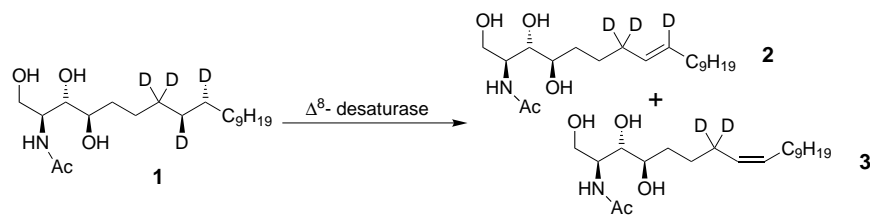
Angew. Chem. **2002**, *114*, 2404–2408

M. Daghighi, L. Hennig, M. Findeisen, S. Giesa, F. Schümer, H. Hennig, A. G. Beck-Sickinger, P. Welzel* 2293–2297

Tetrafunctional Photoaffinity Labels Based on Nakanishi's *m*-Nitroalkoxy-Substituted Phenyltrifluoromethyldiazirine

Keywords: antibiotics • photoaffinity labels • photochemistry • transglycosylase

The simultaneous formation of *E* and *Z* double bonds results from the *syn* elimination of H and/or D atoms from different conformations of 4-hydroxy-sphinganine [D₄]**1**. Δ^8 -Sphingolipid desaturase from *Helianthus annuus* is heterologously expressed in yeast and catalyzes the transformation to *E* olefin **2** (88%) and *Z* olefin **3** (12%).



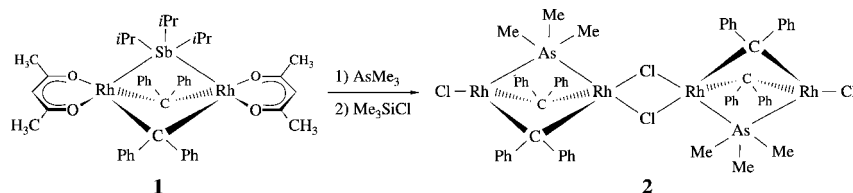
Angew. Chem. **2002**, *114*, 2394–2397

C. Beckmann, J. Rattke, N. J. Oldham,
P. Sperling, E. Heinz,
W. Boland* 2298–2300

Characterization of a Δ^8 -Sphingolipid
Desaturase from Higher Plants: A
Stereochemical and Mechanistic Study on
the Origin of *E,Z* Isomers

Keywords: desaturases • elimination •
enzyme catalysis • isotope effects •
sphingolipids

A tertiary arsane ligand in a bridging position occurs for the first time in the structurally characterized transition-metal complex **2**, which was prepared from **1** by stepwise ligand substitution of both the trialkylstibane and acetylacetonate ligands. The analogous chainlike phosphane-bridged dimer $[\text{ClRh}(\mu\text{-PMe}_3)(\mu\text{-CPh}_2)_2\text{Rh}(\mu\text{-Cl})_2\text{Rh}(\mu\text{-PMe}_3)(\mu\text{-CPh}_2)_2\text{RhCl}]$ has also been isolated and characterized by X-ray crystallography.



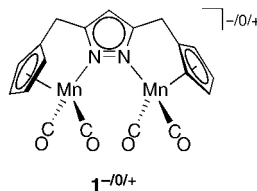
Angew. Chem. **2002**, *114*, 2398–2401

T. Pechmann, C. D. Brandt, C. Röger,
H. Werner* 2301–2303

A New Type of Chainlike Tetranuclear
Rhodium Complexes with PR_3 and AsMe_3
as Bridging Ligands

Keywords: As ligands • bridging ligands •
carbene complexes • P ligands • rhodium

Fast electron transfer between the Mn centers in the mixed-valent complex **1**, a dinuclear analogue of complexes with $\text{Cp}'\text{-N}$ -ligands ($\text{Cp} = \text{C}_5\text{H}_5$), supports the occurrence of cooperative effects in such highly preorganized bimetallic systems. An unusual $\eta^1:\eta^1:\eta^5$ coordination of the pyrazolate group is observed for $\text{K}^+ \text{1}^-$ in the solid state.



Angew. Chem. **2002**, *114*, 2414–2417

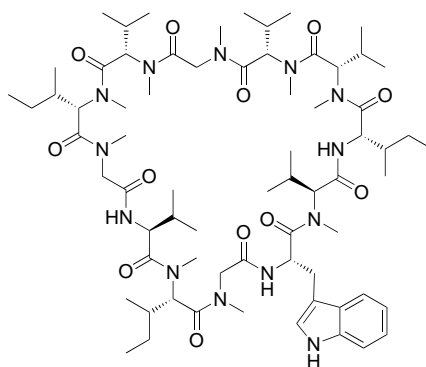
J. C. Röder, F. Meyer,*
E. Kaifer 2304–2306

Bifunctional $\text{Cp} \cap \text{N}$ Complexes—
Unusual Structural Features and
Electronic Coupling in Highly
Preorganized Bimetallic Systems

Keywords: bridging ligands • electronic
structure • manganese • metal–metal
interactions • mixed-valent compounds



Racemization-free coupling of Fmoc-*N*-methyl amino acids on a solid support is quantitative with a new triphosgene-activation method. With this method, the total synthesis of the nematocidal cyclododecapeptide omphalotin A (see picture) was accomplished, which because of its high content of *N*-methyl amino acids had not yet been accessible.



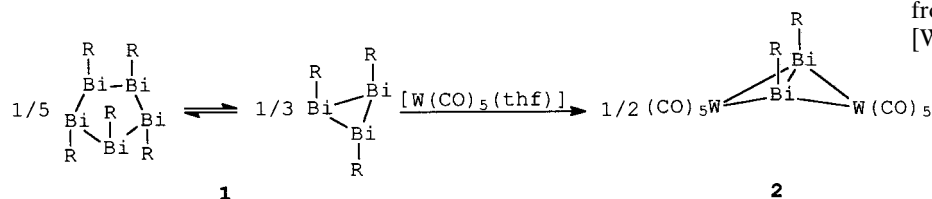
Angew. Chem. **2002**, *114*, 2401–2403

B. Thern, J. Rudolph,
G. Jung* 2307–2309

Total Synthesis of the Nematocidal
Cyclododecapeptide Omphalotin A by
Using Racemization-Free Triphosgene-
Mediated Couplings in the Solid Phase

Keywords: *N*-methyl amino acids •
omphalotin A • peptides • solid-phase
synthesis • total synthesis • triphosgene

The wings of the butterfly structure are widely extended in 2 (see picture, R = Me₃SiCH₂), a complex with a dibismuthene ligand, which coordinates as a “side-on”-bridging, four-electron donor to two tungsten atoms. Complex **2** is formed from the reaction of [W(CO)₅(thf)] with alkylbismuth five- and three-membered rings of cyclobismuthanes **1**, which exist in equilibrium.



Angew. Chem. **2002**, *114*, 2411–2414

L. Balázs, H. J. Breunig,*

E. Lork 2309–2312

Synthesis of the Dibismuthene Complex
[$\{\mu\text{-}\eta^2\text{-(cis-Me}_3\text{SiCH}_2\text{Bi)}_2\}\{\text{W(CO)}_5\}_2$]
from a Cyclobismuthane and
[W(CO)₅(thf)]

Keywords: bismuth • small-ring systems • structure elucidation • tungsten

What's new about complexes 1 and 2, textbook examples of coordination compounds? Quantum-chemical simulations reveal an exceptionally strong sensitivity of their ⁵⁷Fe NMR spectroscopy chemical shifts to the Fe–C bond length, which, in turn, changes noticeably on going from the gas phase to aqueous solution.



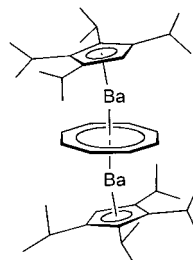
Angew. Chem. **2002**, *114*, 2417–2420

M. Bühl,* F. T. Mauschick, F. Terstegen,
B. Wrackmeyer 2312–2315

Remarkably Large Geometry
Dependence of ⁵⁷Fe NMR Chemical
Shifts

Keywords: density functional calculations • iron • molecular dynamics • NMR spectroscopy • solvent effects

Sublimable without decomposition is the first barium triple-decker sandwich complex [(⁴Cp)Ba(cot)Ba(⁴Cp)] (⁴Cp = C₅H₇Pr₄; cot = cyclooctatetraene; see picture). Short distances (significantly below the sum of Van der Waals radii) between two of the methyl groups of each ⁴Cp ligand indicate a Ba···CH₃ interaction.

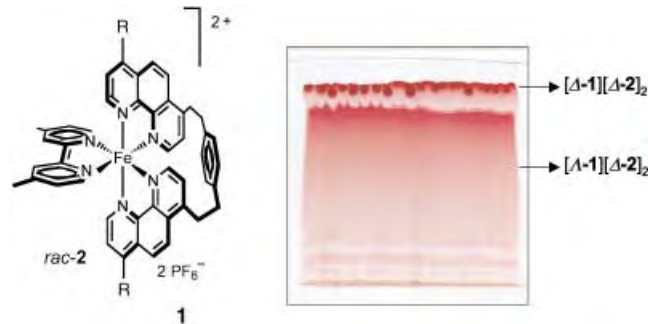


H. Sitzmann,* M. D. Walter,
G. Wolmershäuser 2315–2316

A Triple-Decker Sandwich Complex of Barium

Keywords: alkaline-earth metals • barium • cyclopentadienyl ligands • structure elucidation • triple-decker complexes

Configurational stability is conferred on the complex **1** (R = 4-MeOC₆H₄) by the carefully designed tetradentate bis(1,10-phenanthroline) ligand. The resolution and asymmetric synthesis of **1** were readily achieved by using tris(tetrachlorobenzenediolato)phosphate(v) anions (**2**) as chiral auxiliaries. The picture shows the separation of the enantiomers of **1** by preparative ion-pair thin-layer chromatography.



Angew. Chem. **2002**, *114*, 2423–2425

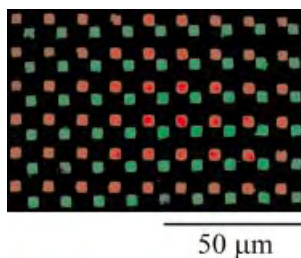
D. Monchaud, J. J. Jodry, D. Pomeranc,
V. Heitz, J.-C. Chambron, J.-P. Sauvage,
J. Lacour* 2317–2319

Ion-Pair-Mediated Asymmetric Synthesis
of a Configurationally Stable
Mononuclear Tris(diimine)–Iron(II)
Complex

Keywords: chiral auxiliaries • chiral resolution • ion pairs • iron • N ligands



High-resolution arrays of antibodies can be prepared in a highly parallel manner by a combination of affinity purification and microcontact printing. Arrays with lateral dimensions of between 100 and 3 μm were prepared by using planar, affinity stamps that were patterned by using various soft lithographic techniques. The fluorescence microscopy image shown demonstrates the placement of anti-chicken and anti-goat antibodies on a glass substrate from a stamp.



Angew. Chem. **2002**, *114*, 2426–2429

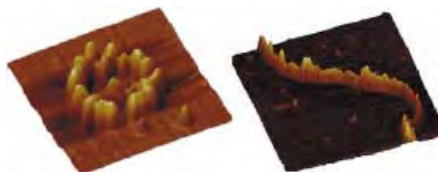
J. P. Renault, A. Bernard, D. Juncker,
B. Michel, H. R. Bosshard,
E. Delamarche* 2320–2323

Fabricating Microarrays of Functional
Proteins Using Affinity Contact Printing

Keywords: antibodies • antigens •
lithography • microcontact printing •
patterning

A crop of gold circles and lines:

Psoralen-functionalized Au nanoparticles incorporated into DNA, and Au-nanoparticle-functionalized poly-L-lysine, yield linear and circular nanowires, respectively, on mica surfaces (see atomic force microscopy images).



Angew. Chem. **2002**, *114*, 2429–2433

F. Patolsky, Y. Weizmann,
O. Lioubashevski,
I. Willner* 2323–2327

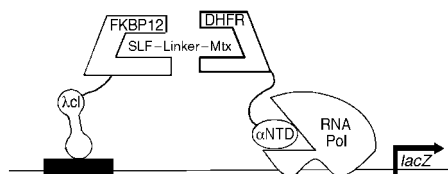
Au-Nanoparticle Nanowires Based on
DNA and Polylysine Templates

Keywords: DNA • gold • intercalation •
nanoparticles • nanostructures •
nanowires



A method for in vivo affinity chromatography,

the yeast three-hybrid assay simplifies protein identification and amplification at the end of affinity panning. The bacterial system described should increase, by several orders of magnitude, the number of protein variants that can be assayed (see picture; SLF = synthetic analogue of FK506; Mtx = methotrexate; FKBP12 = FK506-binding protein 12; DHFR = dihydrofolate reductase; λCI = λ -repressor; αNTD = N-terminal domain of the α -subunit of RNA Pol; RNA Pol = RNA polymerase).



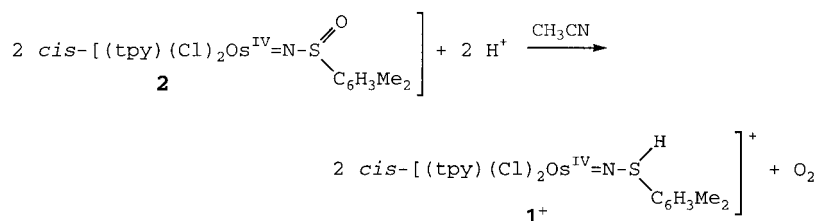
Angew. Chem. **2002**, *114*, 2433–2436

E. A. Althoff,
V. W. Cornish* 2327–2330

A Bacterial Small-Molecule Three-
Hybrid System

Keywords: bioorganic chemistry • gene
expression • protein engineering •
proteomics • signal transduction

Librating oxygen: In a novel example of O_2 evolution/activation based on a ligand, in this case, one electronically activated by the Os–N multiple bond, compound **2** ($\text{tpy} = 2,2':6',2''\text{-terpyridine}$) is converted reversibly into **1**⁺ on addition of H^+ ions. These reactions are remarkable both for their occurrence and for the rates at which they occur.



Angew. Chem. **2002**, *114*, 2436–2439

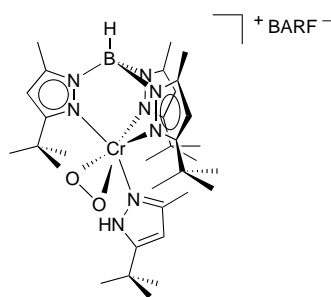
M. H. V. Huynh,* D. E. Morris,
P. S. White, T. J. Meyer* 2330–2333

Proton-Induced, Reversible Evolution of
 O_2 from the Os^{IV} –Sulfoximido Complex
[$\text{Os}^{\text{IV}}(\text{tpy})(\text{Cl})_2[\text{NS}(\text{O})\text{-}3,5\text{-Me}_2\text{C}_6\text{H}_3]$]

Keywords: N ligands • osmium • oxygen
evolution • redox chemistry • S ligands

Binding oxygen: A four-coordinate chromium(II) complex binds O_2 to yield the first structurally characterized chromium(III) superoxo complex. The superoxide ligand is coordinated in a “side-on” fashion (see structure; BARF = tetrakis(3,5-bis(trifluoromethyl)phenyl)borate). This bonding mode seems to be more widespread than commonly appreciated.

Angew. Chem. **2002**, *114*, 2439–2441



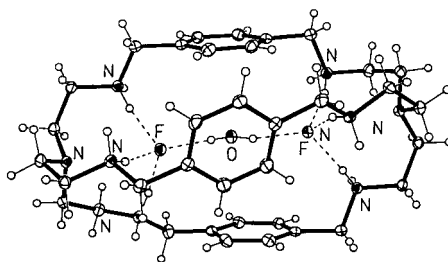
K. Qin, C. D. Incarvito, A. L. Rheingold, K. H. Theopold* 2333–2335

A Structurally Characterized Chromium(III) Superoxide Complex Features “Side-on” Bonding

Keywords: chromium • coordination modes • dioxygen • N ligands • tripodal ligands



Two fluoride ions in a single azacryptand: The two fluoride ions are bridged by a water molecule (see structure) to give an anion-based cascade complex, which mimics the analogous transition-metal cascade complexes with these ligands.



M. A. Hossain, J. M. Llinares, S. Mason, P. Morehouse, D. Powell, K. Bowman-James* 2335–2338

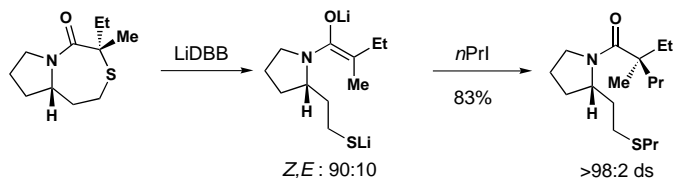
Parallels in Cation and Anion Coordination: A New Class of Cascade Complexes

Keywords: anions • bridging ligands • cascade complex • cryptands • macrocyclic ligands

Angew. Chem. **2002**, *114*, 2441–2444



High diastereoselectivity is achieved in the alkylation of α,α -disubstituted amide enolates to form quaternary carbon products (see scheme; LiDBB = di-*tert*-butyldiphenyllithium). No chelating groups are necessary for stereocontrol in either the enolate-formation or alkylation steps. In many cases, amplification of the alkylation diastereoselectivity above the isomeric ratio of the intermediate enolates is observed.



Angew. Chem. **2002**, *114*, 2444–2447

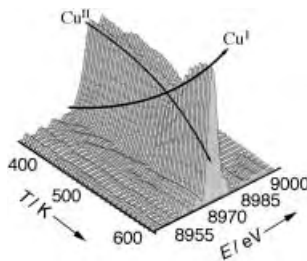
J. M. Manthorpe, J. L. Gleason* 2338–2341

Stereoselective Formation of Quaternary Carbon Centers: Alkylation of α,α -Disubstituted Amide Enolates

Keywords: alkylation • amides • asymmetric synthesis • lactams • quaternary carbon centers



The rate-determining step of the ethylene oxychlorination reaction on $CuCl_2/\gamma-Al_2O_3$ catalyst could be identified by an in situ, time-resolved XANES study. According to these data (see figure; E = photon energy) and the simultaneously determined catalyst activity, the rate-determining step is the oxidation of $CuCl$. The dopant potassium chloride, added to the industrial catalysts, decreases the rate of the reduction step, which becomes the rate-determining step for the $KCl/CuCl_2/\gamma-Al_2O_3$ catalyst.



C. Lamberti,* C. Prestipino, F. Bonino, L. Capello, S. Bordiga, G. Spoto, A. Zecchina, S. Diaz Moreno, B. Cremaschi, M. Garilli, A. Marsella, D. Carmello, S. Vidotto, G. Leofanti 2341–2344

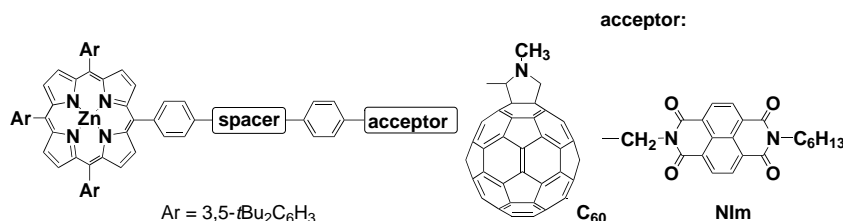
The Chemistry of the Oxychlorination Catalyst: an In Situ, Time-Resolved XANES Study

Keywords: copper • ethylene • oxychlorination • redox chemistry • X-ray absorption spectroscopy

Angew. Chem. **2002**, *114*, 2447–2450



Do electrons prefer to visit planes or spheres? Reorganization energies for intramolecular electron transfer involving a 3D acceptor (C_{60}) and a 2D acceptor (Nlm; see scheme) have been determined. Comparison of reorganization energies for the intra- versus intermolecular electron transfer has provided, for the first time, valuable insight into the intrinsic reorganization energies relating to different molecular shapes.



Angew. Chem. **2002**, *114*, 2450–2453

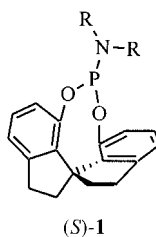
H. Imahori,* H. Yamada, D. M. Guldi,*
Y. Endo, A. Shimomura, S. Kundu,
K. Yamada, T. Okada,* Y. Sakata,
S. Fukuzumi* 2344–2347

Comparison of Reorganization Energies
for Intra- and Intermolecular Electron
Transfer

Keywords: donor–acceptor systems •
electron transfer • fullerenes •
photosynthesis • porphyrinoids



Monodentate phosphorus ligands, too, can be effective: Chiral amine derivatives can be obtained in high enantioselectivities (up to 99.7% *ee*) by the asymmetric hydrogenation of enamides in the presence of rhodium complexes of the chiral spiro phosphorus ligands (*S*)-**1**, the first monodentate P ligands that are effective in this class of reactions.



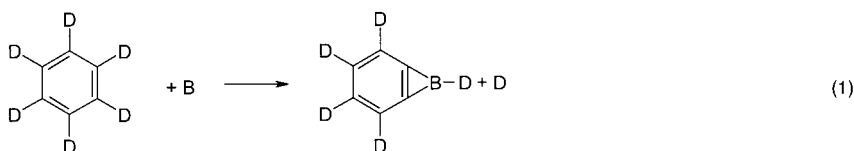
Angew. Chem. **2002**, *114*, 2454–2456

A.-G. Hu, Y. Fu, J.-H. Xie, H. Zhou,
L.-X. Wang, Q.-L. Zhou* ... 2348–2350

Monodentate Chiral Spiro
Phosphoramidites: Efficient Ligands for
Rhodium-Catalyzed Enantioselective
Hydrogenation of Enamides

Keywords: asymmetric catalysis •
homogeneous catalysis • hydrogenation •
P ligands • spiro compounds

A versatile atomic boron versus hydrogen exchange led to the formation of perdeuterated benzoborirene in the gas phase according to Equation (1). It might well be that this concept could also be adapted to form more complex heteroaromatic boron-bearing molecules in the gas phase.



Angew. Chem. **2002**, *114*, 2456–2458

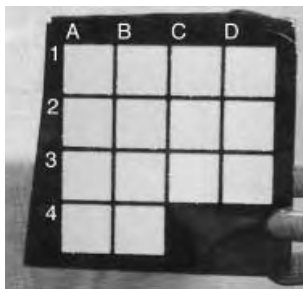
R. I. Kaiser,*
H. F. Bettinger* 2350–2352

Gas-Phase Detection of the Elusive
Benzoborirene Molecule

Keywords: ab initio calculations •
aromaticity • benzene • boron • mass
spectrometry



Scribing in the presence of reactive species enables silicon to be chemomechanically patterned and simultaneously functionalized with monolayers. Arrays of patches of monolayers are created by scribing different regions of silicon in the presence of different reagents, as shown for the homologous series of 1-alkenes from 1-pentene (A1) to 1-octadecene (B4).



Angew. Chem. **2002**, *114*, 2459–2462

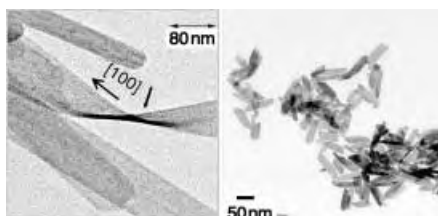
T. L. Niederhauser, Y.-Y. Lua, G. Jiang,
S. D. Davis, R. Matheson, D. A. Hess,
I. A. Mowat, M. R. Linford* 2353–2356

Arrays of Chemomechanically Patterned
Patches of Homogeneous and Mixed
Monolayers of 1-Alkenes and Alcohols on
Single Silicon Surfaces

Keywords: alcohols • alkenes •
monolayers • silicon • surface chemistry



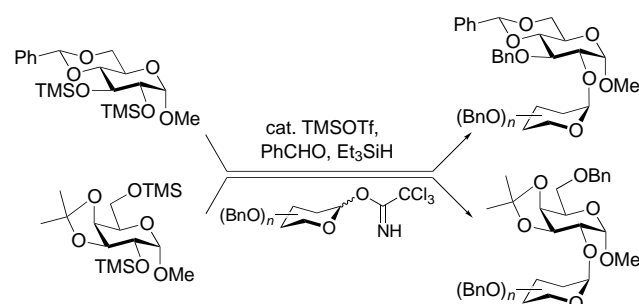
With double jets to nanobelts: Well-defined very thin CdWO_4 nanorods/nanobelts can be easily synthesized by double-jet crystallization in aqueous solution at room temperature in the absence of a polymeric crystallization modifier (see picture, left). Further hydrothermal ripening leads to the self-assembly of the nanorods/nanobelts into raftlike bundles, whereas very thin 2D sheetlike nanocrystals (see picture, right) and 1D nanorods with diameter 2.5 nm are obtained in the presence of double-hydrophilic block copolymers. Both the 1D and 2D polymer-modified species show highly increased fluorescence efficiency.



Angew. Chem. **2002**, *114*, 2462–2466



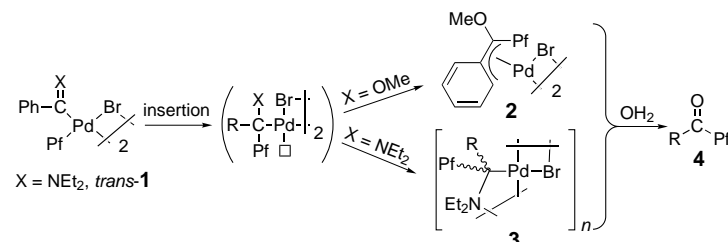
A highly regioselective benzyl and allyl protection of D-hexopyranosides allows their application in the synthesis of biologically potent $\alpha 1 \rightarrow 2$ linked disaccharide derivatives by means of a regioselective one-pot protection–glycosylation (see scheme).



Angew. Chem. **2002**, *114*, 2466–2468

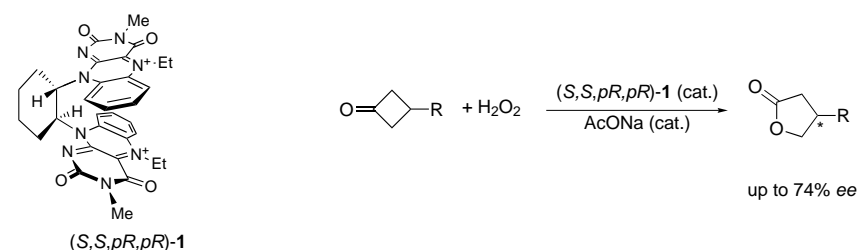


The interaction of an electrophilic carbene carbon atom with the π -electron density of an aryl group favors an intramolecular migratory insertion reaction (see scheme; $\text{Pf} = \text{C}_6\text{F}_5$). This reaction gives alkyl compounds (**2** or **3**) which can be identified prior to their eventual hydrolysis to **4**.



Angew. Chem. **2002**, *114*, 2469–2472

The chiral organocatalyst bisflavin **1** catalyzes the asymmetric Baeyer–Villiger reaction of cyclobutanones with H_2O_2 (see scheme). The corresponding lactones are obtained with up to 74% *ee*.



Angew. Chem. **2002**, *114*, 2472–2474

S.-H. Yu,* M. Antonietti, H. Cölfen,
M. Giersig 2356–2359

Synthesis of Very Thin 1D and 2D CdWO_4
Nanoparticles with Improved
Fluorescence Behavior by Polymer-
Controlled Crystallization

Keywords: block copolymers • crystal
growth • fluorescence •
morphosynthesis • nanoparticles • self-
assembly

C.-C. Wang, J.-C. Lee, S.-Y. Luo,
H.-F. Fan, C.-L. Pai, W.-C. Yang, L.-D. Lu,
S.-C. Hung* 2360–2362

Synthesis of Biologically Potent
 $\alpha 1 \rightarrow 2$ -Linked Disaccharide Derivatives
via Regioselective One-Pot Protection–
Glycosylation

Keywords: carbohydrates • glycosides •
glycosylations • oligosaccharides •
protecting groups

A. C. Albéniz,* P. Espinet,* R. Manrique,
A. Pérez-Mateo 2363–2366

Observation of the Direct Products of
Migratory Insertion in Aryl Palladium
Carbene Complexes and Their
Subsequent Hydrolysis

Keywords: carbenes • hydrolysis •
insertion • palladium • transmetalation

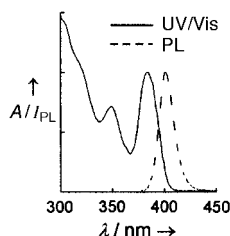
S.-I. Murahashi,* S. Ono,
Y. Imada* 2366–2368

Asymmetric Baeyer–Villiger Reaction
with Hydrogen Peroxide Catalyzed by a
Novel Planar-Chiral Bisflavin

Keywords: asymmetric catalysis •
biomimetic synthesis •
enantioselectivity • lactones • oxidation



Controllable reactivity of Cd precursors in the growth of CdS nanocrystals was achieved by varying the concentration of stabilizing ligand with a noncoordinating solvent. Such tunable reactivity is critical for developing the synthesis of semiconductor nanocrystals to the level of that of CdSe nanocrystals. The high quality of the CdS nanocrystals is indicated by the sharpness of the UV/Vis and photoluminescence spectra (see diagram, A = absorbance, I_{PL} = photoluminescence intensity).



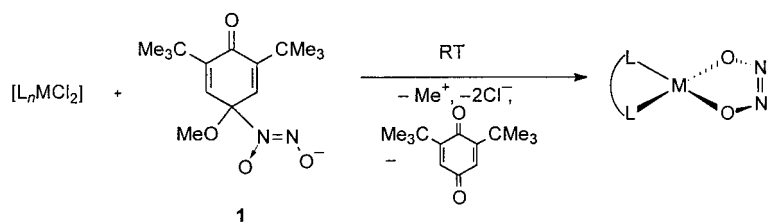
W. W. Yu, X. Peng* 2368–2371

Formation of High-Quality CdS and Other II–VI Semiconductor Nanocrystals in Noncoordinating Solvents: Tunable Reactivity of Monomers

Keywords: cadmium • nanostructures • semiconductors • solvent effects • sulfur

Angew. Chem. **2002**, *114*, 2474–2477

Ligand formed by C–N bond cleavage: Transition-metal-promoted heterolytic cleavage of the C–N bond in **1** results in the formation of five new complexes of *cis* hyponitrite with Group 10 transition metals. The new complexes include $[\text{Ni}(\eta^2\text{-O}_2\text{N}_2)(\text{dppf})]$ (dppf = 1,1'-bis(diphenylphosphanyl)ferrocene) which is structurally characterized and the thermal decomposition of which follows unimolecular kinetics.



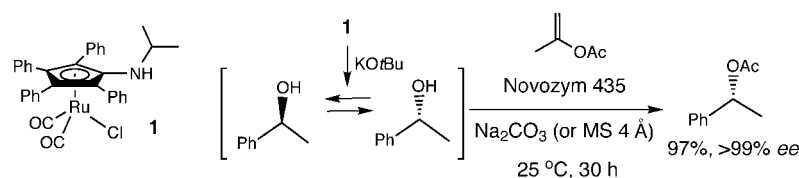
Angew. Chem. **2002**, *114*, 2477–2479

N. Arulsamy, D. S. Bohle,* J. A. Imonigie, S. Levine 2371–2373

An Umpolung Approach to *cis*-Hyponitrite Complexes

Keywords: nickel • nitrogen oxides • O ligands • P ligands • umpolung

Ruthenium–enzyme tandem catalysis: The novel racemization catalyst **1** improves the dynamic kinetic resolution (DKR) of secondary alcohols dramatically. The DKR proceeds at room temperature with isopropenyl acetate as an acyl donor. In addition, the DKR is faster even with much less lipase than in previous DKRs.



Angew. Chem. **2002**, *114*, 2479–2482

J. H. Choi, Y. H. Kim, S. H. Nam, S. T. Shin, M.-J. Kim,* J. Park* 2373–2376

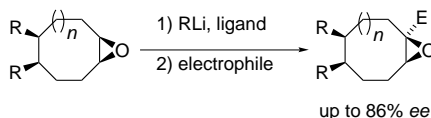
Aminocyclopentadienyl Ruthenium Chloride: Catalytic Racemization and Dynamic Kinetic Resolution of Alcohols at Ambient Temperature

Keywords: asymmetric synthesis • homogeneous catalysis • kinetic resolution • lipases • ruthenium



Simple *meso*-epoxides can be asymmetrically functionalized:

Ligand-assisted direct hydrogen–lithium exchange allows the generation of destabilized oxiranyl lithium species and their subsequent trapping by a wide array of electrophiles (see scheme; E = group formed by addition of electrophile). When carried out in the presence of (–)-sparteine as ligand, this reaction provides a new enantioselective route to epoxides.



D. M. Hodgson,* E. Gras ... 2376–2378

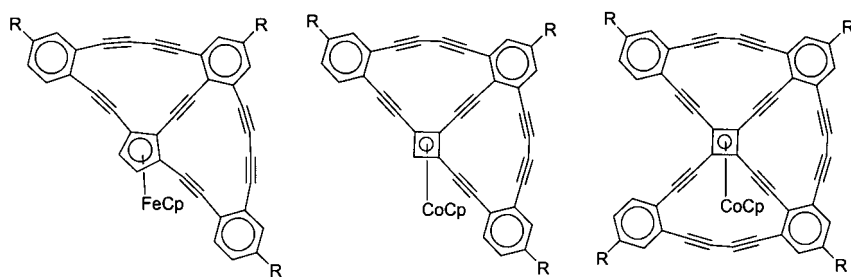
Chiral Epoxides by Desymmetrizing Deprotonation of *meso*-Epoxides

Keywords: asymmetric synthesis • carbanions • epoxides • lithiation

Angew. Chem. **2002**, *114*, 2482–2484



A combination of Pd- and Cu-catalyzed couplings make the half-wheels (see left and middle picture; Cp = C₅H₅) and the seco-wheel (right) shown here accessible. Single-crystal structures of all three target molecules have been obtained.



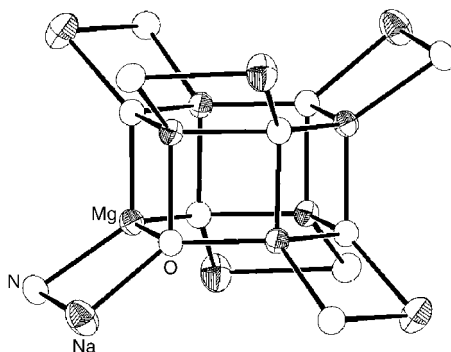
Angew. Chem. **2002**, *114*, 2484–2488

M. Laskoski, W. Steffen, J. G. M. Morton,
M. D. Smith, U. H. F. Bunz* 2378–2382

Synthesis and Structural Characterization
of Organometallic Cyclynes: Novel
Nanoscale, Carbon-Rich Topologies

Keywords: alkynes • copper •
cyclobutadiene complexes •
homogeneous catalysis • palladium

Introducing THF to synergic sodium–magnesium amide mixtures (3 tmpH:1 *n*BuNa:1 Bu₂Mg in a hydrocarbon solution; tmpH = 2,2,6,6-tetramethylpiperidine) has a surprising outcome: it leads to the cleavage of the ether and the formation of S₆-symmetric molecules with (Mg₆O₆·(NaN)₆) cores (see picture).



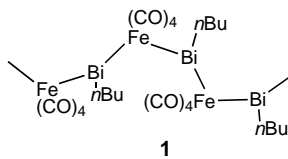
Angew. Chem. **2002**, *114*, 2488–2490

A. M. Drummond, L. T. Gibson,
A. R. Kennedy, R. E. Mulvey,*
C. T. O'Hara, R. B. Rowlings,
T. Weightman 2382–2384

Hexameric Mg–O Stacks with Six THF-
Solvated Sodium Amide Appendages:
“Super” Variants of Inverse Crown Ethers
Generated by Cleavage of THF

Keywords: alkali metals • alkaline-earth
metals • amides • cleavage reactions •
crown compounds

A unique zigzag ...-Bi-Fe-... chain forms the basis of the structure of [*n*BuBiFe(CO)₄]_∞ (**1**; see picture), which was characterized by single-crystal X-ray diffraction. Compound **1** was isolated from the ultrasonication of the dimeric product [{*n*BuBiFe(CO)₄]₂] from the reaction of [Et₄N]₃[Bi{Fe(CO)₄]₄] with *n*BuBr followed by acidification with HOAc.



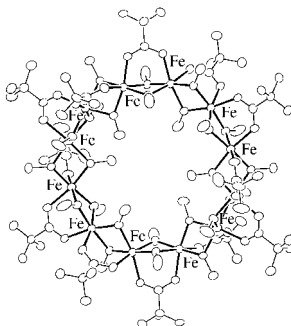
Angew. Chem. **2002**, *114*, 2490–2492

M. Shieh,* Y. Liou, M.-H. Hsu,
R.-T. Chen, S.-J. Yeh, S.-M. Peng,
G.-H. Lee 2384–2386

A Unique Bismuth–Iron Chain Polymer
Containing the ...-Bi-Fe-... Link:
Formation and Structure of
[*n*BuBiFe(CO)₄]_∞

Keywords: bismuth • carbonyl ligands •
iron • metal–metal interactions •
polymers

New wheels: The 1:2 reaction of ferric nitrate with benzoic acid (Ph₂C(OH)COOH) in methanol at pH ≈ 4.0 results in the formation of a new member of the molecular ferric-wheels family with the carboxylatobis(alkoxo) bridging unit. The molecular structure of [{Fe(OMe)₂(Ph₂C(OH)COO)}]₁₂ (see picture) consists of a centrosymmetric ring of 12 Fe^{III} atoms held together by 24 μ₂-methoxide ligands and 12 1,3-bridging carboxylate ligands. The 12 metal ions are nearly coplanar and the ring size is ≈ 11.4 Å. The Mössbauer spectrum and magnetic susceptibility measurements are presented.



Angew. Chem. **2002**, *114*, 2492–2495

C. P. Raptopoulou,* V. Tangoulis,
E. Devlin 2386–2389

[{Fe(OMe)₂(O₂CC(OH)Ph₂)}]₁₂:
Synthesis and Characterization of a New
Member in the Family of Molecular Ferric
Wheels with the Carboxylatobis(alkoxo)
Bridging Unit

Keywords: cluster compounds • ferric
wheels • iron • magnetic properties •
O ligands



An unprecedented yellow polymer

with low-coordinate phosphorus atoms in the backbone has been prepared. The material is soluble in polar organic solvents, and moderate molecular weights ($M_n = 2900 - 10\,500 \text{ g mol}^{-1}$) were estimated from ^{31}P NMR spectroscopic end-group analysis. The possible π -conjugation was investigated by UV/Vis spectroscopy, which revealed a red shift in λ_{max} for the polymer when compared with colorless molecular-model systems (see picture; left: model system, right: new polymer, in THF).



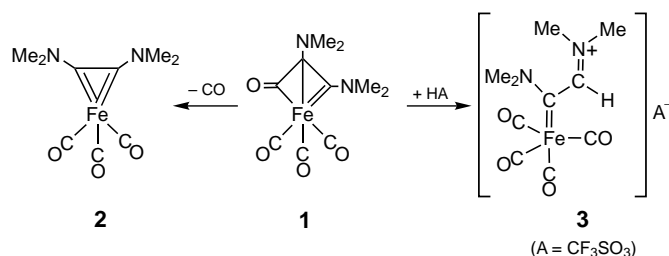
Angew. Chem. **2002**, *114*, 2495–2498

V. A. Wright, D. P. Gates* 2389–2392

Poly(*p*-phenylenephosphaalkene):
A π -Conjugated Macromolecule
Containing P=C Bonds in the Main Chain

Keywords: conjugation •
phosphaalkenes • phosphorus •
polymers • silicon

Intermediate isolated? The reaction of $[\text{Fe}(\text{CO})_5]$ with $\text{Me}_2\text{N}-\text{C}\equiv\text{C}-\text{NMe}_2$ follows an unprecedented associative pathway to give the ferrabicyclobutenone **1**. Complexes such as **1** could be key intermediates in the iron-mediated cyclization of alkynes to cyclopentadienones. Compound **1** undergoes a variety of C–C coupling and C–C-bond-cleavage reactions to afford a multitude of new organoiron compounds including **2** and **3**.



Angew. Chem. **2002**, *114*, 2499–2502

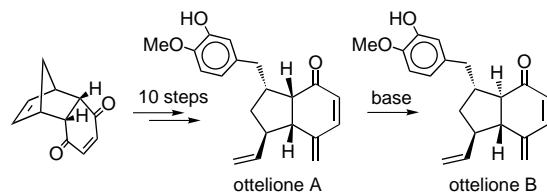
A. C. Filippou,*
T. Rosenauer 2393–2396

A Reaction Pathway of $[\text{Fe}(\text{CO})_5]$ with
Alkynes via Ferrabicyclobutenones

Keywords: alkyne ligands • carbene
ligands • C–C coupling • iron •
metallacycles



The biologically potent antitubercular and anticancer otteliones A and B (see scheme) have been synthesized from readily available starting materials by using a short, simple, efficient, and flexible strategy. The structural ambiguity of the natural products has been resolved.



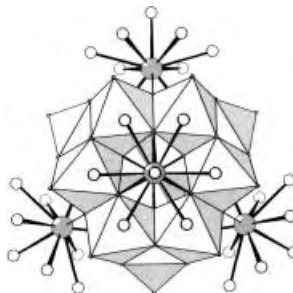
Angew. Chem. **2002**, *114*, 2502–2504

G. Mehta,* K. Islam 2396–2398

Total Synthesis of (\pm)-Otteliones A and B

Keywords: antitumor agents •
configuration determination • natural
products • total synthesis

Six Mo dimers arranged around a central PO_4 tetrahedron form the core of the novel ϵ -Keggin polyoxocation $[\epsilon\text{-PMo}_{12}\text{O}_{36}(\text{OH})_4\{\text{La}(\text{H}_2\text{O})_4\}_4]^{5+}$ (see structure) capped with four $\{\text{La}(\text{H}_2\text{O})_4\}^{3+}$ units. A ^{31}P NMR spectroscopy study shows that the ϵ -Keggin ion is unstable in aqueous solution, and leads to the formation of a polyanion/polycation salt, which is crystallographically characterized.



Angew. Chem. **2002**, *114*, 2504–2507

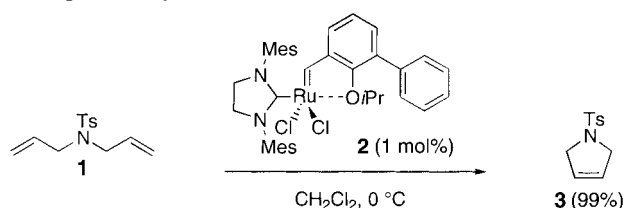
P. Mialane, A. Dolbecq, L. Lisnard,
A. Mallard, J. Marrot,
F. Sécheresse* 2398–2401

$[\epsilon\text{-PMo}_{12}\text{O}_{36}(\text{OH})_4\{\text{La}(\text{H}_2\text{O})_4\}_4]^{5+}$: The
First $\epsilon\text{-PMo}_{12}\text{O}_{40}$ Keggin Ion and Its
Association with the Two-Electron-
Reduced $\alpha\text{-PMo}_{12}\text{O}_{40}$ Isomer

Keywords: Keggin ions • lanthanum •
molybdenum • polyoxometalates • solid-
state structures



Olefin metathesis even at 0 °C! A phenyl substituent in the ruthenium catalyst **2** leads to greatly increased initiation rates in different metathesis reactions, for example, the cyclization of **1** to form **3**.



Angew. Chem. **2002**, *114*, 2509–2511

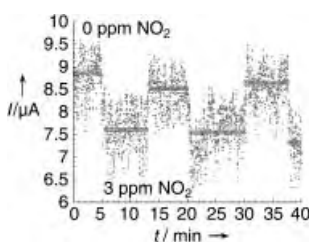
H. Wakamatsu, S. Blechert* 2403–2405

A New Highly Efficient Ruthenium Metathesis Catalyst

Keywords: homogeneous catalysis • metathesis • olefins • ruthenium



Good candidates for miniaturized, ultrasensitive gas sensors in many applications are individual single-crystalline SnO₂ nanoribbons. Here it is shown that they can be used to detect ppm-level concentrations of NO₂ at room temperature under UV illumination. The picture illustrates that they work reliably even near their resolution limit under 365-nm light.



Angew. Chem. **2002**, *114*, 2511–2514

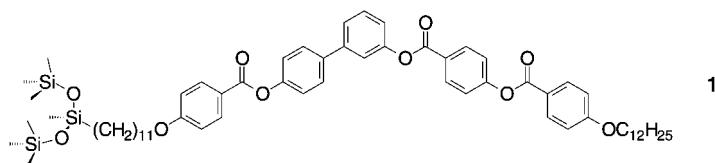
M. Law, H. Kind, B. Messer, F. Kim, P. Yang* 2405–2408

Photochemical Sensing of NO₂ with SnO₂ Nanoribbon Nanosensors at Room Temperature

Keywords: nanoribbons • nanostructures • nanowires • nitrogen dioxide • sensors



In conventional fluids the molecular dipole moments of the individual molecules cancel out, which leads to a macroscopic apolar structure. Directed molecular design using microsegregation and tailoring the molecular shape of compounds such as **1**, can lead to fluid layer structures with a macroscopic polar order.



Angew. Chem. **2002**, *114*, 2514–2518

G. Dantlgraber, A. Eremin, S. Diele, A. Hauser, H. Kresse, G. Pelzl, C. Tschierske* 2408–2412

Chirality and Macroscopic Polar Order in a Ferroelectric Smectic Liquid-Crystalline Phase Formed by Achiral Polyphilic Bent-Core Molecules

Keywords: chirality • ferroelectricity • liquid crystals • mesophases • microsegregation • siloxanes



Supporting information on the WWW (see article for access details).

* Author to whom correspondence should be addressed



Accelerated publications



BOOKS

Coffee Flavor Chemistry	Ivon Flament	<i>U. H. Engelhardt</i>	2413
Structure and Bonding in Crystalline Materials	Gregory S. Rohrer	<i>P. Kroll</i>	2413
Glycochemistry	Peng G. Wang, Carolyn R. Bertozzi	<i>T. Ziegler</i>	2414
Computational Methods in Physics, Chemistry and Biology	Paul Harrison	<i>W. Koch</i>	2416
Handbook of Modern Pharmaceutical Analysis	Satinder Ahuja, Stephen Scypinski	<i>P. Surmann</i>	2416
Object-Oriented Magnetic Resonance	Michael Mehring, Volker A. Weberruß	<i>B. Reif</i>	2417



WEB SITES

http://www.pbglinks.com	Linking Photonic Band Gaps	<i>S. Yang</i>	2419
---	-------------------------------	----------------------	------

SERVICE

• VIPs	2213	• Keywords	2420
• <i>Angewandte's</i> Sister-Journals	2229–2231	• Authors	2421
• Vacancies	A59	• Preview	2422
• Sources	A57		

Don't forget all the Tables of Contents
from 1998 onwards may be still found
on the WWW under:
<http://www.angewandte.org>

Issue 12, 2002 was published online on June 13.

APOLOGY

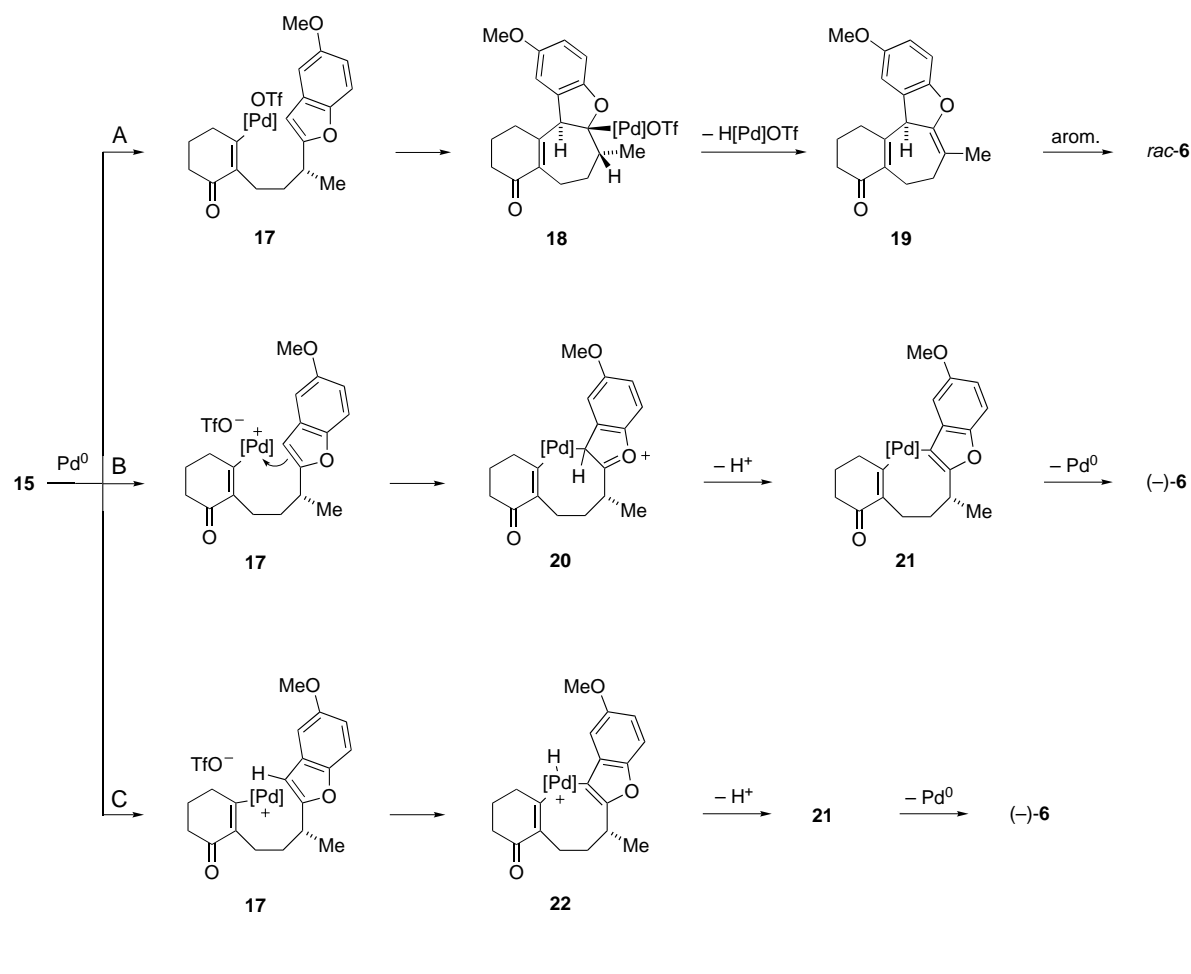
In the Communication “Strongly Acidic and High-Temperature Hydrothermally Stable Mesoporous Aluminosilicates with Ordered Hexagonal Structure” (Z. Zhang, Y. Han, L. Zhu, R. Wang, Y. Yu, S. Qiu, D. Zhao, F.-S. Xiao, *Angew. Chem. Int. Ed.* **2001**, *40*, 1258–1362) the thematically related manuscript “Mesoporous Aluminosilicates with Ordered Hexagonal Structure, Strong Acidity, and Extraordinary Hydrothermal Stability at High Temperatures” (Z. Zhang, Y. Han, F.-S. Xiao, S. Qiu, L. Zhu, R. Wang, Y. Yu, Z. Zhang, B. Zou, Y. Wang, H. Sun, D. Zhao, Y. Wei, *J. Am. Chem. Soc.* **2001**, *123*, 5014–5021) was not cited (and vice versa), although both manuscripts were submitted to the respective journals at the same time. The authors apologize for this mistake.

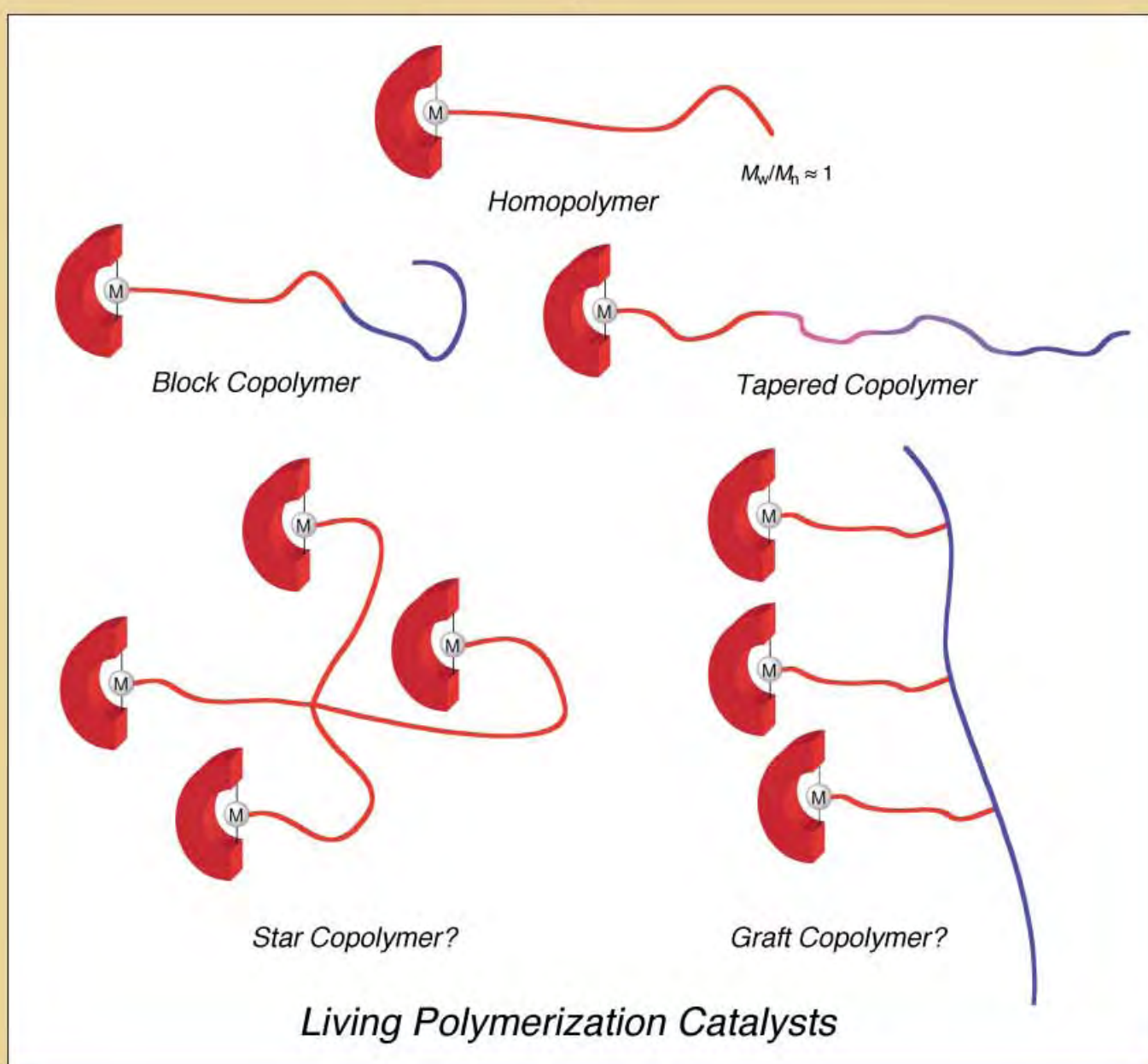
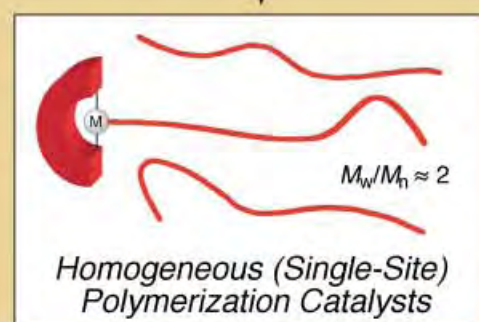
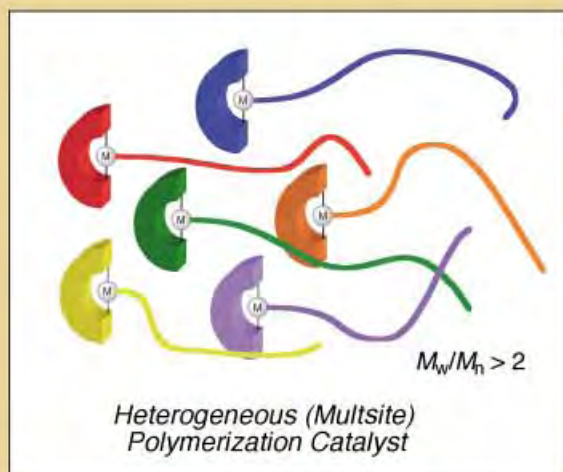
In the Minireview by **P. Cintas** in issue 7, **2002**, pp. 1139–1145, the second paragraph on the right column of page 1142 may mislead some readers, as it suggests that heterochiral peptides are unable to form a helical arrangement. In fact, previous publications (see last paragraph and ref. 52 in ref. [1]) have shown that D,L peptides are capable of forming helical structures, and this fact may be of importance for understanding the development of homochirality starting from heterochiral sequences. The chiral amplification that results from the majority rule (see ref. 40 in ref. [1]) may be large enough for a small excess of majority units to initiate the epimerization of the minority units (L) to the configuration of the majority units (D). Overall, this process, after repetitive cycles, would lead to a preferential helical sense in which the predominant chirality (D) of the units that form the polypeptides is prevalent.^[1,2] This commentary should clarify the discussion of this point in the light of past and recent literature.

[1] M. M. Green, J.-W. Park, T. Sato, A. Teramoto, S. Lifson, R. L. B. Selinger, J. V. Selinger, *Angew. Chem.* **1999**, *111*, 3329–3345; *Angew. Chem. Int. Ed.* **1999**, *38*, 3138–3154.

[2] M. M. Green, J. V. Selinger, *Science* **1998**, *282*, 879.

In the Communication by C. C. Hughes and D. Trauner in Issue 9, **2002**, pp. 1569–1572, the structures of frondosin A and frondosin B were inadvertently exchanged in Scheme 1. The numbering in Scheme 4 was also incorrect: the corrected Scheme is shown below. The editors apologize for these errors.





Catalysts for the Living Insertion Polymerization of Alkenes: Access to New Polyolefin Architectures Using Ziegler–Natta Chemistry

Geoffrey W. Coates,* Phillip D. Hustad, and Stefan Reinartz

Dedicated to Professor Maurice Brookhart and Professor Robert H. Grubbs on the occasion of their 60th birthdays

Coordination–insertion polymerization systems have long been superior to their anionic, cationic, and radical polymerization counterparts with regard to stereochemical control. However, until five years ago, these metal-based insertion methods were inferior to ionic and radical mechanisms in the category of living polymerization, which is simply a polymerization that occurs with rapid initiation and negligible chain termination or transfer. In the last half decade, the living insertion

polymerization of unactivated olefins has emerged as a powerful tool for the synthesis of new polymer architectures. Materials available today by this route range from simple homopolymers such as linear and branched polyethylene, to atactic or tactic poly(α -olefins), to end-functionalized polymers and block copolymers. This review article summarizes recent developments in this rapidly growing research area at the interface of synthetic and mechanistic organometallic chemistry, polymer

chemistry, and materials science. While special emphasis is placed on polymer properties and novel polymeric architectures, most of which were inaccessible just a decade ago, important achievements with respect to ligand and catalyst design are also highlighted.

Keywords: alkenes • block copolymers • homogeneous catalysis • living polymerization • Ziegler–Natta catalysis

1. Introduction

Polymeric materials are currently more indispensable to modern society than at any other point in history. The potential applications of a polymer are determined by its physical and mechanical properties, which in turn are defined by the morphology (solid-state arrangement) of the polymer. Polymer morphology largely depends on the composition and architecture of the polymer. Therefore, the development of synthetic methods for the polymerization of a wide range of monomers with control over the stereochemistry and molecular weight of the resultant polymers is a long-standing scientific challenge. A primary goal of synthetic polymer chemistry that has existed for the last half century is the development of chain-growth polymerization methods that enable consecutive enchainment of monomer units without termination. Such techniques, now known as living polymerizations,^[1] allow both precise molecular weight control as well

as the synthesis of a wide array of polymer architectures.^[2] For example, the initiation of multiple polymer chains from a central core results in the formation of a star-branched polymer, while the consecutive addition of two monomers to a single initiator produces a diblock copolymer.^[3] Living methods also allow the synthesis of end-functional polymers if special initiation and/or quenching methods are employed. Of course, living polymerizations have the liability that each catalyst only forms one chain, in contrast to common alkene polymerization catalysts that can produce thousands of chains each as a result of periodic chain transfer or termination events. (Note: in this review, we refer to living species for alkene polymerization as “catalysts”, not “initiators”, to emphasize the fundamental catalytic event of monomer enchainment, not polymer chain formation.) The real value of living polymerization methods is that they allow the creation of virtually limitless types of new materials from a basic set of available monomers.

Based on annual production volume, polyolefins are by far the most important commercial class of synthetic polymers. Since the initial discoveries of Ziegler^[4] and Natta,^[5] remarkable advances have been reported concerning the control of comonomer incorporation as well as dramatic improvements in activity. Homogeneous olefin polymerization catalysts now exist that are unparalleled in all of polymer chemistry

[*] Prof. Dr. G. W. Coates, P. D. Hustad, Dr. S. Reinartz
Department of Chemistry and Chemical Biology
Baker Laboratory, Cornell University
Ithaca, New York 14853-1301 (USA)
Fax: (+1) 607-255-4137
E-mail: gc39@cornell.edu

concerning the detailed control of macromolecular stereochemistry.^[6] However, olefin insertion catalysts have always been inferior to their other chain-growth counterparts in one respect. While extraordinary advances in living/controlled polymerization have been discovered by using anionic,^[7] cationic,^[8] and radical-based^[9–11] polymerization, until very recently there existed a comparative lack of living olefin polymerization systems. A significant number of advances have been reported in the last half decade, prompting us to review the area of catalysts for alkene polymerization that proceed without appreciable chain transfer or termination. In this review, we only address the living polymerization of unactivated alkenes by insertion methods; ring-opening metathesis polymerization (ROMP), the polymerization of conjugated dienes and acrylates, group transfer polymerization, and CO/alkene copolymerization will not be addressed.

The seven generally accepted criteria for a living polymerization are:

- 1) polymerization proceeds to complete monomer conversion, and chain growth continues upon further monomer addition;
- 2) number average molecular weight (M_n) of the polymer increases linearly as a function of conversion;^[12]
- 3) the number of active centers remains constant for the duration of the polymerization;
- 4) molecular weight can be precisely controlled through stoichiometry;
- 5) polymers display narrow molecular weight distributions, described quantitatively by the ratio of the weight average molecular weight to the number average molecular weight ($M_w/M_n \sim 1$);
- 6) block copolymers can be prepared by sequential monomer addition;
- 7) end-functionalized polymers can be synthesized.^[13]

Few polymerization systems, whether ionic-, radical-, or metal-mediated, that are claimed to proceed by a living mechanism have been shown to meet all of these criteria. This review will therefore include all systems that claim living olefin polymerization, providing that a substantial number of the key criteria have been met.

Common features of alkene polymerization catalyst systems are chain transfer and elimination reactions that terminate the growth of a polymer chain and result in the initiation of a new polymer chain by the catalyst (Scheme 1). For example, in metallocene catalysts, consecutive alkene insertion into the metal–carbon bond connecting the catalyst and polymer chain^[14] proceeds until β -hydrogen and/or β -alkyl elimination occurs.^[15] When alkylaluminum cocatalysts are employed, an additional termination route is chain transfer to the aluminum center.^[15] In many systems, the lifetime of chain formation is on the order of seconds, rendering sequential monomer addition methods for block copolymer synthesis futile. Several strategies have been devised to decrease the rate of chain termination relative to that of propagation such that living systems can be formed. The first consideration in many cases is simply lowering the polymerization temperature of an ordinary non-living catalyst system to achieve living or at least controlled

Geoffrey W. Coates, born in Evansville, Indiana in 1966, obtained a B.A. degree in chemistry from Wabash College in 1989 and a Ph.D. in organic chemistry from Stanford University in 1994. In his thesis work, under the direction of Robert M. Waymouth, he investigated the stereoselectivity of metallocene Ziegler–Natta catalysts. Following his doctoral studies, he was an NSF Postdoctoral Fellow with Robert H. Grubbs at the California Institute of Technology. During the summer of 1997, he joined the Department of Chemistry at Cornell University where he is currently Professor of Chemistry. His main research interests are the design, synthesis, characterization, and applications of polymers with an emphasis on catalytic transformations and the control of stereochemistry.



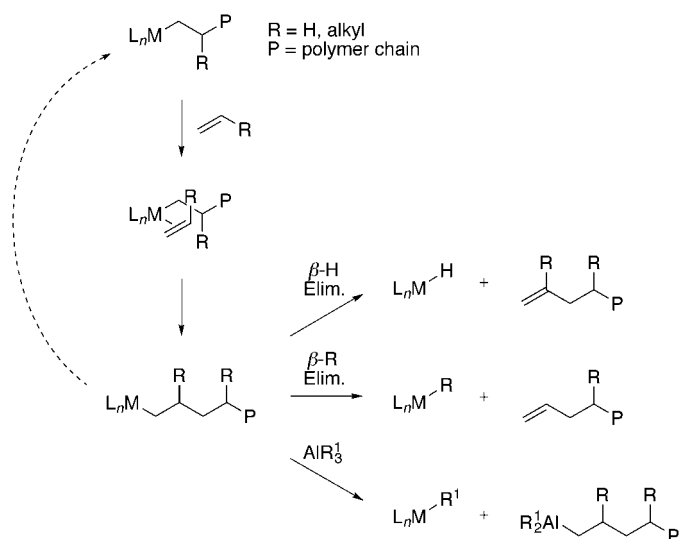
P. D. Hustad

G. W. Coates

S. Reinartz

Phillip D. Hustad, born in Bristol, Tennessee in 1975, obtained a B.S. degree in Chemistry in 1997 from Emory & Henry College in Emory, Virginia. Inspired by undergraduate research with Prof. Koji Nakanishi at Columbia University, he then entered the Ph.D. program in Chemistry at Cornell University. He is currently working under the guidance of Geoffrey W. Coates on the development and applications of new catalysts for living olefin polymerization.

Stefan Reinartz, born in Hilden, Germany in 1972, studied chemistry at Heinrich-Heine-Universität Düsseldorf, Université de Nantes (France), and the University of North Carolina at Chapel Hill (UNC). After obtaining his Diplom in 1998, he returned to UNC, where he earned his Ph.D. in inorganic chemistry in 2001. His dissertation under the direction of Joseph L. Templeton and Maurice Brookhart focused on organometallic platinum chemistry relevant to bond activation processes. He is currently a DAAD Postdoctoral Fellow with Geoffrey W. Coates at Cornell University.



Scheme 1. Mechanisms of propagation and chain transfer in Ziegler-Natta catalyzed olefin polymerization.

behavior. Since β -hydrogen and alkyl elimination processes are unimolecular while propagation is bimolecular, a lowering in temperature more adversely affects elimination processes relative to enchainment. Since precipitation of polymers from solution at low temperatures can hinder the controlled nature of a living polymerization, it is generally advantageous to perform reactions at ambient temperature. Therefore, a second strategy for discovering living systems is to design new catalysts through empirical modification and/or computational methods.^[16] By creating species that are incapable of common termination reactions at room temperature, living catalysts have been devised. A final consideration is to eliminate the use of alkyl aluminum cocatalysts that give the potential for chain-transfer reactions. In this regard, the development of weakly coordinating anions has made significant advances in living olefin polymerization possible.^[17]

2. Vanadium Catalysts for Living Olefin Polymerization

Olefin polymerization emerged in the 1950s as a principal area of organometallic research when Ziegler and Natta and co-workers discovered that titanium chloride in the presence of alkylaluminum compounds was an efficient catalyst for polymerization of ethylene and propylene.^[4, 5] Following this breakthrough, vanadium compounds in combination with alkylaluminum compounds were shown to be active catalysts for the polymerization of olefins. Through modification of ligands and activators, vanadium catalysts were also found to polymerize olefins in a living fashion at low temperatures. The utility of these living systems has been demonstrated through the synthesis of a wide variety of end-functionalized polypropylenes (PPs) and PP-containing block copolymers. However, polymerizations with these systems are limited to temperatures at or below -40°C , and living behavior is restricted to only a few monomers.

2.1. Propylene Polymerization with Vanadium Compounds

In the 1960s, Natta and co-workers discovered that vanadium tetrachloride activated with diethylaluminum chloride produced syndio-enriched polypropylenes at -78°C .^[18] The rate of polymerization was constant for long reaction times (ca. 50 h), and molecular weight increase with time was nearly linear over 25 h. The $[\text{Al}]/[\text{V}]$ ratio had a dramatic effect on the lifetime of active chains; an increase in cocatalyst concentration was mirrored by a decrease in lifetime, implicating chain transfer to aluminum centers as a source of termination. The syndiospecificity of this catalyst was found to be the result of regioselective secondary (2,1) insertion of propylene.^[19] Anisole was also found to have a dramatic effect on both catalytic activity and the average lifetime of active chains.^[20] In later studies, polypropylenes from this catalytic system were found to be unimodal with narrow molecular weight distributions ($M_w/M_n = 1.4 - 1.9$).^[21]

Although this catalytic system produced polypropylenes that were nearly living, the first true example of living olefin polymerization did not appear until over a decade later. In 1979, Doi et al. reported the first catalytic olefin polymerization system to satisfy all the requirements for a living polymerization. The catalyst, $[\text{V}(\text{acac})_3]$ (**1a**; Figure 1; acac = acetylacetonate) activated with Et_2AlCl , produced partially

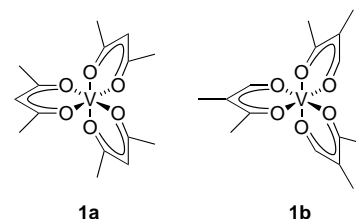
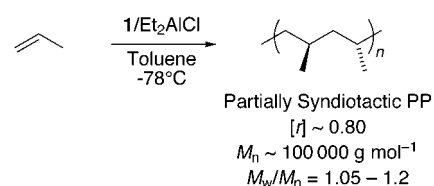


Figure 1. Vanadium catalyst precursors for living olefin polymerization.

syndiotactic polypropylenes (81 % *r* dyads; $[r] = 0.81$)^[15] at -78°C with extremely narrow molecular weight distributions ($M_w/M_n = 1.05 - 1.20$; Scheme 2).^[22, 23] Molecular weight increased linearly with time to values as high as $100\,000\text{ g mol}^{-1}$, and the number of polymer chains remained constant during the course of the reaction. However, the catalyst exhibited living behavior only at temperatures below -65°C ; reactions at temperatures as low as -48°C resulted in polypropylenes with broadened molecular weight distributions ($M_w/M_n = 1.37 - 1.45$). Also, catalytic activity (ca. $4\text{ kg}_{\text{PP}}\text{ mol V}^{-1}\text{ h}^{-1}$) suffered from the fact that only about 4 % of the vanadium centers were active. The nature of the aluminum cocatalyst also had a dramatic effect on polymerization activity, living

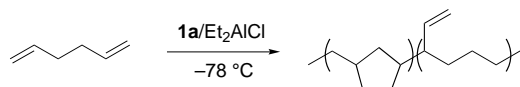


Scheme 2. Living polymerization of propylene with vanadium catalysts.

behavior, and stereoselectivity, suggesting a bimetallic active species. Particularly, use of the more electron-deficient cocatalyst EtAlCl_2 led to an increase in chain transfer to monomer, giving polymers with distributions approaching the theoretical value for polymerizations involving chain transfer ($M_w/M_n = 2.0$).^[23, 24] The activating effect of anisole was also demonstrated for the **1a**/ Et_2AlCl catalyst system.^[25] The additive led to a threefold increase in the number of active vanadium centers without adversely affecting livingness or syndiospecificity.

To address the problem of activation, Doi and co-workers studied a variety of vanadium complexes and found that subtle ligand modifications had dramatic effects on catalytic behavior.^[26–28] Through these studies, complex **1b** was found to be highly active (relative to **1a**) for the living polymerization of propylene (ca. $100 \text{ kg}_{\text{PP}} \text{ mol}_V^{-1} \text{ h}^{-1}$; Scheme 2). The increase in activity was attributed to a greater number of active vanadium centers in the reaction; the number of polymer chains per metal center approached unity for this catalytic system. Again, the polypropylene was partially syndiotactic ($[r] = 0.80$), consistent with a secondary insertion mechanism. The catalyst also displayed living behavior at temperatures as high as -40°C , giving high molecular weight polymers with low polydispersity (M_n up to $100\,000 \text{ g mol}^{-1}$, $M_w/M_n = 1.2–1.4$).

Despite the success of these vanadium catalysts with propylene, living behavior is limited to only a few monomers with this catalytic system. For example, ethylene polymerizations with **1a**/ Et_2AlCl at -78°C gave high molecular weight polyethylenes (PEs; $>300\,000 \text{ g mol}^{-1}$) with molecular weight distributions consistent with the probable distribution for a single-site catalyst ($M_w/M_n = 2.0$).^[29] However, ethylene/propylene copolymerizations were living; reaction of ethylene and propylene with **1b**/ Et_2AlCl at -60°C rapidly produced a very high molecular weight copolymer ($M_n = 1\,020\,000 \text{ g mol}^{-1}$) with a narrow polydispersity ($M_w/M_n = 1.22$).^[30] These catalysts were also found to be inactive for polymerization of higher α -olefins. For example, reaction of 1-pentene with **1a**/ Et_2AlCl resulted in formation of heptane and 3-methylhexane, the products of a single 1-pentene addition to a vanadium–ethyl species with 2,1- and 1,2-regiochemistry, respectively.^[31] No further reaction was detected, presumably due to the sterically congested nature of the catalytic site following the insertion. However, the vanadium system did produce living polymers with 1,5-hexadiene; at -78°C , the diene was polymerized to low molecular weight polymer ($M_n = 6600 \text{ g mol}^{-1}$) with a narrow molecular weight distribution ($M_w/M_n = 1.4$).^[32] This polymer, however, did not possess the typical methylene-1,3-cyclopentane microstructure obtained with other insertion polymerization catalysts. By NMR analysis, the microstructure was determined to contain tetramethylene-1-vinylene units (46 %) as well as methylene-1,3-cyclopentane structures (54 %; Scheme 3). Copolymerization of propylene and 1,5-



Scheme 3. Polymerization of 1,5-hexadiene with a vanadium catalyst.

hexadiene also displayed living behavior. The distribution of the polymer microstructure varied with the mole fraction of hexadiene in the copolymer; high diene content gave equal amounts of the two repeat units, while lower incorporation resulted in exclusive formation of tetramethylene-1-vinylenes. However, the mechanism for formation of this unique polymer is unclear.

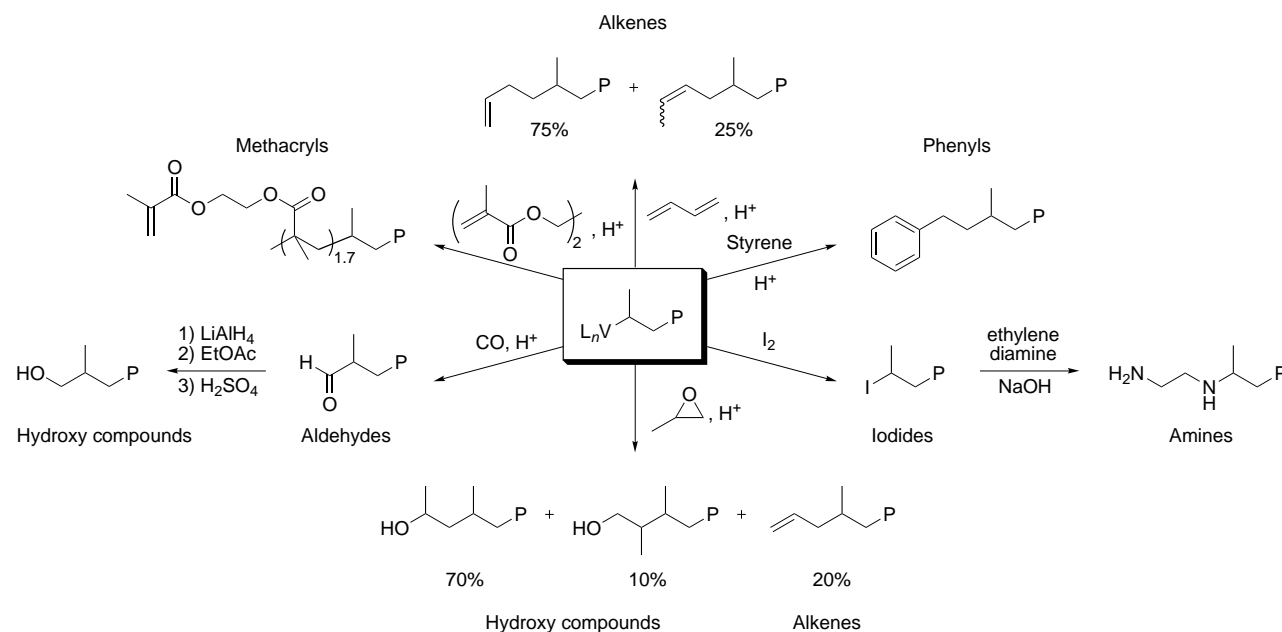
2.2. End-Functionalized Polypropylenes from Vanadium Compounds

Doi and co-workers have demonstrated the utility of the living vanadium catalysts through the synthesis of several tailor-made polymers.^[33–37] By reacting active polymer chains with additives, polypropylenes with a wide variety of functional end groups can easily be prepared with these living catalyst systems (Scheme 4). In addition to providing important mechanistic information, these functional polymers display unique properties and have also been used as macro-initiators for the synthesis of block copolymers.

In an effort to synthesize new end-functionalized polymers, a living vanadium-polypropylene species was quenched with iodine at -78°C to give a monodisperse iodine-functionalized polypropylene ($M_w/M_n = 1.15$).^[33] NMR spectroscopy revealed that the structure of this end group resulted from reaction of I_2 with a secondary alkylvanadium compound, providing evidence for a 2,1 insertion mechanism. The iodine functionality was used to prepare an amine-terminated polypropylene by reacting the polymer with excess ethylenediamine in THF, followed by basic workup.^[35] These polymers have also been used as macroinitiators for the preparation of diblock copolymers (see Section 2.3).

By reacting active living vanadium centers with carbon monoxide, Doi et al. have prepared aldehyde-terminated polypropylenes (Scheme 4).^[38] Again, CO was found to insert quantitatively into secondary vanadium–carbon bonds. This aldehyde functionality has also been used to prepare hydroxy-functionalized polypropylenes by reduction of the aldehyde with LiAlH_4 in Et_2O , followed by acidic hydrolysis.^[36] Hydroxy-terminated polypropylenes were also prepared with moderate success by reaction of an active vanadium species with propylene oxide.^[36] The insertion of the epoxide into the growing polymer chain occurred with decent regioselectivity, preferentially adding at the unsubstituted carbon atom (7/1) to give the secondary alcohol. However, the reaction also yielded a fraction of allyl-terminated polypropylene from an undesirable elimination reaction (20 %).

Polypropylene macromonomers containing methacryl functionality were prepared by addition of ethylene glycol dimethacrylate (EGDM) to a living chain end.^[39] Propylene polymerization was conducted for 1 h at -60°C with the complex **1b**/ Et_2AlCl , giving a low molecular weight polypropylene ($M_n = 3100 \text{ g mol}^{-1}$, $M_w/M_n = 1.13$). Addition of an excess of EGDM to this living chain end at -55°C and reaction for an additional 1 h resulted in quantitative capping of the chain ends without formation of EGDM homopolymer ($M_n = 4000 \text{ g mol}^{-1}$, $M_w/M_n = 1.10$). Both IR and NMR spectroscopy revealed the presence of the methacryl unit in the



Scheme 4. Synthesis of end-functional polypropylenes with a vanadium catalyst.

polymer; interestingly, an average of 1.7 molecules of EGDM were reported to be present per chain.

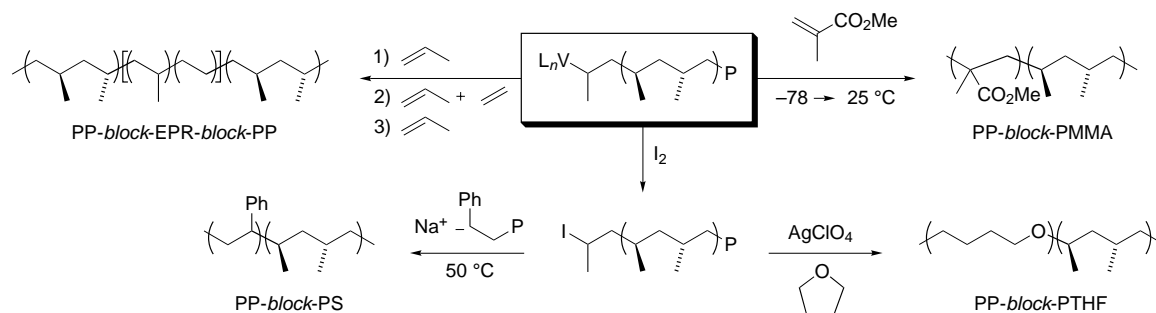
Finally, additives that produce polypropylenes with alkenyl and phenyl end groups were explored by Doi and co-workers.^[36] By adding butadiene to living polypropylene prepared with **1a**/Et₂AlCl, a polymer containing alkene end groups was formed after quenching. NMR spectroscopy showed that the butadiene inserted with both 2,1 and 1,4 regiochemistry, producing polymers with both terminal (75 %) and internal (25 %) olefins. Phenyl-terminated polymers were also prepared in this fashion by addition of styrene to a living polypropylene, which reacts quantitatively with the growing polymer chain without formation of any styrene homopolymer.

2.3. Copolymers and Block Copolymers from Vanadium Compounds

One of the most attractive features of a living catalyst system lies in its ability to produce well-defined block copolymers by sequential monomer addition. Several methods have been described for block copolymer formation using

vanadium catalysts. To this end, Doi and co-workers reported the synthesis of both AB- and ABA-type block copolymers from ethylene and propylene (Scheme 5). As described in Section 2.1, the reaction of **1a**/Et₂AlCl/anisole with propylene at -78°C generates a living polypropylene chain end.^[25] In the presence of propylene, a small amount of ethylene was added to this living chain, resulting in rapid formation of an AB-type copolymer containing syndio-enriched polypropylene and ethylene/propylene rubber (EPR) domains.^[40] A sharp increase in both polymer yield and molecular weight versus time was observed following the ethylene addition. However, these rates quickly returned to values consistent with propylene homopolymerization, indicating that ethylene consumption was complete after a short time. The steady increase in yield and molecular weight following the ethylene addition indicated the continued formation of propylene homopolymer to give an ABA-type triblock copolymer (*syn*PP-*block*-EPR-*block*-*syn*PP).

In addition to providing block copolymers based on non-polar olefins by sequential monomer addition, the vanadium catalysts have also been employed for the synthesis of block copolymers from polar monomers by transforming the living chain end to one capable of initiating a radical or cationic



Scheme 5. Synthesis of block copolymers with a vanadium catalyst; EPR = ethylene/propylene rubber.

polymerization (Scheme 5). Doi et al. discovered that the polymerization of methyl methacrylate (MMA) with **1a**/Et₂AlCl at 25 °C displayed living character during the initial stages of the reaction, giving low molecular weight poly(methyl methacrylate) (PMMA) with a narrow molecular weight distribution ($M_n = 2400 \text{ g mol}^{-1}$, $M_w/M_n = 1.2$).^[34] Copolymerizations of MMA with styrene suggested that the reaction proceeded by a radical pathway. This new method for MMA polymerization was employed for the synthesis of polypropylene/PMMA diblock copolymers. By reacting propylene with **1a**/Et₂AlCl at –78 °C, a living polypropylene chain end was formed ($M_n = 16000 \text{ g mol}^{-1}$, $M_w/M_n = 1.2$). Addition of MMA to the reaction mixture and warming to 25 °C resulted in formation of a higher molecular weight polymer containing a syndio-enriched PMMA segment (15 wt % PMMA, $M_n = 18000 \text{ g mol}^{-1}$, $M_w/M_n = 1.2$).

Another example of this strategy for block copolymer formation was demonstrated in the synthesis of a copolymer with a poly(tetrahydrofuran) (PTHF) domain. As described in Section 2.2, Doi et al. synthesized a monodisperse iodine-terminated polypropylene ($M_n = 16500 \text{ g mol}^{-1}$, $M_w/M_n = 1.15$) by addition of I₂ to a living polypropylene chain end.^[33] This polymer was then dissolved in THF at 0 °C and treated with AgClO₄, causing immediate precipitation of AgI and concomitant formation of a cationic macro-initiator capable of THF polymerization. After 96 h, a monodisperse polymer ($M_w/M_n = 1.14$) of higher molecular weight was isolated. IR and NMR analysis revealed that the polymer contained both polypropylene and PTHF domains.

Finally, tailor-made block copolymers can be prepared by the coupling of iodine-terminated polypropylenes with mono-functional or multifunctional living polymers. Doi et al. exploited this strategy for the synthesis of a well-defined polypropylene–polystyrene diblock copolymer.^[29] Addition of an iodine-terminated polypropylene ($M_n = 22000 \text{ g mol}^{-1}$, $M_w/M_n = 1.14$) to a living polystyrene anion ($M_n = 13000 \text{ g mol}^{-1}$, $M_w/M_n = 1.27$) resulted in formation of a higher molecular weight polymer ($M_n = 35000 \text{ g mol}^{-1}$, $M_w/M_n = 1.25$), consistent with the quantitative coupling of the two component polymers.

3. Rare-Earth Metal Catalysts for Controlled Alkene Polymerization

Schumann, Marks, and co-workers showed as early as 1985 that organolanthanide complexes were promising candidates for living olefin polymerization.^[41] Dimeric Cp*-based hydride complexes **2a–c** (Figure 2; Cp* = pentamethylcyclopentadienyl) were extremely active for the polymerization of ethylene, with turnover numbers of more than 1800 s^{–1} for **2a** at room temperature. Molecular weight distributions of polymers from the lutetium catalyst **2c** were reproducibly less than two ($M_n = 96000\text{–}361000 \text{ g mol}^{-1}$; $M_w/M_n = 1.37\text{–}1.68$), and the average number of polymer chains per lanthanide center for catalysts **2a–c** was always less than one. Based on these observations, it was speculated that these systems were operating in a living fashion. Furthermore,

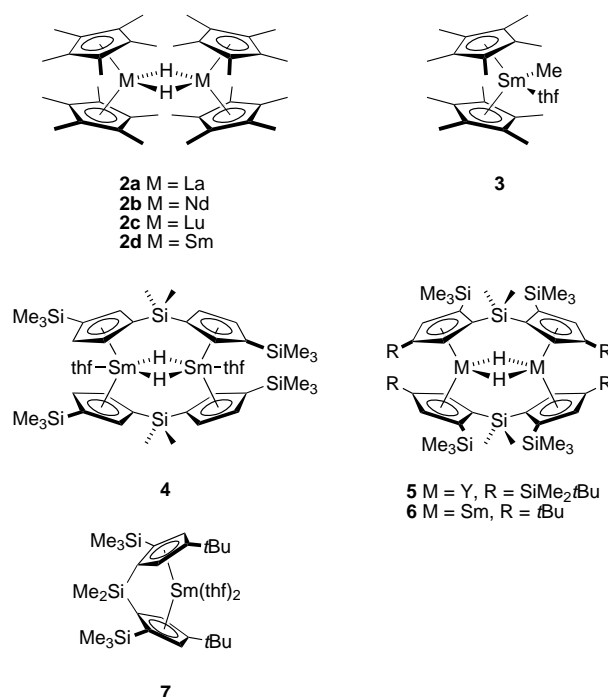
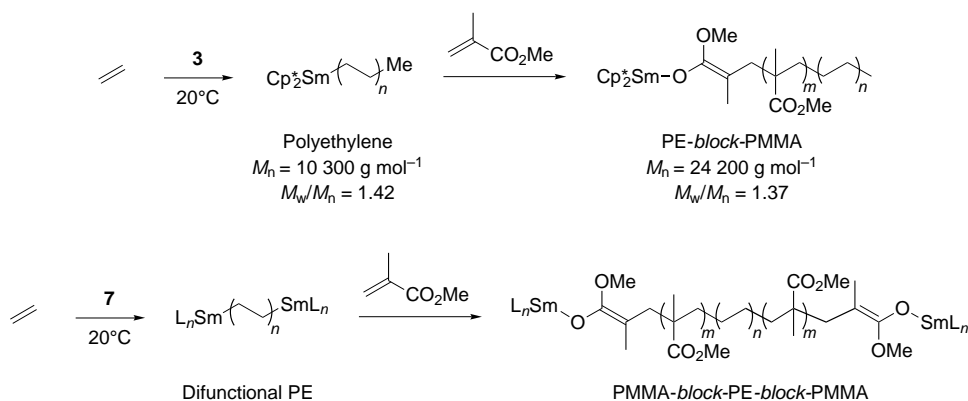


Figure 2. Lanthanide catalysts for living olefin polymerization. THF = tetrahydrofuran.

polymerization at –78 °C with **2b** showed that temperature effects on possible chain termination reactions such as β -hydride elimination were not important ($T = 25^\circ\text{C}$, $t = 5 \text{ s}$, $M_n = 590000 \text{ g mol}^{-1}$; $M_w/M_n = 1.81$; $T = -78^\circ\text{C}$, $t = 600 \text{ s}$, $M_n = 648000 \text{ g mol}^{-1}$; $M_w/M_n = 1.95$). Perfectly living behavior of these hydride catalysts was believed to be impeded by mass-transport effects and initiation-limiting dissociation of the catalyst dimer.

Yasuda and co-workers reported in 1992 that complex **2d** was extremely active for the living, syndiospecific polymerization of MMA ($[r] = 0.97$ at –95 °C, $[r] = 0.91$ at 0 °C) to form high molecular weight polymers (M_n up to 560000 g mol^{–1}) with extremely narrow molecular weight distributions ($M_w/M_n < 1.05$) via a coordination anionic polymerization mechanism.^[42] Immediately following this discovery, the sequential addition copolymerization of ethylene and polar monomers was reported to give block copolymers, implicating a change of mechanism from insertion to coordination anionic during the course of the polymerization.^[43] Since this material has been extensively reviewed elsewhere, we will only highlight the general concept.^[44–47]

In 1992, Yasuda et al. reported that samarium catalyst **3** (Figure 2) could effect the room-temperature block copolymerization of ethylene (insertion mechanism) and several polar monomers (non-insertion mechanism) such as methyl methacrylate, methyl acrylate, ethyl acrylate, δ -valerolactone, and ϵ -caprolactone (CL).^[43] In a typical two-step procedure, ethylene was first polymerized to a reactive polyethylene (PE) ($M_n = 6600\text{–}27000 \text{ g mol}^{-1}$, $M_w/M_n = 1.39\text{–}2.01$) in toluene under atmospheric pressure, followed by the addition of the respective polar monomer to form a linear diblock copolymer with relatively narrow polydispersity (Scheme 6). Reversal of monomer addition did not lead to block copoly-



Scheme 6. Synthesis of polyethylene/poly(methyl methacrylate) diblock and triblock copolymers with samarium catalysts.

mer formation. The resulting materials, such as PE-*block*-PMMA and PE-*block*-poly(CL) showed advantageous materials properties such as deep coloration with dyes when a short polar block was present.

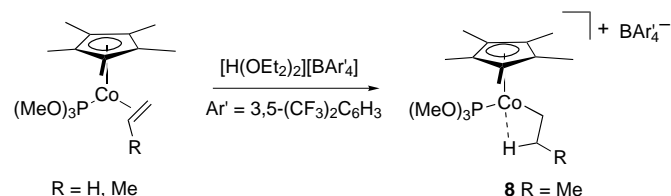
Recently, Yasuda and co-workers developed a binuclear samarium complex **4** (Figure 2) which exhibited high activity for the polymerization of ethylene (M_n up to $50\,000\text{ g mol}^{-1}$; $M_w/M_n = 1.63\text{--}1.68$) and efficiently formed diblock copolymers such as PE-*block*-PMMA (M_n up to $70\,000\text{ g mol}^{-1}$; $M_w/M_n = 1.67\text{--}1.69$) and polyethylene-*block*-poly(CL) ($M_n = 70\,000\text{ g mol}^{-1}$; $M_w/M_n = 1.65$).^[48] Structurally related complexes **5** and **6** (Figure 2) were then applied in the first controlled block copolymerization of 1-hexene and 1-pentene with MMA and CL.^[49] Yasuda and co-workers have also reported new divalent samarium complexes with bridging bis(cyclopentadienyl) (Cp) ligands and applied them in the polymerization of ethylene.^[50] In particular, racemic complex **7** provided encouraging results not only in the formation of polyethylene but also in the polymerization of higher α -olefins to give highly isotactic poly(α -olefins) (e.g. poly(1-pentene): $M_w = 10\,600\text{ g mol}^{-1}$, $M_w/M_n = 1.48$, poly(1-hexene), $M_w = 8300\text{ g mol}^{-1}$, $M_w/M_n = 1.55$). Cyclopolymerization of 1,5-hexadiene resulted in the formation of poly(methylene-1,3-cyclopentane) with a *cis*-ring content of about 50% ($M_w = 28\,500\text{ g mol}^{-1}$; $M_w/M_n = 1.88$). Furthermore, since catalyst **7** operated by a mechanism involving coordination of ethylene to two samarium centers followed by electron transfer to give a telechelic ethylene-bridged dinuclear species, block copolymerization of ethylene and MMA resulted in formation of the triblock PMMA-*block*-PE-*block*-PMMA copolymer (Scheme 6).^[51] Corresponding trivalent lanthanide compounds with bridging bis(Cp) ligands were not found to be superior in polymerization activity.^[52]

It should be mentioned that the organolanthanide complexes discussed here do not entirely meet the generally accepted criteria for living olefin polymerization, especially with respect to molecular weight distribution. However, through the combination of living anionic polymerization of polar monomers with partially controlled olefin insertion polymerization, these systems have found exciting applications in the synthesis of new materials with interesting properties.

4. Cobalt, Niobium, and Tantalum Catalysts for Living Ethylene Polymerization

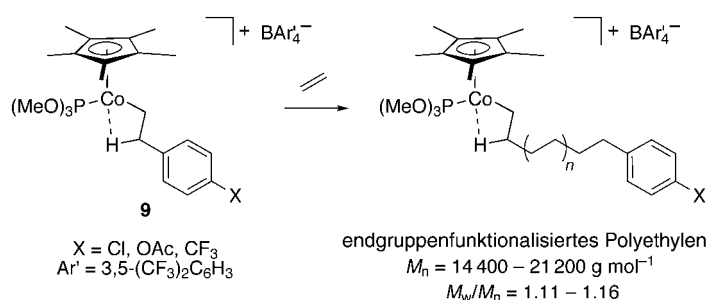
In the beginning of the 1990s, a number of catalyst systems for ethylene polymerization were reported in which the resulting polyethylene displayed a surprisingly narrow molecular weight distribution. The cobalt catalyst **8** ($\text{Ar}' = 3,5\text{-(CF}_3)_2\text{C}_6\text{H}_3$), prepared by protonation of the alkene-bound precursor (Scheme 7), produced polyethylenes with narrow polydispersities for low molecular weight samples ($M_n = 13\,600\text{ g mol}^{-1}$; M_w/M_n

$M_n = 1.17$), while the polydispersity increased for samples of higher molecular weight presumably due to mass transport problems ($M_n = 48\,500\text{ g mol}^{-1}$; $M_w/M_n = 1.71$).^[53] In addition, precipitation of polymer was regarded as a possible catalyst deactivation route.



Scheme 7. Synthesis of cobalt catalysts for olefin polymerization.

Based on this encouraging lead, Brookhart and co-workers subsequently reported a slightly modified cobalt catalyst for living ethylene polymerization and the synthesis of end-functional polyethylenes.^[54] Highly electrophilic cobalt complexes **9**, when exposed to 1 atm of ethylene for 3 h at room temperature followed by hydrogenolysis of the Co-C(alkyl) bond, formed end-functional polyethylenes (M_n up to $20\,000\text{ g mol}^{-1}$) with narrow polydispersities ($M_w/M_n = 1.11\text{--}1.16$) (Scheme 8). ^{13}C NMR analysis of the resulting polymer revealed a polymer microstructure with no branching. The presence of only one terminal methyl resonance signal indicated that the initiating species was the β -aryl-substituted, β -agostic complex (Scheme 8), and not its α -aryl-substituted, β -agostic isomer, in which case the corresponding polymer



Scheme 8. Synthesis of end-functional polyethylenes with cobalt catalysts.

would have displayed two methyl resonance signals (i.e. $\text{CH}_3\text{CH}_2(\text{CH}_2\text{CH}_2)_n\text{CH}(\text{CH}_3)\text{C}_6\text{H}_4\text{X}$). Furthermore, interaction of the functional group with the cobalt center, which could lead to catalyst deactivation, was prevented since the metal center can not migrate past the aryl group. However, broadening of the molecular weight distribution was again observed for higher molecular weight polymers ($M_n > 40\,000\text{ g mol}^{-1}$).

Silyl-functionalized polyethylene could be generated in an analogous fashion with the β -agostic complex $[\text{Cp}^*\{\text{P}(\text{OMe})_3\}\text{CoCH}_2\text{CH}(\mu\text{-H})(\text{CH}_2)_4\text{SiR}_3][\text{BAR}'_4]$ (**10**) ($\text{BAR}'_4 = \text{B}(3,5\text{-(CF}_3)_2\text{C}_6\text{H}_3)_4$). Molecular weights and molecular weight distributions for SiEt_3 -functional polyethylenes compared well with those of the aryl-substituted polymers. However, Me_2SiCl -functional polyethylenes showed lower molecular weight ($M_n = 10\,200\text{ g mol}^{-1}$) and broader molecular weight distribution ($M_w/M_n = 1.41$), presumably due to catalyst poisoning. While these cobalt complexes provided routes to end-functional polyethylenes, there are a number of drawbacks in these systems, namely the relatively low molecular weight of the resulting polymer, rather elaborate catalyst synthesis, and, especially in case of the complex **10**, their high moisture sensitivity.

The next major advance towards living olefin polymerization came in mid-1990s with the development of niobium diene based systems (Figure 3).^[55–57] Since these Group 5 systems are isoelectronic with Group 4 bis(Cp) complexes,

ization upon addition of $\text{B}(\text{C}_6\text{F}_5)_3$. Furthermore, changing the steric bulk of the catalyst system by replacing the Cp^* ligand of **11** with the less hindered Cp ligand resulted in a significant broadening of the molecular weight distribution of the resulting polyethylene ($M_w/M_n = 1.40$), presumably due to inferior catalyst stability.

Following these leads, Mashima and co-workers subsequently synthesized dimethyltantalum complexes **13a–c** (Figure 3). Interestingly, the corresponding niobium complexes decomposed rapidly via carbene intermediates.^[57] Although these tantalum species were inferior to niobium complexes **11** and **12** with respect to catalytic activity and molecular weight distribution of the resulting polymer, they did polymerize olefins in a controlled fashion. Addition of $\text{B}(\text{C}_6\text{F}_5)_3$ to a solution of **13b** at room temperature resulted in formation of the ion-pair $[\text{Cp}^*\text{Ta}(\eta^4\text{-isoprene})\text{Me}][\text{MeB}(\text{C}_6\text{F}_5)_3]$, as suggested by NMR experiments. The in situ generated η^4 -butadiene congener **13a**/ $\text{B}(\text{C}_6\text{F}_5)_3$ was found to be active for the polymerization of ethylene ($1.38\text{ kg}_{\text{PE}}\text{ mol}_{\text{Ta}}^{-1}\text{ h}^{-1}$), and the activity could be enhanced by adding AlEt_3 . When activated with MAO, dimethyl complexes **13a–c** and the corresponding dichloro complexes displayed comparable activities, indicating formation of similar active species.

5. Nickel and Palladium Catalysts for Living Olefin Polymerization

The search for catalyst systems for the living polymerization of α -olefins gained additional momentum by the development of diimine nickel and palladium catalysts in the mid-1990s.^[58] The advantages of these late transition metal systems are multifold. Late metal catalysts allow the copolymerization of functional monomers because of the reduced oxophilicity of the late metal center.^[59] Many of the late metal catalyst precursors are easily accessible, and detailed mechanistic studies have been undertaken since key species such as alkyl olefin complexes can be cleanly generated.

It is worth noting that more than a decade before the discovery of late transition metal catalysts for living polymerization of unactivated olefins, nickel allyl catalysts for living polymerization of conjugated dienes already existed. In 1984, Teyssié and co-workers reported that bis[(η^3 -allyl)(trifluoroacetato)nickel] (**14**) promoted the living polymerization of 1,3-butadiene to poly(1,4-butadiene) with predictable molecular weight and narrow molecular weight distribution ($M_w/M_n = 1.2\text{--}2.0$) at or above room temperature.^[60] Even though conversion of monomer was not complete (77 % at best), the linear increase in number-average molecular weight with conversion was consistent with a living polymerization. Deming and Novak, who utilized catalyst **14** in the polymerization of *tert*-butyl-isocyanide to form the corresponding helical polymers,^[61] took advantage of its living behavior in the polymerization of butadiene to form poly(butadiene)/poly(isocyanide) diblock copolymers (Scheme 9).^[62] Bimetallic nickel initiators were then developed for the synthesis of hydroxytelechelic poly(butadiene) and symmetric poly(isocyanide)-*block*-poly(butadiene)-*block*-poly(isocyanide) tri-

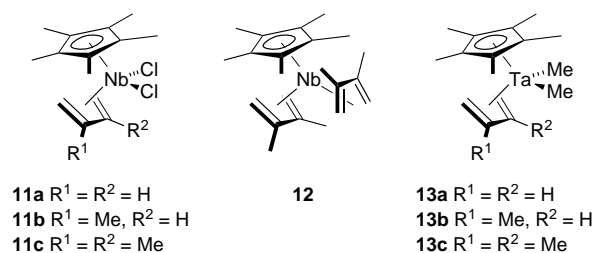
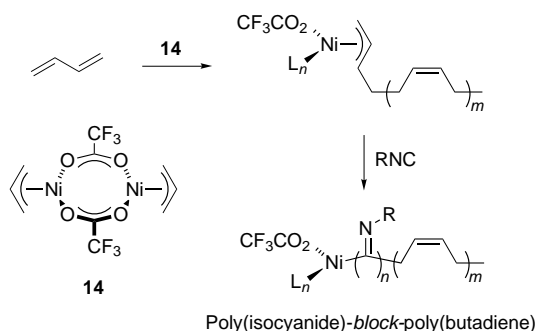


Figure 3. Niobium- and tantalum catalyst precursors for living olefin polymerization.

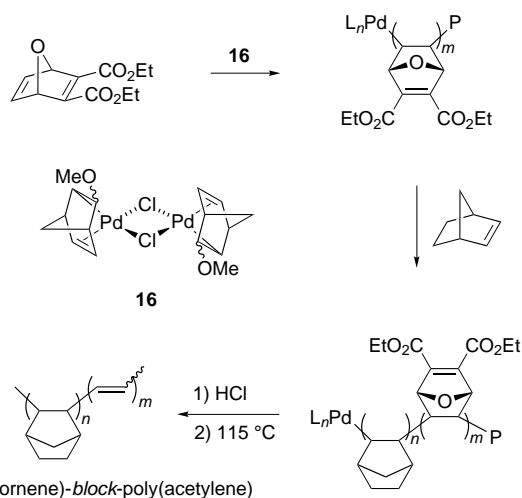
Mashima and co-workers realized that these precursors should be active in olefin polymerization. After an initial paper disclosing the validity of this idea,^[55] living ethylene polymerizations with the niobium diene systems **11a–c**/MAO (MAO = methylaluminoxane) and **12**/MAO were reported in 1994.^[56] Polymerization below 0°C occurred in a living fashion to produce high molecular weight polyethylenes (M_n up to $40\,000\text{ g mol}^{-1}$) with extremely narrow polydispersities (M_w/M_n as low as 1.05). The catalyst precursors were synthesized in low to moderate yields from $[\text{Cp}^*\text{NbCl}_4]$ and two equivalents of the respective allyl Grignard reagent. The substitution pattern of the diene moiety, which is essential for catalytic activity, influenced catalytic performance. For example, catalysts comprising 1,3-butadiene (**11a**) or 2,3-dimethyl-1,3-butadiene (**11c**) displayed approximately equal polymerization activities (38.7 versus $35.2\text{ kg}_{\text{PE}}\text{ mol}_{\text{Nb}}^{-1}\text{ h}^{-1}$) at 20°C , while catalyst **11b** containing the 2-methyl-1,3-butadiene ligand was somewhat less active ($19.2\text{ kg}_{\text{PE}}\text{ mol}_{\text{Nb}}^{-1}\text{ h}^{-1}$). The bis(diene) complex **12** was inactive for ethylene polymer-



Scheme 9. Nickel-catalyzed living copolymerization of butadiene and isocyanides.

block copolymers.^[63] Allylnickel catalysts have also found applications in the living polymerization of functionalized and nonfunctionalized allenes.^[64]

Risse and Mehler reported the living polymerization of norbornene using $[\text{Pd}(\text{MeCN})_4][\text{BF}_4]_2$ (**15**). Poly(norbornene)s with number-average molecular weights up to $30\,000\text{ g mol}^{-1}$ exhibited narrow molecular weight distributions at low monomer conversions; at higher conversions, the distributions broadened.^[65] Using **15**, Risse and Breunig reported the polymerization of ester-functionalized norbornenes. Depending on the nature of the ester substituent, polymers with narrow molecular weight distributions were obtained and block copolymers were synthesized.^[66] Novak and Safir also demonstrated the potential of palladium catalysts for living olefin polymerization in 1995. Hydrocarbon–poly(acetylene) block copolymers were synthesized by living insertion polymerization using extremely robust, air- and moisture-stable alkylpalladium(II) complexes containing σ,π -alkyl ligands (**16**) (Scheme 10).^[67] Polymerization of diethyl 7-oxabicyclo[2.2.1]hepta-2,5-diene-2,3-dicarboxylate, which can be viewed as a protected acetylene monomer, occurred quantitatively with **16** to yield a polymer with an active palladium end group. Subsequent addition of norbornene to this macroinitiator led to the formation of a block copolymer. Upon heating, this material underwent a retro-



Scheme 10. Synthesis of norbornene/acetylene block copolymers with a palladium catalyst.

Diels–Alder reaction, giving a poly(norbornene)-block-poly(acetylene) diblock copolymer.

A major breakthrough in living olefin polymerization occurred in 1995 with the discovery of a new family of late transition metal catalysts by Brookhart and co-workers. Soon after the initial report on the synthesis and polymerization activity of α -diiminepalladium and -nickel complexes,^[68] a subsequent paper appeared demonstrating the use of these nickel systems for the living polymerization of α -olefins.^[69] Catalyst precursor **17** (Figure 4), when activated with MAO in

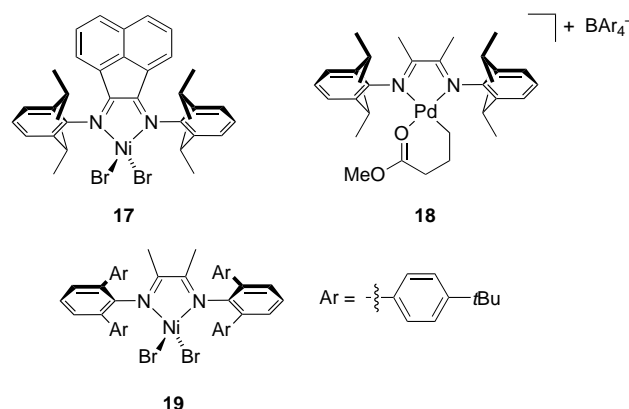
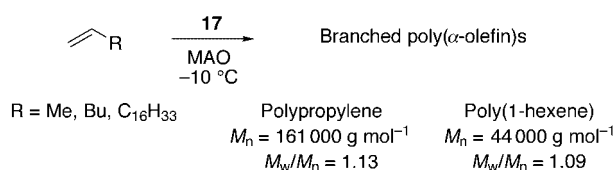


Figure 4. Nickel and palladium α -diimine catalysts and catalyst precursors for living olefin polymerization.

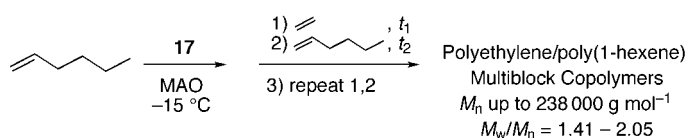
toluene at room temperature, was shown to be very active for the polymerization of α -olefins (turnover frequencies between 300 and 3000 h^{-1}), yielding high molecular weight materials (M_n up to $190\,000\text{ g mol}^{-1}$ for polypropylene) with relatively narrow polydispersities ($1.4 < M_w/M_n < 1.8$). At lower temperatures (-10°C) and low monomer concentrations, polymers with very narrow molecular weight distributions were obtained because undesirable chain transfer reactions were suppressed under these conditions. Accordingly, complex **17**/MAO in toluene under 1 atm of propylene at -10°C yielded high molecular weight polypropylene ($M_n = 161\,000\text{ g mol}^{-1}$, $M_w/M_n = 1.13$; Scheme 11).



Scheme 11. Living polymerization of α -olefins with a nickel diimine catalyst system.

Since chain walking (consecutive β -hydride elimination followed by olefin reinsertion with opposite regiochemistry) is a distinguishing mechanistic feature of palladium and nickel diimine catalysts,^[68, 70, 71] polymerization of ethylene results in a highly branched polymer, while polymerization of higher α -olefins leads to chain straightening, as indicated by a branching content that is lower than expected. The unique combination of living α -olefin polymerization behavior with the formation of chain straightened poly(α -olefin)s provided the

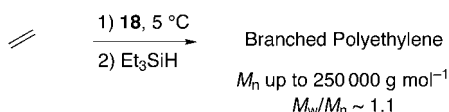
basis for a new strategy for the preparation of elastomeric materials. While polymerization of propylene by **17** formed an amorphous material ($T_g = -16^\circ\text{C}$), polymerization of octadecene led to a polymer with unbranched, crystalline domains ($T_m = 56^\circ\text{C}$). Based on these amorphous and crystalline polymer domains, several diblock and triblock polymers were prepared. A poly(octadecene)-*block*-poly(octadecene-*co*-propylene)-*block*-poly(octadecene) triblock copolymer, for example, consisting of semicrystalline poly(1-octadecene) blocks and an amorphous propylene/octadecene core, displayed elastomeric properties.^[69] Killian and Brookhart also exploited a similar strategy towards synthesis of ethylene/1-hexene multiblock polymers (Scheme 12).^[72] Although some chain transfer in ethylene homopolymerizations



Scheme 12. Synthesis of polyethylene/poly(1-hexene) multiblock copolymers with a nickel diimine catalyst.

with nickel catalyst **17** occurs even at temperatures below 0°C , a successful procedure for the synthesis of these unique multiblock materials was developed. Catalyst **17** in a toluene/1-hexene solution at -15°C was combined with MMAO (MMAO = modified methylaluminoxane), and ethylene was repeatedly added in short pulses. Since 1-hexene polymerization was living under these conditions, the main reaction product was expected to be a multiblock polymer despite some chain transfer. Depending on the time intervals for both ethylene and hexene polymerizations and the number of cycles in which this procedure was repeated, the resulting materials displayed excellent elastomeric properties (elongations of up to 1090 %, tensile strength up to 860 psi).

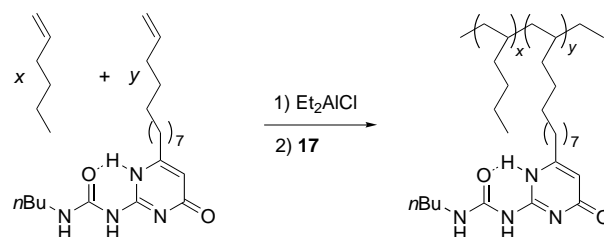
While nickel diimine catalysts did not polymerize ethylene in a living fashion, Gottfried and Brookhart recently reported experimental conditions under which ethylene can be polymerized by palladium catalyst **18** to give amorphous polymers with controlled molecular weights and narrow molecular weight distributions (Scheme 13).^[73] Quenching the reaction mixture with triethylsilane, whereby the $\text{Pd}-\text{C}_{(\text{alkyl})}$ bonds were cleanly converted to saturated end groups, proved crucial to obtaining monodisperse polyethylenes with this catalytic system. When the polymerization was quenched with acidified methanol, chain coupling frequently occurred and the resulting polyethylene displayed a bimodal molecular weight distribution. The polydispersity index of these polyethylenes remained well under 1.1 up to molecular weights of $250\,000\text{ g mol}^{-1}$. The resulting polymers were highly branched (100 branches/1000 C), and the branching number was



Scheme 13. Living polymerization of ethylene with a palladium diimine catalyst.

independent of the polymerization conditions. However, performing the polymerization at lower ethylene pressures (1 atm) resulted in a somewhat broadened molecular weight distribution ($M_w/M_n = 1.27$). Lower ethylene pressures were believed to retard the rate of initiation relative to the rate of propagation since the palladium chelate complex **18** is favored over the corresponding chelate-opened alkyl olefin catalyst resting state. When polymerizations were performed at 27°C , catalyst decay led to a nonlinear increase of the molecular weight over time and broadened molecular weight distributions of the resulting polyethylenes.

The full potential of the nickel and palladium α -diimine systems has not yet been fully explored in the context of living polymerization, and one can only imagine the exciting possibilities for materials synthesis offered by these systems. Possible future challenges involve control over stereochemistry in living α -olefin polymerization with C_2 -symmetric diimine catalysts, as well as the copolymerization of monomers containing functional groups. The following two examples are given to illustrate this point. Non-living syndiospecific polymerization of propylene by α -diimine nickel catalysts has been reported.^[74–77] Rieger and co-workers recently reported the synthesis of extremely bulky C_2 -symmetric nickel and palladium α -diimine complexes and their application in the formation of ultra high molecular weight polyethylenes at ambient temperature. Linear polyethylene of narrow polydispersity ($M_w = 4\,500\,000\text{ g mol}^{-1}$; $M_w/M_n = 1.3$) was obtained with catalyst **19**/MAO, providing an encouraging lead for future investigations.^[78] Taking advantage of the living behavior and functional group tolerance of catalyst **17**, we explored the copolymerization of 1-hexene with a functionalized olefin capable of forming intermolecular hydrogen bonds (Scheme 14).^[79] Ureidopyrimidone (UP) functionalized poly(1-hexene)s with low comonomer content (ca. 2 %) were synthesized in a living fashion ($M_n = 33\,000 - 104\,000\text{ g mol}^{-1}$, $M_w/M_n = 1.2 - 1.4$). These materials display elastomeric properties, indicating the formation of hydrogen-bond crosslinks between polymer chains. It should be pointed out that the resulting polymer is certainly more complex than shown in Scheme 14 because of chain walking.



Scheme 14. Synthesis of ureidopyrimidone-functional poly(1-hexene) with a nickel diimine catalyst.

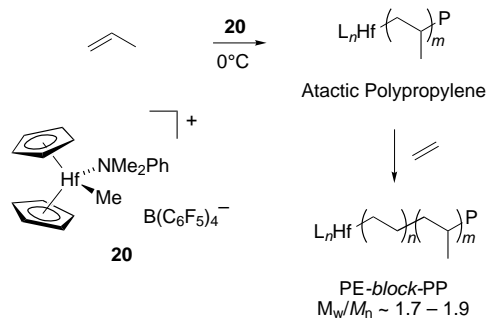
6. Titanium, Zirconium, and Hafnium Catalysts for Living Alkene Polymerization

Given the key advances in the control of polymer stereochemistry and comonomer incorporation over the last two decades,^[6] a significant amount of research in the quest for

living olefin polymerization catalysts has centered on complexes based on the Group 4 metals. Metallocene catalyst systems have been shown to exhibit living behavior at low temperatures by suppressing undesirable β -hydride or β -alkyl eliminations. Recently, non-metallocene systems based on nitrogen and oxygen donor ligands have received considerable attention.^[80] In addition to providing pathways for living olefin polymerization at ambient temperature, these systems have also made possible considerable advances concerning the control of stereochemistry in living olefin polymerization. By combining these long-sought goals, these complexes provide routes to the synthesis of polyolefin materials inaccessible by conventional polymerization methods.

6.1. Metallocene Complexes

Turner and Hlatky demonstrated the synthesis of a block copolymer of propylene and ethylene using a cationic hafnocene that was stable to chain transfer over the lifetime of the polymerization reaction (Scheme 15), even though the



Scheme 15. Synthesis of ethylene/propylene diblock copolymers with a hafnocene catalyst.

obtained polymer molecular weight distributions were not satisfying.^[81] Propylene was first added to a solution of $[\text{Cp}_2\text{HfMe}(\text{PhNMe}_2)][\text{B}(\text{C}_6\text{F}_5)_4]$ (**20**) at 0°C . After consumption of propylene, ethylene was added to the reactor. Based on extraction studies, it was determined that 75% of the polypropylene chains were incorporated into diblock copolymers composed of atactic polypropylene and high-density polyethylene segments. The copolymer could also be synthesized by the reverse monomer addition, that is adding ethylene first, but the molecular weight distribution was higher in this case (1.89 versus 1.72) and the propylene content was lower (30% versus 37%). Due to the relatively short lifetimes of the living polymer chains, triblock copolymers were not efficiently formed.

Bochmann and co-workers reported that $[\text{Cp}^*\text{TiMe}_3]$ (**21**; Figure 5) activated with $\text{B}(\text{C}_6\text{F}_5)_3$ was highly active for the polymerization of propylene to form high molecular weight atactic polypropylene (M_n up to $4\,000\,000\text{ g mol}^{-1}$) that displayed elastomeric properties.^[82] The presence of polymer fractions with very narrow molecular weight distributions ($M_w/M_n = 1.1$) in this MAO-free polymerization system was intriguing, and it was concluded that about half of the active

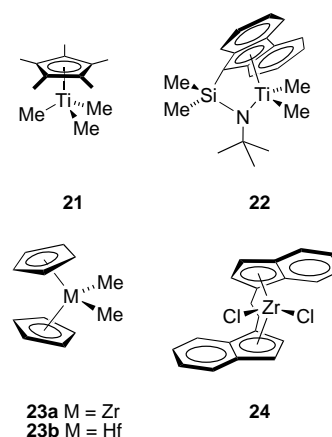


Figure 5. Metallocene catalyst precursors for living olefin polymerization at low temperatures.

titanium centers operated in a living fashion. Polymers with relatively narrow polydispersities ($M_w/M_n = 1.6$) were obtained at room temperature when polymerizations were performed in light petroleum despite reduced catalyst productivity in that solvent. Overall, the **21**/ $\text{B}(\text{C}_6\text{F}_5)_3$ system showed several characteristics of living behavior at room temperature, such as linear increase of polymer yield with both catalyst concentration and time. Addition of AlMe_3 or $\text{Al}i\text{Bu}_3$, even in substoichiometric amounts, dramatically decreased catalytic activity and produced polymers with bimodal molecular weight distributions. Polymerization of 1-hexene under similar conditions gave atactic poly(1-hexene) with broader molecular weight distributions (M_n ca. $10\,000\text{ g mol}^{-1}$, $M_w/M_n \sim 2.4$).^[83]

Based on the notion that β -hydride elimination is negligible in comparison with propagation in standard metallocene–MAO systems at temperatures below -40°C ,^[84] the research groups of Shiono and Fukui investigated olefin polymerization with metallocene or constrained geometry catalysts at very low temperatures. To avoid chain transfer to aluminum, Shiono and co-workers utilized borane activators in their initial study.^[85] The titanium catalyst **22**, when activated with $\text{B}(\text{C}_6\text{F}_5)_3$ at -50°C , produced syndio-enriched polypropylene ($[rrrr] = 0.24$) with narrow molecular weight distributions (M_n up to $20\,000\text{ g mol}^{-1}$, $M_w/M_n = 1.15 - 1.40$), and polymerization of 1-hexene under similar conditions also displayed living behavior. Raising the temperature of the reaction to 0°C resulted in complete deactivation of the catalyst system. By using rigorously dried MAO (free of AlMe_3 impurities), Shiono and co-workers then showed that chain transfer to aluminum caused by residual AlMe_3 could be efficiently suppressed in this system. Accordingly, moderately syndiotactic polypropylene ($[rrrr] = 0.42$) could be produced in a living fashion with **22**/MAO even at 0°C ($M_n = 10\,100\text{ g mol}^{-1}$; $M_w/M_n = 1.35$).^[86]

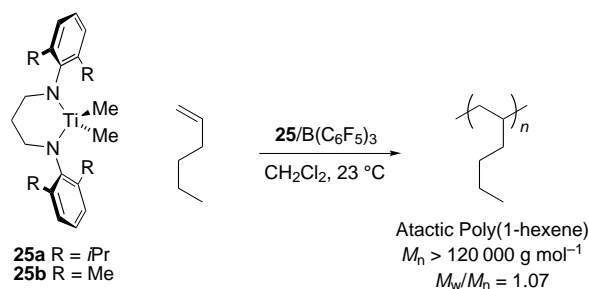
Fukui and co-workers demonstrated that the simple bis(Cp) catalyst **23a** activated with $\text{B}(\text{C}_6\text{F}_5)_3$ was capable of the living polymerization of propylene at -78°C in the presence of $\text{Al}(n\text{Oct})_3$ as scavenger.^[87] The number of polymer chains was found to be constant for the course of the reaction, indicating that chain transfer did not occur at very low temperatures.

While the molecular weights of the resulting polymers were rather low ($M_w < 10\,000 \text{ g mol}^{-1}$), the molecular weight distributions were extremely narrow ($M_w/M_n = 1.06$) and polymer yields increased linearly with time. Carbon monoxide also reacted quantitatively with the living polypropylene chain ends, generating polypropylenes with terminal aldehyde functionality.^[88] Similarly, the hafnium system **23b**/ $\text{B}(\text{C}_6\text{F}_5)_3$, also displayed living behavior at -50°C . Living polymerization of 1-hexene was also observed with the C_2 -symmetric ansa-metallocene system **24**/ $\text{B}(\text{C}_6\text{F}_5)_3$ at -78°C , producing highly isotactic monodisperse poly(1-hexene) ($M_w/M_n = 1.2-1.3$). However, the catalytic activity for this system was low, resulting in only very low molecular weight polymers ($M_n < 5400 \text{ g mol}^{-1}$). Catalyst **24**/ $\text{B}(\text{C}_6\text{F}_5)_3$ did not produce highly isotactic polypropylene in a living fashion at -78°C , presumably due to β -alkyl elimination. Tritto and co-workers have recently shown that **24** exhibits “quasi-living” behavior for ethylene/norbornene copolymerization when activated with MAO.^[89]

Very recently, Fukui and Murata employed the mixed metallocene catalyst system $[\text{Cp}_2\text{ZrMe}_2]/\text{B}(\text{C}_6\text{F}_5)_3/[\text{Cp}^*\text{TiCl}_3]$ for the living polymerization of propylene at -50°C .^[90] Again, reaction of carbon monoxide with a living polypropylene gave aldehyde-functionalized polypropylenes. Fukui and Murata also employed the mixed metallocene catalyst system $[\text{Ph}_2\text{C}(\text{Cp})(\text{fluorenyl})\text{ZrCl}_2]/\text{Al}(\text{nOct})_3/\text{B}(\text{C}_6\text{F}_5)_3/[\text{Cp}^*\text{TiCl}_3]$ for the living syndiospecific polymerization of propylene at -50°C .^[91] Finally, Brekner and co-workers described how “quasi-living” metallocene/MAO systems could be used in the synthesis of cycloolefin copolymers with narrow molecular weight distribution when generated at temperatures between 0°C and 40°C ($M_w/M_n = 1.1-1.4$).^[92]

6.2. Diamido Complexes

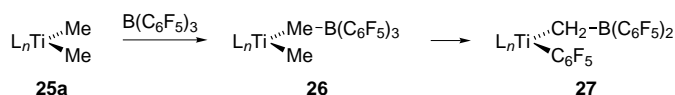
Since the mid-1990s, several Group 4 catalysts with ancillary amido ligands for living olefin polymerization have been described. While these systems are of high academic interest since they are amenable to detailed mechanistic studies, their application in polymer synthesis has so far been limited to atactic polymers of propylene and simple α -olefins. Living polymerization of ethylene has not been reported with these catalysts, and only one example of an olefin block copolymer has been reported. In 1996, McConville and co-workers introduced a new class of diamido catalysts for living olefin polymerization. These tetrahedral dimethyltitanium complexes **25a, b** bearing ancillary propylene-bridged aryl-substituted diamido ligands proved to be highly active catalysts for polymerization of 1-hexene when activated by MAO (Scheme 16). For example, treatment of precatalyst **25a** with MAO at room temperature gave atactic poly(1-hexene) ($M_n = 47\,000 \text{ g mol}^{-1}$, $M_w/M_n = 1.73$). Chain transfer to the aluminum cocatalyst was implicated as the lone source of termination since olefinic resonances were absent from the NMR spectrum of the polymer. By activating the precatalyst with $\text{B}(\text{C}_6\text{F}_5)_3$, chain transfer reactions were eliminated and the polymerization of 1-hexene and higher α -olefins proceeded in living fashion (Scheme 16).^[93] A decrease in the steric



Scheme 16. Living polymerization of 1-hexene with McConville's diamidotitanium catalysts.

bulk of the ligand by replacement of the isopropyl substituents with methyl groups (**25b**) did not substantially influence catalyst performance. Polymerizations run in CH_2Cl_2 led to a dramatic increase in catalytic activity, yielding high molecular weight atactic polymers ($M_n > 120\,000 \text{ g mol}^{-1}$) with narrow molecular weight distributions ($M_w/M_n = 1.07$). This increase in activity was reasoned to be the result of better separation of the assumed catalyst ion-pair in the more polar solvent. On the other hand, polymerization activity decreased in the presence of toluene, presumably due to competitive binding to the active site. Mechanistic studies, including isotopic labeling and iodine quenching reactions, suggested that olefin insertion occurred in a primary (1,2) fashion.^[94]

In a straightforward synthesis, the dimethyltitanium complexes **25a, b** were obtained by Grignard addition to the corresponding dichlorides, which in turn were best synthesized from the silylated diamines $\text{Me}_3\text{SiArN}(\text{CH}_2)_3\text{NArSiMe}_3$ and TiCl_4 . Although attempts to isolate a cationic methyltitanium complex as a model for the presumed active species failed, a few important mechanistic issues concerning catalyst deactivation were addressed in these attempts. Addition of $\text{B}(\text{C}_6\text{F}_5)_3$ to a solution of the dimethyl complex **25a** in pentane led to the precipitation of a catalytically active borane adduct **26** (Scheme 17).^[95] Suspensions of this adduct slowly evolved



Scheme 17. Deactivation pathway observed in McConville's diamidotitanium complexes.

methane to form an inactive methylene-bridged derivative **27** that was characterized by single-crystal X-ray diffraction, thus exemplifying a possible catalyst deactivation pathway (Scheme 17). Shiono and co-workers have recently reported that **25a** also produces polypropylene with low molecular weight distribution using a modified MAO that is free of trialkylaluminum residues.^[96]

Soon after McConville's initial report, Schrock and co-workers reported zirconium complexes with tridentate diamido ligands based on the hypothesis that a propagating four-coordinate cationic species would be more stable than a three-coordinate species.^[97] Since 1997, Schrock and co-workers have developed three different classes of compounds for use in the living, aspecific polymerization of 1-hexene (Figure 6).

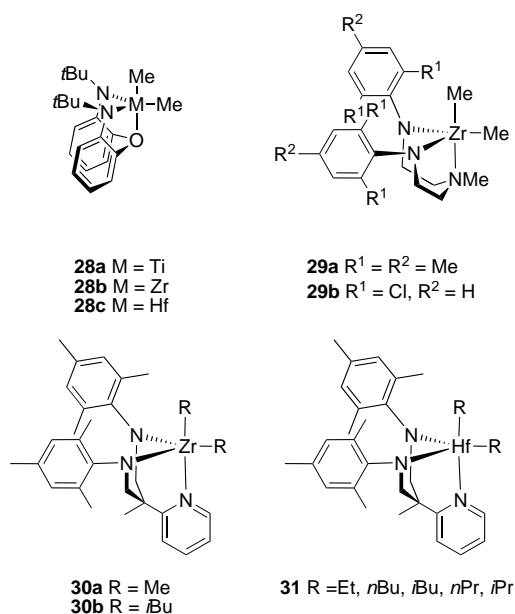


Figure 6. Diamido catalyst precursors for living olefin polymerization.

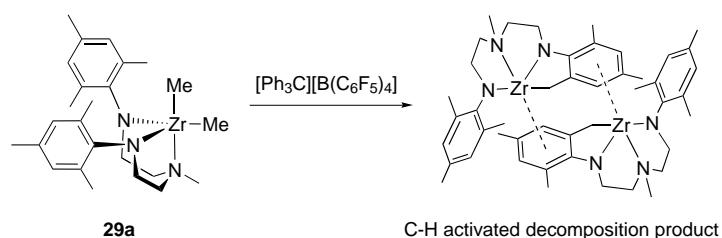
In the first two classes of compounds **28**^[97–101] and **29**,^[102–104] the two amido donor atoms are connected to a central donor (either oxygen or nitrogen), while in the third class **30**/**31**^[105, 106] all three donors are connected to a central carbon atom. Even though living α -olefin polymerization has been restricted almost exclusively to 1-hexene with these catalysts, the resulting polymer molecular weight distributions are among the narrowest known.

In 1997, Schrock and co-workers developed a very bulky and robust tridentate diamido ligand with a central oxygen donor atom.^[97] Group 4 catalyst precursors **28a–c**, incorporating the ligand $[(D_6)tBuN-o-C_6H_4)_2O]^{2-}$ (NON ligand) were prepared by Grignard addition to the corresponding dichloride complexes. The latter were best synthesized from the ligand dianion and $M(NMe_2)_2Cl_2$ and subsequent treatment of the bis(dimethylamido) intermediates with Me_3SiCl . The dimethyl complexes display trigonal-bipyramidal coordination geometry in the solid state with the oxygen donor and one methyl substituent in the apical positions, as demonstrated by X-ray crystallography of **28a** and **28b**.^[100] Methide abstraction from the dimethyl complex **28b** by $B(C_6F_5)_3$ yielded a reasonably stable ion pair, $[(NON)ZrMe][MeB(C_6F_5)_3]$ (**32**), which was characterized in the solid state and by NMR spectroscopy. Both complex **32** as well as the dimethylaniline adduct $[(NON)ZrMe(PhNMe_2)][B(C_6F_5)_4]$ (**33**) were active for the polymerization of ethylene at room temperature ($100\text{ kg}_{PE}\text{ mol}_{Zr}^{-1}\text{ h}^{-1}$ for **32**, $800\text{ kg}_{PE}\text{ mol}_{Zr}^{-1}\text{ h}^{-1}$ for **33**). Catalyst **33** also polymerized 1-hexene to atactic poly(1-hexene) ($200\text{ kg}_{PH}\text{ mol}_{Zr}^{-1}\text{ h}^{-1}$, $M_n = 45\,000\text{ g mol}^{-1}$, $M_w/M_n = 1.2$). By lowering the temperature to 0°C , chain transfer reactions were suppressed, and the polymerization occurred in a living fashion ($M_w/M_n < 1.05$ in the presence of more than 200 equivalents 1-hexene).

Insights into the polymerization mechanism were gained in a labeling study which established predominant 1,2 insertion of the olefin (1-hexene or 1-nonene) as well as β -hydride

elimination as the primary mechanism of chain termination at 40°C .^[98] The rate of β -hydride elimination was slow at 0°C , presumably due to steric crowding around the metal center which prevents the “backing up” of the bulky polymer chain towards the ligand in an olefin–hydride intermediate. Therefore, at lower temperatures, the polymerization proceeded without appreciable chain transfer. When the steric crowding about the metal center was relaxed by replacing the *tert*-butyl substituents with less bulky isopropyl or cyclohexyl groups, the corresponding activated metal dialkyl complexes only oligomerized 1-hexene.^[99] Interestingly, zirconium complexes bearing the structurally-related sulfur donor ligand $[(D_6)tBuN-o-C_6H_4)_2S]^{2-}$ (NSN) were not active for polymerization of 1-hexene.^[107]

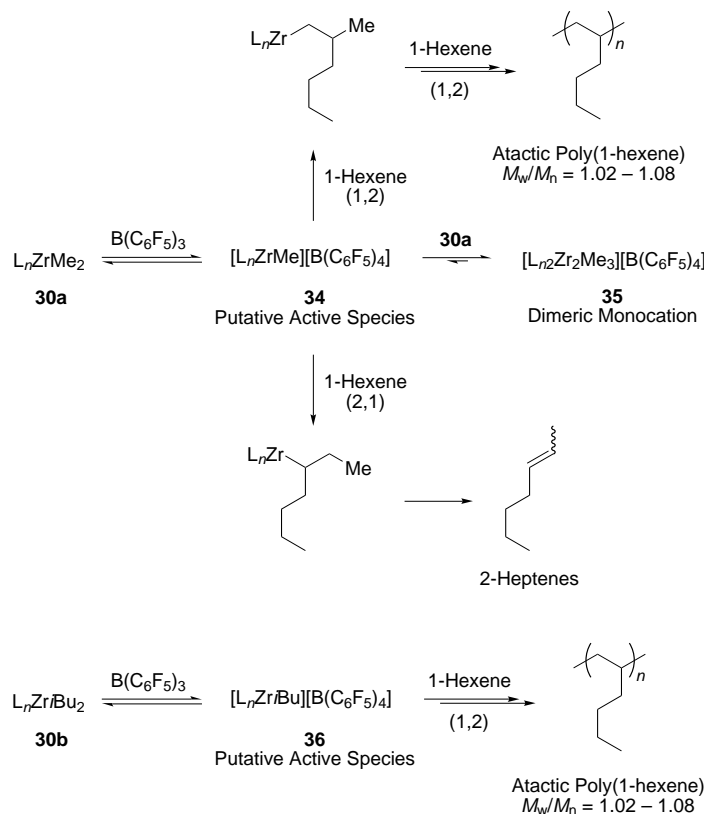
A second class of compounds for living olefin polymerization was introduced by Schrock and co-workers in 1999. Replacing the oxygen in the ligand backbone with an amine donor resulted in the more rigid tridentate complex **29a**.^[102] Activation of **29a** with $[Ph_3C][B(C_6F_5)_4]$ and subsequent reaction with 1-hexene led to the formation of poly(1-hexene) which displayed limited average molecular weight and broader molecular weight distribution than the polymer obtained with the NON system **28**. Subsequent studies revealed that this non-living behavior was caused by catalyst decomposition by C–H activation of one of the mesityl *o*-methyl substituents, producing a dimeric decomposition product that was characterized by X-ray crystallography (Scheme 18).^[103] A similar

Scheme 18. C–H activation as a catalyst deactivation pathway observed in systems based on precursor **29a**.

decomposition pathway of a cationic zirconium complex through C–H bond activation of an adjacent methyl group had previously been uncovered by Horton and co-workers in a structurally related triamido system.^[108] A simple change in aryl substitution from 2,4,6-trimethylphenyl to 2,6-dichlorophenyl prevented C–H activation of the ligand, and a living 1-hexene polymerization catalyst precursor **29b** was obtained.^[103] The polymer generated with catalyst **29b**/ $[Ph_3C][B(C_6F_5)_4]$ at 0°C was of higher molecular weight than that produced with the NON catalysts **28** (M_n up to $79\,000\text{ g mol}^{-1}$), while the molecular weight distribution of the polymer remained extremely narrow (M_w/M_n , 1.01–1.04).

In 2000, Schrock and co-workers reported a third class of compounds for living olefin polymerization. Employing the NNN framework in the form of diamidopyridine ligands (MesNpy), in which the three donor atoms are connected to a central carbon atom, the geometrically rigid zirconium complexes **30a,b** were prepared. An interesting initiator effect was uncovered in 1-hexene polymerization by com-

plexes **30a**, **b**.^[105] Methide abstraction from the dimethyl species **30a** with $[\text{Ph}_3\text{C}][\text{B}(\text{C}_6\text{F}_5)_4]$ was found to be a rather complex process, leading to the formation of the putative active species $[(\text{MesNpy})\text{ZrMe}][\text{B}(\text{C}_6\text{F}_5)_4]$ (**34**) in equilibrium with **30a** and a monocationic dimer $[(\text{MesNpy})_2\text{Zr}_2\text{Me}_3][\text{B}(\text{C}_6\text{F}_5)_4]$ (**35**) (Scheme 19). Solutions of **30a**/ $[\text{Ph}_3\text{C}][\text{B}(\text{C}_6\text{F}_5)_4]$ were active for the polymerization of



Scheme 19. Initiator effect in diamidopyridine catalysts for living olefin polymerization.

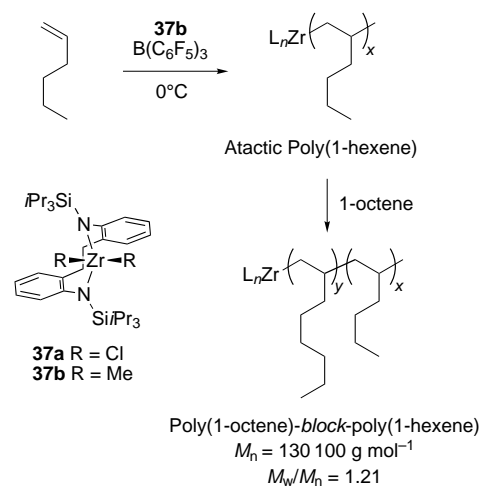
1-hexene, but consumption of 1-hexene was not a first-order process. The average molecular weight of the resulting polymer was 10 times higher than expected assuming quantitative initiation. Furthermore, NMR studies uncovered the formation of 2-heptenes in the reaction, presumably originating from secondary (2,1) insertion of 1-hexene into the active catalyst **34** to give a 3-heptyl species that is susceptible to β -hydride elimination. The larger fraction of the 3-heptyl species β -hydride eliminates and forms heptenes and a catalytically inactive metal species, while the smaller fraction propagates by primary (1,2) insertion. Despite these mechanistic complications, the molecular weight distribution of the resulting poly(1-hexene) was surprisingly narrow with this system ($M_w/M_n < 1.08$).

When the initiating group was changed from methyl to isobutyl (**30b**), activation with $[\text{Ph}_3\text{C}][\text{B}(\text{C}_6\text{F}_5)_4]$ cleanly generated a monomeric species $[(\text{MesNpy})\text{Zr}i\text{Bu}][\text{B}(\text{C}_6\text{F}_5)_4]$ (**36**; Scheme 19). Since dimer formation like in the methyl analogue **30a** did not occur, all the zirconium centers were available for polymerization and consequently no unreacted dialkyl complex **30b** was observed. Although the activated

species **36** decomposed in the absence of monomer by β -hydride elimination, addition of 1-hexene led to a living polymerization. In this case, heptenes were not observed, suggesting that 1-hexene predominantly inserted into the more sterically crowded $\text{Zr}-\text{C}_{(\text{isobutyl})}$ bond in a primary (1,2) fashion, yielding a 2-heptyl species that was relatively stable towards β -hydride elimination. Polymers produced with **30b**/ $[\text{Ph}_3\text{C}][\text{B}(\text{C}_6\text{F}_5)_4]$ displayed molecular weights approximately three times the theoretical value (based on Zr) and molecular weight distributions were again extremely narrow ($M_w/M_n = 1.03$).

Most recently, Schrock and co-workers reported the synthesis, characterization, and polymerization activity of cationic hafnium complexes of the general formula $[(\text{MesNpy})\text{HfR}][\text{B}(\text{C}_6\text{F}_5)_4]$ (**31**; $\text{R} = \text{Et}, n\text{Bu}, i\text{Bu}, n\text{Pr}, i\text{Pr}$).^[106] These compounds displayed a surprising stability towards β -hydride elimination below 10°C , and they promoted the living polymerization of 1-hexene under these conditions. Insertion of 1-hexene into a $\text{Hf}-\text{C}_{(\text{alkyl})}$ bond was found to be about half as fast as for the Zr analogue **30**.

A final example of living olefin polymerization by a group IV catalyst with an ancillary diamido ligand was reported by Kim and coworkers.^[109] Activated versions of these bidentate, aniline precursors **37a**, **b** were active for the polymerization of ethylene, propylene, and higher α -olefins (Scheme 20).



Scheme 20. 1-Hexene/1-octene block copolymer synthesis with a diamido catalyst system.

For example, **37a**/MAO showed an activity of $5300 \text{ kg}_{\text{PE}} \text{ mol}_{\text{Zr}}^{-1} \text{ h}^{-1}$ under 1 atm of ethylene at room temperature. However, the polymers produced with **37a**/MAO at room temperature were polydisperse, low molecular weight materials ($M_n < 9000 \text{ g mol}^{-1}$, $M_w/M_n = 2.09 - 2.35$). Cooling the polymerization to 0°C reduced β -elimination reactions, giving materials of higher molecular weight, but chain transfer to the aluminum cocatalyst again gave polymers with broad molecular weight distributions. However, employing $\text{B}(\text{C}_6\text{F}_5)_3$ as an activator for the dimethyl complex **37b** at 0°C gave high molecular weight atactic polymers with relatively narrow polydispersities. The catalyst system **37b**/ $\text{B}(\text{C}_6\text{F}_5)_3$ at 0°C polymerized 1-hexene with a linear increase in molecular

weight with yield to give atactic poly(1-hexene) with a narrow molecular weight distribution ($M_n = 118\,300\text{ g mol}^{-1}$, $M_w/M_n = 1.23$). The living nature of the polymerization was also demonstrated by the sequential addition of two different α -olefins to form a 1-hexene/1-octene block copolymer ($M_n = 108\,700\text{ g mol}^{-1}$; $M_w/M_n = 1.21$) (Scheme 20).

6.3. Zirconium Amidinates

Although the living vanadium catalysts developed by Doi et al. gave syndio-enriched polypropylenes (Section 2.1), the first catalyst to simultaneously achieve the highly sought goals of livingness and stereoselectivity was reported by Jayaratne and Sita in 2000.^[110] Using an amidinate zirconium catalyst, the living isospecific polymerization of 1-hexene was achieved with high stereoselectivity. By addition of carbodiimides to the Zr–C_(methyl) bond in [Cp*ZrMe₃], catalyst precursors **38a–d** (Figure 7) were easily prepared. When $R^1 \neq R^2$, the resulting

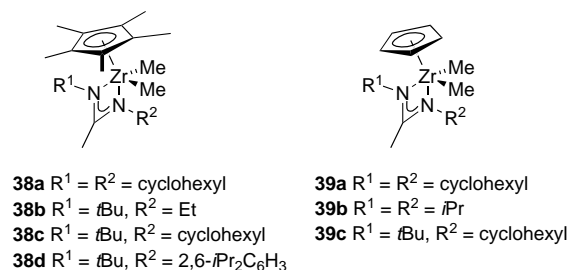
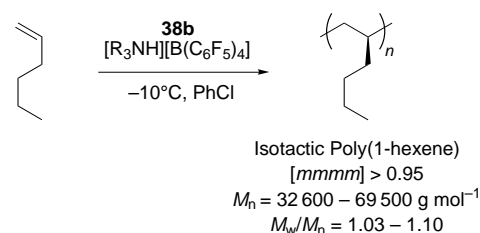


Figure 7. Amidinate catalyst precursors for living polymerization of 1-hexene.

compounds are chiral but variable-temperature ^1H NMR revealed low barriers to racemization. Upon activation with [PhNMe₂H][B(C₆F₅)₄] in chlorobenzene at 0 °C, symmetric complex **38a** was active for the polymerization of 1-hexene, giving a monodisperse polymer ($M_n = 11\,000\text{ g mol}^{-1}$, $M_w/M_n = 1.10$). The narrow molecular weight distribution and the lack of olefinic resonances characteristic of chain transfer indicated the living nature of the polymerization. However, microstructural analysis by ^{13}C NMR revealed the lack of stereochemical control in the polymerization.

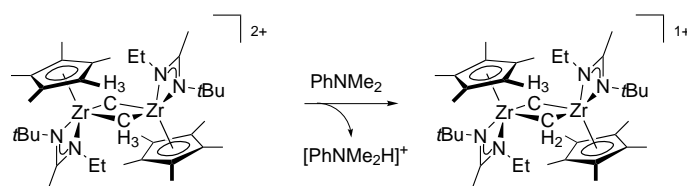
With this encouraging lead, the catalytic properties of C₁-symmetric compounds **38b–d** were evaluated.^[110] Precursors **38c, d** displayed poor activity toward 1-hexene, presumably due to the sterically encumbered nature of the complex. However, the activated complex **38b** proved to be a superior catalyst for the polymerization of 1-hexene at 25 °C (Scheme 21). In addition to an increase in activity and molecular weight, the polymer was also highly isotactic ($[mmmm] > 0.95$). The increase in activity was unfortunately accompanied by a broadening of the molecular weight distribution ($M_w/M_n = 1.50$). However, lowering the polymerization temperature to –10 °C led to higher molecular weight polymers with extremely narrow polydispersities ($M_w/M_n = 1.03\text{–}1.10$) and high stereoselectivities ($[mmmm] > 0.95$). The living character of the polymerization was demonstrated by the linear increase of number-average molecular weight (M_n)



Scheme 21. Living isospecific polymerization of 1-hexene with zirconium amidinate catalysts.

with conversion. Furthermore, addition of a second portion of 1-hexene (180 equiv) to a living polymer chain end ($M_n = 20\,700\text{ g mol}^{-1}$, $M_w/M_n = 1.03$) resulted in formation of a higher molecular weight polymer ($M_n = 35\,400\text{ g mol}^{-1}$, $M_w/M_n = 1.13$).

Although this catalytic system displayed excellent selectivity for production of isotactic poly(1-hexene), the mechanism of stereocontrol was unclear. NMR spectroscopy revealed a small resonance attributed to a *mmmr*-pentad as the only visible stereoerror, consistent with an isotactic stereoblock microstructure.^[110] The high selectivity demonstrated by this system was remarkable considering the low barrier to racemization of precursor **38b**. Sita et al. suggested that the barrier might be higher in the activated complex and the structural defects in the polymer were a consequence of amidinate ring flipping. To shed light on the origin of stereocontrol in this unique system, crystallographic analyses of **38b** and **38b**/[B(C₆F₅)₄] were performed.^[111] Indeed, the more electrophilic metal center of the activated complex resulted in a shortening of the Zr–N bonds, providing evidence that suggests a higher barrier to racemization in the active species. Also, coordination of diethyl ether to the activated complex occurred on the more sterically encumbered face of the catalyst, suggesting that olefin coordination might be preferred at that site. Crystallization in the absence of Lewis bases at low temperatures (–10 °C) provided a dimer with bridging methyl groups comprising a planar four-membered ring, inside of which reside two bridging agostic hydrogen atoms (Scheme 22). The elongated Zr–C_(methyl) bond

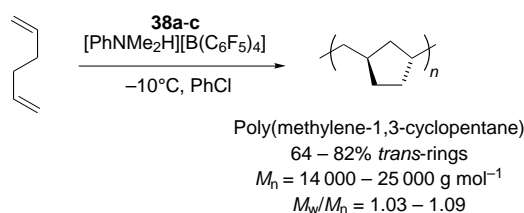


Scheme 22. Potential deactivation pathway in amidinate catalyst systems.

length demonstrated the stabilizing effect of these α -agostic interactions. It was suggested that these bridging α -agostic interactions in dimeric cations might serve to lower the barrier to migratory insertion, as has been proposed for mononuclear complexes.^[14] On the other hand, crystallization of activated complex **38b**/[B(C₆F₅)₄] at 25 °C revealed the formation of a $\mu\text{-CH}_2$, $\mu\text{-CH}_3$ monocationic species, resulting from reduction of one of the metal centers (Scheme 22). This species,

presumably the result of deprotonation of the dimer by dimethylaniline introduced from the cocatalyst, revealed a viable pathway for termination of active centers during the polymerization with this catalytic system.

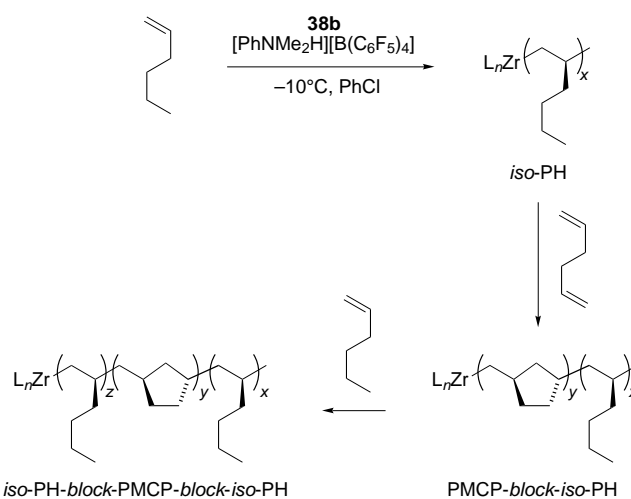
The enormous potential of this living and stereoselective catalyst system lies in its potential for the synthesis of well-defined olefin block copolymers with both crystalline and amorphous domains. Due to the microphase separation of such blocks, these materials have numerous applications as compatibilizers and elastomers. In a demonstration of the utility of this living catalyst system, Sita and co-workers explored the cyclopolymerization of nonconjugated dienes to give living polymers with high melting transitions.^[112] To this end, 1,5-hexadiene was polymerized by the catalyst system **38a–c**/[PhNMe₂H][B(C₆F₅)₄] in chlorobenzene at –10 °C to give poly(methylene-1,3-cyclopentane)s (PMCP) with narrow molecular weight distributions ($M_w/M_n = 1.03–1.09$; Scheme 23). The lack of olefinic resonances in the polymers



Scheme 23. Living cyclopolymerization of 1,5-hexadiene with zirconium amidinate catalysts.

and the linear kinetic relationship ($\ln([M_0]/[M_t])$ versus time) were consistent with a living polymerization. Analysis of the PMCP microstructures showed that the catalysts displayed high selectivity for cyclization (>98%). Selectivity for formation of *trans* rings was mediated by the steric bulk of the catalyst precursor; increasing bulk of the amidinate ligands in the series **38a**→**38b**→**38c** was mirrored by an increase in *trans* ring content and thus the degree of crystallinity ($T_m = 98–102\text{ °C}$). Furthermore, the ligand structure had a huge influence on the tacticity of the PMCP. While precursor **38a** gave an atactic polymer, complex **38b** displayed a high degree of stereocontrol, giving highly isotactic PMCP.

Sita and co-workers exploited the ability of the amidinate zirconium catalysts to produce living polymers with crystalline domains through the synthesis of block copolymers from 1-hexene and 1,5-hexadiene (Scheme 24).^[112] Addition of 1-hexene to the activated complex **38b**/[PhNMe₂H][B(C₆F₅)₄] in chlorobenzene at –10 °C gave a living isotactic poly(1-hexene) ($M_n = 12\,200\text{ g mol}^{-1}$, $M_w/M_n = 1.03$). Addition of 1,5-hexadiene to this living chain end resulted in formation of a higher molecular weight polymer ($M_n = 22\,800\text{ g mol}^{-1}$, $M_w/M_n = 1.05$). The ¹³C NMR spectrum of the material was consistent with both PH and PMCP and showed the highly isotactic nature of the diblock material. This strategy was also applied to the synthesis of a triblock copolymer ($M_n = 30\,900\text{ g mol}^{-1}$, $M_w/M_n = 1.05$) by addition of a second portion of 1-hexene to a living diblock (Scheme 24). Through AFM imaging, the block nature of this unique triblock material was

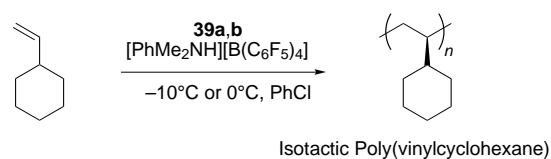


Scheme 24. Synthesis of poly(1-hexene)/PMCP diblock and triblock copolymers with a zirconium amidinate catalyst.

demonstrated. A thin film of the material phase-separated into a morphology composed of PMCP cylinders embedded in a PH matrix.

In 2001, Sita et al. reported a modified class of amidinate catalysts for living olefin polymerization (**39a–c**; Figure 7).^[113] Employing the less bulky Cp ligand, the activated complexes displayed enhanced activities relative to their Cp* counterparts. For example, complex **39b**/[PhNMe₂H][B(C₆F₅)₄] polymerized 1-hexene (200 equiv) to 79% conversion in only 2 min and proceeded to completion in under 10 min to give a monodisperse polymer ($M_n = 20\,800\text{ g mol}^{-1}$, $M_w/M_n = 1.03$). A kinetic study of 1-hexene polymerization with **39c** revealed a linear relationship consistent with a living polymerization, and GPC traces of all reported polymers showed narrow distributions ($M_w/M_n = 1.03–1.09$). While the more exposed nature of the metal center was beneficial in regard to catalytic activity, it had a detrimental effect on stereoselectivity. Unlike complex **38b**, which produced highly isotactic poly(1-hexene)s, polymers from both the achiral compounds **39a, b** and the C₁-symmetric, chiral complex **39c** were atactic, demonstrating the importance of the bulky Cp* ligand for stereodifferentiation.

Given the enhanced activities of these catalysts toward polymerization of 1-hexene, Sita et al. reasoned that these complexes might be capable of polymerization of more sterically encumbered monomers such as vinylcyclohexane.^[113] Indeed, activation of **39a, b** at –10 °C in the presence of vinylcyclohexane resulted in nearly complete conversion to polymer (Scheme 25). Despite the achiral, C_s-symmetric nature of catalyst precursors, the poly(vinylcyclohexane) microstructures in each case were highly isotactic



Scheme 25. Isospecific living polymerization of vinylcyclohexane with a zirconium amidinate catalyst.

($[mmmm] > 95\%$), indicative of a chain-end control mechanism. The linear kinetic relationship and the narrow polydispersities of the polymers ($M_w/M_n = 1.04–1.10$) demonstrated the living nature of the polymerization. This living polymerization was also applied to the synthesis of a new triblock copolymer composed of poly(vinylcyclohexane) and polyhexene domains through a sequential addition approach.

6.4. Amine Bis(phenolate) Complexes

In 1999, a new family of Group 4 complexes bearing amine bis(phenolate) [ONO]- and [ONNO]-type ligands was introduced by Kol, Goldschmidt, and co-workers.^[114] Initial investigations of the C_s -symmetric zirconium compounds **40a** and **41a** (Figure 8) demonstrated the dramatic effect of the extra

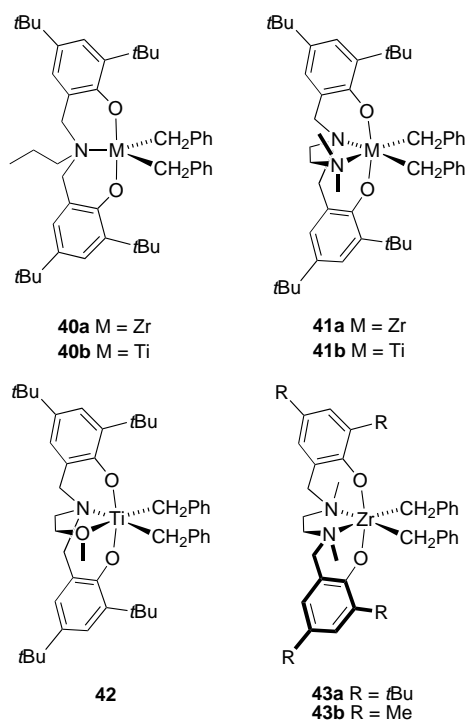
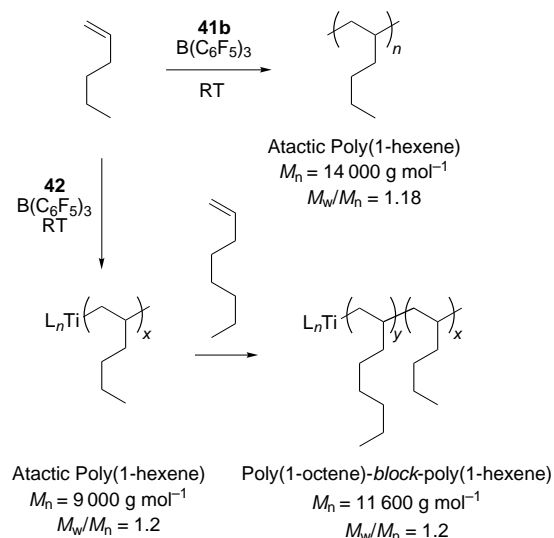


Figure 8. Amine bis(phenolate) catalyst precursors for living olefin polymerization.

donor arm on catalytic activity.^[115] When activated with $B(C_6F_5)_3$ at room temperature, complex **40a** bearing the tridentate [ONO] ligand displayed low activity toward 1-hexene ($23 \text{ kg}_{\text{PH}} \text{ mol}_{\text{Zr}}^{-1} \text{ h}^{-1}$), producing only 1-hexene oligomers (< 20 units/chain). On the other hand, complex **41a**/ $B(C_6F_5)_3$ based on the tetradentate [ONNO] ligand was extremely active for the polymerization ($15\,500 \text{ kg}_{\text{PH}} \text{ mol}_{\text{Zr}}^{-1} \text{ h}^{-1}$), giving high molecular weight poly(1-hexene) with polydispersities consistent with a single-site catalyst ($M_n = 170\,000 \text{ g mol}^{-1}$, $M_w/M_n = 2.2$). The catalytic performance of the titanium complexes **40b** and **41b** was also investigated.^[116] In this case, the activated complex **40b** bearing the [ONO]-type ligand was slightly more active than the [ONNO] complex **41b**, but the polymerization quickly attained a maximum value of molecular weight ($M_n =$

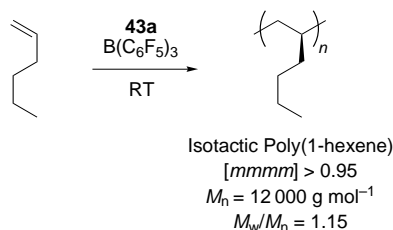
1500 g mol^{-1} , $M_w/M_n \sim 2$). However, the polymerization of 1-hexene with **41b**/ $B(C_6F_5)_3$ bearing the amine donor proceeded in a living fashion ($M_n = 14\,000 \text{ g mol}^{-1}$, $M_w/M_n = 1.18$), giving poly(1-hexene) with a linear increase in molecular weight with time (Scheme 26). As anticipated, NMR spectroscopy revealed the absence of olefinic end groups and the atactic microstructure of the polyhexene. In this case, the presence of the extra donor arm served to suppress chain transfer reactions.



Scheme 26. Living polymerization of 1-hexene and block copolymerization of 1-hexene and 1-octene with amine bis(phenolate)-type catalysts.

With the successes of the extra donor arm of these complexes, Kol, Goldschmidt, and co-workers recently reported a new ligand in this family.^[117] Incorporating an extra oxygen donor, this [ONOO]-type ligand gave the analogous C_s -symmetric titanium species **42** (Figure 8). When activated at room temperature by $B(C_6F_5)_3$, complex **42** proved to be active for polymerization of 1-hexene ($20–35 \text{ kg}_{\text{PH}} \text{ mol}_{\text{Ti}}^{-1} \text{ h}^{-1}$) (Scheme 26). The living behavior of this system was evident by the narrow polydispersities ($M_w/M_n = 1.07–1.12$) and the linear increase of molecular weight with time. Amazingly, this linear relationship was still observed after extremely long reaction times (31 h), giving a high molecular weight poly(1-hexene) ($M_n = 445\,000 \text{ g mol}^{-1}$, $M_w/M_n = 1.12$). The polymerizations also had living character at elevated temperatures, with reactions as high as 65°C giving relatively monodisperse polymers ($M_n = 22\,000 \text{ g mol}^{-1}$, $M_w/M_n = 1.30$). The livingness of this system was also demonstrated through the synthesis of a block copolymer of 1-hexene and 1-octene (Scheme 26). Addition of 1-hexene to **42**/ $B(C_6F_5)_3$ in chlorobenzene at room temperature gave poly(1-hexene) after 3.5 h ($M_n = 9000 \text{ g mol}^{-1}$, $M_w/M_n = 1.2$). After an additional 1.5 h, addition of 1-octene to this living chain end resulted in formation of a higher molecular weight polymer ($M_n = 11\,600 \text{ g mol}^{-1}$, $M_w/M_n = 1.2$) with a ^{13}C NMR spectrum consistent with atactic poly(1-hexene-*block*-1-octene).

With the promising lead of living behavior mediated by an extra amine donor, Kol and co-workers targeted complexes with a new type of [ONNO] ligand with similar functionality but different connectivity, providing catalysts with C_2 symmetry capable of stereocontrol in α -olefin polymerization.^[118] The diamine bis(phenolate) ligands proved excellent for this task, providing C_2 -symmetric complexes (**43a,b**) analogous to the ansa-metallocenes. Complex **43a**, when activated at room temperature by $B(C_6F_5)_3$, proved to be an active catalyst for the polymerization of 1-hexene ($18 \text{ kg}_{\text{PH}} \text{ mol}_{\text{Zr}}^{-1} \text{ h}^{-1}$) (Scheme 27). The linear increase in molecular weight (M_n up to 12000 g mol^{-1}) with conversion and the narrow molecular weight distribution of the polymers ($M_w/M_n = 1.11\text{--}1.15$)



Scheme 27. Living isospecific polymerization of 1-hexene with a diamine bis(phenolate) catalyst.

demonstrated the living nature of the polymerization. Furthermore, ^{13}C NMR spectroscopy revealed that the polymer possessed a highly isotactic microstructure (>95%). The bulky *tert*-butyl substituents of **43a** were crucial to both the livingness and stereoselectivity of the catalytic system; polymerization of 1-hexene with the methyl-substituted complex **43b**/ $B(C_6F_5)_3$ yielded atactic poly(1-hexene) with a broader molecular weight distribution ($M_n = 23\,000 \text{ g mol}^{-1}$, $M_w/M_n = 1.57$).

6.5. Bis(phenoxyimine) and Bis(indolideimine) Complexes

Scientists at Mitsui have discovered that Group IV complexes bearing phenoxyimine ligands are a remarkable class of catalysts for olefin polymerization.^[119] Based on these initial discoveries, several advances in the area of stereoselective as well as living olefin polymerization have been reported. For example, Tian and Coates targeted Mitsui-type complexes (**44a**) for isospecific propylene polymerization. Due to their structural similarities with the ansa-metallocenes, they reasoned that these C_2 -symmetric complexes might be suitable precursors for the isospecific polymerization of α -olefins through a site-control mechanism. Surprisingly, compound **44a**/MAO (Figure 9) produced polypropylenes that were substantially syndiotactic ($[rrrr] = 0.78$).^[120] Microstructural analysis of the resulting polymer revealed that a chain-end mechanism was responsible for the observed stereocontrol. Subsequent studies revealed that this extreme chain end control was enhanced by an unusual secondary insertion

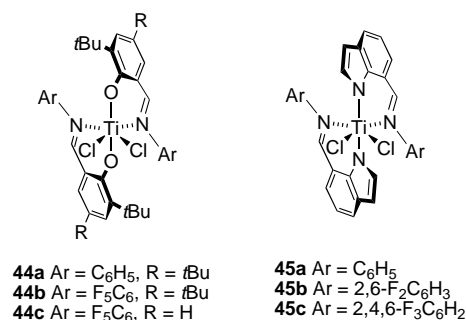
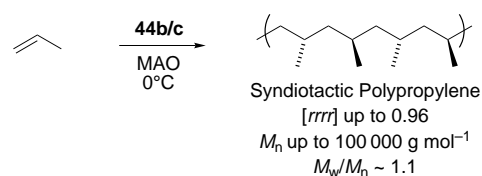


Figure 9. Bis(phenoxyimine) and bis(indolide-imine) catalyst precursors for living olefin polymerization.

mechanism.^[19, 120, 121] However, GPC analyses revealed the lack of molecular weight control in this system ($M_w/M_n \sim 2$).

In an effort to develop improved versions of these phenoxyimine catalysts, Coates and coworkers discovered that simple fluorination of the aniline moiety had a beneficial effect on both catalytic activity and stereoselectivity.^[122] The catalytic system **44b**/MAO was an order of magnitude more active than **44a** and provided highly syndiotactic polypropylene ($[rrrr] = 0.96$; Scheme 28). The polymer exhibited a peak

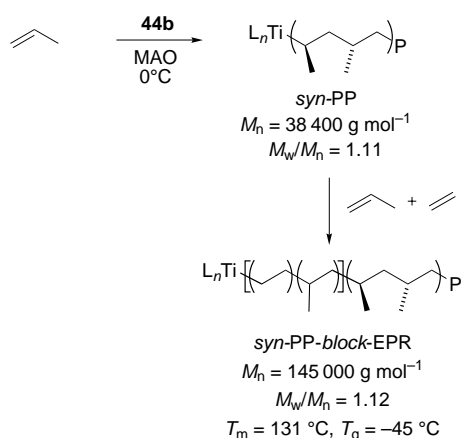


Scheme 28. Highly syndiospecific and living polymerization of propylene with bis(phenoxyimine) catalysts.

melting temperature of 148°C , among the highest values reported for syndiotactic polypropylene. These polymers also displayed narrow molecular weight distributions ($M_w/M_n \sim 1.1$) and were free of olefinic end groups. Not only were β -hydride and β -methyl eliminations suppressed, but the polymerization also proceeded without transfer to the aluminum cocatalyst, a common source of chain transfer in catalytic systems activated by MAO. The living nature of the reaction was demonstrated by the linear relationship of molecular weight and polymer yield. Although a slight deviation from the initial linear relationship was observed at longer reaction times, molecular weight distributions remained narrow ($M_w/M_n = 1.11$) to molecular weights approaching $100\,000 \text{ g mol}^{-1}$. Furthermore, the molecular weight of the polymer was close to the value calculated from the monomer/initiator ratio obtained from the mass of the polymer produced, indicating that each molecule of catalyst produces exactly one polymer chain during the polymerization. Remarkably, polymers with $M_n > 300\,000 \text{ g mol}^{-1}$ were synthesized with fairly narrow molecular weight distributions ($M_w/M_n = 1.34$), and the reactions were also living at room temperature ($M_w/M_n = 1.13$). Fujita and co-workers concurrently reported that the fluorine-containing catalyst system (**44c**/MAO) is also living for propylene polymerization (M_n up to $108\,000 \text{ g mol}^{-1}$, $M_w/M_n = 1.07\text{--}1.14$).^[123] Polymers from this bis(phenoxyimine)

catalyst, which incorporates a single *tert*-butyl substituent on the phenoxy moiety, exhibited somewhat lower syndiotacticity ($[rrrr] = 0.76$) and peak melting temperature ($T_m = 137^\circ\text{C}$) than polymers from **44b**/MAO, although low molecular weight oligomers ($M_n = 2000\text{ g mol}^{-1}$) are nearly perfectly syndiotactic.

Coates and co-workers demonstrated the utility of this living and stereoselective catalyst system through the synthesis of well-defined ethylene/propylene copolymers with crystalline, syndiotactic polypropylene domains (Scheme 29).^[122] Addition of **44b** to a solution of propylene



Scheme 29. Synthesis of ethylene/propylene diblock copolymers with a bis(phenoxyimine) catalyst; EPR = ethylene/propylene rubber.

and MAO at 0°C resulted in the formation of a living polypropylene after 2 h ($M_n = 38\,400\text{ g mol}^{-1}$, $M_w/M_n = 1.11$). Addition to a slight overpressure of ethylene to this living chain end resulted in rapid formation of a higher molecular weight polymer ($M_n = 145\,100\text{ g mol}^{-1}$, $M_w/M_n = 1.12$). The polymer, a *syn*-PP-*block*-EPR diblock copolymer, displayed a T_m of 131°C , while the T_g of the EPR domain was -45°C . Fujita and co-workers have also reported the remarkable, above room temperature living polymerization of ethylene^[124] (M_n up to $400\,000\text{ g mol}^{-1}$, $M_w/M_n = 1.05\text{--}1.13$) and copolymerization of ethylene and propylene using the modified phenoxyimine system **44c**.^[125] Monodisperse ethylene/propylene copolymers with varying propylene content (15–48 mol %) were prepared with **44c**/MAO at 25°C ($M_n > 80\,000\text{ g mol}^{-1}$, $M_w/M_n = 1.07\text{--}1.13$). Diblock and triblock copolymers composed of polyethylene, polypropylene, and ethylene/propylene blocks have also been synthesized with this catalyst system.^[124, 125] For example, a *syn*-PP-*block*-EPR diblock similar to that described above by Coates and co-workers was prepared from reaction of ethylene with a living polypropylene chain ($M_n = 27\,000\text{ g mol}^{-1}$, $M_w/M_n = 1.13$). The resulting copolymer ($M_n = 161\,000\text{ g mol}^{-1}$) displayed a broader molecular weight distribution ($M_w/M_n = 1.51$).^[125]

Fujita and co-workers have also developed a new class of compounds bearing indolide-imine ligands for the living polymerization of ethylene.^[126] When activated by MAO at 25°C , complexes **45a–c** produced polyethylenes with narrow

molecular weight distributions ($M_n = 11\,000\text{--}41\,800\text{ g mol}^{-1}$, $M_w/M_n = 1.11\text{--}1.14$). Increasing electrophilicity of the metal center through fluorination of the ligand led to an increase in activity, with **45c** providing the most active precursor. The living nature of the polymerization was demonstrated for **45c**/MAO by the linear increase in molecular weight with polymer yield. Notably, polymerization with **45c**/MAO at 50°C also produced polyethylene with a fairly narrow polydispersity ($M_w/M_n = 1.24$).

7. Outlook and Summary

The last half-decade has witnessed a renaissance in living olefin polymerization, building rapidly on the foundation set solidly by Doi and co-workers over two decades ago. Today, we have many efficient and selective catalysts available for living olefin polymerization. Polyethylene, as well as atactic, isotactic, and syndiotactic poly(α -olefins) can now be efficiently synthesized in a living manner, allowing the creation of unlimited new polymer architectures, such as block copolymers and end-functional macromolecules. The ability to synthesize such polymers will allow the detailed study of structure–property relationships and their influence on mechanical and physical properties of this new class of materials.

Perhaps the main challenge facing this new field is that these sophisticated (and therefore usually expensive) metal complexes only form one polymer chain during the polymerization reaction, rendering the displacement of current commodity polyolefins by these new materials economically nonviable. Therefore, significant research must be conducted to develop new strategies for the production of multiple polymer chains per initiator. Such approaches will include the development of agents that can cleave the growing polymer chain from the metal but regenerate the catalyst in an active form that can propagate a new polymer molecule. Alternately, other methods for the synthesis of block copolymers from non-living systems must also be pursued. These include: 1) the development of oscillating catalysts that can change their geometries during chain growth;^[127] 2) the transfer of chains between catalysts of differing stereospecificities;^[128] 3) the change of polymerization conditions that affect stereochemistry or comonomer incorporation on a time scale faster than chain growth; and 4) the development of stopped-flow techniques.^[129]

Undoubtedly, the future will witness continued research at this exciting interface of organometallic chemistry and polymer science to the benefit of both fields. It is clear that living systems will allow detailed mechanistic studies of catalysts due to their discrete nature; in return these new catalysts will allow the synthesis and study of a wide range of new polymeric materials.

G.W.C. gratefully acknowledges a Packard Foundation Fellowship in Science and Engineering, a Dreyfus New Faculty Award, an Alfred P. Sloan Research Fellowship, an Arnold and Mabel Beckman Foundation Young Investigator Award, a NSF

CAREER Award, and a Camille Dreyfus Teacher-Scholar Award. S.R. thanks the DAAD for a postdoctoral fellowship.

Received: November 7, 2001 [A 499]

- [1] M. Szwarc, *J. Polym. Sci. Part A* **1998**, 36, IX–XV.
- [2] O. W. Webster, *Science* **1991**, 251, 887–893.
- [3] For leading references on block copolymers, see: a) F. S. Bates, G. H. Fredrickson, *Phys. Today* **1999**, 52, 32–38; b) I. W. Hamley, *The Physics of Block Copolymers*, Oxford University Press, Oxford, **1998**; c) F. S. Bates, *Science* **1991**, 251, 898–905; d) M. Hillmyer, *Curr. Opin. Solid State Mater. Sci.* **1999**, 4, 559–564.
- [4] K. Ziegler, E. Holzkamp, H. Breil, H. Martin, *Angew. Chem.* **1955**, 67, 426.
- [5] G. Natta, P. Pino, P. Corradini, F. Danusso, E. Mantica, G. Mazzanti, G. Moraglio, *J. Am. Chem. Soc.* **1955**, 77, 1708–1710.
- [6] G. W. Coates, *Chem. Rev.* **2000**, 100, 1223–1252.
- [7] *Anionic Polymerization: Principles and Practical Applications* (Ed.: H. L. Hsieh, R. P. Quirk), Marcel Dekker, New York, **1996**.
- [8] *Cationic Polymerizations: Mechanisms, Synthesis, and Applications*, (Ed.: K. Matyjaszewski), Marcel Dekker, New York, **1996**.
- [9] C. J. Hawker, A. W. Bosman, E. Harth, *Chem. Rev.* **2001**, 101, 3661–3688.
- [10] M. Kamigaito, T. Ando, M. Sawamoto, *Chem. Rev.* **2001**, 101, 3689–3746.
- [11] K. Matyjaszewski, J. H. Xia, *Chem. Rev.* **2001**, 101, 2921–2990.
- [12] Molecular weights are most readily measured by using gel permeation chromatography (GPC). This technique determines relative number- and weight-average molecular weights unless the chromatograph is calibrated with monodisperse standards of the polymer being examined. Since there are few commercially available polyolefin standards, especially of block copolymers most molecular weight data in this review are measured relative to polystyrene standards.
- [13] R. P. Quirk, B. Lee, *Polym. Int.* **1992**, 27, 359–367.
- [14] For a leading reference on the mechanism of polymerization of olefins by metallocene catalysts, see: R. H. Grubbs, G. W. Coates, *Acc. Chem. Res.* **1996**, 29, 85–93.
- [15] L. Resconi, L. Cavallo, A. Fait, F. Piemontesi, *Chem. Rev.* **2000**, 100, 1253–1345.
- [16] L. Q. Deng, T. Ziegler, T. K. Woo, P. Margl, L. Y. Fan, *Organometallics* **1998**, 17, 3240–3253.
- [17] E. Y. X. Chen, T. J. Marks, *Chem. Rev.* **2000**, 100, 1391–1434.
- [18] A. Zambelli, G. Natta, I. Pasquon, R. Signorini, *J. Poly. Sci. Part C* **1967**, 2485–2499.
- [19] In a secondary insertion, the monomer inserts into the polymer chain such that the more substituted carbon atom becomes bound to the metal center and the polymer chain becomes attached to the unsubstituted carbon of the alkene.
- [20] A. Zambelli, I. Pasquon, R. Signorini, G. Natta, *Makromol. Chem. Macromol. Chem. Phys.* **1968**, 112, 160–182.
- [21] Y. Doi, M. Takada, T. Keii, *Bull. Chem. Soc. Jpn.* **1979**, 52, 1802–1806.
- [22] Y. Doi, S. Ueki, T. Keii, *Macromolecules* **1979**, 12, 814–819.
- [23] Y. Doi, S. Ueki, T. Keii, *Makromol. Chem. Macromol. Chem. Phys.* **1979**, 180, 1359–1361.
- [24] P. J. Flory, *Principles of Polymer Chemistry*, Cornell University Press, Ithaca, **1953**.
- [25] S. Ueki, Y. Doi, T. Keii, *Makromol. Chem. Rapid Commun.* **1981**, 2, 403–406.
- [26] Y. Doi, S. Suzuki, K. Soga, *Makromol. Chem. Rapid Commun.* **1985**, 6, 639–642.
- [27] Y. Doi, S. Suzuki, K. Soga, *Macromolecules* **1986**, 19, 2896–2900.
- [28] Y. Doi, S. Suzuki, G. Hizal, K. Soga, *Transition Met. Catal. Polym.* **1988**, 182–194.
- [29] Y. Doi, S. Ueki, T. Keii in *Coordination Polymerization* (Eds.: C. C. Price, E. J. Vandenberg), Plenum Press, New York, **1983**.
- [30] Y. Doi, N. Tokuhito, S. Suzuki, K. Soga, *Makromol. Chem. Rapid Commun.* **1987**, 8, 285–290.
- [31] Y. Doi, S. Ueki, S. Tamura, S. Nagahara, T. Keii, *Polymer* **1982**, 23, 258–262.
- [32] Y. Doi, N. Tokuhito, K. Soga, *Makromol. Chem. Macromol. Chem. Phys.* **1989**, 190, 643–651.
- [33] Y. Doi, Y. Watanabe, S. Ueki, K. Soga, *Makromol. Chem. Rapid Commun.* **1983**, 4, 533–537.
- [34] Y. Doi, T. Koyama, K. Soga, *Makromol. Chem. Macromol. Chem. Phys.* **1985**, 186, 11–15.
- [35] Y. Doi, T. Keii, *Adv. Polym. Sci.* **1986**, 73–4, 201–248.
- [36] Y. Doi, G. Hizal, K. Soga, *Makromol. Chem.* **1987**, 188, 1273–1279.
- [37] Y. H. Doi, M. Nunomura, N. Ohgizawa, K. Soga, *Makromol. Chem. Rapid Commun.* **1991**, 12, 245–249.
- [38] Y. Doi, M. Murata, K. Soga, *Makromol. Chem. Rapid Commun.* **1984**, 5, 811–814.
- [39] S. Ueki, H. Furuhashi, N. Murakami, M. Murata, Y. Doi, *Stud. Surf. Sci. Catal.* **1995**, 92, 359–362.
- [40] Y. Doi, S. Ueki, T. Keii, *Makromol. Chem. Rapid Commun.* **1982**, 3, 225–229.
- [41] G. Jeske, H. Lauke, H. Mauermann, P. N. Swepston, H. Schumann, T. J. Marks, *J. Am. Chem. Soc.* **1985**, 107, 8091–8103.
- [42] H. Yasuda, H. Yamamoto, K. Yokota, S. Miyake, A. Nakamura, *J. Am. Chem. Soc.* **1992**, 114, 4908–4910.
- [43] H. Yasuda, M. Furo, H. Yamamoto, A. Nakamura, S. Miyake, N. Kibino, *Macromolecules* **1992**, 25, 5115–5116.
- [44] H. Yasuda, E. Ihara, *Macromol. Chem. Phys.* **1995**, 196, 2417–2441.
- [45] H. Yasuda, E. Ihara, T. Hayakawa, T. Kakehi, *J. Macromol. Sci. Pure Appl. Chem.* **1997**, A34, 1929–1944.
- [46] H. Yasuda, E. Ihara, *Bull. Chem. Soc. Jpn.* **1997**, 70, 1745–1767.
- [47] H. Yasuda, *J. Polym. Sci. Part A* **2001**, 39, 1955–1959.
- [48] G. Desurmont, Y. Li, H. Yasuda, T. Maruo, N. Kanehisa, Y. Kai, *Organometallics* **2000**, 19, 1811–1813.
- [49] G. Desurmont, T. Tokimitsu, H. Yasuda, *Macromolecules* **2000**, 33, 7679–7681.
- [50] E. Ihara, M. Nodono, K. Katsura, Y. Adachi, H. Yasuda, M. Yamagashira, H. Hashimoto, N. Kanehisa, Y. Kai, *Organometallics* **1998**, 17, 3945–3956.
- [51] G. Desurmont, M. Tanaka, Y. Li, H. Yasuda, T. Tokimitsu, S. Tone, A. Yanagase, *J. Polym. Sci. Part A* **2000**, 38, 4095–4109.
- [52] E. Ihara, S. Yoshioka, M. Furo, K. Katsura, H. Yasuda, S. Mohri, N. Kanehisa, Y. Kai, *Organometallics* **2001**, 29, 1752–1761.
- [53] M. Brookhart, A. F. Volpe, Jr., J. M. DeSimone, *Polym. Prepr. Am. Chem. Soc. Div. Polym. Chem.* **1991**, 32, 461–462.
- [54] M. Brookhart, J. M. DeSimone, B. E. Grant, M. J. Tanner, *Macromolecules* **1995**, 28, 5378–5380.
- [55] K. Mashima, S. Fujikawa, H. Urata, E. Tanaka, A. Nakamura, *J. Am. Chem. Soc.* **1993**, 115, 10990–10991.
- [56] K. Mashima, S. Fujikawa, H. Urata, E. Tanaka, A. Nakamura, *J. Chem. Soc. Chem. Commun.* **1994**, 1623–1624.
- [57] K. Mashima, S. Fujikawa, Y. Tanaka, H. Urata, T. Oshiki, E. Tanaka, A. Nakamura, *Organometallics* **1995**, 14, 2633–2640.
- [58] S. D. Ittel, L. K. Johnson, M. Brookhart, *Chem. Rev.* **2000**, 100, 1169–1203.
- [59] L. S. Boffa, B. M. Novak, *Chem. Rev.* **2000**, 100, 1479–1493.
- [60] P. Hadjiandreou, M. Julemont, P. Teyssie, *Macromolecules* **1984**, 17, 2455–2456.
- [61] T. J. Deming, B. M. Novak, *Macromolecules* **1991**, 24, 326–328.
- [62] T. J. Deming, B. M. Novak, *Macromolecules* **1991**, 24, 5478–5480.
- [63] T. J. Deming, B. M. Novak, J. W. Ziller, *J. Am. Chem. Soc.* **1994**, 116, 2366–2374.
- [64] M. Suzuki, T. Takao, N. Sakamoto, I. Tomita, T. Endo, *Polym. J.* **1999**, 31, 1021–1024.
- [65] C. Mehler, W. Risse, *Macromolecules* **1992**, 25, 4226–4228.
- [66] S. Breunig, W. Risse, *Makromol. Chem.* **1992**, 193, 2915–2927.
- [67] A. L. Safir, B. M. Novak, *Macromolecules* **1995**, 28, 5396–5398.
- [68] L. K. Johnson, C. M. Killian, M. Brookhart, *J. Am. Chem. Soc.* **1995**, 117, 6414–6415.
- [69] C. M. Killian, D. J. Tempel, L. K. Johnson, M. Brookhart, *J. Am. Chem. Soc.* **1996**, 118, 11664–11665.
- [70] V. M. Möhring, G. Fink, *Angew. Chem.* **1985**, 97, 982–984; *Angew. Chem. Int. Ed. Engl.* **1985**, 24, 1001–1003.
- [71] Z. Guan, P. M. Cotts, E. F. McCord, S. J. McLain, *Science* **1999**, 283, 2059–2062.
- [72] C. M. Killian, Thesis, University of North Carolina, **1996**.

- [73] A. C. Gottfried, M. Brookhart, *Macromolecules* **2001**, *34*, 1140–1142.
- [74] D. Pappalardo, M. Mazzeo, S. Antinucci, C. Pellecchia, *Macromolecules* **2000**, *33*, 9483–9487.
- [75] C. Pellecchia, A. Zambelli, L. Oliva, D. Pappalardo, *Macromolecules* **1996**, *29*, 6990–6993.
- [76] C. Pellecchia, A. Zambelli, *Macromol. Rapid Commun.* **1996**, *17*, 333–338.
- [77] C. Pellecchia, A. Zambelli, M. Mazzeo, D. Pappalardo, *J. Mol. Catal. A Chem.* **1998**, *128*, 229–237.
- [78] M. Schmid, R. Eberhardt, M. Klinga, M. Leskela, B. Rieger, *Organometallics* **2001**, *20*, 2321–2330.
- [79] L. R. Rieth, R. F. Eaton, G. W. Coates, *Angew. Chem.* **2001**, *113*, 2211–2214; *Angew. Chem. Int. Ed.* **2001**, *40*, 2153–2156.
- [80] G. J. P. Britovsek, V. C. Gibson, D. F. Wass, *Angew. Chem.* **1999**, *111*, 448–468; *Angew. Chem. Int. Ed. Engl.* **1999**, *38*, 428–447.
- [81] H. W. Turner, G. G. Hlatky (Exxon), PCT Int. Appl. 9112285, **1991**.
- [82] J. Sassmannshausen, M. E. Bochmann, J. Rosch, D. Lilge, *J. Organomet. Chem.* **1997**, *548*, 23–28.
- [83] M. C. Murray, M. C. Baird, *J. Mol. Catal. A Chem.* **1998**, *128*, 1–4.
- [84] L. Resconi, F. Piemontesi, G. Francisocono, L. Abis, T. Fiorani, *J. Am. Chem. Soc.* **1992**, *114*, 1025–1032.
- [85] H. Hagihara, T. Shiono, T. Ikeda, *Macromolecules* **1998**, *31*, 3184–3188.
- [86] T. Hasan, A. Ioku, K. Nishii, T. Shiono, T. Ikeda, *Macromolecules* **2001**, *34*, 3142–3145.
- [87] Y. Fukui, M. Murata, K. Soga, *Macromol. Rapid Commun.* **1999**, *20*, 637–640.
- [88] Y. Fukui, M. Murata, *Macromol. Chem. Phys.* **2001**, *202*, 1430–1434.
- [89] J. C. Jansen, R. Mendichi, P. Locatelli, I. Tritto, *Macromol. Rapid Commun.* **2001**, *22*, 1394–1398.
- [90] Y. Fukui, M. Murata, *Macromol. Chem. Phys.* **2001**, *202*, 1473–1477.
- [91] Y. Fukui, M. Murata, *Macromol. Chem. Phys.* **2001**, *202*, 3205–3209.
- [92] H. Cherdron, M.-J. Brekner, F. Osan, *Angew. Makromol. Chem.* **1994**, *223*, 121–133.
- [93] J. D. Scollard, D. H. McConville, *J. Am. Chem. Soc.* **1996**, *118*, 10008–10009.
- [94] J. D. Scollard, D. H. McConville, J. J. Vittal, N. C. Payne, *J. Mol. Catal. A Chem.* **1998**, *128*, 201–214.
- [95] J. D. Scollard, D. H. McConville, S. J. Rettig, *Organometallics* **1997**, *16*, 1810–1812.
- [96] H. Hagimoto, T. Shiono, T. Ikeda, *Macromol. Rapid Commun.* **2002**, *23*, 73–76.
- [97] R. Baumann, W. M. Davis, R. R. Schrock, *J. Am. Chem. Soc.* **1997**, *119*, 3830–3831.
- [98] R. Baumann, R. R. Schrock, *J. Organomet. Chem.* **1998**, *557*, 69–75.
- [99] R. Baumann, R. Stumpf, W. M. Davis, L. C. Liang, R. R. Schrock, *J. Am. Chem. Soc.* **1999**, *121*, 7822–7836.
- [100] R. R. Schrock, R. Baumann, S. M. Reid, J. T. Goodman, R. Stumpf, W. M. Davis, *Organometallics* **1999**, *18*, 3649–3670.
- [101] J. T. Goodman, R. R. Schrock, *Organometallics* **2001**, *20*, 5205–5211.
- [102] L. C. Liang, R. R. Schrock, W. M. Davis, D. H. McConville, *J. Am. Chem. Soc.* **1999**, *121*, 5797–5798.
- [103] R. R. Schrock, P. J. Bonitatebus, Y. Schrodi, *Organometallics* **2001**, *20*, 1056–1058.
- [104] Y. Schrodi, R. R. Schrock, P. J. Bonitatebus, *Organometallics* **2001**, *20*, 3560–3573.
- [105] P. Mehrkhodavandi, P. J. Bonitatebus, R. R. Schrock, *J. Am. Chem. Soc.* **2000**, *122*, 7841–7842.
- [106] P. Mehrkhodavandi, R. R. Schrock, *J. Am. Chem. Soc.* **2001**, *123*, 10746–10747.
- [107] D. D. Graf, R. R. Schrock, W. M. Davis, R. Stumpf, *Organometallics* **1999**, *18*, 843–852.
- [108] A. D. Horton, J. de With, A. J. van der Linden, H. van de Weg, *Organometallics* **1996**, *15*, 2672–2674.
- [109] Y. M. Jeon, S. J. Park, J. Heo, K. Kim, *Organometallics* **1998**, *17*, 3161–3163.
- [110] K. C. Jayaratne, L. R. Sita, *J. Am. Chem. Soc.* **2000**, *122*, 958–959.
- [111] R. J. Keaton, K. C. Jayaratne, J. C. Fettingner, L. R. Sita, *J. Am. Chem. Soc.* **2000**, *122*, 12909–12910.
- [112] K. C. Jayaratne, R. J. Keaton, D. A. Henningsen, L. R. Sita, *J. Am. Chem. Soc.* **2000**, *122*, 10490–10491.
- [113] R. J. Keaton, K. C. Jayaratne, D. A. Henningsen, L. A. Koterwas, L. R. Sita, *J. Am. Chem. Soc.* **2001**, *123*, 6197–6198.
- [114] E. Y. Tshuva, M. Versano, I. Goldberg, M. Kol, H. Weitman, Z. Goldschmidt, *Inorg. Chem. Commun.* **1999**, *2*, 371–373.
- [115] E. Y. Tshuva, I. Goldberg, M. Kol, H. Weitman, Z. Goldschmidt, *Chem. Commun.* **2000**, 379–380.
- [116] E. Y. Tshuva, I. Goldberg, M. Kol, Z. Goldschmidt, *Inorg. Chem. Commun.* **2000**, *3*, 611–614.
- [117] a) E. Y. Tshuva, I. Goldberg, M. Kol, Z. Goldschmidt, *Chem. Commun.* **2001**, 2120–2121; b) E. Y. Tshuva, S. Groysman, I. Goldberg, M. Kol, Z. Goldschmidt, *Organometallics* **2002**, *21*, 662–670.
- [118] E. Y. Tshuva, I. Goldberg, M. Kol, *J. Am. Chem. Soc.* **2000**, *122*, 10706–10707.
- [119] a) S. Matsui, Y. Tohi, M. Mitani, J. Saito, H. Makio, H. Tanaka, M. Nitabaru, T. Nakano, T. Fujita, *Chem. Lett.* **1999**, 1065–1066; b) S. Matsui, M. Mitani, J. Saito, Y. Tohi, H. Makio, H. Tanaka, T. Fujita, *Chem. Lett.* **1999**, 1263–1263; c) S. Matsui, M. Mitani, J. Saito, N. Matsukawa, H. Tanaka, T. Nakano, T. Fujita, *Chem. Lett.* **2000**, 554–555; d) T. Fujita, Y. Tohi, M. Mitani, S. Matsui, J. Saito, M. Nitabaru, K. Sugi, H. Makio, T. Tsutsui, *Eur. Pat. Appl.* 874005 (*Chem. Abstr.* **1998**, *129*, 331166); for a patent regarding Mitsui's research in living alkene polymerization, see: e) M. Mitani, Y. Yoshida, J. Mohri, K. Tsuru, S. Ishii, S. Kojoh, T. Matsugi, J. Saito, N. Matsukawa, S. Matsui, T. Nakano, H. Tanaka, N. Kashiwa, T. Fujita, PCT Int. Appl. WO2001055231 (*Chem. Abstr.* **2001**, *135*, 137852).
- [120] J. Tian, G. W. Coates, *Angew. Chem.* **2000**, *112*, 3772–3775; *Angew. Chem. Int. Ed.* **2000**, *39*, 3626–3629.
- [121] a) J. Saito, M. Mitani, M. Onda, J. Mohri, S. Ishii, Y. Yoshida, T. Nakano, H. Tanaka, T. Matsugi, S. Kojoh, N. Kashiwa, T. Fujita, *Macromol. Rapid Commun.* **2001**, *22*, 1072–1075; b) M. Lamberti, D. Pappalardo, A. Zambelli, C. Pellecchia, *Macromolecules* **2002**, *35*, 658–663; c) P. D. Hustad, J. Tian, G. W. Coates, *J. Am. Chem. Soc.* **2002**, *124*, 3614–3621.
- [122] J. Tian, P. D. Hustad, G. W. Coates, *J. Am. Chem. Soc.* **2001**, *123*, 5134–5135.
- [123] J. Saito, M. Mitani, J. Mohri, S. Ishii, Y. Yoshida, T. Matsugi, S. Kojoh, N. Kashiwa, T. Fujita, *Chem. Lett.* **2001**, 576–577.
- [124] a) J. Saito, M. Mitani, J. Mohri, Y. Yoshida, S. Matsui, S. Ishii, S. Kojoh, N. Kashiwa, T. Fujita, *Angew. Chem., Int. Ed. Engl.* **2001**, *40*, 2918–2920; *Angew. Chem.* **2001**, *113*, 3002–3004; b) M. Mitani, J. Mohri, Y. Yoshida, J. Saito, S. Ishii, K. Tsuru, S. Matsui, R. Furuyama, T. Nakano, H. Tanaka, S. Kojoh, T. Matsugi, N. Kashiwa, T. Fujita, *J. Am. Chem. Soc.* **2002**, *124*, 3327–3336.
- [125] S. Kojoh, T. Matsugi, J. Saito, M. Mitani, T. Fujita, N. Kashiwa, *Chem. Lett.* **2001**, 822–823.
- [126] T. Matsugi, S. Matsui, S. Kojoh, Y. Takagi, Y. Inoue, T. Fujita, N. Kashiwa, *Chem. Lett.* **2001**, 566–567.
- [127] G. W. Coates, R. M. Waymouth, *Science* **1995**, *267*, 217–219.
- [128] For recent examples of stereoblock polymer synthesis using polymer exchange pathways, see: a) J. C. W. Chien, Y. Iwamoto, M. D. Rausch, W. Wedler, H. H. Winter, *Macromolecules* **1997**, *30*, 3447–3458; b) J. C. W. Chien, Y. Iwamoto, M. D. Rausch, *J. Poly. Sci. Part A* **1999**, *37*, 2439–2445; c) S. Lieber, H. H. Brintzinger, *Macromolecules* **2000**, *33*, 9192–9199; d) K. C. Jayaratne, L. R. Sita, *J. Am. Chem. Soc.* **2001**, *123*, 10754–10755.
- [129] B. Liu, H. Matsuoka, M. Terano, *Macromol. Rapid Commun.* **2001**, *22*, 1–24.

Chemical Strategies for Iron Acquisition in Plants

Dorothee Staiger*

Abstract: Iron is an essential element for plant nutrition. Although iron is the fourth most abundant element (3 %) of the earth's crust, it is not readily available because of its low solubility. Therefore, plants need an active mechanism to extract iron from the soil. They have evolved several chemical strategies to acquire iron ions and the physiology of these mechanisms has been known for a long time. Only recently, the use of molecular genetic approaches has led to a biochemical and molecular characterization of the players involved, thus providing an entry to the manipulation of iron uptake in plants.

Introduction

1.1. The Role of Iron in Plant Metabolism

In 1882 the plant physiologist Julius von Sachs became aware of the importance of iron for plant nutrition. He investigated the consequences of submerging roots into an iron-free medium by growing plants in hydroponic cultures. He observed that newly formed leaves remained white because they were not able to produce the green pigment, chlorophyll, and concluded that this disease, chlorosis, is the result of iron deficiency.^[1] This experiment demonstrated that iron is essential for chlorophyll biosynthesis.

The importance of iron for metabolism is founded upon its ability to form two stable ions, Fe^{II} and Fe^{III}. Accordingly, iron ions are involved in most redox processes in the electron transport chains of photosynthesis and respiration which serve to transform energy from electron transport into ATP, the energy source of the cell. Iron is also important for symbiotic nitrogen fixation in root nodules of legumes. Iron is contained in the subunits of the nitrogenase enzyme that reduces N₂ to NH₃, as well as in leghaemoglobin that binds molecular oxygen in the root nodules.

1.2. Threats of Excess Iron

The property of iron ions to catalyze one-electron transitions requires a limitation of the cellular iron concentration since iron promotes the formation of toxic oxygen species. Superoxide anions are formed as intermediates during the reduction of molecular oxygen to H₂O within the cell. These anions reduce Fe^{III} to Fe^{II} (Scheme 1), which in turn catalyze

Reduction of Fe^{III} by superoxide anions



Fenton reaction



Sum: Haber – Weiss reaction



Scheme 1. Toxicity of iron ions within the cell. The Haber – Weiss reaction is the sum of the reduction of Fe^{III} ions by superoxide anions and the Fenton reaction, the Fe^{II}-catalyzed degradation of H₂O₂ to highly reactive hydroxyl radicals.

the decomposition of H₂O₂ to highly reactive hydroxyl radicals (the Fenton reaction), which damage cellular components such as DNA and lipids. Such an excess of reactive oxygen species is designated oxidative stress.^[2, 3] In pea mutants that accumulate excess iron, for example, cell death even occurs, which leads to so-called necrotic lesions in leaves. This situation is analogous to a hereditary disease in humans in which enhanced iron uptake correlates with highly enhanced incidence of liver cancer.

How do plants cope with excess iron? On the one hand, as a preventive means, an antioxidative system destroys superoxide radicals and H₂O₂ before they come into contact with iron. Ironically, iron and heme groups are essential cofactors of the peroxidase and catalase enzymes which decompose H₂O₂. On the other hand, excess iron is stored in a multimeric protein, ferritin, that can accommodate up to 4500 iron ions.^[2]

1.3. Iron Uptake

Control of iron uptake represents another approach the plant can adopt to balance its iron content. Although iron

[*] Dr. D. Staiger
Institute for Plant Sciences
Swiss Federal Institute for Technology
8092 Zurich (Switzerland)
Fax: (+41) 1-632-1081
E-mail: dorothee.staiger@ipw.biol.ethz.ch

ranks fourth (3%) among the elements in the earth's crust, it is not readily available for plant nutrition. Iron primarily occurs in the form of insoluble oxyhydroxide polymers, such as goethite ($\alpha\text{-FeOOH}$) and hematite ($\alpha\text{-Fe}_2\text{O}_3$), which are generated by weathering. Free iron ions occur at neutral pH values only at a concentration of about 10^{-17} M ; ferrous ions that are more soluble are readily oxidized to ferric ions, which again precipitate.^[4] The low solubility of ferric ions therefore does not guarantee a sufficient supply of iron for the roots. Plants therefore require an active mechanism to release iron from Fe^{III} oxide hydrates and to absorb it from the soil.

Iron excess is found mainly on waterlogged soil with anaerobic conditions, such as rice fields. Here, Fe^{III} ions are readily reduced to more soluble Fe^{II} ions. The excess accumulation of Fe^{II} ions in the rice plants results in the well-known bronzing phenomenon, caused by oxidative stress.^[2, 3]

Plants have evolved three chemical strategies to acquire iron: release of protons from the root surface to enhance dissociation of Fe^{III} oxides, reduction, and chelation.^[3, 5] These mechanisms have been well described at the physiological level and several mutants defective in iron uptake have been identified during the last few decades. However, the use of molecular genetic approaches has only recently led to the biochemical and molecular characterization of the players involved.

2. Strategy I: Reduction

Most plants, except the grasses, activate a battery of mechanisms—the so-called strategy I, which should be distinguished from strategy II of the grasses which will be discussed subsequently.^[5]

2.1. Elements of Strategy I

Strategy I plants excrete protons from the root surface to lower the pH value in the immediate vicinity of the root, the so-called rhizosphere. It is likely that this is accomplished by activation of a proton-pumping ATPase, an enzyme that transfers protons through the cell membrane to the outside at the expense of ATP. Acidification of the soil shifts the equilibrium towards dissociation of $[\text{Fe}(\text{OH})_3]$ complexes: lowering the pH value by one unit increases the solubility of Fe^{III} ions by a factor of a thousand.^[6]

Furthermore, the capacity to reduce ferric ions in an NADH-dependent manner increases at the root surface. Ferrous ions are about 10^{16} times more soluble than ferric ions at neutral pH. Ferrous ions are the substrate for a specific uptake system.^[7] In addition, plants increase the surface available for iron uptake by an increased formation of root hairs (appendices of the outermost cell layer). The elements of strategy I are shown in Figure 1. A sensor that measures iron concentration within the plant has remained elusive.

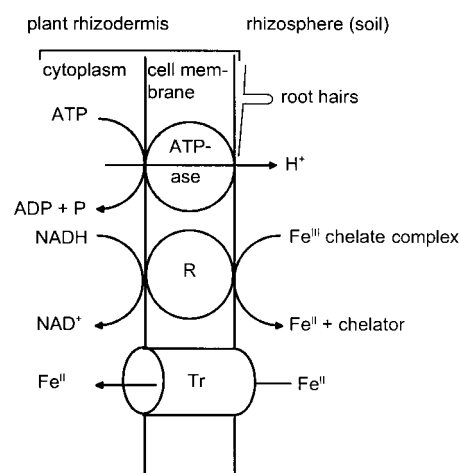


Figure 1. Elements of strategy I (adapted from ref. [5]). The outermost cell layer of the root, the rhizodermis, and the immediate vicinity of the soil, the rhizosphere, are depicted. All plants, except the grasses, respond to iron limitation by acidifying the rhizosphere, increased reduction of an Fe^{III} chelate by an NADH-dependent reductase (R) at the root surface, and Fe^{II} uptake by a specific, inducible uptake system (Tr). Moreover, the root surface is increased through the formation of additional root hairs.

2.2. Identification of Fe^{III} –Chelate Reductase through a Genetic Approach in the Model Plant *Arabidopsis thaliana*

A genetic approach in the model plant *Arabidopsis thaliana* (Figure 2) has led to the identification of components of the iron-uptake system. *Arabidopsis* is a weed of the cruciferous plant family. It has developed into the model system of plant molecular biologists because of its short generation time of a few weeks and its small genome that has been entirely sequenced.^[8]

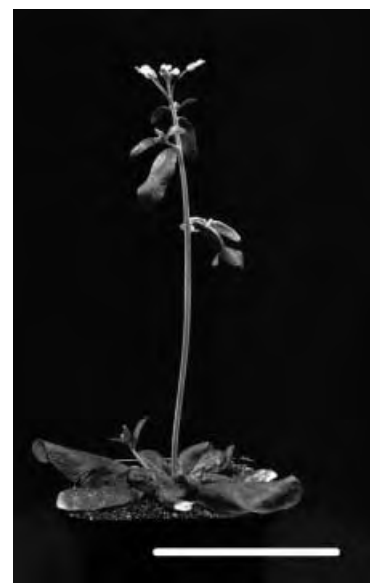


Figure 2. *Arabidopsis thaliana* is a small member of the cruciferous plants. It has developed into the model plant of plant molecular biologists because of its short generation time of a few weeks and its small genome, whose entire sequence is known.^[8] The bar corresponds to 5 cm.

Arabidopsis is a strategy I plant and relies on solubilization of iron by an increased NADH-dependent Fe^{III} -reducing capacity at the root surface. A genetic screen for mutants that do not enhance this Fe^{III} -reducing capacity in times of iron deficiency has been initiated to identify the reducing activity molecularly.^[9] Towards this end, *Arabidopsis* seeds have been treated with ethyl methane sulfonate (EMS), a mutagen that modifies bases of the genome. In the case where such a mutation affects an essential amino acid of a particular protein, a defect is observed in the plant. The offspring of the mutagenized population was screened for individuals with a defect in their iron-reducing capacity by a colorimetric test for the product of the reduction: ferrous ions form a complex with the ferrozine dye whose appearance can be followed photo-metrically at 562 nm.

In this way, three mutants have been identified, *frd1-1*, *frd1-2* and *frd1-3* (*frd* = ferric reductase deficient). These mutants do not show an increased Fe^{III} reductase activity upon iron depletion, in contrast to wild-type plants.^[9] Genetic tests revealed that the three mutations affected the same gene locus.

The identification of the defective gene in these mutants took advantage of a concomitant approach to clone plant Fe^{III} -chelate reductase by homology to the known yeast Fe^{III} -chelate reductase. Towards this end, chemically synthesized oligonucleotides corresponding to conserved regions of the yeast gene were used as starting molecules for enzymatic amplification from the *Arabidopsis* genome by the polymerase chain reaction.^[10]

Indeed, part of an *Arabidopsis* gene was amplified that codes for a putative reductase. The predicted protein shows, among others, homology to human phagocyte NADPH oxidase. This enzyme catalyzes the reduction of O_2 to O_2^- by transferring one electron across the cell membrane onto O_2 . The newly identified *Arabidopsis* protein features hydrophobic regions indicative of localization within a membrane (Figure 3). On the cytosolic sides there are binding sites for the electron donor NADH and the cofactor FAD. The membrane-localized part of the molecule contains binding sites for the heme groups that mediate electron transport to the outside.^[10]

Is this protein indeed connected to the defect in the *frd* mutants? The transformation of the wild-type gene for the

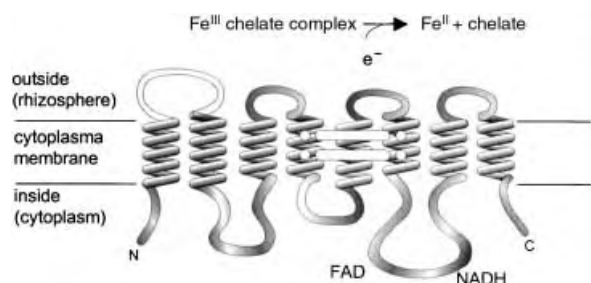


Figure 3. Schematic structure of the Fe^{III} -chelate reductase (adapted from ref. [10]). The reductase has hydrophobic regions indicative of membrane-spanning domains. On the cytosolic site there are binding sites for the electron donor NADH and the cofactor FAD. In the part of the protein that is localized within the membrane there are two histidine residues (open circles) which serve as attachment sites for the heme groups that mediate the electron transport.

Fe^{III} reductase into the *frd1* mutants results in their ability to reduce Fe^{III} ions being restored. Furthermore, point mutations were found in the reductase genes of the mutants that led to defective proteins, which indicated that the *frd* mutations indeed affect the reductase-reducing Fe^{III} centers at the root surface.^[10]

2.3. Identification of Components of the Iron-Uptake System by Functional Complementation of Yeast Mutants

How do Fe^{II} ions formed by this reduction step finally get into the cell? Functional complementation in yeast was applied to identify iron transport proteins (Figure 4). This

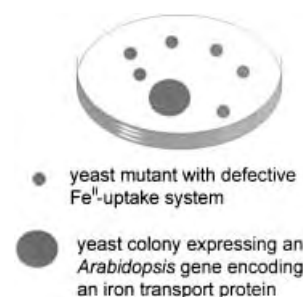


Figure 4. Identification of an *Arabidopsis thaliana* iron-transport protein by functional complementation in yeast. A yeast mutant with a defect in two Fe^{II} -uptake systems grows only poorly on a medium with a low iron concentration and forms small colonies. A number of *Arabidopsis* genes was introduced into this mutant. Colonies that subsequently grow better express an *Arabidopsis* protein mediating Fe^{II} uptake.^[11]

technique relied on a yeast mutant defective in two iron-uptake systems. It grows only poorly on substrates with reduced iron content, as indicated by the formation of small colonies. A collection of *Arabidopsis* genes was introduced into this mutant. Colonies that grow better and thus have a larger diameter should express an *Arabidopsis* protein mediating Fe^{II} uptake.

In this way the *Arabidopsis* protein IRT1 (IRT = iron-regulated transporter) encoding a putative iron-transport protein was isolated.^[11] The derived protein is predicted to have eight membrane-spanning domains. No homology was found to known iron-transport proteins from yeast or the bacterium *Escherichia coli*, which indicates that IRT1 is the prototype of a new class of transport proteins.

The transport properties of IRT1 were tested after heterologous expression in yeast. The measurement of the uptake of radioactive iron ions in the presence and absence of the reductant ascorbate revealed that Fe^{II} ions are the preferred substrate. This observation is consistent with a physiological role for IRT1 in the uptake of Fe^{II} ions, the product of NADH-dependent reduction.^[11] It is frequently observed that not only iron, but other toxic ions also accumulate in the plant in response to iron deficiency. To test whether IRT1 can transport other ions several transition metals were tested for their ability to compete with uptake of radioactive iron ions.^[11] A 10-fold excess of Cd^{II} ions inhibits Fe^{II} uptake, whereas Mn^{II} and Zn^{II} ions are inhibitory only at a 100-fold excess.

These observations suggest that IRT1 may have a broad substrate specificity and may transport toxic ions such as cadmium into the plant.

The importance of single amino acids for the transport process was investigated by site-specific mutagenesis.^[12] Replacement of three histidine residues and a glutamic acid residue by alanine eliminates transport activity, thus indicating that these residues may bind the metal ions during the transport process. Mutation of glutamic acid 103 eliminates the ability to transport zinc, but does not affect the transport of iron, manganese, and zinc ions. Mutation of aspartic acid 100 eliminates the transport of iron and manganese ions. Mutation of aspartic acid 136 also eliminates transport of iron and manganese, and impairs uptake of cadmium ions, thus leaving only zinc ions as a substrate. Thus, single amino acids were indeed determined that convey substrate specificity to the transporter.

This finding represents a first step towards a targeted modification of the transport profile of a protein mediating metal uptake in plants. Such a modified protein ultimately may prove useful to manipulate a plant's metal content by selective uptake of specific cations, such as iron, but elimination of others, such as the toxic cadmium ion.

Recently, a second iron transport protein closely related to IRT1, namely IRT2, was identified in *Arabidopsis*.^[13] Its expression in the yeast mutant led to the uptake of iron and zinc, but not manganese and cadmium. The expression of the *IRT2* gene in the outermost cell layers of the root and in the root hairs suggests that IRT2 may mediate iron uptake from the soil.^[13]

3. Strategy II: Chelation

Grasses, for example, barley and maize, follow strategy II. It is based on chelation, and takes advantage of iron's propensity to form complexes through coordinative bonds. When iron deficiency occurs, the plants synthesize and secrete hexadentate chelators that bind Fe^{III} ions from complexes in the soil and thus keep it in solution.^[3, 5] These chelators are designated "phytosiderophores", in analogy to iron-uptake systems of microorganisms that secrete iron chelators designated as "siderophores", from the Greek "iron bearers".^[14] The complexes of iron with the phytosiderophores are reimported into the root through specialized transport systems (Figure 5).^[15]

The amount of phytosiderophores released into the soil correlates with the plant's tolerance of iron deficiency. Barley is relatively resistant against iron deficiency, whereas rice plants that secrete only a few phytosiderophores are sensitive to iron deficiency (Figure 6).^[5, 16]

3.1. Biosynthesis of Phytosiderophores

Phytosiderophores are produced according to the iron demand in the cell. Under iron limitation, the corresponding biosynthetic enzymes are induced (Scheme 2). L-methionine serves as a precursor molecule that is activated at the expense

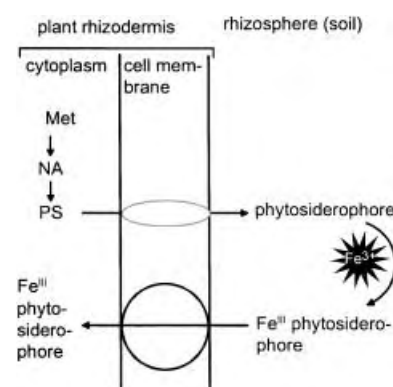


Figure 5. Elements of strategy II (adapted from ref. [5]). The outermost cell layer of the root, the rhizodermis, and the immediate vicinity of the soil, the rhizosphere, are depicted. Grasses respond to iron limitation by synthesis of phytosiderophores (PS) from L-methionine via the non-protein amino acid nicotianamine (NA). The phytosiderophores are released into the rhizosphere and bind Fe^{III} ions. The entire Fe^{III} -phytosiderophore complexes are taken up into the cells of the root surface through a specific, inducible transport system.

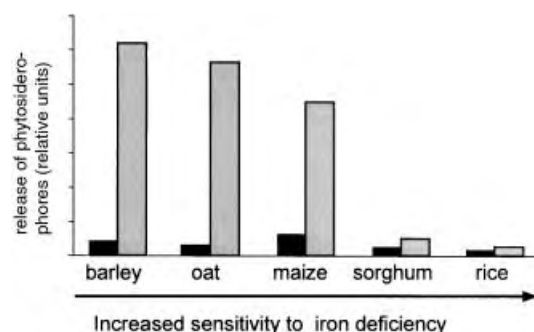
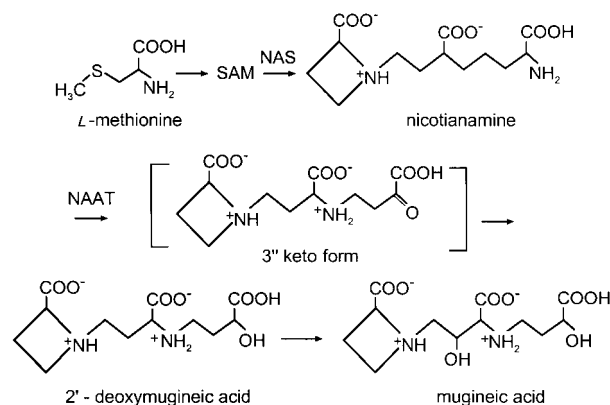


Figure 6. Correlation of the release of phytosiderophores and resistance to iron deficiency (adapted from ref. [5]). The amount of phytosiderophores released into the soil correlates with the plant's tolerance of iron deficiency. Barley is relatively resistant to iron deficiency whereas rice that secretes only a small amount of phytosiderophores is very sensitive to iron deficiency. Black bar: preculture in the presence of iron; gray bar: preculture in the absence of iron.



Scheme 2. Biosynthesis of phytosiderophores (refs. [17–19]). SAM = (S)-adenosylmethionine; NAS = nicotianamine synthase; NAAT = nicotianamine aminotransferase.

of ATP to (S)-adenosylmethionine.^[17, 18] Polymerization of three molecules of (S)-adenosylmethionine and formation of an azetidine ring yields the non-protein amino acid nicotianamine. The enzyme nicotianamine synthase was purified from

barley and cloned. It is a novel protein.^[19] Nicotianamine is converted into the keto form through a transamination catalyzed by nicotianamine aminotransferase and subsequently reduced to 2'-deoxymugineic acid.^[20] The six functional groups serve to bind the Fe^{III} ions as chelates. The introduction of additional hydroxy groups into 2'-deoxymugineic acid yields species-specific derivatives of mugineic acid that are collectively designated phytosiderophores.^[21] The additional hydroxy groups can increase the stability of the Fe^{III}–chelate complexes.^[22]

Interestingly, nicotianamine was found not only in strategy II plants but also in all the plants examined. A mutant with iron-deficiency symptoms has been found in tomato. This mutant is unable to synthesize nicotianamine. Nicotianamine is thought to play a role in the transport of iron ions in strategy I plants such as tomato. It was shown that the mutant has a defect in nicotianamine synthase.^[23] The products of the subsequent reactions are found only in grasses. The transfer of the amino group by nicotianamine aminotransferase is thus the key reaction that distinguishes grasses from the remainder of the plants.^[24]

3.2. Identification of the Uptake System in Fe^{III}–Phytosiderophore Chelate Complexes

Whereas Fe^{III} ions are reduced to the more soluble Fe^{II} form and taken up by transport proteins such as IRT1 in strategy I plants, strategy II plants take up Fe^{III} ions complexed with phytosiderophores.^[5] Recently, the special uptake system for phytosiderophores was identified by taking advantage of the maize *yellow stripe* mutant that cannot take up Fe^{III} phytosiderophores.^[25] Thus, it suffers from iron deficiency and impaired chlorophyll biosynthesis, which results in the characteristic yellow stripes on the leaves. The mutation is caused by insertion of the transposon Ac (activator) into a gene essential for iron uptake. Transposons are DNA sequences that can change their position in the genome. By using this genetic element as a tool, the affected gene was isolated. It codes for a protein with 12 transmembrane domains. Its role in iron transport was investigated in the above-mentioned yeast mutant that is deficient in iron uptake and thus grows poorly under iron limitation. Upon expression of the maize *YSI* gene in the yeast mutant, the mutant is able to form colonies on medium containing Fe^{II}-deoxymugineic acid, which suggests that *YSI* indeed encodes a transporter for Fe^{III} siderophores.^[25]

4. Summary and Perspective

Under iron limitation, strategy II plants, such as the grasses, rely on the production of phytosiderophores, hexadentate ligands, that are able to form complexes with Fe^{III} ions. The Fe^{III}–phytosiderophore complexes are subsequently taken up by the plants with the help of highly specific root-transport systems.^[15] All other plants release protons into the soil to solubilize Fe^{III} ions, which are the substrate of an inducible Fe^{III}–chelate reductase. The product Fe^{II} ion is taken up into

root cells through a specific metal transport protein such as *Arabidopsis* IRT1.^[11] Strategy I is severely impaired on calcareous soils because of the high pH values and the low solubility of Fe^{III} ions. In contrast, phytosiderophores are capable of chelating iron even at higher pH values. This offers an ecological advantage to grasses on calcareous soils relative to strategy I plants.

What are the implications of an increased understanding of iron-uptake processes in plants for human nutrition? Iron deficiency is the most prominent of nutritional disorders.^[26] As plants are the main iron source for the majority of the world's population, enhancing the iron content of crop plants could contribute to alleviate iron deficiency.

A prerequisite to manipulate the iron content is to understand the fate of iron in the entire plant: further issues include details about the translocation of iron within the plant, the distribution of iron to the organelles within the cell as well as regulation of the genes whose products are involved in uptake, distribution, and storage of iron.

To increase the iron content in a useful form for human nutrition iron has to be targeted to those plant organs that provide nutrition. Moreover, an increase in iron uptake by enhanced expression of transport proteins in transgenic plants requires that the simultaneous uptake of unwanted ions such as toxic Cd^{II} is avoided. Another process that relies on the uptake of toxic metal ions is known as phytoremediation, the decontamination of soil and water polluted with heavy metals with the aid of metal-accumulating plants.^[26] In this case, plants should not transport the metal ions from the roots to the shoot in order to keep the biomass for disposal small. Progress in understanding iron uptake obtained with the model plant *Arabidopsis thaliana* provides an entry to these applications.

My thanks go to Dr. Hans-Martin Fischer, Dr. Marcel Bucher, and Prof. Nikolaus Amrhein for helpful discussions, Stephan Lange and Christoph Lippuner for critical reading of the manuscript, and Dr. Dieter Rubli for help with the figures.

Received: November 12, 2001 [M1540]

- [1] P. von Sengbusch, *Botanik*, McGraw-Hill, Hamburg, **1989**.
- [2] J.-F. Briat, S. Lobréaux, *Trends Plant Sci.* **1997**, 2, 187–193.
- [3] J.-F. Briat, I. Fobis-Loisy, N. Grignon, S. Lobréaux, N. Pascal, G. Savoin, S. Thoirion, N. von Wirén, O. van Wuytswinkel, *Biol. Cell* **1995**, 84, 69–81.
- [4] M. L. Guerinot, Y. Yi, *Plant Physiol.* **1994**, 104, 815–820.
- [5] H. Marschner, V. Römhild, M. Kissel, *J. Plant Nutr.* **1986**, 9, 695–713.
- [6] E. L. Connolly, M. L. Guerinot in *Plasma membrane redox systems and their role in biological stress and disease* (Eds.: H. Asard, A. Berczi, R.J. Caubergs), Kluwer Academic, Dordrecht, **1998**, pp. 179–192.
- [7] H. F. Bienfait, *J. Bioenerg. Biomembr.* **1985**, 17, 73–83.
- [8] Arabidopsis Genome Initiative, *Nature* **2000**, 408, 796–815.
- [9] Y. Yi, M. L. Guerinot, *Plant J.* **1996**, 10, 835–844.
- [10] N. J. Robinson, C. M. Procter, E. L. Connolly, M. L. Guerinot, *Nature* **1999**, 397, 694–697.
- [11] D. Eide, M. Broderius, J. Fett, M. L. Guerinot, *Proc. Natl. Acad. Sci. USA* **1996**, 93, 5624–5628.
- [12] E. E. Rogers, D. J. Eide, M. L. Guerinot, *Proc. Natl. Acad. Sci. USA* **2000**, 97, 12356–12360.
- [13] G. Vert, J.-F. Briat, C. Curie, *Plant J.* **2001**, 26, 181–189.
- [14] V. Braun, H. Killmann, *Trends Biochem. Sci.* **1999**, 24, 104–109.

- [15] V. Römheld, H. Marschner, *Plant Physiol.* **1986**, *80*, 175–180.
- [16] S.-i. Takagi, K. Nomoto, T. Takemoto, *J. Plant Nutr.* **1984**, *7*, 469–477.
- [17] S. Shojima, N.-K. Nishizawa, S. Fushiya, S. Nozoe, T. Irifune, S. Mori, *Plant Physiol.* **1990**, *93*, 1497–1503.
- [18] J. F. Ma, K. Nomoto, *Physiol. Plant.* **1996**, *97*, 609–617.
- [19] K. Higuchi, K. Suzuki, H. Nakanishi, H. Yamaguchi, N.-K. Nishizawa, S. Mori, *Plant Physiol.* **1999**, *119*, 471–479.
- [20] M. Takahashi, H. Yamaguchi, H. Nakanishi, T. Shioiri, N.-K. Nishizawa, S. Mori, *Plant Physiol.* **1999**, *121*, 947–956.
- [21] H. Nakanishi, H. Yamaguchi, T. Sasakuma, N.-K. Nishizawa, S. Mori, *Plant Mol. Biol.* **2000**, *44*, 199–207.
- [22] N. von Wirén, H. Khodr, R. C. Hider, *Plant Physiol.* **2000**, *124*, 1149–1157.
- [23] H.-Q. Ling, G. Koch, H. Bäumlein, M. W. Ganal, *Proc. Natl. Acad. Sci. USA* **1999**, *96*, 7098–7103.
- [24] K. Kanazawa, K. Higuchi, N.-K. Nishizawa, S. Fushiya, M. Chino, S. Mori, *J. Exp. Bot.* **1994**, *45*, 1903–1906.
- [25] C. Curie, Z. Panaviene, C. Loulergue, S. L. Dellaporta, J. F. Briat, E. L. Walker, *Nature* **2001**, *409*, 346–349.
- [26] M. L. Guerinot, D. E. Salt, *Plant Physiol.* **2001**, *125*, 164–167.

Available in Print or on CD-ROM!

Hawley's Condensed Chemical Dictionary, 14th Edition

Richard J. Lewis, Jr.

Cloth • ISBN 0-471-38735-5 • 1200 pages • September 2001
\$149 • £95 • €310.98

CD-ROM • ISBN 0-471-05532-8 • \$149.00 • September 2001
\$149 • £95 • €350.09

In its fourteenth edition, Hawley's Condensed Chemical Dictionary once again establishes itself as the world's principal lexicon of industrial chemicals, nomenclature, processes, reactions, products, and related terminology. Scrutinized and extensively revised by internationally renowned chemist and reference author, Richard J. Lewis Sr., this newest edition features updated information on production, usage, and regulatory trends. In addition, the dictionary contains:

- Up-to-date chemical entries, definitions, and cross references
- Web links to new, as well as established, manufacturers and associations
- To-the-point information on natural products, manufacturing processes, and equipment

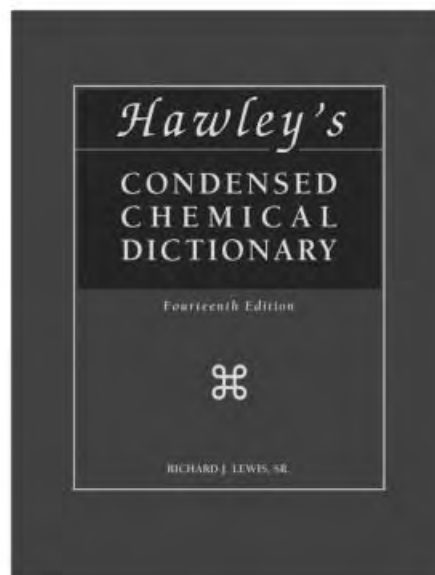
ORDER NOW!

Call: 1-800-225-5945
Email: custserv@wiley.com
www.wiley.com/hawleys
Please refer to code 2-8021 when ordering



Ordering Information for:

Europe, Middle East, Africa & Asia: John Wiley & Sons, Ltd., Tel. +44 (0) 1243 843294, Fax. +44 (0) 1243 843296, E-mail cs-books@wiley.co.uk
Germany, Switzerland & Austria: Wiley-VCH Verlag GmbH, Tel. +49 (0) 6201 606152, Fax. +49 (0) 6201 606184, E-mail service@wiley-vch.de
www.wiley.com www.wileyeurope.com www.wiley-vch.de



Small Interfering RNAs and Their Chemical Synthesis

Ronald Micura*

Only few years ago, it was discovered that RNA plays a fundamental role in post-transcriptional regulation of gene expression. When double-stranded RNA (dsRNA) of around 300 to 1000 base pairs (bp) in length was injected into the nematode *Caenorhabditis elegans*, the specific silencing of genes highly homologous in sequence to the delivered dsRNA was induced.^[1] This phenomenon, termed RNA interference (RNAi), paved the way for a straightforward determination of gene function, once the sequence of the gene was known.^[2]

Mechanism of RNA Interference

Elucidation of the mechanism of RNAi is subject to intensive research. Transfection with dsRNA results in the degradation of the sequence-homologous mRNA, even in only substoichiometric amounts. The initial step is the processing of the dsRNA into fragments of 21–23 nucleotide (nt) strands. These short interfering RNA molecules (siRNA) are the mediators of mRNA degradation, as was recently established by T. Tuschl and co-workers, who demonstrated that chemically synthesized RNA duplexes with the fragment pattern mentioned above are capable of guiding mRNA cleavage.^[3]

These siRNA duplexes readily associate to form target-cleaving RNA protein complexes (target=sense or antisense), which have not been well characterized to date. These complexes are referred to as small interfering ribonucleoprotein particles (siRNPs; Figure 1). The model of Tuschl and co-workers discriminates between two classes of siRNPs; namely, one that cleaves only the antisense and another that cleaves only the sense strand. Depending on the orientation of the duplex within an siRNP, only one of the two siRNA strands is capable of target-RNA recognition (the siRNAs at the proteins which are represented by black rounded rectangles in Figure 1). This model corresponds to earlier findings that certain chemical modifications, such as 2'-aminouridine or 2'-deoxythymidine, are well tolerated in the sense strand, but not in the mRNA cleavage-guiding antisense strand.^[4]

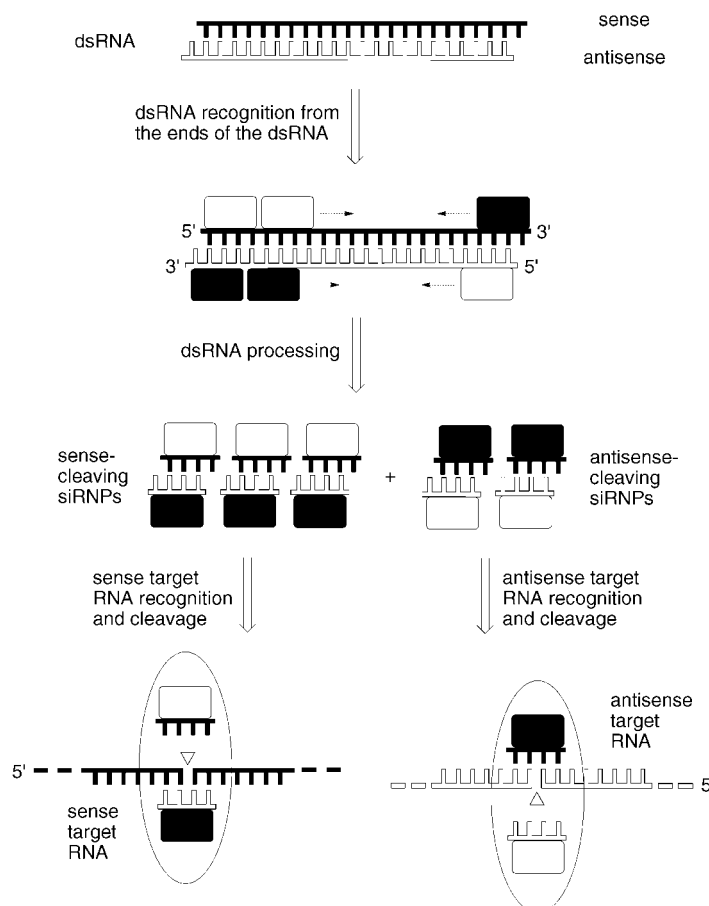


Figure 1. Model for RNA interference (RNAi) proposed by T. Tuschl and co-workers. Small interfering RNAs (siRNA) are the key molecules for targeted RNA cleavage (Figure adapted from reference[3]).

It is suggested that the relative orientation of the siRNA duplex within the siRNP is preserved from the preceding step of dsRNA processing.^[3] The proteins involved, among them a nuclease of the RNase III family, assemble on the dsRNA in an asymmetric fashion and remain at least partly associated with the siRNA products. Thus, the molecular information of directionality is passed on, which results in distinct roles of the siRNA strands, only one being capable of guiding targeted RNA cleavage. The siRNA duplex is thought to be temporarily disrupted during target recognition and reformed after release of the cleaved target RNA. The position of RNA

[*] Dr. R. Micura
Leopold Franzens University
Institute of Organic Chemistry
Innrain 52a, 6020 Innsbruck (Austria)
Fax: (+43) 512-5072892
E-mail: ronald.micura@uibk.ac.at

cleavage relative to the guide siRNA is near the center of the region covered by the 21 or 22 nt siRNA.

Synthetic oligoribonucleotides were also valuable, as it was observed that 21 or 22 nt siRNA duplexes with double nucleotide 3'-overhangs were more efficient in degrading target RNA than similar blunt-ended duplexes.^[3] This observation is consistent with the cleavage pattern of an RNase III-like nuclease activity during dsRNA processing.^[5] It is of further note that dsRNAs of less than 38 bp are inefficient mediators of RNAi, as the reaction rate of siRNA formation is significantly reduced compared with longer dsRNA.^[3]

siRNA in Mammalian Cells

Although RNAi has become routine in many laboratories and has been studied for a wide range of organisms, its use in mammalian cells has long been considered problematic. However, with the understanding of siRNAs as key components in RNAi, the breakthrough for RNAi applications in mammalian cells has followed. The problem was that dsRNA in mammalian cells activates a nonspecific viral defense mechanism, the interferon response, which results in a global shutdown of protein synthesis and leads to cell death.^[6] This pathway masks any sequence-specific effects that might arise from an RNAi pathway. However, the nonspecific pathway requires longer dsRNA, and does not occur with dsRNAs shorter than 30 bp. So, Tuschl and co-workers tested the ability of siRNA to target various luciferase transgenes in mammalian cell cultures (COS-7, NIH/3T3, HeLa, and 293 cells) and indeed observed reproducible, sequence-specific siRNA inhibition, which was easily assayed by luminescence spectroscopy.^[7] In addition, siRNAs were also effective when targeting endogenous genes. Non-sequence-specific effects started to emerge for the transfection with 50 bp and longer RNAs, which suggested that both pathways (RNAi and interferon response) can operate simultaneously. However, gene expression in mammalian cells was not eliminated completely, as it was observed in the reference system of *Drosophila* cells.^[7] That apart, the work above represents a landmark for siRNA as the upcoming gene-silencing methodology which, at this time, seems to be more promising than the alternatives, which include antisense and ribozyme-based strategies.

Two Major Improvements in the Chemical Synthesis of RNA

Chemically synthesized RNA oligonucleotides are key components of RNAi technology. Although the widespread 5'-O-dimethoxytrityl(DMT)-2'-O-*tert*-butyldimethylsilyl(TBDMS) phosphoramidite chemistry enables their synthesis, this method has not reached the level of chemical DNA synthesis in terms of product quality and the accessible oligonucleotide length.^[8, 9] In the need for more robust RNA routine-synthesis strategies, two novel methodologies have been developed and demonstrated to be successful.

The 2'-O-TOM Method

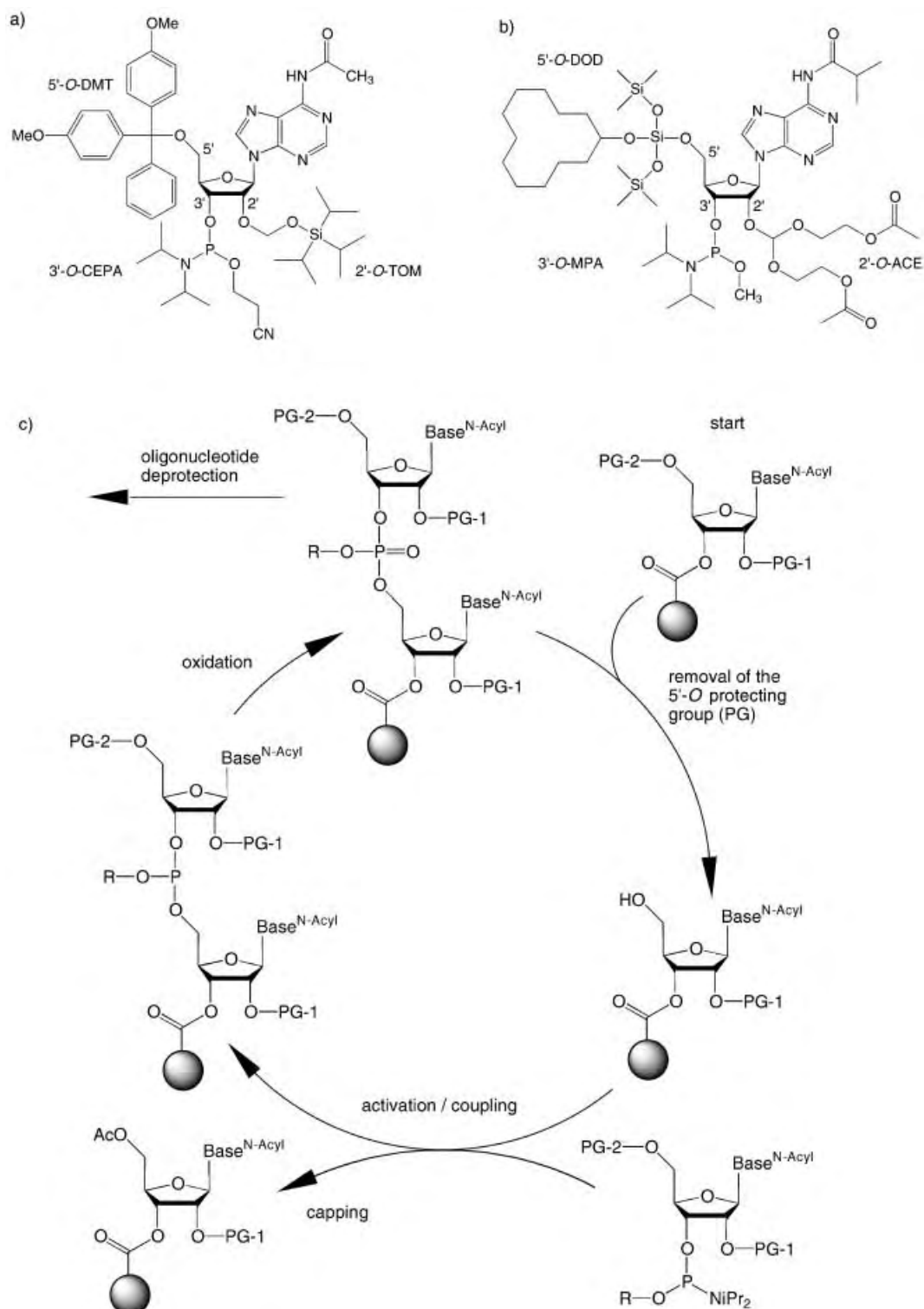
The first improvement was achieved by S. Pitsch and co-workers and maintains the principle of 5'-O-DMT-protection and 3'-O-(2-cyanoethyl)diisopropylphosphoramidite coupling

(Scheme 1 a,c, Table 1). The key feature is the 2'-O-triisopropylsilyloxymethyl (TOM) protecting group of the nucleotide building blocks which was first introduced in 1998, but was recently published with the synthetic details.^[10] The TOM protecting group guarantees an average coupling yield of 99.4% under DNA coupling conditions and the usage of benzylthiotetrazole as activator. This superior coupling behavior, compared to the 2'-O-TBDMS building blocks (typical coupling yield: $\leq 98\%$), can be attributed to the minimal steric demand of the TOM protecting group and allows the synthesis of up to 80mers. Furthermore, the combination of this coupling with the simple *N*-acetyl protection at the exocyclic amino groups of the nucleobases enables a reliable and complete two-step deprotection, first with MeNH₂ in EtOH/H₂O, followed by Bu₄NF in THF, without concomitant degradation of the RNA products. The HPLC chromatograms of these RNA species are comparable to those obtained for the corresponding DNA sequence homologues. The TOM method is offered commercially as an oligoribonucleotide production service, and the nucleotide building blocks are also available commercially, which has contributed to the fast propagation of the method.^[11] This availability resulted, for example, in the development of a solid-phase approach for the preparation of small circular RNA species, and in the usage of a variety of TOM-protected modified nucleoside building blocks.^[12] A further strength of the TOM method is that it can be easily combined with the existing large pool of nucleoside labelling and marker building blocks.

The 2'-O-ACE Method

The second novel method for the chemical synthesis of RNA was introduced by S. Scaringe and co-workers, and represents an impressive strategy which was first communicated in 1998, recently followed by the detailed procedures.^[13] Based on the literature, mildly acidic aqueous conditions were considered the most desirable for the final 2'-O deprotection of the synthesized RNA. The loss of orthogonality in the combination with the 5'-O-DMT group was an obstacle to using a mildly acid-labile 2'-O protecting group. The new RNA synthesis strategy is therefore based on the fluoride-labile 5'-O-bis(trimethylsiloxy)cyclododecyloxysilyl ether (DOD), together with the 2'-O-bis(2-acetoxyethyl)oxy)methyl (ACE) orthoester (Scheme 1 b,c, Table 1). The 3'-OH group is derivatized as the methyl-*N,N*-diisopropylphosphoramidite, as the cyanoethyl group turned out to be unstable with fluoride reagents. The coupling yields are higher than 99%, in less than 90 s and are therefore also superior to those observed for the TBDMS building blocks.

After the oligonucleotide assembly, the phosphate methyl protecting groups are removed with disodium 2-carbamoyl-2-cyanoethylene-1,1-dithiolate trihydrate (S₂Na₂) in DMF (Scheme 2). Then basic conditions (40% aqueous MeNH₂) cause oligonucleotide cleavage from the solid support, along with the removal of the acyl protecting groups on the exocyclic amino groups and, importantly, of the acetyl groups on the 2'-orthoesters. The resulting 2'-O-bis(2-hydroxyethyl-oxy)methyl orthoesters are ten times more acid labile than prior to the removal of the acetyl groups; very mild acidic



Scheme 1. a) Nucleoside building blocks used in the 2'-O-TOM method (other nucleobases: *N*⁴-acetylcytosine, *N*²-acetylguanine, uracil); b) nucleoside building block used in the 2'-O-ACE method (other nucleobases: *N*⁴-acetylcytosine, *N*²-isobutyrylguanine, uracil); c) General scheme for the automated synthesis of oligoribonucleotides. PG = protecting group.

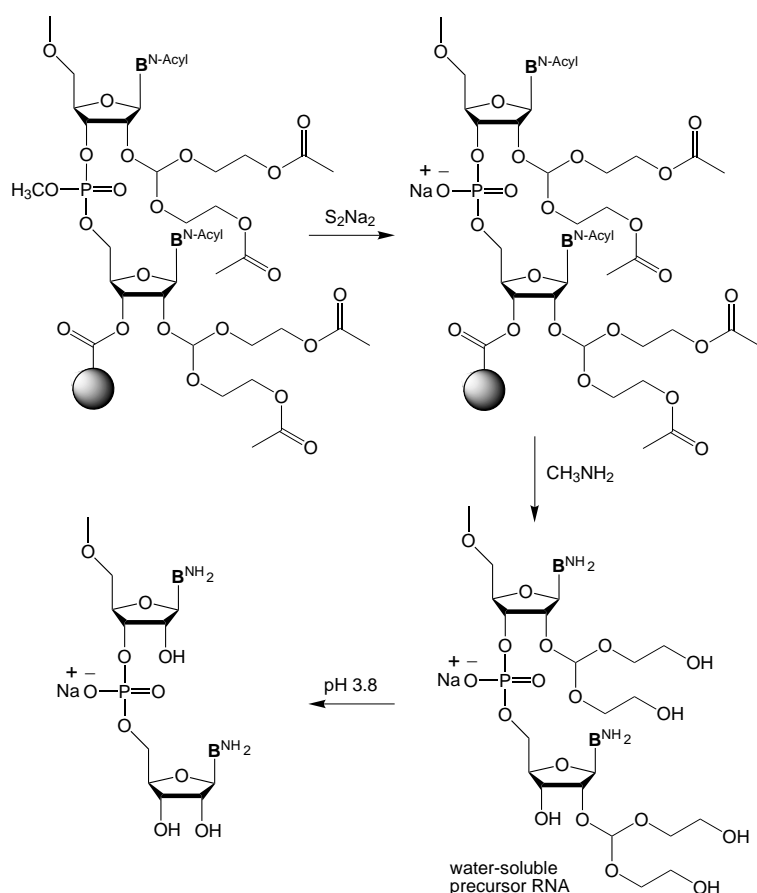
conditions (pH 3.8, 30 min, 60 °C) are therefore required for the final deprotection step. The HPLC chromatograms of the crude RNAs impress by showing hardly any by-products.

Unequivocally, the access to the 2'-O-bis(2-hydroxyethyl-oxy)methyl oligoribonucleotide is a major strength of the new

approach as this precursor RNA is water soluble, can be analyzed by HPLC, and purified if necessary. Of further significance is that the 2'-O-bis(2-hydroxyethyl-oxy)methyl protection of the precursor oligoribonucleotide appears to interrupt secondary structures. This was demonstrated by the synthesis of a 23mer homopolymer of guanosine.^[13d]

Table 1. Conditions for a complete coupling cycle in the 2'-O-TOM method and in the 2'-O-ACE method, and for the subsequent deprotection of the synthesized oligoribonucleotide.

	2'-O-TOM method (1.5 μ mole scale)	2'-O-ACE method (0.2 μ mole scale)
Removal of the 5'-O-PG	4% dichloroacetic acid in 1,2-dichloroethane, 90 s	1.1 M HF/2.9 M triethylamine in dimethylformamide, 35 s
Activation/Coupling	0.25 M benzylthiotetrazole (65 equiv)/0.1 M cyanoethylphosphoramidite (6 equiv) in CH ₃ CN, 90 s	0.5 M ethylthiotetrazole (75 equiv)/0.1 M methylphosphoramidite (15 equiv) in CH ₃ CN, 90 s
Capping	Ac ₂ O/2,6-lutidine/THF (1/1/8; v/v) and <i>N</i> -methylimidazole/THF (16/84; v/v), 60 s	Ac ₂ O/CH ₃ CN (1/9; v/v) and <i>N</i> -methylimidazole/CH ₃ CN (1/9; v/v), 30 s
Oxidation	I ₂ /H ₂ O/pyridine/THF (3/2/20/75; w/w), 45 s	1 M <i>tert</i> -butylhydroperoxide in toluene, 45 s
Oligonucleotide deprotection	1) 10 M MeNH ₂ in EtOH/H ₂ O; 1–24 h, 25–33 °C 2) 1 M Bu ₄ NF · 3 H ₂ O in THF; 1–50 h, 25 °C 3) 1 M Tris · HCl, H ₂ O, pH 7.4	1) 1 M disodium-2-carbamoyl-2-cyanoethylene-1,1-dithiolate trihydrate (S ₂ Na ₂) in DMF; 15 min 2) 40% MeNH ₂ in H ₂ O; 1 h, 55 °C 3) 100 mM tetramethylethylenediamine/acetic acid, pH 3.8; 30 min, 60 °C



Scheme 2. Deprotection of an oligoribonucleotide synthesized by the 2'-O-ACE method proceeds via a water-soluble precursor RNA which cannot form strong secondary structures and is therefore easy to analyze by HPLC.

The 2'-O-ACE method can be used on commercial automated DNA synthesizers after some technical adjustments. This chemistry has been commercialized as an oligoribonucleotide production service, however, the corresponding nucleotide building blocks are not yet commercially available. First reports on the incorporation of nucleoside modifications also exist and, just recently, the combined chemical and enzymatic synthesis of tRNAs for high-throughput crystallization was published.^[14]

Both methodologies, the 2'-O-TOM method and the 2'-O-ACE routes are major improvements in the synthesis of RNA oligonucleotides and offer unprecedented product quality. With respect to the incorporation of modifications, the TOM chemistry appears to have a slight advantage at the moment, as it benefits from the large existing “modifier” pool developed for use with TBDMS. It will be interesting to see if, in the long term, the 2'-O-ACE method is able to take the place of the 5'-O-DMT method, which is now strengthened by the TOM protecting group.

- [1] A. Fire, S. Xu, M. K. Montgomery, S. A. Kostas, S. E. Driver, C. C. Mello, *Nature* **1998**, *391*, 806–811.
- [2] For a Highlight on RNA interference see: a) U. Schepers, T. Kolter, *Angew. Chem.* **2001**, *113*, 2503–2505; *Angew. Chem. Int. Ed.* **2001**, *40*, 2437–2439; for reviews see, for example: b) T. Tuschl, *ChemBioChem* **2001**, *2*, 239–245; c) R. Barnstead, *Curr. Opin. Chem. Biol.* **2001**, *5*, 63–66.
- [3] S. M. Elbashir, W. Lendeckel, T. Tuschl, *Genes Dev.* **2001**, *15*, 188–200.
- [4] S. Parrish, J. Fleenor, S. Xu, C. Mello, A. Fire, *Mol. Cell* **2000**, *6*, 1077–1087.
- [5] E. Bernstein, A. A. Caudy, S. M. Hammond, G. J. Hannon, *Nature* **2001**, *409*, 363–366.
- [6] G. R. Stark, I. M. Kerr, B. R. Williams, R. H. Silverman, R. D. Schreiber, *Annu. Rev. Biochem.* **1998**, *67*, 227–264.
- [7] S. M. Elbashir, J. Harborth, W. Lendeckel, A. Yalcin, K. Weber, T. Tuschl, *Nature*, **2001**, *411*, 494–498.
- [8] G. M. Blackburn, M. Gait, *Nucleic Acids in Chemistry and Biology*, 2nd ed., Oxford University Press, Oxford, UK, **1996**.
- [9] K. K. Ogilvie, K. L. Sadana, E. A. Thompson, M. A. Quilliam, J. B. Westmore, *Tetrahedron Lett.* **1974**, *15*, 2861–2863.
- [10] a) X. Wu, S. Pitsch, *Nucleic Acids Res.* **1998**, *26*, 4315–4323; b) “Ribonucleoside-derivative and method for preparing the same”: S. Pitsch, P. A. Weiss, L. Jenny, US Patent 5,986,084, **1999**; c) S. Pitsch, P. A. Weiss, L. Jenny, A. Stutz, X. Wu, *Helv. Chim. Acta* **2001**, *84*, 3773–3795.
- [11] a) M. Hüniges, C. Rolz, R. Gschwind, R. Peteranderl, F. Berglechner, G. Richter, A. Bacher, H. Kessler, G. Gemmecker, *EMBO J* **1998**, *17*, 4092–4100; b) M. C. Nagan, P. Beuning, K. Musier-Forsyth, C. J. Cramer, *Nucleic Acids Res.* **2000**, *28*, 2527–2534; c) M. Brännvall, N. E. Mikkelsen, L. A. Kirsebom, *Nucleic Acids Res.* **2001**, *29*, 1426–1432.
- [12] Small circular RNA species: a) R. Micura, *Chem. Eur. J.* **1999**, *5*, 2077–2082; b) R. Micura, W. Pils, K. Grubmayr, *Angew. Chem.* **2000**, *112*, 956–959; *Angew. Chem. Int. Ed.* **2000**, *39*, 922–926; modified

- nucleosides: c) R. Micura, W. Pils, C. Höbartner, K. Grubmayr, M.-O. Ebert, B. Jaun, *Nucleic Acids Res.* **2001**, 29, 3997–4005; d) V. Boudou, J. Langridge, A. Van Aerschot, C. Hendrix, A. Millar, P. Weiss, P. Herdewijn, *Helv. Chim. Acta* **2000**, 83, 152–161; e) C. Höbartner, M.-O. Ebert, B. Jaun, R. Micura, *Angew. Chem.* **2002**, 114, 619–623; *Angew. Chem. Int. Ed.* **2002**, 41, 605–609.
- [13] a) S. A. Scaringe, F. E. Wincott, M. H. Caruthers, *J. Am. Chem. Soc.* **1998**, 120, 11 820–11 821; b) S. A. Scaringe, US Patent 6,111,086, **1998**;

- c) S. A. Scaringe, *Methods Enzymol.* **2000**, 317, 3–18; d) S. A. Scaringe, *Methods* **2001**, 23, 206–217.
- [14] Nucleoside modifications: a) M. Meroueh, P. J. Grohar, J. Qiu, J. SantaLucia, Jr., S. A. Scaringe, C. S. Chow, *Nucleic Acids Res.* **2000**, 28, 2075–2083; b) H. M.-P. Chui, M. Meroueh, S. A. Scaringe, C. S. Chow, *Bioorg. Med. Chem.* **2002**, 325–332; tRNAs: c) L. D. Sherlin, T. L. Bullock, T. A. Nissan, J. J. Perona, F. J. Lariviere, O. C. Uhlenbeck, S. A. Scaringe, *RNA* **2001**, 7, 1671–1678.

Hydrides and Iodides of Gold

Margaret-Jane Crawford* and Thomas M. Klapötke*

The synthesis of gold hydrides in the solid state has long been desirable. Despite early investigations by Wiberg et al.,^[1] to prepare AuH₃ utilizing a variety of reducing agents such as LiAlH₄, AlH₃, and LiBH₄, no direct evidence for the elusive AuH₃ could be obtained and only decomposition products, that is, Au and H₂ could be detected. Despite, or possibly because, of the lack of experimental evidence for gold hydrides in the solid state, a considerable number of theoretical studies have probed the structure of AuH and by using density functional methods.^[2–6] Moreover, in the past few years, the chemistry of the gold halides and hydrides has received a great deal of attention, and utilizing a combination of computational and experimental techniques, the structures of many of the gold halides have been shown to agree with earlier structural predictions made by Schwerdtfeger et al.^[5–7]

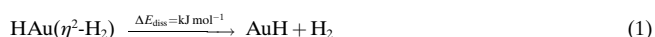
The similar electronegativities ($\chi_{\text{AR}} \text{I} = 2.2$; $\chi_{\text{AR}} \text{H} = 2.2$; $\chi_{\text{AR}} \text{Au} = 2.4$)^[6b] of I and H, makes a comparison between gold hydride and iodide compounds relevant. Whereas AuH is a stable diatomic molecule that has been characterized in the gas phase, and although the analogous diatomic AuX species (X = F, Cl, Br) have been known in the gas phase for some time, it was only very recently that the gas-phase structure of AuI was determined by microwave spectroscopy.^[8] However, whereas AuH was until very recently unknown in the solid state, AuI is a well-known and even commercially available (!) polymer, which is constructed of a zigzag chain with linear I–Au–I units (Figure 1).^[9] The unusual chainlike structure found for AuI can be explained by relativistic effects (as opposed to correlation effects) which show an increased covalency in the Au–I interac-



Figure 1. Solid state structure of gold(I) iodide.

tions.^[10] The structures of AuI₃ and AuH₃, however, were found to be a complex problem, not least because of the decreasing stability of the gold trihalides with increasing mass of the halide.^[11–14] For AuH₃, the lowest-energy isomer was found not to be either the T-shaped or linear structure, but rather, a Y-shaped structure (singlet electronic state) which is better viewed as an adduct between AuH and H₂.

Bayse recently reported detailed quantum-chemical DFT studies of the AuH₃/Au₂H₆ system, and suggested that in AuH₃ the AuH and H₂ units would be only loosely bound together [Eq. (1)].^[3]



Moreover, with respect to the dimerization of AuH₃ to form Au₂H₆, the “classical” square-planar, *D*_{2h} structure of Au₂H₆ was reported to be the only isomer located. The dimerization of both the Y- and T-shaped isomers of AuH₃, which formed *D*_{2h} Au₂H₆, was found in both cases to be an exothermic process by –84 and –305 kJ mol^{–1}, respectively (Figure 2). The bonding in the lowest-energy Y-shaped isomer of AuH₃

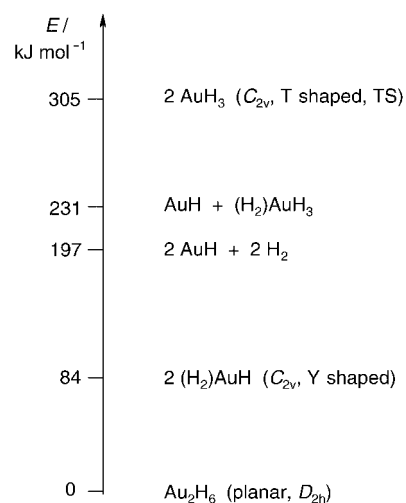


Figure 2. Relative energies of various gold hydride species (TS = transition state).

[*] Dr. M.-J. Crawford, Prof. Dr. T. M. Klapötke
Department of Chemistry
Ludwig-Maximilians University, Munich
Butenadtstrasse 5–13 (Haus D), 81377 Munich (Germany)
Fax: (+49) 89-2180-7492
E-mail: mjc@cup.uni-muenchen.de, tmk@cup.uni-muenchen.de

can be rationalized as consisting of two major donor–acceptor interactions:^[2]

- donation of electron density from the bonding H_2 σ orbital into an empty orbital on the metal center (M),
- back donation of electron density from a filled d_π metal orbital into the antibonding σ^* H–H orbital.

The $\sigma \rightarrow M$ interaction results in both a decrease of the H–H bond strength, and an increase in the H–H bond length with respect to the free H_2 molecule. However, if the back donation $M \rightarrow \sigma^*$ is particularly strong, the H_2 units can be cleaved by oxidative addition, which results in formal oxidation of the metal from $M(n)$ to $M(n+2)$. However, in the case of AuH_3 , oxidative addition does not occur, that is, the H–H bond in the H_2 ligand remains intact.

Recent ground-breaking solid-matrix investigations by Andrews and Wang,^[15] have provided the first experimental evidence for not only $(H_2)AuH$, but also for AuH_5 and the corresponding deuterated analogues. The excellent agreement between calculated and experimentally observed vibrational spectra confirm the existence of the metal–hydride–dihydrogen complex for AuH_3 as opposed to the T-shaped C_{2v} structure which represents a first-order transition state, or the also postulated, but not observed, planar D_{3h} Y-shaped structure (also not a true minimum), or linear $C_{\infty v}$ form of AuH_3 , with the triplet-electronic-state analogues being higher in energy in all cases than the singlet state. The effective stabilization of $(H_2)AuH$ by addition of H_2 forming $(H_2)AuH_3$, resulted in the experimental observation of a further, previously unknown gold hydride.

Certainly, establishing the first gold hydride in the condensed phase was a remarkable experimental achievement and now raises the question, as to whether the synthesis and characterization of one of the last missing members of the AuX/AuX_3 ($X=H, F-I$) series AuI_3 can be achieved. Recently, detailed computational investigations building on initial investigations by Schwerdtfeger et al.^[12] have probed the question as to the structure and stability of gold iodides in the +III oxidation state.^[14] The calculated isomers and their relative energies are shown in Figure 3. Whilst Au_2I_6 was calculated to adopt a D_{2h} gas-phase structure, the potential-energy surface for the monomer AuI_3 is particularly flat. Thus, the Y-shaped form of AuI_3 is a true minimum at B3LYP level

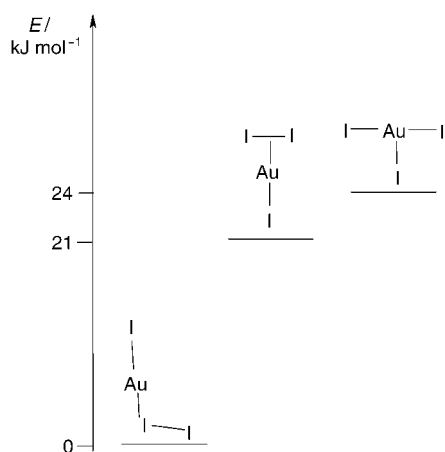


Figure 3. Relative energies of gold(III) iodide species.

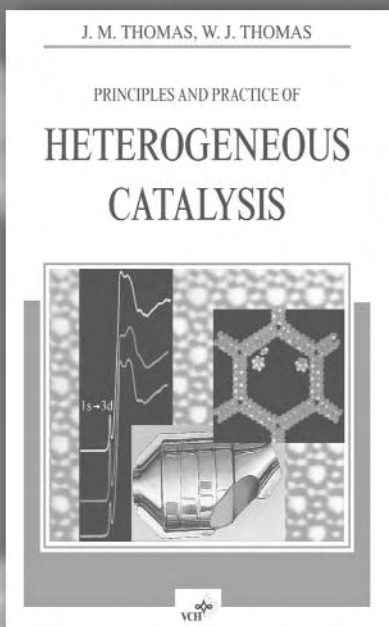
of theory, but a first-order transition state at the MP2 level. In contrast to the lighter gold trihalide homologues, the Y-shaped structure is lower in energy than the T-shaped species (B3LYP level) which in turn corresponds to a first-order transition state (global minimum for AuF_3 , $AuCl_3$, $AuBr_3$ is the T-shaped isomer; the Y-shaped form is a first-order transition state). The Y-shaped molecule (which is favored over the T-shaped form by 3–8 kJ mol^{−1}) in AuI_3 can best be described as $(I_2)AuI$ in an analogous manner to AuH_3 , that is, an I_2 unit is loosely bound to an Au–I moiety. Again, the I–I bond length is only slightly longer than that found in free I_2 , however, the dissociation energy of non-relativistic $(I_2)AuI$ (forming I_2 and AuI) is only +28 kJ mol^{−1}, and as for $(H_2)AuH$, the dissociation energy is only mildly endothermic. However, with relativistic considerations at the CCSD(T) level of theory this value is considerably higher at 97.3 kJ mol^{−1}. However, when a consideration of relativistic effects is taken into account, the Au–I bond length is considerably shortened (by ≈ 0.5 Å) and is rationalized as an increase in the oxidation state of the central Au atom from +I to +III, thus the higher oxidation state is stabilized by relativistic effects.

Static and dynamic Jahn–Teller systems have been used to explain the paradox between the gold trihalides. In AuI_3 the difference in energy between the Y- and T-shaped species is considerably smaller than in AuF_3 , thus making AuI_3 a dynamic Jahn–Teller system. Such distortions are, of course, further increased by relativistic effects. Recently, the global minimum for AuI_3 has been elucidated to be that of a further isomer, the L-shaped form (C_s symmetry), which is a true minimum for all AuX_3 ($X=F-I$) species, but only for AuI_3 is this the lowest energy form.^[14] In the L-shaped isomer the charge transfer from the X_2 unit to the AuX moiety has been calculated to be most pronounced for AuI_3 .

With the successful preparation of gold hydrides in the solid state for the first time, an obvious synthetic target must now be the solid state characterization of a free trialkyl gold compound, such compounds have been extensively investigated both theoretically and experimentally by Hoffmann et al. although never isolated in the solid state.^[16] Finally, very exciting advances have also recently been made in gold chemistry by M. Jansen et al. in the chemistry of auride compounds with the synthesis, isolation, and characterization of cesiumauride ammonia, $CsAu \cdot NH_3$, a crystalline analogue of alkali metals dissolved in ammonia^[17] and K. Seppelt and co-workers with the successful preparation of several binary and ternary gold-xenon complexes.^[18, 19]

- [1] E. Wiberg, H. Neumaier, *Inorg. Nucl. Chem. Lett.* **1965**, 1, 35–37.
- [2] C. A. Bayse, M. B. Hall, *J. Am. Chem. Soc.* **1999**, 121, 1348–1358.
- [3] C. A. Bayse, *J. Phys. Chem. A* **2001**, 105, 5902–5905.
- [4] K. Balasubramanian, M. Z. Liao, *J. Phys. Chem.* **1988**, 92, 361–364.
- [5] P. Schwerdtfeger, P. D. W. Boyd, A. K. Burrell, W. T. Robinson, M. J. Taylor, *Inorg. Chem.* **1990**, 29, 3593–3607.
- [6] a) P. Schwerdtfeger, P. D. W. Boyd, S. Brienne, A. K. Burrell, *Inorg. Chem.* **1992**, 31, 3411–3422; b) P. Schwerdtfeger, *Heteroatom Chem.*, in press.
- [7] P. Schwerdtfeger, M. Dolg, W. H. E. Schwarz, G. A. Bowmaker, P. D. W. Boyd, *J. Chem. Phys.* **1989**, 91, 1762–1774.
- [8] L. M. Reynard, C. J. Evans, M. C. L. Gerry, *J. Mol. Spectrosc.* **2001**, 205, 344–346.

- [9] H. Jagodzinski, *Z. Kristallogr.* **1959**, *112*, 80–87.
 [10] T. Söhnel, H. Hermann, P. Schwerdtfeger, *Angew. Chem.* **2001**, *113*, 4511–4515; *Angew. Chem. Int. Ed.* **2001**, *40*, 4382–4385.
 [11] N. B. Balabanov, J. E. Boggs, *J. Phys. Chem. A* **2001**, *105*, 5906–5910.
 [12] T. Söhnel, R. Brown, L. Kloo, P. Schwerdtfeger, *Chem. Eur. J.* **2001**, *7*, 3167–3173.
 [13] B. Réffy, M. Kolonits, A. Schulz, T. M. Klapötke, M. Hargittai, *J. Am. Chem. Soc.* **2000**, *122*, 3127–3134.
 [14] a) A. Schulz, M. Hargittai, *Chem. Eur. J.* **2001**, *7*, 3657–3670; b) X. Wang, L. Andrews, *J. Phys. Chem. A* **2002**, *106*, 3744–3748.
 [15] X. Wang, L. Andrews, *J. Am. Chem. Soc.* **2001**, *123*, 12899–12900.
 [16] S. Komiya, T. A. Albright, R. Hoffmann, J. K. Kochi, *J. Am. Chem. Soc.* **1976**, *98*, 7255–7265.
 [17] A.-V. Mudring, M. Jansen, J. Daniels, S. Krämer, M. Mehring, J. P. P. Ramalho, H. Romero, M. Parrinello, *Angew. Chem.* **2002**, *114*, 128–132; *Angew. Chem. Int. Ed.* **2002**, *41*, 120–124.
 [18] T. Drews, S. Seidel, K. Seppelt, *Angew. Chem.* **2002**, *114*, 470–473; *Angew. Chem. Int. Ed.* **2002**, *41*, 454–456.
 [19] S. Seidel, K. Seppelt, *Science* **2000**, *290*, 117–118.



Principles and Practice of Heterogeneous Catalysis

J. M. THOMAS, *The Master's Lodge, Peterhouse, Cambridge, UK;*
W. J. THOMAS, *University of Bath, UK*
 3-527-29239-X 1996 XIX, 669 pp
 375 figures 25 tables. SC.
 € 55.00*/DM 107.57/£32.50

Catalysis occupies a pivotal position in the physical and biological sciences. As well as being the mainstay of the chemical industry, it is the means of effecting many laboratory syntheses and the root cause of all enzymatic processes.

This book is an eminently readable introduction to the fundamental

principles of heterogeneous catalysis. Written by world-renowned experts, it explains the vocabulary, grammar and literature of catalysis from the laboratory-oriented model study through to the operating plant.

Didactically skillful and using many lucidly designed figures, the authors present an insightful exposition of all important concepts, new developments and techniques in this rapidly advancing field.

* The €-prices refer to Germany only!

Register now for the free

WILEY-VCH Newsletter!

<http://www.wiley-vch.de/home/pas>

Wiley-VCH · P. O. Box 10 11 611 · 69451 Weinheim, Germany
 Fax: +49 (0) 62 01-60 61 84 · service@wiley-vch.de · www.wiley-vch.de

 **WILEY-VCH**

73901111_vj

Comment on the Communication “Highly Efficient White Organic Electroluminescence from a Double-Layer Device Based on a Boron Hydroxyphenylpyridine Complex” by Wang et al.

Pi-Tai Chou,* Chung-Chih Cheng, Chau-Shuen Chiou, and Guo-Ray Wu

Recently, Liu et al.^[1] developed a new luminescent material, 1,6-bis(2-hydroxy-5-methylphenyl)pyridine, ((mdppy)BF) and investigated its electroluminescent (EL) properties. They claimed that a highly efficient “white-light” device could be produced based on molecular structures incorporating ITO/NPB/(mdppy)BF/LiF/Al configurations (ITO = indium–tin oxide; NPB = *N,N'*-bis(α -naphthyl)-*N,N'*-diphenyl-1,1'-biphenyl-4,4'-diamine). Knowing that the photoluminescence (PL) spectra of solid film for individual (mdppy)BF and NPB were maximized at 445 and 450 nm, respectively, they further attempted to rationalize the results of white-light EL based on the exciplex formation at the interface between NPB and (mdppy)BF. Support for this viewpoint was rendered by the PL spectra of the single-layer co-deposited NPB/(mdppy)BF film in which the emission is qualitatively similar to the EL spectrum at a high ratio of the interface versus the bulk of the two materials.

While the results and interpretation are sound, the EL spectrum illustrated in Figure 4, which is the main frame of ref. [1], deserves more careful examination. Through the course of studies on the weak chemiluminescence and/or electroluminescence we have gained a lot of experience in dealing with the interference of stray, dim light, particularly when the sample emission consists of broad spectral features. When we compared Figure 4 of the article with the spectrum acquired from dim room light (fluorescent lamp) a striking resemblance was apparent. Four major Hg lines (Figure 1 b; 405, 437, 546, and 577 nm) exactly overlap with the peaks in the EL spectrum shown in Figure 4 of ref. [1] (Figure 1 a). The ratios for the respective peaks of Figures 1 a and b are slightly different. This is possibly a result of the different spectral response of the charge coupled detector (CCD, Princeton Instrument, Model 576G/1) and the PR650 spectrometer used in ref. [1].

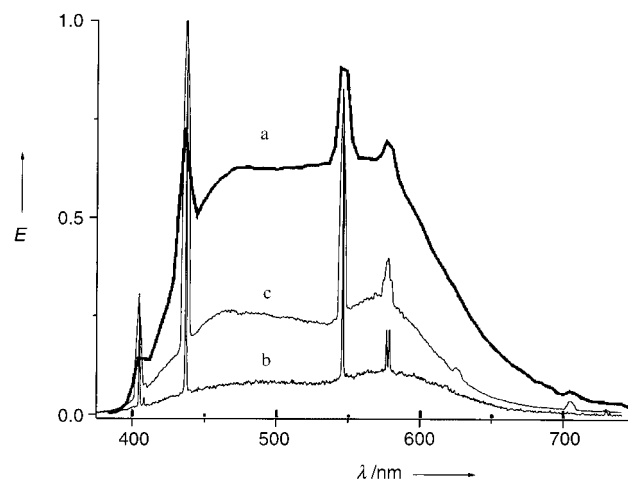


Figure 1. a) The EL spectra taken from Figure 4 of ref. [1]; b) spectrum of the dim room light from a Hg fluorescence lamp; c) similar experimental conditions as in b, except that the slit was adjusted to achieve similar spectral resolution as in a.

The much more sensitive CCD system led to the use of a smaller slit and hence increased the spectral resolution (note the doublet feature on the 577-nm line). Figure 1 c demonstrated the low-resolution spectrum of room light in which the slit had been adjusted so that the bandwidth of the spectral line was similar to that shown in ref. [1]. Again, the match of four spectral lines in Figure 1 a and c is apparent.

The exact match in wavelength for four Hg atomic lines led us to conclude that there existed certain interference from the stray light in the EL spectrum shown in Figure 4 of ref. [1]. Furthermore, there is a lack of photophysical basis to anticipate sharp spectral lines in an EL device consisting of organic dyes in the solid film.

Certainly, without performing a similar EL experiment as that in ref. [1], we cannot and do not intend to make any conclusions regarding the capability of the white-light generation based on the aforementioned device. However, the significance of ref. [1] is mainly in the white light generation using a very simple organic array which is of current importance in developing a light-emitting device. We thus feel this comment is appropriate and timely.

[*] Prof. Dr. P.-T. Chou

Department of Chemistry, National Taiwan University
No.1, Sec., 4 Roosevelt Road, Taipei, Taiwan (ROC)
Fax: (+886)2-2369-5208
E-mail: chop@ccms.ntu.edu.tw

C.-C. Cheng

Department of Chemistry, Fu-Jen Catholic University
No. 510, Chung Cheng Road, Shin Chuang, Taiwan (ROC)

C.-S. Chiou, G.-R. Wu

Department of Chemistry, National Chung-Cheng University
No. 160, San-Hsing, Ming-Hsiung, Chia-Yi, Taiwan (ROC)

[1] Y. Liu, J. Guo, H. Zhang, Y. Wang, *Angew. Chem.* **2002**, *114*, 190–192; *Angew. Chem. Int. Ed.* **2002**, *41*, 182–184.

Reply

Yu Liu, Jianhua Guo, Huidong Zhang, and Yue Wang*

Recently, we reported a new luminescent complex, boron 1,6-bis(2-hydroxy-5-methylphenyl)pyridine fluoride ((mdppy)BF), and a white electroluminescent (EL) device based on (mdppy)BF.^[1] Figure 4 in ref. [1] needs a more careful examination. In fact, we are also trying to explain the EL spectrum feature. Figure 4 was recorded at lower luminance (10 cd m^{-2}). The comment of Chou et al. made us realize that stray light could disturb the EL spectrum feature. In ref. [1] we only presented an EL spectrum at low luminance. We also recorded the EL spectra at higher luminance. Figure 1 shows the EL spectra of the ITO/NPB/(mdppy)BF/LiF/Al device recorded at 30 and 120 cd m^{-2} , respectively. The EL spectrum at the higher luminance level showed a different line shape than that at low luminance because stray light interference is negligible at higher luminance. Before reading the comment of Chou et al., we believed that the EL spectra at low luminance were different to those at higher luminance because exciplex emissions exhibit different characteristics at different luminance levels. Exciplex emission often contains quite complex mechanisms and thus the EL devices that have exciplex emission often show different EL spectra with varying luminance.

The minimum luminance that our PR 650 spectrometer can detect is 1 cd m^{-2} and its measurement error is 2%. The PR 650 spectrometer could not detect the luminance of stray light, so the luminance of the stray light was lower than 1 cd m^{-2} . The EL efficiency and Commission Internationale de l'Eclairage (CIE) coordinates, which were described in ref. [1], were obtained at higher luminance ($> 100 \text{ cd m}^{-2}$). The performance data of the white EL device was precise. Recently, we developed five other boron hydroxyphenyl-pyridine complexes and investigated their EL properties. The five complexes showed similar EL performance to

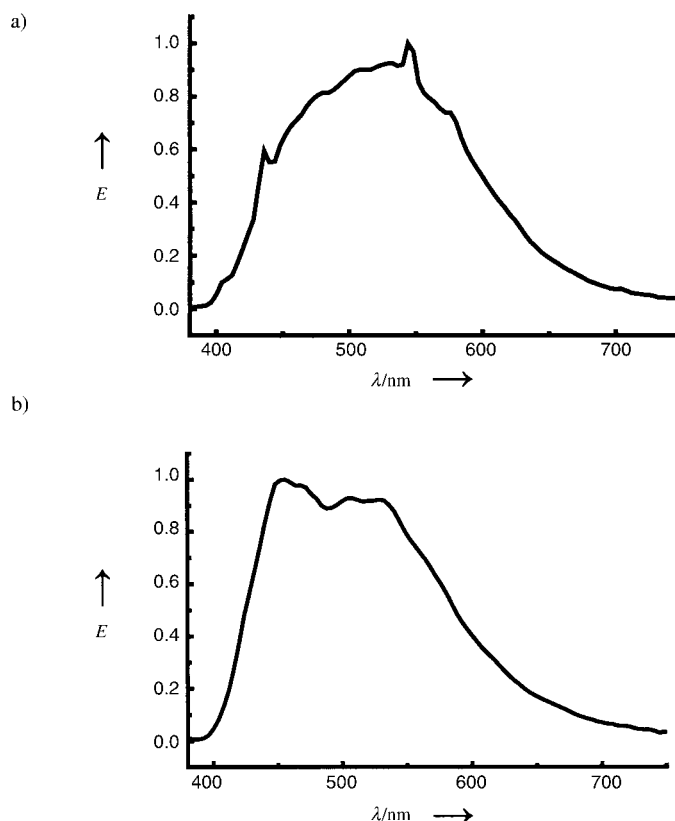


Figure 1. The EL spectra of the ITO/NPB/(mdppy)BF/LiF/Al device at a luminance of a) 30 cd m^{-2} and b) 120 cd m^{-2} .

(mdppy)BF. Boron hydroxyphenyl-pyridine complexes could be used to develop highly efficient white EL devices with simple device structure and material system. We will report our new results in the near future. Finally, we thank Chou et al. for their comment, which helped considerably to clarify the EL spectra that we obtained.

[*] Prof. Dr. Y. Wang, Y. Liu, J. Guo, H. Zhang

Key Laboratory for Supramolecular Structure and Materials of the Ministry of Education
Jilin University
Changchun 130023 (P. R. China)
Fax: (+86) 431-898-0729
E-mail: yuewang@mail.jlu.edu.cn

[1] Y. Liu, J. Guo, H. Zhang, Y. Wang, *Angew. Chem.* **2002**, *114*, 190; *Angew. Chem. Int. Ed.* **2002**, *41*, 182.

The Stable Pentamethylcyclopentadienyl Cation Remains Unknown**

Michael Otto, David Scheschkewitz, Tsuyoshi Kato, Mark M. Midland, Joseph B. Lambert, and Guy Bertrand*

For several years we have been interested by the stabilization of highly reactive species, such as silyl cations,^[1] carbocations,^[2a] carbenes,^[2b] diradicals,^[2c] and antiaromatic heterocycles;^[2d] thus, cyclopentadienyl cations are of special interest for us. The parent compound ($C_5H_5^+$) is supposed to have antiaromatic character,^[3] and the triplet ground state predicted from simple Hückel theory has been confirmed by ESR spectra^[4] and by the latest ab initio calculations.^[5] Like the $C_5H_5^+$ ion the pentamethylcyclopentadienyl cation ($C_5Me_5^+$) is predicted to have a triplet ground state, with the singlet state being 4.2 kcal mol⁻¹ higher in energy.^[5b] Jutzi and Mix^[6] reported that the reaction of bromopentamethylcyclopentadiene with silver tetrafluoroborate or hexafluoroantimonate below -30°C , led to a deep violet solution. In the ^{13}C NMR spectrum, only a broad signal attributed to the solvent was observable, which indicated the triplet nature of the cation. Polymers were formed upon warming this solution, but the pentamethylcyclopentadienyl cation has been trapped by various nucleophiles.

Based on this prior literature, the recent report on the isolation of the pentamethylcyclopentadienyl cation **1** by one of us^[7] was therefore really fascinating and unexpected. The tetrakis(pentafluorophenyl)borate salt of **1** was described as a crystalline material, stable for weeks at room temperature, and that can be left open to the atmosphere without serious decomposition.

There were two major differences between the calculations and observations: the observed C4–C5 bond length (1.51 Å) was 11% longer than the calculated one (1.36 Å), and in contrast to the calculated geometry, which predicted no pyramidalization of C4 and C5, their attached methyl groups protruded appreciably from the plane ($\text{CH}_3\text{--C4--C5--CH}_3$ dihedral angle = 106.9° ; Figure 1). These differences were explained by crystal packing between the anion and the cation, which would pyramidalize C4 and C5, a distortion permitted by the weak π bonding. These would have been noncovalent nonbonded interactions. The resulting deformations would have been a trade off between coulombic attractions and nonbonded repulsions.

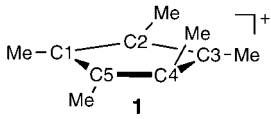
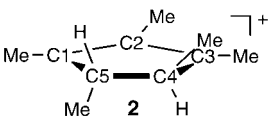
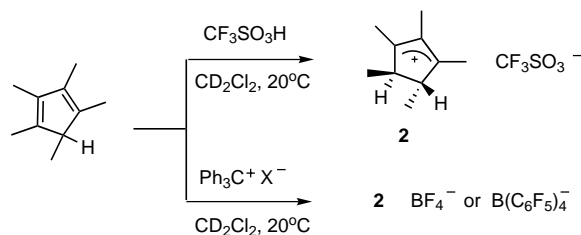
		
^{13}C NMR (ppm)	C1, C3 : 243 and 250 C2 : 153 C4, C5 : 60	C1, C3 : 244.5 C2 : 153.6 C4, C5 : 60.6, JCH = 129.6
Bond lengths (Å)	C1–C2 : 1.41 C2–C3 : 1.39 C3–C4 : 1.48 C4–C5 : 1.51 C1–C5 : 1.50	C1–C2 : 1.40 C2–C3 : 1.40 C3–C4 : 1.49 C4–C5 : 1.54 C1–C5 : 1.50
Dihedral angle ($^\circ$)	Me–C4–C5–Me: 106.9	Me–C4–C5–Me: 106.7

Figure 1. Comparison of ^{13}C NMR chemical shifts and geometric parameters for **1** and **2** (**1**: solid-state NMR spectroscopy and X-ray diffraction study; **2**: solution NMR and calculations).

Although reasonable these explanations were not totally convincing. Moreover, the observed dihedral angle between the methyl groups bonded to C4 and C5 and the C4–C5 bond length were in perfect agreement with a saturated fragment (C4–C5 single bond and the methyl groups in *trans* position). In other words, hydrogen atoms (difficult to observe by X-ray diffraction studies) might have been present on C4 and C5 and therefore the actual structure would be the already known^[8] pentamethylcyclopentenyl cation **2**. This assumption was reinforced by the ^{13}C NMR chemical shift for the C4 and C5 carbons of **1** ($\delta = 60$), which are in the expected range for the corresponding sp^3 carbon atoms of **2** (Figure 1).^[9]

To confirm our hypothesis, we first treated a CD_2Cl_2 solution of pentamethylcyclopentadiene with trifluoromethylsulfonic acid at room temperature (Scheme 1). According to ^1H and ^{13}C NMR spectroscopy, the protonation reaction was extremely clean. The ^1H NMR spectrum fits perfectly with that reported for compound **2**,^[8b] while the $^{13}\text{C}\{^1\text{H}\}$ NMR spectrum ($\delta = 244.5, 153.6, 60.6, 23.6, 14.6, 10.8$ ppm) is also in good agreement with that reported for **1** (Figure 1).^[7] Interestingly, the ^{13}C NMR proton-coupled spectrum indicates that the signal at 60.6 ppm arises from a CH carbon atom [$^1J(\text{CH}) = 129.6$ Hz]. Ab initio calculations (B3LYP/6-31G**) were also carried out on compound **2** and the optimized geometry reproduces reasonably well the experimentally observed parameters for **1** (Figure 1).



Scheme 1.

[*] Prof. G. Bertrand, M. Otto, Dr. D. Scheschkewitz, Dr. T. Kato, Prof. M. M. Midland
UCR-CNRS Joint Research Chemistry Laboratory, UMR 2282
Department of Chemistry
University of California
Riverside, CA 92521-0403 (USA)
Fax: (+1) 909-787-4713
E-mail: gbertran@mail.ucr.edu
Prof. J. B. Lambert
Department of Chemistry
Northwestern University
Evanston, IL 60208-3113 (USA)

[**] Financial support of this work by the CNRS, UCR, RHODIA, and NSF (CHE9983610) is gratefully acknowledged.

We have checked that Cp^*H ($\text{Cp}^* = \text{C}_5\text{Me}_5$) reacts with triphenylmethyl tetrafluoroborate and tetrakis(pentafluorophenyl)borate salts to afford derivative **2** (<50% yield; Scheme 1). This reaction is quite unexpected. Performing the previous experiments in deuterated solvents, or using Cp^*D as a precursor, also leads to **2**, without deuterium atoms on C4 and C5. Therefore, we have to admit that the mechanism of this reaction is still obscure and requires further investigation.

In conclusion, there is no doubt that the reported pentamethylcyclopentadienyl cation **1**^[7] is actually the pentamethylcyclopentenyl cation **2**. However, these recent developments will stimulate further research in this challenging area.

- [1] a) C. A. Reed, *Acc. Chem. Res.* **1998**, *31*, 325; b) J. B. Lambert, Y. Zhao, S. M. Zhang, *J. Phys. Org. Chem.* **2001**, *14*, 370.
 [2] a) T. Kato, H. Gornitzka, A. Baceiredo, W. W. Schoeller, G. Bertrand, *Science* **2000**, *289*, 754; b) D. Bourissou, O. Guerret, F. P. Gabbaï, G. Bertrand, *Chem. Rev.* **2000**, *100*, 39; c) D. Scheschkewitz, H. Amii, H. Gornitzka, W. W. Schoeller, D. Bourissou, G. Bertrand, *Science* **2002**, *295*, 1880; d) G. Bertrand, *Angew. Chem.* **1998**, *110*, 282; *Angew. Chem. Int. Ed.* **1998**, *37*, 270.
 [3] A. D. Allen, T. T. Tidwell, *Chem. Rev.* **2001**, *101*, 1333.
 [4] E. Wasserman, R. S. Hutton, *Acc. Chem. Res.* **1977**, *10*, 27.

- [5] a) H. Jiao, P. v. R. Schleyer, Y. Mo, M. A. McAllister, T. T. Tidwell, *J. Am. Chem. Soc.* **1997**, *119*, 7075; b) B. Reindl, P. v. R. Schleyer, *J. Comput. Chem.* **1998**, *19*, 1402; c) Y. Shiota, M. Kondo, K. Yoshizawa, *J. Chem. Phys.* **2001**, *115*, 9243.
 [6] P. Jutzi, A. Mix, *Chem. Ber.* **1992**, *125*, 951.
 [7] J. B. Lambert, L. Lin, V. Rassolov, *Angew. Chem.* **2002**, *114*, 1487; *Angew. Chem. Int. Ed.* **2002**, *41*, 1429.
 [8] a) P. H. Campbell, N. W. K. Chiu, K. Deugau, I. J. Miller, T. S. Sorensen, *J. Am. Chem. Soc.* **1969**, *91*, 6404; b) D. M. Brouwer, J. A. Van Doorn, *Recl. Trav. Chim. Pays-Bas* **1970**, *89*, 333; c) R. F. Childs, M. Zeya, R. P. Dain, *Can. J. Chem.* **1981**, *59*, 76.
 [9] ¹³C NMR data for the parent cyclopentenyl cation: G. A. Olah, G. Liang, Y. K. Mo, *J. Am. Chem. Soc.* **1972**, *94*, 3544.
 [10] Gaussian 98 (Revision A.7), M. J. Frisch, G. W. Trucks, H. B. Schlegel, G. E. Scuseria, M. A. Robb, J. R. Cheeseman, V. G. Zakrzewski, J. A. Montgomery, R. E. Stratmann, J. C. Burant, S. Dapprich, J. M. Millam, A. D. Daniels, K. N. Kudin, M. C. Strain, O. Farkas, J. Tomasi, V. Barone, M. Cossi, R. Cammi, B. Mennucci, C. Pomelli, C. Adamo, S. Clifford, J. Ochterski, G. A. Petersson, P. Y. Ayala, Q. Cui, K. Morokuma, D. K. Malick, A. D. Rabuck, K. Raghavachari, J. B. Foresman, J. Cioslowski, J. V. Ortiz, A. G. Baboul, B. B. Stefanov, G. Liu, A. Liashenko, P. Piskorz, I. Komaromi, R. Gomperts, R. L. Martin, D. J. Fox, T. Keith, M. A. Al-Laham, C. Y. Peng, A. Nanayakkara, C. Gonzalez, M. Challacombe, P. M. W. Gill, B. G. Johnson, W. Chen, M. W. Wong, J. L. Andres, M. Head-Gordon, E. S. Replogle, J. A. Pople, Gaussian, Inc., Pittsburgh, PA, **1998**.

Comment on the X-Ray Structure of Pentamethylcyclopentadienyl Cation

Thomas Müller*

In a recent communication Lambert and co-workers reported the unusual X-ray structure of singlet pentamethylcyclopentadienyl cation **1**.^[1] Its molecular structure (**1a**, Figure 1) is highly localized with C1–C2 and C2–C3 distances expected for allyl cations (139.3 and 140.5 pm, respectively) and relatively long C1–C5 and C3–C4 bonds (148.2 and 150.0 pm, respectively). The most unusual and striking structural feature of this cation is, however, a very long formal C=C bond (151.0 pm) with strongly *trans* pyramidalized carbon atoms (dihedral angle $\theta(\text{H}_3\text{C}-\text{C}_4-\text{C}_5-\text{CH}_3) = 107^\circ$). It is noteworthy that the sum of the bond angles around the pyramidalized carbon atoms, C4 and C5, are 327.8° and 327.7° , very close to that expected for tetravalent carbon atoms.^[2] Although the authors noted that this unusual geometry of the claimed cation **1** is not supported by theory,^[1, 3] they attribute this distortion to crystal packing forces “permitted by the weak π bonding” between C4 and C5.^[1]

Solid-state ¹³C NMR spectroscopy of the crystalline material gives ¹³C NMR chemical shifts for C1–C3 characteristic for allyl cations ($\delta = 250, 243$ (C1 and C3), 153 ppm (C2)).^[1, 4]

A resonance at $\delta^{13}\text{C} = 60$ ppm was attributed to C4 and C5 (Table 1, entry 9),^[1] a very unusual upfield shifted ¹³C NMR signal for a formally sp^2 -hybridized carbon atom.

The close structural and magnetic similarity of **1a** to allyl cations prompted us to reinvestigate the structure and NMR spectroscopy parameters of **1** and related allyl cations by

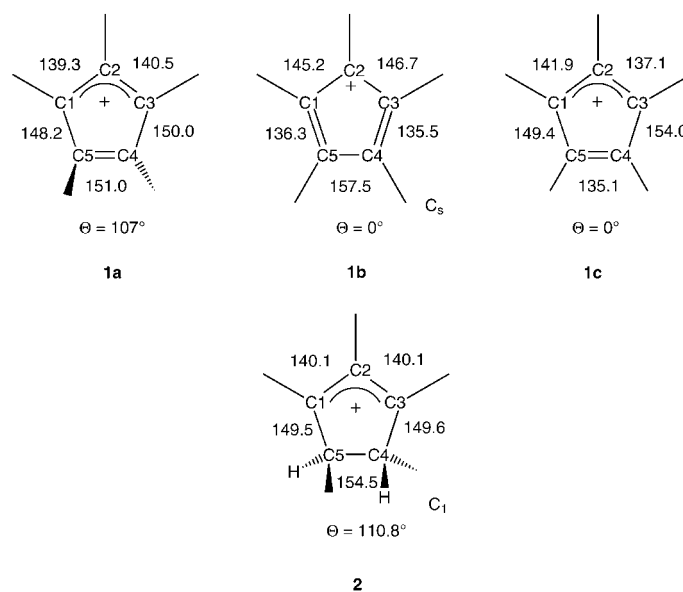


Figure 1. Experimental molecular structure of the cation **1a**^[1] and calculated structures of singlet **1b** (B3LYP/6–31G(d)) and singlet **1c** (CASSCF(4/5)/6–31G(d)) and **2** (B3LYP/6–31G(d)); bond lengths [pm], dihedral angle θ (Me–C4–C5–Me) [$^\circ$].

[*] Dr. T. Müller
 Institut für Anorganische Chemie der Goethe Universität
 Frankfurt/Main
 Marie Curie Strasse 11
 60439 Frankfurt
 Fax: (+49) 69-798-29188
 E-mail: Dr.Thomas.Mueller@chemie.uni-frankfurt.de

Supporting information for this article is available on the WWW under <http://www.angewandte.org> or from the author.

Table 1. Relative energies of compounds **3** and calculated ^{13}C NMR chemical shifts for compounds **1–3** (GIAO/B3LYP/6–311G(d,p)//B3LYP/6–31G(d)).

Entry	Compound	E_{rel} [kcal mol $^{-1}$]	δ $^{13}\text{C}(\text{C1})^{[a]}$	δ $^{13}\text{C}(\text{C2})^{[a]}$	δ $^{13}\text{C}(\text{C3})^{[a]}$	δ $^{13}\text{C}(\text{C4})^{[a]}$	δ $^{13}\text{C}(\text{C5})^{[a]}$
1	3a	0.0				133.0	133.0
2	3b	54.3				181.1	181.1
3	3c	12.6				163.4	163.4
4	3d	58.9				207.7	207.7
5	1b		144.3	282.0	144.2	191.0	204.4
6	1c ^[b]		258.2	154.9	282.6	164.9	176.8
7	2		256.7	158.6	256.7	67.8	69.3
8	2 (X-ray) ^[c]		253.3	156.1	251.1	63.6	62.7
9	1a (exp) ^[d]		243/250	153	243/250	60	60

[a] Calculated relative to tetramethylsilane (TMS): $\sigma(^{13}\text{C}) = 183.8$. [b] A CASSCF(4/5)/6–31G(d) optimized geometry was used. [c] Heavy-atom geometry taken from ref. [1], all 15 methyl hydrogen positions and the C(4)- and C(5)-methine hydrogen positions optimized at B3LYP/6–31G(d). [d] Experimental data for **1a** reported in ref. [1].

quantum-mechanical calculations.^[5] The results suggest that the X-ray structure reported by Lambert and co-workers^[1] is not that of **1** but that of the pentamethylcyclopentenyl cation, **2**.

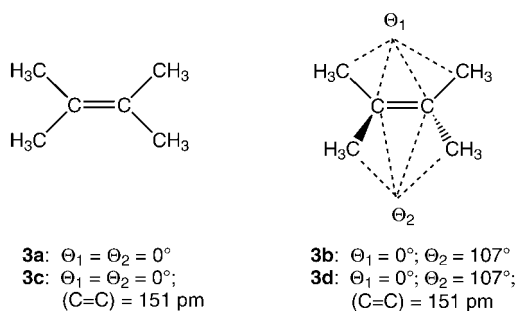
Pyramidalization of a C=C bond is energetically a very unfavorable process. For example, tetramethylethene (**3**) in its equilibrium geometry (**3a**) is lower in energy by 54.4 kcal mol $^{-1}$ than in the pyramidalized structure **3b** (Figure 2, Table 1). The C=C bond in **3b** is slightly elongated upon pyramidalization (134.9 pm (**3a**); 139.9 pm (**3b**) at B3LYP/6–31G(d)^[6]). It is, however, still markedly shorter (by 11.1 pm) than the C4–C5 bond in the crystal structure **1a**. In addition, NMR calculations at the GIAO/B3LYP/6–311G(d,p) level of theory^[7] reveal that this distortion of the C=C bond is connected with a significant *downfield* shift of the ^{13}C NMR chemical shift of the unsaturated carbon atoms ($\Delta\delta = 48.1$ ppm, see Table 1, entries 1 and 2). This is in contrast to the finding by Lambert et al. who report a significant *upfield* shift for the resonance signals of C4 and C5 compared to the expected range for tricoordinate carbon atoms.^[1] Even in the case of a weak π bond, modeled by **3** with a fixed C=C bond of 151 pm (**3c**), the pyramidalization is a quite unfavorable process, (energy difference **3c/3d**: 46.4 kcal mol $^{-1}$) and it results in a *downfield* shift of the ^{13}C NMR resonance of the tricoordinate carbon atoms ($\Delta\delta = 44.3$ ppm).

In Figure 1 the theoretical structures of singlet pentamethylcyclopentadienyl cation (**1b,c**) obtained at different levels of theory are compared with the molecular geometry derived from Lambert and co-worker's X-ray structure (**1a**). In agreement with previous ab initio calculations,^[3c] the DFT optimization of singlet **1** results in a Jahn–Teller-distorted bisallylic structure, **1b**,^[3e] while multi configuration self-consistent-field (MCSCF) calculations^[8] predict the allyl–ene isomer, **1c**, to be more stable.^[1] It is important to notice that

both theoretical singlet structures differ significantly from the experimental geometry **1a**. In particular, the distortions apparent in **1a** destabilize it considerably compared to both isomers **1b** and **1c**. That is, **1a** is higher in energy by 61.3 kcal mol $^{-1}$ and 47.8 kcal mol $^{-1}$ compared to **1b** and **1c**, respectively (at B3LYP/6–311G(d,p)//B3LYP/6–31G(d) (**1a/1b**) and at CASSCF(4,5)/6–31G(d) (**1a/1c**)).^[9] This situation suggests that π bonding in both isomers is no less important than in the regular alkene **3**. Also the calculated ^{13}C NMR chemical shifts for singlet **1b** and **1c** deviate noticeably from the experimental data (Table 1), which indicates that neither **1b** nor **1c** have been obtained.

In sharp contrast, not only the theoretical structure for the permethylated allyl cation **2** closely matches the experimental structure (Figure 1), also the calculated ^{13}C NMR chemical shifts compare favorably with the ^{13}C NMR data provided by Lambert and co-workers (Table 1). The agreement between the calculated NMR chemical shifts for **2** and those determined experimentally is further improved when the NMR calculations employ not the theoretical gas-phase structure, but the experimental structure with hydrogen atoms attached to the carbon atoms C4 and C5,^[10] thus transforming the alleged cation **1** into the cyclopentenyl cation **2** (Table 1).

Quantum-mechanical calculations show that the distortions which are apparent in the unusual structure **1a** strongly destabilize **1**. Therefore, it is unlikely that relatively weak crystal-lattice forces are responsible for the elongated, *trans* pyramidalized formal C=C bond in **1a**. On the other hand, calculations of geometry and ^{13}C NMR chemical-shift parameters for the pentamethylcyclopentene cation **2** are in good agreement with the experimental data reported by Lambert et al. In conclusion, our computational results provide strong evidence that the species obtained by Lambert and co-workers is indeed the pentamethylcyclopentene cation **2**.

Figure 2. Pyramidalization of **3**.

[1] J. B. Lambert, L. Lin, V. Rassolov, *Angew. Chem.* **2002**, *114*, 1487; *Angew. Chem. Int. Ed.* **2002**, *41*, 1429.

[2] Geometrical data are extracted from the Cambridge data base file CCDC-178042.

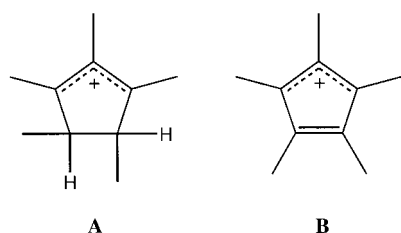
[3] a) A detailed review is given by V. I. Minkin, M. N. Glukhovtsev, B. Y. Simkin, *Aromaticity and Antiaromaticity*, Wiley, New York, **1994**, p. 230; b) M. N. Glukhovtsev, B. Reindl, P. v. R. Schleyer *Mendeleev Commun.* **1993**, 100; c) B. Reindl, P. v. R. Schleyer, *J. Comput. Chem.* **1998**, *19*, 1402; d) Y. Shiota, M. Kondo, K. Yoshizawa, *J. Chem. Phys.* **2001**, *115*, 9243; e) The triplet state, **1(T)**, is however lower in energy than **1b** by 6.1 kcal mol $^{-1}$ (B3LYP/6–31G(d)).

- [4] ^{13}C NMR data for allyl cations: a) G. A. Olah, G. Liang, *J. Am. Chem. Soc.* **1972**, *94*, 8071; b) H. Mayr, G. A. Olah, *J. Am. Chem. Soc.* **1977**, *99*, 510; c) G. A. Olah, H. Mayr, *J. Am. Chem. Soc.* **1976**, *98*, 7333; d) G. A. Olah, P. R. Clifford, Y. Halpern, R. G. Johanson, *J. Am. Chem. Soc.* **1971**, *93*, 4219; e) G. A. Olah, R. J. Spear, *J. Am. Chem. Soc.* **1975**, *97*, 1539.
- [5] All calculations were performed with Gaussian98 Revisions A3–A9, Gaussian, Inc., M. J. Frisch, G. W. Trucks, H. B. Schlegel, G. E. Scuseria, M. A. Robb, J. R. Cheeseman, V. G. Zakrzewski, J. A. Montgomery, R. E. Stratmann, J. C. Burant, S. Dapprich, J. M. Millam, A. D. Daniels, K. N. Kudin, M. C. Strain, O. Farkas, J. Tomasi, V. Barone, M. Cossi, R. Cammi, B. Mennucci, C. Pomelli, C. Adamo, S. Clifford, J. Ochterski, G. A. Petersson, P. Y. Ayala, Q. Cui, K. Morokuma, D. K. Malick, A. D. Rabuck, K. Raghavachari, J. B. Foresman, J. Cioslowski, J. V. Ortiz, A. G. Baboul, B. B. Stefanov, G. Liu, A. Liashenko, P. Piskorz, I. Komaromi, R. Gomperts, R. L. Martin, D. J. Fox, T. Keith, M. A. Al-Laham, C. Y. Peng, A. Nanayakkara, C. Gonzalez, M. Challacombe, P. M. W. Gill, B. G. Johnson, W. Chen, M. W. Wong, J. L. Andres, M. Head-Gordon, E. S. Replogle, J. A. Pople, Gaussian, Inc., Pittsburgh, PA, **1999**.
- [6] a) A. D. Becke, *Phys. Rev. A* **1988**, *38*, 3098; b) A. D. Becke, *J. Chem. Phys.* **1993**, *98*, 5648; c) C. Lee, W. Yang, R. G. Parr, *Phys. Rev. B* **1988**, *37*, 785.
- [7] a) R. Ditchfield, *Mol. Phys.* **1974**, *27*, 789; b) K. Wolinski, J. F. Hilton, P. Pulay, *J. Am. Chem. Soc.* **1982**, *104*, 5667; c) J. R. Cheeseman, G. W. Trucks, T. A. Keith, M. J. Frisch, *J. Chem. Phys.* **1996**, *104*, 5497.
- [8] For an introduction in the methodology see: W. J. Hehre, L. Radom, P. v. R. Schleyer, J. A. Pople, *Ab initio molecular orbital theory*, Wiley, New York, **1986**.
- [9] Calculated from single-point energies using the heavy-atom geometry of **1a** with all 15 hydrogen positions of **1** optimized at B3LYP/6–31G(d).
- [10] Calculated by using the heavy-atom geometry of **1a** with all 17 hydrogen positions of **2** optimized at B3LYP/6–31G(d).

Statement

Joseph B. Lambert*

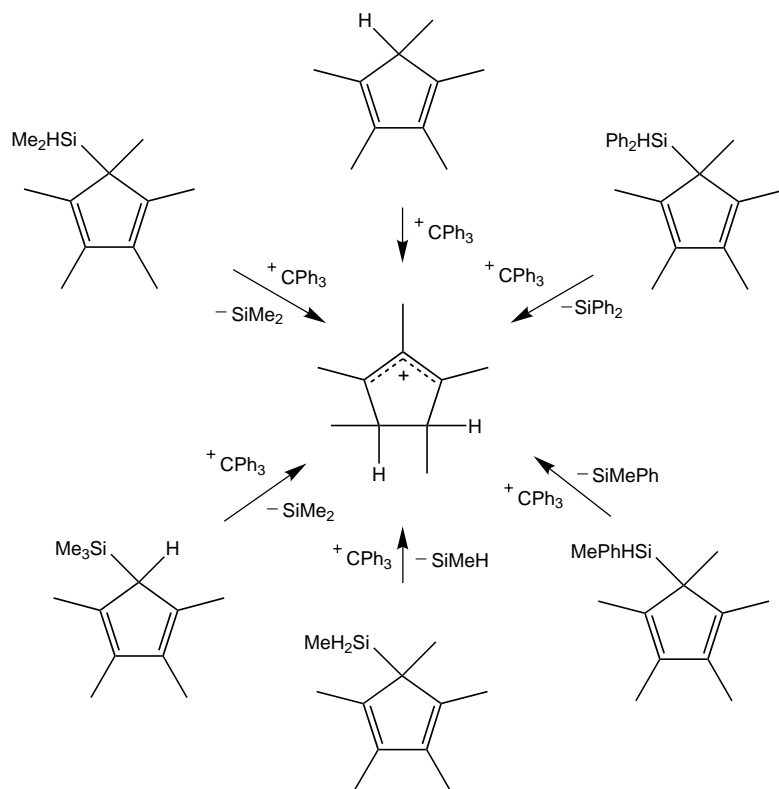
As we conclude in the accompanying Correspondence,^[1] the X-ray structure described recently^[2] is of the pentamethylcyclopentenyl cation (**A**) rather than the pentamethylcyclopentadienyl cation (**B**). The



key resonance of the CH protons in the NMR spectrum of **A** is broad and featureless, inexplicably lacking the expected quartet splitting. In the $^1\text{H}/^{13}\text{C}$ 2D spectrum, the CH group exhibits a weak to negligible cross peak, in contrast to the strong cross peaks for all the methyl groups. Consequently, the methine carbon appears to show no hydrogen connectivity.

In addition to the method of formation described in ref. [2], we previously prepared the same cation by five other methods (Scheme 1), all of which admit of logical pathways to **B** rather than to **A**. Triphenylcarbinol is not a product, only triphenylmethane in each case. We are currently exploring mechanistic pathways that can explain these unusual observations.

Because of the evidence presented in ref. [1], I am retracting the conclusions of ref. [2], which were entirely my



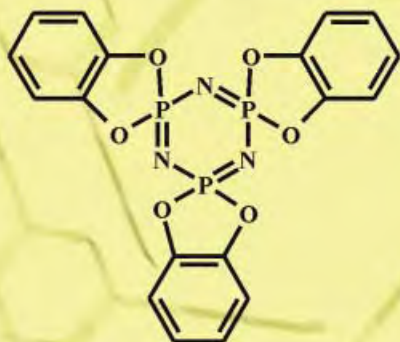
Scheme 1.

own and imply no reflection on the part of my co-workers (whose experimental and theoretical work is valid).

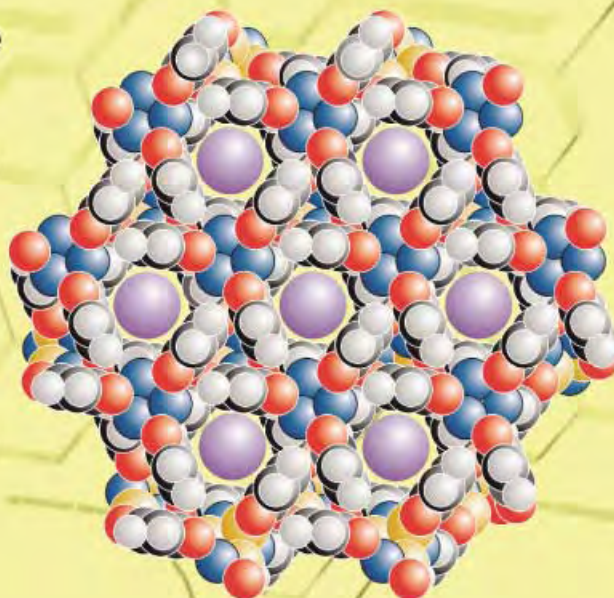
[*] Prof. Dr. J. B. Lambert
Department of Chemistry
Northwestern University
Evanston, Illinois, 60208 (USA)
Fax: (+1)847-491-7713

- [1] M. Otto, D. Scheschkewitz, T. Kato, M. M. Midland, J. B. Lambert, G. Bertrand, *Angew. Chem.* **2002**, *114*, 2379; *Angew. Chem. Int. Ed.* **2002**, *41*, 2275.
- [2] J. B. Lambert, L. Lin, V. Rassolov, *Angew. Chem.* **2002**, *114*, 1487; *Angew. Chem. Int. Ed.* **2002**, *41*, 1429.

phosphazene molecule



channel architecture



I₂



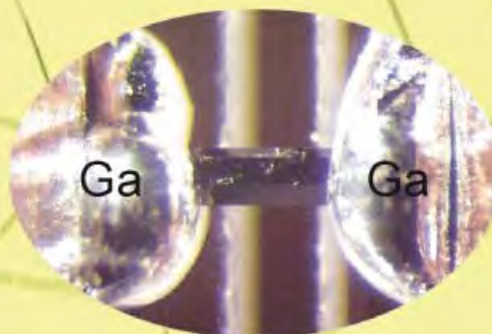
in-diffusion



The trigonal arrangement of phosphazene molecules provides a hexagonal channel structure, wherein iodine forms molecular chains by inward diffusion and crystallization. The iodine chains show electrical conductivity. For more information see the following pages.



chains of iodine



conductivity: $10^{-6} - 10^{-8} \Omega^{-1} \text{m}^{-1}$

Supramolecular-Wire Confinement of I₂ Molecules in Channels of the Organic Zeolite Tris(*o*-phenylenedioxy)cyclotriphosphazene**

Tino Hertzsch, Felix Budde, Edwin Weber, and Jürg Hulliger*

1D arrays of atoms or molecules with the property of conducting charge or photonic energy are considered major components for setting up future devices based on molecular-sized functional units.^[1] Molecular wires typically include conjugated chain-type molecules in solution^[2] and carbon nanotubes.^[3] By use of scanning-probe microscopy techniques, it is possible to prepare atomic arrays in chains or other structures on a substrate.^[4] Recently, potassium-doped fullerene chains were found in channels of an inorganic material.^[5] In crystals of inorganic zeolites, dyes can transport photonic energy.^[6] Dielectric crystalline host structures that provide an ordered array of aligned functional molecules are therefore of general interest to investigate transport properties along or perpendicular to chains of guest molecules.

Here, we report on the synthesis of inclusion crystals of tris(*o*-phenylenedioxy)cyclotriphosphazene (TPP, Figure 1)^[7] and I₂, as well as on the conductivity properties of single TPP · y(I₂) crystals, measured parallel (||) and perpendicular (⊥) to the channel axis of this organic zeolite.

TPP belongs to a growing family of cyclophosphazenes, some of which form channel-type inclusion compounds.^[8] A quasicylindrical channel topology was reported for an inclusion complex with benzene as the guest molecule. Unit cell parameters of $a = 1.804$, $c = 10.054$ Å ($P6_3$ for benzene guest) suggest a channel diameter of ≈ 5 Å^[9] and an interchannel distance of about 12 Å. After the release of benzene, the channel structure was found to be metastable up to a temperature of about 150 °C.^[10] Because of a reversible uptake of guest molecules, hexagonal TPP was recognized as one of the first organic zeolites.

Iodine is a 2D semiconductor^[11] and one of the best characterized n-type molecular donors for the formation of $n \rightarrow \sigma^*$ charge-transfer complexes.^[12] The electrical conductivity in the (b,c) plane, where I₂ molecules form a 2D network, is about 3400 times larger than the conductivity perpendicular to this plane. In supramolecular solid-state structures, chain formation, intercalation, and inclusion in cavities are known.^[13] Sorption and mass-transport properties of a 1D inclusion complex of I₂ in the zeolite MFI were

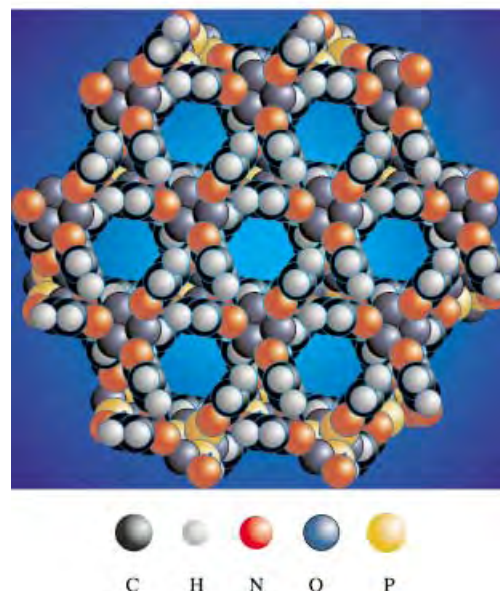
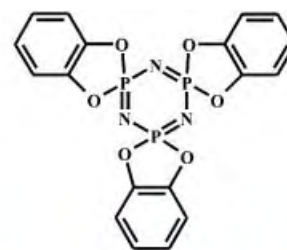


Figure 1. Molecular structure of TPP and the channel topology viewed along the *c* axis (channels with a diameter of about 5 Å). From data in ref. [8].

investigated.^[14] and inclusion of a number of solvents in TPP is known.^[8] Diffusive guest exchange and cocrystallization with nonlinear-optical molecules has recently produced new materials, whose polarity can be explained by a Markov model.^[15] Previous and present results support promising inclusion and zeolite-type properties of TPP, even for atoms (Xe^[10]) and other small species (H₂O, Br₂, CH₃I).

The investigations herein were based upon a single observation: Colorless, transparent, needle-shaped (1–2 mm long) single crystals of TPP · 0.6(THF) (Figure 2a) and some crystals of iodine were brought together in a closed system at room temperature ($p(\text{I}_2) \approx 0.3$ Torr). A few seconds after I₂ was brought into the system (Figure 2b), staining started from the capping faces and extended continuously into the volume of the crystals. After 1–2 days, most crystals were entirely colored (Figure 2c). I₂ inclusion in the crystal with TPP was also obtained by cocrystallization from the vapor phase and from a mesitylene solution. All reactions (I, II, III, see Figure 3) produced hexagonal, dichroitic, purple to black single crystals. The optical density of the crystals varied, depending on the conditions of preparation; hence, the degree of loading could be varied.

With regard to the above-mentioned electronic properties of iodine, it would be desirable to form a closed chain of interacting I₂ molecules along the channels in the TPP. Assuming a van der Waals contact between the I₂ molecules

[*] Prof. Dr. J. Hulliger, T. Hertzsch, F. Budde
Department of Chemistry and Biochemistry
University of Berne
Freiestrasse 3, 3012 Berne (Switzerland)
Fax 00 41 31 631 3993
E-mail: juerg.hulliger@iac.unibe.ch

Prof. Dr. E. Weber
Institute of Organic Chemistry
TU Bergakademie Freiberg
Leipziger Strasse 29, 09599 Freiberg (Germany)

[**] This work was supported by the Swiss National Funds Priority Program on "Functional Supramolecular Materials" (no. 4047-057476/1). E.W. thanks the Fonds der Chemischen Industrie for financial support.

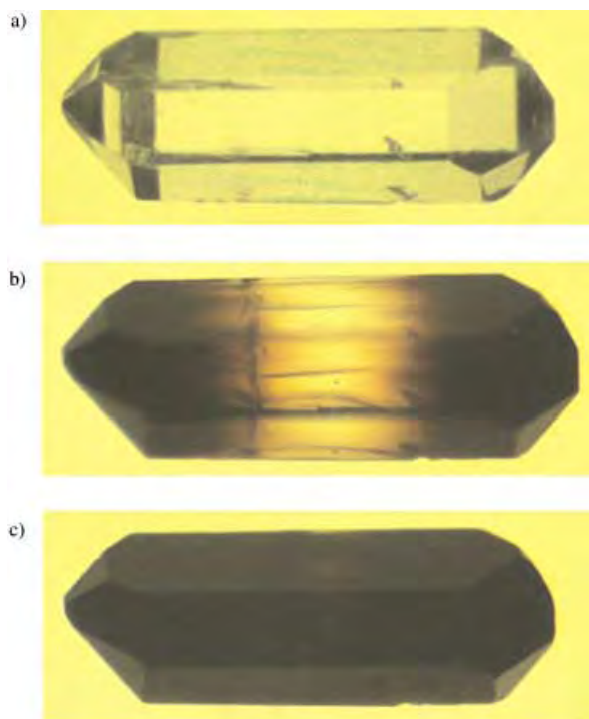


Figure 2. Crystals of $\text{TPP} \cdot x'(\text{THF}) \cdot y(\text{I}_2)$ (typical size: 2 mm) featuring three states of the process of diffusion in and diffusion out of iodine and THF, respectively. a) Initial state; b) early state, in which only capping faces were colored; c) final state, in which iodine has stained crystals up to the center. The figure supports the concept of the counterdiffusion of THF and iodine.

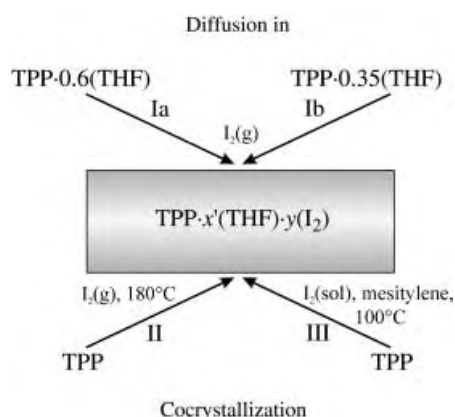


Figure 3. Different routes to the inclusion of I_2 molecules into channels of the TPP zeolite. sol = solvated.

aligned along the channels, the maximum I_2 content would yield $\text{TPP} \cdot y(\text{I}_2)$ crystals, with a value of $y \approx 0.75$.

Table 1 summarizes the chemical composition of all the $\text{TPP} \cdot x'(\text{THF}) \cdot y(\text{I}_2)$ and $\text{TPP} \cdot y(\text{I}_2)$ inclusion crystals we obtained. When diffusion experiments were performed using of $\text{TPP} \cdot 0.6(\text{THF})$ single crystals (Ia), most THF ($x \approx 0.4$) remained in the channels. It was also possible to increase the I_2 content by a partial desorption of the template solvent prior to the diffusion of iodine into the crystal: $\text{TPP} \cdot 0.35(\text{THF})$ crystals (route Ib) contained more iodine than the $\text{TPP} \cdot 0.6(\text{THF})$ material which was exposed to I_2 at the same temperature.

Table 1. Synthetic routes to and chemical compositions of $\text{TPP} \cdot x'(\text{THF}) \cdot y(\text{I}_2)$ and $\text{TPP} \cdot y(\text{I}_2)$ crystals.

Synthetic route	Reaction conditions	Composition of $\text{TPP} \cdot x'(\text{THF}) \cdot y(\text{I}_2)$	Decomposition temperature [$^{\circ}\text{C}$]
Ia	$\text{TPP} \cdot 0.6(\text{THF})$, I_2 , 25°C , 24 h	$x' = 0.4$, $y = 0.16$	230–248
Ib	$\text{TPP} \cdot 0.35(\text{THF})$, I_2 , 25°C , 24 h	$x' = 0.25$, $y = 0.45$	238–249
II	TPP , I_2 , 180°C evacuated	$x' = 0$, $y = 0.40$	244–249
III	TPP , I_2 , mesitylene, 100°C , slow cooling	$x' = 0$, $y = 0.65–0.75$	247–250

Given that 1 mm-long single crystals of $\text{TPP} \cdot x(\text{THF})$ did not disintegrate or crack after diffusion of I_2 into the crystals, we wondered by what type of mechanism the staining and the release of THF might occur simultaneously. Counterdiffusion of THF and I_2 is likely, because it was observed that staining started and progressed from the capping faces only. A mechanism of counterdiffusion was recently proposed^[15] to explain the staining of the volume of $\text{TPP} \cdot x(\text{THF})$ crystals by much larger guest molecules than I_2 (phenyls, biphenyls, stilbenes). However, such a mechanism would involve the channel wall showing some flexibility. A mechanism for solid-state reactions in molecular crystals was recently proposed, which assumed considerable flexibility of molecular lattices.^[16]

Cocrystallization from the vapor phase (route II; Figure 3) needed temperatures of 180°C to provide a sufficiently high vapor pressure of TPP. These crystals obtained by this method were very small and showed a considerably lower I_2 content than those from route Ib. Exploration of reactions I, II, and III showed that cocrystallization from mesitylene (route III) gave rise to the maximum loading. The $\text{TPP} \cdot y(\text{I}_2)$ crystals formed at a starting T of $80–100^{\circ}\text{C}$ had an I_2 content in the range of $x \approx 0.65–0.75$. Here, it is important to note that mesitylene was not co-included with I_2 .

All $\text{TPP} \cdot y(\text{I}_2)$ crystals obtained showed a remarkable thermal stability; according to thermogravimetric (TG) and differential-scanning calorimetry (DSC) measurements, an efficient $\text{I}_2(\text{g})$ loss started above 150°C and decomposition (melting) was observed near $T \approx 250^{\circ}\text{C}$. No significant weight loss caused by I_2 desorption was observed at 25°C , under vacuum, over 12 h of treatment.

Structurally, I_2 molecules are aligned in a parallel fashion (confirmed by the dichroism), and are surrounded by two sets of three phenyl rings, which form a π -electron wall around the I_2 molecule (Figure 1). As reported for complexes with aromatic molecules,^[17] a stabilizing interaction of $\Delta H_f^{\circ} = 8–15 \text{ kJ mol}^{-1}$ is expected to support inclusion-crystal formation. A van der Waals length of 6.8 \AA (I_2) and stacking along a period of TPP molecules of $c \approx 10 \text{ \AA}$ will most likely result in an incommensurate structural relationship between the guest and the host sublattices. Partial loading ($y < 0.75$) can be a source of translational disorder of I_2 along individual channels. X-ray single-crystal and powder data confirmed the structure of the TPP host lattice.^[18]

Electrical measurements on single crystals were performed by contacting them with liquid Ga. A special cell for mounting

small crystals between copper electrodes was constructed, which allowed the crystals to be monitored during measurements. An atmosphere of 1–2 bar $\text{SF}_6(\text{g})$ was used, and conductivity measurements (Keithley electrometer 6517A) were performed on six single crystals of $\text{TPP} \cdot y(\text{I}_2)$ ($y \approx 0.65$ – 0.75 , $T = 25^\circ\text{C}$), which were obtained from two different crystallization attempts (route III, Figure 3). σ_{\parallel} values in the order of 10^{-6} – $10^{-8} \Omega^{-1} \text{m}^{-1}$ were found for a potential of 50 V. However, three of these crystals were exposed to a voltage of 50 V, an increase in the current I (up to a factor of two) was observed with time. In cases where the voltage was 500–1000 V, the conductivity could be enhanced by a factor of 30–300, depending on the individual crystals. For crystals in which a stable current was established after several hours, an anisotropy factor (σ_{\parallel} , σ_{\perp}) of about 30 was measured. This factor provides evidence for a preferred conductivity along I_2 chains in the TPP channels. Further investigation of the nonlinearity and the time dependence of the $I(U)$ function is in progress.

In summary, we present the first example of I_2 molecules being brought into a chainlike configuration, surrounded by a π -donor-type environment, which separates chains laterally. Observed values of the conductivity of $\text{TPP} \cdot y(\text{I}_2)$ are of the same order as those in the (b,c) plane^[11] of iodine ($1.7 \times 10^{-6} \Omega^{-1} \text{m}^{-1}$, 25°C). Efficient sorption of I_2 by the $\text{TPP} \cdot x(\text{THF})$ zeolite crystals may find application in the sensing and removal of radioactive $^{129}\text{I}_2$.^[19]

Experimental Section

^1H NMR spectra were recorded on a Bruker-Spectroscopin AC 300 spectrometer. The UV/Vis spectra were measured on a Cary spectrometer.

Preparation of TPP: Hexachlorocyclophosphazene (recrystallized in heptane), sublimed pyrocatechol, and anhydrous sodium carbonate were mixed in dry THF. The resulting precipitate was filtered off and dried. The product was purified by recrystallization (toluene) and a double sublimation ($p = 10^{-2}$ mbar, $T = 210^\circ\text{C}$).

Preparation of the $\text{TPP} \cdot x(\text{THF})$ clathrate: TPP was dissolved in THF at 60°C . Single crystals up to several millimeters long were obtained by slow cooling (1°C h^{-1}). The ratio of TPP/THF was determined by ^1H NMR spectroscopy ($x \approx 0.60$, Ia). Partially desolvated clathrate crystals were obtained when exposed to vacuum at room temperature for 24 h ($x \approx 0.35$, Ib).

Preparation of inclusion compounds $\text{TPP} \cdot x'(\text{THF}) \cdot y(\text{I}_2)$ (route I): $\text{TPP} \cdot x(\text{THF})$ crystals were sealed in ampoules ($V \approx 3 \text{ cm}^3$) with an excess of iodine and placed into the homogeneous hot zone of a glass oven at a temperature of 25 – 100°C .

Preparation of inclusion compounds $\text{TPP} \cdot y(\text{I}_2)$, route II: Cocrystallization was performed in the gas phase in ampoules ($V \approx 3 \text{ cm}^3$), up to 180°C , with a small temperature gradient between iodine(I) and TPP(s).

Route III: Sublimated TPP and an excess of iodine were dissolved in mesitylene at 80 – 100°C . Black single crystals (III), were obtained by slow cooling (1°C h^{-1}). The ratio of TPP/iodine was measured by UV/Vis spectroscopy, by using three independent series of crystals and standard solutions for iodine. The average content (y) of I_2 varied between 0.65 – 0.75 for different batches. A value of $y = 0.75$ demonstrates that batches with a maximum concentration of iodine could be prepared.

Received: January 2, 2002 [Z18461]

[1] C. Joachim, S. Roth, *Atomic and Molecular Wires*, Kluwer Academic, Dordrecht, 1997.

[2] K. J. Donovan, E. G. Wilson, *Synth. Met.* **1989**, 28, 569–574.

- [3] C. H. Olk, J. P. Heremans, *J. Mater. Res.* **1994**, 9, 927–932.
- [4] R. Wiesendanger, H.-J. Güntherrodt, *STM I, II, Springer Series in Surface Sciences* 20, 28, Springer, Berlin, 1992.
- [5] B. Ye, M. L. Trudeau, D. M. Antonelli, *Adv. Mater.* **2001**, 13, 561–565.
- [6] D. Brühwiler, N. Gfeller, G. Calzaferri, *J. Phys. Chem. B* **1998**, 102, 2923–2929.
- [7] H. R. Allcock, *J. Am. Chem. Soc.* **1964**, 86, 2591–2595.
- [8] H. R. Allcock, L. A. Siegel, *J. Am. Chem. Soc.* **1964**, 86, 5140–5144.
- [9] L. A. Siegel, J. H. van der Hende, *J. Chem. Soc. A*, **1967**, 817–820.
- [10] P. Sozzani, A. Comotti, R. Simonutti, T. Meersmann, J. W. Logan, *Angew. Chem.* **2000**, 112, 2807–2810; *Angew. Chem. Int. Ed.* **2000**, 39, 2695–2699.
- [11] A. S. Balchin, H. G. Drickamer, *J. Chem. Phys.* **1961**, 34, 1948–1949.
- [12] G. DeBoer, J. W. Burnett, M. A. Young, *Chem. Phys. Lett.* **1996**, 259, 368–375.
- [13] M. Noltemeyer, W. Sängler, *Nature* **1976**, 259, 629–632; M. Noltemeyer, W. Sängler, *J. Am. Chem. Soc.* **1980**, 102, 2710–2713; R. D. Bailey, G. W. Drake, M. Grabarczyk, T. W. Hanks, L. L. Hook, W. T. Pennington, *J. Chem. Soc. Perkin Trans. 2* **1997**, 12, 2773–2779; F. H. Herstein, M. Kapon, G. M. Reisner, *Acta Crystallogr. Sect. B* **1985**, 41, 348–354; M. Chachisvilis, I. Garcia-Ochoa, A. Douhal, A. H. Zewail, *Chem. Phys. Lett.* **1998**, 29, 153–159.
- [14] M. Kočirik, J. Kornatowski, V. Masařík, P. Novák, A. Zikánová, J. Maixner, *Microporous Mesoporous Mater.* **1998**, 23, 295–308; G. Wirsberger, H. P. Fritzer, A. Popitsch, G. van der Goor, P. Behrens, *Angew. Chem.* **1996**, 108, 2951–2953; *Angew. Chem. Int. Ed. Engl.* **1996**, 35, 2777–2779.
- [15] T. Hertzsch, S. Kluge, F. Budde, E. Weber, J. Hulliger, *Adv. Mater.* **2001**, 13, 1864–1867.
- [16] G. Kaupp, M. Haak, *Angew. Chem.* **1996**, 108, 2948–2951; *Angew. Chem. Int. Ed. Engl.* **1996**, 35, 2774–2777.
- [17] J. Joens, *J. Org. Chem.* **1989**, 54, 1126–1128.
- [18] H. R. Allcock, M. L. Levin, R. R. Whittle, *Inorg. Chem.* **1986**, 25, 41–47.
- [19] J. Hulliger, T. Hertzsch, patent application, USA, **2001**.

Trapping Energy from and Injecting Energy into Dye–Zeolite Nanoantennae**

Huib Maas and Gion Calzaferri*

The light-harvesting system in green plants is a supra-molecular machine that collects light energy for photosynthesis. The beauty of this photonic antenna has inspired many researchers to examine and even try to mimic it. Different approaches have been used to build artificial photonic antennae.^[1–5] Exciting results based on a host–guest system have been obtained in our group^[6–10] with the host material zeolite L, a hexagonal crystal with one-dimensional channels

[*] Prof. Dr. G. Calzaferri, Dipl.-Chem. H. Maas
Department of Chemistry and Biochemistry
University of Berne
3012 Berne (Switzerland)
Fax: (+41) 31-631-3994
E-mail: Gion.Calzaferri@iac.unibe.ch

[**] This work is part of the Swiss National Science Foundation Project NFP 47 (4047-057481). We thank René Bühler for the synthesis of the zeolite L nanocrystals.

along the crystal axis.^[11–13] As guests we have used a wide range of highly fluorescent dye molecules. The size and shape of these dyes is such that they can enter the free open diameter of the zeolite L channels but they are prevented from forming dimers once inside. In this way we are able to build highly organized systems in which monomeric dyes are present in a high concentration. The distance between the individual dye molecules is in the order of magnitude of the Förster radius for energy transfer,^[14] which enables efficient energy transport in such dye-loaded zeolite L crystals. We have made photonic antennae with two (see Figure 1 A)^[7] and three dyes,^[9] and inverse antennae in which the donors are located at both ends of the crystals and the acceptors in the middle.^[15]

The systems reported so far are able to transport electronic excitation energy radiationless within the zeolite crystal structure. To mimic the natural supra-molecular machine and for a number of technologically interesting applications it would be desirable to lead the collected energy out of the crystals, or to inject energy from the exterior into the dye-loaded crystals. Our suggestions to reach this goal involve stopcock molecules (as shown in Figure 1 B).^[6, 16] These molecules have a stopcock shape with a head that is too big to penetrate the free open diameter of the zeolite channels and a label that is smaller and can enter. The head and the label are connected by a flexible spacer. Herein we show for the first time that such stopcocks can trap electronic excitation energy at the zeolite crystal surface, and inject excitation energy into dye-loaded zeolite L crystals in a complementary arrangement.

The ratio between the internal and the external surface of the zeolite L crystals is proportional to the ratio between the number of molecules that can be inserted in the crystal channels and the number of molecules that can be adsorbed as a monolayer on the external surface. One way of keeping this ratio small is by using small zeolite L crystals; the synthesis of zeolite L crystals with a size of about 30 nm has been reported.^[7, 17] The large external surface of these nanocrystals makes them suitable hosts to show energy transfer from molecules inside the crystals to molecules on the surface and vice versa.

Because the zeolite L crystals have a cylindrical shape, one can distinguish between two external surfaces: the coat, and the base. The coat is vaulted and lacks channel entrances, while the base is flat and contains the channel entrances. These differences give rise to different adsorption affinities.

Scheme 1 shows the dye molecules BTRX and B493/503 we have used as stopcocks. Their head consists of a BODIPY fluorophore, and their label is a succinimidyl ester.^[18] The succinimidyl ester makes the label polar and we know that keto groups form specific interactions to sites inside the channels. Although BTRX and B493/503 have polar groups it is possible to dissolve small amounts in an apolar solvent such as cyclohexane. If a suspension of nanocrystals in the same solvent is then added to this solution, the stopcocks are extracted from the solution onto the polar zeolite surface.

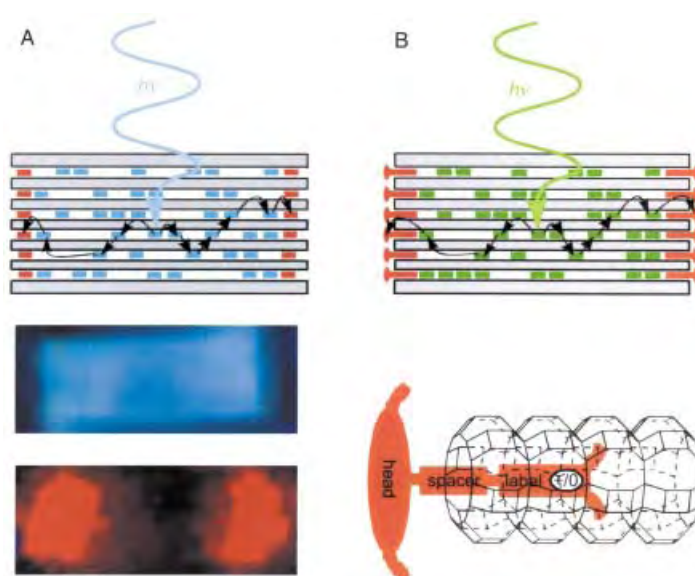
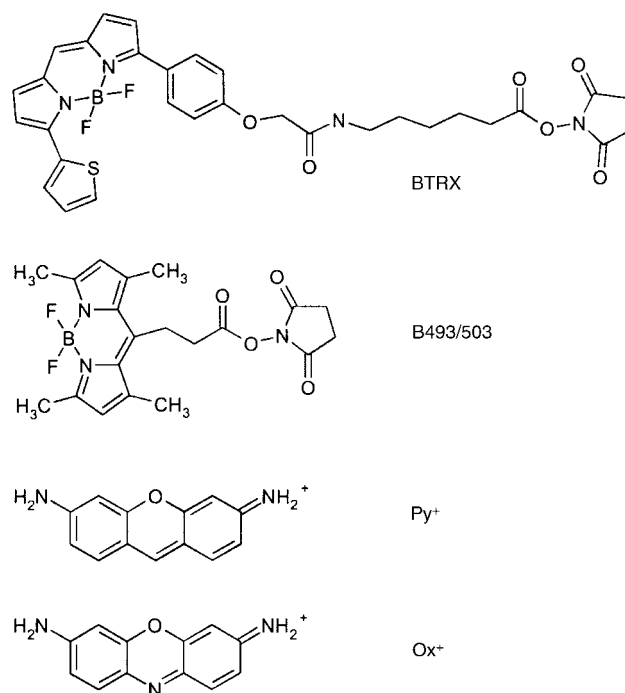


Figure 1. Dye-loaded zeolite L antenna; A) blue-emitting donor molecules inside the zeolite transfer electronic excitation energy to red-emitting acceptor molecules at the left and right of the cylindrical crystal. B) Antenna system with stopcock molecules as external traps and a schematic picture of a stopcock at the end of a zeolite L channel. The stopcock contains a head, a spacer, and a label.



Scheme 1. Dyes examined: BODIPY TR-X SE (BTRX), BODIPY 493/503 SE (B493/503), pyronine⁺ (Py⁺), and oxonine⁺ (Ox⁺).

Owing to the adsorption equilibrium, the more preferred adsorption sites will after some time be predominantly occupied. Thus a difference in adsorption affinity between the coat and the base of the crystals will be pronounced after the adsorption process has reached its equilibrium state. If the dye concentration on the crystal surface becomes too high, aggregation will occur. Aggregates usually quench fluorescence^[19] and it is therefore necessary to work with well-controlled amounts of dye so that only monomers are present.

Energy-transfer experiments were done on the two different systems shown in Figure 2. The Py^+ /BTRX system was used to investigate energy transfer from Py^+ molecules inside the zeolite channels to the BTRX stopcocks, and the Ox^+ /B493/503 system to investigate energy transfer from B493/503 stopcocks to Ox^+ molecules inside the zeolite channels. For these experiments zeolite nanocrystals with a size of about 30 nm were used.

The optical properties of Py^+ -loaded and of BTRX modified nanocrystals are shown in Figure 3A. The spectral overlap integral between the fluorescence spectrum of Py^+ and the excitation spectrum of BTRX is large—a prerequisite for effective energy transfer. Py^+ -zeolite L crystals with different occupational probabilities, p_{Py} , were modified with two BTRX stopcocks per channel. Py^+ was selectively excited at 22000 cm^{-1} . Figure 3B shows the resulting fluorescence spectra for different Py^+ loads. After Py^+ excitation, we can clearly see the fluorescence band of BTRX around 16000 cm^{-1} . It is the result of energy transfer from Py^+ molecules inside the crystals to BTRX molecules on the external surface (Figure 2 top). The dotted spectrum in Figure 3B arises from a sample in which the amount of Py^+ inside the channels is twice the amount of BTRX on the external surface. An increase of the donor concentration leads to a decrease of the mean

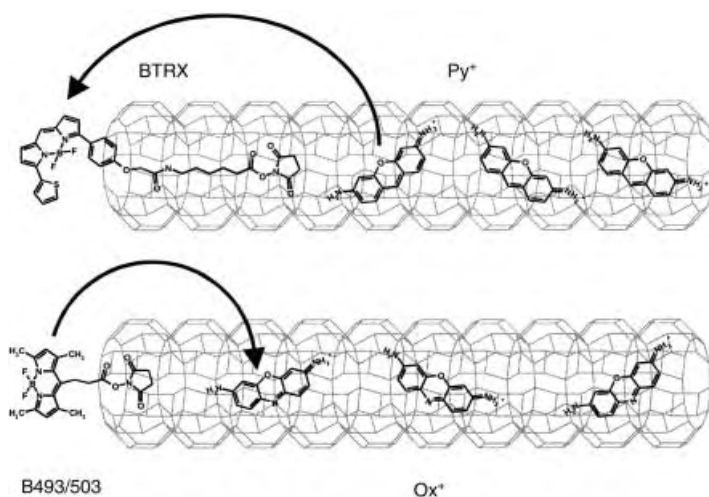


Figure 2. Top: Py^+ -filled zeolite L channels; the ends of the channels are modified with BTRX stopcocks for external trapping of electronic excitation energy. Bottom: Ox^+ -filled zeolite L channels; and the ends of the channels are modified with B493/503 stopcocks for electronic excitation energy injection.

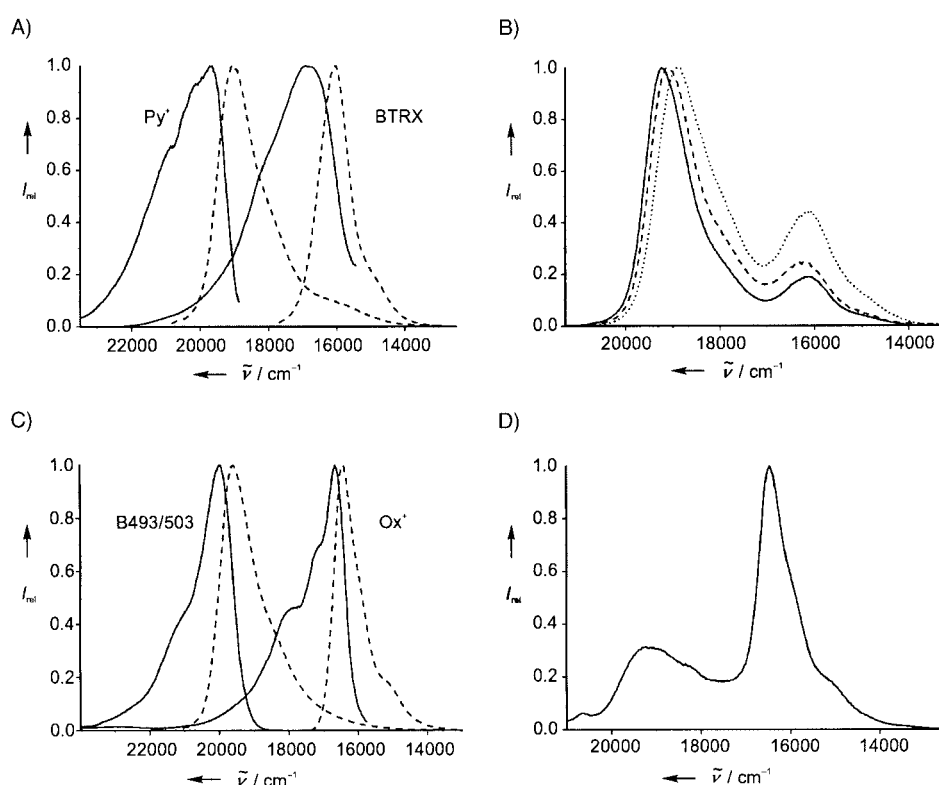


Figure 3. A) Fluorescence (---) and fluorescence excitation (—) spectra of Py^+ in, and BTRX on the external surface of zeolite L nanocrystals; $\epsilon_{\text{Py}^+}(\lambda_{\text{max}}) \approx 83200\text{ cm}^{-1}\text{M}^{-1}$, $\epsilon_{\text{BTRX}}(\lambda_{\text{max}}) \approx 68000\text{ cm}^{-1}\text{M}^{-1}$; $J_{\text{Py}^+-\text{BTRX}} = 3 \times 10^{-10}\text{ cm}^3\text{M}^{-1}$, $p_{\text{Py}} = 0.06$; the crystals with BTRX were modified with two molecules per channel. B) Fluorescence spectra of Py^+ -zeolite L nanocrystals modified with two BTRX per channel. —: $p_{\text{Py}} = 0.02$, ---: $p_{\text{Py}} = 0.06$, ----: $p_{\text{Py}} = 0.10$. C) Fluorescence (---) and fluorescence excitation (—) spectra of Ox^+ in, and of B493/503 on the external surface of zeolite L nanocrystals; $\epsilon_{\text{Ox}^+}(\lambda_{\text{max}}) \approx 84100\text{ cm}^{-1}\text{M}^{-1}$, $\epsilon_{\text{B493/503}}(\lambda_{\text{max}}) \approx 84000\text{ cm}^{-1}\text{M}^{-1}$; $J_{\text{B493/503-Ox}^+} = 1.5 \times 10^{-10}\text{ cm}^3\text{M}^{-1}$, $p_{\text{Ox}^+} = 0.008$; the crystals with B493/503 were modified with one molecule per channel. D) Fluorescence spectra of Ox^+ -zeolite L nanocrystals modified with one B493/503 per channel. All spectra have been scaled to the same height $I_{\text{max}} = 1$.

donor–acceptor and mean donor–donor separation. It is expected that this results in more effective energy transfer, which is what we observe (Figure 3B). We attribute the bathochromic shift of the Py^+ emission band to self-absorption and re-emission.^[8]

The reverse of this external trapping is injection of electronic excitation energy. For this, we need a system, such as the chosen B493/503-modified Ox^+ -zeolite L, in which the donor stopcocks are at both ends and the acceptor molecules are inside the zeolite channels (Figure 2 bottom). We first characterized the Ox^+ -zeolite nanocrystals and the nanocrystals modified with B493/503 separately (Figure 3C). Again the spectral overlap integral between the emission spectrum of B493/503 and the excitation spectrum of Ox^+ is large. The B493/503 stopcocks are excited selectively at 21740 cm^{-1} . We modified Ox^+ -zeolite L crystals with one molecule of B493/503 per channel. The occupational probability of Ox^+ was chosen to be very small (0.008) so that 3.5 times more donor molecules were present than acceptor molecules. After specific excitation of the B493/503 stopcocks at 21740 cm^{-1} the emission spectrum of Figure 3D was obtained, which shows that impressive energy transfer takes place from the B493/503 stopcocks to the Ox^+ molecules. The emission band at 16000 cm^{-1} is due to energy injection from

B493/503. This energy injection works even better than the energy trapping of excited Py^+ molecules by BTRX. The length of the tail of BTRX is 1.8 nm and that of B493/503 is 0.9 nm. The shorter tail of B493/503 allows shorter donor–acceptor separations R_{DA} . Because the Förster energy transfer rate falls off with R_{DA}^{-6} the shorter distance is presumably the main reason for the higher transfer efficiency.

Although the nanocrystals are a good choice for energy-transfer experiments, it is at the present time technically not feasible to examine the organization of the individual dyes with an optical microscope. To visualize this we therefore used large zeolite L crystals of about 2 μm length. Our aim was to establish on which zeolite surface the stopcocks preferably bind and to try to image the energy transfer. Modification of large Py^+ -zeolite L crystals with two BTRX molecules per channel led to the fluorescence microscope images shown in Figure 4. The zeolite crystals were exchanged with Py^+ for very short periods so that the Py^+ molecules could not diffuse far into the zeolite channels. This accounts for why the middle part of the crystals in Figure 4 are dark.

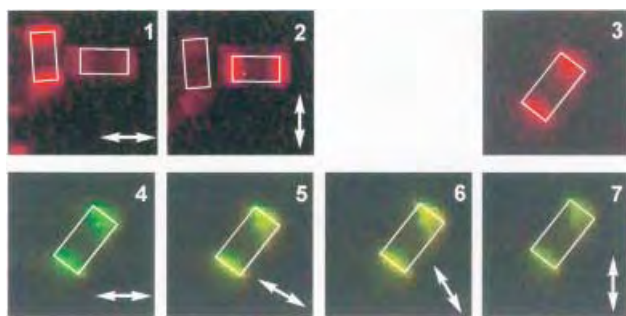


Figure 4. Fluorescence microscope images of 2 μm Py^+ -zeolite L crystals modified with 2 BTRX molecules per channel. The white rectangles indicate single zeolite L crystals. 1, 2) Images of BTRX-modified zeolites after excitation at 545–580 nm and detection with a 610 nm cut-off filter using a polarizer (the direction of the transmitted polarization is indicated by the arrows); 3) image of a crystal detected without polarizer. 4–7) images of the same crystal as in 3) after excitation at 470–490 nm and detection with a 515 nm cut-off filter at different polarizations.

Images 1 and 2 in Figure 4 show the emission after BTRX excitation of two perpendicular lying crystals; the transmitted polarization direction is indicated by the arrows. It is clear that the stopcocks are located at the bottom and top of the cylindrical crystals and that the BTRX emission is polarized perpendicular to the crystal axis. The $S_0 \leftarrow S_1$ transition dipole moment of the BODIPY fluorophore is polarized along the chromophore axis.^[20] Molecular orbital calculations^[10c, 21] reveal that the $S_0 \leftarrow S_1$ transition dipole moment of BTRX is similarly polarized. One would therefore expect an emission perpendicular to the crystal axis when the molecules partly penetrate the zeolite L channels. Images 3–7 in Figure 4 all show the same crystal. Image 3 shows the emission after BTRX excitation and images 4–7 show the emission after Py^+ excitation. The color of the emitted light changes significantly with polarization. Depending on the polarization a green to yellow emission dominates. The yellow color is a mixture of green (Py^+) and red (BTRX) emission. If the Py^+ and the BTRX molecules are differently oriented, different contribu-

tions of red and green occur for the different polarization. For the polarization perpendicular to the crystal axis (as approximately is the case in image 5), the red contribution is largest and the crystals appear yellow.

In conclusion we have shown that electronic excitation energy can be trapped outside and injected into nanoantennae by stopcock molecules that preferably adsorb at the base of the cylindrical zeolite L crystals. This opens the door to a wide range of applications, for example, for mimicking the natural photosynthesis apparatus, for supramolecular nanoprobe, and in dye-sensitized solar cells and light-emitting diodes.^[16]

Experimental Section

Chemically pure zeolite L materials were synthesized and characterized as described in reference [7]. The potassium zeolite L crystals were pretreated by stirring in a buffer of pH 6 for 1 h followed by washing with doubly distilled H_2O three times. Py^+ and Ox^+ were synthesized and purified according to the procedure in reference [10b]. BTRX (BODIPY TR-X SE) and B493/503 (BODIPY 493/503 SE) were obtained from Molecular Probes Inc. and used as received. Py^+ and Ox^+ molecules were inserted in the zeolite L channels by ion exchange from H_2O . An aqueous zeolite L suspension was treated in an ultrasonic bath for 20 min and then added to an aqueous dye solution containing the appropriate amount of dye. The mixture was refluxed for 1 h. Afterwards the dye-loaded crystals were washed twice with MeOH by ultrasonic treatment for 15 min to remove dyes from the external surface. For the adsorption of BTRX and B493/503 the zeolite L crystals were suspended in cyclohexane and sonicated for 20 min. Then a dye solution in cyclohexane with the appropriate amount of dye was added and the mixture was sonicated for 30 min at room temperature. Adsorption of BTRX and B493/503 onto the dye-loaded zeolites did not extract any cationic dyes from inside the zeolite. Solid-state samples were prepared on 16 mm diameter quartz plates for fluorescence measurements which were carried out the same day.

Fluorescence spectra were measured with a Perkin Elmer LS 50B luminescence spectrometer using suitable cut-off filters (Py^+ was excited at 455 nm and detected at 550 nm; BTRX was excited at 550 nm and detected at 690 nm; Ox^+ was excited at 560 nm and detected at 670 nm; B493/503 was excited at 460 nm and detected at 575 nm). Absorption spectra were recorded on a Perkin Elmer Lambda 900 spectrophotometer. Optical microscopy images of fluorescent samples were recorded under an Olympus BX 60 microscope combined with a Kappa CF 20 DCX Air K2 CCD camera with 100 \times magnification using an immersion oil. The light stemming from a mercury lamp was first passed through a 438 nm cut-off filter. It was then passed through appropriate excitation cubes comprising a narrow-band excitation filter, a dichroic mirror, and a cut-off filter. Py^+ was excited between 470 and 490 nm and detected with a cut-off filter at 515 nm, BTRX was excited between 545 and 580 nm and detected with a cut-off filter at 610 nm. By inserting a polarizer in front of the camera the fluorescence images could be examined at different polarizations.

Received: December 5, 2001 [Z18332]

- [1] V. Balzani, S. Campagna, G. Denti, A. Juris, S. Serroni, M. Venturi, *Sol. Energy Mater. Sol. Cells* **1995**, *38*, 159.
- [2] H. Bücher, K. H. Drexhage, M. Fleck, H. Kuhn, D. Möbius, F. P. Schäfer, J. Söndermann, W. Sperling, P. Tillmann, J. Wiegand, *Mol. Cryst.* **1967**, *2*, 199.
- [3] B. A. Gregg, U. Resch, *J. Photochem. Photobiol. A* **1995**, *87*, 157.
- [4] S. E. Webber, *Chem. Rev.* **1990**, *90*, 1469.
- [5] V. Balzani, P. Ceroni, S. Gestermann, M. Gorka, C. Kauffmann, M. Maestri, F. Vögtle, *ChemPhysChem* **2000**, *4*, 224.
- [6] G. Calzaferri, H. Maas, M. Pauchard, M. Pfenniger, S. Megelski, A. Devaux in *Advances in Photochemistry*, Vol. 27 (Ed.: D. C. Neckers), Wiley-VCH, Weinheim, **2002**, in press.
- [7] S. Megelski, G. Calzaferri, *Adv. Funct. Mater.* **2001**, *11*, 277.
- [8] G. Calzaferri, D. Brühwiler, S. Megelski, M. Pfenniger, M. Pauchard, B. Hennessy, H. Maas, A. Devaux, U. Graf, *Solid State Sci.* **2000**, *2*, 421.

- [9] M. Pauchard, A. Devaux, G. Calzaferri, *Chem. Eur. J.* **2000**, *6*, 3456.
 [10] a) N. Gfeller, G. Calzaferri, *J. Phys. Chem. B* **1997**, *101*, 1396; b) N. Gfeller, S. Megelski, G. Calzaferri, *J. Phys. Chem. B* **1999**, *103*, 1250; c) S. Megelski, A. Lieb, M. Pauchard, A. Drechsler, S. Glaus, C. Debus, A. J. Meixner, G. Calzaferri, *J. Phys. Chem. B* **2001**, *105*, 25.
 [11] P. A. Anderson, A. R. Armstrong, A. Porch, P. P. Edwards, L. J. Woodall, *J. Phys. Chem. B* **1997**, *101*, 9892.
 [12] C. Bärlocher, W. M. Meier, D. H. Olsen, *Atlas of Zeolite Framework Types*, Elsevier, Amsterdam, **2001**.
 [13] D. W. Breck, *Zeolite Molecular Sieves*, Wiley, New York, **1974**.
 [14] a) T. Förster, *Ann. Phys. (Leipzig)* **1948**, *6*, 55; b) T. Förster, *Fluoreszenz Organischer Verbindungen*, Vandenhoeck & Ruprecht, Göttingen, **1951**; c) T. Förster in *Comparative Effects on Radiation*, Wiley, New York, **1960**, pp. 300–319.
 [15] M. Pauchard, S. Huber, R. Méallet-Renault, H. Maas, R. Pansu, G. Calzaferri, *Angew. Chem.* **2001**, *113*, 2921; *Angew. Chem. Int. Ed.* **2001**, *40*, 2839.
 [16] G. Calzaferri, M. Pauchard, H. Maas, S. Huber, A. Khatyr, T. Schaafsma, *J. Mater. Chem.* **2002**, *12*, 1.
 [17] a) M. Tsapatsis, T. Okubo, M. Lovallo, M. E. Davis, *Mater. Res. Soc. Symp. Proc.* **1995**, *371*, 21; b) M. Tsapatsis, M. Lovallo, T. Okubo, M. E. Davis, M. Sadakata, *Chem. Mater.* **1995**, *7*, 1734.
 [18] R. P. Haugland, *Handbook of Fluorescent Probes and Research Products*, Molecular Probes Inc., Eugene, **2001**.
 [19] a) M. Kasha, H. R. Rawls, M. A. El-Bayoumi, *Pure Appl. Chem.* **1965**, *11*, 371; b) E. G. McRae, M. Kasha, *J. Chem. Phys.* **1958**, *28*, 721.
 [20] J. Karolin, L. B.-Å. Johansson, L. Strandberg, T. Ny, *J. Am. Chem. Soc.* **1994**, *116*, 7801.
 [21] G. Calzaferri, R. Rytz, *J. Phys. Chem.* **1995**, *99*, 12141.

Sr₄N₃: A Hitherto Missing Member in the Nitrogen Pressure Reaction Series Sr₂N → Sr₄N₃ → SrN → SrN₂**

Yurii Prots, Gudrun Auffermann, Michael Tovar, and Rüdiger Kniep*

In the course of our investigations on the formation and existence of diazenides of strontium,^[1] we developed an analytical method for quantitative nitrogen speciation.^[2] By means of this technique (carrier-gas hot extraction with a controlled temperature program), we could confirm the results of the structure determinations on SrN ($\hat{=}$ (Sr²⁺)₄ [N³⁻]₂ [N₂²⁻]) and Sr[N₂] ($\hat{=}$ (Sr²⁺) [N₂²⁻]). The system was calibrated by using, for example, Sr₂N^[3] (the starting material of the high-pressure synthesis of diazenides).^[1] In the course of our studies, it turned out that Sr₂N, synthesized at ambient pressure, often contains significant portions of diazenide

which were not clearly visible by X-ray or spectroscopic investigations.^[4] In principle, these experimental results would be consistent with a homogeneity range of Sr₂N towards SrN according to (partial) formation of mixed crystals Sr_{2-x}N (complete miscibility in the limits 0 ≤ x ≤ 1), although previous studies^[1] had provided “no indication for homogeneity ranges” of the nitride diazenides. In fact, we now find that at lower N₂ reaction pressure (already above 1 bar), Sr₂N reacts to the hitherto “overlooked” nitride–diazenide Sr₄N₃.

Sr₄N₃, a dark gray powder with metallic luster, was synthesized in autoclaves^[5] by the reaction of Sr₂N with molecular nitrogen (9 bar) at 650 °C for 6 h.^[6] No impurities were detected by X-ray and neutron diffraction investigations^[7] at ambient pressure nor by chemical analysis.^[9] The contents of oxygen, hydrogen, and carbon were below the limits of detection. At constant reaction temperature (650 °C) and time (6 h), the diffraction pattern of Sr₄N₃ was observed up to a reaction pressure of 100 bar amongst the characteristic reflections of SrN. The lattice parameters of Sr₄N₃ and SrN, determined at ambient pressure, remained unchanged within the standard deviations.

The crystal structure of the air- and moisture-sensitive microcrystalline powder of Sr₄N₃ was solved by a combination of X-ray and neutron diffraction.^[7] The observed and calculated neutron diffraction diagram, as well as the difference profile, are given in Figure 1. The crystal structure of Sr₄N₃ is depicted in Figure 2 (center) showing the close

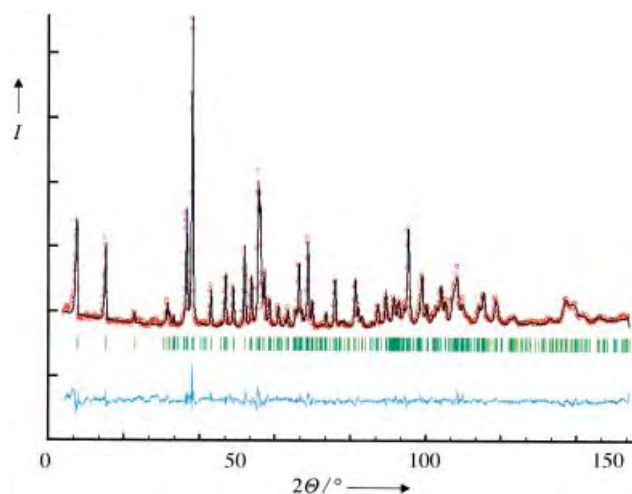


Figure 1. Neutron diffraction diagram of Sr₄N₃ $\hat{=}$ Sr₈[N]₄[N₂] (powder diffractometer E9, HMI Berlin) at 298 K: Observed (red dots), calculated (black solid line), and difference profiles (blue line). The green ticks mark the positions of the Bragg reflections of the monoclinic C-centered cell.^[7]

relation to the starting material Sr₂N (left) and the next higher “pressure stage” SrN (right). The evident structural relation makes it reasonable to suppose the reaction paths during the formation of Sr₄N₃ via an intercalation step.^[10] Thus, these structural chemical facts can easily be described when starting with the subnitride Sr₂N^[3] as the host structure (CdCl₂ type). In the first step of the N₂-pressure induced intercalation which occurs already at about 1 bar (*p*_{N₂}), one half of the octahedral holes ($\square^{(0)}$) between two adjacent layers $\frac{2}{3}$ (Sr_{6/3}N) along [001] in the host structure, are occupied by N₂. Thus, packages of

[*] Prof. Dr. R. Kniep, Dr. Yu. Prots, Dr. G. Auffermann
 Max-Planck-Institut für Chemische Physik fester Stoffe
 Nöthnitzer Strasse 40, 01187 Dresden (Germany)
 Fax: (+49) 351-4646-3002
 E-mail: Kniep@cpfs.mpg.de
 Dr. M. Tovar
 Hahn-Meitner-Institut, Berlin
 Glienicke Strasse 100, 14109 Berlin (Germany)

[**] We thank the Fonds der Chemischen Industrie for financial support, the Hahn-Meitner-Institut for giving us access to the powder diffractometer E9, B. Bayer and A. Völzke for assistance with the chemical analyses.

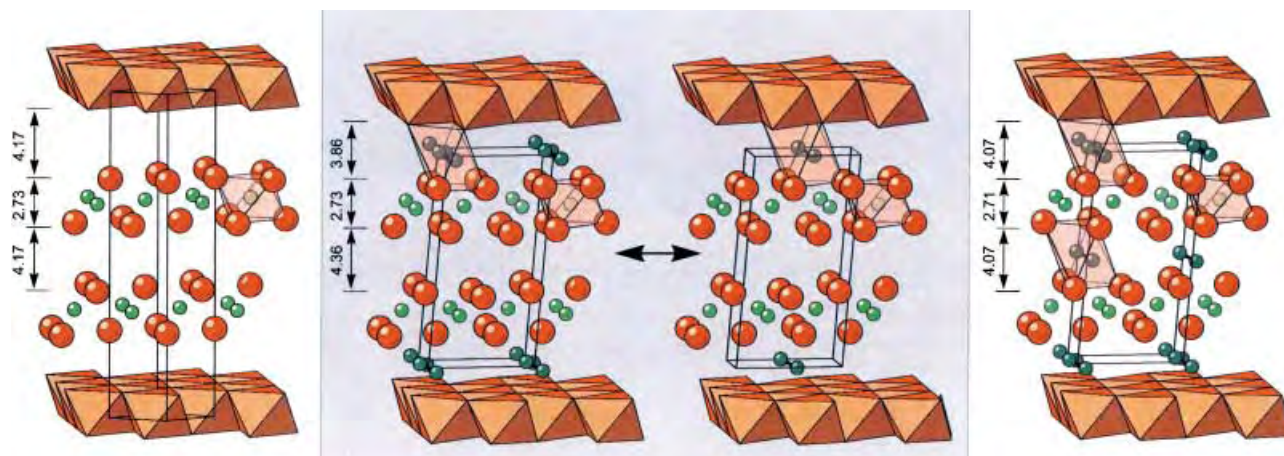
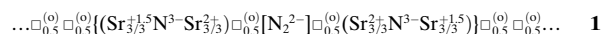


Figure 2. Crystal structures of $\text{Sr}_2\text{N} \cong (\text{Sr}^{+1.5})_2[\text{N}^{3-}]$ (left), $\text{Sr}_4\text{N}_3 \cong (\text{Sr}^{+1.5})_4(\text{Sr}^{2+})_4[\text{N}^{3-}]_4[\text{N}_2^{2-}]$ (center) and $\text{SrN} \cong (\text{Sr}^{2+})_4[\text{N}^{3-}]_2[\text{N}_2^{2-}]$ (right). The top and bottom boundaries of the figures are represented by layers of $\text{Sr}_{6/3}\text{N}$ octahedra centered by $[\text{N}^{3-}]$ (polyhedral representation). Ball-and-stick representation between the polyhedral layers: $\text{Sr}^{+1.5/2+}$: red; $[\text{N}^{3-}]$: light green; $[\text{N}_2^{2-}]$: dark green. Transparent octahedra allow a better orientation. On the assumption of ordered N_2 occupation, the two limiting primitive structures of Sr_4N_3 are emphasized by the gray background; in fact, a C-centered cell with half-occupation of the octahedral holes is found (see text and [7]). The numbers (in Å) correspond to the d values of neighboring Sr layers. Although the thicknesses of the layers of the unoccupied octahedral layers in Sr_4N_3 (4.36 Å) are significantly larger than those in Sr_2N (4.17 Å), the interatomic distances Sr–Sr between the Sr layers are in a comparable order of magnitude (Sr_2N : 4.73; Sr_4N_3 : 4.73, 4.78, and 4.83 Å).

layers $\{(\text{Sr}_{6/3}\text{N})_{0.5}^{(0)}[\text{N}_2]_{0.5}^{(0)}(\text{Sr}_{6/3}\text{N})\}$ are formed leading to the composition Sr_4N_3 . These packages contain the diazenide ion N_2^{2-} ($\text{N}=\text{N}$ bond length: 1.22 Å), and the closely coordinating strontium ions are oxidized from oxidation state +1.5 (host: $(\text{Sr}^{+1.5})_2[\text{N}^{3-}]$) to +2. This results in layered packages with the ionic formula **1**:



The strontium ions at the boundaries of the packages are in the low-valent oxidation state +1.5 and form together with the adjacent $\text{Sr}^{+1.5}$ layers the (metallic) subregions with unoccupied octahedral holes.

In the first intercalation step (formation of Sr_4N_3), the diazenide dumbbells can, in principle, occupy two octahedral holes within the layers (Figure 2 (center)); see also ionic formula **1**). Evidently, the spatial separation of the diazenide layers ($c = 13.76$ Å) makes an alternative occupation of the octahedral holes possible although, within every layer, the same kind of octahedral holes are always occupied. In fact, the diffraction pattern indicates a C-centered space group, thus leading to a half-occupation of all the octahedral holes by the N_2 species.^[7] The octahedral holes between neighboring $\text{Sr}^{+1.5}$ layers remain empty.

X-ray investigations showed that, already at a N_2 reaction pressure of 10 bar ($T = 650^\circ\text{C}$) the second intercalation stage (SrN ; ^[1] Figure 2, right) can be identified besides Sr_4N_3 . For the formation of this state, additionally, one half of the empty octahedral holes between the $\text{Sr}^{+1.5}$ double layers are occupied in an ordered manner: $\{\text{Sr}_4^{+1.5}\text{Sr}_4^{2+}[\text{N}^{3-}]_4[\text{N}_2^{2-}]\} + \text{N}_2 \rightarrow \{\text{Sr}_8^{2+}[\text{N}^{3-}]_4[\text{N}_2^{2-}]\}[\text{N}_2^{2-}]$. The stepwise oxidation of strontium is now finished. At higher N_2 reaction pressure (above 500 bar), besides SrN , the tetragonal diazenide $\text{Sr}[\text{N}_2]$ ^[1] is formed (close structural relationship to the monoclinic $\text{Ba}[\text{N}_2]$),^[11] which is obtained as a single-phase product above 5000 bar (p_{N_2}).

It has already been reported^[1] that SrN and $\text{Sr}[\text{N}_2]$ thermally decompose ($300\text{--}400^\circ\text{C}$) at ambient pressure under argon to give Sr_2N (release of molecular nitrogen). Sr_4N_3 reacts in the same way. Interestingly, in this connection, the analytically ascertained contents of diazenides in Sr_2N ^[2] are obviously caused by “impurities” of Sr_4N_3 . Analytically pure Sr_2N , prepared from the elements at ambient pressure, will certainly be obtained only after additional treatment (650°C) in vacuum (10^{-6} bar). This finding would be consistent, on the basis of the close structural relations, with a deintercalation process, although our investigations on the preservation of topochemical host–guest relations for intercalation and deintercalation in the system Sr–N , are not yet finished.^[10]

Sr_4N_3 belongs to the class of subcompounds with metallic character, a property which, for example, for the binary subnitride Ba_3N ^[12] is described with the following formula: $[\text{Ba}^{2+}]_3[\text{N}^{3-}] \cdot 3e^-$. Applying this to the strontium–subnitride–diazenide results in the formula $(\text{Sr}^{2+})_8[\text{N}^{3-}]_4[\text{N}_2^{2-}] \cdot 2e^-$, which does not reflect the peculiarity of the crystal chemistry of strontium (**1** and Figure 2, center). Therefore, we prefer, for the elucidation of the obviously mixed-valent Sr compound, the formula $(\text{Sr}^{+1.5})_4(\text{Sr}^{2+})_4[\text{N}^{3-}]_4[\text{N}_2^{2-}]$. This formula is not only consistent with the crystal structure, it also makes it readily apparent which of the Sr species, in the course of the reduction process of molecular nitrogen, are oxidized to Sr^{2+} during the formation of the second intercalation stage (SrN ; see Figure 2 right). To answer the question of the real existence of “low-valent” strontium, additional experimental and theoretical studies are necessary.

Received: February 28, 2002 [Z 18792]

- [1] G. Auffermann, Yu. Prots, R. Kniep, *Angew. Chem.* **2001**, *113*, 565–567; *Angew. Chem. Int. Ed.* **2001**, *40*, 547–549.
- [2] G. Auffermann, U. Schmidt, B. Bayer, Yu. Prots, R. Kniep, *Anal. Bioanal. Chem.*, in press.
- [3] N. E. Brese, M. O’Keeffe, *J. Solid State Chem.* **1990**, *87*, 134–140.

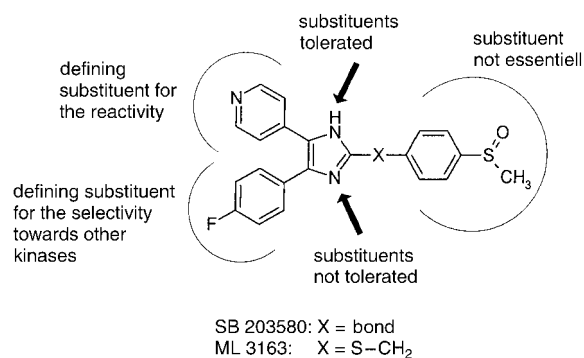
- [4] G. Auffermann, Yu. Prots, R. Kniep, S. F. Parker, S. M. Bennington, *ChemPhysChem.*, in press.
- [5] a) W. Bronger, G. Auffermann, *Chem. Mater.* **1998**, *10*, 2723–2732; b) W. Bronger, G. Auffermann, P. Müller, *J. Less-Common Met.* **1988**, *142*, 243–252.
- [6] Sr_4N_3 was synthesized by heating Sr_2N (prepared at 1120 K from the elements) in a molybdenum boat under a N_2 atmosphere (Messer Griesheim, given purity 99.999%, purified by oxisorb-catridges, Messer Griesheim) for 6 h at 920 K in an autoclave.^[5] An initial pressure of 8 bar (corresponding to a reaction pressure of 9 bar) led to nearly single-phase Sr_4N_3 . The course of the reaction was steadily controlled by a pressure gauge.
- [7] Neutron diffraction experiments were carried out on the powder diffractometer E9 at the reactor BER II of the HMI Berlin. Sr_4N_3 was placed under argon into a cylindrical vanadium container (diameter 8 mm, length 47 mm, wall thickness 0.15 mm) and was closed with a cap containing an indium seal. Crystal structure data derived from neutron diffraction experiments with the wavelength $\lambda = 1.7965 \text{ \AA}$ in the range $2^\circ < 2\theta < 158^\circ$ at 298 K and 2 K: monoclinic, space group $C2/m$, $Z=2$; 298 K: $a = 6.7070(4)$, $b = 3.8280(2)$, $c = 13.7625(8) \text{ \AA}$, $\beta = 96.519(5)^\circ$, $V = 351.05(3) \text{ \AA}^3$; Sr1 in (4i): $x = 0.413(1)$, $z = 0.1413(4)$; Sr2 in (4i): $x = 0.127(1)$, $z = 0.3406(3)$; N1 in (4i): $x = 0.775(1)$, $z = 0.2515(4)$; N2 in (4i): $x = 0.083(1)$, $z = 0.0217(6)$, occupancy factor = 0.5; $R_{\text{profile}} = 0.055$, $R_{\text{Bragg}} = 0.053$, number of observed reflections: 272. 2 K: $a = 6.6886(3)$, $b = 3.8173(2)$, $c = 13.7382(6) \text{ \AA}$, $\beta = 96.447(3)^\circ$, $V = 348.55(3) \text{ \AA}^3$; Sr1 in (4i): $x = 0.4133(7)$, $z = 0.1412(3)$; Sr2 in (4i): $x = 0.1290(7)$, $z = 0.3413(3)$; N1 in (4i): $x = 0.7748(6)$, $z = 0.2483(3)$; N2 in (4i): $x = 0.0850(8)$, $z = 0.0234(4)$, occupancy factor = 0.5; $R_{\text{profile}} = 0.066$, $R_{\text{Bragg}} = 0.047$, number of observed reflections: 261. The refinements were carried out using the program Fullprof.^[8] Further details on the crystal structure investigations may be obtained from the Fachinformationszentrum Karlsruhe, 76344 Eggenstein-Leopoldshafen, Germany (fax: (+49) 7247-808-666; e-mail: crysdata@fiz-karlsruhe.de), on quoting the depositary numbers CSD-412394 and CSD-412395.
- [8] J. Rodriguez-Carvajal, Laboratoire Léon Brillouin, Saclay FULL-PROF.2 K Version 1.9e May, **2001**.
- [9] The nonmetallic components N, O, H, C were quantitatively determined by the carrier-gas hot extraction or combustion technique (TC 436 DR/5, RH 404 and C200CHLH (LECO)): Sr_4N_3 ($N_{\text{exp}} 10.86(8)$, $N_{\text{calcd}} 10.71 \text{ wt\%}$). Si_3N_4 was used as a calibration standard. Impurities of O, H, and C were not detected (limits of detection: $C < 0.1$; $H < 0.005$; $O < 0.05 \text{ wt\%}$). Using a temperature ramping from 500–1500 K, it was not only possible to determine the nitrogen content^[2] in $\text{Sr}_4\text{N}_3 \rightleftharpoons (\text{Sr}^{+1.5})_4(\text{Sr}^{2+})_4[\text{N}^{3-}]_4 [\text{N}_2^{2-}]$ but also to quantify the two different nitrogen species in the molar ratio of 2:1.
- [10] G. Auffermann, Yu. Prots, R. Kniep, unpublished results.
- [11] G. V. Vajenine, G. Auffermann, Yu. Prots, W. Schnelle, R. K. Kremer, A. Simon, R. Kniep, *Inorg. Chem.* **2001**, *40*, 4866–4870.
- [12] P. E. Rauch, A. Simon, *Angew. Chem.* **1992**, *104*, 1505–1506; *Angew. Chem. Int. Ed.* **1992**, *31*, 1519–1521.

Ones, Thiones, and N-Oxides: An Exercise in Imidazole Chemistry**

Stefan Laufer,* Gerd Wagner, and
Dunja Kotschenreuther

*Dedicated to Prof. Dr. Wolfgang Wiegrobe
on the occasion of his 70th birthday*

The inhibition of the proinflammatory cytokines interleukin 1β (IL- 1β) and tumor-necrosis factor α (TNF- α) has been recognized as a rewarding target for the development of tailor-made anti-inflammatory drugs.^[1] Among the most promising small-molecular anticytokine agents are inhibitors of p38 MAP kinase, a serine/threonine-specific kinase involved in the biosynthesis and release of cytokines from immunocells.^[2a] Like other potent inhibitors of p38 MAP kinase, our lead compound ML 3163 was derived from 5-(pyridin-4-yl)imidazole (SB 203 580; Scheme 1), which



Scheme 1. Structural requirements for inhibition of p38 MAP kinase.

binds to the ATP-binding site of the p38 kinase,^[2b] and has demonstrated efficacy in various models.^[2c] In the development of pharmaceuticals, in addition to bioactivity, the issues of bioavailability and toxicity must be addressed. For example, further development of SB 203 580 itself has been obstructed by its liver toxicity, which is caused by interaction with cytochrome P450 (P450).^[2d] Therefore, it is of general interest to the medicinal chemist to have a straightforward synthetic methodology which provides access to a large number of bioactive candidate molecules.

Herein we describe such a versatile synthetic strategy for the ready preparation of numerous structurally diverse

[*] Prof. Dr. S. Laufer, G. Wagner, D. Kotschenreuther
Institute of Pharmacy
Department of Pharmaceutical and Medicinal Chemistry
Eberhard-Karls-University Tübingen
Auf der Morgenstelle 8, 72076 Tübingen (Germany)
Fax: (+49) 7071-29-5037
E-mail: stefan.laufer@uni-tuebingen.de

[**] Thanks to Merckle GmbH, Blaubeuren (Germany) for financial and organizational support, Fonds der Chemischen Industrie (Germany) for financial support, Dr. W. Zimmermann for helpful discussions, and C. Greim for establishing the p38 test assay.

Supporting information for this article is available on the WWW under <http://www.angewandte.org> or from the author.

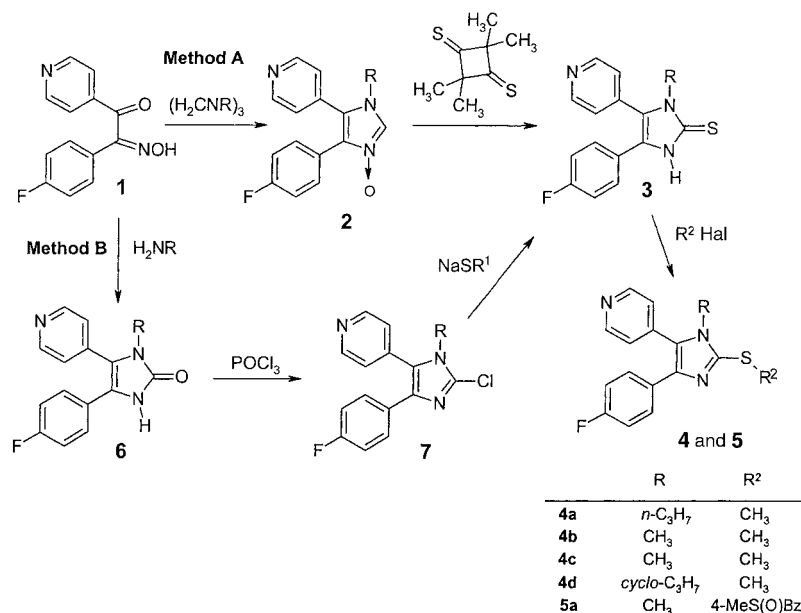
ML 3163 analogues. In this class of compounds (Scheme 1), substituents at the 4 and 5-position of the imidazole core are essential for efficient and selective inhibition of p38 MAP kinase,^[2b,e,f] while substituents at the 1 and 2-position primarily serve to reduce interaction with P450 and to improve cell permeability. To find p38 MAP kinase inhibitors with enhanced cellular activity and diminished toxicity, we have developed a synthetic methodology which provides 1,2,4,5-tetrasubstituted imidazole derivatives, with maximum flexibility in the type of substituents. Most importantly, this synthetic route also allows for the regioselective placement of substituents at the imidazole nitrogen atom; the regiochemistry of substituents at the ring nitrogen atoms being decisive for inhibitory potency (Scheme 1).^[2e,f] As a result of these efforts, several analogues of ML 3163 were identified as anticytokine agents well suited for further development. Moreover, this general method may be applied in the quest for novel ATP-competitive inhibitors for other kinases.

Synthetic approaches towards highly substituted imidazoles are few and often restricted to a fixed pattern of substitution.^[3a-c] Preliminary experiments revealed that direct *N*-methylation of 5-(pyridin-4-yl)imidazoles by various methods predominantly yields the "wrong" regioisomer.^[3d] To obtain tetrasubstituted imidazole derivatives of the desired regiochemistry, and to extend the scope of substituents at the 1-position beyond simple alkyl moieties, we attempted the introduction of *N*-substituents at an earlier synthetic stage. The synthesis of 4/5-alkyl/aryl-substituted imidazole-2-thiones with simple alkyl substituents at the 1-position has been reported, from the corresponding *N*-oxides.^[4a] However, initial attempts to extend the scope of this reaction to the preparation of 5-(pyridin-4-yl)imidazole-2-thiones failed (Scheme 2, Method A). The required *N*-oxides **2** could not be synthesized from 1-(4-fluorophenyl)-2-(pyridin-4-yl)hydroximino-ethan-2-one (**1**) under acidic conditions. Com-

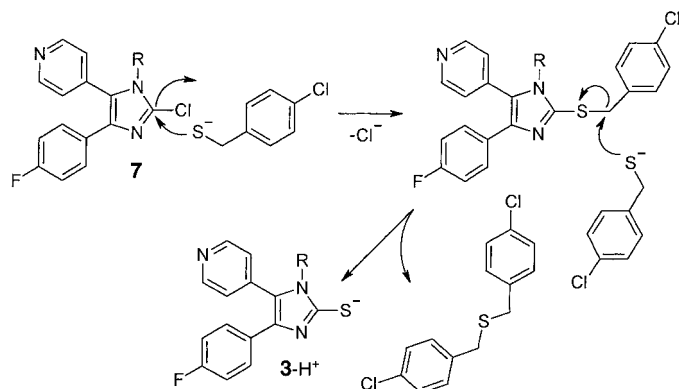
pounds **2** were obtained in good yields only when **1** was treated with the appropriate triazinanes under neutral conditions.^[4b] Unfortunately, this approach was not successful in the case of *N*-phenyl- or *N*-pyridinyltriazinanes (Scheme 2, R = Ph, 3-Pyr). Imidazole *N*-oxides **2** were converted into imidazole-2-thiones **3** by treatment with 2,2,4,4-tetramethylcylobutane-1,3-dithione.^[4a] Here, a much wider array of different substituents in the 1-position was tolerated than previously reported;^[4a] these included favorable functionalities for biological activity (R = cyclopropyl, 3-morpholinopropyl) or toxicity (R = tetramethylpiperidin-4-yl). Subsequent alkylation of imidazole-2-thiones **3**, according to the protocol we had applied in the preparation of ML 3163,^[5] yielded the corresponding 2-alkylsulfanyl imidazoles **4** and **5**.

A second general synthesis of imidazole-2-thiones had to be devised to provide *N*-aryl and *N*-pyridinylimidazole derivatives. This synthetic pathway was based on the conversion of imidazole-2-ones into imidazole-2-thiones via 2-chloroimidazoles (Scheme 2, Method B). According to Lettau, simple *N*-aryl imidazole-2-ones can be prepared from the corresponding α -hydroximinoketones.^[6] However, this method has been limited to imidazole-2-ones bearing at least one simple alkyl substituent at the 4 or 5-position, and was unsuitable for the preparation of 4,5-diphenylimidazole-2-ones.^[6] We managed to overcome these restrictions and application of this strategy afforded 4,5-diphenylimidazole-2-ones as well as the 5-(pyridin-4-yl)imidazole-2-ones **6**. However, under the reaction conditions reported by Lettau, only the starting material was recovered.^[6] A change in the solvent from ethanol to acetonitrile or glacial acetic acid gave the imidazole-2-ones **6** in moderate to high yields. A wide range of different substituents at position 1 was tolerated, including alkyl, cycloalkyl, aryl, heteroaryl, and substituted alkyl, for example, 3-chloropropyl. The latter compound (**6**, R = 3-chloropropyl) served to generate further analogues by nucleophilic modification of the side-chain (e.g. **6**, R = 3-morpholinopropyl).

As immediate synthetic precursors for imidazole-2-thiones, we required the corresponding 2-chloroimidazoles **7** which were readily obtained by chlorination of imidazole-2-ones **6** with phosphorylchloride (Scheme 2).^[7a] The conversion of chloro-substituted (hetero)aromatics into the corresponding aromatic thiols by nucleophilic substitution has been described for electron-deficient polychlorobenzenes, 4-chloropyridine, and 2- and 4-chloroquinolines.^[7b] Much to our surprise, this approach was also successful in the case of the electron-rich 2-chloro-5-(pyridin-4-yl)imidazoles **7**. When compounds **7** were reacted with sodium (4-chlorophenyl)methanethiolate (4.5 equiv), the corresponding imidazole-2-thiones **3** formed in good to moderate yields. This reaction proceeds in two consecutive steps (Scheme 3): First, nucleophilic aromatic substitution affords the 2-(4-chlorobenzylsulfanyl)imidazole. Second, nucleophilic aliphatic substitution effects the cleavage of these thioethers. Bis-



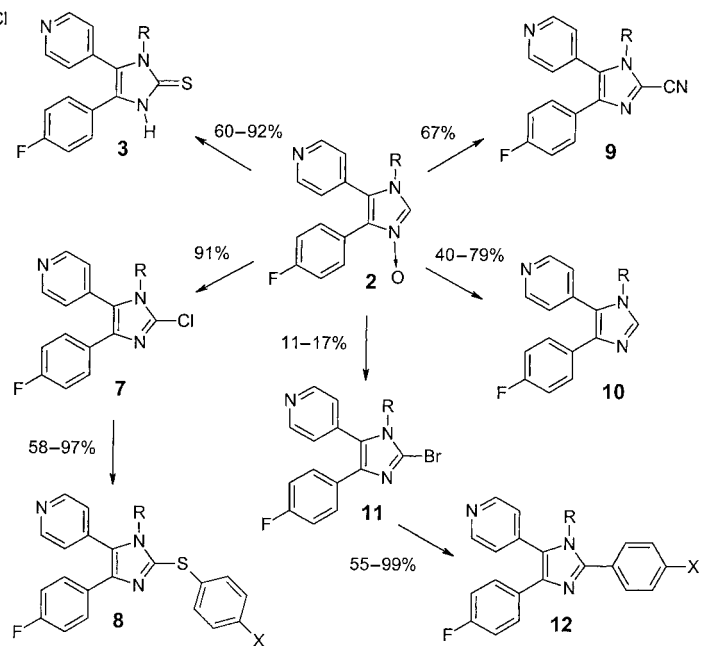
Scheme 2. Preparation of imidazole-2-thiones from imidazole-*N*-oxides (Method A) or imidazole-2-ones (Method B). The imidazole derivative **4c** has a 2-acetylaminopyridinyl group in the 5-position, in place of the shown pyridinyl group.



Scheme 3. Proposed mechanism for the conversion of 2-chloroimidazoles into imidazole-2-thiones, by treatment with (4-chlorophenyl)methanethiolate.

(4-chlorobenzyl)sulfide could be identified by GC–MS as the elimination product of the second step. This observation strongly supports the proposed mechanism. However, this reaction failed in the presence of sterically demanding substituents at the 1-position of 2-chloroimidazoles **7** ($R = 2$ -dimethylaminoethyl, tetramethylpiperidin-4-yl, 3-morpholinopropyl). In one case, 2-(4-chlorobenzylsulfanyl)imidazole was isolated in a very low yield, which indicates that nucleophilic aromatic substitution indeed takes place during the first reaction step. This result prompted us to investigate the general applicability of this reaction to the preparation of imidazolyl sulfides. Compound **7a** ($R = \text{propyl}$) was treated with a reduced amount (2.2 equiv) of sodium (4-chlorophenyl)methanethiolate, to halt the reaction at the level of the corresponding 2-(4-chlorobenzylsulfanyl)imidazole. However, examination of the crude product by GC–MS did not reveal the expected sulfide, but a 4:5 ratio of **7:3a** ($R = \text{propyl}$). This result suggests that nucleophilic heteroaromatic substitution is the rate-limiting step in this reaction scheme. Replacement of sodium (4-chlorophenyl)methanethiolate with three equivalents of sodium ethanethiolate afforded ethylsulfanylimidazole as the only product (yield 74 %). We reasoned that cleavage of the imidazolyl sulfides by nucleophilic aliphatic substitution (step 2) is favored by activating substituents such as a benzyl group, while a simple alkyl group is not sufficient. This finding led us to the synthesis of phenylimidazolyl sulfides **8**, which are not readily accessible by other methods. Treatment of **7** with thiophenol derivatives (2.5 equiv) gave the corresponding phenylimidazolylsulfides **8** in good yields (Scheme 4). Apart from this additional benefit, the strategy of preparing **3** from **6** (Scheme 2, Method B) was complementary to the imidazole-*N*-oxide pathway (Scheme 2, Method A) for two reasons: 1) While Method A fails in the case of (hetero)aromatic amines, these substituents are readily introduced by Method B, and 2) the problems which are encountered with Method B in the case of sterically demanding substituents at the 1-position do not occur in Method A.

During the course of our work directed at the regioselective synthesis of the 1-substituted imidazole-2-thiones **3** via the imidazole-*N*-oxides **2** (Scheme 2, Method A), it became apparent that these *N*-oxides are extremely useful intermediates



Scheme 4. The scope of synthetic transformations of 5-pyridin-4-yl-imidazole-*N*-oxides. In the case of **7**, **8**, and **9**, only the derivatives with $R = \text{propyl}$ were synthesized.

in the synthesis of structurally diverse 5-(pyridin-4-yl)imidazole derivatives modified at the 2-position (Scheme 4). Compound **2a** ($R = \text{propyl}$) was converted into the imidazole-2-carbonitrile **9** with trimethylsilylcarbonitrile.^[8a] Deoxygenation of **2** with PCl_3 yielded the imidazole **10** with only a hydrogen atom in the 2-position.^[8b] This method provides an alternative pathway for the synthesis of known p38 MAP kinase inhibitors such as SB 210313 (**10**, $R = 3$ -morpholinopropyl).^[2f] As with the corresponding imidazole-2-ones **6**, the imidazole-1*N*-oxide **2a** ($R = \text{propyl}$) was chlorinated with phosphorylchloride to give the 2-chloroimidazole **7a**.^[8b] Furthermore, bromination of several *N*-oxides **2** with phosphoryl bromide led to the 2-bromoimidazole derivatives **11**. The crude product of these reactions was a mixture of **10** and **11**, which was separated by column chromatography. Although **11** was obtained in only moderate yields, this approach was the most successful attempt in the preparation of 2-bromo-5-(pyridin-4-yl)imidazole. Alternative methods, for example, treatment of **10** with *N*-bromosuccinimide in acetonitrile, treatment of **10** with Br_2 , or reaction of **6** with SOBr_2 , afforded only traces of **11**. The 2-bromoimidazoles **11** were suitable synthetic precursors for the 1-substituted 2-aryl imidazoles **12**, as **11** underwent nearly quantitative Suzuki coupling with different boronic acids.^[8c] The synthetic importance of **11** in this reaction is underlined by the failure of the corresponding 2-chloroimidazoles **7** to provide 2-aryl imidazoles under Suzuki conditions.

The above synthetic methodology enabled us to prepare a plethora of highly diverse and highly substituted imidazole derivatives from a comparatively small number of starting compounds. In the p38 MAP kinase assay, analogues **4b–d** exceeded the reference compound ML 3163 in biological potency (Table 1). These compounds also efficiently inhibited cytokine release from human monocytes because of their

Table 1. Inhibition of p38 MAP kinase, cytokine release, and cytochrome P450 isoforms by selected compounds.

Compound	p38	IC ₅₀ ± SEM [μM] ^[a]		Inhibition [%] of P450 isoforms ^[b]	
		TNF-α	IL-1β	2D6	3A4
SB 203580	0.29 ± 0.03 (7)	0.59 ± 0.09 (21)	0.037 ± 0.006 (20)	73.1	76.6
ML 3163	4.0 ± 1.0	1.1 ± 0.4 (4)	0.38 ± 0.13 (4)	71.8	87.1
4b	2.2 (1)	2.2 ± 0.9	0.45 ± 0.03	7.8	28.3
4c	0.50 (1)	0.51 ± 0.24 (4)	0.11 ± 0.03 (4)	13.4	16.5
4d	2.2 (1)	1.1 ± 0.3	0.38 ± 0.04	0.7	28.8

[a] Tests were carried out in duplicate, except where the number in brackets denotes otherwise. SEM = Standard error of measurement. [b] Results are from one experiment each, carried out at a test-compound concentration of 10 μM in phosphate buffer (pH 7.4) with DMSO (0.1 %).

favorable cell-penetration properties. In the whole-blood assay, IC₅₀ values (μM) for the most active derivatives **4b** (TNF-α: 5.6 ± 0.95, IL-1β: 1.5 ± 0.7), **4c** (TNF-α: 0.51 ± 0.24, IL-1β: 0.11 ± 0.03), and **4d** (TNF-α: 5.1 ± 0.4, IL-1β: 1.1 ± 0.7) were lower than those of lead compound ML 3163 (TNF-α: 20.3 ± 4.8, IL-1β: 2.78 ± 0.13), and close to the nanomolar range. Finally, the most promising results came from the toxicity screen, in which **4b–d** (Table 1) only moderately interacted with those P450 isoforms most important for drug metabolism.^[9] This profile gives **4b–d** a clear advantage over both SB 203580 and ML 3163, and makes them strong candidates for further development as anti-inflammatory drugs.

Received: November 6, 2001 [Z18173]

- [1] J. C. Lee, A. M. Badger, D. E. Griswold, D. Dunnington, A. Truneh, B. Votta, J. R. White, P. R. Young, P. E. Bender, *Ann. N. Y. Acad. Sci.* **1993**, 696, 149–170; For a review of anti-TNF-α strategies, see: R. C. Newton, C. P. Decicco, *J. Med. Chem.* **1999**, 42, 2296–2314.
- [2] a) J. C. Lee, J. T. Laydon, P. C. McDonnell, T. F. Gallagher, S. Kumar, D. Green, D. McNulty, M. J. Blumenthal, J. R. Heys, S. W. Landvatter, J. E. Strickler, M. M. McLaughlin, I. R. Siemens, S. M. Fisher, G. P. Livi, J. R. White, J. L. Adams, P. R. Young, *Nature* **1994**, 372, 739–746; b) L. Tong, S. Pav, D. M. White, S. Rogers, K. M. Crane, C. L. Cywin, M. L. Brown, C. A. Pargellis, *Nat. Struct. Biol.* **1997**, 4, 311–316; c) A. M. Badger, J. N. Bradbeer, B. Votta, J. C. Lee, J. L. Adams, D. E. Griswold, *J. Pharmacol. Exp. Ther.* **1996**, 279, 1453–1461; d) J. L. Adams, J. C. Boehm, S. Kassis, P. D. Gorycki, E. F. Webb, R. Hall, M. Sorenson, J. C. Lee, A. Ayrton, D. E. Griswold, T. F. Gallagher, *Bioorg. Med. Chem. Lett.* **1998**, 8, 3111–3116; e) T. F. Gallagher, G. L. Seibel, S. Kassis, J. T. Laydon, M. J. Blumenthal, J. C. Lee, D. Lee, J. C. Boehm, S. M. Fier-Thompson, J. W. Abt, M. E. Sorenson, J. M. Smietana, R. F. Hall, R. S. Garigipati, P. E. Bender, K. F. Erhard, A. J. Krog, G. A. Hofmann, P. L. Sheldrake, P. C. McDonnell, S. Kumar, P. R. Young, J. L. Adams, *Bioorg. Med. Chem.* **1997**, 5, 49–64; f) J. C. Boehm, J. M. Smietana, M. E. Sorenson, R. S. Garigipati, T. F. Gallagher, P. L. Sheldrake, J. Bradbeer, A. M. Badger, J. T. Laydon, J. C. Lee, L. M. Hillegass, D. E. Griswold, J. J. Breton, M. C. Chabot-Fletcher, J. L. Adams, *J. Med. Chem.* **1996**, 39, 3929–3937.
- [3] a) K. Ebel, *Methoden Org. Chem. (Houben-Weyl)*, 4. Aufl., Vol. E8c, **1994**, p 1–215; b) J. Kister, G. Assef, G. Mille, J. Metzger, *Can. J. Chem.* **1979**, 57, 813–821; c) P. M. Kochergin, *Russ. J. Gen. Chem.* **1961**, 31, 1010–1012; d) N. J. Liverton, J. W. Butcher, C. F. Claiborne, D. A. Claremon, B. E. Libby, K. T. Nguyen, S. M. Pitzengerger, H. G. Selnick, G. R. Smith, A. Tebben, J. P. Vacca, S. L. Varga, L. Agarwal, K. Dancheck, A. J. Forsyth, D. S. Fletcher, B. Frantz, W. A. Hanlon, C. F. Harper, S. J. Hofsess, M. Kostura, J. Lin, S. Luell, E. A. O'Neill, C. J. Orevillo, M. Pang, J. Parsons, A. Rolando, Y. Sahly, D. M. Visco, S. J. O'Keefe, *J. Med. Chem.* **1999**, 42, 2180–2190.

- [4] a) G. Mloston, T. Gendek, H. Heimgartner, *Helv. Chim. Acta* **1998**, 81, 1585–1595; b) R. Bartnik, W. Hahn, G. Mloston, *Rocz. Chem.* **1977**, 51, 1747.
- [5] S. Laufer, H.-G. Striegel, K. Neher (Merckle GmbH), DE 19842833 A1, **1998** (*Chem. Abstr.* **2000**, 132, 210154).
- [6] H. Lettau, *Z. Chem.* **1970**, 10, 462.
- [7] a) T. Ravindranathan, R. D. Wakharkar, A. B. Landge, *Org. Prep. Proced. Int.* **1986**, 18, 95–98; b) L. Testaferri, M. Tiecco, M. Tingoli, D. Chianelli, M. Montanucci, *Synthesis* **1983**, 751–755.
- [8] a) G. Mloston, M. Celeda, G. K. S. Prakash, G. A. Olah, H. Heimgartner, *Helv. Chim. Acta* **2000**, 83, 728–738; b) I. J. Ferguson, K. Schofield, *J. Chem. Soc. Perkin Trans. 1* **1975**, 275–277; c) D. Wang, J. Haseltine, *J. Heterocycl. Chem.* **1994**, 31, 1637–1639.
- [9] M. Spatzenegger, W. Jaeger, *Drug Metab. Rev.* **1995**, 27, 397–417.

Tetrafunctional Photoaffinity Labels Based on Nakanishi's *m*-Nitroalkoxy-Substituted Phenyltrifluoromethyldiazirine**

Mohammed Daghigh, Lothar Hennig, Matthias Findeisen, Sabine Giesa, Frank Schumer, Horst Hennig, Annette G. Beck-Sickinger, and Peter Welzel*

Photoaffinity labeling has been demonstrated to be a remarkably efficient method for studying the interactions of biologically significant compounds (ligands) with their target macromolecules.^[1] The method allows the identification of the targets (for example, binding proteins) and, also the binding domain within the target protein. An appropriate photoaffinity-labeling compound should contain three structural elements:

- a) a ligand which directs the label to the binding site on the protein,
- b) a photolabile group for attaching to the protein,
- c) an indicator that allows the identification of the labeled peptides after enzymatic digestion of the labeled protein.

[*] Prof. Dr. P. Welzel, M. Daghigh, Dr. L. Hennig
Institut für Organische Chemie
Universität Leipzig
Johannisallee 29, 04103 Leipzig (Germany)
Fax: (+49) 341-9736-559
E-mail: welzel@organik.chemie.uni-leipzig.de

Dr. M. Findeisen, Dr. S. Giesa
Institut für Analytische Chemie
Universität Leipzig
Johannisallee 29, 04103 Leipzig (Germany)

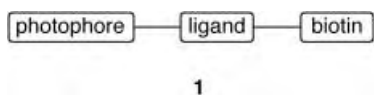
F. Schumer, Prof. Dr. H. Hennig
Institut für Anorganische Chemie
Universität Leipzig
Johannisallee 29, 04103 Leipzig (Germany)

Prof. Dr. A. G. Beck-Sickinger
Institut für Biochemie
Universität Leipzig
Talstrasse 33, 04103 Leipzig (Germany)

[**] We are grateful to Mrs. R. Herold and Mrs. R. Oehme for technical assistance. Financial support by the Deutsche Forschungsgemeinschaft, BC Biochemie GmbH, and the Fonds der Chemischen Industrie is gratefully acknowledged.

Supporting information for this article is available on the WWW under <http://www.angewandte.org> or from the author.

Such an indicator may be a radioactive ligand or a nonradioactive tag such as a biotin group. The latter has the great advantage that it enables the labeling of the target protein and labeled protein fragments to be demonstrated by means of their interaction of biotin with avidin or streptavidin and isolating them by affinity chromatography.^[2] Usually, the probes have the general appearance of **1**, that is, the photolabile group is attached to the ligand to which in turn the biotin tag is connected in a linear arrangement. Thus, the syntheses of these probes are linear and of limited efficiency.



We have now developed the two photoaffinity labeling reagents **7** (Scheme 1 A) and **18** (Scheme 3) which can accommodate the photophore, here an aryl trifluoromethyl-diazirine (a carbene precursor first introduced by Brunner^[3, 4]), the biotin tag, and the ligand attachment site independently.^[5] Any desired ligand can be coupled to the free OH group of **7** and to the squaric ester function of **18** by an appropriate method. In addition, these compounds have two photolabile groupings, the diazirine moiety which generates the carbene intermediate on irradiation at 350 nm^[6] and an alkyl *m*-nitrophenyl ether which undergoes a photo-substitution reaction to yield the corresponding *m*-nitrophenol on irradiation at the same wavelength in mildly basic solution.^[7] As suggested by Nakanishi and co-workers,^[8] the latter reaction can be used to remove both the ligand and the biotin tag from the peptide before mass spectrometric sequencing to avoid complications in its mass spectrometric analysis.

Amine **3** was prepared starting from dimethyl 5-hydroxy-isophthalate (**2**) as described by Nakanishi and co-workers (Scheme 1 A).^[8] The oxidation of **3** with dimethyldioxirane was already known to give the corresponding nitro compound **4a** in a reported yield of 66%. We found the reaction to be rather capricious. In our hands, the method of Krohn et al.^[9] (Zr(OtBu)₄-mediated oxidation with *tert*-butyl hydroperoxide) gave far more reliable results. The yields of **4a** were uniformly in the range of 80%. Oxidative degradation of **4a**^[10] provided aldehyde **4b**, and reduction of the latter with NaBH₄ furnished primary alcohol **4c** in 84% yield. Isocyanate **6** was obtained from (*R*)-malic acid (**5**) as described previously.^[11] The coupling of **6** with primary alcohol **4c** gave urethane **9**, which reacted with the biotin derivative **8** (obtained from the corresponding, commercial diamine and biotin activated with *N,N'*-carbonyldiimidazole (CDI) in pyridine) to give **7** through amide formation and concomitant loss of the protecting group. The ¹H and ¹³C NMR spectra of **7** were fully assigned by H₂H COSY and ¹³C,¹H COSY experiments. The ¹⁹F NMR signal was found at $\delta = 12.65$ ppm (CDCl₃ solution, trifluoroacetic acid (TFA) $\delta = 0$ ppm). The ESI mass spectrum^[12] showed the expected quasi molecular ion peaks.^[13] Compound **7** can be regarded as a broadly applicable biotin-tagged photoaffinity label. We attached **7** to the moenomycin derivative **11b** (obtained from moenomycin A by the azo-coupling/Japp Klingemann route described pre-

viously^[14]) to give **12** (Scheme 1 B), which was fully characterized by ¹H and ¹³C NMR spectroscopy as well as mass spectrometry.^[15]

The photochemistry of the system was studied with model compounds **4c** and **7**. Thus, experiments on an analytical scale (0.76 mmol L⁻¹ in methanol, mercury high-pressure lamp, monochromator, 350 nm) indicate (see the isosbestic points in Figure 1) that **4c** is cleanly converted into the methoxy

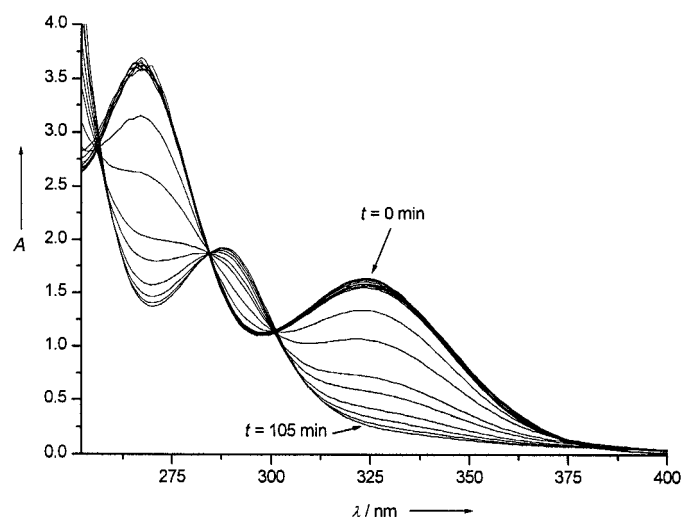


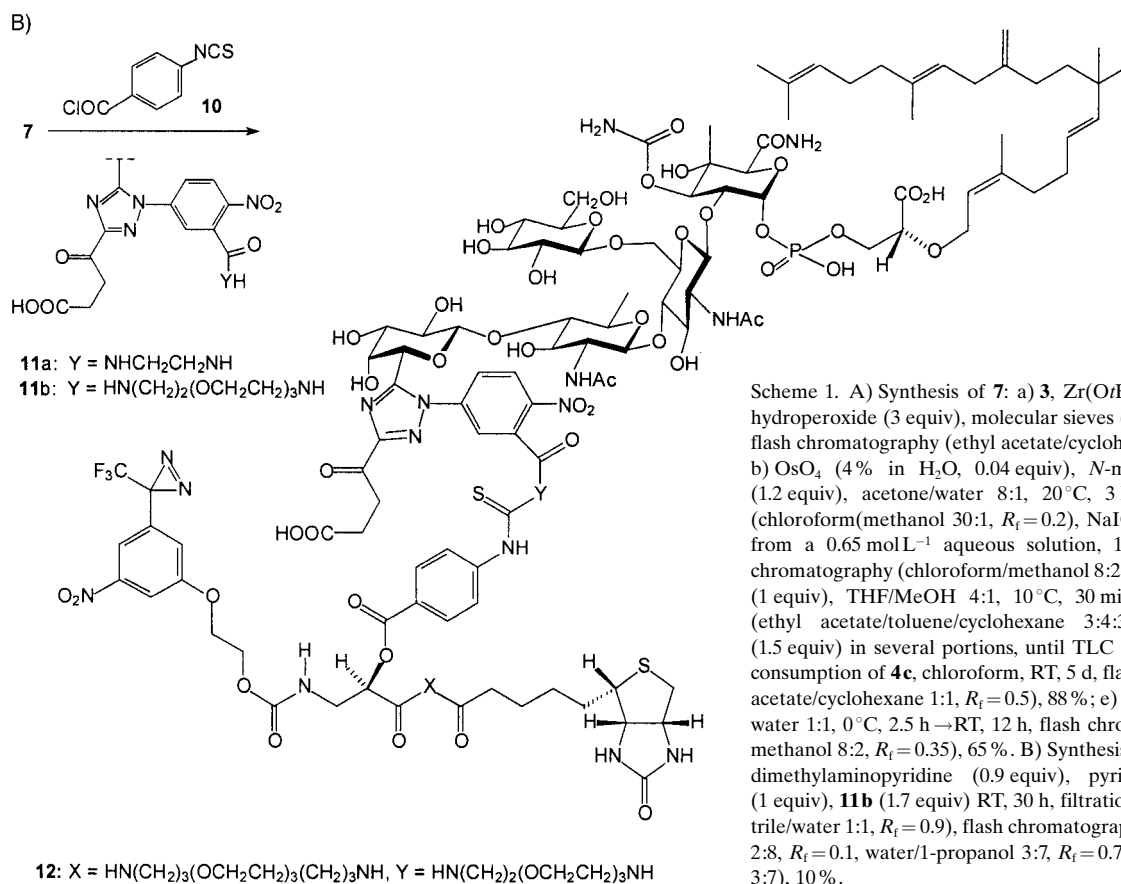
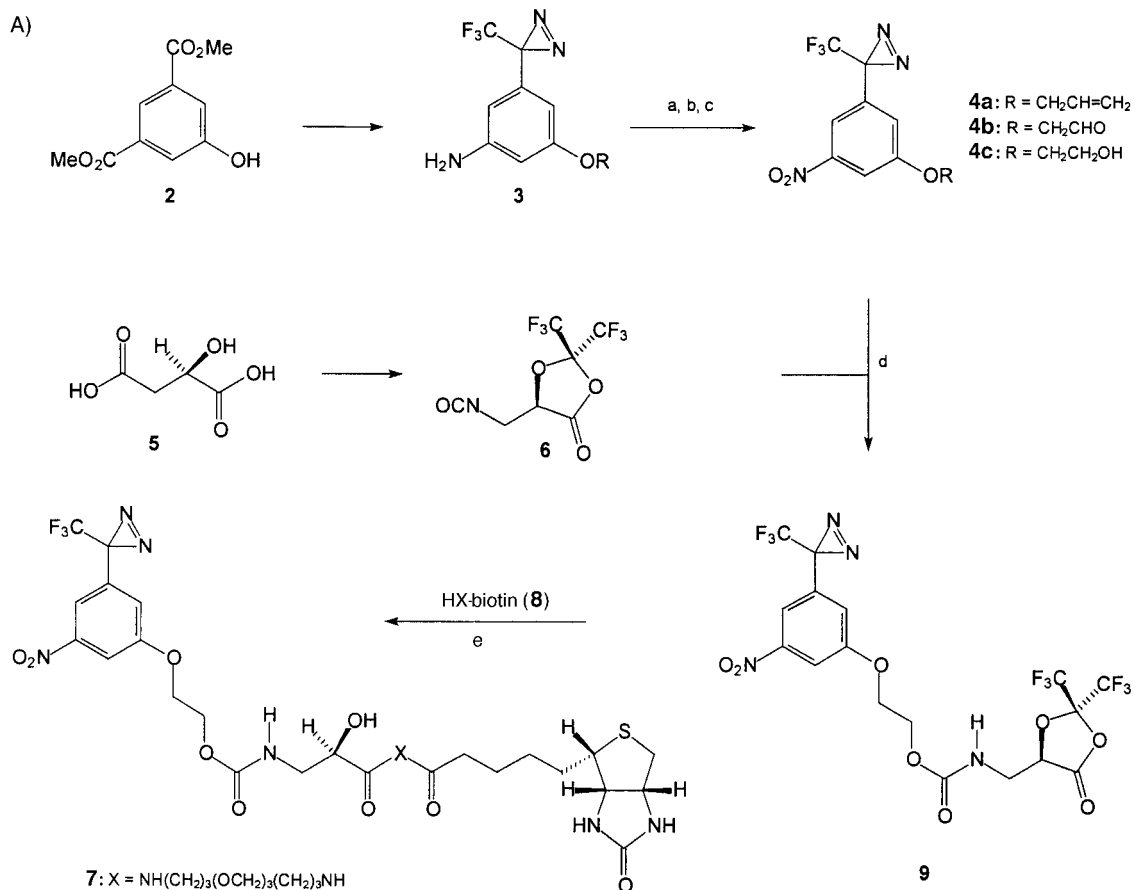
Figure 1. UV/Vis spectroscopic control of the conversion of **4c** into **13**.

derivative **13** (Scheme 2). On a preparative scale, irradiation of **4c** (0.7 mM in methanol, 10 °C, argon atmosphere, 350 nm, Rayonet reactor) furnished the methoxy compound **13** in 70% yield (according to the ¹⁹F NMR spectrum of the reaction mixture). After chromatographic purification, **13** was fully characterized by NMR spectroscopy and mass spectrometry.

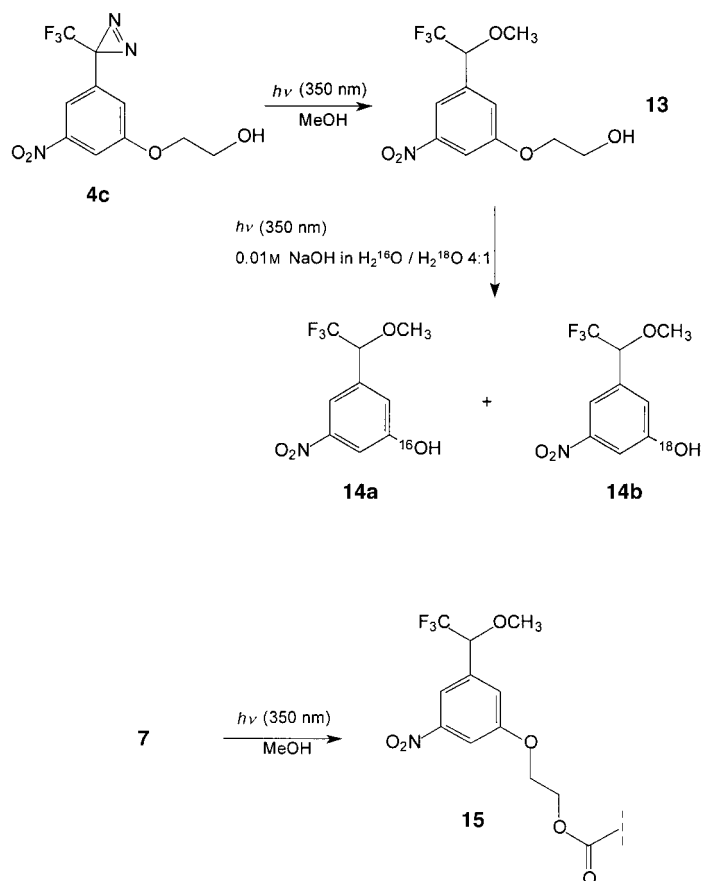
The aromatic photosubstitution by which the *m*-nitroalkoxy derivatives are converted into the corresponding *m*-nitrophenols offers the very promising opportunity to assist mass spectrometric structural elucidation by simply executing the photosubstitution in a mixture of H₂¹⁶O and H₂¹⁸O. We performed the cleavage reaction of **13** in 0.01 mol L⁻¹ NaOH in a 4:1 mixture of H₂¹⁶O and H₂¹⁸O. As Figure 2 shows the 4:1 ratio of H₂¹⁶O and H₂¹⁸O is nicely translated into a 4:1 ratio of the intensities of the molecular ions of the substitution products **14a** and **14b**. Thus, after a photoaffinity labeling experiment, all labeled peptides should be easily recognized by doublets with a mass difference of two in the mass spectra.

We also studied the photodegradation of photolabel **7** on an analytical scale (1.34 mM in methanol) under the conditions described above. The UV spectra are more complicated because of overlapping bands. The difference spectra ($A_{(t)} - A_{(t=0)}$) displayed in Figure 3 have been calculated to separate the absorptions of the reaction site. Figure 3 again nicely shows two isosbestic points indicative of a clean conversion of **7** into **15**.

A second broadly applicable photoaffinity reagent based on a *m*-nitroalkoxy-substituted phenyltrifluoromethyldiazirine (Nakanishi diazirine) was obtained from aldehyde **4b** and amino compound **16** by reductive amination to give secondary



Scheme 1. A) Synthesis of **7**: a) **3**, Zr(OtBu)₄ (0.1 equiv), *tert*-butyl hydroperoxide (3 equiv), molecular sieves (3 Å), CH₂Cl₂, 20 °C, 19 h, flash chromatography (ethyl acetate/cyclohexane 2:8, *R_f* = 0.7), 80 %; b) OsO₄ (4% in H₂O, 0.04 equiv), *N*-methylmorpholine-*N*-oxide (1.2 equiv), acetone/water 8:1, 20 °C, 3 h, flash chromatography (chloroform/methanol 30:1, *R_f* = 0.2), NaIO₄ on silica gel (obtained from a 0.65 mol L⁻¹ aqueous solution, 14 equiv), RT, 24 h, flash chromatography (chloroform/methanol 8:2, *R_f* = 0.8), 74 %; c) NaBH₄ (1 equiv), THF/MeOH 4:1, 10 °C, 30 min, flash chromatography (ethyl acetate/toluene/cyclohexane 3:4:3, *R_f* = 0.4), 84 %; d) **6** (1.5 equiv) in several portions, until TLC analysis showed complete consumption of **4c**, chloroform, RT, 5 d, flash chromatography (ethyl acetate/cyclohexane 1:1, *R_f* = 0.5), 88 %; e) **8** and **9** (1.5 equiv), DME/water 1:1, 0 °C, 2.5 h → RT, 12 h, flash chromatography (chloroform/methanol 8:2, *R_f* = 0.35), 65 %. B) Synthesis of **12**: **7** and **10** (1 equiv), dimethylaminopyridine (0.9 equiv), pyridine, 0 °C, then water (1 equiv), **11b** (1.7 equiv) RT, 30 h, filtration through RP18 (acetonitrile/water 1:1, *R_f* = 0.9), flash chromatography (methanol/chloroform 2:8, *R_f* = 0.1, water/1-propanol 3:7, *R_f* = 0.7, RP18 (acetonitrile/water 3:7), 10 %.



Scheme 2. Photochemical transformations.

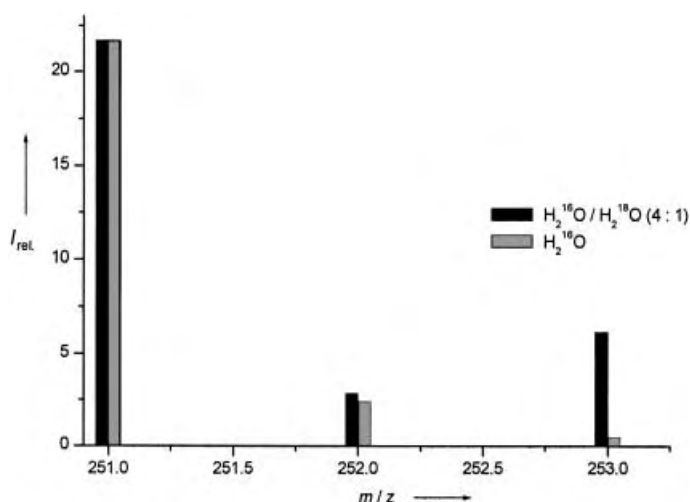


Figure 2. Molecular ions of the photo-substitution product(s) of **13**. Light gray: reaction in H_2^{16}O , black: reaction in 4:1 $\text{H}_2^{16}\text{O}/\text{H}_2^{18}\text{O}$.

amine **17** in 60% yield (Scheme 3). Reaction of **17** with diethyl squarate^[16–18] provided squaric acid ester amide **18**.^[19] As usual for squaric acid amides,^[16] two ^{13}C NMR signals appeared for many carbon atoms, thus indicating the presence of two conformers. Compound **18** can be attached to any suitable ligand with a primary or secondary amino group. Thus, the reaction of **18** with the moenomycin derivative **11a** in a 1:1 mixture of water and methanol at pH 9 furnished

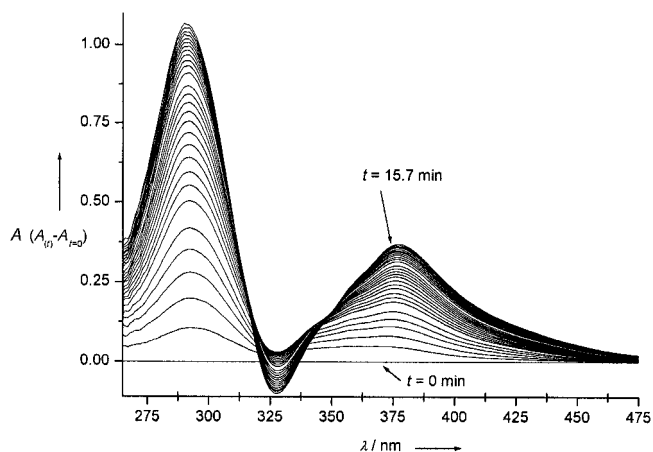


Figure 3. UV/VIS spectroscopic control of the conversion of **7** into **15**, difference spectra $A(t) - A(t=0)$.

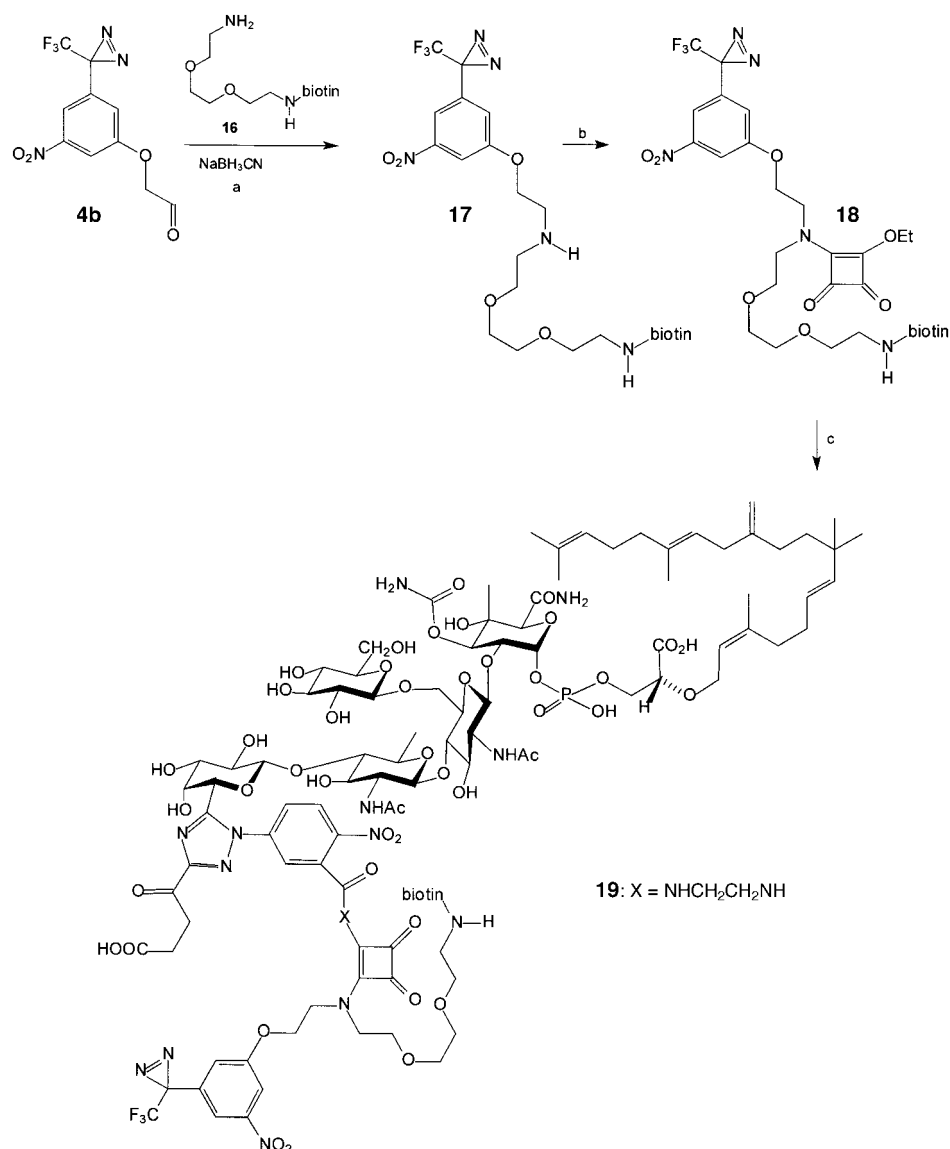
compound **19**, which was characterized by NMR spectroscopy and mass spectrometry.^[20]

Both **12** and **19** have been found to be antibiotically active against a number of *Staphylococcus aureus* strains (minimum inhibitory concentration (MIC): 4.8×10^{-7} and $3.2 \times 10^{-7} \text{ mol L}^{-1}$, respectively)^[21] although to a lower degree than moenomycin A itself.^[22]

In conclusion, we have developed two biotinylated photoaffinity labels based on Nakanishi's diazirine that can be attached to any suitable ligand. The photochemical removal of the ligand and biotin from labeled peptides can be used to introduce a $^{16}\text{O}/^{18}\text{O}$ tag. This should greatly facilitate identification of cross-linked peptides by mass spectrometry. Compounds **12** and **19** are fully equipped for photoaffinity studies. In addition, they have been found to be antibiotically active, and their use in the photoaffinity labeling of their target protein, the transglycosylase domain of penicillin-binding protein 1b,^[23] will be reported in due course.

Received: December 7, 2001 [Z18343]

- [1] F. Kotzyba-Hilbert, I. Kapfer, M. Goeldner, *Angew. Chem.* **1995**, *107*, 1391–1408; *Angew. Chem. Int. Ed. Engl.* **1995**, *34*, 1296–1312; S. A. Fleming, *Tetrahedron* **1995**, *51*, 12479–12520; G. Dormán, *Top. Curr. Chem.* **2001**, *211*, 169–225; G. Dormán, G. D. Prestwich, *Trends Biotechnol.* **2000**, *18*, 64–76.
- [2] *A Laboratory Guide to Biotin-Labeling in Biomolecule Analysis* (Eds.: T. Meier, F. Fahrenholz), Birkhäuser, Basel **1996**.
- [3] J. Brunner, *Annu. Rev. Biochem.* **1993**, *62*, 483–514; T. Weber, J. Brunner, *J. Am. Chem. Soc.* **1995**, *117*, 3084–3095.
- [4] For a comparison of four photoactivatable probes, see P. J. A. Weber, A. G. Beck-Sickinger, *J. Pept. Res.* **1997**, *49*, 375–383.
- [5] See B. A. Gilbert, R. R. Rando, *J. Am. Chem. Soc.* **1995**, *117*, 8061–8066.
- [6] M. Nassal, *Liebigs Ann. Chem.* **1993**, 1510–1523; Y. Ambroise F. Pillon, C. Miokowski, A. Valleix, B. Rousseau, *Eur. J. Org. Chem.* **2001**, 3961–3964, and references therein.
- [7] E. Havinga, M. E. Kronenberg, *Pure Appl. Chem.* **1968**, *16*, 137–152.
- [8] K. Fang, M. Hashimoto, S. Jockusch, N. J. Turro, K. Nakanishi, *J. Am. Chem. Soc.* **1998**, *120*, 8543–8544; M. Hashimoto, Y. Liu, K. Fang, H. Li, G. Campiani, K. Nakanishi, *Bioorg. Med. Chem.* **1999**, *7*, 1181–1194.
- [9] K. Krohn, J. K  pke, H. Rieger, *J. Prakt. Chem.* **1997**, *339*, 335–339.



Scheme 3. Synthesis of **19**: a) **4b** and **16** (1.5 equiv), methanol, TFA (0.2 molL⁻¹ in methanol, adjusting the pH to 7.0), NaCNBH₃ (1 equiv), RT, 32 h, flash chromatography (methanol/chloroform 1:9, *R_f* = 0.1), 60%; b) 3,4-diethoxy-3-cyclobutene-1,2-dione (2.7 equiv), ethanol, RT, 19 h, flash chromatography (methanol/chloroform 2:10, *R_f* = 0.5), 91%; c) **11a**, water/methanol 1:1, Et₃N (adjusting the pH to 9), RT, 5 d, flash chromatography (1-propanol/water 7:2, *R_f* = 0.5), 32%.

- [10] M. Daumas, Y. Vo-Quang, L. Vo-Quang, F. Le Goffic, *Synthesis* **1989**, 64–65.
- [11] T. Rühl, L. Hennig, Y. Hatanaka, K. Burger, P. Welzel, *Tetrahedron Lett.* **2000**, 4, 4555–4558; K. Burger, E. Windeisen, R. Pires, *J. Org. Chem.* **1995**, 60, 7641–7645; R. Pires, K. Burger, *Synthesis* **1996**, 1277–1279, and references therein.
- [12] FT-ICR-MS (Apex II, Bruker Daltonics, water/methanol).
- [13] C₃₄H₄₉F₃N₈O₁₂S (850.86, 850.34), ESI MS: *m/z* = 889.27644 ([*M*+K]⁺), calcd: 889.27743; 873.30178 ([*M*+Na]⁺), calcd: 873.30350.
- [14] U. Kempin, L. Hennig, D. Knoll, P. Welzel, D. Müller, A. Markus, J. van Heijenoort, *Tetrahedron* **1997**, 53, 17669–17690.
- [15] C₁₂₄H₁₇₇F₃N₁₉O₅₂PS₂ (2917.95, 2916.09), ESI MS: *m/z* = 971.02420 ([*M*–3H]³⁻), calcd: 971.02343.
- [16] L. F. Tietze, M. Arlt, M. Beller, K.-H. Glüsenkamp, E. Jähde, M. F. Rajewsky, *Chem. Ber.* **1991**, 124, 1215–1221.
- [17] Review: A. Schmidt, *Synthesis* **1980**, 961–994; L. F. Tietze, C. Schröter, S. Gabius, U. Brinck, A. Goerlach-Graw, H.-J. Gabius, *Bioconjugate Chem.* **1991**, 2, 148–153; V. P. Kamath, P. Diedrich, O. Hindsgaul, *Glycoconjugate J.* **1996**, 13, 315–319; V. Pozsgay, E. Dubois, L. J. Pannell, *J. Org. Chem.* **1997**, 62, 2832–2864; J. Zhang, A. Yergey, J. Kowalak, P. Kováč, *Carbohydr. Res.* **1998**, 313, 15–20.
- [18] A. Buchynskyy, U. Kempin, S. Vogel, L. Hennig, M. Findeisen, D. Müller, S. Giesa, H. Knoll, P. Welzel, *Eur. J. Org. Chem.*, in press.
- [19] C₃₂H₄₀F₃N₇O₁₀S (771.77, 771.25), ESI MS: *m/z* = 772.25759 [*M*+H]⁺, calcd: 772.25822; 794.23993 [*M*+Na]⁺, calcd: 794.24017.
- [20] C₁₀₈H₁₅₁F₃N₁₇O₄₆PS (2543.50, 2541.94), ESI MS: *m/z* = 1269.96424 ([*M*–2H]²⁻), calcd: 1269.96320; 864.30686 ([*M*–3H]³⁻), calcd: 864.30637.
- [21] MIC values were determined by a serial twofold microdilution method (Iso-Sensitest medium, Oxoid). A series of decreasing concentrations of the compound under investigation was prepared in the medium. For inoculations, 1 × 10⁵ cfu mL⁻¹ were used. The MIC values were determined after 24 h at 37 °C (absence of visible turbidity).
- [22] S. Vogel, A. Buchynskyy, K. Stembera, K. Richter, L. Hennig, D. Müller, P. Welzel, F. Maquin, C. Bonhomme, M. Lampilas, *Bioorg. Med. Chem. Lett.* **2000**, 10, 1963–1965, and references therein.
- [23] See K. Stembera, A. Buchynskyy, S. Vogel, D. Knoll, A. A. Osman, J. A. Ayala, P. Welzel, *ChemBioChem*, **2002**, 3, 332–340.

or scrambling of deuterium (>98% D substitution per center). The protocol is highly flexible and the combination of appropriate starting materials allows almost any position to be labeled with hydrogen isotopes. The two additional deuterium atoms at C5 were required to secure the origin of metabolites in the event that both deuterium atoms from C6 and C7 of the precursor acids were removed.

Cells of the transgenic yeast, which express the gene of the Δ^8 -sphingolipid desaturase from sunflower, were grown in the presence of cerulenin and labeled palmitic acids. After alkaline hydrolysis, the released sphingobases were converted by Sanger's reagent into their dinitrophenyl (DNP) derivatives and pre-separated by TLC.^[23] The derivatives could be analyzed as negative ions by ESI MS with very high sensitivity and essentially free from background. By passing through a reversed-phase silica HPLC column (RP-18), the *E* and *Z* isomers of the DNP-modified 4-hydroxy-8-sphingenine were separated and analyzed individually (Figure 1). Both isomers

To determine the position of the remaining deuterium atoms in (8*E*)-4-hydroxy-8-sphingenine, the double bond was oxidized with OsO₄^[27] and the resulting diol cleaved with NaIO₄ under phase-transfer conditions.^[28] The aliphatic cleavage product, decanal, was then analyzed by GC/MS (chemical ionization, *i*-butane). Decanal from the oxidative degradation of (8*E*)-4-hydroxy-8-sphingenine was found to possess one deuterium atom at the carbonyl group,^[29] which demonstrates the simultaneous removal of the C8-D_R and the C9-H_S atoms. Decanal from the oxidative degradation of (8*Z*)-4-hydroxy-8-sphingenine possessed no deuterium atom, which confirmed that the two remaining deuterium isotopes on the metabolite (*m/z* = 482) were located in the polar head of the 4-hydroxy-8-sphingenine at C7 (marker isotopes at C5 of the administered palmitic acid). These findings suggest that both desaturation steps leading to either the 8*E* or the 8*Z* isomer of 4-hydroxy-8-sphingenine involved the *syn* elimination of two vicinal hydrogen atoms. Any influence from

unspecific isomerases of the yeast cells on the *E/Z* ratio of the products could be excluded, since the expression of desaturases from other plants in the same system resulted in different and characteristic *E/Z* mixtures of the unsaturated products.^[22, 23] Moreover, the resulting *E/Z* ratio proved to be sensitive to isotopic substitution at C8 and/or C9 on the saturated precursor and hence is intrinsically linked to the mechanism of desaturation.^[30]

The KIEs of the removal of the hydrogen atoms from C8 and C9 of the sphingolipid precursor were determined by mass spectrometric analysis of the metabolites from racemic [5,5,6- and 5,5,7-D₃]palmitic acids (Scheme 2) fed to the transgenic yeast. All experiments followed the above protocol and were carried out at least in triplicate. Average values of the resulting KIEs are compiled in Table 1.

In contrast to previously studied systems, two distinct and different KIEs were found for the removal of the two hydrogen atoms from C8 and C9 of the saturated precursor en route to the 8*Z* isomer. The KIEs associated with the production of the (8*E*)-isomer follow the usual trend: a large KIE for the removal of the hydrogen atom attacked initially and a low KIE for the subsequent loss of the second hydrogen atom, which is in agreement with the two-step radical mechanism of previously studied desaturases.^[31, 12] Since both isomers are generated by the same enzyme, a uniform mechanism that involves a

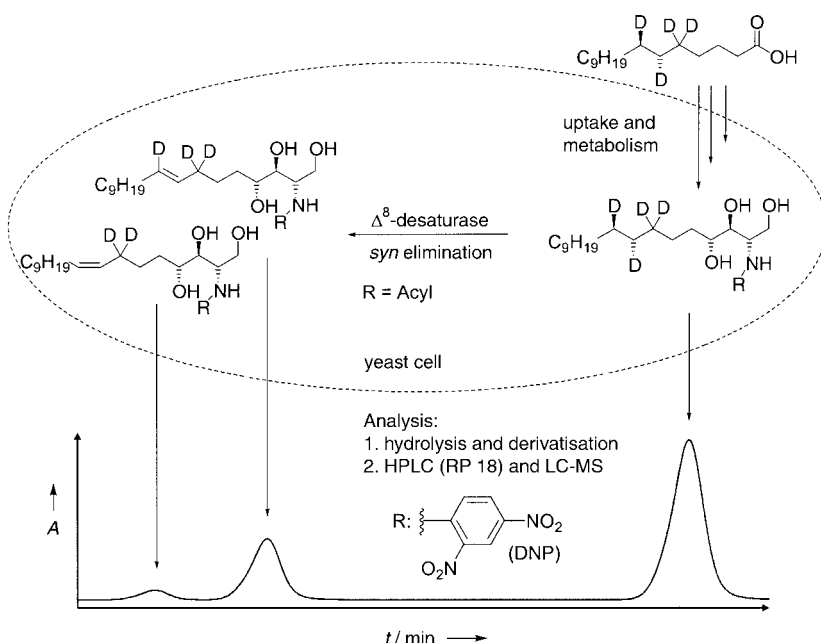


Figure 1. Biosynthesis and desaturation of 4-hydroxysphinganine. Deuterium-labeled palmitic acid from the culture medium enters the transgenic yeast cell and is metabolized via *N*-acyl-4-hydroxysphinganine into acylated (8*E*)- and (8*Z*)-4-hydroxy-8-sphingenine. The *E/Z* isomers of their DNP derivatives were separated by reversed-phase HPLC (RP 18) with UV detection (350 nm).

from the transformation of [5,5,6,7-D₄]-(*6R,7R*)-palmitic acid displayed spectra with an intense [*M* – H][–] pseudomolecular ion, with no further fragmentation. The major isomer, (8*E*)-4-hydroxy-8-sphingenine gave rise to a single [*M* – H][–] ion (*m/z* = 483); the 8*Z* isomer also gave rise to a single ion (*m/z* = 482). In addition, both isomers displayed a weak signal at *m/z* = 480, which corresponded to the [*M* – H][–] ion of unlabeled, natural 4-hydroxy-8-sphingenine. The *E* isomer was formed stereospecifically by the loss of a single deuterium atom along with a single hydrogen atom from C8 and C9, respectively, of the saturated 4-hydroxysphinganine precursor. In contrast, the 8*Z* isomer was generated with simultaneous removal of two deuterium atoms (C8-D_R and C9-D_R) of the saturated precursor.

qucent loss of the second hydrogen atom, which is in agreement with the two-step radical mechanism of previously studied desaturases.^[31, 12] Since both isomers are generated by the same enzyme, a uniform mechanism that involves a

Table 1. KIEs of the desaturation of specifically deuterated sphingolipids.

Δ^8 -Phytosphingenine	Atom	<i>k</i> _{H/D}
<i>E</i> isomer	C8	1.91 ± 0.14
	C9	1.16 ± 0.04
<i>Z</i> isomer	C8	2.07 ± 0.16
	C9	3.79 ± 0.59

KIEs were calculated from the ratio of the intensities of the pseudomolecular ions of [D₃]- and [D₂]phytosphingenine after correction for the abundance of their ¹³C satellite peaks.

transient C-centered radical should hold for both isomers (as shown in Scheme 1). Thus, the C8-H_R atom of a staggered alkyl segment should be exposed directly to the active center of the desaturase if an *E* isomer is to be formed. Following removal of this hydrogen atom, the radical intermediate at C8 could suffer a second electron transfer or undergo a direct β -cleavage with simultaneous transfer of the C9-H_S atom to the reactive center without a significant KIE (Table 1, $k_{H/D} = 1.16 \pm 0.04$). The production of the 8Z isomer requires a *gauche* conformation of the substrate in the relevant area and proceeds with initial hydrogen abstraction from C9 (Figure 1). Since the initial attack on the hydrogen atoms en route to the *E* or *Z* isomers occurred at different methylene groups, a common reactive intermediate (radical) is ruled out. Our data support a mechanism by which the Δ^8 -sphingolipid desaturase directly and independently converts two differently populated conformations of the same substrate with either *anti* or *gauche* orientation about the C8–C9 axis into *E* or *Z* alkenes.

Owing to the simultaneous production of 8*E* and 8*Z* double bonds and to the different KIEs for the production of the two isomers (Table 1), the Δ^8 -sphingolipid desaturase is different from the hitherto studied and stereospecifically operating fatty acid desaturases. Moreover, in the case of the 8*Z* isomer, initial attack is directed onto a hydrogen atom distal to the polar head (C9), while all previously studied desaturases,^[31, 12] including the recently described Δ^4 -*trans*-dihydroceramide desaturase from rat liver,^[32] attack a hydrogen atom of the proximal C atom. Despite these differences, the Δ^8 -sphingolipid desaturase removes, en route to the *E* and *Z* isomers, the hydrogen atoms from exactly the same spatial positions as all other previously studied *E*- or *Z*-selective fatty acid desaturases.^[18, 19] It remains to be seen whether or not *E/Z* mixtures of other desaturases, for example, those from pheromone glands of insects,^[15, 19] follow similar principles and also rely on single enzymes, or whether in these organisms two stereospecifically operating enzymes generate the isomeric mixtures. More work on the mechanistic basis of the Δ^8 -sphingolipid desaturase is required and will be reported soon.

Experimental Section

The open reading frame of a Δ^8 -Sphingolipid desaturase cDNA from *Helianthus annuus* was cloned behind the constitutive ADH1 promotor of the yeast expression vector pVT-U-102 and transformed in *Saccharomyces cerevisiae* INVSc1.^[22] Transgenic yeast cells were cultured for 4 d at 30 °C at OD₆₀₀ ~ 1.0 in a medium containing Cerulenin (25 μ M; Sigma) and [D]palmitic acid (0.25 mM) in complete minimal medium-dropout-uracil (100 mL) with 2% raffinose and 1% tergitol-NP40 (Sigma). Cells were harvested by centrifugation, washed, and directly hydrolyzed (10% Ba(OH)₂ (w/v) in H₂O/Dioxan (1:1), 24 h, 110 °C). The released long-chain sphingobases (LCB) were converted into the DNP derivatives and prepurified by TLC (silica gel 60, CHCl₃/MeOH 9:1 v/v). The configurational isomers of the DNP derivatives were separated by HPLC on reversed-phase silica (RP 18, GROM-SIL 120 ODS-5, 3 μ m, 125 \times 2 mm, ST, Grom, Herrenberg) with a gradient of 0.2 mL min⁻¹ from 60% MeOH/CH₃CN/2-propanol (10:3:1 v/v/v) and 40% water (10 min) to 20% water and, finally 0% water (40 min). The DNP derivatives were analyzed by ESI MS on a Micromass Quattro II mass spectrometer (Micromass, Manchester, UK). Spectra were recorded in the negative-ion mode (source temperature: 100 °C, desolvation temperature: 250 °C, cone voltage: 35 Volt).

Received: January 28, 2002 [Z18587]

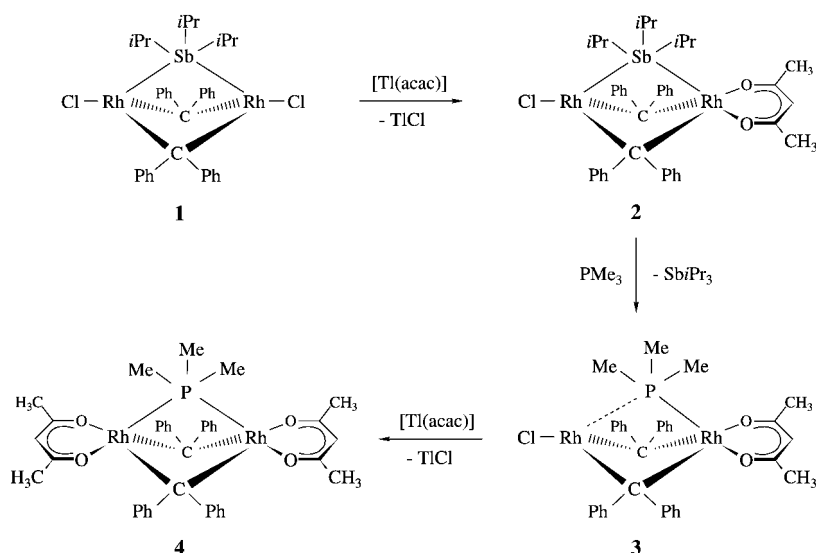
- [1] A. H. Merrill, J. Sweeley, C. C. Sweeley, in *Biochemistry of lipids, lipoproteins and membranes* (Eds.: D. E. Vance, J. E. Vance), Elsevier Science, Amsterdam, **1996**.
- [2] C. K. Y. Ng, K. Carr, M. R. McAinsh, B. Powell, A. M. Hetherington, *Nature* **2001**, *410*, 596.
- [3] H. Imai, M. Ohnishi, K. Hotsubo, M. Kojima, S. Ito, *Biosci. Biotechnol. Biochem.* **1997**, *61*, 351.
- [4] J. A. Broadwater, J. A. Haas, B. G. Fox, *Fett/Lipid* **1998**, *100*, 103.
- [5] P. Sperling, E. Heinz, *Eur. J. Lipid Sci. Technol.* **2001**, *103*, 158.
- [6] J. Shanklin, E. B. Cahoon, *Annu. Rev. Plant Physiol. Plant Mol. Biol.* **1998**, *49*, 611.
- [7] L. Fauconnot, P. H. Buist, *J. Org. Chem.* **2001**, *66*, 1210.
- [8] L. J. Morris, R. V. Harris, W. Kelly, A. T. James, *Biochem. J.* **1968**, *109*, 673.
- [9] Y. Lindqvist, W. J. Huang, G. Schneider, J. Shanklin, *EMBO J.* **1996**, *15*, 4081.
- [10] J. Du Bois, T. J. Mizoguchi, S. J. Lippard, *Coord. Chem. Rev.* **2000**, *200*, 443.
- [11] Y. S. Yang, J. Baldwin, B. A. Ley, J. M. Bollinger, E. I. Solomon, *J. Am. Chem. Soc.* **2000**, *122*, 8495.
- [12] D. Meesapyodsuk, D. W. Reed, C. K. Savile, P. H. Buist, S. J. Ambrose, P. S. Covelio, *Biochemistry* **2000**, *39*, 11948.
- [13] P. H. Buist, B. Behrouzian, *J. Am. Chem. Soc.* **1998**, *120*, 871.
- [14] P. H. Buist, B. Behrouzian, *J. Am. Chem. Soc.* **1996**, *118*, 6295.
- [15] A. Pinilla, F. Camps, G. Fabrias, *Biochemistry* **1999**, *38*, 15272.
- [16] J. L. Abad, F. Camps, G. Fabrias, *Angew. Chem.* **2000**, *112*, 3417; *Angew. Chem. Int. Ed.* **2000**, *39*, 3279.
- [17] B. Behrouzian, P. H. Buist, J. Shanklin, *Chem. Commun.* **2001**, 401.
- [18] A. Svatos, B. Kalinova, W. Boland, *Insect Biochem. Mol. Biol.* **1999**, *29*, 225.
- [19] I. Navarro, I. Font, G. Fabrias, F. Camps, *J. Am. Chem. Soc.* **1997**, *119*, 11335.
- [20] W. Boland, C. Frössl, M. Schöttler, M. Toth, *J. Chem. Soc. Chem. Commun.* **1993**, 1155.
- [21] J. L. Abad, F. Camps, G. Fabrias, *Insect Biochem. Mol. Biol.* **2001**, *31*, 799.
- [22] P. Sperling, A. Blume, U. Zähringer, E. Heinz, *Biochem. Soc. Trans.* **2000**, *28*, 638.
- [23] P. Sperling, U. Zähringer, E. Heinz, *J. Biol. Chem.* **1998**, *273*, 28590.
- [24] F. Schneider, R. Lessire, J. J. Bessoule, H. Juguelin, C. Cassagne, *Biochim. Biophys. Acta* **1993**, *1152*, 243.
- [25] O. Thum, C. Hertweck, H. Simon, W. Boland, *Synthesis* **1999**, 2145.
- [26] C. E. Tucker, P. Knochel, *J. Org. Chem.* **1993**, *58*, 4781.
- [27] H. C. Kolb, M. S. Van Nieuwenhze, K. B. Sharpless, *Chem. Rev.* **1994**, *94*, 2483.
- [28] T. Takata, R. Tajima, W. Ando, *J. Org. Chem.* **1983**, *48*, 4764.
- [29] Oxidative degradation of [7,7,9-D₃]-(*8E*)-phytosphingenine yields a mixture of decanal and [1-D]decanal. The ratio of labeled and unlabeled decanal corresponds to the ratio of labeled and natural (*E*)-4-hydroxy-8-sphingenine prior to the cleavage.
- [30] C6-labeled palmitic acid yields the *E/Z* isomers of 4-hydroxy-8-sphingenine in a ratio of about 6:1, whereas the C7-labeled equivalent gives a lower ratio of the *Z* isomer (ca. 11:1) as a result of high KIE.
- [31] B. Behrouzian, L. Fauconnot, F. Daligault, C. Nugier-Chauvin, H. Patin, P. H. Buist, *Eur. J. Biochem.* **2001**, *268*, 3545.
- [32] C. K. Savile, G. Fabrias, P. H. Buist, *J. Am. Chem. Soc.* **2001**, *123*, 4382.

A New Type of Chainlike Tetranuclear Rhodium Complexes with PR_3 and AsMe_3 as Bridging Ligands**

Thomas Pechmann, Carsten D. Brandt, Cornelia Röger, and Helmut Werner*

Dedicated to Professor Wolfgang Beck on the occasion of his 70th birthday

In the context of our studies on the reactivity of square-planar carbenerhodium(I) compounds $\text{trans}[\text{RhCl}(\text{=CRR}')(\text{L})_2]$ with $\text{L} = \text{PR}_3, \text{AsR}_3, \text{SbR}_3$,^[1] we previously observed that the bis(stibane) derivatives $\text{trans}[\text{RhCl}(\text{=CRR}')(\text{SbiPr}_3)_2]$ generate upon heating dinuclear rhodium(I) complexes with $[\text{Rh}(\mu\text{-SbiPr}_3)\text{Rh}]$ as a building block.^[2] After initial attempts to substitute the triisopropylstibane in **1** by a tertiary phosphane or arsane failed,^[2] we circumvented the difficulties by the sequence of reactions shown in Scheme 1. The crucial observation was that replacing



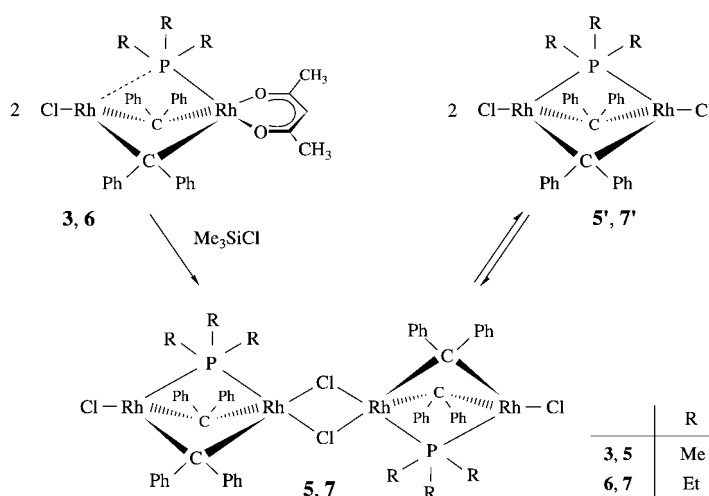
Scheme 1. Indirect substitution of the SbiPr_3 ligands in **1** by PMe_3 and subsequent reaction to give **4**.

one of the chloro ligands in **1** by acetylacetonate (acac) changes the reactivity of the starting material significantly and provides the opportunity to substitute SbiPr_3 for PMe_3 without fragmentation of the dinuclear molecular core. Subsequent reaction of **3** with $[\text{Ti}(\text{acac})]$ affords the symmetrical bis(acac) complex **4** in virtually quantitative yield.^[3]

While both the NMR spectra and the X-ray structure analysis of **3** clearly indicate that the phosphane ligand is in a "semibridging" position,^[3,4] the data for **4** are somewhat

different. The ^{31}P NMR spectrum of **4** displays a sharp triplet (due to $^{31}\text{P} - ^{103}\text{Rh}$ coupling) which does not broaden or split into a doublet of doublets upon cooling the solution in $[\text{D}_8]\text{toluene}$ at -80°C . However, the two $\text{Rh}-\text{P}$ bond lengths (2.2707(7) and 2.5700(8) Å) are not exactly the same, which we explained, taking the NMR data into consideration, by packing effects in the lattice.^[3]

To find out how strongly the anionic ligands influence the binding of the bridging moieties to the metal centers, we studied a variety of substitution reactions of the phosphane-bridged compounds **3** and **4** of which those with Me_3SiCl furnished a breakthrough (Scheme 2). Treatment of **3** with an excess of the chlorosilane in benzene led to a smooth replacement of acac by chloride and gave a red solid **5**, which correctly analyzed as $[\text{Rh}_2\text{Cl}_2(\text{CPh}_2)_2(\text{PMe}_3)_2]$, in 92% yield. The reaction of **6**^[3] with Me_3SiCl in the molar ratio of about 1:200 proceeded analogously and gave the PEt_3 -bridged species **7** in 85% yield. While we anticipated, owing to the ^1H and ^{13}C NMR spectra of **5** and **7**, that both compounds would possess a structure analogous to that of the stibane-bridged complex **1**, the X-ray crystal structure analysis of **5** revealed that in the lattice two dinuclear moieties are connected through two bridging chloro ligands to give a Rh_4 species with a chainlike $\{\text{ClRh}_2\text{Cl}_2\text{Rh}_2\text{Cl}\}$ core (Figure 1).^[5] Moreover, the midpoint of the planar $\text{Rh}(\mu\text{-Cl})_2\text{Rh}$ fragment is a center of symmetry. Besides the $\text{Rh1}-\text{Rh2}$ distance of 2.5054(2) Å, which differs only slightly to that of the stibane-bridged compound **1** (2.5349(5) Å),^[2] the most important structural features of **5** are the $\text{Rh}-\text{P}$ bond lengths of 2.3625(6) Å and 2.4826(6) Å. The difference between these two distances is much less than for the bis(acac) complex **4** indicating that—at least in the crystal lattice—the type of the anionic ligands bonded to the rhodium center influences the position of the bridging phosphane unit. Owing to the similarity of the $\text{Rh}-\text{Rh}$ and $\text{Rh}-\text{P}$ distances, the bond angles of the Rh_2P triangle are nearly the same and deviate only marginally from the 60° value.



Scheme 2. Synthesis of the tetranuclear rhodium complexes **5** and **7**, which are in equilibrium with the dinuclear complexes **5'** and **7'**.

[*] Prof. Dr. H. Werner, Dipl.-Chem. T. Pechmann, Dipl.-Chem. C. D. Brandt, C. Röger, Institut für Anorganische Chemie, Universität Würzburg, Am Hubland, 97074 Würzburg (Germany), Fax: (+49) 931-888-4623, E-mail: helmut.werner@mail.uni-wuerzburg.de

[**] This work was supported by the Deutsche Forschungsgemeinschaft (SFB 347) and the Fonds der Chemischen Industrie.

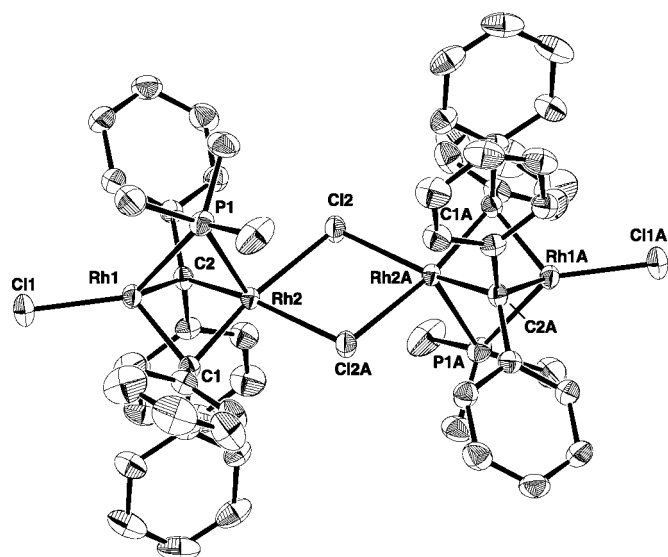


Figure 1. Molecular structure of **5** in the crystal. Selected bond lengths [Å] and angles [°]: Rh1–Rh2 2.5054(2), Rh1–P1 2.4826(6), Rh2–P1 2.3625(6), Rh1–C1 1.988(2), Rh1–C2 1.968(2), Rh2–C1 2.044(2), Rh2–C2 2.051(2), Rh1–Cl1 2.3088(6), Rh2–Cl2 2.4961(5), Cl1–Rh1–Rh2 167.894(19), Cl1–Rh1–P1 135.51(2), Cl1–Rh1–C1 122.43(6), Cl1–Rh1–C2 119.98(6), Rh1–C1–Rh2 76.83(7), Rh1–C2–Rh2 77.08(7), Rh1–P1–Rh2 62.217(15), C1–Rh1–C2 91.09(8), C1–Rh2–C2 87.19(8), C1–Rh1–P1 87.06(6), C2–Rh1–P1 88.43(6), C1–Rh2–P1 89.11(6), C2–Rh2–P1 89.88(6), Rh1–Rh2–Cl2 137.252(14), C1–Rh2–Cl2 170.77(6), C2–Rh2–Cl2 96.33(6), P1–Rh2–Cl2 99.41(2).

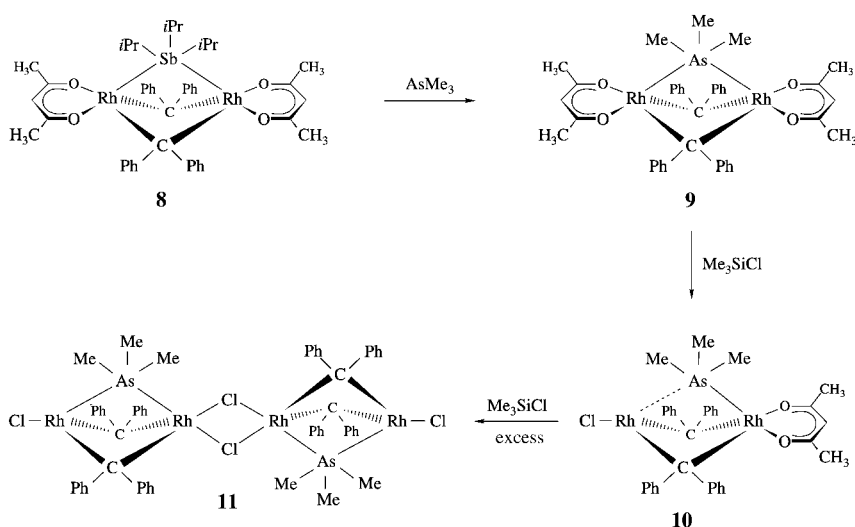
Although cryoscopic measurements with a saturated solution of **5** in benzene confirm that under these conditions the tetranuclear compound is present (calcd: $M_r = 1370.4$; found: $M_r = 1310$), the ^{31}P NMR spectrum of **5** at room temperature (in C_6D_6) is concentration-dependent. The spectrum of a nearly saturated solution (4 mmol L^{-1}) exhibits a somewhat broadened triplet at $\delta = -24.6\text{ ppm}$ which after lowering the concentration to 0.1 mmol L^{-1} transforms into a sharp triplet with a chemical shift of $\delta = -20.4\text{ ppm}$. Since the data in CD_2Cl_2 are quite similar (a broadened triplet being observed at $\delta = -23.1\text{ ppm}$ for a concentrated and a sharp triplet at $\delta = -15.7\text{ ppm}$ for a diluted solution), we conclude that both in benzene and dichloromethane a rapid equilibrium between the Rh_4 and the Rh_2 species exists (see Scheme 2), and that at low concentrations the Rh_2 species **5'** dominates. At -80°C in $[\text{D}_8]\text{toluene}$, the ^{31}P NMR spectrum of **5** displays a doublet of doublets at $\delta = -30.4$ (with $^{31}\text{P} - ^{103}\text{Rh}$ coupling constants of 128.4 and 95.4 Hz) indicating that under these conditions the conversion of **5** to **5'** is inhibited.

After attempts to generate a dinuclear rhodium(I) complex with a trialkylarsane as a bridging ligand by treatment of the stibane derivative **1** with AsMe_3 or AsiPr_3 failed, we succeeded in preparing the “missing link” between the $[\text{Rh}(\mu\text{-SbR}_3)\text{Rh}]$ and $[\text{Rh}(\mu\text{-PR}_3)\text{Rh}]$ compounds in a stepwise manner. Whereas the reaction of **8**^[6] even with a large excess of AsMe_3 in benzene leads to an equilibrium

mixture of **8** and **9**, in hexane as solvent (in which **9** is only sparingly soluble) the arsane-bridged complex **9** is obtained (6 h, 25°C) as a light-brown solid in 85 % yield (Scheme 3). Although **9** can be stored under argon at -25°C for weeks, in solution (benzene or acetone) it decomposes quite rapidly.

Despite its lability, compound **9** reacts with Me_3SiCl (molar ratio 1:1.1) to give the dinuclear complex **10**, which possibly contains the arsane in a semibridging coordination mode. As already observed with the PMe_3 counterparts **3** and **4**, the unsymmetrical species **10** is significantly more stable than **9** and does not decompose in benzene even after storing for three days. Replacing the remaining acac ligand of **10** by chloride is more difficult and, even with a large excess of Me_3SiCl , the formation of **11** occurs only slowly at room temperature. After removal of the volatiles, the dichloro derivative was isolated as a red-brown solid in 91 % yield. As shown by the X-ray crystal structure analysis,^[5] the symmetrical AsMe_3 -bridged compound **11** is isomorphous to **5** and also possesses the midpoint of the $\text{Rh}(\mu\text{-Cl})_2\text{Rh}$ unit as a center of symmetry (Figure 2). For both **5** and **11**, each half-dimer structure is found twice in the asymmetric unit. However, the most noteworthy structural feature of **11** is that in contrast to **5** the terminal Cl-Rh bond length is longer than the Cl-Rh distances in the bridge. For this observation there is no precedence. The two Rh-As bond lengths of **11** differ slightly (2.5475(4) and 2.6731(4) Å) reflecting the inequivalence of the “outer” and “inner” metal centers of the $\{\text{ClRh}_2\text{Cl}_2\text{Rh}_2\text{Cl}\}$ chain. Since the ^1H as well as the ^{13}C NMR spectra of **11** (in CD_2Cl_2) remain unchanged in the temperature range between 193 K and 333 K, we assume that under these conditions no dissociation of the dimeric Rh_4 to the monomeric Rh_2 species takes place.

The results of the present investigation close a gap in the field of coordination chemistry. After it had been supposed for decades that tertiary phosphanes, arsanes, and stibanes behave exclusively as terminal ligands, it was only recently that this postulate became weakened. The preparation of compound **1** (the first “outsider”)^[7] and its SbMe_3 and SbEt_3 analogues^[2] was followed by the isolation and structural characterization of **3** and **4** and has now culminated in the



Scheme 3. Substitution of the SbPr_3 ligands in **8** by AsMe_3 and subsequent reaction to give **11**.

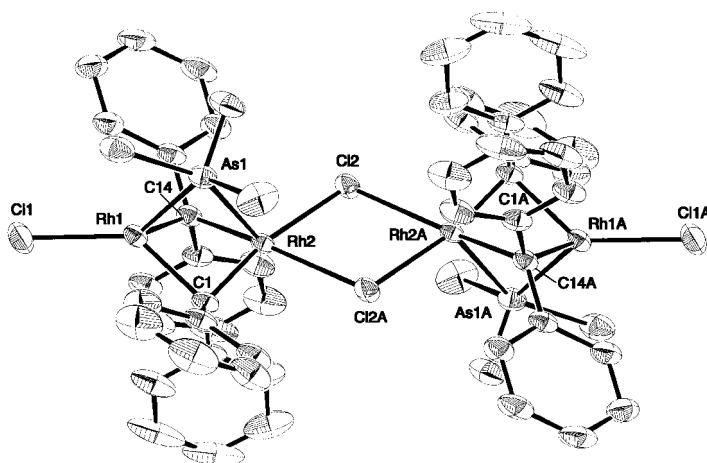


Figure 2. Molecular structure of **11** in the crystal. Selected bond lengths [Å] and angles [°]: Rh1–Rh2 2.8407(3), Rh1–As1 2.5475(4), Rh2–As1 2.6731(4), Rh1–Cl1 2.129(3), Rh1–Cl4 1.934(3), Rh2–Cl1 1.862(3), Rh2–Cl4 2.157(3), Rh1–Cl1 2.5589(8), Rh2–Cl2 2.3667(7), Cl1–Rh1–Rh2 171.03(2), Cl1–Rh1–As1 129.62(2), Cl1–Rh1–Cl1 136.21(7), Cl1–Rh1–Cl4 124.40(8), Rh1–Cl1–Rh2 90.53(10), Rh1–Cl4–Rh2 87.78(10), Rh1–As1–Rh2 65.881(10), Cl1–Rh1–Cl4 77.91(10), Cl1–Rh2–Cl4 78.73(10), Cl1–Rh1–As1 80.97(7), Cl4–Rh1–As1 90.24(8), Cl1–Rh2–As1 82.53(9), Cl4–Rh2–As1 82.40(7), Rh1–Rh2–Cl2 141.653(18), Cl1–Rh2–Cl2 168.26(9), Cl4–Rh2–Cl2 196.61(7), As1–Rh2–Cl2 108.32(2).

synthesis of the first arsane-bridged species **9–11**. As Braunstein and Boag pointed out last year,^[8] a bonding mode such as $[M(\mu-ER_3)M]$ ($E = P, As, Sb$) should not be regarded as thermodynamically unfavorable and, taking both the isolobal analogy of SiR_3^- and PR_3 and the existence of silyl-bridged transition-metal complexes into consideration,^[8] the preparation of **1, 4, 5, 9**, and **11** might only be the first step into a new field. The recent discovery by Reau and Halet et al.^[9] that the phosphorus atom of substituted phospholes is able to bridge two palladium centers undoubtedly supports this prediction.

Experimental Section

5: A solution of **3** (518 mg, 0.69 mmol) in benzene (70 mL) was treated with Me_3SiCl (1 mL, 7.9 mmol) and stirred for 24 h at room temperature. The solvent and excess silane were evaporated in vacuo, the red solid was washed with diethyl ether (2×5 mL) and dried: yield 436 mg (92 %); m.p. 126 °C (decomp); 1H NMR (400 MHz, C_6D_6 , 4 mmol L^{-1} , 293 K): $\delta = 0.88$ ppm (d, $^2J(P,H) = 10.6$ Hz; PCH_3); ^{13}C NMR (100.6 MHz, C_6D_6 , 4 mmol L^{-1} , 293 K): $\delta = 187.8$ (m; CPh_2), 23.5 ppm (d, $^1J(P,C) = 40.0$ Hz; PCH_3); ^{31}P NMR (81.0 MHz, C_6D_6 , 4 mmol L^{-1} , 293 K): $\delta = -24.6$ ppm (br t, $^1J(Rh,P) = 109.4$ Hz); ^{31}P NMR (81.0 MHz, C_6D_6 , 0.1 mmol L^{-1} , 293 K): $\delta = -20.4$ ppm (t, $^1J(Rh,P) = 109.3$ Hz); ^{31}P NMR (81.0 MHz, $[D_8]toluene$, 2 mmol L^{-1} , 293 K): $\delta = -21.3$ ppm (t, $^1J(Rh,P) = 111.9$ Hz); ^{31}P NMR (81.0 MHz, $[D_8]toluene$, 2 mmol L^{-1} , 193 K): $\delta = -30.4$ ppm (dd, $^1J(Rh,P) = 128.4$ and 95.4 Hz).

Compound **7** was prepared as described for **5**, by using **6** (132 mg, 0.17 mmol) and Me_3SiCl (5 mL, 39.4 mmol) as starting materials. Red solid: yield 103 mg (85 %); m.p. 85 °C (decomp); 1H NMR (400 MHz, C_6D_6): $\delta = 0.77$ ppm (m; PCH_2CH_3); ^{13}C NMR (100.6 MHz, C_6D_6): $\delta = 186.7$ (m; CPh_2), 22.0 (d, $^1J(P,C) = 34.3$ Hz; PCH_2), 9.3 ppm (d, $^2J(P,C) = 4.8$ Hz; PCH_2CH_3); ^{31}P NMR (162.0 MHz, C_6D_6 , 293 K): $\delta = 4.8$ ppm (t, $^1J(Rh,P) = 102.5$ Hz).

Compound **9** was prepared from **8** (553 mg, 0.56 mmol) and $AsMe_3$ (108 μL , 1.0 mmol). Light brown solid: yield 408 mg (85 %); m.p. 105 °C (decomp); 1H NMR (200 MHz, C_6D_6 , 293 K): $\delta = 5.50$ (s; CH of acac), 1.95 (s; CH_3 of acac), 0.88 ppm (s; $AsCH_3$); ^{13}C NMR (100.6 MHz, CD_2Cl_2 ,

233 K): $\delta = 188.0$ (s; CO of acac), 172.7 (t, $^1J(Rh,C) = 22.4$ Hz; CPh_2), 99.5 (s; CH of acac), 27.8 (s; CH_3 of acac), 18.0 ppm (s; $AsCH_3$). Compound **10** was prepared analogously as described for **5**, by using **9** (76 mg, 0.09 mmol) and Me_3SiCl (12 μL , 0.10 mmol) as starting materials; reaction time 1 h. Brown solid: yield 62 mg (88 %); m.p. 105 °C (decomp); 1H NMR (400 MHz, C_6D_6 , 293 K): $\delta = 5.41$ (s; CH of acac), 1.89 (s; CH_3 of acac), 0.62 ppm (s; $AsCH_3$); ^{13}C NMR (100.6 MHz, C_6D_6): $\delta = 189.1$ (s; CO of acac), 178.2 (dd, $^1J(Rh,C) = 27.2$ and 20.0 Hz; CPh_2), 101.0 (s; CH of acac), 28.0 (s; CH_3 of acac), 18.6 ppm (s; $AsCH_3$).

Compound **11** was prepared from **10** (75 mg, 0.09 mmol) and excess Me_3SiCl (2 mL, 15.7 mmol) in benzene (2 mL). Red-brown solid: yield 63 mg (91 %); m.p. 120 °C (decomp); 1H NMR (400 MHz, CD_2Cl_2 , 293 K): $\delta = 1.19$ ppm (s; $AsCH_3$); ^{13}C NMR (100.6 MHz, CD_2Cl_2 , 293 K): $\delta = 20.5$ ppm (s; $AsCH_3$).

Received: February 1, 2002 [Z18626]

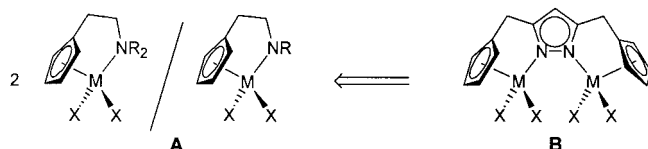
- a) P. Schwab, N. Mahr, J. Wolf, H. Werner, *Angew. Chem.* **1993**, *105*, 1498–1500; *Angew. Chem. Int. Ed. Engl.* **1993**, *32*, 1480–1482; b) H. Werner, P. Schwab, E. Bleuel, N. Mahr, P. Steinert, J. Wolf, *Chem. Eur. J.* **1997**, *3*, 1375–1384.
- a) P. Schwab, N. Mahr, J. Wolf, H. Werner, *Angew. Chem.* **1994**, *165*, 82–84; *Angew. Chem. Int. Ed. Engl.* **1994**, *33*, 97–99; b) P. Schwab, J. Wolf, N. Mahr, P. Steinert, U. Herber, H. Werner, *Chem. Eur. J.* **2000**, *6*, 4471–4478.
- T. Pechmann, C. D. Brandt, H. Werner, *Angew. Chem.* **2000**, *112*, 4069–4072; *Angew. Chem. Int. Ed.* **2000**, *39*, 3909–3911.
- For definition of “semibridging” see: C. Elschenbroich, A. Salzer, *Organometallics*, 2nd ed., VCH, Weinheim, **1992**, p. 225.
- Data for the X-ray structure analyses: **5**: Crystals from benzene, $C_{58}H_{58}Cl_4P_2Rh_4 \cdot 2C_6H_6$ ($M_r = 1526.64$); crystal size $0.4 \times 0.4 \times 0.2$ mm³; monoclinic, space group $P2_1/c$ (no. 14), $a = 22.2854(11)$, $b = 15.1150(7)$, $c = 19.2895(9)$ Å, $\beta = 101.8780(10)^\circ$, $Z = 4$, $V = 6358.4(5)$ Å³, $\rho_{\text{calc}} = 1.595$ g cm⁻³; $T = 173(2)$ K; $2\theta = 50.00^\circ$; 60 158 reflections measured, 11 183 were unique ($R_{\text{int}} = 0.0228$), and 10 525 observed ($I > 2\sigma(I)$); Bruker Smart Apex diffractometer with D8 goniometer equipped with a low-temperature device in ω mode,^[11] Mo K_{α} radiation ($\lambda = 0.71073$ Å), graphite-monochromated; Lp correction. The structure was solved by the Patterson method and refined with the full-matrix, least-squares method; $R_1 = 0.0228$, $wR_2 = 0.0541$ (for 10 525 reflections with $I > 2\sigma(I)$), $R_1 = 0.0249$, $wR_2 = 0.0551$ (for all 11 183 data); data-to-parameter ratio 15.38; residual electron density +0.472/–0.351 e Å⁻³. **11**: Crystals from benzene, $C_{58}H_{58}As_2Cl_4Rh_4 \cdot 2C_6H_6$ ($M_r = 1614.55$); crystal size $0.67 \times 0.66 \times 0.63$ mm³; monoclinic, space group $P2_1/c$ (no. 14), $a = 19.4838(11)$, $b = 15.2521(9)$, $c = 22.4012(13)$ Å, $\beta = 102.5350(10)^\circ$, $Z = 4$, $V = 6498.3(7)$ Å³, $\rho_{\text{calc}} = 1.650$ g cm⁻³; $T = 173(2)$ K; $2\theta = 49.42^\circ$; 73 301 reflections measured, 10 944 were unique ($R_{\text{int}} = 0.0208$), and 10 117 observed ($I > 2\sigma(I)$); Bruker Smart Apex diffractometer with D8 goniometer equipped with a low-temperature device in ω mode,^[11] Mo K_{α} radiation ($\lambda = 0.71073$ Å), graphite-monochromated; Lp correction. The structure was solved by direct methods and refined with the full-matrix, least-squares method; $R_1 = 0.0274$, $wR_2 = 0.0719$ (for 10 117 reflections with $I > 2\sigma(I)$), $R_1 = 0.0300$, $wR_2 = 0.0734$ (for all 10 944 data); data-to-parameter ratio 15.05; residual electron density +0.919/–0.593 e Å⁻³. CCDC-178267 (**5**) and CCDC-178268 (**11**) contain the supplementary crystallographic data for this paper. These data can be obtained free of charge via www.ccdc.cam.ac.uk/conts/retrieving.html (or from the Cambridge Crystallographic Data Centre, 12, Union Road, Cambridge CB2 1EZ, UK; fax: (+44) 1223-336-033; or deposit@ccdc.cam.ac.uk).
- U. Herber, T. Pechmann, B. Weberndörfer, K. Ilg, H. Werner, *Chem. Eur. J.* **2002**, *8*, 309–319.
- K. G. Caulton, *Chemtracts: Inorg. Chem.* **1999**, 592–595.
- P. Braunstein, N. M. Boag, *Angew. Chem.* **2001**, *113*, 2493–2499; *Angew. Chem. Int. Ed.* **2001**, *40*, 2427–2433.
- M. Sauthier, B. Le Guennic, V. Deborde, L. Toupet, J.-F. Halet, R. Reau, *Angew. Chem.* **2001**, *113*, 234–237; *Angew. Chem. Int. Ed.* **2001**, *40*, 228–231.
- The 1H and ^{13}C NMR data of the phenyl groups were omitted for simplicity.
- D. Stalke, *Chem. Soc. Rev.* **1998**, *27*, 171–178.

Bifunctional Cp \cap N Complexes—Unusual Structural Features and Electronic Coupling in Highly Preorganized Bimetallic Systems**

Jens C. Röder, Franc Meyer,* and Elisabeth Kaifer

*Dedicated to Professor Lutz F. Tietze
on the occasion of his 60th birthday*

Complexes of cyclopentadienyl (Cp) ligands with functional amino or amido side chains are currently receiving enormous attention in organometallic chemistry.^[1, 2] While the donor substituent tethered to the Cp moiety usually serves a hemilabile chelate function in generic type **A** complexes, we recently put forward a novel approach in which a pyrazolate group in complexes of type **B** links two Cp units and acts both as an intramolecular N donor and as a bridging group spanning two metal ions.^[3] Such a strategy, that is the formal



Scheme 1. Synthesis of the complex $K^+ 3^-$.

coupling of two N-containing ligand compartments through a functionalized pyrazolate bridge to constitute a preorganized dinuclear scaffold, has successfully been employed for mimicking cooperative effects in biomimetic coordination compounds.^[4] Accordingly, type **B** systems are now expected to give rise to novel organometallic chemistry in which two adjacent metal ions might work in concert. Here we report the first transition metal complex of type **B**, its unusual structural features in the solid state, and characteristics of the metal–metal interaction in the mixed-valent form.

It proved difficult to introduce the parent Cp into the side arms of functionalized pyrazole derivatives such as **1**,^[5] and thus we employed a “protected” form of Cp: attachment of $[CpMn(CO)_3]$ to the pyrazole nucleus was achieved in a $[Pd(PPh_3)_2]/ZnCl_2$ -catalyzed cross-coupling reaction^[6] yielding **2** (Scheme 1).

A single-crystal structure analysis^[7] showed that **2** contains a protonated (noncoordinating) 1*H*-pyrazole heterocycle suitably arranged to potentially interact with the pendant

metal carbonyl fragments. Photolytic decarbonylation of **2** and deprotonation using KOtBu gave $K^+ 3^-$, the first bimetallic complex of type **B**. Its formation can be monitored by IR spectroscopy through the characteristic changes of the CO stretching frequencies (2015/1927 cm^{-1} for **2** versus 1919(1896)/1848(1816) cm^{-1} for **3**).^[8]

Single crystals of $K^+ 3^- \cdot 0.9 THF$ obtained from THF/light petroleum were analyzed by X-ray crystallography.^[9] The asymmetric unit contains four (very similar) dimanganese(II) units of the anticipated constitution—one of which is depicted in Figure 1. The N–Mn–C $_{\text{CO}}$ angles in **3**[–] are rather large (mean value 101.9°) compared to those in other $[CpMn(CO)_2L]$ complexes (L = N-donor ligand; 92.6–98.1° according to a CSD search), indicating a somewhat strained situation in the chelate complex **3**[–].

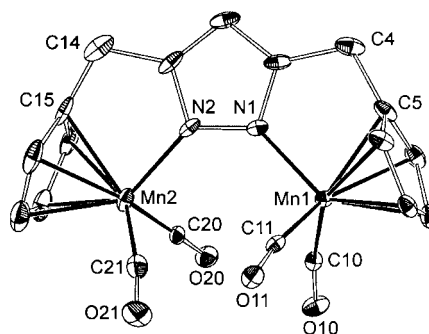


Figure 1. Molecular structure of **3**[–] (30% probability ellipsoids). Selected interatomic distances [\AA] and range of selected bond angles and dihedral angles [$^\circ$]; values for the other three independent molecules in square brackets: Mn1–N1 2.034(4) [2.032(4), 2.066(3), 2.047(4)], Mn2–N2 2.053(4) [2.060(4), 2.053(4), 2.033(4)]; C $_{\text{CO}}$ –Mn–N 98.6(2)–102.9(2) [100.0(2)–103.8(2), 102.3(2)–104.7(2), 96.3(2)–102.8(2)], Mn1–N1–N2–Mn2 27.9(1) [22.3(1), 10.3(1), 34.3(1)].

[*] Prof. Dr. F. Meyer
Institut für Anorganische Chemie
Georg-August-Universität Göttingen
Tammannstrasse 4, 37077 Göttingen (Germany)
Fax: (+49) 551-39-3063
E-mail: franc.meyer@chemie.uni-goettingen.de
Dr. J. C. Röder, Dr. E. Kaifer
Anorganisch-Chemisches Institut
Universität Heidelberg
Im Neuenheimer Feld 270, 69120 Heidelberg (Germany)

[**] Generous support by Prof. Dr. G. Huttner is gratefully acknowledged. We thank the DFG (SFB 247; Graduiertenkolleg-Stipendium to J.C.R.) and the Fonds der Chemischen Industrie for funding.

The bimetallic entities are connected through potassium ions to form a three-dimensional coordination polymer in the solid state. All K^+ ions are involved in unusual $\eta^5 \pi$ interactions with the pyrazolate heterocycle (Figure 2; $d(K-N)$ 2.83–3.07, $d(K-C)$ 3.14–3.52 Å).^[10] Such η^5 coordination to a pyrazolate group is very rare and has only recently been reported in a few cases,^[11] while to the best of our knowledge the $\eta^1:\eta^1:\eta^5$ pyrazolate binding mode observed in **3** is unprecedented.^[12]

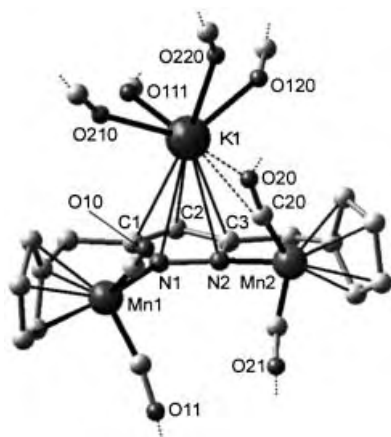


Figure 2. Part of the solid-state structure of $(K^+ 3^-) \cdot 0.9 THF$.

The coordination sphere of two of the four crystallographically distinct K^+ ions is completed by three O atoms of CpMn-bound CO groups and by one THF solvent molecule, while the other two K^+ ions are coordinated to four neighboring carbonyl-O atoms. These latter K^+ ions display a further open coordination site and exhibit a remarkably short additional side-on π contact with one CO ligand that is already end-on-bound to a second K^+ ion (see Figure 2: $d(K1 \cdots C20/O20)$ 3.07/3.14, $d(K2 \cdots C310/O310)$ 3.02/2.95 Å). According to a CSD search these are among the shortest side-on $K^+ \cdots CO$ contacts detected thus far.^[13]

The $Mn^I Mn^I$ compound **3**[−] is easily oxidized, for example, by air. The cyclic voltammogram of **3**[−] in THF reveals two well-separated reversible redox waves at $E_{1/2} = -0.37$ and $E_{1/2} = +0.14$ V (Figure 3),^[14] corresponding to the formation of the

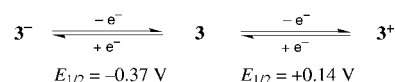
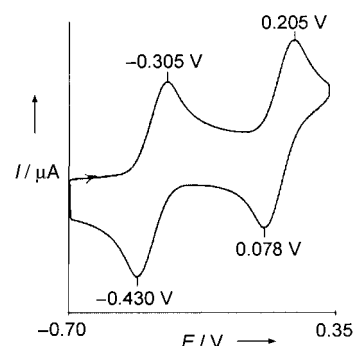


Figure 3. Cyclic voltammogram of **3**[−] (Pt electrode, solvent THF, electrolyte 0.1 M $N^iBu_4^+PF_6^-$; scan speed 200 mV s^{−1}).^[14]

$Mn^I Mn^{II}$ (d^5/d^6) and the oxidized $Mn^{II} Mn^{II}$ (d^5/d^5) species. The rather large separation of these single-electron processes ($\Delta E_{1/2} = 509$ mV) suggests strong electronic coupling and significant stabilization of the mixed-valent compound **3** ($K_{comp} = 3.8 \times 10^8$). A related $Mn^I Zn^{II}$ complex with only one redox-active Mn ion gave a single wave at $E_{1/2} = -0.20$ V in CH_2Cl_2 .^[6c]

Complex **3** can be prepared on a preparative scale by stoichiometric oxidation of **3**[−] with $AgBF_4$ and was isolated as a red powder. It should be noted that **3** is a rare example of a neutral d^5/d^6 mixed-valent complex, which is of particular interest because the absence of charge trapping in nonpolar solvents is expected to favour a high degree of delocalization.

The EPR spectrum of **3** in 2-methyltetrahydrofuran at 293 K shows an 11-line pattern ($g_{iso} = 2.028$; $a(^{55}Mn)_{iso} = 28.3 \times 10^{-4}$ cm^{−1}; Figure 4), confirming the equivalence of the two metal centers on the EPR time scale. A spectrum in frozen solution (123 K), however, indicates localized valency with electron coupling to only one ⁵⁵Mn nucleus. Variable-temperature EPR spectra were measured to locate the coalescence temperature, that is the transition between EPR-localized and -delocalized states (Figure 4). Transition between the isotropic 11-line pattern and a 6-line profile occurs around 185 K, where the solution (2-methyltetrahydrofuran/3-methylcyclopentane 1:4) still retains its fluidity. If one assumes sufficiently slow intramolecular electron transfer at low temperature as the reason, a rough estimate of the activation energy E_{th}^\ddagger and the thermal electron transfer rate k_{th} can be derived from Gagné's approximation [Eq. (1)]:^[15] $E_{th}^\ddagger = 13.6$ kJ mol^{−1} and $k_{th} = 2.5 \times 10^{10}$ s^{−1} at 298 K.

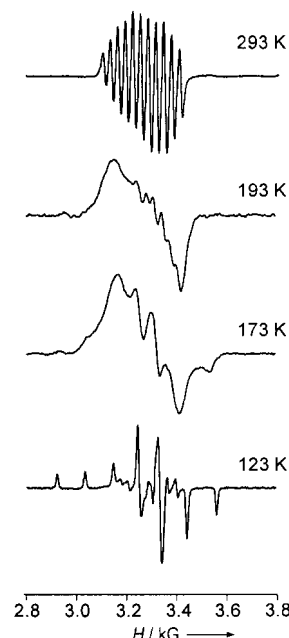


Figure 4. EPR spectra of the mixed-valent complex **3** in 2-methyltetrahydrofuran/3-methylcyclopentane (1:4) at selected temperatures.

$$k_{th} = (kT/h) \exp(-E_{th}^\ddagger/RT) \quad (1)$$

Based on these initial results, a Robin–Day class II assignment may be proposed for **3**. Accordingly, four CO absorptions are observed for the neutral mixed-valent $Mn^I Mn^{II}$ compound **3** (2027, 1952, 1899, and 1827 cm^{−1}), confirming that **3** is a valence-trapped species on the short vibrational time scale (ca. 10^{-12} s).

While the kinetically inert $CpMn(CO)_2$ fragment has frequently been used for the stabilization of unusual molecules^[6] and for the construction of d^5/d^6 mixed-valent systems,^[17] the notorious lability of $[CpMn(CO)_2(L)]$ complexes has generally hampered the isolation and detailed

characterization of systems with “inorganic” ligands L, in particular in the oxidized Mn^{II} forms. In **3**, the rigid chelate arrangement now precludes dissociation, and the π plane of the bridging pyrazolate roughly coincides with the mirror plane of the Mn^{II}(CO)₂ fragment, which is a favorable situation for stabilizing electronic π interactions. A more detailed study of the electronic properties of **3**^{−/0/+} will be reported in due course.

Experimental Section

2: [CpMn(CO)₃] was dissolved in THF and deprotonated with *n*BuLi at −78 °C. The solution was sequentially treated with ZnCl₂, [Pd(PPh₃)₂] (prepared by the reduction of [PdCl₂(PPh₃)₂] with diisobutylaluminum hydride (DIBAH)) and **1**, and stirred for 1 h at −78 °C and at room temperature under exclusion of light for a further 72 h. Following hydrolysis with brine, the tetrahydropyran (THP)-protected product was purified by column chromatography (diethyl ether/light petroleum 1:1, *R*_f = 0.33, yield 44%). The THP protecting group was cleaved with ethanolic HCl, and the product **2** obtained as yellowish crystals from CH₂Cl₂/light petroleum (yield 66% for the second step). Details of the synthetic procedures and full characterization of the compounds will be reported elsewhere.^[7]

K⁺3[−]: A solution of **2** (0.29 g, 0.58 mmol) in THF (200 mL) was irradiated with a high-pressure mercury lamp in a quartz apparatus for 15 min at −40 °C, which caused the reaction mixture to turn deep red. The progress of the reaction was monitored by IR spectroscopy in the CO stretching region (2015, 1927 before irradiation; 1916, 1843 after irradiation). After the mixture had been warmed to room temperature, KO^tBu (0.65 g, 0.58 mmol) was added and the reaction mixture was left to stir for 1 h. All volatile material was then removed under vacuum and the red residue washed with light petroleum and dissolved in a small amount of THF. Slow diffusion of light petroleum into the solution deposited red crystals of K⁺3[−]·0.9THF (yield: 0.18 g, 0.37 mmol, 64%). IR (KBr): $\tilde{\nu}$ = 1911 vs, 1885 m, 1844 vs, 1804 m cm^{−1}; IR (THF): $\tilde{\nu}$ = 1919 vs, 1896 m, 1848 vs, 1816 m cm^{−1}; UV/Vis (THF): $\lambda_{\text{max}}(\epsilon)$ = 400 nm (460 m^{−1} cm^{−1}); MS (FAB): *m/z* (%): 482 (10) [*M*⁺], 443 (20) [*M*⁺ − K], 387 (45) [*M*⁺ − K − 2CO]; elemental analysis: calcd (%) for C₁₉H₁₃KMnN₂O₄ (482.29): C 49.82, H 3.81, N 5.05; found: C 49.24, H 3.81, N 5.04.

Received: February 12, 2002 [Z18699]

- [1] a) J. Okuda, *Comments Inorg. Chem.* **1994**, *16*, 185–205; b) P. Jutzi, U. Siemeling, *J. Organomet. Chem.* **1995**, *500*, 175–185.
- [2] A. L. McKnight, R. M. Waymouth, *Chem. Rev.* **1998**, *98*, 2587–2598.
- [3] J. C. Röder, F. Meyer, H. Pritzkow, *Organometallics* **2001**, *20*, 811–817.
- [4] a) F. Meyer, P. Rutsch, *Chem. Commun.* **1998**, 1037–1038; b) F. Meyer, E. Kaifer, P. Kircher, K. Heinze, H. Pritzkow, *Chem. Eur. J.* **1999**, *5*, 1617–1630; c) J. Ackermann, F. Meyer, E. Kaifer, H. Pritzkow, *Chem. Eur. J.* **2002**, *8*, 247–258.
- [5] J. C. Röder, F. Meyer, M. Konrad, E. Kaifer, H. Pritzkow, *Eur. J. Org. Chem.* **2001**, 4479–4487.
- [6] a) M. E. Huttenloch, J. Diebold, U. Rief, H. H. Brintzinger, *Organometallics* **1992**, *11*, 3600–3607; b) M. Enders, G. Kohl, H. Pritzkow, *J. Organomet. Chem.* **2001**, *622*, 66–73; c) J. C. Röder, F. Meyer, R. F. Winter, E. Kaifer, *J. Organomet. Chem.* **2002**, *641*, 113–120.
- [7] J. C. Röder, F. Meyer, E. Kaifer, unpublished results.
- [8] The two CpMn(CO)₂ moieties in **3**[−] (and also in **3**⁺) are vibrationally coupled, giving rise to a second (less intense) pair of IR bands. See also: C. G. Atwood, W. E. Geiger, *J. Am. Chem. Soc.* **1993**, *115*, 5310–5311.
- [9] Crystal structure of (K⁺3[−])₄·3.6THF (C₇₆H₅₂K₄Mn₈N₈O₁₆·3.6THF, *M*_r = 2188.8): monoclinic, *P*2₁/*c*, *a* = 23.071(5), *b* = 25.404(5), *c* = 15.501(3) Å, β = 91.14(3), *V* = 9083(3) Å³, *Z* = 4, ρ_{calcd} = 1.601 g cm^{−3}, $\mu(\text{MoK}\alpha)$ = 1.33 mm^{−1}, $2\theta_{\text{max}}$ = 54.9°, 20751 independent reflections (*R*_{int} = 0.093), 12009 observed [*I* > 2 σ (*I*)], 1192 parameters; final

*R*1[*I* > 2 σ (*I*)] = 0.076, *wR*2 = 0.127, goodness of fit on *F*² = 1.020, largest difference peak +0.73/−0.48 e Å^{−3}. Data were collected on a Nonius Kappa CCD diffractometer at 200 K using MoK α radiation (λ = 0.71073 Å). The structure was solved by direct methods with the SHELXS-97 and refined with the SHELXL-97 programs. Non-hydrogen atoms were refined in anisotropic models. Hydrogen atoms were placed at calculated positions and allowed to ride on the atoms they are attached to. CCDC 162374 contains the supplementary crystallographic data for this paper. These data can be obtained free of charge via www.ccdc.cam.ac.uk/conts/retrieving.html (or from the Cambridge Crystallographic Data Centre, 12, Union Road, Cambridge CB2 1EZ, UK; fax: (+44) 1223-336-033; or deposit@ccdc.cam.ac.uk).

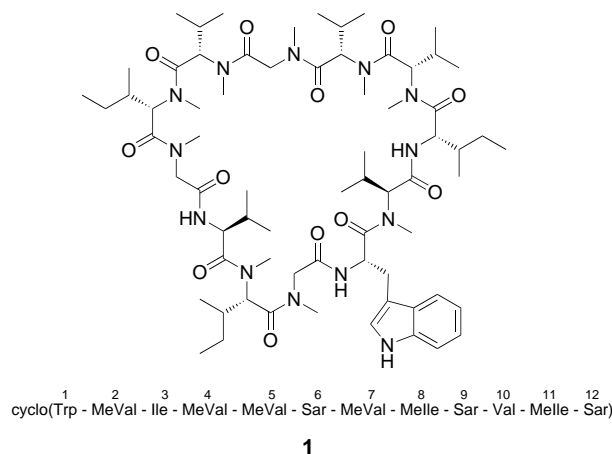
- [10] The average K–C distance is 3.06 Å in CpK and 3.37 Å for K–arene interactions: a) R. E. Dinnebier, U. Behrens, F. Olbrich, *Organometallics* **1997**, *16*, 3855–3858; b) D. L. Clark, J. C. Gordon, J. C. Huffman, R. L. Vincent-Hollis, J. G. Watkin, B. D. Zwick, *Inorg. Chem.* **1994**, *33*, 5903–5911.
- [11] Ru: J. R. Perera, M. J. Heeg, H. B. Schlegel, C. W. Winter, *J. Am. Chem. Soc.* **1999**, *121*, 4536–4537; K: Z. Hu, S. M. Gorun, *Inorg. Chem.* **2000**, *40*, 667–671; Ti: G. B. Deacon, E. E. Delbridge, C. M. Forsyth, B. W. Skelton, A. H. White, *J. Chem. Soc. Dalton Trans.* **2000**, 745–751; Eu: G. B. Deacon, A. Gitlits, P. W. Roesky, M. R. Bürgstein, K. C. Lim, B. W. Skelton, A. H. White, *Chem. Eur. J.* **2001**, *7*, 127–138; Ba: A. Steiner, G. T. Lawson, B. Walfort, D. Leusser, D. Stalke, *J. Chem. Soc. Dalton Trans.* **2001**, 219–221.
- [12] J. E. Cosgriff, G. B. Deacon, *Angew. Chem.* **1997**, *109*, 298–299; *Angew. Chem. Int. Ed. Engl.* **1997**, *37*, 286.
- [13] *d*(K1...C/O) = 3.195/3.023 Å has been observed in K₃[Mn₃(CO)₁₂]: W. Schatz, H.-P. Neumann, B. Nuber, B. Kanellakopoulos, M. L. Ziegler, *Chem. Ber.* **1991**, *124*, 453–463.
- [14] Values versus the saturated calomel electrode (SCE). *i*_{pa}/*i*_{pc} ≈ 1; *i*_{pc}/*v*^{1/2} ≈ constant.
- [15] R. R. Gagné, C. A. Koval, T. J. Smith, M. C. Cimlino, *J. Am. Chem. Soc.* **1979**, *101*, 4571–4580; all symbols have their usual meanings. *k*_{th} is taken to be equal to the EPR lifetime at the coalescence temperature (5.5 × 10⁸ s^{−1}). *E*_{th} is supposed to not change in the given temperature range and adiabatic electron transfer is assumed. See also: a) R. C. Long, D. N. Hendrickson, *J. Am. Chem. Soc.* **1983**, *105*, 1513–1521; b) S. K. Dutta, S. B. Kumar, S. Bhattacharyya, E. R. T. Tiekink, M. Chaudhury, *Inorg. Chem.* **1997**, *36*, 4954–4960.
- [16] a) K. G. Caulton, *Coord. Chem. Rev.* **1981**, *38*, 1–43; b) D. Sellmann, J. Müller, P. Hofmann, *Angew. Chem.* **1982**, *94*, 708–709; *Angew. Chem. Int. Ed. Engl.* **1982**, *21*, 691; c) A. Winter, G. Huttner, L. Zsolnai, P. Kroneck, M. Gottlieb, *Angew. Chem.* **1984**, *96*, 986–987; *Angew. Chem. Int. Ed. Engl.* **1984**, *23*, 975.
- [17] a) R. Gross, W. Kaim, *Inorg. Chem.* **1986**, *25*, 4865–4870; b) W. Kaim, R. Gross, *Comments Inorg. Chem.* **1988**, *7*, 269–285; c) C. A. Atwood, W. E. Geiger, *J. Am. Chem. Soc.* **2000**, *122*, 5477–5485.

Total Synthesis of the Nematicidal Cyclododecapeptide Omphalotin A by Using Racemization-Free Triphosgene-Mediated Couplings in the Solid Phase**

Bernd Thern, Joachim Rudolph, and Günther Jung*

In memory of Ernst Bayer

The natural product omphalotin A (**1**) belongs to a family of cyclic dodecapeptides from the basidiomycete *Omphalotus olearius*.^[1] and shows a selective activity against phytopathogenic nematodes such as *Meloidogyne incognita*.^[1] Under



in vitro conditions, omphalotin A outreaches known nematocides such as ivermectin in potency and selectivity.^[2] The high specificity and structure of **1**, which are unusual for a nematocide, lead to the assumption that a hitherto unknown biological target is responsible for the activity of **1**. To elucidate this target, high amounts of the cyclopeptide are required which cannot be produced by fermentation alone.^[2]

Structurally, the highly lipophilic omphalotin A is closely related to the immunosuppressive cyclosporin therapeutics; nine of its twelve amino acids are N-methylated. This high

degree of methylation results in conformational freedom and complicates chemical syntheses considerably, as the experience from syntheses of cyclosporins illustrates.^[3] The main problems are low coupling yields, side reactions such as diketopiperazine formation or racemization,^[4] and the lability of N-alkylated peptides towards acids.^[5] Despite numerous reports on reagents for the coupling of sterically hindered N-methyl amino acids,^[6] a satisfactory solution for this problem has not yet been found.^[7]

Here we report on the synthesis of **1** using Fmoc amino acids on a polystyrene support with a trityl linker (TCP resin). This linker allows product cleavage under very mild conditions using hexafluoroisopropanol (HFIP).^[8] In view of the acid lability of the products, these mild conditions were crucial.

First, we did model reactions to form all N-methylated peptide bonds in **1** using four different reagents (dicyclohexylcarbodiimide = DCC, triphosgene = BTC, diisopropylcarbodiimide/hydroxyazabenzotriazole = DIC/HOAt, tetramethylfluoroformamidinium hexafluorophosphate = TFFH). As far as coupling efficiency is concerned, the BTC method of Falb et al.^[9] turned out to be far superior (Table 1).

Table 1. Each of the eight N-methylated amide bonds of omphalotin A were formed using four different reagents. In the case of complete conversion, a negative chloranil test showed the absence of secondary amines after one (+ +) or two (+) coupling cycles, respectively. In the case of incomplete conversion (–), the chloranil test was positive even after double coupling cycles. The results were verified by HPLC or HPLC–MS after cleavage from the resin.

N-methylated amide bond ^[a]	TFFH ^[b]	DIC/HOAt ^[c]	DCC ^[d]	BTC ^[e]
Fmoc-Trp-OH → H-MeVal-R	–	+	+	++
Fmoc-Ile-OH → H-MeVal-R	–	–	+	++
Fmoc-Sar-OH → H-MeVal-R	–	++	++	++
Fmoc-MeVal-OH → H-MeVal-R	–	–	–	++
Fmoc-MeVal-OH → H-Melle-R	–	–	–	++
Fmoc-Val-OH → H-Melle-R	–	–	+	++
Fmoc-MeVal-OH → H-MeGly-R	++	++	++	++
Fmoc-Melle-OH → H-MeGly-R	++	++	++	++

[a] R = Phe-TCP-resin; [b] Fmoc AA, TFFH: 5 equiv, DIEA: 10 equiv, 1 h in DMF (AA = amino acid); [c] Fmoc AA, HOAt, DIC, DIEA: 3 equiv, 1 h in DMF; [d] Fmoc AA: 6 equiv, DCC: 3 equiv, 1.5 h in DMF; [e] see ref. [9].

HPLC–MS, however, showed considerable amounts of by-products in the cleavage products from the BTC couplings, as did the HPLC chromatograms published by Falb et al.^[9] Furthermore, the BTC coupling turned out to be useless for the synthesis of longer peptides. After only a few such couplings, no product could be isolated from the TCP resin. On Wang resin with the less acid-labile *p*-alkoxybenzyl linker, quantitative diketopiperazine formation resulted upon Fmoc removal from the dipeptidyl resin with piperidine. Therefore, we decided to use the TCP resin, and to adapt the methodology of the BTC coupling to the properties of this resin.^[10]

For the first successful synthesis of **1**, the following protocol was developed: The N-Fmoc-protected peptidyl–TCP resin is pretreated with diisopropylethylamine (DIEA) and the activation of the Fmoc-N-methyl amino acid is carried out

[*] Prof. Dr. G. Jung, Dipl.-Chem. B. Thern

Institute of Organic Chemistry

University of Tübingen

Auf der Morgenstelle 18, 72076 Tübingen (Germany)

Fax: (+49) 7071-295-560

E-mail: guenther.jung@uni-tuebingen.de

Dr. J. Rudolph

Central Research, Bayer AG

51368 Leverkusen (Germany)

New address: Bayer Corporation

Pharmaceutical Division, Department of Chemistry

400 Morgan Lane, West Haven, CT 06516 (USA)

[**] B.T. received a scholarship from the graduate college "Analytical Chemistry" of the DFG. We are grateful to Dietmar G. Schmid for high-resolution FTICR–MS measurements, to Graeme Nicholson for enantiomeric GC–MS analyses, to Dr. Joachim Wesener for discussions on MS analysis, to Daniel Bischoff for preparative HPLC–MS, and to Heidi Theis and Roman Hanke for experimental assistance.

Supporting information for this article is available on the WWW under <http://www.angewandte.org> or from the author.

at room temperature in THF by addition of BTC and collidine.^[11] This procedure enables us to use BTC on acid-labile TCP resin. Premature cleavage from the resin, which was initially observed during syntheses starting from resin-bound sarcosine, was prevented by limiting the pretreatment of the resin with DIEA, as well as the Fmoc deprotection with piperidine, to the shortest possible duration. An elevated temperature during the coupling reaction was unnecessary, as the presence of the strong base DIEA appears to accelerate the coupling reaction.^[12] By use of these modifications, the formation of by-products was almost completely eliminated. Furthermore, the amount of Fmoc amino acid needed per coupling reaction could be reduced from 5 to 3.5 equivalents without any loss of coupling efficiency.

Even in the exceedingly difficult coupling of Fmoc-MeVal to resin-bound MeVal, quantitative conversion can be observed when the modified BTC activation is used. The coupling of unmethylated Fmoc amino acids, on the other hand, often gave insufficient coupling yields. In these cases, DIC/HOAt or HATU activation led to better results.

Starting from TCP resin preloaded with Fmoc-sarcosine, and using a combination of BTC, DIC/HOAt, and HATU-couplings, the linear dodecapeptide with C-terminal Sar⁶ [Oma(7-6)] was obtained in 84% yield and 90% purity (HPLC, $\lambda = 214$ nm). Only three coupling reactions had to be repeated, whereas the remaining eight were complete after a single coupling cycle (Figure 1). The crude product of the coupling reaction was purified by flash chromatography on silica gel. Diastereomerically pure^[13] omphalotin A was obtained in a cyclization yield of 37% and in an overall yield of 31% with respect to the first loading of the resin with Fmoc-sarcosine.

Analogous syntheses starting from resin-bound Sar⁹ or Sar¹² also yielded **1** in a diastereomerically pure form. A total of 102 mg of pure **1** was synthesized.

The high-resolution ¹H and ¹³C NMR spectra correspond to the data given in the literature.^[1b] The molecular mass determined by ES-FTICR-MS in the ultrahigh-resolution mode corresponds to the theoretical value up to a relative mass error of 2 ppm (Figure 2). Additionally, the identity of the synthetic product was confirmed by co-elution with the natural compound in the analytical HPLC and by comparison of their ES-FTICR-MS fragmentation spectra.

The modified BTC coupling was thus demonstrated to be a highly efficient, experimentally simple and very low-cost method for the coupling of N-methyl amino acids. We showed

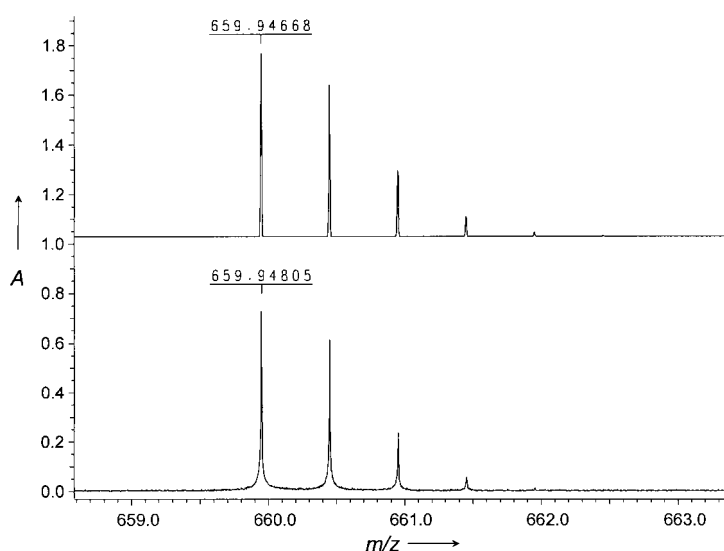


Figure 2. ES-FTICR-mass spectrum of synthetic omphalotin A ($[M+2H]^{2+}$). The upper trace shows the simulation, the lower trace shows the spectrum recorded in the ultrahigh-resolution mode. The relative mass error is 2 ppm.

that the novel BTC activation is racemization free.^[13] Using this solid-phase coupling, we developed a methodology which allows the synthesis of omphalotin A in a very short time and in high yields compared to both solid-phase and solution-phase syntheses of the structurally related cyclosporins. This method is expected to facilitate greatly the synthesis of numerous other N-alkylated peptides such as cyclosporins,^[14] tentoxins, dolastatins, jaspamides, and didemnines.^[7] It has a high potential for automation in the multiple, parallel peptide synthesis^[15] which we are currently investigating. Experiments to improve the efficiency of the BTC method for the coupling of nonmethylated amino acids are also currently under way in our laboratory.

Experimental Section

Fmoc-N-methyl amino acids were prepared according to Freidinger et al.^[16] HOAt and HATU were purchased from Applied Biosystems (Foster City, CA, USA). TFFH was purchased from Advanced ChemTech (Bamberg, Germany). TCP resin was obtained from PepChem (Tübingen, Germany). Preparative HPLC was performed on the "high-throughput purifier" (HTP) coupled to the M-8000 ES-MS (Merck-Hitachi, Darmstadt, Germany) using a C18-RP column (isocratic elution, 62% acetonitrile in H₂O, 0.1% TFA; TFA = trifluoroacetic acid) with MS and UV detection (diode array). ES-FTICR-MS measurements were performed on a Daltonic APEX II spectrometer (Bruker, Bremen, Germany).

The synthesis of **1** starting from Sar⁶ was performed on 238 mg of TCP resin preloaded with Fmoc-sarcosine (0.58 mmol g⁻¹; 138 μ mol; 1 equiv).

BTC coupling: Fmoc-peptidyl resin was deprotected with 20% piperidine/DMF (2 min + 8 min). After washing, the resin was treated with dry THF (1 mL) for 15 min. Meanwhile, the following Fmoc amino acid (483 μ mol; 3.5 equiv) was added to a 68 mM solution of BTC in dry THF (2.4 mL; 1.15 equiv BTC). Sym-collidine (180 μ L; 10 equiv) was added to the clear solution, upon which a precipitate of

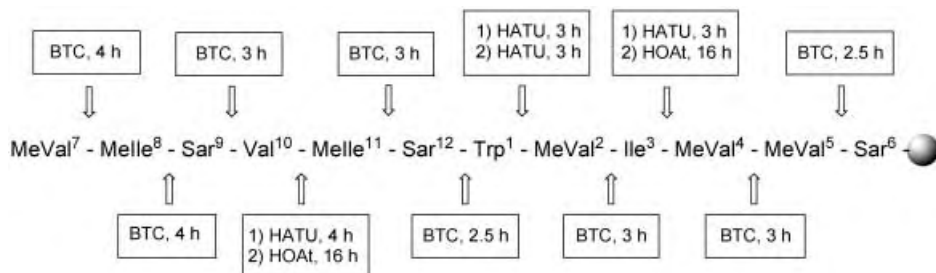


Figure 1. Synthesis outline for the linear dodecapeptide with Sar⁶ [omphalotin A(7-6)]. After the times given, the respective couplings were quantitative (chloranil test, Kaiser test, and/or HPLC). Peak area of the Fmoc-deprotected dodecapeptide (crude product): 90% (HPLC, $\lambda = 214$ nm).

collidinium chloride was formed. DIEA (190 μ L, 8 equiv) was added to the resin, immediately followed by addition of the suspension. The mixture was shaken for the reaction times given in Figure 1, filtered, and washed.

DIC/HOAt coupling: Fmoc amino acid (414 μ mol; 3 equiv) and HOAt (57 mg; 3 equiv) were dissolved in a small volume of CH_2Cl_2 /DMF (1:1). DIC (65 μ L; 3 equiv) was added and the mixture was shaken. After 15 min, this solution was added to the Fmoc-deprotected peptidyl resin (swollen in DMF) and shaken for the reaction times given in Figure 1.

HATU coupling: Fmoc amino acid (552 μ mol; 4 equiv) and HATU (210 mg; 4 equiv) were dissolved in a small volume of CH_2Cl_2 /DMF (1:1). DIEA (190 μ L; 8 equiv) was added and the mixture was shaken. After 15 min, this solution was added to the Fmoc-deprotected peptidyl resin (swollen in DMF) and shaken for the reaction times given in Figure 1.

Cleavage and deprotection: Following Fmoc deprotection, the dodecapeptidyl-TCP resin was washed and HFIP/ CH_2Cl_2 1:5 (5 mL) was added. The suspension was shaken for 15 min, after which the filtrate was collected and evaporated to dryness under reduced pressure. The cleavage procedure was repeated twice. Yield: 155 mg linear dodecapeptide OmA(7-6) (116 μ mol; 84 %), HPLC purity ($\lambda = 214$ nm): 90 %.

This peptide (155 mg; 116 μ mol; 1 equiv) was dissolved in CH_2Cl_2 (400 mL). HOAt (32 mg; 2 equiv), 3-(3-dimethylaminopropyl)-1-ethylcarbodiimide (EDCI; 45 mg; 2 equiv) and DIEA (160 μ L; 8 equiv) were added successively. After stirring for 16 h at RT, 2/3 of the solvent was evaporated under reduced pressure. The organic phase was washed with saturated NaHCO_3 , 8 % citric acid, and brine, dried over Na_2SO_4 , and evaporated to dryness. The cyclopeptide **1** was purified by flash chromatography (silica gel, ethyl acetate/methanol 95:5). Yield: 57 mg **1** (43 μ mol; 31 %).

Analytical data for **1**: ^1H and ^{13}C NMR data of the synthetic omphalotin A correspond to the literature data for the natural compound.^[1b] HR-MS (ES-FTICR-MS): calcd: m/z 659.94668, found: m/z 659.94805 ($[M+2\text{H}]^{2+}$) (Figure 2). For further analytical data and experimental details, see Supporting Information.

Received: February 22, 2002 [Z18750]

- [1] a) A. Mayer, H. Anke, O. Sterner, *Nat. Prod. Lett.* **1997**, *10*, 25–32; b) O. Sterner, W. Etzel, A. Mayer, H. Anke, *Nat. Prod. Lett.* **1997**, *10*, 33–38; c) A. Mayer, H. Anke, O. Sterner, M. Kilian, R. Hain, D. Berg, W. Etzel, H. Gau (Bayer AG), WO 97/20857, **1996**.
- [2] A. Mayer, M. Kilian, B. Hoster, O. Sterner, H. Anke, *Pestic. Sci.* **1999**, *55*, 27–30.
- [3] S. Y. Koo, R. M. Wenger, *Helv. Chim. Acta* **1997**, *80*, 695–705; b) P. Raman, S. S. Stokes, Y. M. Angell, G. R. Flentke, D. H. Rich, *J. Org. Chem.* **1998**, *63*, 5734–5735.
- [4] J. R. McDermott, N. L. Benoiton, *Can. J. Chem.* **1973**, *51*, 2555–2561.
- [5] a) J. Urban, T. Vaisar, R. Shen, M. S. Lee, *Int. J. Pept. Protein Res.* **1996**, *37*, 182–189; b) T. Vaisar, J. Urban, *J. Mass Spectrom.* **1998**, *33*, 505–524.
- [6] a) P. Li, J. C. Xu, *Tetrahedron Lett.* **1999**, *40*, 8301–8304; b) P. Li, J. C. Xu, *J. Org. Chem.* **2000**, *65*, 2951–2958.
- [7] J. M. Humphrey, A. R. Chamberlin, *Chem. Rev.* **1997**, *97*, 2243–2266.
- [8] R. Bollhagen, M. Schmiedberger, K. Barlos, E. Grell, *J. Chem. Soc. Chem. Commun.* **1994**, *22*, 2559–2560.
- [9] F. Falb, T. Yechezkel, Y. Salitra, C. Gilon, *J. Pept. Res.* **1999**, *53*, 507–517. The amino acid is activated with BTC and collidine in THF and reacted with peptidyl resin for 1 h at 50 °C.
- [10] Falb et al.^[9] prepared peptide amides on Rink amide resin which does not allow the formation of diketopiperazines.
- [11] J. Rudolph, G. Jung, B. Thern (Bayer AG), Patent application pending.
- [12] An increase in coupling efficiency by the combination of a weak base for carboxy activation and a stronger base for the coupling reaction has been described for the system DIC/HOAt:L. A. Carpino, A. El-Faham, *Tetrahedron* **1999**, *55*, 6813–6830.
- [13] GC-MS analyses of the totally hydrolysed **1** and of intermediate products were performed on chiral phase (W. König, I. Benecke, N.

Lucht, E. Schmidt, J. Schulze, S. Sievers, *J. Chromatogr.* **1983**, *279*, 555–562). Only negligible amounts of D-amino acids were found (see Supporting Information).

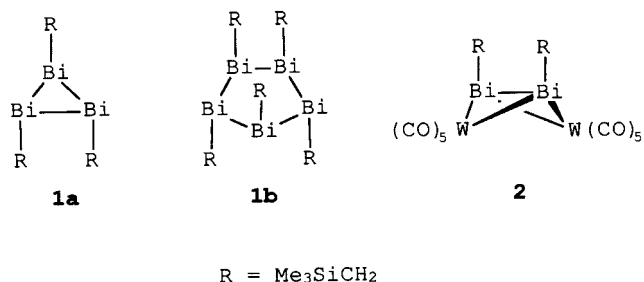
- [14] B. Thern, J. Rudolph, G. Jung, *Tetrahedron Lett.* **2002**, *43*, in press.
- [15] a) *Combinatorial Peptide and Nonpeptide Libraries* (Ed.: G. Jung), Wiley-VCH, Weinheim, **1996**; b) *Combinatorial Chemistry—Synthesis, Analysis and Screening* (Ed.: G. Jung), Wiley-VCH, Weinheim, **1999**.
- [16] R. M. Freidinger, J. S. Hinkle, D. S. Perlow, B. H. Arison, *J. Org. Chem.* **1983**, *48*, 77–81.

Synthesis of the Dibismuthene Complex $[\mu-\eta^2-(cis-\text{Me}_3\text{SiCH}_2\text{Bi})_2]\{\text{W}(\text{CO})_5\}_2$ from a Cyclobismuthane and $[\text{W}(\text{CO})_5(\text{thf})]$

Lucia Balázs, Hans Joachim Breunig,* and Enno Lork

Owing to relativistic effects it is expected that two valence electron pairs of bismuth should be inert.^[1,2] Consequently, Bi^{I} compounds should be relatively stable and their reactivity should differ considerably from that of corresponding compounds the lighter homologues. To date there is little evidence for these effects because true Bi^{I} compounds are rare.^[2] The first organometallic examples are *trans*-dibismuthenes, $\text{RBi}=\text{BiR}$ ^[3] and two cyclobismuthanes, $(\text{RBi})_n$ ($n=3,4$),^[4a] which are protected by very bulky aryl groups or by the $(\text{Me}_3\text{Si})_2\text{CH}$ group, respectively. Recently, the ring compounds $(\text{RBi})_4$ ($\text{R}=(\text{Me}_3\text{Si})_3\text{Si}$) and R_6Bi_8 ($\text{R}=(\text{Me}_3\text{Si})_3\text{Sn}$) were described.^[4b]

Searching for less hindered Bi^{I} compounds, for which the specific properties might emerge more clearly, we have studied the bismuth ring system trimethylsilylmethylbismuth(i) (**1**), whose main components are the new cyclobismuthane **1a**, a three-membered ring, and **1b**, the first bismuth five-membered ring. Three- and five-membered rings are well known in the chemistry of P, As, and Sb.^[5]



[*] Prof. Dr. H. J. Breunig, L. Balázs, Dr. E. Lork
 Universität Bremen
 Institut für Anorganische und Physikalische Chemie
 28334 Bremen (Germany)
 Fax: (+49) 421-218-4042
 E-mail: breunig@chemie.uni-bremen.de

on dilution and heating. As shown in Figure 1 the three- and five-membered rings exist in an approximately 1:1 molar ratio at 5 °C. It is likely that at low temperatures and in the solid state the five-membered ring is the main component.^[10]

The equilibrium between **1a** and **1b** is unusual, since solutions of bis(trimethylsilyl)methylbismuth contain three- and four-membered rings, and trimethylsilylmethylantimony as well as other alkylpnictogen ring systems with “slim” substituents exist in the crystal or in solution almost exclusively as five-membered rings.^[5c] Bulky substituents are usually required for the stabilization of pnictogen three-membered rings; they form in ring–ring equilibria only at much higher temperatures.^[5a]

The unique character of the Bi ring system **1** is exemplified also in the reaction with $[\text{W}(\text{CO})_5(\text{thf})]$, which leads to the dibismuthene complex **2**, a red crystalline compound, which is well soluble in hydrocarbons and melts at 95 °C. The structure of **2** was determined by single-crystal X-ray diffraction.^[11] It is a complex of a *cis*-dibismuthene coordinated “side-on” bridging to two $\text{W}(\text{CO})_5$ units in a bicyclic butterfly structure (Figure 2). The Bi–Bi bond in **2** (3.003(1) Å) is longer than in

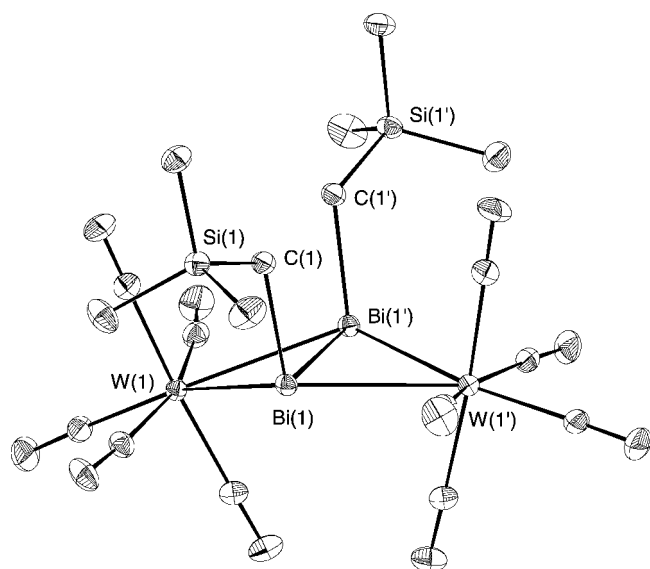


Figure 2. Structure of **2** in the crystal (the ellipsoids represent 30% probability). Selected distances [Å] and angles [°]: Bi(1)–Bi(1') 3.0024(7), Bi(1)–C(1) 2.303(6), Bi(1)–W(1') 3.118(1), Bi(1)–W(1) 3.124(1); C(1)–Bi(1)–Bi(1') 96.2(2), C(1)–Bi(1)–W(1') 103.2(1), Bi(1')–Bi(1)–W(1') 61.34(2), C(1)–Bi(1)–W(1) 104.3(2), Bi(1')–Bi(1)–W(1) 61.15(2), W(1')–Bi(1)–W(1) 117.88(3).

free dibismuthenes $\text{RBi}=\text{BiR}$ with aryl substituents in *trans* positions ($\text{R}=[(\text{Me}_3\text{Si})_2\text{CH}]_3\text{C}_6\text{H}_2$ 2.8206(8),^[3a] $\text{R}=(\text{Me}_3\text{C}_6\text{H}_2)_2\text{C}_6\text{H}_3$ 2.832(1) Å^[3c]), or in the dibismuth complexes $[\text{Bi}_2\{\text{W}(\text{CO})_5\}_3]$ (2.818(3) Å)^[7a] and $[\text{Bi}_2\{\text{Sm}(\text{C}_5\text{Me}_5)_2\}_2]$ (2.851(1) Å).^[7d] It lies in the range of the Bi–Bi single bonds of $(\text{Ph}_2\text{Bi})_2$ (2.990(2) Å),^[12a] $[\text{Et}_2\text{Bi}][\text{Al}(\text{tBu})_3]$ (2.9831(1) Å),^[12b] or $[(\text{Me}_3\text{Si})_2\text{CHBi}]_4$ (2.972(5)–3.042(3) Å^[6]). Also in diphosphene complexes with “side-on” coordination the P–P bond lengths are considerably longer than in free diphosphenes.^[6b] The Bi–W distances in **2**

(3.118(1), 3.124(1) Å) are similar to those in $[\text{Bi}_2\{\text{W}(\text{CO})_5\}_3]$ (3.083(3)–3.134(3) Å).^[7a] They are longer than the Bi–W bond lengths in $[\text{Ph}_3\text{BiW}(\text{CO})_5]$ (2.829 Å),^[13a] $[(\text{Ph}_3\text{P})_2\text{N}][\text{Ph}_2\text{Bi}\{\text{W}(\text{CO})_5\}_2]$ (2.882–2.885 Å),^[13b] and $[(\text{Bi}_2)\text{W}_2(\text{CO})_8][\text{MeBiW}(\text{CO})_5]$ (2.851–3.001 Å).^[7b] The Bi–Bi–C bond angles and the Bi_2W dihedral angles in **2** are 96.4(4) and 155.5°, respectively. Thus, the wings of the butterfly structure are widely extended.

Our recent study of the reaction of $(\text{RSb})_n$ ($n=4, 5$; $\text{R}=\text{Me}_3\text{SiCH}_2$) with $[\text{W}(\text{CO})_5(\text{thf})]$ under very similar conditions allows a very direct comparison of the reactivity of analogous antimony(i) and bismuth(i) compounds. In the case of the reaction of the cyclostibanes no distibene analogue of **2** is formed, instead two Sb atoms of the five-membered ring are coordinated in a terminal fashion and *cyclo*- $[\text{1,3-}\{\text{W}(\text{CO})_5\}_2(\text{RSb})_5]$ is formed.^[14]

With **1** and $[(\text{Me}_3\text{Si})_2\text{CH}_2\text{Bi}]_n$ ($n=3,4$) there are now two cyclic alkylbismuth(i) systems known, and the differences to the lighter homologues are emerging. The unusual preference for three-membered rings in ring–ring equilibria is remarkable. Monomeric alkylbismuth(i) species were not identified. They are, however, possible intermediates in ring–ring transformations or in the formation of **2**.

Experimental Section

All operations were carried out in an argon atmosphere in dry solvents.

1: A Grignard solution prepared from $\text{Me}_3\text{SiCH}_2\text{Cl}$ (10.0 g, 81.6 mmol) and magnesium (2.4 g, 100.9 mmol) in THF (110 mL) was added dropwise to a suspension of Ph_2BiCl (32.2 g, 80.8 mmol) in THF (100 mL). The reaction mixture was stirred for 2 h at 0 °C and for 18 h at room temperature. The THF was removed in vacuum and the residues were extracted with petroleum ether. After the removal of the solvent, $\text{Me}_3\text{SiCH}_2\text{BiPh}_2$ remained as a yellowish oil (30.8 g; 84.7%), which crystallized at room temperature to give colorless needles. HCl gas was introduced for 2 h at 0 °C into a solution of $\text{Me}_3\text{SiCH}_2\text{BiPh}_2$ (28.0 g, 62.2 mmol) in CHCl_3 (130 mL), the mixture was stirred for 30 min, and subsequently the solvent was removed to give $\text{Me}_3\text{SiCH}_2\text{BiCl}_2$ as a yellowish solid (17.5 g; 76.7%). MS (70 eV): m/z (%): 351 (78) $[M^+ - \text{Me}]$, 336 (38) $[M^+ - 2\text{Me}]$, 279 (25) $[M^+ - \text{R}]$, 244 (17) $[\text{BiCl}^+]$, 209 (100) $[\text{Bi}^+]$. LiAlH_4 (2.8 g, 73.0 mmol) was added portionwise to a precooled (–70 °C) solution of $\text{Me}_3\text{SiCH}_2\text{BiCl}_2$ (12.8 g, 34.9 mmol) in Et_2O (200 mL) and the mixture was stirred. Filtration at –30 °C through a precooled frit covered with kieselgur gave a dark red solution from which **1** (9.3 g; 90%) remained as a red solid after the removal of the solvent in vacuum. M.p. 38–40 °C; elemental analyses calcd (%) for $\text{C}_{20}\text{H}_{35}\text{Bi}_3\text{Si}_5$: C 16.22, H 3.74; found: 15.87, H 3.89; ^1H NMR of **1a** (200 MHz, C_6D_6 , 5 °C, TMS): $\delta=0.059$ (s, 9H; CH_3), 0.17 (s, 18H; CH_3), AB spin systems with A: 1.602, B: 1.991 ($^2J(\text{H,H})=12.1$ Hz, 4H; CH_2), 1.765 ppm (s, 2H; CH_2); ^1H NMR of **1b** (200 MHz, C_6D_6 , 5 °C, TMS): $\delta=0.138$ (s, 18H; CH_3), 0.144 (s, 9H; CH_3), 0.173 (s, 18H; CH_3), AB spin systems with A: 2.5515, B: 3.684 ($^2J(\text{H,H})=12.2$ Hz, 4H; CH_2), and A: 2.786, B: 2.933 ($^2J(\text{H,H})=12.3$ Hz, 4H; CH_2), 2.818 ppm (s, 2H; CH_2); MS (CI, NH_3): m/z (%): 975 (3) $[\text{R}_4\text{Bi}_3^+]$, 888 (2) $[\text{R}_3\text{Bi}_3^+]$, 854 (82) $[\text{R}_3\text{Bi}_3^+ - 2\text{Me}]$, 766 (6) $[\text{R}_4\text{Bi}_2^+]$, 400 (100) $[\text{R}_2\text{Bi}^+ + \text{NH}_3]$, 383 (35) $[\text{R}_2\text{Bi}^+]$.

2: A solution of $[\text{W}(\text{CO})_5(\text{thf})]$ (0.44 g, 1.11 mmol) in THF (100 mL) was added to a solution of **1** (1.0 g, 1.1 mmol) at 0 °C in THF (30 mL) and stirred for 3 h at 0 °C. After removal of the solvent the residues were extracted with petroleum ether (60 mL) and the extracts were filtered through a frit covered with kieselgur. Concentration of the solution, followed by cooling to –28 °C gave red crystals of **2**. M.p. 95–96 °C; elemental analysis (%) calcd for $\text{C}_{18}\text{H}_{22}\text{O}_{10}\text{Si}_2\text{W}_2\text{Bi}_2$: C 17.43, H 1.79; found: C 18.01, H 1.86; ^1H NMR (200 MHz, C_6D_6 , 25 °C): $\delta=0.17$ (s, 9H; CH_3), 1.94 ppm (s, 2H; CH_2); ^{13}C NMR (50 MHz, C_6D_6 , 25 °C, TMS): $\delta=1.26$ (s; CH_3), 191.10, 192.02, 200.04 ppm (s, CO); IR (petroleum ether): $\tilde{\nu}=2054, 1956\text{ cm}^{-1}$,

(C=O); MS (CI, NH₃): *m/z* (%): 1239 (8) [*M*⁺], 1152 (25) [*M*⁺ – R], 943 (18) [R₂BiW₂(CO)₁₀]⁺, 707 (100) [R₂BiW(CO)₅]⁺, 324 (29) [W(CO)₅]⁺.

Received: December 21, 2001 [Z18424]

- [1] As a consequence of the spin–orbit coupling the 6p orbitals split into one p(1/2) and two p(3/2) orbitals. The former is spherically symmetric and like the 6s orbital stabilized by relativistic effects. In addition to the inert s electron pair there should be an inert p electron pair and Bi^{II} should be stable in the configuration 6s², 6p(1/2)², 6p(3/2)⁰: P. Pykkö, *Chem. Rev.* **1988**, 88, 563–594.
- [2] *Chemistry of Arsenic, Antimony and Bismuth*, (Ed.: N. C. Norman), Blackie Academic, London, **1998**.
- [3] a) N. Tokitoh, Y. Arai, R. Okazaki, S. Nagase, *Science* **1977**, 277, 78–80; b) N. Tokitoh, *J. Organomet. Chem.* **2000**, 611, 217–227; c) B. Twamley, C. D. Sofield, M. M. Olmstead, P. P. Power, *J. Am. Chem. Soc.* **1999**, 121, 3357–3367.
- [4] a) H. J. Breunig, R. Rösler, E. Lork, *Angew. Chem.* **1998**, 110, 3361–3363; *Angew. Chem. Int. Ed.* **1998**, 37, 3175–3177; b) G. Linti, W. Köstler, *Z. Anorg. Allg. Chem.* **2002**, 628, 63–66.
- [5] a) *The Chemistry of Inorganic Homo- and Heterocycles*, Vol. 2 (Eds.: I. Haiduc, D. Sowerby), Academic Press, London, **1987**; b) H. J. Breunig, R. Rösler, *Chem. Soc. Rev.* **2000**, 29, 403–410; c) A. Silvestru, H. J. Breunig, K. H. Ebert, R. Kaller, *J. Organomet. Chem.* **1995**, 501, 117–121.
- [6] a) K. H. Whitmire, *Adv. Organomet. Chem.* **1998**, 42, 1–145; b) J. Borm, L. Zsolnai, G. Huttner, *Angew. Chem.* **1983**, 95, 1018; *Angew. Chem. Int. Ed. Engl.* **1983**, 22, 977; c) H. Lang, O. Orama, G. Huttner, *J. Organomet. Chem.* **1985**, 291, 293–309; d) K. B. Dillon, V. C. Gibson, J. A. K. Howard, L. J. Sequeira, J. W. Yao, *Polyhedron* **1996**, 15, 4173–4177; e) D. Fenske, H. Schottmüller, *Z. Anorg. Allg. Chem.* **1998**, 624, 443–451.
- [7] a) G. Huttner, U. Weber, L. Zsolnai, *Z. Naturforsch. B* **1982**, 37, 707–710; b) A. M. Arif, A. H. Cowley, N. C. Norman, M. Pakulski, *J. Am. Chem. Soc.* **1985**, 107, 1062–1063; c) A. M. Arif, A. H. Cowley, N. C. Norman, M. Pakulski, *Inorg. Chem.* **1986**, 25, 4836–4840; d) W. J. Evans, S. L. Gonzales, J. W. Ziller, *J. Am. Chem. Soc.* **1991**, 113, 9880–9882; e) W. Clegg, N. A. Compton, R. J. Errington, G. A. Fischer, N. C. Norman, T. B. Marder, *J. Chem. Soc. Dalton Trans.* **1991**, 2887–2895.
- [8] R. E. Schulz, Dissertation, Universität Bremen, Shaker Verlag, Aachen, **1996**.
- [9] a) $\delta = 4.45$ ppm (CH₂); for the CH₃ groups several signals in the region $\delta = 0.07$ – 0.24 ppm are possible.
- [10] *c*(**1a**):*c*(**1b**) = 0.3 in the range from –15 to –80 °C, 0.95 at 5 °C, 2 at 25 °C. The value 0.3 is also observed for a solution of the solid prepared and analyzed at –60 °C. Equilibration occurs only above –15 °C.
- [11] X-ray structure analysis of **2** (C₁₈H₁₀Bi₂O₁₀Si₂W₂): *M*_r = 1240.20; crystal dimensions 0.5 × 0.4 × 0.35 mm³; monoclinic, space group C2/*c*, *a* = 22.809(5), *b* = 8.622(2), *c* = 18.381(4) Å, β = 124.20(3)°, *V* = 2.9897(12) nm³, *Z* = 4, ρ_{calc} = 2.755 Mg m^{–3}, μ = 19.529 mm^{–1}. A crystal was fixed on a glass fiber with Kel-F oil and measured on a STOE-IPDS at –100 °C. With graphite-monochromated MoK α radiation (0.71073 Å) 20417 reflections were measured (2.16 < θ < 26.06°). A total of 2863 reflections remained after averaging (*R*_{int} = 0.0732), and the structure was solved by direct methods. The refinements converged after an empirical (DIFABS) absorption correction at *wR*₂ = 0.0550 (refinement against *F*²) for all 20417 reflections and 160 variables (*R*₁ = 0.0218 for 2863 reflections with *I* > 2 σ (*I*)). Heavy atoms were refined anisotropically and the H atoms were refined with a riding model and a common isotropic temperature factor. Max./min. residual electron densities: 1.317/–0.842 e Å^{–3}. The structure solution and refinement was carried out using SHELX-97^[15] and the Diamond program was used for the graphical representation.^[16] CCDC-175881 (**2**) contains the supplementary crystallographic data for this paper. These data can be obtained free of charge via www.ccdc.cam.ac.uk/conts/retrieving.html (or from the Cambridge Crystallographic Data Centre, 12, Union Road, Cambridge CB2 1EZ, UK; fax: (+44) 1223-336-033; or deposit@ccdc.cam.ac.uk).

- [12] a) F. Calderazzo, R. Poli, G. Pelizzi, *J. Chem. Soc. Dalton Trans.* **1984**, 2365–2369; b) A. Kuczkowski, S. Schulz, M. Nieger, *Angew. Chem.* **2001**, 113, 4351–4353; *Angew. Chem. Int. Ed.* **2001**, 40, 4222–4225.
- [13] a) N. J. Holmes, W. Levason, M. Webster, *J. Organometal. Chem.* **1997**, 545–546, 111–115; b) R. E. Bachman, K. H. Whitmire, *Inorg. Chem.* **1995**, 34, 1542–1551.
- [14] G. Balazs, H. J. Breunig, E. Lork, *Z. Anorg. Allg. Chem.* **2001**, 627, 2666–2668.
- [15] G. M. Sheldrick, SHELX-97, Universität Göttingen, **1997**.
- [16] DIAMOND - Visual Crystal Structure Information System, CRYSTAL IMPACT, Postfach 1251, 53002 Bonn.

Remarkably Large Geometry Dependence of ⁵⁷Fe NMR Chemical Shifts**

Michael Bühl,* Frank T. Mauschick, Frank Terstegen, and Bernd Wrackmeyer

With the continuous improvement of NMR hardware and acquisition techniques, transition-metal NMR spectroscopy is losing much of its formerly exotic character. NMR spectra of nuclei with low NMR receptivity or large quadrupole moments, in compounds hitherto believed to pose insurmountable problems, can now be measured within reasonable time.^[1] One recent example is aqueous [Fe(CN)₅(NO)]^{2–} (**1**), the ⁵⁷Fe chemical shift $\delta(^{57}\text{Fe})$ of which was determined as $\delta = 2004$ ppm.^[1b] What is particularly noteworthy about this result is that this Fe nucleus is significantly shielded with respect to that of [Fe(CN)₆]^{4–} (**2**; $\delta = 2455$ ppm). Both anions are prominent textbook examples in coordination chemistry.^[2] Since an interpretation of this difference in ⁵⁷Fe nuclear magnetic shielding is not straightforward, we resorted to quantum-chemical calculations of these $\delta(^{57}\text{Fe})$ chemical shifts, which have been shown to be accessible with reasonable accuracy at suitable levels of density functional theory (DFT).^[3] Such computations are normally performed for isolated static molecules in their equilibrium geometry at 0 K. For **1** and **2**, such an approach initially afforded computed values, $\delta = 2254$ and 4120 ppm, respectively, which are in rather poor accord with the experimental data obtained in aqueous solution. For the highly charged tetraanion **2** in particular, the error of the DFT value with respect to experiment amounts to more than $\Delta\delta = 1600$ ppm. Evidently, interactions between the complex and the solvent must be taken into account.

[*] Dr. M. Bühl, Dipl.-Chem. F. T. Mauschick, Dr. F. Terstegen
Max-Planck-Institut für Kohlenforschung
Kaiser-Wilhelm-Platz 1, 45470 Mülheim an der Ruhr (Germany)
Fax: (+49) 208-306-2996
E-mail: buehl@mpi-muelheim.mpg.de
Prof. Dr. B. Wrackmeyer
Universität Bayreuth
Universitätsstrasse 30, 95440 Bayreuth (Germany)

[**] This work was supported by the Deutsche Forschungsgemeinschaft. M.B. thanks Prof. W. Thiel for his continuing support. Computations were performed on Compaq XP1000 and ES40 workstations at the MPI Mülheim.

We have recently suggested a computational protocol to model solvent and thermal effects on transition-metal chemical shifts.^[4] The procedure involves DFT-based Car–Parrinello molecular dynamics (CPMD) simulations of the metal complex in a periodic water box, and averaging of the δ values computed for a number of snapshots along the trajectory. For $\delta(^{51}\text{V})$ of vanadate species, relatively small differences between the equilibrium and the averaged values, δ_e and $\delta^{300\text{K}}$, respectively, have been obtained, on the order of a few dozen ppm. To test if such a dynamical approach would be able to describe larger effects, we now report a similar study of $\delta(^{57}\text{Fe})$ values of **1** and **2**, modeled in aqueous solution. Indeed, substantial thermal and solvent effects are obtained, which can be traced back to relatively modest variations in geometrical parameters.

As will be documented elsewhere,^[5] CPMD results for highly charged **2** were plagued by artifacts due to limited box sizes under the periodic boundary conditions. We therefore decided to adopt a dynamical approach without such periodicity, where the metal complex, described by a well-established DFT method, is placed into a large water cluster which is described by a suitable force field.^[6] Similar molecular dynamics simulations, usually with purely force-field based methods, are frequently used to study solvent effects.^[7] Initial simulations were performed for **2** and for $[\text{Fe}(\text{CO})_5]$ (**3**), the standard used in ^{57}Fe NMR spectroscopy, in the gas phase (that is without solvent and at pure DFT level). Figure 1 illustrates the evolution of the averaged magnetic

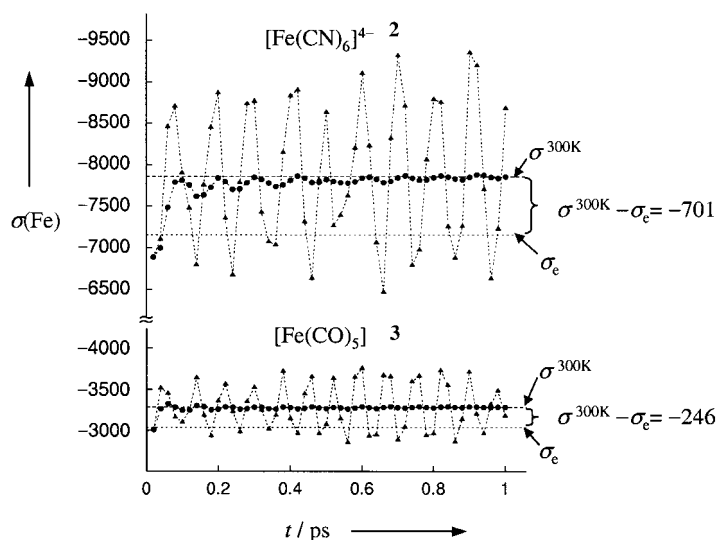


Figure 1. Absolute ^{57}Fe magnetic shielding constants $\sigma(^{57}\text{Fe})$ for $[\text{Fe}(\text{CO})_5]$ (**3**, bottom) and $[\text{Fe}(\text{CN})_6]^{4-}$ (**2**, top), computed for snapshots from a 1 ps MD simulation. Triangles: raw data; circles: running average values (average value up to this point); dashed lines: final average values $\sigma^{300\text{K}}$, dotted lines: equilibrium values σ_e .

shieldings^[8] over 1 ps. On going from the equilibrium value to the average at 300 K, a substantial deshielding is obtained for the ^{57}Fe nucleus in **3**, $\sigma^{300\text{K}} - \sigma_e = -246$, and an even larger one, $\sigma^{300\text{K}} - \sigma_e = -701$, for that in **2**. Thus, the chemical shift of **2** relative to that of **3** increases by 455 ppm upon thermal averaging in the gas phase.^[9] When **2** is placed in an aqueous

environment, in contrast, a similar averaging affords a substantial shielding of the metal nucleus, $\sigma^{300\text{K}} - \sigma_e = +1281$. The resulting δ values are collected in Table 1.

Table 1. ^{57}Fe chemical shifts δ (GIAO-B3LYP) and mean Fe–C distances r [Å] based on molecular dynamics (MD) simulations in vacuo and in aqueous solution.

Level of approximation	$[\text{Fe}(\text{CN})_6]^{4-}$ 2	$[\text{Fe}(\text{CN})_5(\text{NO})]^{2-}$ 1
δ_e (//QM-opt) ^[a]	4120	2254
$\delta^{300\text{K}}$ (//MD) ^[b]	4575	2466
$\delta^{300\text{K}}$ (//MD/ H_2O) ^[c]	2593	2076
$\delta_{\text{Experiment}}/\text{H}_2\text{O}$ ^[d]	2455	2004
r_e (QM-opt) ^[a]	1.973	1.955 ^[e]
$r^{300\text{K}}$ (MD) ^[b]	1.987	1.969 ^[e]
$r^{300\text{K}}$ (MD/ H_2O) ^[c]	1.924	1.943 ^[e]

[a] Isolated molecule, optimized at the BP86/AE1 level. [b] Average values from 1 ps simulations of the isolated molecule at about 300 K. [c] Average values from 1 ps simulations at about 300 K in water. [d] Guadimum counterions, from reference ^[1b]. [e] Only minute differences are found in the mean distances to the cyano groups *trans* and *cis* to the NO ligand.

Inspection of the molecular structures reveals that the deshielding and shielding effects of thermal averaging and solvation, respectively, are paralleled by noticeable elongation and shortening, respectively, of the average Fe–C bond length r (Table 1). As these changes amount to a few pm only, the ^{57}Fe magnetic shielding appeared to be very sensitive to this geometrical parameter. In fact, an explicit computation of the Fe–C bond-length/shielding derivative^[10] in isolated **2** afforded a value of $\partial\sigma(\text{Fe})/\partial r_{\text{FeC}} = -35\,100 \text{ ppm Å}^{-1}$.^[11] In absolute terms, this value is much larger than an experimental estimate for a related complex, $[\text{Co}(\text{CN})_6]^{3-}$, for which $\partial\sigma(\text{Co})/\partial r_{\text{CoC}} = -8000 \text{ ppm Å}^{-1}$ has been deduced^[12] from isotope effects on the metal chemical shift. Most of the gas-to-liquid shift simulated for **2**, $\Delta\delta = -1982 \text{ ppm}$, can thus be attributed to the concomitant shortening of the Fe–C bonds (compare MD and MD/ H_2O entries in Table 1) by $\Delta r = -0.063 \text{ Å}$, which, together with the bond-length/shielding derivative, would correspond to a value of $\Delta\delta = -2211$ (see below for a discussion of the direct solvent effect). The final, simulated $\delta(^{57}\text{Fe})$ value of 2593 ppm in aqueous solution is in reasonable, qualitative accord with that obtained from the experiment ($\delta = 2455 \text{ ppm}$).

Corresponding simulations were performed for the nitrosyl complex **1**, both in the gas phase and in water. The resulting trends in the computed $\delta(^{57}\text{Fe})$ values are qualitatively the same as those just described for **2**, but are much more attenuated (Table 1). For instance, the gas-to-liquid-shift is computed as $\Delta\delta = -390 \text{ ppm}$, about a fifth of that in **2**. The final, simulated $\delta(^{57}\text{Fe})$ value in aqueous solution ($\delta = 2076 \text{ ppm}$) is in good accord with that obtained from the experiment ($\delta = 2004 \text{ ppm}$). Likewise, the observed shielding on going from **2** to **1**, $\Delta\delta = -451 \text{ ppm}$,^[1b] is qualitatively reproduced, at $\Delta\delta = -545 \text{ ppm}$, in the simulations. The latter, apparently, afford a reasonable description of **1** and **2** in aqueous solution.

What is the structure of the solvation shells? Based on purely geometric criteria for the existence of an

O(water)–H···X(ligand) hydrogen bond,^[13] the average numbers of such hydrogen bonds in aqueous **1** and **2** is computed to be 7.4 and 15.3, respectively. The N atoms of the cyano ligands are the sole H-bond acceptors, and no such bonds are formed involving the nitrosyl group in **1**. As expected, the highly charged complex **2** attracts more water molecules than complex **1**.^[14] In both cases, these first solvation shells are not static on the ps time scale of the MD simulations, but show exchange between H-bonded and free water molecules. Interestingly, the direct effect of the coordinated water molecules on the values of $\delta(^{57}\text{Fe})$ is much lower than the aforementioned gas-to-liquid shifts. If, in the snapshots from the aqueous solutions, the water molecules are deleted from the NMR inputs (affording the isolated complexes, but in the geometries of the solvated ones), $\delta^{300\text{K}}$ values of 2448 and 2140 are obtained for **2** and **1**, respectively. These values are much closer to the corresponding MD/H₂O data than to the MD results of the isolated complexes (Table 1). The main effect of hydration on the value of $\delta(^{57}\text{Fe})$ is thus indirect, as it is the concomitant change of the geometrical parameters that governs the solvent effect. The same has been surmised in other cases, for instance for the value of $\delta(^{11}\text{B})$ in aqueous BH_3NH_3 .^[15, 16]

What is, finally, the origin of the stronger shielding of the ^{57}Fe nucleus in **1** relative to that in **2**? In both cases, the magnetic shielding is governed by huge paramagnetic contributions, σ^p . Analysis of the MOs of **2** (in an idealized O_h symmetric structure employing the averaged parameters from the simulation in water) reveals that strong contributions to σ^p can arise from the coupling of each of the triply degenerate HOMOs, through the action of the magnetic operator, with a suitable low-lying virtual MO.^[17] One such combination is depicted in the upper part of Figure 2. The situation is more complicated in **1**, since many of the orbital degeneracies are lifted due to the lower symmetry. For instance, the t_{2g} HOMO in **2** splits into b_1 and e MOs in **1**, with similar energy gaps for the respective, magnetically allowed transitions (Figure 2 bottom). In the nitrosyl complex, however, the metal d contribution to the MOs is significantly reduced with respect to that in **2**. This is consistent with reduced paramagnetic contributions and, thus, an apparent shielding of the ^{57}Fe nucleus in **1**. The lower geometry-sensitivity of the value of $\delta(^{57}\text{Fe})$ in **2** relative to that in **1** is probably also rooted in these reduced paramagnetic contributions.

In summary, we have modeled the ^{57}Fe chemical shifts of iron cyanide complexes in aqueous solution using a dynamical, combined QM/MM approach. To our knowledge, this is the first application of this methodology to transition metal NMR parameters, and complements related schemes based on CPMD simulations. Large thermal and solvation effects on $\delta(^{57}\text{Fe})$ are computed, on the order of 1000 ppm and more, which can be attributed to a remarkable sensitivity of the ^{57}Fe magnetic shielding constant to the Fe–C bond length. It is to be expected that this sensitivity should manifest itself in unusual temperature dependencies or isotope effects on the $\delta(^{57}\text{Fe})$ values of these complexes. Recently,^[1c] the isotope-induced chemical shift $^1\Delta^{12/13}\text{C}(^{57}\text{Fe})$ has been determined for the first time for ferrocene, and work in this direction is in progress for $[\text{Fe}(\text{CN})_6]^{4-}$ (**2**). Insights are obtained into the

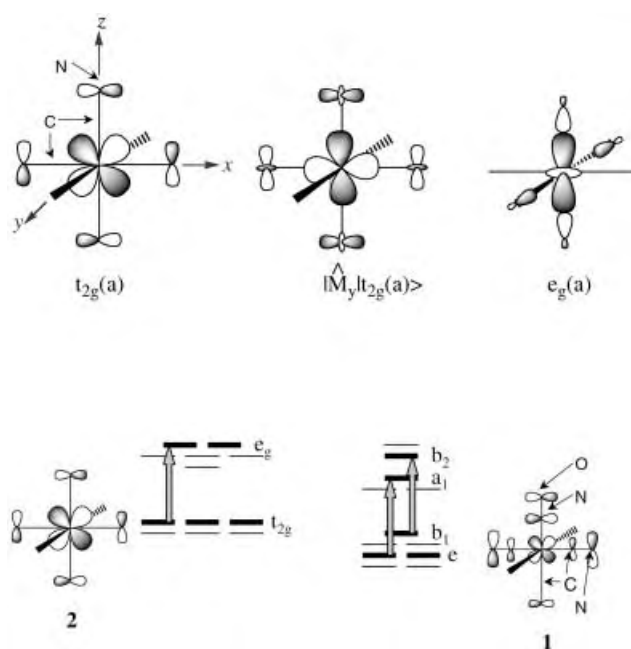


Figure 2. Top: Schematic representation of important MOs of **2**. Left: HOMO; middle: transformed HOMO after action of the angular momentum operator in y direction, \hat{M}_y , on it; right: low-lying virtual orbital suitable for overlap with the transformed HOMO. Bottom: Qualitative scheme of near-frontier MOs in **1** and **2**, including important magnetic transitions (gray arrows, only one for degenerate transitions shown); one of each t_{2g} and e orbitals is also sketched to illustrate the reduced metal d character in the latter.

structure and dynamics of the first solvation shell around the complexes and into the mechanism governing the trend of the values of $\delta(^{57}\text{Fe})$ upon ligand variation. The possibility to model thermal and solvent effects on NMR chemical shifts will certainly broaden the scope of applications beyond those already possible with computations for hypothetical, static molecules.

Received: December 17, 2001 [Z18401]

- [1] For instance: a) B. Wrackmeyer, A. Ayazi, H. E. Maisel, M. Herberhold, *J. Organomet. Chem.* **2001**, 630, 263–265; b) C. Janiak, T. Dorn, H. Paulsen, B. Wrackmeyer, *Z. Anorg. Chem.* **2001**, 627, 1663–1668; c) B. Wrackmeyer, O. L. Tok, M. Herberhold, *Organometallics* **2001**, 20, 5774–5776.
- [2] For instance: N. N. Greenwood, A. Earnshaw, *Chemistry of the Elements*, 2nd ed., Butterworth-Heinemann, Oxford, **1997**.
- [3] a) M. Bühl, *Chem. Phys. Lett.* **1997**, 267, 251–257; review: b) M. Bühl, M. Kaupp, V. G. Malkin, O. L. Malkina, *J. Comput. Chem.* **1999**, 20, 91–105.
- [4] M. Bühl, M. Parrinello, *Chem. Eur. J.* **2001**, 7, 4487–4494.
- [5] M. Bühl, F. T. Mauschick, unpublished results.
- [6] The Fe complexes were calculated at the RI-BP86/AE1 level, that is, using the gradient-corrected functionals of Becke (A. D. Becke, *Phys. Rev. A* **1988**, 38, 3098–3100) and Perdew (J. P. Perdew, *Phys. Rev. B* **1986**, 33, 8822–8824; J. P. Perdew, *Phys. Rev. B* **1986**, 34, 7406), the extended Wachters basis on Fe (A. J. H. Wachters, *J. Chem. Phys.* **1970**, 52, 1033–1036; P. J. Hay, *J. Chem. Phys.* **1977**, 66, 4377–4384), 6–31G* basis on the ligands, and making use of the resolution-of-identity (RI) approximation as implemented in the TURBOMOLE program (R. Ahlrichs, M. Bär, M. Häser, H. Korn, M. Kölmel, *Chem. Phys. Lett.* **1989**, 154, 165–169), together with a medium-sized grid (grid 3) and suitable auxiliary basis sets (K. Eichkorn, O. Treutler, H. Öhm, M. Häser, R. Ahlrichs, *Chem. Phys. Lett.* **1995**, 240, 283; K.

- Eichkorn, F. Weigend, O. Treutler, R. Ahlrichs, *Theor. Chem. Acc.* **1997**, 97, 119–124). Water was described by the CHARMM force field of the MSI-CHARMM 25b2 program (QUANTA98, Molecular Simulations, Inc., 9685 Scranton Rd. San Diego, CA 92121. The published results were generated by using the program CHARMM. This program is distributed by Molecular Simulations Inc.). For the coupling between QM and MM parts, a polarized embedding scheme was used (corresponding to model B in: D. Bakowies, W. Thiel, *J. Phys. Chem.* **1996**, 100, 10580–10594). MD simulations were performed by using the ChemShell program (P. Sherwood, A. H. deVries, *ChemShell - A Shell for Computational Chemistry*, CCLRC Daresbury Laboratory, **1999**, see <http://www.dl.ac.uk>) for NVT ensembles at approximately 300 K. For the aqueous species, the complexes were placed at the center of a spherical water cluster with a diameter of 30 Å, containing a total of 449 water molecules. After a short minimization (100 steps), the outmost layer to a depth of 5 Å from the surface was completely frozen to avoid evaporation of the minidroplet in the subsequent MD run. The aqueous species were simulated for 4 ps with a time step of 1 fs. Data sampling was started after the first 3 ps, which were taken for equilibration. In addition, the O–H distances in the water monomers were frozen with the SHAKE algorithm. Isolated complexes were simulated (after 0.5 ps of equilibration) for 1 ps with a time step of 0.5 fs.
- [7] See for instance: M. Orozco, F. J. Luque, *Chem. Rev.* **2000**, 100, 4187–4225.
- [8] Magnetic shieldings were computed for equilibrium geometries and for snapshots taken from the MD simulations at the GIAO-B3LYP level (see ref. [3a] for details), by employing a medium-sized grid and DZ basis, that is, the augmented Wachters basis on Fe and DZ basis (W. Kutzelnigg, U. Fleischer, M. Schindler in *NMR Basic Principles and Progress*, Vol. 23, Springer, Berlin, **1990**, pp. 165–262) on all other atoms. The use of the smaller DZ basis, rather than the larger basis II (that has been employed, for instance, in ref. [3a]) resulted in relatively small changes of the computed δ values, for instance by $\Delta\delta = 40$ ppm for **2**, but makes the large number of NMR computations for the snapshots more tractable. In the chemical-shift calculations, the 20 nearest solvent water molecules were included explicitly. Representative snapshots were taken every 20 fs. Chemical shifts are reported relative to $[\text{Fe}(\text{CO})_5]$ (**3**), optimized or simulated at the same respective level (σ_{c} and σ_{300K} values –3036.6 and –3282.3, respectively, see Figure 1). Neat **3** is the accepted standard in ^{57}Fe NMR spectroscopy. We have only performed a simulation for the gas phase, not for the liquid, which would be a formidable task in itself, but have used the averaged σ_{300K} value from the gas-phase simulation as a reference value also for the solution studies. It should be kept in mind that this procedure could introduce a systematic error for the computed gas-to-liquid shifts, and that more attention should be paid to the trends in the δ values between **1** and **2**, rather than to their actual values.
- [9] It should be noted that this value only represents the “classical” thermal effect and is not averaged over the zero-point motion. More than qualitative agreement with experiment is not to be expected anyway, due to the rather limited basis sets employed in the computations.
- [10] Obtained by performing NMR computations for a total of four static structures with elongated or compressed Fe–C distances (in steps of 0.02 Å) and a linear fit of the resulting σ values.
- [11] A similar value, 35200 ppm \AA^{-1} , is obtained when the larger basis II is used for the ligands.
- [12] C. J. Jameson, D. Rehder, M. Hoch, *J. Am. Chem. Soc.* **1987**, 109, 2589–2594; this empirical value has been qualitatively reproduced by using theoretical methods similar to those employed in the present study: N. Godbout, E. Oldfield, *J. Am. Chem. Soc.* **1997**, 119, 8065–8069.
- [13] In typical hydrogen-bonded systems containing O–H...O moieties, the O...O distance is smaller than 3.5 Å and the O–H bond is directed towards the second oxygen atom such that the O–H...O angle is larger than 140° (see for instance: E. Schwegler, G. Galli, F. Gygi, *Phys. Rev. Lett.* **2000**, 84, 2429–2432); the same criteria have been applied to the O–H...X moieties in **1** and **2**.
- [14] Counterions, which have not been considered explicitly, are likely to affect the fine structure of the solvation shell, but would probably not change the qualitative picture.

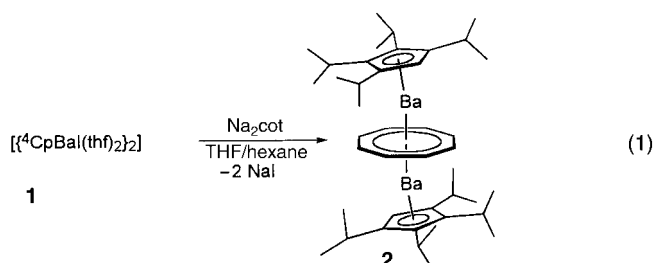
- [15] M. Bühl, T. Steinke, P. v. R. Schleyer, R. Boese, *Angew. Chem.* **1991**, 103, 1179–1180; *Angew. Chem. Int. Ed. Engl.* **1991**, 30, 1160–1161.
- [16] Simple optimization of **2** in a polarizable continuum, as has been done for BH_3NH_3 in ref. [15], also leads to Fe–C bond contraction, but gives much too short Fe–C bond lengths, below 1.90 Å.
- [17] For similar pictorial rationalizations of paramagnetic contributions see, for instance: Y. Ruiz-Morales, T. Ziegler, *J. Phys. Chem. A* **1998**, 102, 3970–3976.

A Triple-Decker Sandwich Complex of Barium

Helmut Sitzmann,* Marc D. Walter, and
Gotthelf Wolmershäuser

While triple-decker sandwich complexes are common in transition-metal chemistry,^[1–8] very few comparable complexes of main-group metals are known that are ionic and show strong bending with centroid-M-centroid angles of 134° ($[\text{Cp}_3\text{Ti}]^-$ ($\text{Cp} = \text{C}_5\text{H}_5$)^[9]), 116° ($[\text{Cp}_3\text{Cs}_2]^-$ ^[10]), 155/152° ($[(\text{C}_5\text{Me}_5)_3\text{Sn}_2]^{+11}$), or 124/130° ($[(\eta^6\text{-C}_7\text{H}_8)_2(\mu, \eta^5\text{-C}_5\text{Me}_5)\text{In}_2]^{+11}$). We showed several years ago that bending in sandwich complexes of the heavy alkaline-earth metals can be eliminated with extremely bulky alkylcyclopentadienyl ligands.^[12]

Herein we report on the first triple-decker complex of barium. At ambient temperature the half-sandwich complex $[\text{CpBa}(\text{thf})_2]$ (**1**; $\text{Cp} = \text{C}_5\text{H}(\text{CHMe}_2)_4$)^[13] reacts slowly with Na_2cot ($\text{cot} = \text{cyclooctatetraene}$) in THF/hexane (5:1) [Eq. (1)]. The colorless product is readily soluble in THF, soluble in toluene, and moderately soluble in pentane. ^1H and



^{13}C NMR spectra show one set of signals for two magnetically equivalent ^4Cp rings (see Experimental Section) and one signal for one cot ligand at $\delta = 6.02$ ppm (^1H) and $\delta = 95.3$ ppm (^{13}C). On exposure to air the microcrystalline compound turns intense yellow immediately, then orange-red within seconds, and finally pale yellow with a strong cot smell.

EI mass spectra show a signal corresponding to a dinuclear $[\text{CpBa}(\text{cot})\text{Ba}^+\text{Cp}]^+$ ion with the correct isotope pattern as well as signals for the fragments $[\text{CpBa}(\text{cot})\text{Ba}]^+$ and

[*] Prof. Dr. H. Sitzmann, Dipl.-Chem. M. D. Walter, Dr. G. Wolmershäuser
FB Chemie der Universität Kaiserslautern
Erwin-Schrödinger-Strasse, 67663 Kaiserslautern (Germany)
Fax: (+49) 631-205-4676
E-mail: sitzmann@chemie.uni-kl.de

[⁴CpBa]⁺. In a sealed capillary under argon the dibarium complex [⁴CpBa(COT)Ba⁴Cp] (**2**) displays a melting range of 224–227 °C. It remained unchanged even after the melt had been heated to 250 °C and could be sublimed above 215 °C in oil pump vacuum.

Heavy alkaline-earth element cot complexes [(cot)ML_n] (M = Ca, Sr, Ba, L = thf, pyridine^[14]) are known, but could not be crystallographically characterized. The analogous ytterbium complex [(cot)Yb(py)₃], however, could be structurally characterized by single-crystal X-ray diffraction.^[15]

The crystal structure of **2**^[16] shows a centrosymmetric triple-decker sandwich complex with essentially planar C₅ and C₈

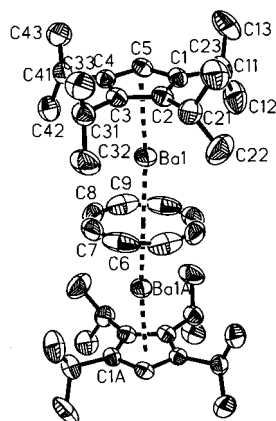


Figure 1. Crystal structure of **2**. Selected distances [Å] and angles [°]: Ba1–C1 2.945(4), Ba1–C2 2.982(4), Ba1–C3 2.993(4), Ba1–C4 2.977(4), Ba1–C5 2.927(4), Ba1–C6 2.998(4), Ba1–C7 2.994(5), Ba1–C8 3.014(4), Ba1–C9 3.000(5), Ba1A–C6 3.003(5), Ba1A–C7 3.015(6), Ba1A–C8 3.016(6), Ba1A–C9 3.007(5), Ba1–Cp_{centroid} 2.71, Ba1–cot_{centroid} 2.40, Cp_{centroid}–Ba1–cot_{centroid} 169.5; angles between ⁴Cp plane/C1–C11 0.7, ⁴Cp plane/C2–C21 3.1, ⁴Cp plane/C3–C31 2.1, ⁴Cp plane/C4–C41 0.2.

complexes of the general formula [(C₅Me₅)Ln(cot)Ln(C₅Me₅)] with a cot middle deck have been structurally characterized for the divalent lanthanides Sm,^[18] Yb, and Eu.^[19] They are bent with Cp_{centroid}–Sm–Cp_{centroid} = 149.3/148.9°, Cp_{centroid}–Eu–Cp_{centroid} = 147.2/149.5°, Cp_{centroid}–Yb–Cp_{centroid} = 161.2/159.5°. Triple-decker sandwich complexes of the trivalent lanthanides cerium, neodymium, and samarium of general formula [(cot'')Ln(cot'')Ln(cot'')] (cot'' = 1,4-(SiMe₃)₂ C₈H₆) could not yet be structurally characterized.^[20]

Experimental Section

Solid Na₂cot (75 mg, 0.5 mmol) was added to a solution of **1** (642 mg, 0.5 mmol) in a mixture of THF (20 mL) and hexanes (5 mL) and the suspension was stirred for two days at ambient temperature. Removal of the solvent in vacuo and extraction of the solid residue with toluene (20 mL), followed by filtration and evaporation gave an ivory powder

(190 mg, 0.22 mmol; 45%), which could be obtained as colorless single crystals suitable for X-ray diffraction from [D₆]benzene. C,H-analysis gave unsatisfactory results due to the extreme air sensitivity of **2**. ¹H NMR (400 MHz, 298 K, C₆D₆): δ = 6.02 (s, 8H; cot), 5.11 (s, 2H; ring-H (⁴Cp)), 2.94 (m, 4H; CHMe₂), 2.84 (m, 4H; CHMe₂), 1.24 (d, ³J(H,H) = 7.2 Hz, 12H; CH₃), 1.21 (d, ³J(H,H) = 7.2 Hz, 12H; CH₃), 1.16 (d, ³J(H,H) = 6.8 Hz, 12H; CH₃), 1.02 ppm (d, ³J(H,H) = 6.8 Hz, 12H; CH₃); ¹³C{¹H} NMR (100 MHz, C₆D₆): δ = 127.5 (s; ring-C), 123.4 (s; ring-C), 101.7 (dt; ring-CH (⁴Cp)), ¹J(C,H) = 155, ⁴J(C,H) = 5 Hz, 95.3 (d, ¹J(C,H) = 158 Hz; cot), 26.9 (CHMe₂), 26.6 (CHMe₂), 25.7 (CH₃), 25.3 (CH₃), 24.1 (CH₃), 23.7 ppm (CH₃); EI-MS (70 eV): *m/z* (%): 846.2 (6) [*M*⁺], 613.0 (74) [*M*⁺ – C₅H(CHMe₂)₄], 371.1 (100) [Ba{C₅H(CHMe₂)₄}⁺].

Received: March 18, 2002 [Z18915]

- [1] H. Werner, *Angew. Chem.* **1977**, *89*, 1–10; *Angew. Chem. Int. Ed. Engl.* **1977**, *16*, 1–10.
- [2] J. W. Lauher, M. Elian, R. H. Summerville, R. Hoffmann, *J. Am. Chem. Soc.* **1976**, *98*, 3218–3224.
- [3] a) W. Siebert, *Angew. Chem.* **1985**, *97*, 924–939; *Angew. Chem. Int. Ed. Engl.* **1985**, *24*, 953; b) W. Siebert, *Adv. Organomet. Chem.* **1993**, *35*, 187–210.
- [4] K. Jonas, W. Rüsseler, K. Angermund, C. Krüger, *Angew. Chem.* **1986**, *98*, 904–905; *Angew. Chem. Int. Ed. Engl.* **1986**, *25*, 927.
- [5] O. J. Scherer, *Acc. Chem. Res.* **1999**, *32*, 751–762.
- [6] M. Stephan, P. Müller, U. Zenneck, H. Pritzkow, W. Siebert, R. N. Grimes, *Inorg. Chem.* **1995**, *34*, 2058–2067.
- [7] P. L. Arnold, F. G. N. Cloke, P. B. Hitchcock, J. F. Nixon, *J. Am. Chem. Soc.* **1996**, *118*, 7630–7631.
- [8] G. E. Herberich, B. Ganter, *Inorg. Chem. Commun.* **2001**, *4*, 100–103.
- [9] D. R. Armstrong, A. J. Edwards, D. Moncrieff, M. A. Paver, P. R. Raithby, M.-A. Rennie, C. A. Russell, D. S. Wright, *J. Chem. Soc. Chem. Commun.* **1995**, 927.
- [10] S. Harder, M. H. Prosenc, *Angew. Chem.* **1996**, *108*, 101–103; *Angew. Chem. Int. Ed. Engl.* **1996**, *35*, 97–99.
- [11] A. H. Cowley, C. L. B. Macdonald, J. S. Silverman, J. D. Gorden, A. Voigt, *Chem. Commun.* **2001**, 175–176.
- [12] H. Sitzmann, T. Dezember, M. Ruck, *Angew. Chem.* **1998**, *110*, 3294–3296; *Angew. Chem. Int. Ed.* **1998**, *37*, 3114–3116.
- [13] H. Sitzmann, F. Weber, M. D. Walter, G. Wolmershäuser, *Organometallics*, submitted.
- [14] D. S. Hutchings, P. C. Junk, W. C. Patalinghug, C. L. Raston, A. H. White, *J. Chem. Soc. Chem. Commun.* **1989**, 973–974.
- [15] A. L. Wayda, I. Mukerji, J. L. Dye, R. D. Rogers, *Organometallics* **1987**, *6*, 1328–1332.
- [16] Crystal structure determination of 2·2C₆D₆: IPDS diffractometer with imaging system (Stoe), MoK_α radiation, λ = 71.073 pm, 2θ_{max} = 51.0°, 359 images with 0° ≤ φ ≤ 359° and Δφ = 1.0°, T = 293(2) K, crystal dimensions 0.48 × 0.40 × 0.16 mm³, monoclinic, space group P2(1)/c (no. 14), lattice parameters (293 K): a = 14.9481(14), b = 9.0286(6), c = 19.430(2) Å, β = 103.846(12)°, V = 2546.0(4) Å³, Z = 4, ρ_{calcd} = 1.307 g cm^{−3}, μ(MoK_α) = 15.69 cm^{−1}, absorption correction with the multi-scan method (MULABS/PLATON 98), transmission factors 0.495 to 0.773, structure solution: direct methods (SIR97), full-matrix least-squares refinement based on F_o² (SHELXL-97), 34 732 reflections, 4729 unique reflections, 261 parameters, R1(2821 F_o > 2σ(F_o)) = 0.0345, wR2(all) = 0.0781, residual electron density +0.688 to −0.662 e Å^{−3}, no disorder, CH and CH₃ groups have been refined as rigid groups with variable torsion angles (C–H = 0.96 Å, C–C–H and H–C–H 109.5°). Further details on the crystal structure investigation may be obtained from the Fachinformationszentrum Karlsruhe, 76344 Eggenstein-Leopoldshafen, Germany (fax: (+49)7247-808-666; e-mail: crysdata@fiz-karlsruhe.de), on quoting the depository number CSD-182290.
- [17] R. A. Williams, K. F. Tesh, T. P. Hanusa, *J. Am. Chem. Soc.* **1991**, *113*, 4843–4851.
- [18] W. J. Evans, R. D. Clark, M. A. Ansari, J. W. Ziller, *J. Am. Chem. Soc.* **1998**, *120*, 9555–9563.
- [19] W. J. Evans, M. A. Johnston, M. A. Greci, J. W. Ziller, *Organometallics* **1999**, *18*, 1460–1464.
- [20] P. Poremba, F. T. Edelman, *J. Organomet. Chem.* **1998**, *553*, 393–395.

Ion-Pair-Mediated Asymmetric Synthesis of a Configurationally Stable Mononuclear Tris(diimine)–Iron(II) Complex**

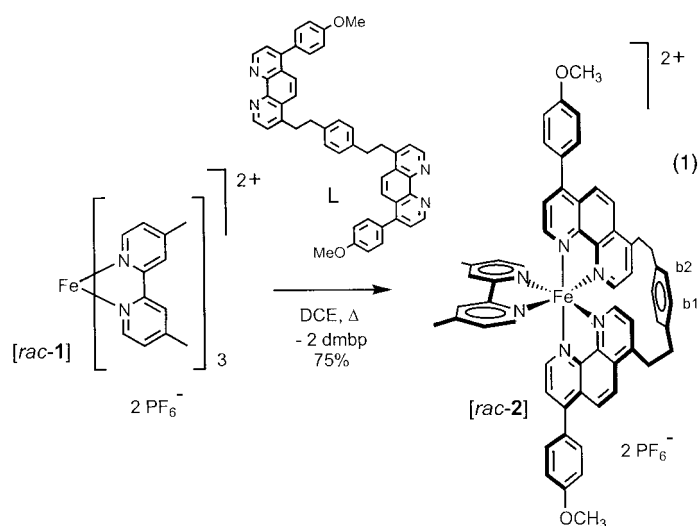
David Monchaud, Jonathan J. Jodry, Didier Pomeranc, Valérie Heitz, Jean-Claude Chambron, Jean-Pierre Sauvage, and Jérôme Lacour*

In memory of André Collet

Chiral mononuclear divalent tris(diimine) complexes of first-row transition metals—keystones of coordination chemistry—are notoriously known for their high chemical but low configurational stability.^[1] The Δ and Λ enantiomers—right- and left-handed propellers, respectively—can be isolated in good enantiomeric purity by efficient resolution procedures.^[1d, 2] However, once dissolved, these derivatives racemize rapidly when no other source of chiral information is present on the ligands^[3] or in the reaction medium.^[4]

Recently, the synthesis of a bis(1,10-phenanthroline) ligand L that forms octahedral complexes with a well-defined axis was reported: simple treatment of $[\text{Fe}(\text{dmbp})_3][\text{PF}_6]_2$ (**1**) [**1**][PF_6]₂, 1.0 equiv, dmbp = 4,4'-dimethyl-2,2'-bipyridine) with L (1.0 equiv) in refluxing 1,2-dichloroethane (DCE) afforded $[\text{Fe}(\text{dmbp})(\text{L})][\text{PF}_6]_2$ (**2**) [**2**][PF_6]₂ in high yield and purity [Eq. (1); for b1 and b2, see Figure 1].^[5] Here we report on the unusual configurational stability of **2**, which can be resolved by simple preparative thin-layer chromatography (TLC), and on its direct asymmetric synthesis by using TRISPHAT anions (see below) as noncovalent chiral auxiliaries (diastereomeric ratio, d.r. > 20:1).

The ease of synthesis of **2** and the rapidity of its formation led us to assume a high chemical stability for **2** [**2**][PF_6]₂. It was then debatable whether an improved chemical stability would also mean an increased configurational stability, so that the Δ and Λ enantiomers might be inert and separable from each other. Previously, the synthesis and resolution of the D_3 -symmetric tris(tetrachlorobenzenediolato)phosphate(v) anion (**3**), known as TRISPHAT, was reported.^[6] In association with mononuclear ruthenium(II) or iron(II)tris(diimine) com-



plexes, it is an efficient NMR chiral-shift, resolving, and asymmetry-inducing agent.^[7] It was therefore foreseen that anion **3** could behave as a NMR chiral-shift reagent for the structurally related complex **2** and possibly lead to its resolution.

Racemic complex **2** was studied in combination with a TRISPHAT salt. In an NMR tube, $[\text{Et}_4\text{N}][\Delta\text{-3}]$ ^[8] was added as a solid to a solution of **2** [**2**][PF_6]₂ in 10% $[\text{D}_6]\text{DMSO}/\text{CDCl}_3$ (Figure 1, spectra (a) and (b)). Efficient separation of the signals of **2** was achieved with small amounts of chiral-shift reagent (1.0–2.5 equiv). Protons H(b1) and H(b2) [see Equation (1)] were most easily monitored, and a rather large difference in chemical shift ($\Delta\delta_{\text{max}} \approx 0.15$ ppm) was observed. A 1:1 ratio of Δ and Λ enantiomers could be measured by direct integration of the respective signals. This 1:1 ratio of the diastereomers $[\Delta\text{-2}][\Delta\text{-3}]_2$ and $[\Lambda\text{-2}][\Delta\text{-3}]_2$ indicated a possible configurational stability of cation **2**. Indeed, it was recently shown that anions **3** act as effective asymmetry inducers on $[\text{Fe}(\text{dmbp})_3]^{2+}$ (**1**); when associated with the labile cationic guest, they control its configuration with high diastereoselectivity (d.r. > 49:1 in CDCl_3 in favor of $[\Delta\text{-1}][\Delta\text{-3}]_2$).^[7b] Two hypotheses could then explain the lack of asymmetric induction observed in the NMR titration experiment (Figure 1, spectrum (b)): poor chiral recognition by **3** or high configurational stability of **2**.

We thus decided to attempt an ion-pair chromatographic resolution, as the physical separation of ion pairs $[\Delta\text{-2}][\Delta\text{-3}]_2$ and $[\Lambda\text{-2}][\Delta\text{-3}]_2$ would prove the second hypothesis to be correct.^[9] Under previously reported conditions,^[7d, e] solutions of [cinchonidinium][$\Delta\text{-3}$] (2.5 equiv) in acetone and of **2** [**2**][PF_6]₂ in CH_2Cl_2 were prepared, mixed, and adsorbed on silica gel plates. Development by elution with CH_2Cl_2 showed a much reduced affinity of salts **2** [**2**][$\Delta\text{-3}$]₂ for silica gel, as they were retained to a much lesser extent than the PF_6^- precursor ($R_f \approx 0$).^[10] Two well-separated bands were obtained ($R_f \approx 0.94$ and 0.84 in analytical TLC), abraded from the glass

[*] Prof. J. Lacour, D. Monchaud, J. J. Jodry
Département de Chimie Organique
Université de Genève
quai Ernest Ansermet 30, 1211 Genève 4 (Switzerland)
Fax: (+41) 22-328-73-96
E-mail: jerome.lacour@chiorg.unige.ch

D. Pomeranc, Dr. V. Heitz, Dr. J.-C. Chambron,^[†] Dr. J.-P. Sauvage
Laboratoire de Chimie Organo-Minérale
UMR CNRS n° 7513, Faculté de Chimie
Institut Le Bel, Université Louis Pasteur
4, rue Blaise-Pascal, 67070 Strasbourg-Cedex (France)

[†] Present address:
Université de Bourgogne
Faculté des Sciences Gabriel, LIMSAG (UMR 5633)
6, Boulevard Gabriel, 21100 Dijon (France)

** We are grateful for financial support of this work by the Swiss National Science Foundation, the Federal Office for Education and Science (COST D11), the Fondation de Famille Sandoz (JL), the EC, the CNRS, and the MENRT (DP).

Supporting information for this article is available on the WWW under <http://www.angewandte.org> or from the author.

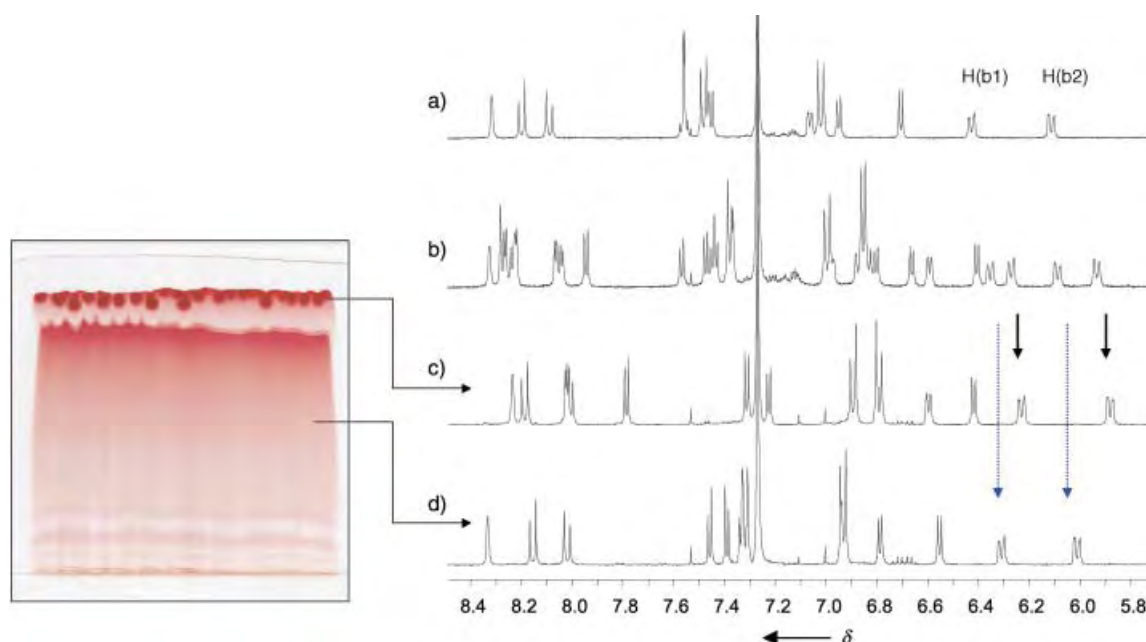


Figure 1. Ion-pair chromatographic resolution of $[rac-2][PF_6]_2$ with [cinchonidinium][$\Delta-3$]. 1H NMR spectra ($\delta = 8.50$ – 5.75) in 10% $[D_6]DMSO/CDCl_3$ of a) $[rac-2][PF_6]_2$; b) $[rac-2][PF_6]_2$ + 2.5 equiv of $[Et_4N][\Delta-3]$, d.r. = 1:1; c) $[\Delta-2][\Delta-3]_2$, d.r. > 49:1; d) $[\Lambda-2][\Delta-3]_2$, d.r. > 49:1.

surface, and stirred in CH_2Cl_2 . The resulting suspensions were filtered and concentrated in vacuo. The 1H NMR spectra revealed two completely different sets of signals corresponding to the resolved Λ and Δ enantiomers of the cation **2** (Figure 1, spectra (c) and (d)). Pure separated diastereomeric ion pairs $[\Delta-2][\Delta-3]_2$ and $[\Lambda-2][\Delta-3]_2$ were thus obtained in good chemical yields (48 and 45%, respectively). A circular dichroism (CD) spectrum of the more strongly eluted fraction (CH_2Cl_2 , ca. $5 \cdot 10^{-6} M$) revealed strong exciton coupling in the $\pi-\pi^*$ region ($\Delta\epsilon_{270} = +73$, $\Delta\epsilon_{300} = -101 M^{-1} cm^{-1}$) and the visible metal-to-ligand charge transfer (MLCT) transitions also showed opposite Cotton effects ($\Delta\epsilon_{479} = -16$, $\Delta\epsilon_{553} = +18 M^{-1} cm^{-1}$). The CD spectrum of the less strongly eluted diastereomer in the 235–600 nm region is essentially the mirror image. These spectra can be assigned to the Δ and Λ configurations of the cationic complex and demonstrate that compounds $[\Delta-2][\Delta-3]_2$ and $[\Lambda-2][\Delta-3]_2$ are the more and less strongly eluted ion pairs, respectively.^[11] We believe that the unusual configurational stability of **2**, evidenced by the 1H NMR spectra shown in Figure 1, is attributable to the bis-bidentate nature of **L**. Racemization of the iron(II) complex implies a complete rearrangement of the system with several decoordination and recoordination steps that result, in particular, in the inversion of the helix formed by **L** within **2**.^[5, 12]

Asymmetric synthesis of configurationally stable mononuclear coordination complexes has recently been the subject of much attention; the classical strategy is the introduction of stereogenic elements on the ligands, which then control—by intramolecular diastereoselective interactions—the configuration around the octahedral metal center.^[3, 13] Temporary covalent interactions between a chiral medium (sugars) and designed achiral ligands can also be used and lead to good selectivities, as shown recently by Shinkai et al.^[14] Having demonstrated the configurational stability of complex **2**, we

reasoned that its asymmetric synthesis could be also possible by using TRISPHAT anions (**3**) as chiral auxiliaries.^[15] We imagined that the configurational ordering induced by anions **3** on the labile $[Fe(dmbp)_3]^{2+}$ precursor **1** could be partially or fully transferred to complex **2** during synthesis. Treatment of a solution of $[1][\Delta-3]_2$ in refluxing CD_2Cl_2 [d.r. 7.25:1 in favor of the homochiral ion pair (1H NMR)^[16]] with **L** (0.94 equiv) afforded the desired complex $[2][\Delta-3]_2$ in quantitative yield. Excellent diastereoselectivity (d.r. > 20:1) was obtained, as a single set of signals corresponding to those of diastereomer $[\Delta-2][\Delta-3]_2$ could be observed in the 1H NMR spectrum of the crude reaction mixture (Figure 2, spectrum (c)).^[17] To our knowledge, this is the first example of high selectivity in the asymmetric synthesis of a stable coordination complex by using diastereoselective interactions restricted to intermolecular forces.

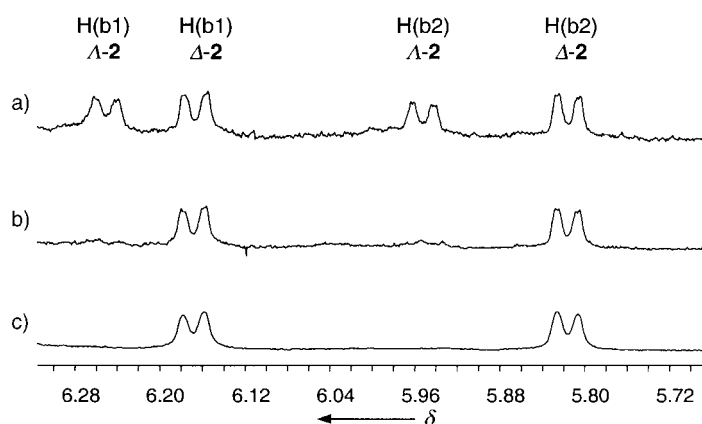
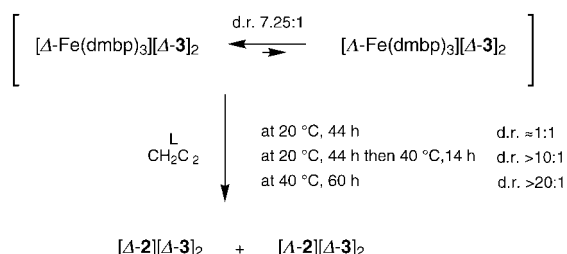


Figure 2. 1H NMR spectra ($\delta = 6.30$ – 5.68) in 10% $[D_6]DMSO/CDCl_3$ of the crude reaction mixture $[1][\Delta-3]_2 + L$. a) After 44 h at $20^\circ C$, d.r. \approx 1:1; b) after 44 h at $20^\circ C$ and 14 h at reflux, d.r. > 10:1; c) after 60 h at reflux, d.r. > 20:1.

It was then of interest to determine the origin—kinetic or thermodynamic—of the selectivity, especially since its value (d.r. > 20:1) is higher than the asymmetric induction of anions **3** on **1** (d.r. = 7.25:1). Several studies were therefore performed to determine the nature of the control. First, pure heterochiral complex $[A-2][A-3]_2$, isolated by chromatographic resolution, was heated to reflux in CD_2Cl_2 , and complete transformation into the homochiral diastereomer $[A-2][A-3]_2$ was observed after 18 h.^[18] Under similar conditions, no change was monitored for solutions of complex $[A-2][A-3]_2$. These results seemed to indicate thermodynamic control, as the high diastereoselectivity of the synthetic reaction could result from equilibration of the diastereomers at elevated temperature. To test this hypothesis, the asymmetric synthesis was attempted again at room temperature (20 °C) rather than at reflux (40 °C). A rather long reaction time (44 h) was required to achieve replacement of two dmbp ligands by L, and the resulting $[2][A-3]_2$ salt was obtained with essentially no selectivity (Scheme 1; d.r. \approx 1:1, Figure 2, spectrum (a)).



Scheme 1.

When the reaction was carried out for 44 h at 20 °C and then 14 h at 40 °C, a high selectivity was again observed in favor of the homochiral complex $[A-2][A-3]_2$ (d.r. > 10:1, Figure 2, spectrum (b)). All these experiments seem to indicate that the reactions performed at room temperature lead to a poor diastereoselectivity under kinetic control, and that heating is required to induce a high degree of configurational ordering under thermodynamic control. The selectivity of the reaction probably results from the preferred homochiral association of three-bladed propellers **2** and **3**.

In conclusion, we have shown that the configurational stability of a tris(diimine)–iron(II) complex can be unusually high for a carefully designed tetradentate ligand and that its resolution and asymmetric synthesis is feasible by using TRISPHAT anions as noncovalent chiral auxiliaries.

Received: December 6, 2001 [Z18336]

- [1] For tris(diimine)–iron(II) complexes, typical inversion barriers are in the range of 20–28 kcal mol^{−1}: a) R. G. Wilkins, *Kinetics and Mechanism of Reactions of Transition Metal Complexes*, 2nd ed., VCH, Weinheim, **1991**; b) L. Seiden, F. Basolo, H. M. Neumann, *J. Am. Chem. Soc.* **1959**, *81*, 3809–3813; c) F. M. Van Meter, H. M. Neumann, *J. Am. Chem. Soc.* **1976**, *98*, 1388–1394; d) A. Yamagishi, *Inorg. Chem.* **1986**, *25*, 55–57.
- [2] F. P. Dwyer, E. C. Gyarfas, *J. Proc. R. Soc. N. S. W.* **1950**, *83*, 263–265; A. Yamagishi, M. Soma, *J. Chem. Soc. Chem. Commun.* **1981**, 539–540.
- [3] J.-L. Pierre, *Coord. Chem. Rev.* **1998**, *178–180*, 1183–1192; A. von Zelewsky, *Coord. Chem. Rev.* **1999**, *190–192*, 811–825; U. Knof,

- A. von Zelewsky, *Angew. Chem.* **1999**, *111*, 312–333; *Angew. Chem. Int. Ed.* **1999**, *38*, 302–322; A. von Zelewsky, O. Mamula, *J. Chem. Soc. Dalton Trans.* **2000**, 219–231.
- [4] S. Kirschner, N. Ahmad, C. Munir, R. J. Pollock, *Pure Appl. Chem.* **1979**, *51*, 913–923; S. Kirschner, I. Bakkar, *Coord. Chem. Rev.* **1982**, *43*, 325–335; S. Kirschner, T. Gish, U. Freeman, Jr., *ACS Symp. Ser.* **1994**, *565*, 303–307; K. Nakashima, S. Shinkai, *Chem. Lett.* **1994**, 1267–1270.
- [5] D. Pomeranc, J.-C. Chambron, V. Heitz, J.-P. Sauvage, *C. R. Acad. Sci. Ser. IIC* **2001**, *4*, 197–200; D. Pomeranc, V. Heitz, J.-C. Chambron, J.-P. Sauvage, *J. Am. Chem. Soc.* **2001**, *123*, 12215–12221.
- [6] J. Lacour, C. Ginglinger, C. Grivet, G. Bernardinelli, *Angew. Chem.* **1997**, *109*, 660–662; *Angew. Chem. Int. Ed. Engl.* **1997**, *36*, 608–609; J. Lacour, C. Ginglinger, F. Favarger, *Tetrahedron Lett.* **1998**, 4825–4828.
- [7] a) J. Lacour, C. Ginglinger, F. Favarger, S. Torche-Halldimann, *Chem. Commun.* **1997**, 2285–2286; b) J. Lacour, J. J. Jodry, C. Ginglinger, S. Torche-Halldimann, *Angew. Chem.* **1998**, *110*, 2522–2524; *Angew. Chem. Int. Ed.* **1998**, *37*, 2379–2380; c) J. Lacour, C. Goujon-Ginglinger, S. Torche-Halldimann, J. J. Jodry, *Angew. Chem.* **2000**, *112*, 3830–3832; *Angew. Chem. Int. Ed.* **2000**, *39*, 3695–3697; d) J. Lacour, S. Torche-Halldimann, J. J. Jodry, C. Ginglinger, F. Favarger, *Chem. Commun.* **1998**, 1733–1734; e) D. Monchaud, J. Lacour, C. Coudret, S. Fraysse, *J. Organomet. Chem.* **2001**, *624*, 388–391.
- [8] Prepared in a similar manner to $[Bu_4N][A-3]$: H. Ratni, J. J. Jodry, J. Lacour, E. P. Kündig, *Organometallics* **2000**, *19*, 3997–3999.
- [9] N. C. Fletcher, F. R. Keene, *J. Chem. Soc. Dalton Trans.* **1999**, 683–690; T. J. Rutherford, P. A. Pellegrini, J. Aldrich-Wright, P. C. Junk, F. R. Keene, *Eur. J. Inorg. Chem.* **1998**, 1677–1688; T. J. Rutherford, F. R. Keene, *J. Chem. Soc. Dalton Trans.* **1998**, 1155–1162, and references therein.
- [10] J. Lacour, S. Barchéath, J. J. Jodry, C. Ginglinger, *Tetrahedron Lett.* **1998**, *39*, 567–570.
- [11] A. J. McCaffery, S. F. Mason, J. Norman, *J. Chem. Soc. A* **1969**, 1428–1441; R. Kuroda, Y. Saito, in *Circular Dichroism: Principles and Applications* (Eds.: K. Nakanishi, N. Berova, R. W. Woody), Wiley, New York, **1994**, pp. 217–258; M. Ziegler, A. von Zelewsky, *Coord. Chem. Rev.* **1998**, *177*, 257–300, and references therein.
- [12] O. Mamula, A. von Zelewsky, T. Bark, H. Stoeckli-Evans, A. Neels, G. Bernardinelli, *Chem. Eur. J.* **2000**, *6*, 3575–3585; H. Muerner, P. Belser, A. von Zelewsky, *J. Am. Chem. Soc.* **1996**, *118*, 7989–7994; H. Muerner, A. von Zelewsky, H. Stoeckli-Evans, *Inorg. Chem.* **1996**, *35*, 3931–3935.
- [13] K. Bernauer, H. Stoeckli-Evans, D. Hugli-Cleary, H. J. Hilgers, H. Abd-el-Khalek, J. Porret, J. J. Sauvain, *Helv. Chim. Acta* **1992**, *75*, 2327–2329; P. Belser, S. Bernhard, E. Jandrasics, A. von Zelewsky, L. De Cola, V. Balzani, *Coord. Chem. Rev.* **1997**, *159*, 1–8; H. Weizman, J. Libman, A. Shanzer, *J. Am. Chem. Soc.* **1998**, *120*, 2188–2189; D.-R. Ahn, T. W. Kim, J.-I. Hong, *J. Org. Chem.* **2001**, *66*, 5008–5011; S. G. Telfer, A. F. Williams, G. Bernardinelli, *Chem. Commun.* **2001**, 1498–1499, and references therein.
- [14] T. Mizuno, M. Takeuchi, I. Hamachi, K. Nakashima, S. Shinkai, *Chem. Commun.* **1997**, 1793–1794; T. Mizuno, M. Takeuchi, I. Hamachi, K. Nakashima, S. Shinkai, *J. Chem. Soc. Perkin Trans. 2* **1998**, 2281–2288; G. Nuding, K. Nakashima, R. Iguchi, T. Ishi-i, S. Shinkai, *Tetrahedron Lett.* **1998**, *39*, 9473–9476; T. Masuda, T. Nagasaki, S. Tamagaki, *Supramol. Chem.* **2000**, *11*, 301–314.
- [15] Chiral counterions can act as efficient asymmetric inducers on labile organometallic complexes: R. M. Yeh, M. Ziegler, D. W. Johnson, A. J. Terpin, K. N. Raymond, *Inorg. Chem.* **2001**, *40*, 2216–2217; J. Lacour, J. J. Jodry, D. Monchaud, *Chem. Commun.* **2001**, 2302–2303, and ref. [7b].
- [16] The diastereoselectivity induced by anions **3** on **1** is lower in CH_2Cl_2 than in $CHCl_3$ because of the higher polarity of dichloromethane: C. Reichardt, *Solvents and Solvent Effects in Organic Chemistry*, 2nd ed., VCH, Weinheim, **1988**.
- [17] A shorter reaction time (24 h) can be used, but to ensure the high diastereoselectivity and complete ligand exchange (see below), a prolonged reaction time (60 h) is best.
- [18] At room temperature in CD_2Cl_2 , no such epimerization was observed by ¹H NMR spectroscopy.

Fabricating Microarrays of Functional Proteins Using Affinity Contact Printing**

Jean Philippe Renault, André Bernard, David Juncker, Bruno Michel, Hans Rudolf Bosshard, and Emmanuel Delamarche*

Phenomena involving the binding between biomolecules are ubiquitous in biology and are essential for cell growth, signal transmission, and immune defense. In the latter system, the binding between antibody and antigen has already been exploited technologically to perform affinity purifications on columns and immunoassays on surfaces.^[1] Recently, the fabrication of microarrays of proteins which require the immobilization of a large number of receptors on a surface have fueled the invention of novel patterning techniques such as pin-spotting and drop-on-demand.^[2] Microarrays of proteins may find utility in proteomics, immunoassays, or for screening libraries of (bio)chemicals. It is at present not clear which patterning method will be the one best suited to pattern proteins on surfaces, but classical lithography does not seem capable of fabricating microarrays of proteins. Soft lithography^[3] offers the possibility of manipulating proteins and other biomolecules by printing them from a micropatterned stamp to a surface^[4] or by depositing them from a liquid using microfluidic networks (μ FNs).^[5] Affinity microcontact printing (α CP)^[6] is a refined soft-lithographic technique that uses an elastomeric stamp made of polydimethylsiloxane (PDMS) and derivatized with binding biomolecules to extract corresponding binding partners from an impure, dilute source for placing them on a surface with spatial control.

Herein, we describe, by using one particular example, how specific binding between biomolecules provides a unique opportunity to make use of self-assembly processes in technology: we propose different variants of α CP to pattern surfaces with ensembles of biomolecules where the pattern on the affinity stamp (α -stamp) is not determined by its topography but by the position of various proteins covalently linked to a planar α -stamp (Figure 1). This modified surface enables the simultaneous capture of different target proteins on the α -stamp from a complex solution (Figure 1A). Thus, the capture step (Figure 1B) directs the assembly of an array of target molecules on the stamp (Figure 1C), which can be

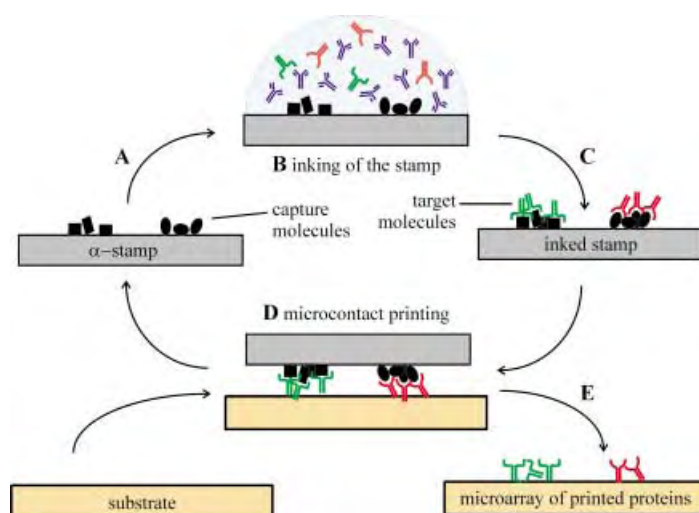


Figure 1. Microarrays of proteins on surfaces can be fabricated using an α -stamp derivatized with various capture sites that can extract target biomolecules from a complex solution and release them on a surface in a single microcontact-printing step. The α -stamp can be reused for several inking and printing cycles.

microcontact-printed onto a substrate in one step (Figure 1D). The α -stamp is recovered at the end of this process, and can be reused.^[6] We opted for protein antigens (entire immunoglobulin G) as capture molecules and antibodies as targets because these binding partners are very specific, can be readily conjugated with fluorescent markers, and of course play an important role in heterogeneous immunoassays.

Affinity stamps are prepared by immobilizing the capture molecules on an “activated stamp” that is reactive towards NH_2 groups of proteins. An activated stamp is made in three steps from a planar layer of PDMS (see the Supporting Information for experimental details). First, silanol groups are created at the PDMS surface using an O_2 plasma.^[7] These silanol groups are subsequently treated with 3-aminopropyltriethoxysilane to create an amino-derivatized surface. These amines are then treated with a homo-bisfunctional cross-linker (BS^3) to produce the activated surface.^[7] The stamps produced in this way are stable for several hours in a dry environment such as a dessicator, and can immobilize monolayers of proteins under mild chemical conditions.^[8, 9] Activated stamps are hydrophilic, with an advancing contact angle with water of approximately 30° , and therefore cannot be locally derivatized at high resolution with solutions of proteins by pin-spotting or ink-jet methods.^[2, 10] Our aim was to prepare α -stamps having arbitrary patterns with dimensions as small as a few micrometers, and we developed various methods to achieve this goal. The first method relies on coupling proteins to small areas of an activated stamp using microwells^[11] (μ -wells; Figure 2). The microwells are anisotropically etched through a 525- μm -thick Si wafer, and can be placed in contact with the activated stamp (Figure 2a). This contact is conformal and seals each microwell individually. Pipetting the desired amount of protein solution into all or a subset of the microwells determines the array of capture molecules formed on the α -stamp (Figure 2b, c). The hydrophobization of the top and bottom faces of the array of

[*] Dr. E. Delamarche, Dr. A. Bernard, D. Juncker, Dr. B. Michel
IBM Research
Zurich Research Laboratory
Säumerstrasse, 4, 8803 Rüschlikon (Switzerland)
Fax: (+41) 1-724-8952
E-mail: emd@zurich.ibm.com

Dr. J. P. Renault, Prof. H. R. Bosshard
Dept. of Biochemistry
University of Zurich
Winterthurerstrasse 190, 8057 Zurich (Switzerland)

[**] This work was partially supported by the Swiss National Science Foundation NFP 36 (grant 31.55308.98) and by the Swiss Federal Office for Education and Science within the BIOTECH European project BIOPATT (BIO4CT980536). We thank I. Caelen and H. Schmid for their help and discussions.

Supporting information for this article is available on the WWW under <http://www.angewandte.org> or from the author.

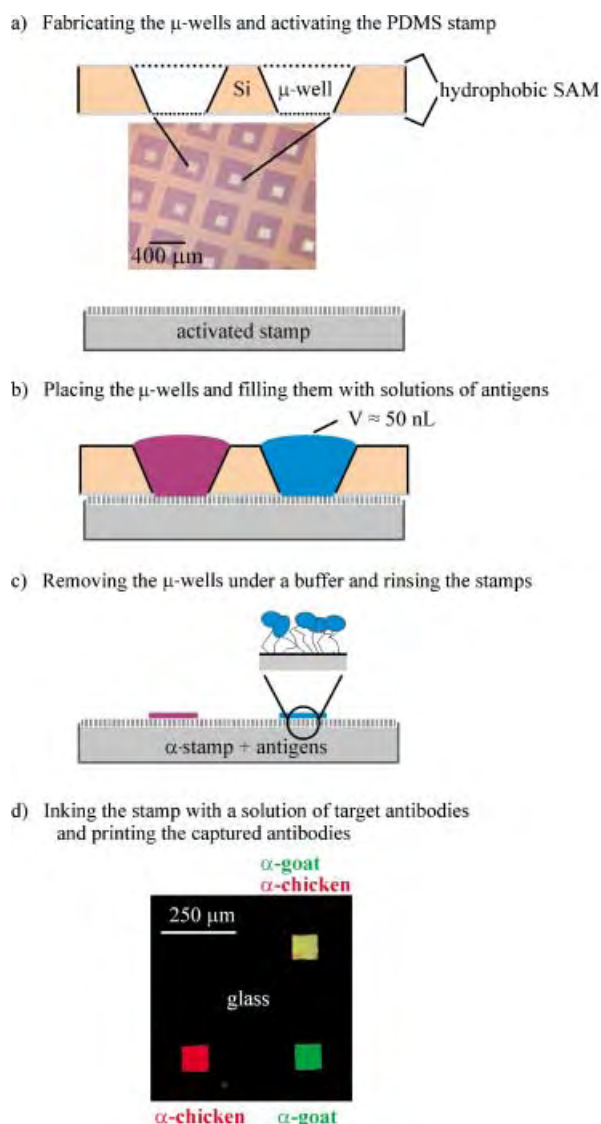


Figure 2. Preparation of a microarray of proteins using an α -stamp patterned with microwells. a) The microwells are formed in a Si wafer, and the PDMS stamp is derivatized with cross-linkers for proteins. b) The contact of the microwells with the activated stamp localizes the attachment of capture molecules from solution to the area of the stamp exposed in each microwell. c) After separating it from the microwells, rinsing and drying, the α -stamp is ready for use. d) The α -stamp in this example had an empty capture site and sites with covalently attached anti-chicken antigens, anti-goat antigens, and protein A. Inking the α -stamp consists of the binding of antibodies (here tagged fluorescently) from solution to their specific antigens on the surface of the stamp. After rinsing and drying the inked α -stamp, the antibodies can be printed onto a glass surface and visualized by fluorescence microscopy.

microwells by using a perfluorinated silane prevents leakage of liquid across the wells.^[12] In addition, the truncated pyramidal shape of the microwells makes it possible to fill them readily. The microwells used here can hold up to 50 nL of solution, and their drying could be controlled on the timescale needed for the coupling reaction. Affinity-capture sites based on the immobilization of protein A, and mouse, goat, and chicken antigens were patterned on an α -stamp by using $100 \times 100 \mu\text{m}^2$ wells (Figure 2d). This α -stamp is inked with a solution of anti-species antibodies (fluorescein iso-

thiocyanate labeled (FITC) anti-goat and tetramethylrhodamine B isothiocyanate linked (TRITC) anti-chicken antibodies) containing a large amount of bovine serum albumin (BSA). Each type of antibody binds in parallel to its specific antigen on the α -stamp during this inking step, and protein A captures both types of antibodies whereas BSA adsorbs elsewhere and prevents nonspecific adsorption on the α -stamp. The target molecules are transferred from the α -stamp to a glass slide during a printing step, and can be visualized as a result of their fluorescence label. The pattern in Figure 2d reveals the expected fluorescence pattern in which the target molecules are placed with high accuracy and contrast on their final substrate.

The preparation of the α -stamp is probably the most critical part of the α CP technique, and dispensing the solution of proteins into the microwells limits the practical resolution of α CP. This limitation can be circumvented by using microfluidic networks (μ FNs) to prepare the α -stamp. We take advantage of the sealing between the channels of a μ FN and a PDMS surface to deposit capture proteins on an intermediate stamp from the microchannels of the μ FN (Figure 3a). This stamp is then contacted with the activated stamp for 10 min. The capture antigens transfer and bind covalently to the surface of the activated stamp in this step (Figure 3b). We verified that the transfer was complete and that it did not alter the pattern by using fluorescently tagged antigens. The fluorescence microscopy images in Figure 3c reveal that the α -stamp prepared with this method can extract an ensemble of fluorescently tagged antibodies and then release them by printing onto a surface several times. The affinity site of line d in this example comprises protein A, for which we noticed that fewer FITC anti-goat antibodies were captured and printed after the third cycle. We speculate that during these consecutive cycles protein A captures both types of antibodies present in the ink with differing efficiencies. The high-resolution potential of μ FNs^[13] is conserved in the fabricated array of antibodies, and the investment in preparing the α -stamp is compensated by reusing it for several cycles of capture and release.^[6]

μ CP is an efficient and low-cost method for patterning proteins with submicrometer resolution.^[14] Since μ CP uses the deposition of proteins from bulk solution on stamps and prints them on a substrate, liquids can be handled simply by manual pipetting without the need for a particular dispensing device. α CP can be extended by using μ CP to form very high-resolution arrays of proteins in the following way. First, a layer of capture antigens is deposited from solution onto a hydrophobic PDMS stamp (Figure 4a). The contact between a patterned Si substrate and the inked stamp releases the proteins from the stamp to the Si surface in the areas of contact (Figure 4b).^[15] This operation is a subtractive transfer of proteins, and does not require structured PDMS stamps; it is therefore insensitive to mechanical deformations as can occur in conventional μ CP.^[16] The patterned antigens are transferred to an activated PDMS stamp in a printing step (Figure 4c). Repeating these steps with careful alignment enables the formation of ensembles of arrays on the α -stamp, each containing one type of capture protein (Figure 4d). The stability of the activating layer on the stamp means there is no

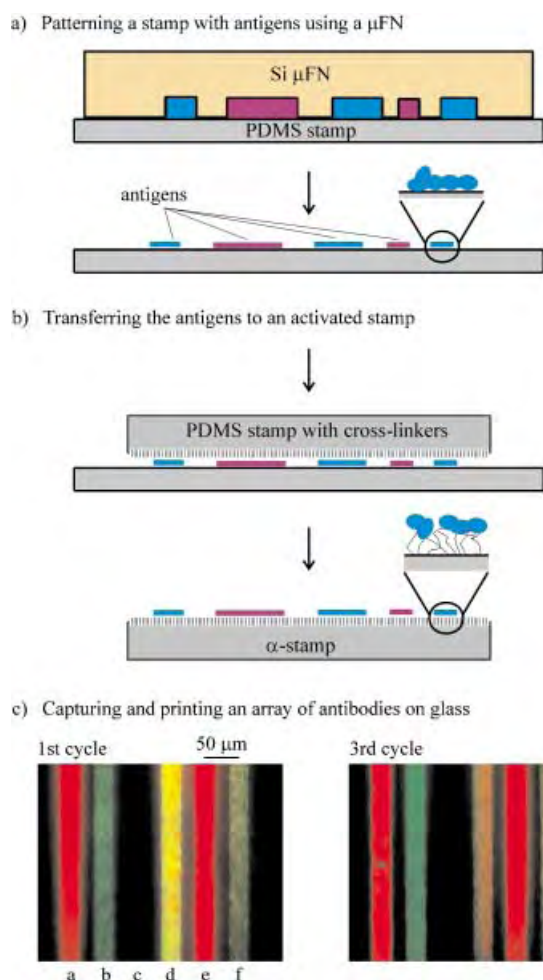


Figure 3. Patterning lines of proteins on a surface with an α -stamp prepared using a μ FN. The μ FN localizes the deposition of capture antigens on an intermediate, nonmodified PDMS stamp (a), which can then transfer and attach the proteins to an activated PDMS stamp (b). The α -stamp is used to capture fluorescently tagged antibodies, and print them as lines onto a glass surface (c). The captured molecules on the α -stamp were chicken IgGs (lines a and e), goat IgGs (lines b and f), protein A (line d), and mouse IgGs (line c). Inking this stamp was done by exposing it to a solution containing BSA (1%), FITC-anti-goat antibodies, and TRITC-anti-chicken antibodies. The fluorescence microscope images reveal that the capture was specific, and the release efficient in providing a high-resolution pattern of printed antibodies even after the α -stamp had been used several times.

need to reactivate the α -stamp between printing steps of the capture proteins if the overall process is shorter than about 2 h. The pattern on the glass substrate in Figure 5a involved two printing steps (done manually) to prepare the α -stamp, and one inking and printing cycle using the α -stamp to yield the "microarray". Specifically, two different antigens (IgGs) from goat and chicken were immobilized on an activated stamp, and used as antigens to extract their respective target antibodies simultaneously from a solution containing FITC-anti-goat and TRITC-anti-chicken antibodies. The captured antibodies were then printed onto the glass substrate in $3 \times 3 \mu\text{m}^2$ areas. This microarray has a density of approximately 10^4 spots of proteins per mm^2 with two types of proteins. The ability of the printed anti-goat antibodies to bind to goat antigens is seen in the AFM image of Figure 5b.

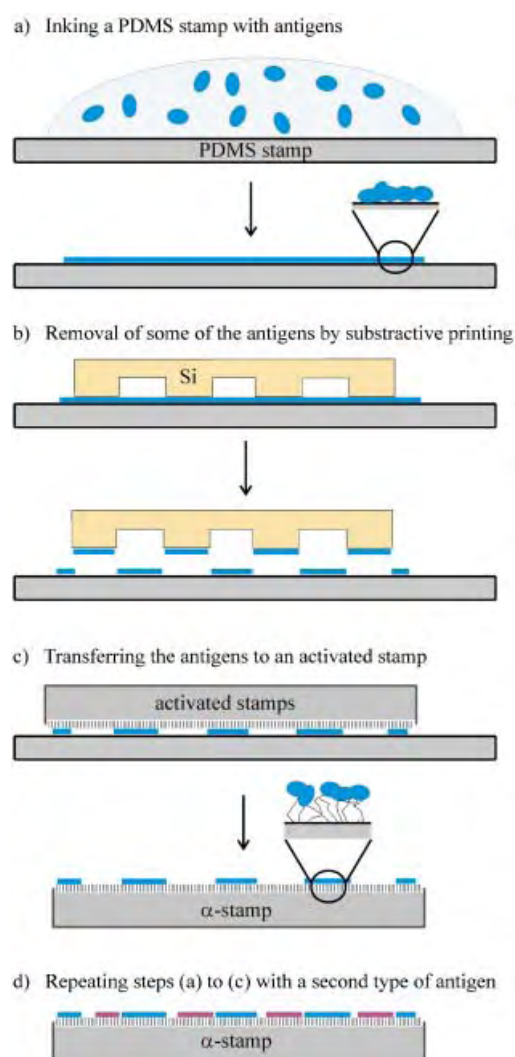


Figure 4. Preparation of an α -stamp by using the deposition of capture proteins from solution and subtractive μ CP. A layer of capture antigens is deposited from solution onto a PDMS stamp (a), and patterned by removing the antigens in some regions of the stamp by subtractive printing (b). The remaining capture antigens are transferred onto an activated stamp (c). Repeating these steps enables several arrays of capture proteins to be successively added to the α -stamp (d).

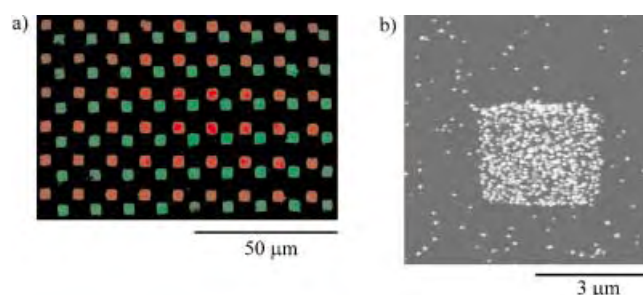


Figure 5. Arrays of anti-chicken antibodies and anti-goat antibodies printed using an α CP having 10^4 equivalent capture sites per mm^2 that consist of immobilized chicken and goat antigens. a) Fluorescence microscope image showing the placement of the TRITC-anti-chicken and FITC-anti-goat antibodies from a stamp onto a glass substrate. b) AFM image obtained on a spot of the array in which the printed anti-goat antibodies bound to Au-labeled goat antigens presented in solution. Detection of this binding was done by staining the Au labels with electroless-deposited silver particles of an average diameter of 80 nm.

The fluorescence data in our experiments indicated that the surface coverage of the final printed layer for each of the three patterning methods presented here is nearly equivalent and reaches about 60 % of the surface coverage obtained by direct deposition of the antibodies from solution. As already described for μ CP and α CP of proteins, the printing process does not compromise the binding efficiency of the printed antibody. This strategy might not be suitable for patterning a large number of different proteins on a surface. However, it can place a few different proteins as adjacent high-density arrays on a surface. Such arrays could find an application for high-throughput screening in which a large number of analytes could be spotted using a subset of the patterned areas. Another possibility for creating high-density immunoassays on planar surfaces is by performing surface immunoassays using many different analytes and capture sites, such as shown in Figure 5. The main limiting factor in using the prepared microarrays for diagnostic purposes could be misplacement of target molecules during the inking of the α -stamp. Such a misplacement, which may induce false positive reactions, can arise from cross-reactions of the target molecules with different capture proteins and/or from nonspecific adsorption on the α -stamp. The former is limited by biological specificity of affinity extraction. The latter can be limited by the systematic use of blocking agents such as BSA. Indeed, for the recognition of goat antigen by the printed array shown in Figure 5a, the recognition signal in the areas with printed anti-chicken antibodies was only 5 % of that in the areas with printed anti-goat antibodies.

In summary, we have illustrated how α CP can complement different patterning methods to produce repeatedly, and in parallel, high resolution arrays of proteins in three simple steps: 1) "inking", 2) rinsing, and 3) printing the stamp on the substrate. Since α -stamps carry the complementary pattern of binding partners specific to the target proteins on their surface, the proteins self-assemble into the predefined array on the stamp surface during inking in solution, and dissociate upon printing. Hence, the (re)production of the target protein arrays is fast and easy. The initial production of the α -stamp is a one-time burden only. We thus believe that the methodology presented is powerful and versatile, and should be useful in detection and fabrication strategies that are based on arrays of proteins.

Received: January 30, 2002
Revised: April 15, 2002 [Z18619]

- [1] *Immunassay* (Eds.: E. P. Diamandis, T. K. Christopoulos), Academic Press, San Diego, CA, **1996**.
- [2] *DNA Microarrays: A Practical Approach* (Ed.: M. Schena), Oxford University Press, Oxford, UK, **1999**.
- [3] a) Y. Xia, G. M. Whitesides, *Angew. Chem.* **1998**, *110*, 568–594; *Angew. Chem. Int. Ed.* **1998**, *37*, 550–575; b) G. M. Whitesides, E. Ostuni, S. Takayama, X. Jiang, D. E. Ingber, *Annu. Rev. Biomed. Eng.* **2001**, *3*, 335–373.
- [4] A. Bernard, E. Delamarche, H. Schmid, B. Michel, H. R. Bosshard, H. Biebuyck, *Langmuir* **1998**, *14*, 2225–2229.
- [5] E. Delamarche, A. Bernard, H. Schmid, B. Michel, H. Biebuyck, *Science* **1997**, *276*, 779–781.
- [6] A. Bernard, D. Fitzli, P. Sonderegger, E. Delamarche, B. Michel, H. R. Bosshard, H. Biebuyck, *Nat. Biotechnol.* **2001**, *19*, 866–869.

- [7] C. Donzel, M. Geissler, A. Bernard, H. Wolf, B. Michel, J. Hilborn, E. Delamarche, *Adv. Mater.* **2001**, *13*, 1164–1167.
- [8] S. C. Lin, F. G. Tseng, H. M. Huang, C. Y. Huang, C. C. Chieng, *Fresenius J. Anal. Chem.* **2001**, *371*, 202–208.
- [9] A. Bernard, H. R. Bosshard, *Eur. J. Biochem.* **1995**, *230*, 416–423.
- [10] a) G. MacBeath, S. L. Schreiber, *Science* **2000**, *289*, 1760–1763; b) H. Zhu, M. Bilgin, R. Bangham, D. Hall, A. Casamayor, P. Bertone, N. Lan, R. Jansen, S. Bidlingmaier, T. Houfek, T. Mitchell, P. Miller, R. A. Dean, M. Gerstein, M. Snyder, *Science* **2001**, *293*, 2101–2105.
- [11] a) J. Hyun, A. Chilkoti, *J. Am. Chem. Soc.* **2001**, *123*, 6943–6944; b) J. S. Hovis, S. G. Boxer, *Langmuir* **2001**, *17*, 3400–3405; c) U. Schobel, I. Coille, A. Brecht, M. Steinwand, G. Gauglitz, *Anal. Chem.* **2001**, *73*, 5172–5179.
- [12] D. Juncker, H. Schmid, A. Bernard, I. Caelen, B. Michel, N. de Rooij, E. Delamarche, *J. Micromech. Microeng.* **2001**, *11*, 532–541.
- [13] E. Delamarche, A. Bernard, H. Schmid, A. Bietsch, B. Michel, H. Biebuyck, *J. Am. Chem. Soc.* **1998**, *120*, 500–508.
- [14] A. Bernard, J. P. Renault, B. Michel, H. R. Bosshard, E. Delamarche, *Adv. Mater.* **2000**, *12*, 1067–1070.
- [15] Z. Yang, A. M. Belu, A. Liebmann-Vinson, H. Sugg, A. Chilkoti, *Langmuir* **2000**, *16*, 7482–7492.
- [16] A. Bietsch, B. Michel, *J. Appl. Phys.* **2000**, *88*, 4310–4318; M. Geissler, A. Bernard, A. Bietsch, H. Schmid, B. Michel, E. Delamarche, *J. Am. Chem. Soc.* **2000**, *122*, 6303–6304.

Au-Nanoparticle Nanowires Based on DNA and Polylysine Templates

Fernando Patolsky, Yossi Weizmann,
Oleg Lioubashevski, and Itamar Willner*

The assembly of ordered nanoparticle architectures is a challenging topic in nanotechnology directed to the construction of nanoscale devices.^[1] Within this broad subject, the conjugation of biomaterials and nanoparticles to yield ordered architectures is a promising route to tailor future sensing and catalytic devices, nanocircuitry, or nanodevices, for example transistors, and computing devices.^[2] DNA is an attractive biomaterial for use as a template in programmed nanoparticle structures. The ability to synthesize nucleic acids of predesigned shapes and composition, the versatile biocatalytic transformations that can be performed on DNA, for example, ligation, scission, or polymerization, enable "cut and paste" procedures to be carried out on the template DNA, thus enabling us to design and manipulate the DNA "mold". Furthermore, the association of metal ions to the DNA phosphate units, or the intercalation of transition-metal complexes or molecular substrates into the DNA provide a means to functionalize the DNA-template and to initiate further chemical transformations on the mold. Nanoparticle–DNA assemblies were organized by the hybridization of nucleic-acid-functionalized metal^[3] or semiconductor nano-

[*] Prof. I. Willner, F. Patolsky, Y. Weizmann, O. Lioubashevski
Institute of Chemistry
The Hebrew University of Jerusalem
Jerusalem 91904 (Israel)
Fax: (+972) 2-652-7715
E-mail: willner@vms.huji.ac.il

particles^[4] with a complementary DNA. Metal nanowires on a template λ -DNA were generated by the initial binding of Ag^+ ions to the DNA, followed by reduction of the ions to yield catalytic sites for the electroless clustering of Ag metal on the DNA. Individual wires with a width of around 50 nm were prepared by this method.^[5] A related approach was applied to grow Pd clusters on a λ -DNA template.^[6] Similarly, CdS-nanoparticles with a positively charged modifying layer were electrostatically attracted to DNA to form a quasi-1D nanoparticle structure.^[7] Here we report a new method to generate Au-nanoparticle wires by the intercalation of psoralen-functionalized Au nanoparticles into a double-stranded DNA, followed by the photochemical covalent attachment of the intercalator with the DNA template.

Amino psoralen (**1**) was covalently-linked to 1.4-nm Au nanoparticles functionalized with a single *N*-hydroxysuccinimide group (Nanoprobes, USA; Equation (1)). (TEM experiments indicate that 5–10% of the particles exhibit a larger diameter, up to 3 nm.)

The resulting intercalator-modified Au nanoparticle was then intercalated with a double-stranded poly A/poly T duplex, of approximately 900 nm length, and the resulting assembly was irradiated with a 12 Watt UV lamp, $\lambda > 360$ nm. Under these conditions, psoralen undergoes a photoinduced $2\pi+2\pi$ cycloaddition with the thymine residues, a process that leads to the covalent attachment of the intercalator to the DNA.^[8] The obtained DNA complex was then deposited on a freshly cleaved mica surface. Figure 1A shows the 3D AFM image of the resulting Au-nanoparticle wire. The imaged area of this wire has a length of around 600–700 nm (the wire extends beyond the imaged area) and a width of approximately 3.5–8 nm (estimated, taking into account the tip diameter, 12 nm, determined by SEM). The height of the nanowire in most of the wire domains is about 4 nm (Figure 1B). The height of 4 nm may be attributed to the intercalation of the Au nanoparticles in a helical mode along the double-stranded perimeter of the template DNA. A few of the wire domains reach a height up to about 8 nm (Figure 1C). These domains may originate from Au nanoparticles of larger sizes, as well as the possible bending or twisted superposition of the nanoparticle wire resulting from its deposition on the mica surface. The intercalated nanoparticles

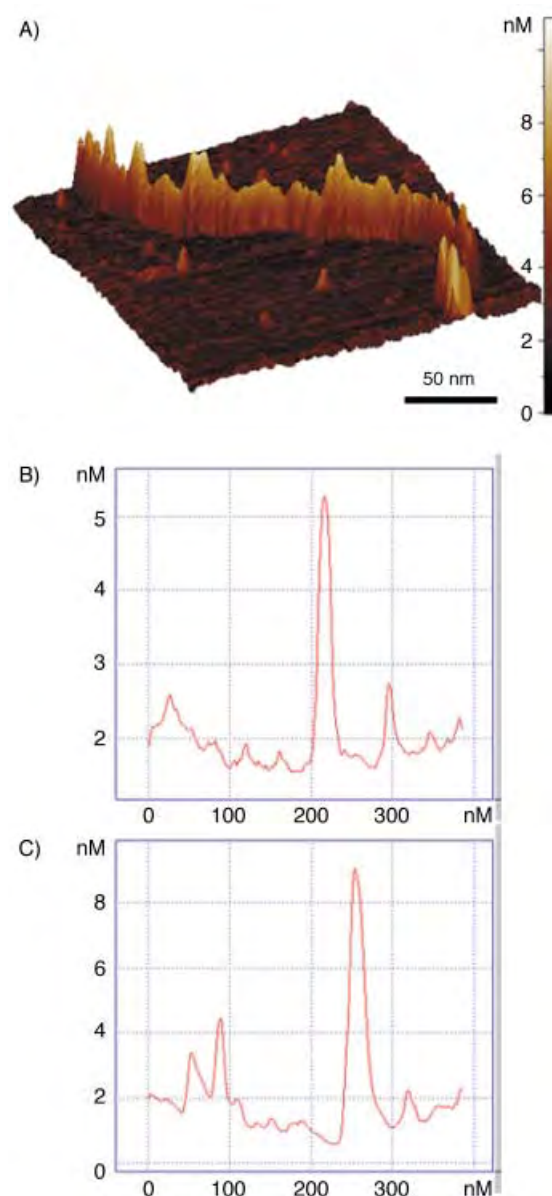
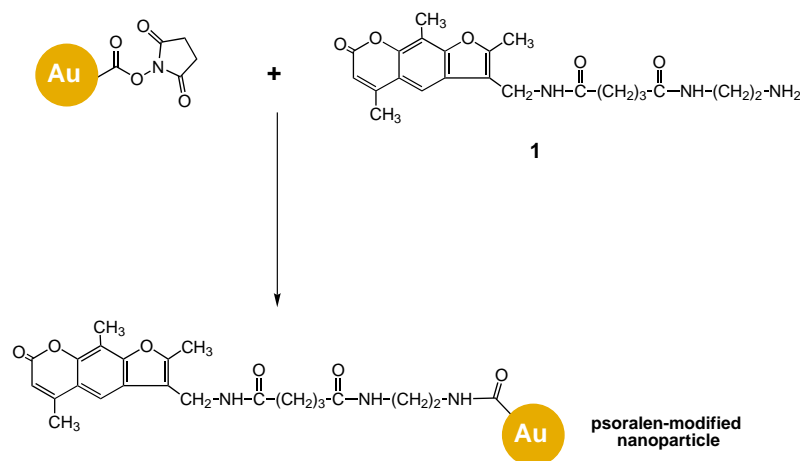


Figure 1. A) AFM image of an Au-nanoparticle wire in the poly A/poly T template. B) Cross-section of the Au-nanoparticle wire in a domain of lower height (high probability). C) Cross-section of the Au-nanoparticle wire in an area of higher height (low probability).



reveal a high-density structure in the template DNA. A similar procedure was employed to incorporate the **1**-functionalized Au nanoparticles into λ -DNA. We find that the Au-nanoparticle wires are formed, yet the density of the particles is substantially lower. Figure 2 shows the AFM image of a collection of λ -DNA templates with the incorporated Au nanoparticles. In contrast to the height observed for the Au nanoparticles incorporated into the poly A/poly T template, we find that the height of the nanoparticles incorporated into the λ -DNA, does not exceed 3.5 nm. This difference may be attributed

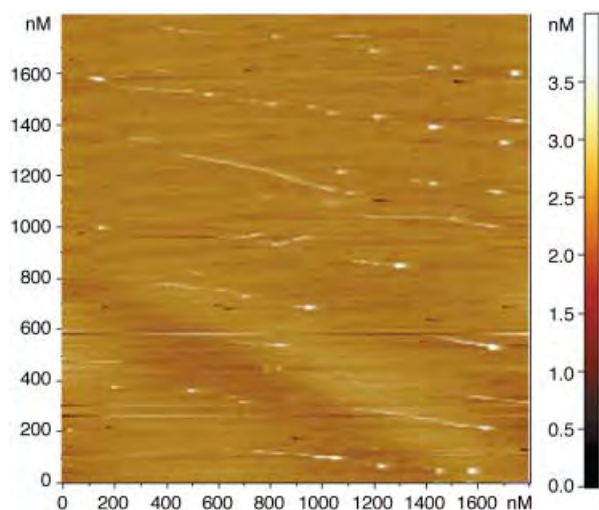


Figure 2. AFM image of Au nanoparticles incorporated in λ -DNA.

to the low-density coverage of the DNA by the particles that prevents the binding of particles on opposite sides of the surface-deposited DNA. It should be noted that the Au-nanoparticle-functionalized λ -DNA is structurally aligned on the mica surface. The alignment mechanism is not fully understood at present. Since we apply an Ar flow to dry the sample drop on the surface, it is plausible that the directional sample drying leads to the aligned structure.

A different approach to generate the Au-nanoparticle wires involves the chemical modification of poly-L-lysine with the Au nanoparticles functionalized with a single *N*-hydroxysuccinimide unit [Eq. (2)].

The deposition of the polylysine functionalized with the Au nanoparticles on a mica surface yields circular nanoparticle arrays. Figure 3 A shows the 3D structure of a circular nanowire that includes a dense assembly of Au nanoparticles. Most of the modified polylysine chains are assembled in a circular structure and no linear Au-nanoparticle wires were detected (Figure 3 B). Nonetheless, not all of the circles reveal a dense packing of the nanoparticles.

The generated circles on the mica surface reveal high stability; they are not washed off the surface with water, and they preserve their 3D structure for at least three months. Figure 3 C shows the histogram of the ring diameter of the Au-nanoparticle rings. The highest frequency is observed for rings with a diameter between 100 nm and 200 nm. A few rings reveal a small diameter of about 50 nm and some of the rings are substantially larger, around 650 nm. The polylysine employed in our study has a molecular weight of 52 000 with a dispersity of approximately 11 %. This information suggests that a polymer chain includes 231 ± 25 monomer units with an average length of about 92 ± 10 nm which implies that each of the Au-nanoparticle circles is generated by several inter-

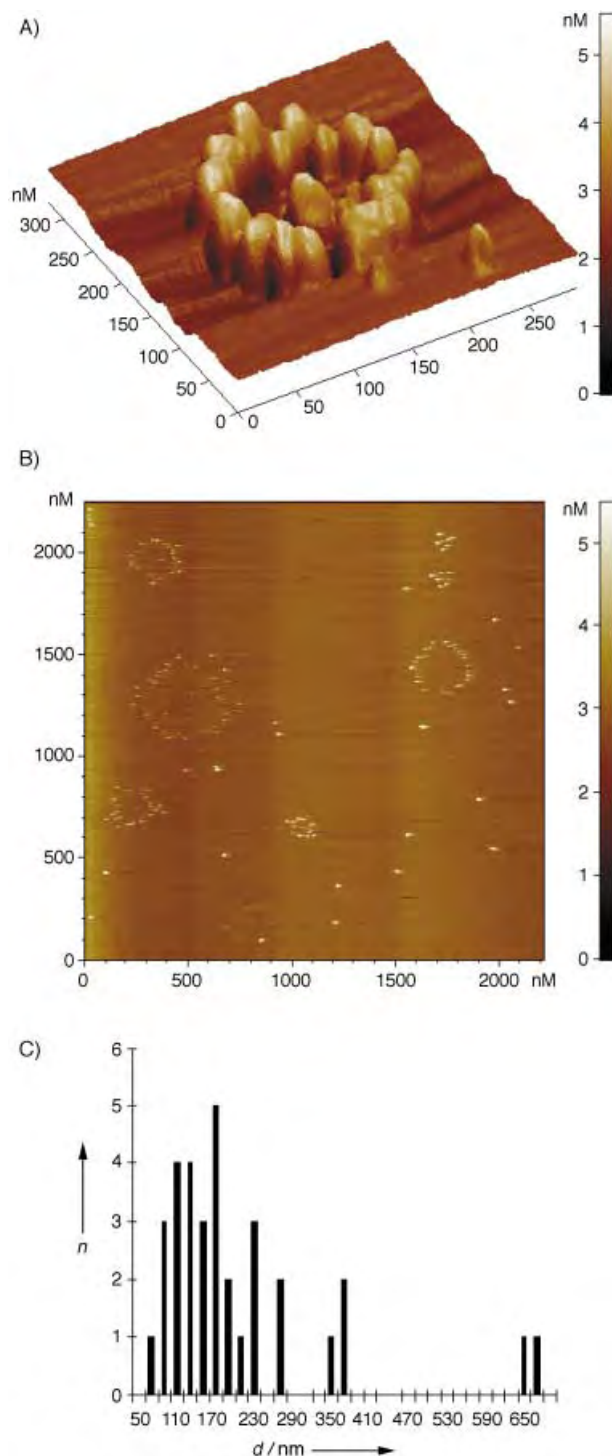
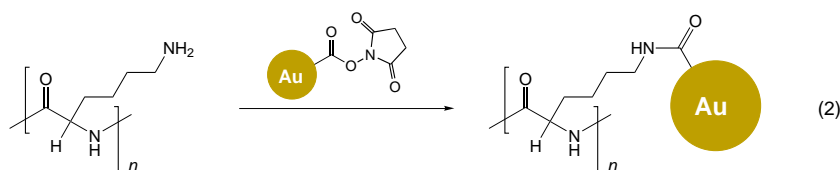


Figure 3. A) AFM image of a circular Au-nanoparticle-functionalized polylysine formed on a mica surface upon evaporation. B) Representative AFM image of Au-nanoparticle-functionalized polylysine rings formed on a mica surface upon evaporation. C) Histogram of the diameter of self-assembled Au-nanoparticle-polylysine circles on a mica surface resulting from evaporation (n = frequency; d = ring diameter).



linked polymer chains. The formation of molecular and macromolecular ring structures on surfaces has been addressed experimentally^[9, 10] and theoretically.^[11, 12] Although there is no unified theory regarding the formation of circular structures on

surfaces, based on the available knowledge, one may suggest a plausible mechanism for the formation of the Au-nanoparticle rings on the surface. The water droplet that includes the modified polylysine, wets the hydrophilic mica surface, and the film formed thins uniformly on the surface upon evaporation.^[13] When it reaches a thickness of several tenths of a nanometer, the aqueous layer reaches the point of instability, which results in film rupture and the formation of droplets. Drying of the droplets that includes the dispersed particles results in the concentration of the material at the edges of the evaporating droplet as a result of a capillary flow of the interior solution to the evaporating edges.^[11a] The diameter of the resulting ring is then controlled by the dimensions of the coalesced droplet, the number of polymer chains confined to the droplet, and the rate of evaporation that is also dominated by the concentration of the polymer in the droplet. The resulting ring is then stabilized on the mica surface by hydrogen bonds and interchain hydrogen bonds. Upon the combing^[14] of the Au-nanoparticle-functionalized polylysine on the mica surface, linear Au-nanoparticle-polymer wires are formed (Figure 4). Thus, the shape of the resulting wire can be controlled by the mode of its deposition on the surface.

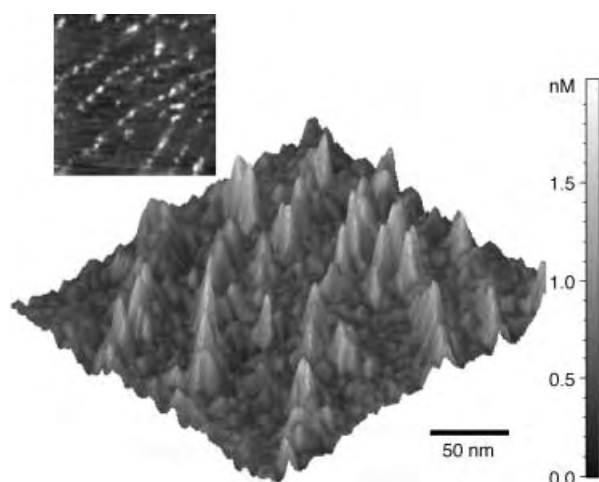


Figure 4. AFM image of Au-nanoparticle-functionalized polylysine formed on a mica surface by the combing method. Inset: 2D image of the Au-nanoparticle structures.

In conclusion, our study has demonstrated the generation of Au-nanoparticle wires on DNA or polylysine as templates. The DNA–Au-nanoparticle wires were generated by a new method that involves the incorporation of an intercalator-functionalized Au nanoparticle into double-stranded DNA, followed by the photochemical cross-linking of the intercalator to the DNA matrix. Another approach included the chemical modification of a polymer chain with the Au nanoparticles, and the surface assembly of the nanoparticle wire. The future enlargement of the nanoparticle wires by catalytic, electroless deposition of metals, is anticipated to yield conductive wires of predesigned width and shape. The future generation of conductive nanorings is particularly exciting, as it would enable the generation of nanoscale magnets by

passing a current through the nanostructures, or eventually, magnetically induced chemical reactions in nanoscale domains. Polylysine and DNA are two oppositely charged polyelectrolytes. Thus, the interaction of DNA or Au-nanoparticle-functionalized DNA with the Au-nanoparticle-tethered polylysine is anticipated to yield further nanoparticle architectures. Preliminary studies indicate that although the Au-nanoparticle rings on the mica surface exhibit high stability, their treatment with the λ -DNA that includes the intercalated Au nanoparticles results in the rupture of the Au-nanoparticle rings. We find that the Au-nanoparticle–polylysine wraps around the negatively charged DNA. This process enhances the coverage of the resulting multi-component Au-nanoparticle wires.

Experimental Section

1-Functionalized Au nanoparticles: Amino psoralen (**1**), (Sigma; 10 μ g, 40 nmol) was mixed with mono-*N*-hydroxysuccinimide-modified Au particle in a Hepes buffer solution (100 μ L; 10 mM, pH 8) for 2 h at room temperature, followed by further incubation for 12 h at 4 °C. The resulting mixture was purified from the excess of **1** using a microspin column (spin column 30, Sigma). The resulting brown solution was further dialyzed against 10 mM Hepes buffer solution using a microdialyzing device (5 kDa cutoff). All procedures were performed in the dark, to prevent photo-degradation of **1**. The **1**-modified Au nanoparticles were characterized by absorption spectroscopy. From their absorption spectrum the spectrum of the pure Au nanoparticles (with the appropriate concentration factor) was subtracted to yield the absorbance band at $\lambda = 360$ nm, characteristic of **1**. From this band the concentration of **1** in the sample was determined, which gave a 1:1 ratio between **1** and the Au nanoparticles, yield 80%.

Poly-L-Lysine–Au-nanoparticle conjugate: Polylysine (52 000 g mol^{−1}, 0.2 nmol) was mixed with *N*-hydroxysuccinimide-activated Au nanoparticles (6 nmol; Nanoprobes, 1.4 nm) in Hepes buffer solution (100 μ L; 30 mM, pH 8) for 12 h at 4 °C. The resulting polylysine/Au-nanoparticle conjugate was purified by spin chromatography using a gel microspin column with the appropriate fractionation range (spin column 100, > 200 bases, Sigma). The resulting brown solution of the polylysine–gold-nanoparticle conjugate was further dialyzed against a Hepes buffer solution (10 mM, pH 8.5) at 4 °C for 4 h, while renewing the dialysis solution every hour, using a microdialyzing device (15 kDa cutoff).

Nanoparticle wires on surfaces: λ -DNA (Sigma) or poly A/poly T (Pharmacia) approximate 0.3×10^{-12} M concentrations were mixed with **1**-modified Au nanoparticles (1 μ m) and incubated at room temperature for 20 min. Afterwards, the mixture was irradiated with a long UV lamp (12 Watt), $\lambda > 360$ nm, for 45 min, while keeping the mixture in an ice bath. The DNA–gold-nanoparticle wires were then separated from unbound **1**–Au-nanoparticle using a microspin column of specific pore-size. A drop of the DNA–gold nanoparticle solution (4 μ L) was placed on a freshly cleaved mica surface, and allowed to evaporate. The surface was then washed with water (20 μ L) and dried with a gentle flow of argon.

The polylysine–Au-nanoparticle circles were prepared by placing a drop (4 μ L) of a 1000-fold-diluted polymer-conjugate solution (ca. 2.5×10^{-9} M) on a freshly cleaved mica surface. The drop was allowed to evaporate, and the surface was washed with triply distilled water (3×100 μ L), and dried under a gentle flow of argon. The sample could be stored for at least 3 months under an argon atmosphere.

The polylysine–Au-nanoparticle wires were prepared by the combing technique.^[14] A drop (4 μ L) was positioned on a glass surface, and this was placed on a freshly cleaved mica surface. The glass was removed and the Au-nanoparticle structures on the mica surface were imaged. Samples were imaged after 5–10 min of evaporation and gentle drying under Argon. Atomic force microscopy (AFM) images were acquired in tapping mode in air by a Smena B instrument (NT-MDT, Russia), with a 30- μ m scanner, and

NSC-16 cantilevers (resonance frequency ~ 180 kHz). Scan rates used were 1.5–2.5 Hz with a cantilever oscillation amplitude of the order of 20–40 nm.

Received: February 5, 2002 [Z18661]

A Bacterial Small-Molecule Three-Hybrid System**

Eric A. Althoff and Virginia W. Cornish*

Affinity chromatography has long been used to identify the protein targets of small-molecule drugs and other biomolecules. Although an essential tool for biochemical research, affinity chromatography can often be labor-intensive and time-consuming. Recently, the yeast three-hybrid assay, a derivative of the two-hybrid assay, was introduced as a straightforward, in vivo alternative to affinity chromatography.^[1,2] In the three-hybrid assay, protein–small molecule interactions are detected by the dimerization of the two halves of a transcriptional activator (TA) through the receptors of the small molecule and subsequent transcription of a reporter gene.^[3–6] For affinity chromatography applications, one ligand–receptor pair is used as an anchor and the other is the small molecule–protein interaction being investigated. Although the yeast three-hybrid assay is quite powerful, a bacterial equivalent would increase the number of proteins that could be tested by several orders of magnitude because the transformation efficiency of *E. coli* is significantly greater than that of *S. cerevisiae*. Furthermore, there may be applications where it is advantageous to test a eukaryotic protein in a prokaryotic environment in which many pathways are not conserved. However, the yeast three-hybrid assay cannot be transferred directly to bacteria. The components of the transcription machinery and the mechanism of transcriptional activation differ significantly between bacteria and yeast. Ligand–receptor pairs often are organism-specific because of cell permeability, toxicity, or other interactions with the cellular milieu. Bacterial two-hybrid assays have only begun to be developed in the past few years^[7] and to date only initial efforts toward the design of a bacterial three-hybrid system have been reported.^[8,9] Herein we report the first robust small-molecule bacterial three-hybrid system—a heterodimer of methotrexate and a synthetic analogue of FK506 that activates transcription in the *E. coli* RNA polymerase two-hybrid system (Figure 1).

We chose to construct our bacterial three-hybrid system from the RNA polymerase two-hybrid system reported by Dove et al. in 1997.^[10] A variety of methods for detecting protein–protein interactions in bacteria are now availa-

- [1] a) C. M. Niemeyer, *Angew. Chem.* **2001**, *113*, 4254–4287; *Angew. Chem. Int. Ed.* **2001**, *40*, 4128–4158; b) A. N. Shipway, E. Katz, I. Willner, *ChemPhysChem* **2000**, *1*, 18–52; c) W. Shenton, S. A. Davies, S. Mann, *Adv. Mater.* **1999**, *11*, 449–452; d) C. A. Mirkin, *Inorg. Chem.* **2000**, *39*, 2258–2272.
- [2] a) Q. H. Liu, L. M. Wang, A. G. Frutos, A. E. Condon, R. M. Corn, L. M. Smith, *Nature* **2000**, *403*, 175–179; b) E. Ben-Jacob, A. Hermon, S. Caspi, *Phys. Lett. A* **1999**, *263*, 199–202.
- [3] a) F. Patolsky, K. T. Ranjit, A. Lichtenstein, I. Willner, *Chem. Commun.* **2000**, 1025–1026; b) T. A. Taton, R. C. Mucic, C. A. Mirkin, R. L. Letsinger, *J. Am. Chem. Soc.* **2000**, *122*, 6305–6306.
- [4] I. Willner, F. Patolsky, J. Wasserman, *Angew. Chem.* **2001**, *113*, 1913–1916; *Angew. Chem. Int. Ed.* **2001**, *40*, 1861–1864.
- [5] E. Braun, Y. Eichen, U. Sivan, G. Ben-Yoseph, *Nature* **1998**, *391*, 775–778.
- [6] a) J. Richter, R. Seidel, R. Kirsch, M. Mertig, W. Pompe, J. Planschke, H. K. Schackert, *Adv. Mater.* **2000**, *12*, 507–510; b) W. E. Ford, O. Harnack, A. Yasuda, J. M. Wessels, *Adv. Mater.* **2001**, *13*, 1793–1797.
- [7] T. Torimoto, M. Yamashita, S. Kowabata, T. Sakata, H. Mori, H. Yoneyama, *J. Phys. Chem. B* **1999**, *103*, 8799–8803.
- [8] Z. Wang, K. Shah, T. M. Rana, *Biochemistry* **2001**, *40*, 6458–6464.
- [9] a) A. P. H. J. Schenning, F. B. G. Benneker, H. P. M. Geurts, X. Y. Liu, R. J. M. Nolte, *J. Am. Chem. Soc.* **1996**, *118*, 8549–8552; b) L. Latterini, R. Blossey, J. Hofkens, P. Vanoppen, F. C. de Schryver, A. E. Rowan, R. J. M. Nolte, *Langmuir* **1999**, *15*, 3582–3588.
- [10] a) S. Maenosono, C. D. Dushkin, S. Saita, Y. Yamaguchi, *Langmuir* **1999**, *15*, 957–965; b) P. C. Ohara, J. R. Heath, W. M. Gelbart, *Angew. Chem.* **1997**, *109*, 1120–1122; *Angew. Chem. Int. Ed.* **1997**, *36*, 1078–1081.
- [11] a) R. D. Deegan, O. Bakajin, T. F. Dupont, G. Huber, S. R. Nagel, T. A. Whitten, *Nature* **1997**, *389*, 827–829; b) U. Thiele, M. Mertig, W. Pompe, *Phys. Rev. Lett.* **1998**, *80*, 2869–2872.
- [12] a) D. Beaglehole, H. K. Christenson, *J. Phys. Chem.* **1992**, *96*, 3395–3403; b) A. S. Padmakar, K. Kargupta, A. Sharma, *J. Chem. Phys.* **1999**, *110*, 1735–1744; c) G. Reiter, *Phys. Rev. Lett.* **1992**, *68*, 75–78.
- [13] a) M. Elbaum, S. G. Lipson, *Phys. Rev. Lett.* **1994**, *72*, 3562–3566; b) N. Samid-Merzel, S. G. Lipson, D. S. Tannhauser, *Phys. Rev. E* **1998**, *57*, 2906–2913.
- [14] J. Hu, M. Wang, H.-U. G. Weier, P. Frantz, W. Kolbe, D. F. Ogletree, M. Salmeron, *Langmuir* **1996**, *12*, 1697–1700.

[*] Prof. V. W. Cornish, E. A. Althoff
Department of Chemistry, Columbia University
New York, NY 10027 (USA)
Fax: (+1) 212-932-1289
E-mail: vc114@columbia.edu

[**] We are grateful for financial support for this work from the National Institutes of Health (grant GM62867) and Columbia University. E.A.A. is a Howard Hughes Medical Institute Predoctoral Fellow. V.W.C. is a Beckman, Burroughs-Wellcome, Dreyfus, and NSF Career New Faculty Awardee. We especially thank A. Hochschild and S. Dove for their guidance as well as for supplying many of the plasmids and strains reported in this work; in addition, we thank Ariad Pharmaceuticals for providing a synthetic protocol for SLF and J. Hu and S. Kopytek for their many helpful suggestions.



Supporting information for this article is available on the WWW under <http://www.angewandte.org> or from the author.

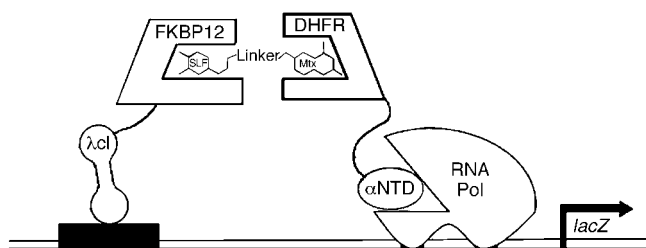


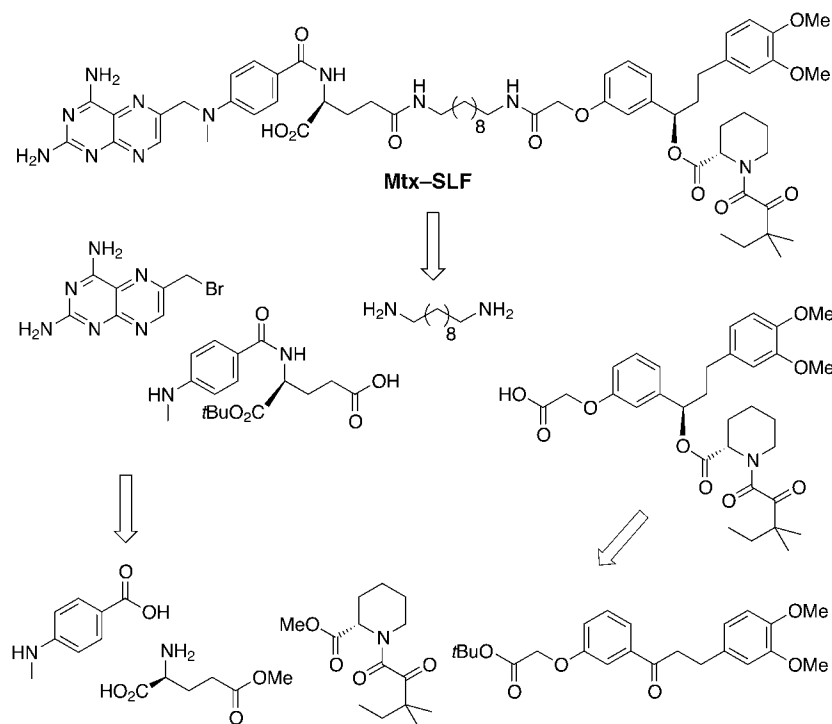
Figure 1. Bacterial RNA polymerase small-molecule three-hybrid system. A bacterial two-hybrid system was developed by Dove and Hochschild based on their observation that λ CI-mediated recruitment of RNA polymerase (RNA Pol) is sufficient to activate gene transcription. Herein we report a three-hybrid variant of this system built around the interaction between the small molecules methotrexate (Mtx) and a synthetic analogue of FK506 (SLF) and their protein receptors, dihydrofolate reductase (DHFR) and FK506-binding protein 12 (FKBP12), respectively. In this assay, the binding site for the DNA-binding protein λ CI is placed upstream of the promoter for a *lacZ* reporter gene. λ CI is fused to FKBP12 and the N-terminal domain of the α -subunit of RNA Pol (α NTD) is fused to DHFR. Thus, upon addition of the small molecule heterodimer Mtx-SLF, the λ CI-FKBP12 and α NTD-DHFR fusion proteins are dimerized, thus activating transcription of the *lacZ* reporter gene.

ble.^[7–14] Generally, these methods are based either on enzyme complementation or transcriptional activation or repression assays. Whereas the enzyme complementation assays are essentially the same as those used in eukaryotes, entirely new transcription-based assays had to be developed for bacteria because the components of the transcription machinery are poorly conserved between eukaryotes and prokaryotes. We chose to adapt the RNA polymerase assay developed by Dove et al. because transcriptional activation in this assay results in a large increase in reporter gene transcription and because reconstitution of transcriptional activation should be largely conformation-independent. Based on their studies of the mechanism of transcriptional activation by λ -repressor (λ CI),^[15] Dove et al. developed an *in vivo* assay for protein–protein interactions based on dimerization of λ CI and the N-terminal domain of the α -subunit of RNA polymerase (α NTD). They showed that this assay could detect the interaction between the proteins Gal4 and Gal11^P as an increase in transcription of a *lacZ* reporter gene.^[16] We used this direct protein–protein interaction as a small-molecule independent positive control in work reported herein. Dove and Hochschild optimized the *lacZ* reporter gene such that dimerization of λ CI and α NTD activates transcription 10–100-fold over basal levels. A variant of this assay that can be run as a *his3* growth selection was recently reported.^[17]

The key to converting this two-hybrid assay into a three-hybrid system was the design of a dimeric ligand that could bridge λ CI and α NTD through the receptors of the ligand. For the bridging small molecule, we chose to prepare a heterodimer of methotrexate (Mtx) and a synthetic analogue of

FK506 (SLF). We call this heterodimer Mtx-SLF. We planned to use Mtx-SLF to dimerize a λ CI-FKBP12 (λ CI-FK506-binding protein 12) protein chimera and an α NTD-DHFR (α NTD-dihydrofolate reductase) protein chimera as shown in Figure 1. Mtx inhibits DHFR with a low picomolar K_i , and the interaction between the two has been extensively studied.^[18, 19] Furthermore, our laboratory recently showed that Mtx could be used successfully in a yeast three-hybrid system.^[6] For the other half of the bridging small molecule, we used SLF. FK506 functions as a natural small-molecule dimerizer, and dimers of FK506 have been developed as artificial chemical inducers of dimerization.^[3, 20] SLF was developed by Ariad Pharmaceuticals as an FK506 analogue; it has a nanomolar affinity for FKBP12, and the interaction between the two has been fully characterized.^[21, 22] Furthermore, SLF homodimers have been used previously in several mammalian three-hybrid systems.^[23]

The retrosynthetic analysis of Mtx-SLF is shown in Scheme 1. The synthesis is based on previous syntheses of Mtx and SLF derivatives and was designed to allow Mtx, SLF, or the linker between them to be varied readily. The Mtx portion of the molecule begins as the γ -methyl ester of L-glutamic acid and is based on previous syntheses of Mtx.^[6, 24] γ -Methyl L-glutamic acid is inexpensive, and the α -carboxylate can be selectively protected as the *tert*-butyl ester by transiently protonating the α -amino group.^[25] The diprotected amino acid is then coupled to 4-(methylamino)benzoic acid by using standard peptide coupling reagents. Finally, the γ -methyl ester is saponified to yield the free acid for further reactions. SLF acid was synthesized as described previously from L-pipecolinic acid in 59% yield over six steps.^[5, 21] The Mtx and SLF portions were then coupled to 1,10-diaminodecane in a three-component peptide coupling reaction. 2,4-



Scheme 1. Retrosynthetic analysis of Mtx-SLF.

Diamino-6-bromomethyl-pteridine is added after this coupling reaction to simplify the purification of the synthetic intermediates. Finally, acid cleavage of the *tert*-butyl ester yielded Mtx-SLF. Thus, the Mtx-SLF heterodimer was prepared from two components in 5% overall yield over the six steps from the γ -methyl ester of L-glutamic acid or 6% overall yield in nine steps from the L-pipecolic acid precursor of SLF.

The next step was the construction of the *E. coli* strain that expresses the λ CI-FKBP12 and α NTD-DHFR fusion proteins and contains the *lacZ* reporter construct. Plasmids that encode the λ CI-FKBP12 and α NTD-DHFR chimeras were prepared from vectors pAC λ CI32 and pBR α LN by using standard molecular biology techniques.^[7] We used the same synthetic *lacZ* reporter, *placOR2-62*, initially reported by the Hochschild group. The reporter *placOR2-62* is maintained in one copy in the chromosome as a prophage and encodes the *lacZ* gene 62 base pairs downstream from the λ CI binding site (Figure 1).^[10] Based on previous results from Kopytek and Hu showing that *tolC*⁻, which encodes a portion of a multidrug-resistance efflux pump (MDR), and *thyA*⁻, which encodes an enzyme upstream of DHFR in the thymidine biosynthesis pathway, mutations improved the viability and tolerance of *E. coli* to Mtx-based molecules, we expected export as well as toxicity of Mtx-SLF to be problematic in *E. coli*.^[26] Thus, we modified the original Hochschild strain KS1 to be *tolC*⁻ to decrease active export of our small molecule by the TolC-dependent MDR efflux pump. At the low concentrations of Mtx-SLF required for the three-hybrid experiments, however, Mtx was not sufficiently toxic to warrant the *thyA*⁻ mutation (data not shown). We introduced the *tolC*⁻ mutation into KS1 by using a standard molecular biology technique for gene transfer, P1vir transduction, from strain SK037.^[26] We call this test strain V674E. Transformation of the plasmids bearing the various λ CI and α NTD fusion proteins into V674E yielded the final experimental strains.

We used standard β -galactosidase assays in liquid culture and on plates^[27] to establish that Mtx-SLF activates transcription of the *lacZ* reporter gene in *E. coli* strain V674E (Figure 2 and Supporting Information). Overnight cultures were used to inoculate fresh LB media that contained Mtx-SLF, IPTG, and the appropriate antibiotics. These cultures were grown, lysed, and assayed for β -galactosidase activity by using *o*-nitrophenyl- β -D-galactopyranoside (ONPG), a chromogenic substrate for β -galactosidase. Cells that express λ CI-FKBP12 and α NTD-DHFR showed sixfold greater activation of *lacZ* transcription at 1 μ M Mtx-SLF and tenfold greater activation at 10 μ M Mtx-SLF than cells that express only λ CI and α NTD. For comparison, the levels of transcriptional activation for the direct protein-protein interaction are 13-fold higher and are unaffected by the concentration of Mtx-SLF in the media. As seen in Figure 3, the levels of transcriptional activation in the three-hybrid system correlate with the concentration of Mtx-SLF in the media. We begin to see transcriptional activation at 0.3 μ M Mtx-SLF, and the levels of activation are still increasing at 10 μ M Mtx-SLF. Concentrations higher than 10 μ M Mtx-SLF cannot be used as the small molecule begins to become toxic to the *E. coli*. Several independent controls establish that transcriptional

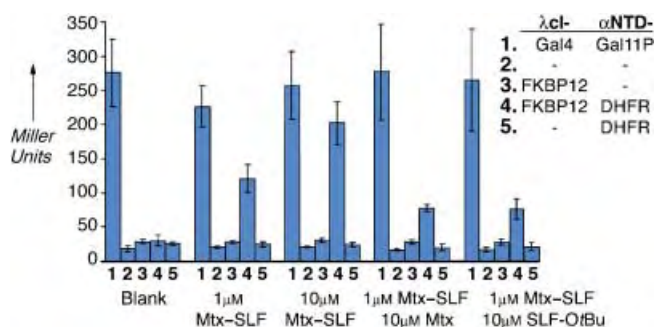


Figure 2. The levels of small-molecule-induced transcriptional activation were quantified by using liquid *lacZ* assays. The strains are assayed in liquid ONPG assays in which the levels of transcriptional activation can be quantified based on the amount of reporter protein β -galactosidase that is produced. Each column corresponds to strain V674E bearing plasmids expressing various λ CI and α NTD fusion proteins: 1, λ CI-Gal4, α NTD-Gal11P; 2, λ CI, α NTD; 3, λ CI-FKBP12, α NTD; 4, λ CI-FKBP12, α NTD-DHFR; 5, λ CI, α NTD-DHFR. Strain 1 is the Gal4-Gal11P direct protein-protein interaction used as a positive control. Strains 2, 3, and 5 lack either DHFR or FKBP12 or both and are used as negative controls to test the assumption that transcriptional activation is dependent on both halves of the Mtx-SLF small molecule. The last two small-molecule concentrations are competition assays in which an excess of one of the ligands for the receptor proteins was used to compete out the positive signal by effectively decreasing the number of successful three-hybrid interactions. The strains were assayed in triplicate from three transformants and standard deviations are shown. The strains are grown in LB medium with IPTG (0.5 mM), ampicillin (100 μ g mL⁻¹), chloramphenicol (6 μ g mL⁻¹), and small molecules at the indicated concentration.

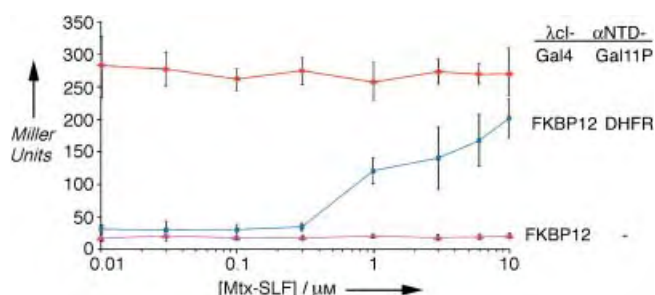


Figure 3. The levels of transcriptional activation depend on the concentration of Mtx-SLF in the bacterial three-hybrid system. The concentrations of Mtx-SLF in the media were varied, and the levels of *lacZ* transcription were quantified in liquid culture by using ONPG. The strains are V674E expressing the following λ CI and α NTD fusion proteins: (●), λ CI-Gal4, α NTD-Gal11P (a direct protein-protein interaction); (▲), λ CI-FKBP12, α NTD (a negative control); and (■), λ CI-FKBP12, α NTD-DHFR (the three-hybrid system). The rate of ONPG hydrolysis was measured in triplicate from three different transformants after growth in LB media that contained IPTG (0.5 mM), ampicillin (100 μ g mL⁻¹), chloramphenicol (6 μ g mL⁻¹), and Mtx-SLF at the indicated concentrations. The standard deviation for each data point is also shown.

activation indeed requires both halves of Mtx-SLF (Figure 2). Neither Mtx, SLF, nor a combination of the two increases the levels of transcription in the three-hybrid system (data not shown). At 1 μ M Mtx-SLF, a tenfold excess of either Mtx or the *tert*-butyl ester of SLF decreased the levels of transcription to about half that with 1 μ M Mtx-SLF alone. Deletion of either DHFR or FKBP12 from the λ CI-FKBP12 and α NTD-DHFR fusion proteins drops the levels of small-molecule-induced transcriptional activation to the background levels observed in cells that express only λ CI and α NTD.

The bacterial small-molecule three-hybrid system described herein should provide a robust platform for high-throughput assays based on protein–small molecule interactions. The Mtx–SLF heterodimeric ligand can be prepared readily and gives a strong transcription readout in the *E. coli* RNA polymerase three-hybrid system. Notably, the levels of transcriptional activation with the Mtx–SLF three-hybrid system are comparable to those with the direct protein–protein interaction, despite the fact that one noncovalent interaction has been replaced with two. The EC_{50} for *lacZ* transcription is greater than the K_D of either Mtx or SLF for FKBP12.^[5] Currently we are carrying out in vitro experiments to examine the relationship between *lacZ* transcription and the K_D of the ligand–receptor interaction. Three-hybrid systems provide an in vivo alternative to affinity chromatography that can be used to evolve proteins that recognize a particular small molecule, to screen a library of small molecules based on binding to a particular protein, or to screen cDNA libraries to find the protein targets of drugs or to classify proteins based on their small-molecule interactions. Because of the high transformation efficiency and rapid doubling time of *E. coli*, this system should increase the number of proteins that can be tested in three-hybrid assays by several orders of magnitude compared with yeast systems. A bacterial assay should be particularly advantageous in molecular evolution experiments in which in the order of 10^8 variants may be necessary to alter protein function. Based on our results, we believe that Mtx will provide a versatile anchor for presenting a variety of different small molecules.

Received: February 4, 2002 [Z18636]

- [1] S. Fields, O. Song, *Nature* **1989**, *340*, 245–246.
- [2] E. Licitra, J. Liu, *Proc. Natl. Acad. Sci. USA* **1996**, *93*, 12817–12821.
- [3] D. Spencer, T. Wandless, S. Schreiber, G. Crabtree, *Science* **1993**, *262*, 1019–1024.
- [4] M. Farrar, J. Alberola-Ila, R. Perlmutter, *Nature* **1996**, *383*, 178–181.
- [5] J. Amara, T. Clackson, V. Rivera, T. Guo, T. Keenan, S. Natesan, R. Pollock, W. Yang, N. Courage, D. Holt, M. Gilman, *Proc. Natl. Acad. Sci. USA* **1997**, *94*, 10618–10623.
- [6] H. Lin, W. Abida, R. Sauer, V. Cornish, *J. Am. Chem. Soc.* **2000**, *122*, 4247–4248.
- [7] J. Hu, M. Kornacker, A. Hochschild, *Methods* **2000**, *20*, 80–94, and references therein.
- [8] S. Firestine, F. Salinas, A. Nixon, S. Baker, S. Benkovic, *Nat. Biotechnol.* **2000**, *18*, 544–547.
- [9] S. Kopytek, R. Standaert, J. Dyer, J. Hu, *Chem. Biol.* **2000**, *7*, 313–321.
- [10] S. Dove, J. Joung, A. Hochschild, *Nature* **1997**, *386*, 627–630.
- [11] S. Michnick, I. Remy, F. Campbell-Valois, A. Vallee-Belisle, J. Pelletier, *Methods Enzymol.* **2000**, *238*, 208–230.
- [12] G. Karimova, J. Pidoux, A. Ullmann, D. Ladant, *Proc. Natl. Acad. Sci. USA* **1998**, *95*, 5752–5756.
- [13] T. Ozawa, S. Nogami, M. Sato, Y. Ohya, Y. Umezawa, *Anal. Chem.* **2000**, *72*, 5151–5157.
- [14] T. Wehrman, B. Kleaveland, J. Her, R. Balint, H. Blau, *Proc. Natl. Acad. Sci. USA* **2002**, *99*, 3469–3474.
- [15] S. Dove, F. Huang, A. Hochschild, *Proc. Natl. Acad. Sci. USA* **2000**, *97*, 13215–13220.
- [16] S. Dove, A. Hochschild, *Genes Dev.* **1998**, *12*, 745–754.
- [17] J. Joung, E. Ramm, C. Pabo, *Proc. Natl. Acad. Sci. USA* **2000**, *97*, 7382–7387.
- [18] S. Benkovic, C. Fierke, A. Naylor, *Science* **1988**, *239*, 1105–1110.
- [19] J. Bolin, D. Filman, D. Matthews, R. Hamlin, J. Kraut, *J. Biol. Chem.* **1982**, *257*, 13663–13672.
- [20] G. Crabtree, S. Schreiber, *Trends Biochem. Sci.* **1996**, *21*, 418–422.

- [21] T. Keenan, D. R. Yeager, N. L. Courage, C. T. Rollins, M. E. Pavone, V. M. Rivera, W. Yang, T. Guo, J. F. Amara, T. Clackson, M. Gilman, D. A. Holt, *Bioorg. Med. Chem.* **1998**, *6*, 1309–1335.
- [22] D. Holt, J. Luengo, D. Yamashita, H. Oh, A. Konialan, H. Yen, L. Rozamus, M. Brandt, M. Bossard, M. Levy, D. Eggleston, J. Liang, L. Schultz, T. Stout, J. Clardy, *J. Am. Chem. Soc.* **1993**, *115*, 9925–9938.
- [23] T. Clackson, *Curr. Opin. Chem. Biol.* **1997**, *1*, 210–218.
- [24] B. Hart, W. Haile, N. Licato, W. Bolanowska, J. McGuire, J. Coward, *J. Med. Chem.* **1996**, *39*, 56–65.
- [25] L. Liu, R. Tanke, M. Miller, *J. Org. Chem.* **1986**, *51*, 5332–5337.
- [26] S. Kopytek, J. Dyer, G. Knapp, J. Hu, *Antimicrob. Agents Chemother.* **2000**, *44*, 3210–3212.
- [27] J. H. Miller, *A Short Course in Bacterial Genetics: A Laboratory Manual and Handbook for Escherichia Coli and Related Bacteria*, Cold Spring Harbor Laboratory Press, Plainview, NY, **1992**.

Proton-Induced, Reversible Evolution of O₂ from the Os^{IV}–Sulfoximido Complex [Os^{IV}(tpy)(Cl)₂{NS(O)-3,5-Me₂C₆H₃}]**

My Hang V. Huynh,* David E. Morris, Peter S. White, and Thomas J. Meyer*

O₂ activation in biological systems is a key step in respiration with O₂ activation achieved by a complex series of steps involving binding to an Fe–heme, electron transfer, and, ultimately, atom transfer to a reducing substrate.^[1] Kinetic difficulties in the electroreduction of O₂ to H₂O in fuel cells create a significant over-voltage which limits

[*] Dr. T. J. Meyer

Associate Director for Strategic Research
Los Alamos National Laboratory, MS A127
Los Alamos, NM 87545 (USA)
Fax: (+1) 505-667-5450
E-mail: tjmeyer@lanl.gov

Dr. M. H. V. Huynh

Director-Funded Postdoctoral Fellow
Los Alamos National Laboratory
Chemistry Division MS J514
Los Alamos, NM 87545 (USA)
Fax: (+1) 505-667-3314
E-mail: huynh@lanl.gov

Dr. D. E. Morris

Actinide, Catalysis, and Separations Group
Chemistry Division MS J514
and the Glenn T. Seaborg Institute for Transactinium Science
Los Alamos National Laboratory
Los Alamos, NM 87545 (USA)

Dr. P. S. White

Department of Chemistry
University of North Carolina at Chapel Hill
Chapel Hill, NC 27599-3290 (USA)

[**] We are grateful to the Laboratory Directed Research and Development Program for support of this research. M.H.V.H. gratefully acknowledges postdoctoral fellowship support from the Director's Office of Los Alamos National Laboratory. Los Alamos National Laboratory is operated by the University of California for the U.S. Department of Energy under Contract W-7405-ENG-36. tpy = 2,2':6',2''-terpyridine.

performance.^[2] Similarly, water oxidation in photosynthesis is a complex process involving multiple electron transfer based on a four-manganese-center cluster.^[3]

The mechanistic difficulties in the reduction of O₂ or the oxidation of water arise from the thermodynamic instability of one-electron intermediates such as OH[•] or the O₂^{•−} ion and the requirement for multiple-electron pathways to avoid them. Mechanisms for the activation or evolution of O₂ must accommodate two oxygen atoms and a net four-electron change.^[4] We report here the remarkable reactions of the *cis* and *trans* isomers of the Os^{IV}–sulfoximido complexes, [Os^{IV}(tpy)(Cl)₂{NS(O)C₆H₃Me₂}] (2; tpy = 2,2':6',6''-terpyridine and C₆H₃Me₂ = 3,5-Me₂C₆H₃), and their Os^{IV}–sulfilimido analogues, [Os^{IV}(tpy)(Cl)₂{NS(H)C₆H₃Me₂}]⁺ (1⁺), towards proton-gain or loss-induced evolution and addition of O₂, respectively.

When *cis*-[Os^{VI}(tpy)(Cl)₂(N)]⁺ is treated with Me₂C₆H₃SH in CH₃CN [Eq. (1)], a rapid reaction occurs to give *cis*-1⁺. Further reaction of 1⁺ with O ← NMe₃ in CH₃CN occurs to give *cis*-2 [Eq. (2)]. An analogous reactivity was reported earlier for the *trans* isomer.^[5]

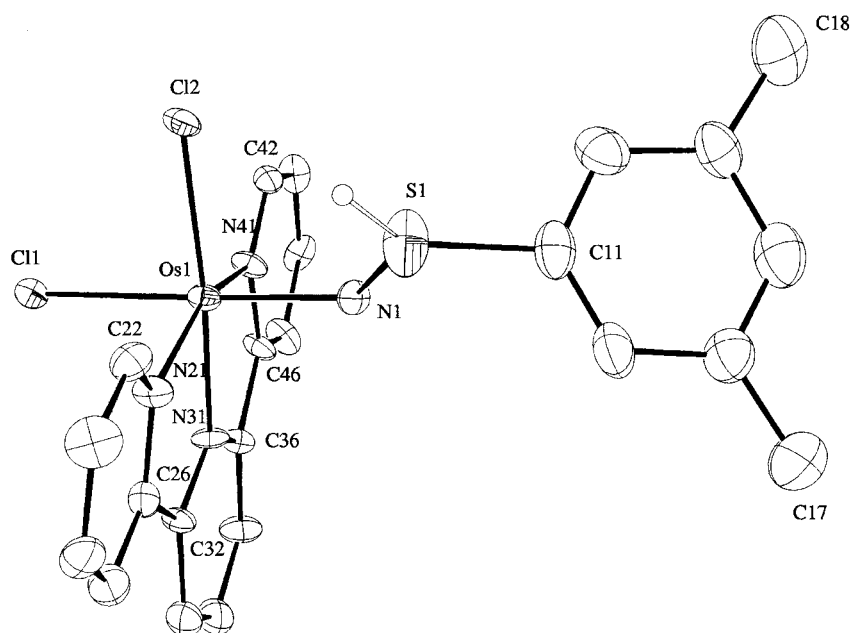


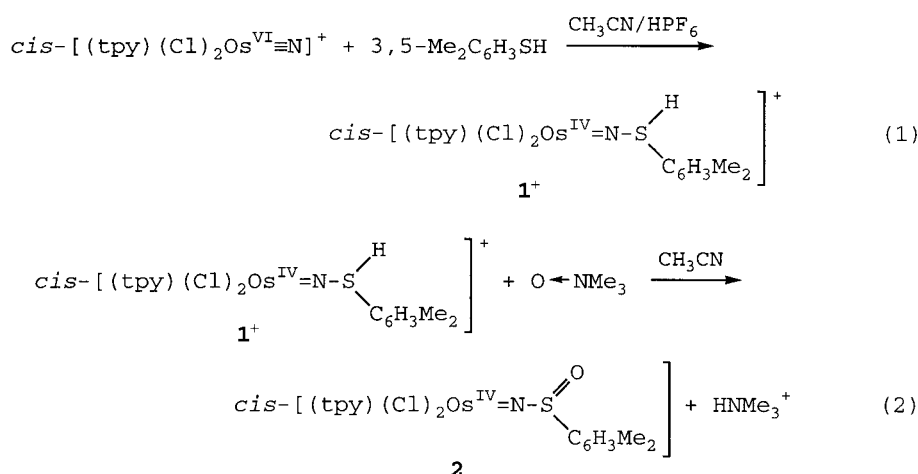
Figure 1. ORTEP diagram (thermal ellipsoids set at the 30% level) and labeling scheme for 1⁺·PF₆[−].

N1–S1 bond lengths of 1.947(11) Å and of 1.645(12) Å, respectively, are consistent with multiple bonding.^[8] The angle N1–S1–C11 102.8(7)° is consistent with pseudo sp³ hybridization at the S atom of the sulfilimido ligand. The Os–N(sulfilimido) bond length, the bent angle Os1–N1–S1 124.6(6)°, and the diamagnetism of the complexes (as shown by ¹H NMR spectroscopy) are all consistent with a d⁴ spin-paired Os^{IV} complex. There are structural similarities with the related Os^{IV} complexes, *cis*-[Os^{IV}(tpm)Cl₂][N(H)N(CH₂)₄O]⁺ (tpm = tris-(pyrazol-1-yl)methane),^[9a] *cis*-[Os^{IV}(tpy)(Cl)(NCCCH₃)]⁺[NN(CH₂)₄O]⁺,^[9a] and *cis*-[Os^{IV}(tpy)(NCCCH₃)₂][NN(CH₂)₄O]²⁺.^[9b]

When one equivalent of HPF₆ as HPF₆·H₂O is added to CH₃CN solutions of either *cis*- or *trans*-2, immediate color changes occur from dark green (λ_{max}(*cis*) = 444, 592, and 696 nm and

λ_{max}(*trans*) = 404, 586, and 714 nm) to bright red (λ_{max}(*cis*) = 460 nm and λ_{max}(*trans*) = 466 nm) with noticeable gas evolution. There is no competition between solvolysis under these conditions. UV/Vis spectral changes with incremental additions of HPF₆ for the *trans* isomer are shown in Figure 2. Based on molar extinction coefficients,^[5–7] the conversion from 2 into 1⁺ is quantitative. The evolved gas was shown to be O₂ by oxygen-electrode measurements. The amount of gas evolved was consistent with the 2:1 ratio in Equation (3).^[10]

Attempts to follow the reaction by stopped-flow mixing were unsuccessful because it is too rapid even at −50 °C in either 2:1 (v/v) CH₃C(O)CH₃:CH₃CN or CH₃C(O)CH₃. Based on the spectral changes in Figure 2, H⁺ is required as a stoichiometric reagent, and the energetics of protonation to



Both *cis* products, 1⁺^[6] and 2,^[7] have been isolated, the former as its PF₆[−] salt, in 95 and 85% yields, respectively. In 10:1 (v/v) CH₃CN:H₂O, 1⁺ undergoes solvolysis in a few minutes to give *cis*-[Os^{IV}(tpy)(Cl)(NCCCH₃)(NSC₆H₃Me₂)]⁺ which undergoes further solvolysis to give *cis*-[Os^{IV}(tpy)(NCCCH₃)₂(NSC₆H₃Me₂)]²⁺ over a few hours. This chemistry will be reported elsewhere.

Compound 1⁺·PF₆[−] was also characterized by X-ray crystallography of crystals grown by slow diffusion of Et₂O into a CH₃CN solution.^[6f] The structure (Figure 1) shows that the distorted octahedral arrangement of ligands at the Os center in the parent nitrido complex is retained in the protonated sulfilimido product. The Os–N(tpy) bond lengths range from 1.992(9) to 2.091(11) Å with the shortest Os–N(tpy) bond *trans* to the longer chloride bond. The Os–N(sulfilimido) and

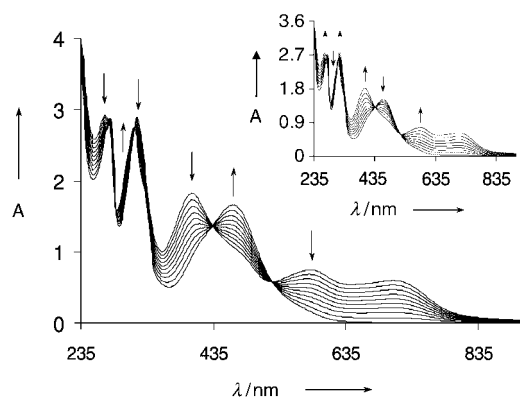
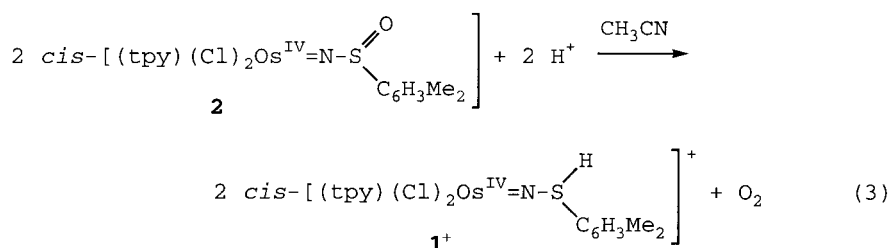


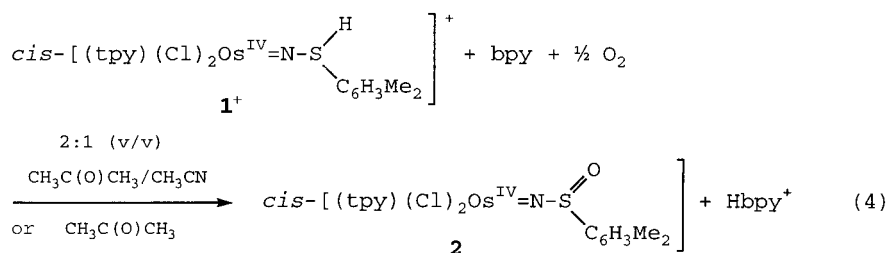
Figure 2. Spectral changes upon sequential addition of aliquots of HPF₆ (60 wt % solution in H₂O) in CH₃CN to 1.13 × 10⁻⁴ M *trans*-**2** in CH₃CN and inset, the reverse reaction between *trans*-**1**⁺ and bpy in air-saturated CH₃CN.



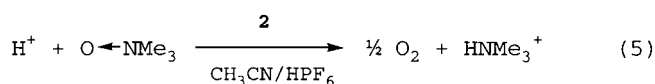
form **1**⁺ are presumably required to drive the reaction to completion. By inference, H⁺ is also required for the activation of the O₂ evolution process, but the mechanistic details remain obscure.

Remarkably, the O₂ evolution chemistry is reversible. When 2,2'-bipyridine (bpy) is added in stoichiometric amount to air-saturated CH₃CN solutions of **1**⁺, the UV/Vis spectrum changes quantitatively to that of **2** (Figure 2 inset). Addition of bpy deprotonates **1**⁺ to give [Os^{IV}(tpy)(Cl)₂(NSC₆H₃Me₂)] which undergoes O₂ oxidation to give **2** [Eq. (4)]. An uptake of O₂ was observed at the oxygen electrode but was difficult to quantify because of the large O₂ background in air-saturated solutions. Attempts to measure the kinetics of these reactions with added bpy by stopped-flow mixing in either 2:1 (v/v) CH₃C(O)CH₃:CH₃CN or CH₃C(O)CH₃ at -50 °C were also unsuccessful because the reactions were too rapid.

It is possible to generate O₂ catalytically from O ← NMe₃ based on the reactions in Equations (2) and (4). Addition of HPF₆ in large excess to **2** in CH₃CN in the presence of 100 equivalents of O ← NMe₃ results in rapid O₂ evolution. The O₂ evolution was quantitative based on O ← NMe₃ as



measured by the oxygen electrode. The net reaction is shown in Equation (5).



Catalytic activation of O₂ towards oxidation of PPh₃ to OPPh₃ in CH₃CN has been reported for *trans*-[Os^{IV}(tpy)(Cl)₂(NS-3,5-Me₂C₆H₃)]PF₆ but is rate limited by O-atom transfer from *trans*-[Os^{IV}(tpy)(Cl)₂(NS(O)C₆H₃Me₂)] (**2**) to PPh₃.^[5]

Initial observations show that the reactivity reported here is general for the series *cis*- or *trans*-[Os^{IV}(tpy)(Cl)₂(NS(O)Ar)]/[Os^{IV}(tpy)(Cl)₂(NS(H)Ar)]⁺ with Ar = 3,5-Me₂C₆H₃, 4-MeC₆H₄, and C₆H₅. It is a novel example of O₂ evolution/activation based on a ligand, in this case, one electronically activated by the Os–N multiple bond. These reactions are remarkable both for their occurrence and for the rates at which they occur.

Received: January 21, 2002 [Z18553]

- [1] a) H. Nohl, A. V. Kozlov, K. Staniek, L. Gille, *Bioorg. Chem.* **2001**, 29, 1–13; b) J. P. Klinman, *J. Biol. Inorg. Chem.* **2001**, 6, 1–13; c) S. Shiva, P. S. Brookes, R. P. Patel, P. G. Anderson, V. M. Darley-Usmar, *Proc. Natl. Acad. Sci. USA* **2001**, 98, 7212–7217; d) A. E. Martell, R. J. Motekaitis, R. Menif, D. A. Rockcliffe, A. Llobet, *J. Mol. Catal. A-Chem.* **1997**, 117, 205–213; e) D. E. Edmondson, B. H. Huynh, *Inorg. Chim. Acta* **1996**, 252, 399–404; f) D. H. Lee, N. Wei, N. N. Murthy, Z. Tyeklar, K. D. Karlin, S. Kaderli, B. Jung, A. D. Zuberbuhler, *J. Am. Chem. Soc.* **1995**, 117, 12498–12513; g) H. Niknahad, S. Khan, P. Obrien, *Chem.-Biol. Interact.* **1995**, 98, 27–44.
- [2] a) I. Yamanaka, K. Otsuka, *J. Chem. Soc. Faraday Trans.* **1993**, 89, 1791–1797; b) I. Yamanaka, K. Otsuka, *J. Alloys Compd.* **1993**, 193, 56–58; c) K. Asano, T. Hibino, H. Iwahara, *J. Electrochem. Soc.* **1995**, 142, 3241–3245; d) H. M. Saffarian, R. Srinivasan, D. Chu, S. Gilman, *J. Electrochem. Soc.* **2001**, 148, A559–A564; e) S. Z. Wang, Y. Jiang, W. Z. Li, J. W. Yan, *Studies in Surf. Sci. and Catal.* **1997**, 112, 401–410.
- [3] a) C. Tommos, G. T. Babcock, *Acc. Chem. Res.* **1998**, 31(1), 18–25; b) V. K. Yachandra, K. Sauer, M. P. Klein, *Chem. Rev.* **1996**, 96, 2927–2950; c) K. Lindberg, L. E. Andreasson, *Biochem.* **1996**, 35(45), 14259–14267; d) P. E. M. Siegbahn, R. H. Crabtree, *J. Am. Chem. Soc.* **1999**, 121, 117–127.
- [4] a) R. A. Binstead, C. W. Chronister, J. F. Ni, C. M. Hartshorn, T. J. Meyer, *J. Am. Chem. Soc.* **2000**, 122, 8464–8473; b) A. S. Arico, A. K. Shukla, H. Kim, S. Park, M. Min, V. Antonucci, *Appl. Surf. Sci.* **2001**, 172, 33–40; c) R. Z. Jiang, D. J. Chu, *J. Electrochem. Soc.* **2000**, 147, 4605–4609; d) M. Odgaard, E. Skou, *Solid State Ionics* **1996**, 86, 1217–1222; e) S. Y. Ye, A. K. Vijh, L. H. Dao, *J. Electroanal. Chem.* **1996**, 415, 115–121.
- [5] M. H. V. Huynh, P. S. White, T. J. Meyer, *J. Am. Chem. Soc.* **2001**, 123, 9170–9171.
- [6] **1**⁺-PF₆: a) elemental analysis calcd (%) for OsC₂₃H₂₁N₄SCl₂PF₆: C 34.90, H 2.67, N 7.08; found: C 35.03, H 2.61, N 7.18; b) cyclic voltammetry in 0.1 M Bu₄NPF₆/CH₃CN (V vs sodium saturated calomel electrode (SSCE)): E_{1/2} (Os^{V/IV}) = +1.21 V and E_{1/2} (Os^{IV/III}) = -0.09 V; c) UV/Vis spectra in CH₃CN λ_{max} [nm] (ε, M⁻¹cm⁻¹): 460 (9.47 × 10³), 314 (1.99 × 10⁴), 272 (2.37 × 10⁴), 228 (3.16 × 10⁴); d) IR (Nujol mull): ν̄ = ν(S–H)

- 1994, $\nu(3,5\text{-Me}_2\text{C}_6\text{H}_3\text{HS})$ 1601 (vs), and 1558 (s) $\nu(\text{tpy})$ 1469 (vs), 1449 (vs), and 1390 cm^{-1} (vs); $\nu(^{14}\text{NS})$ 1023 and $\nu(^{15}\text{NS})$ 991 cm^{-1} ; e) ^1H NMR data (δ = DMSO): 9.0–6.9 (m, 14 aromatic protons (11 H of tpy and 3 H of the aryl group)) 2.3 (s, 6H, methyl protons), 3.4 ppm (s, 1H, proton on the S atom); f) CCDC-177717 (1⁺) contains the supplementary crystallographic data for this paper. These data can be obtained free of charge via www.ccdc.cam.ac.uk/conts/retrieving.html (or from the Cambridge Crystallographic Data Centre, 12, Union Road, Cambridge CB21EZ, UK; fax: (+44) 1223-336-033; or deposit@ccdc.cam.ac.uk).
- [7] 2: a) Elemental analysis calcd (%) for $\text{OsC}_{23}\text{H}_{20}\text{N}_4\text{SOCl}_2$: C 41.76, H 3.05, N 8.47; found: C 42.07, H 3.08, N 8.19; b) cyclic voltammetry in 0.1 M $\text{Bu}_4\text{NPF}_6/\text{CH}_3\text{CN}$ (V vs SSCE): $E_{1/2}(\text{Os}^{\text{V}/\text{IV}}) = 1.23$ V, $E_{1/2}(\text{Os}^{\text{VI}/\text{V}}) = 0.30$ V, $E_{1/2}(\text{Os}^{\text{IV}/\text{III}}) = -0.89$ V, and $E_{1/2}(\text{Os}^{\text{III}/\text{II}}) = -1.19$ V; c) UV/Vis spectra in CH_3CN λ_{max} [nm] (ϵ , $\text{M}^{-1}\text{cm}^{-1}$): 696 (3.17×10^3), 592 (2.79×10^3), 444 (9.16×10^3), 320 (1.32×10^4), 272 (2.07×10^4), 212 (2.73×10^4); d) IR (Nujol mull): $\tilde{\nu} = \nu(3,5\text{-Me}_2\text{C}_6\text{H}_3\text{HS})$ 1603 (vs) and 1578 (s), $\nu(\text{tpy})$ 1477 (vs), 1449 (vs), and 1435 (vs), and $\nu(\text{S=O})$ 1277 cm^{-1} ; e) ^1H NMR (DMSO) δ = 8.95–8.91 (d, 6 and 6'-positions of tpy), 8.64–8.61 (d, 3 and 3'-positions of tpy), 7.83–7.81 (d, 3' and 5'-positions of tpy), 7.48–7.42 (t, 5 and 5'-positions of tpy), 7.44–7.41 (q, 2 and 6-positions of benzene ring), 7.14–7.10 (t, 4 and 4'-positions of tpy), 6.97–6.94 (t, 4'-position of tpy), 6.90 (s, 4-position of benzene ring), and 1.71 ppm (d, 6 methyl protons on benzene ring).
- [8] a) M. H. V. Huynh, P. S. White, T. J. Meyer, *Angew. Chem.* **2000**, *112*, 4267–4270; *Angew. Chem. Int. Ed.* **2000**, *39*, 4101–4104; b) Selected bond lengths and angles of the S-protonated *trans* isomer of the Os^{IV} –sulfilimido (*trans*-1⁺) complex are listed for comparison: Os–N(tpy) 2.015(10), 2.108(9), and 2.129(9) Å (with the shortest Os–N(tpy) bond *trans* to the sulfilimido ligand); Os=N(sulfilimido) 1.906(10) Å; N(1)–S(1) 1.706(9) Å (single bond); $\angle \text{Os}(1)\text{--N}(1)\text{--S}(1)$ 130.4(6) $^\circ$; and $\angle \text{N}(1)\text{--S}(1)\text{--C}(1)$ 101.6(5) $^\circ$.
- [9] a) M. H. V. Huynh, E.-S. El-Samanody, K. D. Demadis, P. S. White, T. J. Meyer, *Inorg. Chem.* **2000**, *39*, 3075–3085; b) M. H. V. Huynh, P. S. White, T. J. Meyer, *Inorg. Chem.* **2001**, *40*, 5231–5235.
- [10] The oxygen produced was measured by a Thermal Orion Model 1230 waterproof dissolved oxygen meter both with and without salinity correction modes. Each measurement of dissolved oxygen was corrected against a blank air-saturated acidic CH_3CN solution.

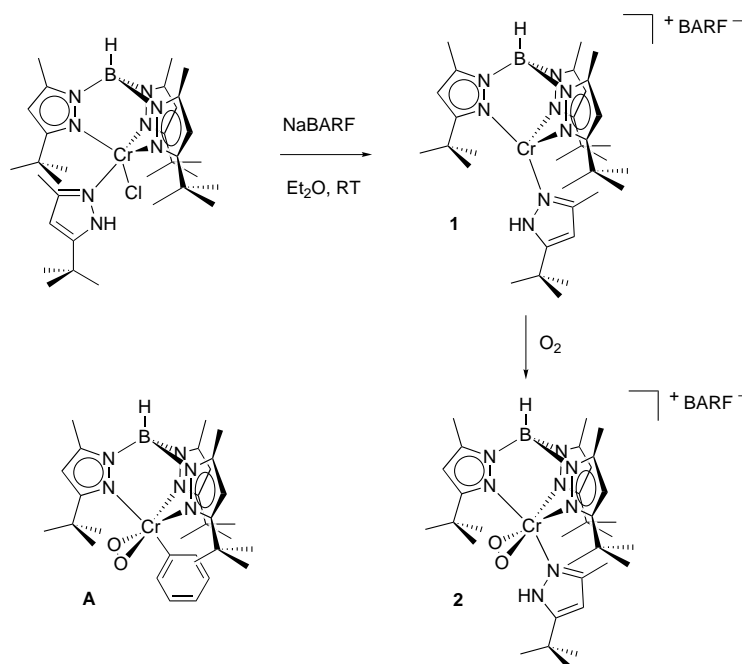
A Structurally Characterized Chromium(III) Superoxide Complex Features “Side-on” Bonding**

Kun Qin, Christopher D. Incarvito, Arnold L. Rheingold, and Klaus H. Theopold*

The coordination chemistry of dioxygen (O_2) is of interest in the context of bioinorganic chemistry and oxidation catalysis. Catalytic transformations utilizing O_2 as the oxidant are considered environmentally benign; however, they typically require “activation” of

the dioxygen by a metal center. Whereas the chemistry of chromium—a common ingredient in oxidation reagents—is replete with high-valent oxo (O^{2-}) or peroxo (O_2^{2-}) compounds, there exist few superoxo complexes of chromium resulting from the binding of gaseous O_2 , and none that have been structurally characterized.^[1] In a recent report on the insertion of O_2 into the chromium–carbon bond of $[\text{Tp}^{\text{tBu,Me}}\text{Cr-Ph}]$ ($\text{Tp}^{\text{tBu,Me}}$ = hydrotris(3-*tert*-butyl-5-methylpyrazolyl)-borate) we provided spectroscopic evidence for a reactive Cr^{III} superoxide intermediate (**A**, Scheme 1), and we proposed a “side-on” bonding mode for the superoxo ligand.^[2] Herein we describe the synthesis and structural characterization of a stable Cr^{III} superoxide complex that supports our earlier assignment.

Key to our investigation was the synthesis of a coordinatively unsaturated Cr^{II} precursor that would not suffer insertion of a coordinated O_2 , for example, into a chromium–carbon bond. Thus we prepared $[\text{Tp}^{\text{tBu,Me}}\text{Cr}(\text{pz}'\text{H})]\text{-BARF}$ (**1**, $\text{pz}'\text{H}$ = 3-*tert*-butyl-5-methylpyrazole, BARF = tetrakis(3,5-bis(trifluoromethyl)phenyl)borate) by reaction of $[\text{Tp}^{\text{tBu,Me}}\text{Cr}(\text{pz}'\text{H})\text{Cl}]$ with NaBARF (see Scheme 1). Complex **1** featured the characteristic *cis*-divacant octahedral structure of four-coordinate $[\text{Tp}^{\text{tBu,Me}}\text{CrX}]$ derivatives;^[3] hence it should be able to coordinate O_2 . Indeed, exposure of a diethyl ether solution of **1** at -78°C to excess O_2 caused a rapid color change from blue to red. Warming to room temperature followed by standard work-up of the reaction mixture yielded $[\text{Tp}^{\text{tBu,Me}}\text{Cr}(\text{pz}'\text{H})(\text{O}_2)]\text{BARF}$ (**2**) as a dark red solid in high yield. The solid-state IR spectrum of **2** showed an O–O stretching vibration at 1072 cm^{-1} . In the product of the reaction of **1** with $^{18}\text{O}_2$ this band was shifted to 1007 cm^{-1} . These values are consistent with an assignment as a superoxo complex of chromium(III).^[4] The effective magnetic moment of **2** ($\mu_{\text{eff}}(295\text{ K}) = 2.8(1)\mu_{\text{B}}$) must result from strong



Scheme 1. Synthesis of precursor **1** and chromium superoxo complex **2**.

[*] Prof. Dr. K. H. Theopold, K. Qin, C. D. Incarvito, Prof. Dr. A. L. Rheingold
Department of Chemistry and Biochemistry
Center for Catalytic Science and Technology
University of Delaware
Newark, DE 19716 (USA)
Fax: (+1) 302-831-6335
E-mail: theopold@udel.edu

[**] This work was supported by a grant from the U.S. Department of Energy.

antiferromagnetic coupling between the Cr^{III} ion (d^3 , $S = 3/2$) and the coordinated superoxide radical ($S = 1/2$).

The most unambiguous method for determining the bonding mode of the dioxygen is of course X-ray crystallography. Fortunately **2** is rather stable and cooling of a CH₂Cl₂ solution to -30°C gave dark red crystals of **2**·CH₂Cl₂ suitable for a structure determination (Figure 1).^[5] The most conspicuous feature is the “side-on” (or η^2 -) coordination of the O₂ ligand.

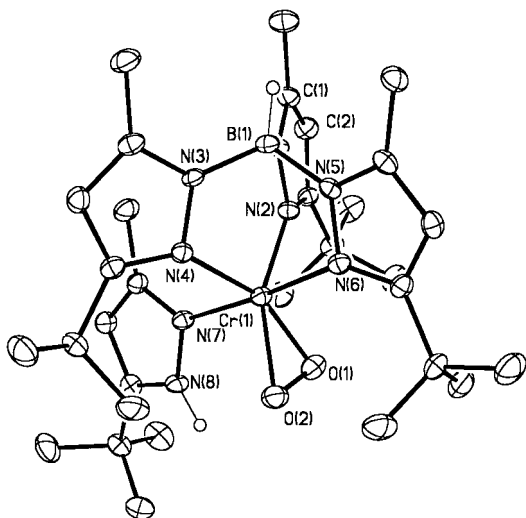


Figure 1. The molecular structure of **2**; the BARF anion has been omitted for clarity. Selected interatomic distances [Å] and angles [°]: Cr(1)–O(1) 1.861(4), Cr(1)–O(2) 1.903(4), O(1)–O(2) 1.327(5), Cr(1)–N(2) 2.069(4), Cr(1)–N(4) 2.080(5), Cr(1)–N(6) 2.080(4), Cr(1)–N(7) 2.063(5); O(1)–Cr(1)–O(2) 41.27(16), O(1)–Cr(1)–N(7) 88.48(18), O(2)–Cr(1)–N(7) 86.76(18).

At 1.861(4) and 1.903(4) Å, respectively, the Cr–O distances are essentially identical. The O(1)–O(2) bond length of 1.327(5) Å puts the ligand squarely into the superoxo category.^[6] The trivalent nature of chromium is also supported by the metal–ligand bond distances. Thus the average Cr–N_{TP} distance of 2.08 Å is significantly shorter than the corresponding value in [Tp^tBu₃MeCr^{II}(pz'H)(Cl)] (2.18 Å); the same holds for the Cr–N_{pzH} bond (2.063(5) Å versus 2.144(7) Å). The orientation of the pyrazole ligand (perpendicular to the CrO₂ plane) puts its NH proton in a position to hydrogen bond to the oxygen atoms.^[7] The relevant distances, namely 2.90 Å (N(8)–O(1)) and 2.80 Å (N(8)–O(2)), are certainly short enough for N–H···O interactions.^[8] However, the N–H–O angles (the hydrogen atom was located and its position refined) of 98.4° (N(8)–H–O(1)) and 109.8° (N(8)–H–O(2)) are rather acute for hydrogen bonds. Furthermore, the N–H stretching vibration of **2** appears as a sharp band at 3446 cm^{−1} in the IR spectrum, which is actually higher than $\nu_{\text{N-H}}$ of **1**. The evidence for substantial hydrogen bonding in **2** is thus ambiguous, and we hesitate to ascribe significant strengthening of the O₂ coordination to it.

Encouraged by the stability of **2**, and in the hopes of gauging electronic effects on the bonding of O₂ to Cr^{II} centers, we then investigated the reactivity of several analogous chromium complexes with dioxygen. Gratifyingly, [Tp^tBu₃MeCr(py)]BARF (py = pyridine), [Tp^tBu₃MeCrCl], and [Tp^tBu₃MeCrOPh] all yielded isolable dioxygen complexes, which have

been characterized by various methods, including IR spectroscopy of the ¹⁶O₂ and ¹⁸O₂ isotopomers. The results are listed in Table 1. The extent of electron transfer to the O₂ unit, as measured by $\nu_{\text{O-O}}$ stretching frequency data, parallels the donor strength of the changing ligand (Ph[−] > PhO[−] > pz'H > py > Cl[−]). Based on the chemical analogy and their spectroscopic similarity, we assume that all of these complexes contain side-on bonded superoxide ligands.

To our knowledge, **2** is the first structurally characterized

Table 1. O–O stretching frequencies of chromium(III) superoxo complexes.

Compound	$\nu(^{16}\text{O} - ^{16}\text{O})$	$\nu(^{18}\text{O} - ^{18}\text{O})$
[Tp ^t Bu ₃ MeCr(Ph)(O ₂)] ^[a]	1027 cm ^{−1}	969 cm ^{−1}
[Tp ^t Bu ₃ MeCr(OPh)(O ₂)]	1068 cm ^{−1}	1009 cm ^{−1}
[Tp ^t Bu ₃ MeCr(pz'H)(O ₂)]BARF (2)	1072 cm ^{−1}	1007 cm ^{−1}
[Tp ^t Bu ₃ MeCr(py)(O ₂)]BARF	1083 cm ^{−1}	1025 cm ^{−1}
[Tp ^t Bu ₃ MeCr(Cl)(O ₂)]	1104 cm ^{−1}	1044 cm ^{−1}

[a] Data from ref. [2].

chromium superoxo complex; it is also a representative of the small, but growing, number of mononuclear “side-on” superoxide complexes.^[9] We wish to suggest that this bonding mode may be more common than is generally assumed. The reactivity of this new class of O₂ complexes, especially with regard to dioxygen activation and oxidation reactions, is currently under investigation.

Experimental Section

1: [Tp^tBu₃MeCr(pz'H)Cl]^[2] (0.530 g 0.82 mmol) was dissolved in Et₂O (30 mL). An Et₂O solution of NaBARF (0.704 g 0.80 mmol) was added at room temperature. The mixture was stirred at room temperature for 48 h. After the solvent was removed, the solid was washed three times with pentane, and then extracted with Et₂O to yield a deep blue solution. Cooling the solution to -30°C overnight produced blue crystals (1.00 g, 80% yield) of **1**. ¹H NMR (250 MHz, CD₂Cl₂): δ = 81.0 (br, 3H), 48.9 (br, 9H), 32.4 (br, 3H), 10.9 (br, 27H), 7.8, 7.6 (12H), 2.8 (9H), −13.9 (1H), and −24.9 ppm (1H); IR (KBr): $\tilde{\nu}$ = 3435 (s, N–H), 2972 (s), 2805 (w), 2556 (w, B–H), 1610 (m), 1541 (s), 1473 (s), 1424 (s), 1354 (vs), 1276 (vs), 1137 (vs), 1063 (s), 887 (s), 838 (s), 806 (m), 716 (s), 682 cm^{−1} (s); UV/Vis (Et₂O): $\lambda_{\text{max}}(\epsilon)$ = 282 (4000), 669 nm (329); m.p.: 186°C; μ_{eff} (295 K) = 5.0(1) μ_{B} ; elemental analysis calcd (%) for C₆₄H₆₆B₂CrF₂₄N₈: C 52.05, H 4.50, N 7.59; found: C 51.75, H 4.66, N 7.53.

2: Compound **1** (0.445 g 0.3 mmol) dissolved in Et₂O (10 mL) was charged into an ampoule. This solution was degassed and cooled to -78°C . Then 1 atm of dry O₂ was admitted into the ampoule while the solution inside was stirred. The deep blue solution turned dark red within 5 min. The solution was kept under the O₂ atmosphere at -78°C overnight. Then the solvent was removed under vacuum, and the remaining solid was extracted with cold CH₂Cl₂. After cooling the concentrated solution to -30°C overnight, 0.325 g (70% yield) of dark red crystals of **2** were obtained. ¹H NMR (250 MHz, CD₂Cl₂): δ = 31.3 (br, 3H), 7.7, 7.6 (s, 12H), 3.5 (br, 27H), 1.7 (br, 9H), −8.9 ppm (br, 9H); IR (KBr): $\tilde{\nu}$ = 3446 (s, N–H), 3020 (w), 2971 (s), 2876 (w), 2565 (w, B–H), 1609 (m), 1546 (s), 1481 (s), 1423 (s), 1354 (vs), 1277 (vs), 1182 (vs), 1128 (vs), 1072 (s), 1046 (m), 1029 (w), 886 (s), 839 (s), 811 (s), 713 (s), 671 cm^{−1} (s); UV/Vis (Et₂O): $\lambda_{\text{max}}(\epsilon)$ = 279 (6150), 445 (714), 566 (407), 624 (264), 926 nm (274); m.p.: 125°C; μ_{eff} (295 K) = 2.8(1) μ_{B} ; elemental analysis calcd (%) for C₆₄H₆₆B₂CrF₂₄N₈O₂: C 50.94, H 4.41, N 7.42; found: C 50.29, H 4.19, N 6.90.

Received: February 18, 2002 [Z18729]

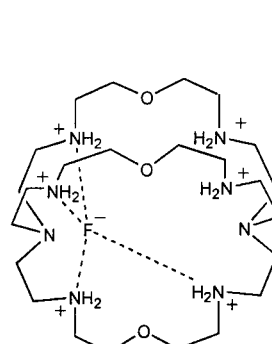
- [1] a) M. H. Dickmann, M. T. Pope, *Chem. Rev.* **1994**, 94, 569; b) S. K. Cheung, C. J. Grimes, J. Wong, C. A. Reed, *J. Am. Chem. Soc.* **1976**, 98, 5028; c) A. Bakac, S. L. Scott, J. H. Espenson, *J. Am. Chem. Soc.* **1995**, 117, 6483.
- [2] A. Hess, M. R. Hörz, L. M. Liable-Sands, D. C. Lindner, A. L. Rheingold, K. H. Theopold, *Angew. Chem. Int. Ed.* **1999**, 111, 126; *Angew. Chem.* **1999**, 38, 166.
- [3] J. L. Kersten, R. R. Kucharczyk, G. P. A. Yap, A. L. Rheingold, K. H. Theopold, *Chem. Eur. J.* **1997**, 3, 1668.
- [4] K. Nakamoto, *Infrared and Raman Spectra of Inorganic and Coordination Compounds*, 3rd ed., Wiley, New York, **1977**, p. 297.
- [5] **2**: monoclinic, $P2_1/c$, $a = 19.1562(15)$, $b = 19.6372(15)$, $c = 19.2621(14)$ Å, $\beta = 99.919(2)^\circ$, $V = 7137.6(9)$ Å³, $\rho_{\text{calc}} = 1.483$ g cm⁻³, $\theta = 1.73\text{--}27.00^\circ$, $\text{MoK}\alpha$, $\lambda = 0.71073$ Å, $T = 173$ K, 33900 reflections, 13653 independent, *SADABS* absorption correction, $\mu = 0.347$ mm⁻¹, max and min transmission: 0.9338 and 0.9338, solved by direct methods and refined by full-matrix least-squares procedures using SHELXTL (5.1), 945 parameters, $R = 0.0749$, $wR = 0.1943$, largest difference peak and hole: 1.027 and -1.301 e Å⁻³. CCDC-179035 (**2**) contains the supplementary crystallographic data for this paper. These data can be obtained free of charge via www.ccdc.cam.ac.uk/conts/retrieving.html (or from the Cambridge Crystallographic Data Centre, 12, Union Road, Cambridge CB2 1EZ, UK; fax: (+44) 1223-336-033; or deposit@ccdc.cam.ac.uk).
- [6] M. H. Gubelmann, A. F. Williams, *Struct. Bonding (Berlin)* **1983**, 55, 1.
- [7] a) Y. Takahashi, M. Hashimoto, S. Hikichi, M. Akita, Y. Moro-oka, *Angew. Chem.* **1999**, 111, 3259; *Angew. Chem. Int. Ed.* **1999**, 38, 3074; b) N. Kitajima, H. Komatsuzaki, S. Hikichi, M. Osawa, Y. Moro-oka, *J. Am. Chem. Soc.* **1994**, 116, 11596.
- [8] A. F. Wells, *Structural inorganic chemistry*, Clarendon, Oxford, **1984**, p. 357.
- [9] a) J. W. Egan, Jr., B. S. Haggerty, A. L. Rheingold, S. C. Sendlinger, K. H. Theopold, *J. Am. Chem. Soc.* **1990**, 112, 2445; b) K. Fujisawa, M. Tanaka, Y. Moro-oka, N. Kitajima, *J. Am. Chem. Soc.* **1994**, 116, 12079; c) X. Zhang, G. R. Loppnow, R. McDonald, J. Takats, *J. Am. Chem. Soc.* **1995**, 117, 7828; d) D. J. E. Spencer, N. W. Aboelella, A. M. Reynolds, P. L. Holland, W. B. Tolman, *J. Am. Chem. Soc.* **2002**, 124, 2108.

Parallels in Cation and Anion Coordination: A New Class of Cascade Complexes**

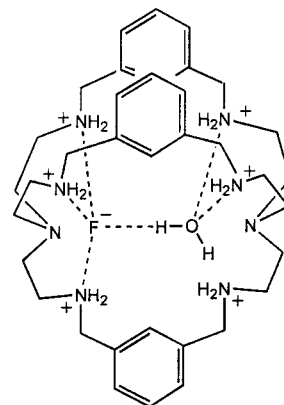
Md. Alamgir Hossain, José M. Llinares, Susan Mason,
Paula Morehouse, Douglas Powell, and
Kristin Bowman-James*

For a number of years it has been speculated that azacryptands capable of binding two metal ions could also serve as hosts for two discrete anions. In the early 1980s Lehn and co-workers proposed that a simple bicyclic azacryptand

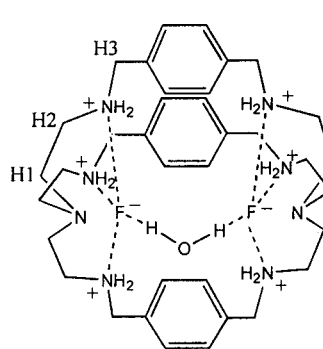
(bis-tren) derived from two tren (tris(2-aminoethyl)amine) units might be capable of encapsulating a bifluoride ion.^[1] Although not considered as “discrete” ions in that regard, bifluoride does consist of two fluoride ions linked by a hydrogen bridge. However, a crystal structure revealed only a single fluoride ion sitting to one side of the cavity (**A**). In 1998



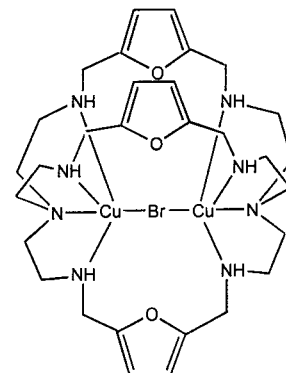
bis-tren(F)
A



MEAcryp(F)(H₂O)
B



PEAcryp(F)₂(H₂O)
C



FuEAcryp(Cu)₂(Br)
D

we observed ditopic anion binding behavior, namely, two discrete encapsulated nitrate ions, for a related azacryptand, MEAcryp.^[2, 3] Our subsequent attempt to sequester either a bifluoride ion or two discrete fluoride ions in the MEAcryp cavity was not successful, although crystallographic results did indicate two residents in the cavity: a molecule of water and a fluoride ion (**B**).^[4, 5]

By very slightly enlarging the cavity size with a *p*-xylyl spacer to give PEAcryp (**L**),^[2] we have at last succeeded in capturing two fluoride ions inside the cavity (**C**), to provide the first example of an azacryptand with two encapsulated fluoride ions. Rather than being linked by a single hydrogen atom, as for a bifluoride ion (F–H–F⁻), a water molecule bridges the two halide ions (F⁻⋯H–O–H⋯F⁻). This additional structural feature adds another dimension to the finding, thus making this complex the first example of an “anion-based cascade complex,” where two spherical anions play the topological role of the two metal ions in traditional cascade complexes. These findings serve to expand the

[*] Prof. K. Bowman-James, Dr. M. A. Hossain, Dr. J. M. Llinares, Dr. S. Mason, P. Morehouse, Dr. D. Powell
Department of Chemistry
University of Kansas
Lawrence, KS 66045 (USA)
Fax: (+1) 785-864-5396
E-mail: kbowman-james@ku.edu

[**] This research was sponsored by the Environmental Management Science Program, Offices of Science and Environmental Management, U.S. Department of Energy under Grant DE-FG-96ER62307.

Supporting information for this article is available on the WWW under <http://www.angewandte.org> or from the author.

increasing number of examples of analogies between traditional transition metal coordination chemistry and anion coordination chemistry, where hydrogen bonding in the latter replaces lone-pair coordination in the former.

Cascade complexes in ditopic aza macrocycles and cryptands are well-documented and were first termed as such over two decades ago.^[6] Normally these complexes consist of monocyclic or bicyclic ligands with two encapsulated metal ions and a bridging anion. More recently, researchers have advanced the field significantly by identifying more readily accessible macrocycles and cryptands derived from Schiff base condensations between amines and aromatic or heterocyclic dialdehydes, followed by simple reductions of the resulting imines to amines.^[7] These ligands form similar types of cascade complexes with metal ions, as in the recently reported dicopper cascade complex of a bis-tren cryptand with a furan spacer (**D**).^[8]

In this first example of an anion-based cascade complex, $[\text{H}_6\text{L}(\text{F})_2(\text{H}_2\text{O})][\text{SiF}_6]_2 \cdot 12\text{H}_2\text{O}$ (**1**), **L** is hexaprotonated, and is surrounded by two external SiF_6^{2-} counterions and twelve molecules of water.^[9–12] Thus, the only fluoride ions in the structure are in the cavity of **L**. Figure 1 shows views looking

Table 1. Interatomic distances and angles for hydrogen-bonding interactions of the encapsulated fluoride ions for **1**.

Atoms	Distance [Å]	Atoms	Distance [Å]
F1...N4	2.6703(14)	F(2)...N(13)	2.6538(14)
F1...N28	2.6042(14)	F(2)...N(19)	2.6820(14)
F1...N33	2.7237(12)	F(2)...N(42)	2.6100(14)
F1...O1S	2.7090(13)	F(2)...O(1S)	2.7168(13)
Atoms	Angle [°]	Atoms	Angle [°]
N4...F1...N28	111.5	N13...F2...N19	97.4
N4...F1...N33	96.7	N13...F2...N42	107.2
N28...F1...N33	97.1	N19...F2...N42	100.3
O1S...F1...N4	99.0	O1S...F2...N13	91.6
O1S...F1...N28	98.5	O1S...F2...N19	111.4
O1S...F1...N33	152.0	O1S...F2...N42	140.6

3.002 Å) which are slightly less than the sum of the van der Waals radii of nitrogen and fluorine atoms (3.02 Å).^[13] The hydrogen bonds from the fluoride ions to the amines range from 2.6 to just above 2.7 Å, with slightly longer hydrogen bonds to the water cascade. The fluoride...fluoride distance is 4.736 Å. The distance between the bridgehead nitrogen atoms (N1 and N16) of **L** is 10.717 Å, which results in an elongated ellipsoidal shape for the cryptand, and is probably the result of the two “guests” in the cavity.

An attempt to isolate a mixed fluoride/chloride complex resulted in a second cryptand structure in which two fluoride ions were found inside the cavity, $[\text{H}_6\text{L}(\text{F})_2(\text{H}_2\text{O})][\text{Cl}]_2[\text{SiF}_6] \cdot 9\text{H}_2\text{O}$ (**2**). Again the fluoride ions are bridged by a water molecule, but two chloride ions and a single SiF_6^{2-} ion serve as counterions, with nine additional water molecules of crystallization.^[14] The isolation of an analogous structure in the presence of competing anions indicates that the fluoride cascade complex represents a preferred structural pattern for fluoride ions with PEAcryp (**L**).

Protonation constants for **L** and binding constants for fluoride ions with **L** were determined by potentiometric methods, and the latter verified by NMR titrations. Although protonation constants for **L** were determined previously by others using Et_4NClO_4 as the electrolyte,^[15] we recalculated the constants using NaTsO (Ts = toluene-4-sulfonyl) as the electrolyte of choice for anion binding studies, as the bulky TsO^- ion is presumed to provide minimal competition for binding. The two series of pK_a values were in good agreement, with the exception of the fifth and sixth protonation steps, for which our values (5.80(4) and 5.68(2)) were almost one unit less than those previously reported (6.7(1) and 6.52(9)).^[15] Earlier studies on the influence of various electrolytes in these systems indicated that higher pK_a values in the lower pH region are observed in the presence of anions with binding capabilities, as would be the case for perchlorate.^[16]

Binding constants were determined by both potentiometric and NMR methods. The potentiometric results indicated two viable models, one with an $[\text{H}_6\text{LF}]^{5+}$ species and the other with an $[\text{H}_6\text{LF}_2]^{4+}$ species at low pH values (maximizing at about pH 4), but not a model where both occurred simultaneously. The system is very complex, however, as a consequence of the proximity of the fifth and sixth protonation constants, and so the actual species present at lower pH values become difficult to define unambiguously. Since the dinuclear

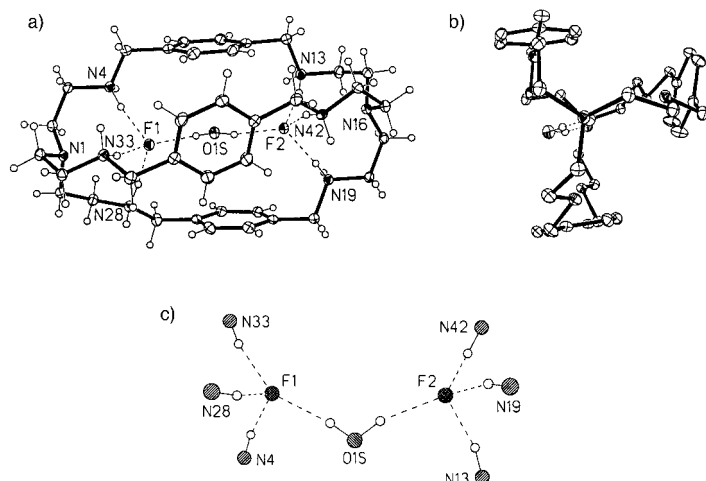


Figure 1. Views of $[\text{H}_6\text{L}(\text{F})_2(\text{H}_2\text{O})]^{4+}$: a) side view showing the water cascade; b) view down the pseudo-threefold axis; c) view showing only the coordination of the fluoride ions. The external anions and the water molecules of crystallization are omitted for clarity.

into the cavity and down the threefold axis (a and b, respectively). The view in Figure 1b shows that the two fluoride ions reside almost in the center of the cavity, with the water bridge somewhat to the outside: F1 is 0.124 Å and F2 is 0.229 Å from a line between N1 and N16. Each fluoride ion is coordinated in a very distorted tetrahedron through hydrogen-bonding interactions to three protonated secondary amines of a given tren unit and the bridging water molecule (Table 1, Figure 1c). The distortion arises from the fact that the water molecule lies between two of the three cryptand “arms,” the N4...N13 and N19...N28 bridges, which results in very large O-F-N angles for the farside bridge (N33...N42) of 152.0 and 140.6°.

The fluoride ions are almost equidistant from their respective bridgehead amines, at distances (2.994 and

results gave better statistics and were chemically plausible, these are taken as the best model (Figure 2). Furthermore, the ditopic model is in agreement with the crystal structure analysis. The results indicated $K_{[H_3LF]/[H_3L][F]} = 3.16(2)$, $\log K_{[H_4LF]/[H_4L][F]} = 3.24(4)$, $\log K_{[H_5LF]/[H_5L][F]} = 3.96(2)$, and

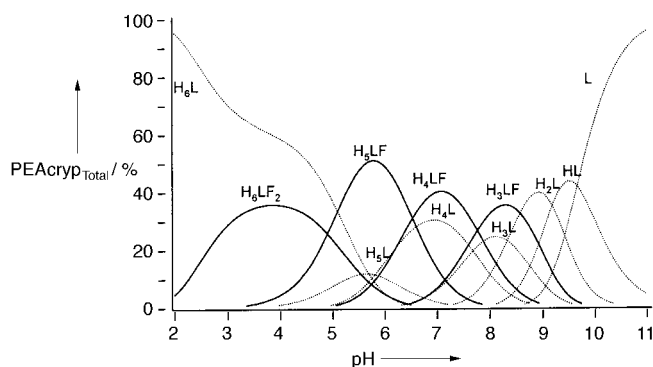


Figure 2. NMR titration curves for the three aliphatic signals of **L**, $\Delta H1$ (\blacktriangle), $\Delta H2$ (\bullet), and $\Delta H3$ (\blacksquare) with NaF in D_2O at $25^\circ C$ and $pD = 5.0 \pm 0.1$.

$\log K_{[H_6LF]/[H_5L][F]} = 6.54(5)$. The NMR results compare favorably with the potentiometric results and yielded $\log K_a = 3.13(5)$ for a 1:1 complex at $pD 5.0$, where potentiometric data indicate that the complex is a mixture of penta- and hexaprotonated receptors. The NMR titration of **L** with NaF at $pD 5.0$ gave the best fit for a 1:1 NaF:**L** ratio (Figure 3), in agreement with a Job's plot performed at $pD 5.0$, which indicated a maximum $\Delta\delta$ value at $0.6 = [L]/([L] + [F^-])$. These results, taken together, tend to indicate that a dinuclear complex is not the primary species in solution, although it may be present at lower pH values.

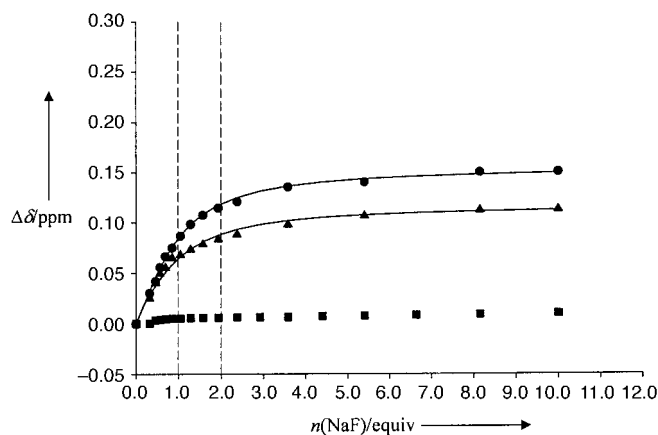


Figure 3. Distribution diagram of the tosylate salt of **L**·NaF (1:1) in 0.1 M NaTsO at 298.1 K.

^{19}F NMR spectroscopy was also used to probe the solution structure of the complex (Figure 4). Two signals are evident at $pH 5.0$: one at $\delta = -78$ ppm, and one at $\delta = -113$ ppm. The former is assigned to an internal fluoride ion, while the latter is characteristic of a solvated or external fluoride ion.^[4] The signal at $\delta = -78$ ppm is still sharp at $pH 5.5$, but quite broad at $pH 6.5$ and 7.0 , and is completely absent at $pH 7.5$. This observation contrasts with that found for the MEACryp

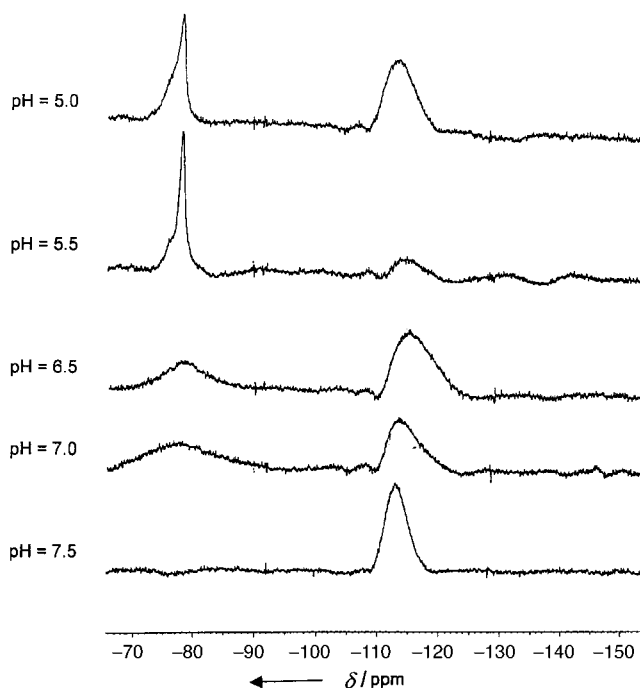


Figure 4. ^{19}F NMR spectra of NaF:PEACryp·6Ts (10 mM) in 0.1 M KT at $-25^\circ C$ in $DMSO:H_2O$ (40:60).

complex (**B**), where only an internally bound fluoride ion was observed between $pH 5.0$ and 6.5 .^[4]

In conclusion, this structure represents the first example of two fluoride ions within an azacryptand cavity. Additionally, a new class of cascade complexes with water as the cascade has been identified, where anions play the topological role of the metal ions. This finding further expands on the analogies between traditional transition metal coordination chemistry and anion coordination chemistry, where hydrogen bonds in the latter fill the role of the coordinate covalent bonds in the former.

Experimental Section

1: PEACryp (**L**) was synthesized according to previously published methods and isolated as the free base.^[5] The fluoride complex was obtained by titrating a solution of **L** in methanol with a 48 % solution of HF to $pH 2.0$. A white crystalline powder formed immediately, which was recrystallized from a mixture of isopropanol and water to yield X-ray quality colorless plates. 1H NMR (500 MHz, $CDCl_3$, TMS): $\delta = 2.87$ (t, 12 H, NCH_2), 3.31 (t, 12 H, NCH_2CH_2), 4.25 (s, 12 H, $ArCH_2$), 7.43 ppm (d, 12 H, ArH); ^{13}C NMR (125 MHz, $CDCl_3$, TMS): $\delta = 45.0$ (NCH_2), 48.8 (NCH_2CH_2), 51.0 ($ArCH_2$), 129.8 (C_{Ar}), 131.9 ppm (CH_{Ar}); FAB-MS: m/z 599 [HL] $^+$, 619 [$H_2L^{2+}+F^-$], 639 [$H_3L^{3+}+2F^-$]. Elemental analysis calcd for ($C_{36}H_{78}N_8F_{14}O_9Si_2$): C 39.70, H 7.21, N 10.28; found: C 39.77, H 7.04, N 10.23.

Potentiometric measurements: The potentiometric titrations were carried out in 0.1 M NaOTs at 298.1 ± 0.1 K. Electromotive force (EMF) data was obtained using an Orion 81–02 electrode. The electrode was calibrated as a hydrogen-ion concentration probe by titration of previously standardized amounts of HCl with CO_2 -free NaOH solutions and determining the equivalent point by the Gran's method, which gives the standard potential E° and the ionic product of water ($pK_w = 13.73(1)$). The computer program SUPERQUAD^[17] was used to calculate the protonation and stability constants. The titration curves for each system were obtained from about 100 experimental points corresponding to at least three measurements taken along the pH range 2.0–11.0. The concentrations of both ligand and

fluoride ions were 1 to 2 mM. The protonation constant of fluoride in water is: $\log K_{\text{HF/F}} = 3.15$.

NMR Measurements: ^1H NMR spectra were recorded on a Bruker AM500 spectrometer at 500 MHz. Binding constants were obtained by NMR titrations of **L** with fluoride from 25 measurements in D_2O at $\text{pD} = 5.0 \pm 0.1$. Initial concentrations were $[\text{L}]^0 = 2 \text{ mM}$ and titrations were performed using aliquots from a 20 mM stock solution of NaF. A solution of the sodium salt of [2,2,3,3- D_4]-3-(trimethylsilyl)propionic acid (TPS) in D_2O in a capillary tube was used as an external reference. The pD value was adjusted with a concentrated solution of TsOH and NaOD in D_2O . All spectra were recorded at room temperature. The association constants K_s were calculated by fitting f to δ_{obs} (consisting of several independent NMR signals) with a 1:1 association model using Sigma Plot software. Equations (1) and (2) were used, where **L** is the ligand and A^- is the anion, and the error limit in K is less than 10%:

$$c = ([\text{A}^-]^0 + [\text{L}]^0 + 1/K_s - \{([\text{A}^-]^0 + [\text{L}]^0 + 1/K_s)^2 - 4[\text{L}]^0[\text{A}^-]^0\}^{1/2})/2 \quad (1)$$

$$f = (\delta_{\text{LA}} - \delta_{\text{L}})c/[\text{L}]^0 + \delta_{\text{L}} \quad (2)$$

The Job's plot was performed by examining different concentration ratios of **L** and NaF in D_2O at $\text{pD} = 5.0 \pm 0.1$, while maintaining the total concentration of the ligand plus NaF at 10 mM. The pD value was adjusted with a concentrated solution of TsOH and NaOD in D_2O . NMR measurements were recorded at room temperature.

Received: October 22, 2001
Revised: April 12, 2002 [Z18101]

- [1] B. Dietrich, J. Guilhem, J.-M. Lehn, C. Pascard, E. Sonveaux, *Helv. Chim. Acta* **1984**, 67, 91–104.
- [2] Nomenclature: M = *m*-xylyl, P = *p*-xylyl, and Fu = furan spacers; E = ethyl links within the tren unit between amine groups; A = amine; cryp = cryptand.
- [3] a) S. Mason, T. Clifford, L. Seib, K. Kuczera, K. Bowman-James, *J. Am. Chem. Soc.* **1998**, 120, 8899–8900; b) T. Clifford, A. Danby, J. M. Llinares, S. Mason, N. W. Alcock, D. Powell, J. A. Aguilar, E. García-España, K. Bowman-James, *Inorg. Chem.* **2001**, 40, 4710–4720.
- [4] T. Clifford, S. Mason, J. M. Llinares, K. Bowman-James, *J. Am. Chem. Soc.* **2000**, 122, 1814–1815.
- [5] J. A. Aguilar, T. Clifford, A. Danby, J. M. Llinares, S. Mason, E. García-España, K. Bowman-James, *Supramol. Chem.* **2001**, 13, 405–417.
- [6] a) J.-M. Lehn, S. H. Pine, E. I. Watanabe, A. K. Willard, *J. Am. Chem. Soc.* **1977**, 99, 6766–6768; b) J.-M. Lehn, *Pure Appl. Chem.* **1980**, 52, 2441–2459.
- [7] a) J. Jazwinski, J.-M. Lehn, D. Lilenbaum, R. Ziessel, J. Guilhem, C. Pascard, *J. Chem. Soc. Chem. Commun.* **1987**, 1691–1692; b) D. McDowell, J. Nelson, *Tetrahedron Lett.* **1988**, 29, 385–386; c) D. Chen, A. E. Martell, *Tetrahedron* **1991**, 47, 6895–6902.
- [8] V. Amendola, E. Bastianello, L. Fabbrizzi, C. Mangano, P. Pallavicini, A. Perotti, A. M. Lanfredi, F. Ugozzoli, *Angew. Chem.* **2000**, 112, 3039–3042; *Angew. Chem. Int. Ed.* **2000**, 39, 2917–2920.
- [9] X-ray data for **1**: A crystal of dimensions $0.64 \times 0.42 \times 0.21 \text{ mm}$ was selected for structural analysis. Crystal data: $M_r = 1161.31$; triclinic space group, $P\bar{1}$, $a = 9.8302(11)$, $b = 15.9973(19)$, $c = 17.417(2) \text{ \AA}$, $\alpha = 84.404(3)^\circ$, $\beta = 89.959(3)^\circ$, $\gamma = 77.098(2)^\circ$, $V = 2656.5(5) \text{ \AA}^3$, $Z = 2$, $\rho_{\text{calcd}} = 1.452 \text{ g cm}^{-3}$, $F(000) = 1232$. A total of 12226 observed reflections ($I > 2\sigma(I)$) were collected. The refinement converged at $R1(F, \text{observed data}) = 0.0443$, and $wR2(F^2, \text{all data}) = 0.1189$, and $\text{GOF} = 0.974$. Diffraction data were collected using a Bruker SMART APEX CCD area detector mounted on a Bruker D8 goniometer using graphite-monochromated $\text{MoK}\alpha$ radiation ($\lambda = 0.71073 \text{ \AA}$) at $100(2) \text{ K}$.^[8] Intensity data were measured as a series of ω and θ oscillation frames each of 0.3° for times of 5 s per frame. The detector was operated in a 512×512 mode and was positioned 5.04 cm from the sample. Coverage of unique data was close to 99.4% complete to 26.00° in θ . Cell parameters were determined from a least-squares fit of 9504 peaks in the range $2.40 < \theta < 30.58^\circ$. Virtually no decay was

observed, based on data obtained for a number of peaks monitored at both the beginning and end of data collection. The data were corrected for absorption by the semi-empirical method.^[9] Lorentz and polarization corrections were applied. The data were merged to form a set of 15608 independent data with $R_{\text{int}} = 0.0248$. The space group was determined by statistical tests, and the structure was solved by direct methods and refined by full-matrix least-squares methods on F^2 .^[10] Hydrogen atom positions were initially determined by geometry and refined by a riding model. Non-hydrogen atoms were refined with anisotropic displacement parameters. CCDC-172118 (**1**) and CCDC-172119 (**2**) contains the supplementary crystallographic data for this paper. These data can be obtained free of charge via www.ccdc.cam.ac.uk/conts/retrieving.html (or from the Cambridge Crystallographic Data Centre, 12, Union Road, Cambridge CB21EZ, UK; fax: (+44) 1223-336-033; or deposit@ccdc.cam.ac.uk).

- [10] Data collection: SMART Software Reference Manual, Bruker-AXS, 6300 Enterprise Dr., Madison, WI 53719-1173, USA, **1994**. Data reduction: SAINT Software Reference Manual, Bruker-AXS, 6300 Enterprise Dr., Madison, WI 53719-1173, USA, **1995**.
- [11] G. M. Sheldrick, SADABS. Program for Empirical Absorption Correction of Area Detector Data, University of Göttingen, Göttingen (Germany), **1996**.
- [12] G. M. Sheldrick, SHELXTL Version 5 Reference Manual, Bruker AXS 5465 E. Cheryl Parkway, Madison, WI 53711-5373, USA, **1994**, using *International Tables for Crystallography, Vol. C*, Kluwer, Boston, **1995**, Tab. 6.1.1.4, 4.2.6.8, and 4.2.4.2.
- [13] N. Alcock in *Bonding and Structure*, Ellis Horwood, West Sussex, England, **1990**, p. 316.
- [14] Synthesis, characterization, and structural results for **2** are given in the Supporting Information.
- [15] Protonation constants for PEAcryp have been reported as $\log K_1 = 9.6(1)$, $\log K_2 = 9.00(4)$, $\log K_3 = 8.62(8)$, $\log K_4 = 7.3(1)$, $\log K_5 = 6.7(1)$, and $\log K_6 = 6.52(9)$ using Et_4NClO_4 as the electrolyte: F. Arnaud-New, S. Fuangswasdi, B. Maubert, J. Nelson, V. McKee, *Inorg. Chem.* **2000**, 39, 573–579.
- [16] R. J. Motekaitis, A. E. Martell, J.-M. Lehn, E.-I. Watanabe, *Inorg. Chem.* **1982**, 21, 4253–4257.
- [17] P. Gans, A. Sabatini, A. Vacca, *J. Chem. Soc. Dalton Trans.* **1985**, 1195–1200.

Stereoselective Formation of Quaternary Carbon Centers: Alkylation of α,α -Disubstituted Amide Enolates**

Jeffrey M. Manthorpe and James L. Gleason*

The stereoselective formation of quaternary carbon centers is one of the most challenging tasks in organic chemistry and can only be achieved using methods which employ some form of carbon–carbon bond forming reaction.^[1] One of the most straightforward methods for the formation of carbon–carbon bonds is the alkylation of an enolate with an alkyl halide and,

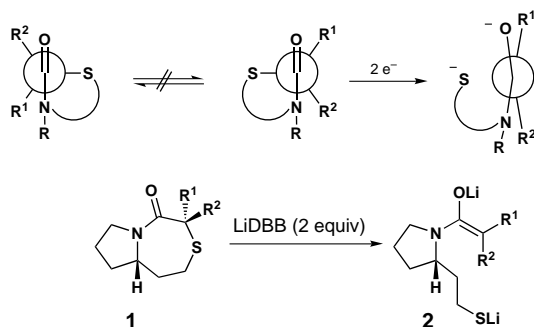
[*] Prof. J. L. Gleason, J. M. Manthorpe
Department of Chemistry
McGill University
801 Sherbrooke St. West, Montreal, QC, H3A 2K6 (Canada)
Fax: (+1) 514-398-3797
E-mail: jim.gleason@mcgill.ca

[**] We thank NSERC, Research Corporation, and Merck Frosst Therapeutic Inc. for support of this research. J.M.M. acknowledges support from FCAR in the form of a postgraduate fellowship.

Supporting information for this article is available on the WWW under <http://www.angewandte.org> or from the author.

indeed, several methods for the stereoselective formation of quaternary carbon centers have been based on this approach.^[2–17] One of the most significant problems in any approach based on enolate alkylation is to control enolate stereochemistry (*E* vs. *Z*). This control is necessary, as it works in tandem with π -facial selectivity to a stereoselective reaction. Many methods solve this problem by employing cyclic enolates or metal chelates.^[2–11] Although this works well, the final alkylation products usually contain specific functional group residues that were necessary to form the cyclic enolate. This often limits the scope of these methods.

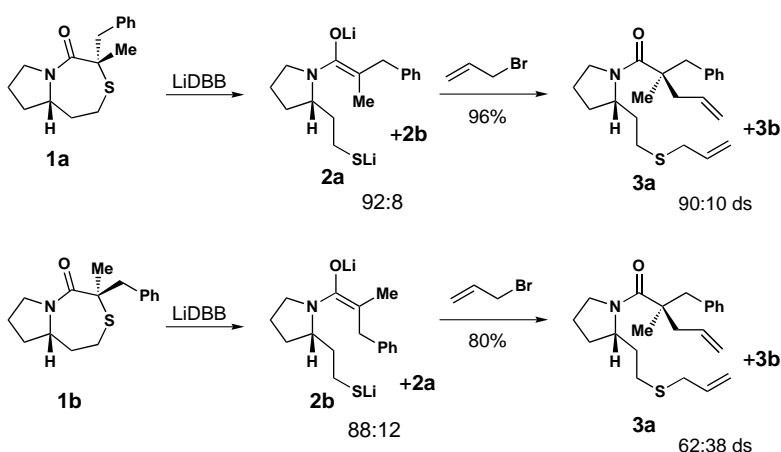
Recently, we reported a method for the preparation of α,α -disubstituted amide enolates by reduction of bicyclic thioglycolate lactams.^[18] This method was based on a simple operational model wherein the bicyclic system constrains the sulfur so that it is held rigidly on one face of the carbonyl plane (Scheme 1). Upon two-electron



Scheme 1. Operational model for the stereocontrolled synthesis of α,α -disubstituted amide enolates **2** by reduction of bicyclic thioglycolate lactams **1**.

reduction, carbon–sulfur bond cleavage occurs to form an enolate dianion and the *E/Z* stereochemistry of the enolate is governed by the relative locations of the α -alkyl groups in the starting lactam. Good to excellent levels of stereocontrol are observed and both *E* and *Z* amide enolates **2** may be prepared (Scheme 1). Importantly, this method removes the requirement for a cyclic enolate or chelating functionality to control enolate stereochemistry; any alkyl groups may be present at the R^1 and R^2 positions. A feature of our design is that the reduction step liberates a chiral auxiliary which is reminiscent of a prolinol amide. Prolinol amides have been used to control stereochemistry in alkylations which form tertiary carbon stereocenters.^[19] Here, we report that high stereoselectivities may be achieved for the formation of quaternary carbon centers by the alkylation of our α,α -disubstituted enolates, which in many cases even exceed the stereoisomer ratio of the intermediate enolates.

As previously reported, reduction of diastereomeric lactams **1a** and **1b** with lithium di-*tert*-butyldiphenylide (LiDBB)^[20] in THF at -78°C affords the corresponding *Z* and *E* enolates with 92:8 and 88:12 selectivity, respectively (Scheme 2).^[18] Addition of allyl bromide to the enolates



Scheme 2. Alkylation to form quaternary carbon stereocenters.

resulted in the formation of C,S-dialkylated products in high yields.^[21] Intriguingly, alkylation of either enolate, **2a** or **2b**, afforded the same major product **3a**. The alkylation of *Z* enolate **2a** showed good stereoselectivity (90:10) which was roughly in line with the ratio of the intermediate enolates. Alkylation of *E* enolate **2b** was only poorly selective (62:38).^[22] Additives had only a modest effect on the alkylation selectivity of the *E* enolate. Conducting the reaction in the presence of 20% hexamethylphosphoramide (HMPA) reversed the stereoselectivity slightly (39:61 ratio), while addition of 1,3-dimethyl-3,4,5,6-tetrahydro-2(1*H*)-pyrimidinone (DMPU, 45%) or LiCl (10 equiv) had minimal effects. The addition of HMPA had no discernable effect on either the yield or the stereoselectivity in the alkylation of the *Z* enolate.

A significant and practical improvement in the stereoselectivity of the alkylation was observed when the *Z* enolates are allowed to react with unactivated alkyl halides [Eq. (1), Table 1]. For instance, reaction of enolate **2a** with ethyl iodide instead of allyl bromide afforded the corresponding product **3c** with 96.5:3.5 diastereoselectivity (93% *de*). Similar selec-

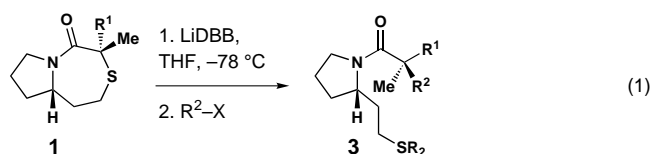


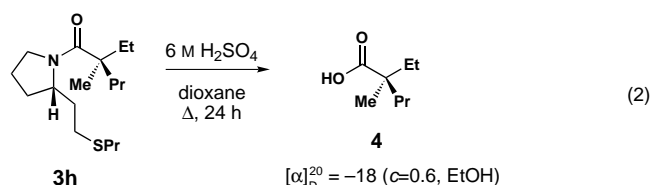
Table 1. Alkylations using unactivated electrophiles [Eq. (1)].

Lactam	R^1	<i>Z/E</i> Ratio of 2 ^[a]	<i>de</i> [%] of 2	R^2X	Product	Yield [%]	<i>de</i> [%] ^[a]
1a	Bn	92:8	84	EtI	3c	89	93
1a	Bn	92:8	84	<i>n</i> BuI	3d	76	> 95
1c	<i>n</i> Pr	87:13	74	EtI	3e	85	89
1c	<i>n</i> Pr	87:13	74	<i>n</i> BuI	3f	71	95
1c	<i>n</i> Pr	87:13	74	<i>i</i> BuI	3g	59 ^[b]	87
1d	Et	90:10	80	<i>n</i> PrI	3h	83	> 95
1e	allyl	87:13	74	EtI	3i	84	88
1e	allyl	87:13	74	BuI	3j	80	91
1f	<i>n</i> Bu	— ^[c]	—	<i>n</i> PrI	3k	88	> 95

[a] Determined by ^{13}C NMR spectroscopy. [b] HMPA (23%) was added during the alkylation step. [c] Not determined.

tivities were observed for a series of *Z* enolates and unactivated *n*-alkyl halides. The yields were high and in most cases the reactions proceeded to completion within 4 h at -78°C without added polar co-solvents.^[23] Branched alkyl halides such as isobutyl iodide were slower to react, but gave acceptable yields at -78°C in the presence of HMPA.^[24] Importantly, in all cases explored with unactivated alkyl iodides the alkylation selectivities were higher than the *Z/E* ratios of the intermediate enolates. This selectivity enhancement presumably has its origin in the low alkylation selectivity of the minor *E* enolates (1:1 selectivity was observed for reaction of **2b** with EtI). From a practical standpoint, the poor selectivity of the *E* enolates is not a significant issue, as a judicious choice of the alkylation sequence can allow stereoisomeric products to be prepared. For example, alkylation products **3f** and **3k** were prepared with high diastereoselectivity by simply inverting the overall alkylation sequence. These molecules are not true diastereomers, as they have different alkyl groups on sulfur. However, upon cleavage of the amide auxiliary (vide infra), the final products were isolated as a pair of enantiomers.

Hydrolysis of the alkylation products proved to be difficult. Heating **3h** in a 1:1 mixture of 6 M H_2SO_4 and dioxane for 24 h resulted in formation of the acid **4** [Eq. (2)] in 18 % yield



along with recovery of 71 % of the starting material. Although this direct hydrolysis was not practical, it did allow the stereochemistry of the alkylation process to be elucidated. Comparison of the optical rotation of **4** with literature data established that the *S* isomer was formed in the alkylation step.^[25] Thus, the alkylation occurs from the top face of the enolate [as drawn in Eq. (2)]. Similar facial selectivity was observed by Evans and Takacs in the reactions of O-alkylated prolinol *Z* amide enolates.^[19a] In the latter case, masking the prolinol hydroxyl group as an ether resulted in a switch in facial selectivity, presumably due to a loss of chelation. Given the similar facial selectivity and that chelation here would require an eight-membered ring, our results seem most consistent with an unchelated enolate.

An effective method for removal of the chiral auxiliary proved to be reductive cleavage. Treatment of the amides with lithium amidotrihydroborate^[26] in THF at reflux [Eq. (3)] afforded the corresponding primary alcohols in high yields (Table 2). The enantiomeric excess of the products was assessed either directly or on the corresponding carboxylic acids (see Table 2 and Supporting Information). In all cases, the enantiomeric excess of the products was consistent with the diastereomeric excess of the alkylation products, indicating that no significant kinetic resolution occurred during the reductive cleavage of the chiral auxiliary.

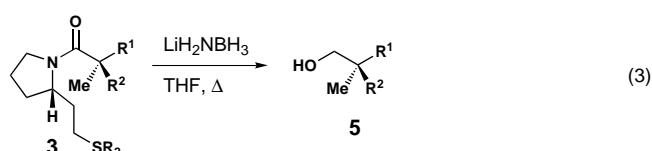


Table 2. Reductive cleavage of the chiral auxiliary with lithium amidotrihydroborate [Eq. (3)].

Amide	R ¹	R ²	Product	Yield [%]	ee [%]
3c	Bn	Et	5a	96	94 ^[a]
3d	Bn	<i>n</i> Bu	5b	97	96 ^[a]
3f	<i>n</i> Pr	<i>n</i> Bu	5c	99	96 ^[b]
3k	<i>n</i> Bu	<i>n</i> Pr	5d	87	95 ^[b]
3j	allyl	<i>n</i> Bu	5e	74	93 ^[b]

[a] Determined by HPLC analysis (Chiracel OD column). [b] Determined by capillary GC analysis (ChirasilDex column) on the corresponding carboxylic acid. Due to peak tailing, the GC analyses are accurate to within $\pm 2\%$.

In conclusion, we have developed a highly stereoselective enolate alkylation process for the generation of quaternary carbon centers. The stereoselectivities are highest for reactions of α,α -disubstituted *Z* amide enolates with unactivated *n*-alkyl iodides. The method is notable in that high selectivities are obtained without the need for cyclic enolates or metal chelates, thus allowing any alkyl group to be incorporated into the final product. The resulting alkylation products may be cleaved in high yield to the corresponding primary alcohols using lithium amidotrihydroborate. Finally, enantiomeric pairs of molecules may be formed simply by inverting the order of alkylation followed by cleavage of the chiral auxiliary. Further studies in this area will focus on the extension of the method to other carbon–carbon bond forming reactions.

Experimental Section

Reduction/alkylation procedure [Eq. (1)]: A solution of LiDBB in THF was added dropwise with a glass syringe to a solution of lactam **1a** (243 mg, 882 μmol , 1 equiv) in THF (8.8 mL) in a Schlenk flask at -78°C until the green color of LiDBB briefly persisted. *n*-Butyl iodide (402 μL , 3.53 mmol, 4.0 equiv) was added dropwise and the solution was stirred at -78°C for 4 h. Saturated ammonium chloride solution (10 mL) was added and the resulting mixture was warmed to room temperature and extracted with ethyl acetate ($3 \times 25\text{ mL}$). The combined organic layers were dried over anhydrous sodium sulfate, filtered, and concentrated. The residue was purified by chromatography on silica gel eluting with 3 % ethyl acetate in hexanes to afford 260 mg of **3d** as a colorless oil in 76 % yield. The product was determined to have $>95\%$ *de* by ^{13}C NMR analysis. ^1H NMR ($\text{C}_6\text{D}_5\text{CD}_3$, 105°C): δ = 6.95–7.08 (m, 5H), 4.24 (m, 1H), 2.93–3.11 (m, 3H), 2.38–2.51 (m, 5H), 1.97–2.16 (m, 2H), 1.07–1.60 (m, 14H), 1.13 (s, 3H), 0.76–0.88 ppm (m, 6H); ^{13}C NMR ($\text{C}_6\text{D}_5\text{CD}_3$, 105°C): δ = 173.8, 138.8, 130.3, 127.7, 126.0, 58.8, 48.2, 46.9, 46.3, 41.3, 34.3, 31.9, 31.8, 29.3, 28.8, 27.0, 25.0, 23.2, 22.6, 21.8, 13.6, 13.2 ppm. C, H, N analysis calcd for $\text{C}_{24}\text{H}_{39}\text{NOS}$: C 73.98, H 10.09, N 3.59; found: C 74.31, H 9.98, N 3.60.

Reductive cleavage of the chiral auxiliary [Eq. (3)]: A solution of *n*-butyllithium in hexanes (2.27 M, 2.39 mL, 5.42 mmol, 3.90 equiv) was slowly added to a stirred solution of diisopropylamine (799 μL , 5.70 mmol, 4.10 equiv) in THF (2.5 mL) at 0°C . After stirring for 10 min, borane–ammonia complex (90 %, 191 mg, 5.56 mmol, 4.0 equiv) was added in one portion. After stirring at 0°C for 15 min the mixture was warmed to 23°C and after 10 min a solution of **3c** (464 mg, 1.39 mmol, 1 equiv) in THF (5 mL) was added with a cannula. The mixture was heated at reflux for

24 h, then cooled to 0 °C, and quenched with aqueous hydrochloric acid (3 M, 5 mL). The resulting mixture was warmed to 23 °C and stirred for 30 min, at which point aqueous sodium hydroxide (3 M, 10 mL) was added. The mixture was stirred at 23 °C for 30 min and extracted with diethyl ether (3 × 20 mL). The combined organic layers were dried over anhydrous sodium sulfate, filtered, and concentrated in vacuo. Column chromatography on silica gel eluting with 30 % diethyl ether in pentane afforded (R)-2-ethyl-2-methyl-2,3-dihydrocinnamyl alcohol **5a** (239 mg, 1.34 mmol, 96 %) as a colorless oil. ¹H NMR (CDCl₃): δ = 7.19–7.31 (m, 5H), 3.33 (s, 2H), 2.61 (AB, 2H, J = 24.6 Hz), 1.58 (bs, 1H), 1.27–1.40 (m, 2H), 0.93 (t, 3H, J = 7.5 Hz), 0.82 ppm (s, 3H); ¹³C NMR (CDCl₃): δ = 139.0, 130.8, 128.1, 126.2, 68.4, 42.8, 39.1, 29.1, 21.0, 8.3 ppm. High-resolution FAB-MS: m/z (M+H): 179.14359 (C₁₂H₁₉O⁺ requires 179.14359). [α]_D²⁵ = –5.9 (c = 14.2, CH₂Cl₂). The product was determined to have 94 % ee by HPLC (Chiralcel OD column, eluting with 1 % 2-propanol in hexanes at 0.7 mL min^{–1}; R_t = 20.5 min (major enantiomer), 22.8 min (minor enantiomer)).

Received: October 26, 2001

Revised: April 11, 2002 [Z18123]

- [1] For reviews, see: a) K. Fuji, *Chem. Rev.* **1993**, 93, 2037; b) E. J. Corey, A. Guzman-Perez, *Angew. Chem.* **1998**, 110, 402; *Angew. Chem. Int. Ed.* **1998**, 37, 388.
- [2] a) A. I. Meyers, M. Harre, R. Garland, *J. Am. Chem. Soc.* **1984**, 106, 1146; b) D. Romo, A. I. Meyers, *Tetrahedron* **1991**, 47, 9503; c) M. D. Groaning, A. I. Meyers, *Tetrahedron*, **2000**, 56, 9843.
- [3] a) A. G. Schultz, M. Macielag, P. Sundararaman, A. G. Taveras, M. Welch, *J. Am. Chem. Soc.* **1988**, 110, 7828; b) A. G. Schultz, *Acc. Chem. Res.* **1990**, 23, 207; c) A. G. Schultz, *Chem. Commun.* **1999**, 1263.
- [4] G. Frater, *Helv. Chim. Acta* **1979**, 62, 2825.
- [5] a) K. Tomioka, K. Ando, Y. Takemasa, K. Koga, *J. Am. Chem. Soc.* **1984**, 106, 2718; b) K. Kato, H. Suemune, K. Sakai, *Tetrahedron* **1994**, 50, 3315.
- [6] M. Ihara, M. Takahashi, H. Niitsuka, N. Taniguchi, K. Yasui, K. Fukumoto, *J. Org. Chem.* **1989**, 54, 5413.
- [7] a) J. Aahman, J. P. Wolfe, M. V. Troutman, M. Palucki, S. L. Buchwald, *J. Am. Chem. Soc.* **1998**, 120, 1918; b) A. Chieffi, K. Kamikawa, J. Ahman, J. M. Fox, S. L. Buchwald, *Org. Lett.* **2001**, 3, 1897.
- [8] a) B. M. Trost, G. M. Schroeder, *J. Am. Chem. Soc.* **1999**, 121, 6759; b) S.-L. You, X.-L. Hou, L.-X. Dai, X.-Z. Zhu, *Org. Lett.* **2001**, 3, 149.
- [9] a) A. Bhattacharya, U.-H. Dolling, E. J. J. Grabowski, S. Karady, K. M. Ryan, L. M. Weinstock, *Angew. Chem.* **1986**, 98, 442; *Angew. Chem. Int. Ed. Engl.* **1986**, 25, 476; b) U.-H. Dolling, P. Davis, E. J. J. Grabowski, *J. Am. Chem. Soc.* **1984**, 106, 446; c) Y. Yamashita, K. Odashima, K. Koga, *Tetrahedron Lett.* **1999**, 40, 2803.
- [10] a) L. E. Overman, J. F. Larrow, B. A. Stearns, J. M. Vance, *Angew. Chem.* **2000**, 112, 219; *Angew. Chem. Int. Ed.* **2000**, 39, 213; b) S. B. Hoyt, L. E. Overman, *Org. Lett.* **2000**, 2, 3241.
- [11] D. Enders, P. Teschner, G. Raabe, J. Runsink, *Eur. J. Org. Chem.* **2001**, 4463.
- [12] S. Hosoi, K. Sekiguchi, M. Enemoto, S. Kobayashi, *Tetrahedron Lett.* **2000**, 41, 6429.
- [13] S. G. Davies, J. C. Walker, *J. Chem. Soc. Chem. Commun.* **1986**, 495.
- [14] P. I. Dalko, Y. Langlois, *J. Org. Chem.* **1998**, 63, 8107.
- [15] T. Hamamoto, T. Katsuki, M. Yamaguchi, *Tetrahedron Lett.* **1986**, 27, 2463.
- [16] D. Enders, A. Zamponi, T. Schäfer, C. Nübling, H. Eichenauer, A. S. Demir, G. Raabe, *Chem. Ber.* **1994**, 127, 1707.
- [17] R. K. Boeckman, D. J. Boehmler, R. A. Musselman, *Org. Lett.* **2001**, 3, 3777.
- [18] J. M. Manthorpe, J. L. Gleason, *J. Am. Chem. Soc.* **2001**, 123, 2091.
- [19] a) D. A. Evans, J. M. Takacs, *Tetrahedron Lett.* **1980**, 21, 4233; b) P. Sonnet, R. R. Heath, *J. Org. Chem.* **1980**, 45, 3137; c) D. A. Evans, R. L. Dow, T. S. Shih, J. M. Takacs, R. Zahler, *J. Am. Chem. Soc.* **1990**, 112, 5290.
- [20] P. K. Freeman, L. L. Hutchinson, *Tetrahedron Lett.* **1976**, 1849.
- [21] Greater than two equivalents of electrophile must be added, as the S- and C-alkylations occur at similar rates.
- [22] The reasons for this dichotomous behavior are unclear. We have been unable to detect significant E/Z isomerization under the reaction

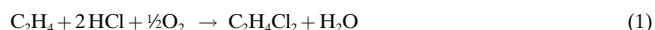
conditions. Other effects such as aggregation state and/or different reactive conformations of the E and Z enolates cannot be ruled out.


- [23] Alkylation of amide enolates with unactivated electrophiles often requires the addition of HMPA or LiCl for useful reaction rates to be observed. For examples see ref. [19] and a) A. G. Myers, B. H. Yang, H. Chen, L. McKinstry, D. J. Kopecky, J. L. Gleason, *J. Am. Chem. Soc.* **1997**, 119, 6496; b) W. Oppolzer, R. Moretti, S. Thomi, *Tetrahedron Lett.* **1989**, 30, 5603.
- [24] Addition of HMPA affected only the reaction rate. Conducting the reaction without HMPA resulted in the identical diastereoselectivity but the yield of **3g** was only 20 %.
- [25] G. Fronza, G. Fogliato, C. Fuganti, P. Grasselli, R. Rigoni, *Tetrahedron* **1996**, 52, 14281.
- [26] a) A. G. Myers, B. H. Yang, D. J. Kopecky, *Tetrahedron Lett.* **1996**, 37, 3623; b) A. G. Myers, B. H. Yang, H. Chen, D. J. Kopecky, *Synlett* **1997**, 5, 457; see also: c) G. B. Fisher, J. C. Fuller, J. Harrison, S. G. Alvarez, E. R. Burkhardt, C. T. Goraliski, B. Singaram, *J. Org. Chem.* **1994**, 59, 6378.

The Chemistry of the Oxychlorination Catalyst: an In Situ, Time-Resolved XANES Study**

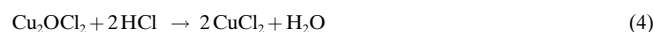
Carlo Lamberti,* Carmelo Prestipino, Francesca Bonino, Luciana Capello, Silvia Bordiga, Giuseppe Spoto, Adriano Zecchina, Sofia Diaz Moreno, Barbara Cremaschi, Marco Garilli, Andrea Marsella, Diego Carmello, Sandro Vidotto, and Giuseppe Leofanti

Almost all of the world production of vinyl chloride today is based on cracking of 1,2-dichloroethane. For many decades, this compound has been produced by catalytic oxychlorination of ethylene with hydrochloric acid and oxygen [Eq. (1)]. The reaction is performed at 490–530 K and 5–6 atm (1 atm ≈ 1.01 × 10⁵ Pa) using both air and oxygen in fluid- or fixed-bed reactors.^[1]



- [*] Dr. C. Lamberti,^[+] C. Prestipino,^[+] F. Bonino, L. Capello,^[+] Prof. Dr. S. Bordiga, Prof. Dr. G. Spoto, Prof. Dr. A. Zecchina
Dipartimento di Chimica IFM
Via P. Giuria 7, 10125 Torino (Italy)
and
INSTM Research unit of Turin University
Fax: (+39) 011-670-7855
E-mail: carlo.lamberti@unito.it
Dr. S. Diaz Moreno
ESRF
BP 220, 38043 Grenoble (France)
B. Cremaschi, M. Garilli, A. Marsella, D. Carmello, S. Vidotto, G. Leofanti^[++]
EVC Technological Centre
Via della Chimica 5, 30175 Porto Marghera/Venezia (Italy)
- [+] Also with INFN UdR di Torino Università (Italy)
- [++] Consultant: Via Firenze 43, 20010 Canegrate/Milano (Italy)
- [**] L.C. was supported by an INFN grant for her stay at the ESRF. We are indebted to R. Weigel for his fundamental support during data acquisition and to M. Sanchez Del Rio for his important support on the complex data handling.
-  Supporting information for this article is available on the WWW under <http://www.angewandte.org> or from the author.

Commercial catalysts are produced by impregnation of γ -alumina with CuCl_2 (4–8 wt % Cu). Other chlorides (mainly alkali or alkaline earth metal chlorides) in variable concentration are also added to make the catalyst more suitable for industrial reactors.^[1–3] In spite of an abundant literature on the subject,^[1–8] a significantly improved knowledge of the system—limited to the basic catalyst (containing only CuCl_2 without additives)—has been achieved only recently.^[4, 6–8] In particular, it has been shown by feeding separately the three reagents that the oxychlorination reaction (1) is catalyzed by a highly dispersed CuCl_2 phase^[4, 6] and follows a three-step redox mechanism: a) chlorination of ethylene by reduction of CuCl_2 to CuCl [Eq. (2)], b) oxidation of CuCl to an oxychloride [Eq. (3)], and c) re-chlorination of this oxychloride with HCl [closure of the catalytic cycle,^[7, 8] Eq. (4)].



However, as no information is available on the true state of the catalyst in the simultaneous presence of all three reagents, it is not possible to identify the rate-determining step of the reaction. Here we report the first temperature-resolved investigation on the oxidation state and activity of the catalyst under true reaction conditions. The aim of the present work is to identify how the chemistry of the copper species controls the catalytic functions and how the presence of potassium (that is, the typical additive of fixed-bed industrial catalysts) modifies the chemical properties of the copper species and thus the catalytic behavior of the catalyst.

The temperature was increased from 373 to 623 K and then decreased again to 373 K to model the wide range of temperature that can be found in the different zones of the fixed-bed reactors at different periods of catalyst lifetime. The oxidation state of the catalyst was monitored by the shift of the Cu_K edge in XANES spectra.^[9] XANES spectroscopy has been shown to be very sensitive to $\text{Cu}^I \rightleftharpoons \text{Cu}^{II}$ changes,^[7, 8, 10–13] and has the further advantage that X-rays are particularly suitable for in situ studies. The present study was performed on the basic catalyst (hereafter Cu5.0), and then it was extended to a catalyst containing also KCl (hereafter K3.6Cu5.0).

The $\text{Cu}^{II} \rightarrow \text{Cu}^I$ reduction can be deduced from the decrease of the white-line intensity (Figure 1a, b) and from the blue shift of the absorption edge, more evident in the first derivative spectra (Figure 1c). A comparison of these XANES spectra with those of model compounds reveals that the low-temperature spectra are close to that of CuCl_2 , while the high-temperature ones are close to that of CuCl .^[14] Quantitative information on the Cu^I and Cu^{II} concentration was obtained from the cross analysis of edge position and maximum of the first derivative spectrum.^[12]

The results obtained on Cu5.0 during the complete temperature cycle are reported in Figure 2a, b. At the starting point (373 K), only Cu^{II} is present and the catalyst is inactive. O_2 conversion and Cu^{II} reduction start in the same temperature range (470–490 K) and progressively increase with temper-

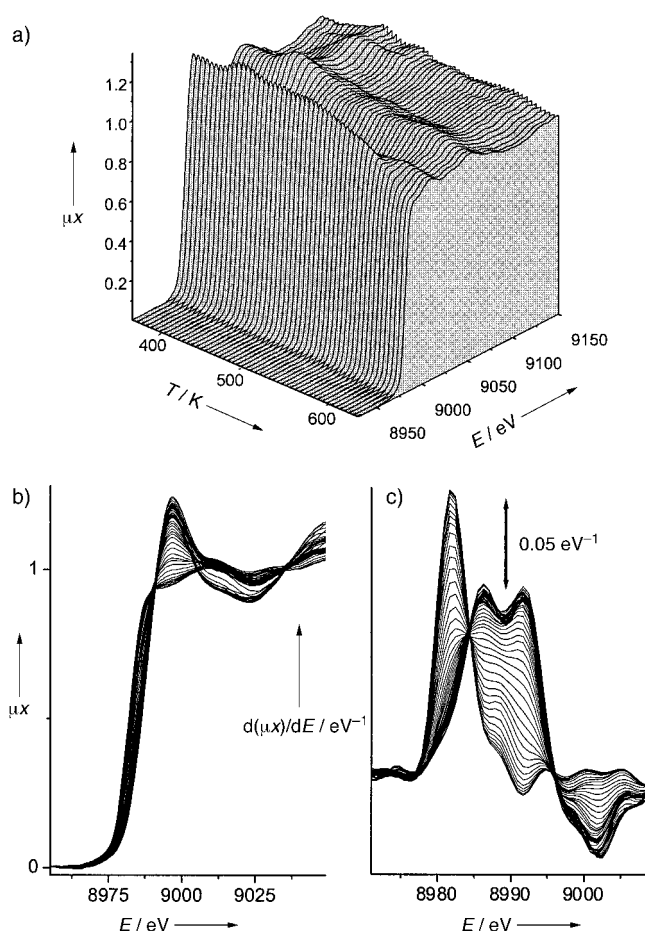


Figure 1. a) Three-dimensional XANES spectra (collected each 30 s) of Cu5.0 during heating from 373 to 623 K with 12 K min^{-1} . b) Front view of the spectra shown in (a). c) Derivative spectra, Fourier filtered to remove the high-frequency noise. E = photon energy, μx = normalized absorption, assuming $\mu x = 1$ at $E = 9035 \text{ eV}$. The presence of two isosbestic points in the XANES (8990 and 9005 eV) and derivative spectra (8984 and 8995 eV) is direct proof for only two species being present on the catalyst in significant amounts: CuCl_2 and CuCl in mutual transformation. The oxychloride formed according to Equation (3) is not detected because the re-chlorination step is too fast.^[15]

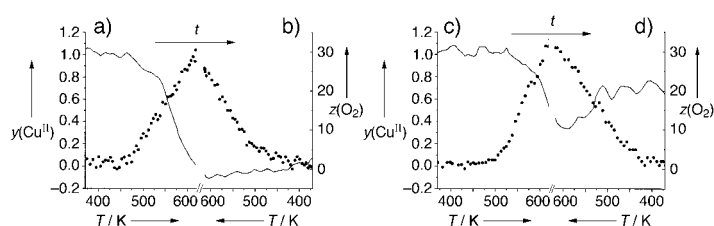


Figure 2. a) O_2 conversion (representative for the catalyst's activity; z , full dots, right axis) and Cu^{II} fraction (y , full line, left axis) for Cu5.0 during temperature ramp-up. b) As diagram (a), but for the temperature ramp-down. c) and d) Equivalent presentations to (a) and (b) for K3.6Cu5.0. The time axis runs in all diagram parts from left to right. $y(\text{Cu}^{II}) = 1 - y(\text{Cu}^I)$, where $y(\text{Cu}^I)$ has been determined by the relative intensity of the first derivative maximum at 8982 eV (Figure 1c) compared to the value obtained on a totally reduced sample.

ature. Cu^{II} reduction becomes complete at 600 K. During the cooling step, the conversion progressively declines and becomes negligible in the 490–470 K range, while the oxidation state of Cu does not change. The results entail that,

at the typical oxychlorination temperature, Cu^{I} dominates and the rate-determining step is the oxidation of CuCl [Eq. (3)]. To understand the low efficiency of the oxidation process, the catalyst was subjected at the end of the cooling step to two different oxidizing treatments at increasing temperatures (373–623 K): one with diluted O_2 , the other with a diluted O_2 –HCl mixture. The first treatment caused the complete Cu^{I} oxidation already at 373 K, while the second left Cu^{I} unchanged up to 550 K, and, even at 623 K, Cu^{I} was still present. This points out that HCl acts as a poison for the Cu^{I} oxidation and is responsible for the prevailing reduced state of copper during the reaction.

Figure 2c, d shows the results of the same experiment performed on K3.6Cu5.0 as catalyst. The $\text{Cu}^{\text{II}} \rightarrow \text{Cu}^{\text{I}}$ reduction began at a slightly higher temperature (around 520 K) and was not complete: 30% of Cu^{II} survived even at 623 K. The activity of this catalyst started around 490 K, that is before the reduction process. During the cooling step, Cu was re-oxidized to a fraction of 80%, and the activity survived down to 450 K.

These results indicate that addition of potassium favors the oxidized state of the catalyst, suggesting that it causes either an increase in the oxidation rate [Eq. (3)] or a decrease in the reduction rate [Eq. (2)].^[15] The decrease in the reduction rate was testified by dosing ethylene alone at 500 K in a pulse reactor (see Figure in the Supporting Information) on K3.6Cu5.0 and Cu5.0 catalysts following a procedure previously reported.^[6] These data imply that the rate-determining step of the oxychlorination reaction (1) catalyzed by K3.6Cu5.0 is the reduction of the active phase.

The deactivating effect of potassium cannot be attributed to a decrease in the copper chloride active surface area, because the Cu dispersion, measured by CO adsorption at room temperature (RT)^[7] on samples previously reduced in H_2 , is the same (Cu5.0: 47%, K3.6Cu5.0: 49%). The effect should be rather ascribed to the formation of a mixed chloride ($\text{K}_x\text{CuCl}_{2+x}$),^[16] which reduces the ability of the active surface to adsorb ethylene and/or transfer two Cl atoms to each ethylene molecule. The formation of the mixed chloride, although not detectable by XRD owing to too small crystal size,^[6] is suggested by IR spectroscopy of adsorbed CO on samples previously reduced in ethylene (Figure 3). The absorption bands are due to the formation of $\text{Cu}^{\text{I}} \cdots \text{CO}$ adducts.^[7, 17] The difference in $\tilde{\nu}(\text{CO})$ (2139 cm^{-1} for Cu5.0 and 2117 cm^{-1} for K3.6Cu5.0) implies that the Cu^{I} ions on the two catalysts belong to different compounds: a totally reduced CuCl salt for sample Cu5.0^[7, 17, 18] and a mixed, partially reduced potassium–copper chloride for sample K3.6Cu5.0. The lower intensity of the bands in Figure 3a reflects the lower ability of this catalyst to be reduced by ethylene, supporting the XANES data.

The moderating effect of potassium on the catalytic activity allows to control the formation of hot spots, associated with the strong exothermicity of the oxychlorination reaction. This explains why loading the industrial reactors with catalysts having a decreasing K/Cu ratio in the direction of the flow of the reactants improves performance and catalyst lifetime. Moreover, the favored oxidized state +2 of Cu minimizes the Cu loss caused by the volatility of Cu^{I} species.

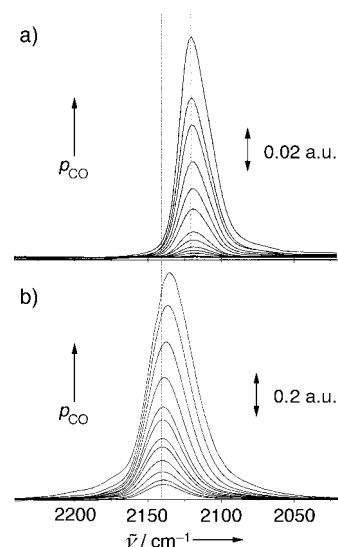


Figure 3. RT IR spectra (same scale) obtained when CO with increasing pressure p_{CO} was dosed on K3.6Cu5.0 (a) or Cu5.0 (b), previously reduced in C_2H_4 at 500 K for 1 h. a.u. = absorbance units.

In conclusions, we could identify the rate-determining step in the ethylene oxychlorination reaction catalyzed by $\text{CuCl}_2/\gamma\text{-Al}_2\text{O}_3$ and clarify and experimentally prove the role of the potassium dopant in catalysts used in fixed-bed industrial reactors: the alkali metal ion modifies the redox properties of the copper species favoring its oxidized state.

Experimental Section

The samples, containing either 5.0 wt % Cu (labeled Cu5.0) or 5.0 wt % Cu plus 3.6 wt % K (labeled K3.6Cu5.0), were prepared from chlorides following the incipient-wetness method.^[4] The experiments were performed by feeding a cell containing a self-supported thin pellet of the catalyst with a diluted mixture of the three reagents ($\text{C}_2\text{H}_4\text{:HCl:O}_2\text{:N}_2 = 100\text{:}36.1\text{:}7.6\text{:}180$), representative of the fixed-bed process. In the course of the experiment the temperature was increased from 373 to 623 K and then decreased again to 373 K. The gas output was analyzed with a Balzer Quadstar 422 quadrupole mass spectrometer. XANES spectra were collected at the ID24 dispersive EXAFS beamline^[19] of the ESRF facility. For IR measurements, performed at RT, a thin self-supporting wafer of the catalyst was prepared and activated under dynamic vacuum at 500 K for 2 h inside an IR cell designed to allow in situ temperature treatments, reagents dosage, evacuation, and CO dosage. The IR spectra were recorded at a 2 cm^{-1} resolution on a BRUKER FTIR 66 spectrometer equipped with a mercury–cadmium–telluride cryodetector.

Received: December 12, 2001
Revised: March 18, 2002 [Z18372]

- [1] a) J. S. Naworski, E. S. Evil, *Applied Industrial Catalysis*, Vol. 1 (Ed.: B. E. Leach), Academic Press, New York, **1983**, p. 239; b) M. N. Newmann in *Encyclopedia of Polymer Science and Engineering*, Vol. 17, Wiley, New York, **1985**, p. 245, and references therein.
- [2] W. D. Mross, *Catal. Rev. Sci. Eng.* **1983**, 25, 591–637.
- [3] A. Arcoya, A. Cortes, X. L. Seoane, *Can. J. Chem. Eng.* **1982**, 60, 55–60.
- [4] a) A. Baiker, W. L. Holstein, *J. Catal.* **1983**, 84, 178–188; b) K. Rollins, P. A. Sermon, *J. Chem. Soc. Chem. Commun.* **1986**, 1171–1172; c) E. M. Fortini, C. L. Garcia, D. E. Resasco, *J. Catal.* **1986**, 99, 12–18; d) P. A. Sermon, K. Rollins, P. N. Reyes, S. A. Lawrence, M. A. Martin Luengo, M. J. Davies, *J. Chem. Soc. Faraday Trans. 1* **1987**, 83, 1347–1353; e) P. S. Sai Prasad, P. Kanta Rao, *J. Chem. Soc.*

- Chem. Commun.* **1987**, 951–952; f) C. L. Garcia, D. E. Resasco, *J. Catal.* **1990**, *122*, 151–165.
- [5] G. Leofanti, M. Padovan, M. Garilli, D. Carmello, A. Zecchina, G. Spoto, S. Bordiga, G. Turnes Palomino, C. Lamberti, *J. Catal.* **2000**, *189*, 91–104, and references therein.
- [6] G. Leofanti, M. Padovan, M. Garilli, D. Carmello, G. L. Marra, A. Zecchina, G. Spoto, S. Bordiga, C. Lamberti, *J. Catal.* **2000**, *189*, 105–116.
- [7] G. Leofanti, A. Marsella, B. Cremaschi, M. Garilli, A. Zecchina, G. Spoto, S. Bordiga, P. Fiescaro, G. Berlier, C. Prestipino, G. Casali, C. Lamberti, *J. Catal.* **2001**, *202*, 279–295.
- [8] G. Leofanti, A. Marsella, B. Cremaschi, M. Garilli, A. Zecchina, G. Spoto, S. Bordiga, P. Fiescaro, C. Prestipino, F. Villain, C. Lamberti, *J. Catal.* **2002**, *205*, 375–381.
- [9] Although the exact position of the X-ray photoelectron edge of an element in a material is also defined by the coordinating ligands and the local symmetry around the absorbing atom the main factor is the oxidation state of this atom.
- [10] a) L. S. Kau, D. J. Spira-Solomon, J. E. Penner-Hahn, K. O. Hodgson, E. I. Solomon, *J. Am. Chem. Soc.* **1987**, *109*, 6433–6442; b) N. J. Blackburn, R. W. Strange, J. Reedijk, A. Volbeda, A. Farooq, A. Karlin, J. Zubieta, *Inorg. Chem.* **1989**, *28*, 1349–1357.
- [11] a) C. Lamberti, G. Spoto, D. Scarano, C. Pazé, M. Salvalaggio, S. Bordiga, A. Zecchina, G. Turnes Palomino, F. D'Acapito, *Chem. Phys. Lett.* **1997**, *269*, 500–508; b) G. Turnes Palomino, P. Fiescaro, S. Bordiga, A. Zecchina, E. Giamello, C. Lamberti, *J. Phys. Chem. B* **2000**, *104*, 4064–4073; c) V. Bolis, S. Maggiorini, L. Meda, F. D'Acapito, G. Turnes Palomino, S. Bordiga, C. Lamberti, *J. Chem. Phys.* **2000**, *113*, 9248–9261.
- [12] a) M. Fernández-García, I. Rodríguez-Ramos, P. Ferreira-Aparicio, A. Guerrero-Ruiz, *J. Catal.* **1998**, *178*, 253–263; b) P. Kappen, J.-D. Grunwaldt, B. S. Hammershøi, L. Tröger, B. S. Clausen, *J. Catal.* **2001**, *198*, 56–65.
- [13] C. Lamberti, G. Turnes Palomino, S. Bordiga, G. Berlier, F. D'Acapito, A. Zecchina, *Angew. Chem.* **2000**, *112*, 2222–2225; *Angew. Chem. Int. Ed.* **2000**, *39*, 2138–2141.
- [14] XANES spectroscopy is one of the most informative techniques for determining oxidation states and local symmetries of transition metal ions [see for example A. Bianconi in *X-Ray Absorption* (Eds.: D. C. Koningsberger, R. Prins), Wiley, New York, **1988**, p. 573]. This is particularly true when model compounds with well-defined oxidation and coordination states are available for comparison. In this regard, the reader should refer to refs. [7, 8]. It has been shown that the spectra of the as-activated catalyst and of the catalyst after interaction with O₂ [that is, at the end of the cycle described in Equations (2)–(4)] are very close to that of the CuCl₂ model compound. In addition, the XANES spectra of the catalyst after interaction with C₂H₄ under static conditions are in fair agreement with that of CuCl, except for a less pronounced 1s→4p transition. This difference has been explained in terms of the high dispersion of the CuCl particles on the reduced catalyst, showing 50 % of surface Cu^I as determined in a combined IR/CO chemisorption study.^[7]
- [15] In a parallel experiment, in which only HCl was dosed to the oxychloride phase, it was demonstrated that the chlorination of the oxychloride occurs already at 373 K. This implies that reaction (4) is immediate at the temperature of interest, thus it is not responsible for the presence of Cu^{II}.
- [16] The ability of potassium and copper to form the phase KCuCl₃ is well known, see for example: N. N. Greenwood, A. Earnshaw, *Chemistry of the Elements*, Pergamon, Oxford, **1986**, p. 1385.
- [17] A. Zecchina, D. Scarano, S. Bordiga, G. Spoto, C. Lamberti, *Adv. Catal.* **2001**, *46*, 265–397, and references therein.
- [18] D. Scarano, P. Galletto, C. Lamberti, R. De Franceschi, A. Zecchina, *Surf. Sci.* **1997**, *387*, 236–242.
- [19] a) http://www.esrf.fr/exp_facilities/ID24/ID24.html; b) M. Hagelstein, A. San Miguel, T. Ressler, A. Fontaine, J. Goulon, *J. Phys. IV* **1997**, *7*, C2–303–308.

Comparison of Reorganization Energies for Intra- and Intermolecular Electron Transfer**

Hiroshi Imahori,* Hiroko Yamada, Dirk M. Guldi,* Yoshito Endo, Akihisa Shimomura, Santi Kundu, Koji Yamada, Tadashi Okada,* Yoshiteru Sakata, and Shunichi Fukuzumi*

The reorganization energy (λ), which is a sum of two terms, inner-sphere reorganization energy, λ_i , and outer-sphere reorganization energy, λ_o , imposes probably the most far-reaching impact on biological electron-transfer (ET) systems.^[1] In particular, the primary ET processes in photosynthesis are all characterized by small reorganization energies.^[2] This situation allows, for instance, forward ET processes to proceed under nearly optimal conditions, that is, near the top region of the Marcus parabola, whereas the highly exergonic and energy-wasting back-ET process is shifted deeply into the inverted region. To achieve small reorganization energies, it is highly desirable for the construction of artificial photosynthetic systems to employ donor–acceptor couples, which offer room for the delocalization of the charges—electrons or

[*] Prof. Dr. H. Imahori

Department of Molecular Engineering
Graduate School of Engineering
Kyoto University
PRESTO, JAPAN Science and Technology Corporation
Sakyo-ku, Kyoto 606-8501 (Japan)
Fax: (+81) 75-751-7279
E-mail: imahori@mee3.moleng.kyoto-u.ac.jp

Dr. habil. D. M. Guldi
Radiation Laboratory
University of Notre Dame
Notre Dame, Indiana 46556 (USA)
Fax: (+1) 574-631-8068
E-mail: guldi.1@nd.edu

Prof. Dr. T. Okada, A. Shimomura, Dr. S. Kundu
Department of Chemistry
Graduate School of Engineering Science
and Research Center for Materials Science at Extreme Conditions
Osaka University
Toyonaka, Osaka 560-8531 (Japan)
Fax: (+81) 6-6850-6244
E-mail: okada@chem.es.osaka-u.ac.jp

Prof. Dr. S. Fukuzumi, Dr. H. Yamada, Y. Endo
Department of Material and Life Science
Graduate School of Engineering
Osaka University
CREST, JAPAN Science and Technology Corporation
Suita, Osaka 565-0871 (Japan)
Fax: (+81) 6-6879-7370
E-mail: fukuzumi@ap.chem.eng.osaka-u.ac.jp

Dr. K. Yamada, Prof. Dr. Y. Sakata
The Institute of Scientific and Industrial Research
Osaka University
Mihoga-oka, Ibaraki, Osaka 567-0047 (Japan)

** This work was supported by COE, Grant-in-Aid for Scientific Research, Specially Promoted Research (No. 10102007), and the Development of Innovative Technology (No. 12310) from Ministry of Education, Sports, Culture, Science and Technology, Japan and by the Office of Basic Energy Sciences of the U.S. Department of Energy. This is document NDRL-4379 from the Notre Dame Radiation Laboratory.



Supporting information for this article is available on the WWW under <http://www.angewandte.org> or from the author.

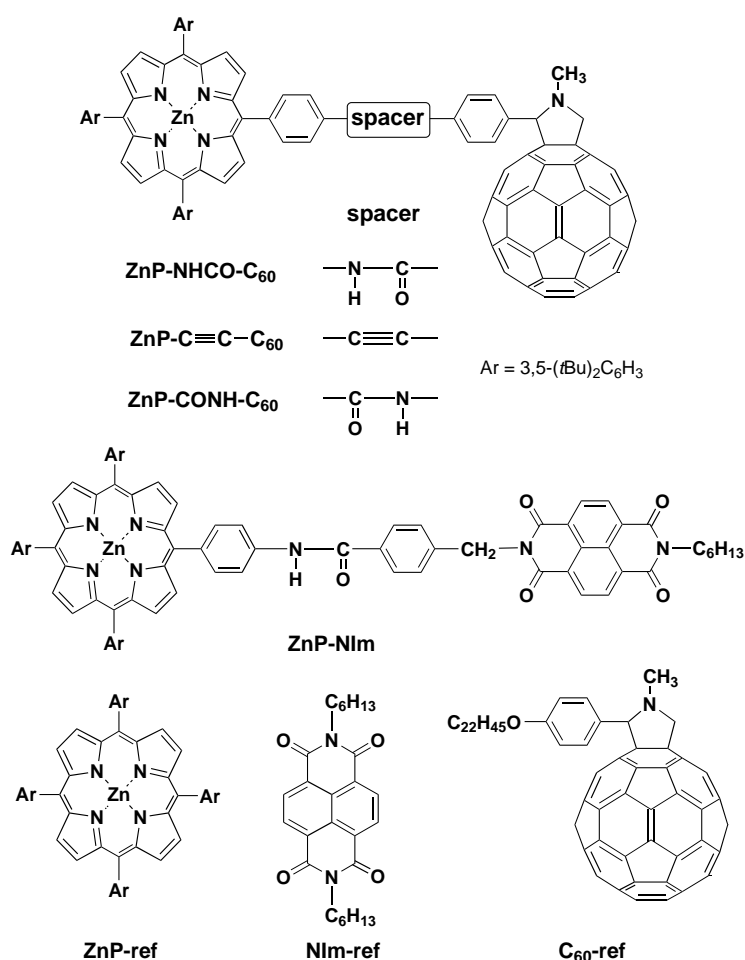
holes—within their structure. In this context, the exceptionally small λ values of porphyrin–fullerene donor–acceptor ensembles, a fact that relates to their delocalized π -electron systems, have great potential.^[3] A quantitative comparison of λ values for intramolecular ET processes of a large 3D π acceptor (i.e., fullerenes) with those of conventional 2D acceptors (i.e., quinones and diimides), which have similar redox potentials and intervening spacers has, however, yet to be reported, mainly as a result of the synthetic challenges involved.^[4–6]

Herein we report the first comprehensive assay of λ values for intramolecular ET involving a 3D acceptor (spherical C_{60}) and a 2D acceptor (planar naphthalenediimide (NIm)); Supporting Information: S1). For this purpose we designed a series of porphyrin-linked C_{60} and NIm ensembles, endowed with similar rigid spacers (–NHCO–, –C≡C–, –CONH–)^[3c, 7–9] as shown in Scheme 1. In addition, we report a quantitative analysis of λ values in intramolecular ET versus intermolecular ET.

Details on the synthesis and characterization of the compounds are provided in the Supporting Information (S2). Importantly, the first reduction potentials of **C₆₀-ref** (–1.02, –1.04, –0.92 V versus Fc/Fc⁺ (Fc = ferrocene) in THF, PhCN, and DMF, respectively)^[3c] are virtually the same as those of **NIm-ref** (–1.15, –1.05, –0.91 V versus Fc/Fc⁺ in THF, PhCN, and DMF, respectively).

Time-resolved transient absorption spectra of the different dyads were measured by pico- and nanosecond laser photolysis in THF, PhCN, and DMF. Upon excitation of, for example, **ZnP-NHCO-C₆₀** with a 532 nm laser pulse (18 ps) in THF, a characteristic broad band at 680 nm assigned to the zincporphyrin radical cation (**ZnP^{•+}**)^[10] appeared. Concomitantly, the porphyrin singlet excited state (**¹ZnP***) absorption at 460 nm decayed, which suggests the transformation of **¹ZnP*-NHCO-C₆₀** into **ZnP^{•+}-NHCO-C₆₀^{•-}**. The presence of **C₆₀^{•-}** (1000 nm) and **ZnP^{•+}** (680 nm) in the molecule was further substantiated by an independent set of complementary nanosecond experiments (Figure 1). By fitting the rise and decay of the fingerprint absorptions to a first-order rate law, the charge separation (CS) rates evolving from **¹ZnP*** to **C₆₀** ($k_{ET(CS)}$) and the charge recombination (CR) rates within the **C₆₀^{•-}/ZnP^{•+}** pairs ($k_{ET(CR)}$) were determined. In THF, the exact values were $2.2 \times 10^{10} \text{ s}^{-1}$ and $2.0 \times 10^6 \text{ s}^{-1}$, respectively. Hereby, the $k_{ET(CS)}$ value agrees well with the corresponding value ($2.0 \times 10^{10} \text{ s}^{-1}$) obtained from the fluorescence lifetime measurements. A similar behavior was also observed for **ZnP-C≡C-C₆₀** ($k_{ET(CS)} = 3.7 \times 10^{10} \text{ s}^{-1}$, $k_{ET(CR)} = 1.5 \times 10^6 \text{ s}^{-1}$) and **ZnP-CONH-C₆₀** ($k_{ET(CS)} = 1.3 \times 10^{10} \text{ s}^{-1}$, $k_{ET(CR)} = 3.7 \times 10^5 \text{ s}^{-1}$).^[3c]

Importantly, in all **ZnP-C₆₀** dyads, the value of charge separation, $k_{ET(CS)}$, is much larger than the value of charge recombination, $k_{ET(CR)}$. This result infers that the CS processes for **ZnP-C₆₀** dyads are in the Marcus top region whereas the CR processes are in the Marcus inverted region.^[3c] Conversely, the $k_{ET(CR)}$ value in the corresponding NIm-based dyad, **ZnP-NIm**, is much larger than the $k_{ET(CS)}$ value as determined



Scheme 1.

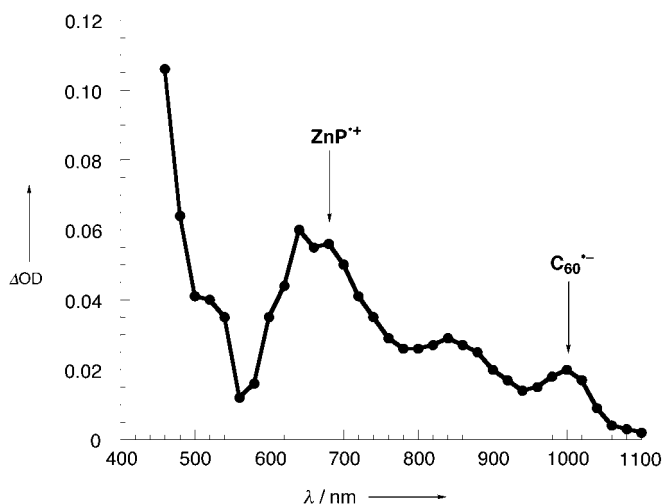


Figure 1. Nanosecond time-resolved transient absorption spectrum of **ZnP-NHCO-C₆₀** excited at 532 nm in THF (absorption ratio of **ZnP**:**C₆₀** = 3:1).

by the picosecond transient absorption spectrum^[11] and the decay of the **¹ZnP*** fluorescence (Supporting Information: S3). This situation means that the CS processes for **ZnP-NIm** are in the Marcus normal region whereas the CR processes are in the Marcus top region. The $k_{ET(CS)}$ and $k_{ET(CR)}$ values of **ZnP-NIm** in THF were determined as $3.9 \times 10^8 \text{ s}^{-1}$

and $2.0 \times 10^{10} \text{ s}^{-1}$, respectively. In more polar PhCN and DMF, a behavior resembling ET was noted for all of the dyads investigated (Table 1).

Table 1. Rate constants (k_{ET}) for charge separation (CS) and charge recombination (CR) and the free energy changes ($-\Delta G_{\text{ET}}^0$)^[a] in porphyrin–fullerene and porphyrin–naphthalenediimide dyads.

THF ($\epsilon_s = 7.58$)		Benzonitrile ($\epsilon_s = 25.2$)		DMF ($\epsilon_s = 36.7$)	
$-\Delta G_{\text{ET}}^0$ [eV]	k_{ET} [s ⁻¹]	$-\Delta G_{\text{ET}}^0$ [eV]	k_{ET} [s ⁻¹]	$-\Delta G_{\text{ET}}^0$ [eV]	k_{ET} [s ⁻¹]
ZnP-NHCO-C₆₀					
CS 0.70	2.2×10^{10} ^[b]	0.70	2.8×10^{10}	0.89	1.3×10^{10} ^[b]
CR 1.37	2.0×10^6	1.34	2.4×10^6	1.17	3.4×10^6
ZnP-C≡C-C₆₀					
CS 0.67	3.7×10^{10} ^[c]	0.69	3.0×10^{10}	[d]	3.0×10^{10} ^[c]
CR 1.40	1.5×10^6	1.35	2.1×10^6	[d]	2.5×10^6
ZnP-CONH-C₆₀					
CS 0.65	1.3×10^{10} ^[c]	0.66	9.5×10^9 ^[e]	0.85	1.3×10^{10} ^[e]
CR 1.42	3.7×10^5 ^[e]	1.38	1.3×10^6 ^[e]	1.21	1.8×10^6 ^[e]
ZnP-NIm					
CS 0.57	3.9×10^8	0.69	[d]	0.90	3.5×10^8 ^[b]
CR 1.50	2.0×10^{10}	1.35	[d]	1.16	[d]

[a] $-\Delta G_{\text{CR}}^0 = E_{\text{ox}}(\text{D/D}^{+}) - [E_{\text{red}}(\text{A/A}^{-})]$, $-\Delta G_{\text{CS}}^0 = \Delta E_{0,0} - (-\Delta G_{\text{CR}}^0)$ where $E_{\text{ox}}(\text{D/D}^{+})$ and $E_{\text{red}}(\text{A/A}^{-})$ are the first oxidation potential of donor and the first reduction potential of acceptor, respectively, and $\Delta E_{0,0}$ is energy of the 0-0 transition between the lowest excited state and the ground state. [b] From ref. [8]. [c] From ref. [9]. [d] Not determined. [e] From ref. [3c].

In the next step we quantified the driving-force dependence on the ET rate constants (k_{ET}), by Equation (1), where V represents the electronic coupling matrix element.^[1] This equation is rewritten to give Equation (2) which is also applied to evaluate the electron-transfer rate constant (k_{ET}).

$$k_{\text{ET}} = \left(\frac{4\pi^3}{h^2 \lambda k_{\text{B}} T} \right)^{1/2} V^2 \exp \left[- \frac{(\Delta G_{\text{ET}}^0 + \lambda)^2}{4 \lambda k_{\text{B}} T} \right] \quad (1)$$

$$k_{\text{B}} T \ln k_{\text{ET}} + \frac{\Delta G_{\text{ET}}^0}{2} = k_{\text{B}} T \ln \left[\left(\frac{4\pi^3}{h^2 \lambda k_{\text{B}} T} \right)^{1/2} V^2 \right] - \frac{\lambda}{4} - \frac{(\Delta G_{\text{ET}}^0)^2}{4\lambda} \quad (2)$$

The driving forces ($-\Delta G_{\text{ET}}^0$) for the intramolecular ET processes were determined accurately, based on the first oxidation potential of the zincporphyrin donor and the first reduction potential of the fullerene/naphthalenediimide acceptors in THF, PhCN, and DMF, together with the energy level of the porphyrin singlet excited state. According to Equation (2), a plot of $k_{\text{B}} T \ln k_{\text{ET}} + (\Delta G_{\text{ET}}^0/2)$ versus $(\Delta G_{\text{ET}}^0)^2$ for **ZnP-NHCO-C₆₀**, **ZnP-C≡C-C₆₀**, and **ZnP-CONH-C₆₀** gives a linear correlation (Supporting Information: S4).^[12] The λ and V values are obtained from the intercept and the slope as $\lambda = 0.59 \pm 0.15 \text{ eV}$ and $V = 7.9 \pm 1.7 \text{ cm}^{-1}$, respectively. A linear correlation was also obtained for **ZnP-NIm** (Supporting Information: S4) which afforded a much larger λ value ($\lambda = 1.41 \pm 0.33 \text{ eV}$) together with a similar V value ($7.8 \pm 3.2 \text{ cm}^{-1}$).^[13] Such an extraordinary large difference in λ between the C₆₀ and NIm dyads is the reason why the ratio of

$k_{\text{ET}(\text{CS})}$ to $k_{\text{ET}(\text{CR})}$ is reversed in the two donor–acceptor systems (Table 1). This result is the first quantitative manifestation that the λ value of a 3D electron acceptor (C₆₀) is, indeed, much smaller than the value of a typical 2D acceptor (NIm).

However, our current conclusion is in sharp contradiction to a previous hypothesis concerning the λ value for an intermolecular electron self-exchange reaction of *t*BuC₆₀⁻/*t*BuC₆₀[•].^[14] In particular, the value of 0.64 eV in PhCN/benzene (1:7 v/v) is quantitatively similar to that seen for the BQ^{•-}/BQ couple (BQ = benzoquinone), 0.74 eV in PhCN.^[14] To shed light on this apparent discrepancy, the λ value of intermolecular electron self-exchange between (**ZnP-ref**)^{•+}/**ZnP-ref** and between (**NIm-ref**)^{•-}/**NIm-ref** was determined by analyzing line-width variations in the ESR spectra (Supporting Information: S5).^[15–17] The line width (ΔB_{pp}) increased with increasing **NIm-ref** concentration (Supporting Information: S6). From the slope of the linear correlation the electron self-exchange rate constant (k_{ex}) was determined.^[16, 18] The Arrhenius plot of k_{ex} at various temperatures (Supporting Information: S7) afforded the activation parameters ($\Delta H^\ddagger = 4.2 \text{ kJ mol}^{-1}$ and $\Delta S^\ddagger = -14 \text{ J K}^{-1} \text{ mol}^{-1}$). The λ values of **ZnP-ref**^{•+}/**ZnP-ref** and **NIm-ref**^{•-}/**NIm-ref** were determined from the rate constant in MeCN at 298 K as 0.30 eV and 0.34 eV, respectively. Both of these λ values are substantially smaller than the value of *t*BuC₆₀⁻/*t*BuC₆₀[•] (0.64 eV). With the λ values of the electron self-exchange reaction of each component in hand, the λ values of intermolecular ET were estimated as the average of the two λ values of electron self-exchange reactions. Importantly, the λ value of the intermolecular ET from **ZnP-ref** to **NIm-ref** (0.32 eV) is appreciably smaller than that seen for the **ZnP-ref**/**C₆₀-ref** couple (0.47 eV).

In summary, our results clearly infer that intermolecular ET between a planar naphthalenediimide (NIm) acceptor and a planar zincporphyrin (ZnP) donor takes place at short separation distances rendering the reorganization energy small. In contrast to such a 2D π system, intermolecular ET involving a spherical 3D π system (C₆₀) is likely to occur at larger distances. An important asset is the effective radius of the acceptor moiety: Even if C₆₀ is held at the same critical distance (i.e., van der Waals contact) as NIm, because of the strong π – π interactions, the effective center-to-center separation is significantly larger. In the case of intramolecular ET systems, the fixed distance, by which the donor and acceptor are separated, allows the intrinsic reorganization energies of a planar and a spherical acceptor to be distinguished. This study has provided for the first time insights into the intrinsic reorganization energies of electron transfer, which relate to different molecular shapes.

Experimental Section

Details on the synthesis and characterization of the compounds are provided in the Supporting Information (S2). Time-resolved fluorescence spectra of the compounds were measured by a single-photon counting method using a second-harmonic generation (SHG, 524 nm) of a semiconductor YLF laser (Lightwave 131-1047-300, FWHM = 20 ps) as an excitation source.^[19] Picosecond transient absorption spectra of **ZnP-NIm** were measured by means of a picosecond dye laser (FWHM 12 ps) pumped

by the second harmonic of a repetitive mode-locked Nd³⁺:YAG laser (Quintel, Picochrome YG-503 C/PTL-10).^[19] The 590-nm output of the dye laser (Rhodamine 6G) was used for excitation. Picosecond laser flash photolysis experiments for **ZnP-C₆₀** dyads were carried out with 532-nm laser pulses from a mode-locked, Q-switched Quintel YG-501 DP ND:YAG laser system (pulse width ~18 ps, 2–3 mJ/pulse).^[3c] The white continuum picosecond probe pulse was generated by passing the fundamental output through a D₂O/H₂O solution. Nanosecond laser-flash photolysis experiments were performed with laser pulses from a Quanta-Ray CDR Nd:YAG system (532 nm, 6 ns pulse width) in a front face excitation geometry.^[3c] A Xe lamp was triggered synchronously with the laser. A monochromator (SPEX) in combination with either a Hamamatsu R 5108 photomultiplier or a fast InGaAs-diode was employed to monitor transient absorption spectra.

Tetramethyl-*p*-benzoquinone (Me₄Q) radical anion was prepared by proportionation reactions of Me₄Q with the dianion obtained by deprotonation of the corresponding hydroquinone with tetrabutylammonium hydroxide.^[14] The self-exchange rate constants between the reference compounds and the corresponding radical anions in CH₃CN at various temperatures are directly determined by analyzing line-width variations of the ESR spectra.^[14] Typically, an aliquot of a stock solution of the Me₄Q radical anion (5.0×10^{-4} M) was added to an ESR tube containing a deaerated CH₃CN solution of various concentrations of **Nlm-ref** (5.0×10^{-4} M to 2.0×10^{-3} M) under an atmospheric pressure of Ar. The ESR spectra of the **Nlm-ref** radical anion were measured at various temperature (–40 to 25 °C) with a JEOL X-band spectrometer (JES-RE1XE). The ESR spectra were recorded under nonsaturating microwave power conditions. The magnitude of modulation was chosen to optimize the resolution and the signal-to-noise (S/N) ratio of the observed spectra, when the maximal slope line width (ΔB_{pp}) of the ESR signals was unchanged with the larger modulation. The *g* values and the hyperfine coupling constants were calibrated with a Mn²⁺ ion marker. The **ZnP-ref** radical cation was produced by the chemical oxidation of **ZnP-ref** with [Ru(bpy)₃]³⁺ ions (bpy = 2,2'-bipyridine).^[20]

Received: January 10, 2002

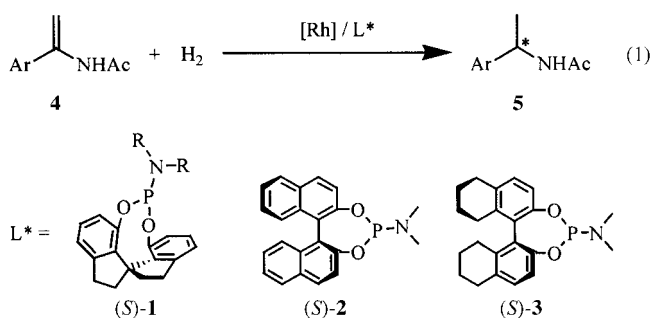
Revised: March 1, 2002 [Z18508]

- [1] a) R. A. Marcus, N. Sutin, *Biochim. Biophys. Acta* **1985**, *811*, 265; b) R. A. Marcus, *Angew. Chem.* **1993**, *105*, 1161; *Angew. Chem. Int. Ed. Engl.* **1993**, *32*, 1111; c) J. R. Winkler, H. B. Gray, *Chem. Rev.* **1992**, *92*, 369; d) H. B. Gray, J. R. Winkler in *Electron Transfer in Chemistry*, Vol. 3 (Ed.: V. Balzani), Wiley-VCH, Weinheim, **2001**, pp. 3–23; e) M. D. Newton, *Chem. Rev.* **1991**, *91*, 767; f) M. D. Newton, *Adv. Chem. Phys.* **1999**, *106*, 303.
- [2] *The Photosynthetic Reaction Center* (Eds.: J. Deisenhofer, J. R. Norris), Academic Press, San Diego, **1993**.
- [3] a) H. Imahori, N. V. Tkachenko, V. Vehmanen, K. Tamaki, H. Lemmetyinen, Y. Sakata, S. Fukuzumi, *J. Phys. Chem. A* **2001**, *105*, 1750; b) V. Vehmanen, N. V. Tkachenko, H. Imahori, S. Fukuzumi, H. Lemmetyinen, *Spectrochim. Acta Part A* **2001**, *57*, 2229; c) H. Imahori, K. Tamaki, D. M. Guldi, C. Luo, M. Fujitsuka, O. Ito, Y. Sakata, S. Fukuzumi, *J. Am. Chem. Soc.* **2001**, *123*, 2607.
- [4] Reorganization energies of diporphyrin dyads for intramolecular ET have been reported. However, no quantitative comparison of the λ values with the corresponding 2D acceptors has been performed. a) A. Harriman, V. Heitz, J.-P. Sauvage, *J. Phys. Chem.* **1993**, *97*, 5940; b) J.-C. Chambron, A. Harriman, V. Heitz, J.-P. Sauvage, *J. Am. Chem. Soc.* **1993**, *115*, 7419; c) J. M. DeGraziano, P. A. Liddell, L. Leggett, A. L. Moore, T. A. Moore, D. Gust, *J. Phys. Chem.* **1994**, *98*, 1758; d) A. Osuka, G. Noya, S. Taniguchi, T. Okada, Y. Nishimura, I. Yamazaki, N. Mataga, *Chem. Eur. J.* **2001**, *7*, 3134.
- [5] a) H. Imahori, K. Hagiwara, T. Akiyama, M. Aoki, S. Taniguchi, T. Okada, M. Shirakawa, Y. Sakata, *Chem. Phys. Lett.* **1996**, *263*, 545; b) D. Kuciauskas, P. A. Liddell, S. Lin, S. G. Stone, A. L. Moore, T. A. Moore, D. Gust, *J. Phys. Chem. B* **2000**, *104*, 4307; c) A. Nakano, A. Osuka, T. Yamazaki, Y. Nishimura, S. Akimoto, I. Yamazaki, A. Itaya, M. Murakami, H. Miyasaka, *Chem. Eur. J.* **2001**, *7*, 3134.
- [6] Farid and Harriman indicated that the rate of charge recombination was affected by the size of the aromatic nucleus. It is highly likely that the effect is a result of changes in reorganization energy. I. R. Gould, D. Ege, J. E. Moser, S. Farid, *J. Am. Chem. Soc.* **1990**, *112*, 4290; A. M. Brun, A. Harriman, S. M. Stephan, *J. Phys. Chem.* **1992**, *96*, 254.
- [7] Although free rotations around the spacer methylene unit in **ZnP-Nlm** and the pyrolidine moiety in **ZnP-C₆₀** are possible, such rotations would not affect the ET rates as much as reported in similar porphyrin–quinone systems. T. Asahi, M. Ohkuchi, R. Matsusaka, N. Mataga, R. P. Zhang, A. Osuka, K. Maruyama, *J. Am. Chem. Soc.* **1993**, *115*, 5665.
- [8] H. Imahori, K. Tamaki, H. Yamada, K. Yamada, Y. Sakata, Y. Nishimura, I. Yamazaki, M. Fujitsuka, O. Ito, *Carbon* **2000**, *38*, 1599.
- [9] K. Yamada, H. Imahori, Y. Nishimura, I. Yamazaki, Y. Sakata, *Chem. Lett.* **1999**, 895.
- [10] C. Luo, D. M. Guldi, H. Imahori, K. Tamaki, Y. Sakata, *J. Am. Chem. Soc.* **2000**, *122*, 6535.
- [11] a) G. P. Wiederrecht, M. P. Niemczyk, W. A. Svec, M. R. Wasielewski, *J. Am. Chem. Soc.* **1996**, *118*, 81; b) R. T. Hayes, M. R. Wasielewski, D. Gosztola, *J. Am. Chem. Soc.* **2000**, *122*, 5563.
- [12] The Marcus plots for **ZnP-CONH-C₆₀** involving CS from the excited porphyrin and **C₆₀** singlet states, and CS from the excited **C₆₀** triplet state, and CR from **C₆₀^{•–}** to **ZnP^{•+}** have been reported.^[3c] The plots in THF, PhCN, and DMF fit well to a single parabolic Marcus curve on the basis of Equation (1), which implies that the classical Marcus theory is valid for both the CS and CR processes in the porphyrin–fullerene linked systems. This result supports the idea that reorganization energies of porphyrin–fullerene systems are virtually the same in the three solvents because of the charge delocalization in porphyrin and fullerene moieties, which would mask the solvent effects on the reorganization energies.^[3c,d] Thus, the λ values are assumed to be similar in **ZnP-NHCO-C₆₀**, **ZnP-C≡C-C₆₀**, and **ZnP-CONH-C₆₀**.
- [13] The *V* values of **ZnP-NHCO-C₆₀**, **ZnP-C≡C-C₆₀**, **ZnP-CONH-C₆₀** (7.9 ± 1.7 cm^{–1}), and **ZnP-Nlm** (7.8 ± 3.2 cm^{–1}) are found to be similar. This result agrees with the similarity in the intervening spacer moieties. We have also reported the linear correlation of logarithmic *k*_{ET} versus edge-to-edge distance (*R*_{ee}) in porphyrin–fullerene linked systems (i.e., porphyrin–fullerene dyads, triads, and tetrad) including **ZnP-CONH-C₆₀** where the decay coefficient factor (β) is 0.6 Å^{–1}. Since the *R*_{ee} values (11.9 Å) are the same in the two systems, the similar *V* values are consistent with the distance dependence of *k*_{ET}. H. Imahori, D. M. Guldi, K. Tamaki, Y. Yoshida, Y. Sakata, S. Fukuzumi, *J. Am. Chem. Soc.* **2001**, *123*, 6617.
- [14] S. Fukuzumi, I. Nakanishi, T. Suenobu, K. M. Kadish, *J. Am. Chem. Soc.* **1999**, *121*, 3468.
- [15] S. Marguet, P. Hapiot, P. Neta, *J. Phys. Chem.* **1994**, *98*, 7136.
- [16] R. Chang, *J. Chem. Educ.* **1970**, *47*, 563.
- [17] The same hyperfine coupling constants give a good fit for the ESR spectra in the presence of **Nlm-ref** using different ΔB_{pp} values. Thus, the observed line broadening because of electron self-exchange was in the slow-exchange region.^[16]
- [18] The *k*_{ex} value was determined using equation: $k_{ex} = 1.52 \times 10^8 (\Delta B_{pp} - \Delta B_{pp}^0) / [(1 - P_i)[\text{Nlm-ref}]]$, where ΔB_{pp} and ΔB_{pp}^0 are the peak-to-peak line widths of the ESR spectra in the presence and absence of **Nlm-ref**, respectively, and *P*_i is a statistical factor which can be taken as nearly zero.^[16]
- [19] H. Imahori, K. Tamaki, Y. Araki, T. Hasobe, O. Ito, A. Shimomura, S. Kundu, T. Okada, Y. Sakata, S. Fukuzumi, *J. Phys. Chem. A* **2002**, *106*, 2803.
- [20] S. Fukuzumi, I. Nakanishi, K. Tanaka, T. Suenobu, A. Tabard, R. Guillard, E. V. Caemelbecke, K. M. Kadish, *J. Am. Chem. Soc.* **1999**, *121*, 785.

Monodentate Chiral Spiro Phosphoramidites: Efficient Ligands for Rhodium-Catalyzed Enantioselective Hydrogenation of Enamides**

Ai-Guo Hu, Yu Fu, Jian-Hua Xie, Hai Zhou,
Li-Xin Wang, and Qi-Lin Zhou*

Optically active α -arylethylamines are an important class of compounds that are widely used in organic and pharmaceutical synthesis, and much effort has been made to develop efficient asymmetric synthetic methods for them.^[1] Asymmetric catalytic hydrogenation of enamides, initiated by Kagan et al.,^[2] provides a direct and convenient route to chiral amine derivatives. However, many well-known chiral diphosphane ligands, such as DIOP, BINAP, and CHIRAPHOS, which are extremely successful in the asymmetric hydrogenation of dehydroamino acid derivatives, do not give high enantioselectivity in the hydrogenation of enamides.^[3, 4] A breakthrough was achieved by Burk et al.^[4a] with the introduction of BPE and DuPHOS ligands, which gave excellent enantioselectivity in the Rh-catalyzed asymmetric hydrogenation of enamides. Lately, some other P ligands were also reported to be efficient in the hydrogenation of enamides.^[4b, 5] However, all ligands that gave a high degree of enantiocontrol are bidentate. To our knowledge, no efficient chiral monodentate ligand has been reported for the asymmetric hydrogenation of enamides, although some monodentate P ligands were successfully used in the hydrogenation of dehydroamino acid derivatives.^[6] Here we describe highly efficient monodentate chiral ligands **1** containing a 1,1'-spirobiindane backbone for the Rh-catalyzed asymmetric hydrogenation of α -arylethylamine derivatives [Eq. (1)] with excellent enantioselectivities (up to 99.7% *ee*).



The chiral monodentate phosphoramidite ligands **1** (abbreviated SIPHOS) were conveniently synthesized in good yields from enantiomerically pure 1,1'-spirobiindane-7,7'-diol, which was easily prepared from 3-methoxybenzaldehyde by using the procedure described by Birman et al.^[7] We demonstrated recently that the Rh complex of (*S*)-**1a** (R = CH₃) is a highly efficient catalyst in the asymmetric hydrogenation of dehydroamino acid and itaconic acid derivatives with up to 99.3 % *ee*. Therefore, we were prompted to investigate the utility of this catalyst in the asymmetric hydrogenation of α -phenylenamide **4a** and an excellent enantioselectivity (up to 98.8 % *ee*) was achieved. This showed, for the first time, that monodentate phosphorus ligands can be effective in the enantiocontrol of asymmetric hydrogenation of enamides.

The results in Table 1 show that the enantioselectivity of the reaction was sensitive to the solvent used, and toluene is the solvent of choice. In contrast, the hydrogen pressure has a negligible influence on the enantioselectivity. For example, in the hydrogenation of **4a** with Rh(*S*)-**1a** catalyst in toluene, the *ee* values of product **5a** at 25 °C under 10 atm and 100 atm H₂ were 96 % and 96.2 %, respectively (Table 1, entries 1 and 2). The investigation of catalyst loading showed that 0.5 mol % catalyst was sufficient to give a high enantioselectivity, while the *ee* value of the product dropped drastically with 0.1 mol % catalyst.

Table 1. Asymmetric hydrogenation of **4a** (Ar=Ph) with [Rh(cod)₂]BF₄/*(S)*-**1a**.^[a]

Entry	Solvent	Cat. [mol %]	<i>ee</i> ^[b] [%]	Config. ^[c]
1	toluene	1	96	<i>S</i>
2 ^[d]	toluene	1	96.2	<i>S</i>
3 ^[e]	toluene	1	98.7	<i>S</i>
4	EtOAc	1	89.8	<i>S</i>
5	acetone	1	83.3	<i>S</i>
6	CH ₂ Cl ₂	1	82.5	<i>S</i>
7	THF	1	80.5	<i>S</i>
8	CH ₃ OH	1	50	<i>S</i>
9 ^[e]	toluene	0.5	98.8	<i>S</i>
10 ^[d]	toluene	0.1	84	<i>S</i>

[a] The reaction was performed at 25 °C with 0.5 mmol of substrate in 5 mL of solvent, P_{H_2} = 10 atm, $[Rh(cod)_2]BF_4/(S)\text{-}\mathbf{1a}$ = 1/2.2 unless otherwise mentioned. Complete conversions were achieved within 12 h. Yields were quantitative. [b] Determined by chiral capillary GC on a Varian Chirasil-L-Val column (25 m). [c] Determined by comparing the optical rotation with the reported value.^[4a] [d] P_{H_2} = 100 atm. [e] T = 5 °C, P_{H_2} = 50 atm.

Catalysts prepared in situ from cationic Rh complexes were active in the asymmetric hydrogenation of enamide **4a** and provided a similar level of enantiocontrol, although the catalyst with a bulkier counteranion needed a longer time for completion of the reaction (Table 2, entries 1, 4, 5). In sharp contrast, the catalyst prepared from the neutral complex $[\{\text{RhCl}(\text{cod})\}_2]$ was completely inert under the same conditions (entry 6). This might imply that the difficult dissociation of chloride hindered the coordination of the substrate to Rh.^[5d, 5e] The influence of ligand structure on the enantioselectivity of the catalysts was also examined in the hydrogenation of **4a**. When the alkyl groups on the nitrogen atom of ligands **1** was changed from methyl ((*S*)-**1a**) to ethyl ((*S*)-**1b**) and isopropyl ((*S*)-**1c**), the enantioselectivity of the

[*] Prof. Dr. Q.-L. Zhou, A.-G. Hu, Y. Fu, J.-H. Xie, H. Zhou, L.-X. Wang
Institute of Elemento-Organic Chemistry
Nankai University
94 Weijin Rd., Tianjin 300071 (China)
Fax: (+86)22-2350-0011
E-mail: qlzhou@public.tpt.tj.cn

[**] We thank the National Natural Science Foundation of China, the Major State Basic Research Development Program (grant No. G2000077506), and the Ministry of Education of China for financial support.


 Supporting information for this article is available on the WWW under <http://www.angewandte.org> or from the author.

Table 2. Asymmetric hydrogenation of **4a**: influence of the structure of the catalyst.^[a]

Entry	Catalyst	<i>T</i> [°C]	<i>t</i> [h] ^[b]	<i>ee</i> [%]	Config.
1	[Rh(cod) ₂]BF ₄ /(<i>S</i>)- 1a	25	12	96	<i>S</i>
2 ^[c]	[Rh(cod) ₂]BF ₄ /(<i>S</i>)- 1a	5	12	98.7	<i>S</i>
3	[Rh(cod) ₂]BF ₄ /(<i>R</i>)- 1a	25	12	96.2	<i>R</i>
4	[Rh(cod) ₂]PF ₆ /(<i>S</i>)- 1a	25	20	96.4	<i>S</i>
5	[Rh(cod) ₂]SbF ₆ /(<i>S</i>)- 1a	25	48	95.3	<i>S</i>
6	[[Rh(cod)Cl] ₂]/(<i>S</i>)- 1a	25	no reaction		
7	[Rh(cod) ₂]BF ₄ /(<i>S</i>)- 1b	25	20	57	<i>S</i>
8	[Rh(cod) ₂]BF ₄ /(<i>S</i>)- 1c	25	24	38	<i>S</i>
9 ^[c]	[Rh(cod) ₂]BF ₄ /(<i>S</i>)- 2	5	12	93	<i>R</i>
10 ^[c]	[Rh(cod) ₂]BF ₄ /(<i>S</i>)- 3	5	12	96	<i>R</i>

[a] Reaction conditions: substrate/catalyst (*S*/*C*) = 100; *P*_{H₂} = 10 atm unless otherwise mentioned. [b] Time for 100 % conversion. [c] *P*_{H₂} = 50 atm.

catalysts was greatly decreased (entries 7 and 8). For comparison, ligand (*S*)-**2**, which was developed by Feringa et al. and was highly efficient in the asymmetric hydrogenation of dehydroamino acid derivatives,^[6d] was investigated, and 93 % *ee* was obtained (entry 9). A difference between (*S*)-**1a** and (*S*)-**2** is that the dihedral angle of the two aromatic planes is larger in the former than in the latter. This might be one of the reasons that (*S*)-**1a** provides a more efficient steric effect around the Rh atom, which improves the enantioselectivity of the catalyst. This rationale is supported by the utility of ligand (*S*)-**3** prepared from H₈-BINOL.^[8] The dihedral angle of the two aromatic planes in (*S*)-**3** should be larger than that in (*S*)-**2**, but smaller than that in (*S*)-**1a**. When the Rh complex of (*S*)-**3** catalyzed the asymmetric hydrogenation of enamide **4a**, 96 % *ee* was achieved (entry 10). This *ee* value lies between those with (*S*)-**1a** (98.7 % *ee*) and (*S*)-**2** (93 % *ee*).

A variety of α -arylenamides can be hydrogenated with Rh/(*S*)-**1a** catalyst to produce the corresponding α -arylamine derivatives with high *ee* values (Table 3). The electronic nature of the phenyl ring of the enamide had little influence on the enantioselectivity of the reaction, while substitution at the *ortho* or *meta* position of the phenyl ring led to a lower *ee* value.

Although several rhodium complexes with monodentate phosphorus ligands have been successfully applied in the

asymmetric hydrogenation of dehydroamino acid and itaconic acid derivatives, the structures of the catalysts are still unknown.^[9] We were able to grow a single crystal of the Rh complex of (*S*)-**1a** suitable for X-ray crystallography. The structure of [Rh(cod){(*S*)-**1a**]₂⁺ is shown in Figure 1.^[10, 11] The complex contains two phosphoramidite ligands **1a**, coordinated to Rh through the P atom. To minimize the steric repulsion, the two ligands have an orientation in which the angle of the two Rh-P-N planes is 43.6°. The Rh-P bond lengths (2.286 Å) in the crystal of [Rh(cod){(*S*)-**1a**]₂⁺ are close to those reported in the Rh complexes of bidentate phosphane ligands.^[12] However, the P-Rh-P angle (95.6°) is distinctly larger than those in Rh complexes of bis-phosphanes.^[12] This may cause the chiral spiro frameworks of the

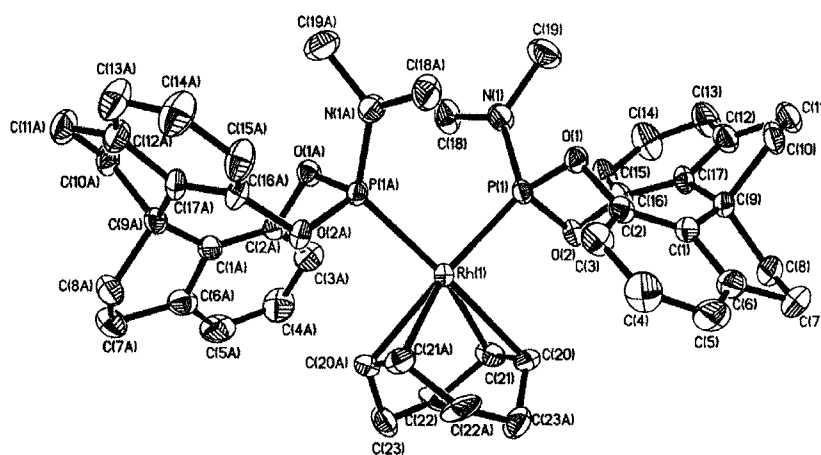


Figure 1. Structure of [Rh(cod){(*S*)-**1a**]₂⁺.

ligands in the transition state to be closer to the substrate coordinated to Rh and enhance the enantiodiscrimination of the catalyst.

In conclusion, we have developed novel and easily prepared chiral spiro phosphorus ligands that provide the first examples of highly efficient monodentate chiral ligands for the asymmetric hydrogenation of enamides. The applications of these ligands in other asymmetric transformations are currently under investigation.

Received: February 20, 2002
Revised: March 22, 2002 [Z18748]

Table 3. Asymmetric hydrogenation of **4** with catalysis by Rh/(*S*)-**1a**.^[a]

Entry	Ar	<i>ee</i> [%] ^[b]	Config. ^[c]
1	C ₆ H ₅ (4a)	98.7	<i>S</i>
2	<i>p</i> -CH ₃ C ₆ H ₄ (4b)	99.7	<i>S</i>
3	<i>m</i> -CH ₃ C ₆ H ₄ (4c)	91.6	<i>S</i>
4	<i>p</i> -CF ₃ C ₆ H ₄ (4d)	98.9	<i>S</i>
5	<i>p</i> -FC ₆ H ₄ (4e)	99.1	<i>S</i>
6	<i>o</i> -FC ₆ H ₄ (4f)	91.1	<i>S</i>
7	<i>p</i> -ClC ₆ H ₄ (4g)	99.3	<i>S</i>
8	<i>p</i> -BrC ₆ H ₄ (4h)	99.5	<i>S</i>
9	2-furanyl (4i)	98.7	<i>S</i>
10	2-thienyl (4j)	95.8	<i>S</i>

[a] Reaction condition: *S*/*C* = 100, *T* = 5 °C, *P*_{H₂} = 50 atm. [b] Determined by chiral capillary GC on a Varian Chirasil-L-Val column (25 m). [c] Determined by comparing the optical rotation with the reported value.^[4a]

- a) M. Nográdi, *Stereoselective Synthesis*, 2nd Ed., VCH, Weinheim, 1995; b) S. E. Denmark, T. Weber, D. W. Piotrowski, *J. Am. Chem. Soc.* **1987**, 109, 2224; c) R. E. Gawley, K. Rein, S. Chemburkar, *J. Org. Chem.* **1989**, 54, 3002; d) L. N. Pridgen, M. K. Mokhallalati, M.-J. Wu, *J. Org. Chem.* **1992**, 57, 1237.
- a) H. B. Kagan, N. Langlois, T. P. Dang, *J. Organomet. Chem.* **1975**, 90, 353; b) D. Sinou, H. B. Kagan, *J. Organomet. Chem.* **1976**, 114, 325.
- a) T. Morimoto, M. Chiba, K. Achiwa, *Chem. Pharm. Bull.* **1992**, 40, 2894; b) N. E. Lee, S. L. Buchwald, *J. Am. Chem. Soc.* **1994**, 116, 5958.
- See also: a) M. J. Burk, Y. M. Wang, J. R. Lee, *J. Am. Chem. Soc.* **1996**, 118, 5142; b) F.-Y. Zhang, C.-C. Pai, A. S. C. Chan, *J. Am. Chem. Soc.* **1998**, 120, 5808.
- a) G. Zhu, X. Zhang, *J. Org. Chem.* **1998**, 63, 9590; b) D. Xiao, Z. Zhang, X. Zhang, *Org. Lett.* **1999**, 1, 1679; c) R. Kuwano, K. Sato, T. Kurokawa, D. Karube, Y. Ito, *J. Am. Chem. Soc.* **2000**, 122, 7614; d) I. D. Gridnev, N. Higashi, T. Imamoto, *J. Am. Chem. Soc.* **2000**, 122, 10486; e) I. D. Gridnev, M. Yashutake, N. Higashi, T. Imamoto, *J. Am.*

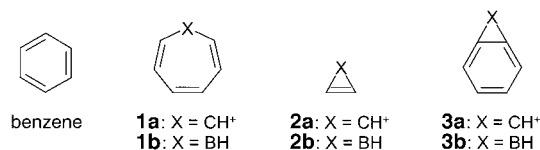
- Chem. Soc.* **2001**, 123, 5268; f) W. Li, X. Zhang, *J. Org. Chem.* **2000**, 65, 5871; g) Y.-Y. Yan, T. V. Rajanbabu, *Org. Lett.* **2000**, 2, 4137.
- [6] a) F. Guillen, J.-C. Fiaud, *Tetrahedron Lett.* **1999**, 40, 2939; b) C. Claver, E. Fernandez, A. Gillon, K. Heslop, D. J. Hyett, A. Martorell, A. G. Orpen, P. G. Pringle, *Chem. Commun.* **2000**, 961; c) M. T. Reetz, G. Mehler, *Angew. Chem.* **2000**, 112, 4047; *Angew. Chem. Int. Ed.* **2000**, 39, 3889; d) M. van den Berg, A. J. Minnaard, E. P. Schudde, J. van Esch, A. H. M. de Vries, J. G. de Vries, B. L. Feringa, *J. Am. Chem. Soc.* **2000**, 122, 11539; e) I. V. Komarov, A. Börner, *Angew. Chem.* **2001**, 113, 1237; *Angew. Chem. Int. Ed.* **2001**, 40, 1197.
- [7] V. B. Birman, A. L. Rheingold, K.-C. Lam, *Tetrahedron: Asymmetry* **1999**, 10, 125.
- [8] D. J. Cram, R. C. Helgeson, S. C. Peacock, L. J. Kaplan, L. A. Domeier, P. Moreau, K. Koga, J. M. Mayer, Y. Chao, M. G. Siegel, D. H. Hoffman, G. D. Y. Sogah, *J. Org. Chem.* **1978**, 43, 1930.
- [9] Orpen and Pringle et al. have reported the X-ray structure of a Pt complex of a monodentate biarylphosphonite (see ref. [6b]).
- [10] Crystal data for $[\text{Rh}(\text{cod})\{(\text{S})\text{-1a}\}_2](\text{OH}) \cdot \text{CH}_2\text{Cl}_2$: $\text{C}_{47}\text{H}_{55}\text{N}_2\text{Cl}_2\text{O}_3\text{P}_2\text{Rh}$, $M_r = 963.68$, $T = 293$ K, tetragonal, space group $P4_12_12$, $a = 10.495(2)$, $b = 10.495(2)$, $c = 42.528(12)$ Å, $V = 4684.1(19)$ Å³, $Z = 4$, 4099 unique reflections, $R1 = 0.0519$. CCDC 179716 contains the supplementary crystallographic data for this paper. These data can be obtained free of charge via www.ccdc.cam.ac.uk/conts/retrieving.html (or from the Cambridge Crystallographic Data Centre, 12, Union Road, Cambridge CB21EZ, UK; fax: (+44) 1223-336-033; or deposit@ccdc.cam.ac.uk).
- [11] The salt of the Rh^I complex obtained as a single crystal was $[\text{Rh}(\text{cod})\{(\text{S})\text{-1a}\}_2](\text{OH})$, instead of expected $[\text{Rh}(\text{cod})\{(\text{S})\text{-1a}\}_2]\text{BF}_4$. This might be because the $[\text{Rh}(\text{cod})_2]\text{BF}_4$ used in the preparation of catalyst contained water of crystallization [Aldrich 33498-7 (2000–2001)]. The single crystal of $[\text{Rh}(\text{cod})\{(\text{S})\text{-1a}\}_2](\text{OH})$ was also tested in the catalytic hydrogenation of **4a**, and 97.6% *ee* (at 10 °C) was obtained.
- [12] a) B. D. Vineyard, W. S. Knowles, M. J. Sabacky, G. L. Bachman, D. J. Weinkauff, *J. Am. Chem. Soc.* **1977**, 99, 5946; b) A. S. C. Chan, J. J. Pluth, J. Halpern, *Inorg. Chim. Acta*, **1979**, 37, L477; c) A. S. C. Chan, J. J. Pluth, J. Halpern, *J. Am. Chem. Soc.* **1980**, 102, 5952.

Gas-Phase Detection of the Elusive Benzoborirene Molecule**

Ralf I. Kaiser* and Holger F. Bettinger*

The cyclic delocalization of π electrons, responsible for the important concepts of aromaticity and antiaromaticity,^[1] has been fascinating ever since the discovery of benzene by Michael Faraday almost 200 years ago.^[2] The π system of benzene can be ported to the five- and seven-membered rings

by removing or introducing a CH^+ unit to result in the cyclopentadienyl anion (C_5H_5^-) and tropylium cation (C_7H_7^+) (**1a**),^[3] Scheme 1), respectively. Volpin et al. suggested that it



Scheme 1. Structures of (potentially) π aromatic compounds.

is possible to generate heteroaromatic homologues of aromatic hydrocarbons by substitution of a CH^+ unit by an isoelectronic BH group.^[4] Borirene **2b**^[5] and 1*H*-borepin **1b**,^[6] first synthesized in a low-temperature argon matrix and in solution, thus resemble the 2π -electron cyclopropenyl cation **2a**^[7] and the 6π -electron tropylium cation **1a**, respectively (Scheme 1). Extension of the 6π -electron system onto a second ring results in benzocyclopropenyl cation **3a** and benzoborirene **3b** as the simplest systems (Scheme 1). Although studied theoretically,^[8] **3a** and **3b** have not yet been observed experimentally.

How could the elusive benzoborirene **3b** be “made” in the laboratory? Ground-state boron and carbon atoms are known to react with a variety of unsaturated systems in crossed-beam experiments by an atom addition–hydrogen elimination mechanism.^[9, 10] This protocol was used very recently to produce **2b** from atomic boron and ethene in the gas phase through reaction (1).^[9a] Here we extend this novel concept and report on the formation of the hitherto unknown benzoborirene **3b**, the isoelectronic boron analogue of the elusive **3a**, through the atom–molecule reaction (2).



This reaction was studied in the gas phase at the molecular level by employing a crossed molecular beam setup.^[11] We prepared a pulsed boron beam by laser ablation of a boron rod and by entraining the ablated atoms in helium gas; this beam perpendicularly crossed a beam of benzene seeded in argon in a scattering chamber at a collision energy of (23.1 ± 0.8) kJ mol^{−1}. The reaction products were detected with a rotatable quadrupole mass spectrometer after electron ionization (EI); the ionizer was suited in an ultra-high-vacuum chamber. Velocity distributions of the product were collected with the time-of-flight (TOF) technique, that is, recording the arrival time of a distinct mass-to-charge ratio (m/z) of the ionized product, at different scattering angles (Figure 1).^[11] Integrating these TOF spectra leads to the laboratory angular distribution.

TOF spectra were recorded at m/z 93 ($^{11}\text{BC}_6\text{D}_5^+$) and 91 ($^{11}\text{BC}_6\text{D}_4^+$). At both mass-to-charge ratios, superimposable spectra were obtained suggesting that the signal at m/z 91 originates from cracking of the parent molecule (m/z 93) in

[*] Dr. R. I. Kaiser
Department of Chemistry
University of York
York YO105DD (UK)
Fax: (+44)1904-432516
E-mail: rik1@york.ac.uk

Dr. H. F. Bettinger
Lehrstuhl für Organische Chemie II
Ruhr-Universität Bochum (Germany)
Fax: (+49)234-3214353
E-mail: Holger.Bettinger@ruhr-uni-bochum.de

[**] This work was supported by the Deutsche Forschungsgemeinschaft (R.I.K.), Academia Sinica (Taiwan), University of York, and the Fonds der Chemischen Industrie through a Liebig Fellowship (H.F.B.), and Professor W. Sander, Bochum, (H.F.B.). We thank Dr. A. Balster (Bochum) for assistance with creating the cover picture and Professors W. Sander and P. von R. Schleyer for helpful discussions.

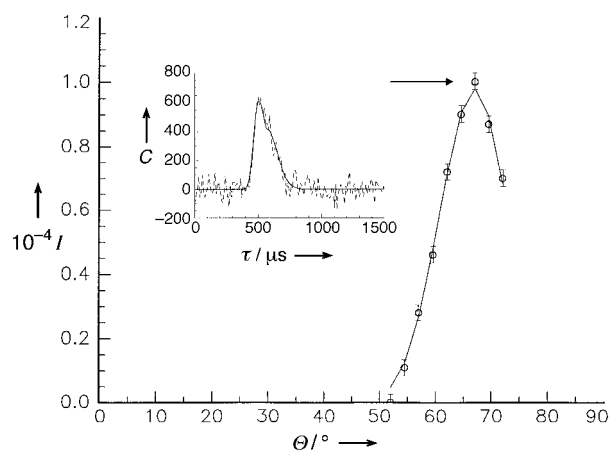


Figure 1. The laboratory angular distribution I at m/z 93 of the $^{11}\text{BC}_6\text{D}_5$ product from the reaction of atomic boron with $[\text{D}_6]\text{benzene}$; the direction of the boron beam is defined as 0° , that of the benzene beam as 90° . The solid line represents the angular distribution obtained from the best-fit center-of-mass angular and translational energy distributions, the open circles the experimental data (I : integrated counts; Φ : laboratory angle; τ : time of flight; C : counts). The time-of-flight spectrum recorded at the center-of-mass angle is shown as an inset (dashed line: experimental data; solid line: best fit from the center-of-mass functions).

the ionizer. Therefore, in accord with Equation (2), a molecule with the gross formula $^{11}\text{BC}_6\text{D}_5$ is formed.^[12] However, our ultimate goal is not only to assign the chemical formula of the reaction product, but to also elucidate the chemical structure of this organoboron species. Therefore it is necessary to extract information on the chemical dynamics and to unravel the underlying reaction mechanism from the experimental data. We achieved this by fitting the TOF spectra and the laboratory angular distribution of the $^{11}\text{BC}_6\text{D}_5$ product at m/z 93. This procedure yields two “best-fit” functions: the center-of-mass translational energy flux distribution $P(E)$ and the angular flux distribution $T(\theta)$ of the products, which are both displayed in Figure 2.^[13]

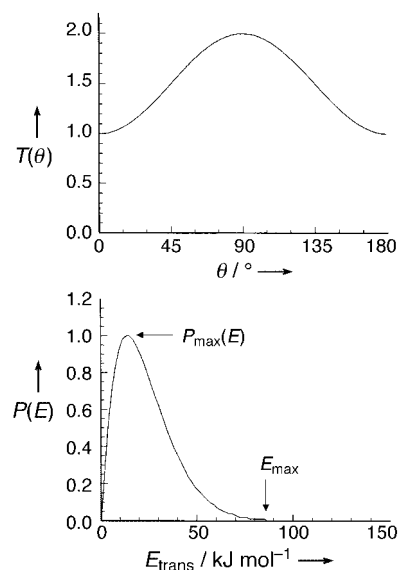


Figure 2. Best fit center-of-mass angular (T , left) and translational energy (P , right) flux distributions of the reaction of atomic boron with $[\text{D}_6]\text{benzene}$ to form benzoborirene plus atomic deuterium. θ : center-of-mass angle; E_{trans} : translational energy.

The maximum translational energy ($E_{\text{max}} = 80 - 90 \text{ kJ mol}^{-1}$) can be used to identify the nature of the products. Here, E_{max} is simply the sum of the reaction exoergicity plus the collision energy. Therefore, if we subtract the latter from E_{max} , the exoergicity of reaction (1) is calculated to be $(62 \pm 5) \text{ kJ mol}^{-1}$. The assignment of the $^{11}\text{BC}_6\text{D}_5$ product is possible by comparing the experimentally determined reaction exoergicity with theoretical data obtained from electronic structure computations for the conceivable reaction products $[\text{D}_5]\text{-3b}$, $[\text{D}_5]\text{-4}$, and $[\text{D}_5]\text{-5}$. Geometries were fully optimized with Gaussian98^[14a] utilizing Becke's^[14b,c] three-parameter hybrid functional in conjunction with the correlation functional of Lee et al.^[14d] and the 6-311 + $G(d,p)$ basis set $[\text{B3LYP}/6\text{-}311 + G(d,p)]$. Second derivatives were obtained analytically and used to compute unscaled harmonic vibrational frequencies and zero-point vibrational energies for the deuterated species. Energies were refined by single-point coupled-cluster computations involving single and double excitations, as well as a perturbative estimate of triple excitations^[14e] in conjunction with Dunning's^[14f] correlation-consistent triple- ζ basis set $[\text{CCSD}(\text{T})/\text{cc-pVTZ}]$ using the MOLPRO program.^[14g-i]

We found $[\text{D}_5]\text{-3b}$ to be the most stable isomer at the $\text{CCSD}(\text{T})/\text{cc-pVTZ}/\text{B3LYP}/6\text{-}311 + G(d,p)$ level of theory, while $[\text{D}_5]\text{-4}$ and $[\text{D}_5]\text{-5}$ are less stable by 131 and 176 kJ mol^{-1} , respectively. Good agreement between the experimental $[(62 \pm 5) \text{ kJ mol}^{-1}]$ and theoretical (69.7 kJ mol^{-1}) reaction energies is reached only for the formation of $[\text{D}_5]\text{-3b}$, while the reactions yielding $[\text{D}_5]\text{-4}$ and $[\text{D}_5]\text{-5}$ are strongly endoergic by 61.5 and $106.3 \text{ kJ mol}^{-1}$, respectively. Therefore, taking into account the collision energy of 23.1 kJ mol^{-1} , formation of $[\text{D}_5]\text{-4}$ and $[\text{D}_5]\text{-5}$ is not feasible under our experimental conditions. Thus, we conclude that benzoborirene $[\text{D}_5]\text{-3b}$ is the sole reaction product at m/z 93. This is the very first time that a boron-bearing aromatic, bicyclic molecule has been synthesized in which the six π electrons can be delocalized over seven atoms. The geometry of $[\text{D}_5]\text{-3b}$ (Figure 3) is very similar to those obtained in previous lower-level calculations.^[8d-f] The nucleus-independent chemical shifts (NICS)^[15a] were computed 1 Å above the ring centers,^[15b-d] and indicate that the aromatic character (based on magnetic criteria) of the six- and three-membered rings [NICS(1.0) values are -9.5 and -15.3 ppm , respectively] is slightly attenuated and intensified, respectively, compared to that of benzene [NICS(1.0) = -10.2] and borirene [NICS(1.0) = -14.4].

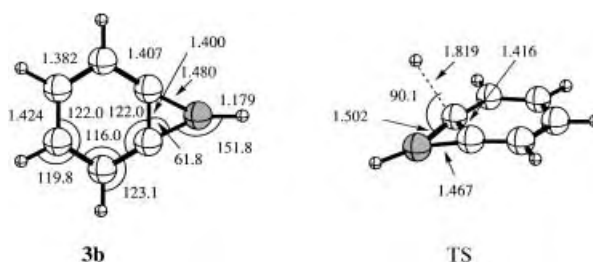


Figure 3. Selected bond lengths [\AA] and bond angles [$^\circ$] for **3b** and the transition state TS as computed at the $\text{B3LYP}/6\text{-}311 + G(d,p)$ level of theory.

Finally, we would like to discuss the reaction mechanism and investigate the angular flux distribution $T(\theta)$ closer. The latter shows a symmetric profile around 90° (see Figure 2); this indicates that the intensity of the flux distribution is the same at a center-of-mass angle θ and at the angle $180^\circ - \theta$. This symmetric shape is characteristic for a bimolecular gas-phase reaction which goes through a reactive intermediate having a lifetime larger than its rotation period.^[11] This intermediate is a $^{11}\text{BC}_6\text{D}_6$ isomer. It is known from reaction (1) that an initial boron addition to the π system is followed by a deuterium migration before the accumulated reaction energy is used for hydrogen ejection.^[9] A feasible reaction path also exists on the $\text{C}_6\text{D}_6\text{B}$ potential energy surface which involves, according to CCSD(T)/cc-pVTZ//B3LYP/6-311+G(d,p) investigations, addition of a boron atom to benzene to yield $\text{C}_6\text{D}_6\text{B}$ ($-34.6 \text{ kJ mol}^{-1}$, 2A) and subsequent [1,2]-D shift to $\text{C}_6\text{D}_5\text{BD}$ ($-253.6 \text{ kJ mol}^{-1}$, 2A') with a barrier (-0.6 kJ mol^{-1} with respect to the reactants) well below the available collision energy of $+23 \text{ kJ mol}^{-1}$. The actual shape of the function $T(\theta)$ reflects the direction in which the hydrogen atom leaves the fragmenting intermediate to form the $^{11}\text{BC}_6\text{D}_5$ product: the peak at 90° is indicative of emission of a deuterium atom perpendicular to the molecular plane of the $^{11}\text{BC}_6\text{D}_5$ moiety.^[11] The translational energy flux distribution $P(E)$ (see Figure 2) provides two additional sets of information on the ejection of the deuterium atom. First, the distribution maximum $P_{\text{max}}(E)$ of $10\text{--}20 \text{ kJ mol}^{-1}$ can give the order of magnitude of the barrier height in the exit channel.^[11] This data suggests a significant geometry and electron density change from the decomposing $^{11}\text{BC}_6\text{D}_6$ intermediate to the products. In other words, the reversed reaction—the addition of a deuterium atom to the $^{11}\text{BC}_6\text{D}_5$ molecule—has an entrance barrier of this order of magnitude. These experimental conclusions are confirmed by electronic structure computations. We find that the barrier for the addition of a deuterium atom to one of the bridgehead carbon atoms of $[\text{D}_5]\text{-3b}$ via the transition state TS has a barrier of 27.4 kJ mol^{-1} . The attacking D atom is oriented roughly perpendicularly to the molecular plane of $[\text{D}_5]\text{-3b}$ in this transition state (Figure 3).

In summary, our study identified for the first time the benzoborirene molecule in the gas phase by a combination of crossed-beam experiments and high-level electronic structure computations. It seems reasonable to assume that the versatile boron–hydrogen exchange reaction can be employed to synthesize even more complex heteroaromatic polycyclic boron-bearing molecules. For instance, the reaction of boron atoms with naphthalene should likely yield a tricyclic heteroaromatic molecule with ten π electrons via the boron versus hydrogen exchange channel.

Received: December 14, 2001 [Z18382]

- [1] a) P. von R. Schleyer, *Chem. Rev.* **2001**, *101*, 1115; b) for a recent compilation of reviews on aromaticity, see: *Chem. Rev.* **2001**, *101* (5).
 [2] M. Faraday, *Philos. Trans. R. Soc. London* **1825**, 440.
 [3] a) W. von E. Doering, L. H. Knox, *J. Am. Chem. Soc.* **1954**, *76*, 3203; b) H. J. Dauben, Jr., F. A. Gadecki, K. M. Harmon, D. L. Pearson, *J. Am. Chem. Soc.* **1957**, *79*, 4557; c) K. M. Harmon in *Carbonium Ions*, Vol. 4 (Eds.: G. A. Olah, P. von R. Schleyer), Wiley, New York, **1973**, pp. 1579–1641.

- [4] M. E. Volpin, Y. D. Koreshkov, V. G. Dulova, D. N. Kursanov, *Tetrahedron* **1962**, *18*, 107.
 [5] L. Andrews, D. V. Lanzisera, P. Hassanzadeh, Y. Hannachi, *J. Phys. Chem. A* **1998**, *102*, 3259.
 [6] A. J. Ashe, J. W. Kampf, Y. Nakadaira, J. M. Pace, *Angew. Chem.* **1992**, *104*, 1267; *Angew. Chem. Int. Ed. Engl.* **1992**, *31*, 1255.
 [7] R. Breslow, J. T. Groves, G. Ryan, *J. Am. Chem. Soc.* **1967**, *89*, 5048.
 [8] a) B. Halton, M. P. Halton, *Tetrahedron* **1973**, *29*, 1717; b) O. Sinanoglu, *Tetrahedron Lett.* **1988**, *29*, 889; c) R. Benassi, S. Ianelli, M. Nardelli, F. Taddei, *J. Chem. Soc. Perkin Trans. 2* **1991**, 1381; d) Z. B. Maksic, M. Eckert-Maksic, K.-H. Pfeifer, *J. Mol. Struct.* **1993**, *300*, 445; e) M. Eckert-Maksic, Z. Glasovac, Z. B. Maksic, I. Zrinski, *Theochem* **1996**, *366*, 173; f) A. Stanger, *J. Am. Chem. Soc.* **1998**, *120*, 12034.
 [9] a) N. Balucani, O. Asvany, Y. T. Lee, R. I. Kaiser, N. Galland, Y. Hannachi, *J. Am. Chem. Soc.* **2000**, *122*, 11234; b) N. Balucani, O. Asvany, Y. T. Lee, R. I. Kaiser, N. Galland, M. T. Rayez, Y. Hannachi, *J. Comput. Chem.* **2001**, *22*, 1359.
 [10] a) R. I. Kaiser, C. Ochsenfeld, M. Head-Gordon, Y. T. Lee, A. G. Suits, *Science* **1996**, *274*, 1508; b) R. I. Kaiser, I. Hahndorf, L. C. L. Huang, Y. T. Lee, H. F. Bettinger, P. von R. Schleyer, P. R. Schreiner, H. F. Schaefer III, *J. Chem. Phys.* **1999**, *110*, 6091.
 [11] R. I. Kaiser, N. Balucani, *Acc. Chem. Res.* **2001**, *34*, 699.
 [12] The following data of the integrated TOF spectra at distinct m/z ratios were derived at an electron energy of 200 eV: m/z 95: <0.01 ; m/z 94: $0.07\text{--}0.08$; m/z 93: 1.0 ; m/z 92: $0.18\text{--}0.23$; m/z 91: $1.3\text{--}1.4$.
 [13] R. I. Kaiser, C. Ochsenfeld, D. Stranges, M. Head-Gordon, Y. T. Lee, *Faraday Discuss.* **1998**, *109*, 183.
 [14] a) Gaussian 98 (Revision A.7): M. J. Frisch, G. W. Trucks, H. B. Schlegel, G. E. Scuseria, M. A. Robb, J. R. Cheeseman, V. G. Zakrzewski, J. A. Montgomery, R. E. Stratmann, J. C. Burant, S. Dapprich, J. M. Millam, A. D. Daniels, K. N. Kudin, M. C. Strain, O. Farkas, J. Tomasi, V. Barone, M. Cossi, R. Cammi, B. Mennucci, C. Pomelli, C. Adamo, S. Clifford, J. Ochterski, G. A. Petersson, P. Y. Ayala, Q. Cui, K. Morokuma, D. K. Malick, A. D. Rabuck, K. Raghavachari, J. B. Foresman, J. Cioslowski, J. V. Ortiz, B. B. Stefanov, G. Liu, A. Liashenko, P. Piskorz, I. Komaromi, R. Gomperts, R. L. Martin, D. J. Fox, T. Keith, M. A. Al-Laham, C. Y. Peng, A. Nanayakkara, C. Gonzalez, M. Challacombe, P. M. W. Gill, B. G. Johnson, W. Chen, M. W. Wong, J. L. Andres, M. Head-Gordon, E. S. Replogle, J. A. Pople, Gaussian, Inc., Pittsburgh, PA, **1998**; b) A. D. Becke, *J. Chem. Phys.* **1993**, *98*, 5648; c) P. J. Stephens, F. J. Devlin, C. F. Chabalowski, M. J. Frisch, *J. Phys. Chem.* **1994**, *98*, 11623; d) C. Lee, W. Yang, R. G. Parr, *Phys. Rev. B* **1988**, *37*, 785; e) K. Raghavachari, G. W. Trucks, J. A. Pople, M. Head-Gordon, *Chem. Phys. Lett.* **1989**, *157*, 479; f) T. H. Dunning, *J. Chem. Phys.* **1989**, *90*, 1007; g) C. Hampel, K. Peterson, H.-J. Werner, *Chem. Phys. Lett.* **1992**, *190*, 1; h) P. J. Knowles, C. Hampel, H.-J. Werner, *J. Chem. Phys.* **1993**, *99*, 5129; i) MOLPRO is a package of ab initio programs written by H.-J. Werner and P. J. Knowles; Version 2000.1 was used.
 [15] a) P. von R. Schleyer, C. Maerker, A. Dransfeld, H. Jiao, N. J. R. van Eikema Hommes, *J. Am. Chem. Soc.* **1996**, *118*, 6317; b) P. von R. Schleyer, H. Jiao, N. J. R. van Eikema Hommes, V. G. Malkin, O. L. Malkina, *J. Am. Chem. Soc.* **1997**, *119*, 12669; c) P. von R. Schleyer, M. Manoharan, Z.-X. Wang, B. Kiron, H. Jiao, R. Puchta, N. J. R. van Eikema Hommes, *Org. Lett.* **2001**, *3*, 2465; d) using the GIAO method (K. Wolinski, J. F. Hinton, P. Pulay, *J. Am. Chem. Soc.* **1990**, *112*, 8251) at the B3LYP/6-311+G(d,p) level of theory.

Arrays of Chemomechanically Patterned Patches of Homogeneous and Mixed Monolayers of 1-Alkenes and Alcohols on Single Silicon Surfaces**

Travis L. Niederhauser, Yit-Yian Lua, Guilin Jiang, Steven D. Davis, Reija Matheson, Deborah A. Hess, Ian A. Mowat, and Matthew R. Linford*

We have previously demonstrated a facile, chemomechanical method of simultaneously functionalizing and patterning silicon with single organic monolayers by scribing it while it is wet with 1-alkenes,^[1] 1-alkynes,^[1] and 1-haloalkanes.^[2] Here we show that this method can be extended to create individual surfaces that have different monolayer coatings in distinct and precisely controlled regions (Figure 1). Like microcontact

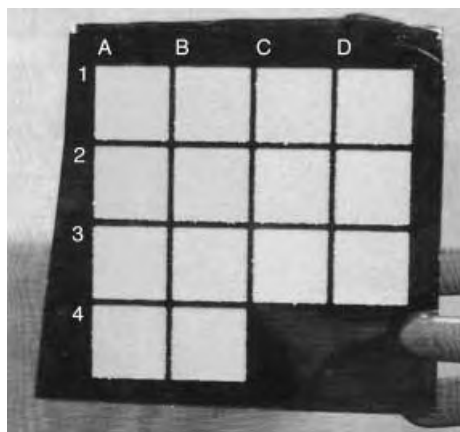


Figure 1. Scribed patches (0.8 × 0.8 cm each) on Si containing the homologous series of 1-alkenes from 1-pentene (A1) to 1-octadecene (B4).

printing, this technique allows multiple, patterned, surface features to be prepared with ease. To create these arrays a Si surface is 1) wet with a reactive compound, 2) scribed in a specific region with a computer-controlled diamond-tipped rod, 3) rinsed with a solvent, and 4) dried. This process is then repeated, without moving the Si surface from its original position, to create monolayer coatings in regions distinct from the first. With this technique we have prepared arrays of functionalized, scribed regions on single Si surfaces of a) the

homologous series of 1-alkenes from 1-pentene to 1-octadecene (a more extensive study than was previously reported^[1]), b) a series of alcohols (providing the first direct evidence for the bonding of alcohols to scribed Si), and c) a series of mixed monolayers on scribed Si from two 1-alkenes or from a 1-alkene and an alcohol (this is the first report of mixed monolayers on scribed Si). Our motivation for studying mixed monolayers is to be able to more easily create surfaces with more than one functional group, or with diluted functionality, as has been demonstrated with mixed monolayers of thiols on gold.^[3] Our desire to study the reactivity of alcohols and other functional groups with scribed silicon stems from our interest in developing it as a substrate for the creation of advanced materials.

As before,^[1, 2] the preparations described herein were performed in the air without any special treatment or degassing of chemicals. The time required to prepare, analyze (especially trends), and chemically modify arrays on single surfaces is much less than that required for the same number of coatings on individual surfaces because some experimental clean-up and analysis steps can be carried out on all array elements simultaneously. In addition, the ability to create surfaces with different monolayer coatings in precisely controlled regions should prove technologically valuable, for example, in creating single surfaces to perform multiple bioassays. Finally, the principles demonstrated herein should allow the preparation of functionalized patterns with smaller features.

We proposed^[1, 2] that scribed and unpassivated^[4] Si react similarly with 1-alkenes, 1-alkynes, and 1-haloalkanes to yield monolayers that are tethered through C–Si bonds, and that these monolayers are structurally similar to those prepared from hydrogen-terminated Si.^[1, 2, 5] Here we propose that scribed and unpassivated Si react similarly with alcohols (and water), which bind to different crystal faces of unpassivated Si through cleavage of O–H bonds to form Si–O and Si–H species.^[6–8] A fraction of the chemisorbed alcohols undergo further fragmentation on Si(111)–(7 × 7) to form Si–C bonds.^[5, 6] These results suggest that Si–O, Si–H, and perhaps Si–C bonds are formed by scribing Si with alcohols and that the chemisorption may be complex.

Other related methods of modifying surfaces include scribing hydrogen-terminated silicon with an AFM tip in the air to produce silicon oxide,^[9] grinding silicon in the presence of reactive chemicals to produce coated silicon particles,^[10] nanoshaving monolayers of thiols on gold while they are immersed in a solution containing a thiol different from the one in the monolayer,^[11] micromachining monolayers on gold with a scalpel blade or a carbon fiber followed by immersion in a thiol solution,^[12] and mechanically scratching surfaces to partition fluid-supported membranes.^[13]

Figure 2 shows X-ray photoelectron spectroscopy (XPS) data and water contact angle measurements from arrays of individually functionalized patches prepared from 1-alkenes on single Si surfaces. The increasing C1s/Si2p XPS signals, which are in good agreement with previously published results from single patches on single surfaces,^[1] and the increase in water contact angles up to the 1-undecene-derived surface indicate an increased carbon loading on the surface. The

[*] Dr. M. R. Linford, Dr. T. L. Niederhauser, Y.-Y. Lua, G. Jiang, S. D. Davis, R. Matheson
Department of Chemistry and Biochemistry
Brigham Young University
Provo, UT 84602 (USA)
Fax: (+1) 801-422-5474
E-mail: mrlinford@chemdept.byu.edu

Dr. D. A. Hess
Evans Texas
Round Rock, TX 78681 (USA)
Dr. I. A. Mowat
Charles Evans & Associates
810 Kifer Rd., Sunnyvale, CA 94086-5203 (USA)

[**] This work was supported by the Petroleum Research Fund.

Supporting information for this article is available on the WWW under <http://www.angewandte.org> or from the author.

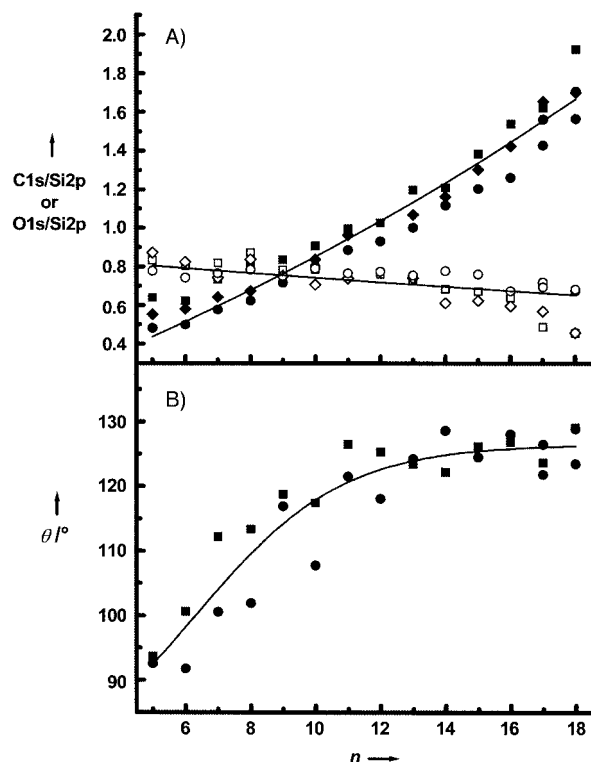


Figure 2. XPS (C1s/Si2p: solid symbols; O1s/Si2p: open symbols) and water contact angle measurements (θ) from arrays of patches prepared from 1-alkenes of different chain lengths (n : 1-alkene chain length, 1-pentene to 1-octadecene). Each symbol type represents data from a different array. Each point in (B) represents the average of two contact angle measurements made on either side of a 10- μ L drop placed on the scribed surface. The solid lines are guides to the eye.

change in contact angles can be attributed, in part, to an increasingly thick hydrocarbon film which acts as a hydrophobic barrier between the more polarizable silicon substrate and water droplets. The similar water contact angles from patches prepared from 1-undecene to 1-octadecene suggest that their outer few Ångströms are the same. Analogous wetting behavior was observed for thiols on gold.^[11] We attribute the high values of and variation in our water contact angles to surface roughness (CH₃-terminated monolayers from long-chain adsorbates on planar substrates have advancing water contact angles of 111–115°.^[14, 15]) The O1s/Si2p ratio as determined by XPS decreases with increasing chain length of the 1-alkene. This result is consistent with greater attenuation through increasingly thick organic films of less energetic O1s photoelectrons compared to more energetic Si2p photoelectrons^[16] from surfaces with constant oxygen levels at their Si–hydrocarbon interfaces.^[1, 2]

Arrays of patches or single patches on individual silicon surfaces both yielded the same results by XPS for silicon scribed with alcohols. These spectra show that 1) there is an approximately linear increase in carbon loading with increasing alkyl chain length, as was found for alkenes,^[1] alkynes,^[1] and alkyl halides,^[2] (see Supporting Information and Figure 2) and 2) high-resolution C1s narrow scans (Figure 3) indicate carbon atoms chemically shifted to higher oxidation states. The chemically shifted components show approximately the expected fraction of the total area for one carbon atom in each

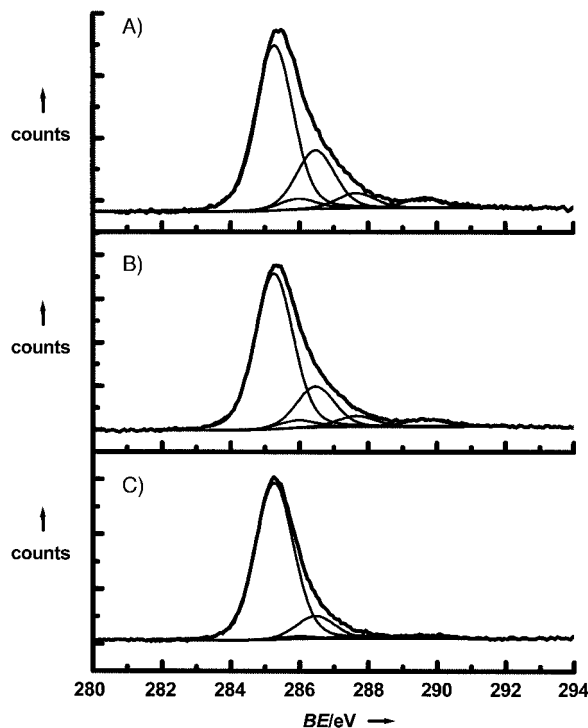


Figure 3. High-resolution XPS C1s narrow scans as a function of electron binding energy (BE) for patches on a silicon surface scribed in the presence of A) 1-propanol, B) 1-butanol, and C) 1-octanol along with peak-fitting results. The area ratios of the two low binding energy peaks to the other peaks are (average of two measurements, errors are half the distance between data points) $2.5 \pm 0.5:1$, $3.0 \pm 0.3:1$, and $6.8 \pm 1.3:1$ for 1-propanol, 1-butanol, and 1-octanol, respectively. All peak widths were fixed at 1.31 eV, which was the value found for the large, unshifted component in the 1-octanol spectrum. The binding energies for the peaks in the fits were set at 285.26, 285.96, 286.47, 287.66, and 289.66 eV. The peak at 285.96 is attributed to the carbon atom secondarily shifted by the presumed carboxyl carbon atom at 289.66 eV.

alkyl chain bonded to one or more oxygen atoms. Surfaces prepared by scribing silicon under 1-propanol, 1-butanol, and 1-octanol were also analyzed by time-of-flight/secondary ion mass spectrometry (TOF-SIMS). The resulting positive and negative ion spectra provide strong evidence for the formation of the expected surface species with three, four, and eight carbon atoms, respectively. Indeed, the 1-propanol-derived surface produces significantly higher levels of C₃H₇⁺, C₃H₇OSi⁺, C₃H₅O⁺, and C₃H₇O⁺ ions than the surfaces derived from 1-butanol and 1-octanol. Similarly, the 1-butanol-derived surface yielded higher levels of C₄H₉⁺, C₄H₉OSi⁺, C₄H₇O⁺, and C₄H₉O⁺ ions and the 1-octanol-derived surface higher levels of C₈H₁₅O⁺ and C₈H₁₇O⁺ than the other surfaces (see Supporting Information).

Figure 4 shows XPS and wetting data from arrays of mixed monolayers on scribed Si prepared from binary solutions of 1-decene and 1-octadecene. As expected, the C1s/Si2p ratio increases with increasing concentration of 1-octadecene in solution. However, in contrast to mixed monolayers of thiols on gold, which often show a strong preference for the adsorption of one thiol over another,^[17] the C1s/Si2p data are fairly linear over the concentrations of 1-octadecene studied. This observation suggests that kinetics, rather than thermodynamics, govern monolayer formation on scribed Si.

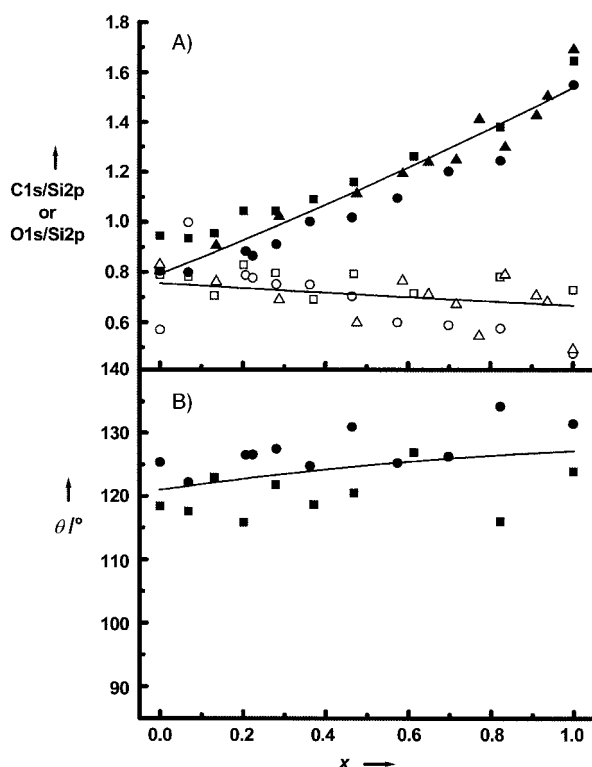


Figure 4. XPS (C1s/Si2p: solid symbols; O1s/Si2p: open symbols) and water contact angle measurements (θ) from arrays of patches prepared from binary solutions of 1-decene and 1-octadecene (x : mole fraction of 1-octadecene). Each symbol type represents data from a different array. Each point in (B) represents the average of two contact angle measurements made on either side of a 10- μ L drop placed on the scribed surface. The solid lines are guides to the eye.

We again attribute the decrease in the O1s/Si2p data to photoelectron attenuation through increasingly thick hydrocarbon films. As expected, the water contact angle data (Figure 4B) suggest there is a small increase in the hydrophobicity of these surfaces as the mole fraction of 1-octadecene in solution increases.

Figure 5 shows XPS and wetting data for arrays of mixed monolayers on single Si surfaces prepared from binary solutions of 1-decene and 1-decanol. XPS and wetting data show there is a decrease in the amount of surface carbon and water contact angles as the mole fraction of 1-decanol increases. (1-Haloalkanes also have lower C1s/Si2p ratios than 1-alkenes with the same number of carbon atoms.^[1,2]) The increase in the amount of surface oxygen shown in Figure 5B is consistent with higher surface concentrations of chemisorbed alcohols.

To better understand the stability of these new materials the arrays were immersed in boiling 0.1M H_2SO_4 for 1 h. After this stability test (open symbols) the concentration of carbon on the surface decreases at higher solution concentrations of 1-decanol (>30%), the surface oxygen concentrations of all of the patches increase (with the greatest increase at highest concentrations of 1-decanol in solution), and the water contact angles decrease (the greatest decrease is again at higher solution concentrations of 1-decanol). These results, especially the large changes in the properties of the 100% 1-decanol-derived patches, are consistent with a model of

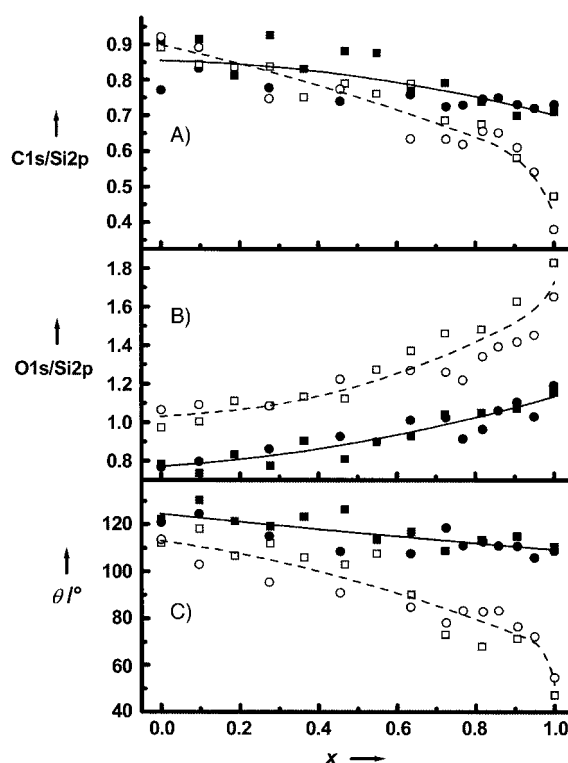


Figure 5. XPS and water contact angle data (θ) for two arrays of patches prepared by scribing under binary solutions of 1-decene and 1-decanol (x : mole fraction 1-decanol) before (solid symbols) and after (open symbols) a stability test (1 h in boiling 0.1M H_2SO_4). Each symbol shape represents data from a different array. The lines are guides to the eye.

hydrolyzable Si–O bonds holding the alkyl chains from 1-decanol and unhydrolyzable Si–C bonds tethering alkyl chains from 1-decene. The contact angle data and residual carbon (by XPS) of 100% 1-decanol monolayers suggest that hydrolysis of the monolayer is incomplete under these conditions or that some of the alcohol molecules bind to the surface through C–Si bonds. Adventitious carbon would also influence these results. In addition, the data in Figure 5 point to some general oxidation of all of the Si–monolayer interfaces during the stability test.

Received: January 25, 2002
Revised: April 15, 2002 [Z18584]

- [1] T. L. Niederhauser, G. Jiang, Y.-Y. Lua, M. J. Dorff, A. T. Woolley, M. C. Asplund, D. A. Berges, M. R. Linford, *Langmuir* **2001**, *17*, 5889–5900.
- [2] T. L. Niederhauser, Y.-Y. Lua, Y. Sun, G. Jiang, G. S. Strossman, P. Pianetta, M. R. Linford, *Chem. Mater.* **2002**, *14*, 27–29.
- [3] C. D. Bain, G. M. Whitesides, *J. Am. Chem. Soc.* **1988**, *110*, 6560–6561.
- [4] R. J. Hamers, Y. Wang, *Chem. Rev.* **1996**, *96*, 1261–1290.
- [5] J. M. Buriak, *Chem. Commun.* **1999**, 1051–1060.
- [6] M. Carbone, M. N. Piancastelli, R. Zanoni, G. Comtet, G. Dujardin, L. Hellner, *Surf. Sci.* **1997**, *370*, L179–L184.
- [7] M. Carbone, M. N. Piancastelli, J. J. Paggel, C. Weindel, K. Horn, *Surf. Sci.* **1998**, *412/413*, 441–446.
- [8] M. P. Casaletto, R. Zanoni, M. Carbone, M. N. Piancastelli, L. Aballe, K. Weiss, K. Horn, *Surf. Sci.* **2000**, *447*, 237–244.
- [9] H. T. Lee, J. S. Oh, S.-J. Park, K.-H. Park, J. S. Ha, H. J. Yoo, J.-Y. Koo, *J. Vac. Sci. Technol. A* **1997**, *15*, 1451–1454.

- [10] "Producing coated particles by grinding in the presence of reactive species: "M. R. Linford, US-A 6,132,801 **2000**.
- [11] S. Xu, G. Liu, *Langmuir* **1997**, *13*, 127–129.
- [12] N. L. Abbott, J. P. Folkers, G. M. Whitesides, *Science* **1992**, *257*, 1380–1382.
- [13] P. S. Cremer, J. T. Groves, L. A. Kung, S. G. Boxer, *Langmuir* **1999**, *15*, 3893–3896.
- [14] C. D. Bain, E. B. Troughton, Y.-T. Tao, J. Evall, G. M. Whitesides, R. G. Nuzzo, *J. Am. Chem. Soc.* **1989**, *111*, 321–335.
- [15] A. Ulman, *An Introduction to Ultrathin Organic Films from Langmuir–Blodgett to Self-Assembly*, Academic Press, Boston **1991**.
- [16] C. D. Bain, G. M. Whitesides, *J. Phys. Chem.* **1989**, *93*, 1670–1673.
- [17] P. E. Laibinis, R. G. Nuzzo, G. M. Whitesides, *J. Phys. Chem.* **1992**, *96*, 5097–5105.

Synthesis of Very Thin 1D and 2D CdWO₄ Nanoparticles with Improved Fluorescence Behavior by Polymer-Controlled Crystallization**

Shu-Hong Yu,* Markus Antonietti, Helmut Cölfen, and Michael Giersig

Nanosized building blocks with lower dimensionality, such as nanotubes, nanowires, nanorods, and ultrathin nanoplatelets have recently experienced a heightened interest.^[1–9] These systems with at least one restricted dimension offer opportunities for investigating the influence of size and dimensionality on optical, magnetic, and electronic properties.^[2] They can also be used as one component for a nanocomposite material to significantly improve the material properties.^[8] Recent efforts have focused on the development of new synthetic routes for preparing nanorods, nanowires, or nanotubes with uniform sizes and aspect ratios, for example, nanorods/nanowires of BaCrO₄,^[3] CdSe,^[4] metal nanorods: Cu,^[5a] Fe,^[5b] Ag,^[5c,d] Au,^[6] FeOOH,^[7] and vanadium oxide nanotubes (VO_x-NTs).^[9] A family of long semiconductor-oxide nanobelts with widths of 30 to 300 nanometers and width-to-thickness ratios of 5 to 10 was successfully synthesized by simply evaporating the desired commercial metal-oxide powders at high temperature.^[2b] The formation of a 2D

BaCrO₄ nanorod monolayer assembly using the Langmuir–Blodgett technique was also reported,^[10] and 2D wurtzite ZnS nanosheets were fabricated by a solution-based template method.^[11]

Recently, tungstate materials have attracted much interest because of their luminescence behavior, structural properties, and potential applications.^[12] Cadmium tungstate (CdWO₄) nanocrystals with a monoclinic wolframite structure are interesting because of their high average refractive index, low radiation damage, low afterglow, and high X-ray absorption coefficient;^[13] they can be used, for instance, as an X-ray scintillator.^[14, 15] Other tungstates with Scheelite structure MWO₄ (M = Ca, Ba, Pb) also display interesting excitonic luminescence, thermoluminescence, and stimulated Raman scattering (SRS) behavior.

To date, the procedure regarded as optimal to prepare CdWO₄ nanorods is a hydrothermal process at 130 °C.^[16] The nanorods of different compositions reported so far generally have rather small aspect ratios (length-to-diameter) of 2–10,^[17] which results in weak symmetry-breaking surface effects. In addition a reverse micelle templating method has recently been used to synthesize uniform BaWO₄ nanorods with diameters of 5 nm and aspect ratios of about 150 by using barium bis(2-ethylhexyl)sulfosuccinate [Ba(AOT)₂] micelles, which are treated with NaAOT microemulsion droplets containing sodium tungstate (Na₂WO₄).^[17] The large excess of surfactants as well as the very low concentration throughout synthesis, however, could restrict the applicability of this procedure.


Herein, we present a facile aqueous-solution route for the synthesis of extremely thin 1D and 2D CdWO₄ nanoparticles with controlled sizes (length, width, thickness) by using a combination of the double-jet injection of simple inorganic reactants and double-hydrophilic block copolymers (DHBCs) as crystal-growth modifiers.

DHBCs have been introduced as very efficient inhibitors and crystal-growth modifiers^[18] and have already shown their potential for the morphosynthesis of calcium carbonate, barium sulfate, calcium phosphates, and zinc oxide crystals.^[19] To differentiate between the influence of process parameters and the chemical influence of the DHBCs, CdWO₄ was crystallized in a set of experiments in the absence of polymer. The X-ray diffraction (XRD) pattern in Figure 1a demonstrates that well-crystallized CdWO₄ particles can be easily synthesized at room temperature, which can be indexed as monoclinic wolframite structure with unit cell parameters $a = 5.029$, $b = 5.859$, $c = 5.074$ Å (JSPDS Card: 14-676). The sharper nature of the diffraction peaks 100, 200, and 002 suggests possible preferential orientation along these directions. In addition, the 010 diffraction peak is very weak and broadened, which indicates that the thickness direction will be along the b axis, which was confirmed by high-resolution (HR) TEM results.

The corresponding TEM image in Figure 2a shows very thin, uniform CdWO₄ nanorods/nanobelts with lengths in the range of 1–2 μm and a uniform width of 70 nm along their entire length (aspect ratio of about 30). No different contrast was observed, which suggests the perfect growth of the nanoparticles and uniform thickness. Large scale, lower-

[*] Dr. S.-H. Yu, Prof. Dr. M. Antonietti, Dr. H. Cölfen
Max Planck Institute of Colloids and Interfaces
Department of Colloid Chemistry
MPI Research Campus Golm, 14424 Potsdam (Germany)
Fax: (+49) 331-567-9502
E-mail: shyu@mpikg-golm.mpg.de
Dr. M. Giersig
Hahn-Meitner-Institut, Abt. Physikalische Chemie
Glienickerstrasse 100, 15109 Berlin (Germany)

[**] We acknowledge financial support by the Max Planck Society and the DFG (SFB 448). S.-H. Yu thanks the Alexander von Humboldt Foundation for granting a research fellowship. H.C. thanks the Dr. Hermann Schnell Foundation for financial support. Th. Goldschmidt AG, Essen is acknowledged for donation of the PEG-*b*-PMAA block copolymer. Dr. Jan Rudloff is thanked for the phosphonation of PEG-*b*-PMAA.

 Supporting information for this article is available on the WWW under <http://www.angewandte.org> or from the author.

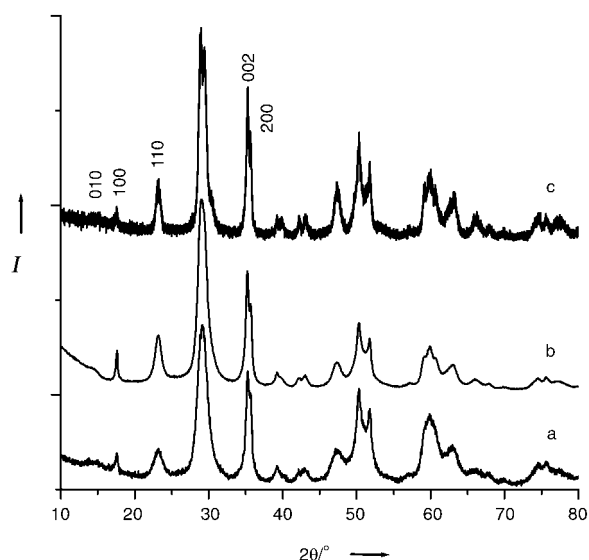


Figure 1. X-ray diffraction patterns of the CdWO_4 samples obtained under different conditions: a) initial solution: 20 mL, pH 5.3, double jet, end solution: $[\text{Cd}^{2+}]/[\text{WO}_4^{2-}] = 8.3 \times 10^{-3} \text{ M}$, at room temperature; b) and c) pH 5.3, double jet, end solution $[\text{Cd}^{2+}]/[\text{WO}_4^{2-}] = 8.3 \times 10^{-3} \text{ M}$, then hydrothermal crystallization: b) 80°C , 6 h; c) 120°C , 6 h.

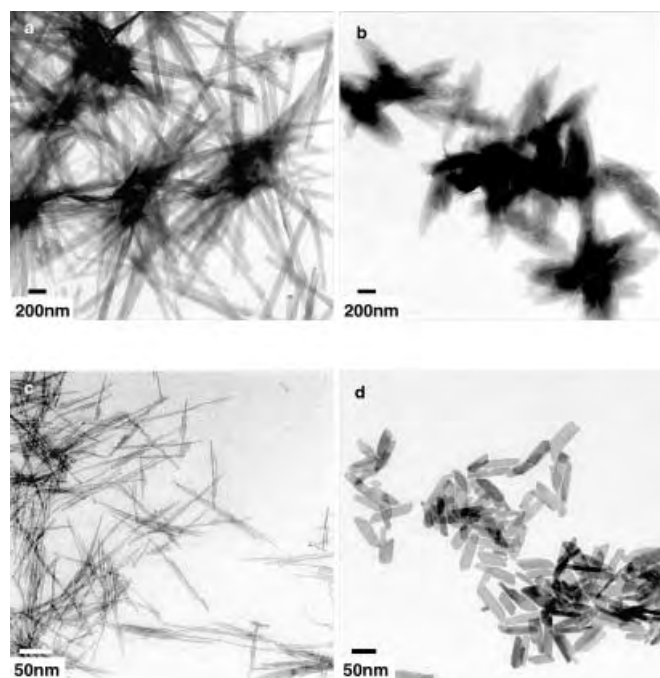


Figure 2. TEM images of the samples obtained under different conditions: a) and b) no additives: a) pH 5.3, double jet, $[\text{Cd}^{2+}]/[\text{WO}_4^{2-}] = 8.3 \times 10^{-3} \text{ M}$ (end solution), at room temperature, b) pH 5.3, double jet, $[\text{Cd}^{2+}]/[\text{WO}_4^{2-}] = 8.3 \times 10^{-3} \text{ M}$ (end solution), then hydrothermal crystallization: 80°C , 6 h, c) pH 5.3, in the presence of PEG-*b*-PMAA (1 g L^{-1}), 20 mL, double jet, $[\text{Cd}^{2+}]/[\text{WO}_4^{2-}] = 8.3 \times 10^{-3} \text{ M}$ (end solution), then hydrothermal crystallization: 80°C , 6 h, d) direct hydrothermal treatment of 20 mL solution containing equal molar $[\text{Cd}^{2+}]/[\text{WO}_4^{2-}] = 8.3 \times 10^{-2} \text{ M}$, pH 5.3, at 130°C , 6 h, in the presence of 1 g L^{-1} PEG-*b*-PMAA- PO_3H_2 (21 %).

magnification TEM images also show that all the longer nanorods/nanobelts tend to aggregate towards nested, star-like clusters (see Supporting Information Figure 1a and Figure 1b). Successive hydrothermal ripening after the dou-

ble-jet reaction leads to a rearrangement of the rods into 2D lens-shaped, raftlike superstructures (Figure 2b) with a resulting lower aspect ratio. The thickness of the rods and the raftlike superstructures was shown to be 6–7 nm by scanning force microscopy (SFM) topography height profiles (see Supporting Information Figures 2a,b). The structure modeling data clearly shows the W octahedra chain within the wolframite structure. The thin nature of the elongated nanoparticles could be related with the chain structure of the W octahedra in the wolframite type structure.^[20] (see Supporting Information Figure 3).

An optional hydrothermal ripening of the CdWO_4 nanorods at different temperatures leads either to further self-assembly into 2D raftlike structures (Figure 2b and Supporting Information Figure 1d) or the formation of 2D single-crystalline nanoplatelets (Figure 2d). The self-organization of the nanorods into 2D structures induced by hydrothermal treatment is very similar to that reported for BaWO_4 and BaCrO_4 nanorods,^[10] but differs significantly from the assembly of the short BaCrO_4 and CdSe nanorods where ribbonlike and vertical rectangular/hexagonal superstructures are favored.^[3a, 4]

There are two reasons for the rods to align parallel,^[17] first, to maximize the entropy of the self-assembled structure of rodlike or nematic objects by minimizing the excluded volume per particle in the array, as first suggested by Onsager,^[21] and second, because of the higher sum of van der Waals forces along the length of a nanorod as compared to its tip.^[6]

The aspect ratio in absence of the polymer is already about 30, which is higher than the previously reported values for BaCrO_4 and CdSe .^[3a, 4] Additionally, these particles are comparably thin, which is important for the mechanical performance in nanocomposites.^[8]

In a second step, the DHBC poly(ethylene glycol)-*block*-poly(methacrylic acid) (PEG-*b*-PMAA) was added to the solvent reservoir before the double-jet crystallization process and the mixture was then hydrothermally ripened at 80°C . Figure 2c shows that in this case, uniform nanofibers with a diameter of 2.5 nm, a length of 100–210 nm, and an aspect ratio of 40–85 can be readily obtained. These nanofibers can now be regarded as “real” 1D objects, since the number of surface atoms is comparable with those embedded within the structure. In addition, it is seen that the single fibers are well separated, which indicates a sufficient steric stabilization brought about by the adsorbed DHBCs. Hydrothermal ripening at 80°C for longer time or at higher temperatures (120°C) results in this case again in a co-alignment of the rods along their axis to form similar raftlike and very thin 2D-superstructures, as described above (see Supporting Information Figures 1c and d).

In addition, a new polymer-driven morphology arises when the partly phosphonated hydrophilic block copolymer PEG-*b*-PMAA- PO_3H_2 (21 %; 1 g L^{-1}) is added at an elevated temperature of 130°C even without using the double-jets but at higher concentrations ($8.3 \times 10^{-2} \text{ M}$) and coupled supersaturation. Figure 2d shows that very thin platelike particles with a width of 17–28 nm, a length of 55–110 nm, and an aspect ratio of 2–4 are obtained by a direct hydrothermal process.

The HRTEM magnification in Figure 3a shows that the particles obtained in the absence of polymer are very thin, as seen by a tilted structure (indicated by the arrow). The nanobelts show the preferential orientation growth in length

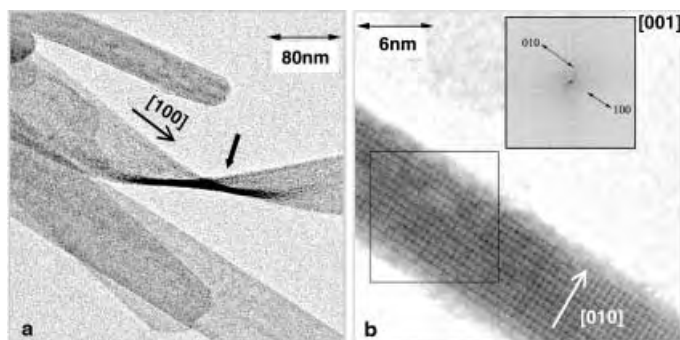


Figure 3. TEM and HRTEM images of the samples obtained under different conditions: a) No additives: pH 5.3, double jet, final solution $[\text{Cd}^{2+}]/[\text{WO}_4^{2-}] = 8.3 \times 10^{-3} \text{ M}$, at room temperature, showing the very thin nanobelts (indicated by the arrow), b) HRTEM image taken along $[001]$, shows the clear lattice fringes of $[100]$ and $[010]$ with spacing 5.86 \AA and 5.02 \AA , respectively. The thickness of the short sheetlike nanoplates is about 8 nm .

along the a axis and width along the c axis (see Supporting Information Figure 2c). The HRTEM image in Figure 3b was taken exactly along the axis $[001]$ of the nanoplatelets, showing clearly the lattice fringes of the $[100]$ and $[010]$ planes. The short sheetlike nanoplatelets with thickness of about 8 nm preferentially grew along $[100]$ and $[001]$. That the crystals along the b axis are thin and much more elongated along the c and a axes is again consistent with the above XRD results.

The slow and controlled reactant addition by the double-jet technique under stirring maintains formation of intermediate amorphous nanoparticles at the jets^[18b] so that nanoparticles are the precursors for further particle growth rather than ionic species, an important difference to previous reports.^[16] This growth mechanism is crucial to obtain the observed nanobelt structure (Figure 2a and Figure 3a). In contrast, the direct mixing of reactants at room temperature under stirring without using the double-jet technique can only produce large aggregates composed of very poorly defined thin platelike particles (data not shown).

Atomic modeling of the exposed crystal surfaces can indicate the structure specificity. The surface structure cleavage of the CdWO_4 crystals (Supporting Information Figure 4) shows that the (100) face contains W octahedral anions in a zigzag orientation, which shows that this face will not be favorable for the adsorption of the negatively charged polymer groups, and leads to the detected fastest growth rate along the $[100]$ direction. A view along the b axis reveals a regular linear alignment of the tungstate clusters and consequently of the Cd^{2+} ions in a favorable orientation for polymer adsorption on the (010) face.

Figure 4 shows the luminescence spectra of the different CdWO_4 nanostructures obtained under different conditions

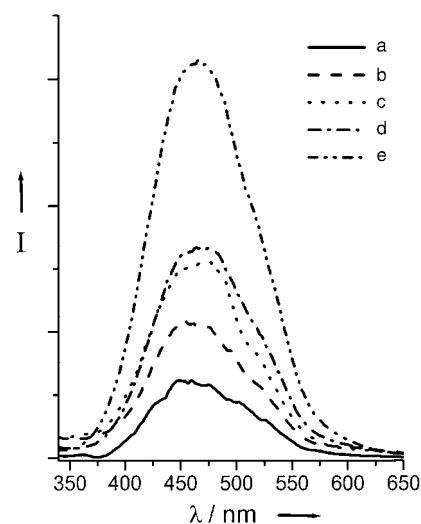


Figure 4. Room temperature photoluminescence spectra of the samples obtained under different conditions: a) pH 5.26, double jet, final solution $[\text{Cd}^{2+}]/[\text{WO}_4^{2-}] = 8.3 \times 10^{-3} \text{ M}$; b) and c) pH 5.26, double jet, final solution $[\text{Cd}^{2+}]/[\text{WO}_4^{2-}] = 8.3 \times 10^{-3} \text{ M}$, then hydrothermal crystallization: b) 80°C , 6 h ; c) 120°C , 6 h ; d) pH 5.3, in the presence of PEG-*b*-PMAA (1 g L^{-1}), 20 mL , double jet, final solution $[\text{Cd}^{2+}]/[\text{WO}_4^{2-}] = 8.3 \times 10^{-3} \text{ M}$, then hydrothermal crystallization: 80°C , 6 h ; e) direct hydrothermal treatment of 20 mL solution containing equal molar $[\text{Cd}^{2+}]/[\text{WO}_4^{2-}] = 8.3 \times 10^{-4} \text{ M}$, pH 5.3, at 130°C , 6 h , in the presence of 1 g L^{-1} PEG-*b*-PMAA- PO_3H_2 (21 %).

and with different polymers, but similar concentrations. The spectral characteristics were very similar to those of the other scheelite tungstate crystals (AWO_4 , $\text{A} = \text{Pb}, \text{Ca}, \text{Ba}, \text{Sr}$).^[22] The absolute luminescence intensity increases with increasing hydrothermal crystallization temperature (Figure 4a–c), and is an indication of the perfection of the crystals. Quite unexpectedly, the luminescence efficiency is further increased in the presence of the different DHBCs (at lower crystallization temperature), where the best-performing system increases in efficiency by a factor of two. This increase is explained by a highly perfected structure where quenching surface defects are suppressed or blocked by the polymers. The increase of luminescence efficiency by blocking of surface states was observed for DHBC-stabilized CdS quantum dots,^[23] and perfecting crystal surfaces by surface-active polymers was described very recently.^[24]

The CdWO_4 nanostructures obtained in the absence of polymer exhibit a blue emission band in the range $400\text{--}550 \text{ nm}$ centered around 460 nm when excited at 253 nm , which agrees well with the data for the single crystals obtained at high temperatures,^[14] but is blue-shifted compared to the reported “intrinsic luminescence” at $480\text{--}490 \text{ nm}$.^[25] The blue-emission structure of all three samples contains at least two or three components. Generally, the presence of Gaussian components indicates that the electronic levels corresponding to relaxed excited states of an emission center belong to a degenerated excited states influenced by some perturbation.^[26] The emission-band shape might be explained considering Jahn–Teller active vibrational modes of t_2 symmetry which influence the WO_4^{2-} complex anion of slightly distorted tetrahedral symmetry to lead to a structured absorption band for the $\text{A}_1 \rightarrow \text{T}_{1(2)}$ transitions.^[26, 27] The decomposition of the

band into individual components results in three Gaussians with their maximum located at 423, 451, and 483 nm, respectively, to give good agreement with the experimental data.^[28] The subsequent hydrothermal treatment leads to the red-shift of the three components (Supporting Information: Figures 5 a,c and Table 1).

Similarly, the deconvolution of the emission spectra of the two samples made in the presence of DHBCs reveal an additional green component at 501 nm or 509 nm, respectively (see Supporting Information Figures 5 d,e and Table 1). The comparable amount of the blue and green emission components can be used, taking advantage of the fact that all the recombination processes are transferred to the green component by an efficient energy transfer through free charge carriers.^[29] Thus the remaining blue emission component is almost free of recombination processes. The decomposition of the band is not unique since the individual Gaussian components strongly overlap which makes the numerical solution rather unstable. The correlation of energy transfer processes in the blue and green emission components in the synthesized particular systems with lower dimensionality deserves further investigation in time and temperature resolved experiments.

In summary, we have found a simple aqueous route to prepare uniform and very thin CdWO₄ nanorods/nanobelts and elongated nanosheets at room temperature starting from simple inorganic reactants by the double-jet crystallization technique. This technique provides nanoparticulate precursors for further crystallization which is in contrast to previously reported techniques. Additionally, application of two different double-hydrophilic block copolymers throughout a hydrothermal ripening process allowed a fine tuning of both crystal morphology and crystal superstructure, for example, 2D raftlike structures could be formed by a hydrothermal ripening process. The prepared structures display a very strong blue/green luminescence at room temperature, where the quantum efficiency is highly improved by addition of the DHBCs. This effect is speculatively attributed to a perfecting of the nanocrystals and/or blocking of quenching surface states by the DHBCs. This approach is expected to form a new general route for the controlled morphosynthesis of tungstate luminescence materials in restricted dimensions, with controllable size and shape, the solid-state optical properties of which are of interest.

Experimental Section

All chemicals were obtained from Aldrich and were used without further purification. A commercial block copolymer PEG-*b*-PMAA (PEG = 3000 g mol⁻¹, PMAA = 700 g mol⁻¹) was obtained from Th. Goldschmidt AG, Essen, Germany. The carboxylic acid groups of this copolymer were partially phosphonated (21%) to give a copolymer with carboxyl and phosphonated groups, PEG-*b*-PMAA-PO₃H₂, according to ref. [18b].

The precipitation of CdWO₄ was carried out in a double-jet reactor thermostated at 25 °C as described previously.^[18c] A solution of distilled water (20 mL) was adjusted to the desired pH 5.3, by using 1 M NaOH or HCl, before it was used for the precipitation of CdWO₄. Under vigorous stirring, 0.1 M CdCl₂ and 0.1 M Na₂WO₄ were injected through capillaries into a Teflon reaction vessel with a reactant supply of 1 mL h⁻¹ for 2 h, which gave a CdWO₄ formation rate of 1.39×10^{-4} M min⁻¹. The reactant supply was stopped after injection for 2 h, and the precipitate was left under

continuous stirring in its mother solution for at least 6 h to ensure complete equilibration. For direct hydrothermal treatment, equal molar CdCl₂ and Na₂WO₄ (1.67×10^{-3} mol) were mixed in block copolymer solution (20 mL, 1 g L⁻¹) under stirring and then the pH value was adjusted to 5.3 by using 1 M HCl.

The above solution was poured into a commercial stainless Teflon-lined autoclave of 40 mL capacity (SANPLATEC Company, Japan) after double-jet reaction. The autoclave was maintained at a certain temperature (80–130 °C) for 6 h, and then air cooled to room temperature. The precipitates were collected and washed with distilled water and dried in air for further characterization.

TEM images were taken with a Zeiss EM 912 Omega microscope. HR-TEM was carried out on a Philips CM 12 microscope operating at 120 kV (equipped with an EDAX 9800 analyzer). Dry powder samples were used for the measurements of X-ray powder diffraction (XRD) using a PDS 120 (Nonius GmbH, Solingen) with CuK_α radiation. The photoluminescence (PL) measurements were performed on a Perkin Elmer Luminescence Spectrometer LS50B at room temperature. Scanning force micrographs (SFM) were obtained from a Digital Instruments Nanoscope III in tapping mode (Digital Instruments Inc., Santa Barbara, CA)). The height profiles of the nanostructures along the solid line were processed by using the Nanoscope software. The samples were prepared by dropping the nanoparticle dispersion onto a freshly cleaved mica substrate. The computer modeling was done with the Cerius² software (Accelrys).

Received: February 5, 2002

Revised: March 25, 2002 [Z 18656]

- [1] C. M. Lieber, *Solid State Commun.* **1998**, *107*, 607.
- [2] a) J. T. Hu, T. W. Odom, C. M. Lieber, *Acc. Chem. Res.* **1999**, *32*, 435; A. M. Morales, C. M. Lieber, *Science* **1998**, *279*, 208; b) Z. W. Pan, Z. R. Dai, Z. L. Wang, *Science* **2001**, *291*, 1947.
- [3] a) M. Li, H. Schnablegger, S. Mann, *Nature* **1999**, *402*, 393; b) S. H. Yu, H. Cölfen, M. Antonietti, *Chem. Eur. J.* **2002**, *8*, in press.
- [4] X. G. Peng, L. Manna, W. D. Yang, J. Wickham, E. Scher, A. Kadavanich, A. P. Alivisatos, *Nature* **2000**, *404*, 59.
- [5] a) J. Tanori, M. P. Pileni, *Adv. Mater.* **1995**, *7*, 862; b) S.-J. Park, S. Kim, S. Lee, Z. G. Khim, K. Char, T. Hyeon, *J. Am. Chem. Soc.* **2000**, *122*, 8581; c) B. A. Korgel, D. Fitzmaurice, *Adv. Mater.* **1998**, *10*, 661; d) Y. Zhou, S. H. Yu, C. Y. Wang, X. G. Li, Y. R. Zhu, Z. Y. Chen, *Adv. Mater.* **1999**, *11*, 850.
- [6] B. Nikoobakht, Z. L. Wang, M. A. El-Sayed, *J. Phys. Chem. B* **2000**, *104*, 8635.
- [7] H. Maeda, Y. Maeda, *Langmuir* **1996**, *12*, 1446.
- [8] E. P. Giannelis, *Adv. Mater.* **1996**, *8*, 29.
- [9] M. E. Spahr, P. Bitterli, R. Nesper, M. Müller, F. Krumeich, H.-U. Nissen, *Angew. Chem.* **1998**, *110*, 1339; *Angew. Chem. Int. Ed.* **1998**, *37*, 1263.
- [10] F. Kim, S. Kwan, J. Akana, P. D. Yang, *J. Am. Chem. Soc.* **2001**, *123*, 4360.
- [11] S. H. Yu, M. Yoshimura, *Adv. Mater.* **2002**, *14*, 296.
- [12] N. Saito, N. Sonoyama, T. Sakata, *Bull. Chem. Soc. Jpn.* **1996**, *69*, 2191.
- [13] H. Lotem, Z. Burshtein, *Opt. Lett.* **1987**, *12*, 561.
- [14] V. A. Pustovarov, A. L. Krymov, B. Shulgin, *Rev. Sci. Instrum.* **1992**, *63*, 3521.
- [15] K. Tanaka, T. Miyajima, N. Shirai, Q. Zhang, R. Nakata, *J. Appl. Phys.* **1995**, *77*, 6581.
- [16] H. Liao, Y. Wang, X. Liu, Y. Li, Y. Qian, *Chem. Mater.* **2000**, *12*, 2819.
- [17] S. Kwan, F. Kim, J. Akana, P. D. Yang, *Chem. Commun.* **2001**, 447.
- [18] a) H. Cölfen, *Macromol. Rapid Commun.* **2001**, *22*, 219, and references therein; b) H. Cölfen, M. Antonietti, *Langmuir* **1998**, *14*, 582; c) M. Sedlak, M. Antonietti, H. Cölfen, *Macromol. Chem. Phys.* **1998**, *199*, 247.
- [19] a) M. Antonietti, M. Breulmann, C. Göltner, H. Cölfen, K. K. Wong, D. Walsh, S. Mann, *Chem. Eur. J.* **1998**, *4*, 2493; b) L. Qi, H. Cölfen, M. Antonietti, *Angew. Chem.* **2000**, *112*, 617; *Angew. Chem. Int. Ed.* **2000**, *39*, 604; c) L. Qi, H. Cölfen, M. Antonietti, M. Lei, J. D. Hopwood, A. J. Ashley, S. Mann, *Chem. Eur. J.* **2001**, *7*, 3526; d) M. Öner, J. Norwig, W. H. Meyer, G. Wegner, *Chem. Mater.* **1998**, *10*, 460; e) H. Cölfen, L. Qi, *Chem. Eur. J.* **2001**, *7*, 106.

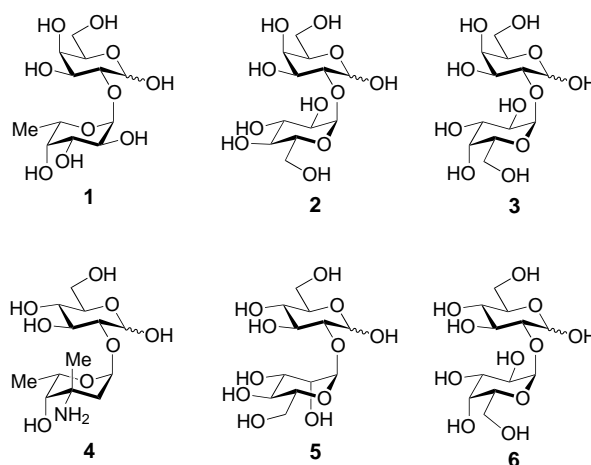
- [20] A. P. Chichagov, V. V. Ilyukhin, N. V. Belov, *Sov. Phys. Dokl.* **1966**, *11*, 11.
 [21] L. Onsager, *Ann. N. Y. Acad. Sci.* **1949**, *51*, 627.
 [22] M. Nikl, P. Bohacek, E. Mihokova, M. Kobayashi, M. Ishii, Y. Usuki, V. Babin, A. Stolovich, S. Zazubovich, M. Bacci, *J. Lumin.* **2000**, *87*, 1136.
 [23] L. Qi, H. Cölfen, M. Antonietti, *Nano. Lett.* **2001**, *1*, 61.
 [24] A. Peytcheva, M. Antonietti, *Angew. Chem.* **2001**, *113*, 3484; *Angew. Chem. Int. Ed.* **2001**, *40*, 3380.
 [25] M. M. Chirilaa, K. T. Stevensa, H. J. Murphyb, N. C. Giles, *J. Phys. Chem. Solids* **2000**, *61*, 675.
 [26] K. Polak, M. Nikl, K. Nitsch, M. Kobayashi, M. Ishii, Y. Usuki, O. Jarolimek, *J. Lumin.* **1997**, *72–74*, 781.
 [27] Y. Toyozawa, M. Inoue, *J. Phys. Soc. Jpn.* **1966**, *21*, 1663.
 [28] M. Springis, V. Tale, I. Tale, *J. Lumin.* **1997**, *72–74*, 784.
 [29] M. Nikl, P. Straková, K. Nitsch, V. Petíek, V. Múka, O. Jarolímek, J. Novák, P. Fabeni, *Chem. Phys. Lett.* **1998**, *291*, 300.

Synthesis of Biologically Potent $\alpha 1 \rightarrow 2$ -Linked Disaccharide Derivatives via Regioselective One-Pot Protection – Glycosylation**

Cheng-Chung Wang, Jinq-Chyi Lee, Shun-Yuan Luo, Hsin-Fang Fan, Chin-Ling Pai, Wei-Chieh Yang, Lung-Dai Lu, and Shang-Cheng Hung*

Dedicated to Professor Chun-Chen Liao
on the occasion of his 60th birthday

$\alpha 1 \rightarrow 2$ -Linked disaccharides are key subunits of numerous biologically potent oligosaccharides, antigens, antibiotics, glycoproteins, and glycolipids. For example, the tumor antigen Globo H,^[1] ABH blood groups,^[2] and human milk oligosaccharides^[3] contain α -L-Fuc(1 \rightarrow 2)-D-Gal (**1**) as a common component. α -D-Glc(1 \rightarrow 2)-D-Gal (**2**) is a structural element of glycoproteins isolated from the body wall of leeches.^[4] α -D-Gal(1 \rightarrow 2)-D-Gal (**3**) is found as the disaccharide repeating unit of *Streptococcus pneumoniae* type 15 antigen.^[5] Vancomycin, a significant glycopeptide antibiotic against gram-positive bacteria, has a disaccharide moiety **4**, which consists of $\alpha 1 \rightarrow 2$ -linked vancosamine with D-glucopyranose.^[6] α -D-Man(1 \rightarrow 2)-D-Glc (**5**) is a typical constituent in the cell membrane of halophilic bacteria.^[7] The glycolipids extracted from *Lactobacillus casei* A.T.C.C. 7469 are composed of α -D-Gal(1 \rightarrow 2)- α -D-Glc(1 \rightarrow 1)-glycerol lipid **6** as the major com-



ponent.^[8] Given the importance of these disaccharide motifs with $\alpha 1 \rightarrow 2$ linkages, there is a need to develop a highly selective protection^[9] of hexopyranosides to generate a free hydroxy group at C2 for their synthesis. To tackle this problem, we describe herein a highly regioselective benzyl or allyl protection of hexopyranosides to the corresponding 2-hydroxy compounds by means of very mild, acid-catalyzed, reductive etherification of their O-trimethylsilylated derivatives with a variety of aldehydes.^[10] Finally, we show their applications in the regioselective one-pot protection – glycosylation to prepare these biologically potent $\alpha 1 \rightarrow 2$ -linked disaccharide derivatives.

The one-pot synthesis of the trimethylsilyl ether **8** from methyl α -D-glucopyranoside **7** in 74% yield was carried out through a combination of 4,6-O-benzylidenation and 2,3-di-O-silylation. Triethylsilane-reductive O3-etherification of **8** with various aryl and α,β -unsaturated aldehydes in the presence of trimethylsilyl trifluoromethanesulfonate (TMSOTf) as the catalyst successfully afforded the corresponding 2-hydroxy compounds **9–15**. Excellent selectivity and yields were observed in comparison with known methods for the regioselective introduction of acyl or alkyl groups in D-glucopyranosides at O3 (Table 1).^[11] Under these acidic conditions, it was observed that the 4,6-O-benzylidene acetal of **8** was not hydrolyzed or opened, and that the double bonds of allyl ethers **14** and **15** were not further reduced. The regiochemistry of **9–15** was determined through the ¹H and ¹H,¹H COSY NMR spectra: H2 was correlated with the proton of the free hydroxy group as well as with H1. The high selectivity is perhaps induced not only by the steric hindrance between the anomeric methoxy group and the 2-OTMS group, but also by the inductive effect of two anomeric oxygen atoms which causes a decrease in the nucleophilicity of O2.

We studied the regioselective etherification in a variety of O-trimethylsilylated pyranosides (Table 2). The highlights include 3-O-benzylation of different protected D-glucopyranosides and α,α' -trehalose, and 6-O-benzylation of β -cyclodextrin as well as of the D-galactopyranosyl derivatives. The 4,6-O-isopropylidene ketal **16**, α -allyl ether **18**, and β -D-thioglucopyranoside **20** were selected to examine the compatibility of substituted groups at the O4, O6, and anomeric positions, and the corresponding 3-OBn compounds **17**, **19**,

[*] Dr. S.-C. Hung, C.-C. Wang, S.-Y. Luo, H.-F. Fan, C.-L. Pai
Institute of Chemistry, Academia Sinica
Taipei 115 (Taiwan)
Fax: (+886) 2-2783-1237
E-mail: chung@chem.sinica.edu.tw
J.-C. Lee, W.-C. Yang, L.-D. Lu
Department of Chemistry, National Tsing Hua University
Hsinchu 300 (Taiwan)

[**] We thank Professor Sunney I. Chan for his helpful discussions. This work was supported by the National Science Council (NSC 90-2323-B-001-008).

Supporting information for this article is available on the WWW under <http://www.angewandte.org> or from the author.

Table 1. Trimethylsilyl trifluoromethanesulfonate activated triethylsilane-reductive O3-etherification of **8** with a variety of aryl and α,β -unsaturated aldehydes.^[a]

Entry	R	T [°C]	t [h]	Product	Yield [%]
1	Ph	−78	0.5	9	94
2	4-OMePh	−78	0.5	10	91
3	3,4-(OMe) ₂ Ph	−78	3	11	87
4	4-ClPh	−78	4	12	77
5	2-naphthyl	−78	2	13	81
6	(<i>E</i>)-MeHC=CH	−86	6.5	14	68
7	(<i>E</i>)-PhHC=CH	−86	6.5	15	87

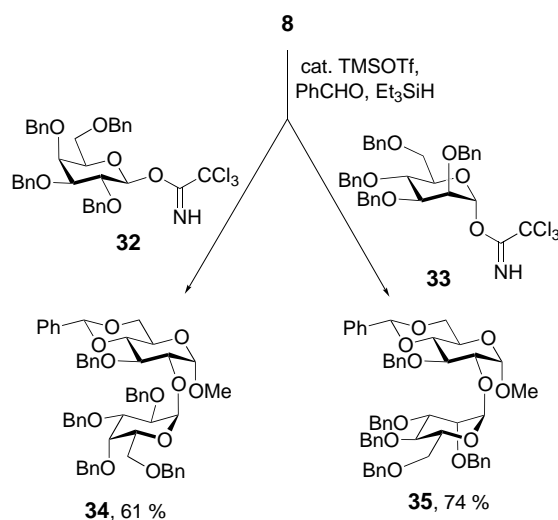
[a] Reagents and conditions: a) PhCH(OMe)₂, CSA, TMSCl, Et₃N, 74%; b) cat. TMSOTf, RCHO, Et₃SiH, CH₂Cl₂. TMS = trimethylsilyl; CSA = camphorsulfonic acid; Tf = trifluoromethanesulfonyl.

Table 2. Trimethylsilyl trifluoromethanesulfonate activated triethylsilane-reductive benzylation of various O-trimethylsilylated sugars with benzaldehyde at −78 °C.

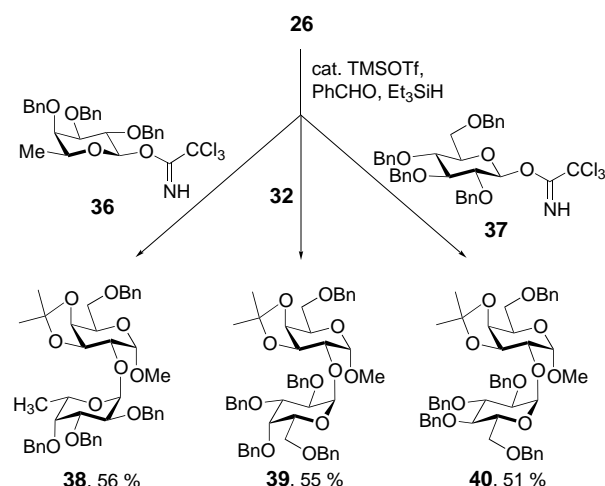
Entry	Silylated sugar	Product	Yield [%]
1			75
2			87
3			86
4			87
5			62
6			96
7			95
8			92
9			91

and **21**, respectively, were obtained in good yields (Table 2, entries 1–3). A similar phenomenon was observed in the α,α' -trehalose derivative **22**: the 3,3'-di-O-benzylated product **23** was produced in high yield under the standard conditions (Table 2, entry 4). No 2-OBn regioisomer was detected in any of the above cases. However, the corresponding 2,3-diols (entries 1–3) and 2,2',3,3'-tetraol (entry 4), which result from the hydrolysis of the bis-OTMS functionalities owing to prolonged reaction times, were isolated in 5–10% yields, which cause a slight drop in the overall yield. Regioselective benzylation of cyclodextrin molecules at various hydroxy groups is a big challenge for synthetic chemists.^[12] Interestingly, we found that the O-trimethylsilylated β -cyclodextrin **24**^[13] successfully delivered the corresponding 6-OBn compound **25** in 62% yield after recrystallization from methanol (Table 2, entry 5). Finally, the 3,4-O-isopropylidene-D-galactopyranosyl sugars **26** and **30** (Table 2, entries 6–9) also displayed excellent regioselectivity as expected to provide the 2-hydroxy compounds **27–29** and **31**, respectively, in very high yields compared to etherifications under basic conditions.^[14]

To the best of our knowledge, the regioselective one-pot protection–glycosylation strategy of carbohydrate molecules has not been studied to date. Since TMSOTf was successfully used as the catalyst in the reductive etherification and it was often the reagent of choice in the coupling reactions of sugars, we investigated this methodology further to prepare the α -linked disaccharide units in one-pot syntheses. The perbenzylated D-galacto (**32**), D-manno (**33**), L-fuco (**36**), and D-glucopyranosyl (**37**) trichloroacetimidates^[15] were selected as glycosyl donors. TMSOTf-catalyzed triethylsilane-reductive benzylation of the D-glucopyranosyl sugar **8** followed by coupling with **32** and **33**^[16] gave the expected α -disaccharides **34** and **35** in 61% and 74% yields, respectively (Scheme 1). Similarly, regioselective one-pot O6-benzylation and O2-glycosylation of **26** with **36**, **32**, or **37** led to the desired products **38** (56%), **39** (55%), or **40** (51%), respectively (Scheme 2). Their α configurations were determined from the coupling constants of the anomeric protons. Compounds **34**,



Scheme 1. Regioselective one-pot benzylation–glycosylation of **8** with the glycosyl donors **32** and **33** to form the α -linked disaccharides **34** and **35**, respectively.



Scheme 2. Regioselective one-pot benzylation-glycosylation of **26** with the glycosyl donors **36**, **32**, and **37** to form the α -linked disaccharides **38**, **39**, and **40**, respectively.

35, **38**, **39**, and **40** are the protected versions of biologically potent disaccharides **6**, **5**, **1**, **3**, and **2**, respectively.

In conclusion, we have successfully developed a highly regioselective benzyl and allyl protection of hexopyranosides, and demonstrated their applications in the synthesis of biologically potent α 1 \rightarrow 2-linked disaccharide derivatives in a regioselective one-pot protection-glycosylation.

Received: January 28, 2002 [Z18593]

- [1] a) F. Burkhart, Z. Zhang, S. Wacowich-Sgarbi, C.-H. Wong, *Angew. Chem.* **2001**, *113*, 1317–1319; *Angew. Chem. Int. Ed.* **2001**, *40*, 1274–1277; b) T. Zhu, G.-J. Boons, *Angew. Chem.* **1999**, *111*, 3704–3707; *Angew. Chem. Int. Ed.* **1999**, *38*, 3495–3497; c) J. M. Lassaletta, R. R. Schmidt, *Liebigs. Ann.* **1996**, 1417–1427; d) M. T. Bilodeau, T. K. Park, S. Hu, J. T. Randolph, S. J. Danishefsky, P. O. Livingston, S. Zhang, *J. Am. Chem. Soc.* **1995**, *117*, 7840–7841.
- [2] a) T. Feizi, *Nature* **1985**, *314*, 53–57; b) B. Wegmann, R. R. Schmidt, *Carbohydr. Res.* **1984**, *184*, 254–261; c) J.-C. Jacquinet, P. Sinaÿ, *Tetrahedron* **1976**, *32*, 1693–1697.
- [3] a) C. Kunz, S. Rudloff, W. Baier, N. Klein, S. Strobel, *Annu. Rev. Nutr.* **2000**, *20*, 699–722; b) M. T. Cancilla, S. G. Penn, J. A. Carroll, C. B. Lebrilla, *J. Am. Chem. Soc.* **1996**, *118*, 6736–6745.
- [4] T. Biswas, A. K. Mukherjee, *Carbohydr. Res.* **1978**, *63*, 173–181.
- [5] M. B. Perry, D. R. Bundle, V. Daoust, D. J. Carlo, *Mol. Immunol.* **1982**, *19*, 235–246.
- [6] a) K. C. Nicolaou, C. N. C. Boddy, S. Bräse, N. Winssinger, *Angew. Chem.* **1999**, *111*, 2230–2287; *Angew. Chem. Int. Ed.* **1999**, *38*, 2096–2152; b) D. H. Williams, B. Bardsley, *Angew. Chem.* **1999**, *111*, 1264–1286; *Angew. Chem. Int. Ed.* **1999**, *38*, 1172–1193; c) C. Thompson, M. Ge, D. Kahne, *J. Am. Chem. Soc.* **1999**, *121*, 1237–1244.
- [7] C. A. A. van Boeckel, P. Westerduin, J. H. van Boom, *Carbohydr. Res.* **1984**, *133*, 219–234.
- [8] S. K. Heatherington, J. Baddiley, *Biochem. J.* **1968**, *107*, 491–496.
- [9] For excellent reviews and books on protecting groups, see: a) K. Jarowicki, P. J. Kocienski, *J. Chem. Soc. Perkin Trans. 1* **2000**, 2495–2527, and references therein; b) J. R. Hanson, *Protecting Groups in Organic Synthesis*, Sheffield Academic Press, Sheffield, **1999**; c) T. W. Greene, P. G. M. Wuts, *Protective Groups in Organic Synthesis*, 3rd ed., Wiley, New York, **1999**; d) M. Schelhaas, H. Waldmann, *Angew. Chem.* **1996**, *108*, 2192–2219; *Angew. Chem. Int. Ed. Engl.* **1996**, *35*,

2056–2083; e) P. J. Kocienski, *Protecting Groups*, Georg Thieme, Stuttgart, **1994**.

- [10] a) S.-C. Hung, S. R. Thopate, F.-C. Chi, S.-W. Chang, J.-C. Lee, C.-C. Wang, Y.-S. Wen, *J. Am. Chem. Soc.* **2001**, *123*, 3153–3154; b) N. Komatsu, *Tetrahedron Lett.* **2001**, *42*, 1733–1736; c) K. Fukase, Y. Fukase, M. Oikawa, W.-C. Liu, Y. Suda, S. Kusumoto, *Tetrahedron* **1998**, *54*, 4033–4050; d) S. Hatakeyama, M. Yoshida, T. Esumi, Y. Iwabuchi, H. Irie, T. Kawamoto, H. Yamada, M. Nishizawa, *Tetrahedron Lett.* **1997**, *38*, 7887–7890; e) N. Komatsu, J.-Y. Ishida, H. Suzuki, *Tetrahedron Lett.* **1997**, *38*, 7219–7222; f) S. Hatakeyama, T. Ikeda, H. Irie, C. Izumi, H. Mori, K. Uenoyama, H. Yamada, M. Nishizawa, *J. Chem. Soc. Chem. Commun.* **1995**, 1959–1960; g) S. Hatakeyama, H. Mori, K. Kitano, H. Yamada, M. Nishizawa, *Tetrahedron Lett.* **1994**, *35*, 4367–4370; h) T. Mukaiyama, K. Wariishi, M. Furuya, S. Kobayashi, *Chem. Lett.* **1989**, 1277–1280; i) M. B. Sassaman, K. D. Kotian, G. K. S. Prakash, G. A. Olah, *J. Org. Chem.* **1987**, *52*, 4314–4319; j) S. Torii, S. Takagishi, T. Inokuchi, H. Okumoto, *Bull. Chem. Soc. Jpn.* **1987**, *60*, 775–776; k) G. A. Olah, T. Yamato, P. S. Iyer, G. K. S. Prakash, *J. Org. Chem.* **1986**, *51*, 2826–2828; l) J.-I. Kato, N. Iwasawa, T. Mukaiyama, *Chem. Lett.* **1985**, 743–746; m) T. Tsunoda, M. Suzuki, R. Noyori, *Tetrahedron Lett.* **1979**, 4679–4680.
- [11] a) J. J. Gridley, A. J. Hacking, H. M. I. Osborn, D. G. Spackman, *Tetrahedron* **1998**, *54*, 14925–14946; b) L. Jiang, T.-H. Chan, *J. Org. Chem.* **1998**, *63*, 6035–6038; c) H. Qin, T. B. Grindley, *J. Carbohydr. Chem.* **1996**, *15*, 95–108; d) D. J. Jenkins, B. V. L. Potter, *Carbohydr. Res.* **1994**, *265*, 145–149; e) P. J. Garegg, I. Kvarnström, A. Niklasson, G. Niklasson, S. T. Svensson, *J. Carbohydr. Chem.* **1993**, *12*, 933–953; f) L. Panza, S. Brasca, S. Riva, G. Russo, *Tetrahedron: Asymmetry* **1993**, *4*, 931–932; g) B. Classon, P. J. Garegg, S. Oscarson, A.-K. Tidén, *Carbohydr. Res.* **1991**, *216*, 187–196; h) S. Kim, H. Chang, W. J. Kim, *J. Org. Chem.* **1985**, *50*, 1751–1752; i) R. Eby, K. T. Webster, C. Schuerch, *Carbohydr. Res.* **1984**, *129*, 111–120.
- [12] L. Jicsinszky, É. Fenyvesi, H. Hashimoto, A. Ueno in *Comprehensive Supramolecular Chemistry*, Vol. 3 (Eds.: J. L. Atwood, J. E. D. Davies, D. D. MacNicol, F. Vögtle, J. Szejtli, T. Osa), Pergamon, Oxford, **1996**, pp. 57–188.
- [13] M. Bukowska, M. Maciejewski, J. Prejzner, *Carbohydr. Res.* **1998**, *308*, 275–279.
- [14] a) R. Eby, C. Schuerch, *Carbohydr. Res.* **1982**, *100*, C41–C43; b) H. M. Flowers, *Carbohydr. Res.* **1982**, *100*, 418–423.
- [15] R. R. Schmidt, W. Kinzy, *Adv. Carbohydr. Chem. Biochem.* **1994**, *50*, 21–121.
- [16] **General Procedure:** A mixture of the trimethylsilyl ether (1.0 equiv), freshly dried molecular sieves (3 Å, 1 mg per 1 mg trimethylsilyl ether), benzaldehyde (1.2 equiv), triethylsilane (1.2 equiv), and dichloromethane (8.5 mL per 1 mmol trimethylsilyl ether) was stirred at room temperature for 30 min under nitrogen. The mixture was cooled to -78°C , trimethylsilyl trifluoromethanesulfonate (0.1 equiv) was slowly added, and the reaction was monitored by TLC. After the starting material was totally consumed, a solution of the glycosyl trichloroacetimidate^[15] (1.2 equiv) in dichloromethane (5 mL per 1 mmol glycosyl donor) and trimethylsilyl trifluoromethanesulfonate (0.3 equiv) were added successively, the system was gradually warmed up to -40°C , and the mixture was stirred at the same temperature overnight. The reaction was quenched with saturated aqueous sodium bicarbonate, and the aqueous phase was extracted with ethyl acetate (3 \times). The combined organic layers were washed with brine, dried over magnesium sulfate, filtered, and evaporated in vacuo. The residue was purified by flash column chromatography to give the expected disaccharide. The yields are summarized in Schemes 1 and 2.

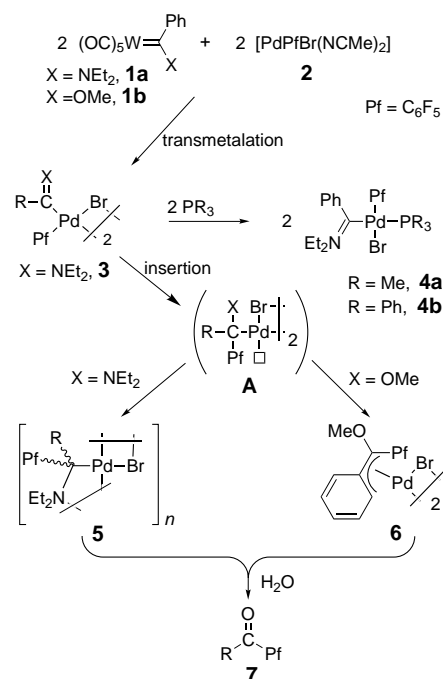
Observation of the Direct Products of Migratory Insertion in Aryl Palladium Carbene Complexes and Their Subsequent Hydrolysis**

Ana C. Albéniz,* Pablo Espinet,* Raúl Manrique, and Alberto Pérez-Mateo

The use of carbene ligands in palladium-catalyzed processes, presumably involving “[PdR(carbene)_n]” intermediates, is becoming increasingly important.^[1] In this context, the understanding of the reactivity of these species, including the interactions between precursors of palladium carbenes,^[2] becomes relevant. The formation of coupling products (R-carbene)⁺ (R=alkyl) from alkyl palladium carbene complexes bearing heterocyclic carbenes C(NR'₂)₂ has been studied before, and theoretical calculations have discounted an alkyl-migration mechanism in favor of a concerted reductive elimination process.^[3] We hypothesized that the course of the reaction might be different for other systems with more electrophilic carbene ligands. The use of aryl in place of alkyl ligands should also facilitate a migratory insertion mechanism, and the use of fluorinated aryl groups might facilitate the observation of intermediates and products. Compared with the rather stable palladium carbene complexes in which the less electrophilic carbene ligands are stabilized by two amino groups (C(NR'₂)₂),^[4] those with carbene ligands stabilized by only one amino group (CR''(NR'₂)) are still rare.^[5] Other heteroatom (for example, CR''(OR')) or nonheteroatom ((CR'₂)) palladium carbenes are very elusive species, although often proposed as intermediates in many Pd-catalyzed reactions.^[6] We report here the unprecedented direct observation of migratory insertion of carbene ligands into a Pd-aryl bond. The Pd complexes containing the hydrocarbonyl ligand formed by insertion can be identified spectroscopically and by their hydrolysis products. In the case of CR''(NR'₂) carbenes, the migratory insertion occurs on isolable and characterizable compounds.

The transformations discussed herein are summarized in Scheme 1. Transmetalation of the carbene ligand from [W(CO)₅(CPhX)] (X = NEt₂, **1a**; X = OMe, **1b**) to [PdBrPf(NCMe)₂] (Pf = C₆F₅, **2**) leads eventually, at very different rates, to the migratory insertion products **5** and **6**. Both **5** and **6** undergo hydrolysis to afford the ketone **7**.

The transfer of a carbene between W and Pd centers has been previously used in the preparation of some palladium diamino carbenes^[7] and, along with the extension described here for monoaminocarbenes, seems a convenient synthetic



Scheme 1. Synthesis, pentafluorophenyl migratory insertion, and hydrolysis of palladium carbene complexes.

route. The possible competition of a Pd-catalyzed carbene dimerization is not evident under controlled stoichiometric conditions.^[2]

Transmetalation with the carbene ligand CPh(NEt₂) affords **3** as an isolable yellowish solid.^[8] The splitting of the bridging ligands with an equimolar amount of tertiary phosphane gives the monomeric derivatives **4**. Both **3** and **4** were characterized spectroscopically and by elemental analysis. The X-ray crystal structure of **4a** was determined (Figure 1). The carbene and pentafluorophenyl groups are in a *cis* arrangement (which suggests that they are the two ligands with the highest *trans* influence) and lie perpendicular to the palladium coordination plane. The bond lengths found in the carbene moiety

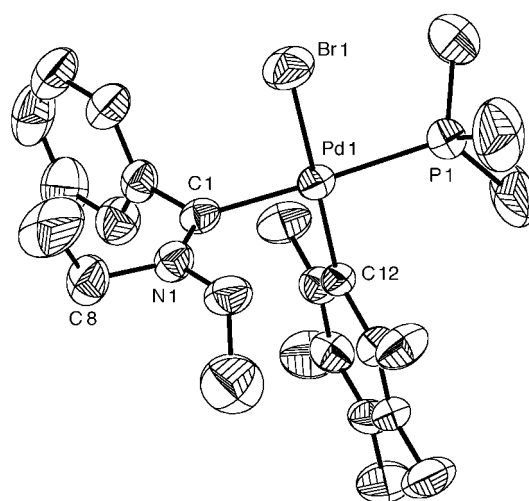


Figure 1. Molecular structure of **4a** (ORTEP plot, hydrogen atoms omitted for clarity). Selected bond lengths [Å] and angles [°]: Pd1-C1 2.030(5), C1-N1 1.291(6), Pd1-C12 2.016(5); Pd1-C1-N1 125.0(4), C1-N1-C8 124.3(4).

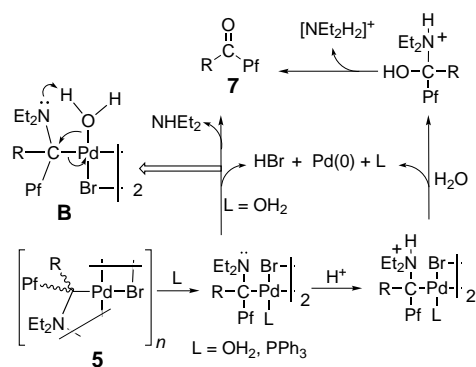
[*] Dr. A. C. Albéniz, Prof. P. Espinet, R. Manrique, A. Pérez-Mateo
Departamento de Química Inorgánica
Facultad de Ciencias, Universidad de Valladolid
Prado de la Magdalena s/n, 47005 Valladolid (Spain)
Fax: (+34)983-42-013
E-mail: espinet@qi.uva.es

[**] This work was supported by the Dirección General de Enseñanza Superior (Ministerio de Educación y Cultura, BQU2001-2015) and the Junta de Castilla y León (VA80/99 and VA17/00B). A fellowship from the Junta de Castilla y León to A.P.-M. is also acknowledged.

Supporting information for this article is available on the WWW under <http://www.angewandte.org> or from the author.

reflect the important donation of the lone pair of electrons on the amino group to the carbene carbon atom: the C=N bond length is consistent with a double bond, and the Pd1–C1 bond is a single one, very similar in length to the Pd–C12 bond. Pd complexes featuring two different monodentate auxiliary ligands (for example, [PdXRL¹]) are extremely rare, as they show a tendency to rearrange to mixtures of the symmetric complexes.

Complexes **3** and **4** decompose in CDCl₃ (very slowly) by migratory insertion. Kinetic experiments carried out with different starting concentrations of **4b** indicate that it disappears by a unimolecular process. The final product of the reaction is the hydrolysis product Pf(Ph)C=O (**7**). An intermediate aminoalkyl palladium complex **5** accumulates in solution during the course of the decomposition of **3**. Compound **5** is clearly observed in the ¹⁹F NMR spectrum, where signals corresponding to the F_{ortho} atom of a C-bound Pf group (ca. δ = –135 ppm) along with the spectral pattern of the ketone **7** slowly appear at the expense of the signals of complex **3** (Pf bound to Pd, ca. δ = –110 ppm). Concomitant *trans/cis* isomerization of **3** is also observed, but both isomers react to give **5** and **7**.^[8, 9] The exact structure of **5** could not be determined because of the impossibility of isolating it as a pure species, but it must accomplish tetracoordination from the unsaturated putative intermediate **A** by forming Br and aminocarbene double bridges. The structures of stoichiometrically related tetrapalladium oligomers (*n* = 4) are well established.^[10] The hydrolysis reaction, which takes several days, possibly occurs on a de-coordinated transient species in equilibrium (**A**) by acid-catalyzed protonation of the appended amino group and external attack of adventitious water in the NMR tube (Scheme 2). Once initiated by traces of acid,



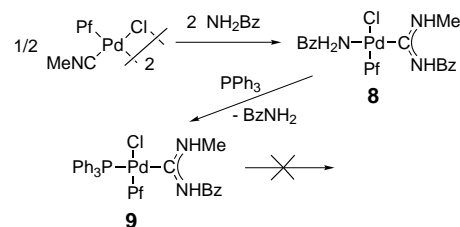
Scheme 2. Hydrolysis of palladium complexes containing a nucleophilic end group in the hydrocarbene ligand.

the hydrolysis produces HBr which further facilitates the reaction. In the case of L = H₂O, intramolecular hydrolysis by the more acidic coordinated water (intermediate **B**) is plausible. These proposals are supported by the following observations: 1) deliberate addition of water to a solution of **3** at the start hardly affects the rate of formation of **5**, but greatly increases its hydrolysis, 2) addition of water to an NMR solution rich in **5** results in its hydrolysis within hours, compared with days for a reference sample, 3) addition of PPh₃ to an NMR solution rich in **5** also accelerates noticeably its hydrolysis compared with a reference sample (PPh₃ should

coordinate better than water, hindering the formation of **B**, while displacing and favoring the formation of de-coordinated amino group). Consistently, **4b** also gives **7** (very slowly), but no inserted intermediate is observed.

No intermediate palladium carbene could be detected with the carbene ligand CPh(OMe), even at low temperatures. The migratory insertion on an unstable palladium carbene analogous to **3** apparently proceeds very fast in this case to give the benzylic derivative **6**, which then hydrolyzes to **7** and the ketal Pf(Ph)C(OMe)₂. The intermediate alkyl complex **A** (Scheme 1, X = OMe) is stabilized by coordination of the double bond to give **6**. Complex **6** decomposes quickly in solution at room temperature, but can be isolated as a crude yellowish solid (unpurified with some reaction by-products) by working at low temperatures. It was identified spectroscopically by NMR spectroscopy. Its ¹H NMR spectrum shows the very characteristic high-field shift for the aromatic proton involved in an η³ Pd-bound benzylic moiety (δ = 5.55 ppm).^[11] We propose an *anti*-Pf stereochemistry for the C-1 allylic carbon atom on the basis of the ¹⁹F NMR spectrum of **6**.^[12] The observation of the ketal Pf(Ph)C(OMe)₂ as a solvolysis product arises from preferential reaction of **6** with methanol, which is generated as a by-product in this reaction and is more nucleophilic than water.

Diaminocarbene derivatives should be less prone to give this reaction pattern. To test this premise, the pentafluorophenyl diaminocarbene derivative [PdPfBr{C(NHMe)(NHCH₂Ph)}(PPh₃)] (**9**), which is analogous to **4b**, was synthesized (Scheme 3).^[13] No change was observed in the NMR spectrum of a solution of **9** in CDCl₃ over 20 days at room temperature; **4b** gives **7** under the same conditions (23% decomposition after 10 days). A solution of **9** kept at 50 °C for 10 days also remains unchanged.



Scheme 3. Synthesis of palladium diaminocarbene complexes.

In summary, a migratory insertion reaction has been described for aryl carbene complexes of palladium. The reaction is intramolecular and is favored by the interaction of an electrophilic carbene carbon atom with the π-electron density of the aryl group and, as the structure of **4a** shows, both groups are appropriately oriented in the ground state. The electrophilicity of the carbene carbon atom is modulated by its substituents: (C(NR₂)₂) << (CR''(NR₂)) < CR''(OR'). The π-electron density on the C_{ipso} atom of the pentafluorophenyl group is lower than in a phenyl ring and the migratory insertion is expected to be slower. As a result, pentafluorophenyl monoaminocarbenes of palladium are stable enough to be characterized, but still sufficiently reactive to provide a nice picture of the migratory insertion reaction.

Experimental Section

All manipulations were carried out by using Schlenk techniques. Complexes **1a**,^[14] **1b**,^[15] **2**,^[16] and **8**^[13] were prepared according to literature methods. All palladium carbene complexes gave satisfactory elemental analyses. Only selected spectroscopic data are included. For full experimental details see the Supporting Information.

trans-3: Equimolar amounts of **1a** and **2** were mixed in MeCN and stirred for 18 h at room temperature. The solvent was evaporated to dryness and the residue was extracted with CHCl₃. The resulting yellow solution was filtered through activated carbon, concentrated (ca. 2 mL), and Et₂O was added. The solution was cooled to –20 °C to afford **3** as a yellow solid. Yield 58%. **trans-3** is a 1.3:1 mixture of *syn* (**3**) and *anti* (**3'**) isomers in solution. ¹H NMR (300 MHz, CDCl₃): δ = 7.38–6.77 (5H; Ph, **3/3'**), 5.23 (dq, *J* = 14.4, 7.2 Hz, 1H; CHH, **3'**), 5.13 (m, 1H; CHH, **3'**), 5.11 (q, 2H; CH₂, **3**), 3.55 (dq, *J* = 14.4, 7.2 Hz, 1H; CHH', **3/3'**), 3.42 (dq, *J* = 14.4, 7.2 Hz, 1H; CHH', **3/3'**), 1.56 (t, *J* = 7.2 Hz, 3H; CH₃, **3**), 1.52 (t, *J* = 7.2 Hz, 3H; CH₃, **3'**), 1.02 (t, *J* = 7.2 Hz, 3H; CH₃, **3'**), 1.01 ppm (t, *J* = 7.2 Hz, 3H; CH₃, **3**). ¹⁹F NMR (282 MHz, CDCl₃, 253 K): δ = –164.0 (m, 1F; *m*-Pf, **3'**), –163.8 (m, 1F; *m*-Pf, **3**), –162.6 (m, 1F; *m*-Pf, **3**), –162.3 (m, 1F; *m*-Pf, **3'**), –160.1 (t, 1F; *p*-Pf, **3**), –160.0 (t, 1F; *p*-Pf, **3'**), –117.9 (m, 1F; *o*-Pf, **3'**), –117.5 (m, 2F; *o*-Pf, **3**), –117.1 ppm (m, 1F; *o*-Pf, **3'**). ¹³C{¹H} NMR (75.4 MHz, CDCl₃, 253 K): δ = 229.24 (s; Pd–C, **3'**), 228.89 ppm (s; Pd–C, **3**).

cis-3: ¹H NMR (300 MHz, CDCl₃): δ = 7.74–7.14 (m, 5H; Ph), 5.32–4.93* (2H; CH₂), 3.60* (2H; CH₂'), 1.64 (t, *J* = 7.2 Hz, 3H; CH₃), 1.09 ppm (m, 3H; CH₃); ¹⁹F NMR (282 MHz, CDCl₃): δ = –165.00 (m, 2F; *m*-Pf), –162.82 (t, 1F; *p*-Pf), –116.65 ppm (m, 2F; *o*-Pf). *Signal overlaps with signals of the *trans* isomers.

Complexes **4a** and **4b** were obtained by the addition of a stoichiometric amount of the phosphane to a solution of **3** in CH₂Cl₂. After 1 h at room temperature, the solvent was evaporated to dryness and *n*-hexane was added to afford, after cooling at –20 °C, pale orange solids.

4a: Yield 50%. ¹H NMR (300 MHz, CDCl₃): δ = 7.30–6.80 (5H; Ph), 4.75 (q, *J* = 7.3 Hz, 2H; CH₂), 3.36 (dq, *J* = 13.6, 6.8 Hz, 1H; CHH'), 3.51 (dq, *J* = 13.6, 6.8 Hz, 1H; CHH'), 1.54 (t, *J* = 6.8 Hz, 3H; CH₃), 1.19 (t, *J* = 9.6 Hz, 9H; PCH₃), 1.08 ppm (t, *J* = 6.8 Hz, 3H; CH₃); ¹⁹F NMR (282 MHz, CDCl₃): δ = –163.82 (m, 1F; *m*-Pf), –162.89 (m, 1F; *m*-Pf), –160.80 (t, 1F; *p*-Pf), –116.51 ppm (m, 2F; *o*-Pf); ³¹P{¹H} NMR (121.4 MHz, CDCl₃): δ = –17.34 ppm (d, ⁴*J*_{FP} = 7.87 Hz); ¹³C{¹H} NMR (75.4 MHz, CDCl₃, 263 K): δ = 244.27 ppm (d, ²*J*_{CP} = 151.3 Hz; Pd–C).

4b: Yield 69%. ¹H NMR (300 MHz, CDCl₃): δ = 7.58–6.95 (20H; Ph), 4.93 (q, *J* = 7.0 Hz, 2H; CH₂), 3.62 (dq, *J* = 13.8, 6.9 Hz, 1H; CHH'), 3.42 (dq, *J* = 13.8, 6.9 Hz, 1H; CHH'), 1.62 (t, *J* = 6.9 Hz, 3H; CH₃), 1.11 ppm (t, *J* = 6.9, 3H; CH₃); ¹⁹F NMR (282 MHz, CDCl₃): δ = –164.63 (m, 1F; *m*-Pf), –163.19 (m, 1F; *m*-Pf), –162.41 (t, 1F; *p*-Pf), –117.20 (m, 1F; *o*-Pf), –116.42 ppm (m, 1F; *o*-Pf); ³¹P{¹H} NMR (121.4 MHz, CDCl₃): δ = 21.73 ppm (d, ⁴*J*_{FP} = 7.15 Hz); ¹³C{¹H} NMR (75.4 MHz, CDCl₃, 263 K): δ = 241.62 ppm (d, ²*J*_{CP} = 142.4 Hz; Pd–C).

5: ¹H NMR (300 MHz, CDCl₃): δ = 7.76–7.63 (5H; Ph), 4.75 (q, *J* = 7.2 Hz, 2H; CH₂), 4.62 (q, *J* = 7.2 Hz, 2H; CH₂'), 1.67 (t, 3H; CH₃), 1.38 ppm (t, 3H; CH₃); ¹⁹F NMR (282 MHz, CDCl₃): δ = –155.90 (m, 2F; *m*-Pf), –142.88 (t, 1F; *p*-Pf), –134.78 ppm (m, 2F; *o*-Pf).

6: A solution of **1b** and **2** in THF was stirred at room temperature for 40 min. Compound **6** was obtained by evaporation to dryness and addition of Et₂O at –20 °C. Yield 32%. ¹H NMR (300 MHz, CDCl₃, 263 K): δ = 8.15–7.30 (m, 4H; Ph), 5.55 (m, 1H; *benz*-η³-Ph), 3.51 ppm (s, 3H; OCH₃); ¹⁹F NMR (282 MHz, CDCl₃, 263 K): δ = –160.64 (m, 2F; *m*-Pf), –150.55 (t, 1F; *p*-Pf), –135.93 (br, 1F; *o*-Pf), –127.54 ppm (br, 1F; *o*-Pf).

7: ¹H NMR (300 MHz, CDCl₃): δ = 7.87 (m, 2H; *o*-Ph), 7.70 (m, 1H; *p*-Ph), 7.54 ppm (m, 2H; *m*-Ph); ¹⁹F NMR (282 MHz, CDCl₃): δ = –160.28 (m, 2F; *m*-Pf), –150.88 (t, 1F; *p*-Pf), –140.30 ppm (m, 2F; *o*-Pf).

Pf(Ph)C(OMe)₂: ¹H NMR (300 MHz, CDCl₃): δ = 7.61 (m, 2H; *m*-Ph), 7.46 (m, 1H; *p*-Ph), 7.34 (m, 2H; *o*-Ph), 3.23 ppm (6H; OCH₃); ¹⁹F NMR (282 MHz, CDCl₃): δ = –162.48 (m, 2F; *m*-Pf), –155.01 (t, 1F; *p*-Pf), –139.35 ppm (m, 2F; *o*-Pf).

9: Two atropisomers were found in solution at room temperature (1.25:1 ratio). Isomer 1: ¹H NMR (300 MHz, CDCl₃): δ = 7.61–7.26 (20H; Ph),

6.70 (m, 1H; HNCH₂Ph), 5.72 (m, 1H; HNMe), 4.30 (d, *J* = 5.0 Hz, 2H; HNCH₂Ph), 3.56 ppm (d, *J* = 4.4 Hz, 3H; HNCH₃); ¹⁹F NMR (282 MHz, CDCl₃): δ = –163.48 (m, 2F; *m*-Pf), –162.36 (t, 1F; *p*-Pf), –117.40 ppm (m, 2F; *o*-Pf); ³¹P{¹H} NMR (121.4 MHz, CDCl₃): δ = 21.30 ppm. Isomer 2: ¹H NMR (300 MHz, CDCl₃): δ = 7.61–7.26 (20H; Ph), 6.49 (m, 1H; HNMe), 5.72 (m, 1H; HNCH₂Ph), 5.36 (d, *J* = 5.2 Hz, 2H; HNCH₂Ph), 2.77 ppm (d, *J* = 4.9 Hz, 3H; HNCH₃); ¹⁹F NMR (282 MHz, CDCl₃): δ = –163.37 (m, 2F; *m*-Pf), –162.29 (t, 1F; *p*-Pf), –117.77 ppm (m, 2F; *o*-Pf); ³¹P{¹H} NMR (121.4 MHz, CDCl₃): δ = 21.69 ppm; ¹³C{¹H} NMR (75.4 MHz, CDCl₃): δ = 198.52 ppm (d, ²*J*_{PC} = 146.4 Hz; Pd–C, both isomers).

X-ray structural analysis of **4a**: a yellow prism (0.2 × 0.12 × 0.05 mm) obtained by slow evaporation of a solution in CH₂Cl₂ was mounted on the tip of a glass fiber. X-ray measurements were made using a Bruker SMART CCD area-detector diffractometer with MoK_α radiation (λ = 0.71073 Å). Crystal data: C₂₀H₂₄BrF₅NPPd, *M*_r = 590.68, monoclinic *P*2(1)/*c*, *a* = 9.168(6), *b* = 19.028(12), *c* = 13.969(9) Å, *a* = γ = 90, β = 102.235(13)°, *V* = 2382(3) Å³, *Z* = 5, ρ_{calcd} = 2.059 g cm^{–3}, *F*(000) = 1460; μ(MoK_α) = 3.211 mm^{–1}. 9864 reflections were collected (1.84° > θ > 21.69°). Intensities were integrated and the structure was solved by direct methods. Full-matrix least-squares refinement (on *F*²) based on 2921 independent reflections converged with 267 variable parameters and no restraints. Non-hydrogen atoms were refined anisotropically and hydrogen atoms were constrained to ideal geometries and refined with fixed isotropic displacement parameters. *R*1 = 0.0316, for *F*² > 2σ(*F*²); *wR*2 = 0.0749. GOF (*F*²) = 0.937. The max/min residual electron density was 0.669/–0.336 e Å^{–3}. CCDC-178512 contains the supplementary crystallographic data for this paper. These data can be obtained free of charge via www.ccdc.cam.ac.uk/contents/retrieving.html (or from the Cambridge Crystallographic Data Centre, 12, Union Road, Cambridge CB21EZ, UK; fax: (+44)1223-336-033; or deposit@ccdc.cam.ac.uk).

Received: February 5, 2002 [Z18657]

- Recent examples: Heck-type and coupling reactions: a) W. A. Herrmann, V. P. W. Böhm, C. W. K. Gstöttmayr, M. Grosche, C.-P. Reisinger, T. Weskamp, *J. Organomet. Chem.* **2001**, 617–618, 616–628, and references therein; b) A. M. Magill, D. S. McGuinness, K. J. Cavell, G. J. P. Britovsek, V. C. Gibson, A. J. P. White, D. J. Williams, A. H. White, B. W. Skelton, *J. Organomet. Chem.* **2001**, 617–618, 546–560; c) E. Peris, J. A. Loch, J. Mata, R. H. Crabtree, *Chem. Commun.* **2001**, 201–202; d) J. Huang, S. P. Nolan, *J. Am. Chem. Soc.* **1999**, 121, 9889–9890; amination reactions: e) S. R. Stauffer, S. Lee, J. P. Stambuli, S. I. Hauck, J. F. Hartwig, *Org. Lett.* **2000**, 2, 1423–1426; f) J. Huang, G. Grasa, S. P. Nolan, *Org. Lett.* **1999**, 1, 1307–1309; asymmetric hydrosilation: g) D. Enders, H. Gielen, *J. Organomet. Chem.* **2001**, 617–618, 70–80; dehalogenation: h) M. S. Viciu, G. A. Grasa, S. P. Nolan, *Organometallics* **2001**, 20, 3607–3612; copolymerization: i) M. G. Gardiner, W. A. Herrmann, C.-P. Reisinger, J. Schwarz, M. Spiegel, *J. Organomet. Chem.* **1999**, 572, 239–247.
- For example, dimerization of a carbene ligand in Group 6 metal–carbene complexes is catalyzed by a diverse range of Pd catalysts: M. A. Sierra, J. C. Amo, M. J. Mancheño, M. Gómez-Gallego, *J. Am. Chem. Soc.* **2001**, 123, 851–861.
- D. S. McGuinness, N. Saendig, B. F. Yates, K. J. Cavell, *J. Am. Chem. Soc.* **2001**, 123, 4029–4040.
- D. Bourissou, O. Guerret, F. P. Gabbaï, G. Bertrand, *Chem. Rev.* **2000**, 100, 39–91.
- a) J. Cámpora, S. A. Hudson, P. Massiot, C. M. Maya, P. Palma, E. Carmona, L. A. Martínez-Cruz, A. Vegas, *Organometallics* **1999**, 18, 5225–5237; b) B. Crociani, R. L. Richards, *J. Organomet. Chem.* **1978**, 154, 65–78, and references therein.
- Some examples: cyclopropanation: a) F. Bernardi, A. Bottoni, G. P. Miscione, *Organometallics* **2001**, 20, 2751–2758; b) C. Rodríguez-García, A. Oliva, R. M. Ortuño, V. Branchadell, *J. Am. Chem. Soc.* **2001**, 123, 6157–6163, and references therein; cine substitution in Stille couplings: c) C. A. Busacca, J. Swestock, R. E. Johnson, T. R. Bailey, L. Musza, C. A. Rodger, *J. Org. Chem.* **1994**, 59, 7553–7556; other processes: d) S. Ogooshi, T. Nishida, T. Shinagawa, H. Kurosawa, *J. Am. Chem. Soc.* **2001**, 123, 7164–7165; e) M. Yoshida, M. Ihara, *Angew. Chem.* **2001**, 113, 636–639; *Angew. Chem. Int. Ed.* **2001**, 40,

- 616–619; f) B. M. Trost, G. J. Tanoury, *J. Am. Chem. Soc.* **1988**, *110*, 1636–1638; g) B. M. Trost, C. R. Self, *J. Am. Chem. Soc.* **1983**, *105*, 5942–5944.
- [7] S.-T. Liu, K. R. Reddy, *Chem. Soc. Rev.* **1999**, *28*, 315–322.
- [8] Several geometrical isomers are possible for complexes **3**. In CDCl_3 , **3** is a mixture of *trans-anti* and *trans-syn* isomers, which correspond to a *trans* arrangement of carbene moieties along the Pd...Pd axis and a relative *syn* or *anti* arrangement of the diethylamino groups relative to the coordination plane. The compound first formed is tentatively assigned (the assignment might be reversed) as *trans-3*, which (both isomers) slowly isomerizes to the *cis* (*syn* and *anti* isomers) and eventually undergoes hydrolysis when kept in solution for several days.
- [9] Decomposition data for **3** (%) after seven days in CDCl_3 at room temperature: *trans-3* (25.9), *cis-3* (26.9), **5** (19.5), **7** (27.7).
- [10] a) A. C. Albéniz, P. Espinet, Y.-S. Lin, *Organometallics* **1996**, *15*, 5003–5009; b) R. Usón, J. Fornies, P. Espinet, E. Lalinde, A. García, P. G. Jones, K. Meyer-Bäse, G. M. Sheldrick, *J. Chem. Soc. Dalton Trans.* **1986**, 259–264.
- [11] a) A. C. Albéniz, P. Espinet, Y.-S. Lin, *Organometallics* **1997**, *16*, 4030–4032; b) L. E. Craswell, J. L. Spencer, *J. Chem. Soc. Dalton Trans.* **1992**, 3445–3452.
- [12] The ^{19}F NMR spectrum of **6** shows two broad signals for the two inequivalent F_{ortho} atoms at $\delta = -135.93$ and -127.54 ppm, which indicate there is restricted rotation of the Pf group about the C–C bond, and hence the Pf group must be located in a sterically crowded position. The chemical shifts for these signals are consistent with a Pf group bound to a carbon atom and closely influenced by the metal center, which also points to an *anti* arrangement of the group.
- [13] **8**: R. Usón, J. Fornies, P. Espinet, R. Navarro, E. Lalinde, *Trans. Met. Chem.* **1984**, *9*, 277–279. Both **8** and **9** are a mixture of atropisomers in solution at room temperature which are derived from hindered rotation about both C(carbene)–N bonds.
- [14] E. O. Fischer, F. R. Kreibl, *Synthetic Methods of Organometallic and Inorganic Chemistry*, Thieme, Stuttgart, **1997**, pp. 129–131.
- [15] E. O. Fischer, U. Schubert, H. Fischer, *Inorg. Synth.* **1979**, *19*, 169–171.
- [16] A. C. Albéniz, P. Espinet, C. Foces-Foces, F. H. Cano, *Organometallics* **1990**, *9*, 1079–1085.

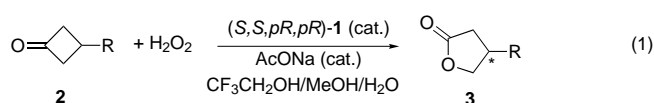
Asymmetric Baeyer–Villiger Reaction with Hydrogen Peroxide Catalyzed by a Novel Planar-Chiral Bisflavin**

Shun-Ichi Murahashi,* Satoshi Ono, and Yasushi Imada*

Metal-free organocatalytic reactions, especially enantioselective ones, have attracted increasing attention as a complement to metal-catalyzed and enzyme-catalyzed reactions.^[1] Organocatalytic reactions have several advantages, for exam-

ple, the availability of structural diversity of the catalysts in optically pure form and their stability under aerobic and aqueous conditions, and the catalysts are often more stable than enzymes.

In 1989 we demonstrated that 5-alkylated flavins can be used as organocatalysts for oxidations based on the precise kinetic study on the recycling step of flavoenzymes.^[2] Thus, the flavin-catalyzed biomimetic oxidations of sulfides and amines with hydrogen peroxide occurs highly efficiently to give the corresponding sulfoxides and nitrones, respectively. A novel method for enantioselective oxidation with organocatalysts can be developed if one can design suitable chiral flavin catalysts. We report herein that a flavin-catalyzed asymmetric Baeyer–Villiger reaction of cyclobutanones can be performed with up to 74% *ee* [Eq. (1)].



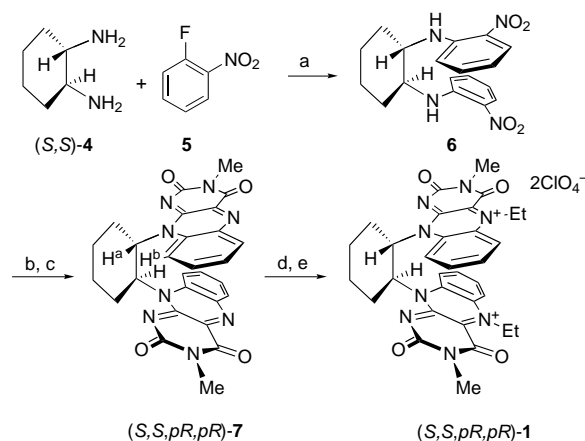
Much attention has been focused on the asymmetric Baeyer–Villiger reaction, because this is the direct route to obtain optically active lactones from cyclic ketones.^[3] Transition-metal catalysts in the asymmetric Baeyer–Villiger reactions of cyclic ketones have been studied extensively: copper with a combination of molecular oxygen and aldehyde,^[4] platinum with H_2O_2 ,^[5] titanium with *tert*-butyl hydroperoxide,^[6] cobalt with urea· H_2O_2 ,^[7] and magnesium^[8] and aluminum^[9] with cumene hydroperoxide; selectivities of up to 77% *ee* were observed. Enantioselective Baeyer–Villiger reactions have been also performed by using microbial whole cell cultures^[10] as well as purified enzymes^[11] with stoichiometric amounts of NADPH as a cofactor.

Catalytic Baeyer–Villiger reactions have been shown to occur in the presence of flavin catalyst,^[12] which is similar to our catalyst.^[2] Therefore, we wanted to design chiral flavin catalysts for enantioselective oxidation reactions. Planar-chiral flavins have been prepared and used for the asymmetric oxidation of sulfides.^[13, 14] However, the synthesis of the catalysts is very tedious because of the need for optical resolution with preparative HPLC. To prepare chiral flavin catalysts simply without optical resolution, we designed planar-chiral C_2 -symmetric bisflavinium perchlorate **1** (Scheme 1), in which each of the flavin moieties blocks one plane of the other flavin moiety. The bisflavin catalyst **1** was prepared in three steps without resolution. Treatment of (*S,S*)-1,2-diaminocyclohexane (**4**) with *o*-fluoronitrobenzene (**5**) gave (*S,S*)-1,2-bis[(2-nitrophenyl)amino]cyclohexane (**6**) in 77% yield. Catalytic hydrogenation of **6** over palladium on charcoal and subsequent treatment with 3-methylalloxan^[15] gave C_2 -symmetric bisflavin **7** in 90% yield [m.p. 223.5–224.6 °C; $[\alpha]_D^{25} = +401$ ($c = 0.20$ in CHCl_3)] in diastereomerically pure form. The stereochemistry was determined by difference NOE experiments of **7**:^[16] irradiation of the H^b proton ($\delta = 8.38$ ppm) caused a 20% enhancement of the signal for H^a ($\delta = 7.30$ ppm) and caused no detectable enhancement of other signals on the cyclohexane ring, from

[*] Prof. Dr. S.-I. Murahashi
Department of Applied Chemistry, Faculty of Engineering
Okayama University of Science
1-1, Ridaicho, Okayama 700-0005 (Japan)
Fax: (+81)86-256-9513
E-mail: murahashi@high.ous.ac.jp

Prof. Dr. Y. Imada, S. Ono
Department of Chemistry, Graduate School of Engineering Science
Osaka University
1-3, Machikaneyama, Toyonaka, Osaka 560-8531 (Japan)
Fax: (+81)6-6850-6224
E-mail: imada@chem.es.osaka-u.ac.jp

[**] This work was supported by the Research for the Future program, the Japan Society for the Promotion of Science.



Scheme 1. Synthesis of **1**. a) K_2CO_3 , EtOH, reflux, 36 h, 77 %; b) H_2 , Pd/C, AcOH, room temperature, 3 h; c) 3-methylalloxan, $\text{B}(\text{OH})_3$, AcOH, 10 h, 90 % over two steps; d) CH_3CHO , NaBH_3CN , $\text{Na}_2\text{S}_2\text{O}_4$, DMF, 60 °C, 3 h; e) HClO_4 , NaNO_2 , NaClO_4 , H_2O , 1 h, 80 % over two steps. DMF = *N,N*-dimethylformamide.

which the (*S,S,pR,pR*) stereochemistry can be deduced. This diastereomer (of three possibilities) was obtained exclusively as a result of rotational restriction between two flavin moieties. The energy minima of the three possible diastereomers were calculated by the semi-empirical molecular-orbital method (AM1).^[17] The energy of (*S,S,pR,pR*)-**7** is the lowest and is 4.6 and 6.5 kcal mol⁻¹ lower than that of (*S,S,pS,pS*)-**7** and (*S,S,pR,pS*)-**7**, respectively. The violet catalyst **1** was obtained upon treatment of **7** with ethanal and NaBH_3CN and subsequent treatment with HClO_4 , NaNO_2 , and NaClO_4 [m.p. 220 °C (dec.)].^[18] The antipode (*R,R,pS,pS*)-**7** was also prepared from (*R,R*)-**4** in a similar manner.

Treatment of 3-phenylcyclobutanone (**2a**; *R* = Ph) with a solution of hydrogen peroxide (30 %) in the presence of bisflavin (*S,S,pR,pR*)-**1** (10 mol %) at -30 °C gave optically active 3-phenyl- γ -butyrolactone (**3a**). The *S* configuration of **3a** was confirmed by comparison of the optical rotation with that reported in the literature.^[19] The enantiomeric excess of **3a** was determined by HPLC analysis with a chiral column (Daicel Chiralpak AS).

The enantioselectivity is strongly dependent on the solvent used. Representative results of the solvent effect on the catalyzed oxidation of **2a** are summarized in Table 1. Higher enantioselectivities were obtained when a protic solvent was used. The reaction in MeOH or a MeOH/water mixture (2:1) gave the lactone (*S*)-**3a** with 35 and 45 % *ee*, respectively, in lower yields, because of the formation of the dimethyl ketal of **2a** (Table 1, entries 3 and 4). The reaction in trifluoroethanol or 1,1,1,3,3,3-hexafluoro-2-propanol gave (*S*)-**3a** with low enantioselectivity, because the noncatalyzed reaction with hydrogen peroxide occurs fast.^[20] When a mixture of solvents ($\text{CF}_3\text{CH}_2\text{OH}/\text{MeOH}/\text{water}$ 6:3:1) was used, both noncatalyzed reaction and ketalization were retarded, and higher enantioselectivity (55 % *ee*) was observed (Table 1, entry 7). Furthermore, a catalytic amount of AcONa was added to trap perchloric acid, which is formed from the reaction of the flavin catalyst with hydrogen peroxide.^[21] Thus, the oxidation of **2a** with hydrogen peroxide in the presence of bisflavin **1**

Table 1. Effect of solvent on the bisflavin-catalyzed asymmetric Baeyer–Villiger reaction of **2a** with H_2O_2 .^[a]

Entry	Solvent	Yield [%]	<i>ee</i> [%] ^[b]
1	CH_2Cl_2	13	8 (<i>S</i>)
2	MeCN	61	22 (<i>S</i>)
3	MeOH	15	35 (<i>S</i>)
4	MeOH/ H_2O (2:1)	17	45 (<i>S</i>)
5	$\text{CF}_3\text{CH}_2\text{OH}$	89	8 (<i>S</i>)
6	$\text{CF}_3\text{CH}_2\text{OH}$ ^[c]	81	31 (<i>S</i>)
7	$\text{CF}_3\text{CH}_2\text{OH}/\text{MeOH}/\text{H}_2\text{O}$ (6:3:1)	52	55 (<i>S</i>)
8	$\text{CF}_3\text{CH}_2\text{OH}/\text{MeOH}/\text{H}_2\text{O}$ (6:3:1) ^[c]	67	63 (<i>S</i>)
9	$\text{CF}_3\text{CH}_2\text{OH}/\text{MeOH}/\text{H}_2\text{O}$ (6:3:1) ^[c,d]	64	62 (<i>R</i>)

[a] A mixture of **2a** (0.2 mmol), (*S,S,pR,pR*)-**1** (0.02 mmol), and H_2O_2 (0.3 mmol) in solvent (1 mL) was stirred at -30 °C for 6 days. [b] Determined by HPLC analysis with a chiral stationary phase (Daicel Chiralpak AS, hexane/2-propanol 9:1). [c] AcONa (0.05 mmol) was added. The reaction was carried out in 0.5 mL of solvent. [d] (*R,R,pS,pS*)-**1** was used as catalyst.

(10 mol %) and AcONa (25 mol %) gave (*S*)-**3a** in 67 % yield with 63 % *ee* (Table 1, entry 8). Without the catalyst **1** no oxidation occurred. The opposite enantiomer (*R*)-**3a** was obtained when (*R,R,pS,pS*)-**1** was used as a catalyst (Table 1, entry 9). A protic solvent is essential to obtain higher enantioselectivity, which indicates that the hydrophobic π - π stacking between the aromatic ring of the catalyst **1** and that of a substrate seems to play an important role in asymmetric induction.^[22, 23] Such a solvent effect is not observed for the metal-catalyzed asymmetric Baeyer–Villiger reaction.^[7]

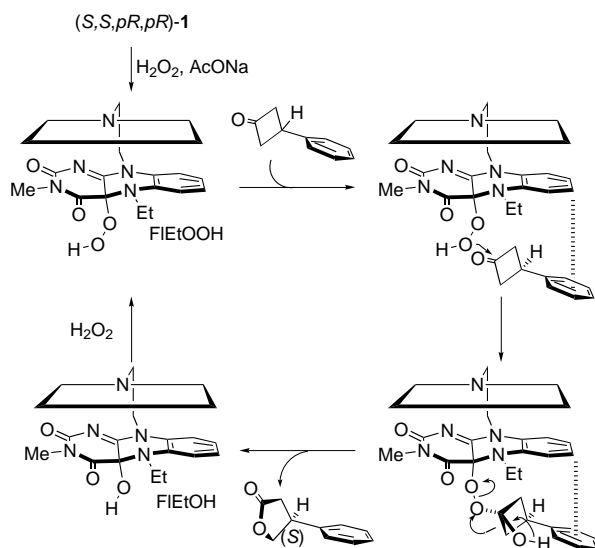
Various 3-aryl-substituted cyclobutanones can be oxidized enantioselectively by using the novel chiral flavin catalyst **1** in the presence of AcONa. Representative results are summarized in Table 2. The enantioselectivity was slightly influenced by the electronic effect of the 3-arylcyclobutanones **2**. The cyclobutanone bearing *p*-bromophenyl group was converted into the lactone **2d** with 68 % *ee*. 3-(4-Fluorophenyl)- γ -butyrolactone (**3f**) was obtained with 74 % *ee* at -50 °C.

Table 2. Asymmetric Baeyer–Villiger reaction of 3-arylcyclobutanones catalyzed by (*S,S,pR,pR*)-**1**.^[a]

Entry	2	<i>R</i>	Yield [%] ^[b]	<i>ee</i> [%] ^[c]
1	b	4-MeOC ₆ H ₄	67	61 (+)
2	c	4-MeC ₆ H ₄	53	62 (+)
3	a	Ph	67	63 (<i>S</i>)
4	d	4-BrC ₆ H ₄	28	68 (+)
5	e	4-ClC ₆ H ₄	34	66 (<i>S</i>)
6	f	4-FC ₆ H ₄	55	65 (+)
7	f	4-FC ₆ H ₄	17 ^[d]	74 (+)

[a] A mixture of substrate **2** (0.6 mmol), **1** (0.06 mmol), AcONa (0.15 mmol), and H_2O_2 (0.9 mmol) in $\text{CF}_3\text{CH}_2\text{OH}/\text{MeOH}/\text{H}_2\text{O}$ (6:3:1, 1.5 mL) was stirred at -30 °C for 6 days. [b] Determined by HPLC analysis with a chiral stationary phase, Daicel Chiralpak AS. [c] The absolute configuration was determined by comparison with reported data.^[19] [d] The reaction was carried out at -50 °C.

The reaction can be rationalized by assuming the mechanism shown in Scheme 2.^[2] The enantioselectivity is induced by face selectivity in the formation of the Criegee adduct. Since one face of the catalyst is completely blocked, the substrate would be attacked by the opposite side of the other



Scheme 2. Mechanism for the bisflavin-catalyzed asymmetric Baeyer–Villiger reaction.

flavin group. The asymmetric induction seems to be induced by hydrophobic π – π stacking between the phenyl ring of the substrate and that of the catalyst to fix the direction of the substrate. Nucleophilic attack of the hydroperoxyflavin at the carbonyl group of the substrate occurs from the opposite side of the phenyl group of the substrate. Thus intramolecular rearrangement occurs antiperiplanar to the leaving group^[3b] to give the (S)- γ -butyrolactone.

In conclusion, we demonstrated that novel planar-chiral bisflavinium perchlorate **1** catalyzes the asymmetric Baeyer–Villiger reaction of cyclobutanones with hydrogen peroxide to give the corresponding optically active lactones with up to 74% ee. This is the first demonstration that organic chiral compounds can catalyze asymmetric Baeyer–Villiger reactions, and will become a trigger to provide future environmentally friendly, clean organocatalytic oxidation reactions.

Received: February 11, 2002 [Z18691]

- [1] P. I. Dalko, L. Moisan, *Angew. Chem.* **2001**, *113*, 3840; *Angew. Chem. Int. Ed.* **2001**, *41*, 3726, and references therein.
- [2] S.-I. Murahashi, T. Oda, Y. Masui, *J. Am. Chem. Soc.* **1989**, *111*, 5002.
- [3] For reviews, see: a) G. R. Krow, *Org. React.* **1993**, *43*, 251; b) M. Renz, B. Meunier, *Eur. J. Org. Chem.* **1999**, 737, and references therein.
- [4] a) C. Bolm, G. Schlingloff, K. Weickhardt, *Angew. Chem.* **1994**, *106*, 1944; *Angew. Chem. Int. Ed. Engl.* **1994**, *33*, 1848; b) C. Bolm, T. K. Luong, G. Schlingloff, *Synlett* **1997**, *10*, 1151.
- [5] A. Gusso, C. Baccin, F. Pinna, G. Strukul, *Organometallics* **1994**, *13*, 3442.
- [6] M. Lopp, A. Paju, T. Kanger, T. Pehk, *Tetrahedron Lett.* **1996**, *37*, 7583.
- [7] T. Uchida, T. Katsuki, *Tetrahedron Lett.* **2001**, *42*, 6911.
- [8] C. Bolm, O. Beckmann, A. Cosp, C. Palazzi, *Synlett* **2001**, 1461.
- [9] C. Bolm, O. Beckmann, C. Palazzi, *Can. J. Chem.* **2001**, *79*, 1593.
- [10] a) V. Alphand, R. Furstoss, *J. Org. Chem.* **1992**, *57*, 1306; b) V. Alphand, R. Furstoss in *Enzyme Catalysis in Organic Synthesis* (Eds.: K. Drauz, H. Waldmann), VCH, Weinheim, **1995**, pp. 745–772.
- [11] C. T. Walsh, Y.-C. J. Chen, *Angew. Chem.* **1988**, *100*, 342; *Angew. Chem. Int. Ed. Engl.* **1988**, *27*, 333.
- [12] C. Mazzini, J. Lebreton, R. Furstoss, *J. Org. Chem.* **1996**, *61*, 8.
- [13] S.-I. Murahashi, *Angew. Chem.* **1995**, *107*, 2670; *Angew. Chem. Int. Ed. Engl.* **1995**, *34*, 2443.

- [14] S. Shinkai, T. Yamaguchi, O. Manabe, F. Toda, *J. Chem. Soc. Chem. Commun.* **1988**, 1399.
- [15] P. Hemmerich, B. Prijs, H. Erlenmeyer, *Helv. Chim. Acta* **1960**, *43*, 372.
- [16] R. Yanada, Y. Yoneda, M. Yazaki, N. Mimura, T. Taga, F. Yoneda, K. Yanada, *Tetrahedron: Asymmetry* **1997**, *8*, 2319.
- [17] M. J. S. Dewar, E. G. Zoebisch, E. F. Healy, J. J. P. Stewart, *J. Am. Chem. Soc.* **1985**, *107*, 3902.
- [18] S. Ghisla, U. Hartmann, P. J. Hemmerich, *Liebigs Ann. Chem.* **1973**, 1388.
- [19] G. Helmchen, G. Nill, *Angew. Chem.* **1979**, *91*, 66; *Angew. Chem. Int. Ed. Engl.* **1979**, *18*, 65.
- [20] a) K. Neimann, R. Neumann, *Org. Lett.* **2000**, *2*, 2861; b) M. C. A. van Vliet, I. W. C. E. Arends, R. A. Sheldon, *Synlett* **2001**, 248.
- [21] Control experiments show that HClO₄-catalyzed Baeyer–Villiger reaction of **2a** in CF₃CH₂OH/MeOH/H₂O at –30 °C gave racemic **3a** in 20% yield after 6 days.
- [22] H. A. Staab, P. Kirsch, M. F. Zipplies, A. Weinges, C. Krieger, *Chem. Ber.* **1994**, *127*, 1653.
- [23] C. A. Hunter, J. K. M. Sanders, *J. Am. Chem. Soc.* **1990**, *112*, 5525.

Formation of High-Quality CdS and Other II–VI Semiconductor Nanocrystals in Noncoordinating Solvents: Tunable Reactivity of Monomers**

W. William Yu and Xiaogang Peng*

Semiconductor nanocrystals are of great interest for both fundamental research and industrial development.^[1, 2] The lack of adequate synthetic methods for nanocrystals of the desired quality is currently a bottleneck in this field.^[3] The relatively successful approaches, including the organometallic approach^[4–8] and its alternatives,^[9–13] are exclusively performed in coordinating solvents. Evidently, only a few compounds can act as the coordinating solvents,^[11] and this makes it extremely challenging to identify a suitable reaction system for growing high-quality nanocrystals in most cases. Here we show that noncoordinating solvents not only are compatible with the synthesis of semiconductor nanocrystals, but also provide tunable reactivity of the monomers by simply varying the concentration of ligands in the solution. The tunable reactivity of the monomers provides a necessary balance between nucleation and growth, which is the key for control over the size and size distribution of the resulting nanocrystals.^[5] In practice, such tunability has great potential to promote the synthesis of various semiconductor nanocrystals to the level of that of the well-developed CdSe

[*] Dr. X. Peng, Dr. W. W. Yu
Department of Chemistry & Biochemistry
University of Arkansas
Fayetteville, AR 72701 (USA)
Fax: (+1) 501-575-4049
E-mail: xpeng@uark.edu

[**] Financial support by the National Science Foundation through CHE0101178 is acknowledged.

Supporting information for this article is available on the WWW under <http://www.angewandte.org> or from the author.

nanocrystals in coordinating solvents. A successful synthetic scheme for high-quality CdS nanocrystals is demonstrated here.

The noncoordinating solvent used in this study was octadecene (ODE), which is a liquid at room temperature and boils at about 320 °C. Oleic acid, a natural surfactant, was chosen as the ligand for stabilizing the nanocrystals and the cationic precursors. For the synthesis of CdS, the precursors were CdO and elemental sulfur, two naturally occurring minerals. For the synthesis of CdS nanocrystals (for details, see Experimental Section), CdO was dissolved in ODE by reaction with oleic acid at elevated temperature. Into this hot solution, a room-temperature solution of elemental sulfur in ODE was injected. The reaction was monitored by UV/Vis absorption and photoluminescence (PL) spectroscopy by taking aliquots from the reaction flask.

The power of noncoordinating solvents is demonstrated by the results shown in Figure 1. All reactions in Figure 1 were performed under identical conditions, except for the concentration of oleic acid in the reaction mixture. With pure oleic acid as coordinating solvent, only a small amount of bulk CdS particles were observed. As the concentration of oleic acid in ODE decreased, the growth rate of the nanocrystals slowed down systematically, and the size distribution of the resulting nanocrystals became significantly narrower at the focus of the size distribution,^[5] as indicated by the sharpness of the first absorption peak of the sharpest spectrum in each series.

Similar results were obtained for the synthesis of ZnSe and CdSe nanocrystals in ODE with oleic acid as ligand. ZnSe nanocrystals, regardless of their size, cannot be formed in pure oleic acid, pure trioctylphosphane oxide (TOPO), or a mixture thereof as coordinating solvent. This even holds for the traditional organometallic approach.^[7] However, using a dilute solution of oleic acid in ODE, we observed the formation of ZnSe nanocrystals with a decent size distribution. In pure fatty acids or mixtures thereof with TOPO, it is not practical to synthesize CdSe nanocrystals with relatively small sizes (< 4 nm).^[11] With ODE as noncoordinating solvent and an appropriate amount of oleic acid as ligand, the size of

CdSe nanocrystals can range from approximately 1.5 to 20 nm in a controllable fashion.

The influence of the concentration of oleic acid on the growth kinetics of CdS nanocrystals (Figure 1) and of other types of semiconductor nanocrystals is dramatic. This influence is the result of the tuned reactivity of the cationic monomers in the noncoordinating solvent, where the term "cationic monomer" refers to all cadmium or zinc species in solution that are not in the form of nanocrystals.^[14] A reaction mixture for the synthesis of CdS in ODE after a given reaction time was separated to two fractions by extraction with CHCl₃/CH₃OH (1:1). Apparently, the CdS nanocrystals are only soluble in the ODE phase, and oleic acid and cadmium oleate are both extracted into the CHCl₃/CH₃OH phase. This separation was confirmed by UV/Vis and FTIR measurements (see Figure 2, left and Supporting Information). After this separation, the concentration of unconverted cadmium

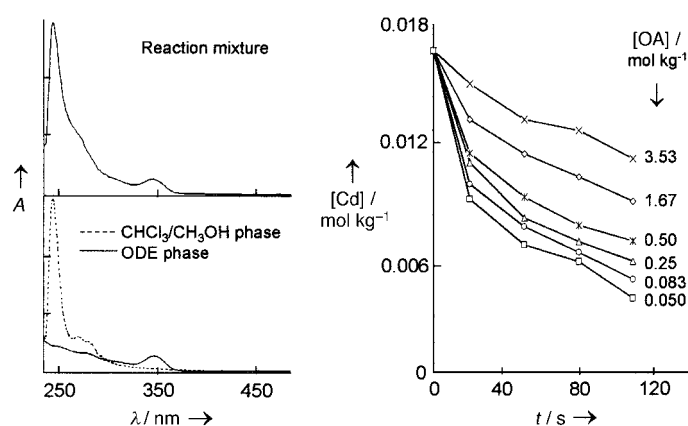


Figure 2. Spectroscopic monitoring of the separation of CdS nanocrystals from oleic acid and unconsumed cadmium oleate (left). Temporal evolution of the monomer concentrations in ODE with different oleic acid concentrations (right). [Cd] = Cd monomer concentration.

oleate in the reaction solution was determined by atomic absorption spectroscopy (Figure 2, right). The concentration of cadmium monomer in the solution dropped very quickly during the first 20 s, and the rate of this depletion increased with decreasing oleic acid concentration (Figure 2, right). From the spectra in Figure 1, one can find that the average size of the nanocrystals about 20 s after the injection decreased systematically with decreasing initial oleic acid concentration. Similar results were obtained for the formation of other types of semiconductor nanocrystals. Hence, it is safe to conclude that the number of nanocrystals (nuclei) formed in the initial nucleation stage increased significantly with increasing initial oleic acid concentration. This conclusion indicates that the reactivity of the monomers in solution increases significantly when the ligand concentration in solution decreases.

In contrast, the depletion rate of the monomers did not change much with a different initial oleic acid concentration after the initiation stage of the reactions, although the remaining monomer con-

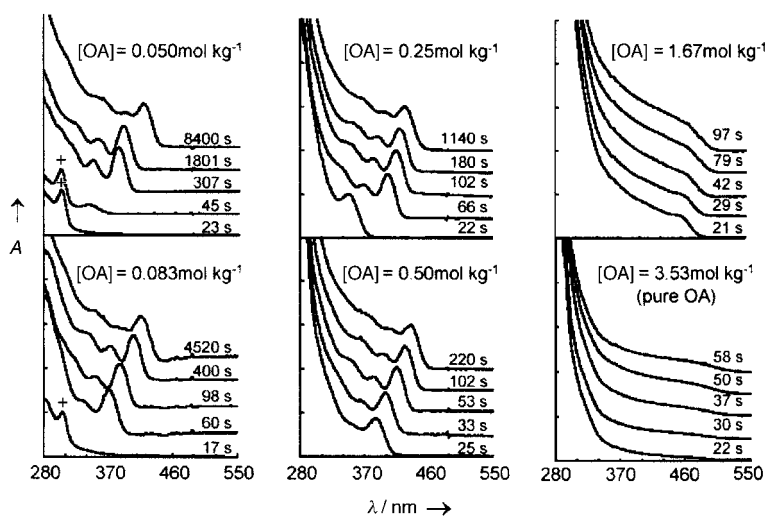


Figure 1. Temporal evolution of the absorption spectrum of the CdS nanocrystals grown in ODE with different oleic acid concentrations [OA]. The absorption peaks of a magic-sized nanocluster are marked +. A = absorbance.

centration was higher for the reactions with a higher oleic acid concentration. Likely, this is caused by two conflicting factors. In comparison to a reaction with a lower ligand concentration, the reactivity of the monomers of a given reaction was lower but the remaining concentration of the monomers was higher.

The influence of the ligand concentration in controlling the size and size distribution of the nanocrystals is dramatic (Figure 1). According to current understanding, control of the size distribution of growing colloidal nanocrystals is achieved by a balance between nucleation and growth. A successful synthetic scheme should start with a fast and short nucleation period, which is followed by a growth stage without either prolonged nucleation or ripening, which is referred as "focusing of size distribution".^[5] If too many nuclei were formed in the initial nucleation period, the remaining monomers would not be sufficient to promote the focusing of size distribution for a sufficient time, and this would result in an undesired Ostwald ripening or defocusing of size distribution. If too few nuclei formed, the growth reaction would be too fast to be controlled to reach the desired size and size distribution. To achieve this essential balance between nucleation and growth, a nearly continuous tunable reactivity of the monomers is desirable. As discussed above, such tunability can be readily achieved by simply altering the ligand concentration in a noncoordinating solvent. This tunability may indicate that the cadmium monomers in the solution at elevated temperatures are not simply cadmium oleate. The number of "nearby" ligands for each cadmium ion may strongly depend on the concentration of the ligands in the bulk solution. Consequently, the reactivity of those cadmium complexes at elevated temperatures varies with the ligand concentration in solution.

To our knowledge, the UV/Vis absorption and photoluminescence (PL) spectra shown in Figure 3 are among the sharpest for CdS nanocrystals reported,^[8, 15, 16] and this

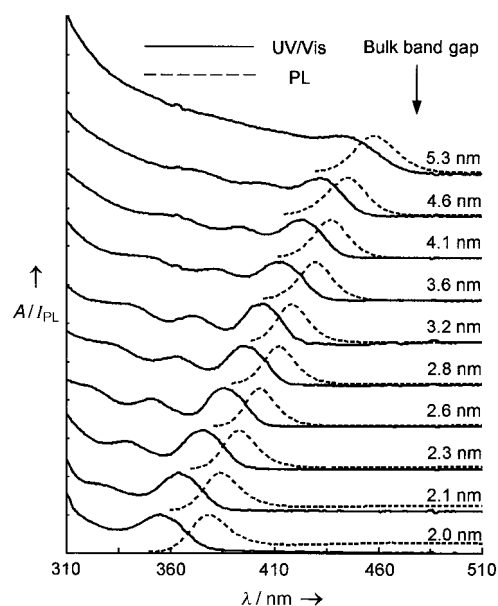


Figure 3. UV/Vis absorption and photoluminescence (PL) spectra of the as-prepared CdS nanocrystals with different sizes. I_{PL} = photoluminescence intensity.

indicates a superior size distribution of the nanocrystals formed in ODE. The achievable size range is also plausible when compared to the existing synthetic schemes.^[8, 15, 16] The approach with a noncoordinating solvent presented here can reproducibly and controllably generate CdS nanocrystals in almost the entire quantum confined size regime (ca. 1–6 nm), with the first exciton absorption peak from 305 nm (likely a magic size, see Figure 1) to about 440 nm. The PL of the CdS nanocrystals is dominated by the band-edge emission, except for those smaller than about 2 nm. Transmission electron microscope (TEM) measurements (Figure 4) confirmed that

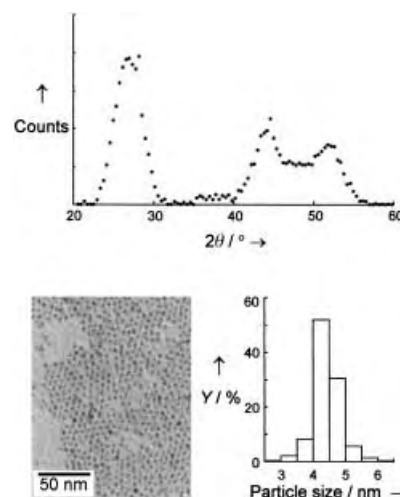


Figure 4. X-ray diffraction pattern (top), TEM image (bottom, left), and the corresponding size-distribution diagram of the CdS nanocrystals (bottom, right).

the size distribution of the as-prepared CdS nanocrystals was nearly monodisperse in the entire size range mentioned above, with a relative standard deviation of 5–15% without any size sorting. The diffraction pattern seems to combine that of wurtzite nanocrystals with one or more zinc blende stacking faults along the *c* axis.^[8] Importantly, the synthesis can also be performed with the reaction system open to air without deteriorating the quality of the nanocrystals (see Supporting Information).

In conclusion, the temporal course of the nucleation and growth of semiconductor nanocrystals can be tuned by simply changing the concentration of the ligands in a noncoordinating solvent. Such flexibility is impossible for a synthesis performed in coordinating solvents. Appropriate reactivity of the monomers, manipulated by varying the ligand concentration in noncoordinating solvent, led to a balance between the two conflicting requirements of a successful synthetic scheme: a fast but short nucleation stage and a slow but long growth stage without Ostwald ripening.^[5] Although this work focused on the synthesis of II–VI semiconductor nanocrystals in ODE, we believe ODE will not be a unique noncoordinating solvent, and other such solvents should be suitable for the synthesis of different types of colloidal nanocrystals. The introduction of noncoordinating solvents further enhances the possibility of implementing green-chemical principles into the design of synthetic schemes for colloidal nanocrystals, which

may become significant for industrial production of those novel materials.^[3] As demonstrated above, the procedure and the chemicals used for the synthesis of high-quality CdS nanocrystals are simple, safe, and inexpensive in comparison to those reported previously.^[8,15,16]

Experimental Section

Typically, a mixture (4 g in total) of CdO (0.0128 g, 0.10 mmol), oleic acid (0.30–21.2 mmol), and technological-grade ODE (Aldrich) was heated to 300 °C. A solution of sulfur (0.0016 g, 0.05 mmol) in ODE was swiftly injected into this hot solution, and the reaction mixture was allowed to cool to 250 °C for the growth of CdS nanocrystals. The synthesis can be carried out under argon or open to air. Aliquots were taken at different time intervals, and UV/Vis and PL spectra were recorded for each aliquot. XRD and TEM measurements were also performed to characterize the crystallinity, size, and size distribution of the resulting crystals. The size-distribution diagrams were obtained by measuring about 500 individual CdS nanocrystalline particles on enlarged photographs. All the measurements were performed on the original aliquots without any size sorting. The unconsumed cadmium precursor was separated from the nanocrystals by the repeated extraction of the reaction aliquots with an equal volume of CHCl₃/CH₃OH (1:1). The extraction process was monitored by a UV/Vis absorption spectrophotometer. The size of the resulting nanocrystals were determined by TEM measurements and literature data on size versus the position of the first sorption peak.^[8,16] The characterization and sample preparation of the nanocrystals, including X-ray diffraction, TEM, PL, and UV/Vis, were reported in a previous paper.^[14] The size distribution was also determined by using the method reported in ref. [14]. The CdSe and ZnSe nanocrystals were synthesized in a similar fashion; the selenium precursor was a solution of selenium/tributylphosphane (1:1.1) in ODE.

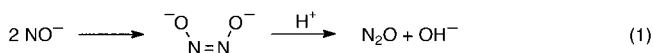
Received: January 31, 2002 [Z18622]

An Umpolung Approach to *cis*-Hyponitrite Complexes**

Navamoney Arulsamy, D. Scott Bohle,*
Jerome A. Imonigie, and Seth Levine

*Dedicated to Professor Karl Wieghardt
on the Occasion of his 60th Birthday*

The reductive dimerization of nitric oxide to give nitrous oxide is an important process both in the remediation of nitrogen-oxide pollutants in flue and exhaust gases by heterogeneous platinum metals,^[1] and in the use of the oxyanions of nitrogen as terminal electron acceptors by dissimilatory bacteria.^[2] In these transformations the key step is the formation of the nitrogen–nitrogen double bond, and here the frequently proposed mechanism is the stereospecific dimerization of nitroxyl, NO[−], to give *cis* hyponitrite, followed by elimination of nitrous oxide, [Eq. (1)].^[3]



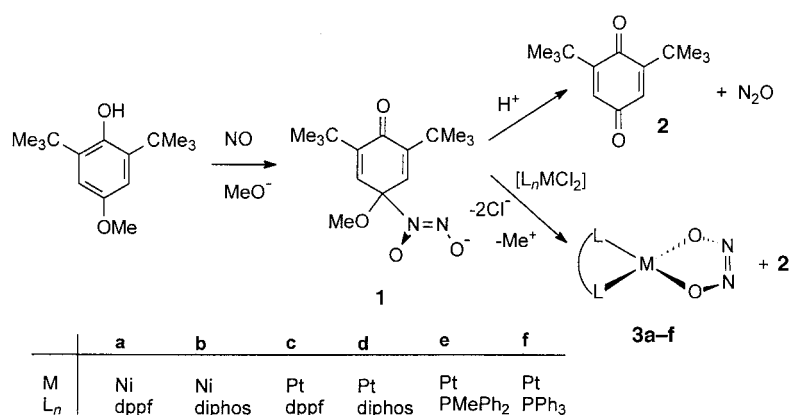
Unlike *trans* hyponitrite, for which there is an extensive and well established structural,^[4] mechanistic,^[5–8] and derivative chemistry,^[9] our knowledge of *cis* hyponitrite is sparse. Although an elegant spectroscopic and structural study of sodium *cis* hyponitrite,^[10,11] derived from the solid-state reaction of sodium oxide and nitrous oxide, established a new benchmark for this area, the reactivity of the free or coordinated dianion remains vaguely outlined. Thus key aspects of the kinetics and mechanism of the decomposition of *cis* hyponitrite, its coordination chemistry, and alkylation remain unknown. Furthermore, there is only a solitary structurally characterized complex of a chelated mononuclear *cis* hyponitrite, [Pt(η²-O₂N₂)(PPh₃)₂], which results from the equally unique oxidative coupling of two nitric oxides by [Pt(PPh₃)₄].^[12–18] Related reactions for different late transition metals are thought to give *trans*-hyponitrite complexes.^[19–21] Herein we describe: 1) a new general method for the introduction and stabilization of *cis* hyponitrite in the coordination sphere of a metal, 2) the structure of one of these complexes, [Ni(η²-O₂N₂)(dppf)], (dppf = 1,1'-bis(diphenylphosphanyl)ferrocene), and 3) the reactivity of these new *cis*-hyponitrite complexes.

We recently described the synthesis of a new class of diazeniumdiolates, RN₂O₂[−], from the base-mediated condensation of 2,4,6-trisubstituted phenols with nitric oxide.^[22] In the course of characterizing one of these derivatives, with R = OMe, **1**, we observed rapid acid-promoted stoichiometric

- [1] Reviews relevant to colloidal nanocrystals: *Acc. Chem. Res.* **1999**, 32(5), 387 (Special Issue for Nanostructures).
- [2] A. P. Alivisatos, *Science* **1996**, 271, 933.
- [3] X. Peng, *Chem. Eur. J.* **2002**, 8, 334.
- [4] X. Peng, L. Manna, W. D. Yang, J. Wickham, E. Scher, A. Kadavanich, A. P. Alivisatos, *Nature* **2000**, 404, 59.
- [5] X. Peng, J. Wickham, A. P. Alivisatos, *J. Am. Chem. Soc.* **1998**, 120, 5343.
- [6] A. J. Nozik, O. I. Micic, *MRS Bull.* **1998**, 23, 24.
- [7] M. A. Hines, P. Guyot-Sionnest, *J. Phys. Chem. B* **1998**, 102, 3655.
- [8] C. B. Murray, D. J. Norris, M. G. Bawendi, *J. Am. Chem. Soc.* **1993**, 115, 8706.
- [9] Z. A. Peng, X. Peng, *J. Am. Chem. Soc.* **2002**, 124, 3343.
- [10] L. Qu, X. Peng, *J. Am. Chem. Soc.* **2002**, 124, 2049.
- [11] L. Qu, Z. A. Peng, X. Peng, *Nano Lett.* **2001**, 1, 333.
- [12] Y.-w. Jun, S.-M. Lee, N.-J. Kang, J. Cheon, *J. Am. Chem. Soc.* **2001**, 123, 5150.
- [13] M. A. Malik, N. Revaprasadu, P. O'Brien, *Chem. Mater.* **2001**, 13, 913.
- [14] Z. A. Peng, X. Peng, *J. Am. Chem. Soc.* **2001**, 123, 1389.
- [15] Z. A. Peng, X. Peng, *J. Am. Chem. Soc.* **2001**, 123, 183.
- [16] T. Vossmeier, L. Katsikas, M. Giersig, I. G. Popovic, K. Diesner, A. Chemseddine, A. Eychmüller, H. Weller, *J. Phys. Chem.* **1994**, 98, 7665.

[*] Prof. Dr. D. S. Bohle, Dr. N. Arulsamy, Dr. J. A. Imonigie, S. Levine
Department of Chemistry
University of Wyoming
Laramie, WY 82071-3838 (USA)
Fax: (+1) 307-766-2807
E-mail: Bohle@uwyo.edu

[**] This research was supported by the National Institutes of Health, the Department of Energy, and the Air Force Office of Scientific Research.



Scheme 1.

decomposition to generate nitrous oxide and 2,6-di-*tert*-butylbenzoquinone (**2**; Scheme 1). This unusual umpolung in the heterolysis of the C–N bond suggested that the reaction might occur for other electrophiles, most notably transition metals. In this case the result proves to be a new approach to *cis*-hyponitrite complexes. Thus the reaction of **1** and divalent Group 10 transition-metal complexes results in the rapid formation of new diamagnetic square-planar *cis*-hyponitrite complexes, **3a–e**, at room temperature in high yield, as well as known *cis*-hyponitrite complex **3f** (Scheme 1, diphos = 1,2-ethanediyldis[(diphenyl)phosphane]). The net transfer of $\text{N}_2\text{O}_2^{2-}$ to a transition metal from a diazeniumdiolate such as **1** is a new reactivity pattern for these reagents which usually form chelates or occasionally reductively nitrosylate metal centers.^[23] Crystallographic characterization of **3a** by single-crystal X-ray diffraction (Figure 1) confirms the chelation of a *cis*-hyponitrite ligand in a square-planar complex. The dppf ligand adopts a common^[24] but compact synclinal staggered configuration with the P(1)–centroid(1)–centroid(2)–P(2)

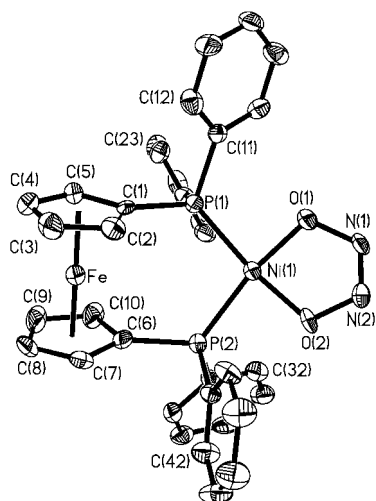


Figure 1. ORTEP representation for **3a** with the hydrogen atoms omitted. Selected bond lengths [Å] and angles [°]: Ni(1)–O(1) 1.820(4), Ni(1)–O(2) 1.818(4), O(1)–N(1) 1.400(6), N(1)–N(2) 1.236(6), N(2)–O(2) 1.385(5), Ni(1)–P(1) 2.180(2), Ni(1)–P(2) 2.205(2); O(1)–Ni(1)–O(2) 83.9(2), Ni(1)–O(1)–N(1) 112.2(3), O(1)–N(1)–N(2) 115.4(4), N(1)–N(2)–O(2) 115.4(5), N(2)–O(2)–Ni(1) 112.9(3), P(1)–Ni(1)–P(2) 101.59(6).

dihedral angle (τ) of 28.5°. Prior structural determinations of *cis*-hyponitrite complexes, $[(\text{H}_3\text{N})_5\text{CoN}(\text{O})\text{NOC}(\text{NH}_3)_5](\text{NO}_3)_4$,^[25] and $[\text{Pt}(\eta^2\text{-O}_2\text{N}_2)(\text{PPh}_3)_2]$,^[12] have proven troublesome and were only refined to conventional *R* factors of 16 and 11 %, respectively, for the more intense data.

Unlike *trans* hyponitrite which is readily protonated or alkylated to give metastable RONNOR or RONNO[−] adducts ($\text{R} = \text{H}^+$ or R^+),^[9] the only known metastable derivatives of *cis* hyponitrite involve O,O chelation or O,N dicoordination to transition-metal centers. Thus *cis* RONNOR or *cis* RONNO[−] are unknown, and the latter have been theoretically predicted to have very low energy barriers for the elimination of RO^- ions

and nitrous oxide.^[9] Electrophiles, such as HCl or Me_3SiCl , readily cleave **3a–f** to return $[\text{L}_2\text{MCl}_2]$ and nitrous oxide. Nitrous oxide is also generated during the thermolysis of **3a–f**, which all exothermally decompose at relatively low temperatures, between 75 and 120 °C, to give black insoluble residues. In addition to their thermal instability the new *cis*-hyponitrite complexes **3a–e** photolytically decompose upon UV irradiation.

To spectrophotometrically follow the kinetics of their thermal decomposition reactions we have incorporated the chelating phosphane ligand dppf in **3a,c**, to act as a visible chromophore. When the ferrocene-based absorption, $\lambda_{\text{max}} = 406 \text{ nm}$ for **3a**, is used to monitor their thermal decomposition in DMF at 40 °C the kinetics are first order in complex alone, with $k = 3.3 \pm 0.2 \times 10^{-4} \text{ s}^{-1}$, and are independent of the initial complex concentration and of added triphenylphosphane, even when the $[\text{PPh}_3]$ is three orders-of-magnitude higher than **3a**. Although there is little solvent effect on the rate of **3a** decomposition, for example, in dimethylacetamide under the above conditions, the decomposition again follows triphenylphosphane-independent first-order kinetics with $k = 3.8 \pm 0.3 \times 10^{-4} \text{ s}^{-1}$. In dichloromethane black insoluble products interfere with the kinetic measurements. Moreover, nitrous oxide release into the gas phase, monitored by the IR absorbance of the $\nu(\text{N}_2\text{O})$ band at 2224 cm^{-1} , also follows the same kinetic profile with $k = 1.5 \pm 1.1 \times 10^{-4} \text{ s}^{-1}$ for the decomposition of **3a** in DMF at 40 °C. Taken together, the kinetics results indicate that the rate-limiting step in the decomposition of **3a** is unimolecular and accompanies release of nitrous oxide. The resulting reactive fragment, formally a terminal oxo complex $[(\text{dppf})\text{NiO}]$, which results from loss of nitrous oxide, is similar to some of the intermediates which have been proposed for carbon dioxide exchange in $[\text{Pt}(\eta^2\text{-O}_2\text{CO})(\text{PPh}_3)_2]$.^[26] In support of the presence of such a proposed reactive intermediate in the decomposition of **3f** we have treated dichloromethane solutions of **3f** at reflux with saturating pressures of carbon dioxide or excess carbon disulfide and find that among the platinum-containing products are $[\text{Pt}(\eta^2\text{-O}_2\text{CO})(\text{PPh}_3)_2]$, and $[\text{Pt}(\eta^2\text{-S}_2\text{CO})(\text{PPh}_3)_2]$, respectively, in addition to $[\text{PtCl}_2(\text{PPh}_3)_2]$.

In summary, a new general method to prepare *cis*-hyponitrite complexes from the diazeniumdiolate compound **1** is described and a high-resolution structure of one such

derivative has been determined. The decomposition of these complexes suggests rate-limiting loss of nitrous oxide leads to unusual and reactive late-transition-metal terminal oxo intermediates.

Experimental Section

3a: [Ni(dppf)Cl₂]₂^[27] (268 mg) dissolved in CH₂Cl₂ (15 mL) was treated in one addition with **1**^[22] (2 equivalents, 249 mg) suspended in methanol (60 mL). Rapidly a deep orange color developed and the solution volume was immediately reduced to ca 10 mL by evaporation at ambient temperatures. The resulting bright orange crystals were isolated by filtration and washed with portions of cold methanol (4 × 10 mL) or until the filtrate was colorless. Recrystallization of this product from dichloromethane/ethanol at room temperature returns 243 mg (93 % yield) of **3a**. Elemental analysis calcd (%) C₃₄H₂₈FeN₂NiO₂P₂ · ½CH₂Cl₂: C 59.26, H 4.05, N 3.88; found: C 59.43, H 4.28, N 3.64; IR (KBr): $\tilde{\nu}$ = 1480 m, 1449 s, 1436 s, 1307 m, 1194 w, 1182 w, 1168 m, 1096 s, 1036 m, 1028 m, 999 w, 983 m, 917 m, 827 w, 799 m, 744.3 s, 692 s, 638 w, 625 m, 556 m, 510, s, 494 s, 471 cm⁻¹ m; ¹H NMR (400 MHz, CD₂Cl₂): δ = 7.84 (m, 8H), 7.52 (m, 4H), 7.42 (t, J = 7.3 Hz, 8H), 4.42 (m, 4H), 4.26 ppm (m, 4H); ³¹P NMR (162 MHz, CD₂Cl₂): δ = 25.0 ppm (s) (UV/Vis: λ_{max} , (ϵ_{max} , M⁻¹cm⁻¹) in CH₂Cl₂: 406 nm (655); differential scanning calorimetry (DSC): ΔH = -802 kcal mol⁻¹ T_{onset} = 75 °C. Crystals suitable for X-ray diffraction were grown from CH₂Cl₂/Et₂O at -15 °C.

Crystal data for **3a**: C₃₅H₂₈Cl₂FeN₂NiP₂O₂, M = 755.99, 143 K, triclinic space group $P\bar{1}$, a = 10.6210(8), b = 11.3831(9), c = 15.515(2) Å, α = 84.021(2), β = 72.745(2), γ = 69.790(1)°, V = 1681.0(3) Å³, Z = 2, ρ_{calcd} = 1.494 Mg m⁻³, $F(000)$ = 772, 426 parameters; R_1 (wR_2) [$I > 2\sigma(I)$] = 0.064 (0.15), $s(\text{GOF})$ = 0.98. Crystals of **3a** were mounted on glass fibers with epoxy resin and diffraction data was collected on a Bruker Smart CCD diffractometer equipped with a sealed molybdenum tube which was monochromated to give λ = 0.71073 Å. The structure was solved using direct methods and refined using full-matrix least-squares on F^2 with SHELXTL. With the exception of the disordered dichloromethane solvate, all non-hydrogen atoms were refined anisotropically with element assignments as described in the text. CCDC-176081 (**3a**) contains the supplementary crystallographic data for this paper. These data can be obtained free of charge via www.ccdc.cam.ac.uk/conts/retrieving.html (or from the Cambridge Crystallographic Data Centre, 12, Union Road, Cambridge CB21EZ, UK; fax: (+44) 1223-336-033; or deposit@ccdc.cam.ac.uk).

Received: February 26, 2002 [Z18780]

- [1] T. R. Ward, R. Hoffmann, M. Shelef, *Surf. Sci.* **1993**, 289, 85.
- [2] B. C. Berks, S. J. Ferguson, J. W. B. Moir, D. J. Richardson, *Biochim. Biophys. Acta* **1995**, 1232, 97.
- [3] M. N. Hughes, *Q. Rev. Chem. Soc.* **1968**, 22, 1.
- [4] N. Arulsamy, D. S. Bohle, J. A. Imonigie, E. S. Sagan, *Inorg. Chem.* **1999**, 38, 2716.
- [5] A. M. Al-Ajlouni, E. S. Gould, *J. Chem. Soc. Dalton Trans.* **2000**, 1239.
- [6] M. R. Goyal, P. Bhatnagar, R. K. Mittal, Y. K. Gupta, *Indian J. Chem. Sect. A* **1989**, 28, 280.
- [7] M. R. Goyal, P. Bhatnagar, R. K. Mittal, Y. K. Gupta, *Indian J. Chem. Sect. A* **1989**, 28, 382.
- [8] M. N. Hughes, P. E. Wimbeldon, G. Stedman, *J. Chem. Soc. Dalton Trans.* **1989**, 533.
- [9] N. Arulsamy, D. S. Bohle, J. A. Imonigie, E. S. Sagan, *J. Am. Chem. Soc.* **2000**, 122, 5539.
- [10] C. Feldmann, M. Jansen, *Angew. Chem.* **1996**, 108, 1807; *Angew. Chem. Int. Ed. Engl.* **1996**, 35, 1728.
- [11] C. Feldmann, M. Jansen, *Z. Anorg. Allg. Chem.* **1997**, 623, 1803.
- [12] S. Bhaduri, B. F. G. Johnson, A. Pickard, P. R. Raithby, G. M. Sheldrick, C. I. Zuccaro, *J. Chem. Soc. Chem. Commun.* **1977**, 354.
- [13] S. Bhaduri, B. F. G. Johnson, C. J. Savory, J. A. Segal, R. H. Walter, *J. Chem. Soc. Chem. Commun.* **1974**, 809.
- [14] S. Cenini, R. Ugo, G. La Monica, S. D. Robinson, *Inorg. Chim. Acta* **1972**, 6, 182.

- [15] R. Ugo, S. Bhaduri, B. F. G. Johnson, A. Khair, A. Pickard, *J. Chem. Soc. Chem. Commun.* **1976**, 694.
- [16] S. Bhaduri, B. F. G. Johnson, A. Khair, I. Ghatak, D. M. P. Mingos, *J. Chem. Soc. Dalton* **1980**, 1572.
- [17] A. R. Middleton, G. Wilkinson, M. B. Hursthouse, N. P. Walker, *J. Chem. Soc. Dalton* **1982**, 663.
- [18] R. J. Puddephatt, P. J. Thompson, *J. Chem. Soc. Dalton* **1976**, 2091.
- [19] B. Jezowska-Trzebiatowska, J. Hanuza, M. Ostern, J. Ziolkowski, *Inorg. Chim. Acta* **1972**, 6, 141.
- [20] H. Okamura, E. Miki, K. Mizumachi, T. Ishimori, *Bull. Chem. Soc. Jpn.* **1976**, 49, 666.
- [21] R. Bau, I. H. Sabherwal, A. B. Burg, *J. Am. Chem. Soc.* **1971**, 93, 4926.
- [22] D. S. Bohle, J. A. Imonigie, *J. Org. Chem.* **2000**, 65, 5685.
- [23] N. Arulsamy, D. S. Bohle, B. Doletski, *Helv. Chim. Acta* **2001**, 84, 3281.
- [24] G. Bandoli, A. Dolmella, *Coord. Chem. Rev.* **2000**, 209, 161.
- [25] B. F. Hoskins, F. D. Whillans, D. H. Dale, D. C. Hodgkin, *J. Chem. Soc. Chem. Commun.* **1969**, 69.
- [26] M. A. Andrews, G. L. Gould, E. J. Voss, *Inorg. Chem.* **1996**, 35, 5740.
- [27] I. R. Butler, W. R. Cullen, T. J. Kim, S. J. Rettig, J. Trotter, *Organometallics* **1985**, 4, 972.

Aminocyclopentadienyl Ruthenium Chloride: Catalytic Racemization and Dynamic Kinetic Resolution of Alcohols at Ambient Temperature**

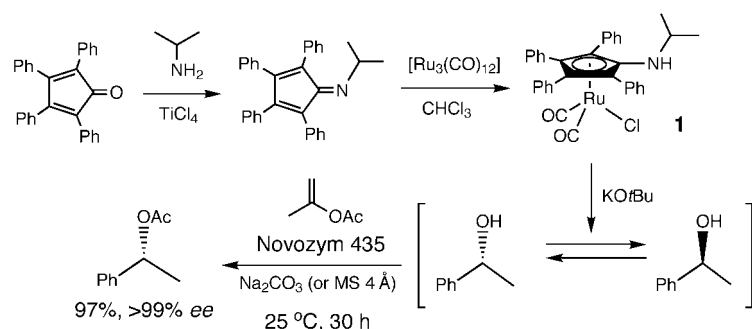
Jun Ho Choi, Yu Hwan Kim, Se Hyun Nam, Seung Tae Shin, Mahn-Joo Kim,* and Jaiwook Park*

Dynamic kinetic resolution (DKR) is an attractive method for the complete transformation of a racemic mixture into a single enantiomer.^[1] The DKR of secondary alcohols is a prominent example, for which transition-metal-catalyzed racemization is coupled with enzymatic acylation.^[2] In particular, Bäckvall and co-workers have introduced a notable catalyst system that provides a wide range of chiral acetates in good yields and excellent optical purities.^[2b-f] However, the catalyst for the racemization of secondary alcohols is activated at high temperature, and needs the corresponding ketones as hydrogen mediators.^[3] Thus, the catalyst system requires a thermally stable lipase; *p*-chlorophenyl acetate has been selected as an acyl donor,^[2c] because oxidation of the starting alcohols occurs when the conventional alkenyl acetates are used as acyl donors.^[4]

[*] Prof. J. Park, Prof. M.-J. Kim, J. H. Choi, Y. H. Kim, S. H. Nam, S. T. Shin
National Research Laboratory of Chirotechnology
Department of Chemistry
Division of Molecular and Life Sciences
Pohang University of Science and Technology (POSTECH)
San 31 Hyoja Dong, Pohang 790-784 (Korea)
Fax: (+82) 54-279-3399
E-mail: mjk@postech.ac.kr, pjw@postech.ac.kr

[**] We are grateful for the financial support from MOST through the NRL program, KOSEF through the Center for Integrated Molecular System, and the Korean Ministry of Education through the BK21 project for our graduate program.

Herein we report a novel ruthenium catalyst that can racemize secondary alcohols efficiently at room temperature without the aid of hydrogen mediators.^[5, 6] Furthermore, the catalytic racemization is compatible with the use of isopropenyl acetate for the DKR of secondary alcohols at room temperature (Scheme 1).



Scheme 1. Synthesis of **1** and DKR of 1-phenylethanol; MS = molecular sieve.

For the synthesis of aminocyclopentadienyl ruthenium chloride (**1**), it was fortunate to select chloroform as the solvent in the reaction of $[\text{Ru}_3(\text{CO})_{12}]$ with the imine prepared from isopropylamine and 2,3,4,5-tetraphenylcyclopentadienone. Attempts at synthesizing the tricarbonyl analogue under various other reaction conditions failed. The molecular structure of **1** was confirmed by X-ray diffraction analysis (Figure 1).^[7]

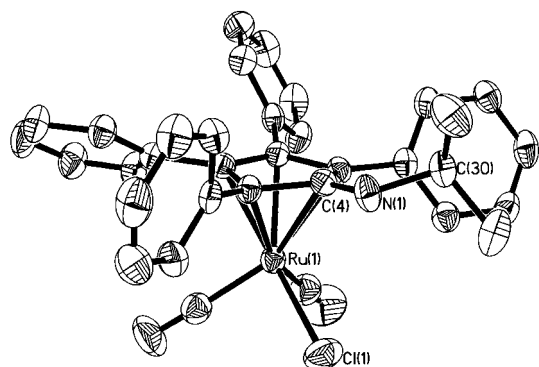


Figure 1. ORTEP plot (thermal ellipsoids set at 50% probability) of the molecular structure of **1**. All hydrogen atoms are omitted for clarity. Selected bond lengths [Å] and angles [°]: Ru(1)–Cl(1) 2.4137(8), Ru(1)–C(4) 2.430(3), N(1)–C(4) 1.339(3), N(1)–C(30) 1.467(3); Cl(1)–Ru(1)–C(4) 86.96(7), Ru(1)–C(4)–N(1) 131.6(2), C(4)–N(1)–C(30) 128.4(2).

Table 2. Dynamic kinetic resolution of 1-phenylethanol.^[a]

Entry	Acyl donor ^[b]	Lipase ^[c] [mg]	Additive ^[d]	T [°C]	t [h]	Acetate [%] ^[e]	ee ^[f] [%]
1	$\text{CH}_2=\text{CHOCOCH}_3$	0.7		25	96	55	98.6
2	$\text{CH}_2=\text{CHOCOCH}_3$	0.7	Na_2CO_3	25	96	89	97.0
3	$\text{CH}_2=\text{C}(\text{CH}_3)\text{OCOCH}_3$	0.7	molecular sieve 4 Å	25	40	98	98.5
4	$\text{CH}_2=\text{C}(\text{CH}_3)\text{OCOCH}_3$	0.7	Na_2CO_3	25	30	97	> 99
5	$\text{CH}_2=\text{C}(\text{CH}_3)\text{OCOCH}_3$	0.7	Na_2CO_3	40	24	95	> 99
6	$\text{CH}_2=\text{C}(\text{CH}_3)\text{OCOCH}_3$	0.7	Na_2CO_3	70	12	90	> 99
7	$p\text{-ClC}_6\text{H}_4\text{OCOCH}_3$ ^[g]	7	Na_2CO_3	25	42	95	> 99

[a] The reactions were carried out with 0.25 mmol of 1-phenylethanol and 4 mol % of **1**, which was activated with 5 mol % of potassium *tert*-butoxide, in dry toluene (0.80 mL) under argon atmosphere. [b] 1.5 equiv of alkenyl acetate [c] Novozym 435. [d] Sodium carbonate (1.0 equiv) or molecular sieve 4 Å (60 mg) was used. [e] The yields were determined by GC. [f] The % ee values were determined by HPLC equipped with a chiral column ((*R,R*) Whelk-01, Merck). [g] 3 equiv.

We expected the generation of a coordinatively unsaturated and active species by the elimination of hydrogen chloride from **1** with a proper base.^[8] Indeed, (*S*)-1-phenylethanol (> 99% ee) was racemized completely within 30 min at 25 °C by the catalytic species generated by the treatment of **1** with potassium *tert*-butoxide. The scope of the catalytic racemization was investigated under various conditions (Table 1): The racemization rate is not affected significantly by the polarity and the coordinating ability of solvents (entries 1–4, though it is slightly slower with acetone). Even without solvent, the racemization is practically completed in 12 h with only 0.3 mol % of **1** (entry 5). Notably, the catalytic species is still active in the presence of vinyl acetate in toluene (entry 6), although the racemization is almost prevented when vinyl acetate alone is employed as a solvent (entry 7).

On the basis of the racemization results, the DKR of 1-phenylethanol was investigated with varying conditions (Table 2): Unexpectedly, the DKR is unsuccessful under the racemization conditions of the entry 6 in Table 1 despite the fact that the lipase itself does not interfere with the catalytic racemization. A breakthrough is the use of sodium carbonate or 4-Å molecular sieve as an additive (Table 2 entries 2 and 3). Isopropenyl acetate is a better acyl donor than vinyl acetate it gives faster and more productive DKR. Increasing temperature makes the DKR faster, but the production of acetophenone increases: 1.6% at 25 °C, 2.5% at 40 °C, and 10.4% at 70 °C (entries 4–6). In the

Table 1. Catalytic racemization of (*S*)-1-phenylethanol at 25 °C after activating **1** with potassium *tert*-butoxide.^[a]

Entry	Solvent	t [h]	ee ^[b] [%]
1	toluene	0.5	0.0
2	CH_2Cl_2	0.5	0.0
3	THF	0.5	0.0
4	acetone	0.5	24.7
5	no solvent ^[c]	12	1.8
6	toluene + vinyl acetate ^[d]	1.0	6.8
7	vinyl acetate	5.0	96.4

[a] (*S*)-1-Phenylethanol (> 99% ee, 0.25 mmol) dissolved in a solvent (0.80 mL) was added to a flask containing **1** (6.2 mg, 4.0 mol %) and potassium *tert*-butoxide (0.013 mmol, 5.2 mol %). [b] Measured by HPLC equipped with a chiral column (Chiralcel OD, Daicel). [c] (*S*)-1-Phenylethanol (> 99% ee, 0.40 mL, 3.3 mmol) was added to a flask containing **1** (6.2 mg, 0.30 mol %) and potassium *tert*-butoxide (0.013 mmol, 0.40 mol %). [d] Toluene (0.80 mL) was mixed with vinyl acetate (0.38 mmol, 1.5 equiv).

DKR with *p*-chlorophenyl acetate, the reaction proceeds more slowly even with ten times more lipase (entry 7). This result clearly shows the advantage of isopropenyl acetate over *p*-chlorophenyl acetate as the acyl donor. Furthermore, the use of isopropenyl acetate makes the isolation of the acylated product much easier than with *p*-chlorophenyl acetate.^[9]

Our catalyst system was effective also for the DKR of other aromatic alcohols and aliphatic alcohols (Table 3): Substituent effects are insignificant in the DKR of aromatic alcohols while the DKR of aromatic alcohols is somewhat faster than that of aliphatic alcohols.

Table 3. Dynamic kinetic resolution of various alcohols.^[a]

Entry	Alcohol ^[b]	<i>t</i> [h]	Acetate ^[b]	ee [%]
1	1-(<i>p</i> -chlorophenyl)ethanol	48	94 %	> 99 ^[c]
2	1-(<i>p</i> -methoxyphenyl)ethanol	48	90 %	> 99 ^[c]
3	1-indanol	48	89 %	95.0 ^[d]
4	1-cyclohexylethanol	72	86 %	> 99 ^[e]
5	2-octanol	72	89 %	90.5 ^[e]

[a] The reactions were carried out with 1.00 mmol of an alcohol under the conditions of the entry 4 in Table 2. [b] Yields of isolated product. [c] By HPLC ((*R,R*) Whelk-01, Merck). [d] By HPLC after hydrolysis to 1-indanol (Chiralcel OD, Daicel). [e] By GC (Chiralcel B-PH, Alltech).

The observations recorded in Table 1 require a mechanism different from those involving simple hydrogen-transfer reactions for the catalytic racemization. In particular, the slow down of the racemization in acetone cannot be explained by the mechanisms involving ketones as hydrogen mediators. It is also notable that acetophenone was produced in only about 7% during the racemization in acetone. Thus, it is proposed that the racemization occurs during the reversible transformation between a ruthenium–alcohol complex (**2**) and a ruthenium–ketone complex (**3**; Scheme 2). The equilibrium would shift towards **2**, which exchanges alcohols rapidly at room temperature. The low yield of acetophenone

during the racemization in acetone is explained by the slow exchange of ketones in **3**. Meanwhile, it is not clear yet why the racemization is inhibited significantly during the DKR without sodium carbonate or molecular sieves. A possible cause for the inhibition is the formation of acetic acid from the reaction of the acetylated lipase and water during the DKR. In a separate experiment, we observed that the racemization of 1-phenylethanol was inhibited by the addition of acetic acid and then recovered slowly by the subsequent addition of sodium carbonate.^[10, 11]

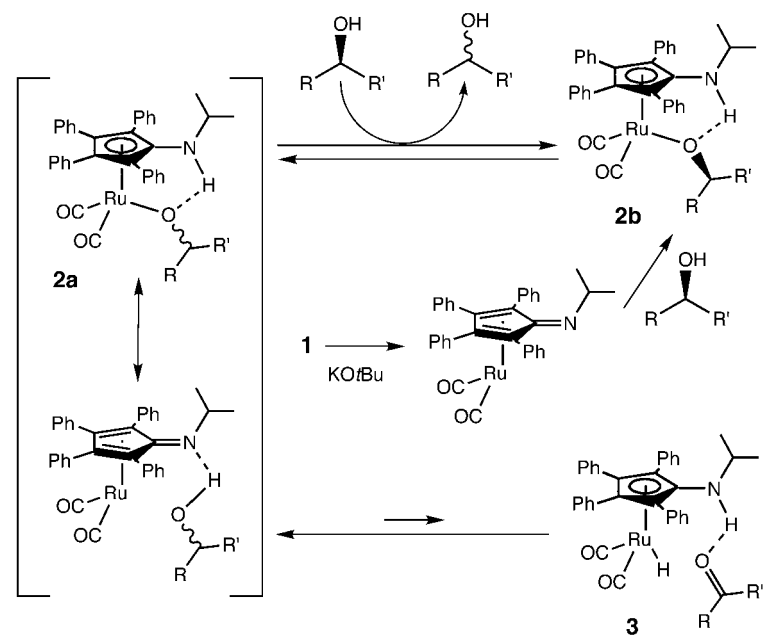
In summary, we have demonstrated highly efficient racemization and DKR of secondary alcohols by the use of a novel ruthenium catalyst compatible with enzymatic resolution. The new mode of our catalytic racemization allows the use of more reactive isopropenyl acetate as an acyl donor and thus much less lipase. Furthermore, the simple method for the preparation of the catalyst can be applied for the development of more practical catalysts.

Experimental Section

1: In a 100-mL flask equipped with a grease-free high-vacuum stopcock, [Ru₃(CO)₁₂] (1.0 g, 1.6 mmol) and the imine (1.0 g, 2.4 mmol) prepared from isopropylamine and 2,3,4,5-tetraphenylcyclopentadienone were dissolved in dry, degassed chloroform (30 mL).^[12] After the flask was filled with Ar and closed, the solution was stirred at 90 °C for 5 days. The reaction mixture was concentrated and purified by chromatography on a silica-gel column to give yellow solid **1** (691 mg, 47% yield). The solid was recrystallized from CH₂Cl₂/Et₂O. m.p. 197 °C (dec.); ¹H NMR (CDCl₃; 300 MHz): δ = 7.57–6.91 (m, 20H), 4.20 (d, *J* = 4.1 Hz, 1H), 3.3–3.23 (m, 1H), 0.86 ppm (d, *J* = 3.2 Hz, 6H); ¹³C NMR (CDCl₃; 75 MHz): δ = 198.4, 144.8, 133.7, 131.9, 130.6, 128.9, 128.7, 128.2, 127.7, 101.4, 81.7, 45.6, 25.2 ppm; IR (KBr, cm⁻¹): ν̄(CO) = 2017 (s), 1963 (s); MS (FAB, *m/z*): 619.6(M⁺); elemental analysis (%) calcd for C₃₄H₂₈NO₂ClRu: C 65.96, H 4.56, N 2.26; found: C 65.77, H 4.60, N 2.11.

Dynamic kinetic resolution of 1-phenylethanol: A solution of potassium *tert*-butoxide (1M in THF; 52 μL, 0.050 mmol) was added to a 50-mL flask equipped with a grease-free high-vacuum stopcock. The THF was removed under vacuum, and the flask was filled with argon. Then, **1** (24.8 mg, 0.04 mmol), Novozym 435 (2.8 mg; Novo Nordisk), Na₂CO₃ (104 mg, 1.00 mmol), a solution of 1-phenylethanol (120 μL, 1.00 mmol) in toluene (3.2 mL), and isopropenyl acetate (168 μL, 1.5 mmol) were added sequentially under argon. After being stirred at 25 °C for 30 h, the reaction mixture was concentrated and purified by chromatography on a silica-gel column (ethyl acetate/hexane 1:8) to give (*R*)-1-phenylethyl acetate (156 mg, 95% yield, >99% ee).

Received: February 14, 2002
Revised: April 22, 2002 [Z18712]



Scheme 2. Proposed mechanism for the catalytic racemization of secondary alcohols.

- [1] For recent reviews, see: a) R. Noyori, M. Tokunaga, K. Kitamura, *Bull. Chem. Soc. Jpn.* **1995**, 68, 36; b) R. S. Ward, *Tetrahedron: Asymmetry* **1995**, 6, 1475; c) S. Cad-dick, K. Jenkins, *Chem. Soc. Rev.* **1996**, 447; d) R. Stürmer, *Angew. Chem.* **1997**, 109, 1221; *Angew. Chem. Int. Ed. Engl.* **1997**, 36, 1173; e) U. T. Strauss, U. Felfer, K. Faber, *Tetrahedron: Asymmetry* **1999**, 10, 107; f) F. F. Huerta, A. B. E. Minidis, J.-E. Bäckvall, *Chem. Soc. Rev.* **2001**, 30, 321.
- [2] a) P. M. Dinh, J. A. Howarth, A. R. Hudnott, J. M. J. Williams, W. Harris, *Tetrahedron Lett.* **1996**, 37, 7623; b) A. L. E. Larsson, B. A. Persson, J.-E. Bäckvall, *Angew. Chem.* **1997**, 109, 1256; *Angew. Chem. Int. Ed. Engl.* **1997**, 36, 1211; c) B. A. Persson, A. L. E. Larsson, M. L. Ray,

- J.-E. Bäckvall, *J. Am. Chem. Soc.* **1999**, *121*, 1645; d) B. A. Persson, F. F. Huerta, J.-E. Bäckvall, *J. Org. Chem.* **1999**, *64*, 5237; e) F. F. Huerta, Y. R. S. Laxmi, J.-E. Bäckvall, *Org. Lett.* **2000**, *2*, 1037; f) F. F. Huerta, J.-E. Bäckvall, *Org. Lett.* **2001**, *3*, 1209; g) J. H. Koh, H. M. Jeong, M.-J. Kim, J. Park, *Tetrahedron Lett.* **1999**, *40*, 6281; h) H. M. Jeong, J. H. Koh, M.-J. Kim, J. Park, *Org. Lett.* **2000**, *2*, 2487; i) H. M. Jeong, J. H. Koh, M.-J. Kim, J. Park, *Org. Lett.* **2000**, *2*, 409; j) M.-J. Kim, D. Lee, E. A. Huh, H. M. Jeong, J. H. Koh, J. Park, *Org. Lett.* **2000**, *2*, 2377; k) M.-J. Kim, Y. K. Choi, M. Y. Choi, M. J. Kim, J. Park, *J. Org. Chem.* **2001**, *66*, 4736.
- [3] In reference [2g], we have reported an exceptional case that does not require hydrogen mediators. However, oxygen, a base, and high reaction temperature were necessary to generate catalytic species.
- [4] In references [2h] and [2i], we have described the use of alkenyl acetates as substrates and acyl donors in the presence of proper hydrogen donors.
- [5] For a review about racemization, see: E. J. Ebbens, G. J. A. Ariaans, J. P. M. Houbiers, A. Braggink, B. Zwanenburg, *Tetrahedron* **1997**, *53*, 9417.
- [6] We have found a catalyst system for the racemization of secondary alcohols at room temperature without the aid of hydrogen mediators. However, the catalyst system requires strong bases, and is not compatible with enzymatic acylation: J. H. Koh, H. M. Jeong, J. Park, *Tetrahedron Lett.* **1998**, *39*, 5544.
- [7] Crystal data for **1**: $C_{34}H_{28}ClNO_2Ru$. $M_r = 619.09$ g mol⁻¹. Orange crystal: size $0.50 \times 0.20 \times 0.20$ mm³, orthorhombic, $a = 20.1560(13)$, $b = 13.2405(9)$, $c = 21.1819(14)$ Å, $\alpha = 90^\circ$, $\beta = 90^\circ$, $\gamma = 90^\circ$, space group *Pbca*, $V = 5652.9(6)$ Å³, $Z = 8$, $T = 223(2)$ K, $\rho_{\text{calcd}} = 1.455$ g cm⁻³, absorption coefficient = 0.681 mm⁻¹. Siemens SMART diffractometer, $\lambda = 0.71073$ Å, scan mode- ω (ω -scan width: 1.92 to 23.33°). 22982 reflections were measured, giving 4077 unique data with $I > 2\sigma(I)$. $R = 0.0252$, $R_w = 0.0592$, GOF = 1.004. CCDC-179224 (**1**) contains the supplementary crystallographic data for this paper. These data can be obtained free of charge via www.ccdc.cam.ac.uk/conts/retrieving.html (or from the Cambridge Crystallographic Data Centre, 12, Union Road, Cambridge CB2 1EZ, UK; fax: (+44) 1223-336-033; or deposit @ccdc.cam.ac.uk).
- [8] For examples of activating catalyst precursors by treatment with proper bases, see: K.-J. Haack, S. Hashiguchi, A. Fujii, T. Ikariya, R. Noyori, *Angew. Chem.* **1997**, *109*, 297; *Angew. Chem. Int. Ed. Engl.* **1997**, *36*, 285, and references therein.
- [9] The separation of the product from unreacted *p*-chlorophenyl acetate is difficult in some cases.^[2c]
- [10] When 5 mol % of acetic acid was added to the mixture given in entry 1 in Table 1, the optical purity of 1-phenylethanol changed only to 69.0% *ee* in 30 min. However, the racemization was completed in 5 h by the subsequent addition of sodium carbonate (1 equiv).
- [11] A related complex, $[(2,5\text{-Ph}_2\text{-3,4-tol}_2(\eta^5\text{-C}_4\text{COH}))Ru(CO)_2\text{-(O}_2\text{CCF}_3)]$, is formed in the reaction of $[(2,5\text{-Ph}_2\text{-3,4-tol}_2(\eta^5\text{-C}_4\text{CO}))Ru(CO)_2]$ and trifluoroacetic acid: C. P. Casey, S. W. Singer, D. R. Powell, R. K. Hayashi, M. Kavana, *J. Am. Chem. Soc.* **2001**, *123*, 1090.
- [12] The imine was prepared in 90% yield according to the procedure described by W. Dai, R. Strinivasan, J. A. Katzenellenbogen, *J. Org. Chem.* **1989**, *54*, 2204. Physical properties of the imine: m.p.: 223°C ; ¹H NMR (CDCl₃): $\delta = 7.25\text{--}6.75$ (m, 20H), $4.08\text{--}4.00$ (m, 1H), 1.04 ppm (d, $J = 3$ Hz, 6H); ¹³C NMR (CDCl₃): $\delta = 165.8, 137.6, 131.9, 130.2, 129.8, 128.2, 127.8, 127.4, 127.2, 127.1, 126.5, 52.3, 24.6$ ppm; MS (FAB, m/z): 425.27 (M^+); elemental analysis (%) calcd for C₃₂H₂₇N: C 90.31, H 6.39, N 3.29; found: C 90.26, H 6.62, N 3.14.

Chiral Epoxides by Desymmetrizing Deprotonation of *meso*-Epoxides**


David M. Hodgson* and Emmanuel Gras

Epoxides are widely utilized as versatile synthetic intermediates, and the epoxide functional group is also found in a number of interesting natural products.^[1] Therefore, the development of efficient (especially asymmetric) methods for the elaboration of epoxides is an important ongoing challenge.^[2] In contrast to chemistry exploiting the electrophilic nature of epoxides, the utility of epoxides as nucleophiles (via oxiranyl anions, eg **1**-Li), first studied by Eisch and Galle,^[3] is less developed.^[4] A current requirement with this latter strategy is that the epoxide must possess an activating substituent (electron-withdrawing, trialkylsilyl, or trialkylstannyl group) attached to the epoxide ring. Electron-withdrawing and trialkylsilyl substituents facilitate the formation of oxiranyl anions by promoting deprotonation (usually lithiation) and prolonging the solution lifetime of these otherwise very labile intermediates. Trialkylstannyl- and sulfinyl-substituted epoxides react with organolithium species (by transmetalation and desulfinylation, respectively) rapidly enough at low temperatures, such that the resultant unstabilized oxiranyl anions can exhibit synthetically useful nucleophilic (rather than carbene-type) reactivity with a range of electrophiles.^[5] Such reactions demonstrate the value of oxiranyl-lithium species as important intermediates in the elaboration of epoxides, but they also indicate the potential limitation of requiring an activated epoxide precursor to carry out the chemistry.

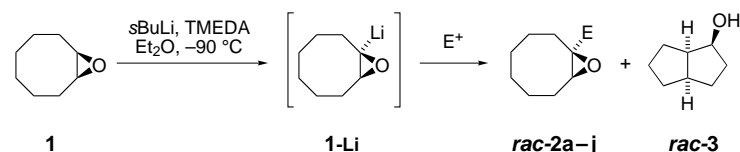
Recently, we showed that direct lithiation of terminal epoxides, followed by electrophile trapping of the nonstabilized oxiranyl anion intermediates, was possible in the presence of a diamine ligand.^[6] However, the reaction was restricted to silylation (with TMSCl; TMS = trimethylsilyl) present during generation of the oxiranyl anion) and deuteration (MeOD as an external electrophile). Here we report the first examples of unactivated epoxides undergoing direct deprotonation to give destabilized (alkyl-substituted) oxiranyl anions, and their subsequent trapping with a range of electrophiles (including C–C-bond formation). Furthermore, a new enantioselective approach to substituted epoxides is demonstrated: symmetry breaking by asymmetric lithiation^[7, 8]—electrophile trapping, at an epoxide functionality fused to eight- and seven-membered rings.

[*] Dr. D. M. Hodgson, Dr. E. Gras
Dyson Perrins Laboratory
University of Oxford
South Parks Road, Oxford, OX1 3QY (UK)
Fax: (+44) 1865-275-674
E-mail: david.hodgson@chem.ox.ac.uk

[**] This work was supported by the Engineering and Physical Sciences Research Council (EPSRC) in the U.K. and by a Marie Curie Fellowship of the European Community (program TMR under contract number HPMF-CT-2000-00558). We also thank the EPSRC National Mass Spectrometry Service Centre for mass spectra, and I. D. Cameron for preliminary observations.

 Supporting information for this article is available on the WWW under <http://www.angewandte.org> or from the author.

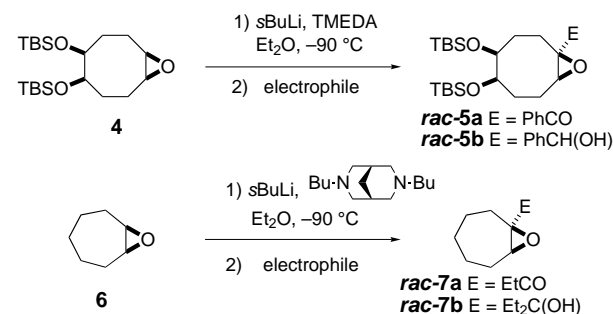
We first sought conditions for the efficient lithiation–deuterium (D) trapping of cyclooctene oxide (**1**; Scheme 1). As previously observed,^[8c] in the absence of a diamine, the



Scheme 1. Lithiation–electrophile trapping of cyclooctene oxide (**1**). a) E = D, 98 % (using CD₃OD); b) E = PhCH(OH) (*d.r.* 1:1^[9]) 80 % (using PhCHO); c) E = PhCO, 56 % (using PhCONMe₂); d) E = EtCH(OH), 48 % (using EtCHO); e) E = Et₂C(OH), 60 % (using Et₂CO); f) E = EtCO, 45 % (using EtCONMe₂); g) E = EtOCO, 40 % (using EtOCOCl, 10 equiv); h) E = Bu₃Sn, 56 % (using Bu₃SnCl); i) E = Me₃Si, 38 % (using Me₃SiCl in situ), 60 % (using Me₃SiCl in situ and 3,7-dibutyl-3,7-diazabicyclo[3.3.1]nonane (DBB)^[10] as ligand); j) E = Me, 60 % (using MeI).

deprotonation of **1** by sBuLi (2.45 equiv) in Et₂O at –90 °C proceeded sluggishly. A reaction time of 1 h, followed by addition of CD₃OD, gave unreacted starting epoxide **1** (56 %), *rac*-**2a** (24 %), and the bicyclic alcohol *rac*-**3** (12 %). Thus, one third of the intermediate oxiranyl-lithium species **1-Li** had already undergone decomposition (by transannular C–H insertion)^[8] under these conditions; this decomposition is an indication of its lability (in the absence of a diamine). However, reaction under otherwise identical conditions, but in the presence of *N,N,N',N'*-tetramethylethylenediamine (TMEDA; 2.5 equiv) resulted in complete reaction of epoxide **1** to give *rac*-**2a** (78 %), along with only 5 % of the bicyclic alcohol *rac*-**3**. Thus, the added ligand appears to both accelerate deprotonation and reduce the rate of decomposition of the oxiranyl anion. Reducing the excess of base used in the deprotonation was obviously desirable, and using sBuLi (1.25 equiv) and TMEDA (1.3 equiv) gave 98 % D incorporation in cyclooctene oxide **1** after 3 h, with no byproducts. This encouraging result led us to examine the reaction of **1-Li**, generated under these conditions, with other electrophiles. Significantly, introduction of a wide array of functionality at an unactivated epoxide carbon atom was found to be possible (Scheme 1).

A preliminary examination of lithiation–electrophile trapping with other epoxides was then undertaken. The methodology was successfully extended to a substituted cyclooctene-oxide substrate **4**^[11] leading to *rac*-**5a** (84 %) and *rac*-**5b** (85 %; Scheme 2). Using DBB as the ligand, the reaction



Scheme 2. Synthesis of substituted cyclooctene and cycloheptene oxides (**4** and **6**).

involving cycloheptene oxide (**6**) yielded the corresponding functionalized epoxides *rac*-**7a** (54 %) and *rac*-**7b** (52 %; Scheme 2).

However, attempted lithiation–deuteration of cyclohexene oxide and cyclopentene oxide with either TMEDA or DBB as the ligand was unsuccessful (the presumed intermediate oxiranyl-lithium species underwent typical carbenoid rearrangements and reductive alkylation).^[12] Electrophile trapping of the oxiranyl anion from an acyclic system was studied using *cis*-5-decene oxide, and (with DBB as the ligand) complete deuteration and partial silylation (using TMSCl in situ) were successful, albeit in low yields (30 % and 18 %, respectively).

As previous studies carried out in this laboratory have shown that the use of a chiral, nonracemic diamine (such as (–)-sparteine)^[7] allows asymmetric deprotonation–rearrangement of epoxides,^[8, 11] we explored enantioselective epoxide functionalization. Using (–)-sparteine as the ligand resulted in electrophile incorporation, in good yields and *ee* values (Table 1). As observed during the asymmetric rearrangements of epoxides,^[8, 11] better *ee* values were achieved when *i*PrLi was used instead of sBuLi (Table 1, entries 4 and 5).

While many powerful methods have been developed for the asymmetric desymmetrization of *meso*-epoxides,^[13] the present work illustrates a different approach, in which a chemical transformation occurs selectively at one of the enantiotopic epoxide termini, but the useful epoxide functional group is retained in the product, resulting in a new method for chiral

Table 1. Enantioselective electrophile trapping—symmetry breaking of *meso*-epoxides.^[a]

Entry	<i>n</i>	R	E	Yield [%]	<i>ee</i> value [%] ^[b]
1	1	H	TMS	72	74
2	1	H	SnBu ₃	60	79 ^[c]
3	1	H	PhCH(OH)	80	76 ^[d]
4	1	H	PhCO	68 (77) ^[e]	77 (86) ^[e]
5	1	H	Et ₂ C(OH)	75 (63) ^[e]	77 (86) ^[e]
6	1	H	EtCH(OH)	74	76 ^[f]
7	1	H	EtCO	67	78
8	1	H	EtOCO	58	81
9	1	OTBS	PhCH(OH)	79	77 ^[d,g]
10	1	OTBS	PhCO	84	74 ^[g]
11	0	H	Et ₂ C(OH)	48	73
12	0	H	EtCO	57	74

[a] Absolute configuration of predominant enantiomer [as shown in Equation (1)] is assigned by analogy with the known sense of asymmetric induction in the deprotonation–rearrangement of the *meso*-epoxides with (–)-sparteine.^[8, 11] [b] Determined by chiral GC (Chrompack-CP-Chiralsil-DEX-CB column) unless otherwise indicated. [c] Determined after reaction with *n*BuLi and trapping with 3-pentanone.^[5a] [d] Determined after MnO₂ oxidation. [e] *i*PrLi was used instead of sBuLi. [f] Determined after Dess–Martin oxidation. [g] Determined by chiral HPLC (Daicel Chiralpak OD column).

epoxide synthesis. A study of other ligands to expand the scope of the process and enhance asymmetric induction, as well as synthetic applications, is currently underway.

Experimental Section

Typical procedure for lithiation–electrophile trapping of cyclooctene oxide (**1**) in the presence of a diamine:

The diamine (2.6 mmol) was added dropwise to a solution of RLi (1.4 M, 2.5 mmol) in Et₂O (8 mL) at –90 °C. This mixture was stirred for 1 h at –90 °C. A solution of cyclooctene oxide (**1**; 2.0 mmol) in Et₂O (2 mL), precooled to –90 °C, was then added rapidly by cannula to the solution of ligand/RLi and the reaction mixture was then stirred at –90 °C for 3 h. Neat electrophile (3.0 mmol) was added dropwise, and the mixture was then allowed to warm to room temperature over 5 h. After quenching with aqueous H₃PO₄ (0.5 M, 25 mL), the organic phase was washed with saturated aqueous NaHCO₃ (25 mL) and brine (25 mL). The aqueous layers were extracted twice with Et₂O (25 mL) and the combined organic phases were dried (MgSO₄) and evaporated under reduced pressure. Purification of the residue by column chromatography (SiO₂, Et₂O, petrol) gave the substituted epoxide.

Received: March 4, 2002 [Z18822]

- [1] I. Erden in *Comprehensive Heterocyclic Chemistry II*, Vol. 1A (Eds.: A. R. Katritzky, C. W. Rees, E. F. V. Scriven), Pergamon, Oxford, **1996**, pp. 97–171.
- [2] a) R. A. Johnson, K. B. Sharpless in *Catalytic Asymmetric Synthesis*, 2nd ed. (Ed.: I. Ojima), Wiley-VCH, New York, **2000**, pp. 231–285; b) T. Katsuki in *Catalytic Asymmetric Synthesis*, 2nd ed. (Ed.: I. Ojima), Wiley-VCH, New York, **2000**, pp. 287–325; c) E. N. Jacobsen, M. H. Wu in *Comprehensive Asymmetric Catalysis* (Eds.: E. N. Jacobsen, A. Pfaltz, H. Yamamoto), Springer, Berlin, **1999**, pp. 649–677.
- [3] J. J. Eisch, J. E. Galle, *J. Am. Chem. Soc.* **1976**, *98*, 4646–4648.
- [4] a) T. Satoh, *Chem. Rev.* **1996**, *96*, 3303–3325; b) Y. Mori, *Rev. Heteroat. Chem.* **1997**, *17*, 183–210.
- [5] a) P. Lohse, H. Loner, P. Acklin, F. Sternfeld, A. Pfaltz, *Tetrahedron Lett.* **1991**, *32*, 615–618; b) T. Satoh, S. Kobayashi, S. Nakanishi, K. Horiguchi, S. Irisa, *Tetrahedron* **1999**, *55*, 2515–2528.
- [6] D. M. Hodgson, S. L. M. Norsikian, *Org. Lett.* **2001**, *3*, 461–463.
- [7] a) D. Hoppe, T. Hense, *Angew. Chem.* **1997**, *109*, 2376–2410; *Angew. Chem. Int. Ed. Engl.* **1997**, *36*, 2282–2316; b) P. Beak, A. Basu, D. J. Gallagher, Y. S. Park, S. Thayumanavan, *Acc. Chem. Res.* **1996**, *29*, 552–560.
- [8] a) D. M. Hodgson, G. P. Lee, *Chem. Commun.* **1996**, 1015–1016; b) D. M. Hodgson, G. P. Lee, *Tetrahedron: Asymmetry* **1997**, *8*, 2302–2306; c) D. M. Hodgson, G. P. Lee, R. E. Marriott, A. J. Thompson, R. Wisedale, J. Witherington, *J. Chem. Soc. Perkin Trans. 1* **1998**, 2151–2161; d) D. M. Hodgson, L. A. Robinson, *Chem. Commun.* **1999**, 309–310; e) D. M. Hodgson, C. R. Maxwell, I. R. Matthews, *Tetrahedron: Asymmetry* **1999**, *10*, 1847–1850; f) D. M. Hodgson, L. A. Robinson, M. L. Jones, *Tetrahedron Lett.* **1999**, *40*, 8637–8640.
- [9] G. A. Molander, K. Mautner, *J. Org. Chem.* **1989**, *54*, 4042–4050.
- [10] K. M. Bertini Gross, Y. M. Jun, P. Beak, *J. Org. Chem.* **1997**, *62*, 7679–7689.
- [11] a) D. M. Hodgson, I. D. Cameron, *Org. Lett.* **2001**, *3*, 441–444; b) D. M. Hodgson, I. D. Cameron, M. Christlieb, R. Green, G. P. Lee, L. A. Robinson, *J. Chem. Soc. Perkin Trans. 1* **2001**, 2161–2174.
- [12] a) J. K. Crandall, M. Apparu, *Org. React. (N. Y.)* **1983**, *29*, 345–443; b) E. Doris, L. Dechoux, C. Mioskowski, *Synlett* **1998**, 337–343.
- [13] For selected reviews and recent contributions, see: a) D. M. Hodgson, A. R. Gibbs, G. P. Lee, *Tetrahedron* **1996**, *52*, 14361–14384; b) E. N. Jacobsen, *Acc. Chem. Res.* **2000**, *33*, 421–431; c) S. Matsunaga, J. Das, J. Roels, E. M. Vogl, N. Yamamoto, T. Iida, K. Yamaguchi, M. Shibasaki, *J. Am. Chem. Soc.* **2000**, *122*, 2252–2260; d) M. J. Södergren, S. K. Bertilsson, P. G. Andersson, *J. Am. Chem. Soc.* **2000**, *122*, 6610–6618; e) W. A. Nugent, *J. Am. Chem. Soc.* **1998**, *120*, 7139–7140; f) S. E. Denmark, P. A. Barsanti, K.-T. Wong, R. A. Stavenger, *J. Org. Chem.* **1998**, *63*, 2428–2429.

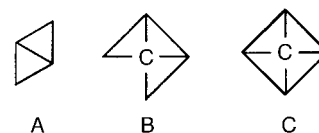
Synthesis and Structural Characterization of Organometallic Cyclines: Novel Nanoscale, Carbon-Rich Topologies**

Matthew Laskoski, Winfried Steffen,
Jason G. M. Morton, Mark D. Smith, and
Uwe H. F. Bunz*

Dedicated to Professor Günther E. Szeimies

“Carbon-rich” defines an exciting area that spans the world of large arenes to that of highly alkynylated structures including carbon wires, peralkynylated π perimeters, graphdiyne segments, dehydroannulenes, and cyclophane derivatives.^[1–9] Carbon-rich organometallic compounds are less explored than their organic counterparts, a tribute to the considerably increased effort in their synthetic access.^[10–14] Aesthetic structures, exciting topologies on the nanometer scale, and their modular synthesis, however, make carbon-rich organometallic compounds attractive. Rewards are expected in materials properties that differ from their organic counterparts, such as electroactivity and potential nonlinear optics (NLO) activity. In addition, large carbon-rich organometallic molecules are often surprisingly soluble and form single crystals, which allows their structural characterization in the solid state,^[13] a feature that is often elusive for their organic counterparts.

Herein we report the synthesis and structural characterization of three novel organometallic cyclines^[10] with an expanded bicyclo[1.1.0]butane (**A**) and a [2.1.0.0^{1,3}]pentane (**B**) topology. In these structures, the C–C single bonds of the



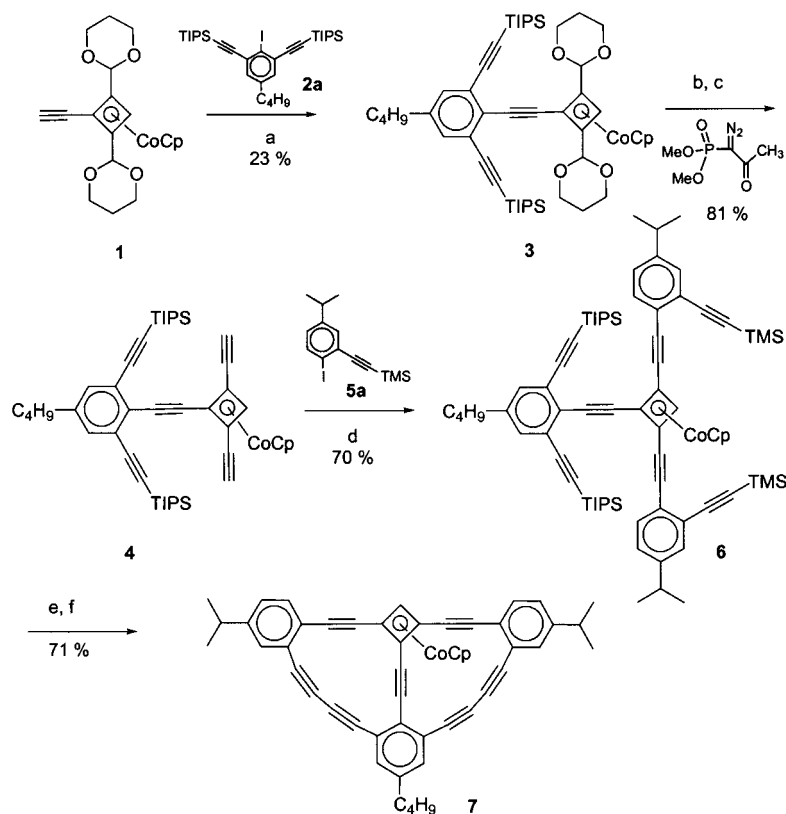
small rings are replaced by alkyne or butadiyne bridges, while the carbon atoms are substituted by benzene rings, cyclobutadiene(cyclopentadienylcobalt) units, or ferrocene centers. Key steps in the synthesis of these targets are the selective *ortho*-metalation of organometallic acetals,^[14] and the conversion of aldehydes into alkynes by the Ohira method.^[15]

Pd-catalyzed coupling of **1**^[14] to the iodide **2a** furnishes **3** in 23 % (Scheme 1). The moderate yield of **3** is a result of the two *meta*-positioned alkyne groups in **2a** between which the iodide is sandwiched. Only the active Hartwig catalyst

[*] Prof. Dr. U. H. F. Bunz, M. Laskoski, W. Steffen, J. G. M. Morton, Dr. M. D. Smith
Department of Chemistry and Biochemistry
The University of South Carolina
Columbia, SC 29208 (USA)
Fax: (+1) 803-777-929-0267
E-mail: bunz@mail.chem.sc.edu

[**] We thank the National Science Foundation for generous support (CAREER award; CHE 99-81765).

Supporting information for this article is available on the WWW under <http://www.angewandte.org> or from the author.



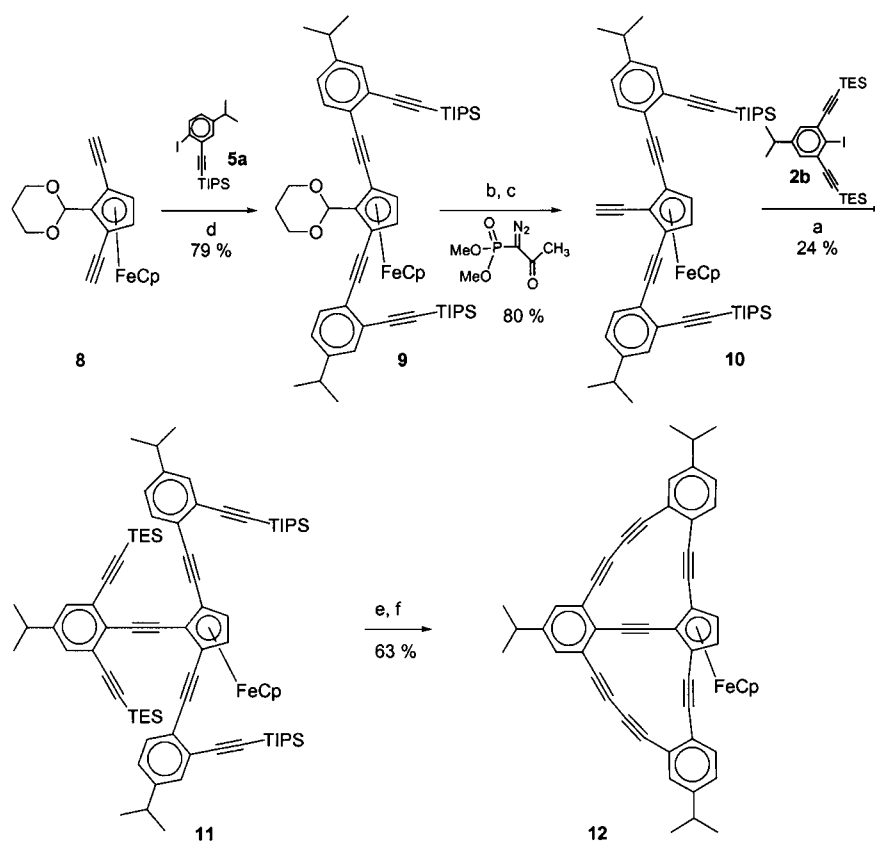
Scheme 1. a) $[\text{Pd}\{\text{P}(o\text{-tolyl})_3\}_2]$, CuI , NEt_3 , THF, 24°C , 12 h; b) p -toluenesulfonic acid, THF, 24°C , 12 h; c) K_2CO_3 , 24°C , 8 h; d) $[\text{Pd}(\text{PPh}_3)_2\text{Cl}_2]$, CuI , piperidine, THF, 24°C , 12 h; e) Bu_4NF , THF, 24°C , 1 h; f) $\text{Cu}(\text{OAc})_2$, CH_3CN , 80°C , 8 h.

$[\text{Pd}\{\text{P}(o\text{-tolyl})_3\}_2]$ ^[14b] with THF as cosolvent^[16] is capable of coupling **1** to **2a**. The coupling product **3** was deketalized and treated with the Ohira–Seyferth reagent $\text{CH}_3\text{C}\equiv\text{OCN}_2\text{P}=\text{O}(\text{OMe})_2$ ^[15] to give the pentayne **4** in 81% yield. Coupling of **4** to **5** furnishes **6** in 70% yield. Desilylation of **6** proceeds with Bu_4NF in THF; the intermediate heptyne was immediately utilized for the coupling step to close the two cyclyne rings to form **7** in 71% yield. The six-step synthesis (**1** \rightarrow **7**) occurs in a respectable overall yield of 9%.

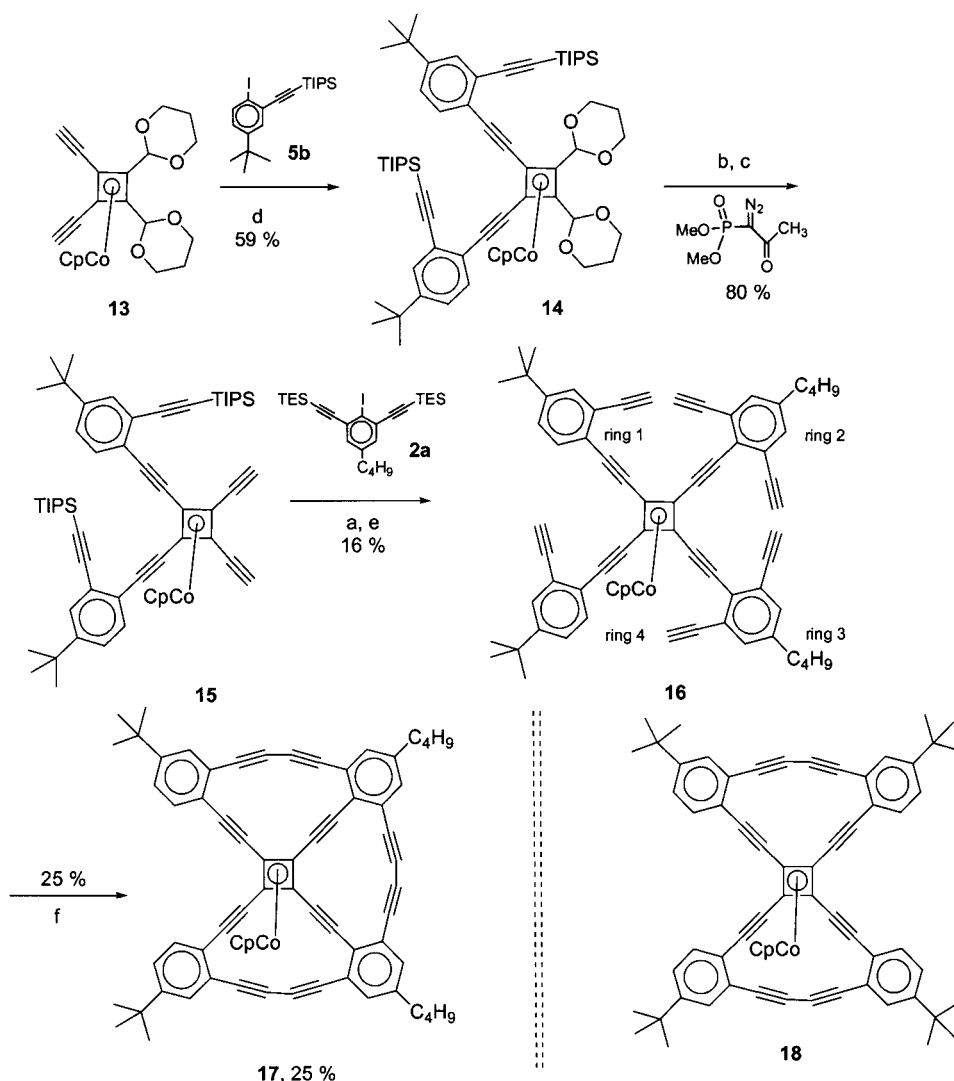
The ferrocene-containing “super-bicyclo[1.1.0]butane” (**12**) was targeted to show the general applicability of the method. Diyne **8** was treated with **5a** under Pd catalysis (Scheme 2) to furnish **9** in 79% yield. Deketalization with *para*-toluenesulfonic acid (TsOH) followed by Ohira alkynylation^[15] transforms **9** into the pentayne **10** in 80%. The critical step is the Pd-catalyzed coupling of **10** to **2b** that furnishes **11** in 24%. The yield of the coupling reaction is only moderate, again as a result of the decreased reactivity the

iodide **2b** experiences as a consequence of being positioned between two alkyne substituents. Deprotection of **11** and a double cyclization using $\text{Cu}(\text{OAc})_2$ in acetonitrile^[15c] gives **12** in 61% yield as stable, dark-red needles.

It was of interest if a “super-tricyclic” structure analogous to **B** was accessible by this method. A retrosynthetic analysis suggests **13** as the starting point for **17** (Scheme 3). Pd-catalyzed coupling of **13** to **5b** gave **14** in 59% yield. Deprotection by TsOH and conversion of the two aldehyde groups into alkyne units proceeded under standard conditions^[15] to give **15** in 80%. The critical step is the double Pd-catalyzed coupling of **15** to **2a** that provided **16** in 17% yield after deprotection with Bu_4NF in THF. The last step in the reaction sequence is the triple ring closure to give **17**, which proceeds in 25% yield. Significant amounts of insoluble and infusible tan-colored solids are formed as by-products. The relatively low yield of this transformation is a consequence of the underlying statistics of the ring-closing reaction. If the alkynes of benzene rings 1 and 4 in **16** couple, **17** cannot form. Instead cross-linking to form insoluble materials prevails. If the ring-closing reaction proceeds statistically, it is expected that 33% of **16** will be lost to the unwanted cyclizations, hence, the highest possible reaction yield is 67%. The actual yield of 25% suggests that each ring forms



Scheme 2. For reactants and conditions see Scheme 1.



Scheme 3. For reactants and conditions see Scheme 1.

in a satisfactory yield of 72%, if the unproductive coupling pathways are corrected for by a simple statistical analysis.

The novel and intriguing structures of the organometallic super-bicyclo[1.1.0]butanes **7** and **12** as well as the super-tricyclo[2.1.0.0^{1,3}]pentane **17** mandated their single-crystal structure analysis.^[17–19] Suitable, coffin-shaped specimens were obtained from mixtures of dichloromethane and hexanes.

ORTEP representations of **7**, **12**, and **17**, and the packing diagram of **12** are shown in Figures 1–3. The bond lengths and bond angles in **7**, **12**, and **17** are in excellent agreement with the reported values for alkynylated cyclobutadiene and cyclopentadienyl complexes.^[13, 20]

The polyne **7** forms a perfect half-wheel. The three radial alkyne units attached to the cyclobutadiene complex are linear. The butadiyne groupings are moderately bent to accommodate the topological requirements of the structure (Figure 1). The substituents (i.e., spokes and periphery of the large hydrocarbon ligand) on the cyclobutadiene complex are considerably less nonplanar than expected for multiply ethynylated complexes of this type.^[13, 20] This effect may be a consequence of the direct interconnection of the three alkyne substituents by a network of cyclyne rings.

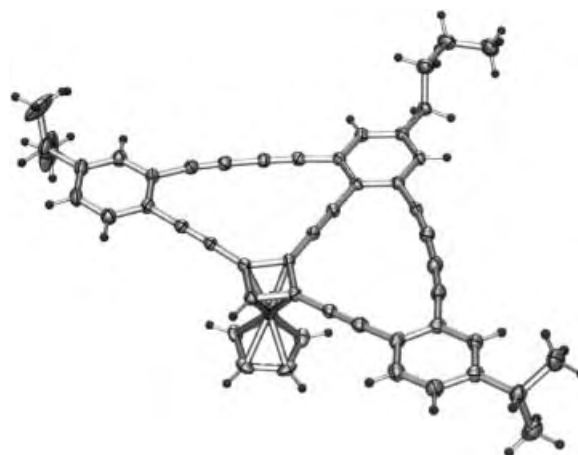


Figure 1. ORTEP representation of the molecular structure of **7**.

tained from dichloromethane/hexane mixtures and an ORTEP representation of **17** is shown in Figure 3a. The molecules of **17** are disordered in the crystal, but the large hydrocarbon ligand is visibly flattened out (Figure 3b)

The ferrocene-based cyclyne **12** (Figure 2) shows considerable in-plane bending of the outer two of the three radial alkyne units, which leads to a slight ruffling of the large hydrocarbon ligand (Figure 2a), similar to that observed in some porphyrins.^[21] This ruffling is caused by the minor mismatch of the circumference of the perimeter compared to the size of the radial spokes, and bears testimony to the way the outer π perimeter adapts to the decreased bond angles (72°) prevalent in the ferrocene module relative to the square cyclobutadiene complexes. The packing of **12** is remarkable and shown in Figure 2b. Six molecules of **12** form a circular arrangement that results in a helical superstructure not observed in the packing of **7**.

The structures of the open congeners of **17** and of the butterfly **18** have been described recently.^[13] In these species the alkyne bridges are bent away from the cyclobutadiene nucleus to accommodate for the electronic influence of the {CpCo} fragment. It was of interest whether the same distortion was visible in the polyne **17**. A suitable specimen was ob-

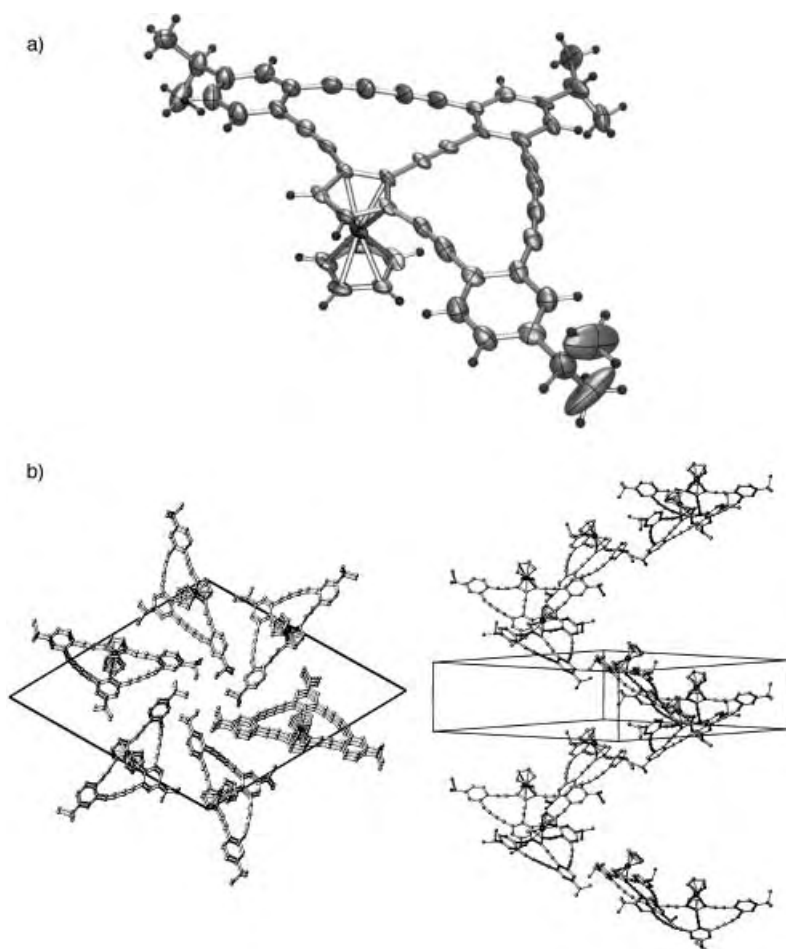


Figure 2. a) ORTEP representation of **12**. b) Packing diagram of **12**. The sixfold axis in which the single molecules of **12** are packed in the solid state is visible.

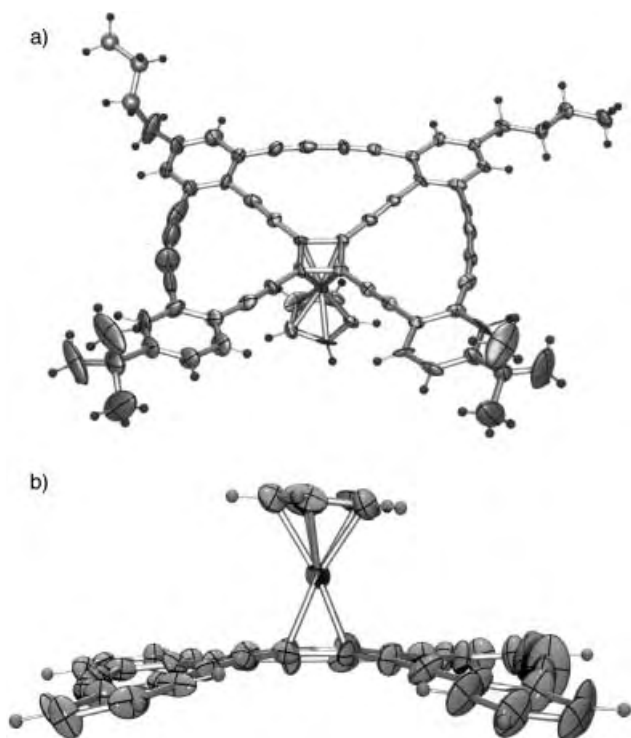


Figure 3. a) ORTEP representation of **17**. b) Side-view ORTEP representation of **17**. Substituents are removed for clarity.

compared to the structure of the butterfly-shaped **18**.^[13] The flattening is particularly pronounced in the back-side of the large ligand, where the third ring is closed. The full wheel with the topology **C** is expected to be planar, as a result of the geometric relationship of the perimeter to the length of the radial spokes.

In conclusion, a series of novel polycyclic carbon-rich organometallic compounds (**7**, **12**, and **17**) has been prepared by a combination of Ohira alkynylations, Pd/Cu-catalyzed couplings, and Cu(OAc)₂-mediated cyclizations. They represent nanoscale versions of **A** and **B**; they have been subjected to single-crystal structure determination and show subtle differences in their structures depending upon the central organometallic core. We will report on the synthesis and characterization of a full wheel with a nanoscale topology of the unknown fenestrane type **C** structure in the future.^[22, 23]

Received: February 20, 2002 [Z18746]

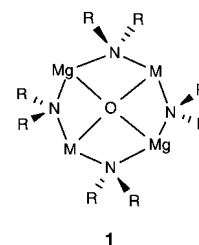
- [1] M. D. Watson, A. Fechtenkötter, K. Müllen, *Chem. Rev.* **2001**, *101*, 1267; A. J. Berresheim, M. Müller, K. Müllen, *Chem. Rev.* **1999**, *99*, 1747; S. Ito, P. T. Herwig, T. Böhme, J. P. Rabe, W. Rettig, K. Müllen, *J. Am. Chem. Soc.* **2000**, *122*, 7698; F. Dötz, J. D. Brand, S. Ito, L. Gherghel, K. Müllen, *J. Am. Chem. Soc.* **2000**, *122*, 7707; T. Weil, U. M. Wiesler, A. Herrmann, R. Bauer, J. Hofkens, F. C. De Schryver, K. Müllen, *J. Am. Chem. Soc.* **2001**, *123*, 8101.
- [2] R. Diercks, J. C. Armstrong, R. Boese, K. P. C. Vollhardt, *Angew. Chem.* **1986**, *98*, 270; *Angew. Chem. Int. Ed. Engl.* **1986**, *25*, 268; P. I. Dosa, C. Erben, V. S. Iyer, K. P. C. Vollhardt, I. M. Wasser, *J. Am. Chem. Soc.* **1999**, *121*, 10430; R. Boese, A. J. Matzger, K. P. C. Vollhardt, *J. Am. Chem. Soc.* **1997**, *119*, 2052.
- [3] R. Dembinski, T. Bartik, B. Bartik, M. Jaeger, J. A. Gladysz, *J. Am. Chem. Soc.* **2000**, *122*, 810.
- [4] C. Kosinski, A. Hirsch, F. W. Heinemann, F. Hampel, *Eur. J. Org. Chem.* **2001**, 3879; B. Leibrock, O. Vostrowsky, A. Hirsch, *Eur. J. Org. Chem.* **2001**, 4401; G. Schermann, T. Grösser, F. Hampel, A. Hirsch, *Chem. Eur. J.* **1997**, *3*, 1105.
- [5] Y. Rubin, T. C. Parker, S. J. Pastor, S. Jalisatgi, C. Boule, C. L. Wilkins, *Angew. Chem.* **1998**, *110*, 1353; *Angew. Chem. Int. Ed.* **1998**, *37*, 1226; N. Jux, K. Holczer, Y. Rubin, *Angew. Chem.* **1996**, *108*, 2031; *Angew. Chem. Int. Ed. Engl.* **1996**, *35*, 1986.
- [6] For an excellent review, see M. M. Haley, J. J. Pak, S. C. Brand, *Top. Curr. Chem.* **1999**, *201*, 82; W. B. Wan, S. C. Brand, J. J. Pak, M. M. Haley, *Chem. Eur. J.* **2000**, *6*, 2044; M. M. Haley, S. C. Brand, J. J. Pak, *Angew. Chem.* **1997**, *109*, 864; *Angew. Chem. Int. Ed. Engl.* **1997**, *36*, 836; J. J. Pak, T. J. R. Weakley, M. M. Haley, *Organometallics* **1997**, *16*, 4505.
- [7] F. Diederich, *Nature* **1994**, *369*, 199; F. Diederich, Y. Rubin, *Angew. Chem.* **1992**, *104*, 1123; *Angew. Chem. Int. Ed. Engl.* **1992**, *31*, 1101; J. D. Tovar, N. Jux, T. Jarrosson, S. I. Khan, Y. Rubin, *J. Org. Chem.* **1997**, *62*, 3432.
- [8] G. J. Palmer, S. R. Parkin, J. E. Anthony, *Angew. Chem.* **2001**, *113*, 2577; *Angew. Chem. Int. Ed.* **2001**, *40*, 2509.
- [9] Y. Tobe, K. Kubota, K. Naemura, *J. Org. Chem.* **1997**, *62*, 3430.
- [10] For an example of an organometallic cyclyne, see J. D. Bradshaw, L. Guo, C. A. Tessier, W. J. Youngs, *Organometallics* **1996**, *15*, 2582.
- [11] G. Scholz, R. Gleiter, F. Rominger, *Angew. Chem.* **2001**, *113*, 2559; *Angew. Chem. Int. Ed.* **2001**, *40*, 2477.

- [12] U. H. F. Bunz, *Top. Curr. Chem.* **1999**, *201*, 131; U. H. F. Bunz, Y. Rubin, Y. Tobe, *Chem. Soc. Rev.* **1999**, 107.
- [13] M. Laskoski, G. Roidl, M. D. Smith, U. H. F. Bunz, *Angew. Chem.* **2001**, *113*, 1508; *Angew. Chem. Int. Ed.* **2001**, *40*, 1460; M. Laskoski, M. D. Smith, J. G. M. Morton, U. H. F. Bunz, *J. Org. Chem.* **2001**, *66*, 5174; U. H. F. Bunz, G. Roidl, M. Altmann, V. Enkelmann, K. D. Shimizu, *J. Am. Chem. Soc.* **1999**, *121*, 10719.
- [14] a) M. Laskoski, J. G. M. Morton, M. D. Smith, U. H. F. Bunz, *Chem. Commun.* **2001**, 2590; b) for the active catalyst $[Pd(P(o\text{-tolyl})_3)_2]$, see F. Paul, J. Patt, J. F. Hartwig, *Organometallics* **1995**, *14*, 3030.
- [15] a) S. Ohira, *Synth. Lett.* **1989**, 19, 561; S. Müller, B. Liepold, G. J. Roth, H. J. Bestmann, *Synlett* **1996**, 521; D. F. Taber, Y. Wang, *J. Am. Chem. Soc.* **1997**, *119*, 22; b) for the diazophosphonate, see D. Seyferth, R. S. Marmor, P. Hilbert, *J. Org. Chem.* **1971**, *36*, 1379; D. G. Brown, E. J. Velthuisen, J. R. Commerford, R. G. Brisbois, T. R. Hoye, *J. Org. Chem.* **1996**, *61*, 2540; c) the most efficient alkyne–alkyne coupling reaction we have utilized so far has been developed by: F. Vögtle, R. Berscheid, *Synthesis* **1992**, 58; P. Siemsen, R. C. Livingston, F. Diederich, *Angew. Chem.* **2000**, *112*, 2740; *Angew. Chem. Int. Ed.* **2000**, *39*, 2633.
- [16] M. M. Haley, personal communication on related transformations.
- [17] For details of X-ray crystallography on **7**, **12**, and **17** see the Supporting Information. Crystal data for **7**: $C_{51}H_{37}Co$, $M_r = 708.74$, triclinic, $P-1$, $a = 10.9507(8)$, $b = 12.1458(8)$, $c = 15.4401(11)$ Å, $\alpha = 86.981(1)^\circ$, $\beta = 79.657(1)^\circ$, $\gamma = 65.458(1)^\circ$, $V = 1837.2(2)$ Å³, $Z = 2$, $\rho_{\text{calcd}} = 1.281$ g cm⁻³. $2\theta_{\text{max}} = 50.2^\circ$; 15359 reflections collected, 6532 independent, 5052 with $I > 2\sigma(I)$. No absorption correction ($\mu = 0.50$ mm⁻¹). $R1$, $wR2$ ($I > 2\sigma(I)$) = 0.0416, 0.814, respectively.
- [18] Crystal data for **12**: $C_{51}H_{36}Fe \cdot 0.25CH_2Cl_2$, $M_r = 725.88$, hexagonal, $P6_3$, $a = 27.174(2)$, $c = 9.1170(7)$ Å, $V = 5830.4(7)$ Å³, $Z = 6$, $\rho_{\text{calcd}} = 1.240$ g cm⁻³. $2\theta_{\text{max}} = 48.2^\circ$; 22326 reflections collected, 5788 independent, 4316 with $I > 2\sigma(I)$. No absorption correction applied ($\mu = 0.46$ mm⁻¹). $R1$, $wR2$ ($I > 2\sigma(I)$) = 0.0623, 0.1231, respectively; GOF = 1.013. 509 parameters refined, 4 restraints (disordered CH_2Cl_2 solvent).
- [19] Crystal data for **17**: $C_{69}H_{59}Co$, $M_r = 939.03$, monoclinic, $P2_1/n$, $a = 10.568(1)$, $b = 35.490(4)$, $c = 15.132(2)$ Å, $\beta = 102.215(3)^\circ$, $V = 5547.0(11)$ Å³, $Z = 4$, $\rho_{\text{calcd}} = 1.124$ g cm⁻³. $2\theta_{\text{max}} = 45.1^\circ$; 21290 reflections collected, 7278 independent, 3104 with $I > 2\sigma(I)$. No absorption correction ($\mu = 0.35$ mm⁻¹). $R1$, $wR2$ ($I > 2\sigma(I)$) = 0.1098, 0.2544, respectively; GOF = 1.008. 605 parameters refined. Molecular disorder corresponding to a 90° rotation around the $Co \cdots Cp_{\text{centroid}}$ vector is present, but could not be modeled as a result of the small fraction (<10%).
- [20] U. H. F. Bunz, V. Enkelmann, *Organometallics* **1994**, *13*, 3823.
- [21] W. Jentzen, M. C. Simpson, J. D. Hobbs, X. Song, T. Ema, N. Y. Nelson, C. J. Medforth, K. M. Smith, M. Veyrat, M. Mazzanti, R. Rammaseul, J. C. Marchon, T. Takeuchi, W. A. Goddard, J. A. Shellnutt, *J. Am. Chem. Soc.* **1995**, *117*, 11085.
- [22] For an example of a hexagonal fenestrane geometry, see W. B. Wan, M. M. Haley, *J. Org. Chem.* **2001**, *66*, 3893.
- [23] For examples of planar carbon and bona fide fenestrane geometries in organic and organometallic chemistry, see D. Röttgers, G. Erker, R. Fröhlich, M. Grehl, S. J. Silvero, I. Hyla-Kryspin, R. Gleiter, *J. Am. Chem. Soc.* **1995**, *117*, 10503; M. Thommen, R. Keese, *Synlett* **1997**, 231; D. Kuck, A. Schuster, R. A. Krause *J. Org. Chem.* **1991**, *56*, 3472; S. Grimme, *J. Am. Chem. Soc.* **1996**, *118*, 1529; D. Kuck, *Chem. Ber.* **1994**, *127*, 409.

Hexameric Mg–O Stacks with Six THF-Solvated Sodium Amide Appendages: “Super” Variants of Inverse Crown Ethers Generated by Cleavage of THF**

Allison M. Drummond, Lorraine T. Gibson, Alan R. Kennedy, Robert E. Mulvey,* Charles T. O’Hara, René B. Rowlings, and Tracy Weightman

s-Block organometallic compounds are known to be thermodynamically unstable with respect to oxidation or hydrolysis (giving oxides or hydroxides). However, under certain kinetic conditions such reactions may not reach completion but instead stop at intermediate composite structures containing metal cations, oxygen-based anions (usually O^{2-} or OH^-), and organic skeletons. This “oxygen encapsulation” phenomenon^[1] has probably existed since these air- and moisture-sensitive compounds first appeared about a century ago, but it is only relatively recently that its detection has become routine (in suitably crystalline samples) through X-ray crystallographic study. Inevitably the proliferation of such studies has meant more structures of this type (mainly formed fortuitously rather than intentionally) coming to light, though the complex factors controlling their formation remain largely in the dark. We are interested in a special class of oxygen-encapsulated compound: inverse crown ethers^[2] are mixed alkali-metal magnesium (or zinc) amides, the amido component of which is derived from the exceptionally bulky amines (2,2,6,6-tetramethylpiperidine (tmpH) or 1,1,1,3,3,3-hexamethyldisilazane (hmds(H))). Their common structure is characterized by octagonal $(NM^1NM^2)_2$ rings (e.g. **1**) which act as square-planar tetrametallic hosts for the encapsulation of a single anion (either O^{2-} or $(O_2)^{2-}$). Herein we describe a “super” variant to these simple, two-dimensional inverse crown ethers in a new class of heterobimetallic amide, the novel three-dimensional cage construction of which includes multiple O^{2-} encapsulation. Moreover we have traced the source of encapsulated O^{2-} ions, often a matter of puzzlement in examples reported previously, to the cleavage of THF solvent molecules used in the reaction.



Originally we set out to synthesize hypothetical $[Na_2Mg_2(tmp)_4(O)_x(O_2)_y]$, the missing entry in the series of

[*] Prof. R. E. Mulvey, A. M. Drummond, Dr. L. T. Gibson, Dr. A. R. Kennedy, C. T. O’Hara, Dr. R. B. Rowlings, T. Weightman
Department of Pure and Applied Chemistry
University of Strathclyde
Glasgow, G1 1XL (UK)
Fax: (+44) 141-552-0876
E-mail: r.e.mulvey@strath.ac.uk

[**] This work was supported by the UK Engineering and Physical Science Research Council through grant award no GR/M78113. We would also thank Professor P. J. Hall (Department of Chemical and Process Engineering, University of Strathclyde) for use of the mass spectrometer, and Professor S. Gambarotta (University of Ottawa) for helpful advice.

known inverse crown ethers $[\text{Li}_2\text{Mg}_2(\text{hmds})_4(\text{O})_x(\text{O}_2)_y]$, $[\text{Li}_2\text{Mg}_2(\text{tmp})_4\text{O}]$, and $[\text{Na}_2\text{Mg}_2(\text{hmds})_4(\text{O})_x(\text{O}_2)_y]$.^[2] This was approached using the standard “synergic” metal amide mixture (3 tmpH:1 *n*BuNa:1 Bu₂Mg) in a hydrocarbon solution). When the solution was exposed to dry oxygen (a proven method of generating inverse crown ethers), no solid product could be obtained from it. This failure prompted us to introduce THF to a fresh reaction mixture, not exposed to oxygen, in anticipation of a solvated inverse crown ether. A vivid change in the color of the solution (yellow to brown) accompanied this addition, as a sign that THF was intimately involved (in a dual role, intact as a ligand and cleaved; see later) in the ensuing reactions. While a THF solvate was produced, it proved to be much more unique in composition and structure than expected, having the formula $[\{\text{NaMg}(\text{tmp})(\text{O})(\text{thf})\}_6]$ (**2**). To test the generality of this new found reaction, we carried out the same procedure but replaced TMPH by the bulky amine diisopropylamine, HN(*i*Pr)₂. By yielding $[\{\text{NaMg}(\text{NiPr}_2)(\text{O})(\text{thf})\}_6]$ (**3**), this second reaction confirmed that a new class of mixed sodium–magnesium amide, sixfold oxygen-encapsulated, had been discovered.

X-ray crystallographic studies established that **2** and **3** are isostructural, so only the data for one structure need to be discussed here. Exhibiting crystallographically imposed *S*₆ symmetry, the molecular structure of **3**^[3] (Figure 1) is hex-

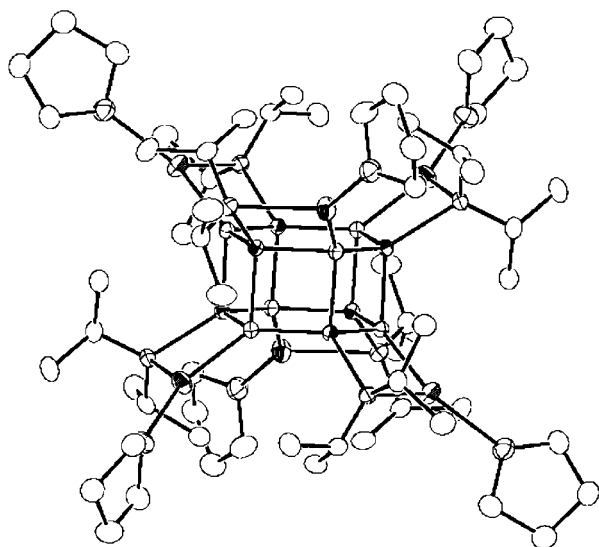


Figure 1. Molecular structure of **3** (atoms drawn as 35% probability ellipsoids; hydrogen atoms omitted for clarity).

americ. Its (MgO)₆ core (Figure 2) comprises two stacked (MgO)₃ trimeric rings. Appended to each of these rings is a set of three *exo*-oriented four-membered Mg–O–Na–N rings, positioned in a staggered fashion with regard to the opposing set. Dative Na–O(thf) bonds complete the structure. To effect ring stacking, the distorted tetrahedral Mg atoms form highly strained (inter-trimer) O–Mg–O' connectivities (mean angle, 92.78°). For the distorted trigonal-planar Na atom, strain is most pronounced at the O–Na–N corner (angle, 88.68(6)°) of the heterometallic–heteroanionic ring. To the best of our knowledge no precedent exists for a simple

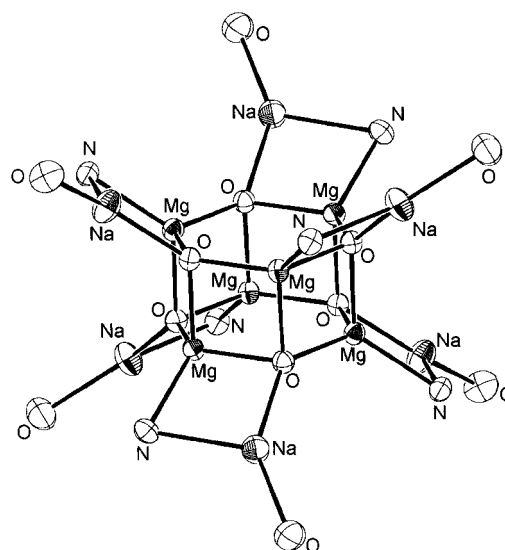
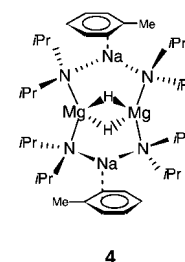


Figure 2. Inorganic core of **3** (atoms drawn as 40% probability ellipsoids).

molecular (MgO)₆ cage. While tetrameric (MgO)₄ cubanes exist (e.g., in the alkoxide $[(\text{CpMgOEt})_4]$ ^[4]), hitherto hexameric cages have only been identified with organoelement ligands isoelectronic to O²⁻ such as imides (e.g., in $[\{(\text{thf})\text{MgN}(\text{Ph})\}_6]$ ^[5]) or phosphanediides (e.g., in $[\{\text{MgP}(\text{Si}t\text{Bu}_3)_6\}]$ ^[6]). There is also a recent report of an odd hexanuclear magnesium diisopropylcarbamato structure with a single encapsulated μ_4 -bonding O²⁻ ion in $[\text{Mg}_6(\text{O}_2\text{CNiPr}_2)_{10}(\text{O})]$.^[7] The structure of **3** follows the pattern running through the whole inverse crown family: the encapsulated “guest” (here O²⁻; elsewhere, O₂²⁻;^[2] H⁻;^[8] Ar⁻;^[2] Ar²⁻;^[2] $[(\text{C}_5\text{H}_3)_2\text{Fe}]^{4-}$ ^[9]) is stabilized predominantly by interaction with Mg, as opposed to M, centers (where M = Li, Na, or K). Covering a narrow range (1.9473(13)–2.0020(14) Å), the Mg–O bond lengths in **3** cannot be compared with their counterparts in $[\text{Na}_2\text{Mg}_2(\text{hmds})_4(\text{O})_x(\text{O}_2)_y]$ ^[2] due to the latter’s contamination with peroxide. The metal–N(diisopropylamide) bond lengths in **3** (for Mg, 2.1324(16) Å; for Na, 2.4040(18) Å) are similar with those in the hydride-encapsulated inverse crown **4** (2.0651(18) and 2.4807(18) Å respectively).^[8] As expected there is a substantial difference in the Na–O bond lengths in **3** reflecting the anionic/dative distinction between the O centers involved (i.e., for O²⁻, 2.1402(15) Å; for THF, 2.2689(18) Å).

In view of the nature of the cages of the structures of **2** and **3**, strictly they should not be classed themselves as inverse crown ethers. Originally the name was coined to describe host–guest *ring* systems, which topologically display an inverse relationship to conventional crown ether complexes, that is, the metal-based host rings are Lewis acidic (cationic), while their oxygen-based guests are Lewis basic (anionic). However, the fact that **2** and **3** are built up of heterobimetallic–amido–oxo “NaMg[N(R₂)O]” monomeric subunits, clearly places them within the developing framework of inverse crown chemistry.



In an attempt to pinpoint the source of the oxide in the hexameric structures, we repeated the preparation of **2** in a vial connected through a heated capillary to a Hiden Analytical Quadrupole mass spectrometer (Warrington, England). After the addition of THF, the reaction mixture was heated and the volatile products blown into the mass spectrometer were subjected to selective ion mass (SIM) analysis. This confirmed the presence of ethylene (parent peak at 28 amu; daughter fragments at 27, 26, and 25 amu). Ethylene is commonly extruded during THF-cleavage processes,^[10] so the origin of the O²⁻ ions in **2** is almost certainly from THF. Fragmentation of THF is a complex matter, the outcome of which can differ depending on many variables such as the metal and the nature of the organyl assailant. Hard organolithium bases are known to deprotonate THF at the α -position, before undergoing a $[\pi 4s + \pi 2s]$ cycloreversion to afford enolate "CH₂=CH-O⁻" and ethylene.^[11] There are also precedents for THF fragmentation leading to M-O-M bridges in organolanthanide chemistry,^[12] and to O²⁻ in other metal^[13] and metalloid^[14] systems. Here the heterobimetallic nature of the inverse crown ether system exacerbates the complexity of the THF fragmentation process, a sign of which is that the filtrates left following the isolation of **2** and **3** darken and degrade to viscous oils in a matter of days. However the salient point is that both new compounds can be prepared reproducibly in a pure crystalline form, and isolated for future synthetic exploration, before the onset of this degradation.

Experimental Section

2 and **3**: In a typical preparation, BuNa, Bu₂Mg, and the relevant amine (5.5:15 mmol) were mixed together in a hydrocarbon solution under a protective argon atmosphere. Dry, distilled THF (5 mL, 62 mmol) was then added and the solution warmed for 30 min. Cooling the solution on the bench (for **2**) or in the refrigerator at -26 °C (for **3**) afforded colorless crystals of **2** or **3**. Yields of first batches isolated were typically 18 or 11 %, respectively. No further solids could be isolated due to degradation of the filtrate solutions. M.p. 330 °C (decomp) and 258 °C (decomp), respectively. Satisfactory analyses (C, H, N) were obtained for both compounds. ¹H NMR (400.13 MHz, [D₆]DMSO, 300 K): **2**: δ = 3.60 (m, 4H; CH₂O-THF), 1.76 (m, 4H; CH₂-THF), 1.57 (m, 2H; γ -CH₂), 1.23 (m, 4H; β -CH₂), 1.02 ppm (s, 12H; CH₃); ¹H NMR (400.13 MHz, [D₈]toluene, 300 K) **3**: δ = 3.35 (m, 4H; CH₂O-THF), 3.26 (septet, 2H; CH), 1.33 (m, 4H; CH₂-THF), 1.20 ppm (d, 12H; CH₃).

Received: February 22, 2002 [Z18755]

[1] A. E. Wheatley, *Chem. Soc. Rev.* **2001**, 30, 265.

[2] R. E. Mulvey, *Chem. Commun.* **2001**, 1049.

[3] Crystal data for **3**: C₆₀H₁₃₂Mg₆N₆Na₆O₁₂; a colorless needle of approximate dimensions 0.55 × 0.10 × 0.10 mm gave a trigonal space group *R*3 \bar{h} , *a* = *b* = 23.8599(6), *c* = 12.1274(4) Å, *V* = 5979.1(3) Å³, *T* = 123 K, *Z* = 3, ρ_{calcd} = 1.178 Mg m⁻³, $2\theta_{\text{max}}$ = 52°, $\text{MoK}\alpha$, λ = 0.71073 Å. The structure was solved, and refined on *F*², using programs of the Shelx family to convergence at *R*1 = 0.0419 (for 2019 reflections with *I* > 2 σ (*I*)), *wR*2 = 0.1177, and *S* = 1.022 for 140 parameters and 2602 unique reflections. Highest residual electron density 0.437 e Å⁻³. Hydrogen atoms were placed in calculated positions and in a riding mode. Compound **2** was found to be isostructural with **3** but contained highly disordered groups at the THF positions which adversely affected the quality of the solution. CCDC-1790244 (**2**) and CCDC-1790245 (**3**) contain the supplementary crystallographic data for this paper. These data can be obtained free of charge via www.ccdc.cam.ac.uk/conts/retrieving.html (or from the

Cambridge Crystallographic Data Centre, 12, Union Road, Cambridge CB2 1EZ, UK; fax: (+44) 1223-336-033; or deposit@ccdc.cam.ac.uk).

- [4] H. Lehmkuhl, K. Mehler, R. Benn, A. Ruffiniska, C. Krüger, *Chem. Ber.* **1986**, 119, 1054.
 [5] T. Hascall, K. Ruhlandt-Senge, P. P. Power, *Angew. Chem.* **1994**, 106, 350; *Angew. Chem. Int. Ed. Engl.* **1994**, 33, 356.
 [6] M. Westerhausen, M. Krofta, A. Pfizner, *Inorg. Chem.* **1999**, 38, 598.
 [7] K.-C. Yang, C.-C. Chang, C.-S.-Yeh, G.-H. Lee, S.-M. Peng, *Organometallics* **2001**, 20, 126.
 [8] D. J. Gallagher, K. W. Henderson, A. R. Kennedy, C. T. O'Hara, R. E. Mulvey, R. B. Rowlings, *Chem. Commun.* **2002**, 376.
 [9] W. Clegg, K. W. Henderson, A. R. Kennedy, R. E. Mulvey, C. T. O'Hara, R. B. Rowlings, D. M. Tooke, *Angew. Chem.* **2001**, 113, 4020; *Angew. Chem. Int. Ed.* **2001**, 40, 3902.
 [10] For example see: R. Duchateau, C. T. van Wee, J. H. Teuben, *Organometallics* **1996**, 15, 2291, and references therein.
 [11] T. Kottke, R. J. Lagow, D. Hoffmann, R. D. Thomas, *Organometallics* **1997**, 16, 789; B. Walford, S. K. Pandey, D. Stalke, *Chem. Commun.* **2001**, 1640.
 [12] T. Dubé, S. Conoci, S. Gambarotta, G. P. A. Yap, *Organometallics* **2000**, 19, 1182.
 [13] H. C. Aspinall, M. R. Tillotson, *Inorg. Chem.* **1996**, 35, 2163.
 [14] W. Köstler, G. Linti, *Eur. J. Inorg. Chem.* **2001**, 1841.

A Unique Bismuth–Iron Chain Polymer Containing the ...-Bi-Fe-... Link: Formation and Structure of [*n*BuBiFe(CO)₄]_∞**

Minghuey Shieh,* Yeantarn Liou, Miao-Hsing Hsu, Rung-Tsang Chen, Shiow-Jane Yeh, Shie-Ming Peng, and Gene-Hsiang Lee

The construction of supramolecules or extended frameworks based on coordination and organometallic complexes is one of the major areas of current research in inorganic and organometallic chemistry.^[1] Nevertheless, this approach has received little attention in the field of organobismuth–transition-metal complexes;^[2] such complexes are of great importance mainly due to their potential applications as catalysts in olefin oxidation and ammoxidation^[3] and as precursors to a variety of electronic materials.^[4] Bismuth has been shown to form the polymer [Et₂Bi(OAr)]_∞ in which the alkoxide ligand bridges the Et₂Bi groups giving a helical chain with no direct Bi–Bi interaction.^[5] For the Bi-Fe-CO system, the polymer [{PhCH₂NMe₃}{(μ-H)Fe₂(CO)₆Bi₂(μ-Cl)₂}]_∞ was

[*] Prof. Dr. M. Shieh, Y. Liou, M.-H. Hsu, R.-T. Chen, S.-J. Yeh

Department of Chemistry
National Taiwan Normal University
Taipei, Taiwan, 116 (Republic of China)
Fax: (+886) 2-2932-4249
E-mail: mshieh@scc.ntnu.edu.tw

Prof. Dr. S.-M. Peng, G.-H. Lee
Department of Chemistry
National Taiwan University
Taipei, Taiwan, 117 (Republic of China)

[**] This work was supported by the National Science Council of Taiwan (NSC 89-2113-M-003-018 to M. S.) and by the National Taiwan Normal University (ORD 91-1).

shown to possess “Bi₂Fe₄” tetrahedral units connected by a chloride ligand, leading to an infinite chain but without a continuous $\cdots\text{Bi-Fe-}\cdots$ interaction.^[6] To date, there are no polymeric complexes that contain an infinite $\cdots\text{Bi-Fe-}\cdots$ contact of any type. We report herein the unprecedented bismuth–iron chain polymer, $[\text{nBuBiFe}(\text{CO})_4]_\infty$ (**1**), which contains the unique zigzag $\cdots\text{Bi-Fe-}\cdots$ chain.

In the preparation of the ring complex $[\text{nBuBiFe}(\text{CO})_4]_2$ (**2**) from the reaction of $[\text{Et}_4\text{N}]_3[\text{Bi}(\text{Fe}(\text{CO})_4)_4]$ with *n*BuBr in MeCN followed by acidification,^[7] we found that ultrasonication of **2** led to the formation of the polymeric product $[\text{nBuBiFe}(\text{CO})_4]_\infty$ (**1**). An X-ray structure analysis of crystals of **1** revealed an unusual mixed-metal chain polymer which is composed of the *n*BuBiFe(CO)₄ groups with a novel $\cdots\text{Bi-Fe-}\cdots$ chain (Figure 1).^[8] To the best of our knowledge, **1** is the first infinite heteroleptic Bi–Fe-bonded chain to be structurally characterized.

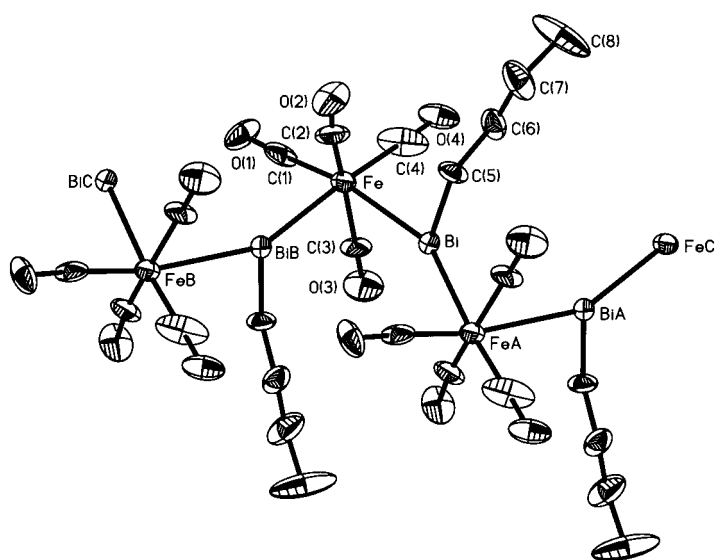


Figure 1. Structure of a segment of the polymer **1** (ORTEP diagram). Selected bond lengths [Å] and angles [°]: Bi–Fe 2.849(5), BiB–Fe 2.771(5), Bi–C(5) 2.20(3), Fe–C(1) 1.80(5), Fe–C(2) 1.74(5), Fe–C(3) 1.81(3), Fe–C(4) 1.80(5), C(5)–C(6) 1.523(19), C(6)–C(7) 1.52(2), C(7)–C(8) 1.51(2), Fe–Bi–FeA 156.46(15), Bi–Fe–BiB 81.47(12), Fe–Bi–C(5) 100.0(9), FeA–Bi–C(5) 93.6(9), Bi–Fe–C(1) 169.5(11), Bi–Fe–C(2) 86.3(15), Bi–Fe–C(3) 79.2(15), Bi–Fe–C(4) 92(2), C(1)–Fe–C(4) 97(3), BiB–Fe–C(1) 88.9(15), BiB–Fe–C(2) 79.0(18), BiB–Fe–C(3) 87.6(11), BiB–Fe–C(4) 174(2).

Noteworthy in **1** is the zigzag $\cdots\text{Bi-Fe-Bi-Fe-}\cdots$ chain with alternating short (2.771(5) Å) and long (2.849(5) Å) Bi–Fe distances and alternating Bi–Fe–Bi and Fe–Bi–Fe angles of 81.47(12)° and 156.46(15)°, respectively. Notably, the neighboring *n*Bu groups are oriented in the *trans* position and the Fe(CO)₄ groups sit in the staggered-like position along the chain. The C–C distance between two “parallel” *n*Bu groups (C(8)–C(8)C) is around 1.96 Å, which is within their van der Waals contact (i.e., 3.4 Å)^[9] indicative of the weak interaction. This intramolecular interaction of the alkyl groups may partly account for the formation of **1**.

Whereas the ring complex **2** is considered as the dimeric product of the monomer $[\text{nBuBiFe}(\text{CO})_4]$ derived from the ionic complex $[\text{nBuBi}(\text{Fe}(\text{CO})_4)_3]^{2-}$,^[7] the polymer **1** can be

viewed as the polymeric product that results from the cleavage (probably by radical processes) of Bi–Fe bonds in **2** upon ultrasonication. The formation of **1** from **2** is reversible. The polymer **1** can be obtained from a solution of **2**, and **1** dissolves in most organic solvents to form the dimeric product **2** in almost quantitative yield. No analogous polymers like **1** were observed when analogous reactions were carried out for Bi compounds with shorter alkyl groups (R = Me, Et). Hence, the freedom of the alkyl groups and the effective crystal packing play an important role in the formation of **1**.

The coordination geometry at the bismuth center in **1** can be described as a pyramidal structure with an uncoordinated lone pair of electrons, which is seen in many other bismuth-containing complexes such as $[\text{R}_2\text{Bi}_2\text{Fe}_2(\text{CO})_8]$,^[7] $[\text{Et}_4\text{N}][\text{Bi-Fe}_3(\text{CO})_{10}]$,^[10] and $[\text{Et}_4\text{N}]_2[\text{Bi}_2\text{Fe}_4(\text{CO})_{13}]$.^[11] However, it is noteworthy that the Fe–Bi–Fe angle (156.46(15)°) is unusually large and the sum of the angles at the bismuth center is about 350°, not far off being planar. These two features are quite different to those of the above-mentioned complexes and the related complex $[\text{EtBi}(\text{Mo}(\text{CO})_3\text{Cp})_2]$.^[12] In the absence of multiple bonding between the Bi and Fe centers in **1**, the lone pair of electrons on the bismuth center may be in an essentially unhybridized p orbital and thus capable of interacting with the *cis*-carbonyl ligands, which might account for the *trans* orientation of the *n*Bu groups and the alternating Bi–Fe bond lengths (2.771(5) versus 2.849(5) Å). In addition, the iron atom is pseudooctahedrally coordinated to two bismuth atoms and four carbonyl groups; the Bi–Fe–Bi angle (81.47(12)°) is smaller than most angles about the iron atom due to the demands of the orientation of the chain and the *n*Bu groups. The Bi–C distance of 2.20(3) Å is similar to those in $[\text{Me}_2\text{Bi}_2\text{Fe}_2(\text{CO})_8]$ (2.28(1) Å)^[13] and $[\text{iBu}_2\text{Bi}_2\text{Fe}_2(\text{CO})_8]$ (2.29(1) Å).^[14] The C–C distances in **1** are in the range of 1.51(2)–1.52(2) Å, which are comparable to those in the related complex $[(\text{iBu})_2\text{Bi}_2\text{Fe}_2(\text{CO})_8]$.^[14] These features reflect the small distortion of the alkyl groups in polymer **1**. Work is in progress to determine the generality of the structure of **1** and to investigate its applications.

Experimental Section

All reactions were performed under an atmosphere of pure nitrogen using standard Schlenk techniques.

1: *n*BuBr (3 mL, 27.94 mmol) was added dropwise to a sample of $[\text{Et}_4\text{N}]_3[\text{Bi}(\text{Fe}(\text{CO})_4)_4]$ (2.54 g, 2.00 mmol) in MeCN (40 mL). The mixed solution was heated at 40–42 °C for 24 h, and the resulting solution was filtered and dried under vacuum to give a residue to which HOAc (10 mL) was added. The mixture was stirred at room temperature for 20 h, and the HOAc was removed under vacuum. The residue was extracted with hexane (40 mL) several times and the hexane extract was showed to contain the dimeric complex **2** (0.30 g).^[7] The hexane solution containing **2** was concentrated, and subsequently ultrasonicated in a water bath with an ultrasonicator (50 Hz, 4 amp, 110 V) for 20 min. The resultant solution was cooled in a freezer to give crystals of $[\text{nBuBiFe}(\text{CO})_4]_\infty$ (**1**). Yield: 0.28 g. IR (nujol): $\tilde{\nu}_{\text{CO}}$ = 2034 (s), 1998 (w), 1983 cm^{−1} (s, br); m.p. 71 °C; elemental analysis (%) calcd for $[\text{nBuBiFe}(\text{CO})_4]_\infty$: C 22.14, H 2.09; found: C 22.12; H 2.10. Polymer **1** decomposed quickly into the dimeric species in most organic solvents.

Received: February 22, 2002 [Z18757]

- [1] a) D. Braga, F. Grepioni, G. R. Desiraju, *Chem. Rev.* **1998**, 98, 1375; b) P. F. H. Schwab, M. D. Levin, J. Michl, *Chem. Rev.* **1999**, 99, 1863; c) S. Leininger, B. Olenyuk, P. J. Stang, *Chem. Rev.* **2000**, 100, 853; d) T. Nakajima, A. Ishiguro, Y. Wakatsuki, *Angew. Chem.* **2001**, 113, 1096; *Angew. Chem. Int. Ed.* **2001**, 40, 1066.
- [2] a) N. C. Norman, *Chem. Soc. Rev.* **1988**, 17, 269–281; b) L. D. Freedman, G. O. Doak, *Chem. Rev.* **1982**, 82, 15; c) N. A. Compton, R. J. Errington, N. C. Norman, *Adv. Organomet. Chem.* **1990**, 31, 91; d) C. Silvestru, H. J. Breunig, H. Althaus, *Chem. Rev.* **1999**, 99, 3277; e) D. F. Shriver, H. D. Kaesz, R. D. Adams, *The Chemistry of Metal Cluster Complexes*, VCH, New York, **1990**.
- [3] C. Coin, T. Zevaco, E. Dunach, M. Postel, *Bull. Soc. Chim. Fr.* **1996**, 133, 913.
- [4] a) P. Majewski, *Adv. Mater.* **1994**, 6, 460; b) R. D. Rogers, A. H. Bond, S. Aguinaga, *J. Am. Chem. Soc.* **1992**, 114, 2960; c) S. Wang, D. B. Mitzi, G. A. Landrum, H. Genin, R. Hoffmann, *J. Am. Chem. Soc.* **1997**, 119, 724; d) A. Ekstrand, M. Nygren, G. Westin, *J. Sol-Gel Sci. Technol.* **1997**, 8, 697; e) F. Soares-Carvalho, P. Thomas, J. P. Mercurio, B. Frit, S. Parola, *J. Sol-Gel Sci. Technol.* **1997**, 8, 759.
- [5] K. H. Whitmire, J. C. Hutchison, A. McKnight, C. M. Jones, *J. Chem. Soc. Chem. Commun.* **1992**, 1021.
- [6] J. R. Eveland, J.-Y. Saillard, K. H. Whitmire, *Inorg. Chem.* **1997**, 36, 4387.
- [7] M. Shieh, Y. Liou, B.-W. Jeng, *Organometallics* **1993**, 12, 4926.
- [8] **1**: $C_8H_6BiFeO_4$, $M_r = 433.98$, monoclinic, space group $C2$, $a = 17.347(6)$, $b = 7.152(2)$, $c = 9.523(5)$ Å, $\beta = 92.96(4)^\circ$, $V = 1179.9(8)$ Å³, $Z = 4$, $\rho_{\text{calc}} = 2.443$ g cm⁻³, $\mu = 16.109$ mm⁻¹, $\lambda = 0.70930$ Å, transmission range 0.54–1.00, crystal dimensions about $0.40 \times 0.50 \times 0.60$ mm³. A total of 1134 unique reflections were collected on a Nonius (CAD-4) diffractometer at 298 K in the 2θ range 2.0–50°. Full-matrix least-squares refinement on F^2 converged to $R = 0.0628$ (all data), 0.0542 ($I > 2\sigma(I)$); $wR = 0.1763$ (all data), 0.1635 ($I > 2\sigma(I)$). All calculations were performed by using SHELXTL packages. CCDC-177971 (**1**) contains the supplementary crystallographic data for this paper. These data can be obtained free of charge via www.ccdc.cam.ac.uk/conts/retrieving.html (or from the Cambridge Crystallographic Data Centre, 12, Union Road, Cambridge CB21EZ, UK; fax: (+44) 1223-336-033; or deposit@ccdc.cam.ac.uk).
- [9] J. E. Huheey, *Inorganic Chemistry*, 3rd ed., Harper&Row, New York, **1983**, p. 258.
- [10] K. H. Whitmire, C. B. Lagrone, M. R. Churchill, J. C. Fetting, L. V. Biondi, *Inorg. Chem.* **1984**, 23, 4227–4232.
- [11] K. H. Whitmire, M. Shieh, C. B. Lagrone, B. H. Robinson, M. R. Churchill, J. C. Fetting, R. F. See, *Inorg. Chem.* **1987**, 26, 2798–2807.
- [12] W. Clegg, N. A. Compton, R. J. Errington, G. A. Fisher, N. C. Norman, N. Wishart, *J. Organomet. Chem.* **1990**, 399, C21.
- [13] K. H. Whitmire, M. Shieh, J. Cassidy, *Inorg. Chem.* **1989**, 28, 3164.
- [14] M. Shieh, Y. Liou, S.-M. Peng, G.-H. Lee, *Inorg. Chem.* **1993**, 32, 2212.

[{Fe(OMe)₂[O₂CC(OH)Ph₂]}₁₂]: Synthesis and Characterization of a New Member in the Family of Molecular Ferric Wheels with the Carboxylatobis(alkoxo) Bridging Unit**

Catherine P. Raptopoulou,* Vassilis Tangoulis, and Eamon Devlin

High-nuclearity transition-metal clusters continue to attract a great deal of interest, partly because of their fascinating physical properties and partly for the architectural beauty of their structures. An interesting subarea of 3d metal cluster chemistry is the small but growing family of molecules that have circular structures. Large cyclic polymetallic clusters are valued for their ability to mimic the properties of linear coordination polymers.^[1] For example, theories developed for analyzing magnetically coupled ring systems have been extensively applied to calculate the thermodynamic properties of 1D materials.^[2] Furthermore, the chemistry of circular molecular clusters is also associated with supramolecular chemistry. Anion and cation recognition provide the possibility of controlling the size of clusters. A representative example of this approach is the ability to address the synthesis of molecular rings by exploiting host–guest interactions with alkali-metal cations, because alkali-metal cations are hosted by rings of different size. Thus, hexairon(III)^[3–5] and hexamanganese(III)^[6] complexes with cyclic M₆O₁₂ cores can easily accommodate Li⁺ and Na⁺ ions, both in the solid state and in solution, whereas Cs⁺ ions require larger rings, such as M₈O₁₆.^[5]

Metal rings have excited mankind since mythological times.^[7] The largest cyclic structure containing exclusively paramagnetic 3d metals is the Ni₂₄^{II} wheel reported by Winpenny and co-workers,^[8] which is approximately an order of magnitude smaller than the giant wheels constructed from molybdate fragments by the Müller group;^[9] a Ni₁₂^{II} wheel is also known.^[10] Large, cyclic, polymetallic arrangements of other 3d metals, either unsupported or supported (by ions or molecules as guests), have been found for chromium(III),^[11] manganese(II),^[12] iron(II),^[13] iron(III),^[12, 14] cobalt(II),^[15] and copper(II).^[16]

Restricting further discussion to the so-called ferric wheels with nuclearities equal to or higher than ten, the structurally characterized complexes that contain O-donor groups as bridging ligands are [{Fe(OMe)₂(O₂CCH₂Cl)}₁₀]^[14a] [{Fe(OMe)₂(O₂CMe)}₁₀]^[14b] [{Fe(OMe)₂L}₁₀]^[14c] where L[–] is

[*] Dr. C. P. Raptopoulou, Dr. E. Devlin
Institute of Materials Science
NCSR “Demokritos”
15310 Ag. Paraskevi Attikis, Athens (Greece)
Fax: (+30) 10-651-9430
E-mail: craptop@ims.demokritos.gr
Dr. V. Tangoulis
Department of Materials Science
University of Patras
26500 Patras (Greece)

[**] We thank Dr. Claudio Sangregorio and the Department of Chemistry of Florence, Italy for the magnetic measurements.

the monoanion of 3-(4-methylbenzoyl)propionic acid, $[\{\text{Fe}(\text{OMe})_2(\text{dbm})\}_{12}]$,^[14d] where dbm[−] is the dibenzoylmethanato ligand, and $[\{\text{Fe}(\text{OH})(\text{XDK})\text{Fe}_2(\text{OMe})_4(\text{O}_2\text{CMe})_2\}_6]$,^[14e] where XDK^{2−} is the ion of *m*-xylylenediamine bis(Kemp's triacid imide). All three $\text{Fe}_{10}^{\text{III}}$ wheels contain chemically equivalent $(\mu\text{-O}_2\text{CR})(\mu\text{-OMe})_2$ units, while the $\text{Fe}_{12}^{\text{III}}$ wheel contains chemically equivalent $(\mu\text{-OMe})_2$ units. The repeating unit in the $\text{Fe}_{18}^{\text{III}}$ cluster, known as the molecular 18-wheeler, comprises a $(\mu\text{-hydroxo})\text{bis}(\mu\text{-carboxylato})\text{diiron(III)}$ moiety linked by an acetate and two methoxide ions to a third iron(III) atom; an acetate and two additional methoxide ligands on this iron center form bridges to the next trinuclear repeating unit in the cluster.^[14e]

The family of ferric wheels with the $(\mu\text{-O}_2\text{CR})(\mu\text{-OR}')_2$ unit is restricted to decanuclear complexes.^[14a–c] We wondered whether change of the carboxylato or/and alkoxo ligands would influence the size of these wheels and permit the isolation of larger wheels. The main driving force behind our efforts was our desire to test the general belief^[8] that it is not possible to generate a large 3d-metal wheel with only one type of bridging interaction. For example, while $\text{Fe}_{10}^{\text{III}}$ wheels can be accurately described as $[\{\text{Fe}(\text{OMe})_2(\text{O}_2\text{CR})\}_{10}]$ ($\text{R} = \text{Me}$, CH_2Cl , $\text{CH}_2\text{CH}_2\text{C}(\text{O})\text{C}_6\text{H}_4\text{Me}$) and Cr_8^{III} wheels^[11] can be described as $[\{\text{CrX}(\text{O}_2\text{CR})\}_8]$ ($\text{X} = \text{F}$, $\text{R} = \text{CMe}_3$; $\text{X} = \text{OH}$, $\text{R} = \text{Ph}$), such a description as an oligomer of a mononuclear fragment is not accurate for larger wheels. For both the $\text{Fe}_{18}^{\text{III}}$ ^[14e] and $\text{Ni}_{24}^{\text{II}}$ ^[8] wheels mentioned above, a more accurate description is as an oligomer of trinuclear building blocks. Herein we report the isolation and characterization of the unique $x = 12$ member of the $[\{\text{Fe}(\text{OR}')_2(\text{O}_2\text{CR})\}_x]$ family of ferric wheels. Since it has been recently pointed out^[8, 16b] that utilization of strong interligand hydrogen bonds might be an important feature in generating large wheel-shaped clusters, we decided to employ carboxylate ligands containing suitable hydrogen-bond donor groups.

The 1:2 reaction of $\text{Fe}(\text{NO}_3)_3 \cdot 9\text{H}_2\text{O}$ with benzilic acid, $\text{Ph}_2\text{C}(\text{OH})\text{COOH}$, in MeOH under reflux at $\text{pH} \approx 4$ gave a microcrystalline solid. Diffusion of Et_2O into the yellow methanolic filtrate resulted in yellow crystals of $[\{\text{Fe}(\text{OMe})_2(\text{O}_2\text{CC}(\text{OH})\text{Ph}_2)\}_{12}] \cdot 2\text{H}_2\text{O} \cdot \text{Et}_2\text{O}$ ($\mathbf{1} \cdot 2\text{H}_2\text{O} \cdot \text{Et}_2\text{O}$) formed over a period of four weeks. The initially precipitated solid was characterized as compound **1** by microanalysis and IR spectroscopy.

Single-crystal X-ray crystallography^[17] showed complex **1** to be a dodecanuclear ferric wheel. The molecular structure (Figure 1) consists of a centrosymmetric ring of twelve Fe^{III} atoms held together by twenty-four μ_2 -methoxo ligands and twelve 1,3-bridging carboxylate ligands. Each iron(III) atom has a distorted octahedral geometry and is joined to its neighbors by edge-sharing methoxide and *cis*-carboxylate bridges. The twelve iron centers are nearly coplanar, with an average deviation of $\approx 0.48 \text{ \AA}$ from the best least-squares plane through them. In contrast, in the cyclic dodecanuclear compound $[\{\text{Fe}(\text{OMe})_2(\text{dbm})\}_{12}]$,^[14d] which contains bis(μ -methoxo) units, the ring defined by the iron(III) atoms is not planar and the structure is best described as a twisted "ribbon".

The benzilate(−1) ion has the possibility of further interaction with the iron(III) centers through the hydroxyl

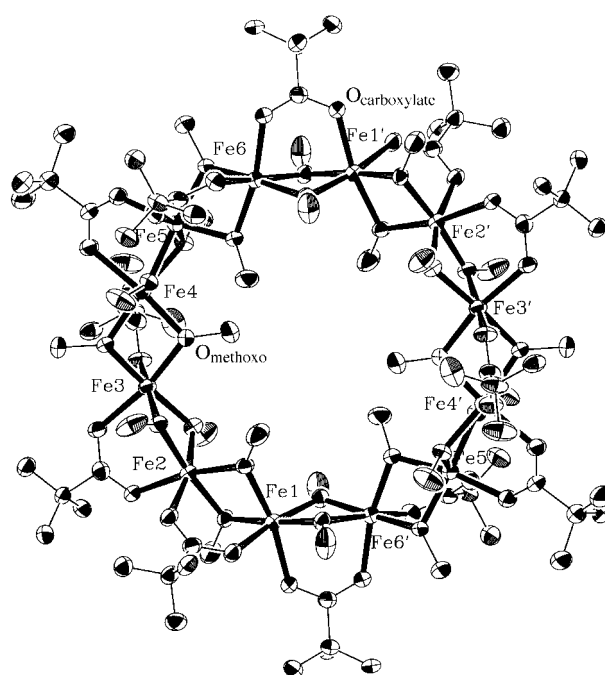


Figure 1. Molecular structure of **1**. For clarity, only the *ipso* carbon atom of each phenyl ring is shown. An inversion center relates the primed atoms to the unprimed ones. Interatomic distances [\AA]: $\text{Fe} \cdots \text{Fe} = 3.013(1) - 11.634(1)$, $\text{Fe}-\text{O}_{\text{methoxo}} = 1.962(5) - 1.990(5)$, $\text{Fe}-\text{O}_{\text{carboxylate}} = 2.001(5) - 2.100(5)$.

oxygen atom, but, in the case of **1**, this potential is not realized and the ligand is merely bidentate, spanning metal–metal vectors in a 1,3-bridging mode.

A side view of **1** is shown in Figure 2. The methoxo ligands are arranged above and below the ring defined by the iron(III) atoms. The benzilate ligands can be divided into two groups of six members each. The carboxylate moieties of the first group almost lie in the plane of the twelve metal ions (average displacement of the carboxylate oxygen atoms: 0.39 \AA), while those of the second group are arranged above and below the metal ring (average displacement of the carboxylate oxygen atoms: 2.35 \AA) in an alternating fashion between the carboxylate groups belonging to the first group.

The closest $\text{Fe} \cdots \text{Fe}$ distances are almost identical in **1** ranging from 3.013 to 3.030 \AA , very similar to those found in $[\{\text{Fe}(\text{OMe})_2(\text{O}_2\text{CCH}_2\text{Cl})\}_{10}]$ ^[14a] (average value: 3.028 \AA) and shorter than the distances found^[14d] in $[\{\text{Fe}(\text{OMe})_2(\text{dbm})\}_{12}]$ (average

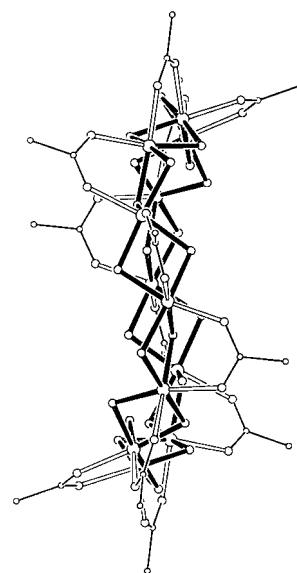


Figure 2. ORTEP diagram of a side view of **1**. Empty bonds show the arrangement of the benzilate(−1) ligands with respect to the mean plane of the iron(III) atoms (larger empty circles).

value: 3.136 Å). The ring size in **1**, calculated by averaging the distances between iron(III) atoms on opposite sides of the ring is 11.41 Å, larger than the 9.80 and 10.34 Å values found in $[\{\text{Fe}(\text{OMe})_2(\text{O}_2\text{CCH}_2\text{Cl})\}_{10}]^{[14a]}$ and $[\{\text{Fe}(\text{OMe})_2(\text{dbm})\}_{12}]^{[14d]}$ respectively. This difference in the ring size between the latter and **1** is a consequence of the difference in the $\text{Fe}\cdots\text{Fe}\cdots\text{Fe}$ angles. These angles range from 142.6 to 146.3° in **1**, very close to the ideal 150° value required by ring-closure considerations for a planar, 12-membered ring, and from 117.3 to 136.2° in $[\{\text{Fe}(\text{OMe})_2(\text{dbm})\}_{12}]^{[14d]}$ (very close to the optimum value of 120° for a structure based on edge-sharing octahedra).

Complex **1** is one of the two largest cyclic ferric clusters yet reported with chemically equivalent bridging units, the other being $[\{\text{Fe}(\text{OMe})_2(\text{dbm})\}_{12}]^{[14d]}$. The small family of the dodecanuclear iron clusters with exclusively O ligation also includes two $\text{Fe}_8^{\text{II}}\text{Fe}_4^{\text{III}}$ oxo/carboxylate complexes;^[18a,b] these two clusters do not have cyclic structures.

The Mössbauer spectrum of a polycrystalline sample of **1** at room temperature (Figure 3) reveals a single quadrupole doublet with an isomer shift of 0.41(1) mm s^{-1} (referenced versus iron foil at room temperature) and a quadrupole

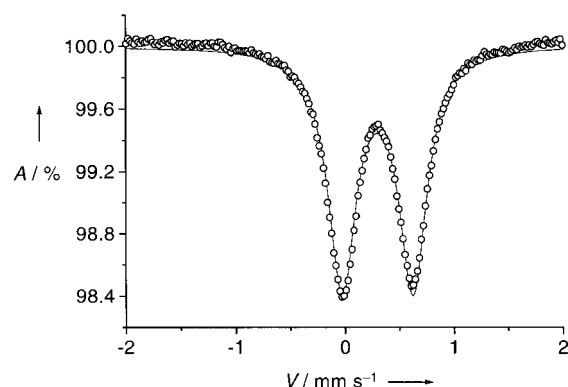


Figure 3. Mössbauer spectrum of polycrystalline **1** at room temperature. — is the best fit to the data with the spectral parameters mentioned in the text.

splitting of 0.65(1) mm s^{-1} . The isomer-shift value is within the range expected for high-spin iron(III) centers in a non-sulfur environment.^[19] The ΔE_Q value indicates a slightly unsymmetrical electric field, consistent with the variations in Fe–O bond distances revealed by the X-ray investigations.^[17] The width at half height is 0.15(1) mm s^{-1} .

The magnetic susceptibility of **1** is indicative of antiferromagnetic interactions between the high-spin iron(III) ions ($S = 5/2$). The broad maximum at 60 K in the curve (Figure 4) can be nicely fit by a Heisenberg $S = 5/2$ quantum chain model with $J = -10.9 \text{ cm}^{-1}$ and $g = 2.00$ ($H = J\sum_i S_i S_{i+1}$).^[20] The departures from the calculated behavior at low temperature arise from a small percentage of paramagnetic impurity. For a ring of N ions, an energy gap $\Delta E \approx 4J/N = 3.6 \text{ cm}^{-1}$ is predicted between the ground state $S = 0$ and the first excited $S = 1$. The calculated J value is close to that found in other dialkoxo-bridged iron(III) complexes with similar Fe–O–Fe angles.^[14a]

In conclusion, the molecular architecture of **1** underscores the ability of synthetic chemistry to enrich our world with

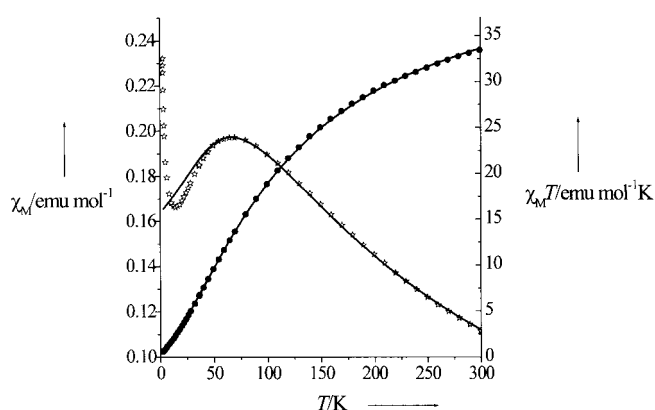


Figure 4. Magnetic susceptibility measurements of **1** in the range 2–300 K at 0.1 T applied magnetic field; (●) refer to $\chi_M T$, stars to χ_M , — represent the best fit to the data.

objects of beauty.^[21] The self-assembly of this complex provides further evidence for the tendency of metal ions linked by alkoxo/hydroxo ligands and *syn,syn* η^2 -carboxylate bridges to form large cyclic molecules. Compound **1** is the largest cyclic ferric cluster yet reported with the carboxylato-bis(alkoxo) bridging unit. It should be stressed that there are no hydrogen bonds in the structure of this cluster, which could stabilize the wheel providing an extra intramolecular force for its formation. We do not know if **1** is the largest ferric wheel containing this type of bridging interaction. Work is in progress for the preparation of other members of the family of $[\{\text{Fe}(\text{OR}')_2(\text{O}_2\text{CR})\}_x]$ wheels by changing the nature of the R, R' groups, while simultaneously we are trying to construct still larger wheels using the “oligomerization of high-nuclearity building blocks” design principle.^[8]

Experimental Section

Solid $\text{Ph}_2\text{C}(\text{OH})\text{COOH}$ (0.23 g, 1.0 mmol) was dissolved in a stirred solution of $\text{Fe}(\text{NO}_3)_3 \cdot 9\text{H}_2\text{O}$ (0.20 g, 0.5 mmol) in hot MeOH (20 mL). The resulting orange-red solution was heated under reflux for 10 min and then the pH value was adjusted to 4 with a solution of LiOH in MeOH. A color change to yellow occurred. The yellow solution was heated further under reflux for 1 h, during which time a yellow precipitate formed. The solid was collected by filtration, washed with cold MeOH and Et_2O (not added to the filtrate) and dried in vacuum, yield 48%; elemental analysis calcd (%) for $\text{C}_{192}\text{H}_{204}\text{O}_{60}\text{Fe}_{12}$ (**1**): C 55.7, H 5.0; found: C 55.6, H 4.9. Yellow crystals of the product were grown by layering the methanolic filtrate with Et_2O ; the formulation $\text{1} \cdot 2\text{H}_2\text{O} \cdot \text{Et}_2\text{O}$ was determined crystallographically, but the analytical sample (consisting of washed and vacuum-dried crystals) was analyzed as solvent-free.

Magnetic susceptibility data were collected on microcrystalline samples of **1** with a Cryogenics S600 SQUID magnetometer with an applied field of 0.1 T and in the temperature range 2–300 K. Data were corrected with the standard procedure for the contribution of the sample holder and diamagnetism of the sample. The Mössbauer spectrum of microcrystalline **1** was measured at room temperature by a conventional constant-acceleration spectrometer equipped with a γ -ray source of ^{57}Co in Rh; isomer shifts were referenced versus a thin α -iron foil at room temperature.

Received: February 28, 2002 [Z18788]

[1] L. J. De Jongh, A. R. Miedema, *Adv. Phys.* **1974**, 23, 1.

[2] C. J. O'Connor, *Prog. Inorg. Chem.* **1982**, 29, 203.

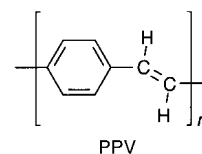
[3] G. L. Abbati, A. Cornia, A. C. Fabretti, W. Malavasi, L. Schenetti, A. Caneschi, D. Gatteschi, *Inorg. Chem.* **1997**, 36, 6443.

- [4] A. Caneschi, A. Cornia, A. C. Fabretti, S. Foner, D. Gatteschi, R. Grandi, L. Schenetti, *Chem. Eur. J.* **1996**, *2*, 1379.
- [5] R. W. Saalfrank, I. Bernt, E. Uller, F. Hampel, *Angew. Chem.* **1997**, *109*, 2596; *Angew. Chem. Int. Ed. Engl.* **1997**, *36*, 2482.
- [6] G. L. Abbati, A. Cornia, A. F. Fabretti, A. Caneschi, D. Gatteschi, *Inorg. Chem.* **1998**, *37*, 1430.
- [7] For example, R. W. Wagner, *Das Rheingold*, Schott, Mainz, **1873**.
- [8] A. L. Dearden, S. Parsons, R. E. P. Winpenny, *Angew. Chem.* **2001**, *113*, 155; *Angew. Chem. Int. Ed.* **2001**, *40*, 152.
- [9] A. Müller, C. Serain, *Acc. Chem. Res.* **2000**, *33*, 2.
- [10] A. J. Blake, C. M. Grant, S. Parsons, J. M. Rawson, R. E. P. Winpenny, *J. Chem. Soc. Chem. Commun.* **1994**, 2363.
- [11] Representative references are: a) I. M. Atkinson, C. Benelli, M. Murrie, S. Parsons, R. E. P. Winpenny, *Chem. Commun.* **1999**, 285; b) N. V. Gerbeleu, Yu. T. Struchkov, G. A. Timco, A. S. Batsanov, K. M. Indrichan, G. A. Popovich, *Dokl. Akad. Nauk. SSSR* **1990**, *313*, 1459; c) E. J. L. McInnes, C. Anson, A. K. Powell, A. J. Thomson, S. Poussereau, R. Sessoli, *Chem. Commun.* **2001**, 89.
- [12] S.-X. Liu, S. Lin, B.-Z. Lin, C.-C. Lin, J.-Q. Huang, *Angew. Chem.* **2001**, *113*, 1118; *Angew. Chem. Int. Ed.* **2001**, *40*, 1084.
- [13] For example, D. Fenske, A. Fischer, *Angew. Chem.* **1995**, *107*, 340; *Angew. Chem. Int. Ed. Engl.* **1995**, *34*, 307.
- [14] a) K. L. Taft, C. D. Delfs, G. C. Papaefthymiou, S. Foner, D. Gatteschi, S. J. Lippard, *J. Am. Chem. Soc.* **1994**, *114*, 823; b) C. Benelli, S. Parsons, G. A. Solan, R. E. P. Winpenny, *Angew. Chem.* **1996**, *108*, 1967; *Angew. Chem. Int. Ed. Engl.* **1996**, *35*, 1825; c) M. Frey, S. G. Harris, J. M. Holmes, D. A. Nation, S. Parsons, P. A. Tasker, R. E. P. Winpenny, *Chem. Eur. J.* **2000**, *6*, 1407; d) A. Caneschi, A. Cornia, A. C. Fabretti, D. Gatteschi, *Angew. Chem.* **1999**, *111*, 1372; *Angew. Chem. Int. Ed.* **1999**, *38*, 1295; e) S. P. Watton, R. Fuhrmann, L. E. Pence, A. Caneschi, A. Cornia, G. L. Abbati, S. J. Lippard, *Angew. Chem.* **1997**, *109*, 2917; *Angew. Chem. Int. Ed. Engl.* **1997**, *36*, 2774.
- [15] P. L. Jones, K. J. Byrom, J. C. Jeffery, J. A. McCleverty, M. D. Ward, *Chem. Commun.* **1997**, 1361.
- [16] a) G. A. Ardizzone, M. A. Angaroni, G. L. Monica, F. Cariatì, S. Cenini, M. Moret, N. Masciocchi, *Inorg. Chem.* **1991**, *30*, 4347; b) C.-H. Chang, K. C. Hwang, C.-S. Liu, Y. Chi, A. J. Carty, L. Scoles, S.-M. Peng, G.-H. Lee, J. Reedijk, *Angew. Chem.* **2001**, *113*, 4787; *Angew. Chem. Int. Ed.* **2001**, *40*, 4651.
- [17] Crystal data for **1**: crystal dimensions 0.15 × 0.30 × 0.60 mm, monoclinic, space group $P2_1/c$, $a = 21.14(1)$, $b = 27.16(1)$, $c = 19.274(9)$ Å, $\beta = 104.99(1)^\circ$, $V = 10689(1)$ Å³, $Z = 2$, $\rho_{\text{calc}} = 1.321$ g cm⁻³, $2\theta_{\text{max}} = 43.8^\circ$, $\text{MoK}\alpha$ ($\lambda = 0.710730$ Å), θ - 2θ scan, $T = 298$ K, 13445 measured reflections, 12909 independent reflections ($R_{\text{int}} = 0.0268$), 12391 reflections included in the refinement. Lorentz, polarization corrections were applied, $\mu = 0.867$ mm⁻¹, $(\Delta/\sigma) = 0.095$, 1262 parameters refined, $R1 = 0.0624$ (for 8482 reflections with $I > 2\sigma(I)$), $wR2 = 0.1453$ (on F^2). Max./min. residual peaks in the final difference map 0.619/−0.414 e Å⁻³. A crystal of **1** was mounted in a glass capillary with drops of mother liquor because of its sensitivity to air exposure. The structure was solved by direct methods using SHELXS-86 and refined by full-matrix least-squares techniques on F^2 using SHELXL-93. All non-hydrogen atoms were refined anisotropically, except for the solvent molecules, which were refined isotropically. All hydrogen atoms were introduced at calculated positions as riding on bonded atoms. CCDC-180394 (**1**) contains the supplementary crystallographic data for this paper. These data can be obtained free of charge via www.ccdc.cam.ac.uk/conts/retrieving.html (or from the Cambridge Crystallographic Data Centre, 12, Union Road, Cambridge CB2 1EZ, UK; fax: (+44) 1223-336-033; or deposit@ccdc.cam.ac.uk).
- [18] a) K. L. Taft, G. C. Papaefthymiou, S. J. Lippard, *Science* **1993**, *259*, 1302; b) A. Caneschi, A. Cornia, S. J. Lippard, G. C. Papaefthymiou, R. Sessoli, *Inorg. Chim. Acta* **1996**, *243*, 295.
- [19] B. P. Murch, F. C. Bradley, P. D. Boyle, V. Papaefthymiou, L. Que, Jr., *J. Am. Chem. Soc.* **1987**, *109*, 7993.
- [20] T. Smith, S. A. Friedberg, *Phys. Rev.* **1968**, *176*, 660.
- [21] R. Hoffmann, *Sci. Am.* **1993**, *268*, 66.

Poly(*p*-phenylenephosphaalkene): A π -Conjugated Macromolecule Containing P=C Bonds in the Main Chain**

Vincent A. Wright and Derek P. Gates*

Approximately twenty years ago, several examples of stable neutral compounds possessing acyclic (p–p) π bonds involving the heavier p-block elements were prepared.^[1] Subsequently, the synthesis, structures, and reactivity of numerous low-coordinate molecules has received extensive study and continues to attract considerable attention.^[2] Despite current interest in the preparation of organic macromolecules possessing π -conjugated backbones,^[3] to our knowledge, the incorporation of heavy-element multiple bonds into a π -conjugated polymer is unprecedented.^[4,5] Furthermore, the incorporation of inorganic elements into the polymer backbone is synthetically challenging and often results in materials with unique properties.^[6] Therefore, the development of methods to prepare π -conjugated polymers containing heavier main-group (p–p) π bonds is of fundamental interest, and may ultimately lead to materials with novel properties.^[7] The poly(*p*-phenylenevinylene)s (PPVs) are an exciting class of luminescent organic macromolecules containing C=C bonds which pose many synthetic challenges.^[3a,c,8] However, the possible incorporation of other stable multiple bonds, such as the well-established P=C moiety,^[9] into the PPV structure has not been explored.^[10] Herein, we report the synthesis and characterization of a poly(*p*-phenylenephosphaalkene), a π -conjugated macromolecule containing phosphorus(III)–carbon double bonds in the polymer backbone.

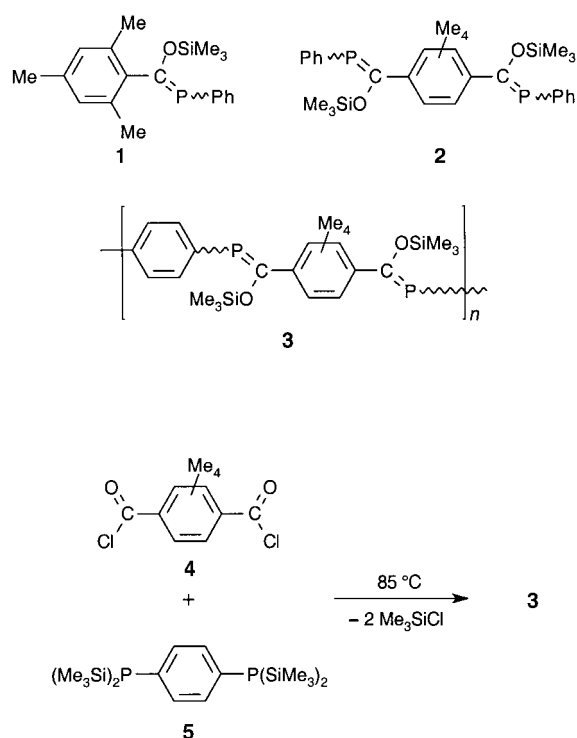


An elegant and general route to phosphorus(III)–carbon double bonds involves the rapid and thermodynamically favorable [1,3]-sigmatropic rearrangement of an acylphosphane to a phosphalkene (Scheme 1).^[1a] From a preparative standpoint, this method is probably the most convenient and versatile route to phosphalkenes with minimal steric protection.^[11] We initiated our investigations by preparing model compounds **1** and **2** for the polymer **3**, under conditions chosen to mimic a typical condensation polymerization. Therefore, phosphalkene **1** was prepared in the absence of solvent by stirring mesitylene-2-carboxylic acid chloride and $\text{PhP}(\text{SiMe}_3)_2$ at 50 °C for several days. Analysis of the reaction mixture by ³¹P NMR spectroscopy showed only two signals

[*] Prof. D. P. Gates, V. A. Wright
Department of Chemistry
University of British Columbia
2036 Main Mall, Vancouver, BC, V6T 1Z1 (Canada)
Fax: (+1) 604-822-2847
E-mail: dgates@chem.ubc.ca

[**] We thank the Natural Sciences and Engineering Research Council (NSERC) of Canada and the University of British Columbia for support of this work, and Prof. M. Wolf for the use of UV/Vis and IR equipment.

Supporting information for this article is available on the WWW under <http://www.angewandte.org> or from the author.



Scheme 1. The [1,3]-sigmatropic rearrangement of an acylphosphane to a phosphalkene.

($\delta = 149.2$, 54 % and 134.0, 46 %), assigned to the *E* and *Z* isomers of **1**, respectively. After distillation (110 °C; 0.1 mmHg), analytically pure **1** was isolated as a pale yellow liquid (yield, 75 %).

Examples of molecules possessing two or more phosphalkene moieties bridged by arylene spacers are uncommon;^[12] furthermore, there are only two previous reports of bis(phosphalkene)s prepared through [1,3]-sigmatropic rearrangement.^[11b, 12b] Thus, we set out to prepare **2** from a concentrated solution of PhP(SiMe₃)₂ (2 equiv) and **4** in THF and hexanes. After several days of heating and monitoring by ³¹P NMR spectroscopy, the PhP(SiMe₃)₂ was completely consumed, and pure **2** (yield, 42 %) was isolated as a colorless powder from a concentrated hexanes solution (–35 °C). Unexpectedly, the ³¹P NMR spectrum of **2** in CDCl₃ shows eight resonances distributed over the regions expected for *E*- (44 %) and *Z*-phosphalkene (56 %) isomers. In addition, there were six resolved signals for OSiMe₃ groups in the ¹H NMR spectrum. Four signals are expected for the three possible isomers (*E,E*; *E,Z*; *Z,Z*), thus, we postulate that the additional NMR signals arise from restricted rotation of the P=C groups about the central aryl plane in **2**.

In order to prepare the target poly(*p*-phenylenephosphalkene), two bifunctional starting reagents (**4** and **5**) were required. The silylated phosphane **5** was prepared by treating 1,4-diphosphanobenzene^[13] with MeLi (4 equiv) in diethyl ether followed by addition of Me₃SiCl (4 equiv).^[14] Analytically pure **5** was obtained as a colorless solid after vacuum sublimation at 100 °C. The thermolysis of **4** and **5** was conducted just above their melting temperature (85 °C) in a vacuum-sealed Pyrex tube. In a typical experiment, after about 24 h the initially colorless, free-flowing liquid was

highly viscous and yellow.^[15] Poly(*p*-phenylenephosphalkene) (**3**) was purified by precipitation of the polymer from a concentrated THF solution with cold hexanes (ca. –30 °C) and subsequent drying in vacuo. The brittle yellow solid (yield, 35 %) was dissolved in C₆D₆ and analyzed by ³¹P NMR spectroscopy, which showed broad overlapping signals for the *E* and *Z* isomers in **3** and for the polymer end groups (see Figure 1).^[16] The ²⁹Si NMR (DEPT) spectrum exhibited three signals ($\delta = 21$ and 18, **3** OSiMe₃; 1.4 ppm (d), **3** P(SiMe₃)₂ end groups) with the signals arising from OSiMe₃ groups in **3** showing similar chemical shifts to those in **1** ($\delta = 21.3$, 18.2 ppm).

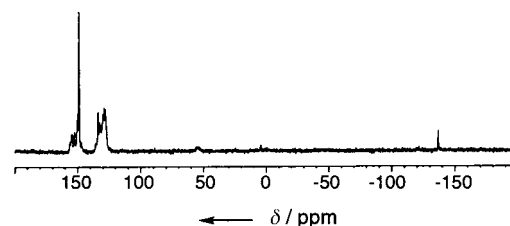


Figure 1. ³¹P NMR spectrum (C₆D₆) of **3** (trial 2) after precipitation with hexanes.

An estimate of the molecular weight (*M_n*) of several samples was obtained from relative integration of the ³¹P NMR signals for P(SiMe₃)₂ end groups and P=C units.^[17] The results are shown in Table 1; samples of **3** had moderate degrees of polymerization (\bar{X}_n , *n* in **3**) between 5 and 21, not

Table 1. Selected characterization data for **1**, **2**, and **3**.

Compound	<i>t</i> _{polym} [h]	\bar{X}_n^*	<i>M_n</i> [*] [g mol ^{–1}]	UV/Vis λ_{max} [nm]	<i>Z/E</i>
1			328	310	0.85
2			550	314	1.27
3 (trial 1)	21	5	2900	328	1.12
3 (trial 2)	27	21	10 500	338	1.14
3 (trial 3)	28	12	6300	334	1.06
3 (trial 4)	34	12	6300	334	1.05

* *M_n* and \bar{X}_n were estimated using end-group analysis (see ref. [17]).

unusual for a step-growth reaction. Moreover, the elemental analyses, including chlorine analysis for two samples, were consistent with the molecular weights estimated from end-group analysis. The ¹³C NMR spectrum exhibited resonances consistent with the assigned structure and, importantly, broad signals for the C=P moiety were detected at $\delta = 212$ and 198 ppm. The infrared spectra of films of **3** were remarkably similar to those for **1**, **2**, and other analogous phosphalkenes.^[11a] The thermal stability of **3** was assessed by thermogravimetric analysis (TGA) under dry helium. The polymer **3** was stable to weight loss up to 190 °C, whereupon approximately 40 % was lost, followed by an additional 20 % at 400 °C. After heating to 800 °C, 40 % of the mass remained as a black solid.

The electronic structure of the new phosphalkenes prepared was probed in THF solution (ca. 10^{–5} M) by using UV/Vis spectroscopy. Few detailed UV/Vis studies have been conducted on phosphalkenes,^[12e, 18] although there are two

possible chromophores; ($n-\pi^*$) and ($\pi-\pi^*$). Typical spectra for the polymer (**3**) and model compounds (**1** and **2**) are shown in Figure 2. Broad absorbances were observed for **1** ($\lambda_{\text{max}} = 310 \text{ nm}$) and **2** ($\lambda_{\text{max}} = 314 \text{ nm}$). Analysis of poly(*p*-phenylenephosphaalkene) (**3**) revealed a broad absorbance ($\lambda_{\text{max}} = 328\text{--}338 \text{ nm}$) and a tail stretching into the visible

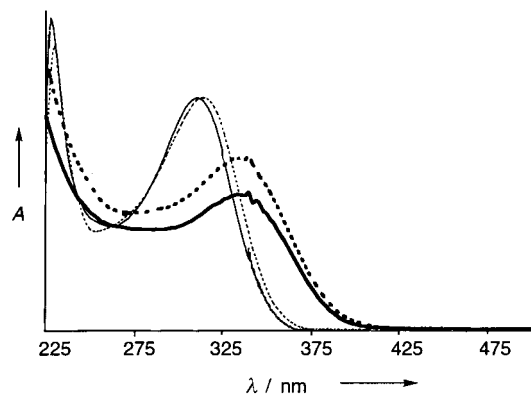


Figure 2. UV/Vis spectra of: **1** —; **2** ---; **3** (trial 3) —; **3** (trial 4) ---.

region. We speculate that the bathochromic shift observed for poly(*p*-phenylenephosphaalkene) compared with **1** and **2** suggests some degree of π -conjugation through the phenylene and $\text{P}=\text{C}$ units. However, the red shift for **3** is less than that for *trans*-PPV compared with *trans*-stilbene (ca. 426 nm vs. 294/307 nm), which we attribute to conformational nonplanarity in the main chain, caused by the bulky C_6Me_4 groups in **3**.^[19, 20] In addition, the breadth of the absorbance for **3** may be caused, in part, by the mixture of isomers present ($Z/E \approx 1.1$; compare *cis*-stilbene (276 nm) and *trans*-stilbene (294/307 nm)),^[20] and/or the polydispersity of the material. Further studies are necessary to confirm the extent of π -conjugation in **3**.

In summary, we have prepared and characterized the first π -conjugated polymer containing $\text{P}=\text{C}$ bonds in the main chain. Future studies will explore the scope of this synthetic methodology and attempt to develop routes to air- and moisture-stable poly(*p*-phenylenephosphaalkene)s.

Experimental Section

All manipulations were performed under a nitrogen atmosphere in a glove box or using standard Schlenk techniques. Assignment of NMR spectra were made with the aid of COSY, APT, HMQC, and HMBC experiments. The *E* and *Z* isomers of **1**, **2**, and **3** were assigned by comparison with analogous systems; the signals arising from the *E* isomer are observed downfield from those of the *Z* isomer in the ^{31}P NMR spectrum.^[11, 21]

1: Bis(trimethylsilyl)phenylphosphane (5.6 g, 22.0 mmol) and mesitylene-2-carboxylic acid chloride (4.0 g, 21.9 mmol) were stirred at 50°C , and over several days quantitative conversion to **1** was observed by ^{31}P NMR spectroscopy. Pure **1** (5.4 g, 75%) was isolated as a pale yellow liquid after vacuum distillation (b.p. 110°C , 0.1 mmHg). **1:** ^{31}P NMR (121.5 MHz, C_6D_6): $\delta = 149.2$ (s, 54%, *E*-**1**), 134.0 ppm (s, 46%, *Z*-**1**); ^1H NMR (400.1 MHz, CDCl_3): *E*-**1**: $\delta = 7.13\text{--}7.01$ (m, 5H; *o*, *m*, *p*-Ph), 6.73 (s, 2H; *m*-Mes), 2.20 (s, 9H; *o*, *p*-CH₃), 0.42 ppm (s, 9H; OSi(CH₃)₃); *Z*-**1**: $\delta = 7.79$ (m, 2H; *o*-Ph), 7.35 (m, 3H; *m*, *p*-Ph), 6.91 (s, 2H; *m*-Mes), 2.48 (s, 6H; *o*-

CH₃), 2.32 (s, 3H; *p*-CH₃), -0.05 ppm (s, 9H; OSi(CH₃)₃); ^{13}C NMR (CDCl_3 , 100.6 MHz): *E*-**1**: $\delta = 197.3$ (d, 1J (C,P) = 49 Hz; C=P), 138.5 (d, 1J (C,P) = 39 Hz; *i*-Ph), 138.0 (d, 2J (C,P) = 9 Hz; *i*-Mes), 137.4 (s; *p*-Mes), 134.2 (d, 3J (C,P) = 5 Hz; *o*-Mes), 133.0 (d, 2J (C,P) = 13 Hz; *o*-Ph), 128.0 (s; *m*-Mes), 127.7 (d, 3J (C,P) = 6 Hz; *m*-Ph), 127.5 (s; *p*-Ph), 21.0 (s; *p*-CH₃), 19.9 (s; *o*-CH₃), 0.3–0.1 ppm (m; OSi(CH₃)₃); *Z*-**1**: $\delta = 210.2$ (d, 1J (C,P) = 41 Hz; C=P), 139.5 (d, 1J (C,P) = 44 Hz; *i*-Ph), 138.1 (s; *p*-Mes), 136.8 (d, 2J (C,P) = 28 Hz; *i*-Mes), 136.5 (d, 3J (C,P) = 8 Hz; *o*-Mes), 133.3 (d, 2J (C,P) = 13 Hz; *o*-Ph), 128.4 (s; *m*-Mes), 128.1 (s; *m*-Ph), 127.5 (s; *p*-Ph), 21.1 (s; *p*-CH₃), 20.7 (s; *o*-CH₃), 0.3–0.1 ppm (m; OSi(CH₃)₃); ^{29}Si NMR (C_6D_6 , 79.5 MHz): $\delta = 21.3$ (s), 18.2 ppm (s); UV/Vis (THF): λ_{max} (ϵ) = 310 nm (6000); IR (neat): $\tilde{\nu} = 2921$ (m), 2853 (m), 1601 (w), 1456 (s), 1377 (m), 1252 (vs), 1187 (vs), 847 cm^{-1} (s); MS (EI, 70 eV): m/z (%): 330 (3), 329 (10), 328 (44) [M^+], 253 (1), 252 (4), 251 (23) [$M^+ - \text{C}_6\text{H}_5$], 148 (9), 147 (100) [$\text{C}_{10}\text{H}_{11}\text{O}$], 74 (5), 73 (72) [$\text{C}_3\text{H}_5\text{Si}$]; elemental analysis: $\text{C}_{19}\text{H}_{25}\text{OSi}$; calcd C 69.48, H 7.67, found C 69.54, H 7.60.

2: To a mixture of bis(trimethylsilyl)phenylphosphane (0.93 g, 3.7 mmol) and **4** (0.47 g, 1.8 mmol) was added hexanes:tetrahydrofuran (5 mL:2 mL) until dissolved. The solution was stirred at 85°C in a closed vessel for a several days and ^{31}P NMR spectroscopy showed quantitative formation of **2**. The solvent was removed in vacuo giving a pale yellow oil, from which **2** was isolated (0.42 g, 42%) as a colorless powder from hexanes at -35°C . **2:** ^{31}P NMR (CDCl_3 , 121.5 MHz): $\delta = 155.2$ (s, 20%), 154.9 (s, 4%), 150.7 (s, 2%), 149.5 (s, 18%), 134.0 (s, 23%), 131.8 (s, 4%), 129.9 (s, 12%), 129.6 ppm (s, 17%); ^1H NMR (CDCl_3 , 300.1 MHz): $\delta = 7.8\text{--}6.9$ (m, 10H; Ph-H), 2.39, 2.38, 2.23, 2.19, 2.11, 2.05, 2.02 (s, 12H; Ar-CH₃), 0.38, 0.31, 0.30 (s; OSi(CH₃)₃, *E* isomers (44%)), -0.09 , -0.10 , -0.15 ppm (s; OSi(CH₃)₃, *Z* isomers (56%)); ^{13}C NMR (CDCl_3 , 75.5 MHz): $\delta = 211.8$ (d, 1J (C,P) = 44 Hz; C=P, *Z*-**2**), 198.6 (d, 1J (C,P) = 49 Hz; C=P, *E*-**2**), 140–137 (m; *i*-Ph and *i*-Ar), 134–132 (m; *o*-Ph), 131–130 (m; *o*-Ar), 128–127 (m; *m*-Ph and *p*-Ph), 19–17 (m; Ar-CH₃), 0.8–0.1 ppm (m; OSi(CH₃)₃); UV/Vis (THF): λ_{max} (ϵ) = 314 nm (28000); IR (neat): $\tilde{\nu} = 3052$ (s), 2956 (vs), 2922 (sh), 1451 (sh), 1432 (s), 1251 (vs), 1192 (vs), 981 (s), 900 (sh), 854 cm^{-1} (vs); MS (EI, 70 eV): m/z (%): 553 (3), 552 (12), 551 (35), 550 (82) [M^+], 475 (4), 474 (6), 473 (26) [$M^+ - \text{Ph}$], 443 (2), 442 (3), 441 (7) [$M^+ - \text{PPhPh}$], 371 (4), 370 (12), 369 (51) [$M^+ - \text{P(Ph)SiMe}_3$], 74 (9), 73 (100) [SiMe_3]; elemental analysis: calcd C 65.42, H 7.32, found C 65.32, H 7.47.

3: The same procedure was followed for each trial (1–4). All glassware was rinsed with Me_3SiCl and flame dried prior to use. Compounds **4** (0.601 g, 2.32 mmol) and **5** (1.00 g, 2.32 mmol) were mixed as finely ground powders, and flame sealed in vacuo in a thick-walled Pyrex tube. The sample was placed in a preheated (85°C) oven, whereupon the solids melted forming a colorless, free-flowing liquid. After 6–8 h, the mixture showed an increase in viscosity and was yellow. The reaction was monitored until the liquid was almost immobile (ca. 24 h), and the yellow/orange material was removed from the oven. The tube was broken, Me_3SiCl was removed in vacuo, and the residue dissolved in a minimum amount of THF (ca. 3 mL). The viscous solution was evenly distributed over the walls of the flask, and cold hexanes (ca. -30°C) were added rapidly to precipitate the polymer as a yellow solid. The hexanes-soluble fraction was removed and the polymer **3** remained (0.384 g, 35%) as a bright yellow glassy solid after drying in vacuo. **3:** ^{31}P NMR (CDCl_3 , 121.5 MHz): $\delta = 157\text{--}149$ (br m; *E*-**3**), 138–124 (br m; *Z*-**3**), -137 ppm (br; $\text{P(SiMe}_3)_2$ end groups; see Table 1 for *Z/E* ratio, and degree of polymerization for each trial). All integrations for end-group analyses are reported with a relaxation delay of 2.0 s; however, spectra were obtained by using 20 s and 30 s delays, and integrals were identical. ^{29}Si NMR (CDCl_3 , 79.5 MHz): $\delta = 21.7\text{--}20.5$ (br m), 18.4–17.0 (br m), 1.4 ppm (d; 1J (Si, P) = 26 Hz, end groups); ^1H NMR (CDCl_3 , 400.1 MHz): $\delta = 7.8\text{--}6.6$ (br m; C_6H_4), 2.5–2.1 (br m; $\text{C}_6(\text{CH}_3)_4$), 0.5– -0.5 ppm (br m; Si(CH₃)₃); ^{13}C NMR (CDCl_3 , 100.6 MHz): $\delta = 211.9$ (br; *Z*-C=P), 197.9 (br; *E*-C=P), 142.0 (br; *i*- C_6Me_4), 139.1 (br; *i*- C_6H_4), 132.4, 130.2 (br; *o*- C_6H_4 , *o*- C_6Me_4), 18.6, 17.5 (br s; $\text{C}_6(\text{CH}_3)_4$), 0.7, 0.2 ppm (br s; OSi(CH₃)₃); UV/Vis (see Table 1); IR (film): $\tilde{\nu} = 2955$ (m), 2921 (m), 2849 (m), 1252 (vs), 1187 (s), 846 cm^{-1} (vs); elemental analysis: $[\text{C}_{24}\text{H}_{34}\text{O}_2\text{P}_2\text{Si}_2]_n + [\text{C}_{26}\text{H}_{43}\text{O}_2\text{P}_2\text{Si}_2\text{Cl}]$; trial 1 calcd ($n = 5$) C 59.80, H 7.32, found C 59.89, H 7.26, trial 3 calcd ($n = 12$) C 60.43, H 7.28, Cl 0.57, found C 60.27, H 7.39, Cl 0.62, trial 4 calcd ($n = 12$) C 60.43, H 7.28, Cl 0.57, found C 59.64, H 7.39, Cl 1.10.

Received: March 7, 2002 [Z18848]

- [1] Selected early breakthroughs in the synthesis of stable compounds containing P=C, P=P, Si=C, Si=Si, P=C bonds: a) G. Becker, *Z. Anorg. Allg. Chem.* **1976**, 423, 242; b) T. C. Klebach, R. Lourens, F. Bickelhaupt, *J. Am. Chem. Soc.* **1978**, 100, 4886; c) M. Yoshifuji, I. Shima, N. Inamoto, K. Hirotsu, T. Higuchi, *J. Am. Chem. Soc.* **1981**, 103, 4587; d) A. G. Brook, F. Abdesaken, B. Gutekunst, G. Gutekunst, R. K. Kallury, *J. Chem. Soc. Chem. Commun.* **1981**, 191; e) R. West, M. J. Fink, J. Michl, *Science* **1981**, 214, 1343; f) G. Becker, G. Gresser, W. Uhl, *Z. Naturforsch. B* **1981**, 36, 16.
- [2] For reviews, see: P. P. Power, *Chem. Rev.* **1999**, 99, 3463; R. Okazaki, N. Tokitoh, *Acc. Chem. Res.* **2000**, 33, 625; M. Yoshifuji, *J. Chem. Soc. Dalton Trans.* **1998**, 3343; L. Weber, *Chem. Ber.* **1996**, 129, 367; N. C. Norman, *Polyhedron* **1993**, 12, 2431; E. Niecke, D. Gudat, *Angew. Chem.* **1991**, 103, 251; *Angew. Chem. Int. Ed. Engl.* **1991**, 30, 217; M. Regitz, *Chem. Rev.* **1990**, 90, 191; R. West, *Angew. Chem.* **1987**, 99, 1231; *Angew. Chem. Int. Ed. Engl.* **1987**, 26, 1201; A. H. Cowley, *Polyhedron* **1984**, 3, 389.
- [3] For reviews, see: a) *Handbook of Conducting Polymers*, 2 ed. (Eds.: T. A. Skotheim, R. L. Elsenbaumer, J. R. Reynolds), Dekker, New York, **1998**; b) A. Kraft, A. C. Grimsdale, A. B. Holmes, *Angew. Chem.* **1998**, 110, 416; *Angew. Chem. Int. Ed.* **1998**, 37, 402; c) W. J. Feast, J. Tsibouklis, K. L. Pouwer, L. Groenendaal, E. W. Meijer, *Polymer* **1996**, 37, 5017; d) U. H. F. Bunz, *Chem. Rev.* **2000**, 100, 1605; e) D. T. McQuade, A. E. Pullen, T. M. Swager, *Chem. Rev.* **2000**, 100, 2537.
- [4] The spontaneous polymerization of PhC≡P has been reported. NMR spectroscopic analysis suggests that the polymer is mainly composed of saturated trivalent phosphane moieties with P=C units being a minor component. D. A. Loy, G. M. Jamison, M. D. McClain, T. M. Alam, *J. Polym. Sci. Part A* **1999**, 37, 129.
- [5] The intriguing polymeric metal, (SN)_n, is a superconductor at 0.26 K, however the electronic structure of this solid-state inorganic material is still under investigation. For a recent review, see: A. J. Banister, I. B. Gorrell, *Adv. Mater.* **1998**, 10, 1415.
- [6] a) I. Mannes, *Angew. Chem.* **1996**, 108, 1712; *Angew. Chem. Int. Ed. Engl.* **1996**, 35, 1602; b) H. R. Allcock, *Adv. Mater.* **1994**, 6, 106; c) J. E. Mark, H. R. Allcock, R. West, *Inorganic Polymers*, Prentice Hall, New Jersey, **1992**.
- [7] For recent examples of conjugated polymers containing inorganic elements, see: M. Altmann, U. H. F. Bunz, *Angew. Chem.* **1995**, 107, 603; *Angew. Chem. Int. Ed. Engl.* **1995**, 34, 569; H. A. Brison, T. P. Pollagi, T. C. Stoner, S. J. Geib, M. D. Hopkins, *Chem. Commun.* **1997**, 1263; N. Matsumi, K. Naka, Y. Chujo, *J. Am. Chem. Soc.* **1998**, 120, 5112; H. Sohn, R. R. Huddleston, D. R. Powell, R. West, K. Oka, X. Yonghua, *J. Am. Chem. Soc.* **1999**, 121, 2935; B. L. Lucht, M. A. Buretea, T. D. Tilley, *Organometallics* **2000**, 19, 3469; S. Yamaguchi, T. Goto, K. Tamao, *Angew. Chem.* **2000**, 112, 1761; *Angew. Chem. Int. Ed.* **2000**, 39, 1695; B. L. Lucht, N. O. St. Onge, *Chem. Commun.* **2000**, 2097.
- [8] J. H. Burroughes, D. D. C. Bradley, A. R. Brown, R. N. Marks, K. Mackay, R. H. Friend, P. L. Burns, A. B. Holmes, *Nature* **1990**, 347, 539.
- [9] See for example: K. B. Dillon, F. Mathey, J. F. Nixon, *Phosphorus: The Carbon Copy*, Wiley, New York, **1998**; R. Appel in *Multiple Bonds and Low Coordination in Phosphorus Chemistry* (Eds.: M. Regitz, O. J. Scherer), Thieme, Stuttgart, **1990**; J. F. Nixon, *Chem. Rev.* **1988**, 88, 1327; F. Mathey, *Acc. Chem. Res.* **1992**, 25, 90; L. Weber, *Eur. J. Inorg. Chem.* **2000**, 2425.
- [10] The poly(azomethines), C=N analogues of PPV, have been known since the 1920s (R. Adams, R. E. Bullock, W. C. Wilson, *J. Am. Chem. Soc.* **1923**, 45, 521) and soluble derivatives exhibiting photoluminescence, liquid crystallinity, high thermal stability, and high tensile strength are known. See for example: P. W. Morgan, S. L. Kwolek, T. C. Pletcher, *Macromolecules* **1987**, 20, 729; T. Matsumoto, F. Yamada, T. Kurosaki, *Macromolecules* **1997**, 30, 3547; O. Thomas, O. Inganäs, M. R. Andersson, *Macromolecules* **1998**, 31, 2676.
- [11] See, for example: a) G. Becker, *Z. Anorg. Allg. Chem.* **1977**, 430, 66; b) G. Becker, O. Mundt, *Z. Anorg. Allg. Chem.* **1978**, 443, 53; c) G. Becker, W. Becker, G. Uhl, *Z. Anorg. Allg. Chem.* **1984**, 518, 21; d) R. Pietschnig, E. Niecke, M. Nieger, K. Airola, *J. Organomet. Chem.* **1997**, 529, 127; e) A. Grünhagen, U. Pieper, T. Kottke, H. W. Roesky, *Z. Anorg. Allg. Chem.* **1994**, 620, 716; f) A. Mack, E. Pierron, T. Allspach, U. Bergsträßer, M. Regitz, *Synthesis* **1998**, 1305.
- [12] See, for example: a) A. Jouaiti, M. Geoffroy, G. Terron, G. Bernardinelli, *J. Chem. Soc. Chem. Commun.* **1992**, 155; b) F. Knoch, R. Appel, H. Wenzel, *Z. Kristallogr.* **1995**, 210, 224; c) A. Jouaiti, M. Geoffroy, G. Terron, G. Bernardinelli, *J. Am. Chem. Soc.* **1995**, 117, 2251; d) H. Kawanami, K. Toyota, M. Yoshifuji, *Chem. Lett.* **1996**, 533; e) S. Shah, T. Concolino, A. L. Rheingold, J. D. Protasiewicz, *Inorg. Chem.* **2000**, 39, 3860.
- [13] E. M. Evleth, L. D. Freeman, R. I. Wagner, *J. Org. Chem.* **1962**, 27, 2192.
- [14] The phosphane (**5**) was mentioned previously, however, detailed synthetic procedures were not described. R. Appel, P. Fölling, B. Josten, W. Schuhn, H. V. Wenzel, F. Knoch, *Z. Anorg. Allg. Chem.* **1988**, 556, 7. Our synthetic procedure and spectroscopic data are provided in the Supporting Information.
- [15] Heating the polymerization mixture for 48 h at 85 °C resulted in an insoluble yellow gel which swelled reversibly in THF. Analysis of the swollen gel by ³¹P NMR spectroscopy showed broad resonances similar to those for the soluble polymer **3**. Presumably, this material is partially cross-linked or high molecular weight **3**.
- [16] Samples of **3** exhibit no change in their NMR spectra after several months of storage in THF solution under an inert atmosphere. Upon exposure to moisture, solutions of **3** rapidly undergo partial hydrolysis, and signals arising from -PH₂ and -PHSiMe₃ end groups were observed by using ³¹P NMR spectroscopy. Excess water results in partial hydrolysis of the O-SiMe₃ side groups giving an enol, which tautomerizes to acylphosphane (δ = -16 ppm; ¹J_{PH} = 232 Hz).
- [17] The molecular weights of **3** were estimated by integration of the P(SiMe₃)₂ and P=C signals in the ³¹P NMR spectrum (relaxation delays of between 2 and 30 s resulted in identical ratios). A statistical (50:50) mixture of C(O)Cl and P(SiMe₃)₂ end groups was assumed; consistent with elemental analysis and the trace of C(O)Cl (δ = 170 ppm) detected in the baseline of the ¹³C NMR spectrum. We speculate that the small resonance at 50 ppm in the ³¹P NMR spectrum of **3** is caused by minor cross-linking of the polymer chains. To date, the sensitivity of **3** towards oxygen and moisture has precluded GPC analysis. Thus far, MALDI-TOF MS has not been successful, perhaps because of the reactivity of **3** with hydroxy-containing matrices.
- [18] H. Kawanami, K. Toyota, M. Yoshifuji, *J. Organomet. Chem.* **1997**, 535, 1.
- [19] Incorporation of 2,3,5,6-tetramethyl-1,4-phenylene units into PPV leads to a blue shift of 20–30 nm in the absorbance spectrum. See S. Chung, D. W. Lee, D. Oh, C. E. Lee, J. Jin, *Acta Polym.* **1999**, 50, 298.
- [20] W. W. Simmons, *The Sadtler Handbook of Ultraviolet Spectra*, Sadtler Research Laboratories, Philadelphia, **1979**.
- [21] For a discussion of the NMR spectra of phosphalkenes see E. Fluck in *Topics in Phosphorus Chemistry*, Vol. 10, Wiley, New York, **1980**, p. 193, and references therein.

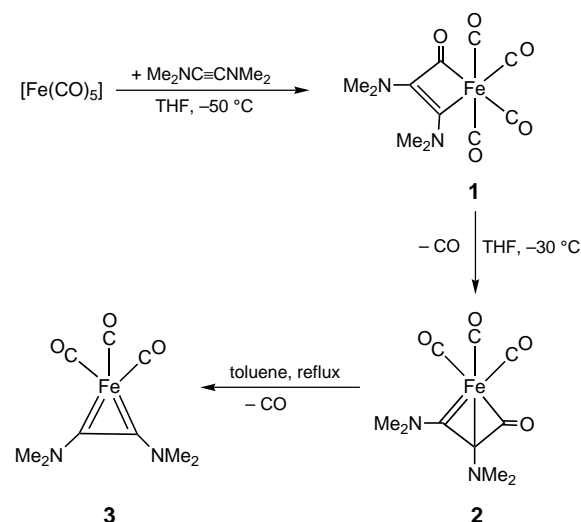
A Reaction Pathway of $[\text{Fe}(\text{CO})_5]$ with Alkynes via Ferrabicyclobutenones**

Alexander C. Filippou* and Torsten Rosenauer

*Dedicated to Professor Gottfried Huttner
on the occasion of his 65th birthday*

Several studies have been carried out on the reactions of $[\text{Fe}(\text{CO})_5]$ with alkynes since the pioneering work of W. Hübel.^[1] These reactions are complex and in general not selective affording a plethora of organometallic complexes and carbocycles.^[1, 2] Common products are the tricarbonyl(η^4 -cyclopentadienone)iron complexes,^[3] which have been widely used in organic synthesis.^[4] The reactions of $[\text{Fe}(\text{CO})_5]$ with alkynes follow a dissociative pathway and need photochemical or high thermal activation because of the large Fe–CO bond dissociation energy.^[5] Along this reaction pathway $[\text{Fe}(\text{CO})_4(\eta^2\text{-alkyne})]$ complexes have been isolated as thermally sensitive solids.^[6] The elementary steps for their conversion into the products remain however unclear. Following our studies on diaminoacetylene complexes^[7] we present here the first example for an associative reaction of $[\text{Fe}(\text{CO})_5]$ with $\text{Me}_2\text{N}-\text{C}\equiv\text{C}-\text{NMe}_2$ to afford a ferrabicyclobutenone and its selective C–C coupling and cleavage reactions to give a multitude of novel organoiron compounds.

Thus, treatment of $[\text{Fe}(\text{CO})_5]$ with $\text{Me}_2\text{N}-\text{C}\equiv\text{C}-\text{NMe}_2$ in THF at -50°C affords a very thermolabile intermediate, which from in situ low-temperature IR and NMR spectroscopy results is suggested to be the ferracyclobutenone **1** (Scheme 1, see Table 1). Complex **1** decarbonylates above about -30°C to give selectively the ferrabicyclobutenone **2**,



Scheme 1.

[*] Prof. Dr. A. C. Filippou, Dipl.-Chem. T. Rosenauer
Institut für Chemie
Humboldt-Universität zu Berlin
Brook-Taylor Strasse 2, 12489 Berlin (Germany)
Fax: (+49)30-2093-6939
E-mail: filippou@chemie.hu-berlin.de

[**] This work was supported by the Deutsche Forschungsgemeinschaft. We thank Dr. B. Ziemer, Dr. G. Kociok-Köhn, and P. Neubauer for the single-crystal X-ray diffraction studies.

which was isolated as an orange, thermally stable solid in 79 % yield (Scheme 1). Complex **2** loses CO either in refluxing toluene or upon melting at 124°C to afford selectively the red alkyne complex **3** in 95 % yield (Scheme 1, Table 1). Compounds **2** and **3**, are the first fully characterized members of two classes of long sought after complexes (Table 1).^[8, 9] The molecular structure of **2** reveals a distorted square-pyramidal complex, in which the C4 and C8 atoms of the ferracycle and two carbonyl ligands (C1–O1, C3–O3) occupy the basal coordination sites (Figure 1).^[10] The four-membered ferracycle is puckered (folding angle $\text{Fe}, \text{C4}, \text{C5}/\text{Fe}, \text{C5}, \text{C8} = 133.0^\circ$).

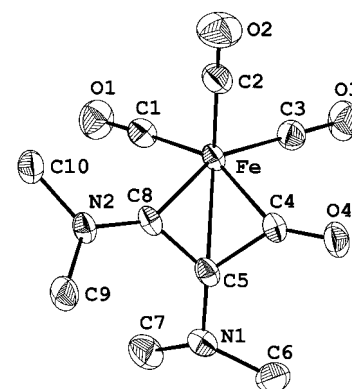


Figure 1. DIAMOND plot of the molecular structure of **2**, hydrogen atoms have been omitted (thermal ellipsoids at the 50 % probability level). Selected bond lengths [Å] and bond angles $^\circ$: Fe–C4 1.933(3), Fe–C5 2.215(2), Fe–C8 1.896(3), C4–C5 1.469(3), C5–C8 1.400(4), C4–O4 1.210(3); C8–Fe–C4 71.91(11), Fe–C4–C5 79.99(15), C4–C5–C8 103.2(2), C5–C8–Fe 82.97(16).

The Fe–C $_{\alpha}$ bond (Fe–C8 1.896(3) Å) is considerably shorter than the Fe–C $_{\beta}$ distance (Fe–C5 2.215(2) Å) and compares well with those of metallacyclic iron–carbene complexes.^[11] This situation suggests in connection with the coplanar arrangement of the atoms Fe, C8, C5, and N2, the planarity of the C $_{\alpha}$ -bonded amino group (sum of the bond angles at N2 359.6°), the short C8–N2 bond (1.306(4) Å) and the short C5–C8 bond (1.400(4) Å) an extensive π -electron delocalization over the atoms Fe, C8, N2, and C5. The C $_{\beta}$ -bonded amino group is not planar as shown by the sum of the bond angles at N1 of 343.1° , and the C5–N1 bond (1.384(3) Å) is intermediate in length between a C–N single (1.46 Å) and C–N double bond (1.27 Å).^[12] The spectroscopic data of **2** also confirm to the solid-state structure (Table 1). Thus, the IR spectrum of **2** in THF displays two characteristic bands at $\tilde{\nu} = 1733$ and 1632 cm^{-1} , which are assigned to the $\nu(\text{C}=\text{O})$ and $\nu(\text{C}_{\beta}\cdots\text{C}_{\alpha}\cdots\text{N})$ vibrations, respectively. The $^{13}\text{C}\{^1\text{H}\}$ NMR spectrum of **2** (CDCl_3 , 25°C) shows a single resonance for the carbonyl ligands at $\delta = 211.4$ suggesting rapid intramolecular CO scrambling and three signals at $\delta = 60.6$, 216.4, and 223.1, which by heteronuclear multiple bond correlation (HMBC) were assigned to the β -, α -, and acyl-carbon atom of the ferrabicyclic, respectively. Furthermore, the variable-temperature ^1H NMR spectra in CDCl_3 (206–298 K) show that complex **2** is fluxional because of hindered rotation of the C $_{\beta}$ -bonded amino group. The activation barrier ΔG^\ddagger for the site exchange of the methyl groups was calculated to be

9.95 kcal mol⁻¹ ($T_c = 215$ K, $\Delta\nu = 152$ Hz). In comparison, rotation of the C_a-bonded amino group is frozen even at ambient temperature giving rise to two methyl proton resonance signals at $\delta = 3.33$ and 3.59 ($\Delta G^\ddagger > 14.4$ kcal mol⁻¹).

The coordination geometry of complex **3** can be described as distorted square pyramidal with two CO ligands (C3–O1, C4–O2) and the alkyne carbon atoms occupying the basal coordination sites (Figure 2).^[10] Distortion results from the

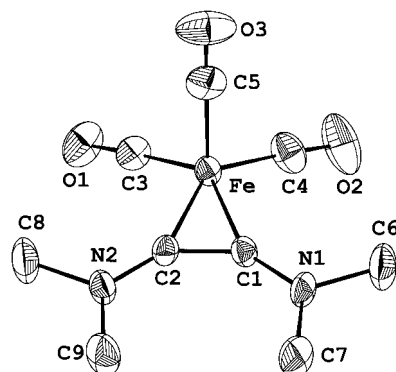
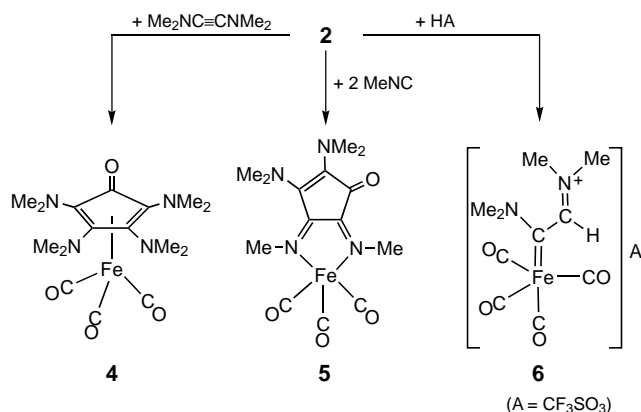


Figure 2. DIAMOND plot of the molecular structure of **3**, hydrogen atoms have been omitted (thermal ellipsoids at the 50% probability level). Selected bond lengths [Å] and bond angles [°]: Fe–C1 1.845(3), Fe–C2 1.844(3), Fe–C3 1.773(4), Fe–C4 1.785(4), Fe–C5 1.787(4), C1–C2 1.375(4), C1–N1 1.318(4), C2–N2 1.333(4); C1–Fe–C2 43.76(14), C3–Fe–C4 98.98(18), C3–Fe–C5 99.68(16), C4–Fe–C5 98.96(18), C_m–Fe–C5 114.87 (C_m denotes the midpoint of the alkyne C–C bond).

small bite angle of the alkyne ligand (43.8(1)°) and the bending of the apical carbonyl ligand (C5–O3) away from the alkyne moiety (C_m–Fe–C5 114.87°, Figure 2). The short Fe–C_{alkyne} bonds (1.844(3) and 1.845(3) Å), the long (C–C)_{alkyne} bond (1.375(4) Å), the short C_{alkyne}–N bonds (1.318(4) and 1.333(4) Å), and the planarity of the coordinated bis(dimethylamino)acetylene unit provide structural evidence for the presence of a four-electron-donor alkyne ligand with extensive π -electron delocalization.^[7] This assignment is supported by the spectroscopic data, such as the IR absorption band of the $\nu(\text{N}\equiv\text{C}\equiv\text{C}\equiv\text{N})$ vibration at 1698 cm⁻¹, the downfield-shifted resonance signal for the alkyne carbon atom at $\delta = 193.8$ ppm, and the hindered rotation of the amino groups, which gives rise to two methyl resonance signals in the ¹H and ¹³C{¹H} NMR spectra at –79 °C (Table 1).^[7] Furthermore the ¹³C{¹H} NMR spectrum of **3** (–79 °C) shows only one carbonyl-carbon resonance at $\delta = 220.5$ ppm indicating a rapid site exchange of the CO ligands on the NMR time scale (Table 1).

Complex **2** is a useful reactive starting material undergoing a variety of selective reactions with nucleophiles.^[13] Thus, treatment of **2** with Me₂N–C≡C–NMe₂ in THF at –50 °C affords selectively the yellow cyclopentadienone complex **4** (Scheme 2, Table 1),^[3d] which provides for the first time experimental evidence for the key role that ferrabicyclobutenones can play in iron-centered [2+2+1] cycloaddition reactions.^[1, 3, 4] Another example of the high reactivity of **2** is the fast reaction with methyl isocyanide (MeNC) in THF at –10 °C to yield, after double isocyanide insertion, the very air-sensitive, black 1,4-diaza-1,3-diene complex **5**, in which



Scheme 2.

Me₂N–C≡C–NMe₂, one carbon monoxide, and two isocyanide molecules have been C–C coupled to give a rare 4,5-diimino-2-cyclopentene-1-one ligand (Scheme 2, Table 1).^[14] Complex **5** adopts a coordination geometry between trigonal bipyramidal and square pyramidal, the carbonyl ligand C7–O3 being the pivot group (Figure 3).^[10] The 1,4-diaza-1,3-diene (DAD) ligand in **5** reveals similar bonding parameters to those of the few other structurally characterized [(DAD)Fe(CO)₃] complexes.^[15]

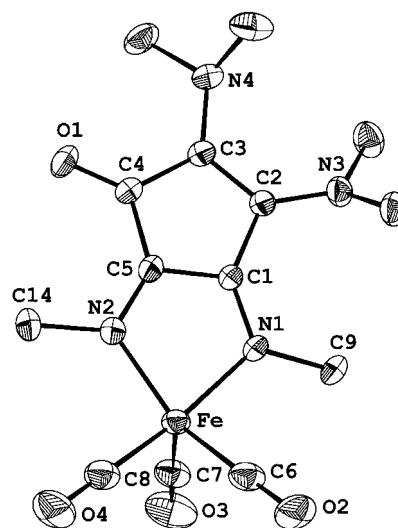


Figure 3. DIAMOND plot of the molecular structure of **5**, hydrogen atoms have been omitted (thermal ellipsoids at the 50% probability level). Selected bond lengths [Å] and bond angles [°]: Fe–N1 1.963(2), Fe–N2 1.928(2), C1–N1 1.316(3), C5–N2 1.318(3), C1–C2 1.487(3), C2–C3 1.391(3), C3–C4 1.487(3), C4–C5 1.487(3), C1–C5 1.412(3), N1–C9 1.470(3), N2–C14 1.473(3), C2–N3 1.367(3), C3–N4 1.391(3); N1–Fe–N2 81.64(9), N1–Fe–C8 165.96(10), N2–Fe–C6 147.94(11).

Complex **2** also reacts with electrophiles as shown by the C–C bond cleavage reaction with CF₃SO₃H in CH₂Cl₂ at 20 °C to afford selectively the orange-yellow aminocarbene complex **6** (Scheme 2, Table 1). Compound **6** is the first reported carbene complex bearing an electron-withdrawing iminium group at the carbene-carbon atom. An almost orthogonal orientation of the carbene-ligand plane (Figure 4; Fe, C5, N1, C8) and the plane of the iminium group

Table 1. Selected analytical data of complexes **1**–**6**.^[a]

[Fe(CO)₅] : IR: $\tilde{\nu}$ = 2019 (s), 1993 cm ^{−1} (vs) ($\nu(\text{C}\equiv\text{O})$).
1 : IR (THF, −50 °C): $\tilde{\nu}$ = 2086 (w), 2034 (s), 2014 cm ^{−1} (vs) ($\nu(\text{C}\equiv\text{O})$); ¹ H NMR ([D ₈]THF, −50 °C, 300.1 MHz): δ = 2.50 (s, 6H, C _β -NMe ₂), 3.39 ppm (broad s, 6H, C _α -NMe ₂); ¹³ C{ ¹ H} NMR ([D ₈]THF, −50 °C, 75.5 MHz): δ = 44.6 (C _β -NMe ₂), 46.0 (broad s, C _α -NMe ₂), 126.6 (C _β), 170.3, 172.0 (C=O, C _α), 204.7 (1 × C≡O), 208.2 (1 × C≡O), 212.8 ppm (2 × C≡O).
2 : IR: $\tilde{\nu}$ = 2035 (vs), 1963 (vs, sh), 1955 (vs) ($\nu(\text{C}\equiv\text{O})$), 1733 (m) ($\nu(\text{C}=\text{O})$), 1632 cm ^{−1} (m) ($\nu(\text{C}\equiv\text{C}\equiv\text{N})$); ¹ H NMR (CDCl ₃): δ = 2.08 (s, 6H, C _β -NMe ₂), 3.33 (s, 3H, C _α -NMe ₄), 3.59 ppm (s, 3H, C _α -NMe ₆); ¹³ C{ ¹ H} NMR (CDCl ₃): δ = 40.4 (C _β -NMe ₂), 43.8 (C _α -NMe ₄), 46.6 (C _α -NMe ₆), 60.6 (C _β), 211.4 (3 × C≡O), 216.4 (C _α), 223.1 ppm (C=O).
3 : yield 95 %, red solid, m.p. 71 °C. IR: $\tilde{\nu}$ = 2011 (s), 1927 (vs) ($\nu(\text{C}\equiv\text{O})$), 1698 cm ^{−1} (m) ($\nu(\text{N}\equiv\text{C}\equiv\text{C}\equiv\text{N})$); ¹ H NMR ([D ₈]toluene, −79 °C): δ = 1.93 (s, 6H, 2 × NMe _A), 2.95 ppm (s, 6H, 2 × NMe _B); ¹³ C{ ¹ H} NMR ([D ₈]toluene, −79 °C): δ = 45.1 (2 × NMe _A), 47.1 (2 × NMe _B), 193.8 (2 × C _{alkyne}), 220.5 ppm (3 × C≡O).
4 : yield 89 %, yellow solid, m.p. 101 °C. IR: $\tilde{\nu}$ = 2030 (s), 1959 (vs) ($\nu(\text{C}\equiv\text{O})$), 1638 cm ^{−1} (m) ($\nu(\text{C}=\text{O})$); ¹ H NMR (CDCl ₃): δ = 2.74 (s, 12H, 2 × NMe ₂), 2.79 ppm (s, 12H, 2 × NMe ₂); ¹³ C{ ¹ H} NMR (CDCl ₃): δ = 41.8 (2 × NMe ₂), 43.8 (2 × NMe ₂), 97.9 (2 × C-NMe ₂), 108.8 (2 × C-NMe ₂), 159.4 (C=O), 211.6 ppm (3 × C≡O).
5 : yield 78 %, black solid, m.p. 93 °C (decomp.). IR: $\tilde{\nu}$ = 2015 (vs), 1941 (vs) ($\nu(\text{C}\equiv\text{O})$), 1670 (m), 1565 (m), 1533 (w), 1505 cm ^{−1} (m) ($\nu(\text{C}=\text{O})$, $\nu(\text{C}=\text{C})$, $\nu(\text{C}=\text{N})$); ¹ H NMR (C ₆ D ₆): δ = 2.03 (s, 6H, NMe ₂), 2.51 (s, 6H, NMe ₂), 3.54 (s, 3H, NMe), 3.97 ppm (s, 3H, NMe); ¹³ C{ ¹ H} NMR (C ₆ D ₆): δ = 41.3 (2C, NMe ₂), 42.9 (2C, NMe ₂), 45.9 (1C, NMe), 47.3 (1C, NMe), 145.6 (1C, C _{ring}), 147.6 (1C, C _{ring}), 148.4 (1C, C _{ring}), 163.9 (1C, C _{ring}), 181.3 (1C, C _{ring}), 216.5 ppm (3 × C≡O).
6 : yield 85 %, orange-yellow solid, m.p. 106 °C (decomp.). IR: $\tilde{\nu}$ = 2053 (s), 1984 (m), 1951 (vs), 1944sh ($\nu(\text{C}\equiv\text{O})$), 1672 (w), 1589 cm ^{−1} (w) ($\nu(\text{C}=\text{N})$); ¹ H NMR (CD ₂ Cl ₂): δ = 3.37(s, broad, 6H, NMe ₂), 3.72 (s, 3H, NMe _A), 3.89 (s, 3H, NMe _B), 8.84 ppm (s, 1H, CH); ¹³ C{ ¹ H} NMR (CD ₂ Cl ₂): δ = 44.1 (very broad, NMe ₂), 48.9 (NMe _A), 51.7 (NMe _B), 150.0 (C(H)NMe ₂), 211.6 (4 × C≡O), 239.6 ppm (Fe=C).

[a] Correct elemental analyses were obtained for complexes **2**–**6**. IR spectra were recorded with a Bruker IFS-55 spectrometer in THF at ambient temperature unless otherwise stated. ¹H and ¹³C{¹H} NMR spectra were recorded on a Bruker AM-300 spectrometer in solution at 25 °C unless otherwise stated.

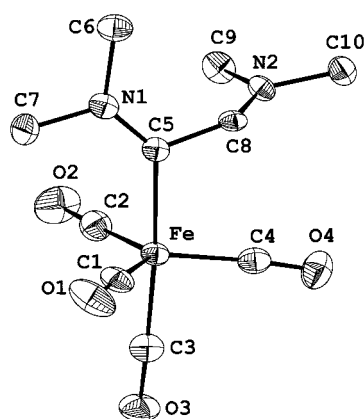


Figure 4. DIAMOND plot of the structure of the cation in **6**, hydrogen atoms have been omitted (thermal ellipsoids at the 50 % probability level). Selected bond lengths [Å] and bond angles [°]: Fe–C5 1.978(6), C5–N1 1.284(9), C5–C8 1.484(9), C8–N2 1.284(8); C5–C8–N2 123.8(6).

(C8,N2,C9,C10), is observed in the trigonal-bipyramidal complex cation (dihedral angle = 83.9°).^[10]

It is not only the unique reaction pathway of [Fe(CO)₅] with Me₂N–C≡C–NMe₂ to give the novel ferrabicyclobutenone **2**

and the experimental evidence that this type of complexes can be the key intermediate in the iron-mediated cyclization of alkynes to cyclopentadienones that merits consideration, but also the diverse reactivity of **2** which provides access to a multitude of new organoiron compounds. Compound **2** is a useful starting material for a multitude of electron-rich ferracycles, which react with electrophiles to give π -electron delocalized systems.

Experimental Section

2: A solution of [Fe(CO)₅] (2.07 g, 10.56 mmol) in THF (90 mL) was treated at −78 °C with Me₂N–C≡C–NMe₂ (0.79 g, 7.04 mmol). The mixture was allowed to warm to room temperature within 3 h and stirred for 1 h. Completion of the reaction was confirmed by IR spectroscopy. The resulting orange solution was evaporated to dryness and the dirty orange residue washed with cold pentane (0 °C; 3 × 10 mL) to remove traces of **4**. The solid was extracted with diethyl ether and the extract filtered to remove some insoluble green material. The filtrate was evaporated to dryness to give complex **2** as an orange, microcrystalline solid. Yield 1.564 g (79 % from Me₂N–C≡C–NMe₂), m.p. 124 °C (decarbonylation to **3**); elemental analysis calcd (%) for C₁₀H₁₂FeN₂O₄ (280.06): C 42.89, H 4.32, N 10.00; found: C 42.79, H 4.41, N 9.71; EI-MS (70 eV): m/z : 280 [M]⁺, 252 [M –CO]⁺, 224 [M –2CO]⁺, 196 [M –3CO]⁺, 168 [M –4CO]⁺, 112 [Me₂NC≡CNMe₂]⁺.

Received: March 19, 2002 [Z18931]

- [1] W. Hübel in *Organic Syntheses via Metal Carbonyls, Vol. 1* (Eds.: I. Wender, P. Pino), Wiley, New York, **1968**, pp. 273–340, and references therein.
- [2] W. R. Fehlhammer, H. Stolzenberg in *Comprehensive Organometallic Chemistry, Vol. 4* (Eds.: G. Wilkinson, F. G. A. Stone, E. W. Abel), Pergamon, Oxford, **1983**, p. 545, and references therein.
- [3] For example: a) E. Weiss, R. Merényi, W. Hübel, *Chem. Ber.* **1962**, *95*, 1170–1178; b) J. L. Boston, D. W. A. Sharp, G. Wilkinson, *J. Chem. Soc.* **1962**, 3488–3494; c) R. B. King, C. A. Harman, *Inorg. Chem.* **1976**, *15*, 879–885; d) C. Wilcox, R. Breslow, *Tetrahedron Lett.* **1980**, *21*, 3241–3242; e) D. Fornals, M. A. Pericàs, F. Serratos, J. Vinaixa, M. Font-Altaba, X. Solans, *J. Chem. Soc. Perkin. Trans.* **1987**, 2749–2752.
- [4] a) A. J. Pearson, A. Perosa, *Organometallics* **1995**, *14*, 5178–5183, and references therein; b) H.-J. Knölker, E. Baum, H. Goesmann, R. Klaus, *Angew. Chem.* **1999**, *111*, 2196–2199; *Angew. Chem. Int. Ed.* **1999**, *38*, 2064–2066, and references therein.
- [5] J. Pearson, J. Cooke, J. Takats, R. B. Jordan, *J. Am. Chem. Soc.* **1998**, *120*, 1434–1440, and references therein.
- [6] J. Cooke, J. Takats, *J. Am. Chem. Soc.* **1997**, *119*, 11088–11089, and references therein.
- [7] A. C. Filippou, B. Lungwitz, G. Kociok-Köhn, *Eur. J. Inorg. Chem.* **1999**, 1905–1910, and references therein.
- [8] To date complexes analogous to **2** have only been postulated as intermediates in metal-centered alkyne–CO coupling reactions: a) T. Mao, Z. Zhang, J. Washington, J. Takats, R. B. Jordan, *Organometallics* **1999**, *18*, 2331–2341; b) M. Barrow, N. L. Cromhout, A. R. Manning, J. F. Gallagher, *J. Chem. Soc. Dalton Trans.* **2001**, 1352–1358.
- [9] To date [M(CO)₃(η^2 -alkyne)] species (M = Fe, Ru, Os) have only been suggested as intermediates to account for the increased reactivity of the complexes [M(CO)₄(η^2 -alkyne)] in carbonyl substitution reactions: a) ref. [5]; b) S. A. Decker, M. Klobukowski, *J. Am. Chem. Soc.* **1998**, *120*, 9342–9355.
- [10] Crystal structure determination of **2**: C₁₀H₁₂FeN₂O₄, M_r = 280.06; orange crystals from diethyl ether upon cooling from 20 → −78 °C, monoclinic, space group $P2_1/c$, a = 8.7893(10), b = 9.359(3), c = 15.2880(14) Å, α = γ = 90, β = 98.530(8)°, V = 1243.6(4) Å³, Z = 4, ρ_{calcd} = 1.496 g cm^{−3}, T = 180(2) K, $2\theta_{\text{max}}$ = 65.8°, μ = 1.216 mm^{−1}, $F(000)$ = 576, 5571 reflections, 2180 unique reflections, 154 param-

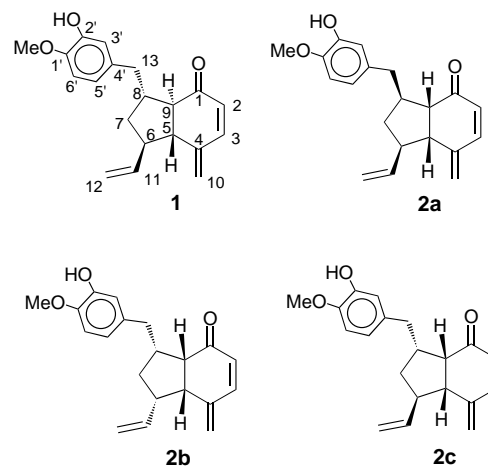
ters, GOF = 1.081, $R_1 = 0.0463$ [$I > 2\sigma(I)$], $wR_2 = 0.1350$, min./max. residual electron density $-0.989/0.599 \text{ e } \text{\AA}^{-3}$. Crystal structure determination of **3+4**: $\text{C}_9\text{H}_{12}\text{FeN}_2\text{O}_3$, $M_r = 252.05$ (**3**), $\text{C}_{16}\text{H}_{24}\text{FeN}_4\text{O}_4$, $M_r = 392.24$ (**4**); orange cocrystals of **3** and **4** (molar ratio 1/1: chromatographic work-up of the product mixture of the reaction of $[\text{Fe}_2(\text{CO})_9]$ with $\text{Me}_2\text{N}-\text{C}\equiv\text{C}-\text{NMe}_2$ containing the complexes **2**, **3**, **4** and $[\text{Fe}_2(\text{CO})_6(\mu-\text{CNMe}_2)_2]$ led to a fraction containing **3** and **4** from which the cocrystals were grown from a pentane solution upon cooling from $20 \rightarrow -30^\circ\text{C}$), triclinic, space group $P\bar{1}$, $a = 8.831(2)$, $b = 8.944(2)$, $c = 21.354(5) \text{ \AA}$, $\alpha = 97.26(3)^\circ$, $\beta = 95.31(3)^\circ$, $\gamma = 113.20(3)^\circ$, $V = 1519.0(7) \text{ \AA}^3$, $Z = 2$, $\rho_{\text{calc}} = 1.409 \text{ g cm}^{-3}$, $T = 160(2) \text{ K}$, $2\theta_{\text{max}} = 52.48^\circ$, $\mu = 1.005 \text{ mm}^{-1}$, $F(000) = 672$, 13 771 reflections, 5573 unique reflections, 361 parameters, GOF = 1.008, $R_1 = 0.0461$ [$I > 2\sigma(I)$], $wR_2 = 0.1311$, min./max. residual electron density $-0.504/0.524 \text{ e } \text{\AA}^{-3}$. Crystal structure determination of **5**: $\text{C}_{14}\text{H}_{18}\text{FeN}_4\text{O}_4$, $M_r = 362.17$; violet crystals from pentane upon cooling from $20 \rightarrow -78^\circ\text{C}$, triclinic, space group $P\bar{1}$, $a = 8.6326(12)$, $b = 10.222(2)$, $c = 11.114(3) \text{ \AA}$, $\alpha = 113.15(2)^\circ$, $\beta = 105.499(17)^\circ$, $\gamma = 99.58(3)^\circ$, $V = 827.2(3) \text{ \AA}^3$, $Z = 2$, $\rho_{\text{calc}} = 1.454 \text{ g cm}^{-3}$, $T = 180(2) \text{ K}$, $2\theta_{\text{max}} = 53.9^\circ$, $\mu = 0.936 \text{ mm}^{-1}$, $F(000) = 376$, 5758 reflections, 3512 unique reflections, 209 parameters, GOF = 1.068, $R_1 = 0.0451$ [$I > 2\sigma(I)$], $wR_2 = 0.1324$, min./max. residual electron density $-0.631/0.685 \text{ e } \text{\AA}^{-3}$. Crystal structure determination of **6**: $\text{C}_{11}\text{H}_{13}\text{F}_3\text{FeN}_2\text{O}_7\text{S}$, $M_r = 430.14$; yellow crystals upon diffusion of diethyl ether in THF at 20°C , triclinic, space group $P\bar{1}$, $a = 6.6594(17)$, $b = 10.490(3)$, $c = 12.988(4) \text{ \AA}$, $\alpha = 102.87(4)^\circ$, $\beta = 100.02(3)^\circ$, $\gamma = 95.78(3)^\circ$, $V = 861.8(4) \text{ \AA}^3$, $Z = 2$, $\rho_{\text{calc}} = 1.658 \text{ g cm}^{-3}$, $T = 180(2) \text{ K}$, $2\theta_{\text{max}} = 50.48^\circ$, $\mu = 1.062 \text{ mm}^{-1}$, $F(000) = 436$, 5674 reflections, 2892 unique reflections, 226 parameters, GOF = 1.109, $R_1 = 0.0776$ [$I > 2\sigma(I)$], $wR_2 = 0.2197$, min./max. residual electron density $-0.725/1.778 \text{ e } \text{\AA}^{-3}$. Instruments: STOE STADI-4 four-circle diffractometer with scintillation counter (**2** and **5**) and STOE-IPDS diffractometer with area detector (**3** and **6**) at $\lambda(\text{MoK}\alpha) = 0.71073 \text{ \AA}$. CCDC-181665–181668 contains the supplementary crystallographic data for this paper. These data can be obtained free of charge via www.ccdc.cam.ac.uk/conts/retrieving.html (or from the Cambridge Crystallographic Data Centre, 12, Union Road, Cambridge CB21EZ, UK; fax: (+44) 1223-336-033; or deposit@ccdc.cam.ac.uk).

- [11] a) J. Park, J. Kim, *Organometallics* **1995**, *14*, 4431–4434; b) R. Schobert, *J. Organomet. Chem.* **2001**, *617–618*, 346–359; c) N. Le Gall, D. Luat, J.-Y. Salaün, H. des Abbayes, L. Toupet, *J. Organomet. Chem.* **2001**, *617–618*, 483–494; d) Theoretical studies are currently in progress to elucidate the nature of the Fe-C β interaction in **2**.
- [12] a) C. Sandorfy in *The Chemistry of the Carbon-Nitrogen Double Bond* (Ed.: S. Patai), Interscience, London, **1970**.
- [13] Additional evidence for the Lewis acidic character of **2** is the formation of adducts with Lewis bases such as PMe_3 . The resulting octahedral ferracyclobutenones $\text{mer}/\text{fac}-[\text{Fe}(\text{CO})_3\text{PMe}_3(\eta^1:\eta^1\text{-C}(\text{NMe}_2)\text{C}(\text{NMe}_2)\text{C}(\text{O}))]$ are related to **1**: T. Rosenauer, A. C. Filippou, unpublished results.
- [14] a) N. Obata, T. Takizawa, *Tetrahedron Lett.* **1969**, 3403–3406; b) N. Obata, T. Takizawa, *Chem. Commun.* **1971**, 587–588; c) R. Breslow, F. A. McCormick, C. Werner, *Tetrahedron Lett.* **1999**, *40*, 2447–2448.
- [15] M. W. Kokkes, D. J. Stufkens, A. Oskam, *J. Chem. Soc. Dalton Trans.* **1983**, 439–445.

Total Synthesis of (\pm)-Otteliones A and B**

Goverdhan Mehta* and Kabirul Islam

The isolation of the two diastereomeric otteliones A and B from the widely occurring but little studied fresh water plant *Ottelia alismoides*, and the determination of their structures, which include a unique 4-methylenecyclohex-2-enone substructure, was reported in 1998.^[1] Collaborative efforts between US and Egyptian scientists, who employed high-field NMR spectroscopy techniques and modeling studies, led to the stereostructure **1** for ottelione B. However, the



structure of ottelione A could not be assigned unambiguously, and both **2a** and **2b** were considered as likely formulations, the former being more likely.^[1] In 2000, scientists at Rhône-Poulenc Rohrer reinterpreted^[2] the NMR spectroscopic data and proposed an alternate stereostructure **2c** for ottelione A (RPR 112378). Otteliones have attracted much attention as they exhibit remarkable, broad-ranging biological activity.^[1–4] Chinese scientists have reported the antitubercular effect of extracts of *Ottelia alismoides*, which is rich in otteliones, and have shown in clinical trials that two cases of bilateral tuberculosis of the cervical lymph gland were cured in three months.^[3] At the National Cancer Institute, in vitro screening against a panel of 60 human cancer cell lines showed that otteliones exhibited cytotoxicity at nM–pM levels.^[1, 4] More recent results have shown that ottelione A is an efficient inhibitor of tubulin polymerization ($\text{IC}_{50} = 1.2 \text{ }\mu\text{M}$) and is able to disassemble preformed microtubules in a manner reminiscent of the colchicines, vinblastine, and vincristine.^[2] The cytotoxicity of otteliones can be attributed to the presence of

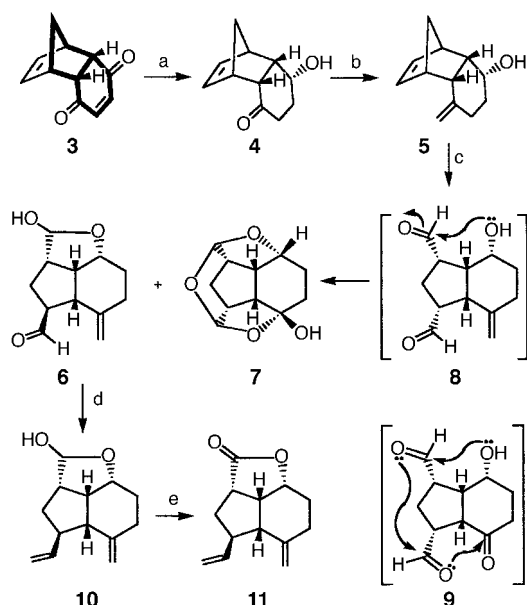
[*] Prof. G. Mehta, K. Islam
Department of Organic Chemistry, Indian Institute of Science
Bangalore-560012 (India)
Fax: (+91) 80-360-0936
E-mail: gm@orgchem.iisc.ernet.in

[**] We would like to thank Professor Thomas R. Hoyer for the NMR spectroscopic data for the otteliones for comparison purposes. K.I. thanks the CSIR (India) for a research fellowship.

Supporting information for this article is available on the WWW under <http://www.angewandte.org> or from the author.

the unique electrophilic 4-methylenecyclohex-2-enone moiety that engages the sulfhydryl groups of the cysteine residues on the tubulin and disrupts the microtubule dynamics; this suggests a mechanism of action similar to that of T138067, a cytotoxic molecule with antitumor activity that reacts specifically with cysteine residue 239 in β -tubulin and is proposed to bind in the close vicinity of the colchicine-binding site.^[2, 5–7] In view of the structural ambiguity and complexity, exceptional therapeutic potential, and the desirability to access analogues, otteliones have aroused considerable synthetic interest. The presence of four contiguous stereogenic centers, the *cis*-hydrindane moiety with side chains at C6 and C8, and the rare and sensitive 4-methylenecyclohex-2-enone functionality make otteliones challenging synthetic targets. We report herein the first total synthesis of racemic otteliones A and B through a short and flexible strategy that fully secures their structure and has potential for accessing diverse analogues.^[8, 9]

The key to our synthetic strategy towards otteliones **1** and **2** was the choice of the readily available Diels–Alder adduct **3** of cyclopentadiene and benzoquinone as the starting point (Scheme 1).^[10] We recognized that **3** embodies a readily

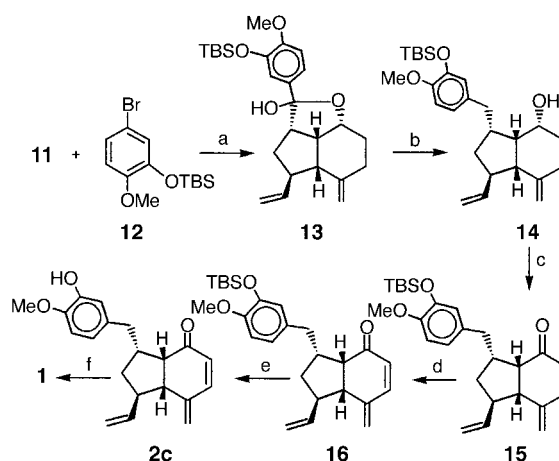


Scheme 1. Reagents and conditions: a) LiAlH_4 , Et_2O , 0°C , 78%; b) $\text{Zn}-\text{TiCl}_4-\text{CH}_2\text{Br}_2$, CH_2Cl_2 , 0°C , 71%; c) 1) O_3 , MeOH , -78°C ; 2) Me_2S , room temperature, 70%; d) $\text{Ph}_3\text{PCH}_3^+\text{I}^-$, $n\text{BuLi}$, THF , 0°C , 89%; e) PCC , CH_2Cl_2 , 0°C , 91%. PCC = pyridinium chlorochromate.

extractable *cis*-hydrindane framework (see bold lines in **3**) whose functionalities can be differentiated and elaborated in a regio- and stereoselective manner to the substitution and functionalization pattern of the natural products. Lithium aluminum hydride reduction of **3** led to both 1,4- and 1,2-reduction to furnish the tricyclic hydroxy ketone **4**.^[11] Lombardo methylenation^[12] of **4** smoothly delivered **5** and set the stage for unraveling the hydrindane moiety. Controlled ozonolysis of **5** delivered **6** and **7** (8:1).^[11] The major product of the reaction, the lactol aldehyde **6** originated through the intramolecular capture of one of the aldehyde moieties of the

intermediate dialdehyde **8** by the appropriately positioned α -hydroxy group and concomitant epimerization of the second aldehyde group to the thermodynamically more stable *exo* orientation. The minor product of the ozonolysis reaction, the dome-shaped pentacyclic ether **7**, was derived through a cascade intramolecular acetalization process in the intermediate keto dialdehyde **9**, which is formed through the oxidative cleavage of both olefinic bonds of **5** (Scheme 1). Wittig olefination of **6** installed the vinyl side chain of **10** with the correct stereochemistry. PCC oxidation of lactol **10** delivered the crystalline lactone **11** whose stereostructure corresponded to the revised^[2] formulation **2c** of ottelione A and was fully secured through single-crystal X-ray structure determination.

We next focused on the introduction of the benzylic side chain at C8 by utilizing the lactone functionality of **11**. The organolithium reagent derived from **12** readily added to **11** to furnish **13**, which was further deoxygenated through lithium/ammonia reduction (Scheme 2). This protocol also released the hydroxy group at C1 to yield **14**. PCC oxidation of **14** to the cyclohexanone **15** was straightforward and set the stage for the generation of the crucial 4-methylenecyclohex-2-



Scheme 2. Reagents and conditions: a) $n\text{BuLi}$, THF , $-78^\circ\text{C} \rightarrow \text{RT}$, 82%; b) Li , liquid NH_3 , THF , -33°C , 63%; c) PCC , CH_2Cl_2 , 0°C , 89%; d) 1) LHMDS , PhSeCl , THF , -78°C ; 2) H_2O_2 (30%), CH_2Cl_2 , 0°C , 61% over two steps; e) TBAF , THF , 0°C , 68%; f) DBU , benzene, 65°C , 83%. DBU = 1,8-diazabicyclo[5.4.0]undec-7-ene, LHMDS = lithium 1,1,1,3,3,3-hexamethyldisilazane, TBAF = tetrabutylammonium fluoride.

enone moiety, which was produced through the phenylselenation–selenoxide elimination sequence to give **16** (Scheme 2). Finally, fluoride-mediated cleavage of the TBS protecting group in **16** furnished ottelione A (**2c**), whose spectra are identical to those of the natural product.^[1, 2] Synthetic **2c** smoothly underwent epimerization at C9 on exposure to base (DBU) to give ottelione B (**1**), whose spectra match those of the natural product (Scheme 2).

To summarize, we have delineated an 11-step, regio- and stereocontrolled synthesis of the biologically potent natural products otteliones A and B from commercially available starting materials in 5.4% overall yield, and have thus fully secured their structures. Our approach is concise and flexible,

amenable to scale-up, geared to provide access to analogues, and involves only one protecting-group manipulation.^[13]

Received: March 12, 2002 [Z18878]

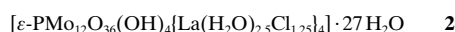
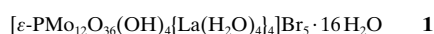
- [1] S. E. N. Ayyad, A. S. Judd, W. T. Shier, T. R. Hoye, *J. Org. Chem.* **1998**, 63, 8102.
- [2] C. Combeau, J. Provost, F. Lanceli, Y. Tournoux, F. Prod'homme, F. Herman, F. Lavelle, J. Leboul, M. Vuilhorgne, *Mol. Pharm.* **2000**, 57, 553.
- [3] H. Li, H. Li, X. Qu, Y. Shi, L. Guo, Z. Yuan, *Zhongguo Zhongyao Zazhi (Chin. J. Chin. Mater. Med.)* **1995**, 20, 115, 128.
- [4] J. Leboul, J. Prevost, French Patent WO96/00205, **1996** [*Chem. Abstr.* **1996**, 124, 242296].
- [5] The 4-methylenecyclohex-2-enone moiety has been rarely reported,^[6] and therefore the interaction of this electrophilic chromophore with biological systems has remained unexplored.
- [6] a) D. F. Murray, M. W. Baum, M. Jones, *J. Org. Chem.* **1986**, 51, 1; b) M. E. Jung, H. L. Rayle, *Synth. Commun.* **1994**, 24, 197; c) H. Wild, *J. Org. Chem.* **1994**, 59, 2748.
- [7] For the details of the interaction of tubulin with drugs and alkylating agents, see: a) R. Kuriyama, H. Sakai, *J. Biochem. (Tokyo)* **1974**, 76, 651; b) R. F. Luduena, M. C. Roach, *Biochemistry* **1981**, 20, 4444; c) B. Shan, J. C. Medina, E. Shanta, W. P. Franckmoelle, T. C. Chau, R. M. Learned, M. R. Narbut, D. Stott, P. Wu, J. C. Jean, T. Rosen, P. B. Timmermans, H. Beckmann, *Proc. Natl. Acad. Sci. USA* **1999**, 96, 5686.
- [8] Our synthetic efforts towards the otteliones began towards the end of 1998, and were initially targeted towards **2a**,^[9a] the then favored structure^[1] of ottelione A, and subsequently towards the other possible formulation **2b**.^[9b] In January 2001, we became aware^[2] of the alternate formulation **2c**, and efforts were directed towards this target. We have completed the total synthesis of **2a–c** and several other diastereomers of otteliones A and B. Spectral data of **2a,b** did not match those of the natural product ottelione A (K. Islam, unpublished results).
- [9] a) G. Mehta, D. S. Reddy, *Chem. Commun.* **1999**, 2193; b) G. Mehta, K. Islam, *Synlett* **2000**, 1473; for other approaches to the otteliones, see: L. Trembleau, L. Patiny, L. Ghosez, *Tetrahedron Lett.* **2000**, 41, 6377.
- [10] a) O. Diels, J. M. Blom, W. Koll, *Justus Liebigs Ann. Chem.* **1925**, 443, 247; b) R. C. Cookson, E. Crundwell, R. R. Hill, J. Hudec, *J. Chem. Soc.* **1964**, 3062.
- [11] All new compounds reported herein are racemic and fully characterized on the basis of IR and ¹H and ¹³C NMR spectroscopic data, mass spectrometry, and elemental analyses (see Supporting Information).
- [12] L. Lombardo, *Tetrahedron Lett.* **1982**, 23, 4293.
- [13] Although the plant *Ottelia alismoides* is regarded as a weed and is widely distributed along irrigation canal linings and rice fields in the Afro-Asian region, otteliones A and B are present only at ppm levels; thus synthetic access through practical routes is necessary to evaluate their biological potential.

[ε-PMo₁₂O₃₆(OH)₄{La(H₂O)₄}]⁵⁺: The First ε-PMo₁₂O₄₀ Keggin Ion and Its Association with the Two-Electron-Reduced α-PMo₁₂O₄₀ Isomer

Pierre Mialane, Anne Dolbecq, Laurent Lisnard, Alain Mallard, Jérôme Marrot, and Francis Sécheresse*

Dedicated to Professor Dr. Gilbert Hervé

Polyoxometalates, often considered as soluble metal oxides, have long attracted interest because of their large field of applications, especially in the domain of heterogeneous catalysis.^[1] The famous Keggin ion [α-PMo₁₂O₄₀]^{3−} was isolated nearly 200 years ago. Isomerization formally results from successive 60° rotations of the four basic Mo₃O₁₃ groups. Although the five isomers α, β, γ, δ, and ε of the Keggin structure have been postulated, only the α^[2] and β^[3] isomers of PMo₁₂O₄₀ have been structurally characterized to date. However, the ε-Keggin structure has been encountered in related compounds which are either polyoxocations, with an Al^{III}₁₂ core and a central tetrahedral Al^{III},^[4] Ga^{III}, or Ge^{III}^[5] center, or polyoxoions with Mo^V₂ and V^V₂ cores. In the case of Mo and V derivatives,^[6] the highly negatively charged structure is stabilized by electrophilic capping groups. The Mo^V₂O₄₀ skeleton has been crystallographically characterized in four polyoxometalates: the [(C₅Me₅Rh^{III})₈(Mo^V₁₂O₃₆)(Mo^{VI}O₄)]²⁺ complex^[7] has a central Mo^{VI}O₄^{2−} tetrahedron and eight Rh^{III} capping centers, the [NaMo₁₆(OH)₁₂O₄₀]^{7−}^[8, 9] and [H₂Mo₁₆(OH)₁₂O₄₀]^{6−}^[8] polyoxometalates are stabilized by four capping Mo^{VI}O₃ units and have a central cavity encapsulating a sodium cation and two protons, respectively. Finally, the most recent example is the [Mo₁₂O₃₀(OH)₁₀H₂{Ni(H₂O)₃}]₄ cluster^[10] with two central protons and four Ni^{II} capping centers. These compounds highlight the capacity of the ε-{Mo₁₂O₄₀} core to encapsulate various guests. We report here the synthesis and characterization of the first ε-Keggin cation with a central phosphorous atom, stabilized by four {La(H₂O)₄}³⁺ capping groups. This cation was isolated in the three different salts **1**, **2** and **3**:



Compound **1** is the bromide salt of the [ε-PMo₁₂O₃₆(OH)₄{La(H₂O)₄}]⁵⁺ polyoxocation. Compounds **2** and **3** have chloride ions directly bound to the capping La³⁺ centers; **2** is a neutral compound while **3** has an [α-PMo₁₂O₄₀]^{5−} ion as the counterion.

Compounds **1** and **2** were characterized by ³¹P NMR, IR, and UV/Vis spectroscopy, elemental analysis, potentiometric

[*] Prof. F. Sécheresse, Dr. P. Mialane, Dr. A. Dolbecq, L. Lisnard, A. Mallard, Dr. J. Marrot
Institut Lavoisier, IREM, UMR 8637
Université de Versailles Saint-Quentin
45 Avenue des Etats-Unis, 78035 Versailles (France)
Fax: (+33)1-39-25-43-81
E-mail: secheresse@chimie.uvsq.fr

titrations, and the structures of compounds **1–3** were determined by single-crystal X-ray diffraction.^[11] In a typical experiment, a solution of Mo^V, freshly prepared by the reduction of sodium molybdate by hydrazine in acidic medium, is mixed with a solution of Mo^{VI}O₄^{2–}, H₂PO₄[–] ions and an excess of La³⁺ ions. Red cubic crystals of **1** form by slow evaporation of an hydrobromic acid solution while crystals of **2** are obtained from a reaction mixture containing chloride ions. The blue color of the filtrate can be attributed to the presence of either high-nuclearity species often known as “molybdenum blues” and extensively studied by Müller et al.^[12] or to partially reduced PMo₁₂O₄₀ species. Attempts to synthesize compounds **1** and **2** in absence of Mo^{VI}O₄^{2–} ions have failed. Indeed, potentiometric titrations have shown that both compounds contain 8 Mo^V and 4 Mo^{VI} centers. This result is unexpected, all the previously characterized ϵ -Keggin molybdenum complexes containing only Mo^V ions. As no intervalence Mo^V→Mo^{VI} charge-transfer bands have been observed by electronic absorption spectroscopy (**1** and **2** are red), it is assumed that the Mo^V centers form Mo^V–Mo^V diamagnetic pairs. Both **1** and **2** contain the ϵ -Mo₁₂O₄₀ core, derived formally from the α -Keggin isomer by rotation of all four Mo₃O₁₃ groups by 60° around the C₃ axes. The twelve Mo ions lie on the vertices of a truncated tetrahedron (Figure 1 b) and form six Mo–Mo pairs. Because of the cubic symmetry of

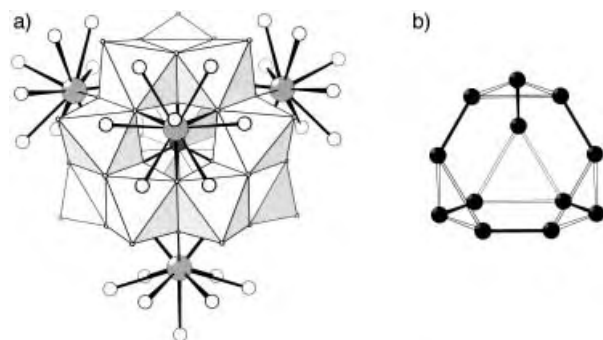


Figure 1. a) Polyhedral representation of the ϵ -Keggin core in **1** capped with four {La(H₂O)₄}³⁺ groups. Six of the terminal oxygen atoms of the water molecules on the La³⁺ ions have half occupancy factors; b) disposition of the twelve Mo atoms, the Mo–Mo pairs are linked in black.

the structure, the four Mo^V–Mo^V and the two Mo^{VI}–Mo^{VI} pairs have been found disordered ($d_{\text{Mo–Mo}} = 2.697(3) - 2.780(1)$ Å). The central cavity accommodates a PO₄ tetrahedron with P–O bonds (1.59(1) Å) in the expected range. The overall *T_d* symmetry of the ϵ -[Mo₁₂O₄₀] structure is maintained by the aggregation of four stabilizing La³⁺ units on the four faces of the truncated tetrahedron defined by the twelve Mo centers (Figure 1a). The La³⁺ ions are bound to the Keggin core by three oxygen atoms. In **1**, their coordination sphere is completed by four water molecules, three of which are disordered over two positions. Seven-coordinate La³⁺ ions are not commonly observed but a few examples have been described.^[13] Furthermore, in **1**, five disordered bromide ions are located in the voids left by the Keggin polyoxocations. The overall charge of the Keggin unit is thus 5+ which implies the presence of four protons on four of the twelve μ_2 -O atoms.

Because of the high symmetry of the cation, these protons cannot be located and are assumed to be delocalized on the overall structure. The detailed formula of the ϵ -Keggin cation in **1** is thus [ε-PMo₈^VMo₃₆^{VI}O₃₆(OH)₄La(H₂O)₄]₄. In **2**, the chloride counterions, which are better ligands than bromide ions, are directly bound to the La³⁺ ions and substitute five of the disordered water molecules ($d_{\text{La–Cl}} = 2.75(1)$ Å).

Compound **1** dissolves readily in water to give dark red solutions. The ³¹P NMR spectrum reveals two resonances δ_1 and δ_2 , located at $\delta = 1.37$ and 0.91, respectively, and with relative intensities 1:5 (Figure 2 a). The evolution of the NMR

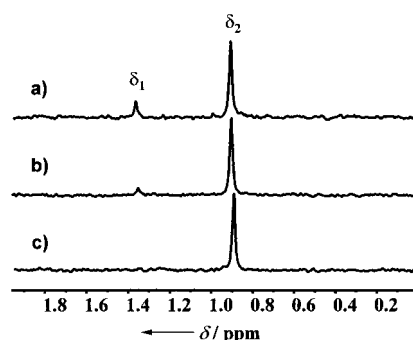
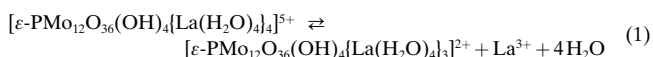


Figure 2. ³¹P NMR spectra of an aqueous solution of [ε-PMo₁₂O₃₆(OH)₄{La(H₂O)₄]₅⁺ (ε-PMo₁₂) to which LaCl₃ was added; the ratios of initial concentrations were a) [La³⁺]:[ε-PMo₁₂]⁰ = 0:1, b) [La³⁺]:[ε-PMo₁₂]⁰ = 0.3:1, c) [La³⁺]:[ε-PMo₁₂]⁰ = 0.8:1.

spectrum after the addition of increasing amounts of LaCl₃ in the solution (Figure 2) has been compared to a similar experiment where LaCl₃ is replaced by NaCl. When NaCl is added, the spectrum remains unchanged while the addition of LaCl₃ has a dramatic effect on the δ_1 line, which progressively decreases and completely disappears. These results show that the Keggin ion is involved in an equilibrium with La³⁺ ions. Considering the evidence of only two ³¹P NMR peaks, we can propose the following equilibrium [Eq. (1)].



The smallest peak (δ_1) is thus attributed to the species with three capping La³⁺ ions while the remaining peak (δ_2) is assigned to the parent ion. From these data the value of the related apparent constant of the equilibrium is $K = 2.4 \times 10^{-4}$ mol L^{–1}. Furthermore, as **1** and **2** have identical ³¹P NMR spectra, it is thus likely that in water the chlorine atoms of **2** are rapidly exchanged with water molecules to give the fully hydrated ions.

When a solution of **2** is left in air at room temperature for several days, a brown powder, totally insoluble in water and in the most usual organic solvents, slowly precipitates which shows that the ϵ -Keggin ion can be readily oxidized. A few dark brown crystals of the oxidation product **3** have been obtained from an aqueous KCl solution of **2**. A single-crystal analysis has shown that, unexpectedly, **3** is a composite of the ϵ cation and an α -Keggin isomer of PMo₁₂O₄₀. As the nonreduced α isomer (0_a) readily decomposes at pH > 2 and

the four-electron-reduced β isomer (IV_β) is more stable than the IV_α isomer in aqueous solution,^[14] it can be postulated that in **3** the α isomer is the two-electron-reduced $[\alpha\text{-PMo}_{12}\text{Mo}_{10}\text{O}_{40}]^{5-}$ (II_α) Keggin ion. Both isomers, the ε - and α -Keggin ions thus play the role of counterions to each other, an unprecedented feature in the chemistry of polyoxometalates. Three chlorine atoms have been found disordered on the four capping La^{3+} groups, which can be explained by the high concentration of chlorine ions in the medium (0.2 M). Concomitantly, three disordered potassium ions have been located in the structure. The geometrical features of the ε -Keggin ions, especially the mean values for the bond valence sum calculations^[15] on the $\mu_2\text{-O}$ atoms, are maintained, which shows that the degree of protonation of the ε -Keggin ion in **2** remains unchanged in **3**. In the α -Keggin ion, the two Mo^{V} units among the twelve Mo centers are delocalized on the overall structure, as usually observed for two-electron-reduced Keggin structures.^[2c, 16] The 3D structure of **3** is remarkable, columns of ε -Keggin polyoxometalates, positively charged, alternate with columns of α -Keggin ions, negatively charged (Figure 3). The positions of the ions, along the

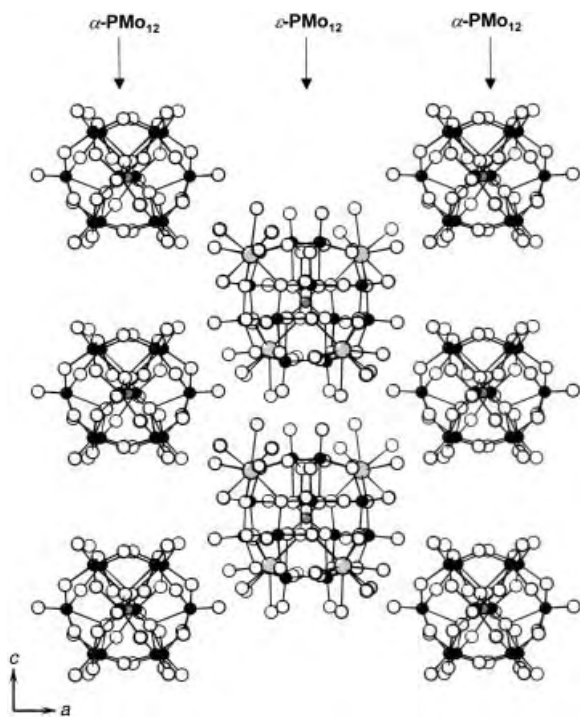


Figure 3. View of the columns of ε - and α -Keggin ions in **3**.

c axis, are shifted from a cationic column to an anionic column, to optimize the cation–anion interactions and obtain the most compact structure. The 3D arrangement can thus be described as a pseudo CsCl structure, which is not surprising considering that the anionic and cationic species can be approximated to spheres of comparable radii (~ 6 Å).

The mechanism of the formation of **3** from **2** involves several intermediates but it can be assumed that in solution, as shown by the NMR spectroscopic studies, two species are in equilibrium, one with four and the other with three capping La^{3+} ions. The loss of one capping La^{3+} ion destabilizes the

ε cation which is more easily oxidized in solution by air, and slowly decomposes to form the II_α Keggin anion. This anion, once formed, precipitates as the totally insoluble salt **3**. This hypothesis was confirmed by the direct synthesis of a mixed salt of the two Keggin derivatives by adding a stoichiometric amount of II_α to a solution of **2**, stabilized by a small quantity of LaCl_3 . A microcrystalline brown precipitate, compound **4**, immediately formed the IR spectrum and X-ray diffraction powder patterns of which are similar to the experimental IR spectrum and to the simulated powder pattern, respectively, of **3** (Figure 4). The microanalysis of **4** is consistent with the formula $[\varepsilon\text{-PMo}_{12}\text{O}_{36}(\text{OH})_4\{\text{La}(\text{H}_2\text{O})_4\}_4][\alpha\text{-PMo}_{12}\text{O}_{40}] \cdot 31\text{H}_2\text{O}$. Compound **4** is thus the analogue of **3** without chloride and potassium ions. Both compounds crystallize in the same crystal lattice, imposed by the large Keggin polyanions and polycations. Similarly **4** can be also synthesized by adding a solution of II_α to an aqueous solution of **1**.

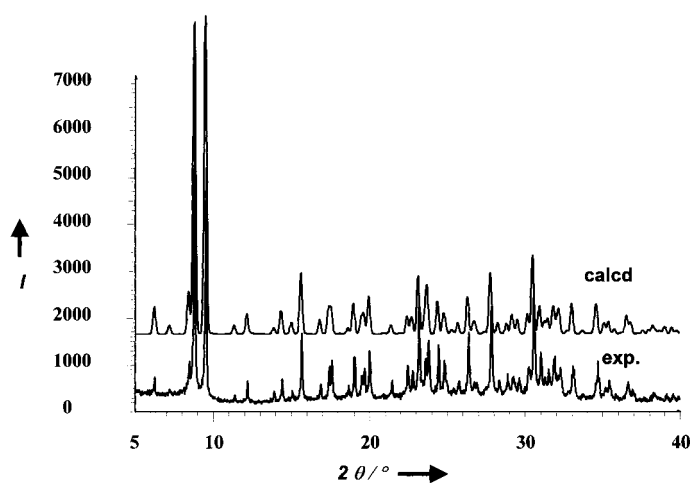


Figure 4. Comparison of the experimental X-ray diffraction powder pattern of **4** and the simulated powder pattern of **3**.

In summary, a novel polyoxocation with the rare ε -Keggin structure has been obtained and characterized. The polyoxocation is soluble in water and can be precipitated with the two-electron-reduced $[\alpha\text{-PMo}_{12}\text{O}_{40}]^{5-}$ Keggin ion to form a composite salt. The crystallization of the ε -Keggin ion in concentrated chloride solutions has shown that the water molecules bound to the lanthanum ions are labile and can be substituted by chloride ions. The functionalization of the ε -Keggin ion could thus be possible by reaction with various ligands, either inorganic (SCN^- , CN^- ...) or organic.

Experimental Section

1: A solution of $[\text{Mo}_2\text{O}_4(\text{H}_2\text{O})_4]^{2+}$ 0.2 M was prepared by dissolving $\text{Na}_2\text{MoO}_4 \cdot 2\text{H}_2\text{O}$ (0.5 g, 2 mmol) in 4 M HBr (10 mL) followed by the addition of $\text{N}_2\text{H}_4 \cdot 2\text{H}_2\text{O}$ (26 μL , 0.5 mmol). The solution was stirred overnight. To this red solution 1 M Na_2MoO_4 (0.5 mL, 0.5 mmol) and 0.1 M NaH_2PO_4 (2.1 mL, 0.21 mmol) was added dropwise. Meanwhile, a solution of La^{3+} ions was obtained by dissolution of La_2O_3 (4.07 g, 12.5 mmol) in HBr 4 M (18.75 mL, 75 mmol). The pH value was adjusted to 1.5 by addition of 8 M NaOH. The dark green reaction mixture was stirred for 15 min, filtered, and then allowed to stand at room temperature for crystallization. After two weeks dark red cubic crystals of **1** (0.114 g, 15% yield, based on

Mo) suitable for X-ray diffraction were collected by filtration and washed with ethanol. It should be noted that the yield of the synthesis is not significantly improved when a stoichiometric amount of Mo^{VI} ions is added in the synthesis. IR: $\tilde{\nu}$ = 999(w), 989(w), 966(w), 930(s), 917(s), 811(m), 766(s), 748(sh), 693(w), 603(m), 518(w), 503(w), 477 cm⁻¹ (w); UV/Vis spectra (H₂O): $\lambda_{\text{max}}(\epsilon)$ = 432 (14100), 292 nm (42200); elemental analysis calcd (%) for H₇₂Br₃La₄Mo₁₂O₇₂P: Br 11.78, La 16.39, Mo 33.97, P 0.91; found Br 11.13, La 15.81, Mo 34.01, P 1.08.

2: A solution of [Mo₂O₄(H₂O)₄]²⁺ 0.2 M was prepared by dissolving Na₂MoO₄·2H₂O (0.5 g, 2 mmol) in 4 M HCl (10 mL) followed by the addition of N₂H₄·2H₂O (26 μ L, 0.5 mmol). The solution was stirred overnight. To this red solution was added dropwise 1 M Na₂MoO₄ (0.5 mL, 0.5 mmol), 0.1 M NaH₂PO₄ (2.1 mL, 0.21 mmol), and then LaCl₃·7H₂O (9.28 g, 25 mmol) dissolved in water (30 mL). The pH value was adjusted to 1.5 by addition of 8 M NaOH. The dark green reaction mixture was stirred for 15 min, filtered and then allowed to stand at room temperature for crystallization. After two weeks dark red cubic crystals of **2** (0.148 g, 21 % yield, based on Mo) suitable for X-ray diffraction studies were filtered and washed with ethanol. The IR spectra of **1** and **2** have the same characteristic bands; elemental analysis calcd (%) for H₁₀₀Cl₃La₄Mo₁₂O₈₆P: Cl 5.23, La 16.38, Mo 33.95, P 0.91; found Cl 5.78, La 16.39, Mo 33.52, P 1.32.

Single crystals of **3:** Solid KCl (0.149 g, 2.0 mmol) was added to a solution of **2** (0.050 g, 1.45 $\times 10^{-5}$ mol) dissolved in water (10 mL). The solution (pH 3.4) was stirred for 5 min and then allowed to stand in air. After a week a few dark brown parallelepiped crystals of **3**, mixed with an unidentified brown powder, were collected by filtration, washed with ethanol and dried with diethyl ether.

II₄: The two-electrons-reduced [α -PMo₁₂O₄₀]⁵⁻ (II₄) ion was synthesized by electrolysis on a platinum electrode at a steady potential (−0.1 V versus standard calomel electrode (SCE)) of a solution of [PMo₁₂O₄₀]³⁻ in HClO₄ 1 M/1,4-dioxane (50/50).^[14] The degree of reduction was controlled by polarography. The acid salt H₃II₄·~20H₂O was precipitated with concentrated HCl, filtered, and dried in air.

4: As solutions of **2** have been found to be air sensitive, the reaction was performed under a nitrogen atmosphere using standard Schlenk techniques. A solution of H₃II₄·~20H₂O (0.065 g, 2.95 $\times 10^{-5}$ mol) in degassed water (5 mL) was added dropwise to a solution of **2** (0.100 g, 2.95 $\times 10^{-5}$ mol) and LaCl₃·7H₂O (0.011 g, 2.95 $\times 10^{-5}$ mol) in degassed water (5 mL). A dark brown precipitate (0.130 g, yield 87%) immediately formed, which was collected by filtration and washed with water and ethanol. IR: $\tilde{\nu}$ = 1055(w), 1018(w), 985(w), 963(w), 935(s), 904(sh), 863(sh), 817(s), 766(s), 693(w), 603(m), 518(w), 503(w), 477 cm⁻¹ (w); elemental analysis calcd (%) for H₁₀₂La₄Mo₂₄O₁₂₇P₂: La 10.88, Mo 45.12, P 1.21; found La 10.90, Mo 45.04, P 1.45, Cl 0.04.

Chemical analyses: redox back titrations for the determination of the amount of Mo^V ions is based on the oxidation of Mo^V by Ce⁴⁺ ions. The sample (about 30 mg) was dissolved in water (20 mL) and excess Ce⁴⁺ ion solution (0.05 M); the excess Ce⁴⁺ ion was titrated potentiometrically with Fe²⁺ ions (0.05 M) using a 702 SM Titrino.

NMR measurements: ³¹P NMR spectra were recorded at 278 K on a Bruker AC-300 spectrometer operating at 121.5 MHz in 5 mm tubes. ³¹P chemical shifts are referenced to the external standard 85 % H₃PO₄. The initial concentration of **1** was [ϵ -PMo₁₂]⁰ = 8.5 $\times 10^{-3}$ M. Increasing amounts of a solution of LaCl₃ ([La³⁺]⁰ = 0.17 M) were added in the NMR tube.

Received: March 1, 2002

Revised: April 8, 2002 [Z18804]

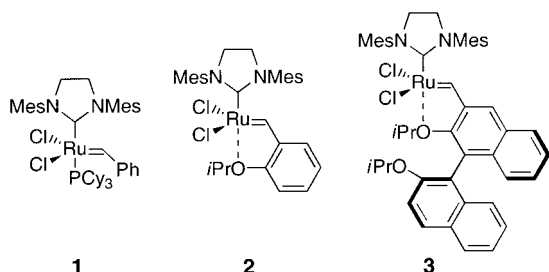
- [1] a) *Polyoxometalates: From Platonic solid to Anti-Retroviral Activity* (Eds.: M. T. Pope, A. Müller), Kluwer Academic Publishers, Dordrecht, **1994**; b) M. T. Pope, A. Müller, *Angew. Chem.* **1991**, 103, 56; *Angew. Chem. Int. Ed. Engl.* **1991**, 30, 34; c) *Chem. Rev.* **1998**, 1–389 (Special issue on Polyoxometalates, Guest Ed. C. Hill).

- [2] a) See for example for the structure of [α -PMo₁₂O₄₀]³⁻: J. C. A. Boeyens, G. J. McDougal, J. Van, R. Smit, *J. Solid State Chem.* **1976**, 18, 191; b) for the structure of the one-electron-reduced anion: A. Prout, S. Taunier, V. Artero, F. Robert, R. Thouvenot, P. Gouzerh, *Chem. Commun.* **1996**, 2195; c) for the two-electron-reduced anion: R. Neier, C. Trojanowski, R. Mattes, *J. Chem. Soc. Dalton Trans.* **1995**, 2521.
- [3] J. N. Barrows, G. B. Jameson, M. T. Pope, *J. Am. Chem. Soc.* **1985**, 107, 1771.
- [4] a) G. Johansson, *Ark. Kemi* **1963**, 20, 305; b) G. Johansson, *Ark. Kemi* **1963**, 20, 321; c) W. O. Parker, R. Millini, I. Kiricsi, *Inorg. Chem.* **1997**, 36, 571.
- [5] A. P. Lee, B. L. Philips, M. M. Olmstead, W. H. Casey, *Inorg. Chem.* **2001**, 40, 4485.
- [6] H. Ichida, K. Nagai, Y. Sasaki, M. T. Pope, *J. Am. Chem. Soc.* **1989**, 111, 586.
- [7] H. K. Chae, W. G. Klemperer, D. E. Paez Loyo, V. W. Day, T. A. Eberspacher, *Inorg. Chem.* **1992**, 31, 3189.
- [8] M. I. Khan, A. Müller, S. Dillinger, H. Bögge, Q. Chen, J. Zubieta, *Angew. Chem.* **1993**, 105, 1811; *Angew. Chem. Int. Ed. Engl.* **1993**, 32, 1780.
- [9] M. I. Khan, Q. Chen, J. Salta, C. J. O'Connor, J. Zubieta, *Inorg. Chem.* **1996**, 35, 1880.
- [10] A. Müller, C. Beugholt, P. Kögerler, H. Bögge, S. Bud'ko, M. Luban, *Inorg. Chem.* **2000**, 39, 5176.
- [11] Crystal data and structure refinements for **1**: a dark red cubic crystal (0.18 \times 0.18 \times 0.16 mm) was analyzed with a Siemens SMART three-circle diffractometer equipped with a CCD bidimensional detector using MoK α monochromatized radiation (λ = 0.71073 Å). Cubic, space group *P*4₃*m*, *a* = 12.2256(1) Å, *V* = 1827.30(3) Å³, *Z* = 1, ρ_{calcd} = 2.757 g cm⁻³, $\mu(\text{MoK}\alpha)$ = 7.105 mm⁻¹, *F*(000) = 1370, 13173 reflections measured, of which 1030 were independent, 57 refined parameters, *R* = 0.0572, *wR*₂ = 0.1474. **2**: a dark red crystal (0.34 \times 0.22 \times 0.22 mm); cubic, space group *P*4₃*m*, *a* = 12.4193(1) Å, *V* = 1915.54(3) Å³, *Z* = 1, ρ_{calcd} = 2.437 g cm⁻³, $\mu(\text{MoK}\alpha)$ = 4.344 mm⁻¹, *F*(000) = 1280, 8636 reflections measured, of which 990 were independent, 69 refined parameters, *R* = 0.0701, *wR*₂ = 0.1766. **3**: a dark brown plate (0.14 \times 0.12 \times 0.04 mm); tetragonal, space group *P*4̄, *a* = 20.2354(2), *c* = 12.3785(2) Å, *V* = 5068.6(1) Å³, *Z* = 2, ρ_{calcd} = 3.182 g cm⁻³, $\mu(\text{MoK}\alpha)$ = 4.857 mm⁻¹, *F*(000) = 4460, 23474 reflections measured, of which 7289 were independent, 399 refined parameters, *R* = 0.0657, *wR*₂ = 0.1248. All the molybdenum and phosphorus atoms of the Keggin ions were refined anisotropically while the potassium, oxygen, and chlorine atoms were refined by using isotropic temperature factors. For **1**, **2**, and **3**, data reduction was performed with the SAINT software. The absorption correction was based on multiple and symmetry-equivalent reflections in the data set using the SADABS program based on the method of Blessing. The structures were solved by direct methods and refined by full-matrix least-squares using the SHELX-TL package. Further details on the crystal structure investigations may be obtained from the Fachinformationszentrum Karlsruhe, 76344 Eggenstein-Leopoldshafen, Germany (fax: (+49) 7247-808-666; e-mail: crysdata@fiz-karlsruhe.de), on quoting the depository numbers CSD-412375 (**1**), -412376 (**2**), and -412377 (**3**).
- [12] A. Müller, J. Meyer, E. Krickemeyer, E. Diemann, *Angew. Chem.* **1996**, 108, 1296; *Angew. Chem. Int. Ed. Engl.* **1996**, 35, 1206.
- [13] a) W. J. Evans, R. E. Golden, J. W. Ziller, *Inorg. Chem.* **1993**, 32, 3041; b) O. Poncelet, L. G. Hubert-Pfalzgraf, J.-C. Daran, R. Astier, *J. Chem. Soc. Chem. Commun.* **1989**, 1846.
- [14] J.-M. Fruchart, P. Souchay, *C. R. Hebd. Seances Acad. Sci. Ser. C* **1968**, 266, 1571.
- [15] N. E. Brese, M. O'Keeffe, *Acta Crystallogr. Sect. B* **1991**, 47, 192.
- [16] a) A. Müller, E. Krickemeyer, M. Penk, V. Wittneben, J. Döring, *Angew. Chem.* **1990**, 102, 85; *Angew. Chem. Int. Ed. Engl.* **1990**, 29, 88; b) N. Casañ-Pastor, P. Gomez-Romero, G. B. Jameson, L. C. W. Baker, *J. Am. Chem. Soc.* **1991**, 113, 5658.

A New Highly Efficient Ruthenium Metathesis Catalyst**

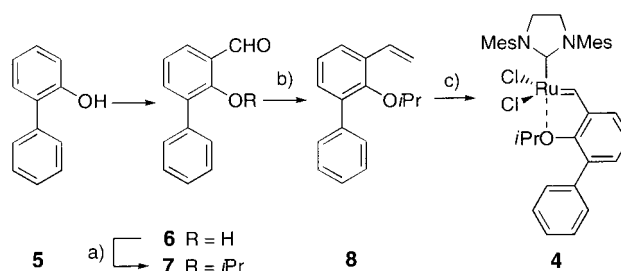
Hideaki Wakamatsu and Siegfried Blechert*

Catalytic olefin metathesis has recently become a powerful tool for carbon—carbon-bond formation in organic chemistry.^[1] Over the last three years it has been demonstrated that ruthenium alkylidenes that bear N-heterocyclic carbene ligands, for example, **1** and similar analogues, exhibit extraordinary activity and stability.^[2] Studies on the mechanism of olefin metathesis reactions have also been described.^[2e,f] Phosphane-free catalyst **2**^[3] has also recently been developed and studied. This catalyst possesses superior general reactivity toward electron-deficient olefins^[4a,b,d] and is readily modified for attachment to solid supports,^[4c,e] thus leading to enhanced recyclability^[4c] and even to efficient metathesis in methanol and water.^[4c] We have also prepared catalyst **3** with the aim of promoting asymmetric induction in metathesis reactions.^[5]



No asymmetric induction was found. However, activity studies^[5] demonstrated a relative reactivity order of **3** > **1** > **2**. BINOL-derived **3** also exhibited a similar shelf stability to **1** and **2**. Herein we report the synthesis and catalytic activity of **4** (Scheme 1), a precatalyst with a markedly greater efficiency in metathesis processes than either **1**, **2**, or **3**.

At first, encouraged by the success of the BINOL-based catalyst **3**, we were interested in determining which structural units in the ligand were responsible for the high initiation rates observed. Extensive studies indicated that the presence of steric bulk adjacent to the chelating isopropoxy moiety was critical. Therefore it seemed logical to synthesize complex **4** as shown in Scheme 1. 2-Hydroxybiphenyl-3-carbaldehyde (**6**) was synthesized from commercially available phenol **5**, according to the literature procedure.^[6] Ligand **8** was obtained by sequential alkylation and Wittig olefination of **6**. The bright green complex **4** could be produced in good yield by the reaction of **1** with **8** (2 equiv), and was purified by flash chromatography. At this point, the potential of **4** in the ring-closing metathesis (RCM) of tosylamide **9** was tested. When these reactions were carried out at 0 °C in the presence of



Scheme 1. Synthesis of catalyst **4**. a) *i*PrBr, NaH, DMF, 50 °C, 82 %; b) $\text{Ph}_3\text{P}^+\text{CH}_3\text{Br}^-$, *t*BuOK, Et_2O , 0 °C, 88 %; c) **1** (1 equiv), **8** (2 equiv), CuCl (1 equiv), CH_2Cl_2 , 40 °C, 71 %.

1 mol% of catalyst, **4** showed a dramatic improvement in activity over **1** and **3** (Figure 1). At room temperature, the reaction catalyzed by **4** was too fast for convenient accurate

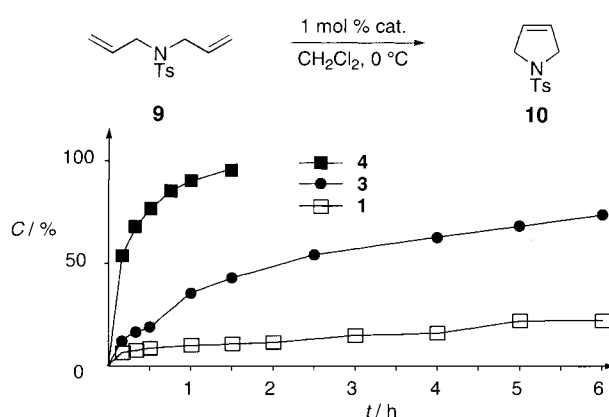
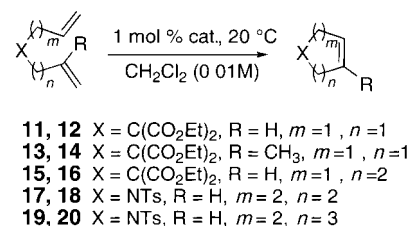


Figure 1. RCM at 0 °C in the presence of catalyst **1**, **3**, and **4**.

measurement. No conversion with catalyst **2** was observed at 0 °C. Consequently in all further metathesis reactions it made more practical sense to compare the new alkylidene **4** with benchmark catalyst **1** instead of with the more sluggish styrene ether based **2**.^[5] It was also observed that as little as 0.05 mol% of **4** could induce cyclization of **9** in 80% yield. The catalyst retained the same activity after being exposed to air in the solid state for one week.

The RCM of miscellaneous substrates was also examined and gave impressive results (Scheme 2, Table 1). The superior activity of complex **4** over complex **1** could be established in all cases.

The applicability of **4** in other metathesis reactions was also tested. The results of cross metathesis (CM) of **21** and **22**



Scheme 2. Various ring-closing metathesis reactions in the presence of catalyst **1** and **4**.

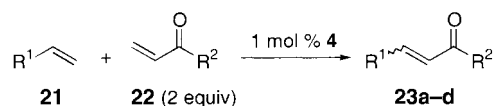
[*] Prof. Dr. S. Blechert, Dr. H. Wakamatsu
 Institut für Chemie, Technische Universität Berlin
 Strasse des 17. Juni 135, 10623 Berlin (Germany)
 Fax: (+49)30-3142-3619
 E-mail: blechert@chem.tu-berlin.de

[**] This work was supported by the Fonds der Chemischen Industrie.

Table 1. Ring-closing metathesis in the presence of **1** and **4**.

Entry	Substrate	Product	Catalyst	time [min]	Yield [%]
1	9	10	4	≪ 10	99
2	9	10	1	60	99
3	11	12	4	≪ 10	99
4	11	12	1	90	99
5	13	14	4	40	99
6	13	14	1	240	99
7	15	16	4	≪ 10	99
8	15	16	1	90	99
9	17	18	4	≪ 10	99
10	17	18	1	60	99
11	19	20	4	≪ 10	99
12	19	20	1	240	93

(Scheme 3) are shown in Table 2. These reactions were carried out at 20 °C in the presence of 1 mol % of catalyst. The reaction of **21a** with **22a** in the presence of **4** yielded **23a** after only 15 minutes (Table 2, entry 1). Under identical



21a: R¹ = (CH₂)₃OBz **22a:** R² = OMe
21b: R¹ = (CH₂)₄OTBS **22b:** R² = Me

Scheme 3. Cross metathesis in the presence of catalyst **1** and **4**.

Table 2. Cross metathesis of **21** and **22**.^[a]

Entry	21	22	Catalyst	time [min]	Yield [%]	(<i>E</i>)- 23 /(<i>Z</i>)- 23
1	a	a	4	15	93	97:3
2	a	a	1	180	86 (12) ^[b]	97:3
3	a	b	4	20	82	99:1
4 ^[c]	b	a	4	20	91	99:1
5	b	b	4	40	90	99:1

[a] All reactions were carried out at 20 °C in CH₂Cl₂ (0.05 M). [b] Conversion after 15 min in parenthesis. [c] Catalyst (2.5 mol %).

conditions, the reaction catalyzed by **1** took 3 h to reach completion, and the conversion after 15 minutes was 12 % (Table 2, entry 2). The efficiency of **4** relative to **1** in ring-opening cross metathesis processes was also tested (Table 3).

Oxanorbornene derivatives *exo*-4,10-dioxatricyclo[5.2.1.0]-dec-8-ene-dione, protected *exo*-3-hydroxymethyl-(bicyclo[2.2.1]hept-5-en-2-yl)-methanol, and its *endo* carbocyclic analogue were treated with allyltrimethylsilane (**24**) at 20 °C in the presence of a minute quantity of catalyst (minimum 0.005 mol %) to give ring-opened products **25**. These reactions highlight the vast difference in activity between **1** and **4**, which could also be seen in the ring-opening metathesis polymerization (ROMP) of cyclooctadiene.^[7] We found the times taken to reach complete conversion of the monomer depended strongly on the reaction conditions, particularly the extent to which oxygen is excluded, but not on the batch of **1** (either purchased from commercial sources or synthesized in our laboratories). For instance, in ROMP reactions with **1**, times of between 30 to over 60 minutes were required, whereas reaction times for **4** were always significantly shorter. Figure 2

Table 3. Ring-opening cross metathesis with **24** (1 equiv) in the presence of catalysts **4** and **1**.^[a]

Entry	25	Catalyst	time [min]	Yield [%]
1 ^[b]	a	4	30	99
2 ^[b]	a	1	30	20 ^[c,d]
3	b	4	5	97
4	b	1	5	1 ^[c,e]
5	c	4	10	87
6	c	1	10	5 ^[c,f]

[a] Conditions: 20 °C, catalyst (0.005 mol %), CH₂Cl₂ (0.05 M). [b] Catalyst (0.025 mol %). [c] Conversions determined by ¹H NMR spectroscopic analysis. [d] Yield = 94 % after 2.5 h. [e] Yield = 92 % after 3 h. [f] Yield = 75 % after 3 h.

represents an example that clearly demonstrates the difference in terms of reactivity between **1** and **4** in a ROMP reaction under identical conditions.

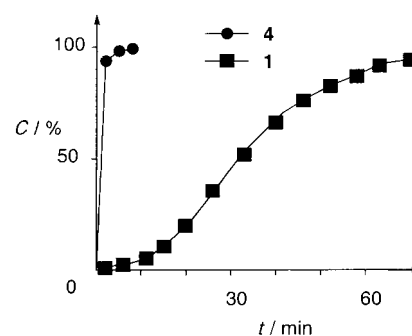


Figure 2. ROMP of cycloocta-1,5-diene in the presence of catalysts **1** and **4**. Conditions: 20 °C, monomer/catalyst ratio 300:1, catalyst = 0.5 mM, CD₂Cl₂ as solvent. Conversion was determined by ¹H NMR.

In an attempt to ascertain the exact cause of the extraordinary activity of precatalyst **4**, the RCM of **9** was monitored under various conditions. At first, parallel experiments were conducted in the presence of **4** (0.01 mol %) in both the presence and absence of ligand **8** (0.1 mol %); however, **10** was obtained in the same yield and reaction time in both cases. Following this, **9** was cyclized by using **4** (1 mol %) in the presence of PCy₃ (1 mol %) and also by using **1** (1 mol %) in the presence of ligand **8** (1 mol %). In the case of the reaction promoted by **4**, the final yield was unchanged, although conversion times were considerably longer. In the latter case, yield and reaction speed were independent of added **8**. We surmise from these results that in the case of catalyst **4**, the active 14-electron species proposed by Grubbs and co-workers^[2f] must be speedily produced by relatively fast dissociation of the bulky ligand **8**, and that in the presence of substrate or added PCy₃, reassociation of **8** to ruthenium metal is slow. Therefore, it is thought that a relatively large proportion of the precatalyst is converted into the active species in solution, thus leading to excellent activity.



In conclusion, we have succeeded in the development of the ruthenium-based metathesis catalyst **4**, which exhibits excellent metathesis activity, without any loss of stability in air. These findings once again demonstrate that seemingly small variations in ligand structure can result in significant improvements in catalysis.

Experimental Section

4: CuCl (21 mg, 0.22 mmol) and then **1** (168 mg, 0.20 mmol) in CH₂Cl₂ (4 mL total) were added to a solution of **8** (94 mg, 0.39 mmol) in CH₂Cl₂ (16 mL) in a glove box. This reaction mixture was stirred for 1 h at 40 °C. The reaction mixture was concentrated in vacuo. The residue was dissolved in a minimum volume of CH₂Cl₂, passed through a Pasteur pipette containing a plug of cotton, and concentrated in vacuo. The residue was purified by flash chromatography on silica gel (4:1 hexane/MTBE) to afford **4** (99 mg, 71 %). ¹H NMR (CD₂Cl₂): δ = 0.81 (d, *J* = 6.2 Hz, 6H), 2.15–2.72 (br, 18H), 4.16 (s, 4H), 4.36 (septet, *J* = 6.2 Hz, 1H), 6.92 (dd, *J* = 0.9, 7.3 Hz, 1H), 6.99 (t, *J* = 7.5 Hz, 1H), 7.06 (br, 4H), 7.31–7.42 (m, 6H), 16.60 ppm (s, 1H); ¹³C NMR (CD₂Cl₂): δ = 19.6, 20.5, 51.2, 77.0, 120.9, 123.1, 127.3, 128.1, 128.6, 128.8, 128.9, 131.1, 132.8, 137.8, 138.5, 138.9, 139.3, 147.7, 148.5, 209.8, 297.4 ppm; IR (film): ν̄ = 3492 (br), 1702 (w), 1605 (w), 1481 (m), 1449 (m), 1422 (m), 1263 (s), 1105 (m) cm⁻¹; HRMS *m/z* calcd for C₃₇H₄₂ON₂Cl₂Ru: [M⁺] 702.1711, found: 702.1719; elemental analysis calcd (%) for C₃₇H₄₂ON₂Cl₂Ru · 1/2 H₂O: C 62.44, H 6.09, N 3.94; found: C 62.32; H 5.97, N 3.88.

Received: April 22, 2002 [Z19143]

Photochemical Sensing of NO₂ with SnO₂ Nanoribbon Nanosensors at Room Temperature**

Matt Law, Hannes Kind, Benjamin Messer, Franklin Kim, and Peidong Yang*

A major area of application for nanowires and nanotubes is likely to be the sensing of important molecules, either for medical or environmental health purposes. The ultrahigh surface-to-volume ratios of these structures make their electrical properties extremely sensitive to surface-adsorbed species, as recent work has shown with carbon nanotubes,^[1, 2] functionalized silicon nanowires and metal nanowires.^[3, 4] Chemical nanosensors are interesting because of their potential for detecting very low concentrations of biomolecules or pollutants on platforms small enough to be used in vivo or on a microchip. Here we report the development of photochemical NO₂ sensors that work at room temperature and are based on individual single-crystalline SnO₂ nanoribbons.

Tin dioxide is a wide-bandgap (3.6 eV) semiconductor. For n-type SnO₂ single crystals, the intrinsic carrier concentration is primarily determined by deviations from stoichiometry in the form of equilibrium oxygen vacancies, which are predominantly atomic defects.^[5] The electrical conductivity of nanocrystalline SnO₂ depends strongly on surface states produced by molecular adsorption that results in space-charge layer changes and band modulation.^[6] NO₂, a combustion product that plays a key role in tropospheric ozone and smog formation, acts as an electron-trapping adsorbate on SnO₂ crystal faces and can be sensed by monitoring the electrical conductance of the material. Because NO₂ chemisorbs strongly on many metal oxides,^[7] commercial sensors based on particulate or thin-film SnO₂ operate at 300–500 °C to enhance the surface molecular desorption kinetics and continuously “clean” the sensors.^[8] The high-temperature operation of these oxide sensors is not favorable in many cases, particularly in an explosive environment. We have found that the strong photoconducting response of individual single-crystalline SnO₂ nanoribbons makes it possible to achieve equally favorable adsorption–desorption behavior at room temperature by illuminating the devices with ultraviolet (UV) light of energy near the SnO₂ bandgap. The active desorption process is thus photoinduced molecular desorption (Figure 1).^[9]

- [1] a) M. Schuster, S. Blechert, *Angew. Chem.* **1997**, *109*, 2124; *Angew. Chem. Int. Ed. Engl.* **1997**, *36*, 2036; b) S. K. Armstrong, *J. Chem. Soc. Perkin Trans. 1* **1998**, 371; c) R. H. Grubbs, S. Chang, *Tetrahedron* **1998**, *54*, 4413; d) A. Fürstner, *Angew. Chem.* **2000**, *112*, 3140; *Angew. Chem. Int. Ed.* **2000**, *39*, 3012; e) T. M. Trnka, R. H. Grubbs, *Acc. Chem. Res.* **2001**, *34*, 18–29.
- [2] a) W. A. Herrmann, M. Speigler, W. C. Schattenmann, T. Westcamp, *Angew. Chem.* **1998**, *110*, 2631; *Angew. Chem. Int. Ed.* **1998**, *37*, 2490; b) W. A. Herrmann, T. Westcamp, L. Ackermann, F. J. Kohl, A. Fürstner, *Tetrahedron Lett.* **1999**, *40*, 4787; c) J. Huang, E. D. Stevens, S. P. Nolan, J. L. Pedersen, *J. Am. Chem. Soc.* **1999**, *121*, 2674; d) M. Scholl, S. Ding, C. W. Lee, R. H. Grubbs, *Org. Lett.* **1999**, *1*, 953; e) M. S. Sanford, M. Ulman, R. H. Grubbs, *J. Am. Chem. Soc.* **2001**, *123*, 749; f) M. S. Sanford, J. A. Love, R. H. Grubbs, *J. Am. Chem. Soc.* **2001**, *123*, 6543.
- [3] a) S. B. Garber, J. S. Kingsbury, B. L. Gray, A. H. Hoveyda, *J. Am. Chem. Soc.* **2000**, *122*, 8168; b) S. Gessler, S. Randl, S. Blechert, *Tetrahedron Lett.* **2000**, *41*, 9973.
- [4] a) S. Randl, S. Gessler, H. Wakamatsu, S. Blechert, *Synlett* **2001**, 430; b) S. Imhof, S. Randl, S. Blechert, *Chem. Commun.* **2001**, 1692; c) S. Randl, N. Buschmann, S. J. Connon, S. Blechert, *Synlett* **2001**, 1547; d) S. Randl, S. J. Connon, S. Blechert, *Chem. Commun.* **2001**, 1796; e) S. J. Connon, S. Blechert, *Bioorg. Med. Chem. Lett.* **2002**, in press.
- [5] H. Wakamatsu, S. Blechert, *Angew. Chem.* **2002**, *114*, 832; *Angew. Chem. Int. Ed.* **2002**, *41*, 794.
- [6] M. M. G. Antonisse, B. H. M. Snellink-Ruël, A. C. Ion, J. F. J. Engbersen, D. N. Reinhoudt, *J. Chem. Soc. Perkin Trans. 2*, **1999**, 1211.
- [7] C. W. Bielawski, R. H. Grubbs, *Angew. Chem.* **2000**, *112*, 3025; *Angew. Chem. Int. Ed.* **2000**, *39*, 2903.

[*] Prof. P. Yang, M. Law, Dr. H. Kind, B. Messer, F. Kim
Department of Chemistry
University of California, Berkeley
Berkeley, CA 94720-1460 (USA)
Fax: (+1) 510-642-7301
E-mail: p_yang@uclink.berkeley.edu

[**] This work was supported by the Camille and Henry Dreyfus Foundation, 3M Corporation, the National Science Foundation, and the University of California, Berkeley. P.Y. is an Alfred P. Sloan Research Fellow. Work at the Lawrence Berkeley National Laboratory was supported by the Office of Science, Basic Energy Sciences, Division of Materials Science of the US Department of Energy. We thank the National Center for Electron Microscopy for the use of their facilities.

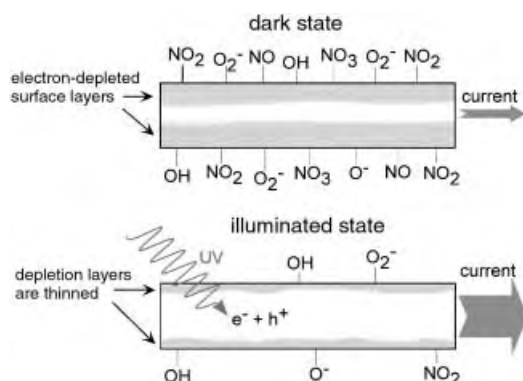


Figure 1. A schematic longitudinal cross-section of a nanoribbon in the dark and in UV light. In the illuminated state, photogenerated holes recombine with trapped electrons at the surface, desorbing NO_2 and other electron-trapping species: $h^+ + \text{NO}_{2(\text{ads})}^- \rightarrow \text{NO}_{2(\text{gas})}$. The space charge layer thins, and the nanoribbon conductivity rises. Ambient NO_2 levels are tracked by monitoring changes in conductance in the illuminated state.

SnO_2 nanoribbons were synthesized using a simple thermal deposition process.^[10–12] The nanoribbons are single crystalline with a rutile structure. Field emission scanning electron microscopy (FE-SEM) and transmission electron microscopy (TEM) imaging (Figure 2) reveal they are tens of μm long

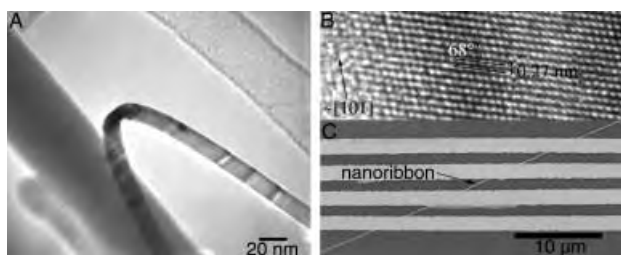


Figure 2. A) Low-resolution TEM image of a thin SnO_2 nanoribbon. The short side of the rectangle is visible near the twist. B) HRTEM image looking down onto the (010) side surface plane near the edge of a nanoribbon, with the lattice spacing and growth direction indicated in agreement with ref. [10]. The angle between the (101) and (011) plane is 68° . C) Typical FE-SEM image of a NO_2 -sensing nanoribbon device on an insulating substrate.

with rectangular cross sections, typically 80–120 nm wide and 10–30 nm thick. High-resolution (HRTEM) analysis confirms that they grow approximately along the [101] direction and present the (101) and (010) rutile planes as surface facets along the growth axis and the (201) plane on the ends. The as-synthesized nanoribbons were deposited from ethanol solution onto prefabricated gold electrodes in a four-terminal configuration, and SEM imaging was used to ensure that only a single nanowire bridged the electrodes of each sample (Figure 2C). The samples were electrically connected to a Keithley source-measure unit and mounted in a home-made test chamber for gas sensing measurements.

We analyzed the optoelectronic response of these devices in air and NO_2 environments in order to probe their chemical-sensing abilities. The behavior of a representative nanoribbon is shown in Figure 3A. In the dark and in pure air (troughs of blue curve), the nanoribbons had resistances ranging from 500 M Ω to 12 G Ω .^[13] When exposed to UV light with a

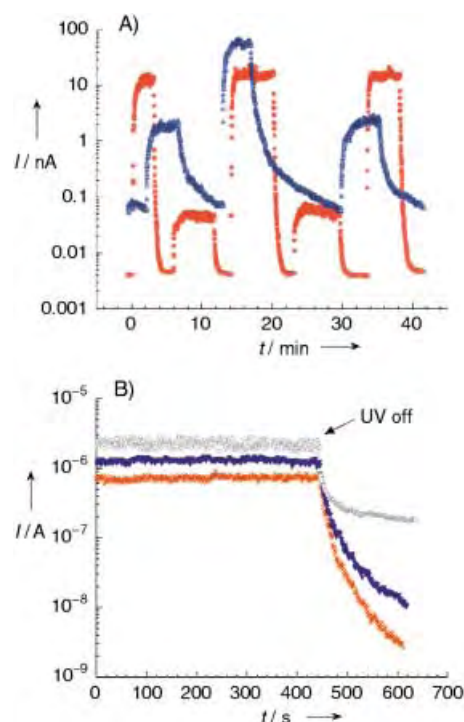


Figure 3. A) Photoresponse of a single nanoribbon in pure air (blue) and 100 ppm NO_2 (red). The large peaks of both curves correspond to 254 nm UV illumination, the small peaks to 365 nm illumination, and the troughs to dark current. The blue-to-red signal ratio is 45:1 under 365 nm light and 4:1 under 254 nm light. Note the shorter decay times in the presence of NO_2 . Bias is 1.0 V. B) Initial decay of the 254 nm photoresponse for a nanoribbon in 8×10^{-5} mbar vacuum (gray), air (blue), and 100 ppm (red) NO_2 . 99.9% decay in vacuum took over 4 h, while the signals in air and NO_2 decayed fully in about 300 and 200 s, respectively. Bias is 0.5 V.

wavelength of 254 nm (intensity = 0.63 mW cm^{-2} ; large peak of blue curve), which corresponds to an energy significantly greater than the SnO_2 bandgap (345 nm), the nanosensor conductance increased by three to four orders of magnitude and stabilized within 1–2 min. The conductance rise is due both to the generation of photocurrent, which directly increases the number of free carriers within the device, and to photodesorption of surface species (mostly O_2^- and H_2O -derived),^[14] with a concomitant thinning of the electron depletion layer near the nanoribbon surface. This phenomenon was also observed recently in ZnO nanowires.^[15]

The effect was fully reversible when the light was turned off, with 99.9% decay of the photoresponse in 300–500 s. Illumination with 365 nm radiation (intensity = 0.5 mW cm^{-2} ; small peaks of blue curve in Figure 3A) also resulted in a photoresponse, typically a 10- to 100-fold increase in the nanoribbon conductance, with slightly faster rise and decay constants than in the 254 nm case. The effect of the 365 nm radiation, which corresponds to an energy slightly smaller than the bandgap, is likely due to the presence of surface states that populate the energy gap. The photoswitching behavior was reproducible at both UV wavelengths indefinitely.

When the nanoribbons were tested in an atmosphere of 100 ppm NO_2 in air (Matheson Tri-Gas), resistance values were higher for all three states—dark, 254-exposed and 365-

exposed (red curve in Figure 3A)—compared to their respective values in pure air. The photoresponse decays were also significantly faster in 100 ppm NO₂, with 99.9% falloffs in 35–50 s. This faster decay rate can be attributed to the strong adsorption and electron-trapping interaction of NO₂ on SnO₂ surfaces. Figure 3B shows the photocurrent decay for a single nanosensor in vacuum, air, and 100 ppm NO₂ environments after exposure to a 254 nm light source. Decay times get shorter and dark currents smaller in the sequence vacuum → air → 100 ppm NO₂, which reflects the availability of gas-phase molecules for adsorption and the better oxidizing ability of NO₂ relative to O₂. Comparing the two curves in Figure 3A shows that the current/conductance difference between the device operating in air and in 100 ppm NO₂ was larger under 365 nm than under 254 nm illumination, so that greater sensitivity to NO₂ occurred using the longer wavelength. The precise reason for this tendency is unknown, but it was observed for all samples and the best nanosensors were operated under continuous 365 nm light during sensing experiments. Note that UV is vital for sensing, as NO₂ adsorption is irreversible in the dark. Figure 4 plots the response ratios of nine of the nanosensors to concentrations of NO₂ from 2–100 ppm.

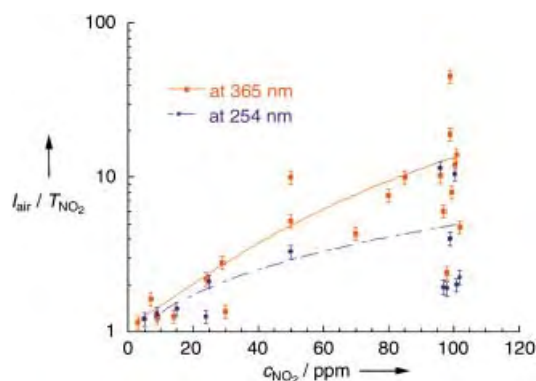


Figure 4. Responses for nine samples at different NO₂ concentrations. Only those samples with response ratios ($I_{\text{air}}/I_{\text{NO}_2}$) greater than 8 at 100 ppm NO₂ were tested at lower concentrations. The fits to the data are suggestive only, as the individual nanoribbons showed nonlinear sensing behavior.

The nature of the electrical contacts between the SnO₂ nanoribbons and the gold electrodes is important to understanding the behavior of these devices, since the contacts dictate whether the metal–semiconductor junctions or the semiconducting nanoribbons themselves are responsible for the photochemical response. Rectifying current (I) versus voltage (V) behavior was observed for many of the nanosensors, indicating that the contacts act as metal–semiconductor Schottky diodes. This suggests that the overall current response in many of the nanowire sensors resulted from four combined effects: 1) photoconductivity of the nanoribbon, 2) NO₂ adsorption on the nanoribbon, 3) photoresponse of the junctions, and 4) modulation of the Schottky potential barriers due to NO₂ activity in the junction regions. Thus, for the samples with non-ohmic contacts, sensing was a collective effect of the nanoribbon and the junctions.

Although most of the nanoribbon sensing devices showed rectifying behavior, samples with ohmic contacts have also been tested with nearly linear I - V characteristics under 254 nm irradiation (Figure 5A). Experiments with these samples (Figure 5B) gave clear evidence that the nanoribbon is the active sensing element when the contacts are ohmic. This suggests that the nanoribbons may dominate the photochemical response even in the non-ohmic devices.

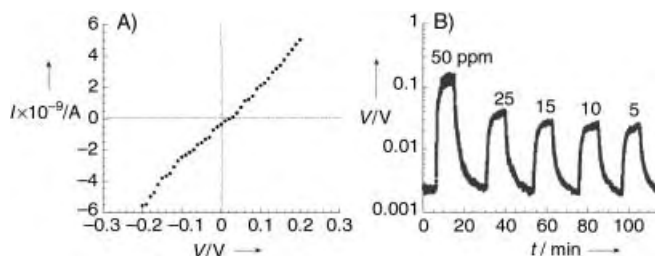


Figure 5. A) A nanoribbon device showing nearly ohmic behavior under 254 nm UV light in 100 ppm NO₂. In this case, the device properties depend predominantly on the nanoribbon itself. B) Cycling the nanoribbon between decreasing concentrations of NO₂ (peaks) and 8×10^{-5} mbar vacuum (troughs) under 254 nm UV light. The resolution limit of the sensor is 5–10 ppm. Current was held constant at 5 nA.

To determine the behavior of the nanosensors under realistic operating conditions, they were cycled through different NO₂ concentrations under continuous 365 nm illumination and in gas flows of 150 sccm (standard cubic centimeters per minute). The devices showed greater sensitivity to low NO₂ concentrations (<15 ppm), while higher concentrations caused smaller signal changes as the nanoribbon surface became saturated with NO₂. In addition, the signal noise decreased at higher concentrations.

The resolution limit achieved by these nanoribbons fell between 2 and 10 ppm for the six samples that showed response ratios of 8 or better at 100 ppm NO₂ under 365 nm light. Figure 6 shows the conductance response of one nanosensor cycled between pure air and 3 ppm NO₂. Even with the low signal-to-noise ratio, current steps can be clearly distinguished as the NO₂ was turned on and off. This behavior was stable for more than 20 cycles without appreciable drift and

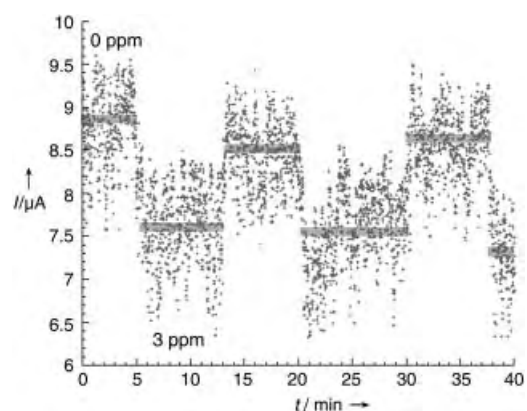


Figure 6. Cycling a nanosensor near its resolution limit under 365 nm light. NO₂ concentrations are indicated. Horizontal bars are signal averages. The average signal difference for the three cycles is 16%. Bias is 0.5 V.

with response times of less than one minute. The average response ratio at 3 ppm NO₂ was 1.16.

Individual SnO₂ nanoribbons are small, fast and sensitive devices for detecting ppm-level NO₂ at room temperature under UV light. These nanodevices can be operated under laboratory conditions over many cycles without loss of sensitivity. The advantages of low-temperature, potentially drift-free operation make SnO₂ nanoribbons good candidates for miniaturized, ultrasensitive gas sensors in many applications. Further sensitivity increases should be achievable by using thinner nanoribbons, developing ohmic SnO₂–metal contacts and decorating these structures with catalysts. With such innovations, the chemical detection of single molecules on nanowires may soon be within reach.

Received: February 22, 2002 [Z18752]

- [1] a) J. Kong, N. Franklin, C. Wu, S. Pan, K. J. Cho, H. Dai, *Science* **2000**, 287, 622; b) R. J. Chen, N. R. Franklin, J. Kong, J. Cao, T. W. Tombler, Y. Zhang, H. Dai, *Appl. Phys. Lett.* **2001**, 79, 2258.
- [2] P. G. Collins, K. Bradley, M. Ishigami, A. Zettl, *Science* **2000**, 287, 1801.
- [3] Y. Cui, Q. Wei, H. Park, C. M. Lieber, *Science* **2001**, 293, 1289.
- [4] F. Favier, E. C. Walter, M. P. Zach, T. Benter, R. M. Penner, *Science* **2001**, 293, 2227.
- [5] C. G. Founstadt, R. H. Rediker, *J. Appl. Phys.* **1971**, 42, 2911.
- [6] O. V. Safonova, M. N. Rumyantseva, L. I. Ryabova, M. Labeau, G. Delabouglise, A. M. Gaskov, *Mater. Sci. Eng. B* **2001**, 85, 43.
- [7] See for example: a) V. E. Henrich, P. A. Cox, *The Surface Science of Metal Oxides*, Cambridge University Press, Cambridge, **1994**; b) J. Tamaki, M. Nagaishi, Y. Teraoka, N. Miura, N. Yamazoe, L. Moriya, Y. Nakamura, *Surf. Sci.* **1989**, 221, 183.
- [8] N. Barsan, M. S. Berberich, W. Goepel, *Fresenius J. Anal. Chem.* **1999**, 365, 287.
- [9] E. Comini, A. Cristalli, G. Faglia, G. Sberveglieri, *Sens. Actuators B* **2000**, 65, 260.
- [10] Z. R. Dai, Z. W. Pan, Z. L. Wang, *Solid State Commun.* **2001**, 118, 351.
- [11] M. Huang, Y. Wu, H. Feick, N. Tran, E. Weber, P. Yang, *Adv. Mater.* **2001**, 13, 113.
- [12] M. Huang, S. Mao, H. Feick, H. Yan, Y. Wu, H. Kind, E. Weber, R. Russo, P. Yang, *Science* **2001**, 292, 1897.
- [13] Resistivity estimates were made difficult by uncertainties in the cross-sectional area of a nanoribbon dispersed across the electrodes of a device. Dark values in air fell from 1 to 500 Ω cm. The resistivity values of the nanoribbons are highly dependent on ambient light levels, the chemical state of the surface and the quality of the electrical contacts; they cannot be directly compared with bulk values. We therefore use only conductance values here.
- [14] N. Yamazoe, J. Fuchigami, M. Kishikawa, T. Seiyama, *Surf. Sci.* **1978**, 86, 335.
- [15] H. Kind, H. Yan, B. Messer, M. Law, P. Yang, *Adv. Mater.* **2002**, 14, 158.

Chirality and Macroscopic Polar Order in a Ferroelectric Smectic Liquid-Crystalline Phase Formed by Achiral Polyphilic Bent-Core Molecules**



Gert Dantlgraber, Alexei Eremin, Siegmund Diele, Anton Hauser, Horst Kresse, Gerhard Pelzl, and Carsten Tschierske*

Materials with a macroscopic polar order have a variety of useful properties, such as piezo- and pyroelectricity and second-order nonlinear optical activity^[1, 2] Especially ferroelectric (FE) and antiferroelectric (AF) liquid crystalline (LC) materials are of great interest, because they can be rapidly switched between different states by means of external electrical fields.^[3, 4] These properties makes them useful for numerous applications, such as electrooptic devices, information storage, switchable NLO (nonlinear optic) devices and light modulators, which may be of interest for optical computing and other future technologies. At first, smectic LC phases with tilted arrangements of nonracemic chiral rodlike and disclike molecules have been used for this purpose and for a long time molecular chirality appeared to be essential for obtaining such materials.^[3] However, the discovery by Niori et al. that bent-core mesogenic compounds (banana-shaped molecules) without molecular chirality, can also organize in fluid smectic phases with a polar order opened a new area in the field of LC research.^[5, 6] The polar structure of the smectic layers of such molecules is provided by the dense directed packing of their bent aromatic cores. However, to escape from a macroscopic polar order the bent direction in adjacent layers is antiparallel, so that the layer polarization alternates from layer to layer, which leads to a macroscopic apolar AF structure.^[7] In most cases of such mesophases the molecules are additionally tilted relative to the layer normal.^[8] Therefore these phases (also known as “B2”-phases) can be described as tilted smectic phases (SmC) with a polar order of the molecules (P) within the layers, and an antiparallel polarization in adjacent layers (A), which leads to the notation SmCP_A. Because the molecules in adjacent layers can have either a synclinic (molecules in adjacent layers are tilted in the same direction, C_S) or an anticlinic (molecules in adjacent layers are tilted in opposite directions, C_A) interlayer correlation, the four different phase structures shown in Figure 1 may result for such mesophases.^[7] Usually, the AF phases represent the ground states, whereas the FE states (SmC_SP_F and SmC_AP_F) can only be achieved after

[*] Prof. Dr. C. Tschierske, G. Dantlgraber
Institute of Organic Chemistry
Martin-Luther-University Halle-Wittenberg
Kurt-Mothes-Strasse 2, 06120 Halle (Germany)
Fax: (+49) 345-55-27223
E-mail: tschierske@chemie.uni-halle.de

A. Eremin, Dr. S. Diele, Dr. A. Hauser, Prof. Dr. H. Kresse,
Prof. Dr. G. Pelzl
Institute of Physical Chemistry
Martin-Luther-University Halle-Wittenberg

[**] This work was supported by the Deutsche Forschungsgemeinschaft and the Fonds der Chemischen Industrie.

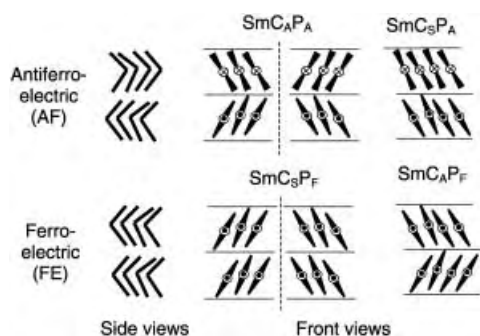
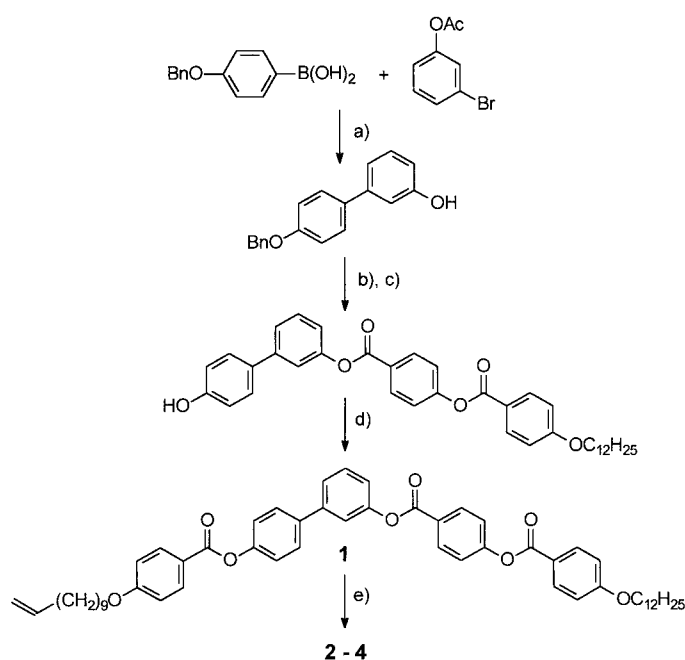


Figure 1. The four possible states of SmCP phases that are distinguished by the relative tilt sense and the polar order in adjacent layers. The notations C_S and C_A refer to synclinal and anticlinal tilt while P_F and P_A refer to ferroelectric (FE) and antiferroelectric (AF) polar order in adjacent layers.^[7]

applying a sufficiently strong external electric field. They are not stable and relax back to the AF state after the electric field is switched off. Only recently first examples of ferroelectric switchable mesophases were reported for a few special bent-core molecules. Remarkably, the materials showing this special switching behavior in fluid smectic phases (SmCP phases) are chiral molecules or their mixtures.^[9] Ferroelectric switching was also observed for higher-ordered “banana phases”, for a “B7” phase formed by a racemic mixture^[10] of bent molecules and for a “B5” phase formed by achiral molecules.^[11] Here we report first examples of nonchiral molecules forming a ferroelectric switchable fluid smectic phase (SmCP_F phase). They are a novel type of polyphilic liquid crystal^[2, 12] composed of three incompatible units: A bent rigid aromatic core,^[13] two flexible alkyl chains, and a bulky oligosiloxane unit^[14] at one end.

The synthesis of these molecules is shown in Scheme 1 and the phase-transition temperatures obtained by polarized-light optical microscopy and differential scanning calorimetry (DSC) are summarized in Table 1.^[18] The parent compound **1** of this series, composed only of the rigid bent-core unit and two terminal hydrocarbon chains shows a conventional SmCP_A-phase with a typical AF switching behavior, which is characterized by the occurrence of two polarization peaks in the switching current response. This phase is only monotropic [metastable, phase sequence: Cr 108 (SmCP_A 98) Iso], but hydrosilylation^[14d] leads to the ternary block molecules **2–4** which show significantly increased stabilities of their mesophases, despite that the oligosiloxane units are very bulky and therefore are expected to reduce the mesophase stability. Instead, the mesophase stability is nearly independent of the size of the siloxane units. Even for molecule **4**, with a branched trisiloxane unit, nearly the same transition temperature is found. All siloxane derivatives **2–4** form mesophases which are quite distinct from that of the parent compound **1** and all other known liquid-crystalline phases. Typically, they appear from the isotropic liquid state as fractal nuclei which coalesce to a grainy unspecific texture which is completely dark (optically isotropic) between crossed polarizers, showing only very small irregularly distributed bright spots. The most remarkable feature is that in these mesophases domains of opposite handedness can be distinguished. Rotating the



Scheme 1. Synthesis of compounds **1–4**. a) cat. $[Pd(PPh_3)_4]$, $NaHCO_3$, H_2O , glyme, reflux, 8 h;^[15] b) 4-(4-dodecyloxybenzoyloxy)benzoic acid,^[13] CMC, DMAP, CH_2Cl_2 , 20 °C, 24 h;^[16] c) H_2 , Pd/C, AcOEt, 20 °C, 24 h;^[16] d) 4-(10-undecene-1-yloxy)benzoic acid,^[17] CMC, DMAP, CH_2Cl_2 , 20 °C, 24 h;^[16] e) R_3SiH (R is shown in Table 1), Karstedt's catalyst, toluene, 20 °C, 30 min;^[14d] CMC = *N*-cyclohexyl-*N'*-(2-morpholinoethyl)carbodiimide methyl *p*-toluenesulfonate; DMAP = 4-dimethylaminopyridine

Table 1. Transition temperatures (T) and corresponding enthalpy values [in square brackets] of the compounds **2–4**.^[a]

Compound	R_3Si-	T [°C]	$[\Delta H/kJ mol^{-1}]$
2	$Me_3SiOSiMe_2-$	Cr 77 [17.0]	SmCP _A 118 [23.5]
3	$Me_3Si(OSiMe_2)_2-$	Cr 70 [29.3]	SmCP _F 115 [24.3]
4	$(Me_3SiO)_2SiMe-$	Cr 63 [8.9]	SmCP _F 116 [21.1]

[a] Abbreviations: Cr = crystalline solid state; SmCP_A = antiferroelectrically switchable smectic mesophase in which the molecules are tilted with respect to the layer normal and have a polar order within the layers; SmCP_F = ferroelectrically switchable smectic mesophase in which the molecules are tilted with respect to the layer normal and have a polar order within the layers; Iso = isotropic liquid phase. Transition temperatures and enthalpies were determined by DSC (Perkin-Elmer DSC-7, first heating scan, rate: 10 K min⁻¹) and confirmed by polarized-light optical microscopy.

analyzer by a small angle (5–10°) dark and more bright domains become visible. If the analyzer is rotated in the opposite direction the brightness of the domains is reversed (Figure 2). The light transmission does not change if the sample is rotated. This effect has already been reported for the “B4” phase,^[19] which actually represents a soft crystal, and the “Sm1”-phase which also seems to have a three-dimensional superstructure though only a simple layer structure is found by X-ray diffraction.^[20] However, in contrast to these

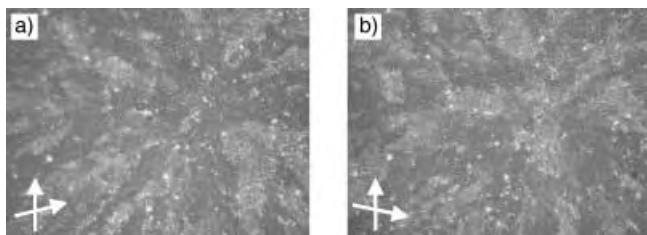


Figure 2. Texture of the mesophase of compound **4** ($T = 105\text{ }^{\circ}\text{C}$) obtained by cooling the isotropic liquid without applied field. The photographs were taken with polarizer and analyzer slightly uncrossed to distinguish domains of opposite chirality. Changing the direction of the analyzer as indicated by the arrows [compare (a) and (b)] reverses the brightness of the domains. The brightness of the images is strongly enhanced to make the different regions visible.

phases, in the mesophases of **2–4** the transparent blue color which is typical for B4 and Sm1 phases cannot be observed, and these mesophases are highly fluid, like conventional SmA and SmC phases.

X-ray investigations (non-oriented samples, Guinier camera) confirm the presence of a well-defined layer structure by the appearance of a sharp layer reflection and its higher orders (up to the 4th order) with $d = 4.4\text{ nm}$ for compound **4**. For this compound the diffuse scattering in the wide-angle range has a very asymmetric profile in which two maxima can be separated, one maximum at 0.45 nm corresponds to the mean distance between the fluid alkyl chains and the second one with a maximum at about 0.7 nm corresponding to the mean distance between the disordered siloxane units. This is an indication of a fluid nanosegregated organization. It can be assumed that because of the significantly larger space required by the siloxane units compared to the rest of the molecule the molecules should adapt an antiparallel end-to-end packing within the layers. In this way the siloxane units build up their own sublayers, which leads to the triple-layer structure shown in Figure 3. The effective molecular length L

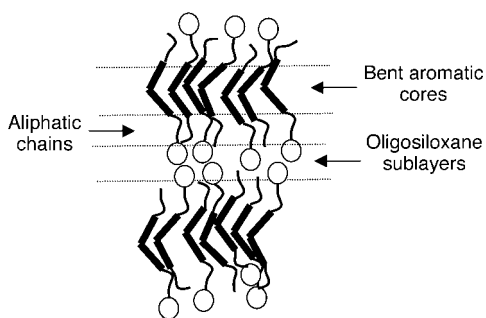


Figure 3. Proposed triple-layer organization of the molecules **3** and **4** in the SmCP_F state.

is around 5.5 nm , which is significantly larger than the layer spacing found in X-ray measurements. This result is in line with the proposed monolayer structure in which the molecules are additionally tilted by an angle of about $30\text{--}35$ degrees with respect to the layer normal.

In the next step electrooptical investigations were carried out in a transparent sandwich-type capacitor cell consisting of two indium-tin-oxide (ITO) coated glass plates. The repola-

rization current in response to an applied triangular-wave field^[21] shows two peaks for the disiloxane derivative **2** (AF switching) and only one peak for compounds **3** and **4**, as typical for FE switching (Figure 4). Compound **4** was inves-

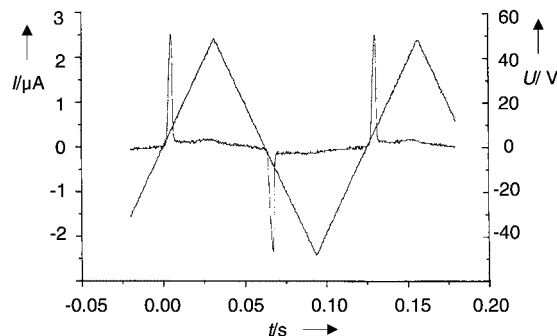


Figure 4. Switching current response in the mesophase of compound **4** on applying a triangular-wave voltage at $104\text{ }^{\circ}\text{C}$ in a $10\text{ }\mu\text{m}$ non-coated ITO cell (EHC, Japan) at a frequency of 1 Hz .

tigated in more detail. Even at very low frequency (0.02 Hz) we observed only one very sharp current response peak, corresponding to a high value of the spontaneous polarization of 700 nCcm^{-2} . This one-peak response is found in every case, independent of the sample preparation. It is a strong indication for an FE switching behavior which is additionally supported by optical observations of the switching process.

If the isotropic liquid is slowly cooled under an applied dc electric field ($10\text{ V }\mu\text{m}^{-1}$) a texture with many circular domains appears (Figure 5a). In these domains the smectic layers are circularly arranged around the center of the domains. The characteristic feature of these domains are extinction crosses, whereby the direction of the extinction brushes corresponds to the direction of the optical axes of the smectic layers. In these bright birefringent field-induced circular domains the extinction crosses are rotated by $70\text{--}80^{\circ}$ clockwise or anticlockwise depending on the sign of the applied field. This angle corresponds to twice the tilt angle. It should be emphasized that the extinction crosses remain unchanged if the field is switched off, that means, there is no relaxation of the switched state as observed in the AF phases. This bistable switching clearly points to an FE ground state, which confirms the results of the current-response measurements. In this FE ground state the correlation between adjacent smectic layers is synclinic (SmC_SP_F).

If however, an alternating field (ac, $10\text{ V }\mu\text{m}^{-1}$, 200 Hz) is applied during cooling the isotropic liquid, the appearing mesophase shows in addition to a weakly birefringent fanlike texture also weakly birefringent circular domains (Figure 5b). In these domains the extinction crosses coincide with the direction of polarizer and analyzer. On applying an electric field the extinction crosses do not rotate, although a switching process is clearly visible. In this case the ferroelectric ground state can be explained by an anticlinic packing of the molecules in adjacent layers (SmC_AP_F).

In contrast to the states obtained under the influence of an external electric field, there is obviously no birefringence if the smectic phase is formed without such an applied field, that

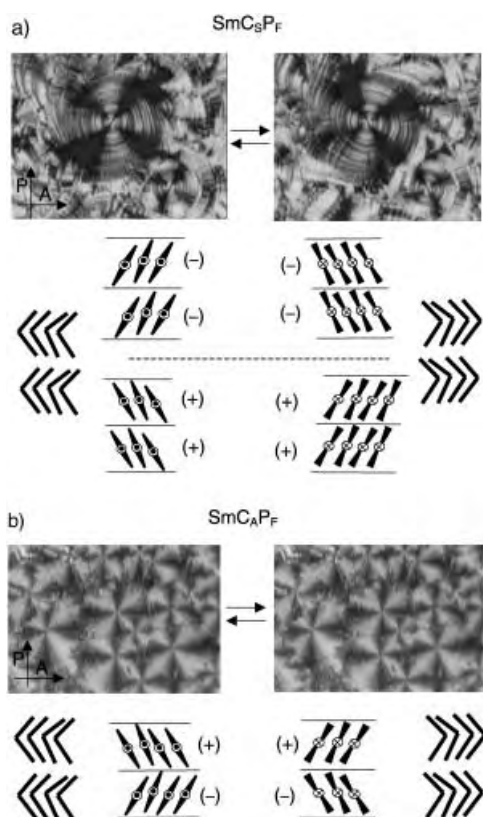


Figure 5. Switching behavior observed between crossed polarizers. a) Texture obtained by cooling the isotropic liquid under an electric dc field of $10 \text{ V } \mu\text{m}^{-1}$. The extinction cross of the circular domains does not coincide with the crossed polarizers. By switching the electric field between $+1.5 \text{ V } \mu\text{m}^{-1}$ (left-hand side) and $-1.5 \text{ V } \mu\text{m}^{-1}$ (right-hand side) the extinction cross rotates by an angle of $70\text{--}80^\circ$ (sample thickness: $10 \text{ } \mu\text{m}$; $T = 70^\circ\text{C}$)^[22] b) Texture obtained by cooling the isotropic liquid under an electric ac field of $10 \text{ V } \mu\text{m}^{-1}$ (200 Hz). The extinction crosses coincide with the crossed polarizers and do not rotate on applying an electric field (sample thickness: $10 \text{ } \mu\text{m}$; $T = 70^\circ\text{C}$).

is, this phase seems to be optically uniaxial. However, the polar order and the tilted organization of the molecules in the layers would require an optical biaxiality of this phase, that is, a birefringence is expected to occur. Another characteristic feature of this texture is the existence of domains with opposite chirality (see above). These findings point to the presence of a helical arrangement of the molecules with the helix axis perpendicular to the substrate surfaces, whereby the pitch of this helix is different from the wavelength of the visible light and the helix-sense is different in regions with opposite chirality. The helix axis can occur perpendicular to the layer planes (SmC*-like) or parallel to the layer planes (TGB-like). Both helical superstructures would lead to optical uniaxiality of the phases and would allow a compensation of the layer polarity on a macroscopic scale by retaining a nearly parallel alignment of the bent directions of the molecules in adjacent layers.

In summary, the mesophase presented here is the first FE switchable SmCP phase which is formed by achiral bent-core mesogens. Additionally, the materials have interesting properties which could be of use in applications; they are stable, have a low conductivity, and their mesophases occur at

comparatively low temperatures. The appearance of siloxane sublayers seems to have an essential influence on the preference of a parallel alignment of the molecular bent directions in adjacent layers. Usually, the packing of the bent molecules in adjacent layers is antiparallel (AF), which provides synclinal interlayer interfaces (see side views in Figure 1). These easily allow interlayer fluctuations and are therefore entropically favorable. In the FE state the parallel molecular bent directions in adjacent layers lead to anticlinical interlayer interfaces between them, which are disfavored because they suppress the interlayer fluctuations. Decoupling the layer interfaces by the siloxane sublayers reduces or inhibits these interlayer penetrations and therefore their importance for the molecular organization is reduced, which allows a ferroelectric order more easily.^[23] The importance of the decoupling of the layers is also shown in that reducing the number of siloxane units gives rise to AF properties (compounds **1** and **2**). This decoupling may also be responsible for the possibility to control the relative tilt direction of the molecules in adjacent layers (synclinal versus anticlinical) by changing the type of the applied electric field (dc versus ac). Additionally, it should be pointed out that the supra-molecular organization of these molecules is strongly influenced not only by external fields, but also by the interactions with the substrate surfaces, which all together define the system as a whole.

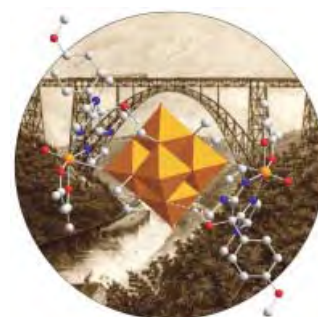
Received: March 19, 2002 [Z18929]

- [1] M. C. Petty, M. R. Bryce, D. Bloor, *Introduction to Molecular Electronics*, Edward Arnold, London, **1995**.
- [2] a) B. I. Ostrovskii *Structure and Bonding*, **1999**, 94, 200; b) T. Goldacker, V. Abetz, R. Stadler, I. Erukhimovich, L. Leibler, *Nature* **1999**, 398, 137.
- [3] H.-S. Kitzerow, C. Bahr, *Chirality in Liquid Crystals*, Springer, Berlin, **2001**.
- [4] S. T. Lagerwall, *Ferroelectric and Antiferroelectric Liquid Crystals*, Wiley-VCH, Weinheim, **1999**.
- [5] T. Niori, F. Sekine, J. Watanabe, T. Furuwara, H. Takezoe, *J. Mater. Chem.* **1996**, 6, 1231.
- [6] A related effect was observed in mixtures of side-chain polymers and low molecular-weight mesogens: E. A. Soto Bustamante, S. V. Yablonskii, B. I. Ostrovskii, L. A. Beresnev, L. M. Blinov, W. Haase, *Liq. Cryst.* **1996**, 21, 829.
- [7] D. R. Link, G. Natale, R. Shao, J. E. MacLennan, N. A. Körblöva, D. M. Walba, *Science* **1997**, 278, 1924.
- [8] An orthogonal phase is reported in ref. [6] and was also reported for a rigid bent-core molecule: A. Eremin, S. Diele, G. Pelzl, H. Nadas, W. Weissflog, J. Salfetnikova, H. Kresse, *Phys. Rev. E* **2001**, 64, 51707.
- [9] a) E. Gorecka, D. Pociecha, F. Araoka, D. R. Link, M. Nakata, J. Thisayukta, Y. Takanishi, J. Watanabe, H. Takezoe, *Phys. Rev. E* **2000**, 62, R4524; b) M. Nakata, D. R. Link, J. Thisayukta, Y. Takanishi, K. Ishikawa, J. Watanabe, H. Takezoe, *J. Mater. Chem.* **2001**, 11, 2694; c) M. Nakata, D. R. Link, F. Araoka, J. Thisayukta, Y. Takanishi, K. Ishikawa, J. Watanabe, H. Takezoe, *Liq. Cryst.* **2001**, 28, 1301.
- [10] D. M. Walba, E. Körblöva, R. Shao, J. E. MacLennan, D. R. Link, M. A. Glaser, N. A. Clark, *Science* **2000**, 288, 2181.
- [11] H. Nadas, W. Weissflog, A. Eremin, G. Pelzl, S. Diele, B. Das, S. Grande, *J. Mater. Chem.* **2002**, 12, 1316.
- [12] C. Tschierske *J. Mater. Chem.* **2001**, 11, 2646.
- [13] D. Shen, A. Pegenau, S. Diele, I. Wirth, C. Tschierske, *J. Am. Chem. Soc.* **2000**, 122, 1593.
- [14] Siloxane units were used for several calamitic polyphilic mesogens, for example, a) M. Ibn-Elhaj, H. Möhwald, M. Z. Cherkaoui, R. Zniber,

- Langmuir* **1998**, *14*, 504; b) P. Sebastiao, S. Mery, M. Sieffert, J. F. Nicoud, Y. Galerne, D. Guillon, *Ferroelectrics* **1998**, *212*, 133; c) H. J. Coles, S. Meyer, P. Lehmann, R. Deschenaux, I. Jauslin, *J. Mater. Chem.* **1999**, *9*, 1085; d) G. H. Mehl, J. W. Goodby, *Chem. Ber.* **1996**, *129*, 521.
- [15] a) N. Miyaura, T. Yanagi, A. Suzuki, *Synth. Commun.* **1981**, *11*, 513; b) N. Miyaura, A. Suzuki, *Chem. Rev.* **1995**, *95*, 2457; c) M. Hird, G. W. Gray, K. J. Toyne, *Mol. Cryst. Liq. Cryst.* **1991**, *206*, 187.
- [16] C. Tschierske, H. Zschke, *J. Prakt. Chem.* **1989**, *331*, 365.
- [17] N. W. Adams, J. S. Bradshaw, J. M. Bayona, K. E. Markides, M. L. Lee, *Mol. Cryst. Liq. Cryst.* **1987**, *147*, 43.
- [18] All analytical data are in accordance with the proposed structure, for example, compound **4**: ^1H NMR (400 MHz, CDCl_3) δ = 8.30 (d, J = 8.8 Hz, 2H, Ar-H), 8.15 (d, J = 8.8 Hz, 4H, Ar-H), 7.64 (d, J = 8.6 Hz, 2H, Ar-H), 7.49 (d, J = 5.3 Hz, 2H, Ar-H), 7.46–7.45 (m, 1H, Ar-H), 7.38 (d, J = 8.6 Hz, 2H, Ar-H), 7.29 (d, J = 8.6 Hz, 2H, Ar-H), 7.23–7.20 (m, 1H, Ar-H), 7.00 (d, J = 9.0 Hz, 2H, Ar-H), 6.97 (d, J = 9.0 Hz, 2H, Ar-H), 4.04 (t, J = 6.6 Hz, 4H, OCH_2), 1.82 (m, 4H, CH_2), 1.45 (m, 4H, CH_2), 1.36–1.28 (m, 30H, CH_2), 0.89 (t, J = 6.6 Hz, 3H, CH_3), 0.46 (t, J = 7.4 Hz, 2H, Si- CH_2), 0.10 (s, 18H, Si- CH_3), 0.06 ppm (s, 3H, Si- CH_3); ^{13}C NMR (100 MHz, CDCl_3) δ = 164.78, 164.34, 164.18, 163.75, 163.51, 155.46, 151.28, 150.81, 142.08, 137.66, 132.34, 132.23, 131.74, 129.75, 128.95, 128.15, 126.82, 124.58, 122.11, 122.04, 121.44, 120.94, 120.48, 120.35, 114.27, 68.39, 68.32, 33.21, 31.92, 29.65, 29.63, 29.62, 29.57, 29.37, 29.36, 29.12, 29.09, 26.00, 25.98, 23.08, 22.69, 17.65, 14.12, 1.88, –0.23 ppm; elemental analysis calcd (%) for $\text{C}_{63}\text{H}_{88}\text{O}_{10}\text{Si}_3$: C 69.44 %, H 8.14; found C 69.33 %, H 8.12.
- [19] a) G. Heppke, D. D. Parghi, H. Sawade, *Liq. Cryst.* **2000**, *27*, 313; b) J. Thisayukta, H. Takezoe, J. Watanabe, *Jpn. J. Appl. Phys.* **2001**, *40*, 3277.
- [20] a) J. Thisayukta, Y. Nakayama, S. Kawauchi, H. Takezoe, J. Watanabe, *J. Am. Chem. Soc.*, **2000**, *122*, 7441; b) J. Thisayukta, H. Niwano, H. Takezoe, J. Watanabe, *J. Mater. Chem.* **2001**, *11*, 2717.
- [21] Determined by the three angular wave method as described in ref. [4].
- [22] Two distinct enantiomeric configurations, which differ in the tilt-direction and the direction of the polar axes of the molecules in the smectic layers (+/+ and –/–), are possible for the SmC_sP_F state.^[7] They occur in different regions within the sample, in which the extinction crosses rotate either clockwise or anticlockwise.
- [23] Quite similarly, decreasing the temperature reduces the out-of-layer fluctuations and could lead to a transition from an AF to FE order as recently shown for a B5-phase.^[11]

COVER PICTURE

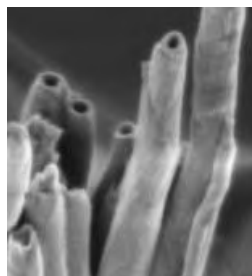
The cover picture shows a polyhedral representation of a polyoxovanadate core $\{V_6O_{13}(OMe)_6\}^{2-}$, which is linked to two vanadyl moieties. These are coordinated through the N_2O_2 donor set of organic ligands, which additionally stabilize the hexavanadate through two hydrogen bonds. This compound can be considered as “bridging the gap” between polyoxometalates and classic coordination compounds. Fittingly, in the background, is Müngsten railway bridge near Wuppertal, Germany, which links the towns of Remscheid and Solingen. The bridge, which was built in 1897, at a height of 107 m, an arch width of 170 m, and a total length of 500 m was considered an engineering masterpiece of its time in Europe. More about the successful linkage of two important classes of compounds is reported in the communication by M. Piepenbrink, M. U. Triller, N. H. J. Gorman, and B. Krebs on pp. 2523 ff.



REVIEW

Contents

Since the discovery of the carbon nanotubes in 1991, much effort has been made to find nanotubes and other anisotropic nanomaterials. This interest is caused by the outstanding structural characteristics of such materials that are combined with promising physical and chemical properties. This review focuses on the advances made in oxidic nanotubes, such as vanadium oxide nanotubes (see picture) and nanorods, and highlights the most important synthetic trends.



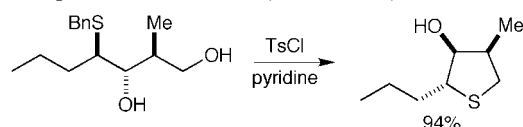
G. R. Patzke, F. Krumeich,
R. Nesper* 2446–2461

Oxidic Nanotubes and Nanorods—
Anisotropic Modules for a Future
Nanotechnology

Keywords: nanomaterials • nanorods •
nanotubes • oxides • solvothermal
synthesis

Angew. Chem. **2002**, *114*, 2554–2571

Cyclization reactions involving thiiranium and thiolanium ion intermediates lead to highly substituted saturated O, N, and S heterocycles in high yield and with complete stereocontrol (see scheme).



Angew. Chem. **2002**, *114*, 2572–2593

D. J. Fox, D. House,*
S. Warren* 2462–2482

Mechanisms of Sulfanyl (RS) Migrations:
Synthesis of Heterocycles

Keywords: cyclization • heterocycles •
rearrangement • sulfanyl groups •
thiiranium ions

ESSAY

Out of the Blue: The noble colors blue and purple were highly regarded in the past because of their rarity. Thus ancient civilizations invented blue and purple pigments, such as, Egyptian Blue (see amulet shown), Chinese Blue, and Chinese Purple, all of which contain alkaline-earth metals and copper. It is shown how their synthesis may have been developed in ancient times: an understanding of stoichiometry, the control of reaction temperature, and the hypothesis of knowledge transfer are essential.



Angew. Chem. **2002**, *114*, 2595–2600

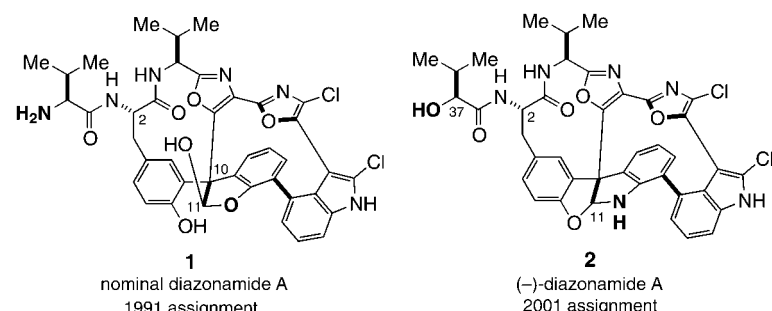
H. Berke* 2483–2487

Chemistry in Ancient Times: The
Development of Blue and Purple
Pigments

Keywords: alkaline-earth metals •
dyes/pigments • history of science

HIGHLIGHTS

Revision of the structure originally proposed for the antimitotic natural product diazonamide A (**2**) was required after the recent synthesis of polycycle (**1**); the total synthesis of **2** still remains elusive. However, there is much to learn from the significant synthetic contributions and innovative strategies developed to date.



Angew. Chem. **2002**, *114*, 2601–2606

T. Ritter, E. M. Carreira* ... 2489–2495

The Diazonamides: The Plot Thickens

Keywords: antitumor agents •
atropisomerism • natural products •
structure elucidation • total synthesis

VIPs

The following communications are “Very Important Papers” in the opinion of two referees. They will be published shortly (that marked with a diamond will be published in the next issue). Short summaries of these articles can be found on the *Angewandte Chemie* homepage at the address <http://www.angewandte.org>

Highly Selective Transport of Organic Compounds by Using Supported Liquid Membranes Based on Ionic Liquids

L. C. Branco, J. G. Crespo,
C. A. M. Afonso* ◆

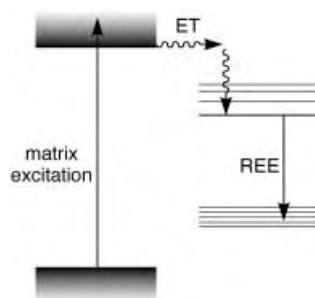
Atom-Transfer Tandem Radical Cyclization Reactions Promoted by Lewis Acids

D. Yang,* S. Gu, H.-W. Zhao,
N.-Y. Zhu

Metallabenzenes and Valence Isomers: Synthesis and Characterization of a Platinabenzene

V. Jacob, T. J. R. Weakley,
M. M. Haley*

Matrix excitation above the band-gap energy enables lanthanide ions in host–guest systems to be sensitized (see scheme; ET = energy transfer; REE = rare earth emission). The enhanced luminescence of the enclosed lanthanide ions gives characteristic linelike emission spectra.



H. Maas, A. Currao,
G. Calzaferri* 2495–2497

Encapsulated Lanthanides as
Luminescent Materials

Keywords: energy transfer • glasses •
lanthanides • luminescence • zeolites

Angew. Chem. **2002**, *114*, 2607–2608

COMMUNICATIONS

Doing a stretch in zeolites: Usually molecular sieves selectively process and yield the fastest diffusing, least bulky molecule. When sieves were identified that seemed to selectively yield, adsorb, and stabilize isomers with a larger diameter, the term “inverse shape selectivity” was coined. Molecular simulations indicate that these sieves preferentially yield molecules because of entropic effects, which favor those molecules that have the shortest effective length. In narrow zeolite pores linear molecules are stretched whereas in wide pores they can be coiled (see diagram).



Angew. Chem. **2002**, *114*, 2609–2612

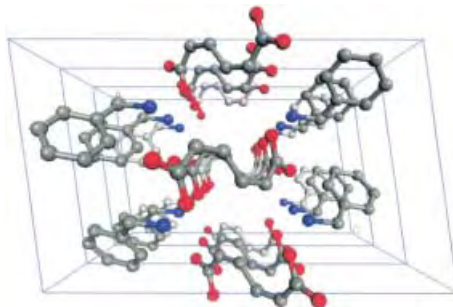
M. Schenk, S. Calero, T. L. M. Maesen,
L. L. van Benthem, M. G. Verbeek,
B. Smit* 2499–2502

Understanding Zeolite Catalysis: Inverse
Shape Selectivity Revised

Keywords: alkanes • heterogeneous
catalysis • molecular modeling • shape
selectivity • zeolites



Stacking made to order: Weak intermolecular interactions such as 2D hydrogen-bonding networks, aromatic-ring stacking, and CH/π or halogen–halogen interactions account for the columnar organization of muconic and sorbic acid derivatives in the crystalline state (see picture). When the stacking distance is close to 5 Å these 1,3-dienes undergo topochemical polymerization upon irradiation.



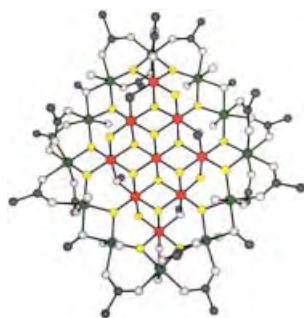
Angew. Chem. **2002**, *114*, 2612–2615

A. Matsumoto,* K. Sada,* K. Tashiro,*
M. Miyata,* T. Tsubouchi, T. Tanaka,
T. Odani, S. Nagahama, T. Tanaka,
K. Inoue, S. Saragai,
S. Nakamoto 2502–2505

Reaction Principles and Crystal Structure
Design for the Topochemical
Polymerization of 1,3-Dienes

Keywords: crystal engineering •
polymerization • solid-state reactions •
supramolecular chemistry •
topochemistry

Beautiful offspring: Manganese/oxide/carboxylate-cluster chemistry continues to surprise with its rich variety of structural types. Here a new Mn_{21} cluster (see picture Mn^{4+} (red), Mn^{3+} (green)) with a $12\text{Mn}^{\text{III}}9\text{Mn}^{\text{IV}}$ oxidation level and an approximately planar core is reported.



Angew. Chem. **2002**, *114*, 2616–2618

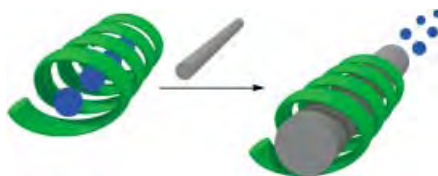
J. T. Brockman, J. C. Huffman,
G. Christou* 2506–2508

A High Nuclearity, Mixed-Valence
Manganese(III,IV) Complex:
 $[\text{Mn}_{21}\text{O}_{24}(\text{OMe})_8(\text{O}_2\text{CCH}_2\text{tBu})_{16}(\text{H}_2\text{O})_{10}]$

Keywords: cluster compounds • magnetic
properties • manganese • mixed-valent
compounds • structure elucidation

Common-or-garden starch can render single-walled carbon nanotubes (SWNTs) readily soluble in water. The secret is to preorganize the linear amylose component in the starch into a helix with iodine prior to bringing the SWNTs on the scene.

The SWNTs displace the iodine molecules in a “pea-shooting” type of mechanism (see scheme). After some physical cajoling of the aqueous solution containing the starch–SWNT complex, a fine “bucky paper” is formed. Spitting in the aqueous solution, followed by sitting around for a few hours, also enables equally fine “bucky paper” to be harvested.



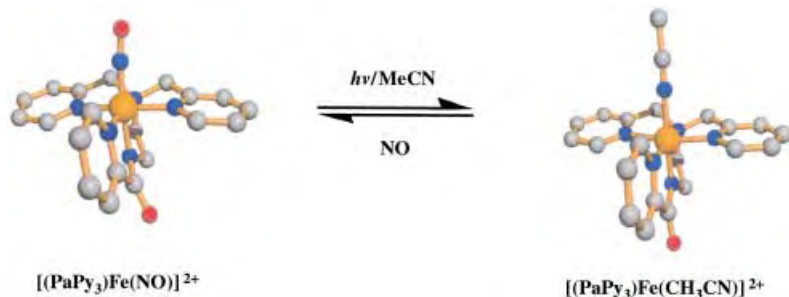
A. Star, D. W. Steuerman, J. R. Heath, J. F. Stoddart* 2508–2512

Starched Carbon Nanotubes

Keywords: amylose • hydrophobic interactions • molecular recognition • nanotubes • self-assembly

Angew. Chem. **2002**, *114*, 2618–2622

Reversible NO binding in acetonitrile is observed in the non-heme Fe^{III} complex [Fe(PaPy₃)(NO)](ClO₄)₂ (see scheme). The NO moiety is photolabile, and can dissociate from this complex under very mild conditions. The carboxamido nitrogen donor *trans* to NO appears to play a crucial role in the observed photolability. (PaPy₃ = *N*-[*N,N*-bis(2-pyridylmethyl)aminoethyl]-2-pyridinecarboxamide).



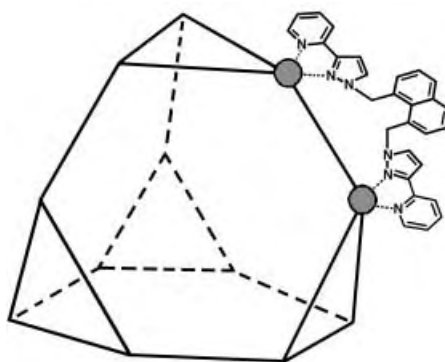
A. K. Patra, R. Afshar, M. M. Olmstead, P. K. Mascharak* 2512–2515

The First Non-Heme Iron(III) Complex with a Ligated Carboxamido Group That Exhibits Photolability of a Bound NO Ligand

Keywords: iron • nitric oxide • N ligands • photolability

Angew. Chem. **2002**, *114*, 2622–2625

Instead of the expected tetrahedral M₄L₆ cage, a far more complicated M₁₂L₁₈ cage forms when the bridging ligand shown reacts with Co^{II} ions. The dodecanuclear cage has the topology of a tetrahedron in which all four vertices are truncated to reveal triangular faces. A bridging ligand spans each of the 18 edges of the metal cage, and all 12 metal–tris(chelate) centers are homochiral. [BF₄][–] ions are located in the large central cavity and in the two-dimensional cavities at the center of each face.



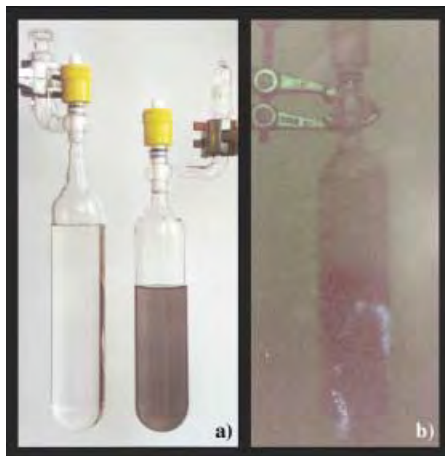
Z. R. Bell, J. C. Jeffery, J. A. McCleverty, M. D. Ward* 2515–2518

Assembly of a Truncated-Tetrahedral Chiral [M₁₂(μ-L)₁₈]²⁴⁺ Cage

Keywords: cage compounds • host–guest systems • N ligands • self-assembly • supramolecular chemistry

Angew. Chem. **2002**, *114*, 2625–2628

Small flashes (b) occur during the freezing of triethylgallium samples in liquid nitrogen, and on warming from -196°C this is accompanied by decomposition (a). This effect was observed during the determination of the crystal structures of GaMe_3 and GaEt_3 , which both show intermolecular interactions between their electron-deficient gallium atoms and the alkyl groups of neighboring molecules.



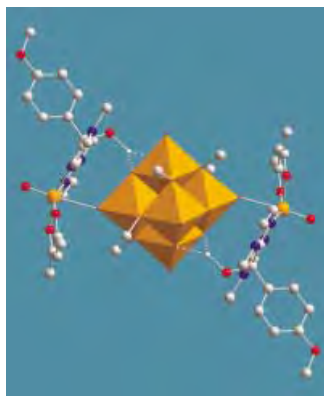
Angew. Chem. **2002**, *114*, 2629–2633

N. W. Mitzel,* C. Lustig, R. J. F. Berger,
N. Runeberg 2519–2522

Luminescence Phenomena and Solid-State Structures of Trimethyl- and Triethylgallium

Keywords: ab initio calculations • gallium • luminescence • photochemistry • solid-state structures

Cluster catalysts for directed oxygen transfer? In attempts towards the creation of novel catalytic systems for directed oxygen-transfer processes a novel type of polyoxometalate cluster containing vanadium was synthesized. The first example of a polyoxovanadate composed of a hexavanadate molecular center and two reactive, exchangeable, vanadium-centered complexes which are tilted towards the polyoxometalate center is presented (see picture).



Angew. Chem. **2002**, *114*, 2633–2635

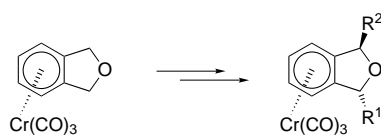
M. Piepenbrink, M. U. Triller,
N. H. J. Gorman, B. Krebs* . 2523–2525

Bridging the Gap between Polyoxometalates and Classic Coordination Compounds: A Novel Type of Hexavanadate Complex

Keywords: coordination chemistry • N ligands • polyoxometalates • structure elucidation • vanadium



A completely stereoselective synthesis of pharmacologically relevant *trans*-1,3-disubstituted dihydroisobenzofurans utilizes the surprising selectivity during the benzylic deprotonation of a silylated [phthalan– $\text{Cr}(\text{CO})_3$] complex (see scheme).



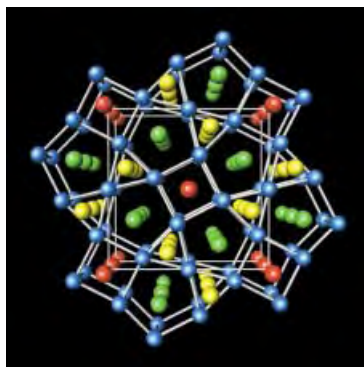
Angew. Chem. **2002**, *114*, 2635–2638

S. Zemolka, J. Lex,
H.-G. Schmalz* 2525–2528

Benzylic *endo*-Alkylation of Phthalan– $\text{Cr}(\text{CO})_3$ Complexes via Temporary Silylation: An Entry to *trans*-1,3-Disubstituted Dihydroisobenzofurans

Keywords: alkylation • arenes • chromium • deprotonation • enantioselectivity

Quaternary rhodium borides of general formula $\text{A}_2\text{MRh}_5\text{B}_2$ (see picture: Mg green, Mn red, Rh blue, B yellow) offer a nice playground for combined synthetic–theoretical investigations. The relative robustness of the underlying structure type allows various adjustments of the valence-electron concentration to be explored. In synthesizing new magnetic materials by following a chemical theory of cooperative magnetic phenomena, it is demonstrated how physical properties, such as antiferromagnetic or ferromagnetic behavior can be understood, predicted, and, eventually, realized.



Angew. Chem. **2002**, *114*, 2638–2642

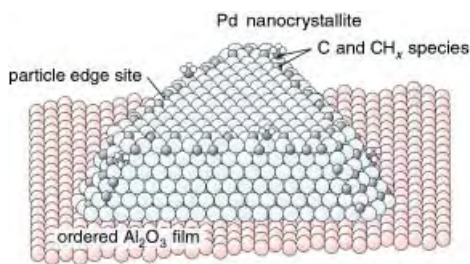
R. Dronskowski,* K. Korczak,
H. Lueken, W. Jung 2528–2532

Chemically Tuning between Ferromagnetism and Antiferromagnetism by Combining Theory and Synthesis in Iron/Manganese Rhodium Borides

Keywords: borides • density functional calculations • intermetallic phases • magnetism • solid-state structures

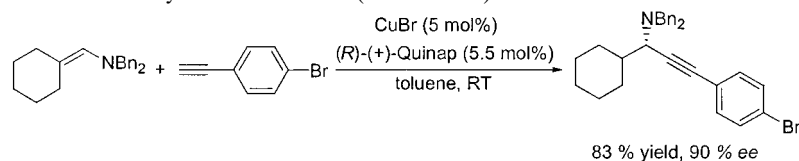
Catalytically active nanoparticle

sites: Different catalytic activity of different active sites coexisting on a supported nanoparticle has been directly observed using molecular-beam techniques and in situ surface vibrational spectroscopy. For methanol decomposition on a supported Pd model catalyst (see picture), it is shown that carbon–oxygen-bond breakage and dehydrogenation occur as competing reaction pathways at particle defects and on regular facets, respectively.



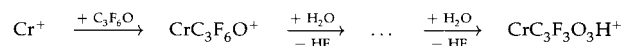
Angew. Chem. **2002**, *114*, 2643–2646

Enantiomerically enriched, functionalized, and protected propargylamines are obtained under mild conditions in a new copper(I)/Quinap-catalyzed addition reaction of alkynes to enamines (see scheme).



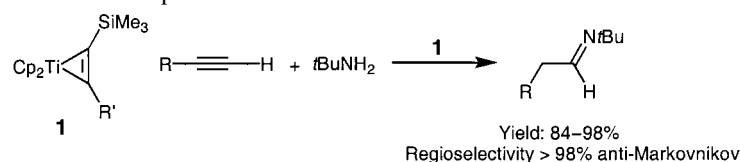
Angew. Chem. **2002**, *114*, 2651–2654

Despite being unreactive towards many neutral compounds even in the sense of association, Cr^+ undergoes gas-phase adduct formation with hexafluoroacetone. In the presence of water, the monoadduct undergoes three consecutive C–F bond hydrolysis reactions, which may be followed, after complexation of water, by even a fourth C–F bond cleavage (see scheme).



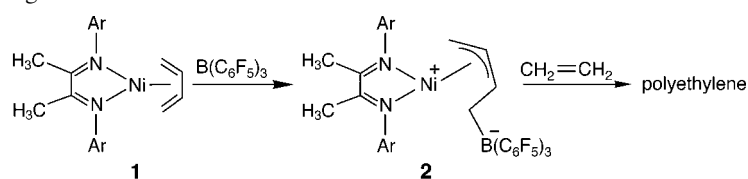
Angew. Chem. **2002**, *114*, 2648–2651

Titanocene- η -alkyne complexes such as **1** are efficient catalysts for the hydroamination of terminal alkynes to imines (see scheme; R = alkyl, R' = SiMe_3 or Ph). Excellent yields of imines and good to excellent regioselectivities for the anti-Markovnikov products were obtained.



Angew. Chem. **2002**, *114*, 2646–2648

Addition of $\text{B}(\text{C}_6\text{F}_5)_3$ to the butadiene ligand in **1** leads to the zwitterionic complex **2** (characterized by single-crystal X-ray diffraction; Ar = 2,6-diisopropylphenyl), which is an active catalyst for the polymerization of ethylene. The formation of **2** could have model character for an activation pathway for homogeneous Ziegler–Natta catalysts of late transition metals without σ -alkyl ligands.



Angew. Chem. **2002**, *114*, 2662–2664

S. Schauermaun, J. Hoffmann,
V. Johánek, J. Hartmann, J. Libuda,*
H.-J. Freund 2532–2535

Catalytic Activity and Poisoning of
Specific Sites on Supported Metal
Nanoparticles

Keywords: heterogeneous catalysis •
kinetics • molecular beams • supported
catalysts • surface chemistry

C. Koradin, K. Polborn,
P. Knochel* 2535–2538

Enantioselective Synthesis of
Propargylamines by Copper-Catalyzed
Addition of Alkynes to Enamines

Keywords: alkynes • asymmetric
synthesis • C–H activation •
heterogeneous catalysis •
propargylamines

U. Mazurek, D. Schröder,
H. Schwarz 2538–2541

Hydrolytic Activation of C–F Bonds in
the Gas Phase by Intrinsically Unreactive
Chromium Cations

Keywords: C–F activation • chromium •
gas-phase reactions • hydrolysis • mass
spectrometry

A. Tillack, I. Garcia Castro,
C. G. Hartung, M. Beller* .. 2541–2543

Anti-Markovnikov Hydroamination of
Terminal Alkynes

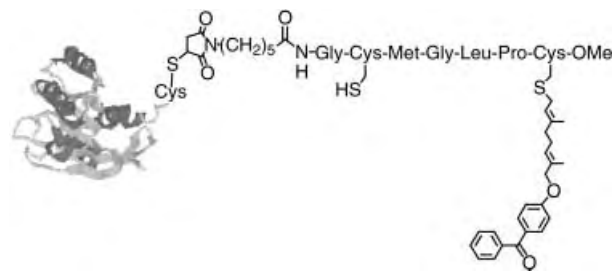
Keywords: alkynes • homogeneous
catalysis • hydroamination •
metallocenes • titanium

J. W. Strauch, G. Erker,* G. Kehr,
R. Fröhlich 2543–2546

Formation of a Butadienenickel-Based
Zwitterionic Single-Component Catalyst
for Ethylene Polymerization: An
Alternative Activation Pathway for
Homogeneous Ziegler–Natta Catalysts
of Late Transition Metals

Keywords: diene ligands • homogeneous
catalysis • nickel • polymerization •
Ziegler–Natta catalysis

The combination of organic synthesis with cell biology provides access to a chimera of the signal-transducing Ras protein, which contains a photoactivatable benzophenone group in its isoprenoid membrane anchor, yet retains biological activity. The semisynthetic protein is a new tool to address open questions concerning the mechanism of selective plasma membrane localization of Ras and to identify putative binding partners of Ras.



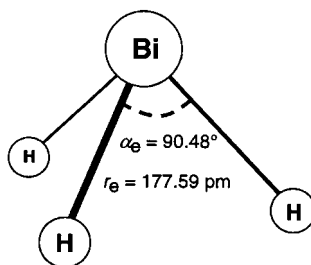
Angew. Chem. **2002**, *114*, 2655–2658

J. Kuhlmann,* A. Tebbe, M. Völkert,
M. Wagner, K. Uwai,
H. Waldmann* 2546–2550

Photoactivatable Synthetic Ras Proteins:
“Baits” for the Identification of Plasma-
Membrane-Bound Binding Partners of
Ras

Keywords: lipoproteins •
photoactivation • protein engineering •
signal transduction

Fact! That is the answer to the question posed in the title. Over 40 years passed before the synthesis of bismuthine (BiH_3 ; see picture) by Amberger was confirmed successfully. High-resolution IR and millimeter-wave spectroscopy as well as ab initio calculations now provide a detailed picture of the molecular structure of this compound.



Angew. Chem. **2002**, *114*, 2659–2661

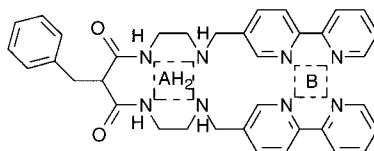
W. Jerzembeck, H. Bürger,*
L. Constantin, L. Margulès, J. Demaison,
J. Breidung, W. Thiel 2550–2552

Bismuthine BiH_3 : Fact or Fiction? High-
Resolution Infrared, Millimeter-Wave,
and Ab Initio Studies

Keywords: ab initio calculations •
bismuth • hydrides • IR spectroscopy •
rotational spectroscopy

Shedding light on the environment:

An auxillary light-emitting fragment (coumarin-343) binds to a Cu^{II} ion in the right-hand compartment (B) of the ligand shown and its fluorescence is “switched off”. If the pH value is raised from 7 to ≥ 11 the metal moves to the left compartment (A), which imposes a square stereochemistry and forces dissociation of the indicator, thus “switching on” the fluorescence. The pH-driven metal translocation is reversible and can be carried out for many cycles.



Angew. Chem. **2002**, *114*, 2665–2668

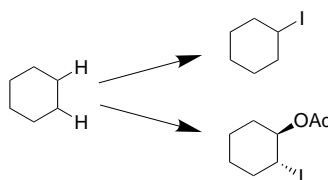
V. Amendola, L. Fabbri,* C. Mangano,
H. Miller, P. Pallavicini, A. Perotti,
A. Taglietti 2553–2556

Signal Amplification by a Fluorescent
Indicator of a pH-Driven Intramolecular
Translocation of a Copper(II) Ion

Keywords: copper • fluorescent probes •
molecular devices • N ligands • transition
metals

You can also choose from alkanes!

Either mono- or bifunctional iodo derivatives can be prepared from alkanes (see scheme) in an efficient and selective manner by using $\text{PhI}(\text{OAc})_2$, I_2 , and an alcohol.



Angew. Chem. **2002**, *114*, 2668–2670

J. Barluenga,* F. González-Bobes,
J. M. González 2556–2558

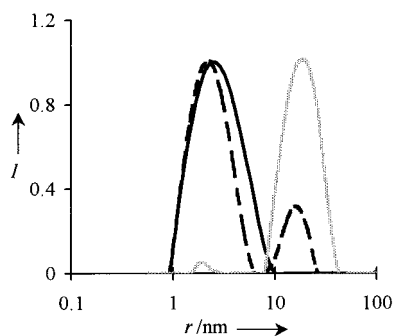
Activation of Alkanes upon Reaction
with $\text{PhI}(\text{OAc})_2 - \text{I}_2$

Keywords: alkanes • C–H activation •
iodination • iodine • photochemistry



In situ dynamic light scattering (DLS) and high-resolution transmission electron microscopy (HRTEM) can be used, in conjunction with other techniques, to improve our understanding of the mechanism of zeolite formation. The effects of aging and hydrothermal pre-treatment of precursors cause variations in the size distribution (see diagram; r = particle size, I = intensity) and relative crystallinity of the as-prepared zeolitic materials.

Angew. Chem. **2002**, *114*, 2670–2673



S. Mintova,* N. H. Olson, J. Senker,
T. Bein* 2558–2561

Mechanism of the Transformation of
Silica Precursor Solutions into Si-MFI
Zeolite

Keywords: dynamic light scattering •
electron microscopy • silicon • zeolites



The *syn* and *anti* topoisomers of fused subphthalocyanine dimers were synthesized and characterized. The space-filling model of the *anti* topoisomer is depicted. These compounds are the first step towards the synthesis of larger curved π surfaces.



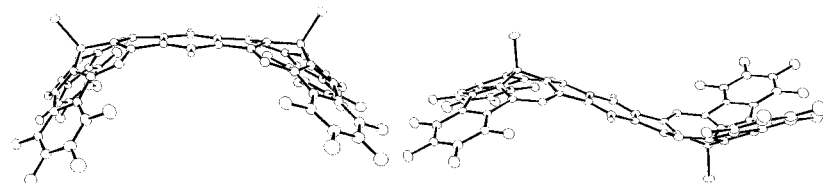
C. G. Claessens, T. Torres* .. 2561–2565

Synthesis, Separation, and
Characterization of the Topoisomers of
Fused Bicyclic Subphthalocyanine
Dimers

Keywords: boron • electronic
spectroscopy • macrocycles •
phthalocyanines

Angew. Chem. **2002**, *114*, 2673–2677

The structures of *cis* and *trans* forms of a binuclear subphthalocyanine (SubPc) have been determined by X-ray crystallography (see pictures). Electronic absorption and magnetic circular dichroism spectra of these dimers are similar in shape, but the Q band of the *trans* isomer appears at longer wavelength than that of the *cis* isomer by about 3–4 nm.



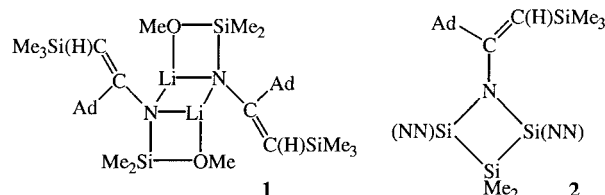
Angew. Chem. **2002**, *114*, 2677–2680

T. Fukuda, J. R. Stork, R. J. Potucek,
M. M. Olmstead, B. C. Noll,
N. Kobayashi,* 2565–2568
W. S. Durfee* 2565–2568

cis and *trans* Forms of a Binuclear
Subphthalocyanine

Keywords: boron • electronic
spectroscopy • macrocycles •
phthalocyanines • structure elucidation

A novel reaction of a thermally stable silylene with **1**, obtained by regio- and stereospecific insertion of the α -halogen-free adamantyl cyanide into the Li–C bond of the bis(silyl)methyl compound $\text{Li}[\text{CH}(\text{SiMe}_2\text{OMe})(\text{SiMe}_3)]$, yielded the new azatrisilacyclobutane **2**. NN = 1,2-[(*i*BuCH₂)N]₂C₆H₄.



Angew. Chem. **2002**, *114*, 2680–2683

F. Antolini, B. Gehrhus,* P. B. Hitchcock,
M. F. Lappert* 2568–2571

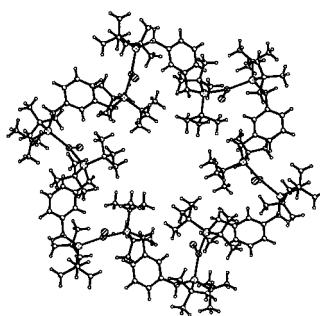
Synthesis and Structure of an
Azatrisilacyclobutane and Its Precursor,
a Novel Lithium Enamide Having a
Tricyclic (LiNSiO)₂ Skeleton

Keywords: allylic compounds •
heterocycles • insertion • silicon •
silylenes



With an outside diameter of approximately 2 nm, the title complex comprises six copper chloride moieties bridged by six 1,3-(CH₂PtBu₂)₂C₆H₄ ligands (see X-ray crystal structure). The solution properties of the resulting 48-atom macrocycle have been studied by variable-temperature NMR and UV/Vis spectroscopy, as well as by electrochemical studies.

Angew. Chem. **2002**, *114*, 2683–2685



E. D. Blue, T. B. Gunnoe,*
N. R. Brooks 2571–2573

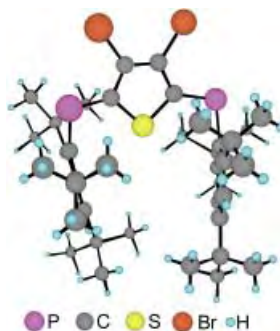
Synthesis, Spectroscopy, and Solid-State Structural Characterization of the Hexanuclear Copper Macrocycle [Cu₆Cl₆(μ-PCHP)₆]

Keywords: copper • electrochemistry • fluorescence • macrocycles • phosphane ligands



The first diphosphaheteroquinoid compound, which contains two low-coordinate phosphorus atoms and a thienoquinoid skeleton (see picture), was isolated as air-stable orange crystals. Its quinoid nature was confirmed by X-ray crystallography and cyclic voltammetry, which revealed the expected redox behavior.

Angew. Chem. **2002**, *114*, 2686–2688



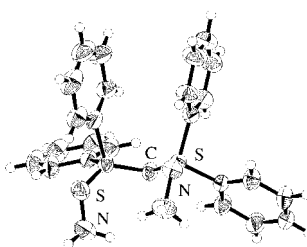
F. Murakami, S. Sasaki,
M. Yoshifuji* 2574–2576

Synthesis, Structure, and Redox Properties of Diphosphathienoquinones

Keywords: phosphalkenes • quinones • radical ions • redox chemistry • sulfur heterocycles

Double ylidic character in the S-C-S bonds is apparent from the single-crystal X-ray analysis of the title compound (see structure). This electronic configuration was supported by ab initio calculations on a model compound in which the phenyl groups were replaced by methyl groups.

Angew. Chem. **2002**, *114*, 2688–2690



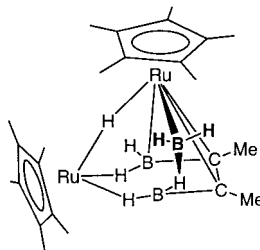
T. Fujii, T. Ikeda, T. Mikami, T. Suzuki,
T. Yoshimura* 2576–2578

Synthesis and Structure of (MeN)Ph₂S=C=SPh₂(NMe)

Keywords: bond theory • carbanions • multiple bonds • sulfur • ylides

Make the weak bonds first: Addition of carbon to a metallaborane rather than a metal to a carborane permits the isolation of metallacarboranes with a) identical compositions and different shapes, b) an exocluster bridging boryl group (see picture), and c) isomers with two CMe or CH and CEt fragments.

Angew. Chem. **2002**, *114*, 2690–2693



H. Yan, A. M. Beatty,
T. P. Fehlner* 2578–2581

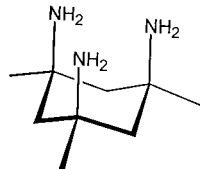
Reaction of 2-Butyne with *nido*-[1,2-(Cp*RuH)₂B₃H₇]: Improved Kinetic Control Leads to Metallacarboranes of Novel Composition and Structure

Keywords: alkynes • boranes • cluster compounds • metallacarboranes • ruthenium



A “two-protons-plus-one-lone-pair” bifurcated relationship is adopted by the amine groups in the amino equivalent of Kemp's triacid (see structure). Intramolecular proton transfer occurs in the aminolysis of three esters with this triamine, whereas two diamines, studied for comparison, switch abruptly from intramolecular to intermolecular proton transfer, depending upon the ester reactivity. The triamine offers attractive possibilities as a framework for bioorganic modeling.

Angew. Chem. **2002**, *114*, 2693–2696



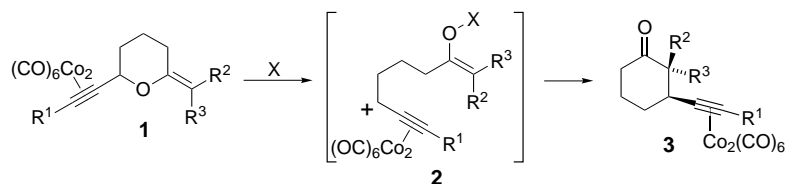
F. M. Menger,* J. Bian,
V. A. Azov 2581–2584

A 1,3,5-Triaxial Triaminocyclohexane: The Triamine Corresponding to Kemp's Triacid

Keywords: amines • enzyme models • hydrogen bonds • reaction mechanisms



Simultaneous generation of an enolate and Nicholas carbocation unit (**2**) occurs on treatment of enol ether–cobalt complexes **1** with Lewis acids (X). Subsequent cyclization provides α -functionalized β -alkynyl cycloalkanones **3** in a regiospecific fashion. The scope of this rearrangement process is discussed, as is the stereoselectivity of α -alkyl incorporation.



Angew. Chem. **2002**, *114*, 2696–2699

D. R. Carbery, S. Reignier, J. W. Myatt,
N. D. Miller, J. P. A. Harrity* 2584–2587

Development of a Co-Mediated
Rearrangement Reaction

Keywords: alkyne ligands •
carbocations • cobalt • cyclization • enol
ethers

The nature of oxide-supported metal catalysts may change in oxidizing conditions: Studies on the correlation between the Rh phase in the structure of the Rh/Al₂O₃ catalyst and the catalytic performance for the reduction of NO by H₂ to N₂ (on reduced, metallic sites) and N₂O (on oxidized sites) reveal that the phases of the supported metal species can be interconverted on time scales that can be deterministic in terms of the activity and selectivity of the catalysts.

Angew. Chem. **2002**, *114*, 2699–2701

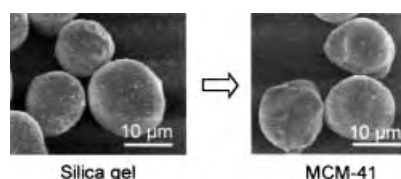
M. A. Newton, A. J. Dent,
S. Diaz-Moreno, S. G. Fiddy,
J. Evans* 2587–2589

Rapid Phase Fluxionality as the
Determining Factor in Activity and
Selectivity of Highly Dispersed, Rh/Al₂O₃
in deNO_x Catalysis

Keywords: heterogeneous catalysis •
nanostructures • rhodium • structure–
activity relationships • X-ray absorption
spectroscopy

Pores for order: Particles of silica gel can be transformed into MCM-41 without losing their size and shape by a low-temperature hydrothermal treatment (see electron micrographs). This method allows easy preparation of custom-tailored materials for chromatography and separation.

Angew. Chem. **2002**, *114*, 2702–2704



T. Martin, A. Galarneau, F. Di Renzo,*
F. Fajula, D. Plee 2590–2592

Morphological Control of MCM-41 by
Pseudomorphic Synthesis

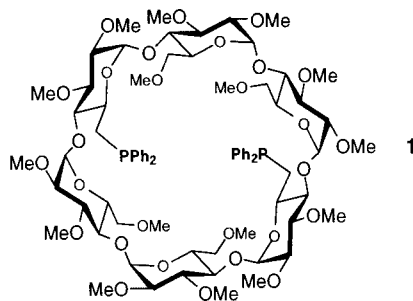
Keywords: microporous materials •
particles • pseudomorphism • silicates •
zeolites



Are α -cyclodextrin cavities chlorophillic? The α -CD-derived diphosphane **1**, a ligand which shows a marked tendency to act as a *trans*-spanning chelator, provides an answer to this question.

Reaction of **1** with a variety of transition metal chlorides systematically afforded complexes in which the M–Cl bond(s) is(are) captured by the cavity and results in weak interactions between the sequestered Cl atoms and inwardly oriented C–H bonds. The shortest H–5...Cl distance in the Pd complex is 2.64(2) Å.

Angew. Chem. **2002**, *114*, 2705–2708



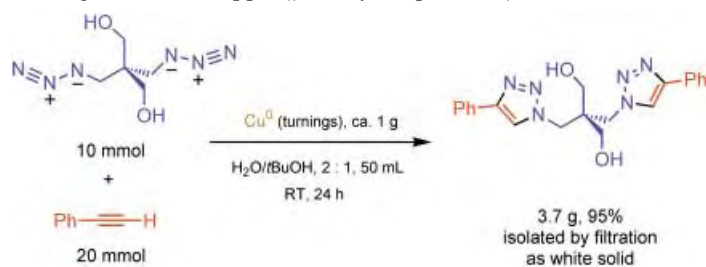
E. Engeldinger, D. Armspach,* D. Matt,*
P. G. Jones, R. Welter 2593–2596

A Cyclodextrin Diphosphane as a First
and Second Coordination Sphere
Cavitand: Evidence for Weak
C–H...Cl–M Hydrogen Bonds within
Metal-Capped Cavities

Keywords: chelates • cyclodextrins •
metallocavities • noncovalent
interactions • phosphanes



By simply stirring in water, organic azides and terminal alkynes are readily and cleanly converted into 1,4-disubstituted 1,2,3-triazoles through a highly efficient and regioselective copper(I)-catalyzed process (see scheme for an example).



Angew. Chem. **2002**, *114*, 2708–2711

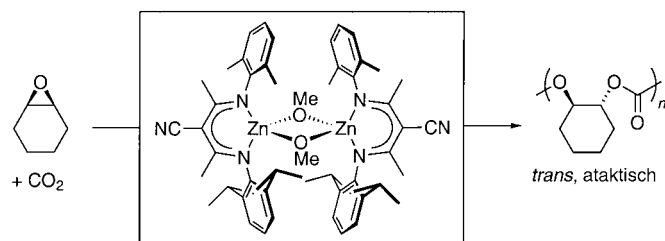
V. V. Rostovtsev, L. G. Green,
V. V. Fokin,*
K. B. Sharpless* 2596–2599

A Stepwise Huisgen Cycloaddition
Process: Copper(I)-Catalyzed
Regioselective “Ligation” of Azides and
Terminal Alkynes

Keywords: azides • copper •
cycloaddition • homogeneous catalysis •
nitrogen heterocycles



CO₂ is perhaps the most attractive carbon-based feedstock owing to its abundance and low toxicity. Utilization of this contributor to global warming is a long-standing goal. Reported here are new single-site β -diiminate zinc catalysts that exhibit unprecedented activities for CO₂/epoxide polymerization (see scheme).



Angew. Chem. **2002**, *114*, 2711–2714

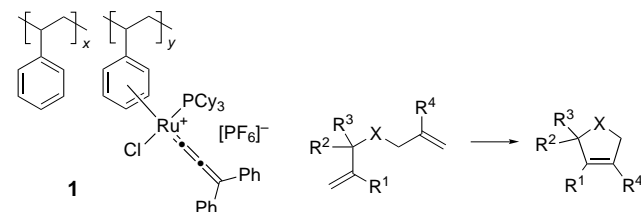
D. R. Moore, M. Cheng, E. B. Lobkovsky,
G. W. Coates* 2599–2602

Electronic and Steric Effects on Catalysts
for CO₂/Epoxide Polymerization: Subtle
Modifications Resulting in Superior
Activities

Keywords: carbon dioxide fixation •
green chemistry • homogeneous
catalysis • ligand effects • ring-opening
polymerization



Styrene as ligand and support: An excellent polymer-supported ruthenium catalyst **1** has been developed in which the benzene rings of polystyrene are utilized as ligands to immobilize the ruthenium onto the polymer. In the presence of **1**, ring-closing olefin metathesis proceeded smoothly to afford adducts in high yields. Furthermore, the catalyst was recovered quantitatively by filtration, and could be reused without loss of activity.



Angew. Chem. **2002**, *114*, 2714–2716

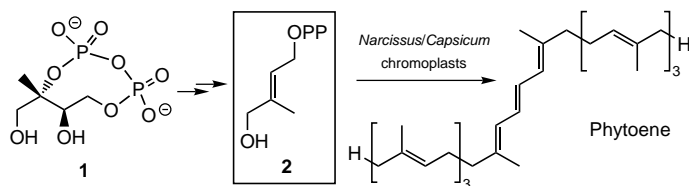
R. Akiyama, S. Kobayashi* . 2602–2604

A Novel Polymer-Supported Arene–
Ruthenium Complex for Ring-Closing
Olefin Metathesis

Keywords: alkenes • metathesis •
microencapsulation • ruthenium •
supported catalysts



The missing link in the new deoxyxylulose phosphate metabolic pathway leading to the biosynthesis of plant terpenoids has been identified. The intermediate between the cyclic diphosphate **1** and the basic isoprenoid building blocks dimethylallyl diphosphate and isopentenyl diphosphate has been shown for the first time to be (*E*)-4-hydroxy-3-methylbut-2-enyl diphosphate (**2**) by incorporation of tritium-labeled **2** into phytoene.



Angew. Chem. **2002**, *114*, 2716–2719



Supporting information on the WWW
(see article for access details).



Accelerated publications

W. Gao, R. Loeser, M. Raschke,
M. A. Dessoy, M. Fulhorst,
H. Alpermann, L. A. Wessjohann,*
M. H. Zenk* 2604–2607

(*E*)-4-Hydroxy-3-methylbut-2-enyl
Diphosphate: An Intermediate in the
Formation of Terpenoids in Plant
Chromoplasts

Keywords: biosynthesis • diphosphates •
isoprenes • isotopic labeling • terpenoids

* Author to whom correspondence should be addressed



BOOKS

Bioninformatics – From Genome to Drugs.

Thomas Lengauer

Andrew H. Davis 2609

Organobismuth Chemistry

Hitomi Suzuki,
Yoshihiro Matano

K. Seppelt 2610

Metal Oxygen Cluster

John B. Moffat

H. Knözinger 2611

Extraction of Metals from Soils and Waters

D. Max Roundhill

R. Ludwig 2611



WEB SITES

<http://www.ch.cam.ac.uk/c2k/>

The Best Chemistry
Sites?

M. Müller 2615

SERVICE

• VIPs	2426	• Authors	2617
• Angewandte's Sister-Journals	2437–2439	• Preview	2618
• Keywords	2616		

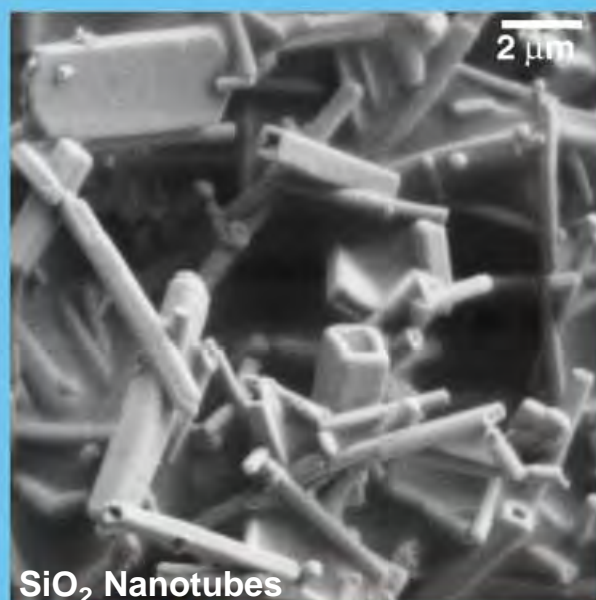
**Don't forget all the Tables of Contents
from 1998 onwards may be still found
on the WWW under:
<http://www.angewandte.org>**

Issue 13, 2002 was published online on July 1.

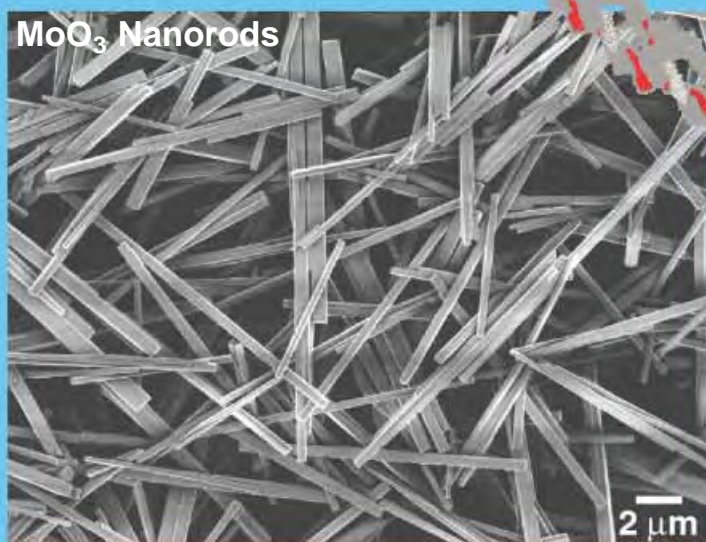
CORRIGENDA

In the book review on *Voodoo Science: the road from foolishness to fraud* by N. J. Turro (*Angew. Chem.* **2002**, *41*, 1069), the references were inadvertently omitted. The editorial office apologizes for this, and the references are now given.

- [1] T. S. Kuhn, *The Nature of Scientific Revelutions*, 2nd ed., University of Chicago Press, Chicago, IL, **1970**.
- [2] a) N. J. Turro, *Angew. Chem.* **2000**, *112*, 2343; *Angew. Chem. Int. Ed.* **2000**, *39*, 2255; b) N. J. Turro, *Angew. Chem.* **2000**, *98*, 872; *Angew. Chem. Int. Ed. Engl.* **1986**, *25*, 882.
- [3] R. Ehrlich, *Nine Crazy Ideas in Science*, Princeton University Press, Princeton, NJ, **2001**.
- [4] M. Shermer, *Why People Believe Weird Things*, Freeman, NY, **1997**.
- [5] W. Gratzer, *The Undergrowth of Science*, Oxford University Press, Oxford, **2000**.
- [6] I. Langmuir, *Phys. Today*, **1989**, *42*, 36



Oxidic nanotubes and nanorods are accessible now in various systems with well-developed morphology. Structural versatility as well as anisotropic chemical and physical properties are unique characteristics that make them promising materials.



Oxidic Nanotubes and Nanorods—Anisotropic Modules for a Future Nanotechnology

Greta R. Patzke, Frank Krumeich, and Reinhard Nesper*

The discovery of carbon nanotubes in 1991 is a milestone in nanomaterials research. Since then, more and more anisotropic nanoparticles have been detected and characterized. The development of nanodevices might benefit from the distinct morphology and high aspect ratio of nanorods and nanotubes as these can be functionalized in unique ways such as incorporation of nanorods in nanotubes. Downscaling a broad range of materials to 1D nanoscopic structures is currently the focus of a rapidly growing scientific community. Developing general pathways to this goal would transfer a wide variety of properties to the nanoscale—a spec-

trum of phenomena so diverse that it would cover not only inorganic systems but all of materials science. Synthesis of real functional materials, however, always involves considerable synthetic ingenuity, interdisciplinary collaboration, as well as technological and economical realism. The major topic of this review is to provide a survey of recent progress in the synthesis of oxidic nanotubes and nanorods—with their non-oxidic counterparts briefly highlighted—and to outline the major synthetic routes leading to them. With the challenges of synthesizing bulk oxidic materials in mind, the establishment of trustworthy and uncomplicat-

ed ways of providing them as anisotropic nano-modules on an industrial scale appears to be more or less serendipity. Of the methods utilized in nanotube and nanorod synthesis solvothermal processes have emerged as powerful tools for generalizing and systematizing controlled syntheses of nano-morphologies. The flexibility and reliability of this synthetic approach is demonstrated here for the transformation of transition-metal oxides into high-quality anisotropic nanomaterials.

Keywords: nanorods • nanotubes • nanomaterials • oxides • solvothermal synthesis •

1. Introduction

Entering the world of nanomaterials has become an exciting challenge for chemists, physicists, and materials scientists. During the final decade of the last century, a vast knowledge about the synthesis and properties of various nanoparticles and nanocomposites was collected, with new insights and discoveries emerging almost on a daily basis.

Now expectations concerning the application of nanomaterials as the upcoming functional materials for the 21st Century are rising: the technological limits of today's micro-devices are already becoming apparent. Thus, downscaling conventional technologies by at least an order of magnitude would be the next logical step, and nanoparticles are the perfect building blocks for this purpose. This revolutionary development offers completely new dimensions when it

comes to the production of nanodevices: a drastic reduction in the necessary amount of functional materials—and therefore also of price and toxicity—could turn production processes which are considered laborious and environmentally harmful into elegant “white technologies”. The dimensions of nanoparticles, located between those of molecules and conventional microelectronics, allow mimicking of nature's efficient ways of managing with less when it comes to chemical and physical processing.

Moreover, physical and chemical properties of substances can be considerably altered when they are exhibited on a nanoscopic scale, and this phenomenon opens up a completely new perspective for materials design that benefits from the introduction of particle size as a new, powerful parameter.^[1]

So what can stop us from getting rid of our old-fashioned techniques and shrinking them down to the economically and practically preferable nanoscale?

First of all, the multitude of nanoparticles known and their syntheses have to be mastered. This includes the scaling up of known laboratory-scale syntheses into reliable, standard manufacturing procedures for nanomaterials with uniform, monodisperse morphologies. This alone is not enough: once

[*] Prof. Dr. R. Nesper, Dr. G. R. Patzke, Dr. F. Krumeich
Laboratory of Inorganic Chemistry
ETH Hönggerberg–HCI
8093 Zürich (Switzerland)
Fax: (+41) 1-632-1149
E-mail: nesper@inorg.chem.ethz.ch

readily available, these particles should then be improved by means of coating and functionalization. Moreover, there are still many substance classes remaining—especially three-and-more-element systems such as oxidic high-temperature superconductors—that have yet to be transformed into nanoscale materials. But even if all these problems have been mastered, there is another task left that must be tackled to make technological applications possible: addressing and alignment of single particles which is necessary, for example, in nanocapacitors or nanotransistors.

For alignment and functionalization procedures, nanoparticles with an anisotropic morphology are certainly advantageous. Especially nanotubes possess several different areas of contact (borders, inner and outer surfaces, and structured tube walls) that in principle can be functionalized in several ways. Their basic hollow morphology is almost directly associated with their usage as nanoscale host materials.

The most prominent examples of nanotubes are certainly the carbon nanotubes. Detailed information about the full scale of their potential and practical applications can be found in a series of review articles devoted to this topic.^[2] In this regard, the up-and-coming class of oxidic nanotubes might offer even more properties and advantages leading directly to new technological applications.

But their non-hollow counterparts—nanorods and nanowires—should not be missing in a future “nano-toolbox” filled with functional nanoparticles that can be combined to design new devices. Nanorods and nanowires need not be stabilized by any kind of incorporated templating material, and the

synthetic requirements for their production are surprisingly flexible. Oxidic nanorods are currently a major topic in nanoscopic research activities, and the chase for binary oxidic nanorods has been successful all over the periodic table.

Ordered arrays of both nanotubes and nanorods are accessible in principle. The combination of nanotubes and nanorods by the *tube-in-tube* or the *rod-in-tube* approach would be an outstandingly elegant means of intrinsic functionalization taking advantage both of the inner surface of nanotubes and the high aspect ratio of nanorods.

The ongoing success on all frontiers of nanomaterials research makes it more and more difficult to keep up to date with all new achievements and to derive general trends that could be the main pathways to future technology. So this article is intended to give a concise and useful survey of recent progress in synthesis and characterization of oxidic nanotubes and nanorods in combination with highlights from other materials classes. Even a short scan of novel publications concerning these topics clearly reveals that solvothermal synthesis is one of the most powerful tools providing access to distinct morphologies of nanomaterials. Selected recent examples from our laboratory illustrate the straightforward applicability of this strategy upon the production of both nanotubes and nanorods that are uniformly and quantitatively produced either in the presence of a template or via a self-organization process in solution. Sometimes it is uncomplicated “chimie douce” (soft chemistry) that provides the best results—with remarkable reliability, selectivity, and efficiency that can rarely be achieved with conventional methods.

Greta R. Patzke, born in Bremen, Germany, in 1974, studied chemistry in Hannover. She received her PhD for work on chemical transport reactions under the supervision of Professor M. Binnewies in 1999, and then she moved to the ETH Zürich to carry out work towards her habilitation. Her research interests are focused on the synthesis of nanomaterials, their structural characterization, and the application of their novel properties.



G. R. Patzke



F. Krumeich



R. Nesper

Frank Krumeich, born in Bad Hersfeld (Germany) in 1960, studied chemistry at the Justus-Liebig-Universität in Giessen and finished his doctorate 1990 with Professor R. Gruhn. After five years at the Universität Bonn and one year at the Institut für Angewandte Chemie in Berlin-Adlershof, he came to the ETH Zürich in 1997. He specializes in structural characterization by TEM methods. Besides nanomaterials, his research interests comprise bronze-type Nb-W oxides and quasicrystals (dodecahedral tantalum tellurides).

Reinhard Nesper, born in Elze/Hannover (Germany) in 1949, studied chemistry at the Universität Münster and then moved to the Max-Planck-Institut für Festkörperforschung in Stuttgart where he received his PhD under the supervision of Professor H.-G. von Schnering. Apart from a period of research with Professor Roald Hoffmann at Cornell University in 1984, he was a member of the scientific staff at the Max-Planck-Institut Stuttgart from 1978 to 1990. In 1989, he received his habilitation at the Universität Stuttgart and in 1990 he accepted the chair of inorganic chemistry at the ETH Zürich. His main areas of interest are solid-state chemistry, structure determination, and the electronic structure of solids as well as new materials, nanostructures, structure–property relationships, and models for structure formation.

2. Nanotubes

The discovery of the carbon nanotubes (CNT) by Iijima in 1991^[3] in conjunction with the outstanding physical and chemical properties of this novel material has put the scientific community into a kind of continuous gold-rush mood. Up to now, immense efforts have been undertaken worldwide to optimize the synthesis, to characterize the structure, and to determine the properties of the CNTs. In addition to multi-walled CNTs, it was also possible to produce single-walled CNTs, consisting of only one concentric graphite-type layer, by co-vaporizing carbon and transition metals.^[4] Various applications of CNTs have been investigated, for example, as gas detectors,^[5] as field emitters,^[6] as tips for scanning-probe microscopy,^[7] as quantum wires,^[8] and as electromechanical devices, just to mention a few.^[9, 10] For a while, they also seemed to be very attractive as storage devices for hydrogen,^[11] however, the earlier results could not be verified in later experiments and finally part of the storage capacity was traced back to metal impurities.^[12] Semiconducting CNTs may be structurally altered in such a way that each tube becomes an electronic rectifying device,^[13] while metallic CNTs are presumably able to transfer enormous current densities.^[14] Of course, if CNTs would be available in large amounts at low costs, they would be an extremely versatile, novel, lightweight, high-stability material in many respects. Last but not least, it should be mentioned that the elastic properties of CNTs are beyond those of all industrial materials, utilized so far.^[15]

As a side-branch of this ongoing research in the field of CNTs, structurally related nanotubes of boron nitride (BN)^[16] and boron carbide (BC)^[17] have been found and microscopically characterized. Furthermore, an intensive search for tubular variants of other phases has been started.^[18] These studies led to the successful preparation of nanotubular forms of several oxides, which are the focus of this review, as well as of chalcogenides, which will be covered briefly. In other inorganic systems, the tubular morphology is quite rare: NiCl₂ nanotubes were observed as a unique example of a tubular halogen compound.^[19] Metallic nanotubes are accessible from bismuth,^[20] and, furthermore, membranes consisting of gold^[21] and nickel^[22] nanotubes, exhibiting interesting transport and magnetic properties can be obtained by using microporous alumina as a template. In addition, nanotubes of tellurium were prepared recently.^[23]

In general, tubular phases cover a wide range of size, extending from mm-long hollow fibers down to nanotubes with a diameter of only a few nm. Consequently, electron-microscopy methods are the most indispensable tools for the characterization of structure and morphology.^[24] As an example for oxides, needle-shaped niobium oxide crystals can be regarded as macroscopic tubes since there are channels along the needle axis.^[25] This structure is most likely a result of defects, which arise under the non-equilibrium growth conditions during the preparation by chemical transport. Other examples are the hollow needles of W₁₈O₄₇^[26] and ZnO.^[27]

It is noteworthy that similar phenomena have also been observed in other systems, such as in minerals, for example,

tochinolite 2Fe_{1-x}S · 1.7[(Mg_{0.7}Al_{0.3})(OH)₂],^[28] in rare-earth sialons,^[29] in Ag₂Se,^[30] as well as in misfit layer structures.^[31] The size of other tubular oxides, such as those of titanium and vanadium, is about three orders of magnitude smaller than these microtubes, and these materials are therefore designated as oxide nanotubes. Although there is a wide agreement among scientists that the use of the term *nanotube* is restricted for the description of a material with a corresponding morphology, recently some misunderstanding has regrettably been caused by its use for specifying columnar structures, such as Na₂V₃O₇^[32] or MoS₂I_{0.33}.^[33] Certainly, this misuse should be avoided. Under these circumstances, it is noteworthy that S. Iijima, the discoverer of the CNTs, had designated them in his first papers modestly as microtubules of graphitic carbon. The term *nanotube* was not introduced into the literature until the following year.

At the present stage, it is important to discriminate between isolated and aggregated or fused nanotubes on the one hand and between cylinder-like tubes and scrolls on the other hand. There are a few distinct differences between the latter two such as topological flexibility, which is much larger for nanoscrolls, and dimensionality considerations. Whereas cylinder-like nanotubes are one-dimensional, nanoscrolls are still composed of layers which may have a considerable expansion when unscrolled. In this respect, scrolls may adopt one- and/or two-dimensional properties.

2.1. Vanadium Oxide Nanotubes

Considering the importance of vanadium oxide in catalysis, in electrochemistry, and as a functional ceramic, the fabrication of this material in nanostructured form and with anisotropic morphology appears to be a particularly attractive goal. The first successful approach to make a tubular vanadium oxide was with the use of carbon nanotubes as a template.^[34] It was possible by exploitation of surface-tension effects to coat the CNTs externally with crystalline layers of a V₂O₅-like structure.

A fundamentally new type of vanadium oxide nanotubes (VO_x-NTs) was obtained by a soft-chemistry synthesis involving an amine with long alkyl chains as a molecular, structure-directing template.^[35] This material which is available in gram amounts is mostly constructed in a scroll-like fashion. The tube diameters can be tuned from a few nanometers in the conventional VO_x-NTs up to several hundreds of nm in a new type discovered recently. VO_x-NTs are easily accessible in high yield by treating a vanadium(v) oxide precursor with an amine (C_nH_{2n+1}NH₂ with 4 ≤ n ≤ 22) or an α,ω-diaminoalkane (H₂N[CH₂]_nNH₂ with 14 ≤ n ≤ 20), followed by hydrolyzation, aging of the gel, and a hydrothermal reaction. The possibility of using V₂O₅, VOCl₃,^[36] or HVO₃^[37] as the vanadium source instead of a vanadium(v) alkoxide provides a low-cost alternative. Recently, the first VO_x-NTs that contain an aromatic amine were obtained with phenylpropylamine.^[38]

The lengths of the VO_x-NTs vary in the range 0.5–15 μm and the outer diameters in the range 15–150 nm. Interestingly, tubes obtained with monoamines tend to form thin tube walls consisting of rather few layers (2–10), whereas diamines

predominantly lead to tubes with comparatively thick walls, consequently comprising a much larger number of layers (>10). As a rule, the VO_x -NTs have open ends (Figure 1 a); closed tubes are scarcely observed. Vanadium oxide layers between which protonated template molecules are embedded build up the tube walls. As a result, the distance between the VO_x layers increases with increasing length of the amine or diamine applied, and interlayer distances between approximately 1.7 and 3.8 nm can be achieved in a controllable way.

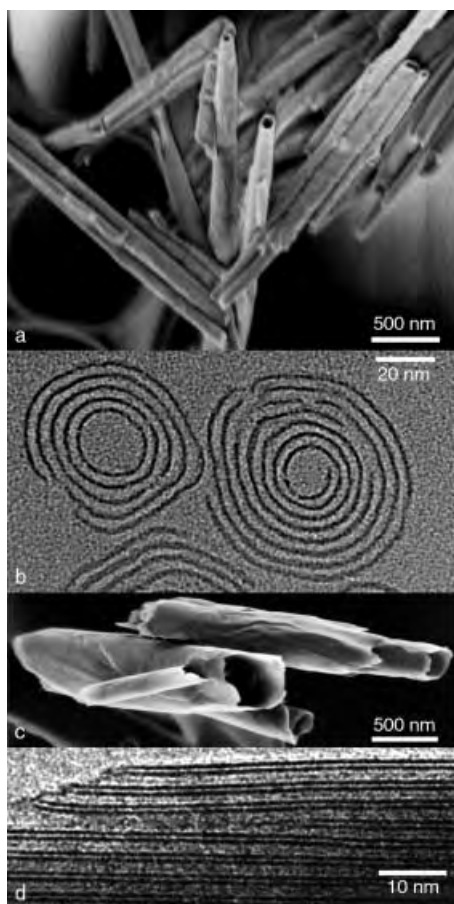


Figure 1. a) SEM image of vanadium oxide nanotubes, containing undecylamine as template (C_{11} - VO_x -NTs). The tube tips are open. b) TEM image of the cross-sectional structure of C_{16} - VO_x -NTs. The NT on the left consists of five concentric VO_x layers, that on the right of a scrolled single layer. Gaps appear at several sites in the VO_x layers. c) SEM image of vanadium oxide nanotubes obtained by addition of ammonia during the synthesis (N-VO_x -NTs). d) TEM image of the structure within the tube walls of a N-VO_x -NT. Two different interlayer distances (~ 0.9 nm, ~ 2.0 nm, template: dodecylamine) appear alternately.

Both possible types of nanotubes, namely those built up by closed concentric cylinders and those formed by scrolling one or more layers, appear in this system (Figure 1 b). Most VO_x -NTs are combinations of both pure structural types and show defects, for example, gaps in the VO_x layers inside the walls.^[39] The VO_x layers are crystalline as confirmed by X-ray and electron diffraction, and a 2D square lattice with a length of about 0.62 nm can describe their structure. All present experimental evidence shows that the structure of the VO_x layers is the same in all types of VO_x -NTs as well as in

$\text{BaV}_7\text{O}_{16} \cdot x\text{H}_2\text{O}$.^[40] X-ray diffraction (XRD) patterns of VO_x -NTs simulated with a structural model based on this layer structure agree well with the experimentally observed ones.^[41] These layers have the composition V_7O_{16} . They consist of two sheets of VO_5 square pyramids pointing in opposite directions, and the sheets are connected by VO_4 tetrahedra (Figure 2).

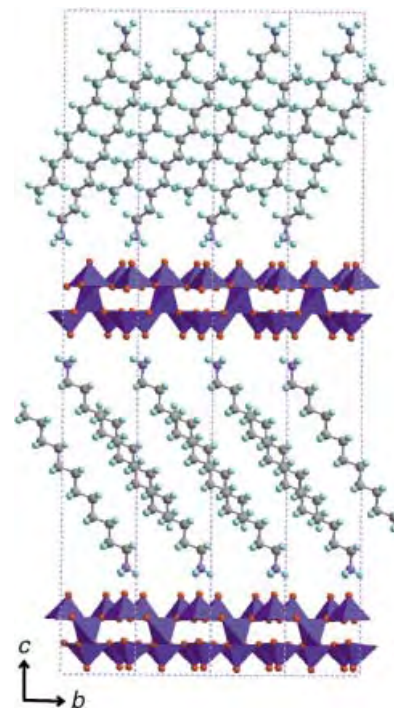


Figure 2. Structural model for the layers inside the walls of the VO_x -NTs.

Because of the scroll-type morphology, the VO_x -NTs exhibit a remarkable structural flexibility that distinguishes them from most other nanotube systems. Various exchange reactions in which the tubular morphology is well preserved are feasible. Intercalated monoamines can be substituted by diamines simply by mixing a suspension of the VO_x -NTs with the respective diamine.^[42] Furthermore, a certain amount of the monoamine can be exchanged reversibly by various metal ions, for example, Na^+ , K^+ , Ca^{2+} , Sr^{2+} , Fe^{2+} , or Co^{2+} .^[43] The possibility to insert lithium electrochemically opens up some new perspectives for battery applications; specific capacities up to 200 mA h g^{-1} have been measured by several research groups.^[44] However, the morphological flexibility is a drawback in this case and leads to rapid decay of the tubular morphology. Other materials turn out to be more stable under the electrochemical redox cycles.^[45]

A novel type of vanadium oxide nanotube has been obtained by adding ammonia during the hydrolysis step of the synthesis.^[46] These tubes have a much larger diameter, typically around 200 nm (Figure 1 c). The main characteristic is the structure inside the rather thin tube wall that consists of two different, alternating, interlayer distances (Figure 1 d). The larger separation is a result of the embedded amine molecules whereas it is assumed that the NH_4^+ ion is located in the narrow layers. Most likely, the structure with the shorter interlayer distance is stiffer than that with the array of amine

molecules and thus impedes bending, so causing the larger diameter of these tubes compared to the conventional VO_x -NTs. To our knowledge this type of layer structure with a regular arrangement of alternating short and long interlayer distances has been observed in a tubular phase here for the first time.

2.2. Titanium Oxide Nanotubes

Titanium oxide nanotubes (TiO_2 -NTs) are accessible with varying structure and size following different routes. The first synthesis reported used a polymer mold, on which titanium oxide was deposited electrochemically.^[47] The TiO_2 -NT preparation in porous alumina, applying different titanium precursors, represents a similar approach.^[48] The use of organic gelators generates supramolecular assemblies that form TiO_2 -NTs after calcination.^[49] Furthermore, polymer fibers can be used as templates: after coating with titanium oxide by a sol-gel method and removing the polymer thermally, TiO_2 -NTs are obtained.^[50] Another synthesis route is the anodic oxidation of titanium.^[51] In these cases, the TiO_2 -NTs are up to some 10 μm long and have an outer diameter of 100–200 nm while the actual wall thickness depends on the synthesis conditions applied.

TiO_2 -NTs with a much smaller size have recently been synthesized by a surprisingly simple procedure. TiO_2 with anatase or rutile structure was treated with NaOH and subsequently with HCl.^[52] The resulting TiO_2 -NTs are 50–200 nm long and their diameter is about 10 nm (Figure 3a).

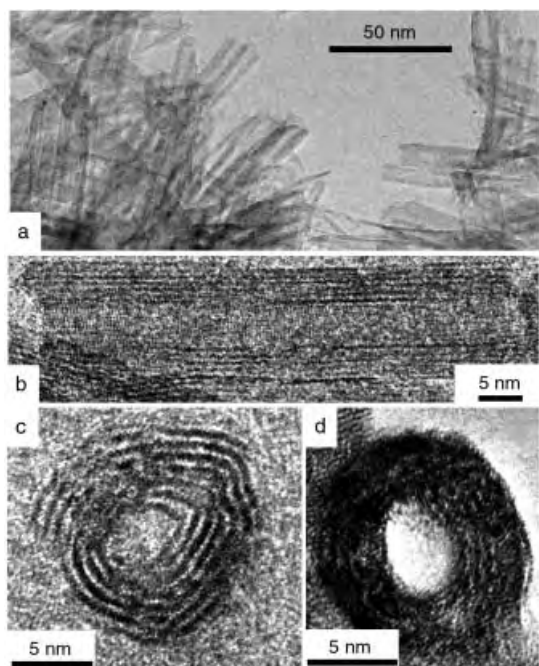


Figure 3. a) TEM image of TiO_2 nanotubes. b) HRTEM image of a well-developed, ~ 50 nm long NT with a diameter of ~ 10 nm. Lattice fringes can be seen. c) TEM image of the cross-section of a scroll-like NT. Projection along the tube axis is obtained by an embedding method for TEM preparation. d) Tube fragment that by chance is oriented parallel to the incident electron beam. This light area in the center demonstrates that the tube core is empty.

The high resolution (HR) TEM image (Figure 3b) of such a TiO_2 -NT shows that the tubes have an inner core and walls. The presence of lattice fringes indicates the crystalline structure of TiO_2 -NTs. Parallel fringes in the walls correspond to a distance of about 7 nm, which can also be detected as a broad reflection by X-ray and electron diffraction. The observed weak reflections indicate that the TiO_2 -NTs are built in a layered titanate structure.^[53, 54] The reflections of anatase, which have been detected in previous investigations,^[52] are most likely caused by impurities. Views of the tube cross-section (Figure 3c) show a spiral arrangement of the dark fringes in the walls.^[54] This observation requires a special TEM preparation technique that fixes the pre-orientation of the tubes by embedding them in a resin and preserves the orientation in the course of the thinning procedure.^[55] The resin is apparently able to fill the tube core by capillary action, and thus the contrast of an amorphous material is observed in the tube center. On the other hand, the TEM image of a tube fragment, which is by chance oriented in the appropriate direction, shows a bright contrast in its center indicating an open channel (Figure 3d). Since the TiO_2 -NTs are rather stable during thermal treatment, an application in catalysis or as a material supporting catalytic metal particles seems more probable than the use of the thermally unstable VO_x -NTs.

2.3. Other Oxidic Nanotubes

Tubular forms of silicon oxide appear in different types and sizes. It is long known that the fibrous asbestos minerals serpentine and chrysotile comprise a tubular structure that consists of curved layers.^[56] For instance, the layer structure of $[\text{Mg}_3(\text{OH})_4(\text{Si}_2\text{O}_5)]$ contains sheets of MgO_6 octahedra on one side and SiO_4 tetrahedra on the other side. This structural anisotropy causes the bending of the layers. A comprehensive TEM investigation of various chrysotile samples revealed the co-existence of fibers with spiral structures and with concentric layer structures.^[57] These structural characteristics are surprisingly similar to those typical for VO_x -NTs.

In contrast to the crystalline silicate minerals, the walls of artificial tubular SiO_2 phases are generally amorphous. Silica nanotubes can be obtained by template-assisted soft chemistry routes,^[58] similar to that leading to mesoporous M41-S materials,^[59] or by a high-temperature approach.^[60] Well-developed silica nanotubes with large diameter (up to 200 nm) and rather thin tube walls are formed by an interesting method using organic molecules as templates.^[61] Derivates of cholesterol gelatinize organic solvents, and some of the resulting xerogels consist of tubular structures. The sol-gel polymerization of tetraethoxysilane occurs on the surface of these cylindrical templates, and SiO_2 -NTs form after calcination. Large nanotubes of SiO_2 and TiO_2 are formed by calcination of fiberlike crystals of $[\text{Pt}(\text{NH}_3)_4](\text{HCO}_3)_2$ coated with $\text{Si}(\text{OEt})_4$ or $\text{Ti}(\text{OEt})_4$.^[62] The tube walls consist of amorphous silicon- or titanium oxide, respectively, while the inner core is partly filled with Pt nanoparticles (Figure 4). Owing to the shape of the template-

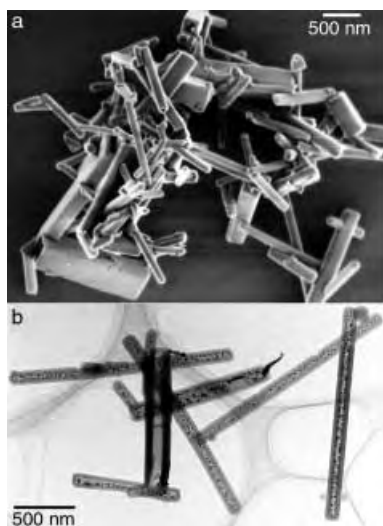


Figure 4. a) SEM image and b) TEM image of silica nanotubes filled with Pt particles, recognizable as dark spots in (b).

ing $[\text{Pt}(\text{NH}_3)_4](\text{HCO}_3)_2$ single crystals, the tube cross-sections are often rectangular.

A widely applicable route to inorganic nanotubes is to use CNTs as templates.^[63] The CNTs were coated with a thin film of secondary material that builds up the tube wall after removal of the carbon. Besides vanadium oxide nanotubes (Section 2.1), this procedure generates tubular forms of SiO_2 , Al_2O_3 ,^[64] MoO_3 , RuO_2 ,^[65] and ZrO_2 .^[66] Of course, such secondary coatings may generally be applied to any kind of suitable primary nanoparticle to generate so-called core-shell nanosystems.

2.4. Ordering Arrays of Nanotubes

Aligned nanotubular arrays have been synthesized for different materials since the remarkable work on the MCM mesoporous phases.^[67] Long known and well explored is the electrochemical route to nanotubular aluminum oxide which is prepared by anodic oxidation of Al films.^[68] These porous aluminum oxide membranes can be used as a template to generate nanotube or nanorod arrays of various materials. After depositing the second material from the gas phase, by sol-gel reactions, or by other methods, the aluminum oxide is dissolved by alkaline treatment. Outstanding examples of arrays generated by this route are those of oxodic nanotubes of TiO_2 ,^[69] In_2O_3 , Ga_2O_3 ,^[70] BaTiO_3 , and PbTiO_3 ,^[71] as well as of nanorods of ZnO , MnO_2 , WO_3 , Co_3O_4 , and V_2O_5 .^[72] In this context it is interesting to note that both growth and decomposition as well as dissolution of solids may lead to the formation of arrays of aligned nanotubes or nanorods.

Quite recently, well-ordered beautiful submicrometer tubular arrays of elemental silicon have been prepared by a combination of lithographic and HF etching techniques.^[73] Utilizing such arrays as chemical containers for the precipitation of secondary materials from the gas phase leads in many cases to the formation of secondary nanotubes or nanorods inside the primary tunnel systems.^[74] If the primary matrix is dissolved, isolated secondary nanotubes or nanorods

are created. A more comprehensive exploration of the rapidly growing research on nanoparticle arrays, however, is beyond the scope of this article.^[75]

2.5. Chalcogenide Nanotubes

Microtubules of misfit layer compounds, for example, in the systems $(\text{BiS})_{1+\delta}(\text{NbS}_2)_n$ ^[76] and PbNb_2S_5 ,^[77] have been known for a long time. Their typical diameter is in the range of a few microns, thus somewhat larger than what we would call nanotubes today. In 1992, shortly after the discovery of the CNTs, the first chalcogenide nanotubes were found for WS_2 by Tenne et al.^[78] Multiwalled WS_2 nanotubes can conveniently be prepared in large amounts by treating needlelike WO_{3-x} crystals with H_2 and H_2S .^[79] Alternatively, they are accessible by a chemical transport reaction^[80] and by the pyrolysis of composites of WS_2 and intercalated cetyltrimethylammonium cations.^[81] Similar to the CNTs, WS_2 -NTs can function as tips in scanning-probe microscopy.^[82]

MoS_2 nanotubes were synthesized for the first time in 1995,^[83] and in the following years, a variety of synthetic routes has been developed for MoS_2 nanotubes.^[84] Remarkably, a part of the tungsten content (~ 10 atom %) in the WS_2 nanotubes can be substituted by niobium, thereby generating novel mixed $(\text{W,Nb})\text{S}_2$ nanotubes.^[85] Most recently, NbS_2 , TaS_2 ,^[86] MoSe_2 , and WSe_2 ^[87] nanotubes were prepared for the first time. Here, the formation of the tubular morphology occurs during the reduction of the corresponding triselenides or selenometallates, by hydrogen. Furthermore, it is possible to coat CNTs with layers of WS_2 ^[88] and NbS_2 .^[89] NbS_2 nanotubes have been modeled in advance and predicted to be stable, but the energy for bending is higher than in CNTs.^[90] Similar calculations revealed that multiwalled chalcogenide nanotubes are more stable than single-walled, and, in the case of MoS_2 - and WS_2 -NTs these multiwalled NTs are semiconductors.^[91] As the latter sulfides are excellent lubricant additives, their nanoparticulate forms were tested to see if they have similar properties and gave quite promising results.^[92] A further step towards an application of these materials is the possibility to store hydrogen electrochemically in MoS_2 nanotubes.^[93]

A novel method for the synthesis of nanotubes of semi-conducting and other chalcogenides involves organic agents. A colloid of a metastable InS phase has been obtained from $t\text{Bu}_3\text{In}$ and H_2S in an organic solvent in the presence of benzenethiol which acts as a catalyst.^[94] As a by-product, InS nanotubes were generated. Nanotubes and nanowires of CdSe and CdS could be prepared in the presence of a surfactant.^[95] In these tubes, the walls comprise nanocrystalline particles of CdSe or CdS , respectively. GaSe nanotubes have also been modeled and predicted to be stable.^[96] A novel representative for nanotubes with a quite complex structure is generated by self-assembly in a colloid containing PbS nanoparticles, a polymer (poly(ethylene oxide)), and a surfactant (sodium dodecylsulfate).^[97] The presence of nanotubes in this colloid was detected by means of SEM and TEM (Figure 5). Their tube walls comprise well-developed layers of PbS nanoparticles that are embedded in the organic matrix structure.

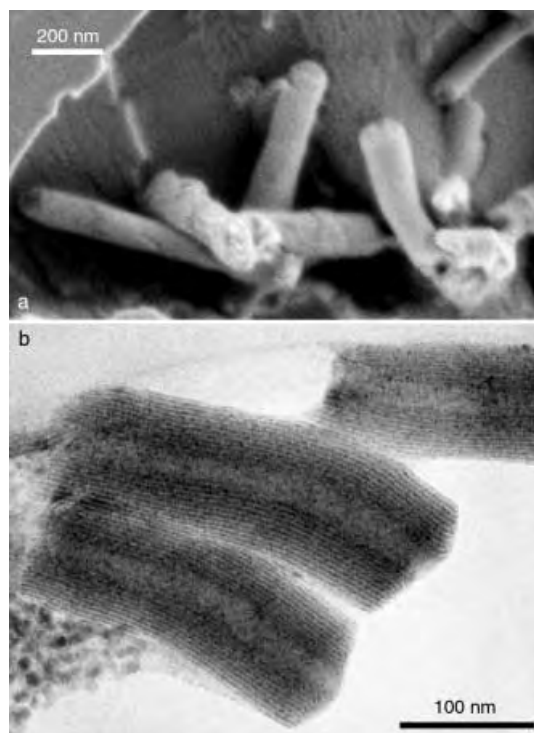


Figure 5. a) SEM image and b) TEM image of PbS nanotubes. Layers of PbS nanoparticles, which can be seen as lines with dark contrast, appear in the tube walls.

Similar to the vanadium oxide nanotubes, these PbS nanotubes also have a composite structure with an organic and an inorganic part.

2.6. Predicted Kinetically Stable Nanotubes

In addition to theoretical investigations already mentioned, there are a number of predictions that suggest quite interesting targets for the experimental chemist: a) the famous semiconductor laser material gallium nitride,^[98] b) phosphorus,^[99] c) silicide as well as silane forms (Figure 6a),^[100] and d) GeH.^[101] Also SiO₂ in form of silsesquioxane has recently been explored theoretically and found to form stable tubular nano arrangements.^[102]

We have calculated possible models for V₂O₅ nanotubes as an approximation to the more complicated wall structures which have been determined for the real VO_x nanoscrolls.^[35] A completely new set of potential parameters has been determined based on a series of density function calculations of binary and ternary vanadium oxides. Different coordination numbers had to be taken into account as well as a discrimination between vanadyl and bridging oxygen atoms (Figure 6b).^[103]

It should be noted here, that quite frequently authors argue that general similarities to CNTs, that is, the existence of graphite-related six-ring nets, should be a prerequisite for nanotube formation. According to our experimental experience and theoretical investigations, we predict that in principle all layered materials should be convertible into tubular arrangements under suitable reaction conditions whether they form six-membered rings or are linked in other ways. If layers of a lamellar material are being separated from each other by some chemical or physical means, and if the interaction of the individual layers with their coordination shells is weak enough, there should always be the possibility of

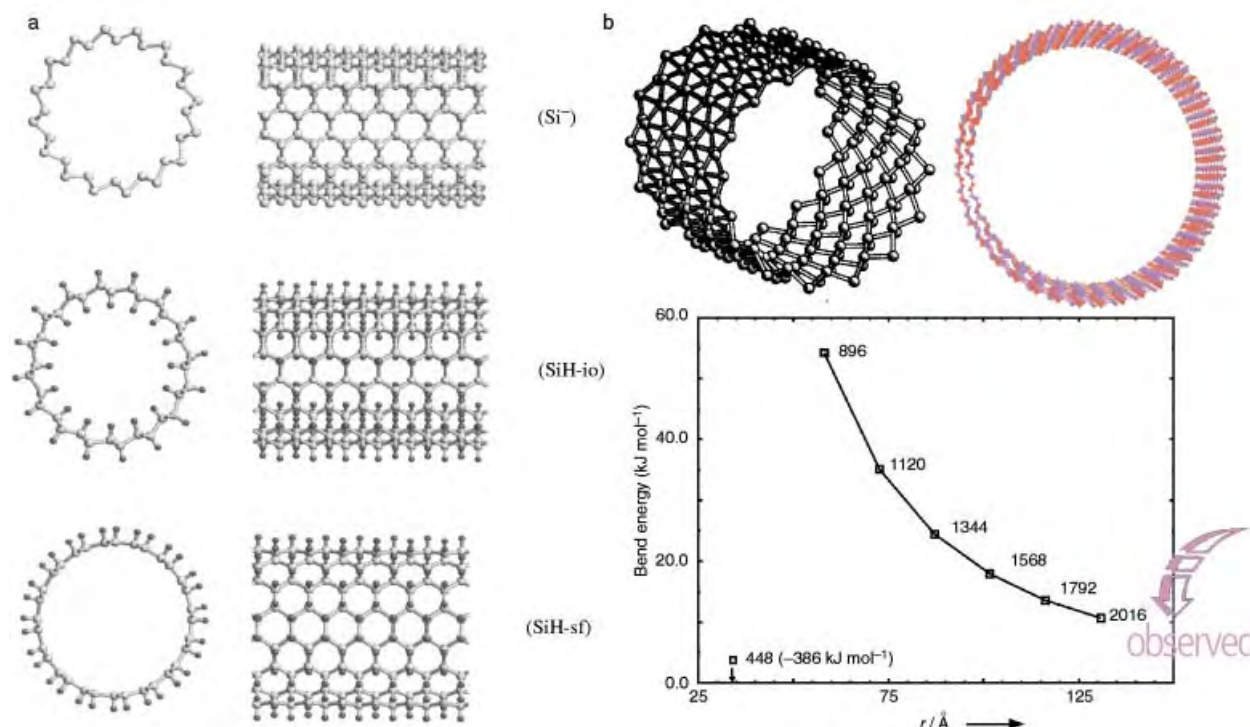


Figure 6. Predicted structures for nanotubes of a) silicides and silanes (Copyright© 2001 by APS)^[100] and b) V₂O₅. Bond energies ΔE_{bend} of V₂O₅ double-layer tubes versus radius of the tubes with respect to the flat double layers (unit cell composition V₆O₂₀): $\Delta E_{\text{bend}} = E_{\text{tube}} / \text{number of cells} - E_{\text{layer}}$. Both E_{tube} and E_{layer} were obtained by lattice energy minimization of the corresponding structures (ref. [103]). At each energy point, the total number of atoms in the tube is given.

self-contacts, that is, scroll formation. In the case of charged layers, this may be enhanced by local charge cancellation as a result of template coordination, for example.

3. Nanorods

Inorganic nanotubes in general are promising materials with unique properties, but they also have a common small drawback: they are rather rare—especially when it comes to complex or oxidic materials. In many synthesis processes nanorod formation frequently seems to compete with nanotube formation. Even if a reaction fulfills all prerequisites and passes through all the intermediates that are expected for the synthesis of a nanotube, the final product may still be a nanorod. Nanorods are surely morphologically less versatile host particles than nanotubes because they lack an accessible inner volume, but nevertheless, they have other advantages, such as enhanced thermal stability. So, if the sophisticated synthetic goal of producing hollow anisotropic nanostructures is sacrificed, then a wide range of synthetic routes opens up to deliver nanobelts, nanowires, and nanorods with almost any desired dimensions and aspect ratios. Redox-active materials, semiconductors, and metals can all be designed from such nanomaterials which might serve in a future nanotechnology, for example, as electronic, optical, or other functional materials.

For the sake of clarity, all non-hollow anisotropic inorganic nanostructures will be addressed as “nanorods” in the following, may they have been termed rod, fiber, wire, or filament before. First, we want to discuss briefly the most important classes of inorganic nanorods, including metals, semiconductors, and carbon-containing materials, each one illustrated by a few recent, impressive synthetic examples. Then, we will turn to the topic of oxidic nanorods with emphasis on the various synthetic strategies that are employed to trigger the growth of many different oxides in 1D nanoscopic arrangements. Finally, new results concerning molybdenum oxide nanorods will illustrate the power of solvothermal synthesis, which, at present, is one of the most convenient strategies used for the design of new nanomaterials.

3.1. Inorganic Nanorods, Fibers, and Filaments

The majority of investigations dealing with inorganic nanorods is focused on the following areas: metallic nanorods, semiconductor nanorods, carbide- or nitride-based nanorods, carbon nanorods, and oxidic nanorods.

In the field of metallic nanorods, highly anisotropic nanoparticles of noble metals have attracted considerable interest as a result of their possible applications in optical, electronic, and mechanical nanodevices. Silver and selenium nanorods, for example, are generated easily and flexibly by simple reactions in aqueous solution at room temperature.

- The preparation of long, continuous silver nanowires is possible by a photochemical process employing treatment of an AgBr emulsion with a special developer containing

silver nitrate. The shape of the rods is controlled by the photographic process.^[104]

- Either silver nanorods or nanowires with specific aspect ratios are accessible by reduction of preformed metal-salt seeds with ascorbic acid in the presence of a surfactant. A crucial parameter here is the pH value of the reaction mixture.^[105]
- Selenium nanowires are formed in the course of an unconventional bioinorganic synthesis including the reduction of selenate to selenium by the protein cytochrome c_3 as a key step.^[106] There are indications that the catalytic function of this enzyme also accelerates other reduction reactions that provide nanoparticles.
- A whole series of metal and semiconductor rods of different quality has been generated inside of carbon nanotubes.^[10, 107]

Once suitable sets of nanoparticles have been established they may have to be arranged in ordered arrays—a process which is essential for some applications. Recent success in the self-assembly of gold nanorods points out that soon these challenges might be mastered. Gold nanorods with an aspect ratio of 4.6:1, which have been prepared electrochemically and by precipitation methods, self-assemble into one-, two-, and three-dimensional structures. The latter can even be extended into superlattices of nanorods.^[108]

Semiconductor nanorods are in the focus of current research interests.^[109] In this field, the groups of Lieber and Alivisatos have contributed important synthetic strategies providing systematic approaches that can be applied to the synthesis of other materials.

- Laser-assisted catalytic growth is utilized to prepare a whole class of nanowires such as binary III-V materials (GaAs, GaP,...), ternary III-V materials (GaAs/P, InAs/P), binary II-VI compounds and binary SiGe alloys.^[110] Equilibrium phase diagrams can be used to predict catalysts and growth conditions. In this way, single-crystalline nanowires with diameters as small as 3 nm can be rationally synthesized.
- A morphological series of CdSe nanocrystals including nanorods is accessible in a predictable but completely different way: Thermal decomposition of organometallic precursors in a hot mixture of trioctylphosphane oxide and hexylphosphonic acid. The various shapes are basically controlled by the ratio between the two additives which influences the relative growth rates of different faces of the emerging CdSe crystals.^[111]

Carbon-based nanorods are a third major area of interest in nanorod research. It has turned out that SiC nanorods possess outstanding mechanical properties that make them promising candidates for any kind of reinforcement in the design of composite materials. Again, the variety of possible synthetic approaches and the successful mastering of the crucial alignment step can be demonstrated by two recent examples:

- The reaction of aligned carbon nanotubes with SiO at 1400 °C affords highly aligned SiC nanorods with well-separated, nanowire tips. Moreover, these arrays exhibit excellent field emission properties together with a unique combination of elasticity and strength.^[112]

- β -SiC nanorods with diameters from 10 to 40 nm and lengths up to several micrometers are available even at temperatures 1000 °C lower than the above mentioned synthesis: hydrothermal reactions can also be applied for carbide-nanorod formation, and in the case of SiC the starting materials are SiCl_4 , CCl_4 , and Na.^[113]

3.2. Oxidic Nanorods

Oxidic nanoparticles are essential for the design of superconductors, semiconductors, sensors, and many other devices in a future nanotechnology. Therefore, a general synthetic access is needed for their large-scale preparation. From the scientific point of view, transforming the manifold of technically relevant oxidic materials into 1D nanostructures offers fundamental opportunities for investigating the effect of size and dimensionality on their collective optical, magnetic, and electronic properties.

Oxidic nanorods in particular have raised scientific interest because of the observation of high critical current densities in nanorod-superconductor composites, such as MgO nanorods incorporated in $\text{AgBi}_2\text{Sr}_2\text{CaCu}_2\text{O}_8$.^[114] The introduction of nanorods improves the performance of the superconductor dramatically and is thus an important step towards large-scale applications, because the critical current densities need to be enhanced considerably in these materials.

Table 1 contains a survey of recent research activities concerning the synthesis of oxidic nanorods. A closer look at

the multitude of available materials, however, reveals the general trends and, moreover, certain challenges that remain to be tackled:

- First of all, the variety of different synthetic routes is obvious. There are many quite successful strategies employed for specific targets, but: there is no general guideline that could be consulted for the design of any kind of desired novel nanorods.
- This problem could be overcome by the concise study of the underlying mechanistic processes that lead to the formation of 1D nanoscopic structures. Up to now, only a minority of the publications in this area really deliver synthetic guidelines and explanations that can be productively applied to the synthesis of other classes of nanorods. To save the extensive optimization work that precedes many brilliant nanorod syntheses, it is necessary to devote more efforts on fundamental mechanistic studies. Such attempts will certainly be favored by joint collaborations on mechanistic investigations in catalysis, biomineralization, and nanosciences.
- Nevertheless, there are some major synthetic methods that are often successfully employed for nanorod formation: gas-phase reaction methods, solvothermal routes, template-directed as well as liquid-crystal assisted syntheses, various solution-based techniques, and sonochemically driven reactions are widely used. So when it comes to the development of new nanorod syntheses, there are at least some principal pathways that are likely to be successful. For many oxides, gas-phase thermochemical syntheses seem to prevail, however, a continuous search for low-temperature alternatives is under way.

Table 1. Synthetic routes for oxidic nanorods (published since 1995).

Oxide	Synthetic route	Ref.	Oxide	Synthetic route	Ref.
BaCrO_4	Fusion of reverse micelles and microemulsion droplets	[122]	MnO_2	Template method with alumina membranes	[127]
BaSO_4	Precipitation from aqueous solution in presence of polymers	[123]	MnO_2	Hydrothermal synthesis	[142]
BaWO_4	Reversed micelle templating method	[124]	MoO_3	Template-directed reaction of molybdic acid and subsequent leaching process	[143]
CdO	Evaporation of metal oxide powders at high temperatures	[125]	MoO_3	Templating against carbon nanotubes	[65]
CdWO_4	Hydrothermal treatment of CdCl_2 and Na_2WO_4	[126]	MoO_2	Templating against carbon nanotubes	[65]
Co_3O_4	Template method with alumina membranes	[127]	PbTiO_3	Sol-gel electrophoresis, deposition in polycarbonate membrane	[144]
CuO	Room temperature reaction of $\text{CuCl}_2 \cdot 2\text{H}_2\text{O}$ and NaOH with PEG 400	[128]	RuO_2	Templating against carbon nanotubes	[65]
Fe_2O_3	Thin-film processing method	[129]	Sb_2O_3	Microemulsion method for the system AOT–water–toluene ^[a]	[145]
Fe_3O_4	Sonication of aqueous iron(II) acetate in the presence of β -cyclodextrin	[130]	Sb_2O_3	Microemulsion method for the system AOT–water–toluene ^[a]	[145]
Ga_2O_3	DC arc discharge of GaN powders in Ar/ O_2 mixture	[131]	Sb_2O_3	Templating against carbon nanotubes	[65]
Ga_2O_3	Gas reaction method starting from Ga and O_2 at 780 °C	[132]	SnO_2	Annealing of powders generated from inverse microemulsions	[146]
Ga_2O_3	Physical evaporation at 300 °C from a bulk gallium target	[133]	SnO_2	Evaporation of metal oxide powders at high temperatures	[125]
Ga_2O_3	DC arc discharge (GaN, graphite, nickel powder)	[134]	SiO_2	Helical mesostructured tubules from Vortex-Assisted Surfactant Templates	[147]
Ga_2O_3	Electric arc discharge of GaN powders mixed with Ni and Co	[135]	TiO_2	Sol-gel template method employing alumina membranes	[148]
Ga_2O_3	Heating of Ga with SiO_2 powder and a Fe_2O_3 catalyst	[136]	V_2O_5	Vanadium pentoxide gels	[149]
GeO_2	Carbon-nanotube confined reaction of metallic Ge	[137]	V_2O_5	Templating against carbon nanotubes	[65]
In_2O_3	Evaporation of metal oxide powders at high temperatures	[125]	WO_3	Templating against carbon nanotubes	[65]
In_2O_3	Growth from Au droplets	[138]	YBCO	Laser ablation of a high T_c superconductor $\text{YBa}_2\text{Cu}_3\text{O}_7$	[150]
IrO_2	Templating against carbon nanotubes	[65]	ZnO	Gas reaction employing Zn and H_2O	[151]
$\text{K}_2\text{Ti}_6\text{O}_{13}$	Calcination of KF and TiO_2	[139]	ZnO	Evaporation of metal oxide powders at high temperatures	[125]
MgO	Vapor-solid growth process with in situ generated Mg vapor	[114]	ZnO	Catalyzed epitaxial growth	[152]
MgO	Heating of MgCl_2 at 750 °C in mixture gas (Ar/ H_2) ^[b]	[140]	ZnO	Self-organization of nanoparticles	[153]
$\text{Mg}(\text{OH})_2$	Solvothermal treatment of Mg, H_2O , and ethylenediamine	[141]			

[a] AOT = sodium bis(2-ethylhexyl)sulfosuccinate. [b] The quartz apparatus is probably the oxygen source.

- In recent years, rapid progress has been made in the transformation of binary oxides into anisotropic 1D nano-scale morphologies—but the series of binary oxidic nanorods is far from complete. Even if this goal has been fulfilled, the great variety of ternary and higher oxidic nanorods still remains to be discovered—and with them possible drastic enhancements of their manifold properties which are already fascinating in the bulk materials.

Three recent publications reveal how the main synthetic strategies are employed in an elegant and effective way.^[115] Solvothermal syntheses will be treated in the next section.

High-temperature evaporation of metal oxides: This surprisingly uncomplicated technique starts out from commercially available oxides of zinc, tin, indium, cadmium, and gallium which are placed at the center of an alumina tube that is subsequently inserted in a tube furnace.^[125] The evaporation temperatures are determined on the basis of the melting point of the oxides. As a result, perfectly shaped nanobelts of the semiconducting oxides are deposited. They exhibit wire-like nanostructures with remarkable lengths that even extend to the millimeter scale.

Reverse micelle- and micro-emulsion templating synthesis: This technique was utilized to generate uniform oxide materials such as BaWO₄ nanorods.^[124] The problem of particle alignment is tackled during the synthesis, because as-made assemblies consisting of arrangements in side-by-side geometry are formed. Similar nanorod superstructures of BaWO₄ are also produced as Langmuir–Blodgett monolayer assemblies.

Sonochemical processing of aqueous solutions: Magnetite nanorods are accessible by straightforward ultrasound irradiation of aqueous iron(II) acetate solutions in the presence of β -cyclodextrin which acts as a size-stabilizing agent. The starting material is converted quantitatively into nanorods by three hours of sonication.^[130]

3.3. Solvothermal Synthesis of Molybdenum Oxide Nanorods: A Case Study

Solvothermal synthesis is one of the most powerful strategies employed in nanochemistry. Especially when exposed to supercritical conditions, many starting materials undergo quite unexpected reactions that are often accompanied by the formation of nanoscopic morphologies, which are not accessible by classical routes.

Another benefit from solvothermal synthesis is the wide variety of parameters that can be chosen and combined: reaction temperatures close to room temperature or as high as several 100 °C, variations in pH value of the systems, choice and concentration of solvents, introduction and removal of templates and other additives, choice of different autoclave geometries, etc.^[116] Combinatorial methods might be a suitable approach towards systematization of these parameter fields—but the problem of subsequent scale-up procedures always remains to be solved after a breakthrough in solvothermal combinatorial synthesis.

If, however, a standard procedure for solvothermal formation of nanoparticles has been established, then these

solvothermal reactions are outstandingly efficient (almost 100 % conversion of the starting material), time-saving, and experimentally effortless, such as the low-cost synthesis of vanadium oxide nanotubes (see Section 2.1).^[36]

3.3.1. Nanorods of α -MoO₃·H₂O and MoO₃: Template-Directed versus Template-Free Solvothermal Syntheses

The solvothermal syntheses of MoO₃·H₂O^[143] and MoO₃ nanorods^[117] are especially suitable to demonstrate the differences in template-directed and template-free solvothermal approaches—and the effectiveness of these pathways.

When planning a solvothermal synthesis of nanoparticles with a distinct anisotropic morphology, it is always convenient to start from an educt with a layered structure, especially when a template is involved. Therefore, both of the nanorod syntheses discussed here have the same starting material in common: yellow molybdic acid, MoO₃·2H₂O. This precursor is cheap, easy to synthesize in large amounts, and air and moisture stable. The layered structure of this host compound facilitates direct intercalation of template molecules such as neutral primary amines with long alkyl chains. Yellow molybdic acid consists of [MoO₅(H₂O)] octahedra connected in infinite layers with water molecules intercalated in between.^[118] There are two kinds of differently bound water molecules which can be removed in a topotactical reaction proceeding in two steps.^[119] This reaction sequence, however, is observed neither during MoO₃·H₂O nanorod formation nor in the template-free route leading to nanorods of MoO₃. So how do these reactions proceed?

3.3.2. Template-Directed Formation of MoO₃·H₂O Nanorods

The synthesis of MoO₃·H₂O nanorods is basically carried out in two steps. First, MoO₃·2H₂O undergoes an intercalation of amines and a lamellar composite material is formed. This intermediate is then treated with HNO₃, and a leaching process takes place which removes the amine from the intercalation compound. As a result, template-free MoO₃·H₂O nanofibers are quantitatively formed.

The first step includes addition of amine and distilled water, followed by aging at room temperature for at least 48 hours. The subsequent hydrothermal treatment is remarkably insensitive towards changes in time. The temperature may range between 100 and 120 °C: no matter how long the duration of the hydrothermal treatment (from 1 up to 14 days), the lamellar phase is always formed. At higher reaction temperatures, more caution must be exercised when choosing the appropriate reaction time. Finally, the intercalation process is completely inhibited at 180 °C. So there is a relatively wide window of possible reaction parameters. The lamellar product for dodecylamine as an intercalate can be expressed by the general formula (C₁₂H₂₈N)_{0.5}MoO_{3.25} and exhibits interlayer distances of 2.76 nm (Figure 7a). Generally, several long-chained primary amines (C_nH_{2n+1}NH₂ with 11 ≤ n ≤ 16) can serve as templates.

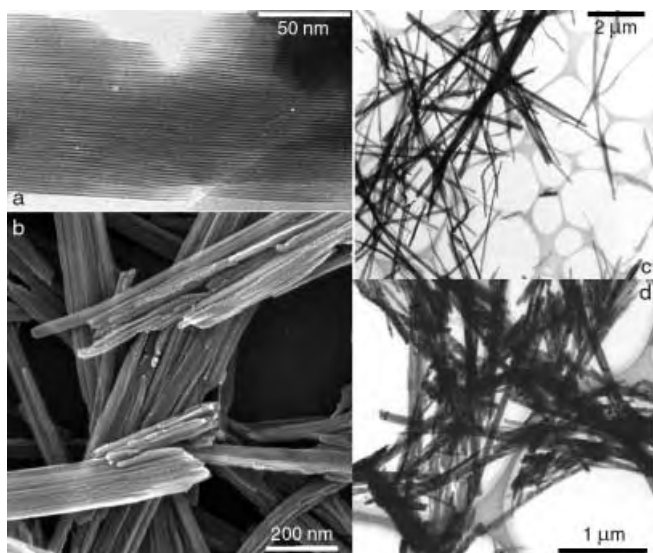


Figure 7. a) TEM image of the layered molybdenum oxide amine composite containing dodecylamine as a template. b) SEM image of several bundles of $\text{MoO}_3 \cdot \text{H}_2\text{O}$ fibers. c) Representative TEM image of $\text{MoO}_3 \cdot \text{H}_2\text{O}$ fibers consisting of smaller filaments. d) Representative TEM image of molybdenum oxide fibers after heating at 400°C in air for several hours.

During the second step the template is leached out again to give the final product. For this purpose, stirring the mixture for 2 days at room temperature with 33 % HNO_3 is sufficient. At first glance, the formation of a mesoporous material could reasonably be expected, however, a morphological transformation is observed instead: The lamellar composite material is turned into fibers, which corresponds to the conversion of a 2D into a 1D nanoscopic material. As a result, $\text{MoO}_3 \cdot \text{H}_2\text{O}$ fibers with an approximate diameter around 140 nm and an average length of 5 μm are formed (Figure 7c), which exhibit an interesting morphological feature: SEM micrographs reveal that they indeed form bundles of agglomerated smaller filaments with diameters ranging from 20 to 50 nm (Figure 7b).

This filament-like shape in the nanoscale dimension leads to the exposure of a large fraction of the atoms to the surface. Thus, these materials are promising candidates for the development of new catalytic materials. Molybdenum oxides are indeed important and effective catalysts in alcohol^[120] and methane oxidation.

Finally, the fibers withstand thermal treatment at 400°C . Their morphology remains almost unchanged, although they are converted into MoO_3 (Figure 7d). There is, however, a much more simple and elegant route to quickly generate large amounts of MoO_3 nanorods.

3.3.3. Template-Free Formation of MoO_3 Nanorods

The synthetic procedure for the direct transformation of $\text{MoO}_3 \cdot 2\text{H}_2\text{O}$ into MoO_3 nanorods can be outlined quite briefly: autoclave treatment of the starting material with small amounts of a solvent, preferably an acid, results in the quantitative formation of fibrous MoO_3 . The progress of the reaction can even be monitored optically, because the yellow molybdic acid is turned into the blue nanorod material. This

process combines two benefits that seem to be rather contradictory at first sight: although the reaction in general is remarkably stable towards changes in parameters, the morphology of the emerging rods can still be controlled by varying the conditions! So what is going on with the yellow molybdic acid here?

In a standard procedure, $\text{MoO}_3 \cdot 2\text{H}_2\text{O}$ is simply treated with diluted glacial acetic acid in an autoclave (180°C , 7 days). Plain nanorods with an average diameter of 100–150 nm and lengths on the microscale (3–8 μm) are formed quantitatively (Figure 8). After washing off the acid and drying in air, the product is pure.

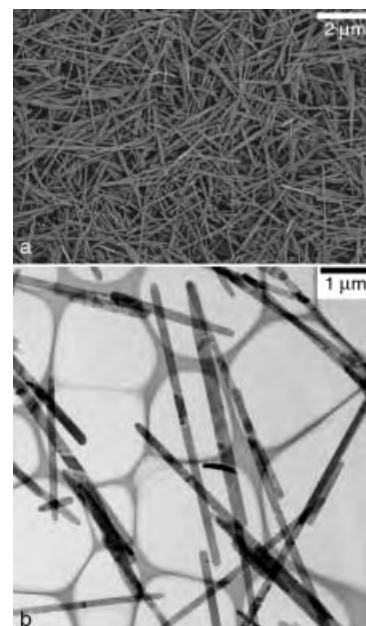


Figure 8. a) SEM and b) TEM images of MoO_3 fibers after 7 days of hydrothermal treatment in acetic acid.

The parameters time and temperature can be chosen from a wide range. Systematic investigations indicate the minimum experimental requirements necessary for the formation of nanorods: At 80°C , practically no product formation can be observed, because most of the yellow molybdic acid is dissolved. Complete dissolution of the starting material without any product formation occurs when the temperature is raised to 180°C with the reaction time limited to 1 day. Thus, the onset of the reaction requires temperatures around 90°C and at least two or three days reaction time. Figure 9 shows the transition from finely shaped to thicker rods when the temperature is increased stepwise from 90°C to 180°C . Thus, the morphology of the rods can be directed by appropriate choice of temperatures below 180°C .

From a mechanistic point of view, the fact that the educt is first dissolved completely and then precipitates again clearly excludes any kind of topotactic reaction. Consequently, the connection between success of solvothermal treatment and pre-structured layers in the educt is lost here, which suggests that much more anisotropic morphologies may be generated in this straightforward fashion. Therefore, a thorough investigation is under way to generalize the underlying reaction principle and so to exploit it for the synthesis of other nanomaterials.

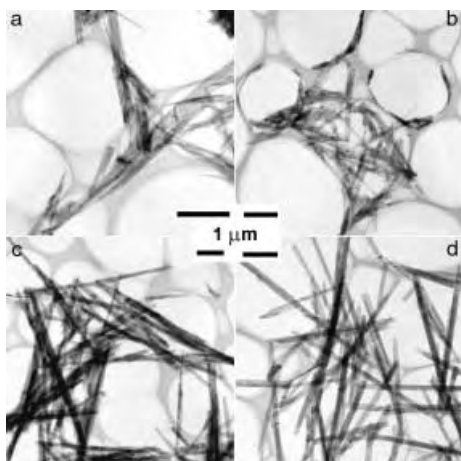


Figure 9. Representative TEM images of MoO_3 nanorods after 3 days of hydrothermal treatment in acetic acid at different temperatures: a) 90 °C, b) 120 °C, c) 150 °C, d) 180 °C.

The pH value of the reaction mixture is an even more powerful factor than the temperature when nanorods of specific diameters are to be synthesized. By appropriate choice of an acidic solvent, nanorod diameters ranging from the microscopic scale down to about 100 nm are accessible. The MoO_3 fibers can gradually be tuned by changing the diluted acid (Figure 10). This principle can be used to meet the specific needs of industrial applications and it can be further refined by combination with the influence of temperature on the morphology.

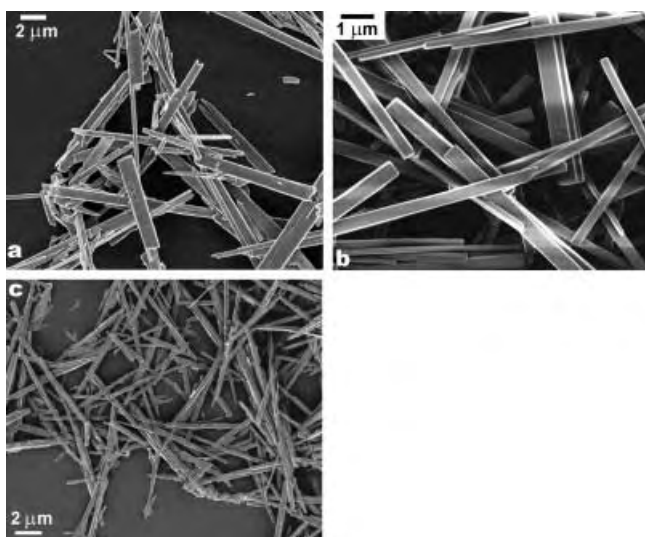


Figure 10. SEM images of MoO_3 nanorods showing the effect of acid addition: a) H_2SO_4 , b) HCl , c) salicylic acid.

In summary, these $\text{MoO}_3 \cdot 2\text{H}_2\text{O}$ –solvent systems are confined to a few elementary components. Therefore, they are predestined for fundamental studies elucidating the mechanisms of solvothermal processes. The products exhibit a distinct anisotropic morphology in almost 100% yield with no particle agglomerations. Therefore, morphological changes related to variation of parameters can be detected unambiguously and immediately. In principle, MoO_3 nanorods are

formed in an outstandingly high yield within a very wide scope of experimental conditions with little synthetic effort. Thus, this synthetic approach is a good and stable candidate for industrial manufacturing in scaled-up processes.

3.4. General Trends in Nanotube and Nanorod Syntheses

“Trained serendipity” is surely one of the most reliable companions of chemists. The “training”, of course, is a profound chemical knowledge combined with naïve curiosity and freeflying fantasy. Though we are far beyond betting on chance synthetic chemistry still requires an element of luck, and this is especially true for designing the nano regime. Quasicrystals and fullerenes could have been detected long before the eighties but have simply been in the shadow of other scientific discoveries and went unnoticed. Some general trends are emerging in the design of nanotubes and nanorods:

- Growth out of nanoscopic catalyst drops as realized for CNTs and for semiconductor nanorods
- Condensation or polymerization inside or outside of nanotubular structures
- Scrolling of layered materials either starting directly from the bulk solids or from lamellar intermediates
- Nanorod formation on ion exchange in nanotubular or lamellar materials—cation against H^+ ions—leading to a densification of morphology
- Stacking of tori (rings) in a freestanding manner or aided by nanotubes or rods
- Moulding by use of tenside template solutions or liquid-crystal structures with or without external fields
- Sonication in suitable solvents. Surprisingly, acid treatment of single-walled CNTs under supersonication can lead to formation of carbon rings and tori.^[121]

The general trick of course would be a surface-directed growth process if one knew and could design selected surface coverages under synthesis conditions. This technique would go much beyond biomineralization because it is not restricted to the use of “biomolecules”. Furthermore, this fundamental problem in materials design, catalysis, biomineralization, and nanoelectronics will benefit from the interdisciplinary exchange of ideas circumventing historical research borders.

4. Summary and Outlook

Despite of being mainly focused on oxidic systems, this review clearly reveals the vast amount of knowledge that has been gained in the last ten years on anisotropic nanoscopic materials and the enormous potential these materials have for nanotechnology. The discovery of the carbon nanotubes in 1991 has catalyzed a fruitful and still growing interest in nanotubes and nanorods, both in application-oriented industrial as well as in basic research. Although carbon nanotubes are still the most widely investigated examples for such materials, especially regarding potential applications, the world-wide search in other systems is steadily increasing this structural family. This growing diversity is not only because of an extension of the systems investigated but also to the skillful

application of a wide range of different synthetic methods. Prominent among them are soft chemistry routes that involve sol–gel reactions and that frequently employ organic molecules as structure-directing templates. For example, such procedures are utilized to generate nanotubes of vanadium and titanium oxide as well as molybdenum oxide fibers. This approach is outstanding because of the high yield and the high purity of the products. Another versatile method is the use of pre-structured materials. They are acting as structure-directing templates as well, but the term *template* is used here to designate a nano- or even microstructured material rather than a molecule as in the case of the above-mentioned soft chemistry routes. These templates can be anisotropic particles themselves, such as carbon nanotubes or polymer fibers, which are coated with a second material and are removed afterwards. Alternatively, the template can be a porous material, such as aluminum oxide, in which the pores are filled with a second material. After dissolution of the aluminum oxide, the nanotubes or nanorods remain. It is this inventiveness concerning new sophisticated synthetic pathways that promises to be the basis for the discovery of many more new and useful anisotropic materials.

However, it is not only the synthetic capability that has increased immensely in recent years, but also the optimization of the analytical tools and their wide availability that contribute to a better characterization of these materials. For instance, without electron microscopes with high resolution, several of the nanotubular phases might have slipped the attention of the researchers.

The interesting physical and chemical properties of strongly anisotropic materials, such as, nanotubes and nanorods quite often differ from those of the corresponding bulk material and those of isotropic nanoparticles. The usefulness of these properties for various applications is mentioned in this review. However, it must be stated that this is only the beginning. Because of ongoing attempts to further miniaturize electronic, optical, and mechanical components, there is a need for materials that could be used as building blocks in the size region of a few nanometers. Considering these perspectives, we are sure that the role of nanotubes and nanorods in a future nanotechnology can hardly be overestimated.

In a much more advanced stage of technology well-designed nanoparticles may then become the larger hosts for molecular devices—molecular in the original meaning of the term. For further optimization of presently utilized materials, nanotechnology anyhow is an imperative.

Our research was generously supported by the ETH Zurich (TEMA – Templated Materials), by the Swiss National Science Foundation (MaNEP – Materials with Novel Electronic Properties), and by the National Research Program “Supramolecular Functional Materials”.

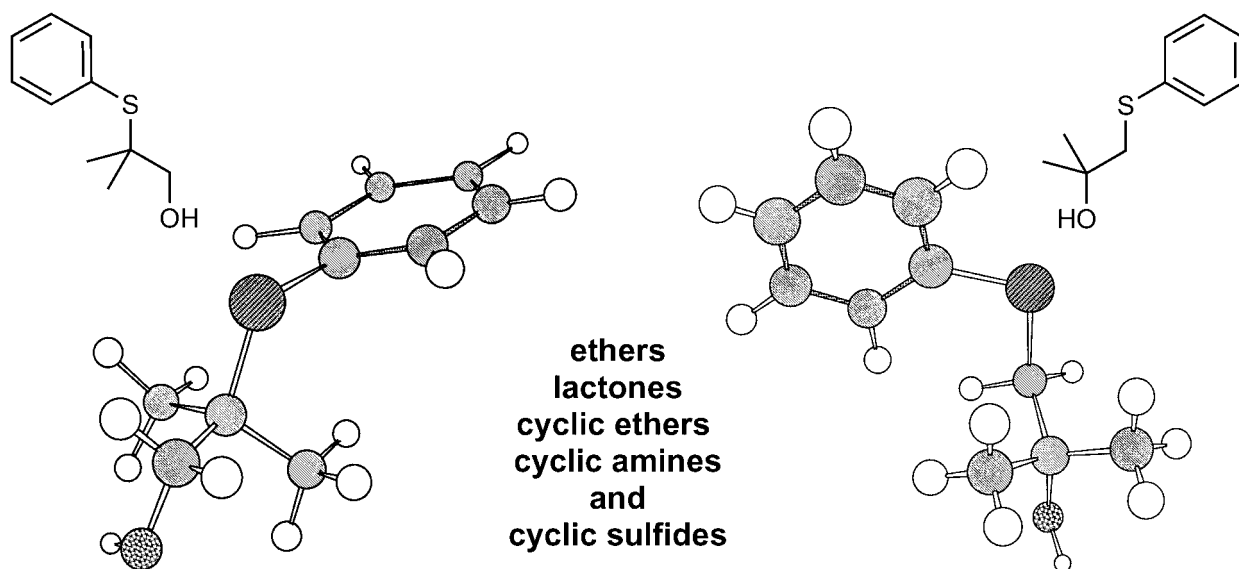
Received: December 13, 2001 [A 506]

- [1] C. N. R. Rao, A. K. Cheetham, *J. Mater. Chem.* **2001**, *11*, 2887; C. N. R. Rao, G. U. Kulkarni, P. J. Thomas, P. P. Edwards, *Chem. Eur. J.* **2002**, *8*, 29.

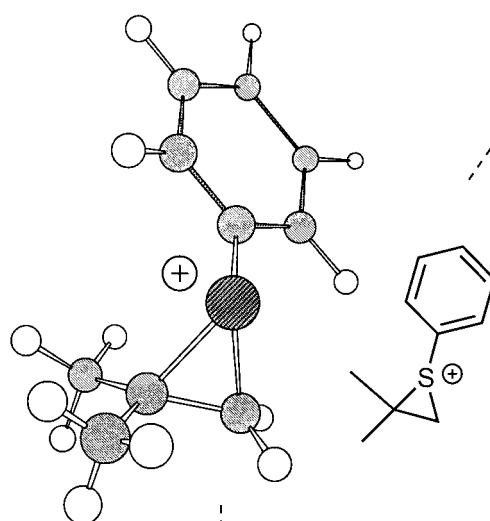
- [2] P. M. Ajayan, *Chem. Rev.* **1999**, *99*, 1787; N. Grobert, *Nachr. Chem. Tech. Lab.* **1999**, *47*, 768; P. M. Ajayan, O. Z. Zhou, *Top. Appl. Phys.* **2001**, *80*, 391.
- [3] S. Iijima, *Nature* **1991**, *354*, 56.
- [4] S. Iijima, *Nature* **1993**, *363*, 603; D. S. Bethune, C. H. Kiang, M. S. De Vries, G. Gorman, R. Savoy, J. Vazques, R. Beyers, *Nature* **1993**, *363*, 605.
- [5] J. Kong, N. R. Franklin, C. Zhou, M. G. Chapline, S. Peng, K. Cho, H. Dai, *Science* **2000**, *287*, 622; P. G. Collins, K. Bradley, M. Ishigami, A. Zettl, *Science* **2000**, *287*, 1801.
- [6] A. G. Rinzler, J. H. Hafner, P. Nikolaev, L. Lou, S. G. Kim, D. Tomanek, P. Nordlander, D. T. Colbert, R. E. Smalley, *Science* **1995**, *269*, 1550; W. A. de Heer, A. Chatelain, D. Ugarte, *Science* **1995**, *270*, 1179; Q. H. Wang, A. A. Setlur, J. M. Lauerhaas, J. Y. Dai, E. W. Seelig, R. P. H. Chang, *Appl. Phys. Lett.* **1998**, *72*, 2912.
- [7] H. J. Dai, J. H. Hafner, A. G. Rinzler, D. T. Colbert, R. E. Smalley, *Nature* **1996**, *384*, 147.
- [8] M. H. Devoret, H. J. Dai, A. Thess, R. E. Smalley, L. J. Gerlings, *Nature* **1997**, *386*, 474.
- [9] P. Pocharal, Z. L. Wang, D. Ugarte, W. A. de Heer, *Science* **1999**, *283*, 1513.
- [10] C. N. R. Rao, B. C. Satishkumar, A. Govindaraj, M. Nath, *Chem-PhysChem* **2001**, *2*, 79.
- [11] A. C. Dillon, K. M. Jones, T. A. Bekkedahl, C. H. Kiang, D. S. Bethune, M. J. Heben, *Nature* **1997**, *386*, 377.
- [12] M. Hirscher, M. Becher, M. Haluska, U. Dettlaff-Weglikowska, A. Quintel, G. S. Duesberg, Y.-M. Choi, P. Downes, M. Hulman, S. Roth, I. Stepanek, P. Bernier, *Appl. Phys. A* **2001**, *72*, 129; C. Zandonella, *Nature* **2001**, *410*, 734.
- [13] P. Lambin, A. Fonseca, J. P. Vigneron, J. B. Nagy, A. A. Lucas, *Chem. Phys. Lett.* **1995**, *245*, 85; A. Fonseca, E. A. Perpète, P. Galet, B. Champagne, J. B. Nagy, J. M. André, P. Lambin, A. A. Lucas, *J. Phys. B* **1996**, *25*, 4915; V. Meunier, L. Henrad, P. Lambin, *Phys. Rev. B* **1998**, *57*, 2591; G. Treboux, P. Lapstun, K. Silverbruck, *J. Phys. Chem.* **1999**, *103*, 1871.
- [14] R. Saito, G. Dresselhaus, M. S. Dresselhaus, *Physical Properties of Carbon Nanotubes*, World Scientific, Singapur, **1998**; T. W. Ebbesen, H. J. Lezec, H. Hiura, J. W. Bennett, H. F. Ghaemi, T. Thio, *Nature* **1996**, *382*, 54.
- [15] M. M. J. Treacy, T. W. Ebbesen, J. M. Gibson, *Nature* **1996**, *381*, 678.
- [16] W. Han, Y. Bando, K. Kurahima, T. Sato, *Appl. Phys. Lett.* **1998**, *73*, 3085; D. Goldberg, W. Han, Y. Bando, L. Bourgeois, K. Kurahima, T. Sato, *J. Appl. Phys.* **1999**, *86*, 2364; E. Bengu, L. D. Marks, *Phys. Rev. Lett.* **2001**, *86*, 2385.
- [17] B. C. Satishkumar, A. Govindaraj, K. R. Harikumar, J.-P. Zhang, A. K. Cheetham, C. N. R. Rao, *Chem. Phys. Lett.* **1999**, *300*, 473.
- [18] W. Tremel, *Angew. Chem.* **1999**, *111*, 2311; *Angew. Chem. Int. Ed.* **1999**, *38*, 2175; R. Tenne, A. K. Zettl, *Top. Appl. Phys.* **2001**, *80*, 81; R. Nesper, G. Patzke, *Nachr. Chem. Tech. Lab.* **2001**, *49*, 886; R. Tenne, *Prog. Inorg. Chem.* **2001**, *50*, 269.
- [19] Y. Rosenfeld Hachon, E. Grunbaum, R. Tenne, J. Sloan, J. L. Hutchison, *Nature* **1998**, *395*, 336.
- [20] Y. Li, J. Wang, Z. Deng, Y. Wu, X. Sun, D. Yu, P. Yang, *J. Am. Chem. Soc.* **2001**, *123*, 9904.
- [21] C. J. Brumlik, C. R. Martin, *J. Am. Chem. Soc.* **1991**, *113*, 3174; C. R. Martin, M. Nishizawa, K. Jirage, M. Kang, *J. Phys. Chem. B* **2001**, *105*, 1925; S. B. Lee, C. R. Martin, *Chem. Mater.* **2001**, *13*, 3236.
- [22] J. Bao, C. Tie, Z. Xu, Q. Zhou, D. Shen, Q. Ma, *Adv. Mater.* **2001**, *13*, 1631.
- [23] B. Mayers, Y. Xia, *Adv. Mater.* **2002**, *14*, 279.
- [24] The transmission electron microscopy (TEM) images shown in this paper were recorded on a CM30 microscope (Philips, Eindhoven, acceleration voltage 300 kV, point resolution 0.2 nm). Scanning electron microscopy (SEM) was performed on a LEO 1530 Gemini, which was operated at low voltage (usually 1 kV) to avoid charging of the uncoated, as-synthesized samples. The SEM image in Figure 7b was taken with an Hitachi S-900 microscope (courtesy of Dr. Martin Müller, ETH Zürich).
- [25] G. Heurung, R. Gruehn, *Z. Anorg. Allg. Chem.* **1982**, *491*, 101.
- [26] W. B. Hu, Y. Q. Zhu, W. K. Hsu, B. H. Chang, M. Terrones, N. Grobert, H. Terrones, J. P. Hare, H. W. Kroto, D. R. M. Walton, *Appl. Phys. A* **2000**, *70*, 231.

- [27] L. Vayssieres, K. Keis, A. Hagfeldt, S.-E. Lundquist, *Chem. Mater.* **2001**, *13*, 4395.
- [28] G. A. Kakos, T. W. Turney, T. B. Williams, *J. Solid State Chem.* **1994**, *108*, 102.
- [29] R. Lauterbach, W. Schnick, *J. Mater. Sci.* **2000**, *35*, 3793.
- [30] J. Hu, B. Deng, Q. Lu, K. Tang, R. Jiang, Y. Qian, G. Zhou, H. Cheng, *Chem. Commun.* **2000**, 715.
- [31] E. Makovicky, B. G. Hyde, *Struct. Bonding (Berlin, Ger.)* **1981**, *46*, 101.
- [32] P. Millet, J. Y. Henry, F. Mila, J. Galy, *J. Solid State Chem.* **1999**, *147*, 676.
- [33] M. Remskar, A. Mrzel, Z. Skraba, A. Jesih, M. Ceh, J. Demšar, P. Stadelmann, F. Levy, D. Mihailovic, *Science* **2001**, *292*, 479.
- [34] P. M. Ajayan, O. Stephan, P. Redlich, C. Colliex, *Nature* **1995**, *375*, 564.
- [35] R. Nesper, M. E. Spahr, M. Niederberger, P. Bitterli, Int. Patent Appl. PCT/CH97/00470, **1997**; M. E. Spahr, P. Bitterli, R. Nesper, M. Müller, F. Krumeich, H.-U. Nissen, *Angew. Chem.* **1998**, *110*, 1339; *Angew. Chem. Int. Ed.* **1998**, *37*, 1263; F. Krumeich, H.-J. Muhr, M. Niederberger, F. Bieri, B. Schnyder, R. Nesper, *J. Am. Chem. Soc.* **1999**, *121*, 8324; H.-J. Muhr, F. Krumeich, U. P. Schönholzer, F. Bieri, M. Niederberger, L. J. Gauckler, R. Nesper, *Adv. Mater.* **2000**, *12*, 231.
- [36] R. Nesper, H.-J. Muhr, M. Niederberger, Int. Patent Appl. PCT/CH00/00570, **2000**; M. Niederberger, H.-J. Muhr, F. Krumeich, F. Bieri, D. Günther, R. Nesper, *Chem. Mater.* **2000**, *12*, 1995.
- [37] M. Niederberger, Dissertation No. 13971, ETH, Zürich, **2000**.
- [38] F. Bieri, F. Krumeich, H.-J. Muhr, R. Nesper, *Helv. Chim. Acta* **2001**, *84*, 3015.
- [39] F. Krumeich, H.-J. Muhr, M. Niederberger, F. Bieri, R. Nesper, *Z. Anorg. Allg. Chem.* **2000**, *626*, 2208.
- [40] X. Wang, L. Liu, R. Bontchev, A. J. Jacobson, *Chem. Commun.* **1998**, 1009.
- [41] M. Wörle, J. de Onate, H.-J. Muhr, F. Bieri, R. Nesper, *Chimia* **1999**, *53*, 336; M. Wörle, F. Krumeich, H.-J. Muhr, F. Bieri, R. Nesper, unpublished results.
- [42] F. Krumeich, H.-J. Muhr, M. Niederberger, F. Bieri, M. Reinoso, R. Nesper, *Mater. Res. Soc. Symp. Proc.* **2000**, *581*, 393.
- [43] J. M. Reinoso, H.-J. Muhr, F. Krumeich, F. Bieri, R. Nesper, *Helv. Chim. Acta* **2000**, *83*, 1724.
- [44] M. E. Spahr, P. Stoschitzki-Bitterli, R. Nesper, O. Haas, P. Novák, *J. Electrochem. Soc.* **1999**, *146*, 2780; S. Nordlinder, K. Edström, T. Gustafsson, *Electrochem. Solid-State Lett.* **2001**, *4*, A129; A. Doble, K. Ngala, S. Yang, P. Y. Zavalij, M. S. Whittingham, *Chem. Mater.* **2001**, *13*, 4382.
- [45] M. E. Spahr, Dissertation Nr. 12281, ETH, Zürich, **1997**.
- [46] K. S. Pillai, F. Krumeich, H.-J. Muhr, M. Niederberger, R. Nesper, *Solid State Ionics* **2001**, *141–142*, 185.
- [47] P. Hoyer, *Langmuir* **1996**, *12*, 1411.
- [48] H. Imai, Y. Takei, K. Shimizu, M. Matsuda, H. Hirahima, *J. Mater. Chem.* **1999**, *9*, 2971; M. Zhang, Y. Bando, K. Wada, *J. Mater. Sci. Lett.* **2001**, *20*, 167; S. M. Liu, L. M. Gan, L. H. Liu, W. D. Zhang, H. C. Zeng, *Chem. Mater.* **2002**, *14*, 1391.
- [49] S. Kobayashi, K. Hanabusa, N. Hamasaki, M. Kimura, H. Shirai, *Chem. Mater.* **2000**, *12*, 1523.
- [50] R. A. Caruso, J. H. Schattka, A. Greiner, *Adv. Mater.* **2001**, *13*, 1577.
- [51] D. Gong, C. A. Grimes, O. K. Varghese, W. Hu, R. S. Singh, Z. Chen, E. C. Dickey, *J. Mater. Res.* **2001**, *16*, 3331.
- [52] T. Kasuga, M. Hiramutsu, A. Hoson, T. Sekino, K. Niihara, *Langmuir* **1998**, *14*, 3160; T. Kasuga, M. Hiramutsu, A. Hoson, T. Sekino, K. Niihara, *Adv. Mater.* **1999**, *11*, 1307.
- [53] G. H. Du, Q. Chen, R. C. Che, Z. Y. Yuan, L. M. Peng, *Appl. Phys. Lett.* **2001**, *79*, 3702.
- [54] K. S. Pillai, F. Krumeich, R. Nesper, unpublished results.
- [55] E. Müller, F. Krumeich, *Ultramicroscopy* **2000**, *84*, 143.
- [56] F. Liebau, *Structural Chemistry of Silicates*, Springer, Berlin, **1995**.
- [57] K. Yada, *Acta Crystallogr. Sect. A* **1971**, *27*, 659.
- [58] H.-P. Lin, C.-Y. Mou, S.-B. Liu, *Adv. Mater.* **2000**, *12*, 103.
- [59] C. T. Kresge, M. E. Leonowicz, W. J. Roth, J. C. Vartuli, J. S. Beck, *Nature* **1992**, *359*, 710.
- [60] Z. L. Wang, R. P. Gao, J. L. Gole, J. D. Stout, *Adv. Mater.* **2000**, *12*, 1938.
- [61] J. H. Jung, Y. Ono, S. Shinkai, *Langmuir* **2000**, *16*, 1643.
- [62] C. Hippe, M. Wark, E. Lork, G. Schulz-Ekloff, *Microporous Mesoporous Mater.* **1999**, *31*, 235.
- [63] R. A. Caruso, M. Antonietti, *Chem. Mater.* **2001**, *13*, 3272.
- [64] B. C. Satishkumar, A. Govindaraj, E. M. Vogl, L. Baumallick, C. N. R. Rao, *J. Mater. Res.* **1997**, *12*, 604.
- [65] B. C. Satishkumar, A. Govindaraj, M. Nath, C. N. R. Rao, *J. Mater. Chem.* **2000**, *10*, 2115.
- [66] C. N. R. Rao, B. C. Satishkumar, A. Govindaraj, *Chem. Commun.* **1997**, 1581.
- [67] J. S. Beck, J. C. Vartuli, W. J. Roth, M. E. Leonowicz, C. T. Kresge, K. D. Schmidt, C. T. W. Chu, D. H. Olson, E. W. Sheppard, S. B. McCullen, J. B. Higgins, J. C. Schlenker, *J. Am. Chem. Soc.* **1992**, *114*, 10834.
- [68] L. Pu, X. Bao, J. Zou, D. Feng, *Angew. Chem.* **2001**, *113*, 1538; *Angew. Chem. Int. Ed.* **2001**, *40*, 1490.
- [69] J. C. Hulthen, C. R. Martin, *J. Mater. Chem.* **1997**, *7*, 1075.
- [70] B. Cheng, E. T. Samulski, *J. Mater. Chem.* **2001**, *11*, 2901.
- [71] B. A. Hernandez, K.-S. Chang, E. R. Fisher, P. K. Dorhout, *Chem. Mater.* **2002**, *14*, 480.
- [72] B. B. Lakshmi, P. K. Dorhout, C. R. Martin, *Chem. Mater.* **1997**, *9*, 857.
- [73] A. Birner, R. B. Wehrspohn, U. M. Gösele, K. Busch, *Adv. Mater.* **2001**, *13*, 377.
- [74] L.-C. Qin, X. Zhao, K. Hirahara, Y. Miyamoto, Y. Ando, S. Iijima, *Nature* **2000**, *408*, 50.
- [75] L. Dai, A. W. H. Mau, *Adv. Mater.* **2001**, *13*, 899; G. Gu, G. Philipp, X. Wu, M. Burghard, A. M. Bittner, S. Roth, *Adv. Funct. Mater.* **2001**, *11*, 295.
- [76] L. C. Otero-Díaz, R. Withers, A. Gómez-Herrero, T. R. Welberry, S. Schmid, *J. Solid State Chem.* **1995**, *115*, 274; A. Gómez-Herrero, A. R. Landa-Cánovas, S. Hansen, L. C. Otero-Díaz, *Micron* **2000**, *31*, 587.
- [77] D. Bernaerts, S. Amelinckx, G. Van Tendeloo, J. Van Landuyt, *J. Cryst. Growth* **1997**, *172*, 433; D. Bernaerts, S. Amelinckx, G. Van Tendeloo, J. Van Landuyt, *J. Phys. Chem. Solids* **1997**, *58*, 1807.
- [78] R. Tenne, L. Margulis, M. Genut, G. Hodes, *Nature* **1992**, *360*, 444.
- [79] R. Tenne, M. Homyonfer, Y. Feldman, *Chem. Mater.* **1998**, *10*, 3225; A. Rothschild, G. L. Frey, M. Homyonfer, R. Tenne, M. Rappaport, *Mater. Res. Innovations* **1999**, *3*, 145; A. Rothschild, J. Sloan, R. Tenne, *J. Am. Chem. Soc.* **2000**, *122*, 5169; A. Rothschild, R. Popovitz-Biro, O. Lourie, R. Tenne, *J. Phys. Chem. B* **2000**, *104*, 8976; Y. Q. Zhu, W. K. Hsu, N. Grobert, B. H. Chang, M. Terrones, H. Terrones, H. W. Kroto, D. R. M. Walton, *Chem. Mater.* **2000**, *12*, 1190.
- [80] M. Remškar, Z. Škraba, M. Regula, C. Ballif, R. Sanjinés, F. Lévy, *Adv. Mater.* **1998**, *10*, 246.
- [81] Y. D. Li, X. L. Li, R. R. He, J. Zhu, Z. X. Deng, *J. Am. Chem. Soc.* **2002**, *124*, 1411.
- [82] A. Rothschild, S. R. Cohen, R. Tenne, *Appl. Phys. Lett.* **1999**, *75*, 5169.
- [83] Y. Feldman, E. Wasserman, D. J. Srolovitz, R. Tenne, *Science* **1995**, *267*, 222.
- [84] M. Remškar, Z. Škraba, F. Cléton, R. Sanjinés, F. Lévy, *Appl. Phys. Lett.* **1996**, *69*, 351; M. Zelinski, P. K. Dorhout, *J. Am. Chem. Soc.* **1998**, *120*, 734; W. K. Hsu, B. H. Chang, Y. Q. Zhu, W. Q. Han, H. Terrones, M. Terrones, N. Grobert, A. K. Cheetham, H. W. Kroto, D. R. M. Walton, *J. Am. Chem. Soc.* **2000**, *122*, 10155; M. Nath, A. Govindaraj, C. N. R. Rao, *Adv. Mater.* **2001**, *13*, 283.
- [85] Y. Q. Zhu, W. K. Hsu, M. Terrones, S. Firth, N. Grobert, R. J. H. Clark, H. W. Kroto, D. R. M. Walton, *Chem. Commun.* **2001**, 121.
- [86] M. Nath, C. N. R. Rao, *J. Am. Chem. Soc.* **2001**, *123*, 4841.
- [87] M. Nath, C. N. R. Rao, *Chem. Commun.* **2001**, 2236.
- [88] R. L. D. Whitby, W. K. Hsu, C. B. Boothroyd, P. K. Fearon, H. W. Kroto, D. R. M. Walton, *ChemPhysChem* **2001**, *2*, 620.
- [89] Y. Q. Zhu, W. K. Hsu, H. W. Kroto, D. R. M. Walton, *Chem. Commun.* **2001**, 2184.
- [90] G. Seifert, H. Terrones, M. Terrones, T. Frauenheim, *Solid State Commun.* **2000**, *115*, 635.
- [91] G. Seifert, H. Terrones, M. Terrones, G. Jungnickel, T. Frauenheim, *Solid State Commun.* **2000**, *114*, 245; G. Seifert, T. Köhler, R. Tenne, *J. Phys. Chem. B* **2002**, *106*, 2497.

- [92] L. Rapoport, Y. Feldman, M. Homyonfer, H. Cohen, J. Sloan, J. L. Hutchison, R. Tenne, *Wear* **1999**, 229, 975; M. Chhowalla, G. A. J. Amaratunga, *Nature* **2000**, 407, 164; C. Drummond, N. Alcantar, J. Israelachvili, R. Tenne, Y. Golan, *Adv. Funct. Mater.* **2001**, 11, 348.
- [93] J. Chen, N. Kuriyama, H. Yuan, H. T. Takeshita, T. Sakai, *J. Am. Chem. Soc.* **2001**, 123, 11813.
- [94] J. A. Hollingsworth, D. M. Poojary, A. Clearfield, W. E. Buhro, *J. Am. Chem. Soc.* **2000**, 122, 3562.
- [95] C. N. R. Rao, A. Govindaraj, F. L. Deepak, N. A. Gunari, M. Nath, *Appl. Phys. Lett.* **2001**, 78, 1853.
- [96] M. Cote, M. L. Cohen, D. J. Chadi, *Phys. Rev. B* **1998**, 58, R4277.
- [97] E. Leontidis, T. Kyprianidou-Leodidou, F. Krumeich, W. Caseri, unpublished results.
- [98] S. M. Lee, Y. H. Lee, Y. G. Hwang, J. Elsener, D. Porezag, T. Frauenheim, *Phys. Rev. B* **1999**, 60, 7788.
- [99] G. Seifert, T. Frauenheim, *J. Korean Phys. Soc.* **2000**, 37, 89.
- [100] G. Seifert, T. Köhler, K. U. Urbassek, E. Hernández, T. Frauenheim, *Phys. Rev. B* **2001**, 63, 193409.
- [101] G. Seifert, T. Köhler, Z. Hajnal, T. Frauenheim, *Solid State Commun.* **2001**, 119, 653.
- [102] D. Wichmann, K. Jug, *J. Phys. Chem. B* **1999**, 103, 10087.
- [103] M. Brändle, R. Nesper, unpublished results. Lattice energy minimizations of the V_2O_5 double layer tubes (space group $P4mmm$) and the planar V_2O_5 double layer (space group $Pmmm$) employed a DFT-parametrized shell model potential for vanadium oxides. The tubes and the double layers were arranged in periodic orthorhombic boxes. Both were allowed to relax freely within their space group constraints and under constant pressure conditions along the tube axis and the layer plane directions. Shell model parameters were obtained from fitting to the energy gradients of optimized and distorted vanadium oxide clusters that were saturated with OH groups. The saturation was chosen so that the total electron count of the cluster and the formal charge of the vanadium ions (+5) were correct. Cluster energies and gradients were obtained from DFT/B3LYP calculations with a DZP basis set for H and V and a TZP basis set for O (A. Schäfer, H. Horn, R. Ahlrichs, *J. Chem. Phys.* **1992**, 97, 2571). TURBOMOLE (R. Ahlrichs, M. Bär, M. Häser, H. Horn, C. Kölmel, *Chem. Phys. Lett.* **1995**, 162, 165; O. Treutler, R. Ahlrichs, *J. Chem. Phys.* **1995**, 102, 346) was used for the DFT calculations. GULP was used for the fitting and for all periodic calculations (J. D. Gale, *J. Chem. Soc., Faraday Trans.* **1997**, 93, 629). The clusters $[VO(OH)_3] (C_{3v})$ and $[VO(OH)_3]_2 (C_{3v})$ (both clusters with trigonal tetracoordination of V) and $V_6O_{21}H_{12} (C_{2v})$, $V_6O_{20}H_{10} (C_{2v})$, $[V_6O_{20}H_{10}]_2 (C_{3v})$, $V_3O_7H_{11} (C_s)$ and $[V_3O_7H_{11}]_2 (C_s)$ (all clusters with pyramidal pentacoordination of V).
- [104] S. Liu, J. Yue, A. Gedanken, *Adv. Mater.* **2001**, 13, 656.
- [105] N. R. Jana, L. Gearheart, C. J. Murphy, *Chem. Commun.* **2001**, 617.
- [106] A. Abdelouas, W. L. Gong, W. Lutze, J. A. Shelnut, R. Franco, I. Moura, *Chem. Mater.* **2000**, 12, 1510.
- [107] P. Chen, X. Wu, J. Lin, K. L. Tan, *J. Phys. Chem.* **1999**, 22, 4559; Z. I. Zhang, B. Li, Z. J. Shi, Z. N. Gu, Z. Q. Xue, L.-M. Peng, *J. Mater. Res.* **2000**, 15, 2658.
- [108] B. Nikoobakht, Z. L. Wang, M. A. El-Sayed, *J. Phys. Chem. B* **2000**, 104, 8635; B. R. Martin, D. J. Dermody, B. D. Reiss, M. Fang, L. A. Lyon, M. J. Natan, T. E. Mallouk, *Adv. Mater.* **1999**, 11, 1021.
- [109] Y. Wu, H. Yan, M. Huang, B. Messer, J. H. Song, P. Yang, *Chem. Eur. J.* **2002**, 8, 1260.
- [110] X. Duan, C. M. Lieber, *Adv. Mater.* **2000**, 12, 298.
- [111] L. Manna, E. C. Scher, A. P. Alivisatos, *J. Am. Chem. Soc.* **2000**, 122, 12700.
- [112] Z. W. Pan, H.-L. Lai, F. C. K. Au, X. Duan, W. Zhou, W. Shi, N. Wang, C.-S. Lee, N.-B. Wong, S.-T. Lee, S. Xie, *Adv. Mater.* **2000**, 12, 1186.
- [113] K. Tang, Y. Qian, *Appl. Phys. Lett.* **1999**, 75, 507.
- [114] P. D. Yang, C. M. Lieber, *Science* **1996**, 273, 1836.
- [115] A recent paper reports the synthesis of various oxide nanorods by a combination of a sol–gel reaction and electrophoretic deposition.
- S. J. Limmer, S. Seraji, T. P. Chou, C. Nguyen, G. Cao, *Adv. Funct. Mater.* **2002**, 12, 59.
- [116] K. Byrappa, M. Yoshimura, *Handbook of Hydrothermal Technology*, Noyes, Park Ridge, N.J., **2001**.
- [117] G. R. Patzke, F. Krumeich, R. Nesper, unpublished results.
- [118] I. Bösch, B. Krebs, *Acta Crystallogr. Sect. B* **1974**, 30, 1795.
- [119] J. R. Günter, *J. Solid State Chem.* **1972**, 5, 354.
- [120] W. Zhang, S. T. Oyama, *J. Phys. Chem.* **1996**, 100, 10759.
- [121] R. Martell, H. R. Shea, P. Avouris, *Nature* **1999**, 398, 299.
- [122] M. Li, H. Schnablegger, S. Mann, *Nature* **1999**, 402, 393.
- [123] L. Qi, H. Cölfen, M. Antonietti, M. Li, J. D. Hopwood, A. J. Ashley, S. Mann, *Chem. Eur. J.* **2001**, 7, 3526.
- [124] S. Kwan, F. Kim, J. Akana, P. Yang, *Chem. Commun.* **2001**, 447.
- [125] Z. W. Pan, Z. R. Dai, Z. L. Wang, *Science* **2001**, 291, 1947.
- [126] H.-W. Liao, Y.-F. Wang, X.-M. Liu, Y.-D. Li, Y.-T. Qian, *Chem. Mater.* **2000**, 12, 2819.
- [127] B. B. Lakshmi, C. J. Patrissi, C. R. Martin, *Chem. Mater.* **1997**, 9, 2544.
- [128] W. Wang, Y. Zhan, G. Wang, *Chem. Commun.* **2001**, 727.
- [129] N. Beermann, L. Vayssieres, S.-E. Lindquist, A. Hagfeldt, *J. Electrochem. Soc.* **2000**, 147, 2456.
- [130] R. Kumar, Y. Koltypin, X. N. Xu, Y. Yeshurun, A. Gedanken, I. Felner, *J. Appl. Phys.* **2001**, 89, 6324.
- [131] Y. C. Choi, W. S. Kim, Y. S. Park, S. M. Lee, D. J. Bae, Y. H. Lee, G.-S. Park, W. B. Choi, N. S. Lee, G. M. Kim, *Adv. Mater.* **2000**, 12, 746.
- [132] J. Y. Li, Z. Y. Qiao, X. L. Chen, L. Chen, Y. G. Cao, M. He, H. Li, Z. M. Cao, Z. Zhang, *J. Alloys Compd.* **2000**, 306, 300.
- [133] H. Z. Zhang, Y. C. Kong, Y. Z. Wang, X. Du, Z. G. Bai, J. J. Wang, D. P. Yu, Y. Ding, Q. L. Hang, S. Q. Feng, *Solid State Commun.* **1999**, 109, 677.
- [134] W. Q. Han, P. Kohler-Redlich, F. Ernst, M. Rühle, *Solid State Commun.* **2000**, 115, 527.
- [135] G.-S. Park, W.-B. Choi, J.-M. Kim, Y. C. Choi, Y. H. Lee, C.-B. Lim, *J. Crystal Growth* **2000**, 220, 494.
- [136] C. C. Tang, S. S. Fan, M. L. de la Chapelle, P. Li, *Chem. Phys. Lett.* **2001**, 333, 12.
- [137] Y. Zhang, J. Zhu, Q. Zhang, Y. Yan, N. Wang, X. Zhang, *Chem. Phys. Lett.* **2000**, 317, 504.
- [138] C. Liang, G. Meng, Y. Lei, F. Philipp, L. Zhang, *Adv. Mater.* **2001**, 13, 1330.
- [139] G. L. Li, M. Liu, G. H. Wang, *J. Mater. Res.* **2001**, 16, 3614.
- [140] Z. Cui, G. W. Meng, W. D. Huang, G. Z. Wang, L. D. Zhang, *Mater. Res. Bull.* **2000**, 35, 1653.
- [141] Y. Li, M. Sui, Y. Ding, G. Zhang, J. Zhuang, C. Wang, *Adv. Mater.* **2000**, 12, 818.
- [142] X. Wang, Y. Li, *J. Am. Chem. Soc.* **2002**, 124, 2880.
- [143] R. Nesper, F. Krumeich, M. Niederberger, A. Baiker, F. Eigenmann, Eur. Patent Appl. 01810072.7, **2001**; M. Niederberger, F. Krumeich, H.-J. Muhr, M. Müller, R. Nesper, *J. Mater. Chem.* **2001**, 11, 1941.
- [144] S. J. Limmer, S. Seraji, M. J. Forbess, Y. Wu, T. P. Chou, C. Nguyen, G. Cao, *Adv. Mater.* **2001**, 13, 1269.
- [145] L. Guo, Z. Wu, T. Liu, W. Wang, H. Zhu, *Chem. Phys. Lett.* **2000**, 318, 49.
- [146] Y. Liu, C. Zheng, W. Wang, Y. Zhan, G. Wang, *J. Crystal Growth* **2001**, 233, 8.
- [147] W.-J. Kim, S.-M. Yang, *Adv. Mater.* **2001**, 13, 1191.
- [148] M. Zhang, Y. Bando, K. Wada, *J. Mater. Sci. Lett.* **2001**, 20, 167.
- [149] J. Livage, *Chem. Mater.* **1991**, 3, 578.
- [150] Y. F. Zhang, Y. H. Tang, X. F. Duan, Y. Zhang, C. S. Lee, N. Wang, I. Bello, S. T. Lee, *Chem. Phys. Lett.* **2000**, 323, 180.
- [151] J. Y. Li, X. L. Chen, H. Li, M. He, Z. Y. Qiao, *J. Crystal Growth* **2001**, 233, 5.
- [152] M. H. Huang, S. Mao, H. Feick, H. Yan, Y. Wu, H. Kind, E. Weber, R. Russo, P. Yang, *Science* **2001**, 292, 1897.
- [153] C. Pacholski, A. Kornowski, H. Weller, *Angew. Chem.* **2002**, 114, 1234; *Angew. Chem. Int. Ed.* **2002**, 41, 1188.

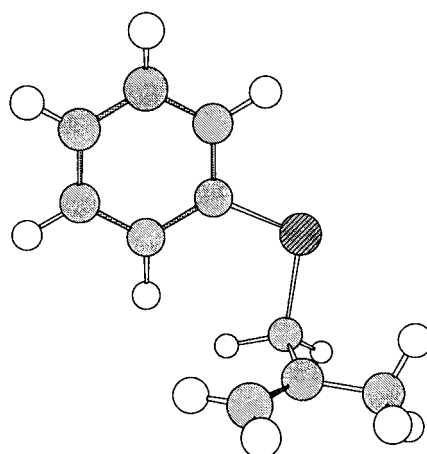


thiiranium
and
thiolanium
ions



molecular
modeling

thermodynamic
vs
kinetic
control



allylic sulfides
and
allylic alcohols

Mechanisms of Sulfanyl (RS) Migrations: Synthesis of Heterocycles

David J. Fox, David House,* and Stuart Warren*

Thiiranium (episulfonium) ions had been acknowledged as reaction intermediates for many years, but it was not until 1977 that Nicolaou demonstrated systematically that these reactive heterocyclic cations could be trapped by carboxylic acids to give lactones. In the years that followed this report, extensive research greatly extended the scope of this reaction, particularly with regard to the methods for generating thiiranium ions, the types of nucleophiles that are compatible with this reaction, and the selectivity involved in the cyclization reactions. For many years we have been using thiiranium ions for the synthesis of saturated heterocycles. Whereas Nicolaou's method relied on electrophilic sulfonylation of alkenes, we have generated thiiranium ions by displacement of a

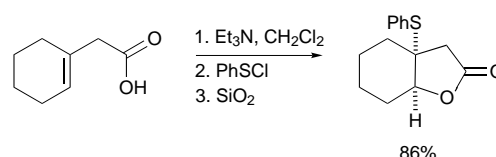
leaving group with neighboring-group participation by a sulfanyl group. Many of the examples we have reported are of cyclizations that are reversible and so where two (and in some cases more) products can result, the outcome of the reactions provides fundamental information about the relative stability of different heterocyclic ring systems. This Review will begin with a brief introduction to sulfanyl participation as a method for generating thiiranium (and thiolanium) ions, and will go on to explore the idea of using sulfanyl migrations in synthesis. Initially, emphasis will be placed on mechanisms of [1,2] sulfanyl migrations: we will look specifically at [1,2] sulfanyl migrations (usually PhS) with elimination, substitution, and cyclization. Emphasis will then shift to the factors that affect the

outcome of cyclization reactions. In particular, we will cover cyclizations with hydroxy nucleophiles and examine situations in which there are more than one hydroxy nucleophile present. We will also examine cyclizations with other nucleophiles, namely amines and sulfides. After our discussion of [1,2] sulfanyl migrations, we will look very briefly at the scope of [1,4] sulfanyl participation, before finally drawing up some guidelines that (we hope) will help other organic chemists take advantage of the rearrangement reactions that the sulfanyl group has to offer.

Keywords: cyclization • heterocycles • rearrangement • sulfanyl groups • thiiranium ions

1 Introduction

In 1977 Nicolaou reported a lactonization procedure of unsaturated carboxylic acids with phenylsulfenyl chloride.^[1] This "sulfenyl–lactonization" reaction is shown in Scheme 1. The reaction of phenylsulfenyl chloride with alkenes was already known to produce thiiranium ions,^[2] but for the first time it was demonstrated that these useful intermediates could be trapped to produce a range of lactones. Following this report, numerous examples were published in which thiiranium ions from alkene precursors were trapped.^[3]



Scheme 1. Sulfenyl/lactonization procedure of Nicolaou and co-workers.

In 1975, we published our first results on the use of thiiranium ions for the preparation of allylic sulfides.^[4] Our procedure was different to that of Nicolaou and Lysenko: the thiiranium ions were generated by treatment of 2-phenylsulfanyl alcohols with a sulfonic acid. One of our earliest observations was that these thiiranium ions generated from 2-phenylsulfanyl alcohols tended to react by [1,2] phenylsulfanyl migration (see Section 2). The aim of this Review is to collect, for the first time, our results of the use of sulfanyl migrations in stereoselective organic synthesis and to rationalize the products that are formed in these reactions.

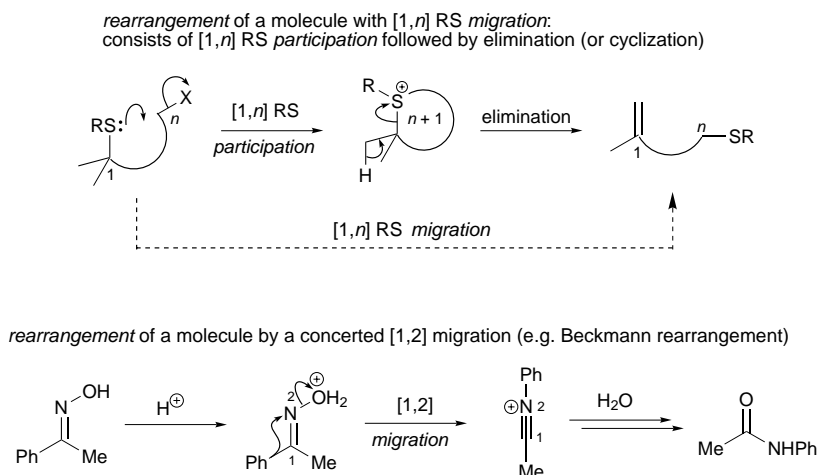
[*] Dr S. Warren, Dr D. J. Fox
University Chemical Laboratory
Lensfield Road, Cambridge CB2 1EW (UK)
Fax: (+44) 1223-336-913
E-mail: sw134@cam.ac.uk

Dr D. House
Dyson Perrins Laboratory
South Parks Road, Oxford OX1 3QY (UK)
E-mail: david.house@hotmail.com

We will use the terms *participation*, *migration*, and *rearrangement* throughout the discussion to describe reactions of thiiranium ions and so at this point we need to define precisely what they mean to us:

- **[1,*n*] RS participation** refers to the nucleophilic displacement of a leaving group by a 1,*n*-related sulfanyl group (RS) to give a (1+*n*)-membered cyclic cationic intermediate. In most cases *n* will be 2 and hence thiiranium ions will be produced, although brief mention will be made of [1,4] participation from which thiolanium ions result.
- **[1,*n*] RS migration** refers to the actual movement of the sulfanyl group. Sulfanyl migrations are mechanistically different from most carbon migrations^[*] (e.g. the Beckmann rearrangement^[5]) since the migration occurs in two separate steps (Scheme 2): first, [1,*n*] participation to give a cyclic intermediate, and second, cleavage of the C1–S bond either by nucleophilic attack or elimination.

[*] Clearly, not all carbon migrations are concerted. Phenyl groups, for example, may migrate in a stepwise fashion via bridged phenonium ion intermediates.



Scheme 2. Illustration of [1,*n*] RS participation, [1,*n*] RS migration, and rearrangement.

- **Rearrangement** refers to an overall reaction in which the sulfanyl group moves from C1 to C*n*. A rearrangement will normally involve a [1,*n*] migration and either a cyclization or an elimination.

During the discussion we hope to demonstrate the effectiveness of using a sulfanyl group (RS) as a tool for constructing allylic and heterocyclic compounds with, in most

Stuart Warren was born in Hertfordshire in England in 1938 and brought up in Cheshire. He did his first degree and Ph.D. (with Dr. Malcolm Clark) at Cambridge University and postdoctoral work with Prof. Frank Westheimer at Harvard University. In 1971 he was appointed as a lecturer at Cambridge University and as a teaching fellow at Churchill College and was promoted to reader in 2000. His research is centered on asymmetric synthesis with phosphorus and sulfur, and he has a special interest in rearrangement reactions. His interest in teaching has been expressed in several text books and in courses given in industry and was recognized by the Royal Society of Chemistry and Cambridge University with teaching awards. In 2002 he was awarded the Bader prize by the Royal Society of Chemistry.



S. Warren



D. Fox



D. House

David Fox was born in 1972 in Leamington Spa, Warwickshire (UK). In 1994 he gained a degree in chemistry from the University of Oxford. He remained in Oxford to carry out research on asymmetric addition reactions of organometallic reagents to carbonyl compounds under the direction of Prof. Stephen Davies, leading to a D.Phil. in 1998. He then moved to Cambridge, to the laboratories of Dr Stuart Warren, where is working on sulfanyl migration reactions and phosphane oxide chemistry.

David House was born in 1974 in Nuneaton, Warwickshire (UK). In 1996 he gained a degree in chemistry from the University of Cambridge. He remained in Cambridge to carry out research on phenylsulfanyl migration reactions under the direction of Dr Stuart Warren, leading to a Ph.D. in 1999. He then moved to Geneva, where he spent 12 months in the laboratories of Prof. E. Peter Kündig working on the synthesis and reactions of planar chiral (arene)chromium tricarbonyl complexes. He is currently working as a research associate at the University of Oxford with Dr Timothy Donohoe on the Birch reduction of aromatic heterocycles.

cases, total control over the product stereochemistry. Generally, the phenylsulfanyl group ($R = \text{Ph}$) is used, as this provides molecules with a chromophore to aid in chromatographic separations, but alkyl sulfanyl groups, the pyridylsulfanyl group, and even sulfanyl (SH) behave in much the same way (see Section 5.2).

The phenylsulfanyl group is tolerant of many oxidizing agents, for example, olefins can be dihydroxylated in the presence of a PhS group,^[6] diols may even be cleaved with sodium periodate without oxidation of sulfur^[7] (more aggressive oxidants such as *meta*-chloroperbenzoic acid, however, rapidly effect oxidation to sulfoxide and even sulfone.^[8]) Figure 1 summarizes some of the principal strategies that we

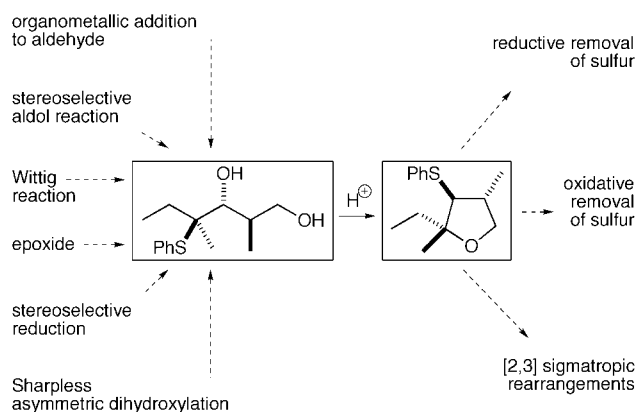


Figure 1. Strategies for the synthesis of cyclization precursors.

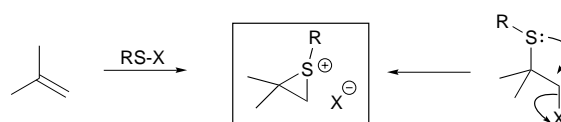
have used for the construction of compounds that contain the phenylsulfanyl group. Our syntheses of sulfanyl compounds are not included in this Review: we will concern ourselves only with the outcome of the rearrangement reactions themselves.

Once the sulfanyl group has served its purpose, it can be removed easily from the molecules (Figure 1) by reductive (e.g. Raney nickel) or oxidative methods (e.g. oxidation to sulfoxide followed by *syn* elimination) or by [2,3] sigmatropic rearrangements of the derived sulfoxides or sulfonium ylides. These are processes that may also introduce new functionality or stereochemistry into the molecule.

2 Mechanisms of Sulfanyl Migrations

2.1 Generation and Structure of Thiiranium Ions

As we have shown, thiiranium ions are normally generated in one of two ways (Scheme 3): 1) treatment of alkenes with a sulfur electrophile (usually RSCl), or 2) nucleophilic displacement of a good leaving group (often H_2O) with neighboring-group participation by sulfur. Both methods will be encountered throughout the ensuing discussion.



Scheme 3. Generation of thiiranium ions.

Thiiranium ions are reactive intermediates and are not generally isolable. However, in certain cases thiiranium ions have been isolated with non-nucleophilic counterions, especially SbCl_6^- and BF_4^- , as fine crystalline powders with sharp melting points (although they decompose on melting).^[9] X-ray crystallographic data have recently been collected for the thiiranium ions **1** and **2**, which bear *tert*-butyl substituents in a *cis* and *trans* arrangement, respectively.^[10] The data shown in Figure 2 highlight the long C–S bond and the narrow C–S–C angle. ^1H and ^{13}C NMR spectra have also been recorded for thiiranium ions (in dichloromethane at 20°C): characteristic proton resonances occur in the range 3.7–4.8 ppm.^[9, 10]

As reactive intermediates, thiiranium ions normally decompose in one of two ways:^[*] 1) loss of a β proton to form allylic sulfides, or 2) nucleophilic capture (Scheme 4). Although we will discuss allylic sulfide formation by proton loss, the majority of our article will focus on the second reaction, nucleophilic capture. Nucleophilic attack on thiiranium ions is

[*] Lucchini et al. have shown that thiiranium ions may also decompose by ring expansion to thietanium ions, although this slow reaction has only been observed for “stable” thiiranium ions and is not dealt with in this Review.^[11]

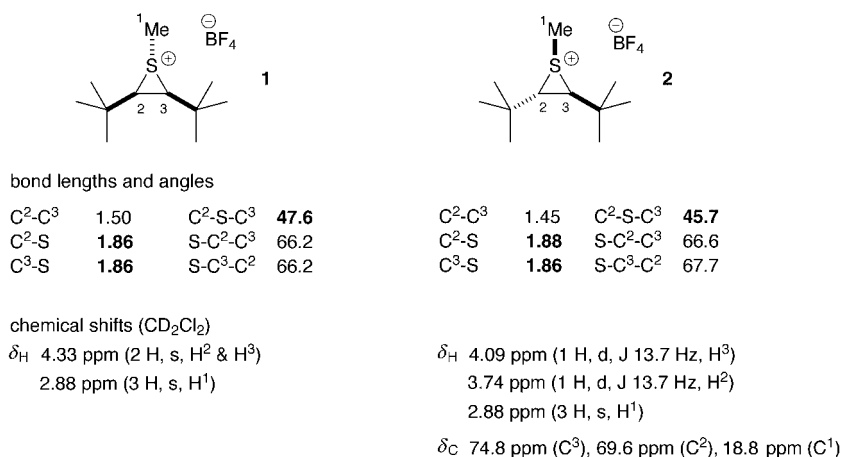
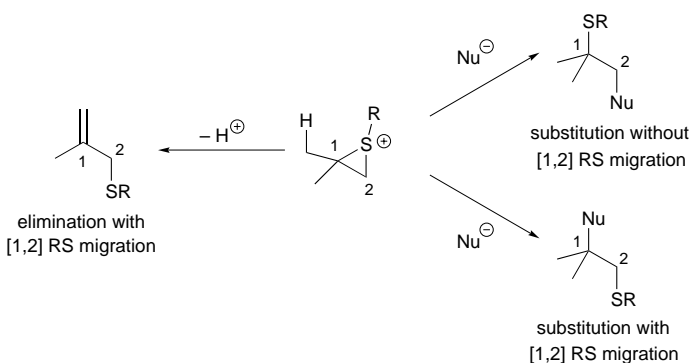


Figure 2. Selected data for thiiranium ions.



Scheme 4. Reactions of thiiranium ions.

often irreversible and two possible regioisomeric products may be formed; the product distribution will necessarily reflect the relative rates of reaction at the two electrophilic sites. In our own work however, most examples of nucleophilic attack are reversible and so the product ratios are determined by thermodynamic factors. Both the reversible and irreversible cases will be discussed in detail.

2.2 Elimination Reactions of Thiiranium Ions with [1,2] RS Migration

2.2.1 [1,2] RS Migration from 2-Phenylsulfanyl Alcohol Precursors

We begin our discussion with elimination reactions of thiiranium ions and with a simple thiiranium ion precursor, 2-phenylsulfanyl alcohol **3**. Treatment of this secondary alcohol with *p*-toluenesulfonic acid in benzene (5 min) gives a single product, the allylic sulfide **4** (Scheme 5a).^[4] Proton loss occurs only from the more substituted end of the

thiiranium ion (H^A) and consequently the sulfanyl group has undergone a [1,2] PhS migration. Similar behavior is observed for the primary alcohol **5**: again the sole product is that formed by [1,2] PhS migration (Scheme 5a).^[12] In both cases the sulfanyl group has moved to a less substituted carbon atom and to simplify discussion we refer to this process as a “downhill” migration. Downhill migration of a sulfanyl group from a secondary to a primary center is also possible, although slightly more vigorous conditions are needed: 1 equiv TsOH, refluxing toluene, 4–6 hr (Scheme 5a).^[12]

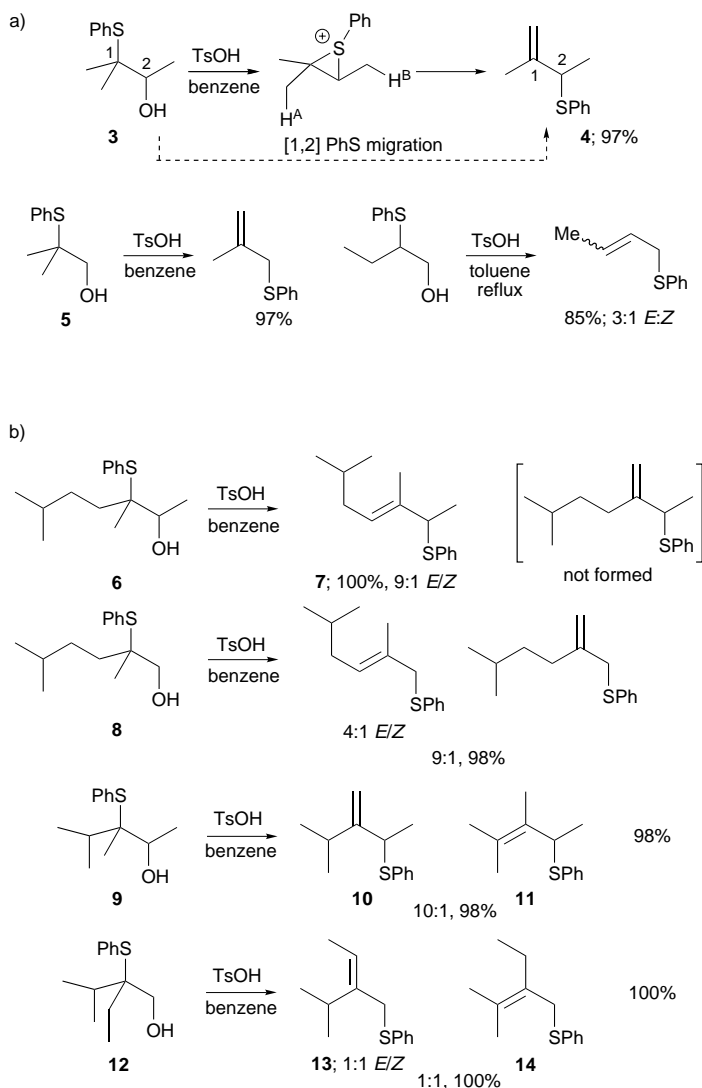
When the migration origin is unsymmetrically substituted, as in alcohol **6**, two different products of downhill migration may be formed (Scheme 5b).^[12] For tertiary to secondary migrations, regioselectivity is generally excellent. Alcohol **6** gives a single regioisomer of allylic sulfide **7** (*E/Z* 9:1) on treatment with acid in benzene. The primary alcohol **8**, with a primary migration terminus, rearranges slightly less selectively. If the migration origin bears a secondary substituent (e.g. isopropyl) both regio- and stereocontrol are impaired (Scheme 5b). Secondary alcohol **9** rearranges to give the regioisomeric allylic sulfides **10** and **11** (10:1) and the primary alcohol **12** gives only a 1:1 mixture of regioisomers **13** and **14**. For the cases in which regioisomeric products can be formed, the mixtures are thought to be dependent on steric crowding in the transition state for allylic sulfide formation.

More highly functionalized allylic sulfides have also been generated in this way. For example, the stable enamine **16** could be prepared by rearrangement of the 2-phenylsulfanyl alcohol **15** (prepared by an *anti*-selective aldol reaction) (Scheme 6a).^[13] “Flat” (secondary to secondary) and “uphill” migrations are generally not possible unless there is an extra driving force for the reaction. This driving force can be provided by a “sacrificial” silyl group; thus alcohols **17** and **18** undergo flat and uphill migrations, respectively (Scheme 6b).^[14] The silyl group stabilizes the cation that results from the [1,2] migration by the β -silyl effect. “Flat” migrations can also be driven forward by unsaturated ester formation from lactones. For example, the lactone **19** was converted into the unsaturated ester **20** by treatment with *p*-toluenesulfonic acid in butanol (Scheme 6c).^[15, 16]

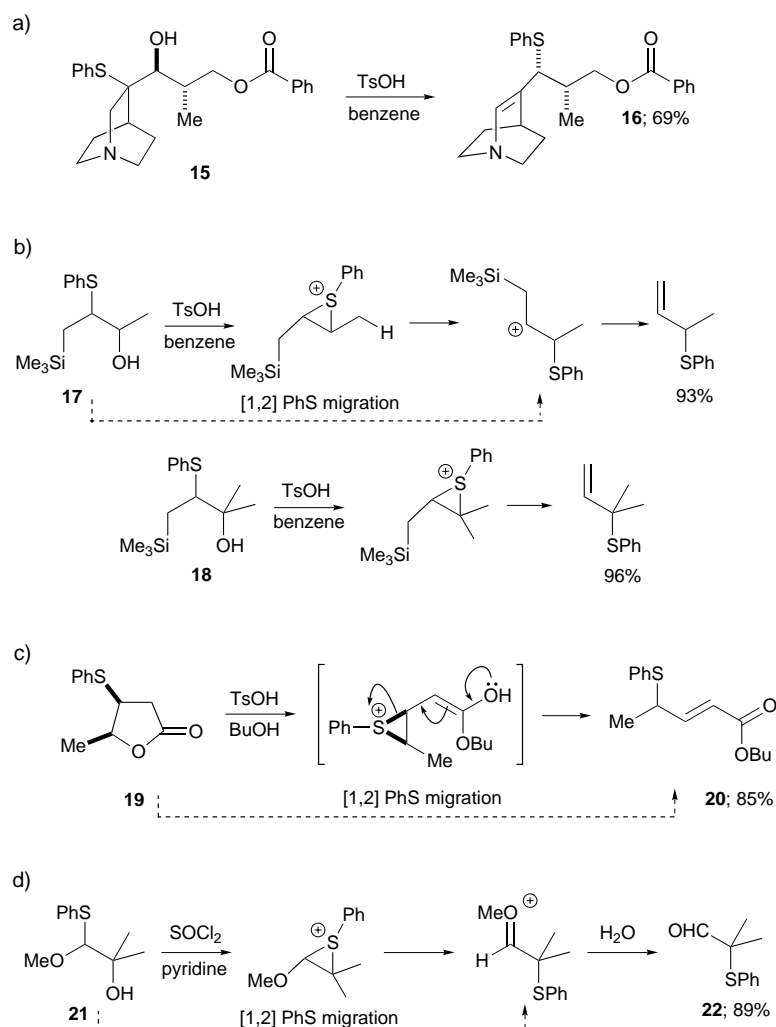
The final example in this section is a remarkable [1,2] RS migration commonly referred to as the de Groot rearrangement.^[17, 18] Treatment of tertiary alcohols such as **21** with thionyl chloride generates a chlorosulfite, which is rapidly displaced by the neighboring sulfanyl group to give a thiiranium ion substituted with an ether oxygen atom (Scheme 6d). By analogy with the β -silyl effect, the [1,2] PhS migration is completed in a second step in a formally uphill sense by π -bond formation of the ether oxygen atom. After hydrolysis of the oxonium ion, a 2-phenylsulfanyl aldehyde **22** is generally obtained in excellent yield.

2.2.2 Isomerization of Allylic Sulfides: The [1,3] RS Migration

In the preceding section, almost all the reaction products were allylic sulfides. These allylic sulfides may undergo a second sulfur-promoted rearrangement: a [1,3] RS migration in which the sulfur group will again move to a less substituted



Scheme 5. a) Elimination reactions with downhill migration; b) selectivity in the formation of allylic sulfides.



Scheme 6. a) Formation of a "stable" enamine by [1,2] PhS migration; b) elimination reactions with flat and uphill migration; c) flat migration driven by unsaturated ester formation; d) de Groot rearrangement (an uphill [1,2] PhS migration).

carbon atom. This reaction has been shown by crossover experiments to be a radical process (Scheme 7a).^[19] Generally, the [1,3] RS migration is so efficient, even in daylight, that for the isolation of the allylic sulfides formed directly from the [1,2] RS migration it is necessary to exclude light if the [1,3] RS migration is to be prevented. Unlike the acid-catalyzed formation of allylic sulfides by [1,2] RS migration, the [1,3] RS migration is reversible and so equilibrium ratios result.

Use of the tandem [1,2]/[1,3] PhS migration considerably increases the scope of the allylic sulfide synthesis, since a common precursor (e.g. alcohols **3**, **9**, **17**, and **18**) can give either of the two allylic sulfides (**4**, **10**, **25**, and **27**) or (**23**, **24**, **26**, and **28**), respectively (Scheme 7b).^[20] Clearly the [1,3] PhS is not observed in some allylic sulfides because the two rearranged compounds are the same.

Paquette and co-workers have recently made use of this rearrangement for the preparation of the functionalized cyclopentanone **29** (Scheme 7c).^[21] We have also used the [1,3] PhS migration to equilibrate double bond isomers of alkenes. Wittig reactions of the aldehydes **22** and **31** gave the allylic sulfides **30** and **32**, respectively, as a mixture of *E* and *Z*

isomers. On prolonged exposure to daylight, solutions of both dienes were equilibrated to give (*E*)-**30** and (*E,E*)-**32**, respectively, as single geometrical isomers (Scheme 7d).^[7]

2.2.3 Allylic Alcohol Synthesis: Coupled [1,2] RS Migrations and [2,3] Evans–Mislow Rearrangements

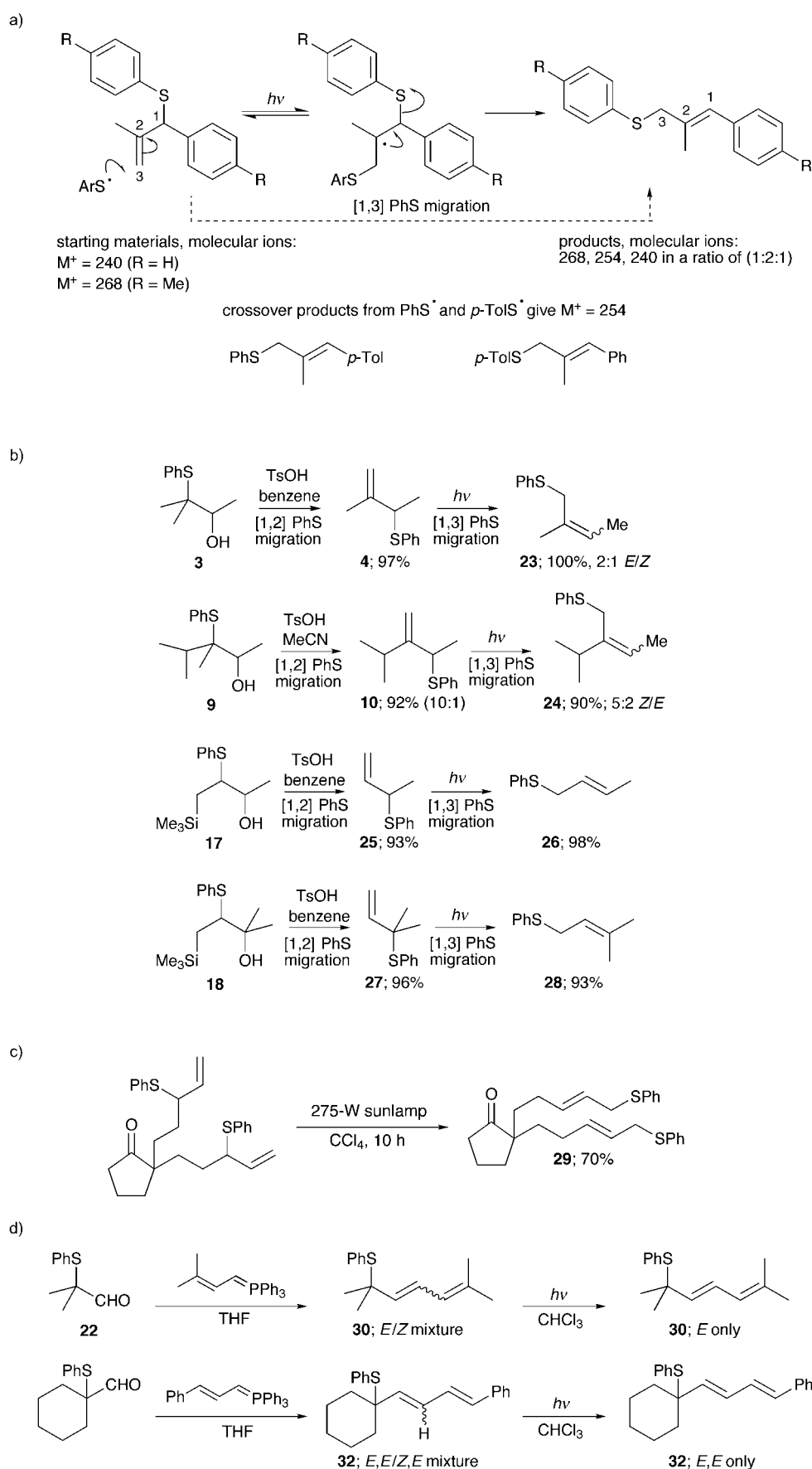
We have shown how the [1,2] PhS migration has been used to prepare allylic sulfides. Oxidation of the allylic sulfides produced in this reaction to allylic sulfoxides enables us to take advantage of yet another sulfur-promoted rearrangement: the Evans–Mislow rearrangement.^[22] The combination of these two rearrangements provides an efficient route to diastereomerically pure allylic alcohols with 1,4-related stereogenic centers with control over the intervening double-bond geometry. For example, treatment of the alcohol **33** (derived from an *anti*-selective aldol reaction) with *p*-toluenesulfonic acid results in the stereospecific formation of allylic sulfide **34** (Scheme 8).^{[23][*]} Oxidation of sulfide **34** with sodium periodate followed by treatment with a thiophile (NaSPh) leads to the *syn* allylic alcohol **35**. Complete control over the 1,4-related stereogenic centers is possible because both rearrangements are stereospecific. Similarly, the allylic sulfide **36** was oxidized with sodium borate and rearranged to give the allylic alcohol **37**.^[24]

2.3 Nucleophilic Attack on Thiiranium Ions

2.3.1 Nucleophilic Attack on Thiiranium Ions Derived from Alkenes

So far we have shown thiiranium ions that are generated by using sulfur as a nucleophile. However, an alternative approach is to react an alkene with an electrophilic source of sulfur. The most common sulfur electrophiles used for this purpose are sulfonyl chlorides (RSCl). Initially, a thiiranium ion is formed, and in the absence of added nucleophiles, the chloride counterion attacks the thiiranium ion, thus producing regioisomeric mixtures of β -chlorosulfides.^[25] These chlorosulfides tend to be rather unstable and are generally not isolated or separated. Despite the difficulty in handling these compounds, β -chlorosulfides may be dehydrated with good regioselectivity to give allylic sulfides. For example, geranyl benzyl ether **38** undergoes chemoselective sulfonylation to give the β -chlorosulfide regioisomers **39** and **40** (Scheme 9a).^[26] Treatment of this mixture with camphorsulfonic acid (CSA) gave the allylic sulfide **41**. The high regioselectivity observed in the elimination is a consequence of the

[*] The stereochemistry of the [1,2] PhS migration is discussed in Section 3.1.1.



elimination, which proceeds via a thiiranium ion intermediate, as already discussed.

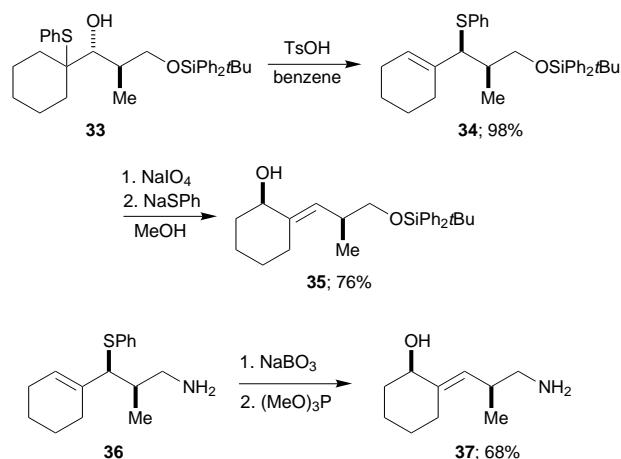
Besides undergoing elimination reactions, β -chlorosulfides can undergo nucleophilic substitution reactions. For example, treatment of the previous mixture of β -chlorosulfide regioisomers **39** and **40** with silica gel gives the β -hydroxysulfide **42** in which the sulfanyl group has undergone a [1,2] migration (Scheme 9b).^[26] By analogy with our previous observations we note that reaction has occurred exclusively at the more substituted end of the thiiranium ion, thus promoting a downhill sulfanyl migration. Similarly, treatment of the alkene **43** with phenylsulfenyl chloride followed by sodium acetate in acetic acid gave the β -acetoxysulfide **44** as a single isomer, again the products of downhill migration (Scheme 9c).^[27]

2.3.2 Nucleophilic Attack on Thiiranium Ions Derived from 2-Phenylsulfanyl Alcohols

In Section 2.2.1 we discussed the dehydration of a simple 2-phenylsulfanyl alcohol **3** to give a single allylic sulfide regioisomer by treatment with *p*-toluenesulfonic acid in benzene solution. If this experiment is performed with ethanol as the solvent, none of the allylic sulfide **4** is formed; instead, ethyl ether **45** is formed by nucleophilic attack of ethanol on the intermediate thiiranium ion (Scheme 10a).^[20] Isomeric ether **46** is not produced, which reflects the reversible nucleophilic trapping of the thiiranium ion: the thiiranium ion can be regenerated by protonation of the ether oxygen atom and sulfur participation.

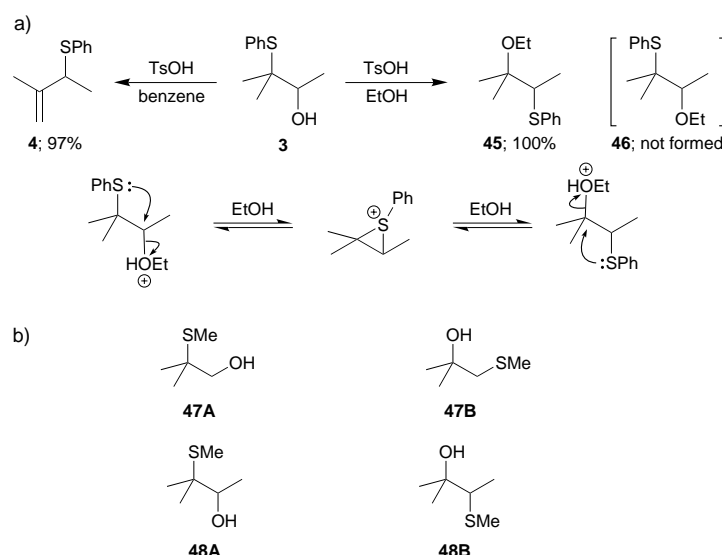
Given that this reaction is thermodynamically control-

Scheme 7. a) Mechanistic probe of the [1,3] PhS migration; b) tandem [1,2] and [1,3] PhS migrations; c) example of a double [1,3] PhS migration; d) use of the [1,3] PhS migration to equilibrate alkene double bond geometry.



Scheme 8. Stereocontrolled allylic alcohol synthesis by tandem [1,2] PhS migration and [2,3] Evans–Mislow rearrangement.

led, we need to account for the difference in stabilities of the two ethers **45** and **46**. To this end we performed semiempirical molecular modeling calculations on some



Scheme 10. a) Nucleophilic attack under thermodynamic control; b) isomeric 2-methylsulfanyl alcohols compared by PM3 semiempirical molecular-modeling.

simple isomeric compounds, with very interesting results. The calculations involved the comparisons of the enthalpies of formation of sulfide isomers **47A** and **47B** and of **48A** and **48B** (Scheme 10b).^[*] Table 1 shows the values of ΔH_f (from the elements) calculated for these molecules in the

Table 1. Calculated gas phase enthalpies of formation for sulfide isomers: **47A**, **47B** and **48A**, **48B**.

Compound	$\Delta H_f(298\text{ K})$ [kcal mol ⁻¹]	No. of conformations
47A	– 62.1 to – 58.7	8
47B	– 68.8 to – 63.8	11
48A	– 66.4 to – 61.6	22
48B	– 69.0 to – 64.3	24

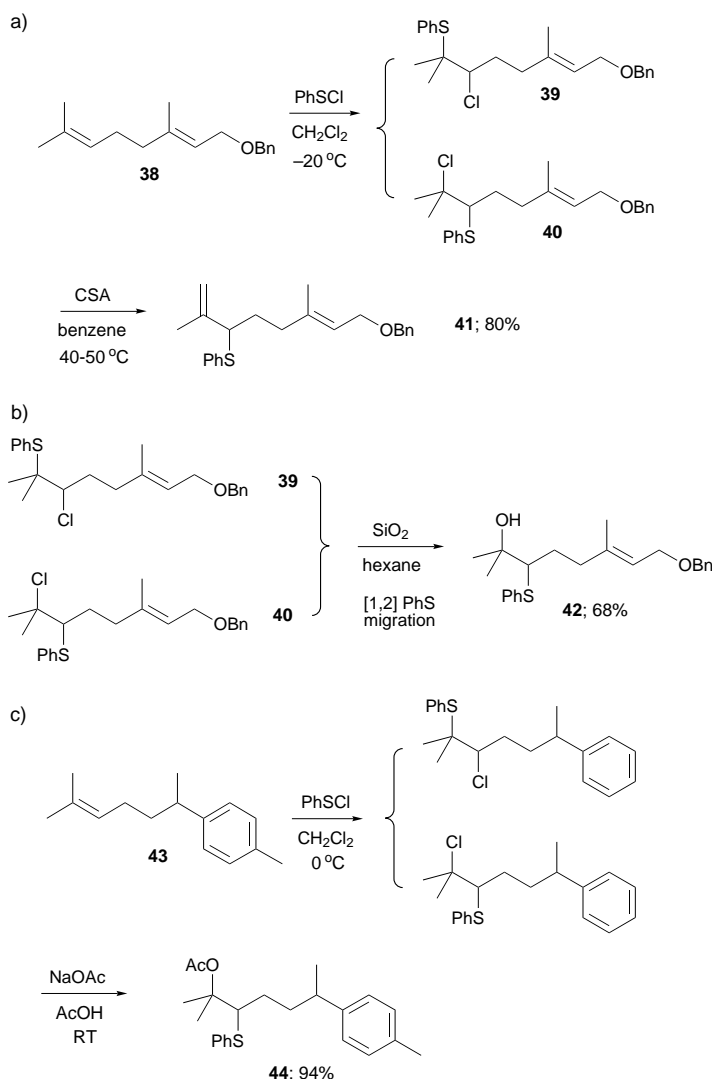
gas phase at 298 K. Although we are not comparing Gibbs free energies (ΔG_f) (no entropy term), the results are nevertheless interesting; in both cases the more stable isomer has the sulfur substituent on the less substituted carbon atom. We believe this enthalpy difference to be a fundamental driving force for sulfur to move “downhill” in our [1,2] RS migrations under thermodynamic control.

Out of interest, we calculated the enthalpies of formation for isobutyl alcohol, *tert*-butyl alcohol, isobutyl thiol, and *tert*-butyl thiol (Table 2). Whilst these calculations must be interpreted cautiously (given the lack of gas-phase thermo-

Table 2. Calculated gas-phase enthalpies of formation for alcohol and thiol isomers.

Compound	$\Delta H_f(298\text{ K})$ [kcal mol ⁻¹]
<i>i</i> BuOH	– 69.9
<i>t</i> BuOH	– 71.3
<i>i</i> BuSH	– 20.3
<i>t</i> BuSH	– 17.9

[*] Calculations were performed with CS MOPAC Pro version 5.0 with a PM3 basis set.



Scheme 9. a) Dehydration of β -chlorosulfides; b) nucleophilic attack of water onto thiiranium ions; c) nucleophilic attack of acetate onto thiiranium ions.

chemical data) it is interesting to see that isobutyl thiol is predicted to be the lower-energy isomer, whereas *tert*-butyl alcohol is lower in energy than isobutyl alcohol.

3 Cyclization Reactions with [1,2] RS Migration by Using Oxygen Nucleophiles

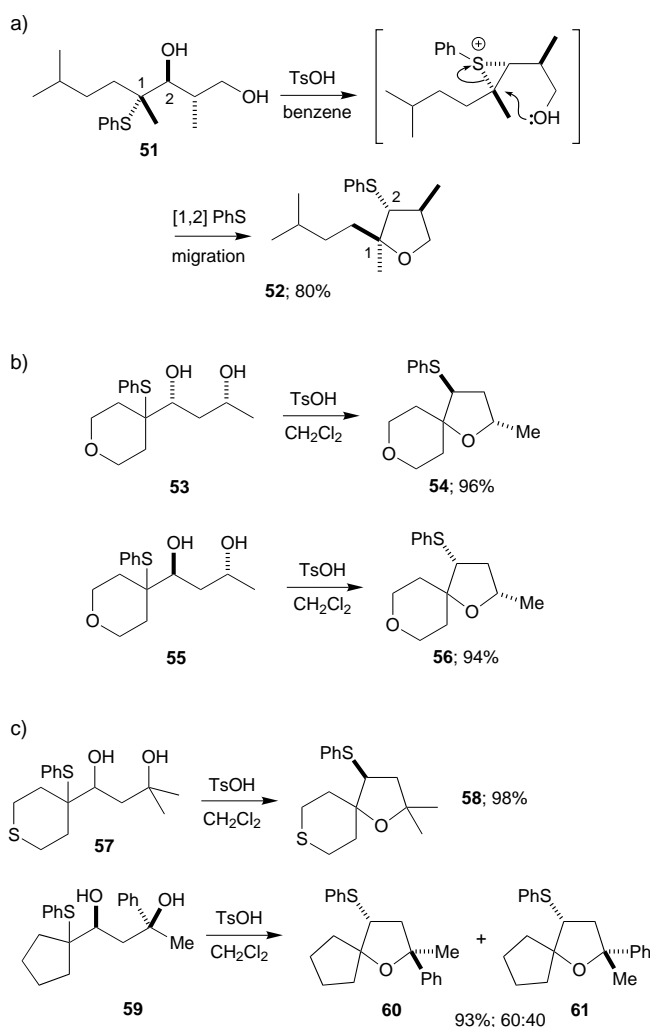
In Section 2.2.3 we discussed the preparation of allylic alcohols by using a [1,2] RS migration with elimination to give allylic sulfides, which underwent [2,3] sigmatropic rearrangement after oxidation to sulfoxides. If the diol **49**, rather than the protected diol **33**, was treated with *p*-toluenesulfonic acid, the reaction followed an altogether different course: cyclization occurred to give the tetrahydrofuran (THF) **50** as the only product of the reaction (Scheme 11).^[23] The remainder of this Review will focus on the use of thiiranium ions to prepare saturated heterocycles in high yields and, in almost all cases, with complete stereocontrol.

3.1 Cyclizations of Alcohols through Intramolecular Attack of Thiiranium Ions

3.1.1 Stereochemistry of Cyclization Reactions

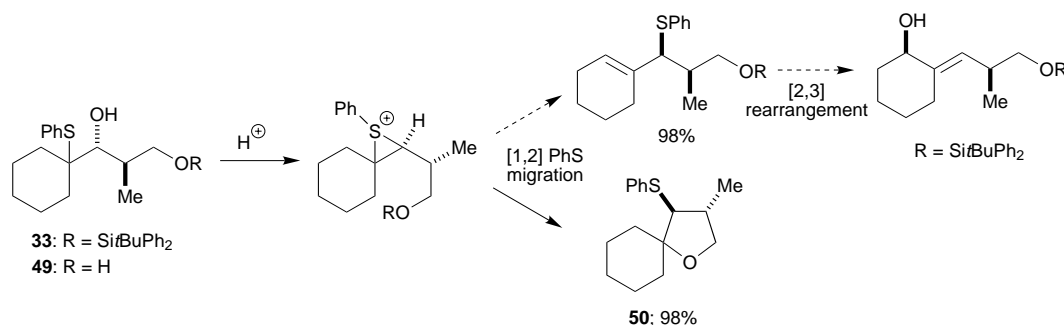
We were able to show that cyclizations through intramolecular attack onto thiiranium ions occur with complete inversion of configuration at the migration origin and terminus.^[28] For example, treatment of the diol **51** with an acid catalyst gave the THF **52** with the stereochemistry indicated in Scheme 12a. Though at first this may seem to be an obvious observation, nucleophilic substitution at a tertiary carbon center would normally proceed by an S_N1 mechanism with loss of stereochemical integrity. Here the long C–S bond means that the electrophilic carbon atom can adopt a near-planar geometry and the cyclization may occur via a “loose” S_N2 -type transition state. Table 3 illustrates the generality of this cyclization reaction: notably, in all cases products are formed in high yield and without loss of stereochemical integrity. Even sulfanyl (SH) groups undergo the [1,2] RS migration, albeit more slowly.^[29]

By preparing compounds with a secondary hydroxy group as the nucleophile, we were able to show that no epimerization of this stereogenic center occurs during the cyclization reaction (**53** → **54** and **55** → **56**, Scheme 12b).^[30] The real test,



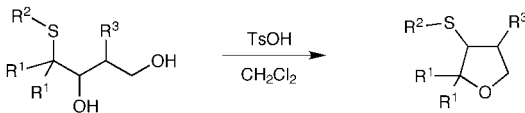
Scheme 12. Stereochemical outcome of cyclization reactions: a) inversion occurs at migration origin and terminus; b) no epimerization of nucleophilic secondary hydroxy group occurs; c) no dehydration occurs with tertiary hydroxy groups but benzylic tertiary hydroxy groups are prone to epimerization.

however, came when a tertiary hydroxy group was used as the nucleophile. Tertiary alcohol **57** gave **58** on treatment with acid (Scheme 12c).^[30] Remarkably, dehydration is not a competing pathway in this reaction! The benzylic tertiary alcohol **59** also showed no sign of dehydration, though epimerization of this stereogenic center resulted in the formation of the THFs **60** and **61** (60:40).



Scheme 11. Rearrangements with [1,2] PhS migration with subsequent elimination or cyclization.

Table 3. Examples of THF synthesis by [1,2] RS Migration.



R ¹	R ²	R ³	THF	Yield
Me	H	H		96%
Me	Bn	H		96%
Me	H	<i>syn</i> -Me	<i>syn</i>	95%
Me	H	<i>anti</i> -Me	<i>anti</i>	98%
–CH ₂ CH ₂ (NMe)CH ₂ CH ₂ –	Ph	<i>anti</i> -Me	<i>anti</i>	85%
–CH ₂ CH ₂ OCH ₂ CH ₂ –	Ph	<i>syn</i> -Me	<i>syn</i>	94%
–CH ₂ CH ₂ SC ₂ H ₄ CH ₂ –	Ph	<i>anti</i> -Me	<i>anti</i>	99%
–CH ₂ CH ₂ SC ₂ H ₄ CH ₂ –	Ph	<i>syn</i> -Me	<i>syn</i>	99%
<i>c</i> -C ₈ H ₁₆	Ph	<i>anti</i> -Me	<i>anti</i>	76%
<i>c</i> -C ₁₂ H ₂₄	Ph	<i>anti</i> -Me	<i>anti</i>	100%

3.1.2 Cyclization of 1,3-Diols: Kinetic vs Thermodynamic Control

In the preceding section we discussed the cyclization onto thiiranium ions to give “rearranged” THFs. (By “rearranged” we mean a product formed by a [1,2] RS migration. Conversely, “unrearranged” products are formed without [1,2] RS migration). We have rather overlooked the possibility of the alternative cyclization onto the less substituted end of the thiiranium ion to give unrearranged oxetanes as products (e.g. **62** → **63** in contrast to **62** → **64**, Scheme 13a). Since these cyclizations are reversible, the formation of oxetanes is doubly disadvantaged on account of the strain energy of a four-membered ring and the sulfur group not having migrated downhill.

The question of the relative rates of the two cyclizations remained unanswered, however, and so non-equilibrating conditions were sought to gain further insight into the reaction mechanism. We prepared cyclic sulfites of 1,3-diols and studied their decomposition by sulfanyl participation and loss of SO₂ and subsequent cyclization of the oxyanion onto the thiiranium ion.^[31] A ratio of 14:86 for **65/66** represents the kinetic distribution for the cyclization of oxyanion **67** (Scheme 13b). Clearly this need not be the same ratio as for cyclization in acid, but it is a good model since no equilibration can occur under basic conditions. Similarly, the cyclic sulfite prepared from diol **68** decomposed to give **69** and **70** (25:75).

We found that oxetanes could be prepared as the sole products from 1,3-diols under modified Mitsunobu conditions by using Ziram (zinc dimethyldithiocarbamate)^[32] (Scheme 13c).^[31] Although the role of Ziram in this reaction remains unclear, it seems likely that it prevents the sulfur group from displacing the phosphorus leaving group, thus allowing the secondary hydroxy group to act as the nucleophile in an unprecedented fashion. Brief exposure of these oxetanes to acid results in total conversion into THFs, for example, **71** → **72** (Scheme 13c).

If we make the migration origin a secondary center, the cyclization should be less beneficial because in both the starting material and product the sulfur is bound to an equally substituted carbon atom (“flat” migration). It turns out that the stereochemistry plays the deciding role in these cycliza-

tions.^[28] Diol **73** rearranges to give **74** with 2,3-*anti*, 3,4-*anti* stereochemistry (Scheme 13d). Diol **75** gives the THF **76** with 2,3-*syn*, 3,4-*anti* stereochemistry, but the diastereomeric diol **77** does not give the corresponding (2,3-*anti*,3,4-*syn*)-**78**, only decomposition products (Scheme 13d). Presumably, the eclipsing interaction that results from the development of 3,4-*syn* stereochemistry severely destabilizes the transition state for cyclization. A 1,3-diol with a primary migration origin does not result in any cyclization, regardless of the stereochemistry. In this case, THF formation would require the sulfanyl group to move to a more highly substituted carbon atom which, as we have already mentioned, is a thermodynamically unfavorable process.

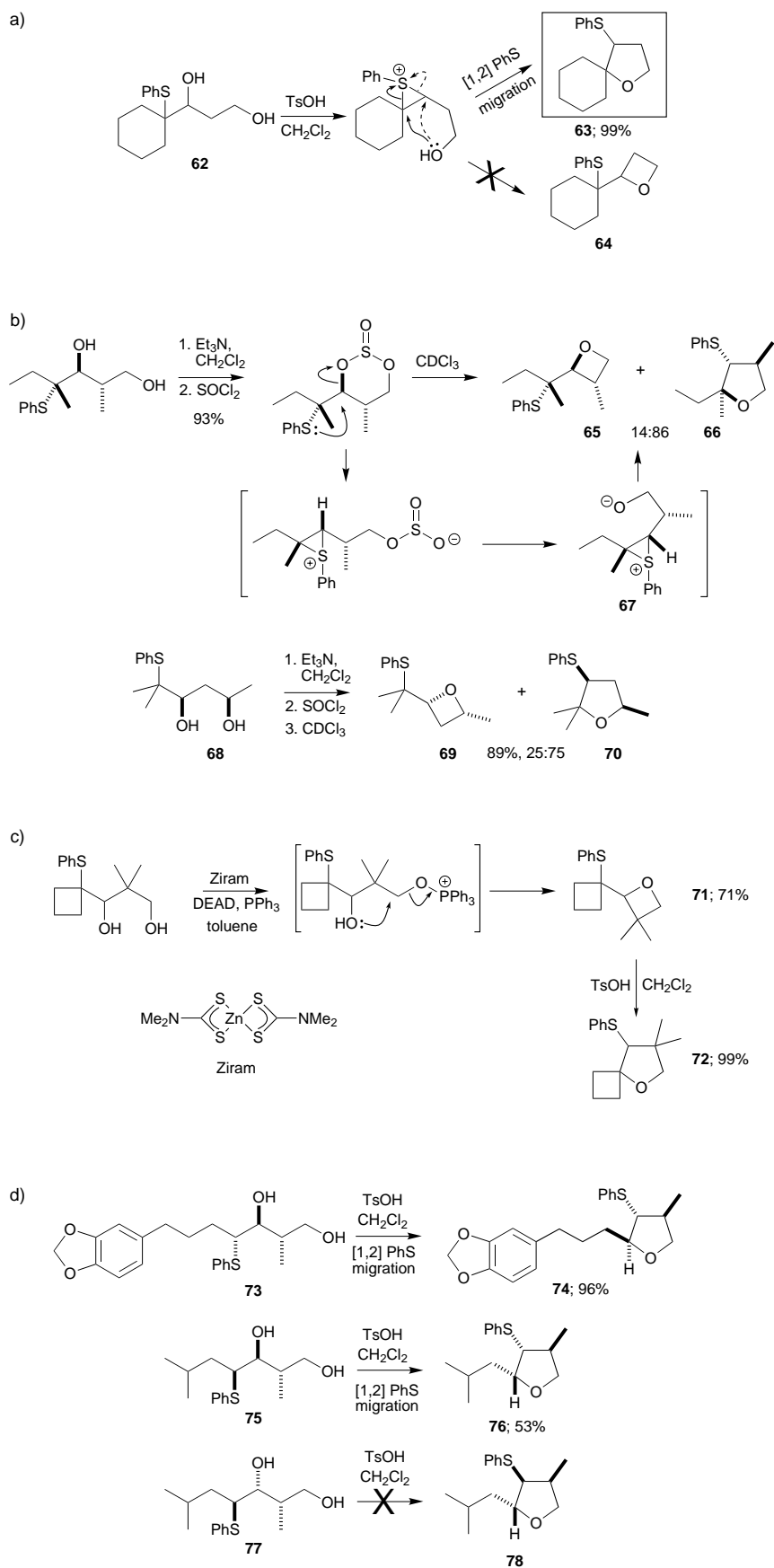
In a closely related series of experiments, Williams and Phillips prepared highly substituted THFs from diol precursors; however the alcohol and sulfanyl functionalities are transposed to give 1,4-diols with an intervening 2-phenyl-sulfanyl group (Scheme 14a).^[33] The cyclizations (e.g. **79** → **80**) were triggered by treating these compounds with a hard methylating agent (e.g. dimethyl sulfate). In this way the same thiiranium ions are formed and in all of the cases reported THFs are obtained as the sole product, that is, no oxetane is present (Scheme 14a). The juxtaposition of the hydroxy and sulfanyl groups means that these cyclizations occur *without* [1,2] PhS migration, but with retention of configuration.

Fallis and Tuladhar prepared oxygen heterocycles by generating thiiranium ions from alkenes.^[34] Interestingly, attempts to cyclize 3-buten-1-ol by treatment with phenyl-sulfonyl chloride and diisopropylethylamine (to neutralize HCl production and prevent equilibration) led only to the alcohol **81** in which the thiiranium ion had been captured by a chloride ion rather than by the tethered nucleophile (Scheme 14b). In light of the previous discussion, the reason for this is clear: for the sulfanyl group to migrate downhill (secondary to primary center) an oxetane must be formed and intermolecular capture by a chloride ion is clearly faster than the 4-*exo-tet* cyclization to the oxetane.

Knight and co-workers have prepared THFs by a related approach in which iodine was used as the electrophile.^[35, 36] For example when the alkene **82** was treated with iodine in acetonitrile, the highly substituted THF **83** was obtained (Scheme 14c).

3.1.3 Cyclizations of 1,4 Diols: THFs and THPs

Perhaps a more interesting cyclization is that of the 1,4-diol **84**; in this case the two possible products are either an unrearranged THF **85** or a rearranged tetrahydropyran (THP) **86** (Scheme 15a). Both types of heterocycle are frequently encountered and so the factors that determine their relative stability might be expected to be more subtle than for the THF vs oxetane. It turns out that THP **86**, the product of downhill [1,2] PhS migration, is formed as the sole product when diol **84** is treated with acid.^[37] Why should the THP **86** be more stable than THF **85**? We believe that the answer again lies in the position of the sulfanyl group: in THP **86** the sulfur group has moved downhill to a secondary center and the oxygen atom has now become bonded to a tertiary center. In the THF **85** the situation is reversed. If the 1,4-diol **84** is



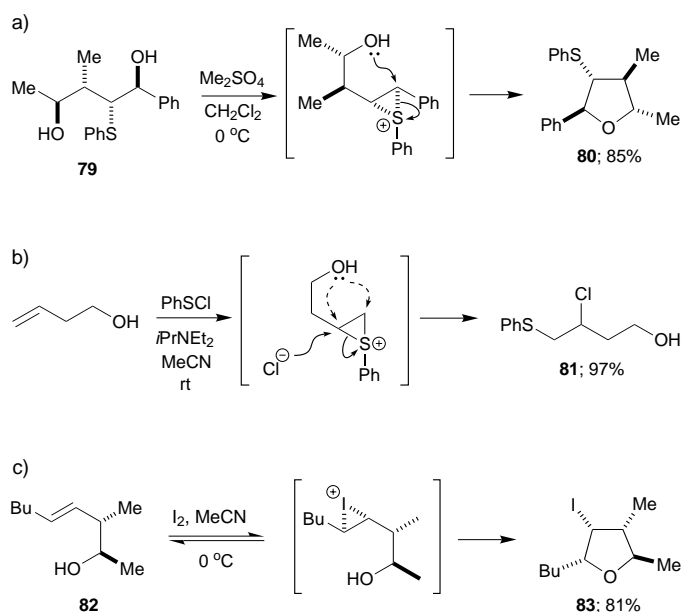
Scheme 13. a) Oxetanes are not formed in acid-catalyzed cyclization reactions; b) oxetanes may be formed under kinetic conditions; c) unusual oxetane synthesis under modified Mitsunobu conditions; d) scope and limitations of THF synthesis with flat migrations.

treated with *p*-toluenesulfonyl chloride instead of acid, the *rearranged* THF **86** is no longer formed. Instead the *unrearranged* THF **85** is formed as a result of tosylation of the primary hydroxy group and the secondary hydroxy group acting as the nucleophile (Scheme 15b).^[37] We were again able to demonstrate why the unrearranged product had not been isolated from the acid-catalyzed reaction; treating this THF with acid caused equilibration to give only the product of [1,2] RS migration, THP **86**.

Together with Fallis and co-workers, we studied the sulfenyletherification of several 4-penten-1-ols.^[38] The parent alkene **87** gives the THF **88** as a single product in 84% yield; in this case the sulfanyl group is bound to a primary center, in the THF alternative **89** it is bound to a secondary center (Scheme 15c). If Baldwin's rules^[39] are invoked (these cyclizations are under kinetic control), then the outcome of this reaction represents a pure 5-*exo-tet* cyclization, as opposed to a hybrid 6-*exo/7-endo-tet* cyclization. Accordingly, the trisubstituted alkene **90** gave only THP **91**, which avoids the sulfanyl group occupying a tertiary position (Scheme 15c).^[38] In a similar way, Clive et al. have studied the capture of seleniranium ions by oxygen nucleophiles, in this case phenols.^[40] Interestingly, the alkene **92** cyclizes on treatment with phenylselenenyl chloride to give the benzodihydrofuran **93** with the phenylselenenyl group bound to a primary center (Scheme 15d). On the other hand, cyclization of the dimethyl homologue **94** gives the benzodihydropyran **95** with the phenylselenenyl group occupying a secondary center (rather than a tertiary center if the alternative product was formed).

3.1.4 Cyclizations of 1,*n*-Diols (*n* = 2, 5, and 6): Limitations of Cyclization Reactions

To investigate further the scope of cyclization reactions of tethered alcohols onto thiiranium ions, 1,*n*-diols (*n* = 2, 5, and 6) were prepared.^[37] The 1,2-diol **96** gave the allylic sulfide **97** on treatment with acid (Scheme 16a). Perhaps unsurprisingly, neither of the two possible cyclization products, epoxide **98** or oxetane **99**, were formed. The unstable epoxide **98** could be prepared by an alternative route and on treatment with



Scheme 14. a) Williams' THF synthesis occurs without [1,2] PhS migration; b) sulfenylation of 3-buten-1-ol does not produce an oxetane or THF; c) Knight's iodoetherification reaction conditions.

acid rearranged quantitatively to the allylic sulfide **97** (Scheme 16a). Clearly, ring strain in these small-ring heterocycles makes allylic sulfide **97** the most favorable product. The 1,5-diol that might be expected to cyclize with [1,2] PhS migration to give the oxepane **100**, in fact gives the unrearranged THP **101** as the major product, along with some of the allylic sulfide **102** (Scheme 16b). Ring strain in the seven-membered ring is clearly sufficient to override the inherent preference for downhill migration. Attempting to favor the cyclization by incorporation of a *Z* olefin in the side chain (diol **103**) resulted only in the formation of dihydropyran **104** (Scheme 16b). Finally, attempts to prepare oxocane **105** no longer result in cyclization; instead the thiiranium ion formed in this reaction decomposes by elimination to give allylic sulfide **106** (Scheme 16c). The chain has become too long for cyclization to be efficient.

3.2 Higher Levels of Competition: Cyclization with Triol Substrates

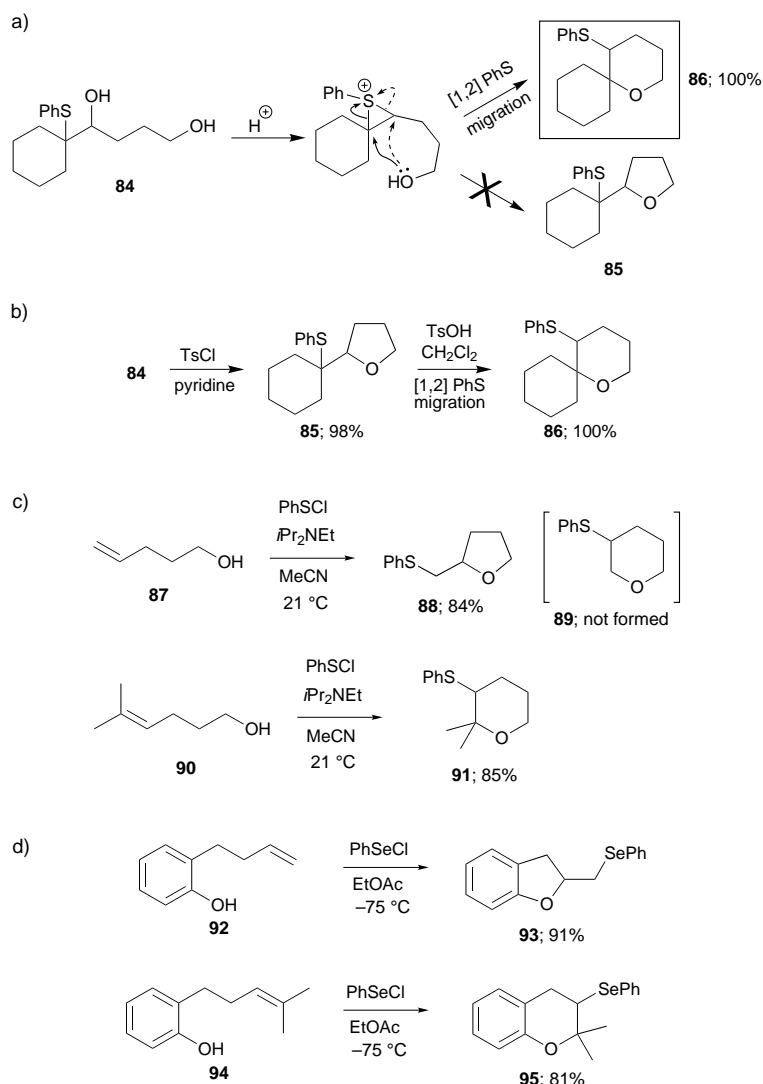
In this section we look at more complicated cyclizations: substrates with two competing nucleophiles. In each of these reactions there will, in principle, be four possible products. Either one of the oxygen nucleophiles present could cyclize onto either end of a thiiranium ion. By studying these reactions we could investigate the subtle factors that stabilize one ring system over another.

3.2.1 Competition between Primary Hydroxy End Groups of Branched Side Chains

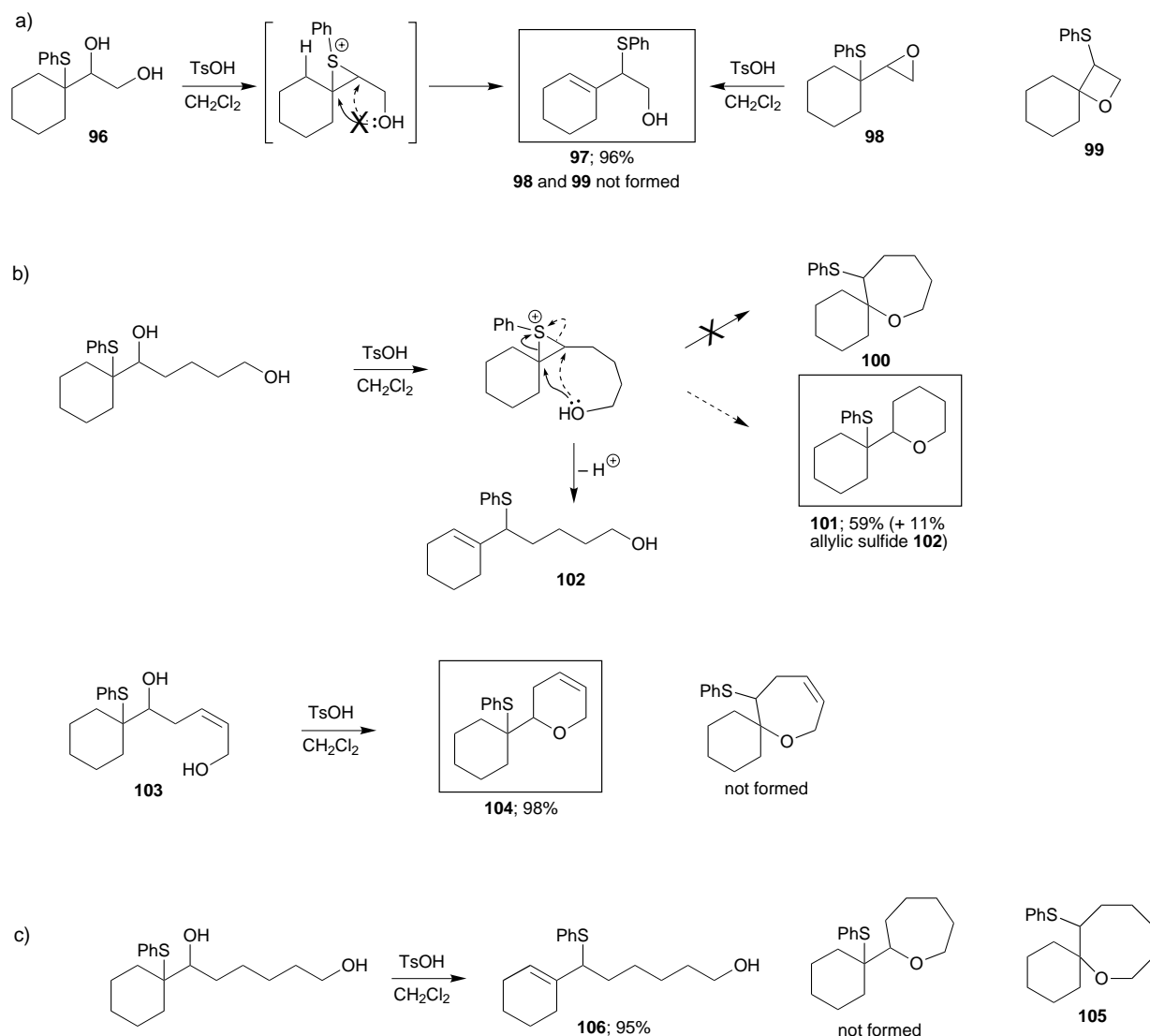
When triol **107**, which contains two diastereotopic hydroxy groups, was cyclized, two products could result,

depending on which hydroxy group was involved in the cyclization.^[*] The result is that only the *anti* THF **108** is formed in quantitative yield (Scheme 17a).^[41] Increasing the length of one of the side chains of triol **107** gives two diastereomeric triols: *anti*-**109** and *syn*-**111** (Scheme 17b). This time, each cyclization can give a rearranged THF or a rearranged THP, again depending on which of the two primary hydroxy groups is involved in the cyclization.^[41] Treatment of *anti* triol **109** with *p*-toluenesulfonic acid gave exclusively the *anti* THP **110**. However, treatment of the *syn* diastereoisomer **111** with acid led to the formation of the *anti* THF **112**. Together, these reactions established the importance of the ring stereochemistry: 3,4-*syn* stereochemistry in THFs is unfavorable because the groups are eclipsed, and a

[*] Clearly, two diastereomeric oxetanes could also result by cyclization onto the less substituted end of the thiiranium ion, but, as we have already seen, these compounds are much less stable than the THFs.



Scheme 15. a) Competing THF and THP formation under thermodynamic control; b) evidence for [1,2] PhS migrations being under thermodynamic control; c) competing THF and THP formation under kinetic control; d) competing THF and THP formation under kinetic control with a selenium electrophile.



Scheme 16. Limitations of cyclization reactions: a) epoxides and oxetanes are not formed under acid catalysis; b) THPs are formed without [1,2] PhS migration instead of the oxepane alternatives; c) oxocanes and larger rings sizes are not favorable.

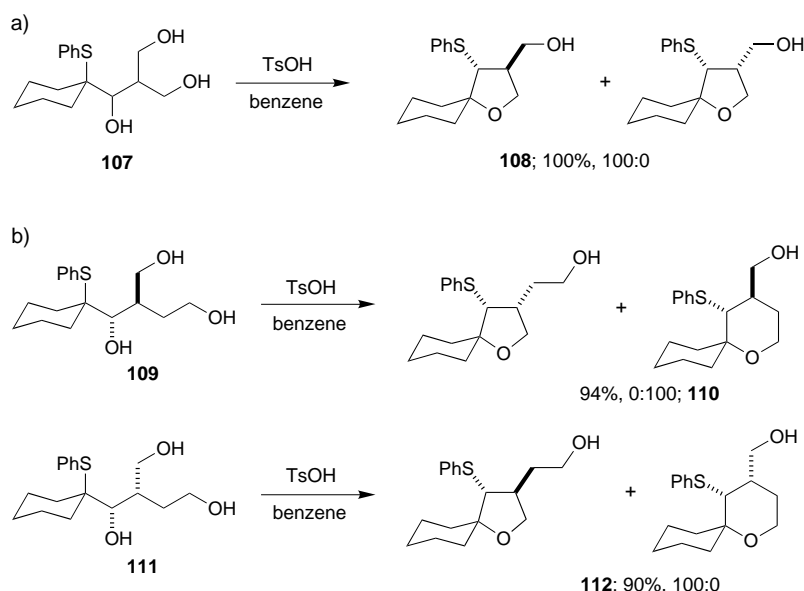
3,4-*syn* relationship in the THP would necessitate that one of the substituents be axial.

3.2.2 Competition between Primary Hydroxyl Endgroups of Separate Side Chains

In a series of closely related experiments, we looked at cyclizations onto thiiranium ions in which two separate side chains were terminated by a primary hydroxy group each. An orthogonal protecting group strategy was used to prepare authentic samples of the different cyclization products to establish unequivocally the structure of the products from these competitive cyclization reactions. These reactions were mostly designed to probe the importance of substitution pattern on ring stability. Triol **113** could produce either THF **114** or THF **115** by [1,2] PhS migration (Scheme 18a).^[42] It was shown that the major product was the more highly substituted THF **114**. This has been attributed to a thermody-

namic manifestation of the Thorpe–Ingold effect.^[43, 44] By removing the methyl group from the side chain (triol **116**) it was assumed that the Thorpe–Ingold effect would be minimized and that the product balance would be altered. Indeed the balance was completely altered, and the major product was the THF **117** in which the sulfur group has migrated onto the side chain rather than onto the ring.

In a second series of experiments, competitions were set up between five- and six-membered rings. For example, triol **118** could cyclize to produce either THF **119** or THP **120** (Scheme 18b).^[45] Once again the major product was shown to be the more highly substituted heterocycle **119**. The final variation made to this series of compounds was the addition of a pair of *gem* methyl groups to the left-hand side chain to give triol **121**. It was assumed that this substitution would reverse the selectivity to favor the THP **123**. This hypothesis was correct: a complete reversal in THF/THP selectivity was



Scheme 17. a) Competition between diastereotopic hydroxy nucleophiles: *anti* THF is the thermodynamic product; b) stereochemistry can be more important than ring size.

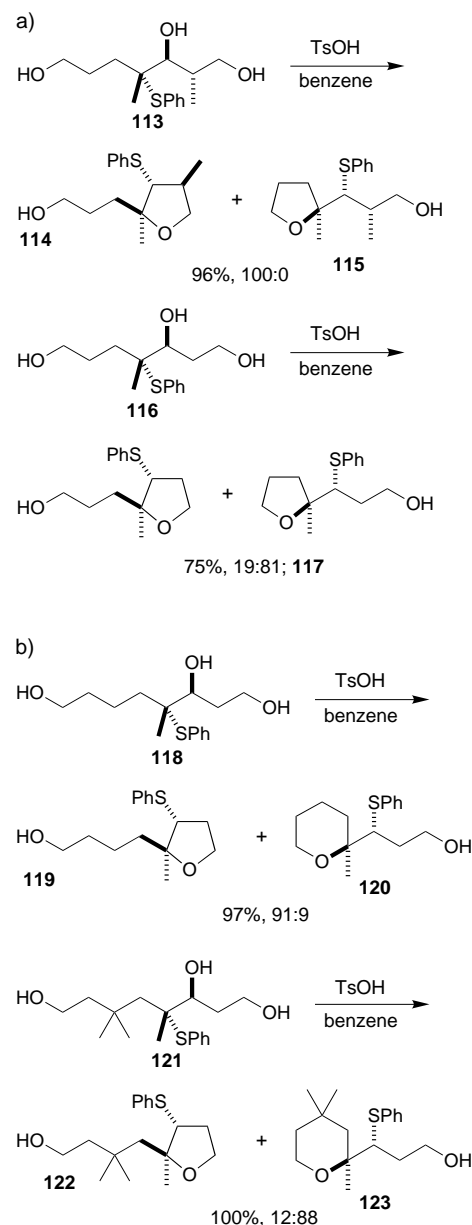
observed from 91:9 (**119/120**) to 12:88 (**122/123**).^[*] The conclusion of these experiments was that ring size (five- or six-membered) is relatively unimportant in deciding the outcome of the reaction; the degree of substitution of the rings is a more important consideration.

3.2.3 Competition between Primary and Secondary Hydroxy Groups in the Same Side Chain

Recently we have studied the cyclization reactions of triols with all three hydroxy groups in the same chain. Four triols **124**, **126**, **128**, and **130** were prepared by asymmetric dihydroxylation and stereocontrolled reduction and rearranged by treatment with *p*-toluenesulfonic acid in refluxing dichloromethane. In each case the thermodynamic products were found to be the THFs **125**, **127**, **129**, and **131**, respectively (Scheme 19a).^[6]

In contrast to the rearrangement of the branched triols **109** and **111** (Scheme 17 b) ring size has become more important than the relative stereochemistry. Now that the two substituents are 2,4- rather than 3,4-related, a 2,4-*syn* THF is preferred to the alternative 2,4-*anti* THP (Scheme 19a), in which one of the two substituents would enter an axial environment. More interestingly though, the 2,4-*anti* THF is preferred to the 2,4-*syn* THP, in which both groups could now be equatorial. We presume in this case that the factor that governs the outcome of the cyclization (the degree of substitution being equal for both rings) is the *gem*-disubstituted migration origin. In the THP, one of the C–C bonds is forced to be axial; presumably the 1,3-diaxial interactions are too severe and the flatter THF ring is preferred.

[*] It is possible in this case that equilibrium was not reached.

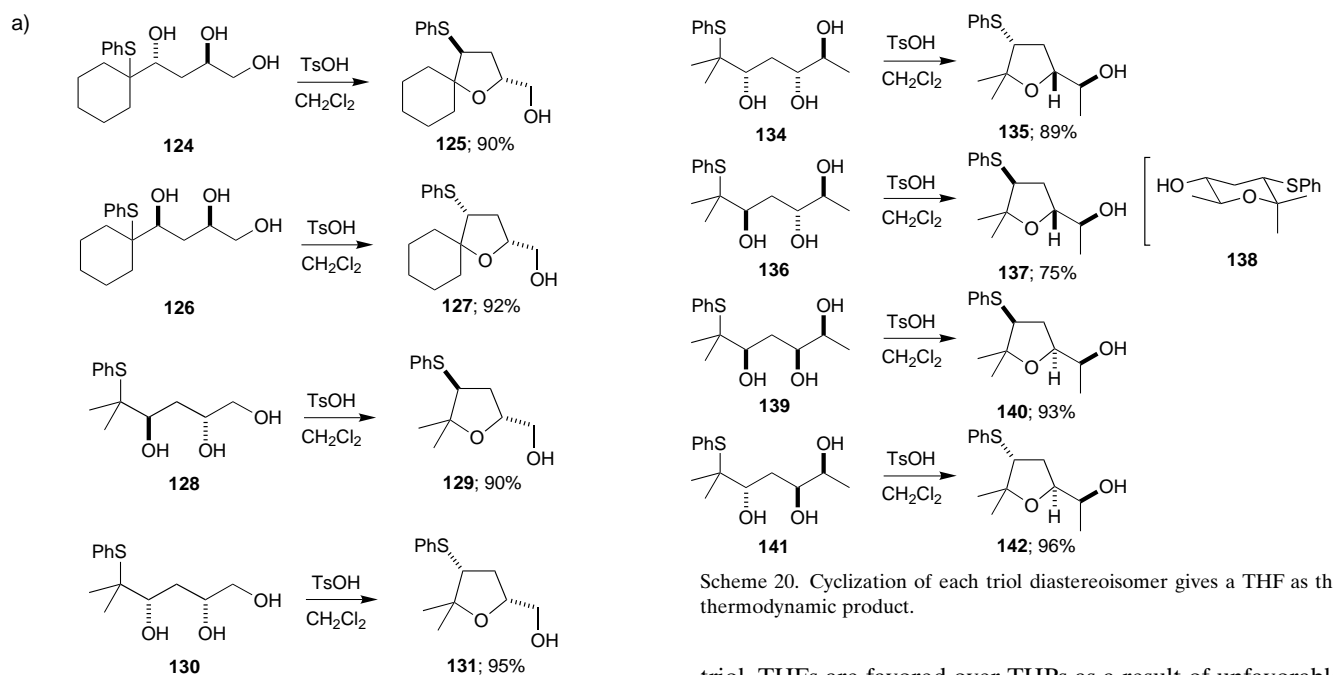


Scheme 18. a) The Thorpe–Ingold effect plays a role in determining the outcome of the cyclization; b) The Thorpe–Ingold effect can reverse the outcome of a competitive cyclization reaction.

By following these cyclizations by ¹H NMR spectroscopy, it could be shown that the products of the reaction were very time-dependent, that is, equilibrium was reached slowly.^[6] For example, rearrangement of triol **128** in CDCl₃ at 40 °C gave three products (unrearranged THF **133**, rearranged THF **129**, and rearranged THP **132**) and starting material after two hours (Scheme 19b). After nine hours, the THF **129/132** ratio in the mixture was approximately 1:1; after 36 hours, THF **129** was present with only a trace amount of THP **132**.

3.2.4 Competition between Two Secondary Hydroxy Groups in the Same Side Chain

In the final experiments in this series, the four diastereomeric triols **134**, **136**, **139**, and **141**, which contain three

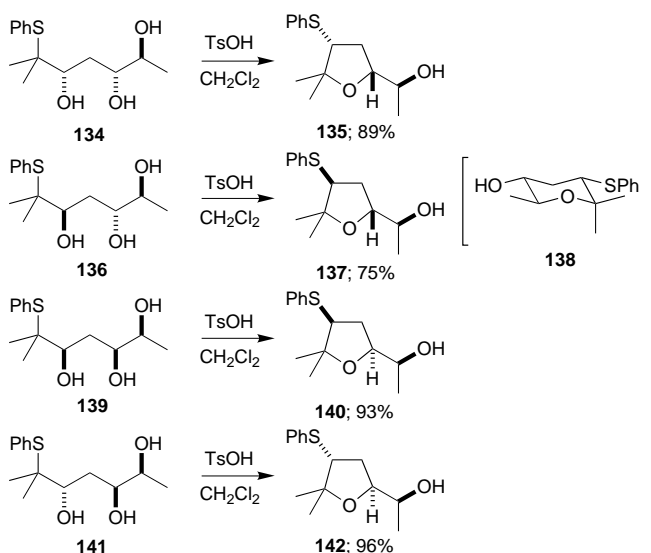


Scheme 19. a) THFs as thermodynamic products from competitive cyclization reactions; b) four possible outcomes of a competition experiment: no oxetane is observed but initially all three products may be observed by ^1H NMR spectroscopic analysis.

secondary hydroxy groups in the same side chain, were prepared.^[46] This would prove to be the most conclusive test of the relative influence of ring size and stereochemistry. Again it was found that THFs **135**, **137**, **140**, and **142** were produced in very high yields under thermodynamic control (Scheme 20). Only in the case of triol **136** with 2,4-*anti*, 4,5-*anti* stereochemistry was any THP isolated. In this case, THP **138**, which has the maximum number of equatorial substituents, accounted for 17 % of the final product mixture. It seems sensible therefore that 1,3-diaxial interactions that result from an axial methyl group should strongly disfavor THP formation in these types of compounds.

3.2.5 Kinetic Control in Competitive Cyclizations

In Sections 3.2.3 and 3.2.4, we saw that 2,4,5-triols that bear a phenylsulfanyl group at C1 rearrange to THFs as thermodynamic products, independent of the stereochemistry of the

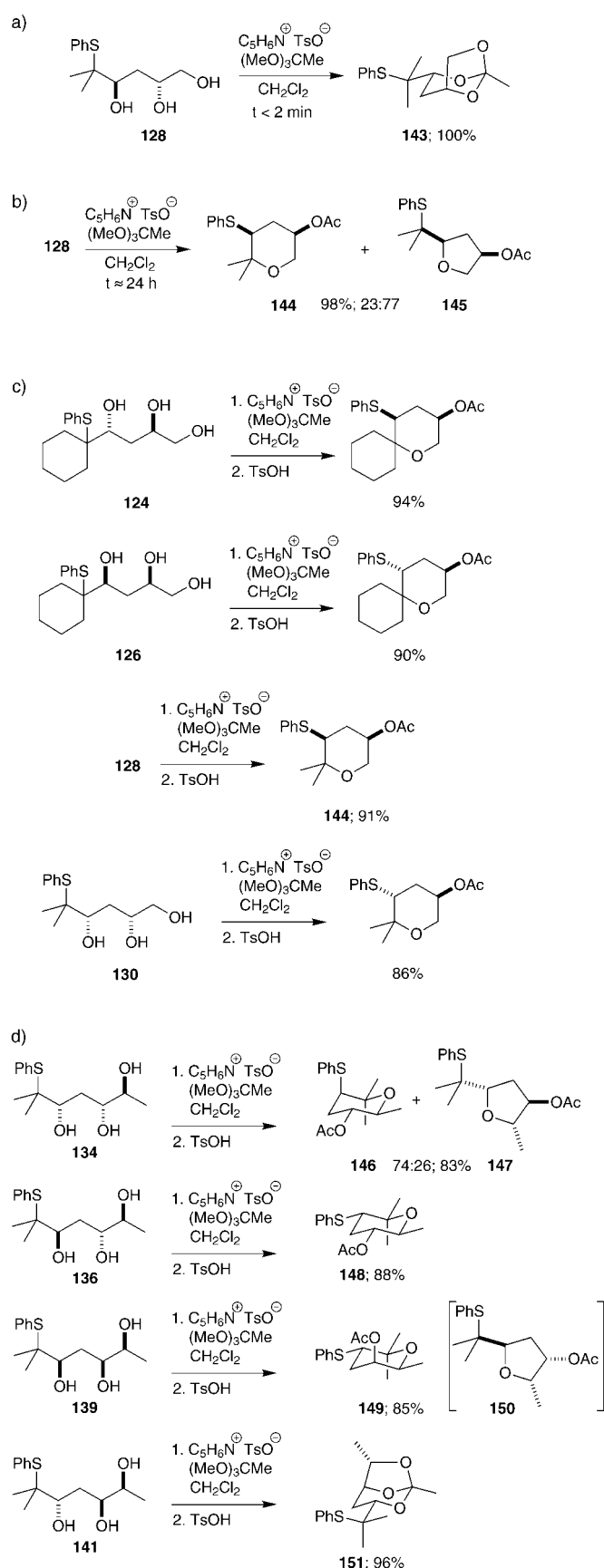


Scheme 20. Cyclization of each triol diastereoisomer gives a THF as the thermodynamic product.

triol. THFs are favored over THPs as a result of unfavorable 1,3-diaxial interactions in the THPs. The same triols were rearranged by using a reagent system specially developed to protect the secondary hydroxy nucleophile and activate the secondary hydroxy leaving group simultaneously.^[47] The reagents used were trimethyl orthoacetate and pyridinium *p*-toluenesulfonate (PPTS, $\text{p}K_{\text{a}} \sim 5.5$). The choice of acid is very important: orthoesters are known to exchange under general acid catalysis,^[48] but we believe that the acid-catalyzed rearrangement of 2-phenylsulfanyl alcohols is a specific acid-catalyzed process (the hydroxy group is protonated before displacement by the sulfanyl group). Generation of a leaving group under these mild conditions ensures that there is no competing direct rearrangement.

Treatment of the *anti* triol **128** under the conditions described gives the bicyclic orthoester **143** after a very short reaction time ($t < 2$ min) (Scheme 21 a). However, if the triol **128** is reacted for a longer period ($t \sim 24$ h), two different products are formed: rearranged THP **144** and unrearranged THF **145** (Scheme 21 b). By following this experiment by ^1H NMR spectroscopy and performing a series of control experiments, we could show that the two heterocycles are formed under kinetic control and that the product ratio is independent of reaction time. The results of this experiment complement our earlier studies on cyclic sulfites (Section 3.1.3) and the kinetic analysis of the competing formation of THFs and THPs. This model provides a true kinetic ratio for the acid-catalyzed cyclization, as the nucleophile is a hydroxy group rather than the oxanion in the cyclic sulfite reactions.

This important mechanistic observation may appear to be useless for synthetic purposes because of the product mixtures that are formed. On the contrary, treatment of the product mixtures with *p*-toluenesulfonic acid leads to complete equilibration to the protected THP **144** in which the sulfanyl group has moved “downhill” (Scheme 21 c).^[47] For the triols **124**, **126**, **128**, and **130** (from Section 3.2.3), which contain a primary hydroxy group, this reaction proved to be general (Scheme 21 c).



Scheme 21. a) Formation of an unusual bicyclic orthoester; b) acid-catalyzed rearrangement of a triol under kinetic control; c) two-step rearrangement of triols to give protected THPs as thermodynamic products; d) scope and limitation of the two-step rearrangement of triols.

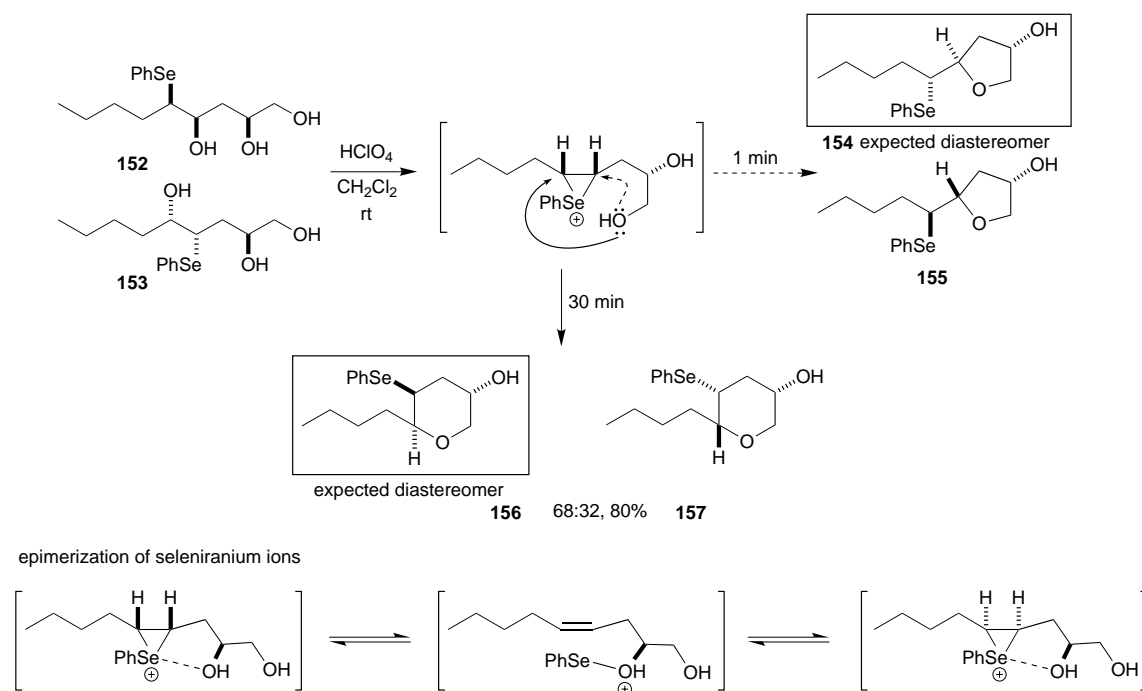
The triols **134**, **136**, **139**, and **141** (see Section 3.2.4), which contain three secondary hydroxy groups, revealed that this two-step route to protected THPs is not without limitations (Scheme 21 d).^[46] Depending on the stereochemistry, different products are observed. Rearrangement and equilibration of the 2,4-*syn*, 4,5-*anti* triol **134** gave only a 74:26 mixture of the rearranged THP **146** and unrearranged THF **147**. The inference in this case could be that it is unfavorable for the sulfur group to occupy an axial position, indeed it could be sufficiently unfavorable that it can partly overcome the driving force for “downhill” migration. The 2,4-*anti*, 4,5-*anti* triol **136** behaved quite differently; after equilibration of an initial THF/THP mixture, the only product identified was the THP **148** with the methyl, acetoxy, and phenylsulfanyl groups all occupying equatorial positions (Scheme 21 d). The 2,4-*syn*, 4,5-*syn* triol **139** gave, after the two-step reaction sequence, the THP **149** with an axial acetate (the alternative THF **150** contains an unfavorable 2,3-*syn* relationship) (Scheme 21 d). Finally, the 2,4-*anti*, 4,5-*syn* diastereoisomer **141** gave only the bicyclic orthoester **151** after prolonged treatment with trimethyl orthoacetate and PPTS.

Gruttadauria et al. have examined competitive cyclizations of a series of hydroxyselenides and sulfides.^[49–52] When the triols **152** and **153** (which form the same intermediate seleniranium ion) were treated with perchloric acid in dichloromethane at room temperature, the two diastereomeric THFs **154** and **155** were produced after one minute (Scheme 22).^[50] These THFs are unrearranged products (i.e. products in which no [1,2] PhSe migration has occurred). However, if the reaction was run for 30 minutes, unrearranged THPs **156** and **157** were produced. Clearly the THPs are the thermodynamic products of this reaction. To explain the fact that diastereomeric products are formed, the authors proposed that one of the hydroxy groups might interact with the selenium atom of the seleniranium ion intermediate to the extent that the C–Se bonds are broken to give a transient alkene. This would allow rotation to occur and a second addition of the selenium onto the opposite face of the alkene. The equilibration of seleniranium ions represents one of main differences between cyclizations with selenium and sulfur compounds.

4 Cyclization with Sulfur and Nitrogen Nucleophiles

4.1 Synthesis of Sulfur-Containing Heterocycles

The use of thiiranium ions to promote cyclization reactions has been extended to include thiols as nucleophiles.^[53, 54] The 1,*n*-hydroxythiols **158**–**160** were prepared by Mitsunobu displacement of the primary alcohol of the corresponding 1,*n*-diol by using Ziram followed by reduction with lithium aluminum hydride (Scheme 23 a). This route could not be used to prepare the 1,3-hydroxythiol; as we saw in Section 3.1.2, this reaction gives oxetanes instead (Scheme 13 c).^[53] However, aldol reaction of aldehyde **31** with the lithium enolate of ethyl dithioacetate followed by reduction did give the required 1,3-hydroxythiol **161** (Scheme 23 b). On treatment with acid, the 1,3-hydroxythiol **161** gave the spirocyclic



Scheme 22. Cyclizations involving seleniranium ions.

thiolane **162**, which belongs to a class of compounds that is not well-known (Scheme 23c).^[54] None of the thietane **163** was detected.

The second member of the series, 1,4-hydroxythiol **158**, rearranged to give not the expected thiane **164**, but instead the unrearranged thiolane **165** (Scheme 23d).^[54] This is exactly the opposite situation to the analogous alcohol **84** cyclization in which the rearranged THP **86** is formed. Our criteria for sulfur moving “downhill” can no longer be applied in this case because two sulfur atoms are present. The primary sulfide nucleophile is necessarily moving “uphill” and so this must counteract the tendency of the tertiary sulfanyl group to move “downhill”. In this seemingly subtle example, the deciding factor is likely to be the adverse 1,3-diaxial interactions that would be present in the thiane **164**. As expected the 1,5-hydroxythiol **159** does not give the thiepane **166**, instead the unrearranged thiane **167** is formed.^[54] This must reflect the increased strain in the seven-membered ring (Scheme 23e). Finally, as we saw for the 1,6-diol, the 1,6-hydroxythiol **160** undergoes elimination to give the allylic sulfide **168** because the side chain has now become too long for cyclization to compete with elimination (Scheme 23f).^[54]

It is not yet clear whether the cyclization reactions with sulfur nucleophiles are under kinetic or thermodynamic control. Sulfides are much less basic than ethers and so once formed, the heterocycles might not be reopened. An alternative approach to thiolanes by using [1,4] participation of a benzylsulfanyl (BnS) group is discussed in Section 5.2.

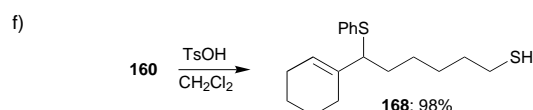
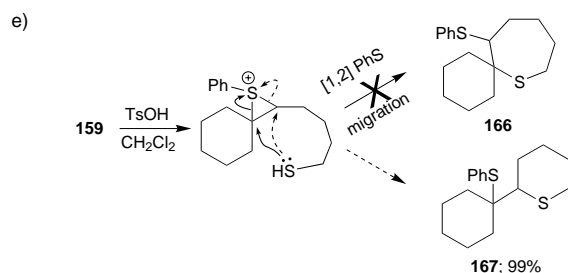
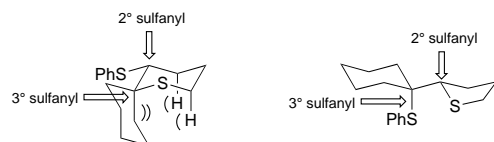
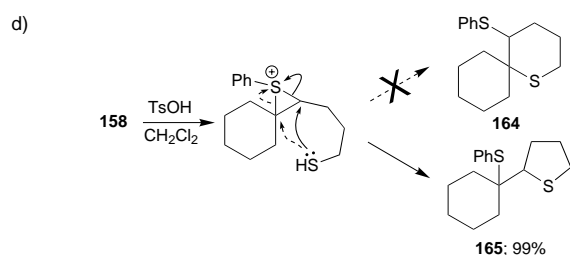
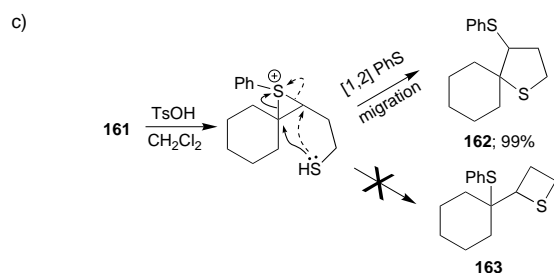
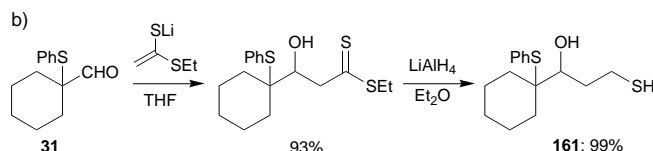
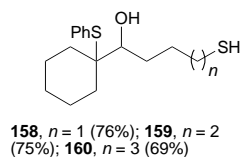
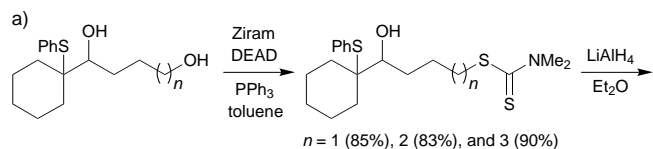
4.2 Synthesis of Nitrogen-Containing Heterocycles

The synthesis of nitrogen heterocycles by sulfanyl migration presents a real challenge. Within the acidic reaction con-

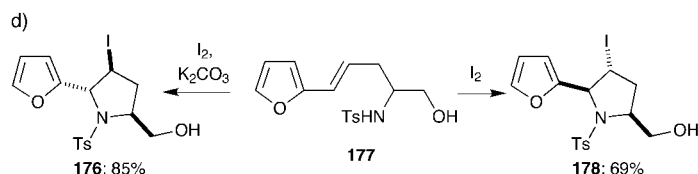
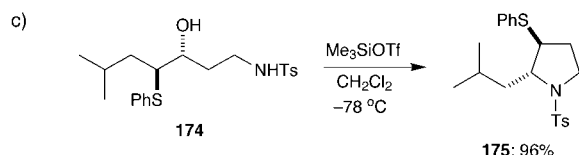
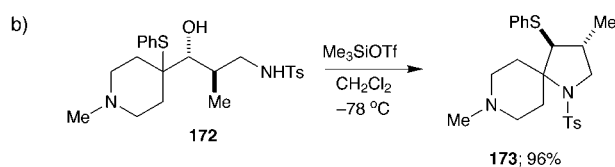
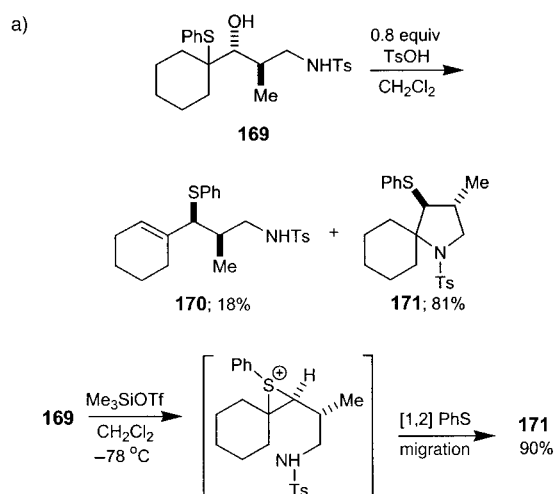
ditions used to generate thiiranium ions, any amine nucleophiles will be protonated and hence their nucleophilicity removed. A successful strategy would require the generation of a leaving group under non-acidic conditions (a subject of current research) or the fine-tuning of the basicity of the nitrogen atom with minimal detriment to its nucleophilicity. Sulfonamides were found to satisfy this second criterion partially.^[24] Treatment of sulfonamide **169** with *p*-toluenesulfonic acid in dichloromethane gives some of the allylic sulfide **170**, together with the pyrrolidine **171**, but use of trimethylsilyl triflate gives the protected pyrrolidine **171** in satisfactory yield (Scheme 24a).

The synthesis of protected pyrrolidines with trimethylsilyl triflate is quite general, for example, amine functionality in the substrate is tolerated (e.g. **172** → **173**, Scheme 24b) and “flat” migrations are also possible (e.g. **174** → **175**, Scheme 24c), as was the case for certain cyclic ethers.^[24] Table 4 shows some other examples of this reaction; enantiomerically pure starting materials could be prepared by an Evans *syn*-selective asymmetric aldol reaction^[55, 56] and products with 3,4-*syn* stereochemistry are possible.

Knight et al. have published details of their iodine-induced cyclizations by using nitrogen nucleophiles.^[57] A particularly interesting example was the treatment of sulfonamide **177** with iodine under basic conditions to give the 2,5-*anti* pyrrolidine **176** and under acidic conditions to give the 2,5-*syn* pyrrolidine **178** (Scheme 24d). The authors rationalized this observation by invoking the participation of the furan oxygen atom in the base-catalyzed cyclization. Our attempts to use carbon nucleophiles to trap thiiranium ions have so far met with only limited success. Edstrom and Livinghouse have reported the reaction of electron-rich arene nucleophiles with thiiranium ions in the presence of silver salts.^[58]



Scheme 23. a) Synthesis of 1, n -hydroxythiols ($n \neq 3$); b) synthesis of 1,3-hydroxythiols; c) rearrangement of 1,3-hydroxythiols to give thiolanes; d) 1,4-hydroxythiols give thiolanes without [1,2] PhS migration; e) 1,5-hydroxythiols give thiolanes without [1,2] PhS migration; f) 1, n -hydroxythiols with $n > 5$ rearrange to allylic sulfides.



Scheme 24. a) Trimethylsilyl triflate promoted cyclization with a sulfonamide nucleophile; b) pyrrolidine formation; c) flat migrations may be tolerated in pyrrolidine formation; d) iodine-promoted pyrrolidine formation.

Table 4. Examples of Me₃SiOTf-promoted pyrrolidine synthesis with [1,2] PhS migration.

R	Yield
<i>c</i> -C ₅ H ₈	96 % (> 98 % <i>ee</i>)
<i>c</i> -C ₆ H ₁₀	99 %
-CH ₂ CH ₂ (NMe)CH ₂ CH ₂ -	89 %

5 Thiolanium Ions and [1,4] RS Participation

Until now the discussion has been mostly centered around thiiranium ions formed by [1,2] sulfanyl participation, which is by far the most common example of sulfur participation. Sulfur is also known to participate to give thietanium,^[59, 60] thiolanium,^[61, 62] and thianium ions.^[62, 63] We concern ourselves here with only thiolanium ions, as sulfur participation to give

four- and six-membered rings is kinetically less favorable and consequently less well documented.

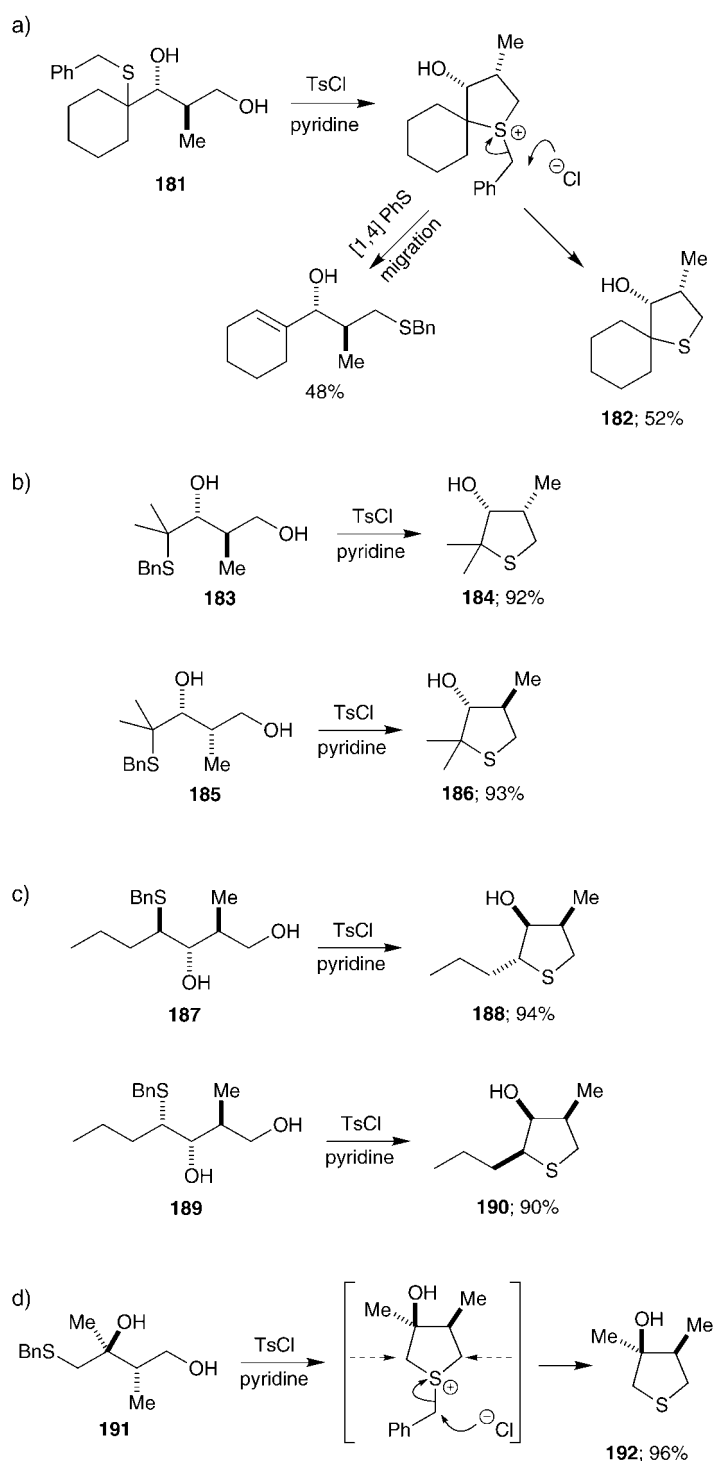
5.1 Elimination Reactions of Thiolanium Ions

In Section 3 we discussed the 1,3-diol **49** and noted that this compound provided the link between elimination and cyclization reactions of thiiranium ions: on treatment with acid, the free diol cyclizes, whereas the primary protected compound **33** undergoes elimination (Scheme 11). If diol **49** is treated with *p*-toluenesulfonyl chloride instead of acid, an altogether different pathway is followed (Scheme 25).^[37] The primary hydroxy group is first tosylated; in a second step sulfur participates in a [1,4] fashion through a five-membered ring to give the thiolanium ion **179**. With no suitably placed nucleophiles, elimination occurs to give the allylic alcohol **180** in which the sulfanyl group has undergone a [1,4] migration.

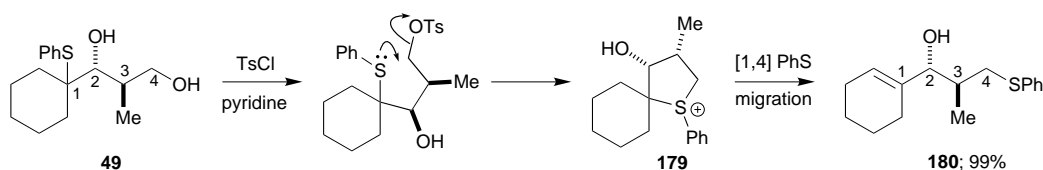
5.2 Thiolane Synthesis by Debenzylation of Thiolanium Ions

The choice of R in [1,2] RS migration reactions is largely irrelevant. Most commonly, R = Ph because it provides a chromophore to aid in chromatographic processes. Alkylsulfanyl (R = Me, Et, *t*Bu), benzylsulfanyl, and even sulfanyl (R = H) groups have also been used successfully.^[29] TsCl-promoted [1,4] PhS migration of the benzylsulfanyl diol **181** opened up yet another reaction pathway. Not only does elimination occur onto the thiolanium ion, but the chloride ion released in the reaction also debenzylates the thiolanium ion to give the some of the thiolane **182** (Scheme 26a).^[64] With a view to increasing the yields of thiolane formed in these reactions, acyclic sulfides were also examined (elimination of an axial proton from within the cyclohexane ring is particularly favorable). From *anti* diol **183** and *syn* diol **185** thiolanes *syn*-**184** and *anti*-**186** were formed in yields of 92 % and 93 %, respectively (Scheme 26b).^[64] Table 5 shows that sterically crowded thiolanes may also be formed by using this reaction.

Secondary sulfides also perform well in this reaction: *anti* sulfide **187** and *syn* sulfide **189** were converted into thiolanes **188** and **190** in yields of 94 % and 90 % yields, respectively (Scheme 26c).^[64] Amazingly, even primary sulfides are well behaved in this reaction: the sulfide *anti*-**191** gives thiolane *syn*-**192** on treatment with *p*-toluene-

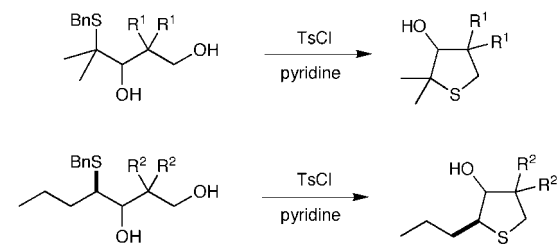


Scheme 26. a) Alternative thiolane synthesis in the presence of a benzylsulfanyl group; b) the stereochemistry is not affected in the [1,4] BnS migration; c) flat migrations are tolerated in cyclizations with [1,4] BnS migration of primary sulfides.



Scheme 25. [1,4] PhS migration proceeds via a thiolanium ion intermediate.

Table 5. Examples of thiolane synthesis by [1,4] BnS participation and debenzylation.



R ¹	R ²	Stereochemistry	Thiolane	Yield
H	–	n/a		93 %
Me	–	n/a		94 %
–	H	<i>anti</i>	<i>anti</i>	94 %
–	H	<i>syn</i>	<i>syn</i>	91 %
–	Me	<i>anti</i>	<i>anti</i>	96 %

sulfonyl chloride, despite there being three appealing sites for an S_N2 reaction (Scheme 26d).

5.3 [1,4] PhS Migration as an Alternative Route to THFs

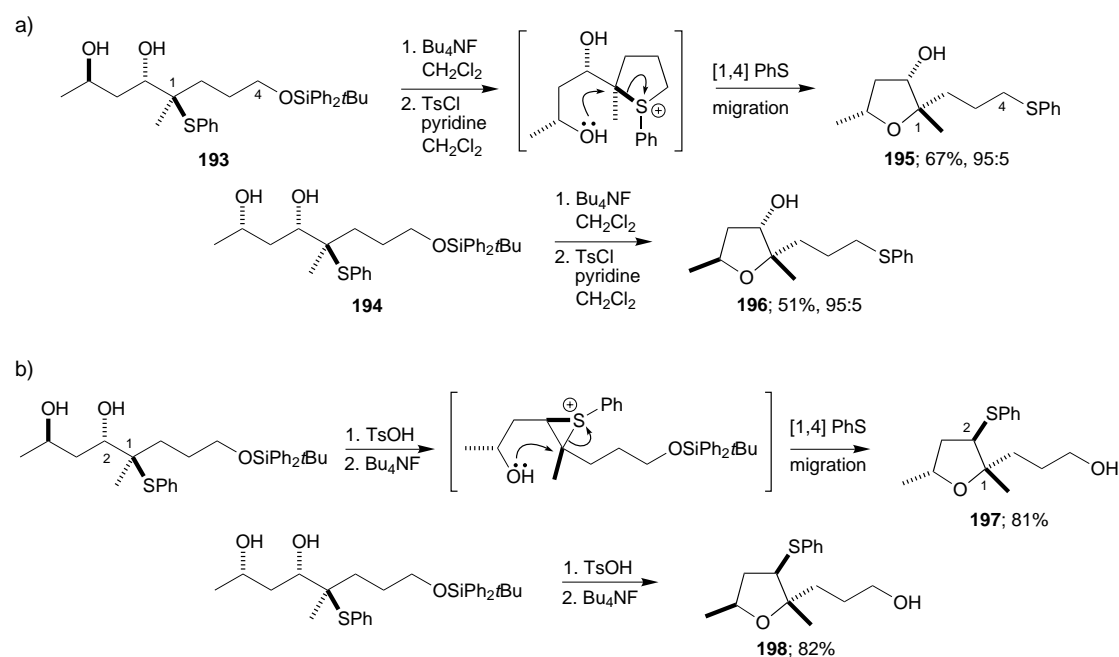
A logical extension to the [1,4] RS participation is to introduce suitably placed nucleophiles to permit cyclization by a [1,4] RS migration. Primary protected triols *anti*-**193** and *syn*-**194** could be prepared by a short sequence of reactions that included an aldol reaction and a stereocontrolled reduction. Deprotection of these triols (TBAF) and treatment with *p*-toluenesulfonyl chloride led to the highly substituted THFs **195** and **196**, albeit in rather modest yields (Scheme 27a).^[65] The cyclization was shown to be stereospecific (NOESY) with inversion at the migration origin as expected. The minor isomers formed in these reactions are believed to

be the C2 epimers formed by ring opening and reclosing of the thiolanium ion, a process that we have never observed for thiiranium ion mediated cyclizations. To prove that these compounds had not been formed by the normal [1,2] PhS pathway, the protected triols were rearranged with *p*-toluenesulfonic acid and deprotected to give the isomeric THFs **197** and **198** (OH-, PhS-exchanged, and different stereochemical series) (Scheme 27).

6 Summary and Outlook

The strategy of migrating functional groups represents a useful and efficient method in organic synthesis. The sulfanyl group enjoys a prominent role in rearrangement reactions; perhaps no other element in the periodic table offers as diverse a potential for rearrangement reactions. We have shown how [1,2], [1,3], and [1,4] sulfanyl migrations can bring about rearrangements in a high-yielding and stereocontrolled fashion. One of the main aims of this Review has been to highlight the kinds of molecules that can be prepared by using the strategy of sulfanyl migration: this method is particularly suited to the stereocontrolled synthesis of five- and six-membered saturated heterocycles and functionalized alkenes with 1,4-related stereogenic centers. From the examples encountered in this Review, some general guidelines for cyclizations can be drawn:

- Only THFs and THPs are formed under equilibrating conditions; epoxides, oxetanes, and saturated oxygen heterocycles with seven or more atoms have never been observed.
- THFs with 3,4-*syn* stereochemistry are thermodynamically unfavorable; if a THF or THP alternative is available, this is likely to be the major product.



Scheme 27. a) Capture of thiolanium ions by hydroxy nucleophiles—an alternative stereocontrolled THF synthesis; b) synthesis of isomeric THFs by [1,2] PhS migration.

- *gem*-Dialkyl substitution on a cyclizing side chain may stabilize a product according to the Thorpe–Ingold effect.
- In situations in which the same *gem*-dialkyl pair are present in a THF or a THP, a THF is likely to result.

Received: September 11, 2001 [A 491]

- [1] K. C. Nicolaou, Z. Lysenko, *J. Chem. Soc. Chem. Commun.* **1977**, 293.
- [2] a) N. Kharasch, C. M. Buess, *J. Am. Chem. Soc.* **1949**, 71, 2724; b) W. H. Mueller, P. E. Butler, *J. Org. Chem.* **1967**, 32, 2925; c) W. H. Mueller, *Angew. Chem.* **1969**, 81, 475; *Angew. Chem. Int. Ed. Engl.* **1969**, 8, 482; d) W. A. Thaler, W. H. Mueller, P. E. Butler, *J. Am. Chem. Soc.* **1968**, 90, 2069; e) W. H. Mueller, P. E. Butler, *J. Am. Chem. Soc.* **1968**, 90, 2075; f) W. A. Thaler, *J. Org. Chem.* **1969**, 34, 871; g) D. C. Owsley, G. K. Helmkamp, S. N. Spurlock, *J. Am. Chem. Soc.* **1969**, 91, 3606; h) W. H. Mueller, *Angew. Chem.* **1969**, 81, 475; i) W. A. Smit, M. Z. Krimer, E. A. Vorob'eva, *Tetrahedron Lett.* **1975**, 2451; j) G. Capozzi, O. De Lucchi, V. Lucchini, G. Modena, *Tetrahedron Lett.* **1975**, 2603; k) S. Ikegami, J. I. Ohishi, Y. Shimizu, *Tetrahedron Lett.* **1975**, 3923.
- [3] W. A. Smit, A. S. Gybin, V. S. Bogdanov, *Tetrahedron Lett.* **1978**, 1085.
- [4] P. Brownbridge, S. Warren, *J. Chem. Soc. Chem. Commun.* **1975**, 820.
- [5] R. E. Gawley, *Org. React.* **1988**, 35, 1.
- [6] D. House, F. Kerr, S. Warren, *Chem. Commun.* **2000**, 1779.
- [7] D. House, S. Warren, unpublished results.
- [8] L. M. Rossi, P. Trimarco, *Synthesis* **1978**, 465.
- [9] A. S. Gybin, W. A. Smit, V. S. Bogdanov, *Tetrahedron Lett.* **1980**, 21, 383.
- [10] R. Destro, V. Lucchini, G. Modena, L. Pasquato, *J. Org. Chem.* **2000**, 65, 3367.
- [11] V. Lucchini, G. Modena, L. Pasquato, *J. Am. Chem. Soc.* **1991**, 113, 6600.
- [12] P. Brownbridge, S. Warren, *J. Chem. Soc. Perkin Trans. 1* **1977**, 2272.
- [13] I. Coldham, S. Warren, *J. Chem. Soc. Perkin Trans. 1* **1992**, 2303.
- [14] P. Brownbridge, I. Fleming, A. Pearce, S. Warren, *J. Chem. Soc. Chem. Commun.* **1976**, 751.
- [15] P. Brownbridge, P. G. Hunt, S. Warren, *Tetrahedron Lett.* **1983**, 25, 3391.
- [16] P. Brownbridge, J. Durman, P. G. Hunt, S. Warren, *J. Chem. Soc. Perkin Trans. 1* **1986**, 1947.
- [17] A. de Groot, B. J. M. Jansen, *Tetrahedron Lett.* **1981**, 22, 887.
- [18] A. de Groot, B. J. M. Jansen, *Synthesis* **1985**, 434.
- [19] P. Brownbridge, S. Warren, *J. Chem. Soc. Perkin Trans. 1* **1976**, 2125.
- [20] a) P. Brownbridge, S. Warren, *J. Chem. Soc. Chem. Commun.* **1975**, 820; b) P. Brownbridge, S. Warren, *J. Chem. Soc. Perkin Trans. 1* **1977**, 1131.
- [21] S. Usui, J.-I. Ohishi, Y. Shimizu, L. A. Paquette, *Tetrahedron Lett.* **1999**, 40, 3495.
- [22] D. A. Evans, G. C. Andrews, *Acc. Chem. Res.* **1974**, 7, 147.
- [23] V. K. Aggarwal, I. Coldham, S. McIntyre, S. Warren, *J. Chem. Soc. Perkin Trans. 1* **1991**, 451.
- [24] I. Coldham, S. Warren, *J. Chem. Soc. Perkin Trans. 1* **1993**, 1637.
- [25] G. H. Schmid, M. S. Strukelj, S. Dalipi, M. D. Ryan, *J. Org. Chem.* **1987**, 52, 2403.
- [26] Y. Masaki, K. Hashimoto, K. Kaji, *Tetrahedron Lett.* **1978**, 4539.
- [27] Y. Masaki, K. Hashimoto, S. Kazhuiko, K. Kaji, *J. Chem. Soc. Chem. Commun.* **1979**, 855.
- [28] V. K. Aggarwal, I. Coldham, S. McIntyre, F. H. Sansbury, M. J. Villa, S. Warren, *Tetrahedron Lett.* **1988**, 29, 4885.
- [29] J. Eames, R. V. H. Jones, S. Warren, *Tetrahedron Lett.* **1996**, 37, 4823.
- [30] J. Eames, M. A. Delasheras, S. Warren, *Tetrahedron Lett.* **1996**, 37, 4077.
- [31] J. Eames, S. Warren, *Tetrahedron Lett.* **1996**, 37, 3525.
- [32] P. Rollin, *Tetrahedron Lett.* **1986**, 27, 4169.
- [33] D. R. Williams, J. G. Phillips, *Tetrahedron* **1986**, 42, 3013.
- [34] S. M. Tuladhar, A. G. Fallis, *Tetrahedron Lett.* **1987**, 28, 523.
- [35] J. M. Barks, D. W. Knight, C. J. Seaman, G. G. Weingarten, *Tetrahedron Lett.* **1994**, 35, 7259.
- [36] S. P. Bew, J. M. Barks, D. W. Knight, R. J. Middleton, *Tetrahedron Lett.* **2000**, 41, 4447.
- [37] L. Djakovitch, J. Eames, R. V. H. Jones, S. McIntyre, S. Warren, *Tetrahedron Lett.* **1995**, 36, 1723.
- [38] P. Bird, J. Eames, A. G. Fallis, R. V. H. Jones, M. Roddis, C. F. Sturino, S. O'Sullivan, S. Warren, M. S. Westwell, J. Worrall, *Tetrahedron Lett.* **1995**, 36, 1909.
- [39] J. E. Baldwin, *J. Chem. Soc. Chem. Commun.* **1976**, 734.
- [40] D. L. J. Clive, G. Chittattu, N. J. Curtis, W. A. Kiel, C. K. Wong, *J. Chem. Soc. Chem. Commun.* **1977**, 725; cyclizations via seleniranium ions have been extensively reviewed, see: M. Tiecco, *Top. Curr. Chem.* **2000**, 208, 7.
- [41] F. H. Sansbury, S. Warren, *Tetrahedron Lett.* **1992**, 33, 539.
- [42] S. McIntyre, S. Warren, *Tetrahedron Lett.* **1990**, 31, 3457.
- [43] J. T. Edward, E. Cooke, T. C. Paradellis, *Can. J. Chem.* **1982**, 60, 2546.
- [44] J. R. Snyder, A. S. Serianni, *Carbohydr. Res.* **1991**, 210, 21.
- [45] S. McIntyre, F. H. Sansbury, S. Warren, *Tetrahedron Lett.* **1991**, 32, 5409.
- [46] D. House, F. Kerr, S. Warren, *Chem. Commun.* **2000**, 1783.
- [47] D. J. Fox, D. House, F. Kerr, S. Warren, *Chem. Commun.* **2000**, 1781.
- [48] E. H. Cordes, H. G. Bull, *Chem. Rev.* **1974**, 74, 581.
- [49] M. Gruttadauria, P. Lo Meo, R. Noto, *Tetrahedron* **1999**, 55, 4769.
- [50] M. Gruttadauria, R. Noto, *Tetrahedron Lett.* **1999**, 40, 8477.
- [51] M. Gruttadauria, P. Lo Meo, R. Noto, *Tetrahedron* **1999**, 55, 14097.
- [52] M. Gruttadauria, C. Aprile, S. Riela, R. Noto, *Tetrahedron Lett.* **2001**, 42, 2213.
- [53] J. Eames, R. V. H. Jones, S. Warren, *Tetrahedron Lett.* **1996**, 37, 707.
- [54] J. Eames, S. Warren, *J. Chem. Soc. Perkin Trans. 1* **1999**, 2783.
- [55] K. Chibale, S. Warren, *J. Chem. Soc. Perkin Trans. 1* **1995**, 2411.
- [56] a) D. A. Evans, J. Bartoli, T. L. Shih, *J. Am. Chem. Soc.* **1981**, 103, 2127; b) J. R. Gage, D. A. Evans, *Org. Synth.* **1989**, 68, 77.
- [57] D. W. Knight, A. L. Redfern, J. Gilmore, *Tetrahedron Lett.* **1998**, 39, 8909.
- [58] E. Edstrom, T. Livinghouse, *J. Chem. Soc. Chem. Commun.* **1986**, 279.
- [59] E. L. Eliel, W. H. Pearson, L. M. Jewell, A. G. Abatjoglou, *Tetrahedron Lett.* **1980**, 21, 331.
- [60] A. R. Dunn, R. J. Stoodley, *J. Chem. Soc. Perkin Trans. 1* **1972**, 2509.
- [61] B. D. Tilak, R. B. Mitra, C. V. Deshpande, *Tetrahedron Lett.* **1965**, 3569.
- [62] V. Cere, S. Pollicino, A. Fava, *Tetrahedron* **1996**, 52, 5989.
- [63] I. Izquierdo, M. T. Plaza, F. Aragon, *Tetrahedron: Asymmetry* **1996**, 7, 2567.
- [64] J. Eames, N. Kuhnert, R. V. H. Jones, S. Warren, *Tetrahedron Lett.* **1998**, 39, 1247.
- [65] J. Eames, N. Kuhnert, S. Warren, *Synlett* **1999**, 1215.

Chemistry in Ancient Times: The Development of Blue and Purple Pigments

Heinz Berke*

Dedicated to Professor Roald Hoffmann on the occasion of his 65th birthday

1. The World of Colors and the Antique Blue and Purple Pigments

Colors are fascinating. At first man only saw the quality and variety of colors in nature, but later tried to make them himself. That is why a special relationship exists between man and colors, both through perception and through expression.^[1] Both are linked to aesthetics and have influenced the arts in various ways throughout the history of mankind. As a result, colored substances and pigments were highly valued and much sought after in ancient times as raw materials for the arts.

In prehistoric times and in the antiquity, the availability of these substances was the key problem, directly linked to their accessibility. Earth colors were readily available at all times as they could be directly taken from the soil. They were, for example, used in cave paintings. Looking at these paintings, it is striking that no blue color is found. In general, organic or mineral sources for stable blue dyes and pigments are exceptionally rare.

In ancient times, the rare blue mineral pigments could be mined to the major part only from deposits that were difficult to access. Even later civilizations often suffered from shortages of stable blue pigments. This situation did not change until the 19th century when industrialization led to the chemical mass production of dyes and pigments. The shortage of blue pigments most probably caused their high idealistic and materialistic esteem. The first blue mineral pigment that was both accessible to mankind and truly stable, was most likely lapis lazuli ($(\text{Na,Ca})_8[\text{SiAlO}_4]_6(\text{S}_2\text{O}_7)$; S_3^{2-} or S_2^{2-} chromophores embedded into sodalite cages).^[2] This precious stone was mined in the antiquity in the area of today's Afghanistan. The demand for blue pigments was also met by using the more abundant mineral azurite, a basic copper carbonate. The less stable azurite is found, for example, as a component in layers of paint of Chinese art objects from pre-Christian times. In these times, one was also able to prepare

blue-colored glazes and glasses by the use of cobalt minerals. The blue glaze of the tiles of Babylon's Istar gate contain significant amounts of cobalt.^[3] To a certain extent smalt, a cobalt–aluminum spinel compound, was used in ancient Egypt.^[4]

The blue pigments used in pre-industrial times all suffered from specific restrictions that hindered their broader application. The lack of a blue pigment that could be used universally, apparently resulted in the development of methods to produce stable blue materials. These methods also include the production of Maya Blue^[5] used by Indian civilizations, which is based on indigo stabilized by intercalation into clays.

People's efforts to enhance the availability and quality of blue pigments by producing them themselves began in pre-dynastic ancient Egypt more than 5200 years ago.^[6] At that time a pigment was created which is known today as Egyptian Blue ($\text{CaCuSi}_4\text{O}_{10}$).^[7–13] Traces of the compound have been found in artifacts such as a small plate from 3600 BC for an olive oil container, which certifies the quality of the oil blessed by the goddess Iset. Egyptian civilizations used Egyptian Blue frequently over the next millennia. The golden age of its use was most likely the period of the New Kingdom (1580–1085 BC), which coincides with the most productive period of artwork in ancient Egypt. Among the most remarkable pieces from this time are the crown of Nefertete and the Talatat stones of the temple of her husband Echnaton, both painted using Egyptian Blue.^[6, 14]

Even before the collapse of the Egyptian Empire Egyptian Blue reached the ancient Greek and Roman civilizations.^[9] Egyptian Blue was also widely used in Mesopotamia and in the area of today's Iran. Concurrently it became a commodity for the Romans. In his legendary work "De Architectura" from 24 AD, the Roman architect Vitruvius published a recipe for Egyptian Blue, known to the Romans as *caeruleus*, and also mentioned its production in factories. Together with the end of the Roman Empire, the knowledge of Egyptian Blue was lost.

Blue pigments also played an important role in China's historical development. While the already mentioned azurite was used in ancient times as mineral blue pigment, cobalt oxide found use in glazes and glasses. Azurite, relatively abundant in China, was mined mainly to produce copper and copper alloys.^[15] However there was no mineral blue for universal use in ancient China as azurite is rather unstable and

[*] Prof. Dr. H. Berke
Anorganisch-chemisches Institut
Universität Zürich
Winterthurerstrasse 190, 8057 Zürich (Switzerland)
Fax: (+41) 1-635-6802
E-mail: hberke@aci.unizh.ch

the staining by cobalt oxide is limited to special applications. These disadvantages apparently triggered within the Chinese civilization the start of the industrial–chemical development and production of blue pigments with enhanced properties. The answers to this challenge are Chinese Blue and Chinese Purple, also known as Han Blue and Han Purple.^[16] Compared with Egyptian Blue these pigments contain the homologue element barium instead of calcium.^[8, 17, 18] They are chemical compounds of the composition $\text{BaCuSi}_4\text{O}_{10}$ ^[19] and $\text{BaCuSi}_2\text{O}_6$.^[20]

The samples investigated so far came from blue and purple octagonal dye rods, most probably used as a commodity for paint production.^[16, 18] Chinese Blue and Purple were also found in pigment layers from the Terracotta Army (Figure 1)^[6, 14, 18, 21] or applied for the staining of glasses.^[22] Some samples date back to the “Warring States” period (479–221 BC). The Blue and Purple were most commonly used during the Q’in and Han dynasties (221 BC–220 AD).^[16, 21] Later use has not yet been proven.



Figure 1. Sample of the Terracotta Army Xi'an, China. Left: a group of terracotta soldiers. Top right: fragments of the purple trousers of a soldier (fragment 003–92). Bottom right: A microscopic view (enlargement 500-times) of a cross section of its pigment layer. The displayed part has a horizontal extension of 0.22 mm. The pigment layer contains grains of Chinese Purple and Cinnabar. Under the pigment layer there is a dark lacquer and under that the terracotta.

2. Three Pigments—One Chemistry

As Egyptian Blue, Chinese Blue, and Chinese Purple are all alkaline-earth-metal copper silicates, they are chemically related compounds. Samples of the compounds are shown in Figure 2. Egyptian and Chinese Blue even have the same copper and silicate stoichiometry and the same microscopic structure. They are also very similar macroscopically, crystals of both compounds show the same appearance.^[7, 17] Their structures contain four-membered $(\text{SiO})_4$ rings and oxygen bridges linking different rings in such a way that four four-membered rings form an eight-membered ring.^[6, 19] The infinite layered assembly of the rings shows puckering (Figure 3), with the remaining terminal oxygen atoms of the SiO_4 tetrahedra functioning as coordination sites for the metal ions. Between two opposing four-membered rings lies a Cu^{2+} ion in a square-planar environment. The Cu^{2+} ions occupy half of



Figure 2. Egyptian Blue ($\text{CaCuSi}_4\text{O}_{10}$; left), Chinese Blue ($\text{BaCuSi}_4\text{O}_{10}$; middle), and Chinese Purple ($\text{BaCuSi}_2\text{O}_6$; right). Egyptian Blue and Chinese Blue appear very similar under comparable conditions. That they appear different here is a result of the samples being of different particle size. Small particles lead to lightening in tone. The sample of Egyptian Blue consists of coarse crystalline material, while Chinese Blue was ground.

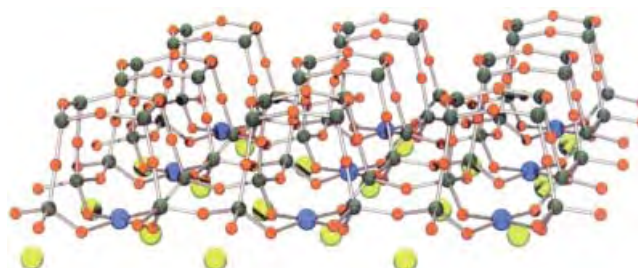


Figure 3. Schematic representation of a puckered layer of $\text{MCuSi}_4\text{O}_{10}$ ($\text{M} = \text{Ca}, \text{Ba}$) with Cu^{2+} ions (blue) in square-planar environment. The coordination sphere of the M^{2+} ions (yellow) is extended to eight-coordination by binding to a neighboring layer (O red, Si green).

the holes and are arranged in rows. Eight-coordinate M^{2+} ions (Ca^{2+} , Ba^{2+}) occupy the remaining half of the hole sites and additionally interconnect two neighboring silicate sheets. The Cu^{2+} ions in both Egyptian and Chinese Blue have virtually identical environments. As the Cu^{2+} ions are the chromophores responsible for the blue color,^[23] both compounds show very similar color properties.

Comparing compositions, Chinese Purple ($\text{BaCuSi}_2\text{O}_6$) contains two equivalents of SiO_2 less than the blue compounds. It appears during the reaction leading to Chinese Blue and is therefore a kinetic product.^[6] Even though Chinese Purple also forms a layered arrangement, the structural motifs differ significantly from those of Egyptian and Chinese Blue. The condensation process to give silicate frameworks stops with the formation of islands of $\text{Si}_4\text{O}_{12}^{8-}$ rings; Cu_2 units hold these rings together to build up $\text{Cu}_2\text{Si}_4\text{O}_{12}^{4-}$ layers (Figure 4). Barium ions are located in

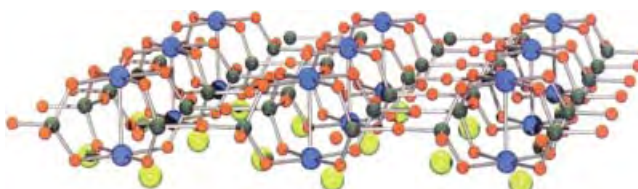


Figure 4. Layered structure of Chinese Purple $\text{BaCuSi}_2\text{O}_6$. The main feature is the Cu_2 unit (blue) which is held together by four bridging SiO_2 moieties from the four-membered silicate rings (Ba yellow, O red, Si dark green).

between the sheets and interconnect them in a way similar to that of Chinese Blue. The unusual and unique feature of this compound is the Cu–Cu bond with a bond length of 2.73 Å, very close to the reference compound copper acetate (Cu₂(acetate)₄, 2.64 Å).^[6, 18, 20] Thus, the early Chinese chemists—whether they deserve this title on closer inspection remains doubtful—were the first to prepare a chemical compound containing a metal–metal bond.

The instability of Chinese Purple is to a great extent attributable to the presence of the Cu–Cu bond. For example, the compound is sensitive not only to mineral acids but also to oxalic acid. This might be the reason why microorganisms that excrete oxalate or oxalic acid are suspected to contribute to the decay of works of art.^[24] Chinese Purple is also thermally less stable than Chinese Blue as it decomposes at 1200 °C within 4 hours to generate a green-black glass. It is likely that Chinese Blue is formed to some extent as the reactions in Equations (1) and (2) take place.^[6, 18]



Chinese Blue is stable under these conditions, but Egyptian Blue decomposes at 1000 °C^[7] to a green-black mixture of copper oxide, tridymite, and glass. This property sets strong restrictions to a successful syntheses of the compound because temperature control is required. It also caused in ancient times the need to develop special processing methods for the production of compact bodies of Egyptian Blue such as amulets, seals or bricks (Figure 5). As simple casting was not possible, these objects had to be made by complicated multistep sintering processes.



Figure 5. Amulet of dwarfish god Bes consisting of compact Egyptian Blue, 24th Dynasty (Property of the author).

3. Complex Experimentation

The ancient task of developing methods to produce Egyptian Blue, Chinese Blue, and Chinese Purple faced more than the general problems normally associated with chemical synthesis. In the case of Egyptian Blue the starting materials,

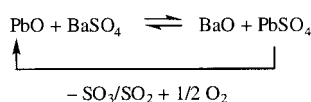
lime, sand, and copper minerals (azurite, malachite), were easily accessible in ancient times.^[7] In some places,^[25] azurite is even found as a mixture together with lime and sand. Such a three-component mixture might have been used directly for the synthesis, but how the preparations were developed remains unknown. We can only speculate that this favorable natural circumstance might have promoted the early chemical approaches. From our experience in chemistry today we know that any basic discovery by chance is only a first step towards useful products. Following the first discovery of Egyptian Blue, it was necessary to work out the stoichiometry of raw materials and flux additives for the pseudo-sintering process, as well as physical and chemical conditions for the synthesis. This was surely a tedious development lasting generations. However, it is important to note that, based on our own archeometric measurements as well as those of other groups, the composition of Egyptian Blue samples is quite constant over 4000 years. This indicates that it was soon realized how important it was to use constant proportions of the raw materials. For example, the blue pigment of Nefertete's crown has a composition very close to CaCuSi₄O₁₀.^[6] Nevertheless, some investigations have shown that ancient samples of Egyptian Blue often contain wollastonite (CaSiO₃), because too much lime and quartz were used.^[11]

The synthesis of Egyptian Blue became more efficient by the use of a flux additive. As independent experiments demonstrate, this also significantly enhances the quality of the product. Specifically, papyrus ash (consisting mainly of K₂CO₃), NaCl, and the ancient trona (a mixture of Na₂CO₃, Na₂SO₄, and NaCl from the Wadi Atrun)^[7, 9, 12] were used in ancient times. This important refinement of the production method was without doubt the result of lengthy empirical developments. Additionally, the synthesis requires a supply of air and a firing temperature between 800 and 900 °C. In the time of the Old Kingdom (3197–2778 BC) this was realized by blowing air in through pipes. Later this was replaced by bellows. Direct ways to measure the temperature (like thermometers) were unknown to ancient Egyptian civilizations so other criteria were relied upon to indicate whether the correct temperature had been reached. Since the production methods were empirical, specialized personnel was required for development and realization. As a result, a good technical “infrastructure” and a high degree of craftsmanship was necessary.

The production of Chinese Blue and Chinese Purple is even more complex than that for Egyptian Blue. One factor is that the phase diagram for BaO/CuO/SiO₂ shows at least four phases, so strict control of the amounts of the starting materials is necessary to obtain pure products. The two historically relevant phases that may be also found as mixtures have a Ba:Cu ratio of 1:1. It is unclear to what extent the formation of mixtures was planned to generate different color tones. The formation of mixtures may, however, happen independently of the raw-material stoichiometries, because BaCuSi₂O₆ is formed first as the kinetic product. BaCuSi₄O₁₀ is the product of a comparatively slow subsequent reaction. High temperatures (≈1000 °C) were needed to produce both pigments and this temperature had to be maintained for a significant time, in particular to obtain pure BaCuSi₄O₁₀.^[8, 17]

clearly, the synthesis required substantial technical demands, as it still does today.

The greatest problem for the production of Chinese Blue and Chinese Purple however was the barium source. Independent experiments have shown that the use of witherite (BaCO_3) leads to products of satisfactory quality, but witherite is very rare and was not readily available in ancient China. Nevertheless some samples indicate its use. If baryte (BaSO_4) is used in a mixture with quartz and copper minerals, only small amounts of blue or purple barium–copper silicates form.^[6, 14, 18] Chinese chemists nevertheless found a brilliant trick to circumvent these problems: they added lead salts (lead carbonate or lead oxide) that catalyze a dismutase reaction leading to the in situ decomposition of BaSO_4 (Scheme 1). Since PbSO_4 decomposes already at 1000°C (much lower than the 1560°C needed for BaSO_4 !), it is reasonable to assume that the PbO formed is performing catalysis, while BaO is removed from the equilibrium as Chinese Blue and Chinese Purple are formed.



Scheme 1. Decomposition of BaSO_4 with lead catalysis.

There is still no answer to the fundamental question as to why Chinese chemists considered including barium minerals into their syntheses. It is not an absolutely impossible idea to assume that these pigments were discovered in a totally independent way by applying the rare barium minerals. This is not very convincing though if an alternative theory is taken into account that will be presented in the following section. In either case, the use of barium minerals requires mineralogical knowledge to be aware that these substances are special materials. Some general interest in barium minerals related to glass production is recorded in China since the Warring States period.^[22, 26]

4. Technology Transfer

It was already mentioned that the use of Egyptian Blue had spread all over the Mediterranean area by the first millennium BC and was employed by many civilizations. Egyptian Blue of high quality was obtained at this time and as long as no compact bodies had to be produced, the physical and chemical conditions for the synthesis were relatively easy to attain. Additionally, the raw materials were easily available. The situation was fundamentally different for Chinese Blue and Chinese Purple at the beginning of the Warring States period. The syntheses of these color pigments were much harder concerning restrictions imposed by restraints from the stoichiometry, the more difficult physical conditions, and the availability of the raw materials. This explains why it seems quite unlikely that the invention of these pigments was accomplished in a convergent manner more or less *ab initio*. Knowledge about the many conditions for the syntheses, which includes the restrictions arising from the available raw

materials, had to merge together at the same time in one experiment to successfully generate the pigments.

On this basis, it seems more likely to assume that the production methods for Chinese Blue and Chinese Purple were developed stepwise and that they were based on the methods to produce Egyptian Blue. From today's perspective, the blue compounds only differ because of the chemically minor variation of the alkaline-earth metal. Considering the knowledge of the times, the modification of Egyptian Blue has to be viewed as a big step as there was no knowledge of atoms and molecules or even the periodic table. Therefore, a very tedious empirical approach was the only alternative.

Further facts support the hypothesis about the relationship between Egyptian Blue and the Chinese pigments. Two antique objects made from Egyptian Blue, a cup and a sistrum from Hasanlu in Iran,^[12, 27] both first of all demonstrate the use of this synthetic pigment in regions far to the East of Egypt. Additionally, these objects show a chemical variation of Egyptian Blue ($\text{CaCuSi}_4\text{O}_{10}$), since they at least to some extent contain the strontium analogue $\text{SrCuSi}_4\text{O}_{10}$.^[28] It seems quite reasonable that the replacement of calcium by strontium was not planned but instead happened by chance. But still it happened and most probably based on the knowledge about Egyptian Blue.

The question remains as to how knowledge about Egyptian Blue spread. It might have happened along the Silk Road which was the only existing link between the Mediterranean and the Far-East. Historians suppose that the Silk Road, that also passes through Iran, was used from at least 1000 BC. This is much earlier than the occurrence of Chinese Blue and Chinese Purple during the Warring States period. In principle, other similar transfer events give further support to this idea of a technology transfer along the Silk Road. However, in such other cases the information was transferred in the other direction from the Far-East to the Mediterranean. Examples include the transfer of knowledge about silk^[29] and paper^[30] production.

As was already shown, some difficulties with the barium–copper silicate chemistry could not be solved on the basis of Egyptian knowledge alone. Additionally, independent developments were required. The invention of Chinese Blue and Chinese Purple is therefore an admirable technical–chemical feat. The pigment syntheses are excellent examples of the positive influence of science and technology on society, in this case related to chemistry and accompanied by technology transfer. Focusing on ancient Egypt, this occurrence is a well known fact.^[31] Constantly striving for improvement is generally seen in the ancient Chinese civilization, as well.^[32]

Firstly, I would like to thank my partner during many of these studies, Dr. Hans-Georg Wiedemann, Stäfa, Switzerland, who introduced me to the field of ancient blue pigments. I would also like to thank professor Roald Hoffmann, Cornell University, Ithaca, USA, for encouraging me to write this article and for his many useful suggestions. Furthermore, I am indebted to Prof. Ernst Peter Fischer, Universität Konstanz, for work on the manuscript. Finally, I would like to acknowledge a number of scientific institutes and museums that made these studies possible by the loan of original samples. Without these

analyses the historical conclusions drawn in this article would not have been possible. I am furthermore grateful to Catharina Blänsdorf, Bayerisches Landesamt für Denkmalpflege, Munich, for the photographs of Figure 1.

- [1] H. Zollinger, *Color, a multidisciplinary approach*, Wiley-VCH, Weinheim, **1999**; M. Pastoreau, *Blue: the history of a color*, Princeton University Press, Princeton **2001**.
- [2] D. Reinen, G. G. Lindner, *Chem. Soc. Rev.* **1999**, 28, 75.
- [3] J. Marzahn, *Das Istar-Tor von Babylon*, Staatliche Museen zu Berlin—Preussischer Kulturbesitz, Philipp von Zabern, Mainz, **1995**; R. Koldewey, *Das wieder erstehende Babylon*, 5. Aufl., Beck, Munich, **1990**; *Handwerk und Technologie im Alten Orient: ein Beitrag zur Geschichte der Technik im Altertum*, Internat. Tagung Berlin 1991 (Ed.: R.-B. Wartke) Philipp von Zabern, Mainz, **1994**.
- [4] W. Noll, K. Angst, *Neues Jahrb. Mineral. Monatsh.* **1975**, 5, 209.
- [5] M. José-Yacamán, L. Rendon, J. Arenas, M. C. S. Puche, *Science* **1996**, 273, 223; D. Reinen, *Chem. Unserer Zeit*, **1996**, 30, 312.
- [6] H. G. Wiedemann, H. Berke, *Chemical and Physical Investigations of Egyptian and Chinese Blue and Purple*, *Proceedings of the Conf. Polychromy of the Terracotta Army of the First Chinese Emperor Qin Shihuangdi*, Xian, **1999**, p. 13.
- [7] G. Bayer, H. G. Wiedemann, *Sandoz Bulletin* **1976**, 40, 20.
- [8] H. G. Wiedemann, G. Bayer, A. Reller, *Actes de Table Ronde Ravello Edipuglia*, Bari, Italy, **1997**, p. 195.
- [9] J. Riederer in *Artists Pigments. A Handbook of their History and Characteristics*, Vol. 3 (Ed.: E. W. Fitzhugh), Oxford University Press, Oxford, **1997**, p. 23.
- [10] M. S. Tite, M. Bimson, M. R. Cowell, *Adv. Chem. Ser.* **1984**, 205, 215.
- [11] H. Jaksch, W. Seipel, K. L. Weiner, A. El Goresy, *Naturwissenschaften* **1983**, 50, 525.
- [12] W. T. Chase in *Science and Archeology* (Ed.: R. H. Brill), MIT Press, Cambridge, MA, **1971**, p. 80.
- [13] A. P. Laurie, W. F. P. McClintock, F. D. Miles, *Proceedings of the Royal Academy* **1914**, 89, 419.
- [14] S. Bouherour, H. Berke, H. G. Wiedemann, *Chimia*, **2001**, 55, 942.
- [15] P. J. Golas in *Science and Civilization in China*, Vol. 5 (Ed.: J. Needham) Cambridge University Press, Cambridge, U.K., **1999**.
- [16] E. W. FitzHugh, L. A. Zycherman, *Stud. Conserv.* **1983**, 28, 15; E. W. FitzHugh, L. A. Zycherman, *Stud. Conserv.* **1992**, 37, 145.
- [17] H. G. Wiedemann, G. Bayer in *Conservation of Ancient Sites on the Silk Road: Proceedings of an International Conference on the Conservation of Grotto Sites, Mogao Grottoes, Dunhuang, The People's Republic of China* (Ed.: N. Angnew), Los Angeles: Getty Conservation Institute, **1997**, p. 379.
- [18] H. Berke, H. G. Wiedemann, *EASTM* **2000**, 17, 94.
- [19] A. Pabst, *Acta Crystallogr.* **1959**, 12, 733.
- [20] L. W. Finger, R. M. Hazen, R. J. Hemley, *Am. Mineral.* **1989**, 74, 952; J. Janczak, R. Kubiak, *Acta Crystallogr. Sect. C* **1992**, 48, 1299.
- [21] C. Thieme, E. Emmerling, C. Herm, Y. Q. Wu, T. Zhou, Zh. Zhang in *Techna—Monographs in Material and Society 2, CIMTEC Conference Proceedings, Florence, Italy July 1994* (Ed.: P. Vincenzini), Faenza, **1995**, p. 591; C. Herm, C. Thieme, E. Emmerling, Y. Q. Wu, T. Zhou, Zh. Zhang, *Techna—Monographs in Materials and Society 2, CIMTEC Conference Proceedings, Florence, Italy July 1994* (Ed.: P. Vincenzini), Faenza, **1995**, p. 675.
- [22] R. H. Brill, S. S. C. Tong, D. Dohrenwend, in *Scientific Research in Early Chinese Glass* (Eds.: R. H. Brill, J. H. Martin), The Corning Museum of Glass, **1991**, p. 31.
- [23] D. Ajo, G. Pozza, G. Chiari, F. De Zuane, M. Favaro, *Journal of Cultural Heritage* **2000**, 1, 393.
- [24] H. G. Wiedemann, A. Reller, I. Lamprecht, *Proc. II. Internat. Symposium: The oxalate films in the conservation of works of art*, Milan, **1996**, p. 355.
- [25] L. Heck, *Metalla (Bochum)* **1999**, 6.1, 13.
- [26] J. Needham, *Science and Civilization in China, Part III, Vol. 5*, Cambridge University Press, Cambridge, U.K., **1976**.
- [27] O. W. Muscarella, *The Metropolitan Museum of Art Bulletin* **1966**, 25, 121.
- [28] H. G. Wiedemann, E. Doehne, D. Stulik, F. D. Preusser, *Proc. 28th Intern. Symposium on Archeometry, 1992*, Los Angeles, CA, **1992**, 143.
- [29] H. G. Wiedemann, *Chinesische Seide*, Wiedemann c/o Mettler Instrumente AG, Greifensee, Switzerland, **1984**; W. Cheng, *History of Textile Technology of Ancient China*, New York, USA, **1992**; A. A. Ierusalimskaja, B. Borkopp, *Von China nach Byzanz: frühmittelalterliche Seiden aus der Staatlichen Ermitage Sankt Petersburg*, Bayerisches Nationalmuseum, Munich, Germany **1996**; J. C. Y. Watt, A. E. Wardwell, *When silk was gold: Central Asian and Chinese textiles*, Abrams, New York, USA, **1996**.
- [30] W. E. Scott, J. C. Abbott in collaboration with S. Trosset, *Properties of paper: an introduction*, Tappi Press, Atlanta, USA, **1995**.
- [31] M. Clagett, *Ancient Egyptian Science, Vol. 1*, American Philosophical Society, Philadelphia, USA, **1989**.
- [32] J. Needham, *Science and Civilization in China, Part I—XIII*, Cambridge University Press, Cambridge U.K., **1974–1999**.

The Diazonamides: The Plot Thickens**

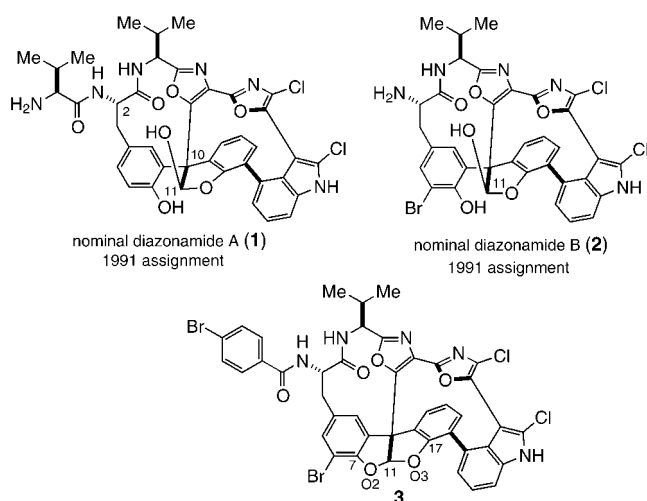
Tobias Ritter and Erick M. Carreira*

The role of total chemical synthesis as a tool for the structure elucidation of natural products has been largely supplanted by X-ray crystallographic and NMR spectroscopic methods. For the most part, in this respect, synthesis has remained indispensable only as a means to confirm absolute or relative stereochemical assignments, in particular when the imprimatur of an X-ray crystallographic assignment is absent. Thus, it seems quite striking that, in this day and age, synthesis studies lead to a significant structural revision of a new class of biologically active natural products. The disclosure in 1991 of diazonamides A and B (Scheme 1) immediately aroused the attention of the scientific community as a consequence of the unusual structures of these natural products and their impressive activity against human cancer-cell lines. That the structure elucidation was carried out using modern spectroscopic means and was crowned by X-ray crystallographic analysis of a simple derivative of diazon-

amide B (**3**) would seem to have foreclosed any doubt on the assignment and provided a green light to subsequent studies, focused exclusively on devising a workable synthesis strategy. The synthetic community rose to the challenge, crafting a number of innovative strategies to key intermediates to the presumed structure of diazonamides A and B.^[1]

Recently, Harran and co-workers at South Western Medical Center at Dallas documented the successful synthesis of **1**.^[2] Not only is their strategy notable for its innovation and expediency, but also for an important revelation: the structure of diazonamides was incorrectly assigned. Herein we provide a brief account of the synthetic work by Harran as well as the accompanying detective work which allowed the subsequent corrected assignment to be made.^[3] Moreover, despite the fact that, in retrospect, the assigned structure was incorrect, analysis of the studies reported and strategies developed to date are included, as there is much to be learned from them. These include the strategies documented by the groups of Magnus,^[4] Nicolaou,^[5] Vedejs,^[6] Wipf,^[7] and Wood.^[8]

The piquant story commences with the isolation of diazonamides A and B from the colonial ascidian *Diazona chinensis*. Diazonamide A possesses potent in vitro activity against HCT-116 human colon carcinoma and B-16 marine melanoma cancer-cell lines (IC₅₀ values less than 15 ng mL⁻¹).^[9] Transformation of diazonamide B to the corresponding *p*-bromobenzamide **3** provided a crystalline derivative suitable for X-ray crystallographic analysis. The diphenylacetal group in **3** was thought to result from the net dehydration occurring during derivatization. On the basis of a small coupling of the C11 proton to a D₂O-exchangeable proton, diazonamide B was thus assigned as the hemiacetal at the C11 atom. The spectroscopic similarity in ¹H and ¹³C NMR, UV, and IR spectra indicated the same polycyclic nucleus for the diazonamide A framework. Incorporation of a valine residue at the C2 amino group reconciles the proposed structure with the observed high-resolution mass spectrum, in which it had also been assumed that, during HRMS measurement, loss of water converts the hemiacetal into the acetal. Given the spectroscopic data amassed, the structural assignment was deemed to be established fact. The shortage of natural material with which to perform further pharmacological studies as well as the unprecedented molecular architecture, whose retrosynthetic deconvolution and subsequent reconstitution would result in innovative reactions, render the diazonamides ideal targets for synthesis studies. The



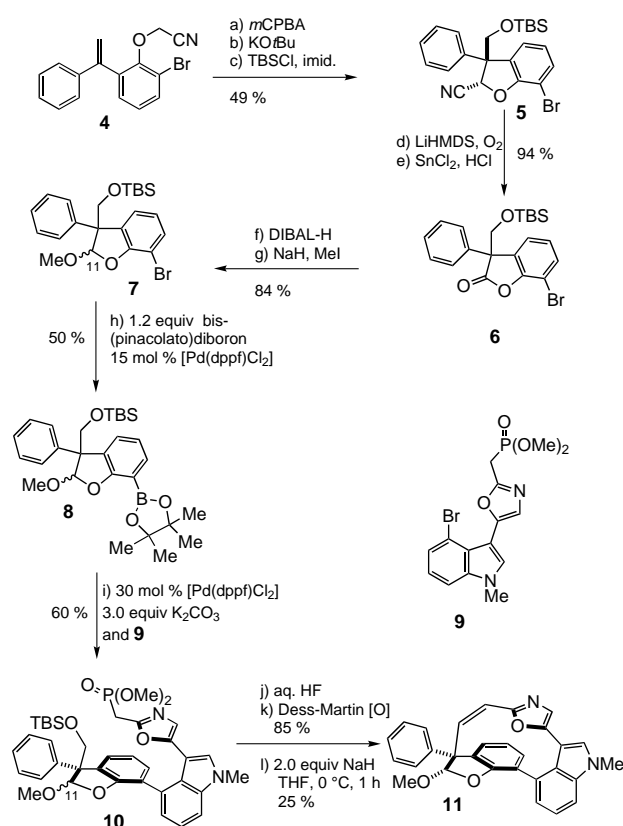
Scheme 1. Original assignments of the structures of nominal diazonamides A (**1**) and B (**2**) as well as the crystallographically determined structure of the *p*-bromobenzamide derivative **3**.

[*] Prof. Dr. E. M. Carreira, T. Ritter
Laboratorium für Organische Chemie
ETH Hönggerberg, HCI, 8093 Zürich (Switzerland)
Fax: (+41)1-632-1328
E-mail: carreira@org.chem.ethz.ch

[**] We are grateful to the Fonds der Chemischen Industrie for providing a Kekulé Stipendium to T.R.

key problems associated with the core stem from the halogenated heterocyclic framework found in a single atropisomeric form and the triaryl acetaldehyde at its epimer center at the C10 atom.

The construction of the quaternary C10 center and the heterocyclic core in a single atropisomeric form was addressed in an early model system by Nicolaou (Scheme 2). Treatment



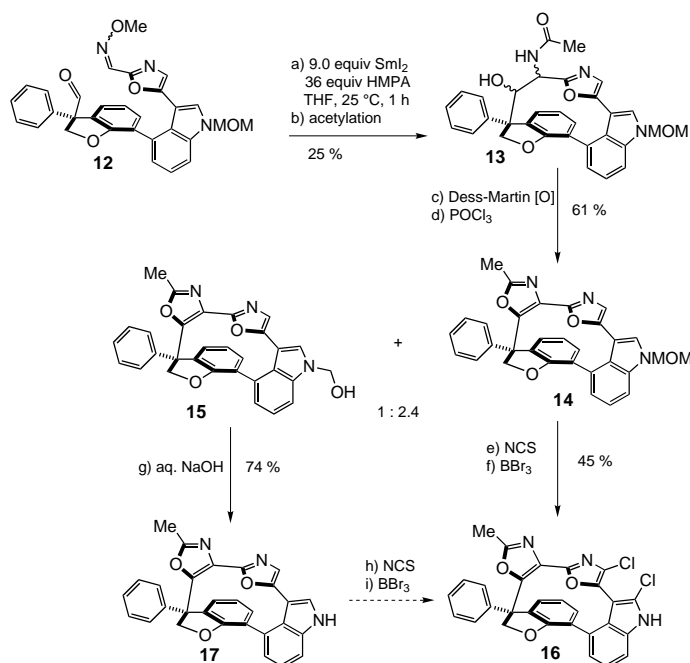
Scheme 2. Horner–Wadsworth–Emmons cyclization strategy (Nicolaou et al.).

of diaryl alkene **4** with *m*CPBA affords an epoxide which subsequently undergoes regioselective nucleophilic 5-*exo-tet* opening^[10] by the nitrile enolate to furnish a cyanoalcohol which is protected to yield **5**. Following oxidation to the benzofuranone **6** and lactone semireduction, methylation proceeds to give **7** as a stereoisomeric mixture. As subsequently observed, see below, the stereochemistry of the lactol was critical in the subsequent macrocyclization.

After converting the aryl bromide **7** into the boronate **8** using the method developed by Ishiyama et al.,^[11] Suzuki coupling of **8** to the phosphonate **9** affords **10** in 30% overall yield from **7**, as a mixture of four isomers which arises from C11 epimers and atropisomerism. The protected alcohol group in **10** is converted into the corresponding aldehyde, which undergoes Horner–Wadsworth–Emmons cyclization at 0 °C to give the desired macrocycle **11** as a single atropisomer and a single epimer at the C11 center in 25% yield. It is interesting to note that only one of the diastereomeric starting aldehydes participates in the ring closure. Thus, in analogy with the classic synthesis of erythronolide,^[12] the

success or failure of the macrocyclization is coupled to stereochemical features of the intervening chain.

In a subsequent approach, Nicolaou et al. examined a strategy in which ring closure is effected using an intramolecular pinacol cyclization reaction of an aldehyde and an oxime (Scheme 3). To avoid the problems observed in the

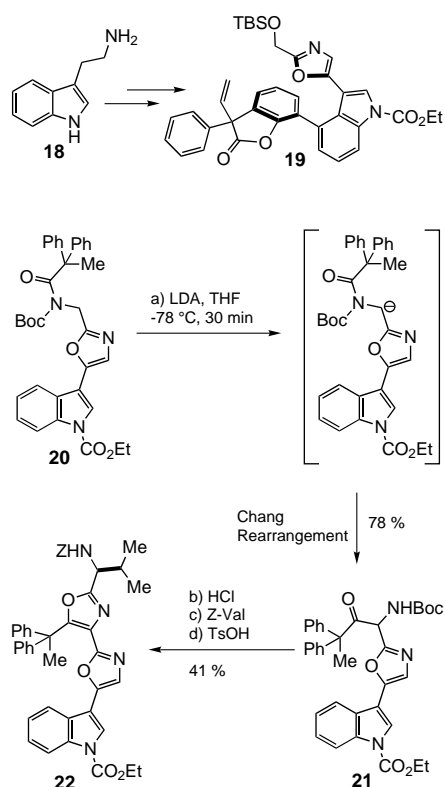


Scheme 3. Pinacol–cyclization strategy (Nicolaou et al.).

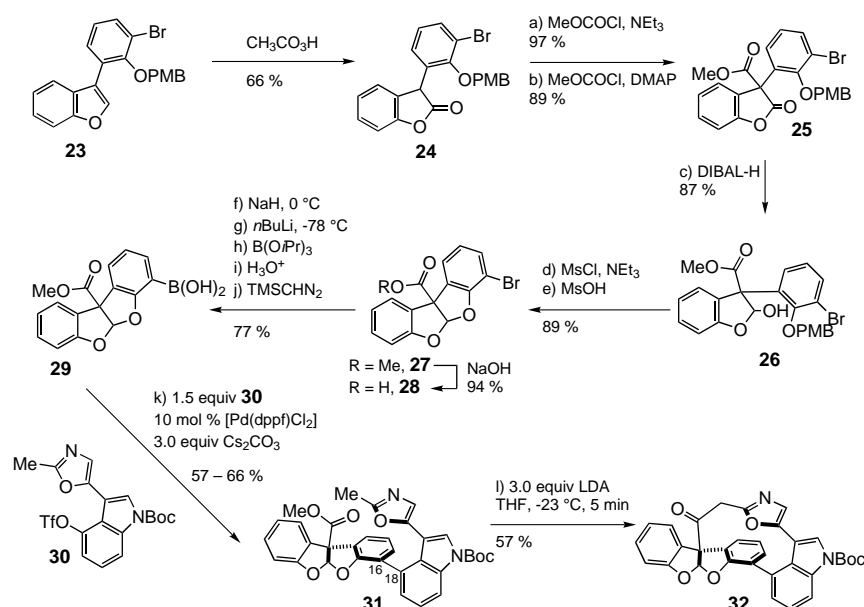
earlier route arising from the stereochemistry at the C11 center, the dihydrobenzofuran **12** was synthesized. Treatment of the aldehyde/oxime with SmI_2 in HMPA/THF gives an aminoalcohol, which on *N*-acetylation furnishes **13** in 25% overall yield. Oxidation and oxazole formation provides **14** and **15** as a 2.4:1 mixture. Chlorination and indole deprotection of **14** provides **16** in 45%. Conversion of **15** into **17** (74% yield) gives access to additional quantities of **16**.

In the route of Wipf et al., a related disconnection plan is envisioned for the construction of the macrocycle, albeit with a distinct, innovative approach to the precursors (Scheme 4). After establishing a synthesis of benzofuranone **19**, Wipf utilizes a clever application of the Chang rearrangement^[13] to afford the protected amino ketone **21**, which is subsequently converted into the requisite oxazole. Thus, deprotonation of **20** at -78°C with LDA cleanly provides aminoketone **21** in superb yield (78%) through smooth rearrangement of the intermediate carbanion. In the three steps that follow, bisoxazole **22** is efficiently obtained.

In the approach of Vedejs et al., the same region of the molecule is chosen for retrosynthetic unraveling of the macrocycle, which in the synthetic direction relies on a Dieckmann-like cyclization reaction (Scheme 5). The preparation of the cyclization precursor commences with oxidation of **23** and acylation of the resulting **24** with methylchloroformate (57% yield) using the method of Black et al.,^[14] a

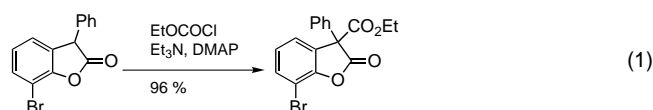


Scheme 4. Modified Chang rearrangement (Wipf et al.).



Scheme 5. Imino-Dieckmann cyclization (Vedejs et al.).

synthetic step similar to that documented by Moody et al. in simple model studies toward the diazonamides [Eq. (1)].^[15]



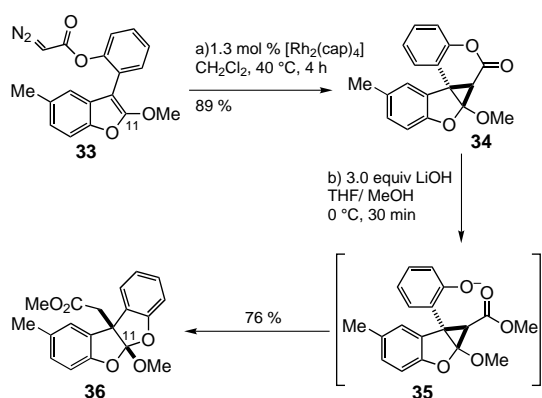
Chemoselective reduction of the resulting lactone **25**, mesylation, and subsequent treatment with methanesulfonic

acid furnishes the requisite dibenzoacetal **27** in 77% yield. The required aryl boronic acid **29** is prepared in 72% overall yield from **27** by saponification of the methyl ester, halogen–lithium exchange and treatment with triisopropyl borate, hydrolysis of the boronic ester, and reintroduction of the methyl ester. In the subsequent Suzuki coupling, aryl boronic acid **29** is allowed to react with aryl triflate **30** by utilizing catalytic [Pd(dppf)Cl₂] and Cs₂CO₃ as the base. The use of this base led to significant rate acceleration and improved yields to 57–66%. NMR spectroscopic studies reveal that the two atropisomers interconvert at room temperature, with a value for the barrier of rotation around the C16–C18 biaryl axis of $\Delta G^\ddagger = 15.5 \text{ kcal mol}^{-1}$. This result is noteworthy, considering the lack of ready interconversion at room temperature between atropisomers **10** in an earlier synthesis (Scheme 2). Treatment of **31** with LDA leads to the Dieckmann-like reaction, which furnishes the expected macrocycle **32** in 57% yield as a single atropisomer. X-ray crystallographic analysis established that the cyclization affords an intermediate with the desired stereochemistry.

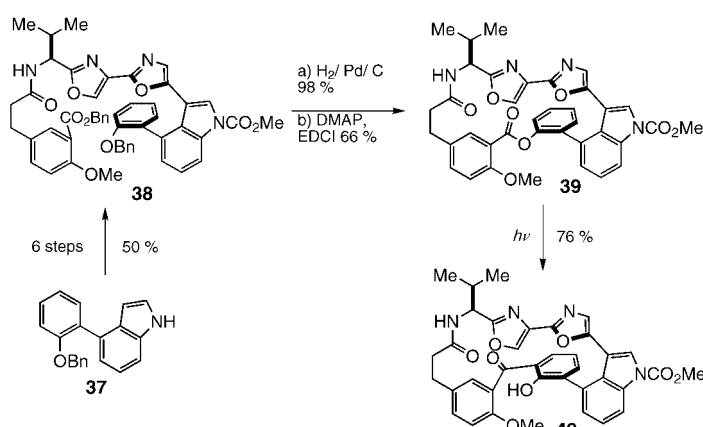
In the studies of Nicolaou and Vedejs discussed above, enolate chemistry was relied upon for the installation of the quaternary center at C10; by contrast Wood et al. documented a clever and elegant approach in a model study. Intramolecular cyclopropanation of a benzofuran, followed by an anion-induced ring fragmentation, leads to a key structure (Scheme 6). The diazoacetate **33** is subjected to rhodium(II)-catalyzed cyclopropanation to afford pentacycle **34** in excellent yield (89%). Subsequent treatment of **34** with LiOH initiates ring opening and rearrangement to the orthoester **36**, which incorporates the requisite quaternary center. The use of a transition-metal-catalyzed cyclopropanation reaction opens the possibility to prepare the key precursors in an optically active form; indeed, preliminary work using Doyle's catalyst^[16] revealed that the optically active cyclopropane **34** can be formed in 45% *ee*.

A significant departure from the macrocyclization strategies that involve carbanionic intermediates is proffered by the bold, innovative strategy developed by Magnus et al.

In this approach, photo-Fries rearrangement of **39** was used for the construction of the diazonamide framework. The precursor lactone **39** is efficiently synthesized in only eight linear steps from indole **37** (Scheme 7). Following debenzoylation of **38** (98%), the macrolactone **39** was obtained, by using the Keck modification^[17] of the Steglich esterification^[18] procedure, in 66% yield, as a 1.5:1 mixture of atropisomers. The macrolactone underwent photo-rearrangement to afford **40** as two atropisomers (2:1) in 76% yield.



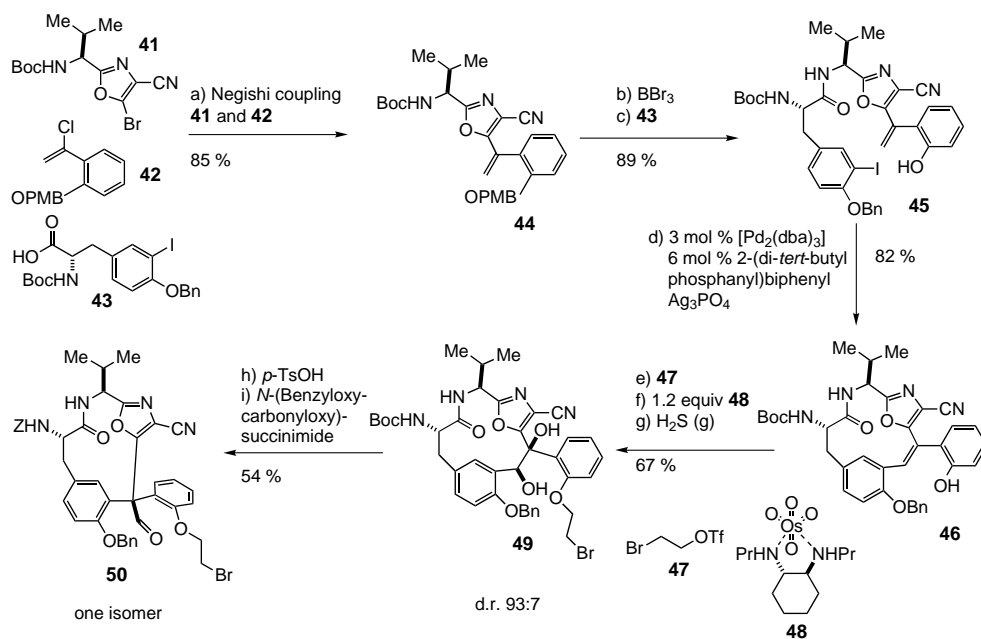
Scheme 6. Cyclopropanation–ring-opening strategy (Wood et al.).



Scheme 7. Photo-Fries rearrangement strategy (Magnus et al.).

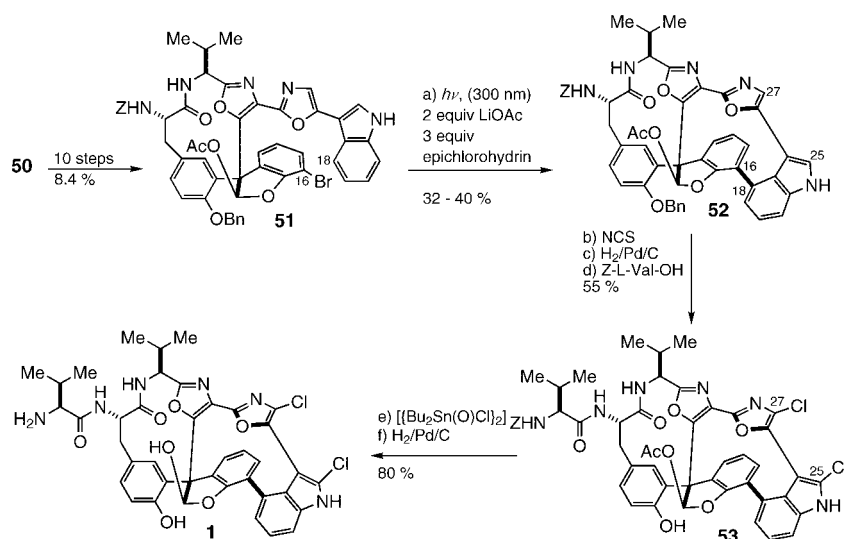
In the Harran approach, the problem of forming the macrocycle is efficiently tackled by focusing on the triaryl acetaldehyde epicenter. In this elegant, imaginative strategy, introduction of the core macrocycle is effected in a highly convergent manner by construction of the bond-linking rings **E** and **F** (Scheme 1), by proceeding from advanced, densely functionalized fragments. The selection of this key bond disconnection was critical, leading to the successful development of a synthesis of the nominal diazonamide **A** (**1**).

The bromooxazole **41** and the vinylchloride **42** were coupled by use of a Negishi coupling reaction^[19] in 85% yield (Scheme 8). Following removal of the *N*-Boc- and *O*-PMB protecting groups, the iodotyrosine derivative **43** participated in amide-bond formation to furnish **45**. In the ring-closing reac-

Scheme 8. Early steps of the total synthesis of nominal **1** (Harran et al.).

tion, Heck coupling of the iodoolefin **45** afforded the macrocyclic framework **46** in a remarkable 82% yield. An important observation from the study of the cyclization reaction is that the use of 2-(di-*tert*-butylphosphanyl)biphenyl generated a robust Pd complex that allows the reaction to be executed with low catalyst loading; moreover, all other phosphane ligands used inhibit the reaction. A working hypothesis that guided the development of the successful cyclization is a mechanistic model in which macrocyclization is facilitated by proceeding from **45** through a preorganized intermediate involving a palladium(II) phenoxide. After derivatization of the phenol **46** as its 2-bromoethyl ether, the latter was treated with the dihydroxylation reagent **48**, (formed with OsO₄ and (1*S*,2*S*)-*N,N'*-bis(3,3-dimethylbutyl)cyclohexane-1,2-diamine^[20]) to afford the glycol **49** in 67% overall yield. The use of this osmium reagent is necessary to override the intrinsic bias of the molecule to undergo dihydroxylation with opposite-face selectivity and to ensure that the correct stereochemistry is established (93:7 d.r.). Pinacol rearrangement of the diol **49** under acidic conditions then furnished the triaryl acetaldehyde **50** as a single stereoisomer in excellent yield (54%) after amine carbamoylation.

Conversion of the nitrile into the desired substituted oxazole, along with the necessary functionalization of the core, was effectively carried out (ten steps, 8.4% yield) to give the aryl bromide **51** (Scheme 9). This aryl bromide is then the precursor for a second macrocyclization reaction which is carried out by a clever application of the photochemical method developed by Witkop et al.^[21] A possible reaction pathway is an intramolecular photoinduced electron transfer from the indole chromophore to the adjacent bromoarene and biradical collapse to form the C16–C18 bond. It has to be pointed out that this macrocyclization, which is carried out in 32–40% yield, forms **52** as a single atropisomer, thus the asymmetry associated with the diazonamide polycycle follows



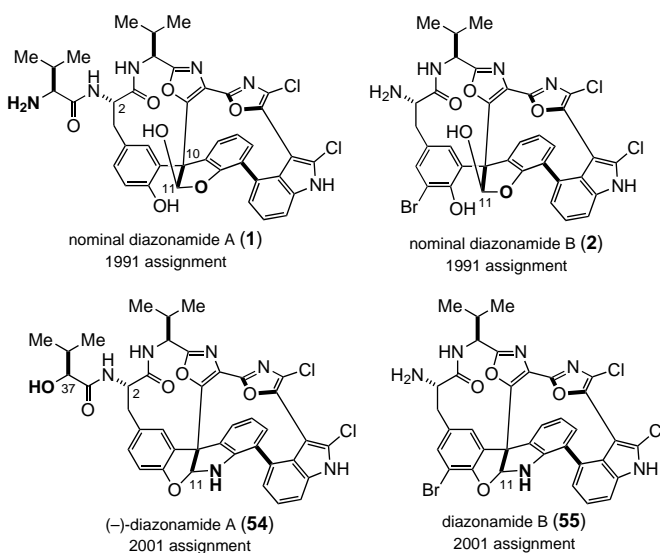
Scheme 9. Late steps of the total synthesis of nominal **1** (Harran et al.).

from the stereochemical control in the early steps of the route. Chlorination of **52** with *N*-chlorosuccinimide at C27 and C25 proceeded smoothly. Stannoxane-catalyzed deacetylation of the acetyl hemiacetal and final hydrogenolysis (80%) culminated in the total synthesis of the nominal diazonamide **A** (**1**).

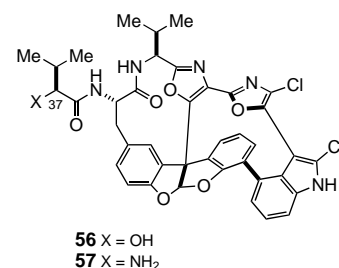
Surprisingly, subsequent structural analysis revealed that the material obtained from the synthesis study differed from that isolated from natural sources. Thus, both the ^1H NMR spectrum and the notable chemical instability of the synthetic material were telling; the synthetic material consists of a 4:1 mixture of C11 lactol epimers, a feature that was not observed with the natural product. Moreover, in contrast to the behavior of diazonamide A, the susceptibility of the synthetic material to degradation prevented further detailed characterization. Harran et al. reasoned that a correct structure for diazonamide A would need to reconcile the observed exact mass of 765.1998 amu with a closely related polycyclic framework. Careful reexamination of the original characterization procedure was critical, as acidic hydrolysis of diazonamide A had not yielded valine as anticipated.^[22] Thus, the first feature that seemingly had to be corrected was the fact that the C2 side chain of diazonamide A might have been misassigned. Detailed NMR spectroscopic analysis then suggested that the C2 side chain incorporates a hydroxy group rather than an amino group, as originally assigned. This $\text{NH}_2 \rightarrow \text{OH}$ exchange requires a adjustment to correct for the corresponding 1-Dalton increase in molecular mass.

In an impressive logical breakthrough, it was reasoned that the observed exact mass of 743.0340 amu for natural diazonamide B (**55**) is more consistent with the molecular formula of $\text{C}_{35}\text{H}_{25}\text{N}_6\text{O}_4\text{Cl}_2\text{Br}$ ($[M^+ + \text{H}] = 743.0576$) than with the mass corresponding to the structure originally assigned to diazonamide B (**2**) ($[M + \text{H}]^+ - \text{H}_2\text{O} = 744.0416$) with the formula $\text{C}_{35}\text{H}_{26}\text{N}_5\text{O}_6\text{Cl}_2\text{Br}$. This can be reconciled with the crystallographic data if a protonated nitrogen atom in diazonamide B

was mistaken for an oxygen atom. Careful analysis of the X-ray crystallographic data is revealing: the observed C7–O2 bond length of 1.371 Å does not deviate from common aryl C–O bond lengths, whereas the length of the C17–O3 bond (1.433 Å) is longer than the maximal value (1.409 Å) observed for similar bond types. The large thermal motion of the O3 atom also suggests an element with fewer electrons and a larger covalent radius. Based on these results and on a ^1H – ^{15}N NMR correlation spectrum (HSQC) of diazonamide A, Harran et al. then concluded that the structure of the diazonamides is more properly assigned as the C11 diaryl aminoral. Thus structures **54** and **55** are most consistent with the available data. Of course, the absolute stereochemistry of the α -hydroxy acid side chain at C2 remains to be assigned, a feature which current synthetic efforts will surely secure.

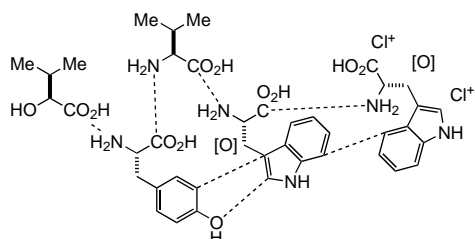


Given the fact that, within experimental error, model compound **56** (prepared from (*S*)-hydroxy isovaleric acid) and diazonamide A (**54**) are equipotent in in vitro cytotoxicity assays, Harran has suggested that the natural product is of the *S* configuration at the C37 center. The synthetic alcohol **56** is about 16 times more potent than its C37 epimer and more than 50 times more potent than the corresponding amine **57** in



the inhibition of the growth of human ovarian adenocarcinoma OVCAR-3 in vitro.

While analyzing the correct structure of diazonamide A, Harran et al. have speculated about its biosynthesis. Retro-spectively, it is plausible that the diazonamide polycycle is biosynthetically constructed from four natural amino acids (Scheme 10). In this respect, the core can be traced back to an oxidized ditryptophan unit which is oxidatively coupled to a tyrosine residue.



Scheme 10. Biosynthesis proposed by Harran et al. [O] = oxidation.

The scientific merit of the studies by various research groups outlined above rests above all in the discoveries and contributions made in the field of synthetic methods. However, one cannot help but also confess some amazement: The diazonamide story reminds us that the synthetic chemistry of natural products at the cutting edge can be counted on to have surprises in store for its practitioner, not only in the hidden treasures it reveals but also in the impact on biology. The revised structures will again challenge organic chemists as targets for synthesis. The modular aspects of the strategies reported to access the nominal diazonamides are certainly flexible enough to provide potential access routes to the natural product. However, anyone who has partaken in a synthetic challenge of this magnitude knows that even the slightest structural change in an advanced intermediate of a synthetic route can have substantial repercussions for the success or failure of the route. The $\text{NH}_2 \rightarrow \text{OH}$ exchange in the revised diazonamide structure cannot be considered trite, and one can look forward to continuing studies into this synthetic challenge and its culmination.

Abbreviations

cap	caprolactamate
mCPBA	meta-chloroperbenzoic acid
dba	trans,trans-dibenzylideneacetone
Dess–Martin [O]	Dess–Martin periodinane
DIBAL-H	diisobutylaluminum hydride
DMAP	4-dimethylaminopyridine
DMF	N,N-dimethylformamide
DMSO	dimethylsulfoxide
dppf	1,1'-bis(diphenylphosphanyl)ferrocene
EDCI	1-(3-dimethylaminopropyl)-3-ethylcarbodiimide hydrochloride
HMPA	hexamethylphosphoramide
imid.	imidazole
LDA	lithium diisopropylamide

LiHMDS	lithium hexamethyldisilazide
MOM	methoxymethyl
Ms	methanesulfonyl
MS	molecular sieves
NCS	N-chlorosuccinimide
PMB	p-methoxybenzyl
TBAF	tetra-n-butylammonium fluoride
TBSCl	tert-butyldimethylsilyl chloride
TMS	trimethylsilyl
TsOH	p-toluenesulfonic acid
Z	benzyloxycarbonyl

- a) M. C. Bagley, C. J. Moody, A. G. Pepper, *Tetrahedron Lett.* **2000**, *41*, 6901–6904; b) M. C. Bagley, S. L. Hind, C. J. Moody, *Tetrahedron Lett.* **2000**, *41*, 6897–6900; c) F. Lach, C. J. Moody, *Tetrahedron Lett.* **2000**, *41*, 6893–6896; d) A. Boto, M. Ling, G. Meek, G. Pattenden, *Tetrahedron Lett.* **1998**, *39*, 8167–8170; A. Radspieler, J. Liebscher, *Synthesis* **2000**, 745–750; H. C. Hang, E. Drotleff, G. I. Elliot, T. A. Ritsema, J. P. Konopelski, *Synthesis* **1999**, 398–400; J. P. Konopelski, J. M. Hottenroth, H. M. Oltra, E. A. Veliz, Z. C. Yang, *Synlett* **1996**, 609–611.
- a) J. Li, S. Jeong, L. Esser, P. G. Harran, *Angew. Chem.* **2001**, *113*, 4901–4904; *Angew. Chem. Int. Ed.* **2001**, *40*, 4765–4770; b) J. Li, X. Chen, A. W. G. Burgett, P. G. Harran, *Angew. Chem.* **2001**, *113*, 2754–2757; *Angew. Chem. Int. Ed.* **2001**, *40*, 2682–2685; c) X. Chen, L. Esser, P. G. Harran, *Angew. Chem.* **2000**, *112*, 967–970; *Angew. Chem. Int. Ed.* **2000**, *39*, 937–940; d) S. Jeong, X. Chen, P. G. Harran, *J. Org. Chem.* **1998**, *63*, 8640–8641.
- J. Li, A. W. G. Burgett, L. Esser, C. Amezcua, P. G. Harran, *Angew. Chem.* **2001**, *113*, 4906–4909; *Angew. Chem. Int. Ed.* **2001**, *40*, 4770–4773.
- a) P. Magnus, C. Lescop, *Tetrahedron Lett.* **2001**, *42*, 7193–7196; b) J. D. Kreisberg, P. Magnus, E. G. McIver, *Tetrahedron Lett.* **2001**, *42*, 627–629; c) P. Magnus, E. G. McIver, *Tetrahedron Lett.* **2000**, *41*, 835–838; d) F. Chan, P. Magnus, E. G. McIver, *Tetrahedron Lett.* **2000**, *41*, 831–834; e) P. Magnus, J. D. Kreisberg, *Tetrahedron Lett.* **1999**, *40*, 451–454.
- a) K. C. Nicolaou, S. A. Snyder, K. B. Simonsen, A. E. Koumbis, *Angew. Chem.* **2000**, *112*, 3615–3620; *Angew. Chem. Int. Ed.* **2000**, *39*, 3473–3478; b) K. C. Nicolaou, X. Huang, N. Giuseppone, P. Bheema Rao, M. Bella, M. V. Reddy, S. A. Snyder, *Angew. Chem.* **2001**, *113*, 4841–4845; *Angew. Chem. Int. Ed.* **2001**, *40*, 4705–4709.
- a) E. Vedejs, M. A. Zajac, *Org. Lett.* **2001**, *3*, 2451–2454; b) E. Vedejs, D. A. Barda, *Org. Lett.* **2000**, *2*, 1033–1035; c) E. Vedejs, J. Wang, *Org. Lett.* **2000**, *2*, 1031–1032.
- a) P. Wipf, J. L. Methot, *Org. Lett.* **2001**, *3*, 1261–1264; b) P. Wipf, F. Yokokawa, *Tetrahedron Lett.* **1998**, *39*, 2223–2226.
- D. E. Fuerst, B. M. Stoltz, J. L. Wood, *Org. Lett.* **2000**, *2*, 3521–3523.
- N. Lindquist, W. Fenical, G. D. Van Duyne, J. Clardy, *J. Am. Chem. Soc.* **1991**, *113*, 2303–2304.
- G. Stork, L. D. Cama, D. R. Coulsen, *J. Am. Chem. Soc.* **1974**, *96*, 5268–5270.
- T. Ishiyama, M. Murata, N. Miyaara, *J. Org. Chem.* **1995**, *60*, 7508–7510.
- R. B. Woodward, E. Logusch, K. P. Nambiar, K. Sakan, D. E. Ward, B.-W. Au-Yeung, P. Balaram, L. J. Browne, P. J. Card, C. H. Chen, R. B. Chênevert, A. Fliri, K. Frobel, H.-J. Gais, D. G. Garratt, K. Hayakawa, W. Heggie, D. P. Hesson, D. Hoppe, I. Hoppe, J. A. Hyatt, D. Ikeda, P. A. Jacobi, K. S. Kim, Y. Kobuke, K. Kojima, K. Krowicki, V. J. Lee, T. Leutert, S. Malchenko, J. Martens, R. S. Matthews, B. S. Ong, J. B. Press, T. V. Rajan Babu, G. Rousseau, H. M. Sauter, M. Suzuki, K. Tatsuta, L. M. Tolbert, E. A. Truesdale, I. Uchida, Y. Ueda, T. Uyehara, A. T. Vasella, W. C. Vladuchick, P. A. Wade, R. M. Williams, N.-C. Wong, *J. Am. Chem. Soc.* **1981**, *103*, 3213–3215.
- S. D. Lee, T. H. Chan, K. S. Kwon, *Tetrahedron Lett.* **1984**, *25*, 3399–3402.
- T. H. Black, S. M. Arrivo, J. S. Schumm, J. M. Knobloch, *J. Org. Chem.* **1987**, *52*, 5425–5430.

- [15] C. J. Moody, K. J. Doyle, M. C. Elliott, T. J. Mowlem, *J. Chem. Soc. Perkin Trans. 1* **1997**, 16, 2413–2419.
- [16] M. P. Doyle, D. C. Forbes, *Chem. Rev.* **1998**, 98, 911–935.
- [17] E. P. Boden, G. E. Keck, *J. Org. Chem.* **1985**, 50, 2394–2395.
- [18] B. Neises, W. Steglich, *Angew. Chem.* **1978**, 90, 556–557; *Angew. Chem. Int. Ed. Engl.* **1978**, 17, 522–524.
- [19] T. Takahashi, M. Kotori, R. Fisher, Y. Nishihara, K. Nakajima, *J. Am. Chem. Soc.* **1995**, 117, 11039–11040.
- [20] S. Hanessian, P. Meffre, M. Girard, S. Beaudoin, J.-Y. Saneau, Y. Bennani, *J. Org. Chem.* **1993**, 58, 1991–1993.
- [21] a) O. Yonemitsu, P. Cerutti, B. Witkop, *J. Am. Chem. Soc.* **1966**, 88, 3941–3945; b) H. G. Theuns, H. B. M. Lenting, C. A. Salemink, H. Tanaka, M. S. Shibata, K. Ito, R. J. J. C. Lousberg, *Heterocycles* **1984**, 22, 2007–2011.
- [22] N. Lindquist, Dissertation, University of California (San Diego, USA), **1989**.

Encapsulated Lanthanides as Luminescent Materials

Huib Maas, Antonio Currao, and Gion Calzaferri*

Dedicated to Professor Roald Hoffmann on the occasion of his 65th birthday

Materials which embed organic dyes, rare earth ions, complexes, or quantum dots in a matrix with specifically tailored chemical and optical properties provide a challenging approach to novel chemical and optical applications. These materials have the potential to be used in microoptics, optoelectronics, laser materials, solar cells, sensors, battery electrodes, and photocatalysis. In this article we focus on lanthanides encapsulated in zeolites, glass films derived from sol–gel processes, and semiconductors.

The research work on the unique luminescent properties of rare earth elements hosted in different matrixes is strongly motivated by their technological importance in optoelectronic devices.^[1] The materials emit over the entire spectral range of interest: near infrared (NIR; Nd³⁺, Er³⁺), red (Eu³⁺, Pr³⁺, Sm³⁺), green (Er³⁺, Tb³⁺), and blue (Tm³⁺, Ce³⁺). Their optical transitions involve 4f orbitals, which are well shielded from their chemical environment by 5s² and 5p⁶ electrons. The f–f transitions are parity forbidden and, as a result, the absorption coefficients are very low and the emissive rates are slow, which results in long-lived and linelike emission bands. As a consequence, direct excitation of the lanthanide ions is unfavorable. The comparatively fast thermal relaxation of the excitation energy is a problem when using lanthanide ions for luminescence. This nonradiative relaxation may occur by interaction of the electronic levels of the lanthanide ion with suitable vibrational modes of the environment.^[2] The efficiency of these processes depends on the energy gap between the ground and excited states as well as the vibrational energy of the oscillators. For example,

when solvents containing OH groups are coordinated to lanthanide ions, efficient nonradiative deactivations take place through vibronic coupling with the vibrational states of the OH oscillators. Replacement of the OH oscillators by low-frequency OD oscillators, diminishes the vibronic deactivation pathway.^[3] Different ways to overcome the difficulties of low absorptivity and thermal relaxation have been used. We show the apparently most important ones in Figure 1:

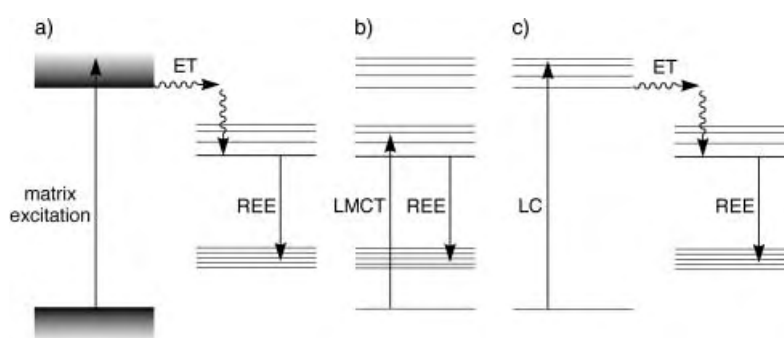


Figure 1. Three paths to efficient lanthanide luminescence (ET = energy transfer; REE = rare earth emission; LMCT = ligand → metal charge transfer absorption; LC = ligand-centered absorption). a) A matrix is excited above the band-gap energy and, after energy transfer, the lanthanide ion emits. b) Ligand → metal charge-transfer absorption can lead to an excited lanthanide ion which luminesces. c) Ligand-centered absorption excites a ligand which transfers its electronic excitation energy to a lanthanide ion that fluoresces.

a) matrix excitation followed by energy transfer to the lanthanide ion, b) ligand → metal charge transfer followed by lanthanide f–f emission, and c) ligand-centered absorption followed by energy transfer to the lanthanide ion.

We first discuss the use of coordinating ligands as sensitizers. After absorption of light by the ligands, the electronic excitation energy is transferred and results in a luminescence of the lanthanide ion (see Figure 1c). A possibility, given by Vögtle, Balzani, and co-workers, is to use a specially designed dendrimer which is able to play the role of the ligand for the lanthanide ions but which is also capable of working as an

[*] Prof. Dr. G. Calzaferri, Dipl.-Chem. H. Maas, Dr. A. Currao
University of Bern
Department of Chemistry and Biochemistry
Freiestrasse 3, 3012 Bern (Switzerland)
Fax: (+41) 31-631-3994
E-mail: gion.calzaferri@iac.unibe.ch

- [15] C. J. Moody, K. J. Doyle, M. C. Elliott, T. J. Mowlem, *J. Chem. Soc. Perkin Trans. 1* **1997**, 16, 2413–2419.
- [16] M. P. Doyle, D. C. Forbes, *Chem. Rev.* **1998**, 98, 911–935.
- [17] E. P. Boden, G. E. Keck, *J. Org. Chem.* **1985**, 50, 2394–2395.
- [18] B. Neises, W. Steglich, *Angew. Chem.* **1978**, 90, 556–557; *Angew. Chem. Int. Ed. Engl.* **1978**, 17, 522–524.
- [19] T. Takahashi, M. Kotori, R. Fisher, Y. Nishihara, K. Nakajima, *J. Am. Chem. Soc.* **1995**, 117, 11039–11040.
- [20] S. Hanessian, P. Meffre, M. Girard, S. Beaudoin, J.-Y. Saneau, Y. Bennani, *J. Org. Chem.* **1993**, 58, 1991–1993.
- [21] a) O. Yonemitsu, P. Cerutti, B. Witkop, *J. Am. Chem. Soc.* **1966**, 88, 3941–3945; b) H. G. Theuns, H. B. M. Lenting, C. A. Salemink, H. Tanaka, M. S. Shibata, K. Ito, R. J. J. C. Lousberg, *Heterocycles* **1984**, 22, 2007–2011.
- [22] N. Lindquist, Dissertation, University of California (San Diego, USA), **1989**.

Encapsulated Lanthanides as Luminescent Materials

Huib Maas, Antonio Currao, and Gion Calzaferri*

Dedicated to Professor Roald Hoffmann on the occasion of his 65th birthday

Materials which embed organic dyes, rare earth ions, complexes, or quantum dots in a matrix with specifically tailored chemical and optical properties provide a challenging approach to novel chemical and optical applications. These materials have the potential to be used in microoptics, optoelectronics, laser materials, solar cells, sensors, battery electrodes, and photocatalysis. In this article we focus on lanthanides encapsulated in zeolites, glass films derived from sol–gel processes, and semiconductors.

The research work on the unique luminescent properties of rare earth elements hosted in different matrixes is strongly motivated by their technological importance in optoelectronic devices.^[1] The materials emit over the entire spectral range of interest: near infrared (NIR; Nd³⁺, Er³⁺), red (Eu³⁺, Pr³⁺, Sm³⁺), green (Er³⁺, Tb³⁺), and blue (Tm³⁺, Ce³⁺). Their optical transitions involve 4f orbitals, which are well shielded from their chemical environment by 5s² and 5p⁶ electrons. The f–f transitions are parity forbidden and, as a result, the absorption coefficients are very low and the emissive rates are slow, which results in long-lived and linelike emission bands. As a consequence, direct excitation of the lanthanide ions is unfavorable. The comparatively fast thermal relaxation of the excitation energy is a problem when using lanthanide ions for luminescence. This nonradiative relaxation may occur by interaction of the electronic levels of the lanthanide ion with suitable vibrational modes of the environment.^[2] The efficiency of these processes depends on the energy gap between the ground and excited states as well as the vibrational energy of the oscillators. For example,

when solvents containing OH groups are coordinated to lanthanide ions, efficient nonradiative deactivations take place through vibronic coupling with the vibrational states of the OH oscillators. Replacement of the OH oscillators by low-frequency OD oscillators, diminishes the vibronic deactivation pathway.^[3] Different ways to overcome the difficulties of low absorptivity and thermal relaxation have been used. We show the apparently most important ones in Figure 1:

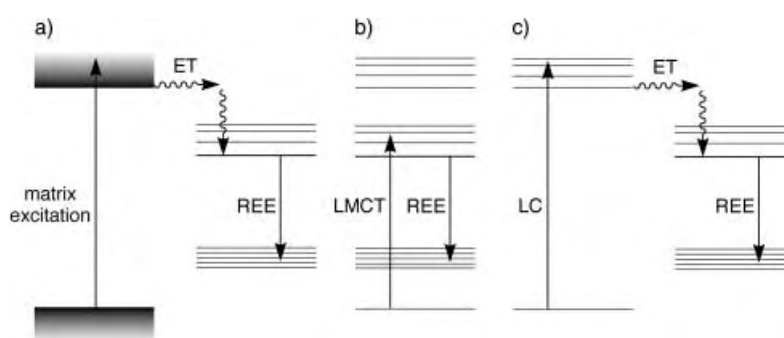


Figure 1. Three paths to efficient lanthanide luminescence (ET = energy transfer; REE = rare earth emission; LMCT = ligand → metal charge transfer absorption; LC = ligand-centered absorption). a) A matrix is excited above the band-gap energy and, after energy transfer, the lanthanide ion emits. b) Ligand → metal charge-transfer absorption can lead to an excited lanthanide ion which luminesces. c) Ligand-centered absorption excites a ligand which transfers its electronic excitation energy to a lanthanide ion that fluoresces.

a) matrix excitation followed by energy transfer to the lanthanide ion, b) ligand → metal charge transfer followed by lanthanide f–f emission, and c) ligand-centered absorption followed by energy transfer to the lanthanide ion.

We first discuss the use of coordinating ligands as sensitizers. After absorption of light by the ligands, the electronic excitation energy is transferred and results in a luminescence of the lanthanide ion (see Figure 1 c). A possibility, given by Vögtle, Balzani, and co-workers, is to use a specially designed dendrimer which is able to play the role of the ligand for the lanthanide ions but which is also capable of working as an

[*] Prof. Dr. G. Calzaferri, Dipl.-Chem. H. Maas, Dr. A. Currao
University of Bern
Department of Chemistry and Biochemistry
Freiestrasse 3, 3012 Bern (Switzerland)
Fax: (+41) 31-631-3994
E-mail: gion.calzaferri@iac.unibe.ch

antenna.^[4] The dendrimer was used as a light-harvesting ligand for enhancing the NIR luminescence of the Nd³⁺ ion.

Zeolites possess pore structures and these enable them to act as host for molecules and ions. The cations present in the pores of the zeolites have a charge-compensating function and can generally be exchanged. Rare earth ions and some of their complexes can be inserted by ion exchange.^[5] Ligands can protect the lanthanide ions from the water molecules present in zeolites under ambient conditions.^[2a] The zeolite framework itself, which consists of a corner-sharing network of tetrahedrally coordinated TO₄ units (T = Si, Al, P, Ga, B, Be, Ti), only has low vibration quanta which are not expected to contribute much to nonradiative deactivation of the excited state of the lanthanide ion. Ligands containing organic chromophores can be used to excite the lanthanide ion by the mechanisms shown in Figure 1b and 1c.^[2a, 5b] However, conventional ligands do not usually give rise to inert complexes because the lanthanide ions are unable to form strong coordination complexes as a result of their electronic configuration.^[2b] Depending on the solvent, this situation leads to a competition of the coordination sites between the ligands and solvent molecules. Lanthanide ions inside zeolite pores that are not complexed must be excited by sensitization of another species. For this, one can use, for example, Ce³⁺ ions which have allowed f-d transitions.^[6] Intrazeolite transitions, which occur at about 180 nm in the UV spectrum, have been reported to sensitize lanthanide ions.^[5a] It is not clear, however, to what extent charge-transfer transitions between the zeolite framework oxygen atoms and metal cations, which were found to be important in other cases, play a role in these materials.^[7]

Another strategy is to use the high porosity of glass films derived from sol–gel processes by incorporating inorganic lumophores, such as lanthanide cryptate or other macrocycles, as light-harvesting centers.^[8] These efficiently collect photons and subsequently transfer their energy to the lanthanide ions to produce intense luminescence. The luminescence can be activated or enhanced by the presence of a molecule to be sensed. The target molecule must diffuse through the porous network of the film and bind to the lanthanide ion, thus increasing the emission of the light-harvesting centers. The sensors work by simply monitoring the emission intensity from the lanthanide centers. The advantageous mechanical and chemical stability, as well as the optical transparency of sol–gel matrixes, has been investigated as optical pH sensors based on luminescent lanthanide complexes.^[9] Very recently, an enhanced fluorescence has been reported^[10] from Eu³⁺-doped silica gels in which CdS nanoparticles were adsorbed onto the pore surface of the gels. The CdS colloids were able to enhance the photoluminescence of the europium ions by energy transfer, even in the gel state.

Another way to minimize the difficulties of low absorptivity and nonradiative relaxation is by encapsulating the lanthanide ions in a semiconducting matrix. Charge carriers in a semiconductor can recombine at a lanthanide-related trap site in the matrix and transfer their recombination energy to the lanthanide ion, which then becomes excited and subsequently emits. Therefore, the lanthanides have been studied as emission amplifiers for semiconductors, which have an

intrinsic indirect bandgap, such as silicon.^[11] Er³⁺-doped silicon nanoparticles have been prepared by copolyolysis of disilane and a volatile erbium complex. These materials show a characteristic NIR photoluminescence of the Er³⁺ ion at 1540 nm.^[12] The charge carriers can be generated optically, which results in photoluminescence, or electrically, which gives electroluminescence. Both processes have been observed at room temperature in Eu³⁺-doped thin films of GaN grown on Si substrates.^[13] Conde-Gallardo et al. showed that the semiconducting nature of TiO₂ grown by the sol–gel method on glass and on a crystalline silicon substrate provides a suitable environment for enhancing the luminescence of the Eu³⁺ ion.^[14] Excitation above the bandgap energy of the Eu³⁺–TiO₂ layers on glass or on silicon lead to intense Eu³⁺ emission. The process seems to correspond to the mechanism shown in Figure 1a. Excitation below the bandgap energy mainly caused some weak luminescence from a TiO₂ defect.

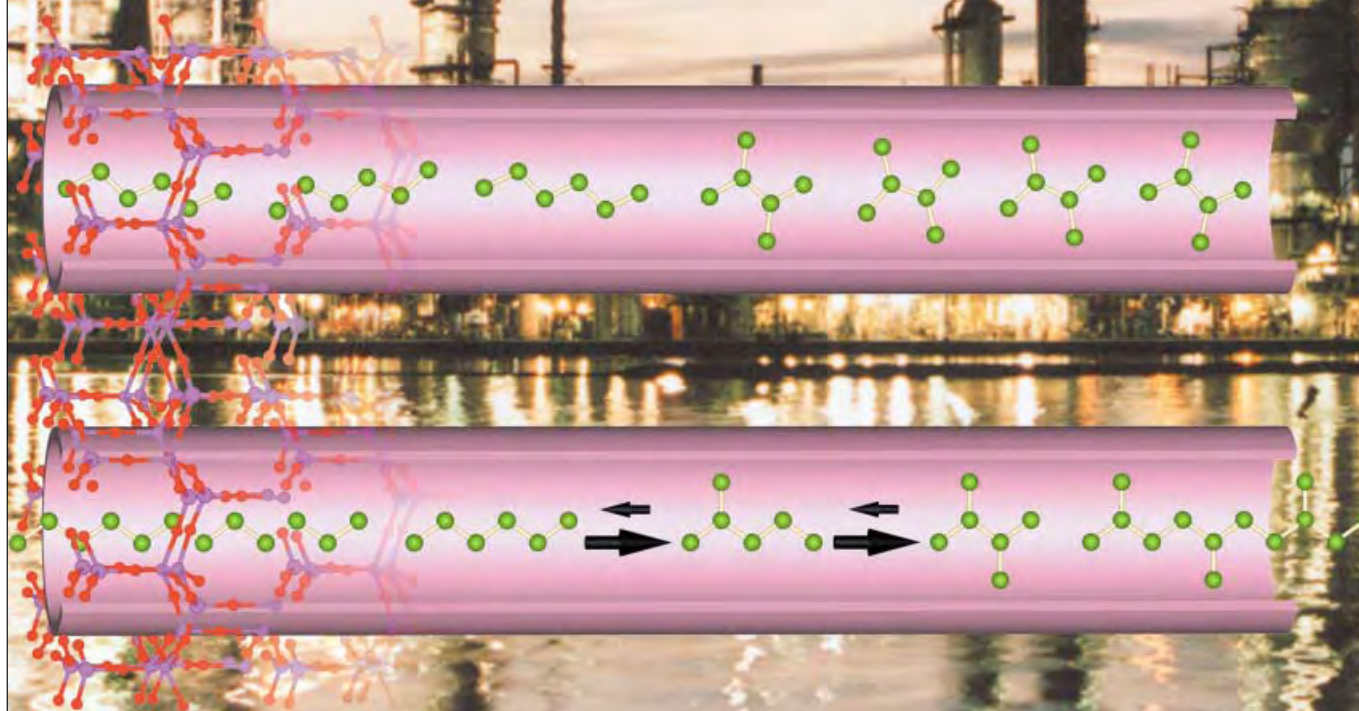
Thermally stable and ordered mesoporous metal oxides (for example, TiO₂, ZrO₂, Al₂O₃, SiTiO₄, ZrTiO₄) are interesting and attractive host matrixes. Stucky and co-workers reported a simple and versatile synthesis for materials with a pore size of up to 14 nm.^[15] They used amphiphilic block copolymers as structure-directing agents in non-aqueous solutions. Hexagonal or cubic mesostructures have been obtained, depending on the agent used. These mesoporous oxides contain nanocrystalline domains within relatively thick amorphous walls. For example, a well-ordered cubic array of TiO₂ mesopores of about 7–8 nm in size and a wall structure composed of 1–5-nm anatase nanocrystallites embedded in an amorphous titanium oxide matrix was obtained by this procedure.^[16] This interesting two-phase wall structure of ordered TiO₂ nanoparticles was successfully tested as a host for Eu³⁺ ions.^[17] A cubic mesostructured matrix of titanium dioxide with a three-dimensional array of embedded anatase nanocrystals was doped with high concentrations of Eu³⁺ ions (up to 8 mol %). The semiconducting anatase nanocrystallites were found to sensitize the Eu³⁺ activator, which leads to an energy-transfer system shown in Figure 1a) that produces a bright red luminescence (ca. 614 nm). Most amazing is the simple preparation by dip-coating and subsequent heat treatment of such films. These films were reported to have a self-assembled framework, high surface area, and to be air and moisture stable.

- [1] T. Jüstel, H. Nikol, C. Ronda, *Angew. Chem.* **1998**, *110*, 3250–3271; *Angew. Chem. Int. Ed.* **1998**, *37*, 3084–3103.
- [2] a) Y. Wada, T. Okubo, M. Ryo, T. Nakazawa, Y. Hasegawa, S. Yanagida, *J. Am. Chem. Soc.* **2000**, *122*, 8583–8584; b) N. Sabbatini, M. Guardigli, J.-M. Lehn, *Coord. Chem. Rev.* **1993**, *123*, 201–228.
- [3] N. Sabbatini, S. Dellonte, M. Ciano, A. Bonazzi, V. Balzani, *Chem. Phys. Lett.* **1984**, *107*, 212–216.
- [4] F. Vögtle, M. Gorka, V. Vicinelli, P. Ceroni, M. Maestri, V. Balzani, *ChemPhysChem* **2001**, *2*, 769–773.
- [5] a) T. Jüstel, D. U. Wiechert, C. Lau, D. Sendor, U. Kynast, *Adv. Funct. Mater.* **2001**, *11*, 105–110; b) I. L. V. Rosa, O. A. Serra, E. J. Nassar, *J. Lumin.* **1997**, *72–74*, 532–534.
- [6] U. Kynast, V. Weiler, *Adv. Mater.* **1994**, *6*, 937–941.
- [7] a) R. Seifert, A. Kunzmann, G. Calzaferri, *Angew. Chem.* **1998**, *110*, 1604–1606; *Angew. Chem. Int. Ed.* **1998**, *37*, 1521–1524; b) R. Seifert, R. Rytz, G. Calzaferri, *J. Phys. Chem. A* **2000**, *104*, 7473–7483.

- [8] a) C. M. Rudzinski, A. M. Young, D. G. Nocera, *J. Am. Chem. Soc.* **2002**, *124*, 1723–1727; b) “Chemosensors of Ion and Molecule recognition” W. K. Hartmann, M. A. Mortellaro, D. G. Nocera, Z. Pikramenou in *NATO ASI Ser. Ser. C* **1997**, *492*, 159–176; c) J. I. Dulebohn, B. Van Vlierberge, K. A. Berglund, R. B. Lessard, J.-A. Yu, D. G. Nocera, *Mater. Res. Soc. Symp. Proc.* **1990**, *180*, 733–740.
- [9] S. Blair, M. P. Lowe, C. E. Mathieu, D. Parker, P. K. Senanayake, R. Katakya, *Inorg. Chem.* **2001**, *40*, 5860–5867.
- [10] S. T. Selvan, T. Hayakawa, M. Nogami, *J. Non-Cryst. Solids* **2001**, *291*, 137–141.
- [11] A. Polman, *J. Appl. Phys.* **1997**, *82*, 1–39.
- [12] J. St. John, J. L. Coffey, Y. Chen, R. F. Pinizzotto, *J. Am. Chem. Soc.* **1999**, *121*, 1888–1892.
- [13] J. Heikenfeld, M. Garter, D. S. Lee, R. Birkhahn, A. J. Steckl, *Appl. Phys. Lett.* **1999**, *75*, 1189–1191.
- [14] A. Conde-Gallardo, M. García-Rocha, I. Hernández-Calderón, R. Palomino-Merino, *Appl. Phys. Lett.* **2001**, *78*, 3436–3438.
- [15] P. Yang, D. Zhao, D. I. Margolese, B. F. Chmelka, G. D. Stucky, *Nature* **1998**, *396*, 152–155.
- [16] a) P. Yang, D. Zhao, D. I. Margolese, B. F. Chmelka, G. D. Stucky, *Chem. Mater.* **1999**, *11*, 2813–2826; b) P. Alberius-Henning, K. L. Frindell, R. C. Hayward, E. J. Kramer, B. F. Chmelka, G. D. Stucky, *Chem. Mater.*, submitted.
- [17] K. L. Frindell, M. H. Bartl, A. Popitsch, G. D. Stucky, *Angew. Chem.* **2002**, *114*, 1001–1004; *Angew. Chem. Int. Ed.* **2002**, *41*, 959–962.

Entropy strikes again

Anyone who has experience in moving house [the *Angewandte* team has just done this!] knows that those boxes filled with small books are the heaviest, because these small objects pack so easily. The same entropy effect explains the catalytic selectivity towards the formation of branched hydrocarbons in zeolites. The pink tubes represent the zeolite pores at high loading in which effective size differences between linear and branched molecules (top tube) determine the selectivity (bottom tube).



For more information
see the following pages.

Understanding Zeolite Catalysis: Inverse Shape Selectivity Revised**

Merijn Schenk, Sofia Calero, Theo L. M. Maesen, Lucas L. van Benthem, Martijn G. Verbeek, and Berend Smit*

The molecular aspect of shape selectivity in zeolites is one of the key factors in zeolite science and technology of which a better understanding is required. The prediction of even qualitative aspects of a product distribution for a given reaction in a particular zeolite would be a significant step forward.^[1] In this respect the work of Santilli et al.,^[2] which introduced the concept of inverse shape selectivity, can be seen as an important step. Inverse shape selectivity was used to explain the high yield of dibranched alkanes in AFI-type of zeolites. This concept is one of the first, apparently successful attempts, to predict some aspects of a product distribution by using molecular simulations. Traditional shape selectivity states, for example, that molecules will not (*trans*-)form if they are too bulky to fit inside a channel of a zeolite. Therefore, selectivity can be obtained by selecting zeolites with different channel sizes. Santilli et al. argued that the inverse process could also result in shape selectivity: those molecules form that have an optimal fit within the channels. For example, a difference in combustion properties (octane value) provides an economic incentive to prefer the formation of branched paraffins to linear paraffins. The concept of inverse shape selectivity tells us that this demand can be met by using zeolites that afford a maximum difference in Gibbs free energy between the branched and linear isomers. Using state-of-the-art simulation techniques and force fields, Santilli et al. demonstrated that their idea correlated perfectly with the measured selectivity. More importantly, Santilli et al.'s concept could be used to predict the optimal structure of a zeolite.

The initial motivation of our work was to redo and further refine the calculations of Santilli et al. by using more advanced simulation techniques and improved force fields. Whereas the simulations of Santilli et al. were limited to the energetic contributions, our approach, which uses the configurational-bias Monte Carlo (CBMC), allows computations of the entropic contributions as well.^[3] In addition, Santilli et al.

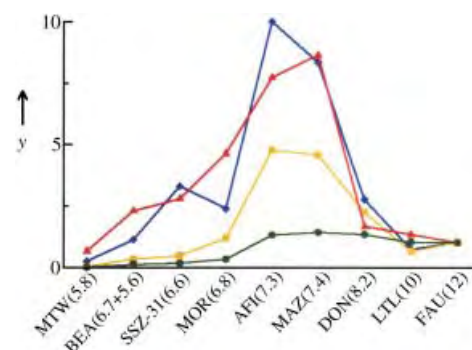


Figure 1. Experimental and simulated normalized DMB/*n*-C₆ yield ratios (*y*) for various zeolite structures at *T* = 577 K and *P* = 3000 kPa. The ratios were normalized by setting the value for the FAU-type zeolite at one. The experimental ratios (red) were determined from *n*-C₁₆ hydroconversion experiments,^[2] the calculated ratios were taken from simulated adsorption isotherms of 2,2-DMB/*n*-C₆ (yellow) and 2,3-DMB/*n*-C₆ (blue) or from Henry coefficients (green). The numbers in parentheses are the average pore sizes [Å]. DMB = dimethylbutane, *n*-C₆ = *n*-hexane.

used the CVFF force field. Macedonia and Maginn have since shown that this force field is not particularly suited for simulating branched paraffins,^[4] for example, the CVFF force field does not reproduce the step that is clearly visible in the measured isotherms of isobutane adsorption by MFI-type silica at approximately half the loading.^[2] The force field we used does describe the adsorption isotherms of linear and branched alkanes in MFI quantitatively.

To our surprise, these "improved" simulations predict that the free energies of the linear and branched isomers in the "optimal" zeolites are nearly identical (see Figure 1). This result suggests that none of the "optimal" zeolites would favor the formation of branched alkanes. This prediction is in marked disagreement with the significant differences in selectivity observed experimentally. This situation suggests that the initial success of the predictions of Santilli et al. may have resulted from a fortuitous cancellation of errors. More importantly, our results also question the molecular interpretation of Santilli et al., that an optimum match between a branched molecule and the zeolite channel induces the selectivity. Here, we will demonstrate that the molecular basis of inverse shape selectivity is related to entropic effects inside the zeolite pores under conditions where the zeolites are (almost) fully saturated.

An important assumption in the calculations of Santilli et al. is that at reaction conditions the loading is sufficiently low, such that alkane–alkane interactions can be ignored. To test this assumption, we have computed adsorption isotherms for various C₁₆ isomers, which is the reactant of the reaction of interest. Figure 2 shows a binary isotherm (577 K) of equal amounts of 2,5,8,11-tetramethyldodecane (a *teM*-C₁₂) and *n*-C₁₆ in AFI-type pores. At low pressures there is little difference between the loading of the isomers, which is consistent with our observation that the free energies of these isomers at low loading are similar. However, if we consider the loading under reaction conditions (3 × 10³ kPa), the adsorption isotherm shows that these pores are fully saturated with reactants. In addition, the AFI-type pores strongly prefer the adsorption of the shortest, most compact molecule, *teM*-C₁₂, to that of the longer molecule, *n*-C₁₆. Similar simulations

[*] Prof. B. Smit, Drs. M. Schenk, Dr. S. Calero, L. L. van Benthem, M. G. Verbeek
Department of Chemical Engineering
University of Amsterdam
Nieuwe Achtergracht 166, 1018 WV Amsterdam (The Netherlands)
Fax: (+31)20-525-5604
E-mail: B.Smit@science.uva.nl
Dr. T. L. M. Maesen
ChevronTexaco
Energy Research and Technology
100 Chevron Way, Richmond, CA 94802-0627 (USA)

[**] These investigations are supported in part by the Netherlands Research Council for Chemical Sciences (CW) with financial aid from the Netherlands Technology Foundation (STW) and by the Netherlands Organization for Scientific Research (NWO) through PIONIER, and by the Stichting Nationale Computer Faciliteiten (National Computing Facilities Foundation) for the use of the supercomputer facilities. We thank the European Commission for a Marie Curie Individual Research Fellowship (to S.C.), and Christiaan Meijer for assistance with the artwork.

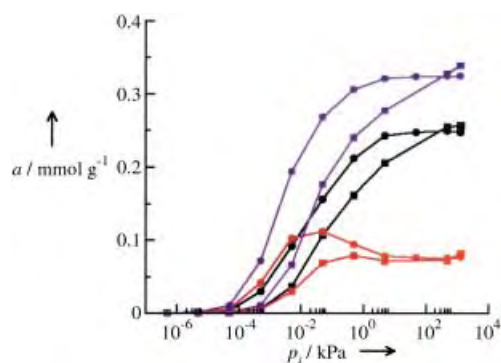


Figure 2. Simulated adsorption isotherms of equal amounts of teM-C₁₂ (black) and n-C₁₆ (red) in AFI- (●) and DON-type (■) pores at $T = 577$ K. The total loading is given in purple. The grand canonical Monte Carlo simulations have been performed using the CBMC technique as described in Vlugt et al.^[9] A united atom force field has been used to describe the alkane–alkane interactions and the zeolite–alkane interactions. The parameters can be found in ref. [9]. AFI and DON have 1D linear pores with average channel diameters of 7.3 and 8.2 Å, respectively.

of different pore structures show that also the other systems are fully saturated with reactant under reaction conditions. These results clearly indicate that a key assumption underlying the mechanism of inverse shape selectivity does not hold. An alternative mechanism is therefore needed.

Since teM-C₁₂ is the most likely source for dimethylbutane (DMB), and dimethyltetradecane (dM-C₁₄) the most likely source for *n*-hexane (n-C₆),^[5,6] it would be tempting to conclude that the DMB/*n*-C₆ ratio in the hydrocracking products is related to the differences in free energy of formation of these highly branched C₁₆ isomers. However, Figure 2 also shows that similar differences in free energy are observed for the DON structure, which has a much larger pore diameter but does not yield a high DMB/*n*-C₆ ratio.^[7] These results demonstrate that at reaction conditions the zeolites are saturated with bulky C₁₆ isomers, which have a very low diffusion coefficient, hence the exchange between gas phase and adsorbed phase will be extremely slow. Therefore we cannot assume that the adsorbed phase is in thermodynamic equilibrium with the gas phase. However, this does imply that the adsorbed phase will exhibit an intracrystalline thermodynamic equilibrium, that is, the zeolite will preferentially form those isomers that have the lowest free energy of formation at the conditions of interest. In other words, the product molecules are trapped sufficiently long in the zeolite

that they will hydroisomerize towards their intracrystalline thermodynamic equilibrium distribution. If this assumption holds, the product distribution is determined by the relative intracrystalline Gibbs free energies of formation at reaction conditions. Since we do not know the composition of the various isomers at these conditions, we cannot compute these free energies exactly. The free energies can be approximated if we assume that the dominant factor is that the zeolite is completely saturated with hydrocarbons, and that the exact composition of the hydrocarbons is of secondary importance. In the structures of interest the molecules align nose to tail, and since the molecules only see the tail and nose of their neighbors it is of secondary importance whether the rest of the molecule is big or small.

We estimate the Gibbs free energy of formation of the hexane isomers by a binary mixture of 2,2- or 2,3-dimethylbutane (2,2-DMB or 2,3-DMB) and *n*-hexane (n-C₆) at reaction conditions and compute the relative free energies of these two components. In Figure 1 these DMB/*n*-C₆ ratios are plotted for various zeolite structures. For small-pore zeolites the branched products are too bulky to form, giving selectivity towards the linear isomers. For the large-pore zeolites the linear and branched molecules are equally likely to form. An optimal selectivity is obtained for zeolites with pore size of approximately 7 Å. This observation is exactly what is found experimentally.^[2]

A molecular explanation of our observation is shown in Figure 3. Talbot^[8] has shown that if we pack molecules in a 1D pore, at high pressures the smallest molecule will expel the bigger molecule. This is a purely entropic effect. A real zeolite is not a pure 1D system, therefore it is important to introduce

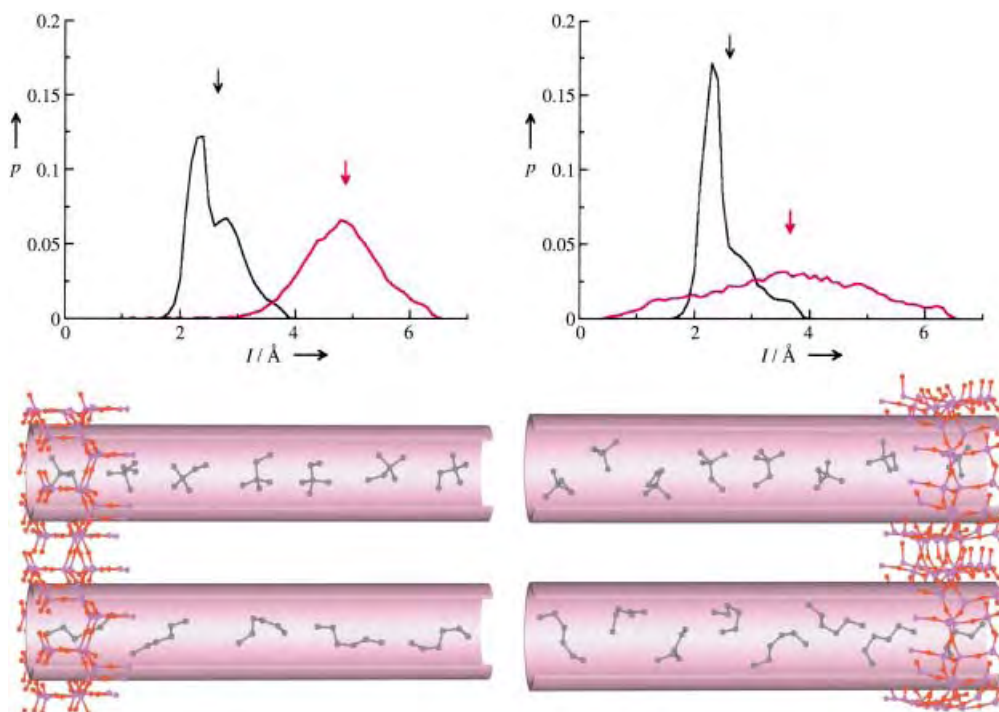


Figure 3. Adsorption of linear and branched hexane isomers in AFI (left) and AET (right). The “snapshots” show some typical conformations of the linear and branched isomers. In the smaller tube (AFI) the linear isomers are stretched while in the wider tube (AET) coiled conformations are also observed. Top: the projected end-to-end distance distribution of *n*-hexane (red) and 2,2-DMB (black), the arrows indicate the effective size of the molecules.

the effective size of a molecule, which is defined as the end-to-end distance projected on the center line of the channel. Figure 3 shows the distribution of this distance for a large (AET) and optimal pore size (AFI). In the large-pore structure we observe for the linear isomer a very broad distribution, reflecting all possible conformations (curled and stretched) of this isomer. Hence, the effective size of the linear and branched isomer is nearly identical. If we reduce the size of the channel, this distribution is dominated by the stretched conformations, which increases the effective size of the linear isomers. Because the effective size of the linear isomer is large, these molecules are expelled at *high* pressure.

An important difference between the concept of inverse shape selectivity and our entropic explanation is the role of the zeolite. Inverse shape selectivity indicates that one should look at those zeolites, which have an optimal “match” for the branched isomer. In our mechanism the role of the zeolite is to provide an environment in which the length differences between the linear and branched isomers are maximum, which translates into an optimal pore diameter. For a given pressure, the maximum selectivity is determined by the relative effective sizes of the alkane molecules. The details of the channel structure are in this mechanism of secondary importance. This situation suggests that we can “optimize” any zeolite structure by tuning its diameter. In Figure 4 we have performed this optimization for several known zeolite structures by changing the pore diameters by a simple scaling factor. Of course, such an optimization cannot be performed in practice, but does illustrate our point that irrespective of the details of the zeolite a similar optimal selectivity is obtained for nearly identical channel dimensions. At lower temperatures or higher pressures the entropy effect is more pronounced and a better selectivity could be expected. The results shown in Figure 4 are at lower temperatures than those in Figure 1 (403 K versus 577 K). The data at these lower temperatures give significantly higher selectivities. A similar effect can be expected from an increase of the pressure.

Two conclusions of practical importance can be drawn from our work. We have shown that there is a thermodynamic limit to the maximum selectivity that can be obtained for these types of reactions. This limit implies that any novel zeolite

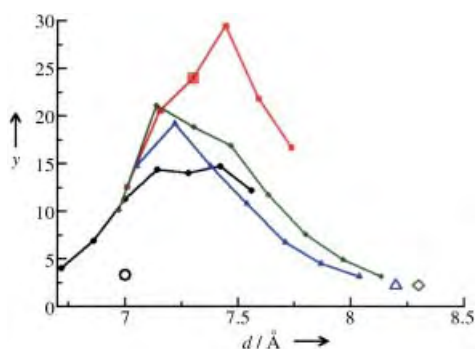


Figure 4. Normalized 2,2-DMB/*n*-C₆ yield ratios (with respect to the FAU selectivity) for some “optimized” pore structures at *T* = 403 K and *P* = 1000 kPa. The size of MOR- (black, pore too small), AFI- (red, optimal), AET- (green, too wide), and DON-type (blue, too wide) channels was adjusted by scaling the coordinates. The open symbols represent the zeolite structures before resizing. MOR was first made circular before the scaling was applied.

structures will have a selectivity towards branched paraffins which is at best similar to the selectivity of MAZ and AFI. A more successful approach to increase the selectivity would be to operate at higher pressure or lower temperatures, since the entropy effect is more pronounced at these conditions.

Received: February 1, 2002 [Z18631]

- [1] J. Weitkamp, S. Ernst, L. Puppe in *Catalysis and Zeolites* (Eds.: J. Weitkamp, L. Puppe), Springer, Berlin, **1999**, pp. 326–376.
- [2] D. S. Santilli, T. V. Harris, S. I. Zones, *Microporous Mater.* **1993**, *1*, 329–341.
- [3] D. Frenkel, B. Smit *Understanding molecular simulations*, 2nd ed., Academic Press, San Diego, **2002**.
- [4] M. D. Macedonia, E. J. Maginn, *Mol. Phys.* **1999**, *96*, 1375–1390.
- [5] J. Weitkamp, S. Ernst, *Catal. Today* **1994**, *19*, 107–150.
- [6] J. A. Martens, P. A. Jacobs in *Zeolite Microporous Solids: Synthesis, Structure, and Reactivity* (Eds.: E. G. Derouane, F. Lemos, C. Naccache, F. Ramão-Ribeiro), Kluwer, Amsterdam, **1992**, pp. 511–529.
- [7] M. Yoshikawa, P. Wagner, M. Lovallo, K. Tsuji, T. Takewaki, C.-Y. Chen, L. W. Beck, C. Jones, M. Tsapatsis, S. I. Zones, M. E. Davis, *J. Phys. Chem. B* **1998**, *102*, 7139–7147.
- [8] J. Talbot, *AIChE J.* **1997**, *43*, 2471–2479.
- [9] T. J. H. Vlucht, R. Krishna, B. Smit, *J. Phys. Chem. B* **1999**, *103*, 1102–1118.

Reaction Principles and Crystal Structure Design for the Topochemical Polymerization of 1,3-Dienes

Akikazu Matsumoto,* Kazuki Sada,* Kohji Tashiro,* Mikiji Miyata,* Takashi Tsubouchi, Toshihiro Tanaka, Toru Odani, Sadamu Nagahama, Tomoyuki Tanaka, Katsunari Inoue, Seishi Saragai, and Shinsuke Nakamoto

Crystal engineering is the planning of the properties and functions of crystalline materials by using preorganized molecules.^[1] This process involves the control of crystal

- [*] Dr. A. Matsumoto, Dr. T. Tanaka, T. Odani
Department of Applied Chemistry
Graduate School of Engineering, Osaka City University
and PRESTO-JST
Sugimoto, Sumiyoshi-ku, Osaka 558-8585 (Japan)
Fax: (+81) 6-6605-2981
E-mail: matsumoto@chem.eng.osaka-cu.ac.jp
- Dr. K. Sada, Prof. Dr. M. Miyata, T. Tanaka, K. Inoue
Department of Material and Life Science
Graduate School of Engineering, Osaka University
2-1 Yamadaoka, Suita, Osaka 565-0871 (Japan)
E-mail: sadatcm@mbx.nc.kyushu-u.ac.jp
miyata@ap.chem.eng.osaka-u.ac.jp
- Prof. Dr. K. Tashiro, Dr. S. Saragai, S. Nakamoto
Department of Macromolecular Science
Graduate School of Science, Osaka University
Toyonaka, Osaka 560-0043 (Japan)
E-mail: ktashiro@chem.sci.osaka-u.ac.jp

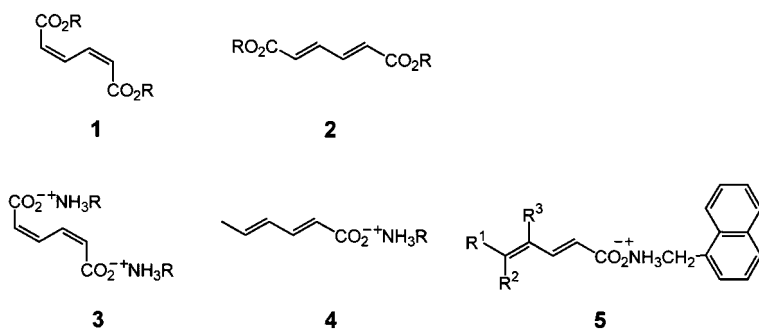
T. Tsubouchi, S. Nagahama
Department of Applied Chemistry
Graduate School of Engineering, Osaka City University
Sugimoto, Sumiyoshi-ku, Osaka 558-8585 (Japan)

Supporting information for this article is available on the WWW under <http://www.angewandte.org> or from the author.

packing based on information from the chemical structure of the molecules and is required to clarify the correlation between the structure and functions. Topochemical polymerization, which is one of the most important functions of crystalline materials, is the specific crystal-to-crystal reaction to give a unique chain structure and a polymer single crystal that cannot be manufactured by solution polymerization or by recrystallization of a preformed polymer from its solution or melt. This technique is very useful in developing nanomaterials and devices in constrained media including layers, channels, and solid surfaces.^[2] It is well known that some limited diyne and olefin monomers undergo topochemical polymerization,^[3–7] but other monomers have long been believed not to polymerize in a topochemical manner. In fact, no designer crystal has been reported for the 1,3-diene monomers, despite the pioneering work by Tieke et al. reported in the 1980s regarding the radiation polymerization of several layered compounds in the crystalline state.^[8] In recent years we have studied the solid-state photopolymerization of various 1,3-diene monomers, including the esters and alkylammonium salts of the (*Z,Z*)- and (*E,E*)-muconic and sorbic acids, which proceeds by means of a topochemical reaction mechanism.^[9–13] The polymer crystals obtained were characterized as organic intercalation materials.^[14, 9]

Here we propose principles for the topochemical polymerization of 1,3-diene monomers to predict the polymerization reactivity and design crystalline polymer materials. Currently, topochemical polymerization is opened not only to the diyne library, but also to the larger and more popular diene library. This is a first step in the rational design for the topochemical polymerization of diene monomers, moving away from the trial-and-error approach. Diene polymerization has potential for the construction of advanced organic materials in the solid state, because the topochemical polymerization of diyne and diene monomers provides different types of polymers, that is, conjugate and nonconjugate polymers, respectively, which could be used as molecular devices for optics and optoelectronics.

We have investigated the molecular packing in the crystals of many diene monomers that can or cannot undergo topochemical polymerization. All the muconic and sorbic acid derivatives with *Z,Z* and *E,E* configurations (**1–4**, Scheme 1) have similar molecular conformations in the crystalline state, that is, they are *s-trans* dienes with a highly planar structure.^[14] The stacking structure of the monomers was evaluated by using the following parameters (Figure 1):^[15] the intermolecular distance between carbon atoms that react



Scheme 1. Diene monomers examined in this study.

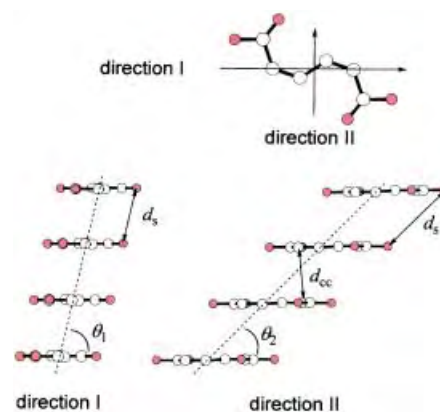


Figure 1. Definition of stacking parameters used for the prediction of the topochemical polymerization reactivity. d_{cc} is the intermolecular distance between the 2 and 5' carbon atoms. d_s is the stacking distance between the adjacent monomers in a column. θ_1 and θ_2 are the angles between the stacking direction and the molecular plane in orthogonally different directions. The view from direction I is parallel to a vector through the 2 and 5 carbon atoms of the diene moieties.

to make a new bond during the topochemical polymerization (d_{cc}), the stacking distance along the column (d_s), and the angles between the stacking direction and the molecular plane in orthogonally different directions (θ_1 and θ_2). The values of the parameters determined for the monomers **1–4** are summarized in Table 1.^[16]

Table 1. Stacking structure of the topochemically polymerizable muconic and sorbic acid derivatives in the crystals.

Monomer	R	d_{cc} [Å]	d_s [Å]	θ_1 [°]	θ_2 [°]
1	ethyl	3.79	4.93	79	49
1	4-chlorobenzyl	3.57	5.12	82	44
3	benzyl	4.24	4.86	67	55
3	2-chlorobenzyl	4.19	4.94	62	52
4	2-methylbenzyl	5.35	5.00	28	60
4	4-methylbenzyl	5.43	4.93	24	61
4	1-naphthylmethyl	5.37	4.99	29	61
4	–R– = <i>p</i> -xylylene	5.47	4.99	25	60
Lithium sorbate	–	5.69 ^[a]	5.04 ^[a]	7 ^[a]	32 ^[a]
5a	$R^1 = R^2 = R^3 = H$	5.31	4.95	29	61
5d	$R^1 = R^2 = CH_3, R^3 = H$	3.30	4.90	87	42

[a] Calculated from the crystal structure reported in [ref. 22].

The polymerizable monomer crystals exhibit d_{cc} values in the range between 3.6 and 5.7 Å, and the distance increases in the order of monomer species **1** < **3** < **4**. The θ_1 and θ_2 values are also dependent on the monomer structure. In contrast, all the d_s values are in an exclusively limited region of 4.9–5.1 Å. Figure 2 shows the relationship between the d_s and θ_2 values. The blue curve is calculated for the closest packing of the planar molecules with a thickness of 3.5 Å and θ_1 of 90°. For esters **1** and **2**, the plots are situated near the calculated curve because of the closest packing of the planar molecules in the crystals. In contrast, the ammonium derivatives often favor structures other than the columnar structure which results in the scattered points far from the calculated curve. This is caused by the diversity in the hydrogen bond pattern including one-dimensional ladders and two-dimensional sheets, depend-

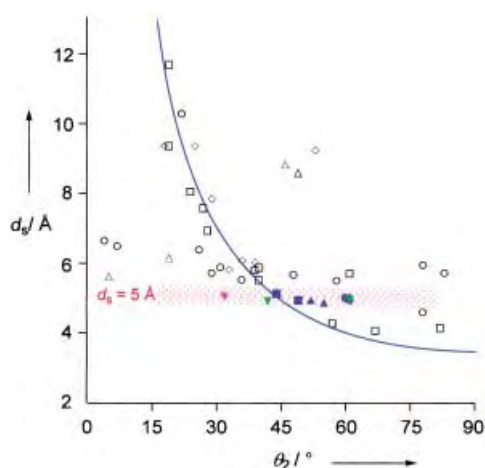


Figure 2. Relationship between the d_s and θ_2 values for the 1,3-diene monomers in the crystals. (\square) **1**, (\diamond) **2**, (\triangle) **3**, (\circ) **4**, and (∇) **5**; data for lithium sorbate (\blacklozenge) reported by Schlitter and Beck.^[22] Closed and open symbols represent polymerizable and nonpolymerizable monomers, respectively.

ing on the structure of the N-substituted groups. Several monomers have smaller d_{cc} and d_s values, and although this appears to be advantageous for the polymerization, they are actually nonpolymerizable (see also Supporting Information). For example, the diethyl ester of **1** has an alternative crystal structure at a low temperature as a result of the first-order phase transition,^[17] which seriously affects the polymerization reactivity; this monomer polymerizes quite rapidly at room temperature, but not at all below -45°C . The stacking parameters of **1** ($R = \text{Et}$) determined at a low temperature ($d_{cc} = 3.88 \text{ \AA}$, $d_s = 4.25 \text{ \AA}$, $\theta_1 = 80^\circ$, and $\theta_2 = 57^\circ$) are very similar to those given in Table 1 for the polymerizable structure. In this way, a slight change in the d_s value from 4.93 to 4.25 \AA or a deviation from the shaded red zone in Figure 2 diminishes the polymerization reactivity of the diethyl ester of **1**.

Which factor determines the polymerization reactivity? We emphasize the importance of the d_s value for the topochemical polymerization process. Namely, the stacking distances of the polymerizable monomers are close to the values of the repeating unit, that is, a fiber period of polymer chains with a fully stretched conformation, produced along with a crystallographic axis in the crystals. The fiber period for the ethyl ester polymer of **1** was determined to be 4.84 \AA from the X-ray diffraction data gathered for the polymer single crystal.^[10] If the polymerization proceeds for monomers with d_s values greater or smaller than 5 \AA , then the monomer molecules have to translate along the stacking axis during the polymerization. When d_s is close to the fiber period of the resulting polymer, monomer molecules rotate with the minimum translational movement and make a bond between the 2 and 5' carbon atoms.

The principles of diene polymerization seem to be similar to those for diynes, which are already well established,^[4] but the former are more sensitive to structural changes in the monomer crystals. This results from the difference in the planar and linear molecular shapes of dienes and diynes, respectively, that is, the direction of the π orbital of the

reacting moieties. Because the structural factors of diene polymerization in the crystalline state are not as straightforward as those for diyne polymerization, the discovery and generalization of the former has lagged behind.

The next question is how to make a suitable stacking distance of 5 \AA for the polymerization in the crystals of the diene monomers. Some "supramolecular synthons"^[19] are available for the topochemical polymerization of the ammonium and ester derivatives of the 1,3-diene carboxylic acids: two-dimensional hydrogen bond networks, aromatic ring stacking, and CH/π or halogen–halogen interactions (Figure 3). It is noteworthy that a naphthylmethylammonium

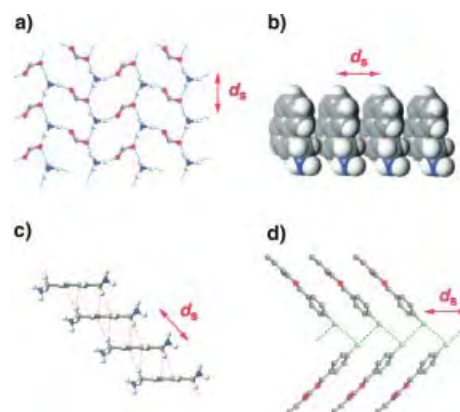


Figure 3. Supramolecular synthons for the molecular stacking with a 5 \AA distance, which is appropriate for the topochemical polymerization of the 1,3-diene monomers. a) Two-dimensional hydrogen bond network formed between primary ammonium and carboxylate groups, which act as triple hydrogen bond donors and acceptors, respectively. b) Aromatic ring stacking. The benzyl and naphthylmethyl moieties are packed in the crystals with a herringbone or γ -type structure. c) CH/π interaction between aromatic and benzyl groups. In the naphthylmethylammonium crystals, interactions between the π and aromatic or benzylic hydrogen atoms are observed. In the crystals of benzylammonium, 4-methylbenzylammonium, and *p*-xylylenediammonium crystals, an interaction of π -electrons with the benzylic hydrogen atoms is important. d) Halogen–halogen zigzag chains. The validity of this interaction has been proved by the chlorine atom substitution of the benzyl ester of **1**.^[23] Similar halogen chains are also observed in the crystals of the chloro-substituted benzylammonium salts of **3**.

counterion enforces a robust layer structure in which diene carboxylic acid molecules are arranged in a fashion appropriate for the polymerization. These crystals show the synergetic effects of the two-dimensional hydrogen bond network, aromatic stacking, and CH/π interaction.^[20, 21] Furthermore, we tested the polymerization reactivity of several diene carboxylic acids other than the muconic and sorbic acids. All the substituted diene monomers **5a–5e** (Scheme 1 and Table 2) polymerized by means of a topochemical polymerization mechanism to give the corresponding stereoregular polymers under photoirradiation in the crystalline state. The crystal structures and molecular packing (**5a** and **5d** in Table 1) were again similar to those of other polymerizable sorbate and muconate monomers which indicates that the polymerization principles are valid for a variety of diene monomers.

Here we have proposed reaction principles for the topochemical polymerization of 1,3-diene monomers in the crystalline state. In the crystals of polymerizable monomers,

Table 2. Topochemical polymerization of **5** under UV irradiation for 8 h in the crystalline state.

Monomer	R ¹	R ²	R ³	Yield [%]
5a	H	H	H	88
5b	(CH ₂) ₂ CH ₃	H	H	20
5c	(CH ₂) ₃ CH ₃	H	H	24
5d	CH ₃	CH ₃	H	67
5e	CH ₃	H	CH ₃	11
4	CH ₃	H	H	98

diene molecules stack in a columnar structure with an exclusively limited stacking distance of 5 Å, a value close to the repeating distance of the monomer units in the resulting polymer chain and appropriate for the polymerization by a topochemical reaction mechanism. We have also identified supramolecular synthons for constructing the desired monomer stacking in the crystals by using weak intermolecular interactions such as the two-dimensional hydrogen bond networks, aromatic ring stacking, and CH/π or halogen–halogen interactions.

Experimental Section

The muconic and sorbic acid derivatives used in this work were prepared by the methods described in previous papers.^[9, 11, 12] The reaction of malonic acid and acrolein was used to prepare *trans*-2,4-pentadienoic acid;^[24] subsequent reaction with 1-naphthylmethylamine gave **5a** quantitatively. Precursor carboxylic acids for **5b–5e** were synthesized by the reaction of triethylphosphonoacetate with the corresponding unsaturated aldehydes followed by hydrolysis.

Typical procedure: To NaH (1.42 g, 0.036 mmol) in dry THF was added triethylphosphonoacetate (7.1 mL, 0.036 mmol), and then 3-methyl-2-butenal (3.0 g, 0.036 mmol) in THF was added dropwise over 1 h. The reaction mixture was stirred overnight. Silica gel column chromatography (hexane/ethyl acetate 10:1) provided ethyl 2-*trans*-5-methyl-2,4-hexadienoate. After hydrolysis with KOH, 2-*trans*-5-methyl-2,4-hexadienoic acid was isolated as a yellowish powder. Yield 2.65 g (60%). The quantitative reaction with 1-naphthylmethylamine provided **5b**, which was recrystallized from methanol.

Photoirradiation was carried out with a high-pressure Hg lamp (Toshiba SHL-100-2, 100 W) at a distance of 10 cm through a Pyrex filter. The polymer yield was determined gravimetrically after any unreacted monomer had been removed with methanol or chloroform. Single-crystal X-ray data were collected on a Rigaku RAXIS RAPID diffractometer or Nonius Kappa CCD system with MoK_α radiation (λ = 0.71073 Å) or CuK_α radiation (λ = 1.5418 Å) and a graphite monochromator. The structures were solved by direct methods with the programs SIR88 and SIR92 and refined by using full-matrix least-squares procedures. All the calculations were performed with the CrystalStructure crystallographic software package of Molecular Structure Corporation or maXus of Mac Science, Japan.

Received: December 28, 2001 [Z18449]

- [1] a) G. M. J. Schmidt, *Pure Appl. Chem.* **1971**, 27, 647; b) G. R. Desiraju, *Crystal Engineering: The Design of Organic Solids*, Elsevier, Amsterdam, **1989**; c) V. Enkelmann, G. Wegner, K. Novak, K. B. Wagener, *J. Am. Chem. Soc.* **1993**, 115, 10390; d) A. Matsumoto, T. Odani, K. Sada, M. Miyata, K. Tashiro, *Nature* **2000**, 405, 328; see also, M. D. Ward, *Nature* **2000**, 405, 293; e) K. Tanaka, F. Toda, *Chem. Rev.* **2000**, 100, 1025; f) M. Alberecht, M. Lutz, A. L. Spek, G. van Koten, *Nature* **2000**, 406, 970; see also, J. W. Steed, *Nature* **2000**, 406, 943; g) M. Irie, S. Kobatake, M. Horichi, *Science* **2001**, 291, 1769; see also, J. R. Scheffer, C. Scott, *Science* **2001**, 291, 1712; h) G. R. Desiraju, *Nature* **2001**, 412, 397; i) B. Moulton, M. J. Zaworotko, *Chem. Rev.* **2001**, 101, 1629.
- [2] a) Y. Lu, Y. Yang, A. Sellinger, M. Lu, J. Huang, H. Fan, R. Haddad, G. Lopez, A. R. Burns, D. Y. Sasaki, J. Shelnut, C. J. Brinker, *Nature*

- 2001**, 410, 913; see also, G. D. Stucky, *Nature* **2001**, 410, 885; b) T. Aida, K. Tajima, *Angew. Chem.* **2001**, 113, 3919; *Angew. Chem. Int. Ed.* **2001**, 40, 3803; c) K. Morigaki, T. Baumgart, A. Offenhausser, W. Knoll, *Angew. Chem.* **2001**, 113, 1841; *Angew. Chem. Int. Ed.* **2001**, 40, 172; d) Y. Okawa, M. Aono, *Nature* **2001**, 409, 683; e) Y. Okawa, M. Aono, *J. Chem. Phys.* **2001**, 115, 2317.
- [3] G. Wegner, *Pure Appl. Chem.* **1977**, 49, 443.
- [4] V. Enkelmann, *Adv. Polym. Sci.* **1984**, 63, 91.
- [5] M. Hasegawa, *Adv. Phys. Org. Chem.* **1995**, 30, 117.
- [6] G. W. Coates, A. R. Dunn, L. M. Henling, J. W. Ziller, E. B. Lobkovsky, R. H. Grubbs, *J. Am. Chem. Soc.* **1998**, 120, 3641.
- [7] J. Xiao, M. Yang, J. W. Lauher, F. W. Fowler, *Angew. Chem.* **2000**, 112, 2216; *Angew. Chem. Int. Ed.* **2000**, 39, 2132.
- [8] a) B. Tieke, *J. Polym. Sci., Polym. Chem. Ed.* **1984**, 22, 391; b) B. Tieke, G. Chapuis, *J. Polym. Sci., Polym. Chem. Ed.* **1984**, 22, 2895; c) B. Tieke, G. Chapuis, *Crystallographically Ordered Polymers*, Vol. 337 (Ed.: D. J. Sandman), ACS Symposium Series, Washington DC, **1987**, pp. 61; d) B. Tieke, *Colloid Polym. Sci.* **1985**, 263, 965; e) B. Tieke, *Adv. Polym. Sci.* **1985**, 71, 79; f) B. Tieke, G. Chapuis, *Mol. Cryst. Liq. Cryst.* **1986**, 137, 101. In this literature the crystal structures of the monomer and polymer are shown for derivatives of sorbic acid. The stacking distance between the monomers (ca. 4.9 Å), which is estimated from the crystal structure data in the literature, agrees well with our conclusion.
- [9] A. Matsumoto, T. Odani, *Macromol. Rapid Commun.* **2001**, 22, 1195, and references therein.
- [10] K. Tashiro, A. N. Zadorin, S. Saragai, T. Kamae, A. Matsumoto, K. Yokoi, S. Aoki, *Macromolecules* **1999**, 32, 7946.
- [11] A. Matsumoto, T. Odani, M. Chikada, K. Sada, M. Miyata, *J. Am. Chem. Soc.* **1999**, 121, 11 122.
- [12] A. Matsumoto, S. Nagahama, T. Odani, *J. Am. Chem. Soc.* **2000**, 122, 9109.
- [13] S. Nagahama, A. Matsumoto, *J. Am. Chem. Soc.* **2001**, 123, 12 176.
- [14] We do not have sufficient crystal data for the *E,Z* monomers to discuss at the present because of the difficult isolation of pure isomers and single crystals.
- [15] In the previous papers θ_1 and θ_2 were defined in an alternative way. Formerly, direction I was parallel to a vector through the 2 and 3 carbon atoms (4 and 5 carbon atoms) for the *Z,Z* monomers and the 2 and 4 carbon atoms (3 and 5 carbon atoms) for the *E,E* monomers. However, it was not convenient for nonplanar molecules. Therefore, the values of θ_1 and θ_2 in this study are different from the previously reported values for some monomers. The present method is unambiguous and valid even for nonplanar 1,3-butadiene derivatives.
- [16] In Table 1 the data for the topochemically polymerizable monomers are shown. Supporting information is available for the nonpolymerizable monomers; see also, refs. [11], [17], [18], and [23].
- [17] S. Saragai, K. Tashiro, S. Nakamoto, T. Kamae, A. Matsumoto, T. Tsubouchi, *Polym. J.* **2001**, 33, 199.
- [18] S. Saragai, K. Tashiro, S. Nakamoto, A. Matsumoto, T. Tsubouchi, *J. Phys. Chem. B* **2001**, 105, 4155.
- [19] a) G. R. Desiraju, *Angew. Chem.* **1995**, 107, 2540; *Angew. Chem. Int. Ed. Engl.* **1995**, 34, 2311; b) A. Nangia, G. R. Desiraju, *Top. Curr. Chem.* **1998**, 198, 57.
- [20] a) G. R. Desiraju, T. Steiner, *The Weak Hydrogen Bond in Structural Chemistry and Biology*, Oxford University Press, Oxford, **1999**; b) T. Steiner, *Angew. Chem.* **2002**, 114, 50–80; *Angew. Chem. Int. Ed.* **2002**, 41, 48–76; *J. Am. Chem. Soc.* **2002**, 124, in press.
- [21] M. Nishio, M. Hirota, Y. Umezawa, *The CH/π Interaction: Evidence, Nature, and Consequences*, Wiley, New York, **1998**.
- [22] S. M. Schlitter, H. P. Beck, *Chem. Ber.* **1996**, 129, 1561. In this paper the authors speculated that the polymerization proceeds in the direction of the *c*-axis. However, the polymerization probably proceeds along the *b*-axis, and consequently, d_p should be regarded as 5.04 Å. The small θ_1 and θ_2 values are disadvantageous for the polymerization, and they require rotational change in the conformation of the monomer molecules during polymerization. This would result in the collapse of the crystals, as reported in the paper.
- [23] A. Matsumoto, T. Tanaka, T. Tsubouchi, K. Tashiro, S. Saragai, S. Nakamoto, in preparation.
- [24] P. J. Jessup, C. B. Petty, J. Roos, L. E. Overman, *Org. Synth. Coll. Vol.* **1988**, 6, 95.

**A High Nuclearity, Mixed-Valence Manganese(III,IV) Complex:
[Mn₂₁O₂₄(OMe)₈(O₂CCH₂tBu)₁₆(H₂O)₁₀]****

Jonathan T. Brockman, John C. Huffman, and George Christou*

High-nuclearity manganese carboxylate clusters have been attracting intense interest during the last several years from scientists in various disciplines. This is because of a combination of factors, not least their aesthetic qualities and their unusual magnetic properties.^[1, 2] The latter arise from their large, and often abnormally large, ground-state spin values, which, in combination with significant easy-axis-type magnetoanisotropy, leads to Mn clusters exhibiting the new magnetic phenomenon of single-molecule magnetism.^[2] This property is the ability of discrete molecules to exhibit the superparamagnet-like property of slow magnetization relaxation and thus to behave as magnets below their blocking temperature by exhibiting magnetization versus field hysteresis.^[3, 4] The first single-molecule magnet (SMM) was [Mn₁₂O₁₂(O₂CMe)₁₆(H₂O)₄] (**1**), which possesses an *S* = 10 ground state.^[3, 5] and a number of other Mn_x SMMs have since been discovered.^[1, 2, 6–9]

As part of a continuing effort to prepare new clusters with large *S* values that might be SMMs, we have been exploring new reactions of **1**, or its derivatives, such as [Mn₁₂O₁₂(O₂CCH₂tBu)₁₆(H₂O)₄] (**2**), which can readily be prepared from **1** by a ligand-substitution procedure.^[10] A solution of **2** in CH₂Cl₂ was treated with an equal volume of MeOH, and the solution concentrated by slow evaporation over several days. After a brown solid was removed by filtration, black crystals of [Mn₂₁O₂₄(OMe)₈(O₂CCH₂tBu)₁₆(H₂O)₁₀] (**3**) formed over few days. The yield is very low (~3%) but the reaction has been reproduced several times. The structure of **3** (Figure 1, top)^[11] consists of an Mn core that is approximately planar and is ligated on the periphery by 16 μ-O₂CCH₂tBu groups and 10 H₂O molecules. The complex is trapped valence, the Mn^{III} ions being the outer Mn6–Mn11 atoms and their symmetry-related partners; the complex has crystallographic C_i symmetry. The Mn^{III} ions were identified by their metric parameters and Jahn–Teller distortions. As expected, the Jahn–Teller elongated Mn^{III}–O bonds (2.135(9)–2.323(8) Å) are significantly longer than the other Mn^{III}–O bonds (1.858(7)–1.981(8) Å). The Mn^{IV}–O bonds are in a narrower range (1.838(7)–1.956(8) Å). The 21 Mn ions are not all in the same plane: the nine Mn^{IV} ions (Mn1–Mn5) and two Mn^{III} ions (Mn8) are co-planar, but the two Mn₅

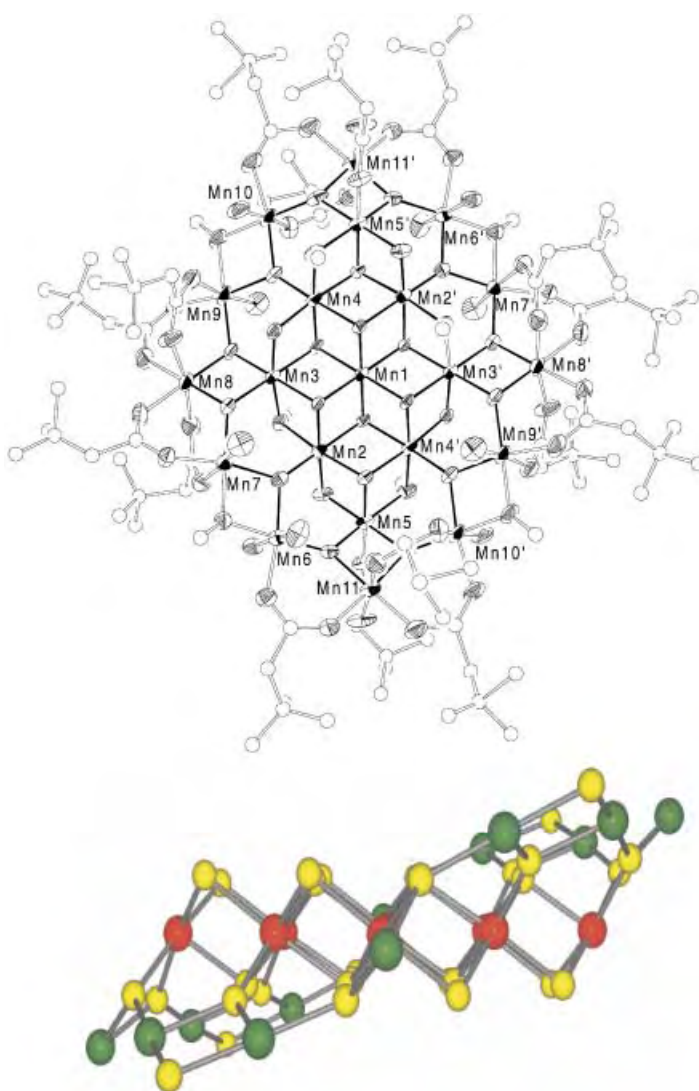


Figure 1. Top: ORTEP plot of the molecular structure of complex **3** (the thermal ellipsoids are set at 50% probability). Bottom: side view showing Mn⁴⁺ (red), Mn³⁺ (green), and O (yellow) atoms to emphasize the planar central Mn₁₁ unit.

crescents (Mn7, Mn6, Mn11, Mn10, Mn9) at top and bottom are slightly above and below this plane (Figure 1, bottom). The central oxide-bridged Mn₉ unit is reminiscent of the planar CdI₂-type sheet structure, as indeed is known for Mn^{IV} in the mineral lithiophorite (Al, Li) MnO₂(OH)₂.^[12, 13] Thus, a useful description of the [Mn₂₁O₂₄(OMe)₈] core is as a CdI₂-like [Mn₉^{IV}O₂₀] sheet held within a non-planar [Mn₁₂^{III}O₁₂] ring. This description relates the Mn₂₁ structure to that of **1** and **2**, which can be described as a [Mn₄^{IV}O₄] cube held with a non-planar [Mn₈^{III}O₈] ring (Figure 2).^[5, 14, 15] Complex **3** also has similarity to [Mn₁₉O₁₂(OC₂H₂OMe)₁₄(HOC₂H₂OMe)₁₀], which also has an approximately planar Mn₁₉ topology but all the metal ions are Mn^{II} centers.^[16] Similarly, complex **3** is also related to the [Fe₁₇O₄(OH)₁₆(heidi)₈(H₂O)₁₂]³⁺ and [Fe₁₉O₆(OH)₁₄(heidi)₁₀(H₂O)₁₂]⁺ (heidiH₃ = N(CH₂CO₂H)₂(CH₂OH)(CH₂CH₂OH)) clusters with planar Fe_x cores.^[17, 18]

The magnetic properties of **3** were investigated by solid-state magnetic susceptibility (χ_M) measurements in the 1.8 to 300 K range and DC fields up to 7 Tesla. The $\chi_M T$ value

[*] Prof. Dr. G. Christou, J. T. Brockman
Department of Chemistry
University of Florida
Gainesville, FL 32611-7200 (USA)
Fax: (+1) 352-392-6737
E-mail: christou@chem.ufl.edu
Dr. J. C. Huffman
Molecular Structure Center
Department of Chemistry
Indiana University, Bloomington, IN 47405-7102 (USA)

[**] This work was supported by the U.S. National Science Foundation (Grant CHE-0123603).

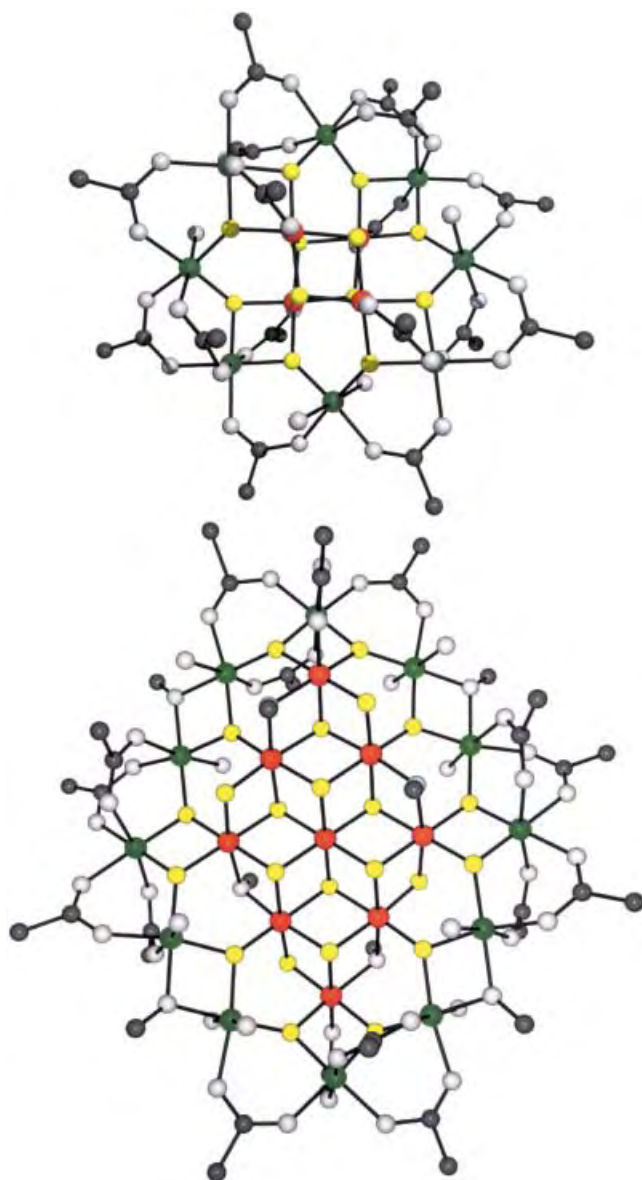


Figure 2. Comparison of the structures of Mn_{12} (top) and Mn_{21} (bottom) compounds. Color scheme: Mn^{4+} (red), Mn^{3+} (green), O^{2-} (yellow), other types of O atom (off-white), C (black).

steadily decreases from $42.1 \text{ cm}^3 \text{ K mol}^{-1}$ at 300 K to $19.0 \text{ cm}^3 \text{ K mol}^{-1}$ at 25.0 K, and then decreases more rapidly to $4.47 \text{ cm}^3 \text{ K mol}^{-1}$ at 2.00 K (Figure 3). The data strongly suggest predominantly antiferromagnetic exchange interactions within **3**. To determine the ground state, magnetization versus field and temperature data were collected in the 1–7 T and 1.9–10 K ranges and fitted by a matrix-diagonalization method to a model that assumes only the ground state is populated and includes axial zero-field splitting ($S_z^2 D$).^[8] The best fit gave $S = 13/2$, $g = 1.79$, and $D = -0.53 \text{ cm}^{-1}$. Comparable fits were obtained with $S = 15/2$, $g = 1.55$, $D = -0.40 \text{ cm}^{-1}$, and $S = 11/2$, $g = 2.10$, $D = -0.75 \text{ cm}^{-1}$, but were rejected owing to their unreasonable g value. The obtained $S = 13/2$ value is reasonable given that the $\text{Mn}^{\text{IV}} \cdots \text{Mn}^{\text{IV}}$ and $\text{Mn}^{\text{IV}} \cdots \text{Mn}^{\text{III}}$ interactions within the sheetlike structure are expected to be antiferromagnetic, but that spin frustration^[19] within the triangular M_3 units will prevent maximum spin

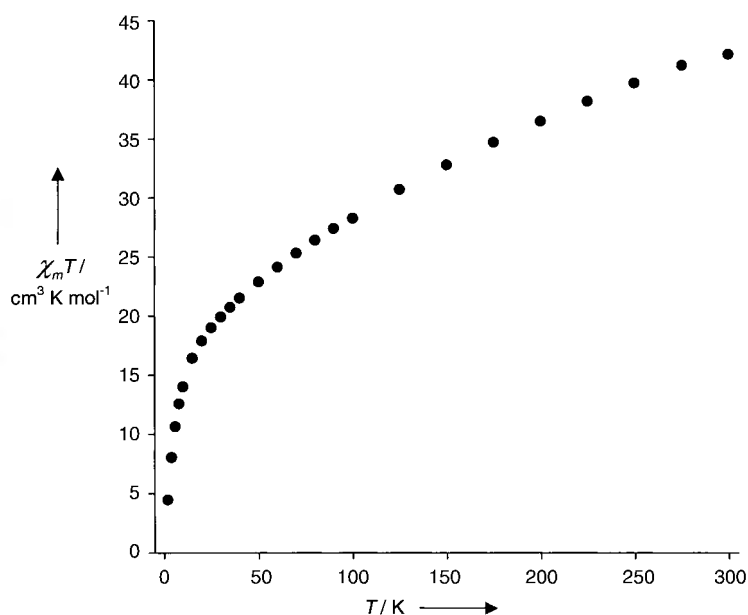


Figure 3. Plot of χ_{MT} versus T for complex **3**.

compensation to give a $S = 1/2$ ground state. In $[\text{Mn}_{12}\text{O}_{12}(\text{O}_2\text{CR})_{16}(\text{H}_2\text{O})_4]$ complexes, the acute angles within the central $[\text{Mn}_4^{\text{IV}}\text{O}_4]$ cubane lead to ferromagnetic $\text{Mn}^{\text{IV}} \cdots \text{Mn}^{\text{IV}}$ interactions and a correspondingly higher ($S = 10$) ground state, even though the nuclearity of Mn_{12} clusters is almost half that of **3**.

The relatively large S and D values suggested **3** might display the slow magnetization relaxation of a single-molecule magnet, and preliminary AC magnetic susceptibility studies were therefore performed in a 3.5 G field oscillating at frequencies up to 1500 Hz. No significant out-of-phase (χ''_{M}) signal was observed at temperatures $> 1.8 \text{ K}$ (the limit of our instrument), which suggests that further studies at lower temperatures are required.

In summary, the methanolysis of **2** in $\text{MeOH}/\text{CH}_2\text{Cl}_2$ has led to an interesting new structural type in higher-oxidation-state Mn cluster chemistry, a disk-like Mn_{21} mixed-valent complex. Mn chemistry continues to surprise and astound with the remarkable variety and aesthetic beauty of its molecular offspring.

Experimental Section

A brown solution of $2 \cdot \text{CH}_2\text{Cl}_2 \cdot \text{MeCN}$ (0.50 g, 0.18 mmol) in CH_2Cl_2 (50 mL) was treated with MeOH (50 mL). The solution was allowed to slowly concentrate by evaporation over 5 days, during which time a brown precipitate was obtained. The solid was removed by filtration and the filtrate maintained for two more days at room temperature to give well-formed black crystals of $3 \cdot 10\text{H}_2\text{O}$ in about 3% yield. Despite the low yield, the reaction is reproducible, although the quality of the black crystals varies. Solid dried in vacuo analyzed as solvent-free, elemental analysis: (%) calcd for $\text{C}_{104}\text{H}_{220}\text{Mn}_{21}\text{O}_{74}$: C 32.80, H 5.82; found for dried sample: C 32.99, H 5.55; selected IR data (KBr pellet): $\tilde{\nu} = 1634(\text{s})$, 1559 (w), 1539 (w), 1477 (w), 1456 (w), 1436 (w), 1410 (m), 1384 (s), 1275 (w), 1232 (w), 1121 (m), 1033 (m), 667 (m), 596 (br, s), 503 cm^{-1} (w). The brown powder has an IR spectrum similar to that of the crystals, but could not be purified to our satisfaction. Thus, only the black crystals were employed for characterization and study.

Received: February 18, 2002 [Z18727]

- [1] G. Aromi, S. M. J. Aubin, M. A. Bolcar, G. Christou, H. J. Eppley, K. Folting, D. N. Hendrickson, J. C. Huffman, R. C. Squire, H.-L. Tsai, S. Wang, M. W. Wemple, *Polyhedron* **1998**, *17*, 3005–3020.
- [2] G. Christou, D. Gatteschi, D. N. Hendrickson, R. Sessoli, *MRS Bull.* **2000**, *25*, 66–71.
- [3] R. Sessoli, D. Gatteschi, A. Caneschi, M. A. Novak, *Nature* **1993**, *365*, 141–143.
- [4] H. J. Eppley, H.-L. Tsai, N. de Vries, K. Folting, G. Christou, D. N. Hendrickson, *J. Am. Chem. Soc.* **1995**, *117*, 301–317.
- [5] R. Sessoli, H.-L. Tsai, A. R. Schake, S. Wang, J. B. Vincent, K. Folting, D. Gatteschi, G. Christou, D. N. Hendrickson, *J. Am. Chem. Soc.* **1993**, *115*, 1804–1816.
- [6] S. M. J. Aubin, M. W. Wemple, D. M. Adams, H.-L. Tsai, G. Christou, D. N. Hendrickson, *J. Am. Chem. Soc.* **1996**, *118*, 7746–7754.
- [7] E. K. Brechin, J. Yoo, M. Nakano, J. C. Huffman, D. N. Hendrickson, G. Christou, *Chem. Commun.* **1999**, 783–784.
- [8] J. Yoo, E. K. Brechin, A. Yamaguchi, M. Nakano, J. C. Huffman, A. L. Maniero, L.-C. Brunel, K. Awaga, H. Ishimoto, G. Christou, D. N. Hendrickson, *Inorg. Chem.* **2000**, *39*, 3615–3623.
- [9] C. Boskovic, E. K. Brechin, W. E. Streib, K. Folting, D. N. Hendrickson, G. Christou, *Chem. Commun.* **2001**, 467–468.
- [10] J. Yoo, A. Yamaguchi, M. Nakano, J. Krzystek, W. E. Streib, L.-C. Brunel, H. Ishimoto, G. Christou, D. N. Hendrickson, *Inorg. Chem.* **2001**, *40*, 4604–4616.
- [11] Crystal structure data for $3 \cdot 10\text{H}_2\text{O}$: $\text{C}_{104}\text{H}_{240}\text{Mn}_{21}\text{O}_{84}$, $M_r = 3988.70$, triclinic, space group $P\bar{1}$, $a = 12.4031(5)$, $b = 19.0808(7)$, $c = 19.6760(7)$ Å, $\alpha = 108.149(1)^\circ$, $\beta = 90.450(1)^\circ$, $\gamma = 106.773(1)^\circ$, $V = 4212.11$ Å³, $T = 111$ K, $Z = 1$, 64219 reflections collected, 19399 unique ($R_{\text{av}} = 0.099$), $R(F) = 0.0503$ and $R_w(F) = 0.0506$ using 5975 reflections with $I > 2.33\sigma(I)$. CCDC-177268 contains the supplementary crystallographic data for this paper. These data can be obtained free of charge via www.ccdc.cam.ac.uk/conts/retrieving.html (or from the Cambridge Crystallographic Data Centre, 12, Union Road, Cambridge CB21EZ, UK; fax: (+44) 1223-336-033; or deposit@ccdc.cam.ac.uk).
- [12] A. D. Wadsley, *Acta Crystallogr.* **1952**, *5*, 676–680.
- [13] The structure of chalcophanite ($\text{ZnMn}_3\text{O}_7 \cdot 3\text{H}_2\text{O}$) is similar, but one in every seven Mn^{IV} sites is vacant. A. D. Wadsley, *Acta Crystallogr.* **1955**, *8*, 165–172.
- [14] Z. Sun, D. Ruiz, N. R. Dilley, M. Soler, J. Ribas, K. Folting, M. B. Maple, G. Christou, D. N. Hendrickson, *Chem. Commun.* **1999**, 1973–1974.
- [15] M. Soler, P. Artus, K. Folting, J. C. Huffman, D. N. Hendrickson, G. Christou, *Inorg. Chem.* **2001**, *40*, 4902–4912.
- [16] I. A. M. Pohl, L. G. Westin, M. Kritikos, *Chem. Eur. J.* **2001**, *7*, 3439–3445.
- [17] A. K. Powell, S. L. Heath, D. Gatteschi, L. Pardi, R. Sessoli, G. Spina, F. Del Giallo, F. Pieralli, *J. Am. Chem. Soc.* **1995**, *117*, 2491–2502.
- [18] J. C. Goodwin, R. Sessoli, D. Gatteschi, W. Wernsdorfer, A. K. Powell, S. L. Heath, *J. Chem. Soc. Dalton Trans.* **2000**, 1835–1840.
- [19] J. K. McCusker, H. G. Jang, S. Wang, G. Christou, D. N. Hendrickson, *Inorg. Chem.* **1992**, *31*, 1874–1880.

Starched Carbon Nanotubes**

Alexander Star, David W. Steuerman, James R. Heath, and J. Fraser Stoddart*

Dedicated to Professor David N. Reinhoudt on the occasion of his 60th birthday

Since their discovery^[1] in 1993, single-walled carbon nanotubes (SWNTs) have found numerous applications^[2] in chemistry and physics on account of their anisotropic shapes (diameters of around 1 nm and lengths of micrometers), remarkable strengths and elasticities, and unique physical properties, for example, high thermal and electrical conductivities. By contrast, and despite their clear potential, SWNTs have not yet been fully integrated into biological systems,^[3] mainly because of the considerable difficulty in rendering them soluble in aqueous solutions.

Initially, the challenge of achieving soluble SWNTs in organic solvents was addressed by their covalent modification—examples include both end-group^[4] and side-wall^[5] functionalization. Covalent modification, however, has the disadvantage that it impairs their physical properties. For these, and other reasons, we have been attracted by a supramolecular approach^[6] to the solubilization problem—namely, the noncovalent functionalization of SWNTs by wrapping polymers around them in the knowledge that desired features can be grafted onto the polymers, prior to their being self-assembled around the SWNTs. Considerable progress^[6, 7] has been made in the use of synthetic polymers to render SWNTs soluble in organic solvents. However, while some water-soluble polymers^[8] and surfactants^[9] can bring aqueous solubilities to SWNTs, they may not be as biocompatible as would be desirable.

It was for this reason, amongst others, that we decided to explore the possibility of solubilizing SWNTs in aqueous solutions of starch.^[10] We knew from our knowledge of the supramolecular chemistry of fullerenes^[11] that cyclodextrins (CDs) of the appropriate dimensions (γ -CD commonly and δ -CD occasionally), and in the correct stoichiometries, will dissolve fullerenes (C_{60} and C_{70} , for example) in water.^[12] CDs are the macrocyclic analogues^[13] of starch. The connection is clear. Here, we report 1) that common starch, provided it is activated toward complexation by wrapping itself helically around small molecules, will transport SWNTs competitively into aqueous solutions, 2) that the process is sufficiently reversible at high temperatures to permit the separation of SWNTs in their supramolecular starch-wrapped form by a series of physical manipulations from amorphous carbon, and 3) that the addition of glucosidases to these starched carbon nanotubes results in the precipitation of the SWNTs from aqueous solution.

[*] Prof. J. F. Stoddart, Dr. A. Star, D. W. Steuerman, Prof. J. R. Heath
Department of Chemistry and Biochemistry
University of California, Los Angeles
405 Hilgard Avenue, Los Angeles, CA 90095-1569 (USA)
Fax: (+1) 310-206-1843
E-mail: stoddart@chem.ucla.edu

[**] This work was funded by the Office of Naval Research and by the National Science Foundation.

Starch and, in particular its linear component, amylose form^[10] inclusion complexes with a wide range of guest molecules. Amylose is composed of α -1,4 linkages between D-glucopyranose residues, and adopts^[14] a left-handed helical conformation (Figure 1a) in aqueous solution. It forms inclusion complexes as a result of hydrophobic interactions between guest molecules and the cylindrical cavity inside the amylose helix, which typically comprises around six α -D-glucopyranose residues per turn. The cavity diameter of the amylose helix is a variable dimension that allows the

biopolymer to adapt itself and accommodate the variety of differently proportioned guest molecules with which it is known^[15] to complex. In the knowledge that amylose can adjust its helical dimensions according to the size of the guest, we have carried out molecular dynamics (MD) calculations^[16] to probe the nature of the interactions between a short (6,6)-SWNT and an amylose fragment (maltooctaose) containing eight repeating α -1,4-D-glucopyranose residues. These calculations lend support to the formation of a supramolecular complex (Figure 1b) in which the maltooctaose wraps itself helically in a left-handed fashion around the nanotube. The hydrophobic faces of the D-glucopyranose residues (more precisely H-3 and H-5 in Figure 1a) interact with the hydrophobic surface of the nanotube leaving the three hydroxy groups on C-2, C-3, and C-6 to orient themselves so that they point outwards into the aqueous phase surrounding the complex and form hydrogen bonds to the water molecules coating its hydrophilic surface.

Our initial experiments, which were carried out on starch, revealed that, although SWNTs are not soluble in an aqueous solution of starch, they are soluble in an aqueous solution of a starch–iodine complex. We interpret these observations as suggesting that the initial preorganization of the amylose in starch into a helical conformation by iodine—or, indeed, by small organic molecules—prepares the way for a single carbon nanotube or bundles (Figure 1c) thereof to displace the many small molecules inside the helix by a “pea-shooting” type of mechanism, whereby enthalpic gain from favorable van der Waals interactions is aided and abetted by an entropy-driven process. In search of evidence for this theory, we examined the ability of iodine complexes of the separate components—amylose (the linear one) and amylopectin (the branched one)—of starch^[10] to solubilize SWNTs in water. While the amylose–iodine complex is just about as good as the starch–iodine complex, the amylopectin–iodine complex does not solubilize SWNTs in water. Like amylose, amylopectin contains α -1,4-linked D-glucopyranose chains. These chains, however, carry branches at C-6 on approximately every 25 D-glucopyranose residues, which also have the α configuration. The result is a very large molecular weight, dendrimer-like, glucan which does not complex with iodine nearly as well as does amylose in aqueous solution. The amylopectin–iodine complex is a dull-red color by comparison, in keeping with its impaired ability to form an inclusion complex with iodine, and hence with SWNTs. It seems, however, that the presence of amylopectin, along with amylose in starch, enhances the ability of the latter to form water-soluble complexes with SWNTs that are stable for long periods of time. Presumably the highly branched amylopectin molecules can interact favorably with the amylose-wrapped SWNTs and thus stabilize them in aqueous solution.

Amylose can apparently solubilize SWNTs directly in water because of the presence of complexed *n*BuOH molecules in most commercially available samples. Analysis of such a sample in D₂O by ¹H NMR spectroscopy confirms the presence of *n*BuOH (minimum of 10% by wt). The broad singlet for the methyl protons in *n*BuOH complexed by amylose is centered on $\delta = 0.90$ ppm, in contrast with that in free *n*BuOH, which is better resolved and resonates at

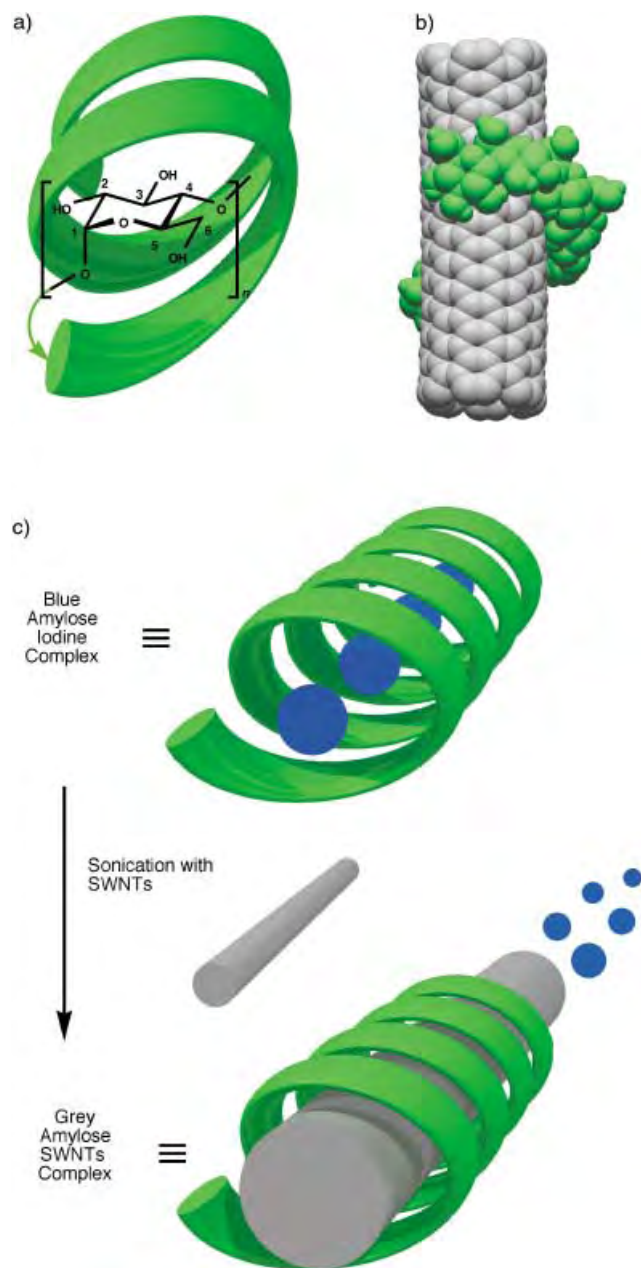


Figure 1. a) Schematic representation of the left-handed helix adopted by amylose when it complexes with small molecules. One α -1,4-linked D-glucopyranose residue, with its numbering system is overlaid on the helix. b) Space-filling representation of the result of computer modeling (molecular mechanics and molecular dynamics simulations using the solvation model for water) between a short (6,6)-SWNT and maltooctaose. c) Schematic representation of the “pea-shooting” type of mechanism whereby carbon nanotubes displace iodine molecules from the amylose helix.

$\delta = 0.87$ ppm. This upfield shift, which is consistent with literature data^[17] for helical amylose complexes with small organic molecules, has served as an additional probe in our present studies. Upon addition of an excess of iodine to the amylose-*n*-butanol complex in D₂O, a deep-blue color is formed and the ¹H NMR signal for the Me protons in the *n*BuOH molecules appears at $\delta = 0.87$ ppm. Similar spectroscopic behavior was observed during solubilization of SWNTs in a solution of the amylose-*n*-butanol complex in D₂O. Thus, both iodine and *n*BuOH molecules can be used as templates for the preorganization of amylose as a left-handed helix prior to its solubilizing SWNTs in water.

The release of iodine during the solubilization of SWNTs in an aqueous solution of the blue amylose-iodine complex is evident from a comparison (Figure 2) of UV/Vis spectra.

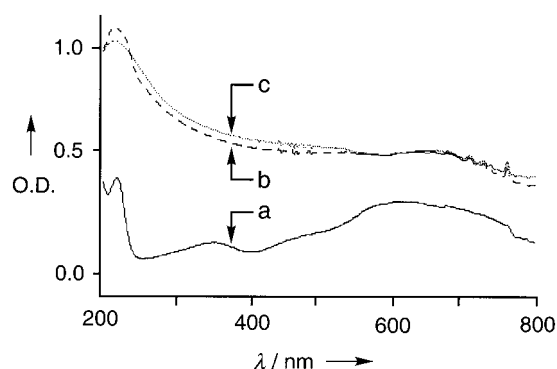


Figure 2. UV/Vis Spectra recorded in water of the blue amylose-iodine complex (a, full line), the amylose-SWNT complex obtained from the amylose-iodine complex (b, dashed line) and the amylose-*n*-butanol complex (c, dotted line); O.D. = optical density.

Figure 2a shows the multiple absorptions present^[18] in the UV/Vis spectrum of the amylose-iodine complex in water. These absorptions are eradicated upon solubilization of SWNTs in an aqueous solution of the amylose-iodine complex, and the blue coloration is lost. Moreover, SWNTs solubilized in water with amylose, using two different templates (iodine and *n*BuOH), show very similar UV/Vis spectra (see Figure 2b and c, respectively). These spectra reveal small features which are characteristic of SWNTs prepared by the high-pressure carbon monoxide (HiPco) process.^[19]

We have also investigated the starch-wrapped SWNTs by atomic force microscopy (AFM) following spin-evaporation of a drop of their aqueous solution on mica. AFM images show (Figure 3) small bundles of starched nanotubes which are covered profusely with amorphous polysaccharide. Excess of free starch—probably amylopectin in the main—is also evidently associated with the starch-wrapped SWNTs.

The consequences of enzymatic hydrolysis on the integrity of the starch-wrapped SWNTs in water has been investigated using the commercially available amyloglucosidase^[20] from *Rhizopus* mold. Addition of this enzyme to an aqueous solution of the starch-wrapped SWNTs results in the precipitation of all the nanotubes inside 10 minutes, as indicated by light-scattering measurements (Figure 4a) and also by changes (Figure 4b) that are clearly visible with the naked



Figure 3. An AFM image of isolated bundles of starch-wrapped SWNTs on a mica surface. Amorphous polysaccharide material is seen to aggregate with the nanotubes mostly at junctions between bundles.

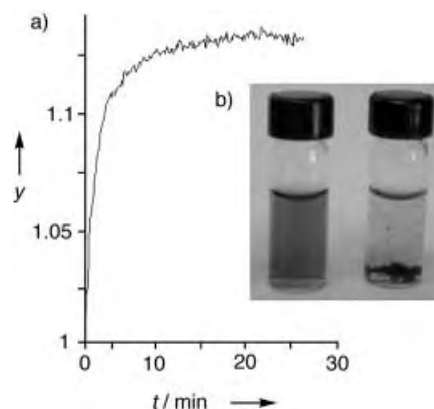
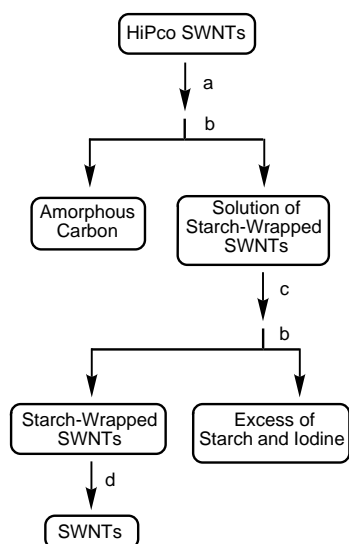


Figure 4. Enzymatic hydrolysis of the starch-SWNT complex. a) Changes (y is the refraction in arbitrary units) in light scattering upon addition of amyloglucosidase and b) a photograph of vials containing the complex before (left) and after (right) addition of the enzyme.

eye. ¹H NMR spectroscopy was also used to follow the enzymatic hydrolysis of starch-wrapped SWNTs in D₂O. The spectrum of the starch-SWNT complex in D₂O, which, although severely broadened—probably because of the presence of ferromagnetic particles carried over from the process used to produce the SWNTs—changes during the course of an hour to another broad spectrum, which corresponds to that of glucose.

The fact that the supramolecular chemistry which operates between SWNTs and amylose can be conducted under physical, chemical, or biological control constitutes an important scientific development^[21] with implications for both carbon nanotube and starch research. At the simplest practical level, it is now easy to purify SWNTs cheaply, under ambient conditions, using readily available starch complexes. A protocol for the cleaning up of SWNTs with starch is given in Scheme 1. Furthermore, given the recent progress^[22] in the



Scheme 1. Proposed scheme for purification of SWNTs in water with starch. a) Sonication (water bath—Branson model 1510, 40 kHz) in water with starch–iodine complex; b) centrifugation (3300 rpm, 15 min); c) heating to boiling, whereupon the starch-wrapped SWNTs precipitates out of solution. The resulting starch-wrapped SWNTs are water-soluble up to concentrations of 3 g L^{-1} following sonication for 1 min. d) Addition of amyloglucosidase and incubation at room temperature for 18 h, followed by filtration through a PTFE membrane filter and washings with water.

separation of enantiomeric fullerenes, by using amylose-based chromatographic techniques, the possibility of employing amylose in some shape or form to differentiate between enantiomeric carbon nanotubes displaying right- and left-handed helicities is a prospect that can now at least be contemplated. Finally, opportunities clearly exist to form complexes between SWNTs and a range of different amylose derivatives, so enabling their deeper integration with other biosystems.

Experimental Section

Commodities: Soluble starch (for iodometry) was from Fisher Scientific. Amylose, purchased from Aldrich contains more than 10 % of *n*BuOH and so is “activated” toward the solubilization of SWNTs in water. Amylopectin (from potato starch) was obtained from Fluka. SWNTs, produced by the literature method,^[19] were used as received from Rice University. Amyloglucosidase from *Rhizopus* mold (activity, 23 U mg^{-1}) was purchased from Sigma.

Solubilization of SWNTs in water: An aqueous solution of a starch–iodine complex was prepared by saturating a water-soluble starch solution (10 g L^{-1}) with an excess of iodine overnight. SWNTs (10 mg) were dispersed in the resulting blue solution (42 mL) of the starch–iodine complex (containing 400 mg of starch) by agitation, followed by mild (no more than 5 min) ultrasonication. A black residue separates from the starch-wrapped SWNTs on centrifugation at 3300 rpm for 15 min. After repeating this cycle again on the residue, the amount of amorphous carbon removed was about 4 mg. The combined aqueous solutions were heated to boiling, whereupon the starch-wrapped SWNTs precipitated out of solution. The excess of starch and iodine was removed by centrifugation and decantation. The precipitate was redissolved in water (42 mL) by sonication (1 min) and the aqueous solution (which was now stable on boiling) was concentrated by evaporation over three successive cycles that involved further centrifugation, decantation, and sonication, to yield ultimately starch-wrapped SWNTs (12 mg). This product, which can be dissolved in water up to a concentration of 3 g L^{-1} , was subsequently shown by enzymatic hydrolysis^[20] of the starch to be an approximate 5:1 mixture

(by wt) of starch and SWNTs, respectively. When this procedure was repeated using amylose the stability of the amylose complex with SWNTs in water was lower than that when starch was employed. The use of amylopectin resulted in very much reduced complex stabilities.

Preparation of the starch-wrapped SWNTs for AFM: The sample preparation for AFM was accomplished by placing a newly cleaved mica wafer in a base (KOH) bath to ensure hydrophilicity. A solution of the starch–nanotube complex was sonicated for 60 s before being dropped onto the wafer. Finally, this wafer was spun at 4000 rpm for 30 s and then rinsed in water. The topographical data were recorded with a Digital Instruments Multimode AFM with a high-resolution stage, controlled by a Nanoscope IIIa scanning probe microscope controller with a Nanoscope Extender. The images were recorded with standard tips in tapping mode at a scan rate of 0.5 Hz.

Enzymatic hydrolysis of starch-wrapped SWNTs: Starch-wrapped SWNTs (3.3 mg) were dissolved in 0.1 M sodium acetate buffer (pH 4.75) in D_2O (1 mL) and 10 μL of an enzyme solution (10 mg mL^{-1} in the buffer) were added. ^1H NMR spectra (360 MHz) were recorded every 20 min until the hydrolysis of the starch was completed (after 16 h). In this experiment, and also in a control with starch alone, the singlet ($\delta = 1.96\text{ ppm}$) for the acetoxy groups in the buffer solution was used as an internal reference for estimating the relative amounts of starch and glucose.^[23] Following hydrolysis,^[24] the insoluble SWNTs were isolated by filtration through a PTFE membrane filter (0.2 μm) and, after washing (water) and drying, the purified “bucky paper” (0.5 mg) was isolated.

Received: February 26, 2002 [Z18778]

- [1] S. Iijima, T. Ichihashi, *Nature* **1993**, 363, 603–605.
- [2] P. M. Ajayan, *Chem. Rev.* **1999**, 99, 1787–1799.
- [3] For examples of the immobilization of biomolecules on carbon nanotubes motivated by the prospect of making new kinds of biosensor materials, see: a) F. Balavoine, P. Schultz, C. Richard, V. Mallouh, T. W. Ebbesen, C. Mioskowski, *Angew. Chem.* **1999**, 111, 2036–2039; *Angew. Chem. Int. Ed.* **1999**, 38, 1912–1915; b) R. J. Chen, Y. Zhang, D. Wang, H. Dai, *J. Am. Chem. Soc.* **2001**, 123, 3838–3839.
- [4] a) J. Liu, A. G. Rinzier, H. Dai, J. H. Hafner, R. K. Bradley, P. J. Boul, A. Lu, T. Iverson, K. Shelimov, C. B. Huffman, F. Rodriguez-Macias, Y.-S. Shon, T. R. Lee, D. T. Colbert, R. E. Smalley, *Science* **1998**, 280, 1253–1256; b) J. Chen, M. A. Hamon, H. Hu, Y. Chen, A. M. Rao, P. C. Ehlund, R. C. Haddon, *Science* **1998**, 282, 95–98.
- [5] P. J. Boul, J. Liu, E. T. Mickelson, C. B. Huffman, L. M. Ericson, I. W. Chiang, K. A. Smith, D. T. Colbert, R. H. Hauge, J. L. Margrave, R. E. Smalley, *Chem. Phys. Lett.* **1999**, 310, 367–372.
- [6] A. Star, J. F. Stoddart, D. Steuerman, M. Diehl, A. Boukai, E. Wong, X. Yang, S.-W. Chung, H. Choi, J. R. Heath, *Angew. Chem.* **2001**, 113, 1771–1775; *Angew. Chem. Int. Ed.* **2001**, 40, 1721–1725.
- [7] Polymers that have been used to prepare composites with SWNTs include polymethylmethacrylate, see: a) M. Yudasaka, M. Zhang, C. Jabs, S. Iijima, *Appl. Phys. A* **2001**, 71, 449–451; b) C. Stephan, T. P. Nguyen, M. Lamy de la Chapelle, S. Lefrant, C. Journet, P. Bernier, *Synth. Met.* **2000**, 108, 139–149. Polymers have also been used to prepare composites with multiwalled nanotubes, see: c) M. S. P. Shaffer, A. H. Windle, *Adv. Mater.* **1999**, 11, 937–941; d) Z. Jin, X. Sun, G. Xu, S. H. Goh, W. Ji, *Chem. Phys. Lett.* **2000**, 318, 505–510. Recently, polymers have been used in the spinning of SWNTs into long fibers, see: e) B. Vigolo, A. Penicaud, C. Coulon, C. Sauder, R. Paillet, C. Journet, P. Bernier, P. Poulin, *Science* **2000**, 290, 1331–1334. For composite materials formed between nanotubes and poly(metaphenylenevinylene), see: f) S. A. Curran, P. M. Ajayan, W. J. Blau, D. L. Carroll, J. N. Coleman, A. B. Dalton, A. P. Davey, A. Drury, B. McCarthy, S. Maier, A. Strevant, *Adv. Mater.* **1998**, 10, 1091–1093; g) S. A. Curran, A. P. Davey, J. N. Coleman, A. B. Dalton, B. McCarthy, S. Maier, A. Drury, D. Gary, M. Brennan, K. Ryder, M. Lamy de la Chapelle, C. Journet, P. Bernier, H. J. Byrne, D. Carroll, P. M. Ajayan, S. Lefrant, W. Blau, *Synth. Met.* **1999**, 103, 2559–2562; h) J. N. Coleman, A. B. Dalton, S. Curran, A. Rubio, R. C. Barklie, W. J. Blau, *Adv. Mater.* **2000**, 12, 213–216.

- [8] M. J. O'Connell, P. Boul, L. M. Ericson, C. Huffman, Y. Wang, E. Haroz, C. Kuper, J. Tour, K. D. Ausman, R. E. Smalley, *Chem. Phys. Lett.* **2001**, *342*, 265–271.
- [9] G. S. Duesberg, J. Muster, V. Krstic, M. Burghard, S. Roth, *Appl. Phys. A* **1998**, *67*, 117–119.
- [10] a) P. Collins, R. Ferrier, *Polysaccharides: Their Chemistry*, Wiley, Chichester, **1995**, pp. 478–523; b) J. Lehmann, *Carbohydrates: Structure and Biology*, Thieme, Stuttgart, **1998**, pp. 98–103; c) D. B. Thompson, *Carbohydr. Polym.* **2000**, *43*, 223–239.
- [11] For an excellent review on supramolecular fullerene chemistry, see: F. Diederich, M. Gómez-López, *Chem. Soc. Rev.* **1999**, *28*, 263–277.
- [12] a) T. Anderson, K. Nilsson, M. Sundahl, G. Westman, O. Wennerström, *J. Chem. Soc. Chem. Commun.* **1992**, 604–606; b) W. Kutner, P. Boulas, K. M. Kadish, *J. Electrochem. Soc.* **1992**, *139*, 243C; c) M. Sundahl, T. Andersson, K. Nilsson, O. Wennerström, G. Westman, *Synth. Met.* **1993**, *56*, 3252–3257; d) D. D. Zhang, Q. Liang, J. W. Chen, M. K. Li, S. S. Wu, *Supramol. Chem.* **1993**, *3*, 235–238; e) Á. Buvári-Barcza, T. Braun, L. Barcza, *Supramol. Chem.* **1994**, *4*, 131–135; f) Z.-i. Yoshida, H. Takekuma, S.-i. Takekuma, Y. Matsubara, *Angew. Chem.* **1994**, *106*, 1658–1660; *Angew. Chem. Int. Ed. Engl.* **1994**, *33*, 1597–1599; g) D. D. Zhang, J. W. Chen, Y. Ying, R. F. Cai, X. L. Shen, S. H. Wu, *J. Inclusion Phenom.* **1993**, *16*, 245–253; h) Y. Liu, L. F. Wang, D. D. Zhang, *Chin. Sci. Bull.* **1995**, *40*, 1759–1760; i) C. Y. Jin, D. D. Zhang, T. Oguma, S. X. Qian, *J. Inclusion Phenom.* **1996**, *24*, 301–310; j) T. Furuishi, T. Endo, H. Nagase, H. Ueda, T. Nagai, *Chem. Pharm. Bull.* **1998**, *46*, 1658–1659; k) Á. Buvári-Barcza, J. Rohonczy, N. Rozlosnik, T. Gilányi, B. Szabó, G. Lovas, T. Braun, L. Barcza, *J. Chem. Soc. Perkin Trans. 2* **2001**, 191–196.
- [13] See *Chem. Rev.* **1998**, *98*, 1741–2076 for a special issue on cyclodextrins.
- [14] a) W. Hinrichs, G. Buettner, M. Steifa, C. Betzel, V. Zabel, B. Pfannmueller, W. Saenger, *Science* **1987**, *238*, 205–208; b) R. C. Teitelbaum, S. L. Ruby, T. J. Marks, *J. Am. Chem. Soc.* **1978**, *100*, 3215–3217; c) R. E. Rundle, *J. Am. Chem. Soc.* **1947**, *69*, 1769–1772, and references therein.
- [15] The inner diameters that have been reported (by electron diffraction studies on crystalline amylose complexes or so-called V-amylose) are 4.5, 6.0, and up to 7–8 Å: a) Y. Yamashita, *J. Polym. Sci. Part A* **1965**, *3*, 3251–3260; b) Y. Yamashita, N. Hirai, *J. Polym. Sci. Part A2* **1966**, *4*, 161–171; c) Y. Yamashita, K. Monobe, *J. Polym. Sci. Part A2* **1971**, *9*, 1471–1481.
- [16] Molecular dynamics (MD) simulations, based on the AMBER force field, using the solvation model for water, were achieved within MacroModel. The assembly was allowed to equilibrate over the course of a 100 ps (1.5 fs time step) MD simulation at 300 K, before providing the superstructure displayed in Figure 1b. For conformational analysis of an amylose fragment (maltoheptaose) in water, see: J. Shimada, H. Kaneko, T. Takada, S. Kitamura, K. Kajiwara, *J. Phys. Chem. B* **2000**, *104*, 2136–2147.
- [17] J. Kadokawa, Y. Kaneko, H. Tagaya, K. Chiba, *Chem. Commun.* **2001**, 449–450.
- [18] It has been shown that in the amylose–iodine complex, the iodine molecules exist as polyiodide chains and are composed of I_3^- and I_5^- subunits which combine to form four dominant polyiodide chains (I_9^{3-} , I_{11}^{3-} , I_{13}^{3-} , and I_{15}^{3-}) and give different absorption spectra when complexed inside the amylose. The absorption maxima associated with these chains appear at 480–510, 610–640, 690–720, and 730–760, respectively. See: X. Yu, C. Houtman, R. H. Atalla, *Carbohydr. Res.* **1996**, *292*, 129–141.
- [19] I. W. Chiang, B. E. Brinson, A. Y. Huang, P. A. Willis, M. J. Bronikowski, J. L. Margrave, R. E. Smalley, R. H. Hauge, *J. Phys. Chem. B* **2001**, *105*, 8297–8301.
- [20] Among the numerous enzymes that will hydrolyze starch, there is amylglucosidase, an exoamylase which attacks all the α -1,4 and α -1,6 glucosidic linkages to produce glucose. For more information about the properties of this and other glucosidases, see: T. Yamamoto, *Enzyme Chemistry and Molecular Biology of Amylases and Related Enzymes*, CRC, Boca Raton, FL, USA, **1995**, pp. 3–201. α -Amylase, which is present in human saliva, is an endoamylase that attacks the α -1,4 glucosidic linkages in starch randomly and so reduces the lengths of the glucan chains. Indeed, we have found that aqueous solutions of starch-SWNTs are stable for weeks provided you do not spit on them! Addition of saliva to these solutions leads to precipitation of the carbon nanotubes after several hours.
- [21] Just as this manuscript was about to be submitted, we learned of a simple procedure for dispersing SWNTs in aqueous solutions of the acidic polysaccharide, Gum Arabic, produced by Acacia Senegal trees. See: R. Bandyopadhyaya, E. Nativ-Roth, O. Regev, R. Yerushalmi-Rozen, *Nano Lett.* **2002**, *2*, 25–28.
- [22] C. Yamamoto, T. Hayashi, Y. Okamoto, S. Ohkubo, T. Kato, *Chem. Commun.* **2001**, 925–926.
- [23] Enzymatic hydrolysis of starch-wrapped SWNTs has also been followed by carrying out light-scattering measurements recorded on a Jasco J-715 spectrophotometer with a 1-cm fluorescence cell. In this experiment, an enzyme solution (2 μ L of 10 mg mL⁻¹) was added to the starch-wrapped SWNTs in aqueous solution at a concentration of 0.5 mg mL⁻¹ (Figure 4a).
- [24] In the case of the enzymatic hydrolysis of starch, the combined intensities for the anomeric protons (H_a and H_b) of D-glucopyranose equal that for the anomeric protons (H_b) in starch. However, the glucose produced on treating the starch-wrapped SWNTs integrates for significantly more than the complexed starch. It is well known that proton signals in polymer-wrapped SWNTs are not only broadened but reduced in their intensities by this kind of complexation. See: ref. [8].

The First Non-Heme Iron(III) Complex with a Ligated Carboxamido Group That Exhibits Photolability of a Bound NO Ligand**

Apurba K. Patra, Raman Afshar, Marilyn M. Olmstead, and Pradip K. Mascharak*

Dedicated to Professor Karl Wieghardt on the occasion of his 60th birthday

Nitric oxide (NO) is the first gaseous molecule known to act as a biological messenger and it participates in several important functions including control of blood pressure, neurotransmission, and inhibition of tumor growth.^[1] The tumoricidal property of NO has raised interest in the use of organic^[1] and metal–nitrosyl complexes^[2] that release NO upon illumination as agents in photodynamic therapy (PDT).^[3] Such compounds can deliver NO to biological targets on demand and are preferred over conventional photodynamic agents such as photofrin in treating malignant tumors with hypoxic locales. In recent years, iron–nitrosyl complexes such as Na₂[Fe(CN)₅NO]^[4] and Roussin's salts^[5]

[*] Prof. Dr. P. K. Mascharak, Dr. A. K. Patra, R. Afshar
Department of Chemistry and Biochemistry
University of California
Santa Cruz, CA 95064 (USA)
Fax: (+1) 831-459-2935
E-mail: pradip@chemistry.ucsc.edu

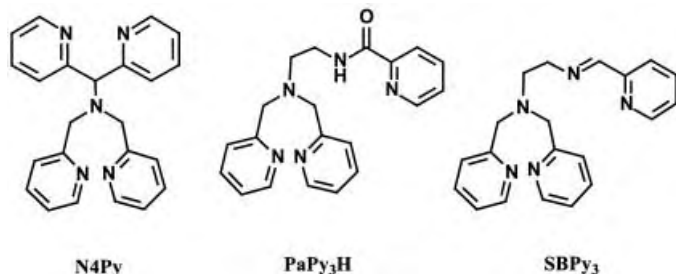
Dr. M. M. Olmstead
Department of Chemistry
University of California
Davis, CA 95616 (USA)

[**] Financial support from the NSF (CHE-9818492) and NIH (GM 61636) is gratefully acknowledged. The Bruker SMART 1000 diffractometer was funded in part by an NSF Instrumentation Grant CHE-9808259.

Supporting information for this article is available on the WWW under <http://www.angewandte.org> or from the author.

have been studied extensively as prospective NO-releasing agents in PDT.

Although a survey of the coordination chemistry of NO clearly reveals its preference for Fe^{II} centers, the binding of NO to Fe^{III} centers has been reported in a few heme^[6] and non-heme^[7, 8] species. Recently, we reported the low-spin Fe^{III} complex [Fe(PaPy₃)(CH₃CN)][ClO₄]₂ (**1**) which binds to a



variety of ligands, through replacement of the solvent (acetonitrile) molecule.^[9] Herein, we report that **1** readily reacts with NO to afford [Fe(PaPy₃)(NO)][ClO₄]₂ (**2**) and that **2** rapidly loses NO upon exposure to light in solvents such as CH₃CN (thus re-forming **1**). Binding of NO at the non-heme Fe^{III} center in **1** is completely reversible and the bound NO is photolabile. We believe that the photolability of NO observed with **2** is related to the coordinated carboxamido nitrogen atom, which provides extra stability to the Fe^{III} center.^[10] To prove this hypothesis we have also synthesized the Fe^{III} complex of the Schiff base SBPy₃, a ligand identical to PaPy₃H except for the presence of an imine group in place of the carboxamide moiety. The low-spin Fe^{III} complex [Fe-(SBPy₃)(dmf)][ClO₄]₃ (**3**) is spontaneously reduced to the corresponding Fe^{II} species [Fe(SBPy₃)(CH₃CN)][ClO₄]₂ in CH₃CN and exhibits no affinity toward NO. The behavior of **3** in CH₃CN is similar to that of the iron complex containing the N4Py ligand, as reported by Feringa and co-workers.^[11]

When purified NO gas is passed through a solution of **1** in CH₃CN, its purple color rapidly turns red showing the formation of the NO adduct **2**. Since the bound NO in **2** is labile in CH₃CN under light, we have synthesized **2** by an alternative method. A slurry of [Fe(dmf)₆][ClO₄]₃ and PaPy₃H (1:1) in MeOH, was stirred with one equivalent of a mild base, in this case, triethylamine, at 45 °C. The mixture became homogeneous and reddish purple within 30 min. Passage of NO through this solution caused rapid precipitation of red microcrystalline **2** in good yield. The IR spectrum of **2** displays an NO stretch at 1919 cm⁻¹, which is within the range (1822–1937 cm⁻¹) expected for an {Fe–NO}⁶-type complex.^[6b, 8b] The ¹H NMR spectrum of **2** (prepared and run in the dark) clearly indicates its *S* = 0 ground state (see Supporting Information). The structure of the cation of **2** is shown in Figure 1.^[12] The Fe^{III} center is in a distorted octahedral geometry. The *tert*-amine and the three pyridine nitrogen atoms comprise the equatorial plane, with the carboxamido nitrogen atom and the NO ligand occupying the axial positions; the Fe–N–O bond is almost linear (Fe–N6–O2 = 173.1(2)°). Although the average Fe–N_{py} and Fe–N_{amine} bond lengths of **2** are similar to those in **1**, the Fe–N_{amido} bond

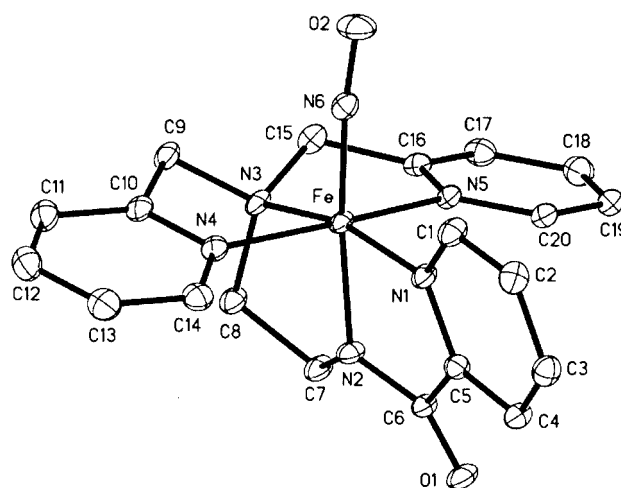


Figure 1. ORTEP diagram of [Fe(PaPy₃)(NO)]²⁺, the cation of **2**, showing the atom labeling scheme. All H atoms and the CH₃CN molecule present as solvent of crystallization have been omitted for clarity. Selected bond lengths [Å] and bond angles [°]: Fe–N1 1.978(2), Fe–N2 1.9009(19), Fe–N3 1.972(2), Fe–N4 1.982(2), Fe–N5 1.983(2), Fe–N6 1.677(2), N6–O2 1.139(3); Fe–N6–O2 173.1(2), N6–Fe–N2 174.35(9), N1–Fe–N2 81.18(8), N1–Fe–N3 165.68(8), N1–Fe–N4 97.13(9), N1–Fe–N5 95.88(8), N2–Fe–N3 84.58(8), N2–Fe–N4 91.82(8), N2–Fe–N5 84.35(8), N3–Fe–N4 81.79(9), N3–Fe–N5 84.13(8), N3–Fe–N6 97.54(9), N4–Fe–N5 165.71(8), N4–Fe–N6 93.67(9), N5–Fe–N6 90.64(9).

(1.901(2) Å) is longer than that in **1** (1.826(3) Å). There is evidence of appreciable double bond character in the Fe–N(O) bond (1.677(2) Å), much like that observed in other {Fe–NO}⁶ species.^[6b, 8b]

When the red solution of **2** in CH₃CN is kept in the dark, the electronic absorption spectrum (rapid scan) does not change appreciably, even after 48 h (see Supporting Information). However, when the cuvette is exposed to light (50 W tungsten lamp), the color changes rapidly to purple (namely, the color of **1**).^[13] Clean isosbestic points are observed in successive electronic absorption spectra (Figure 2). Conversely, when NO is introduced into the cuvette, the color slowly goes back to red (the color of **2**, see Supporting Information).

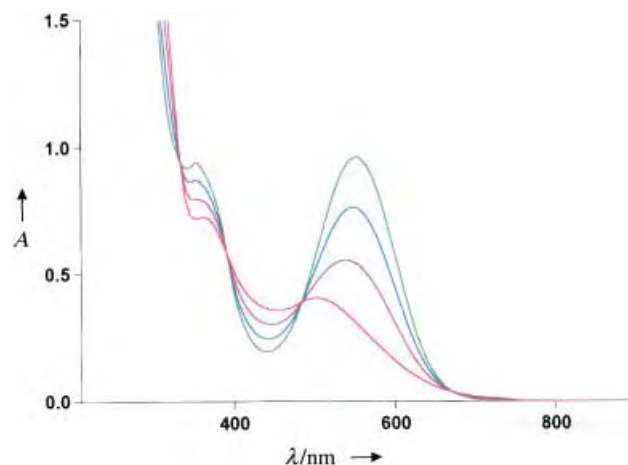


Figure 2. Conversion of [Fe(PaPy₃)(NO)][ClO₄]₂ (**2**, red trace) into [Fe(PaPy₃)(CH₃CN)][ClO₄]₂ (**1**, green trace) in CH₃CN under illumination with a 50 W tungsten lamp (*t*_{1/2} = 45 s).

The low-spin Fe^{III} complex [Fe(SBPY₃)(dmf)][ClO₄]₃ (**3**) has been isolated from the reaction of [Fe(dmf)₆][ClO₄]₃ and SBPY₃ (1:1) in MeOH. Isolation of this Fe^{III} complex is only possible from MeOH since it precipitates out from this solvent immediately on formation. When **3** is dissolved in CH₃CN or DMF, the red solution rapidly turns purple as a consequence of the spontaneous reduction of **3** to the corresponding Fe^{II} complex [Fe(SBPY₃)(solvent)][ClO₄]₃ (see Supporting Information). As a consequence of this rapid formation, crystals of **3** suitable for structural studies were not obtained. However, analytical and spectral data clearly establish the identity of this compound. We have synthesized the purple diamagnetic Fe^{II} complex [Fe(SBPY₃)(CH₃CN)][BF₄]₂ (**4**) and characterized it by X-ray crystallography (see Supporting Information).^[14] Complex **4** exhibits a half-wave potential (*E*_{1/2}) of 1.01 V (versus the saturated calomel electrode, SCE) in CH₃CN. Clearly, the SBPY₃ ligand stabilizes the Fe^{II} center much like N4Py (*E*_{1/2} of [Fe(N4Py)(CH₃CN)][ClO₄]₂ in CH₃CN = 1.01 V versus SCE) and hence, in both cases, one obtains the Fe^{II} complex rather easily. In the present case, complex **3** is amenable for isolation because of its low solubility in methanol.

Notably, **3** does not bind NO under any conditions. Since both **1** and **3** are low-spin, the ground-state electronic configuration is not responsible for this difference. There is a difference, however, in their redox potential; the *E*_{1/2} value for **1** in CH₃CN is 0.21 V (versus SCE). The presence of just one carboxamido nitrogen atom around the Fe^{III} center in **1** stabilizes the +3 oxidation state of iron by approximately 0.8 V relative to **3** or [Fe(N4Py)(CH₃CN)][ClO₄]₂. It appears, therefore, that a more stabilized Fe^{III} center (such as that in **1**) is required for NO binding and the photolability of the bound NO molecule (as in the NO adduct of **1**). Since the bound NO in **2** is *trans* to the carboxamido nitrogen atom, it also appears that a negatively charged donor center is another requirement for the photolability of the bound NO molecule. Reversible binding of NO has been observed at the non-heme Fe^{III} site in the microbial enzyme nitrile hydratase.^[15, 16] This Fe^{III} center is coordinated to carboxamido nitrogen atoms in the equatorial plane, and is stabilized to a great extent.^[17] Additionally, in the NO-bound “dark” form, NO is *trans* to a negatively charged cystinato sulfur donor and the enzyme releases NO upon illumination.

In conclusion, [Fe(PaPy₃)(NO)][ClO₄]₂ (**2**) is the first example of an {Fe–NO}⁶-type iron–nitrosyl species with a carboxamido nitrogen atom as a donor.^[18] It is also the first non-heme Fe^{III} species that binds NO reversibly and exhibits the photolability of a bound NO moiety under very mild conditions. Photokinetic studies of **2** and related complexes are ongoing.

Experimental Section

All reactions were carried out in an inert N₂ atmosphere.

2: A slurry of [Fe(dmf)₆][ClO₄]₃ (0.23 g, 0.29 mmol) in MeOH (10 mL) was added to a stirred solution of PaPy₃H (0.10 g, 0.29 mmol) in MeOH (10 mL), followed by the addition of triethylamine (0.03 g, 0.3 mmol) diluted in MeOH (2 mL). The reaction mixture was then stirred at 45 °C for 30 min, by which time a reddish purple solution was obtained. Purified NO gas was then introduced into the flask, and a red-colored complex

precipitated out immediately. It was then filtered, washed with anhydrous Et₂O, and dried under vacuum (0.095 g, 52 % yield). Crystals of [Fe(PaPy₃)(NO)][ClO₄]₂·CH₃CN (**2**·CH₃CN), suitable for X-ray diffraction, were grown in the dark by diffusion of Et₂O into a solution of the complex in CH₃CN. Elemental analysis calcd for C₂₂H₂₃Cl₂FeN₇O₁₀ (**2**·CH₃CN): C 39.31, H 3.45, N 14.59; found: C 39.28, H 3.51, N 14.60; FT-IR (KBr): $\tilde{\nu}$ = 3082(w), 2932(w), 2867(w), 1919(s), 1642(s), 1609(m), 1453(m), 1385(m), 1289(w), 1228(w), 1090(s), 765(m), 623(m); UV/Vis (CH₃CN, prepared in dark conditions) λ_{max} /nm (ϵ in M⁻¹cm⁻¹) = 500 (1040), 365 (1840); ¹H NMR (500 MHz, CD₃CN): δ = 8.99 (d, 1H), 8.51 (t, 1H), 8.28 (d, 1H), 8.14 (t, 2H), 8.04 (m, 1H), 7.73 (d, 2H), 7.44(t, 2H), 6.72 (d, 2H), 5.02 (dd, 4H), 3.73 (d, 2H), 3.68 (d, 2H) ppm.

3: A solution of [Fe(dmf)₆][ClO₄]₃ (0.50 g, 0.63 mmol) in MeOH (20 mL) was slowly added to a solution of SBPY₃ (0.21 g, 0.63 mmol) in MeOH (10 mL) and stirred. Complex **3** rapidly precipitated from the reaction mixture as a red microcrystalline solid which was filtered, washed with anhydrous Et₂O, and dried under vacuum (0.26 g, 57 % yield). Elemental analysis calcd for C₂₄H₃₂Cl₃FeN₆O₁₄ (**3**·MeOH): C 36.45, H 4.08, N 10.63; found: C 36.31, H 4.11, N 10.73; selected IR frequencies (cm⁻¹, KBr disk): $\tilde{\nu}$ = 3425(br, m), 3072(w), 2932(w), 2791(w), 1650(m), 1602(m), 1479(w), 1437(m), 1291(m), 1090(vs), 774(s), 620(s); UV/Vis (CH₃CN) λ_{max} /nm (ϵ in M⁻¹cm⁻¹) = 545 (sh, 1500), 445 (sh, 2470), 390 (sh, 4240), 345 (5420). X-band EPR spectrum in 1:1 methanol/acetone glass (86 K): *g* = 2.313, 2.157, 1.933 (see Supporting Information).

4: A solution of [Fe(H₂O)₆][BF₄]₂ (0.20 g, 0.6 mmol) in MeOH (10 mL) was added to a solution of SBPY₃ (0.20 g, 0.6 mmol) in MeOH (7 mL). The deep purple solution was stirred for 1 h, at which point CH₃CN (3 mL) was added. Anhydrous Et₂O was then allowed to diffuse into this mixture at 4 °C. Magenta plates of [Fe(SBPY₃)(CH₃CN)][BF₄]₂·½Et₂O·½CH₃OH (**4**·½Et₂O·½CH₃OH) were isolated after 4 days (0.27 g, 70 % yield). Elemental analysis calcd for C₂₄H₃₀B₂F₈FeN₆O (**4**·½Et₂O·½CH₃OH): C 44.48, H 4.67, N 12.97; found: C 44.21, H 4.81, N 12.73; selected IR frequencies (cm⁻¹, KBr disk): $\tilde{\nu}$ = 3427(br, m), 1605(m), 1460(m), 1294(w), 1054(vs), 771(m), 523(m). UV/Vis (CH₃OH) λ_{max} /nm (ϵ in M⁻¹cm⁻¹) = 570 (4030), 395 (5690), 280 (8730), 257 (11 870); UV/Vis (CH₃CN) λ_{max} /nm (ϵ in M⁻¹cm⁻¹) = 557 (6780), 385 (10 560), 280 (10 820), 252 (16 830); ¹H NMR (500 MHz, CD₃CN): δ = 9.28 (s, 1H), 8.97 (d, 1H), 8.31 (d, 1H), 8.24 (t, 1H), 7.80 (m, 3H), 7.42 (d, 2H), 7.09 (t, 2H), 6.56 (d, 2H), 4.82 (dd, 4H), 3.82 (t, 2H), 3.18 (t, 2H) ppm.

Received: March 21, 2002 [Z18954]

- a) *Methods in Nitric Oxide Research* (Eds.: M. Feelisch, J. S. Stamler), Wiley, Chichester, **1996**; b) E. Culotta, D. E. Koshland, *Science* **1992**, 258, 1862–1865.
- a) P. C. Ford, J. Bourassa, K. Miranda, B. Lee, I. Lorkovic, S. Boggs, S. Kudo, L. Laverman, *Coord. Chem. Rev.* **1998**, 171, 185–202; b) M. J. Clarke, J. B. Gaul, *Struct. Bonding* **1993**, 81, 147–181.
- a) R. Ackroyd, C. Kelty, N. Brown, M. Reed, *Photochem. Photobiol.* **2001**, 74, 656–669; b) R. K. Pandey, *J. Porphyrins Phthalocyanines* **2000**, 4, 368–373.
- a) R. J. Singh, N. Hogg, F. Neese, J. Joseph, B. Kalyanaraman, *Photochem. Photobiol.* **1995**, 61, 325–330; b) S. Kudo, J. L. Bourassa, S. E. Boggs, Y. Sato, P. C. Ford, *Anal. Biochem.* **1997**, 247, 193–202.
- a) J. Bourassa, W. DeGraff, S. Kudo, D. A. Wink, J. B. Mitchell, P. C. Ford, *J. Am. Chem. Soc.* **1997**, 119, 2853–2860; b) J. L. Bourassa, P. C. Ford, *Coord. Chem. Rev.* **2000**, 200, 887–900.
- a) M. K. Ellison, W. R. Scheidt, *J. Am. Chem. Soc.* **1999**, 121, 5210–5219; b) W. R. Scheidt, Y. J. Lee, K. J. Hatano, *J. Am. Chem. Soc.* **1984**, 106, 3191–3198.
- C. Hauser, T. Glaser, E. Bill, T. Weyhermuller, K. Wieghardt, *J. Am. Chem. Soc.* **2000**, 122, 4352–4364.
- a) C. A. Grapperhaus, A. K. Patra, M. S. Mashuta, *Inorg. Chem.* **2002**, 41, 1039–1041; b) D. Schweitzer, J. J. Ellison, S. C. Shoner, S. Lovell, J. A. Kovacs, *J. Am. Chem. Soc.* **1998**, 120, 10996–10997.
- J. M. Rowland, M. Olmstead, P. K. Mascharak, *Inorg. Chem.* **2001**, 40, 2810–2817.
- D. S. Marlin, P. K. Mascharak, *Chem. Soc. Rev.* **2000**, 29, 69–74.
- a) G. Roelfes, M. Lubben, K. Chen, R. Y. N. Ho, A. Meetsma, S. Genseberger, R. M. Hermant, R. Hage, S. K. Mandal, V. G. Young, Jr., Y. Zang, H. Kooijmann, A. L. Spek, L. Que, Jr., B. L.

- Feringa, *Inorg. Chem.* **1999**, 38, 1929–1936; b) M. Lubben, A. Meetsma, E. C. Wilkinson, B. L. Feringa, L. Que, Jr., *Angew. Chem.* **1995**, 107, 1610–1612; *Angew. Chem. Int. Ed. Engl.* **1995**, 34, 1512–1514.
- [12] Crystal data for $[\text{Fe}(\text{PaPy}_3)(\text{NO})][\text{ClO}_4]_2 \cdot \text{CH}_3\text{CN} (2 \cdot \text{CH}_3\text{CN})$: red plates, $0.48 \times 0.40 \times 0.02 \text{ mm}^3$, orthorhombic, space group *Pbca*, $a = 7.740(3)$, $b = 21.990(9)$, $c = 30.634(11) \text{ \AA}$, $V = 5214(3) \text{ \AA}^3$, $Z = 8$, $\rho_{\text{calcd}} = 1.713 \text{ Mg m}^{-3}$, $2\theta_{\text{max}} = 60^\circ$, $\mu(\text{Mo K}\alpha) = 0.855 \text{ mm}^{-1}$, ω scans, $\lambda = 0.71073 \text{ \AA}$; the data were collected at 91(2) K on a Bruker SMART 1000 diffractometer; a total of 69800 reflections were measured, of which 7591 were independent ($R_{\text{int}} = 0.051$) and included in the refinement; min./max. transmission = 0.684/0.983; solution by direct methods (SHELXL-97, Sheldrick, **1990**); refinement by full-matrix least-squares based on F^2 (SHELXL-97, Sheldrick, **1997**); 380 parameters, $R1 = 0.0628$, $wR2 = 0.1270$ for all data; $R1 = 0.0476$ computed for 6082 observed data ($I > 2\sigma(I)$).
- [13] A cuvette containing a 0.4 mm solution of **2** in CH_3CN was placed 5 cm from a 50 W tungsten lamp for 30 s intervals and the absorption spectra were monitored on a Cary 50 spectrophotometer in fast-scan mode (spectra shown in Figure 2). The rate of NO release was slower ($t_{1/2} = 1.5 \text{ min}$) when a 20 W tungsten lamp was used. NO release upon illumination was also observed with solutions of **2** in DMF and water. In the solid state, **2** is very stable towards light (no observed decomposition over a period of months).
- [14] a) Crystal data for $[\text{Fe}(\text{SBPy}_3)(\text{CH}_3\text{CN})][\text{BF}_4]_2 \cdot \frac{1}{2} \text{Et}_2\text{O} \cdot \frac{1}{2} \text{CH}_3\text{OH} (4 \cdot \frac{1}{2} \text{Et}_2\text{O} \cdot \frac{1}{2} \text{CH}_3\text{OH})$: magenta-colored platelike crystals, $0.44 \times 0.29 \times 0.05 \text{ mm}^3$, monoclinic, space group *C2/c*, $a = 38.398(15)$, $b = 11.859(5)$, $c = 12.783(5) \text{ \AA}$, $\beta = 103.422(8)^\circ$, $V = 5662(4) \text{ \AA}^3$, $Z = 8$, $\rho_{\text{calcd}} = 1.520 \text{ Mg m}^{-3}$, $2\theta_{\text{max}} = 61^\circ$, $\mu(\text{Mo K}\alpha) = 0.616 \text{ mm}^{-1}$, ω scans, $\lambda = 0.71073 \text{ \AA}$; the data were collected at 91(2) K on a Bruker SMART 1000 diffractometer; a total of 37587 reflections were measured, of which 8565 were independent ($R_{\text{int}} = 0.067$) and included in the refinement; min./max. transmission = 0.773/0.970; solution by direct methods (SHELXL-97, Sheldrick, **1990**); refinement by full-matrix least-squares based on F^2 (SHELXL-97, Sheldrick, **1997**); 372 parameters, $R1 = 0.1023$, $wR2 = 0.1759$ for all data; $R1 = 0.0607$ computed for 5681 observed data ($I > 2\sigma(I)$); b) CCDC-181941 (complex **2**) and CCDC-181942 (complex **4**) contain the supplementary crystallographic data for this paper. These data can be obtained free of charge via www.ccdc.cam.ac.uk/conts/retrieving.html (or from the Cambridge Crystallographic Data Centre, 12, Union Road, Cambridge CB21EZ, UK; fax: (+44)1223-336-033; or deposit@ccdc.cam.ac.uk).
- [15] S. Nagashima, M. Nakasako, N. Dohmae, M. Tsujimura, K. Takio, M. Odaka, M. Yohda, N. Kamiya, I. Endo, *Nature Struct. Biol.* **1998**, 5, 347–351.
- [16] a) M. Odaka, K. Fujii, M. Hoshino, T. Noguchi, M. Tsujimura, S. Nagashima, N. Yohda, T. Nagamune, I. Inoue, I. Endo, *J. Am. Chem. Soc.* **1997**, 119, 3785–3791; b) T. Noguchi, M. Hoshino, M. Tsujimura, M. Odaka, I. Inoue, I. Endo, *Biochemistry*, **1996**, 35, 16777–16781.
- [17] a) P. K. Mascharak, *Coord. Chem. Rev.* **2002**, 225, 201–214; b) J. C. Noveron, M. M. Olmstead, P. K. Mascharak, *J. Am. Chem. Soc.* **2001**, 123, 3247–3259; c) J. C. Noveron, M. M. Olmstead, P. K. Mascharak, *Inorg. Chem.* **1998**, 37, 1138–1139.
- [18] An $[\text{Fe}(\text{NO})]^{7-}$ -type iron–nitrosyl complex with a carboxamido nitrogen atom has been reported; see: M. Ray, A. P. Golombek, M. P. Hendrich, G. P. A. Yap, L. M. Liable-Sands, A. L. Rheingold, A. S. Borovik, *Inorg. Chem.* **1999**, 38, 3110–3115.

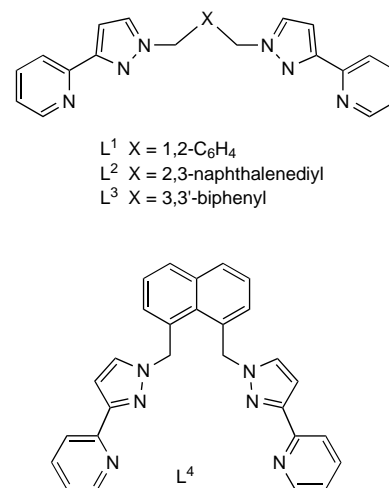
Assembly of a Truncated-Tetrahedral Chiral $[\text{M}_{12}(\mu\text{-L})_{18}]^{24+}$ Cage**

Zöe R. Bell, John C. Jeffery, Jon A. McCleverty, and Michael D. Ward*

One of the most active areas of research in metallo-supramolecular chemistry at present is the assembly of polyhedral cage complexes from labile metal centers and multidentate bridging ligands.^[1] Apart from the intrinsic appeal of the structures, they are of interest both for understanding the mechanisms of the assembly process which lead to their formation and for the host–guest chemistry associated with their large central cavities.^[1]

Tetradentate ligands with two bidentate chelating termini are commonly used in this area. When these coordinate to octahedral metal centers in the absence of any other ligands, the resulting complex must have a metal:ligand ratio of 2:3, as found in dinuclear triple helicates with three bridging ligands.^[2] The next member of this series is the M_4L_6 tetrahedron, in which a bridging ligand spans each edge of a tetrahedral array of metal ions. This type of structure has been extensively studied recently,^[3–6] and there is a well-developed host–guest chemistry based on the binding of counterions or solvent molecules in the tetrahedral cavities. The only three-dimensional cage of which we are aware with a higher nuclearity but with the same M_2L_3 ratio is the cube $[\text{Ni}_8(\text{tab})_{12}]^{16+}$ (tab = 1,2,3,4-tetraaminobutane);^[7] in 1997 we described a (two-dimensional) circular M_8L_{12} helicate with an anion encapsulated in the central cavity.^[8]

Our recent work in this area is based on ligands such as L^1 – L^3 which contain two bidentate pyrazolylpyridine units linked to an aromatic core through two methylene spacers.^[3,9] With cobalt(II) ions these ligands form $[\text{Co}_4\text{L}_6]^{8+}$ cages which bind



[*] Prof. M. D. Ward, Dr. Z. R. Bell, Dr. J. C. Jeffery, Prof. J. A. McCleverty
 School of Chemistry
 University of Bristol
 Cantock's Close, Bristol BS8 1TS (UK)
 Fax: (+44)117-929-0509
 E-mail: mike.ward@bristol.ac.uk

[**] We thank the EPSRC for financial support.

anions in the central cavity. With the shorter ligands L^1 and L^2 the central anion (perchlorate or tetrafluoroborate) is completely encapsulated and tightly bound in the central cavity, and in fact acts as a template for the assembly of the cage around it.^[3] With the larger bridging ligand L^3 , in contrast, the anions in the cavity exchange freely with those outside through large cavities in the center of each face.^[9] In seeking to prepare a related tetrahedral cage with a cavity of intermediate size, for the purposes of investigating the size selectivity of anion binding, we prepared ligand L^4 in which the spacer is a 1,8-naphthyl unit. Unexpectedly, this reacts with cobalt(II) and zinc(II) ions to generate dodecanuclear cage complexes $[M_{12}(\mu-L^4)_{18}]X_{24}$ (where X = perchlorate or tetrafluoroborate) in which each of the 18 bridging ligands spans an edge of a truncated-tetrahedral M_{12} array.

The ligand L^4 was prepared^[10] by reaction of 1,8-bis(bromomethyl)naphthalene with 3-(2-pyridyl)pyrazole by using the procedure we have described before for related ligands.^[3, 9] Reaction of L^4 with $Co(O_2CCH_3)_2 \cdot 4H_2O$ in MeOH in a 3:2 ratio afforded an orange solution from which a precipitate was obtained on addition of aqueous $NaBF_4$. Crystallization by diffusion of ethyl acetate vapor into a solution of the complex in DMF/MeCN afforded X-ray quality crystals of a material whose elemental analysis, as expected, was consistent with the empirical formula $[Co_2(L^4)_3][BF_4]_4$.

The crystal structure is shown in Figures 1–3.^[11] The core of the structure is a truncated tetrahedral array of 12 metal ions; this polyhedron is generated by truncating each of the four vertices of a tetrahedron to reveal a triangular face. Each of the four faces of the initial tetrahedron therefore becomes a hexagon, and the polyhedron accordingly contains four triangular and four hexagonal faces (Figure 1). This is a very

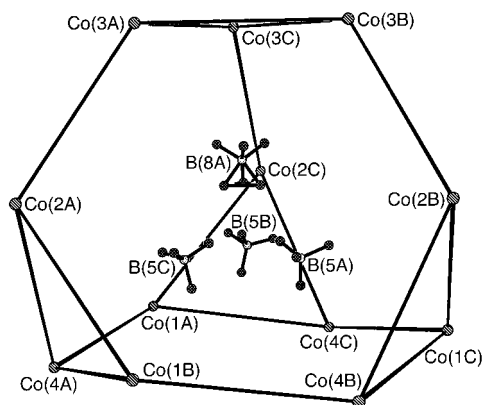


Figure 1. Section of the crystal structure of $[Co_{12}(L^4)_{18}][BF_4]_{24}$ showing the dodecanuclear cage of Co^{II} ions and the four encapsulated anions.

rare structural type in metal cage complexes: discrete $[Sn_{12}]^{12-}$ ionic clusters of this structure occur in the Zintl compounds $CaNa_{10}Sn_{12}$ and $SrNa_{10}Sn_{12}$,^[12] and a dodacnuclear “capsule” with this arrangement of metal ions was formed by hydrogen-bonding association of four approximately planar triangular, trinuclear complex units.^[13]

The $Co \cdots Co$ separations along each of the 18 edges lie in the range 9.22–9.36 Å. Every cobalt(II) ion is coordinated by a

meridional arrangement of three pyridyl and three pyrazolyl donors from the three bidentate chelating units. All $Co-N$ bonds are in the range 2.1–2.2 Å. All twelve cobalt(II) centers within each complex molecule have the same chirality; the crystal as a whole is, however, racemic. The space-filling view (Figure 2) emphasises how the ligands are entwined around each other, with extensive aromatic π -stacking interactions between overlapping naphthyl units of the ligands; columnar stacks of eight naphthyl units occur around the periphery of the complex. In the solid state the complex has only one threefold axis, but the idealized symmetry is T , similar to those of the M_4L_6 tetrahedral cages in which all four metal ions are homochiral.^[3, 14]

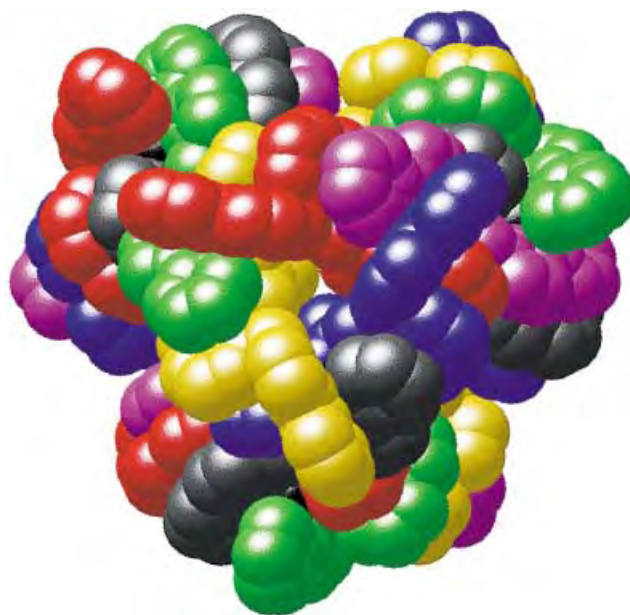


Figure 2. Space-filling view of the complex cation of $[Co_{12}(L^4)_{18}][BF_4]_{24}$.

The central cavity of the cage contains four tetrafluoroborate anions (of which one is disordered, with six F atom positions evident with a site occupancy of two-thirds in each; Figure 1). The boron atoms of these four anions describe an approximate tetrahedron with $B \cdots B$ separations of about 5.3 Å. The proximity of these anions results in $F \cdots F$ contacts between adjacent anions of 3.25 Å (based on the three ordered anions only). In addition, the two-dimensional cavities at the center of the triangular and hexagonal faces all contain a tetrafluoroborate anion (Figure 3). This situation results in nonbonded $F \cdots C$ separations of 3.0–3.3 Å, possibly involving weak $C-H \cdots F$ hydrogen-bonding interactions.^[15] Counterions are often found occupying the two-dimensional cavities at the center of circular helicate complexes^[7, 16] and the three-dimensional cavities at the center of cage complexes;^[1, 3–6, 17] with anions bound in both two-dimensional (on the surface) and three-dimensional (at the center) cavities, $[Co_{12}(\mu-L^4)_{18}][BF_4]_{24}$ displays both types of behavior. Whether these anions are acting as templates without which the $[Co_{12}(\mu-L^4)_{18}]^{24+}$ cage could not form is not yet known.

Electrospray mass spectra (at a variety of cone voltages) of a solution of redissolved crystals of the complex in DMF

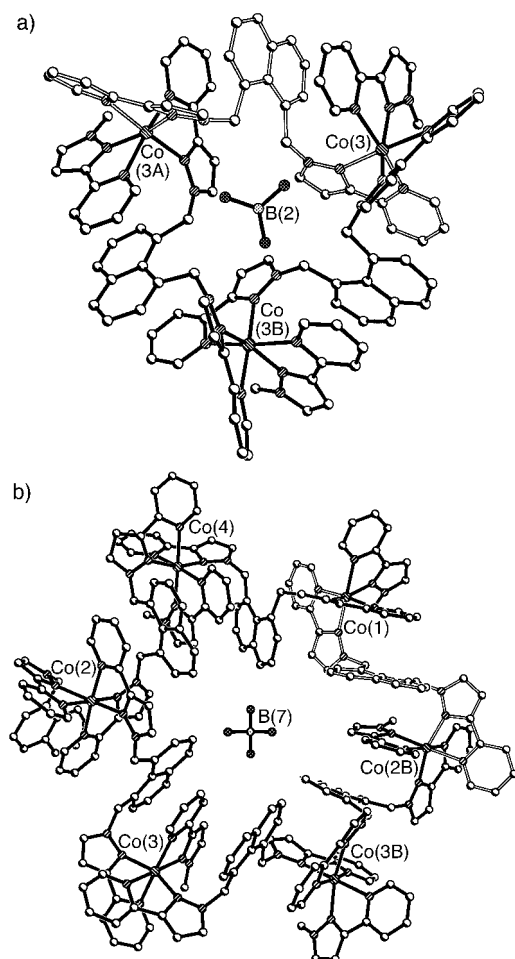


Figure 3. Sections of the crystal structure of $[\text{Co}_{12}(\text{L}^4)_{18}][\text{BF}_4]_{24}$ showing a) the view looking onto a triangular face, and b) the view looking onto a hexagonal face. One ligand has been shaded differently in each figure for clarity. In each case there is a $[\text{BF}_4]^-$ ion in the cavity at the center of the face.

showed only peaks at low m/z values, most of which were not readily assignable. Decomposition of the complex in solution under these conditions was clear from some signals (for example $[\text{HL}^4]^+$ at m/z 443, and $[\text{Co}(\text{L}^4)]^{2+}$ at m/z 250). MALDI-TOF and Fourier transform ion cyclotron resonance (FT-ICR) spectra gave similar results and also failed to show any peaks consistent with retention of the cage structure. ^1H NMR spectroscopy provided further evidence that the cage structure dissociates in solution. The intact cage has two different types of edge (12 around the triangular faces, and the remaining 6 on the hexagonal faces), with each edge having twofold symmetry. We would therefore expect to see two independent ligand halves, that is, 22 proton environments for the intact cage. The spectrum recorded at -20°C in $[\text{D}_6]\text{DMSO}/\text{CD}_3\text{CN}$ shows at least 36 paramagnetically shifted proton environments in the range $\delta = 10\text{--}110$ ppm, which is characteristic of the ligands coordinated to cobalt(II) ions,^[18] as well as signals in the $\delta = 6\text{--}10$ ppm region characteristic of free ligand. The spectrum becomes even more complicated at higher temperatures. Fragmentation of the cage clearly occurs in this strongly coordinating solvent; the cage is not soluble in less well-coordinating solvents.

Finally, we note that we have observed essentially identical structures with zinc(II) in place of cobalt(II) ions, and also with a perchlorate as counterion in place of tetrafluoroborate. Details of these structural determinations, and studies on whether alternative (nontetrahedral) guest anions give similar cages, will be reported in due course.

Received: March 18, 2002

Revised: April 25, 2002 [Z18916]

- [1] Recent reviews: a) D. L. Caulder, K. N. Raymond, *Acc. Chem. Res.* **1999**, 32, 975; b) D. L. Caulder, K. N. Raymond, *J. Chem. Soc. Dalton Trans.* **1999**, 1185; c) M. Fujita, *Chem. Soc. Rev.* **1998**, 27, 417; d) G. F. Swiegers, T. J. Malefetse, *Chem. Eur. J.* **2001**, 7, 3637; e) B. J. Holliday, C. A. Mirkin, *Angew. Chem.* **2001**, 113, 2076; *Angew. Chem. Int. Ed.* **2001**, 40, 2022; f) S. Leininger, B. Olenyuk, P. J. Stang, *Chem. Rev.* **2000**, 100, 853; g) R. W. Saalfrank, E. Uller, B. Demleitner, I. Bernt, *Struct. Bonding* **2000**, 96, 149.
- [2] a) C. R. Rice, S. Wörl, J. C. Jeffery, R. L. Paul, M. D. Ward, *J. Chem. Soc. Dalton Trans.* **2001**, 550; b) M. Albrecht, *Chem. Soc. Rev.* **1998**, 27, 281; c) C. Piguet, G. Bernardinelli, G. Hopfgartner, *Chem. Rev.* **1997**, 97, 2005.
- [3] a) J. S. Fleming, K. L. V. Mann, C.-A. Carraz, E. Psillakis, J. C. Jeffery, J. A. McCleverty, M. D. Ward, *Angew. Chem.* **1998**, 110, 1315; *Angew. Chem. Int. Ed.* **1998**, 37, 1279; b) R. L. Paul, Z. R. Bell, J. C. Jeffery, J. A. McCleverty, M. D. Ward, *Proc. Natl. Acad. Sci. USA* **2002**, 99, 4883.
- [4] a) R. W. Saalfrank, R. Burak, A. Breit, D. Stalke, R. Herbst-Irmer, J. Daub, M. Porsch, E. Bill, M. Mütther, A. X. Trautwein, *Angew. Chem.* **1994**, 106, 1697; *Angew. Chem. Int. Ed. Engl.* **1994**, 33, 1621; b) R. W. Saalfrank, N. Low, B. Demleitner, D. Stalke, M. Teichert, *Chem. Eur. J.* **1998**, 4, 1305.
- [5] Recent examples from Raymond's research group: a) D. W. Johnson, K. N. Raymond, *Inorg. Chem.* **2001**, 40, 5157; b) A. J. Terpin, M. Ziegler, D. W. Johnson, K. N. Raymond, *Angew. Chem.* **2001**, 113, 161; *Angew. Chem. Int. Ed.* **2001**, 40, 157; c) M. Ziegler, J. J. Miranda, U. N. Andersen, D. W. Johnson, J. A. Leary, K. N. Raymond, *Angew. Chem.* **2001**, 113, 755; *Angew. Chem. Int. Ed.* **2001**, 40, 733.
- [6] a) E. J. Enemark, T. D. P. Stack, *Angew. Chem.* **1998**, 110, 977; *Angew. Chem. Int. Ed.* **1998**, 37, 932; b) S. Mann, G. Huttner, L. Zsolnai, K. Heinze, *Angew. Chem.* **1996**, 108, 2983; *Angew. Chem. Int. Ed. Engl.* **1996**, 35, 2808.
- [7] A. Zimmer, D. Kuppert, T. Weyhermüller, I. Müller, K. Hegetschweiler, *Chem. Eur. J.* **2001**, 7, 917.
- [8] P. L. Jones, K. J. Byrom, J. C. Jeffery, J. A. McCleverty, M. D. Ward, *Chem. Commun.* **1997**, 1361.
- [9] R. L. Paul, S. M. Couchman, J. C. Jeffery, J. A. McCleverty, Z. R. Reeves, M. D. Ward, *J. Chem. Soc. Dalton Trans.* **2000**, 845.
- [10] A mixture of 1,8-bis(bromomethyl)naphthalene (1.049 g, 3.3 mmol), 3-(2-pyridyl)pyrazole (1.02 g, 7.03 mmol), aqueous $n\text{Bu}_4\text{OH}$ (40% wt/wt, 0.16 mL), aqueous NaOH (2.34 g dissolved in 5.5 cm³ of water), and toluene (35 cm³) was heated with vigorous stirring at 85°C for 24 h. After cooling, the organic layer was separated, washed with water, and dried over MgSO_4 . Removal of solvent yielded a brown oil which was purified by recrystallization from dichloromethane/hexane to yield L^4 as an off-white solid (yield: 0.52 g, 36%). EIMS: m/z : 442 $[\text{M}^+]$. ^1H NMR (CDCl_3): δ = 8.56 (2H, d; pyridyl H^6), 7.86 (2H, d; naphthyl H^2/H^7 or H^4/H^5), 7.84 (2H, d; pyridyl H^3), 7.64 (2H, m; pyridyl H^4), 7.39 (2H, t; naphthyl H^3/H^6), 7.19 (2H, d; naphthyl H^4/H^5 or H^2/H^7), 7.12 (2H, m; pyridyl H^5), 7.07 (2H, d; pyrazolyl H^5), 6.80 (2H, d; pyrazolyl H^4), 5.87 ppm (4H, s; CH_2). Elemental analysis calcd for $\text{C}_{28}\text{H}_{22}\text{N}_6$: C 76.3, H 4.9, N 19.3%; found: C 76.0, H 5.0, N 19.0%.
- [11] Crystal data for $[\{\text{Co}_4(\text{L}^4)_6\}][\text{BF}_4]_8 \cdot 0.5 \text{EtOAc} \cdot 2 \text{DMF} \cdot 12 \text{MeCN} \cdot 0.33 \text{H}_2\text{O}]_3$: M_r = 12822.57, trigonal, space group $R\bar{3}$, a = 41.167(5), c = 82.016(9) Å, V = 120374(23) Å³, Z = 6; ρ_{calcd} = 1.061 g cm⁻³; crystal dimensions 0.5 × 0.45 × 0.4 mm³; $\mu(\text{MoK}\alpha)$ = 0.318 mm⁻¹. 175 784 data were collected ($2\theta_{\text{max}}$ = 45°) at 123 K on a Bruker-AXS SMART diffractometer with a CCD area detector; after merging these gave 34966 unique data (R_{int} = 0.0922). An empirical absorption correction

was applied using SADABS. The structure was solved and refined using the SHELX-97 suite of programs^[19]; refinement of 2418 parameters converged at $R_1 = 0.129$, $wR_2 = 0.359$. The complex lies on a threefold axis such that only four of the metal ions are unique. The metal ions and the ligand C and N atoms were refined with anisotropic thermal parameters, as were some of the $[\text{BF}_4]^-$ counterions; the remaining counterions and all of the (largely disordered) solvent atoms were refined isotropically. Of the expected eight $[\text{BF}_4]^-$ ions in the asymmetric unit, six were well defined; two are on threefold axes such that only one-third of the anion is in the asymmetric unit (and in one of these the F atom positions are disordered); and one only refined adequately with site occupancies of 50 % for all atoms, making 7.166 anions. The remainder could not be located and it is assumed that they are in the regions of the crystal where there is extensive disorder of lattice solvent molecules; the formulation given above for solvent molecules is necessarily an approximation. CCDC-181453 contains the supplementary crystallographic data for this paper. These data can be obtained free of charge via www.ccdc.cam.ac.uk/conts/retrieving.html (or from the Cambridge Crystallographic Data Centre, 12, Union Road, Cambridge CB2 1EZ, UK; fax: (+44) 1223-336-033; or deposit@ccdc.cam.ac.uk).

- [12] S. Bobev, S. C. Sevov, *Inorg. Chem.* **2001**, *40*, 5361.
- [13] I. M. Müller, R. Robson, F. Separovic, *Angew. Chem.* **2001**, *113*, 4519; *Angew. Chem. Int. Ed.* **2001**, *40*, 4385.
- [14] T. Beissel, R. E. Powers, T. N. Parac, K. N. Raymond, *J. Am. Chem. Soc.* **1999**, *121*, 4200.
- [15] a) F. Grepioni, G. Cojazzi, S. M. Draper, N. Scully, D. Braga, *Organometallics* **1998**, *17*, 296; b) G. Desiraju, T. Steiner, *The weak hydrogen bond in structural chemistry and biology*, OUP, Oxford, **1999**.
- [16] B. Hasenknopf, J.-M. Lehn, B. O. Kneisel, G. Baum, D. Fenske, *Angew. Chem.* **1996**, *108*, 1987; *Angew. Chem. Int. Ed. Engl.* **1996**, *35*, 1838.
- [17] a) D. W. Johnson, K. N. Raymond, *Inorg. Chem.* **2001**, *40*, 5157; b) M. Scherer, D. L. Caulder, D. W. Johnson, K. N. Raymond, *Angew. Chem.* **1999**, *111*, 1690; *Angew. Chem. Int. Ed.* **1999**, *38*, 1588.
- [18] E. C. Constable, C. E. Housecroft, T. Kulke, C. Lazzarini, E. R. Schofield, Y. Zimmermann, *J. Chem. Soc. Dalton Trans.* **2001**, 2864.
- [19] a) G. M. Sheldrick, SHELXS-97, Program for the Solution of Crystal Structures, University of Göttingen, Göttingen (Germany), **1997**; b) G. M. Sheldrick, SHELXS-97, Program for the Solution of Crystal Structures, University of Göttingen, Göttingen (Germany), **1997**.

Luminescence Phenomena and Solid-State Structures of Trimethyl- and Triethylgallium**

Norbert W. Mitzel,* Christian Lustig,
Raphael J. F. Berger, and Nino Runeberg

Dedicated to Professor Dr. Rainer Mattes on the occasion of his 65th birthday

Trialkylgallium compounds are widely used as precursors in chemical vapor deposition (CVD) processes for the generation of thin layers of gallium semiconductor compounds such as GaAs or GaN.^[1] Although triethylgallium (GaEt₃) was first described in 1932,^[2] to date there have been no reports about its remarkable luminescent behavior and decomposition upon cooling to liquid-nitrogen temperature, which we present herein. We also investigate these phenomena in the context of the solid-state structures of this class of compounds.

We observed intriguing luminescence phenomena and decomposition of GaEt₃, when we attempted to degas a 100-mL sample (electronic grade purity) to transfer part of it under vacuum for a crystal-growth experiment in the course of structure determination. A large number of little flashes were observed during the freezing process in liquid nitrogen, but even more intense flashes occurred after removing the coolant (Figure 1b). The light emissions start about one minute after the sample is removed from the coolant, that is, when the temperature is between –180 and –150 °C, and stop when the sample reaches an average temperature of about –100 °C. The light emission is accompanied by a sound resembling the cracking of ice, which indicates the origin of the effect; triboluminescence^[3] caused by breaking of the GaEt₃ crystals.

Triboluminescence occurs in certain crystalline phases when mechanical stress is applied (in our case because of thermal contraction or expansion of the polycrystalline sample). The light emission in these cases is said to be caused by the charge separation over the new surfaces generated by breaking a crystal, the discharge of such accumulated charge, and the subsequent excitation of the gas between the new



Figure 1. a) Two samples of GaEt₃. Left: a pure sample; Right: a sample after 15 freeze–thaw cycles under argon, b) the triboluminescence flashes which occur upon warming a sample of GaEt₃ under argon that had been frozen in liquid nitrogen.

surfaces. This explanation is consistent with our observation that GaEt₃ samples handled under inert gases (He, Ne, Ar, Xe) show luminescence, and that the observed emission spectrum (Figure 2) contains the atomic emission spectrum of the corresponding noble gas. Only for xenon were other lines observed, but these could not be identified to date. This observation is fully consistent with other reports on the dependence of triboluminescence spectra on the present gas atmosphere.^[3]

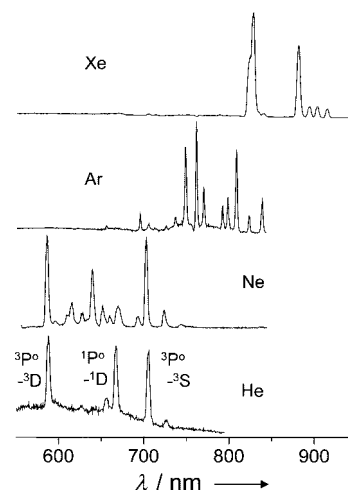


Figure 2. Luminescence spectra of GaEt₃ under different inert gases, recorded about 1 min after removing a 100-mL sample from cooling (–196 °C). For the lower spectrum (He), an assignment of some lines is given.

The decomposition of the sample with emission is easily seen by a blackening of the liquid, which becomes darker after each freeze–thaw cycle (Figure 1a). In a neon atmosphere, the strongest decomposition is observed. Finally a fine, black

[*] Priv.-Doz. Dr. N. W. Mitzel,^[+] Dipl.-Chem. C. Lustig, Dipl.-Chem. R. J. F. Berger
Anorganisch-chemisches Institut
Technische Universität München
Lichtenbergstrasse 4, 85747 Garching (Germany)
E-mail: mitzel@uni-muenster.de
Dr. N. Runeberg
University of Helsinki
P.O. Box 55 (A.I. Virtasen aukio 1), 00014 (Finland)

[+] New address:
Institut für Anorganische und Analytische Chemie
Westfälische Wilhelms-Universität Münster
Wilhelm-Klemm-Strasse 8, 48149 Münster (Germany)
Fax: (+49)251-83-36007

[**] This work was supported by the Deutsche Forschungsgemeinschaft, Fonds der Chemischen Industrie, and the Leonhard-Lorenz-Stiftung. Generous support from Professor H. Schmidbaur (Garching) is gratefully acknowledged. We thank Dr. D. Kovalev and co-workers (Physik Department, Technische Universität München) for help with recording the luminescence spectra.

precipitate of elemental Ga settles after standing for a few days. Thus, this physical effect of luminescence is accompanied by a chemical change of the sample. To understand this decomposition in more detail, we repeated the freeze–thaw cycles about 100 times with a small sample of neat GaEt₃ in an NMR spectroscopy tube and measured the ¹H and ¹³C NMR spectra before and after this treatment. Small amounts of ethane and even smaller amounts of ethene could be detected. The gases could be accumulated and isolated by repeating the experiment about 30 times with a 100-mL sample and pumping the volatile components through a series of cold traps on a high vacuum line. Tiny amounts of ethane and ethene passed through a –78 °C trap and were identified by gas-phase IR spectroscopy and NMR spectroscopy. Apart from the black precipitate (which is finely divided gallium), no other decomposition product was found, in particular no dihydrogen gas or butane (from dimerized ethyl substituents of the GaEt₃). Decomposition of the homologous AlEt₃ by photochemical processes is known to yield elemental aluminum and ethane^[4] and therefore we anticipated a similar process in our case. This process parallels the photochemical initialization of chemical reactions by triboluminescence, such as detonations, which were previously reported.^[5]

We could verify this hypothesis by directly exposing GaEt₃ in a glass tube to a neon discharge, to simulate the conditions of discharge and light emission involved in triboluminescence. In these experiments samples of liquid GaEt₃ at –78 °C and solid GaEt₃ at –110 °C were placed in a neon atmosphere (about 5 mbar), which was excited about 5 cm above the GaEt₃ surface by applying a weak, high frequency field, so that the typical red neon light was observable. Under these conditions the same decomposition products (ethane, traces of ethene, and a small amount of a black gallium precipitate) were observed.

To date we could not find other gallium alkyls showing triboluminescence under these conditions, but we have tested only tri-*n*-butylgallium, tri-*tert*-butylgallium, and trimethylgallium. The reason for this different behavior can be rationalized by the solid-state structures, as GaEt₃ is the only compound crystallizing in an acentric and polar space group, which was often described as a prerequisite for triboluminescence^[6] and the crystals of most triboluminescent compounds are found to adopt acentric space groups (exceptions are known, but are disputed).^[3] By contrast to GaEt₃, GaMe₃ crystallizes centrosymmetrically and both butylgallium compounds are glassy solids.

Mechanical energy is the source of energy for the observed triboluminescence in GaEt₃, but without application of external mechanical stress. For an improved understanding of the cracking of the galliumtrialkyl compounds during freezing and thawing, we looked at the thermal contraction of these compounds. GaEt₃ and GaMe₃ undergo an enormous shrinkage during the liquid–solid phase transition. According to our crystallographic data (see below) the density in the solids at –130 °C is 24.5 % and 26.2 % higher

than that of liquid GaEt₃ ($\rho(30\text{ °C}) = 1.058\text{ g cm}^{-3}$) and GaMe₃ ($\rho(25\text{ °C}) = 1.151\text{ g cm}^{-3}$), respectively.^[7] For GaEt₃ we observed an almost linear increase in density of 12 % while cooling the liquid from +30 to –82 °C, a spontaneous rise in density of 10 % during the liquid–solid phase transition at –82 °C, but only a small thermal contraction of 2 % in the solid state of GaEt₃ by further cooling to –145 °C. These density changes were determined by crystallographic measurement of the cell dimensions at five temperatures between –85 °C (i.e. near the melting point of –82 °C, $\rho = 1.307\text{ g cm}^{-3}$) and –145 °C ($\rho = 1.331\text{ g cm}^{-3}$). This large shrinkage during solidification probably builds up the strain that is later released by cracking of the crystals, which leads to the observed triboluminescence. The reason for the relatively high density of the solids of GaEt₃ and GaMe₃ becomes obvious from their crystal structures, which will now be described.

The solid-state structure of GaEt₃ (Figure 3) is quite complicated,^[8] as it comprises layers of wavelike networks of the four independent molecules in the unit cell. The Ga atoms are between 2.50 and 3.16 Å away from the H atoms of their next neighbors. The corresponding Ga···C distances, which describe the relevant contacts, lie between 3.087–3.593 Å. Each of the Ga atoms is weakly coordinated by two such intermolecular Ga···C contacts, apart from Ga1, which is involved in only one such short interaction. Note that the Ga atoms form contacts to both sorts of C atoms, methylene and methyl carbon atoms, of the neighboring molecules. All GaEt₃ molecules are present in conformations with almost planar GaC₆ skeletons and no gauche conformation for CCGaC units occurs. Three of the four molecules are found in a propeller-like arrangement and only the GaEt₃ molecule containing Ga3 does not adopt approximate C₃ symmetry and has two ethyl groups pointing towards each another. The wide Ga–C–C angles (between 113.3(2) and 118.8(2)°) resemble the B–C–C angles in the structure of solid

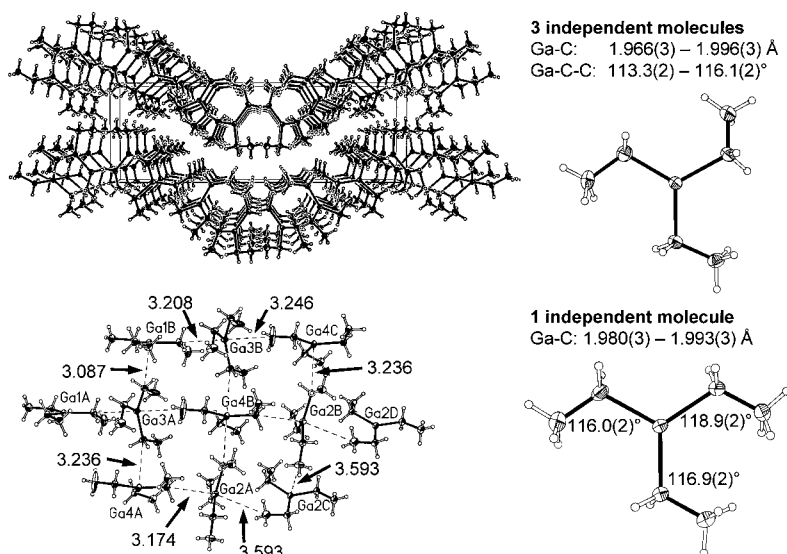


Figure 3. Crystal structure of GaEt₃. Upper left: layers of GaEt₃ wavelike arranged networks; lower left: part of one of the layers showing the connectivity of the network; right: the four independent molecules and their geometries.

BEt₃ (118.7–119.3°), which was explained by hyperconjugation of the boron p orbital into C–H orbitals.^[9]

With the structure determination and ab initio calculations of a GaMe₃ dimer, we wanted to provide more detailed knowledge about the intermolecular forces responsible for the thermal contraction of the gallium alkyls in general and thus the triboluminescence of GaEt₃. The crystal structure of GaMe₃ was unknown to date, as well as the structure of BMe₃, while the structures of the other trimethyl compounds of the group 13 elements are described. By chance, the determination of the structure of GaMe₃ was simultaneously and independently undertaken by two other groups but, interestingly, two different structures of GaMe₃ were obtained; a monoclinic one ($\rho(-143^\circ\text{C}) = 1.444\text{ g cm}^{-3}$, space group *C2/c*, two independent molecules) in the hands of Boese, Parsons, and co-workers^[10] and a tetragonal one from our experiments ($\rho(-140^\circ\text{C}) = 1.453\text{ g cm}^{-3}$, space group *P4₂/n*, Figure 4).^[8] Boese and co-workers also determined the structure of BMe₃.^[10] With these newly established data, the structures of the trimethyl compounds of the group 13 elements are found to differ markedly from one another: BMe₃ is monomeric,^[10] AlMe₃ crystallizes as a dimer with two bridging methyl units, with short Al–C distances and four-coordinate Al atoms,^[11, 12] whereas InMe₃^[13] and TlMe₃^[14] are arranged into tetramers with considerably longer metal–carbon distances, with the metal atoms adopting a primary trigonal-planar coordination, while the weaker intermolecular interactions are in perpendicular direction to the primary coordination plane.

Our tetragonal structure of GaMe₃ is closely related to the structures of InMe₃ and TlMe₃, which are also tetragonal and tetrameric. The gallium atoms in GaMe₃ are planar (sum of angles about Ga 359.9°) and weakly coordinated to a methyl group of a neighboring molecule, with Ga⋯H distances between 2.95–2.96 Å and a Ga⋯C distance of 3.134 Å. Surprisingly this distance is longer than that of InMe₃ (In⋯C 3.083(12) Å)^[13] and shorter than in TlMe₃ (Tl⋯C 3.16 Å).^[14] The interactions between the metal atoms and the methyl groups of molecules of other tetramers are much longer than those within the tetramers (In⋯C 3.558(15) and Tl⋯C 3.31 Å) and are even longer in GaMe₃ (3.647(3) Å). These weak contacts arrange the GaMe₃ tetramers into endless 2D networks.

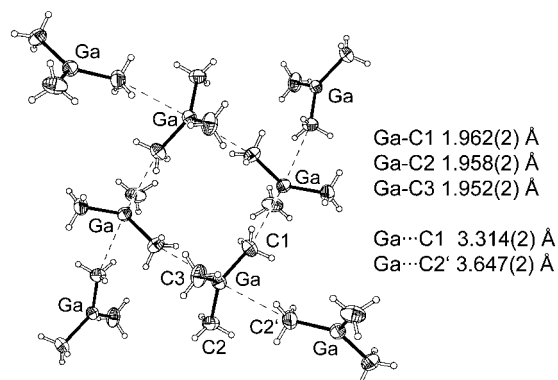


Figure 4. A tetramer of GaMe₃ and its connectivity in the layers of tetragonal crystals.

Although less symmetrical, the monoclinic structure of GaMe₃^[10] can also be described as containing tetrameric units (Ga⋯C 3.069 and 3.210 Å), which are also part of a large 2D network formed by longer Ga⋯C contacts of 3.234 and 3.523 Å, but these rather similar distances make a clear distinction between the longer and shorter distances impossible. In our tetragonal structure of GaMe₃ the order of Ga–C bond lengths is fully consistent with the involvement of the respective methyl groups in secondary bonding. They are: Ga–C3 1.952(3) Å (no Ga⋯C contact), Ga–C2 1.958(2) Å (weak Ga⋯C2' contact of 3.647(2) Å) and Ga–C1 1.962(2) Å (short Ga⋯C(1)' contact of 3.314(2) Å). They are only marginally shorter than in gaseous GaMe₃ (1.967(2) Å),^[12] which shows that the intermolecular interactions do not strongly distort the structure of the monomers.

As no detailed investigations on the cause of these interactions have been reported to date, we performed quantum chemical calculations. For computational feasibility we chose to model the interactions in the tetrameric structure by only considering a dimer of GaMe₃, that is, to model only one of the interactions between a Ga center and the methyl group of another GaMe₃ molecule. The structure of the GaMe₃ dimer was optimized and the interaction energy analyzed at the local MP2/TZVP level.^[15] The optimized structure is shown in Figure 5 and, apart from a slight twist, the geometry appears to be very similar to a fragment of the tetrameric unit in the crystal. The calculated intermolecular

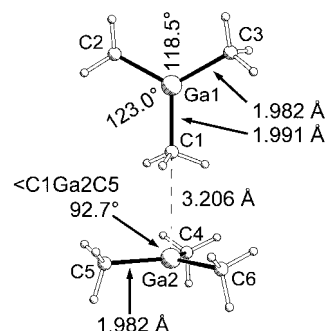


Figure 5. Calculated geometry of the dimer of GaMe₃ (LMP2/TZVP).

Ga⋯C distance is in the dimer 3.206 Å and 3.134(1) Å in the tetramer of solid, tetragonal GaMe₃. The calculations reproduce the slight elongation of the Ga–C bond of the coordinated methyl group involved in the dimer/tetramer formation, as well as the staggered arrangement of the hydrogen atoms in this methyl group, relative to the GaC₃ skeleton of the neighboring GaMe₃ molecule. The calculated interaction energy between the GaMe₃ molecules is 11.4 kJ mol^{−1}.

The interaction energy obtained at the LMP2 level can be partitioned into the following components: The SCF contribution, which should contain the major part of any covalent, ionic, or electrostatic contributions. This contribution is calculated to be 3.4 kJ mol^{−1}. The remaining part is the correlation contribution of the interaction energy and it can be separated into different classes, according to referen-

ce [15a]. The calculated attractive contributions for dispersion are 7.5 kJ mol^{-1} , for ionic excitations 4.2 kJ mol^{-1} , and for exchange dispersion 0.0 kJ mol^{-1} . In addition, there is a repulsive contribution of -3.8 kJ mol^{-1} , which corresponds to the reduced intramonomer correlation when the monomers approach each other. As the SCF interaction can be reproduced by a model, which only takes into account the classical electrostatic interactions between the GaMe_3 monomers without any induction or dispersion effects,^[16] we conclude that the interaction has no covalent character, but consists of dispersion and ionic correlation contributions, as well as classical electrostatic contributions.

The topology of the electron density in the region of this $\text{Ga} \cdots \text{C}$ interaction shows a bond-critical point on the line connecting the Ga atom and the C atom of the neighboring methyl group. This point indicates that there is no interaction of the agostic type which would require $\text{Ga} \cdots \text{H}$ interactions with bond-critical points between Ga and H atoms.^[17] Furthermore, the calculated Ga-C-H angles at the interacting methyl group are only slightly wider than the other Ga-C-H angles in the dimer.

We showed a connection between weak intermolecular forces leading to a large temperature dependence of the density and thus to mechanical properties, which causes the triboluminescence of GaEt_3 , as this crystallizes in an polar, acentric space group and which is distinct from the non-triboluminescent GaMe_3 . Many details remain still unclear and deserve further investigation. These include the chemistry involved in the decomposition of GaEt_3 and the interaction of GaEt_3 with xenon.

Received: July 23, 2001

Revised: April 22, 2002 [Z17564]

- [1] a) R. Dötzer, G. Raab, E. Todt, G. Urban, *Chem. Ing. Tech.* **1964**, *36*, 616–637; b) R. A. Kovar, H. Derr, D. Brandau, J. O. Callway, *Inorg. Chem.* **1975**, *14*, 2809–2814; c) K. M. Coward, A. C. Jones, A. Steiner, J. F. Bickley, M. E. Pembler, N. M. Boag, S. A. Rushworth, L. M. Smith, *J. Mater. Chem.* **2000**, *10*, 1875–1880.
- [2] L. M. Dennis, W. Patnode, *J. Am. Chem. Soc.* **1932**, *54*, 182–189.
- [3] L. M. Sweeting, *Chem. Mater.* **2001**, *13*, 854–870.
- [4] W. H. Glaze, T. L. Brewer, A. C. Ranade, *J. Organomet. Chem.* **1970**, *25*, C6–C8.
- [5] J. E. Field, *Acc. Chem. Res.* **1992**, *25*, 489–496.
- [6] F. A. Cotton, L. M. Daniels, P. Huang, *Inorg. Chem.* **2001**, *40*, 3576–3578.
- [7] “Organogallium Compounds”: *Gmelin Handbook of Inorganic and Organometallic Chemistry*, 8th ed., Springer, Berlin, **1995**.
- [8] Crystal data for GaMe_3 and GaEt_3 : Single cylindrical crystals of GaMe_3 and GaEt_3 of 0.3-mm diameter were grown in the cryostream of a Nonius DIP 2020 diffractometer by slowly cooling the melt sealed in a thin-walled glass capillary after establishing a solid–liquid equilibrium and optically selecting a single suitable seed crystal by repeated crystallization–melting cycles. Intensity corrections were applied using the program SCALEPACK.^[18] The structures were solved by direct methods and refined by least-squares methods on F^2 .^[19] C and Ga atoms were refined with anisotropic thermal displacement factors, H atoms isotropically (all CH_3 groups in GaMe_3 were restrained to have local C_3 symmetry, in GaEt_3 only one CH_3 group had to be restrained to local tetrahedral symmetry). GaMe_3 : GaC_3H_9 , tetragonal, $P4_2/n$, $a = 12.9532(3)$, $c = 6.2588(1) \text{ \AA}$, $\beta = 90.8522(5)^\circ$, $V = 1050.13(4) \text{ \AA}^3$, $Z = 8$, $\rho_{\text{calc}} = 1.453 \text{ g cm}^{-3}$, $\lambda = 0.71073 \text{ \AA}$, $2\theta_{\text{max}} = 63^\circ$, $T = 133(2) \text{ K}$, $\mu = 5.059 \text{ mm}^{-1}$, 28820 measured and 1684 independent reflections ($R_{\text{int}} = 0.041$). $F(000) = 464$, 110 parameters, $R_1 = 0.0336$ for 1526 reflections with $F_o > 4\sigma(F_o)$ and $wR_2 = 0.0882$ for all 1684 data. Max./min. residual peaks $-0.62/0.70 \text{ e \AA}^{-3}$. GaEt_3 : $\text{GaC}_6\text{H}_{15}$, monoclinic, Pc , $a = 8.4514(1)$, $b = 25.1534(3)$, $c = 7.4473(1) \text{ \AA}$, $V = 1582.98(3) \text{ \AA}^3$, $Z = 8$, $\rho_{\text{calc}} = 1.317 \text{ g cm}^{-3}$, $\lambda = 0.71073 \text{ \AA}$, $2\theta_{\text{max}} = 55^\circ$, $T = 133(2) \text{ K}$, $\mu = 3.375 \text{ mm}^{-1}$, 62175 measured and 6946 independent reflections ($R_{\text{int}} = 0.0218$). $F(000) = 656$, 485 parameters, $R_1 = 0.0249$ for 6806 reflections with $F_o > 4\sigma(F_o)$ and $wR_2 = 0.0602$ for all 6946 data. Max./min. residual peaks $-0.36/0.28 \text{ e \AA}^{-3}$. The structure of GaEt_3 was refined as a racemic twin with the major component contributing 53.3(10)%. CCDC-163477 (GaMe_3) and CCDC-163478 (GaEt_3) contain the supplementary crystallographic data for this paper. These data can be obtained free of charge via www.ccdc.cam.ac.uk/conts/retrieving.html (or from the Cambridge Crystallographic Data Centre, 12, Union Road, Cambridge CB2 1EZ, UK; fax: (+44) 1223-336-033; or deposit@ccdc.cam.ac.uk).
- [9] R. Boese, D. Bläser, N. Niederprüm, M. Nüsse, W. A. Brett, P. von R. Schleyer, M. Bühl, N. J. R. van Eikema Hommes, *Angew. Chem.* **1992**, *104*, 356–358; *Angew. Chem. Int. Ed. Engl.* **1992**, *31*, 314–316.
- [10] R. Boese, D. Bläser, M. Prager, S. Parsons, C. M. Morrison, personal communications, **2001**.
- [11] a) E. L. Amma, R. E. Rundle, *J. Am. Chem. Soc.* **1958**, *80*, 4141–4145; b) A. J. Blake, S. Craddock, *J. Chem. Soc. Dalton Trans.* **1990**, 2393–2396.
- [12] G. S. McGrady, J. F. C. Turner, R. M. Ibberson, M. Prager, *Organometallics* **2000**, *19*, 4398–4401.
- [13] G. M. Sheldrick, W. S. Sheldrick, *J. Chem. Soc. A* **1970**, 28–30.
- [14] B. Beagley, D. G. Schmidling, I. A. Steer, *J. Mol. Struct.* **1974**, *21*, 437–444.
- [15] a) MOLPRO is a package of ab initio programs written by H.-J. Werner and P. J. Knowles, with contributions from R. D. Amos, A. Berning, D. L. Cooper, M. J. O. Deegan, A. J. Dobbyn, F. Eckert, C. Hampel, G. Hetzer, T. Leininger, R. Lindh, A. W. Lloyd, W. Meyer, M. E. Mura, A. Nicklaß, P. Palmieri, K. Peterson, R. Pitzer, P. Pulay, G. Rauhut, M. Schütz, H. Stoll, A. J. Stone, T. Thorsteinsson; b) N. Runeberg, M. Schütz, H.-J. Werner, *J. Chem. Phys.* **1999**, *110*, 7210–7215.
- [16] a) ORIENT version 3.2 by A. J. Stone with contributions from A. Dullweber, M. P. Hodges, P. L. A. Popelier, D. J. Wales; b) A. J. Stone, *Chem. Phys. Lett.* **1981**, *83*, 233–239.
- [17] P. L. A. Popelier, G. Logothetis, *J. Organomet. Chem.* **1998**, *555*, 101–111.
- [18] Z. Otwinowski, W. Minor, *Methods Enzymol.* **1997**, *276*, 307–326.
- [19] SHELXTL 5.01, Siemens Analytical X-Ray Instrumentation Inc. Madison, WI, **1995**.

Bridging the Gap between Polyoxometalates and Classic Coordination Compounds: A Novel Type of Hexavanadate Complex

Markus Piepenbrink, Michael U. Triller, Neville H. J. Gorman, and Bernt Krebs*

Dedicated to Professor Roald Hoffman on the occasion of his 65th birthday

Polyoxometalates have gained great interest because of their remarkable chemical properties and their enormous potential shown in fields of catalytic, technical, and medical applications.^[1] During the last decade, the research in this rapidly growing area has focused on the design of new compounds, among them many in interdisciplinary fields between solid-state chemistry, material science, and organic synthesis.^[2, 3] To find new pathways for the synthesis of catalysts and to understand the mechanistic background of catalysis, one of the most challenging tasks is the development of novel selective and highly efficient catalytic systems containing polyoxoanions.^[4] Therefore, our group has focused on the design of novel polyoxometalate catalysts for directed oxygen-transfer processes.^[5]

In comparison to the extensive work on polyoxomolybdates and polyoxotungstates, considerably less research has been conducted in the field of polyoxovanadates. Among the structural types known in this area, the $\{V_6O_{19}\}^{n-}$ core is extremely rare.^[6] A small number of compounds containing this structural motif (with tris(alkoxo) ligands as the only substituents) have been reported.^[7] In addition, some polyoxometalate-supported organometallic complexes have been synthesized and characterized where heterometal fragments (Cp^*M^{2+}) ($Cp^* = C_5Me_5$, $M^{2+} = Rh, Ir$) cap the hexavanadate core.^[8] These few species represent the only structurally characterized vanadium clusters incorporating the Lindqvist structure type ($\{V_6O_{19}\}^{n-}$).

Herein we present the first example of a $\{V_6O_{19}\}^{n-}$ core that is substituted by two vanadyl moieties ligated by exchangeable ligands. With this new approach of combining polyoxometalate chemistry and classic coordination chemistry we hope to enhance the catalytic potential of polyoxovanadates. The coordination sphere of the two scaffolding vanadyl moieties resembles the structural motif in the active site of vanadium-containing haloperoxidases.^[9] These vanadium centers are ligated by the new ligand bis(1-methylimidazol-2-yl)-4-methoxyphen-1-ylmethanol (bmimp) and are attached to the hexavanadate core by oxygen atom bridges. The two vanadyl complexes cap the polyoxovanadate and are tilted towards the polyoxometalate unit (Figure 1). This tilt is facilitated by a hydrogen bond originating from the ligand OH-group towards one edge of a VO_6 octahedron.

$[VO(bmimp)(acac)]_2[V_6O_{13}(OCH_3)_6]$ (**1**; acac = acetylacetonate) was synthesized in methanolic solution by adding

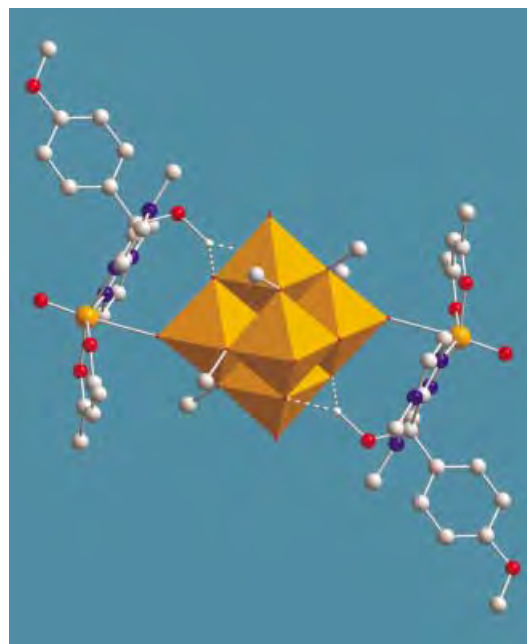


Figure 1. The polyoxovanadate core $\{V_6O_{13}(OMe)_6\}^{2-}$ linked to two vanadyl moieties containing organic ligands (polyhedral view).

$[VO(acac)_2]$ to bmimp. After one day, orange prismatic crystals were obtained and characterized by X-ray diffraction.^[10] The hexavanadate located in the center of the molecular structure consists of six VO_6 octahedra which build up an octahedron of the Lindqvist type (Figure 2). The oxygen

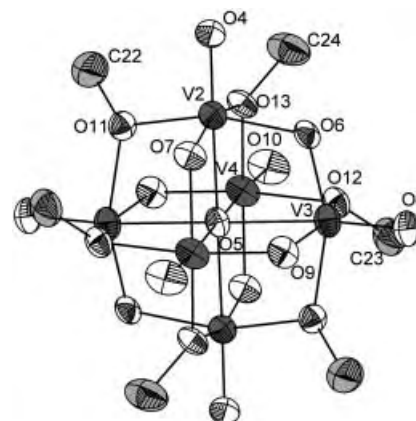


Figure 2. Central molecular part of the structure of **1** (thermal ellipsoids set at 50 % probability). Selected bond lengths [Å]: V2–O4 1.624(3), V2–O5 2.224(1), V2–O6 1.897(3), V2–O7 1.752(4), V2–O13 2.034(3).

framework contains four oxygen atoms bound to vanadium centers by double bonds (O8, O10), six μ_2 -oxo bridges (O6, O7, O9), one central oxygen atom (O5), and six μ_2 -alkoxo bridging methanol oxygen atoms (O11, O12, O13). The incorporation of methanol into polyoxovanadates has been described previously.^[7a]

The hexavanadate core can formally be regarded as a $\{V_6O_{13}(OMe)_6\}^{2-}$ ion. As part of this subunit, one terminal oxygen atom O4 forms a bridge to the outer-shell vanadium atom. Remarkably, the observed distance between V2 and O4 is 1.624(3) Å, which is expected for vanadyl bonds ($V=O$), whereas the V1–O4 bond is unusually long (2.381(3) Å), a

[*] Prof. Dr. B. Krebs, M. Piepenbrink, M. U. Triller, N. H. J. Gorman
Westfälische Wilhelms-Universität Münster
Institut für Anorganische und Analytische Chemie
Wilhelm-Klemm-Strasse 8, 48149 Münster (Germany)
Fax: (+49) 251-833-8366
E-mail: krebs@uni-muenster.de

result of being *trans* to the oxo group O1 (Figure 3). The atom V1 has a distorted-octahedral coordination environment. The two nitrogen atoms of the bidentate ligand bmimpmp together

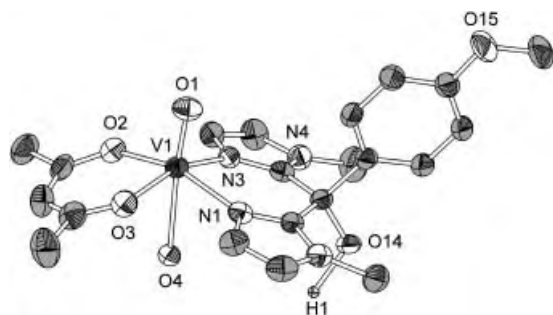


Figure 3. Coordination sphere of V1 and the organic ligand system (thermal ellipsoids set at 50% probability).

with the two oxygen atoms of the acetylacetonate ligand form the equatorial plane; the atom V1 is located 0.376 Å above this N₂O₂ plane.

Compound **1** exhibits interesting structure-determining hydrogen-bonding interactions. The hydrogen atom H1 of the ligand bmimpmp forms a hydrogen bond with O7 (1.717 Å) and O9 (1.893 Å) of the hexavanadate cluster thus tilting the ligand bmimpmp towards the hexavanadate cluster (see Figure 1). This effect results in a V1–O4–V2 angle of 154.6°, which deviates considerably from 180°.

According to our experience in polyoxometalate molecular science the calculation of oxidation states by using bond-valence parameters for solids is a particularly suitable method to determine whether or not the distribution of the oxidation states is disordered. Application of the parameters presented by Brese and O'Keeffe resulted in $V_{V1} = 3.994$ (by using bond-valence parameters of O for N) and 4.209 (by using bond-valence parameter for N without considering the vanadium oxidation state).^[11] The oxidation states of the three vanadium atoms forming the polyoxovanadate core were calculated to be $V_{V2} = 5.092$, $V_{V3} = 5.070$, and $V_{V4} = 5.078$. Therefore we propose the vanadium atoms V2, V3, and V4 to exist in the +v oxidation state, leading to a net charge of –2 for the polyoxometalate cluster, which is counterbalanced by the two formally positively charged vanadyl moieties (V^{IV}). This configuration is in accord with cyclic voltammetry measurements.

A number of experiments are prompted by the results presented herein. Variation of the scaffolding vanadyl moieties offers a way to fine tune potential catalytic properties of the polyoxovanadate unit. We have already started to synthesize new ligand systems with similar coordination sites. Furthermore, ligand-exchange experiments appear to be successful. Since the hydrogen bond facilitates the tilt of the ligand towards the polyoxometalate core, control over the protonation state might allow for discrimination between different substrates in catalysis by using the hydrogen bond as a molecular switch. By linking transition-metal complexes containing asymmetric organic ligands to the described hexavanadate species, it should be possible to generate a series of new compounds containing steric information for better directed oxygen-transfer processes. These compounds

would also serve as models to clarify catalytic mechanisms in polyoxometalate chemistry.

Experimental Section

bmimpmp: In a three-neck flask equipped with a dropping funnel, a gas inlet, and a gas outlet, 1-methylimidazole (75.4 mmol, 6 mL) was dissolved in dry diethyl ether (200 mL) under a protective argon atmosphere and cooled to –78 °C. *n*-Butyllithium (75.4 mmol, 47 mL, 1.6 M in hexane) was added dropwise. The reaction mixture was allowed to warm to 0 °C to complete deprotonation. After cooling to –78 °C, 4-methoxyethylbenzoate (prepared by acid-catalyzed esterification of 4-methoxybenzoic acid with ethanol) was slowly added dropwise. The reaction mixture was allowed to warm to 0 °C over a period of 12 h and then quenched with water (50 mL). The phases were separated and the aqueous phase extracted with diethyl ether (2 × 30 mL) and CHCl₃ (3 × 30 mL). The combined colorless organic phases were dried over MgSO₄. The solvent was removed under reduced pressure to leave a colorless oil from which the crude product precipitates as a white solid upon storage of the oil at –20 °C. Recrystallization from acetone and CHCl₃ yields colorless crystals (yield: 4.5 g, 40%). Elemental analysis (%) calculated for C₁₆H₁₈N₄O₂: C 64.41, H 6.08, N 18.78; found: C 64.13, H 6.20, N 18.65; ¹H NMR (300 MHz, CDCl₃, TMS): δ = 3.38 (s, 6H; CH₃), 3.77 (s, 3H; OCH₃), 6.82 (d, ³J(H,H) = 9 Hz, 2H; CH_{im}), 6.84 (d, ³J(H,H) = 1 Hz, 2H; CH_{ph}), 6.93 (d, ³J(H,H) = 1 Hz, 2H; CH_{ph}), 6.98 ppm (d, ³J(H,H) = 9 Hz, 2H; CH_{im}); ¹³C NMR (75 MHz, CDCl₃, TMS): δ = 34.5 (CH₃), 55.1 (OCH₃), 76.4 (COH), 113.5 (CH_{ph}), 123.2 (CH_{ph}), 125.7 (CH_{im}), 128.5 (CH_{im}), 134.0 (C_{ph}), 148.4 (C_{im}), 192.9 ppm (COMe); IR (KBr pellet; 4000–400 cm^{–1}): $\tilde{\nu}$ = 2954 (m), 1609 (m), 1587 (w), 1511 (s), 1481 (m), 1405 (m), 1251 (s), 1055 (m), 1035 (m), 756 (s), 683 (w), 594 (w); MS (70 eV): *m/z* (%): 299 (20) [M⁺+H], 298 (100) [M⁺], 191 (32) [C₉H₁₁N₄O⁺].

1: bmimpmp (0.2 mmol, 59 mg) and triethylamine (3 drops) were dissolved in methanol (5 mL) and [VO(acac)₂] (0.8 mmol, 212 mg) was added. The reaction mixture was stirred for 12 h. From the resulting orange solution, orange rhombical crystals suitable for X-ray diffraction grew upon leaving the solution to stand for one day (yield: 36.7 mg, 24%). IR (KBr pellet; 4000–400 cm^{–1}): $\tilde{\nu}$ = 3408 (m, br), 3118 (w), 3079 (w), 2920 (m), 2811 (w), 1606 (m), 1586 (s), 1524 (s), 1507 (s), 1443 (m), 1374 (s), 1282 (m), 1252 (m), 1185 (w), 1158 (m), 1146 (m), 1070 (m), 1032 (s, br), 987 (m), 956 (vs), 920 (vs), 839 (m), 784 (m), 756 (s), 733 (m), 660 (m), 594 (m), 542 (w), 499 (w), 463 (w), 443 (m); cyclic voltammetry (saturated in methanol (<1 mm), supporting electrolyte tetrabutylammonium hexafluorophosphate 100 mM): Measurement taken at a Perkin-Elmer 263A Potentiostat with a glassy-carbon working electrode, Ag/AgCl reference electrode, and Pt counter electrode. An irreversible oxidation peak at 130 mV was found corresponding to the V^{IV}/V^V redox couple.

Received: January 21, 2002 [Z18545]

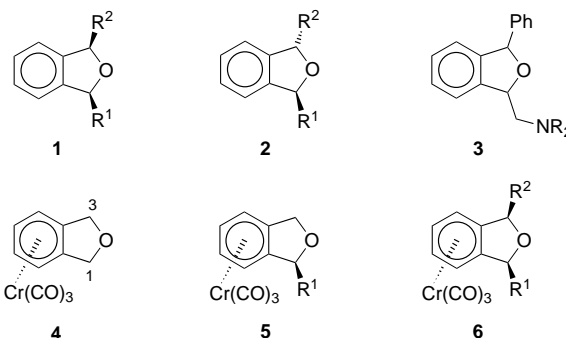
- [1] a) *Polyoxometalate Chemistry* (Eds.: M. T. Pope, A. Müller), Kluwer, Dordrecht, **2001**; b) "Polyoxometalates": *Chem. Rev.* **1998**, *98*, 1–389.
- [2] a) R. L. La Duca, Jr., R. Ratkowski, R. S. Rarig, Jr., J. Zubieta, *Inorg. Chem. Commun.* **2001**, *4*, 621–625; b) H. Weiner, R. G. Finke, *J. Am. Chem. Soc.* **1999**, *121*, 9831–9842; c) J. R. Galán-Mascarós, C. Giménez-Saiz, S. Triki, C. J. Gómez-García, E. Coronado, L. Ouahab, *Angew. Chem.* **1995**, *107*, 1601–1603; *Angew. Chem. Int. Ed. Engl.* **1995**, *34*, 1460–1462.
- [3] a) Y. Zhang, J. R. D. DeBord, C. J. O'Connor, R. C. Haushalter, A. Clearfield, J. Zubieta, *Angew. Chem.* **1996**, *108*, 1067–1069; *Angew. Chem. Int. Ed. Engl.* **1996**, *35*, 989–991; b) J. T. Rijssenbeck, D. J. Rose, R. C. Haushalter, J. Zubieta, *Angew. Chem.* **1997**, *109*, 1049–1052; *Angew. Chem. Int. Ed. Engl.* **1997**, *36*, 1008–1010; c) D. Hagman, C. Sangregorio, C. J. O'Connor, J. Zubieta, *J. Chem. Soc. Dalton Trans.* **1998**, 3707–3709.
- [4] a) R. Neumann, M. Dahan, *Nature* **1997**, *388*, 353; b) A. M. Khenkin, R. Neumann, *Angew. Chem.* **2000**, *112*, 4254–4256; *Angew. Chem. Int. Ed.* **2000**, *39*, 4088–4090; c) H. Weiner, R. G. Finke, *J. Am. Chem. Soc.* **1999**, *121*, 9831–9842; d) C. L. Hill, X. Zhang, *Nature* **1995**, *373*, 324–326.
- [5] a) M. Bösing, A. Nöh, I. Loose, B. Krebs, *J. Am. Chem. Soc.* **1998**, *120*, 7252–7259; b) M. Bösing, I. Loose, H. Pohlmann, B. Krebs, *Chem. Eur. J.* **1997**, *3*, 1232–1237.

- [6] P. Gouzerh, A. Proust, *Chem. Rev.* **1998**, 98, 77–112, and references therein
- [7] a) Q. Chen, D. P. Goshorn, C. P. Scholes, X. Tan, J. Zubieta, *J. Am. Chem. Soc.* **1992**, 114, 4667–4681; b) A. Müller, J. Meyer, H. Bögge, A. Stammler, A. Botar, *Z. Anorg. Allg. Chem.* **1995**, 621, 1818–1831.
- [8] H. K. Chae, W. G. Klemperer, V. W. Day, *Inorg. Chem.* **1989**, 28, 1423–1424.
- [9] a) A. Messerschmidt, L. Prade, R. Wever, *Biol. Chem.* **1997**, 378, 309–315; b) M. Weyand, H.-J. Hecht, M. Kieß, M.-F. Liaud, H. Vilter, D. Schomburg, *J. Mol. Biol.* **1999**, 293, 595–611.
- [10] Crystal-structure analysis for **1**: Single-crystal X-ray diffraction data were collected on a Bruker Nonius Smart diffractometer with a CCD detector ($\lambda(\text{CuK}\alpha) = 1.54184 \text{ \AA}$) at 200(2) K, crystal dimensions $0.16 \times 0.12 \times 0.06 \text{ mm}^3$. Structure solution was achieved by applying direct statistical methods of phase determination using the SHELXS program, and full-matrix least-squares refinements were performed using the SHELXL-97 software: Monoclinic, space group $P2_1/c$, $a = 15.132(3)$, $b = 15.934(3)$, $c = 13.290(3) \text{ \AA}$, $\beta = 98.78(3)^\circ$, $V = 3166.8(11) \text{ \AA}^3$, $\rho_{\text{calcd}} = 1.708 \text{ g cm}^{-3}$, $2\theta_{\text{max}} = 51.9^\circ$, total collected reflections 18280, unique reflections 5858, $R_{\text{int}} = 0.0786$, $\mu = 1.218 \text{ mm}^{-1}$, $R_1 = 0.0597$ and $wR_2 = 0.1539$ for $I > 2\sigma(I)$, $R_1 = 0.0878$ and $wR_2 = 0.1627$ for all reflections, 425 total parameters, $\text{Goof} = 0.967$ on $|F^2|$, max./min. residual electron density $1.131 / -0.555 \text{ e \AA}^{-3}$. CCDC-176210 (**1**) contains the supplementary crystallographic data for this paper. These data can be obtained free of charge via www.ccdc.cam.ac.uk/Contents/retrieving.html (or from the Cambridge Crystallographic Data Centre, 12, Union Road, Cambridge CB21EZ, UK; fax: (+44) 1223-336-033; or deposit@ccdc.cam.ac.uk).
- [11] N. E. Brese, M. O'Keeffe, *Acta Crystallogr. Sect. B* **1991**, 47, 192–197. The oxidation state of atom i is given by $\sum_j v_{ij} = V$ with $v_{ij} = \exp[(R_{ij} - d_{ij})/b]$. Here b is taken to be a “universal” constant equal to 0.37 \AA , v_{ij} is the valence of a bond between two atoms i and j , R_{ij} is given by the empirical parameters, and d_{ij} is the observed length of the bond.

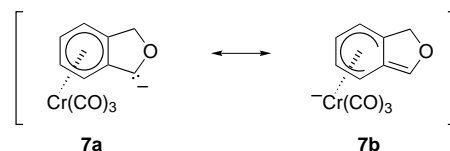
Benzylic *endo*-Alkylation of Phthalan–Cr(CO)₃ Complexes via Temporary Silylation: An Entry to *trans*-1,3-Disubstituted Dihydroisobenzofurans**

Saskia Zemolka, Johann Lex, and Hans-Günther Schmalz*

Substituted 1,3-dihydroisobenzofurans (phthalans) represent an interesting class of compounds owing to their promising pharmacological potential,^[1] but they have received only little attention from synthetic chemists in the past.^[2] In particular, almost no general methods are available for the stereoselective synthesis of *cis*- or *trans*-1,3-disubstituted derivatives of type **1** and **2**, respectively.^[3] With regard to the usefulness of such compounds as intermediates for the synthesis of bioactive oxonanes^[4] and the established biological activity of compounds of type **3**,^[5] the search for efficient stereoselective entries to 1,3-disubstituted phthalans remains a challenging task.



In 1989, Davies and co-workers reported the preparation of a few *cis*-configured compounds of type **1** ($R^1, R^2 = \text{Me}, \text{D}$) starting from the [phthalan–Cr(CO)₃] complex **4**.^[6] In two successive benzylic deprotonation/alkylation steps, **4** can be transformed (via *rac*-**5**) into bis-*exo*-alkylated complexes of type **6**, from which the free ligands **1** are easily obtained by oxidative decomplexation.^[6] The method exploits both the ability of the Cr(CO)₃ fragment to stabilize a negative charge in the benzylic position^[7] and the strong steric effect of the metal fragment (shielding of the *endo* face).^[7b, 8] The stabilization of the anionic intermediate **7a** derived from **4** by benzylic deprotonation can be understood in terms of the resonance structure **7b** in which the charge is delocalized to the Cr(CO)₃ unit (Scheme 1).^[9]



Scheme 1. Resonance structures of the benzylic anion derived from **4**.

In the course of our research on the application of chiral arene–Cr(CO)₃ complexes in the stereoselective synthesis of bioactive compounds,^[10] we were interested in using the silylated complex **8** as a building block for the synthesis of new 1,3-disubstituted phthalans. Compound **8** was selected since it is easily prepared, even in the optically active form,^[11] from the parent complex **4**. Herein we disclose the results of a study which has led to the discovery of some unexpected, remarkably selective transformations and to the development of an efficient and completely stereoselective route to 1-*endo*-alkylated complexes and to *trans*-1,3-disubstituted phthalans.

When complex *rac*-**8** was treated with *t*BuLi at low temperatures (–100 to –78 °C) followed by quenching of the resulting anion with different electrophiles, we were surprised to find that the 1,1-disubstituted products (*rac*-**11**) were formed with complete regio- and diastereoselectivity (Table 1). Evidently, the deprotonation of *rac*-**8** does not, as

[*] Prof. Dr. H.-G. Schmalz, S. Zemolka, Dr. J. Lex^[+]
Institut für Organische Chemie, Universität zu Köln
Greinstrasse 4, 50939 (Germany)
Fax: (+49) 221-470-3064
E-mail: schmalz@uni-koeln.de

[**] This work was supported by Aventis Pharma Deutschland GmbH and the Fonds der Chemischen Industrie. The authors thank Dr. H. Schmickler and Dr. M. Schäfer for their invaluable support with advanced NMR spectroscopic and MS spectrometric techniques. Gifts of chemicals from Aventis and Chemetall AG are gratefully acknowledged.

[+] X-ray crystallographic analysis.

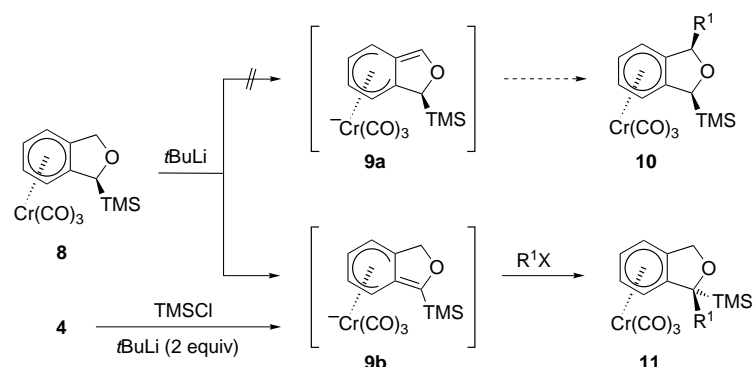
Supporting information for this article is available on the WWW under <http://www.angewandte.com> or from the author.

Table 1. Preparation of 1,1-disubstituted complexes of type *rac-11* according to Scheme 2.

Starting material	Electrophile (R ¹ X)	Method ^[a]	Product	R ¹	Yield [%] ^[b]
<i>rac-8</i>	MeI	A	<i>rac-11a</i>	Me	76
<i>rac-8</i>	allyl bromide	A	<i>rac-11b</i>	allyl	80
<i>rac-8</i>	<i>n</i> BuI	A	<i>rac-11c</i>	<i>n</i> Bu	83
<i>rac-8</i>	TMSCl	A	<i>rac-11d</i>	TMS	72
<i>rac-8</i>	TBSOC ₅ H ₁₀ I	A	<i>rac-11e</i>	TBSOC ₅ H ₁₀	54
<i>rac-8</i>	BnOCOCl	A	<i>rac-11f</i>	CO ₂ Bn	57
4	MeI	B	<i>rac-11a</i>	Me	96
4	allyl bromide	B	<i>rac-11b</i>	allyl	99
4	<i>n</i> BuI	B	<i>rac-11c</i>	<i>n</i> Bu	78
4	H ₂ O	B	<i>rac-11g</i>	H	96
4	MeOD	B	<i>rac-11h</i>	D	83

[a] Method A: *rac-8*, THF, *t*BuLi (1.1 equiv), $-100 \rightarrow -78^\circ\text{C}$, 1 h, then R¹X (2.5–5 equiv), $-78 \rightarrow -45^\circ\text{C}$, 1–5 h (TLC control), then H₂O quench and extractive workup; method B: **4**, THF, TMSCl (1.01 equiv), -100°C , then *t*BuLi (2.2 equiv), 2 h, $-100 \rightarrow -78^\circ\text{C}$, then R¹X (3 equiv), $-78 \rightarrow -50^\circ\text{C}$, 1–3.5 h (TLC control). [b] Yield of isolated product after

originally anticipated (see below), lead to the intermediate *rac-9a* (Scheme 2). Instead, the isomeric benzylic anion *rac-9b* is generated, which is subsequently alkylated by the



Scheme 2. Unexpected formation of 1,1-disubstituted complexes of type **11** by deprotonation/alkylation of **8**. For details see Table 1.

electrophile (R¹X) from the unhindered *exo* face. Thus, the bulky TMS group ends up in the *endo* position with respect to the Cr(CO)₃ fragment, as found in the X-ray crystal structures of **11a** and *rac-11d* (Figure 1).^[12]

Starting from **4**, the preparation of 1,1-disubstituted complexes of type *rac-11* could also be carried out in an efficient one-pot procedure (Scheme 2): treatment of a solution of **4**

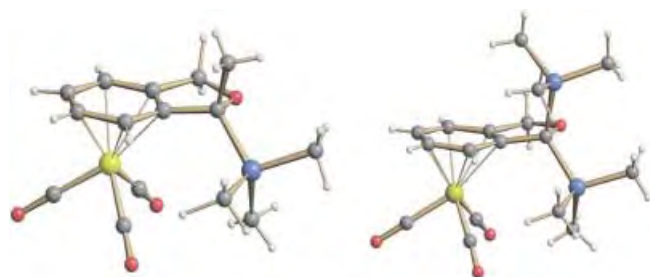
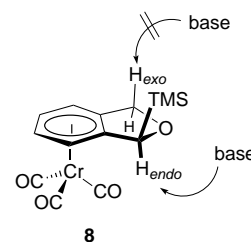


Figure 1. Structure of **11a** (left) and *rac-11d* (right) in the crystalline state.^[12]

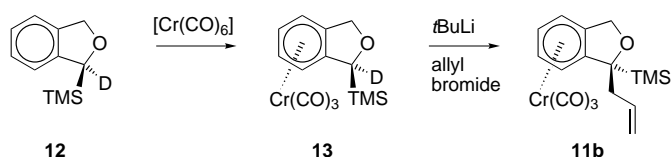
and TMSCl (1 equiv) in THF with *t*BuLi (2 equiv) at low temperatures (-100 to -78°C) under in situ quench (ISQ) conditions^[11, 13] directly afforded a deep red solution of the benzylic anion (*rac-9b*), which could be quenched (as before) with different electrophiles to give the products usually even in better yields than in the former two-step procedure (Table 1).

The clean access to compounds of type **11** opened interesting perspectives for further transformations (see below). However, we were puzzled by the fact that deprotonation of **8** with *t*BuLi selectively affords the intermediate **9b**, even at -100°C (i.e. kinetic control). We had expected the isomeric species **9a** to be formed, anticipating the benzylic deprotonation of **8** to occur from the *exo* face.^[14] Clearly, **9b** is thermodynamically more stable than **9a** as a result of the α -silyl effect.^[15] The question was whether an *endo* deprotonation had occurred at the highly hindered silylated position of **8** (H_{endo} at C1) or if **9b** was possibly formed by rearrangement of **9a** generated by a “standard” *exo* deprotonation at the unhindered opposite benzylic position (H_{exo} at C3) (Schemes 2 and 3).



Scheme 3. Deprotonation (3-*exo* versus 1-*endo*) of complex **8**.

To distinguish between these two possibilities, we decided to employ the deuterated derivative *rac-13* (*rac*-[D]₁**8**) in a deprotonation/alkylation sequence. Compound *rac-13* was prepared by diastereoselective complexation ([Cr(CO)₆], *n*Bu₂O/THF, reflux) of *rac-12*,^[16] which in turn was obtained from *rac-11h* by oxidative decomplexation. When *rac-13* was deprotonated with *t*BuLi at -78°C and the resulting anion was quenched with allyl bromide, the completely dedeuterated product *rac-11b* was isolated in 69% yield (Scheme 4).^[17] This result clearly demonstrates that, in contrast to established arene–Cr(CO)₃ chemistry,

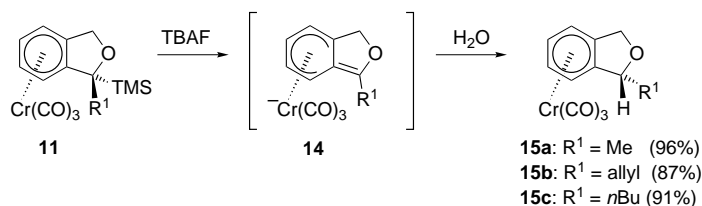


Scheme 4. Proof of the 1-*endo*-deprotonation of **8** by using the deuterated derivative **13**. The experiment was carried out with the racemic compounds. Reagents and conditions: step 1: [Cr(CO)₆] (1.08 equiv), *n*Bu₂O/THF (10:1), 155°C , 27 h; step 2: *t*BuLi (1.1 equiv), THF, -78°C , 2 h, then allyl bromide (2 equiv), 2 h.

the deprotonation of *rac-8* indeed proceeds from the *endo* face (at the silylated position). Most likely, the enhanced acidity at C1 as a result of the TMS substituent overcompensates the shielding of the *endo* face by the Cr(CO)₃ fragment in this specific case (Scheme 3).^[18]

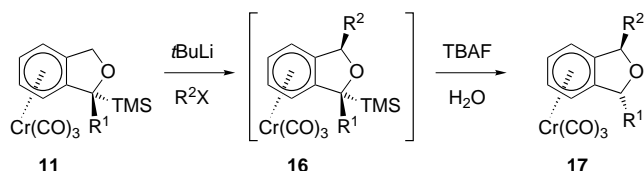
Desilylation of compounds of type *rac-11* with tetrabutylammonium fluoride (TBAF) in the presence of water furnished the monosubstituted complexes *rac-15* as pure *endo*

diastereomers in excellent yields through diastereoselective protonation of the intermediate anion *rac*-**14** from the *exo* face (Scheme 5).^[19]



Scheme 5. Desilylation of complexes of type **11** leads to *endo*-alkylated products of type **15** through *exo* protonation of the intermediate **14**. Reagents and conditions: THF, H₂O, 0 °C, TBAF (3 equiv), 10 min, room temperature, 12 h.

The newly developed, unique entry to *endo*-alkylated products prompted us to investigate the possibility of utilizing the silylated complexes *rac*-**11** in the synthesis of *trans*-1,3-disubstituted phthalans. Indeed, after subjecting complexes of type *rac*-**11** to the typical deprotonation/alkylation conditions and direct desilylation of the intermediates *rac*-**16**, the *trans*-1,3-disubstituted complexes *rac*-**17** were obtained as pure diastereomers (Scheme 6, Table 2). The expected *trans* con-



Scheme 6. One-pot synthesis of *trans*-1,3-disubstituted phthalan complexes of type **17**. For details, see Table 2.

Table 2. Preparation of *trans*-1,3-disubstituted complexes of type *rac*-**17** according to Scheme 6.^[a]

Starting material	Electrophile (R ² -X)	Product	R ¹	R ²	Yield [%] ^[b]
<i>rac</i> - 11a	allyl bromide	<i>rac</i> - 17a	Me	allyl	91
<i>rac</i> - 11a	<i>n</i> BuI	<i>rac</i> - 17b	Me	<i>n</i> Bu	76
<i>rac</i> - 11a	BnBr	<i>rac</i> - 17c	Me	Bn	72
<i>rac</i> - 11a	MeSSMe	<i>rac</i> - 17d	Me	S-Me	67
<i>rac</i> - 11a	Et ₂ NCOCi	<i>rac</i> - 17e	Me	CONe ₂	56
<i>rac</i> - 11a	EtOCOCi	<i>rac</i> - 17f	Me	CO ₂ Et	56 ^[c]
<i>rac</i> - 11b	<i>n</i> BuI	<i>rac</i> - 17g	allyl	<i>n</i> Bu	50
<i>rac</i> - 11b	MeI	<i>rac</i> - 17h	allyl	Me	77
<i>rac</i> - 11c	BnBr	<i>rac</i> - 17i	<i>n</i> Bu	Bn	77

[a] THF, *t*BuLi (1.1 equiv), −78 °C, 2 h, then R²X (2–4 equiv), −78 → −10 °C, 1 to 5 h (TLC control), then H₂O, room temperature, 0 °C, then TBAF (1.5–7.5 equiv), room temperature, 12 h; extractive workup. [b] Yield of isolated product after chromatographic purification. [c] Inverse addition: the anion was added at −78 °C to R²X in THF, then 2 h, −78 °C.

figuration of the products was unequivocally proven by means of X-ray crystallographic analysis in the cases of *rac*-**17b** and *rac*-**17f** (Figure 2)^[12] and NMR spectroscopic correlations.

To demonstrate the applicability of the developed methodology in the preparation of nonracemic compounds, the chirogenic step (i.e. the deprotonation of the prochiral complex **4**) was performed enantioselectively^[11] by using the

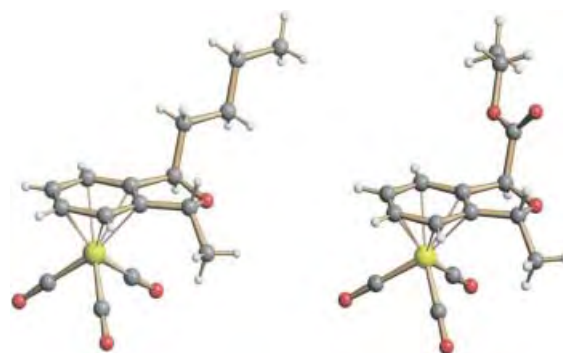
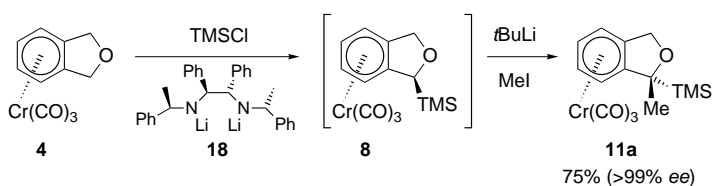


Figure 2. Structure of *rac*-**17b** (left) and *rac*-**17f** (right) in the crystalline state.^[12]

chiral amide base **18**.^[20] Therefore, **4** was treated with **18** (1 equiv) in the presence of TMSCl (ISQ conditions) at −100 °C, and the intermediate **8** (formed in situ) was directly converted by deprotonation with *t*BuLi and an electrophilic quench (MeI) into complex **11a**^[12] with >99% *ee* (HPLC) in 75% yield (Scheme 7, Figure 1).^[21] By combining the transformations shown in Scheme 7 (**4**→**11**) and Scheme 6 (**11**→**17**) the diastereo- and enantioselective synthesis of *trans*-1,3-disubstituted phthalan complexes can be carried out through a short and efficient sequence of two one-pot procedures.



Scheme 7. One-pot, enantioselective synthesis of **11a**. Reagents and conditions: TMSCl (1.01 equiv), **18** (1.08 equiv), THF, −100 °C, then slow addition of **4** in THF, −95 → −85 °C, 45 min., then *t*BuLi (2.3 equiv), −78 °C, 1 h, MeI (5 equiv), 1 h.

In conclusion, we have succeeded in elaborating a general, practical, and fully stereoselective entry to *trans*-1,3-dialkylated dihydroisobenzofurans. The method exploits the remarkable and unexpected finding that the deprotonation of **8** occurs at the substituted benzylic position (from the *endo* face!). Our current investigations are aimed at the application of this method to the synthesis of more sophisticated systems related to bioactive natural products.

Received: February 7, 2002 [Z18667]

- [1] a) A prominent example of a bioactive phthalan is the antidepressant citalopram; see: B. G. Pollock, *Expert Opin. Pharmacother.* **2001**, *2*, 681; b) R. G. Lovey, A. J. Elliott, J. J. Kaminski, D. Loebenberg, R. M. Parmegiani, D. F. Rane, V. M. Girijavallabhan, R. E. Pike, H. Guzik, B. Antonacci, T. Y. Tomaine, *J. Med. Chem.* **1992**, *35*, 4221.
- [2] a) W. Friedrichsen in *Advances in Heterocyclic Chemistry*, Vol. 37 (Ed.: A. R. Katritzky), Academic Press, London, **1999**, p. 1; b) B. A. Keay, P. W. Dibble in *Comprehensive Heterocyclic Chemistry II*, Vol. 2 (Eds.: A. R. Katritzky, C. W. Rees, E. F. V. Scriven), Pergamon, London, **1996**, p. 395.
- [3] a) D. F. Ewing, C. Len, G. Mackenzie, G. Ronco, P. Villa, *Tetrahedron: Asymmetry* **2000**, *11*, 4995; b) D. F. Ewing, N.-E. Fahmi, C. Len, G.

- Mackenzie, A. Pranzo, *J. Chem. Soc. Perkin Trans. 1* **2000**, 3561; c) B. Chao, D. C. Dittmer, *Tetrahedron Lett.* **2000**, 41, 6001.
- [4] a) M. C. Elliott, C. J. Moody, T. J. Mowlem, *Synlett* **1993**, 909; b) D. S. Brown, M. C. Elliott, C. J. Moody, T. J. Mowlem, *J. Chem. Soc. Perkin Trans. 1* **1995**, 1137.
- [5] For antiseecretory and antihistamine activities, see: a) S. Ram, A. K. Saxena, P. C. Jain, G. K. Patnaik *Indian J. Chem. Sect. B* **1984**, 23, 1261; b) M. W. Klohs, F. J. Petracek (Dart Industries Inc.), US Patent 3471519, **1969** [*Chem. Abstr.* **1969**, 71, 124212].
- [6] S. J. Coote, S. G. Davies, D. Middlemiss, A. Naylor, *J. Organomet. Chem.* **1989**, 379, 81.
- [7] For reviews, see: a) S. G. Davies, S. J. Coote, C. L. Goodfellow in *Advances in Metal-Organic Chemistry*, Vol. 2 (Ed.: L. S. Liebeskind), JAI, London, **1989**, p. 1; b) S. G. Davies, T. D. McCarthy in *Comprehensive Organometallic Chemistry II*, Vol. 12 (Eds.: E. W. Abel, F. G. A. Stone, G. Wilkinson), Pergamon, New York, **1995**, p. 979.
- [8] a) H.-G. Schmalz, S. Siegel in *Transition Metals for Organic Synthesis*, Vol. 1 (Eds.: M. Beller, C. Bolm), Wiley-VCH, Weinheim, **1998**, p. 550; b) M. Uemura in *Advances in Metal-Organic Chemistry*, Vol. 2 (Ed.: L. S. Liebeskind), JAI, London, **1989**, p. 195.
- [9] a) A. Pfletschinger, T. K. Dargel, H.-G. Schmalz, W. Koch, *Chem. Eur. J.* **1999**, 5, 537; b) C. A. Merlic, J. C. Walsh, D. J. Tantillo, K. N. Houk, *J. Am. Chem. Soc.* **1999**, 121, 3596.
- [10] For selected recent work, see: a) F. Dehmel, H.-G. Schmalz, *Org. Lett.* **2001**, 3, 3579; b) D. Hörstermann, H.-G. Schmalz, G. Kociok-Köhn, *Tetrahedron* **1999**, 55, 6905; c) T. Geller, H.-G. Schmalz, J. W. Bats, *Tetrahedron Lett.* **1998**, 39, 1537; d) K. Schellhaas, H.-G. Schmalz, J. W. Bats, *Chem. Eur. J.* **1998**, 4, 57; e) H.-G. Schmalz, A. Majdalani, *Synlett* **1997**, 1303.
- [11] a) R. A. Ewin, N. S. Simpkins, *Synlett* **1996**, 317; b) R. A. Ewin, A. M. MacLeod, D. A. Price, N. S. Simpkins, A. P. Watt, *J. Chem. Soc. Perkin Trans. 1* **1997**, 401; for a review, see: c) S. E. Gibson (née Thomas), E. G. Reddington, *Chem. Commun.* **2000**, 989.
- [12] For details of the crystal structure analyses of compounds *rac-11d*, *11a*, *rac-17b*, and *rac-17f*, see Supporting Information. CCDC-179013 (*rac-11d*), CCDC-179014 (*11a*), CCDC-179015 (*rac-17b*), and CCDC-179016 (*rac-17f*) contain the supplementary crystallographic data for this paper. These data can be obtained free of charge via www.ccdc.cam.ac.uk/conts/retrieving.html (or from the Cambridge Crystallographic Data Centre, 12, Union Road, Cambridge CB2 1EZ, UK; fax: (+44) 1223-336-033; or deposit@ccdc.cam.ac.uk).
- [13] D. A. Price, N. S. Simpkins, A. M. MacLeod, A. P. Watt, *J. Org. Chem.* **1994**, 59, 1961.
- [14] a) T. Volk, D. Bernicke, J. W. Bats, H.-G. Schmalz, *Eur. J. Inorg. Chem.* **1998**, 1883; b) J. Blagg, S. J. Coote, S. G. Davies, B. E. Mobbs, *J. Chem. Soc. Perkin Trans. 1* **1986**, 2257.
- [15] D. J. Peterson, *Organomet. Chem. Rev. Sect. A* **1972**, 7, 295.
- [16] A diastereomeric mixture of *rac-13* and *rac-11h* (7.5:1) was formed, which was easily separated by chromatography.
- [17] In this case, a by-product (19%) of type **10** was obtained which indicates a strong kinetic isotope effect (abstraction of D_{endo} at C1 versus H_{exo} at C3).
- [18] A participation of the ring oxygen atom (as a coordinating site) in the *endo* deprotonation step is likely, as other benzylic silylated [arene-Cr(CO)₃] complexes do not exhibit such behavior; see, for example: J. Blagg, S. J. Coote, S. G. Davies, D. Middlemiss, A. Naylor, *J. Chem. Soc. Perkin Trans. 1* **1987**, 689.
- [19] For other examples of *exo*-protonation of Cr(CO)₃-complexed benzylic anions, see refs. [10a, e], as well as: H.-G. Schmalz, S. Siegel, D. Bernicke, *Tetrahedron Lett.* **1998**, 39, 6683.
- [20] The base **18** was prepared from *R*-(+)-1-phenylethylamine; see: N. S. Simpkins, K. Bambridge, M. J. Begley, *Tetrahedron Lett.* **1994**, 35, 3391.
- [21] The absolute configuration of **11a** was determined by X-ray crystal-structure analysis^[12] and confirmed the expected results.^[11b]

Chemically Tuning between Ferromagnetism and Antiferromagnetism by Combining Theory and Synthesis in Iron/Manganese Rhodium Borides**

Richard Dronskowski,* Karol Korczak, Heiko Lueken, and Walter Jung

Dedicated to Professor Welf Bronger on the occasion of his 70th birthday

Cooperative magnetic phenomena such as ferromagnetism and antiferromagnetism have not only made up an enormously rich synthetic and theoretical playground for generations of solid-state physicists and chemists,^[1, 2] they also form the material basis of the most critical key technology of today's information society, namely data storage and data retrieval.^[3, 4] Fortunately enough, within the last two decades modern high-level electronic-structure calculations of the density-functional type have proven to be able to reproduce a number of essential observables (e.g., magnetic moments) in many (inter)metallic magnets with satisfying accuracy, thereby offering a first step in an atomistic understanding of these magnetic properties. Only recently, however, has it been shown that a more chemically oriented theoretical framework, intended to offer semiquantitative signposts for the synthesis of new cooperative magnets, can be constructed simply by identifying bonding "fingerprints" which are characteristic for either metallic ferromagnets or antiferromagnets.^[5, 6]

When a nonmagnetic ("spin-restricted") band-structure calculation is performed on a typical ferromagnet such as bcc-Fe, a crystal orbital Hamilton population (COHP) bonding analysis yields *antibonding* Fe–Fe interactions at the Fermi level (Figure 1, top left), which indicates an electronic instability. Upon spontaneous spin polarization ("spin-unrestricted" calculation), bcc-Fe undergoes a distortion, but instead of the atoms the electrons rearrange themselves.^[7] Thus, spontaneous magnetization makes the spin-up (α) and spin-down (β) electrons inequivalent, thereby reducing the electronic symmetry, which annihilates the antibonding states and, consequently, lowering the overall energy and the bonding energy by a few percent (Figure 1, top right).^[5, 6] For antiferromagnetism, things are a little bit more subtle. A corresponding nonmagnetic band-structure calculation on a typical antiferromagnet such as bcc-Cr results in the Fermi level being positioned exactly between the bonding and

[*] Prof. Dr. R. Dronskowski, K. Korczak, Prof. Dr. H. Lueken
Institut für Anorganische Chemie
Rheinisch-Westfälische Technische Hochschule
Professor-Pirlet-Strasse 1, 52056 Aachen (Germany)
Fax: (+49) 241-80-92288
E-mail: dronsk@HAL9000.ac.rwth-aachen.de
Prof. Dr. W. Jung
Institut für Anorganische Chemie
der Universität zu Köln
Greinstrasse 6, 50939 Köln (Germany)

[**] It is a pleasure to thank Dipl.-Chem. Uwe Couhorn, Dipl.-Chem. Yasemin Kurtulus, and Dr. Bernhard Eck for assistance as well as the Fonds der Chemischen Industrie for their support.

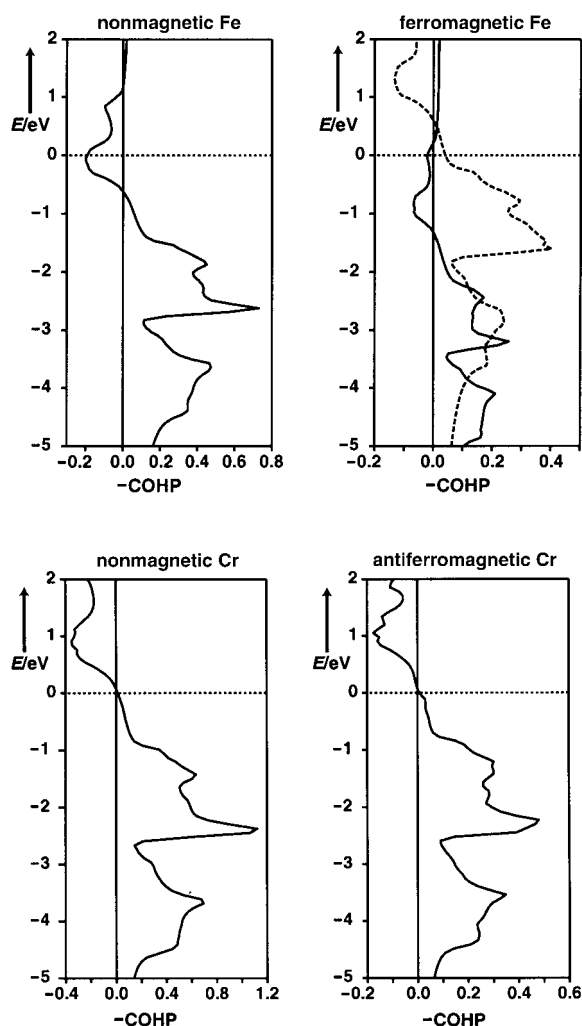


Figure 1. Top: COHP analysis of Fe–Fe bonding in nonmagnetic bcc-Fe (left) and in ferromagnetic, spin-polarized bcc-Fe (right; α spin lattice (—), β spin lattice (---)). Bottom: COHP analysis of Cr–Cr bonding in nonmagnetic bcc-Cr (left) and in antiferromagnetic, spin-polarized bcc-Cr (right); the Fermi levels (horizontal dotted lines) have been set to zero.

antibonding states, that is, in the *nonbonding* region (Figure 1, bottom left). This situation does not alter very much when a real antiferromagnetic calculation is performed; the states around the Fermi level remain nonbonding, the strength of interatomic bonding stays very much the same,^[6, 8] and it is only the slightly changing slope of the COHP close to the Fermi level that reminds us of a well-known instability in extended solids^[9] (Figure 1, bottom right). To successfully create new metallic ferromagnets and antiferromagnets, the synthetic recipe^[6, 8] for all transition metals and their alloys reads as follows: *Try to adjust the Fermi level of the material under investigation so as to position it within the antibonding states (ferromagnets) or nonbonding states (antiferromagnets) of the magnetically active atoms, that is, those atoms which have narrow band widths in their elemental forms.* Here are some examples for such a *tuning* of the valence-electron concentration by means of either an electronic enrichment or depletion:

The quaternary family of intermetallic phases $A_2MRh_5B_2$ (M =metal) which crystallize in an ordered, substitutional

variant of the $Ti_3Co_5B_2$ structure type, is especially well-suited to exploit these ways of chemical thinking since the overall structure is robust enough to allow a number of chemical substitutions to take place by skillful syntheses.^[10] We will discuss the structural peculiarities using the example of $Mg_2MnRh_5B_2$, an electron-poor representative of this rich family of compounds, all of which crystallize in the space group $P4/mbm$. Within the tetragonal unit cell (see Figure 2,

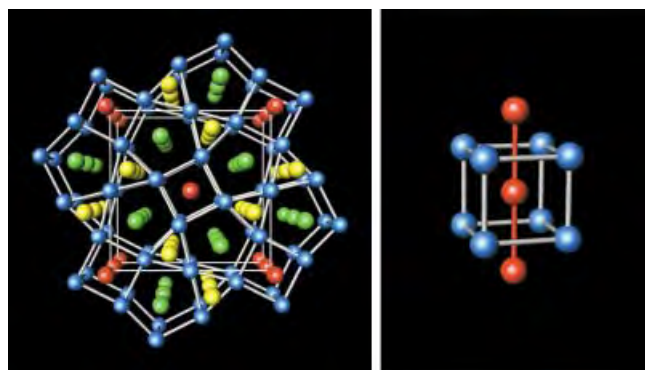


Figure 2. Left: perspective view of the $Mg_2MnRh_5B_2$ crystal structure along the [001] axis with magnesium atoms in green, manganese atoms in red, rhodium atoms in blue, and boron atoms in yellow; right: tetragonal rhodium prisms (blue) around manganese atoms (red).

left), there are trigonal, tetragonal, and pentagonal rhodium prisms stacked on top of each other along the [001] direction. While the triangular prisms are centered by boron atoms, the pentagonal prisms accommodate magnesium atoms; the tetragonal prisms contain the magnetically important manganese atoms (see also Figure 2, right). As a result, there are quasi 1D Mn–Mn chains running along the c axis with intrachain distances of about 2.91 Å while the interchain distances are on the order of 6.60 Å.

Magnetic susceptibility measurements on $Mg_2MnRh_5B_2$ immediately revealed Curie–Weiss behavior $\chi_{mol} = C/(T - \Theta_P)$ for temperatures above 160 K with a Weiss constant $\Theta_P = -130$ K and a Curie constant $C = 1.61 \times 10^{-5} \text{ m}^3 \text{ K mol}^{-1}$.^[10] The latter number corresponds to a paramagnetic moment of $3.2 \mu_B$ per Mn atom while the former indicates considerable *antiferromagnetic* Mn–Mn exchange interactions. Nonetheless, characteristic features for 1D magnetic behavior are not obvious. Around 3 K, a maximum in χ_{mol} is observed at magnetic fields $B_0 < 0.1$ T. Not too surprisingly, nonmagnetic band-structure calculations on $Mg_2MnRh_5B_2$ fully corroborate the experimental findings. As shown in the left part of Figure 3, the Fermi level in the COHP analysis is clearly positioned in the region of *nonbonding* Mn–Mn interactions, just like in the antiferromagnetic archetype (bcc-Cr). Thus, a tendency for antiferromagnetic spin ordering is indicated by both experiment and theory. To computationally describe this (so far still unknown) antiferromagnetic structure of $Mg_2MnRh_5B_2$ using the simplest model, we doubled the short tetragonal axis and switched to a spin-polarized band-structure calculation. Starting from a rough estimate for the antiparallel spin ordering on the neighboring Mn atoms (ca. $\pm 2 \mu_B$) and a net moment of zero, the spin-polarized

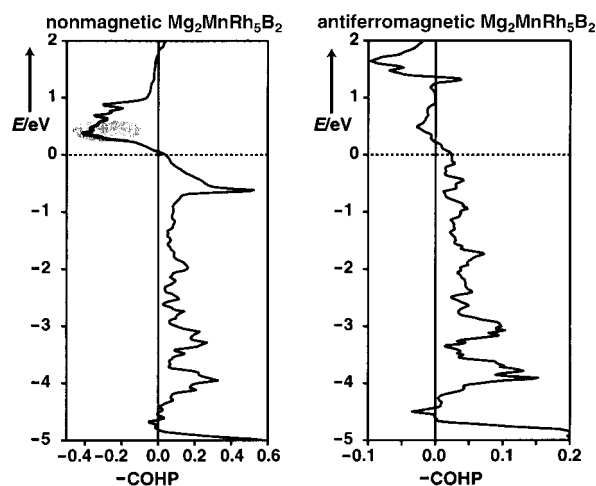


Figure 3. COHP analysis of Mn–Mn bonding in nonmagnetic $\text{Mg}_2\text{MnRh}_5\text{B}_2$ (left) and in antiferromagnetic, spin-polarized $\text{Mg}_2\text{MnRh}_5\text{B}_2$ (right). The Fermi levels (horizontal dotted lines) have been set to zero. The shaded COHP region in the left part symbolizes a hypothetical electronic enrichment by three electrons.

calculation in fact keeps to both the zero net moment and the antiferromagnetic ordering, and it converges to a self-consistent saturation moment of $3.23 \mu_B$ on Mn; all the other atoms are magnetically almost inactive. As expected from the antiferromagnetic archetype (bcc-Cr), in the COHP analysis the nonbonding Mn–Mn states close to the Fermi level (see right part of Figure 3) of the antiferromagnetic calculation remain practically untouched.

Keeping in mind the above-mentioned recipe for synthesizing metallic ferromagnets and antiferromagnets, it is straightforward to predict how to chemically create a new *ferromagnet* starting from the antiferromagnetic $\text{Mg}_2\text{MnRh}_5\text{B}_2$ with 62 valence electrons per formula unit (2×2 (Mg), 1×7 (Mn), 5×9 (Rh), 2×3 (B)). Supposing a rigid-band behavior will hold upon chemical substitution, the experimentalist needs to shift the Fermi level up by increasing the valence-electron concentration such that the new Fermi level will cut through the strongly antibonding states around +0.4 eV as given in the preceding Figure 3 (left, shaded region). A numerical COHP integration shows that such an increase corresponds to *three* additional electrons per formula unit, to be realized by replacing Mg with Sc and Mn with Fe, such that “ $\text{Sc}_2\text{FeRh}_5\text{B}_2$ ” with 65 valence electrons per formula unit (2×3 (Sc), 1×8 (Fe), 5×9 (Rh), 2×3 (B)) should do.^[11]

Fortunately, $\text{Sc}_2\text{FeRh}_5\text{B}_2$ can indeed be prepared by classic high-temperature chemical synthesis, similar to the case of the manganese compound.^[10] The susceptibility measurement reveals that $\text{Sc}_2\text{FeRh}_5\text{B}_2$ is, in fact, *ferromagnetic* below $T_C = 450$ K. A constant magnetization is easily reached for temperatures below 300 K at applied fields $B_0 > 2$ T with a maximum value of $3.3 \mu_B$ per Fe at 1.7 K. The magnetization above T_C as a function of temperature and applied field is more complicated than would be expected for a simple ferromagnet; Curie–Weiss behavior is not observed. The shape of the corresponding Fe–Fe COHP analysis within a nonmagnetic electronic-structure calculation (see Figure 4, left) is very similar to predictions. In harmony with the

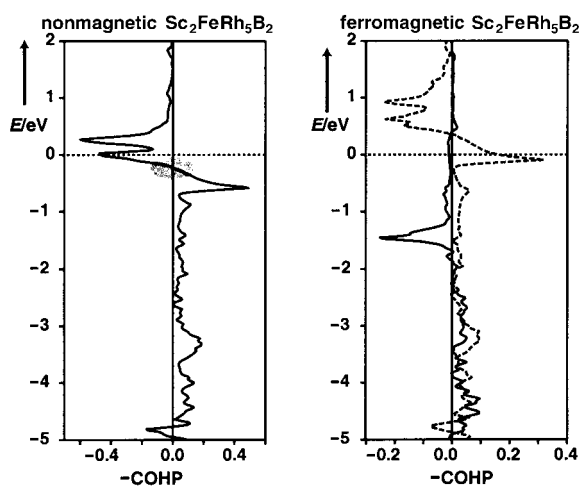


Figure 4. COHP analysis of Fe–Fe bonding in nonmagnetic $\text{Sc}_2\text{FeRh}_5\text{B}_2$ (left) and in ferromagnetic, spin-polarized $\text{Sc}_2\text{FeRh}_5\text{B}_2$ (right). The Fermi levels (horizontal dotted lines) have been set to zero. The shaded COHP region in the left part symbolizes a hypothetical electronic depletion by three electrons.

ferromagnetic properties of $\text{Sc}_2\text{FeRh}_5\text{B}_2$, there are strongly *antibonding* Fe–Fe interactions around the Fermi level, which remind us of the scenario in the ferromagnetic archetype (bcc-Fe, see above). One may also expect that spin-polarization will remove these antibonding interactions at the Fermi level, thereby lowering the total energy. To do so, the spin-polarized band-structure calculation of $\text{Sc}_2\text{FeRh}_5\text{B}_2$ was started from a small extra moment (ca. $1 \mu_B$) on the Fe atom and then iterated to self-consistency. As a result, the theoretical saturation moment is $3.96 \mu_B$ while the individual moments (μ_B) are -0.05 for Sc, 2.93 for Fe, 0.25 for Rh1, 0.08 for Rh2, and 0.02 for B. Note that one 4d atom, namely Rh1, is somewhat involved in the magnetic interactions. As predicted, the formerly antibonding Fe–Fe interactions at the Fermi level are no longer visible in a spin-polarized COHP analysis (Figure 4, right), just like for bcc-Fe.

Adopting a similar strategy to that for the antiferromagnetic Mn compound, we can try to plan further synthetic steps on the basis of the non-spin-polarized Fe–Fe COHP analysis of ferromagnetic $\text{Sc}_2\text{FeRh}_5\text{B}_2$ (see again Figure 4, left). It is clear from the Figure that a further electronic *enrichment* will populate more antibonding states which destabilize the structure; in fact, the attempt to increase the valence-electron concentration through substituting Sc atoms by Zr atoms does not lead to alternative ferromagnets but to perovskite-related phases. On the other hand, an electronic *depletion* of ferromagnetic $\text{Sc}_2\text{FeRh}_5\text{B}_2$, for example, by three electrons, would position the Fermi level back into a region of *nonbonding* metal–metal interactions (shaded region in Figure 4, left) which is the fingerprint of an antiferromagnetic material. In other words, a chemical reduction of ferromagnetic $\text{Sc}_2\text{FeRh}_5\text{B}_2$ by three electrons would result in an *antiferromagnetic* alloy, regardless of the magnetic nature of the transition element.

We can come up with two crucial experiments testing the above reasoning, both of which involve a readjusted valence-electron concentration of the intermetallic alloy. In the first

case, we start from the composition $\text{Sc}_2\text{FeRh}_5\text{B}_2$ (65 valence electrons) and lower it by three electrons by substituting Fe for Mn and a partial substitution of Rh for Ru. For example, the hypothetical formula “ $\text{Sc}_2\text{MnRu}_2\text{Rh}_3\text{B}_2$ ” with 62 valence electrons per formula unit (2×3 electrons for Sc, 1×7 for Mn, 2×8 for Ru, 3×9 for Rh, and 2×3 for B) would be such a candidate for antiferromagnetism.

As a matter of fact, $\text{Sc}_2\text{MnRu}_2\text{Rh}_3\text{B}_2$ can be synthesized by standard methods (see below) in quantitative yields;^[12] its magnetization properties are shown in Figure 5. As predicted, the new phase shows *antiferromagnetic* properties, very much resembling isoelectronic $\text{Mg}_2\text{MnRh}_5\text{B}_2$. The Weiss constant Θ_p of $\text{Sc}_2\text{MnRu}_2\text{Rh}_3\text{B}_2$ is around -300 K, and the paramagnetic moment corresponds to $2.3 \mu_B$ per Mn atom.

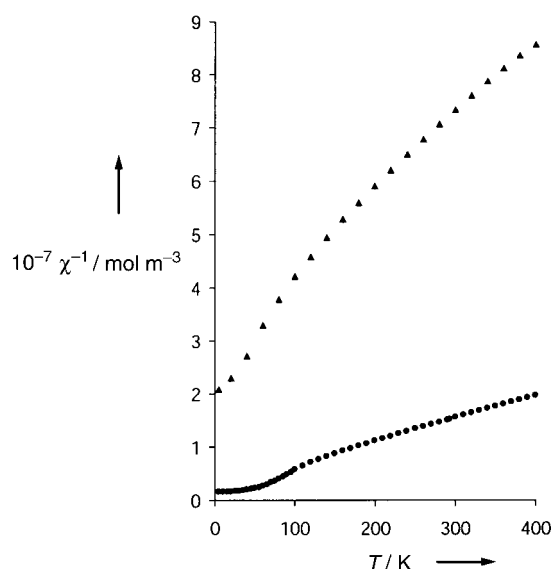


Figure 5. Plots of the reciprocal molar susceptibilities of $\text{Sc}_2\text{MnRu}_2\text{Rh}_3\text{B}_2$ (▲) and $\text{Sc}_2\text{FeRu}_3\text{Rh}_2\text{B}_2$ (●) as a function of the temperature.

But there is also an alternative way of electronically depleting the 65-electron alloy $\text{Sc}_2\text{FeRh}_5\text{B}_2$, not touching upon the chemical nature of the magnetically active transition metal: To do so, the substitution only involves the Rh sublattice in which *three* of the five Rh atoms are replaced by Ru atoms, thus the synthetic antiferromagnetic target would be “ $\text{Sc}_2\text{FeRu}_3\text{Rh}_2\text{B}_2$ ”, again corresponding to 62 valence electrons per formula unit (2×3 electrons for Sc, 1×8 for Fe, 3×8 for Ru, 2×9 for Rh, and 2×3 for B).

Fortunately, $\text{Sc}_2\text{FeRu}_3\text{Rh}_2\text{B}_2$ is also synthetically accessible in almost quantitative yield.^[13] Its magnetic properties (Figure 5) prove that the new material is indeed an *antiferromagnet*, as predicted on the basis of the rigid-band model and the associated COHP diagram. The experimental data reveal that the Weiss constant lies at about -90 K while the paramagnetic moment is $4.0 \mu_B$ per Fe atom. Thus, it is clear that the magnetic type of behavior of both $\text{Sc}_2\text{MnRu}_2\text{Rh}_3\text{B}_2$ and $\text{Sc}_2\text{FeRu}_3\text{Rh}_2\text{B}_2$ is solely a function of the electron filling, that is, an electron concentration which positions the Fermi level in nonbonding Mn–Mn or Fe–Fe states.

In conclusion, we have exemplified how to understand experimental findings, in terms of the bonding properties of magnetically active transition-metal atoms in complex intermetallic alloys, such as $\text{Mg}_2\text{MnRh}_5\text{B}_2$ and $\text{Sc}_2\text{FeRh}_5\text{B}_2$. We have also shown that the magnetic properties of $\text{Sc}_2\text{MnRu}_2\text{Rh}_3\text{B}_2$ and $\text{Sc}_2\text{FeRu}_3\text{Rh}_2\text{B}_2$ (and possibly many other intermetallic phases) can be predicted by the shape of COHP diagrams as a function of the electronic energy. From what has been said so far, it seems clear that related, isostructural intermetallic phases with 63 or 64 valence electrons will be interesting candidates for competition between antiferromagnetic (62 electrons) and ferromagnetic (65 electrons) exchange interactions. Corresponding, yet to be synthesized, intermetallic phases with fewer than, say, 62 electrons, should not exhibit strong magnetic phenomena because the Fermi level would be positioned in bonding M–M states in which there is no tendency for electronic distortions in terms of spontaneous spin polarization. Isostructural intermetallic phases with more than 65 electrons are probably impossible to realize synthetically.

Experimental Section and Theoretical Methodology

All intermetallic compounds were synthesized by classic solid-state chemical routes (elemental components, closed containers, high temperatures, and arc melting procedures).^[10] The products were structurally characterized by a combination of single-crystal/powder X-ray diffraction and neutron diffraction. The crystallographic lattice parameters of $\text{Mg}_2\text{MnRh}_5\text{B}_2$, $\text{Sc}_2\text{MnRu}_2\text{Rh}_3\text{B}_2$, and $\text{Sc}_2\text{FeRu}_3\text{Rh}_2\text{B}_2$ were determined from powder. Internal coordinates of $\text{Mg}_2\text{MnRh}_5\text{B}_2$ were assumed to be identical with $\text{Mg}_2\text{FeRh}_5\text{B}_2$ because of their excellent lattice match; these combined spatial parameters were used for the electronic-structure calculation on $\text{Mg}_2\text{MnRh}_5\text{B}_2$. For $\text{Sc}_2\text{FeRh}_5\text{B}_2$, all structural parameters were determined from single-crystal diffractometry and were used, without modification, for the theoretical part. Magnetic susceptibilities were determined between 2 and 400 K at $B_0 = 0.5$ T using a SQUID magnetometer MPMS-5S (Quantum Design, San Diego, USA). Corrections for diamagnetic and conduction-electron contributions were not applied. For $\text{Sc}_2\text{MnRu}_2\text{Rh}_3\text{B}_2$ and $\text{Sc}_2\text{FeRu}_3\text{Rh}_2\text{B}_2$, the tendency for Curie–Weiss behavior becomes only apparent at $T > 300$ K. This region has thus been used to estimate the corresponding C and Θ_p values.

Band-structure calculations were performed using Linear Muffin–Tin Orbital (LMTO) theory^[14] within the local (spin) density approximation (LDA and LSDA).^[15] All calculations were checked for convergence of energies, orbital moments, integrated COHP values and magnetic moments with respect to the number of k points used in the reciprocal-space integrations. The program used was TB-LMTO4.7.^[16] Crystal Orbital Hamilton Population (COHP) analysis^[17] is a partitioning scheme for the band-structure energy (sum of the energies of the Kohn–Sham orbitals) in terms of orbital-pair contributions. COHP analysis, while in many ways analogous to crystal orbital overlap population (COOP) analysis used in extended Hückel calculations,^[18] provides a quantitative measure of bond strengths and is probably more appropriate for a first-principles calculation. All COHP curves are presented here in a format similar to COOP curves: positive values are bonding, and negative antibonding (i.e., we are plotting $-\text{COHP}$ instead of COHP).

Received: February 18, 2002 [Z18728]

- [1] S. Chikazumi, *Physics of Ferromagnetism*, Clarendon Press, Oxford, 1997.
- [2] H. Lueken, *Magnetochemie*, Teubner, Stuttgart, Leipzig, 1999.
- [3] R. C. O’Handley, *Modern Magnetic Materials*, Wiley, New York, 2000.
- [4] R. Dronskowski, *Adv. Funct. Mater.* **2001**, 11, 27.

- [5] G. A. Landrum, R. Dronskowski, *Angew. Chem.* **1999**, *111*, 1482; *Angew. Chem. Int. Ed.* **1999**, *38*, 1390.
- [6] G. A. Landrum, R. Dronskowski, *Angew. Chem.* **2000**, *112*, 1598; *Angew. Chem. Int. Ed.* **2000**, *39*, 1560.
- [7] Some aspects of the scenario upon onset of magnetism (antibonding character of degenerate highest crystal orbital, symmetry lowering of the underlying wavefunction upon spin polarization) resemble the classic Jahn–Teller case; however, since only electronic coordinates are involved, the term “electronic” Jahn–Teller instability is probably more appropriate.
- [8] A. Decker, G. A. Landrum, R. Dronskowski, *Z. Anorg. Allg. Chem.* **2002**, *628*, 303.
- [9] In fact, the change in slope of the COHP is similar to what is observed in the classical Peierls distortion of a 1D chain of H atoms. In the present case, however, only electronic coordinates are involved such that the (admittedly questionable) term “electronic” Peierls instability is better suited.
- [10] E. A. Nagelschmitz, W. Jung, R. Feiten, P. Müller, H. Lueken, *Z. Anorg. Allg. Chem.* **2001**, *627*, 523.
- [11] A perceptive reviewer raised the question whether an alternative structural distortion to a nonmagnetic form might also be possible; indeed, such “conventional” distortion could be expected to equally reduce or remove the antibonding M–M states. Nonetheless, we believe that the purely electronic distortion through spin polarization is the preferred choice for the ferromagnetic transition metals and their alloys since it is evidently connected with a smaller energetic penalty. If the latter becomes too large, for example, during the attempted electronic enrichment of $\text{Sc}_2\text{FeRh}_3\text{B}_2$ with even stronger antibonding Fe–Fe interactions (see text), the alternative structural distortion takes over.
- [12] $\text{Sc}_2\text{MnRu}_3\text{Rh}_3\text{B}_2$ lattice parameters from Guinier measurements: $a = 9.3909(5) \text{ \AA}$, $c = 3.0170(3) \text{ \AA}$; the structure has also been confirmed from single-crystal data.
- [13] $\text{Sc}_2\text{FeRu}_3\text{Rh}_3\text{B}_2$ lattice parameters from Guinier measurements: $a = 9.3319(9) \text{ \AA}$, $c = 3.0101(5) \text{ \AA}$; a corroborating refinement from single-crystal data has also been performed. There are small traces of an additional phase (probably Ru_4Fe) present in the powdery material; Ru_4Fe has been observed by D. V. Sokol'skii, L. M. Kurashvili, A. F. Burtsev, K. K. Kuzembaev, *Russ. J. Phys. Chem.* **1987**, *61*, 293.
- [14] O. K. Andersen, *Phys. Rev. B* **1975**, *12*, 3060; O. K. Andersen, O. Jepsen, *Phys. Rev. Lett.* **1984**, *53*, 2571; “Tight-Binding Approach to Computational Materials Science”: O. K. Andersen, C. Arcangeli, R. W. Tank, T. Saha-Dasgupta, G. Krier, O. Jepsen, I. Dasgupta, *Mater. Res. Soc. Symp. Proc.* **1998**, *491*, 3.
- [15] U. von Barth, L. Hedin, *J. Phys. C* **1972**, *5*, 1629.
- [16] G. Krier, O. Jepsen, A. Burkhardt, O. K. Andersen, The TB-LMTO-ASA program, version 4.7.
- [17] R. Dronskowski, P. E. Blöchl, *J. Phys. Chem.* **1993**, *97*, 8617; see also website <http://www.cohp.de>
- [18] T. Hughbanks, R. Hoffmann, *J. Am. Chem. Soc.* **1983**, *105*, 3528.

Catalytic Activity and Poisoning of Specific Sites on Supported Metal Nanoparticles**

Swetlana Schauermaun, Jens Hoffmann, Viktor Johánek, Jens Hartmann, Jörg Libuda,* and Hans-Joachim Freund

Typically, heterogeneous catalysts are based on nanometer-sized active particles, dispersed on an inert support material. In many cases it is assumed that the unique reactivities of such surfaces arise from the simultaneous presence of different active sites. On a molecular level, however, knowledge of the reaction kinetics of such systems is scarce (see e.g. refs. [1, 2] and references therein).

Herein, we present first direct evidence for the different activity of coexisting sites on a well-defined supported-nanoparticle system. As a model reaction we choose the decomposition of methanol on well-ordered Pd crystallites. For this reaction system two competing decomposition pathways exist (Figure 1): whereas dehydrogenation to CO

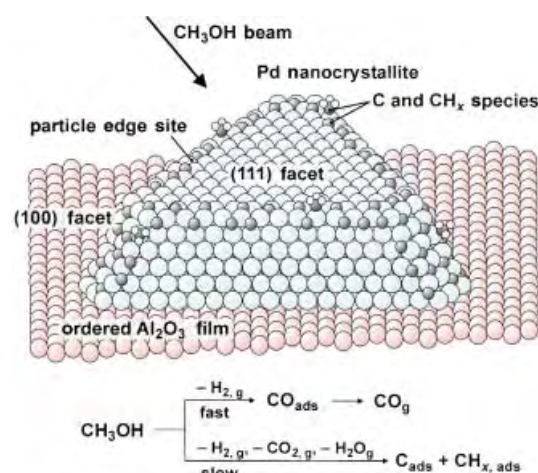


Figure 1. Schematic representation of the supported Pd nanoparticles and the blocking of defect sites by carbon species during methanol decomposition.

represents the dominating reaction channel,^[3, 4] slow carbon–oxygen-bond breakage leads to formation of adsorbed carbon and CH_x species.^[4–6] With increasing carbon coverage the rate of carbon–oxygen-bond breakage drops rapidly, whereas the kinetics of dehydrogenation is hardly affected. We show that on ordered Pd crystallites these carbon and hydrocarbon species preferentially block defect sites on the particles such as particle edges and steps (see Figure 1). From this, we conclude that activity for carbon–oxygen-bond breakage is

[*] Dr. J. Libuda, Dipl.-Chem. S. Schauermaun, Dipl.-Phys. J. Hoffmann, Dr. V. Johánek, Dipl.-Ing. J. Hartmann, Prof. Dr. H.-J. Freund
Fritz-Haber-Institut der Max-Planck-Gesellschaft
Faradayweg 4–6
14195 Berlin (Germany)
Fax: (+49) 30-8413-4309
E-mail: libuda@fhi-berlin.mpg.de

[**] We acknowledge support of this project by the Max-Planck Society and the Deutsche Forschungsgemeinschaft through the Priority Program 1091.

drastically enhanced at the particle defect sites, whereas this is not the case for the dehydrogenation pathway. This type of detailed investigation is made possible by two factors:

1) We employed a supported model catalyst, which, in contrast to real catalysts, is characterized by a lower and controllable level of complexity and which is suitable for the application of most surface-science experimental techniques (see refs. [1, 2, 7, 8] and references therein). The model surface used is based on a well-ordered Al_2O_3 film on a $\text{NiAl}(110)$ single crystal.^[9] On this model support, Pd particles are grown under well-controlled conditions in ultra-high vacuum (UHV). The geometric and electronic structure as well as the adsorption properties of these particles have been characterized extensively.^[10–14] Briefly, the Pd aggregates represent well-shaped crystallites with an average size of approximately 6 nm. They grow in the (111) orientation and predominantly expose (111) facets as well as a small fraction of (100) facets. In Figure 2a a scanning tunneling microscopy (STM) image of the Pd particles is shown and a schematic model is displayed in Figure 1. Further structural details can be found in the literature.^[13]

2) Kinetic measurements were made on these model surfaces by using molecular-beam techniques (e.g. refs. [2, 15, 16]) which provide a unique way to derive detailed kinetic information, for example, by enabling us to modulate reactant fluxes in a flexible way, determine exact

reaction probabilities, or detect reaction products in a collision-free manner. To perform such experiments on supported model catalysts, we used a molecular-beam system which allows up to three beams to cross on the sample surface and perform time-resolved reflection–absorption IR spectroscopy (TR-RAIRS) and angle resolved/integrated gas–phase detection, simultaneously.^[17] Recently, we have applied the molecular-beam approach to the CO oxidation on supported model catalysts.^[18, 19] Here, we focus on the methanol decomposition as a first example of a more complex reaction system.

In brief, molecular adsorption of methanol is followed by the formation of methoxy species on the Pd particles. This first intermediate is stable up to temperatures of 200 K. At higher temperatures, decomposition proceeds by two competing reaction pathways. Dehydrogenation as the dominating reaction channel results in rapid formation of CO. Depending on the rate of CO formation and desorption (i.e. the surface temperature), a significant steady-state coverage of adsorbed CO is built up, which can be monitored by in situ TR-RAIRS (IR at 440 K: $\tilde{\nu}(\text{C}=\text{O}) = 1900, 1840 \text{ cm}^{-1}$).

As a second pathway, we observe slow breakage of the carbon–oxygen bonds, which leads to the formation of adsorbed carbon and hydrocarbon species. This assumption is corroborated by two observations: First, weak features in the C–H-stretching-frequency region (IR: $\tilde{\nu} = 2945, 2830 \text{ cm}^{-1}$) indicate the presence of CH_x -species. Such hydrocarbon species have been shown to be stable up to 500 K.^[5] Second, in a temperature programmed desorption (TPD) experiment we observe desorption of hydrocarbons ($M_r = 15, 700 \text{ K}$) and recombinative desorption of CO ($M_r = 28, 800 \text{ K}$), which is characteristic for the presence of atomic carbon.^[20]

It is essential to note that during exposure of the catalyst to CO under identical conditions no carbon formation is observed.^[18] From this we infer that the carbon deposits do not originate from CO decomposition, but from breakage of the C–O bond during the methanol dehydrogenation process.

The question arises: where on the nanoparticles are the carbon deposits located? This question is answered by RAIRS with CO as a probe molecule. The corresponding spectra for the pristine Pd particles and after prolonged exposure to methanol are compared in Figure 2b.

For the pristine sample (Figure 2b), the spectrum is dominated by a sharp absorption feature at 1960 cm^{-1} (1) with a broad low-frequency shoulder (2; $1930–1840 \text{ cm}^{-1}$) and an additional weak feature at 2080 cm^{-1} (3). Previously, the features between 1930 cm^{-1} and 1840 cm^{-1} (2) have been assigned to CO adsorbed on bridge and hollow sites predominantly on Pd(111), and the absorption peak at 2080 cm^{-1} (3) to on-top CO.^[11, 12] A detailed comparison with previous work shows that the prominent absorption band at 1960 cm^{-1} (1) originates from a superposition of bridge-bonded CO on (100) facets and CO adsorbed at defect sites, such as particle edges or steps.^[11, 12] The contribution of (100) facets, however, is expected to be small because these facets are the minor fraction and because of their tilted geometry (as a consequence of the surface selection rule, IR absorption is attenuated on small, tilted facets, e.g. ref. [21]). Following these arguments, we assume that the absorption feature at 1960 cm^{-1} is dominated by CO adsorbed on defect sites,

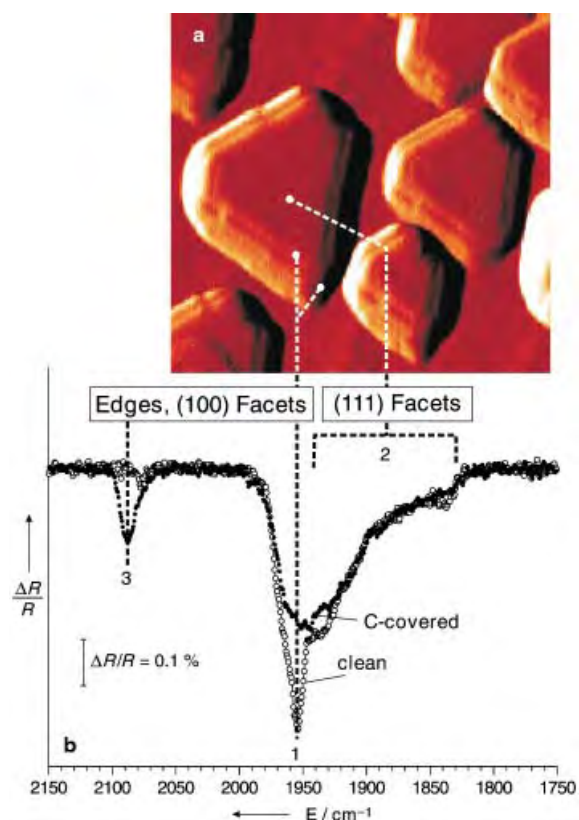


Figure 2. a) STM image of the Pd particles grown at 300 K on $\text{Al}_2\text{O}_3/\text{NiAl}(110)$ ($20 \text{ nm} \times 20 \text{ nm}$), from ref. [17]; b) RAIR spectra for CO adsorbed on $\text{Pd}/\text{Al}_2\text{O}_3/\text{NiAl}(110)$ (sample temperature 100 K, after CO exposure at 300 K); R = reflectivity open symbols: immediately after preparation; solid symbols: after prolonged exposure to methanol at 440 K.

mainly on steps and particle edges (see Figure 1). Note, however, that the signals are expected to be strongly modified by dipole-coupling effects.^[22] As a consequence, the relative intensities do not directly reflect the relative abundance of the corresponding sites, but the defect feature at high frequency can gain intensity at the expense of the regular absorption signal at lower frequency.

After extended exposure to methanol, drastic changes are observed in the spectrum for the adsorbed CO (Figure 2b). The defect peak at 1960 cm⁻¹ (1) vanishes almost completely, whereas the absorption signal in the on-top region (3) strongly increases (2090 cm⁻¹). All other features in the spectrum, in particular the region below 1950 cm⁻¹ (regular facets), remain practically unchanged. Although the dipole-coupling effects mentioned above preclude a straightforward quantification, it is apparent from these observations that adsorption at particle defect sites (i.e. steps and edges) is blocked by carbon species formed by carbon–oxygen-bond breakage. We conclude that these carbon species formed by the decomposition of methanol preferentially accumulate at defect sites.

Next the effect of carbon accumulation on the kinetics of both reaction pathways was investigated. Carbon formation results in a slowly decreasing CO absorption capacity, which allows us to follow the process in situ by TR-RAIRS. To quantify the surface fraction covered by carbon, we calibrate the integral CO absorption as a function of coverage (θ_{CO} : fraction of Pd surface sites covered by CO; note that in RAIRS there is no simple relation between coverage and absorption because of the dipole-coupling effects^[21]). To do so, we combine a CO sticking-coefficient measurement and a TR-RAIRS experiment. The calibration curve is used to estimate the surface fraction covered by carbon as a function of exposure time to methanol ($\theta_{\text{C}}(t) = \theta_{\text{CO}}(0) - \theta_{\text{CO}}(t)$, $\theta_{\text{CO}}(0)$: initial CO coverage). It is apparent that the initial rate of carbon formation is high, but drops rapidly with increasing carbon coverage (the calculated rates of carbon formation $r_{\text{C}} = d(\theta_{\text{CO}}(0) - \theta_{\text{CO}}(t))/dt$ are given in Figure 3). From this observation we conclude that the carbon–oxygen-bond breakage is fast only at the defect sites, which are preferen-

tially blocked during the reaction, but not at the regular facet sites.

The next question to ask is whether the second reaction pathway, that is, the methanol dehydrogenation, is affected by carbon accumulation in a similar manner? For experimental reasons,^[23] the dehydrogenation rate is determined in an isotope-exchange experiment combined with surface detection by TR-RAIRS. The setup comprises a ¹²CH₃OH beam and a ¹³CH₃OH beam of equal intensity. Switching between the two beams, we follow the exchange between the dehydrogenation products ¹²CO and ¹³CO (IR at 440 K: $\tilde{\nu}(\text{C=O}) = 1900, 1840 \text{ cm}^{-1}$; $\tilde{\nu}(\text{C=O}) = 1860, 1800 \text{ cm}^{-1}$) and determine the time constants for CO exchange τ_{CO} on the clean and the partially carbon-covered catalyst. Moreover, we can use the steady-state coverages of CO (see above) to derive the corresponding rates of CO formation (or methanol dehydrogenation) as $r_{\text{CO}} = \theta_{\text{CO}} \tau_{\text{CO}}^{-1}$ (Figure 3).

It is apparent that whereas the rate of carbon–oxygen-bond breakage drastically decreases with increasing carbon coverage, the rate constant for CO exchange remains nearly unaffected by this process. The decrease in the dehydrogenation rate simply reflects the decrease in the carbon-free Pd surface area. Quantitatively, we find that the ratio between the rates of dehydrogenation and carbon–oxygen-bond breakage $r_{\text{CO}}/r_{\text{C}}$ increases from 30 on the pristine sample to approximately 1000 on the carbon-contaminated sample.

In conclusion we have presented the first direct evidence for the different activity of various reactive sites coexisting on a well defined supported metal catalyst. Combining molecular-beam methods and TR-RAIRS, we have investigated the kinetics of methanol decomposition on well-ordered Pd crystallites. Two competing reaction pathways are observed, the rapid dehydrogenation to give CO and the slow carbon–oxygen-bond breakage leading to formation of carbon and hydrocarbon species. Employing CO as a probe molecule, it is shown the carbon-oxygen bond breakage occurs preferentially at particle step and edge sites, whereas this is not the case for dehydrogenation.

Experimental Section

All experiments were performed in a UHV molecular beam apparatus at the Fritz-Haber-Institute (Berlin) which allows up to three beams to be crossed on the sample surface.^[17] The CH₃OH beam (Merck, >99.8%) and the ¹³CH₃OH beam (Cambridge Isotope Laboratories, >99%) are generated by effusive multichannel-array sources. For all methanol experiments the surface temperature was 440 K and the beam intensity was $5.3 \times 10^{14} \text{ molecules cm}^{-2} \text{ s}^{-1}$. The RAIR spectra in Figure 2 were recorded (at 100 K after CO saturation at 300 K) before and after exposure to a methanol dose of $2.5 \times 10^{18} \text{ molecules cm}^{-2}$. The rates given in Figure 3 for the partially carbon-covered sample correspond to a similar methanol dose. For the isotope-exchange experiments, beam modulation was provided by computer-controlled shutters located inside the second pumping stages of the beam sources. For coverage calibration, CO sticking-coefficient measurements were performed using a quadrupole mass spectrometer (ABB Extrel) and a beam generated from a supersonic expansion ($2.2 \times 10^{13} \text{ molecules cm}^{-2} \text{ s}^{-1}$, sample temperature 300 K). All IR spectra were acquired employing a vacuum FT-IR spectrometer (Bruker IFS 66v) at a spectral resolution of 2 cm⁻¹.

The aluminum oxide film was prepared by sputtering and annealing of a NiAl(110) single crystal, followed by an oxidation and annealing procedure, the details of which are given elsewhere.^[9] Cleanliness and quality of the oxide film was checked by LEED (low-energy electron diffraction) and

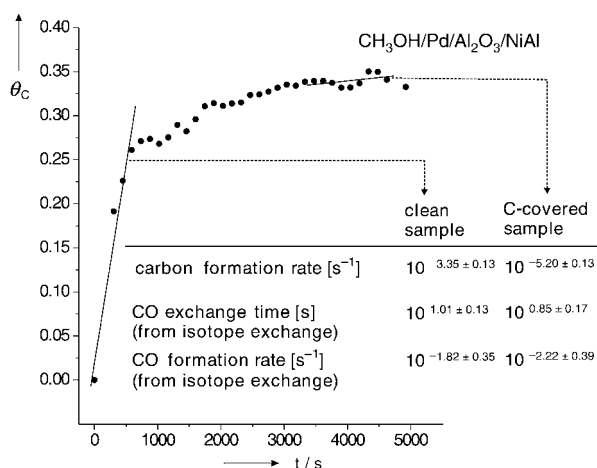


Figure 3. Estimated carbon coverage as a function of exposure time t to the methanol beam (derived from TR-RAIRS, surface temperature of 440 K), $\theta_{\text{C}} = \theta_{\text{CO}}(0) - \theta_{\text{CO}}(t)$ per monolayer, and calculated rates of carbon formation (carbon–oxygen-bond breakage) and CO formation (dehydrogenation).

AES (auger electron spectroscopy). Before the experiment, Pd (>99.9%) was deposited by evaporation from a rod by using a commercial evaporator (Focus, EFM 3) based on electron bombardment (Pd coverage: $2.7 \times 10^{15} \text{ cm}^{-2}$, sample temperature: 300 K). The evaporator flux was calibrated by a quartz microbalance prior to use. After preparation the Pd particles were stabilized by oxygen and CO exposure as discussed previously.^[13, 24]

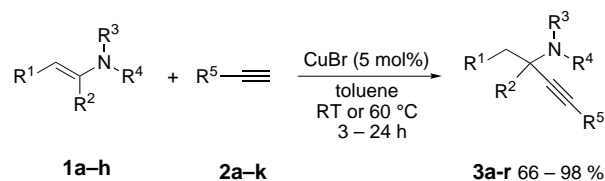
Received: March 1, 2002 [Z18807]

- [1] V. P. Zhdanov, B. Kasemo, *Surf. Sci. Rep.* **2000**, 39, 25, and references therein.
- [2] C. R. Henry, *Surf. Sci. Rep.* **1998**, 31, 231, and references therein.
- [3] G. A. Kok, A. Noordermeer, B. E. Nieuwenhuys, *Surf. Sci.* **1983**, 135, 65.
- [4] R. P. Holroyd, M. Bowker, *Surf. Sci.* **1997**, 377–379, 786.
- [5] M. Rebholz, N. Kruse, *J. Chem. Phys.* **1991**, 95, 7745.
- [6] J.-J. Chen, Z.-C. Jiang, Y. Zhou, B. R. Chakraborty, N. Winograd, *Surf. Sci.* **1995**, 328, 248.
- [7] H.-J. Freund, *Angew. Chem.* **1997**, 109, 444; *Angew. Chem. Int. Ed. Engl.* **1997**, 36, 452.
- [8] K. Hayek, B. Jenewein, B. Klotzer, W. Reichl, *Top. Catal.* **2001**, 12, 25, and references therein.
- [9] J. Libuda, F. Winkelman, M. Bäumer, H.-J. Freund, T. Bertrams, H. Neddermeyer, K. Müller, *Surf. Sci.* **1994**, 318, 61.
- [10] M. Bäumer, H.-J. Freund, *Prog. Surf. Sci.* **1999**, 61, 127.
- [11] K. Wolter, O. Seiferth, H. Kühlenbeck, M. Bäumer, H.-J. Freund, *Surf. Sci.* **1998**, 399, 190.
- [12] M. Frank, M. Bäumer, *Phys. Chem. Chem. Phys.* **2000**, 2, 4265.
- [13] I. Meusel, J. Hoffmann, J. Hartmann, M. Heemeier, M. Bäumer, J. Libuda, H.-J. Freund, *Catal. Lett.* **2001**, 71, 5.
- [14] S. Shaikhutdinov, M. Frank, M. Bäumer, S. D. Jackson, R. Oldman, J. C. Hemminger, H.-J. Freund, *Catal. Lett.* in press.
- [15] M. P. D'Evelyn, R. J. Madix, *Surf. Sci. Rep.* **1984**, 3, 413.
- [16] M. Asscher, G. A. Somorjai in *Atomic and Molecular Beam Methods*, Vol. 2 (Ed.: G. Scoles), Oxford University Press, Oxford, **1988**, p. 489.
- [17] J. Libuda, I. Meusel, J. Hartmann, H.-J. Freund, *Rev. Sci. Instrum.* **2000**, 71, 4395.
- [18] J. Libuda, I. Meusel, J. Hoffmann, J. Hartmann, L. Piccolo, C. R. Henry, H.-J. Freund, *J. Chem. Phys.* **2001**, 114, 4669.
- [19] I. Meusel, J. Hoffmann, J. Hartmann, J. Libuda, H.-J. Freund, *J. Phys. Chem. B* **2001**, 105, 3567.
- [20] V. Matolin, M. Rebholz, N. Kruse, *Surf. Sci.* **1991**, 245, 233.
- [21] F. M. Hoffmann, *Surf. Sci. Rep.* **1983**, 3, 107.
- [22] P. Hollins, *Surf. Sci. Rep.* **1992**, 16, 51.
- [23] The fragmentation pattern of CH_3OH which like CO contains m/z 28 as a main fragment and the low reaction probabilities prevent rate measurements by quadrupole mass spectrometry.
- [24] S. Shaikhutdinov, M. Heemeier, J. Hoffmann, I. Meusel, B. Richter, M. Bäumer, H. Kühlenbeck, J. Libuda, H.-J. Freund, R. Oldman, S. D. Jackson, C. Konvicka, M. Schmid, P. Varga, *Surf. Sci.* **2002**, 501, 270.

Enantioselective Synthesis of Propargylamines by Copper-Catalyzed Addition of Alkynes to Enamines**

Christopher Koradin, Kurt Polborn, and Paul Knochel*

Propargylamines are important as both synthetic intermediates for the preparation of polyfunctional amino derivatives and as biologically active compounds.^[1] Their preparation in enantiomerically enriched form is therefore of great importance. Although several diastereo- and enantioselective syntheses have been developed,^[2] until now no metal-catalyzed enantioselective synthesis of propargylamines is known.^[3] We report herein a new copper(I)-catalyzed enantioselective addition of alkynes^[4] to enamines. First, we examined the racemic synthesis of propargylamines by metal-complex catalysis. Various metal salts, including $\text{Sc}(\text{OTf})_3$, $\text{Zn}(\text{OTf})_2$, $\text{Yb}(\text{OTf})_3$, and Cu^{I} and Cu^{II} salts,^[5] were tested as catalysts. Copper(I) and copper(II) bromide proved to give the fastest conversions. We chose test enamines^[6] with readily removable protecting groups such as an allyl or a benzyl group. Enamines **1a–h** (1.2–1.5 equiv) reacted readily with terminal alkynes **2a–k** in toluene in the presence of copper(I) bromide (5 mol%) to give propargylic amines of type **3** (Scheme 1, Table 1) under mild reaction conditions.



Scheme 1. Synthesis of propargylamines by the addition of alkynes to enamines.

A range of functionalized alkynes that bear a methoxy group, a double bond, a nitrile group, a chloride, a silyloxy group, an acetal, or a silyl functionality were successfully used (Table 1, entries 1–8). In the case of nitrile **2d**, the reaction required 5 h at 60 °C for complete conversion. Disubstituted enamines tend to be more reactive than trisubstituted enamines (Table 1, entries 10/15 or entries 12/17). In the case of the cyclic enamine **1h**, which is in equilibrium with a dimeric structure,^[7] the reaction was carried out for 3 h at 80 °C (Table 1, entry 18).

After this study, which showed the broad scope of the reaction, we turned our attention to the enantioselective

[*] Prof. Dr. P. Knochel, C. Koradin, Dr. K. Polborn
Department Chemie, Ludwig-Maximilians-Universität
Butenandtstrasse 5-13, Haus F, 81377 München (Germany)
Fax: (+49)89-2180-7680
E-mail: paul.knochel@cup.uni-muenchen.de

[**] We thank the Deutsche Forschungsgemeinschaft (Leibniz program). C.K. thanks BASF AG (Ludwigshafen) for a fellowship. We also thank Chemetall GmbH (Frankfurt) and BASF AG (Ludwigshafen) for the generous gift of chemicals.

Supporting information for this article is available on the WWW under <http://www.angewandte.org> or from the author.

Table 1. Propargylamines of type **3** obtained by the copper(I) bromide catalyzed addition of alkynes **2** to enamines **1**.

Entry	1	2	R ⁵	3	Yield [%] ^[a]
1	a	a	Ph	a	75
2	a	b	CH ₂ OMe	b	84
3	a	c	1-cyclohexenyl	c	77
4	a	d	(CH ₂) ₃ CN	d	82 ^[b]
5	a	e	(CH ₂) ₃ Cl	e	78
6	a	f	CH ₂ OTBDPS	f	93
7	a	g	CH(OEt) ₂	g	66
8	a	h	TMS	h	70

9	b	a	Ph	i	82
10	b	i	<i>n</i> Hex	j	75
11	b	j	H	k	69

12	c	a	Ph	l	98

13	d	a	Ph	m	94 ^[b]
14	d	k	<i>p</i> -BrPh	n	90 ^[b]

15	e	i	<i>n</i> Hex	o	80 ^[b]

16	f	i	<i>n</i> Hex	p	82

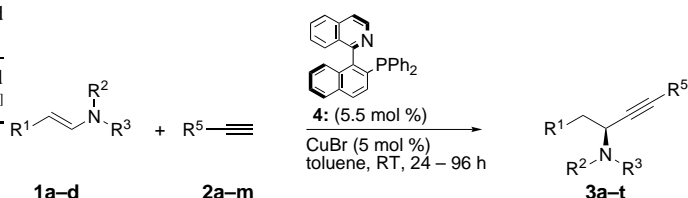
17	g	a	Ph	q	75 ^[b]

18	h	a	Ph	r	86 ^[c]

[a] Yield of isolated analytically pure product. [b] The reaction was performed at 60 °C. [c] The reaction was performed at 80 °C. TBDPS = *tert*-butyldiphenylsilyl, TMS = trimethylsilyl.

addition reaction. Copper(I) bromide was used to test various chiral ligands, for example, diphosphanes, aminophosphanes, and diamines. We found that Quinap (**4**)^[8] in combination with CuBr gave the best results (Scheme 2, Table 2).

Thus, the reaction of phenylacetylene (**2a**) and the enamine **1a** in the presence of copper(I) bromide (5 mol %) and (*R*)-



Scheme 2. Enantioselective synthesis of propargylamines by using copper(I) bromide and Quinap as the catalytic system.

(+)-Quinap (5.5 mol %) in toluene at room temperature (24 h) afforded the propargylamine **3a** in 78 % yield and with 83 % *ee*. Polyfunctional propargylamines that bear a chloride, an OTBDPS, or a nitrile group can be prepared with 54–72 % *ee* (Table 2, entries 4–6). The use of the β -disubstituted

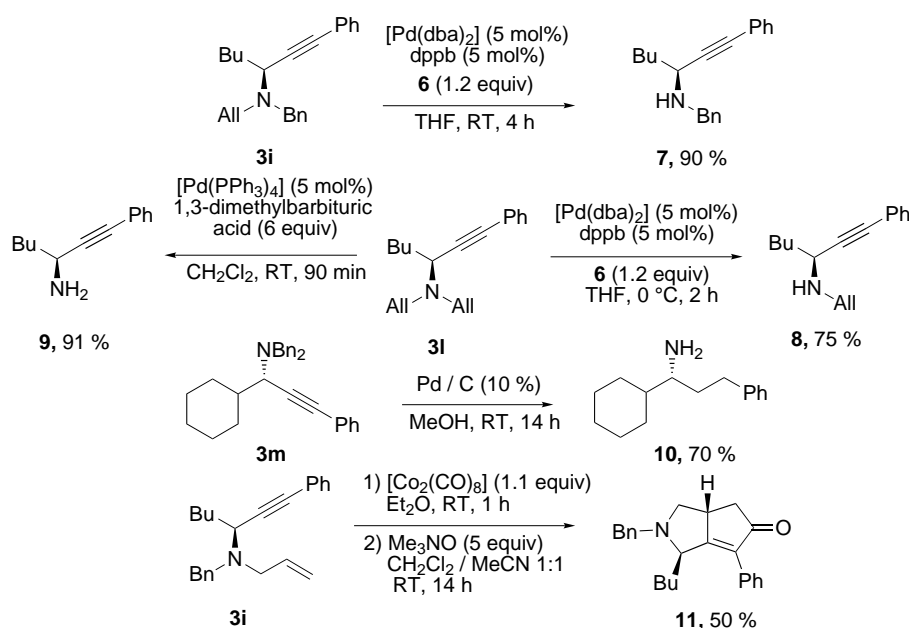
Table 2. Enantioselective synthesis of propargylamines **3** by the copper(I) bromide/Quinap-catalyzed addition of alkynes **2** to enamines **1**.

Entry	1	2	R ⁵	3	Yield [%] ^[a]	<i>ee</i> [%] ^[b]
1	a	a	Ph	a	78	83
2	a	b	CH ₂ OMe	b	76	55
3	a	c	1-cyclohexenyl	c	84	74
4	a	d	(CH ₂) ₃ CN	d	50	54
5	a	e	(CH ₂) ₃ Cl	e	58	60
6	a	f	CH ₂ OTBDPS	f	85	72
7	a	h	TMS	h	73	86 ^[c]
8	b	a	Ph	i	91	82 ^[d]
9	c	a	Ph	l	99	77 ^[d]
10	d	a	Ph	m	79	88
11	d	k	<i>p</i> -BrPh	n	83	90
12	a	l	3-pyridyl	s	57	70
13	a	m	2-pyridyl	t	73	70

[a] Yield of isolated analytically pure product. [b] Enantiomeric excess determined by HPLC with a Chiralcel OD-H column (*n*-heptane/*i*PrOH). [c] Enantiomeric excess determined after conversion into **3a**: 1) TBAF; 2) PhI, Pd⁰ (cat.), Cu^I (cat.), 77 % overall yield. [d] Enantiomeric excess determined after deprotection to the secondary amine.^[11] TBAF = tetrabutylammonium fluoride.

enamine **1d** and 1-bromo-4-ethynylbenzene (**2k**) furnished the corresponding propargylamine **3n** in 83 % yield with the highest enantioselectivity (90 % *ee*; Table 2, entry 11). The propargylamines **3s** and **3t**, which bear heterocyclic rings (Table 2, entries 12 and 13) were prepared with 70 % *ee*.

To the best of our knowledge, this is the first report of a copper-catalyzed asymmetric reaction with Quinap as the chiral ligand. We were able to isolate the complex $[\text{BrCu}(\text{Quinap})]_2$ (**5**) as a yellow, air-stable solid, which has been characterized by X-ray crystallographic analysis (Figure 1).^[9] The complex has a dimeric structure with the typical planar four-membered $\text{Cu}_2(\mu\text{-Br})_2$ ring. The coordination spheres of both copper atoms are distorted tetrahedra, but they are not identical. The Cu1–N1 distance (2.348 Å) is much shorter than the



Scheme 3. Selective transformations of propargylamines. dppb = Diphenylphosphanylbutane, dba = dibenzylideneacetone.

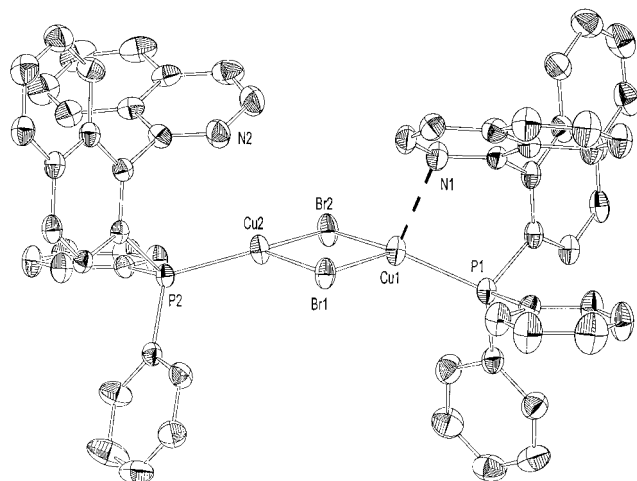


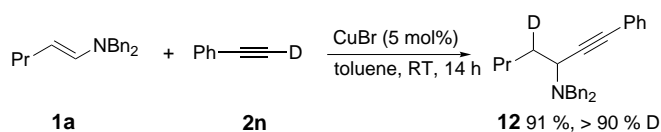
Figure 1. Structure of the complex $[\text{BrCu}(\text{Quinap})]_2$ (**5**) in the solid state (the hydrogen atoms and crystallized solvents are omitted for clarity). Selected bond lengths [Å] and angles [°]: Cu1–Br1 2.4728(8), Cu2–Br2 2.4150(8), Cu1–P1 2.199(2), Cu2–P2 2.1827(13); P2–Cu2–Br2 129.28(4), P2–Cu2–Br1 122.75(4), Br2–Cu2–Br1 104.18(3).

Cu2–N2 distance (2.725 Å). In both cases, the long Cu–N distances indicate the absence of direct bonding, but they are shorter than the sum of the van der Waals radii of Cu and N. Interestingly, the P and the N atoms of the two Quinap molecules are *cis*-oriented, in contrast to monodentate P–N complexes of CuBr.^[10]

The propargylamines **3** obtained can be selectively deprotected by known methods.^[11, 12] Treatment of the mixed allyl benzyl propargylamine **3i** with thiosalicylic acid (**6**) in the presence of a palladium(0) catalyst ($[\text{Pd}(\text{dba})_2]$ (5 mol %) and dppb (5 mol %) leads to the monobenzylated propargylamine **7** in 90 % yield (Scheme 3). The monoallylated amine **8** can be obtained from **3i** in 75 % yield by using the same catalyst. Furthermore, the absolute configuration of the

propargylamine **3i** was determined by its transformation into the amine **9** by using the method of Guibé and co-workers,^[12] and comparison of its optical rotation with literature data.^[2e, 13] Primary amines can be obtained by hydrogenation of the propargylamines **3** in good yields. For example, the amine **3m** is hydrogenated to the amine **10** in 70 % yield. To demonstrate further synthetic applications, the allyl-protected amine **3i** was used in a Pauson–Khand reaction.^[14] Treatment with $[\text{Co}_2(\text{CO})_8]$ (1.1 equiv), followed by oxidation with Me_3NO (5 equiv) afforded the bicyclic compound **11** as a single diastereoisomer in 50 % yield.^[15]

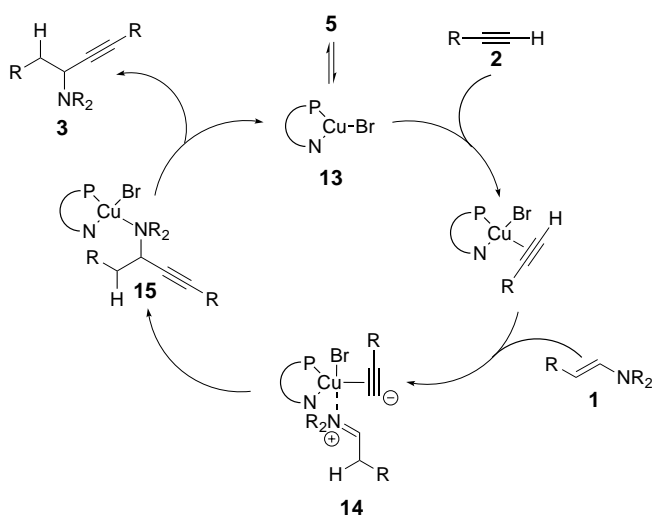
Preliminary mechanistic studies showed that the acetylenic deuterium atom of $[\text{D}]$ phenylacetylene (**2n**) is transferred to the β position of the enamine **1a** (> 90 % deuterium incorporated), leading to **12** in 91 % yield (Scheme 4).



Scheme 4. Deuterium incorporation in propargylic amines.

We suggest the tentative mechanism described in Scheme 5. The dimeric copper complex **5** dissociates to afford the monomeric copper species **13**, which after successive complexation of alkyne **2** and enamine **1** results in the zwitterionic intermediate **14**. After intramolecular transfer of the alkyne moiety to the immonium ion, the copper-complexed product **15** is formed. Decomplexation produces the free propargylamine **3** and regenerates the catalyst **13**.

In summary, we have reported the first copper(II)/Quinap-catalyzed addition of functionalized alkynes to enamines in



Scheme 5. Proposed mechanism.

high yields with up to 90 % *ee*. The mild reaction conditions, the broad scope of the reaction, and the selective deprotection of the propargylamine products show the potential synthetic utility of this method. Further synthetic and mechanistic investigations of this new asymmetric reaction are currently underway.

Experimental Section

Typical procedures:

a) **3m**: CuBr (22 mg, 0.15 mmol, 5 mol %) was suspended in toluene (3 mL) in a 25-mL Schlenk tube under argon. A solution of **1d** (1.049 g, 3.60 mmol, 1.2 equiv), **2a** (0.306 g, 3.00 mmol, 1.0 equiv), and *n*-decane (0.300 g, 2.11 mmol) as internal standard in toluene (3 mL) was added at room temperature. The reaction mixture was stirred for 24 h at room temperature and then for 3 h at 60 °C. Standard workup and purification by column chromatography (SiO₂, pentane/Et₂O 98:2) afforded the desired product as a white solid (1.115 g, 2.83 mmol, 94 %).

b) (–)-**3a**: CuBr (3.6 mg, 0.025 mmol, 5 mol %) and (*R*)-(+)-Quinap (12.1 mg, 0.0275 mmol, 5.5 mol %) were suspended in toluene (2 mL) in a 10-mL Schlenk tube under argon. After 30 min, a solution of **1a** (0.173 g, 0.65 mmol, 1.3 equiv), **2a** (0.051 g, 0.50 mmol, 1.0 equiv) and *n*-decane (0.050 g, 0.35 mmol) as internal standard in toluene (2 mL) was added at room temperature. After stirring for 24 h, standard workup and purification by column chromatography (SiO₂, pentane/Et₂O 98:2) yielded **3a** as a colorless oil (0.144 g, 0.39 mmol, 78 %).

Received: March 28, 2002 [Z19004]

- [1] a) M. A. Huffman, N. Yasuda, A. E. DeCamp, E. J. J. Grabowski, *J. Org. Chem.* **1995**, 60, 1590; b) M. Konishi, H. Ohkuma, T. Tsuno, T. Oki, G. D. VanDuyne, J. Clardy, *J. Am. Chem. Soc.* **1990**, 112, 3715.
- [2] a) J. R. Hauske, P. Dorff, S. Julin, G. Martinelli, J. Bussolari, *Tetrahedron Lett.* **1992**, 33, 3715; b) M. Kolb, J. Barth, *Angew. Chem.* **1980**, 92, 753; *Angew. Chem. Int. Ed. Engl.* **1980**, 19, 725; c) H. Braun, F. P. Schmidtchen, A. Schneider, H. Simon, *Tetrahedron* **1991**, 47, 3329; d) M. J. Burk, J. E. Feaster, *J. Am. Chem. Soc.* **1992**, 114, 6266; e) D. Enders, J. Schankat, *Helv. Chim. Acta* **1995**, 78, 970; f) J. Blanchet, M. Bonin, A. Chiaroni, L. Micouin, C. Riche, H.-P. Husson, *Tetrahedron Lett.* **1999**, 40, 2935; g) C. Fischer, E. M. Carreira, *Org. Lett.* **2001**, 3, 4319.
- [3] R. Noyori, *Asymmetric Catalysis in Organic Synthesis*, Wiley, New York, **1994**.

- [4] For a very efficient Zn-catalyzed enantioselective addition of alkynes to aldehydes, see: a) N. K. Anand, E. M. Carreira, *J. Am. Chem. Soc.* **2001**, 123, 9687; b) E. El-Sayed, N. K. Anand, E. M. Carreira, *Org. Lett.* **2001**, 3, 3017; c) D. E. Frantz, R. Faessler, C. S. Tomooka, E. M. Carreira, *Acc. Chem. Res.* **2000**, 33, 373; d) D. E. Frantz, R. Faessler, E. M. Carreira, *J. Am. Chem. Soc.* **2000**, 122, 1806.
- [5] For a copper(I) chloride catalyzed reaction of alkynes with enamines, see: a) K. C. Brannock, R. D. Burpitt, J. G. Thweatt, *J. Org. Chem.* **1963**, 28, 1462; see also: b) J. J. McNally, M. A. Youngman, S. L. Dax, *Tetrahedron Lett.* **1998**, 39, 967; M. A. Youngman, S. L. Dax, *Tetrahedron Lett.* **1997**, 38, 6347.
- [6] K. Taguchi, F. H. Westheimer, *J. Org. Chem.* **1971**, 36, 1570.
- [7] P. Beeken, F. W. Fowler, *J. Org. Chem.* **1980**, 45, 1336.
- [8] a) J. M. Valk, G. A. Whitlock, T. P. Layzell, J. M. Brown, *Tetrahedron: Asymmetry* **1995**, 6, 2593; b) E. Fernandez, K. Maeda, M. W. Hooper, J. M. Brown, *Chem. Eur. J.* **2000**, 6, 1840.
- [9] Crystal data for **5**: *M*_r = 1287.82, orthorhombic, space group C₂₂1, *a* = 15.549(3), *b* = 16.989(2), *c* = 42.706(7) Å, *V* = 11 281(3) Å³, *Z* = 8, ρ_{calcd} = 1.516 Mg m^{−3}, MoKα radiation (λ = 0.71073 Å), μ = 2.366 mm^{−1}. Data were collected on a NONIUS MACH3 system at 295 K. The structure was solved by direct methods and refined on *F*_o² by full-matrix least-squares methods (SHELXS-86, SHELXL-93). All non-hydrogen atoms were refined anisotropically. *R*1 = 0.0374, *ωR*2 = 0.0834 for all data with *I* > 2σ(*I*). CCDC-182716 contains the supplementary crystallographic data (excluding structure factors) for this paper. These data can be obtained free of charge via www.ccdc.cam.ac.uk/conts/retrieving.html (or from the Cambridge Crystallographic Data Centre, 12, Union Road, Cambridge CB2 1EZ, UK; fax: (+44) 1223-336-033; or deposit@ccdc.cam.ac.uk).
- [10] a) J. Qiong-Hua, L. De-Liang, W. Yu-Xian, X. Xin-Quan, *Acta Crystallogr.* **1998**, C54, 948; b) J. Zukerman-Schpector, E. E. Castellano, A. E. Mauro, M. R. Roveri, *Acta Crystallogr.* **1986**, C42, 302.
- [11] a) S. Lemaire-Audoire, M. Savignac, J. P. Genêt, *Tetrahedron Lett.* **1995**, 36, 1267; b) S. Lemaire-Audoire, M. Savignac, C. Dupuis, J. P. Genêt, *Bull. Soc. Chim. Fr.* **1995**, 132, 1167.
- [12] F. Garro-Helion, A. Mertouk, F. Guibé, *J. Org. Chem.* **1993**, 58, 6109.
- [13] All chiral propargylamines **3** showed the same sign of optical rotation.
- [14] N. Jeong in *Transition Metals for Organic Synthesis*, Vol. 1, (Eds.: M. Beller, C. Bolm), Wiley-VCH, Weinheim, **1998**, 560.
- [15] The stereochemistry of **11** was established by analysis of NOE data.

Hydrolytic Activation of C–F Bonds in the Gas Phase by Intrinsically Unreactive Chromium Cations**

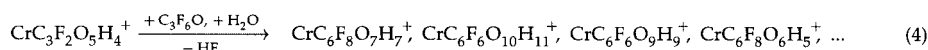
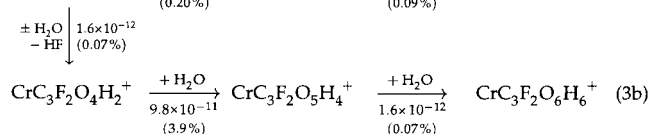
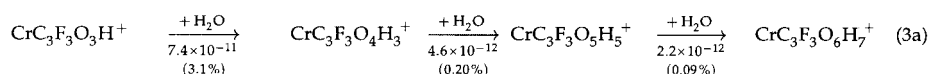
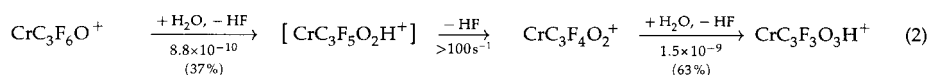
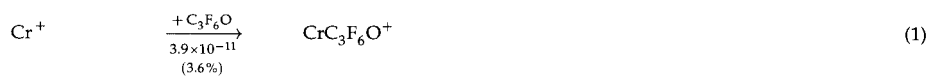
Ulf Mazurek, Detlef Schröder, and Helmut Schwarz*

To the best of our knowledge, hydrolytic activation of C–F bonds in the gas phase has hitherto been unknown.^[1] Moreover, considering the facts that 1) thermalized chromium cations are generally unreactive in the gas phase,^[2–6] 2) C–F bonds show a bond-dissociation energy of 105–110 kcal mol^{−1}^[7, 8] thus being more stable than any other C–X bond, and 3) hexafluoroacetone is commercially available in the forms of sesqui- and trihydrates, which means it is

[*] Prof. Dr. H. Schwarz, Dipl.-Chem. U. Mazurek, Dr. D. Schröder
Institut für Chemie, Technische Universität Berlin
Straße des 17. Juni 135, 10623 Berlin (Germany)
Fax: (+49) 30-314-21102
E-mail: Helmut.Schwarz@www.chem.tu-berlin.de

[**] This work was supported by the Deutsche Forschungsgemeinschaft and the Fonds der Chemischen Industrie.

stable against hydrolysis, one would not expect the contact of Cr^+ with hexafluoroacetone and water in the gas phase to cause any chemical reaction. Nonetheless, in the course of another study^[6] we realized that chemical reactions are indeed observed, as summarized in Equations (1)–(4).



Following its formation [Eq. (1)], the monoadduct $\text{CrC}_3\text{F}_6\text{O}^+$ undergoes F/OH exchange [Eq. (2)] and facile HF loss, thus forming $\text{CrC}_3\text{F}_4\text{O}_2^+$. The short-lived intermediate $\text{CrC}_3\text{F}_5\text{O}_2\text{H}^+$ cannot be observed directly. A second F/OH exchange transforms $\text{CrC}_3\text{F}_4\text{O}_2^+$ into $\text{CrC}_3\text{F}_3\text{O}_3\text{H}^+$, and subsequent complexation of water [Eq. (3)] yields $\text{CrC}_3\text{F}_3\text{O}_4\text{H}_3^+$. At this point, the reaction sequence bifurcates. While complexation of additional water molecules [Eq. (3a)] dominates the product spectrum, a smaller fraction of ions lose a fourth molecule of HF prior to further water addition [Eq. (3b)]. Figure 1 shows the temporal evolution of the ion concentrations from Cr^+ through $\text{CrC}_3\text{F}_2\text{O}_4\text{H}_2^+$.

While the addition of water to $\text{CrC}_3\text{F}_3\text{O}_4\text{H}_3^+$ to yield $\text{CrC}_3\text{F}_3\text{O}_5\text{H}_5^+$ and eventually $\text{CrC}_3\text{F}_3\text{O}_6\text{H}_7^+$ dominates the reaction system, $\text{CrC}_3\text{F}_2\text{O}_5\text{H}_4^+$ formed from $\text{CrC}_3\text{F}_2\text{O}_4\text{H}_2^+$

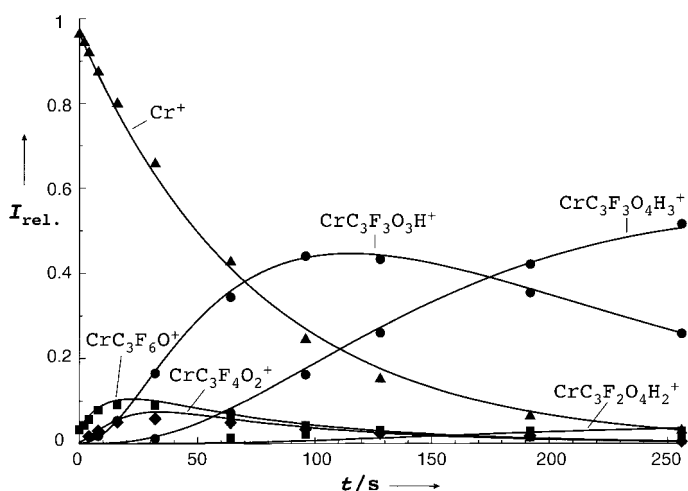


Figure 1. Complexation of thermalized chromium cations at a hexafluoroacetone pressure of 1.0×10^{-7} mbar and initial reactions with background water. For clarity, some data points close to the abscissa as well as side products were omitted.

constitutes a second bifurcation point of the reaction sequence. To a lesser extent, $\text{CrC}_3\text{F}_2\text{O}_5\text{H}_4^+$ continues to complex water molecules [Eq. (3b)]; to a larger extent, however, partially hydrolyzed Cr^+ -hexafluoroacetone diadducts, predominantly $\text{CrC}_6\text{F}_8\text{O}_7\text{H}_7^+$ and $\text{CrC}_6\text{F}_6\text{O}_{10}\text{H}_{11}^+$, are formed [Eq. (4)]. These diadducts are susceptible to further F/OH exchange.^[9] Additional F/OH exchange reactions that transform the cations $\text{CrC}_3\text{F}_3\text{O}_3\text{H}^+$, $\text{CrC}_3\text{F}_3\text{O}_4\text{H}_3^+$, and $\text{CrC}_3\text{F}_3\text{O}_5\text{H}_5^+$ shown in Equation (3a) in a “diagonal-mode” fashion into their congeners $\text{CrC}_3\text{F}_2\text{O}_4\text{H}_2^+$, $\text{CrC}_3\text{F}_2\text{O}_5\text{H}_4^+$, and $\text{CrC}_3\text{F}_2\text{O}_6\text{H}_6^+$, respectively, [Eq. (3b)] could not be proven beyond doubt. Figure 2 shows the temporal evolution of the ion concentrations starting from $\text{CrC}_3\text{F}_3\text{O}_3\text{H}^+$. Three aspects of the complex reaction sequence shall be addressed in more detail.

a) The first three of the hydrolysis reactions are more efficient than any following transformation by at least one order of magnitude. Furthermore, the very first C–F bond activation constitutes the rate-limiting hydrolysis reaction, thus indicating remarkable synergistic effect: the more C–F bonds that are transformed into C–O bonds, the more facile the next C–F bond cleavage (up to $n = 3$).

b) The structures of the observed cations may be governed either by pure complexation of the chromium cation or by insertion of the metal ion into one of the bonds of the ligand. Deliberate decomposition of $\text{CrC}_3\text{F}_3\text{O}_3\text{H}^+$, however, implies that no metal insertion into a C–C or C–F bond has taken place during the first three C–F bond cleavage steps.^[10] Furthermore, $\text{CrC}_3\text{F}_3\text{O}_4\text{H}_3^+$ was found to lose only water in an analogous experiment, thus supporting the previous results. We conclude that the C–F bond activation reported herein does not proceed through the “harpoon” mechanism

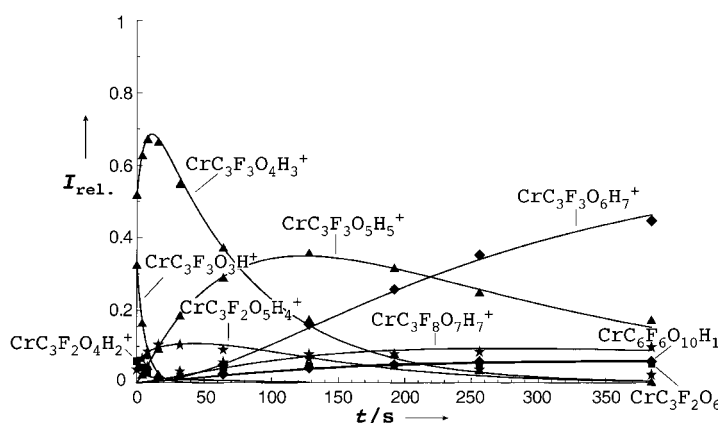


Figure 2. Hydrolysis of $\text{CrC}_3\text{F}_6\text{O}^+$ at a water pressure of 5.0×10^{-8} mbar. As a result of the fast rate of the first hydrolysis steps, the reactions could only be followed by starting with $\text{CrC}_3\text{F}_3\text{O}_3\text{H}^+$. For clarity, some data points close to the abscissa as well as side products were omitted. Of the partially hydrolyzed diadducts, only their major representatives $\text{CrC}_6\text{F}_8\text{O}_7\text{H}_7^+$ and $\text{CrC}_6\text{F}_6\text{O}_{10}\text{H}_{11}^+$ are shown.

postulated for both lanthanoid cations^[11, 12] and Ca^+ .^[13] If the ligand $\text{C}_3\text{F}_3\text{O}_3\text{H}$ is assumed to possess the structure of trifluoropyruvic acid, one may conclude that 1) the keto group of hexafluoroacetone remains unchanged, 2) one of the trifluoromethyl groups is completely hydrolyzed and eventually turned into a carboxylic acid group, and 3) both the newly formed carboxylic acid group and the other (unchanged) trifluoromethyl group chelate the chromium cation, whereas the keto group does not interact for steric reasons. c) Both HF losses from $\text{CrC}_3\text{F}_5\text{O}_2\text{H}^+$ [Eq. (2)] and $\text{CrC}_3\text{F}_5\text{O}_4\text{H}_3^+$ [Eq. (3)] may proceed through two alternative pathways: intramolecularly formed HF may readily dissociate from the complex in a unimolecular reaction as a result of its weak coordination or the HF loss may be assisted by an additional water molecule coordinating to the complex^[6, 14, 15] in a bimolecular reaction. In an FT-ICR mass spectrometer, unimolecular dissociations originate from metastable parent ions, which cannot be detected in general. A bimolecular reaction, however, cannot proceed with unlimited rate. Consequently, we postulate that the unobserved cation $\text{CrC}_3\text{F}_5\text{O}_2\text{H}^+$ loses HF in an unimolecular reaction. A bimolecular reaction would have to occur with a reaction efficiency of 5500 % (!) of the collision rate to account for the observed ion intensities' temporal evolution. In contrast, the observed cation $\text{CrC}_3\text{F}_5\text{O}_4\text{H}_3^+$ loses HF in a bimolecular reaction. The rate constants reported in Equations (2) and (3) were calculated accordingly.

To summarize, we were able to activate the strong C–F bond by interaction with an intrinsically unreactive cation. This activation was sufficient to facilitate hydrolysis of the C–F bond. Most remarkably, considering the relatively inefficient Cr^+ –hexafluoroacetone adduct formation, the even lower reactivity of Cr^+ towards water^[6] is essential for the reactions reported herein. If the association of water and Cr^+ was more efficient, the chromium cations would be consumed by this reaction and would no longer be available for activating hexafluoroacetone. A systematic study of structurally related compounds (e.g., trifluoroacetone) will be necessary to reveal whether the hitherto single observation of a cation-assisted hydrolytic C–F bond activation can be transformed into a general concept.^[33]

Experimental Section

Chemicals: Methane (Linde, 99.95 %) and metallic chromium (Balzers, >99.9 %) were used as purchased. Tap water was used without further purification. The water was added into a half-micro test tube directly connected to the gas-inlet system of the mass spectrometer and degassed by two freeze-pump-thaw cycles. Hexafluoroacetone was liberated from its sesquihydrate (Merck-Schuchardt, >97 %) by reaction and additional dehydration with phosphorus pentoxide (P_4O_{10}) by adopting established procedures.^[16–19]

Mass spectrometer: All experiments were performed on a Bruker Spectrospin CMS-47X FT-ICR mass spectrometer whose setup and operation have been described previously^[20, 21] as well as pressure measurement in the reaction cell^[22] and both generation and study of chromium cations.^[4–6] The background pressure in the reaction cell was 2.0×10^{-9} mbar. Reaction conditions: 1) adduct formation [Eq. (1)]: methane-thermalized cations $^{52}\text{Cr}^+$, $\text{C}_3\text{F}_6\text{O}$ pressure 1.0×10^{-7} mbar, maximum reaction time 256 s; 2) hydrolysis reactions [Eq. (2)]: $\text{CrC}_3\text{F}_6\text{O}^+$ was generated by pulsing-in $\text{C}_3\text{F}_6\text{O}$ to $^{52}\text{Cr}^+$ and subsequent isolation, effective water pressure 3.0×10^{-9} mbar, maximum reaction time 12 s; 3) complex-

ation by water [Eq. (3)]: $\text{CrC}_3\text{F}_6\text{O}^+$ generated by pulsing-in and isolation as before, water pressure 5.0×10^{-8} mbar, maximum reaction time 384 s; 4) connectivity of $\text{CrC}_3\text{F}_5\text{O}_3\text{H}^+$: the ion was generated by pulsing-in $\text{C}_3\text{F}_6\text{O}$ to Cr^+ and subsequent reaction with background water; the ion of interest was isolated and subjected to a CID experiment^[23] in the presence of 7.0×10^{-8} mbar of argon.

Analysis of results: Reaction sequences were derived from the temporal evolution of ion intensities and complementary double-resonance experiments.^[24] Reaction kinetics were analyzed by using a computer program that determines rate constants and distribution ratios based on the experimentally observed temporal evolution of ion intensities, and a flexible kinetic model.^[25] Unless otherwise noted, the reaction rate constants are reported as effective bimolecular rate constants in units of $\text{cm}^3 \text{molecules}^{-1} \text{s}^{-1}$ whereas reaction efficiencies ϕ in parenthesis are given as fractions of the measured bimolecular rate constants and the gas-kinetic collision rates^[28] according to the capture theory.^[26, 27] The absolute error of the experimentally determined rate constants is in the range of ± 30 %, ^[22] whereas the relative rates are more precise (± 10 %).^[22] The rate constant of the formation of the monoadduct formation [Eq. (1)] is thought to be more imprecise (± 40 %) as a result of the rough estimation of the polarizability of hexafluoroacetone. The effective water pressure is only one and a half times the background pressure, thus the same wider error margin is assessed for the reactions shown in Equation (2).

Received: March 6, 2001 [Z18838]

- [1] On April 9, 2002, a SciFinder search for the keywords “C–F bond activation gas phase” by using the search menu “Explore by Research Topic” returned seven references. Of these, only four (refs. [11–13, 29]) refer to C–F bond activation at all; none of the returned references relates to hydrolysis.
- [2] S. W. Buckner, J. R. Gord, B. S. Freiser, *J. Am. Chem. Soc.* **1988**, *110*, 6606–6612.
- [3] J. B. Schilling, J. L. Beauchamp, *Organometallics* **1988**, *7*, 194–199.
- [4] U. Mazurek, D. Schröder, H. Schwarz, *Collect. Czech. Chem. Commun.* **1998**, *63*, 1498–1512.
- [5] U. Mazurek, H. Schwarz, *Inorg. Chem.* **2000**, *39*, 5586–5590.
- [6] U. Mazurek, D. Schröder, H. Schwarz, *Eur. J. Inorg. Chem.* **2002**, in press.
- [7] K. P. C. Vollhardt, N. E. Schore, *Organische Chemie*, 3rd ed., Wiley-VCH, Weinheim, **2000**, p. 88.
- [8] M. B. Smith, J. March, *March's Advanced Organic Chemistry*, 5th ed., Wiley, New York, **2001**, p. 911.
- [9] The complexation of $\text{CrC}_3\text{F}_5\text{O}_3\text{H}_4^+$ with another molecule of hexafluoroacetone or its hydrate(s) as summarized in Equation (4) is supposed to originate from hexafluoroacetone hydrate formation. It is plausible that this hydrate formation, in turn, originates from pulsing hexafluoroacetone into the reaction cell. Supposedly, the hydrates stick to the walls of the reaction cell more efficiently than hexafluoroacetone itself does.
- [10] $\text{CrC}_3\text{F}_5\text{O}_3\text{H}^+$ was subjected to a CID experiment^[23] in the presence of argon (7.0×10^{-8} mbar). The fragment ions observed were mostly Cr^+ , as well as CrF^+ , CrF_2^+ , and their hydrolysis products^[6]. Chromium-free cations and cationic organochromium complexes were not detected. Our interpretation refers to the chelate structure of $\text{CrC}_3\text{F}_5\text{O}_3\text{H}^+$ discussed in more detail in the text. Upon decomposition, kinetically excited $\text{CrC}_3\text{F}_5\text{O}_3\text{H}^+$ cations may lose Cr^+ when colliding with argon. However, upon collision with background water, one or more of the chelation-weakened C–F bonds might be broken, thus causing the formation of CrF^+ or CrF_2^+ , or CrOH^+ or Cr(OH)_2^+ , respectively, and HF, besides the corresponding neutral organic fragment.
- [11] C. Heinemann, N. Goldberg, I. C. Tornieporth-Oetting, T. M. Klappötke, H. Schwarz, *Angew. Chem.* **1995**, *107*, 225–229; *Angew. Chem. Int. Ed. Engl.* **1995**, *34*, 213–217.
- [12] H. H. Cornehl, G. Hornung, H. Schwarz, *J. Am. Chem. Soc.* **1996**, *118*, 9960–9965.
- [13] J. N. Harvey, D. Schröder, W. Koch, D. Danovich, S. Shaik, H. Schwarz, *Chem. Phys. Lett.* **1997**, *278*, 391–397.
- [14] D. K. Bohme, *Int. J. Mass Spectrom. Ion Processes* **1992**, *115*, 95–110.
- [15] A. J. Chalk, L. Radom, *J. Am. Chem. Soc.* **1997**, *119*, 7573–7578.

- [16] A. L. Henne, J. W. Shepard, E. J. Young, *J. Am. Chem. Soc.* **1950**, 72, 3577–3579.
- [17] R. N. Haszeldine, *J. Chem. Soc.* **1953**, 3565–3573.
- [18] R. N. Haszeldine, *J. Chem. Soc.* **1954**, 1273–1279.
- [19] A. T. Morse, P. B. Ayscough, L. C. Leitch, *Can. J. Chem.* **1955**, 33, 453–457.
- [20] K. Eller, H. Schwarz, *Int. J. Mass Spectrom. Ion Processes* **1989**, 93, 243–257.
- [21] K. Eller, W. Zummack, H. Schwarz, *J. Am. Chem. Soc.* **1990**, 112, 621–627.
- [22] D. Schröder, H. Schwarz, D. E. Clemmer, Y. Chen, P. B. Armentrout, V. I. Baranov, D. K. Böhme, *Int. J. Mass Spectrom. Ion Processes* **1997**, 161, 175–191.
- [23] R. B. Cody, S. C. Burnier, B. S. Freiser, *Anal. Chem.* **1982**, 54, 96–101.
- [24] M. B. Comisarow, V. Grassi, G. Parisod, *Chem. Phys. Lett.* **1978**, 57, 413–416.
- [25] U. Mazurek, H. Schwarz, *ICR Kinetics*, v. 3.0.1, TU Berlin, Berlin, **1998**, available upon request.
- [26] T. Su, W. J. Chesnavich, *J. Chem. Phys.* **1982**, 76, 5183–5185.
- [27] T. Su, *J. Chem. Phys.* **1988**, 89, 5355.
- [28] Parameters: water: dipole moment 1.854 D,^[30] polarizability $1.45 \times 10^{-24} \text{ cm}^3$,^[30] relative ion gauge sensitivity 0.97;^[31] hexafluoroacetone: dipole moment 0.395 D,^[32] polarizability $7.5 \times 10^{-24} \text{ cm}^3$ (estimation based on the data for acetone and fluorinated methanes $\text{CH}_n\text{F}_{4-n}$ ^[30]), relative ion gauge sensitivity 2.59.^[31]
- [29] J. N. Harvey, D. Schröder, W. Koch, D. Danovich, S. Shaik, H. Schwarz, *Chem. Phys. Lett.* **1997**, 273, 164–170.
- [30] *CRC Handbook of Chemistry and Physics*, 79th ed. (Ed.: D. R. Lide), CRC Press, Boca Raton, FL, **1998**.
- [31] J. E. Bartmess, R. M. Georgiadis, *Vacuum* **1983**, 33, 149–153.
- [32] J. U. Grabow, N. Heineking, W. Stahl, *Z. Naturforsch. A* **1991**, 46, 229–232.
- [33] **Note added in proof** (June 3, 2002): Since the submission of this paper several publications have appeared on C–F bond activation; see for example: K. Uneyama, H. Amii, *J. Fluorine Chem.* **2002**, 114, 127–131; K. Guennou de Cadenet, R. Rumin, F. Y. Pétilon, D. S. Yufit, K. W. Muir, *Eur. J. Inorg. Chem.* **2002**, 639–657; D. Zhang, C. Liu, S. Bi, *J. Phys. Chem. A* **2002**, 106, 4153–4157.

Anti-Markovnikov Hydroamination of Terminal Alkynes**

Annegret Tillack, Ivette Garcia Castro,
Christian G. Hartung, and Matthias Beller*

*Dedicated to Professor Dr. Lutz F. Tietze
on the occasion of his 60th birthday*

Imines are of significant importance as intermediates for the synthesis of various amines and carbonyl compounds. In general, the synthesis of imines includes amination of a suitable aldehyde or ketone. A more atom-efficient route is the direct hydroamination of alkynes.^[1] This method has the additional advantage that no water is produced as a by-

product. Hence, various domino reactions (e.g. direct nucleophilic addition of organometallic reagents) are possible, which do not work in the presence of water.

The homogeneously catalyzed intermolecular hydroamination of alkynes is known to proceed in the presence of Hg and Tl salts,^[2] alkali metals (Cs),^[3] Ti,^[4] Zr,^[5] Nd,^[6] U, and Th^[7] complexes. In addition, complexes of late-transition metals (such as Ru, Pd,^[8] and Rh^[9]) have been used as catalysts for this transformation. Clearly, catalysts based on cheap and easily available titanium and zirconium complexes offer significant advantages compared to those based on toxic metals (Hg, Tl) or more expensive (U, Th, Ru, Pd, and Rh) complexes.

Recently, important progress in the intermolecular hydroamination of alkynes with titanium complexes was made by Johnson and Bergman^[10] and by Doye and co-workers.^[4] While the former group developed the modified titanium complex $[\text{Cp}(\text{ArNH})(\text{py})\text{Ti}=\text{NAr}]$ (Cp = cyclopentadienyl, py = pyridyl) and used it for the reaction of 2,6-dimethylaniline and diphenylacetylene, the latter group described an efficient and general method for the hydroamination of various internal alkynes using dimethyltitanocene as a catalyst. Bytschkov and Doye showed that the turnover frequency of this catalyst can be enhanced by using microwaves.^[4c] Kinetic measurements by Bergman^[10] and Doye^[11] also established a general mechanism of the dimethyltitanocene-catalyzed intermolecular hydroamination of alkynes. Surprisingly little attention was paid to the hydroamination of terminal alkynes using titanium catalysts,^[12] although the regioselective, sequential amination and hydroxylation of compounds that are unsaturated at the terminal position is one of the most challenging goals for industrial catalysis. Herein we report the first example of a titanocene-catalyzed anti-Markovnikov hydroamination of terminal aliphatic alkynes.

Some time ago we started a program on catalytic amination reactions of olefins and alkynes.^[13, 9] Inspired by the work of Doye and Bergman, we also recently looked for easily available and stable titanocene complexes. Here, titanocene alkyne complexes of the type $[\text{Cp}_2\text{Ti}(\eta^2\text{-Me}_3\text{SiC}\equiv\text{CR})]$ (Rosenthal's catalyst)^[14] appeared to be suited as amination catalysts.^[15] These complexes ($[\text{Cp}_2\text{Ti}(\eta^2\text{-Me}_3\text{SiC}\equiv\text{CSiMe}_3)]$ **1**^[14a] and $[\text{Cp}_2\text{Ti}(\eta^2\text{-Me}_3\text{SiC}\equiv\text{CPh})]$ **2**^[14b]) are easily synthesized by reaction of titanocene dichloride with the corresponding silylated alkyne.

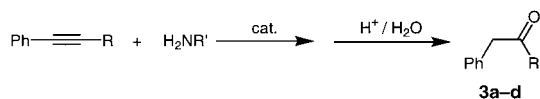
Compared to previously used titanocene precatalysts, the titanacyclopentene complexes **1** and **2** are safe and stable under argon at room temperature for many months in German version. Indeed, hydroamination of internal alkynes (diphenylacetylene, 1-phenylpropyne) with aniline or *tert*-butylamine proceeds in excellent yields in the presence of **1** (81–98% yield after hydrolysis with HCl, Table 1). As shown in Table 2, different terminal aliphatic alkynes react with *tert*-butylamine with extremely high regioselectivity (>98%), in high yields (84–98%), and within a short time (2–24 h), by using 0.5–2.5 mol % of catalyst **1**, to give the imines **4a–e** and **5**. Although the reactions proceed smoothly with 0.5 mol % of catalyst, we used 2.5 mol % in general because of the shorter reaction time.

Pleasingly, only the anti-Markovnikov products were obtained, which is explained by the selective formation of the

[*] Prof. Dr. M. Beller, Dr. A. Tillack, Dr. I. Garcia Castro,
Dr. C. G. Hartung
Institut für Organische Katalyseforschung (IfOK)
Universität Rostock e.V.
Buchbinderstrasse 5–6, 18055 Rostock (Germany)
Fax: (+49)381-466-9324
E-mail: matthias.beller@ifok.uni-rostock.de

[**] We acknowledge financial support of this project from the Deutsche Forschungsgemeinschaft (DFG) and the state of Mecklenburg-West Pomerania. C. Mewes, Dr. C. Fischer, H. Baudisch, and S. Buchholz are thanked for their excellent technical support.

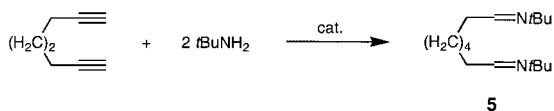
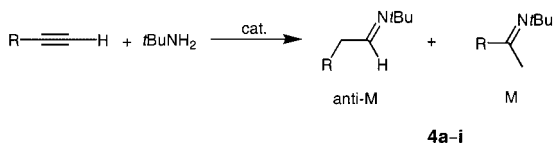
Table 1. Intermolecular hydroamination of internal alkynes in the presence of **1**.^[a]


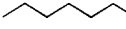
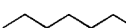


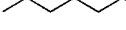
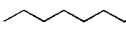
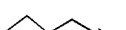



Alkyne R	Amine R'	Mole % cat.	<i>T</i> [°C]	Conversion [%]	Yield [%] ^[b]
Ph	<i>t</i> Bu	3.0	100	100	84 (3a)
Ph	Ph	3.0	140	95	92 (3b)
CH ₃	<i>t</i> Bu	3.0	100	100	81 (3c)
CH ₃	Ph	2.0	140	100	98 (3d)

[a] Toluene, 24 h, amine/alkyne = 1.5:1. [b] Determination of yield of the corresponding ketone after hydrolysis of the imine (5% HCl) was by gas chromatography with an internal standard.

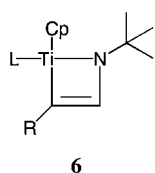
Table 2. Hydroamination of terminal aliphatic alkynes with *tert*-butylamine in the presence of **1**.



Entry	Alkyne	Mole % cat.	<i>T</i> [°C]	<i>t</i> [h]	Amine/ Alkyne	Yield [%] (anti-M/M) ^[a]	
1		2.5	85	2	1.5:1	90 (>99:1)	4a
2		2.5	85	2	1.5:1	97 (87:1)	4b
3		1.0	85	24	1.5:1	98 (89:1)	4b
4	 ^[b]	0.5	85	24	1.5:1	60 (75:1)	4b
5	 ^[c]	2.5	85	24	1.5:1	92 (83:1)	4b
6		2.5	85	24	1.5:1	93 (63:1)	4c
7		2.5	85	24	1.2:1	84 (63:1)	4d
8		2.5	85	24	1.5:1	88 (100:0)	4e
9		5.0	100	2	4.0:1	92 (100:0)	5

[a] GC yield determined with an internal standard (hexadecane or dodecane).

[b] 64% conversion. [c] Catalyst: **2**, anti-M/M = anti-Markovnikov/Markovnikov.



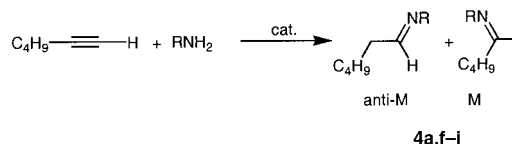
azatitanacyclobutene **6**. Here, the ligand L represents either another cyclopentadienyl ligand, an amine, or an alkyne, because free cyclopentadiene is observed in most GC spectra of the reaction mixtures.

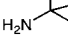
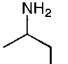
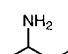
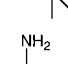
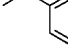
6 In agreement with the binding constant of the different alkynes, catalyst **1** is slightly more active than catalyst **2** (Table 2, entries 2 and 5). Interestingly, the dihydroamination of diynes, for example, 1,7-octadiyne (entry 9), proceeds smoothly. In the presence of an excess of amine (amine/alkyne = 4:1), both triple bonds react

selectively with anti-Markovnikov regiochemistry to yield the 1,8-bisimine **5**. Phenylacetylene also reacts with high regioselectivity to give the anti-Markovnikov product. Unfortunately, a preparative isolation of the corresponding linear imine was not possible because of side reactions during distillation of this product.

Apart from *tert*-butylamine, other aliphatic (*sec*-butylamine, 3,3-dimethyl-2-butylamine), benzylic amines (α -methylbenzylamine), and aniline react with 1-hexyne to give imines in high yields (Table 3). Except when using aniline, the

Table 3. Hydroamination of 1-hexyne with different amines in the presence of **1**.



Amine	Mole % cat.	<i>T</i> [°C]	<i>t</i> [h]	Amine/ Alkyne	Yield [%] (anti-M:M) ^[a]
	2.5	85	2	1.5:1	90 (>99:1) 4a
	5.0	85	24	1.5:1	86 (3:1) 4f
	2.5	85	24	1.5:1	96 (4:1) 4g
	5.0	100	24	1.2:1	79 (2:1) 4h
	5.0	100	24	1.2:1	94 (1:3) 4i

[a] GC yield determined with internal standard (hexadecane or dodecane).

anti-Markovnikov products were obtained preferentially. However, the observed regioselectivity is lower than that obtained with *tert*-butylamine, which demonstrates the importance of steric factors for the selective formation of the azitanacyclobutene **6**. Nevertheless, steric bulk is not the only important factor influencing the regiochemical outcome of the reaction, as shown by the hydroamination of 1-hexyne with aniline.

In summary, we have introduced titanocene–alkyne complexes as new catalysts for the hydroamination of internal and terminal alkynes. This class of titanium complexes is easily available, stable, and can be used in a safe and practical manner. The reactions of terminal alkynes with aliphatic amines proceed highly selectively in the presence of catalyst **1** or **2**, to give the corresponding primary anti-Markovnikov functionalized imines in good to excellent yields. Even higher selectivities for anti-Markovnikov aminations might be expected by using sterically more hindered titanocenes.

Experimental Section

Chemicals were obtained from Aldrich, Fluka (solvents), Acros, and Strem and, unless otherwise noted, were used without further purification.

Amines were distilled from CaH_2 . Alkynes were degassed, flushed with argon, and stored over molecular sieves (4 Å). All experiments were carried out under an argon atmosphere.

Catalysts **1** and **2** were synthesized according to a literature procedure.^[14a,b] Imines **4b–h** and **5** were isolated after distillation of the crude hydroamination mixtures and were characterized by NMR spectroscopy, MS, IR spectroscopy, and elemental analyses. Identification of all other products was performed by comparison with authentic products. Compounds **4a** and **4i** were synthesized according to the procedures in references [16] and [9], respectively.

Example of a typical hydroamination experiment (**4b**, Table 2, entry 2): A solution of 1-octyne (3.2 mL, 2.4 g, 21.5 mmol) and *tert*-butylamine (3.5 mL, 2.4 g, 32.2 mmol) was treated with **1** (0.15 g, 0.43 mmol, 2 mol % in toluene (6 mL). This mixture was heated to 85 °C and distilled under vacuum after 24 h. Product **4b** was obtained at 48–49 °C (0.1 mbar); yield: 2.9 g (75 %, >98 % (GC) anti-Markovnikov product); ¹H NMR (400 MHz, CDCl_3): δ = 0.85 (t, 3H, CH_3), 1.14 (s, 9H, C- CH_3), 1.21–1.34 (m, 8H, CH_2), 1.46 (m, 2H, CH_2), 2.20 (m, 2H, CH_2), 7.56 ppm (t, ³J = 5.35 Hz, 1H, CH); ¹³C NMR (100 MHz, CDCl_3): δ = 14.0 (CH_3), 22.6, 26.4, 29.1, 29.2 (CH_2), 29.6 (C- CH_3), 31.7, 36.4 (CH_2), 56.4 (C_q), 159.3 ppm (CH); IR (neat): $\nu_{\text{C=N}}$: 1671 cm^{-1} ; MS (EI, 70 eV): m/z = 184 [M^+ +1], 183 [M^+], 168 [M^+ - CH_3], 99 [$\text{C}_7\text{H}_{15}^+$], 84 [$\text{C}_6\text{H}_9\text{NCH}^+$], 57 [C_4H_9^+]; elemental analysis $\text{C}_{12}\text{H}_{25}\text{N}$ calcd (%) C 78.62, H 13.74, N 7.64; found C 78.19, H 13.99, N 7.42.

Received: December 21, 2001 [Z18425]

- [1] Reviews: a) M. Nobis, B. Driessen-Hölscher, *Angew. Chem.* **2001**, *113*, 4105–4108; *Angew. Chem. Int. Ed.* **2001**, *40*, 3983–3986; b) T. E. Müller, M. Beller, *Chem. Rev.* **1998**, *98*, 675–703; c) J.-J. Brunet, D. Neibecker in *Catalytic Heterofunctionalization* (Eds.: A. Togni, H. Grützmaier), Wiley-VCH, Weinheim, **2001**, pp. 91–141; d) T. E. Müller, M. Beller in *Transition Metals for Organic Synthesis, Vol. 2* (Eds.: M. Beller, C. Bolm), Wiley-VCH, Weinheim, **1998**, pp. 316–330; e) E. Haak, S. Doye, *Chem. Unserer Zeit* **1999**, *33*, 297–303; f) J. J. Brunet, D. Neibecker, F. Niedercorn, *J. Mol. Catal.* **1989**, *49*, 235–259; g) R. Taube in *Applied Homogeneous Catalysis with Organometallic Compounds, Vol. 1* (Eds.: B. Cornils, W. A. Herrmann), Wiley-VCH, Weinheim, **1996**, S. 507–520.
- [2] a) J. Barluenga, F. Aznar, *Synthesis* **1975**, 704–705; b) J. Barluenga, F. Aznar, *Synthesis* **1977**, 195–196; c) J. Barluenga, F. Aznar, R. Liz, R. Rodes, *J. Chem. Soc. Perkin Trans. 1* **1980**, 2732–2737.
- [3] D. Tzalis, C. Koradin, P. Knochel, *Tetrahedron Lett.* **1999**, *40*, 6193–6195.
- [4] a) E. Haak, I. Bytschkov, S. Doye, *Angew. Chem.* **1999**, *111*, 3584–3586; *Angew. Chem. Int. Ed.* **1999**, *38*, 3389–3391; b) E. Haak, S. Doye, *Org. Lett.* **2000**, *2*, 1935–1937; c) I. Bytschkov, S. Doye, *Eur. J. Org. Chem.* **2001**, 4411–4418; d) E. Haak, I. Bytschkov, S. Doye, *Eur. J. Org. Chem.* **2002**, 457–463.
- [5] a) A. M. Baranger, P. J. Walsh, R. G. Bergman, *J. Am. Chem. Soc.* **1993**, *115*, 2753–2763; b) P. J. Walsh, A. M. Baranger, R. G. Bergman, *J. Am. Chem. Soc.* **1992**, *114*, 1708–1719.
- [6] Y. Li, T. J. Marks, *Organometallics* **1996**, *15*, 3770–3772.
- [7] a) A. Haskel, T. Straub, M. S. Eisen, *Organometallics* **1996**, *15*, 3773–3775; b) M. S. Eisen, T. Straub, A. Haskel, *J. Alloys Compd.* **1998**, *271*–273, 116–122; c) T. Straub, A. Haskel, T. G. Neyroud, M. Kapon, M. Botoshansky, M. S. Eisen, *Organometallics* **2001**, *20*, 5017–5035.
- [8] a) M. Tokunaga, M. Eckert, Y. Wakatsuki, *Angew. Chem.* **1999**, *111*, 3416–3419; *Angew. Chem. Int. Ed.* **1999**, *38*, 3222–3225; b) M. Tokunaga, Y. Wakatsuki, *J. Synth. Org. Chem. Jpn.* **2000**, *58*, 587–596; c) M. Heider, J. Henkelmann, T. Ruehl, *Eur. Pat. Appl.* EP 646571, **1995** [*Chem. Abstr.* **1995**, *123*, 22925s]; d) Y. Uchimaru, *Chem. Commun.* **1999**, 1133–1134; e) I. Kadota, A. Shibuya, L. Mpaka Lutete, Y. Yamamoto, *J. Org. Chem.* **1999**, *64*, 4570–4571.
- [9] C. G. Hartung, A. Tillack, H. Trauthwein, M. Beller, *J. Org. Chem.* **2001**, *66*, 6339–6343.
- [10] J. S. Johnson, R. G. Bergman, *J. Am. Chem. Soc.* **2001**, *123*, 2923–2924.
- [11] F. Pohlki, S. Doye, *Angew. Chem.* **2001**, *113*, 2361–2364; *Angew. Chem. Int. Ed.* **2001**, *40*, 2305–2308.

- [12] a) Y. Shi, J. T. Ciszewski, A. L. Odom, *Organometallics* **2001**, *20*, 3967–3969; b) C. Cao, J. T. Ciszewski, A. L. Odom, *Organometallics* **2001**, *20*, 5011–5013.
- [13] a) M. Beller, M. Eichberger, H. Trauthwein, *Angew. Chem.* **1997**, *109*, 2306–2308; *Angew. Chem. Int. Ed. Engl.* **1997**, *36*, 2225–2227; b) M. Beller, H. Trauthwein, M. Eichberger, C. Breindl, T. E. Müller, A. Zapf, *J. Organomet. Chem.* **1998**, *566*, 277–285; c) M. Beller, H. Trauthwein, M. Eichberger, C. Breindl, T. E. Müller, *Eur. J. Inorg. Chem.* **1999**, 1121–1132; d) M. Beller, O. R. Thiel, H. Trauthwein, C. G. Hartung, *Chem. Eur. J.* **2000**, *6*, 2513–2522; e) A. Tillack, H. Trauthwein, C. G. Hartung, M. Eichberger, S. Pitter, A. Jansen, M. Beller, *Monatsh. Chem.* **2000**, *131*, 1327–1334; f) M. Beller, H. Trauthwein, M. Eichberger, C. Breindl, J. Herwig, T. E. Müller, O. R. Thiel, *Chem. Eur. J.* **1999**, *5*, 1306–1319; g) H. Trauthwein, A. Tillack, M. Beller, *Chem. Commun.* **1999**, 2029–2030.
- [14] a) V. V. Burlakov, U. Rosenthal, P. V. Petrovskii, V. B. Shur, M. E. Vol'pin, *Organomet. Chem. USSR* **1988**, *1*, 526; b) V. V. Burlakov, U. Rosenthal, R. Beckhaus, A. V. Polyakov, Y. T. Struchkov, G. Oehme, V. B. Shur, M. E. Vol'pin, *Organomet. Chem. USSR* **1990**, *3*, 237–238; c) A. Tillack, C. Lefebvre, N. Peulecke, D. Thomas, U. Rosenthal, *Tetrahedron Lett.* **1997**, *38*, 1533–1534; d) N. Peulecke, D. Thomas, W. Baumann, C. Fischer, U. Rosenthal, *Tetrahedron Lett.* **1997**, *38*, 6655–6656; e) N. Peulecke, A. Ohff, P. Kosse, A. Tillack, A. Spannenberg, R. Kempe, W. Baumann, V. V. Burlakov, U. Rosenthal, *Chem. Eur. J.* **1998**, *4*, 1852–1861; f) S. Pulst, F. G. Kirchbauer, B. Heller, W. Baumann, U. Rosenthal, *Angew. Chem.* **1998**, *110*, 2029–2031; *Angew. Chem. Int. Ed.* **1998**, *37*, 1915–1927; g) P. Arndt, A. Spannenberg, W. Baumann, S. Becke, U. Rosenthal, *Eur. J. Inorg. Chem.* **2001**, 2885–2890; Rosenthal's catalysts are now commercially available from Fluka.
- [15] N. Peulecke, Ph.D. thesis, Rostock, **1997** describes an amination of trimethylsilylacetylene and phenylacetylene with aniline in the presence of **1** with a maximum yield of 50 %. However, other amines, such as *tert*-butylamine, do not react.
- [16] N. Y. Grigor'eva, I. M. Avrutov, O. A. Pinsker, O. N. Yudina, A. I. Lutsenko, A. M. Moiseenkov, *Izv. Akad. Nauk SSSR Ser. Khim.* **1985**, *8*, 1824–1835.

Formation of a Butadienenickel-Based Zwitterionic Single-Component Catalyst for Ethylene Polymerization: An Alternative Activation Pathway for Homogeneous Ziegler–Natta Catalysts of Late Transition Metals**

Joachim W. Strauch, Gerhard Erker,* Gerald Kehr, and Roland Fröhlich

Homogeneous Ziegler–Natta catalysis has become very important in recent years.^[1] In addition to the many reported catalysts based on metallocenes with metals from Group 4 and related systems, a variety of Ziegler–Natta systems of late

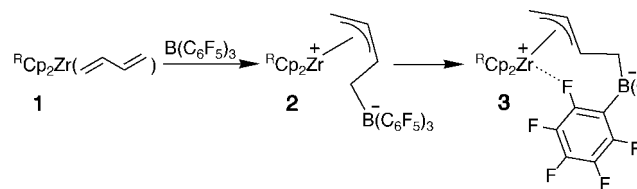
[*] Prof. Dr. G. Erker, Dipl.-Chem. J. W. Strauch, Dr. G. Kehr, Dr. R. Fröhlich^[+]
Organisch-Chemisches Institut der Universität
Westfälische Wilhelms-Universität Münster
Corrensstrasse 40, 48149 Münster (Germany)
Fax: (+49)251-833-36503
E-mail: erker@uni-muenster.de

[+] X-ray crystal structure analysis.

[**] This work was supported by the Fonds der Chemischen Industrie (and the BMBF) and the Deutsche Forschungsgemeinschaft.

transition metal catalysts have significantly contributed to the expansion of this field, especially those derived from complexes with chelating imine ligands.^[2] In all such systems, regardless of whether they are based on the early or late d-metal components, the catalytically active species is an alkylmetal complex cation L_nMR^+ (or its ion-pair equivalent^[3]). In the case of the ubiquitous use of methylalumoxane (MAO) activation, this is usually generated in situ by alkylation of the corresponding metal dihalide derivative, followed by transfer of an alkyl anion equivalent. A variety of other activator components, for example $B(C_6F_5)_3$, R_3C^+ , or R_3NH^+ ,^[4] have also been used successfully for this purpose.

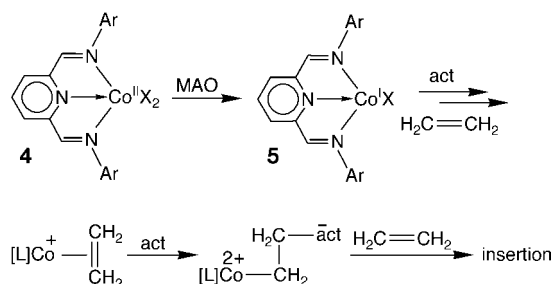
We have previously developed an alternative method of activation of homogeneous Ziegler–Natta catalysts containing metallocenes with transition metals from Group 4 and related systems: Treatment of the butadienezirconocene complexes **1** with $B(C_6F_5)_3$ results in the formation of the zwitterionic metallocene systems **3** (Scheme 1). These systems are active neutral single-component catalysts for olefin



Scheme 1. Formation of **3** by addition of $B(C_6F_5)_3$ to **1**.

polymerization that do not require the addition of further activating components.^[5] The systems **3** have allowed some detailed mechanistic studies of the alkene C–C coupling steps taking place at such catalyst systems.^[6] We report here, to our knowledge for the first time, the preparation of a related zwitterionic “butadiene-borate” Ziegler–Natta catalyst system of a late transition metal by addition of the electrophilic borane $B(C_6F_5)_3$ to a butadienenickel(0) complex.

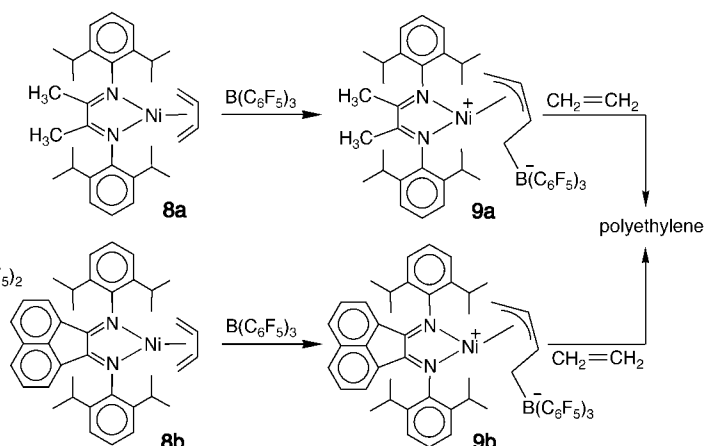
This development may be of specific importance in view of some recent observations made with late transition metal Ziegler–Natta catalysts. Treatment of bis(imine)halogenocobalt(II) chelate complexes **4** with MAO^[7,8] led to the reduction to the respective Co^I complexes **5** rather than to alkylation (Scheme 2).^[9,10] Subsequent alkylation of **5** followed by methyl anion abstraction must then lead to a σ -alkyl ligand free cation which can be considered a direct precursor of the active catalyst species, although it lacks the essential metal–



Scheme 2. Reduction of **4** to give **5** and subsequent alkylation.

carbon σ bond.^[11] One potential explanation for the observed catalytic olefin polymerization features of this system is based on the assumption that the activating Lewis acid might have been added to a cationic intermediate $[L]_nCo(ethylene)^+$ complex (see Scheme 2). Our new reaction, in which a bis(imine)nickel chelate complex participates, represents a vinylogous analogue of such an activation pathway in which a σ -alkyl group does not participate.

Treatment of $\{[biacetyl]bis(2,6\text{-diisopropylphenylimine})\}-NiBr_2\}$ with the oligomeric “butadiene-magnesium” reagent^[12] gave the known (η^4 -butadiene)nickel complex (**8a**; Scheme 3).^[13] The addition of $B(C_6F_5)_3$ ^[14] to **8a** took place cleanly to yield the chelate complex **9a** (81 % yield of isolated



Scheme 3. Formation of the catalysts **9a** and **9b** for the polymerization of ethylene.

product). Single crystals of **9a** for the X-ray structure analysis were obtained from benzene (Figure 1). The structure of **9a** shows the presence of the bis(imine) chelate ligand stabilizing the central Ni atom (Ni–N1 1.920(1), Ni–N2 1.951(1) Å). The C=N bonds in the five-membered metallacycle are short (C11–N1/C21–N2 1.289(2), C11–C21 1.493(2) Å). The planes of the bulky aryl groups are rotated considerably from the plane of the central metallacycle, but in different directions (dihedral angles C14–C13–N1–C11 $-107.4(2)^\circ$, C24–C23–N2–C21 $76.0(2)^\circ$), a structural feature that evidently occurs because of the unsymmetrical substitution pattern at the remaining ligand at the Ni center. The bulky $B(C_6F_5)_3$ reagent adds regioselectively at the terminal C4 carbon atom of the former butadiene ligand (C4–B 1.672(3) Å); the *cisoid* arrangement of the butadiene framework is preserved. Thus **9a** contains an *anti*-configured monosubstituted η^3 -allyl ligand (*Z*-configured at the C2–C3 bond). The bulky borate group is rotated as much as possible away from the core of the nickel complex^[15] (Ni–C3–C4–B $176.0(1)^\circ$, the Ni–C4 distance is 2.803(2) Å). The Ni–C1 (2.007(2) Å) and Ni–C3 bonds (2.048(2) Å) are slightly longer than the central Ni–C2 bond (1.968(2) Å) of the (π -allyl)nickel group. C1 and C3 of the π -allyl group lie almost in the bis(imine)nickel plane (N1–Ni–C3 $169.1(1)^\circ$, N2–Ni–C1 $172.4(1)^\circ$). The C1–C2 and C2–C3 bonds are equal in length (1.401(3) Å, C1–C2–C3 $120.4(2)^\circ$), the C3–C4 bond as expected is longer (1.490(3) Å).

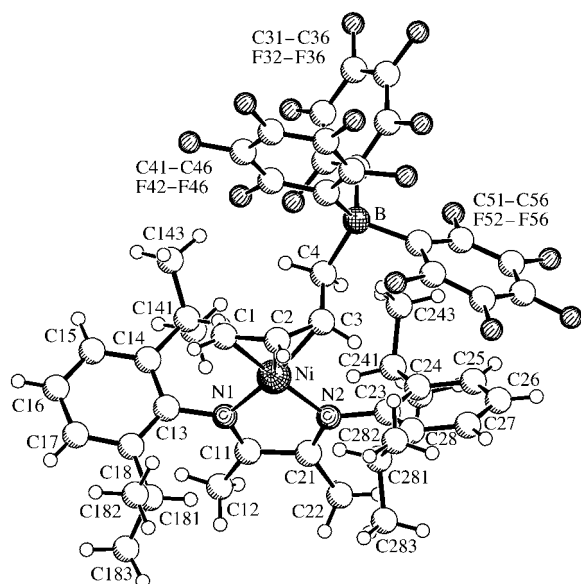


Figure 1. Structure of complex **9a**. Selected bond lengths [Å] and angles [°]: Ni–C1 2.007(2), Ni–C2 1.968(2), Ni–C3 2.048(2), Ni–C4 2.803(2), Ni–N1 1.920(1), Ni–N2 1.951(1), C1–C2 1.401(3), C2–C3 1.401(3), C3–C4 1.490(3), C4–B 1.672(3), B–C31 1.659(3), B–C41 1.665(3), B–C51 1.653(3), N1–C13 1.448(2), N1–C11 1.289(2), C11–C21 1.493(2), C21–N2 1.289(2), N2–C23 1.449(2); C1–Ni–C2 41.3(1), C1–Ni–C3 73.7(1), C1–Ni–N1 103.5(1), C1–Ni–N2 172.4(1), C2–Ni–C3 40.8(1), C2–Ni–N1 141.2(1), C2–Ni–N2 131.4(1), C3–Ni–N1 169.1(1), C3–Ni–N2 101.1(1), N1–Ni–N2 82.7(1), Ni–C1–C2 67.9(1), Ni–C2–C1 70.9(1), Ni–C2–C3 72.7(1), Ni–C3–C2 66.5(1), Ni–C3–C4 103.7(1), C1–C2–C3 120.4(2), C2–C3–C4 127.2(2), C3–C4–B 114.4(1), C13–N1–Ni 124.7(1), C11–N1–Ni 114.5(1), C11–N1–C13 120.8(1), N1–C11–C21 114.5(2), C11–C21–N2 114.2(1), C23–N2–Ni 126.2(1), C21–N2–Ni 113.4(1), C21–N2–C23 120.2(1); for further values see text.

NMR spectra indicate an analogous structure of complex **9a** in solution. The signal patterns of the two bis(imine) ligands differ owing to the presence of the substituted η^3 -allyl ligand (^1H and ^{13}C NMR: signals of the methyl groups at $\delta = 1.16/1.15$ and $19.5/18.4$ ppm, respectively). The π -allyl group shows characteristic ^{13}C NMR resonances at $\delta = 54.3$ (C1), 110.9 (C2), and 100.7 ppm (C3), and there is a broad signal ($\delta = 26$ ppm) corresponding to the C4 atom bound to the boron atom. The ^1H NMR spectrum of **9a** shows the typical signals for π -allyl groups at $\delta = 2.57$ (1- H_{syn}), 2.69 (1- H_{anti}), and 4.88 (2- H_{meso}) with typical coupling constants of 7.2 Hz ($^3J(\text{H}_{\text{syn}}, \text{H}_{\text{meso}})$) and 14.3 Hz ($^3J(\text{H}_{\text{anti}}, \text{H}_{\text{meso}})$), and signals of the diastereotopic hydrogen atoms 4-H/4-H' at $\delta = 2.00$ and 1.03 ppm. The acenaphthenequinonebis(imine)-derived complex **9b** was prepared analogously. It shows very similar spectroscopic features, and thus must be considered to have an analogous *anti*-configured π -allyl unit.

Complexes **9a** and **9b** are active Ziegler–Natta single-component catalysts for ethylene polymerization, which do not require the presence of an additional activator component; however, some triisobutylaluminum was added as a “scrubbing agent” in the experiments on a preparative scale, as is usually done to prevent catalyst deactivation by hydrolysis pathways at the very low metal complex concentrations that were employed. At 25 °C and a monomer pressure of 2 bar, polyethylene (PE) was formed with the **9a** catalyst with an activity (*a*) of 159 kg(PE)mol(Ni) $^{-1}$ h $^{-1}$ bar(ethene) $^{-1}$. The catalyst **9b** is

only slightly less active under the same conditions (*a* = 106). The resulting polyethylene has a branched structure, as typically formed with such homogeneous organometallic Ziegler–Natta nickel catalysts.^[2, 16]

The catalysts **9a** and **9b** are the first examples of the successful application of the metal/butadiene/borane activation method to generate active homogeneous Ziegler–Natta catalyst systems based on typical late transition metal complexes. The isolated and structurally characterized complexes may be structurally and chemically related to the active intermediates in the recently disclosed “alkyl group free” Ziegler–Natta systems (Scheme 2).^[7, 8] It appears that the addition of an activator component, such as $\text{B}(\text{C}_6\text{F}_5)_3$ or even potentially MAO, to a suitable metal alkene π complex might be a suitable general method for forming (or generating in situ) active homogeneous Ziegler–Natta-type catalysts for alkene polymerization.

Experimental Section

9a: A solution of $\text{B}(\text{C}_6\text{F}_5)_3$ (198 mg, 387 μmol) in toluene (15 mL) was added dropwise with stirring to a solution of the butadienenickel complex **8a** (200 mg, 387 μmol) in toluene (15 mL) at -78°C . The mixture was warmed to room temperature and then stirred for 2 h. The solvent was removed in vacuo and the residue suspended in pentane (20 mL). The product was collected by filtration, washed with pentane (2×20 mL), and dried in vacuo. Yield of **9a**: 321 mg (81%), m.p. 212 °C (decomp); elemental analysis (%) calcd for $\text{C}_{50}\text{H}_{46}\text{BF}_{15}\text{N}_2\text{Ni}$ (1029.4): C 58.34, H 4.50, N 2.72; found: C 58.64, H 4.81, N 2.76; ^1H NMR ($[\text{D}_8]\text{toluene}$, 600 MHz, 298 K): $\delta = 7.26$ (t, 1H), 7.09 (d, 1H), 7.05 (m, 2H), 6.96 (2d, 2H; aryl), 4.88 (m, 1H; $^3J = 14.3$ Hz and 7.2 Hz, allyl 2-H), 4.21 (br., 1H; 3-H), 2.69 (d, 1H; 1- H_{anti}), 2.57 (d, 1H; 1- H_{syn}), 2.00, 1.03 (br. each 1H, 4-H/H') 3.73, 2.98, 2.64, 2.29 (sept., each 1H; $-\text{CHMe}_2$), 1.57, 1.49, 1.12, 1.01, 0.98, 0.97, 0.92, 0.77 (d, each 3H; $-\text{CH}(\text{CH}_3)_2$), 1.16, 1.15 ppm (s, 3H each, $\text{N}=\text{C}-\text{CH}_3$); ^{13}C NMR ($[\text{D}_6]\text{benzene}$, 150.8 MHz, 298 K): $\delta = 173.1$, 172.5 ($-\text{C}=\text{N}-$), 148.1 ($^1J_{\text{CF}} = 240$ Hz), 138.4 ($^1J_{\text{CF}} = 250$ Hz), 136.7 ($^1J_{\text{CF}} = 250$ Hz); *o*-, *p*-, *m*- $\text{B}(\text{C}_6\text{F}_5)_3$), 143.1, 141.1 (arom. C1), 138.2, 137.6, 137.5, 136.0 (arom. C2, C6), 128.0, 127.8, 124.2, 124.1, 123.8, 123.5 (arom. CH), 110.9 (allyl-C2), 100.7 (C3), 54.3 (C1), ~ 26 (br., C4), 30.6, 29.5, 29.1, 28.6 ($-\text{CHMe}_2$), 24.4, 24.2, 24.0, 23.9, 23.3, 22.7, 22.2, 22.1 ($-\text{CH}(\text{CH}_3)_2$), 19.5, 18.4 ppm ($-\text{N}=\text{C}-\text{CH}_3$).

X-ray crystal structure analysis of **9a**: $\text{C}_{50}\text{H}_{46}\text{BF}_{15}\text{N}_2\text{Ni} \cdot 0.5\text{C}_6\text{H}_6$, $M_r = 1068.46$, dark red crystal $0.50 \times 0.40 \times 0.30$ mm, $a = 14.550(1)$, $b = 23.070(1)$, $c = 15.141(1)$ Å, $\beta = 99.91(1)^\circ$, $V = 5006.5(5)$ Å 3 , $\rho_{\text{calcd}} = 1.418$ g cm $^{-3}$, $\mu = 4.82$ cm $^{-1}$, empirical absorption correction via SORTAV ($0.795 < T < 0.869$), $Z = 4$, monoclinic, space group $P2_1/n$ (no. 14), $\lambda = 0.71073$ Å, $T = 198$ K, ω and φ scans, 31 004 reflections collected ($\pm h, k, l$), $(\sin \theta)/\lambda = 0.65$ Å $^{-1}$, 11 452 independent ($R_{\text{int}} = 0.035$) and 9345 observed reflections ($I > 2\sigma(I)$), 659 refined parameters, $R = 0.040$, $wR^2 = 0.93$, max. residual electron density ± 0.43 e Å $^{-3}$, hydrogen atoms calculated and refined as riding atoms. Data set was collected with a Nonius Kappa CCD diffractometer, equipped with a rotating anode generator Nonius FR 591, for programs used see reference [17].

CCDC-180390 contains the supplementary crystallographic data for this paper. These data can be obtained free of charge via www.ccdc.cam.ac.uk/conts/retrieving.html (or from the Cambridge Crystallographic Data Centre, 12 Union Road, Cambridge CB2 1EZ, UK; fax: (+44) 1223-336033; or deposit@ccdc.cam.ac.uk).

9b: Treatment of **8b** (200 mg, 326 μmol) with $\text{B}(\text{C}_6\text{F}_5)_3$ (16.7 mg, 326 μmol) was carried out analogously to that for **9a**. Yield **9b**: 334 mg (91%), m.p. 182 °C (decomp); elemental analysis (%) calcd for $\text{C}_{50}\text{H}_{46}\text{BF}_{15}\text{N}_2\text{Ni}$ (1125.5): C 61.90, H 4.12, N 2.49; found: C 62.09, H 4.57, N 2.40; ^1H NMR ($[\text{D}_6]\text{benzene}$, 600 MHz, 298 K): $\delta = 7.40$ (t, 1H), 7.20 (d, 1H), 7.19–7.13 (m, 4H; Ph), 7.13, 7.08, 6.62, 6.59, 6.54, 6.47 (acenaphth. H), 5.10 (1H; allyl 2-H), 4.64 (1H; 3-H), 2.99 (1H; 1- H_{anti}), 2.87 (1H; 1- H_{syn}), 2.32, 1.45 (br., each 1H; 4-H/H'), 4.04, 3.41, 3.17, 2.84 (sept., each 1H; $-\text{CHMe}_2$), 1.57, 1.53, 1.45, 1.20, 1.03, 0.96, 0.77, 0.74 ppm (d, each 3H; $-\text{CH}(\text{CH}_3)_2$).

Polymerization reactions: A 1-L glass autoclave was charged with toluene (200 mL) and triisobutylaluminum (0.5 mL). The mixture was stirred (700 rpm), thermostated at 25 °C, and saturated with ethylene (2 bar). The polymerization reaction was started by the injection of a solution of the respective zwitterionic complex in toluene, generated in situ by treatment of **8a** or **8b** (ca. 35 μ mol) with an equimolar amount of $B(C_6F_5)_3$ in toluene (8 mL). After 1 h the reaction was quenched by adding aqueous HCl in methanol (15 mL). The polymer was precipitated with additional methanol (100 mL), collected by filtration, washed with 6N aqueous HCl (100 mL), water (200 mL), acetone (50 mL), and then dried in vacuo.

Received: March 20, 2002 [Z18937]

- [1] H.-H. Brintzinger, D. Fischer, R. Mülhaupt, B. Rieger, R. M. Waymouth, *Angew. Chem.* **1995**, *107*, 1255–1283; *Angew. Chem. Int. Ed. Engl.* **1995**, *34*, 1143–1170.
- [2] G. J. P. Britovsek, V. C. Gibson, D. F. Wass, *Angew. Chem.* **1999**, *111*, 448–468; *Angew. Chem. Int. Ed.* **1999**, *38*, 428–447; S. D. Ittel, L. K. Johnson, M. Brookhart, *Chem. Rev.* **2000**, *100*, 1169–1203.
- [3] X. Yang, C. L. Stern, T. J. Marks, *J. Am. Chem. Soc.* **1994**, *116*, 10015–10031.
- [4] H. Sinn, W. Kaminsky, *Adv. Organomet. Chem.* **1980**, *18*, 99–149; X. Yang, C. L. Stern, T. J. Marks, *J. Am. Chem. Soc.* **1991**, *113*, 3623–3625; J. C. W. Chien, W.-M. Tsai, M. D. Rausch, *J. Am. Chem. Soc.* **1991**, *113*, 8570–8571; M. Bochmann, A. J. Jaggar, J. C. Nicholls, *Angew. Chem.* **1990**, *102*, 830–832; *Angew. Chem. Int. Ed. Engl.* **1990**, *29*, 780–782; review: E. Y.-X. Chen, T. J. Marks, *Chem. Rev.* **2000**, *100*, 1391–1434.
- [5] B. Temme, G. Erker, J. Karl, H. Luftmann, R. Fröhlich, S. Kotila, *Angew. Chem.* **1995**, *107*, 1867–1869; *Angew. Chem. Int. Ed. Engl.* **1995**, *34*, 1755–1757; review: G. Erker, *Acc. Chem. Res.* **2001**, *34*, 309–317.
- [6] M. Dahlmann, G. Erker, M. Nissinen, R. Fröhlich, *J. Am. Chem. Soc.* **1999**, *121*, 2820–2828; M. Dahlmann, G. Erker, K. Bergander, *J. Am. Chem. Soc.* **2000**, *122*, 7986–7998.
- [7] T. M. Kooistra, Q. Knijnenburg, J. M. M. Smits, A. D. Horton, P. H. M. Budzelaar, A. W. Gal, *Angew. Chem.* **2001**, *113*, 4855–4858; *Angew. Chem. Int. Ed.* **2001**, *40*, 4719–4722.
- [8] V. C. Gibson, M. J. Humphries, K. P. Tellmann, D. F. Wass, A. J. P. White, D. J. Williams, *Chem. Commun.* **2001**, 2252–2253.
- [9] Electron transfer had previously been observed or used in activation processes of metallocene Ziegler–Natta catalysts: R. F. Jordan, *Adv. Organomet. Chem.* **1991**, *32*, 325–387.
- [10] For recent evidence of electron-transfer processes occurring in $B(C_6F_5)_3$ activation chemistry see, for example: C. J. Harlan, T. Hascall, E. Fujita, J. R. Norton, *J. Am. Chem. Soc.* **1999**, *121*, 7274–7275; C. J. Beddows, A. D. Burrows, N. G. Connelly, M. Green, J. M. Lynam, T. J. Paget, *Organometallics* **2001**, *20*, 231–233; R. J. Kwaan, C. J. Harlan, J. R. Norton, *Organometallics* **2001**, *20*, 3818–3820.
- [11] For a formally related homogeneous alkyl-free Group 4 metal Ziegler–Natta catalyst see: J. Cano, P. Royo, M. Lanfranchi, M. A. Pellinghelli, A. Tiripicchio, *Angew. Chem.* **2001**, *113*, 2563–2565; *Angew. Chem. Int. Ed.* **2001**, *40*, 2495–2497; J. Jin, D. R. Wilson, E. Y.-x. Chen, *Chem. Commun.* **2002**, 708–709, and references therein.
- [12] H. Yasuda, Y. Kajihara, K. Mashima, K. Nagasuna, K. Lee, A. Nakamura, *Organometallics* **1982**, *1*, 388–396, and references therein.
- [13] J. C. M. Sinnema, G. H. B. Fendesak, H. tom Dieck, *J. Organomet. Chem.* **1990**, *390*, 237–250.
- [14] A. G. Massey, A. J. Park, *J. Organomet. Chem.* **1964**, *2*, 245–250; A. G. Massey, A. J. Park in *Organometallic Synthesis*, Vol. 3, (Eds.: R. B. King, J. J. Eisch), Elsevier, New York, **1986**, p. 461.
- [15] For structurally related metallocene complexes with metals of Group 4 see: J. Karl, G. Erker, R. Fröhlich, *J. Organomet. Chem.* **1997**, *535*, 59–62; M. Dahlmann, G. Erker, R. Fröhlich, O. Meyer, *Organometallics* **2000**, *19*, 2956–2967.
- [16] The resulting polyethylene contains mostly methyl branches, as expected: L. K. Johnson, C. M. Killian, M. Brookhart, *J. Am. Chem. Soc.* **1995**, *117*, 6414–6415; C. M. Killian, D. J. Tempel, L. K. Johnson, M. Brookhart, *J. Am. Chem. Soc.* **1996**, *118*, 11664–11665; C. M. Killian, L. K. Johnson, M. Brookhart, *Organometallics* **1997**, *16*,

2005–2007; B. L. Small, M. Brookhart, *J. Am. Chem. Soc.* **1998**, *120*, 7143–7144; S. A. Svejda, L. K. Johnson, M. Brookhart, *J. Am. Chem. Soc.* **1999**, *121*, 10634–10635; NMR characterization: G. B. Galland, R. F. de Souza, R. S. Mauler, F. F. Nunes, *Macromolecules* **1999**, *32*, 1620–1625.

- [17] Programs used: data collection COLLECT (B. V. Nonius, **1998**), data reduction Denzo-SMN (Z. Otwinowski, W. Minor, *Methods in Enzymol.* **1997**, *276*, 307–326), absorption correction SORTAV (R. H. Blessing, *Acta Crystallogr. Sect. A* **1995**, *51*, 33–37; R. H. Blessing, *J. Appl. Crystallogr.* **1997**, *30*, 421–426), structure solution SHELXS-97 (G. M. Sheldrick, *Acta Crystallogr. Sect. A* **1990**, *46*, 467–473), structure refinement SHELXL-97 (G. M. Sheldrick, Universität Göttingen, **1997**), graphics SCHAKAL (E. Keller, Universität Freiburg, **1997**).

Photoactivatable Synthetic Ras Proteins: “Baits” for the Identification of Plasma-Membrane-Bound Binding Partners of Ras**

Jürgen Kuhlmann,* Andreas Tebbe, Martin Völkert, Melanie Wagner, Koji Uwai, and Herbert Waldmann*

The regulation of cell growth and differentiation by proteins of the Ras superfamily^[1] requires the correct subcellular distribution of the small GTP-binding proteins (GTP = guanosine triphosphate).^[2] The biological function of Ras is strictly dependent on its correct translocation to the plasma membrane, and this localization is directly linked to posttranslational S-farnesylation and S-palmitoylation of Ras.^[3]

The real mechanism of translocation is still the subject of debate. On the one hand for K-Ras^B, which embodies a polycationic hexalysine stretch and a farnesyl thioether at the C terminus, a model was proposed in which unspecific but highly anionic “sites” (formed at least in part by the lipid bilayer) at the plasma membrane instead of a classical specific proteinaceous receptor are responsible for association of this Ras isoform with the plasma membrane.^[4] On the other hand for H- and N-Ras, which have S-farnesyl and S-palmitoyl substituents at the C terminus, a membrane-trapping model^[5] was postulated in which a prenyl protein specific palmitoyl-

- [*] Dr. J. Kuhlmann, Dipl.-Biochem. A. Tebbe, Dipl.-Biochem. M. Wagner
Max-Planck-Institut für molekulare Physiologie
Abteilung Strukturelle Biologie
Otto-Hahn-Strasse 11, 44227 Dortmund (Germany)
Fax: (+49) 231-133-1435
E-mail: juergen.kuhlmann@mpi-dortmund.mpg.de
Prof. Dr. H. Waldmann, Dipl.-Chem. M. Völkert, Dr. K. Uwai
Max-Planck-Institut für molekulare Physiologie
Abteilung Chemische Biologie
Otto-Hahn-Strasse 11, 44227 Dortmund (Germany)
and
Fb. 3, Organische Chemie, Universität Dortmund
Otto-Hahn-Strasse 6, 44227 Dortmund (Germany)
Fax: (+49) 231-133-2499
E-mail: herbert.waldmann@mpi-dortmund.mpg.de

[**] We thank Christine Nowak for excellent technical assistance, Lilianna Wielitzer for help with the UV exposure system, and Fred Wittinghofer for continuous encouragement. The work was supported by the Fonds der Chemischen Industrie and the Alexander von Humboldt Foundation.

transferase (PTase) is located in the plasma membrane. However, these proposals have been challenged by recent findings that suggest that K-Ras and H-/N-Ras traffic to the cell surface through different routes and that palmitoyl substitution of the H- and N-isoform occurs in the endoplasmic reticulum.^[6]

In addition, the correlation of subcompartmentation of the plasma membrane^[7] with signal transduction events has received increasing attention. Thus, H-Ras is enriched in membrane domains with high levels of sphingolipids and cholesterol (rafts),^[8] whereas K-Ras shows a random distribution in the plasma membrane.^[6] To unravel the mechanisms that direct Ras localization and to identify putative binding partners of Ras in the plasma membrane or other intracellular compartments, new tools that go beyond the techniques available from regular biological methodology alone are urgently needed.

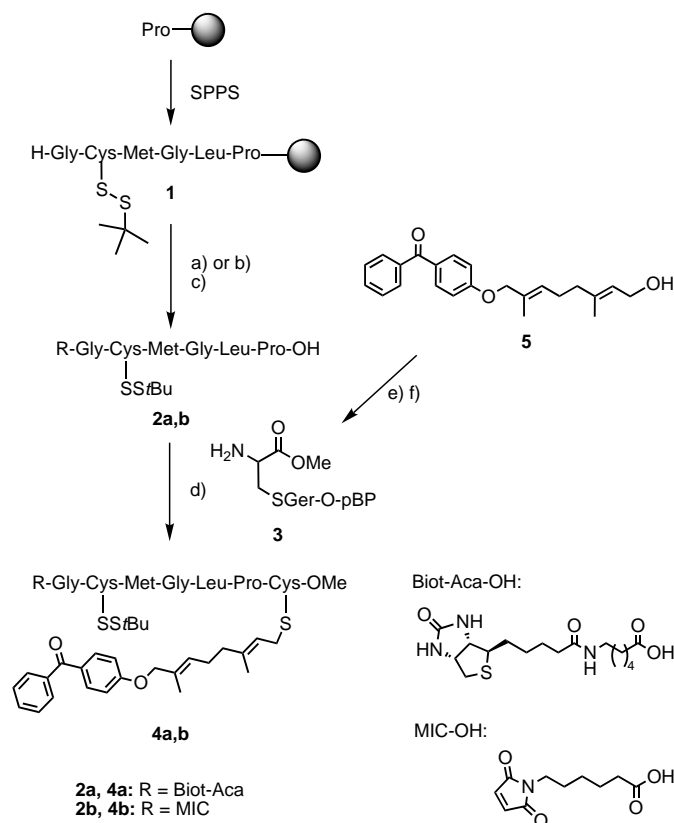
In addressing this challenge, we have synthesized Ras lipopeptides and a Ras protein that incorporate a photoactivatable isoprenoid thioether. Our evaluations demonstrated that the lipopeptides will be suitable "baits" for covalent coupling of proteins, whereas the protein construct demonstrated biological activity required to trap Ras binding partners.

As suitable chemical tools for covalent trapping and identification of possible membrane-embedded binding partners of the Ras-proteins, lipopeptides were considered that meet the following requirements:

1. They should embody the characteristic C-terminal amino acid sequence of the Ras protein that is in contact with the membrane and most likely also with a putative binding partner. To fulfill this criterion, the C-terminal heptapeptide sequence of N-Ras was chosen which terminates in a S-farnesyl-substituted cysteine methyl ester.^[9]
2. The peptides should be selectively localized to and stably inserted into the plasma membrane of cells, in our case by insertion of a palmitoylatable cysteine residue that is located at the C terminus of N-Ras. This cysteine was masked as a *tert*-butyl disulfide, which can be cleaved readily by treatment with dithiothreitol. The cysteine thiol functional group liberated is readily derivatized with a palmitoyl group, and the resulting S-palmitoyl- and S-farnesyl-substituted Ras peptide is selectively localized at the plasma membrane.^[10, 11]
3. The conjugate should contain a group that can be photoactivated,^[12] preferably incorporated into the membrane-embedded isoprenoid residue. For this purpose the benzophenone group (BP) was chosen as an established photophore.^[13, 14]
4. They should carry a group that allows the isolation and detection of the covalently crosslinked products by established methods. For this purpose the biotin label was chosen because it can serve both as a tag for product enrichment and as a detection label.
5. The synthesis strategy should give access to photoactivatable lipopeptides for the labeling experiments and to protein–lipopeptide conjugates, which can be used to determine the activity of the lipopeptides. The maleimidecaproic acid (MIC) group was chosen to couple the

lipopeptide to a Ras mutant with a C-terminal cysteine residue.^[15, 16] Such peptides were required to demonstrate that the conjugate is selectively directed to the plasma membrane and that the photophore does not significantly influence the binding to a putative Ras binding protein, if at all.

These criteria are met by the peptides **4a** and **4b**, which were synthesized as shown in Scheme 1. The N-terminal hexapeptide of the Ras sequence was synthesized efficiently



Scheme 1. Solid-phase synthesis of the hexapeptides **2a/b** and fragment coupling with the BP-labeled isoprenyl-derivatized cysteine **3**. a) Biot-Aca-OH, HBTU, HOBT, DIPEA, DMF; b) MIC-OH, HBTU, HOBT, DIPEA, DMF; c) TFA in CH_2Cl_2 (10 %), **2a**: 62 %, **2b**: 33 %; d) **3**, EDCl, HOBT, CH_2Cl_2 , **4a**: 43 %, **4b**: 55 %; e) NCS, DMS, CH_2Cl_2 ; f) CysOMe · HCl, NH_3 , MeOH, 66 % over two steps. BP = benzophenone, SPPS = solid-phase peptide synthesis, DEAD = diethylazodicarboxylate, HBTU = 2-(1*H*-benzotriazole-1-yl)-1,1,3,3-tetramethyluronium hexafluorophosphate, HOBT = 1-hydroxybenzotriazole, DIPEA = diisopropylethylamine, DMF = *N,N*-dimethylformamide, DMS = dimethyl sulfide, EDCl = 1-ethyl-3-(3-dimethylaminopropyl)carbodiimide hydrochloride, NCS = *N*-chlorosuccinimide.

on a solid support. The peptide was linked to the polymeric carrier through the chlorotriptyl (chlorotriphenylmethyl) linker, and Fmoc-protected amino acids were employed for chain elongation. After assembly of the hexapeptide and N-terminal deprotection, either biotinylaminocaproic acid (Biot-Aca-OH) or maleimidecaproic acid (MIC-OH) were introduced followed by release of the Biot-Aca- and MIC-labeled peptides **2a** and **2b** from the solid support. Both compounds were isolated in high yields and then coupled with the S-alkylated cysteine methyl ester **3** to yield the target peptides **4a** and **4b**. In **3** the terminal isoprene unit of the farnesyl

group has been replaced by the benzophenone photophore, which approximates it in size and lipophilicity. The lipid-modified and benzophenone-labeled cysteine methyl ester **3** was synthesized by conversion of allyl alcohol **5**^[17] into the corresponding allyl chloride and subsequent nucleophilic substitution with cysteine methyl ester (Scheme 1).

The synthesis strategy is both efficient and flexible. The chosen combination of solid-phase and solution synthesis and the assembly of the target peptides from building blocks that can be varied readily opens up the opportunity to generate a variety of further analogues rapidly if required. Furthermore, variation of the photophore is straightforward. Thus, a variety of suitable tools for further biological investigations can be generated efficiently by means of this approach. To investigate if the benzophenone isoprenoid groups could be applied to the photoaffinity labeling of Ras interaction partners, we performed exposure experiments with solutions of lipopeptide **4a** (1.6 μ M) and bovine serum albumin (BSA; 8 μ M). The reaction mixture was exposed to UV light and samples were taken before exposure to UV light, and after 5, 15, 30, and 60 min of exposure. The time course of the reaction was analyzed by SDS-PAGE and Western Blot. Biotinylated BSA was detected by incubation with a streptavidine–alkaline phosphatase conjugate and subsequent enzymatic reaction. The benzophenone moiety was stable in the absence of UV irradiation, whereas exposure to 300–400-nm light led to rapid photoactivation and coupling of the lipopeptide to BSA (Figure 1). Five minutes of exposure to UV light were sufficient for maximum biotinylation of the BSA sample.

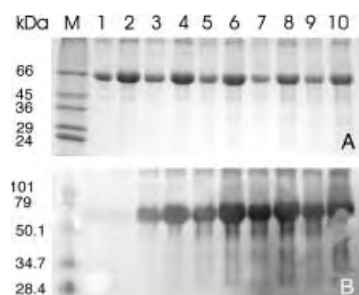


Figure 1. Coupling of biotinylated lipopeptide with BSA. A solution of lipopeptide **4a** (10 μ M) and a fivefold excess of BSA were exposed to UV light, and samples were taken before (1, 2) and 5 min (3, 4), 15 min (5, 6), 30 min (7, 8), and 60 min (9, 10) after start of irradiation. Aliquots corresponding to 3 μ g (1, 3, 5, 7, 9) and 5 μ g (2, 4, 6, 8, 10) of BSA were applied in SDS-PAGE (A) and Western Blot (B).

Utilization of lipopeptides with a benzophenone isoprenoid group for the affinity labeling of Ras-interaction proteins requires that the replacement of the farnesyl group by a geranyl benzophenone moiety does not prevent the recognition of the lipopeptides by receptors or modifying enzymes for Ras. We generated a lipoprotein by coupling oncogenic N-Ras mutant N-RasG12V Δ 181 (which has a truncated C terminus) with lipopeptide **4b** (which corresponds to the native C-terminus of N-Ras with a free palmitoylation site and a geranyl benzophenone instead of the farnesyl thioether at the last amino acid residue) as shown in Scheme 1. The reaction of the MIC group of the lipopeptide with the free cysteine

residue at position 181 of the N-Ras mutant proceeded almost quantitatively.

N-RasG12V Δ 181 terminates in a free cysteine residue, which selectively reacts with the MIC group. The coupling product was extracted by treatment with Triton-X114 and purified by ion-exchange chromatography. Gel electrophoresis gave a single band for the hydrophobic protein (Figure 2). Mass spectrometric analysis (Figure 3) gave rise to signals for the coupling product without the *S*-*tert*-butyl protecting group at the cysteine group, which can be substituted with a palmitoyl group (N-RasG12V^{CysGerBP}, 21 659 Da), and a smaller signal for the coupling product with the protecting group (21 747 Da). These data verify a 1:1 stoichiometry for the protein–lipopeptide coupling product. Specific reaction of MIC lipopeptide **4b** with the C-terminal cysteine (Cys181) of N-RasG12V Δ 181 was validated by tryptic digestion of the chimeric protein with trypsin and chymotrypsin. ESI-MS and MALDI-TOF analysis of the proteolytic products excluded significant formation of lipopeptide thioethers with Cys51, Cys80, or Cys118 of N-RasG12V Δ 181 (data not shown).

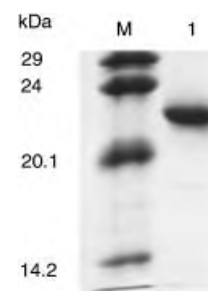


Figure 2. Characterization of the coupling product of N-RasG12V Δ 181 with lipopeptide **4a** by SDS-PAGE. SDS-PAGE of the coupling product shows a protein band with an apparent mass of 22 kDa and a purity > 90%.

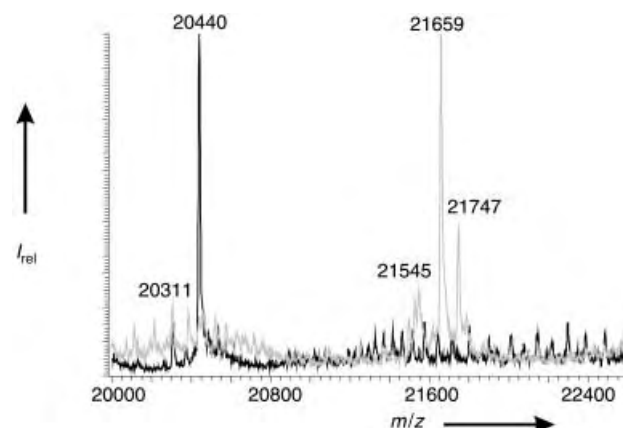


Figure 3. Characterization of the coupling product of N-RasG12V Δ 181 with lipopeptide **4a** by ESI MS. Mass spectra of N-RasG12V Δ 181 (black) and the coupling product of N-RasG12V Δ 181 with lipopeptide **4a** (gray). The base peak in the spectra corresponds to the theoretical mass of the N-RasG12V Δ 181 that has been truncated at the C terminus (20 440 Da). The minor peak at 20 311 Da can be assigned to N-RasG12V Δ 181 without the N-terminal Met1 (theoretical mass: 20 309 Da). The MS spectrum of the coupling product shows a major peak at 21 659 Da and a minor peak at 21 747 Da. These signals match the masses of the coupling product N-RasG12V Δ 181–**4a** after and before removal of the *S*-*tert*-butyl protecting group, respectively.

The rat pheochromocytoma cell line PC12 can be induced to differentiate by oncogenic Ras mutants.^[18] This effect can be correlated to the transforming potential of Ras mutants in a microinjection assay.^[19] To ensure that benzophenone lipopeptides are applicable as photoaffinity probes for the identification of Ras receptors and modifiers, we analyzed the

differentiating potential of the oncogenic coupling product of N-RasG12V Δ 181 and the benzophenone lipopeptide **4b** and compared it with the efficiency of N-RasG12V full-length protein and the “natural” chimera with a C-terminal farnesyl thioether (N-RasG12V^{CysFar}) to induce the corresponding morphological pattern in PC12 cells. Gratifyingly, the lipoprotein with the benzophenone isoprenoid moiety induced neurite-like outgrowths in PC12 cells (Figure 4), thus indicating biological activity of the protein. This result implies that the construct with a geranyl benzophenone thioether and a carboxymethylation at the C terminus is sufficient to address the oncogenic chimera to its functional location, which includes palmitoylation of the free cysteine of the lipopeptide moiety.

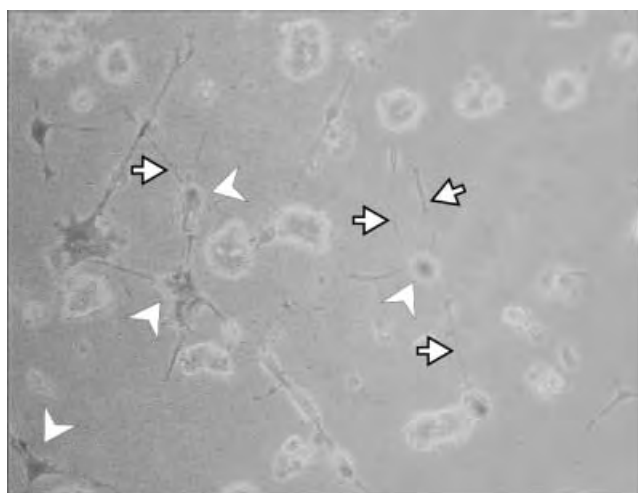


Figure 4. Differentiation of PC12 cells by N-RasG12V^{CysGerBP}. Overlay of a phase contrast and fluorescence microscopy image of PC12 cells after co-injection of 100 μ M oncogenic Ras construct and FITC-dextran. Only cells with a fluorescent marker (dark cell body, white arrowheads) have formed neurite-like outgrowths (black-bordered white arrows). FITC = fluorescein isothiocyanate.

The data show that the potential of the benzophenone derivative to induce neurite-like outgrowths is approximately one third of the values recorded for N-RasG12V (full length) or N-RasG12V^{CysFar} (Figure 5). This activity is sufficient to allow the successful execution of biological experiments, including photoactivation studies.

Our results demonstrate that introduction of a benzophenone group as a photoactivatable ligand in the isoprenoid moiety of Ras-lipopeptides does not obstruct the ability of a corresponding oncogenic Ras-lipoprotein chimera to differentiate PC12 cells. Furthermore, photochemical activation of the benzophenone can be initiated by exposure to near-UV light (350–360 nm), thus limiting photodamage of the protein targets. Therefore, probes such as peptide **4a** with the C-terminal peptide sequence of Ras-proteins, a benzophenone isoprenoid substitution of the farnesyl group, and a suitable affinity tag (e.g. biotin) are promising tools for the isolation of Ras-modifying enzymes and Ras-interaction partners, in particular of plasma-membrane-localized proteins.

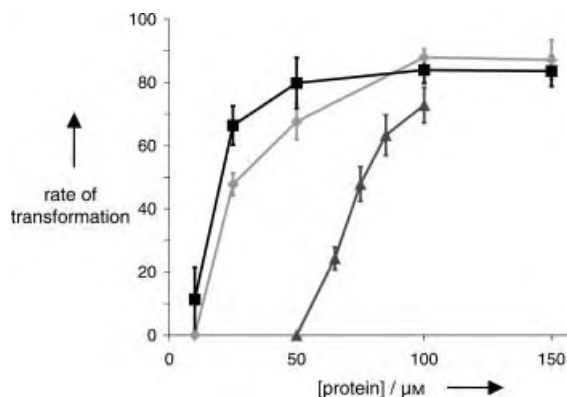


Figure 5. Differentiation efficiency of oncogenic N-Ras constructs. PC12 cells were microinjected with a protein solution that contained N-RasG12V^{CysGerBP} (▲), N-RasG12V^{CysFar} (◆), and full-length N-RasG12V (■) in the given concentrations.

Studies with green fluorescent protein constructs of Ras proteins have promoted the idea that it is the hydrophobically modified C terminus of the Ras isoforms that determines targeting and localization,^[6, 20] whereas the G domain is less important for targeting the protein. The Ras C terminus is flexible and was not resolved in the crystal structures of the protein^[21, 22] and its complexes^[23] nor in the NMR spectroscopic analysis of H-Ras.^[24] Therefore, it is most probable that affinity tags presenting the Ras C terminus are sufficient for recognition by and binding to putative receptors and modifiers.

By combining the power of organic synthesis with cell biology numerous synthetic lipopeptide and lipoprotein “baits” are accessible. For instance different natural or non-natural hydrophobic modifications, alternative affinity tags, or radiolabels may be introduced or the entire peptide backbone may be replaced by a nonpeptide scaffold, thereby opening up a multitude of possible applications. The combination of chemical synthesis, cell biology, and elaborated biochemical and mass spectrometric approaches delineated herein should provide a new powerful approach to solve some of the most prevailing problems and answer open questions concerning signal transduction through Ras proteins.

Received: January 7, 2002 [Z18487]

- [1] L. Van Aelst, M. Barr, S. Marcus, Polverino, A. M. Wigler, *Proc. Natl. Acad. Sci. USA* **1993**, 90, 6213–6217.
- [2] A. Wittinghofer, *Biol. Chem.* **1998**, 379, 933–937.
- [3] A. Wittinghofer, H. Waldmann, *Angew. Chem.* **2000**, 112, 4360–4383; *Angew. Chem. Int. Ed.* **2000**, 39, 4193–4214.
- [4] M. O. Roy, R. Leventis, J. R. Silvius, *Biochemistry* **2000**, 39, 8298–8307.
- [5] S. Shahinian, J. R. Silvius, *Biochemistry* **1995**, 34, 3813–3822.
- [6] A. Apolloni, I. A. Prior, M. Lindsay, R. G. Parton, J. F. Hancock, *Mol. Cell. Biol.* **2000**, 20, 2475–2487.
- [7] D. A. Brown, E. London, *J. Biol. Chem.* **2000**, 275, 17221–17224.
- [8] S. Roy, R. Luetterforst, A. Harding, A. Apolloni, Etheridge, M. E. Stang, B. Rolls, J. F. Hancock, R. G. Parton, *Nat. Cell Biol.* **1999**, 1, 98–105.
- [9] J. F. Hancock, A. I. Magee, J. E. Childs, C. J. Marshall, *Cell* **1989**, 57, 1167–1177.
- [10] H. Waldmann, M. Schelhaas, E. Nagele, J. Kuhlmann, A. Wittinghofer, Schroeder, J. R. Silvius, *Angew. Chem.* **1997**, 109, 2334–2337; *Angew. Chem. Int. Ed. Engl.* **1997**, 36, 2238–2241.

- [11] H. Schroeder, R. Leventis, S. Rex, M. Schelhaas, E. Nagele, H. Waldmann, J. R. Silvius, *Biochemistry* **1997**, *36*, 13102–13109.
- [12] F. Kotzyba-Hibert, I. Kapfer, M. Goeldner, *Angew. Chem.* **1995**, *107*, 1391–1408; *Angew. Chem. Int. Ed. Engl.* **1995**, *34*, 1296–1312.
- [13] T. A. Kale, C. Raab, N. Yu, D. E. Dean, M. D. Distefano, *J. Am. Chem. Soc.* **2001**, *123*, 4373–4381.
- [14] G. Dorman, G. D. Prestwich, *Trends Biotechnol.* **2000**, *18*, 64–77.
- [15] B. Bader, K. Kuhn, D. J. Owen, H. Waldmann, A. Wittinghofer, J. Kuhlmann, *Nature* **2000**, *403*, 223–226.
- [16] K. Kuhn, D. J. Owen, B. Bader, A. Wittinghofer, J. Kuhlmann, H. Waldmann, *J. Am. Chem. Soc.* **2001**, *123*, 1023–1035.
- [17] D. M. Marecak, Y. Horiuchi, H. Arai, M. Shimonaga, Y. Maki, T. Koyama, K. Ogura, G. D. Prestwich, *Bioorg. Med. Chem. Lett.* **1997**, *7*, 1973–1978.
- [18] D. Bar-Sagi, J. R. Feramisco, *Cell* **1985**, *42*, 841–848.
- [19] R. H. Cool, G. Schmidt, C. U. Lenzen, H. Prinz, D. Vogt, A. Wittinghofer, *Mol. Cell. Biol.* **1999**, *19*, 6297–6305.
- [20] E. Choy, V. K. Chiu, J. Silletti, M. Feoktistov, T. Morimoto, D. Michaelson, I. E. Ivanov, M. R. Philips, *Cell* **1999**, *98*, 69–80.
- [21] A. M. de Vos, L. Tong, M. V. Milburn, P. M. Matias, J. Jancarik, S. Noguchi, S. Nishimura, K. Miura, E. Ohtsuka, S. H. Kim, *Science* **1988**, *239*, 888–893.
- [22] E. F. Pai, W. Kabsch, U. Krengel, K. C. Holmes, J. John, A. Wittinghofer, *Nature* **1989**, *341*, 209–214.
- [23] K. Scheffzek, M. R. Ahmadian, W. Kabsch, L. Wiesmuller, A. Lautwein, F. Schmitz, A. Wittinghofer, *Science* **1997**, *277*, 333–338.
- [24] K. Yamasaki, G. Kawai, Y. Ito, Y. Muto, J. Fujita, T. Miyazawa, S. Nishimura, S. Yokoyama, *Biochem. Biophys. Res. Commun.* **1989**, *162*, 1054–1062.

Bismuthine BiH₃: Fact or Fiction? High-Resolution Infrared, Millimeter-Wave, and Ab Initio Studies**

Wolfgang Jerzembeck, Hans Bürger,*
Lucian Constantin, Laurent Margulès, Jean Demaison,
Jürgen Breidung, and Walter Thiel

Standard Inorganic Chemistry textbooks^[1] report that bismuthine, BiH₃, is a common although unstable Group 15 hydride. Typically only the boiling point^[2] of +16.8°C is mentioned for characterization. Apart from the early observation of a “volatile bismuth hydride” by Paneth in 1918,^[3] its relevance in analytical chemistry,^[4] and a mass spectrometric

study,^[5] all experimental information on BiH₃ (synthesis, isolation, and vapor pressure) originates from the report by Amberger in 1961.^[2] To the best of our knowledge nobody has to date been able to repeat Amberger’s (admittedly presumptuous) synthesis of BiH₃ by decomposition of CH₃BiH₂ at –55 to –45°C, or to develop an alternative route to this compound. Hence, unlike the case of the short-lived monohydride BiH,^[6] neither the structure nor the vibrational spectrum of BiH₃ have been determined experimentally.

We report herein the successful repetition of Amberger’s synthesis of BiH₃ and its unambiguous characterization by independent, modern spectroscopic methods, which are supported by ab initio calculations. Our particular interest in BiH₃ concerns those structural and spectroscopic properties that are expected to be unique for BiH₃. First, BiH₃ should have the smallest H–X–H bond angle (ca. 90.0°) of any of the hydrides of the composition XH₂ and XH₃ (Figure 1). In the vibrational ground state, BiH₃ should thus be an oblate symmetric top ($I_a = I_b < I_c$) extremely close to the spherical top ($I_a = I_b = I_c$) limit, even more so than SbH₃.^[7] In vibrationally excited states it may switch to a prolate symmetric top with $I_a < I_b = I_c$. Therefore it should reveal, with unprecedented distinction, particular ground and excited state rotational energy patterns that require appropriate reductions of the rotational–vibrational Hamiltonian.^[8] Owing to the near-rectangular H–Bi–H angle, the heavy central atom, the expected small HBi/BiH’ coupling, and the large anharmonicity of the BiH stretching motion, BiH₃ would also be a prototype molecule for local mode behavior.^[9]

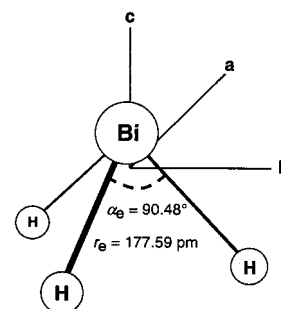


Figure 1. Molecular structure of BiH₃ with principal axes of inertia indicated; α_e , r_e = bond angle and length in the equilibrium structure.

After numerous failures we were able to repeat the reported synthesis^[2] and eventually obtained apparently pure BiH₃ in quantities sufficient to enable us to carry out gas-phase infrared (IR) and millimeter-wave (MMW) measurements over periods of minutes to hours. In brief, we first prepared Bi(CH₃)₃ from BiCl₃ and CH₃MgI, and then reacted this with BiCl₃ to give CH₃BiCl₂ by using standard procedures.^[10] CH₃BiCl₂ was then reduced with LiAlH₄ in di-*n*-butyl ether at –78°C to give CH₃BiH₂ whose disproportionation at –55 to –45°C yielded BiH₃ along with methylbismuthanes. Some hydrogen, which formed by decomposition of the hydrides, was pumped off while the reaction mixture was cooled by using liquid nitrogen. Thereafter this mixture was allowed to warm to about –50°C and volatile material expanded into cooled absorption cells until a total vapor pressure of between 10 and 100 Pa was reached.

IR spectra were recorded in the region for stretching fundamentals $\nu_1(A_1)/\nu_3(E)$ at about 1700 cm^{–1} with a resolution of 4.4×10^{-3} cm^{–1} (Figure 2), and in the region for bending modes $\nu_2(A_1)/\nu_4(E)$ at about 750 cm^{–1} with a resolution of 6.6×10^{-3} cm^{–1} (Figure 3).^[11] An external dou-

[*] Prof. Dr. H. Bürger, Dr. W. Jerzembeck
Anorganische Chemie
Bergische Universität Wuppertal
42097 Wuppertal (Germany)
Fax: (+49)202-439-2901
E-mail: buerger1@uni-wuppertal.de

Dr. L. Constantin, Dr. L. Margulès, Dr. J. Demaison
Laboratoire de Physique des Lasers, Atomes et Molécules
Université de Lille 1
59655 Villeneuve d’Ascq (France)
Dr. J. Breidung, Prof. Dr. W. Thiel
Max-Planck-Institut für Kohlenforschung
45470 Mülheim (Germany)

[**] We thank the German–French PROCOPE program and the PICS 599 project for support. We also thank Prof. H. Stoll, Stuttgart, for helpful discussions.

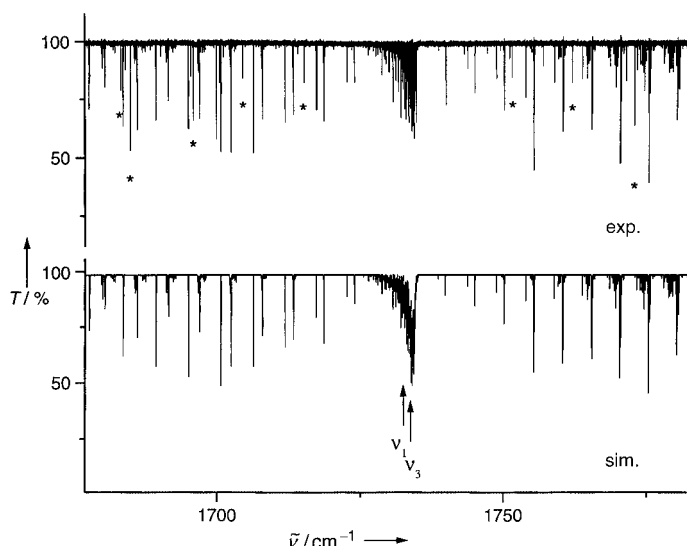


Figure 2. The ν_1 and ν_3 bands of BiH_3 . Lines denoted by an asterisk in the experimental spectrum (top) are attributed to residual H_2O in the interferometer. In the simulated spectrum (bottom) the band centers are indicated by arrows.

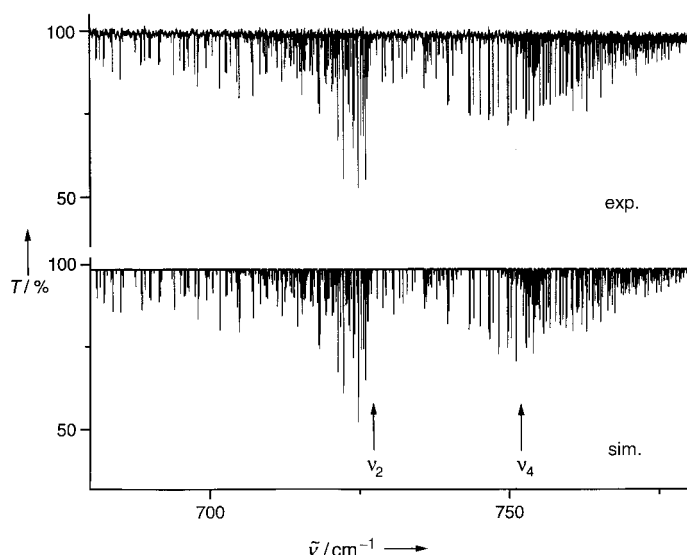


Figure 3. The ν_2 and ν_4 bands of BiH_3 : Experimental (top) and simulated spectrum (bottom; band centers are indicated by arrows).

ble-jacketed glass cell (inner diameter 70 mm, 120 cm long) equipped with NaCl windows and cooled to -40°C was used. At a total pressure of about 100 Pa data were collected for periods of 10–30 min before absorptions assignable to BiH_3 disappeared and it was necessary to recharge the cell. We confirm Amberger's observation^[2] that deposited metallic Bi accelerates the decomposition of BiH_3 significantly. Altogether 30 and 76 scans were collected in the ν_1/ν_3 and ν_2/ν_4 spectral regions, respectively. The analysis of the spectra established that essentially all observed absorption lines could be assigned to the ν_1 , ν_2 , ν_3 , and ν_4 bands of $^{209}\text{BiH}_3$ (Bi is a monoisotopic element).

Since the analysis of the spectra required highly accurate constants of the ground vibrational state we also measured rotational $J=1\leftarrow 0$, $2\leftarrow 1$, $4\leftarrow 3$, and $8\leftarrow 7$ transitions in the 158, 317, 633, and 1260 GHz ranges, respectively.^[12] The

$J=8\leftarrow 7$, $K=3^+$ transition is illustrated in Figure 4. The observed nuclear quadrupole hyperfine structure is in agreement with a spin $I=9/2$ for ^{209}Bi . Rotational and vibrational (ground-state combination difference) data, including 210 combinations with $\Delta K\neq 0$ providing C_0 , were merged and fitted.^[13]

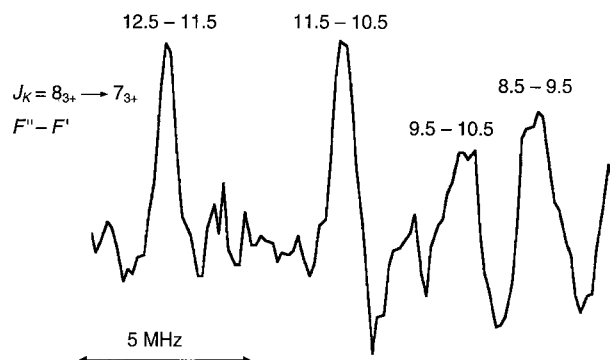


Figure 4. Part of the $J_K=8_{3+}\leftarrow 7_{3+}$ transition of BiH_3 , split by quadrupole hyperfine structure, between the upper components 3^+ of the split $K=3$ sublevels. ($F''-F'$) components are labeled.

The rotational–vibrational analyses of the ν_1/ν_3 ^[14] and ν_2/ν_4 bands,^[15] which will be reported in detail elsewhere, yield the vibrational wavenumbers and, among other constants, the vibrational corrections to the ground state rotational constants (B_0-B_e , C_0-C_e) which can be used to calculate the equilibrium rotational constants (B_e , C_e) and to derive the equilibrium geometry (r_e), Table 1.

Since the experimental data differ from published ab initio results^[16,17] by more than is nowadays tolerable, we have performed novel ab initio calculations^[18–28] at highly correlated levels by using several large basis sets and different relativistic pseudopotentials for the Bi atom (small-core pseudopotentials with and without counterpoise corrections, large-core pseudopotentials with and without core polarization potential). We will provide a full account of the results of these calculations elsewhere, here we only present the geometries, rotational constants, and fundamental wavenumbers at the highest theoretical level applied^[18] and compare them with their experimental counterparts (Table 1).

Table 1. Molecular parameters of BiH_3 (all derived from this work).

	Experiment	Ab initio calculation
ν_1 [cm^{-1}]	1733.2547	1746 ^[a]
ν_2 [cm^{-1}]	726.6990	737 ^[a]
ν_3 [cm^{-1}]	1734.4669	1758 ^[a]
ν_4 [cm^{-1}]	751.2386	761 ^[a]
B_0 [cm^{-1}]	2.6416	2.6257 ^[b]
C_0 [cm^{-1}]	2.6010	2.6024 ^[b]
B_e [cm^{-1}]	2.6709	2.6517 ^[c]
C_e [cm^{-1}]	2.6297	2.6274 ^[c]
$r_0(\text{BiH})$ [pm]	178.52	179.16
$\alpha_0(\text{HBiH})$ [$^\circ$]	90.50	90.07
$r_e(\text{BiH})$ [pm]	177.59	178.29 ^[c]
$\alpha_e(\text{HBiH})$ [$^\circ$]	90.48	90.08 ^[c]

[a] Harmonic wavenumbers from CCSD(T), anharmonicity corrections from MP2.^[18] [b] Equilibrium values from CCSD(T), vibrational corrections from MP2.^[18] [c] From CCSD(T).^[18]

The agreement of experimental (Figure 2, top and Figure 3, top) and simulated spectra (Figure 2, bottom and Figure 3, bottom) proves unambiguously that the observed spectra originate from BiH₃, and moreover that the rotational–vibrational analyses are correct and the determined molecular constants reliable and meaningful. The results of our ab initio calculations are consistent with the experimental data (Table 1) and thus offer further support for the experimental assignments.

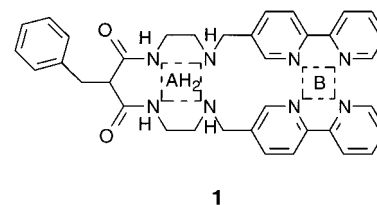
In conclusion, we have confirmed that Amberger obtained BiH₃ in his demanding (and thus presumably to date unrepeated) synthesis. We have determined for the first time accurate molecular constants for BiH₃ from IR and MMW spectra as well as accurate r_0 and r_e structures, vibrational energies, and the pattern of rotational and rotational–vibrational energies. The experimental results are in agreement with those from high-level ab initio calculations.

Received: March 22, 2002 [Z18958]

- [1] A. F. Holleman, E. Wiberg, N. Wiberg, *Lehrbuch der Anorganischen Chemie*, de Gruyter, Berlin, **1995**; N. N. Greenwood, A. Earnshaw, *Chemistry of the Elements*, Pergamon, Oxford, **1984**.
- [2] E. Amberger, *Chem. Ber.* **1961**, *94*, 1447–1452.
- [3] a) F. Paneth, *Ber. Dtsch. Chem. Ges.* **1918**, *51*, 1704–1728; b) F. Paneth, E. Winternitz, *Ber. Dtsch. Chem. Ges.* **1918**, *51*, 1728–1743.
- [4] See, for example: a) M. Thompson, B. Pahlavanpur, S. J. Walton, G. F. Kirkbright, *Analyst* **1978**, *103*, 705–713; b) K. Fujita, T. Takada, *Talanta* **1986**, *33*, 203–207.
- [5] F. E. Saalfeld, H. J. Svec, *Inorg. Chem.* **1963**, *2*, 46–50.
- [6] a) A. M. R. P. Bopegedera, C. R. Brazier, P. F. Bernath, *Chem. Phys. Lett.* **1989**, *162*, 301–305; b) R.-D. Urban, P. Polomsky, H. Jones, *Chem. Phys. Lett.* **1991**, *181*, 485–490; c) E. H. Fink, K. D. Setzer, D. A. Ramsay, M. Vervloet, J. M. Brown, *J. Mol. Spectrosc.* **1990**, *142*, 108–116; d) H. G. Hedderich, P. F. Bernath, *J. Mol. Spectrosc.* **1993**, *158*, 170–176.
- [7] L. Fusina, G. Di Lonardo, P. De Natale, *J. Chem. Phys.* **1998**, *109*, 997–1003.
- [8] K. Sarka, D. Papoušek, J. Demaison, H. Mäder, H. Harder in *Vibration-Rotational Spectroscopy and Molecular Dynamics*, (Ed.: D. Papoušek), World Scientific, Singapore, **1997**, pp. 116–238.
- [9] In local modes, X–H stretching excitation energy of XH_n molecules is localized the more in one single X–H bond the higher the excitation (typically in overtones), and dynamic symmetry lowering (XH₃→XH/H₂, C_{3v}→C_s) occurs. See, for example: a) M. S. Child, L. Halonen, *Adv. Chem. Phys.* **1984**, *57*, 1–58; b) L. Halonen, *Adv. Chem. Phys.* **1998**, *104*, 49–179; c) P. Jensen, *Mol. Phys.* **2000**, *98*, 1253–1285; d) T. Lukka, L. Halonen, *J. Chem. Phys.* **1994**, *101*, 8380–8389.
- [10] R. Marquardt, *Ber. Dtsch. Chem. Ges.* **1887**, *20*, 1518–1523.
- [11] Bruker 120 HR interferometer, Globar source, KBr beam splitter, MCT 800 and MCT 600 detectors, respectively, in the ν_1/ν_3 and ν_2/ν_4 regions, low pass filters, wavenumber precision $<1 \times 10^{-3} \text{ cm}^{-1}$, quoted resolution is 1/maximum optical path difference.
- [12] Between 150 and 650 GHz the rotational spectrum was measured by using phase-locked backward-wave oscillators as sources. At 1260 GHz a far-IR laser-sideband spectrometer was used.
- [13] A standard Hamiltonian complete to sextic centrifugal distortion constants, comprising off-diagonal elements taking into account $\Delta K = \pm 3$ interactions, and considering Bi nuclear quadrupole ($I=9/2$) and spin-rotation effects was used.
- [14] ν_1/ν_3 : Coriolis constants $C\zeta^z = -0.0230 \text{ cm}^{-1}$ and $\sqrt{2}B\Omega_{13}\zeta_{13}^y = \pm 0.0666 \text{ cm}^{-1}$ are small. $\sigma(\text{fit})$ is $0.66 \times 10^{-3} \text{ cm}^{-1}$ over 564 observations with $J'_{\text{max}} = 10$.
- [15] The $\nu_2=1$ and $\nu_4=1$ states are strongly coupled, with x,y Coriolis resonance dominating: $\sqrt{2}B\Omega_{24}\zeta_{24}^y = 1.8193 \text{ cm}^{-1}$. Moreover, $l(2,2)$, $l(2,-1)$, and $l(2,-4)$ interactions are present. $\sigma(\text{fit})$ is $0.56 \times 10^{-3} \text{ cm}^{-1}$ over 514 observations with $J'_{\text{max}} = 10$.
- [16] a) P. Schwerdtfeger, L. J. Laakkonen, P. Pyykkö, *J. Chem. Phys.* **1992**, *96*, 6807–6819; b) P. Schwerdtfeger, G. A. Heath, M. Dolg, M. A. Bennett, *J. Am. Chem. Soc.* **1992**, *114*, 7518–7527; c) D. Dai, K. Balasubramanian, *J. Chem. Phys.* **1990**, *93*, 1837–1846.
- [17] J. Breidung, W. Thiel, *J. Mol. Spectrosc.* **1995**, *169*, 166–180.
- [18] The molecular geometry of BiH₃ (C_{3v} symmetry) was optimized at the CCSD(T) level of theory^[19] by using counterpoise-corrected energies.^[20] The innermost core electrons of the Bi atom (1s–4f) were replaced by a relativistic pseudopotential,^[21] whereas the remaining 23 electrons in the Bi atom were treated explicitly by employing a (12s12p9d3f2g)/[6s6p4d3f2g] basis set.^[21] The aug-cc-pVQZ basis^[19] was used for the H atoms. All electrons outside the Bi core were correlated. At the CCSD(T) equilibrium geometry the harmonic force field was calculated numerically from corresponding counterpoise-corrected energies. Anharmonic normal coordinate force fields were determined at the MP2 level^[19] without counterpoise corrections by employing the same basis sets as above and by using a finite difference procedure.^[22] The CCSD(T) and MP2 calculations were performed with the Molpro2000^[23] and Gaussian98^[24] program systems, respectively.
- [19] Abbreviations: CCSD(T) = coupled-cluster method with single and double excitations^[25] and a perturbational treatment of triple excitations;^[26] MP2 = Møller–Plesset second-order perturbation theory;^[27] aug-cc-pVQZ = augmented correlation-consistent polarized valence quadruple zeta basis.^[28]
- [20] S. F. Boys, F. Bernardi, *Mol. Phys.* **1970**, *19*, 553–566.
- [21] B. Metz, H. Stoll, M. Dolg, *J. Chem. Phys.* **2000**, *113*, 2563–2569.
- [22] W. Schneider, W. Thiel, *Chem. Phys. Lett.* **1989**, *157*, 367–373.
- [23] Molpro2000 is a package of ab initio programs written by H.-J. Werner and P. J. Knowles, with contributions from R. D. Amos, A. Bernhardsson, A. Berning, P. Celani, D. L. Cooper, M. J. O. Deegan, A. J. Dobbyn, F. Eckert, C. Hampel, G. Hetzer, T. Korona, R. Lindh, A. W. Lloyd, S. J. McNicholas, F. R. Manby, W. Meyer, M. E. Mura, A. Nicklass, P. Palmieri, R. Pitzer, G. Rauhut, M. Schütz, H. Stoll, A. J. Stone, R. Tarroni, T. Thorsteinsson.
- [24] Gaussian 98 (Revision A.9), M. J. Frisch, G. W. Trucks, H. B. Schlegel, G. E. Scuseria, M. A. Robb, J. R. Cheeseman, V. G. Zakrzewski, J. A. Montgomery, R. E. Stratmann, J. C. Burant, S. Dapprich, J. M. Millam, A. D. Daniels, K. N. Kudin, M. C. Strain, O. Farkas, J. Tomasi, V. Barone, M. Cossi, R. Cammi, B. Mennucci, C. Pomelli, C. Adamo, S. Clifford, J. Ochterski, G. A. Petersson, P. Y. Ayala, Q. Cui, K. Morokuma, D. K. Malick, A. D. Rabuck, K. Raghavachari, J. B. Foresman, J. Cioslowski, J. V. Ortiz, A. G. Baboul, B. B. Stefanov, G. Liu, A. Liashenko, P. Piskorz, I. Komaromi, R. Gomperts, R. L. Martin, D. J. Fox, T. Keith, M. A. Al-Laham, C. Y. Peng, A. Nanayakkara, C. Gonzalez, M. Challacombe, P. M. W. Gill, B. G. Johnson, W. Chen, M. W. Wong, J. L. Andres, M. Head-Gordon, E. S. Replogle, J. A. Pople, Gaussian, Inc., Pittsburgh, PA, **1998**.
- [25] G. D. Purvis III, R. J. Bartlett, *J. Chem. Phys.* **1982**, *76*, 1910–1918.
- [26] K. Raghavachari, G. W. Trucks, J. A. Pople, M. Head-Gordon, *Chem. Phys. Lett.* **1989**, *157*, 479–483.
- [27] C. Møller, M. S. Plesset, *Phys. Rev.* **1934**, *46*, 618–622.
- [28] R. A. Kendall, T. H. Dunning, Jr., R. J. Harrison, *J. Chem. Phys.* **1992**, *96*, 6796–6806.

Signal Amplification by a Fluorescent Indicator of a pH-Driven Intramolecular Translocation of a Copper(II) Ion**

Valeria Amendola, Luigi Fabbrizzi,* Carlo Mangano, Hamish Miller, Piersandro Pallavicini, Angelo Perotti, and Angelo Taglietti



The translocation of a metal ion in a reversible and repeatable manner from one compartment to the other within a ditopic ligand could lead to mechanical work at the molecular level.^[1] This possibility gives rise to a new class of potential artificial molecular machines,^[2] thus adding to the possibilities based on rotaxanes and catenanes.^[3,4] Movement of metal ions, which takes place following a predetermined pathway, can be induced by different stimuli, such as a variation of the redox potential,^[5,6] or a pH change.^[7] The use of pH as the stimulus is especially convenient as it involves a rather mild perturbation and does not cause degradation of the system, and hence its operation can be repeated at will, indefinitely. This situation is not always the case with the more drastic and destructive processes which involve an auxiliary oxidation and reduction reaction. The essential requirements for the occurrence of a pH-driven metal translocation process are that 1) one of the two coordinating compartments (A) also shows a distinct acid–base behavior (for example, through the $AH_n \rightleftharpoons A^{n-} + nH^+$ equilibrium), and that 2) the coordinating tendencies of the two compartments decrease along the series $A^{n-} \gg B \gg AH_n$, where B is the second compartment that does not display acid–base behavior, at least in the investigated pH interval. Thus, at a pH value in which AH_n dominates, the metal ion stays in compartment B. On the other hand, when the pH value is increased and AH_n deprotonates, the metal ion moves to the more appealing compartment A^{n-} . The metal ion moves back to B on decreasing the pH value. In the case of transition metal ions, a change in the compartment typically modifies the stereochemistry and the ligand field experienced by the cation, thus altering its electronic structure and spectral features. Ultimately, the displacement of the metal ion is signaled by a color change of the solution. We show here that the position of the metal ion in the ditopic system can be determined by the powerful signal of a fluorescent indicator (which is present at a very low concentration) provided that the indicator is able to interact selectively with the metal ion.

The envisaged ditopic ligand **1** contains two distinct tetradentate compartments: A and B. The donor set of A consists of two secondary amine and two secondary amide nitrogen atoms. As the amide group itself possesses poor or no

coordinating tendencies, the neutral form AH_2 is expected to display minimum binding tendencies towards the chosen metal ion, Cu^{II} . On the other hand, at neutral or slightly alkaline pH values, the amide group deprotonates in the presence of divalent late-transition-metal ions to give rise to a very strong donor group: thus, the doubly deprotonated A^{2-} compartment is expected to establish especially intense metal–ligand interactions and give rise to a very stable complex with a square geometry. Compartment B is constituted by two 2,2'-bipyridine (bpy) fragments, which display fairly good binding tendencies towards Cu^{II} ions. Complexes of the $[Cu^{II}(bpy)_2]^{2+}$ type tend to be five coordinate, the remaining coordination site being occupied by a solvent molecule or by a coordinating anion. Thus, it appears that the required sequence of affinity ($A^{2-} \gg B \gg AH_2$) is established and that the Cu^{II} ion can be translocated between B and A and vice versa over a defined pH range.

We used a dioxane/water mixture (4:1) as the solvent. Pure water could not be used because of the precipitation of Cu^{II} complexes in alkaline conditions. We carried out potentiometric titration experiments and, through nonlinear least-squares treatment of titration data,^[8] we calculated the formation constants of the species present in equilibrium between pH 2 and 12. We were then able to draw the corresponding distribution curves (Figure 1).

Two major metal-containing species are present in alkaline conditions in a solution containing equimolar amounts of **1** (LH_2) and Cu^{II} ions. A species $[Cu^{II}(LH_2)]^{2+}$ reaches its maximum abundance (80 %) at pH 7.4, and a species $[Cu^{II}(L)]$ reaches 100 % abundance at $pH \geq 11$.

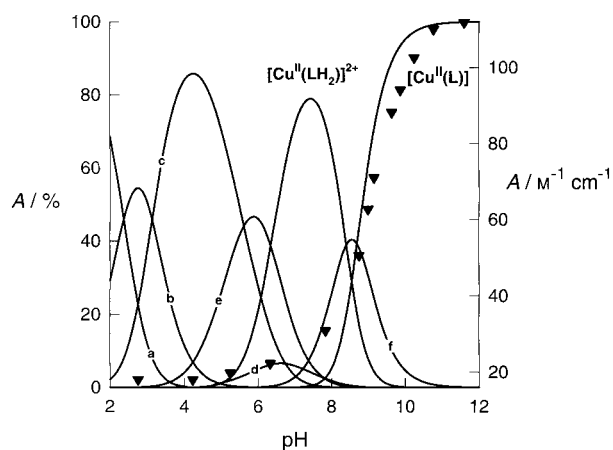


Figure 1. Concentration of the species present at the equilibrium in a solution containing equimolar amounts of **1** ($=LH_2$) and Cu^{2+} ions; profiles **a**, **b**, **c**, and **d** refer to the variously protonated forms of LH_2 (from LH_6^{4+} to LH_3^+). Profile **e** refers to the metal-containing protonated species $[Cu^{II}(LH_3)]^{3+}$. Profile **f** refers to the metal-containing species $[Cu^{II}(LH_2)(OH)]^+$. Full triangles give the molar absorptance of the d–d band ($\lambda_{max} = 502$ nm) of the $[Cu^{II}(L)]$ complex.

[*] Prof. L. Fabbrizzi, Dr. V. Amendola, Dr. C. Mangano, Dr. H. Miller, Dr. P. Pallavicini, Prof. A. Perotti, Dr. A. Taglietti
Dipartimento di Chimica Generale
Università di Pavia
via Taramelli 12, 27100 Pavia (Italy)
Fax: (+39)0382-528-544
E-mail: luigi.fabbrizzi@unipv.it

[**] This work was supported by the European Union (RT Network Molecular Level Devices and Machines: Contract HPRN-CT-2000-00029) and by the Italian Ministry of University and Research (PRIN—Progetto “Dispositivi Supramolecolari”).

Noticeably, the absorption spectrum of the blue solution at pH 7.4 (Figure 2) is very similar to that of a solution of the $[\text{Cu}^{\text{II}}(\text{bpy})_2]^{2+}$ model complex. This observation indicates that the metal ion stays in compartment B. Moreover, the mass spectra (ESI) recorded at this pH value display peaks at m/z 776, 778, and 780 which correspond to $[\text{Cu}^{\text{II}}(\text{LH}_2)]^+$, $[\text{Cu}^{\text{II}}(\text{LH}_2)]^+$, and $[\text{Cu}^{\text{II}}(\text{LH}_2)]^+$, as expected.

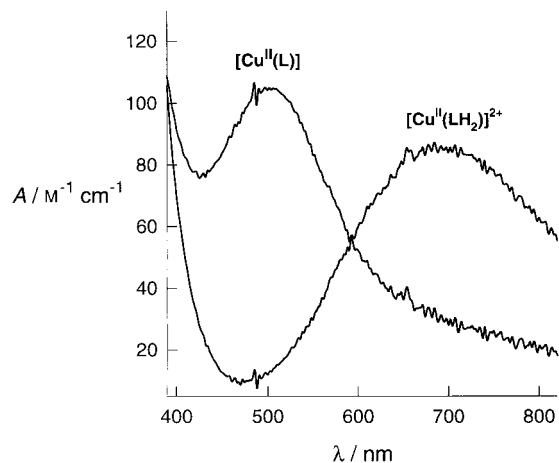


Figure 2. d-d spectra of the $[\text{Cu}^{\text{II}}(\text{LH}_2)]^{2+}$ complex (blue, Cu^{2+} stays in compartment B) and of the $[\text{Cu}^{\text{II}}(\text{L})]^{2+}$ complex (pink/violet, Cu^{2+} stays in compartment A).

On the other hand, adjusting the pH value to 12 by the addition of standard base makes the solution become pink/violet. The color and the absorption spectrum are similar to that observed for the model complex with a tetradentate ligand containing two deprotonated amide groups and two amine groups ($\text{NH}_2\text{CH}_2\text{CH}_2\text{NH}(\text{CO})\text{CH}_2\text{CH}_2\text{CH}_2\text{NH}(\text{CO})\text{CH}_2\text{CH}_2\text{NH}_2$ (dioxo-2,3,2-tet)). This evidence suggests that the metal ion in the species dominating at $\text{pH} \geq 11$ ($[\text{Cu}^{\text{II}}(\text{L})]$) is located in compartment A^{2-} (Figure 2). Further evidence is derived from pH-dependent spectrophotometric measurements. In particular, the intensity of the band at 502 nm superimposes well on the abundance profile of the $[\text{Cu}^{\text{II}}(\text{L})]$ species. Moreover, the ESI mass spectrum recorded at pH 12 displays the signal of the expected species, $[\text{Cu}^{\text{II}}(\text{L}) + \text{Na}]^+$, with m/z 698, 700 (Na^+ comes from the added standard base). The solution turns blue again on addition of standard acid back to pH 7.4, which indicates that the reverse translocation has taken place. The direct and reverse translocation processes can be repeated at will, in principle indefinitely. The detection limit is determined by the progressive dilution of the solution, which arises as a result of the consecutive addition of the standard solutions of acid and base.

The rate of the metal ion translocation, both direct and reverse, could be determined by stopped-flow spectrophotometric experiments. In particular, the B-to-A metal ion displacement could be monitored through the development of the absorption band at 502 nm, which corresponds to the formation of the pink/violet $[\text{Cu}^{\text{II}}(\text{L})]$ species. The absorbance versus time profile strictly fits a first-order kinetics, with a lifetime τ of 0.54 ± 0.05 s. The first-order A-to-B transloca-

tion, investigated through the decay of the band at 502 nm, exhibits a lifetime τ of 0.58 ± 0.05 s. First-order patterns observed for both direct and reverse processes indicate the intramolecular nature of the translocation. No details are available on the intimate mechanism of the processes. It is probable that the minor species which forms at pH 8.5 plays some role. The formula $[\text{Cu}^{\text{II}}(\text{L})\text{OH}]^+$ is assigned to this singly charged species: the hydroxide ion results from the deprotonation of the water molecule bound to the Cu^{II} ion in the five-coordinate complex in compartment B.

The reversible translocation can be followed through a more powerful signal, fluorescence, by making use of an auxiliary light-emitting fragment, namely coumarin-343 (FIH, **2**). This molecule is a protic acid, since it contains a carboxylic acid group, whose pK_A value in the 4:1 dioxane/water solution is 7.30 ± 0.02 . The undissociated form FIH is strongly fluorescent, with an emission band centered at $\lambda_{\text{max}} = 490$ nm; the emission band of the dissociated form (FI^-) is less intense (fluorescence intensity (I_F) is 75 % that of FIH) and is blue-shifted to 471 nm (λ_{max}). Thus, a solution of coumarin-343 (for example, 2×10^{-6} M) is fluorescent over the entire pH range, even if a change in the I_F and λ_{max} values is observed in the pH 6.5–8.5 range. If the same solution is also made 4×10^{-4} M in the copper(II) complex of **1** (a concentration 220 times higher than that of FIH), the pH dependence of the fluorescence intensity corresponding to the FIH and FI^- bands changes drastically.

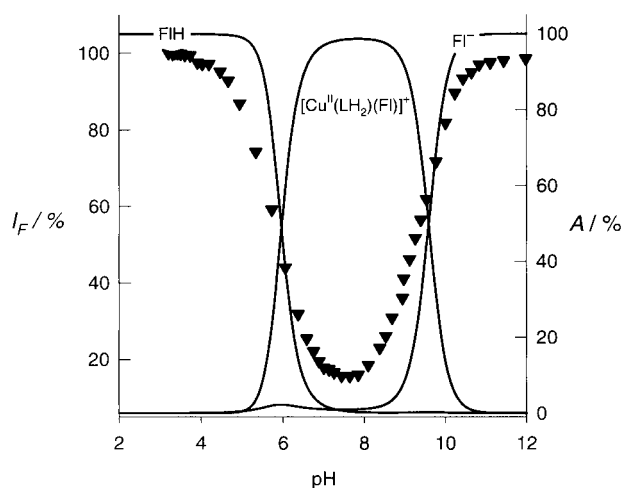
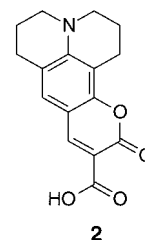


Figure 3. Full triangles (left vertical axis) indicate the fluorescence intensity (I_F) of a solution containing 2×10^{-6} M coumarin-343 (**2**) and 4×10^{-4} M of the $[\text{Cu}^{\text{II}}(\text{LH}_2)]^{2+}/[\text{Cu}^{\text{II}}(\text{L})]$ complex: values of the descending arm of the well-shaped profile refer to the emission band at 490 nm (emitting fragment: coumarin-343, undissociated form, FIH); values of the ascending arm refer to the emission band at 471 nm (emitting fragment: dissociated form, FI^-). I_F values are normalized. Solid lines (right vertical axis) give the pH dependance of the concentration of FIH, $[\text{Cu}^{\text{II}}(\text{LH}_2)(\text{FI})]^+$, and FI^- in the same solution. Moving up from pH 7, by the absence of fluorescence (bottom of the well) signals that the Cu^{II} ion stays in compartment B, while the presence of fluorescence signals that the Cu^{II} ion is in compartment A.

pH 7–8, then it increases again (according to a well-shaped profile) to reach a plateau at pH > 11.5. This behavior can be accounted for by assuming that in the pH interval where the well of the I_F plot is present, the $[\text{Cu}^{\text{II}}(\text{LH}_2)(\text{H}_2\text{O})]^{2+}$ species forms and the carboxylate group of FI^- replaces the water molecule coordinated to the Cu^{II} center in the B compartment. The binding of FI^- to the transition metal ion causes a quenching of the fluorescence, through either an electron-transfer or an energy-transfer process. At pH > 11.5, when more than 99.8% of the metal has translocated to the A^{2-} site, a planar complex is formed, which, as a result of the very strong in-plane interaction, does not exhibit any affinity towards further ligands. As a consequence, FI^- is released to the solution and displays its full fluorescence. Thus, B-to-A translocation is signaled by the switching-on of the fluorescence. On the other hand, A-to-B translocation, induced by adjusting the pH value back to 7–8, is signaled by the switching-off of the fluorescence. One can switch the pH values back and forth many times and, as a result of the high efficiency of the fluorescence signal, the occurrence of the reversible translocation can be perceived each time, both visually and instrumentally.

A binding constant of 5.5 ± 0.1 log units was found from the spectrofluorimetric data for the equilibrium: $[\text{Cu}^{\text{II}}(\text{LH}_2)(\text{H}_2\text{O})]^{2+} + \text{FI}^- \rightleftharpoons [\text{Cu}^{\text{II}}(\text{LH}_2)(\text{FI})]^+ + \text{H}_2\text{O}$. Thus, it was possible to draw the distribution diagram shown in Figure 3. This plot indicates that the $[\text{Cu}^{\text{II}}(\text{LH}_2)(\text{FI})]^+$ adduct begins to form at pH 4.5, which causes fluorescence quenching (left arm of the well, \blacktriangledown). On the other hand, a decrease in the $[\text{Cu}^{\text{II}}(\text{LH}_2)(\text{FI})]^+$ concentration, which is associated with a translocation to A, corresponds to the release of the FI^- light-emitting species and to the generation of fluorescence (right arm of the well, \blacktriangledown).

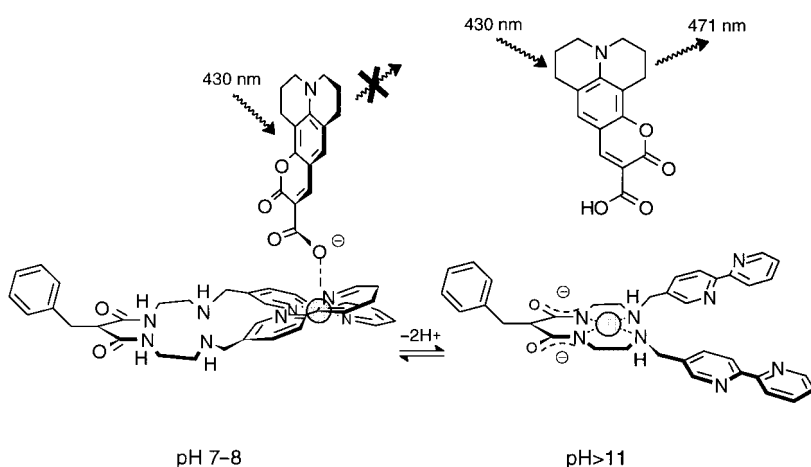
Scheme 1 provides a pictorial sketch of the hypothesized stereochemical aspects of metal translocation and of complexation/decomplexation of FI^- . It has to be noted that metal displacement in a previously described pH-driven Cu^{II} translocation experiment involved drastic rearrangement and folding of the ligating framework.^[9] In the present case, each compartment displays a distinct coordinating behavior and does not interfere with metal binding by the other compartment.

Translocation of a transition metal ion between the unequivalent compartments of a ditopic ligand is an interesting switching process, which can be read by monitoring a variety of properties (spectroscopic, magnetic, electrochemical). Among these properties, fluorescence is undoubtedly one of the most advantageous, as it is visual and can be detected instrumentally with extreme sensitivity. A rational, but very time consuming, way to profit from fluorescence involves the synthesis of ligands, to whose framework a given fluorophore has been covalently bound. However, this approach can be highly perturbative, as the sterically hindering fluorogenic substituent may strongly reduce the rate of metal-ion movement. In a reported example,^[7] the covalent linking of a fluorescent fragment (anthracene) to the framework of the ditopic ligand made the translocation rate of the metal ion (Ni^{II}) decrease by an order of magnitude with respect to a system without steric hinderance (the τ value varied from hundreds of milliseconds to seconds). On the other hand, the use of an auxiliary fluorescent indicator that possesses coordinating tendencies is not perturbative at all, particularly because it is present at an extremely low concentration (220 times lower than that of the $[\text{Cu}^{\text{II}}(\text{LH}_2)]^{2+}$ complex). Moreover, in spite of the fact that FI^- binds only a small fraction of $[\text{Cu}^{\text{II}}(\text{LH}_2)]^{2+}$ ions, a powerful ON/OFF signal is detected even after many cycles and remarkable dilution. The only prerequisite the designer should address is that of the two compartments: one should provide coordinative unsaturation and the other should not. Fluorescent indicators recently experienced a revival in the sensing of recognition events.^[10] In particular, coumarin-343 has been used as an OFF/ON indicator to signal the recognition of HCO_3^- ions by a dicopper(II) bis-tren cryptate (tren = tris(2-ethylamino)-amine).^[11] It appears now that fluorescent indicators can also be profitably utilized to signal the movements occurring at the molecular level and to monitor the working of molecular machines.

Experimental Section

Ligand **1** was synthesized through the Schiff-base reaction of 6-benzyl-1,4,8,11-tetraazaundecane-5,8-dione^[7] (1 mmol) with 5-(2,2')-bipyridine-carboxyaldehyde^[12] (2 mmol) in ethanol (20 mL, room temperature, 24 h), followed by in situ reduction with an excess of NaBH_4 (0.8 g). The solvent was removed from the reaction mixture on a rotary evaporator and the solid residue was treated with 0.1M NaOH (20 mL). Extraction with CH_2Cl_2 , drying with MgSO_4 , and removal of the solvent under vacuum gave the desired product as a solid in 35% yield. Elemental analysis calcd (%) for $\text{C}_{36}\text{H}_{38}\text{N}_8\text{O}_2$: C 70.37, H 6.18, N 18.23; found C 70.41, H 6.16, N 18.20. MS (ESI): m/z : 615 [**1** + H^+]; ^1H NMR (CDCl_3): δ = 8.72 (d, 2H, Ar-H), 8.60 (s, 2H, Ar-H), 8.48 (t, 2H, Ar-H), 7.78 (m, 4H, Ar-H), 7.1–7.3 (m, 9H, Ar-H), 6.95 (brt, 2H, CONH), 3.79 (s, 4H, NHCH_2 -bipyridine), 3.38–3.20 (m, 7H, $\text{CONHCH}_2\text{CH}_2 + \text{PhCH}_2\text{CH}$), 2.65 (m, 4H, CONHCH_2), 2.15 (br, CH_2NHCH_2).

Received: December 27, 2001
Revised: April 22, 2002 [Z18443]



Scheme 1.

- [1] J.-M. Lehn, *Supramolecular Chemistry, Concepts and Perspectives*, VCH, Weinheim, 1995, pp. 124–127.
- [2] V. Amendola, L. Fabbri, C. Mangano, P. Pallavicini, *Acc. Chem. Res.* **2001**, 34, 488–493.

- [3] V. Balzani, A. Credi, F. M. Raymo, J. F. Stoddart, *Angew. Chem.* **2000**, *112*, 3484–3530; *Angew. Chem. Int. Ed.* **2000**, *39*, 3348–3391.
 [4] J.-P. Sauvage, *Acc. Chem. Res.* **1998**, *31*, 611–619.
 [5] L. Zelikovitch, J. Libman, A. Shanzler, *Nature* **1995**, *374*, 790–792.
 [6] T. R. Ward, A. Lutz, S. P. Parel, J. Ensling, P. Güttlich, P. Buglyó, C. Orvig, *Inorg. Chem.* **1999**, *38*, 5007–5017.
 [7] V. Amendola, L. Fabbri, C. Mangano, P. Pallavicini, A. Perotti, A. Taglietti, *J. Chem. Soc. Dalton Trans.* **2000**, 185–189.
 [8] P. Gans, A. Sabatini, A. Vacca, *Talanta* **1996**, *43*, 1739–1753.
 [9] V. Amendola, C. Brusoni, L. Fabbri, C. Mangano, H. Miller, P. Pallavicini, A. Perotti, A. Taglietti, *J. Chem. Soc. Dalton Trans.* **2001**, 3528–3533.
 [10] E. V. Anslyn, *Acc. Chem. Res.* **2001**, *34*, 963–972.
 [11] L. Fabbri, A. Leone, A. Taglietti, *Angew. Chem.* **2001**, *113*, 3156–3159; *Angew. Chem. Int. Ed.* **2001**, *40*, 3066–3069.
 [12] V. Balzani, V. Polin, E. Schmohel, *Synthesis* **1998**, *3*, 321–324.

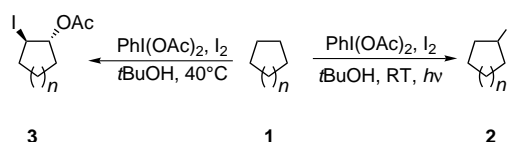
Activation of Alkanes upon Reaction with $\text{PhI}(\text{OAc})_2 - \text{I}_2^{**}$

José Barluenga,* Francisco González-Bobes, and José M. González

Carbon–hydrogen-bond-activation reactions are challenging processes in organic synthesis.^[1] Halogenation reactions have been thoroughly studied and widely practiced and provide a simple and classic way to functionalize hydrocarbons.^[2] However, the iodination of alkanes has been a particularly elusive reaction and still remains as an active research area.^[3] The endothermic nature of the overall process has been invoked to explain the failure of a radical-chain approach to accomplish this reaction.^[4, 5] While performing β -scission reactions of cycloalkanols,^[6] we noticed that (diacetoxyiodo)benzene $[\text{PhI}(\text{OAc})_2]$ ^[7] gave rise to a mixture of compounds, where iodocyclohexane (**2b**) was found as the major product, resulting from an activation of the cyclohexane used as solvent.

Herein we report new approaches to selectively produce either iodoalkanes **2** or 1-acetoxy-2-iodocycloalkanes **3** from readily available hydrocarbons **1**. The products **2** and **3** arise from single and double formal C–H-bond-activation reactions, respectively. This unique reaction manifold can be tuned by treating alkanes **1** with $\text{PhI}(\text{OAc})_2$, iodine (I_2), and *tert*-butylalcohol (*t*BuOH) simply by using photochemical or thermal conditions (Scheme 1).

Our initial studies with cyclohexane (**1b**) showed that the presence of an alcohol is necessary for an efficient alkane activation. *t*BuOH was found to be the most effective of all the alkanols tested. Thus, cycloalkanes were cleanly converted



Scheme 1. Photochemical and thermal reactivity of hydrocarbons with $\text{PhI}(\text{OAc})_2 - \text{I}_2$.

into the corresponding iodinated derivatives, under irradiation conditions (2×100 W lamps), in high yield, under relatively mild conditions, and in rather short reaction times. In addition, toluene (**1e**) also gives benzyl iodide (**2e**) as the sole reaction product.^[8] Linear alkanes react affording mixtures of monoiodinated derivatives in good combined yield, showing high selectivity for secondary positions (Table 1).

An outstanding feature of this iodine(III)-induced activation of alkanes was observed when carrying out the reactions under thermal instead of photochemical conditions.^[9] In this case, bifunctional compounds **3** were obtained as major, or even single, reaction products (Scheme 1, Table 2). The global

Table 1. Synthesis of iodoalkanes **2** from alkanes **1**.^[a]

Entry	Alkane (1)	Concentration [M] ^[b]	Reaction time [h]	Product (2)	Yield [%] ^[c]
1		0.04	1.5		98
2		0.04	4		97
3		0.02	6		92
4		0.02	8		85 ^[d]
5		0.02	1		92 ^[e]
6		0.04	4		85 ^[f]

[a] All reactions performed with the following stoichiometry: $\text{PhI}(\text{OAc})_2$ (1 equiv), I_2 (1.1 equiv), *t*BuOH (1 equiv). The alkane was used as solvent. [b] Referred to iodine. [c] GC yield unless otherwise specified. [d] Compound **2d** was isolated in 80% yield upon column chromatography with *n*-hexane as eluant. [e] Determined by ^1H NMR spectroscopy. [f] Proportions of isomers (determined by GC): **2g**:**2h** = 1:1.5, **2f**:**2g** + **2h** = 1:15.

[*] Prof. Dr. J. Barluenga, F. González-Bobes, Dr. J. M. González
 Instituto de Química Organometálica “Enrique Moles”
 Unidad Asociada al C.S.I.C.
 Universidad de Oviedo
 33071 Oviedo (Spain)
 Fax: (+34) 98-510-3450
 E-mail: barluenga@sauron.quimica.uniovi.es

[**] This research was supported by DGES (Grant PB97-1271). F.G.-B. thanks FICYT for a fellowship.

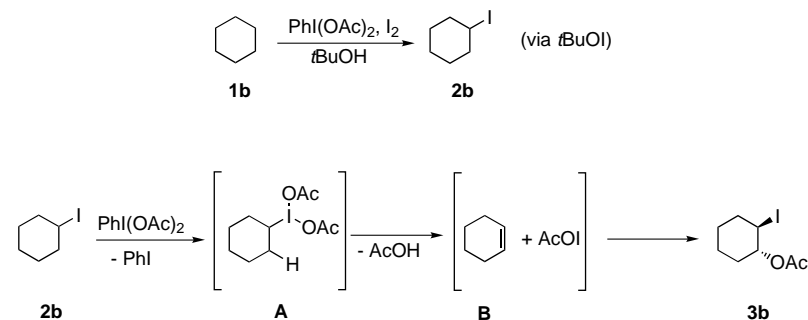
Table 2. Synthesis of 1-acetoxy-2-iodocycloalkanes **3** from cycloalkanes **1**.^[a]

Entry	Cycloalkane (1)	PhI(OAc) ₂ ^[b]	Product (3)	Yield [%] ^[c]
1		3.5		71
2		2		92
3		2		47
4		3		65

[a] All reactions performed with 1.1 equivalent of I₂. The alkane was used as solvent. Reaction time 14 h. [b] Molar ratio [PhI(OAc)₂]:*t*BuOH = 1:1. [c] Isolated yield referred to I₂.

transformation formally represents a direct and unprecedented diastereoselective 1,2-functionalization of an alkane. All the reactions were performed under ambient light at 40 °C (bath temperature) and different amounts of PhI(OAc)₂ were required to obtain fair to excellent yields of compounds **3**. When cycloheptane (**1c**) was employed as substrate in the reaction, a ring contraction was observed, affording the unexpected methylcyclohexane derivative **3c** in 47% yield (Table 2).

For the basis of a mechanistic proposal, an initial formation of intermediate species of hypoiodite nature, which result from the interaction of the PhI(OAc)₂–I₂ system and an alcohol, is widely accepted.^[10] Thus, generation of *tert*-butylhypoiodite (*t*BuOI) could be reasonably invoked to promote the synthesis of the observed iodoalkanes **2** by a radical-chain mechanism.^[4] The formation of the bifunctional derivatives **3** could be explained assuming a ligand transfer from PhI(OAc)₂ to the iodoalkane **2** previously formed,^[11, 12] which gives rise to (diacetoxyiodo)alkane species (**A**; Scheme 2), which are in general unstable. An elimination reaction to generate an olefin (**B**), followed by addition of the



Scheme 2. Proposed reaction mechanism.

acetylhypoiodite formed “in situ” would account for the observed *trans* diastereoselectivity in which 1-acetoxy-2-iodocycloalkanes **3** are obtained (Scheme 2).

In conclusion, a new method amenable for the selective mono- and bifunctionalization of alkanes has been described, under mild, simple and efficient conditions. The reported examples leading to the synthesis of bifunctional derivatives constitute the first diastereoselective vicinal activation reaction of a hydrocarbon. Further investigations concerning the interaction of iodine(III) species with alkanes are in progress.

Experimental Section

All reactions were carried out under a positive pressure of nitrogen. Alkanes **1** were dried under reflux over sodium, distilled under nitrogen, and purged with argon to remove oxygen traces prior to their use.

3b: Iodine (1.1 mmol, 280 mg) and *t*BuOH (2 mmol, 0.2 mL) were sequentially added to a suspension of PhI(OAc)₂ (2 mmol, 644 mg) in **1b** (25 mL). The resulting mixture was stirred at 40 °C (bath temperature) for 14 h. The mixture was allowed to cool and then quenched with sodium thiosulfate (5% solution in water, 25 mL). The mixture was transferred to a separating funnel, the aqueous layer was reserved and the organic one distilled under reduced pressure to recover excess **1b**. The distillation residue was diluted with diethyl ether (20 mL), mixed with the previously reserved aqueous layer and extracted. The aqueous phase was further extracted with diethyl ether (3 × 20 mL). The combined organic layers were washed with NaOH (5% solution in water, 2 × 40 mL), brine (2 × 40 mL), and dried over sodium sulfate. The solvent was removed at reduced pressure. The resulting liquid was further purified by column chromatography (hexane/ethyl acetate 25/1) to give **3b** as a pale yellow liquid (245 mg, 92%).

Received: February 18, 2002
Revised: March 27, 2002 [Z18726]

- [1] For leading references: a) *Activation of unreactive bonds and organic synthesis* (Ed.: S. Murai), Springer, Berlin, **1999**; b) C. Jia, T. Kitamura, Y. Fujiwara, *Acc. Chem. Res.* **2001**, *34*, 633–639; c) W. D. Jones, *Science* **2000**, *287*, 1942–1943; d) G. Dyker, *Angew. Chem.* **1999**, *111*, 1808–1822; *Angew. Chem. Int. Ed.* **1999**, *38*, 1698–1712; e) S. S. Stahl, J. A. Labinger, J. E. Bercaw, *Angew. Chem.* **1998**, *110*, 2298–2311; *Angew. Chem. Int. Ed.* **1998**, *37*, 2180–2192.
- [2] a) For a review: E. S. Huyser in *The Chemistry of the Carbon-Halogen Bond, Part 1* (Ed.: S. Patai), Wiley, New York, **1973**, pp. 549–607; b) For a list of reagents, with references, see: R. C. Larock in *Comprehensive Organic Transformations*, VCH, New York, **1989**, pp. 311–313.
- [3] a) P. R. Schreiner, O. Lauenstein, E. D. Butova, A. A. Fokin, *Angew. Chem.* **1999**, *111*, 2956–2958; *Angew. Chem. Int. Ed.* **1999**, *38*, 2786–2788; b) O. Lauenstein, A. A. Fokin, P. R. Schreiner, *Org. Lett.* **2000**, *2*, 2201–2204; c) A. A. Fokin, O. Lauenstein, P. A. Gunchenko, P. R. Schreiner, *J. Am. Chem. Soc.* **2001**, *123*, 1842–1847.
- [4] D. D. Tanner, G. C. Gidley, *J. Am. Chem. Soc.* **1968**, *90*, 808–809.
- [5] L. Liguori, H.-R. Bjørsvik, A. Bravo, R. Fontana, F. Minisci, *Chem. Commun.* **1997**, 1501–1502.
- [6] J. Barluenga, F. González-Bobes, S. R. Ananthoju, M. A. García-Martín, J. M. González, *Angew. Chem.* **2001**, *113*, 3491–3494; *Angew. Chem. Int. Ed.* **2001**, *40*, 3389–3392.
- [7] For reviews on (diacetoxyiodo)benzene, see: a) H. Togo, M. Katohgi, *Synlett* **2001**, 565–581; b) P. J. Stang, V. V. Zhdankin, *Chem. Rev.* **1996**, *96*, 1123–1178; c) A. Vavoglis, *Chem. Soc. Rev.* **1981**, *10*, 377–407.
- [8] To our knowledge a direct and efficient iodination of toluene is almost without precedent. Previously, a

34 % yield was reported in the preparation of **2e** from **1e** and *t*BuOCl/HgI₂, see reference [4].

- [9] None of the bifunctional derivatives **3** were observed when performing the reaction under photochemical conditions, even using an excess of PhI(OAc)₂. For instance, when **1a** was treated with PhI(OAc)₂ (2 equiv), I₂ (1.1 equiv), and *t*BuOH (2 equiv) under the influence of light at room temperature, only the formation of **2a** was observed after 8 h, the excess PhI(OAc)₂ was recovered.
- [10] For recent evidence: a) J. Madsen, C. Viuf, M. Bols, *Chem. Eur. J.* **2000**, *6*, 1140–1146; b) J. L. Courtneidge, J. Luszyk, D. Pagé, *Tetrahedron Lett.* **1994**, *35*, 1003–1006.
- [11] J. Gallos, A. Varvoglis, *J. Chem. Soc. Perkin Trans. 1* **1983**, 1999–2002.
- [12] We have observed that **2b** was cleanly converted into **3b** under comparable thermal conditions, thus providing additional evidence for the proposed mechanism.

Mechanism of the Transformation of Silica Precursor Solutions into Si-MFI Zeolite

Svetlana Mintova,* Norman H. Olson, Jürgen Senker, and Thomas Bein*

*Dedicated to Professor Jens Weitkamp
on the occasion of his 60th birthday*

The mechanisms governing the transformation of precursor solutions or gels into zeolitic materials are still not fully understood.^[1–5] The scientific challenge is to understand these mechanisms to enhance synthetic control for the design of new zeolite structures, and for the preparation of novel assemblies such as films, monoliths, and functional nanostructures.

The crystal growth of silicalite-1—a microporous polymorph with MFI topology—has received considerable attention because it can serve as model system for a fundamental understanding of the mechanism of zeolite formation.^[6–9] The nanoscale organosilicate clusters in the precursor solutions used for the synthesis of nanosized MFI-type zeolite have been observed with techniques such as dynamic light scattering (DLS),^[6] nuclear magnetic resonance (NMR),^[7,8] small-angle X-ray scattering (SAXS),^[9,10] and high-resolution transmission electron microscopy (HRTEM).^[11–13] It appears that nanoscale species with a size of about 3–4 nm are formed in the precursor solutions before long-range order is established.^[14,15] Additional information about the structure, particle size, and shape of the silicate species in the MFI-precursor solutions containing organic additives was obtained by using

NMR spectroscopy^[16] and in situ SAXS measurements.^[9,10] These studies suggest that the aggregation of the primary units is an important step in the nucleation process, and that it depends on many factors, such as the alkalinity of the precursor solution, the type of silica source, and aging time. However, structural information regarding the initial framework species assembled from molecular precursors is still very limited.

In previous studies we have investigated the nucleation and growth processes of zeolites A (LTA) and Y (FAU) (using the tetramethylammonium (TMA) ion) by HRTEM.^[11] It was observed that the crystalline structures nucleate in amorphous gel aggregates existing in the colloidal aqueous solutions, and that these gel aggregates are completely converted into crystalline products after extended reaction times.

Herein, we examine the formation of the colloidal precursor solution and the crystal growth of Si-MFI by in situ DLS combined with ²⁹Si solid-state NMR spectroscopy, HRTEM, and other techniques.

A clear precursor solution, prepared for the synthesis of Si-MFI zeolite, was aged at room temperature on an orbital shaker for 24 h (A24h) to 30 days (A30d). Samples were heated to 90 °C and then examined by in situ DLS measurements. A major advantage of the in situ study is the elimination of invasive procedures that may modify the crystallization process of the Si-MFI zeolite. Figure 1 shows

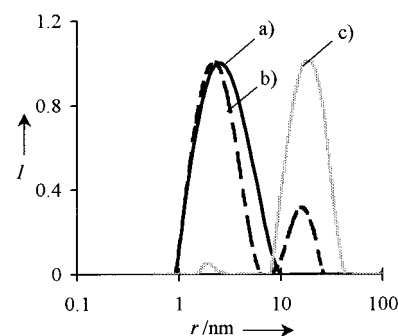


Figure 1. DLS data of TPA-silica precursor solutions: a) aged for 24 h (A24h) at room temperature, and after heating for b) 4 min (A24hH4m) and c) 6 h (A24hH6) at 90 °C. The distribution function analysis (DFA) is displayed as scattering intensity per unweighted particle size classes (I = scattering intensity).

the particle size (r) distribution of the precursor solution aged for 24 h (A24h), and for samples heated to 90 °C for 4 min (A24hH4m) and 6 h (A24hH6). Prior to heating, the presence of sub-colloidal particles with sizes in the range of about 1–10 nm is observed in the A24h sample. These particles are shown to be amorphous by X-ray diffraction. After hydrothermal treatment of solution A24h for only 4 min (Figure 1b), an increase of the scattering intensity is observed, due to the presence of a second generation of particles with mean radius of about 15 nm (sample A24hH4m; Figure 1b). The two particle populations present in these samples are quite diverse, the first having a mean radius of about 2.3 nm and the second having a radius of about 15 nm. By increasing the heating time from 4 min to 6 h (sample A24hH6; Figure 1c), the peak indicative for the presence of sub-colloidal

[*] Dr. S. Mintova, Prof. T. Bein, Dr. J. Senker
Department of Chemistry
University of Munich
Butenandtstrasse 5–11, 81377 Munich (Germany)
Fax: (+49) 89-2180-7622
E-mail: svetlana.mintova@cup.uni-muenchen.de
tbein@cup.uni-muenchen.de

Dr. N. H. Olson
Department of Biology
Purdue University
West Lafayette, IN 47907 (USA)

particles (~ 2.3 nm) is diminished, whereas the peak representing the new generation of particles (~ 15 nm) becomes more pronounced. The solid products extracted by high-speed centrifugation from the samples A24h and A24hH4m were shown by X-ray analysis to be entirely amorphous, while sample A24hH6 displays Bragg reflections corresponding to the MFI-type structure.^[17] The XRD pattern of sample A24h is similar to that depicted in Figure 3a.

After aging the TPA-silica precursor solution for 30 days at room temperature (sample A30d), particles with a radius of between 1 and 15 nm are formed (Figure 2a). The solution

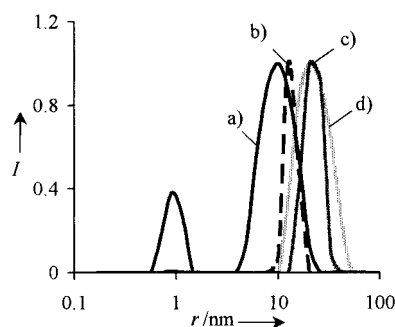


Figure 2. DLS data of TPA-silica precursor solutions: a) aged for 30 days (A30d) at RT, and after heating for b) 2 h (A30dH2), c) 3 h (A30dH3), and d) 4 h (A30dH4) at 90 °C. The DFA is displayed as scattering intensity per unweighted particle size classes.

remained clear over this extended time period. From the particle size distribution data of this sample, we can conclude that the primary sub-colloidal units are consumed during the long aging period, and that a new particle population is formed. The distribution depicted in Figure 2a shows that upon aging for 30 days, the precursor species rearrange into two distinct particulate forms, with mean radii of about 1 nm and 10 nm, respectively. These particles exhibit X-ray scattering, suggesting the onset of crystalline order of the MFI structure (Figure 3a). After hydrothermal treatment of the samples for 2, 3, and 4 h, the particle size distribution curves show the disappearance of the sub-colloidal fraction (~ 1 nm) in favor of the formation of larger particles with radii between 10 and 60 nm (Figure 2b, c, d). The appearance of diffraction lines suggests the emergence of crystalline MFI-type zeolite in sample A30dH2, (Figure 3b), with a fully crystalline sample obtained after hydrothermal treatment for 3 h (A30dH3) (Figure 3c).

Analysis by HRTEM supports the results of the X-ray analysis, as formation of crystalline Si-MFI is clearly observed in sample A30d (Figure 4a). This

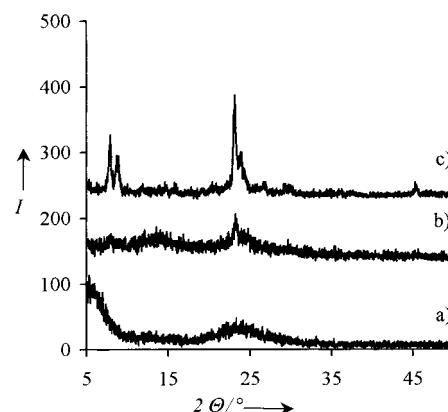


Figure 3. Powder diffraction patterns of a) a precursor solution aged for 30 days (A30d) at room temperature, and after hydrothermal treatment at 90 °C for b) 2 h (A30dH2) and c) 3 h (A30dH3).

HRTEM image reveals, for the first time, the presence of solid objects with a mean radius in the range of 2–10 nm having crystalline fringes corresponding to the MFI structure. Further evidence of the significant crystallinity of the nano-sized particles in sample A30d was obtained from IR spectroscopy. Freeze-dried samples of A30d and A30dH3, prepared in KBr pellets, yielded distinct absorptions at 459 and 557 cm^{-1} for A30dH3, while A30d shows two bands shifted to higher frequencies, at 462 and 580 cm^{-1} . The

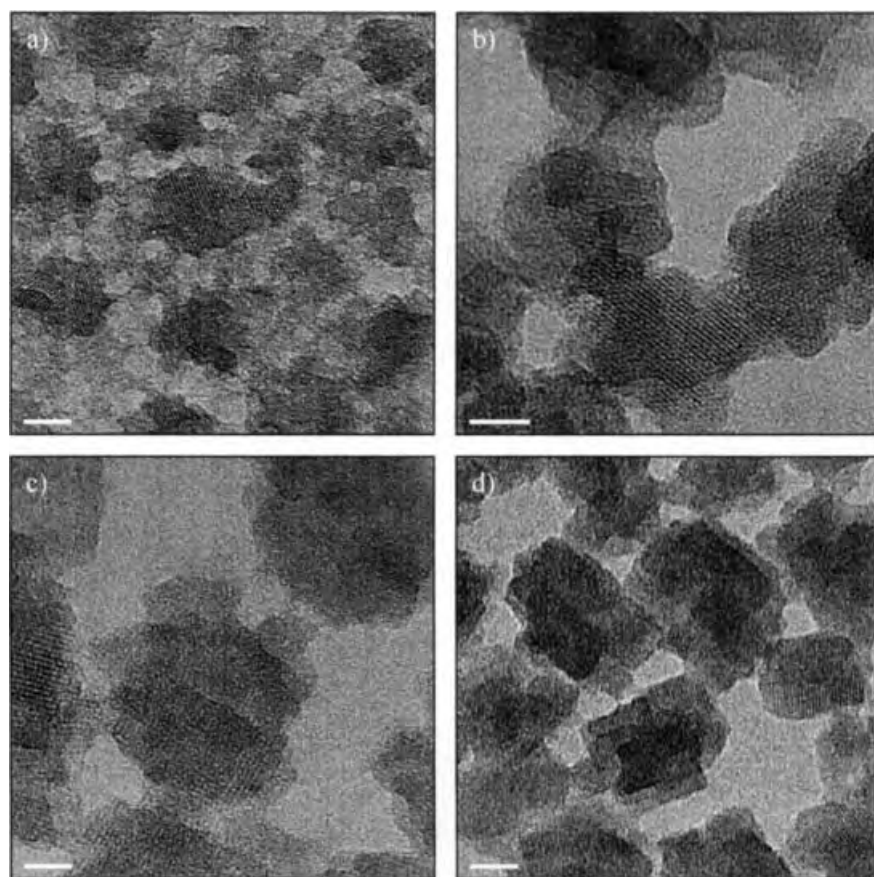


Figure 4. HRTEM images of nanosized particles extracted from a) a TPA-silica precursor solution aged for 30 days (A30d) at room temperature, and after heating for b) 2 h (A30dH2), c) 3 h (A30dH3), and d) 4 h (A30dH4) at 90 °C. Scale bar = 10 nm. (See Experimental Section for details).

frequency shift can be ascribed to the small size of silicate particles containing double 5-rings, while the different ratios between the two bands ($\sim 560/\sim 460\text{ cm}^{-1}$) suggest a lower degree of crystallinity in the A30d sample than in the hydrothermally treated A30dH3 sample.^[15] These data confirm that the MFI topology can be formed by aging at room temperature. Notably, the particles are very stable during the sample purification process, which includes one-step centrifugation and ultrasonic redispersion in doubly distilled water.

A complementary ^{29}Si solid-state NMR investigation was performed with the solution A30d and freeze-dried particles of sample A30dH3. Sharp ^{29}Si NMR signals are observed between $\delta = -71.2$ and -98 ppm in sample A30d; these are attributed to Q^0 , Q^1 , Q^2 , and Q^3 units of small silicate species in the liquid phase (Figure 5a). In addition, two broad signals

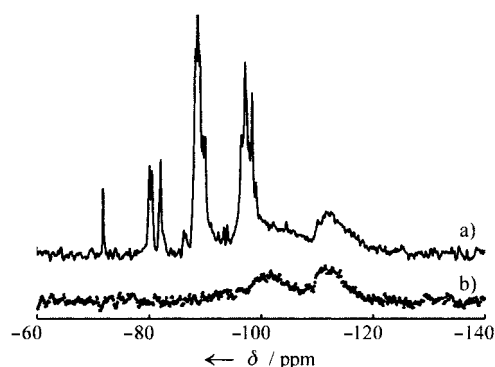


Figure 5. ^{29}Si NMR spectra of a) the as-prepared TPA-silica precursor solution aged for 30 days (A30d) at room temperature and b) the freeze-dried MFI crystalline sample collected from the solution heated at 90°C for 3 h (A30dH3).

at $\delta = -101.5$ and -112.2 ppm are also observed, indicating the presence of species with mainly Q^3 and Q^4 sites, which correspond to larger condensed polysilicate units in the solid nanoparticles (Figure 5a). The difference in the width of the signals measured for this sample is attributed to the presence of Q^0 , Q^1 , Q^2 , and Q^3 silicate species mainly in the liquid phase, and Q^3 and Q^4 units in the solid phase. In the freeze-dried crystalline MFI sample A30dH3 (Figure 5b), two broad resonance signals are detected with chemical shifts of $\delta = -101.5$ and -112.2 ppm, respectively. The intensity of the two resonance signals, assigned to Q^3 and Q^4 units, is similar. This is probably due to a high concentration of Q^3 silicon existing at the external surface of the nanoparticles, and at internal defects. Since the position and the intensity of the two signals at $\delta = -101.5$ and -112.2 ppm in the liquid and solid samples are similar it is suggested that they are due to the presence of crystalline Si-MFI type nanoparticles in both cases.

During hydrothermal treatment of sample A30d, the crystalline particles grow until the small sub-colloidal particles ($\sim 1\text{ nm}$) are completely consumed. The DLS data provide information on the consumption of the nanometer-scale precursor crystalline particles, and the formation of the larger MFI crystals, which display mono-modal particle size distribution (Figure 2). The size distribution measured for sample A30dH3 (3 h HT treatment) is sharper than that for

sample A30dH4 (4 h), which is probably due to a more homogeneous distribution of round-shaped colloidal crystals in the former. TEM images of the extracted particles from these samples are shown in Figure 4b, c, and d. The particles in all three samples are single crystals with the expected lattice fringes of MFI-type zeolite. No intergrowth of different lattice orientations is observed, indicating that each crystal was generated from one single-crystalline nanoparticle existing in the aged solution. The Si-MFI crystals obtained from samples A30dH2 and A30dH3 are cauliflower-shaped, while the individual particles in sample A30dH4 have the platelike coffin morphology typical for MFI-type crystals. The formation of crystalline MFI zeolite is more rapid from the solution aged for 30 days (about 3 h) than that obtained after aging for only 24 h (about 6 h). Very effective crystal growth was achieved in the aged precursor solution, where the nutrient pool consists of the sub-colloidal MFI particles formed at room temperature, which resembles Ostwald ripening during crystal growth processes.

In conclusion, we have shown how DLS, HRTEM, and other data provide information about the formation and consumption of particles in reactive organosilica solutions leading to nanoscale crystalline Si-MFI particles. Most strikingly, sub-colloidal precursor particles crystallize within 1 to 30 days at room temperature to form the MFI topology. Additional heating leads to the formation of a second larger crystal-size population at the expense of the sub-colloidal crystals. These findings strongly suggest that the aging step in zeolite synthesis leads to the formation of nanoscale crystalline particles, or domains of the desired zeolite phase. This provides a clear understanding of the paramount importance of such low-temperature pre-treatment steps in zeolite synthesis.

Experimental Section

Nanosized Si-MFI crystals were prepared from clear solutions with a molar composition: $9\text{ TPAOH} : 25\text{ SiO}_2 : 530\text{ H}_2\text{O} : 100\text{ EtOH}$. Tetraethoxysilane (TEOS, 98%; Aldrich), tetrapropylammonium hydroxide (TPAOH; Aldrich) and doubly distilled water were used as starting materials. The precursor solution was aged on an orbital shaker (180 rpm) at room temperature for between 24 h and 30 days. Further crystallization was carried out in a quartz cuvette mounted in the DLS instrument with an internal heater set to 90°C for up to 6 h. All samples with different times of aging and crystallization are specified in Table 1.

In situ DLS was used (ALV-NIBS/HPSS) to investigate the polycondensation process of TEOS in a concentrated aqueous solution of TPAOH at room temperature, and upon hydrothermal treatment at 90°C . The back scattering geometry (scattering angle 173° , HeNe laser with 3 mW output power at 632.8 nm wavelength) permits measurements at high sample

Table 1. Conditions for the preparation of Si-MFI zeolite.

Sample ^[a]	Aging time	Crystallization time
A24h	24 h	–
A24hH4m	24 h	4 min
A24hH6	24 h	6 h
A30d	30 days	–
A30dH2	30 days	2 h
A30dH3	30 days	3 h
A30dH4	30 days	4 h

[a] Abbreviations: A = aged sample; H = hydrothermally treated sample.

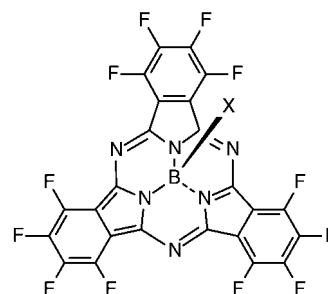
concentration, because a complete penetration of the incident light through the sample was not required. The distribution function analysis (DFA) data were used to investigate multi-modal particle size distributions in the liquid samples. HRTEM images were recorded by using a Philips CM 200 FEG TEM operated at 200 kV. The ^{29}Si MAS experiments were carried out with 4 mm ZrO_2 rotors in a commercial double resonance probe using a DSX advance impulse spectrometer (Bruker DSX Avance 500) working at a resonance frequency of 99.369 MHz. The samples were examined by using a single-pulse acquisition. The 90° pulse length and the recycle delay were set to 3.0 μs and 40 s. The XRD measurements were performed on a Scintag XDS 2000 diffractometer using $\text{CuK}\alpha$ radiation. IR spectra were recorded from KBr pellets on a Bruker Equinox 55 spectrometer. Prior to the XRD and IR measurements, nanosized crystals were separated from the mother liquor by one-step centrifugation at 20000 rpm for 1 h, and redispersed in an ultrasonic bath in doubly distilled water for 2 h prior to further investigations. Solid products were obtained by freeze-drying of the centrifuged samples.

Received: January 24, 2002 [Z18579]

Synthesis, Separation, and Characterization of the Topoisomers of Fused Bicyclic Subphthalocyanine Dimers**

Christian G. Claessens and Tomás Torres*

Subphthalocyanines (SubPcs, **1**)—lower homologues of phthalocyanines—are nonplanar cone-shaped aromatic macrocycles comprising three N-fused diiminoisindoline units around a boron atom core.^[1] The 14 π -electron system



1a X = Cl
1b X = OPh

characteristic of these compounds confers interesting optical properties that have been exploited in the fields of dyes, nonlinear optics, and photonic devices.^[1] Moreover, these properties may be fine-tuned since the axial (X) and peripheral positions in SubPcs (see **1**) can be easily functionalized or derivatized.^[1] On the other hand, the intrinsic chirality of subphthalocyanines with C_3 or C_1 symmetries represents^[2] also a promising feature that enhances their potential as building blocks for the construction of complex molecules.^[1]

One focus of our current efforts is the stepwise synthesis of extended π surfaces.^[3] Thus, we have recently described the preparation of heterobinuclear azaporphyrinic systems^[4a] as well as multinuclear annulene–phthalocyanines.^[4b] In this regard, although fused binuclear phthalocyanine dimers are well-known,^[5] only one example of a fused subphthalocyanine dimer analogue, whose characterization data (^1H NMR and UV/Vis spectroscopy) do not agree with any of the characteristic features described herein, has been claimed.^[6]

[*] Prof. T. Torres, Dr. C. G. Claessens
Departamento de Química Orgánica
Facultad de Ciencias
Universidad Autónoma de Madrid
Cantoblanco, 28049 Madrid (Spain)
Fax: (+34)91-397-3966
E-mail: tomas.torres@uam.es

[**] This work was supported by the CICYT (Spain; research project MAT-99-0180) and the European Community (contract HPRN-CT-2000-00020). C.G.C. thanks the CICYT for a “Ramon y Cajal” contract. We thank César J. Pastor Montero from the Servicio Interdepartamental de Investigación de la Universidad Autónoma de Madrid for the X-ray structure elucidation. Editorial Note: See also following communication in this issue: T. Fukuda, J. R. Stork, R. J. Potucek, M. M. Olmstead, B. C. Noll, N. Kobayashi, W. S. Durfee, *Angew. Chem.* **2002**, *114*, 2677; *Angew. Chem. Int. Ed.* **2002**, *41*, 2565.

Supporting information for this article is available on the WWW under <http://www.angewandte.org> or from the author.

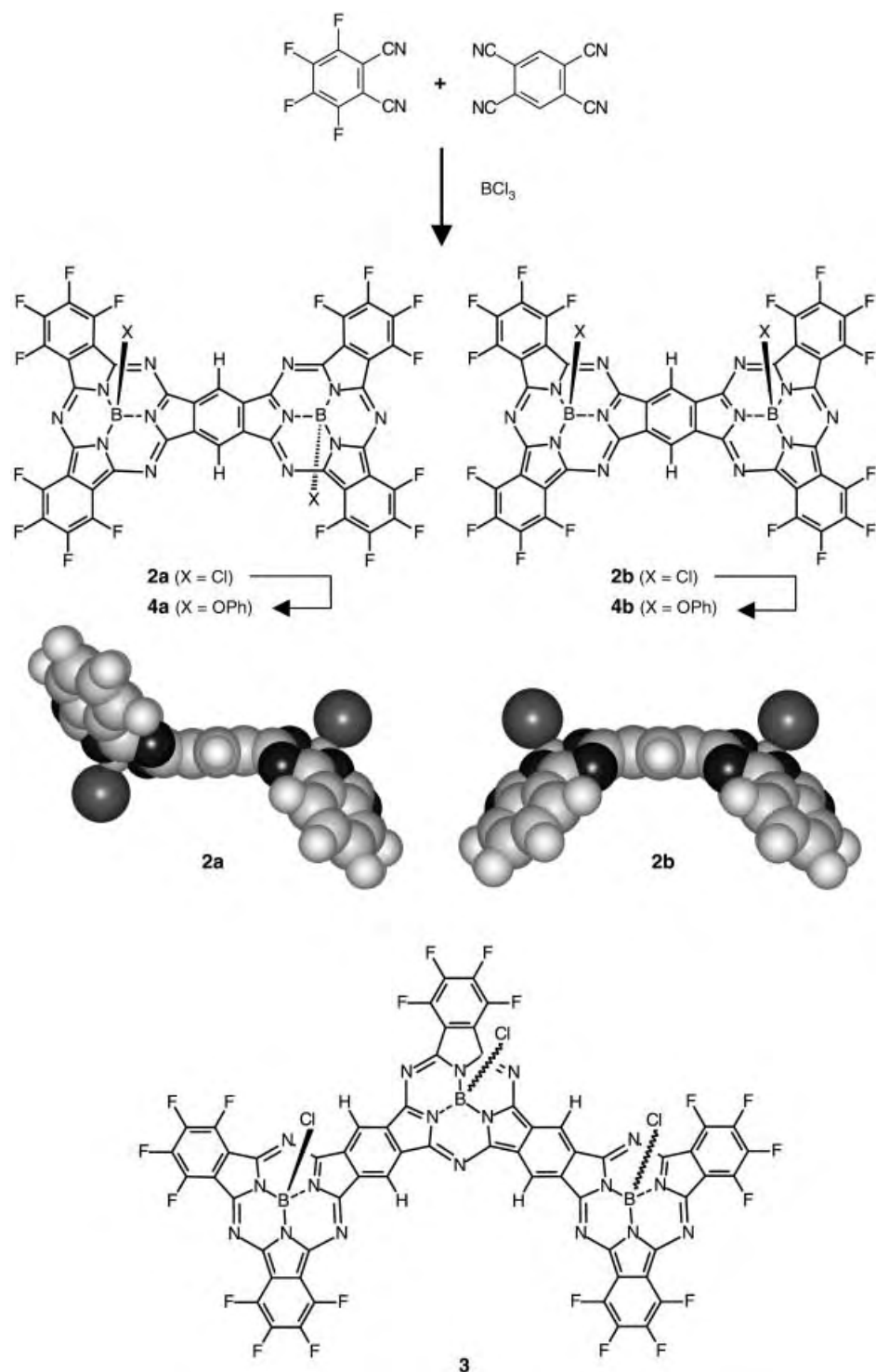
- [1] C. S. Cundy, M. S. Henty, R. J. Plaisted, *Zeolites* **1995**, *15*, 400.
- [2] P.-P. E. A. de Moor, T. P. M. Beelen, B. U. Komanschek, R. A. van Santen, *Micropor. Mesopor. Mater.* **1998**, *21*, 263.
- [3] S. L. Burkett, M. E. Davis, *Chem. Mater.* **1995**, *7*, 920.
- [4] M. Tsapatsis, M. Lovallo, M. E. Davis, *Micropor. Mater.* **1996**, *5*, 381.
- [5] M. W. Anderson, J. R. Agger, J. T. Thornton, N. Forsyth, *Angew. Chem.* **1996**, *108*, 1301; *Angew. Chem. Int. Ed. Engl.* **1996**, *35*, 1210.
- [6] a) A. E. Persson, B. J. Schoeman, J. Sterte, J.-E. Otterstedt, *Zeolites* **1994**, *14*, 557; b) B. J. Schoeman, *Zeolites* **1997**, *18*, 97; c) B. J. Schoeman, *Micropor. Mesopor. Mater.* **1998**, *22*, 9; d) T. A. M. Twomey, M. Mackay, H. P. C. E. Kuipers, R. W. Thompson, *Zeolites* **1994**, *14*, 162.
- [7] C. E. A. Kirschhock, R. Ravishankar, F. Verspeurt, P. J. Grobet, P. A. Jacobs, J. A. Martens, *J. Phys. Chem.* **1999**, *103*, 4965.
- [8] S. L. Burkett, M. E. Davis, *J. Phys. Chem.* **1994**, *98*, 4647.
- [9] a) P.-P. E. A. de Moor, T. P. M. Beelen, R. A. van Santen, *J. Phys. Chem.* **1999**, *103*, 1639; b) P.-P. E. A. de Moor, T. P. M. Beelen, R. A. van Santen, L. W. Beck, M. E. Davis, *J. Phys. Chem.* **2000**, *104*, 7600.
- [10] a) R. I. Walton, F. Millange, D. O'Hare, A. T. Davies, G. Sanker, C. R. A. Catlow, *J. Phys. Chem.* **2001**, *105*, 83; b) R. I. Walton, D. O'Hare, *J. Phys. Chem.* **2001**, *105*, 91.
- [11] a) S. Mintova, N. Olson, V. Valtchev, T. Bein, *Science* **1999**, *283*, 958; b) S. Mintova, N. Olson, T. Bein, *Angew. Chem.* **1999**, *111*, 3400; *Angew. Chem. Int. Ed.* **1999**, *38*, 3201.
- [12] O. Regev, Y. Cohen, E. Kehat, Y. Talmon, *Zeolites* **1994**, *14*, 314–319.
- [13] O. Terasaki, *Molecular Sieves: Science and Technology*, Vol. 2 (Eds.: H. G. Karge, J. Weitkamp), Springer, Berlin, **1999**, p. 71.
- [14] B. J. Schoeman, *Zeolites* **1997**, *18*, 97.
- [15] a) R. Ravishankar, C. E. A. Kirschhock, B. J. Schoeman, P. Vanoppen, P. J. Grobet, S. Storck, W. F. Maier, J. A. Martens, F. C. De Schryver, P. A. Jacobs, *J. Phys. Chem. B* **1998**, *102*, 2633; b) R. Ravishankar, C. E. A. Kirschhock, P.-P. Knops-Gerrits, E. J. P. Feijen, P. J. Grobet, P. Vanoppen, F. C. De Schryver, G. Miehe, H. Fuess, B. J. Schoeman, P. A. Jacobs, J. A. Martens, *J. Phys. Chem. B* **1999**, *103*, 4960; c) C. E. A. Kirschhock, R. Ravishankar, L. Van Looveren, P. A. Jacobs, J. A. Martens, *J. Phys. Chem. B* **1999**, *103*, 4972; d) C. E. A. Kirschhock, R. Ravishankar, P. A. Jacobs, J. A. Martens, *J. Phys. Chem. B* **1999**, *103*, 11021; e) C. E. A. Kirschhock, V. Buschmann, S. Kremer, R. Ravishankar, C. J. Y. Houssin, B. L. Mojet, R. A. van Santen, P. J. Grobet, P. A. Jacobs, J. A. Martens, *Angew. Chem.* **2001**, *113*, 2707; *Angew. Chem. Int. Ed.* **2001**, *40*, 2637.
- [16] a) S. D. Kinrade, C. T. G. Knight, D. L. Pole, R. T. Syvitski, *Inorg. Chem.* **1998**, *37*, 4272; b) S. D. Kinrade, C. T. G. Knight, D. L. Pole, R. T. Syvitski, *Inorg. Chem.* **1998**, *37*, 4278.
- [17] M. M. J. Treasy and J. B. Higgins, *Collection of Simulated XRD Powder Patterns of Zeolites*, 4th rev. ed., Elsevier, Dordrecht, **2001**, p. 234.

Herein we report on the synthesis of fused subphthalocyanine dimers (Scheme 1), and show for the first time that this kind of binuclear system is actually formed as a mixture of two topoisomers that have been separated and characterized.

The dichloro-SubPc dimers **2a** and **2b** (Scheme 1) were synthesized by statistical condensation of ten equivalents of tetrafluorophthalonitrile and one equivalent of 1,2,4,5-benzenetetracarboxitrile in the presence of three equivalents of boron trichloride according to a procedure similar to the one

described in reference [7]. After purification by column chromatography on silica gel, bright blue dimers **2a** and **2b** (Scheme 1) and purple SubPc **1a** were obtained in 9, 11, and 43 % yield, respectively. Very small quantities of a mixture of the dark blue trimer **3**, which theoretically consists of three topoisomers (*syn,syn*, *syn,trans*, and *trans,trans*), were also isolated.

¹H NMR spectra of topoisomers **2a** and **2b** showed a singlet at $\delta = 10.48$ and 10.46 ppm, respectively, corresponding to the



Scheme 1. Synthesis of compounds **2a,b**, **3a–c**, and **4a,b**.

protons attached to the central benzene ring.^[8] These very high chemical shifts indicate unambiguously the aromatic character of the junction between the two subphthalocyanine halves of the molecules. The small difference between the chemical shifts corresponding to each topoisomer shows that the geometry of the molecule does not influence very much the ring currents. The UV/Vis spectra (Figure 1) of dimers **2a** and **2b** revealed the presence of the expected B and Q bands characteristic of porphyrazines. Both spectra showed a Q-band region composed of 1) a sharp band at 693 and 692 nm, respectively, whose intensity ($\lg(\epsilon)=4.9$) is comparable to that of Pcs, and 2) three less intense bands at about 660, 630, and 600 nm, whose intensity ($\lg(\epsilon)=4.4-4.5$) is comparable to that of SubPcs. The UV/Vis spectrum of trimer **3** shows a very intense ($\lg(\epsilon)=4.9$) Q band at 755 nm along with smaller bands at shorter wavelength (Figure 1). The huge shifts for the Q band (118–119 nm for **2a** and **2b**, and 181 nm for **3a–c**, with respect to the position of the Q band in SubPc **1a**) along with their higher intensity clearly indicate that the SubPc subunits within the dimers and trimers are fully conjugated.^[9]

The substitution of the chlorine atom in the axial position of dimers **2a** and **2b** by a bulkier group, such as a phenoxy group, allowed the assignment of the resulting topoisomers **4a** and **4b** (Scheme 1). Thus, the previous reaction between 1,2,4,5-benzenetetracarbonitrile and tetrafluorophthalonitrile was performed and the crude reaction product was treated with phenol at 120 °C overnight (Scheme 1). Dimers **4a** and **4b**

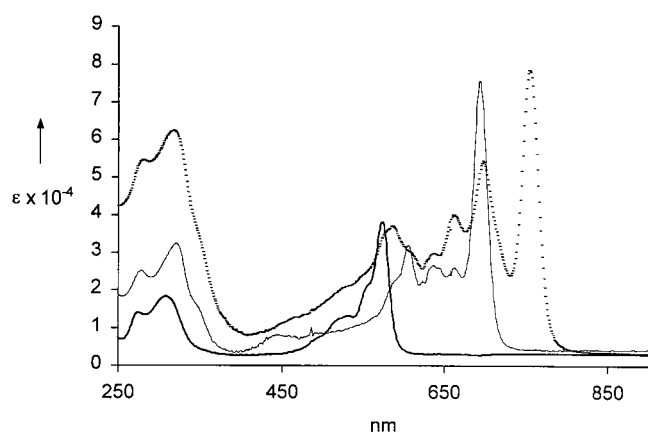


Figure 1. UV/Vis spectra of compounds **2b**, **1b**, and **3a–c** in chloroform.

were obtained, after purification by column chromatography, in 6 and 7% yields, respectively. Symmetrical SubPc **1b** was isolated in 34% yield and single crystals suitable for X-ray crystallography were obtained by slow evaporation from a solution of **1b** in acetone.^[10] The X-ray crystal structure of SubPc **1b** (Figure 2) is very similar to those of other SubPcs in the few examples reported,^[11] thus demonstrating the rigid character of the cone-shaped macrocyclic core that remains virtually unchanged.^[1]

However, remarkably, the packing in the solid state is (Figure 3) very different from the ones already observed and shows infinite one-dimensional hydrogen-bonded arrays of SubPcs. Two subPcs are intermolecularly connected by two C–H...F hydrogen bonds between protons H2 and H3 and fluorine atoms F3 and F4, respectively (See Figure 2 and 3).^[12]

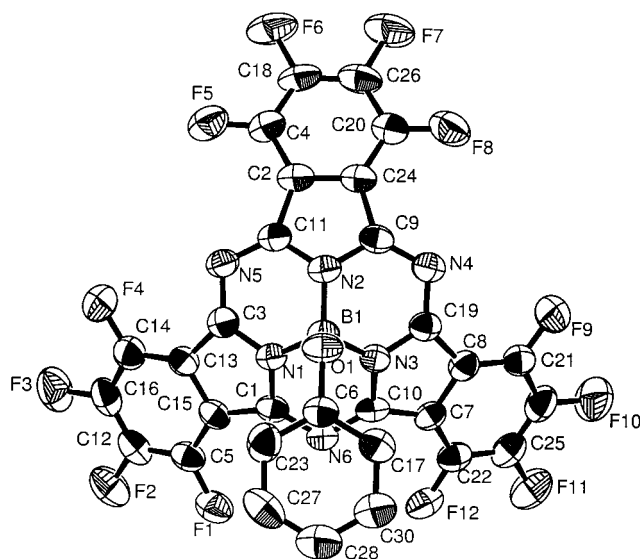


Figure 2. Structure of the subphthalocyanine **1b** (ORTEP representation).

¹H NMR spectra of compounds **4a** and **4b** both exhibit a singlet at $\delta = 10.40$ and 10.36 ppm, respectively, in a similar way as **2a** and **2b**. Moreover, all three spectra corresponding to **4a**, **4b**, and **1b** showed signals at $\delta = 6.8$ – 5.3 ppm corresponding to the protons on the phenyl group. In particular, the *ortho* aromatic protons close to the SubPc ring give rise to very shielded doublets at $\delta_1 = 5.36$, $\delta_2 = 5.49$, and $\delta_3 = 5.31$ ppm in **4a**, **4b**, and **1b**, respectively, as a consequence of the strong ring currents produced by the aromatic SubPc moieties. The chemical shift difference $\Delta\delta = \delta_2 - \delta_1 =$

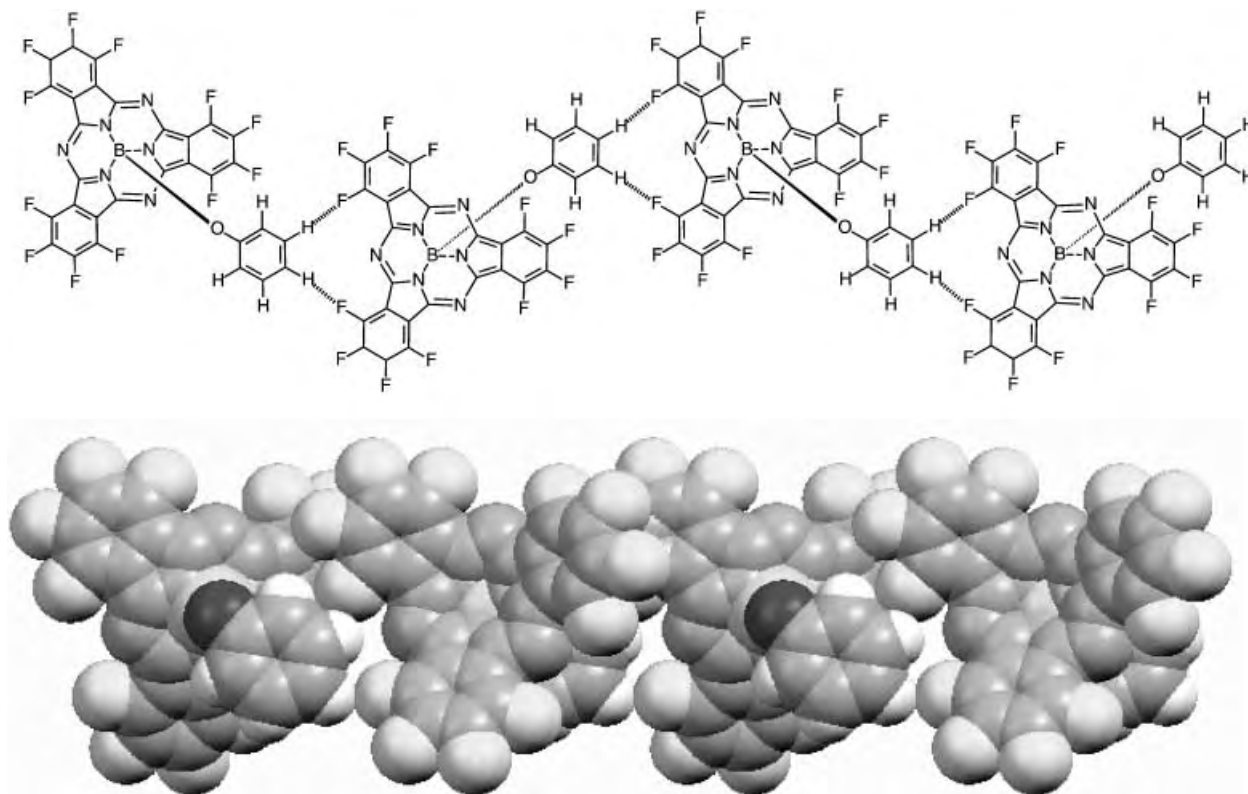


Figure 3. Schematic and CPK structure of the one-dimensional H-bonded array of subphthalocyanines in the X-ray crystal structure of **1b**.

0.13 ppm may be interpreted on the basis of computer-generated CPK models of topoisomers **4a** and **4b** (Figure 4).^[13]

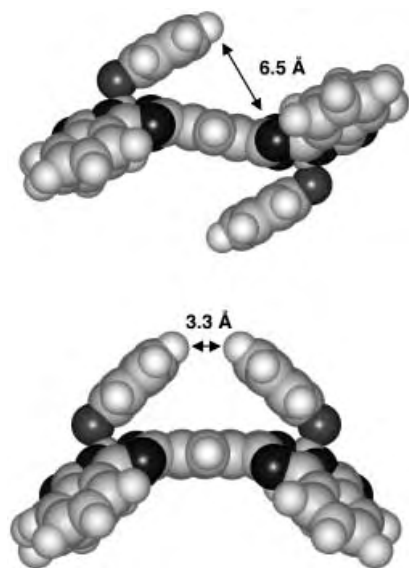


Figure 4. Computer-generated CPK models of the *syn* and *anti* topoisomers of dimer **2**, showing the shortest possible distances between the axial phenyl ring and the closest atom in the other half of the dimer.

In the *anti* topoisomer, the protons of the axial phenyl ring of one SubPc half are located^[14] at a distance ≥ 6.5 Å from the closest atoms of the other SubPc half, showing that these protons should give rise to ^1H NMR signals very similar to the ones of SubPc **1b**. On the other hand, the protons of the axial phenyl ring in the *syn* topoisomer are located^[14] at a distance ≥ 3.3 Å from the closest atoms of the other phenyl ring, thus showing a possible magnetic dipolar interaction between the two phenyl rings. In this way we propose the following model in which the *anti* isomer is **4a** ($\delta_1 \approx \delta_3$) and the *syn* isomer is **4b** ($\delta_2 \neq \delta_3$).^[15] Subsequently, it was shown that dimers **2a** and **2b**, when treated individually with phenol, gave rise to **4a** and **4b**, respectively. It was then possible to ascertain that **2a** and **2b** were *anti* and *syn* topoisomers, respectively.

In conclusion, we have synthesized and fully characterized the fused subphthalocyanine dimers **2a,b** and **4a,b**. The careful examination of NMR and X-ray data allowed the assignment of the structure of the topoisomers *anti* **4a** and *syn* **4b**. Chemical derivatization of **2a** and **2b** into **4a** and **4b** allowed the assignment of the topoisomers *anti* **2a** and *syn* **2b**. This represents, we believe, a first step towards the stepwise synthesis of larger fully conjugated SubPc structures.

Experimental Section

Compounds **1a**, **2a**, **2b**, and **3a–c**: BCl_3 (10.1 mL of a 1 M solution in *p*-xylene) was added dropwise to a solid mixture of tetrafluorophthalonitrile (561 mg, 2.81 mmol) and 1,2,4,5-benzenetetracarboxitrile (50 mg, 0.28 mmol). The reaction mixture was refluxed for three hours and after cooling down to room temperature, was flushed with argon. The resulting dark purple slurry was then evaporated under vacuo and subjected to various column chromatographies on silica gel using acetone/hexane (1:0 to 1:4, v/v). Four main fractions were collected; order of elution: **1a**, **2a**, **2b**, **3**;

note that the elution order of **2a** and **2b** is swapped when toluene/hexane mixtures are employed.

SubPc **1a**: Purple powder, 260 mg (43 %); see Supporting Information.

Dimer **2a**: Blue reddish powder, 27 mg (9 %); m.p. $> 250^\circ\text{C}$; ^1H NMR (300 MHz, CDCl_3 , 25°C): $\delta = 10.48$ ppm (s); IR (KBr): $\tilde{\nu} = 1539, 1487, 1400, 1285, 1225, 1165, 1115, 1067, 1020, 962, 858, 789, 638, 592, 557\text{ cm}^{-1}$; UV/Vis (CHCl_3): $\lambda_{\text{max}}(\text{lg}(\epsilon)) = 693$ (4.9), 661 (4.4), 635 (4.4), 604 (4.5), 592 (sh), 441 (3.7), 319 (4.5), 278 nm (4.4); MALDI-TOF: m/z : 1070.7 [M^+] and [$M^+ + \text{H}$]; HR-LSIMS calcd for $\text{C}_{42}\text{H}_{21}\text{N}_{12}\text{F}_{16}\text{B}_2\text{Cl}_2$: [M^+]: m/z : 1069.9833, found 1069.9845; elemental analysis calcd (%) for $\text{C}_{42}\text{H}_{21}\text{N}_{12}\text{F}_{16}\text{B}_2\text{Cl}_2$: C 47.10, H 0.19, N 15.69; found: C 47.56, H 0.26, N 15.25.

Dimer **2b**: Blue reddish powder, 33 mg (11 %); m.p. $> 250^\circ\text{C}$; ^1H NMR (300 MHz, CDCl_3 , 25°C): $\delta = 10.46$ ppm (s); IR (KBr): $\tilde{\nu} = 1535, 1481, 1400, 1273, 1219, 1165, 1111, 1070, 1016, 966, 856, 795, 708, 658, 586\text{ cm}^{-1}$; UV/Vis (CHCl_3): $\lambda_{\text{max}}(\text{lg}(\epsilon)) = 692$ (4.9), 662 (4.4), 636 (4.4), 605 (4.5), 592 (sh), 441 (3.9), 320 (4.5), 278 nm (4.4); MALDI-TOF: m/z : 1071.7 [M^+] and [$M^+ + \text{H}$]; HR-LSIMS calcd for $\text{C}_{42}\text{H}_{21}\text{N}_{12}\text{F}_{16}\text{B}_2\text{Cl}_2$: [M^+]: m/z : 1069.9833, found 1069.9825; elemental analysis calcd (%) for $\text{C}_{42}\text{H}_{21}\text{N}_{12}\text{F}_{16}\text{B}_2\text{Cl}_2$: C 47.10, H 0.19, N 15.69; found: C 47.61, H 0.31, N 15.51.

Trimer **3**: Dark blue powder, 6 mg (3 %); m.p. $> 250^\circ\text{C}$; ^1H NMR (300 MHz, CDCl_3 , 25°C): $\delta = 10.58$ (s), 10.53 (s), 10.51 (s), 10.48 (s), 10.44 ppm (s); IR (KBr): $\tilde{\nu} = 1733, 1625, 1537, 1517, 1483, 1402, 1281, 1220, 1166, 1112, 1058, 1017, 858, 794, 706, 653, 578\text{ cm}^{-1}$; UV/Vis (CHCl_3): $\lambda_{\text{max}}(\text{lg}(\epsilon)) = 755$ (4.9), 697 (4.6), 661 (4.5), 637 (4.4), 585 (4.5), 317 (4.6), 280 nm (4.6); MALDI-TOF: m/z : 1495.6 [M^+]; HR-LSIMS calcd for $\text{C}_{60}\text{H}_{18}\text{N}_{18}\text{F}_{20}\text{B}_3\text{Cl}_3$: [M^+]: m/z : 1493.9892, found 1493.9936; elemental analysis calcd (%) for $\text{C}_{60}\text{H}_{18}\text{N}_{18}\text{F}_{20}\text{B}_3\text{Cl}_3$: C 48.19, H 0.27, N 16.86; found: C 48.54, H 0.41, N 16.33.

Compounds **1b**, **4a**, and **4b**: A mixture of phenol (500 mg, 5.3 mmol) and the crude product from the previous reaction was warmed up to 120°C overnight. The resulting solid was then subjected to various column chromatographies on silica gel using dichloromethane, ethyl acetate/hexane (1/4), and acetone/hexane (1:0 to 1:4, v/v).

Subphthalocyanine **1b**: Purple powder, 224 mg (34 %); see Supporting Information.

Dimer **4a**: Dark blue powder, 20 mg (6 %); m.p. $> 250^\circ\text{C}$; ^1H NMR (300 MHz, CDCl_3 , 25°C): $\delta = 10.40$ (s, 2H), 6.75–6.60 (m, 6H), 5.36 ppm (d, $J = 7.6$ Hz, 4H); IR (KBr): $\tilde{\nu} = 1529, 1477, 1393, 1275, 1213, 1161, 1107, 1080, 968, 899, 702, 644, 598\text{ cm}^{-1}$; UV/Vis (CHCl_3): $\lambda_{\text{max}}(\text{lg}(\epsilon)) = 688$ (4.9), 657 (4.4), 631 (4.4), 600 (4.5), 587 (sh), 441 (3.7), 319 (4.4), 274 nm (4.3); MALDI-TOF: m/z : 1186.9 [M^+] and [$M^+ + \text{H}$]; HR-LSIMS calcd for $\text{C}_{54}\text{H}_{12}\text{N}_{12}\text{F}_{16}\text{B}_2\text{O}_2$: [M^+]: m/z : 1187.1137, found 1187.1146; elemental analysis calcd (%) for $\text{C}_{54}\text{H}_{12}\text{N}_{12}\text{F}_{16}\text{B}_2\text{O}_2$: C 54.67, H 1.02, N 14.17; found: C 55.11, H 1.32, N 13.77.

Dimer **4b**: Dark blue powder, 23 mg (7 %); m.p. $> 250^\circ\text{C}$; ^1H NMR (300 MHz, CDCl_3 , 25°C): $\delta = 10.36$ (s, 2H), 6.905–6.72 (m, 6H), 5.49 ppm (d, $J = 8.2$ Hz, 4H); IR (KBr): $\tilde{\nu} = 1531, 1477, 1396, 1265, 1225, 1103, 995, 903, 760, 708, 644, 594\text{ cm}^{-1}$; UV/Vis (CHCl_3): $\lambda_{\text{max}}(\text{lg}(\epsilon)) = 689$ (4.9), 657 (4.4), 631 (4.4), 601 (4.5), 586 (sh), 441 (3.9), 319 (4.5), 273 nm (4.5); MALDI-TOF: m/z : 1186.8 [M^+] and [$M^+ + \text{H}$]; HR-LSIMS calcd for $\text{C}_{54}\text{H}_{12}\text{N}_{12}\text{F}_{16}\text{B}_2\text{O}_2$: [M^+]: m/z : 1186.1137, found 1186.1190; elemental analysis calcd (%) for $\text{C}_{54}\text{H}_{12}\text{N}_{12}\text{F}_{16}\text{B}_2\text{O}_2$: C 54.67, H 1.02, N 14.17; found: C 54.95, H 1.27, N 13.64.

Received: February 20, 2002 [Z18749]

- [1] C. G. Claessens, D. González-Rodríguez, T. Torres, *Chem. Rev.* **2002**, 102, 835–853.
- [2] a) C. G. Claessens, T. Torres, *Tetrahedron Lett.* **2000**, 41, 6361–6365; b) N. Kobayashi, *Coord. Chem. Rev.* **2001**, 219–221, 99–123.
- [3] a) J. O. Jeppesen, K. Takimiya, F. Jensen, T. Brimert, K. Nielsen, N. Thorup, J. Becher, *J. Org. Chem.* **2000**, 65, 5794–5805; b) G. E. M. Maguire, E. S. Meadows, C. L. Murray, G. W. Gokel, *Tetrahedron Lett.* **1997**, 38, 6339–6342.
- [4] a) G. De la Torre, M. V. Martínez-Díaz, P. R. Ashton, T. Torres, *J. Org. Chem.* **1998**, 63, 8888–8893; b) E. M. García-Frutos, F. Fernández-Lazaro, E. M. Maya, P. Vázquez, T. Torres, *J. Org. Chem.* **2000**, 65, 6841–6846.

- [5] a) N. Kobayashi, T. Fukuda, D. Lelievre, *Inorg. Chem.* **2000**, *39*, 3632–3637; b) K. Ishii, N. Kobayashi, Y. Higashi, T. Osa, D. Lelievre, J. Simon, S. Yamauchi, *Chem. Commun.* **1999**, 969–970; c) N. Kobayashi, H. Lam, W. A. Nevin, P. Janda, C. C. Leznoff, T. Koyama, A. Monden, H. Shirai, *J. Am. Chem. Soc.* **1994**, *116*, 879–890; d) D. Lelievre, L. Bosio, J. Simon, J.-J. André, F. Bensebaa, *J. Am. Chem. Soc.* **1992**, *114*, 4475–4479; e) N. Kobayashi, M. Numao, R. Kondo, S. Nakajima, T. Osa, *Inorg. Chem.* **1991**, *30*, 2241–2244; f) E. S. Dods-worth, A. B. P. Lever, P. Seynour, C. C. Leznoff, *J. Phys. Chem.* **1985**, *89*, 5698–5705.
- [6] N. Kobayashi, *J. Chem. Soc. Chem. Commun.* **1991**, 1203–1205.
- [7] R. S. Nohr, J. G. MacDonald (Kimberly-Clark Worldwide, Inc., USA), PCT Int. Appl. WO 0,071,621 **2000** [*Chem. Abstr.* **2001**, *134*, 18557].
- [8] These low-field proton signals at $\delta \approx 10.5$ ppm were not reported in reference [6].
- [9] Few examples have been described of intramolecular interactions between phthalocyanine subunits in related binuclear phthalocyanine systems in which the two Pc moieties are connected through benzene rings.^[5] In these cases, the Q band undergoes a shift to the red, which has been attributed to the enlargement of the π -conjugated system, with concomitant splitting of the Q band as a consequence of intramolecular electronic coupling between the Pc subunits. However, in these cases, both red-shifting and splitting were much smaller than observed in the present study for SubPc dimers **2** and trimers **3**.
- [10] CCDC-179556 (**1b**) contains the supplementary crystallographic data for this paper. These data can be obtained free of charge via www.ccdc.cam.ac.uk/conts/retrieving.html (or from the Cambridge Crystallographic Data Centre, 12, Union Road, Cambridge CB2 1EZ, UK; fax: (+44) 1223-336-033; or deposit@ccdc.cam.ac.uk).
- [11] a) R. Potz, M. Göldner, H. Hückstädt, U. Cornelissen, A. Tutaß, H. Homborg, *Z. Anorg. Allg. Chem.* **2000**, *626*, 588–596; b) J. R. Stork, R. J. Potucek, W. S. Durfee, B. C. Noll, *Tetrahedron Lett.* **1999**, *40*, 8055–8058; c) M. K. Engel, J. Yao, H. Maki, H. Takeuchi, H. Yonehara, C. Pac, *Kawamura Rikagaku Kenkyusho Hokoku* **1997**, *9*, 53–65; d) K. Kasuga, T. Idehara, M. Handa, Y. Ueda, T. Fujiwara, K. Isa, *Bull. Chem. Soc. Jpn.* **1996**, *69*, 2559–2563; e) M. Hanack, J. Rauschnabel, *Tetrahedron Lett.* **1995**, *36*, 1629–1632; f) H. Kietai, *Monatsh. Chem.* **1974**, *105*, 405–418.
- [12] Two types of intermolecular hydrogen bonds were found in the X-ray crystal structure of SubPc **1b**: 1) C27–H2–F3a defined by $d(C \cdots F) = 3.265$ Å, $d(H \cdots F) = 2.667$ Å, $(C-H \cdots F) = 167^\circ$ and 2) C28–H3–F4b defined by $d(C \cdots F) = 3.432$ Å, $d(H \cdots F) = 2.533$ Å, $(C-H \cdots F) = 143^\circ$.
- [13] The CPK models were generated on the basis of the X-ray crystal structure of compound **1b**. They do not correspond to any energy minimum.
- [14] For both the *anti* and *syn* isomers, the distances were calculated after tilting the phenyl ring towards the other half of the dimer (see Figure 4).
- [15] We discarded any possible intermolecular interactions or aggregation since the ¹H NMR chemical shifts as well as the UV bands are not sensitive to changes of concentration.

cis and *trans* Forms of a Binuclear Subphthalocyanine**

Takamitsu Fukuda, Jay R. Stork, Richard J. Potucek, Marilyn M. Olmstead, Bruce C. Noll, Nagao Kobayashi,* and William S. Durfee*

In 1972 Mellor and Ossko^[1] reported the synthesis and spectroscopic characterization of the boron-containing subphthalocyanine (SubPc) macrocycle; the cone shape of SubPcs was confirmed by X-ray crystallography shortly thereafter.^[2] After a nearly 20 year hiatus, interest in these unusual systems was renewed when one of us (N.K.) published the synthesis and spectroscopic study of a binuclear SubPc in which two SubPc units shared a central benzene ring.^[3] As was subsequently pointed out, the bowl shape of the SubPc should result in *cis* and *trans* forms of the binuclear species, having C_{2v} and C_{2h} molecular symmetry, respectively.^[4]

We report here on the synthesis of a variation of the original binuclear SubPc, the separation of the *cis* and *trans* binuclear forms, and their spectroscopic and structural characterization (Scheme 1). In the original procedure 4-*tert*-butylphthalonitrile and 1,2,4,5-tetracyanobenzene were allowed to react in a 20:1 ratio with BBr_3 . We have replaced the 4-*tert*-butylphthalonitrile with tetrafluorophthalonitrile to prevent the formation of positional isomers that the 4-*tert*-butyl substituent engenders, and to reduce the number of benzo units that can undergo halogenation, an unavoidable side reaction when BBr_3 or BCl_3 is used in SubPc syntheses.^[5] We also report the X-ray crystal structure analysis of the perfluorinated monomer,^[6] derived from the cyclotrimerization of tetrafluorophthalonitrile, which is unavoidably the major product of the reaction.^[7]

[*] Prof. Dr. Dr. N. Kobayashi, T. Fukuda

Department of Chemistry
Graduate School of Science
Tohoku University
Sendai 980-8578 (Japan)
Fax: (+81) 22-217-9279

E-mail: nagaok@mail.cc.tohoku.ac.jp

Prof. W. S. Durfee, J. R. Stork, R. J. Potucek

Department of Chemistry
Buffalo State College
1300 Elmwood Avenue, Buffalo, NY 14222-1095 (USA)
Fax: (+1) 716-878-4028

E-mail: durfeews@buffalostate.edu

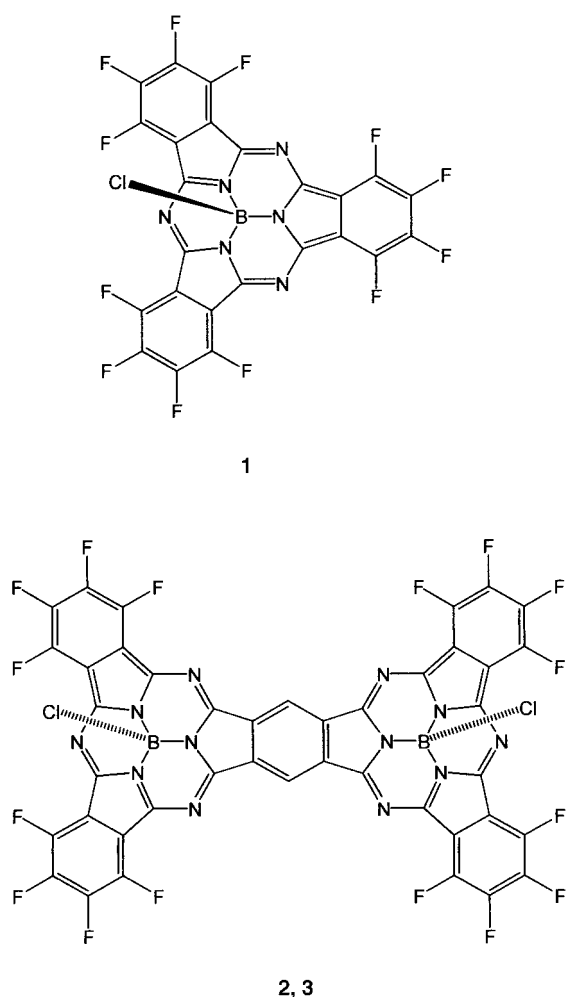
Dr. M. M. Olmstead

Department of Chemistry
University of California
One Shields Avenue, Davis, CA 95616-5298 (USA)

Dr. B. C. Noll

Department of Chemistry and Biochemistry
University of Colorado at Boulder
Boulder, CO 80309-0215 (USA)

[**] This work was supported by the Donors of the Petroleum Research Fund, administered by the American Chemical Society, the Research Foundation of the State University of New York (W.S.D.), the Daiwa Anglo-Japanese Foundation (N.K.), and a Grant-in-Aid for JSPS fellows (T.F.). Editorial Note: See also preceding communication in this issue: C. G. Claessens, T. Torres, *Angew. Chem.* **2002**, *114*, 2673; *Angew. Chem. Int. Ed.* **2002**, *41*, 2561.



Scheme 1. The structures of **1**, **2** (*cis*), and **3** (*trans*).

Figure 1 shows the X-ray structures of compounds **1**, **2** (*cis* form), and **3** (*trans* form). The structures^[8] of the three compounds show how the tetrahedral boron center forces a cupped geometry on the delocalized ring system. In each molecule, the boron atom is nearly 0.6 Å out of the plane of its three bonded nitrogen atoms. In the *cis*-SubPc **2**, the combination of two cupped monomer units leads to a full hemispherical molecule large enough to encircle the hemisphere of C_{60} . In the *trans*-SubPc **3**, the molecule has crystallographic inversion symmetry and forms a novel S-shaped molecule. Highly efficient and appealing packing arrangements result from the mutual fit of projections of one molecule into the cavity of its neighbor (Figure 2). Although the near absence of hydrogen atoms (0 H in **1**, 2 H in **2** and **3**) plays a part, and solvated CH_2Cl_2 molecules are present in the structures of **2** and **3**, the efficiency of the packing can be appreciated from the volume/non-H atoms of 13.0 Å³ in **1**, 14.3 Å³ in **2**, and 14.5 Å³ in **3**.

Figure 3 shows the electronic absorption, magnetic circular dichroism (MCD) spectra, and calculated electronic spectra (AM1 calculations using HyperChem Software^[9]) for **2** and **3**. Compared with the

spectra of monomeric **1**, the Q band of the dimer has more structure and is shifted to the red by about 120 nm, suggesting delocalization of electrons over the whole molecule. Both **2** and **3** show similar spectra; however, the Q band of **3** (*trans* form) appears at longer wavelength than that of **2** (*cis* form) by about 3–4 nm, and the absorbance at a shorter wavelength side of the Soret band is higher for **3**. The MCD peaks in the Q-band region correspond closely to the absorption peaks (Faraday *B* terms), characteristic of systems lacking degenerate states. Since the molecules have either C_{2v} (**2**) or C_{2h} (**3**) symmetry, the doubly degenerate bands of monomeric **1** with C_{3v} symmetry^[10] split into two bands close in energy, and transitions into these orbitals give rise to pairs of intense oppositely signed *B* terms in the MCD spectra.^[11] Thus, in the Q-band region, bands at about 690–695 and 600–605 nm can be safely assigned to the split Q_{00} transitions.^[12] The theoretical spectra reproduce these experimental characteristics. Although not shown, the Q and Soret bands of **1** were calculated at 555 and 550 nm with an oscillator strength (*f*) value of 0.515 and 0.503, and at 336 and 332 nm with an *f* value

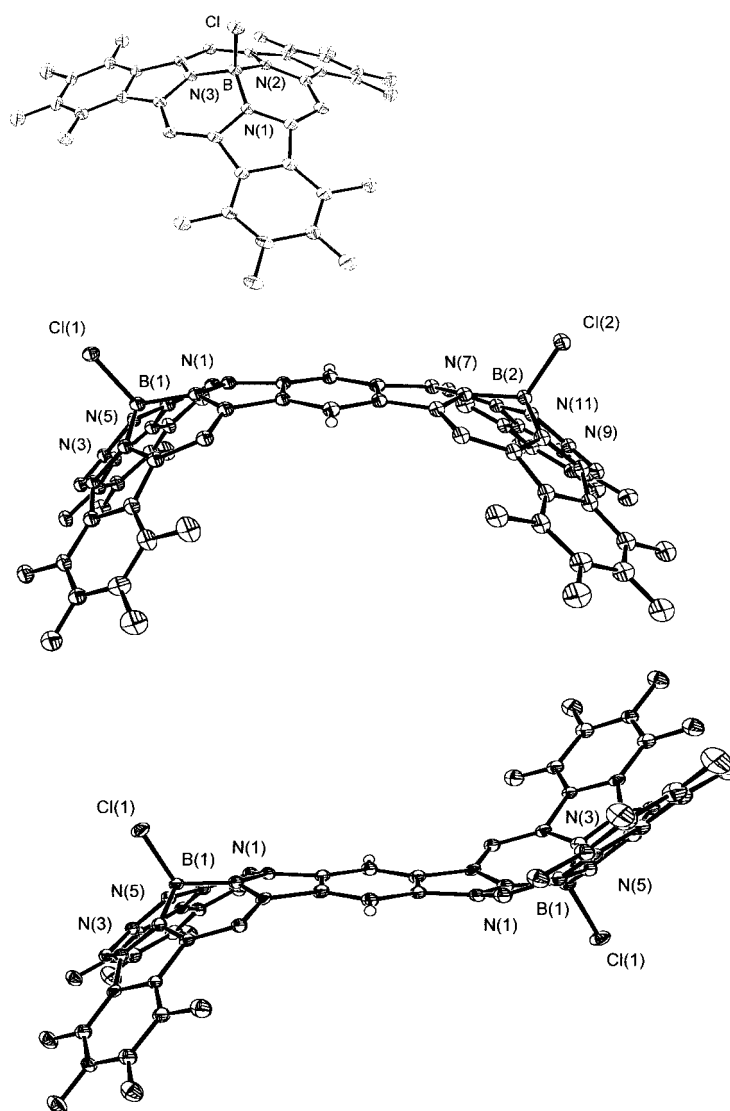


Figure 1. The X-ray crystal structures of **1** (top), **2** (middle), and **3** (bottom). Only the atoms of the boron coordination sphere are labeled.

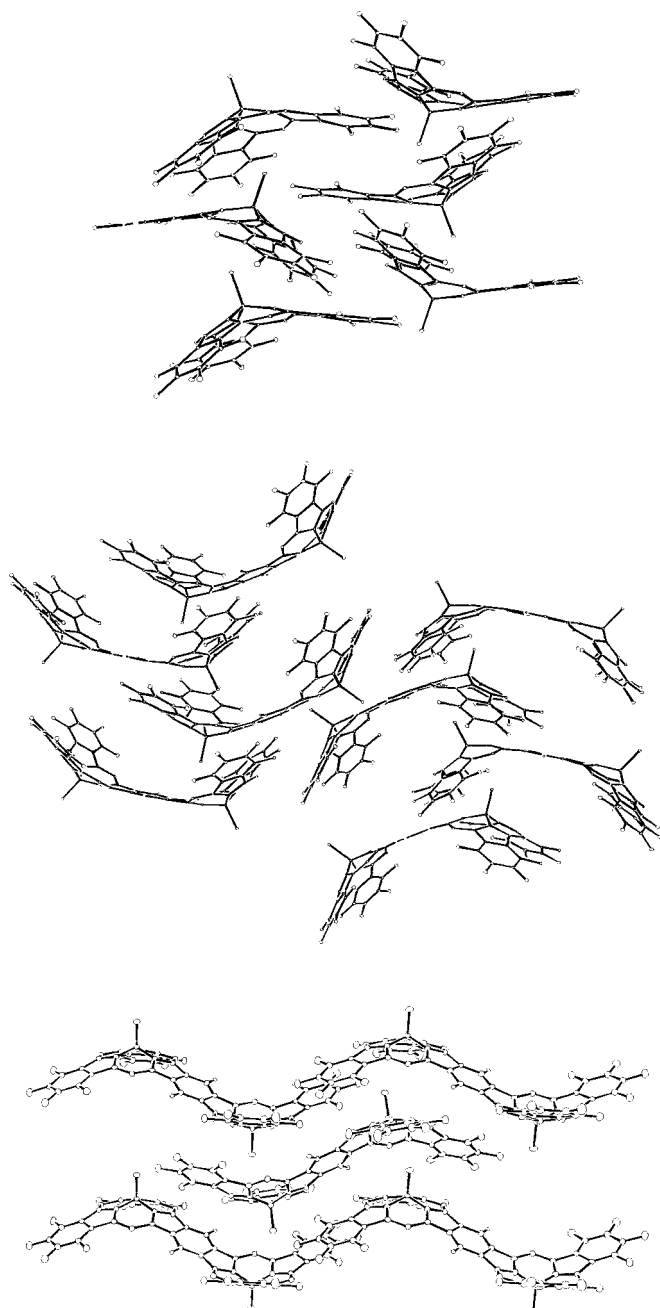


Figure 2. Crystal packing of **1** (top), **2** (middle), and **3** (bottom).

of 0.350 and 0.325, respectively. As shown in Figure 3, both **2** and **3** are expected to have intense split Q bands. The Q band of longest wavelength of the *trans* isomer **3** was calculated to lie at longer wavelength than that of the *cis* isomer **2**. In addition, compared to the *cis* isomer, for the *trans* isomer many intense transitions were calculated at the shorter wavelength side of the Soret band. These results match nicely with observations.

In conclusion, we have separated the *cis* and *trans* isomers of a binuclear SubPc and characterized both isomers by various spectroscopic methods and X-ray crystallography. The electronic absorption and MCD spectra of these dimers are similar in shape, but the Q band of the *trans* isomer appeared at longer wavelength than that of the *cis* isomer by about

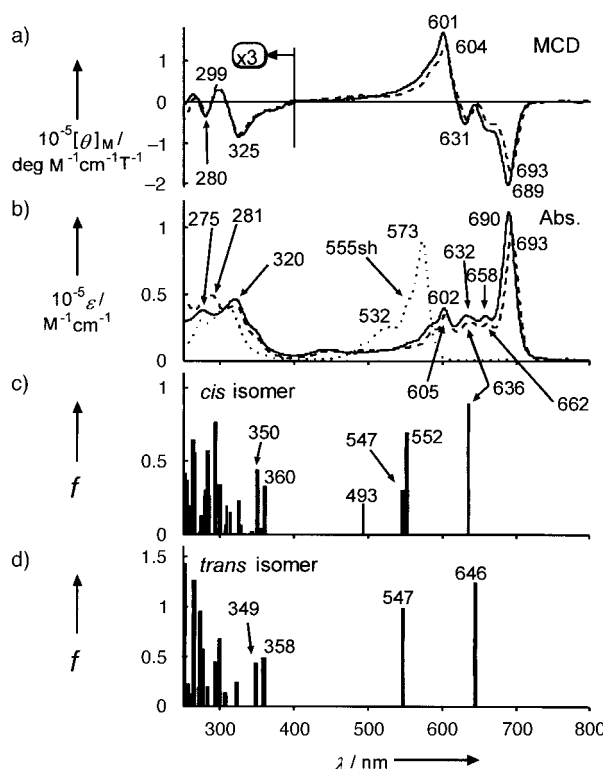


Figure 3. MCD (a) and electronic absorption spectra (b) of **2** (solid lines) and **3** (broken lines) in chloroform, and calculated electronic spectra for **2** (c) and **3** (d). Coordinates from the X-ray data of **2** and **3** were used for the calculations. The electronic absorption spectrum of monomeric **1** is shown as a dotted line in b.

3–4 nm, and the shorter wavelength side of the Soret band of the *trans* isomer was stronger than that of the *cis* isomer. These characteristics were reproduced by quantum-mechanical calculations.

Experimental Section

Tetrafluorophthalonitrile (2.0 g, 10 mmol) and 1,2,4,5-benzenetetracarbonitrile (0.089 g, 0.50 mmol) were cooled in 1,2,4-trichlorobenzene (20 mL) to approximately 12 °C. Eight to ten drops of BCl_3 , condensed by using a dropping cold finger, were added and the reaction mixture was heated to reflux (214 °C) for 30 min. The solvent was then removed by vacuum distillation. The crude product was adsorbed onto silica and purified by flash chromatography on silica with toluene/hexanes (1:20 v/v) as eluent. When **1** (the major product) had eluted the polarity was gradually increased with toluene and the dimer fractions were collected. To obtain pure samples of **2** and **3** it was necessary to chromatograph the dimer mixture at least two more times on silica, eluting with toluene/hexanes (1:1). By comparing X-ray data, we found that the *cis* isomer was eluted first.^[7] The purity of the samples used for spectroscopy was confirmed by HPLC and TLC. Slow evaporation of a solution of **1** in toluene produced crystals suitable for X-ray diffraction. Crystals of **2** and **3** were obtained by layering solutions of the respective compound in dichloromethane with cyclohexane and allowing the slow mixing of the two phases.

Received: March 11, 2002 [Z18862]

- [1] A. Meller, A. Ossko, *Monatsh. Chem.* **1972**, 103, 150.
- [2] H. Kietaihl, *Monatsh. Chem.* **1974**, 153, 405.
- [3] N. Kobayashi, *J. Chem. Soc. Chem. Commun.* **1991**, 1203.
- [4] N. Kobayashi, *J. Porphyrins Phthalocyanines* **1999**, 3, 453; C. G. Claessens, D. González-Rodríguez, T. Torres, *Chem. Rev.* **2002**, in press.

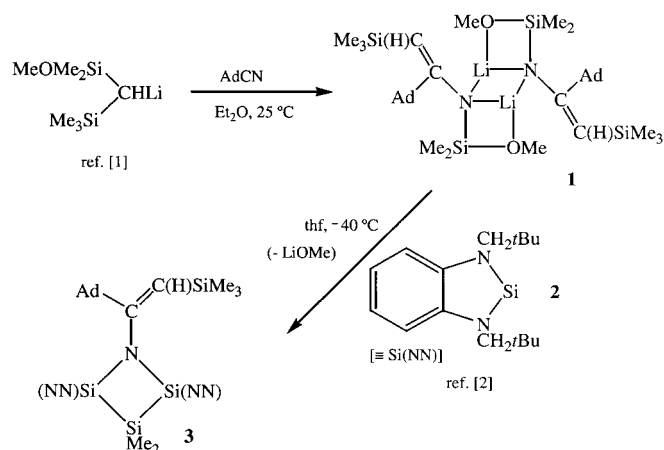
- [5] M. Geyer, F. Plenzig, J. Rauschnabel, M. Hanack, B. del Rey, Á. Sastre, T. Torres, *Synthesis* **1996**, 1139.
- [6] R. A. Kipp, J. A. Simon, M. Beggs, H. E. Ensley, R. H. Schmehl, *J. Phys. Chem. A* **1998**, *102*, 5659.
- [7] Representative data. **1**: Yield: 51%; m.p. > 300 °C; UV/Vis (CHCl₃): λ_{max} ($\epsilon \times 10^{-4}$) = 573 (8.96), 555(sh), 532 (2.59), 309 (4.04), 275 (3.03) nm; FAB-MS (*m*-nitrobenzyl alcohol): calcd for C₂₄BClF₁₂N₆: *m/z*: 646 [*M*⁺]. *cis* Isomer **2**: Yield: < 1%; m.p. > 320 °C; ¹H NMR (300 MHz, CDCl₃): δ = 10.47 ppm (s, 2H, arom); IR (KBr): $\tilde{\nu}$ = 2959, 2926, 2857, 1732, 1534, 1483, 1262, 1221, 1165, 1107, 1019, 965, 801, 771, 745, 706, 660, 581, 419 cm⁻¹; UV/Vis (CHCl₃): λ_{max} ($\epsilon \times 10^{-4}$) = 690 (11.1), 658 (3.39), 632 (3.40), 602 (3.94), 443 (0.86), 320 (4.61), 275 (3.81) nm; HR-FAB-MS: calcd for C₄₂H₃B₂Cl₂F₁₆N₁₂: [*M*⁺ + H]: *m/z*: 1070.9911, found 1070.9927. TLC (silica), *R*_f = 0.53 (toluene/hexane, 1:1). *trans* Isomer **3**: Yield: < 1%; m.p. > 320 °C; ¹H NMR (300 MHz, CDCl₃): δ = 10.49 ppm (s, 2H, arom); IR (KBr): $\tilde{\nu}$ = 2924, 2957, 2855, 1717, 1534, 1483, 1271, 1221, 1165, 1109, 1019, 992, 965, 704, 642, 592, 419 cm⁻¹; UV/Vis (CHCl₃): λ_{max} ($\epsilon \times 10^{-4}$) = 693 (6.43), 662 (1.90), 636 (1.96), 605 (2.39), 448 (0.51), 320 (2.78), 281 (3.35) nm; HR-FAB-MS: calcd for C₄₂H₃B₂Cl₂F₁₆N₁₂: [*M*⁺ + H]: *m/z*: 1070.9911, found 1070.9905. TLC (silica), *R*_f = 0.43 (toluene/hexane, 1:1).
- [8] Crystal data for the SubPc **1**: 0.06 × 0.17 × 0.22 mm, monoclinic, *P*₂₁/*c*, *a* = 11.2997(11), *b* = 10.6022(11), *c* = 19.1563(19) Å, β = 95.507(7)°, *V* = 2284.4(4) Å³, *Z* = 4, ρ_{calcd} = 1.880 Mg m⁻³, $2\theta_{\text{max}}$ = 52.7°, λ = 0.71073 Å, ω scans, 170(2) K, 20288 measured, 4664 independent reflections included in the refinement, Lorentzian but no absorption corrections performed (μ = 0.297 mm⁻¹, min./max. transmission = 0.937/0.982), solved by direct methods (SHELXS-90), refined by using SHELXL-97, 397 parameters, no H atoms, *R* = 0.0948, *wR* = 0.1055 for all data refined against $|F^2|$, residual electron density max./min. 0.32/−0.31 e Å⁻³. Crystal data for the *cis*-SubPc dimer · 2 CH₂Cl₂ **2**: 0.04 × 0.04 × 0.40 mm, monoclinic, *P*₂₁/*c*, *a* = 14.4237(13), *b* = 31.630(3), *c* = 10.2000(10) Å, β = 101.354(3)°, *V* = 4562.4(7) Å³, *Z* = 4, ρ_{calcd} = 1.807 Mg m⁻³, $2\theta_{\text{max}}$ = 56.6°, λ = 0.71073 Å, ω scans, 91(2) K, 37305 measured, 6637 independent reflections included in the refinement, Lorentzian and absorption corrections (SADABS) performed (μ = 0.495 mm⁻¹, min./max. transmission = 0.826/0.980), solved by direct methods (SHELXS-90), refined by using SHELXL-97, 743 parameters, H atoms constrained, *R* = 0.1135, *wR* = 0.1586 for all data refined against $|F^2|$, residual electron density max./min. 1.18/−0.85 e Å⁻³. Crystal data for the *trans*-SubPc dimer · 3.25 CH₂Cl₂ **3**: 0.03 × 0.12 × 0.16 mm, triclinic, *P* $\bar{1}$, *a* = 10.8638(11), *b* = 13.4945(15), *c* = 17.2990(18) Å, α = 107.608(4), β = 91.300(5), γ = 101.347(4)°, *V* = 2360.8(4) Å³, *Z* = 2, ρ_{calcd} = 1.805 Mg m⁻³, $2\theta_{\text{max}}$ = 50.7°, λ = 0.71073 Å, ω scans, 91(2) K, 22234 measured, 8623 independent reflections included in the refinement, Lorentzian but no absorption corrections performed (μ = 0.537 mm⁻¹, min./max. transmission = 0.919/0.984), solved by direct methods (SHELXS-90), refined by using SHELXL-97, 743 parameters, H atoms constrained, *R* = 0.1198, *wR* = 0.1937 for all data refined against $|F^2|$, residual electron density max./min. 1.02/−0.95 e Å⁻³. CCDC-181314 (**1**), CCDC-181315 (**2**), and CCDC-181316 (**3**) contain the supplementary crystallographic data for this paper. These data can be obtained free of charge via www.ccdc.cam.ac.uk/conts/retrieving.html (or from the Cambridge Crystallographic Data Centre, 12 Union Road, Cambridge CB2 1EZ, UK; fax: (+44) 1223-336033; or deposit@ccdc.cam.ac.uk).
- [9] HyperChem Pro software package, Hypercube, Inc. Gainesville, FL, USA, **1997**.
- [10] N. Kobayashi, T. Ishizaki, K. Ishii, H. Konami, *J. Am. Chem. Soc.* **1999**, *121*, 9096.
- [11] a) A. Tajiri, J. Winkler, *Z. Naturforsch.* **1983**, *38a*, 1263; b) A. Kaito, T. Nozawa, T. Yamamoto, M. Hatano, Y. Orii, *Chem. Phys. Lett.* **1977**, *52*, 154.
- [12] Similar spectra have been reported for a planar dinuclear phthalocyanine that shares a common benzene ring (N. Kobayashi, T. Fukuda, D. Lelièvre, *Inorg. Chem.* **2000**, *39*, 3632).

Synthesis and Structure of an Azatrisilacyclobutane and Its Precursor, a Novel Lithium Enamide Having a Tricyclic (LiNSiO)₂ Skeleton**

Floria Antolini, Barbara Gehrhuis,* Peter B. Hitchcock, and Michael F. Lappert*

We report results that have a bearing on two diverse but related and currently topical areas of organometallic chemistry. The first concerns insertion of an α -hydrogen-free nitrile into an Li–C bond, and specifically of 1-adamantyl cyanide (AdCN) into the chiral bis(silyl)methyl compound Li[CH(SiMe₂OMe)(SiMe₃)]^[1] to yield the lithium enamide **1**. The second deals with the insertion of the thermally stable bis(amino)silylene Si[(NCH₂tBu)₂C₆H₄-1,2] (Si(NN)) **2**^[2] into an Li–N bond, and particularly of Si(NN) into **1** to afford the azatrisilacyclobutane **3**, in which a transient insertion product **4** is a plausible intermediate.

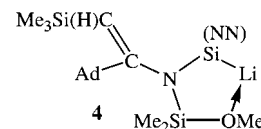
The reactions and conditions leading to the new colorless crystalline compounds **1** and **3** are summarized in Scheme 1.



Scheme 1. Synthesis of **3** via **1**.

The yields (**1**, 64%; **3**, 50%) of X-ray quality crystalline materials were not optimized. Each of **1** and **3** revealed the parent molecular ion in the EI mass spectra and gave satisfactory microanalyses and multinuclear NMR spectra.

The crystalline lithium enamide **1** is a centrosymmetric dimer (Figure 1).^[3] It has a rhomboidal, planar (LiN)₂ core (the endocyclic angles at the Li atoms are wider than those at the N



[*] Dr. B. Gehrhuis, Prof. M. F. Lappert, Dr. F. Antolini, Dr. P. B. Hitchcock
School of Chemistry, Physics and Environmental Science
University of Sussex
Brighton, BN1 9QJ (UK)
Fax: (+44) 1273-677-196
E-mail: B.Gehrhuis@sussex.ac.uk, M.F.Lappert@sussex.ac.uk

[**] We thank the EU and the University of Bologna for provision of a studentship for F.A. and the EPSRC for the award of an Advanced Fellowship for B.G. and for other support.

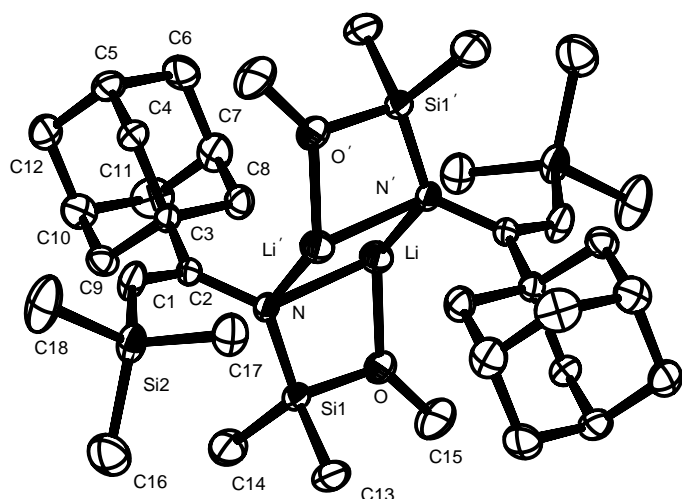


Figure 1. Molecular structure of **1** with selected bond lengths [Å] and angles [°]: Li–N 2.179(3), Li–N' 1.977(3), N–C2 1.401(2), C2–C1 1.353(2), Li–O 1.917(3); Li–N–Li' 75.86(14), N–Li–N' 104.14(14).

atoms), which is the center of a fused tricyclic ladder structure. The outer planar four-membered LiNSiO rings have endocyclic angles ranging from 77.4(1)° at Li to 99.5(1)° at Si. As a result of the intramolecular coordination of the OMe group to Li, the Li–N bond is slightly longer than the Li–N' bond (2.179(3) and 1.977(3) Å, respectively). The Li–O distance of 1.917(3) Å is appropriate for a donor–acceptor bond (cf., 1.933(3) Å in [Li(μ -N(SiMe₃)C(Ph)=C(H)SiMe₃)(thf)]₂).^[4] The other geometric parameters are unexceptional (cf., ref. [3]). The hydrogen atom and the adamantyl groups are arranged in a cisoid fashion about each C=C bond; that is, **1** is the *Z* isomer.

The molecular structure of the azatrisilacyclobutane **3** is shown in Figure 2.^[3] At its core is a puckered Si₃N ring which is folded by 18.4° on the N1–SiMe₂ vector; the silylene moieties point slightly towards each other, and the neopentyl groups at the nitrogen atoms are *cis*-orientated, away from the center of the molecule. Likewise, the bulky SiMe₃ and adamantyl substituents on the C=C fragment connected to the almost planar N1 (sum of angles 357.75°) point away from the molecule to give exclusively the *E* isomer of **3**, in contrast to **1**.

The Si1–Si3 (2.3578(9) Å) and Si2–Si3 (2.3592(8) Å) distances in the Si₃N ring are at the lower end of values reported for comparable tetrasilacycles (2.363–2.445 Å).^[5] The endocyclic Si–N bond lengths are slightly longer than those within the silylene moiety. The internal angles of the Si₃N ring range from 75.39(3)° at the central silicon atom Si3 to 110.46(9)° at the N atom. The transannular Si...Si distance of 2.884 Å is much longer than the 2.511 Å of the sterically hindered (*t*Bu₂Si)₃.^[6] This can be compared to related Si₃N ring derivatives (R₂Si)₃NC₆H₁₁ (R = *i*Pr or *t*Bu; no experimental data were given; Table 1).^[7] The bonding parameters of crystalline **3** are also in good agreement with the calculated values for the parent (H₂Si)₃NH (Si1...Si1' 2.87, Si1–Si2 2.354, Si1–N 1.742 Å, and Si1–N–Si1'

111.1°).^[8, 9] No structural information is available for the azatrisilacyclobutanes (Me₂Si)₃NM(N₃)[CH(SiMe₃)₂]₂ (M = Ge and Sn), which were obtained by treatment of M[CH(SiMe₃)₂]₂ with N₃(SiMe₂)₃N₃.^[10, 11] Only a few other X-ray-characterized compounds with Si₃X (X ≠ Si) ring structures have been described (Cambridge data base); X = C,^[12–15] X = N,^[7] X = Ge,^[5, 16] X = O,^[17, 18] and X = Te.^[19]

The pathway leading to the lithium compound **1** (first step in Scheme 1) is likely to be similar to that described for the conversion of Li[CH(SiMe₃)₂] and *t*BuCN into the η^3 -1-azaallyllithium compound **1**.^[4, 20] The substitution of an SiMe₃ group in Li[CH(SiMe₃)₂] by SiMe₂OMe introduces an element of asymmetry and also an available intramolecular donor site; hence, there are a number of new features. The first is that the formation of **1** involves selective 1,3-migration from C to N of the SiMe₂OMe (rather than the SiMe₃) group; the second is the preference for the enamidolithium tautomer in **1** (cf., **1**). Both are attributed to the presence in **1** of the strong MeO → Li bond. For comparison, reference is made to

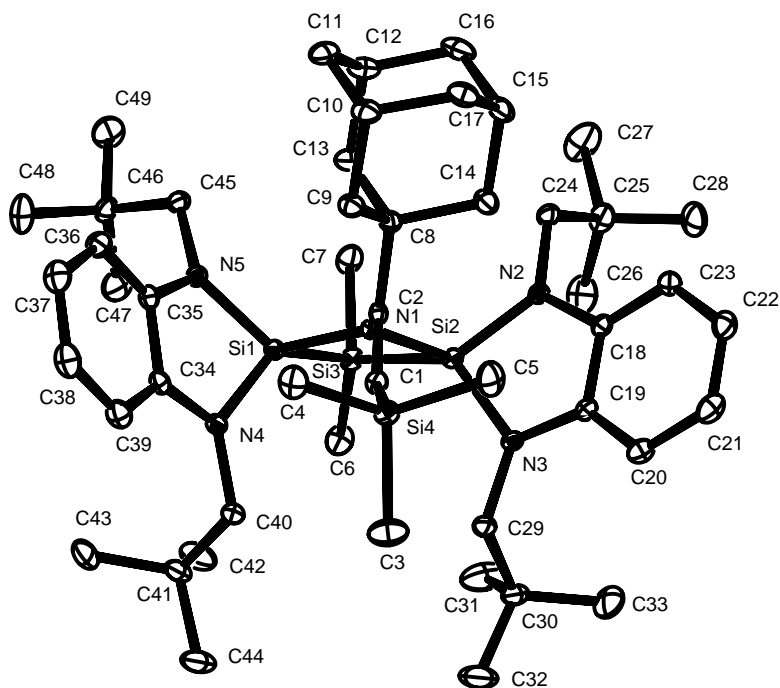
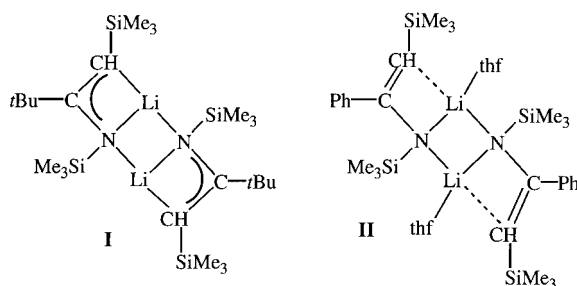


Figure 2. Molecular structure of **3** with selected bond lengths [Å] and angles [°]: Si1–N1 1.7576(18), Si1–Si3 2.3578(9), Si2–Si3 2.3592(8), Si1–N5 1.733(2), Si1–N4 1.746(2), Si2–N1 1.753(2), Si2–N3 1.745(2), N1–C2 1.459(3), C1–C2 1.352(3); N5–Si1–N4 90.56(9), N2–Si2–N3 91.03(9), N1–Si1–Si3 85.39(6), N1–Si2–Si3 85.44(6), Si1–Si3–Si2 75.39(3), Si2–N1–Si1 110.46(9).

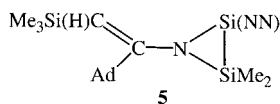
Table 1. Selected bond lengths [Å] and angles [°] for **3** and related azatrisilacyclobutanes (R₂Si)₃NC₆H₁₁.^[7]

NSi _a Si _b Si _c	R = <i>i</i> Pr	R = <i>t</i> Bu	3
Si _a –Si _b	2.362(2)	2.365(2)	2.3592(8)
Si _b –Si _c	2.377(2)	2.393(2)	2.3578(9)
Si _a –N	1.757(4)	1.758(2)	1.7534(18)
Si _c –N	1.757(4)	1.768(3)	1.7576(18)
Si _a –N–Si _c	109.5(2)	109.5(2)	110.46(9)
N–Si _a –Si _b	88.2(1)	88.2(2)	85.44(6)
N–Si _c –Si _b	87.7(1)	87.7(1)	85.39(6)
Si _a –Si _b –Si _c	74.5(1)	74.5(1)	75.39(3)

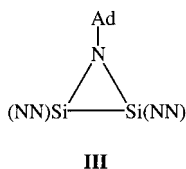
the similar situation in **II**,^[4] which has additional thf ligands. Finally, steric reasons are probably the origin of stereospecific formation of **1** as the *Z* isomer.



We recently examined the facile reactions between the silylene Si(NN) (**2**) and various alkali metal alkyls, a silyl, and amides that contain Li–C, Li–Si, or M–N (M = Li, Na, K) bonds. In general, **2** was readily inserted into the appropriate M–X bond to give the metal silyl M[Si(NN)X],^[21, 22] except for X = N(SiMe₃)₂, for which M[Si(NN)N(SiMe₃)₂] was the transient intermediate along the pathway to the metal amide M[N(SiMe₃)₃Si(NN)SiMe₃] (M = Li, Na, K).^[21] Hence, we anticipated that the reaction between the lithium enamide **1** and Si(NN) would lead to the insertion product **4**. We suggest



molecule of Si(NN) to give the stable azatrisilacyclobutane **3**. A structure related to **5** is **III**, obtained from Si(NN) and $\text{AdN}_{3, [23]}$ and facile insertion of Si(NN) into the Si–C bond of



the *Z* arrangement is attributed to **1** having reacted in solution as the η^3 -1-azaallyllithium tautomer; such behavior is amply precedented.^[4]

In conclusion, we have synthesized two novel compounds **1** and **3**, established their structures, and provided suggestions relating to plausible intermediates. These results contribute to the current interest in metal 1-azaallyls^[25] and stable bis(amino)silylenes.^[26, 27]

Experimental Section

1: AdCN (0.44 g, 2.74 mmol) was added in small portions to a solution of Li[CH(SiMe₂OMe)(SiMe₃)] (0.5 g, 2.74 mmol) in diethyl ether (60 mL) at ambient temperature. The mixture was stirred for 12 h. The volatile materials were removed in vacuo, and the residual solid was extracted into hot toluene. After filtration and concentration, the solution was set aside at ambient temperature to yield colorless crystals of **1** (0.6 g, 64 %). Elemental analysis (%) calcd for C₃₆H₆₈Li₂N₂O₂Si₄: C 62.7, H 4.06, N 9.97; found: C 60.7, H 4.03, N 9.76. M.p. 130 °C (decomp.). ¹H NMR (C₆D₅CD₃, 500.13 MHz, 348 K): δ = 0.17 (s, 15H, SiMe₃ and SiMe₂), 1.63, 1.75 and 1.95 (brs, 16H, AdCN), 3.20 (s, 3H, MeO), 4.49 (s, 1H, CH allylic);

¹³C NMR (C₆D₅CD₃, 125.76 MHz, 348 K): δ = 1.45 (SiMe₃), 20.94 (SiMe₂), 29.76 (CH, AdCN), 37.58 (CH₂, AdCN), 49.49 (MeO), 97.56 (CH allyl), 179.42 (CN); ⁷Li NMR (C₆D₅CD₃, 298 K): δ = -1.88; ²⁹Si NMR (C₆D₅CD₃, 99.36 MHz, 298 K): δ = -13.38, -9.35; EI-MS: *m/z* (%): 687 (10) [*M*]⁺, 337 (25) [*M* - Li]⁺.

3: A solution of **2** (0.41 g, 1.51 mmol) in THF (25 mL) was added dropwise to a cooled (-40°C) solution of **1** (0.26 g, 0.76 mmol) in THF (20 mL). The reaction mixture was allowed to warm to ambient temperature and stirred for 12 h. The volatile substances were removed in vacuo. The residue was crystallized from pentane/Et₂O at 15°C to give white crystals of **3** (0.32 g, 50 %). Elemental analysis (%) calcd for C₄₀H₈₃N₅Si₄: C 68.9, H 9.79, N 7.58; found: C 68.2, H 9.56, N 8.19. M.p. $270-275^{\circ}\text{C}$. ¹H NMR (C₆D₆, 300.13 MHz): δ = 0.16 (s, 9H, SiMe₃), 0.63 and 0.80 (s, 6H, SiMe₂, diastereotopic), 1.00 and 1.07 (s, 36H, *t*Bu), 1.24 (s, 6H, CH₂ Ad), 1.60–1.68 (q, 6H, CH₂, Ad), 1.88 (s, 3H, CH, Ad), 3.25, 3.28, 3.39, 3.42, 3.59, 3.63 (two overlapping signals), and 3.66 (2 AB type, 8H, CH₂), 4.77 (s, 1H, =CH), 6.69–6.86 (m, 8H, phenyl); ¹³C NMR (C₆D₆, 75.47 MHz): δ = -0.94 and 2.00 (SiMe₂, diastereotopic), 2.70 (SiMe₃), 29.51 (CH₂, Ad), 29.54 and 29.60 (CMe₃) 35.04 and 35.29 (CMe₃), 36.97 and 41.36 (CH₂, Ad), 53.46 and 55.06 (CH₂, SiN₂), 109.98 , 111.22 , 116.88 , 117.71 , 138.28 and 140.08 (phenyl), 120.01 (=CH), 165.58 (=CN); ²⁹Si NMR (C₆D₆, 99.36 MHz): δ = -28.86 (SiMe₂), -19.95 (SiN₂), -13.05 (SiMe₃); EI-MS: *m/z* (%): 853 (100) [*M*]⁺.

Received: March 1, 2002 [Z18805]

- [1] T. F. Bates, S. A. Dandekar, J. L. Longlet, K. A. Wood, R. D. Thomas, *J. Organomet. Chem.* **2000**, 595, 87.
- [2] B. Gehrhuis, P. B. Hitchcock, M. F. Lappert, J. Heinicke, R. Boese, D. Bläser, *J. Organomet. Chem.* **1996**, 521, 211.
- [3] Crystallographic data for **1**: [[Li(Me₂OMe)SiNC(Ad)CHSiMe₃]₂], *M_r* = 687.16, triclinic, space group *P*1̄ (no. 2), *a* = 9.4839(3), *b* = 11.3455(3), *c* = 11.5638(3) Å, *α* = 112.266(2), *β* = 95.250(2), *γ* = 112.675(2)°, *V* = 1020.53(5) Å³, *Z* = 1, λ(MoK_α) = 0.71073 Å, *μ* = 0.18 mm⁻¹. Data were collected at 173(2) K on a KappaCCD diffractometer; 4766 independent reflections (*R*_{int} = 0.049), 4317 reflections with *I* > 2σ(*I*), refined using SHELXL-97,^[28] *R*1 = 0.050 and *wR*2 (all data) = 0.132. CCDC-176979 contains the supplementary crystallographic data for this paper. These data can be obtained free of charge via www.ccdc.cam.ac.uk/conts/retrieving.html (or from the Cambridge Crystallographic Data Center, 12, Union Road, Cambridge CB2 1EZ, UK; fax: (+44) 1223-336-033; or deposit@ccdc.cam.ac.uk). Crystallographic data for **3**: [[Me₃SiC(H)C(Ad)N][Si(NCH₂Bu)^t]₂C₆H₄]₂[SiMe₃]], *M_r* = 854.56, monoclinic, space group *P*2₁/c (no. 14), *a* = 10.6544(3), *b* = 23.1542(4), *c* = 21.3560(6) Å, *β* = 96.083(1)°, *V* = 5238.7(2) Å³, *Z* = 4, λ(MoK_α) = 0.71073 Å, *μ* = 0.15 mm⁻¹. Data were collected at 173(2) K on a KappaCCD diffractometer; 9183 independent reflections (*R*_{int} = 0.052), 7188 reflections with *I* > 2σ(*I*), refined using SHELXL-97,^[28] *R*1 = 0.049 and *wR*2 (all data) = 0.126. CCDC-176609 contains the supplementary crystallographic data for this paper. These data can be obtained free of charge via www.ccdc.cam.ac.uk/conts/retrieving.html (or from the Cambridge Crystallographic Data Center, 12, Union Road, Cambridge CB2 1EZ, UK; fax: (+44) 1223-336-033; or deposit@ccdc.cam.ac.uk).
- [4] P. B. Hitchcock, M. F. Lappert, M. Layh, D.-S. Liu, R. Sablong, T. Shun, *J. Chem. Soc. Dalton Trans.* **2000**, 2301.
- [5] H. Suzuki, K. Okabe, R. Kato, N. Sato, Y. Fukuda, H. Watanabe, M. Goto, *Organometallics* **1993**, 12, 4833.
- [6] A. Schäfer, M. Weidenbruch, K. Peters, H. G. von Schnering, *Angew. Chem.* **1984**, 96, 311; *Angew. Chem. Int. Ed. Engl.* **1984**, 23, 302.
- [7] M. Goto, *Kagaku Gijutsu Kenkyusho Hokoku* **1991**, 86, 127.
- [8] R. S. Grev, H. F. Schaefer III, *J. Am. Chem. Soc.* **1987**, 109, 6577.
- [9] C. Liang, L. C. Allen, *J. Am. Chem. Soc.* **1991**, 113, 1878.
- [10] T. Ohtaki, W. Ando, *Chem. Lett.* **1994**, 1061.
- [11] T. Ohtaki, Y. Kabe, W. Ando, *Heteroat. Chem.* **1994**, 5, 313.
- [12] M. Weidenbruch, J. Hamann, K. Peters, H. G. von Schnering, H. Marsmann, *J. Organomet. Chem.* **1992**, 441, 185.
- [13] M. Weidenbruch, J. Hamann, S. Pohl, W. Saak, *Chem. Ber.* **1992**, 125, 1043.

- [14] D. Bravo-Zhivotovskii, Y. Apeloig, Y. Ovchinnikov, V. Igonin, Y. T. Struchkov, *J. Organomet. Chem.* **1993**, *446*, 123.
- [15] Y. Apeloig, D. Bravo-Zhivotovskii, M. Bendikov, D. Danovich, M. Botoshansky, T. Vakul'skaya, M. Voronkov, R. Samoilova, M. Zdravkova, V. Igonin, V. Shklover, Yu. T. Struchkov, *J. Am. Chem. Soc.* **1999**, *121*, 8118.
- [16] H. Suzuki, Y. Fukuda, N. Sato, H. Ohmori, M. Goto, H. Watanabe, *Chem. Lett.* **1991**, 853.
- [17] H. Watanabe, E. Tabei, M. Goto, Y. Nagai, *J. Chem. Soc. Chem. Commun.* **1987**, 522.
- [18] M. Unno, H. Masuda, H. Matsumoto, *Bull. Chem. Soc. Jpn.* **1998**, *71*, 2449.
- [19] M. Weidenbruch, A. Grybat, W. Saak, E. M. Peters, K. Peters, *Monatsh. Chem.* **1999**, *130*, 157.
- [20] P. B. Hitchcock, M. F. Lappert, D.-S. Liu, *J. Chem. Soc. Chem. Commun.* **1994**, 2637.
- [21] B. Gehrhus, P. B. Hitchcock, M. F. Lappert, J. C. Slootweg, *Chem. Commun.* **2000**, 1427.
- [22] X. Cai, B. Gehrhus, P. B. Hitchcock, M. F. Lappert, J. C. Slootweg, *J. Organomet. Chem.* **2002**, *643–644*, 272; X. Cai, B. Gehrhus, P. B. Hitchcock, M. F. Lappert, J. C. Slootweg, *J. Organomet. Chem.* **2002**, *651*, 149.
- [23] B. Gehrhus, P. B. Hitchcock, M. F. Lappert, *Z. Anorg. Allg. Chem.* **2001**, *627*, 1048.
- [24] B. Gehrhus, P. B. Hitchcock, M. F. Lappert, *Organometallics* **1997**, *16*, 4861.
- [25] C. F. Caro, M. F. Lappert, P. G. Merle, *Coord. Chem. Rev.* **2001**, *219–221*, 605.
- [26] M. Haaf, T. A. Schmedake, R. West, *Acc. Chem. Res.* **2000**, *33*, 704.
- [27] B. Gehrhus, M. F. Lappert, *J. Organomet. Chem.* **2001**, *617–618*, 209.
- [28] G. M. Sheldrick, SHELXL-97, Program for Crystal Structure Refinement, University of Göttingen, Göttingen (Germany), **1997**.

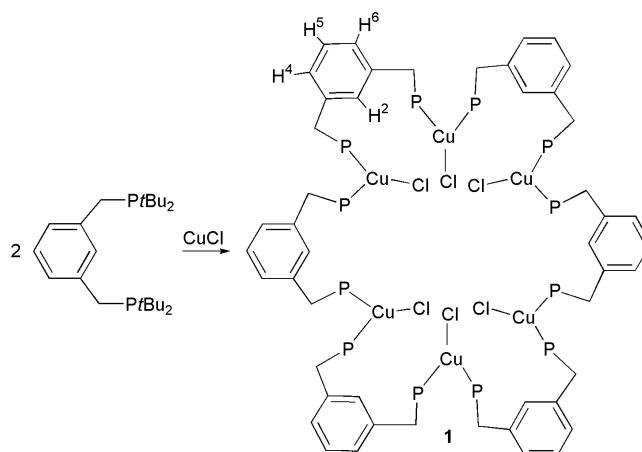
Synthesis, Spectroscopy, and Solid-State Structural Characterization of the Hexanuclear Copper Macrocycle $[\text{Cu}_6\text{Cl}_6(\mu\text{-PCHP})_6]^{**}$

Elizabeth D. Blue, T. Brent Gunnoe,* and Neil R. Brooks

The study of late-transition-metal complexes with electron counts of d^8 – d^{10} has been of significant interest as a result of their interesting photophysical and photoredox chemistry.^[1–7] Extensive study of d^{10} systems has allowed an increased understanding of, and control over, photophysical properties, and it has been suggested that the rich luminescent behavior of many closed-shell systems arises from weak metal–metal interactions.^[1–3, 5, 8, 9] Increasing interest in the preparation and

study of late-transition-metal polynuclear systems stems, in part, from possible applications as therapeutic agents (e.g., photocleavage of DNA), photovoltaics, photocatalysts, and tunable chemical sensors.^[2, 10–12] One challenge to both the study and the understanding of the properties of late-transition-metal polynuclear complexes is the controlled preparation of new structural motifs. Tetranuclear copper cubanes have been the focus of some attention for Group 11 transition metals,^[4] and other polynuclear copper complexes with variable structural patterns are of interest and have been reported.^[13–19] Closely related to work reported herein are penta- and tetranuclear copper macrocycles and recently reported high nuclearity gold systems.^[12, 20–22] We now report the synthesis and characterization (including solid-state X-ray diffraction analysis) of a novel hexanuclear copper macrocycle of the type $[\text{Cu}_6\text{Cl}_6(\mu\text{-PCHP})_6]$ (PCHP = 1,3- $(\text{CH}_2\text{PrBu}_2)_2\text{C}_6\text{H}_4$).

The reaction of CuCl with the bisphosphane 1,3- $(\text{CH}_2\text{PrBu}_2)_2\text{C}_6\text{H}_4$ (PCHP) in a 1:2 stoichiometry yields the hexanuclear complex $\text{Cu}_6\text{Cl}_6(\mu\text{-PCHP})_6$ (**1**; Scheme 1). Sim-



Scheme 1. Preparation of the macrocycle $\text{Cu}_6\text{Cl}_6(\mu\text{-PCHP})_6$ (**1**; P = PrBu_2).

ilar to reactions of aryl Cu^I compounds with bis(diphenylphosphanyl)methane in which metal:ligand stoichiometry is important, slow addition of the CuCl to a solution (CH_2Cl_2) of the PCHP ligand is important to the success of the reaction.^[23] Complex **1** is a macrocycle that incorporates 48 atoms into the large ring structure (if the aryl moieties are each counted as contributing 3 atoms to the macrocycle) and in which each copper atom is bound by phosphorus atoms from two different PCHP ligands. Complex **1** was characterized by elemental analysis, X-ray crystallography, cyclic voltammetry experiments, as well as UV/Vis, ^1H , ^{13}C , and ^{31}P NMR spectroscopy.

Broad resonances in the ^1H NMR spectrum of **1** at room temperature in CD_2Cl_2 reveal a fluxional process. At -10°C sharp resonances are observed with a singlet at $\delta = 8.68$ ppm (aromatic H2), doublets at $\delta = 8.25$ and 7.04 ppm (aromatic H4 and H6), a triplet at $\delta = 7.13$ ppm (aromatic H5), multiplets at approximately $\delta = 3.0$ ppm corresponding to the methylene protons, and four phosphane $t\text{Bu}$ resonances between $\delta = 1.0$ and 1.8 ppm. The aromatic C2–H2 bonds

[*] Prof. T. B. Gunnoe, E. D. Blue
Department of Chemistry
North Carolina State University
Campus Box 8204, Raleigh, NC 27695-8204 (USA)
Fax: (+1) 919-515-8909
E-mail: brent_gunnoe@ncsu.edu

Dr. N. R. Brooks
X-ray Crystallographic Laboratory, Department of Chemistry
University of Minnesota, Minneapolis, MN 55455 (USA)

[**] T.B.G. and E.D.B. acknowledge North Carolina State University for support of this research and Professors Stefan Franzen and Jim Martin for use of UV/Vis and Fluorometer instrumentation. PCHP = 1,3- $(\text{CH}_2\text{PrBu}_2)_2\text{C}_6\text{H}_4$

Supporting information for this article is available on the WWW under <http://www.angewandte.org> or from the author.

remain intact as indicated by the downfield resonance at $\delta = 8.68$ ppm. However, agostic bonding is unlikely because of the distance from the copper centers.^[24] The ^1H NMR spectrum obtained at -10°C is consistent with C_6 molecular symmetry, with all six PCHP ligands equivalent and a lack of mirror symmetry (all methylene protons and *t*Bu groups are inequivalent). At temperatures greater than -10°C a fluxional process introduces mirror symmetry, as shown by the methylene and *t*Bu protons becoming equivalent in the ^1H NMR spectra (consistent with overall D_{6h} symmetry; $\Delta G^\ddagger = 51\text{ kJ mol}^{-1}$). At temperatures less than -10°C the ^1H NMR spectra broaden, presumably as a result of the conversion from C_6 to lower molecular symmetry. However, the resonances are broad down to -70°C , and the slow exchange regime has not been accessed. The ^{31}P NMR spectra (CD_2Cl_2) obtained between -10°C and room temperature are consistent with the suggested fluxionality of complex **1**. At -10°C the ^{31}P NMR spectrum of **1** reveals an AB pattern ($^2J_{\text{PP}} = 126\text{ Hz}$) with resonances at $\delta = 38.6$ and 36.4 ppm , consistent with C_6 molecular symmetry (that is, the two phosphorus atoms on each copper atom are inequivalent). Warming a solution of **1** in C_6D_6 to 70°C results in coalescence of the signals into a single broad phosphane resonance.

Cyclic voltammetry of complex **1** in dichloromethane reveals an irreversible oxidation at $E_{\text{p,a}} = 1.04\text{ V}$ ($E_{\text{p,a}}$ = anodic peak potential; irreversible at scan rates up to 1 V s^{-1}). The observation of a single oxidation could imply little electronic communication between copper redox centers. A second irreversible oxidation is observed at $E_{\text{p,a}} = 1.75\text{ V}$ that is presumably a consequence of the formation of decomposition products. The electronic absorption spectrum of **1** in CH_2Cl_2 reveals maximum absorption at 232 nm ($\epsilon = 1.07 \times 10^5\text{ L mol}^{-1}\text{ cm}^{-1}$). Similar absorptions of related bisphosphane Cu^{I} complexes have been attributed to metal–metal $3d \rightarrow 4s$ transitions.^[25] The emission spectrum of complex **1** in CH_2Cl_2 shows maximum absorption at 354 nm .

The solid-state structure of **1** was studied by X-ray diffraction (Figures 1 and 2).^[26] The copper clusters possess crystallographically imposed hexagonal symmetry, and there are two crystallographically distinct cluster molecules per unit

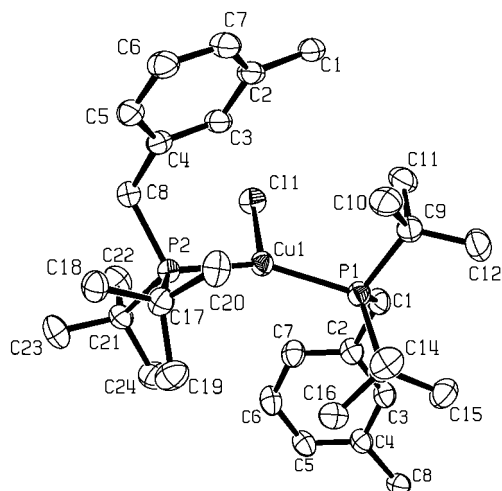


Figure 1. Structure of a section of complex **1** with thermal ellipsoids at the 50% level.

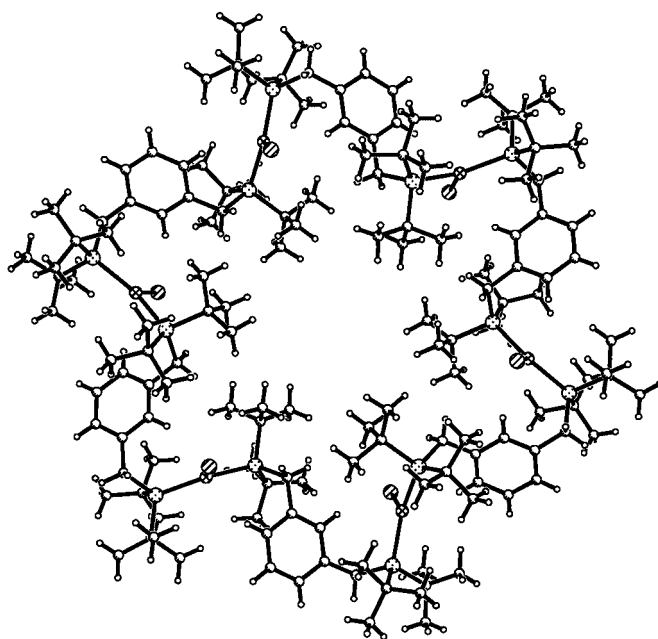


Figure 2. Structure of a single molecule of **1**.

cell. The macrocycles are stacked one directly over another to form a cylinder with an open cavity. At the center of the cylinder are infinite chains of disordered acetonitrile molecules, which coincide with the threefold symmetry axis. Disordered CH_2Cl_2 molecules occupy sites within the channel as well as surrounding the periphery of the clusters. There are nine molecules of CH_2Cl_2 and one molecule of MeCN per copper macrocycle. The inside diameter of the cylinder is approximately 4.5 \AA while the outside diameter of the macrocycle is approximately 24 \AA (Figure 3). No suitable

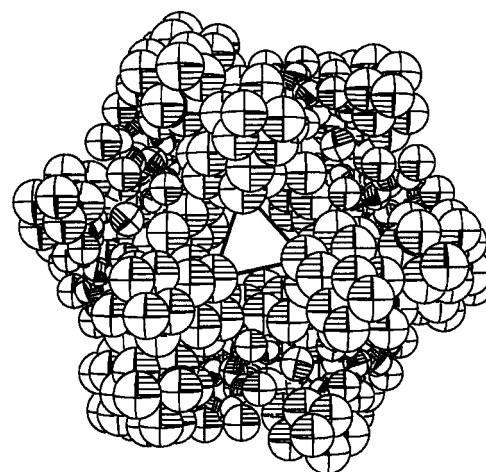


Figure 3. Structure of complex **1** with thermal ellipsoids at the 100% probability level illustrating the inside channel of the solid-state structure.

disorder model could be found for the solvent molecules (CH_2Cl_2 and CH_3CN) so their associated electron density was removed with the SQUEEZE function of PLATON (see Supporting Information). The Cu1-P1 and Cu-P2 bond lengths are $2.2598(4)$ and $2.639(5)\text{ \AA}$ ($2.2591(5)$ and $2.2627(5)\text{ \AA}$ for the second unique molecule), and the

Cu1–Cl1 bond length is 2.3235(5) Å (2.3293(5) Å for the second unique molecule). The copper coordination geometry is best described as distorted trigonal planar with P2–Cu1–P1, P2–Cu1–Cl1, and P1–Cu1–Cl1 bond angles of 147.100(17), 107.385(16), and 105.46(17)° (146.284(18), 106.747(17), and 106.969(17)° for the second unique molecule), respectively. The sum of the bond angles around Cu1 is 359.95(3)° (360.00(3)° for the second unique molecule).

In related Cu^I systems with chelating bis(dicyclohexylphosphanyl)methane ligands, the formation of three-coordinate binuclear complexes with close copper–copper contacts is observed in the solid-state.^[25] In contrast, binuclear four-coordinate copper centers with bridging bis(diphenylphosphanyl)methane ligands have longer copper···copper separations as do three-coordinate systems with (*i*Pr)₂PCH₂P(*i*Pr)(H) ligands.^[27, 28] The large bite angle of the PCHP ligand affords the higher nuclearity (compared with the bi- and trinuclear systems discussed immediately above) hexanuclear copper complex **1**, and the unique geometry effectively insulates the complex from close intramolecular Cu···Cu interactions. Additionally, the steric bulk of the *t*Bu groups prevents intermolecular Cu···Cu interactions in the solid-state (and presumably in solution). Therefore, assignment of the emission to any form of copper···copper interaction can be reliably ruled out.

In summary, the new hexanuclear copper complex [Cu₆Cl₆(μ-PCHP)₆] has been synthesized and fully characterized. The novel macrocyclic structure is a result of the large bite angle of the PCHP ligand, as indicated by an X-ray crystallographic study. In addition, the solution-phase dynamics of complex **1** have been studied by variable-temperature NMR spectroscopy.

Experimental Section

1. The 1,3-(CH₂PrBu)₂C₆H₄ ligand (0.4144 g, 1.05 mmol) was dissolved in CH₂Cl₂ (ca. 30 mL). A CuCl suspension (0.0523 g, 0.528 mmol in CH₂Cl₂ (ca. 20 mL) was added dropwise to this solution. The resulting mixture was stirred overnight, and the solvent volume was then reduced under vacuum to approximately 10 mL. The product was precipitated upon addition of hexanes (approximately 10 mL) and isolated by vacuum filtration through a medium porosity frit. The resulting white solid was washed with hexanes and diethyl ether and dried under vacuum (0.160 g, 0.054 mmol, 61 %). Full characterization details can be found in the Supporting Information.

Received: February 4, 2002 [Z18643]

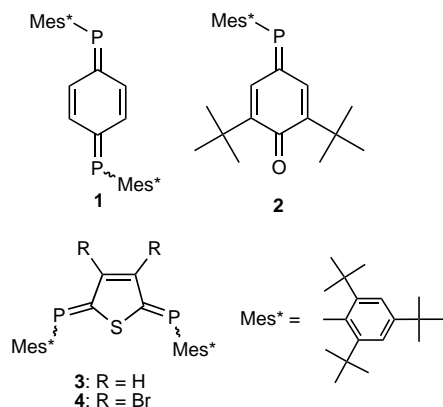
- [1] K. M. Merz, R. Hoffmann, *Inorg. Chem.* **1988**, 27, 2120.
- [2] V. W.-W. Yam, K. K.-W. Lo, *Chem. Soc. Rev.* **1999**, 28, 323.
- [3] P. Pykkö, *Chem. Rev.* **1997**, 97, 597.
- [4] P. C. Ford, *Coord. Chem. Rev.* **1994**, 132, 129.
- [5] V. Balzani, A. Juris, M. Venturi, S. Campagna, S. Serroni, *Chem. Rev.* **1996**, 96, 759.
- [6] A. P. Zipp, *Coord. Chem. Rev.* **1988**, 84, 47.
- [7] D. M. Roundhill, H. B. Gray, C.-M. Che, *Acc. Chem. Res.* **1989**, 22, 55.
- [8] R. M. Sullivan, J. D. Martin, *J. Am. Chem. Soc.* **1999**, 121, 10092.
- [9] V. W.-W. Yam, E. C.-C. Cheng, *Angew. Chem.* **2000**, 112, 4410; *Angew. Chem. Int. Ed.* **2000**, 39, 4240.
- [10] V. W.-W. Yam, S. W.-K. Choi, K. K.-W. Lo, W.-F. Dung, R. Y.-C. Kong, *J. Chem. Soc. Chem. Commun.* **1994**, 2379.
- [11] V. W.-W. Yam, C.-K. Li, C.-L. Chan, *Angew. Chem.* **1998**, 110, 3041; *Angew. Chem. Int. Ed.* **1998**, 37, 2857.

- [12] V. W.-W. Yam, E. C.-C. Cheng, *Gold Bull.* **2001**, 34, 20.
- [13] G. A. Ardizzone, M. A. Angaroni, G. La Monica, F. Cariati, M. Moret, N. Masciocchi, *J. Chem. Soc. Chem. Commun.* **1990**, 1021.
- [14] H. Hope, P. P. Power, *Inorg. Chem.* **1984**, 23, 936.
- [15] T. Chivers, A. Downard, M. Parvez, G. Schatte, *Organometallics* **2001**, 20, 727.
- [16] D. Nobel, G. van Koten, A. L. Spek, *Angew. Chem.* **1989**, 101, 211; *Angew. Chem. Int. Ed. Engl.* **1989**, 28, 208.
- [17] H. Hartl, F. Mahdjour-Hassan-Abadi, *Angew. Chem.* **1984**, 96, 359; *Angew. Chem. Int. Ed. Engl.* **1984**, 23, 378.
- [18] F. Mahdjour-Hassan-Abadi, H. Hartl, J. Fuchs, *Angew. Chem.* **1984**, 96, 497; *Angew. Chem. Int. Ed. Engl.* **1984**, 23, 514.
- [19] P. P. Power, *Prog. Inorg. Chem.* **1991**, 39, 75.
- [20] S. Gambarotta, C. Floriani, A. Chiesi-Villa, C. Guastini, *J. Chem. Soc. Chem. Commun.* **1983**, 1156.
- [21] V. W.-W. Yam, E. C.-C. Cheng, Z.-Y. Zhou, *Angew. Chem.* **2000**, 112, 1749; *Angew. Chem. Int. Ed.* **2000**, 39, 1683.
- [22] V. W.-W. Yam, E. C.-C. Cheng, K.-K. Cheung, *Angew. Chem.* **1999**, 111, 193; *Angew. Chem. Int. Ed.* **1999**, 38, 197.
- [23] a) A. Camus, N. Marsich, G. Pellizer, *J. Organomet. Chem.* **1983**, 259, 367; b) reaction in a 1:1 stoichiometry results in the formation of a copper cubane complex, unpublished results with a 1:2 PCHP:CuCl ratio.
- [24] D. G. Gusev, M. Madott, F. M. Dolgushin, K. A. Lyssenko, M. Y. Antipin, *Organometallics* **2000**, 19, 1734.
- [25] C.-M. Che, Z. Mao, V. M. Miskowski, M.-C. Tse, C.-K. Chan, K.-K. Cheung, D. L. Phillips, K.-H. Leung, *Angew. Chem.* **2000**, 112, 4250; *Angew. Chem. Int. Ed.* **2000**, 39, 4084.
- [26] Crystal data for **1**: Crystals were grown by slow diffusion of hexanes into a solution of **1** in CH₂Cl₂. Colorless block (0.30 × 0.26 × 0.22 mm³), rhombohedral, space group *R* $\bar{3}$, *a* = 41.098(2), *c* = 20.5124(13) Å, *V* = 30 005(3) Å³, ρ_{calc} = 1.251 g cm⁻³, $2\theta_{\text{max}}$ = 54.98°, $\text{Mo}_{\text{K}\alpha}$, λ = 0.71073 Å, 173(2) K, of 62 796 reflections collected, 15 284 are independent and 11 493 have *I* > 2σ(*I*). Residuals [*I* > 2σ(*I*)] *R*1 = 0.0325, *wR*2 = 0.0811. The structure was solved and refined using SHELXTL-plus V5.10 (SHELXTL-Plus V5.10, Bruker Analytical X-Ray Systems, Madison, WI, 1998). Solvent molecules found in the voids of the structure were found to be disordered. There are CH₂Cl₂ molecules located close to metal–organic clusters, which are moderately disordered. There also appears to be highly disordered MeCN molecules located along the center of the tubular cavity. All electron density associated with the solvent molecules was artificially removed with the SQUEEZE function of the PLATON program. (A. L. Spek, *Acta. Crystallogr. Sect. A* **1990**, 46, C34; A. L. Spek, PLATON, A Multipurpose Crystallographic Tool, Utrecht University, Utrecht, The Netherlands, 2000). This electron density was the equivalent to 54 CH₂Cl₂ and 6 MeCN molecules, which were included in the final calculation of molecular weight, density, and associated parameters per unit cell, leaving a void of 8818 Å³. CCDC-176679 contains the supplementary crystallographic data for this paper. These data can be obtained free of charge via www.ccdc.cam.ac.uk/contents/retrieving.html (or from the Cambridge Crystallographic Data Centre, 12, Union Road, Cambridge CB2 1EZ, UK; fax: (+44) 1223-336-033; or deposit @ccdc.cam.ac.uk).
- [27] J. Díez, M. P. Gamasa, J. Gimeno, A. Tiripicchio, M. T. Camellini, *J. Chem. Soc. Dalton Trans.* **1987**, 1275.
- [28] D. J. Brauer, P. C. Knüppel, O. Stelzer, *Chem. Ber.* **1987**, 120, 81.

Synthesis, Structure, and Redox Properties of Diphosphathienoquinones**

Fumiki Murakami, Shigeru Sasaki, and Masaaki Yoshifuji*

Although a variety of π -conjugated molecules containing low-coordinate phosphorus atoms is known,^[1] only two stable phosphaquinoide compounds have been reported: diphosphaquinone **1** by Märkl et al.^[2] and phosphaquinoine **2** by us.^[3] Diphosphathienoquinones **3** are expected to be more stable than **1** and still behave chemically and physically as a quinoid compound, since so-called heteroquinoid, molecules which contain a heteroatom such as sulfur in place of one endocyclic C=C bond of quinoid compounds, generally have higher stability than their benzenoid counterparts without losing the inherent properties of the quinoid system.^[4] Here we report a general synthetic route for diphosphaquinones and diphosphathienoquinones, and the synthesis, structure, and redox properties of the first diphosphathienoquinone **4**.

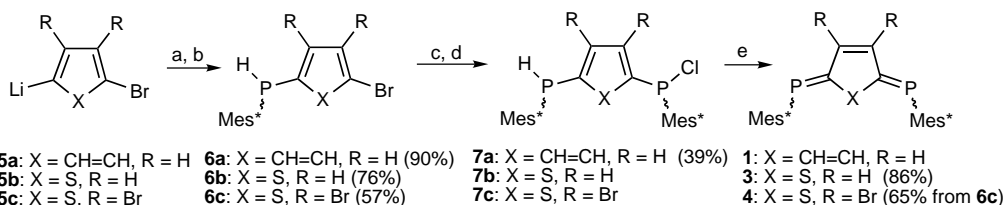


[*] Prof. Dr. M. Yoshifuji, Dr. F. Murakami, Dr. S. Sasaki
Department of Chemistry
Graduate School of Science
Tohoku University
Aoba, Sendai 980-8578 (Japan)
Fax: (+81) 22-217-6562
E-mail: yoshifuji@mail.cc.tohoku.ac.jp

[**] Financial support by Grant-in-Aid for Scientific Research from the Ministry of Education, Culture, Sports, Science, and Technology (Nos. 12740335, 08454193, and 09239101) is gratefully acknowledged. F.M. thanks the Japan Society for the Promotion of Science for a JSPS Postdoctoral Fellowship. The authors also thank the Instrumental Analysis Center for Chemistry, Graduate School of Science, Tohoku University, for the measurement of 500 MHz NMR and mass spectra. This work was partially carried out in Advanced Instrumental Laboratory for Graduate Research of Department of Chemistry, Graduate School of Science, Tohoku University.

Supporting information for this article is available on the WWW under <http://www.angewandte.org> or from the author.

Diphosphaquinone **1** was prepared by dechlorination of 1,4-bis(chlorophosphanyl)benzene with zinc, but the product was contaminated with secondary phosphanes because of over-reduction.^[2] To synthesize diphosphaquinones selectively, we employed 1,6-dehydrochlorination of (chlorophosphanyl)-phosphanylbenzene or -thiophene precursors **7** as the final step (Scheme 1). Compounds **7** were prepared by stepwise introduction of phosphanyl and chlorophosphanyl groups on the aromatic ring by reaction of the corresponding aryllithium



Scheme 1. Synthesis of a diphosphaquinone and diphosphathienoquinones. a) Mes*PCl₂, Et₂O, -78 °C, b) LiAlH₄, Et₂O, 0 °C, c) *t*BuLi (**7a**, **7b**) or *n*BuLi (**7c**), Et₂O, -78 °C, d) Mes*PCl₂, Et₂O, -78 °C, e) KH, [18]crown-6, THF, room temperature.

with Mes*PCl₂^[5] (Mes* = 2,4,6-tri-*tert*-butylphenyl) and obtained as mixtures of diastereomers. Deprotonation of **7a** and **7b** with an excess of potassium hydride in the presence of [18]crown-6 afforded diphosphaquinone **1** and diphosphathienoquinone **3** as inseparable 1:1 mixtures of (*E*)-**1** (δ_p = 261 ppm) and (*Z*)-**1** (δ_p = 263 ppm) and of (*E,Z*)-**3** (δ_p = 209 ppm (d, $J(P,P)$ = 264 Hz), 192 ppm (d, $J(P,P)$ = 264 Hz)) and (*Z,Z*)-**3** (δ_p = 197) isomers. To enhance the preference for the *Z,Z* isomer by steric repulsion between the bulky Mes* and other substituents, bromine atoms were introduced into the 3- and 4-positions of the thiophene ring, and **7c** was dehydrochlorinated to afford air-stable orange prisms of **4** as a single *Z,Z* isomer.

The ¹H NMR spectrum (500 MHz, CD₂Cl₂) of **4** reflected its highly symmetrical structure, and only three signals corresponding to aromatic, *o*-*t*Bu, and *p*-*t*Bu protons were observed. The ¹³C NMR spectrum (126 MHz, CD₂Cl₂) was also indicative of a symmetrical structure, and three signals corresponding to the C atoms close to the phosphorus atoms were observed as a pseudotriplet, typical of an AXX' pattern.^[6] The ³¹P NMR chemical shifts of diphosphathienoquinones (*E,Z*)-**3**, (*Z,Z*)-**3**, and **4** were observed upfield relative to those of diphosphaquinones **1** and phosphaquinoine **2**. The molecular structure of **4** was further studied by X-ray crystallography (Figure 1) and compared with that of thienylphosphane **6c**. The two exocyclic P=C bonds adopt a *Z* configuration with bond lengths of 1.712(2) and 1.714(2) Å, which are longer than those of typical sterically protected phosphalkenes (ca. 1.68 Å)^[7] but comparable to that of phosphaquinoine **2** (1.705(2) Å). The structural change of the five-membered ring from an "aromatic" thiophene to a thienoquinoid structure was revealed by comparing **4** with **6c**. The single bonds C1–C2, C3–C4, C4–S1, and S1–C1 were longer than the corresponding values of **6c** by 0.049, 0.060, 0.031, and 0.024 Å, respectively, while the double bond C2–C3 was shorter by 0.063 Å. The five-membered ring and two exocyclic phosphorus atoms are planar with a maximum

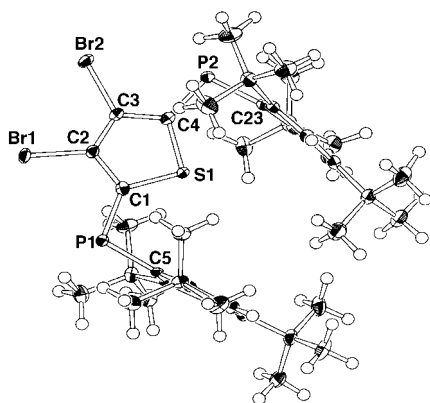


Figure 1. ORTEP plot of **4** with 50% probability thermal ellipsoids. Selected bond lengths [Å] and angles [°]: P1–C1 1.712(2), P2–C4 1.714(2), C1–C2 1.416(3), C2–C3 1.359(3), C3–C4 1.415(3), C4–S1 1.743(2), C1–S1 1.751(2), C5–P1–C1 98.1(1), C23–P2–C4 100.6(1), P1–C1–C2 126.0(2), P1–C1–S1 126.0(1), C2–C1–S1 108.0(2), C1–C2–C3 115.2(2), C2–C3–C4 114.3(2), C3–C4–S1 108.8(2), P2–C4–C3 124.7(2), P2–C4–S1 126.4(1), C4–S1–C1 93.6(1), S1–C1–C2 108.0(2).

deviation from the least-squares plane of 0.0209 Å (C3). However, two *p*-*t*Bu groups are located very close to each other, and the whole diphosphathienoquinoid skeleton is twisted as a result of steric repulsion between them (C5–P1–P2–C23 torsion angle 29.7°).

In analogy with most other quinoid molecules, **4** was expected to be reduced stepwise to the dianion via a radical anion (semiquinone). This was confirmed by cyclic voltammetry of **4** (Figure 2), in which the first reversible ($E_{1/2} = -1.50$ V versus Ag/Ag⁺) and the second irreversible ($E_p = -2.49$ V) redox waves were observed. The first reduction

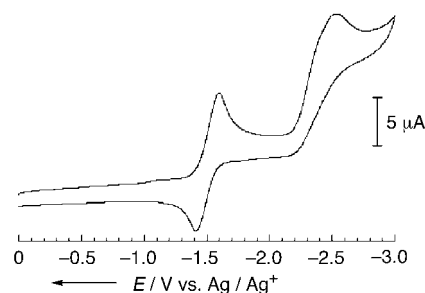


Figure 2. Cyclic voltammogram of **4** at 293 K. Conditions: 10^{−4} M in THF with 0.1 M *n*Bu₄NClO₄ as a supporting electrolyte; working electrode: glassy carbon; counter electrode: Pt wire; reference electrode: Ag/0.01 M AgNO₃ in acetonitrile with 0.1 M *n*Bu₄NClO₄ ($E_{1/2}$ (ferrocene/ferricinium) = 0.180 V); scan rate: 50 mV s^{−1}.

potential, which was significantly lower than those of typical phosphalkenes (ca. −2.2 V),^[8] and the second are very close to that of phosphquinone **2** ($E_{1/2} = -1.55$ V, $E_p = -2.45$), but the radical anion of **4** has enhanced stability. The EPR spectrum of **4**^{•−} obtained by reduction of **4** with sodium metal (Figure 3a) in THF at 293 K consisted of four lines resulting from hyperfine coupling (hfc) with two nonequivalent ³¹P nuclei ($a(P1) = 9.3$, $a(P2) = 2.1$ mT, $g = 2.007$). The EPR spectrum of the frozen solution at 77 K (Figure 3b) was interpreted by assuming axial symmetric hfc and g tensors with a dominant contribution from $a_{||}(P1)$ (27.7 mT) and other

minor contributions.^[9] As observed for phosphquinone **2**, the isotropic and anisotropic hfc constants were much larger than those of radical anions of typical phosphalkenes but very close to those of phosphanyl radicals^[10] which suggests significant localization of an unpaired electron on the 3p orbital of one phosphorus atom (P1; 69% by comparison with atomic hfc constants^[11]) and considerable contribution of thiophene-bearing localized phosphorus radical and anion centers. Further synthetic studies on phosphathienoquinoid and phosphquinoid molecules are in progress.

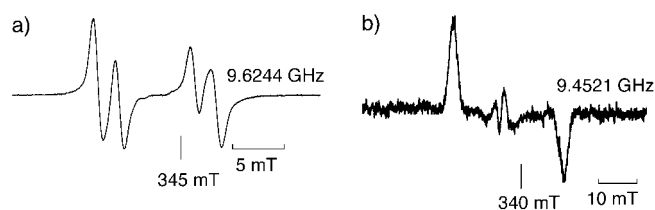


Figure 3. EPR spectra obtained at 295 K (a) and 77 K (b) after reduction of **4** with sodium metal in THF.

Experimental Section

7c: A solution of *tert*-butyllithium (2.1 mL, 1.50 M in *n*-pentane) was added to a solution of **6c** (669 mg, 1.12 mmol) in diethyl ether (15 mL) at 0 °C. The solution was stirred for 20 min at 0 °C and added to a solution of Mes*PCl₂ (417 mg, 1.20 mmol) in diethyl ether (15 mL) at −78 °C. After stirring for 30 min at −78 °C and 10 h at 20 °C, the mixture was washed with saturated NaCl solution, dried over anhydrous MgSO₄, and concentrated to afford crude **7c** almost quantitatively. **7c**: colorless crystals; ³¹P NMR (81 MHz, CDCl₃): δ = 68.8 (s), −67.4 (d, $J(P,H) = 229$ Hz), 68.1 (s), −65.8 ppm (d, $J(P,H) = 230$ Hz).

4: A solution of **7c** in THF (10 mL) was added to a suspension of KH (192 mg, 40 wt% dispersion in mineral oil) and [18]crown-6 (766 mg, 2.90 mmol) in THF (10 mL) at 20 °C, and the mixture was refluxed for 30 min. Excess KH was decomposed with water (ca. 10 mL) at room temperature, and the mixture was washed with saturated NaCl solution, dried over anhydrous MgSO₄, and purified by column chromatography (Al₂O₃/benzene) and recrystallization from benzene to give **4** (578 mg, 0.729 mmol, 65%). **4**: orange plates (benzene), m.p. 173.0–175.0 °C (decomp); ¹H NMR (500 MHz, CD₂Cl₂): δ = 7.25 (4H, brs, arom-*m*), 1.32 (36H, s, C(CH₃)₃-*o*) 1.20 ppm (18H, s, C(CH₃)₃-*p*); ¹³C{¹H} NMR (126 MHz, CD₂Cl₂): δ = 172.37 (AXX', $^1J(P,C) + ^3J(P',C) = 73.6$ Hz, P=C), 154.76 (s, Mes*-*o*), 151.37 (s, Mes*-*p*), 134.90 (AXX', $^1J(P,C) + ^3J(P',C) = 54.2$ Hz, Mes*-*ipso*), 128.74 (AXX', $^2J(P,C) + ^3J(P',C) = 43.3$ Hz, quinone-3), 122.61 (s, Mes*-*m*), 38.46 (s, C(CH₃)₃-*o*), 35.28 (s, C(CH₃)₃-*p*), 33.05 (AXX', $^4J(P,C) + ^5J(P',C) = 6.8$ Hz, C(CH₃)₃-*o*), 31.49 ppm (s, C(CH₃)₃-*p*); ³¹P NMR (81 MHz, CD₂Cl₂): δ = 211.2 ppm (s); UV/Vis (hexanes): λ_{max} (lgε) = 466 (4.39), 370 (3.72), 274 nm (3.91); FABMS *m/z* (%): 794 (56) [*M*⁺+4], 792 (91) [*M*⁺+2], 790 (45) [*M*⁺], 713 (8) [*M*⁺+2−Br], 711 (5) [*M*⁺−Br], 57 (62) [*t*Bu⁺]; HRMS (70 eV, EI): found: *m/z* 790.2114; calcd for C₄₀H₅₈P₂SBr₂: 790.2101.

Crystal data of **4**: C₄₀H₅₈P₂SBr₂, $M_r = 792.71$, red prisms from benzene, crystal dimensions 0.25 × 0.25 × 0.20 mm³. $T = 115$ K, triclinic, space group *P* $\bar{1}$ (no. 2), $a = 11.531(2)$, $b = 18.982(4)$, $c = 10.273(5)$ Å, $\alpha = 95.462(9)$, $\beta = 115.92(3)$, $\gamma = 82.28(2)^\circ$, $V = 2002(1)$ Å³, $Z = 2$, $\rho_{\text{calc}} = 1.315$ g cm^{−3}, $\mu = 2.188$ mm^{−1}, $F(000) = 828.00$, 6920 reflections measured ($2\theta_{\text{max}} = 51.1^\circ$), $R_{\text{int}} = 0.030$; 6920 observed reflections [$I > 0.00\sigma(I)$], 639 variable parameters. $R = 0.037$, $R_w = 0.043$, GOF $S = 1.27$ for observed reflections [$I > 0.00\sigma(I)$] and $R1 = 0.030$ for [$I > 2.00\sigma(I)$]. The maximum and minimum peaks on the final difference Fourier map corresponded to 0.34 and −0.43 e Å^{−3}. CCDC-180101 (**4**) and -180102 (**6c**) contain the supplementary crystallographic data for this paper. These data can be obtained free of charge via www.ccdc.cam.ac.uk/conts/retrieving.html (or from the

Cambridge Crystallographic Data Centre, 12, Union Road, Cambridge CB2 1EZ, UK; fax: (+44) 1223-336-033; or deposit@ccdc.cam.ac.uk).

Received: March 5, 2002 [Z18830]

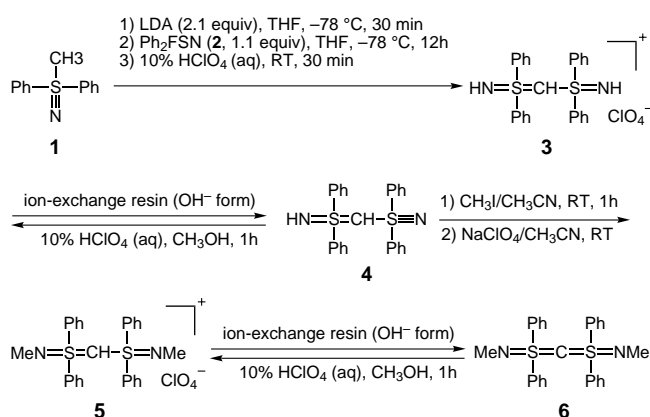
- [1] *Multiple Bonds and Low Coordination in Phosphorus Chemistry* (Eds.: M. Regitz, O. J. Scherer), Georg Thieme, Stuttgart, **1990**.
- [2] G. Märkl, R. Hennig, K. M. Raab, *Chem. Commun.* **1996**, 2057–2058.
- [3] S. Sasaki, F. Murakami, M. Yoshifuji, *Angew. Chem.* **1999**, *111*, 351–354; *Angew. Chem. Int. Ed.* **1999**, *38*, 340–343.
- [4] K. Takahashi, *Pure Appl. Chem.* **1993**, *65*, 127–134; K. Yui, H. Ishida, Y. Aso, T. Otsubo, F. Ogura, A. Kawamoto, J. Tanaka, *Bull. Chem. Soc. Jpn.* **1989**, *62*, 1547–1555.
- [5] M. Yoshifuji, I. Shima, N. Inamoto, K. Hirotsu, T. Higuchi, *J. Am. Chem. Soc.* **1981**, *103*, 4587–4589; M. Yoshifuji, I. Shima, N. Inamoto, K. Hirotsu, T. Higuchi, *J. Am. Chem. Soc.* **1982**, *104*, 6167.
- [6] I. J. Colquhoun, W. McFarlane, *J. Chem. Soc. Dalton Trans.* **1982**, 1915–1921.
- [7] R. Appel in *Multiple Bonds and Low Coordination in Phosphorus Chemistry* (Eds.: M. Regitz, O. J. Scherer), Georg Thieme, Stuttgart, **1990**, pp. 157–219.
- [8] M. Geoffroy, A. Jouaiti, G. Terron, M. Cattani-Lorente, Y. Ellinger, *J. Phys. Chem.* **1992**, *96*, 8241–8245.
- [9] Tentative assignments: $g = 2.007$, $a(P1) = 9.3$, $a(P2) = 2.1$ mT, $g_{\perp} = 2.010$, $g_{\parallel} = 2.003$, $a_{\perp}(P1) = 0.8$, $a_{\parallel}(P1) = 27.7$, $a_{\perp}(P2) = 2.2$, $a_{\parallel}(P2) = 1.2$ mT.
- [10] M. Geoffroy, E. A. C. Lucken, C. Mazeline, *Mol. Phys.* **1974**, *28*, 839–845; B. Çetinkaya, A. Hudson, M. F. Lappert, H. Goldwhite, *J. Chem. Soc. Chem. Commun.* **1982**, 609–610.
- [11] J. R. Morton, K. F. Preston, *J. Magn. Reson.* **1978**, *30*, 577–582.

Synthesis and Structure of (MeN)Ph₂S=C=SPh₂(NMe)

Takayoshi Fujii, Tomio Ikeda, Toshie Mikami, Tetsuya Suzuki, and Toshiaki Yoshimura*

(X)R₂S=C=SR₂(X) can be regarded as the isoelectronic carbon analogue of the [(X)R₂S=N=SR₂(X)]⁺ ion (R = Ar, alkyl; X = lone pair, NH, O).^[1] There has, however, been little reported on this compound to date.^[2] In view of its chemical properties and structural features, investigation of this compound has posed an interesting challenge. Herein, we report the first synthesis, isolation, and crystal structure of (MeN)Ph₂S=C=SPh₂(NMe) (**6**), prepared by the α -proton abstraction of a new type of iminosulfonium ylide [(MeN)Ph₂S=CH-SPh₂(NMe)]⁺ (Scheme 1).

[*] Prof. Dr. T. Yoshimura, Dr. T. Fujii, T. Ikeda, T. Mikami, T. Suzuki
Department of Material Systems Engineering
and Life Science
Faculty of Engineering
Toyama University
Gofuku, Toyama 930-8555 (Japan)
Fax: (+81) 76-445-6850
E-mail: yosimura@eng.toyama-u.ac.jp



Scheme 1. Synthesis of **6**.

α -Lithiation of methyldiphenyl- λ^6 -sulfanenitrile (**1**)^[3a] with lithium diisopropylamide (LDA), followed by treatment with fluorodiphenyl- λ^6 -sulfanenitrile (**2**)^[3b] and acidification with perchloric acid afforded **3** in 66% yield. This compound was further treated with ion-exchange resin IRA-410 (OH⁻ form) to give **4**^[4–6] almost quantitatively. The reaction of **4** with methyl iodide in CH₃CN at room temperature and then treatment with NaClO₄ afforded precursor **5**, which was isolated in 26% yield by recrystallization from MeOH and diethyl ether.^[7] The desired compound **6** was prepared in essentially quantitative yield by passing a methanolic solution of **5** through a column of the above basic resin.^[6] The compositions of **3–6** were identified by NMR (except for **4**) and IR spectroscopy, as well as elemental analysis, and the molecular structures of **5** and **6** were determined by X-ray crystallographic analysis (Figure 1 and 2).^[8]

The X-ray structure of **6** indicates the following characteristic properties (Figure 2). Each sulfur center is associated with one imido and two phenyl groups, in a pseudo-tetrahedral arrangement. The bond angles N1-S1-C1 and

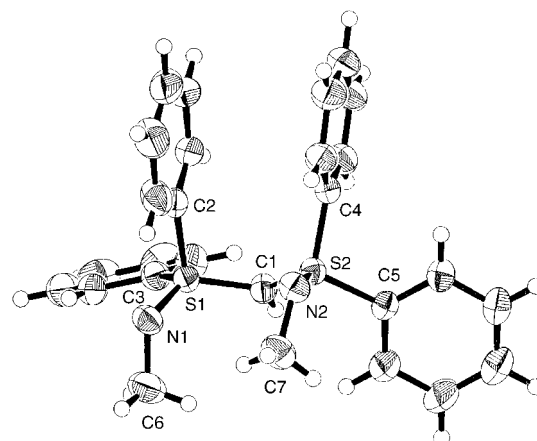


Figure 1. ORTEP drawing of **5** (50% probability thermal ellipsoids for all non-hydrogen atoms, perchlorate anion is omitted for clarity). Selected bond lengths [Å] and angles [°]: S1-N1 1.526(2), S1-C1 1.695(2), S1-C2 1.780(3), S1-C3 1.802(3), S2-N2 1.531(2), S2-C1 1.691(2), S2-C4 1.788(3), S2-C5 1.802(3), N1-C6 1.479(4), N2-C7 1.469(4); N1-S1-C1 123.1(1), N1-S1-C2 103.4(1), N1-S1-C3 112.5(1), C1-S1-C2 107.8(1), C1-S1-C3 102.4(1), C2-S1-C3 106.6(1), N2-S2-C1 119.6(1), N2-S2-C4 103.4(1), N2-S2-C5 115.4(1), C1-S2-C4 110.7(1), C1-S2-C5 102.1(1), C4-S2-C5 104.9(1), S1-N1-C6 117.3(2), S2-N2-C7 118.0(2), S1-C1-S2 118.0(1).

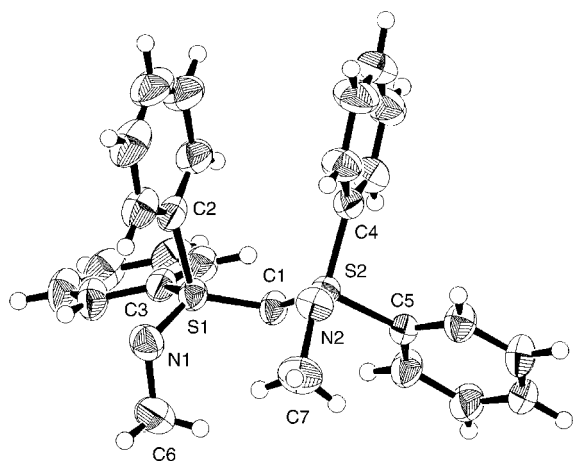


Figure 2. ORTEP drawing of **6** (50 % probability thermal ellipsoids for all non-hydrogen atoms). Selected bond lengths [Å] and angles [°]: S1–N1 1.553(10), S1–C1 1.635(4), S1–C2 1.801(2), S1–C3 1.802(4), S2–N2 1.550(8), S2–C1 1.636(2), S2–C4 1.799(4), S2–C5 1.808(4), N1–C6 1.464(4), N2–C7 1.470(5); N1–S1–C1 124.1(2), N1–S1–C2 102.2(2), N1–S1–C3 110.6(3), C1–S1–C2 115.4(1), C1–S1–C3 101.9(3), C2–S1–C3 100.5(1), N2–S2–C1 128.1(2), N2–S2–C4 101.1(3), N2–S2–C5 110.1(3), C1–S2–C4 111.6(1), C1–S2–C5 102.1(1), C4–S2–C5 101.0(3), S1–N1–C6 115.2(2), S2–N2–C7 115.7(3), S1–C1–S2 116.8(2).

N2–S2–C1 (124.1(2) and 128.1(2)°, respectively), those involving the bridging C1 atom, are considerably larger than the other sulfur-centered bond angles (N–S–C; av. 106.0°, C–S–C; av. 105.4°). The bonds between the sulfur centers and the bridging carbon atom are of similar size, as are the two terminal S–N bonds, and the four bonds between the sulfur centers and phenylic carbon atoms. The bridging S–C1 bonds in **6** (1.635(4) and 1.636(2) Å) are shorter than their counterparts in **5** (1.695(2) and 1.691(2) Å) and in iminosulfonium phenacylide (1.672(2) Å^[3a]). In contrast, the terminal S1–N1 and S2–N2 bonds (1.553(10) and 1.550(8) Å, respectively) are slightly longer than those in **5** (1.526(2) and 1.531 Å) and in iminosulfonium phenacylide (1.538(2) Å^[3a]). Interestingly, the S1–C1–S2 angle in **6** (116.8(2)°) is almost the same as the corresponding angle in **5** (118.0(1)°), and is indicative of sp² hybridization of the C1 atom. These findings suggest that the S1–C1–S2 bonds have double ylidic character, such as is found in carbodiphosphoranes, R₃P=C=PR₃,^[9] and thus the canonical Lewis structures of **B–E** are anticipated (Scheme 2).

To evaluate the electronic structure of **6**, ab initio calculations were carried out on a model compound, (MeN)-Me₂S=C=SMe₂(NMe) (**7**), where the phenyl groups in **6** are all replaced by methyl groups.^[10] Calculations by geometry optimization, the natural population analysis (NPA), and

the natural bond orbital (NBO) analyses were performed at the B3LYP/6-311 + G(2d,p) level.^[11] There is a reasonably good agreement between the bond lengths and angles of the N–S–C–S–N unit in the optimized structure (Figure 3), and

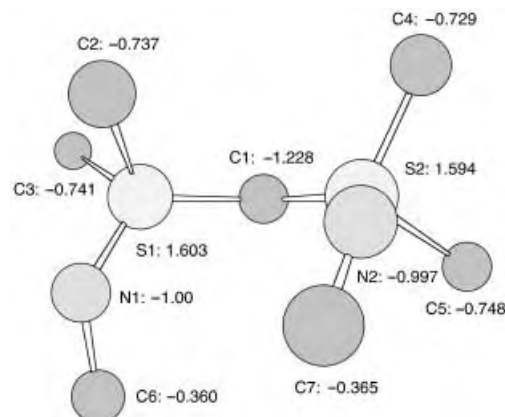


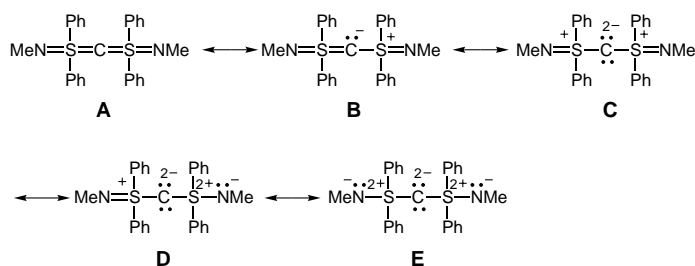
Figure 3. View of the B3LYP/6-311 + G(2d,p) optimized structure and charge distribution (natural charge analysis) of **7** (all hydrogen atoms are omitted for clarity). Selected bond lengths [Å] and angles [°]: S1–N1 1.565, S1–C1 1.646, S1–C2 1.824, S1–C3 1.831, S2–N2 1.567, S2–C1 1.650, S2–C4 1.819, S2–C5 1.836, N1–C6 1.460, N2–C7 1.465; N1–S1–C1 124.9, N1–S1–C2 99.4, N1–S1–C3 111.5, C1–S1–C2 117.6, C1–S1–C3 100.8, C2–S1–C3 100.3, N2–S2–C1 129.6, N2–S2–C4 99.1, N2–S2–C5 112.5, C1–S2–C4 110.8, C1–S2–C5 102.0, C4–S2–C5 99.2, S1–N1–C6 117.1, S2–N2–C7 118.1, S1–C1–S2 120.0.

those in the X-ray structure of **6**. As indicated by NPA and NBO analysis, the N–S–C–S–N unit in **7** has strongly polarized S–C and S–N bonds. The NPA charges at the two sulfur atoms, the two nitrogen atoms, and the central carbon atom are calculated to be +1.603 (S1), +1.594 (S2), –1.000 (N1), –0.997 (N2), and –1.228 (C1), respectively. The NBO procedure for identifying bonds and lone pairs of the N–S–C–S–N unit in **7** clearly showed ten σ bonds and six lone pairs. Therefore, the canonical structure **E** in Scheme 2 shows the best Lewis representation of the electronic configuration of **6**. The pσ and p lone pairs of the central carbon atom (C1) are highly depleted, with occupancies of 1.74e and 1.52e. NBO second-order perturbation analysis^[11b, 12] of **7** indicates five strong orbital interactions of the lone pair (p-LP, pσ-LP) at the central carbon atom with the antibonding σ* orbitals of the S–N and S–C bonds, and the interaction of a lone pair at each terminal nitrogen atom with σ*_{S–C} and σ*_{S–N} orbitals. These results indicate that ionic bonding, as well as LP(C1) → σ* and LP(N) → σ* negative hyperconjugation exist in **7**.

In conclusion, the synthesis of **6** represents the first successful preparation of an organosulfur compound containing the S^{VI}=C=S^{VI} unit, the molecular structure of which has been determined. In addition, the electronic structure of **7**, a model compound based on **6**, was predicted by ab initio molecular calculations.

Experimental Section

3: Lithium diisopropylamide (4.2 mL of 2.0 M solution in heptane/THF/ethylbenzene, 8.4 mmol) was added dropwise at –78 °C to a solution of **1** (861 mg, 4.0 mmol) in THF (50 mL) and stirred for 30 min. A solution of **2** (965 mg, 4.4 mmol) in THF (10 mL) was then added. The mixture was stirred for 12 h at –78 °C, warmed up to room temperature, and then



Scheme 2. Structural representation of **6**.

quenched with 10% perchloric acid (10 mL) and then extracted with CH_2Cl_2 . The solvent was evaporated under reduced pressure, and the residue was washed with MeOH and then recrystallized from EtOH/Et₂O to give colorless crystals of **3** (1.36 g, 66% yield), m.p. 175–176 °C. ¹H NMR (400 MHz, CD₃CN): δ = 5.08 (s, 1H), 7.59–7.64 (m, 8H), 7.69–7.74 (m, 4H), 8.02–8.06 ppm (m, 8H); ¹³C NMR (100 MHz, CD₃CN): δ = 49.3, 127.9, 131.0, 135.2, 140.8 ppm; IR (KBr): $\tilde{\nu}$ = 3315, 3269, 3094, 3062, 1095 cm⁻¹; elemental analysis calcd for C₂₅H₂₃ClN₂O₄S₂: C 58.30, H 4.50, N 5.44; found: C 58.29, H 4.46, N, 5.46.

5: A mixture of **4** (414 mg, 1.0 mmol) and methyl iodide (187 μL , 3 mmol) in acetonitrile (10 mL) was stirred at room temperature for 1 h. A solution of sodium perchlorate (184 mg, 1.5 mmol) in acetonitrile (10 mL) was added, and then the solvent was evaporated under reduced pressure. The residue was dissolved in water (10 mL) and extracted with CH_2Cl_2 . After removal of the solvent, the residue was purified by recrystallization from MeOH/Et₂O to afford **5** as colorless crystals (152 mg),^[7] m.p. 184–185 °C. ¹H NMR (400 MHz, CD₃CN): δ = 2.75 (s, 6H), 5.18 (s, 1H), 7.52–7.57 (m, 8H), 7.65–7.70 (m, 4H), 7.87–7.90 ppm (m, 8H); ¹³C NMR (100 MHz, CD₃CN): δ = 30.4, 39.3, 128.9, 131.0, 135.3, 136.8 ppm; IR (KBr): $\tilde{\nu}$ = 2917, 2872, 2803, 1194, 1091 cm⁻¹; elemental analysis calcd for C₂₇H₂₇ClN₂O₄S₂: C 59.71, H 5.01, N 5.16; found: C 59.72, H 4.97, N, 5.17.

6: A solution of **5** (100 mg) in methanol was passed through a column of Amberlite IRA-410 ion-exchange resin (strong base, OH⁻ form) followed by evaporation of the solvent to give **6** as a pale yellow powder (74 mg, 98%), m.p. 163–164 °C. ¹H NMR (400 MHz, CDCl₃): δ = 2.62 (s, 6H), 7.28–7.35 (m, 12H), 8.00 ppm (dd, J_1 = 8.0 Hz, J_2 = 1.4 Hz, 8H); ¹³C NMR (100 MHz, CDCl₃): δ = 30.1, 39.7, 127.7, 128.3, 130.5, 144.4 ppm; IR (KBr): $\tilde{\nu}$ = 2947, 2840, 2776, 1147 cm⁻¹; elemental analysis calcd for C₂₇H₂₆N₂S₂: C 73.26, H 5.92, N 6.33; found: C 73.11, H 5.99, N, 6.29.

Received: March 7, 2002 [Z18842]

- [1] a) S. Oae, T. Numata, T. Yoshimura in *The Chemistry of the Sulfonium Groups*, Part 2 (Eds.: S. Patai, C. J. M. Stirling), Wiley, Chichester, **1981**, chap. 15, and references therein; b) T. Yoshimura, T. Fujii, S. Murotani, S. Miyoshi, T. Fujimori, M. Ohkubo, S. Ono, H. Morita, *J. Organomet. Chem.* **2000**, *611*, 272–279, and references therein.
- [2] Attempts to prepare R₂S–C=SR₂ from [R₂S–CH₂–SR₂]²⁺ or [R₂S=CH–SR₂]⁺ ions (R = Me, Et) were unsuccessful; see: C. P. Lillya, E. F. Miller, P. Miller, *Int. J. Sulfur Chem.* **1971**, *1*, 89–96.
- [3] a) T. Fujii, T. Suzuki, T. Sato, E. Horn, T. Yoshimura, *Tetrahedron Lett.* **2001**, *42*, 6151–6154; b) T. Yoshimura, M. Ohkubo, T. Fujii, H. Kita, Y. Wakai, S. Ono, H. Morita, C. Shimasaki, E. Horn, *Bull. Chem. Soc. Jpn.* **1998**, *71*, 1629–1637, and references therein.
- [4] Compound **4** could not be isolated from the reaction mixture of lithiated **1** and **2**, and was therefore isolated by converting it into the corresponding perchloric salt **3** upon treatment with perchloric acid (See Experimental Section).
- [5] Unexpectedly, ¹³C NMR spectra of **4** showed only one set of phenyl groups, and methyne proton and carbon resonances were not observed in the temperature range –80 to 100 °C in CD₃OD and [D₆]DMSO. IR and elemental analyses were consistent with the structure of **4**, although the structure of **4** in the solution is still not certain. **4**: m.p. 155–156 °C; IR (KBr): $\tilde{\nu}$ = 1259 cm⁻¹ (S=N); elemental analysis calcd for C₂₅H₂₂N₂S₂: C 72.43, H 5.35, N 6.76; found: C 72.36, H 5.38, N, 6.77.
- [6] Compounds **4** and **6** are considerably basic. Treatment of **4** and **6** with perchloric acid afforded, almost quantitatively, **3** and **5**, respectively.
- [7] The side products in the reaction with methyl iodide were **3** and the *N*-monomethylated compound, [(MeN)Ph₂S=CH–SPh₂(NH)]⁺ [ClO₄]⁻ (**8**). The structure of **8** is still preliminary as it has been difficult to effect the separation of **3** and **8** successfully.
- [8] Crystal data for **5**: C₂₇H₂₇ClN₂O₄S₂, M_r = 547.09, monoclinic, space group $P2_1/n$, Z = 4, a = 12.769(6), b = 16.503(4), c = 14.031(6) Å, β = 115.99(3)°, V = 2657(1) Å³, ρ_{calcd} = 1.367 cm⁻³. X-ray diffraction data were collected on a Rigaku AFC7R diffractometer with graphite monochromated MoK α radiation (λ = 0.71069 Å) at 296 K, and the structure was solved by direct methods (SIR 92) and expanded using Fourier techniques (DRIFT). The final cycle of full-matrix least-squares refinement was based on 5006 observed reflections ($I > 3\sigma(I)$) and 338 variable parameters and converged to R = 0.050 and R_w =

0.071. **6**: C₂₇H₂₆N₂S₂, M_r = 442.64, monoclinic, space group $P2_1/n$, Z = 4, a = 7.40(5), b = 15.63(8), c = 20.36(6) Å, β = 91.6(5)°, V = 2352(20) Å³, ρ_{calcd} = 1.250 cm⁻³. X-ray diffraction data were collected on a Rigaku AFC7R diffractometer with graphite monochromated MoK α radiation (λ = 0.71069 Å) at 296 K, and the structure was solved by direct methods (SIR 92) and expanded using Fourier techniques (DRIFT). The final cycle of full-matrix least-squares refinement was based on 4039 observed reflections ($I > 3\sigma(I)$) and 280 variable parameters and converged to R = 0.042 and R_w = 0.058. CCDC-180279 (**5**) and CCDC-180280 (**6**) contain the supplementary crystallographic data for this paper. These data can be obtained free of charge via www.ccdc.cam.ac.uk/conts/retrieving.html (or from the Cambridge Crystallographic Data Centre, 12, Union Road, Cambridge CB21EZ, UK; fax: (+44) 1223-336-033; or deposit@ccdc.cam.ac.uk).

- [9] For Ph₃P=C=PPh₃, see: a) A. T. Vincent, P. J. Wheatley, *J. Chem. Soc. Dalton Trans.* **1972**, 617–622; b) G. E. Hardy, J. I. Zink, W. C. Kaska, J. C. Baldwin, *J. Am. Chem. Soc.* **1978**, *100*, 8001–8002.
- [10] Gaussian 98 (Revision A.9), M. J. Frisch, G. W. Trucks, H. B. Schlegel, G. E. Scuseria, M. A. Robb, J. R. Cheeseman, V. G. Zakrzewski, J. A. Montgomery, R. E. Stratmann, J. C. Burant, S. Dapprich, J. M. Millam, A. D. Daniels, K. N. Kudin, M. C. Strain, O. Farkas, J. Tomasi, V. Barone, M. Cossi, R. Cammi, B. Mennucci, C. Pomelli, C. Adamo, S. Clifford, J. Ochterski, G. A. Petersson, P. Y. Ayala, Q. Cui, K. Morokuma, D. K. Malick, A. D. Rabuck, K. Raghavachari, J. B. Foresman, J. Cioslowski, J. V. Ortiz, B. B. Stefanov, G. Liu, A. Liashenko, P. Piskorz, I. Komaromi, R. Gomperts, R. L. Martin, D. J. Fox, T. Keith, M. A. Al-Laham, C. Y. Peng, A. Nanayakkara, C. Gonzalez, M. Challacombe, P. M. W. Gill, B. G. Johnson, W. Chen, M. W. Wong, J. L. Andres, M. Head-Gordon, E. S. Replogle, J. A. Pople, Gaussian, Inc., Pittsburgh, PA, **1998**.
- [11] a) NBO version 3.1, E. D. Glendeling, A. E. Reed, J. E. Carpenter, F. Weinhold; b) A. E. Reed, L. A. Curtiss, F. Weinhold, *Chem. Rev.* **1988**, *88*, 899–926, and references therein; c) A. E. Reed, F. Weinhold, *J. Chem. Phys.* **1985**, *83*, 1736–1740.
- [12] a) A. E. Reed, P. von R. Schleyer, *J. Am. Chem. Soc.* **1987**, *109*, 7362–7371; b) A. E. Reed, A. P. von R. Schleyer, *Inorg. Chem.* **1988**, *27*, 3969–3987; c) A. E. Reed, P. von R. Schleyer, *J. Am. Chem. Soc.* **1990**, *112*, 1434–1445, and references therein.

Reaction of 2-Butyne with *nido*-[1,2-(Cp*₂RuH)₂B₃H₇]: Improved Kinetic Control Leads to Metallocarboranes of Novel Composition and Structure**

Hong Yan, Alicia M. Beatty, and Thomas P. Fehlner*

The conventional route to metallocarboranes proceeds in a sequence of steps leading from polyborane to carborane to metallocarborane.^[1–4] Although a fruitful strategy, it is also one in which strong bonds are formed before weak ones. Access to more diverse chemistry might arise by adoption of the reverse strategy, that is, formation of B–B/B–M before B–C/M–C bonds, thereby generating the most stable products

[*] Prof. T. P. Fehlner, Dr. H. Yan, Dr. A. M. Beatty
Department of Chemistry and Biochemistry
University of Notre Dame
Notre Dame, IN 46556 (USA)
Fax: (+1) 219-631-6652
E-mail: fehlner.1@nd.edu

[**] This work was supported by the National Science Foundation CHE 9986880. Cp* = C₅Me₅.

last. Having in hand an efficient, general route to metal-laboranes by the reaction of monocyclopentadienyl metal chlorides with monoboranes, we were in a position to test this hypothesis.^[5] Insertion of an alkyne into a metallaborane has precedence but, in the absence of efficient routes to metal-laboranes, has not been extensively explored.^[6–8] The results described below illustrate the increased scope of metal-laborane chemistry accessible when kinetic barriers are significantly lowered.

Reaction of *nido*-[1,2-(Cp*RuH)₂B₃H₇] (**1**; Cp* = η^5 -C₅Me₅)^[9] with excess 2-butyne at room temperature yields a major product, **2**, and two minor ones, **3** and **4** (Scheme 1). The major product results from addition of the alkyne followed by loss of H₂. The spectroscopic data were not consistent with formation of a single 9 skeletal-electron-pair (sep) *nido* 7-framework-atom cluster as suggested by the molecular formula of **2**^[10, 11] and it took a solid-state structure determination^[12] (Figure 1) to show that the cluster framework adopted by **2** is a *nido* 6-framework-atom cluster. The seventh atom, boron, is found as an exopolyhedral BH₂ fragment bridging an apical Ru-basal boron edge giving *nido*-[1,2-(Cp*Ru)₂(μ -H)(μ -BH₂)-4,5-Me₂-4,5-C₂B₂H₄] (**2**).

Formally, the BH₂ fragment on **2** is a one-electron ligand and **2** has an 8 sep count appropriate for its shape. The NMR spectra and the structure data show that the BH₂ fragment forms a BHB interaction with the terminal hydrogen atom of the basal boron atom it bridges, thus, **2** can also be considered to possess an exopolyhedral BH₃ unit. Although **2** is unique, related compounds are: a metallaborane with a terminal BH₂PR₃ fragment;^[13] a ferraborane with a BH₃ unit replacing the hydrogen atom of a B-H-B bridge;^[14] and a compound with a BX fragment bridging two metal atoms.^[15]

Addition of the alkyne to **1** and loss of BH₃ gives [1,2-(Cp*RuH)₂-4,5-Me₂-4,5-C₂B₂H₄] (**3**) as a minor product. The structure of an analogue of **3** which has different substituents on the carbon atoms was reported earlier to provide a contrast to the reaction of isoelectronic [1,2-(Cp*Rh)₂B₃H₇] with alkynes leading to catalytic cyclotrimerization.^[16] Considerably more surprising is the isolation of [1,2-(Cp*RuH)₂-4-Et-

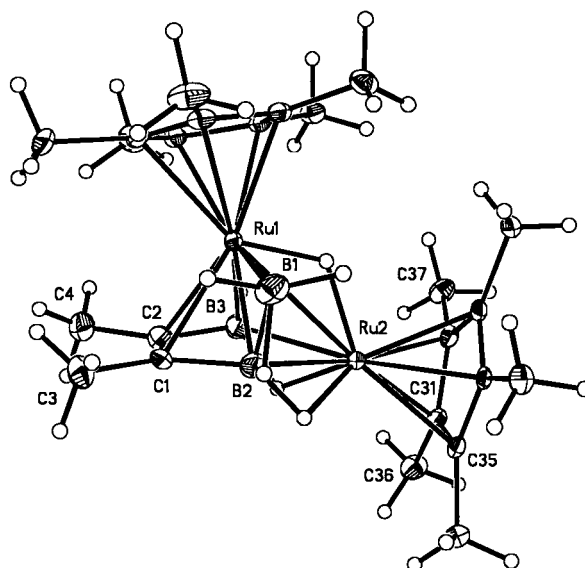
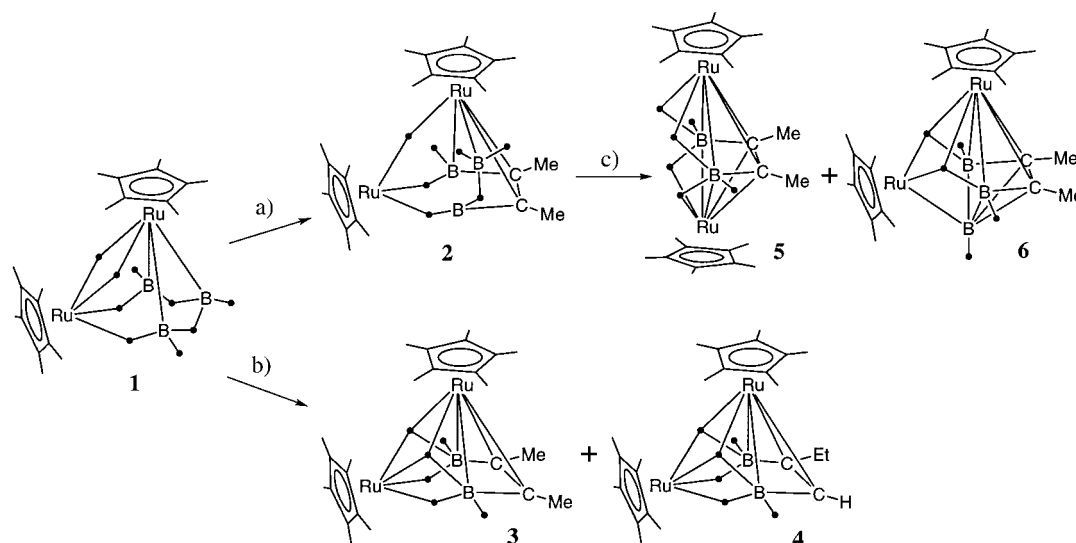


Figure 1. Molecular structure of **2**. Selected bond lengths [Å]: Ru1-B2 2.155(5), Ru1-B1 2.278(6), Ru1-C2 2.292(5), Ru1-B3 2.332(5), Ru1-Ru2 2.9134(5), C1-C2 1.391(8), C1-C3 1.508(7), C1-B2 1.558(7), B1-B2 1.760(9), Ru2-B2 2.293(6), Ru2-B3 2.327(6), C2-C4 1.519(7), C2-B3 1.520(8).

4,5-C₂B₂H₅] (**4**), a product that would be expected to arise from 1-butyne. No detectable 1-butyne was present in the reagent used and, although the isomerization of internal alkenes to terminal alkenes by boranes is well known,^[17] similar isomerization of alkynes is not. However, **4** is clearly a product of the reaction of **1** with 2-butyne. Related complex chemistry occurs when the alkenyl pentaborane formed from B₅H₉ and 2-butyne is converted thermally into 2-Me-3-Et-2-CB₃H₇.^[18] Although mechanistically suggestive, the high reaction barrier makes it unlikely that an alkenyl borane is a precursor to either **3** or **4**.

Heating **2** generates *nido*-[1,7-(Cp*Ru)₂-4,5-Me₂-4,5-C₂B₂H₆] (**5**) and *closo*-[1,2-(Cp*RuH)₂-4,5-Me₂-4,5-C₂B₃H₃] (**6**). Complex **5** has a molecular formula identical to **3** but very different spectroscopic properties. A solid-state structure^[12]



Scheme 1. Conditions; a), b) 2-butyne, room temperature, 24 h, THF; c) 85 °C, 25 h, toluene. ● = H.

(Figure 2) shows it to be a cluster geometric isomer of **3**. Both are 8 sep clusters based on a pentagonal-bipyramidal geometry. Compound **3** has a vacant 5-connect vertex, common for a polyborane, whereas **5** has a vacant 4-connect vertex,

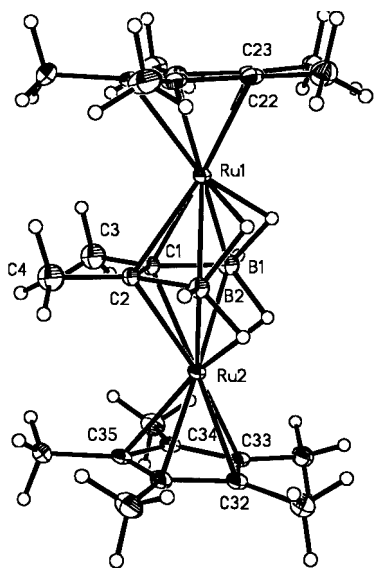


Figure 2. Molecular structure of **5**. Selected bond lengths [Å]: Ru1-C1 2.197(7), Ru1-C2 2.271(8), Ru1-B1 2.290(8), Ru1-B2 2.425(8), Ru2-C1 2.200(7), Ru2-C2 2.284(8), Ru2-B1 2.286(8), Ru2-B2 2.424(8), B1-C1 1.543(12), B2-C2 1.593(12), C1-C2 1.455(11), C1-C3 1.512(11), C2-C4 1.503(12), Ru1-Ru2 3.6383(5).

unusual for a polyborane. Both are stable up to 90 °C. Observation of **3** and **5** in the same reaction system under different conditions is a clear demonstration of kinetic control. The solid-state structure of **6**^[12] (Figure 3) reveals a *closo* geometry consistent with its sep = 8. Along with loss of H₂, the exopolyhedral borane of **2** has reentered the skeletal network.

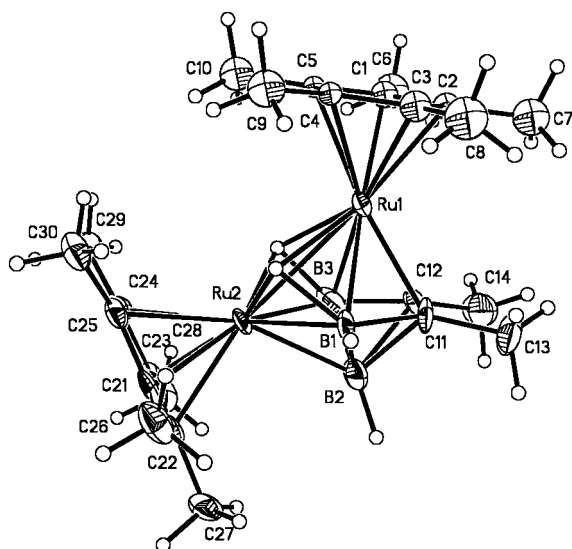


Figure 3. Molecular structure of **6**. Selected bond lengths [Å]: Ru1-C12 2.170(9), Ru1-C11 2.206(10), Ru2-B2 2.172(11), Ru2-B3 2.180(11), Ru2-B1 2.196(9), Ru1-Ru2 2.8832(9), B1-C11 1.573(13), B1-B2 1.802(17), B2-C11 1.738(15), B2-C12 1.751(14), B2-B3 1.813(18), B3-C12 1.582(14), C11-C12 1.411(15), C11-C13 1.512(13), C12-C14 1.541(13).

This work clearly demonstrates that combining metal and boron before carbon permits access to metallacarboranes of types not previously seen. The work constitutes part of a continuing realization of the potential of the inorganometallic chemistry of boron.^[19]

Experimental Section

2–4: MeC≡CMe (0.8 g, 14.8 mmol) was added to an orange solution of **1** (150 mg, 0.29 mmol)^[9] in THF (40 mL). Reaction for 24 h at ambient temperature, removal of solvent and excess alkyne, and chromatography (silica gel, ICN 32-63 D, hexane:toluene = 20:1) gave **2** (83.8 mg, 51 %): ¹H (400 MHz, 22 °C, [D₆]benzene; t = terminal): δ = 4.44 (br, 1 H, B-Ht), 3.70 (br, 1 H, B-Ht), 3.63 (br, 1 H, B-Ht), 1.93 (s, 3 H, Me), 1.82 (s, 15 H, Cp*), 1.80 (s, 3 H, Me), 1.61 (s, 15 H, Cp*), –3.25 (br d, J = 65 Hz, 1 H, B-H-B), –11.02 (pcq = partially collapsed quartet, 1 H, B-H-Ru), –14.92 (s, 1 H, Ru-H-Ru), –14.94 ppm (br, 1 H, B-H-Ru); ¹¹B (128 MHz, 22 °C, [D₆]benzene): δ = 26.1, 20.1, 11.4 ppm (all br 1:1:1); ¹³C (125 MHz, 22 °C, [D₆]benzene): δ = 10.76 (Cp*), 12.17 (Cp*), 15.01 (Me), 19.98 (Me), 88.71 (Cp*), 93.73 (Cp*), 111.50 (br, C-B), 128.30 ppm (br, C-B); FAB-MS: 563 (100 %, [M⁺ – 4 H]); IR (KBr): $\tilde{\nu}$ = 2411, 2461 cm^{–1} (ν_{B-H}); then **3** (27.4 mg, 17 %): ¹H (400 MHz, 22 °C, [D₆]benzene): δ = 2.12 (s, 6 H, Me), 2.05 (br, 1 H, B-Ht), 1.87 (s, 15 H, Cp*), 1.78 (s, 15 H, Cp*), –11.52 (br, s, 2 H, Ru-H-Ru), –12.57 ppm (br, 2 H, B-H-Ru); ¹¹B (128 MHz, 22 °C, [D₆]benzene): δ = –16.2 ppm (br); ¹³C (125 MHz, 22 °C, [D₆]benzene): δ = 11.49 (Cp*), 12.42 (Cp*), 21.20 (Me), 86.71 (Cp*), 90.37 (Cp*), 108.52 ppm (br, C-B); MALDI-MS: 555 ([M⁺]); IR (KBr): $\tilde{\nu}$ = 2427 (ν_{B-H}); then **4** (13 mg, 8 %): ¹H (400 MHz, 22 °C, [D₆]benzene): δ = 4.40 (brs, 1 H, CH), 2.31 (m, 2 H, CH₂), 2.09 (br, 1 H, B-Ht), 1.99 (br, 1 H, B-Ht), 1.85 (s, 15 H, Cp*), 1.79 (s, 15 H, Cp*), 1.45 (t, ³J(H,H) = 7.4 Hz, 3 H, CH₃), –11.67 (s, 1 H, Ru-H-Ru), –11.83 (s, 1 H, Ru-H-Ru), –12.18 (brs, 1 H, B-H-Ru), –12.60 ppm (brs, 1 H, B-H-Ru); ¹¹B (128 MHz, 22 °C, [D₆]benzene): δ = –18.2, –14.7 ppm (all br 1:1); ¹³C (125 MHz, 22 °C, [D₆]benzene): δ = 11.73 (Cp*), 12.38 (Cp*), 20.79 (Me), 33.18 (CH₂), 86.63 (Cp*), 91.14 (Cp*), 97.54 (br, B-C-H) and 118.77 ppm (br, C-B); MALDI-MS: 555 ([M⁺]); IR (KBr): $\tilde{\nu}$ = 2436 (ν_{B-H}).

5 and 6: **2** (96 mg, 0.17 mmol) in toluene (20 mL) was heated for 25 h at 85 °C under N₂. After removal of the solvent and chromatography (silica gel, ICN 23-60 D, hexane) gave **6** (44.2 mg, 46 %): ¹H (400 MHz, 22 °C, [D₆]benzene): δ = 3.82 (pcq, 3 H, B-Ht), 2.13 (s, 6 H, Me), 2.07 (s, 15 H, Cp*), 1.68 (s, 15 H, Cp*), –11.12 ppm (sbr 2 H, B-H-Ru); ¹¹B (128 MHz, 22 °C, [D₆]benzene): δ = 11.07 (d, ²J(B,H) = 145 Hz, 2 B), 8.72 ppm (d, ²J(B,H) = 145 Hz, 1 B); ¹³C (125 MHz, 22 °C, [D₆]benzene): δ = 11.52 (Cp*), 12.29 (Cp*), 21.25 (Me), 86.24 (Cp*), 87.80 (br, C-B), 93.95 ppm (Cp*); FAB: 563.3 (100 %, [M⁺ – 2 H]); IR (KBr): $\tilde{\nu}$ = 2477 (ν_{B-H}); and (hexane:toluene = 20:1) gave **5** (19.8 mg, 21 %): ¹H (400 MHz, 22 °C, [D₆]benzene): δ = 2.41 (s, 6 H, Me), 1.66 (s, 30 H, Cp*), 1.18 (br, 2 H, B-H-B), –10.07 ppm (brs, 4 H, B-H-Ru); ¹¹B (128 MHz, 22 °C, [D₆]benzene): δ = –32.9 ppm (br); ¹³C (125 MHz, 22 °C, [D₆]benzene): δ = 10.92 (Cp*), 21.00 (Me), 84.63 ppm (Cp*); FAB: 553 (100 %, [M⁺ – 2 H]); IR (KBr): $\tilde{\nu}$ = 2420 (ν_{B-H}).

Received: February 27, 2002 [Z18785]

- [1] M. F. Hawthorne, D. C. Young, P. A. Wegner, *J. Am. Chem. Soc.* **1965**, 87, 1818.
- [2] M. F. Hawthorne, G. B. Dunks, *Science* **1972**, 178, 462.
- [3] R. N. Grimes, *Pure Appl. Chem.* **1982**, 54, 43.
- [4] C. A. Plumb, L. G. Sneddon, *Organometallics* **1992**, 11, 1681.
- [5] T. P. Fehlner, *Organometallics* **2000**, 19, 2643.
- [6] R. N. Grimes, *Pure Appl. Chem.* **1974**, 39, 455.
- [7] E. J. Ditzel, X. L. R. Fontaine, N. N. Greenwood, J. D. Kennedy, Z. Sisan, B. Stfbr, M. Thornton-Pett, *J. Chem. Soc. Chem. Commun.* **1990**, 1741.
- [8] J. Bould, N. P. Rath, L. Barton, J. D. Kennedy, *Organometallics* **1998**, 17, 902.
- [9] X. Lei, M. Shang, T. P. Fehlner, *J. Am. Chem. Soc.* **1999**, 121, 1275.
- [10] K. Wade, *Adv. Inorg. Chem. Radiochem.* **1976**, 18, 1.

- [11] D. M. P. Mingos, D. J. Wales, *Introduction to Cluster Chemistry*, Prentice Hall, New York, 1990.
- [12] CCDC-180080–180082 (**2**, **5**, **6**) contains the supplementary crystallographic data for this paper. These data can be obtained free of charge via www.ccdc.cam.ac.uk/conts/retrieving.html (or from the Cambridge Crystallographic Data Centre, 12, Union Road, Cambridge CB2 1EZ, UK; fax: (+44) 1223-336-033; or deposit@ccdc.cam.ac.uk).
- [13] P. McQuade, K. Hupp, J. Bould, H. Fang, N. P. Rath, R. L. Thomas, L. Barton, *Inorg. Chem.* **1999**, *38*, 5415.
- [14] O. Hollander, W. R. Clayton, S. G. Shore, *Chem. Commun.* **1974**, 604.
- [15] H. Braunschweig, T. Wagner, *Angew. Chem.* **1995**, *107*, 904; *Angew. Chem. Int. Ed. Engl.* **1995**, *34*, 825.
- [16] H. Yan, A. M. Beatty, T. P. Fehlner, *Angew. Chem.* **2001**, *113*, 4630; *Angew. Chem. Int. Ed.* **2001**, *40*, 4498.
- [17] H. C. Brown, *Hydroboration*, Benjamin, New York, 1962.
- [18] R. Wilczynski, L. G. Sneddon, *Inorg. Chem.* **1981**, *20*, 3955.
- [19] *Inorganometallic Chemistry* (Ed.: T. P. Fehlner), Plenum, New York, 1992.

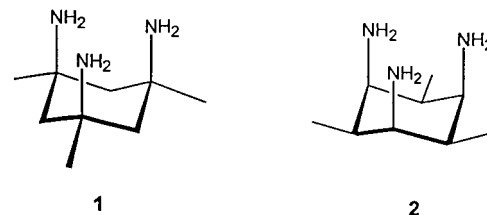
A 1,3,5-Triaxial Triaminocyclohexane: The Triamine Corresponding to Kemp's Triacid**

Fredric M. Menger,* Jianwei Bian, and Vladimir A. Azov

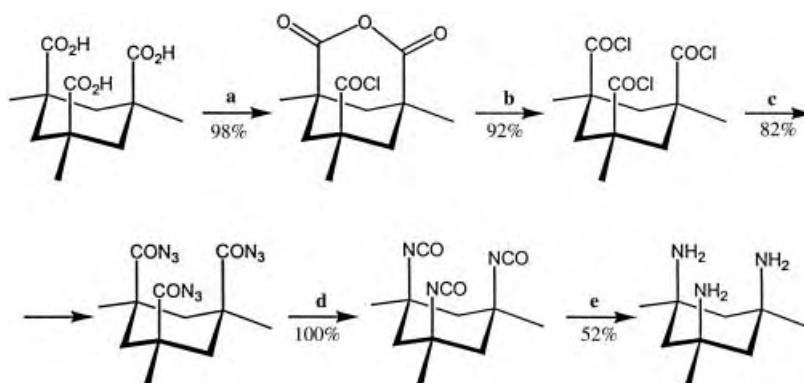
Kemp's triacid is a cyclohexane derivative in which 1,3,5-*cis* methyl groups force three 1,3,5-*cis* carboxy groups into an all-axial conformation.^[1] In the two decades since its inception, Kemp's triacid has served as a useful framework for the design of enzyme models. For example, an aliphatic monoamide of Kemp's triacid hydrolyzes in only minutes at neutral pH and 22 °C because of enzyme-like catalysis by a neighboring carboxy group.^[2] Herein, we examine the properties of triamine **1**, an analogue of Kemp's triacid which has, until now, escaped synthesis.

cis,cis-1,3,5-Triaminocyclohexane^[3] was first prepared in 1957 and, a decade later, its metal complexes were inves-

tigated.^[4] More pertinently, triamine **2**, an isomer of our compound, was previously synthesized and examined,^[5] which provided us with a valuable comparison.^[6] As will be seen, the two systems (**1** and **2**) differ substantially in their basicity and nucleophilicity.



The synthesis of triamine **1**, which started with the addition of 2–4 g Kemp's triacid to SOCl₂, is given in Scheme 1. The product was, however, not the desired triacid chloride but the anhydride/acid chloride. Fortunately, this difficulty could be circumvented with the aid of a literature procedure in which an anhydride is converted into two acid chlorides.^[7] The key



Scheme 1. Synthesis of triamine **1**: a) SOCl₂, ether, RT, b) ZnCl₂, CHCl₂OCH₃, reflux, c) NaN₃, Bu₄NBr, CH₂Cl₂/H₂O, 0 °C, d) dioxane, reflux, e) 37 % HCl, THF, reflux, then Dowex 550A OH[−], CH₃OH.

step, a stereospecific tris-Curtius rearrangement of triazide (purified chromatographically with CHCl₃), proceeded with high yield in refluxing dioxane or toluene (caution!).^[8] The resulting triisocyanate was hydrolyzed under harsh conditions (37 % HCl/THF), from which the trihydrochloride salt precipitated. Treatment with an ion-exchange resin released the free triamine **1** (m.p. of hydrate 86–90 °C), which was characterized by ¹H and ¹³C NMR spectroscopy, MS, elemental analysis, and X-ray crystallography.^[9]

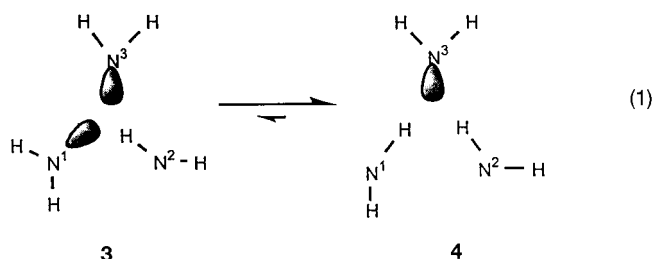
X-ray analyses of the crystalline triamine **1**, **1**·1HCl, and the diacetyl derivative established in each case a preference for three axial nitrogen atoms. Only the **1**·3HCl adopted a conformation with three equatorial nitrogens caused, no doubt, by electrostatic repulsion among the three cationic ammonium groups. A similar dependence of conformation upon the protonation level of triamine **2**, as deduced by NMR spectroscopy, was reported previously.^[5] Three factors favor axial nitrogen atoms: a) the slightly smaller size of an amino group relative to a methyl group,^[10] b) hydrogen bonding among the amine groups, and c) a beneficial antiperiplanar σ_{C-H}–σ_{C-N}^{*} interaction.^[11]

[*] Prof. F. M. Menger, J. Bian, Dr. V. A. Azov
Department of Chemistry
Emory University
Atlanta, GA 30322 (USA)
Fax: (+1) 404-727-6586
E-mail: menger@emory.edu

[**] This research was supported by the National Institutes of Health Grant 21457. We thank Dr. Ken Hardcastle and Bao Do of the Emory X-ray Crystallography Laboratory for the X-ray structures and Dr. Denis Liotta and Dr. James P. Snyder for the use of the Silicon Graphics computer.

Supporting information for this article is available on the WWW under <http://www.angewandte.org> or from the author. CCDC-183190 to CCDC-183202 contain the supplementary crystallographic data for this paper. These data can be obtained free of charge via www.ccdc.cam.ac.uk/conts/retrieving.html (or from the Cambridge Crystallographic Data Centre, 12, Union Road, Cambridge CB2 1EZ, UK; fax: (+44) 1223-336-033; or deposit@ccdc.cam.ac.uk).

The X-ray structure of the parent triamine is noteworthy in that it revealed the spatial disposition of the three amino groups when forced into a 1,3,5-triaxial relationship. Of the two rotameric states, namely the “one-proton-plus-two-lone-pairs” (**3**) and the “two-protons-plus-one-lone-pair” (**4**), the latter was observed exclusively [Eq. (1)]. Conformer **4** has $N^1 \cdots N^3$, $N^2 \cdots N^3$, and $N^1 \cdots N^2$ distances of 3.00, 2.98, and 3.17 Å, respectively, and $N^1H \cdots N^3$ and $N^2H \cdots N^3$ distances of 2.2 Å. N-H-N angles are non-colinear (138°).



Molecular modeling is consistent with the X-ray analytical information. Conformer searches were first carried out with MacroModel using the Monte Carlo method with the MMFFs force field.^[12] The lowest energy triaxial and triequatorial conformers were then reoptimized using density functional theory at the B3LYP/6-31G(d,p) level (Gaussian 98).^[13, 14] The calculations indicate the following for triamine **1**: a) The conformer with triaxial amine groups is 6.2 kcal mol⁻¹ lower in energy than the conformer with triequatorial amine groups, b) the “two-protons-plus-one-lone-pair” configuration is 1.9 kcal mol⁻¹ lower in energy than the “one-proton-plus-two-lone-pairs” configuration. It seems intuitively reasonable that formation of weak bifurcated hydrogen bonds^[15] in **4** should be favored over **3** because, among other factors, this avoids the electron–electron repulsion in **3**.

Further characterization of **1** included titrimetric determination of the pK_a values in water (Table 1). Monoprotonation data indicate that **1** is an unusually strong base ($pK_1 > 12$),

Table 1. pK_a values of triamines **1** and **2**.

Triamine	pK_1	pK_2	pK_3
1	> 12	8.5	5.0
2 ^[a]	7.8	6.7	5.2

[a] Data taken from ref. [5].

whereas **2** is an unusually weak base ($pK_1 = 7.8$). The latter was ascribed to “disruption to the ideal hydrogen-bonded network present in the free triamine caused by protonation”.^[5] We prefer to attribute the low pK_a value in **2** to impaired solvation of the $-NH_3^+$, caused by the two methyl groups buttressing the group on either side. This explanation allows us to rationalize the high basicity of **1** in terms of a favorable $-NH_2 \cdots -NH_3^+$ hydrogen bond. NMR spectroscopic studies showed that, even at -80°C in methylene chloride, an $-NH_3^+$ proton is shuffled rapidly among all the amine groups, but it was not possible, despite repeated attempts, to prove

that the mechanism is an intramolecular “proton circulation”, free from an intermolecular contribution.

Triamine **1** forms crystalline complexes with Cu^{2+} , Zn^{2+} , Ni^{2+} , and Co^{3+} ions, which, according to X-ray analysis, are octahedral in nature (consistent with complexes based on *cis,cis*-triaminocyclohexane^[4] and inositol derivatives^[16]). Triamine **1** also forms a crystalline 1:1 complex with Kemp’s triacid; the corresponding X-ray structure shows two amino groups perched directly above the three carboxy groups with salt bridging occurring between the amino–carboxy group pairs.

The strong basicity of triamine **1** suggested an abnormally high nucleophilicity worthy of investigation. Thus, we quantified the affinity of the triamine **1** toward an ester (*p*-nitrophenyl acetate) in an aprotic solvent (chlorobenzene) at 25.0°C . These conditions were selected because, three decades ago, we had studied the kinetics of such ester aminolyses in detail.^[17] As seen in Table 2, aminolysis of *p*-nitrophenyl

Table 2. Reaction order in amine for the aminolyses of *p*-nitrophenyl acetate (pNPA) *p*-cyanophenyl acetate (pCyPA), and *p*-chlorophenyl acetate (pChPA) by various amines in an aprotic solvent.^[a]

Amine	pNPA	pCyPA	pChPA
triamine 1	first	first	first ^[b]
<i>n</i> -butylamine	second	second	second
<i>tert</i> -butylamine	second		
<i>trans</i> -1,2-diaminocyclohexane	second		
$\text{NH}_2(\text{CH}_2)_2\text{NH}_2$	second	second	second
$\text{NH}_2(\text{CH}_2)_3\text{NH}_2$	first	second	second
$\text{NH}_2(\text{CH}_2)_4\text{NH}_2$	first	second	second
$\text{NH}_2(\text{CH}_2)_5\text{NH}_2$	second	second	second

[a] Runs were carried out in chlorobenzene at 25.0°C . [ester] = $0.9 \times 10^{-4}\text{ M}$ with triamine **1** and $4\text{--}6 \times 10^{-4}\text{ M}$ with other amines. [triamine **1**] = $2.1\text{--}18 \times 10^{-3}\text{ M}$. Reactions (monitored spectrophotometrically at 360 or 400 nm for pNPA and 290 nm for pCyPA and pChPA) were run to infinity. Pseudo-first-order plots were linear for at least two half-lives. Five rate constants were usually determined to ascertain each of the eighteen reactions orders. [b] Carried out at 58.5°C .

acetate by excess **1** is cleanly first order in the amine (i.e. a plot of k_{obs} vs. [amine] is linear with zero intercept). In sharp contrast, aminolyses by excess *n*-butylamine and *tert*-butylamine are cleanly second order in the amine (i.e. plots of k_{obs} vs. [amine]² are linear with zero intercepts).^[18] Second-order dependence on the amine is traditionally explained by a general-base mechanism in which one amine removes a proton from the other nucleophilic amine.^[19] Nitrogen–nitrogen proton transfer occurs intramolecularly with triamine **1**, which accounts for its first-order behavior in the amine.

Since intramolecularity is an issue with **1**, we also inspected the reactivity of four diamines ($\text{H}_2\text{N}(\text{CH}_2)_n\text{NH}_2$ where $n = 2\text{--}5$). The aminolyses are second order in amine for $n = 2$ and 5, but first order for $n = 3$ and 4 (Table 2). Clearly, spatial effects^[20] determine whether or not an intramolecular proton transfer is kinetically profitable. To understand these effects better, MacroModel conformer searches were used to define the lowest energy species with short $\text{N} \cdots \text{N}$ distances (ca. 3.0 Å). The $n = 2$ diamine has a sharp, debilitating N-H-N

angle of 112° (compared to 137–157° for the other diamines and for **1** itself). A more linear N-H-N trajectory for the $n = 2$ diamine, possible only in the bimolecular mode, is thus preferred. Although the $n = 5$ diamine does not suffer from a similar angular constraint, its monomolecularity is disfavored by enthalpic and entropic factors, which are well known to impede cyclizations of larger rings.^[21, 22]

Aminolysis of less reactive esters, the *p*-cyanophenyl and *p*-chlorophenyl acetates, is quite different. The reaction of both esters with the $n = 3$ and $n = 4$ diamines are second order in amine (Table 2). Evidently, the intramolecular proton transfer, which occurs with the nitrophenyl ester, fails to operate competitively here when these two amines attack the *p*-cyanophenyl and *p*-chlorophenyl esters. Although a change in mechanism with structure is commonplace, an overt increase in reaction order with a small reactivity difference (e.g. the cyanophenyl ester is only about threefold less reactive than the nitrophenyl ester) is unprecedented. The unusual conversion from an *intramolecular* to an *intermolecular* general-base mechanism reveals a concept of substantial relevance to enzymology: A mechanistic pathway favored by a particular catalyst geometry may become kinetically inoperative, and be replaced by a different pathway, because of only a minor change in substrate reactivity.^[23] Of course, the point at which the change of mechanism occurs depends upon the particular catalyst/nucleophile. Because triamine **1** retains (uniquely!) its “first-order-in-amine” status throughout the series (Table 1), the compound must possess a geometry and rigidity favorable for intramolecular proton transfer, even with the less reactive substrates.

Further information was obtained from the actual rate constants given in Table 3. Note that only rate constants of the same kinetic order (i.e. either overall second or third order) can be legitimately compared. Superficially, it appears that triamine **1** is a fivefold poorer nucleophile than the $n = 3$ and $n = 4$ diamines. The amine groups of **1** are, however, bonded to tertiary carbon atoms. A comparison of k_3 values for *n*-butylamine and *tert*-butylamine (3.8 and 0.007 min⁻¹M⁻², respectively) shows that steric effects within the nucleophile can be substantial. Adjusting for the rate difference seen in these k_3 values, one can estimate that **1** is in fact a more powerful nucleophile than the $n = 3$ and $n = 4$ diamines by two orders of magnitude (this difference might, of course, stem in part from a high basicity of **1**). However, the diamine rates themselves contain an intramolecular catalytic component. To

improve our understanding of the diamine catalysis, we plotted $k_{\text{obs}}/[\text{amine}]$ versus $[\text{amine}]$ for *n*-butylamine [see Eq. (2)] and used the error limits of the negligible value of the intercept to obtain a maximum possible k_2 value. This k_2 value is one to two orders of magnitude smaller than the accurately known k_2 values for the $n = 3$ and $n = 4$ diamines in Table 3. By combining comparisons, one finds that triamine **1** reflects a minimum inherent catalysis, over and above that of *n*-butylamine, of about three to four orders of magnitude (by contrast, triamine **2** is reported to have an impaired reactivity^[5], probably because of steric effects).

$$k_{\text{obs}} = k_2 [\text{amine}] + k_3 [\text{amine}]^2 \quad (2)$$

Of course, triamine **1** is also special because it is the only amine investigated that maintains a first-order dependence on amine with all three esters.

In summary, we have synthesized triamine **1**, a system in which three amine groups are fixed in 1,3-diaxial relationships. X-ray analysis and theoretical models show that the three amines have a “two-protons-plus-one-lone-pair” bifurcated relationship. Because of this hydrogen-bonded network, triamine **1** is highly basic and, unlike four diamines studied for comparison, it maintains an *intramolecular* general-base catalysis with three related esters. The kinetics also reveal a remarkable dependency of rates and mechanism upon slight variations in substrate reactivity, an observation relevant to the field of enzyme mechanism.

Received: February 28, 2002
Revised: April 22, 2002 [Z18793]

Table 3. Overall second-order (k_2) and third-order (k_3) rate constants for the aminolysis of three esters by various amines.^[a]

Amine	pNPA		pCyPA		pChPA
	k_2	k_3	k_2	k_3	
triamine 1	1.1		0.31		
<i>n</i> -butylamine		3.8		1.5	0.06
<i>tert</i> -butylamine		0.007			
<i>trans</i> -1,2-diaminocyclohexane		5.1			
NH ₂ (CH ₂) ₂ NH ₂		38		8.8	0.31
NH ₂ (CH ₂) ₃ NH ₂	6.3			22	0.42
NH ₂ (CH ₂) ₄ NH ₂	5.3			18	0.34
NH ₂ (CH ₂) ₅ NH ₂		27		8.2	0.31

[a] See Table 2 for reaction conditions. k_2 in units of min⁻¹M⁻¹, and k_3 in units of min⁻¹M⁻². Rates are not corrected for statistical factors.

- [1] D. S. Kemp, K. S. Petrakis, *J. Org. Chem.* **1981**, 46, 5140.
- [2] F. M. Menger, M. Ladika, *J. Am. Chem. Soc.* **1988**, 110, 6794.
- [3] F. Lions, K. V. Martin, *J. Am. Chem. Soc.* **1957**, 79, 1572.
- [4] R. A. D. Wentworth, J. J. Felten, *J. Am. Chem. Soc.* **1968**, 90, 621.
- [5] D. Parker, K. Senanayake, J. Vepsäläinen, S. Williams, A. S. Batsanov, J. A. K. Howard, *J. Chem. Soc. Perkin Trans. 2* **1997**, 1445.
- [6] For an inositol derivative with 1,3,5-triamino groups, see M. Weber, B. Morgenstern, K. Hegetschweiler, *Helv. Chim. Acta* **2001**, 84, 571.
- [7] F. Johnson, K. G. Paul, D. Favara, R. Ciabatti, U. Guzzi, *J. Am. Chem. Soc.* **1982**, 104, 2190.
- [8] H. A. Staab, G. Gabel, C. Krieger, *Chem. Ber.* **1987**, 120, 269. K. A. Lukin, J. Li, P. Eaton, N. Kanomata, J. Hain, E. Punzalan, R. Gilardi, *J. Am. Chem. Soc.* **1997**, 119, 9591. A sample in a melting-point tube vigorously decomposed at 118–120 °C.
- [9] ¹H NMR (400 MHz, CHCl₃, 25 °C): δ = 1.10 (s, 9H); 1.33–1.38 (d, 3H), 1.54–1.58 (d, 3H), 1.92 ppm (bs, 6H); ¹³C NMR (75 MHz, CHCl₃, 25 °C): δ = 35.9, 51.1, 51.3 ppm; HRMS analysed for C₉H₂₁N₃ [*M* + Li] 178.1896, found 178.1891; elemental analysis: calcd for C₉H₂₁N₃·2H₂O: C 52.14, H 12.15, N 20.27; found C 52.62, H 11.78, N 20.01.
- [10] E. L. Eliel, S. H. Wilen, *Stereochemistry of Organic Compounds*, Wiley-Interscience, New York, **1994**.
- [11] A. J. Kirby, *The Anomeric Effect and Related Stereoelectronic Effects at Oxygen*, Springer, Berlin, **1983**. P. Deslongchamps, *Stereoelectronic Effects in Organic Chemistry*, Pergamon, Oxford, **1983**.
- [12] F. Mohamadi, N. G. Richards, W. C. Guida, R. Liskamp, M. Lipton, C. Caufield, G. Chang, T. Hendrickson, W. C. Still, *J. Comput. Chem.* **1990**, 11, 440.
- [13] A. D. Becke, *J. Chem. Phys.* **1993**, 98, 5648; C. Lee, W. Yang, R. G. Parr, *Phys. Rev. B* **1988**, 37, 785.
- [14] Gaussian 98 (Revision A.7), M. J. Frisch, G. W. Trucks, H. B. Schlegel, G. E. Scuseria, M. A. Robb, J. R. Cheeseman, V. G. Zakrzewski, J. A. Montgomery, R. E. Stratmann, J. C. Burant, S. Dapprich, J. M.

- Millam, A. D. Daniels, K. N. Kudin, M. C. Strain, O. Farkas, J. Tomasi, V. Barone, M. Cossi, R. Cammi, B. Mennucci, C. Pomelli, C. Adamo, S. Clifford, J. Ochterski, G. A. Petersson, P. Y. Ayala, Q. Cui, K. Morokuma, D. K. Malick, A. D. Rabuck, K. Raghavachari, J. B. Foresman, J. Cioslowski, J. V. Ortiz, B. B. Stefanov, G. Liu, A. Liashenko, P. Piskorz, I. Komaromi, R. Gomperts, R. L. Martin, D. J. Fox, T. Keith, M. A. Al-Laham, C. Y. Peng, A. Nanayakkara, C. Gonzalez, M. Challacombe, P. M. W. Gill, B. G. Johnson, W. Chen, M. W. Wong, J. L. Andres, M. Head-Gordon, E. S. Replogle, J. A. Pople, Gaussian, Inc., Pittsburgh, PA, **1998** (compiled to run under Windows OS).
- [15] G. A. Jeffrey, *An Introduction to Hydrogen Bonding*, Oxford University Press, New York, **1997**, p. 22.
- [16] M. Weber, D. Kuppert, K. Hegetschweiler, V. Gramlich, *Inorg. Chem.* **1999**, *38*, 859.
- [17] F. M. Menger, *J. Am. Chem. Soc.* **1966**, *88*, 3081; F. M. Menger, J. H. Smith, *J. Am. Chem. Soc.* **1972**, *94*, 3824. For more recent references, see A. B. Maude, A. Williams, *J. Chem. Soc. Perkin Trans. 2* **1995**, 691; H. J. Koh, S. I. Kim, B. C. Lee, I. Lee, *J. Chem. Soc. Perkin Trans. 2* **1996**, 1353.
- [18] The reactions of *n*-butylamine and aliphatic diamines with phenyl acetate in water are both first order in the amine. T. C. Bruice, R. G. Willis, *J. Am. Chem. Soc.* **1965**, *87*, 531.
- [19] M. L. Bender, *Mechanism of Homogeneous Catalysis from Protons to Proteins*, Wiley-Interscience, New York, **1971**.
- [20] X. Duan, S. Scheiner, *J. Am. Chem. Soc.* **1992**, *114*, 5849.
- [21] A. J. Kirby, *Adv. Phys. Org. Chem.* **1980**, *17*, 183.
- [22] B. Capon, *Quart. Rev. Chem. Soc.* **1964**, *18*, 45.
- [23] F. M. Menger, *Acc. Chem. Res.* **1985**, *18*, 128; F. M. Menger, *Adv. Mol. Model.* **1988**, *1*, 189; F. M. Menger, *Proc. Natl. Acad. Sci. USA*, submitted.

Development of a Co-Mediated Rearrangement Reaction**

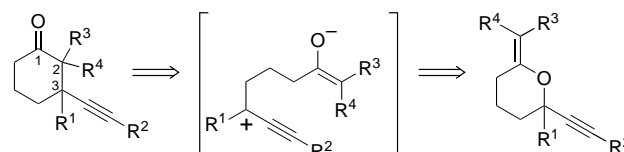
David R. Carbery, Serge Reignier, James W. Myatt, Neil D. Miller, and Joseph P. A. Harrity*

Dedicated to Professor Peter L. Pauson

The conjugate addition of organocuprates to enones represents an important fundamental approach to the elaboration of carbonyl-containing compounds through a C–C

bond-forming reaction.^[1] This process is extremely versatile for alkyl, alkenyl, and aryl group incorporation, however, the inclusion of an alkynyl unit in this fashion is much more limited.^[2] Nonetheless, the conjugate addition of alkynyl alanes does take place in the presence of a Ni catalyst.^[3] Additionally, the use of Lewis acids such as aluminum tris(2,6-diphenylphenoxide) (ATPH),^[4] silyl triflates,^[5] and iodotrimethylsilane^[6] can promote the conjugate addition of alkynyl metal compounds to cyclic enones, although the employment of β -substituted substrates generally prevents addition completely or leads to very poor product yields.

We envisaged a strategically different approach to these compounds (Scheme 1), whereby disconnection of the C2–C3 bond in the cyclic ketone would generate an enolate bearing a



Scheme 1. Retrosynthetic analysis of the formation of cyclic ketones through an enol ether rearrangement.

distal propargylic carbocation. We further surmised that this intermediate might be generated from a cyclic enol ether. To aid scission of the propargylic C–O bond of the enol ether, we examined the effect of the hexacarbonyldicobalt unit on the alkyne because of its ability to stabilize positive charge at the α -position strongly.^[7] Notably, related intramolecular additions of enolates to cobalt-stabilized carbocations have been reported, however, these studies required the propargyl ether and enolate moieties to be prepared independently and in a linear fashion. Furthermore, problems associated with regiochemical enolate formation can result in poor cyclization regioselectivity.^[8] We anticipated that the proposed rearrangement technique would overcome some of these problems whilst providing a direct method for the preparation of α -substituted products from appropriately armed enol ether substrates. We report herein our initial findings on the scope of the rearrangement process for the synthesis of β -alkynyl substituted cyclic ketones.

We embarked on this study by examining the rearrangement of readily available and easily handled *gem* dichloro substituted enol ethers. These compounds were prepared from the corresponding lactones following the method of Lakhri and Chapleur (Scheme 2).^[9] Addition of an alkynyl zinc reagent to commercially available **1** provided keto esters **3a** and **3b**; the homologous compound **3c** was prepared in a similar manner from **2**. Substituted δ -lactones **4a,b** were generated by a Luche reduction and saponification before ring closure. The quaternary substituted analogue **5** was prepared by an analogous procedure but with alkylation of **3b** using MeLi/TiCl₄^[10] in the initial step. ϵ -Lactone **6** was prepared from keto ester **3c** by a similar route. With the key intermediates lactones **4–6** in hand, we prepared the corresponding enol ethers in one step using PPh₃/CCl₄.^[9] Finally, exposure of the enol ethers to octacarbonyldicobalt at room

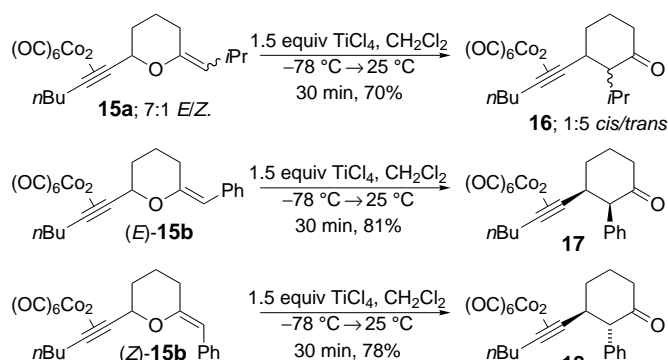
[*] Dr. J. P. A. Harrity, D. R. Carbery, Dr. S. Reignier, J. W. Myatt
Department of Chemistry
University of Sheffield
Brook Hill, Sheffield S3 7HF (UK)
Fax: (+44) 114-273-8673
E-mail: j.harrity@sheffield.ac.uk

Dr. N. D. Miller
Department of Medicinal Chemistry, Neurology CEDD
GlaxoSmithKline Research and Development
Gunnels Wood Road, Stevenage, Hertfordshire SG1 2NY (UK)

[**] The authors are grateful to the EPSRC and GlaxoSmithKline for a studentship (D.R.C.), Pfizer central research for an unrestricted grant (J.W.M.), and the Leverhulme Trust for a research fellowship (S.R.). We also thank Simon Thorpe and Sue Bradshaw for assistance in acquiring spectroscopic data.

Supporting information for this article is available on the WWW under <http://www.angewandte.org> or from the author.

isomers (Scheme 4; major isomer tentatively assigned as *trans*) in high yield.^[18] In contrast to **15a**, the individual *E/Z* isomers of **15b** were readily separable by column chromatography, which allowed the rearrangement of each isomer to be studied individually. To our surprise, we found that the rearrangement of complexes **15b** proceeded stereospecifically such that (*E*)-**15b** provided the *cis*-substituted ketone **17**, whereas the *trans*-substituted ketone **18** was formed exclusively from (*Z*)-**15b**.^[19, 20]



Scheme 4. Transformation of enol complexes **15** to alkynyl ketones.

The origin of these different stereochemical outcomes is intriguing. At present, we are pursuing three possible rationales: 1) Rearrangement of complexes **15a** is mechanistically distinct from that of **15b**. 2) Enol ether isomerization (*E* ↔ *Z*) proceeds rapidly for **15a** (or the intermediate metal enolate) such that the relative ratios of *cis/trans*-**16** are determined by relative rates of rearrangement of each enol(ate) isomer. 3) Product **16** isomerizes under the reaction conditions.^[21]

In conclusion, we report a novel approach to β -alkynyl substituted cyclic ketones through a cobalt-mediated rearrangement reaction of cyclic enol ethers. This technique allows the direct and regiospecific α -incorporation of dichloro-, ester, aryl, and alkyl substituents which can be readily controlled by judicious choice of the enol ether substituent.

Experimental Section

Typical experimental procedure as exemplified by the rearrangement of complex **7b**: To a solution of **7b** (2.0 g, 3.75 mmol) in CH_2Cl_2 (20 mL) at 0 °C was added TiCl_4 (616 μL , 10.0 mmol, 1.5 equiv) by syringe under nitrogen. The reaction mixture was stirred at 0 °C for 10 min and quenched by addition of saturated aqueous NaHCO_3 solution. The reaction mixture was poured into water, extracted with CH_2Cl_2 , dried with MgSO_4 , and the solvent removed in vacuo. Recrystallization of the crude complex afforded **11b** as a deep red solid (1.95 g, 97%), m.p. 77.1–78.3 °C; ^1H NMR (400 MHz, CDCl_3): δ = 0.99 (3H, t, J = 7.2 Hz), 1.46–1.56 (2H, m), 1.58–1.72 (2H, m), 1.75–1.86 (1H, m), 2.06–2.24 (3H, m), 2.64 (1H, dd, J = 9.0, 1.2 Hz), 2.91–3.04 (2H, m), 3.18 (1H, td, J = 14.4, 5.8 Hz), 3.63 ppm (1H, dd, J = 11.4, 3.7 Hz); ^{13}C NMR (100.6 MHz, CDCl_3): δ = 13.9, 22.7, 24.1, 32.7, 33.9, 34.5, 35.5, 57.0, 92.9 (2 × C), 101.2, 194.3, 199.8 ppm (br); $\tilde{\nu}$ = 2962 (s), 2936 (s), 2875 (s), 2092 (s), 2036 (s), 2022 (s), 1739 cm^{-1} (s); HR-MS calcd for $\text{C}_{18}\text{H}_{16}\text{O}_7\text{Cl}_2\text{Co}_2$: 531.8937, found: 531.8941.

Received: February 11, 2002

Revised: April 22, 2002 [Z18688]

- [1] a) B. H. Lipshutz, S. Sengupta, *Org. React.* **1992**, *41*, 135; b) P. Perlmutter, *Conjugate Addition Reactions in Organic Synthesis*, Pergamon, Oxford, **1992**.
- [2] This moiety is often included in mixed cuprates as a nontransferable ligand: a) E. J. Corey, D. J. Beames, *J. Am. Chem. Soc.* **1972**, *94*, 7210; b) G. H. Posner, M. J. Chapdelaine, C. M. Lentz, *J. Org. Chem.* **1979**, *44*, 3661.
- [3] a) R. T. Hansen, D. B. Carr, J. Schwartz, *J. Am. Chem. Soc.* **1978**, *100*, 2244; b) J. Schwartz, D. B. Carr, R. T. Hansen, F. M. Dayrit, *J. Org. Chem.* **1980**, *45*, 3053.
- [4] K. Maruoka, I. Shimada, H. Imoto, H. Yamamoto, *Synlett* **1994**, 519.
- [5] a) S. Kim, J. H. Park, S. Y. Jon, *Bull. Korean Chem. Soc.* **1995**, *16*, 783; b) S. Kim, J. H. Park, *Synlett* **1995**, 163.
- [6] M. Eriksson, T. Ilieski, M. Nilsson, M. Olsson, *J. Org. Chem.* **1997**, *62*, 182.
- [7] a) K. M. Nicholas, *Acc. Chem. Res.* **1987**, *20*, 207; b) A. J. M. Caffyn, K. M. Nicholas in *Comprehensive Organometallic Chemistry II*, Vol. 12 (Eds.: E. W. Abel, F. G. A. Stone, G. Wilkinson, L. S. Hegeudus), Pergamon, Oxford, **1995**, p. 685.
- [8] a) E. Tyrrel, P. Heshmam, L. Sarrazin, *Synlett* **1993**, 769; b) P. Magnus, P. Carter, J. Elliot, R. Lewis, J. Harling, T. Pitterna, W. E. Bauta, S. Fortt, *J. Am. Chem. Soc.* **1992**, *114*, 2544; c) for an alternative approach which uses oxonium ion stabilization see: A. B. Smith III, P. R. Verhoest, K. P. Minibiole, J. J. Lim, *Org. Lett.* **1999**, *1*, 909; d) A. B. Smith III, K. P. Minibiole, P. R. Verhoest, T. J. Beauchamp, *Org. Lett.* **1999**, *1*, 913.
- [9] M. Lakhri, Y. Chapleur, *J. Org. Chem.* **1994**, *59*, 5752.
- [10] M. T. Reetz, K. Kessler, S. Schmidtberger, B. Wenderoth, R. Steinbach, *Angew. Chem.* **1983**, *95*, 1003; *Angew. Chem. Int. Ed. Engl.* **1983**, *22*, 989.
- [11] For a review on the preparation of cobalt-alkyne complexes see: R. S. Dickson, P. J. Fraser, *Adv. Organomet. Chem.* **1974**, *12*, 323.
- [12] The addition of Lewis acids to noncomplexed enol ether substrates did not result in rearrangement to the corresponding ketones, but returned starting materials together with the products of alkene isomerization.
- [13] Mild Lewis acids such as AgOTf and $\text{Yb}(\text{OTf})_3$ were unsuccessful in mediating the reaction and returned starting material even after prolonged reaction times. For an excellent overview on Lewis acid strength and selectivity see: S. Kobayashi, T. Busujima, S. Nagayama, *Chem. Eur. J.* **2000**, *6*, 3491.
- [14] The reduced reaction rates of Ph versus *n*Bu substituted alkynes may also be caused by the delocalization of positive charge in the cationic intermediate. We thank a referee for this suggestion.
- [15] Although the full scope of this methodology must await further study, it does not appear to be applicable to the rearrangement reaction of five-membered cyclic substrates. Indeed, all efforts to promote the rearrangement reaction of dichloro, ester, and unsubstituted enol ethers failed and complex mixtures were returned in all cases examined. The failure of these substrates to perform well under the rearrangement conditions is perhaps not surprising as the cyclization of the intermediate enolate/Nicholas carbocation can be classified as a 5-(enolendo)-*exo*-trig process, which is disfavored on stereoelectronic grounds: J. E. Baldwin, M. J. Lusch, *Tetrahedron* **1982**, *38*, 2939.
- [16] A. Takahashi, Y. Kirio, M. Sodeoka, H. Sasai, M. Shibasaki, *J. Am. Chem. Soc.* **1989**, *111*, 643.
- [17] S. V. Ley, B. Lygo, H. M. Organ, A. Wonnacott, *Tetrahedron* **1985**, *41*, 3825.
- [18] Assignment of the *cis/trans*-**16** NMR spectrum was made based on 400 MHz COSY ^1H NMR spectroscopy of the demetalated *cis* isomer **20**; see Supporting Information for spectra and details.
- [19] *E/Z* Enol ether assignments of **15a** and **15b** were made by comparison to ^1H NMR spectroscopic data reported in reference [16]. The configuration of isomers (*E*)/(*Z*)-**15a** could also be assigned on the basis of the chemical shifts of the ^{13}C NMR signal arising from the carbon atom β to the ether oxygen: D. Barillier, M. P. Strobel, L. Morin, D. Paquer, *Tetrahedron* **1983**, *39*, 767.
- [20] The configurations of **17** and **18** were assigned by measurement of the coupling constants of the protons at the benzylic position. These data were found to be in good agreement with those of similar disubstituted cyclohexanones: a) M. Rettig, A. Sigrist, J. Rétey, *Helv. Chim. Acta* **2000**, *83*, 2246; b) E. Hatzigrigoriou, L. Wartski, J. Seyden-Penne, E.

Toromanoff, *Tetrahedron* **1985**, *41*, 5045. Spectral and analytical data for all new compounds can be found in the Supporting Information. CCDC-177450 (**7a**) and CCDC-177451 (**11a**) contain the supplementary crystallographic data for this paper. These data can be obtained free of charge via www.ccdc.cam.ac.uk/conts/retrieving.html (or from the Cambridge Crystallographic Data Centre, 12, Union Road, Cambridge CB21EZ, UK; fax: (+44) 1223-336-033; or deposit@ccdc.cam.ac.uk).

- [21] Subjection of individual isomers *cis*- and *trans*-**16** to 1.5 equiv TiCl_4 at $-78^\circ\text{C} \rightarrow 25^\circ\text{C}$ for 90 min resulted in only slight (ca. 5–10%) isomerization at the α center. Therefore, the lack of stereospecificity in **15a** \rightarrow **16** cannot be fully explained by rapid equilibration at the α -alkyl moiety of the product.

Rapid Phase Fluxionality as the Determining Factor in Activity and Selectivity of Highly Dispersed, $\text{Rh}/\gamma\text{-Al}_2\text{O}_3$ in deNO_x Catalysis**

Mark A. Newton, Andrew J. Dent, Sofia Diaz-Moreno, Steven G. Fiddy, and John Evans*

Rhodium has for many years been a primary component in the make up of auto-exhaust catalysts because of its ability to catalyze the selective reduction of NO_x to N_2 .^[1,2] A historical view of this type of system is of an active, but essentially static, phase comprising particulate metal; it is from this axiom that studies of metal single crystals^[2] have been accepted as models of macroscopic catalyst behavior. However, it has been established by IR^[3] and XAFS^[4] (X-ray absorption fine structure) spectroscopy that small rhodium particles (on alumina) undergo

corrosive chemisorption to yield a mononuclear $\{\text{Rh}^{\text{I}}(\text{CO})_2\}$ species. In addition, the oxidation of $\text{Rh}/\text{Al}_2\text{O}_3$ under an atmosphere of air and oxygen has also been demonstrated by XAFS.^[5] Recently, using in situ, microreactor-based, energy-dispersive EXAFS (EDE)^[6] and mass spectrometry^[7] we have used the improved time resolution of these techniques to demonstrate that Rh on alumina is rapidly oxidized by NO.^[8] Herein we utilize these procedures to probe the correlation between metal structure and catalytic performance for the reduction of NO by H_2 .

Figure 1 shows the total NO conversion and N_2O (mass 44) production as a function of reaction temperature and feedstock composition. The net conversions and selectivity of the

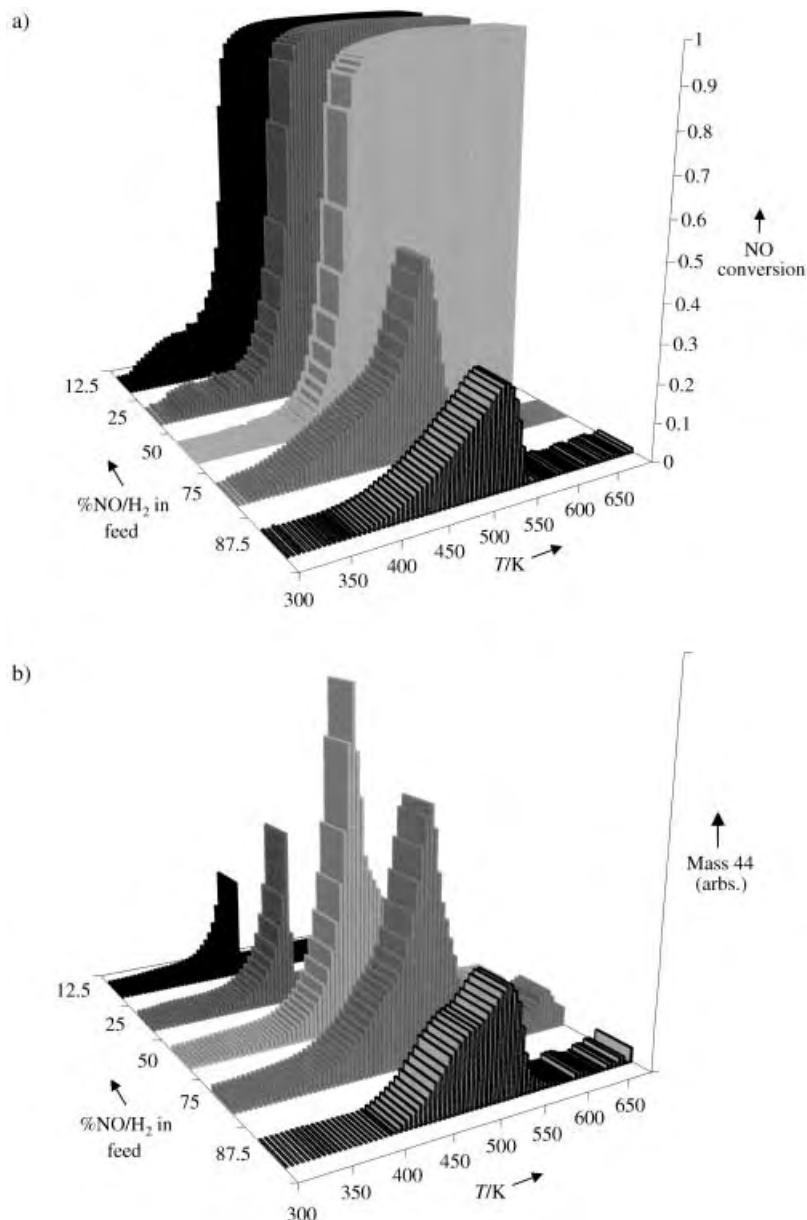


Figure 1. a) NO conversion as a function of reaction temperature and active feedstock composition in the reduction of NO/He by H_2/He over 5 wt % $\text{Rh}/\gamma\text{-Al}_2\text{O}_3$ catalysts derived from $\text{RhCl}_3 \cdot 3\text{H}_2\text{O}$: catalyst charge: 20 mg; $\text{NO}-\text{H}_2/\text{He}=4/96$; total gas flow = 10 mL min^{-1} , GHSV ca. $\sim 10^4\text{ h}^{-1}$. b) N_2O production (mass 44) as a function of reaction temperature and active feedstock composition in the reduction of NO by H_2 over 5 wt % $\text{Rh}/\gamma\text{-Al}_2\text{O}_3$ catalysts derived from $\text{RhCl}_3 \cdot 3\text{H}_2\text{O}$: conditions as for Figure 1a.

[*] Prof. J. Evans, M. A. Newton, S. G. Fiddy

Department of Chemistry
University of Southampton
Southampton, SO17 1BJ (UK)
Fax: (+44) 2380-593-781
E-mail: je@soton.ac.uk

A. J. Dent
CLRC Daresbury Laboratory
Warrington, WA4 4AD (UK)

S. Diaz-Moreno
The European Synchrotron Radiation Facility (ESRF)
38043 Grenoble (France)

[**] This work was funded under the "Catalysis and Chemical Processes initiative of the EPSRC" and through a "long-term project" allocation of beamtime by the ESRF. We thank the EPSRC (MAN) and ICI (SGF) for postdoctoral funding. The technical skills of John James, Melanie Hill, Sebastian Pasternak, and Ralph Wiegel, are gratefully acknowledged as is the beamline (ID 24) stewardship of Dr. Sakura Pascarelli.

catalyzed process are very sensitive functions of the feedstock composition. The “light off” temperature for the reaction increases as the feedstock with NO proportion until the maximum level of NO conversion drops away markedly as the levels of NO are further increased. Also, as NO levels are increased the catalyst selectivity tends toward the production of N_2O rather than the desired N_2 .

Figure 2 shows k^3 -weighted Rh K-edge EDE derived in situ during a typical experiment (in this case for the reaction of a feedstock of composition $NO/H_2/He = 1/3/96$), and Table 1 details the results of the analysis in EXCURV98.^[9] Reduction in H_2 and purging in He results in an EXAFS signature attributed to particulate Rh. However, under the mixture of $NO/He = 4/96$ at 300 K the EDE is clearly not that of metallic

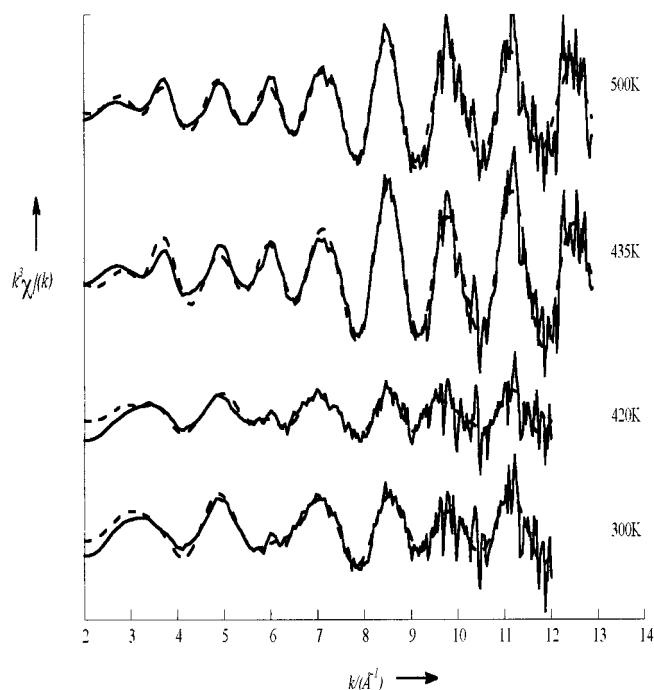


Figure 2. Representative k^3 -weighted EDE spectra derived during the reaction of 5 wt% Rh/ γ - Al_2O_3 catalysts for a reaction of a feedstock of composition $NO/H_2/He = 1/3/96$ at the temperatures indicated. Each spectrum (solid line) is acquired in 500 ms. The dashed line is the theoretical fit derived from an explicit analysis by using EXCURV 98.

Table 1. Elemental coordination (N_x^s), bond length (R), and statistical parameters derived from explicit analysis of the EDE spectra shown in Figure 2. Errors in coordination for the oxidic spectra should be regarded as between 15–20%; those pertaining to particulate systems about 10–15%. Errors in bond length determination are estimated at about 2%.

T [K]	Scatterer (s)	N_x^s	R [Å]	$2\sigma^2$ [Å ²]	k_{min}	k_{max}	R [%]
300	O	2.4	2	0.005	2	12	47.6
	Rh	2.7	2.63	0.011			
	Rh	1.9	3.76	0.013			
420	O	2.5	1.99	0.007	2	12	56.6
	Rh	2.4	2.64	0.013			
	Rh	2.2	3.75	0.015			
435	Rh	8.3	2.65	0.014	2	13	36.2
	Rh	3.4	3.74	0.015			
500	Rh	7.9	2.64	0.015	2	13	35.3
	Rh	3	3.73	0.017			

Rh, consistent with a previous report.^[5] Even at room temperature, the particulate metal phase has been replaced by a new, oxidic phase (elemental coordination: $N_1^{Rh} \approx 2.7$). By 420 K the Rh phase has oxidized even further with a distinct reduction in high k EXAFS intensity. This situation changes rapidly thereafter such that at a temperature 15 K higher (435 K) the EXAFS derived from the sample has reverted to a metallic state with N_1^{Rh} of about 8.

Figure 3 shows in more detail the variation of N_1^{Rh} as a function of reaction temperature and feedstock composition and it is clear that the variations in N_1^{Rh} mirror the total conversion and N_2O production character displayed in Figure 1. The operational phase of the supported Rh catalyst is also therefore a sensitive function of feedstock composition

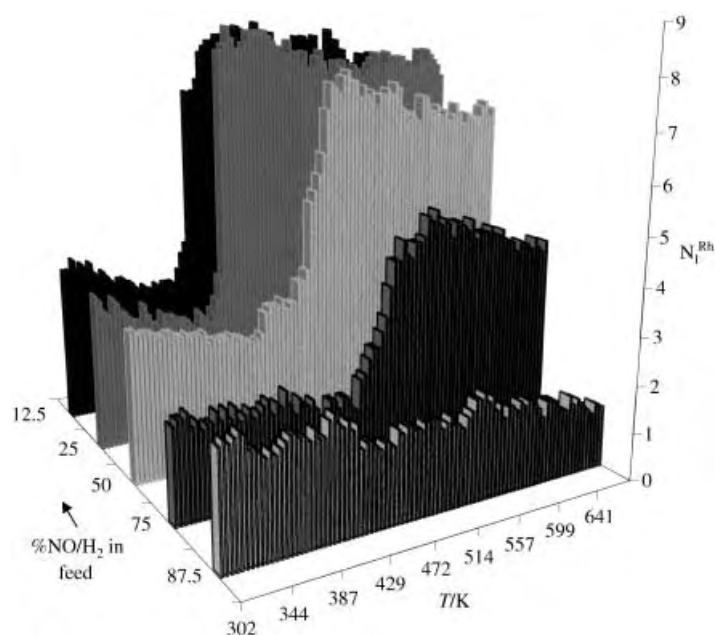


Figure 3. Variation in N_1^{Rh} derived from analysis of alternate EDE spectra collected during NO reduction by H_2 over 5 wt% Rh/ γ - Al_2O_3 catalysts as a function of feedstock composition and reaction temperature (conditions as in Figures 1 a and b).

and reaction temperature. As the feedstock is made progressively more oxidizing (increased NO fraction) the formation of particulate Rh is retarded and is not observed at all up to 673 K when the active feedstock mix is $NO/H_2/He = 3.5/0.5/96$. However, even when particulate Rh is observed to be generated the determined value of N_1^{Rh} does not exceed about 8 indicative of nanoparticulate particles containing between 70 and 150 atoms.^[10] Furthermore, these processes are observed to be entirely reversible upon the cooling of the system under the feedstock.

More reducing conditions promote Rh particle formation at progressively lower temperatures that tend towards the limit of the intrinsic stability (under H_2) of the oxidic phase that forms spontaneously at low temperature under NO .^[8] However, it is the decomposition of this phase that is the precursor of significant NO conversion. It is this phase transition that is also the source of the transient production of N_2O rather than any surface chemistry intrinsic to extended metal surfaces:

below a NO/H₂ ratio of 1, once particulate Rh becomes predominant, a very rapid curtailment of N₂O production is observed. Recent catalytic and infrared work^[11] have already suggested that the formation of N₂O requires the presence of both metallic Rh and oxidized Rh sites. This is consistent with our observations for the NO/H₂/He = 2/2/96 gas stream. These results show directly that the presence of rapid phase altering processes can control the behavior of highly dispersed supported metal catalysts rather than the intrinsic surface chemistry of the bulk metal. We have already shown that such processes may occur when nanoparticulate Rh is exposed to both NO^[8] and O₂.^[12] Interestingly, Rh thin foils and single crystals have been reported to oxidize beyond the surface ad-layer under O₂ above 500 K.^[13] A consequence of these phenomena is that the phase of the supported metal at a given gas composition and temperature can be far from static and may result from a dynamic equilibrium between processes that lead to oxidation and those that reductively reform the particulate metal. While oxidation of these Rh/Al₂O₃ catalysts by NO/He = 4/96 is rapid at room temperature, re-reduction of the NO oxidized Rh sites by H₂/He = 4/96 was evident only above 400 K.^[8] It is this differential that is directly responsible for the activity and selectivity of the catalyst. These processes may be related to the relatively poor performance of the three-way exhaust catalyst in, for instance, the lean burn conditions,^[14] currently favored by the automobile industry on efficiency and environmental grounds; this present study models one component of this.

As can be seen in Figure 1 a, the increase in catalytic activity over a relatively small temperature range is very marked. The rapid oxidative processes may be understood in terms of fundamental, and possibly adiabatic,^[15] dissociative chemistry (occurring in the zero coverage limit) on metallic Rh particles.^[8] As such we may delineate a set of broad criteria for such a system to develop as follows: 1) dissociative adsorption is facile and highly exothermic, rapidly injecting a large amount of energy into the supported metallic nano-cluster; 2) there are poorly effective means for the particle to release this energy through interaction with the gaseous phase or through the particle-support interface; 3) the particles themselves are not large enough to provide an effective energy sink that prevents particle collapse, that is high dispersion; and 4) subsequent reaction with the gaseous environment may result in a new, stable, phase rather than sintering to larger metallic particles.

In summary we have shown that in the limit of high dispersion the nature of oxide-supported metal catalysts may change in oxidizing conditions. Indeed, we have shown that the phases of a supported metal species can be interconverted on time scales that can be deterministic in terms of the activity and selectivity of such catalysts; in this specific case, the selectivity of the reduction of NO by H₂ to N₂ (on reduced, metallic sites) and N₂O (on oxidized sites) can be directly correlated with the phase of the rhodium.

Experimental Section

Aqueous impregnation of RhCl₃·3H₂O to γ-Al₂O₃ was used to make 5 wt % Rh catalysts. Samples were dried overnight before being calcined

for 6 h at 773 K and then sieved to give a 100 μm fraction. Finally the samples were reduced for 5 h at 573 K under flowing H₂. No attempt to prevent exposure of the sample to air was made prior to it (20 mg) being loaded into quartz tubes (i.d. 3 mm, wall thickness ca. 0.2 mm) and secured in place by using 5 mm long quartz wool plugs. These were then loaded into a microreactor described previously.^[6–8] Typical exposure times were 1 ms for I₀ and 3–5 ms for the sample.

EDE measurements were carried out at the ID24 source at the ESRF Grenoble, using an asymmetrically cut Si[111] monochromator in Laue configuration^[16] and a masked, Peltier cooled, CCD detector. Energy calibration was referenced with a Rh foil.

Once loaded into a microreactor the samples were purged with He, re-reduced in H₂ at 373 K, and subsequently purged in He again. This procedure resulted in the formation of particulate Rh with a first-shell Rh coordination (N^{Rh}₁) of about 6.5. During catalytic reactions these samples were then exposed to varying compositions of 4% NO/He and 4% H₂/He at a constant flow rate of 10 mL min^{−1} (gas hourly space velocity (GHSV) ≈ 10000 h^{−1}) whilst being heated at 10 K min^{−1} from room temperature to 673 K. Simultaneously EDE measurements were recorded at a typical rate of 10 spectra min^{−1} with individual spectra being collected with typical acquisition times of about 500 ms. The reactor was interfaced to a Balzers mass spectrometer station multiplexed to measure sample temperature (from a Eurotherm temperature controller) and 16–20 masses simultaneously. Data reduction and analysis was carried out by using PAXAS^[17] and EXCURV98.^[9] N₂O and CO₂ were differentiated through their fragmentation and M²⁺ patterns.

Received: December 27, 2001

Revised: April 24, 2002 [Z18437]

- [1] K. C. Taylor, *Catal. Rev. Sci. Eng.* **1993**, 35, 481.
- [2] B. E. Nieuwenhuys, *Adv. Catal.* **2000**, 44, 259.
- [3] A. C. Yang, C. W. Garland, *J. Phys. Chem.* **1957**, 61, 1504; P. Basu, D. Panyatov, J. T. Yates, *J. Phys. Chem.* **1987**, 91, 3133.
- [4] H. F. T. Van't Blik, J. B. A. D. Van Zon, T. Huizinga, J. C. Vis, D. C. Koningsberger, R. Prins, *J. Phys. Chem.* **1983**, 87, 2264.
- [5] H. A. Martens, R. Prins, H. Zandbergen, D. C. Koningsberger, *J. Phys. Chem.* **1988**, 92, 1903; J. H. A. Martens, R. Prins, D. C. Koningsberger, *J. Phys. Chem.* **1989**, 93, 3179.
- [6] S. G. Fiddy, M. A. Newton, A. J. Dent, G. Salvini, J. M. Corker, S. Turin, T. Campbell, J. Evans, *Chem. Commun.* **1999**, 851.
- [7] M. A. Newton, D. G. Burnaby, A. J. Dent, S. Diaz-Moreno, J. Evans, S. G. Fiddy, T. Neisius, S. Pascarelli, S. Turin, *J. Phys. Chem. A* **2001**, 105, 5965.
- [8] T. Campbell, A. J. Dent, S. Diaz-Moreno, J. Evans, S. G. Fiddy, M. A. Newton, S. Turin, *Chem. Commun.* **2002**, 304.
- [9] N. Binsted EXCURV98, CCLRC Daresbury Laboratory computer program, **1998**.
- [10] A. Jentys, *Phys. Chem. Chem. Phys.* **1999**, 1, 4059.
- [11] T. Chafik, D. I. Konarides, X. E. Verykios, *J. Catal.* **2000**, 190, 446.
- [12] M. A. Newton, A. J. Dent, S. Diaz-Moreno, B. Jyoti, S. G. Fiddy, J. Evans, *J. Phys. Chem. B*, submitted.
- [13] C. H. F. Feden, D. W. Goodman, D. S. Blair, P. J. Berlowitz, G. B. Fisher, S. H. Oh, *J. Phys. Chem.* **1988**, 92, 1563; J. Koshy, *Thin Solid Films* **1978**, 51, L17; G. L. Kellogg, *J. Catal.* **1985**, 92, 167.
- [14] R. Burch, P. J. Millington, *Catal. Today* **1995**, 26, 185.
- [15] H. Neinhuis, *Surf. Sci. Rep.* **2002**, 45, 1.
- [16] M. Hagelstein, C. Ferraro, U. Hatje, T. Ressler, W. Metz, *J. Synchrotron Radiat.* **1998**, 5, 1396.
- [17] N. Binsted, PAXAS: Program for the analysis of X-ray adsorption spectra, University of Southampton, **1988**.

Morphological Control of MCM-41 by Pseudomorphic Synthesis

T. Martin, A. Galarneau, F. Di Renzo,* F. Fajula, and D. Plee

The development of micelle-templated silicas (MTS) has represented one of the most original fields of materials research since the seminal papers from the Kresge and Beck groups on MCM-41 and MCM-48.^[1, 2] The self-assembly of surfactant aggregates and mineral species can be controlled to provide stable mesoporous materials with extremely narrow pore-size distributions. Several recent reviews show the advances in the preparation of ordered porous oxides,^[3–5] as well as their applications in catalysis.^[6–8]

Adsorbents with narrow pore-size distribution at the nanometer scale allow new applications to be devised for the separation of large organic molecules. MCM-41 silicas have been proposed as possible stationary phases for size-exclusion chromatography,^[9] normal-phase HPLC,^[10] capillary gas chromatography,^[11] and enantioselective HPLC.^[12, 13]

The control of the size and shape of the adsorbent particles is an essential condition for any chromatographic application: particle-size scattering affects separation and plate height. Indeed, the preparation of spheres of MTS with predetermined monodispersed size has been the target of several research groups. Positive results have been obtained by introducing surfactant templates in classical preparations of silica gel with controlled grain size. In this way, spheres of MTS have been prepared from water–alcohol systems,^[14, 15] by controlled hydrolysis,^[16, 17] or by spray-drying techniques.^[18] A frequent drawback of these methods is the need to simultaneously optimize the conditions for the synthesis of the desired silica–surfactant mesophase and for the successful formation of monodispersed spheres. This situation restrains the experimental conditions and makes a fine tuning of the properties of MTS, such as, pore size and topology, wall thickness, and aluminum content, difficult. It would be expedient to independently optimize the properties of the particles and the properties of the micelle-templated phase. Herein, a method to achieve this result by transformation of preformed spheres of silica gel into MTS is proposed.

The synthesis procedure is directly adapted from the synthesis of MCM-41,^[1, 2] by using commercial spheres of silica gel as the source of silica. Lichrosphere 100 (Merck) was stirred in an alkaline solution of cetyltrimethylammonium bromide (CTAB), the molar composition of the system being 1 SiO₂/0.25 NaOH/0.1 CTAB/20 H₂O. After 30 min stirring at room temperature, the system was put in an autoclave at 388 K for 24 h. The parent silica (Lichrosphere 100) and the

recovered solid share the same spherical morphology and granulometric distribution (Figure 1). However, while the parent silica is amorphous, the CTAB-treated solid presents the characteristic X-ray powder diffraction pattern of MCM-41.

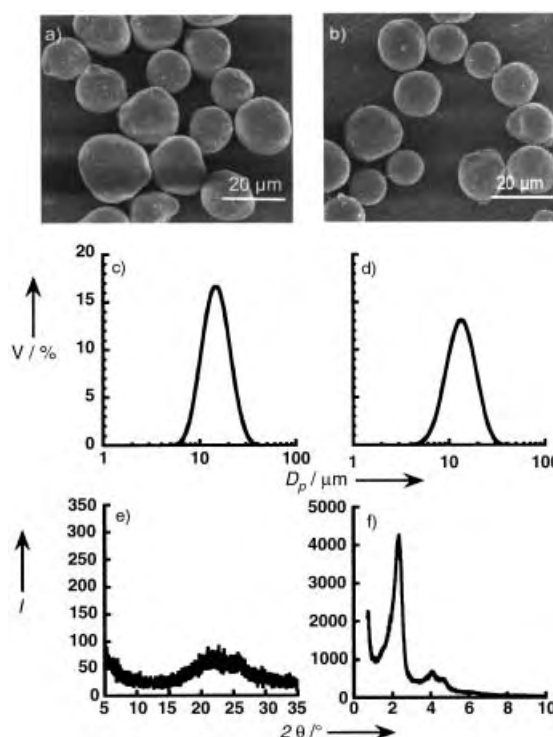


Figure 1. Pseudomorphic transformation of silica gel to MCM-41. Micrographs (a, b), granulometric distributions; the distribution is given in volume *V* as a function of particle diameter *D_p* (c, d), and powder diffraction patterns (e, f) for Lichrosphere 100 (Merck) before (e) and after (f) treatment with CTAB solution.

This transformation corresponds to the definition of pseudomorphism from mineralogy: a pseudomorph is an altered mineral the form of which has the outward appearance of another mineral species. In our case, the MCM-41 grains are pseudomorphs of the silica gel grains.

The pattern of the pseudomorphic transformation can be monitored by X-ray diffraction and nitrogen sorption experiments (Table 1). The adsorption pattern of the parent silica (BK385), which corresponds to a broad pore-diameter distribution centered around 8.5 nm, is completely lost after 15 min at 388 K (Figure 2). This latter material presents a

Table 1. Properties of cetyltrimethylammonium (CTA) treated silica BK385 (Akzo-Nobel).

Time at 388 K [h]	CTA/SiO ₂ ^[a] (w/w)	<i>Y</i> _{CTA} ^[b]	<i>Y</i> _{Si} ^[c]	<i>V</i> _{mp} ^[d] [cm ³ g ^{−1}]	<i>S</i> _{BET} ^[e] [m ² g ^{−1}]	<i>a_c</i> ^[f] [nm]	<i>D</i> _g ^[g] [nm]	<i>t</i> ^[h] [nm]
0.25	0.66	0.92	0.66	0.63	890	5.4	3.7	1.3
1	0.72	0.95	0.62	0.75	980	4.8	3.7	1.0
168	0.81	0.98	0.57	0.89	1078	4.4	3.7	0.8

[a] Composition. [b] Yield of CTA (from thermogravimetric weight loss). [c] Yield of silica (from thermogravimetric weight loss). [d] Structural pore volume. [e] BET surface area. [f] Cell parameter. [g] Pore diameter. [h] Wall thickness at different treatment times.

[*] Dr. F. Di Renzo, T. Martin, Dr. A. Galarneau, Dr. F. Fajula
Laboratoire de Matériaux Catalytiques
et Catalyse en Chimie Organique, UMR 5618
8, Rue de l'Ecole Normale, 34296 Montpellier Cedex 05 (France)
Fax: (+33) 467-144-349
E-mail: direnzo@cit.enscm.fr
Dr. D. Plee
GRL, Atofina, RN117
B.P.34, 64170 Lacq (France)

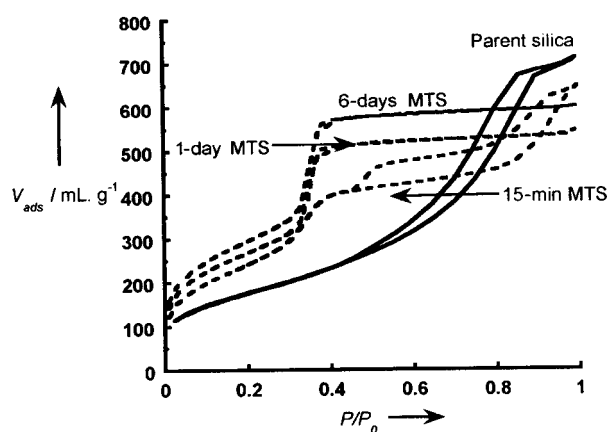


Figure 2. Evolution of the N_2 adsorption/desorption isotherms during the transformation of silica BK385 (Akzo-Nobel) into MCM-41 upon treatment at 388 K for the indicated time. Molar composition 1 SiO_2 /0.25 NaOH/0.1 CTAB/20 H_2O . Samples calcined at 823 K in air.

reversible type IV isotherm with a sharp step around p/p^0 0.37, typical of the structural mesoporosity of MCM-41, and a secondary porosity corresponding to a broad distribution of mesopores with a diameter larger than 20 nm. The desorption around p/p^0 0.45 indicates that a part of the secondary mesoporosity is accessible through the smaller structural mesopores. The sample incorporates 92 % of the available surfactant (Table 1) and presents two broad X-ray diffraction peaks, which correspond to an MCM-41 with poor long-range order^[19] (or/and thick walls on short-range order) and could be indexed according to a hexagonal cell with $a = 5.4$ nm (Table 1).

The amount of incorporated surfactant and the loss of the adsorption pattern of the parent silica suggest that nearly the whole silica is transformed into MCM-41 after 15 min. The secondary porosity corresponds to the volume between the small grains of MCM-41 with poor long-range order formed by nucleation at the pore–silica interface of the parent material. Heterogeneous nucleation of MCM-41 has been reported.^[20] Nevertheless, even if MCM-41 formation is initiated on the surface, the mechanism here is different because MCM-41 is formed by the dissolution of the particles themselves. These intermediates evolve to ordered MCM-41 at longer treatment times by internal reorganization, which is often the case in such material synthesis.^[21] In the process, the lattice parameter decreases whereas the pore size remains constant, in agreement with a decrease of the wall thickness (Table 1). Thinner-wall materials present a higher surfactant/

silica ratio, as shown by the increase of the yield of surfactant, which is virtually nominal at the end of the treatment.

The conservation of the shape and size of the initial system suggests that further transfer of silica from the parent phase to the micelle-templated phase takes place inside the pores of the grains. Each grain behaves like a microreactor in which silica is dissolved by the alkaline solution and silicate species interact with the surfactant to form MTS. In the initial phases of the synthesis, the silica/surfactant ratio inside the grain is higher than the overall composition of the system, which accounts for the formation of a micelle-templated phase with thick silica walls and poor long-range order. Further equilibration with the surfactant-rich and the silica-poor outer solution results in the formation of more-ordered MCM-41 which occupies a larger pore volume and proportionally decreases the secondary mesoporosity.

Starting from parent silica BK385, nearly the whole mesopore volume has the structural porosity of MCM-41 and virtually no secondary mesoporosity is left after seven days. This is not the case for all possible parent silica. In the Table 2, the properties of MCM-41 formed from different parent silica by using the same composition and amount of treatment solution are reported. The grain morphology of the parent silica is always conserved, whereas the structural properties of the final MCM-41 only depend on the composition of the synthesis system and are not affected by the different sources of silica. The secondary mesoporosity does depend on the pore volume of the parent silica. For sources of silica with a pore volume larger than the porosity of the final MCM-41, some secondary porosity is left among the crystallites of MCM-41.

On the contrary, for parent silica with a low initial pore volume, the grain cannot accommodate the forming MCM-41 and bursts during the treatment. Fragmentation of the grain takes place by spalling of the fast-reacting outer rim (Figure 3a). Another instance of grain fragmentation is induced by the use of very alkaline treatment solutions. In this case the dissolution of the parent silica is faster than the diffusion of surfactant inside the grain, and the core of the grain becomes mechanically unstable. Another kind of change of morphology can occur with very long synthesis time (treatments for up to one month have been tested). When the final MCM-41 is left in the mother solution, Ostwald ripening occurs between the MCM-41 crystallites which form the macroscopic grain. Some crystals grow at the expense of others, protrude out of the particles and form spaghetti-like fibers with, in most cases, a hexagonal section (Figure 3b).

Table 2. Properties of calcined MCM-41 synthesized from different silica sources.

Silica source	Average grain size [μm]	Morphology	$V_{mp}^{[a]}$ [$cm^3 g^{-1}$]	$V_p^{[b]}$ [$cm^3 g^{-1}$]	$a_c^{[c]}$ [nm]	$D^{[d]}$ [nm]
Nucleosil (Macherey-Nagel)	5	spheres	0.78	0.93	4.5	3.9
Lichrosphere 60 (Merck)	10	spheres	0.86	0.91	4.7	3.8
Lichrosphere 100 (Merck)	15	spheres	0.82	1.00	4.7	3.6
sylopol (Grace)	50	spheroids	0.76	0.80	4.8	3.9
silica gel (Fluka 60)	130	splinters	0.74	0.80	4.7	3.8
BK385 (Akzo-Nobel)	1	dendrites	0.89	0.93	4.4	3.7
sipernat	< 1	dendrites	0.79	1.08	4.4	3.8

[a] Structural pore volume. [b] Total pore volume ($p/p^0 = 0.98$). [c] Cell parameter. [d] Pore diameter.

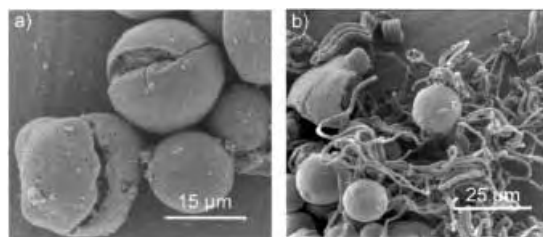


Figure 3. Examples of loss of morphology in unfavorable conditions. a) Blasted grains as a result of low porous volume of the parent silica. b) Long treatment time, Ostwald ripening occurs and spaghetti-like nanocrystallites grow out from the particles.

Pseudomorphic synthesis is a good method to separately optimize the morphology of the grain and the structural properties of MCM-41. The experimental conditions for the treatment with the surfactant solution can be varied widely. The thickness of the MTS walls can be adjusted by changing the alkalinity of the synthesis mixture.^[22] The aluminum content, relevant for catalytic applications, can be controlled by either using a silica aluminum oxide as the silica source or by adding the desired amount of sodium aluminate to the reaction mixture. Quite ordered materials were formed with a Si:Al ratio down to 7:1 in the reaction mixture (5.5:1 in the solid formed). The pore size was varied up to 12 nm by adding a swelling agent (1,3,5-trimethyl benzene) to the reaction mixture, as described elsewhere.^[23]

Pseudomorphic synthesis was successfully applied to a wide range of particle sizes and morphologies (Table 2) which makes this procedure suitable for the preparation of materials with specific morphological requirements. Besides, for chromatographic applications, this procedure was successfully applied to the large-scale preparation of monodispersed spheres of MCM-41. This method could eventually be applied to macroscopic objects such as membranes or films. However, the stress generated during synthesis can lead to mechanical instability and should be taken into account while choosing the porosity of the parent silica and the experimental conditions.

Experimental Section

MTS materials were prepared in a steel autoclave where reactants were mixed in the following proportions 1 SiO₂/0.1–0.4 NaOH/0.05–0.1 cetyltrimethylammonium bromide/0–1.3 1,3,5-trimethyl benzene/0–0.1 NaAlO₂/20–80 H₂O. Reactants were mechanically stirred (400 rpm) for half an hour at room temperature and put carefully in autoclave and left at 388 K for between 15 min to 1 month. (Therefore, heating rate was not monitored and it is expected that the 15-min synthesis does not reach the target temperature). The resulting solids were recovered by filtration, washed with water, and dried at 353 K overnight. Materials were then calcined under air flow at 823 K for 8 h. Materials were then characterized by

powder X-ray diffraction (CuK α radiation, CGR Theta 60 diffractometer with Inel drive), N₂ sorption at 77 K (Micromeritics ASAP 2000), thermogravimetric analyses (Setaram 90C) and scanning electron microscopy (Hitachi). Pore diameters have been evaluated from adsorption data according to Broekhoff and De Boer^[24] and wall thicknesses from diffraction and adsorption data according to Galarneau et al.^[25] The volume of the structural porosity has been measured above the pore-filling step of the MCM-41 isotherm and the total mesopore volume includes all pores with diameter lower than 50 nm. The authors gladly acknowledge the contribution of D. Cot for electron microscopy.

Received: March 18, 2002 [Z18920]

- [1] C. T. Kresge, M. E. Leonowicz, W. J. Roth, J. C. Vartuli, J. S. Beck *Nature* **1992**, 359, 710.
- [2] J. S. Beck, J. C. Vartuli, W. J. Roth, M. E. Leonowicz, C. T. Kresge, K. D. Schmitt, C. T. W. Chu, D. H. Olson, E. W. Sheppard, S. B. McCullen, J. B. Higgins, J. L. Schlenker, *J. Am. Chem. Soc.* **1992**, 114, 10834.
- [3] M. E. Raimondi, J. M. Seddon, *Liq. Cryst.* **1999**, 26, 305.
- [4] F. Schüth, *Chem. Mater.* **2001**, 13, 3184.
- [5] F. Di Renzo, A. Galarneau, P. Trems, F. Fajula in *Handbook of Porous Materials* (Eds.: F. Schüth, K. Sing, J. Weitkamp), Wiley-VCH, **2002**, in press.
- [6] A. Corma, *Chem. Rev.* **1997**, 97, 249.
- [7] D. Brunel, *Microporous Mesoporous Mater.* **1999**, 27, 329.
- [8] D. Trong On, D. Desplandier-Giscard, C. Danumah, S. Kaliaguine, *Appl. Catal. A* **2001**, 222, 299.
- [9] A. A. Kurganov, K. K. Unger, T. Issaeva, *J. Chromatogr. A* **1996**, 753, 177.
- [10] M. Grün, A. A. Kurganov, S. Schacht, F. Schüth, K. K. Unger, *J. Chromatogr. A* **1996**, 740, 1.
- [11] M. Raimondo, G. Perez, M. Sinibaldi, A. De Stefanis, A. A. Tomlinson, *Chem. Commun.* **1997**, 1343.
- [12] C. Thoenen, K. van de Walle, I. F. J. Vankelecom, P. A. Jacobs, *Chem. Commun.* **1999**, 1841.
- [13] C. Thoenen, J. Paul, I. F. J. Vankelecom, P. A. Jacobs, *Tetrahedron: Asymmetry* **2000**, 11, 4819.
- [14] Q. Huo, J. Feng, F. Schüth, G. D. Stucky, *Chem. Mater.* **1997**, 9, 14.
- [15] M. Grün, I. Lauer, K. K. Unger, *Adv. Mater.* **1997**, 7, 254.
- [16] H. Yang, G. Vovk, N. Coombs, I. Sokolov, G. A. Ozin, *J. Mater. Chem.* **1998**, 8, 743.
- [17] C. Boissière, A. Van der Lee, A. El Mansouri, A. Larbot, E. Prouzet, *Chem. Commun.* **1999**, 2047.
- [18] P. J. Bruinsma, A. Y. Kim, J. Liu, S. Baskaran, *Chem. Mater.* **1997**, 9, 2507.
- [19] S. Schacht, M. Janicke, F. Schüth, *Microporous Mesoporous Mater.* **1998**, 22, 485.
- [20] J. Liu, A. Y. Kim, J. W. Virden, B. C. Bunker, *Langmuir* **1995**, 11, 689.
- [21] A. Galarneau, F. Di Renzo, F. Fajula, L. Mollo, B. Fubini, M. F. Ottaviani, *J. Colloid Interface Sci.* **1998**, 201, 105.
- [22] N. Coustel, F. Di Renzo, F. Fajula, *J. Chem. Soc. Chem. Commun.* **1994**, 967.
- [23] D. Desplandier-Giscard, A. Galarneau, F. Di Renzo, F. Fajula, *Stud. Surf. Sci. Catal.* **2001**, 135, 06-P-27.
- [24] J. C. P. Broekhoff, J. H. De Boer, *J. Catal.* **1967**, 9, 15.
- [25] A. Galarneau, D. Desplandier, R. Dutartre, F. Di Renzo, *Microporous Mesoporous Mater.* **1999**, 27, 297.

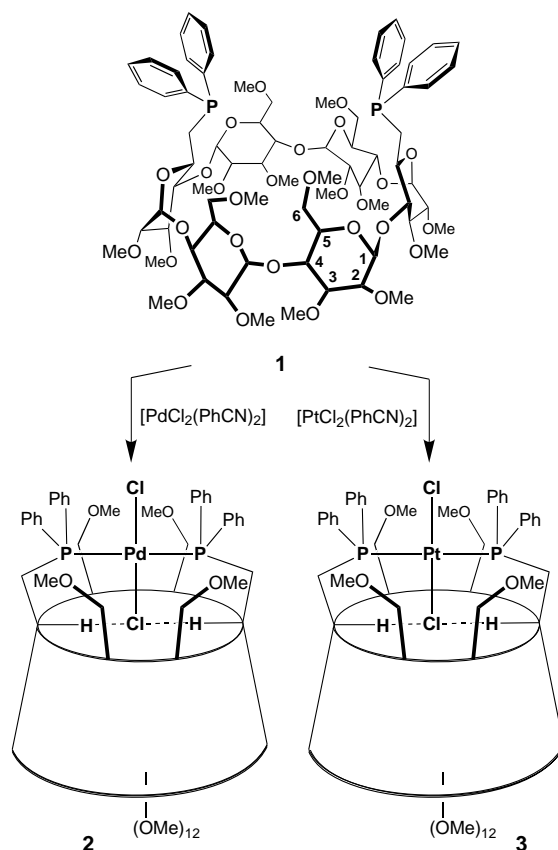
A Cyclodextrin Diphosphane as a First and Second Coordination Sphere Cavitand: Evidence for Weak C–H...Cl–M Hydrogen Bonds within Metal-Capped Cavities

Eric Engeldinger, Dominique Armspach,*
Dominique Matt,* Peter G. Jones, and Richard Welter

Metallocavitands are coordination compounds that provide the opportunity to study host–guest interactions between metal-bonded substrates and the internal part of a molecular cavity.^[1–11] Those in which a metal center is rigidly held above the entrance of an opened cavity are particularly promising since they may force the latter to form a second coordination sphere with certain ligands.^[12, 13] Through coordination, the sequestered fragments are subjected to restricted movement and their controlled positioning is expected to allow specific, weak interactions to operate.

Modified cyclodextrins are amongst the most studied molecular cavities, in particular for their ability to form inclusion complexes with a large range of substrates in water.^[14–16] Many interesting applications derive from this property,^[17–21] but to date little structural data are available about weak, noncovalent interactions involving the inwardly pointing CH bonds.^[22] On the other hand, the systematic weak interglucose C-6-H(*n*)...O-5(*n* + 1) hydrogen bonds which contribute to the stability of the structures of methylated CDs are well documented.^[23, 24] We have recently shown that chelating diphosphanes built on an α -cyclodextrin scaffold such as **1** constitute unique probes for examining substitution reactions occurring at a confined metal center.^[13] In the course of our investigations on the coordination properties of such diphosphanes, we have now found that upon complexation M–Cl fragments are systematically included in the CD cavity, the chlorine atom(s) being noncovalently bonded in an unprecedented way to inner-cavity CH groups.

Cavitand **1**^[13] bears two short phosphane units ideally suited for forming *trans*-chelate complexes with d⁸ metals. Thus, reaction of **1** with [PdCl₂(PhCN)₂] afforded complex **2** in approximately 40% yield (Scheme 1, Table 1).^[25, 26] All NMR data are consistent with a twofold molecular symmetry, while the formation of a monomeric species was inferred from the FAB mass spectrum which displays a strong peak at *m/z* 1710 with the appropriate isotopic profile for the corresponding [M+H]⁺ ion. The presence in the ¹³C NMR spectrum of a



Scheme 1. *trans*-Binding behavior of **1**. Synthesis of **2** and **3**.

virtual triplet for the PCH₂ carbon atoms ($J(\text{PC}) + {}^3J(\text{PC}) = 23 \text{ Hz}$) is in keeping with *trans*-arranged phosphorus atoms.^[27] The platinum analogue **3** which was obtained from [PtCl₂(PhCN)₂] is characterized by a $J(\text{Ppt})$ coupling constant of 2637 Hz, typical of a *trans* configuration (Table 1). The *trans*-spanning behavior of **2** was confirmed by an X-ray diffraction study (Figure 1). The most striking feature of this structure is the presence of a Pd–Cl bond that points inside the cyclodextrin cone with the chlorine atom located near the two inner H-5 atoms of the phosphorus-substituted glucose units. A separation of 2.64(2) Å can be calculated for H-5...Cl by assuming a C-5-H-5 bond length of 0.95 Å. A clear indication of a weak CH...Cl interaction arises from the ¹H NMR spectra of both complexes (**2** and **3**), which show that two H-5 atoms have undergone a significant low-field shift of approximately 0.8 ppm(!), with respect to the free ligand.

A further illustration of the “chlorophilic” binding behavior of cyclodextrin **1** is provided by its reaction with [PdClMe(cod)] (cod = cycloocta-1,5-diene), which results in quantitative formation of **4** (Scheme 2, Table 2). Again diphosphane **1** behaves as a *trans*-binding ligand, as can easily be deduced from the presence of a triplet for the methyl group (${}^3J(\text{PH}) = 6.0 \text{ Hz}$) in the ¹H NMR spectrum. As for the complexes described above, the two H-5 atoms close to the phosphorus atoms are significantly low-field shifted relative to their counterparts in free **1** ($\Delta\delta = +1.35 \text{ ppm}$). Furthermore, 2D ROESY spectra unambiguously confirmed the spatial proximity of the methyl group and the PPh₂ groups, hence establishing the preference of the cavity for the

[*] Dr. D. Armspach, Dr. D. Matt, E. Engeldinger
Laboratoire de Chimie Inorganique Moléculaire
Université Louis Pasteur, UMR 7513 CNRS
1 rue Blaise Pascal, 67008 Strasbourg Cedex (France)
Fax: (+33) 90-241-719
E-mail: darmaspach@chimie.u-strasbg.fr
dmatt@chimie.u-strasbg.fr

Prof. P. G. Jones
Institut für Anorganische und Analytische Chemie
der Technischen Universität
Hagenring 30, 38106 Braunschweig (Germany)
Prof. R. Welter
Laboratoire DECMET
Université Louis Pasteur, UMR 7513 CNRS
4 rue Blaise Pascal, 67070 Strasbourg Cedex (France)

Table 1. Selected analytical data.

2: yellow powder, yield 40 % after column chromatography (SiO₂, CH₂Cl₂/MeOH, 94:6, v/v). *R_f* (CH₂Cl₂/MeOH, 94:6, v/v)=0.31; m.p. 185 °C (decomp); ¹H NMR (200 MHz, CDCl₃, 25 °C): δ = 2.67 (br d, ²J_{H-6a,H-6b} = 10.3 Hz; H-6a^{A,D}), 2.85 (s, 6H; CH₃O-6), 3.20 (s, 6H; CH₃O-6), 3.47 (s, 6H; OCH₃), 3.49 (s, 6H; OCH₃), 3.52 (s, 6H; OCH₃), 3.61 (s, 6H; OCH₃), 3.65 (s, 6H; OCH₃), 3.78 (s, 6H; OCH₃), 3.06–4.11 (m, 32H; H-2, H-3, H-4, H-5^{B,C,E,F}, H-6a^{B,C,E,F}, H-6b), 4.78 (d, ³J_{H-1,H-2} = 2.7 Hz, 2H; H-1), 5.01 (d, ³J_{H-1,H-2} = 3.0 Hz, 2H; H-1), 5.13 (d, ³J_{H-1,H-2} = 3.5 Hz, 2H; H-1), 5.13 (br t, ³J = 10.1 Hz, 2H; H-5^{A,D}), 7.33–7.43 (m, 12H; H_{meta} and H_{para}), 7.55–7.63 (m, 4H; H_{ortho}), 8.07–8.16 ppm (m, 4H; H_{ortho}); ¹³C{¹H} NMR (50.3 MHz, CDCl₃, 25 °C): δ = 34.94 (virtual t, ¹J_{C,P} + ³J_{C,P} = 23.0 Hz; C-6^{A,D}), 57.50, 57.73 (CH₃O-6), 58.94, 59.13 (× 2) (CH₃O-2), 61.13, 61.50, 61.82 (CH₃O-3), 70.02 (C-4^{A,D}), 70.61, 70.80 (C-6^{B,C,E,F}), 71.33, 71.46 (C-5^{B,C,E,F}), 80.28, 80.64, 80.77, 81.23 (× 2), 81.69, 81.75, 83.36 (C-2, C-3, C-4^{B,C,E,F}), 89.90 (virtual t, ²J_{C,P} + ⁴J_{C,P} = 11.5 Hz; C-5^{A,D}), 98.27 (× 2) (C-1^{B,C,E,F}), 100.77 (C-1^{A,D}), 127.51 (virtual t, ³J_{C,P} + ⁵J_{C,P} = 11.5 Hz; C_{meta}), 128.07 (virtual t, ³J_{C,P} + ⁵J_{C,P} = 9.8 Hz; C_{meta}), 130.10 (s; C_{para}), 130.56 (s; C_{para}), 133.48 (virtual t, ²J_{C,P} + ⁴J_{C,P} = 11.5 Hz; C_{ortho}), 135.71 ppm (virtual t, ²J_{C,P} + ⁴J_{C,P} = 13.2 Hz; C_{ortho}) (the C_{ipso} atoms could not be identified); ³¹P{¹H} NMR (121.5 MHz, CDCl₃, 25 °C): δ = 11.9 ppm (s); elemental analysis (%): calcd for C₇₆H₁₁₀Cl₂O₂₈P₂Pd (1710.95): C 53.35, H 6.48; found: C 53.36, H 6.29; MS (FAB): *m/z* (%): 1710.2 (33) [*M*+H]⁺, 1675.2 (17) [*M*–Cl]⁺, 1638.2 (13) [*M*–2Cl]⁺.

3: pale yellow, yield: 41 % after column chromatography (SiO₂, CH₂Cl₂/MeOH 94:6, v/v). *R_f* (CH₂Cl₂/MeOH, 94:6, v/v)=0.31; m.p. 218 °C (decomp); ¹H NMR (200 MHz, CDCl₃, 25 °C): δ = 2.62 (d, ²J_{H-6a,H-6b} = 10.7 Hz; H-6a^{A,D}), 2.88 (s, 6H; CH₃O-6), 3.19 (s, 6H; CH₃O-6), 3.46 (s, 6H; OCH₃), 3.48 (s, 6H; OCH₃), 3.52 (s, 6H; OCH₃), 3.60 (s, 6H; OCH₃), 3.64 (s, 6H; OCH₃), 3.78 (s, 6H; OCH₃), 3.05–4.08 (m, 32H; H-2, H-3, H-4, H-5^{B,C,E,F}, H-6a^{B,C,E,F}, H-6b), 4.76 (d, ³J_{H-1,H-2} = 2.6 Hz, 2H; H-1), 5.00 (d, ³J_{H-1,H-2} = 2.9 Hz, 2H; H-1), 5.13 (d, ³J_{H-1,H-2} = 3.4 Hz, 2H; H-1), 5.18 (br t, ³J = 9.7 Hz, 2H; H-5^{A,D}), 7.32–7.44 (m, 12H; H_{meta} and H_{para}), 7.58–7.64 (m, 4H; H_{ortho}), 8.09–8.16 ppm (m, 4H; H_{ortho}); ¹³C{¹H} NMR (50.3 MHz, CDCl₃, 25 °C): δ = 36.55 (virtual t, ¹J_{C,P} + ³J_{C,P} = 21.5 Hz; C-6^{A,D}), 57.53, 57.86 (CH₃O-6), 58.94, 59.20, 59.30 (CH₃O-2), 61.13, 61.50, 61.86 (CH₃O-3), 69.99 (C-4^{A,D}), 70.54, 70.84 (C-6^{B,C,E,F}), 71.39 (× 2) (C-5^{B,C,E,F}), 80.28, 80.74 (× 2), 81.26 (× 2), 81.69 (× 2), 83.39 (C-2, C-3, C-4^{B,C,E,F}), 89.10 (virtual t, ²J_{C,P} + ⁴J_{C,P} = 11.5 Hz; C-5^{A,D}), 98.21, 98.27 (C-1^{B,C,E,F}), 100.67 (C-1^{A,D}), 127.42 (virtual t, ³J_{C,P} + ⁵J_{C,P} = 9.8 Hz; C_{meta}), 127.97 (virtual t, ³J_{C,P} + ⁵J_{C,P} = 9.8 Hz; C_{meta}), 130.17 (s; C_{para}), 130.56 (s; C_{para}), 133.55 (virtual t, ²J_{C,P} + ⁴J_{C,P} = 11.5 Hz; C_{ortho}), 135.71 (virtual t, ²J_{C,P} + ⁴J_{C,P} = 11.5 Hz; C_{ortho}) (the C_{ipso} atoms could not be identified); ³¹P{¹H} NMR (121.5 MHz, CDCl₃, 25 °C): δ = 7.8 (s with Pt satellites, ¹J_{Pt,P} = 2637 Hz); elemental analysis (%) calcd for C₇₆H₁₁₀Cl₂O₂₈P₂Pt·0.5 C₆H₆ (1799.61+39.06): C 51.61, H 6.19; found: C 51.64, H 6.08; MS (FAB): *m/z* (%): 1799.7 (0.1) [*M*+H]⁺, 1763.8 (0.5) [*M*–Cl]⁺. The molecular structure was confirmed by an X-ray analysis.

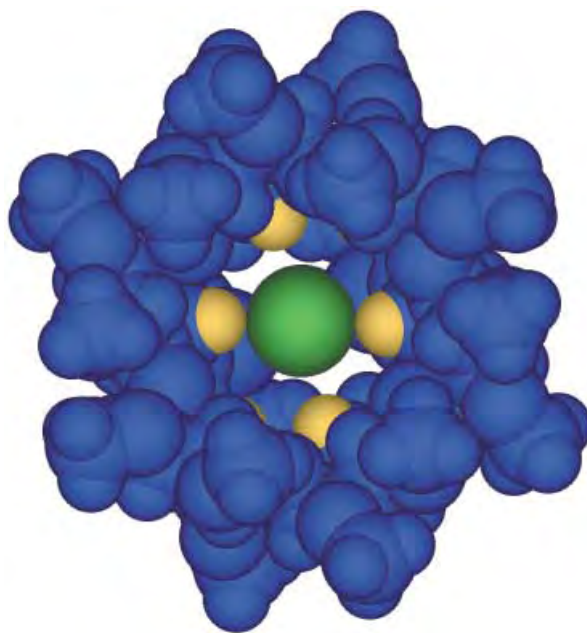
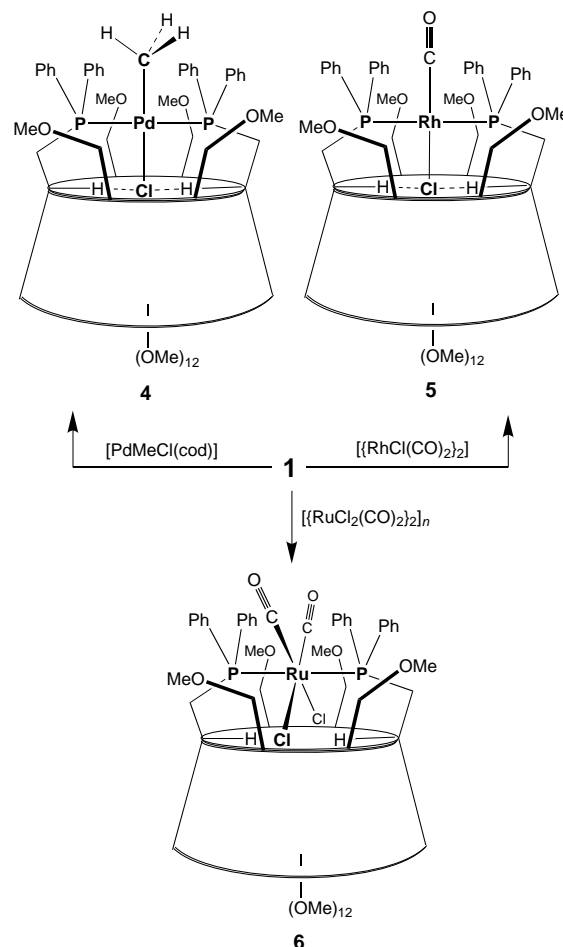


Figure 1. X-ray structure (space-filling model) of the C₂-symmetric complex **2**. View from the bottom showing the Cl(2) atom in green and the H-5 atoms in yellow (two of them are hidden). The butanone molecule included inside the CD has been omitted for clarity. Selected bond lengths [Å] and angle [°]: Pd–Cl(1) 2.2908(19), Pd–Cl(2) 2.2875(19), Pd–P 2.3619(13); P–Pd–P 171.81(7). Shortest H–5⋯Cl(2) distances: 2.64(2) Å.



Scheme 2. Selective entrapment of M–Cl bonds inside an α-cyclodextrin cavity.

polarized Pd–Cl moiety rather than for the less-polar Pd–alkyl group. Selective inclusion of the M–Cl bond in the cavity was also observed for the rhodium complex **5** obtained by reaction of **1** with [{RhCl(CO)₂}]₂ (Table 2). The H-5 atoms in the β position to the P atoms are shifted to 0.96 ppm.

The ability of cavitant **1** to bind M–Cl fragments seems to be a general trend, even when the diphosphane is incorporated into higher coordination spheres. Thus, reaction of **1** with [RuCl₂(CO)₂]_n in boiling ethoxyethanol afforded the octahedral *trans,cis,cis*-complex **6** in approximately 70 % yield, together with trace amounts of another, unidentified complex (Scheme 2, Table 2).^[28] The infrared spectrum of **6** displays two strong carbonyl bands, as expected for two *cis*-coordinated carbonyl groups. The ¹H NMR spectrum is consistent with a C₂-symmetric molecule and reveals that in this case, two pairs of H-5 atoms are involved in hydrogen bonding with the Cl atoms.^[29] The stereochemistry

Table 2. Selected analytical data.

4: yellow powder, yield: 76%; R_f ($\text{CH}_2\text{Cl}_2/\text{MeOH}$, 94:6, v/v) = 0.31; m.p. 178 °C (decomp); ^1H NMR (500 MHz, C_6D_6 , 25 °C): δ = 0.02 (t, $^3J_{\text{H-P}}$ = 6.0 Hz, 3H; PdCH_3), 2.77 (m, 2H; H-6a^{A,D}), 3.20 (s, 6H; OCH_3), 3.22 (s, 6H; OCH_3), 3.30 (s, 6H; OCH_3), 3.31 (s, 6H; OCH_3), 3.33 (s, 6H; OCH_3), 3.39 (s, 6H; OCH_3), 3.86 (s, 6H; $\text{CH}_3\text{O-6}$), 3.88 (s, 6H; $\text{CH}_3\text{O-6}$), 3.13–4.71 (32H; H-2, H-3, H-4, H-5^{B,C,E,F}, H-6a^{B,C,E,F}, H-6b), 5.05 (d, 3J = 2.6 Hz, 2H; H-1), 5.22 (d, 3J = 3.1 Hz, 2H; H-1), 5.40 (d, 3J = 3.5 Hz, 2H; H-1), 5.98 (brt, 3J = 9.5 Hz, 2H; H-5^{A,D}), 6.86–7.25 (m, 12H; H_{meta} and H_{para}), 7.70–7.73 (m, 4H; H_{ortho}), 7.88–7.91 ppm (m, 4H; H_{ortho}); $^{13}\text{C}\{^1\text{H}\}$ NMR (50.3 MHz, C_6D_6 , 25 °C): δ = 4.51 (PdCH_3), 37.30 (virtualt, $^1J_{\text{C-P}} + ^3J_{\text{C-P}}$ = 24.7 Hz; C-6^{A,D}), 57.00, 57.36 ($\text{CH}_3\text{O-6}$), 59.19, 59.56, 60.05 ($\text{CH}_3\text{O-2}$), 60.96, 61.39, 62.11 ($\text{CH}_3\text{O-3}$), 70.00 (C-4^{A,D}), 72.27, 72.34 (C-5^{B,C,E,F}), 72.41, 72.50 (C-6^{B,C,E,F}), 81.35, 81.58 ($\times 2$), 81.88, 82.30, 82.47, 82.83, 84.17 (C-2, C-3, C-4^{B,C,E,F}), 88.80 (virtualt, $^2J_{\text{C-P}} + ^4J_{\text{C-P}}$ = 9.9 Hz; C-5^{A,D}), 98.33, 98.43 (C-1^{B,C,E,F}), 101.09 (C-1^{A,D}), 128.00 (virtualt, $^3J_{\text{C-P}} + ^5J_{\text{C-P}}$ = 9.8 Hz; C_{meta}), 128.43 (virtualt, $^3J_{\text{C-P}} + ^5J_{\text{C-P}}$ = 9.8 Hz; C_{meta}), 129.70 (s; C_{para}), 130.39 (s; C_{para}), 131.11 (d, $^1J_{\text{C-P}} + ^3J_{\text{C-P}}$ = 39.6 Hz; C_{ipso}), 133.54 (virtualt, $^2J_{\text{C-P}} + ^4J_{\text{C-P}}$ = 11.5 Hz; C_{ortho}), 136.00 (virtualt, $^2J_{\text{C-P}} + ^4J_{\text{C-P}}$ = 13.2 Hz; C_{ortho}), 137.77 ppm (virtualt, $^1J_{\text{C-P}} + ^3J_{\text{C-P}}$ = 39.6 Hz; C_{ipso}); $^{31}\text{P}\{^1\text{H}\}$ NMR (121.5 MHz, CDCl_3 , 25 °C): δ = 19.4 ppm (s); elemental analysis (%) calcd for $\text{C}_{77}\text{H}_{113}\text{ClO}_{28}\text{P}_2\text{Pd}$ (1690.53): C 54.71, H 6.74; found: C 54.48, H 6.45; MS (FAB): m/z (%): 1690.6 (17) $[\text{M}]^+$, 1675.5 (10) $[\text{M} - \text{CH}_3]^+$, 1653.6 (15) $[\text{M} - \text{Cl}]^+$, 1638.6 (9) $[\text{M} - \text{CH}_3 - \text{Cl}]^+$.

5: orange-yellow powder, yield: 64%; R_f ($\text{CH}_2\text{Cl}_2/\text{MeOH}$, 94:6, v/v) = 0.30; m.p. 182 °C (decomp); IR (KBr): $\tilde{\nu}$ = 1976 cm^{-1} ($\text{C}=\text{O}$); ^1H NMR (500 MHz, C_6D_6 , 25 °C): δ (assignment by COSY) = 2.84 and 3.65 (br AB, 4H, H-6^{A,D}), 3.16 (s, 6H, OCH_3), 3.19 (d, 2H, H-2^{B,E} or C^F), 3.20 (d, 2H, H-2^{A,D}), 3.21 (d, 2H, H-2^{C,F} or B^E), 3.22 (s, 6H, OCH_3), 3.25 (s, 6H, OCH_3), 3.28 and 4.40 (AB, 2J = 10.6 Hz, 4H, H-6^{C,F} or B^E), 3.32 (s, 6H, OCH_3), 3.33 (d, 2H, H-4^{A,D}), 3.39 (s, 6H, OCH_3), 3.44 (s, 6H, OCH_3), 3.61 (d, 2H, H-3^{C,F} or B^E), 3.65 and 4.33 (AB, 2J = 10.6 Hz, 4H, H-6^{B,E} or C^F), 3.80 (s, 6H, $\text{CH}_3\text{O-6}$), 3.87 (s, 6H, $\text{CH}_3\text{O-6}$), 4.08 (t, 3J = 8.8 Hz, 2H, H-4^{B,E} or C^F), 4.14 (t, 3J = 9.1 Hz, 2H, H-3^{A,D}), 4.15 (t, 3J = 8.8 Hz, 2H, H-4^{C,F} or B^E), 4.47 (brd, 3J = 9.3 Hz, 2H, H-5^{C,F} or B^E), 4.55 (brd, 3J = 9.3 Hz, 2H, H-5^{B,E} or C^F), 5.11 (d, $^3J_{\text{H-1,H-2}}$ = 2.6 Hz, 2H, H-1^{A,D}), 5.19 (d, $^3J_{\text{H-1,H-2}}$ = 2.9 Hz, 2H, H-1^{B,E} or C^F), 5.36 (d, $^3J_{\text{H-1,H-2}}$ = 3.3 Hz, 2H, H-1^{C,F} or B^E), 5.59 (brt, 3J = 9.7 Hz, 2H, H-5^{A,D}), 6.95–7.25 (m, 12H, H_{meta} and H_{para}), 7.78–7.82 (m, 4H, H_{ortho}), 8.17–8.21 ppm (m, 4H, H_{ortho}); $^{13}\text{C}\{^1\text{H}\}$ NMR (125.8 MHz, C_6D_6 , 25 °C): δ = 35.83 (virtualt, $^1J_{\text{C-P}} + ^3J_{\text{C-P}}$ = 22.4 Hz, C-6^{A,D}), 57.25, 57.41 ($\text{CH}_3\text{O-6}$), 59.14, 59.30, 59.44 ($\text{CH}_3\text{O-2}$), 61.25, 61.72, 62.12 ($\text{CH}_3\text{O-3}$), 70.78 (C-4^{A,D}), 71.95, 72.32

(C-5^{B,C,E,F}), 72.12, 72.49 (C-6^{B,C,E,F}), 81.15, 81.63, 81.70 ($\times 2$), 81.88, 81.78, 82.84, 84.12 (C-2, C-3, C-4^{B,C,E,F}), 89.23 (virtualt, $^2J_{\text{C-P}} + ^4J_{\text{C-P}}$ = 10.4 Hz, C-5^{A,D}), 98.31, 98.81 (C-1^{B,C,E,F}), 101.37 (C-1^{A,D}), 127.97 (virtualt, $^3J_{\text{C-P}} + ^5J_{\text{C-P}}$ = 9.6 Hz, C_{meta}), 128.49 (virtualt, $^3J_{\text{C-P}} + ^5J_{\text{C-P}}$ = 9.6 Hz, C_{meta}), 129.69 (s, C_{para}), 130.36 (s, C_{para}), 133.35 (virtualt, $^2J_{\text{C-P}} + ^4J_{\text{C-P}}$ = 12.0 Hz, C_{ortho}), 134.54 (virtualt, $^1J_{\text{C-P}} + ^3J_{\text{C-P}}$ = 44.2 Hz, C_{ipso}), 135.58 (virtualt, $^2J_{\text{C-P}} + ^4J_{\text{C-P}}$ = 13.6 Hz, C_{ortho}), 140.68 ppm (virtualt, $^1J_{\text{C-P}} + ^3J_{\text{C-P}}$ = 42.6 Hz, C_{ipso}); NMR $^{31}\text{P}\{^1\text{H}\}$ (121.5 MHz, C_6D_6 , 25 °C): δ = 17.9 ppm (d, $^1J_{\text{Rh-P}}$ = 132 Hz); elemental analysis (%) calcd for $\text{C}_{77}\text{H}_{110}\text{ClO}_{29}\text{P}_2\text{Rh} \cdot \text{C}_6\text{H}_6$ (1700.02 + 78.11): C 56.07, H 6.58; found: C 56.20, H 6.62; MS (FAB): m/z (%): 1679.4 (12) $[\text{M} - \text{Cl} + \text{O}]^+$, 1670.4 (5) $[\text{M} - \text{CO}]^+$, 1663.4 (3) $[\text{M} - \text{Cl}]^+$, 1635.5 (19) $[\text{M} - \text{CO} - \text{Cl}]^+$.

6: yellow; yield: 61%; R_f ($\text{CH}_2\text{Cl}_2/\text{MeOH}$, 94:6, v/v) = 0.31; m.p. 145–147 °C; ^1H NMR (400 MHz, CDCl_3 , 25 °C): δ (assignment by COSY) = 2.54 (m, 2H; H-6a^{A,D}), 2.83 (s, 6H; $\text{CH}_3\text{O-6}$), 2.95 (dd, $^3J_{\text{H-1,H-2}}$ = 2.7 Hz, $^3J_{\text{H-2,H-3}}$ = 10.0 Hz, 2H; H-2^{A,D}), 3.06 (t, $^3J_{\text{H-3,H-4}}$ = $^3J_{\text{H-4,H-5}}$ = 9.2 Hz, 2H; H-4^{A,D}), 3.12 (dd, $^3J_{\text{H-1,H-2}}$ = 2.9 Hz, $^3J_{\text{H-2,H-3}}$ = 9.6 Hz, 2H; H-2^{B,E} or C^F), 3.15 (dd, 2H; H-6a^{C,F} or B^E), 3.17 (dd, 2H; H-2^{C,F} or B^E), 3.36 (dd, $^2J_{\text{H-6a,H-6b}}$ = 11.9 Hz, $^3J_{\text{H-5,H-6b}}$ = 1.5 Hz, 2H; H-6b^{C,F} or B^E), 3.39 (s, 6H; $\text{CH}_3\text{O-6}$), 3.43 (s, 6H; OCH_3), 3.47 (s, 6H; OCH_3), 3.50 (s, 6H; OCH_3), 3.60 (s, 6H; OCH_3), 3.65–3.75 (3 overlapping dd, 6H; H-6a^{B,E} or C^F, H-3^{A,D}, and H-4^{B,E} or C^F), 3.66 (s, 6H; OCH_3), 3.69 (s, 6H; OCH_3), 3.75–3.82 (3 overlapping dd, 6H; H-3^{B,E} or C^F, H-3^{C,F} or B^E, H-4^{C,F} or B^E), 3.93 (m, $^2J_{\text{H-6b,H-6a}}$ = 11.5 Hz, 2H; H-6b^{A,D}), 3.97 (dt, 3J = 10.8 Hz, 2H; H-5^{B,E} or C^F), 4.36 (dt, 3J = 9.5 Hz, 2H; H-5^{C,F} or B^E), 4.45 (d, 3J = 2.7 Hz, 2H; H-1^{A,D}), 4.57 (brd, 3J = 7.0, 2H; H-6b^{B,E} or C^F), 4.97 (brt, 3J = 9.5 Hz, 2H; H-5^{A,D}), 5.06 (d, 3J = 2.9 Hz, 2H; H-1^{B,E} or C^F), 5.11 (d, 3J = 3.1 Hz, 2H; H-1^{C,F} or B^E), 7.30–7.40 (m, 12H; H_{meta} and H_{para}), 7.48–7.53 (m, 4H; H_{ortho}), 7.89–7.95 ppm (m, 4H; H_{ortho}); $^{13}\text{C}\{^1\text{H}\}$ NMR (50.3 MHz,

CDCl_3 , 25 °C): δ = 33.50 (virtualt, $^1J_{\text{C-P}} + ^3J_{\text{C-P}}$ = 28.0 Hz; C-6^{A,D}), 57.10, 58.15 ($\text{CH}_3\text{O-6}$), 58.61, 58.84, 59.07 ($\text{CH}_3\text{O-2}$), 61.20, 61.27, 61.43 ($\text{CH}_3\text{O-3}$), 70.58 (C-4^{A,D}), 71.03, 71.17 (C-6^{B,C,E,F}), 70.67, 71.39 (C-5^{B,C,E,F}), 78.93, 79.95, 80.80 ($\times 2$), 81.69, 81.98, 82.83, 83.72 (C-2, C-3, C-4^{B,C,E,F}), 92.21 (virtualt, $^2J_{\text{C-P}} + ^4J_{\text{C-P}}$ = 9.9 Hz; C-5^{A,D}), 97.26, 99.32, 102.21 (C-1), 127.94 (virtualt, $^3J_{\text{C-P}} + ^5J_{\text{C-P}}$ = 11.5 Hz; C_{meta}), 128.30 (virtualt, $^3J_{\text{C-P}} + ^5J_{\text{C-P}}$ = 8.2 Hz; C_{meta}), 129.74 (s; C_{para}), 130.43 (s; C_{para}), 131.35 (virtualt, $^2J_{\text{C-P}} + ^4J_{\text{C-P}}$ = 9.8 Hz; C_{ortho}), 132.79 (virtualt, $^1J_{\text{C-P}} + ^3J_{\text{C-P}}$ = 42.8 Hz; C_{ipso}), 134.76 (virtualt, $^2J_{\text{C-P}} + ^4J_{\text{C-P}}$ = 11.5 Hz; C_{ortho}), 139.94 (virtualt, $^1J_{\text{C-P}} + ^3J_{\text{C-P}}$ = 46.2 Hz; C_{ipso}), 193.66 ppm (t, $^2J_{\text{C-P}}$ = 12 Hz; CO); $^{31}\text{P}\{^1\text{H}\}$ NMR (121.5 MHz, CDCl_3 , 25 °C): δ = 12.4 (s); elemental analysis (%) calcd for $\text{C}_{78}\text{H}_{110}\text{O}_{30}\text{P}_2\text{Cl}_2\text{Ru} \cdot 0.5\text{CH}_2\text{Cl}_2$ (1761.62 + 42.47): C 52.26, H 6.20; found: C 52.18, H 6.43; MS (FAB): m/z (%): 1763.4 (8) $[\text{M} + \text{H}]^+$, 1735.4 (30) $[\text{M} - \text{CO} + \text{H}]^+$, 1706.4 (20) $[\text{M} - 2\text{CO}]^+$, 1699.4 (35) $[\text{M} - \text{Cl} - \text{CO}]^+$.

of the complex and the presence of both M–Cl bonds inside the cavity was confirmed by an X-ray study (Figure 2). The solid-state structure exhibits some disorder that is characterized by two possible orientations of the “ $\text{Ru}(\text{CO})_2\text{Cl}_2$ ” cross which rotates by approximately 37° about the P–P axis on switching from one rotamer to the other (isomer ratio 80:20). In other words, the chlorine atoms compete for the central position inside the cyclodextrin. Both rotamers deviate somewhat from ideal C_2 symmetry. In the major one (Figure 2) the Cl(2) atom is close to four consecutive H-5 atoms ($\text{H} \cdots \text{Cl}$ separation ranging from 2.75(2) to 3.00(2) Å), while Cl(1) interacts with the two remaining H-5 atoms (2.84(2) and 2.88(2) Å). Clearly the weakness of the individual $\text{Cl} \cdots \text{H-5}$ interactions favors easy reorientation of the M–Cl bonds within the upper part of the cavity. A general survey on the occurrence of $\text{CH} \cdots \text{Cl}$ hydrogen bonds in molecular structures indicates that such interactions take place only with

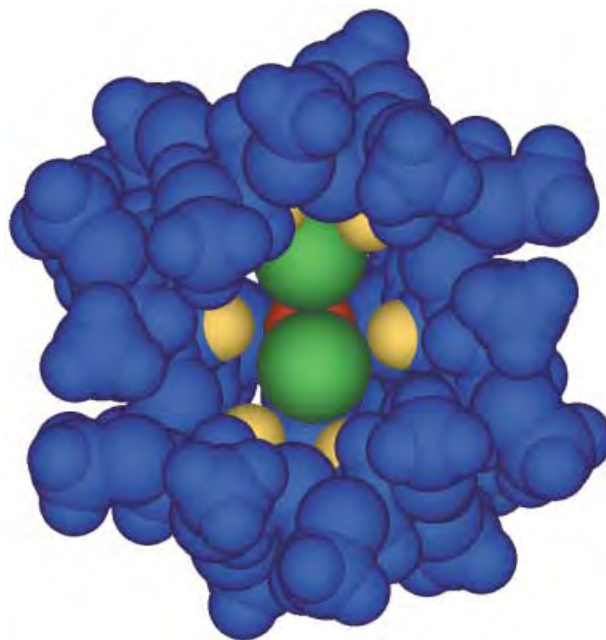


Figure 2. Molecular structure of **6** (major isomer). View from the bottom showing the chlorine atoms in green (Cl(1) down, Cl(2) up), the H-5 atoms in yellow, and the ruthenium atom in red. The included benzene molecule has been omitted for clarity. Selected bond lengths [Å]: Ru–P 2.423(2) and 2.425(2), Ru–Cl(1) 2.408(3), Ru–Cl(2) 2.355(3); shortest Cl(1) \cdots H-5 distances: 2.75(2), 2.80(2), 2.84(2), 3.00(2); shortest Cl(2) \cdots H-5 distances: 2.84(2) and 2.88(2).

Cl atoms having a marked anionic character.^[30] This feature is also realized, but to a lesser extent, in the M–Cl bonds of complexes **2–6**.

The present study illustrates for the first time the ability of an α -cyclodextrin cavity to recognize a transition metal M–Cl bond through weak Cl...H-5 interactions in the solid state as well as in solution. The fact that such subtle interactions could be observed in non-aqueous media is a consequence of the absence of stronger competing supramolecular forces, such as the hydrophobic effect, which usually plays a prevailing role in the formation of CD inclusion complexes. Overall these results illustrate the potential of modified cyclodextrins as second-sphere ligands.

Received: March 25, 2002 [Z18970]

- [1] Y. Rondelez, M.-N. Rager, A. Duprat, O. Reinaud, *J. Am. Chem. Soc.* **2002**, *124*, 1334.
- [2] M. T. Reetz, J. Rudolph, R. Goddard, *Can. J. Chem.* **2001**, *79*, 1806.
- [3] M. Flauaus, M. Herzing, A. Köllhofer, M. Laly, H. Plenio, *Eur. J. Org. Chem.* **2001**, 1061.
- [4] S. Steyer, C. Jeunesse, D. Armspach, D. Matt, J. Harrowfield in *Calixarenes 2001* (Eds.: Z. Asfari, V. Böhmer, J. M. Harrowfield, J. Vicens), Kluwer Academic Publishers, Dordrecht, **2001**, p. 513.
- [5] S. Blanchard, L. Le Clainche, M.-N. Rager, B. Chansou, J.-P. Tugagues, A. F. Duprat, Y. Le Mest, O. Reinaud, *Angew. Chem.* **1998**, *110*, 2861; *Angew. Chem. Int. Ed.* **1998**, *37*, 2732.
- [6] C. Wieser-Jeunesse, D. Matt, A. De Cian, *Angew. Chem.* **1998**, *110*, 3027; *Angew. Chem. Int. Ed.* **1998**, *37*, 2861.
- [7] B. R. Cameron, S. J. Loeb, G. P. A. Yap, *Inorg. Chem.* **1997**, *36*, 5498.
- [8] V. C. Gibson, C. Redshaw, W. Clegg, M. R. J. Elsegood, *J. Chem. Soc. Chem. Commun.* **1995**, 2371.
- [9] R. Deschenaux, M. M. Harding, T. Ruch, *J. Chem. Soc. Perkin Trans. 2* **1993**, 1251.
- [10] H. K. A. C. Coolen, P. W. N. M. van Leeuwen, R. J. M. Nolte, *Angew. Chem.* **1992**, *104*, 906; *Angew. Chem. Int. Ed. Engl.* **1992**, *31*, 905.
- [11] F. Corazza, C. Floriani, A. Chiesi-Villa, C. Guastini, *J. Chem. Soc. Chem. Commun.* **1990**, 640.
- [12] M. Lejeune, C. Jeunesse, D. Matt, N. Kyritsakas, R. Welter, J.-P. Kintzinger, *J. Chem. Soc. Dalton Trans.* **2002**, 1642.
- [13] E. Engeldinger, D. Armspach, D. Matt, *Angew. Chem.* **2001**, *113*, 2594; *Angew. Chem. Int. Ed.* **2001**, *40*, 2526.
- [14] M. V. Rekharasy, Y. Inoue, *Chem. Rev.* **1998**, *98*, 1875.
- [15] K. A. Connors, *Chem. Rev.* **1997**, *97*, 1325.
- [16] D. Armspach, D. Matt, A. Harriman, *Eur. J. Inorg. Chem.* **2000**, 1147.
- [17] M. T. Reetz, *Catal. Today* **1998**, *42*, 399.
- [18] M. T. Reetz, S. R. Waldvogel, *Angew. Chem.* **1997**, *109*, 870; *Angew. Chem. Int. Ed. Engl.* **1997**, *36*, 865.
- [19] S. A. Negopodiev, J. F. Stoddart, *Chem. Rev.* **1998**, *98*, 1959.
- [20] R. Breslow, S. D. Dong, *Chem. Rev.* **1998**, *98*, 1997.
- [21] M. R. Craig, M. G. Hutchings, T. D. W. Claridge, H. L. Anderson, *Angew. Chem.* **2001**, *113*, 1105; *Angew. Chem. Int. Ed.* **2001**, *40*, 1071.
- [22] K. B. Lipkowitz, *Chem. Rev.* **1998**, *98*, 1829.
- [23] T. Aree, I. Uson, B. Schulz, G. Reck, H. Hoier, G. M. Sheldrick, W. Saenger, *J. Am. Chem. Soc.* **1999**, *121*, 3321.
- [24] T. Steiner, W. Saenger, *Carbohydr. Res.* **1996**, *282*, 53.
- [25] Some insoluble material, presumably of oligomeric nature, was also formed during this synthesis. However, this is not the case for complexes **4–6** which were obtained from starting complexes containing very good leaving groups.
- [26] Crystal structure analysis of **2**·C₄H₈O: crystals suitable for X-ray diffraction were obtained by slow diffusion of pentane into a butanone solution of the complex. Crystal data: $M_r = 1782.98$, hexagonal, space group $P6_522$, $a = b = 14.8846(3)$, $c = 67.0615(15)$ Å, $V = 12867.0(5)$ Å³, $Z = 6$, $\rho_{\text{calcd}} = 1.381$ g cm⁻³, $\text{MoK}\alpha$ radiation ($\lambda = 0.71073$ Å), $\mu = 0.395$ mm⁻¹. Data were collected on a Bruker SMART 1000 CCD system at 133(2) K. The structure was solved by direct methods and refined on F_o^2 by full-matrix least squares (program SHELXL-97, G. M. Sheldrick, University of Göttingen). All non-hydrogen atoms were refined anisotropically; hydrogen atoms were included using a

riding model. The absolute configuration (and thus the enantiomeric space group assignment) was determined by a Flack x parameter of $-0.07(3)$. Refinement proceeded to $wR2 = 0.1025$ for all 5529 reflections and $R1 = 0.0413$ for data with $I > 2\sigma(I)$. The compound crystallizes with a butanone molecule positioned inside the cyclodextrin cavity. CCDC-181579 contains the supplementary crystallographic data for this paper. These data can be obtained free of charge via www.ccdc.cam.ac.uk/conts/retrieving.html (or from the Cambridge Crystallographic Data Centre, 12, Union Road, Cambridge CB21EZ, UK; fax: (+44) 1223-336-033; or deposit@ccdc.cam.ac.uk).

- [27] C. A. Bessel, P. Aggarwal, A. C. Marschilok, K. J. Takeuchi, *Chem. Rev.* **2001**, *101*, 1031.
- [28] Crystal structure analysis of **6**·C₆H₆: crystals suitable for X-ray diffraction were obtained by slow diffusion of pentane into a benzene solution of the complex; $M_r = 1839.68$, orthorhombic, space group $P2_12_12_1$, $a = 15.353(2)$, $b = 24.313(2)$, $c = 26.952(3)$ Å, $V = 10060.9(19)$ Å³, $Z = 4$, $\rho_{\text{calcd}} = 1.211$ g cm⁻³, $\text{MoK}\alpha$ radiation ($\lambda = 0.71073$ Å), $\mu = 0.311$ mm⁻¹. Data were collected on a Kappa CCD Enraf Nonius system at 173(2) K. The structure was solved by direct methods and refined on F_o^2 by full-matrix least squares (program SHELXL-97, G. M. Sheldrick, University of Göttingen). All non-hydrogen atoms were refined anisotropically; hydrogens were included using a riding model. The absolute structure was determined by refining Flack's x parameter ($x = -0.01(4)$). $R1 = 0.0830$ and $wR2 = 0.2096$ for 12112 data with $I > 2\sigma(I)$. The compound crystallizes with a benzene molecule included inside the cyclodextrin cavity. CCDC-181578 contains the supplementary crystallographic data for this paper. These data can be obtained free of charge via www.ccdc.cam.ac.uk/conts/retrieving.html (or from the Cambridge Crystallographic Data Centre, 12, Union Road, Cambridge CB21EZ, UK; fax: (+44) 1223-336-033; or deposit@ccdc.cam.ac.uk).
- [29] The behavior of the CD cavity towards the "RuCl₂(CO)₂" unit strongly contrasts with that of a recently reported *p*-tert-butylcalix[4]-arene-derived diphosphane. Upon complexation, the latter favors inclusion of a "Ru–CO" rod over that of a "Ru–Cl" fragment; see reference [6].
- [30] O. Kennard, R. Taylor, *J. Am. Chem. Soc.* **1982**, *104*, 5063.

A Stepwise Huisgen Cycloaddition Process: Copper(0)-Catalyzed Regioselective "Ligation" of Azides and Terminal Alkynes**

Vsevolod V. Rostovtsev, Luke G. Green,
Valery V. Fokin,* and K. Barry Sharpless*

Huisgen 1,3-dipolar cycloadditions^[1] are exergonic fusion processes that unite two unsaturated reactants and provide fast access to an enormous variety of five-membered hetero-

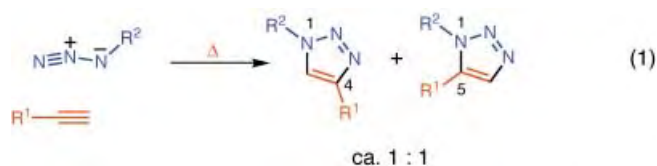
[*] Prof. V. V. Fokin, Prof. K. B. Sharpless, Dr. V. V. Rostovtsev, Dr. L. G. Green
Department of Chemistry and
the Skaggs Institute for Chemical Biology
The Scripps Research Institute, BCC-315
10550 N. Torrey Pines Rd., La Jolla, CA 92037 (USA)
Fax: (+1) 858-784-7562
E-mail: fokin@scripps.edu, sharples@scripps.edu

[**] We thank the National Institute of General Medical Sciences, the National Institutes of Health (GM 28384), the National Science Foundation (CHE-9985553), and the W. M. Keck Foundation for financial support. We also thank Dr. F. Himo, Prof. L. Noodleman, Prof. Flavio Grynszpan, and Prof. M. G. Finn for helpful discussions.

Supporting information for this article is available on the WWW under <http://www.angewandte.org> or from the author.

cycles.^[2] The cycloaddition of azides and alkynes to give triazoles^[3] is arguably the most useful member of this family. However, likely because of concerns about the safety of working with organic azides, synthetic chemists, in both pure and applied fields, have not given this transformation the special attention it deserves. Although the actual cycloaddition step may be faster and/or more regioselective for 1,3-dipoles other than azide, the latter is by far the most convenient to introduce and to carry hidden through many synthetic steps. Indeed, it appears to be the only three-atom dipole which is nearly devoid of side reactions.

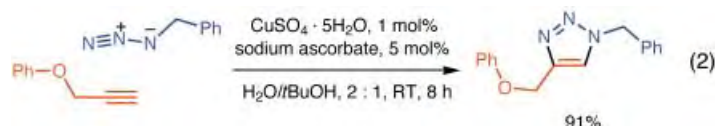
Azides usually make fleeting appearances in organic synthesis: they serve as one of the most reliable means to introduce a nitrogen substituent through the reaction $-R-X \rightarrow [R-N_3] \rightarrow R-NH_2$. The azide intermediate is shown in brackets because it is generally reduced straightaway to the amine.^[4] Despite this “azidophobia”, we have learned to work safely with azides because they are the most crucial functional group for click chemistry endeavors.^[5] Ironically, what makes azides unique for click chemistry purposes is their extraordinary stability toward H_2O , O_2 , and the majority of organic synthesis conditions.^[6] The spring-loaded nature of the azide group remains invisible unless a good dipolarophile is favorably presented.^[7] However, even then the desired triazole-forming cycloaddition may require elevated temperatures and, usually results in a mixture of the 1,4 and 1,5 regioisomers [Eq. (1)].^[1, 8]



Since efforts to control this 1,4- versus 1,5-regioselectivity problem have so far met with varying success,^[9] we were pleased to find this copper(I)-catalyzed reaction sequence which regiospecifically unites azides and terminal alkynes to give only 1,4-disubstituted 1,2,3-triazoles.^[10] The process is experimentally simple and appears to have enormous scope.

While a number of copper(I) sources can be used directly (see below), we found that the catalyst is better prepared in situ by reduction of Cu^{II} salts, which are less costly and often purer than Cu^I salts ($CuSO_4 \cdot 5H_2O$ serves well). As the reductant, ascorbic acid and/or sodium ascorbate proved to be excellent^[11] for they allow preparation of a broad spectrum of 1,4-triazole products in high yields and purity at 0.25–2 mol% catalyst loading. The reaction appears to be very forgiving and does not require any special precautions. It proceeds to completion in 6 to 36 hours at ambient temperature in a variety of solvents, including aqueous *tert*-butyl alcohol or ethanol and, very importantly, water with no organic co-solvent.^[12] Although most experiments were performed at near neutral pH values, the catalysis seems to proceed well at pH values ranging from approximately 4 to 12. In other words, this is a very robust catalytic process, which is so insensitive to the usual reaction parameters as to strain credulity.^[13]

The reaction between phenyl propargyl ether and benzylazide in the presence of 5 mol% of sodium ascorbate and 1 mol% of copper(II) sulfate in a 2:1 mixture of water and *tert*-butyl alcohol furnished the 1,4-disubstituted triazole product in 91% yield after stirring for eight hours at room temperature in a capped scintillation vial, but otherwise with no effort to exclude oxygen [Eq. (2)]. The regiochemistry of the product was established by NOE experiments and confirmed by an X-ray crystallographic analysis.^[14] For comparison, the thermal reaction (neat, 92 °C, 18 h) between these substrates gives both regioisomers in a ratio of 1.6:1 in favor of the 1,4 isomer.



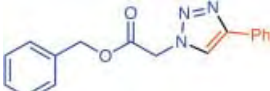
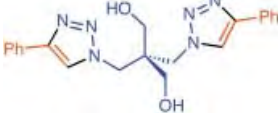
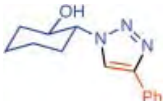
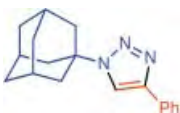
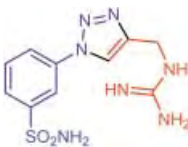
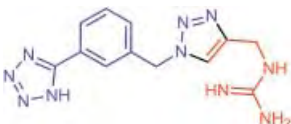
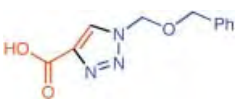
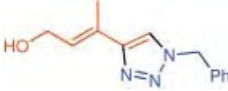
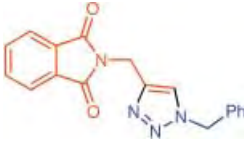
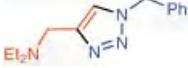
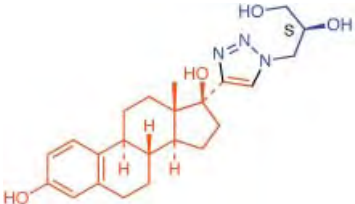
The scope of this copper-catalyzed triazole synthesis is partly revealed by the examples in Table 1; the lack of functional group interference is especially noteworthy. These triazoles are obtained by using a procedure which generally involves little more than stirring the reagents and filtering off pure products. Various substituted primary, secondary, tertiary, and aromatic azides readily participate in this transformation. Tolerance for variations in the acetylene component is also excellent.

Copper(I) salts, for example, CuI , $CuOTf \cdot C_6H_6$, and $[Cu(NCCH_3)_4][PF_6]$, can also be used directly in the absence of a reducing agent. These reactions usually require acetonitrile as co-solvent and one equivalent of a nitrogen base (for example, 2,6-lutidine, triethylamine, diisopropylethylamine, or pyridine). However, formation of undesired by-products, primarily diacetylenes, bis-triazoles, and 5-hydroxytriazoles, was often observed.^[10, 15] This complication with the direct use of Cu^I species was minimized when 2,6-lutidine was used, and exclusion of oxygen further improved product purity and yield.^[16] Even though a broad range of both acetylene and azide components react readily in the acetonitrile system, we prefer the even more reliable and simple Cu^{II} /ascorbate aqueous system (with or without co-solvents and amine buffers/additives).

Our mechanistic proposal for the catalytic cycle is shown in Scheme 1. It begins unexceptionally with formation of the copper(I) acetylide **I**^[17] (as expected, no reaction is observed with internal alkynes), but then gets interesting. Extensive density functional theory calculations^[18] offer compelling evidence which strongly disfavors—by about 12–15 kcal—the concerted [2+3] cycloaddition (B-direct) and points to a stepwise, annealing sequence (B-1 \rightarrow B-2 \rightarrow B-3, hence the term “ligation”), which proceeds via the intriguing six-membered copper-containing intermediate **III**.^[19]

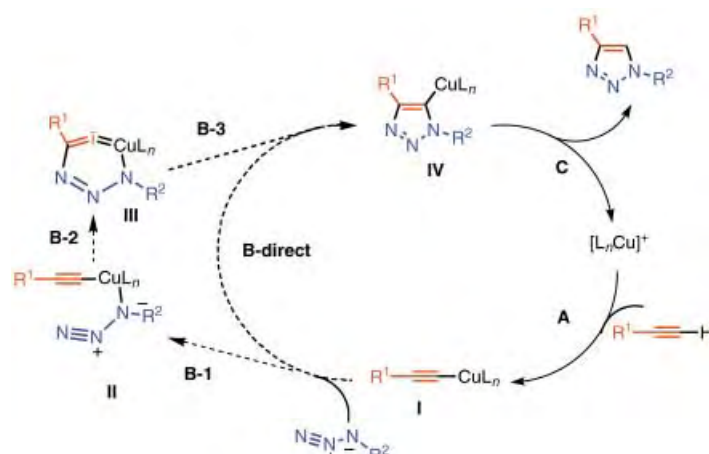
In conclusion, the Cu^I -catalyzed transformation described here—a high-yielding and simple to perform “fusion” process leading to a thermally and hydrolytically stable triazole connection—is an ideal addition to the family of click reactions. The process exhibits broad scope and provides

Table 1. Synthesis of 1,4-disubstituted 1,2,3-triazoles catalyzed by Cu^I ions in the presence of ascorbate.^[a]

Entry	Product	Yield [%]
1		92
2		93
3		82
4		84
5		91
6		88
7		88
8		84
9		88
10		90
11		94

[a] All reactions were carried out in water with *tert*-butyl alcohol as co-solvent, 0.25–0.5 M in reactants, with 1 mol % of CuSO₄ and 10 mol % of sodium ascorbate, and were complete in 12–24 h.

1,4-disubstituted 1,2,3-triazole products in excellent yields and near perfect regioselectivity. The fact that this “unstoppable” reactivity^[20] of copper(I) acetylides with organic azides remained unrevealed until now, despite the great body of research on copper-mediated organic synthesis over the last



Scheme 1. Proposed catalytic cycle for the Cu^I-catalyzed ligation.

seventy years, is extraordinary. It can only be attributed to the often irrational fear of azides and is just another indication of the untapped potential of this underappreciated functional group. Above all, what this new catalytic process seems to offer is an unprecedented level of selectivity, reliability, and scope for those organic synthesis endeavors which depend on the creation of covalent links between diverse building blocks. Several studies which highlight the capabilities of the process, as well as studies hoping to achieve better mechanistic understanding of its unique reactivity features, are currently underway and will be reported in due course.

Experimental Section

General procedure (entry 11, Table 1): 17-ethynylestradiol (888 mg, 3 mmol) and (*S*)-3-azidopropane-1,2-diol (352 mg, 3 mmol) were suspended in a 1:1 mixture of water and *tert*-butyl alcohol (12 mL). Sodium ascorbate (0.3 mmol, 300 μ L of freshly prepared 1 M solution in water) was added, followed by copper(II) sulfate pentahydrate (7.5 mg, 0.03 mmol, in 100 μ L of water). The heterogeneous mixture was stirred vigorously overnight, at which point it cleared and TLC analysis indicated complete consumption of the reactants. The reaction mixture was diluted with water (50 mL), cooled in ice, and the white precipitate was collected by filtration. After washing the precipitate with cold water (2 \times 25 mL), it was dried under vacuum to afford 1.17 g (94 %) of pure product as an off-white powder. M.p. 228–230 °C. Elemental analysis calcd for C₂₃H₃₁N₃O₄: C 64.02, H 7.71, N 9.74 %; found: C 64.06, H 7.36, N 9.64 %. ¹H NMR ([D₆]DMSO) δ = 8.97 (s, 1H), 7.77 (s, 1H), 6.95 (d, *J* = 8.3 Hz, 1H), 6.45 (dd, *J* = 8.3, 2.3 Hz, 1H), 6.41 (d, *J* = 2.3 Hz, 1H), 5.13 (m, 1H), 5.09 (d, *J* = 2.9 Hz, 1H), 4.83 (m, 1H), 4.46 (m, 1H), 4.21 (m, 1H), 3.81 (m, 1H), 3.26 (m, 1H), 2.67 (m, 2H), 2.35 (m, 1H), 2.08 (m, 1H), 1.96 (m, 1H), 1.89–1.77 (m, 3H), 1.63 (m, 1H), 1.48–1.12 (m, 6H), 0.91 (s, 3H), 0.74 ppm (s, 1H); ¹³C NMR ([D₆]DMSO) δ = 154.8, 153.8, 137.2, 130.4, 126.0, 123.3, 114.9, 112.7, 81.1, 70.6, 70.4, 63.2, 52.6, 47.5, 46.7, 43.2, 37.2, 32.6, 29.3, 27.2, 26.1, 23.6, 14.4 ppm.

Received: April 29, 2002 [Z19191]

- [1] a) R. Huisgen in *1,3-Dipolar Cycloaddition Chemistry* (Ed.: A. Padwa), Wiley, New York, **1984**, pp. 1–176; b) A. Padwa in *Comprehensive Organic Synthesis*, Vol. 4 (Ed.: B. M. Trost), Pergamon, Oxford, **1991**, pp. 1069–1109; c) for a review of asymmetric 1,3-dipolar cycloaddition reactions, see K. V. Gothelf, K. A. Jorgensen, *Chem. Rev.* **1998**, 98, 863–909; d) for a review of synthetic applications, see J. Mulzer, *Org. Synth. Highlights* **1991**, 77–95.

- [2] a) W.-Q. Fan, A. R. Katritzky in *Comprehensive Heterocyclic Chemistry II, Vol. 4* (Eds.: A. R. Katritzky, C. W. Rees, E. F. V. Scriven), Pergamon, Oxford, **1996**, pp. 101–126; b) R. N. Butler in *Comprehensive Heterocyclic Chemistry II, Vol. 4* (Eds.: A. R. Katritzky, C. W. Rees, E. F. V. Scriven), Pergamon, Oxford, **1996**, pp. 621–678; c) K. Banert, *Chem. Ber.* **1989**, *122*, 911–918.
- [3] a) R. Huisgen, *Pure Appl. Chem.* **1989**, *61*, 613–628; b) R. Huisgen, G. Szeimies, L. Moebius, *Chem. Ber.* **1967**, *100*, 2494–2507; c) W. Lwowski in *1,3-Dipolar Cycloaddition Chemistry, Vol. 1* (Ed.: A. Padwa), Wiley, New York, **1984**, chap. 5; d) J. Bastide, J. Hamelin, F. Texier, V. Q. Ven, *Bull. Soc. Chim. Fr.* **1973**, 2555–2579; J. Bastide, J. Hamelin, F. Texier, V. Q. Ven, *Bull. Soc. Chim. Fr.* **1973**, 2871–2887.
- [4] Although applications which utilize the unique reactivity offered by the azide group itself are rare, delightful exceptions can be found the following works: a) P. Desai, K. Schildknecht, K. A. Agrios, C. Mossman, G. Milligan, J. Aube, *J. Am. Chem. Soc.* **2000**, *122*, 7226–7232; b) K. Banert, *Targets Heterocycl. Syst.* **1999**, *3*, 1–32; K. Banert, *Liebigs Ann./Recl.* **1997**, 2005–2018; c) W. H. Pearson, W.-K. Fang, *Isr. J. Chem.* **1997**, *37*, 39–46; d) J. Cao, M. C. T. Fyfe, J. F. Stoddart, *J. Org. Chem.* **2000**, *65*, 1937–1946; e) B. Carboni, A. Benali, M. Vaultier, *J. Org. Chem.* **1993**, *58*, 3736–3741, and references therein.
- [5] H. C. Kolb, M. G. Finn, K. B. Sharpless, *Angew. Chem.* **2001**, *113*, 1198–1220; *Angew. Chem. Int. Ed.* **2001**, *40*, 2004–2021.
- [6] Organic azides, particularly in the aliphatic series, are exceptionally stable toward the common reactive chemicals on the Earth's surface, which range from dioxygen and water to the aqueous solutions of highly functionalized organic molecules which make up living cells: E. Saxon, C. R. Bertozzi, *Science* **2000**, *287*, 2007–2010; K. L. Kiick, E. Saxon, D. A. Tirrel, C. R. Bertozzi, *Proc. Natl. Acad. Sci. USA* **2002**, *99*, 19–24.
- [7] In fact, it was the razor sharp reactivity window for this cycloaddition process which spawned our “in situ click chemistry” ideas—an approach which recently resulted in the discovery of the most potent noncovalent inhibitor of acetylcholinesterase known to date: W. G. Lewis, L. G. Green, F. Grynszpan, Z. Radic, P. R. Carlier, P. Taylor, M. G. Finn, K. B. Sharpless, *Angew. Chem.* **2002**, *114*, 1095–1099; *Angew. Chem. Int. Ed.* **2002**, *41*, 1053–1057.
- [8] Unless the acetylene component is attached to an electron-withdrawing group such as a carbonyl or perfluoroalkyl group: J. Bastide, O. Henri-Rousseau, *Bull. Chim. Soc. Fr.* **1973**, 2294–2296; N. P. Stepanova, N. A. Orlova, V. A. Galishev, E. S. Turbanova, A. A. Petrov, *Zh. Org. Khim.* **1985**, *21*, 979–983; N. P. Stepanova, V. A. Galishev, E. S. Turbanova, A. V. Maleev, K. A. Potekhin, E. N. Kurkutova, Yu. T. Struchkov, A. A. Petrov, *Zh. Org. Khim.* **1989**, *25*, 1613–1618; D. Clarke, R. W. Mares, H. McNab, *J. Chem. Soc. Perkin Trans. I* **1997**, 1799–1804.
- [9] P. Zanirato, *J. Chem. Soc. Perkin Trans. I* **1991**, 2789–2796; D. J. Hlasta, J. A. Ackerman, *J. Org. Chem.* **1994**, *59*, 6184–6189; C. A. Booth, D. Philp, *Tetrahedron Lett.* **1998**, *39*, 6987–6990; S. J. Howell, N. Spencer, D. Philp, *Tetrahedron* **2001**, *57*, 4945–4954; W. L. Mock, T. A. Irra, J. P. Wepsiec, M. Adhya, *J. Org. Chem.* **1989**, *54*, 5302–5308; W. L. Mock, *Top. Curr. Chem.* **1995**, *175*, 1–24; J. Chen, J. Rebek, Jr., *Org. Lett.* **2002**, *4*, 327–329; J. W. Wijnen, R. A. Steiner, J. B. F. N. Engberts, *Tetrahedron Lett.* **1995**, *36*, 5389–5392; M. P. Repasky, W. L. Jorgensen, *Faraday Discuss.* **1998**, *110*, 379–389.
- [10] While this manuscript was in preparation, an independent account of copper-catalyzed synthesis of 1,4-triazoles from azides and terminal acetylenes on solid support was reported: C. W. Tornøe, C. Christensen, M. Meldal, *J. Org. Chem.* **2002**, *67*, 3057.
- [11] For a review of reactions of L-ascorbic acid with transition metals, see M. B. Davies, *Polyhedron* **1992**, *11*, 285–321, and references therein; redox properties of ascorbic acid are summarized in C. Creutz, *Inorg. Chem.* **1981**, *20*, 4449.
- [12] The starting materials do not need to be dissolved in the reaction solvent. The reaction seems to proceed just as efficiently as long as adequate stirring is maintained.
- [13] Amazingly, even Cu⁰ can be used as a source of the catalytic species. Although these reactions may take longer to proceed to completion, the experimental procedure is exceedingly simple. For example, bis-triazole shown in entry 2 (Table 1) was obtained in quantitative yield after stirring the corresponding azide and acetylene components for 24 h with about 1 g of coiled copper metal turnings. The turnings were removed at the end of the reaction, and the pure white product was collected by simple filtration.
- [14] CCDC 186236 contains the supplementary crystallographic data for this paper. These data can be obtained free of charge via www.ccdc.cam.ac.uk/conts/retrieving.html (or from the Cambridge Crystallographic Data Centre, 12, Union Road, Cambridge CB21EZ, UK; fax: (+44) 1223-336-033; or deposit@ccdc.cam.ac.uk).
- [15] For a recent summary of the reactions of copper(I) complexes with dioxygen, see S. Schindler, *Eur. J. Inorg. Chem.* **2000**, 2311–2326 and A. G. Blackman, W. B. Tolman in *Structure and Bonding, Vol. 97* (Ed: B. Meunier), Springer, Berlin, **2000**, pp. 179–211.
- [16] For example, ethyl propiolate and benzylazide furnished the corresponding 1,4-triazole in 55% yield when this procedure was used, but only a trace amount of the product was obtained with one equivalent of triethylamine and without exclusion of oxygen.
- [17] G. van Koten, J. G. Noltes in *Comprehensive Organometallic Chemistry, Vol. 2* (Ed.: G. Wilkinson), Pergamon, Oxford, **1982**, chap. 14, p. 720.
- [18] F. Himo, T. Lovell, V. Rostovtsev, V. V. Fokin, K. B. Sharpless, L. Noodleman, unpublished results.
- [19] M. P. Doyle, M. A. McKevey, T. Ye in *Modern Catalytic Methods for Organic Synthesis with Diazo Compounds*, Wiley, New York, **1997**, pp. 163–248.
- [20] The reaction proceeded equally well even in human plasma (protein loading 65–85 mg mL⁻¹, C_{azide} = C_{alkyne} = 5 mM; C_{Cu⁺} = 100 μM), which indicates that the copper species remained available for the catalysis despite being heavily bound to plasma proteins.

Electronic and Steric Effects on Catalysts for CO₂/Epoxide Polymerization: Subtle Modifications Resulting in Superior Activities**



David R. Moore, Ming Cheng, Emil B. Lobkovsky, and Geoffrey W. Coates*

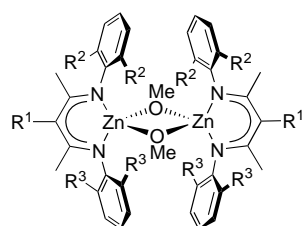
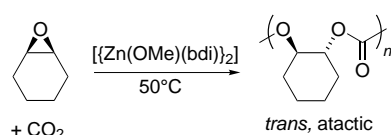
Carbon dioxide is an attractive chemical feedstock. In addition to the fact that CO₂ is an inexpensive substance of practically inexhaustible supply, it is also nonflammable and exhibits low toxicity.^[1–3] Since CO₂ is believed to contribute significantly to global warming, its removal from the atmosphere has added environmental benefits. Consequently, the alternating copolymerization of carbon dioxide with epoxides to aliphatic polycarbonates has been a topic of increasing

[*] Prof. G. W. Coates, D. R. Moore, M. Cheng, E. B. Lobkovsky
Department of Chemistry and Chemical Biology
Baker Laboratory, Cornell University
Ithaca, NY 14853-1301 (USA)
Fax: (+1) 607-255-4137
E-mail: gc39@cornell.edu

[**] This work was generously supported by the NSF (Career Award CHE-9875261). We thank the Cornell University Center for Biotechnology and Eastman Chemicals for partial support of this research. This work made use of the Cornell Center for Materials Research Shared Experimental Facilities, supported through the NSF Materials Research Science and Engineering Centers program (DMR-0079992). G.W.C. gratefully acknowledges a Packard Foundation Fellowship in Science and Engineering, an Alfred P. Sloan Research Fellowship, an Arnold and Mabel Beckman Foundation Young Investigator Award, and a Camille Dreyfus Teacher-Scholar Award. D.R.M. is grateful for a Corning Foundation Science Fellowship.

interest over the past decade.^[4] Not only do these polymers exhibit interesting material properties, but they have the additional environmental advantage that they biodegrade under composting conditions.^[5, 6] Thus the development of efficient and versatile catalysts that can enchain CO₂ with a range of epoxides remains a significant scientific goal.

In 1969, Inoue first reported that ZnEt₂/H₂O mixtures catalyzed the copolymerization of propylene oxide and CO₂.^[7] Although these original catalysts exhibited extremely low activities, requiring days to make appreciable amounts of polymer, they represent a truly remarkable achievement in the field of CO₂ utilization. Detailed information of the active species is not available owing to the heterogeneous nature of the catalyst, but propagation sites are generally thought to consist of zinc alkoxide and carbonate propagating species. In the ensuing two decades, a substantial amount of work was reported regarding the development of related heterogeneous catalyst mixtures for epoxide/CO₂ polymerization.^[4, 8, 9] In the past decade, significantly improved catalysts for cyclohexene oxide (CHO)/CO₂ copolymerization were reported, including chromium porphyrins,^[10–12] discrete zinc phenoxides,^[13–17] and ZnO/fluorinated carboxylic acids.^[18] We recently discovered β -diiminate zinc alkoxides ([{Zn(OMe)(bdi)}₂]; Scheme 1), as



	R ¹	R ²	R ³
[{Zn(OMe)(bdi-1)} ₂]	H	Et	Et
[{Zn(OMe)(bdi-2)} ₂]	CN	Et	Et
[{Zn(OMe)(bdi-3)} ₂]	CN	Et	<i>i</i> Pr
[{Zn(OMe)(bdi-4)} ₂]	CN	Me	<i>i</i> Pr

Scheme 1. Epoxide/CO₂ copolymerization with [{Zn(OMe)(bdi)}₂] catalysts.

well as zinc carboxylates, that exhibit unprecedented rates for CHO/CO₂ polymerization under mild reaction conditions.^[19, 20] In addition, these were the first catalysts reported for the living synthesis of high molecular weight polymers from epoxides and CO₂. Subsequent work centered on the development of chiral imine/oxazoline ligated complexes for the enantioselective copolymerization of epoxides with CO₂.^[21] One of the key design features of these complexes is a permanent ligand set that remains bound to the active zinc center throughout the polymerization and thus improves its catalytic behavior.

Mechanistic studies involving [{Zn(OR)(bdi)}₂] complexes revealed that subtle ligand modifications led to dramatic differences in catalytic activity. For example, the 2,6-substituents of the aryl group have a profound effect on activity; small methyl and large *n*-propyl groups result in inactivity, while ethyl and isopropyl groups result in excellent activity.^[20] Preliminary kinetic studies have revealed that the polymerizations are second order in [Zn(OR)(bdi)] which suggests a bimetallic enchainment of monomer. Therefore, we interpret the inactivity of complexes bearing *ortho*-methyl groups to result from a strongly bound dimer, while the inactivity of complexes bearing *ortho*-*n*-propyl groups stems from the high energy of the bimetallic transition state required for enchainment. Given the fact that extremely subtle steric effects produced such dramatically different catalytic activities, we embarked on the investigation of unsymmetrically substituted complexes in search of improved activities. In addition, we sought to understand the effect of electronic perturbation of the ligand on polymerization rate.^[22, 23] Herein, we report a significantly improved class of single-site catalysts for CHO/CO₂ polymerization as a result of these studies.

Under the premise that a more electron-deficient zinc center would increase the reaction rate due to more efficient epoxide coordination, we investigated the addition of an electron-withdrawing cyano group to the β -diiminate ligand (Scheme 1). Ligand (bdi-2)H was synthesized by the deprotonation of (bdi-1)H followed by reaction with *p*-toluenesulfonylcyanide.^[24] The complexes [{Zn(μ -OMe)(bdi-1)}₂]^[20] and [{Zn(μ -OMe)(bdi-2)}₂] were made by reaction of the ligand with ZnEt₂ followed by reaction with methanol.^[25] In Table 1, we report the data for alternating copolymerization of CHO and CO₂ with [{Zn(μ -OMe)(bdi)}₂], with ligands (bdi-1)H and (bdi-2)H. Reactions were

Table 1. Combined ligand effects on CHO/CO₂ copolymerization.^[a]

Complex	<i>t</i> [min]	CO ₂ pressure [psi/MPa]	TON ^[b]	TOF ^[c] [h ⁻¹]	<i>g</i> _{poly} <i>g</i> _M ⁻¹ [h ⁻¹]	Carbonate linkages [%] ^[d]	<i>M</i> _n [kg mol ⁻¹] ^[e]	<i>M</i> _w / <i>M</i> _n ^[e]
[{Zn(μ -OMe)(bdi-1)} ₂]	120	100/0.69	478	239	518	96	23.7	1.14
[{Zn(μ -OMe)(bdi-2)} ₂]	10	100/0.69	282	1690	3670	93	17.8	1.08
[{Zn(μ -OMe)(bdi-3)} ₂]	10	100/0.69	362	2170	4710	89	22.8	1.11
[{Zn(μ -OMe)(bdi-4)} ₂]	10	100/0.69	382	2290	4980	90	22.9	1.09
[CrCl(tfpp)]/DMAP ^[f]	1080	3300/23	3120	173	472	97	3.9	1.16
[Zn(O-2,6-F ₂ C ₆ H ₃) ₂ ·THF] ₂ ^[g]	2880	800/5.5	365	8	17	> 99	42.0	6.0
HO ₂ CCH=CHCO ₂ (CH ₂) ₂ C ₆ F ₁₃ /ZnO ^[h]	1440	2000/14	216	4	9	93	17.0	6.4

[a] All of the [{Zn(μ -OMe)(bdi)}₂] polymerizations were performed in neat cyclohexene oxide with [monomer]/[Zn] = 1000 at 50 °C. [b] Turnover number; moles of CHO consumed per mole of metal. [c] Turnover frequency; moles of CHO consumed per mole of metal per hour. [d] Calculated by integration of methine resonances in the ¹H NMR spectrum of polymer (CDCl₃, 300 MHz). [e] Determined by gel permeation chromatography, calibrated with polystyrene standards in tetrahydrofuran. [f] tfpp = tetrafluorophenylporphyrin, DMAP = 4-dimethylaminopyridine; data from ref. [11] (*T* = 110 °C). [g] Data from ref. [16] (*T* = 80 °C). [h] Data from ref. [18] (*T* = 100 °C).

run to moderate conversions ($\approx 40\%$) in neat epoxide to emphasize differences in reactivity, although reactions in THF and toluene at longer reaction times proceed to near quantitative conversion. $[\{\text{Zn}(\mu\text{-OMe})(\text{bdi-1})\}_2]$ is an adequate catalyst over the course of 2 hours and produces monodisperse carbonate polymer with a turnover frequency of 239 h^{-1} . In a short 10-minute reaction, $[\{\text{Zn}(\mu\text{-OMe})(\text{bdi-1})\}_2]$ produces only a trace amount of polymer. In contrast, $[\{\text{Zn}(\mu\text{-OMe})(\text{bdi-2})\}_2]$ exhibits substantially higher activity for the polymerization, with a turnover frequency of 1690 h^{-1} . Although the polymer is still monodisperse, the percentage of carbonate linkages is slightly lower (93%).

During our prior copolymerization studies of CHO and CO_2 , we found that the $[\{\text{Zn}(\text{OMe})(\text{bdi})\}_2]$ complex containing 2-ethyl-6-isopropylphenyl groups exhibits superior activity to those with either 2,6-diisopropylphenyl or 2,6-diethylphenyl groups.^[20] We therefore believed that further modification of the ligand geometry could provide an optimal active site for monomer enchainment to result in dramatically improved activities. To probe this we decided to synthesize complexes with ligands bearing different aryl groups. Unsymmetrical ligands were synthesized by refluxing two different anilines (one equivalent of each) plus one equivalent of 2,4-pentanedione in acidic ethanol. Isolation of the unsymmetrical ligands was accomplished through repeated crystallization from ethanol. Cyanation of the ligands and complex synthesis was performed as previously described to give the complexes $[\{\text{Zn}(\mu\text{-OMe})(\text{bdi-3})\}_2]$ and $[\{\text{Zn}(\mu\text{-OMe})(\text{bdi-4})\}_2]$ in 25% and 18% yield, respectively (Scheme 1). The unsymmetrical ligand allows for two potential dimeric complex structures, where the diisopropylphenyl substituents are either *syn* or *anti* to each other. A steric argument would suggest the molecules would rather crystallize to alleviate unnecessary repulsions. A single-crystal X-ray diffraction study^[26] was performed on $[\{\text{Zn}(\mu\text{-OMe})(\text{bdi-4})\}_2]$ and interestingly, the dimeric zinc methoxide aligns the more bulky isopropyl groups adjacent to one another causing minor distortion of the dimer versus symmetrical complexes (Figure 1). The Zn–Zn separation is

2.98 \AA , and each zinc atom adopts a distorted tetrahedral geometry. The six-membered chelate is fairly planar (a slight boat-shaped conformation is achieved) with a Zn deviation of 0.64 \AA from the plane defined by N(1)–N(2)–C(4). The Zn–O bond lengths are 1.94 and 1.98 \AA , and the bond angles of N(1)–Zn(1)–N(2) and O(1)–Zn(1)–O(1A) are 94.19° and 80.89° , respectively. It is unclear why $[\{\text{Zn}(\text{OMe})(\text{bdi-4})\}_2]$ dimerizes and then crystallizes in this fashion, although ^1H NMR spectra of both $[\{\text{Zn}(\mu\text{-OMe})(\text{bdi-3})\}_2]$ and $[\{\text{Zn}(\mu\text{-OMe})(\text{bdi-4})\}_2]$ show a mixture of the two dimeric structures in C_6D_6 solution. We therefore propose that the sterically disfavored dimeric structure is merely more crystalline.

To the best of our knowledge, $[\{\text{Zn}(\mu\text{-OMe})(\text{bdi-3})\}_2]$ and $[\{\text{Zn}(\mu\text{-OMe})(\text{bdi-4})\}_2]$ exhibit the highest reported activity for CHO/ CO_2 copolymerization. Table 1 gives polymerization data for these compounds, as well as literature data for competing catalysts. At 50°C and 100 psi (0.69 MPa) of CO_2 the catalysts exhibit turnover frequencies of 2170 and 2290 h^{-1} . The polymers produced are nearly identical with $\approx 90\%$ carbonate linkages, $M_n = 23000\text{ Da}$, and molecular weight distributions of ≈ 1.1 . Despite the small presence of polyether linkages, these complexes are inactive for the homopolymerization of CHO over one day. We are currently investigating the mechanistic issues as to why polyether linkages are observed, while CHO homopolymer is not synthesized.

In conclusion, we have systematically improved the activity of β -diiminate zinc methoxide complexes for CHO/ CO_2 copolymerization. $[\{\text{Zn}(\mu\text{-OMe})(\text{bdi-4})\}_2]$ exhibits the highest reported activity for this reaction. In addition, these complexes offer new opportunities for control of molecular weights and block copolymer synthesis owing to the living nature of the copolymerizations. The well-defined nature of the complexes provides excellent opportunities to probe the mechanism of the polymerization steps in detail, and these studies are currently underway. Work is also centered on employing these catalysts for the polymerization of new classes of epoxides with CO_2 , as well as other monomers.

Received: March 4, 2002 [Z18816]

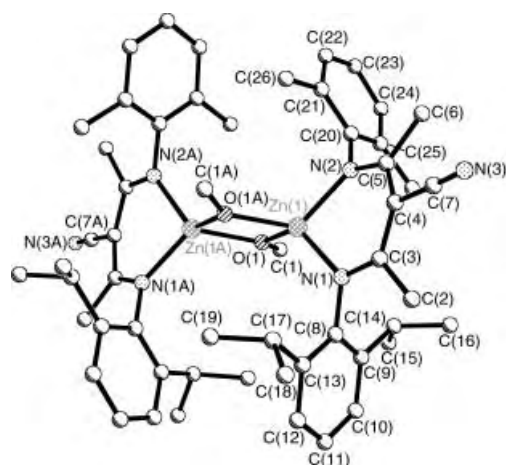


Figure 1. X-ray crystal structure of $[\{\text{Zn}(\mu\text{-OMe})(\text{bdi-4})\}_2]$. Selected bond lengths [\AA] and bond angles [$^\circ$]: Zn(1)–N(1) $2.003(2)$, Zn(1)–N(2) $1.997(2)$, Zn(1)–O(1) $1.9427(17)$, Zn(1)–O(1A) $1.9780(17)$, O(1)–C(1) $1.408(3)$; O(1)–Zn(1)–O(1A) $80.89(7)$, N(1)–Zn(1)–N(2) $94.19(8)$, N(1)–Zn(1)–O(1A) $116.38(8)$, N(2)–Zn(1)–O(1) $119.85(8)$, Zn(1)–O(1)–Zn(1A) $99.11(7)$, C(1)–O(1)–Zn(1) $131.5(2)$, C(1)–O(1)–Zn(1A) $128.2(2)$.

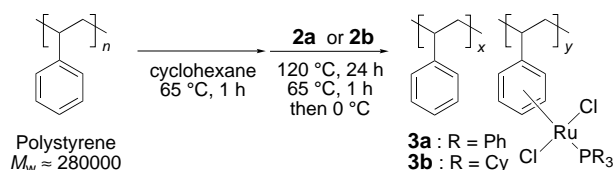
- [1] H. Arakawa, M. Aresta, J. N. Armor, M. A. Barteau, E. J. Beckman, A. T. Bell, J. E. Bercaw, C. Creutz, E. Dinjus, D. A. Dixon, K. Domen, D. L. DuBois, J. Eckert, E. Fujita, D. H. Gibson, W. A. Goddard, D. W. Goodman, J. Keller, G. J. Kubas, H. H. Kung, J. E. Lyons, L. E. Manzer, T. J. Marks, K. Morokuma, K. M. Nicholas, R. Periana, L. Que, J. Rostrup-Nielsen, W. M. H. Sachtler, L. D. Schmidt, A. Sen, G. A. Somorjai, P. C. Stair, B. R. Stults, W. Tumas, *Chem. Rev.* **2001**, *101*, 953–996.
- [2] W. Leitner, *Angew. Chem.* **1995**, *107*, 2391–2405; *Angew. Chem. Int. Ed. Engl.* **1995**, *34*, 2207–2221.
- [3] W. Leitner, *Coord. Chem. Rev.* **1996**, *153*, 257–284.
- [4] For reviews on epoxide/ CO_2 copolymerizations, see: a) D. J. Darensbourg, M. W. Holtcamp, *Coord. Chem. Rev.* **1996**, *153*, 155–174; b) M. S. Super, E. J. Beckman, *Trends Polym. Sci.* **1997**, *5*, 236–240; c) A. Rokicki, W. Kuran, *J. Macromol. Sci. Rev. Macromol. Chem. Phys.* **1981**, *C21*, 135–186.
- [5] M. Okada, *Prog. Polym. Sci.* **2002**, *27*, 87–133.
- [6] S. Y. Yang, X. G. Fang, L. B. Chen, *Polym. Adv. Technol.* **1996**, *7*, 605–608.
- [7] S. Inoue, H. Koinuma, T. Tsuruta, *J. Polym. Sci. Part B: Polym. Lett.* **1969**, *7*, 287–292.

- [8] M. Ree, J. Y. Bae, J. H. Jung, T. J. Shin, *J. Polym. Sci. Part A: Polym. Chem.* **1999**, 37, 1863–1876.
- [9] L. B. Chen, *Macromol. Symp.* **1992**, 59, 75–82.
- [10] W. J. Kruper, D. V. Dellar, *J. Org. Chem.* **1995**, 60, 725–727.
- [11] S. Mang, A. I. Cooper, M. E. Colclough, N. Chauhan, A. B. Holmes, *Macromolecules* **2000**, 33, 303–308.
- [12] L. M. Stamp, S. A. Mang, A. B. Holmes, K. A. Knights, Y. R. de Miguel, I. F. McConvey, *Chem. Commun.* **2001**, 2502–2503.
- [13] D. J. Darensbourg, M. W. Holtcamp, *Macromolecules* **1995**, 28, 7577–7579.
- [14] D. J. Darensbourg, S. A. Niezgoda, J. D. Draper, J. H. Reibenspies, *J. Am. Chem. Soc.* **1998**, 120, 4690–4698.
- [15] D. J. Darensbourg, M. W. Holtcamp, G. E. Struck, M. S. Zimmer, S. A. Niezgoda, P. Rainey, J. B. Robertson, J. D. Draper, J. H. Reibenspies, *J. Am. Chem. Soc.* **1999**, 121, 107–116.
- [16] D. J. Darensbourg, J. R. Wildeson, J. C. Yarbrough, J. H. Reibenspies, *J. Am. Chem. Soc.* **2000**, 122, 12487–12496.
- [17] M. B. Dinger, M. J. Scott, *Inorg. Chem.* **2001**, 40, 1029–1036.
- [18] M. S. Super, E. Berluche, C. Costello, E. J. Beckman, *Macromolecules* **1997**, 30, 368–372.
- [19] M. Cheng, E. B. Lobkovsky, G. W. Coates, *J. Am. Chem. Soc.* **1998**, 120, 11018–11019.
- [20] M. Cheng, D. R. Moore, J. J. Reczek, B. M. Chamberlain, E. B. Lobkovsky, G. W. Coates, *J. Am. Chem. Soc.* **2001**, 123, 8738–8749.
- [21] M. Cheng, N. A. Darling, E. B. Lobkovsky, G. W. Coates, *Chem. Commun.* **2000**, 2007–2008. For a prior system, see: K. Nozaki, K. Nakano, T. Hiyama, *J. Am. Chem. Soc.* **1999**, 121, 11008–11009.
- [22] G. W. Coates, M. Cheng, PCT Int. Appl. WO 2000008088, **2000** [*Chem. Abstr.* **2000**, 132, 152332].
- [23] M. Cheng, Ph. D. Thesis, Cornell University, August 2000.
- [24] E. J. Corey, Z. Wang, *Tetrahedron Lett.* **1993**, 34, 4001–4004.
- [25] The syntheses and detailed characterization of complexes reported in this paper will be reported separately (manuscript in preparation).
- [26] CCDC 180471 ([Zn(μ -OMe)(bdi-4)]₂) contains the supplementary crystallographic data for this paper. These data can be obtained free of charge via www.ccdc.cam.ac.uk/conts/retrieving.html (or from the Cambridge Crystallographic Data Centre, 12, Union Road, Cambridge CB21EZ, UK; fax: (+44) 1223-336-033; or deposit@ccdc.cam.ac.uk).

arene–ruthenium complexes are air- and moisture-sensitive, expensive, and cannot be recovered in many cases, immobilized catalysts are expected to solve these problems. Although several polymer-supported ruthenium complexes have been reported,^[7] however, these are not without problems, such as tedious procedures for the preparation of the complexes, low activity compared with the original catalysts, and difficulty of applying the catalysts to other reactions. Therefore, development of more versatile polymer-supported ruthenium complexes is strongly demanded. Herein, we describe a novel polymer-supported arene–ruthenium complex that is recovered quantitatively and reused for ring-closing olefin metathesis and other reactions.

Our idea is to utilize the benzene rings of polystyrene as ligands to immobilize arene–metal complexes. However, it is known that arene-displacement reactions at Ru^{II} centers are often sluggish.^[8] Thus, we carefully chose [$\text{Ru}(\eta^6\text{-C}_6\text{H}_5\text{CO}_2\text{Et})\text{Cl}_2$]₂ (**1**) as the starting material, because it was reported that an intramolecular arene exchange proceeded in good yield using **1** instead of [$\text{Ru}(\eta^6\text{-p-cymene})\text{Cl}_2$]₂.^[9] Dimer **1** was easily prepared according to the literature procedure,^[8, 9] and treatment of **1** with triphenylphosphane or tricyclohexylphosphane gave [$\text{Ru}(\eta^6\text{-C}_6\text{H}_5\text{CO}_2\text{Et})(\text{PR}_3)_2\text{Cl}$] (**2a**: R = Ph, **2b**: R = Cy) quantitatively.

Preparation of the polymer-supported arene–ruthenium complexes using **2** was successfully performed based on a procedure which is similar in part to that of formation of microcapsules (Scheme 1).^[10, 11] All other methods we tested



Scheme 1. Synthesis of polymer-supported [(arene)RuCl₂(PR₃)] (**3**).



A Novel Polymer-Supported Arene–Ruthenium Complex for Ring-Closing Olefin Metathesis**

Ryo Akiyama and Shū Kobayashi*

Arene–ruthenium complexes are very useful precatalysts for several organic reactions, such as transfer hydrogenation,^[1] Diels–Alder reaction,^[2] olefin cyclopropanation,^[3] enol formate formation,^[4] cyclization of dienylalkyne,^[5] and olefin metathesis.^[6] While the catalysts prepared from the

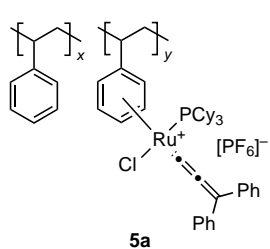
did not give satisfactory results. The structure of the polymer-supported arene–ruthenium complexes was confirmed by NMR spectroscopic analysis. We measured the ³¹P swollen-resin magic-angle spinning (SR-MAS) NMR spectra^[12] of the catalysts, and only one peak arising from PR₃ (**3a** R = Ph: δ = 25.7 ppm, **3b** R = Cy: δ = 28.5 ppm) coordinating to the ruthenium was observed.^[13] From these results, we concluded that the catalyst was supported as [(arene)RuCl₂(PR₃)] (polymer-supported [(arene)RuCl₂(PR₃)] (**3**; PS-RuCl₂(PR₃))). To our knowledge, this is the first example of a polymer-supported ruthenium catalyst, in which the benzene rings of the polymer coordinated to the ruthenium to immobilize the catalyst onto the polymer.

PS-RuCl₂(PR₃) was used in the ring-closing olefin metathesis (RCM). We prepared a polymer-supported cationic ruthenium–allenylidene complex according to the Dixneuf and Fürstner method.^[6b,c] PS-RuCl₂(PPh₃) (**3a**), tricyclohexylphosphane (PCy₃), 1,1-diphenyl-2-propynol (**4**), and sodium hexafluorophosphate (NaPF₆) were mixed in several solvents, and the mixture was stirred for 1 h under reflux. Signals of the

[*] Prof. Dr. S. Kobayashi, R. Akiyama
Graduate School of Pharmaceutical Sciences
The University of Tokyo
CREST, Japan Science and Technology Corporation (JST)
Hongo, Bunkyo-ku, Tokyo 113-0033, (Japan)
Fax: (+81) 3-568-40634
E-mail: skobayas@mol.f.u-tokyo.ac.jp

[**] This work was partially supported by a Grant-in-Aid for Scientific Research from the Japan Society of the Promotion of Science (JSPS). R.A. thanks the JSPS fellowship for Japanese Junior Scientist.

Supporting information for this article is available on the WWW under <http://www.angewandte.org> or from the author.



^{31}P SR-MAS NMR spectra of the activated ruthenium catalyst (**5a**) thus prepared were observed at 50.8 and -144.0 ppm.^[14] We then tested **5a** in the RCM of *N,N*-diallyl-*p*-toluenesulfonamide (**6**) in hexane (Table 1). It was found that the choice of solvents was

crucial. While the desired product was obtained in good yield in the first run in *i*PrOH:hexane (1:1), the activity of the catalyst decreased significantly in the second and third runs

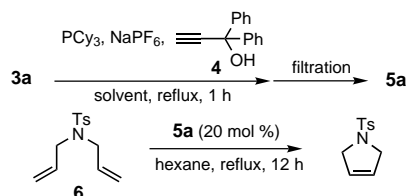


Table 1. Effect of solvents in the preparation of the active catalyst.

Entry	Solvent	Yield [%] (Recovery [%])		
		1st	2nd	3rd
1	<i>i</i> PrOH	8 (quant)	9 (quant)	—
2	<i>i</i> PrOH:hexane (1:1)	78 (quant)	48 (quant)	16 (quant)
3	<i>i</i> PrOH:hexane (1:10)	42 (quant)	69 (quant)	71 (quant)
4	<i>i</i> PrOH:hexane (1:10) ^[a]	49 (98)	72 (quant)	77 (quant)

[a] **3b** was used instead of **3a**.

(entry 2). On the other hand, the yield of the desired product was very low in *i*PrOH (entry 1). In *i*PrOH:hexane (1:10), moderate yields were obtained. The activity of the catalyst was maintained even after the third use (entries 3 and 4).^[15]

To increase the yields, we examined the reactivation conditions of the recovered catalysts in RCM reactions (Table 2). After careful investigation, the best results were obtained when a mixture of the recovered catalyst, PCy_3 , and **4** was stirred for 1 h under reflux and, after addition of NaPF_6 ,

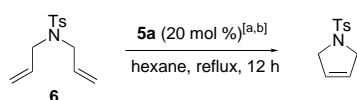


Table 2. Reactivation conditions of the catalyst.

Entry	Method (Conditions)		Yield [%]		
			1st	2nd	3rd
1	A	(PCy ₃ , 4 , reflux, 1 h)	40	72	77
2	B	(PCy ₃ , NaPF ₆ , 4 , RT, 12 h)	63	56	49
3	C	(PCy ₃ , 4 reflux, 1 h then NaPF ₆ , RT, 12 h)	69	73	85
4 ^[c]	C		75	81	98 ^[f]
5 ^[c,d]	C		71	85	88
6 ^[c,e]	C		97	18	12
7 ^[c,g]			80		

[a] Catalyst **5a** was reactivated under method A–C in *i*PrOH:hexane (1:10). [b] Recovery of catalysts was quantitative. [c] Hexane:toluene (10:1) was used as a solvent in RCM. [d] 10 mol % of **5a** were used. [e] 5 mol % of **5a** were used. [f] 4th; 83 % (recovery: quant), 5th; 82 % (recovery: quant), 6th; 89 % (recovery: quant), 7th; 92 % (recovery: quant). [g] [*p*-cymene] $\text{RuCl}(\text{PCy}_3)(\text{C}=\text{C}=\text{CPh}_2)^+[\text{PF}_6]^-$ was used instead of **5a**.

further stirred for 12 h at room temperature (method C). We tested several other examples of the PS–Ru-catalyzed RCM of olefins (Table 3).^[11] Six-membered rings as well as five-membered rings were smoothly formed under these conditions, while sterically hindered diethyl diallylmalonate was less reactive (entry 4). Recovery of the catalyst was quanti-

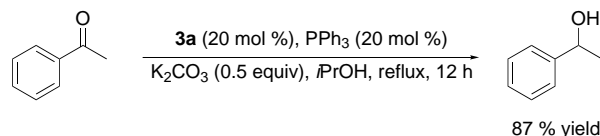
Table 3. Ring-closing olefin metathesis using **5a**.^[a]

Entry	Substrate	Product	Yield [%]
1			98
2			92
3			57 ^[b]
4			72
5			66
6			82

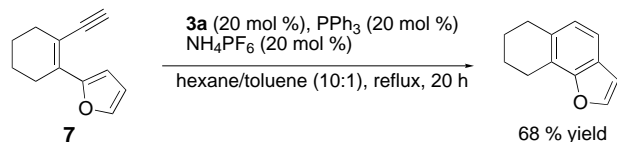
[a] All reactions were carried out using **5a** (20 mol %) in hexane:toluene (10:1) under reflux conditions for 12 h; Ts = tosyl [b] Reaction was carried out for 24 h.

tative in all cases, and the recovered catalyst could be reused without loss of activity. In addition, the structure of the recovered catalyst was confirmed by ^{31}P SR-MAS NMR spectroscopic analysis. Signals were observed at 50.8 and -144.0 ppm, which are consistent with those of the original catalyst **5a**.

Catalyst **3a** was successfully used in other reactions. Acetophenone was reduced smoothly in the presence of **3a** to afford the corresponding alcohol in high yield (Scheme 2). In addition, **3a** catalyzed the cyclization of the dienylalkyne **7** in good yield (Scheme 3).



Scheme 2. Hydrogenation of acetophenone using **3a**.



Scheme 3. Cyclization of dienylalkyne using **3a**.

In summary, we have accomplished the first immobilization of arene–ruthenium complexes onto the benzene rings of polystyrene. The polymer-supported catalyst (PS– RuCl_2 –

(PPh₃) has been successfully used in RCM and other ruthenium(II)-catalyzed reactions. In all cases, the reactions proceeded in high yields, and the catalyst was recovered quantitatively by simple filtration and reused. Further investigation to apply P,S-RuCl₂(PPh₃) to other ruthenium(II)-catalyzed reactions is now in progress.

Received: March 11, 2002 [Z18867]

- [1] a) S. Hashiguchi, A. Fujii, J. Takehara, T. Ikariya, R. Noyori, *J. Am. Chem. Soc.* **1995**, *117*, 7562; b) R. Noyori, S. Hashiguchi, *Acc. Chem. Res.* **1997**, *30*, 97; c) Y. Jiang, Q. Jiang, X. J. Zhang, *J. Am. Chem. Soc.* **1998**, *120*, 3817.
- [2] a) D. L. Davies, J. Fawcett, S. A. Garratt, D. A. Russell, *Chem. Commun.* **1997**, 1352; b) D. Carmona, C. Cativiela, S. Elipse, F. J. Lahoz, M. P. Lamata, M. P. L.-R. Víu, L. A. Oro, C. Vega, F. Viguri, *Chem. Commun.* **1997**, 2352.
- [3] a) F. Simal, A. Demonceau, A. F. Noels, *Tetrahedron Lett.* **1998**, *39*, 3493; b) F. Simal, J. Dominique, A. Demonceau, A. F. Noels, *Tetrahedron Lett.* **1999**, *40*, 1653.
- [4] M. Neveaux, C. Bruneau, P. H. Dixneuf, *J. Chem. Soc. Perkin Trans. 1* **1991**, 1197.
- [5] A. M. Craig, E. P. Malinda, *J. Am. Chem. Soc.* **1996**, *118*, 11319.
- [6] For ring-closing olefin metathesis see: a) E. L. Dias, R. H. Grubbs, *Organometallics* **1998**, *17*, 2758; b) A. Fürstner, M. Picquet, C. Bruneau, P. H. Dixneuf, *Chem. Commun.* **1998**, 1315; c) A. Fürstner, M. Liebl, C. W. Lehmann, M. Picquet, R. Kunz, C. Bruneau, D. Touchard, P. H. Dixneuf, *Chem. Eur. J.* **2000**, *6*, 1847; For ring-opening metathesis polymerization see: d) A. Hafner, A. Mühlebach, P. A. van der Schaaf, *Angew. Chem.* **1997**, *109*, 2213; *Angew. Chem. Int. Ed. Engl.* **1997**, *36*, 2121; e) A. Demonceau, A. W. Stumpf, E. Saive, A. F. Noels, *Macromolecules* **1997**, *30*, 3127.
- [7] For ring-closing olefin metathesis see: a) M. Ahmed, A. G. M. Barrett, D. C. Braddock, S. M. Cramp, P. A. Procopiou, *Tetrahedron Lett.* **1999**, *40*, 8657; b) Q. Yao, *Angew. Chem.* **2000**, *112*, 4060; *Angew. Chem. Int. Ed.* **2000**, *39*, 3896; c) S. C. Schürer, S. Gessler, N. Buschmann, S. Blechert, *Angew. Chem.* **2000**, *112*, 4060; *Angew. Chem. Int. Ed.* **2000**, *39*, 3898; d) J. S. Kingsbury, S. B. Garber, J. M. Giftos, B. L. Gray, M. M. Okamoto, R. A. Farrer, J. T. Fourkas, A. H. Hoveyda, *Angew. Chem.* **2001**, *113*, 4381; *Angew. Chem. Int. Ed.* **2001**, *40*, 4251; For asymmetric hydrogenation see: e) Q. H. Fan, C. Y. Ren, C. H. Yeung, W. H. Hu, A. S. C. Chan, *J. Am. Chem. Soc.* **1999**, *121*, 7407; f) T. Ohkuma, H. Takeno, R. Noyori, *Adv. Synth. Catal.* **2001**, *343*, 369; g) Q. H. Fan, G. J. Deng, C. C. Lin, A. S. C. Chan, *Tetrahedron: Asymmetry* **2001**, *12*, 1241; For other reactions see: h) N. E. Leadbeater, K. A. Scott, L. J. Scott, *J. Org. Chem.* **2000**, *65*, 3231; i) N. E. Leadbeater, *J. Org. Chem.* **2001**, *66*, 2168.
- [8] M. A. Bennett, A. K. Smith, *J. Chem. Soc. Dalton Trans.* **1974**, 233.
- [9] B. Therrien, T. R. Ward, M. Pilkington, C. Hoffmann, F. Gilardoni, J. Weber, *Organometallics* **1998**, *17*, 330.
- [10] a) M. Donbrow, *Microcapsules and Nanoparticles in Medicine and Pharmacy*, CRC Press, Boca Raton, **1992**; b) S. Kobayashi, S. Nagayama, *J. Am. Chem. Soc.* **1998**, *120*, 2985; c) S. Nagayama, M. Endo, S. Kobayashi, *J. Org. Chem.* **1998**, *63*, 6094; d) S. Kobayashi, M. Endo, S. Nagayama, *J. Am. Chem. Soc.* **1999**, *121*, 11229; e) S. Kobayashi, T. Ishida, R. Akiyama, *Org. Lett.* **2001**, *3*, 2649; f) R. Akiyama, S. Kobayashi, *Angew. Chem.* **2001**, *113*, 3575; *Angew. Chem. Int. Ed.* **2001**, *40*, 3469.
- [11] Experimental details are shown in Supporting Information.
- [12] The usefulness of the SR-MAS NMR technique for structure determination of resins directly, without cleavage from polymer supports has been demonstrated through the development of several useful reactions using the cross-linked polystyrene-based resins in the solid-phase in our laboratories. a) S. Kobayashi, R. Akiyama, T. Furuta, M. Moriwaki, *Molecules Online* **1998**, *2*, 35; b) S. Kobayashi, R. Akiyama, H. Kitagawa, *J. Comb. Chem.* **2000**, *3*, 196, and references therein. See also ref. [10e] and [10f].

- [13] We prepared [Ru(η^6 -*p*-cymene)(PPh₃)Cl₂] and measured ³¹P NMR spectrum of this complex (δ = 23.1 ppm); [Ru(η^6 -*p*-cymene)(P-Cy₃)Cl₂] δ = 26.0 ppm.^[6c]
- [14] ³¹P SR-MAS NMR (CDCl₃): 50.8 (PCy₃), –144.0 ppm (PF₆[–]). Solid PPh₃ (δ = –8.4 ppm) was used as an external standard. ³¹P NMR of monomeric ruthenium complex was measured in ref. [6c]. ³¹P NMR (CDCl₃): 58.8 (PCy₃), –140.8 ppm (PF₆[–]). See also A. Fürstner, O. Guth, A. Düffels, G. Seidel, M. Liebl, B. Gabor, R. Mynott, *Chem. Eur. J.* **2001**, *7*, 4811.
- [15] That no leaching of ruthenium metal occurred was confirmed by fluorescence X-ray analysis.

(E)-4-Hydroxy-3-methylbut-2-enyl Diphosphate: An Intermediate in the Formation of Terpenoids in Plant Chromoplasts**

Wenyun Gao, Reik Loeser, Maja Raschke, Marco A. Dessoy, Michael Fulhorst, Henriette Alpermann, Ludger A. Wessjohann,* and Meinhard H. Zenk*

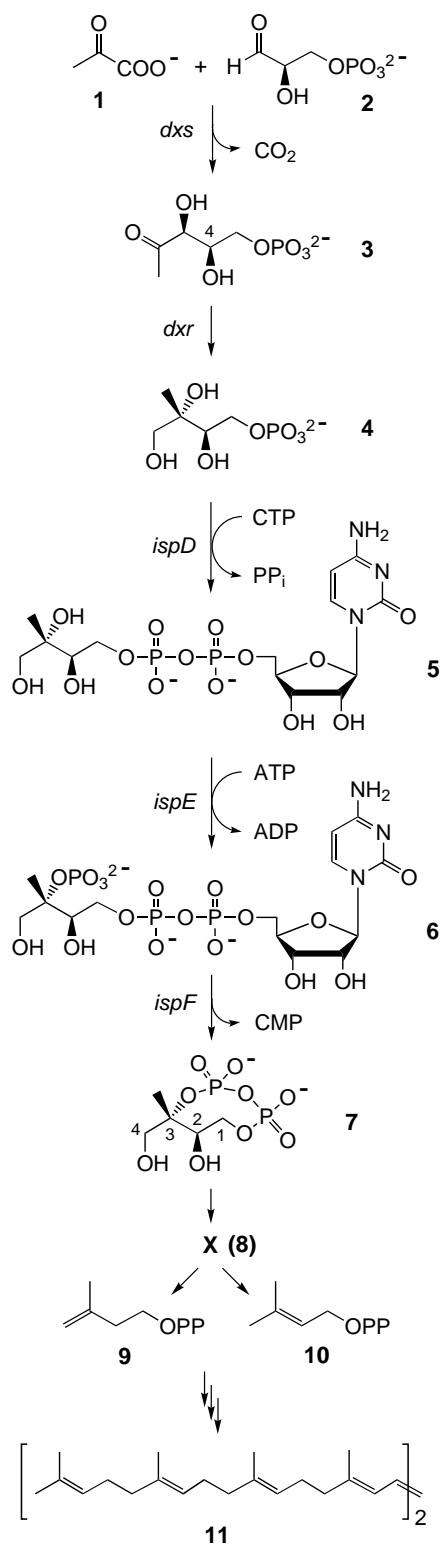
Nature's terpenoids, with over 35000 known members, constitute compounds that are either essential for life (namely, cholesterol, vitamins) or represent secondary products, such as chemical attractants, defense compounds, and antibiotics. Until recently, terpenoids were assumed to be formed exclusively by the mevalonate pathway.^[1] It has now been shown that an alternative metabolic route exists in plastids of higher plants and in the majority of bacteria. This pathway leads from pyruvate (**1**) and D-glyceraldehyde-3-phosphate (**2**) via 1-deoxy-D-xylulose phosphate (**3**, DXP, Scheme 1) and the intermediates **4**–**7** to the key metabolites isopentenyl diphosphate (**9**, IPP) and dimethylallyl diphosphate (**10**, DMAPP), which are essential to all organisms.^[2] The cyclic diphosphate **7** has been proven to be a precursor to **9** and **10** in the alternative pathway and thus to plastidic isoprenoids, mainly phytoene (**11**).^[3] This reaction involves a threefold, possibly stepwise, dehydroxylation at carbon atoms C-2, C-3, and C-4 of **7**.

On comparative phytochemical grounds, we postulated that (E)-4-hydroxy-3-methylbut-2-enyl diphosphate (**8**, Schemes 1 and 2) is a likely intermediate in the deoxyxylulose phosphate pathway between **7** and **9/10**.^[4] This hydroxylated hemiterpene is seen biogenetically in numerous plant-derived products, such as the plant hormone **13**, the glucoside of (E)-2-

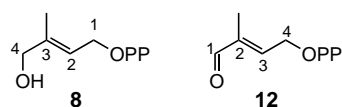
[*] Prof. Dr. L. A. Wessjohann, R. Loeser, M. A. Dessoy, M. Fulhorst
Institut für Pflanzenbiochemie
Weinberg 3, 06120 Halle/Saale (Germany)
Fax: (+49)345-5582-1309
E-mail: wessjohann@ipb-halle.de

Prof. Dr. M. H. Zenk, Dr. W. Gao, M. Raschke, H. Alpermann
Biozentrum, Universität Halle
Weinbergweg 22, 06120 Halle/Saale (Germany)
Fax: (+49)345-5527-301
E-mail: zenk@biozentrum.uni-halle.de

[**] This research was supported by Deutsche Forschungsgemeinschaft, Bonn. W.G. is supported by the Alexander von Humboldt-Foundation and M.A.D. by the German Academic Exchange Service (DAAD).

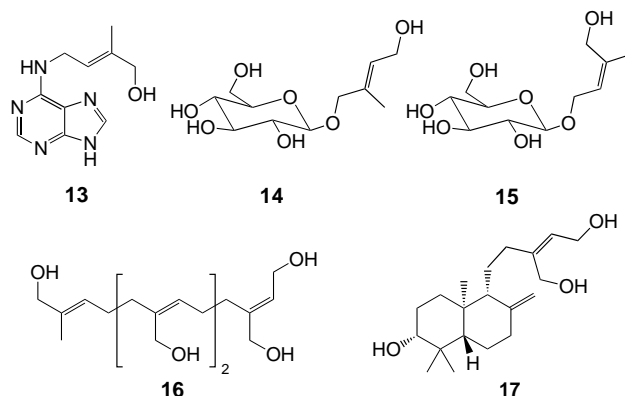


Scheme 1. Deoxyxylulose phosphate (DXP) pathway for the biosynthesis of terpenoids.



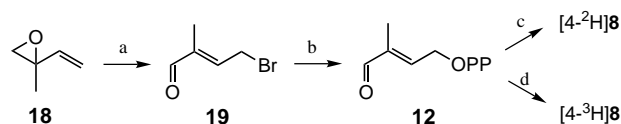
Scheme 2. Proposed late intermediates X (**8**) and **12** of the DXP-isoprenoid pathway.

methylbut-2-ene-1,4-diol(**14**), another glucoside of *Z* isomer **15**, and many other secondary plant products, such as **16** and **17** (Scheme 3).^[5]



Scheme 3. Natural products which may be (partially) derived from intermediate **8** or its IPP analogue.

To test the postulated intermediacy, the labeled diphosphates of **8** were synthesized from the new aldehyde **12** (Scheme 4), which itself is a postulated intermediate (see below). This strategy allowed the convenient introduction of



Scheme 4. Synthesis of **12**, [$4\text{-}^2\text{H}$]**8**, and [$4\text{-}^3\text{H}$]**8**. Reagents and conditions: a) CuBr_2 (2.1 equiv), Li_2CO_3 (1.4 equiv), $\text{CHCl}_3/\text{EtOAc}$ (1:1), 90°C , 20 min, 87%; b) $(n\text{Bu}_4\text{N})_2\text{H}_2\text{P}_2\text{O}_7$ (3 equiv), CH_3CN , 0 to 22°C , 2.5 h, ionic exchange (Na^+), 42% (the yield of **12**, which is obtained within solid sodium(hydrogen) carbonate buffer, was determined by quantitative ^{31}P NMR spectroscopy in NaHCO_3 -buffered water using phenylphosphonic acid as the internal standard); c) NaB^2H_4 (2 mol equiv), $\text{H}_2\text{O}/\text{MeOH}$ (2:1), RT, 2 h, 16%; d) NaB^3H_4 (0.5 mol equiv), $\text{H}_2\text{O}/\text{MeOH}$ (2:1), RT, 2 h, 19%.

tritium or deuterium as the last step in the synthesis. Aldehyde **12** was obtained in a two-step preparation starting from commercially available 2-methyl-2-vinyloxirane (**18**)^[6] following a modification of the method of Davisson et al.^[7] It should be noted that the usual counterion exchange of tetra-*n*-butylammonium to ammonium is not advisable in this case because ammonia addition to the enal moiety can occur. The target compound **8** was obtained as the [$4\text{-}^2\text{H}$]- or [$4\text{-}^3\text{H}$]-labeled form by reduction of **12** with NaB^2H_4 or NaB^3H_4 , respectively.

To test the postulated role of **8** as a biosynthetic intermediate between **7** and **9/10**, chromoplasts from *Narcissus pseudonarcissus* and *Capsicum annuum* were supplied with [$4\text{-}^3\text{H}$]**8** in the presence of a phosphatase inhibitor (NaF), an energy source (adenosine-5'-triphosphate (ATP)/ Mg^{2+}), and a reductant (the reduced form of nicotinamide adenine dinucleotide (NADPH)). The incubations were performed as previously published and terpenoids were isolated from the incubation mixture by extraction with ethyl acetate.^[3]

In the presence of chromoplasts, [4-³H]**8** is rapidly converted in the incubation mixture and radioactivity accumulates in the ethyl acetate phase (Table 1). 50% of the

Table 1. Conversion of [4-³H]**8** [nmol, from radioactivity] into ethyl acetate soluble material ("lipids") containing phytoene (**11**) by *N. pseudonarcissus* and *C. annuum* chromoplasts.^[a]

<i>t</i> [min]	<i>N. pseudonarcissus</i>		<i>C. annuum</i>	
	lipids	11	lipids	11
0	0	0	0	0
10	0.4	0.2	0.2	0.1
30	0.6	0.3	0.4	0.2
60	0.8	0.4	0.6	0.3
120	1.1	0.6	0.7	0.4
240	1.3	0.7	0.8	0.4

[a] Incubation mixture (total volume: 500 μ L): 2.6 μ M [4-³H]**8**, 100 mM tris(hydroxymethyl)aminomethane \cdot HCl (Tris \cdot HCl) buffer (pH 7.6), 2 mM MnCl₂, 10 mM MgCl₂, 5 mM NaF, 2 mM NADP⁺, 1 mM NADPH, 6 mM ATP, 2 mg chromoplast protein, 30 °C.

radioactivity in the ethyl acetate fraction was located in phytoene (**11**), which is the main metabolite synthesized from the more distant precursor **7**.^[3] The remaining 50% of the radioactivity from [4-³H]**8** in that fraction was found in various carotenoids. Phosphorylated intermediates other than **8**, **9**, and **10** were barely detected after HPLC analysis of the aqueous phase (for the HPLC conditions, see ref. [3]). The almost quantitative transformation of labeled **8** into plastidic terpenoids in these taxonomically separate plant species demonstrates for the first time the intermediacy of **8** in the terpenoid pathway in higher plants.

Short term (5–20 min) application of [¹⁴C]**7** to both chromoplast preparations resulted in the incorporation of this cyclic diphosphate into terpenoids,^[3] but upon HPLC analysis of the aqueous phase, radioactivity was clearly seen to transiently accumulate in an intermediate (up to 25% of the total supplied [¹⁴C]**7**) in both the *Narcissus* and *Capsicum* chromoplasts (Figure 1). Phosphatase or chemical hydrolysis^[8] of this labeled compound yielded an allylic alcohol, which corresponded to synthetic (*E*)-2-methyl-2-butene-1,4-diol (various chromatographic analyses).^[4b] This observation is consistent with the intermediacy of **8** in the conversion of **7** into **9/10** in plants. The methylerythritol found in the *Capsicum* system (Figure 1a) is a result of the action of NaF-insensitive phosphatases on **7**.

During the course of this investigation, three research groups reported that **8** accumulates in *Escherichia coli* mutants overexpressing the *GcpE* (*IspG*) gene,^[9, 10] and in bacterial mutants that are deficient in the *LytB* (*IspH*) gene.^[11] Most probably **8** represents a novel intermediate in the deoxyxylulose phosphate pathway, and is likely the missing link **X**^[12] in the formation of **9/10** from **7** (Scheme 1 and Scheme 2). Compound **8** was synthesized previously in unlabeled form by different, more lengthy, routes.^[13]

Aldehyde **12** has been postulated in the hypothetical mechanism of the conversion of **7** into **8** mediated by the *IspG* gene product.^[9] It was also reported that the in vivo conversion of [U-¹³C₅]1-deoxy-D-xylulose resulted in a 5:1 mixture of [U-¹³C₅]**9** and [U-¹³C₅]**10**.^[14] This ratio was not

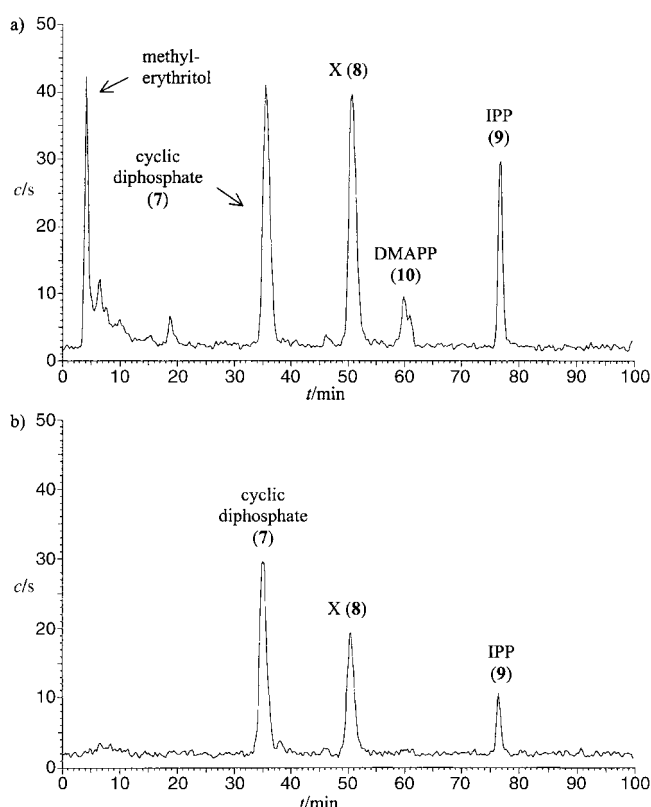


Figure 1. HPLC radiogram of an aliquot of an assay mixture containing the [¹⁴C]**7** and chromoplasts from either a) *C. annuum* or b) *N. pseudonarcissus*. The incubation conditions were as described in ref. [3]. Retention times: methylerythritol: 4.5 min, cyclic diphosphate **7**: 35 min, diphosphate **8**: 50 min, DMAPP **10**: 60 min, IPP **9**: 77 min.

observed by us during the time course of the conversion of **8** into **9** and **10** by chromoplast and bacterial preparations. One discrepancy between the bacterial and the plant systems, however, still needs clarification. While it has been shown that the label from [4-²H]**3** is retained exclusively in the dimethylallyl diphosphate starter unit in the bacterial system,^[15, 16] the dimethylallyl diphosphate starter unit in the plant system (*Catharanthus roseus*) is completely devoid of the deuterium label.^[17] However, feeding experiments using a different plant system, *Eucalyptus globulus*, show that the deuterium label is retained in the dimethylallyl diphosphate starter unit.^[12] No plausible explanation can yet be given for this discrepancy that may reflect different metabolic routes within the plant kingdom.

The demonstration of the rapid and unequivocal transformation of synthetic **8** into isoprenes of the phytoene type and with transition from **7** through **8** to **9/10** in plant chromoplasts provides evidence that **8** is indeed the biologically active intermediate in this pathway present in plastids of higher plants.^[20]

Experimental Section

Isolation of chromoplasts from *C. annuum* and *N. pseudonarcissus*, incorporation experiments with isotope-labeled substrates, and isolation of phytoene and HPLC analyses of phosphorylated metabolites were conducted exactly as previously published.^[3] [3-¹⁴C, Me-¹⁴C]**7** was prepared as described^[18] from [U-¹⁴C₃]**1** and unlabeled **2**. The specific activity

achieved was $103 \mu\text{Ci} \mu\text{mol}^{-1}$. The genes *dxs*, *ispC*, *ispD*, *ispE*, and *ispF* were amplified by the polymerase chain reaction from *Escherichia coli* DNA and were functionally expressed as His-tag fusion proteins to facilitate purification.

12: Bromoaldehyde **19** was prepared in 87% yield from **18** (4.20 g, 50.0 mmol) according to the method of Gray.^[6] Freshly prepared pyrophosphoric acid^[7] was immediately titrated to pH 5.3 with approximately 20% (w/w) aqueous tetra-*n*-butylammonium hydroxide. After lyophilization, bis(tetra-*n*-butylammonium) dihydrogen pyrophosphate was quantitatively obtained as a white, highly hygroscopic solid. This product (9.91 g, 15.0 mmol) was dissolved in dry acetonitrile (20 mL) under a nitrogen atmosphere. The resulting clear solution was then cooled to 0°C and neat **19** (0.815 g, 5.0 mmol) added. While stirring, the reaction was allowed to warm up to room temperature over 2.5 h. The reaction mixture was poured into a cold, aqueous solution (50 mL) of sodium hydroxide (0.60 g, 15.0 mmol) and the acetonitrile partially evaporated under vacuum. The remaining aqueous solution was passed through a column of approximately 30 exchange equivalents of Lewatit SP 112 WS cation exchange resin (Na^+ form). The column was eluted with three column volumes of a 1:49 mixture (v/v) of isopropyl alcohol and 1.8 mM sodium bicarbonate. The eluent was lyophilized to dryness to yield a fluffy solid. The crude material was purified by means of HPLC^[19] (YMC-Pack R&A; 250 \times 20 mm, ODS 120A, 5 μm , 1.8 mM sodium bicarbonate eluent). The eluent was lyophilized to dryness to yield a white fluffy solid. Negative mode ESI MS-MS: m/z : 259 $[M - H]^-$, 241 $[M - H - \text{H}_2\text{O}]^-$, 177 $[\text{H}_3\text{P}_2\text{O}_7]^-$, 159 $[\text{HP}_2\text{O}_6]^-$, 79 $[\text{PO}_3]^-$; ^1H NMR (400 MHz, D_2O): δ = 9.34 (s, 1H; H-1), 6.85 (t, J = 5.3 Hz, 1H; H-3), (4.7–4.9, 1H and HDO overlap from solvent), 1.72 ppm (s, 3H; CH_3); ^{31}P NMR (162 MHz, H_2O): δ = -5.75 (d, J = 22 Hz), -10.89 ppm (dt, J_{PP} = 22 Hz, J_{HP} = 7.7 Hz).

[4- ^2H]8**:** Aldehyde **12** (20 mg, 77 μmol) was reduced in a 2:1 mixture of water and methanol (0.21 mL) at pH 9 with NaB^3H_4 (6.4 mg, 154 μmol) at room temperature (2 h) and the reaction product was purified by ion-exchange chromatography on DEAE Sephadex (3.2 mg, 16%). Negative mode ESI MS-MS data: m/z : 262 $[M - H]^-$, 244 $[M - H - \text{H}_2\text{O}]^-$, 177 $[\text{H}_3\text{P}_2\text{O}_7]^-$, 164 $[M - H - \text{H}_3\text{PO}_4]^-$, 159 $[\text{HP}_2\text{O}_6]^-$, 97 $[\text{H}_2\text{PO}_4]^-$, 79 $[\text{PO}_3]^-$; ^1H NMR data (400 MHz, D_2O): δ = 5.66 (t, J = 7 Hz, 1H; H-2), 4.55 (dd appearing as pseudo-triplet, J_{HH} = J_{HP} = 7 Hz, 2H; H-1), 4.01 (s, 1H; H-4), 1.72 ppm (s, 3H; CH_3).

[4- ^3H]8**:** This was prepared by reduction of **12** with NaB^3H_4 and purified in the same way as 4-deuterated **8** (19% yield). The specific activity achieved was $1.56 \mu\text{Ci} \mu\text{mol}^{-1}$.

Received: April 25, 2002 [Z19170]

[1] For reviews, see: a) N. Qureshi, J. W. Porter, *Biosynthesis of Isoprenoid Compounds*, Vol. 1, Wiley, New York, **1981**, pp. 47–94; b) D. V. Banthorpe, B. V. Charlwood, M. J. O. Francis, *Chem. Rev.* **1972**, 72, 115–155; c) K. Bloch, *Steroids* **1992**, 57, 378–382; d) T. J. Bach, *Lipids* **1995**, 30, 191–202.

[2] For reviews, see a) W. Eisenreich, M. Schwarz, A. Cartayrade, D. Arigoni, M. H. Zenk, A. Bacher, *Chem. Biol.* **1998**, 5, R221–R233;

b) M. Rohmer in *Comprehensive Natural Product Chemistry*, Vol. 2 (Ed.: D. Cane), Pergamon, Oxford, **1999**, pp. 45–68; c) M. Schwarz, D. Arigoni in *Comprehensive Natural Product Chemistry*, Vol. 2 (Ed.: D. Cane), Pergamon, Oxford, **1999**, pp. 367–399; d) F. Rohdich, K. Kis, A. Bacher, W. Eisenreich, *Curr. Opin. Chem. Biol.* **2001**, 5, 535–540.

[3] M. Fellermeier, M. Raschke, S. Sagner, J. Wungsintaweekul, C. A. Schuhr, S. Hecht, K. Kis, T. Radykewicz, P. Adam, F. Rohdich, W. Eisenreich, A. Bacher, D. Arigoni, M. H. Zenk, *Eur. J. Biochem.* **2001**, 268, 6302–6310.

[4] a) M. Fellermeier, PhD thesis, Ludwig-Maximilian-Universität München, **2000**; b) C. Latzel, PhD thesis, Ludwig-Maximilian-Universität, München, **2000**.

[5] *Dictionary of Natural Products*, Chapman and Hall, London, **2001**; for compound **13**, see: D. S. Letham, *Life Sci.* **1963**, 41, 569–573; **14**: M. Nicoletti, L. Tomassini, S. Foddai, *Planta Med.* **1992**, 58, 472; **15**: M. Messerer, P. Winterhalter, *Nat. Prod. Lett.* **1995**, 5, 241–244; **16**: A. B. Gutierrez, J. C. Oberti, P. Kulanthaivel, W. Herz, *Phytochemistry* **1985**, 24, 2967–2971; **17**: H. Rimpler, I. Christiansen, *Z. Naturforsch. C* **1977**, 32, 724–730.

[6] G. M. Gray, *Synthesis* **1983**, 488–489.

[7] V. J. Davisson, A. B. Woodside, T. R. Neal, K. E. Stremler, M. Muehlbacher, C. D. Poulter, *J. Org. Chem.* **1986**, 51, 4768–4779.

[8] B. L. Jones, J. W. Porter in *Methods in Enzymology*, Vol. 110 (Eds.: J. H. Law, H. C. Rilling), Academic Press, London, **1985**, pp. 209–220.

[9] S. Hecht, W. Eisenreich, P. Adam, S. Amslinger, K. Kis, A. Bacher, D. Arigoni, F. Rohdich, *Proc. Natl. Acad. Sci. USA* **2001**, 98, 14837–14842.

[10] M. Seemann, N. Campos, M. Rodríguez-Concepción, E. Ibañez, T. Duvold, D. Tritsch, A. Boronat, M. Rohmer, *Tetrahedron Lett.* **2002**, 43, 1413–1415.

[11] M. Hintz, A. Reichenberg, B. Altincicek, U. Bahr, R. M. Gschwind, A.-K. Kollas, E. Beck, J. Wiesner, M. Eberl, H. Jomaa, *FEBS Lett.* **2001**, 509, 317–322.

[12] C. Rieder, B. Jaun, D. Arigoni, *Helv. Chim. Acta* **2000**, 83, 2504–2513.

[13] a) M. Wolff, M. Seemann, C. Grosdemange-Billiard, D. Tritsch, N. Campos, M. Rodríguez-Concepción, A. Boronat, M. Rohmer, *Tetrahedron Lett.* **2002**, 43, 2555–2559; b) J. L. Ward, M. H. Beale, *J. Chem. Soc. Perkin Trans. 1* **2002**, 710–712.

[14] F. Rohdich, S. Hecht, K. Gärtner, P. Adam, C. Krieger, S. Amslinger, D. Arigoni, A. Bacher, W. Eisenreich, *Proc. Natl. Acad. Sci. USA* **2002**, 99, 1158–1163.

[15] J. L. Giner, B. Jaun, D. Arigoni, *Chem. Commun.* **1998**, 1857–1858.

[16] L. Charon, J.-F. Hoeffler, C. Pale-Grosdemange, L. M. Lois, N. Campos, A. Boronat, M. Rohmer, *Biochem. J.* **2000**, 346, 737–742.

[17] D. Arigoni, W. Eisenreich, C. Latzel, S. Sagner, T. Radykewicz, M. H. Zenk, A. Bacher, *Proc. Natl. Acad. Sci. USA* **1999**, 96, 1309–1314.

[18] C. A. Schuhr, S. Hecht, K. Kis, W. Eisenreich, J. Wungsintaweekul, A. Bacher, F. Rohdich, *Eur. J. Org. Chem.* **2001**, 3221–3226.

[19] D. Zhang, C. D. Poulter, *Anal. Biochem.* **1993**, 213, 356–361.

[20] Note added in proof: Two recent papers pre-published electronically include other syntheses of **8**: D. T. Fox, C. D. Poulter, *J. Org. Chem.* **2002**, ASAP; S. Amslinger, K. Kis, S. Hecht, P. Adam, F. Rohdich, D. Arigoni, A. Bacher, W. Eisenreich, *J. Org. Chem.* **2002**, ASAP.

EDITORIAL

Angewandte Weekly—Back to the Future!

In 1898, in its 11th year, the frequency of publication of *Angewandte Chemie* was increased from fortnightly to weekly, and it continued to appear in this rhythm until 1939. In the following decades the publication frequency was altered several times, most recently in 1994, when production was changed from 12 to 24 issues per year. Now it is planned, from 2003, in the 115th year, to return to weekly publication.

**More often not thicker:
48 issues in 2003!**

After two years of in-depth discussions over the past and future of the journal, the Editorial Board and the International Advisory Board, as well as the Governing Board of the German Chemical Society (GDCh) and the publishers, decided in favor of doubling the number of issues published per year, so that from 2003, 48 issues will appear.

No future without history! *Angewandte Chemie*'s past was illuminated in the first issue of 1988, celebrating the centenary of the journal, and the Editorials from this issue can be perused at your leisure on our Homepage if they are not otherwise available. The last twenty years I know well from my experience here, and they are distinguished by the internationalization of the journal, which in part reflects the internationalization of science. At the start of my time as an editor of *Angewandte Chemie*, at the beginning of the 1980s, I hung—perhaps influenced through my postdoc time in the USA—a map of North America on my office wall. I could mark the place of origin of every manuscript that came from North America with a flag, in 1982 there was only one per month; from Japan we received only one every two months! This year I have hung up a large map of East Asia—this was long overdue considering the number of manuscripts that we receive from Japan, and is today of vital importance to keep

track of the place of origin of the rapidly increasing number of manuscripts from the other countries in this region, and in particular the People's Republic of China. Table 1 shows the number of manuscripts received in the years 1982, 1992, and 2002 (for the first six months!); the non-German contribution increased from 23 % in 1982, to 56 % in 1992, and to 84 % this year, and in the past 20 years the total number of manuscripts received per year has increased more than sevenfold!

Table 1. Number of manuscripts received by *Angewandte Chemie* in 1982, 1992, and 2002 (first six months) by country. In 1992 the preliminary decision was made to increase the publication frequency from 12 to 24 issues in 1994.

	1982 (12 months)	1992 (12 months)	2002 (6 months)
Germany	251	302	188
USA	11	136 ^[a]	241
Canada	4		18
Japan	6	51 ^[b]	177
Great Britain	5	33	53
France	11	42	39
Switzerland/Austria	7	23	28
rest Western Europe	17	69	134 ^[c]
rest of world	16	35	304 ^[d]
Total	328	691	1182

[a] USA and Canada. [b] Total East Asia. [c] Of these: Spain 49, Italy 25, Netherlands 17. [d] Of these: P.R. China 164, South Korea 49, India 45, Taiwan 12.

The growth in manuscript submissions is one factor, continued increase in quality is another. The rejection rate has increased from 18 % in 1982, to 43 % in 1992, to 59 % in 2001. In the same period the impact factor rose from 4.167 to 5.974 and now stands at 8.255 (see Figure 1); since 1996 it has remained at over 8, which, considering the huge increase in

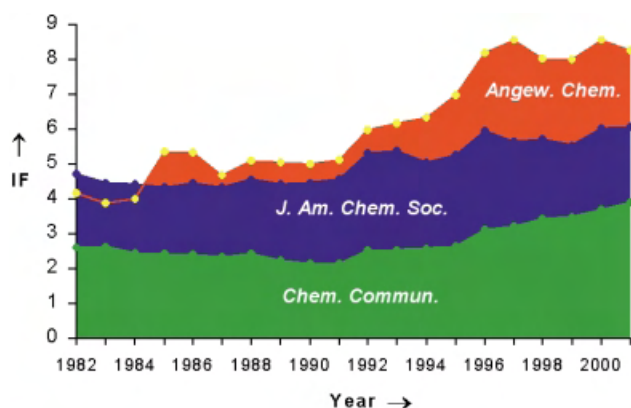


Figure 1. Development of the Impact Factors (IF) of *Chemical Communications*, the *Journal of the American Chemical Society*, and *Angewandte Chemie* 1982–2001.

the number of communications (not reviews!) published per year in this time, from 521 to 868 (+ 67%), was not expected.

The picture of the journal described by these numbers would be incomplete without the many innovations that have consistently made *Angewandte Chemie* more attractive for both readers and authors. As early as 1976 the detailed table of contents was introduced in which each article is described with a short text and, when possible, an appropriate graphic. Similarly the “trade mark” *Angewandte Chemie* cover picture has been with us since 1979. The changes made in the last decade are outlined in Table 2. Naturally the change to weekly publication will be accompanied by further improvements to the journal.

Table 2. Innovations in *Angewandte Chemie* since 1991.

1991	New section “Highlights”
1992	Electronic manuscript administration
1993	On-screen editing of manuscripts
1994	Preview of the next issue
1995	Formation of the International Advisory Board
	Keywords to every article
	Article Finder
1997	Frontispiece for Reviews and the Communications section
1998	Press information to every issue
	Online Supporting Information for Communications
1999	Electronic full text available through Wiley InterScience
	Very Important Papers (VIPs) flagged
2000	New section “Essays”
	<i>Angewandte Chemie</i> in Medline
2001	New sections “Minireviews” and “Web Sites”
2002	Accelerated publications
	Online submission of manuscripts

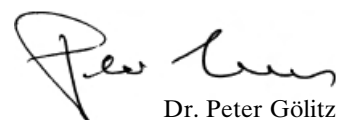
Why weekly issues and not thicker issues? This question was also posed in 1993 as the change to fortnightly from monthly publication was being discussed, and on that occasion I wrote in an Editorial in the August 1993 issue: “When the latest issue is delivered, the typical curiosity-driven reader finds an hour or so to leaf through the journal and skim this or that chemical tidbit. A survey a few years ago showed that the informative table of contents was perused most intensely.” For this reason from next year this section will be even more attractive, and for authors

Free color in the table of contents

the use of color in the table of contents will be free of charge (this comes into force immediately). I continued “When this initial curiosity is satisfied, the issue is set aside for a while. The reader can refer colleagues to articles and join in discussions knowing that he or she must read this or that article thoroughly in a quiet moment. Students, in particular, neglect this task at their peril as examinations approach. Many other readers, however, are all too often surprised by the new issue, and the cycle starts again. Reading habits will not be affected if each issue is thicker or the publication frequency increases.” In one respect reading habits have changed drastically; today many readers look first “online” where smaller units are even more important. The curiosity-driven “reading hour” may not be possible every day, however, curiosity can be (or must be) satisfied on a weekly basis. Readers thus use their subscription (or that of their institution) more intensively, each article receives more attention. For these reasons the decision was made for more frequent rather than thicker issues. A benefit for authors is that we can publish articles in less than a month in the future should the need occur.

In 1994 as *Angewandte Chemie* increased publication frequency from 12 to 24 issues per year J. Fraser Stoddart (University of California, Los Angeles) predicted the journal would be appearing on a weekly basis by the turn of the millennium. He was wrong, but not by much. In the future we will no doubt need to further improve the selection of articles to be published, make the presentation, especially online, even more reader friendly, and remain true to our program as outlined by Wilhelm Foerst, Editor-in-Chief from 1933 to 1969: “A rousing force emanates from important findings, which, in turn inspires receptive natures to strive after achievements of their own. We produce our journal for such people. And we seek out these ‘avant-garde’. This constitutes our entire program.”

“At the turn of the millennium *Angewandte* will be weekly.”
J. Fraser Stoddart, 1993


Dr. Peter Göllitz

PS: Recently the first Impact Factors for *ChemBioChem* and *ChemPhysChem*, the two daughter journals of *Angewandte Chemie* were announced by the Institute of Scientific Information, and in both cases these were far better than could be anticipated for such new journals. For *ChemBioChem* the Impact Factor 2.920 is well above those of other bio(in)organic journals (*Bioorganic and Medicinal Chemistry* and the corresponding Letters journal, for example, have Impact Factors of 1.798 and 1.747, respectively). *ChemPhysChem* with 4.217 is far ahead of all the other (broad based) journals in physical chemistry/chemical physics including both *Journal of Physical Chemistry A and B* (2.630 and 3.379), the *Journal of Chemical Physics* (3.147), *Chemical Physical Letters* (2.364), and *PCCP* (1.787).

Impact Factors of *ChemBioChem* and *ChemPhysChem*: 2.920 and 4.217, respectively

COVER PICTURE

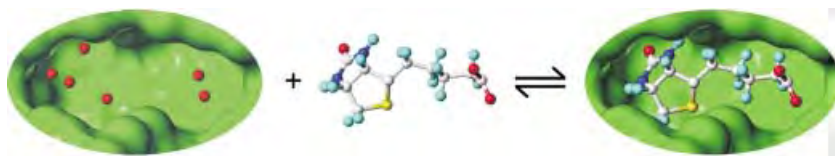
The cover picture shows the interior of a red-figure kylix (440–430 BC, British Museum London) which shows the brilliant exploits of Theseus, the Greek mythology hero. In the center, Theseus is shown defeating the infamous Minotaur within the labyrinth. On the right, the hero raises his hand against Sciron, below whom the turtle is visible. Next clockwise, are shown the bull of Marathon, the punishment of Sinis, the slaying of the sow Phaea, the battle of Cercyon, and finally the punishment of Procrustes. The labors of Theseus are no different from the accomplishments of today's synthetic chemists working in total synthesis. One such endeavor, the total synthesis of the CP molecules with its challenges, twists and turns, and dead-ends, but also its rewards, is compared to the conquest of the Minotaur by Theseus in the Review by K. C. Nicolaou and P. S. Baran on p. 2678 ff.



REVIEWS

Contents

Biological activity at the molecular level involves the binding of a small-molecule ligand to a macromolecular receptor, usually a protein, in aqueous solution (see scheme). Enthalpic and entropic contributions arising from inter- and intra-molecular effects determine the affinity of both binding partners towards each other. Affinity as a key element in life sciences—how well is this quantity understood today?



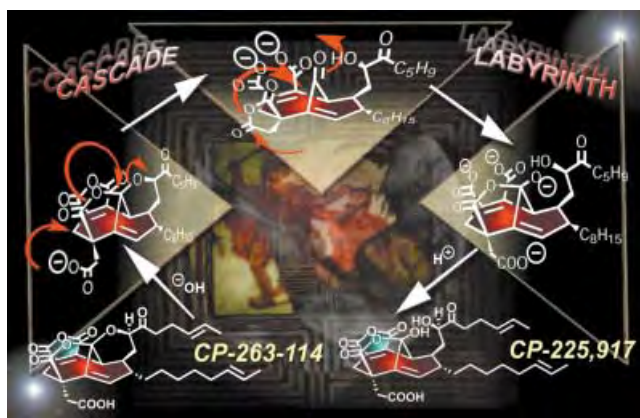
Angew. Chem. **2002**, *114*, 2764–2798

H. Gohlke, G. Klebe* 2644–2676

Approaches to the Description and Prediction of the Binding Affinity of Small-Molecule Ligands to Macromolecular Receptors

Keywords: binding affinity • calorimetry • drug research • protein–ligand interactions • scoring function

Total synthesis programs directed toward complex molecules may take the form of unrelentless campaigns in which the synthetic chemist is faced with unprecedented challenges and unforeseen obstacles, but which often lead to invaluable fundamental knowledge and powerful new technologies. Here the authors describe one of the most arduous and rewarding endeavors in total synthesis of modern times—the synthesis of the CP molecules (see scheme)—and compare it to the Greek mythology's Labyrinth and the conquest of the Minotaur by Theseus.



Angew. Chem. **2002**, *114*, 2800–2843

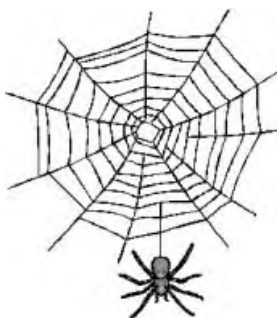
K. C. Nicolaou,* P. S. Baran 2678–2720

The CP Molecule Labyrinth: A Paradigm of How Endeavors in Total Synthesis Lead to Discoveries and Inventions in Organic Synthesis

Keywords: CP molecules • natural products • organic synthesis • synthetic methods • total synthesis

Transgenic goats to spin webs! The silk of spider nets (see picture) possesses unique mechanical properties. By using suitable microbiological methods, a structurally similar fiber protein has recently been prepared that, after spinning, exhibits comparable strength and elasticity to natural spider silk. The American firm Nexia Biotechnology plans to use transgenic goats to express this silk protein in their milk.

Angew. Chem. **2002**, *114*, 2845–2847



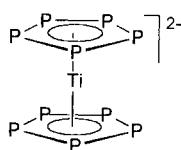
S. Kubik * 2721–2723

High-Performance Fibers from Spider Silk

Keywords: gene technology • mechanical properties • polymers • protein design • spider silk

The P_5 rings of the first inorganic metallocene, $[Ti(\eta^5-P_5)_2]^{2-}$ (see picture) are generated from white phosphorus in a selective reaction. The steric and electronic properties of these rings provide the remarkable stability of this unprecedented sandwich complex.

Angew. Chem. **2002**, *114*, 2847–2848



H. Sitzmann * 2723–2724

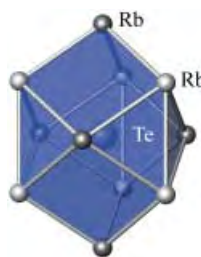
The Decaphosphatitanocene Dianion—A New Chapter in the Chemistry of Naked Polyphosphorus Ligands

Keywords: cyclopentadienyl ligands • metallocenes • phosphorus • P ligands • sandwich complexes • titanium

COMMUNICATIONS

At least four different polymorphic forms are possible for the previously uncharacterized compound Rb_2Te . One form is a metastable phase at room temperature and two are high-temperature phases; in one of the latter, the Te atoms are coordinated in the form of an Edshammar polyhedron (see picture). Rb_2Te is therefore unique within the di(alkali metal) monotellurides.

Angew. Chem. **2002**, *114*, 2849–2854



K. Stöwe,* S. Appel 2725–2730

Polymorphic Forms of Rubidium Telluride Rb_2Te

Keywords: polymorphism • rubidium • solid-state structures • structure elucidation • tellurium

VIPs

The following communications are “Very Important Papers” in the opinion of two referees. They will be published shortly (those marked with a diamond will be published in the next issue). Short summaries of these articles can be found on the *Angewandte Chemie* homepage at the address <http://www.angewandte.org>

Atom-Transfer Tandem Radical Cyclization Reactions Promoted by Lewis Acids

D. Yang, S. Gu, H.-W. Zhao, N.-Y. Zhu ◆

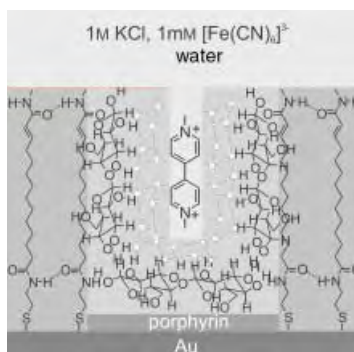
Metallabenzenes and Valence Isomers: Synthesis and Characterization of a Platinabenzene

V. Jacob, T. J. R. Weakley, M. M. Haley*

Stereoselective Synthesis of β -D-Mannopyranosides with Reactive Mannopyranosyl Donors Possessing a Neighboring Electron-Withdrawing Group

R. R. Schmidt,*
A. A.-H. Rahmann, S. Jonke
E. S. H. El Ashry* ◆

In hydrophobic nanometer clefts in membranes, ridge molecules, such as cellobiose, can be anchored for months. They do not diffuse into the neighboring bulk water and electrolytes from the bulk water do not penetrate the immobilized layer. In the presence of dimethyl viologen, cycling of the Au electrode potential causes the viologen molecules to stir the anchored molecules out of the cleft and into the bulk water (see picture: the bulk water phase does not penetrate the hydrate layer but the viologen molecules can).



G. Li, K. Doblhofer,
J.-H. Fuhrhop* 2730–2734

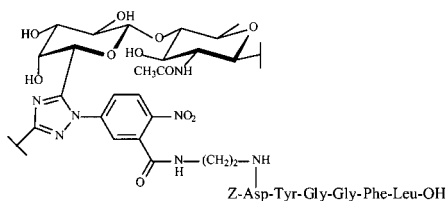
Irreversible Adsorption of Cellobiose, Ascorbic Acid, and Tyrosine to Hydrophobic Surfaces in Water and Their Separation by Molecular Stirring

Keywords: cyclic voltammetry • membranes • nanostructures • self-assembly

Angew. Chem. **2002**, *114*, 2855–2859



Carbohydrate coupling at any desired peptide carboxylate moiety is possible with a highly selective biocatalytic route for the synthesis of carbohydrate–peptide conjugates (see picture).



N. Wehofskey, R. Löser, A. Buchynskyy,
P. Welzel, F. Bordusa* 2735–2738

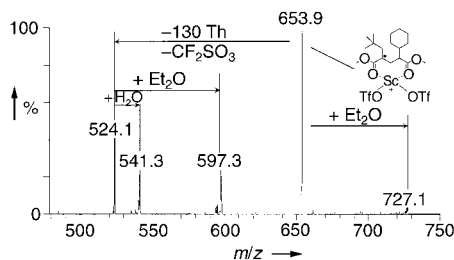
Synthesis of Neo-Peptidoglycans: An Unexpected Activity of Proteases

Keywords: chemoenzymatic synthesis • enzyme catalysis • glycopeptides • proteases • substrate mimetics

Angew. Chem. **2002**, *114*, 2859–2863



A useful tool for the investigation of synthetically important tributyltin-mediated radical chain reactions is electrospray ionization mass spectrometry (ESIMS). A microreaction system is coupled online to the ESI source. Transient radicals were detected unambiguously by using MS/MS methods (see picture).



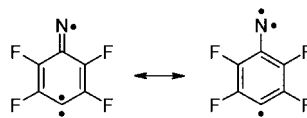
J. Griep-Raming, S. Meyer, T. Bruhn,
J. O. Metzger* 2738–2742

Investigation of Reactive Intermediates of Chemical Reactions in Solution by Electrospray Ionization Mass Spectrometry: Radical Chain Reactions

Keywords: carbocations • mass spectrometry • radicals • reactive intermediates • scandium

Angew. Chem. **2002**, *114*, 2863–2866

Elements of a carbene and a nitrene are linked by a common delocalized π electron in the molecule described here (see picture). The organic high-spin molecule with a quartet ground state could be photochemically generated and spectroscopically characterized in an argon matrix at 3 K.



H. H. Wenk, W. Sander* 2742–2745

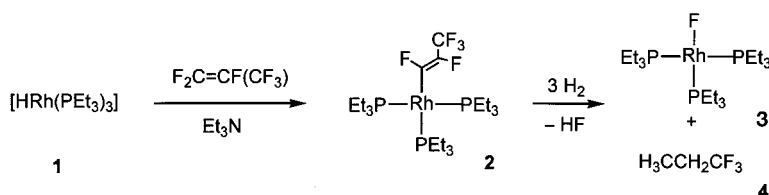
2,3,5,6-Tetrafluorophenyl nitren-4-yl: A Quartet-Ground-State Nitrene Radical

Keywords: density functional calculations • high-spin molecules • matrix isolation • nitrenes • radicals

Angew. Chem. **2002**, *114*, 2873–2876



Rapid and regioselective C–F bond activation of hexafluoropropene occurs on reaction with **1**. Treatment of the resulting complex **2** with hydrogen yields the rhodium fluoro complex **3** and 1,1,1-trifluoropropane (**4**).



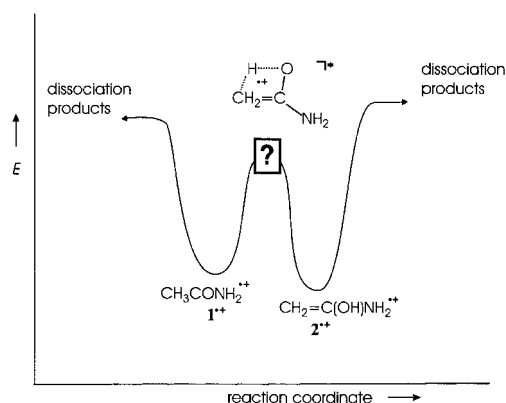
T. Braun,* D. Noveski, B. Neumann,
H.-G. Stammer 2745–2748

Conversion of Hexafluoropropene into 1,1,1-Trifluoropropane by Rhodium-Mediated C–F Activation

Keywords: alkenes • C–F activation • fluorinated ligands • fluorine • rhodium

Angew. Chem. **2002**, *114*, 2870–2873

By using a new “titration” technique, the activation barrier for the strictly unimolecular 1,3-hydrogen migration $1^{*+} \rightarrow 2^{*+}$ has been determined (0.74 ± 0.06 eV; see reaction profile). With this technique the internal energy of 1^{*+} is controlled by variable photoionization of acetamide and the chemistry of the resulting enol ion 2^{*+} is then probed by structure-specific ion–molecule reactions.



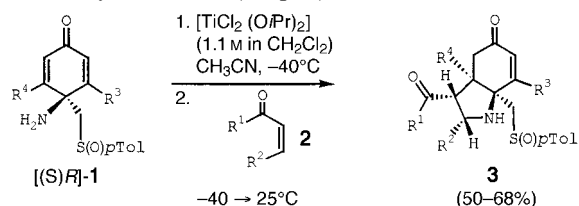
Angew. Chem. **2002**, *114*, 2867–2870

D. Schröder,* J. Loos, R. Thissen,
O. Dutuit, P. Mourgues, H.-E. Audier,
C. Lifshitz, H. Schwarz 2748–2751

Barrier Height Titration by Tunable
Photoionization Combined with Chemical
Monitoring: Unimolecular Keto/Enol
Tautomerization of the Acetamide Cation
Radical

Keywords: electron transfer • hydrogen
transfer • mass spectrometry •
photoionization • tautomerism

New stereogenic centers are generated in the $[\text{TiCl}_2(\text{OiPr})_2]$ -catalyzed reaction of $[(S)R]$ -(*p*-tolylsulfinyl)methyl]-*p*-quinamines **1** with α,β -unsaturated ketones **2** to give hydroindole-substituted systems **3** in a domino process. Up to four stereogenic centers are formed in the reaction of cycloalkenones and up to five when acyclic enones (2 equiv) are used.



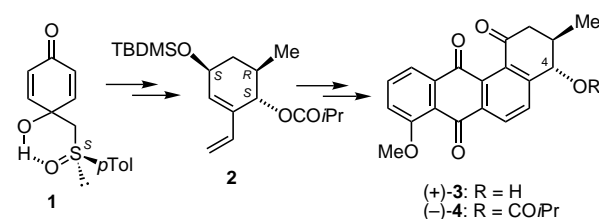
Angew. Chem. **2002**, *114*, 2877–2879

M. C. Carreño,* M. Ribagorda,
G. H. Posner 2753–2755

Titanium-Promoted Stereoselective
Synthesis of Hydroindolones from *p*-
Quinamines by Domino Conjugate
Additions

Keywords: Michael addition • nitrogen
heterocycles • quinamines • sulfoxides •
titanium

The tetracyclic skeleton of C4-oxygenated angucyclinone-type antibiotics rubiginones **A₂** ((+)-**3**) and **C₂** ((-)-**4**) is constructed by Diels–Alder reaction of a racemic sulfinyl-substituted methyl juglone and the enantiopure vinyl cyclohexene **2**, which is prepared in nine steps and in 26% overall yield from sulfinyl-substituted *p*-quinol **1**. TBDMS = *tert*-butyldimethylsilyl.



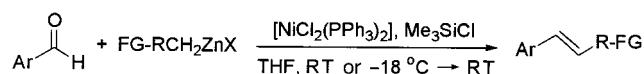
Angew. Chem. **2002**, *114*, 2879–2881

M. C. Carreño,* M. Ribagorda,
Á. Somoza, A. Urbano* 2755–2757

Enantioselective Total Synthesis of
Angucyclinone-Type Antibiotics
Rubiginones **A₂** and **C₂**

Keywords: antibiotics • asymmetric
synthesis • cycloaddition • quinones •
sulfoxides

Stereoselective alkenylated compounds are formed from the reaction of organozinc halides and aldehydes (see scheme; FG = functional group). Under mild conditions, and in the presence of a silylating agent, the Ni-catalyzed procedure gives *E*-alkenes and *E*-stilbenes in excellent yield.



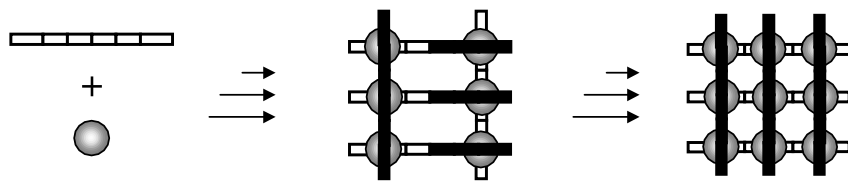
Angew. Chem. **2002**, *114*, 2881–2884

J.-X. Wang,* Y. Fu, Y. Hu . . . 2757–2760

Carbon–Carbon Double-Bond
Formation from the Reaction of
Organozinc Reagents with Aldehydes
Catalyzed by a Nickel(II) Complex

Keywords: aldehydes • alkenes •
homogeneous catalysis • nickel •
organozinc reagents

A $[3 \times 3]$ Ag^+ , metallogrid self-assembles by a highly complex mechanism involving several intermediates, which may be generated at different metal/ligand stoichiometries. Extensive NMR spectroscopic studies have allowed the unraveling of the structure of these species and have revealed that the final grid entity presents high structural robustness and that the last assembly step (see scheme) occurs with strong cooperativity.



Angew. Chem. **2002**, *114*, 2884–2888

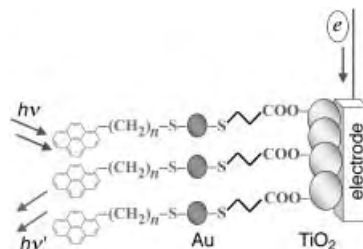
A. Marquis, J.-P. Kintzinger, R. Graff,
P. N. W. Baxter, J.-M. Lehn* 2760–2764

Mechanistic Features, Cooperativity, and Robustness in the Self-Assembly of Multicomponent Silver(I) Grid-Type Metalloarchitectures

Keywords: complexation mechanism • cooperative effects • self-assembly • silver • supramolecular chemistry



Suppressing the charge-transfer quenching with an externally applied electrochemical bias results in a fluorescence enhancement of a fluorophore (pyrene) on a gold nanoparticle surface (see scheme). At positive bias the fluorophore is totally quenched on the gold surface while at negative bias (less than -0.5 V) it becomes highly fluorescent.



Angew. Chem. **2002**, *114*, 2888–2891

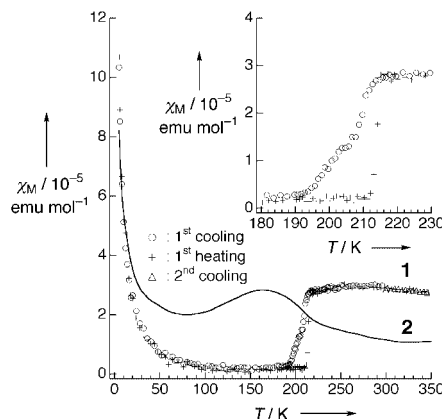
P. V. Kamat,* S. Barazzouk,
S. Hotchandani 2764–2767

Electrochemical Modulation of Fluorophore Emission on a Nanostructured Gold Film

Keywords: fluorescence • gold nanoparticles • nanostructures • organic–inorganic hybrid composites • spectroelectrochemistry



Chains change: Novel valence-ordering structures of the ground states of MMX chain compounds, $[\text{Pt}_2(\text{RCS}_2)_4\text{I}]_\infty$ (**1**: $\text{R} = n\text{Bu}$, **2**: $\text{R} = \text{Et}$), are determined by low-temperature crystal-structure analyses to be $-\text{Pt}^{2+}-\text{Pt}^{3+}-\text{I}^--\text{Pt}^{3+}-\text{Pt}^{2+}-\text{I}^-$. Magnetic susceptibility measurements of **1** (see graph) revealed an abrupt drop in magnitude from a 1D antiferromagnetic spin system to a spin-singlet state accompanying a first-order phase-transition around 210 K. This result is in contrast to the spin degree of freedom of **2** that survived down to 2 K.



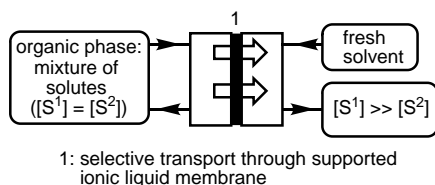
Angew. Chem. **2002**, *114*, 2891–2895

M. Mitsumi,* K. Kitamura, A. Morinaga,
Y. Ozawa, M. Kobayashi, K. Toriumi,*
Y. Iso, H. Kitagawa,
T. Mitani 2767–2771

Valence-Ordering Structures and Magnetic Behavior of Metallic MMX Chain Compounds

Keywords: conducting materials • electronic structure • magnetic properties • mixed-valent compounds • phase transition

Continuous separation of organic compounds is possible by selective transport through a supported liquid membrane, which contains the room-temperature ionic liquid 1-*n*-butyl-3-methylimidazolium hexafluorophosphate immobilized in the porous structure of a hydrophilic polyvinylidene fluoride membrane. A mixture (1:1 molar ratio) of the isomeric amines diisopropylamine (S^1) and triethylamine (S^2) was continuously fractionated over 14 days without any observable decrease in selectivity (see scheme).



Angew. Chem. **2002**, *114*, 2895–2897

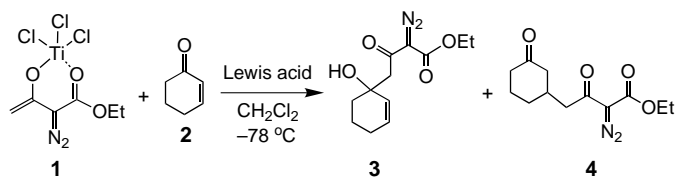
L. C. Branco, J. G. Crespo,
C. A. M. Afonso* 2771–2773

Highly Selective Transport of Organic Compounds by Using Supported Liquid Membranes Based on Ionic Liquids

Keywords: amines • ionic liquids • membranes • selective transport • separation processes



The selective generation of 1,2- and 1,4-addition products (3 and 4, respectively) in the addition of Ti^{IV} enolates **1** to α,β -unsaturated carbonyl compounds **2** can be almost completely controlled by the choice of Lewis acid. The high selectivity for 1,4 addition when the enones are activated by TiCl_4 or SnCl_4 is probably a result of the bridging chlorine atoms.



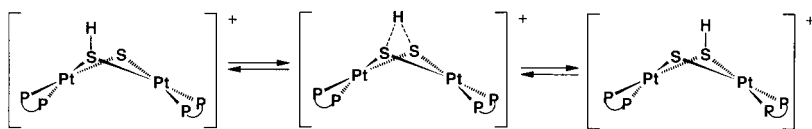
Angew. Chem. **2002**, *114*, 2897–2898

G. Deng, X. Tian, Z. Qu,
J. Wang* 2773–2776

Lewis Acid Controlled Regioselective 1,2 and 1,4 Reaction of α,β -Unsaturated Carbonyl Compounds with Ti^{IV} Enolates Derived from α -Diazo β -Keto Carbonyl Compounds

Keywords: addition • diazo compounds • enones • Lewis acids • Michael addition

Despite the weakness of $\text{S}\cdots\text{H}\cdots\text{S}$ interactions and the fact that they have rarely been reported in transition-metal compounds, variable-temperature NMR data and theoretical calculations provide evidence for fast intramolecular proton exchange between the bridging sulfur atoms in the complexes $[\text{Pt}_2\{\text{Ph}_2\text{P}(\text{CH}_2)_n\text{PPh}_2\}_2(\mu\text{-S})(\mu\text{-SH})]\text{ClO}_4$ ($n = 2, 3$; see scheme).



Angew. Chem. **2002**, *114*, 2900–2902

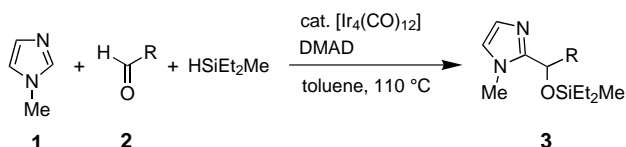
G. Aullón, M. Capdevila, W. Clegg,
P. González-Duarte,* A. Lledós,*
R. Mas-Ballesté 2776–2778

First Evidence of Fast $\text{S}\cdots\text{H}\cdots\text{S}$ Proton Transfer in a Transition Metal Complex

Keywords: hydrogen bonds • platinum • proton transfer • S ligands



A significant increase in yield is observed when DMAD is added to the reaction of 1-methylimidazole (**1**) with aldehydes **2** and diethylmethylsilane in the presence of a catalytic amount of $[\text{Ir}_4(\text{CO})_{12}]$ to produce 2-(1-diethylmethylsiloxyalkyl)-imidazoles **3**. DMAD = dimethyl acetylenedicarboxylate.



Angew. Chem. **2002**, *114*, 2903–2905

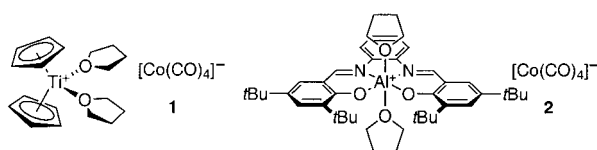
Y. Fukumoto, K. Sawada, M. Hagihara,
N. Chatani, S. Murai* 2779–2781

$[\text{Ir}_4(\text{CO})_{12}]$ -Catalyzed Coupling Reaction of Imidazoles with Aldehydes in the Presence of a Hydrosilane to Give 2-Substituted Imidazoles

Keywords: aldehydes • alkylation • imidazoles • iridium • silanes



Efficient carbonyl insertion into C–O and C–N bonds using $[\text{Lewis acid}]^+[\text{Co}(\text{CO})_4]^-$ complexes **1** and **2** gives regio- and stereoselective carbonylation of a variety of epoxides and aziridines to yield β -lactones and β -lactams, respectively. Both transformations are proposed to occur by the same mechanism, yielding products with inversion of configuration at the site of CO insertion.



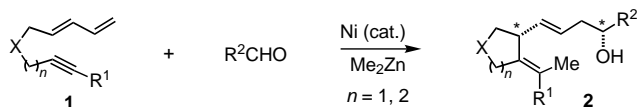
Angew. Chem. **2002**, *114*, 2905–2908

V. Mahadevan, Y. D. Y. L. Getzler,
G. W. Coates* 2781–2784

$[\text{Lewis Acid}]^+[\text{Co}(\text{CO})_4]^-$ Complexes: A Versatile Class of Catalysts for Carbonylative Ring Expansion of Epoxides and Aziridines

Keywords: carbonylation • cobalt • lactams • lactones • ring-opening polymerization

A four-component reaction: A nickel catalyst promotes the conjugate addition of Me_2Zn and a carbonyl compound to 1, ω -dienynes **1** at the terminal positions of the alkyne and the diene moieties, respectively; the through-space interactions of the alkyne and diene groups ensure C–C coupling at the internal positions. The products **2** are obtained in good yields and with excellent 1,5-diastereoselectivity and stereoselectivity about the exocyclic double bond.



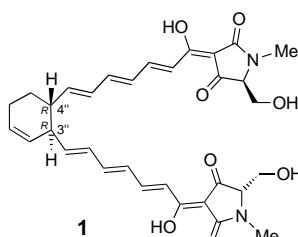
Angew. Chem. **2002**, *114*, 2908–2910

A. Ezoe, M. Kimura,* T. Inoue, M. Mori, Y. Tamaru* 2784–2786

Remarkably High 1,5-Diastereoselectivity in a Nickel-Catalyzed Conjugate Addition of Me_2Zn and Carbonyl Compounds to 1, ω -Dienynes with Through-Space Coupling

Keywords: aldehydes • alkynes • dienes • ketones • nickel • zinc

Only through total synthesis could the absolute configuration of the 3'',4'' ring junction of the polyenol tetramic acid polypeptin C (**1**) be unambiguously established. Key features of the synthesis include a double Swern oxidation, double Stille coupling, and a double Takai olefination.



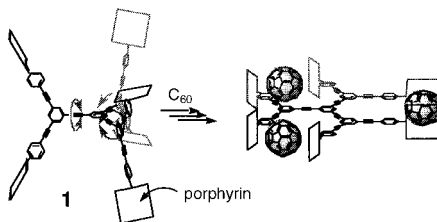
Angew. Chem. **2002**, *114*, 2910–2914

D. A. Longbottom, A. J. Morrison, D. J. Dixon, S. V. Ley* 2786–2790

Total Synthesis of Polypeptin C and Determination of the Absolute Configurations at the 3'',4'' Ring Junction

Keywords: alkenes • lactams • natural products • total synthesis

Treble clefs: The dendritic porphyrin receptor **1** has three fullerene-binding clefts, each of which consists of two face-to-face-oriented porphyrins. [60]Fullerene guests bind to each subunit, successively suppressing the rotational freedom (“domino” effect) and the guest-binding proceeds according to positive homotropic allostery. As expected, the binding constant achieved in this system is large.



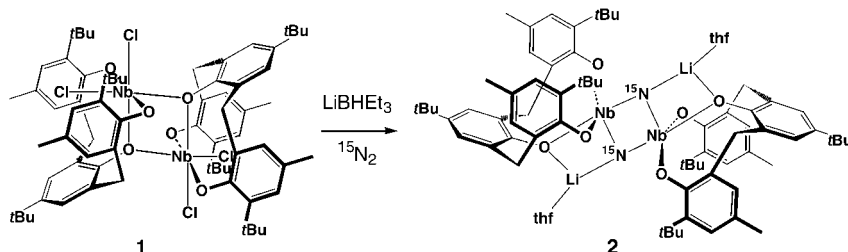
Angew. Chem. **2002**, *114*, 2914–2916

M. Ayabe, A. Ikeda, Y. Kubo, M. Takeuchi, S. Shinkai* 2790–2792

A Dendritic Porphyrin Receptor for C_{60} Which Features a Profound Positive Allosteric Effect

Keywords: allostery • fullerenes • host–guest systems • porphyrinoids • zinc

Nitrogen splits: The reaction of the linked aryloxide–niobium complex **1** with a hydride reagent under 1 atm of N_2 gave the nitride-bridging dimer **2**. The origin of the nitride ligands has been confirmed to be N_2 by repeating the experiment under an atmosphere of $^{15}\text{N}_2$.



Angew. Chem. **2002**, *114*, 2916–2918

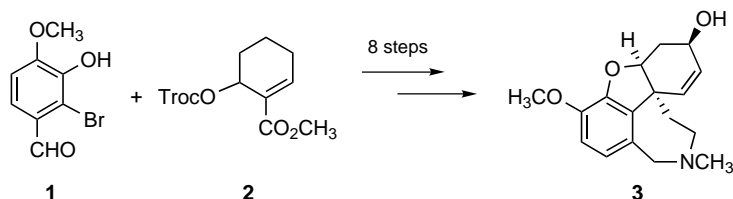
H. Kawaguchi,* T. Matsuo .. 2792–2794

Dinitrogen-Bond Cleavage in a Niobium Complex Supported by a Tridentate Aryloxide Ligand

Keywords: hydrides • niobium • nitrides • nitrogen fixation • O ligands



An effective sequence: Palladium-catalyzed asymmetric allylic alkylation, Heck cyclization, and diastereoselective allylic oxidation were used in the total synthesis of (–)-galanthamine (**3**) in 14.8% overall yield (from **1** and **2**, Troc = 2,2,2-trichloroethoxycarbonyl) and with 96% *ee*. This improved procedure provides the shortest and most efficient nonbiomimetic synthesis of the acetylcholinesterase inhibitor.



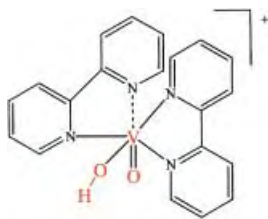
Angew. Chem. **2002**, *114*, 2919–2921

B. M. Trost,* W. Tang 2795–2797

An Efficient Enantioselective Synthesis of (–)-Galanthamine

Keywords: alkylation • allylic compounds • asymmetric synthesis • natural products • palladium

HYSCORE with a vanadium core: Examples of monomeric metal compounds containing the *cis*-[M(=O)(OH)]ⁿ⁺ unit, namely the V^{IV}O²⁺ complexes [V^{IV}O(OH)(bipy)₂][BF₄] (**1**; see picture) and [V^{IV}O(OH)(phen)₂][BF₄·H₂O] (**2**·H₂O), were isolated and structurally characterized. The continuous wave EPR and 2D ESEEM (HYSCORE; hyperfine sublevel correlation) spectroscopy parameters obtained for **1** and **2**·H₂O provide spectroscopic signatures that enable the assignment of the *cis*-[V^{IV}O(OH)]⁺ center in biomolecules.



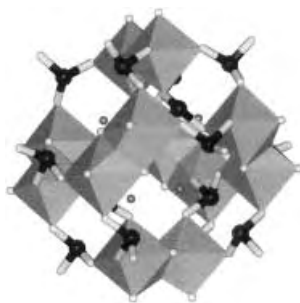
E. J. Tolis, M. J. Manos, A. J. Tasiopoulos, C. P. Raptopoulou, A. Terzis, M. P. Sigalas,* Y. Deligiannakis,* T. A. Kabanos* 2797–2801

Monomeric Compounds Containing the *cis*-[V(=O)(OH)]⁺ Core

Keywords: bioinorganic chemistry • density functional calculations • EPR spectroscopy • ESEEM spectroscopy • hydroxy ligands • vanadium

Angew. Chem. **2002**, *114*, 2921–2925

An unexplored family of polyoxometalates has evolved through the synthesis and structural characterization of the first examples of Mo^V sulfite heteropolyanions. The dodecanuclear molybdenum(v) sulfite exhibits a unique structural motif among polyoxometalates (see picture; gray polyhedra represent Mo^VO₆ octahedral units, black, white, and gray balls are sulfur, oxygen, and nitrogen atoms, respectively).



M. J. Manos, J. D. Woollins, A. M. Z. Slawin,* T. A. Kabanos* 2801–2805

Polyoxomolybdenum(v) Sulfite Complexes: Synthesis, Structural, and Physical Studies

Keywords: cluster compounds • molybdenum • polyoxometalates • sulfite

Angew. Chem. **2002**, *114*, 2925–2929

Big rings and nanocleavage: Whereas a variety of molybdenum oxide based nanoobjects can be obtained by self-assembly concomitant with a variety of modifications of a parent cluster system under alterable boundary conditions, drastic changes—comparable to a molecular-scissors-type activity—can even cause splitting of the parent cluster to (large) fragments which subsequently can be linked in fascinating ways even with the option of generating giant cluster collectives (see picture {Mo₂^{*}} ≡ {Mo₂^{VI/V}O₇(H₂O)}^{3–}).



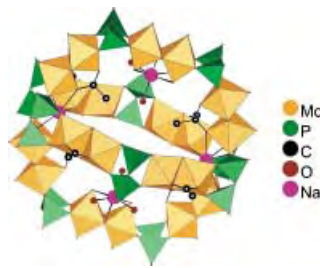
Angew. Chem. **2002**, *114*, 2929–2932

L. Cronin, C. Beugholt, E. Krickemeyer, M. Schmidtman, H. Bögge, P. Kögerler, T. K. K. Luong, A. Müller* 2805–2808

“Molecular Symmetry Breakers” Generating Metal-Oxide-Based Nanoobject Fragments as Synthons for Complex Structures: [Mo₁₂₈Eu₄O₃₈₈H₁₀(H₂O)₈₁]₂^{20–}, a Giant-Cluster Dimer

Keywords: cluster compounds • europium • molybdenum • nanochemistry • polyoxometalates • symmetry breaking

Interconnecting rings: The first pyrophosphate/ Mo^{V} complex $\text{Na}_{24}\{\text{Na}_4(\text{H}_2\text{O})_6 \subset [(\text{Mo}_2\text{O}_4)_{10}(\text{P}_2\text{O}_7)_{10}(\text{CH}_3\text{COO})_8(\text{H}_2\text{O})_4]\} \cdot 97\text{H}_2\text{O}$ is synthesized in mild conditions, and has been characterized by X-ray diffraction (see polyhedral representation) and ^{31}P NMR spectroscopy. This molecular compound is formed of two nearly perpendicular interconnected wheels, an unprecedented topology for an inorganic compound.



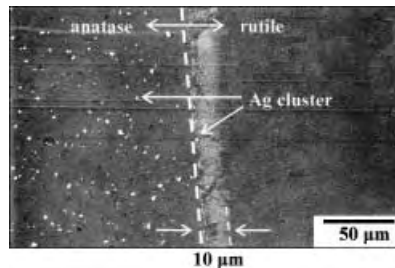
C. du Peloux, P. Mialane, A. Dolbecq, J. Marrot, F. Sécheresse * ... 2808–2810

Mo^V/Pyrophosphate Polyoxometalate:
An Inorganic Cryptate

Keywords: cryptands • host–guest systems • molybdenum • phosphates • polyoxometalates • sodium

Angew. Chem. **2002**, *114*, 2932–2934

Coupling of anatase and rutile TiO_2 in a bilayer form significantly increases photocatalytic activity relative to the individual components. Reducing the dimensions of the junction to the charge-separation distance is of importance in increasing this activity. The interfacial electron transfer from anatase to rutile ($<10\text{ }\mu\text{m}$) was revealed by labeling and visualizing the reduction sites by deposition of Ag nanoparticles (see picture).



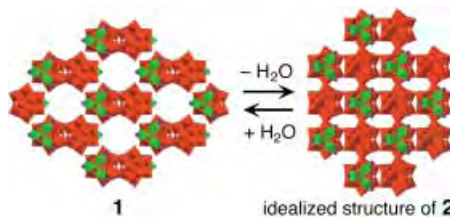
T. Kawahara, Y. Konishi, H. Tada,* N. Tohge, J. Nishii, S. Ito ... 2811–2813

A Patterned TiO_2 (Anatase)/ TiO_2 (Rutile) Bilayer-Type Photocatalyst: Effect of the Anatase/Rutile Junction on the Photocatalytic Activity

Keywords: heterogeneous catalysis • semiconductors • sol–gel processes • thin films

Angew. Chem. **2002**, *114*, 2935–2937

Molecular sieving to take your breath away: The breathing ionic crystal **1** is synthesized by the complexation of Keggin-type $[\alpha\text{-SiW}_{12}\text{O}_{40}]^{4-}$ (red) polyoxometalate with a macro cation $[\text{Cr}_3\text{O}(\text{OOCH})_6(\text{H}_2\text{O})_3]^+$ (green and white). The water of crystallization is easily removed from **1** by evacuation to form a guest-free phase **2**. Compound **2** reversibly adsorbs small alcohols and nitriles as well as water, while longer-chain alcohols and nitriles were excluded, which shows the novel molecular sieving of small hydrophilic molecules by **2**.



S. Uchida, M. Hashimoto, N. Mizuno * 2814–2817

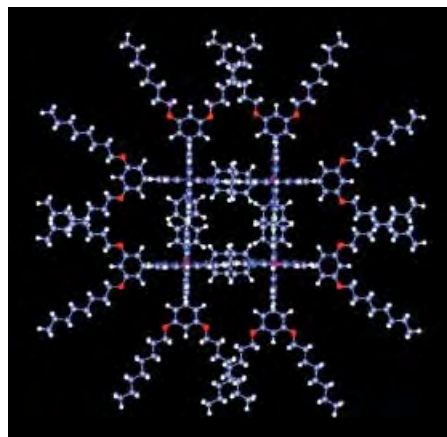
A Breathing Ionic Crystal Displaying Selective Binding of Small Alcohols and Nitriles: $\text{K}_3[\text{Cr}_3\text{O}(\text{OOCH})_6(\text{H}_2\text{O})_3] \cdot [\alpha\text{-SiW}_{12}\text{O}_{40}] \cdot 16\text{H}_2\text{O}$

Keywords: alcohols • hydrophilicity • microporous materials • nitriles • polyoxometalates

Angew. Chem. **2002**, *114*, 2938–2941



Box clever: A very stable box-shaped cyclic tetramer (see picture) was formed from *meso*-pyridyl substituted *meso*–*meso*-linked zinc(II) diporphyrin, in which the porphyrin subunits are held in a rigorous perpendicular orientation.



A. Tsuda, T. Nakamura, S. Sakamoto, K. Yamaguchi, A. Osuka * .. 2817–2821

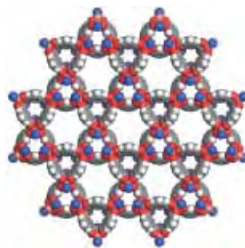
A Self-Assembled Porphyrin Box from *meso*–*meso*-Linked Bis{5-*p*-pyridyl-15-(3,5-di-octyloxyphenyl)porphyrinato zinc(II)}

Keywords: chirality • porphyrinoids • self-assembly • zinc

Angew. Chem. **2002**, *114*, 2941–2945

Self-assembly of triangular nanoscale secondary building units affords a Kagomé lattice (see picture) that exhibits room-temperature magnetic hysteresis. This phenomenon is caused by spin frustration imparted by the triangular lattice topology, which is exemplified by direct comparison to a network having the same composition, but different topology.

Angew. Chem. **2002**, *114*, 2945–2948



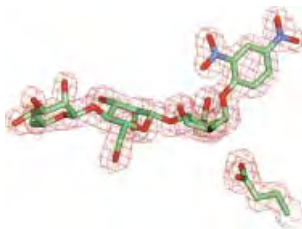
B. Moulton, J. Lu, R. Hajndl,
S. Hariharan,
M. J. Zaworotko* 2821–2824

Crystal Engineering of a Nanoscale
Kagomé Lattice

Keywords: crystal engineering • Kagomé
lattice • magnetic properties •
nanostructures • self-assembly



The conformational reaction pathway for β -mannosidases proposed here is distinct from that of glucosidases and cellulases. The proposal is based on substrate distortions along the reaction pathway of a β -mannosidase (see picture) that were revealed by X-ray crystallography and are close in conformational space to known β -mannosidase inhibitors.



V. M.-A. Ducros, D. L. Zechel,
G. N. Murshudov, H. J. Gilbert, L. Szabó,
D. Stoll, S. G. Withers,
G. J. Davies* 2824–2827

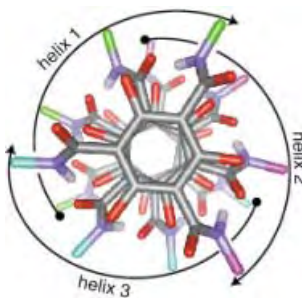
Substrate Distortion by a β -Mannanase:
Snapshots of the Michaelis and Covalent-
Intermediate Complexes Suggest a $B_{2.5}$
Conformation for the Transition State

Keywords: enzyme catalysis •
glycosylation • inhibitors •
mannosidases • X-ray diffraction

Angew. Chem. **2002**, *114*, 2948–2951



Chiral side chains installed into the stacks of overcrowded arenes enforce helical conformations (see picture). The assembly process can be directed with electric fields as a result of a dipole moment parallel to the stacking direction. In concentrated solutions, superhelices emerge that reflect circularly polarized light.



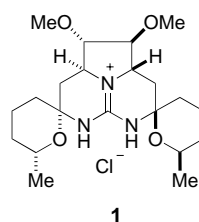
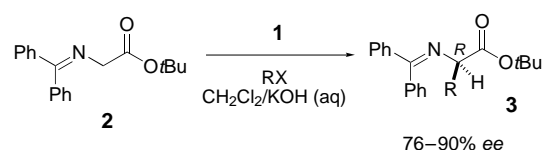
M. L. Bushey, A. Hwang, P. W. Stephens,
C. Nuckolls* 2828–2831

The Consequences of Chirality in
Crowded Arenes—Macromolecular
Helicity, Hierarchical Ordering, and
Directed Assembly

Keywords: helical structures • hydrogen
bonds • molecular recognition • polar
order • self-assembly

Angew. Chem. **2002**, *114*, 2952–2955

The enantioselective alkylation of the Schiff base 2 was carried out in the presence of a novel phase-transfer catalyst, the guanidine-containing pentacyclic compound **1**. The product **3** was obtained with enantiomeric excesses of 76–90% (see scheme).



T. Kita, A. Georgieva, Y. Hashimoto,
T. Nakata, K. Nagasawa* ... 2832–2834

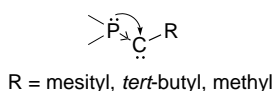
C_2 -Symmetric Chiral Pentacyclic
Guanidine: A Phase-Transfer Catalyst for
the Asymmetric Alkylation of *tert*-Butyl
Glycinate Schiff Base

Keywords: alkylation • asymmetric
synthesis • phase-transfer catalysis •
synthetic methods

Angew. Chem. **2002**, *114*, 2956–2958



An electronic spectator in stable carbenes: A weak π -donor substituent such as a phosphanyl group brings enough stabilization to singlet phosphanyl-(mesityl)carbenes prepared by photolysis of diazo precursors that the mesityl group remains an electronic spectator. The carbenes are sufficiently stable to allow characterization of the phosphanyl(*tert*-butyl)- and even phosphanyl(methyl)carbenes (see picture) by NMR spectroscopy (mesityl = 2,4,6-trimethylphenyl).



E. Despagne, H. Gornitzka,
A. B. Rozhenko, W. W. Schoeller,
D. Bourissou, G. Bertrand* 2835–2837

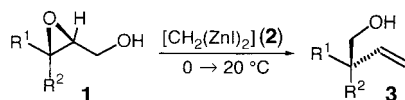
Stable Non-Push–Pull
Phosphanylcarbenes: NMR Spectroscopic
Characterization of a Methylcarbene

Keywords: carbenes • phosphorus •
reactive intermediates • substituent
effects

Angew. Chem. **2002**, *114*, 2959–2961



Retention of the configuration is observed in the pinacol-type rearrangement of 2,3-epoxy alcohols **1** in the presence of bis(iodozincio)methane (**2**). The 1,3-migration of the hydroxymethyl group affords an intermediate 2-hydroxyaldehyde, which is methylenated by **2** in situ to give homoallyl alcohol **3**.



S. Matsubara,* H. Yamamoto,
K. Oshima 2837–2840

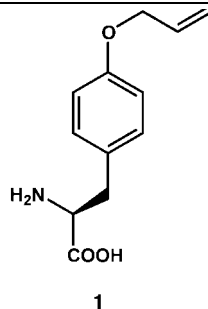
**Stereoselective Pinacol-Type
Rearrangement of 2,3-Epoxy Alcohols
with Retention of Configuration
Mediated by Bis(iodozincio)methane**

Keywords: asymmetric synthesis • Lewis acids • nucleophiles • rearrangement • zinc

Angew. Chem. **2002**, *114*, 2961–2964



Synthetic anchor: An incorporated allyl group may act in this way to allow protein modification in a site-specific fashion. The nonnatural amino acid *O*-allyl-L-tyrosine (**1**) has been site-specifically incorporated into protein in *E. coli*. The yield of full-length mutant Z-domain protein is 5.6 mg L⁻¹, in comparison to 9.2 mg L⁻¹ of native Z-domain protein. A high-resolution mass spectrum suggests the fidelity for the incorporation of **1** is better than 99.8%.



Z. Zhang, L. Wang, A. Brock,
P. G. Schultz* 2840–2842

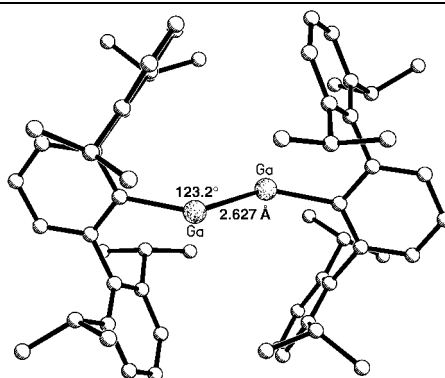
**The Selective Incorporation of Alkenes
into Proteins in *Escherichia coli***

Keywords: allylic compounds • amino acids • biosynthesis • protein expression • protein modifications

Angew. Chem. **2002**, *114*, 2964–2966



A Ga–Ga bond order considerably less than unity in the “digallene” Ar'GaGaAr' (Ar' = 2,6-Dipp₂C₆H₃, Dipp = 2,6-*i*Pr₂C₆H₃; see structure) is indicated by its structure and solution behavior.



N. J. Hardman, R. J. Wright,
A. D. Phillips, P. P. Power* .. 2842–2844

**Synthesis and Characterization of the
Neutral “Digallene” Ar'GaGaAr' and Its
Reduction to Na₂Ar'GaGaAr' (Ar' = 2,6-
Dipp₂C₆H₃, Dipp = 2,6-*i*Pr₂C₆H₃)**

Keywords: aryl substituents • gallium • metal-metal interactions • structure elucidation

Angew. Chem. **2002**, *114*, 2966–2968



Supporting information on the WWW
(see article for access details).

* Author to whom correspondence should be addressed



Accelerated publications



BOOKS

Nomenclature of Organic Compounds	Robert B. Fox, Warren H. Powell	<i>K.-H. Hellwich</i> 2845
Cross-Coupling Reactions – A Practical Guide	Norio Miyaura	<i>L. J. Goossen</i> 2845
Stereochemistry	David G. Morris	<i>H. M. Muchall</i> 2846
Nanoscale Materials in Chemistry	Kenneth J. Klabunde	<i>A. Mews</i> 2847
Drug-Membrane Interactions	Joachim K. Seydel, Michael Wiese	<i>J.-H. Fuhrhop</i> 2848



WEB SITES

http://www.webreactions.net	A Free and Fast Chemical Reaction Search	<i>U. Iserloh</i> 2851
---	---	------------------------------

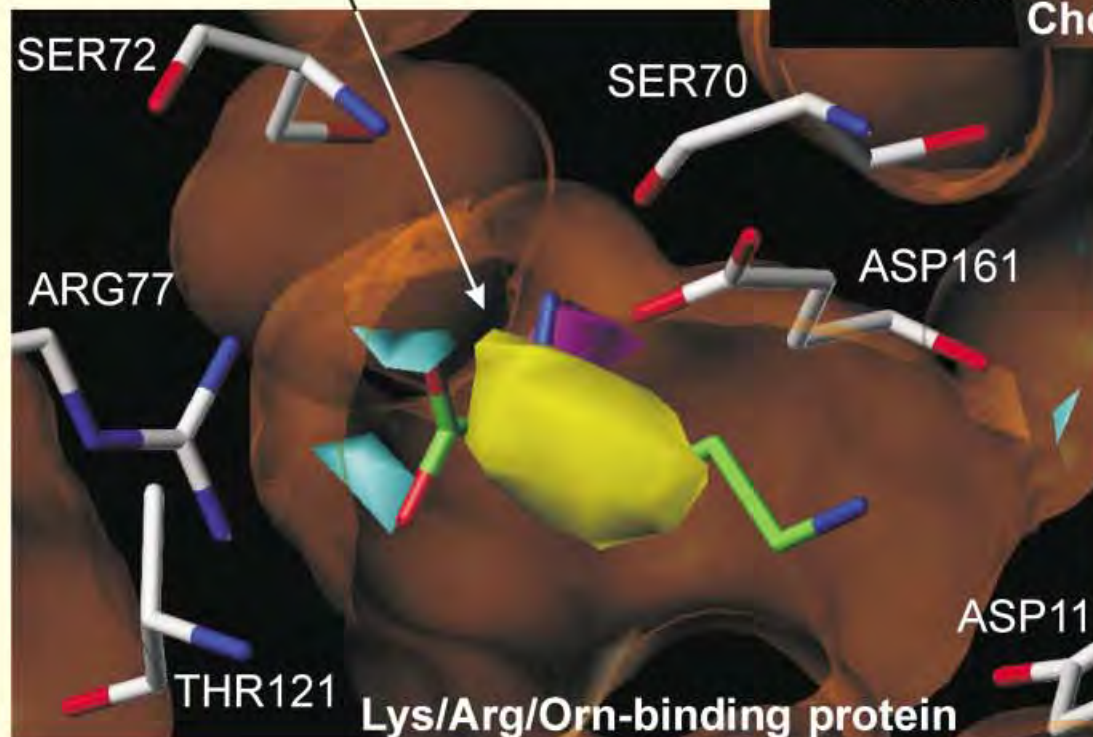
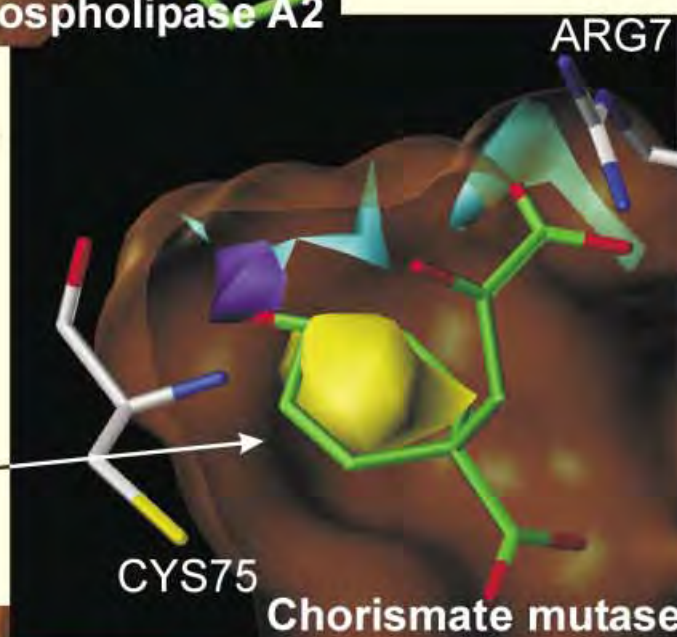
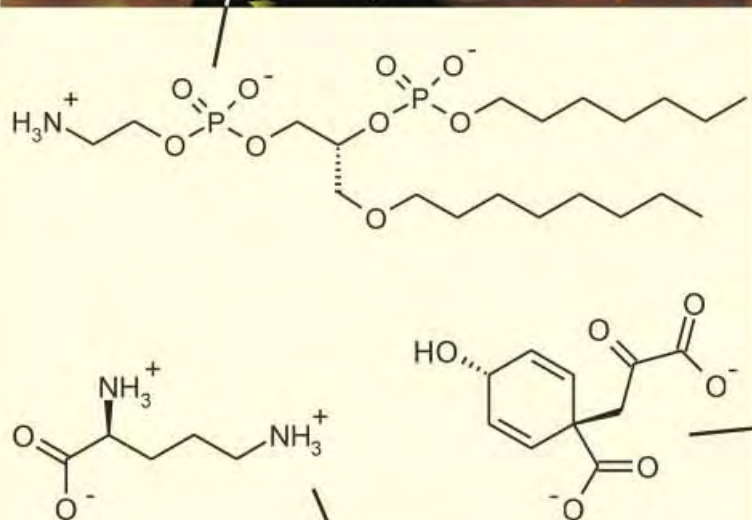
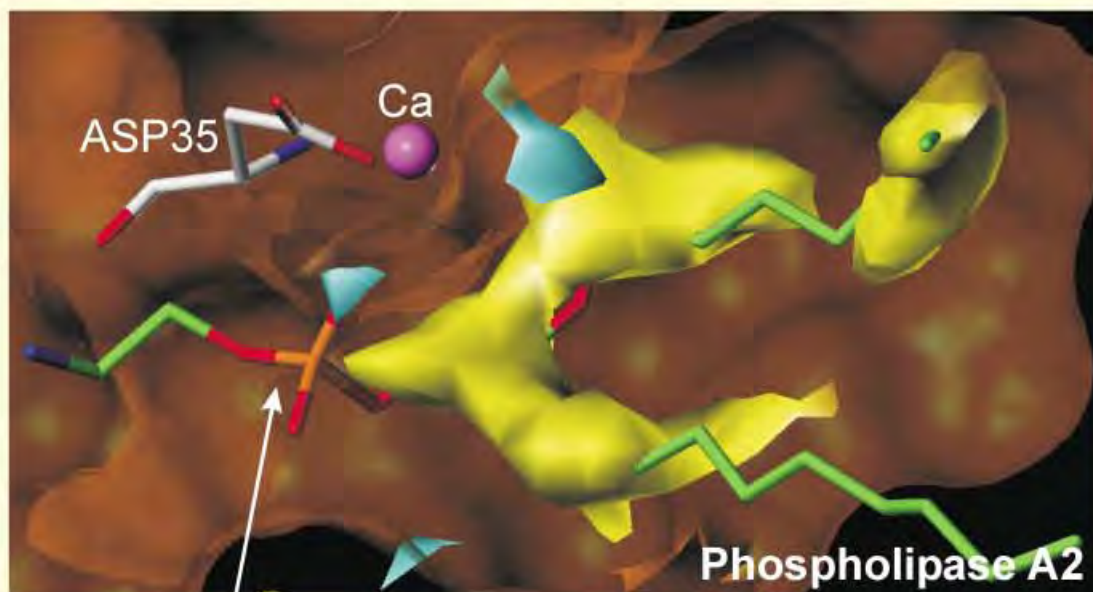
SERVICE

• VIPs	2624	• Keywords	2852
• <i>Angewandte's</i> Sister-Journals	2635 – 2637	• Authors	2853
• Sources	A67	• Preview	2854
• Vacancies	A71		

Don't forget all the Tables of Contents from 1998 onwards may be still found on the WWW under:
<http://www.angewandte.org>

Issue 14, 2002 was published online on July 15.

Spatially resolved identification of favorable protein–ligand interactions in binding pockets



Color code of isopleths:
 aliphatic C
 Carboxylate O
 Hydroxy O
 Amino N

Approaches to the Description and Prediction of the Binding Affinity of Small-Molecule Ligands to Macromolecular Receptors

Holger Gohlke and Gerhard Klebe*

The influence of a xenobiotic compound on an organism is usually summarized by the expression *biological activity*. If a controlled, therapeutically relevant, and regulatory action is observed the compound has potential as a drug, otherwise its toxicity on the biological system is of interest. However, what do we understand by the biological activity? In principle, the overall effect on an organism has to be considered. However, because of the complexity of the interrelated processes involved, as a simplification primarily the “main action” on the organism is taken into consideration. On the molecular level, biological activity corresponds to the binding of a (low-molecular weight) compound to a macromolecular receptor, usually a protein. Enzymatic reactions or signal-transduction cascades are thereby

influenced with respect to their function for the organism. We regard this binding as a process under equilibrium conditions; thus, binding can be described as an association or dissociation process. Accordingly, *biological activity* is expressed as the *affinity* of both partners for each other, as a thermodynamic equilibrium quantity. How well do we understand these terms and how well are they theoretically predictable today? The holy grail of rational drug design is the prediction of the biological activity of a compound. The processes involving ligand binding are extremely complicated, both ligand and protein are flexible molecules, and the energy inventory between the bound and unbound states must be considered in aqueous solution. How sophisticated and reliable are our experimental approaches to

obtaining the necessary insight? The present review summarizes our current understanding of the binding affinity of a small-molecule ligand to a protein. Both theoretical and empirical approaches for predicting binding affinity, starting from the three-dimensional structure of a protein–ligand complex, will be described and compared. Experimental methods, primarily microcalorimetry, will be discussed. As a perspective, our own knowledge-based approach towards affinity prediction and experimental data on factorizing binding contributions to protein–ligand binding will be presented.

Keywords: binding affinity · calorimetry · drug research · protein–ligand interactions · scoring function

1. Introduction

Mutual molecular recognition is the starting point for almost all processes in biological systems. More than 100 years ago, this fact was first recognized by Emil Fischer, who wrote “*that enzyme and glycoside must fit together like a key and a lock in order to initiate a chemical action upon each other*”.^[3] Also Paul Ehrlich’s statement “*Corpora non agunt nisi fixata*”^{[**][4]} is—in a somewhat extended form^[5, 6]—the basis for the scientific explanation of drug action. As a

consequence, the geometrical and chemical complementarity of small molecules (termed *ligands* in the following) and their macromolecular biological target structures (mostly proteins, termed *receptors* in the following) influences metabolic or signal-transduction pathways, and thus initiates a physiological effect.

In recent years, knowledge of the relationship between molecular structure and biological effects has prompted a fundamental change of the methods used in modern drug research. Molecular biological techniques identify receptor dysfunction or failures in regulation as possible causes of a disease. Furthermore, they help to isolate proteins in a purified form, the three-dimensional structure of which is subsequently determined using X-ray structural analysis,^[7, 8] NMR spectroscopy,^[9–11] or cryoelectron microscopy.^[12–15] In addition, the number of characterized protein sequences is currently growing at a dramatic rate as a result of several genome-sequencing projects.^[16–19] This provides a platform for

[*] Prof. Dr. G. Klebe, Dr. H. Gohlke
Institut für Pharmazeutische Chemie
Philipps-Universität Marburg
Marbacher Weg 6, 35032 Marburg (Germany)
Fax: (+49) 6421-282-8994
E-mail: klebe@mail.uni-marburg.de

[**] “The bodies do not act if they are not bound.”

the development of improved techniques to predict protein function^[20–24] and their three-dimensional structure.^[25, 26] Furthermore, enhanced methods for crystal-structure analysis^[27–30] are currently being developed and computational procedures are being applied to identify and select new biological targets.^[31–33] As a result of these efforts, in the near future an enormously expanded range of structurally and functionally characterized molecular targets will become available for drug therapy.^[34]

The development of a new drug, which can take up to 15 years and consume about half a billion dollars,^[35–37] can be divided into several phases.^[38, 39] The process starts with an initial search for a lead structure, that is, a ligand with a detectable affinity for a given receptor. This step is followed by several stages of optimization. The increase in affinity and selectivity of a ligand towards its biological target must be accompanied by an optimization of beneficial pharmacokinetic properties. This involves the absorption of the drug, its distribution and metabolism in the body, along with its excretion and toxicity.^[40–42] The actual validation of a drug is subsequently performed in several phases of clinical trials.

The rapid and reliable identification of potent, high-affinity ligands is of utmost importance in view of the overwhelming number of characterized receptors expected from the genome projects.^[43, 44] Given the limited resources available, the proof of concept for the relevance of a particular therapeutic target has to be assessed in the early phase of drug development. Presently, there are two complementary approaches in the search for new lead structures: *experimental* (high-throughput) *screening*,^[45, 46] involving the in vitro testing of large compound libraries, and *virtual screening*^[47, 48] or *rational design*,^[49–51] which is based on available information about the structure of the biological target and/or already characterized ligands.

Experimental random screening originated from methods of traditional drug research. Large compound libraries of synthetic and natural compounds are tested for possible activity in a bioassay, independent of their actual chemical structure.^[52, 53] In recent years, this method has been promoted extensively by the use of robotic systems to achieve high-throughput testing^[54] along with methodological developments towards combinatorial chemistry,^[55–59] and automated parallel synthesis. Using these techniques, libraries with several tens of thousands of compounds can be easily synthesized in a short time starting from a few reagents. However, the hit rates obtained by these time- and cost-intensive methods, also termed “irrational” because of their untargeted character (“as many as possible and as rapidly as possible”), are frequently less than one tenth of a percent of the number of compounds tested.^[60, 61] Moreover, this method usually ignores knowledge of the features of the biological target. As a consequence, nonrandom or targeted approaches to screening have been developed. Here, the test compounds are preselected by computer methods to maximize their pairwise diversity, for example with respect to chemical properties,^[62] the expected favorable pharmacokinetic behavior,^[63, 64] or the biological target molecule.^[65–69]

Rational drug design follows a different approach. Starting from a known or hypothetical mode of action or binding mechanism, a lead structure is rationally designed and subsequently tested experimentally. The obtained results are fed back into a design cycle as new information (Figure 1).^[51, 70] Impressive results have been obtained with this strategy, as presented, for example, in the recently published studies on the discovery of inhibitors of DNA gyrase^[71] or matrix metalloproteinase 13.^[72] Although this approach is still in its infancy and has only recently profited from advances in computer technology and methodology,^[73, 74] there are already

Holger Gohlke, born 1972, studied chemistry in Darmstadt and completed his Diplomarbeit in 1997 under the supervision of Prof. F. W. Lichtenthaler. He obtained his doctorate in 2000 with Prof. G. Klebe, Philipps-Universität Marburg, where he developed methods for the prediction of protein–ligand interactions. Currently, he is working as a Feodor Lynen Research Fellow with Prof. D. A. Case at the Scripps Research Institute, La Jolla, USA. His research interests are in the area of computational chemistry and computer-aided drug design.



H. Gohlke



G. Klebe

Gerhard Klebe, born 1954, studied chemistry at the University of Frankfurt and obtained his doctorate in physical chemistry. As a Studienstiftung scholar he spent a year in Grenoble, France, at the CNRS and ILL working on experimental electron-density determinations. After postdoctoral positions in crystallography (H. Fuess and H. B. Bürgi), he joined BASF-AG in Ludwigshafen, where he was responsible for molecular modeling and crystallography in drug research. He obtained his Habilitation in pharmaceutical and structural chemistry at the University of Heidelberg in 1992. In the summer of 1996, he was appointed full Professor for Pharmaceutical Chemistry at the University of Marburg. The focus of his research is directed towards various aspects of drug design, in particular the interaction of small-molecule ligands with proteins. The presently applied methods involve molecular biology and protein chemistry, crystallography, bioinformatics and software development, application of drug-design methods, microcalorimetry, and the synthesis of initial lead structures.

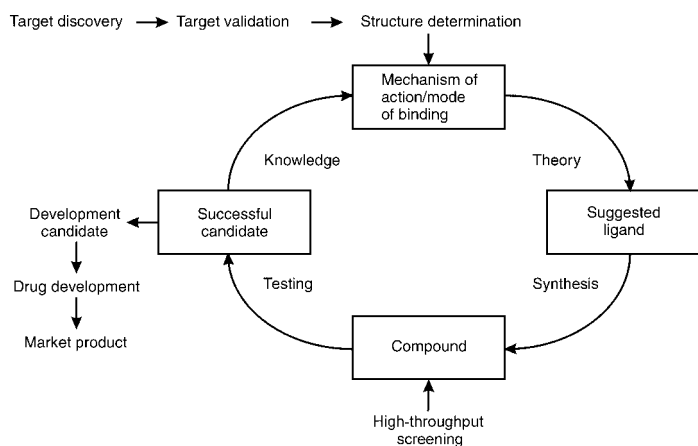


Figure 1. General approach for the rational design of inhibitors. Starting with discovered or previously synthesized compounds and biological testing, information about the mechanism of action or binding mode is used as a starting point for a subsequent design cycle assisted by computational methods.

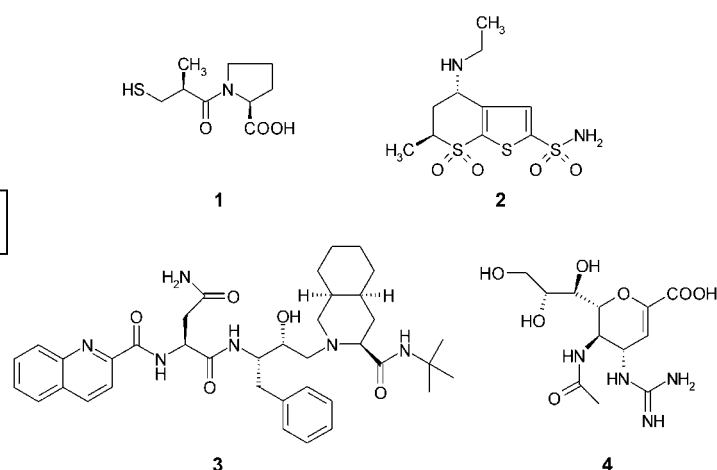
a fair number of examples in which the development and optimization of drug candidates have strongly profited from this approach^[75–79] (Table 1).

Table 1. Proteins, for which inhibitors were discovered or optimized by rational drug design.

Protein	References
aldose reductase	[80, 81]
calmodulin	[82]
carboanhydrase	[83–86]
cyclooxygenase-2	[87, 88]
elastase	[89–91]
FKBP12	[92, 93]
gyrase	[94]
HIV protease	[95–103]
papain	[104]
purine nucleoside phosphatase	[105]
renin	[106–109]
reverse transcriptase	[110–117]
selectin	[118–121]
sialidase (neuraminidase)	[122–132]
streptavidin	[133–136]
thermolysin	[137]
thrombin	[138–145]
thymidylate synthase	[146]

Furthermore, a number of drugs have already been introduced into therapy, which were discovered by this strategy, or where rational design has played a key role in the discovery process, for example, the angiotensin-converting-enzyme (ACE) inhibitor captopril (**1**),^[147] the carboanhydrase inhibitor dorzolamide (**2**),^[77] the HIV-protease inhibitors saquinavir (**3**), indinavir, ritonavir, and nelfinavir,^[148] and the sialidase inhibitors zanamivir (**4**) and oseltamivir (Scheme 1).^[149]

The strategy to be followed in rational design depends on whether the three-dimensional structure of the biological target molecule is known or not. In the latter case, “quantitative structure–activity relationships” (QSAR methods)^[150–154] can be used to establish a relationship between



Scheme 1. Drugs used in therapy, whose development was significantly supported by rational design.

molecular structure and biological activity for a series of active compounds. These models do not only explain the relative differences among the observed affinities, but also allow an affinity prediction for unknown compounds. An alternative procedure is the generation of a pharmacophore model from a series of active compounds.^[155] Here, the molecular properties of the active compounds are represented in geometric terms, which are a prerequisite for biological activity. In a subsequent step new, potentially active, candidate molecules are retrieved from a compound library that obey the pharmacophore hypothesis.^[156] In addition, the results from QSAR methods provide some insight into the structural requirements of the receptor responsible for the derived structure–activity relationship. This information can also be used to generate mini- or pseudoreceptor models.^[157–160]

The gradually increasing number of structurally characterized macromolecular receptors^[2] (Figure 2) provides the basis for any *structure-based design* of active compounds. Receptor geometries are predominantly determined by crystal-structure analysis. The obtained geometries are assumed to be relevant also for the conditions in solution.^[161–166] Using information about the properties of the ligand-binding site along with the assumption, based on the lock-and-key

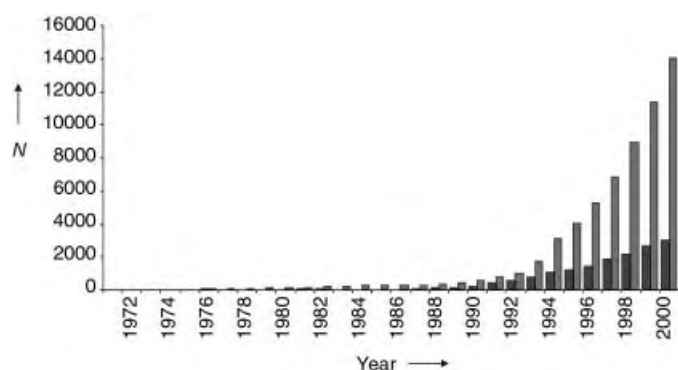


Figure 2. Total number of entries *N* stored in the protein databank PDB^[2] (light gray bars) and entries newly deposited every year (dark gray bars; status January, 2001).

principle, that a potent ligand must exhibit significant structural and chemical complementarity with the binding pocket, two strategies for computer-aided drug design are possible: in de novo design, novel leads are generated in the binding pocket starting from prepositioned seed atoms or fragments that are subsequently grown into entire molecules.^[167, 168] Alternatively, a compound library can be screened for ligands in agreement with the binding-site requirements. The individual molecules are flexibly docked into the binding site.^[169] In both cases, a fast *prediction of ligand affinity* towards the receptor is the most crucial step: only if this assessment is performed with acceptable accuracy and reliability can new leads be discovered by computational methods. This latter strategy is known as virtual screening.^[47, 48, 170] Besides considerably reducing the time and costs of the development, more importantly, the structural insights and affinity information learned can be used subsequently for lead *optimization*.

Two aspects determine the success of computer-aided structure-based ligand design: the generation of reasonable ligand-binding modes (*configuration-generation problem*) and the recognition of those binding modes that correspond best to the experimentally given situation based on a reasonable estimate of the expected binding affinity (*structure and affinity prediction problem*).^[171] An objective test of docking methods performed in 1997^[172] confirmed the assumption that recognizing near-native geometries and predicting their affinities could be achieved only with limited success,^[173–175] whereas the problem of generating reasonable ligand orientations is considered to be virtually resolved,^[50, 176] at least for proteins with rather rigid binding pockets, not involving any water molecules in binding and without any change in protonation state of either ligand or protein upon binding.^[177]

In this review, our current knowledge of the description and prediction of binding affinities of small-molecule ligands to proteins will be summarized. In addition, we will present some of our own recent results on this topic which, on the one hand, give a better understanding of the thermodynamic aspects of ligand binding and, on the other hand, provide a clear improvement in computer docking and virtual screening.

2. Binding Affinity as a Result of Inter- and Intramolecular Contributions—Macroscopic Effects Resulting from Microscopic Events

2.1. 3D Receptor–Ligand Structures—Windows to the World of Interactions

3D structures of receptors (and ligands) do not only form the basis for structure-based drug design. Many of the aspects of ligand-binding described in the following would still be only superficially understood if we did not have the facilities to study them on a molecular level. Protein crystallography,^[7, 8, 178] complemented by high-resolution NMR spectroscopy,^[9–11] provides us with the required information about the arrangement of the atoms in space.

With respect to the study of protein–ligand complexes, it must be kept in mind that X-ray diffraction hardly differentiates between isotopes and elements of similar atomic number because of their comparable diffraction power. Except for protein structures at very high resolution, the positions of terminal N and O atoms, for example, in asparagine and glutamine, can only be assigned on the basis of a self-consistent hydrogen-bond network. Similar problems occur for the imidazole ring of histidine which can adopt two virtually indistinguishable orientations. Moreover, the positions of the poorly diffracting hydrogen atoms remain undetermined. This is of particular importance in the case of H atoms of conformationally flexible groups (for example, hydroxy or amino groups), as well as for groups that can be (de)protonated. However, a consistent picture of the localization of (polar) H atoms and the adopted protonation state can usually be assigned by analyzing the atoms in the neighborhood.^[179, 180]

The relevance of the protein geometry obtained by crystal-structure analysis is mainly determined by the quality of the studied crystals. Resolutions below 1.5 Å (coinciding with the mean length of a covalent bond) are rarely obtained for protein crystals; values between 2 and 3 Å are more usual. Atomic resolution is achieved below 1.2 Å. Along with techniques for experimental phase determination, insights into the electronic structure of molecules^[181, 182] and the localization of polar H atoms can be achieved. The estimated standard-deviation value in atomic coordinates is inherently related to resolution, for example, for a resolution of 2.5 Å this value is about 0.4 Å.^[183–185] This has to be considered whenever intermolecular interactions are discussed on the basis of protein crystal structures.

Furthermore, crystallography performs an averaging in time and space of the individual molecules forming the crystals.^[163] Crystal contacts between neighboring molecules can result in intermolecular interactions, which may affect parts of a structure. Besides positional disorder, which results in distinct occupancies of alternative atomic positions, dynamic disorder also results from thermal motion of the atoms about their equilibrium positions. Even for atoms with an average Debye–Waller factor (B factor) of 20 Å², the mean atomic displacement from equilibrium amounts to 0.5 Å. Moreover, because of time and space averaging during data collection and the requirement for an unperturbed periodic arrangement, only spatially restricted atoms contribute constructively to diffraction and thus only their positions can subsequently be located.

This applies especially to water molecules which can make up to 70 % of the number of atoms in a protein crystal.^[186, 187] While the water molecules of the first hydration shell surrounding protein or ligand are generally well-ordered, their mobility increases with their distance from the molecular surface.^[188]

Moreover, multiple binding modes of ligands can occur as a result of spatial averaging. In such situations, the same ligand can occupy several energetically equivalent orientations in the binding pocket. This case is especially true for weakly binding ligands. In addition, deviating binding modes can occur in different polymorphic forms of the crystalline state. Under

kinetically controlled conditions^[190–192] deviating packing arrangements can be formed, which result in different crystal structures of distinct physicochemical properties.^[189] In the case of crystals of proteins or protein–ligand complexes, these “polymorphs” are usually referred to as “different crystal forms”. Nevertheless, often they exhibit deviating (enzymatic) properties; for example, depending on the crystallization conditions, lipase crystals can be obtained in an “open” or “closed” form.^[166]

In summary, any referral to “the” crystal structure of a compound or protein–ligand complex has to be regarded with some care in the light of these effects that could lead to multiple crystal forms.

2.2. Factors Determining Ligand–Receptor Binding Affinity

The selective binding of a small-molecule ligand to a particular protein is determined by a mutual structural and energetic recognition.^[193–195] Ligands can interact either covalently or noncovalently with their biological target.

The noncovalent, reversible association of receptor (R) and ligand (L) to form a receptor–ligand complex (R'L') generally occurs in an aqueous, electrolyte-containing solution [Eq. (1)].



Under thermodynamic equilibrium conditions, this reaction is determined by the standard Gibbs free energy (or free enthalpy, used in the following) of binding ΔG° . This quantity is related to the experimentally determined association constant K_A (or its reciprocal dissociation or inhibition constants, K_D or K_i , respectively) [Eq. (2)]. ΔG° is composed of an enthalpic (ΔH°) and an entropic ($T\Delta S^\circ$) portion. T refers to the absolute temperature.^[196, 197] In place of ΔG° , the term (binding) affinity is used to describe the tendency of a molecule to form a complex with another one.

$$K_A = K_D^{-1} = K_i^{-1} = \frac{[R'L']}{[R][L]} \quad (2)$$

$$\Delta G^\circ = -RT \ln K_A = \Delta H^\circ - T\Delta S^\circ$$

According to Equation (3), with μ_i^0 as the chemical standard potential of the species i , ΔG° can also be understood as a function to describe the stability of the complex with respect to free ligand and uncomplexed receptor.^[198, 199]

$$\Delta G^\circ = \mu_{R'L'_{\text{aq.}}}^\circ - (\mu_{R_{\text{aq.}}}^\circ + \mu_{L_{\text{aq.}}}^\circ) \quad (3)$$

Experimentally determined inhibition constants fall into a range between 10^{-2} and 10^{-12} M, which corresponds to a Gibbs free standard enthalpy of binding of -10 to -70 kJ mol⁻¹ at $T = 298$ K.^[194] A change in free enthalpy of 5.7 kJ mol⁻¹ at this temperature alters the inhibition constant by one order of magnitude. A comparison of affinities of reversibly binding ligands shows that the increase in binding affinity is about 6.3 kJ mol⁻¹ per atom for molecules with up to 15 non-

hydrogen atoms. Moreover, for larger ligands the affinity is only slightly dependent on the molecular weight.^[200]

It is generally accepted that electrostatic interactions determine noncovalent ligand–receptor binding. They comprise salt bridges, hydrogen bonds, dipole–dipole interactions, and interactions with metal ions. Furthermore, solvation and desolvation contributions, and the mutual spatial complementarity in van der Waals interactions are of utmost importance.^[199, 201–203] The latter aspect has been summarized by Dunitz and Gavezotti in the context of attractive or repulsive interactions in molecular crystals as “empty space is wasted space”.^[204] Similar considerations have been found for protein–ligand complexes.^[93] Additional effects are determined by intramolecular changes of receptor ($R \rightarrow R'$ and ligand ($L \rightarrow L'$) during complex formation.^[194, 195]

2.2.1. Electrostatic Interactions

Pauling already highlighted the importance of hydrogen bonding^[205, 206] for the structures of proteins and their ligand complexes.^[207] Nevertheless, even today, no consensus view on the relative contribution of hydrogen bonding to the thermodynamics of protein folding and ligand binding has been established.^[208–211]

Hydrogen bonds result from an electrostatic attraction between a hydrogen atom bound to an electronegative atom X (usually N or O) and an additional electronegative atom Y or a π -electron system. Distances of 2.5–3.2 Å between hydrogen-bond donor X and acceptor Y and X–H...Y angles of 130–180° are typically found.^[206] Whereas no or only a slight dependency of the hydrogen-bond strength with angular changes are observed in the range of $180 \pm 30^\circ$,^[212] shorter distances down to 2.3 Å result in a more covalent bond character and a larger binding energy,^[213] although, the latter aspect does not hold in general.^[214, 215]

As a result of the electrostatic nature, the strength of a hydrogen bond depends on its microscopic environment: the shielding of electrostatic interactions depends on the local dielectric constant ϵ of the surrounding medium, which means that the Coulombic interaction energy is proportional to ϵ^{-1} . While ϵ values of 1–20 (mostly 2–8) are assumed for the protein interior, the value at the protein periphery, next to the surrounding water, is about 80.^[216, 217] Furthermore, in close proximity to polar groups a higher dielectric constant is expected compared to a nonpolar environment.^[218] This also applies to more conformationally flexible regions of the protein.^[219] Therefore, buried hydrogen bonds are regarded as more important for protein–ligand interactions than those formed in solvent-exposed regions.^[220, 221]

The importance of water in the overall inventory of interactions is further indicated by the fact that only 1–2% of all buried N–H and C=O groups of protein amide bonds do not form a hydrogen bond.^[222] Prior to complex formation, the functional groups of the uncomplexed receptor and the free ligand are involved in hydrogen bonds to surrounding water molecules in the solvent. In the complex, they are replaced by hydrogen bonds of comparable strength formed between the ligand and the receptor. It is hence the *difference* in the free enthalpies of these contributions to the hydrogen-bond

inventory that ultimately determines whether hydrogen bonding contributes to binding affinity or not.^[223–225] Buried polar groups of a ligand or protein that remain unpaired are thus regarded as highly detrimental to complex formation.^[220] As an upper limit in such unfavorable situations, a free-enthalpy contribution of 29 kJ mol^{−1} has been estimated.^[226] On the other hand, these considerations underline why electrostatic interactions and hydrogen bonds are frequently the predominant contribution to the *specificity* of molecular recognition.^[201, 210]

At physiological pH values (ca. 7.4), it is assumed that in proteins the guanidine side chain of arginine ($pK_a = 12.5$) and the terminal amino group of lysine ($pK_a = 10.8$) are protonated, whereas the carboxy groups of aspartic ($pK_a = 3.9$) and glutamic acid ($pK_a = 4.1$) are deprotonated (pK_a values according to reference [227]). Even more complex to predict are the properties of histidine residues ($pK_a = 6.5$). Their exact protonation state will depend upon the dielectric conditions imposed by the local environment. These can change upon ligand binding (Figure 3).^[228, 229] If the bound ligand provides a sterically suitable arrangement of groups oppositely charged to the protein residues, attractive electrostatic interactions, so-called “salt bridges”, can be formed (Figure 4).^[230]

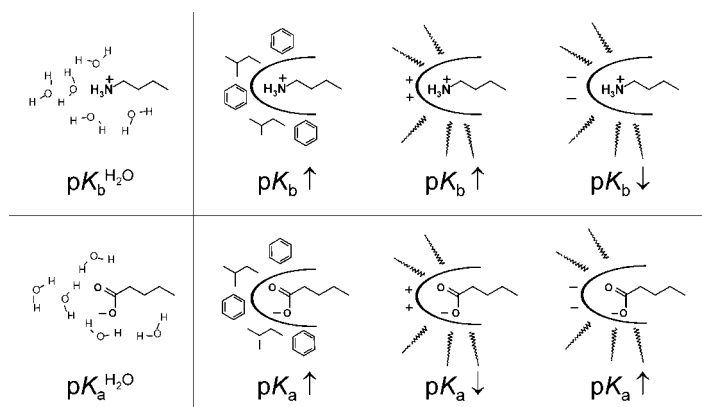


Figure 3. Impact of the protein environment on the pK_b values of a basic ligand group (upper row) and pK_a values of an acidic ligand group (lower row) compared to aqueous solution ($pK_b^{\text{H}_2\text{O}}$ and $pK_a^{\text{H}_2\text{O}}$).

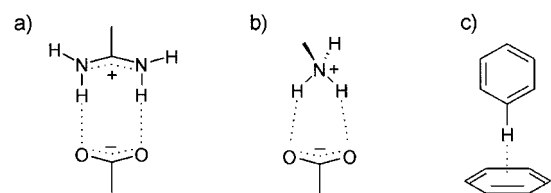


Figure 4. Examples of patterns of special hydrogen bonds: a), b) bidentate ionic (“salt bridges”), c) C–H... π interaction.

The contributions of hydrogen bonds and salt bridges to binding affinity have been estimated, however, the derived values must be considered with respect to the origin of these data. Evidence from protein-mutation studies suggest values for the interaction between uncharged partners of $\Delta G^\circ = -5 \pm 2.5$ kJ mol^{−1}.^[210, 223, 231] Similar values originate from investigations of structures and solution energies of crystalline cyclic dipeptides^[232] and studies estimating the contribution of

intramolecular hydrogen bonds to the stability of proteins.^[233–235] In contrast, values of -10 – -20 kJ mol^{−1} have been reported for charge-assisted hydrogen bonds and salt bridges.^[231, 236] The interpretation of the experimentally determined “apparent” binding contributions suffers from one important problem common to all these studies: the measured quantities correspond to the “intrinsic” contribution of an interaction only if superimposed effects can be excluded.^[231, 237, 238] For example, the contribution of a hydrogen bond was initially reported by Williams and co-workers to be about -25 kJ mol^{−1}.^[239, 240] Later, this estimate was reduced to -1 to -7 kJ mol^{−1} because of incorporation of initially neglected effects.^[241, 242] Similarly, Andrews et al. overestimated the contribution of hydrogen bonds to complex formation because they assumed too large values for the entropic contributions that are detrimental to binding.^[203]

Hydrogen bonds also influence ligand binding by their strong directional nature. Besides theoretical^[243] and spectroscopic investigations, the analysis of crystal data primarily provides important information about their geometry.^[244, 245] Carbonyl and carboxylate oxygen atoms form interactions mainly along the direction of their lone-pair electrons;^[246, 247] for carboxylates the lone-pairs in the *syn* position are preferred to those with *anti* orientation.^[244, 248, 249] A comprehensive compilation of the geometries of nonbonding interactions observed in crystalline solids is given in the IsoStar database^[250] (Figure 5).

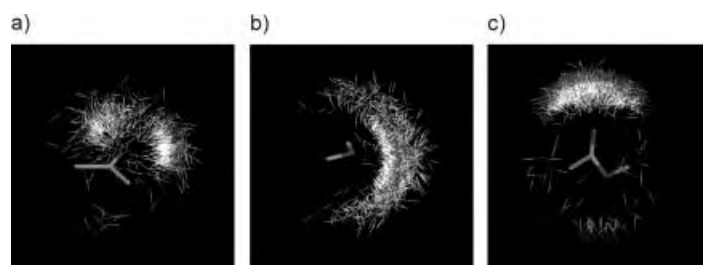


Figure 5. Composite picture of intermolecular interactions as observed in the crystal packing of small molecules compiled in the database IsoStar.^[250] Shown are the arrangements of hydroxy groups around aliphatic ketones (a), aliphatic ethers (b), and aliphatic esters (c) as central groups.

Much weaker, but equally directional^[251] hydrogen bonds are known between C–H...O, C–H...N, C–H... π -systems, and C–H...Cl^[252–256] that also occur in more hydrophobic regions of proteins. Significant contributions to ligand-binding affinity also arise from so-called π – π interactions^[257, 258] between aromatic groups of ligands and side chains such as phenylalanine, tyrosine, or tryptophan.^[259–261] Furthermore, interactions between cations, such as tetraalkylated amines, and aromatic residues are observed.^[262–264] The latter play a significant role in the binding of positively charged ligands to the nicotinic acetylcholine receptor.^[265, 266] Interestingly, comparative calculations on the strength of salt bridges versus cation– π systems in aqueous solution revealed an up to 10 kJ mol^{−1} greater contribution to binding affinity by the latter type of interactions.^[267] Coordinative bonds of ligand functional groups (e.g. hydroxamates, carboxylates, phosphates, thiols) to protein-bound metal ions also stabilize

receptor–ligand complexes.^[268, 269] “More subtle” electrostatic contributions such as dipole–induced dipole, dipole–quadrupole, and quadrupole–quadrupole interactions to protein–ligand binding were found in highly resolved carbonic anhydrase II–ligand complexes. There, the electrostatic interactions were modified systematically by replacing the benzyl hydrogen atoms with fluorine atoms in *N*-(4-sulfamylbenzoyl)benzylamine.^[270]

2.2.2. Solvation and Desolvation

In biological systems, molecular recognition between two molecules takes place in an aqueous environment. Thus, in addition to its role in the energetics of hydrogen bonds, as described in the previous section, water has an additional influence on the formation of protein–ligand complexes.^[271–273]

In the condensed bulk phase, water molecules form a network of three to four hydrogen bonds per molecule.^[205] Similar behavior is also found for about 80% of the water molecules that mediate interactions between protein and ligand, as evidenced by the analysis of 19 highly resolved crystal structures of protein–ligand complexes.^[274] Assuming optimal geometry for these solvent-mediated interactions, a contribution to binding affinity of -10.5 to -12.5 kJ mol⁻¹^[275, 276] and -7 kJ mol⁻¹^[277] has been estimated. The latter value results from an entropic contribution (-30 J mol⁻¹ K⁻¹, corresponding to 9 kJ mol⁻¹ for $-T\Delta S$ at 298 K)^[278] and an enthalpic contribution (-16 kJ mol⁻¹)^[279] which corresponds to the transfer of a water molecule from the bulk phase into the binding epitope.

Analyzing the topography of the surrounding molecular surfaces, it becomes evident that interstitial water molecules in the protein–ligand interface preferentially occupy cavities in the protein surface and less frequently reside in depressions on the ligand surface (Figure 6).^[277, 280, 281] A series of highly

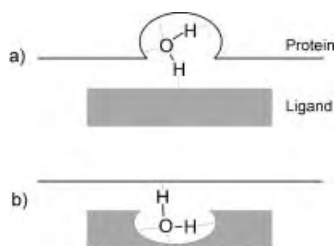


Figure 6. Schematic representation of water molecules mediating an interaction between protein and ligand; a) more frequently observed situation with a water molecule strongly bound to the protein; b) water molecule that is more strongly bound to the ligand (Figure adapted from reference [277]).

resolved crystal structures of the oligopeptide-binding protein (OppA) accommodating different Lys-xxx-Lys ligands (xxx: natural and non-natural amino acids)^[282, 283] shows that, in these complexes, water molecules act as mediators to complement the side-chain residues xxx of different size, whereas the protein structure (apart from the rotation of the side chain in Glu32) remains almost unchanged (Figure 7).



Figure 7. Superposition of the binding pockets extracted from four complex structures of the oligopeptide binding protein (OppA; white) with ligands Lys-xxx-Lys; for each example only the central xxx residue is shown in a different color (orange: Ala (PDB-Code 1jet), violet: Trp (PDB-Code 1jev), green: Glu (PDB-Code 1jeu), light blue: Lys (PDB-Code 2olb)). The water molecules are displayed as spheres with corresponding colors. The rigidity of the binding pocket (apart from Glu32) is obvious, together with a cluster formation of several water molecules.

However, the water molecules do not move without restriction within the ligand-binding pocket. In each case, they occupy energetically favorable, partially conserved positions (Figure 7).^[277, 284–286] Interestingly, the binding constants vary in total by only one order of magnitude even for the exchange Trp → Ala and Lys → Glu as xxx.^[283]

The unique role of water compared to other solvents—forming a tetrahedrally connected network and simultaneously occupying only an exceptionally small molecular volume^[287–289]—also emerges in the desolvation of proteins and ligands upon complex formation. This step involves not only the rupture and reformation of hydrogen bonds to functional groups, but also the reorganization of the water structure at the interface. This is reflected both in the enthalpic and entropic contributions to the binding affinity.^[240, 290–293]

The fact that the transfer of a nonpolar compound or a nonpolar surface portion into water is a) highly unfavorable, b) associated with a reduction in entropy at room temperature, and c) correlated to an increase in heat capacity has been summarized as the “hydrophobic effect”.^[233, 294–298] First introduced by Frank and Evans^[299, 300] the “iceberg model” assumes that during the hydration of a nonpolar compound a *reduction* in the number of hydrogen bonds between water molecules occurs, but that water molecules next to the interface form *stronger* hydrogen bonds than those in the bulk water phase. Accordingly, Silverstein et al.^[301] calculated a free enthalpy of $\Delta G = 2.0$ kJ mol⁻¹ for the cleavage of a hydrogen bond in pure water, whereas the same step involving water molecules in the first solvation sphere around argon atoms requires a free enthalpy of $\Delta G = 2.6$ kJ mol⁻¹. This effect results in a clathrate-type restructuring of the adjacent

water shell along with a partial immobilization of the water molecules.^[302–304]

Whereas the enthalpic contribution almost cancels out for this process at room temperature (fewer but stronger hydrogen bonds instead of many such bonds of medium strength), the entropy decreases because of a higher ordering of the water molecules.^[301] This step is entropically disfavored, but only up to a critical temperature T_s which depends on the nature of the compound to be transferred. At T_s the entropic contribution to the transfer vanishes.^[297, 302] On the opposite side, for $T < T_s$, the burial of a hydrophobic surface upon complex formation corresponds to a favorable entropy-driven process ($\Delta H \approx 0$, $\Delta S > 0$). This view is supported by spectroscopic studies of surface-specific vibrations of molecular arrangements at the $\text{CCl}_4/\text{H}_2\text{O}$ or hydrocarbon/ H_2O interface. Although these studies indicate rather weak hydrogen bonds among the water molecules at the phase interface, the molecules mutually orient because of interactions with the organic phase.^[305]

This classical view, however, is not generally accepted.^[298, 302] An alternative approach does not regard the structuring of the water molecules as the main reason for hydrophobic interactions. Instead, it involves a positive enthalpy resulting from the rupture of several hydrogen bonds in order to create a cavity in the water structure that subsequently accommodates the nonpolar compound.^[306, 307] In agreement with this hypothesis, calorimetric measurements found that contributions of 25–100% of the protein–ligand binding enthalpy originate from solvent reorganization.^[308]

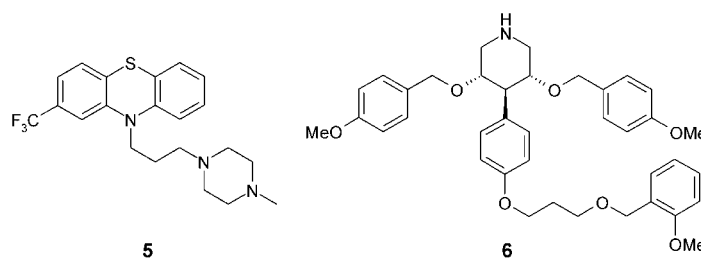
The contribution of hydrophobic interactions to the free enthalpy in protein folding or protein–ligand complex formation can be regarded as proportional to the size of the hydrophobic surface buried during these processes.^[309–314] This allows quantitative characterization of the effects involved.^[315, 316] Solubility studies of hydrocarbons in water revealed -0.10 to $-0.14 \text{ kJ mol}^{-1} \text{ \AA}^{-2}$ as a contribution to hydrophobic interactions.^[309, 310, 317, 318] The correlation of the hydrophobic surface buried upon receptor–ligand binding with experimentally determined binding affinities revealed values of -0.11 to $-0.24 \text{ kJ mol}^{-1} \text{ \AA}^{-2}$ as contributions to the free enthalpy.^[240, 319, 320] The burial of a methyl group ($\approx 25 \text{ \AA}^2$) contributes -2.75 to -6 kJ mol^{-1} , thus increasing the association constants at 298 K by a factor of 3–11. In contrast, however, values of -0.08 to $-0.64 \text{ kJ mol}^{-1} \text{ \AA}^{-2}$ were determined in mutation studies for the influence of hydrophobic interactions on the stability of proteins.^[321–324] Again, most values obtained suggest larger contributions compared with those resulting from solubility studies. This finding can be explained by a cooperative effect (see Section 2.2.4).^[325] Once such effects are neglected, the sole consideration of the size of the buried surface reveals the reported higher contributions per \AA^2 . Huang and Chandler have recently suggested that for small hydrophobic molecules a scaling with molecular volume is more appropriate, whereas for larger hydrophobic molecules scaling with the molecular surface reveals a better correlation.^[326]

Hydrophobic interactions are also regarded as the main driving force for conformational changes of the receptor upon ligand binding. This induced fit can be viewed as a “collapse”

of the receptor about the ligand.^[199] As an extreme case, the binding of trifluoperazine (**5**) to Ca^{2+} calmodulin induces a conformational change of the protein from an extended to a compact form (Figure 8).^[327] Crystal structures of 3,4,5-substituted piperidine derivatives (e.g. **6**) bound to renin show an induced adaptation of the binding pocket to accommodate the attached substituents (Scheme 2).^[328] Similar cases have been described for protein–ligand complexes of aldose reductase^[329] and glycogen phosphorylase.^[330]

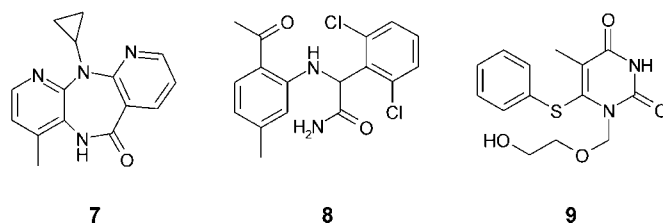


Figure 8. Superposition of the N-terminal domains of calmodulin as uncomplexed (dark gray: PDB code 1lin) and ligand-bound enzyme (light gray: PDB code 3cln). The four bound trifluoperazine molecules (**5**) indicate the induced collapse of the protein upon ligand binding. Only the backbone trace of the protein is shown in each case.



Scheme 2. Ligands of Ca^{2+} -calmodulin (**5**) and renin (**6**) that induce an adaptation of the protein binding pocket.

A comparable orientation of drugs with rather deviating shapes in the same binding pocket originates from induced-fit adaptations as a consequence of favorable hydrophobic interactions. An impressive example is the binding of nevirapin (**7**), α -APA (**8**), or HEPT (**9**; Scheme 3) to HIV-1 reverse transcriptase.^[331] While none of the C- α atoms shift position by more than 2.7 \AA , any structural adaptation of the protein is a response to changes in the substitution pattern of



Scheme 3. Inhibitors of HIV-1 reverse transcriptase.

the inhibitors (Figure 9).^[199] HIV-1 reverse transcriptase has to adapt its conformation consecutively while binding to the substrate RNA. Accordingly, it can be assumed that the observed inhibitor binding freezes different “snapshots” along this conformational transition path.

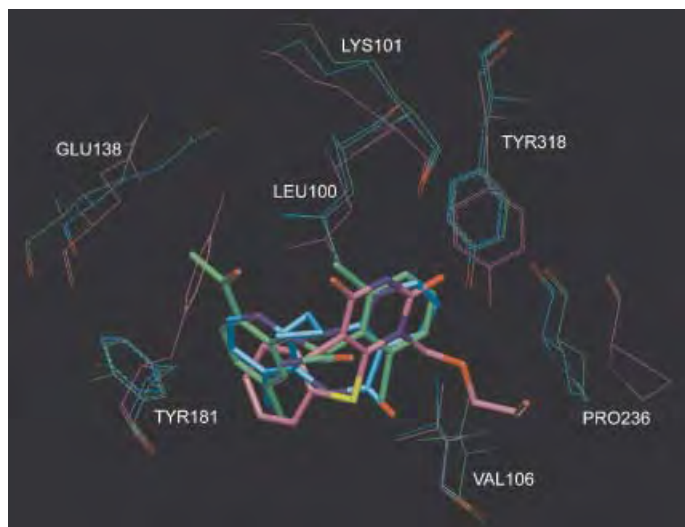


Figure 9. Induced fit of the binding pocket of HIV-1 reverse transcriptase resulting from the binding of nevirapin (7; cyan: PDB-Code 1vrt), α -APA (8; green: PDB-Code 1vru) and HEPT (9; violet: PDB-Code 1rti). The protein residues are color coded similar to the ligands. For clarity, only the amino acids which are next to the ligands in a sphere of $< 4 \text{ \AA}$ and are involved in pronounced conformational changes upon binding of the different ligands are shown.

2.2.3. Intramolecular Changes of Ligand and Receptor

Upon complex formation, the change in degrees of freedom of the different components involved results in a change of entropy.^[332] If the complex formation, neglecting any involved water molecules, is regarded as a bimolecular association step, each component loses three degrees of translation and rotation, while six new vibrational degrees of freedom are created.^[290, 333–335] Although partitioning of the standard enthalpy into individual contributions is formally impossible for such processes in solution,^[336] this simplification provides first insights into the influence of flexibility and mobility of protein and ligand on complex formation.^[332]

The application of the Sackur–Tetrode approach or Trouton’s Rule^[337] requires the arguable assumption^[338] that the results are transferable to solution processes^[198, 339]. If so, for the *complete* immobilization of a molecule a loss in entropy of about $-420 \text{ J mol}^{-1} \text{ K}^{-1}$ results.^[340] However, losses about half this size ($\approx -200 \text{ J mol}^{-1} \text{ K}^{-1}$ ^[290, 333, 334, 343] corresponding to 60 kJ mol^{-1} at 298 K) were found experimentally. The difference can be attributed to the residual mobility of molecules in the complex. The latter is estimated by considering the experimentally observed motion in the crystals (e.g. lysozyme^[341] or insulin^[342]) or the entropy changes involved in inter- and intramolecular reactions. Even smaller contributions of $9\text{--}45 \text{ kJ mol}^{-1}$ were found by Searle and Williams for the melting or sublimation of hydrocarbons or polar organic

molecules.^[292] This is in agreement with results for the association of rigid cyclic dipeptides in the solid, liquid, and gas phases.^[344] Hermans and Wang calculated 29 kJ mol^{-1} (at 300 K) for the free enthalpy of binding of benzene to a lysozyme-T4 mutant resulting from the partial loss of translational and rotational degrees of freedom. This calculation also allowed the estimation of the remaining free space in the binding pocket available for motion of the benzene molecule. Positional deviations of 0.6 \AA in atomic coordinates and $10\text{--}15^\circ$ in rotation about the normal vector of the ring plane were found as root-mean-square deviations in a mutual superposition.^[345]

Upon binding, conformational mobility is restricted, reducing the internal degrees of freedom of rotatable bonds. Such entropic contributions to the free enthalpy of binding were suggested to fall into a range between 0.5 kJ mol^{-1} ,^[236] 2.5 kJ mol^{-1} ,^[292, 343] and $4\text{--}6 \text{ kJ mol}^{-1}$,^[290, 333, 334] at 298 K. For amino acids, the probabilities of rotameric states were calculated based on observed conformational distributions of solvent-exposed side chains in protein crystals. These probabilities were used to estimate the entropy loss for the restriction of their conformational mobility.^[346, 347] Contributions to the free enthalpy from 0 (for Ala, Gly, Pro) to 8.7 kJ mol^{-1} (for Gln), with a mean value of 3.7 kJ mol^{-1} per residue, were suggested.

Experimental evidence indicates that ligands frequently retain considerable residual mobility in the bound state. An *increase* in mobility of the protein can even favorably influence the free binding enthalpy.^[348] Residual mobility is found, for example, for the binding of camphane, adamantane, or thiocamphor to cytochrome P450_{cam}.^[349] Without forming a hydrogen bond, the ligands rotate freely in the binding pocket. They are, therefore, hydroxylated nonselectively. The binding of DNA to the C-terminal domain of topoisomerase 1^[350] demonstrates that complex formation is not solely associated with a restriction of molecular mobility. While some of the protein residues become more highly ordered, others become more mobile. For the binding of a hydrophobic mouse pheromone to mouse major urinary protein, NMR relaxation studies^[351] showed that an increase in protein backbone entropy reveals a considerable *favorable* contribution to the free enthalpy of binding, which is of the same order of magnitude as other contributions. Similarly, Weber et al.^[134, 352] observed by crystallographic and thermodynamic studies of natural and synthetic streptavidin inhibitors that the ligand with the highest binding affinity also experiences the largest residual mobility in the complex.

An alternative strategy to compensate for entropic losses caused by ligand immobilization results from conformational preorganization in solution. In the case of the thrombin inhibitor D-Phe-Pro-boro-Arg,^[353] a “hydrophobic collapse”^[354] in aqueous solution minimizes the hydrophobic surface of the D-Phe and Pro side chains. At the same time, a conformation is adopted that strongly resembles the receptor-bound conformation.^[355] Interestingly, an inverse “hydrophilic collapse” of the immune suppressors CsA and FK506 is made responsible for their high membrane permeability and suggests a formulation of the administered drugs in olive oil.^[356]

Besides entropic contributions, enthalpic differences between solution and receptor-bound conformations of a ligand also influence the free binding enthalpy. Comparing computed force-field energies of the protein-bound conformations with those of the global minima in vacuum revealed differences between 0–167 kJ mol⁻¹ for 33 compounds, with a mean value of 67 kJ mol⁻¹.^[357] For three different dihydrofolate reductase inhibitors, an unfavorable conformational energy contribution to binding of 112–296 kJ mol⁻¹ has been calculated.^[358] These unrealistically high values result from a comparison of the receptor-bound conformers with those in the gas phase. However, such a comparison is of no relevance. Similar studies based on conformational ensembles produced from a solvation model suggest that conformational enthalpy differences amount to less than 12 kJ mol⁻¹, thus slightly disfavoring the receptor-bound state.^[359] In addition, Vieth et al. found that the spatial orientation of “anchor points” responsible for ligand binding to the protein coincide well in protein-bound conformations with those of minimum-energy structures.^[360] In several cases, conformations were also found for ligands which deviate slightly from those in the crystal structure, but have a significantly lower conformational energy.

It has to be considered that the anisotropic molecular environment of the protein perturbs the energy barriers separating different conformational (rotational) states. For example, this influence has been described by comparing the enzyme-bound conformation of methotrexate (an inhibitor of dihydrofolate reductase) with that adopted in its small-molecule crystal structure.^[361] This polarization effect has to be considered in the development of advanced force fields.^[362]

2.2.4. Additivity, Cooperativity, and Enthalpy–Entropy Compensation

Approaches based on group additivities [Eq. (4)] or the additivity of free enthalpy components [Eq. (5)] are frequently applied to understand and predict protein–ligand interactions. In this respect, pioneering work was performed by Andrews et al.^[203] and Lau and Pettitt.^[363]

$$\Delta G = \Delta G_{\text{CH}_3} + \Delta G_{\text{OH}} + \Delta G_{\text{phenyl}} + \dots \quad (4)$$

$$\Delta G = \Delta G_{\text{H-bridge}} + \Delta G_{\text{solvation}} + \Delta G_{\text{conformation}} + \dots \quad (5)$$

Already the variation in the absolute contributions discussed in the previous section demonstrates that this partitioning is not possible in a straightforward way. Strict application of statistical thermodynamics shows^[364] that the free energy (free enthalpy) is a global property of the system under consideration. It thus depends on the total configuration space of the system. Hence, while separation of energy into (pairwise) individual contributions is a reasonable first approximation, this is, in principle, not valid for entropy^[332] and free energy.^[365] As a state function, the free energy is path independent, however, this does not apply for its components, as confirmed by nonadditivity in mutation studies.^[237, 238, 366–368] A separation into individual components is possible if the total system under investigation is separated into mutually

independent subsystems.^[364] The latter is questionable, especially for biological systems featuring weak, noncovalent interactions which lead to many nearly identical (macroscopic) states.^[369]

As an alternative, one can focus on the partitioning of the most dominant part of the free energy [Eq. (6)]^[365, 369, 370]:

$$\Delta G = \Delta H_{\text{H-bridge}} + \Delta H_{\text{solvation}} + \Delta H_{\text{conformation}} + \dots + T\Delta S \quad (6)$$

This strategy has been used, for example, for the calculation of “intrinsic binding energies” from free enthalpies of binding of molecules with groups A, B, or A + B to a protein.^[237, 291]

An impressive example for nonadditivity—also^[371, 372] termed “cooperativity”—becomes apparent for the correlation of the “hydrophobic free enthalpy” with the solvent-inaccessible, nonpolar surface. Protein mutation studies and studies on ligand binding show that the hydrophobic effect obviously promotes stability and binding in aqueous solution to a large extent as suggested by solvent transfer measurements (see Section 2.2.2).^[315] However, the burial of a part of a hydrophobic molecular surface at a binding site can induce a simultaneous cooperative enhancement of neighboring electrostatic interactions.^[325, 372]

The contribution of the standard enthalpy ΔH° and entropy ΔS° to the free (binding) enthalpy ΔG° [Eq. (1)] can be determined directly from microcalorimetry^[373] or van’t Hoff plots of affinity measurements at different temperatures^[374] (see Section 4). Generally, these experiments do not indicate any direct correlation between ΔH° and ΔG° . Thus, any interpretation or prediction of binding properties solely based on enthalpic considerations must be inadequate.^[194] A possible exception might be given for series of closely related ligands with very similar entropic contributions.

The clear correlation between ΔH° and ΔS° (“enthalpy–entropy compensation”) is obviously an intrinsic property of weak intermolecular interactions.^[242, 336] This correlation is generally observed in (supramolecular) host–guest^[375] and receptor–ligand complexes.^[293, 376, 377] However, this form of compensation is by no means a “general” principle.^[378, 379] It can be interpreted that an enhancement of intermolecular binding is accompanied by a loss in degrees of freedom of mobility and vice versa. Its existence is of particular importance for the prediction of receptor–ligand interactions: whereas the individual enthalpic and entropic contributions can vary over large ranges, the total change in free enthalpy is frequently close to zero. As a consequence, small *relative* errors in the prediction of ΔH° and ΔS° can have significant influence on ΔG° .

3. Theoretical Approaches to the Prediction of Binding Affinities

Studies on the prediction of binding affinities can be divided into two major categories:

- If the *3D structure of the biological target molecule is not known* the (often qualitative) prediction of the binding affinity of new ligands is based on the comparison with known reference structures such as endogenous ligands or

previously synthesized compounds.^[150, 151, 380, 381] The considerable importance^[382] of these methods arises from the fact that many pharmacologically important targets are membrane-bound proteins, such as G-protein-coupled receptors (GPCR),^[383, 384] ion channels,^[385] or transport proteins.^[386–388] As, apart from a few examples, no experimentally determined 3D structure of sufficient accuracy is available for these systems, usually only indirectly obtained models can be used.

- If the 3D structure of the receptor is known, binding affinity predictions are performed considering geometrical and chemical complementarity between ligands and biological targets.^[173–175, 198, 389–394] Because of the steadily growing number of spatially characterized receptors (Figure 2), an increasing impact of the latter strategy is to be expected in the near future.

In this review, we focus on methods exploiting the 3D structure of the receptor. As, however, comparative molecular-field analyses (3D QSAR) yield surprisingly good affinity predictions, merely by learning from the information provided by a ligand-training set, these methods will be briefly discussed in the following.

3.1. Approaches without Knowledge of the Receptor Structure

Affinity prediction of ligands in the absence of information about the receptor structure assumes that similarity in biological response is reflected by chemical similarity of the ligands.^[380] Approaches that compare molecules on the one- or two-dimensional level^[395] by means of topological descriptors consider the presence or absence of functional groups by associated bit vectors (so-called fingerprints). They will not be discussed here. Similarly, methods based on substructure mapping,^[396] pharmacophore searches,^[397] and superpositioning of ligands will not be considered.^[398–400] Usually, these methods predict the expected binding affinity only on a qualitative scale.

In contrast, quantitative predictions can be obtained from Quantitative Structure–Activity Relationships (QSAR).^[150] A correlation between structure and biological properties (e.g. affinity or selectivity) of a molecule is determined with respect to physicochemical and structural parameters. Classical 2D-QSAR methods, established by Hansch and Fujita^[401] or Free and Wilson,^[402] suffer from the fact that only data sets of structurally similar ligands can be studied and the spatial structure, essential for the understanding of receptor–ligand interactions, is only vaguely or indirectly considered.^[403]

This limitation is relieved in 3D-QSAR methods:^[152, 404] relative differences in the spatial structure of individual ligands are correlated with a known target property, such as binding affinity. As a prerequisite, the bioactive conformations of all ligands have to be considered to be aligned with each other, which best reflects their assumed arrangement in the binding pocket.^[398] A conformationally rigid example in the data set could be used as a reference structure for a subsequent molecular superpositioning.^[405] Equally well, conformations taken from known protein–ligand com-

plexes,^[406, 407] or functional groups in agreement with a pharmacophore hypothesis can be used.^[408, 409] Besides atom- or group-based superposition methods, molecular fields are used to maximize their mutual similarity, in particular in flexible alignments.^[398, 400]

In the following, a short description of current 3D-QSAR methods will be given, with emphasis on CoMFA (Comparative Molecular Field Analysis) and related developments. Comprehensive reviews in this field have been given by Kubinyi,^[150, 151] Sanz et al.,^[410] and van der Waterbeemd.^[411]

- The 3D-grid-based CoMFA method,^[405] developed from DYLOMMS,^[412] compares a series of molecules in terms of molecular energy fields. It subsequently correlates field differences with differences in the dependent target property, for example, the binding affinity. In its original implementation, steric and electrostatic interaction energies are calculated for all molecules in the data set at the intersections of a grid containing all molecules. This approach assumes that entropic contributions are constant across the data set used for the analysis. For each molecule n , this QSAR results in the Equation (7):

$$\text{Affinity}_n = k + \alpha_1 S_{n,1} + \dots + \alpha_M S_{n,M} + \beta_1 E_{n,1} + \dots + \beta_M E_{n,M} \quad (7)$$

The indices $1, 2, \dots, M$ reflect the respective grid points, and $S_{n,1}, \dots, S_{n,M}$ and $E_{n,1}, \dots, E_{n,M}$ describe steric and electrostatic energies at these points. The coefficients $\alpha_1, \dots, \alpha_M$ and β_1, \dots, β_M are obtained from a system of linear equations by partial least-squares analysis.^[413, 414] Binding affinities of new molecules, not included in the training set, can be predicted using the derived model.

While steric and electrostatic fields account for only enthalpic contributions, attempts have been described to reflect entropic contributions through the characterization of hydrophobic properties.^[415] These approaches include fields based on HINT (Hydrophobic Interaction),^[416, 417] molecular lipophilic potentials (MLP),^[316] GRID fields^[418] based on an H₂O or a DRY probe, or desolvation energy fields calculated with DelPhi.^[419]

- Alternative molecular interaction fields are applied in CoMSIA (Comparative Molecular Similarity Indices Analysis).^[420] Here, Gaussian functions are used to describe steric, electrostatic, and hydrophobic similarities. Similarly, hydrogen-bond donor and acceptor properties are considered.^[244, 421] Compared to CoMFA, this approach avoids particularly steep potentials next to molecular surfaces. Thus, similarity indices are also determined close to the molecules.
- The HASL approach (Hypothetical Active-Site Lattice)^[422] is another grid-based 3D-QSAR technique. It tries to attribute partial activities to grid points within the van der Waals volume of the ligands. The sum of the values at all grid points assigned to one molecule reflects the parameter to be correlated.
- In the Compass method,^[423] molecular interaction fields are calculated in the proximity of the van der Waals surface of the considered molecules, thus focusing on the area likely to be involved in receptor–ligand binding. In addition, the number of descriptors is largely reduced. A QSAR model is

then generated using a back-propagation neural network. Subsequently, this model is further improved by iteratively generating and superimposing conformations of the molecules in the data set.

- In contrast to the previous methods, APEX-3D avoids molecular interaction fields.^[424] Instead, a relationship between structural properties and observed activity is automatically established in a stepwise fashion. Molecules with similar activity are analyzed for corresponding 2D-topological or 3D-topographical patterns. Using logical programming, pharmacophores are identified which provide the basis for molecular superpositioning. Finally, a 3D-QSAR model is generated based on physicochemical properties of the pharmacophoric groups and global molecular properties such as hydrophobicity and molar refraction.
- The YAK method^[158] is based on studies by Höltje and Kier.^[425] Putative amino acid residues are placed in space using a set of ligands to generate a so-called pseudoreceptor. YAK selects and orients the amino acid side chains automatically. If available, crystallographic information, data from sequence analysis of homologous proteins, or mutation studies can be considered. This selection and positioning is iteratively optimized until the computed interaction energies best reflect the affinity data of the ligand under investigation. Finally, a pseudoreceptor is constructed by linking the placed amino acids with poly-Gly fragments.

3.2. Approaches Based on Knowledge of the Receptor Structure

The success of docking and de novo design methods strongly depends on the prediction of binding affinity, purely based on the spatial orientation of a ligand in the binding site.^[174, 175, 426] The fundamentals of statistical thermodynamics used to calculate binding affinity are critically summarized in references [173, 198]. Reviews on applications are given in references [174, 175, 389–391, 394, 427, 428]. The determination of molecular interaction fields based on the known receptor structure is reviewed in reference [429]. References [430, 431] consider special applications and advances in force fields used in this context. A review on the handling of electrostatics in macromolecular systems is found in references [216, 432–436], whereas references [437–445] summarize the advances in calculating free enthalpy and entropy in the context of the thermodynamic perturbation theory.

In the following, the methods are classified and described with respect to their methodological background. This separation is not always strict, as several techniques combine different approaches.

3.2.1. Free-Energy-Perturbation Calculations and Linear Free-Energy Approaches

From a thermodynamic point of view, the rigorous prediction of relative free energies of binding of ligands to proteins results from free-energy-perturbation (FEP) calcu-

lations [Eq. (8)]^[446] or thermodynamic integration (TI) [Eq. (9)],^[447] with explicit consideration of solvent molecules and flexibility of both the receptor and the ligand.^[173, 390, 426]

$$\Delta F = F_1 - F_0 = -k_B T \ln \left\langle \exp \left(-\frac{H_1(\vec{X}) - H_0(\vec{X})}{k_B T} \right) \right\rangle_0 \quad (8)$$

$$\Delta F = F_1 - F_0 = \int_0^1 \left\langle \frac{\partial H_\lambda(\vec{X})}{\partial \lambda} \right\rangle_\lambda d\lambda \quad (9)$$

The basis for these approaches is given by the relationship between the Helmholtz free energy F of a system and the ensemble average of an energy function describing the system under consideration.^[444, 448, 449] $H_\lambda(\vec{X})$ is the energy of the system as a function of the coordinates (\vec{X}) of the particles in configuration space and a coupling parameter λ , k_B is the Boltzmann factor, and T the absolute temperature. The indices “0” and “1” represent $\lambda = 0$ and $\lambda = 1$, respectively. The configurational ensemble averages are taken either from Monte Carlo (MC)^[450] or molecular-dynamics (MD) simulations.^[451] As the difference between free *enthalpy* and free *energy* corresponding to the product of pressure and volume change experienced in an isothermal and isobaric reaction is negligible for processes in solution, free enthalpies are also available.

The method is suitable for studying individual contributions to the free energy/enthalpy on an atomic level or on the level of individual subsystems, such as ligand or protein.^[238, 452, 453] However, it frequently encounters problems concerning the general applicability, which are caused by limited or insufficient sampling of the configuration space, the accuracy of the applied force fields, and the dependence of the results on the protocols used for simulation.^[437, 438, 454] Moreover, long simulation runs are required and they can only allow for minor chemical differences in the ligands if their relative free energies/enthalpies are to be predicted reliably.^[455–458] Some case studies, together with more recent approaches, will be mentioned.

- Postma et al.^[448] and Jorgensen and Ravimohan^[459] used FEP-MD and FEP-MC simulations to predict relative free-energy differences for the binding of benzamidine and *p*-fluorobenzamidine to trypsin,^[460] or for a set of peptidic inhibitors to thermolysin.^[225] In the latter case, a remarkable agreement between *predicted* and experimental values has been achieved,^[461] although only minor structural modifications (exchange of NH to O by CH₂) of the ligands were studied. For example, the addition of a phenyl ring to an inhibitor obviously did not result in full convergence of the computed energies, even after 400 ps simulation time. Compared to experiment, the predicted relative free energy had the wrong sign.^[457] Moreover, Graffner-Nordberg et al. stress that *all* processes combined with ligand binding—such as a change in protonation state—must be considered in the computed energies.^[229] A comprehensive review of examples used for the prediction of protein–ligand affinities is given in reference [442].
- Ota and Brunger^[462] combined non-Boltzmann sampling of configuration space with TI (NBTI). The advantage of this so-called umbrella sampling results from an artificially enhanced ligand flexibility caused by reduced internal

barriers to rotation and a thus augmented sampling of configuration space. Compared to classical TI, smaller deviations between calculated and experimental relative free energies are obtained for benzamidine or benzylamine binding to trypsin.^[463]

- While standard free-energy calculations require time-consuming sampling of configuration space for *each* ligand modification individually, Gerber et al. suggest a simultaneous consideration of an entire *set* of modifications in one single MD simulation.^[464] Assuming a linear separation of individual contributions, the derivative of each individual interaction with respect to the coupling parameter λ is determined analytically. Thus the initial gradients in free-energy contributions at $\lambda = 0$ allow the estimation of the contributions in the final state $\lambda = 1$. Although this method reduces computational efforts by a factor of 10^{-3} , simulations of the binding of trimethoprim-based inhibitors to dihydrofolate reductase and NADPH did not reveal a significant correlation between computed and experimental results.
- Oostenbrink et al.^[465] used a “single-step perturbation” method to estimate relative free binding energies of endogenous and xenobiotic ligands to the estrogen receptor.^[466] Instead of the usual FEP or TI calculations being performed for each ligand, an artificial reference molecule is simulated to generate a configuration ensemble that is representative of all ligands under consideration. Using Equations (8) and (9), the relative free enthalpy between two (real) ligands is calculated using the ΔG difference of the ligands with respect to the artificial reference molecule. Although the computational effort is reduced by a factor of 4–6 with respect to classical TI and mean deviations from experiment of 1.7 kJ mol^{-1} are obtained, it has to be considered that, for four out of five cases, ligand structural variations were limited to the presence or absence of hydroxy or methyl groups.
- Guo et al.^[467] introduced a method in which the coupling parameter λ is handled as a dynamic variable. It develops together with the atomic coordinates of the system following Newton’s law of motion. For a series of related ligands using a set of λ s, relative free energies of binding are simultaneously computed. In the simulation, the different portions of the ligands all interact with the surrounding protein, but none of the ligands “takes notice” of any other one. An efficient mapping of configuration space is achieved with a significant reduction in computational effort.^[468]
- To circumvent the problems occurring in classical free-energy simulations by using large, structurally diverse sets of ligands, a semiempirical method was developed by Åquist et al.^[469, 470] They calculated absolute free energies of binding by considering MD simulations of two physical states. Polar and nonpolar contributions to the free energy are approximated linearly, by taking mean values from simulations of the ligand and protein–ligand complex in water. Required weighting parameters are calibrated using binding affinities of known complexes. However, this adjustment of energy contributions and the scaling of the weighting parameters depends on the simulation condi-

tions and the system setup,^[471, 472] and, accordingly, the general scope of the method appears limited.^[473]

- Jorgensen and co-workers go one step further, by using an equation of the form (10):^[474, 475]

$$\Delta G = \sum_i c_i \xi_i + \text{const} \quad (10)$$

The physicochemical parameters ξ_i reflect ensemble average values obtained from MD or MC simulations. The parameters comprise, for example, the number of hydrogen bonds formed or the size of the buried hydrophobic, hydrophilic, and aromatic surface patches. The c_i values are adjusted by multiple linear regression using a training data set. In this respect the method can be classified as a regression-based approach (see Section 3.2.3). However, for the study of HEPT and nevirapin analogues binding to HIV-1 reverse transcriptase, differently composed Equations (10) were found, depending on the compilation of the training set.^[475] This raises some suspicion about the general applicability and transferability of the approach.

3.2.2. Force-Field-Based Methods and Approaches Based on Additive Free-Enthalpy Contributions

The approaches described in this section assume partitioning of the free enthalpy of ligand-to-receptor binding into a sum of individual contributions [Eq. (5)] (for this assumption, see Section 2.2.4).^[173, 198, 426] Starting from a “master equation” (ME), individual terms are defined on physicochemical grounds, whilst avoiding any cross correlations among them. Furthermore, unlike the methods described in the previous section (Section 3.2.1), all free-energy contributions are no longer derived as *ensemble* mean values, but taken from a single (or a few) generic structure(s). This is an important limiting approximation.^[173]

- Modeling intermolecular interactions of protein–ligand complexes by simple molecular-mechanics force-field calculations in vacuum reflects purely enthalpic contributions to the free enthalpy of binding.^[194, 426] By considering only van der Waals and electrostatic interactions, along with some intramolecular energy contributions, correlations with experimentally determined binding affinities have been obtained for series of closely related ligands, in which entropic contributions can be assumed to be constant.^[476–480] In one example, the result obtained without the explicit consideration of solvent was explained by the predominance of van der Waals interactions and solvent-independent electrostatic contributions.^[481]
- A straightforward approach to including solvent effects in the “master equation” which describes ligand–receptor binding is the use of atom-based solvation parameters,^[311, 312, 314] usually scaled to the surface portion of protein and ligand that is buried upon complex formation. The methods of Vajda et al.,^[482] Weng et al.,^[483] Williams and co-workers,^[240, 241, 484] Krystek et al.,^[485] and Novotny et al.^[486] consider contributions that are adverse to binding as additional terms, which originate from the loss of translational, rotational, and torsional degrees of freedom of the molecules (see Section 2.2.3). Krystek et al., Vajda

et al., and Weng et al. modeled the intermolecular interactions by Coulombic interactions using a distance-dependent dielectric constant; Williams and co-workers used intrinsic binding contributions of functional groups instead. For flexible ligands, Vajda et al. additionally^[482] determined the energy difference experienced by *intramolecular* interactions of the molecule in the free and the bound state.

- The contribution of electrostatic interactions in the presence of water can be determined as an “averaged-field” approximation or continuum representation of the solvent by solving the linearized Poisson–Boltzmann equation^[216] with the method of finite differences^[487] or finite elements.^[488] In this context, *polar* interaction energies of receptor, ligand, and receptor–ligand complex are compared to each other and determined with respect to the surrounding solvent, by considering the molecules (with discrete atomic charges) as regions of low dielectricity embedded in a medium of higher dielectric constant.^[432] The *nonpolar* contribution to desolvation is assumed to be proportional to the size of the surface of both molecules buried upon complex formation. Entropic contributions attributed to the loss of mobility and flexibility are modeled as described in the previous section. Based on this concept, methods to predict free enthalpy of binding were suggested by Froloff et al.,^[489] Zhang and Koshland,^[490] Hofmann et al.,^[491] Politicelli et al.,^[492] and Shoichet et al.^[493] Instead of the Poisson–Boltzmann approach, Zou et al.^[494] used the “generalized Born Model” (GB/SA) of Still et al.^[495] for the calculation of polar interaction energies.
- In the MM/PBSA method^[440, 496, 497] and related approaches,^[498–500] the free enthalpies for a molecular species are given by Equation (11):

$$\langle G \rangle = \langle E_{\text{MM}} \rangle + \langle G_{\text{PBSA/GBSA}} \rangle - TS_{\text{MM}} \quad (11)$$

E_{MM} reflects the mean molecular-mechanical energy, $G_{\text{PBSA/GBSA}}$ is the free enthalpy of (de)solvation obtained by solving the Poisson–Boltzmann equation (PB) or using the generalized Born approach (GB) and a surface-dependent term (SA). Both contributions are obtained by averaging over a sample of representative geometries extracted from a MD trajectory of the species under investigation with explicit consideration of water molecules and counter ions. The term $-TS_{\text{MM}}$ stands for the entropic contributions of the considered species, taken from a quasi-harmonic or normal mode analysis of the MD trajectory. The large scope of applications of this method demonstrates^[501–504] that the properties of protein–ligand complexes exhibiting extensive structural differences can be studied.

- Alternatively, an implicit consideration of the contributions from solvation and desolvation can also be determined directly by molecular mechanics.^[505] Thereby, the free solvation energy attributed to a functional group or amino acid residue is determined using the free solvation energy of the same group when part of a small molecule. This latter solvation contribution has to be reduced by an amount related to the exclusion of solvent molecules caused by their replacement by other atoms of the macromolecular system.

3.2.3. Regression-Based Approaches

As described in the previous section, regression-based approaches—also called “empirical scoring functions”—assume an additivity of individual terms to the total free enthalpy. However, the individual contributions (weighting factors or coefficients) of the separate terms describing the independent variables in the regression equation are determined either by multiple linear regression, partial least-squares regression^[414] or a neural-network analysis,^[506] using a training set of crystallographically resolved receptor–ligand complexes, together with experimentally determined binding affinities. Based on empirical concepts, the explanation of the obtained contributions along with their ability to predict unknown binding affinities justifies the initially assumed partitioning of the free enthalpy. Common to all regression-based methods, the results obtained as well as their transferability to new compound classes depend considerably on the compilation of the training set.^[173] Furthermore, contributions of phenomena rarely observed in the experimental data, which frequently enough are the unfavorable ones, will be described insufficiently by the regression analysis.

- The archetype of an empirical scoring function for protein–ligand interactions was developed by Böhm (SCORE1).^[507] Using a training data set of 45 protein–ligand complexes, the regression analysis with respect to experimentally determined affinities results in a cross-validated standard deviation of 9.3 kJ mol^{−1}. In this analysis, the sum of contributions to hydrogen bonds, ionic interactions, buried nonpolar surface regions, and the loss of (intra)molecular mobility has been considered. Expanding this training set to 82 complexes and considering the degree of burial of hydrogen bonds in the binding epitope along with special terms for aromatic and unfavorable electrostatic interactions, a standard deviation of 8.8 kJ mol^{−1} has been achieved for a prediction data set (SCORE2).^[508] These analyses also showed that the (relative) contributions of the individual terms depend on the compilation of the training set. The same holds for different strategies in partitioning the free enthalpy.

A similar approach has been described by Eldridge et al.^[509] (82 complexes in the training set, ChemScore) and Wang et al.^[510] (170 complexes in the training set, SCORE). Compared to Böhm’s approach,^[507, 508] Eldridge et al.^[509] handle contributions for intramolecular flexibility differently and Wang et al.^[510] classify hydrogen bonds as “strong, moderate, and weak”, including the occurrence of interstitial water molecules as mediators of interactions. An “evolutionary test” demonstrates^[510] that the resulting coefficients only converge if a set of more than 100–120 protein–ligand complexes, which deviate sufficiently in the types of intermolecular interactions, is used for analysis. Murray et al.^[511] improved the predictive power of the scoring function obtained by Eldridge et al.^[509] with respect to a *selected* protein including additional information through Bayesian statistics.

- In their “VALIDATE” approach, Head et al.^[512] use electrostatic and steric interaction energies from AMBER,^[513] an HlogP-based^[514] octanol–water partition coefficient, polar

and nonpolar contact surfaces, and a term to describe intramolecular flexibility. The coefficients for the various contributions were derived based on 55 protein–ligand complexes by means of a partial least-squares^[414] or a neuronal-net analysis. Both strategies result in regression equations that can hardly be interpreted in physical terms. Their relevance, in particular with respect to ligand *optimization*, is thus rather limited.

- In studies of Takamatsu and Itai^[515] (29 avidine ligand complexes in the training set), Venkatarangan and Hopfinger^[516] (23 glycogen phosphorylase–inhibitor complexes in the training set), and Viswanadham et al.^[517] (11 HIV-1 protease–inhibitor complexes in the training set), AMBER interaction energies between protein and ligand^[513] were combined with additional terms to describe hydrophobic interactions and other entropic contributions. The individual coefficients were again determined by multiple linear regression.
- Rognan et al.,^[518] Bohacek and McMartin,^[519] and Kasper et al.^[520] also developed empirical scoring functions tailored towards *one* particular protein. In the first case, training sets of five crystallographically determined HLA-A*0201 peptide–inhibitor complexes and 37 modeled H-2K^k peptide–inhibitor complexes were used to reparameterize the scoring function of Eldridge et al.^[509] Bohacek and McMartin used only nine characterized thermolysin–inhibitor complexes for calibration and considered only the number of hydrogen bonds or hydrophobic contacts in their scoring function. Kasper et al. used an approach similar to Equation (11) scaling, however, the different contributions relative to a training set of 11 peptide–chaperone DnaK complexes.
- In contrast to the functions described above, Jain developed a function^[521] that is continuously differentiable. Terms to describe hydrophobic and polar complementarity of receptor and ligand are modeled combining a Gaussian and a sigmoidal function. Only ligand-dependent contributions are used for handling entropic considerations. The analysis is based on 34 protein–ligand complexes in the training set.

3.2.4. Knowledge-Based Approaches

Knowledge-based approaches are based on the idea that a sufficiently large data sample can serve to derive rules and general principles inherently stored in this knowledge base.^[522] Accordingly, the development of a knowledge-based scoring function at an atomic level is based upon observed frequency distributions of typical interactions in experimentally determined structures: in any system, only those interactions that are close to the frequency maxima of the interactions in the knowledge base are considered to be favorable. This approach has been successfully applied in the field of protein-fold prediction.^[523–525] Using the concept of the “inverse Boltzmann law”,^[526] the frequency distributions of interatomic interactions, derived from protein crystal structures, are converted into “potentials of mean force” or “knowledge-based potentials”. Although the thermodynamic foundation of this procedure^[365, 527–529] and the terminology

used^[530] have been debated, the results obtained by these approaches are superior to those obtained by molecular-mechanics force fields.^[531–534]

Recently, the following approaches have been published on protein–ligand systems:

- Verkhivker et al.^[535] derived distance-dependent knowledge-based pair potentials for a data set of 30 HIV-1, HIV-2, and SIV protease–inhibitor complexes. These potentials were combined with desolvation terms for ligand and protein using atom-based parameters.^[536] To estimate contributions arising from the conformational immobilization of protein side chains, a method introduced by Pickett and Sternberg has been adapted.^[346] Differences in binding affinities of several HIV-1 protease–inhibitor complexes can be reproduced by this concept.
- Surface patches of *pairs* of interacting atoms buried upon complex formation are computed by Wallqvist et al.^[537] in terms of frequency distributions from a set of 38 protein–ligand crystal structures. Atom-based statistical preferences are produced by normalizing with the product of buried surfaces of the corresponding *individual* atoms. Using two parameters calibrated by experimental binding affinities of the training-set molecules, binding affinities of ten additional HIV protease–inhibitor complexes were predicted with a standard deviation of 6.3 kJ mol^{−1}.
- DeWitte and Shakhnovich^[538] used 17 or 109 crystal structures, respectively, from the protein data bank (PDB)^[2] to develop “interatomic-interaction free energies” (SMoG-Score) for ligands that bind to the surface of a protein or into binding pockets. Using a Metropolis–Monte Carlo-based^[450] construction procedure, ligands are generated and energetically ranked in the binding pocket. The method has been applied to complexes of purine nucleoside phosphorylase, the SH3 domain, and HIV-1 protease.
- Muegge and Martin^[539] produced “Helmholtz free interaction energies” (“PMF” score; potential of mean force) from 697 crystallographically determined protein–ligand complexes by using 16 protein and 34 ligand atom types, respectively. Implicit contributions of water are considered using a specific volume correction term^[540] and sampling atom distances up to 12 Å to produce the pair-distribution functions. For a test set of 77 protein–ligand complexes studied crystallographically, a deviation of 1.8 log units in reproducing the experimentally determined binding constants is found.
- Mitchell et al.^[541] published pair potentials (BLEEP) derived from 820 protein–ligand atom-pair distributions based on the “inverse Boltzmann approach”. The analysis included hydrogens initially positioned by the program HBPlus.^[222] As reference state, a semi-empirical Ne–Ne pair potential, suggested by Ng et al.^[542], has been used. In addition, the consideration of water molecules as part of the protein has been tested. For 90 diverse protein–ligand complexes a correlation coefficient of 0.74 (a standard deviation is not reported) is achieved for experimentally determined affinities.^[543]
- The scoring function DrugScore, developed by us,^[544] (see Section 5) is composed of distance-dependent pair poten-

tials and solvent-accessible-surface-dependent singlet potentials. They are computed using distribution functions retrieved from 1376 protein–ligand complexes as stored in the ReliBase data base.^[545] For 55 well-distributed protein–ligand complexes determined by crystal-structure analysis, a deviation of 1.8 log units from experimentally determined inhibition constants has been found.^[546]

3.2.5. Consensus Scoring and Filter Functions

Although not satisfactory from a scientific point of view, a pragmatic strategy to enhance the reliability of predicted binding affinities results from the simultaneous consideration of several scoring functions. Charifson et al.^[547] used a logical AND operation to combine the scoring of ChemScore,^[509] the AMBER-based^[513] function in DOCK,^[548] and the “piecewise linear potential” function^[549]. In a virtual screening assay using three different target enzymes, this consensus scoring function allowed the retrieval of known active inhibitors from a set of randomly selected molecules with a significantly improved reliability. So and Karplus averaged the predictions of up to five different QSAR methods and showed that the combined predictions were superior to the results obtained from the individual evaluations.^[550] Using seven different target proteins for virtual screening, Stahl and Rarey^[551] considered a combination of terms from PLP score^[549] and SCORE1.^[507] They implemented this function into the docking program FlexX^[552] to achieve overall more robust enrichment rates. Interestingly enough, in several cases the combined function does not achieve the same (high) enrichment rates as obtained with the original functions. Terp et al.^[553] even proceeded a step further by correlating the scores of eight functions by using a PLS analysis with experimentally determined binding affinities for a heterogeneous data set of 120 crystallographically determined protein–ligand complexes. Compared to the Consensus Scoring suggested by Charifson et al., the latter approach provides *quantitative* predictions of binding properties. Applying this model to predict affinities of 120 docked MMP inhibitors revealed deviations of less than one log unit for pK_i values in 49 % of the cases.

Because of the way in which they are derived (see Section 3.2.3) regression-based methods evaluate predominantly those favorable interactions *most frequently* exhibited in crystal structures of protein–ligand complexes. However, to recognize and disfavor those protein–ligand geometries occasionally produced by computational docking but which are not in agreement with the experimental evidence, Stahl and Böhm suggested the usage of “filter functions”.^[220] These functions cope, for example, with situations in which polar atoms are buried upon binding but do not form appropriate hydrogen bonds, or where hydrophobic cavities in the protein–ligand binding epitope are generated.

3.2.6. Approaches to the Location of Interactions in Space

Assuming a successful partitioning of binding affinity into individual (additive) contributions (see Section 2.2.4), methods for locating favorable interaction sites can play an

important role in the optimization of ligands in the binding pocket.

- The archetypical method in this area is Goodford’s GRID program.^[418, 554] It is based on a tailored force field. Regions in the binding pocket are contoured in terms of the interaction energies that various probes experience at the intersections of a regularly spaced grid. Such probes could be, for example, water, amino or carboxy groups, or hydrophobic groups (DRY).
- Similar concepts, but based on crystal data are used in the X-SITE^[555] and SuperStar^[556, 557] methods. The X-SITE method uses spatial contact distributions derived from 163 triatomic fragments to highlight favorable interaction sites in a binding pocket. The distributions were retrieved from 83 high-resolution protein structures (without ligands). SuperStar uses spatial information stored in IsoStar.^[250] This latter database comprises nonbonded interactions compiled from crystal data of small molecules in the CSD.^[1] These data are subsequently used to calculate probability densities for contacts with atoms of functional groups (such as ammonium nitrogen atoms, carbonyl oxygen atoms, methyl carbon atoms, ...) at the intersections of a grid embedded into the protein binding pocket.
- Similarly, the knowledge-based pair potentials implemented into DrugScore can be used to identify hot spots of binding^[544] (see Section 5) using appropriate probe atoms (such as aliphatic carbon, carboxylate, carbonyl, hydroxy-oxygen, amino nitrogen...)^[546]
- In contrast, the MCSS (Multiple-Copy Simultaneous-Search) approach^[558] based on the CHARMM force field^[559] distributes probe molecules such as acetamide, methanol, acetate, or propane at favorable positions in the binding pocket. The method has been extended to study flexible regions in the binding pocket.^[560]
- The PROFEC (Pictorial Representation of Free-Energy Changes) approach of Radmer and Kollman^[561] and enhancements of Pearlman^[562] (OWFEG, One-Window Free-Energy Grid) are based on FEP calculations. Two MD trajectories are used to determine free-enthalpy changes resulting from the placement of an atom or group at *different* locations around an inhibitor, both in solution and at the protein binding site.

3.2.7. Comparison of the Various Approaches

A comparison of the developed methods with respect to quality and speed is difficult. First of all, there is not yet a generally accepted data set for establishing and testing a new method. The hardware requirements and the necessary data input preparation for the different approaches are difficult to compare. Moreover, frequently enough the authors have studied a limited set of examples with respect to the scope of the biological systems considered. Accordingly, a reliable assessment of the different methods is difficult. Despite these limitations, the published methods for affinity prediction summarized in Sections 3.2.1–3.2.4 are compared in Table 2 from a methodological point of view. In addition, relationships to other studies or methods are listed.

Table 2. Comparison of the methods for the prediction of binding affinity of receptor–ligand complexes with knowledge of the 3D receptor geometry discussed in Sections 3.2.1–3.2.4.

First author (method name)	Refer- ence	Cross references ^[a]	Method ^[b]	Number of test systems ^[c]	SD ^[d]	Time	Comments
Wong	[460]	–	FEP-MD	2	2.2	–	replacement of benzamide by <i>p</i> -fluorobenzamide and mutation of Gly216Ala in trypsin
Reddy	[564]	–	FEP-MD	2	3.6	–	replacement of a formyl group with a propargyl group
Bash	[225]	[461]	FEP-MD	2	0.5	–	replacement of a NH group with an O atom
McCarrick	[457]	–	FEP-MD	3	8.4	–	substitution of phenyl rings
Ota	[463]	[462]	NBTI	2	1.7	–	improved sampling of the configurational space; replacement of benzamide with benzylamine
Gerber	[464]	–	derivations of the free energy single-step FEP-MD	2 × 36	–	acceleration by 1000 ^{–1}	no significant correlation between experimental and calculated affinities
Oostenbrink	[465]	[466]	λ -dynamic approach	5	3.3 ^[e]	acceleration by 5 ^{–1}	substitution of hydroxy and methyl groups in four of the five ligands.
Guo	[467]	[468]		4	2.1	–	replacement of benzamide with <i>p</i> -aminobenzamide, <i>p</i> -methylbenzamide, <i>p</i> -chlorobenzamide
Åquist	[469]	[471–473]	LIE	18	3.9	–	SD value of Model 6 in Table 2 from reference [470]
Rizzo	[475]	[474]	LIE/LR	2 × 20	3.9	–	different regression equations each according to composition of the data sets
Grootenhuis	[476]	[477, 479]	CHARMM energy	35	8.3	2–5 min per compound	SD value from Protocol 8, Table 3
Hollway	[478]	–	MM2X energy	15	5.7	–	SD for test set from Table 2
Vajda	[482]	[486]	ME based	9 + 3 + 5 + 9	5.4	–	SD for test set from Table 1
Wenig	[483]	[482]	ME based	9 + 10 + 8	≈ 4.2	–	investigation of protein–protein complexes
Williams	[484]	[240, 241]	ME based	1	≈ 11.4	–	SD estimated from errors of individual contributions
Krystek	[485]	–	ME based	9	16.7	–	SD estimated from errors of individual contributions
Checa	[481]	–	AMBER energy + PBE	7	3.3	–	AMBER energy alone correlated equally significantly
Frolloff	[489]	–	PBE + ASP	3 + 5	> 42	–	SD for test set from Table 2 in ref. [489]; systematic error
Zhang	[490]	–	PBE + ASP	9 × 7	2.1	–	9 mutants of isocitrate dehydrogenase as protein components
Kuhn	[502]	[440, 497]	PBE + ASP	1	16.7	–	SD for the biotin/avidin complex
Hoffmann	[491]	[565]	CHARMM + PBE + ASP	10	–	“several h for 100 compounds”	improvement in the placing of docked geometries as target
Pollicelli	[492]	–	PBE + ASP	4	56.4	–	SD for test sets from Tables 1 and 2; systematic error
Shoichet	[493]	[548, 566]	Born equation + ASP	5	20.9	–	SD for test set in Table III; systematic error
Zou	[494]	[566]	GB/SA	6	6.3	10 s per compound	SD for parameter set 1 in Tables 2 and 3
Böhm (SCORE1)	[507]	[565, 567]	regression based	45	9.3	“several compounds per second”	cross-validated SD for function 2
Böhm (SCORE2)	[508]	[565, 567]	regression based	82 + 12	8.8	–	SD for test set from Table 3
Eldridge (ChemScore)	[509]	[511]	regression based	82 + 20 + 10	8.7	–	cross-validated SD for total training set from Table 8
Wang (SCORE)	[510]	[568]	regression based	170	6.3	–	cross-validated SD for total training set from Table 6
Head (VALIDATE)	[512]	–	regression based	51 + 14 + 13 + 11	6.3	–	cross-validated SD for total training set from Table 2
Takamatsu	[515]	–	regression based	29	–	–	calibration solely on avidin complexes
Hopfinger	[516]	–	regression based	15	–	–	calibration solely on glycogen phosphorylase complexes
Viswanadhan	[517]	–	regression based	11	2.4	–	calibration solely on HIV-1 protease complexes
Rognan	[518]	[509]	regression based	5 + 37	3.1 or 5.1	–	calibration on HLA-A*0201 and H-2-K ^b complexes; SD given in each case.
Bohacek	[519]	–	regression based	9	2.3	–	calibration solely on thermolysin inhibitors
Kasper	[520]	–	regression based	11	1.7	–	calibration solely on DnaK–Heptapeptide complexes
Jain	[521]	–	regression based	34	5.7	–	cross-validated SD for function “F”
Verkhivker	[535]	–	knowledge based	7	–	–	derivation and test of the function solely on HIV and SIV proteases
Wallqvist	[537]	[569]	knowledge based	8	6.3	–	SD for calibration set in Table 3
DeWitte (SMoG-Score)	[538]	–	knowledge based	17 + 8 + 11	–	–	no SD value given
Muegge (PMF-Score)	[539]	[570, 571]	knowledge based	77	10.3	–	SD for test set 6 in Table 4
Mitchell (BLEEP)	[541]	[543, 572]	knowledge based	90	–	–	no SD value given
Gohlke (DrugScore)	[544]	[546]	knowledge based	71	9.2	0.2 s per compound	SD for test set “Böhm1998” in Table 2

[a] Listed are references to related work or applications of the method in other programs. [b] For detailed explanations of the methods listed see text. FEP–MD = free-energy perturbation/molecular dynamics, NBTI = non-Boltzmann thermodynamic integration, LIE = linear interaction energy, ME = master equation, PBE = Poisson–Boltzmann equation, ASP = atomic solvation parameter, GB/SA = generalized Born approach, LR = linear regression. [c] The number of protein–ligand complexes used for validation in the individual test sets are reported. [d] The standard deviation between calculated and experimental binding affinities are reported (in kJ mol^{–1}; a temperature of 298 K was assumed for conversion of binding affinities given in logarithmic units). [e] Given is the mean deviation for *relative* free binding energies.

Currently, only a few comparative studies on the evaluation of affinity prediction methods are available. In all published comparisons^[547, 551, 563] enrichment rates achieved in virtual screening are used to assess the quality of the predictions but not the accuracy of the achieved affinity predictions. These studies conclude that, currently, no general-purpose function is available. Depending on the type of target protein and the predominating protein–ligand interactions, the best-suited method has to be selected based on some preliminary tests.

4. Experimental Approaches to Describing Binding Affinity

4.1. Indirect Methods

Binding affinities are usually determined in a binding assay. In the case of enzyme reactions, the influence on enzyme kinetics is followed by means of a readily detectable physical property (e.g. absorption, fluorescence, or fluorescence polarization of one of the reaction partners). The inhibition or binding constant of a ligand is subsequently derived indirectly, by considering the changes in concentration or changes in enzyme kinetics, respectively. For receptor binding studies, inhibitor binding is recorded by the replacement of the ligand with potent, suitably labeled compounds. In all cases, an indirect determination of the binding constant and, accordingly, the free binding enthalpy ΔG° is performed. The partitioning of standard enthalpy ΔH° and standard entropy ΔS° to ΔG° [Eq. (2)] can be determined using van't Hoff plots of affinity measurements at different temperatures.^[573]

In recent years, a large variety of physicochemical methods has been established for the quantitative determination of protein–ligand binding; they are currently being developed further. In this review, only a few such methods will be discussed exemplarily. Plasmon resonance spectroscopy can detect binding of a ligand to a protein immobilized on a solid support or, vice versa, of a protein to a ligand attached to the support by an appropriate anchor group.^[574–576] In particular, the “on” and “off” rates of binding can be studied using this method. A number of NMR spectroscopic pulse sequences have been developed to detect binding through signal shifts or by recording the transfer of magnetization between protein and ligand.^[577–582] Mass spectrometry allows conclusions about the stability and binding affinity of protein–ligand complexes by determining complex dissociation as a function of the measurement parameters (e.g. acceleration voltage).^[583] Under such conditions, the binding parameters are recorded by excluding the solvent environment. This provides valuable complementary information to the other methods.^[584] Furthermore, atomic-force microscopy has been used to determine the strength of protein–ligand interactions by a controlled rupture of the studied complexes.^[585]

4.2. Direct Measurement of Thermodynamic Parameters

Direct access to binding affinities is accomplished through microcalorimetric measurements.^[373] Because of its impor-

tance for the understanding of the thermodynamics of ligand binding, this method will be discussed in more detail. In isothermal titration calorimetry (ITC), a ligand is added in a stepwise fashion at constant temperature to a buffered solution of the receptor. The overall heat of reaction generated upon complex formation is recorded.^[586] The association constant K_A (and, accordingly, ΔG°), together with the stoichiometry of the ligand–receptor binding process are also available. In addition, the binding constant can be computed from the shape of the titration curve. The enthalpic portion of the binding process can be derived from the integrated heat of reaction, the entropic contribution $T\Delta S^\circ$ can be calculated from the difference between ΔH° and ΔG° . Reliable shape analysis of the titration curve requires binding constants of $<10^9 \text{ M}^{-1}$. To measure compounds of higher affinity, the detection range can be extended by the displacement of a lower affinity ligand.^[587–589] Alternatively, for larger affinities the binding constants can also be taken from other experiments (e.g. enzyme kinetics).

The heat of reaction measured in an ITC experiment comprises all intermediate and transient reactions that are superimposed on the binding process. Measuring under different buffer conditions elucidates whether a proton transfer step is involved in the binding process.^[586, 590–592] The functional groups of the protein or ligand can experience changes in protonation state upon complex formation. As a result, the transfer of a ligand from aqueous solution to the protein environment can strongly affect the dielectric properties of the local environment of these groups, resulting in a significant shift of pK_a (pK_b) values (Figure 3). The measured total enthalpy ΔH_{total} is thus composed of the reaction enthalpy ΔH_{bind} and the enthalpy attributed to the proton exchange reaction with the buffer medium ΔH_{ion} . As different buffers exhibit different ionization enthalpies,^[593] this process can be readily detected by measuring under several buffer conditions [Eq. (12)]^[586]

$$\Delta H_{\text{total}} = \Delta H_{\text{bind}} + n \Delta H_{\text{ion}} \quad (12)$$

The stoichiometry of the protonation reaction is available from n , with the sign of n indicating whether protonation or deprotonation of the ligand and protein groups is occurring.

From van't Hoff plots used to analyze affinity data measured at different temperatures, only that part of the binding enthalpy can be extracted that refers directly to the parameters which determine the observed measurement signal (e.g. absorption, fluorescence quenching). This means that only for a direct transformation of the system from a properly defined incipient state (ligand and protein separated) to a final state (protein–ligand complex) the extracted enthalpy is equivalent to the value of ΔH_{bind} obtained by ITC. No intermediate (e.g. conformational) states are allowed to occur, nor should other steps (e.g. change in the protonation state) be superimposed onto the binding process.^[594] In biological systems, ΔG usually shows only a low temperature dependence (see below). Thus, a reliable determination of enthalpy and entropy is hardly possible from van't Hoff plots.

The interpretation of ITC results gives rise to a number of interesting aspects, especially with respect to structural details

of receptor–ligand binding.^[197] In addition to the detection of superimposed protonation reactions, the confirmation of a virtually temperature-independent value of ΔG° as a result of a pronounced enthalpy–entropy compensation has to be emphasized (see Section 2.2.4).

Further access to structural interpretations is provided by the determination of heat-capacity changes ΔC_p . ITC measurements carried out at different temperatures show a strong temperature dependence of ΔH° and, conversely, of $T\Delta S^\circ$ for most biological systems. In such cases, analogous van't Hoff plots show a nonlinear behavior of $\Delta G^\circ/T$ as a function of the reciprocal temperature. In contrast to enthalpy and entropy changes, ΔC_p is virtually temperature independent in the range usually accessible to biological systems. Negative values are found in general for protein–ligand complexes. Accordingly, the complex exhibits lower heat capacity compared to the sum of the free components. With respect to enthalpy and entropy, this general behavior means that, with increasing temperature, protein–ligand binding becomes increasingly exothermic and simultaneously entropically less favorable. Any interpretation in terms of enthalpy- or entropy-driven binding must therefore be considered in the light of the applied temperature conditions. Several models have been discussed in the literature that correlate heat-capacity changes with the hydrophobic surface accessible to water molecules prior to binding but buried upon protein–protein complex formation or protein folding.^[590, 595–600] Similar surface-dependent contributions were found for the transfer of hydrophobic solvent molecules from the water phase into their pure phase (see Section 2.2.2). If this empirical correlation model is applied to the binding of small ligands to their receptors, the values calculated for ΔC_p are too small.^[601–603] Accordingly, the experimentally determined heat capacity of the complex formation is smaller than the value predicted in comparison to the separated components, if the model used only considers the surface contributions buried upon complex formation. To calculate such surface contributions, the relevant structure of the free and ligand-bound protein has to be known. In general, crystal structures are used for this purpose. Therefore, for the binding of a small-molecule ligand to its receptor, the surface-dependent release of the hydration shells cannot provide the sole contribution to the change in heat capacity. Conformational transitions of the binding partners or differences in the excitable vibrational modes of the macromolecular structures arising from complex formation have been discussed as additional explanations.^[604–606] The deviations are, however, also observed for conformationally rigid proteins such as trypsin^[607] and obviously represent a general phenomenon in protein–ligand binding. Thus, it appears likely that they involve water which is ubiquitously present in all binding processes. Liggins and Privalov^[608] assume that the enthalpic contributions to binding resulting from hydrogen bonds formed in the complex are exaggerated. The enthalpy of dehydration necessary for complex formation is also included in this contribution. At the interface of a binding pocket and bulk solvent, the assumption of complete dehydration is probably an overestimate. More likely, even after protein binding, polar ligand groups still influence the water structure in the local proximity. This effect leads to reduced desolvation

contributions which could possibly influence the heat-capacity changes. It might explain the discrepancies in the empirical relationships established for protein-folding experiments and the calculated and the measured ΔC_p values for ligand–protein complexes.

Further information on heat capacities and their changes can be obtained from DSC measurements (differential scanning calorimetry).^[594] The system under investigation is heated under virtually adiabatic conditions at a constant rate and the temperature change in the sample is recorded. Usually, these measurements are performed to study protein stability with respect to denaturation. These studies give important insights into the conformational behavior of biological systems in the investigated temperature interval. Deviations from a constant heat absorption indicate changes in the intramolecular packing of the proteins or structural fluctuations and conformational rearrangements.^[591, 609] The binding of a ligand to a protein influences its stability and heat capacity, which is expressed in pronounced changes of the DSC thermogram^[610–613] and supports the interpretation of the interaction between the binding partners.^[614–616]

5. Characterization and Evaluation of Ligand Binding with a Knowledge-Based Scoring Function

In the following, our own knowledge-based scoring function DrugScore will be briefly described. It is used to predict binding modes and affinities, and it can be applied to identify, in graphical terms, regions in the protein binding pocket that are favorable for interactions.^[544, 546]

For the development of DrugScore, the structural information of 1376 crystallographically determined protein–ligand complexes was retrieved from the database ReliBase. Subsequently, this information was converted into statistical preferences based on 17 atom types.^[545] The requirement to consider both specific interactions and entropy-dependent solvent contributions prompted us to use two terms: a distance-dependent atom–atom pair preference sampled up to 6 Å atom–atom distances (Figure 10), and a singlet preference dependent on the solvent-accessible surface of protein and ligand, both in the bound or unbound state. Definition of an appropriate reference state, to which the atom-type-specific distribution functions relate, is crucial for

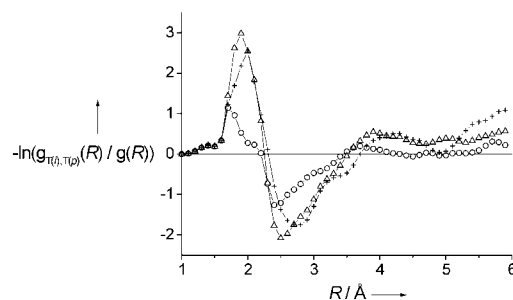


Figure 10. Examples of knowledge-based pair potentials between polar and charged (O.co2-N.pl3 (+), O.3-O.co2 (Δ), O.3-O.3 (○)) ligand and protein atoms as a function of distance. The first atom-type symbol refers to the ligand, the second to the protein.

the information stored in the respective preferences. In case of the pair preferences, a state based on a compact protein–ligand configuration with mean nonspecific interactions was selected. For the singlet preferences, a reference state with complete separation of protein and ligand was used. To evaluate a given protein–ligand binding mode, the various pair interactions and singlet contributions arising from all protein and ligand atoms were summed. Enthalpic and entropic contributions resulting from purely intramolecular effects were not considered.

Using an approximative grid-based method to compute the solvent-accessible surface, little computing time is required to evaluate each protein–ligand configuration. Because of the restriction to non-hydrogen atoms in the derivation of the pair preferences, no assumptions on possible protonation states are required using DrugScore. A triangular function is used for smoothing the pair and singlet distributions initially obtained from the structural data (“moving-window technique”). It should sufficiently “soften” the preferences to tolerate inherent deviations from ideal geometry caused by limited accuracy of protein crystal-structure analyses or limited precision of docked protein–ligand binding modes. As no protein- or ligand-type-specific training data set was used for the development of the function, its general applicability can be assumed.

To assess the reliability of DrugScore to identify near-native protein–ligand binding modes out of a number of clearly deviating geometries, data sets of 91 and 68 complexes were analyzed. Up to 500 protein–ligand configurations were produced with FlexX.^[552] In 80% of the cases, the best-ranked ligand binding modes show an rms deviation of <2.0 Å from the crystal-structure reference (native pose). With respect to the data set of 91 complexes, this corresponds to an improvement of 35% compared to the ranking obtained with the scoring function originally implemented in FlexX

(Figure 11). Similarly, convincing results were obtained considering binding modes generated with DOCK.^[566, 617]

In the context of a virtual screening study on human carbonic anhydrase II (hCAII),^[618] the complex structures of two novel inhibitors (**10**, **11**; Scheme 4) discovered by means of a computer simulation were determined crystallographically. This allowed us to assess directly by experiment the binding modes which had been predicted in advance using DrugScore or the original scoring function in FlexX. As

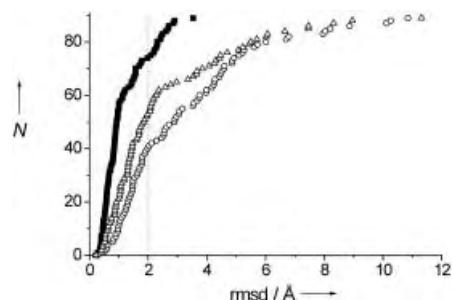
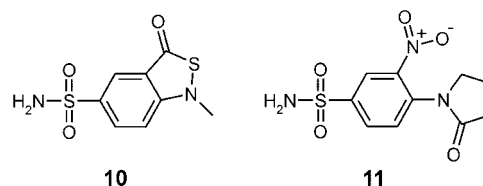


Figure 11. Accumulated number N of best-ranked docking solutions for 91 protein–ligand complexes as a function of the rms deviation with respect to the crystallographic reference structure. The ranking is based on the scoring function in FlexX (○) or DrugScore (△). For comparison, the accumulated number of complexes considering the best generated geometry, disregarding its actual rank, is plotted (■). This distribution indicates the limit an ideal scoring function could achieve.



Scheme 4. Inhibitors discovered as a part of a virtual screening approach on hCAII.^[618]

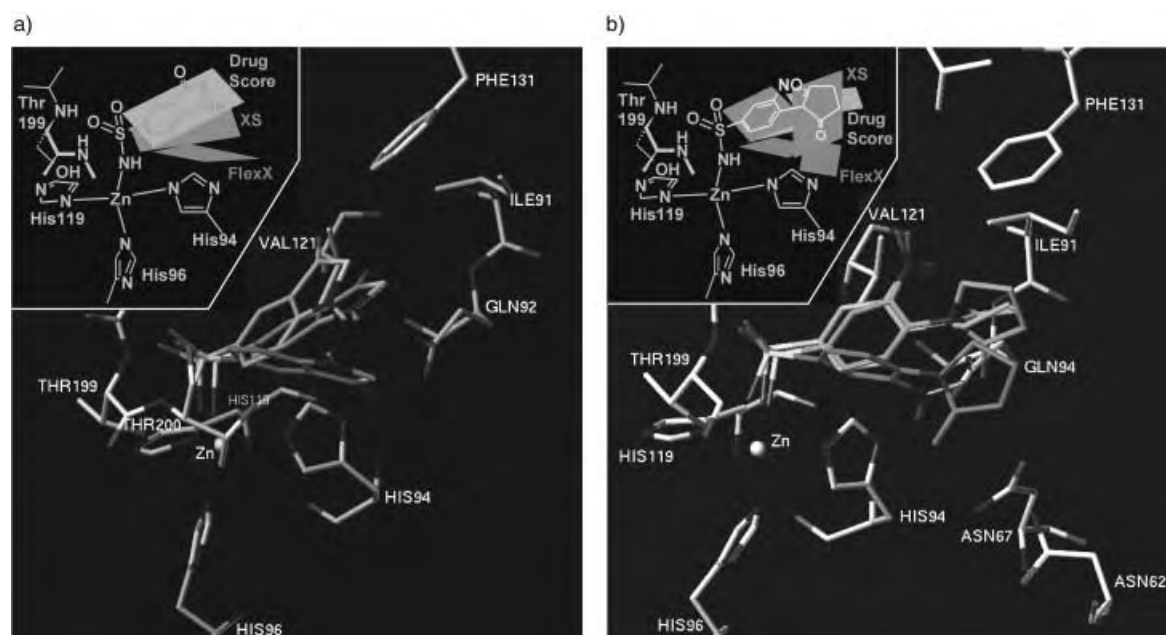


Figure 12. Superposition of the crystal structures (medium gray) and best-ranked docking solutions by DrugScore (light gray) and the scoring function in FlexX (dark gray) of two inhibitors [a): **10**, b): **11**]. They were discovered in virtual screening on hCAII.^[618]

Figure 12 shows, the binding geometry predicted by DrugScore (rmsd value relative to the crystal structure: 1.2 Å for **10**; 1.4 Å for **11**) falls significantly closer to the experimentally observed geometry than does the solution proposed by FlexX, which suggests a configuration with an rmsd relative to the crystal structure of 2.2 Å for **10** and 2.7 Å for **11**. A reliable identification of near-native binding modes is not only of the utmost importance for subsequent ligand optimization, but also a prerequisite for the prediction of binding affinities. Importantly enough, such arrangements have to be produced by docking programs.

The validation of DrugScore with respect to affinity prediction was based on six data sets compiled from crystallographically determined protein–ligand complexes and three data sets with binding modes generated by FlexX. In the case of 16 serine protease–inhibitor complexes (X-ray structures), an r^2 value of 0.86 and a standard deviation of 0.95 logarithmic units was achieved compared to experimental affinities. For a set of 64 thrombin and trypsin inhibitors docked into the respective proteins, an r^2 value of 0.48 and a standard deviation of 0.71 log units was revealed. The deviations matched the experimental error.

“Hot spots” of binding can be calculated by using different probe atoms, using the distance-dependent pair preferences. The results can be visualized in terms of isocontour surfaces. They intuitively highlight favorable regions in the binding pocket suitable for a particular ligand-atom type (Figure 13 and frontispiece). They support ligand optimization and help to establish a protein-based pharmacophore hypothesis that can subsequently be used to screen for candidate molecules in compound libraries.

The prediction of hot spots has been validated using 159 protein–ligand complexes. Through the application of five probe atoms, the atom type observed in the crystal structure could be predicted correctly in 74% of the cases. Requesting only an atom type of appropriate physicochemical properties revealed correct predictions in 85% of the cases. Mapping the protein binding pocket of hCAII with GRID,^[418] SuperStar,^[556] LUDI,^[619] and DrugScore, carried out as part of a virtual screening study,^[618] demonstrated that all methods qualitatively identify the same regions in space, however with different relative weightings.

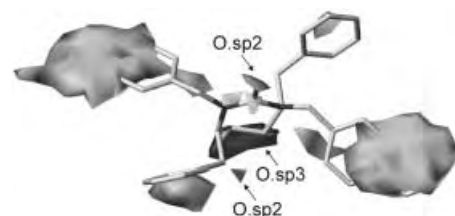
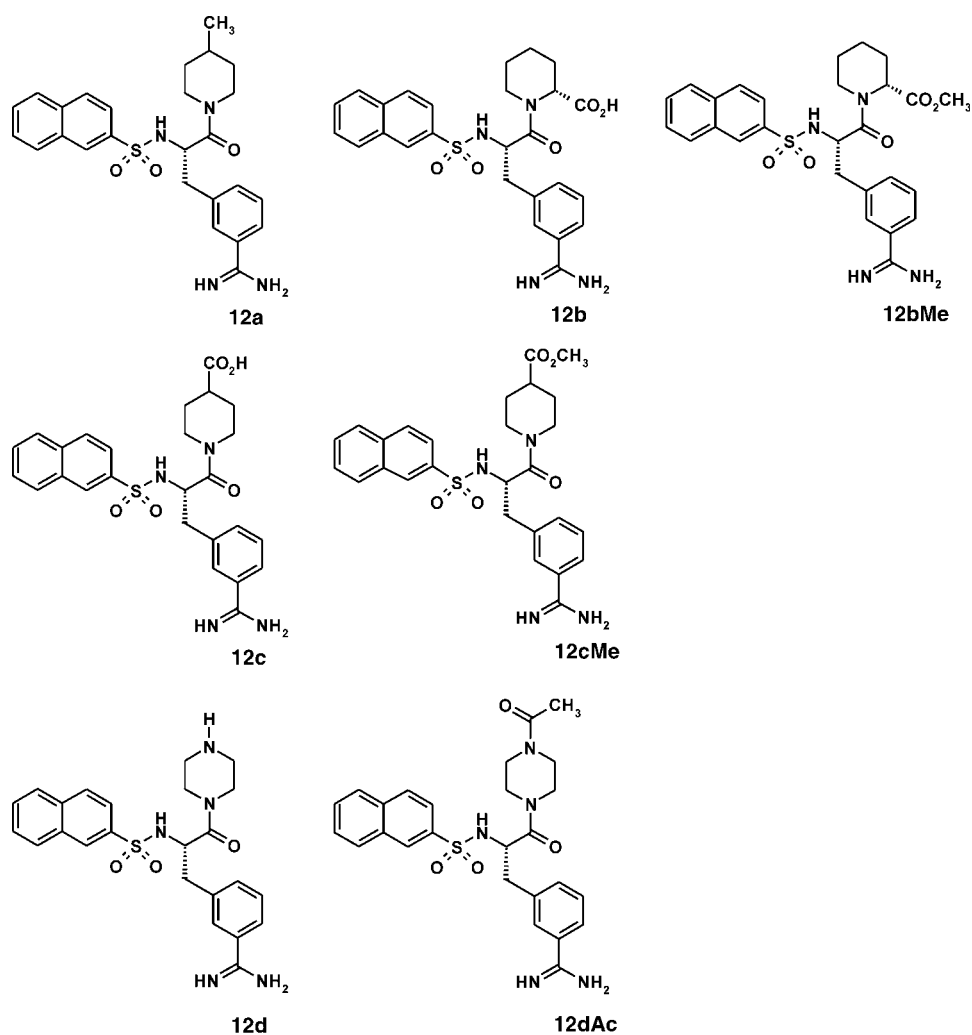


Figure 13. Hot spots in the binding pocket of HIV-1 protease (PDB code 1hrv) based on knowledge-based pair potentials in DrugScore. Values beyond a predefined threshold are isocontoured and shown together with the ligand XK263 from Merck for comparative purposes. Regions favorable for aromatic carbon atoms are colored in light gray, for carbonyl oxygen atoms in midgray, and for hydroxy groups in dark gray.

6. Factorization of Thermodynamic Contributions to Ligand Binding Using an Example of Serine Protease Inhibitors

Inhibitor binding to trypsin and thrombin, studied in our group, should serve as an example for the partitioning of affinity-determining factors.^[607] A series of structurally related benzamidine inhibitors (**12a**–**12dAc**, Scheme 5) and the development compounds napsagatran (**13**), CRC220 (**14**),



Scheme 5. Structurally related inhibitors of trypsin and thrombin.

inogatran (**15**), and melagatran (**16**; Scheme 6) have been investigated by crystallography and microcalorimetry.

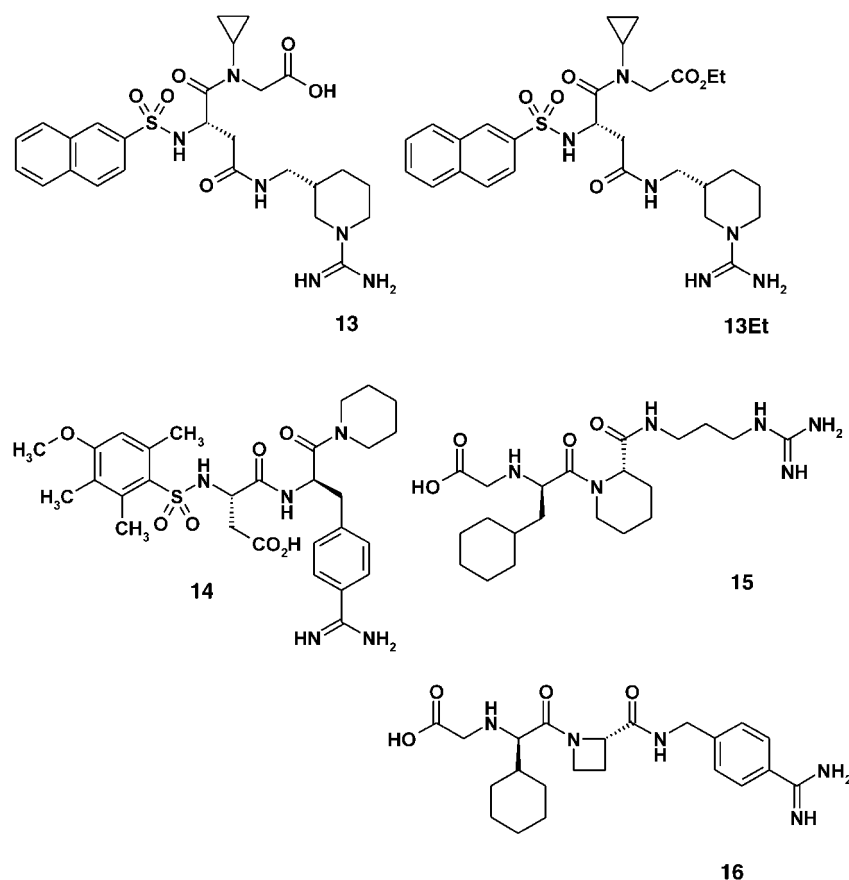
Crystal-structure determination revealed uniform binding modes of all ligands with a salt bridge between the ligand amidino groups and Asp 189. Further interactions are formed between the central amide or sulfonamide groups and the protein carbonyl and amide NH groups of Gly 216 and 219. In detail, however, interesting deviations are observed that allow important conclusions with respect to thermodynamics.

Interestingly, the 2-carboxy derivative **12b** and napsagatran (**13**) acquires a proton upon protein binding, whereas the piperazine derivative **12d** releases a proton upon binding. The closely related 4-carboxy derivative **12c** remains deprotonated at the acid group during the binding process. The same observation holds for CRC220 (**14**); also here the acid group of the central aspartate remains deprotonated. The apparent pK_a shifts of the groups involved, which show very similar pK_a values in water, can be explained by examining binding modes of the different ligands. For CRC220, the carboxylate group is oriented away from the binding pocket towards the solvent (Figure 14); accordingly, this group remains partially solvated and the local dielectric conditions closely resemble those in the bulk water phase. For **12b** and napsagatran, the acid groups are protonated and point towards the catalytic serine. They obviously donate hydrogen bonds to the protein (Figure 14). The environment has such a strong influence on the local dielectric conditions (induced dielectric fit) that the pK_a values of the carboxy groups involved are shifted by more than four log units. The 4-carboxy group in **12b**, which does

not change its deprotonated state upon binding, packs with parallel orientation next to the hydrophobic ring plane of the catalytic histidine. The induced pK_a shift caused by this environment is obviously not sufficient to protonate this acid group. The terminal amino group of **12d** with a pK_a value of 7.5 is partially protonated in the buffer medium of pH = 7.8, however, it binds in the deprotonated form. The hydrophobic protein environment reinforces a pK_a shift of this basic group towards smaller values.

The partitioning of enthalpic and entropic binding contributions for the free acids and esters **12b/12bMe** and **12c/12cMe** provides an instructive example. The inhibitors with the functional groups in the 4 position differ by more than 8 kJ mol⁻¹ in ΔG° (**12c**: -35.5, **12cMe**: -43.6 kJ mol⁻¹), and the higher affinity of the ester is attributed to a stronger enthalpic binding (ΔH° ; **12c**: -26.8, **12cMe**: -39.6 kJ mol⁻¹), whereas the entropic contributions $T\Delta S^\circ$ are comparable (**12c**: +8.7, **12cMe**: +4.0 kJ mol⁻¹). The enthalpically reduced binding of the acid at 25 °C can be explained by an unfavorable desolvation energy: the acid loses hydrogen-bonding partners for two polar acceptors (oxygen atoms), and is transferred from aqueous solution to the protein, whereas, the ester must only compensate for the desolvation of one carbonyl oxygen atom. The bridging ester oxygen atom exhibits practically no basic properties.^[620] For the analogous pair with carboxylate and ester groups in the 2 position, a reverse correlation is observed. Here, acid and ester groups possess almost equal affinities (ΔG° ; **12b**: -36.4, **12bMe**: -37.0 kJ mol⁻¹). However, the free acid is now enthalpically

favorable, the enthalpy contribution of the ester is significantly less exothermic (ΔH° ; **12b**: -46.7, **12bMe**: -16.9 kJ mol⁻¹). For entropic reasons, the binding of the acid is now significantly less favorable ($T\Delta S^\circ$; **12b**: -10.6, **12bMe**: -20.6 kJ mol⁻¹). Upon binding, the protonated acid group in **12b** forms an enthalpically favored hydrogen bond to the protein (see above). At the same time, this part of the molecule loses residual mobility caused by immobilization by this additional hydrogen bond in the binding pocket. This fact results in a less favorable entropic contribution. The reduced temperature factors observed in the crystal structure for this part of the molecule **12b** further support this observation. The piperazine **12d** and the acetyl derivative **12dAc** exhibit very similar binding affinities (ΔG° ; **12d**: -40.8, **12dAc**: -42.7 kJ mol⁻¹). After correcting for the superimposed deprotonation step of **12d**, similar contributions are observed for ΔH° and $T\Delta S^\circ$ in both cases (ΔH° ; **12d**: -32.9, **12dAc**: -34.4, $T\Delta S^\circ$; **12d**: -7.9, **12dAc**: -8.2 kJ mol⁻¹). Both the free amine and the protected acetyl compound possess one polar atom in this group capable of forming hydrogen bonds. As in the bound state, no hydrogen bonds are formed to the protein in



Scheme 6. Development compounds which bind to trypsin and thrombin.

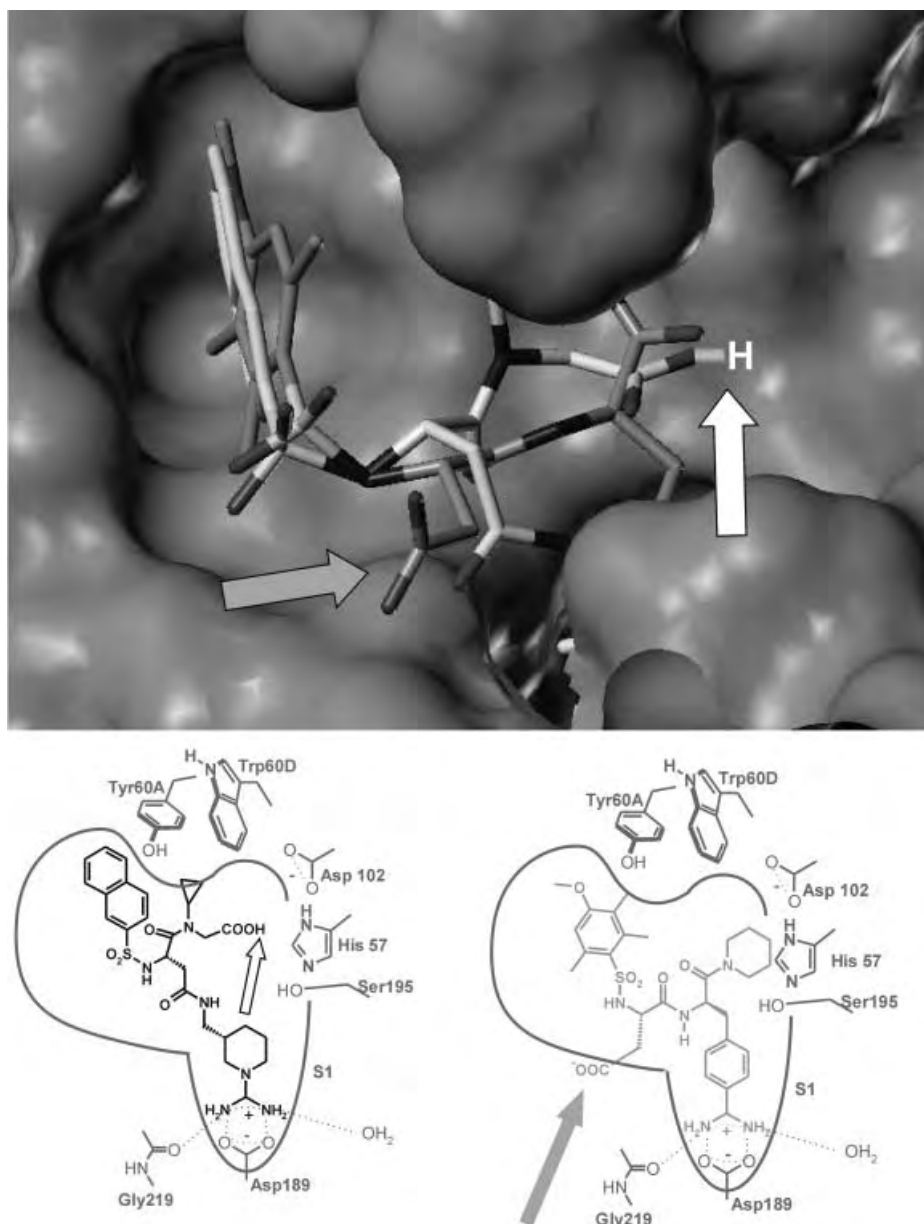


Figure 14. Schematic binding mode (bottom) of napsagatran (**13**) and CRC220 (**14**) to thrombin. The crystallographically determined binding geometries (light: napsagatran, white arrow indicates the protonated carboxylate group; dark: CRC220, gray arrow shows the deprotonated acid group) are superimposed.

either case; this results in an unfavorable desolvation, obviously with comparable thermodynamic contributions for both groups. Additional compounds investigated in this series confirm the discussed trends.

A comparison of the heat-capacity changes is equally interesting. In all cases, a strongly negative ΔC_p is observed, which means that ΔH° becomes increasingly exothermic with rising temperature and, as ΔG° is essentially temperature independent, the binding process becomes entropically less favorable. The surface portions that are buried upon binding were derived from the known crystal structures of the corresponding ligand–protein complexes. As thrombin and trypsin are described as relatively rigid proteins, the surface portions of the uncomplexed protein were calculated using the structure of the protein simply by removing the bound

ligand. If the empirical correlation derived from protein folding (see above) is applied to estimate ΔC_p , the ΔC_p values predicted are too low. Obviously, smaller heat capacities are observed experimentally for the complexes than expected from solvation-dependent surface contributions alone. Presumably, the additional factors described above must be considered for a detailed structural interpretation of ΔC_p . Surprisingly, in contrast to trypsin, a sodium-specific dependence of ΔC_p is found for thrombin. An according allosteric regulation of thrombin is known, however, this ion-specific effect cannot yet be explained in structural terms.

7. Summary and Outlook

The affinity of a small-molecule ligand for a macromolecular receptor usually serves as a criterion to define the biological activity of the respective compound. It is determined by electrostatic interactions between the ligand and the receptor, together with contributions from solvation and desolvation, and the spatial complementarity of both binding partners. Additional influences arise from changes in the number of degrees of freedom and conformational changes of ligand and receptor experienced upon complex formation. Understanding of the determining enthalpic and entropic contributions to binding is a prerequisite for affinity predictions.

The methods of virtual screening and rational drug design require rapid and reliable methods for affinity prediction. In this contribution we have described and classified known theoretical approaches with respect to their methodological foundations. Significant differences in computational requirements and the general scope of the methods have been addressed. The pragmatic combination of several scoring methods as in the so-called consensus approaches indicates that, at present, no general-purpose method is available that adequately considers all above-described relevant contributions to ligand–receptor binding. However, advantages have recently been achieved for the (rapid) prediction of binding affinity by means of newly developed knowledge-based scoring functions.

Physicochemical techniques to quantitatively characterize ligand–receptor binding have been developed and further

enhanced in recent years. In particular, direct access to thermodynamic parameters by means of microcalorimetry provides new insights into the thermodynamic foundations of binding affinity. Supported by the structural characterization of ligand–receptor complexes, it is possible to factorize binding affinity into individual contributions. However, the described examples of serine–protease inhibitors demonstrate that steps superimposed on the binding process must be considered and adequately handled.

With the increase in structural information and binding data about receptor–ligand complexes, further advances in the understanding and the description of binding affinity can be expected. This will improve our methods for its prediction. In particular, current approximations—such as the complete disregard of changes in protonation state of the binding partners upon complex formation, the consideration of receptors as rigid entities, the neglect of allosteric effects, and the to date inadequate handling of water molecules in ligand binding—will be the starting points for new developments.

Abbreviation list

ASP	atomic solvation parameters
CSD	Cambridge Structural Databank, a database of crystal structures of small molecules ^[1]
FEP–MD	free-energy-perturbation calculations/molecular dynamics
GB/SA	generalized Born approach
LIE	linear interaction energy
ME	master equation
NBTI	non-Boltzmann thermodynamic integration
PBE	Poisson–Boltzmann equation
PDB	protein database ^[2]
PLS	partial least-squares method
QSAR	quantitative structure–activity relationships
rmsd	root-mean-square deviation in the Cartesian coordinates of mutually corresponding atoms in two molecules

Received: 22nd October 2001 [A 497]

- [1] F. H. Allen, J. E. Davies, J. J. Galloy, O. Johnson, O. Kennard, C. F. Macrae, E. M. Mitchell, G. F. Mitchell, J. M. Smith, D. G. Watson, *J. Chem. Inf. Comput. Sci.* **1991**, *31*, 187–204.
- [2] F. C. Bernstein, T. F. Koetzle, G. J. Williams, E. E. Meyer, Jr., M. D. Brice, J. R. Rodgers, O. Kennard, T. Shimanouchi, M. Tasumi, *J. Mol. Biol.* **1977**, *112*, 535–542.
- [3] E. Fischer, *Ber. Dtsch. Chem. Ges.* **1894**, *27*, 2985–2993.
- [4] P. Ehrlich, *Lancet* **1913**, *II*, 445–451.
- [5] D. E. Koshland, *Proc. Natl. Acad. Sci. USA* **1958**, *44*, 98–104.
- [6] D. E. Koshland, *Angew. Chem.* **1994**, *106*, 2468–2472; *Angew. Chem. Int. Ed. Engl.* **1994**, *33*, 2375–2378.
- [7] J. P. Glusker, M. Lewis, M. Rossi, *Crystal Structure Analysis for Chemists and Biologists*, VCH, Weinheim, **1994**.
- [8] J. Drenth, *Principles of Protein X-ray Crystallography*, Springer, New York, **1999**.
- [9] K. Wüthrich, *NMR of Proteins and Nucleic Acids*, Wiley, New York, **1986**.
- [10] G. Siegal, J. van Duynhoven, M. Baldus, *Curr. Opin. Chem. Biol.* **1999**, *3*, 530–536.
- [11] G. M. Clore, A. M. Gronenborn, *Science* **1991**, *252*, 1390–1399.
- [12] W. Kühlbrandt, K. A. Williams, *Curr. Opin. Chem. Biol.* **1999**, *3*, 537–543.
- [13] M. H. Stowell, A. Miyazawa, N. Unwin, *Curr. Opin. Struct. Biol.* **1998**, *8*, 595–600.
- [14] W. Chiu, A. McGough, M. B. Sherman, M. F. Schmid, *Trends Cell Biol.* **1999**, *9*, 154–159.
- [15] W. Baumeister, C. S. Alasdair, *Trends Biochem. Sci.* **2000**, *25*, 624–631.
- [16] F. S. Collins, A. Patrinos, E. Jordan, A. Chakravarti, R. Gesteland, L. Walters, E. Fearon, L. Hartwell, C. H. Langley, R. A. Mathies, M. Olson, A. J. Pawson, T. Pollard, A. Williamson, B. Wold, K. Buetow, E. Branscomb, M. Capecchi, G. Church, H. Garner, R. A. Gibbs, T. Hawkins, K. Hodgson, M. Knotek, M. Meisler, G. M. Rubin, L. M. Smith, M. Westerfield, E. W. Clayton, N. L. Fisher, C. E. Lerman, J. D. McInerney, W. Nebo, N. Press, D. Valle, *Science* **1998**, *282*, 682–689.
- [17] G. M. Rubin, M. D. Yandell, J. R. Wortman, G. L. Gabor Miklos, C. R. Nelson, I. K. Hariharan, M. E. Fortini, P. W. Li, R. Apweiler, W. Fleischmann, J. M. Cherry, S. Henikoff, M. P. Skupski, S. Misra, M. Ashburner, E. Birney, M. S. Boguski, T. Brody, P. Brokstein, S. E. Celniker, S. A. Chervitz, D. Coates, A. Cravchik, A. Gabrielian, R. F. Galle, W. M. Gelbart, R. A. George, L. S. Goldstein, F. Gong, P. Guan, N. L. Harris, B. A. Hay, R. A. Hoskins, J. Li, Z. Li, R. O. Hynes, S. J. Jones, P. M. Kuehl, B. Lemaitre, J. T. Littleton, D. K. Morrison, C. Mungall, P. H. O'Farrell, O. K. Pickeral, C. Shue, L. B. Vossell, J. Zhang, Q. Zhao, X. H. Zheng, F. Zhong, W. Zhong, R. Gibbs, J. C. Venter, M. D. Adams, S. Lewis, *Science* **2000**, *287*, 2204–2215.
- [18] S. Broder, J. C. Venter, *Annu. Rev. Pharmacol. Toxicol.* **2000**, *40*, 97–132.
- [19] See edition “The Human Genome”: *Nature* **2001**, *409*, 813–958.
- [20] E. M. Marcotte, M. Pellegrini, H. Ng, D. W. Rice, T. O. Yeates, D. Eisenberg, *Science* **1999**, *285*, 751–753.
- [21] F. Lottspeich, *Angew. Chem.* **1999**, *111*, 2630–2647; *Angew. Chem. Int. Ed.* **1999**, *38*, 2477–2492.
- [22] J. H. Wang, R. M. Hewick, *Drug Discovery Today* **1999**, *4*, 129–383.
- [23] A. Danchin, *Curr. Opin. Struct. Biol.* **1999**, *9*, 363–367.
- [24] C. A. Orengo, A. E. Todd, J. M. Thornton, *Curr. Opin. Struct. Biol.* **1999**, *9*, 374–382.
- [25] D. R. Westhead, J. M. Thornton, *Curr. Opin. Biotechnol.* **1998**, *9*, 383–389.
- [26] B. Rost, *Structure* **1998**, *6*, 259–263.
- [27] S. K. Burley, S. C. Almo, J. B. Bonanno, M. Capel, M. R. Chance, T. Gaasterland, D. Lin, A. Sali, F. W. Studier, S. Swaminathan, *Nat. Genet.* **1999**, *23*, 151–157.
- [28] I. Uson, G. M. Sheldrick, *Curr. Opin. Struct. Biol.* **1999**, *9*, 643–648.
- [29] D. J. Diller, M. R. Redinbo, E. Pohl, W. G. J. Hol, *Proteins* **1999**, *36*, 526–541.
- [30] D. J. Diller, E. Pohl, M. R. Redinbo, B. T. Hovey, W. G. J. Hol, *Proteins* **1999**, *36*, 512–525.
- [31] D. A. Jones, F. A. Fitzpatrick, *Curr. Opin. Chem. Biol.* **1999**, *3*, 71–76.
- [32] J. Skolnick, J. S. Fetrow, *Trends Biotechnol.* **2000**, *18*, 34–39.
- [33] F. Spaltmann, M. Blunck, K. Ziegelbauer, *Drug. Discovery Today* **1999**, *4*, 17–26.
- [34] J. Drews in *Human Disease—from Genetic Causes to Biochemical Effects* (Eds.: J. Drews, S. Ryser), Blackwell, Berlin, **1997**, pp. 5–9.
- [35] G. A. Petsco, *Nature* **1996**, *384*, 7–9.
- [36] J. Drews, *Drug Discovery Today* **2000**, *5*, 2–4.
- [37] J. Drews, *Nat. Biotechnol.* **1996**, *14*, 1516–1518.
- [38] R. B. Silvermann, *Medizinische Chemie für Organiker, Biochemiker und Pharmazeutische Chemiker*, VCH, Weinheim, **1994**.
- [39] H.-J. Böhm, G. Klebe, H. Kubinyi, *Wirkstoffdesign*, Spektrum, Heidelberg, **1996**.
- [40] O. H. Chan, B. H. Stewart, *Drug Discovery Today* **1996**, *1*, 461–473.
- [41] D. A. Smith, H. van de Waterbeemd, *Curr. Opin. Chem. Biol.* **1999**, *3*, 373–378.
- [42] A. P. Watt, D. Morrison, D. C. Evans, *Drug Discovery Today* **2000**, *5*, 17–24.

- [43] D. B. Searls, *Drug Discovery Today* **2000**, 5, 135–143.
- [44] G. R. Lenz, H. M. Nash, S. Jindal, *Drug. Discovery Today* **2000**, 5, 145–156.
- [45] M. H. Beydon, A. Fournier, L. Drugeault, J. Becquart, *J. Biomol. Screening* **2000**, 5, 13–22.
- [46] R. P. Hertzberg, A. J. Pope, *Curr. Opin. Chem. Biol.* **2000**, 4, 445–451.
- [47] W. P. Walters, M. T. Stahl, M. A. Murcko, *Drug Discovery Today* **1998**, 3, 160–178.
- [48] *Virtual Screening for Bioactive Molecules, Vol. 10* (Eds.: H.-J. Böhm, G. Schneider), Wiley-VCH, Weinheim, **2000**.
- [49] I. D. Kuntz, *Science* **1992**, 257, 1078–1082.
- [50] I. D. Kuntz, E. C. Meng, B. K. Shoichet, *Acc. Chem. Res.* **1994**, 27, 117–123.
- [51] D. B. Boyd, *Mod. Drug Discovery* **1998**, 6, 41–48.
- [52] E. M. Gordon, M. A. Gallop, D. V. Patel, *Acc. Chem. Res.* **1996**, 29, 144–154.
- [53] T. Carell, E. A. Wintner, J. Rebek, Jr., *Angew. Chem.* **1994**, 106, 2162–2164; *Angew. Chem. Int. Ed. Engl.* **1994**, 33, 2061–2064.
- [54] J. G. Houston, M. Banks, *Curr. Opin. Biotechnol.* **1997**, 8, 734–740.
- [55] N. K. Terrett, M. Gardner, D. W. Gordon, R. J. Kobylecki, J. Steele, *Tetrahedron* **1995**, 51, 8135–8173.
- [56] F. Balkenhohl, C. von dem Bussche-Hünnefeld, A. Lansky, C. Zechel, *Angew. Chem.* **1996**, 108, 2436–2488; *Angew. Chem. Int. Ed. Engl.* **1996**, 35, 2289–2337.
- [57] S. Kauffman, A. D. Ellington, *Curr. Opin. Chem. Biol.* **1999**, 3, 256–259.
- [58] A. Dömling, I. Ugi, *Angew. Chem.* **2000**, 112, 3300–3344; *Angew. Chem. Int. Ed.* **2000**, 39, 3169–3210.
- [59] S. F. Oliver, C. Abell, *Curr. Opin. Chem. Biol.* **1999**, 3, 299–306.
- [60] R. Lahana, *Drug Discovery Today* **1999**, 4, 447–448.
- [61] M. A. Sills, *Drug Discovery Today* **1998**, 3, 304–312.
- [62] W. A. Warr, *J. Chem. Inf. Comput. Sci.* **1997**, 37, 134–140.
- [63] D. E. Clark, S. D. Pickett, *Drug Discovery Today* **2000**, 5, 49–58.
- [64] J. F. Blake, *Curr. Opin. Biotechnol.* **2000**, 11, 104–107.
- [65] J. H. Van Drie, M. S. Lajiness, *Drug Discovery Today* **1998**, 3, 274–283.
- [66] L. Weber, S. Wallbaum, C. Broger, K. Gubernator, *Angew. Chem.* **1995**, 107, 2452–2454; *Angew. Chem. Int. Ed. Engl.* **1995**, 34, 2280–2282.
- [67] C. M. Murray, S. J. Cato, *J. Chem. Inf. Comput. Sci.* **1999**, 39, 46–50.
- [68] S. J. Teague, A. M. Davis, P. D. Leeson, T. Oprea, *Angew. Chem.* **1999**, 111, 3962–3967; *Angew. Chem. Int. Ed.* **1999**, 38, 3743–3748.
- [69] S. L. Schreiber, *Science* **2000**, 287, 1964–1969.
- [70] *Designing Bioactive Molecules* (Eds.: Y. C. Martin, P. Willet, S. R. Heller), American Chemical Society, Washington, **1999**.
- [71] H.-J. Böhm, M. Böhringer, D. Bur, H. Gmüender, W. Huber, W. Klaus, D. Kostrewa, H. Kühne, T. Lübbers, N. Meunier-Keller, F. Müller, *J. Med. Chem.* **2000**, 43, 2664–2674.
- [72] J. M. Chen, F. C. Nelson, J. I. Levin, D. Mobilio, F. J. Moy, R. Nilakantan, A. Zask, R. Powers, *J. Am. Chem. Soc.* **2000**, 122, 9648–9654.
- [73] B. Buzbee, *Science* **1993**, 261, 852–853.
- [74] J. Couzin, *Science* **1998**, 281, 762.
- [75] G. Klebe, *Period. Biol.* **1998**, 100 (Suppl. 2), 93–98.
- [76] H. Kubinyi, *Curr. Opin. Drug Discovery Dev.* **1998**, 1, 4–15.
- [77] J. Greer, J. W. Erickson, J. J. Baldwin, M. D. Varney, *J. Med. Chem.* **1994**, 37, 1035–1054.
- [78] D. B. Boyd, *Rev. Comput. Chem.* **1990**, 1, 355–371.
- [79] R. E. Babine, S. L. Bender, *Chem. Rev.* **1997**, 97, 1359–1472.
- [80] D. H. Harrison, K. M. Bohren, G. A. Petsko, D. Ringe, K. H. Gabbay, *Biochemistry* **1997**, 36, 16134–16140.
- [81] L. Costantino, G. Rastelli, K. Vescovini, G. Cignarella, P. Vianello, A. D. Corso, M. Cappiello, U. Mura, D. Barlocco, *J. Med. Chem.* **1996**, 39, 4396–4405.
- [82] I. R. Hardcastle, M. G. Rowlands, J. Houghton, I. B. Parr, G. A. Potter, M. Jarmann, K. J. Edwards, C. A. Laughton, J. O. Trent, S. Neidle, *J. Med. Chem.* **1995**, 38, 241–248.
- [83] A. Scozzafava, C. T. Supuran, *J. Med. Chem.* **2000**, 43, 3677–3687.
- [84] P. A. Boriack-Sjodin, S. Zeitlin, H. H. Chen, L. Crenshaw, S. Gross, A. Dantanarayana, P. Delgado, J. A. May, T. Dean, D. W. Christianson, *Protein Sci.* **1998**, 7, 2483–2489.
- [85] L. R. Scolnick, A. M. Clements, J. Liao, L. Crenshaw, M. Hellberg, J. May, T. R. Dean, D. W. Christianson, *J. Am. Chem. Soc.* **1997**, 119, 850–851.
- [86] A. Jain, G. M. Whitesides, R. S. Alexander, D. W. Christianson, *J. Med. Chem.* **1994**, 37, 2100–2105.
- [87] A. S. Kalgutkar, B. C. Crews, S. W. Rowlinson, A. B. Marnett, K. R. Kozak, R. P. Remmel, L. J. Marnett, *Proc. Natl. Acad. Sci. USA* **2000**, 97, 925–930.
- [88] C. I. Bayly, W. C. Black, S. Leger, N. Ouimet, M. Ouellet, M. D. Percival, *Bioorg. Med. Chem. Lett.* **1999**, 9, 307–312.
- [89] C. A. Veale, J. R. Damewood, G. B. Steelman, C. Bryant, B. Gomes, J. Williams, *J. Med. Chem.* **1995**, 38, 86–97.
- [90] R. J. Cregge, S. L. Durham, R. A. Farr, S. L. Gallion, C. M. Hare, R. V. Hoffman, M. J. Janusz, H. O. Kim, J. R. Koehl, S. Mehdii, W. A. Metz, N. P. Peet, J. T. Pelton, H. A. Schreuder, S. Sunder, C. Tardif, *J. Med. Chem.* **1998**, 41, 2461–2480.
- [91] P. R. Bernstein, D. Andisik, P. K. Bradley, C. B. Bryant, C. Ceccarelli, J. R. Damewood, R. Earley, P. D. Edwards, S. Feeney, B. C. Gomes, B. J. Kosmider, G. B. Steelman, R. M. Thomas, E. P. Vacek, C. A. Veale, J. C. Williams, D. J. Wolanin, S. A. Woolson, *J. Med. Chem.* **1994**, 37, 3313–3326.
- [92] M. B. Andrus, S. L. Schreiber, *J. Am. Chem. Soc.* **1993**, 115, 10420–10421.
- [93] P. S. Dragovich, J. E. Barker, J. French, M. Imbacuan, V. J. Kalish, C. R. Kissinger, D. R. Knighton, C. T. Lewis, E. W. Moomaw, H. E. Parge, L. A. Pelletier, T. J. Prins, R. E. Showalter, J. H. Tatlock, K. D. Tucker, J. E. Villafranca, *J. Med. Chem.* **1996**, 39, 1872–1884.
- [94] T. Lubbers, P. Angehrn, H. Gmünder, S. Herzig, J. Kulhanek, *Bioorg. Med. Chem. Lett.* **2000**, 10, 821–826.
- [95] A. Tossi, I. Bonin, N. Antcheva, S. Norbedo, F. Benedetti, S. Miertus, A. C. Nair, T. Malier, F. Dal Bello, G. Palu, D. Romeo, *Eur. J. Biochem.* **2000**, 267, 1715–1722.
- [96] A. K. Ghosh, K. Krishnan, D. E. Walters, W. Cho, H. Cho, Y. Koo, J. Trevino, L. Holland, J. Buthod, *Bioorg. Med. Chem. Lett.* **1998**, 8, 979–982.
- [97] T. Y. Lee, V. D. Le, D. Y. Lim, Y. C. Lin, G. M. Morris, A. L. Wong, A. J. Olson, J. H. Elder, C. H. Wong, *J. Am. Chem. Soc.* **1999**, 121, 1145–1155.
- [98] H. I. Skulnick, P. D. Johnson, P. A. Aristoff, J. K. Morris, K. D. Lovasz, W. J. Howe, K. D. Watenpugh, M. N. Janakiraman, D. J. Anderson, R. J. Reischer, T. M. Schwartz, L. S. Banitt, P. K. Tomich, J. C. Lynn, M.-M. Horng, K.-T. Chong, R. R. Hinshaw, L. A. Dolak, E. P. Seest, F. J. Schwende, B. D. Rush, G. M. Howard, L. N. Toth, K. R. Wilkinson, T. J. Kakuk, C. W. Johnson, S. L. Cole, R. M. Zaya, G. L. Zipp, P. L. Possert, R. J. Dalg, W.-Z. Zhong, M. G. Williams, K. R. Romines, *J. Med. Chem.* **1997**, 40, 1149–1164.
- [99] G. V. DeLuca, S. Erickson Viitanen, P. Y. S. Lam, *Drug Discovery Today* **1997**, 2, 6–18.
- [100] S. Thaisrivongs, D. L. Romero, R. A. Tommasi, M. N. Janakiraman, J. W. Strohbach, S. R. Turner, C. Biles, R. R. Morge, P. D. Johnson, P. A. Aristoff, P. K. Tomich, J. C. Lynn, M. M. Horng, K. T. Chong, R. R. Hinshaw, W. J. Howe, B. C. Finzel, K. D. Watenpugh, *J. Med. Chem.* **1996**, 39, 4630–4642.
- [101] S. H. Reich, M. Melnick, M. J. Pino, M. A. Fuhry, A. J. Trippe, K. Appelt, J. F. Davies II, B. W. Wu, L. Musick, *J. Med. Chem.* **1996**, 39, 2781–2794.
- [102] M. D. Varney, K. Appelt, V. Kalish, M. R. Reddy, J. Tatlock, C. L. Palmer, W. H. Romines, B. W. Wu, L. Musick, *J. Med. Chem.* **1994**, 37, 2274–2284.
- [103] M. A. Navia, R. D. Tung, P. R. Chaturvedi, B. G. Rao, J. A. Partaledis, E. E. Kim, *FASEB J.* **1996**, 10, 2436.
- [104] H. M. Cheng, P. Keitz, J. B. Jones, *J. Org. Chem.* **1994**, 59, 7671–7676.
- [105] J. A. Montgomery, S. Niwas, J. D. Rose, J. A. Secrist III, Y. S. Babu, C. E. Bugg, M. D. Erion, W. C. Guida, S. E. Ealick, *J. Med. Chem.* **1993**, 36, 55–69.
- [106] M. S. Plummer, A. Shahripour, J. S. Kaltenbronn, E. A. Lunney, B. A. Steinbaugh, J. M. Hamby, H. W. Hamilton, T. K. Sawyer, C. Humblet, A. M. Doherty, M. D. Taylor, G. Hingorani, B. L. Batley, S. T. Rapundalo, *J. Med. Chem.* **1995**, 38, 2893–2905.
- [107] J. Rahuel, V. Rasetti, J. Maibaum, H. Rueger, R. Goshke, N. C. Cohen, S. Stutz, F. Cummin, W. Fuhrer, J. M. Wood, M. G. Grutter, *Chem. Biol.* **2000**, 7, 493–504.

- [108] B. A. Lefker, W. A. Hada, A. S. Wright, W. H. Martin, I. A. Stock, G. K. Schulte, J. Pandit, D. E. Danley, M. J. Ammirati, S. F. Sneddon, *Bioorg. Med. Chem. Lett.* **1995**, *5*, 2623–2626.
- [109] A. B. Smith III, R. Akaishi, D. R. Jones, T. P. Keenan, M. C. Guzman, R. C. Holcomb, P. A. Sprengeler, J. L. Wood, R. Hirschmann, M. K. Holloway, *Biopolymers* **1995**, *37*, 29–53.
- [110] C. Mao, E. A. Sudbeck, T. K. Venkatachalam, F. M. Uckun, *Biochem. Pharmacol.* **2000**, *60*, 1251–1265.
- [111] R. Silvestri, M. Artico, G. De Martino, E. Novellino, G. Greco, A. Lavecchia, S. Massa, A. G. Loi, S. Doratiotto, P. La Colla, *Bioorg. Med. Chem.* **2000**, *8*, 2305–2309.
- [112] M. Artico, R. Silvestri, E. Pagnozzi, B. Bruno, E. Novellino, G. Greco, S. Massa, A. Ettore, A. G. Loi, F. Scintu, P. La Colla, *J. Med. Chem.* **2000**, *43*, 1886–1891.
- [113] C. Mao, E. A. Sudbeck, T. K. Venkatachalam, F. M. Uckun, *Antiviral Chem. Chemother.* **1999**, *10*, 233–240.
- [114] E. A. Sudbeck, C. Mao, R. Vig, T. K. Venkatachalam, L. Tuel-Ahlgren, F. M. Uckun, *Antimicrob. Agents Chemother.* **1998**, *42*, 3225–3233.
- [115] R. Vig, C. Mao, T. K. Venkatachalam, L. Tuel-Ahlgren, E. A. Sudbeck, F. M. Uckun, *Bioorg. Med. Chem.* **1998**, *6*, 1789–1797.
- [116] I. Kang, J. H. Wang, *J. Biol. Chem.* **1994**, *269*, 12024–12031.
- [117] D. W. Zaharevitz, R. Gussio, A. Wiegand, R. Jalluri, N. Pattabiraman, G. E. Kellogg, L. A. Pallansch, S. S. Yang, R. W. Buckheit, *Med. Chem. Res.* **1999**, *9*, 551–564.
- [118] T. P. Kogan, B. Dupré, K. M. Keller, I. L. Scott, H. Bui, R. V. Market, P. J. Beck, J. A. Voytus, B. M. Revelle, D. Scott, *J. Med. Chem.* **1995**, *38*, 4976–4984.
- [119] C. M. Huwe, T. J. Woltering, J. Jiricek, G. Weitz-Schmidt, C. H. Wong, *Bioorg. Med. Chem.* **1999**, *7*, 773–788.
- [120] C. H. Wong, F. Moris-Varas, S.-C. Hung, T. G. Marron, C.-C. Lin, K. W. Gong, G. Weitz-Schmidt, *J. Am. Chem. Soc.* **1997**, *119*, 8152–8158.
- [121] M. von Itzstein, P. Colman, *Curr. Opin. Struct. Biol.* **1996**, *6*, 703–709.
- [122] M. von Itzstein, J. C. Dyason, S. W. Oliver, H. F. White, W.-Y. Wu, G. B. Kok, M. S. Pegg, *J. Med. Chem.* **1996**, *39*, 388–391.
- [123] J. C. Wilson, R. J. Thomson, J. C. Dyason, P. Florio, K. J. Quelch, S. Abo, M. von Itzstein, *Tetrahedron: Asymmetry* **2000**, *11*, 53–73.
- [124] N. R. Taylor, A. Cleasby, O. Singh, T. Skarzynski, A. J. Wonacott, P. W. Smith, S. L. Sollis, P. D. Howes, P. C. Cherry, R. Bethell, P. Colman, J. Varghese, *J. Med. Chem.* **1998**, *41*, 798–807.
- [125] P. W. Smith, S. L. Sollis, P. D. Howes, P. C. Cherry, I. D. Starkey, K. N. Copley, H. Weston, J. Sciscinski, A. Merritt, A. Whittington, P. Wyatt, N. Taylor, D. Green, R. Bethell, S. Madar, R. J. Fenton, P. J. Morley, T. Pateman, A. Beresford, *J. Med. Chem.* **1998**, *41*, 787–797.
- [126] G. Taylor, *Curr. Opin. Struct. Biol.* **1996**, *6*, 830–837.
- [127] S. Singh, M. J. Jedrzejewski, G. M. Air, M. Luo, W. G. Laver, W. J. Brouillette, *J. Med. Chem.* **1995**, *38*, 3217–3225.
- [128] W. Lew, X. Chen, C. U. Kim, *Curr. Med. Chem.* **2000**, *7*, 663–672.
- [129] V. R. Atigadda, W. J. Brouillette, F. Duarte, Y. S. Babu, S. Bantia, P. Chand, N. Chu, J. A. Montgomery, D. A. Walsh, E. Sudbeck, J. Finley, G. M. Air, M. Luo, G. W. Laver, *Bioorg. Med. Chem.* **1999**, *7*, 2487–2497.
- [130] J. B. Finley, V. R. Atigadda, F. Duarte, J. J. Zhao, W. J. Brouillette, G. M. Air, M. Luo, *J. Mol. Biol.* **1999**, *293*, 1107–1119.
- [131] J. N. Varghese, P. W. Smith, S. L. Sollis, T. J. Blick, A. Sahasrabudhe, J. L. McKimm-Breschkin, P. M. Colman, *Structure* **1998**, *6*, 735–746.
- [132] C. U. Kim, W. Lew, M. A. Williams, H. T. Liu, L. J. Zhang, S. Swaminathan, N. Bischofberger, M. S. Chen, D. B. Mendel, C. Y. Tai, W. G. Laver, R. C. Stevens, *J. Am. Chem. Soc.* **1997**, *119*, 681–690.
- [133] B. A. Katz, C. R. Johnson, R. T. Cass, *J. Am. Chem. Soc.* **1995**, *117*, 8541–8547.
- [134] P. C. Weber, M. W. Pantoliano, D. M. Simons, F. R. Salemme, *J. Am. Chem. Soc.* **1994**, *116*, 2717–2727.
- [135] B. A. Katz, *Biomol. Eng.* **1999**, *16*, 57–65.
- [136] B. A. Katz, B. Liu, R. Cass, *J. Am. Chem. Soc.* **1996**, *118*, 7914–7920.
- [137] B. P. Morgan, D. R. Holland, B. W. Matthews, P. A. Bartlett, *J. Am. Chem. Soc.* **1994**, *116*, 3251–3260.
- [138] K. Hilpert, J. Ackermann, D. W. Banner, A. Gast, K. Gubernator, P. Hadvary, L. Labler, K. Müller, G. Schmid, T. B. Tschopp, H. van de Waterbeemd, *J. Med. Chem.* **1994**, *37*, 3889–3901.
- [139] J. J. Slon-Usakiewicz, J. Sivaraman, Y. Li, M. Cygler, Y. Konishi, *Biochemistry* **2000**, *39*, 2384–2391.
- [140] S. Hanessian, E. Balaux, D. Musil, L. L. Olsson, I. Nilsson, *Bioorg. Med. Chem. Lett.* **2000**, *10*, 243–247.
- [141] M. Li, Z. Lin, M. E. Johnson, *Bioorg. Med. Chem. Lett.* **1999**, *9*, 1957–1962.
- [142] H. J. Böhm, D. W. Banner, L. Weber, *J. Comput. Aided Mol. Des.* **1999**, *13*, 51–56.
- [143] J. Wagner, J. Kallen, C. Ehrhardt, J. P. Evenou, D. Wagner, *J. Med. Chem.* **1998**, *41*, 3664–3674.
- [144] P. Burkhardt, P. Taylor, M. D. Walkinshaw, *J. Mol. Biol.* **1998**, *277*, 449–466.
- [145] U. Obst, D. W. Banner, L. Weber, F. Diederich, *Chem. Biol.* **1997**, *4*, 287–295.
- [146] B. Shoichet, R. Stroud, D. Santi, I. Kuntz, K. Perry, *Science* **1993**, *259*, 1445–1450.
- [147] *The Practice of Medicinal Chemistry* (Ed.: C. G. Wermuth), Academic Press, London, **1996**.
- [148] J. P. Vacca, J. H. Condra, *Drug Discovery Today* **1997**, *2*, 261–272.
- [149] P. Wutzler, *Infection* **2000**, *28*, 261–266.
- [150] *3D QSAR in Drug Design: Theory, Methods and Applications* (Ed.: H. Kubinyi), Escom, Leiden, **1993**.
- [151] *3D QSAR in Drug Design: Recent Advances* (Eds.: H. Kubinyi, G. Folkers, Y. C. Martin), Kluwer/Escom, Leiden, **1997**.
- [152] T. I. Oprea, C. L. Waller, *Rev. Comput. Chem.* **1997**, *11*, 127–182.
- [153] G. Greco, E. Novellino, Y. C. Martin, *Rev. Comput. Chem.* **1997**, *11*, 183–240.
- [154] *Chemometric Methods in Molecular Design, Vol. 2* (Ed.: H. van de Waterbeemd), Wiley-VCH, Weinheim, **1995**.
- [155] Y. C. Martin in *Designing Bioactive Molecules* (Eds.: Y. C. Martin, P. Willett, S. R. Heller), American Chemical Society, Washington, **1999**.
- [156] D. P. Marriot, I. A. Dougall, P. Meghani, Y. Liu, D. R. Flower, *J. Med. Chem.* **1999**, *42*, 3210–3216.
- [157] J. P. Snyder, S. N. Rao, K. F. Koehler, A. Vedani in *3D QSAR in Drug Design. Theory, Methods and Applications* (Ed.: H. Kubinyi), Escom, Leiden, **1993**, pp. 336–354.
- [158] A. Vedani, P. Zbinden, J. P. Snyder, P. A. Greenidge, *J. Am. Chem. Soc.* **1995**, *117*, 4987–4994.
- [159] M. Gurrath, G. Müller, H.-D. Höltje in *3D QSAR in Drug Design. Recent Advances* (Eds.: H. Kubinyi, G. Folkers, Y. C. Martin), Kluwer/Escom, Dordrecht, **1998**, p. 135–157.
- [160] A. Schafferhans, G. Klebe, *J. Mol. Biol.* **2001**, *307*, 407–427.
- [161] M. S. Doscher, F. M. Richards, *J. Biol. Chem.* **1963**, *238*, 2399–2406.
- [162] C. C. F. Blake, R. Cassels, C. M. Dobson, F. M. Poulsen, R. J. P. Williams, K. S. Wilson, *J. Mol. Biol.* **1981**, *147*, 73–95.
- [163] A. T. Brünger, *Nat. Struct. Biol.* **1997**, *4* (NMR Suppl.), 862–865.
- [164] A. L. Margolin, *Trends Biotechnol.* **1996**, *14*, 223–230.
- [165] A. Mozzarelli, G. L. Rossi, *Annu. Rev. Biophys. Biomol. Struct.* **1996**, *25*, 343–365.
- [166] A. L. Margolin, M. A. Navia, *Angew. Chem.* **2001**, *113*, 2262–2281; *Angew. Chem. Int. Ed.* **2001**, *40*, 2205–2222.
- [167] M. A. Murcko, *Rev. Comput. Chem.* **1997**, *11*, 1–66.
- [168] D. E. Clark, C. W. Murray, J. Li, *Rev. Comput. Chem.* **1997**, *11*, 67–125.
- [169] T. Lengauer, M. Rarey, *Curr. Opin. Struct. Biol.* **1996**, *6*, 402–406.
- [170] H. J. Böhm, M. Stahl, *Curr. Opin. Chem. Biol.* **2000**, *4*, 283–286.
- [171] G. M. Verkhivker, D. Bouzida, D. K. Gehlhaar, P. A. Rejto, S. Arthurs, A. B. Colson, S. T. Freer, V. Larson, B. A. Luty, T. Marrone, P. W. Rose, *J. Comput. Aided Mol. Des.* **2000**, *14*, 731–751.
- [172] J. S. Dixon, *Proteins* **1997**, *Suppl. 1*, 198–204.
- [173] Ajay, M. A. Murcko, *J. Med. Chem.* **1995**, *38*, 4953–4967.
- [174] R. M. A. Knegtel, P. D. J. Grootenhuys in *3D QSAR in Drug Design. Ligand Protein Interactions and Molecular Similarity* (Eds.: H. Kubinyi, G. Folkers, Y. C. Martin), Kluwer/Escom, Dordrecht, **1998**, pp. 99–114.
- [175] T. I. Oprea, G. R. Marshall in *3D QSAR in Drug Design. Ligand Protein Interactions and Molecular Similarity* (Eds.: H. Kubinyi, G. Folkers, Y. C. Martin), Kluwer/Escom, Dordrecht, **1998**, pp. 3–17.
- [176] B. Kramer, M. Rarey, T. Lengauer, *Proteins* **1999**, *37*, 145–156.
- [177] H. A. Carlson, J. A. McCammon, *Mol. Pharmacol.* **2000**, *57*, 213–218.

- [178] N. E. Chayen, T. J. Boggon, A. Casetta, A. Deacon, T. Gleichmann, J. Habash, S. J. Harrop, J. R. Helliwell, Y. P. Nieh, M. R. Peterson, J. Raftery, E. H. Snell, A. Hädener, A. C. Niemann, D. P. Siddons, V. Stojanoff, A. W. Thompson, T. Ursby, M. Wulff, *Q. Rev. Biophys.* **1996**, 29, 227–278.
- [179] R. W. W. Hoofst, C. Sander, G. Vriend, *Proteins* **1996**, 26, 363–376.
- [180] J. E. Nielsen, G. Vriend, *Proteins* **2001**, 43, 403–412.
- [181] S. Longhi, M. Czjzek, C. Cambillau, *Curr. Opin. Struct. Biol.* **1998**, 8, 730–737.
- [182] R. Flaig, T. Koritsanszky, R. Soyka, L. Häming, P. Luger, *Angew. Chem.* **2001**, 113, 368–371; *Angew. Chem. Int. Ed.* **2001**, 40, 355–359.
- [183] A. A. Kossiakoff, M. Randal, J. Guenot, C. Eigenbrot, *Proteins* **1992**, 14, 65–74.
- [184] A. Wlodawer, J. Nachman, G. L. Gilliland, W. Gallagher, C. J. Woodward, *J. Mol. Biol.* **1987**, 198, 469–480.
- [185] P. Dauber-Osguthorpe, V. A. Roberts, D. J. Osguthorpe, J. Wolff, M. Genest, A. T. Hagler, *Proteins* **1988**, 4, 31–47.
- [186] M. Levitt, B. H. Park, *Structure* **1993**, 1, 223–226.
- [187] O. Carugo, D. Bordo, *Acta Crystallogr. Sect. D* **1999**, 55, 479–483.
- [188] P. A. Karplus, C. Faerman, *Curr. Opin. Struct. Biol.* **1994**, 4, 770–776.
- [189] T. Beyer, G. M. Day, S. L. Price, *J. Am. Chem. Soc.* **2001**, 123, 5086–5094.
- [190] J. Bernstein, *Prog. Clin. Biol. Res.* **1989**, 289, 203–215.
- [191] P. Verwer, F. J. J. Leusen, *Rev. Comput. Chem.* **1998**, 12, 327–365.
- [192] J. D. Dunitz, J. Bernstein, *Acc. Chem. Res.* **1995**, 28, 193–200.
- [193] J. M. Lehn, *Angew. Chem.* **1988**, 100, 91–116; *Angew. Chem. Int. Ed. Engl.* **1988**, 27, 89–112.
- [194] H.-J. Böhm, G. Klebe, *Angew. Chem.* **1996**, 108, 2750–2778; *Angew. Chem. Int. Ed. Engl.* **1996**, 35, 2589–2614.
- [195] G. Klebe, H.-J. Böhm, *Period. Biol.* **1998**, 100 (Suppl. 2), 77–83.
- [196] E. di Cera, *Thermodynamic Theory of Site-Specific Binding Processes in Biological Macromolecules*, Cambridge University Press, Cambridge, **1995**.
- [197] *Drug–Receptor Thermodynamics: Introduction and Applications* (Ed.: R. B. Raffa), Wiley, Chichester, **2001**.
- [198] M. K. Gilson, J. A. Given, B. L. Bush, J. A. McCammon, *Biophys. J.* **1997**, 72, 1047–1069.
- [199] A. M. Davis, S. J. Teague, *Angew. Chem.* **1999**, 111, 778–792; *Angew. Chem. Int. Ed.* **1999**, 38, 737–749.
- [200] I. D. Kuntz, K. Chen, K. A. Sharp, P. A. Kollman, *Proc. Natl. Acad. Sci. USA* **1999**, 96, 9997–10002.
- [201] A. Fersht, *Enzyme Structure and Mechanism*, Freeman, New York, **1985**.
- [202] P. M. Dean, *Molecular Foundations of Drug–Receptor Interaction*, Cambridge University Press, Cambridge, **1987**.
- [203] P. R. Andrews, D. J. Craik, J. L. Martin, *J. Med. Chem.* **1984**, 27, 1648–1657.
- [204] J. D. Dunitz, A. Gavezotti, *Acc. Chem. Res.* **1999**, 32, 677–684.
- [205] G. A. Jeffrey, W. Saenger, *Hydrogen Bonding in Biological Structures*, Springer, Berlin, **1991**.
- [206] G. A. Jeffrey, *An Introduction to Hydrogen Bonding*, Oxford University Press, New York, **1997**.
- [207] L. Pauling, R. B. Corey, *Proc. Natl. Acad. Sci. USA* **1951**, 37, 729–740.
- [208] K. P. Murphy, S. J. Gill, *J. Mol. Biol.* **1991**, 222, 699–706.
- [209] A. Yang, K. A. Sharp, B. Honig, *J. Mol. Biol.* **1992**, 227, 889–900.
- [210] A. R. Fersht, *Trends Biochem. Sci.* **1987**, 12, 301–304.
- [211] Q. Zou, S. M. Habermann-Rottinghaus, K. P. Murphy, *Proteins* **1998**, 31, 107–115.
- [212] H. Adalsteinsson, A. H. Maulitz, T. C. Bruice, *J. Am. Chem. Soc.* **1996**, 118, 7689–7693.
- [213] T. Steiner, W. Saenger, *Acta Crystallogr. Sect. B* **1994**, 50, 348–357.
- [214] Z. Wang, H. Luecke, Y. Nanhua, F. Quioco, *Nat. Struct. Biol.* **1997**, 4, 519–522.
- [215] A. Warshel, A. Papazyan, P. A. Kollman, *Science* **1995**, 269, 102–104.
- [216] B. Honig, A. Nicholls, *Science* **1995**, 268, 1144–1149.
- [217] T. Simonson, G. Archontis, M. Karplus, *J. Phys. Chem. B* **1999**, 103, 6142–6156.
- [218] H. Nakamura, *Q. Rev. Biophys.* **1996**, 29, 1–90.
- [219] W. Rocchia, E. Alexov, B. Honig, *J. Phys. Chem. B* **2001**, 105, 6507–6514.
- [220] M. Stahl, H.-J. Böhm, *J. Mol. Graphics Modell.* **1998**, 16, 121–132.
- [221] C. Beeson, N. Pham, G. Shipps, T. A. Dix, *J. Am. Chem. Soc.* **1993**, 115, 6803–6812.
- [222] I. K. McDonald, J. M. Thornton, *J. Mol. Biol.* **1994**, 238, 777–793.
- [223] P. R. Connelly, R. A. Aldape, F. J. Bruzzese, S. P. Chambers, M. J. Fitzgibbon, M. A. Fleming, S. Itoh, D. J. Livingston, M. A. Navia, J. A. Thomson, K. P. Wilson, *Proc. Natl. Acad. Sci. USA* **1994**, 91, 1964–1968.
- [224] D. Grobelny, U. B. Goli, R. E. Galardy, *Biochemistry* **1989**, 28, 4948–4951.
- [225] P. A. Bash, U. C. Singh, F. K. Brown, R. Langridge, P. A. Kollman, *Science* **1987**, 235, 574–576.
- [226] A. R. Fersht, J. S. Shindler, W. C. Tsui, *Biochemistry* **1980**, 19, 5520–5524.
- [227] R. M. C. Dawson, D. C. Elliott, W. H. Elliot, K. M. Jones, *Data for Biochemical Research*, Oxford University Press, Oxford, **1969**.
- [228] J. Antosiewicz, J. A. McCammon, M. K. Gilson, *Biochemistry* **1996**, 35, 7819–7833.
- [229] M. Graffner-Nordberg, J. Marelus, S. Ohlsson, A. Persson, G. Swedberg, P. Andersson, S. E. Andersson, J. Åqvist, A. Hallberg, *J. Med. Chem.* **2000**, 43, 3852–3861.
- [230] X. Barril, C. Aleman, M. Orozco, F. J. Luque, *Proteins* **1998**, 32, 67–79.
- [231] A. R. Fersht, J. P. Shi, J. Knill-Jones, D. M. Lowe, A. J. Wilkinson, D. M. Blow, P. Brick, P. Carter, M. M. Y. Waye, G. Winter, *Nature* **1985**, 314, 235–238.
- [232] S. M. Habermann, K. P. Murphy, *Protein Sci.* **1996**, 5, 1229–1239.
- [233] K. A. Dill, *Biochemistry* **1990**, 29, 7133–7155.
- [234] J. S. Thorson, E. Chapman, E. C. Murphy, P. G. Schultz, J. K. Judice, *J. Am. Chem. Soc.* **1995**, 117, 1157–1158.
- [235] J. Fernandez-Recio, A. Romero, J. Sancho, *J. Mol. Biol.* **1999**, 290, 319–330.
- [236] M. A. Hossain, H.-J. Schneider, *Chem. Eur. J.* **1999**, 5, 1284–1290.
- [237] D. E. Otzen, A. R. Fersht, *Protein Eng.* **1999**, 12, 41–45.
- [238] J. Gao, K. Kuczera, B. Tidor, M. Karplus, *Science* **1989**, 244, 1069–1072.
- [239] A. J. Doig, D. H. Williams, *J. Am. Chem. Soc.* **1992**, 114, 338–343.
- [240] M. S. Searle, D. H. Williams, U. Gerhard, *J. Am. Chem. Soc.* **1992**, 114, 10697–10704.
- [241] D. H. Williams, M. S. Searle, J. P. Mackay, U. Gerhard, R. A. Maplestone, *Proc. Natl. Acad. Sci. USA* **1993**, 90, 1172–1178.
- [242] D. H. Williams, M. S. Westwell, *Chem. Soc. Rev.* **1998**, 27, 57–63.
- [243] M. S. Gordon, J. H. Jensen, *Acc. Chem. Res.* **1996**, 29, 536–543.
- [244] G. Klebe, *J. Mol. Biol.* **1994**, 237, 212–235.
- [245] F. H. Allen, *Acta Crystallogr. Sect. A* **1998**, 54, 758–771.
- [246] J. Kroon, J. A. Kanters, J. G. C. M. van Duijneveldt-van de Rijdt, F. B. van Duijneveldt, J. A. Vliegenhardt, *J. Mol. Struct.* **1975**, 24, 109–129.
- [247] P. Murray-Rust, J. P. Glusker, *J. Am. Chem. Soc.* **1984**, 106, 1018–1025.
- [248] M. Tintelnot, P. Andrews, *J. Comput. Aided Mol. Des.* **1989**, 3, 67–84.
- [249] S. M. Roe, M. M. Teeter, *J. Mol. Biol.* **1993**, 229, 419–427.
- [250] I. J. Bruno, J. C. Cole, J. P. Lommerse, R. S. Rowland, R. Taylor, M. L. Verdonk, *J. Comput. Aided Mol. Des.* **1997**, 11, 525–537.
- [251] J. C. Cole, R. Taylor, M. L. Verdonk, *Acta Crystallogr. Sect. D* **1998**, 54, 1183–1193.
- [252] R. Taylor, O. Kennard, *J. Am. Chem. Soc.* **1982**, 104, 5063–5070.
- [253] S. Harder, *Chem. Eur. J.* **1999**, 5, 1852–1861.
- [254] G. R. Desiraju, *Acc. Chem. Res.* **1996**, 29, 441–449.
- [255] S. Tsuzuki, K. Honda, T. Uchimaru, M. Mikami, K. Tanabe, *J. Am. Chem. Soc.* **2000**, 122, 11450–11458.
- [256] M. Brandl, M. S. Weiss, A. Jabs, J. Sühnel, R. Hilgenfeld, *J. Mol. Biol.* **2001**, 307, 357–377.
- [257] C. A. Hunter, J. K. M. Sanders, *J. Am. Chem. Soc.* **1990**, 112, 5525–5534.
- [258] S. K. Burley, G. A. Petsko, *Science* **1985**, 229, 23–28.
- [259] U. Samanta, D. Pal, P. Chakrabarti, *Acta Crystallogr. Sect. D* **1999**, 55, 1421–1427.
- [260] C. A. Hunter, J. Singh, J. M. Thornton, *J. Mol. Biol.* **1991**, 218, 837–846.
- [261] G. B. McGaughey, M. Gagné, A. K. Rappé, *J. Biol. Chem.* **1998**, 273, 15458–15463.

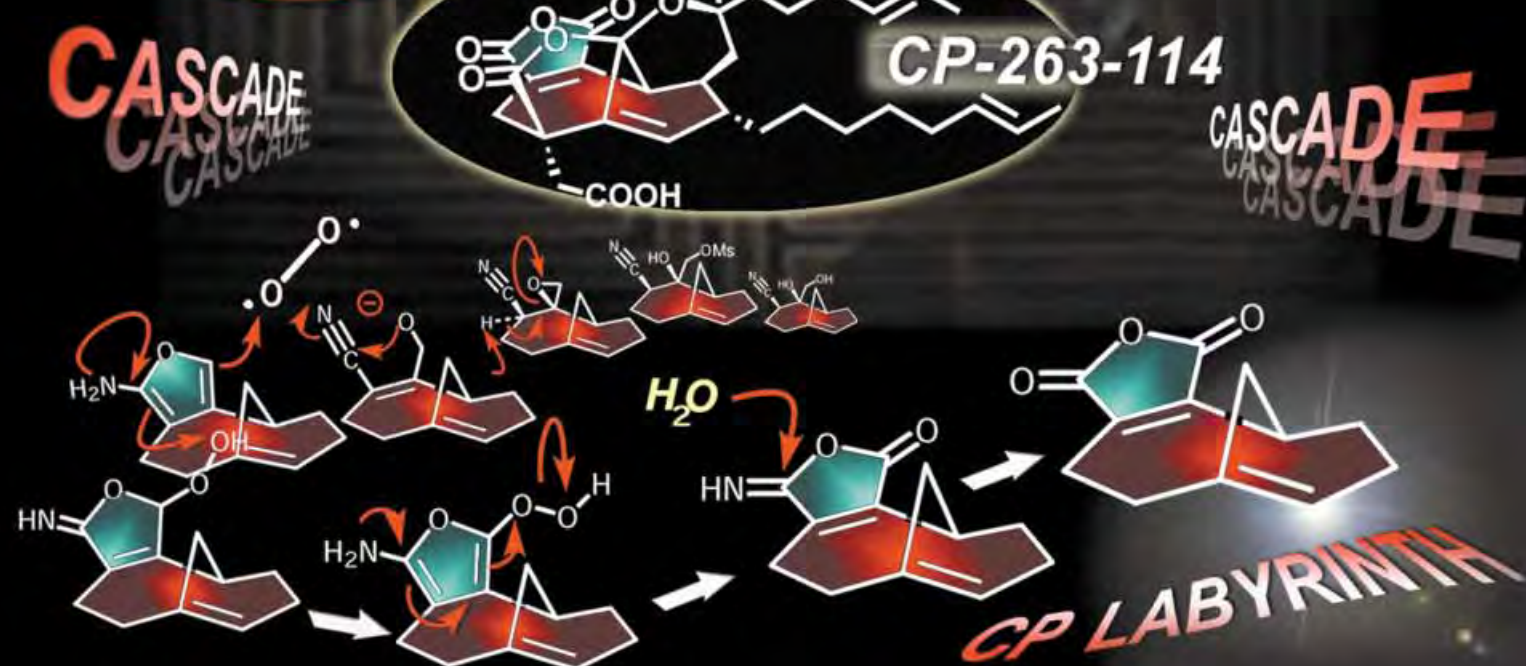
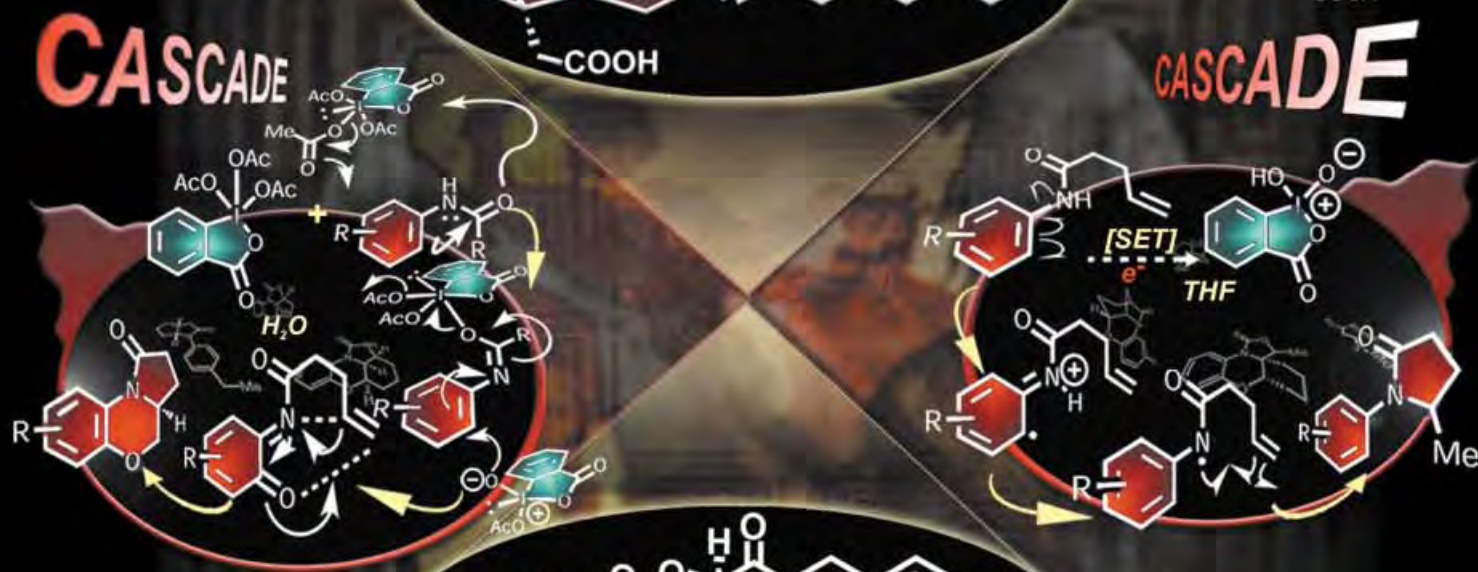
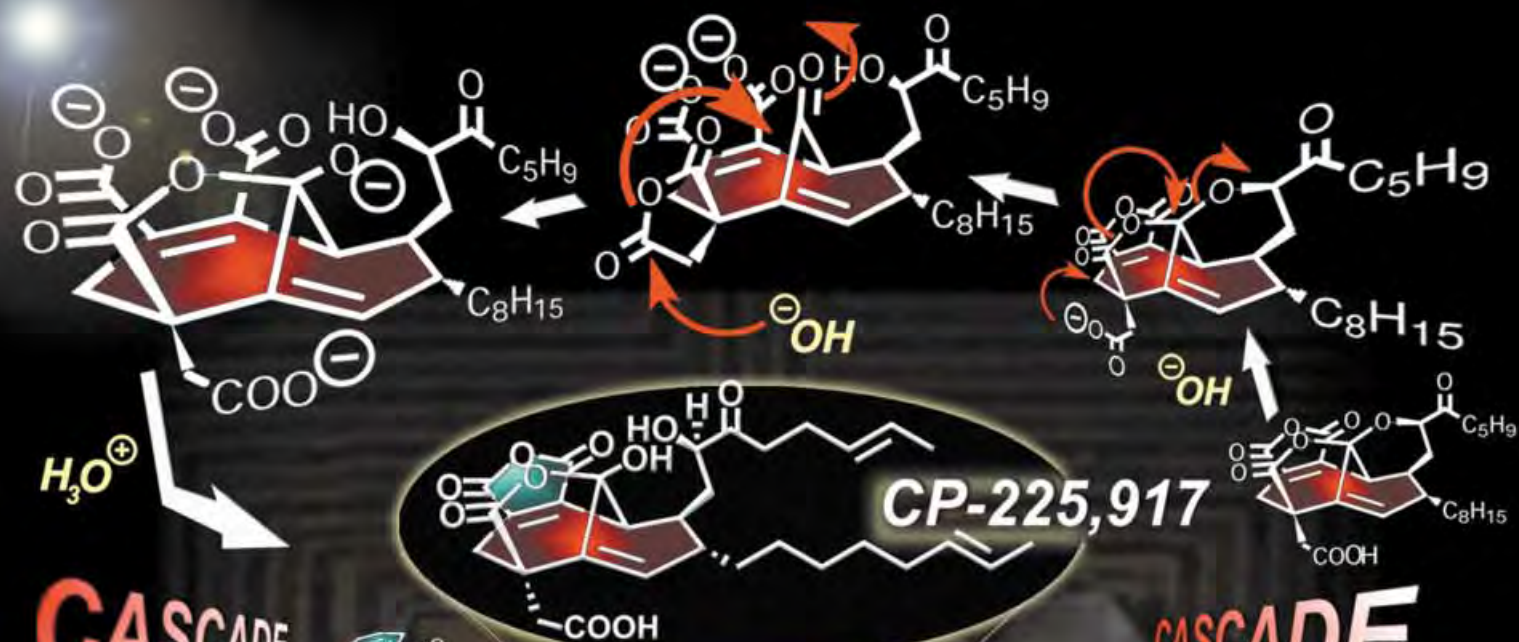
- [262] D. A. Dougherty, *Science* **1996**, 271, 163–168.
- [263] J. C. Ma, D. A. Dougherty, *Chem. Rev.* **1997**, 97, 1303–1324.
- [264] E. V. Pletneva, A. T. Laederach, D. B. Fulton, N. M. Kostic, *J. Am. Chem. Soc.* **2001**, 123, 6232–6245.
- [265] J. D. Schmitt, *Curr. Med. Chem.* **2000**, 7, 749–800.
- [266] K. Brejc, W. J. van Dijk, R. V. Klaasen, M. Schuurmans, J. van der Oost, A. B. Smit, T. K. Sixma, *Nature* **2001**, 411, 269–276.
- [267] J. P. Gallivan, D. A. Dougherty, *J. Am. Chem. Soc.* **2000**, 122, 870–874.
- [268] M. M. Harding, *Acta Crystallogr. Sect. D* **1999**, 55, 1432–1443.
- [269] M. M. Harding, *Acta Crystallogr. Sect. D* **2000**, 56, 857–867.
- [270] C.-Y. Kim, J. S. Chang, J. B. Doyon, T. T. Baird, C. A. Fierke, A. Jain, D. W. Christianson, *J. Am. Chem. Soc.* **2000**, 122, 12 125–12 134.
- [271] R. U. Lemieux, *Acc. Chem. Res.* **1996**, 29, 373–380.
- [272] J. Israelachvili, H. Wennerstrom, *Nature* **1996**, 379, 219–225.
- [273] D. G. Covell, A. Wallqvist, *J. Mol. Biol.* **1997**, 269, 281–297.
- [274] C. S. Poornima, P. M. Dean, *J. Comput. Aided Mol. Des.* **1995**, 9, 500–512.
- [275] H. Wang, A. Ben-Naim, *J. Med. Chem.* **1996**, 39, 1531–1539.
- [276] A. Ben-Naim, *Statistical Thermodynamics for Chemists and Biochemists*, Plenum, New York, **1992**.
- [277] J. E. Ladbury, *Chem. Biol.* **1996**, 3, 973–980.
- [278] J. D. Dunitz, *Science* **1994**, 264, 670.
- [279] *Structural-Based Drug Design: Thermodynamics, Modeling and Strategy* (Ed.: P. R. Connelly), Landes, Austin, **1997**.
- [280] C. S. Poornima, P. M. Dean, *J. Comput. Aided Mol. Des.* **1995**, 9, 513–520.
- [281] L. A. Kuhn, M. A. Siani, M. E. Pique, C. L. Fisher, E. D. Getzoff, J. A. Trainer, *J. Mol. Biol.* **1992**, 228, 13–22.
- [282] J. R. H. Tame, A. J. Wilkinson, *Science* **1994**, 264, 1578–1581.
- [283] J. R. H. Tame, S. H. Sleight, A. J. Wilkinson, J. E. Ladbury, *Nat. Struct. Biol.* **1996**, 3, 998–1001.
- [284] C. S. Poornima, P. M. Dean, *J. Comput. Aided Mol. Des.* **1995**, 9, 521–531.
- [285] M. L. Raymer, P. C. Sanschagrin, W. F. Punch, S. Venkataraman, E. D. Goodman, L. A. Kuhn, *J. Mol. Biol.* **1997**, 265, 445–464.
- [286] D. Ringe, C. Mattos, *Med. Res. Rev.* **1999**, 19, 321–331.
- [287] *Water, a Comprehensive Treatise, Vol. 1–7* (Ed.: F. Franks), Plenum, New York, **1972–1982**.
- [288] D. Eisenberg, W. Kauzmann, *The Structure and Properties of Water*, Oxford University Press, Oxford, **1969**.
- [289] R. Ludwig, *Angew. Chem.* **2001**, 113, 1856–1876; *Angew. Chem. Int. Ed.* **2001**, 40, 1809–1827.
- [290] M. Page, *Angew. Chem.* **1977**, 89, 456–467; *Angew. Chem. Int. Ed. Engl.* **1977**, 16, 449–459.
- [291] W. P. Jencks, *Proc. Natl. Acad. Sci. USA* **1981**, 78, 4046–4050.
- [292] M. S. Searle, D. H. Williams, *J. Am. Chem. Soc.* **1992**, 114, 10 690–10 697.
- [293] E. Grunwald, C. Steel, *J. Am. Chem. Soc.* **1995**, 117, 5687–5692.
- [294] C. Tanford, *The Hydrophobic Effect: Formation of Micelles and Biological Membranes*, Wiley, New York, **1980**.
- [295] A. Ben-Naim, *Hydrophobic Interactions*, Plenum, New York, **1980**.
- [296] A. Ben-Naim, *Solvation Thermodynamics*, Plenum, New York, **1987**.
- [297] K. A. T. Silverstein, A. D. J. Haymet, K. A. Dill, *J. Am. Chem. Soc.* **1998**, 120, 3166–3175.
- [298] W. Blokzijl, J. B. F. N. Engberts, *Angew. Chem.* **1993**, 105, 1610–1648; *Angew. Chem. Int. Ed. Engl.* **1993**, 32, 1545–1579.
- [299] H. S. Frank, M. W. Evans, *J. Chem. Phys.* **1945**, 13, 507.
- [300] G. Nemethy, H. A. Scheraga, *J. Chem. Phys.* **1962**, 36, 3401.
- [301] K. A. T. Silverstein, A. D. J. Haymet, K. A. Dill, *J. Am. Chem. Soc.* **2000**, 122, 8037–8041.
- [302] N. Muller, *Acc. Chem. Res.* **1990**, 23, 23–28.
- [303] A. Pertsemidlis, A. M. Saxena, A. K. Soper, T. Head-Gordon, R. M. Glaeser, *Proc. Natl. Acad. Sci. USA* **1996**, 93, 10 769.
- [304] K. E. Laidig, V. Daggett, *J. Phys. Chem.* **1996**, 100, 5616–5619.
- [305] L. F. Scatena, M. G. Brown, G. L. Richmond, *Science* **2001**, 292, 908–912.
- [306] R. L. Mancera, *J. Comput. Aided Mol. Des.* **1996**, 10, 321–326.
- [307] K. P. Murphy, P. L. Privalov, S. J. Gill, *Science* **1990**, 247, 559.
- [308] M. C. Chervenak, E. J. Toone, *J. Am. Chem. Soc.* **1994**, 116, 10 533–10 539.
- [309] C. Chothia, *Nature* **1974**, 248, 338–339.
- [310] C. Chothia, J. Janin, *Nature* **1975**, 256, 705–708.
- [311] T. Ooi, M. Oobatake, G. Nemethy, H. A. Scheraga, *Proc. Natl. Acad. Sci. USA* **1987**, 84, 3086–3090.
- [312] D. Eisenberg, A. D. McLachlan, *Nature* **1986**, 319, 199–203.
- [313] C. N. Pace, *J. Mol. Biol.* **1992**, 226, 29–35.
- [314] J. Wang, W. Wang, S. Huo, M. Lee, P. A. Kollman, *J. Phys. Chem. B* **2001**, 105, 5055–5067.
- [315] D. H. Williams, B. Bardsley, *Perspect. Drug Discovery Des.* **1999**, 17, 43–59.
- [316] P. Carrupt, B. Testa, P. Gaillard, *Rev. Comput. Chem.* **1997**, 11, 241–315.
- [317] J. A. Reynolds, D. B. Gilbert, C. Tanford, *Proc. Natl. Acad. Sci. USA* **1974**, 71, 2925–2927.
- [318] R. B. Hermann, *J. Phys. Chem.* **1972**, 76, 2754.
- [319] A. Nicholls, K. A. Sharp, B. Honig, *Proteins* **1991**, 11, 281–296.
- [320] P. D. Ross, M. V. Rekharsky, *Biophys. J.* **1996**, 71, 2144–2155.
- [321] L. Serrano, J.-L. Neira, J. Sancho, A. R. Fersht, *Nature* **1992**, 356, 453–455.
- [322] J. T. Kellis, K. Nyberg, A. R. Fersht, *Biochemistry* **1989**, 28, 4914–4922.
- [323] D. Shortle, W. E. Stites, A. K. Meeker, *Biochemistry* **1990**, 29, 8033–8041.
- [324] M. Matsumura, W. J. Becktel, B. W. Matthews, *Nature* **1988**, 334, 406–410.
- [325] G. J. Sharman, M. S. Searle, B. Benhamu, P. Groves, D. H. Williams, *Angew. Chem.* **1995**, 107, 1644–1646; *Angew. Chem. Int. Ed. Engl.* **1995**, 34, 1483–1485.
- [326] D. M. Huang, D. Chandler, *Proc. Natl. Acad. Sci. USA* **2000**, 97, 8324–8327.
- [327] M. Vandonselaar, R. A. Hickie, J. W. Quail, L. T. J. Delbaere, *Nat. Struct. Biol.* **1994**, 1, 795–801.
- [328] H. P. Märki, W. Fischli, A. Binggeli, V. Breu, D. Bur, J. P. Clozel, A. D'Arcy, F. Grüninger, R. Gülller, G. Hirth, T. Lave, S. Mathews, M. Müller, C. Oefner, H. Stadler, E. Vieira, M. Wilhelm, W. Wostl, *9th RSC-SCI Medicinal Chemistry Symposium* (Cambridge, UK), **1997**.
- [329] A. Urzhumtsev, F. Tete-Favier, A. Mitschler, J. Barbanton, P. Barth, L. Urzhumtseva, J. F. Biellmann, A. Podjarny, D. Moras, *Structure* **1997**, 5, 601–612.
- [330] S. E. Zographos, N. G. Oikonomakos, K. E. Tsitsanou, D. D. Leonidas, E. D. Chrysina, V. T. Skamnaki, H. Bischoff, S. Goldmann, K. A. Watson, L. N. Johnson, *Structure* **1997**, 5, 1413–1425.
- [331] J. Ren, R. Esnouf, E. Garman, D. Somers, C. Ross, I. Kirby, J. Keeling, G. Dardy, Y. Jones, D. Stuart, D. Stammers, *Nat. Struct. Biol.* **1995**, 2, 293–302.
- [332] G. P. Brady, K. A. Sharp, *Curr. Opin. Struct. Biol.* **1997**, 7, 215–221.
- [333] M. I. Page, W. P. Jencks, *Proc. Natl. Acad. Sci. USA* **1971**, 68, 1678–1683.
- [334] M. I. Page, *Chem. Soc. Rev.* **1973**, 2, 295–323.
- [335] J. M. Sturtevant, *Proc. Natl. Acad. Sci. USA* **1977**, 74, 2236–2240.
- [336] J. D. Dunitz, *Chem. Biol.* **1995**, 2, 709–712.
- [337] P. W. Atkins, *Physikalische Chemie*, VCH, Weinheim, **1990**.
- [338] K. P. Murphy, D. Xie, K. Thompson, M. Arnzel, E. Freire, *Proteins* **1994**, 18, 63–67.
- [339] J. Janin, *Proteins* **1996**, 24, R1–R2.
- [340] J. Janin, *Proteins* **1995**, 21, 30–39.
- [341] J. Doucet, J. P. Benoit, *Nature* **1987**, 325, 643.
- [342] D. L. D. Caspar, J. Clarage, D. M. Salunke, M. Clarage, *Nature* **1988**, 332, 659–662.
- [343] A. V. Finkelstein, J. Janin, *Protein Eng.* **1989**, 3, 1–3.
- [344] G. P. Brady, K. A. Sharp, *Biophys. J.* **1997**, 72, 913–927.
- [345] J. Hermans, L. Wang, *J. Am. Chem. Soc.* **1997**, 119, 2707–2714.
- [346] S. D. Pickett, M. J. Sternberg, *J. Mol. Biol.* **1993**, 231, 825–839.
- [347] A. J. Doig, M. J. E. Sternberg, *Protein Sci.* **1995**, 4, 2247–2251.
- [348] J. D. Forman-Kay, *Nat. Struct. Biol.* **1999**, 6, 1086–1087.
- [349] R. Raag, T. L. Poulos, *Biochemistry* **1991**, 30, 2674–2684.
- [350] L. Yu, C. X. Zhu, Y. C. Tse-Dinh, S. W. Fesik, *Biochemistry* **1996**, 35, 9661–9666.
- [351] L. Zidek, M. V. Novotny, M. J. Stone, *Nat. Struct. Biol.* **1999**, 6, 1118–1121.
- [352] P. C. Weber, J. J. Wendoloski, M. W. Pantoliano, F. R. Salemme, *J. Am. Chem. Soc.* **1992**, 114, 3197–3200.
- [353] M. S. L. Lim, E. R. Johnston, C. A. Kettner, *J. Med. Chem.* **1993**, 36, 1831–1838.

- [354] R. A. Wiley, D. H. Rich, *Med. Res. Rev.* **1993**, *13*, 327–384.
- [355] B. Testa, P. A. Carrupt, P. Gaillard, F. Billois, P. Weber, *Pharm. Res.* **1996**, *13*, 335–343.
- [356] M. A. Navia, P. R. Chaturvedi, *Drug Discovery Today* **1996**, *1*, 179–189.
- [357] M. C. Nicklaus, S. Wang, J. S. Driscoll, G. W. A. Milne, *Bioorg. Med. Chem.* **1995**, *3*, 411–428.
- [358] M. J. Spark, D. A. Winkler, P. R. Andrews, *Int. J. Quantum Chem.* **1982**, *9*, 321.
- [359] J. Bostrom, P. O. Norrby, T. Liljefors, *J. Comput. Aided Mol. Des.* **1998**, *12*, 383–396.
- [360] M. Vieth, J. D. Hirst, C. L. Brooks III, *J. Comput. Aided Mol. Des.* **1998**, *12*, 563–572.
- [361] D. Mastropaolo, A. Camerman, N. Camerman, *J. Med. Chem.* **2001**, *44*, 269–273.
- [362] T. A. Halgren, W. Damm, *Curr. Opin. Struct. Biol.* **2001**, *11*, 236–242.
- [363] W. F. Lau, B. M. Pettitt, *J. Med. Chem.* **1989**, *32*, 2542–2547.
- [364] A. E. Mark, W. F. van Gunsteren, *J. Mol. Biol.* **1994**, *240*, 167–176.
- [365] A. Ben-Naim, *J. Chem. Phys.* **1997**, *107*, 3698–3706.
- [366] G. F. Ackers, F. R. Smith, *Annu. Rev. Biochem.* **1985**, *54*, 597–629.
- [367] A. Horovitz, *J. Mol. Biol.* **1987**, *196*, 733–735.
- [368] J. A. Wells, *Biochemistry* **1990**, *29*, 8509–8515.
- [369] K. A. Dill, *J. Biol. Chem.* **1997**, *272*, 701–704.
- [370] G. P. Brady, K. A. Sharp, *J. Mol. Biol.* **1995**, *254*, 77–85.
- [371] G. K. Ackers, M. L. Doyle, D. Myers, M. A. Daugherty, *Science* **1992**, *255*, 54–63.
- [372] D. H. Williams, A. J. Maguire, W. Tsuzuki, M. S. Westwell, *Science* **1998**, *280*, 711–714.
- [373] T. Wieseman, S. Wiliston, J. Brandts, L. Lin, *Anal. Biochem.* **1989**, *179*, 131–137.
- [374] R. Hitzemann, *Trends Pharmacol. Sci.* **1988**, *9*, 408.
- [375] A. F. D. de Namor, M.-C. Ritt, M.-J. Schwing-Weill, F. Arnaud-Neu, D. F. V. Lewis, *J. Chem. Soc. Faraday Trans.* **1991**, *87*, 3231–3239.
- [376] P. Gilli, V. Ferretti, G. Gilli, P. A. Borea, *J. Phys. Chem.* **1994**, *98*, 1515–1518.
- [377] C. T. Calderone, D. H. Williams, *J. Am. Chem. Soc.* **2001**, *123*, 6262–6267.
- [378] E. Gallicchio, M. M. Kubo, R. M. Levy, *J. Am. Chem. Soc.* **1998**, *120*, 4526–4527.
- [379] K. Sharp, *Protein Sci.* **2001**, *10*, 661–667.
- [380] G. Klebe in *Rational Molecular Design in Drug Research* (Eds.: T. Liljefors, F. S. Jorgensen, P. Krosgaard-Larsen), Munksgaard, Copenhagen, **1998**, pp. 151–160.
- [381] H. Kubinyi, *Drug Discovery Today* **1997**, *2*, 457–467.
- [382] K. H. Kim, G. Greco, E. Novellino, *Perspect. Drug Discovery Des.* **1998**, *12*, 257–315.
- [383] M. Gurrath, *Curr. Med. Chem.* **2001**, *8*, 1605–1648.
- [384] S. Halazy, *Expert Opin. Ther. Pat.* **1999**, *9*, 431–446.
- [385] B. Fontaine, E. Plassart-Schiess, S. Nicole, *Mol. Aspects Med.* **1997**, *18*, 415–463.
- [386] S. J. Oh, H. J. Ha, D. Y. Chi, H. K. Lee, *Curr. Med. Chem.* **2001**, *8*, 999–1034.
- [387] P. Schloss, D. C. Williams, *J. Psychopharmacol.* **1998**, *12*, 115–121.
- [388] R. J. Vandenberg, *Clin. Exp. Pharmacol. Physiol.* **1998**, *25*, 393–400.
- [389] J. A. McCammon, *Curr. Opin. Struct. Biol.* **1998**, *8*, 245–249.
- [390] J. R. H. Tame, *J. Comput. Aided Mol. Des.* **1999**, *13*, 99–108.
- [391] M. R. Reddy, V. N. Viswanadhan, M. D. Erion in *3D QSAR in Drug Design: Ligand Protein Interactions and Molecular Similarity* (Eds.: H. Kubinyi, G. Folkers, Y. C. Martin), Kluwer/Escom, Leiden, **1998**, pp. 85–98.
- [392] J. D. Hirst, *Curr. Opin. Drug Discovery Dev.* **1998**, *1*, 28–33.
- [393] P. A. Kollman, *Curr. Opin. Struct. Biol.* **1994**, *4*, 240–245.
- [394] H. Gohlke, G. Klebe, *Curr. Opin. Struct. Biol.* **2001**, *11*, 231–235.
- [395] R. D. Brown, Y. C. Martin, *J. Chem. Inf. Comput. Sci.* **1996**, *36*, 572–584.
- [396] C. Humblet, J. B. Dunbar, *Annu. Rep. Med. Chem.* **1993**, *28*, 275–284.
- [397] P. Willett, *J. Mol. Recognit.* **1995**, *8*, 290–303.
- [398] G. Klebe in *3D QSAR in Drug Design. Theory, Methods and Applications* (Ed.: H. Kubinyi), Escom, Leiden, **1993**, pp. 173–199.
- [399] M. G. Bures in *Practical Application of Computer-Aided Drug Design* (Ed.: P. S. Charifson), Marcel Dekker, New York, **1997**, pp. 39–72.
- [400] C. Lemmen, T. Lengauer, *J. Comput. Aided Mol. Des.* **2000**, *14*, 215–232.
- [401] C. Hansch, T. Fujita, *J. Am. Chem. Soc.* **1964**, *86*, 1616–1626.
- [402] S. M. Free, J. W. Wilson, *J. Med. Chem.* **1964**, *7*, 395–399.
- [403] K. H. Kim in *3D QSAR in Drug Design. Theory, Methods and Applications* (Ed.: H. Kubinyi), Escom, Leiden, **1993**, pp. 619–642.
- [404] G. Greco, E. Novellino, Y. C. Martin in *Designing Bioactive Molecules* (Eds.: Y. C. Martin, P. Willett, S. R. Heller), American Chemical Society, Washington, **1998**, pp. 219–251.
- [405] R. D. Cramer III, D. E. Patterson, J. D. Bunce, *J. Am. Chem. Soc.* **1988**, *110*, 5959.
- [406] C. L. Waller, T. I. Oprea, A. Giolitti, G. R. Marshall, *J. Med. Chem.* **1993**, *36*, 4152.
- [407] A. Golbraikh, P. Bernard, J. R. Chrétien, *Eur. J. Med. Chem.* **2000**, *35*, 123–136.
- [408] G. R. Marshall, C. D. Barry, H. E. Bosshard, R. A. Dammkoehler, D. A. Dunn in *Computer-Assisted Drug Design* (Eds.: E. C. Olson, R. E. Christofferson), American Chemical Society, Washington, **1979**, pp. 205–226.
- [409] Y. C. Martin, M. G. Bures, E. A. Danaher, J. DeLazzer in *Trends in QSAR and Molecular Modelling 92* (Ed.: C.-G. Wermuth), Escom, Leiden, **1993**, pp. 20–27.
- [410] *QSAR and Molecular Modelling: Concepts, Computational Tools and Biological Applications* (Eds.: F. Sanz, J. Giraldo, F. Manaut), Prous, Barcelona, **1995**.
- [411] *Chemometric Methods in Molecular Design, Vol. 2* (Ed.: H. van de Waterbeemd), VCH, Weinheim, **1995**.
- [412] R. D. Cramer III, J. D. Bunce in *QSAR in Drug Design and Toxicology* (Eds.: D. Hadzi, B. Jerman-Blasiz), Elsevier, Amsterdam, **1987**.
- [413] P. Geladi, B. R. Kowalski, *Anal. Chim. Acta* **1986**, *185*, 1–17.
- [414] S. Wold, E. Johansson, M. Cocchi in *3D QSAR in Drug Design. Theory, Methods and Applications* (Ed.: H. Kubinyi), Escom, Leiden, **1993**.
- [415] G. Folkers, A. Merz in *Lipophilicity in Drug Action and Toxicology, Vol. 4* (Eds.: V. Pliska, B. Testa, H. van de Waterbeemd), VCH, Weinheim, **1996**, pp. 219–232.
- [416] G. E. Kellogg, D. J. Abraham, *J. Comput. Aided Mol. Des.* **1991**, *5*, 545.
- [417] G. E. Kellogg, J. C. Burnett, D. J. Abraham, *J. Comput. Aided Mol. Des.* **2001**, *15*, 381–393.
- [418] P. J. Goodford, *J. Med. Chem.* **1985**, *28*, 849–857.
- [419] DelPhi/Solvation, Molecular Simulations Inc., San Diego, CA, **1995**.
- [420] G. Klebe, U. Abraham, T. Mietzner, *J. Med. Chem.* **1994**, *37*, 4130–4146.
- [421] G. Klebe, U. Abraham, *J. Comput. Aided Mol. Des.* **1999**, *13*, 1–10.
- [422] A. Doweyko, *J. Med. Chem.* **1988**, *31*, 1396–1406.
- [423] A. N. Jain, K. Koile, D. Chapman, *J. Med. Chem.* **1994**, *37*, 2315–2327.
- [424] V. E. Golender, E. R. Vorpapel in *3D QSAR in Drug Design. Theory, Methods and Applications* (Ed.: H. Kubinyi), Escom, Leiden, **1993**, pp. 137–149.
- [425] H.-D. Höltje, L. B. Kier, *J. Pharm. Sci.* **1974**, *63*, 1722–1725.
- [426] D. Joseph-McCarthy, *Pharm. Ther.* **1999**, *84*, 179–191.
- [427] H.-J. Böhm, M. Stahl, *Med. Chem. Res.* **1999**, *9*, 445–462.
- [428] P. Bamborough, F. E. Cohen, *Curr. Opin. Struct. Biol.* **1996**, *6*, 236–241.
- [429] R. C. Wade in *3D QSAR in Drug Design, Vol. 2* (Eds.: H. Kubinyi, G. Folkers, Y. C. Martin), Kluwer, Dordrecht, **1998**, pp. 486–505.
- [430] I. T. Weber, R. W. Harrison in *3D QSAR in Drug Design, Vol. 2* (Eds.: H. Kubinyi, G. Folkers, Y. C. Martin), Kluwer, Dordrecht, **1998**, 115–127.
- [431] T. Liljefors in *3D QSAR in Drug Design, Vol. 2* (Eds.: H. Kubinyi, G. Folkers, Y. C. Martin), Kluwer, Dordrecht, **1998**, 3–17.
- [432] A. Warshel, A. Papazyan, *Curr. Opin. Struct. Biol.* **1998**, *8*, 211–217.
- [433] M. K. Gilson, *Curr. Opin. Struct. Biol.* **1995**, *5*, 216–223.
- [434] D. Bashford, D. A. Case, *Annu. Rev. Phys. Chem.* **2000**, *51*, 129–152.
- [435] M. Orozco, F. J. Luque, *Chem. Rev.* **2000**, *100*, 4187–4225.
- [436] M. Schaefer, H. W. T. van Vlijmen, M. Karplus, *Adv. Protein Chem.* **1998**, *51*, 1–57.

- [437] P. A. Kollman, *Acc. Chem. Res.* **1996**, 29, 461–469.
- [438] P. Kollman, *Chem. Rev.* **1993**, 93, 2395–2417.
- [439] P. A. Kollman, K. M. Merz, Jr., *Acc. Chem. Res.* **1990**, 23, 246–252.
- [440] P. A. Kollman, I. Massova, C. Reyes, B. Kuhn, S. Huo, L. Chong, M. Lee, T. Lee, Y. Duan, W. Wang, O. Donini, P. Cieplak, J. Srinivasan, D. A. Case, T. E. Cheatham III, *Acc. Chem. Res.* **2000**, 33, 889–897.
- [441] W. P. Reinhardt, M. A. Miller, L. M. Amon, *Acc. Chem. Res.* **2001**, 34, 607–614.
- [442] M. R. Reddy, M. D. Erion, A. Agarwal, *Rev. Comput. Chem.* **2000**, 16, 217–304.
- [443] W. L. Jorgensen, *Acc. Chem. Res.* **1989**, 22, 184–189.
- [444] T. P. Straatsma, *Rev. Comput. Chem.* **1996**, 9, 81–127.
- [445] H. Meirovitch, *Rev. Comput. Chem.* **1998**, 12, 1–74.
- [446] J. G. Kirkwood, *J. Chem. Phys.* **1935**, 3, 300–313.
- [447] R. J. Zwanzig, *J. Chem. Phys.* **1954**, 22, 1420–1426.
- [448] J. P. M. Postma, H. J. C. Berendsen, J. R. Haak, *Faraday Symp. Chem. Soc.* **1981**, 17, 55–67.
- [449] B. L. Tembe, J. A. McCammon, *Comput. Chem.* **1984**, 4, 281–283.
- [450] N. Metropolis, A. W. Rosenbluth, M. N. Rosenbluth, A. H. Teller, E. Teller, *J. Chem. Phys.* **1953**, 21, 1087–1092.
- [451] W. F. van Gunsteren, H. J. C. Berendsen, *Angew. Chem.* **1990**, 102, 1020–1055; *Angew. Chem. Int. Ed. Engl.* **1990**, 29, 992–1023.
- [452] S. Boresch, M. Karplus, *J. Mol. Biol.* **1995**, 254, 801–807.
- [453] G. Archontis, T. Simonson, M. Karplus, *J. Mol. Biol.* **2001**, 306, 307–327.
- [454] D. L. Beveridge, F. M. DiCapua, *Annu. Rev. Biophys. Biophys. Chem.* **1989**, 18, 431–492.
- [455] D. A. Pearlman, *J. Phys. Chem.* **1994**, 98, 1487–1493.
- [456] S. Sen, L. Nilsson, *J. Comput. Chem.* **1999**, 20, 877–885.
- [457] M. A. McCarrick, P. A. Kollman, *J. Comput. Aided Mol. Des.* **1999**, 13, 109–121.
- [458] M. L. Plouffe Price, W. L. Jorgensen, *J. Am. Chem. Soc.* **2000**, 122, 9455–9466.
- [459] W. L. Jorgensen, C. Ravimohan, *J. Chem. Phys.* **1985**, 83, 3050–3054.
- [460] C. F. Wong, J. A. McCammon, *J. Am. Chem. Soc.* **1986**, 108, 3830–3831.
- [461] K. M. Merz, P. A. Kollman, *J. Am. Chem. Soc.* **1989**, 111, 5649–5658.
- [462] N. Ota, A. T. Brunger, *Theor. Chem. Acc.* **1997**, 98, 407–435.
- [463] N. Ota, C. Stroupe, J. M. S. Ferreira-da-Silva, S. A. Shah, M. Mares-Guia, A. T. Brunger, *Proteins* **1999**, 37, 641–653.
- [464] P. R. Gerber, A. E. Mark, W. F. van Gunsteren, *J. Comput. Aided Mol. Des.* **1993**, 7, 305–323.
- [465] B. C. Oostenbrink, J. W. Pitera, M. M. H. van Lipzig, J. H. N. Meerman, W. F. van Gunsteren, *J. Med. Chem.* **2000**, 43, 4594–4605.
- [466] H. Liu, A. E. Mark, W. F. van Gunsteren, *J. Phys. Chem.* **1996**, 100, 9485–9494.
- [467] Z. Guo, C. L. Brooks, X. Kong, *J. Phys. Chem. B* **1998**, 102, 2032–2036.
- [468] S. Banba, Z. Guo, C. L. Brooks III, *J. Phys. Chem. B* **2000**, 104, 6903–6910.
- [469] J. Åquist, C. Medina, J. E. Samuelsson, *Protein Eng.* **1994**, 7, 385–391.
- [470] T. Hansson, J. Marelus, J. Åquist, *J. Comput. Aided Mol. Des.* **1998**, 12, 27–35.
- [471] J. Wang, R. Dixon, P. A. Kollman, *Proteins* **1999**, 34, 69–81.
- [472] H. A. Carlson, W. L. Jorgensen, *J. Phys. Chem.* **1995**, 99, 10667–10673.
- [473] I. D. Wall, A. R. Leach, D. W. Salt, M. G. Ford, J. W. Essex, *J. Med. Chem.* **1999**, 42, 5142–5152.
- [474] A. C. Pierce, W. L. Jorgensen, *J. Med. Chem.* **2001**, 44, 1043–1050.
- [475] R. C. Rizzo, J. Tirado-Rives, W. L. Jorgensen, *J. Med. Chem.* **2001**, 44, 145–154.
- [476] P. D. J. Grootenhuys, P. J. M. van Galen, *Acta Crystallogr. Sect. D* **1995**, 51, 560–566.
- [477] P. D. J. Grootenhuys, S. P. van Helden in *Computational Approaches in Supramolecular Chemistry* (Ed.: G. Wipff), Kluwer, Dordrecht, **1994**, pp. 137–149.
- [478] M. K. Holloway, J. M. Wai, T. A. Halgren, P. M. Fitzgerald, J. P. Vacca, B. D. Dorsey, R. B. Levin, W. J. Thompson, L. J. Chen, S. J. de-Solms, N. Gaffin, A. K. Ghosh, E. A. Giuliani, S. L. Graham, J. P. Guare, R. W. Hungate, T. A. Lyle, W. M. Sanders, T. J. Tucker, M. Wiggins, C. M. Wiscount, O. W. Woltersdorf, S. D. Young, P. L. Darke, J. A. Zugay, *J. Med. Chem.* **1995**, 38, 305–317.
- [479] D. Joseph-McCarthy, J. M. Hogle, M. Karplus, *Proteins* **1997**, 29, 32–58.
- [480] I. V. Kurinov, R. W. Harrison, *Nat. Struct. Biol.* **1994**, 1, 735–743.
- [481] A. Checa, A. R. Ortiz, B. de Pascual-Teresa, F. Gago, *J. Med. Chem.* **1997**, 40, 4136–4145.
- [482] S. Vajda, Z. Weng, R. Rosenfeld, C. DeLisi, *Biochemistry* **1994**, 33, 13977–13988.
- [483] Z. Weng, S. Vajda, C. DeLisi, *Protein Sci.* **1996**, 5, 614–626.
- [484] D. H. Williams, J. P. L. Cox, A. J. Doig, M. Gardener, U. Gerhard, P. T. Kaye, A. R. Lal, I. A. Nicholls, C. J. Salter, R. C. Mitchell, *J. Am. Chem. Soc.* **1991**, 113, 7020–7030.
- [485] S. Krystek, T. Stouch, J. Novotny, *J. Mol. Biol.* **1993**, 234, 661–679.
- [486] J. Novotny, R. E. Bruccoleri, F. A. Saul, *Biochemistry* **1989**, 28, 4735–4749.
- [487] J. Warwicker, H. C. Watson, *J. Mol. Biol.* **1982**, 157, 671–679.
- [488] R. J. Zauhar, R. S. Morgan, *J. Mol. Biol.* **1985**, 186, 815–820.
- [489] N. Froloff, A. Windemuth, B. Honig, *Protein Sci.* **1997**, 6, 1293–1301.
- [490] T. Zhang, D. E. Koshland, *Protein Sci.* **1996**, 5, 348–356.
- [491] D. Hoffmann, B. Kramer, T. Washio, T. Steinmetzer, M. Rarey, T. Lengauer, *J. Med. Chem.* **1999**, 42, 4422–4433.
- [492] F. Polticelli, P. Ascenzi, M. Bolognesi, B. Honig, *Protein Sci.* **1999**, 8, 2621–2629.
- [493] B. K. Shoichet, A. R. Leach, I. D. Kuntz, *Proteins* **1999**, 34, 4–16.
- [494] X. Zou, Y. Sun, I. D. Kuntz, *J. Am. Chem. Soc.* **1999**, 121, 8033–8043.
- [495] W. C. Still, A. Tempczyk, R. C. Hawley, T. Hendrickson, *J. Am. Chem. Soc.* **1990**, 112, 6127–6129.
- [496] I. Massova, P. A. Kollman, *Perspect. Drug Discovery Des.* **2000**, 18, 113–135.
- [497] J. Srinivasan, T. E. Cheatham, P. Cieplak, P. A. Kollman, *J. Am. Chem. Soc.* **1998**, 120, 9401–9409.
- [498] Y. N. Vorobjev, J. C. Almagro, J. Hermans, *Proteins* **1998**, 32, 399–413.
- [499] B. Jayaram, D. Sproun, M. A. Young, D. L. Beveridge, *J. Am. Chem. Soc.* **1998**, 120, 10629–10633.
- [500] G. Archontis, T. Simonson, M. Karplus, *J. Mol. Biol.* **2001**, 306, 307–327.
- [501] C. M. Reyes, P. A. Kollman, *J. Mol. Biol.* **2000**, 297, 1145–1158.
- [502] B. Kuhn, P. A. Kollman, *J. Am. Chem. Soc.* **2000**, 122, 3909–3916.
- [503] T. Lee, P. A. Kollman, *J. Am. Chem. Soc.* **2000**, 122, 4385–4393.
- [504] J. Wang, P. Morin, W. Wang, P. A. Kollman, *J. Am. Chem. Soc.* **2001**, 123, 5221–5230.
- [505] T. Lazaridis, M. Karplus, *Proteins* **1999**, 35, 133–152.
- [506] J. Gasteiger, J. Zupan, *Angew. Chem.* **1993**, 105, 510–536; *Angew. Chem. Int. Ed. Engl.* **1993**, 32, 503–527.
- [507] H. J. Böhm, *J. Comput. Aided Mol. Des.* **1994**, 8, 243–256.
- [508] H. J. Böhm, *J. Comput. Aided Mol. Des.* **1998**, 12, 309–323.
- [509] M. D. Eldridge, C. W. Murray, T. R. Auton, G. V. Paolini, R. P. Mee, *J. Comput. Aided Mol. Des.* **1997**, 11, 425–445.
- [510] R. Wang, L. Liu, L. Lai, Y. Tang, *J. Mol. Model.* **1998**, 4, 379–394.
- [511] C. W. Murray, T. R. Auton, M. D. Eldridge, *J. Comput. Aided Mol. Des.* **1998**, 12, 503–519.
- [512] R. D. Head, M. L. Smythe, T. I. Oprea, C. L. Waller, S. M. Green, G. R. Marshall, *J. Am. Chem. Soc.* **1996**, 118, 3959–3969.
- [513] S. J. Weiner, P. A. Kollman, D. A. Case, U. C. Singh, C. Ghio, G. Alagona, S. Profeta, P. Weiner, *J. Am. Chem. Soc.* **1984**, 106, 765–784.
- [514] C. Hansch, A. Leo, *Substituent Constants for Correlation Analysis in Chemistry and Biology*, Wiley, New York, **1979**.
- [515] Y. Takamatsu, A. Itai, *Proteins* **1998**, 33, 62–73.
- [516] P. Venkatarangan, A. J. Hopfinger, *J. Med. Chem.* **1999**, 42, 2169–2179.
- [517] V. N. Viswanadhan, M. R. Reddy, A. Wlodawer, M. D. Varney, J. N. Weinstein, *J. Med. Chem.* **1996**, 39, 705–712.
- [518] D. Rognan, S. L. Laue-moller, A. Holm, S. Buus, V. Tschinke, *J. Med. Chem.* **1999**, 42, 4650–4658.
- [519] R. S. Bohacek, C. McMartin, *J. Am. Chem. Soc.* **1994**, 116, 5560–5571.
- [520] P. Kasper, P. Christen, H. Gehring, *Proteins* **2000**, 40, 185–192.
- [521] A. N. Jain, *J. Comput. Aided Mol. Des.* **1996**, 10, 427–440.

- [522] W. Bibel, S. Hölldobler, T. Schaub, *Wissensrepräsentation und Inferenz: Eine grundlegende Einführung*, Vieweg, Braunschweig, **1993**.
- [523] R. L. Jernigan, I. Bahar, *Curr. Opin. Struct. Biol.* **1996**, *6*, 195–209.
- [524] A. E. Torda, *Curr. Opin. Struct. Biol.* **1997**, *7*, 200–205.
- [525] S. Vajda, M. Sippl, J. Novotny, *Curr. Opin. Struct. Biol.* **1997**, *7*, 222–228.
- [526] M. J. Sippl, *Curr. Opin. Struct. Biol.* **1995**, *5*, 229–235.
- [527] H. B. Bürgi, J. D. Dunitz, *Acta Crystallogr. Sect. B* **1988**, *44*, 445–448.
- [528] P. D. Thomas, K. A. Dill, *J. Mol. Biol.* **1996**, *257*, 457–469.
- [529] A. V. Finkelstein, A. M. Gutin, A. Y. Badretdinov, *Proteins* **1995**, *23*, 151–162.
- [530] W. A. Koppensteiner, M. J. Sippl, *Biochemistry* **1998**, *63*, 247–252.
- [531] T. Lazaridis, M. Karplus, *J. Mol. Biol.* **1999**, *288*, 477–487.
- [532] J. Moult, *Curr. Opin. Struct. Biol.* **1997**, *7*, 194–199.
- [533] A. V. Finkelstein, *Curr. Opin. Struct. Biol.* **1997**, *7*, 60–71.
- [534] M. J. E. Sternberg, P. A. Bates, L. A. Kelley, R. M. MacCallum, *Curr. Opin. Struct. Biol.* **1999**, *9*, 368–373.
- [535] G. Verkhivker, K. Appelt, S. T. Freer, J. E. Villafranca, *Protein Eng.* **1995**, *8*, 677–691.
- [536] K. A. Sharp, A. Nicholls, R. Friedman, B. Honig, *Biochemistry* **1991**, *30*, 9686–9697.
- [537] A. Wallqvist, R. L. Jernigan, D. G. Covell, *Protein Sci.* **1995**, *4*, 1881–1903.
- [538] R. S. DeWitte, E. I. Shakhnovich, *J. Am. Chem. Soc.* **1996**, *118*, 11733–11744.
- [539] I. Muegge, Y. C. Martin, *J. Med. Chem.* **1999**, *42*, 791–804.
- [540] I. Muegge, *J. Comput. Chem.* **2001**, *22*, 418–425.
- [541] J. B. O. Mitchell, R. A. Laskowski, A. Alex, J. M. Thornton, *J. Comput. Chem.* **1999**, *20*, 1165–1176.
- [542] K.-C. Ng, W. J. Meath, A. R. Allnatt, *Mol. Phys.* **1979**, *37*, 237–253.
- [543] J. B. O. Mitchell, R. A. Laskowski, A. Alex, M. J. Forster, J. M. Thornton, *J. Comput. Chem.* **1999**, *20*, 1177–1185.
- [544] H. Gohlke, M. Hendlich, G. Klebe, *J. Mol. Biol.* **2000**, *295*, 337–356.
- [545] M. Hendlich, *Acta Crystallogr. Sect. D* **1998**, *54*, 1178–1182.
- [546] H. Gohlke, M. Hendlich, G. Klebe, *Perspect. Drug Discovery Des.* **2000**, *20*, 115–144.
- [547] P. S. Charifson, J. J. Corkerey, M. A. Murcko, W. P. Walters, *J. Med. Chem.* **1999**, *42*, 5100–5109.
- [548] E. C. Meng, B. K. Shoichet, I. D. Kuntz, *J. Comput. Chem.* **1992**, *13*, 505–524.
- [549] D. K. Gehlhaar, G. M. Verkhivker, P. A. Rejto, C. J. Sherman, D. B. Fogel, S. T. Free, *Chem. Biol.* **1995**, *2*, 317–324.
- [550] S.-S. So, M. Karplus, *J. Comput. Aided Mol. Des.* **1999**, *13*, 243–258.
- [551] M. Stahl, M. Rarey, *J. Med. Chem.* **2001**, *44*, 1035–1042.
- [552] M. Rarey, B. Kramer, T. Lengauer, G. Klebe, *J. Mol. Biol.* **1996**, *261*, 470–489.
- [553] G. E. Terp, B. N. Johansen, I. T. Christensen, F. S. Jorgensen, *J. Med. Chem.* **2001**, *44*, 2333–2343.
- [554] D. N. A. Boobbyer, P. J. Goodford, P. M. McWhinnie, R. C. Wade, *J. Med. Chem.* **1989**, *32*, 1083–1094.
- [555] R. A. Laskowski, J. M. Thornton, C. Humblet, J. Singh, *J. Mol. Biol.* **1996**, *259*, 175–201.
- [556] M. L. Verdonk, J. C. Cole, R. Taylor, *J. Mol. Biol.* **1999**, *289*, 1093–1108.
- [557] M. L. Verdonk, J. C. Cole, P. Watson, V. Gillet, P. Willett, *J. Mol. Biol.* **2001**, *307*, 841–859.
- [558] A. Miranker, M. Karplus, *Proteins* **1991**, *11*, 29–34.
- [559] A. D. MacKerell, D. Bashford, M. Bellott, R. L. Dunbrack, J. D. Evanseck, M. J. Field, S. Fischer, J. Gao, H. Guo, S. Ha, D. Joseph-McCarthy, L. Kuchnir, K. Kucera, F. T. K. Lau, C. Mattos, S. Michnick, T. Ngo, D. T. Nguyen, B. Prodhom, W. E. Reiher, B. Roux, M. Schlenkrich, J. C. Smith, R. Stote, J. Straub, M. Watanabe, J. Wiorkiewicz-Kuczera, D. Yin, M. Karplus, *J. Phys. Chem. B* **1998**, *102*, 3586–3616.
- [560] C. M. Stultz, M. Karplus, *Proteins* **1999**, *37*, 512–529.
- [561] R. J. Radmer, P. A. Kollman, *J. Comput. Aided Mol. Des.* **1998**, *12*, 215–227.
- [562] D. A. Pearlman, *J. Med. Chem.* **1999**, *42*, 4313–4324.
- [563] C. Bissantz, G. Folkers, D. Rognan, *J. Med. Chem.* **2000**, *43*, 4759–4767.
- [564] M. R. Reddy, R. J. Bacquet, D. Zichi, D. A. Matthews, K. M. Welsh, T. R. Jones, S. Freer, *J. Am. Chem. Soc.* **1992**, *114*, 10117–10122.
- [565] M. Rarey, B. Kramer, T. Lengauer in *Proceedings of the 3rd International Conference on Intelligent Systems for Molecular Biology* (Cambridge, UK, **1995**), pp. 300–308.
- [566] I. D. Kuntz, J. M. Blaney, S. J. Oatley, R. Langridge, T. E. Ferrin, *J. Mol. Biol.* **1982**, *161*, 269–288.
- [567] H. J. Böhm, *J. Comput. Aided Mol. Des.* **1992**, *6*, 61–78.
- [568] P. Tao, L. Lai, *J. Comput. Aided Mol. Des.* **2001**, *15*, 429–446.
- [569] A. Wallqvist, D. G. Covell, *Proteins* **1996**, *25*, 403–419.
- [570] I. Muegge, Y. C. Martin, P. J. Hajduk, S. W. Fesik, *J. Med. Chem.* **1999**, *42*, 2498–2503.
- [571] H. Sookhee, R. Andreani, A. Robbins, I. Muegge, *J. Comput. Aided Mol. Des.* **2000**, *14*, 435–448.
- [572] I. Nobeli, J. B. O. Mitchell, A. Alex, J. M. Thornton, *J. Comput. Chem.* **2001**, *22*, 673–688.
- [573] R. Hitzemann, *Trends Pharmacol. Sci.* **1988**, *9*, 408–411.
- [574] H. Roos, R. Karlsson, H. Nilshans, A. Persson, *J. Mol. Recognit.* **1998**, *11*, 204–210.
- [575] J. Piehler, A. Brecht, G. Gauglitz, C. Maul, S. Grabley, M. Zerlin, *Biosens. Bioelectron.* **1997**, *12*, 531–538.
- [576] R. L. Rich, D. G. Mysza, *Curr. Opin. Biotechnol.* **2000**, *11*, 54–61.
- [577] R. P. Hicks, *Curr. Med. Chem.* **2001**, *8*, 627–650.
- [578] J. M. Moore, *Biopolymers* **1999**, *51*, 221–243.
- [579] B. Meyer, T. Weimar, T. Paters, *Eur. J. Biochem.* **1997**, *246*, 705–709.
- [580] W. Jahnke, L. B. Perez, C. G. Paris, A. Strauss, G. Fendrich, C. M. Nalin, *J. Am. Chem. Soc.* **2000**, *122*, 7394–7395.
- [581] W. Jahnke, S. Rüdiger, M. Zurini, *J. Am. Chem. Soc.* **2001**, *123*, 3149–3150.
- [582] M. Mayer, B. Meyer, *Angew. Chem.* **1999**, *111*, 1824–1844; *Angew. Chem. Int. Ed.* **1999**, *38*, 1784–1788.
- [583] T. D. Veenstra, *Biophys. Chem.* **1999**, *79*, 63–79.
- [584] A. A. Rostom, J. H. R. Tame, J. E. Ladbury, C. V. Robinson, *J. Mol. Biol.* **2000**, *296*, 269–279.
- [585] A. Janshoff, M. Neitzert, Y. Oberdörfer, H. Fuchs, *Angew. Chem.* **2000**, *112*, 3346–3374; *Angew. Chem. Int. Ed.* **2000**, *39*, 3212–3237.
- [586] I. Jelesarov, H. R. Bosshard, *Biochemistry* **1994**, *33*, 13321–13328.
- [587] R. G. Khalifah, F. Zhang, J. S. Parr, E. S. Rowe, *Biochemistry* **1993**, *32*, 3058–3066.
- [588] D. D. Hu, M. R. Eftink, *Biophys. Chem.* **1994**, *49*, 233–239.
- [589] B. W. Sigurskjold, C. R. Berland, B. Svensson, *Biochemistry* **1994**, *33*, 10191–10199.
- [590] K. P. Murphy, D. Xie, K. C. Garcia, L. M. Amzel, E. Freire, *Proteins* **1993**, *15*, 113–120.
- [591] J. Gomez, E. Freire, *J. Mol. Biol.* **1995**, *252*, 337–350.
- [592] G. C. Kresheck, L. B. Vitello, J. E. Erman, *Biochemistry* **1995**, *34*, 8398–8405.
- [593] J. J. Christensen, L. D. Hansen, R. M. Izatt, *Handbook of Proton Ionization Heats and Related Thermodynamic Quantities*, Wiley, New York, **1976**.
- [594] I. Jelesarov, H. R. Bosshard, *J. Mol. Recognit.* **1999**, *12*, 3–18.
- [595] K. P. Murphy, E. Freire, *Adv. Protein Chem.* **1992**, *43*, 313–361.
- [596] R. S. Spolar, J. R. Livingstone, M. T. Record, Jr., *Biochemistry* **1992**, *31*, 3947–3955.
- [597] P. R. Connelly, J. A. Thomson, *Proc. Natl. Acad. Sci. USA* **1992**, *89*, 4781–4785.
- [598] G. I. Makhatadze, P. L. Privalov, *Adv. Protein Chem.* **1995**, *47*, 307–425.
- [599] B. M. Baker, K. P. Murphy, *J. Mol. Biol.* **1997**, *268*, 557–569.
- [600] C. McNemar, M. E. Snow, W. T. Windsor, A. Prongay, P. Mui, R. Zhang, J. Durkin, H. V. Le, P. C. Weber, *Biochemistry* **1997**, *36*, 10006–10014.
- [601] N. J. Faergeman, B. W. Sigurskjold, B. B. Kragelund, K. V. Andersen, J. Knudsen, *Biochemistry* **1996**, *35*, 14118–14126.
- [602] G. A. Holdgate, A. Tunnicliffe, W. H. Ward, S. A. Weston, G. Rosenbrock, P. T. Barth, I. W. Taylor, R. A. Pauptit, D. Timms, *Biochemistry* **1997**, *36*, 9663–9673.
- [603] R. Perozzo, I. Jelesarov, H. R. Bosshard, G. Folkers, L. Scapozza, *J. Biol. Chem.* **2000**, *275*, 16139–16145.
- [604] M. V. Botuyan, D. A. Keire, C. Kroen, D. G. Gorenstein, *Biochemistry* **1993**, *32*, 6863–6874.

- [605] J. E. Ladbury, J. G. Wright, J. M. Sturtevant, P. B. Sigler, *J. Mol. Biol.* **1994**, 238, 669–681.
- [606] H. Berglund, M. Wolf-Watz, T. Lundback, S. van den Berg, T. Hard, *Biochemistry* **1997**, 36, 11 188–11 197.
- [607] F. Dullweber, M. T. Stubbs, J. Stürzebecher, D. Musil, G. Klebe, *J. Mol. Biol.* **2001**, 313, 593–614.
- [608] J. R. Liggins, P. L. Privalov, *Proteins* **2000**, Suppl., 50–62.
- [609] P. L. Privalov, S. A. Potekhin, *Methods Enzymol.* **1986**, 131, 4–51.
- [610] K. Takahashi, H. Fukada, *Biochemistry* **1985**, 24, 297–300.
- [611] A. Shrake, P. D. Ross, *J. Biol. Chem.* **1990**, 265, 5055–5059.
- [612] L. N. Lin, A. B. Mason, R. C. Woodworth, J. F. Brandts, *Biochemistry* **1994**, 33, 1881–1888.
- [613] F. Conejero-Lara, P. L. Mateo, *Biochemistry* **1996**, 35, 3477–3486.
- [614] K. G. Davis, S. E. Plyte, S. R. Robertson, A. Cooper, G. G. Kneale, *Biochemistry* **1995**, 34, 148–154.
- [615] S. V. Litvinovich, K. C. Ingham, *J. Mol. Biol.* **1995**, 248, 611–626.
- [616] V. V. Filimonov, V. V. Rogov, *J. Mol. Biol.* **1996**, 255, 767–777.
- [617] S. Makino, I. D. Kuntz, *J. Comput. Chem.* **1997**, 18, 1812–1825.
- [618] S. Grüneberg, B. Wendt, G. Klebe, *Angew. Chem.* **2001**, 113, 404–408; *Angew. Chem. Int. Ed.* **2001**, 40, 389–393.
- [619] H. J. Böhm, *J. Comput. Aided Mol. Des.* **1992**, 6, 593–606.
- [620] H. J. Böhm, S. Brode, U. Hesse, G. Klebe, *Chem. Eur. J.* **1996**, 2, 1509–1513.
-



The CP Molecule Labyrinth: A Paradigm of How Endeavors in Total Synthesis Lead to Discoveries and Inventions in Organic Synthesis

K. C. Nicolaou* and Phil S. Baran

Dedicated to Mrs. Niki Goulandris for her outstanding contributions to humanity and Planet Earth on the occasion of the opening of the GAIA Center for Environmental Research and Education at the Goulandris Natural History Museum in Athens, Greece.

Imagine an artist carving a sculpture from a marble slab and finding gold nuggets in the process. This thought is not a far-fetched description of the work of a synthetic chemist pursuing the total synthesis of a natural product. At the end of the day, he or she will be judged by the artistry of the final work and the weight of the gold discovered in the process. However, as colorful as this description of total synthesis may be, it does not entirely capture the essence of the endeavor, for there is much more to be told, especially with regard to the contrast of frustrating failures and exhilarating moments of discovery. To fully appreciate the often

Herculean nature of the task and the rewards that accompany it, one must sense the details of the enterprise behind the scenes. A more vivid description of total synthesis as a struggle against a tough opponent is perhaps appropriate to dramatize these elements of the experience. In this article we describe one such endeavor of total synthesis which, in addition to reaching the target molecule, resulted in a wealth of new synthetic strategies and technologies for chemical synthesis. The total synthesis of the CP molecules is compared to Theseus' most celebrated athlos (Greek for exploit, accomplishment): the conquest of the dread-

ed Minotaur, which he accomplished through brilliance, skill, and bravery having traversed the famous labyrinth with the help of Ariadne. This story from Greek mythology comes alive in modern synthetic expeditions toward natural products as exemplified by the total synthesis of the CP molecules which serve as a paradigm for modern total synthesis endeavors, where the objectives are discovery and invention in the broader sense of organic synthesis.

Keywords: CP molecules • natural products • synthetic methods • total synthesis

1. Prologue

"Athens had been at war with Crete. Although the war was over, Minos (King of Crete), ruled the seas and Athens had to pay an awful tribute as a condition for peace. Minos sought revenge for the death of his son and demanded that every nine years the Athenians send him fourteen of their children—7 girls and 7 boys. Once in Crete, the young men and women

were sent into the maze-like labyrinth to face the deadly Minotaur who was half man, half bull.

Each year the children were selected by lot, and as all of Athens mourned they set sail for Crete on a ship with black sails. Theseus, the son of Aegeus (King of Athens), was very brave and had had many adventures already. Theseus resolved to become one of the young men chosen, so that he might slay the Minotaur and put an end to the horrible sacrifice. Aegeus reluctantly agreed to let Theseus go, and asked that Theseus change the sails to white for the journey home if he was successful in his plan to kill the Minotaur.

When the fourteen arrived in Crete, they were entertained at the enormous and colourful palace of Minos. The next day, they were to be sent into the intricate mazes of the labyrinth, home of the deadly Minotaur, from which there was no escape...

That night at dinner, listening to the exploits and adventures of Theseus, Ariadne—daughter of King Minos—fell in love with him. Not wanting to see Theseus killed, Ariadne vowed to find a way to help him. The next morning, as they

[*] Prof. Dr. K. C. Nicolaou, Dr. P. S. Baran
Department of Chemistry and
The Skaggs Institute for Chemical Biology
The Scripps Research Institute
10550 North Torrey Pines Road, La Jolla, CA 92037 (USA)
Fax: (+1) 858-784-2469
E-mail: kcn@scripps.edu
and
Department of Chemistry and Biochemistry
University of California, San Diego
9500 Gilman Drive, La Jolla, CA 92093 (USA)

were being led to the labyrinth, Ariadne gave Theseus a ball of string. She told Theseus to tie the string to the inside of the door, and it would help him find his way back if he was able to kill the Minotaur. She also brought him a sword, which he hid underneath his cape.

After winding his way through twists and turns, Theseus came upon the lair of the Minotaur. In the narrow passageways, they battled until Theseus was triumphant. Theseus began to rewind the ball of string, retracing his steps until he found his way back to the entrance and the other young men and women. Ariadne was waiting for them on the other side. She hid them until nightfall, and in the dark helped them escape to their ship. In exchange for helping him, Ariadne asked that Theseus take her with him and make her his wife, and Theseus happily agreed.

On their return trip to Athens, the ship stopped at the island of Naxos for the night. What happened next, and why it happened is a bit unclear. Either through trickery or too much frivolity (for Naxos was the island of Dionysus, after all) the group became forgetful. The next morning, Theseus set sail with the other Athenians leaving poor Ariadne asleep on the beach. At this point, there are two distinctly different versions of the tale. One version finds Ariadne so distraught that she takes her own life. The other version, which I like to believe, leaves Ariadne happy with Dionysus, living out her days on Naxos.

Away from Naxos, Theseus' forgetfulness remained, and despite his promise to his father, he neglected to change the sails on his ship from black to white. At Cape Sounion, Aegeus watched hopefully every day for the safe return of his son. Spotting the ship, with black sails flying, Aegeus presumed the worst and threw himself from the cliffs to his death and the water below. Today this water is known as the Aegean Sea.^[1]

This tale from Greek Mythology has inspired writers as well as artisans from the days of classical Greece to the twentieth century (Figure 1). Many morals can be found in this story, but in total synthesis, perhaps, the play comes alive more vividly and truly than in other endeavors. The virtues of total synthesis and its practice have been amply discussed in a recent account from our group.^[2] The purpose of this article is to dramatize the endeavor by relating its characters to those of the Theseus and Minotaur myth and, in so doing, offer valuable lessons and inspirations to ensuing generations of chemists. Most importantly, we wish to add to this tale the elements of discovery and invention in the face of adversity. The conquest of the demonic molecule (the Minotaur) by total synthesis (the labyrinth) represents not only an isolated, albeit creative, accomplishment, but moreover one which is accompanied by often abrupt twists and turns and showers of scientific discoveries, inventions, and technological advances (treasures found, tricks invented, skills developed in the labyrinth) with associated rewards and benefits (Ariadne, freeing Athens from the awful sacrifice). Most practitioners of the art of total synthesis, particularly graduate students and postdoctoral fellows, may identify with Theseus and his teammates. They may also recognize their supervisor in the form of King Aegeus. Some may even hint at the evil King Minos as a more fitting description of their supervisors! Many more comparisons and experiences may come alive later on in the article as you read on.

We will now introduce the main characters of the play as it often unfolds in laboratories engaged in total synthesis endeavors. The mighty "molecular Minotaur," the CP molecules, were discovered by a group at Pfizer headed by Takushi Kaneko in the 1990s. Here is how the world at large learned of these compounds in 1995:

K. C. Nicolaou, born in Cyprus and educated in England and the USA, is currently Chairman of the Department of Chemistry at The Scripps Research Institute where he holds the Darlene Shiley Chair in Chemistry and the Aline W. and L. S. Skaggs Professorship in Chemical Biology as well as Professor of Chemistry at the University of California, San Diego. His impact on chemistry, biology, and medicine flows from his works in organic synthesis described in over 550 publications and 70 patents and his dedication to chemical education as evidenced by his training of more than 350 graduate students and postdoctoral fellows. His recent book titled Classics in Total Synthesis, which he co-authored with Erik J. Sorensen, is used around the world as a teaching tool and source of inspiration for students and practitioners of organic synthesis.



K. C. Nicolaou



P. S. Baran

Phil S. Baran was born in Denville, New Jersey in 1977. He received his B.S. in chemistry from New York University while conducting research under the guidance of Professors D. I. Schuster and S. R. Wilson, exploring new realms in fullerene science. Upon entering The Scripps Research Institute as a graduate student in chemistry in 1997, he joined the laboratory of Professor K. C. Nicolaou where he immediately embarked on the total synthesis of the CP molecules. His primary research interest involves natural product synthesis as an enabling endeavor for the discovery of new fundamental concepts in chemistry and their application to chemical biology. He is currently engaged in a postdoctoral position with Professor E. J. Corey at Harvard University.

“New natural products have unusual structures

Fermentation broths of a still-unidentified fungus have yielded two compounds that are promising leads to drugs for lowering serum cholesterol and treating cancer. In addition to their medicinal promise, the two compounds have unusual structures that make them attractive synthetic targets.

Takushi Kaneko, manager of natural products discovery at Pfizer's research laboratories, Groton, Conn., reported the discoveries and structure proofs made by 15 of the firm's researchers at the April International Conference on Biotechnology of Microbial Products in Oiso, Japan. The two compounds are known so far only by their Pfizer code numbers, CP-225,917 and CP-263,114. The Pfizer workers call the microorganism that elaborates the compounds, “an unidentified fungus isolated from juniper twigs in Texas.” They have deposited samples of the organism at the American Type Culture Collection under the accession number ATCC74256. Both compounds inhibit the enzymes squalene synthase and farnesyl protein transferase. Squalene synthase catalyzes condensation of two molecules of the C₁₅ sesquiterpenoid farnesyl pyrophosphate to squalene, with presqualene pyrophosphate as a step on the way. This reaction is one in the overall biosynthesis of cholesterol. The hope is that such compounds will lead to new cholesterol-lowering drugs.

Farnesyl protein 1 transferase mediates farnesylation of the protein p21, which is the product of the *ras* oncogene. A one-amino acid mutation of p21 renders it permanently activated, so that it pushes regulation of cell growth and division out of control. Here, the hope is that the Pfizer compounds will inhibit a step that may be essential to p21 activity and thus to the carcinogenic process.

Both compounds are members of a class called nonadrides, which are natural products featuring nine-membered rings with carboxylic acid groups on adjacent carbons cyclized to anhydrides. The Pfizer team determined the structures of the compounds from high-resolution fast-atom-bombardment mass spectrometry and two-dimensional nuclear magnetic resonance techniques.

In addition, the compounds are bicyclic and violate Bredt's rule, which states that bridgehead atoms of polycyclic compounds cannot be double-bonded. The rule was put forth in 1902 by organic chemistry professor Julius Bredt at the University of Aachen, Germany. Kaneko notes that synthetic chemists have since devised ingenious ways to violate Bredt's rule, but that such compounds are rare in nature.

Another source of strain in the molecules occurs because the apical carbon atom of the bicyclic structure is a carbonyl. But this strain is relieved by conversion to an sp³ hybridized carbon atom by formation of a lactol ring with a neighboring carboxyl group of one compound, and by formation of a lactol/ketal with the carboxyl and a neighboring hydroxyl group in the other compound.^[3]

To say the least, this report^[3] was intriguing to us as it was to many other synthetic chemists, but our enthusiasm for a total synthesis program was curtailed by the lack of a hard-core publication committed to their structures. Indeed, the very unusual connectivities revealed in the *C&E News* article^[3] cast a shadow of doubt over their structures. Prudence



Figure 1. a) Representations of the exploits of Theseus. In the center, the hero is confronting the Minotaur (440–430 BC, interior of a red-figure kylix, British Museum, London). Copyright The British Museum. b) Minotaur, Paris, January 1, 1928 by Pablo Picasso, Musée National d'Art Moderne, Centre National d'Art et de Culture Georges Pompidou, Paris. Copyright CNAC/MNAM/Dist. Réunion des Musées Nationaux/Art Resource, NY, Musée National d'Art Moderne, Centre Georges Pompidou, Paris, France. 2001 Estate of Pablo Picasso/Artists Rights Society (ARS), New York.

dictated that we should wait for a while; besides, the group was busy with several other projects including a number dealing with much larger molecules and, therefore, these small “guys” could be put on the shelf for a time.

Little did we know then how much these small “guys” had in store for us when we finally paid proper attention to them. That occurred in 1997 when the definitive paper^[4] on the CP molecules from the Kaneko group appeared in the *Journal of the American Chemical Society*. Approximately two years later, the battle against the Minotaur was over with the triumphant Theseus having succeeded in the “kill.”^[5] Here is how *Science* magazine described the athlos in its *News of the Week* section in 1999:

“40 Steps to a Chemical Synthesis Summit

Like mountaineers who set off to scale ever more challenging peaks, organic chemists over the past half-century have tested the limits of their skills by attempting to synthesize increasingly complicated natural molecules, such as antibiotics and steroid hormones. The most fiendishly complex targets have taken synthesis labs a decade or more to conquer. With the completion of each new project, labs scan the horizon for even higher peaks. And in the past 2 years, few mountaintops were more tantalizing than a pair of jellyfish-shaped molecules found in 1997 in a fungus.

One enticement was the anticancer and cholesterol-lowering properties of the natural compounds, called CP molecules. The other was their complexity. The molecules' compact structure, crammed with chemical groups, made them “diabolical” targets, says K. C. Nicolaou, an organic chemist at The Scripps Research Institute in La Jolla and the University of California, San Diego. But in the 1 June issue of *Angewandte Chemie*, Nicolaou and his colleagues report having scaled that demonic peak: They have performed the first-ever complete synthesis of the CP molecules.

“It's an extremely impressive accomplishment,” says Samuel Danishefsky, whose own group at Columbia University in New York City was closing in on the same goal. Other recently synthesized molecules have been more than four times the size of the CPs, which have 31 carbon atoms each. But Danishefsky says the CP molecules require particular finesse. “The functional groups bump into each other so that it's difficult to work on one portion of the molecule without affecting another part,” he says.

“The CP molecules originally attracted attention when researchers at the pharmaceutical giant Pfizer showed that they inhibited the work of a cancer-causing gene known as *Ras*, which is overactive in up to 80% of human cancers. CP molecules, it turns out, block the addition of a chemical group known as a farnesyl group onto the *Ras* gene, a key step in its activation. Other more potent farnesyl blockers have been discovered, says Takushi Kaneko, a medicinal chemist at Pfizer's research center in Groton, Connecticut, who helped nail down the structure of the CP molecules. However, the new synthetic work could still prove vital, he says, by allowing chemists to manufacture CP analogues that may prove even more potent and also easier to produce than the CPs themselves.

Getting this far was a nearly two-year slog. In all, it took more than 40 chemical steps and many grams of starting materials to make milligrams of the molecules, which consist of a core ring of nine carbon atoms bearing three more oxygen-containing ring systems. On two occasions the group had progressed to key intermediate compounds along the way, only to find that although they were only a few bonds away from the complete structure they could not forge the final links.

The final attempt that got them to the summit took three key steps. First, the researchers had to convert a linear hydrocarbon precursor molecule into the nine-membered ring at the core of each CP molecule. They turned to a well-known ring-forming process known as an intramolecular Diels–

Alder reaction and tweaked the reaction conditions to coax the precursor to adopt the correct ring-shaped structure.

For the next step, the Scripps researchers developed a set of novel “cascade” reactions. Cascade reactions run through a staccato of intermediate steps, each one automatically producing the right materials and conditions for the next, before ending up at a final product. The researchers used two of their cascade reactions to fuse two additional five-membered carbon- and oxygen-containing ring systems to opposite sides of the core. A final summit push, which consisted of a flurry of reactions provided them with CP-263,114, the more stable of the pair of CP molecules.

However, they also wanted to make its partner, CP-225,917, which differs only in that one of the three attached rings is broken, and the frayed ends capped with hydroxy groups. Trying to coax the stable CP-263,114 into a more unstable form proved very difficult. After numerous attempts, the team designed another cascade reaction which finished the job. When the resulting compound passed muster in a structure-determining NMR spectrometer, the climb was complete. Atop the mountain, says Scripps Ph.D. student Phil Baran, “it feels like a 200-ton anvil has lifted off my back.”

Yet in some ways the work was just beginning. Now the hunt is on to come up with CP analogues that are more potent and simpler to make. The Scripps team is also launching studies of the detailed biological effects of the CPs and their derivatives. Of course, the search is also on for new molecular mountains to climb.”^[6]

How did it all happen and what was discovered and developed in the process? The answers to these and other intriguing questions will be found below as we take you behind the scenes and into the trenches of this battle against the CP molecules, the “molecular Minotaur” of our story.

2. The Intrigue and Lure of the CP Molecules to the Synthetic Chemist

Within the realm of molecular architectures of natural products, the CP molecules (**1** and **2**, Figure 2) occupy an intriguing position not because of their size but instead by virtue of the bond connectivities they display. Thus, the core structure of CP-263,114 (**1**), which consists of only 18 atoms, masters two five-membered rings, two six-membered rings, one seven-membered ring, and one nine-membered ring as well as several unusual and sensitive functionalities, including a maleic anhydride moiety, a γ -hydroxylactone, an internal ketal, a tetrahydropyran system, a bridgehead double bond, and a quaternary center (Scheme 1). While each of these structural features and the five stereogenic centers adorning this target poses its own synthetic challenge, it is the orchestration of the sequence by which one would have to construct them within the whole and maintain their integrity until the end that would present the major challenge to the molecule's total synthesis. In other words, this demonic molecular structure was well fortified and defended by a panoply of barricades whose defensive shield the synthetic chemist would have to overcome in a fierce struggle (see

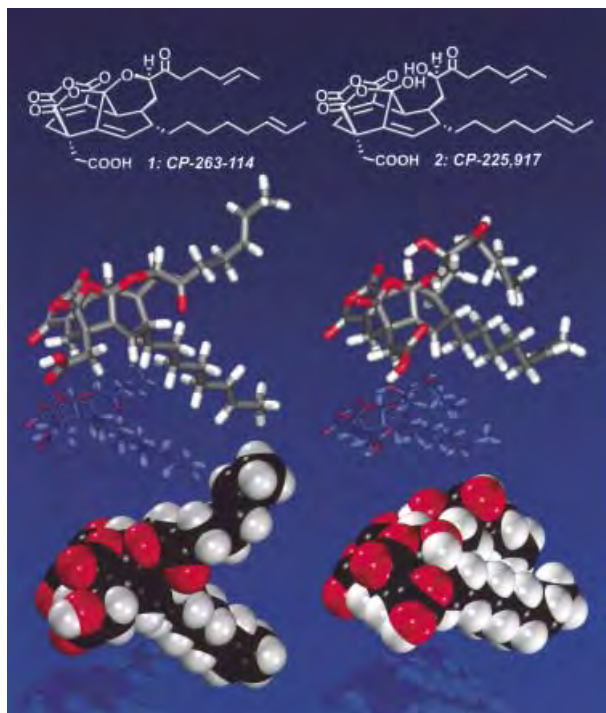
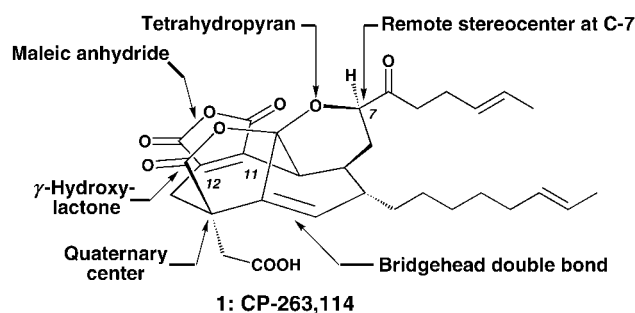


Figure 2. Molecular structures and computer-generated models of the CP molecules.



Scheme 1. Challenging structural elements of the CP molecules.

Figure 3). The outcome of the contest would surely depend on the resourcefulness, courage, and stamina of the daring, “would be conqueror”, chemist. Our first shy steps toward the CP molecules were taken in 1996 with the intention of exploring possible pathways to their general core structure.

3. Entry to the Labyrinth: An Intramolecular Diels–Alder Approach versus a Divinylcyclopropane [3,3] Sigmatropic Rearrangement Strategy

As with many molecules, entry into the synthetic labyrinth of the CP molecules was possible from several gates (exit would prove another matter, of course!). We chose two approaches for initial scouting and feasibility evaluation.

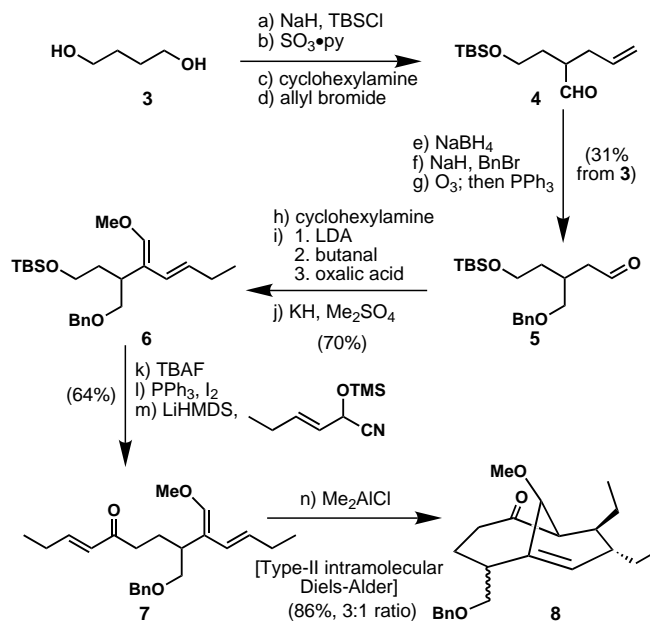
The first approach to the core of the CP molecules called upon the venerable Diels–Alder reaction, specifically a type-II version,^[7] to weave an appropriately designed open-chain precursor into a bicyclo[4.3.1] system **8** whose resemblance to



Figure 3. The “graduate student’s view” of the CP molecules guarded by the dreaded Minotaur.

the CP-molecule structure was not only credible but also encouraging (Scheme 2).^[8] The high yield and exclusive stereochemical outcome of this cycloaddition reaction leading to the desired carbon framework added considerable weight to the potential and possible virtues of such an entry into the anticipated synthetic campaign.

In the meantime, a second foray into the labyrinth was being explored (Scheme 3).^[9] This strategy was designed



Scheme 2. The Diels–Alder approach to the CP core: a model study.

based on an initial carbenoid addition to a double bond followed by a Claisen rearrangement and a final S_H2 reaction. This rather elegant sequence proved rewarding in that all key steps proceeded as planned, but somewhat disappointing with regard to the stereochemical outcome of the final, radical-based S_H2 process. That step led to the wrong stereochemical arrangement at the quaternary center (**21**, Scheme 3).

Was there an error in the planning of this last operation? Specifically, what would the outcome have been in this reaction had we utilized the epimer of the precursor **19**? The

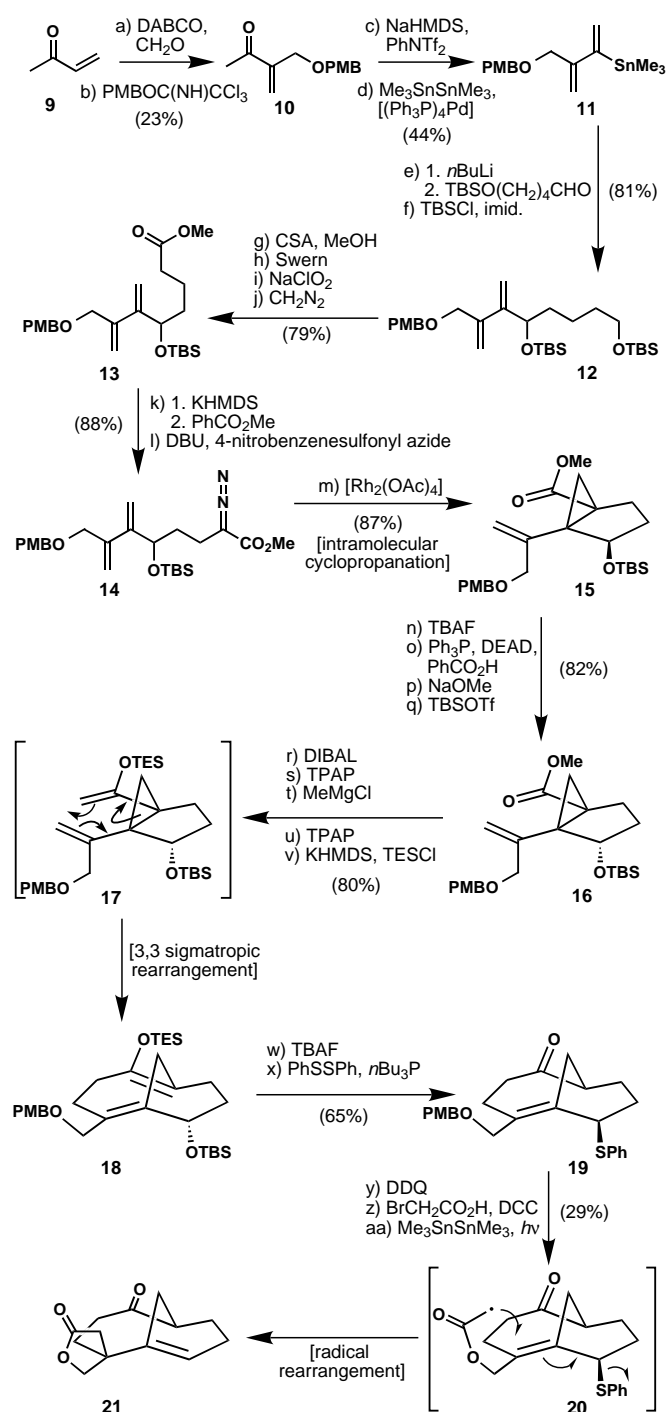
answer to this question will remain unknown in the absence of the experiment, even though one can hypothesize that if the radical S_H2' process proceeds by a *syn* mechanism (as appears from the observed stereochemistry of the product) then reversing the stereochemistry of the leaving group (assuming no other factor intervenes) may result in the formation of the desired product.^[9] On the other hand, it is likely that regardless of the absolute configuration of the carbon atom carrying the phenylthio group, approach of the acetate radical would take place from the convex face of the molecule. While insufficient information in the literature then and now prevents us from “betting the ranch” on such a prediction, the incident underscores the importance of mechanistically driven rational synthetic design. Incidentally, we may now revisit this question as a part of our recent interests in the chemistry initiated by related S_N2' -type reactions of *cis*-1,2-dichlorocyclobutene as an entry into novel molecular diversity.^[10]

As for the choice of entrance into the CP-molecule labyrinth, the dilemma was solved by the disappointing stereochemical result of the latter approach, which tilted the balance in favor of the intramolecular type-II Diels–Alder reaction. In the meantime, the definitive paper and the Kaneko structures of the CP molecules was about to appear in the literature,^[4] so the commitment was made to pursue the molecules as worthy challenges for total synthesis. It was both fortunate and timely (for me, K.C.N.) that a young man by the name of Phil S. Baran was entering the graduate program at Scripps in the same year. At the age of 19, Phil Baran decided to join my group and willingly accepted the CP-molecule challenge. He was destined to become the “Theseus” of this total synthesis story.

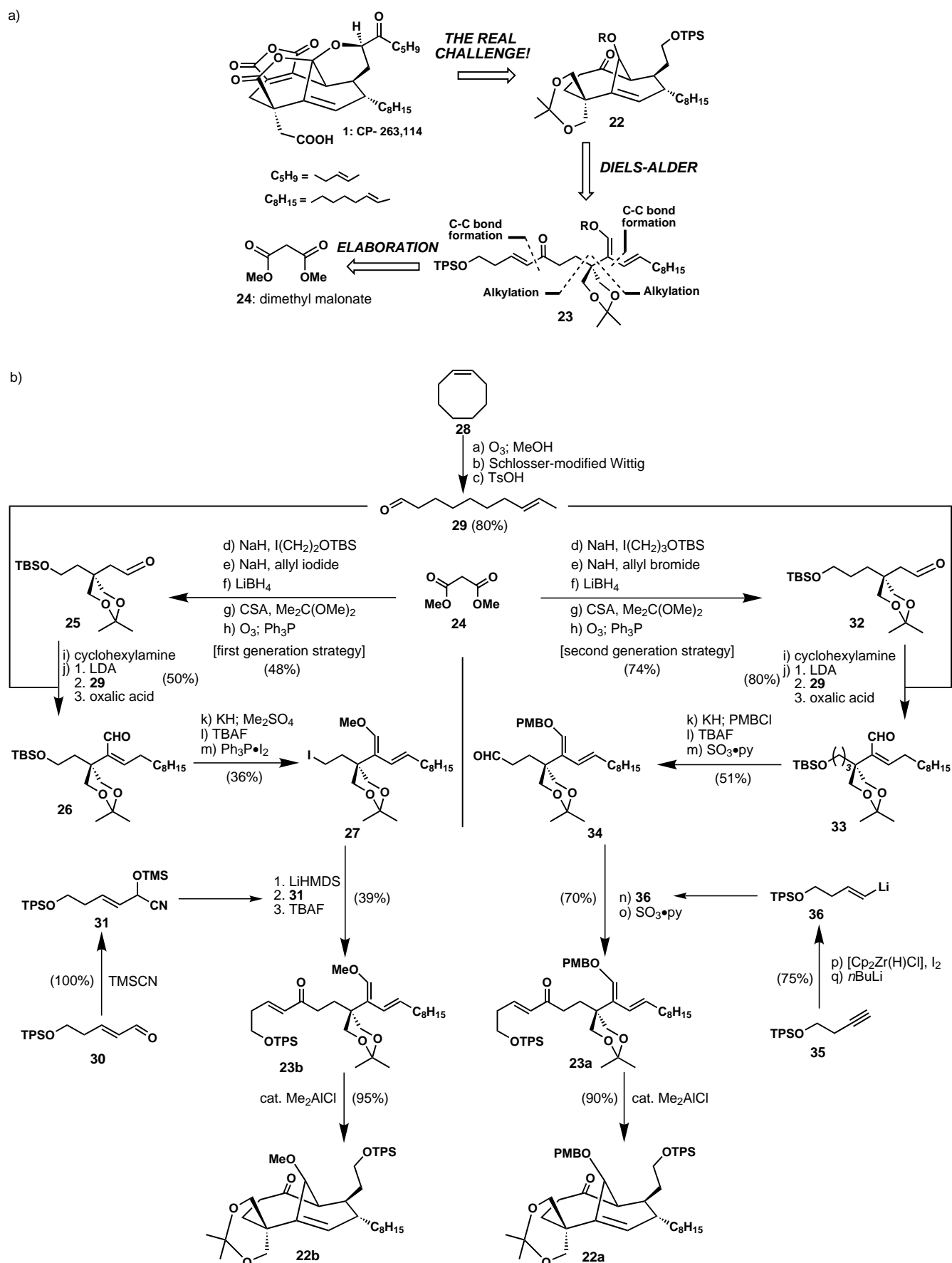
4. Evolution of the Intramolecular Type-II Diels–Alder Strategy to the CP-Molecule Core Structure

Armed with the positive results of the Diels–Alder model study described above, we proceeded to design a more appropriate intermediate for eventual incorporation into a synthetic blueprint capable of reaching the target natural products and streamlining a synthetic route. The general retrosynthetic strategy and the evolution of this plan are shown in Scheme 4.

Our original retrosynthetic analysis entailed the use of the key intermediate **22** whose disassembly to the prochiral precursor **23** became apparent upon recalling the intramolecular type-II Diels–Alder reaction. The obligatory simplification of precursor **23** relied upon two alkylation reactions, two crucial carbon–carbon bond-forming reactions, and a directed aldol reaction to disconnect the molecule as indicated in Scheme 4a. The execution of this plan is shown in Scheme 4b (left). The requisite building blocks **25**, **29**, and **31** were constructed expeditiously from dimethylmalonate (**24**), cyclooctene (**28**), and aldehyde **30**, respectively. Anion formation from the imine generated from aldehyde **25** and cyclohexylamine followed by addition of aldehyde **29** and elimination of H_2O from the resulting product led to the α,β -



Scheme 3. The sigmatropic rearrangement approach to the CP core: a model study.



Scheme 4. a) General retrosynthetic analysis of the CP molecules. b) First and second generation intramolecular type-II Diels – Alder routes to the CP-core structures **22a** and **22b**.

unsaturated aldehyde **26**, whose elaboration to iodide **27** required a second anion generation, quenching with Me_2SO_4 , and desilylation-iodonation. The alkylation of the anion of cyanohydrin **31** with iodide **27** was accomplished only in low yield to afford, upon hydrolysis, enone-diene **23b**, whose Me_2AlCl -catalyzed Diels–Alder reaction proceeded smoothly to give the coveted bicyclo[4.3.1] system **22b**.

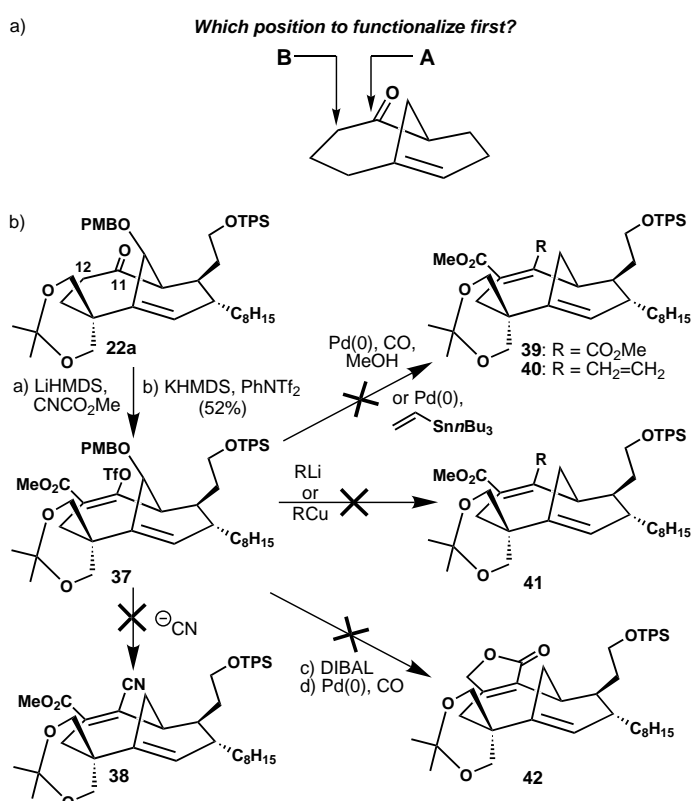
This early success gave us the confidence that a sufficiently elaborated system such as **22** could be reached by the chosen route. However, this route needed to be refined because of the low yielding alkylation step involving the sterically encumbered iodide **27** and because of questions regarding the suitability of the methoxy group as a surrogate to the required bridgehead functionality.

Accordingly, a second approach (Scheme 4b, right) in which a different coupling strategy for the initial building blocks was devised and executed, this time targeting a PMB derivative of the bridgehead hydroxy group. A similar sequence was followed as before except for the final connection which was now made by coupling vinyl lithium **36** with aldehyde **34**. The efficiency of the overall scheme proved quite satisfactory, and hundreds of grams of the key bicyclic system **22a** were synthesized, thus keeping the supply lines for waging battle constantly filled.

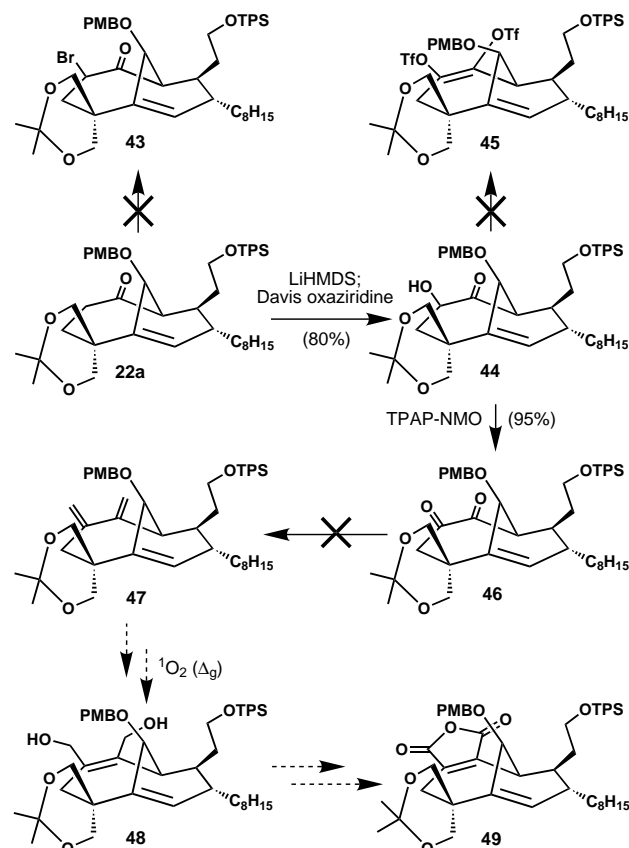
5. The Maleic Anhydride Hurdle

Of the various functionalities adorning the periphery of the CP skeleton, we first decided to investigate and develop a reliable method for the synthesis of the maleic anhydride moiety. Little did we know that this seemingly innocent structural unit would pose one of the most arduous challenges in the CP synthetic labyrinth. Our initial approaches were all flawed in that they attempted to operate first on the more hindered position A (Scheme 5a) after the less hindered carbon atom adjacent to the ketone moiety (position B) had been functionalized. This strategy occupied us for several months because of the ease of alkylation of the ketone enolate with a variety of electrophiles. Several attempts to convert vinyl triflate **37** (easily obtained from ketone **22a**) into suitable anhydride precursors were plagued with unpredicted failures (Scheme 5b), despite success in simple model systems. For several weeks, in parallel to the streamlining of the Diels–Alder sequence (see Section 4), these studies continued as multiple reaction conditions and catalysts were screened in hopes of opening one of the reaction pathways. Thus, conjugate addition–elimination reactions^[11] on **37** (for example, **37** → **38**) failed, as did palladium-catalyzed coupling reactions^[12] (for example, **37** → **39** or **40**), organometallic additions (**37** → **41**), and a DIBAL reduction–carboxymethylation^[13] pathway (**37** → **42**).

Other strategies were then pursued from **22a** and the easily accessible hydroxyketone **44**, as shown in Scheme 6. Having failed to selectively brominate **22a** to **43**, we turned to the hydroxylation of **22a**, a transformation that was smoothly carried out with Davis' oxaziridine^[14] to generate **44**. Formation of ditriflate **45** as an attempt to advance intermediate **44** failed, but oxidation of the latter compound (**44**) with



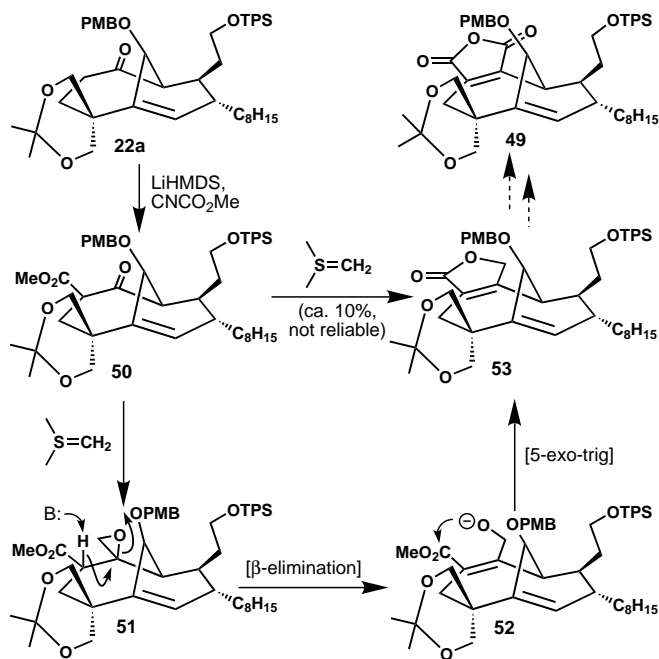
Scheme 5. a) Installation of the maleic anhydride moiety (substituents deleted for clarity). b) Unsuccessful attempts to functionalize triflate **37** toward the maleic anhydride moiety.



Scheme 6. Other failed attempts to access potentially useful precursors to the maleic anhydride moiety.

TPAP/NMO^[15] led to diketone **46**. Hopes that diketone **46** could be funneled into a pathway leading to a maleic anhydride intermediate (**46** → **47** → **48** → **49**) were, however, dashed by failure at the start: diketone **46** was unwilling to be a player in this scenario, resulting in another dead-end situation.

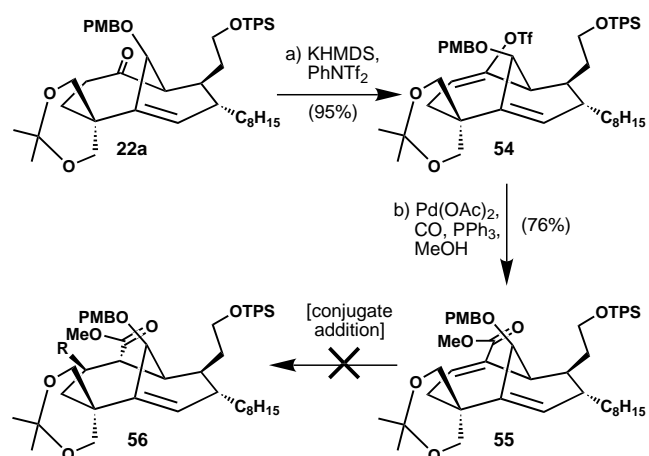
A sulfur ylide-based epoxidation^[17] of keto-ester **50** (readily obtained from ketone **22a**, Scheme 7) then shed a glimpse of light on our endeavors. The expectation was that the initially formed epoxide **51** would suffer β -elimination to furnish



Scheme 7. Attempted epoxidation of ketone **50** leads to butenolide **53**, albeit in low yield, which forced us to abandon this route.

alkoxy ester **52**, whose collapse to the potential maleic anhydride precursor **53** was deemed inevitable. This hypothesis was indeed borne out by the initial experiments, with butenolide **53** being observed in about 10% yield. The euphoric feeling of finally arriving at something resembling the anhydride moiety was soon squelched, however, as we were unable to improve the reaction, despite several repeated attempts. It was now mid-September, 1997.

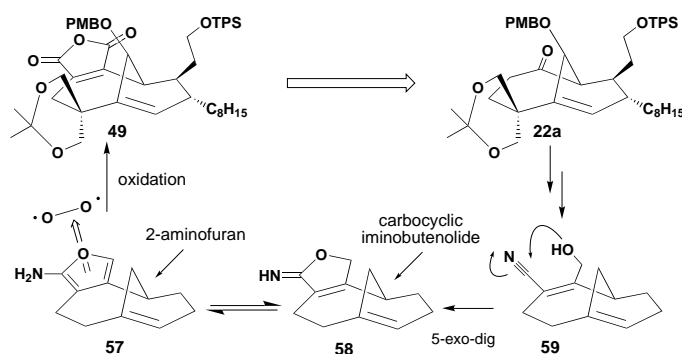
Studies to construct the anhydride were then temporarily halted as finishing touches and optimization of the 13-step sequence to the Diels–Alder product **22a** were undertaken (Scheme 4b). Studies directed toward solving the maleic anhydride problem resumed in the beginning of December, 1997, and continued in the same fashion (functionalization of position A and then position B, Scheme 5a) until Christmas eve of that year when we decided to explore the functionalization of position B first (Scheme 8). Thus, ketone **22a** was converted into the vinyl triflate **54** which was then submitted to Pd-catalyzed carboxymethylation to furnish the α,β -unsaturated ester **55**. This transformation represented the first reliable synthesis of a compound (that is, **55**) bearing a useful carbon functionality at position B, and, at this point, conjugate addition strategies^[11] to provide intermediates of type **56** were



Scheme 8. Successful synthesis of the α,β -unsaturated ester **55**, which, however, turns out to be another dead-end.

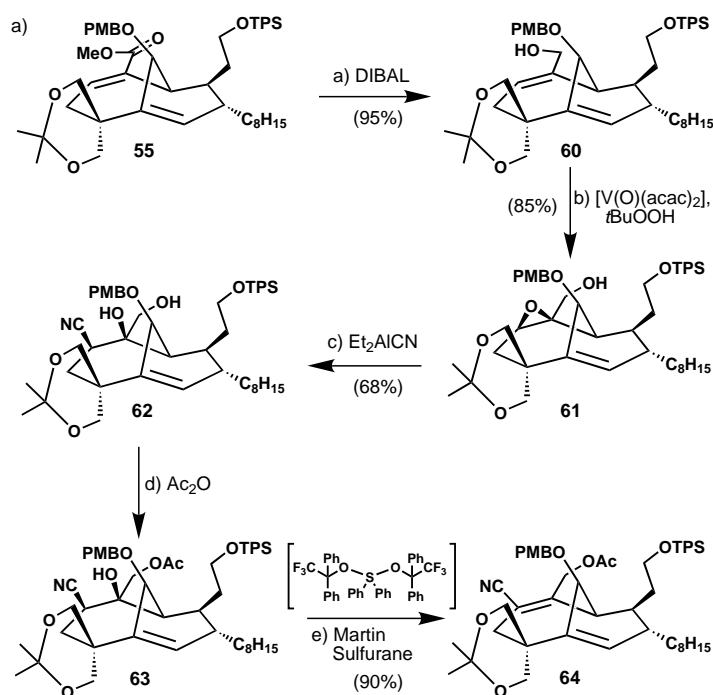
evaluated. All attempts toward this goal failed, however, adding further frustration to those gloomy days. A new plan was clearly needed to extricate ourselves from this rather miserable predicament.

Shortly before New Year's eve, 1997, a rather daring strategy towards the anhydride moiety was conceived of as shown in Scheme 9. We envisaged the use of an unprecedented 2-aminofuran^[17] moiety as a “molecular sponge” to



Scheme 9. Novel designed strategy for the conversion of ketone **22a** into anhydride **49**. (Substituents in structures **57**–**59** have been deleted for clarity.)

harvest oxygen and lead to the maleic anhydride moiety after expulsion of ammonia. On the basis of Dewar's pioneering calculations,^[18] access to the requisite 2-aminofuran (**57**) was envisaged from the iminobutenolide **58**. This idea was inspired by the previous observation of butenolide **53** (Scheme 7) which suggested that a β -elimination pathway could, in principle, permit access to this rare chemical species. Thus, the projected synthetic pathway was directed towards **59** whose generation from ketone **22a** was considered feasible. With the α,β -unsaturated ester in hand, we proceeded at a furious pace which reached a climax at 2:00 a.m. on January 1, 1998, wherein we had synthesized the cyanodiols **62** (Scheme 10a). Soon thereafter, and much to our surprise, we established the unorthodox stereochemistry ($-\text{CN}$, $-\text{OH}$ *cis* to each other) of the compound as suggested by NOE experiments. There are three possible mechanistic rationales



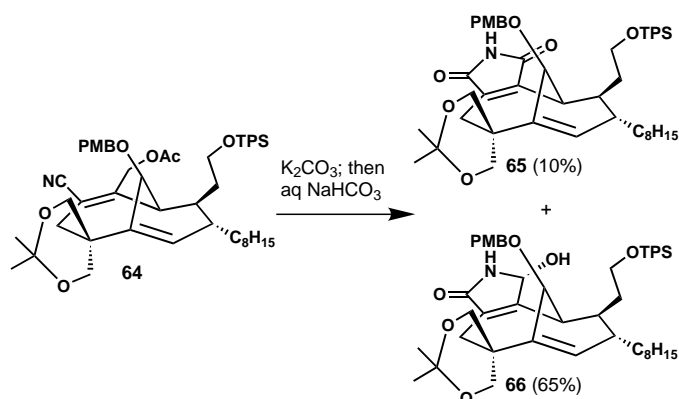
Scheme 10. a) Arrival at the cyanoacetate **64**. b) Three possible mechanistic explanations for the observed “unorthodox” stereoselectivity of the cyanide addition to **61a**.

for this unexpected stereochemical outcome: in the first (Scheme 10b, top), our favored scenario, a molecule of Et_2AlCN ^[19] reacts with the hydroxyl group of **61** furnishing complex **61a**, which suffers nucleophilic attack by cyanide from the more accessible convex site made possible by considerable weakening of one of the epoxide C–O bonds.

This mode of attack would then be accompanied by the observed retention of stereochemistry at C-12 (CP numbering). In the second scenario, the initially formed complex **61a** (Scheme 10b) is envisioned to undergo intramolecular rearrangement, by inversion of configuration, to afford oxetane **61b**, whose reaction with cyanide by inversion is expected to lead to the observed product **62**. In the third scenario (Scheme 10b, bottom) a concave mode of attack by cyanide on complex **61a** is postulated to afford the now inverted cyanodiol **61c** which, under the reaction conditions, suffers epimerization to the observed cyanodiol **62**.

Irrespective of the mechanism of this transformation, formation of **62** was good news because we could now test our iminobutenolide hypothesis. In anticipation of that event, and after scaling up the sequence, the push forward was uninterrupted, and within two days we arrived at the precious acetoxyacetonide precursor **64** by mono-acetylation of **62**, followed by a dehydration facilitated by the Martin sulfurane^[20] (**62** → **63** → **64**, Scheme 10a). One of us (K.C.N.) will never forget the scene in the laboratory on that day in January 1998, who upon arrival at 8:00 a.m. found the other (P.S.B.) fast asleep on his desk with a clean NMR spectrum of compound **64** by his side. It was classic brilliance and characteristic dedication from the team working on this project!

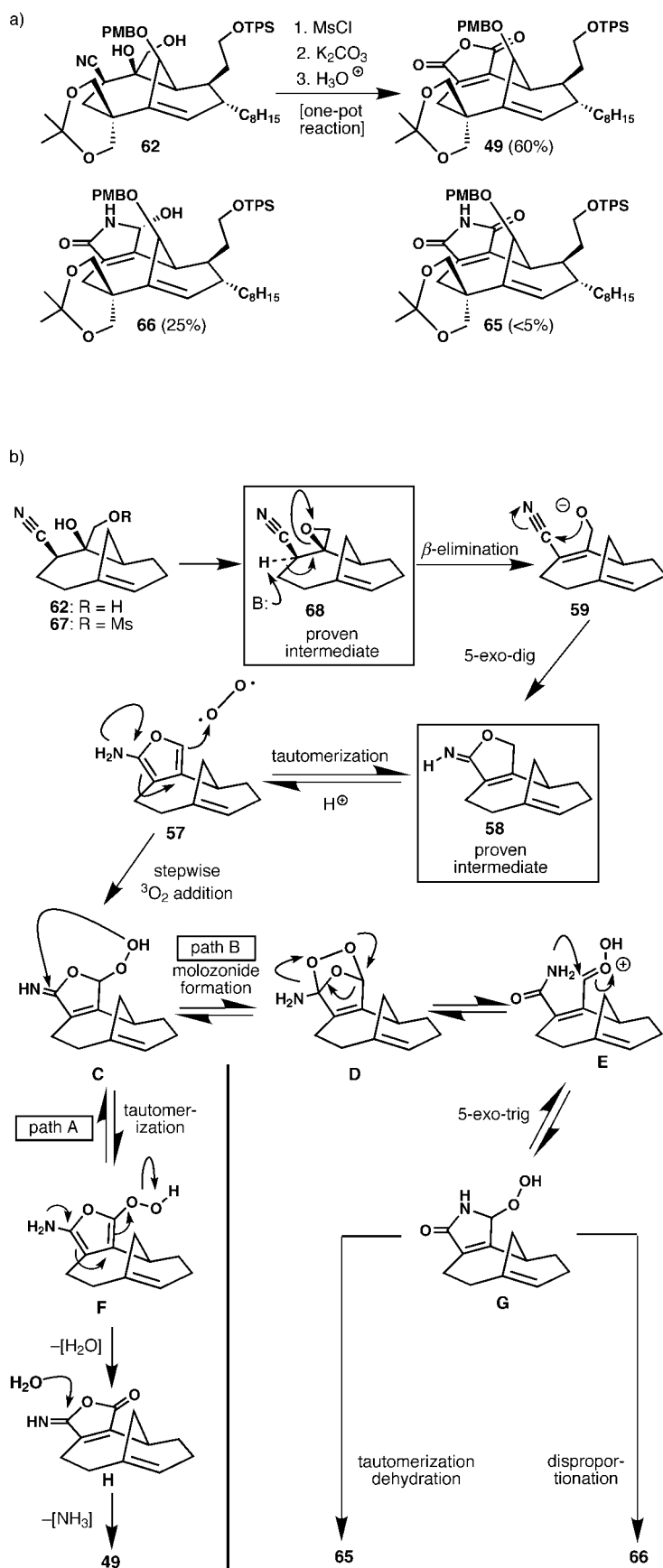
Later that day, the crucial experiment towards iminobutenolide **58** (Scheme 9) was carried out. Scheme 11 tells the rest of the story—disappointing, but interesting! Basic (K_2CO_3) hydrolysis of **64** followed by mildly basic workup (NaHCO_3)



Scheme 11. First attempt to reach the anhydride leads to the maleimide **65** and an unknown by-product, which was later determined to be **66**.

led to two compounds, neither of which was the coveted maleic anhydride **49**. Instead, we discovered that we synthesized maleimide **65** (ca. 10% yield) along with an unknown major product, which was later characterized as a single isomer of the hydroxyamide **66**.

We shall return shortly to the discussion of the mechanistic aspects of these remarkable transformations; but first back to the main issue at hand, the maleic anhydride moiety and its construction. It would take another seven weeks before we finally found reliable conditions for the conversion of cyanodiol **62** into maleic anhydride **49** (Scheme 12a). In this one-pot reaction involving exposure of **62** to mesyl chloride/triethylamine followed by addition of K_2CO_3 and oxalic acid



Scheme 12. a) The “magic” of the maleic anhydride cascade. Conversion of **62** into **49**. b) Proposed mechanistic underpinnings in the conversion of **62** into **49**, **65**, and **66**. (Substituents have been deleted from the structures for clarity.)

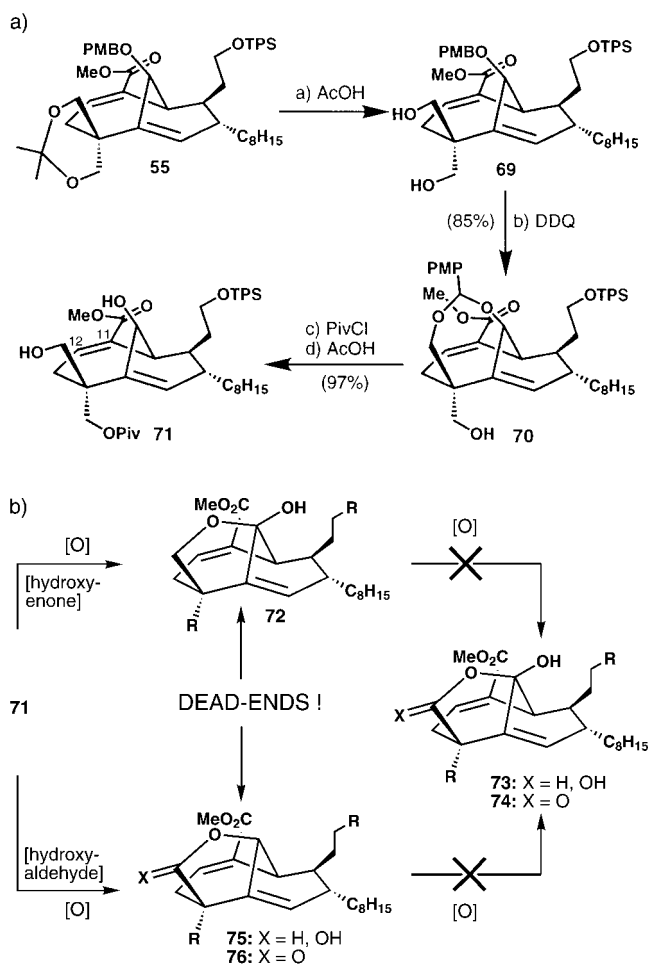
workup, the following chemical transformations were accomplished: 1) primary mesylate formation; 2) epoxide formation; 3) β -elimination rupturing the epoxide; 4) 5-exo-dig cyclization to an iminobutenolide; 5) double oxygenation; and 6) hydrolysis/expulsion of ammonia. Scheme 12b presents a plausible mechanistic rationale for these transformations which explain the formation of the observed final products **49**, **65**, and **66**.

Despite the extraordinary chemistry involved in this cascade in which maleic anhydride is formed,^[21] we restrained ourselves from submitting a paper describing the work until later on in 1998 when further progress toward the CP molecules was made. Notwithstanding the relief and excitement of designing and executing a remarkable cascade reaction to synthesize the maleic anhydride moiety within the CP molecule, we were cognizant of the fact that we were still far away from the center of the CP labyrinth. Sure enough, more challenging hurdles and unpredictable twists, turns, and puzzles were waiting ahead of us, as we shall see in the upcoming sections of the tale.

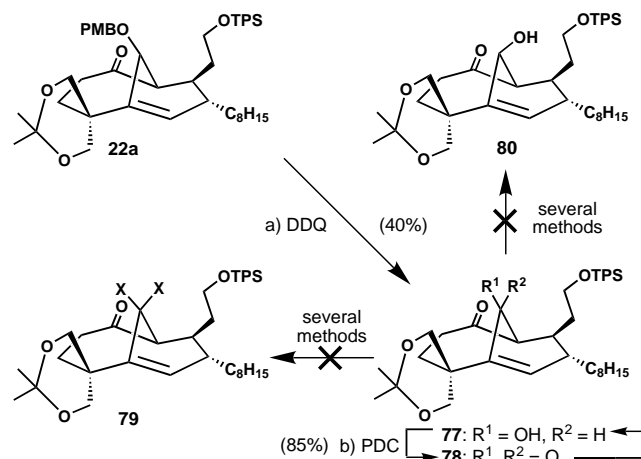
6. The γ -Hydroxylactone Hurdle

Having secured the maleic anhydride moiety, we then decided to turn our attention to the γ -hydroxylactone system of the CP molecules. Seemingly, the construction of this moiety boils down to oxidizing the appropriate carbon atoms to their highest oxidation state. This task turned out, however, not to be so trivial. The underlying challenges of the γ -hydroxylactone construction surfaced rather quickly after synthesizing the model 1,4-diol **71** (Scheme 13a). As shown in Scheme 13b, we were only able to isolate partially oxidized, yet unproductive, forms of the γ -hydroxylactone upon attempted oxidation of this 1,2-diol. For example, if we used oxidants capable of selective oxidation of the bridgehead position, rapid closure to hemiketal **72** was always observed. Alternative oxidants capable of selectively oxidizing the primary alcohol also led to dead-ends in the form of lactol **75** and lactone **76**, which were resistant to further oxidation at the bridgehead position. Other 1,4-diols that differed at positions C-11 and C-12 exhibited similar stubbornness toward oxidizing agents, which forced us, ultimately, to search for an alternative pathway.

Since the stereochemistry of the bridgehead hydroxy group was crucial to the “locked” structures **75** and **76** (Scheme 13b), our first impulse was to invert the stereochemistry at that center. Another option to avoid the “locking up” of partially oxidized intermediates would have been a sequence in which the bridgehead carbon atom was oxidized to the ketone and protected while the primary alcohol was still engaged in the acetonide functionality. These ideas were tested starting with ketone **22a** as shown in Scheme 14, but unfortunately failed. Thus, the bridgehead hydroxy group could not be inverted, neither by a Mitsunobu reaction^[22] nor through an oxidation/reduction sequence, with the latter protocol



Scheme 13. a) Synthesis of the model 1,4-diol system **71**, in preparation for the construction of the γ -hydroxylactone moiety. b) The “lock-up” problem of oxidizing the 1,4-diol system to a γ -hydroxylactone moiety.



Scheme 14. Failed attempts to protect the bridgehead enone or invert the bridgehead hydroxy group.

leading to the same starting alcohol. Furthermore, enone **78** could not be protected under a variety of conditions.

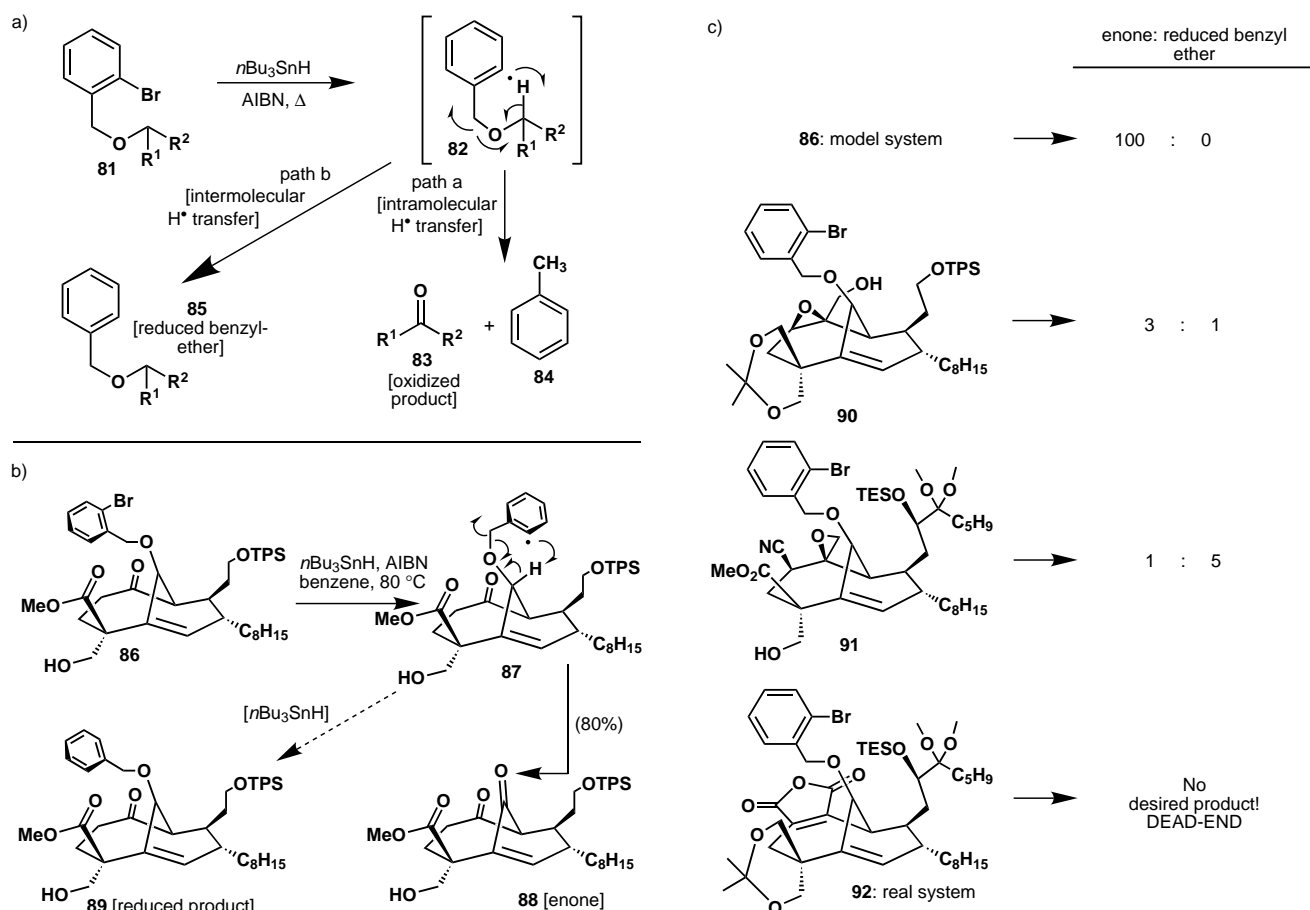
When one of us took a trip downstairs to discuss this problem with Professor Erik Sorensen, he drew our attention to a paper by D. P. Curran and H. Yu which introduced a unique self-oxidizing protecting group to organic synthesis based on the radical chemistry of the *o*-bromobenzyl ether

group (Scheme 15a).^[23] Without the intermediacy of a free hydroxy group at the bridgehead position we would no longer have to worry about “locked” structures! Eager to implement this novel idea to the solution of the thorny γ -hydroxylactone problem, we synthesized substrate **86** as a model system and subjected it to the Curran conditions (Scheme 15c). Much to our delight upon exposure of **86** to the radical debromination conditions we observed a clean oxidation to enone **88** which was exclusively formed in 80% yield. No detectable amounts of the undesired reduced benzyl ether **89** could be seen. The path now appeared clear towards the γ -hydroxylactone! Unfortunately, as is often the case in total synthesis, our hopes were soon crushed when we found that more advanced substrates containing the maleic anhydride moiety, or its progenitor functionalities, failed to follow the same path, but led instead to either the reduced benzyl ether or decomposition products. Scheme 15c summarizes the results with a number of such substrates, with the real intermediate **92** leading to no desired product whatsoever, bringing us once again to a halt.

We went back to the drawing board and devised a strategy which was predicated on the ring-chain tautomerization of hydroxy ketones (Scheme 16a).^[24] Specifically, we reasoned that the locked hemiketal (for example, **94**, Scheme 16a), readily available from structures of type **93**, might be intercepted by an oxidant in its open hydroxy-enone form (**95**) and lead to a dicarbonyl system (namely, **96**) which, after hydration, would lead to the γ -hydroxylactol **97** or even possibly to the γ -hydroxylactone **98** after further oxidation. To test this hypothesis we subjected the easily obtainable 1,4-diol **99** (Scheme 16b) to excess DMP^[25] in CH_2Cl_2 for 16 h, at which point we were delighted to encounter the desired γ -hydroxylactol **100**. We then found that TEMPO/NaOCl^[26] was a suitable oxidant to carry out the further oxidation to the corresponding γ -hydroxylactone **101**. In a custom with which we soon became all too familiar, this simple model study failed to prepare us for the surprise that lay ahead. When we employed as a substrate the more advanced 1,4-diol system **102**, which was identical to the model compound **99** except for the fact that it was now harboring the maleic anhydride moiety, the DMP-mediated oxidation failed to proceed beyond the hemiketal “locked” stage (Scheme 16c). After a number of failed attempts to coax this reaction in the right direction, a linear path to construct the γ -hydroxylactone moiety was pursued (see Scheme 17a).^[27] In retrospect, this strategy, which was based on conventional protecting-group manipulations, set us back a number of months even though it succeeded in furnishing the most advanced CP intermediate (namely, **107**) at the time.^[27] Soon afterwards, however, we were to realize that the anhydride moiety would not tolerate the conditions required to install the “upper” side chain, as indicated in substrates **108** and **109** (Scheme 17b). It was time for a new strategy and the team retreated to earlier intermediates for some serious planning.

7. Selecting a Strategy for the First Serious Assault on the CP Molecules

After coming to the realization that the “upper” side chain would have to be installed prior to maleic anhydride



Scheme 15. a) Curran's self-oxidizing protecting group. b) Model study to reach a bridgehead enone utilizing Curran's self-oxidizing protecting group proves successful. c) Summary of attempts to reach the bridgehead enone utilizing the self-oxidizing protecting group.

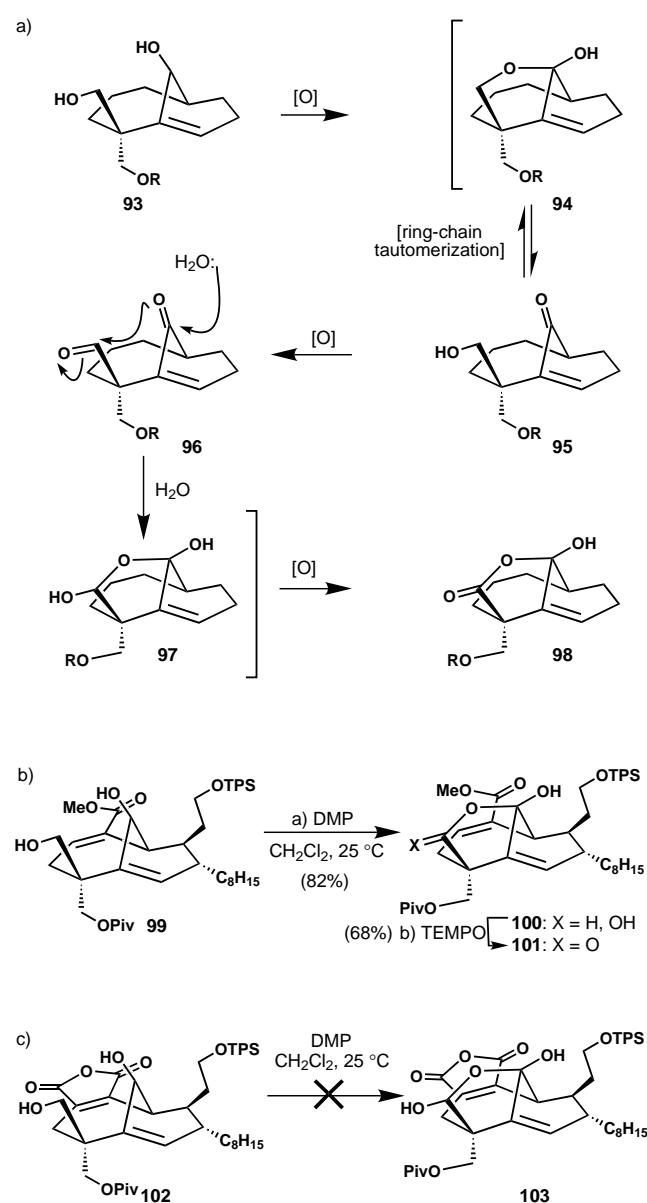
formation, and with two potential methods to construct the γ -hydroxylactone at our disposal (DMP-mediated cascade and the linear approach), we prepared, starting from the Diels–Alder product **22a**, a series of CP-core aldehydes (**111**–**114**, Scheme 18a) for coupling with lithiodithiane **110a**. In our first attempt, we employed ketoaldehyde **111**, which mainly gave us one diastereomeric product (ca. 11:1 ratio of diastereomers) of the corresponding hydroxyketone (**115**). To determine the configuration of the newly generated center at C-7 of the latter compound it was necessary to prepare tetrahydropyran derivative **122**, via intermediates **120** and **121** (Scheme 18b). The NOE signals observed in the ^1H NMR spectrum of this rigidified structure (**122**) confirmed our wish for the 7(*R*) configuration as desired for the CP molecules. This remarkable degree of stereocontrol may be explained by commissioning lithium complexation with both carbonyl groups of **111**, thereby fixing the conformation of the aldehyde in a favorable position to yield the desired product (Figure 4).^[28] As seen in Scheme 18a, the selectivities observed in other cases (aldehydes **112**–**114**) where such a chelation possibility does not exist were either diminished or skewed in the direction of the wrong, 7(*S*) isomer (**117** and **118**).

With a reliable method for the attachment of the “upper” side chain at our disposal, we were now able to charter a route towards the advanced key intermediate **129** (Scheme 19). Key events en route to **129** included a Pd-catalyzed carboxymethylation of the vinyl triflate derived from ketone **123**, a highly

stereoselective epoxidation of the allylic double bond of **125**, and, of course, the efficient formation of the maleic anhydride moiety (**127**→**128**). The structure of **129** was firmly established by X-ray crystallographic analysis.

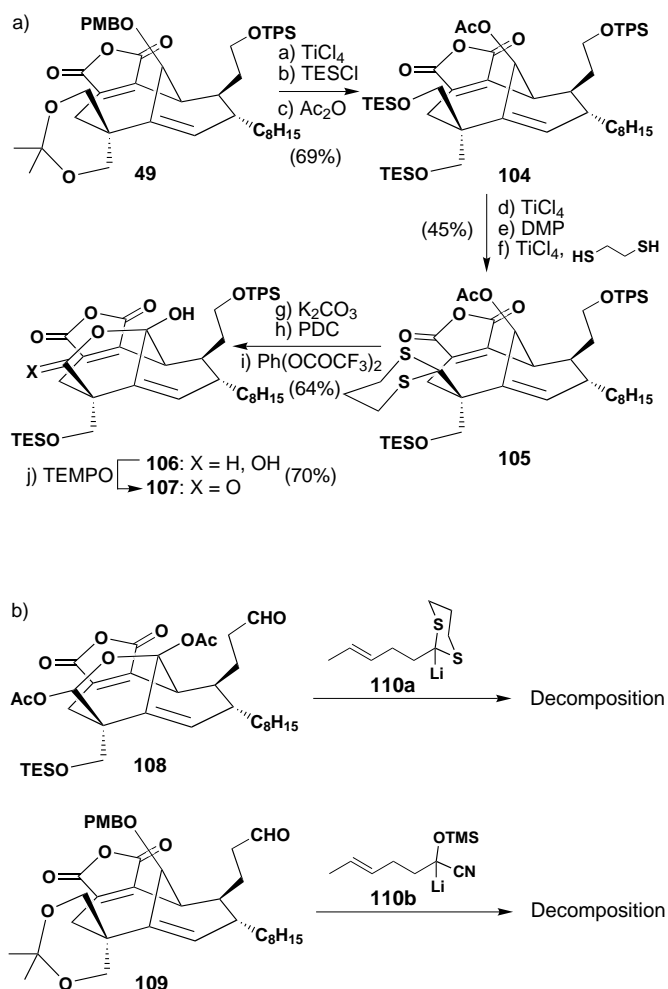
Arrival at key intermediate **129** constituted a somewhat historical event in the CP project, in that we marked this compound as the embarking point for any new excursions. The decision to use **129** as the “beachhead” for all future operations was taken not only because of the intermediate's attractiveness as a readily available and fertile substrate, but also partly because of our frustrating failures with numerous other plans to make substantial forward progress. Indeed, more than ten variations of such strategies were devised and explored, only to lead to dead-ends as summarized in Scheme 20.

The decision to abandon the linear, protecting group-based route to the γ -hydroxylactone moiety was critical, because it allowed us to focus on a more daring and concise approach to this functionality. Given the risky nature of the new scheme, part of the research group remained loyal to the linear approach for a while longer, only to return later to join the main effort on the new strategy. What happened next is a notable example of rational design, although the ideas were considered risky and long-shots. However, a good mix of rational thinking, intuition, desperation, and courage brought us victorious to the next stage. Intuitively we felt that the DMP-based oxidation cascade to produce the γ -hydroxylac-



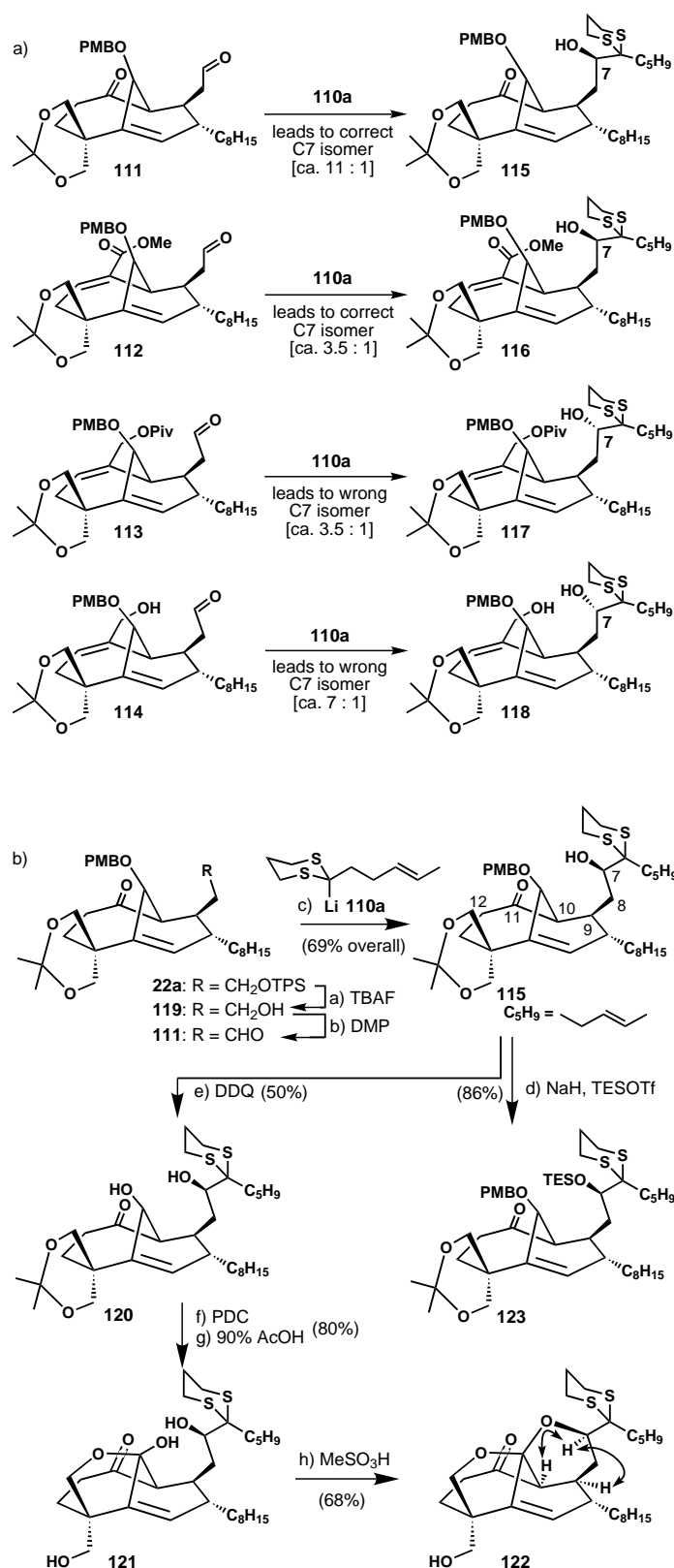
Scheme 16. a) General concept for tandem oxidation of **93** to the corresponding γ -hydroxylactone (**98**) based on the ring-open chain tautomerization of hemiketals. (Substituents have been deleted for clarity, [O] = oxidant.) b) The DMP oxidation cascade of 1,4-diols: proof of principle. c) DMP oxidation cascade of 1,4-diols fails in the presence of the maleic anhydride moiety.

tone system deserved another chance. Our inspiration to try again (having failed before, see Scheme 16) was drawn from the prior observation of the influence the upper side chain had on the reactivity of the core's functionalities and vice versa. Specifically, it was reasoned by analogy that, perhaps, a complete upper side chain such as in **129**, our "beachhead" compound, might exert enough remote influence so as to favorably coax the equilibrium between the closed and open forms of the lactol chain involved in the DMP-oxidation cascade (in contrast to the case with a truncated upper side chain where the lactol remained stubbornly closed, Scheme 16). Unlikely as it seemed, this proposition was viewed almost as a last resort, but since it would only take five steps from **129** to test it, we considered it worthy of pursuit.



Scheme 17. a) Stepwise construction of the γ -hydroxylactone moiety in the presence of the maleic anhydride moiety. b) Chemical reactivity of the anhydride moiety renders side-chain extension by organometallic addition to aldehydes a nonpractical proposition.

At the beginning of November, 1998, we arrived at the coveted hydroxylactol **132** by the route shown in Scheme 21 a. However, no matter how large an excess of DMP in CH_2Cl_2 at room temperature was used in our attempts to oxidize this intermediate further than the lactolaldehyde stage, its hemiketal moiety remained defiantly closed and intact (Scheme 21 b, top). In the midst of their desperation and hope, Yong-Li Zhong and Phil postulated that raising the temperature might persuade the lactol to reveal its primary alcohol, thus rendering it susceptible to oxidation by DMP. They proceeded to design, in complete secrecy (from K.C.N.), an experiment in which hydroxylactol **132** was to be heated in refluxing benzene with excess DMP! It is fair to say at this juncture that had they informed me of their intention to heat DMP at such temperatures, I would have most likely instructed them against this course of action in light of the assumption that DMP could possibly be explosive at high temperatures. Their plot was, therefore, perfect and they got away with it. The first signs of success came when traces of the desired γ -hydroxylactol aldehyde **134** (Scheme 21 b, middle) were detected by NMR spectroscopy despite a rather messy and distressing thin-layer chromatography (TLC) picture.



Scheme 18. a) Extending the upper side-chain. The addition of lithium dithiane to CP-core aldehydes occurs with remarkable remote stereo-control. b) Construction of key intermediate **115** and confirmation of its C-7 stereochemistry by NOE studies on a rigid descendant (**122**). Arrows in structure **122** indicate observed NOEs.

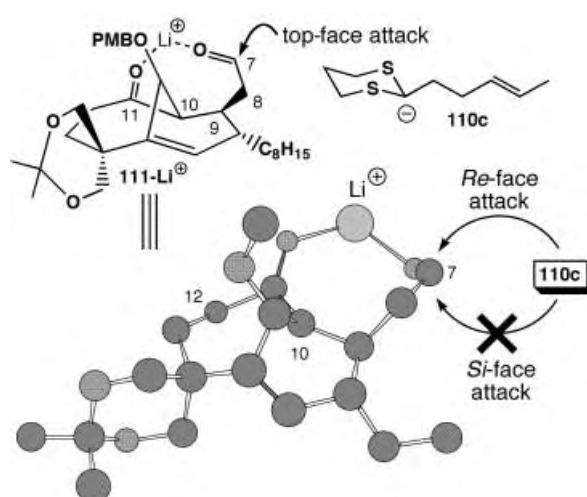
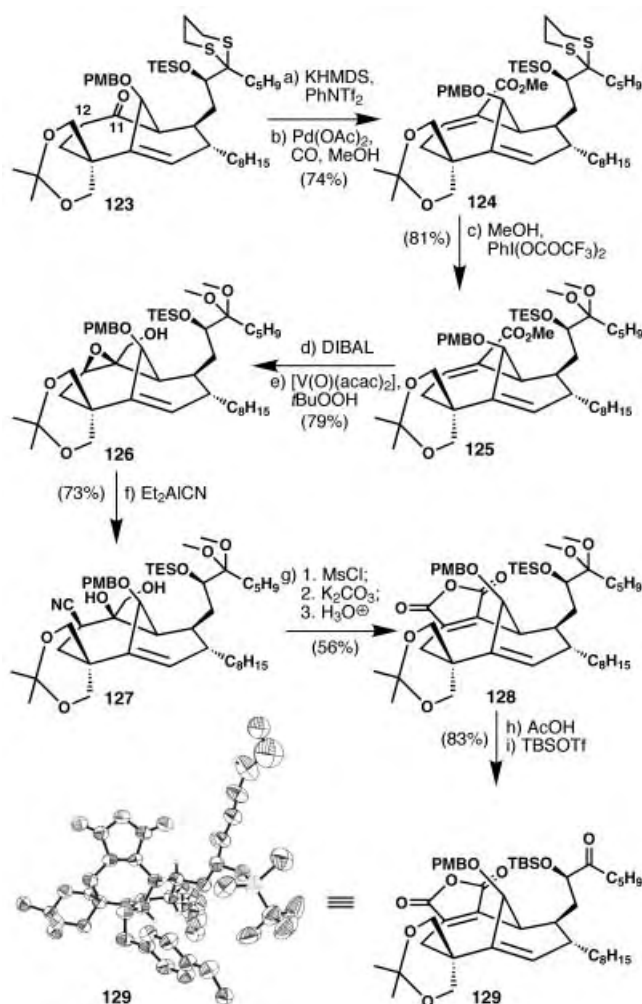
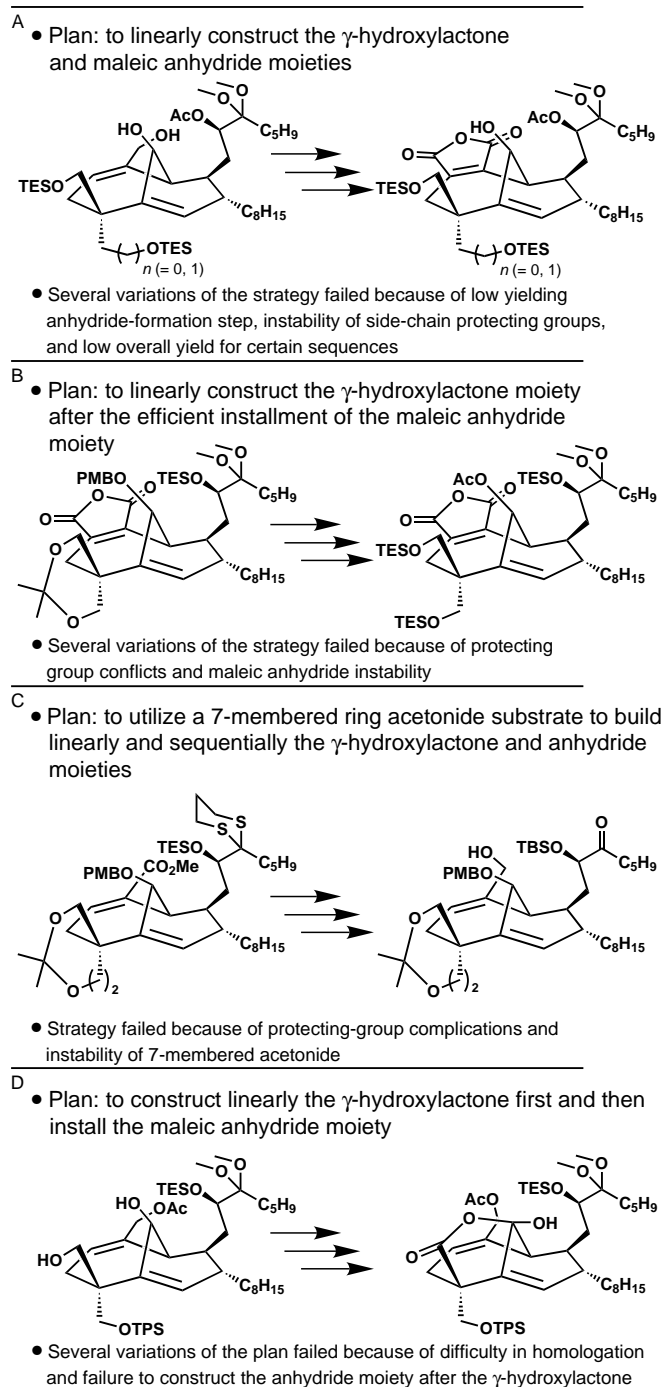


Figure 4. MM3-minimized structure of keto-aldehyde **111** chelated to a lithium cation (Li⁺). Such an interaction explains why the *Si*-face is blocked from attack of the incoming dithiane anion.



Scheme 19. Synthesis and X-ray structure of advanced key intermediate **129**.

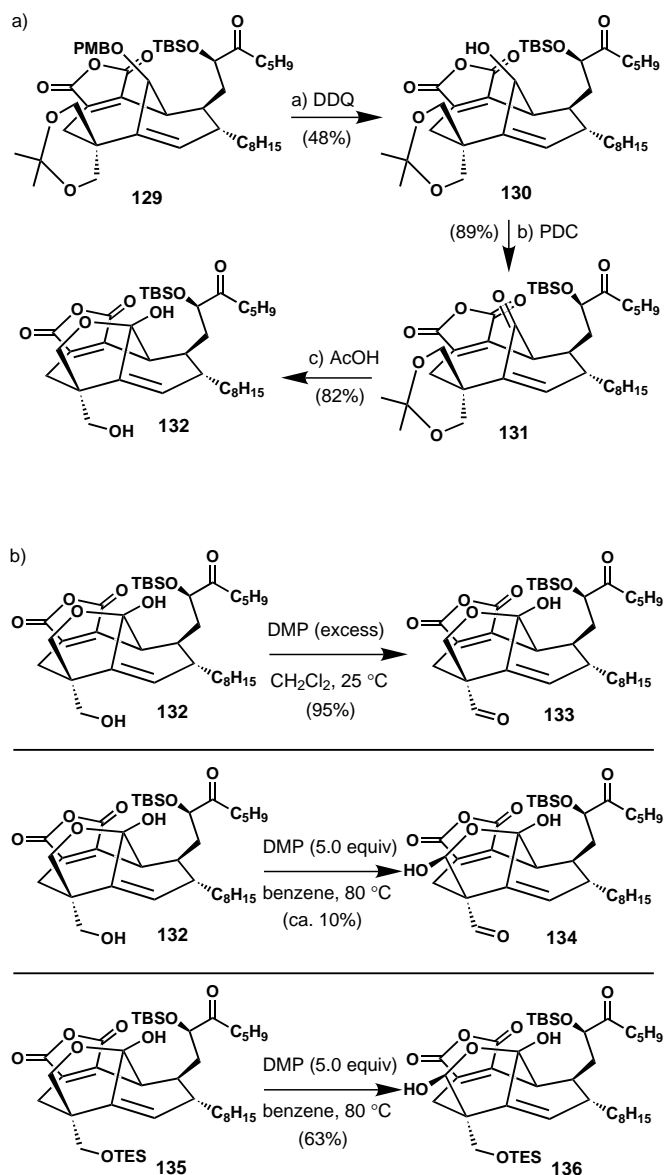
Guided by their impulses, they rushed to perform the next logical experiment which was to employ the TES-protected lactol **135** (Scheme 21 b, bottom) as a substrate in the reaction.



Scheme 20. Summary of selected failed attempts to break through a stalemate.

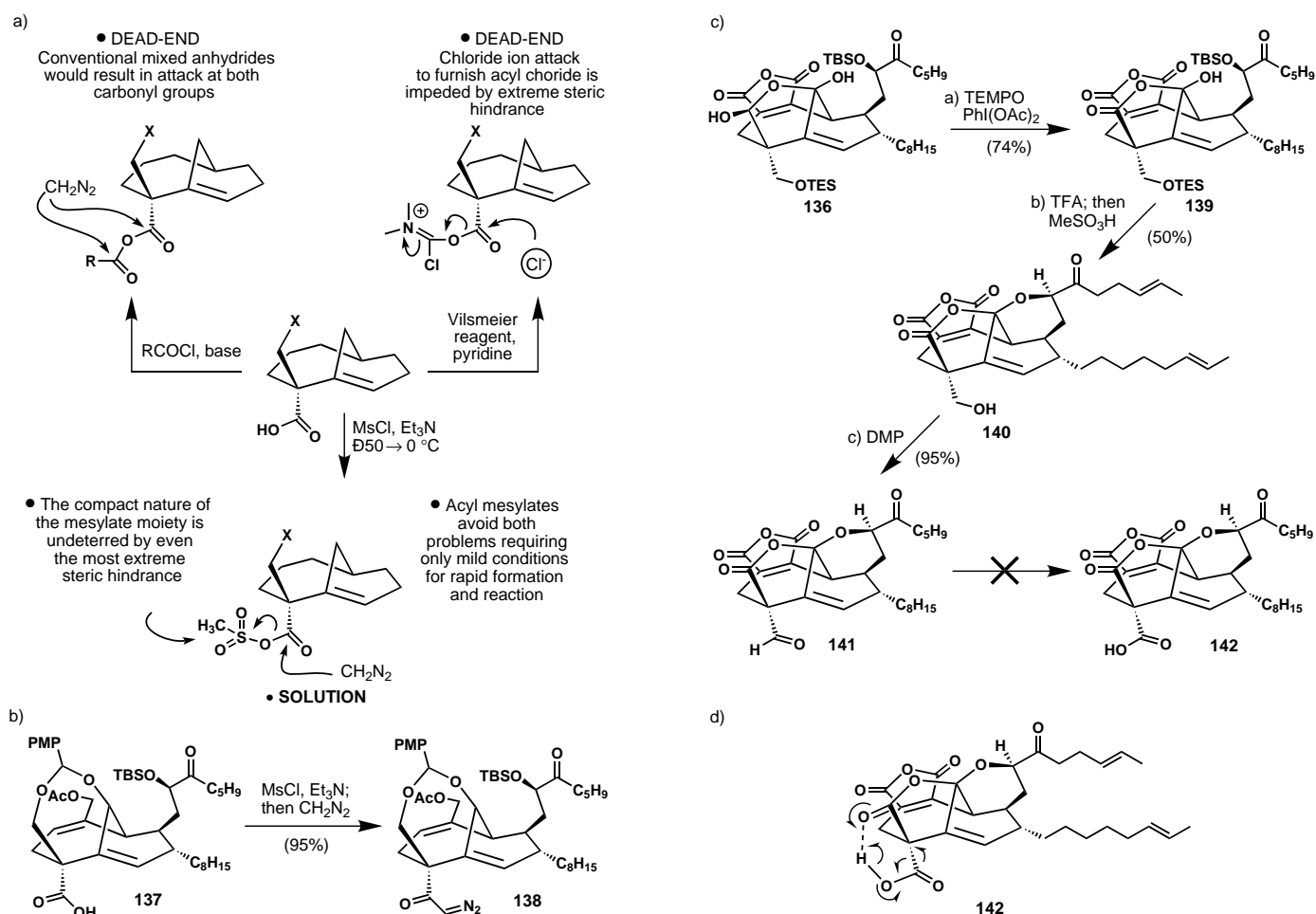
Happily they observed the formation of the desired product, compound **136**, in 63 % yield. That was when I (K.C.N.) heard about their daring escapades with high-temperature DMP oxidations. In retrospect I am, of course, glad that I did not interfere with this part of the expedition which brought us within striking distance of the “Minotaur,” the CP molecules.

From the last intermediate (**136**, Scheme 21 b, bottom) all that remained to reach the target molecules was only a few functional group adjustments and a one-carbon homologation of the projected carboxylic acid side chain, or so it seemed.



Scheme 21. a) Synthesis of **132** from **129**. b) Discovery of the DMP-mediated cascade of **135**. Top: excess DMP at ambient temperature oxidizes the primary alcohol but fails to produce any γ -hydroxylactol; middle: DMP at 80 °C gives encouraging signs with hydroxylactol **132**; bottom: DMP at 80 °C produces γ -hydroxylactol **136** in satisfactory yield from protected lactol **135**.

In anticipation of the upcoming Arndt–Eistert homologation^[29] (the last important operation of projected synthesis) we had been simultaneously conducting model studies with relevant systems to streamline the process. We soon realized that the toolbox of known carboxyl-activation methods which were needed in order to access a diazoketone from a carboxylic acid was inadequate for addressing the sterically demanding CP-based systems (Scheme 22 a). Faced with this challenge we resorted to what synthetic chemists have learned they must do in such circumstances: invent a new and improved method. We rationalized that a relatively small reagent such as a sulfene (generated in situ from MsCl and Et₃N) would not only be able to penetrate the steric shield of the CP system and engage the carboxylic acid as an acyl sulfonate, but also that the latter moiety would be at least as



Scheme 22. a) Difficulties in producing the required sterically hindered diazoketone for Arndt–Eistert homologation lead to the consideration of mixed acyl mesylates as candidates for carboxyl activation. b) Demonstration of the principle of the activation of hindered carboxylic acids by mesylation and synthesis of sterically congested diazoketones from mixed acyl mesylates. c) Synthesis of “Christmas compound” **141** and the elusive carboxylic acid **142**. d) Proposed mechanism (most likely radical) for the rapid decomposition of the γ -hydroxylactone-carboxylic acid **142**.

reactive as the corresponding acyl chloride. Thus, on December 14, 1998, the model compound **137** (Scheme 22b) was exposed to $\text{MsCl}/\text{Et}_3\text{N}$ at 0°C for 10 minutes at which point an ethereal solution of CH_2N_2 was added and the resulting mixture was stirred for another 20 minutes at that temperature. To our delight, a clean conversion of **137** into the corresponding diazoketone (**138**, Scheme 22b) was obtained in 95% yield. With an expedient solution to the problem at hand and eager to engage the “Minotaur” in a final battle, we postponed exploration of the scope and generality of this new method until the synthesis was complete (see Section 11.1).

Returning to the total synthesis, the oxidation of γ -hydroxylactone **136** proceeded in the presence of TEMPO/ $\text{PhI}(\text{OAc})_2$ ^[30] to furnish the γ -hydroxylactone **139** in good yield (Scheme 22c). Acid-induced removal of both silicon protecting groups from **139**, followed by dehydration under the Pfizer conditions^[4] led to the formation of the pyran-alcohol system **140**. The excitement was now hard to contain!

With full confidence that we would soon be finished with the CP molecules (**1** and **2**) at our feet, our plan was to strive for **1** first and then investigate proper protecting groups to access **2**. In fact, we were so sure of our imminent success that we drafted a communication detailing the total synthesis; it

was only missing the yield of the last two steps. The “Minotaur” was finally engaged (Figure 5)! Unfortunately, that was not to be, at least not yet! What we expected to be a nice Christmas present turned out to be the agony of defeat. Once again the “Minotaur” proved defiant. Thus, alcohol **140** was converted into aldehyde **141**, the so-called “Christmas compound” (Scheme 22c). This aldehyde seemed to be endowed with a peculiar instability toward oxidation conditions aimed at its conversion into the coveted carboxylic acid (**142**). Even the mildest of methods, such as the NaClO_2 -based procedure, proved futile and on Christmas eve, 1998, all we had in our hands was an NMR spectrum of what appeared to be a mixture of at least 30 compounds resulting from extensive decomposition. My (K.C.N.) first reaction was to attribute this failure to the “inadequate” experimental skills of my co-workers; after all, I said, “This is a textbook example of the easiest transformations in organic chemistry!” However, despite repeated attempts, including the use of alternative oxidants and trials to trap the carboxylic acid as the methyl ester, we were consistently unsuccessful. I was wrong and I apologized profusely to my very capable co-workers! A possible explanation for this catastrophe is shown in Scheme 22d. An intramolecular hydrogen bond could activate

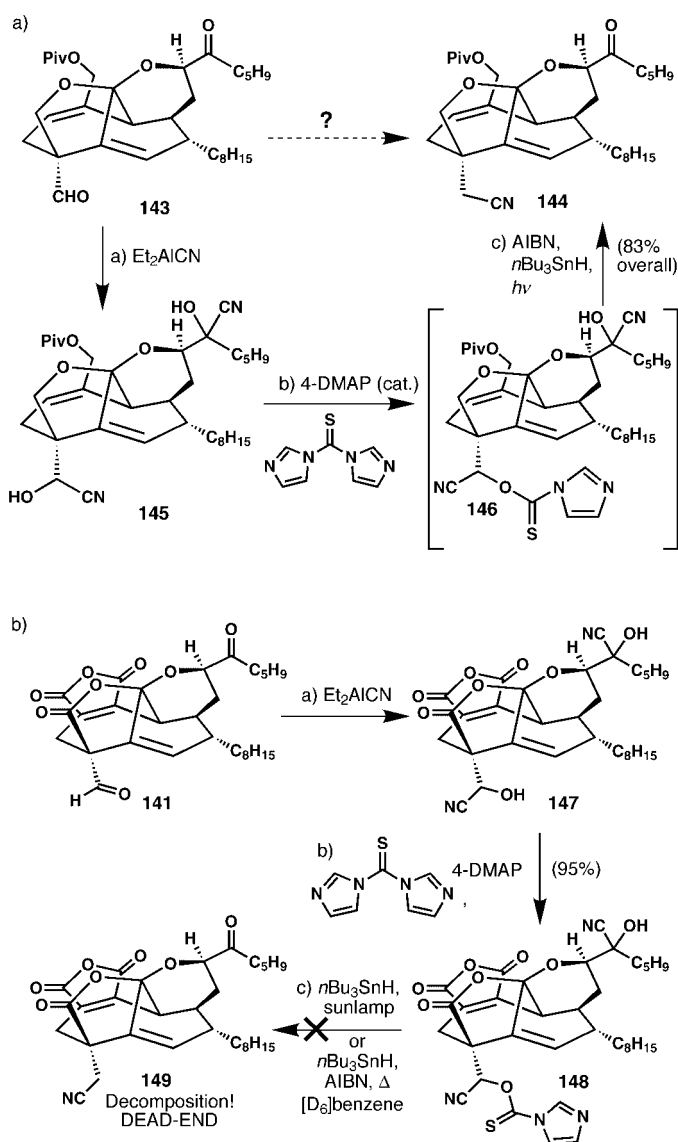


Figure 5. “Christmas compound” **141**. A final blow at the “Minotaur” misses its mark.

both functional groups involved and lead to a nucleophilic attack or decarboxylation.

Convinced of our inability to secure the desired carboxylic acid **142** by direct oxidation of the aldehyde **141** or through other conventional and disadvantage-laden sequences, we quickly formulated an alternative strategy which required a new method for its implementation. Since aldehyde **141** was relatively stable, why not attempt to homologate it without ever going through the intermediate carboxylic acid, which, after all, was at the root of the problem. A mild method for deoxygenating a cyanohydrin would be sufficient to test this hypothesis and so a model study (Scheme 23a) was designed for this purpose.

The idea worked beyond our wildest imagination in that not only the cyanohydrin formation/deoxygenation sequence proceeded in excellent overall yield, but the initially interfering ketone functionality was regenerated smoothly during the radical-induced deoxygenation step. Armed with this key information, we rushed to apply the method to the real system, aldehyde **141**, only to be reminded of the lesson that many had learned before us: “model is model, real is real.” As shown in Scheme 23b, although the first two steps of the newly developed sequence worked beautifully (**141** → **147** → **148**), the method failed miserably in its final stage and left us confronted with yet another dead end. By then we knew that the maleic anhydride moiety was intolerant of radical chemistry and so we learned to stay away from it in the future. Nevertheless, the experience was rewarding in that it led us to develop a rather general method for the mild homologation of hindered aldehydes in the presence of ketones, as well as providing us with some interesting insights into the reactivity of cyanohydrins and the mechanisms involved. We will return to a description of this methodology

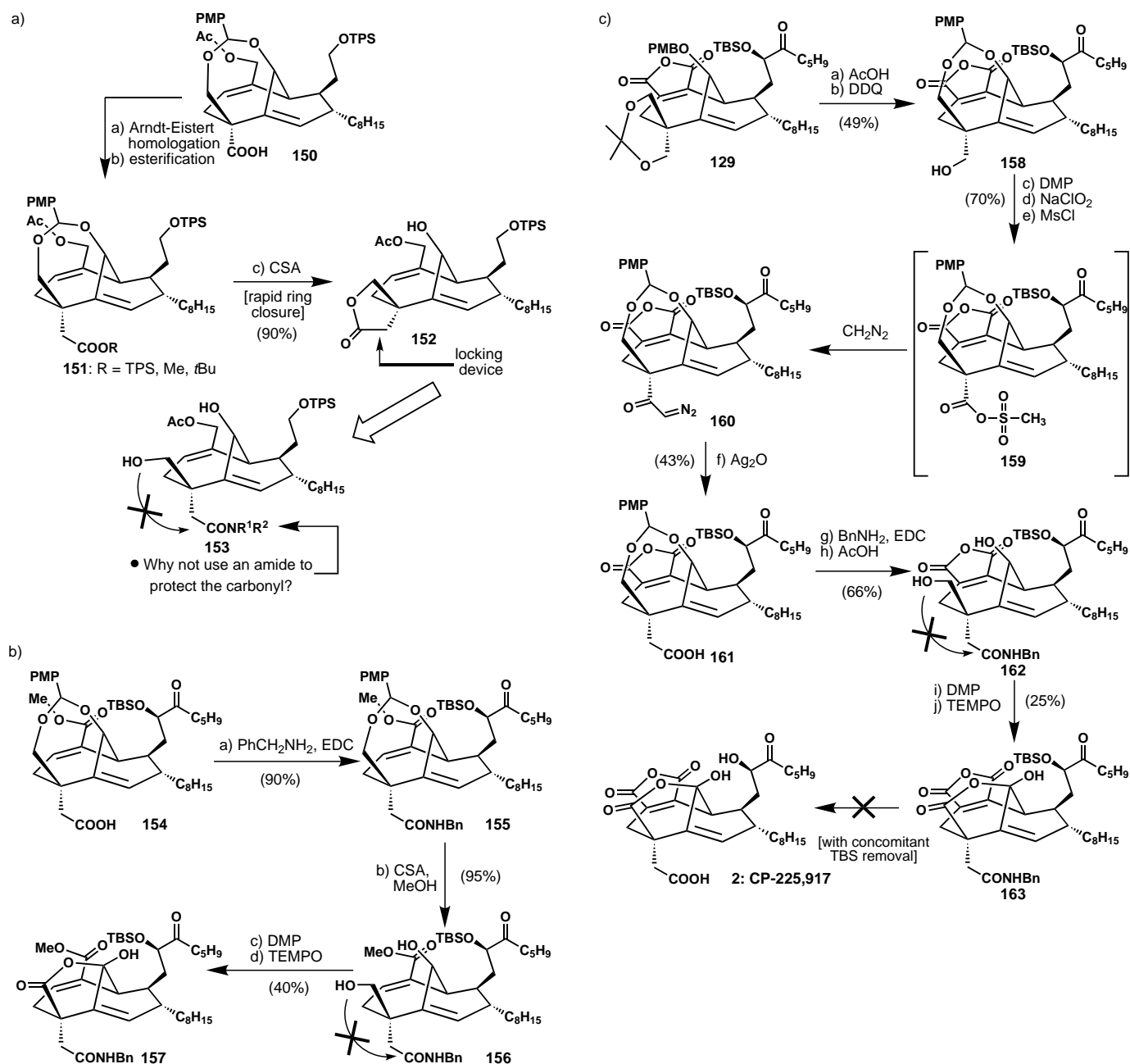


Scheme 23. a) A successful model study for the one-carbon homologation of aldehydes to nitriles brings new hope for the completion of the CP-molecule total synthesis. b) Failure in the real system: the maleic anhydride moiety proves too sensitive for radical chemistry involved in deoxygenation.

later in this article. After a few days of frustrating, last-resort experiments with aldehyde **143**, we decided that it was time for a drastically new approach which we would base on the latest reconnaissance information available.

8. The Second Assault at the CP Molecules

With the latest string of failures, most of the CP-team members were rather depressed; some were even convinced that the “beachhead” compound **129** would never lead to the CP molecules. These feelings persisted only for a few days at the beginning of 1999 while we were scrutinizing our problems and contemplating new plans. Upon realizing that homologation would have to precede lactol construction, we proceeded to investigate several esters of the general type **151** (Scheme 24a) which were easily derived from compound



Scheme 24. a) Dead-end locked structures led us to the amide strategy. b) This strategy allowed the 1,4-diol system to be kept open. c) One-step away from the CP molecules: failure to hydrolyze the benzyl amide **163**.

150 by Arndt–Eistert homologation and esterification. The idea was to see whether we could liberate the 1,4-diol system of **151** and construct from it the γ -hydroxylactone. However, as soon as the benzylidene group was removed from such esters, the structure would rapidly collapse into the γ -lactone system **152**. This result was again a dead-end, another “check” by the molecule, for no matter what we tried, this locking device would not open! If a way existed to shield the homologated carboxylic acid function from attack by the nearby primary alcohol, it would certainly solve this problem. Several options were evaluated, including complete reduction of the carboxylic acid group to the corresponding alcohol followed by protection, as well as a number of other homologation protocols. All of these options either added

significantly to the length of the synthesis or were plagued by low yields relative to the venerable Arndt–Eistert homologation sequence. In the midst of this chaos when everyone was following their own intuition, I (K.C.N.) approached Phil and asked what strategy he was following. “I have an idea,” he said. “It’s simple.” What he had in mind was the use of an amide as a protecting group for the carboxylic acid—a much less reactive functionality than an ester and, therefore, one that would, hopefully, restrain the structure of the 1,4-diol into an open form.

Since there was precedent for mild activation and cleavage of benzyl amides^[31] we targeted first the 1,4-diol system **156**. Within 24 hours of its conception, Phil and Zhong demonstrated the viability of this strategy with the synthesis, on

February 8, 1999, of model benzyl amide γ -hydroxylactone **157** as shown in Scheme 24b. With this success, a great new hope was given to the team and the project had a new lease on life. Efforts began in earnest to construct the real system **163** (Scheme 24c). Within a week the team had reached this new “beachhead” starting from advanced key intermediate **129** following the route shown in Scheme 24c. With 30 mg of benzylamide **162**, we felt confident that we would soon arrive at the CP molecules. Our excitement was heightened even further when we successfully arrived at compound **163** and secured conditions to remove the benzylamide group from appropriate CP model systems. Only a single step was now separating us from the Minotaur. However, once again he deftly evaded our sword, cleverly maneuvering his way out of its path (Figure 6). The fragility of the intact CP molecule was simply too much for any hydrolysis conditions to succeed and we were left in “check” once again, with only a protected form of CP-225,917 (**2**). Further strategies and tactics were needed to continue the campaign.



Figure 6. Final dashes at the Minotaur (benzylamide **162** and heterocycle **208**) are thwarted by unanticipated maneuvers by the monster.

A thorough literature search led to a number of other possible amides^[32–35] as alternatives for what we had in mind (Scheme 25a). We first investigated the aniline amide (anilide) since the conditions reported by Martin and Franz^[32] for its cleavage were remarkably mild. As shown in Scheme 25b, we arrived at the anilide-diol **165** in short order, and upon treatment of the latter compound with DMP we isolated a compound with polarity (TLC) and HRMS data that were consistent with those expected for the γ -hydroxylactone **168** (oxidation of **167**, Scheme 25b)! Analysis of the ^1H NMR spectrum of this product, however, raised serious doubts, since not only was the bridgehead olefinic proton

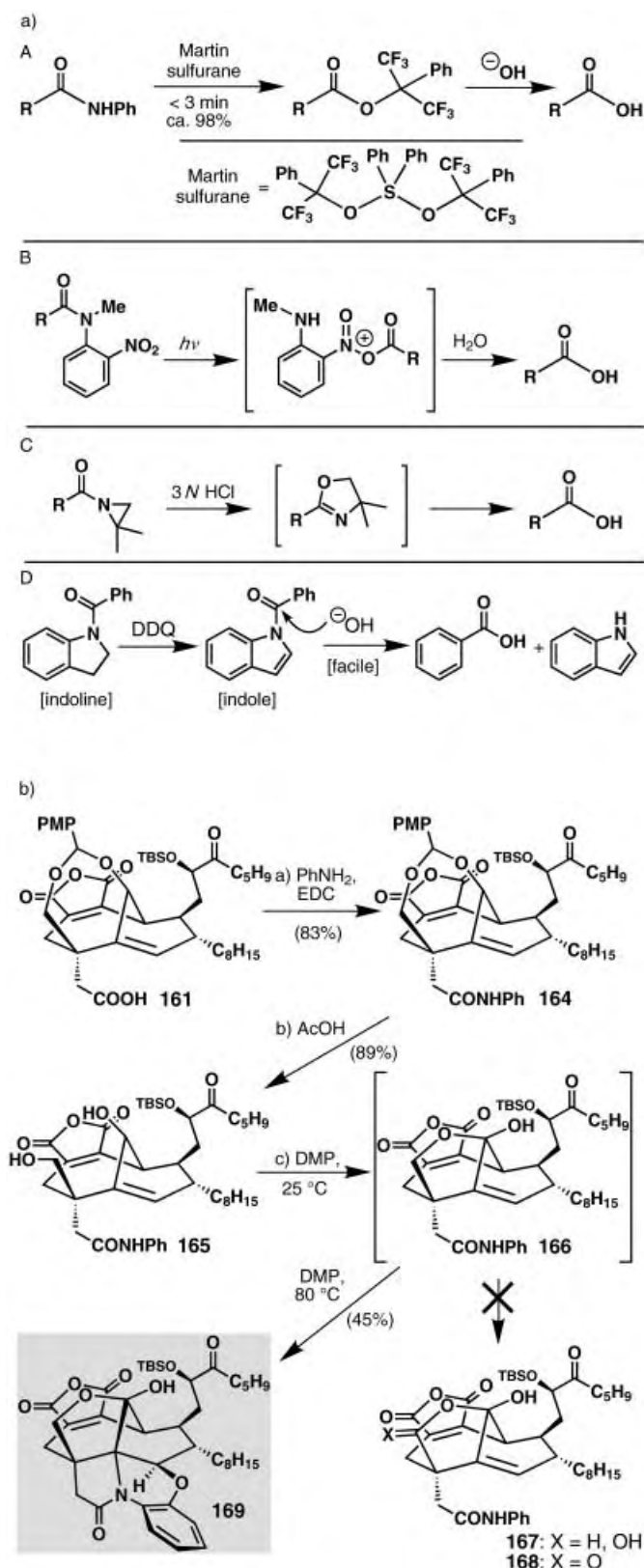
missing but there seemed to be one extra proton. After scaling up the reaction, we were able to obtain clean ^1H and ^{13}C NMR spectra which definitely led us to conclude that we did not have anything resembling lactone **168**. The Minotaur remained unscathed once again (Figure 6)! What, however, was the structure of this strange compound? After several 2D NMR experiments and careful mechanistic reasoning we finally secured the structure of the “mystery compound” as the remarkable polycycle **169**. Was this the Minotaur’s hidden treasure, or simply another road block? Either way, it did not help us at the time and we decided to put this strange discovery on the shelf (but not under the carpet!) until after the total synthesis was complete. Even more disheartening were the failures shown in Scheme 25c, which cast further doubt on the wisdom of the amide strategy and its potential for success.

Early one morning, after another failure, I (K.C.N.) called Phil to my office, sat him down and said, “This project is always in shambles, and it is very painful to everyone. I think we should cut our losses and just forget about the CP molecules. I would not think any less of you if you stop now.” Phil’s eyes widened and he immediately declared, “Impossible, I will never stop until CP has fallen and I know Zhong feels the same way. This is what a PhD is all about, isn’t it?” “OK, good, you passed the test. Now you can go back to work...”

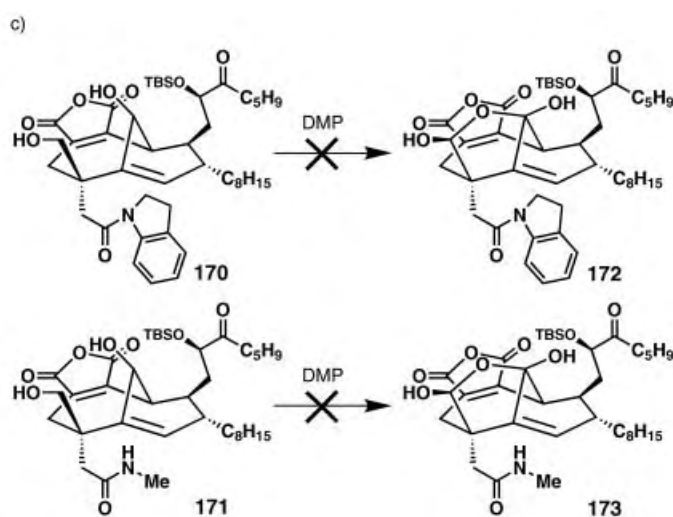
9. Third and Final Assault on the CP Molecules

It was now the beginning of March, 1999, and we were desperately searching for a new strategy. Before another retrosynthetic analysis could be drafted, however, we needed answers to a number of strategic questions as shown in Scheme 26. Since we realized that the DMP cascade to construct the γ -hydroxylactone moiety would have to precede homologation of the carboxylic acid side chain, our concerns now focused on suitable protecting groups for lactol **136** (Scheme 26). After experimenting with a variety of different protecting groups for about a week we realized that it was not such a straightforward proposition, and we were sent back to the drawing board for yet another re-evaluation by the very failures of such strategies (some explorations in that direction that ended in dead-ends are shown in Scheme 26). In the meantime, we dispatched a communication to *Organic Letters* detailing our explorations in the CP project leading to an advanced model compound, but we did not mention the revised protocol for γ -hydroxylactone construction involving DMP at high temperatures.^[27] At this juncture, we had no idea that we would confront the Minotaur and conquer the CP labyrinth in only a couple of weeks!

The key insight which led us out of the maze was hidden within the structure of one of the CP molecules itself. Suddenly we came to realize that, perhaps, nature herself had been giving us a clue on how to answer our protecting-group problems all along! Throughout the campaign we had observed that CP structures in the open lactol form (CP-225,917, **2**) were less stable on silica gel and to most reaction conditions than the corresponding closed pyran derivatives (CP-263,114, **1**). Therefore, we targeted the easily accessible and less-fragile “closed” lactol **177** for synthesis (Scheme 26).



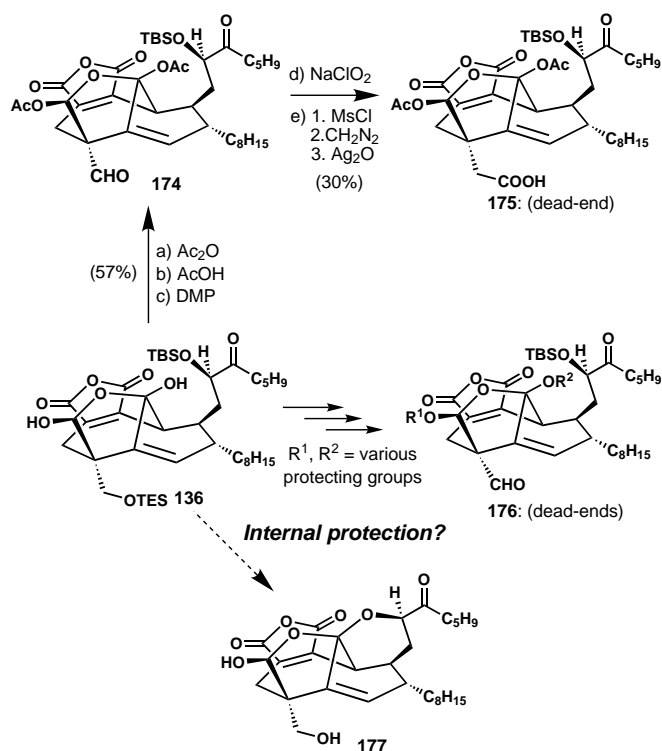
Scheme 25. a) Alternative amide-based protection strategies which were evaluated: A) use of Martin sulfuran for the conversion of amides into esters and carboxylic acids;^[32] B) a photolabile amide group;^[33] C) the Meyer's aziridine ring-expansion method;^[34] and D) Barton's "latent" heteroaromaticity principle for the protection/deprotection of carboxylic acids.^[35] b) Another roadblock or a hidden treasure? Serendipitous isolation of the unusual polycycle **169**. c) Additional failures of the amide strategy led to re-evaluation of the plans.



The clear risk associated with this strategy was that we would, most likely, only be able to access CP-263,114 (**1**), since the conversion of **1** into **2** was not known at that time.

Nevertheless, we proceeded forward thinking that, after all, accessing one of the CP molecules would be better than none at all! The final retrosynthesis was drafted as shown in Scheme 27 a. Thus, based on all our intelligence gathering we projected CP-263,114 (**1**) arising from indoline derivative **178** (see Scheme 25 a D for the rationale), whose origins were traced back to compounds **177** and **136**. We began, starting in late March 1999, working at a furious pace towards the implementation of the new plan. During this period, I (K.C.N.) would often find Zhong and Phil either fast asleep in the mornings or working in eight-hour shifts exchanging material back and forth. As one rested, the other worked; my contribution was to bring them occasional sustenance in the form of sandwiches in the lab! The drive to the indoline amide **185** is depicted in Scheme 27 b. A key discovery occurred when we submitted lactol **177** to a DMP oxidation in dichloromethane, and upon workup we isolated the desired product **179** along with a substantial amount of the ill-fated "Christmas compound" **141**. Although we clearly had no use for the latter compound (**141**) its isolation indicated to us that the hydroxy compound **179** was behaving as a normal lactol, and thus we would not have to employ TEMPO (see Section 6) in the late stage of the synthesis to convert it into the desired lactone. The latter oxidant, although mild, is not as easy to handle, while DMP and its by-products are rather conveniently removed upon completion of the reaction. Capitalizing on our previous observations with DMP, we then proceeded to employ benzene as solvent instead of dichloromethane in an effort to "tame" its reactivity and permit the isolation of lactol **179** as the major product and thus avoid the extraneous, albeit informative, lactone **141**.

In the days approaching the synthesis of the indoline **185** we were all camped out in the laboratory with great expectations. We eagerly anticipated the synthesis of this compound (**185**) since we had prepared an authentic sample from natural CP-263,114 (**1**) (Scheme 27 c). Identical samples would give us the



Scheme 26. The evolution of the internal protection strategy.

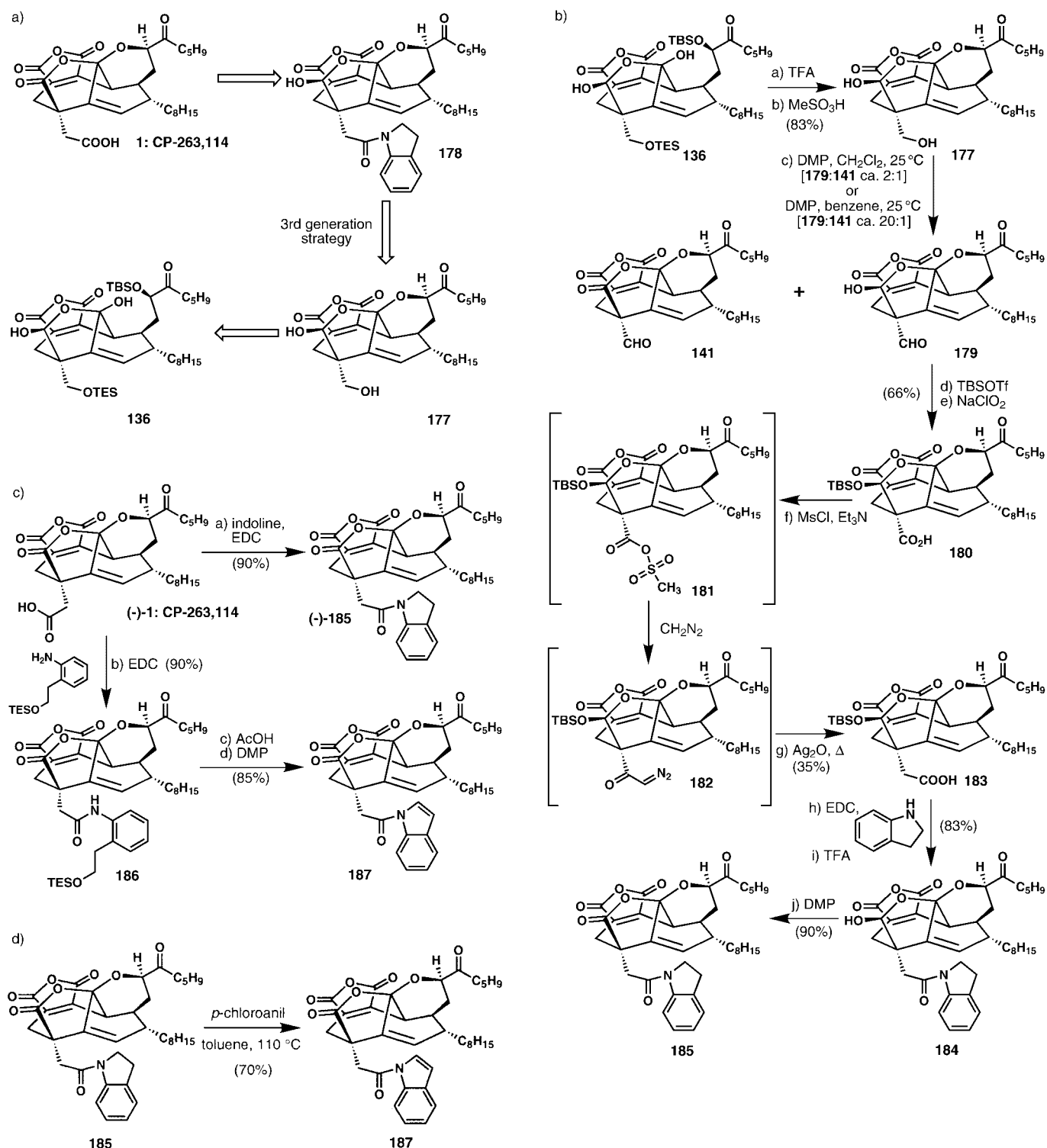
first indication that the total synthesis was in sight, and that the Pfizer structural assignment,^[4] based on NMR spectroscopy alone, was correct. At 8:30 pm on April 7, 1999, the CP team dragged me (K.C.N.) down to the first floor of the Beckman building in front of the NMR instrument. "You have to see this," said Phil with a big smile on his face. "This had better be good," I said as we were riding the elevator en route to the NMR room. On the screen were two spectra side by side; the upper spectrum was that of the naturally derived while the lower spectrum reflected the signals of a 1:1 mixture of synthetic indoline lactol **184** and indoline lactone **185**. Although that final reaction was performed only on a 100 μ g scale and the NMR spectrum showed a 1:1 mixture of starting material and product, it was clear from the spectra and from TLC and HPLC analysis that synthetic **185** was identical to naturally derived **185**! The Minotaur was, this time, not only sighted in the still misty horizon (see Figure 3) but, as it turned out, fatally wounded (see bleeding Minotaur, Figure 7).

But there was still much more work to be completed before we could declare victory. We immediately began a barrage of model studies focusing on the key oxidative conversion of the indoline to its indole counterpart. Simultaneously, we prepared the authentic indole (**187**) from the natural product (CP-263,114, **1**) for comparison purposes. After about 30 hours of continuous searching, we identified *p*-chloroanil as the most mild and likely candidate for the key conversion of **185** into **187**. With more of the synthetic indoline **185** in hand, we set up the reaction in refluxing toluene using excess *p*-chloroanil and to our delight we obtained the coveted synthetic indole **187** (Scheme 27d) which was identical to that prepared from the natural product (Scheme 27c).

Figure 7. Synthetic indoline amide **185** matches a naturally derived sample (**185**). The deadly wounded Minotaur is falling!^[71]

It was April 10, 1999, and we were poised to complete the total synthesis. Only one step remained: hydrolysis of the indole moiety. We reasoned that LiOH would be the most appropriate reagent to accomplish this transformation by virtue of its mild nature and unique solubility and nucleophilicity. Before attempting the reaction with the precious sample of synthetic indole **187**, we decided to conduct a number of model studies. These rather simple experiments, whose primary aim was to probe the stability of the maleic anhydride and hydroxy ketone moieties, turned out to be surprisingly informative. There were several issues which needed to be addressed concerning the treatment of these compounds with base, namely: 1) to what extent, if any, would epimerization of the carefully installed C-7 center take place?; 2) would destructive enolization of the α -hydroxy ketone occur to give a mixture of regioisomeric hydroxy ketones?; and 3) how would the fragile maleic anhydride moiety hold up to the basic conditions? To our dismay we found that treatment of the advanced key intermediate **129** with LiOH (10 equiv) in THF/water followed by workup with NaH₂PO₄ led to a 3:2 mixture of C-7 epimers (**129**:**188**) as observed by ¹H NMR spectroscopy after only 1 h of exposure (Scheme 28). Halting the reaction after 30 minutes afforded a 4:1 mixture of epimers, the major of which was still **129**. As troubling as this result was, it was likely to get worse we thought, for in the real system we would also be faced with the potentially destructive isomerization of the α -hydroxy ketone system. With these issues in mind, we submitted the hydroxy ketone **189** to the same conditions (LiOH, 10 equiv, THF/water; then workup with NaH₂PO₄), and much to our delight found that the α -hydroxy ketone system was still intact with almost no epimerization (>50:1 **189**:**190** by ¹H NMR spectroscopy) after 1 h. After 3 h the ratio was still a remarkable 10:1 in favor of **189**.

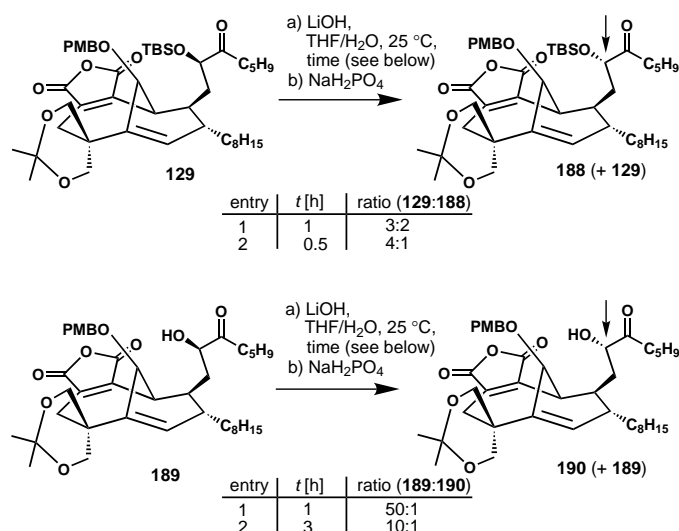
Based on these reassuring model studies, we next proceeded to test the robustness of CP-263,114 (**1**) itself under the



Scheme 27. a) Third generation retrosynthetic analysis of the CP molecules (**1** and **2**). b) Synthesis of indoline amide **185**. c) Synthesis of **185** and **187** from the natural product **1**. d) Synthesis of **187** from **185** through the action of *p*-chloroanil.

basic conditions of the projected final hydrolysis step. Although we were optimistic about the result of this experiment, we were not fully prepared for its outcome. The starting CP molecule (**1**) did not survive the reaction conditions at all, being rapidly transformed to its sister CP molecule (**2**)! Pleasingly the C-7 stereocenter of the CP structure remained intact. Furthermore, since a method existed for the conversion of **2** into **1**, we immediately realized that this

time, perhaps, we had the “Gods” on our side (just as Theseus had in his battle against the Minotaur) in our final assault against the dreaded Minotaur. Before we tell, however, the final tale, we must draw attention to the fascinating mechanistic underpinnings of this interesting base-induced transformation of CP-263,114 (**1**) to CP-225,917 (**2**) as shown in Scheme 29a. This operation commencing with **1** represents a unique cascade reaction sequence since it accomplishes



Scheme 28. Model studies before the final LiOH hydrolysis of the indole derivative to CP-225,917 (**2**).

temporary masking of the maleic anhydride (as its dianion), basic opening of the γ -hydroxylactone, deprotonation of the C-29 carboxylic acid, and reconstitution of **2** upon acidic quench.

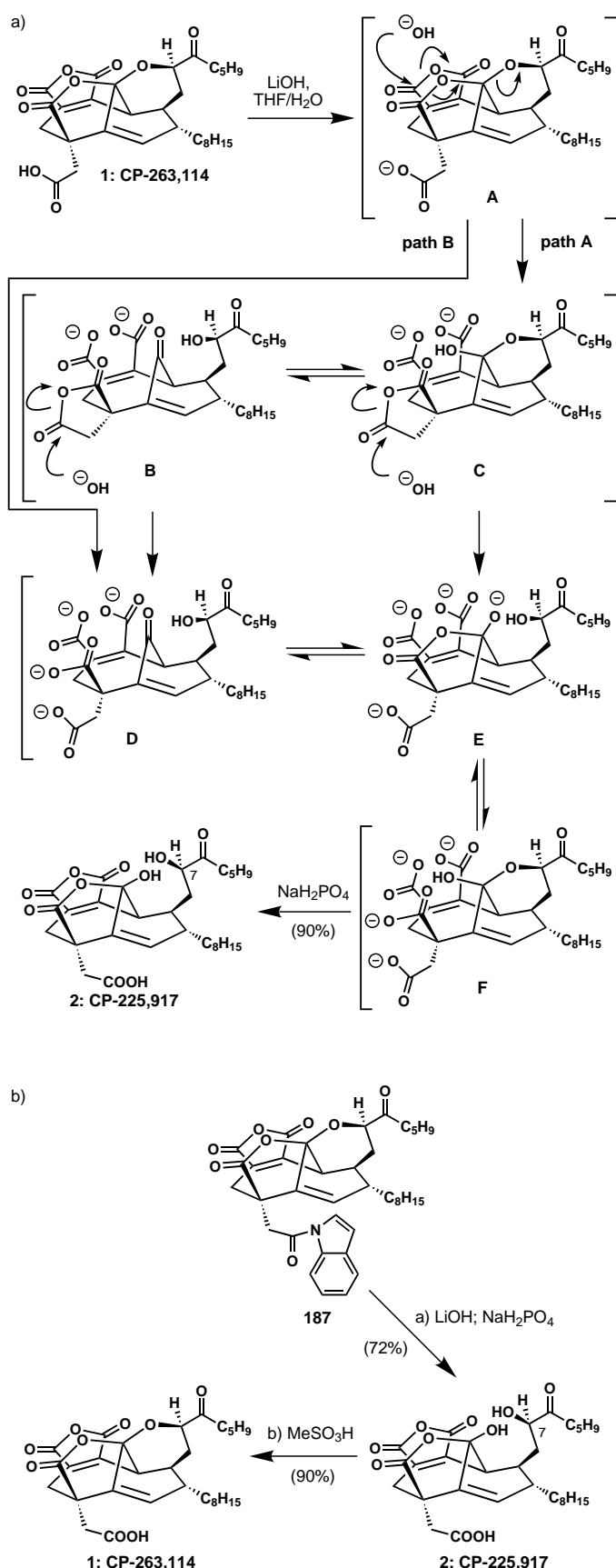
Having practiced the final act, with all the necessary preparations complete, we sharpened our sword and engaged with the Minotaur for the last time. The final reaction was set up at 1:00 a.m. on April 12, 1999. A few hours later it was done (Scheme 29b)! I (K.C.N.) was to learn of the athlos upon my arrival in the lab at 8:00 a.m. that day. Needless to say, pure adrenaline kept Phil and Zhong awake past the successful isolation of CP-225,917 (**2**) and its subsequent conversion into CP-263,114 (**1**).

Within 24 hours of that final blow, two communications were dispatched to *Angewandte Chemie*.^[5a,b] The triumphant team is shown in Figure 8b celebrating their accomplishment with smiles and grins.

Frequently in the endeavors of total synthesis, arrival at the target molecule marks the final act, but not in this case, for it was clear that we had struck gold on several occasions during our journey to the center of the labyrinth. It was time to consolidate the gains made during the campaign and to fully exploit the many inventions and discoveries found during this campaign. In the next sections we will discuss some of these exploits and new synthetic technologies, beginning with the establishment of the absolute configuration of the CP molecules by asymmetric synthesis.

10. Asymmetric Synthesis of CP Molecules

Attempts by ourselves and others to crystallize naturally derived heavy-atom derivatives of the CP molecules to decipher their absolute configuration by X-ray crystallographic analysis had been thwarted by the inability to grow suitably ordered crystals. Therefore, we turned our attention



Scheme 29. a) Conversion of CP-263,114 (**1**) into CP-225,917 (**2**). The remarkable LiOH cascade hydrolysis and postulated mechanistic underpinnings. b) April 12, 1999: The total synthesis of the CP molecules (**1** and **2**) is complete.



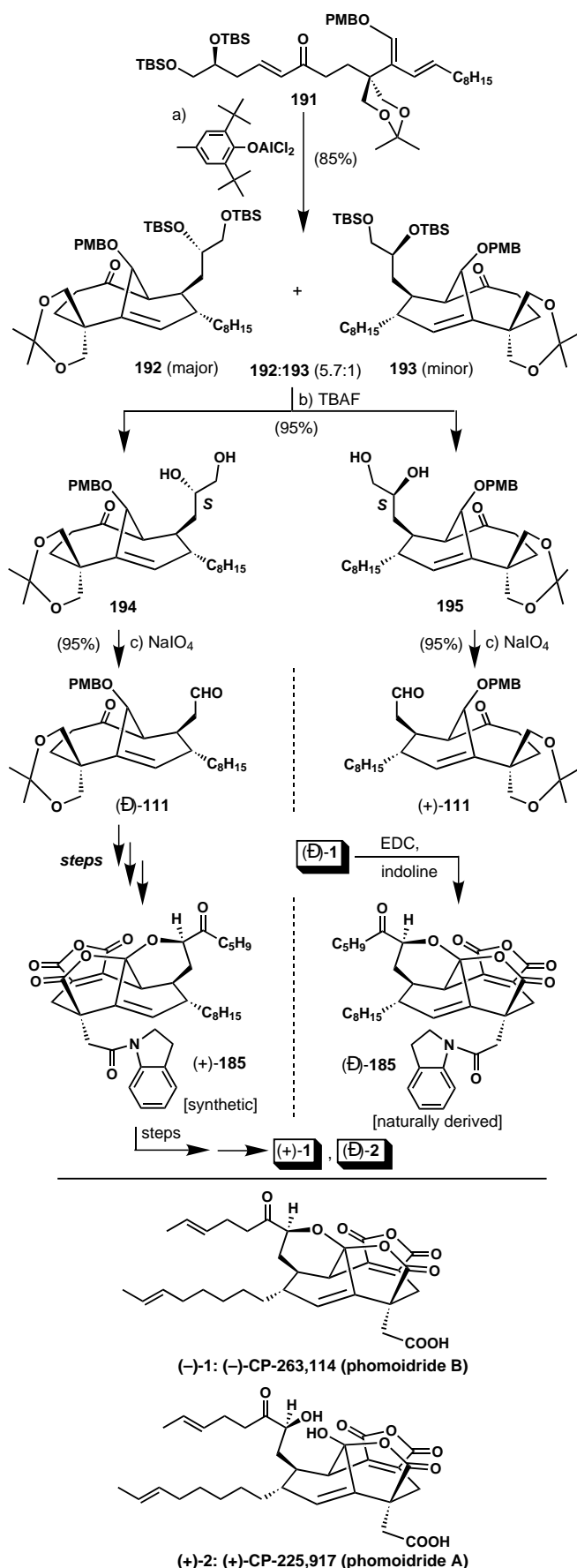
Figure 8. Top: left: In front of the “CP battlefield”, K. C. Nicolaou (left) and Phil S. Baran (right); right: Conquest outside the lab, Phil S. Baran (left) and Yong-Li Zhong (right). Bottom: The triumphant “CP team” shortly after the completion of the feat (from left to right): Ha-Soon Choi, Won-Hyung Yoon, Kin Chiu Fong, Yong-Li Zhong, Phil S. Baran, and Yun He. K. C. Nicolaou is seated.

to determining the absolute configuration of these compounds through chemical synthesis. Our asymmetric total synthesis of the CP molecules, which served to establish their absolute configuration, is summarized in Scheme 30.^[5c] The hallmark of this strategy is the combined use of substrate- and reagent-based control of stereoselectivity.

Shortly after this disclosure, three additional syntheses of the CP molecules appeared from the Shair,^[36] Fukuyama,^[37] and Danishefsky^[28] groups. All three of these syntheses were elegantly conceived and masterfully executed. The syntheses by the groups of Shair^[36] and Fukuyama^[37] also confirmed our absolute configuration assignments.

11. Mining the Gold: Discovery and Invention of New Synthetic Technologies

After traversing the CP-synthetic labyrinth and having marked the points of interest, we set forth to investigate the scope, generality, and mechanistic aspects of the various designed and discovered reactions. These explorations snowballed, for as we garnered mechanistic insights we were able to move to the next step by designing further strategies and

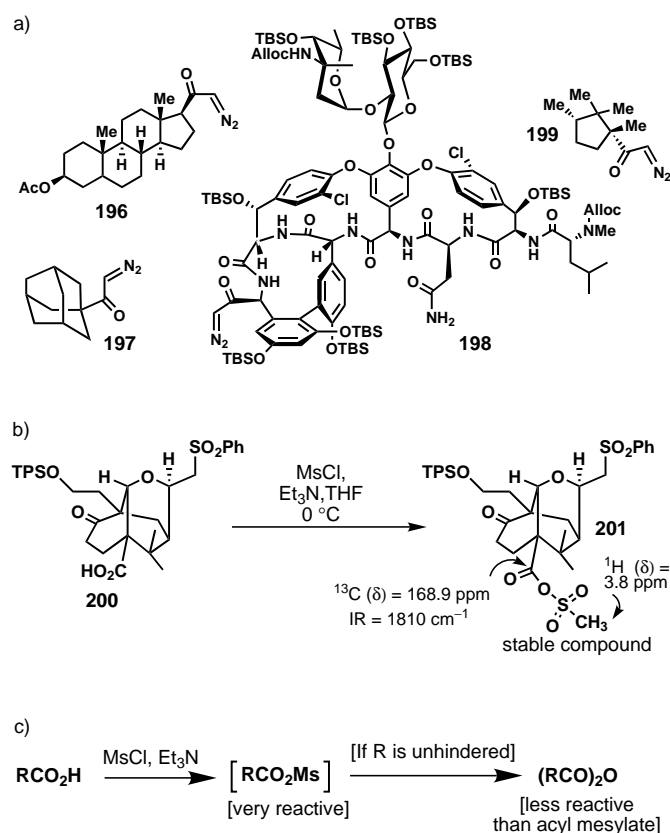


Scheme 30. Asymmetric total synthesis of the CP molecules (top) and assignment of their absolute configuration (bottom).

processes and by calling upon old reagents to perform new reactions. In the following sections we discuss, in approximate chronological order, the synthetic technologies developed during these investigations.

11.1. Acyl Mesylates and the Synthesis of Sterically Hindered Diazoketones

The use of acyl mesylates as novel acyl chloride surrogates for highly hindered carboxylic acids as mentioned above (Scheme 22b) was aptly demonstrated by the synthesis of a variety of hindered ketones (Scheme 31a) on molecular



Scheme 31. a) Examples of hindered diazoketones prepared by the acyl mesylate technology. b) First isolation and characterization of an acyl mesylate (**201**). c) Carbonyl activation, particularly useful in sterically hindered systems.

scaffolds of numerous types, including steroids (**196**) and the vancomycin family of antibiotics (**198**).^[38] In addition, we were able to isolate the first stable acyl mesylate (**201**), enabling a full elucidation of the physical properties for this chemical entity (Scheme 31b).^[38] These studies also shed light on the unexplored chemistry of these highly reactive species (shown in generalized format in Scheme 31c), indicating the differential products that one can expect based on the nature of the molecule onto which this reactive group is attached.^[38]

11.2. Homologation of Sterically Hindered Aldehydes via Cyanohydrin Formation

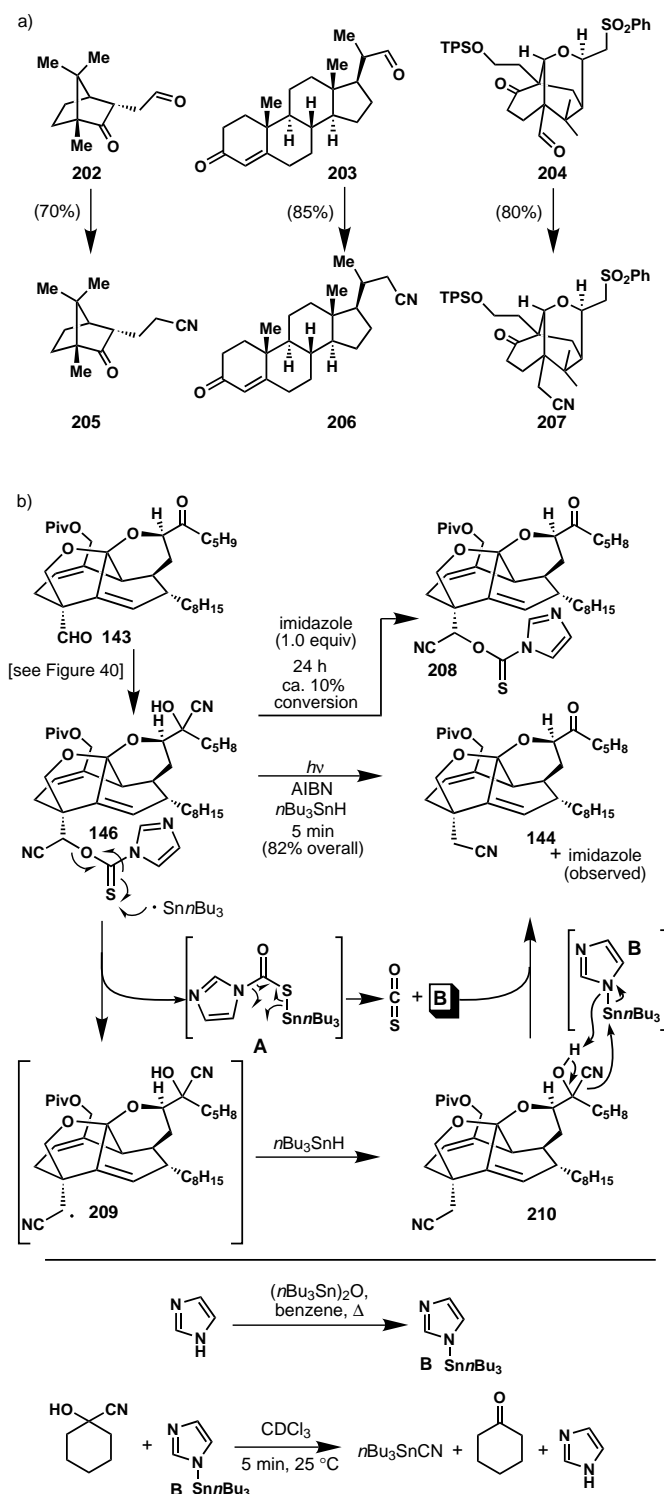
Our struggle to add one carbon to the “Christmas compound” **141**, led to the development of a novel strategy for the homologation of sterically hindered aldehydes even in the presence of ketones and other electrophilic functionalities as mentioned earlier in the context of Scheme 23a. After demonstrating the generality and scope of the process (Scheme 32a for selected examples in substrate classes of historical significance)^[39] we also conducted experiments to confirm the unique mechanism by which it operates (Scheme 32b), providing validation of the specific role played by each reagent in the process, as well as insight into the reactivity of cyanohydrins and their potential use as masking devices for ketones.^[39]

11.3. The DMP- and IBX-Cascade Reactions for the Synthesis of Heterocycles from Anilides, Urethanes and Ureas

The intrigue of the unexpected reaction of DMP with substrate **166** producing the unusual heterocycle **169** (see, Scheme 25b) soon sent us out on an expedition to investigate it further. What was the mechanism of this unprecedented transformation, its prerequisites, scope and generality? Having suspected that the essential requirement for the substrate in this reaction were the anilide and olefinic functionalities, we focused on such substrates. Our first explorations were disappointing and gave only very low yields of the desired products (Scheme 33a). We reasoned that embedding the olefin portion in a ring system might boost the efficiency of the reaction due to reduced conformational freedom and increased electron density. Indeed, this modification proved to be crucial for accessing complex polycyclic systems in synthetically useful yields (Scheme 33b).

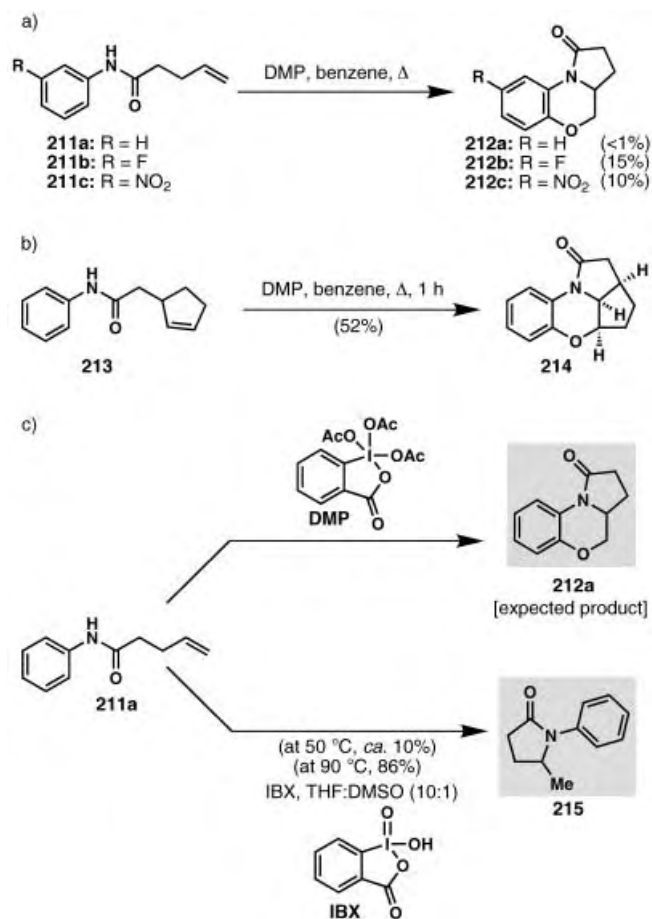
Simultaneously we investigated how the precursor to DMP, IBX (2-iodoxybenzoic acid), might react with such anilides. Perhaps these examples would furnish the same polycycles more efficiently. THF:DMSO (10:1), rather than benzene, was employed as a solvent due to solubility considerations and by analogy to alcohol oxidations performed with IBX. When we conducted the reaction at 50°C with the simple substrate **211a**, instead of forming the polycycle **212a**, we isolated the γ -lactam **215** in 10% yield (Scheme 33c). Upon increasing the reaction temperature to 90°C , remarkably efficient conversion to **215** was observed. In fact, this result was initially received with considerable skepticism by one us (KCN). Could it be that inadequate experimental technique led to this bizarre finding or had we discovered another unique reaction? And how is it that no one had ever reported such reactions with iodine(v)-based reagents or hypervalent iodine compounds in general? It was time to consider this issue from a more global perspective.

Scheme 34a depicts a sampling of iodine(III) and (v)-based reagents. While the chemistry of iodine(III)-based reagents has been extensively explored, iodine (v)-based reagents have been mainly relegated to the realm of alcohol oxidation and a



Scheme 32. a) Examples of selective homologation of ketoaldehydes using the cyanohydrin technology. b) Mechanistic aspects of the cyanohydrin-based homologation of sterically hindered aldehydes in the presence of ketones.

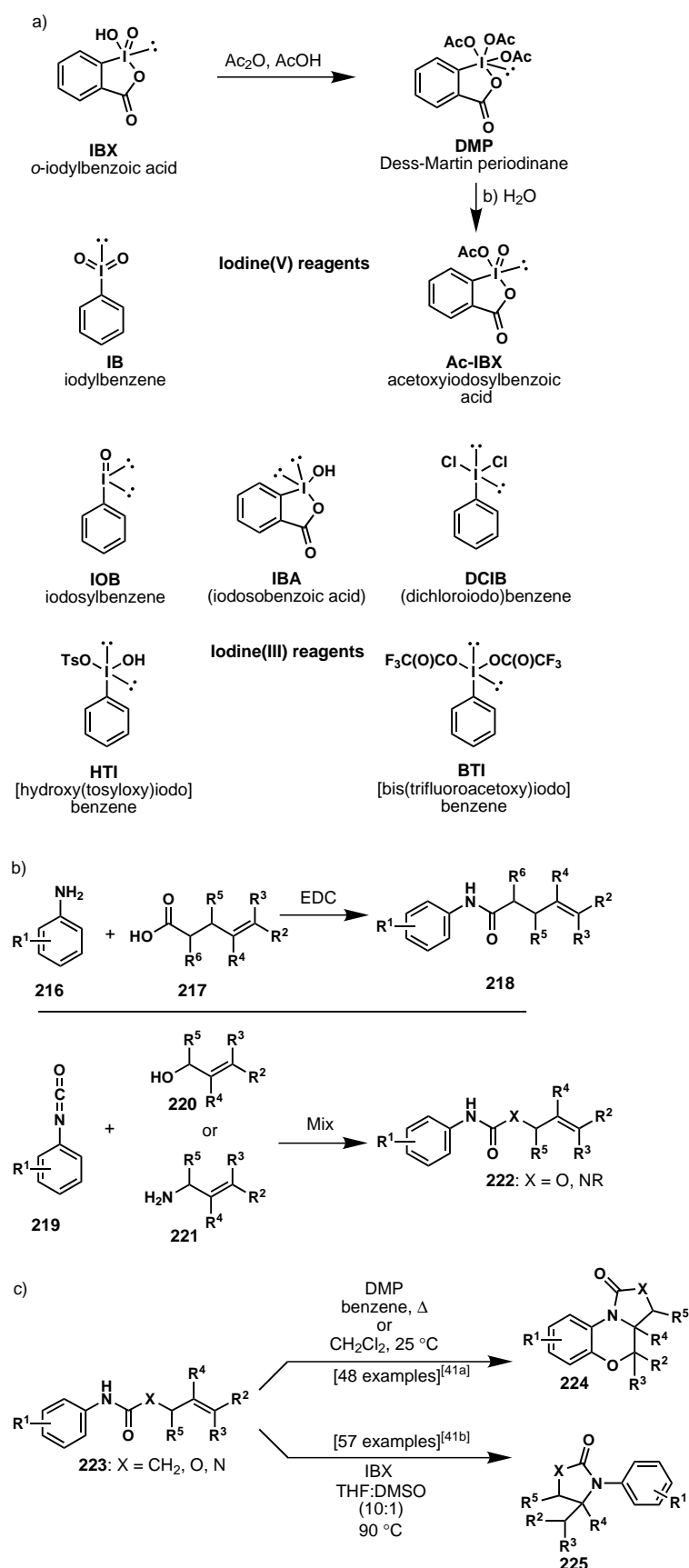
number of closely related processes. For instance, in Varvoglis' 223 page treatise^[40] on hypervalent iodine reagents, only 10 pages are dedicated to the reactions of iodine(v)-based reagents (5 pages deal with alcohol oxidations and 5 pages deal with the use of these reagents as co-oxidants in selenium- and vanadium-catalyzed reactions); the remainder



Scheme 33. a) First attempts to construct polycycles using DMP prove disappointing. b) Using more substituted olefins in the DMP cascade led to synthetically useful yields of heterocycles. c) Discovery of the IBX-cyclization reaction.

focuses on the more popular iodine(III)-manifold. Therefore, we proceeded to rapidly explore the scope and generality of these transformations to determine whether they were simply anomalies or more desirably, useful synthetic transformations.

Since the starting materials for DMP- and IBX-cyclizations were the same, we were able to evaluate the utility of both reactions in parallel. The library of anilides to be used as substrates was rapidly expanded by utilizing a series of simple building blocks as shown in Scheme 34b. We quickly and firmly established the structural parameters required for the reactions to proceed, namely the presence of an anilide moiety and an olefinic system in close proximity. We suspected, however, that the reaction could be extended into the realm of olefinic urethanes and ureas. Indeed, both the DMP- and IBX-cyclizations could be expanded to furnish diverse heterocycles using urethanes and ureas as starting materials (Scheme 34b and c). It took a few days before we realized the potential of the gold mine that we had unearthed!^[41] Because of the excitement which was generated from these discoveries our initial forays into this new territory were not entirely focused and we often went back and forth between studying new reactions of DMP and IBX, always having as our guide mechanistic hypotheses. We will attempt to recount these discoveries in the correct chronological order



Scheme 34. a) Selected hypervalent iodine (III and V) reagents and their relationships. b) The simple preparation of starting amide scaffolds (top) was then extended to the diverse and commercially available phenyl isocyanates and allylic alcohols/amines (bottom). c) General formulas for the remarkably general DMP and IBX reactions.

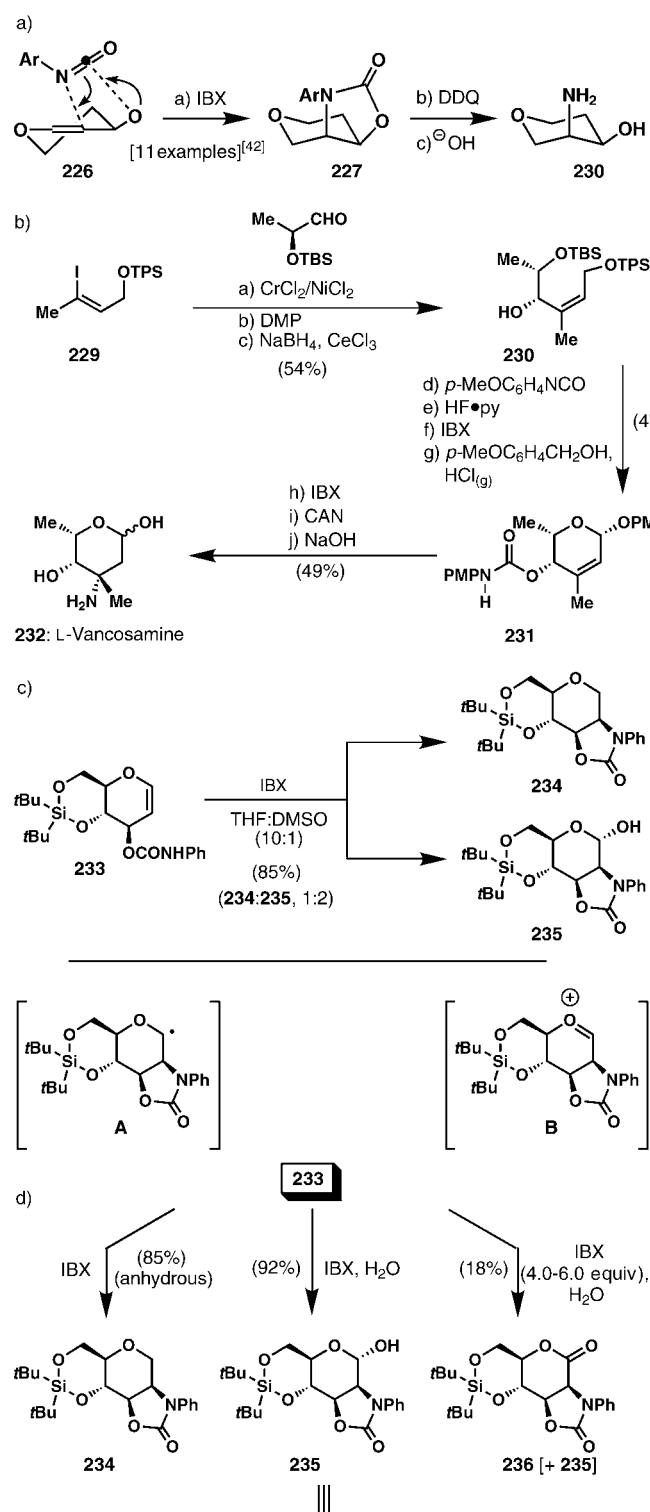
and, thus, we will return to the DMP-cyclization and its mechanism later on; for now we were intrigued by the IBX-cyclization.

11.4. IBX-Mediated Synthesis of Amino Sugars

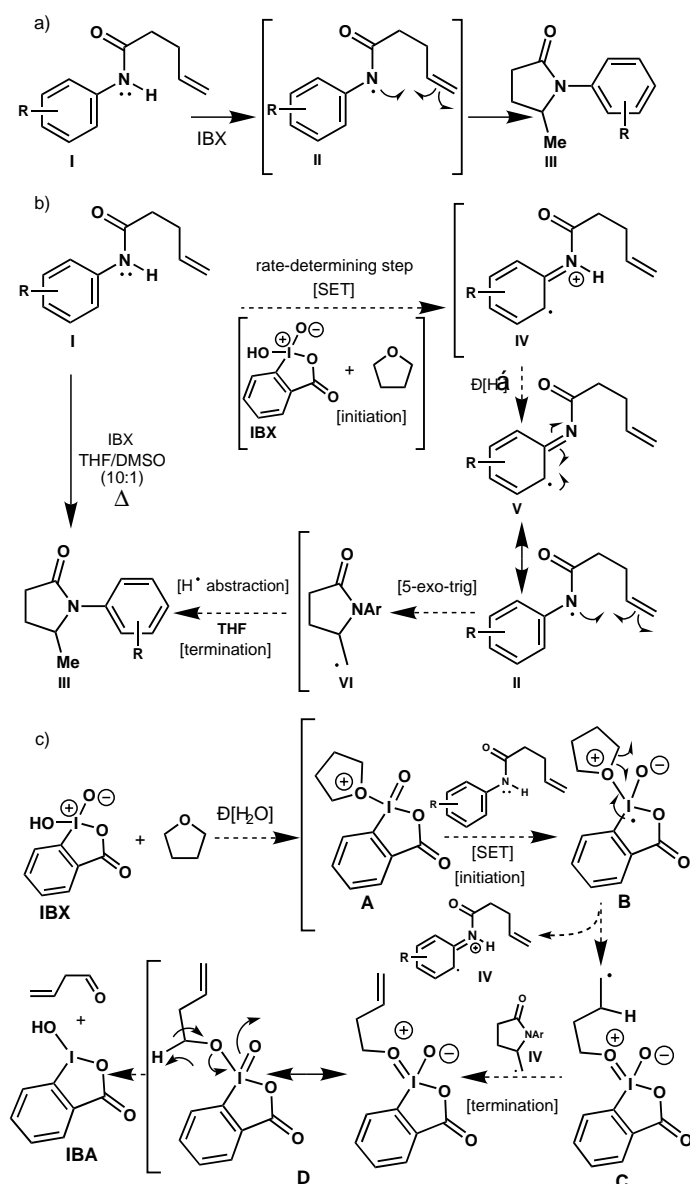
The efficiency with which a latent *cis*-1,2-amino alcohol functionality could be generated from an allylic alcohol by the newly discovered IBX reaction inspired us to investigate this process in the context of carbohydrate scaffolds (Scheme 35a). The expedient preparation of amino sugars and analogues thereof is a worthy synthetic goal since these compounds represent an important class of biologically active molecules. Thus, we were able to access a number of such amino sugars in high yield with complete stereocontrol by using the removable *p*-methoxyphenyl group on the nitrogen center. As a demonstration of its power, the reaction was employed in a concise and efficient synthesis of L-vancosamine (**232**) as shown in Scheme 35b.

The IBX reaction tantalized us further when we employed the glycol urethane **233** as a substrate (Scheme 35c). Instead of isolating 1-deoxyamino-sugar **234** exclusively, as expected, we also observed formation of the aminosugar derivative **235** as a minor product (ca. 1:2 ratio). We hypothesized that the latter compound (**235**) must be arising from attack of water upon an oxonium species such as **B** (Scheme 35c). We then reasoned that if we controlled the amount of water in the reaction system, we might be able to direct the reaction pathway to either 1-deoxyamino sugars or amino sugars at will. Indeed, this line of reasoning was sound since glycol **233** (and a number of other glycol systems) could be reliably converted in high yield to a 1-deoxyamino sugar (for example, **234**) or amino sugar derivatives (for example, **235**) just by controlling the amount of water present (Scheme 35d). In addition, these tunable cascade reactions could be set to provide amino sugar lactones such as **236** by using additional oxidant; however, it was more efficient to oxidize the amino sugars in a separate operation to achieve the same goal (namely, **235** \rightarrow **236**).

Following our work with amino sugars,^[42] we began to think more deeply about the mechanism of the IBX-induced cyclization reaction. The evolution of our understanding of this reaction is shown in Scheme 36. Our first mechanistic postulate for this reaction involving amide-based radicals (Scheme 36a) was accurate, yet rather simplistic. It was H. Martin R. Hoffman that first alerted us to the possibility that these reactions may be following a single-electron transfer (SET) pathway and we, therefore, proposed the mechanism shown in Scheme 36b for this process. The formulation of the possible nature of the IBX·THF complex (Scheme 36c), and the isotope labeling, kinetic,



Scheme 35. a) Application of the IBX cyclization to amino sugar synthesis, Ar = *p*-methoxyphenyl. b) Synthesis of **232** using IBX-based amino sugar synthesis. c) Reaction of **233** with IBX leads to a mixture of **234** and **235**, presumably via radical **A** and oxonium species **B**. d) Synthesis of 1-deoxy amino sugars, amino sugars, and amino sugar lactones from **233** and glycalurethanes.

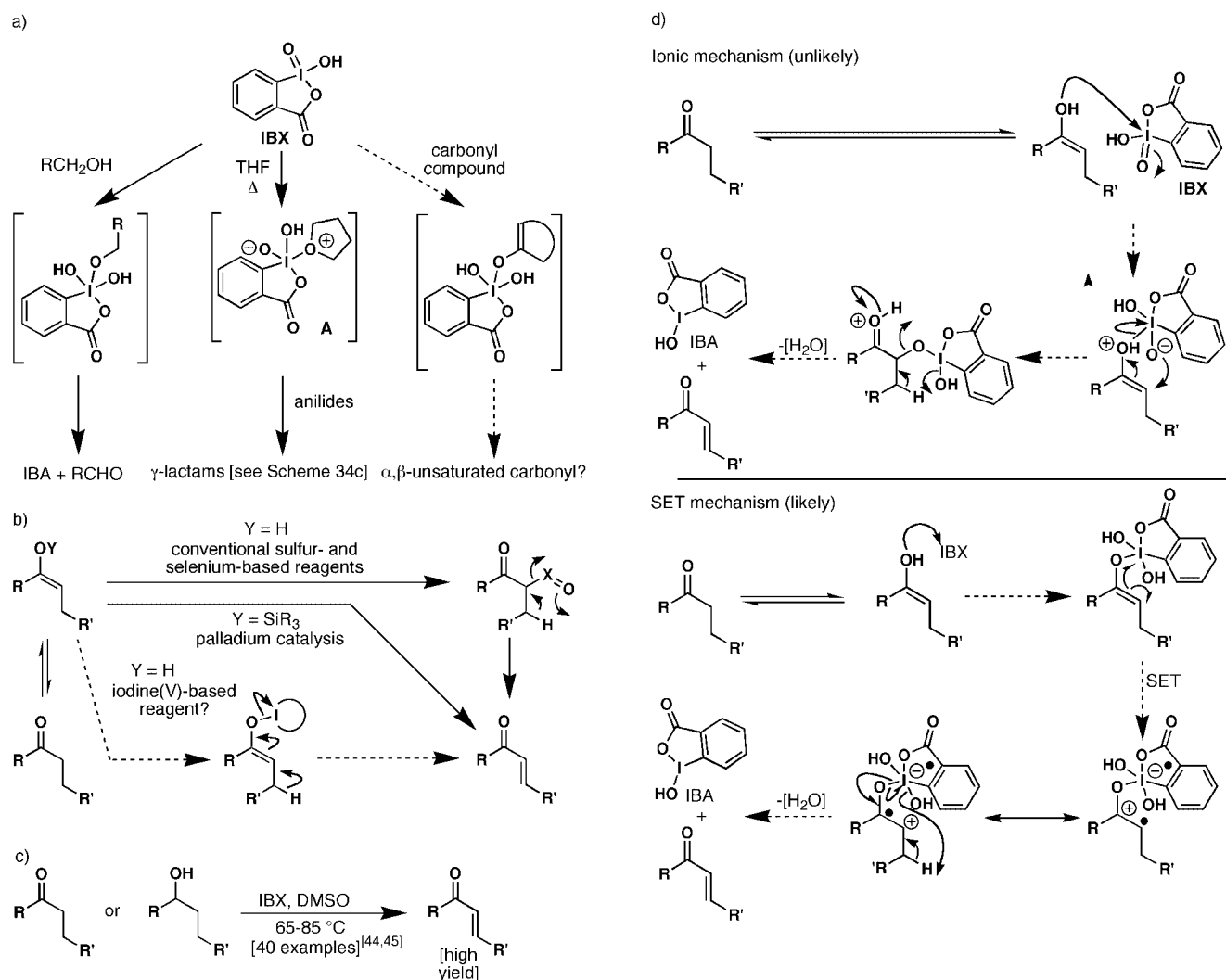


Scheme 36. Evolution of our mechanistic rationale for the SET-based IBX-mediated cyclization of anilides and related compounds (a and b) and plausible role of the solvent (THF) in these reactions (c).

electrochemical, and NMR studies would not come until a few months later.^[43] Only then would we recognize the full potential of IBX as a general and highly controllable SET reagent.

11.5. IBX-Mediated Introduction of Unsaturation Adjacent to Carbonyl Compounds

With an increased but still incomplete level of understanding of the reactivity of IBX, we pondered what other types of molecules might complex to IBX. Alcohols were known to form complexes with IBX to give the corresponding oxidized species (Scheme 37a). In addition, we had found that THF presumably forms some sort of complex with IBX (Scheme 37a). Would a carbonyl compound in its enol form



Scheme 37. a) Original considerations of IBX reactivity lead to a b) mechanistically inspired design of the IBX-based process for introduction of α,β -unsaturation adjacent to a carbonyl system. c) The IBX-mediated dehydrogenation of carbonyl compounds. d) Possible ionic- (top) and SET-based (bottom) mechanisms for the dehydrogenation of carbonyl compounds by IBX.

also form a complex with IBX? If so, would it lead to the corresponding α,β -unsaturated system? This expectation was probably far-fetched at the time. After all, if IBX could accomplish this transformation, why had no one reported it in the last hundred years of the reagent's history? The expectation was that if IBX could possibly trap a carbonyl compound in its enol tautomer, its fate just might be oxidation to the corresponding α,β -unsaturated compound.

The first example of introducing α,β -unsaturation adjacent to a carbonyl function with IBX was performed on May 9, 2000. When Zhong and Phil told me the news, I (K.C.N.) was again skeptical, but clandestinely excited at the same time! As shown in Scheme 37b, our mechanistic reasoning (right or wrong!) paid off with an efficient method for the synthesis of a variety of α,β -unsaturated compounds. Furthermore, since IBX is a very capable oxidant of alcohols, we could proceed in a one-pot process to form an α,β -unsaturated carbonyl compound from an alcohol in high overall yield (Scheme 37c). It was found that a large number of protecting groups and other sensitive functionalities are well tolerated

including nitrogen-based heterocycles and amides. Simple primary alcohols can even be oxidized to the corresponding, often sensitive, α,β -unsaturated aldehydes in high yield.^[44,45]

As it turned out, the initially proposed ionic pathway (Scheme 37d) had to be revised to a SET-based mechanism (Scheme 37d).^[45] We shall now return to the DMP cyclization, and the detailed study of its mechanism which led to the development of a number of additional synthetic technologies.

11.6. New Synthetic Technologies for the Construction of *p*-Quinones, *o*-Imidoquinones, and Complex Molecular Architectures Thereof

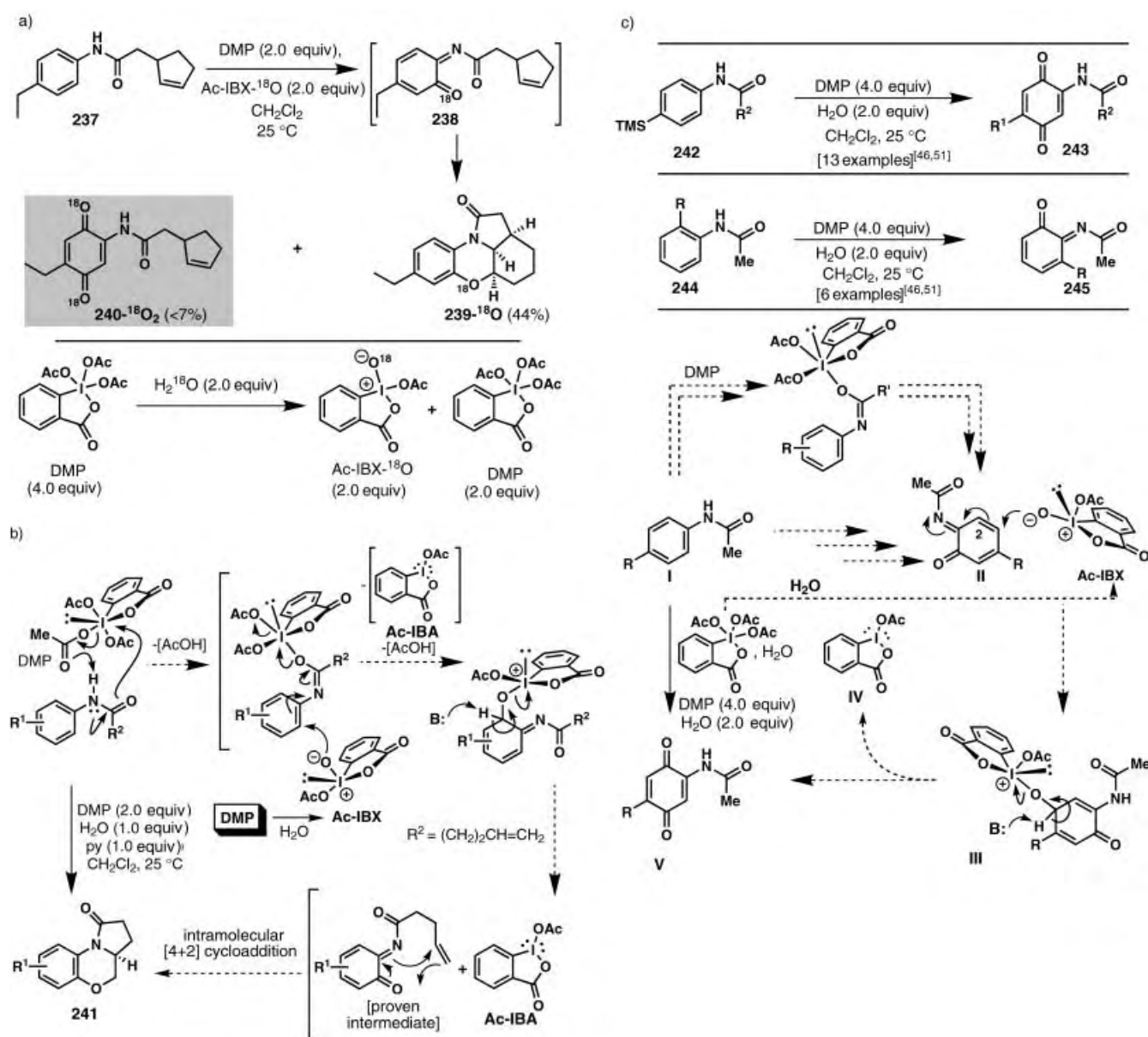
Without much data, we knew that our first analyses of the mechanism of the DMP cascade reaction were speculative and, indeed, were soon proven to be rather primitive. After extensive optimization studies we took note of the special influence of water on the reaction. Through control experi-

ments and isotope labeling studies (Scheme 38a) we were able to arrive at the mechanism shown in Scheme 38b. The remarkable feature of this reaction is that it involves two different iodine(v) reagents, DMP and Ac-IBX, working together. This synergistic reactivity was verified since no reaction occurs when an excess of DMP or Ac-IBX alone are employed. A detailed study of the DMP cyclization also led to a revised protocol which allows the reaction to proceed in dichloromethane at room temperature.^[43]

During the course of our mechanistic studies of the DMP reaction we stumbled onto the ^{18}O -labeled *p*-quinone by-product **240- ^{18}O** (Scheme 38a). We had not observed this type of product earlier because of the higher temperatures employed in the original conditions, which are apparently detrimental to the survival of such species. Logic dictated that if we deleted the appended olefin in the starting anilide we

could, potentially, maximize the yield of the *p*-quinone compound. The pronounced utility and widespread occurrence of the quinone moiety in nature and medically important agents prompted us to explore this possibility. To our delight, we found that a number of 4-substituted anilides could be easily oxidized to the corresponding *p*-quinones in good yields (Scheme 38c top). Although 3-substituted anilides gave unpredictable results, their 2-substituted counterparts gave rise to the corresponding *o*-imidoquinones in high yield (Scheme 38c middle). This procedure represented the first general synthesis of these rather rare species.^[46]

From labeling studies (Scheme 38a) it is clear that two molecules of Ac-IBX are involved in *p*-quinone formation. As shown in Scheme 38c bottom, we postulated that an *o*-imidoquinone (**II**) is actually the precursor to a *p*-quinone (**V**) upon attack of an additional molecule of Ac-IBX. In the



Scheme 38. a) ^{18}O -labeling studies with the DMP cascade reaction. b) Proposed mechanistic underpinnings of the DMP-mediated polycyclization of olefinic aryl amides. c) Synthesis of *p*-quinones from 4-substituted anilides (top), synthesis of *o*-imidoquinones from 2-substituted anilides (middle), and postulated mechanistic rationale for the oxidation of *o*-imidoquinones to *p*-quinones using DMP (bottom).

a)

245

246

b)

247

248

249

250

c)

251

252

253

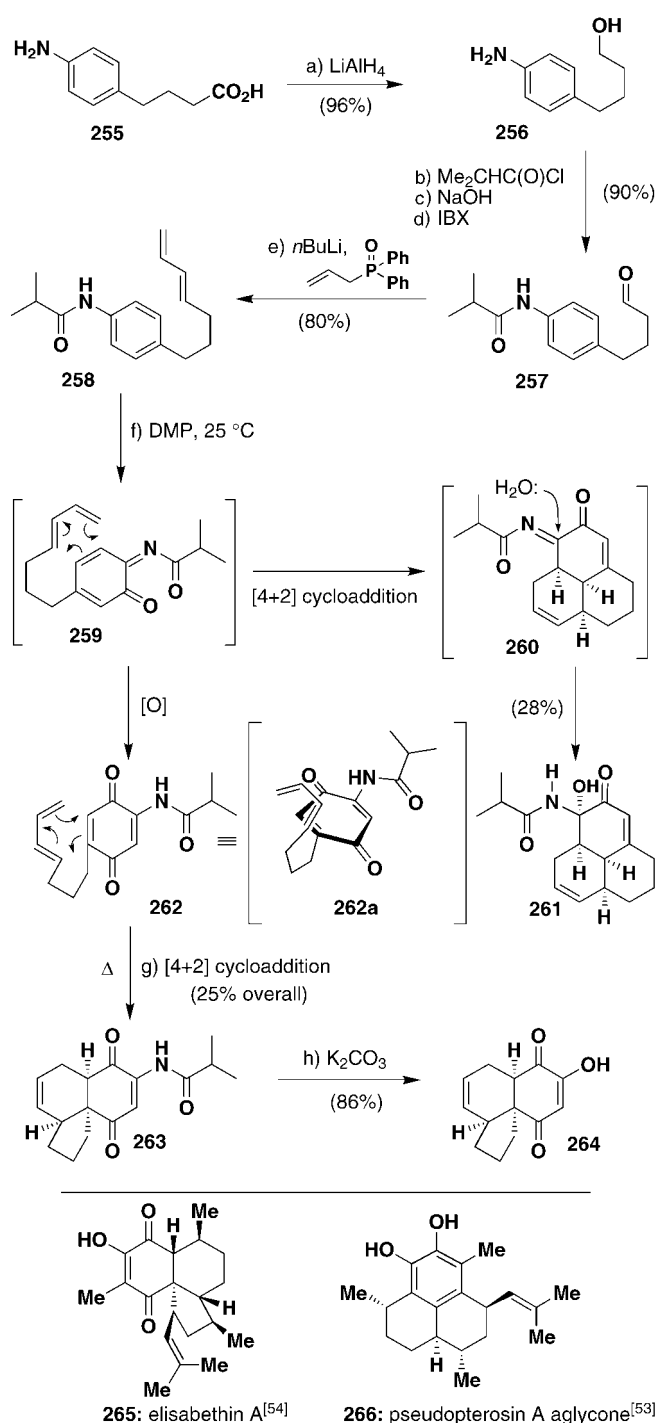
254

d)

256

255

To explore this novel prospect, we designed and synthesized anilide diene **258** as shown in Scheme 40. In line with our expectations, exposure of this substrate to DMP and H₂O in CH₂Cl₂ at ambient temperature led to ketohydroxyamide **261** and quinone **262** in 28 and 25 % yield, respectively. The novel ketohydroxyamide **261** was presumably generated through hydration of the initially formed Diels–Alder adduct **260**. Interestingly, the ketohydroxyamide **261** and its derivatives closely resemble the pseudopterosin family of natural products (for example, pseudopserosin A aglycon, **266**,



Scheme 40. Rapid entry into complex molecular architectures resembling those of pseudopterosin A aglycon and elisabethin A from anilides and DMP.

Scheme 40).^[53] Upon heating, the initially formed quinone **262** was quantitatively converted, by an intramolecular Diels–Alder reaction, into the tricyclic system **263**. The latter framework embodies the full carbocyclic skeleton of the naturally occurring substance elisabethin A (**265**).^[54] It is interesting to note that the structures of these two seemingly unrelated natural product classes (pseudopterosin A and elisabethin A) are produced by the same organism just as the present DMP-initiated cascade furnishes both complex

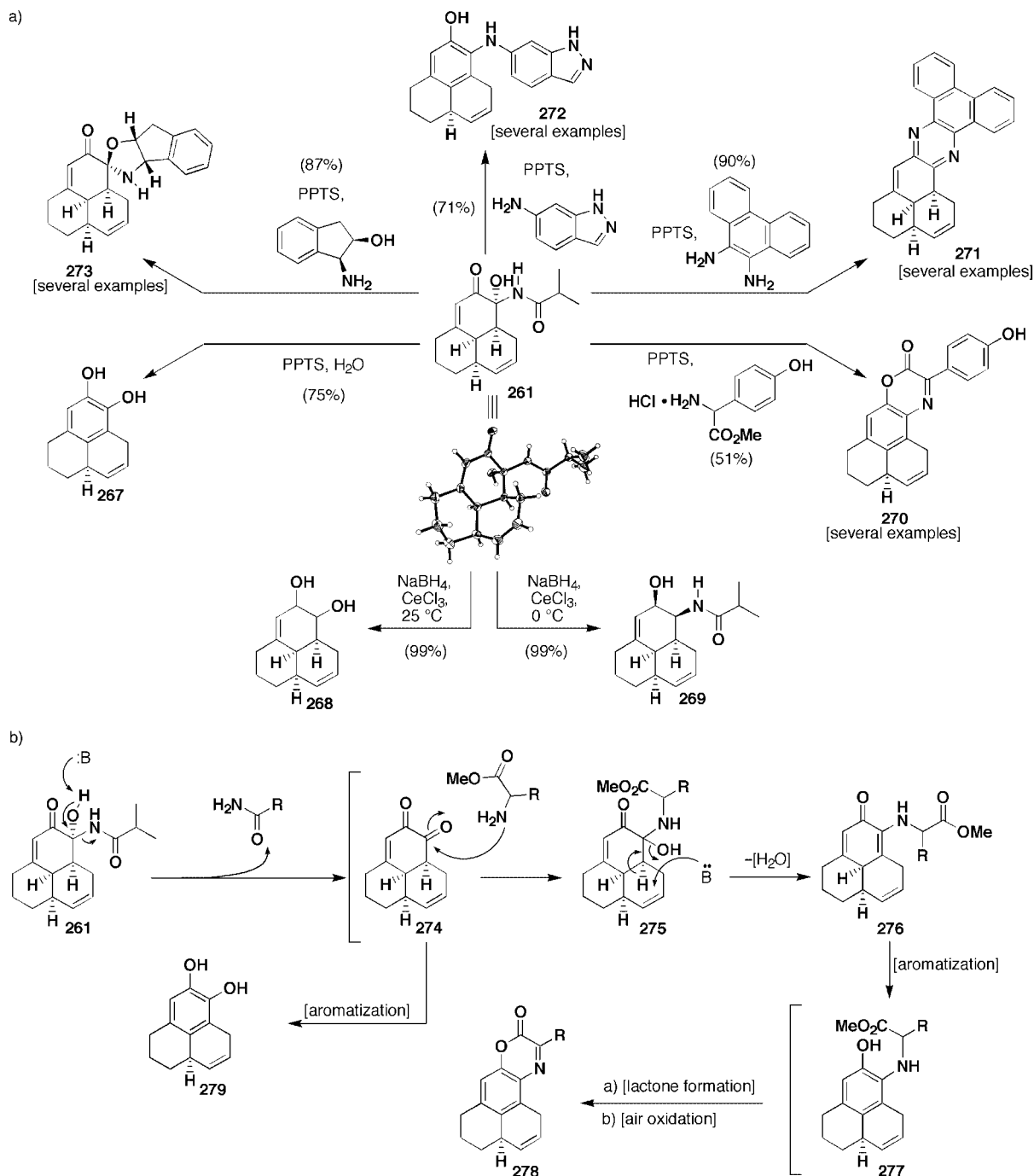
pseudopterosin- and elisabethin-like structures (**261** and **263**) in the same pot.

The ready availability of ketohydroxyamide **261**, coupled with the scarcely investigated chemistry of this moiety,^[55] enticed us to explore its reactivity and synthetic potential. It was soon found that ketohydroxyamide **261** undergoes a diverse range of novel transformations leading to a set of unusual products (Scheme 41 a). These reactions revealed that, despite its misleading appearance, this substance does not always react as a simple protected α -diketone, but has its own chemical identity. Thus, exposure of ketohydroxyamide **261** to PPTS in aqueous media led to diphenol **267** in 75 % yield, whereas treatment with sodium borohydride in the presence of cerium chloride furnished either a mixture of diastereomeric alcohols **268** (99 %, ca. 1:1 ratio, 25°C) or the hydroxyamide **269** (99 %, single isomer, 0°C) depending upon the temperature. Reaction of **261** with C-terminal-protected amino acid derivatives led, through an interesting cascade reaction (Scheme 41 b), to heteroannulation, to furnish complex polycyclic scaffolds (**270**, **278**). The combination of ketohydroxyamide **261** with 1,2-diamines led smoothly to polycyclic pyrazines (**271**), whereas aromatic amines reacted with **261** to afford aniline derivatives (**272**) in high yield. Unusual heterocyclic spiro systems (**273**) were formed when 1,2-amino alcohols were employed in this reaction.

11.7. Benzylic Oxidation with IBX

Parallel to the extensive investigations in the DMP arena, we were also exploring new reactions mediated by IBX. Since we had come to the conclusion that IBX behaved as a general SET reagent, we rationalized that the oxidation of carbon atoms adjacent to aromatic systems should also be possible. As mechanistically illustrated in Scheme 42 a, stepwise SET oxidation of a substituted toluene (**280**) leading to the stabilized benzylic cation (**283**) might trigger such a process by subsequent oxidation with another molecule of IBX to furnish the corresponding substituted benzaldehydes (**281**). The mild nature of IBX and its observed chemoselectivity in other transformations made this proposal particularly enticing.

This plan worked (Scheme 42 b)! Within a few weeks of its discovery, Phil and Zhong utilized this new reaction to complete a series of examples to demonstrate its scope and generality.^[56] Significantly, and in contrast to conventional methods, the reaction tolerated the presence of a variety of sensitive and oxidation-prone functional groups (Scheme 42 b). Moreover, over-oxidation of the resulting aldehydes was never observed. A subsequent, more-detailed mechanistic analysis of this process led us to consider several other possible pathways as shown in Scheme 42 c.^[45] It is also tempting to evolve our rationale and consider another mechanism for the IBX-mediated oxidation of benzylic positions based on literature precedent for aryl π -iodine complexes and their role in single electron transfer redox reactions^[57] (Scheme 43).

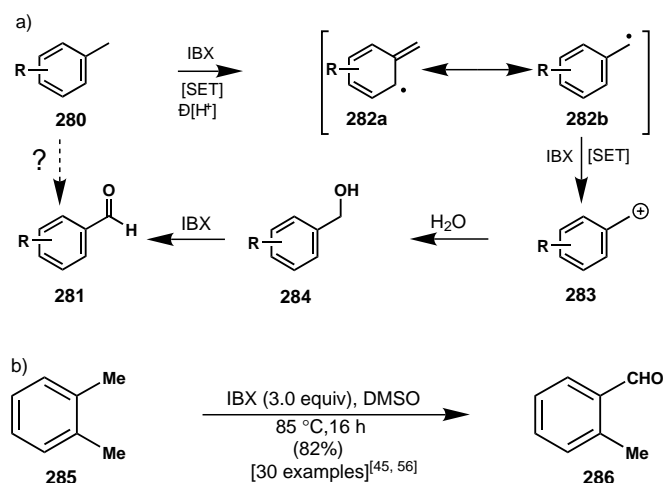


Scheme 41. a) Remarkable reactivity of the unique ketohydroxyamide **261**, and b) postulated mechanism for the cascade heterocyclic annulation of **261** to polycycles **278**.

11.8. A Serendipitous Discovery Leads to an Exploration of the Chemistry of α -Sulfonated Ketones

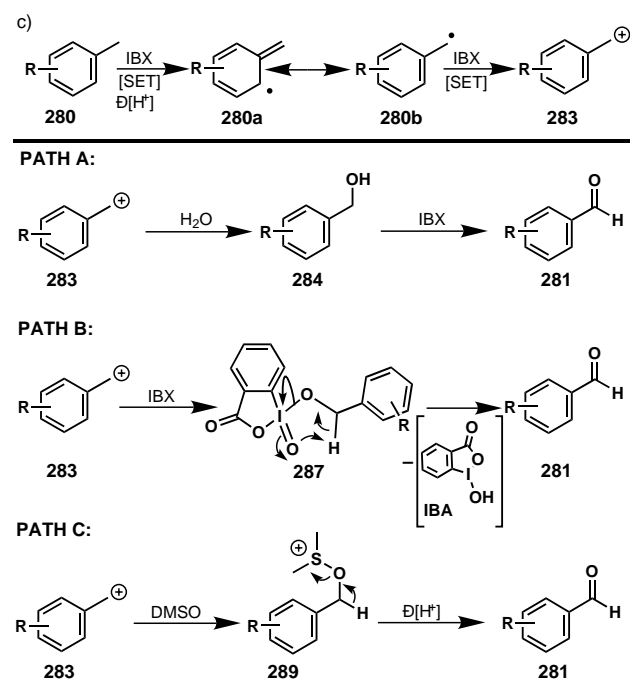
Around the same time that we had unearthed the ability of IBX to mediate the dehydrogenation of carbonyl compounds we had also discovered the potential of α -sulfonated ketones in organic synthesis. How does this seemingly unrelated finding relate to the study of iodine(v) reagents? Early one morning, I (K.C.N.) suggested to Phil and Zhong that they consider the reaction of IBX with epoxides. The hope, as illustrated in Scheme 44a, A, for the case of cyclooctene

oxide, was that nucleophilic attack by IBX itself upon the epoxide moiety (**297**) followed by dehydrogenation would eventually lead to the highly oxidized system **298** in one pot. The proposed reaction was immediately set up with IBX, but there was no change. When we added catalytic amounts of TsOH we observed the formation of a trace amount of a new, strongly UV-active product. This compound turned out to be the α -tosylated ketone **299**. When the reaction was run again with stoichiometric amounts of TsOH we obtained sulfonyloxy ketone **299** in high yield. We were immediately excited by this finding and after a thorough literature search we



FUNCTIONAL GROUPS TOLERATED:

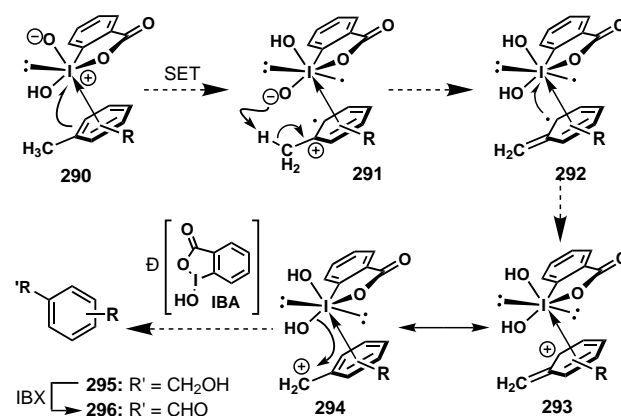
- Olefins
- Amides, carbamates
- N- and O-containing heterocycles
- α,β -Unsaturated and aryl aldehydes



Scheme 42. a) Mechanistically inspired design of an IBX-mediated benzylic oxidation process. b) The IBX-mediated oxidation of benzylic positions. c) Alternative mechanisms postulated for the IBX-mediated benzylic oxidation.

confirmed our suspicions that indeed this was a new route to these types of compounds. It did not take long before we realized the potential of these now readily available intermediates in organic synthesis, particularly in solid-phase chemistry. Initial solution-phase studies (Scheme 44a, B) were promising; especially exciting was the unique synthesis of heterocycle **305**.

In considering the potential of the readily available α -sulfonated ketones, the well-known and fertile chemistry of α -halo ketones came to mind. Despite their versatile nature, however, α -halo ketones cannot easily be attached to solid



Scheme 43. Postulated concerted mechanism for the IBX-mediated benzylic oxidation.

supports for exploitation as precursors to molecular diversity by solid-phase and combinatorial methods. In contrast to the α -halo ketone solid-phase limitations, we found that α -sulfonated ketones can be readily formed on resins by employing sulfonic acid polymers. This advantage of α -sulfonated ketones, coupled with their stability and sometimes unique chemistry,^[58] prompted us to investigate them further. Thus, by tapping into the rich chemistry of related sulfonyloxy ketones,^[59] and by introducing our own modifications, we envisaged the naissance of a seamless and novel linker which would provide access to a wide ranging library of structural types.^[60]

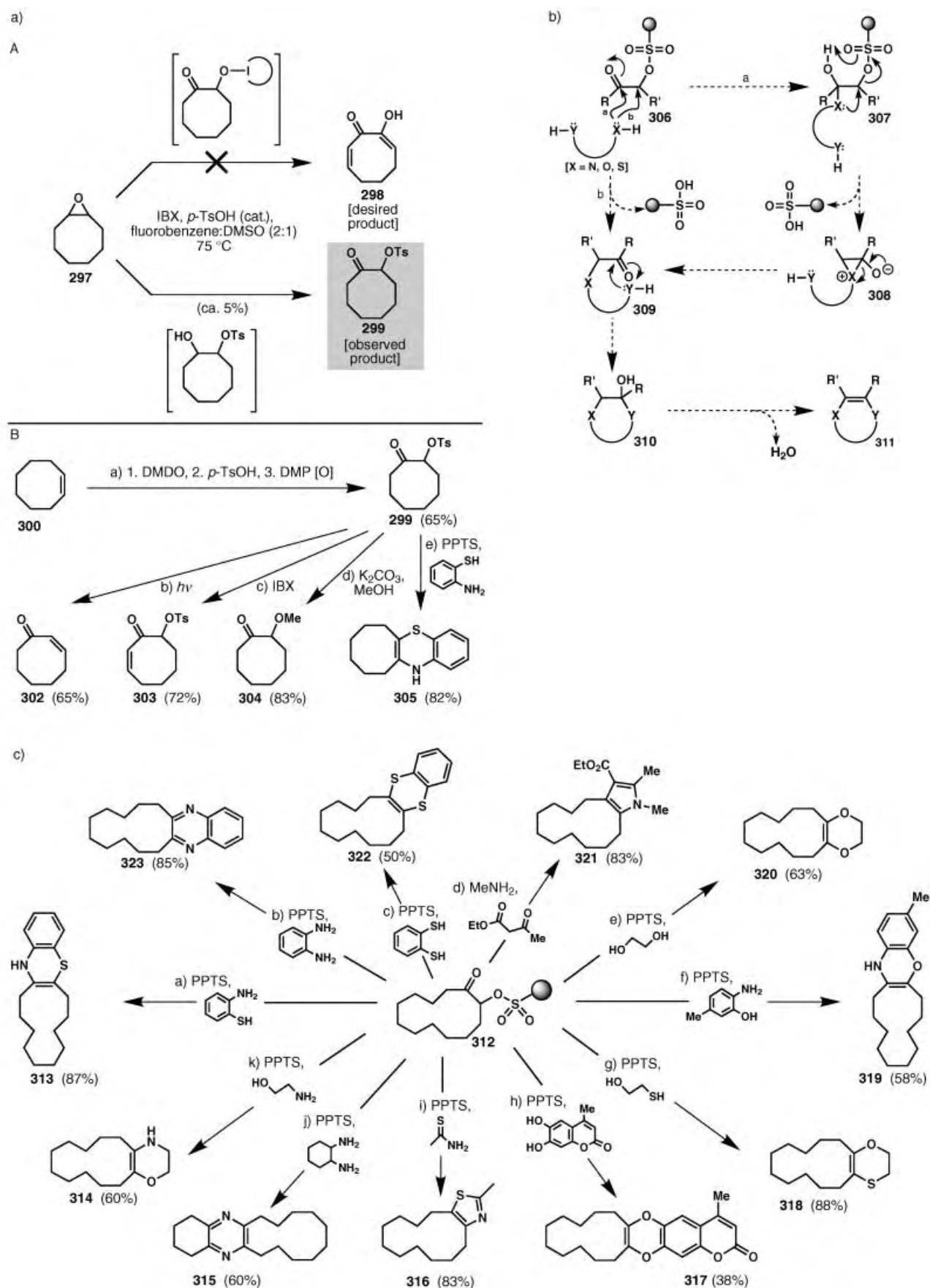
Confident that our solid-bound α -sulfonyloxy ketones were emulating their solution-phase relatives, we evaluated a strategy for the release of heterocycles from the solid support. Pleasingly, we found that this heterocycle-release concept, as depicted in Scheme 44b, allows for the generation of a plethora of ubiquitous heterocycles. Scheme 44c offers a snapshot of some of the explored possibilities.^[60, 61]

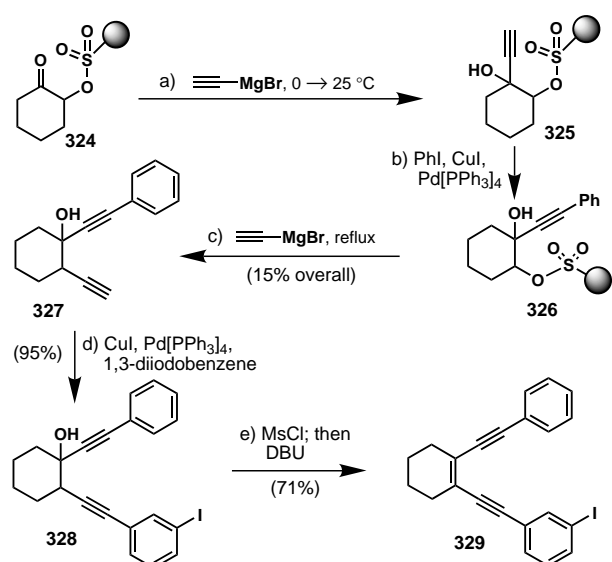
We also investigated the efficiency of carbon–carbon bond forming reactions using α -sulfonyloxy ketones, and given the importance of enediynes and related systems, we set out to develop conditions which would permit the synthesis of such compounds. A unique strategy was then developed to generate libraries of dialkynols (stable precursors to enediynes). An example of this technology leading to the enediyne **329** is shown in Scheme 45.^[61]

The story of α -sulfonyloxy ketones stands as an example of how an unexpected by-product and a little imagination can lead to the development of new chemistry. The moral of the story is that one should not be too quick to sweep unexpected observations under the carpet when they do not serve one's immediate purposes. Rather, one should look at such discoveries from a broader perspective and with curiosity to fuel further explorations into their mechanism and synthetic potential.

11.9. Selectivity in IBX-Mediated Reactions

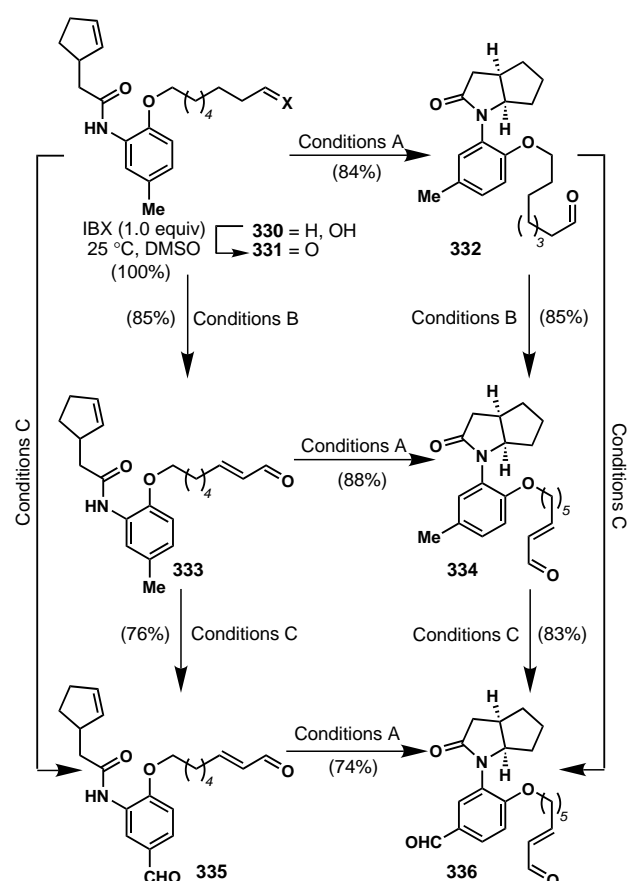
The demonstrated ability of IBX to induce N-centered radical generation (from anilides and with subsequent cycli-





Scheme 45. Synthesis of enediyne **329** from α -sulfonyloxy ketone **324**.

zation reactions), dehydrogenation of carbonyl compounds, and oxidation adjacent to aromatic systems dictated the need to determine the selectivity of the reagent in these reactions. How controllable are these processes in a setting where they are all conceivably possible? Scheme 46 answers this impor-



Scheme 46. Selective chemical transformations with IBX. Reaction conditions A: IBX (2.2 equiv), THF: DMSO (10:1), 85 °C, 8 h; B: IBX (2.0 equiv), TsOH (0.2 equiv), PhF:DMSO, 65 °C, 5 h; C: (3.0 equiv), DMSO, 90 °C, 2 h.

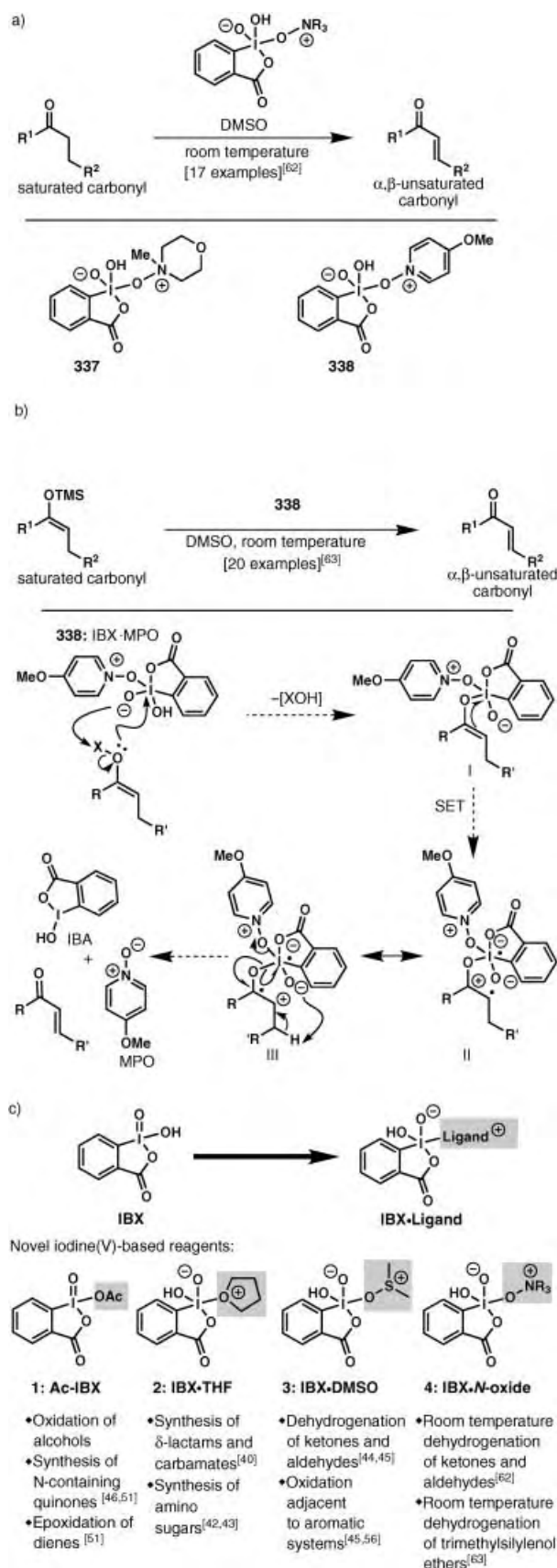
tant question with the synthesis and reactions of alcohol-amide **330** which was designed to probe this issue. Using only three standard sets of conditions, substrate **330** could be easily converted into any of the compounds **331**–**336** as desired. This series of reactions ably illustrates the ease with which IBX-mediated oxidations can be manipulated to furnish a diverse spectrum of highly functionalized products.^[56]

The fact that we could heat compound **333** (conditions A, Scheme 46) in a sealed tube with IBX at 90 °C in THF/DMSO and observe no benzylic oxidation or carbonyl dehydrogenation intrigued us. In the same vein, why, when there was no THF present (conditions B, Scheme 46), did the γ -lactam-forming process seem to shut off? Such questions piqued our earlier suspicions concerning the role of the solvent in these IBX reactions and led us to hypothesize that the solvent actually formed a discrete complex with IBX leading to the dramatic reactivity patterns observed.

11.10. Modifying the Iodine(v) Nucleus of IBX With Different Ligands: Room Temperature Dehydrogenation of Carbonyl Compounds

The possibility that a solvent molecule was forming a complex with IBX was first confirmed qualitatively. Thus, when a solution of IBX in DMSO was heated to 80 °C for a few minutes and then cooled down, the resulting complex was capable of carbonyl dehydrogenation at room temperature,^[62] in contrast to IBX which had merely been dissolved in DMSO at room temperature. Since the conversion of this last reaction was not so high, we began to explore the effect of other ligands on the process. After extensive explorations we found that NMO is a suitable ligand for IBX; it forms a complex at room temperature (as clearly observed by ¹H NMR spectroscopy) and accomplishes room-temperature dehydrogenations in good yields. It was May 12, 2001, when Tamsyn Montagnon, a newly arrived postdoctoral fellow from England, informed me (K.C.N.) of this remarkable advance.^[62]

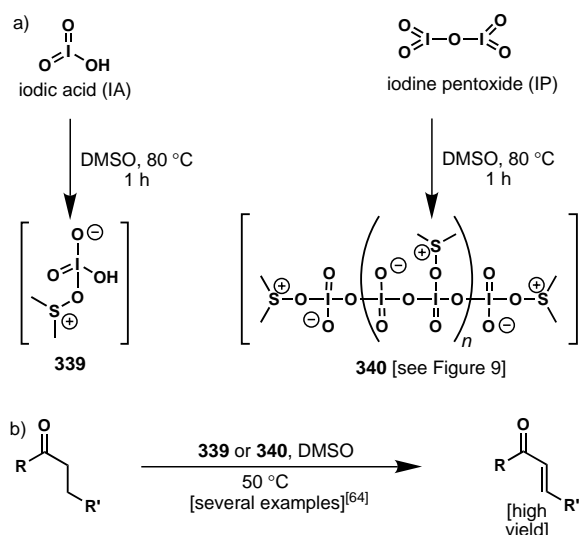
It was again hard to believe, but a clear ¹H NMR spectrum of the IBX · NMO complex left very little doubt of what was happening. Further optimization of the reaction led to the identification of 4-methoxypyridine-*N*-oxide (MPO) as a remarkably efficient ligand for effecting room-temperature dehydrogenation of a wide range of carbonyl compounds.^[62] The applications of this new and mild reagent (IBX · MPO) were extended to encompass a highly efficient and rapid oxidation of trimethylsilylenol ethers to the corresponding enones (Scheme 47b).^[63] Taken in combination, these new methods compliment each other's strengths and allow for a remarkably diverse set of ketones and aldehydes to be converted into their α,β -unsaturated congeners in high yields. Overall, these developments and the new appreciation they brought of the chemical characteristics of IBX ushered in a new paradigm for modifying the iodine(v) nucleus through ligand tailoring as a means to control its reactivity profile (Scheme 47c).



Scheme 47. a) N-oxide ligands on IBX allow for the room-temperature dehydrogenation of carbonyl compounds. b) New methodology extends the utility of N-oxide ligands on IBX to the room-temperature dehydrogenation of trimethylsilylenol ethers. c) Access to novel iodine(v)-based reagents by changing the ligand employed on IBX.

11.11. The Use of Iodic Acid and Iodine Pentoxide in Organic Synthesis

One day in July 2001, while pondering the reactivity of IBX we had an epiphany of sorts. It had always been bothersome to us that the use of IBX in industrial applications would likely be hampered by its high molecular weight, expense, and fear of detonation at high temperature ($> 200^\circ\text{C}$). What exactly is the role of the aromatic moiety in IBX, we asked. Could its removal offer reagents with far higher atom efficiency? With the aromatic moiety simply deleted while maintaining the same oxidation state for iodine as in IBX, would we still be able to accomplish, for instance, carbonyl dehydrogenation? The most simple iodine(v) reagents, iodic acid (HIO_3 , IA) and its anhydride, iodine pentoxide (I_2O_5 , IP) were immediately acquired and investigated experimentally to answer these questions. [64] From our studies with IBX, we reasoned that our best chance for success would be to preform the corresponding DMSO complexes as shown in Scheme 48 a. Remarkably and to our utter amazement, these DMSO complexes



Scheme 48. a) Preparation of IP- and IA-DMSO complexes. b) Their use to introduce α,β -unsaturation into carbonyl compounds.

(**339** and **340**) were indeed capable of the dehydrogenation of carbonyl compounds at rather moderate temperatures ($45-65^\circ\text{C}$) and in high yield (Scheme 148b). Notwithstanding their extensive use in industrial applications [64] and their commercial availability, [65] IA and IP have rarely been employed in organic synthesis. Their industrial applications and studies conducted at elevated temperatures [66] strongly suggest these are particularly stable oxidants. This feature is perhaps related to the extensive secondary bonding networks present in these solids which is at least partially maintained in solution. To improve our understanding of the nature of these iodine(v)–DMSO complexes, we prepared crystalline **340** by lyophilization of a solution of IP in DMSO. [64] X-ray crystallographic analysis of this crystalline solid revealed its remarkable helical structure and provided the first physical confirmation of our long-held hypothesis that DMSO activates these species by acting as a ligand and complexing with the iodine(v) nucleus (Figure 9).

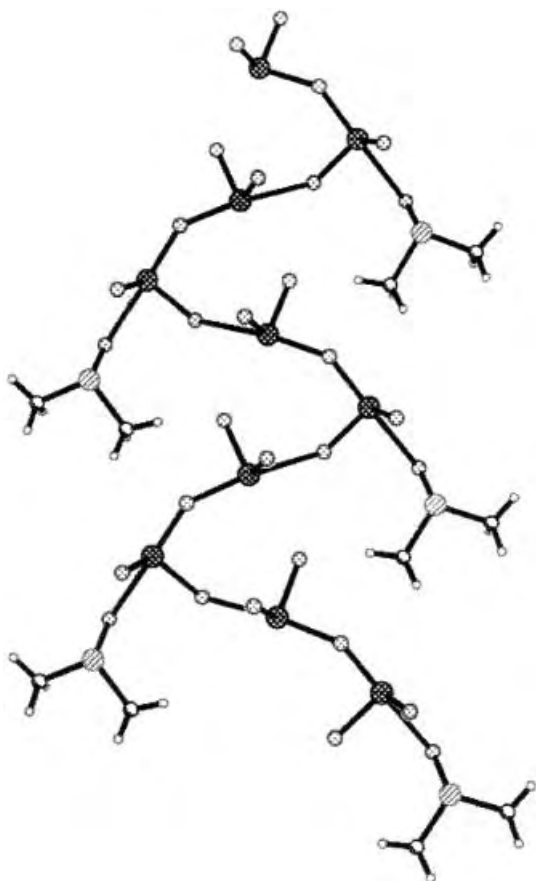


Figure 9. ORTEP representation of the helical IP-DMSO complex structure.

12. Conclusion

In this article, we described our experiences with CP-263,114 (**1**) and CP-225,917 (**2**), two molecules whose conquest by total synthesis was enriched with a surplus of discoveries and inventions in organic synthesis (for a timeline of the main milestone events in this synthetic labyrinth, see Figure 10). Their unusual molecular connectivities and highly sensitive nature added to the lure of their challenge, and were instrumental in stimulating new chemistry by raising the bar at a level unattainable by existing methodology. Rising to this challenge, a team of dedicated graduate students and post-doctoral fellows battled for approximately two years through a “synthetic labyrinth” until the “Minotaur” fell in the face of their unwavering persistence and resourceful attacks. A number of new synthetic strategies and synthetic technologies were invented to get through and accomplish the final goal, and many more synthetic methods were discovered in the process and in follow-up studies. Among the most prominent of these reactions are the maleic anhydride cascade, the DMP-mediated cascade oxidation of 1,4-diols to construct the γ -hydroxylactone, the mixed acyl-sulfonyl anhydride method for activating sterically hindered carboxylic acids, the cyanohydrin-based homologation of sterically hindered aldehydes, the cascade hydrolysis of **1** to **2**, and finally the myriad of

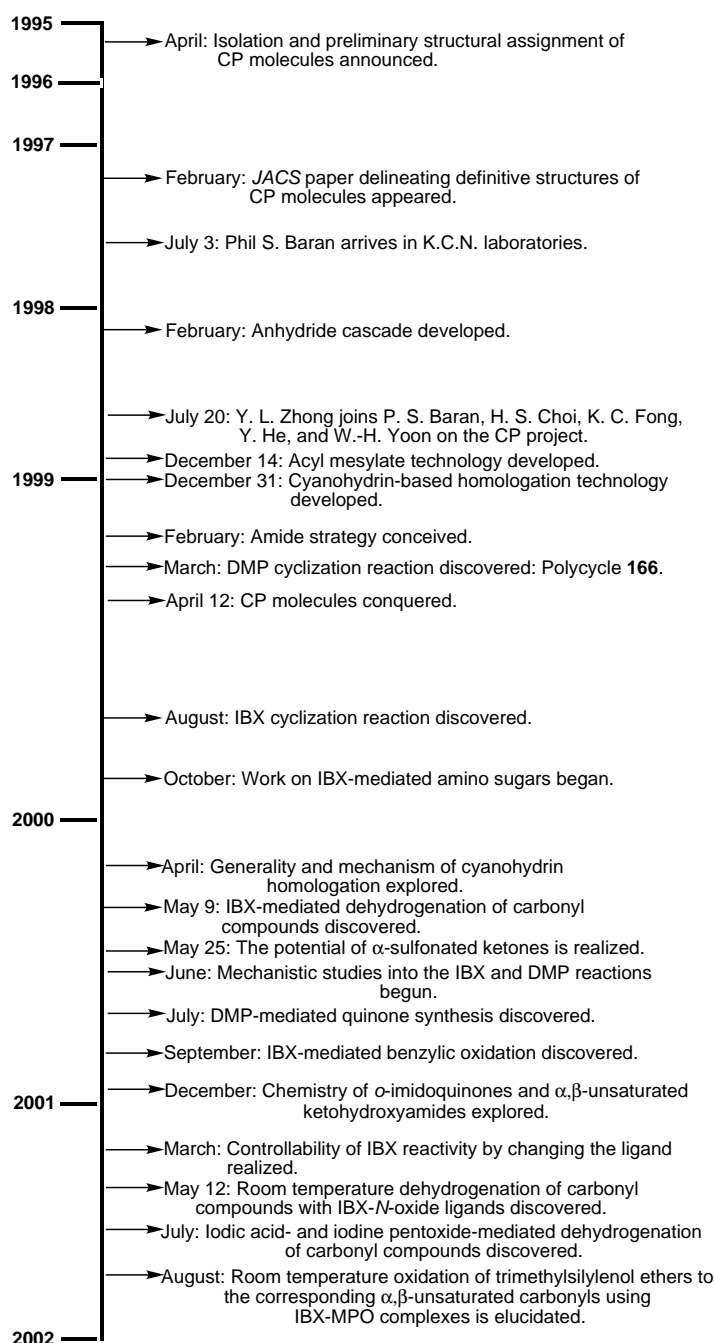


Figure 10. Timeline of an adventure in scientific discovery: The CP labyrinth.

new reactions based on iodine(v) chemistry and spin-offs thereof.

The highly fertile and interwoven studies of synthetic strategy and synthetic methodology inspired by these “demonic” target molecules are a luminous example of how total synthesis should be performed these days. Indeed, this example provides ample demonstration of the attractiveness of total synthesis endeavors as a means to discover and develop science, particularly in the fields of new synthetic methodology and strategy. Another rich and rewarding approach to total synthesis of natural products is to blend it with chemical biology studies. Examples of such endeavors

from these laboratories include the enediyne,^[68] epothilone,^[69] and vancomycin^[70] projects, all of which evolved and grew so that they were accompanied by a number of significant contributions to biology and medicine.

Overall, endeavors in total synthesis, if practiced wisely, are hard to match in terms of yield of basic science and the development of useful applications in biology and medicine, not to mention the opportunity they provide to train young men and women in the art of chemical synthesis. What determines the yield of such benefits is often encoded within the program and depends on many factors, admittedly including serendipity and good luck. However, the practitioner can optimize this yield by rational reasoning and imagination so as to maximize the opportunity, beginning with the prudent selection of the target molecule. The entire enterprise should be based on the premise of not only reaching the destination, but most importantly, collecting “goods and wisdom” along the way.

In closing this article we wish for more targets like the CP molecules, so that they can challenge and sharpen the minds and skills of new “Theseus”.^[71] Nature certainly has them, and it will be up to us to find them and pursue them, and in so doing learn the valuable lessons they hold in store for us. For nature, in her designs, is the supreme master, and thriving to mimic her efficiency and elegance is a most rewarding endeavor.

Abbreviations

Ac	acetyl
acac	acetylacetyl
AIBN	2,2'-azobisisobutyronitrile
Alloc	allyloxycarbonyl
Bn	benzyl
Bz	benzoyl
CAN	cerium ammonium nitrate
CSA	10-camphorsulfonic acid
DABCO	1,4-diazabicyclo[2.2.2]octane
DBU	1,8-diazabicyclo[5.4.0]undec-7-ene
DDQ	2,3-dichloro-5,6-dicyano-1,4-benzoquinone
DEAD	diethyl azodicarboxylate
DIBAL	diisobutylaluminum hydride
4-DMAP	4-dimethylaminopyridine
DMDO	2,2-dimethyldioxirane
DMF	<i>N,N</i> -dimethylformamide
DMP	Dess–Martin periodinane
DMPU	<i>N,N</i> -dimethylpropyleneurea
DMSO	dimethylsulfoxide
EDC	1-(3-dimethylaminopropyl)-3-ethylcarbodiimide
HMDS	bis(trimethylsilyl)amide
IBA	iodosobenzoic acid
IBX	<i>o</i> -iodoxybenzoic acid
imid	imidazole
LDA	lithium diisopropylamide
Ms	methanesulfonyl
NMO	4-methylmorpholine- <i>N</i> -oxide
PDC	pyridinium dichromate
Piv	pivaloyl

PMB	<i>p</i> -methoxybenzyl
PMP	<i>p</i> -methoxyphenyl
PPTS	pyridinium 4-toluenesulfonate
Ts	4-toluenesulfonyl
py	pyridine
TBAF	tetra- <i>n</i> -butylammonium fluoride
TBS	<i>tert</i> -butyldimethylsilyl
TEMPO	2,2,6,6-tetramethyl-1-piperidinyloxy
TES	triethylsilyl
Tf	trifluoromethanesulfonate
TFA	trifluoroacetic acid
THF	tetrahydrofuran
TMS	trimethylsilyl
TPAP	tetra- <i>n</i> -propylammonium perruthenate
TPS	<i>tert</i> -butyldiphenylsilyl

It is with enormous pride and pleasure that we wish to thank our collaborators whose names appear in the references and whose contributions made the described work possible and enjoyable. We gratefully acknowledge the National Institutes of Health (USA), Merck&Co., DuPont, Schering Plough, Pfizer, Hoffmann–La Roche, GlaxoWellcome, Rhone–Poulenc Rorer, Amgen, Novartis, Abbott Laboratories, Bristol Myers Squibb, Boehringer Ingelheim, Zeneca, CaPCURE, the George E. Hewitt Foundation, the Skaggs Institute for Chemical Biology, and the National Science Foundation (fellowship to P.S.B.) for supporting our research programs. We are also grateful for generous contributions by Dr. T. Montagnon and Mr. S. A. Snyder in the assembly of this manuscript.

Received: December 21, 2001 [A 509]

- [1] Anonymous, <http://www.magicaljourneys.com/theseus.html>.
- [2] K. C. Nicolaou, D. Vourloumis, N. Winssinger, P. S. Baran, *Angew. Chem.* **2000**, *112*, 46; *Angew. Chem. Int. Ed.* **2000**, *39*, 44.
- [3] S. Stinson, *Chem. Eng. News* **1995**, *73*(21), 29.
- [4] T. T. Dabrah, T. Kaneko, W. Massefski, Jr., E. B. Whipple, *J. Am. Chem. Soc.* **1997**, *119*, 1594.
- [5] a) K. C. Nicolaou, P. S. Baran, Y.-L. Zhong, H.-S. Choi, W. H. Yoon, Y. He, K. C. Fong *Angew. Chem.* **1999**, *111*, 1774; *Angew. Chem. Int. Ed.* **1999**, *38*, 1669; b) K. C. Fong, Y. He, W. H. Yoon, H.-S. Choi, *Angew. Chem.* **1999**, *111*, 1778; *Angew. Chem. Int. Ed.* **1999**, *38*, 1676; c) K. C. Nicolaou, J.-K. Jung, W. H. Yoon, Y. He, Y.-L. Zhong, P. S. Baran, *Angew. Chem.* **2000**, *112*, 1899; *Angew. Chem. Int. Ed.* **2000**, *39*, 1829; d) K. C. Nicolaou, J. Jung, W. H. Yoon, K. C. Fong, H.-S. Choi, Y. He, Y.-L. Zhong, P. S. Baran, *J. Am. Chem. Soc.* **2002**, *124*, 2183; e) K. C. Nicolaou, P. S. Baran, Y.-L. Zhong, K. C. Fong, H.-S. Choi, *J. Am. Chem. Soc.* **2002**, *124*, 2190; f) K. C. Nicolaou, Y.-L. Zhong, P. S. Baran, J. Jung, H.-S. Choi, W. H. Yoon, *J. Am. Chem. Soc.* **2002**, *124*, 2202.
- [6] R. F. Service, *Science* **1999**, *284*, 1598.
- [7] B. R. Bear, S. M. Sparks, K. J. Shea, *Angew. Chem.* **2001**, *113*, 864; *Angew. Chem. Int. Ed.* **2001**, *40*, 820.
- [8] K. C. Nicolaou, M. W. Härter, L. Boulton, B. Jandeleit, *Angew. Chem.* **1997**, *109*, 1243; *Angew. Chem. Int. Ed. Engl.* **1997**, *36*, 1194.
- [9] K. C. Nicolaou, M. H. D. Postema, N. D. Miller, G. Yang, *Angew. Chem.* **1997**, *109*, 2922; *Angew. Chem. Int. Ed. Engl.* **1997**, *36*, 2821.
- [10] K. C. Nicolaou, J. A. Vega, G. Vassilikogiannakis, *Angew. Chem.* **2001**, *113*, 4573; *Angew. Chem. Int. Ed.* **2001**, *40*, 4441.
- [11] P. Perlmutter, *Conjugate Addition Reactions in Organic Synthesis*, Pergamon, Oxford, **1992**, p. 376.

- [12] J. Tsuji, *Palladium Reagents and Catalysts*, Wiley, New York, **1995**, p. 560.
- [13] G. T. Crisp, A. G. Meyer, *J. Org. Chem.* **1992**, *57*, 6972.
- [14] F. A. Davis, M. S. Haque, *Adv. Oxygenated Processes* **1990**, *2*, 61.
- [15] S. V. Ley, J. Norman, W. P. Griffith, S. P. Marsden, *Synthesis* **1994**, *7*, 639.
- [16] E. J. Corey, M. Chaykovsky, *J. Am. Chem. Soc.* **1965**, *87*, 1345.
- [17] D. J. Lythgoe, I. McClenaghan, C. A. Ramsden, *J. Heterocycl. Chem.* **1993**, *30*, 113; for the elegant use of related amidofurans in synthesis, see A. Padwa, M. Dimitroff, B. Liu, *Org. Lett.* **2000**, *2*, 3233 and references therein.
- [18] N. Bodor, M. J. S. Dewar, A. J. Harget, *J. Am. Chem. Soc.* **1970**, *92*, 2929.
- [19] W. Nagata, M. Yoshioka, T. Okumura, *Tetrahedron Lett.* **1966**, 847.
- [20] J. C. Martin, J. A. Franz, R. J. Arhart, *J. Am. Chem. Soc.* **1974**, *96*, 4604.
- [21] K. C. Nicolaou, P. S. Baran, R. Jautelat, Y. He, K. C. Fong, H.-S. Choi, W. H. Yoon, Y.-L. Zhong, *Angew. Chem.* **1999**, *111*, 532; *Angew. Chem. Int. Ed.* **1999**, *38*, 549.
- [22] D. L. Hughes, *Org. React.* **1992**, *42*, 335.
- [23] D. P. Curran, H. Yu, *Synthesis* **1992**, 123.
- [24] a) J. E. Whiting, J. T. Edward, *Can. J. Chem.* **1971**, *49*, 3799; b) C. D. Hurd, W. Saunderson, *J. Am. Chem. Soc.* **1952**, *74*, 5324.
- [25] a) D. B. Dess, J. C. Martin, *J. Org. Chem.* **1983**, *48*, 4155; b) D. B. Dess, J. C. Martin, *J. Am. Chem. Soc.* **1991**, *113*, 7277; c) S. D. Meyer, S. L. Schreiber, *J. Org. Chem.* **1994**, *59*, 7549.
- [26] P. L. Anelli, C. Biffi, F. Montanari, S. Quici, *J. Org. Chem.* **1987**, *52*, 2559.
- [27] K. C. Nicolaou, Y. He, K. C. Fong, W. H. Yoon, H.-S. Choi, Y.-L. Zhong, P. S. Baran, *Org. Lett.* **1999**, *1*, 63.
- [28] For similar observations, see Q. Tan, S. J. Danishefsky, *Angew. Chem.* **2000**, *112*, 4683; *Angew. Chem. Int. Ed.* **2000**, *39*, 4509.
- [29] F. Arndt, B. Eistert, *Ber. Dtsch. Chem. Ges.* **1935**, *68B*, 200.
- [30] A. D. Mico, R. Margarita, L. Parlanti, A. Vescou, G. Piancatelli, *J. Org. Chem.* **1997**, *62*, 6974.
- [31] Successful removal of the benzylamide on model substrates was realized using protocols described in the following articles: D. A. Evans, P. H. Carter, C. J. Dinsmore, J. C. Barrow, J. L. Katz, D. W. Kung, *Tetrahedron Lett.* **1997**, *38*, 4535; D. L. Flynn, R. E. Zelle, P. A. Grieco, *J. Org. Chem.* **1983**, *48*, 2424.
- [32] J. C. Martin, J. A. Franz, *J. Am. Chem. Soc.* **1975**, *97*, 6137.
- [33] D. Ramesh, R. Wieboldt, A. P. Billington, K. B. Carpenter, G. P. Hess, *J. Org. Chem.* **1993**, *58*, 4599.
- [34] A. I. Meyers, D. L. Temple, D. Haidukewych, E. D. Mihelich, *J. Org. Chem.* **1974**, *39*, 2787.
- [35] M. J. V. De Oliveira Baptista, A. G. M. Barrett, D. H. R. Barton, M. Girijavallabhan, R. C. Jennings, J. Kelly, V. J. Papadimitriou, J. V. Turner, N. A. Usher, *J. Chem. Soc. Perkin Trans. 1* **1977**, 1477.
- [36] C. Chuo, M. E. Layton, S. M. Sheehan, M. D. Shair, *J. Am. Chem. Soc.* **2000**, *122*, 7424.
- [37] W. Nobuaki, T. Itoh, T. Fukuyama, *J. Am. Chem. Soc.* **2000**, *122*, 7825.
- [38] K. C. Nicolaou, P. S. Baran, Y.-L. Zhong, H.-S. Choi, K. C. Fong, Y. He, W. H. Yoon, *Org. Lett.* **1999**, *1*, 883.
- [39] K. C. Nicolaou, G. Vassilikogiannakis, R. Kranich, P. S. Baran, Y.-L. Zhong, S. Natarajan, *Org. Lett.* **2000**, *2*, 1895.
- [40] A. Varvoglis, *Hypervalent Iodine In Organic Synthesis*, Academic Press, New York, **1997**, p. 223; for other reviews, see a) T. Wirth, U. H. Hirt, *Synthesis* **1999**, 1271; b) A. Varvoglis, S. Spyroudis, *Synlett* **1998**, 221; c) T. Kitamura, Y. Fujiwara, *Org. Prep. Proced. Int.* **1997**, *29*, 409; d) P. J. Stang, V. V. Zhdankin, *Chem. Rev.* **1996**, *96*, 1123; e) R. M. Moriarty, R. K. Vaid, *Synthesis* **1990**, 431.
- [41] a) K. C. Nicolaou, Y.-L. Zhong, P. S. Baran, *Angew. Chem.* **2000**, *112*, 636; *Angew. Chem. Int. Ed.* **2000**, *39*, 622; b) K. C. Nicolaou, Y.-L. Zhong, P. S. Baran, *Angew. Chem.* **2000**, *112*, 639; *Angew. Chem. Int. Ed.* **2000**, *39*, 625.
- [42] K. C. Nicolaou, P. S. Baran, Y.-L. Zhong, J. A. Vega, *Angew. Chem.* **2000**, *112*, 2625; *Angew. Chem. Int. Ed.* **2000**, *39*, 2525.
- [43] K. C. Nicolaou, P. S. Baran, R. Kranich, Y.-L. Zhong, K. Sugita, N. Zou, *Angew. Chem.* **2001**, *113*, 208; *Angew. Chem. Int. Ed.* **2001**, *40*, 202.
- [44] K. C. Nicolaou, Y.-L. Zhong, P. S. Baran, *J. Am. Chem. Soc.* **2000**, *122*, 7596.
- [45] K. C. Nicolaou, T. Montagnon, P. S. Baran, Y.-L. Zhong, *J. Am. Chem. Soc.* **2002**, *124*, 2245.
- [46] K. C. Nicolaou, K. Sugita, P. S. Baran, Y.-L. Zhong, *Angew. Chem.* **2001**, *113*, 213; *Angew. Chem. Int. Ed.* **2001**, *40*, 207.
- [47] N. Matsumoto, T. Tsuchida, M. Umekita, N. Kinoshita, H. Iinuma, T. Sawa, M. Hamada, T. Takeuchi, *J. Antibiot.* **1997**, *50*, 900; N. Matsumoto, H. Iinuma, T. Sawa, T. Takeuchi, S. Hirano, T. Yoshioka, M. Ishizuka, *J. Antibiot.* **1997**, *50*, 906; N. Matsumoto, N. Agata, H. Kuboki, H. Iinuma, T. Sawa, T. Takeuchi, K. Umezawa, *J. Antibiot.* **2000**, *53*, 637.
- [48] Total synthesis from other research groups: H. Oka, T. Yoshinari, T. Murai, K. Kuwamura, F. Satoh, K. Funaiishi, A. Okura, H. Suda, M. Okanishi, Y. Shizuri, *J. Antibiot.* **1991**, *44*, 486.
- [49] N. Matsumoto, A. Ariga, S. To-E, H. Nakamura, N. Agata, S.-I. Hirano, J.-I. Inoue, K. Umezawa, *Bioorg. Med. Chem. Lett.* **2000**, *10*, 865; O. Block, G. Klein, H.-J. Altenbach, D. J. Brauer, *J. Org. Chem.* **2000**, *65*, 716; P. Wipf, P. D. G. Coish, *J. Org. Chem.* **1999**, *64*, 5053; L. Alcaraz, G. Macdonald, J. Ragot, N. J. Lewis, R. J. K. Taylor, *Tetrahedron* **1999**, *55*, 3707; for the first total synthesis, see N. Matsumoto, H. Iinuma, T. Sawa, T. Takeuchi, *Bioorg. Med. Chem. Lett.* **1998**, *8*, 2945.
- [50] Total syntheses from other research groups: C. J. Moody, E. Swann, *Tetrahedron Lett.* **1993**, *34*, 1987; H. Suda, M. Ohkubo, K. Matsunaga, S. Yamamura, W. Shimomoto, N. Kimura, Y. Shizuri, *Tetrahedron Lett.* **1993**, *34*, 3797.
- [51] K. C. Nicolaou, K. Sugita, P. S. Baran, Y.-L. Zhong, *J. Am. Chem. Soc.*, in press.
- [52] K. C. Nicolaou, Y.-L. Zhong, P. S. Baran, K. Sugita, *Angew. Chem.* **2001**, *113*, 2203; *Angew. Chem. Int. Ed.* **2001**, *40*, 2145.
- [53] S. A. Look, W. Fenical, G. Matsumoto, J. Clardy, *J. Org. Chem.* **1986**, *51*, 5140; W. Fenical, *J. Nat. Prod.* **1987**, *50*, 1001; S. A. Look, W. Fenical, *Tetrahedron* **1987**, *43*, 3363; for synthetic studies, see E. J. Corey, S. E. Lazerwith, *J. Am. Chem. Soc.* **1998**, *120*, 12777, and references therein.
- [54] A. D. Rodriguez, E. Gonzalez, S. D. Huang, *J. Org. Chem.* **1998**, *63*, 7083.
- [55] To the best of our knowledge, there have been no reported synthetic studies of α,β -unsaturated ketohydroxyamides such as **258**, except for a brief study of the related 3-bromo-2-hydroxy-2-acetamidocyclohexanone, see K. M. Ermolaev, V. I. Maimind, *Biol. Akt. Soedin.* **1968**, 142.
- [56] K. C. Nicolaou, P. S. Baran, Y.-L. Zhong, *J. Am. Chem. Soc.* **2001**, *123*, 3183.
- [57] F. Lehmann, A. Pedro, *J. Med. Chem.* **1972**, *15*, 404.
- [58] S. S. Simons, Jr., M. Pons, D. F. Johnson, *J. Org. Chem.* **1980**, *45*, 3084.
- [59] R. V. Hoffman, *Tetrahedron* **1991**, *47*, 1109.
- [60] K. C. Nicolaou, P. S. Baran, Y.-L. Zhong, *J. Am. Chem. Soc.* **2000**, *122*, 10246.
- [61] K. C. Nicolaou, T. Montagnon, T. Ulven, P. S. Baran, Y.-L. Zhong, F. Sarabia, *J. Am. Chem. Soc.* **2002**, *124*, 5718.
- [62] K. C. Nicolaou, T. Montagnon, P. S. Baran, *Angew. Chem.* **2002**, *114*, 1035; *Angew. Chem. Int. Ed.* **2002**, *41*, 993.
- [63] K. C. Nicolaou, D. L. F. Gray, T. Montagnon, S. T. Harrison, *Angew. Chem.* **2002**, *114*, 1038; *Angew. Chem. Int. Ed.* **2002**, *41*, 996.
- [64] K. C. Nicolaou, T. Montagnon, P. S. Baran, *Angew. Chem.* **2002**, *114*, 1444; *Angew. Chem. Int. Ed.* **2002**, *41*, 1386.
- [65] A Scifinder Scholar search uncovered hundreds of uses, including the following: nonlinear optics: D. N. Nikogosyan, G. G. Gurzadyan, *Kvantovaya Elektron. (Moscow)* **1987**, *14*, 1529; C. D. Lack, T. M. Thomas, Q. Ye, *PCT Int. Appl.* **2001**, 23 [CA Abstract No. 135:154189]; semi-conductors: K. Anderson, M. Hamalainen, M. Malmquist, H. Roos, *PCT Int. Appl.* **1999**, 133 [CA Abstract No. 132:20747]; biosensors: I. E. Vermeir, H. H. Goossens, F. Vandekerckhove, W. P. Gomes, *J. Electrochem. Soc.* **1992**, *139*, 1389; electrochemistry: T. R. Green [CA Abstract No. 134:316180].
- [66] IA and IP are available from a number of suppliers including Aldrich.
- [67] For instance, crystalline IP is prepared by sublimation of powdered IP at 250°C, see K. Selte, A. Kjekshus, *Acta Chem. Scand.* **1970**, *24*, 1912.

- [68] a) K. C. Nicolaou, W.-M. Dai, *Angew. Chem.* **1991**, *103*, 1453; *Angew. Chem. Int. Ed. Engl.* **1991**, *30*, 1387; b) K. C. Nicolaou, W.-M. Dai, S.-C. Tsay, V. A. Estevez, W. Wrasidlo, *Science* **1992**, *256*, 1172; c) K. C. Nicolaou, P. Stabila, B. Asmaeli-Azad, W. Wrasidlo, A. Hiatt, *Proc. Natl. Acad. Sci. USA* **1993**, *90*, 3142.
- [69] a) K. C. Nicolaou, F. Roschangar, D. Vourloumis, *Angew. Chem.* **1998**, *110*, 2120; *Angew. Chem. Int. Ed.* **1998**, *37*, 2014; b) K. C. Nicolaou, A. Ritzén, K. Namoto, *Chem. Commun.* **2001**, 1523.
- [70] a) K. C. Nicolaou, C. N. C. Boddy, S. Bräse, N. Winssinger, *Angew. Chem.* **1999**, *111*, 2230; *Angew. Chem. Int. Ed.* **1999**, *38*, 2097; b) K. C. Nicolaou, R. Hughes, S.-Y. Cho, N. Winssinger, C. Smethurst, H. Labischinski, R. Endermann, *Angew. Chem.* **2000**, *112*, 3981; *Angew. Chem. Int. Ed.* **2000**, *39*, 3823; c) K. C. Nicolaou, S. Y. Cho, R. Hughes, N. Winssinger, C. Smethurst, H. Labischinski, R. Endermann, *Chem. Eur. J.* **2001**, *7*, 3798; d) K. C. Nicolaou, R. Hughes, S. Y. Cho, N. Winssinger, H. Labischinski, R. Endermann, *Chem. Eur. J.* **2001**, *7*, 3824.
- [71] *Greek Mythology* (Ed.: Techni S. A.), Athens, **1998**.
-

High-Performance Fibers from Spider Silk**

Stefan Kubik*

An insect trapped in a spider net has usually no chance of escape. Although a spider net is composed of the smallest amount of ultrathin fibers, it effectively captures rapidly flying insects without breaking, leaving the prey entangled. This ability is largely explained by the mechanical properties of the spider silk, the major component of the spider-net fibers. Spider silk is an unusually tearproof, strong, and elastic fiber protein that is only surpassed in these properties by some modern synthetic high-performance polymers.^[1] Table 1

Table 1. Selected properties of some natural and synthetic fibers.^[1]

	Density [g cm ⁻³]	Elasticity modulus [GPa]	Tenacity [GPa]	Strain break [%]	Toughness [MJ m ⁻³]
nylon 6,6	1.1	5	0.95	18	80
kevlar 49	1.4	130	3.6	3	50
dragline of <i>A. diadematus</i>	1.3	10	1.1	27	160
silk of the moth <i>B. mori</i>	1.3	7	0.6	18	70
wool	1.3	0.5	0.2	50	60
high-tensile steel	7.8	200	1.5	1	6

shows that the orb-web-spinning spider *Araneus diadematus* produces a silk for the dragline and the radiating spokes of the net the strength of which approaches that of high-tensile steel while being significantly more extensible, as well as lighter. Although highly ordered poly(*p*-phenyleneterephthalamide) fibers (Kevlar) are stronger than spider silk and almost as light, they are also significantly less elastic. Moreover, spider silk is hydrophilic, yet not water soluble, and biodegradable.

This comparison clearly demonstrates that spider silk is a highly interesting fiber for, for example, medicinal applications or the production of light and strong composite materials. In contrast to the textile silk that is traditionally produced by cultivation of the silk moth *Bombyx mori*, the isolation of larger amounts of spider silk from the natural resources is not feasible, however, because of the territorial nature of spiders. Alternatively, spider silk can be synthesized

using microbiological methods but, in spite of various attempts, to date no material has thus been produced that is able to compete with natural silk. Only recently, researchers from Nexia Biotechnologies, in cooperation with the Materials Science Team of the U.S. Army, described the successful synthesis of a spider-silk protein with similar mechanical properties to the natural counterpart, by transfer of the corresponding gene into suitable mammalian cells.^[2] A larger scale production of synthetic spider silk thus becomes practicable.

Orb-web spiders produce up to seven different types of silk, which are optimized for different applications in net spinning or cocoon wrapping.^[1, 3] One of the best-investigated spider silks is the one in the dragline, because of its interesting mechanical properties. The nonprotein content of this silk is <1%,^[3] so that investigations on the molecular origins of its mechanical properties can focus on the fiber protein itself. The silk of a dragline usually contains more than one type of protein, however. For the dragline of the two most-studied orb-web-spinning spiders *Nephila clavipes* and *Araneus diadematus*, two and four protein components have been identified, respectively: spidroin I (MaSpI) and spidroin II (MaSpII),^[4] from the former and ADF-1 to ADF-4 from the latter.^[5] The amino acid sequence of all of these proteins has been elucidated with the help of recombinant DNA technology.^[4, 5] In spite of differences in their exact primary structures, all protein chains feature common characteristic sequence motifs of alanine-rich regions that alternate with regions containing mostly glycine. X-ray diffraction and FT-IR spectroscopic investigations indicated that the alanine-rich regions are located in crystalline domains of the silk fiber with a β -sheet structure. The glycine-rich chain segments adopt a much less ordered secondary structure, in which turns or helices can occur locally that are stabilized by hydrogen bonds.^[1, 4] Glutamine residues in the amorphous regions of the polymer chains are responsible for the hydrophilic nature of the spider silk.^[1] The resulting overall protein structure resembles that of synthetic elastomers, in which rigid cross-linked sites alternate with flexible, randomly oriented polymer-chain segments. The origins of the elastic properties of spider silk and synthetic elastomers are therefore very similar: strain caused by an external source induces orientation in the flexible chain segments, whereby the degree of extension depends largely on the length of the chains in the amorphous regions. Releasing the strain causes the extended regions to return to the less ordered structure because of the associated

[*] Priv.-Doz. Dr. S. Kubik
Institut für Organische Chemie und Makromolekulare Chemie
Heinrich-Heine-Universität
Universitätsstrasse 1, 40225 Düsseldorf (Germany)
Fax: (+49) 211-81-14788
E-mail: kubik@uni-duesseldorf.de

[**] I thank Professor Dr. H. Ritter for a critical reading of this manuscript.

entropy gain (Figure 1). In addition to the primary structure of the protein, the tertiary and quaternary structures that arise during the spinning process in Nature also strongly influence the properties of the silk, and all have to be reproduced optimally to prepare fibers with similar mechanical properties to spider silk.

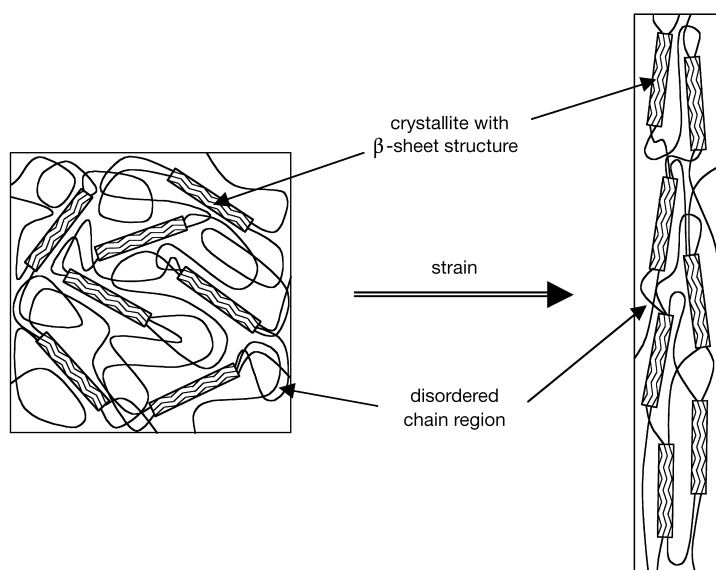


Figure 1. Schematic representation of the three-dimensional structure of a spider-silk dragline, and the effect of mechanical strain on this structure.

Although microbiological syntheses of proteins are state of the art today, the production of fiber proteins with a highly repetitive amino acid sequence remains problematic.^[6] One reason is the occurrence of repetitive sequences in the gene for the protein causes a genetic instability. Furthermore, repetitive sequences in the complementary mRNA chains can induce undesirable secondary structures that hinder translation. Finally, fiber proteins often contain certain amino acids in high amounts (in the spider-silks, alanine and glycine) and cells therefore have to provide an extensive pool of the corresponding tRNAs for effective protein synthesis. These limitations cause the molecular weight distribution of spider-silk proteins synthesized by transgenic *E. coli* bacteria to be highly heterogeneous with a significant amount of prematurely terminated chains.^[7] Transfected yeast^[8] or plants such as tobacco or potatoes^[9] have been shown to be more suitable for a synthesis of the spider-silk protein, but all these strategies had the disadvantage that the product accumulated inside the cell, for example, in the endoplasmic reticulum of plant cells, which necessitated a number of steps for isolation. The strategy proposed by the team of Nexia Biotechnologies to use suitable mammalian cells specialized for the secretion of proteins for the synthesis of spider silk thus represents a significant advancement over previous work.^[2] These cells have the advantage that they release the protein during synthesis into the surrounding solution, from which it can be isolated easily. Moreover, the cells are more closely related to the epithelial cells that produce silk proteins in the glands of the spiders, and they are therefore better suited to an error-free protein synthesis.

The mammalian cell lines used consisted of bovine mammary cells (MAC-T) and hamster kidney cells (BHK), into which partial cDNA encoding a spider-silk protein (MaSpI, MaSpII, or ADF-3) was transferred.^[2] Afterward, these cells were able to produce the corresponding protein, however, the combination of BHK and ADF-3 gave the best results. Because the cells were transfected with partial cDNA, the molecular weight of the protein synthesized was 60 kD, and was thus significantly lower than the average molecular weight (M_w) of natural spider-silk proteins, which can reach 740 kD.^[10] Although a transfer of cDNA multimers into the cells resulted in the expression of proteins with the expected higher molecular weights, synthesis proceeded less effectively, an observation that was ascribed to the above-mentioned reasons. The investigations on fiber processing thus focused on ADF-3 weighing 60 kD. This protein was produced continuously in a hollow-fiber culture system in a total amount of 12 g (ca. 20 μ g per 10⁶ cells per day). Afterward, it was enriched by precipitation with ammonium sulfate, and purified chromatographically. The product was readily soluble in phosphate-buffered saline, an important advantage for processing, and a significant difference to spider-silk proteins produced by *E. coli* or yeast.^[7, 8]

In the silk gland of orb-web-spinning spiders, the silk protein is dissolved in a concentrated lyotropic liquid-crystalline solution. During extrusion, the silk assembles into fibers without the need for strong mechanical forces,^[11] a process that differs from the industrial spinning of many synthetic polymers. Hereby, a polymer, often dissolved in an appropriate solvent, is extruded into a coagulation bath through an opening of suitable diameter, and the mechanical properties of the fiber formed are improved afterward by an external postspinning draw. Although the natural spider-silk protein can, in principle, be processed by a method similar to industrial spinning,^[12] the fiber thus obtained possesses mechanical properties which are inferior to those of the natural starting material. This effect is partly attributed to the need to use the denaturing hexafluoroisopropanol as a solvent, which perturbs the secondary structure of the protein too strongly, and thus the preorganization of the protein chains during spinning. In contrast, an aqueous solution of the synthetic ADF-3 protein produced by BHK could be processed,^[2] which resulted in a fiber with a diameter of 20 μ m after postspinning draw, whose morphology, stiffness, and extensibility compared favorably with the ones of the natural dragline silk of *Araneus diadematus*. Only the strength tenacity remained lower, yet it did approach that of fibers spun from regenerated spider silk (Table 2).^[12] Considering that the molecular weight of the protein used for the preparation of the fiber is lower than that of the natural fiber

Table 2. Comparison of selected properties of natural, regenerated, and synthetic spider silk.

	Elasticity modulus [GPa]	Tenacity [GPa]	Strain break [%]
dragline of <i>N. clavipes</i> ^[1]	22	1.3	12
dragline of <i>A. diadematus</i> ^[1]	10	1.1	27
regenerated silk of <i>N. clavipes</i> ^[12]	8	0.32	
synthetic ADF-3 ^[2, 15]	13	0.26	43

protein, and that only a single component of the dragline silk was used, the reported results are impressive. It is expected that, by optimizing the process, possibly in combination with a deliberate variation of the primary structure of the protein,^[13] fibers that are almost indistinguishable from natural spider silk will be accessible. Nexia Biotechnologies manufactures these fibers under the brand name BioSteel. For the production of larger amounts, they plan to use transgenic goats that express the silk protein in their milk.^[14] Applications of spider silk are anticipated in areas where high mechanical strength, in combination with biodegradability, of fibers and films produced thereof are advantageous, for example, in medicine. The presented results show that a production of high-performance polymers on the basis of spider silk is a promising prospect for the very close future.

- [1] J. M. Gosline, P. A. Guerette, C. S. Ortlepp, K. N. Savage, *J. Exp. Biol.* **1999**, *202*, 3295–3303.
 [2] A. Lazaris, S. Arcidiacono, Y. Huang, J.-F. Zhou, F. Duguay, N. Chretien, E. A. Welsh, J. W. Soares, C. N. Karzas, *Science* **2002**, *295*, 472–476.

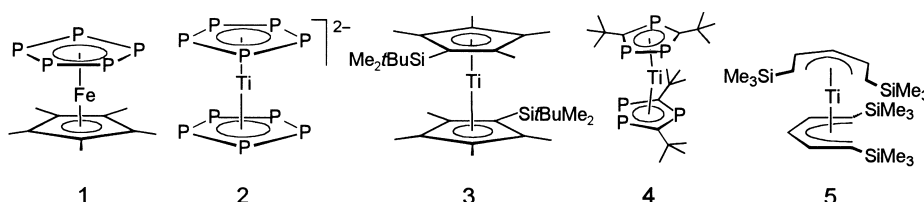
- [3] S. Schulz, *Angew. Chem.* **1997**, *109*, 324–327; *Angew. Chem. Int. Ed. Engl.* **1997**, *36*, 314–327.
 [4] R. V. Lewis, *Acc. Chem. Res.* **1992**, *25*, 392–398.
 [5] P. A. Guerette, D. G. Ginzinger, B. H. F. Weber, J. M. Gosline, *Science* **1996**, *272*, 112–115.
 [6] J. P. O'Brien, *Trends Polym. Sci.* **1993**, *1*, 228–232.
 [7] S. R. Fahnestock, S. L. Irwin, *Appl. Microbiol. Biotechnol.* **1997**, *47*, 23–32.
 [8] S. R. Fahnestock, L. A. Bedzyk, *Appl. Microbiol. Biotechnol.* **1997**, *47*, 33–39.
 [9] J. Scheller, K.-H. Gührs, F. Grosse, U. Conrad, *Nat. Biotechnol.* **2001**, *19*, 573–577.
 [10] C. Jackson, J. P. O'Brien, *Macromolecules* **1995**, *28*, 5975–5977.
 [11] F. Vollrath, D. P. Knight, *Nature* **2001**, *410*, 541–548.
 [12] A. Seidel, O. Liivak, S. Calve, J. Adaska, G. Ji, Z. Yang, D. Grubb, D. B. Zax, L. W. Jelinski, *Macromolecules* **2000**, *33*, 775–780.
 [13] J. P. O'Brien, S. R. Fahnestock, Y. Termonia, K. H. Gardner, *Adv. Mater.* **1998**, *10*, 1185–1195.
 [14] P. Cohen, *New. Sci.* **1998**, *160*(2155), 11. Also see: www.nexiabiochem.com.
 [15] The dimension gpd (grams per denier) used for the modulus of elasticity and tenacity in reference [2] was converted into GPa according to $(\text{gpd} \cdot \delta) / 11.33 \delta$, whereby a value of 1.3 g cm^{-3} was assumed for the density (H.-G. Elias, *Makromoleküle*, Vol. 2, 5th ed., Hüthig & Wepf, Basel, **1992**, p. 522).

The Decaphosphatitanocene Dianion—A New Chapter in the Chemistry of Naked Polyphosphorus Ligands

Helmut Sitzmann*

Even before those progressive researchers had thought about sandwich complexes, ferrocene had already formed from iron and cyclopentadiene, had been collected,^[1] and was awaiting discovery. When $[(\text{C}_5\text{Me}_5)\text{TiCl}_3]$ was distilled from the products of a TiCl_4 -catalyzed olefin isomerization reaction forty years ago,^[2] the affinity of transition metals to this prototype of a pentaalkylcyclopentadienyl ligand became apparent and fueled the boom in cyclopentadienyl complex chemistry.

The interest in transition-metal-promoted self-assembly of five-membered-ring ligands extended to Group 15 at the end of the 1980s, when the dinuclear iron complex $[(\text{C}_5\text{Me}_5)\text{Fe}(\text{CO})_2]_2$ was allowed to react with white phosphorus.^[3] The resulting product, namely pentamethylpentaphosphaferrocene (**1**), stimulated the newly emerging area of P_n complexes



and awakened the idea of bis(pentaphosphacyclopentadienyl) metal complexes (often referred to as decaphosphametallo-cenes).^[4]

While steric protection is not available to prevent aggregation of decaphosphametallo-cenes, electrostatic repulsion is. When Ellis and Urnėžius et al.^[5] treated the bis(naphthalene)titanium dianion with 2.5 equivalents of P_4 at low temperature, the decaphosphatitanocene dianion $[\text{Ti}(\eta^5\text{-P}_5)_2]^{2-}$ (**2**) was formed in high yield as the $2[\text{Na}([18]\text{crown-6})]^+$ salt.^[5]

Whereas the known metallocene dianions that have been generated by electrochemical reduction are highly labile species,^[6] **2** is unreactive with carbon monoxide, xylol isocyanide, or trimethylphosphite, is stable in solution under an atmosphere of pure dioxygen, can be handled in air, and is only slowly attacked by wet pyridine. Crystalline samples of $(\text{PPh}_4^+)_2$ and $(\text{Ph}_3\text{PNPPH}_3^+)_2$ salts of **2** melt at 213–215

[*] Prof. Dr. H. Sitzmann
 FB Chemie der Universität Kaiserslautern
 Erwin-Schrödinger-Strasse, 67663 Kaiserslautern (Germany)
 Fax: (+49) 631-205-2187
 E-mail: sitzmann@chemie.uni-kl.de

(decomp) and 319–323 °C (decomp), respectively. The nature of the cation has little influence on the ^{31}P NMR singlet resonance of **2**, which is observed between $\delta = 60$ and 63 ppm.

The stability of **2** is attributed in part to steric properties of the *cyclo*- P_5 ligand. The plane of this relatively large ring has to move quite close to the metal to allow typical Ti–P bond lengths of 256 pm. The distance of 360 pm between the two P_5 rings in the fully eclipsed molecule **2** is therefore much shorter than the value of 402 pm observed for centrosymmetric $[\text{Ti}(\text{C}_5\text{Me}_4\text{SiMe}_2t\text{Bu})_2]$ (**3**)^[7] and provides steric shielding of the Ti center.

Even more important for the stability and for the diamagnetic ground state of **2** are the electronic properties of the *cyclo*- P_5 ligand. $\eta^5\text{-P}_5$ is a weaker donor, but much stronger acceptor than the cyclopentadienyl ligand, according to density functional computations.^[5] Diamagnetism has also been found for the hexaphosphatitanocene $[\text{Ti}(\text{P}_3\text{C}_2t\text{Bu}_2)_2]$ (**4**).^[8] The small p, π overlap of the phosphorus atoms results in a closer spacing of the ligand π orbitals and places the empty π orbitals low enough in energy to encourage mixing with the titanium 3d HOMO and formation of a metal–ring δ bond. This electron delocalization facilitates spin pairing to form a diamagnetic ground state.^[8] In contrast, the titanocene derivative **3** possesses two unpaired electrons.^[7] Similar steric and electronic arguments have been used to explain the stability and the singlet ground state of “open” titanocenes such as $[\text{Ti}(\text{C}_5\text{H}_5(\text{SiMe}_3)_2)_2]$ (**5**).^[9]

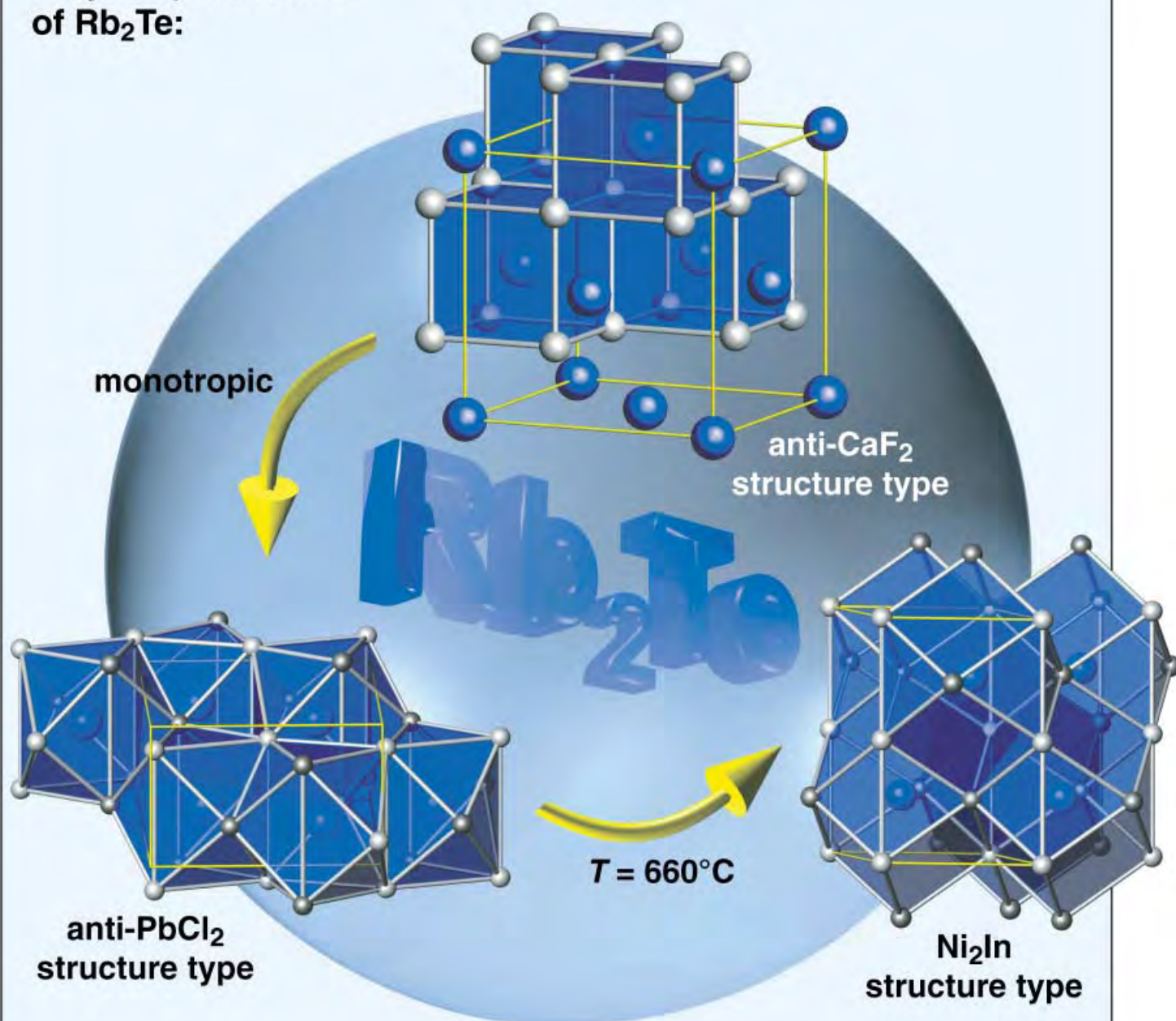
Treatment of **2** with potassium pentamethylcyclopentadienide or 1,4,7-triazacyclononane in pyridine leads to the formation of the free P_5^- ion, as indicated by a ^{31}P NMR signal at $\delta = 468$ ppm. If this reactivity of **2** can be developed into a clean process, **2** may not only become a source of the *cyclo*- P_5 ligand, but possibly also of titanium complexes with one P_5 ring. Some of the questions to be answered in future concern the redox behavior of **2** and the possibility of stacking

reactions in which **2** is used as a nucleophile analogously to the anionic sandwich complexes with boron heterocycles.^[10]

The selective formation of P_5 rings from P_4 , and the surprising stability of **2** most likely indicate that the decaphosphatitanocene dianion acts as the energetic sink in a complicated reaction mixture. This feature can be related to the ligand properties of *cyclo*- P_5 and is probably not restricted to the titanium complex. It will therefore be highly interesting to search for decaphosphametalloocene mono- and especially dianions of other metals, preferably among Groups 4–7 and possibly including second- and third-row transition metals.

- [1] Pauson mentioned (P. L. Pauson, *J. Organomet. Chem.* **2001**, 637–639, 3–6) that S. A. Miller had had ferrocene for about three years before his publication with J. A. Tebbboth and J. F. Tremaine appeared in 1952, but a research team at Union Carbide had collected ferrocene as a “yellow sludge” from clogged iron pipes of a cyclopentadiene crack process even earlier.
- [2] H. Röhl, E. Lange, T. Göbl, G. Roth, *Angew. Chem.* **1962**, 62, 155; *Angew. Chem. Int. Ed. Engl.* **1962**, 1, 117.
- [3] O. J. Scherer, T. Brück, G. Wolmershäuser, *Angew. Chem.* **1987**, 99, 59; *Angew. Chem. Int. Ed. Engl.* **1987**, 26, 59. Pentaarsaferrocenes have been obtained by similar procedures: O. J. Scherer, C. Blath, G. Wolmershäuser, *J. Organomet. Chem.* **1990**, 387, C21–C24.
- [4] M. Baudler, S. Akpapgolu, D. Ouzounis, F. Wasgestian, B. Meinigke, H. Budzikiewicz, H. Münster, *Angew. Chem.* **1988**, 100, 288–289; *Angew. Chem. Int. Ed. Engl.* **1988**, 27, 280–281.
- [5] E. Urnėžius, W. W. Brennessel, C. J. Cramer, J. E. Ellis, P. von R. Schleyer, *Science* **2002**, 295, 832–834.
- [6] A. J. Bard, E. Garcia, S. Kukharensko, V. Strelets, *Inorg. Chem.* **1993**, 32, 3528–3531.
- [7] P. B. Hitchcock, F. M. Kerton, G. A. Lawless, *J. Am. Chem. Soc.* **1998**, 120, 10264–10265.
- [8] F. G. N. Cloke, J. C. Green, J. R. Hanks, J. F. Nixon, J. L. Suter, *J. Chem. Soc. Dalton Trans.* **2000**, 3534–3536.
- [9] a) R. D. Ernst, *Chem. Rev.* **1988**, 88, 1255–1291; b) R. D. Ernst, *Comm. Inorg. Chem.* **1999**, 21, 285, and references therein.
- [10] M. Stefan, P. Müller, U. Zenneck, H. Pritzkow, W. Siebert, R. N. Grimes, *Inorg. Chem.* **1995**, 34, 2058–2067.

Polymorphic forms of Rb_2Te :



The polymorphic form of Rb_2Te that is metastable at room temperature crystallizes in the anti- CaF_2 structure type. Upon warming, it converts irreversibly into the anti- PbCl_2 type. Above $T = 660^\circ\text{C}$, Rb_2Te adopts a Ni_2In -type structure.

In the given polymorph series, the coordination number of the Te atom increases from 8 (cubic), through 9 (double-capped trigonal prism), to 11 (Edshammam polyhedra), which is uncharacteristic of a high-temperature polymorph series.

For more information, see the following pages.

Polymorphic Forms of Rubidium Telluride Rb₂Te**

Klaus Stöwe* and Stephan Appel

The crystal structures of the di(alkali-metal) monochalcogenides A₂Q are known for all the compounds with A = Li–Cs and Q = O–Te, except for one. All the structurally characterized compounds, except the cesium chalcogenides, crystallize in a fluorite-type structure^[1–4] under normal conditions, whereas the cesium chalcogenides, except Cs₂O, which can be assigned to the anti-CdCl₂ type,^[5] crystallize in an anti-PbCl₂-type structure.^[4, 6] The exception mentioned above is the compound Rb₂Te, whose structure has not yet been reported in the literature. On the basis of poor data, complicated diagrams were obtained from diffraction experiments, but they could not be indexed.^[7] This is as a result of the difficulties in the synthesis and the instability of the substance.^[4] Within the scope of our investigations into ternary alkali rare-earth tellurides, we also intended to use the compound Rb₂Te as a flux during synthesis. We therefore considered a characterization of Rb₂Te as a necessary prerequisite.

We developed special laboratory glassware for the synthesis of the highly unstable Rb₂Te.^[8] The apparatus allows the single-phase preparation of all alkali chalcogenides. During synthesis of Rb₂Te from its elements in liquid ammonia, the product was formed as a yellow-green powder after extraction of the excess rubidium metal. A light-yellow product is obtained after prolonged extraction with ammonia. The ammonia solution above the product is light-blue in color during the whole extraction process as a result of the dissolved rubidium metal. From this observation, together with the occurrence of Bragg peaks in the powder diffraction pattern that indicate foreign phases, we deduced that the light-yellow product has a lower Rb content than the yellow-green substance. The phase composition of the products was analyzed by means of X-ray powder diffraction, and their thermal stability was determined by means of differential thermal analysis (DTA).

DTA of the yellow-green thermally untreated product obtained from liquid ammonia (i.e. the stoichiometric compound) shows several phase transitions (Figure 1): above 200 °C it slowly undergoes an irreversible transformation, which ends at about 470 °C (heating rate of 5 °C min^{−1}). The irreversibility of the phase transition can be concluded from the cooling curve: the exothermic effect of the heating curve in the temperature range below 500 °C is no longer observed. Furthermore, this effect is also not observed when the sample is reheated, and even samples that have been annealed for several days at 200 °C do not undergo a retransformation.

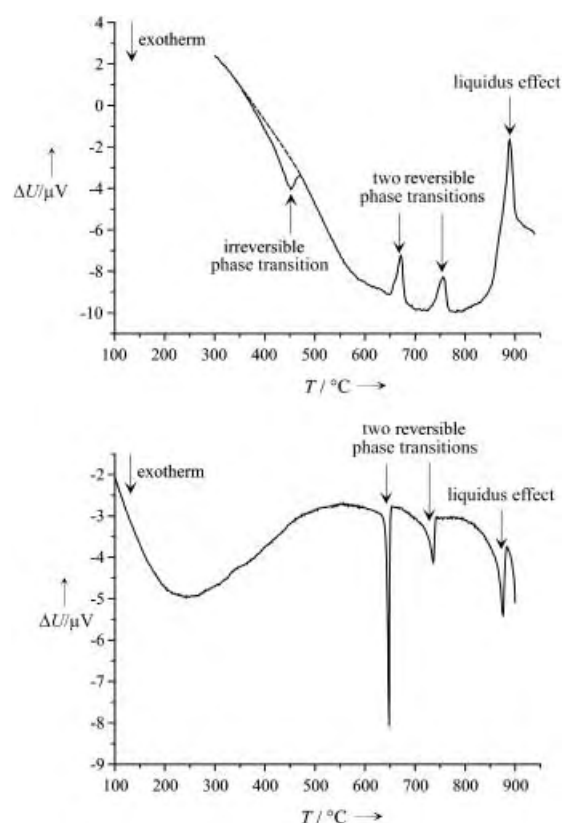


Figure 1. DTA of Rb₂Te. We used cubic, thermally untreated ω -Rb₂Te, which transformed irreversibly into orthorhombic α -Rb₂Te and then into β - and γ -Rb₂Te. Rb₂Te melts congruently at 880 °C. Top: heating curve (heating rate 5 °C min^{−1}). Under these conditions, the $\omega \rightarrow \alpha$ transition is temporarily delayed and not complete until 470 °C. Bottom: cooling curve (cooling rate 5 °C min^{−1}). There is no retransformation into the cubic phase.

Herein, the phase that is metastable at room temperature is termed the ω modification^[*] and the stable phase is referred to as the α modification. A complete $\omega \rightarrow \alpha$ transformation is already observed after annealing at 350 °C for 24 h. The α modification transforms reversibly at 660 °C into β -Rb₂Te, which is transformed further into γ -Rb₂Te at 745 °C. The congruent melting point is attained at 880 °C.

Structure analysis was carried out on powder samples, and the diffraction patterns were interpreted with the aid of programs for reflection-profile analysis and Rietveld refinement (see Experimental Section). When the yellow-green product was analyzed, the diffraction patterns of the different modifications did not show any Bragg peaks of foreign phases. According to the diffraction experiments, the ω modification that is metastable at room temperature crystallizes in an anti-CaF₂-type structure with the space group $Fm\bar{3}m$ and the lattice parameter $a = 849.02(3)$ pm, isotypic to the other rubidium monochalcogenides and also to lithium-, sodium-, and potassium monochalcogenides. On the other hand, the α -Rb₂Te modification that is stable at room temperature forms the anti-PbCl₂-structure type with the space group $Pnma$ and the lattice parameters $a = 896.60(3)$, $b = 557.15(2)$, and $c = 1095.43(3)$ pm. The α phase, however, can only be obtained

[*] Priv.-Doz. Dr. K. Stöwe, Dr. S. Appel
Anorganische und Analytische Chemie und Radiochemie, FR 8.14
Universität des Saarlandes
Postfach 15 11 50, 66041 Saarbrücken (Germany)
Fax: (+49) 681-302-4233
E-mail: k.stoewe@mx.uni-saarland.de

[**] Chemistry of rubidium telluride, Part 1. This work was supported by the Fonds der Chemischen Industrie.

[*] The authors are aware that there is no consistent system for the designation of polymorphic forms.^[9]

as the single-phase product when using the yellow-green product that has undergone little or no extraction with ammonia. After annealing and transformation into the modification that is stable at room temperature, the light-yellow product shows, in addition to the α -Rb₂Te Bragg peaks, further low-intensity peaks of additional phases in the diffraction pattern. These peaks can be assigned to the neighboring phase Rb₅Te₃. We can conclude from this result that the ω modification has a larger compositional width than the other modifications. Transformation into the α modification again results in a second phase with a lower Rb content than Rb₂Te. This result is reinforced by reexamination of the Rb–Te phase diagram by DTA measurements, which will be reported elsewhere. These investigations show that based on thermal effects, the light-yellow product can be ranged in a molar composition of $0.333 < x(\text{Te}) < 0.4$.

The two observed structure types show different anion coordination environments: The Te atoms in ω -Rb₂Te with the Li₂O structure are surrounded by eight Rb atoms in the form of a cube. In α -Rb₂Te with the anti-cotunnite or PbCl₂ structure, nine Rb atoms surround the Te atoms in the shape of a distorted threefold-capped trigonal prism (Figure 2). This phase transition is well known in the literature; however, it is pressure- and not temperature-induced. For example, the difluorides of Ca, Cd, Sr, Eu, Ba, and Pb^[10, 11] or the dioxides of Ce, Th, and Pu^[12, 13] show this phase transition. It follows the pressure-coordination rule and represents the only known type of phase transition with a change in coordination number from 8 to 9.^[14] In the case of Rb₂Te we can deduce by following the Ostwald rule that synthesis in liquid ammonia at first generates a metastable modification with low density, which is transformed into the denser stable modification at higher temperatures.

The structural degrees of freedom that refer to the lattice parameter relations of the orthorhombic cotunnite-structure type (space group *Pnma*) have already been analyzed and plotted in structure maps such as that shown in Figure 3.^[15–17] Beck and Beyer showed that the ionic representatives of the PbCl₂ type can always be assigned to one of exactly three POPS-topologies (POPS = Periodic Zero Potential Surface)^[18] which means that a further subdivision of the structure map is possible. By extending the structure map to the di(alkali-metal) monochalcogenides that crystallize in the anti-cotunnite type, it will become apparent that they belong to the PbCl₂ family and not to the SbSI family. The lower part of Figure 3 shows how α -Rb₂Te changes its position in the structure map with increasing temperature: During the thermal expansion, the point for α -Rb₂Te moves to a zone of intermetallic Co₂P-type compounds. At the temperature of the phase transition into the hexagonal modification β -Rb₂Te ($T_U = 660^\circ\text{C}$), there are large discontinuities in the lattice parameters *b* and *c* after the transformation of the hexagonal cell into an orthorhombic setting (Figure 4, top), which is also noticeable in the structure map. The lattice parameter *a* as well as the molar volume (Figure 4, bottom) show hardly any discontinuities, which points to a relatively large displacive and only a small reconstructive character in the transformation (see discussion below on the symmetry relations between the space groups).

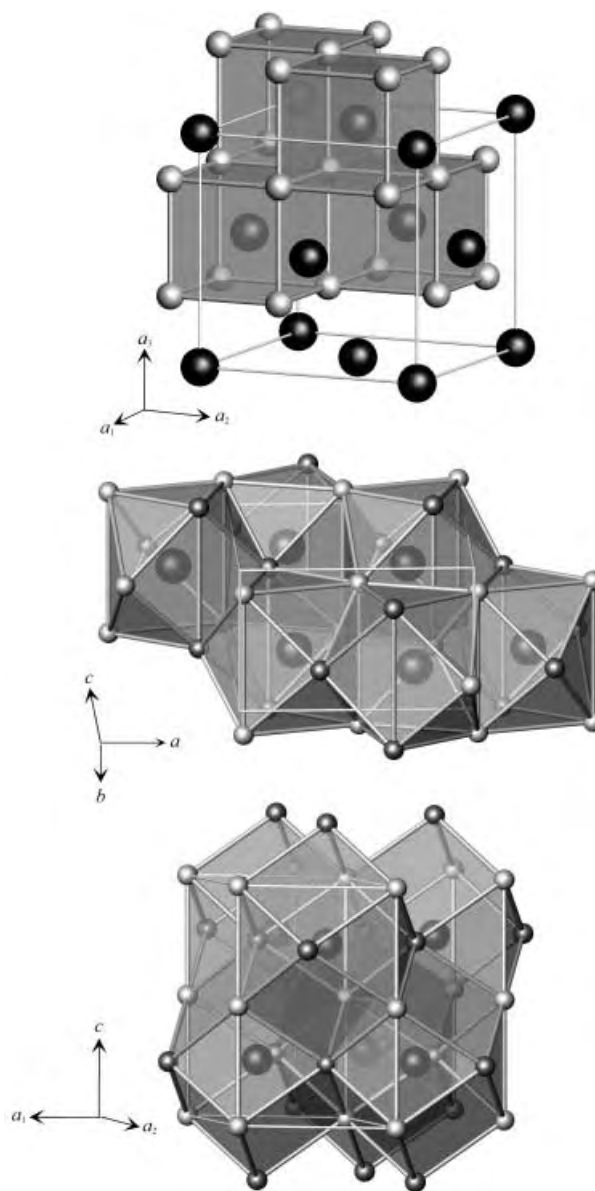


Figure 2. Crystal structures of ω -Rb₂Te (anti-CaF₂ type, top), α -Rb₂Te (anti-PbCl₂ type, middle), and β -Rb₂Te (Ni₂In type, bottom); Te: big, dark-gray spheres; Rb: small, light- and medium-gray spheres.

The X-ray diffraction pattern of the high-temperature phase above $T = 680^\circ\text{C}$ can be indexed in an orthorhombic crystal system, but also in a hexagonal system. The hexagonal lattice parameter relations as well as the peak intensities indicate the Ni₂In-structure type for this modification. The space group of this type is *P6₃/mmc* and for β -Rb₂Te the lattice parameters $a = 611.10(5)$ and $c = 919.0(1)$ pm have been refined for $T = 680^\circ\text{C}$. The Ni₂In-structure type is a filled NiAs-type structure and features relatively high coordination numbers of the atoms. Thus Rb(1) in β -Rb₂Te is surrounded by 12 + 2 neighbors in the form of a double-capped hexagonal prism in which the close neighbors are six Rb(2) and six Te atoms at equal distances, whereas the caps of the prism are formed by two slightly more distant Rb(1) atoms. The coordination environments of Rb(2) and Te are geometrically

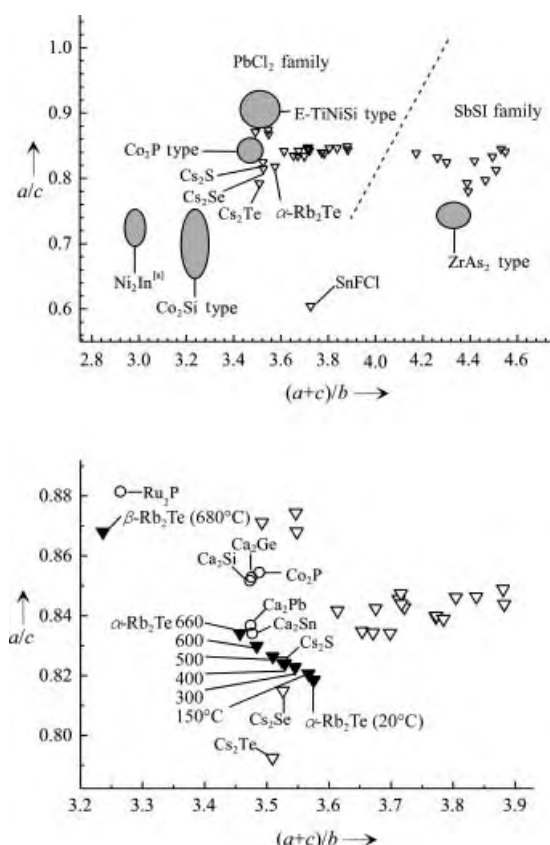


Figure 3. Extended structure map of the PbCl_2 -type according to Jeitschko.^[17] The regions of the covalent and the intermetallic compounds are marked in gray and partly scaled down. Top: overview. Bottom: detail with thermal behavior of Rb_2Te .^[4, 6, 17, 18, 20, 25] [a] Ni_2In does not belong to the PbCl_2 -structure type; however, transformed data have been added to the diagram,^[26] as this crystal structure represents the aristotype of the anti- PbCl_2 -structure type.

equal: 11 neighbors surround these atoms in form of a fivefold-capped trigonal prism. This belongs to the class of Edshammar polyhedra and is denoted ^{11}E .^[19] The $\beta\text{-Rb}_2\text{Te}$ structure can therefore be described as a hexagonally closest packed arrangement of Edshammar polyhedra with central $\text{Rb}(2)$ atoms (Figure 2). This is similar to the NiAs -structure type; however, in this case all Edshammar polyhedra remain empty.

The large displacive component in the transformation of the anti-cotunnite- into the Ni_2In -structure type also becomes clear when comparing the two structure types by examining the $\beta\text{-Rb}_2\text{Te}$ structure in the $[1\bar{1}0]$ direction (Figure 5). The structure relations between the two types can also be illustrated by a group–subgroup relation of the two space groups, as already described by Trübenbach^[20] (Scheme 1). The space group $P6_3/mmc$ represents the supergroup, whose symmetry can be reduced to the space group of the PbCl_2 type in a “translationengleichen” step of index 3 and a “klassengleichen” step of index 2. The $[1\bar{1}0]$ direction of the Ni_2In type corresponds to the b axis after transformation into the orthorhombic crystal system. We thus obtain a picture of the two structures that accentuates the sheet character of the edge-sharing trigonal prisms of the Rb atoms coordinated to

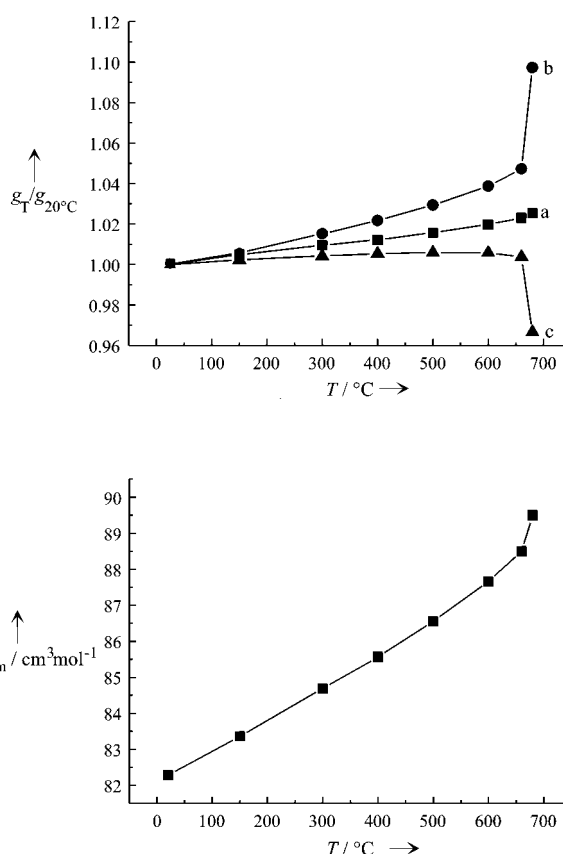


Figure 4. Anisotropic thermal expansion behavior of Rb_2Te , including the region of the $\alpha \rightarrow \beta$ phase transition (transformed parameters). Top: relative lattice parameters. Bottom: molar volume.

the Te atoms. In the Ni_2In type, these prisms are not trigonally but fivefold-capped; two further atoms are added to the coordination environment during the reduction of the folding towards planar sheets.

Based on the observations concerning the coordination numbers, we can expect that this type of phase transition can also be induced by pressure. Thus, BaF_2 not only shows the fluorite-to-cotunnite transition at $p = 3.0$ GPa, but also a second transition to the anti- Ni_2In type above 12 GPa.^[21] Further examples for this high-pressure polymorphism series are the compounds Na_2Te and Na_2S : their transition pressures are $p = 2.3$ GPa and 7 GPa (fluorite-to-cotunnite type) and $p = 5.3$ GPa and 16 GPa (cotunnite-to- Ni_2In type), respectively.^[22, 23] As a high-temperature variant of the PbCl_2 type, the Ni_2In type appears, for example, for the compound MnCoGe .^[24] During the $\alpha \rightarrow \beta$ transition in Rb_2Te , besides the increase in the coordination numbers, the interatomic distances also increase, which corresponds to the pressure–distance paradox (typical for high pressure phases). At the same time, the density decreases (typical for high-temperature phases) during phase transition from $\rho_{\text{calcd}} = 3.373(1) \text{ g cm}^{-3}$ at $T = 660^\circ\text{C}$ to $\rho_{\text{calcd}} = 3.336(1) \text{ g cm}^{-3}$ at $T = 680^\circ\text{C}$.

The crystal structure of the fourth modification, $\gamma\text{-Rb}_2\text{Te}$, which is stable above 745°C (second high-temperature modification), could not be determined so far. Powder-diffraction patterns have been taken at 750 to 770°C ; however

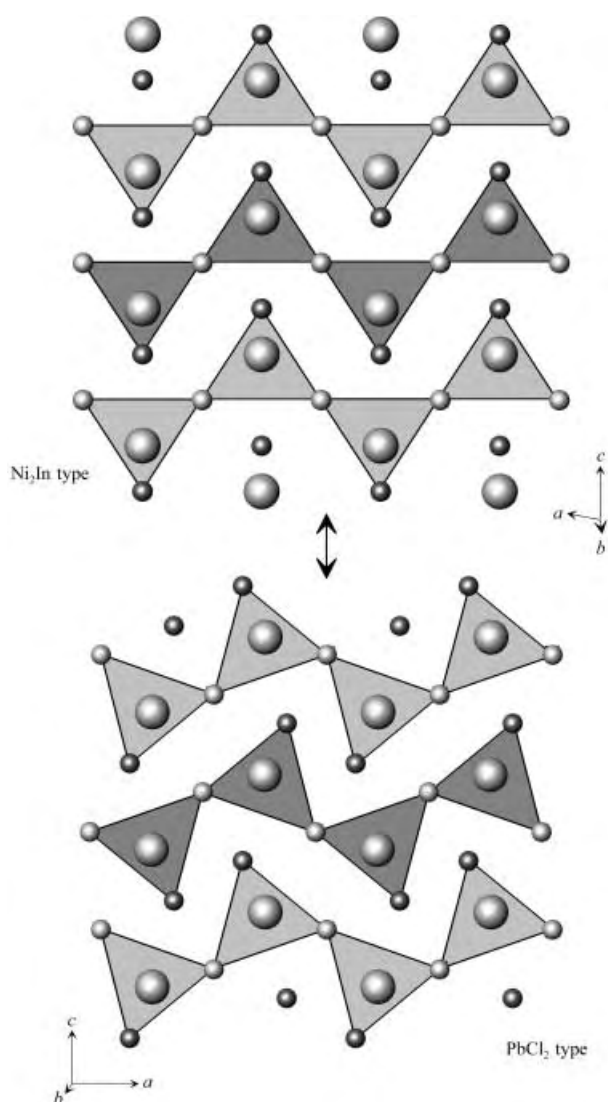


Figure 5. High-temperature-phase β - Rb_2Te (Ni_2In type) and the modification that is stable at room temperature (α - Rb_2Te , PbCl_2 type) with a perspective in the $[1\bar{1}0]$ direction. Te = large spheres, $\text{Rb}(1)$ = small light-grey spheres, $\text{Rb}(2)$ = medium grey spheres.

the quality of these measurements must be improved in the future to obtain a better signal-to-noise ratio. A problem is that at these temperatures the glass wall of the capillary is no longer inert towards the sample over extended periods of time. Furthermore, the reversible phase transition $\beta \rightarrow \gamma$ is often incomplete. Further evidence for the existence of a fourth modification of the congruent melting compound Rb_2Te is seen in the $\text{Rb}-\text{Te}$ phase diagram, for example, corresponding two-phase regions are observed in DTA experiments.

Our studies of the compound Rb_2Te provided some very surprising results. This compound, whose structure has not been characterized for many years, is an exception within the di(alkali-metal) monochalcogenides, as it can exist in two modifications at room temperature: a metastable modification of the anti-fluorite type and a stable modification of the anti-cotunnite type. Synthesis experiments with Cs_2Te showed that the product formed during synthesis in liquid ammonia is

amorphous (X-ray diffraction experiments) and transforms immediately to the anti- PbCl_2 type when annealed. Another unique observation is the existence of further polymorphic high-temperature phases for Rb_2Te . The structure type of one of these phases (β - Rb_2Te) has only been found among the tellurides only for Na_2Te as a high-pressure phase above $p = 5.3 \text{ GPa}$.^[22] Besides the structure of the second high-temperature phase, we are currently analyzing the high-pressure polymorphic forms of Rb_2Te . Furthermore, we are working on a more specific explanation of the polymorphic relations of Rb_2Te by means of quantum-theory calculations. The results of these experiments will be discussed separately.

$P6_3/mmc$	X (2a)	0	0	0	
\downarrow	Y (2c)	$\frac{1}{3}$	$\frac{2}{3}$	$\frac{1}{4}$	
\downarrow	X (2d)	$\frac{1}{3}$	$\frac{2}{3}$	$\frac{3}{4}$	
$a+b, -a+b, c$					
\downarrow	$Cmcm$	X (4a)	0	0	0
\downarrow		X (4c)	0	$y \sim \frac{1}{3}$	$\frac{1}{4}$
\downarrow		Y (4c)	0	$y \sim \frac{2}{3}$	$\frac{1}{4}$
\downarrow	$k2$				
\downarrow	$-(\frac{1}{4}, \frac{1}{4}, 0)$				
\downarrow	$(Pm\bar{c}n)$	X (4c)	$x \sim 0$	$\frac{1}{4}$	$z \sim \frac{1}{4}$
\downarrow	$Pnma$	X (4c)	$x \sim \frac{1}{4}$	$\frac{1}{4}$	$z \sim \frac{7}{12}$
		Y (4c)	$x \sim \frac{1}{4}$	$\frac{1}{4}$	$z \sim \frac{1}{12}$

Scheme 1. Structural relation between α - and β - Rb_2Te in the form of group-subgroup relations between the space groups of the two polymeric forms.

Experimental Section

Synthesis of Rb_2Te : The synthesis of Rb_2Te was carried out in Duran laboratory glassware described in Ref. [8] from the elements (Rb from Chempur, purity 99.9%; Te from Alpha, purity 99.99999%) in liquid ammonia with a small excess of rubidium. Because rubidium as well as the product are very air-sensitive, both reagents were handled in a glovebox (Braun) in an inert Ar atmosphere. To eliminate the excess rubidium, the raw product was extracted with liquid ammonia in a special glass apparatus. The ampoules were subsequently sealed under high-vacuum conditions.

DTA: Rb_2Te was transferred into silica-glass ampoules in a glovebox and these were sealed under high-vacuum conditions. The heating and the cooling curves were plotted with a simultaneous thermal analyzer (STA409, Netzsch) with heating rates of $2-5^\circ\text{C min}^{-1}$. The transition temperatures were taken from the heating curves by extrapolation of the peak-onset temperatures, the melting temperature by determination of the peak maximum of the liquidus effect.

X-ray characterization: All diffraction patterns were taken from powder samples filled into silica capillaries with an outer diameter of 0.2–0.3 mm and under an Ar atmosphere. To reduce the absorption coefficient, the substance was diluted with Si or silica-glass powder. The intensity measurements were carried out on an automatic four-circle diffractometer with a quartz crystal monochromator and a position-sensitive detector (OED50S, Braun) filled with an argon–methane mixture. A Seifert MZ4-type goniometer was used. The diffraction patterns were evaluated with the programs FORMFIT,^[27] WIN-Rietveld,^[28] and GSAS.^[29] For high-temperature diffraction measurements we used a heating device on the powder diffractometer, consisting of an electrically heatable corundum fork, a Pt/Rh–Pt thermoelement, an aluminum cap, and X-ray-amorphous Kapton foil. The temperature was regulated with an electronic controller (HTC9634, Huber). The temperature regulation was calibrated up to about 700°C by thermal dilatation of NaCl , and the temperature scale was checked by means of the phase transition of potassium chromate at 665°C .

Structure refinement: ω - Rb_2Te : cubic, space group $Fm\bar{3}m$, $a = 849.02(3) \text{ pm}$, $V = 6.1200(6) \times 10^8 \text{ pm}^3$, $\rho_{\text{calcd}} = 3.2401(3) \text{ g cm}^{-3}$, $\text{Cu K}\alpha_1$ radi-

ation ($\lambda = 154.056$ pm), $T = 20^\circ\text{C}$, 21 measured reflections ($2\theta_{\text{max}} = 94^\circ$, $\Delta 2\theta = 0.01^\circ$), no absorption correction, refinement program: WIN-Rietveld,^[28] background: linear interpolation, peak profile function: pseudo-Voigt, zero-point shift: $\Delta 2\theta = -0.017(3)^\circ$, 18 refined parameters ($\text{Rb}_2\text{Te} + \text{Si}$), $R_p = 3.79\%$, $R_{wp} = 4.87\%$, atomic sites: Rb (8c) $\frac{1}{4}\frac{1}{4}\frac{1}{4}$, Te (4a) 000. $\alpha\text{-Rb}_2\text{Te}$: orthorhombic, space group $Pnma$, $a = 896.60(3)$ pm, $b = 557.15(2)$ pm, $c = 1095.43(3)$ pm, $V = 5.4722(4) \times 10^8$ pm³, $\rho_{\text{calcd}} = 3.624(1)$ g cm⁻³, $\text{Cu}_{\text{K}\alpha 1}$ radiation ($\lambda = 154.056$ pm), $T = 20^\circ\text{C}$, 263 measured reflections ($2\theta_{\text{max}} = 94^\circ$, $\Delta 2\theta = 0.01^\circ$), no absorption correction, refinement program: GSAS,^[29] background: Chebyshev function with 36 coefficients, peak profile function: modified Thompson–Cox–Hastings pseudo-Voigt, zero-point shift: $\Delta 2\theta = -0.003(1)^\circ$; 20 refined parameters (without background), $R_p = 2.54\%$, $R_{wp} = 3.31\%$, atomic coordinates of all atoms at the site (4c) $x\frac{1}{4}z$: $x(\text{Rb}(1)) = 0.0271(3)$, $z(\text{Rb}(1)) = 0.1784(2)$, $x(\text{Rb}(2)) = 0.1534(2)$, $z(\text{Rb}(1)) = 0.5728(2)$, $x(\text{Te}) = 0.2483(2)$, $z(\text{Te}) = 0.8860(1)$. Furthermore, diffraction patterns were taken at higher temperatures with a heating fork (Table 1), $2\theta_{\text{max}} = 65^\circ$, refinement program:

Table 1. Lattice parameters, unit cell and molar volumes of $\alpha\text{-Rb}_2\text{Te}$ at different temperatures.

$T [^\circ\text{C}]$	a [pm]	b [pm]	c [pm]	V_{EZ} [$\times 10^6$ pm ³] ^[a]	V_{mol} [cm ³ mol ⁻¹]
20	896.28(1)	556.90(1)	1094.98(3)	546.54(3)	82.282(5)
150(3)	900.70(5)	560.13(3)	1097.52(5)	553.71(9)	83.36(1)
300(3)	904.83(6)	565.37(3)	1099.65(6)	562.5(1)	84.69(1)
400(3)	907.25(6)	569.01(3)	1100.83(6)	568.3(1)	85.56(1)
500(5)	910.36(4)	573.28(1)	1101.58(3)	574.91(5)	86.553(8)
600(5)	914.02(4)	578.47(1)	1101.29(3)	582.29(5)	87.665(8)
660(5)	916.9(1)	583.23(4)	1099.21(8)	587.8(1)	88.50(2)

[a] The maximum volume deviation is $dV = V(da/a + db/b + dc/c)$.

WIN-Rietveld,^[28] $\beta\text{-Rb}_2\text{Te}$: hexagonal, space group $P6_3/mmc$, $a = 611.10(5)$ pm, $c = 919.0(1)$ pm, $V = 2.9723(7) \times 10^8$ pm³, $\rho_{\text{calcd}} = 3.336(1)$ g cm⁻³, $\text{Cu}_{\text{K}\alpha 1}$ radiation ($\lambda = 154.056$ pm), $T = 680^\circ\text{C}$, 28 measured reflections ($2\theta_{\text{max}} = 60^\circ$, $\Delta 2\theta = 0.01^\circ$), no absorption correction, refinement program: GSAS,^[29] background: Chebyshev function with 36 coefficients, peak profile function: modified Thompson–Cox–Hastings pseudo-Voigt, zero-point shift: $\Delta 2\theta = -0.018(3)^\circ$; 12 refined parameters (without background), $R_p = 3.39\%$, $R_{wp} = 4.34\%$, atomic sites: Rb(1) (2a) 000, Rb(2) (2d) $\frac{1}{2}\frac{1}{2}\frac{1}{2}$, Te (2c) $\frac{1}{2}\frac{1}{2}\frac{1}{2}$.

Received: October 30, 2001
Revised: April 9, 2002 [Z18134]

- [1] E. Zintl, A. Harder, B. Dauth, *Z. Elektrochem.* **1934**, *40*, 588.
- [2] P. Touzain, M. Cailliet, *Rev. Chim. Miner.* **1971**, *8*, 277.
- [3] K. May, *Z. Kristallogr.* **1936**, *94*, 412.
- [4] H. Sommer, R. Hoppe, *Z. Anorg. Allg. Chem.* **1977**, *429*, 118.
- [5] K. R. Tsai, P. M. Harris, E. N. Lassette, *J. Phys. Chem.* **1956**, *60*, 338.
- [6] I. Schewe-Miller, P. Böttcher, *Z. Kristallogr.* **1991**, *196*, 137.
- [7] W. Klemm, H. Sodomann, P. Langmesser, *Z. Anorg. Allg. Chem.* **1939**, *241*, 281.
- [8] K. Stöwe, S. Appel-Colbus, *Z. Anorg. Allg. Chem.* **1999**, *625*, 1647.
- [9] International Union of Pure and Applied Chemistry, *Nomenclature of Inorganic Chemistry*, 2nd ed., Butterworths, London, **1970**, p. 90.
- [10] L. Gerward, J. Staun Olsen, S. Steenstrup, M. Malinowski, S. Asbrink, W. Waskowska, *J. Appl. Crystallogr.* **1992**, *25*, 578.
- [11] D. P. Dandekar, J. C. Jamieson, *Trans. Am. Crystallogr. Assoc.* **1969**, *19*.
- [12] S. J. Dulcos, Y. K. Vohra, A. L. Ruoff, A. Jayaraman, G. P. Espinosa, *Phys. Rev B* **1988**, *38*, 7755.
- [13] J. P. Dancusse, E. Gering, S. Heathman, U. Benedict, *High Pressure Res.* **1990**, *2*, 381.

- [14] J. M. Leger, J. Haines, *Eur. J. Solid State Inorg. Chem.* **1997**, *34*, 785.
- [15] C. P. Shoemaker, D. P. Shoemaker, *Acta Crystallogr.* **1965**, *18*, 900.
- [16] J. Flahaut, F. Thévet, *J. Solid State Chem.* **1980**, *32*, 365.
- [17] W. Jeitschko, *Acta Crystallogr. Sect. B* **1968**, *24*, 930.
- [18] H. P. Beck, T. Beyer, *Z. Kristallogr.* **1997**, *212*, 565.
- [19] S. Lidin, M. Sommer, T. Popp, H.-G. von Schnering, *Angew. Chem.* **1992**, *104*, 936; *Angew. Chem. Int. Ed. Engl.* **1992**, *31*, 924.
- [20] P. Trübenbach, Diplomarbeit, Erlangen, **1980**.
- [21] J. M. Leger, J. Haines, A. Atouf, O. Schulte, S. Hull, *Phys. Rev. B* **1995**, *52*, 13247.
- [22] I. Schewe-Miller, PhD Thesis, Stuttgart, **1990**; H. J. Beister, I. M. Schewe, K. Syassen, P. Böttcher, Abstract of IUCR XV Conference, Bordeaux, **1990**.
- [23] A. Vegas, A. Grzechnik, K. Syassen, I. Loa, *Acta Crystallogr. Sect. B* **2001**, *57*, 151.
- [24] W. Jeitschko, *Acta Crystallogr. Sect. B* **1975**, *31*, 1187.
- [25] E. Dönges, *Z. Anorg. Allg. Chem.* **1959**, *263*, 112.
- [26] F. Laves, H. J. Wallbaum, *Z. Angew. Min.* **1942**, *4*, 17.
- [27] R. Haberkorn, ERLRAY Program for the Interpretation of X-ray Powder-Diffraction Patterns, Dudweiler, **1998**.
- [28] Siemens Analytical X-ray Systems, Sigma-C GmbH, WIN-Rietveld Version 2.54, Madison, USA, **1992–1997**.
- [29] A. C. Larson, R. B. Von Dreele, GSAS, General Structure Analysis System, Los Alamos National Laboratory, USA, **1994**.

Irreversible Adsorption of Cellobiose, Ascorbic Acid, and Tyrosine to Hydrophobic Surfaces in Water and Their Separation by Molecular Stirring

Guangtao Li, Karl Doblhofer, and Jürgen-Hinrich Fuhrhop*

Hydrophobic nanometer clefts, which are accessible from bulk water, play a role as reactive centers of enzymes and receptors.^[1] In these cavities, host molecules and substrates accumulate, the size of the cavity as well as the stereochemically arrangement of hydrogen bonds seem to play a dominant role in the specific binding of the molecules.^[2] Computer modeling shows that a few water layers are immobilized on the hydrophobic membrane surfaces^[3] and increasing dipolar interactions were measured.^[4] With respect to the strong binding of water-soluble substrates to hydrophobic surfaces, we found out experimentally, that rigid molecules with a hydrophobic and a hydrophilic edge remained fixed in hydrophobic nanometer clefts for months and did not diffuse into the neighboring bulk water. *trans*-1,2-Dihydroxycyclo-

- [*] Prof. J.-H. Fuhrhop, Dr. G. Li
Freie Universität Berlin
FB Biologie, Chemie, Pharmazie
Institut für Chemie/Organische Chemie
Takustrasse 3, 14195 Berlin (Germany)
Fax: (+49) 30-838-55589
E-mail: fuhrhop@chemie.fu-berlin.de
Dr. K. Doblhofer
Fritz-Haber-Institut der Max-Planck-Gesellschaft
Faradayweg 4–6, 14195 Berlin (Germany)

hexane with two equatorial OH groups shows this effect very clearly, whereas the *cis* diastereomer with only one axial OH group was not anchored at all. As an arrangement with two neighboring equatorial OH groups fits well geometrically into hexagonal ice, whereas an equatorial – axial pair does not, we have explained this observation by an immobilization of the diol in the hydrophobic nanometer clefts.^[5] There are model molecular dynamic (MD) calculations for the immobilization of water on hydrophobic walls.^[6] We now report 1) a number of important natural substances and analogues, which are also tightly anchored in hydrophobic nanometer clefts, 2) electrolytes (KCl, ferricyanide), which do not penetrate into the immobilized layer of adsorbed molecules from bulk water, and 3) the effect of dimethyl viologen, which, upon performance of cyclic voltammetry (CV), stirs the anchored molecules into the bulk water.

As described earlier, the membrane clefts were formed in two consecutive self-assembly steps.^[5a-c] First, four-fold symmetrically substituted porphyrins were deposited flat onto a gold surface. Long-chain hydrosulfides then formed monolayers of upright-standing molecules on the gold surface around the porphyrins. The carbonic acid or sulfide-containing porphyrins **3–6** were used (self-assembly time: 2 days), and octadecanethiol (**1**; ODT) or the diamide **2** (2 h) served as amphiphiles. The amphiphile **1** produced fluid, and **2** rigid lipid monolayers. They corresponded to fluid or form-stable nanometer clefts, respectively^[6] (Figure 1). If these coated

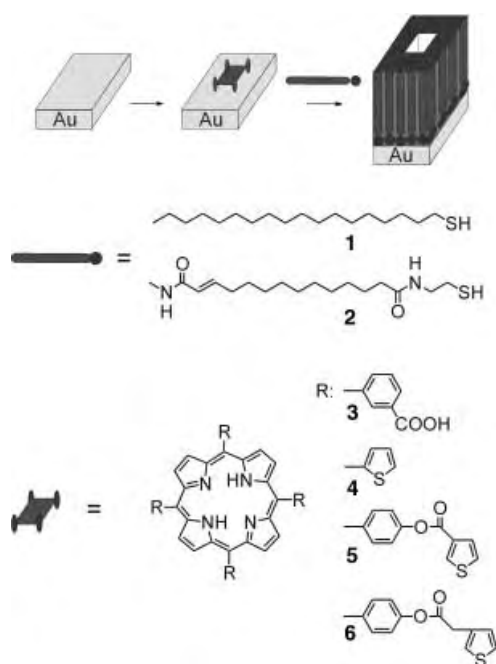


Figure 1. Scheme of the two-step self-assembly process and the substances used for producing clefts with a porphyrin base and a lipid membrane.

gold electrodes were plunged into an aqueous solution of ferricyanide (1 mM) and potassium chloride (1M), both porous membranes allowed cyclic voltammograms of the $[\text{Fe}(\text{CN})_6]^{4-}/[\text{Fe}(\text{CN})_6]^{3-}$ couple in bulk water to be recorded. Attempts to extinguish the fluorescence of anionic porphyrins at the bottom of cleft with cationic manganese(III) porphyrins

in the bulk solution showed that both big and small porphyrin ligands penetrated through the fluid membrane, whereas the clefts in rigid membranes did not let the big porphyrins in. The sketch in Figure 1 shows the formation of the pores, which were closed as described above by employing a 0.1M *trans*-1,2-dihydroxycyclohexane solution.^[5a-c]

Here, we describe the results of CV experiments, which show:

- that tyrosine, ascorbic acid, cellobiose, and related molecules block the membrane clefts for several days in contact with bulk water so that no electron transport at all takes place from the electrode to ferricyanide in bulk water
- that the blocking effect is abolished, when 1 % of maltose is added to the cellobiose
- that the clefts, closed by the cellobiose, will re-open, if the CV is carried out in the presence of dimethyl viologen.

The fluid as well as the rigid hydrophobic monolayers with 2-nm clefts were established on a gold electrode (surface: 30 mm² of medium roughness). The CV curves of ferricyanide (10^{-3} M) were measured in aqueous KCl solution (1M). The current amounted to about 50 % of that measured with naked gold electrodes under the same conditions. Neither the extent of coverage nor the conductivity of the clefts can, however, be derived from this result. Savéant co-workers developed a theory for the experimental finding that the magnitude and shape of the CV curves hardly change, when 50 % of the electrode surface is covered with lipid monolayers.^[7] The density of the clefts cannot be determined by CV. Attempts to characterize the holes by AFM or STM measurements also failed. We could not differentiate between the usual etch holes in the gold surface^[8] and membrane gaps. If the gold electrodes were completely covered with ODT **1** the current between the electrode and the redoxactive ions would be totally blocked. The cyclic voltammograms (“50%”) measured after the two-step self-assembly, resembled, as already reported by Savéant and co-workers, qualitatively and quantitatively those measured for the naked, dumbbell-shaped electrode. In our case, when there was a large amount of bound porphyrin the CV curves were symmetrical and the difference between the peak potentials small. The number of porphyrin gaps could be substantially lowered by substitution upon longer self-assembly times in the second step, for example, 4 h with ODT **1**, the differences between the peak potentials then increased (> 300 mV) and the CV curves became asymmetric (Figure 2, curves 2). When the porphyrin coverage became very low, the area “enclosed” by the CV curves disappeared (not shown). The voltammogram, typical for linear diffusion (for the naked electrode) was replaced by the “polar” curve typical for radial diffusion.^[9, 10] The voltammograms of Figure 2 curves 2 represent intermediate stages. The increasing differences of the peak potentials at a constant porphyrin concentration can be attributed to a slowing down of the electron transport from the gold electrode to the ferricyanide ions and vice versa.^[11–13] Nothing can be said about the conductivity of the water enclosed in the pores (clefts) or about air bubbles which might possibly remain in them. Cyclic voltammograms were reproducible within a low margin of error, when the electrodes and membranes were both been pre-treated in the same manner.

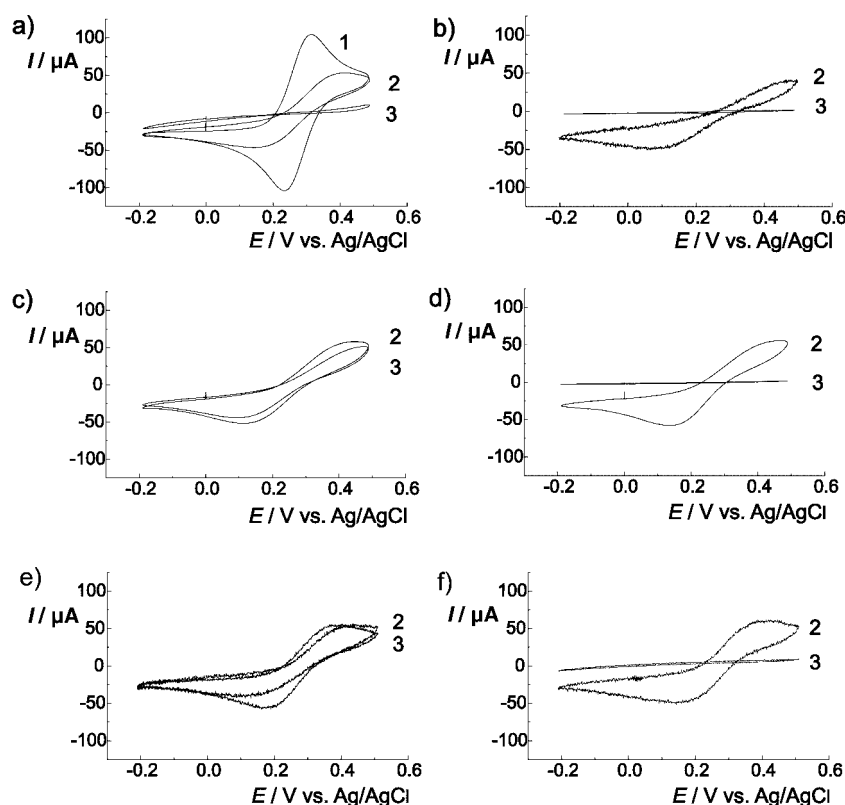


Figure 2. Cyclic voltammograms of 1) an aqueous solution of ferricyanide ions (10^{-3} M; 1 M KCl) measured at 100 mV s^{-1} , 2) with a naked gold electrode with an ODT (a–d) or diamide 2 (e,f) covered monolayer, which show open clefts, and 3) after an ex situ treatment with 0.1 M of the following solutes and washing with water: a) ascorbic acid (ODT 1), b) tyrosine (ODT 1), c) maltose (ODT 1), d) cellobiose (ODT 1), e) maltose (diamide 2), f) cellobiose (diamide 2).

We then abandoned our attempts to characterize the surface area and properties of the membrane pores by CV measurements. After all, we only needed evidence of the blocking and opening processes of the pores.

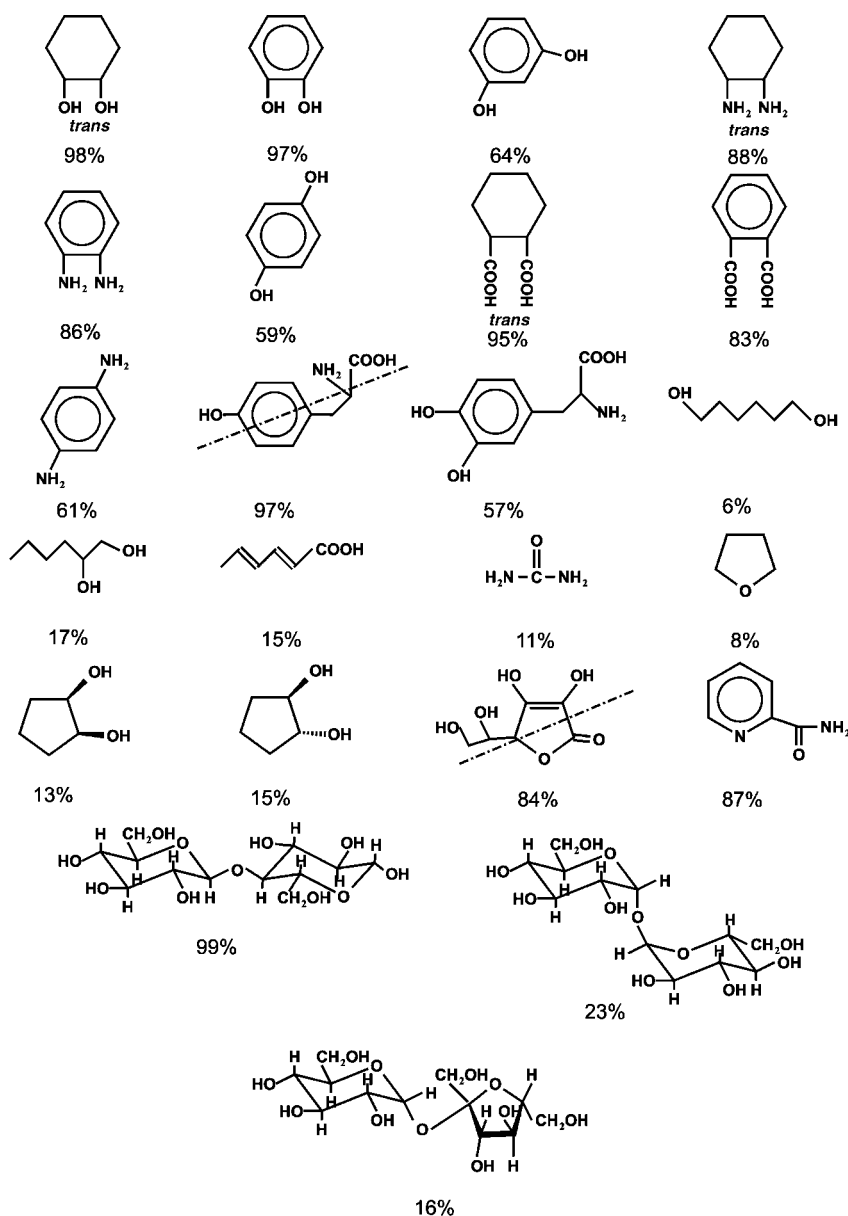
Both the fluid and the rigid clefts were closed by simply plunging the electrode into a 0.1 M aqueous solution of the organic solutes (Figure 2 a–f, curves 3). The electron transport from the electrode to ferricyanide ions in the bulk water was cut off for at least four days and up to six months. This was the case, although the electrode was thoroughly washed with distilled water and the clefts were in direct contact with the bulk water which did not contain any organic solutes. This effect was not observed with $[\text{Ru}(\text{NH}_3)_6]^{2+}$ ions in the same solution and with the same electrodes. We attribute this result to the fact that neither the $[\text{Ru}(\text{NH}_3)_6]^{2+}$ nor the $[\text{Fe}(\text{CN})_6]^{3-}$ complex could penetrate the layer of irreversibly adsorbed molecules. In the case of the ruthenium complex, a tunneling current was, however, still possible. Owing to an electron-transfer velocity thousand times higher than that of ferricyanide,^[9, 10] the electrons clearly overcame the water barrier on the way from the ruthenium complex to the electrode. Electron transfer from the gold electrode to the slowly reacting ferricyanide can, however, no longer be detected.

Scheme 1 summarizes the relative effectiveness of the used solutes. Figure 2 shows typical CVs before the treatment with different 0.1 M solutions and approximately 2–3 h afterwards. In the case of effective blocking molecules, the strength of the

current measured (at a potential of 0.4 V) decreased to values between $<0.1\%$ and 2% of the original value, the speed of the electron transfer from the ferricyanide to the gold as well as the Faraday current, however, dropped to almost zero.^[11–13] Only rigid, cyclic molecules with water-soluble substituents on the ring plane had a blocking effect (*trans*-1,2-dihydroxycyclohexane, -diamine, -dicarboxylate, and the analogous benzene derivatives, cellobiose, ascorbic acid). Open-chain compounds or carbocycles with flexible conformations (e.g. ascorbic acid, glycerol, *trans*-1,2-dihydroxycyclopentane) had as negligible effects as rigid cyclohexane derivatives with axial substituents (*cis*-1,2-dihydroxycyclohexane, maltose). Charged molecules with the right stereochemistry were just as active as electroneutral molecules.

We then tried to re-open the pores for the electron transport from the electrode to the ferricyanide ions. Addition of $>10\%$ of ethanol or some hydrochloric acid ($\text{pH} < 3$) to the bulk water removed the blockade within a few minutes. Once the pores were opened, they could only be closed again by removing the electrode from the KCl/ $\text{K}_3[\text{Fe}(\text{CN})_6]$ solution, washing it, and plunging it into a 0.1 M solution of the solutes given in Scheme 1. We call this procedure ex situ addition. Direct addition of one of the blocking compounds to the electrolyte solution (“in situ”) had only a minor effect, which, moreover, disappeared immediately upon rinsing the electrode with a KCl/ $\text{K}_3[\text{Fe}(\text{CN})_6]$ solution without the organic solute. Figure 3 shows the in situ effect of the cellobiose, which amounts to about 80% of the ex situ blocking observed. Maltose had no effect at all neither ex situ nor in situ. The result of the in situ experiment suggests, that the blocking solution in the membrane clefts must be free of electrolytes. We relate the disturbing influence of the electrolytes on the blocking effect to the destruction of the ordered hydrate structures within the membrane clefts. As the ex-situ-produced blocking effect remained active in contact with electrolyte solution for days, we also conclude that no ions diffused from the bulk water into the hydrate structures of the nanometer clefts.

This situation changed, when 10^{-3} M of dimethyl viologen was added to the bulk water and several CV cycles between $+0.5$ and -0.8 V (against Ag/AgCl) were executed with the electrode. After about 12 cycles, the pores were totally free and the CV appeared in the same form as before the blocking (Figure 4). Control CV experiments with ferricyanide and potassium chloride in the bulk water, but without dimethyl viologen, led to no opening effect whatsoever. We suppose that the narrow dimethyl viologen molecule is drawn into the pore’s electrolyte-free (!) hydrate water through a long-distance effect of the electric field, and is then repelled and moved laterally by the changes of the electrode potential. Possibly a pyridinium ring is reduced reversibly and re-



Scheme 1. Blocking effect of 0.1M solutions of the indicated solutes for the electron transport of ferricyanide ions in the bulk water. The percentages indicated correspond to the measured relative current: $I_{\text{rel}} = [(I_{\text{open}} - I_{\text{blocked}})/I_{\text{open}}] \times 100\%$ at open (I_{open}) and blocked (I_{blocked}) pores at 0.4 V.

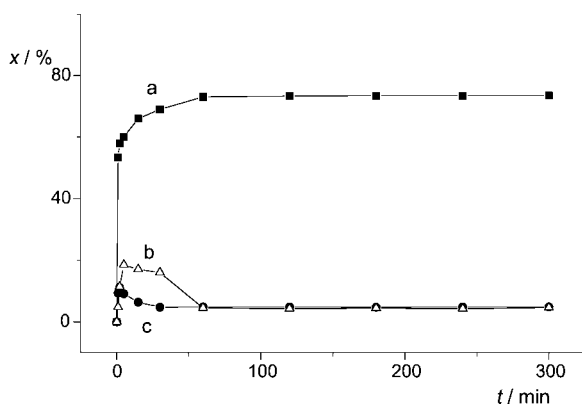


Figure 3. In situ experiments with ODT-covered electrodes, which contained open clefts a) after adding cellobiose (0.1M) to the $\text{KCl}/[\text{Fe}(\text{CN})_6]^{3-}$ solution, b) after adding maltose, and c) test experiment with the naked electrode.

oxidized during these cycles. In any case, the molecule is permanently changing its position and orientation and acts as a molecular stirring rod. The adsorbate is thus transported into the bulk water. All opening processes (ethanol, hydrochloric acid, stirring with dimethyl viologen) were completely and repeatedly reversed by simply plunging the electrode ex situ into a 0.1M solution of cellobiose.

In the case of cellobiose, we also found that only the pure compound had a blocking effect. If, in an ex situ experiment, $>1\%$ of maltose was added, no significant reduction of the current from the electrode to the ferricyanide was measured. Pure cellobiose was, under the same conditions, a perfect blocker. No differences at all could be detected here between the fluid and rigid membrane clefts made of ODT **1** or diamide **2**, respectively.

The experimental results show that planar, rigid molecules, such as, glucose or phenols stick so firmly to fluid as well as to rigid lipid membranes, that bulk water at pH 7 is not able to remove them for several days. This tight attachment can only be effected by allowing an ordering process of several hours.^[5, 14] It can be stopped by adding either a small amount of a structure-breaking substance or electrolytes. The stirring effect of the dimethyl viologen during the CV indicates that the volume of water in the membrane cleft does not contain any electrolytes, as otherwise the electric field of the electrode could not attract the dication. We cannot give a plausible explanation for the water insolubility of the cellobiose, ascorbic acid, etc. anchored to the hydrophobic membrane.

There must be a very close contact between the membrane and the dissolved organic compounds, which permanently hinders the penetration of bulk water into the gap. The medium path lengths for a water molecule in 8-nm³ clefts, are possibly so short, that the trapped molecules adopt the properties of a solid.^[14] The model shown in Figure 5 summarizes our observations for cellobiose. The hydrophobic side of the glucose units is adsorbed to the walls of the membrane cleft and fixed by both hydrogen bonds and an immobile hexagonal hydrate cover.^[5, 15] A single axial OH group or one percent of an α -glycoside (maltose) suffices to disturb the lengthy anchoring process of the molecules. The cyclic changing of the electrode potential changes the potential of one of the cleft walls, and attracts dimethyl viologen molecules strongly enough for them to penetrate the immobilized water volume.

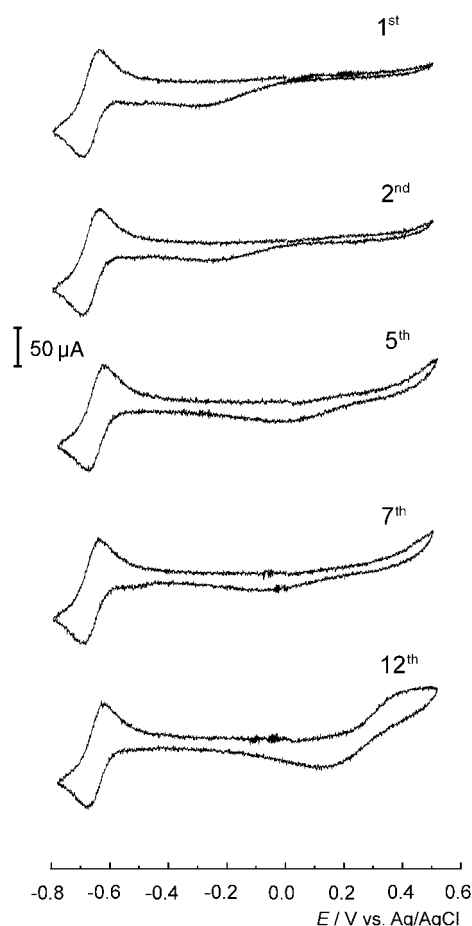


Figure 4. Consecutive cyclic voltammograms, which demonstrate the opening of tyrosine-blocked clefts in the presence of 10^{-3} M dimethyl viologen (see text).

In conclusion, the adsorption processes described above are practically irreversible in neutral water and therefore novel and of interest in their own right. They could, however, also play an important role in biological recognition processes, for example of glycoproteins on membrane surfaces. High, thermodynamic binding constants can hardly be expected from hydrocarbons and hydrophobic walls in aqueous media. Freezing and thawing rigid hydrates in membrane clefts seems to be a plausible operation in the light of our results. The

anchoring of water-soluble redox systems (tyrosine, ascorbic acid) in water volumes of a few cubic nanometers also helps in the construction of supramolecular systems for the photolytic water splitting.^[16]

Received: November 7, 2001

Revised: February 22, 2002 [Z18179]

- [1] D. Voet, J. G. Voet, *Biochemie*, VCH, Weinheim, **1992**, p. 311, 354 (Enzyme); D. Voet, J. G. Voet, *Biochemie*, VCH, Weinheim, **1992**, p. 876 (DNA); D. Voet, J. G. Voet, *Biochemie*, VCH, Weinheim, **1992**, p. 259 (Glycoproteine).
- [2] G. A. Jeffrey, W. Saenger, *Hydrogen Bonding in Biological Structures*, Springer, Berlin, **1991**.
- [3] R. G. Nuzzo, D. L. Allara, *J. Am. Chem. Soc.* **1983**, *105*, 4481.
- [4] A. Ulman, *An Introduction to Ultrathin Organic Films*, Academic Press, San Diego, **1991**.
- [5] a) J.-H. Fuhrhop, T. Bedurke, M. Gnade, J. Schneider, K. Doblhofer, *Langmuir* **1997**, *13*, 455; b) W. Fudickar, J. Zimmermann, L. Ruhlmann, J. Schneider, B. Roeder, U. Siggel, J.-H. Fuhrhop, *J. Am. Chem. Soc.* **1999**, *121*, 9539; c) M. Skupin, G. Li, W. Fudickar, J. Zimmermann, B. Roeder, J.-H. Fuhrhop, *J. Am. Chem. Soc.* **2001**, *123*, 3454.
- [6] M. Vossen, F. Forstmann, *J. Chem. Phys.* **1995**, *101*, 2379.
- [7] C. Amatore, J.-M. Savéant, D. Tessier, *J. Electroanal. Chem.* **1983**, *147*, 39.
- [8] E. Delamarche, B. Michel, H. A. Biebuyck, C. Gerber, *Adv. Mater.* **1996**, *8*, 719.
- [9] O. Chailapakul, R. M. Crooks, *Langmuir* **1993**, *9*, 884.
- [10] O. Chailapakul, R. M. Crooks, *Langmuir* **1995**, *11*, 1329.
- [11] M. T. Carter, G. K. Rowe, J. N. Richardson, L. M. Tender, R. H. Terrill, R. W. Murray, *J. Am. Chem. Soc.* **1995**, *117*, 2896.
- [12] A. J. Bard, L. R. Faulkner, *Electrochemical Methods: Fundamentals and Applications*, Wiley, New York, **2001**.
- [13] C. E. D. Chidsey, *Science* **1991**, *251*, 919.
- [14] F. Franks, *Pure Appl. Chem.* **1987**, *59*, 1189.
- [15] J. Lu, M. E. Green, *J. Phys. Chem. B* **1999**, *103*, 2776.
- [16] G. Li, W. Fudickar, M. Skupin, A. Klyszcz, C. Draeger, M. Lauer, J.-H. Fuhrhop, *Angew. Chem.* **2002**, *119*, 1907; *Angew. Chem. Int. Ed.* **2002**, *41*, 1829.

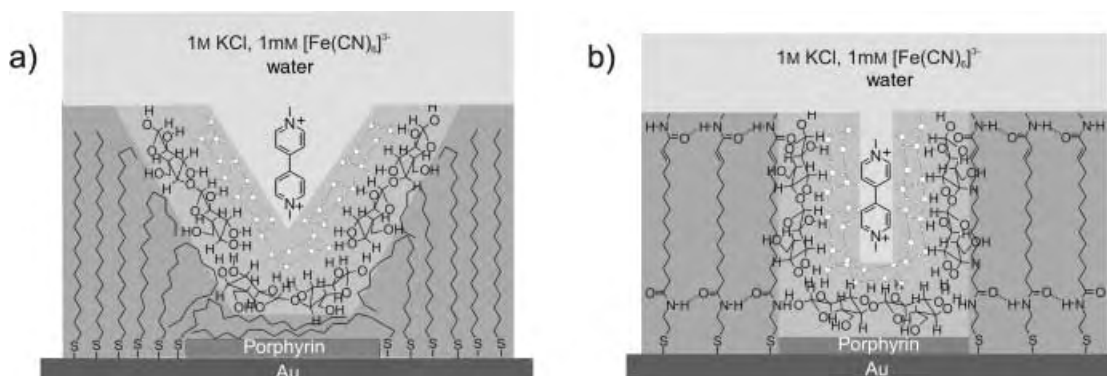


Figure 5. Model of the hydrated, immobile cellobiose layer in hydrophobic membrane clefts a) in a fluid ODT layer, and b) in a rigid layer of amphiphilic diamides (e.g., **2**). The aqueous bulk phase with KCl and ferricyanide does not mix with the hydrate cover, but the dimethyl viologen molecule penetrates and acts as molecular stirrer.

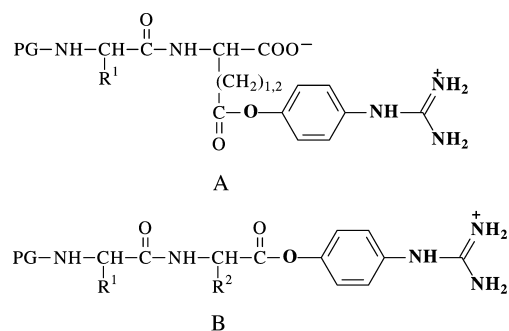
Synthesis of Neo-Peptidoglycans: An Unexpected Activity of Proteases**

Nicole Wehofsky, Reik Löser, Andrij Buchynskyy, Peter Welzel, and Frank Bordusa*

Glycations represent one of the most widespread “post-synthesis” modifications of polypeptides modulating the structure, stability, and biological activity of the carrier molecule. The involvement of glycopeptides in adhesion, differentiation, and growth of cells or the association with cancer-cell lines results in a great biological and pharmaceutical interest in these compounds and their analogues.^[1] Isolation from natural sources or preparation by recombinant DNA techniques, however, usually leads to conjugates with an altered or inhomogeneous carbohydrate content. Currently, only chemical and chemoenzymatic strategies provide access to well-defined carbohydrate–peptide conjugates. Despite the large number of useful synthesis methods, the high complexity, hydrophilicity, and acid- and, in some cases, base-lability of the carbohydrate part, however, make synthesis of these compounds a vast challenge that is far from any routine.^[2]

Herein we report a biocatalytic method allowing the selective acylation of N-glycans with amino acids and peptides. Like the known transglutaminase approach,^[3] this novel strategy enables glutamine (Gln) moieties to be modified with structurally diverse carbohydrates. Moreover, the approach is not restricted to Gln, but is also effective for asparagine (Asn) derivatives. Even conjugates with the carbohydrate moiety linked to the C terminus of the peptide can be prepared by this method. The hallmark of the approach is the use of an ordinary protease as the biocatalyst, for example, clostripain from *Clostridium histolyticum*, which is combined with a novel iso-type of substrate mimetics which are used as the amino acid or peptide precursors. Similar to the known linear-type substrate mimetics,^[4] the iso-type analogues bear a site-specific ester leaving group, for example, the 4-guanidinophenyl ester moiety (OGp), that mediates the acceptance of non-specific acyl residues by the original highly Arg-specific protease. However, to direct the intrinsic

synthesis activity of the enzyme to the side chain of Asp and Glu, the OGp group is linked to the ω -carboxylate of the two amino acids instead of being at the C terminus of the peptide (Scheme 1). This different architecture was found to shift the synthesis activity of the biocatalyst from the α -carboxy group of the peptide towards that of Asp and Glu residues of the side chains enabling the formation of a broad spectrum of N-linked neo-peptidoglycans.



Scheme 1. General structure of iso-type (A) and the classical linear-type substrate mimetics (B). The site-specific 4-guanidinophenyl ester moiety (OGp) is highlighted in bold letters. PG = protecting group; R¹, R², individual side chains.

The capability of clostripain to acylate N-glycans was investigated. For this purpose, reactions with simple monomeric N-glycans, such as, D-glucosamine (**1a**), D-galactosamine (**2**), and muramic acid (**3**), and the classical linear-type substrate mimetic Boc-Phe-Gly-Gly-OGp (Boc = *tert*-butoxycarbonyl) acting as the acyl donor were performed. The OGp moiety was selected because of its known mimic function which was shown to mediate the acceptance of non-specific (non Arg containing) peptides by clostripain.^[4c, 5] The reactions were performed in buffered aqueous solution at pH 8.0 containing 10 % DMF and concentrations of peptide, carbohydrate, and enzyme of 2 mM, 20 mM, and 20 μ M, respectively.^[6] As revealed by HPLC, incubation times between 30 and 40 min led to complete ester consumption in all cases finally resulting in product yields of 68 % (for **1a**), 70 % (**2**), and 64 % (**3**). The synthesis products have been identified by saponification experiments, mass spectrometry, and NMR spectroscopy following their isolation.^[7] Importantly, only single-acylated carbohydrates were found in all instances. Accordingly, except hydrolyzed peptide ester no further side products could be detected. That the coupling failed with the amine-blocked *N*-acetyl-D-glucosamine (**1b**) indicates an exclusive *N*-acylation of the carbohydrates by the enzyme which is in agreement with the NMR spectroscopy data of the products and their resistance towards saponification as well.

The capability of the approach to mediate the coupling of N-glycans to the side chain carboxy groups of Asp and Glu was investigated. For this goal, at least two essential conditions must be fulfilled; 1) overcoming the original Arg specificity of the protease and 2) direction of the intrinsic synthesis activity of the enzyme from the C α -carboxylate (backbone) to that of the side chain of Asp and Glu. Both requisites might be achieved by shifting the OGp moiety from the C α - to the ω -carboxylate of the peptide precursor. To test

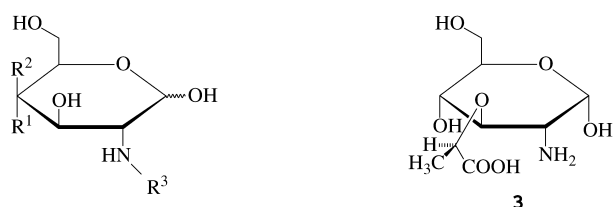
[*] Dr. F. Bordusa, Dr. N. Wehofsky
Max-Planck Society
Research Unit “Enzymology of Protein Folding”
Weinbergweg 22, 06120 Halle/Saale (Germany)
Fax: (+49) 345-551-1972
E-mail: bordusa@enzyme-halle.mpg.de

Dipl.-Chem. A. Buchynskyy, Prof. P. Welzel
University of Leipzig
Department of Organic Chemistry
Johannisallee 29, 04103 Leipzig (Germany)

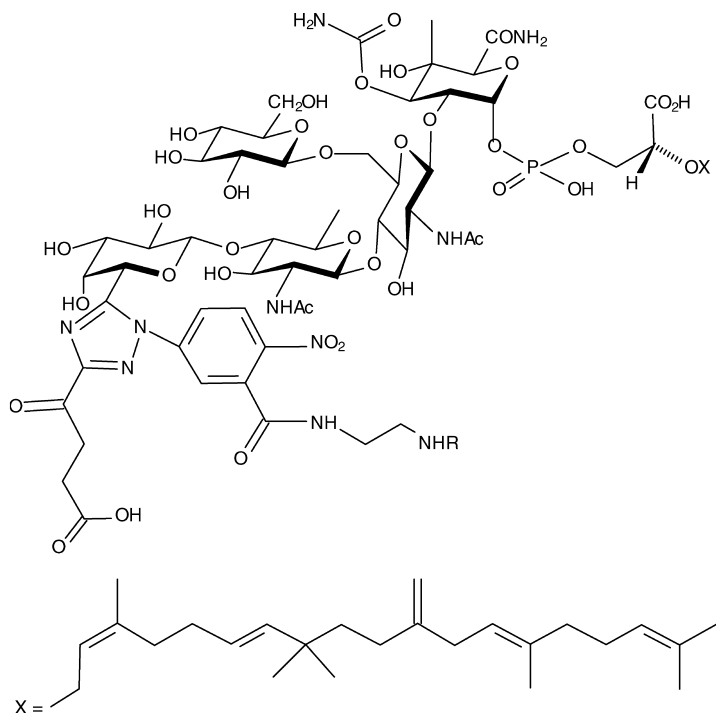
Dipl.-Biochem. R. Löser
University of Leipzig
Institute of Biochemistry
Talstrasse 33, 04103 Leipzig (Germany)

[**] This work has been supported by the Deutsche Forschungsgemeinschaft DFG (Innovationskolleg “Chemisches Signal und biologische Antwort” and BO 1770/1-1) and Fonds der Chemischen Industrie (P.W. and Liebig-scholarship to F.B.).

Supporting information for this article is available on the WWW under <http://www.angewandte.org> or from the author.



- 1a:** $R^1 = \text{OH}$, $R^2 = \text{H}$, $R^3 = \text{H}$
1b: $R^1 = \text{OH}$, $R^2 = \text{H}$, $R^3 = \text{acetyl}$
2: $R^1 = \text{H}$, $R^2 = \text{OH}$, $R^3 = \text{H}$



- 4a:** $R = \text{H}$
4b: $R = \text{phenylacetyl}$

this hypothesis, we initially used the simple amino acid derivatives Z-Glu(OGp)-OH and Z-Asp(OGp)-OH as precursors (Z = benzyloxycarbonyl). Synthesis of the esters can be achieved in a similar way to that of the C α -esterified analogues by using an inverse protecting-group strategy for the carboxy groups of Asp and Glu.^[8] The enzymatic reactions themselves were performed under exactly the same conditions and with the reactant concentrations as described above for Boc-Phe-Gly-Gly-OGp. Similarly, HPLC, NMR spectroscopy, mass spectrometry, and saponification experiments were utilized for product analysis. In addition, the blocked amino component **1b** was used as a probe to verify the selectivity of syntheses. The yields of reactions are summarized in Table 1 and document that both amino acid esters show productive binding at the active site of the enzyme which results in the formation of appropriate N-linked neopeptidoglycans. Only reactions with **1b** gave no products, which indicates an exclusive N-acylation as has been verified by NMR spectroscopy and saponification experiments. In the case of all other carbohydrates (**1a**, **2**, **3**), product yields within

Table 1. Product yields of the clostripain-catalyzed carbohydrate–amino acid coupling reactions.^[a]

Acyl donor	Carbohy- drate acceptor	Product	Yield [%]
Z-Asp(OGp)-OH	1a		72
Z-Asp(OGp)-OH	2		73
Z-Asp(OGp)-OH	3		71
Z-Glu(OGp)-OH	1a		67
Z-Glu(OGp)-OH	2		68
Z-Glu(OGp)-OH	3		67

[a] Conditions were as described in ref. [6]. Concentrations: [donor] = 2 mM, [acceptor] = 20 mM, [clostripain] = 20 μM .

a range of 67–73 % were obtained corresponding with those found for Boc-Phe-Gly-Gly-OGp.

Owing to the apparent independence of this approach to the structure and type of the acyl donor, we investigated its ability to modify Asp-derived peptides instead of a single Asp moiety. As a model, the Leu-enkephalin sequence Z-Asp-Tyr-Gly-Gly-Phe-Leu-OH was selected. Its biological relevance is because the glycosylation of a related peptide drastically increases its affinity to opiate receptors.^[9] The precursor peptide Z-Asp(OGp)-Tyr-Gly-Gly-Phe-Leu-OH was synthesized by standard solid-phase peptide synthesis on Wang resin employing the Fmoc strategy (Fmoc = 9-fluorenylmethoxycarbonyl). To allow ester modification, Z-Asp(OGp(Boc)₂)-OH was used in the last coupling step. Cleavage of the peptide

from the resin by trifluoroacetic acid (TFA) treatment simultaneously deprotected the Tyr side chain and the OGp moiety leading to the peptide ester ready for enzymatic synthesis. An enzyme concentration of 20 μM and an incubation time of less than 15 min with all other reaction conditions and reactant concentrations unchanged led to complete peptide ester consumption resulting in product yields of 70% (for **1a**), 69% (**2**), and 66% (**3**). Except hydrolyzed peptide ester no further side products could be detected while the selectivity of reactions was verified as described above.

Finally, we demonstrated the ability of the method to couple carbohydrates of higher complexity. For this purpose, reactions with a synthetic amino-functionalized moenomycin A analogue **4a**^[10] and the four amino acid and peptide precursors were performed. For synthesis-economy reasons the latter have been used in 1.25-fold excess over **4a** in concentrations of 25 mM and 20 mM, respectively. All other reaction conditions were kept unchanged including the low content of organic solvent. After 1 h and complete ester consumption the reactions were terminated and analyzed by HPLC and mass spectrometry. Figure 1 shows selected HPLC

micelles (critical micelle concentration (CMC) of non-modified moenomycin: 0.5 mM at pH 6.8).^[11] At present, it remains an open question whether the formation of micelles or the increase in complexity of the carbohydrate scaffold contributes to this effect. Assuming that micelle formation decreases at least the rate of diffusion and, thus, hinders the moenomycin attack of the acyl-enzyme intermediate, these results indicate to a rather broad acceptance by the enzyme of highly complex and usually non-micelle N-glycans.

In summary, we have described an efficient method for the synthesis of a wide variety of N-linked neo-peptidoglycans by exploiting the protease/substrate mimetics-based methodology. The approach allows selective coupling of carboxylate moieties derived from Asp and Glu side chains as well as the C-terminus of peptides with both simple monomeric and highly complex acid- and base-labile carbohydrate derivatives under extraordinary mild reaction conditions with yields ranging between 24 and 73%. Because of the known independence of the classical substrate mimetics approach of the individual acyl moiety,^[4] a high flexibility of the synthesis method towards the sequence of the peptide

precursor, at least of those derived from the linear-type derivatives can be expected. Only the presence of specific Arg residues within the peptide may lead to undesired cleavage reactions.^[12] In such an instance the use of a side chain protected Arg moiety seems to offer a promising escape. In any case, to our knowledge there is no other enzyme system that shows a similar synthetic flexibility towards both the peptide and carbohydrate part. These characteristics make the new approach a powerful and rather general one for the synthesis of N-linked neo-peptidoglycans and amino acid-carbohydrate building blocks.

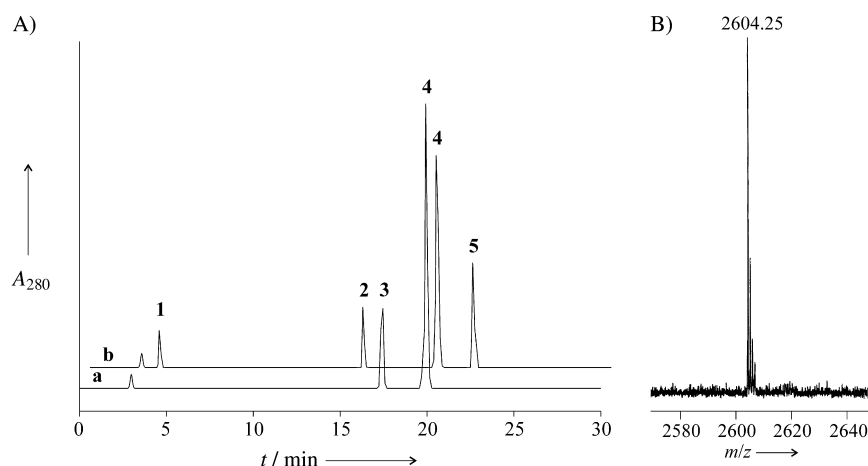


Figure 1. Analysis of the clostripain-catalyzed coupling of Z-Asp(OGp)-Tyr-Gly-Gly-Phe-Leu-OH with moenomycin A (**4a**) by HPLC (A) and MALDI-TOF mass spectrometry (B).^[7] A) a) Before addition of enzyme; b) after 30 min. 1) released 4-guanidinophenol; 2) Z-Asp-Tyr-Gly-Gly-Phe-Leu-OH; 3) Z-Asp(OGp)-Tyr-Gly-Gly-Phe-Leu-OH; 4) moenomycin A; 5) Z-Asp(moenomycin)-Tyr-Gly-Gly-Phe-Leu-OH. A_{280} = absorbance at 280 nm. B) Mass calcd: 2602.96.

profiles that illustrate the well-defined course of catalysis for the reaction of the peptide precursor with **4a**. Similar to reactions using the monomeric carbohydrates, only the formation of single-acylated **4a** could be observed. As for the efficiency of synthesis, for reactions with Boc-Phe-Gly-Gly-OGp 24%, with Z-Asp(OGp)-Tyr-Gly-Gly-Phe-Leu-OH and Z-Glu(OGp)-OH 26%, and with Z-Asp(OGp)-OH 29% of the desired product could be obtained. On the contrary, N-phenylacetyl-moenomycin derivative (**4b**), which was used to verify the selectivity of the enzyme, gave no products. Compared to the yields of about 70% for the monomeric carbohydrates (**1a**, **2**, **3**), the use of the bulky moenomycin derivative clearly decreases the efficiency of synthesis. However, moenomycin is not only a complex carbohydrate, but also an amphiphilic compound with a strong tendency to form

Received: November 14, 2001
Revised: April 5, 2002 [Z18217]

- [1] Reviews: a) P. M. St. Hilaire, M. Meldal, *Angew. Chem.* **2000**, *112*, 1210–1228; *Angew. Chem. Int. Ed.* **2000**, *39*, 1162–1179; b) O. Seitz, *ChemBioChem* **2000**, *1*, 214–246; c) R. A. Dwek, *Chem. Rev.* **1996**, *96*, 683–720; d) H. Lis, N. Sharon, *Eur. J. Biochem.* **1993**, *218*, 1–27; e) A. Varki, *Glycobiology* **1993**, *3*, 97–130.
- [2] Reviews: a) H. Herzner, T. Reipen, M. Schultz, H. Kunz, *Chem. Rev.* **2000**, *100*, 4495–4537; b) G. Arsequell, G. Valencia, *Tetrahedron: Asymmetry* **1999**, *10*, 3045–3094; c) C. M. Taylor, *Tetrahedron* **1998**, *54*, 11317–11362.
- [3] a) S.-C. B. Yan, F. Wold, *Biochemistry* **1984**, *23*, 3759–3765; b) D. Ramos, P. Rollin, W. Klaffke, *Angew. Chem.* **2000**, *112*, 406–408; *Angew. Chem. Int. Ed.* **2000**, *39*, 396–398.
- [4] a) V. Schellenberger, H.-D. Jakubke, N. P. Zapevalova, Y. V. Mitin, *Biotechnol. Bioeng.* **1991**, *38*, 104–108; b) H. Sekizaki, K. Itoh, E. Toyota, K. Tanizawa, *Chem. Pharm. Bull.* **1996**, *44*, 1577–1579, 1585–1587; c) F. Bordusa, D. Ullmann, C. Elsner, H.-D. Jakubke, *Angew. Chem.* **1997**, *109*, 2563–2565; *Angew. Chem. Int. Ed.* **1997**, *36*, 2473–2475; d) M. Thormann, S. Thust, H.-J. Hofmann, F. Bordusa,

- Biochemistry* **1999**, *38*, 6056–6062; e) V. Cеровsky, J. Kockskämper, H. G. Glitsch, F. Bordusa, *ChemBioChem* **2000**, *2*, 126–129.
- [5] a) R. Günther, F. Bordusa, *Chem. Eur. J.* **2000**, *6*, 463–467; b) R. Günther, A. Stein, F. Bordusa, *J. Org. Chem.* **2000**, *65*, 1672–1679.
- [6] The enzymatic reactions were performed in a total volume of 0.5 mL containing 0.1 M *N*-(2-hydroxyethyl)piperazine-*N'*-(2-ethanesulfonic acid) (Hepes), pH 8.0, 0.1 M NaCl, 0.01 M CaCl₂, 10 % (v/v) dimethylformamide (DMF) at 25 °C. The amino acid and peptide esters were dissolved in 10 % aqueous DMF while the carbohydrates were suspended in the appropriate buffer. Readjusting to pH 8.0 was achieved by adding NaOH. After mixing the reactants the reactions were initiated by addition of pre-incubated enzyme (1 mM DL-dithiothreitol, 2.5 mM CaCl₂ in water for 2 h). After defined time intervals the reactions were stopped by addition of trifluoroacetic acid (1 % solution) and further analyzed as described in ref. [7]. To control for spontaneous reactions, parallel reactions without enzyme were analyzed in all cases. On the basis of these controls, non-enzymatic synthesis could be ruled out and the extent of spontaneous hydrolysis of the acyl donor esters was found to be less than 5 %.
- [7] The reactions were analyzed under optimized conditions by reversed-phase HPLC (LiChrospher, 5 µm, 125 × 3 mm; Merck). Detection was at 254 nm (monomeric carbohydrates) or 280 nm (moenomycin, Leu-enkephalin derivative). Mass spectra were recorded for separated and lyophilized probes by using MALDI-TOF (MALDI 5 V5.1.2, Kratos Kompakt) or ESI (Apex II/7 Tesla, Bruker-Daltonics) ionization. NMR spectroscopy (GEMINI 300, Varian) was used to verify the identity of the reactants and products (except moenomycin and its conjugates). Saponification experiments were performed by incubating the synthesis products in 50 % aqueous methanol (pH 11) for 1 h and analysis by HPLC.
- [8] For the synthesis of linear-type substrate mimetics see: N. Müller, F. Bordusa, *Anal. Biochem.* **2000**, *286*, 86–90, and references therein. The isomeric Z-Glu/Asp(OGp)-OH esters were prepared by condensation of Z-Glu/Asp-OtBu and 4-[*N'*,*N'*-bis(Boc)-guanidino]phenol (ratio 1:2) using *N*-[(dimethylamino)-1*H*-1,2,3-triazolo[4,5*b*]pyridine-1-ylmethylene]-*N*-methylmethanaminium hexafluorophosphate *N*-oxide (HATU) as the coupling reagent, *N*-ethyl-diisopropylamine as the general base, and DMF as the solvent at 0 °C. Treatment of the protected amino acid diester products with TFA resulted in the Boc/*t*Bu-cleavage leading to the final Z-Glu/Asp(OGp)-OH esters. The identity and purity of the esters were checked by analytical HPLC, NMR spectroscopy, and thermospray mass spectrometry. By using that optimized synthesis method, the isomeric esters were not formed.
- [9] R. E. Rodriguez, F. D. Rodriguez, M. P. Sacristan, J. L. Torres, G. Valencia, J. M. G. Anton, *Neurosci. Lett.* **1989**, *101*, 89–94.
- [10] a) U. Kempin, L. Hennig, D. Knoll, P. Welzel, D. Müller, A. Markus, J. van Heijenoort, *Tetrahedron* **1997**, *53*, 17669–17690; b) A. Anikin, A. Buchynskyy, U. Kempin, K. Stempera, P. Welzel, G. Lantzsch, *Angew. Chem.* **1999**, *111*, 3931–3935; *Angew. Chem. Int. Ed.* **1999**, *38*, 3703–3707.
- [11] G. Lantzsch, H. Binder, H. Heerklotz, P. Welzel, G. Klose, *Langmuir* **1998**, *14*, 4095–4104.
- [12] N. Wehofsky, S. W. Kirbach, M. Haensler, J.-D. Wissmann, F. Bordusa, *Org. Lett.* **2000**, *2*, 2027–2030.

Investigation of Reactive Intermediates of Chemical Reactions in Solution by Electrospray Ionization Mass Spectrometry: Radical Chain Reactions**

Jens Griep-Raming, Sven Meyer, Torsten Bruhn, and Jürgen O. Metzger*

Dedicated to Professor Hans J. Schäfer on the occasion of his 65th birthday


The reaction mechanism is the detailed, step-by-step description of a chemical reaction. Most chemical reactions take place through a complex sequence of steps via reactive intermediates. The most important reactive intermediates in organic chemical reactions in solution are carbocations, carbanions, carbenes, and radicals. Of course, chemists have been able to detect these intermediates indirectly by chemical and physical methods, and spectroscopic methods are available to study them directly and in detail.^[1] For example, Olah investigated carbocations in “magic acid” solutions under nonreaction conditions.^[2] Transient carbocations that contained an appropriate chromophore were studied by using UV spectroscopy.^[3, 4] Radicals were explored by ESR spectroscopy and in appropriate cases by CIDNP (chemically induced dynamic nuclear polarization), and UV spectroscopy.^[5, 6] However, it seems to be most remarkable that these methods (there may be some exceptions) are not generally suited to detect and to study these reactive intermediates directly in reaction solutions, for example, of a radical chain reaction. Furthermore, substrates, intermediates, and final products cannot be monitored by using these methods. Additional measurements have to be applied to do so. Clearly, it would be of great importance to have a simple method available to study a reaction by monitoring substrates and all intermediates and final products formed, and especially to detect and characterize simultaneously and directly the reactive intermediates. Such a method could give new and important insights in our understanding of reactions and their mechanisms. Furthermore, the method should be applicable to micro amounts of substrates and should allow a high throughput, thus contributing to a sustainable development.^[7]

Recently, electrospray ionization mass spectrometry (ESIMS)^[8] has been successfully applied to the investigation of some chemical reactions in solution. The investigations were mostly performed offline, for example, with the oxidation of tetrahydropterins to radical cations,^[9] homogeneously catalyzed reactions such as the Suzuki reaction,^[10] and the

[*] Prof. Dr. J. O. Metzger, Dipl.-Chem. S. Meyer, Dipl.-Chem. T. Bruhn
Fachbereich Chemie, Carl von Ossietzky Universität Oldenburg
Carl-von-Ossietzky-Strasse 9–11, 26111 Oldenburg (Germany)
Fax: (+49) 441-798-3329
E-mail: juergen.metzger@uni-oldenburg.de

Dr. J. Griep-Raming
Thermo Finnigan MAT GmbH
Barkhausenstrasse 2, 28197 Bremen (Germany)

[**] We thank the Deutsche Forschungsgemeinschaft for financial support of this work.

 Supporting information for this article is available on the WWW under <http://www.angewandte.org> or from the author.

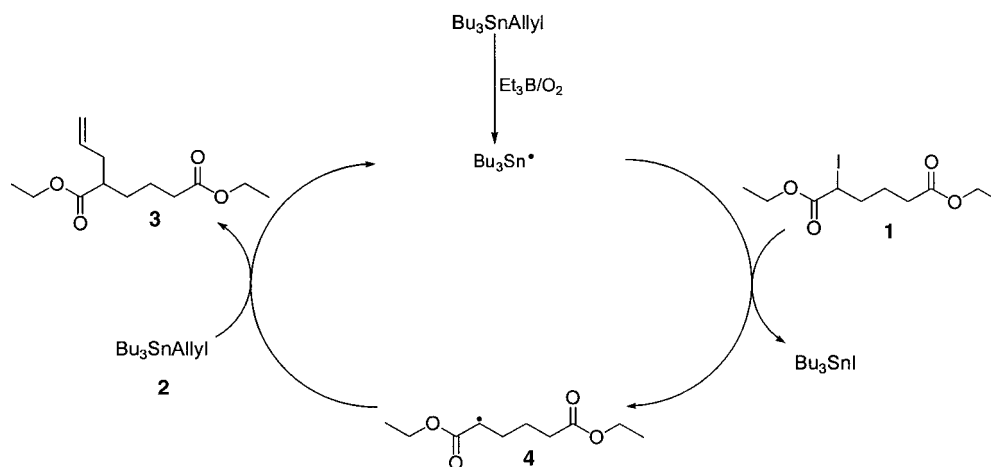
palladium-catalyzed oxidative self-coupling of aryl boronic acids.^[11] Arakawa et al. used an online ESIMS system in which a flow-through photoreaction cell was attached to an electrospray interface. They detected intermediates of photochemical reactions of some transition-metal complexes that have a lifetime of a few minutes.^[12] The oxidation of iron(II) bleomycin with iodosylbenzene was studied online and some intermediate species could be detected.^[13] Chen and co-workers used ESIMS to generate and isolate the active species of homogeneously catalyzed reactions such as Ziegler–Natta polymerization^[14] or olefin metathesis^[15] and studied the reaction with the substrate in the gas phase. Feichtinger and Plattner used the same technique to investigate the formation and reactions of the active species of epoxidation catalysts, for example, oxomanganese–salen complexes.^[16] We described the possibility of detecting stable radicals in solution by ESIMS^[17] and we now report herein our results on the detection of transient radicals in radical chain reactions.

There are many synthetically important radical chain reactions in solution.^[18] However, there is no method available to detect and to study directly the transient radicals in these reactions. Radicals are neutral species and neutral species can normally not be detected by ESIMS. However, it is well known that radical reactions can be mediated by Lewis acids if the substrate is a Lewis base that can chelate the metal atom of the Lewis acid in solution.^[19] We have recently shown that dialkyl glutarates form complexes with Lewis acids such as LiClO_4 , MgBr_2 , and $\text{Sc}(\text{OTf})_3$ in solution in diethyl ether.^[20] We thought that these complexes, for example, of $\text{Sc}(\text{OTf})_3$ should dissociate to form a chelate complex cation and a triflate anion, thus allowing the detection of the complexed ester by ESIMS.^[21] This detection was possible: diethyl 2-iodoadipate (**1**; Scheme 1) was mixed with $\text{Sc}(\text{OTf})_3$ (1.2 equiv) in diethyl ether and very intense ESI mass spectra were obtained which showed monomeric and dimeric complex ions of adipate **1** (Figure 1 a).^[22] The fact that in addition to monomeric also dimeric complex ions $[\mathbf{1}_2 \cdot \text{Sc}_2(\text{OTf})_5]^+$ are observed, which provides evidence for the respective dimeric complexes in solution, is already an important and new result, because up to now dimeric complexes in $\text{Sc}(\text{OTf})_3$ -mediated radical reactions have not been considered. In the presence of

$\text{Sc}(\text{OTf})_3$, adipate **1** reacts with allyltributyltin (**2**) in diethyl ether to give diethyl 2-allyladipate (**3**) via the radical intermediate **4** (Scheme 1).

For the investigation by ESIMS, this reaction was performed by mixing a solution of iodoester **1** and $\text{Sc}(\text{OTf})_3$ in diethyl ether saturated with air and a solution of **2** and Et_3B under argon. The solutions were mixed by using an effective micromixer, which was coupled online to the ESI mass spectrometer.^[23] The reaction times could be varied by the flow rate and/or the length of the transfer capillary between the mixer and the ion source.^[24] Substrate **1** and product **3** could easily be detected and monitored by ESIMS. Most remarkably, a heterodimer complex ion of substrate and product $[\mathbf{1} \cdot \mathbf{3} \cdot \text{Sc}_2(\text{OTf})_5]^+$ (m/z 1405) was detected. However, an intermediate radical complex ion $[\mathbf{4} \cdot \text{Sc}(\text{OTf})_2]^+$ with an expected mass of m/z 544 could not be observed unambiguously because of chemical noise^[25] in the mass spectrum (Figure 1 b). That can easily be understood because the quasi-stationary concentration of the radical in the radical chain reaction is estimated to be approximately 10^{-7} M, four orders of magnitude lower than the concentration of the substrate **1** and of the product **3**. The signal of the intermediate radical ion is expected to disappear in the chemical noise. However, the intermediate radical **4** could be detected as a monomeric complex ion $[\mathbf{4} \cdot \text{Sc}(\text{OTf})_2]^+$ by using the MS/MS technique^[8] to filter out the signal of interest from baseline noise (Figure 1 c).^[26] From this observation, we deduced that **4** also should occur in the reaction solution as a heterodimer complex with substrate **1** and the respective ion should be detectable by MS/MS, which would thus provide additional, independent, and unambiguous evidence for the intermediate radical. The MS/MS spectrum of the heterodimer complex ion of substrate and radical $[\mathbf{1} \cdot \mathbf{4} \cdot \text{Sc}_2(\text{OTf})_5]^+$ (m/z 1364) was indeed observed (Figure 1 d). Two main and characteristic fragmentations of this ion are evident: dissociation by loss of the neutral radical complex $\mathbf{4} \cdot \text{Sc}(\text{OTf})_3$ gives the substrate complex ion $[\mathbf{1} \cdot \text{Sc}(\text{OTf})_2]^+$ (m/z 671) and, complementarily, loss of the neutral substrate complex $\mathbf{1} \cdot \text{Sc}(\text{OTf})_3$ gives the radical complex ion $[\mathbf{4} \cdot \text{Sc}(\text{OTf})_2]^+$ (m/z 544).

The tributyltin hydride or tris(trimethylsilyl)silane-mediated addition of alkyl iodides to alkenes is another syntheti-



Scheme 1. Triethylborane/oxygen-initiated radical chain reaction of **2** with **1** to give adipate **3** via radical **4**.

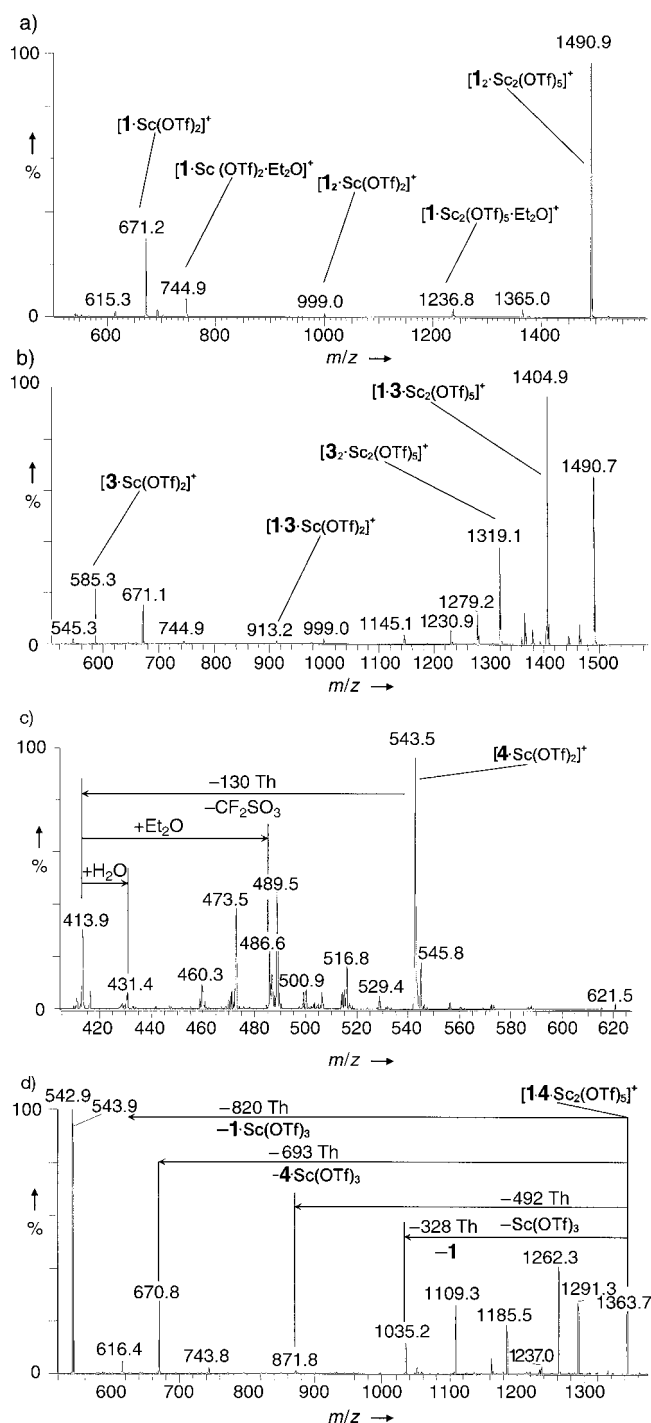
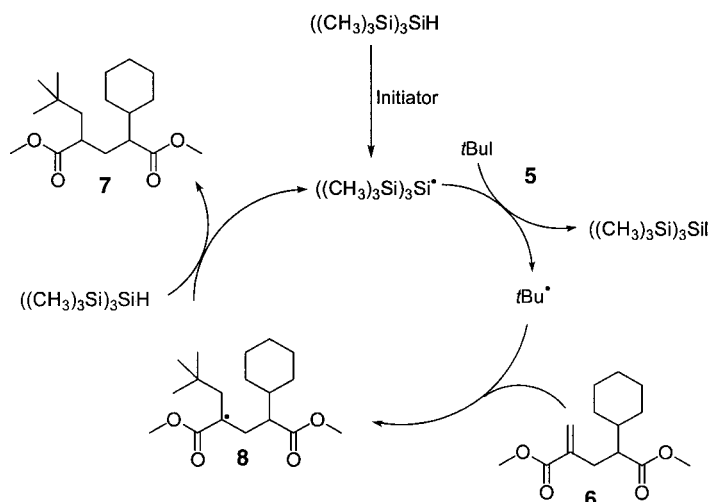


Figure 1. a) Positive-mode ESI mass spectrum of a solution of **1** in the presence of $\text{Sc}(\text{OTf})_3$ in diethyl ether. Monomeric $[\mathbf{1} \cdot \text{Sc}(\text{OTf})_2]^+$ (m/z 671) and dimeric $[\mathbf{1}_2 \cdot \text{Sc}_2(\text{OTf})_5]^+$ (m/z 1491) complex ions are observed. b) Positive-mode ESI mass spectrum of the reaction solution of **1** and **2** in the presence of $\text{Sc}(\text{OTf})_3$ in diethyl ether; new signals (compare with Figure 1 a) are observed and assigned to the product **3**: $[\mathbf{3} \cdot \text{Sc}(\text{OTf})_2]^+$ (m/z 585), $[\mathbf{3}_2 \cdot \text{Sc}_2(\text{OTf})_5]^+$ (m/z 1319), and the heterodimer complex ion $[\mathbf{1} \cdot \mathbf{3} \cdot \text{Sc}_2(\text{OTf})_5]^+$ (m/z 1405). c) The MS/MS spectrum of the radical complex ion $[\mathbf{4} \cdot \text{Sc}(\text{OTf})_2]^+$ (m/z 544) of the same reaction solution shows the characteristic fragmentation of CF_2SO_3 (-130 Th (Thomson)) to give fragment ion m/z 414 accompanied by adduct ions with H_2O (m/z 432) and diethyl ether (m/z 488), which are formed by ion–molecule reactions in the ion trap.^[27] d) The MS/MS spectrum of the substrate–radical complex ion $[\mathbf{1} \cdot \mathbf{4} \cdot \text{Sc}_2(\text{OTf})_5]^+$ (m/z 1364) of the same reaction solution shows fragmentation to give the substrate complex ion $[\mathbf{1} \cdot \text{Sc}(\text{OTf})_2]^+$ (m/z 671) and the radical complex ion $[\mathbf{4} \cdot \text{Sc}(\text{OTf})_2]^+$ (m/z 544).

cally important radical reaction.^[28, 29] The addition of *tert*-butyl iodide (**5**) to dimethyl 2-cyclohexyl-4-methyleneglutarate (**6**) mediated by $(\text{Me}_3\text{Si})_3\text{SiH}$ gives the addition product **7** in good yields (Scheme 2).^[20] We studied this reaction by ESIMS and could easily monitor substrate **6** and product **7** (Figure 2a). We could also detect the intermediate adduct radical **8** by MS/MS as complex ion $[\mathbf{8} \cdot \text{Sc}(\text{OTf})_2]^+$ and independently as heterodimer $[\mathbf{6} \cdot \mathbf{8} \cdot \text{Sc}_2(\text{OTf})_5]^+$ (Figure 2b,c).^[30]



Scheme 2. Tris(trimethylsilyl)silane-mediated addition of *tert*-butyl iodide (**5**) to glutarate **6** to give stereoselectively **7** via adduct radical **8**.^[20]

The detection of the heterodimer radical complex ions in $\text{Sc}(\text{OTf})_3$ -mediated radical reactions provides information that can not be obtained by other techniques and may be important for the stereochemical outcome, for example, of the hydrogen transfer to radical **8**.^[20] This information can only be obtained by ESIMS because this technique allows all ionic species in solution to be detected and characterized by their MS/MS spectrum.

In conclusion, we have shown for the first time that transient radicals in radical chain reactions can be detected unambiguously by ESIMS. Furthermore, substrates and products can easily be monitored. New insights have been obtained in the mechanism of $\text{Sc}(\text{OTf})_3$ -mediated radical chain reactions. The method seems to be generally applicable to the investigation of reactions in solution and to the detection of intermediates, and most importantly, of reactive intermediates. For example, we have been studying the dissociation of carbon–heteroatom bonds as the rate-determining step of $\text{S}_{\text{N}}1$ and $\text{E}1$ reactions. All significant effects described in textbooks of organic chemistry could easily be demonstrated by direct measurement of the carbocations and the respective anions formed in the dissociation equilibrium. The method can be applied to all reactions in solution, as long as the species of interest are ionic species or can be ionized.^[17]

Received: February 13, 2002 [Z18704]

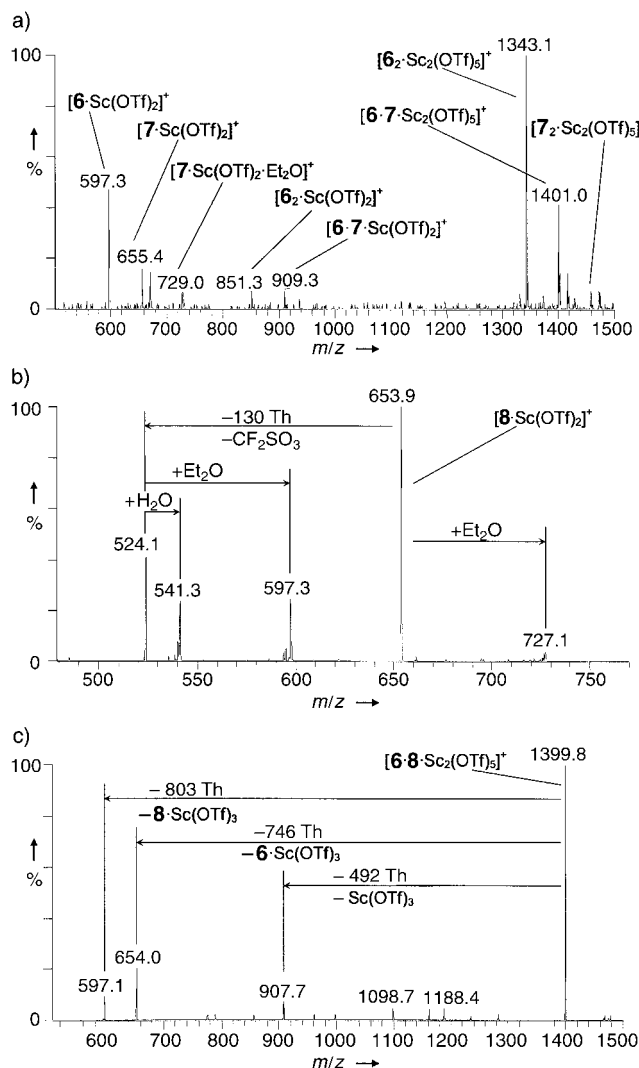


Figure 2. a) Positive-mode ESI mass spectrum of the tris(trimethylsilyl)silane-mediated addition of *tert*-butyl iodide to **6** in the presence of $\text{Sc}(\text{OTf})_3$ in diethyl ether to give the addition product **7** (see Supporting Information). Monomeric and dimeric complex ions of substrate **6** (m/z 597, 851, 1343), product **7** (m/z 655, 729, 1457), and heterodimer complex ions of **6** and **7** (m/z 909, 1401) are observed. A signal of the intermediate radical complex ion (m/z 654) is not evident. b) The MS/MS of the ion at m/z 654 shows the fragmentation of the radical complex ion $[\mathbf{8} \cdot \text{Sc}(\text{OTf})_2]^+$. The loss of CF_2SO_3 (-130 Th) and the attachment of H_2O and diethyl ether to the complex ions is characteristic.^[31] c) The MS/MS spectrum of the ion at m/z 1400 shows the loss of $\mathbf{8} \cdot \text{Sc}(\text{OTf})_3$ (803 Th) to give $[\mathbf{6} \cdot \text{Sc}(\text{OTf})_2]^+$ (m/z 597) (see Figure 2a), and loss of $\mathbf{6} \cdot \text{Sc}(\text{OTf})_3$ (746 Th) to give $[\mathbf{8} \cdot \text{Sc}(\text{OTf})_2]^+$ (m/z 654) (see Figure 2b).

- [1] M. B. Smith, J. March, *March's Advanced Organic Chemistry*, 5th ed., Wiley, New York, 2001, pp. 218–273.
- [2] G. A. Olah, *Angew. Chem.* **1995**, *107*, 1519–1532; *Angew. Chem. Int. Ed. Engl.* **1995**, *34*, 1393–1405.
- [3] *Carbonium Ions, Vol. 1* (Eds.: G. A. Olah, P. von R. Schleyer), Interscience Publishers, New York, 1968; "Carbokationen, Carbokationen-Radikale": D. Lenoir, H.-U. Siehl, *Methoden der Organischen Chemie (Houben-Weyl)*, 4th ed. 1952–, Vol. E19c, pp. 35–43.
- [4] H. Mayr, *Angew. Chem.* **1990**, *102*, 1415–1428; *Angew. Chem. Int. Ed. Engl.* **1990**, *29*, 1371–1384.
- [5] J. K. Kochi, *Free Radicals*, Wiley, New York, 1973.
- [6] J. Fossey, D. Lefort, J. Sorba, *Free Radicals in Organic Chemistry*, Wiley, New York, 1995, pp. 5–18.
- [7] M. Eissen, J. O. Metzger, E. Schmidt, U. Schneidewind, *Angew. Chem.* **2002**, *114*, 402–425; *Angew. Chem. Int. Ed.* **2002**, *41*, 414–436.

- [8] *Electrospray Ionization Mass Spectrometry—Fundamentals, Instrumentation and Applications* (Ed.: R. B. Cole), Wiley, New York, 1997.
- [9] a) A. Schäfer, B. Fischer, H. Paul, R. Bosshard, M. Hesse, M. Viscontini, *Helv. Chim. Acta* **1992**, *75*, 1955–1964; b) A. Schäfer, H. Paul, B. Fischer, M. Hesse, M. Viscontini, *Helv. Chim. Acta* **1995**, *78*, 1763–1776.
- [10] A. Aliprantis, J. Canary, *J. Am. Chem. Soc.* **1994**, *116*, 6985–6986.
- [11] M. A. Aramendia, F. Lafont, M. Moreno-Manas, R. Pleixats, A. Roglans, *J. Org. Chem.* **1999**, *64*, 3592–3594.
- [12] a) R. Arakawa, S. Tachiyashiki, T. Matsuo, *Anal. Chem.* **1995**, *67*, 4133–4138; b) R. Arakawa, F. Matsuda, G.-e. Matsubayashi, T. Matsuo, *J. Am. Soc. Mass Spectrom.* **1997**, *8*, 713–717, and references therein.
- [13] J. W. Sam, X.-J. Tang, R. S. Magliozzo, J. Peisach, *J. Am. Chem. Soc.* **1995**, *117*, 1012–1018.
- [14] D. Feichtinger, D. A. Plattner, P. Chen, *J. Am. Chem. Soc.* **1998**, *120*, 7125–7126.
- [15] a) C. Adlhart, C. Hinderling, H. Baumann, P. Chen, *J. Am. Chem. Soc.* **2000**, *122*, 8204–8214; b) C. Adlhart, P. Hofmann, P. Chen, *Helv. Chim. Acta* **2000**, *83*, 3306–3311; c) M. Volland, C. Kiener, P. Chen, P. Hofmann, *Chem. Eur. J.* **2001**, *7*, 4621–4632.
- [16] D. Feichtinger, D. Plattner, *Chem. Eur. J.* **2001**, *7*, 591–599.
- [17] a) J. O. Metzger, J. Griep-Raming, *Eur. J. Mass Spectrom.* **1999**, *5*, 157–163; b) J. Griep-Raming, J. O. Metzger, *Anal. Chem.* **2000**, *72*, 5665–5668.
- [18] *Radicals in Organic Synthesis* (Eds. P. Renaud, M. P. Sibi), Wiley-VCH, Weinheim, 2001.
- [19] P. Renaud, M. Gerster, *Angew. Chem.* **1998**, *110*, 2704–2722; *Angew. Chem. Int. Ed.* **1998**, *19*, 2562–2722.
- [20] a) A. Hayen, R. Koch, J. O. Metzger, *Angew. Chem.* **2000**, *112*, 2898–2900; *Angew. Chem. Int. Ed.* **2000**, *39*, 2758–2761; b) A. Hayen, R. Koch, W. Saak, D. Haase, J. O. Metzger, *J. Am. Chem. Soc.* **2000**, *122*, 12458–12468.
- [21] It has been shown that nonpolar organic compounds such as alkenes can be ionized in ESIMS by adding transition-metal salts, for example, AgNO_3 to form π complexes: E. Bayer, P. Gfrörer, C. Rentel, *Angew. Chem.* **1999**, *111*, 1046–1049; *Angew. Chem. Int. Ed.* **1999**, *38*, 992–995.
- [22] The experiments were carried out on an LCQ mass spectrometer (Thermo Finnigan, San José, CA, USA). The standard ESI source of the LCQ was used with a stainless-steel metal capillary (110 μm i.d., 240 μm o.d., 120.5 mm length, Metal Needle Kit, Thermo Finnigan). Notably, we cannot draw a direct conclusion from the signal intensities to the relative concentration of the respective species in solution because of the characteristics of the ion trap. Some experiments have been performed on a FT-ICR mass spectrometer Apex II (Bruker Daltonics) and gave the exact masses of the monomeric and dimeric complex ions of substrates and of the products. We thank Dr. J. R. Wesener (Bayer AG) for the possibility of performing these measurements.
- [23] Adipate **1** (20 μmol , 1×10^{-3} M) and scandium triflate (24 μmol , 1.2 equiv) were dissolved in diethyl ether (20 mL). The solution was cooled to 0°C and saturated with air by using a glass syringe. A solution of triethyl borane (50 μmol , 2.5 equiv) and allyltributyltin (100 μmol , 5 equiv) was prepared in diethyl ether (20 mL) under argon. The solutions were mixed using a dual syringe pump feeding in a micromixer with a low dead volume that was coupled directly to the ESI source.
- [24] The volume of the spray capillary (120.5 mm length, 110 μm i.d.) is about 1.14 μL . The flow rate can be varied from 2.5 to 100 $\mu\text{L min}^{-1}$. Thus, the direct connection of the mixer with the spray capillary allows reaction times from 0.7 to 28 s. Longer reaction times are easily possible by using a fused-silica transfer capillary of variable length between the mixer and the spray capillary. Mass spectra were measured at reaction times of approximately 1 s up to some minutes.
- [25] Of course, there is a peak at m/z 544, which falls in the intensity range of chemical noise.
- [26] To detect transient radical cation $[\mathbf{4} \cdot \text{Sc}(\text{OTf})_2]^+$ by MS/MS, the parent ion (m/z 544) was collected for up to 2000 ms in the ion trap (isolation width 1.5 m/z) and then fragmented by collision (CID) with a background gas (in this case, helium). The MS/MS spectrum given in Figure 1c) was obtained. The analogous MS/MS experiment was

performed to detect heterodimer radical cation $[1 \cdot 4 \cdot \text{Sc}_2(\text{OTf})_5]^+$ at m/z 1364 (Figure 1 d). Control experiments of substrate **1** and product **3** in the presence of $\text{Sc}(\text{OTf})_3$ showed no signals that could be assigned to the proposed radical intermediate in the case of the heterodimer radical complex ion. In the case of the monomer radical complex ion, the substrate **1** showed signals that can be assigned to this ion, possibly by homolytic cleavage of the C–I bond in the heated capillary. However, the intensity of these signals is only about one tenth of that in the case of the reaction.

- [27] The water and diethyl ether adduct complex ions $([\text{M} \cdot \text{Sc}(\text{OTf})_2 \cdot \text{H}_2\text{O}]^+)$, $([\text{M} \cdot \text{Sc}(\text{OTf})_2 \cdot \text{Et}_2\text{O}]^+)$ indicate two special features: a rising front peak flank and a negative mass shift. Both phenomena are observed only with quadrupole ion trap analyzers and with particularly unstable (easily fragmentable) ions.
- [28] W. B. Motherwell, D. Crich, *Free Radical Chain Reactions in Organic Synthesis*, Academic Press, London, **1992**, pp. 179–212.
- [29] C. Chatgililoglu in *Radicals in Organic Synthesis* (Eds. P. Renaud, M. P. Sibi), Wiley-VCH, Weinheim, **2001**, pp. 28–49.
- [30] Glutarate **6** (20 μmol , $1 \cdot 10^{-3} \text{ M}$), scandium triflate (24 μmol , 1.2 equiv), and *tert*-butyl iodide (80 μmol , 4 equiv) were dissolved in diethyl ether (20 mL). The solution was cooled to 0°C and saturated with air by using a glass syringe. A solution of triethyl borane (50 μmol , 2.5 equiv) and tris(trimethylsilyl)silane (80 μmol , 4 equiv) was prepared in diethyl ether (20 mL) under argon. The reaction and measurement were performed as described in refs. [23] and [26]. The MS/MS spectrum of m/z 654 ($[8 \cdot \text{Sc}(\text{OTf})_2]^+$, Figure 2b) and of m/z 1400 ($[6 \cdot 8 \cdot \text{Sc}_2(\text{OTf})_5]^+$, Figure 2c) were obtained. Control measurements of substrate **6** and product **7** in the presence of $\text{Sc}(\text{OTf})_3$ showed no signals that can be assigned to the monomeric and heterodimeric radical complex ions.
- [31] The shape of the peak at m/z 597 provides unambiguous evidence for the addition of diethyl ether to the complex ion with m/z 524; see also ref. [27].

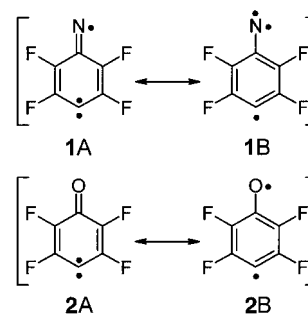
2,3,5,6-Tetrafluorophenylnitren-4-yl: A Quartet-Ground-State Nitrene Radical**

Hans Henning Wenk and Wolfram Sander*

*Dedicated to Professor Walter Siebert
on the occasion of his 65th birthday*

The interaction of unpaired electrons coupled by conjugated π -systems has been studied intensively during the last decade.^[1–3] Also, a few heterospin systems combining different spin-carrying units within one molecule have been described. As these studies were aimed at the development of molecular magnets,^[4] stable organic radicals were utilized, which were coupled to photochemically generated nitrene^[5, 6] or carbene^[7–9] units through *m*- or *p*-phenylene linkers. Systems containing highly reactive radicals (e.g. the phenyl radical) in addition to a nitrene or carbene have not been investigated so far. A molecule of this type is 2,3,5,6-

tetrafluorophenylnitren-4-yl (**1**), which is formally generated by substituting a nitrogen atom for an oxygen atom in tetrafluorooxocyclohexadienylidene (**2**).



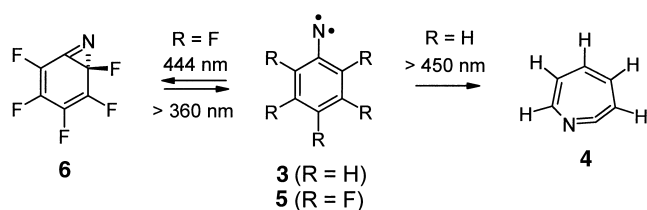
For compound **2**, a triplet ground state has been determined experimentally by using ESR^[10] and IR spectroscopy^[11], as well as theoretically based on quantum-chemical calculations. The electronic structure of **2** can be described by the resonance structures **2A** (carbene) and **2B** (phenyl/phenoxy diradical). For the nitrene radical **1**, which bears an additional unpaired electron, DFT calculations predict a quartet ground state 2.7 kcal mol^{−1} below the lowest doublet state (UB3LYP/6-311G(d,p) + ZPE). The electronic structure of **1** is also qualitatively represented by two resonance structures: structure **1A** corresponds to a combination of a carbene with an iminyl radical, structure **1B** to that of a nitrene and a phenyl radical. Two electrons are localized in the σ plane, one at the nitrogen atom (iminyl radical), the other at the C4 atom of the phenyl ring (phenyl radical). The third unpaired electron is delocalized over the π system and exhibits high spin densities at the nitrogen atom as well as at the C4 atom. Thus, **1** can be represented by the electronic structure of a delocalized carbene (**1A**) and a delocalized nitrene (**1B**), which share a common π electron. Both carbenes and nitrenes have similar structures: open-shell systems with triplet ground states, and thus the parallel alignment of the spins of all three electrons is energetically most favorable; this leads to a quartet ground state.

Photolysis of aryl azides in cryogenic matrices is a well-established method for the generation of triplet aryl nitrenes.^[12–14] Short-wavelength irradiation of aryl iodides has recently been applied to generate various fluorinated phenyl radicals and didehydrobenzenes, which were studied by matrix-isolation spectroscopy.^[15, 16] Therefore, 4-iodo-2,3,5,6-tetrafluoroazidobenzene (**7**; see Scheme 2) was used as a precursor for **1**. The perfluorinated system was chosen because, in contrast to the unsubstituted phenylnitrene (**3**),^[12, 17] for 2,6-difluorinated phenylnitrene derivatives the irreversible ring expansion to the corresponding didehydroazepine (**4**; Scheme 1) was not observed under the conditions of matrix isolation.^[13, 14, 18] Instead, 2,6-difluorophenylnitrene and pentafluorophenylnitrene (**5**) react reversibly to the azirine derivatives (**6**) upon irradiation with light of wavelength 444 nm.^[14]

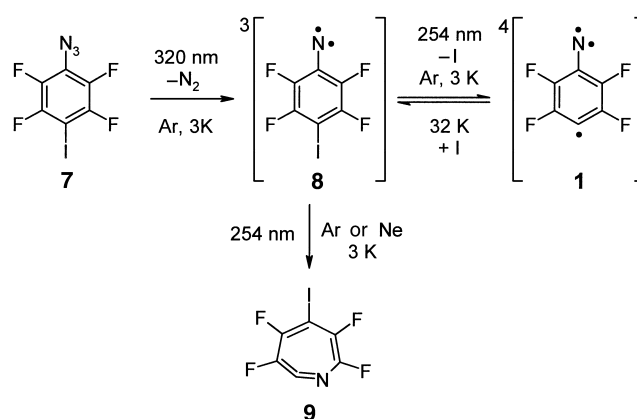
The IR spectrum of **7**, matrix isolated in solid argon at 3 K, exhibits the characteristic $\nu(\text{NN})$ vibration of the azido group at 2131 cm^{−1} (Figure 1 a). The absorptions of **7** disappear upon

[*] Prof. Dr. W. Sander, Dipl.-Chem. H. H. Wenk
Lehrstuhl für Organische Chemie II
Ruhr-Universität Bochum
44780 Bochum (Germany)
Fax: (+49) 234-321-4353
E-mail: wolfram.sander@ruhr-uni-bochum.de

[**] This work was financially supported by the Deutsche Forschungsgemeinschaft and the Fonds der Chemischen Industrie. We thank Professor W. T. Borden for the discussion of the high-spin system.



Scheme 1. Difference in reactivities between unfluorinated and fluorinated phenylnitrenes.



Scheme 2. Photoreaction of **7** and the subsequent chemistry.

Table 1. IR spectroscopic data of T-8.

Mode	Symmetry	$\tilde{\nu}_{\text{exp.}} [\text{cm}^{-1}]^{\text{[a]}}$	$I_{\text{rel.,exp.}}^{\text{[a,b]}}$	$\tilde{\nu}_{\text{calcd}} [\text{cm}^{-1}]^{\text{[c]}}$	$I_{\text{rel.,calcd}}^{\text{[b,c]}}$
15	a_1	599.4	0.07	599.1	0.01
16	b_1	—	—	610.4	0.00
17	a_2	—	—	644.3	0.00
18	b_1	—	—	669.3	0.00
19	b_2	—	—	738.1	0.00
20	a_1	817.3	0.37	811.8	0.23
21	b_2	958.0	1.00	969.8	0.54
22	a_1	—	—	1125.3	0.00
23	b_2	—	—	1146.8	0.00
24	b_2	—	—	1287.1	0.00
25	a_1	1283.5	0.14	1294.1	0.06
26	a_1	1332.2	0.42	1338.8	0.18
27	a_1	1398.2	0.14	1404.1	0.13
28	b_2	1444.7	0.85	1458.2	1.00
29	b_2	1521.6	0.85	1545.9	0.54
30	a_1	1597.3	0.18	1607.3	0.27

[a] Argon matrix, 3 K. [b] Relative intensity based on the most intense absorption. [c] Calculated at the UB3LYP/6–311G(d,p) level of theory, unscaled. The assignment is tentative and is based on band positions and intensities.

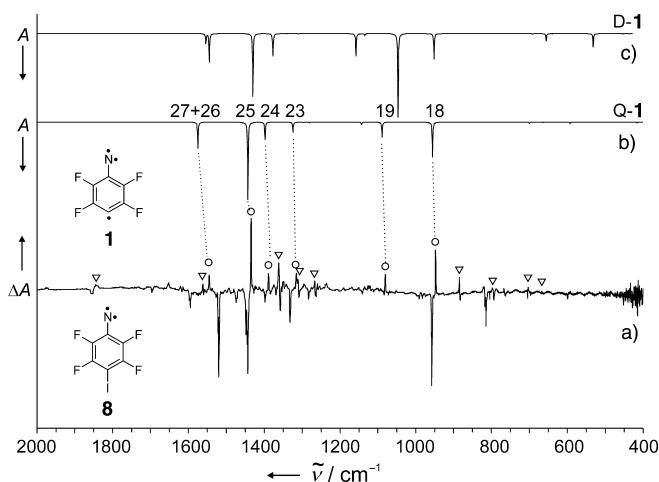


Figure 2. Photochemistry of T-8. a) Difference spectrum. Bands pointing upwards appear, bands pointing downwards disappear upon irradiation of T-2 in an argon matrix at 3 K with light of wavelength 254 nm. Band set A is marked with circles, set B with triangles. b) Calculated (UB3LYP/6–311G(d,p), unscaled) spectrum of quartet nitrene radical Q-1. c) Calculated (UB3LYP/6–311G(d,p), unscaled) spectrum of doublet nitrene radical D-1.

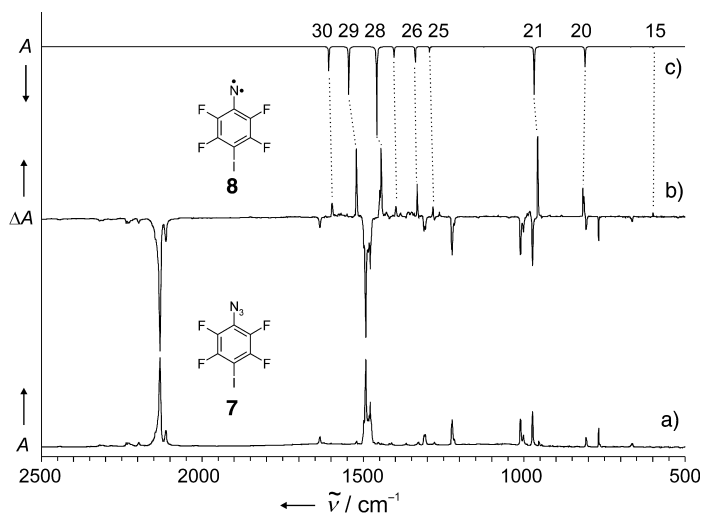


Figure 1. Photochemistry of **7**. a) IR spectrum of **7** (Ar, 3 K). b) Difference spectrum. Bands pointing upwards appear, bands pointing downwards disappear upon irradiation with light of wavelength 320 nm for 17 h. c) Calculated (UB3LYP/6–311G(d,p), unscaled) spectrum of 4-iodo-2,3,5,6-tetrafluorophenylnitrene T-8.

photolysis with light of 320 nm wavelength, while a new compound with intense IR bands at 958, 1445, and 1522 cm^{-1} is formed concurrently. In the UV/Vis spectrum the reaction is accompanied by decrease of the absorption of **7** at 238 nm and the formation of new bands at 257, 293, and 310 nm, as well as two broad absorptions in the 320–360 nm and 390–460 nm region. The new species does not exhibit the characteristic IR absorptions of a didehydroazepine^[12, 17] or an azirine^[14] (which are potential photoproducts of phenylnitrene derivatives), however it does show the typical ESR signals of a triplet nitrene^[19] with the zero-field parameters $|D/hc| = 1.103\text{ cm}^{-1}$ and $|E/hc| = 0.012\text{ cm}^{-1}$. Therefore, the spectrum of the newly formed compound is assigned to the triplet 4-iodo-2,3,5,6-tetrafluorophenylnitrene T-8 (Scheme 2). This interpretation is supported by the calculated IR spectrum, which nicely reproduces the experimental data (Figure 1 b,c, Table 1).

Subsequent monochromatic short-wavelength irradiation with light of wavelength 254 nm results in a decrease of the bands of T-8 and formation of new absorptions, which are assigned to two sets of bands A and B by comparison of the relative intensities in several experiments (Figure 2a). Data set A exhibits IR absorptions in the region from 948 to 1546 cm^{-1} which decrease again upon annealing of the matrix at 32 K, reforming T-8. The UV spectrum does not yield additional information because of rapid deterioration of the optical quality of the matrix upon short wavelength irradiation. The reversibility of the reaction upon annealing of the

matrix indicates cleavage of the C-I bond, and the observed IR spectrum is in excellent agreement with the calculated spectrum of quartet nitrene radical **Q-1** (Figure 2b, Table 2). In contrast, there is less agreement with the calculated data for the doublet state **D-1** (Figure 2c), especially in the region between 900 and 1100 cm⁻¹.

Table 2. IR spectroscopic data of the quartet nitrene radical **Q-1**.

Mode	Symmetry	$\tilde{\nu}_{\text{exp.}}$ [cm ⁻¹] ^[a]	$I_{\text{rel.,exp.}}$ ^[a,b]	$\tilde{\nu}_{\text{calcd}}$ [cm ⁻¹] ^[c]	$I_{\text{rel.,calcd}}$ ^[b,c]
18	<i>b</i> ₂	948.0	0.52	956.4	0.45
19	<i>a</i> ₁	1080.4	0.15	1089.6	0.20
20	<i>b</i> ₂	—	—	1143.5	0.03
21	<i>a</i> ₁	—	—	1280.6	0.01
22	<i>b</i> ₂	—	—	1296.9	0.00
23	<i>a</i> ₁	1315.2	0.19	1324.5	0.13
24	<i>a</i> ₁	1389.0	0.15	1398.8	0.23
25	<i>b</i> ₂	1434.7	1.00	1443.5	1.00
26	<i>b</i> ₂	1545.5	0.15	1575.4	0.34

[a]–[c] See footnotes for Table 1

The second photoproduct **B**, which does not decrease upon annealing of the matrix, has a prominent absorption at 1854 cm⁻¹. The $\nu(\text{C}=\text{N})$ vibration of didehydroazepine **4**, which arises upon photolysis of azidobenzene in cryogenic matrices in addition to phenylnitrene **3**, is observed at a similar frequency.^[12, 17] When the experiment is carried out in a neon matrix, **B** is the exclusive product of the short-wavelength irradiation of **T-8**, while nitrene radical **Q-1** is not observed (Figure 3).^[20] This allows us to unambiguously

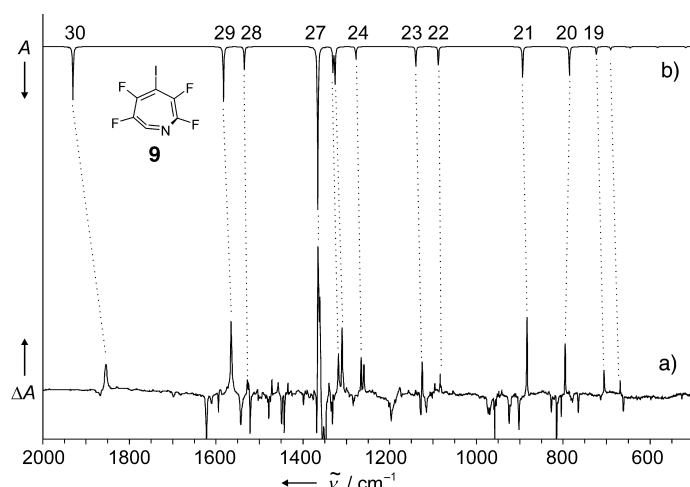


Figure 3. Photochemistry of **T-2**. a) Difference spectrum. Bands pointing upwards appear, bands pointing downwards disappear upon irradiation of **T-2** in a neon matrix at 3 K with light of wavelength 254 nm. b) Calculated (B3LYP/6-311G(d,p), unscaled) spectrum of didehydroazepine (**3**).

distinguish the absorption spectra of **A** and **B**. In particular, it can be discounted that the IR band at 884 cm⁻¹, the assignment of which to **1** would complicate the discrimination between doublet-**1** and quartet-**1** based on IR spectra, is caused by the nitrene radical.

The absorption at 1854 cm⁻¹ indicates rearrangement of **T-8** to the ring-expanded 5-iodo-3,4,6,7-tetrafluorodidehydroazepine (**9**; see Scheme 2) upon photolysis with light of wave-

length 254 nm, although it was established by theoretical^[18] as well as experimental^[13, 14] studies that this reaction should not occur for 2,6-difluorinated phenylnitrenes in cryogenic matrices. In solution a significantly increased barrier for this reaction was observed with less fluorinated starting materials.^[21] Nevertheless, comparison with the calculated spectrum of **9** confirms that the formation of the seven-membered ring is apparently possible in this case (Figure 3, Table 3). According to calculations (B3LYP/6-311G(d,p) + ZPE), the reaction **T-8** → **9** is endothermic by 7.5 kcal mol⁻¹.

Table 3. IR spectroscopic data of **9**.

Mode	$\tilde{\nu}_{\text{exp.}}$ [cm ⁻¹] ^[a]	$I_{\text{rel.,exp.}}$ ^[a,b]	$\tilde{\nu}_{\text{calcd}}$ [cm ⁻¹] ^[c]	$I_{\text{rel.,calcd}}$ ^[b,c]
18	669.1	0.05	691.1	0.02
19	706.1	0.13	724.2	0.05
20	795.9	0.31	786.3	0.18
21	883.7	0.50	894.5	0.19
22	1083.7	0.09	1088.2	0.11
23	1125.5	0.19	1141.0	0.12
24	1259.9	0.16	1278.7	0.08
		1266.1	0.21	
25	1310.1	0.43	1326.5	0.23
26	1318.5	0.24	1332.0	0.15
27	1361.2	0.64	1367.0	1.00
		1365.4	1.00	
28	1528.0	0.06	1535.7	0.14
29	1565.7	0.48	1583.7	0.34
30	1854.1	0.16	1930.3	0.33

[a] Neon matrix, 3 K. [b, c] See footnotes for Table 1.

Comparison of the calculated geometries of tetrafluorooxocyclohexadienylidene (**2**) and the nitrene radical **1** shows that there is not only a formal resemblance of both compounds (Figure 4). With the exception of the C=O and C=N bonds,

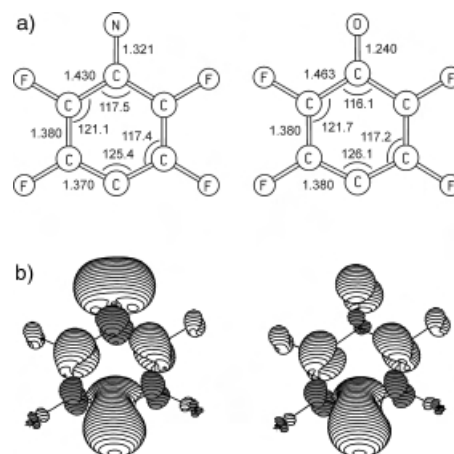


Figure 4. Comparison of the calculated geometries (a) and spin density distributions (b) in nitrene radical **Q-1** and carbene **T-2** (UB3LYP/6-311G(d,p)). Bond lengths [Å], bond angles [°].

the structures of **1** and **2** are almost identical, the differences in C–C bond lengths and bond angles being well below 0.1 Å and 2°, respectively. The spin-density distribution also reflects the similarity of both molecules, with differences appearing only at the nitrogen and oxygen atoms (Figure 4). In the carbene **2** the spin density at the oxygen atom is predominantly

localized in the p orbital perpendicular to the ring plane, while in **1** the highest spin density is in the ring plane.

Photolysis of 4-iodo-2,3,5,6-tetrafluoroazidobenzene (**7**) offers an access to the until now unknown C₆F₄N potential energy surface and to the unusual high-spin nitrene radical **1**. The influence of different topologies and substituents on the spin state of nitrene radicals will be investigated in future studies.

Experimental Section

Matrix experiments were carried out according to standard techniques^[22] using a Sumitomo Heavy Industries RDK-408D closed-cycle cryostat. The lowest temperature available with this system is 2.7 K. Matrices were produced by codeposition of a large excess of neon or argon (Messer-Griesheim, 99.9999%) and the substance to be isolated on top of a cold CsI window. During deposition of argon matrices the temperature of the window was maintained at 30 K. Argon matrices for ESR spectroscopy were deposited at 13 K on a 2 mm OFHC-copper rod, cooled by an APD-HC2 closed-cycle cryostat. IR spectra were recorded with a Bruker Equinox 55 FTIR spectrometer with a resolution of 0.5 cm⁻¹ in the range of 400–4000 cm⁻¹. ESR spectra were recorded with a Bruker Elexsys E500 spectrometer. Irradiations were carried out with a Gräntzel low-pressure mercury lamp (254 nm) and an Osram HBO-500-W/2 high-pressure mercury arc lamp in an Oriel housing with quartz optics, a dichroic mirror, and a Schott cutoff filter (320 nm). DFT calculations were performed with the Gaussian 98 suite of programs.^[23]

4-Iodo-2,3,5,6-tetrafluoroaniline: Yellow HgO (12.8 g, 59.1 mmol) was added to a solution of 2,3,5,6-tetrafluoroaniline (12.8 g, 77.6 mmol) in ethanol (200 mL). The solution was vigorously stirred and iodine (19.8 g, 78.0 mmol) added. The mixture was stirred overnight and filtered over celite. After addition of Na₂SO₃ (1 g) the solution was concentrated to a residual volume of 50 mL using a rotary evaporator. Water (200 mL) was added and the precipitate was filtered off. Recrystallization from 25% ethanol in water and subsequent drying in vacuo yielded 4-iodo-2,3,5,6-tetrafluoroaniline (16.2 g, 55.7 mmol, 72%) as dark crystals. MS: *m/z*(%): 291 (*M*⁺, 100), 164 (50), 144 (25), 137 (60), 127 (30), 117 (25), 69 (20).

4-Iodo-2,3,5,6-tetrafluoroazidobenzene (**7**): 4-Iodo-2,3,5,6-tetrafluoroaniline (3.0 g, 10.3 mmol) was dissolved in trifluoroacetic acid (30 mL) and cooled to 0 °C. A solution of sodium nitrite (0.81 g, 11.7 mmol) in water (15 mL) was slowly added while stirring and cooling with an ice bath. The solution was stirred for further 15 min at 0 °C. A solution of sodium azide (0.75 g, 11.5 mmol) in water (15 mL) was added to the stirred solution, which was subsequently stirred for 1 h at room temperature. After addition of ether (100 mL) the organic phase was washed with water and dilute aqueous NaOH, dried (Na₂SO₄), and evaporated. Chromatography (silica/pentane) yielded **7** (2.18 g, 67%) as a colorless oil. MS: *m/z* (%): 317 (*M*⁺, 10), 289 (30), 162 (100), 127 (30), 117 (20), 112 (10), 98 (25), 69 (25). ¹³C NMR (CDCl₃, 50 MHz): δ = 66.3 (t, *J* = 28.0 Hz), 120.5 (tt, *J* = 2.9 Hz, 12.3 Hz), 140.0 (dm, 256.4 Hz), 147.2 ppm (dm, 248.1 Hz). IR (Ar, 3 K): $\tilde{\nu}$ (%): 2229.9 (5), 2196.8 (5), 2130.9 (100), 2112.4 (18), 1634.5 (10), 1492.2 (95), 1478.4 (49), 1307.6 (15), 1223.2 (31), 1012.1 (31), 1001.9 (13), 974.3 (39), 955.3 (6), 807.8 (11), 768.3 (22), 664.5 cm⁻¹(5).

Received: February 1, 2002 [Z18625]

- [1] a) H. Iwamura, *Adv. Phys. Org. Chem.* **1990**, 179–253; b) H. Iwamura, *J. Phys. Org. Chem.* **1998**, 11, 299–304.
- [2] D. A. Dougherty, *Acc. Chem. Res.* **1991**, 24, 88–94.
- [3] A. Rajca, *Chem. Rev.* **1994**, 94, 871–893.
- [4] *Magnetism: Molecules to Materials* (Eds.: J. S. Miller, M. Drillon), Wiley-VCH, Weinheim, **2001**.
- [5] P. M. Lahti, B. Esat, R. Walton, *J. Am. Chem. Soc.* **1998**, 120, 5122–5123.
- [6] P. M. Lahti, B. Esat, Y. Liao, P. Serwinski, J. Lan, R. Walton, *Polyhedron* **2001**, 20, 1647–1652.
- [7] K. Matsuda, H. Iwamura, *Chem. Commun.* **1996**, 1131–1132.
- [8] K. Matsuda, H. Iwamura, *Mol. Cryst. Liq. Cryst.* **1997**, 306, 89–94.
- [9] K. Matsuda, G. Ulrich, H. Iwamura, *J. Chem. Soc. Perkin Trans. 2* **1998**, 1581–1588.

- [10] H. H. Wenk, R. Hübert, W. Sander, *J. Org. Chem.* **2001**, 66, 7994–7999.
- [11] W. Sander, R. Hübert, E. Kraka, J. Grafenstein, D. Cremer, *Chem. Eur. J.* **2000**, 6, 4567–4579.
- [12] J. C. Hayes, R. S. Sheridan, *J. Am. Chem. Soc.* **1990**, 112, 5879–5881.
- [13] I. R. Dunkin, P. C. P. Thomson, *J. Chem. Soc. Chem. Commun.* **1982**, 1192–1193.
- [14] J. Morawietz, W. Sander, *J. Org. Chem.* **1996**, 61, 4351–4354.
- [15] H. H. Wenk, A. Balster, W. Sander, D. A. Hrovat, W. T. Borden, *Angew. Chem.* **2001**, 113, 2356–2359; *Angew. Chem. Int. Ed.* **2001**, 40, 2295–2298.
- [16] H. H. Wenk, W. Sander, *Chem. Eur. J.* **2001**, 7, 1837–1844.
- [17] O. L. Chapman, J. P. Le Roux, *J. Am. Chem. Soc.* **1978**, 100, 282–285.
- [18] W. T. Borden, W. L. Karney, *J. Am. Chem. Soc.* **1997**, 119, 3347–3350.
- [19] M. S. Platz in *CRC Handbook of Organic Photochemistry, Vol. II* (Ed.: J. C. Scaiano), CRC Press, Boca Raton, FL, USA, **1989**, S. 373–393.
- [20] In contrast, photolysis of fluorinated diiodobenzene derivatives leads to the corresponding radicals and diradicals in solid neon but not in argon, see references [15,16].
- [21] N. P. Gritsan, A. D. Gudmundsdottir, D. Tigelaar, Z. D. Zhu, W. L. Karney, C. M. Hadad, M. S. Platz, *J. Am. Chem. Soc.* **2001**, 123, 1951–1962.
- [22] I. R. Dunkin, *Matrix Isolation Techniques: A Practical Approach*, Oxford University Press, Oxford, **1998**.
- [23] Gaussian 98 (Revision A.7), M. J. Frisch, G. W. Trucks, H. B. Schlegel, G. E. Scuseria, M. A. Robb, J. R. Cheeseman, V. G. Zakrzewski, J. A. Montgomery, R. E. Stratmann, J. C. Burant, S. Dapprich, J. M. Millam, A. D. Daniels, K. N. Kudin, M. C. Strain, O. Farkas, J. Tomasi, V. Barone, M. Cossi, R. Cammi, B. Mennucci, C. Pomelli, C. Adamo, S. Clifford, J. Ochterski, G. A. Petersson, P. Y. Ayala, Q. Cui, K. Morokuma, D. K. Malick, A. D. Rabuck, K. Raghavachari, J. B. Foresman, J. Cioslowski, J. V. Ortiz, A. G. Baboul, B. B. Stefanov, G. Liu, A. Liashenko, P. Piskorz, I. Komaromi, R. Gomperts, R. L. Martin, D. J. Fox, T. Keith, M. A. Al-Laham, C. Y. Peng, A. Nanayakkara, C. Gonzalez, M. Challacombe, P. M. W. Gill, B. G. Johnson, W. Chen, M. W. Wong, J. L. Andres, M. Head-Gordon, E. S. Replogle, J. A. Pople, Gaussian, Inc., Pittsburgh, PA, **1998**.

Conversion of Hexafluoropropene into 1,1,1-Trifluoropropane by Rhodium-Mediated C–F Activation**

Thomas Braun,* Daniel Noveski, Beate Neumann, and Hans-Georg Stammer

Interest in the activation of carbon–fluorine bonds by transition metal centers has been increasing dramatically over the last decade.^[1] Recent discoveries include the stoichiometric^[2] and catalytic^[3, 4] derivatization of aromatic compounds

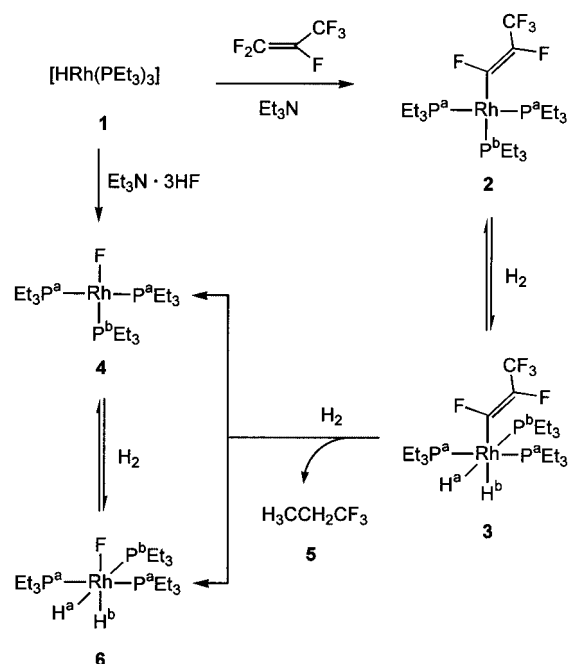
[*] Dr. T. Braun, Dipl.-Chem. D. Noveski, B. Neumann, Dr. H.-G. Stammer
Fakultät für Chemie
Universität Bielefeld
Postfach 100131, 33501 Bielefeld (Germany)
Fax: (+49) 521-106-6026
E-mail: thomas.braun@uni-bielefeld.de

[**] This work was supported by the Deutsche Forschungsgemeinschaft (grant BR-2065/1-2) and the Fonds der Chemischen Industrie. We thank Professor G.-V. Röschenthaler for a gift of hexafluoropropene and DMC² for a loan of RhCl₃. T.B. also thanks Professor P. Jutzi for his generous support.

Supporting information for this article is available on the WWW under <http://www.angewandte.org> or from the author.

by C–F activation.^[1] One of the major achievements was the catalytic conversion of hexafluorobenzene into pentafluorobenzene with [HRh(PMe₃)₄] as catalyst.^[4] However, there are only a few examples of the activation of a C–F bond in fluorinated olefins reported.^[1c, 5–8] The reactions include the activation of hexafluoropropene with [H₂Ir(PPh₃)₂]₃PW₁₂O₄₀, which led to the generation of a propenyl complex.^[5b] The formation of organofluorine compounds by C–F activation of olefins, followed by derivatization and cleavage reactions within the coordination sphere of the metal is even less developed.^[1c, 6–8] With regard to the defluorination of perfluorinated olefins, Jones et al. reported that hexafluoropropene can be converted into propane by using seven equivalents of [(η⁵-C₅Me₅)₂ZrH₂]. The reaction initially forms the complex [(η⁵-C₅Me₅)₂ZrHC₃H₇], which is then allowed to react with hydrogen to yield propane.^[6] In a recent report Whittlesey et al. described the reaction of hexafluoropropene with a ruthenium dihydride, which led to a mixture of lower fluorinated olefins.^[7]

Herein we describe the selective conversion of a perfluorinated olefin into a partially fluorinated alkane by metal-induced hydrodefluorination exclusively at the double bond.^[2e] We show that hexafluoropropene can selectively and under very mild conditions be activated at a rhodium center to give the propenyl complex **2** (Scheme 1). On treatment of **2** with hydrogen, the fluorinated vinyl unit is converted into a nonfluorinated alkyl group, and 1,1,1-trifluoropropane (**5**) together with the rhodium fluoride complex **4** is obtained.



Scheme 1. The synthesis and reactivity of **2**.

Treatment of the rhodium hydrido complex **1** with hexafluoropropene in benzene in the presence of triethylamine results in the fast and regioselective formation of the C–F activation product **2** (Scheme 1). Note that treatment of

[HRh(CO)(PPh₃)₃] with tetrafluoroethene leads to the insertion of the olefin into the rhodium–hydrogen bond.^[9] The proposed structure for **2** is supported by the ³¹P and ¹⁹F NMR spectroscopic data (Table 1). The spectra are of higher order, and coupling constants have been determined by simulation of the ³¹P NMR spectrum by using the program g-NMR (Figure 1).^[10] The ¹⁹F NMR spectrum shows three resonance

Table 1. Selected spectroscopic data for **2–6**; ¹H NMR: 500 MHz, ¹⁹F NMR: 470.4 MHz, ³¹P NMR 202.4 MHz; labeling of atoms as in Scheme 1.

2 :	¹⁹ F NMR (C ₆ D ₆): δ = –64.5 (m, 3F; CF ₃), –95.4 (dm, ³ J(F,F) = 117.7 Hz, 1F; CF), –174.4 ppm (dm, ³ J(F,F) = 117.1 Hz, 1F; CF); ³¹ P NMR (C ₆ D ₆): δ = 18.5 (m, P ^b), 15.5 ppm (m, P ^a).
3 :	¹ H NMR (C ₆ D ₆): δ = –11.3 (dm, ² J(P ^b ,H) ≈ 150 Hz, 1H; H ^a), –12.0 ppm (dm, ¹ J(Rh,H) ≈ 20 Hz, 1H; H ^b); ¹⁹ F NMR (C ₆ D ₆): δ = –63.6 (m, 3F; CF ₃), –87.2 (dm, ³ J(F,F) = 118.9 Hz, 1F; CF), –166.2 ppm (dm, ³ J(F,F) = 118.2 Hz, 1F; CF); ³¹ P NMR (C ₆ D ₆): δ = 28.5 (dm, ¹ J(Rh,P) ≈ 98 Hz; P ^a), 11.8 ppm (m; P ^b).
4 :	¹⁹ F NMR ([D ₈]toluene, 213 K): δ = –277 ppm (dm, br, ¹ J(P ^b ,F) ≈ 188 Hz); ³¹ P NMR ([D ₈]toluene, 213 K): δ = 45.2 (ddt, ² J(P,F) = 187.0, ¹ J(Rh,P) = 180.2, ² J(P,P) = 42.2 Hz; P ^b), 25.1 ppm (ddd, ¹ J(Rh,P) = 138.3, ² J(P,F) = 22.0, ² J(P,P) = 42.2 Hz; P ^a).
5 :	¹ H NMR (C ₆ D ₆): δ = 0.58 (t, ³ J(H,H) = 7.5 Hz, 3H; CH ₃), 1.45 ppm (m, 2H; CH ₂); ¹⁹ F NMR (C ₆ D ₆): δ = –69.1 ppm (t, ³ J(F,H) = 10.4 Hz).
6 :	¹ H NMR (C ₆ D ₆): δ = –9.6 (dm, ² J(P ^b ,H) = 154.7 Hz, 1H; H ^a), –24.9 ppm (ddm, ² J(F,H) ≈ 94, ¹ J(Rh,H) = 20 Hz, 1H; H ^b); ¹⁹ F NMR (C ₆ D ₆): δ = –274 ppm (m, br); ³¹ P NMR (C ₆ D ₆): δ = 28.9 (ddm, ¹ J(Rh,P) = 107.7, ² J(P,P) = 18.4 Hz; P ^a), 12.2 ppm (m; P ^b).

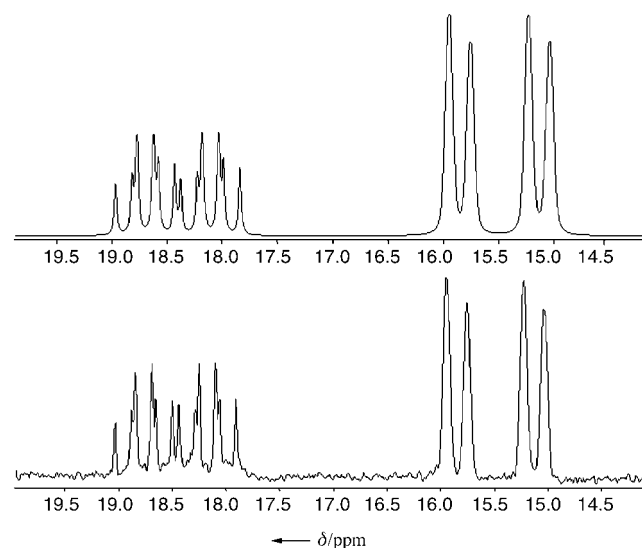


Figure 1. ³¹P NMR spectrum of complex **2**; observed (bottom) and simulated (top) using the following coupling constants (Hz): ¹J(Rh,P^a) = 145.7, ³J(P^a,F) = 6.0, ⁴J(P^a,F) = 4.6, ⁵J(P^a,F) = 4.0, ²J(P^a,P^b) = 39.1, ¹J(Rh,P^b) = 119.3, ³J(P^b,F) = 27.2, ⁴J(P^b,F) = 0.2, ⁵J(P^b,F) = 0.1 Hz; labeling of atoms as in Scheme 1.

signals at δ = –64.5, –95.4, and –174.4 ppm with a ratio 3:1:1, and thus reveals the presence of the propenyl ligand. The chemical shifts and the coupling constants of the olefinic fluorine atoms (*J* = 117.1 Hz) indicate their *trans* orientation.^[5b, 11] The configuration at the double bond in **2** was confirmed by an X-ray diffraction analysis at low temperature (Figure 2).^[12] The rhodium–carbon bond in **2** (2.029(4) Å) is

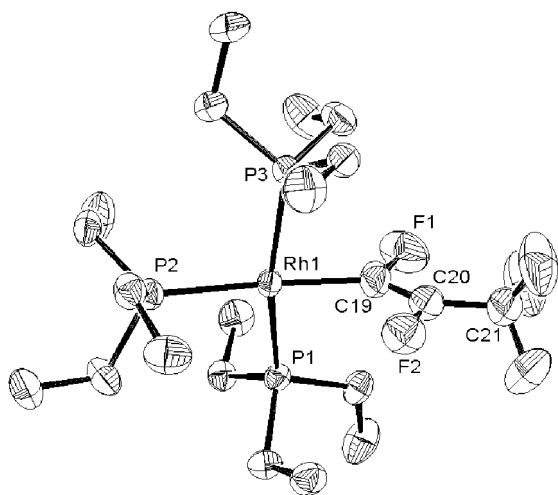


Figure 2. Molecular structure of **2** (ORTEP plot) in the crystal. Selected bond lengths [Å] and angles [°]: Rh1–C19 2.029(4), C19–C20 1.303(7), C19–F1 1.429(5), C20–F2 1.423(6); Rh1–C19–F1 120.8(3), Rh1–C19–C20 130.5(4), C20–C19–F1 108.7(4), C19–C20–F2 114.0(4), C19–C20–C21 136.8(6), C21–C20–F2 109.2(5).

shorter than the corresponding bond in the rhodium(i) complex *trans*-[Rh{C(CN)=C(C₆H₄OMe)₂}(CO)(PiPr₃)₂] (**7**; 2.106(4) Å), which bears a nonfluorinated vinyl ligand.^[13] The C–C double bond in **2** (1.303(7) Å) is likewise shorter than the C–C double bond **7** (1.367(3) Å), but is comparable to the C–C double bond length in hexafluoropropene (1.31 Å), which was determined by electron diffraction in the vapor phase.^[13, 14]

Upon addition of hydrogen to a solution of **2** in C₆D₆ at 300 K a new set of signals emerges in the NMR spectra, which corresponds to the dihydrido complex **3**. Compound **3** could not be isolated in the solid state, and a solution of **3** is only stable for about 30 min at room temperature. Under vacuum, **3** loses hydrogen, and the re-formation of **2** is observed. The ¹H NMR spectrum of **3** exhibits resonance signals for the hydrido ligands at $\delta = -11.3$ (²*J*(P,H_{trans}) \approx 150 Hz) and -12.0 ppm. This finding confirms the *cis-mer* configuration and indicates the presence of an anionic bound carbon ligand *trans* to one of the hydrido ligands.^[4, 15, 16] The ³¹P NMR spectrum is of higher order and shows two multiplets at $\delta = 28.5$ and $\delta = 11.8$ ppm with a phosphorus–phosphorus coupling constant ²*J*(P,P) of about 25 Hz, which is consistent with the presence of a Rh^{III} compound (Table 1).^[15–17]

In the presence of hydrogen, the formation of the compounds **4–6** is observed after a reaction time of 30 min. The presence of a base (Et₃N or Cs₂CO₃) has almost no influence on the product distribution. Assignments in the NMR spectra are partially based on ³¹P–¹H and ¹H–¹H COSY NMR spectra. The ¹⁹F NMR spectrum of **4** at 213 K displays a broad doublet at $\delta = -277$ ppm with a coupling constant of ²*J*(P,F_{trans}) \approx 188 Hz, which is consistent with a nonbridging fluoro ligand *trans* to a phosphane ligand.^[18] The ³¹P NMR spectrum shows two signals at $\delta = 45.2$ and $\delta = 25.1$ ppm for the phosphorus nuclei with the expected coupling pattern (Table 1).^[15, 16, 18a] The ¹H and ³¹P NMR spectroscopic data for **6** resemble those for *cis-mer*-[RhCl(H)₂(PEt₃)₃].^[15] The fluorine bound to the rhodium center displays an additional

coupling ²*J*(H,F_{trans}) \approx 94 Hz in the ¹H NMR spectrum and a broad signal at $\delta = -274$ ppm in the ¹⁹F NMR spectrum.^[18] The formation of 1,1,1-trifluoropropane (**5**) was confirmed by ¹H and ¹⁹F NMR spectroscopy by comparison with an authentic sample. The yield is 80% according to the ¹⁹F NMR spectrum.

The fluoro complex **4** can also be synthesized by reaction of **1** with Et₃N · 3HF, which is a mild source of HF.^[2c, 21] Treatment of a solution of **4** with hydrogen affords compound **6**, which under vacuum converts back to **4**.

One possible mechanism for the C–F activation of the perfluorinated olefin is by loss of HF from an alkyl compound, which was initially formed by insertion.^[1c, 5b] Other possibilities include an electron transfer mechanism or a base-induced, nucleophilic reaction pathway.^[19] The formation of **5** might involve α -fluoro- and β -fluoro-elimination reactions with concomitant formation of HF and subsequent hydrogenation of the generated propynyl ligand or of trifluoropropyne.^[2e, 6, 20] However, a direct cleavage of the Rh–C bond by hydrogen followed by repeated C–F activation and analogous Rh–C cleavage steps by hydrogen is also conceivable.^[4] Mechanistic investigations concerning both the activation of the C–F bond in perfluoropropene and the formation of **5** are in progress.

In conclusion, we have demonstrated the direct conversion of a fluorinated alkenyl unit into a nonfluorinated alkyl group by selective rhodium-mediated C–F activation starting from hexafluoropropene. There is no indication for a defluorination of the trifluoromethyl group. To the best of our knowledge, it is the first example for a selective and complete hydrodefluorination of a perfluorinated olefin, for which only the fluorine atoms at the double bond have been removed.^[6, 22] Moreover, dihydrogen has been used for the reduction of the perfluorovinyl ligand after the activation of the olefin with a rhodium hydrido complex. Note that in the zirconium-mediated conversion of hexafluoropropene into propane a zirconium hydride is the main hydrogen source.^[6] We believe that the reaction described offers a new and general method for preparing hydrofluorocarbons, some of which are of current interest as compounds with less or no ozone depletion potential.^[23]

Received: April 5, 2002 [Z19051]

- [1] a) J. Burdeniuc, B. Jedlicka, R. H. Crabtree, *Chem. Ber.* **1997**, *130*, 145–154; b) T. G. Richmond in *Top. Organomet. Chem.* **1999**, *3*, 243–269; c) J. L. Kiplinger, T. G. Richmond, C. E. Osterberg, *Chem. Rev.* **1994**, *94*, 373–431; d) E. F. Murphy, R. Murugavel, H. W. Roesky, *Chem. Rev.* **1997**, *97*, 3425–3468.
- [2] a) R. Dagani, *Chem. Eng. News* **2001**, 79(9), 40–43; b) B. L. Edlbach, B. M. Kraft, W. D. Jones, *J. Am. Chem. Soc.* **1999**, *121*, 10327–10331; c) T. Braun, S. P. Foxon, R. N. Perutz, P. H. Walton, *Angew. Chem.* **1999**, *111*, 3543–3545; *Angew. Chem. Int. Ed.* **1999**, *38*, 3326–3329; d) M. I. Sladek, T. Braun, B. Neumann, H.-G. Stämmler, *J. Chem. Soc. Dalton Trans.* **2002**, 297–299; e) B. M. Kraft, R. J. Lachicotte, W. D. Jones, *J. Am. Chem. Soc.* **2001**, *123*, 10973–10979.
- [3] a) C. W. K. Gstöttmayr, T. Weskamp, W. A. Herrmann, *Angew. Chem.* **2001**, *113*, 3500–3503; *Angew. Chem. Int. Ed.* **2001**, *40*, 3387–3389; b) Y. Kiso, K. Tamao, M. Kumada, *J. Organomet. Chem.* **1973**, *50*, C12–C13; c) Y. Ishii, N. Chatani, S. Yorimitsu, S. Murai, *Chem. Lett.*

- 1998, 157–158; d) T. Braun, R. N. Perutz, M. I. Sladek, *Chem. Commun.* **2001**, 2254–2255.
- [4] M. Aizenberg, D. Milstein, *J. Am. Chem. Soc.* **1995**, *117*, 8674–8675.
- [5] a) H. Peterson, J. T. Golden, R. G. Bergman, *Organometallics* **1999**, *18*, 2005–2020; b) A. R. Siedle, R. A. Newmark, *Organometallics* **1989**, *8*, 1442–1450.
- [6] B. M. Kraft, R. J. Lachicotte, W. D. Jones, *J. Am. Chem. Soc.* **2000**, *122*, 8559–8560.
- [7] M. S. Kirkham, M. F. Mahon, M. K. Whittlesey, *Chem. Commun.* **2001**, 813–814.
- [8] a) P. L. Watson, T. H. Tulip, I. Williams, *Organometallics* **1990**, *9*, 1999–2009; b) L. A. Watson, D. V. Yandulov, K. G. Caulton, *J. Am. Chem. Soc.* **2001**, *123*, 603–611; c) S. A. Strazisar, P. T. Wolczanski, *J. Am. Chem. Soc.* **2001**, *123*, 4728–4740.
- [9] G. Yagupsky, C. K. Brown, G. Wilkinson, *J. Chem. Soc. Chem. Commun.* **1969**, 1244–1245.
- [10] P. H. M. Budzelaar, g-NMR, Version 4.1, Adept Scientific plc, Letchworth, **2001**.
- [11] T. Braun, B. Blöcker, V. Schorlemer, B. Neumann, A. Stämmler, H.-G. Stämmler, *J. Chem. Soc. Dalton Trans.* **2002**, 2213–2218.
- [12] Data for the X-ray structure analysis of **2**: $C_{21}H_{45}F_3P_3Rh$ ($M_r = 588.39$): crystal dimensions $0.40 \times 0.10 \times 0.08$ mm, monoclinic, $P2_1/n$, $a = 10.1568(6)$, $b = 14.5420(9)$, $c = 19.5829(12)$ Å, $\beta = 104.311(10)^\circ$, $Z = 4$, $V = 2802.6(3)$ Å³, $\rho_{\text{calc}} = 1.394$ g cm⁻³, $T = 183(2)$ K, $\theta_{\text{max}} = 24.99^\circ$, $\text{MoK}\alpha$ radiation ($\lambda = 0.71073$ Å), 12648 reflections collected, 4808 were unique ($R_{\text{int}} = 0.0403$), Siemens Smart CCD diffractometer, semiempirical absorption corrections (from equivalents, $\text{min./max. transmission } 0.9373/0.7350$), $\mu = 0.820$ mm⁻¹. The structure was solved by direct methods (SHELXTL PLUS) and refined with the full-matrix least-squares methods on F^2 (SHELX-97). Final R_1 , wR_2 values on all data: 0.0508, 0.1019. R_1 , wR_2 values for 3852 reflections with $I_o > 2\sigma(I_o)$: 0.0388, 0.0953, goodness-of-fit on F^2 1.067, data-to-parameter ratio 13.1, residual electron density $+0.755/-0.722$ e Å⁻³. CCDC-179384 (**2**) contains the supplementary crystallographic data for this paper. These data can be obtained free of charge via www.ccdc.cam.ac.uk/conts/retrieving.html (or from the Cambridge Crystallographic Data Centre, 12, Union Road, Cambridge CB21EZ, UK; fax: (+44) 1223-336-033; or deposit@ccdc.cam.ac.uk).
- [13] M. Laubender, H. Werner, *Angew. Chem.* **1998**, *110*, 158–160; *Angew. Chem. Int. Ed.* **1998**, *37*, 150–152.
- [14] P. W. Allen, L. E. Sutton, *Acta Crystallogr.* **1950**, *3*, 46–72.
- [15] A. Koch, J. Bargon, *Inorg. Chem.* **2001**, *40*, 533–539.
- [16] B. A. Messerle, C. L. Sleight, M. G. Partridge, S. B. Duckett, *J. Chem. Soc. Dalton Trans.* **1999**, 1429–1436.
- [17] So far, we have not been successful in simulating the ³¹P NMR spectrum of **4**, as the signals are obscured by resonance signals of a small amount of compound **6**.
- [18] a) J. Gil-Rubio, B. Weberndörfer, H. Werner, *J. Chem. Soc. Dalton Trans.* **1999**, 1437–1444; b) J. Vicente, J. Gil-Rubio, D. Bautista, *Inorg. Chem.* **2001**, *40*, 2636–2637.
- [19] Concerning the mechanism of C–F activation reactions see, for example: a) T. Braun, L. Cronin, C. L. Higgitt, J. E. McGrady, R. N. Perutz, M. Reinhold, *New. J. Chem.* **2001**, *25*, 19–21; b) M. K. Whittlesey, R. N. Perutz, M. H. Moore, *Chem. Commun.* **1996**, 787–788; c) L. Edelbach, W. D. Jones, *J. Am. Chem. Soc.* **1997**, *119*, 7734–7742.
- [20] T. G. Richmond, *Angew. Chem.* **2000**, *112*, 3378–3380; *Angew. Chem. Int. Ed.* **2000**, *39*, 3241–3244.
- [21] N. A. Jasim, R. N. Perutz, *J. Am. Chem. Soc.* **2000**, *122*, 8685–8639.
- [22] a) C. G. Krespan in *Chemistry of Organic Fluorine Compounds II* (Eds.: M. Hudlicky, E. E. Pavlath), American Chemical Society, Washington, DC, **1995**, pp. 297–320.
- [23] a) T. Hiyama, *Organofluorine Compounds*, Springer, Berlin, **2000**, p. 196; b) A. R. Ravishankara, A. A. Turnipseed, N. R. Jensen, S. Barone, M. Mills, C. J. Howard, S. Solomon, *Science* **1994**, *263*, 71–75.

Barrier Height Titration by Tunable Photoionization Combined with Chemical Monitoring: Unimolecular Keto/Enol Tautomerization of the Acetamide Cation Radical**

Detlef Schröder,* Jessica Loos, Roland Thissen, Odile Dutuit, Philippe Mourgues, Henri-Edouard Audier, Chava Lifshitz, and Helmut Schwarz

Dedicated to Professor Petr Čárský on the occasion of his 60th birthday

The keto/enol tautomerization is generally assumed to proceed easily. The rapid equilibration of keto and enol tautomers in solution is due to solvent-mediated proton-transfer catalysis. In aprotic solvents, the isomerization is slowed down and simple enols can exhibit significant lifetimes.^[1] In the gas phase, keto and enol isomers hardly interconvert at all at ambient internal energies because the barriers associated with intramolecular 1,3-hydrogen migration are rather large, generally exceeding 2 eV.^[2] Furthermore, for simple, nonconjugated carbonyl compounds, the keto forms are thermochemically more stable (Table 1).^[3,4]

Three features are associated with the ionization of carbonyl compounds to the corresponding cation radicals.^[5]

Table 1. Relative stabilities (in eV)^[a] of neutral and ionized keto and enol tautomers.^[b]

	Neutral	Cation radical
acetaldehyde (CH ₃ CHO)	0.42	–0.66
acetone (CH ₃ COCH ₃)	0.43	–0.60
acetic acid (CH ₃ COOH)	1.20 ^[c]	–0.89
acetamide (CH ₃ CONH ₂)	1.07	–0.82 ^[d]
methyl acetate (CH ₃ COOCH ₃)	1.18 ^[c]	–1.08

[a] $\Delta_f H^\circ(\text{enol}) - \Delta_f H^\circ(\text{keto})$. [b] Taken from ref. [6] unless noted otherwise. [c] Calculated G2 value taken from ref. [4]; also see ref. [3]. [d] Calculated G2 value taken from ref. [10].

[*] Dr. D. Schröder, Dipl.-Chem. J. Loos, Prof. Dr. H. Schwarz
Institut für Chemie
Technischen Universität Berlin
10623 Berlin (Germany)
Fax: (+49) 30-314-21102
E-mail: df@www.chem.tu-berlin.de
Dr. R. Thissen, Dr. O. Dutuit
Laboratoire de Chimie Physique, Bât. 350
Université Paris-Sud
91405 Orsay (France)
Dr. P. Mourgues, Dr. H.-E. Audier
Laboratoire des Mécanismes Réactionnels - DCMR
Ecole Polytechnique
91128 Palaiseau Cedex (France)
Prof. Dr. C. Lifshitz
Department of Physical Chemistry
Hebrew University, Givat Ram
Jerusalem 91904 (Israel)

[**] This work was supported by the Deutsche Forschungsgemeinschaft, the Fonds der Chemischen Industrie, and the Gesellschaft von Freunden der Technischen Universität Berlin. Continuous support by the technical staff of LURE, Orsay, is appreciated. D.S. thanks the Laboratoire de Chimie Physique at the Université Paris Sud for a visiting professorship.

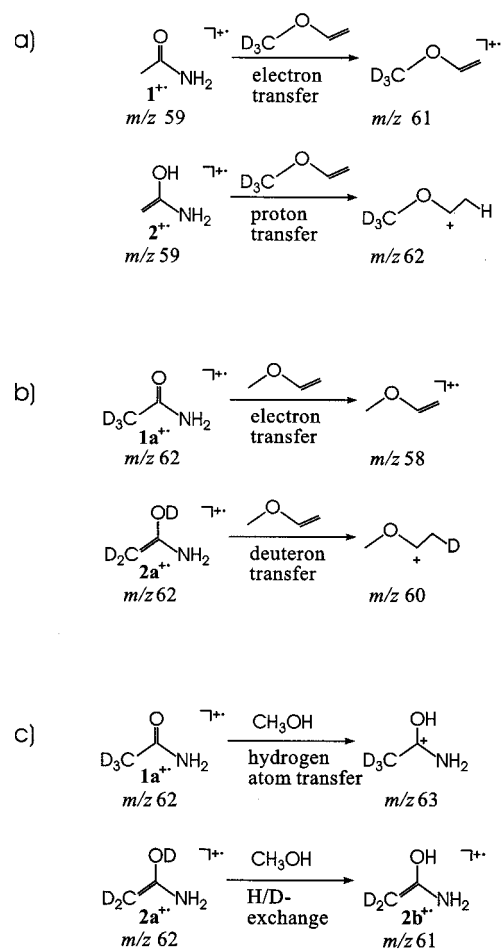
First, keto forms exhibit larger ionization energies (IEs) than the corresponding enols. This difference can be rationalized in a simple manner: ionization of the strong, polarized C=O bond of the keto form is much more difficult than ionization of the donor-substituted, electron-rich C=C bond in the enol. As a consequence, the relative stabilities of keto and enol tautomers tend to reverse for the cation radicals (Table 1). The second effect is indirectly related to the higher IE of the keto form in that the adjacent bonds are significantly weakened upon ionization. In the case of acetone, for example, the bond dissociation energy of $D_{298}(\text{CH}_3\text{CO}-\text{CH}_3) = 3.50$ eV of the neutral molecule drops to $D_{298}(\text{CH}_3\text{CO}^+-\text{CH}_3) = 0.82$ eV in the cation radical.^[6] Finally, although cationization often facilitates hydrogen migrations,^[7] the barriers associated with 1,3-H transfers in ionized keto/enol pairs remain substantial, often similar to those in the neutral keto/enol isomers.^[8, 9] Consequently, unimolecular isomerization of the ionized keto form to the more stable enol tautomer may effectively be impossible because upon increasing the internal energy of the molecular ion facile α -bond cleavages prevent the system from surmounting the activation barrier of a 1,3-H migration.

Recently, however, some of us reported evidence for the occurrence of an unimolecular keto/enol tautomerization in the ionized acetamide $1^{+\bullet}$.^[10] In these experiments, ion cyclotron resonance (ICR) mass spectrometry was used to investigate the bimolecular reactivity of mass-selected $1^{+\bullet}$ in the gas phase with several neutral reagents which specifically probe ion structures ("chemical monitoring"). These experiments reveal that electron ionization (EI) of neutral acetamide leads to an approximate 1:2 mixture of $1^{+\bullet}$ and its enol isomer $2^{+\bullet}$. Based on the above considerations, this therefore would imply that the keto/enol tautomerization $1^{+\bullet} \rightleftharpoons 2^{+\bullet}$ is particularly favored over other carbonyl compounds. Although this view was fully supported by ab initio calculations at the G2 level of theory, the experiment itself bears some ambiguities. Specifically, 1) as electron ionization (20–70 eV) was used, the internal energy of the ions formed is poorly defined, 2) it is rather difficult to rigorously exclude the occurrence of tautomerization due to bimolecular reactions upon or shortly after ionization,^[11–13] and 3) the reagents used as structure-specific chemical monitors may themselves induce the rearrangement of $1^{+\bullet}$ to the more stable enol ion $2^{+\bullet}$, thereby obscuring the interpretation of the kinetic data obtained in ICR experiments.

How can we probe experimentally the barrier of the reaction $1^{+\bullet} \rightarrow 2^{+\bullet}$ more directly? Clearly, one needs 1) an ionization method that permits a better control of the internal energy imparted to the resulting cation radicals, 2) some time delay allowing the unimolecular isomerization $1^{+\bullet} \rightarrow 2^{+\bullet}$ to occur, and 3) a specific indicator for the presence of $2^{+\bullet}$ even in an excess of $1^{+\bullet}$. The solution was accomplished by combining photoionization using monochromatized synchrotron radiation with chemical monitoring by means of tandem mass spectrometry. Thus, ionization of neutral acetamide with photons of adjustable energies allows control of the internal energy content of the initially formed $1^{+\bullet}$, time-delayed mass-selection provides ample time (ca. 60 μs) for the interconversion $1^{+\bullet} \rightarrow 2^{+\bullet}$ to take place, and appropriate ion–molecule

reactions can then be employed to afford enol-specific product ions which are detected eventually. The last challenge was most difficult to tackle because $1^{+\bullet}$ is more energetic than $2^{+\bullet}$, such that many neutral molecules specifically react with $1^{+\bullet}$, while only a few enol-specific processes were identified. After extensive screening of several neutral reagents by means of ICR experiments,^[14] methyl vinyl ether (MVE) and methanol were found as suitable reagents for the photo-ionization studies, provided appropriate labeling is applied to distinguish isobaric ions.

Herein we focus on the major products of these reactions with a particular emphasis on the products of enol-specific reactions. The ion–molecule reaction of $1^{+\bullet}$ with MVE mostly leads to electron transfer, that is $\text{MVE}^{+\bullet} + 1$, whereas the enol $2^{+\bullet}$ undergoes proton transfer to form $[\text{MVE} + \text{H}]^+$ (Scheme 1a).^[15] As the mass resolution of the quadrupole



Scheme 1. Differences in the reactions of the keto form $1^{+\bullet}$ and of the enol form $2^{+\bullet}$ of acetamide and of the deuterated compounds $1\text{a}^{+\bullet}$ and $2\text{a}^{+\bullet}$ with $[\text{D}_3]\text{MVE}$ (a), MVE (b), and methanol (c).

analyzers used in the photoionization experiments excludes separation of isobaric masses, a deuterated neutral reagent ($\text{CD}_3\text{OCH}=\text{CH}_2$, $[\text{D}_3]\text{MVE}$) was required to avoid accidental mass overlap of the decisive enol-specific product $[\text{MVE} + \text{H}]^+$ with $1^{+\bullet}$ and $2^{+\bullet}$ (all m/z 59). With the deuterated precursor ions, the reactions of the keto $1\text{a}^{+\bullet}$ (electron transfer) and the enol $2\text{a}^{+\bullet}$ (deutron transfer) are clearly distinguished for

unlabeled MVE (Scheme 1b). Finally, with methanol, the keto $1a^{++}$ preferentially abstracts a hydrogen atom from the neutral reagent to yield protonated acetamide $[1a+H]^+$, whereas the enol $2a^{++}$ does not react in this manner; rather, simple H/D exchange takes place to yield the enol-specific product $2b^{++}$ (Scheme 1c).

Based on these findings, the following experiment^[16] was designed to probe the unimolecular keto/enol tautomerization $1^{++} \rightleftharpoons 2^{++}$. Neutral acetamide is photoionized in the source by using synchrotron radiation, the molecular ion is mass-selected with the first quadrupole Q1, interacted with the neutral reagent in the octopole at a collision energy of 0.25 ± 0.15 eV, while setting the analyzer Q2 to monitor the formation of the corresponding enol-specific product. In all three cases studied (Scheme 1), notable onsets of “enol reactivity” are observed at photon energies of about 10.5 eV.^[18] Specifically, a threshold of 10.42 ± 0.05 eV evolves for the formation of the enol-specific product $[[D_3]MVE+H]^+$ (m/z 62) in the reaction of 1^{++} and/or 2^{++} (m/z 59) with the deuterated ether (Figure 1a),^[19] 10.51 ± 0.1 eV for the formation of the enol-specific product $([MVE+D])^+$, m/z 60 in the

reaction of deuterated ions $1a^{++}$ and/or $2a^{++}$ (m/z 62) with unlabeled MVE (Figure 1b), and 10.50 ± 0.2 eV for the formation of the enol-specific product ($2b^{++}$, m/z 61) in the reaction of $1a^{++}$ and/or $2a^{++}$ (m/z 62) with methanol (Figure 1c). Control experiments further confirm that the enol 2^{++} , independently generated by the McLafferty rearrangement upon dissociative photoionization of valeramide,^[20] does not show such a threshold behavior; instead, “enol reactivity” is observed as soon as the ions are formed in the source.^[21]

An essential feature as well as a unique advantage of the present experiments is that only the photon energy is varied while all other parameters are kept constant. Hence, the mere observation of reactivity thresholds in Figure 1a–c must be associated with some distinct photon-energy-dependent phenomenon in the ionization process. In particular, any kind of bimolecularly catalyzed keto/enol tautomerization cannot account for this effect. Of course, some barriers might be involved in the interaction with the neutral reagents in the octopole; however, if this were the case, one would not expect essentially identical thresholds for the reactions of two different neutral molecules. Furthermore, the independently generated enol 2^{++} should then exhibit a similar threshold behavior, which is not observed experimentally (see above). Finally, the photoelectron spectrum (PES) of acetamide does not indicate any state-specific effects at the threshold of “enol reactivity” in that the PES is featureless and smoothly drops around 10.5 eV. Therefore, we assign the thresholds in Figure 1 to the onsets of the unimolecular keto/enol tautomerizations $1^{++} \rightarrow 2^{++}$ and $1a^{++} \rightarrow 2a^{++}$. The slightly, but yet significantly larger threshold of the deuterated ion $1a^{++}$ lends further support to this interpretation because it is fully consistent with the operation of a primary kinetic isotope effect in the keto/enol tautomerization of ionized acetamide.^[10] Accordingly, these particular thresholds can be regarded as a direct measure of the activation barrier associated with the unimolecular keto/enol tautomerization of ionized acetamide.

To position these results within the energetics of acetamide, the appearance energies (AEs) of the primary photoion fragments were determined. Perfectly consistent with literature data,^[22] the photoion and photoelectron spectra give $IE(1) = 9.68 \pm 0.03$ eV (9.71 ± 0.03 eV for $1a$). Upon increasing the photon energy, the parent ion persists up to about 11 eV, where several dissociative photoionization reactions become possible. The lowest thresholds are observed for the formation of the ammonium ion ($AE(NH_4^+) = 10.76 \pm 0.07$ eV) concomitant with loss of a neutral C_2HO^\bullet radical and for the generation of the distonic isomer of ionized methylamine^[23] ($AE(\bullet CH_2NH_3^+) = 10.77 \pm 0.05$ eV) accompanied by the loss of carbon monoxide. At slightly higher energies, α -C–C bond cleavage to yield $CH_3^\bullet + CONH_2^+$ becomes feasible with $AE(CONH_2^+) = 11.00 \pm 0.04$ eV. The alternative α -cleavage ($CH_3CO^+ + NH_2^\bullet$) requires $AE(CH_3CO^+) = 11.24 \pm 0.05$ eV. Finally, loss of ammonia concomitant with the formation of ionized ketene has an $AE(CH_2CO^+) = 11.13 \pm 0.07$ eV. For a compound as small as acetamide, it is in fact quite surprising to encounter a situation in which five competing fragmentation channels appear in an energy window of less than 0.5 eV (Scheme 2). Accordingly,

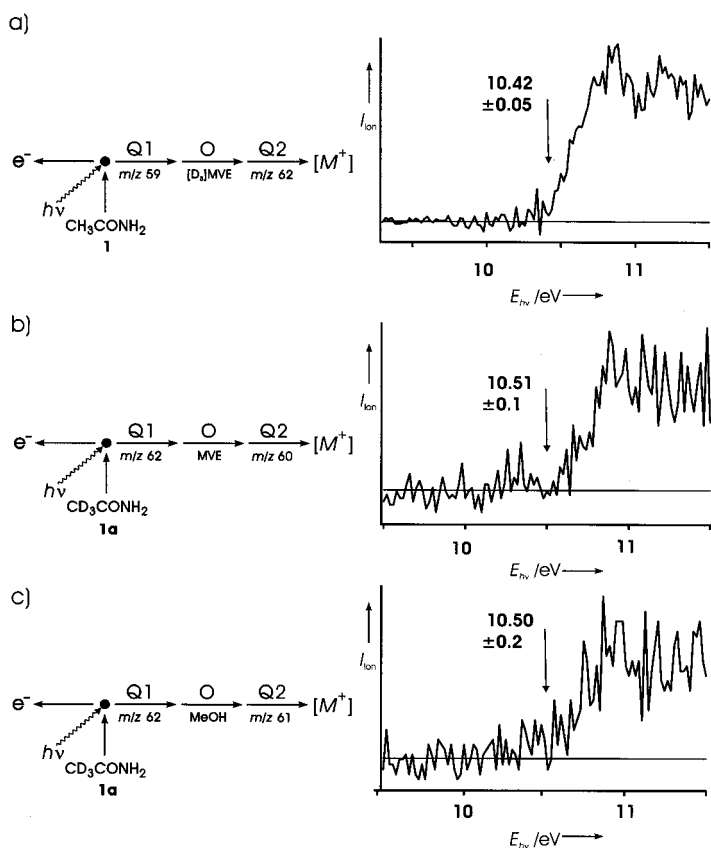
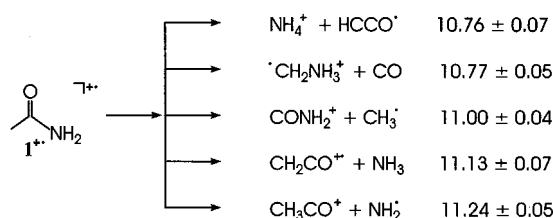


Figure 1. Photoionization experiments of acetamide with delayed chemical monitoring of the enolization in the cation radical (see Scheme 1 for the monitored reactions). Ion intensity (I_{ion}) as a function of photon energy (E_{ph}) for a) the enol-specific product ion at m/z 62 formed in the reaction of mass-selected $1^{++}/2^{++}$ (m/z 59) with $CD_3OCH=CH_2$ ($[D_3]MVE$), b) the enol-specific product ion at m/z 60 formed in the reaction of mass-selected $1a^{++}/2a^{++}$ (m/z 62) with $CH_3OCH=CH_2$ (MVE), and c) the enol-specific product ion at m/z 61 formed in the reaction of mass-selected $1a^{++}/2a^{++}$ (m/z 62) with methanol. The thresholds given as arrows are averages of several independent experiments. Note that these experiments do not employ coincidence techniques.



Scheme 2. Five competing fragmentation channels of acetamide.

the various channels are expected to compete strongly with each other, and more detailed investigations are required for a quantitative description of the fragmentation behavior of ionized acetamide.

In the present context, however, it is sufficient to note that the enol-specific reactions occur below the thresholds of all dissociation channels of 1^+ . The fragment ions are therefore unlikely to interfere with the chemical monitoring technique applied here. Combined with the IEs of the neutral molecules, the thresholds of the enol reactivities therefore imply effective barrier heights of 0.74 ± 0.06 eV for 1^+ and 0.80 ± 0.10 eV for $1a^+$. While the G2 calculations imply a somewhat larger barrier (1.16 eV),^[10] the experimental data are preliminary in that the thermal energies of the reactants have been included so far.

From a more general perspective, the present results demonstrate that the combination of photoionization experiments with chemical monitoring provides a new, powerful method for the direct experimental determination of barrier heights in unimolecular isomerizations of gaseous ions. In marked contrast to femtosecond dynamics,^[24] this technique deliberately includes a time delay in the microsecond regime to allow isomerization to occur. Furthermore, the method is a priori applicable to all ionic species which can be formed in sufficient yields, and it could also be applied to fragment ions formed upon dissociative photoionization. Admittedly, however, the signal-to-noise ratios in Figure 1 are not yet ideal, and we are aiming towards improvement. Furthermore, ongoing coincidence studies and parallel dynamical modeling should reveal the detailed energetics of the various fragmentation channels with explicit reference to competition, thereby hopefully providing a solid benchmark for an “entire” potential-energy surface to be used for the assessment of contemporary ab initio methods with the claim of “chemical accuracy”.^[25]

Received: March 7, 2002 [Z18845]

- [1] C. S. Chin, B. Lee, S. Kim, J. Chun, *J. Chem. Soc. Dalton Trans.* **1991**, 443.
- [2] D. Lee, C. K. Kim, B.-S. Lee, I. Lee, B. C. Lee, *J. Comput. Chem.* **1997**, 18, 56–69, and references therein.
- [3] S. Sklenak, Y. Apeloig, Z. Rappoport, *J. Am. Chem. Soc.* **1998**, 120, 10359–10364.
- [4] R. E. Rosenberg *J. Org. Chem.* **1998**, 63, 5562–5567.

- [5] N. Heinrich, G. Frenking, W. Koch, H. Schwarz, *J. Am. Chem. Soc.* **1986**, 108, 593–600.
- [6] “Gas Phase Ion and Neutral Thermochemistry”: S. G. Lias, J. E. Bartmess, J. F. Liebman, J. L. Holmes, R. D. Levin, W. G. Mallard, *J. Phys. Chem. Ref. Data Suppl.* **1988**, 1, 17.
- [7] D. Kuck, *Int. J. Mass Spectrom.* **2002**, 213, 101–144, and references therein.
- [8] a) G. Bouchoux, *Mass Spectrom. Rev.* **1988**, 7, 1–39; b) G. Bouchoux, *Mass Spectrom. Rev.* **1988**, 7, 203–255.
- [9] For tautomerism in the acetamide enolate ion, see: M. C. Hare, S. S. Marimanikkupam, S. R. Kass, *Int. J. Mass Spectrom.* **2001**, 210/211, 153–163.
- [10] P. Mourgues, J. Chamot-Rooke, H. Nedev, H.-E. Audier, *J. Mass Spectrom.* **2001**, 36, 102–104.
- [11] H.-E. Audier, D. Leblanc, P. Mourgues, T. B. McMahon, S. Hammerum, *J. Chem. Soc. Chem. Commun.* **1994**, 2329–2330.
- [12] T. D. Fridgen, J. M. Parnis, *Int. J. Mass Spectrom.* **1999**, 190/191, 181–194, and references therein.
- [13] M. A. Trikoupi, P. C. Burgers, P. J. A. Rutink, J. K. Terlouw, *Int. J. Mass Spectrom.* **2001**, 210/211, 489–502.
- [14] These experiments were conducted by Audier et al., Palaiseau, in the same manner as those described in ref. [10].
- [15] In the corresponding ICR experiments with thermalized ions, the major product of the enol ion 2^+ with MVE is $\text{C}_3\text{H}_5\text{NO}_2^+$, corresponding to loss of a methyl radical from the encounter complex $[2^+\cdots\text{MVE}]$. At elevated kinetic energies such as those used in CERISES, however, this product disappears in favor of $[\text{MVE}+\text{H}]^+$.
- [16] The experiments were performed with the CERISES apparatus mounted to the beam line SA 63 of the SuperACO synchrotron radiation source at LURE, Orsay. CERISES is a photoionization mass spectrometer with a threshold electron detector and a quadrupole/octopole/quadrupole (QOQ) device for the detection and manipulation of photocations.^[17] In the present experiments, acetamide was introduced into the ion source of CERISES and ionized with monochromatic photons of variable energies. Then, the molecular ion was mass-selected using Q1, interacted with the neutral molecule of interest admitted into the octopole ion guide at pressures in the mTorr regime and a collision energy of 0.25 ± 0.15 eV, while detecting the enol-specific products using Q2. Note that none of the present experiments employed the coincidence capabilities of CERISES. Therefore, the molecular ions formed in the source bear a distribution of internal energies (E_{int}) ranging from $E_{\text{int}}=0$ to $E_{\text{int}}=E_{\text{hv}} - \text{IE}(1)$, where E_{hv} is the photon energy.
- [17] O. Dutuit, C. Alcaraz, D. Gerlich, P. M. Guyon, J. W. Hepburn, C. Metayer-Zeitoun, J. B. Ozenne, T. Weng, *Chem. Phys.* **1996**, 209, 177–194.
- [18] The onsets were determined by extrapolation of the linear part of the initially rising signal-to-noise level. The values given in the text are averages of several independent measurements.
- [19] The data in Figure 1a is corrected for the ^{13}C contribution of the charge-transfer reaction of 1^+ with $[\text{D}_3]\text{MVE}$ leading to m/z 61.
- [20] See: J. Loos, D. Schröder, W. Zummack, H. Schwarz, R. Thissen, O. Dutuit, *Int. J. Mass Spectrom.* **2002**, 214, 105–128, and references therein.
- [21] Labeled variants (e.g. $[4,4\text{-D}_2]\text{valeramide}$) were used to afford the corresponding $[\text{O-D}]\text{enol}$.
- [22] See, Chemistry WebBook database of NIST: <http://webbook.nist.gov/chemistry/>.
- [23] T. Drewello, N. Heinrich, W. P. M. Maas, N. M. M. Nibbering, T. Weiske, H. Schwarz, *J. Am. Chem. Soc.* **1987**, 109, 4810–4818.
- [24] a) F. Fernandez-Alonso, B. D. Bean, J. D. Ayers, A. E. Pomerantz, R. N. Zare, L. Banares, F. J. Aoiz, *Angew. Chem.* **2000**, 112, 2860–2864; *Angew. Chem. Int. Ed.* **2000**, 39, 2748–2752; b) S. De Feyter, E. W.-G. Diau, A. H. Zewail, *Angew. Chem.* **2000**, 112, 263–266; *Angew. Chem. Int. Ed.* **2000**, 39, 257–260.
- [25] *Quantum-mechanical prediction of thermochemical data*, (Ed.: J. Cioslowski), Kluwer, Dordrecht, **2001**.

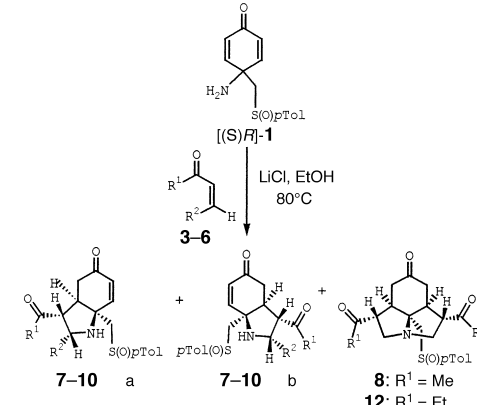
Titanium-Promoted Stereoselective Synthesis of Hydroindolones from *p*-Quinamines by Domino Conjugate Additions**

M. Carmen Carreño,* María Ribagorda, and Gary H. Posner

Stereocontrolled additions to conjugated double bonds included in domino processes^[1] offer the opportunity to prepare structurally complex molecules from simple materials. In spite of the high synthetic potential of 4,4-disubstituted cyclohexadienones, these multifunctional materials have hardly been exploited in asymmetric synthesis.^[2] Their use in domino Michael type additions for the synthesis of polycyclic compounds^[3] is limited to a report from our laboratory: heterocyclic cage compounds were synthesized stereoselectively from [(*S*)/*R*]-[(*p*-tolylsulfinyl)methyl]-*p*-quinols or the analogous *p*-quinamines^[4] upon reaction with 2-trimethylsilyloxyfuran, which initially acts as a nucleophile. The ambident nature of *p*-quinamines suggested that a domino sequence could be initiated by taking advantage of the nucleophilic amino group. We report herein the reaction of *p*-quinamines **1** and **2**^[4] with α,β -unsaturated ketones **3–6** to give rise to hydroindole or azatricyclic frameworks in a sequence of two or four stereoselective conjugate additions (Tables 1 and 2). The overall process opens an easy and convergent access to hydroindole systems, which are commonly found in alkaloids.^[5]

Enantiopure [(*S*)/*R*]-4-[(*p*-tolylsulfinyl)methyl]-*p*-quinamines **1** and **2** were synthesized from *p*-benzoquinoneimine monoacetals,^[6] which are easily accessible by anodic oxidation of *N*-Boc-*p*-methoxyanilines, by addition of the α -lithiocarbanion derived from [(*S*)/*R*]-methyl-*p*-tolylsulfoxide and hydrolysis of the acetal and *N*-Boc protecting groups.^[4] The LiCl-assisted reaction of **1** with methyl vinyl ketone (**3**) afforded a mixture of hexahydroindole-5-ones **7a**, **7b**, octahydropyrroloindolone **8**, and recovered **1** (Table 1, entry 1). The formation of compounds **7** is assumed to proceed through a conjugate addition of the NH₂ group of **1** to **3**, followed by a second intramolecular 1,4 addition of the resulting enol to the cyclohexadienone from the face that contains the nitrogen substituent. This cyclization step leads to the formation of equal amounts of the two diastereomers **7a** and **7b**, since the prochiral electrophilic carbon atoms of **1** are not differentiated under these conditions. The diastereoselective formation of the C3a stereogenic center in each case was not unexpected, since the efficiency of the vicinal amino group in

Table 1. Reactions of **1** with enones in the presence of LiCl.^[a]



Entry	Enone	Equiv	R ¹	R ²	Products	Ratio ^[b] [%] ^[c]
1	3	1.1	Me	H	7a : 7b : 8	30(23):30(23):10 ^[d]
2	3	2	Me	H	8	100(52)
3	4	1.2	–CH ₂ CH ₂ –		9a : 9b	50(40):50(22)
4	5	1.2	–CH ₂ CH ₂ CH ₂ –		10a : 10b	50(27):50(16)

[a] Reagents and conditions: enone, LiCl, EtOH, 30 min, then **1**, 10 h, reflux. [b] Determined by ¹H NMR spectroscopic analysis of the crude product. [c] Yield after flash column chromatography. [d] 30% of **1** was recovered.

directing the face selectivity of conjugate additions in *p*-quinamines^[4] had been previously pointed out. With an excess of enone **3** (Table 1, entry 2), the reaction proceeds via **7a** and **7b**, with a subsequent nucleophilic attack of the nitrogen atom on a second equivalent of **3**, and followed finally by a new intramolecular and stereoselective conjugate addition to the remaining cyclohexenone moiety to afford compound **8** exclusively.

LiCl-promoted reaction of *p*-quinamine **1** with cycloalkenones **4** and **5** allowed the isolation of compounds **9a** and **9b** (Table 1, entry 3) and **10a** and **10b** (Table 1, entry 4), respectively. Four new stereogenic centers resulted from this domino process, with only two diastereomers being formed in each case. Although the reaction was very stereoselective, full stereocontrol and complete conversion of starting material remained a challenge. An efficient desymmetrization of the prochiral cyclohexadienone fragment had been observed in organoaluminum additions to sulfinyl-substituted *p*-quinols.^[7] With this in mind, various Lewis acids (AlMe₃, AlMe₂Cl, BF₃·OEt₂, TiCl₄, [Ti(O*i*Pr)₄], [TiCl(O*i*Pr)₃], [TiCl₂(O*i*Pr)₂]) were screened with *p*-quinamine **1** and cyclopentenone (**4**) as substrates.

We were delighted to observe the complete transformation of the starting materials into diastereomer **9a** (Table 2, entry 1) in the presence of [TiCl₂(O*i*Pr)₂].^[8] Subsequent studies revealed that **1** reacted in a similar way with other enones. Thus, the octahydrocarbazole **10a**^[9] was the major product obtained from cyclohexenone **5** (Table 2, entry 2), and hexahydroindolone **11a** resulted from ethyl vinyl ketone (**6**) (Table 2, entry 3) together with azatricyclic derivative **12** (75:25, Table 1). The use of **6** (2 equiv) led to diastereomerically pure compound **12**, which was assumed to proceed from **11a** (Table 2, entry 4). 3-Methyl-substituted *p*-quinamine [4*S*,(*S*)]-**2a** behaved similarly in the presence of [Ti-

[*] Prof. M. C. Carreño, Dr. M. Ribagorda
Departamento de Química Orgánica (C-I), Universidad Autónoma Cantoblanco, 28049 Madrid (Spain)
Fax: (+34)91-397-3966
E-mail: carmen.carrenno@uam.es

Prof. G. H. Posner
Department of Chemistry, Johns Hopkins University
Remsen Hall, 3400 N. Charles Street, Baltimore, MD 21218 (USA)

[**] This work was supported by the Dirección General de Investigación Científica y Técnica (Grant PB98-0062).

Supporting information for this article is available on the WWW under <http://www.angewandte.org> or from the author.

Table 2. Reactions of **1** and **2a** with α,β -unsaturated ketones in the presence of $[\text{TiCl}_2(\text{OiPr})_2]$.

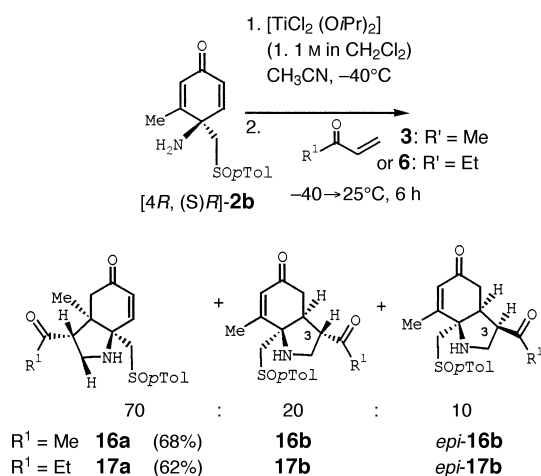
Entry	1–2	Enone	Equiv	R ¹	R ²	R ³	Compound	Yield [%] ^[a]
1	1	4	1.2	–CH ₂ CH ₂ –	H	H	9a	60
2	1	5	1.2	–CH ₂ CH ₂ CH ₂ –	H	H	10a ^[b]	60
3	1	6	1.1	Et	H	H	11a ^[c]	51
4	1	6	2	Et	H	H	12 ^[d]	72
5	2a	6	1.1	Et	H	Me	13a	54
6	2a	4	1.2	–CH ₂ CH ₂ –	Me	Me	14a	50
7	2a	5	1.2	CH ₂ CH ₂ CH ₂ –	Me	Me	15a	54

[(S)-**1**]: R³ = H
[4S, (S)-**2a**]: R³ = Me

[a] Yield after flash column chromatography. [b] Compound **10b** (10%) was detected in the crude reaction mixture. [c] Compound **12** (see Table 1, 25%) was detected in the crude mixture.

$\text{Cl}_2(\text{OiPr})_2$. Upon reaction with ethyl vinyl ketone (**6**), pure diastereomer **13a** was formed (Table 2, entry 5), and cycloalkenones **4** and **5** yielded tricyclic derivatives **14a** and **15a** (Table 2, entries 6 and 7), respectively.

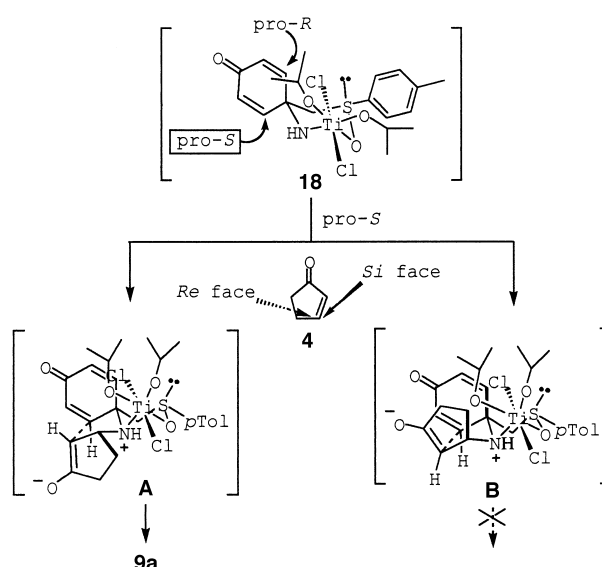
Interestingly, *p*-quinamine [4*R*, (S)-**2b**] evolved under these conditions into a 70:20:10 mixture of **16a**, **16b**, and *epi*-**16b** (Scheme 1) upon reaction with methyl vinyl ketone



Scheme 1. Reaction of **2b** with acyclic enones **3** and **6** in the presence of $[\text{TiCl}_2(\text{OiPr})_2]$.

(**3**), from which **16a** could be isolated pure in 68% yield. Compound **16a** must result from two conjugate additions; the second occurs from the less electrophilic methyl-substituted position of the cyclohexadienone moiety. Similar results were obtained in the reaction of **2b** with **6** (Scheme 1).

The remarkable level of diastereotopic bond selection observed in the cyclohexadienone moiety of **1** with $[\text{TiCl}_2(\text{OiPr})_2]$ suggested a chelation-controlled intramolecular conjugate addition from a species such as **18** (Scheme 2). The chelate formed between the nitrogen atom of **1** and the sulfinyl oxygen atom shows a rigid bipyramidal structure,^[10] with the apical Cl and the pseudoequatorial OiPr groups



Scheme 2. Favored transition state for the reaction of *p*-quinamine **1** with cyclopentenone.

pointing to the spirane moiety. These substituents hinder any nucleophile from approaching the pro-*R* double bond, thereby directing the internal nucleophile to approach from the less hindered face of the pro-*S* electrophilic carbon atom (Scheme 2, transition state **A**).

The *trans* arrangement of the substituents C3/C3a of **9a** is in agreement with the most stable *trans* relationship^[11] of approaching donor and acceptor in **A**. Reaction with cycloalkenones had an additional difficulty as a result of having *Re* and *Si* faces. Approach at the *Si* face (see **B**) shows a destabilizing 1,3-*syn* diaxial interaction, which would make such an attack difficult.^[12]

In summary, we have disclosed Ti-promoted stereoselective domino conjugate additions of [(S)-*p*-(*p*-tolylsulfinyl)methyl]quinamines to α,β -unsaturated ketones. Up to four new stereogenic centers are generated in a single reaction vessel when cycloalkenones are used in the reaction and up to five when two equivalents of acyclic enones used. The method allows quaternary centers to be created efficiently with a single configuration through consistent asymmetric induction.

Received: February 15, 2002 [Z18717]

- [1] Reviews: a) L. F. Tietze, F. Haunert in *Stimulating Concepts in Chemistry* (Eds.: M. Shibasaki, J. F. Stoddart, F. Voegtli), Wiley-VCH, Weinheim, **2000**, pp. 39–64; b) L. F. Tietze, *Chem. Rev.* **1996**, *96*, 115–136; c) P. J. Parsons, C. S. Penkett, A. J. Shell, *Chem. Rev.* **1996**, *96*, 195–206; d) G. H. Posner, *Chem. Rev.* **1986**, *86*, 831–834.
- [2] a) S. F. Martin, C. L. Campbell, *J. Org. Chem.* **1988**, *53*, 3184–3190; b) H. Fujioka, S. Kitagaki, N. Ohno, H. Kitagawa, Y. Kita, K. Matsumoto, *Tetrahedron: Asymmetry* **1994**, *5*, 333–336; c) Y. Take-moto, S. Kuraoka, N. Hamaue, K. Aoe, H. Hiramoto, Ch. Iwata, *Tetrahedron* **1996**, *52*, 14177–14188; d) B. L. Feringa, M. Pineschi, L. A. Arnold, R. Imbos, A. H. M. De Vries, *Angew. Chem.* **1997**, *109*, 2733–2736; *Angew. Chem. Int. Ed. Engl.* **1997**, *36*, 2620–2623; e) P. Wipf, W. Li, *J. Org. Chem.* **1999**, *64*, 4576–4577; f) D. Bland, G. Chambournier, V. Dragan, D. J. Hart, S. Lacoutiere, *Tetrahedron* **1999**, *53*, 8953–8966; g) R. Imbos, M. H. G. Brilman, M. Pineschi, B. L. Feringa, *Org. Lett.* **1999**, *1*, 623–625.

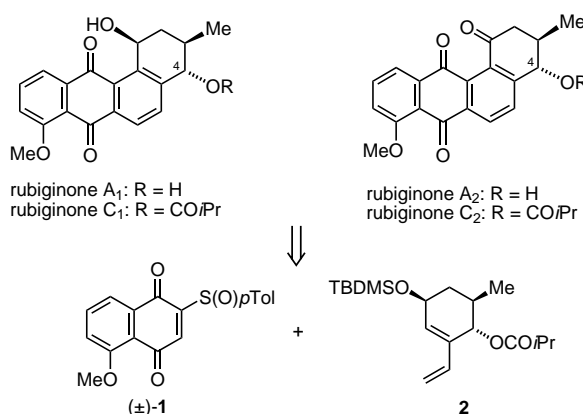
- [3] Acyclic dienones: H. Hagiwara, A. Okano, H. Uda, *J. Chem. Soc. Chem. Commun.* **1985**, 1047–1047.
- [4] M. C. Carreño, M. C. García Luzón, M. Ribagorda, *Chem. Eur. J.* **2002**, 8, 208–216.
- [5] “MTP International Review of Sciences”: *Alkaloids, Ser. I, Vol. 9* (Ed.: K. Wiesner), Butterworths, London, **1973**.
- [6] M. C. Carreño, M. Ribagorda, *J. Org. Chem.* **2000**, 65, 1231–1234.
- [7] a) M. C. Carreño, M. Pérez González, M. Ribagorda, J. Fischer, *J. Org. Chem.* **1996**, 61, 6758–6759; b) M. C. Carreño, M. Pérez González, M. Ribagorda, K. N. Houk, *J. Org. Chem.* **1998**, 63, 3687–3693.
- [8] M. T. Reetz in *Titanium in Organic Synthesis* (Ed.: M. Schlosser), Wiley, New York, **1994**, chap. 3, pp. 198–282.
- [9] The structure of **10a** was established by X-ray diffraction. CCDC-179112 contains the supplementary crystallographic data for this paper. These data can be obtained free of charge via www.ccdc.cam.ac.uk/conts/retrieving.html (or from the Cambridge Crystallographic Data Centre, 12, Union Road, Cambridge CB2 1EZ, UK; fax: (+44) 1223-336-033; or deposit@ccdc.cam.ac.uk).
- [10] a) R. O. Duthaler, A. Hafner, *Chem. Rev.* **1992**, 92, 807–832, and references therein.
- [11] a) A. Barco, S. Benetti, G. Spalluto, A. Casolari, G. P. Pollini, V. Zanirato, *J. Org. Chem.* **1992**, 57, 6279–6286; b) R. A. Bunce, E. J. Wamsley, J. D. Pierce, A. J. Shellhamer, Jr., R. E. Drumright, *J. Org. Chem.* **1987**, 52, 464–466.
- [12] D. P. Curran, H. Qi, N. C. DeMello, C.-H. Lin, *J. Am. Chem. Soc.* **1994**, 116, 8430–8341.

Enantioselective Total Synthesis of Angucyclinone-Type Antibiotics Rubiginones A₂ and C₂**

M. Carmen Carreño,* María Ribagorda, Álvaro Somoza, and Antonio Urbano*

The wide range of biological properties associated with the angucyclinone antibiotics has stimulated great interest in these compounds.^[1] Among the angucyclinone subclass, rubiginones A and C are unique owing to the hydroxy function at C4 (Scheme 1). Moreover, rubiginones C₁ and C₂ represent the only natural angucyclinones that have an ester substituent at the same carbon center. Rubiginones A and C were isolated from the fermentation broth of *Streptomyces griseorubiginosus* and exhibited potentiation of vincristine-induced cytotoxicity against multidrug-resistant tumor cells.^[2] Rubiginone A₂, also named fujianmycin B^[3] or SNA-8073-B,^[4] is claimed to be useful in the treatment of AIDS and Alzheimer's disease.^[5] The absolute stereochemistry of all rubiginones has been determined by the *O*-methylmandelate method.^[6]

The angularly fused tetracyclic skeleton of angucyclinones has been synthesized regioselectively by several methods, which are summarized in an excellent recent review article.^[7]



Scheme 1. Retrosynthetic analysis of rubiginones A and C.

The most general strategy employed is based on the Diels–Alder reaction between a substituted naphthoquinone and a vinyl cyclohexene. Although several efficient total syntheses of angucyclinones have focused on racemic forms,^[8] only a few asymmetric syntheses have been described so far.^[9] Recently, we reported an asymmetric approach to angucyclinones based on the reaction of an enantiopure sulfinyl-substituted 1,4-naphthoquinone and a chiral racemic vinyl cyclohexene.^[10] The sulfoxide group on the quinone framework promoted a double induction in the Diels–Alder reactions which led to the efficient kinetic resolution of the diene partner. This method has been applied to the enantioselective preparation of differently substituted natural angucyclinone derivatives.^[11] Despite the numerous synthetic efforts towards this family of compounds, to the best of our knowledge no total synthesis of C4-oxygenated derivatives have been reported to date.

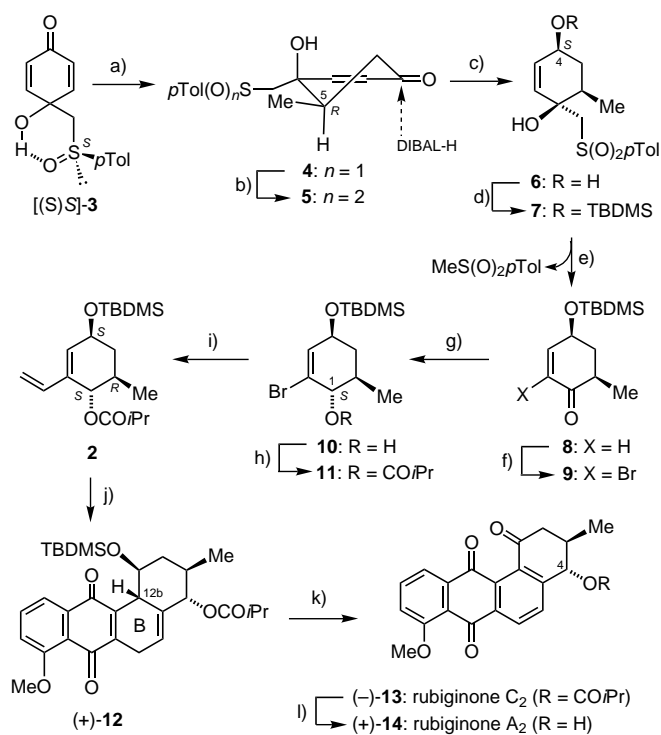
We describe herein the first enantioselective total synthesis of rubiginones A₂ and C₂ based on the Diels–Alder reaction of 5-methoxy-2-(*p*-tolylsulfinyl)-1,4-naphthoquinone (**1**) and enantiopure vinyl cyclohexene **2**, which bears all the stereogenic centers present in the natural products (Scheme 1). The quinone is used in the racemic form because the role of the sulfoxide in this approach is limited to controlling the regioselectivity of the Diels–Alder reaction and facilitating the recovery of the quinone structure after the cycloaddition by pyrolytic elimination. The enantiopure diene **2** was synthesized from [(*S*)-5-(*p*-tolylsulfinyl)methyl]-*p*-quinol (**3**) by means of a stereocontrolled conjugate addition of AlMe₃ as the key step (Scheme 2).

Thus, highly chemo- and diastereoselective conjugate addition of AlMe₃ to [(*S*)-5-(*p*-tolylsulfinyl)methyl]-*p*-quinol (**3**)^[12] afforded derivative **4**, which has the *R* configuration at the new C5 stereogenic center.^[13] Compound **4** was further transformed into the sulfone **5** with MCPBA. Reduction of the carbonyl group of **5** with DIBAL-H provided **6**. The stereoselective reduction of **5** must be a consequence of its rigid structure and the small size of DIBAL-H, whose axial attack at the cyclohexenone ring was expected. The *S* absolute configuration at C4 of **6** was confirmed through the formation of the corresponding Mosher's esters.^[14] After protection of **6** as the TBDMS derivative **7**, and elimination of methyl *p*-tolylsulfone by a Cs₂CO₃-promoted retrocondensation, ketone **8** was obtained in 87% yield. The treatment of **8** with Br₂ and Et₃N yielded

[*] Prof. M. C. Carreño, Dr. A. Urbano, Dr. M. Ribagorda, Á. Somoza
Departamento de Química Orgánica (C-I), Universidad Autónoma
Cantoblanco, 28049 Madrid (Spain)
Fax: (+34)91-397-3966
E-mail: carmen.carrenno@uam.es, antonio.urbano@uam.es

[**] We thank the DGICYT (Grant PB98-0062) for financial support and the MEC and CAM for fellowships to M.R. and A.S.

Supporting information for this article is available on the WWW under <http://www.angewandte.org> or from the author.



Scheme 2. Enantioselective total synthesis of rubiginones **A**₂ and **C**₂: a) AlMe_3 , CH_2Cl_2 , -78°C , 4 h, 65%; b) MCPBA, CH_2Cl_2 , 0°C , 30 min, 96%; c) DIBAL-H, THF, -78°C , 30 min, 99%; d) TBDMSOTf, 2,6-lutidine, CH_2Cl_2 , 0°C , 2 h; e) Cs_2CO_3 , CH_3CN , room temperature, 17 h, 87% over two steps; f) Br_2 , CCl_4 , 0°C , then Et_3N , room temperature, 32 h, 80%; g) LiAlH_4 , THF, -100°C , 30 min; h) $i\text{PrCOCl}$, DMAP, CH_2Cl_2 , 1 h, 79% over two steps; i) $[\text{Pd}(\text{PPh}_3)_4]$, $[\text{CH}_2=\text{CHSnBu}_3]$, toluene, 90°C , 24 h, 78%; j) (\pm)-**1** (2 equiv), CH_2Cl_2 , reflux, 24 h, 52%; k) $h\nu$, air, room temperature, 16 h, 35%; l) K_2CO_3 , THF/MeOH, room temperature, 90 min, 91%. MCPBA = *meta*-chloroperoxybenzoic acid; DIBAL-H = diisobutylaluminum hydride; TBDMSOTf = *tert*-butyldimethylsilyl trifluoromethanesulfonate; DMAP = 4-dimethylaminopyridine.

the α -bromoenone **9**, whose stereoselective reduction with LiAlH_4 at -100°C afforded (1*S*)-**10** and its 1*R* epimer (93:7). The *S* absolute configuration at C1 of the major epimer was again confirmed after transformation of **10** into the Mosher's esters.^[14] Finally, protection of **10** as the isobutyrate derivative **11** and Stille coupling with tributylvinylstannane gave rise to vinyl cyclohexene **2** with the appropriate absolute configuration present at the three stereogenic centers in the natural products.

With enantiopure diene **2** in hand, we undertook the regioselective construction of the tetracyclic skeleton of the rubiginones (Scheme 2) through the Diels-Alder reaction with racemic 5-methoxy-2-(*p*-tolylsulfinyl)-1,4-naphthoquinone (**1**).^[15] After heating the mixture of **1** and **2** in CH_2Cl_2 at reflux for 24 h, we obtained the unstable tetracyclic quinone (+)-**12** as the sole diastereoisomer. Compound **12** results from the spontaneous elimination of the sulfoxide in the initially formed cycloadduct. The stereoselective formation of C12b was expected according to the preferred approach of the dienophile from the face of the diene *anti* to the bulky allylic OTBDMS substituent.^[16]

Several attempts to aromatize the B ring of (+)-**12** with DDQ (2,3-dichloro-5,6-dicyano-1,4-benzoquinone), DBU

(1,8-diazabicyclo[5.4.0]undec-7-ene), or K_2CO_3 were unsuccessful and gave rise to complex reaction mixtures. Serendipitously, we found that the exposure of (+)-**12** to daylight under solvent-free conditions,^[17] afforded **13** in 35% yield ($[\alpha]_D^{20} = -57$ ($c = 0.5$ in CHCl_3)) which gave physical and spectroscopic data identical to those of natural (–)-rubiginone **C**₂ ($[\alpha]_D^{20} = -61$ ($c = 0.5$ in CHCl_3)).^[12] This unprecedented one-pot transformation involves three consecutive reactions of (+)-**12** in a very efficient way: aromatization of the B ring, deprotection of the silyl group, and oxidation of the resulting carbinol to give the corresponding benzylic ketone group. Finally, hydrolysis of the isobutyric ester at C4 of (–)-**13** with $\text{K}_2\text{CO}_3/\text{MeOH}/\text{THF}$ afforded **14** in 91% yield ($[\alpha]_D^{20} = +78$ ($c = 0.2$ in CHCl_3)), which was identical to natural (+)-rubiginone **A**₂.^[18]

In summary, we have reported the first total enantioselective synthesis of the C4-oxygenated angucyclinones rubiginones **A**₂ and **C**₂ based on the asymmetric Diels-Alder reaction of the enantiopure vinyl cyclohexene (+)-**2** and the racemic methoxy-substituted sulfinylnaphthoquinone **1**. The successful route involved the chemo- and stereoselective addition of AlMe_3 to [(*S,S*)-[(*p*-tolylsulfinyl)methyl]-*p*-quinol (**3**) and the elimination of the chiral sulfoxide as methyl *p*-tolylsulfone as the key steps for the synthesis of enantiopure (1*S*,4*S*,6*R*)-**2**, which was obtained over 9 steps in 26% overall yield. The total synthesis of natural angucyclinones (–)-**13** and (+)-**14** was completed after a cycloaddition/sulfoxide elimination process, through a practical light-induced sequence that involved partial aromatization, OTBDMS deprotection, and oxidation of derivative (+)-**12** over 11 steps from *p*-quinol **3** with >95% *ee* in 4.8 and 4.4% overall yield for rubiginones **C**₂ and **A**₂, respectively.

Received: March 21, 2002 [Z18944]

- a) R. H. Thomson, *Naturally Occurring Quinones IV*, 4th ed., Blackie Academic & Professional, London, **1996**, pp. 519–544; b) J. Rohr, R. Thiericke, *Nat. Prod. Rep.* **1992**, *9*, 103–137.
- M. Oka, H. Kamei, Y. Hamagishi, K. Tomita, T. Miyaki, M. Konishi, T. Oki, *J. Antibiot.* **1990**, *43*, 967–976.
- R. W. Rickards, J. P. Wu, *J. Antibiot.* **1985**, *38*, 513–515.
- K. Kimura, F. Kanou, H. Koshino, M. Uramoto, M. Yoshihama, *J. Antibiot.* **1997**, *43*, 967–976.
- K. Kimura, F. Kano, K. Kurosawa, M. Yoshihama, JP 06234693 **1994** [*Chem. Abstr.* **1995**, *122*, 8155].
- M. Oka, M. Konishi, T. Oki, *Tetrahedron Lett.* **1990**, *31*, 7473–7474.
- K. Krohn, J. Rohr, *Top. Curr. Chem.* **1997**, *188*, 127–195.
- a) D. MaI, H. N. Roy, *J. Chem. Soc. Perkin Trans. 1* **1999**, 3167–3171; b) M. L. Patil, H. B. Borate, D. E. Ponde, B. M. Bhawal, V. H. Deshpande, *Tetrahedron Lett.* **1999**, *40*, 4437–4438; c) K. Krohn, J. Micheel, M. Zukowski, *Tetrahedron* **2000**, *56*, 4753–4758; d) K. A. Parker, Q.-J. Ding, *Tetrahedron* **2000**, *56*, 10249–10254; e) T. Rozek, J. H. Bowie, S. M. Pyke, B. W. Skelton, A. H. White, *J. Chem. Soc. Perkin Trans. 1* **2001**, 1826–1830; f) G. A. Kraus, N. Zhang, A. Melekhev, J. H. Jensen, *Synlett* **2001**, 521–522; g) K. Krohn, P. Frese, *Tetrahedron Lett.* **2001**, *42*, 681–682; h) K. Krohn, *Eur. J. Org. Chem.* **2002**, 1351–1362, and references therein.
- a) M. Yamaguchi, T. Okuma, A. Horiguchi, C. Ikeura, T. Minami, *J. Org. Chem.* **1992**, *57*, 1647–1649; b) D. S. Larsen, M. D. O'Shea, S. Brooker, *Chem. Commun.* **1996**, 203–204; c) K. Kim, V. A. Boyd, A. Sobti, G. A. Sulikowski, *Isr. J. Chem.* **1997**, *37*, 3–22; d) G. Matsuo, Y. Miki, M. Nakata, S. Matsumura, K. Toshima, *J. Org. Chem.* **1999**, *64*, 7101–7106; e) F. L. Andrews, D. S. Larsen, L. Larsen, *Aust. J. Chem.*

- 2000, 53, 15–24; f) T. Matsumoto, H. Yamaguchi, M. Tanabe, Y. Yasui, K. Suzuki, *Tetrahedron Lett.* **2000**, 41, 8393–8396; g) G. B. Caygill, D. S. Larsen, S. Brooker, *J. Org. Chem.* **2001**, 66, 7427–7431.
- [10] M. C. Carreño, A. Urbano, J. Fischer, *Angew. Chem.* **1997**, 109, 1695–1697; *Angew. Chem. Int. Ed. Engl.* **1997**, 36, 1621–1623.
- [11] a) M. C. Carreño, A. Urbano, C. Di Vitta, *Chem. Commun.* **1999**, 817–818; b) M. C. Carreño, A. Urbano, C. Di Vitta, *Chem. Eur. J.* **2000**, 6, 906–913.
- [12] Compound [(S)S]-3 was synthesized according to the procedure reported for the (S)R enantiomer, by reaction of 4,4-dimethoxy-2,5-cyclohexadienone with the lithium anion derived from [(S)S]-methyl-*p*-tolylsulfoxide followed by acetal hydrolysis with aqueous oxalic acid: M. C. Carreño, M. Pérez González, K. N. Houk, *J. Org. Chem.* **1997**, 62, 9128–9137.
- [13] M. C. Carreño, M. Pérez González, M. Ribagorda, K. N. Houk, *J. Org. Chem.* **1998**, 63, 3687–3693.
- [14] J. A. Dale, H. S. Mosher, *J. Am. Chem. Soc.* **1973**, 95, 512–519.
- [15] M. C. Carreño, J. L. García Ruano, A. Urbano, *Synthesis* **1992**, 651–653.
- [16] M. C. Carreño, A. Urbano, C. Di Vitta, *J. Org. Chem.* **1998**, 63, 8320–8330.
- [17] K. Krohn, F. Ballwanz, W. Baltus, *Liebigs Ann. Chem.* **1993**, 911–913.
- [18] Different values of the optical rotation of the natural product are reported in the literature: (+)-rubiginone A₂: [α]_D²⁰ = +92 (*c* = 0.5 in CHCl₃),^[2] (+)-fujianmycin B: [α]_D²⁰ = +50 (*c* = 0.176 in CHCl₃),^[3] and (+)-SNA-8073-B: [α]_D²⁰ = +47 (*c* = 0.141 in CHCl₃).^[4] The enantiomeric excess of our synthetic (+)-14 was shown to be > 95% after transformation into the corresponding Mosher esters.^[14]

Carbon–Carbon Double-Bond Formation from the Reaction of Organozinc Reagents with Aldehydes Catalyzed by a Nickel(II) Complex**

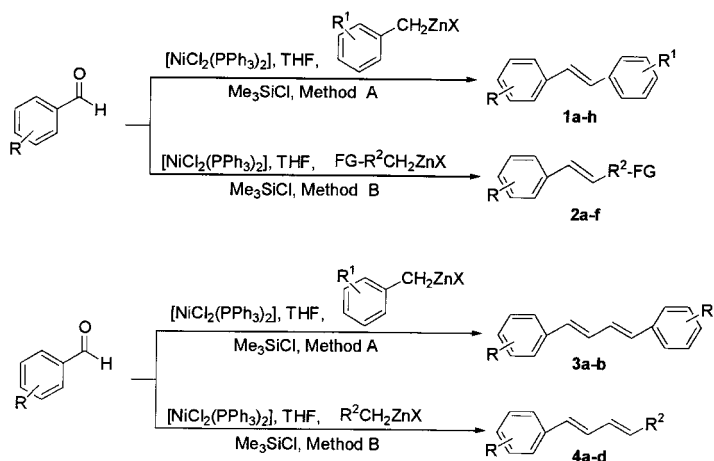
Jin-Xian Wang,* Ying Fu, and Yulai Hu

Reactions that form carbon–carbon bonds are of the utmost importance in modern organic synthesis, and the development of new methods to form such bonds is still a formidable challenge for organic chemists. It is well known that reactions forming C=C bonds have been extensively used in the synthesis of various polyfunctional unsaturated compounds and natural products, while some applications in combinatorial chemistry have also been described. Many methods have been developed for C=C bond formation such as Wittig reactions,^[1] reductive coupling of carbonyl compounds,^[2] self-coupling of α -lithiated benzylic sulfones,^[3] and condensation of aldehyde tosylhydrazones with stabilized carbanions.^[4] More recently, new procedures for the synthesis

of stilbenes have been reported, in which aldehyde tosylhydrazones were treated with benzotriazole-stabilized carbanions,^[5] trimethyl borate/lithium *tert*-butoxide, trialkylboranes, and alkylboron chlorides.^[6]

Organozinc complexes are powerful reagents for the formation of carbon–carbon bonds.^[7] Recently, transition-metal-catalyzed coupling reactions of halides with organozinc complexes have been reported.^[8] In addition, we have reported that the nitro group of 1-aryl-2-nitroethenes can be substituted by organozinc halides, using [Ni(acac)₂] (acac = acetylacetonato) as a catalyst in the presence of a tertiary amine, to give 1-aryl-1-alkenes in excellent yields.^[9]

The reaction of alkylzinc reagents and carbonyl compounds represents one of the most reliable methods to prepare optically active secondary alcohols.^[10, 11] Herein we show that *E*-stilbenes can be formed by the reaction of organozinc halides with aryl aldehydes in the presence of a silylating agent and using [NiCl₂(PPh₃)₂] as the catalyst. To our knowledge, the formation of C=C bonds by the reaction of aldehydes and organozinc reagents, using this catalyst in the presence of chlorotrimethylsilane, is yet to be reported. Herein, we report that a number of *E*-alkenes can be obtained by this route. To investigate the scope and limitations of this new reaction for the synthesis of *E*-alkenes, various aldehydes and organozinc reagents, including some functionalized species, have been utilized as substrates (Scheme 1). The results are summarized in Table 1.



Scheme 1.

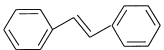
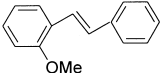
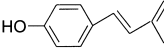
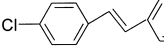
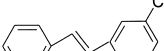

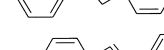
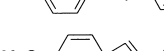
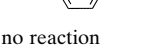

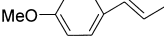
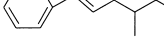
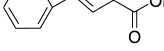
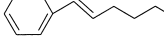
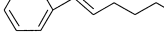
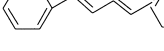
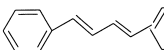
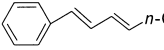
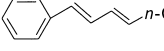
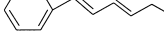
We observed that certain organozinc reagents worked best at particular reaction conditions. For the benzylic zinc halides, reactions at room temperature gave the corresponding *E*-stilbenes in good-to-excellent yields after 8 h (78–92 %, entries 1–8). However, when alkylzinc iodides were used, yields of *E*-alkenes were optimized by carrying out reactions at –18 °C, and then warming to room temperature (54–89 %, entries 10–15, 18–21). Both electron-withdrawing and electron-donating substituents on the phenyl ring, such as methyl, chloro, bromo, benzyloxy, hydroxy, and methoxy, are tolerated in these reactions and generally have little effect on product yield, except for 2,4-dinitrobenzaldehyde which gave no olefination product (entries 2–11 and 17). Where organo-

[*] Prof. J.-X. Wang, Y. Fu, Dr. Y. Hu
Institute of Chemistry, Department of Chemistry
Northwest Normal University
Lanzhou 730070 (P. R. China)
Fax: (+86) 931-776-8159
E-mail: wangjx@nwnu.edu.cn

[**] This work was supported by the National Natural Science Foundation of China and the Northwest Normal University Science and Technology Development Foundation of China.

Supporting information for this article is available on the WWW under <http://www.angewandte.org> or from the author.

Table 1. Nickel(II)-catalyzed alkenylation of functionalized organozinc reagents with aldehydes.[a]

Entry	Ar	FG-R or Aryl	X	Temp. [°C]	Time [h]	Product[b]	Yield[c] [%]
1	Ph	Ph	Cl	RT	8	 1a	88
2	2-MeOPh	Ph	Cl	RT	8	 1b	79
3	4-HOPh	Ph	Cl	RT	8	 1c	78
4	4-ClPh	Ph	Br	RT	8	 1d	87
5	Ph	3-ClPh	Br	RT	8	 1e	81
6	Ph	3-BrPh	Br	RT	8	 1f	63
7	Ph	4-BrPh	Br	RT	8	 1g	85
8	4-MeOPh	Ph	Cl	RT	8	 1h	92
9	2,4-(O ₂ N) ₂ Ph	Ph	Br	RT	8	no reaction	0
10	4-MeOPh	<i>n</i> -C ₇ H ₁₅ -	I	-18-RT	12	 2a	68
11	4-MeOPh	Cl(CH ₂) ₃ -	I	-18-RT	12	 2b	63
12	Ph	 2c	I	-18-RT	12		61
13	Ph	EtO ₂ CCH ₂ -	I	-18-RT	12	 2d	66
14	Ph	Br(CH ₂) ₃ -	I	-18-RT	12	 2e	65
15	Ph	<i>n</i> -C ₄ H ₉ -	I	-18-RT	12	 2f	68
16	PhCH=CH ₂ -	Ph	Cl	RT	8	 3a	89
17	PhCH=CH ₂ -	3-ClPh	Br	RT	8	 3b	74
18	PhCH=CH ₂ -	<i>n</i> -C ₆ H ₁₃ -	I	-18-RT	12	 4a	62
19	PhCH=CH ₂ -	<i>n</i> -C ₇ H ₁₅ -	I	-18-RT	12	 4b	60
20	PhCH=CH ₂ -	 4c	I	-18-RT	12		54
21	PhCH=CH ₂ -	<i>n</i> -C ₅ H ₁₁ -	I	-18-RT	12	 4d	65

[a] All reactions were conducted on the following scale: 10 mmol aldehydes, 11 mmol organozinc reagents, 0.3 mmol catalyst [NiCl₂(PPh₃)₂] in THF (20 mL). [b] All products were characterized by IR and ¹H NMR spectroscopy, as well as mass spectrometry. [c] Yields of isolated products.

zinc halides were functionalized by chloro, bromo, and ester moieties, the corresponding *E*-alkenes also contained these groups (entries 11, 13, and 14). Interestingly, the unsaturated double bond of phenylacrylic aldehyde could also be introduced into the products in moderate-to-good yields (entries 16–21). We also found that these reactions tolerated different molecular structures of RZnX; for example, under

the same conditions, the use of sterically hindered complexes with branched functionalities gave the desired products in moderate yields (entries 12 and 20).

One advantage of this reaction, which makes it a particularly attractive synthetic procedure, is its regioselectivity. The double bond is formed between the carbonyl carbon atom of the aldehyde and the carbon atom of the organozinc

reagent. The reaction is also stereoselective; in all cases only the *E*-alkenes were isolated after chromatography.

In the well-studied Wittig reaction, stilbenes are usually formed in moderate-to-high yield as a mixture of *E* and *Z* isomers, together with triphenylphosphine oxide as a by-product.^[1a] Although the *E*:*Z* ratio can be changed by varying some of the reaction conditions,^[12, 13] recent studies indicate that the *E*:*Z* ratio is unchanged by varying the concentration, mode of addition, or molar ratio of the aldehyde and ylide.^[14] Slight variations were seen by changing the substituents in the aldehyde and aryl alkylidene triphenylphosphorane precursors. The use of an aldehyde as its enamine derivative can limit possible side reactions to give *E*-stilbenes in high yields.^[1a] Our experimental results showed that this reaction is highly stereoselective and only gives *E*-alkenes selectively.

Based on our experimental results and other related studies,^{[15], [16]} we propose the general reaction mechanism shown in Scheme 2. The first step of this mechanism is the reaction of $[\text{NiCl}_2(\text{PPh}_3)_2]$ (**1**) with the functionalized organozinc reagent **2**, to form $[\text{FG-ArCH}_2\text{NiCl}(\text{PPh}_3)_2]$ (**3**). The second step is 1,2-addition of **3** to an aromatic aldehyde **4**, which is activated by chlorotrimethylsilane,^[17] to give nickel complex **6**. The loss of **1** from **6**, in the presence of chlorotrimethylsilane, yields secondary silyl ethers **7**, which have been isolated.^[18] Compounds **7** can also be detected in the reaction by GC-MS. Loss of Me_3SiOH from **7** gives the final *E*-alkenes product **8**.

In conclusion, we have developed a new and convenient method for the efficient and highly stereoselective synthesis of *E*-alkenes from the corresponding aldehydes and functionalized organozinc reagents in the presence of a silylating agent and a catalytic quantity of $[\text{NiCl}_2(\text{PPh}_3)_2]$. The main advantages of this new method are high stereoselectivity, tolerance to unsaturated and polyfunctional groups, simple operation

procedure, and excellent product yields, all under relatively mild reaction conditions.

Experimental Section

Typical procedure: Method A: Benzylzinc halides (11 mmol) were prepared following Knochel's procedure.^[19] $[\text{NiCl}_2(\text{PPh}_3)_2]$ (0.2 g, 0.3 mmol) in THF (2 mL) was added to a solution of benzylzinc halides in THF at 0 °C. After stirring the mixture for 2 min, the temperature was allowed to reach room temperature. A solution of benzaldehyde (1.06 g, 10 mmol) and Me_3SiCl (2.18 g, 20 mmol) in THF (10 mL) was then added dropwise. The reaction mixture was stirred at room temperature for 8 h. *E*-stilbenes were obtained by column chromatography on silica gel using petroleum/ethyl acetate as an eluent. All products were characterized by IR, ^1H NMR, and mass spectroscopy.

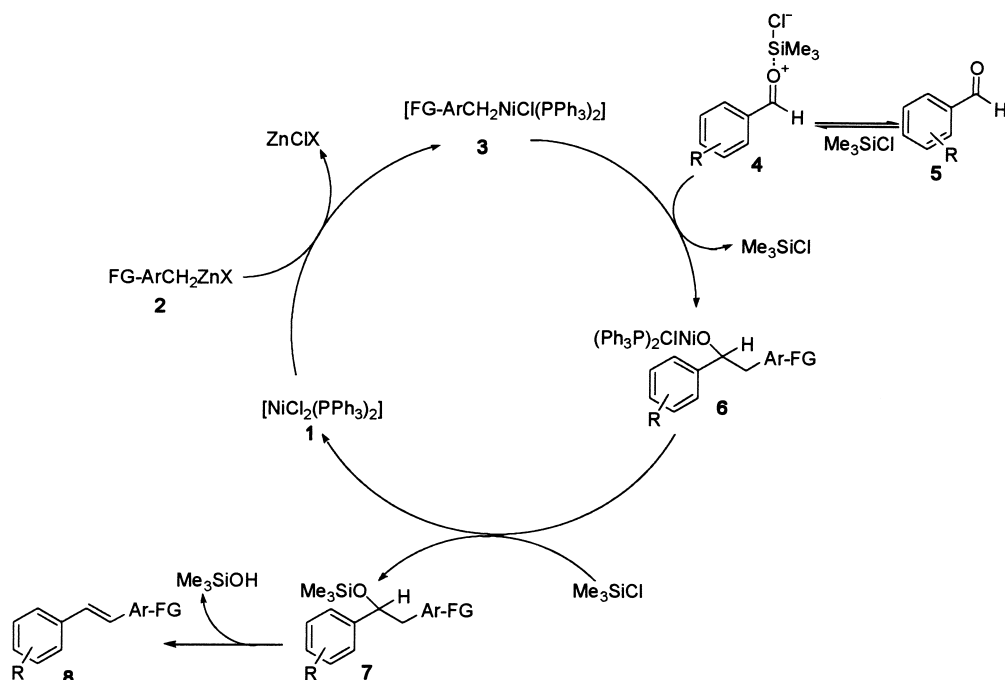
1b: ^1H NMR (400 MHz, CDCl_3): δ = 7.62–7.50 (m, 4H; Ar-H), 7.39–7.19 (m, 4H; Ar-H), 7.10 (d, $^3J(\text{H,H})$ = 16.6 Hz, 1H; =CH), 6.94 (dd, $^3J(\text{H,H})$ = 18.6 Hz, $^3J(\text{H,H})$ = 7.0 Hz, 2H; =CH, Ar-H), 3.88 ppm (s, 3H; OCH_3); IR (KBr): $\tilde{\nu}$ = 3017, 2969, 2841, 1600, 1591, 1569, 1483, 1466, 1241, 1030, 965, 753, 691 cm^{-1} ; MS (70 eV): m/z (%): 210 (100) [M^+], 195 (4) [$M^+ - \text{CH}_3$], 179 (13) [$M^+ - \text{OCH}_3$], 165 (40) [$M^+ - \text{OCH}_3 - \text{CH}_2$], 152 (12) [$M^+ - \text{OCH}_3 - \text{C}_2\text{H}_5$], 139 (4) [$M^+ - \text{OCH}_3 - \text{C}_3\text{H}_7$], 128 (2) [$M^+ - \text{OCH}_3 - \text{C}_4\text{H}_9$], 115 (3) [$M^+ - \text{OCH}_3 - \text{C}_5\text{H}_{11}$], 104 (17) [$M^+ - \text{OCH}_3 - \text{C}_6\text{H}_{13}$], 91 (24) [$\text{C}_6\text{H}_5\text{CH}^+ + 1$], 77 (3) [C_6H_5^+].

2a: ^1H NMR (400 MHz, CDCl_3): δ = 7.32 (dt, $^3J(\text{H,H})$ = 8.2 Hz, $^4J(\text{H,H})$ = 2.0 Hz, 2H; Ar-H), 6.80 (dt, $^3J(\text{H,H})$ = 8.8 Hz, $^4J(\text{H,H})$ = 1.8 Hz, 2H; Ar-H), 6.28 (d, $^3J(\text{H,H})$ = 15.8 Hz, 1H; H-1), 6.02 (dt, $^3J(\text{H,H})$ = 15.8 Hz, $^4J(\text{H,H})$ = 7.2 Hz, 1H; H-2), 3.77 (s, 3H, OCH_3), 2.17 (q, 2H, $^3J(\text{H,H})$ = 6.6 Hz), 1.41–1.08 (m, 10H, CH_2), 0.88 ppm (t, $^3J(\text{H,H})$ = 6.4 Hz, 3H; CH_3); IR (neat): $\tilde{\nu}$ = 2927, 2855, 1610, 1511, 1465, 1370, 1301, 1241, 1098, 964, 831, 725 cm^{-1} ; MS (70 eV): m/z (%): 232 (M^+ , 17.5), 147(100), 134 (22.5), 121, (46.8), 91 (24), 77 (7.0).

2b: ^1H NMR (400 MHz, CDCl_3): δ = 7.27 (dt, $^3J(\text{H,H})$ = 8.8 Hz, $^4J(\text{H,H})$ = 2.2 Hz, 2H; Ar-H), 6.84 (m, 2H; Ar-H), 6.37 (d, $^3J(\text{H,H})$ = 16.0 Hz, 1H; H-1), 6.01 (dt, $^3J(\text{H,H})$ = 15.8 Hz, $^4J(\text{H,H})$ = 7.0 Hz, 1H; H-2), 3.77 (s, 3H, OCH_3), 3.55 (t, $^3J(\text{H,H})$ = 6.6 Hz, 2H; CH_2), 2.35 (q, $^3J(\text{H,H})$ = 6.8 Hz, 2H; CH_2), 1.95–1.74 ppm (m, 2H, CH_2); IR (neat): $\tilde{\nu}$ = 2996, 2934, 2861, 1610, 1512, 1461, 1240, 1170, 1037, 960, 800, 725, 685, 651 cm^{-1} ; MS (70 eV): m/z (%): 214 (1) [$M^+ + 4$], 213 (3) [$M^+ + 3$], 212 (3) [$M^+ + 2$], 211 (9) [$M^+ + 1$], 210 (21) [M^+], 175 (2), 161 (2), 147 (100), 121 (51), 91 (35), 77 (14).

3b: ^1H NMR (400 MHz, CDCl_3): δ = 7.46 (t, $^3J(\text{H,H})$ = 7.6 Hz, 3H; Ar-H), 7.36 (t, $^3J(\text{H,H})$ = 7.6 Hz, 2H; Ar-H), 7.32–7.20 (m, 4H; Ar-H), 6.98 (ddd, $^3J(\text{H,H})$ = 19.8 Hz, $^4J(\text{H,H})$ = 10.6 Hz, $^4J(\text{H,H})$ = 4.1 Hz, 1H), 6.94 (ddd, $^3J(\text{H,H})$ = 19.8 Hz, $^4J(\text{H,H})$ = 10.6 Hz, $^4J(\text{H,H})$ = 4.1 Hz, 1H; CH=), 6.72 (ddd, $^3J(\text{H,H})$ = 20.5 Hz, $^4J(\text{H,H})$ = 11.4 Hz, $^4J(\text{H,H})$ = 5.3 Hz, 1H; CH=), 6.61 ppm (ddd, $^3J(\text{H,H})$ = 21.2 Hz, $^4J(\text{H,H})$ = 11.5 Hz, $^4J(\text{H,H})$ = 4.6 Hz, 1H; CH=); MS (70 eV): m/z (%): 243 (3.4) [$M^+ + 3$], 242 (19.8) [$M^+ + 2$], 241 (13.1) [$M^+ + 1$], 240 (62.1) [M^+], 205 (100) [$M - \text{Cl}$].

4c: ^1H NMR (400 MHz, CDCl_3): δ = 7.45–7.19 (m, 5H; Ar-H), 6.82 (dd, $^3J(\text{H,H})$ = 16.8 Hz, $^4J(\text{H,H})$ = 10.2 Hz, 1H; H-1), 6.53 (t, $^3J(\text{H,H})$ = 16.8 Hz, 1H; H-2), 6.25 (dd, $^3J(\text{H,H})$ = 15.2 Hz, $^4J(\text{H,H})$ = 10.2 Hz, 1H; H-3), 5.80 (dt, $^3J(\text{H,H})$ = 15.0 Hz, $^4J(\text{H,H})$ = 7.0 Hz, 1H; H-4), 2.10 (q, $^3J(\text{H,H})$ = 7.0 Hz, 2H; CH_2), 1.46–1.25 (m, 10H, CH_2), 0.88 ppm (t, $^3J(\text{H,H})$ = 6.2 Hz, 3H; CH_3); IR (neat): $\tilde{\nu}$ = 2926, 2855, 1636, 1606, 1511, 1465, 1370, 1250, 1037, 962, 838, 765 cm^{-1} ; MS (70 eV): m/z (%): 243



Scheme 2. General mechanism for a nickel(II)-catalyzed alkenylation of aldehydes with functionalized organozinc reagents.

(1) [$M^+ + 1$], 242 (5) [M^+], 197 (2), 183 (1), 169 (1), 157, (1), 143 (47), 128 (28), 117 (7), 104 (2), 91 (13), 77 (5), 57 (100), 41 (57).

Method B: Under an argon atmosphere, a mixture of zinc dust (0.85 g, 13 mmol), 1,2-dibromoethane (0.19 g, 1.0 mmol), and THF (2 mL) was heated in a three-necked flask to 60–70 °C for 2–3 min and then cooled to room temperature. Chlorotrimethylsilane (0.1 mL) was added, and the mixture was stirred at room temperature for 15 min. A solution of RI (12 mmol) in THF (10 mL) was then added, and the mixture was stirred for 12 h at 35 °C. The resulting RZnI solution was then added to another three-necked flask, in which [$\text{NiCl}_2(\text{PPh}_3)_2$] (0.2 g, 0.3 mmol) and THF (2 mL) had been previously heated at 60 °C for 2 min. The resulting mixture was cooled to –18 °C. A solution of aldehyde (10 mmol) and chlorotrimethylsilane (20 mmol) in THF (10 mL) was added over a few minutes and the mixture was allowed to warm to room temperature. After stirring the mixture for 12 h, saturated aqueous solution of NH_4Cl (10 mL) and Et_2O (10 mL) were added and the mixture was stirred for 10 min. The organic layer was separated, dried over anhydrous MgSO_4 , and concentrated. The product was isolated from the crude reaction mixture by column chromatography on silica gel using petroleum ether/ethyl acetate as the eluent.

Received: December 28, 2001

Revised: April 11, 2002 [Z 18460]

- [1] a) K. B. Becker, *Synthesis* **1983**, 341–368; b) O. H. Wheeler, H. N. Batlle de Pabon, *J. Org. Chem.* **1965**, 30, 1473–1477; c) A. R. Macquire in *Comprehensive Organic Functional Group Transformations* (Eds.: A. R. Katritzky, O. Meth-Cohn, C. W. Rees) Pergamon, New York, **1995**.
- [2] J. E. McMurry, M. P. Fleming, *J. Am. Chem. Soc.* **1974**, 96, 4708–4709.
- [3] L. Engman, *J. Org. Chem.* **1984**, 49, 3559–3563.
- [4] E. Vedejs, J. M. Dolphin, W. T. Stolle, *J. Am. Chem. Soc.* **1979**, 101, 249–251.
- [5] A. R. Katritzky, D. O. Tymoshenko, S. A. Belyakov, *J. Org. Chem.* **1999**, 64, 3332–3334.
- [6] a) G. W. Kabalka, J. T. Maddox, E. Bogas, *J. Org. Chem.* **1994**, 59, 5530–5531; b) G. W. Kabalka, Z. Wu, Y. Ju, *Tetrahedron* **2001**, 1663–1670.
- [7] P. Knochel, J. J. Almerna Perea, P. Jones, *Tetrahedron*, **1998**, 54, 8275–8319.
- [8] a) R. Giovannini, T. Studemann, A. Devasa-Gayaraj, G. Dussin, P. Knochel, *J. Org. Chem.* **1999**, 64, 3544–3553; b) B. H. Lipshutz, P. A. Blomgren, S.-K. Kim, *Tetrahedron Lett.* **1999**, 40, 197–200; c) H. Avedissian, L. Berinlon, G. Cahiez, P. Knochel, *Tetrahedron Lett.* **1998**, 39, 6163–6166.
- [9] Y. Hu, J. Yu, S. Yang, J.-X. Wang, Y. Yin, *Synlett.* **1998**, 1213–1214.
- [10] a) K. Soai, S. Niwa, *Chem. Rev.* **1992**, 92, 833–856; b) R. Noyori, M. Kitamura, *Angew. Chem.* **1991**, 103, 34–48; *Angew. Chem. Int. Ed. Engl.* **1991**, 30, 49–69.
- [11] a) P. I. Dosa, G. C. Fu, *J. Am. Chem. Soc.* **1998**, 120, 445–446; b) C. Lutz, P. Jones, P. Knochel, *Synthesis* **1999**, 312–316.
- [12] G. Drefahl, D. Lorenz, G. Schnitt, *J. Prakt. Chem.* **1964**, 23, 143–148.
- [13] A. W. Johnson, V. L. Kyllingstad, *J. Org. Chem.* **1966**, 31, 334–336.
- [14] H. Yamataka, K. Nagareda, K. Ando, T. Hanafusa, *J. Org. Chem.* **1992**, 57, 2865–2869.
- [15] C. Alvisi, S. Casolari, A. L. Costa, M. Ritani, E. Tagliavini, *J. Org. Chem.* **1998**, 63, 1330–1333.
- [16] R. Latouche, F. Texier-Boullet, J. Hamelin, *Tetrahedron Lett.* **1991**, 32, 1179–1182.
- [17] a) E. Nakamura, S. Aoki, K. Sekiya, H. Oshino, I. Kuwajima, *J. Am. Chem. Soc.* **1987**, 109, 8056–8066; b) C. R. Johnson, T. G. Marren, *Tetrahedron Lett.* **1987**, 28, 27–30.
- [18] Spectroscopic data for **7**: ^1H NMR (400 MHz, CDCl_3): δ = 7.42 (dd, $^3J(\text{H,H})$ = 8.2 Hz, $^3J(\text{H,H})$ = 1.8 Hz; 1 H), 6.89 (t, $^3J(\text{H,H})$ = 7.4 Hz; 1 H), 6.77 (d, $^3J(\text{H,H})$ = 8.2 Hz; 1 H), 5.09 (t, $^3J(\text{H,H})$ = 6.0 Hz; 1 H), 3.77 (s, 3 H), 1.58 (s, 2 H), 1.24 (s, 8 H), 0.84 (t, $^3J(\text{H,H})$ = 6.6 Hz; 3 H), 0.06 ppm (s, 9 H); ^{13}C NMR (100 MHz, CDCl_3): δ = 155.4, 134.3, 127.4, 126.7, 120.4, 109.8, 68.3, 39.0, 31.8, 29.2, 26.0, 22.7, 14.1, 0.0 ppm; MS (70 eV): m/z (%): 296 ($M^+ + 2$, 0.5), 281 (5), 211 (100), 181 (5), 136 (4), 122 (4), 92 (4), 74 (16).
- [19] S. C. Berk, M. C. P. Yeh, N. Jeong, P. Knochel, *Organometallics* **1990**, 9, 3053–3064.

Mechanistic Features, Cooperativity, and Robustness in the Self-Assembly of Multicomponent Silver(I) Grid-Type Metalloarchitectures

Annie Marquis, Jean-Pierre Kintzinger, Roland Graff, Paul N. W. Baxter, and Jean-Marie Lehn*

Self-organization processes allow the spontaneous but controlled generation of complex organic or inorganic architecture on the basis of the molecular information stored in the components, and its processing through the interactional algorithms defined by specific molecular recognition events.^[1, 2] Such processes connect input components with output entity(ies), with a fidelity/reliability depending on the robustness of the program, that is, its ability to resist interference from factors other than the directing/dominant coding interactions.

While in equilibrium conditions, the process ideally leads to the preferential formation of a given entity under thermodynamic control/pressure; input and output species may be linked by complex mechanistic pathways and involve the generation of kinetic species that may or may not be direct intermediates. Such is the case, for instance, in the final formation of the thermodynamically favored circular helicates following kinetically favored triple-helical complexes.^[3]

Although it is crucial to gain insight into the mechanistic, thermodynamic, and kinetic features of the self-organization process, only few such studies have been reported.^[4] Whereas the preferential, ideally exclusive, formation of a given entity is usually pursued, various factors may interfere with the dominant code and complicate the issue. Thus, considering the self-assembly of inorganic grid architectures, which makes use of specifically designed ligands and of strong metal-ion coordination interactions, $[2 \times 2]$ -,^[5] $[3 \times 3]$ -,^[6] and $[4 \times 4]$ -^[7] type entities form exclusively. However, with a pentadentate ligand, both an incomplete $[4 \times 5]\text{Ag}^+_{20}$ grid and a quadruple helicate are simultaneously generated in place of the full $[5 \times 5]\text{Ag}^+_{25}$ entity, because of the interplay of various structural factors.^[8] On the other hand, such cases also stress that when different “Boltzmann species” are thus formed, provided they are well defined, diversity ensues, an attractive feature of multiple outputs^[9] in a self-assembly process. To gain understanding of the self-organization pathways, it is first necessary to identify the species that may form and then try to define their role in the process. In particular, features such as

[*] Prof. Dr. J.-M. Lehn, Dr. A. Marquis, Dr. P. N. W. Baxter

Laboratoire de Chimie Supramoléculaire
ISIS-Université Louis Pasteur
4, rue Blaise Pascal, 67000 Strasbourg (France)
Fax: (+33)390-241-117
E-mail: lehn@chimie.u-strasbg.fr

Dr. J.-P. Kintzinger
Laboratoire de RMN de la Matière Condensée
CNRS-Université Louis Pasteur
4, rue Blaise Pascal, 67000 Strasbourg (France)

Dr. R. Graff
Service Commun de RMN
Université Louis Pasteur
1, rue Blaise Pascal, 67000 Strasbourg (France)

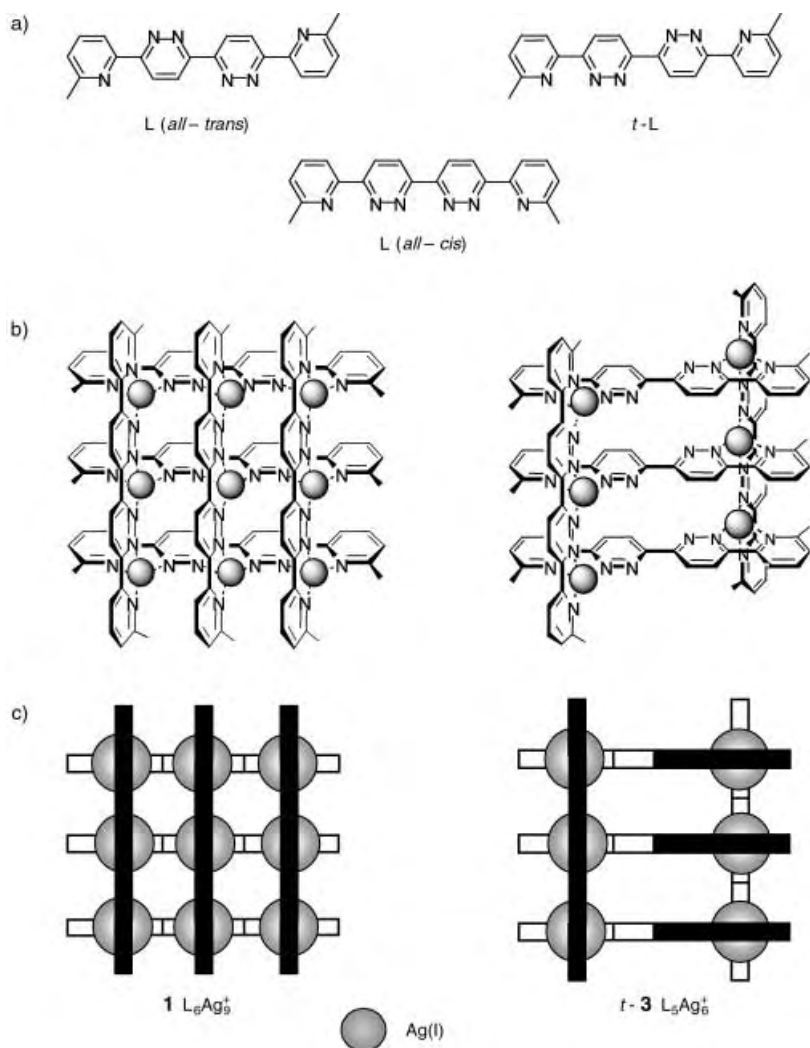


Figure 1. a) Definition of the form of the ligand L used; b) structures of the grid complexes **1** and $t-3$; c) schematic representations of the grid complexes; the white bars denote the parts of the ligands “behind” the silver cations, and the black bars represent those “in front”.

nonlinearity, cooperativity, and structural switching events are of great interest.

The self-assembly of the $[3 \times 3]$ -grid-type complex L_6Ag^+ (**1**; Figure 1) from the tritopic L ligand and Ag^I ions was reported earlier.^[6] We have now investigated the nature of the species which is progressively generated as increasing amounts of metal ions are added to a solution of the ligand,^[10] monitoring the evolution of the resulting mixtures by 1H and ^{109}Ag NMR spectroscopy.^[11] Noting that there may be several assembly pathways and assuming that the final multiligand multimetallic entity **1** builds up by stepwise connection of ligand molecules and metal ions, the identified species of lower ligand numbers and nuclearities should lie on the self-assembly hypersurface, either directly on the mechanistic pathway or on a bifurcation.

The $[3 \times 3]$ L_6Ag^+ grid (**1**) forms immediately and cleanly when a stoichiometric amount of silver(I) is added to a solution of the ligand L (Ag^+/L 9/6). To obtain good reference points, the 1H and ^{109}Ag NMR spectroscopic data for **1** itself were first analyzed in detail. In agreement with the earlier

spectral results,^[6] they allowed a clear identification, by their characteristic chemical shift, of three types of silver cations: “corner”, “edge”, and “center”.

Progressive addition of $AgCF_3SO_3$ to a solution of ligand L leads to very pronounced changes in the 1H NMR spectrum over the titration range until the stoichiometry of **1** is reached, at which only this grid complex is present (Figure 2).

At a low Ag^+/L ratio a mixture of many species is observed, most of which could not be identified, except for one type of complex which predominates at $Ag/L \approx 1:1$ and presents characteristic 1H NMR signals, spread into the $\delta = 6.5–7.0$ ppm and 9.7 ppm regions (Figure 2a). The ^{109}Ag NMR spectroscopic data comprise two signals corresponding to Ag^+ ions in the “corner” position and one signal for an ion in an “edge” position. Together with the detailed analysis of the 1H NMR spectroscopic measurements,^[11] the results point to the presence, among other species, of at least two complexes of $L_nAg_n^+$ type, probably having an intertwined structure and with all ligands in a transoid arrangement around the central C–C bond. The complexes could be a triangular $L_3Ag_3^+$ and a square $L_4Ag_4^+$ ^[14] species, in analogy to earlier observations of coexisting Cu^I complexes of such types (see structures **2**($n=3$) and **2**($n=4$), Figure 3).^[15, 16]

At $Ag^+/L \approx 6:5$, another discrete complex is almost exclusively formed (Figure 2c). Extensive

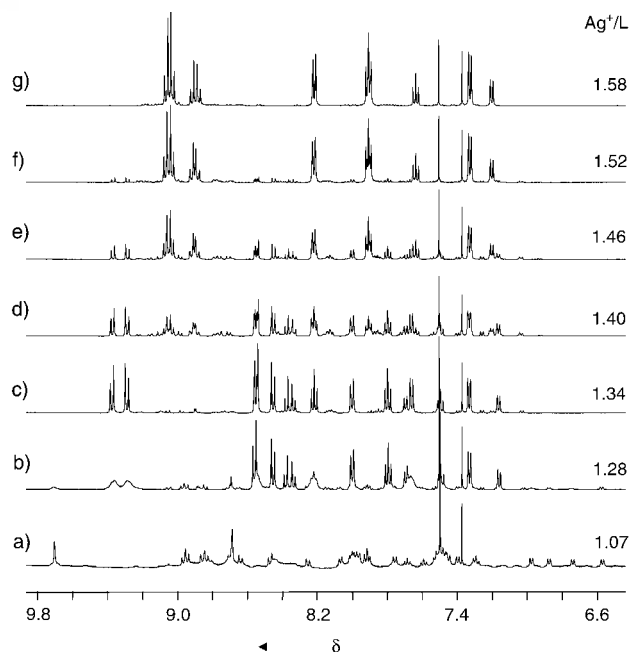


Figure 2. 500 MHz 1H NMR spectra of ligand L in the course of the titration by $AgCF_3SO_3$; solvent: $CDCl_3/CD_3NO_2$ 25/75. The spectra c) and g) at ratios 1.34 and 1.58 correspond to almost pure $L_5Ag_5^+$, **3**, and $L_6Ag_6^+$, **1**, respectively. Because of the small quantities of salt introduced, there may be a significant discrepancy between the Ag^+/L ratio indicated and the actual stoichiometry of the species observed, e.g. for **3**, $L_5Ag_5^+$, traces b) and c).

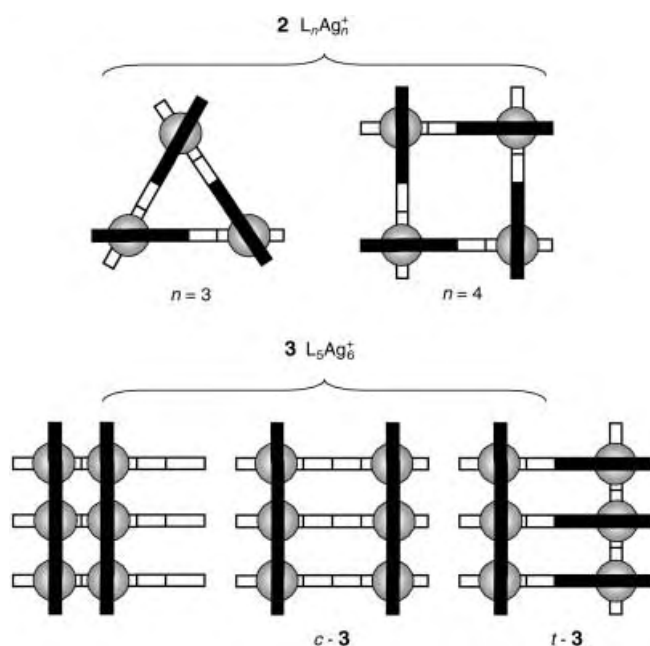


Figure 3. Schematic representation of different forms of the two types of species $L_nAg_n^+$, **2** ($n = 3, 4$), and $L_5Ag_6^+$, **3**; in the complex **3**, bottom left, the terminal pyridine units of the horizontal ligands are expected to be in a transoid orientation to the neighboring pyridazine. For **2**, only forms with “corner” Ag^+ ions are shown.

measurements and analysis of 1H and ^{109}Ag 2D NMR spectra and relaxation times allow the unambiguous identification of the complex as a species of $L_5Ag_6^+$ composition, in agreement with the titration stoichiometry. The silver NMR spectroscopic data indicate the presence of two sets of ^{109}Ag -coupled proton signals corresponding to “corner” and “edge” silver cations, respectively. Together with the 1H NMR spectroscopic data^[17] and taking into account that the transoid conformation around the central C–C bond in **L** is much preferred over the cisoid one,^[12, 13] the structure **t-3** (see Figure 1 b,c) can be assigned to $L_5Ag_6^+$; in **t-3**, the ligands in the set of three (shown as “horizontal”) are in the form *t-L*, presenting a transoid conformation around the central C–C bond, whereas the other two ligands (shown as “vertical”), are in the cisoid form *c-L*. The 1H NMR spectrum in Figure 2b displays exchange-broadened signals for the two cisoid ligands of the **t-3** species. A 2D exchange map shows that the partner(s) in this ligand-exchange reaction is (are) a different species from the $L_nAg_n^+$ complexes mentioned above. This process allows the formation of the *c-L* $_5Ag_6^+$ (**c-3**) entity (Figure 3) which is a prerequisite for the generation of the final grid $L_6Ag_9^+$ (**1**; see also below).^[16]

Further addition of salt leads to the conversion of this intermediate **3** into the final $L_6Ag_9^+$ $[3 \times 3]$ grid (**1**) displaying its characteristic spectrum. It is seen in the distribution diagram for the two main species identified (**1** and **3**; Figure 4) that the formation of $L_6Ag_9^+$ is highly nonlinear. Examination of the proton NMR spectra indicates that there are only small amounts $\leq 10\%$ of other, intermediate, complex(es) formed along the path from **3** to **1**, which cannot interconvert directly but must undergo dissociation/reassociation processes with rotation around the central C–C bond of three **L** ligands.

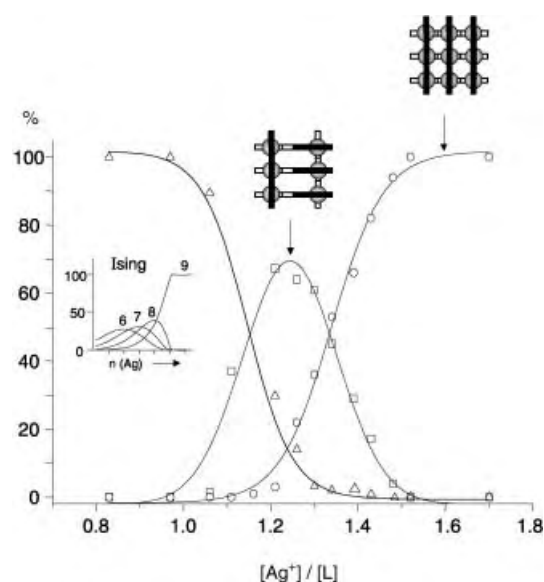


Figure 4. Distribution curves of the species **1**, $L_6Ag_9^+$, (□), the *t-3* form of $L_5Ag_6^+$ (○) and all the others (Δ; by difference) in the course of the titration of **L** by $AgCF_3SO_3$ in CD_3Cl/CD_3NO_2 25/75, determined by integration of characteristic 200 MHz 1H NMR signals for the two complexes. The inset shows part of the distribution curves of the species containing 6–9 silver ions for a statistical non-cooperative Ising model with nine independent sites.

These minor species may be other forms of $L_5Ag_6^+$ (see Figure 3). The behavior observed implies overall positive cooperativity in the formation of $L_6Ag_9^+$ from $L_5Ag_6^+$, with three Ag^+ ions and a ligand molecule binding in a single overall step. In contrast, assuming an Ising model with nine independent (non-cooperative) sites, the distribution curves would demonstrate the formation of the complexes with seven and eight cations, which were not observed in the course of the titration.

Addition of salt much beyond the $L_6Ag_9^+$ stoichiometry, up to four equivalents (six ions to one ligand), did not lead to further changes in the 1H NMR spectrum. Thus, the final $[3 \times 3]$ grid (**1**) is stable to a large excess of Ag^+ ions. This behavior indicates that the $L + Ag^+$ system displays high robustness^[18] with respect to formation of $L_6Ag_9^+$. Conversely, the intermediate entity $L_5Ag_6^+$, which appears and disappears without being directly on the pathway, may be considered as an anomaly, as it exists only in a restricted range of Ag^+ concentrations during the process.

Figure 3 shows a selection of the complexes of type $L_nAg_n^+$ (**2**) and $L_5Ag_6^+$ (**3**) among the many complexes of different compositions and structures that can, in principle, form in the course of the titration.

Formally, conversion of the *trans* species *t-L* $_5Ag_6^+$ (**t-3**) into the corresponding *cis* form *c-L* $_5Ag_6^+$ (**c-3**; Figure 3), where three transoid ligands (*t-L*) become cisoid ones (*c-L*), generates three complexation sites and triggers the binding of three Ag^+ ions and a ligand **L** molecule in a single overall step. *c-L* $_5Ag_6^+$ is expected to be about 20 kcal mol^{−1} less stable than *t-L* $_5Ag_6^+$.^[12] On the other hand, the complexation of a single Ag^+ ion by a 9,10-phenanthroline (phen) and a 2,2'-bipyridine (bipy) unit may be estimated to provide an association free energy of about 15 kcal mol^{−1}, so that binding

of three Ag^+ ions and a ligand L (*all-trans*) by $c\text{-L}_5\text{Ag}^+$ to form L_6Ag^+ , should correspond to about 45 kcal mol⁻¹ binding free energy.^[19] This gross estimate^[19b] does not take into account the weaker binding to a pyridazine nitrogen compared to a pyridine one, nor the electrostatic interactions between the charged coordination sites, nor the stacking interactions between the ligands.

In the L_5Ag^+ entity, the ligands in the set of three, shown as “horizontal”, must be all three either in the *t*-L or in the *c*-L form, as in *t*-3 and *c*-3 respectively; no species with mixed forms [(*c*-L)₂(*t*-L)] or [(*c*-L)(*t*-L)₂] can exist. Thus, cooperativity lies on one hand in the simultaneous “preparation” of the three central sites for binding and on the other hand in the fact that in the incoming L molecule all three sites are rigidly connected, so that binding to one of them forces binding to the other two.^[20] Conversion of one site in $t\text{-L}_5\text{Ag}^+$ from *t* into *c* implies *t* → *c* conversion of the other two, which amounts to an effective increase in affinity from no binding at these two sites to binding at two single phen-type sites (about 2 × (20/2) kcal mol⁻¹).^[19] This factor formally represents the free-energy term $\Delta\Delta G$ by which the affinity of the L_5Ag^+ species for further Ag^+ binding is raised when the first site becomes occupied.^[21] It may be regarded as the coupling between the first binding event and the two subsequent ones. Such a value is qualitatively in line with the very uneven species distribution (Figure 4), in which the starting $t\text{-L}_5\text{Ag}^+$ and the final L_6Ag^+ are highly predominant and the two intermediate species containing seven and eight Ag^+ ions only form in a (very) small amount. These features imply a high cooperativity between the sites, corresponding to a switching process between the two entities.^[22] Positive cooperativity has been observed in helicate formation^[23] as well as in other nonbiological systems.^[4b, 24] In view of the complexity of the conversion of L_5Ag^+ into L_6Ag^+ , it is not possible at this stage to provide a more quantitative analysis of the cooperativity^[21, 22] nor to analyze it in terms of site-specific contributions.^[25]

The present results provide insight into the nature of the species that may be involved in the mechanistic pathway(s) for the self-assembly of the [3 × 3] metallogrid (1) and also hint at how complex such a process is. The results reveal the robustness of the structural program leading to 1, as well as the overall cooperative nature of the system. Both characteristics, together with the reversible exploration of the free-energy hypersurface, are of basic significance for the dynamic behavior of supramolecular devices and materials.^[18]

Received: October 19, 2001

Revised: April 18, 2002 [Z18083]

- [1] a) J.-M. Lehn, *Supramolecular Chemistry: Concepts and Perspectives*, VCH, Weinheim, 1995, chap. 9, p. 139; b) D. S. Lawrence, T. Jiang, M. Levett, *Chem. Rev.* 1995, 95, 2229; c) D. Philp, J. F. Stoddart, *Angew. Chem.* 1996, 108, 1242; *Angew. Chem. Int. Ed. Engl.* 1996, 35, 1154.
- [2] For recent reviews on metal-ion-mediated self-assembly, see for example: a) P. N. W. Baxter in *Comprehensive Supramolecular Chemistry*, Vol. 9 (Eds.: J. L. Atwood, J. E. D. Davies, D. D. MacNicol, F. Vögtle, J.-M. Lehn), Pergamon, Oxford, 1996, chap. 5, p. 165; E. C. Constable in *Comprehensive Supramolecular Chemistry*, Vol. 9 (Eds.:

- J. L. Atwood, J. E. D. Davies, D. D. MacNicol, F. Vögtle, J.-M. Lehn), Pergamon, Oxford, 1996, chap. 6, p. 213; M. Fujita in *Comprehensive Supramolecular Chemistry*, Vol. 9 (Eds.: J. L. Atwood, J. E. D. Davies, D. D. MacNicol, F. Vögtle, J.-M. Lehn), Pergamon, Oxford, 1996, chap. 7, p. 253; b) R. F. Saalfrank, I. Bernt, *Curr. Opin. Solid State Mater. Sci.* 1998, 3, 407; c) B. Olenyuk, A. Fechtenkötter, P. J. Stang, *J. Chem. Soc. Dalton Trans.* 1998, 11, 1707; d) M. Fujita, *Polym. Mater. Sci. Eng.* 1999, 80, 27; e) D. L. Caulder, K. N. Raymond, *J. Chem. Soc. Dalton Trans.* 1999, 8, 1185; f) C. Piguet, *J. Inclusion Phenom. Macrocyclic Chem.* 1999, 34, 361; g) G. F. Swiegers, T. J. Malefetse, *Chem. Rev.* 2000, 100, 3483; h) S. Leininger, B. Olenyuk, P. J. Stang, *Chem. Rev.* 2000, 100, 853.
- [3] B. Hasenknopf, J.-M. Lehn, N. Boumediene, E. Leize, A. Van Dorselaer, *Angew. Chem.* 1998, 110, 3458; *Angew. Chem. Int. Ed.* 1998, 37, 3265.
- [4] See for instance: a) C. Piguet, G. Bernardinelli, B. Bocquet, A. Quattropiani, A. F. Williams, *J. Am. Chem. Soc.* 1992, 114, 7440; b) A. Marquis-Rigault, A. Dupont-Gervais, P. N. W. Baxter, A. Van Dorselaer, J.-M. Lehn, *Inorg. Chem.* 1996, 35, 2307; c) A. Marquis-Rigault, A. Dupont-Gervais, A. Van Dorselaer, J.-M. Lehn, *Chem. Eur. J.* 1996, 2, 1395; d) M. D. Levin, P. J. Stang, *J. Am. Chem. Soc.* 2000, 122, 7428. a) M. T. Youinou, N. Rahmouni, J. Fischer, J. A. Osborn, *Angew. Chem.* 1992, 104, 771; *Angew. Chem. Int. Ed. Engl.* 1992, 31, 733; b) P. N. W. Baxter, J.-M. Lehn, B. O. Kneisel, D. Fenske, *Chem. Commun.* 1997, 2231; c) G. S. Hanan, D. Volkmer, U. S. Schubert, J.-M. Lehn, G. Baum, D. Fenske, *Angew. Chem.* 1997, 109, 1929; *Angew. Chem. Int. Ed. Engl.* 1997, 36, 1842; d) D. M. Bassani, J.-M. Lehn, K. Fromm, D. Fenske, *Angew. Chem.* 1998, 110, 2534; *Angew. Chem. Int. Ed.* 1998, 37, 2364.
- [6] P. N. W. Baxter, J.-M. Lehn, J. Fischer, M.-T. Youinou, *Angew. Chem.* 1994, 106, 2432; *Angew. Chem. Int. Ed. Engl.* 1994, 33, 2284.
- [7] A. M. Garcia, F. Romero-Salguero, D. M. Bassani, J.-M. Lehn, G. Baum, D. Fenske, *Chem. Eur. J.* 1999, 5, 1803.
- [8] P. N. W. Baxter, J.-M. Lehn, G. Baum, D. Fenske, *Chem. Eur. J.* 2000, 6, 4510.
- [9] J.-M. Lehn, *Chem. Eur. J.* 2000, 6, 2097.
- [10] As the grid complex 1 forms and is stable in nitromethane, but is destroyed in coordinating solvents such as acetonitrile, the titrations were performed in a mixture of $\text{CDCl}_3/\text{CD}_3\text{NO}_2$ 25/75 for solubility reasons. The presence of small amounts of water does not significantly affect the formation of the grids. Typical procedure: A suspension of the ligand (5.4 mg; 15.9 μmol) was prepared in 500 μL of the solvent $\text{CDCl}_3/\text{CD}_3\text{NO}_2$ 25/75. Half of the amount of AgCF_3SO_3 salt required for generating the [3 × 3] grid (3 mg; 12 μmol) was initially added to solubilize all the ligand. The titrating agent was a solution containing a 3-fold excess of AgCF_3SO_3 (18 mg; 71.5 μmol) with respect to the stoichiometry of the complete grid, in 250 μL of the same solvent, containing the amount of ligand (2.7 mg; 8 μmol) required to keep its concentration constant during the titration. Aliquots (10 μL) of the metal salt solution were added to the ligand and the ¹H NMR spectra were recorded after each addition, when the thermodynamic equilibrium was assumed to be reached (no change in the NMR spectrum). CDCl_3 was filtrated over basic alumina, then kept over molecular sieves 3 Å; CD_3NO_2 was dried over molecular sieves. The ligand and silver triflate were dried under vacuum and heating, and the silver salt was protected from light.
- [11] ¹H NMR spectra were recorded on a Bruker AC 200 or Bruker ARX 500 spectrometer. The ¹⁰⁹Ag NMR signals were observed by a ¹H/¹⁰⁹Ag 2D HMBC gradient-accelerated procedure on a BRUKER ARX 500 spectrometer using a 5 mm inverse broadband probe and nominal 90° pulses of 36 μs for ¹⁰⁹Ag nuclei and 10 μs for ¹H nuclei. Although no long-range ¹H/¹⁰⁹Ag spin coupling is observed in 1D ¹H NMR spectra, correlations between hydrogen atoms and silver atoms are observed with transfer delays in the range 0.1–0.2 s.
- [12] In 2,2'-bipyridine, the transoid form is calculated to be about 6–8 kcal mol⁻¹ more stable than the cisoid one.^[13] The difference in stability between these two forms should be at least as large in the 3,3'-bipyridazine unit present in L. As a consequence, the L_5Ag^+ species *t*-3 of *C*_{2h} symmetry, with a transoid conformation around the central C–C bond of the three neighboring *t*-L ligands, should be about 20 kcal mol⁻¹ more stable than the corresponding *C*_{2v} species *c*-3, in which the same three ligands are in the cisoid form represented in

structure *c*-L (see Figure 1). Similar considerations hold for the complexes L_nAg^+ (2 Figure 3, top).

- [13] S. T. Howard, *J. Am. Chem. Soc.* **1996**, *118*, 10269; A. Göller, U.-W. Grummt, *Chem. Phys. Lett.* **2000**, *321*, 399.
- [14] For examples of related intertwined structures of $[2 \times 2]$ grids, see: C. S. Campos-Fernández, R. Clérac, K. R. Dunbar, *Angew. Chem.* **1999**, *111*, 3685; *Angew. Chem. Int. Ed.* **1999**, *38*, 3477; X.-H. Bu, H. Morishita, K. Tanaka, K. Biradha, S. Furusho, M. Shionoya, *Chem. Commun.* **2000**, 971.
- [15] P. N. W. Baxter, J.-M. Lehn, K. Rissanen, *Chem. Commun.* **1997**, 1323.
- [16] Several attempts to obtain useful electrospray mass spectral data for the mixtures of Ag^+ complexes and for the final grid **1** were unfortunately fruitless, in contrast to studies of mixtures of related Cu^+ complexes.^[15]
- [17] These data involve a) mutual relaxation cross-peaks between the methyl groups of the three transoid ligands, and b) significant differences in T_1 relaxation times of the central pyridazine hydrogens in the transoid (2.1 s) and in the cisoid (1.3 s) ligands.
- [18] J.-M. Lehn in *Supramolecular Science: Where It Is and Where It Is Going* (Eds.: R. Ungaro, E. Dalcanele), Kluwer, Amsterdam, **1999**, p. 287.
- [19] a) As a first approximation, one may assume that free bipy and 9,10-phenanthroline (phen) are models for binding to a transoid and a cisoid site respectively in ligand L. Then, binding of one free ligand L (*all-trans*) and three Ag^+ ions to the $L_3Ag_3^+$ species *c*-**3** may be estimated to amount to a free energy of about 45 kcal mol⁻¹, corresponding to the formation of three mixed-ligand Ag^+ (bipy,phen) complexes, which would each provide a binding free energy of $[Ag^+(bipy)_2/2 + Ag^+(phen)_2/2] = 10/2 + 20/2 = 15$ kcal mol⁻¹.^[19c] Note that the difference between binding of Ag^+ to a single phen and a single bipy $(20-10)/2 = 5$ kcal mol⁻¹ should compare to a cisoid into transoid conversion that is, 6–8 kcal mol⁻¹.^[12] b) we realize that this data “torturing” may already be going too far... Molecular-mechanics Universal-Force-Field calculations provide an energy difference of about 50 kcal mol⁻¹ between *c*-**3** and *t*-**3**; E. Ruiz, unpublished work. *Ab initio* calculations on different complexes have been undertaken; G. Corongiu, P. Nava, work in progress; c) this corresponds to complexation in acetonitrile: W. J. Peard, R. T. Pflaum, *J. Am. Chem. Soc.* **1958**, *80*, 1593.
- [20] For a discussion of the enthalpic component in positive cooperativity brought in by structural tightening, see: C. T. Calderone, D. H. Williams, *J. Am. Chem. Soc.* **2001**, *123*, 6262.
- [21] $\Delta\Delta G$ provides in principle a direct quantitative measure (when it can be accurately determined) of cooperativity: S. Forsén, S. Linse, *Trends Biochem. Sci.* **1995**, *20*, 495.
- [22] I. Tinoco, Jr., K. Sauer, J. C. Wang, *Physical Chemistry*, Prentice-Hall, Upper Saddle River, **1995**, pp. 638–648.
- [23] A. Pfeil, J.-M. Lehn, *J. Chem. Soc. Chem. Commun.* **1992**, 838; T. M. Garrett, U. Koert, J.-M. Lehn, *J. Phys. Org. Chem.* **1992**, *5*, 529. For another process see E. Leize, A. Van Dorsselaer, R. Krämer, J.-M. Lehn, *J. Chem. Soc. Chem. Commun.* **1993**, 990.
- [24] S. Shinkai, M. Ikeda, A. Sugasaki, M. Takeuchi, *Acc. Chem. Res.* **2001**, *34*, 394, and references therein.
- [25] E. Di Cera, *Chem. Rev.* **1998**, *98*, 1563.

Electrochemical Modulation of Fluorophore Emission on a Nanostructured Gold Film**

Prashant V. Kamat,* Said Barazzouk, and Surat Hotchandani

Fluorophore-bound gold nanoparticles can serve as a probe in biological systems, provide basic understanding of molecular-level interactions of a surface-bound organic moiety,^[1–4] and contribute to the development of biological tracers as well as optoelectronic devices.^[5–8] In a fluorophore–gold nanoassembly the charge transfer interaction between the two components plays an important role as it dictates the pathways by which the excited state deactivates. For example, in the case of 1-aminomethylpyrene the transfer of lone-pair electrons to gold nanoparticles led to a fluorescence enhancement.^[9] On the other hand, the fluorescence emission of a pyrenylthiol ((1-pyrenyl)-6-oxaheptanethiol) was quenched through charge transfer upon binding to the gold nanoparticles.^[10]


Gold nanoparticles capped with organic molecules have a unique ability to retain the charge when subjected to an electric field. Their ability to display quantized charging has been demonstrated by Murray and coworkers.^[6, 11] Control of charging of the gold nanocore thus becomes an important factor if one is interested in modulating the interaction between the gold nanocore and a surface-bound fluorophore. In order to systematically assess the effect of charging on the photochemistry of surface-bound molecules, we have conducted spectroelectrochemical measurements using nanostructured gold films that were functionalized with a pyrenylthiol and have succeeded in modulating the fluorescence using an externally applied electrochemical bias. The possibility of achieving electrochemical modulation of the fluorescence of a gold-surface-bound fluorophore opens up new avenues to design sensors, displays, and biological probes.

Earlier studies have shown that fluorophores bound to bulk metal surfaces are nonfluorescent.^[1, 12–14] Both energy transfer and electron transfer processes are considered to be major deactivation pathways for the excited fluorophore on metal surfaces. Our recent study has shown the possibility of achieving a photoinduced electron transfer in colloidal suspensions of pyrenylthiol-functionalized gold nanoparti-

[*] Dr. P. V. Kamat, S. Barazzouk
Notre Dame Radiation Laboratory
Notre Dame, IN 46556-0579 (USA)
Fax: (+1) 574-631-8068
E-mail: pkamat@nd.edu

Dr. S. Hotchandani
Groupe de Recherche en Énergie et Information Biomoléculaires
Université du Québec à Trois-Rivières
Trois-Rivières, PQ, G9A 5H7 (Canada)

[**] We thank Mr. Binil I. Ipe and Dr. K. George Thomas of the Regional Research Laboratory, Trivandrum, India, for a sample of (1-pyrenyl)-6-oxaheptanethiol. The research described here was supported by the Office of Basic Energy Science of the Department of Energy. This is contribution no. NDRL 4354 from the Notre Dame Radiation Laboratory. S.B. and S.H. acknowledge support of the Natural Sciences and Engineering Research Council of Canada.

 Supporting information for this article is available on the WWW under <http://www.angewandte.org> or from the author.

cles.^[10] If indeed the gold particles act as electron acceptors, it should be possible to modulate the electron transfer quenching of the excited fluorophore by charging the gold nanoparticle at an electrode surface. The charging of organo-capped gold nanoparticles has been demonstrated by monitoring the shift of the plasmon band to lower energies.^[15] However, the shift in the plasmon band was too small (5–9 nm) to resolve these charging effects. Surface-bound fluorophores, on the other hand, provide a new way to monitor the charging events.

In the present study, we have functionalized gold nanoparticles with two different thiols at the same time; one contained a fluorophore (pyrene) and the other a carboxylic acid residue. The latter (sulfanylpropionic acid) served to link the gold nanoparticles to the TiO₂ surface. The electrode preparation is illustrated in Scheme 1. A similar strategy of using difunctional surface modifiers to link different nanoparticles has been demonstrated earlier.^[16–18] The presence of sulfanylpropionic acid also helps to distribute the pyrene moieties around the gold nanocore with minimal intermolecular interactions. Based on the concentration and particle size we estimate an average of about 20 pyrene moieties per gold nanoparticle.

Figure 1 shows the absorption spectra of an OTE/TiO₂ electrode before (b) and after (a) modification with pyrene-functionalized gold nanoparticles. Within minutes of insertion of the OTE/TiO₂ electrode into the THF solution containing the functionalized gold nanoparticles **1** we can observe changes in the electrode coloration. The transparent electrode quickly turns dark purple, thereby confirming the binding of the gold nanoparticles. The electrodes were repeatedly washed with THF to remove any unbound gold nanoparticles. The AFM image (see Figure 1 of the Supporting Information) reveals a highly porous morphology with particle domains of 100 nm diameter. The electrode shows a broad absorption in the visible region with a maximum around 530 nm. This absorption is characteristic of the surface plasmon band of gold nanoparticles and is possibly broadened because of their interaction with the TiO₂ film. Because of the strong

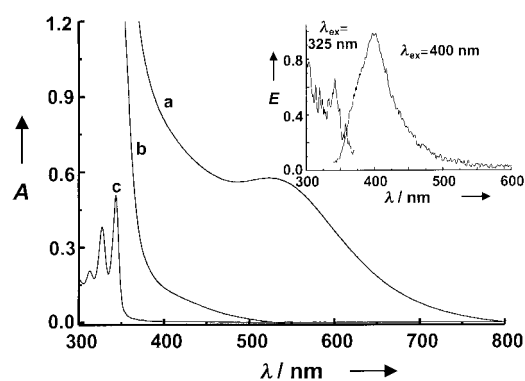


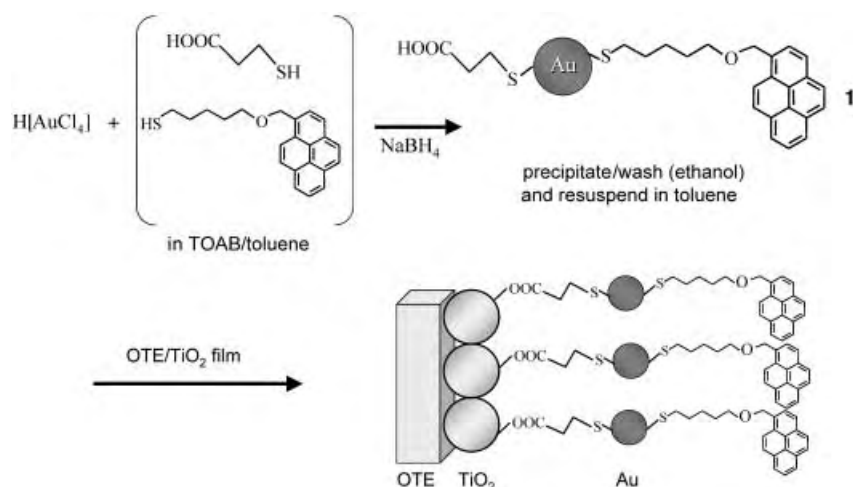
Figure 1. Absorption spectra of a) OTE/TiO₂/1, b) OTE/TiO₂, and c) (1-pyrenyl)-6-oxaheptanethiol in THF. The inset shows the excitation and emission spectra of the OTE/TiO₂/1 electrode recorded at no applied electrochemical bias. The excitation and monitoring wavelengths for these two spectra were 325 nm and 400 nm, respectively.

absorbance of TiO₂ in the UV region, we could not further resolve the pyrene absorption bands.

In the inset of Figure 1 the excitation and emission spectra of the OTE/TiO₂/1 electrode are shown. The electrode exhibits weak emission (monitoring wavelength $\lambda = 400$ nm) with a maximum around 395 nm. As discussed in our previous study,^[10] most of the emission of surface-bound pyrene is quenched by the gold nanocore. Decreased singlet lifetime as well as formation of the oxidation product, pyrene radical cation, indicated the ability of gold nanoparticles to accept electrons from excited pyrene.^[19]

The weak fluorescence seen in Figure 1 stems from pyrene moieties that do not undergo quenching on the gold surface. The excitation spectrum in the inset ($\lambda_{\text{ex}} = 325$ nm) shows the absorption response in the UV (corresponding to the absorption bands at 342, 320, and 314 nm), thereby confirming that the emission arises from surface-bound pyrene. (The front-face geometry as well as the low emission yield limited the resolution of the absorption bands in the excitation spectra.) Another interesting observation was the absence of excimer emission bands in the spectrum of **1** bound to a TiO₂ surface (inset of Figure 1). This contrasts with the observation in colloidal suspension in which we observed excimer emission arising from intermolecular interactions on the gold surface (see Figure 2 of the Supporting Information). The absence of pyrene excimer emission in the film suggests that the molecular movement of the excited-state pyrene moieties is significantly restricted when they are assembled on the TiO₂ surface.

Spectroelectrochemical experiments were conducted using a thin-layer electrochemical cell in a spectrofluorimeter with front-face geometry. Figure 2 shows the emission spectra of OTE/TiO₂/1 at different applied potentials. In a previous study we had shown that gold particles deposited on a nanostructured TiO₂ film permit the flow of electrons following Fermi level equi-



Scheme 1. Functionalization of gold nanoparticles with a pyrenylthiol and their binding to a nanostructured TiO₂ film. TOAB = tetraoctylammonium bromide, OTE = optically transparent electrode.

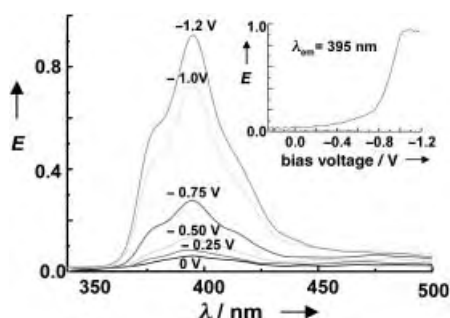
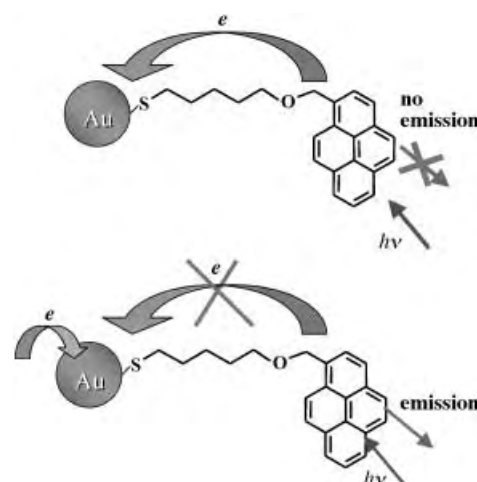


Figure 2. Emission spectra of OTE/TiO₂/1 at different applied potentials using an excitation wavelength of 325 nm. The electrode was maintained at a set potential (0 to −1.2 V vs SCE, electrolyte: 0.1 M tetrabutylammoniumperchlorate in acetonitrile) for 5 min before recording the individual emission spectrum. The inset shows the fluorescence response of OTE/TiO₂/1 at 395 nm during the electrochemical scan.

bration.^[20] Moreover, the pyrene-modified electrodes can also exhibit sensitized photocurrent response when subjected to photoexcitation (Figure 3 of the Supporting Information). As we bias the electrode to negative potentials we observe an increase in the emission yield. It is important to note that the overall shape of the emission band essentially remains the same. This in turn suggests that the photoactive species that contribute to the emission remain unperturbed. As we bias the electrode to more negative potentials, the gold particles become charged and fewer pyrene moieties interact with the gold surface. At potentials around −1.2 V we completely suppress the interaction between the fluorophore and the gold nanocore, and we achieve saturation in the emission increase. We were able to restore more than 90% of the quenched emission by simply charging the gold nanoparticle with an externally applied electrochemical bias. The fluorescence response (at 395 nm) of OTE/TiO₂/1 recorded during an electrochemical scan is shown in the inset of Figure 2. By controlling the applied electrochemical potential one can modulate the pyrene fluorescence at a desired level.

The fact that the spectral features of the pyrene emission hardly change during the sweep of the electrochemical potential suggests that the biasing of the electrode to negative potentials does not cause any pyrene desorption. This aspect was independently confirmed by testing the electrolyte solution from the cell for pyrene emission after the application of a negative bias. The absorption spectrum of the electrode recorded after the spectroelectrochemical experiments did not indicate any deterioration of the film. These results confirm that an externally applied electrochemical bias does not cause any desorption of the surface-bound fluorophore. Its role remains modulation of the excited state dynamics of the surface-bound pyrene.

Scheme 2 illustrates the excited state behavior of surface-bound pyrene in the absence and presence of an applied bias. We expect a majority of the surface-bound pyrene moieties to actively participate in the electron transfer quenching at 0 V or under no electrochemical bias. As we sweep the potential to more negative values, the gold nanocores become charged, thus shifting the quasi-Fermi level to a more negative potential. The quantized charging effects studied with organo-capped gold nanoparticles suggest that the potential shift



Scheme 2. Deactivation of excited surface-bound pyrene a) before and b) after charging the gold nanocore.

amounts to about 0.1 V per accumulated electron.^[11] Hence, the electron transfer from excited pyrene molecules to the gold nanocore experiences a barrier as we apply a negative electrochemical bias. Surface binding of pyrene to the gold surface through an amine group leads to a similar enhancement in the fluorescence yield.^[9] Transfer of lone-pair electrons from the amine group to the gold nanocore resulted in the suppression of the intramolecular quenching process between amine and pyrene moieties.

Basic understanding of the photophysical properties of a surface-bound molecule is important to elucidate the charge transfer interactions as well as the microsurroundings near the metal nanocore. The possibility of electrochemically modulating the fluorescence of a fluorophore on a nanostructured gold electrode opens up new avenues to probe interfacial charge transfer processes. These fluorescence modulation studies also demonstrate the possibility of utilizing noble metal–fluorophore nanoassemblies for sensor and display applications.

Experimental Section

The original procedure^[21] for preparing gold colloids in an organic medium was modified. An aqueous solution of hydrogen tetrachloroaurate(III) hydrate (0.023 g, 0.06 mmol in 2 mL) was mixed with a solution of TOAB (0.1366 g, 0.25 mmol) in 5 mL toluene. The biphasic mixture was vigorously stirred until all the tetrachloroaurate was transferred into the organic layer. A solution of sulfanylpuronic acid (5 mg) and (1-pyrenyl)-6-oxaheptanethiol (3 mg) in 1 mL toluene was added to the gold solution (Au/S molar ratio 1:1). (The preparation of the pyrenylthiol was described earlier.^[10]) After stirring for 2–3 min, a solution of sodium tetrahydroborate (0.1 M) in water (2 mL) was added, and the mixture was stirred for 3 h. The organic layer was separated off and concentrated to 2.5 mL in a rotavap. After addition of ethanol (150 mL), the mixture was cooled to 273 K for 12 h and then in ice–salt mixture for 2–3 h to 255 K. The functionalized gold nanoparticles which settled at the bottom of the flask were filtered and washed with ethanol (5 × 250 mL). The dark brown powder composed of nanoparticles 2–3 nm diameter in size was redispersible in toluene and other organic solvent such as THF.

Colloidal TiO₂ was prepared by hydrolyzing titanium(IV) isopropoxide in water containing acetic acid. The OTEs were cut (1 × 5 cm) from a Pilkington TEC glass (glass plate coated with indium tin oxide). The OTE/TiO₂ electrodes were prepared by casting a thin film of colloidal TiO₂ on OTE plates and drying in air. Scanning electron micrographs show an

assembly of TiO₂ particles 20–30 nm diameter in size, that is of highly porous morphology. After annealing at 673 K for 1 h the electrodes were modified with pyrene-functionalized gold nanoparticles by immersing into a THF solution of the nanoparticles overnight. The electrodes were washed thoroughly with THF to remove any unbound gold nanoparticles. These electrodes are referred to as OTE/TiO₂/1.

Absorption spectra were recorded with a Shimadzu 3101 spectrophotometer, transmission electron micrographs (TEM) with a Hitachi H600 transmission electron microscope. For the spectroelectrochemical experiments a Princeton applied research model 175 galvanostat/potentiostat was used, details of which can be found elsewhere.^[22] The fluorescence from the nanostructured gold film was monitored with an SLM S-8000 photon-counting spectrofluorimeter in a front-face geometry. The other components of the cell were a Pt counter electrode, a saturated calomel reference electrode (SCE) and acetonitrile containing 0.1 M tetrabutylammonium perchlorate (TBAP) as electrolyte.

Received: December 27, 2001
Revised: May 6, 2002 [Z18441]

- [1] O. V. Makarova, A. E. Ostafin, H. Miyoshi, J. R. Norris, D. Meisel, *J. Phys. Chem. B* **1999**, *103*, 9080.
- [2] A. C. Templeton, W. P. Wuelfing, R. W. Murray, *Acc. Chem. Res.* **2000**, *33*, 27.
- [3] A. N. Shipway, E. Katz, I. Willner, *PhysChemPhys* **2000**, *1*, 18.
- [4] X. M. Zhao, Y. N. Xia, G. M. Whitesides, *J. Mater. Chem.* **1997**, *7*, 1069.
- [5] J. J. Hickman, D. Ofer, P. E. Laibinis, G. M. Whitesides, M. S. Wrighton, *Science* **1991**, *252*, 688.
- [6] S. Chen, R. S. Ingram, M. J. Hostetler, J. J. Pietron, R. W. Murray, T. G. Schaaff, J. T. Khoury, M. M. Alvarez, R. L. Whetten, *Science* **1998**, *280*, 2098.
- [7] R. Elghanian, J. J. Storhoff, R. C. Mucic, R. L. Letsinger, C. A. Mirkin, *Science* **1997**, *277*, 1078.
- [8] W. P. McConnell, J. P. Novak, L. C. Brousseau III, R. R. Fuierer, R. C. Tenent, D. L. Feldheim, *J. Phys. Chem. B* **2000**, *104*, 8925.
- [9] K. G. Thomas, P. V. Kamat, *J. Am. Chem. Soc.* **2000**, *122*, 2655.
- [10] B. I. Ipe, K. G. Thomas, S. Barazzouk, S. Hotchandani, P. V. Kamat, *J. Phys. Chem. B* **2002**, *106*, 18.
- [11] S. Chen, R. W. Murray, *J. Phys. Chem. B* **1999**, *103*, 9996.
- [12] P. Avouris, B. N. J. Persson, *J. Phys. Chem.* **1984**, *88*, 837.
- [13] K. Saito, *J. Phys. Chem. B* **1999**, *103*, 6579.
- [14] T. Pagnot, D. Barchiesi, G. Tribillon, *Appl. Phys. Lett.* **1999**, *75*, 4207.
- [15] A. C. Templeton, J. J. Pietron, R. W. Murray, P. Mulvaney, *J. Phys. Chem. B* **2000**, *104*, 564.
- [16] P. V. Kamat, M. de Lind, S. Hotchandani, *Isr. J. Chem.* **1993**, *33*, 47.
- [17] D. Lawless, S. Kapoor, D. Meisel, *J. Phys. Chem.* **1995**, *99*, 10329.
- [18] M. Brust, J. Fink, D. Bethell, D. J. Schiffrin, C. Kiely, *J. Chem. Soc. Chem. Commun.* **1995**, 1655.
- [19] The oxidation potential of excited pyrene is around –1.5 V versus NHE, which thermodynamically favors transfer of electrons to gold nanoparticles ($E_F = 0.5$ V).
- [20] V. Subramanian, E. Wolf, P. V. Kamat, *J. Phys. Chem. B* **2001**, *105*, 11439.
- [21] M. Brust, M. Walker, D. Bethell, D. J. Schiffrin, R. Whyman, *J. Chem. Soc. Chem. Commun.* **1994**, 801.
- [22] P. V. Kamat, I. Bedja, S. Hotchandani, L. K. Patterson, *J. Phys. Chem. B* **1996**, *100*, 4900.

Valence-Ordering Structures and Magnetic Behavior of Metallic MMX Chain Compounds**

Minoru Mitsumi,* Kouhei Kitamura, Ayumi Morinaga, Yoshiki Ozawa, Mototada Kobayashi, Koshiro Toriumi,* Yasuhito Iso, Hiroshi Kitagawa, and Tadaoki Mitani

Recently, 1D halogen-bridged mixed-valence dinuclear metal complexes, so-called MMX chain compounds, have attracted significant attention as quasi-1D electronic systems characterized by strong electron–phonon, electron–electron, and magnetic interactions. Only two families of MMX chain compounds, namely $[[A_4[Pt_2(pop)_4X] \cdot nH_2O]_\infty]$ ($pop = P_2O_5H_2^{2-}$, $A = Li, K, Cs, NH_4$, $X = Cl, Br, I$)^[1] and $[[M_2(dta)_4I]_\infty]$ ($dta = CH_3CS_2^-$, $M = Ni, Pt$)^[2] have been reported. These compounds are 1D chain systems based on a mixed-valence dinuclear unit with a formal oxidation number of +2.5 and a metal–metal bond with a formal bond order of 1/2. An important feature of MMX chain compounds is the increase in internal degrees of freedom upon introducing a dinuclear unit in the mixed-valence state. This property enables a variety of electronic structures, represented by the extreme valence-ordering states shown in Figure 1. These valence-ordering structures would be classified based on the periodicity of the 1D chains as follows. The averaged valence (AV) and charge-polarization (CP) states, in which the periodicity of 1D chains is M–M–X–, correspond to a metallic state with an effective half-filled conduction band mainly composed of $M-Md\sigma^* - Xp_z$ -hybridized orbitals or to the Mott–Hubbard semiconducting state. In contrast, the periodicity of 1D chains in the charge density wave (CDW) and alternate charge-polarization (ACP) states is doubled, and these electronic structures are regarded as Peierls and spin-Peierls states,^[3] respectively.

Kitagawa et al. have reported that $[[Pt_2(dta)_4I]_\infty]$ exhibits metallic conducting behavior above 300 K in an AV state.^[2d] On the results of a ¹²⁹I Mössbauer spectroscopic study, the valence-ordering structure of this compound at temperatures

[*] Dr. M. Mitsumi, Prof. Dr. K. Toriumi, K. Kitamura, A. Morinaga, Prof. Dr. Y. Ozawa, Prof. Dr. M. Kobayashi
Department of Material Science
Himeji Institute of Technology
3-2-1 Kouto, Kamigori-cho, Hyogo 678-1297 (Japan)
Fax: (+81) 791-58-0155
E-mail: mitsumi@sci.himeji-tech.ac.jp, toriumi@sci.himeji-tech.ac.jp
Y. Iso, Prof. Dr. H. Kitagawa,^[+] Prof. Dr. T. Mitani
Japan Advanced Institute of Science and Technology
Tatsunokuchi, Ishikawa 923-1292 (Japan)

[+] Current address: Department of Chemistry
University of Tsukuba
Tsukuba 305-8571 (Japan)

[**] This work was supported by a Grants-in-Aids for Scientific Research (10740307 and 09440232) and Priority Areas “Metal-Assembled Complexes” (11136244) from the Ministry of Education, Science, Sports and Culture, Japan. M.M. gratefully appreciates Prof. Dr. N. Sakai for use of the SQUID magnetometer. M = metal center, X = halogen.



Supporting information for this article is available on the WWW under <http://www.angewandte.org> or from the author.

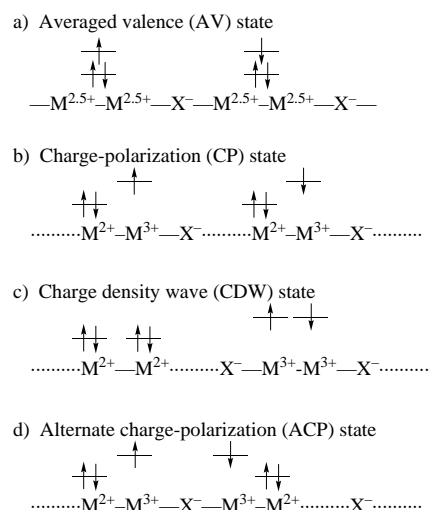


Figure 1. Schematic representation of electronic and lattice structures of the MMX chain compound, where the electrons occupy the Md_{z^2} orbitals.

below 80 K was concluded to be an ACP state. However, no loss in the spin degree of freedom for this system has yet been observed. Recently, we studied the crystal structure and solid-state properties of $[(Pt_2(EtCS_2)_4I)_\infty]$, and revealed a metal–semiconductor (M–S) transition at $T_{M-S}=205$ K, above which the remarkable thermal vibration of a bridging iodine atom in the AV state was observed.^[4] This compound shows diffuse scattering corresponding to a twofold repetition length of the Pt–Pt–I– unit above T_{M-S} . Diffuse scattering begins to convert into superlattice reflections below 140 K. These superlattice reflections are considered to have originated from a CDW or ACP state. The spin degree of freedom, however, persisted down to 2 K.

We report the structural phase-transition, valence-ordering structure and magnetic properties of a new metallic MMX chain compound, $[(Pt_2(nBuCS_2)_4I)_\infty]$ (**1**), as well as its transport properties and an efficient chemical synthesis. This compound clearly exhibits an abrupt drop in the magnetic susceptibility, similar to the spin-Peierls transition, accompanying a first-order phase transition at about 210 K. We have also performed a crystal structure analysis of $[(Pt_2(EtCS_2)_4I)_\infty]$ (**2**) at 48 K which included superlattice reflections to determine its valence-ordering structure in the low-temperature phase. This work has clarified the correlation between the crystal structures and magnetic properties of **1** and **2**.

Black needle crystals of **1** were grown by the slow cooling of a toluene–*n*-hexane solution of equimolar amounts of $[Pt_2(nBuCS_2)_4]$ and $[Pt_2(nBuCS_2)_4I_2]$.^[5]

Differential scanning calorimetry (DSC) measurements of **1** were carried out in the temperature range of 153–443 K. Two peaks of latent heat corresponding to the first-order phase transition were observed in the temperature ranges of 204–212 K and 318–323 K, which revealed the existence of three phases, the low-temperature (LT), room-temperature (RT), and high-temperature (HT) phases.

Compound **1** exhibits relatively high electrical conductivity ($17\text{--}83\text{ Scm}^{-1}$) at room temperature, comparable to the conductivity of $[(Pt_2(dta)_4I)_\infty]$ (ca. 13 Scm^{-1})^[2d] and **2** ($5\text{--}30\text{ Scm}^{-1}$).^[4] The temperature dependence of electrical resis-

tivity ρ , indicates metallic conduction in the HT phase above the transition temperature, $T_{M-S}=325$ K. The LT and RT phases show semiconducting behavior with activation energies of 134 and 255 meV, respectively. The thermoelectric power S , was also measured in the temperature range of 200–400 K. The HT phase shows almost temperature-independent behavior of S ($-10\text{ }\mu\text{V K}^{-1}$), which indicates the existence of a half-filled metallic band.^[6] Below $T_{M-S}=325$ K, S slightly decreases with decreasing temperature, and reaches a minimum value of $-16\text{ }\mu\text{V K}^{-1}$ near 270 K and then, as is characteristic of semiconductors, increases. Furthermore, ρ and S exhibit sharp increases at around 210 K.

ORTEP diagrams of **1** in the RT and LT phases are shown in Figure 2. Compound **1** undergoes a first-order phase-transi-

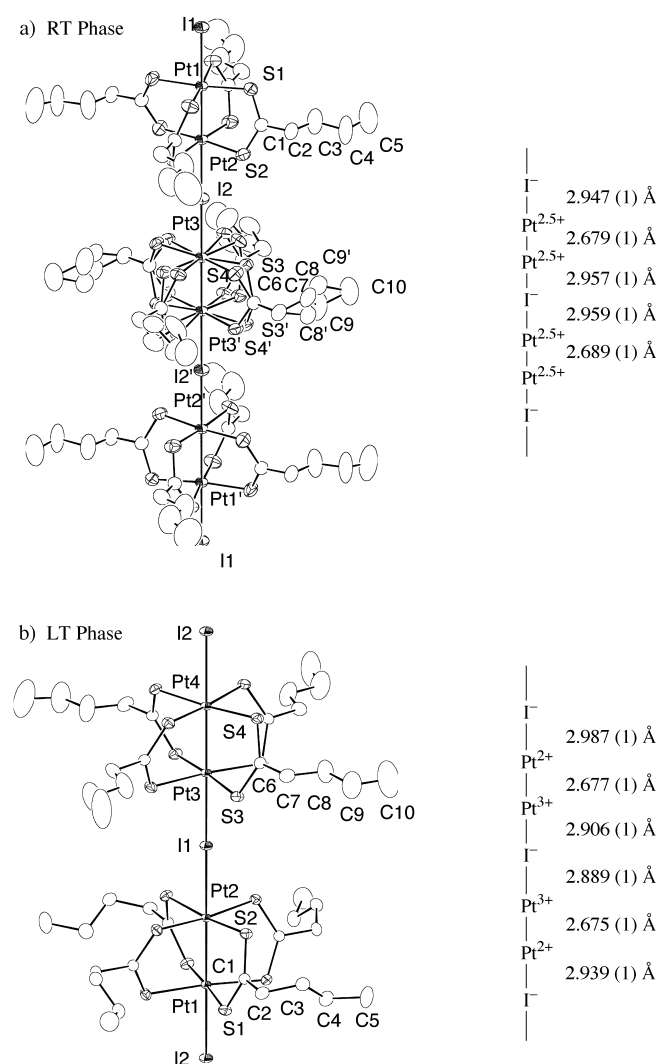


Figure 2. ORTEP diagrams (thermal ellipsoids set at the 50% probability level) and relevant interatomic distances of **1**: a) RT phase (298 K), b) LT phase (167 K).

tion at 204–212 K, where the space group changes from $I4/m$ in the RT phase to $P4/n$ in the LT phase. In both phases, the crystal consists of a neutral 1D chain with a Pt–Pt–I– repeating unit lying on the crystallographic fourfold axis parallel to the *c* axis. The periodicity of the crystal lattice in the 1D chain

direction, however, changes from threefold with a Pt–Pt–I-period in the RT phase to twofold in the LT phase. In the RT phase, all the iodine atoms are located near the midpoint between two diplatinum units and the three crystallographically independent Pt–I bonds are nearly equivalent (2.947 (1), 2.957 (1), and 2.959 (1) Å). Generally, a Pt²⁺–I[−] separation is greater than a Pt³⁺–I[−] separation as the d_{z²} orbital of a Pt²⁺ site is occupied by a pair of electrons. Therefore, the difference between Pt–I bonds enables us to determine the valence state of Pt atoms. The observed Pt–I bonds indicate a valence-ordering structure close to the AV state. The shortest interchain S⋯S distance is S2⋯S2 (1/2 − x, 1/2 − y, 1/2 − z) = 5.121(4) Å, which indicates the absence of interchain S⋯S contacts. In the LT phase, however, there are two Pt–I groups. The shortest Pt–I bonds (2.889(1), 2.906(1) Å) are about 0.07 Å shorter than the longest Pt–I bonds (2.939(1), 2.987(1) Å), though the two Pt–Pt bonds are equivalent (2.675(1) and 2.677(1) Å). As judged by Pt–Pt and Pt–I bonds, the valence-ordering structure in the LT phase can be regarded as an ACP state.

To clarify which valence-ordering structure can be adopted in the ground state of **2**, crystal-structure analysis at 48 K was preformed, which included superlattice reflections (Figure 3). When superlattice reflections are included the space group

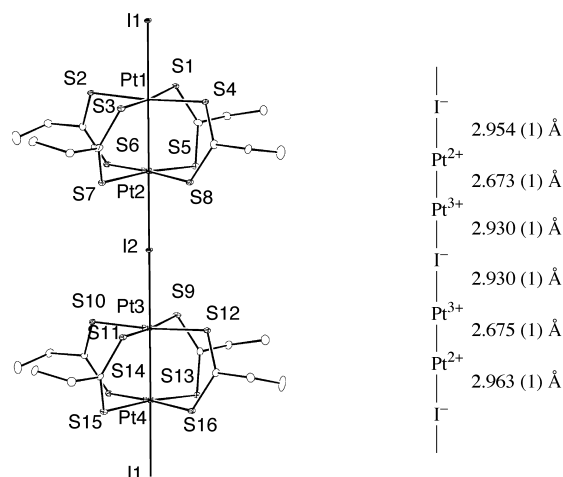


Figure 3. ORTEP diagram (thermal ellipsoids set at the 50% probability level) and relevant interatomic distances of **2** at 48 K.

changes from *C*2/*c* to *P*1̄. Periodicity along the 1D chain direction is a twofold Pt–Pt–I- period. Though the two Pt–Pt bonds are equivalent (2.673(1), 2.675(1) Å), the shortest Pt–I distances (2.930(1), 2.930(1) Å) are about 0.02–0.03 Å smaller than the longest Pt–I bonds (2.954(1), 2.963(1) Å). Judging from the Pt–Pt and Pt–I bonds, the valence-ordering structure of **2** at low temperature can be concluded to be an ACP state, similar to the structure of **1** in the LT phase. These valence-ordering structures are consistent with theoretical predictions by Borshch et al. based on semiempirical quantum-chemical band calculations.^[7]

The temperature dependence of the magnetic susceptibility χ_M , of crystalline samples of **1** was measured in the temperature range of 5–350 K under a magnetic field *H* of

1 T. Results are shown in Figure 4, along with those for **2**.^[4] The χ_M of **1** in the RT phase is on the order of 2.9×10^{-5} emu mol^{−1}, which is in accordance with results from EPR measurements (ca. 2×10^{-5} emu mol^{−1}).^[8] This value is

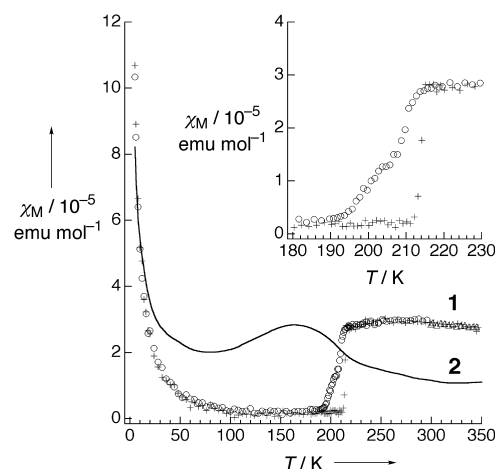


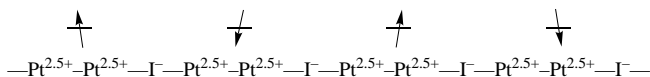
Figure 4. Temperature dependence of the χ_M of **1**: ○ 1st cooling, + 1st heating, △ 2nd cooling (inset expansion between 180 and 230 K); — magnetic susceptibility of **2**.^[4]

smaller by approximately one or two orders of magnitude than those of typical 1D antiferromagnetic spin systems with $S = 1/2$,^[9] which indicates that antiferromagnetic coupling between unpaired electrons on the Pt³⁺ sites is very large. The tail, observed in the χ_M versus *T* plot below around 30 K, may arise from paramagnetic centers originating from impurities and/or lattice defects. The estimated Curie spin concentration is 0.14%. The most striking feature is an abrupt drop in the χ_M of **1** to the spin-singlet state, with hysteresis, around the first-order phase transition.^[10] The electrical and magnetic transitions observed in **1** are similar to *N*-methyl-*N*-ethyl-morpholinium bis-7,7,8,8-tetracyano-*p*-quinodimethanide [MEM(TCNQ)₂], which shows two phase transitions, a metal-semiconductor transition at 335 K and a spin-Peierls transition at 19 K.^[3] The abrupt drop of χ_M in **1** is quite similar to spin-Peierls transitions. The observed magnetic behavior of **1**, however, seems to be well described not by the spin-Peierls transition, but by the regular electronic Peierls transition. This situation is suggested as the transition is first order in nature, the transition temperature is very high, and sharp increases in ρ and *S* are observed at the transition. The origin of lattice distortion is attributable to electron–phonon interactions.

χ_M of **2** is of the order of $1–3 \times 10^{-5}$ emu mol^{−1} in the temperature range of 50–350 K (Figure 4).^[4] Although the AV to ACP phase transition was observed around $T_{M-S} = 205$ K, an abrupt drop in χ_M has not been observed for **2**, which indicates that the spin degree of freedom persists down to 2 K, similar to [Pt₂(dta)₄I]_∞.^[12d] This quite remarkable difference in the magnetic behaviors of **1** and **2** is attributed to the degree of lattice distortion in the 1D MMX chains, as shown in Figure 5. X-ray crystal structure analyses revealed that differences between Pt³⁺–I[−] and Pt²⁺–I[−] bonds of **1** (ca. 0.07 Å) are remarkably larger than those for **2** (0.02–0.03 Å).

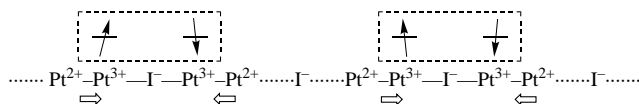
Dynamic valence-ordering state (metallic or semiconductive)

a) one-dimensional antiferromagnetic ordering



Static valence-ordering state (semiconductive)

b) one-dimensional antiferromagnetic ordering



c) spin singlet

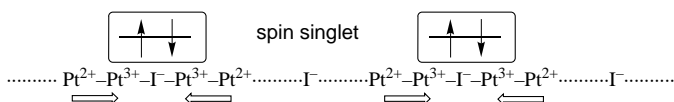


Figure 5. Schematic representation of the valence-ordering and spin states of $[\text{Pt}_2(\text{RCS}_2)_4]_\infty$ ($\text{R} = n\text{Bu}$ (**1**) and Et (**2**)). a) high- and room-temperature phases of **1**, and **2** at room temperature; b) low-temperature phase of **2**; c) low-temperature phase of **1**.

As these distance differences correspond to the lattice distortion of a 1D MMX chain, it is reasonable to consider that the alternation of an exchange interaction in **1** increases with an increase in lattice distortion, resulting in the spin-singlet state of the low-temperature ACP state.

Experimental Section

1: The compounds $[\text{Pt}_2(n\text{BuCS}_2)_4]$ (41 mg, 0.044 mmol) and $[\text{Pt}_2(n\text{BuCS}_2)_4\text{I}_2]$ (52 mg, 0.044 mmol) were dissolved in toluene (3 mL) at 70 °C and then *n*-hexane (4 mL) was added.^[5] After being slowly cooled to 2 °C, black needles separated from the solution and were collected by suction filtration and washed with acetone: yield 78 mg (84 %). Elemental analysis (%) calcd for $\text{C}_{20}\text{H}_{36}\text{IPt}_2\text{S}_8$: C 22.88, H 3.46; found: C 22.91, H 3.46; UV/Vis/NIR (KBr): $\lambda_{\text{max}} = 1110, 560, 403, 304 \text{ nm}$.

X-ray crystallography for **1** and **2**: Data for **1** were collected at 298 and 167 K on an Enraf Nonius CAD4 diffractometer with graphite-monochromated MoK_α radiation ($\lambda = 0.71069 \text{ \AA}$). A numerical absorption correction was applied to all intensity data. The structures were solved by direct methods (SIR92)^[11a] and refined by full-matrix least-squares on F^2 (SHELXL-97).^[11b] All calculations were performed with the teXsan crystallographic software package.^[11c] Crystal data for **1** at 298 K: $\text{C}_{20}\text{H}_{36}\text{IPt}_2\text{S}_8$, $M_r = 1050.07$, black needle, $0.26 \times 0.13 \times 0.12 \text{ mm}$, tetragonal, space group $I4/m$, $a = 13.525(1)$, $c = 25.773(2) \text{ \AA}$, $V = 4714.4(4) \text{ \AA}^3$, $Z = 6$, $\rho_{\text{calcd}} = 2.219 \text{ g cm}^{-3}$, $F(000) = 2958$, $\mu(\text{MoK}_\alpha) = 10.380 \text{ mm}^{-1}$, $2\theta_{\text{max}} = 59.9^\circ$. 7272 reflections were measured, of which 3512 were unique ($R_{\text{int}} = 0.0274$). All non-hydrogen atoms were refined anisotropically. The ligand moiety (S3, S4, C7, and C8) of one of the three diplatinum units in the RT phase is disordered on the mirror plane that is perpendicular to the 1D chain and passes through the midpoint of the Pt3 and Pt3' atoms. $wR2 = 0.1177$, $S = 1.035$ (all data), $R1(1710 \text{ reflections with } I > 2\sigma(I)) = 0.0344$, 132 parameters, min./max. residual electron density $-3.70/0.79 \text{ e \AA}^{-3}$, min./max. transmission $0.2577/0.3376$. **1** at 167 K: $\text{C}_{20}\text{H}_{36}\text{IPt}_2\text{S}_8$, $M_r = 1050.07$, black needle, $0.19 \times 0.14 \times 0.13 \text{ mm}$, tetragonal, space group $P4/n$, $a = 13.419(5)$, $c = 17.072(10) \text{ \AA}$, $V = 3074(2) \text{ \AA}^3$, $Z = 4$, $\rho_{\text{calcd}} = 2.268 \text{ g cm}^{-3}$, $F(000) = 1972$, $\mu(\text{MoK}_\alpha) = 10.612 \text{ mm}^{-1}$, $2\theta_{\text{max}} = 60.0^\circ$. 4992 reflections were measured, of which 4501 were unique ($R_{\text{int}} = 0.046$). All non-hydrogen atoms were

refined anisotropically while all hydrogen atoms were placed at their idealized positions. $wR2 = 0.0907$, $S = 1.057$ (all data), $R1(3209 \text{ reflections with } I > 2\sigma(I)) = 0.0324$, 145 parameters, min./max. residual electron density $-3.36/1.20 \text{ e \AA}^{-3}$, min./max. transmission $0.2482/0.3224$.

Crystal data for **2**: $\text{C}_{12}\text{H}_{20}\text{IPt}_2\text{S}_8$, $M_r = 937.88$, black plate, $0.20 \times 0.12 \times 0.07 \text{ mm}$, triclinic, space group $P\bar{1}$, $a = 9.652(1)$, $b = 15.481(1)$, $c = 15.685(1) \text{ \AA}$, $\alpha = 98.972(2)$, $\beta = 103.516(2)$, $\gamma = 97.610(3)^\circ$, $V = 2215.8(3) \text{ \AA}^3$, $Z = 4$, $\rho_{\text{calcd}} = 2.811 \text{ g cm}^{-3}$, $F(000) = 1716$, $\mu(0.5609 \text{ \AA}) = 7.97 \text{ mm}^{-1}$, $2\theta_{\text{max}} = 60.0^\circ$. Data were collected at 48 K under vacuum ($5.5 \times 10^{-4} \text{ Pa}$) using synchrotron radiation (22.10 keV, $\lambda = 0.5609 \text{ \AA}$) and the MAC Science low-temperature vacuum X-ray camera equipped with an imaging plate (IP) area detector at the BL02B1 beamline of the SPring-8 facility. The frames were indexed and the reflections integrated using DENZO and subsequently scaled using SCALEPACK.^[12] 20594 unique reflections were measured ($R_{\text{int}} = 0.065$). The structure was solved by direct methods (SIR97)^[11d] and refined by full-matrix least-squares on F^2 (SHELXL-97).^[11b] All calculations were performed with the teXsan crystallographic software package.^[11c] $wR2 = 0.1837$, $S = 1.033$ (all data), $R1(11901 \text{ reflections with } I > 2\sigma(I)) = 0.0537$, 415 parameters, min./max. residual electron density $-6.780/6.919 \text{ e \AA}^{-3}$ (peaks are in the vicinity of a Pt1 position). All non-hydrogen atoms were refined anisotropically while all hydrogen atoms were placed at their idealized positions. Crystallographic data (excluding structure factors) for the structures reported in this paper have been deposited with the Cambridge Crystallographic Data Centre as supplementary publication nos. CCDC-177479–177481 contains the supplementary crystallographic data for this paper. These data can be obtained free of charge via www.ccdc.cam.ac.uk/conts/retrieving.html (or from the Cambridge Crystallographic Data Centre, 12, Union Road, Cambridge CB2 1EZ, UK; fax: (+44) 1223-336-033; or deposit@ccdc.cam.ac.uk).

Magnetic susceptibility data of **1** was measured using a Quantum Design MPMS-5SH SQUID magnetometer. Correction for core diamagnetism was made using half the sum of the observed diamagnetism for $[\text{Pt}_2(n\text{BuCS}_2)_4]$ and $[\text{Pt}_2(n\text{BuCS}_2)_4\text{I}_2]$. DC electrical conductivity measurements of **1** were made on several single crystals using a four-probe technique. The thermoelectric power was measured through a dynamic differential method using two sets of Au(Fe)-chromel thermocouples ($76 \mu\text{m} \varnothing$).

Received: January 17, 2002

Revised: March 19, 2002 [Z18539]

- [1] a) C.-M. Che, F. H. Herstein, W. P. Schaefer, R. E. Marsh, H. B. Gray, *J. Am. Chem. Soc.* **1983**, *105*, 4604–4607; b) M. Kurmoo, R. J. H. Clark, *Inorg. Chem.* **1985**, *24*, 4420–4425; c) R. J. H. Clark, M. Kurmoo, H. M. Dawes, M. B. Hursthouse, *Inorg. Chem.* **1986**, *25*, 409–412; d) L. G. Butler, M. H. Zietlow, C.-M. Che, W. P. Schaefer, S. Sridhar, P. J. Grunthaner, B. I. Swanson, R. J. H. Clark, H. B. Gray, *J. Am. Chem. Soc.* **1988**, *110*, 1155–1162; e) B. I. Swanson, M. A. Stroud, S. D. Conradson, M. H. Zietlow, *Solid State Commun.* **1988**, *65*, 1405–1409; f) M. A. Stroud, H. G. Drickamer, M. H. Zietlow, H. B. Gray, B. I. Swanson, *J. Am. Chem. Soc.* **1989**, *111*, 66–72; g) M. Yamashita, S. Miya, T. Kawashima, T. Manabe, T. Sonoyama, H. Kitagawa, T. Mitani, H. Okamoto, R. Ikeda, *J. Am. Chem. Soc.* **1999**, *121*, 2321–2322.
- [2] a) C. Bellitto, A. Flamini, L. Gastaldi, L. Scaramuzza, *Inorg. Chem.* **1983**, *22*, 444–449; b) C. Bellitto, G. Dessy, V. Fares, *Inorg. Chem.* **1985**, *24*, 2815–2820; c) M. Yamashita, Y. Wada, K. Toriumi, T. Mitani, *Mol. Cryst. Liq. Cryst.* **1992**, *216*, 207–212; d) H. Kitagawa, N. Onodera, T. Sonoyama, M. Yamamoto, T. Fukawa, T. Mitani, M. Seto, Y. Maeda, *J. Am. Chem. Soc.* **1999**, *121*, 10068–10080.
- [3] a) J. W. Bray, L. V. Interrante, I. S. Jacobs, J. C. Bonner in *Extended Linear Chain Compounds*, Vol. 3 (Ed.: J. S. Miller), Plenum, New York, **1983**, pp. 353–415, and references therein; b) M. Kurmoo, M. A. Green, P. Day, C. Bellitto, G. Staulo, F. L. Pratt, W. Hayes, *Synth. Met.* **1993**, *55–57*, 2380–2385.
- [4] M. Mitsumi, T. Murase, H. Kishida, T. Yoshinari, Y. Ozawa, K. Toriumi, T. Sonoyama, H. Kitagawa, T. Mitani, *J. Am. Chem. Soc.* **2001**, *123*, 11179–11192.

- [5] $[\text{Pt}_2(\text{nBuCS}_2)_4]$ and $[\text{Pt}_2(\text{nBuCS}_2)_4\text{I}_2]$ were prepared by the similar procedures with literature methods using toluene and *n*-hexane.^[4]
- [6] P. M. Chaikin, R. L. Greene, S. Etamad, E. Engler, *Phys. Rev. B* **1976**, *13*, 1627–1632.
- [7] S. A. Borshch, K. Prassides, V. Robert, A. O. Solonenko, *J. Chem. Phys.* **1998**, *109*, 4562–4568.
- [8] H. Tanaka, K. Marumoto, S. Kuroda, M. Mitsumi, K. Toriumi, unpublished results.
- [9] O. Kahn, *Molecular Magnetism*, VCH, New York, **1993**, pp. 251–286.
- [10] Field dependence of χ_M of **1** was also measured near the phase-transition temperature under the magnetic field of $H = 1\text{--}5\text{ T}$. No variation was observed up to 5 T.
- [11] a) A. Altomare, G. Casciarano, C. Giacovazzo, A. Guagliardi, M. C. Burla, G. Polidori, M. Camalli, *J. Appl. Crystallogr.* **1994**, *27*, 435 (SIR92); b) G. M. Sheldrick, SHELXL-97, University of Göttingen, Göttingen (Germany), **1997**; c) Crystal Structure Analysis Package, Molecular Structure Corporation, **1985**, **1999**; d) A. Altomare, M. C. Burla, M. Camalli, G. L. Casciarano, C. Giacovazzo, A. Guagliardi, A. G. G. Moliterni, G. Polidori, R. Spagna, *J. Appl. Crystallogr.* **1999**, *32*, 115–119 (SIR97).
- [12] Z. Otwinowski, W. Minor, *Methods Enzymol.* **1997**, *276*, 307–326.

Highly Selective Transport of Organic Compounds by Using Supported Liquid Membranes Based on Ionic Liquids**

Luís C. Branco, João G. Crespo, and Carlos A. M. Afonso*

The selective separation of organic compounds is a critical issue in the chemical industry. In case of readily crystallized molecules, selective crystallization is the most practical method for selective separation, whereas for solutes that are liquid at room temperature, separation by fractional distillation, solvent extraction, or chromatographic methods are more convenient. Some of the above-mentioned methods are technically demanding, involve considerable energy costs, and/or result in large amounts of waste solvents. Membranes, defined as permeable and selective barriers between two phases, have been successfully applied in a large diversity of separation processes, including bioseparations, in which classical separation methods are less convenient, undesirable or even not applicable. The reason for the successful use of membrane-based separation processes stems from the fact

that these processes have a high energy efficiency, can be used under moderate temperature and pressure conditions, do not require any additional separating agents or adjuvants, and therefore they are regarded as environmentally friendly.^[1] Solute extraction and recovery by using supported liquid membranes is recognized as one of the most promising membrane-based processes. In a supported liquid-membrane system, a defined solvent or solvent/carrier solution is immobilized inside the porous structure of a polymeric or ceramic membrane, which separates the feed phase (in which the solutes of interest are solubilized) from the receiving phase (in which these solutes will be transferred and, eventually, concentrated). This configuration has attracted a great deal of interest because the amount of solvent/carrier needed is minimal, the solvent/carrier is continuously regenerated as a result of solute transport to the receiving phase, and loss of the solvent/carrier phase is negligible if an appropriate supported liquid membrane is designed.^[2] The use of a room-temperature ionic liquid (RTIL) as an immobilized phase in the supporting membrane between two organic phases in the feed and the receiving compartments is particularly interesting owing to the nonvolatile character of RTILs and their solubility in the surrounding phases, which allows very stable supported liquid membranes to be obtained without any observable loss of the RTIL to the atmosphere or the contacting phases. Herein we show the potential for continuous separation of organic compounds based on the selective transport through supported liquid membranes that contain RTILs.

RTILs that involve a 1,3-dialkylimidazolium cation are attracting increasing interest as new media, mainly because of the advantage of being nonvolatile. Depending on the anion and on the alkyl group of the imidazolium cation, the RTIL can solubilize supercritical CO_2 (scCO_2), a large range of polar and nonpolar organic compounds, and also transition-metal complexes. Simultaneously, they have low miscibility with water, alkanes, and dialkyl ethers^[3] and are insoluble in scCO_2 .^[4] As a result of these properties, they are emerging as an alternative recyclable, environmentally benign, reaction medium for chemical transformations, including transition-metal catalysis^[3] and biocatalysis.^[3f, 5] Their use has also been successfully extended as a potential stationary phase for gas chromatography,^[6] in pervaporation,^[7] and for the substitution of traditional organic solvents (OS) in aqueous–OS^[7a, 8] and OS– scCO_2 biphasic extractions.^[4, 9] It is assumed that the 1,3-dialkylimidazolium RTIL are not a statistical aggregate of anions and cations, but instead a more organized structure that contains polar and nonpolar regions as a result of the formation of weak interactions, mainly as hydrogen bonds, with 2-H of the imidazolium ring.^[10] The above information prompted us to study the potential of using RTIL in supported liquid membranes for selective separation processes.

To illustrate the concept, and as a result of transport studies with representative organic functional compounds, we used a mixture of the organic isomeric amines hexylamine, diisopropylamine, and triethylamine (1:1:1 molar ratio) in diethyl ether in side A of the cell (Figure 1). The two sides of the cell were separated by the RTIL 1-*n*-butyl-3-methylimidazolium hexafluorophosphate ($[\text{bmim}][\text{PF}_6]$) immobilized in the por-

[*] Prof. C. A. M. Afonso, L. C. Branco, Prof. J. G. Crespo
Departamento de Química, Centro de Química Fina e Biotecnologia
Faculdade de Ciências e Tecnologia, Universidade Nova de Lisboa
2829-516 Caparica (Portugal)
Fax: (+351) 21-294-8550
E-mail: cma@dq.fct.unl.pt

[**] This work was supported by the European Commission (contract QLK3-CT-1999-01213) and the Fundação para a Ciência e Tecnologia (project PRAXIS/C/QUI/10069/98). We also acknowledge Raquel Fortunato for the technical support with the membranes and for helpful discussions.

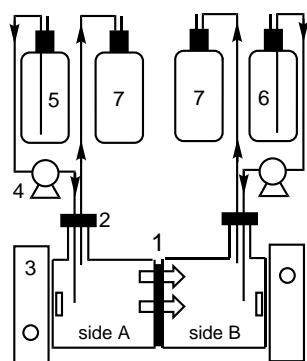


Figure 1. Scheme of the cell used in batch (without pumps) and continuous systems: volume of each side of the cell = 30 mL; 1) supported liquid membrane ($A = 8.5 \text{ cm}^2$); 2) septa (without pumps) or connection to the pumps; 3) magnetic stirrer; 4) pumps; 5) feed solution containing the solutes; 6) receiving solution containing fresh solvent; 7) collection bottle.

ous structure of a polyvinylidene fluoride (PVDF) hydrophilic membrane. Diethyl ether was used as the receiving phase in compartment B. The transport of the primary, secondary, and tertiary amines to compartment B was then monitored (Figure 2).

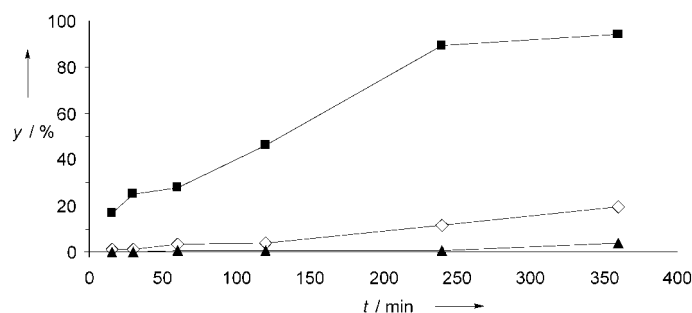


Figure 2. Percentage of recovery of each amine in compartment B of the cell, for batch operation. \diamond hexylamine; \blacksquare diisopropylamine (DIIPA); \blacktriangle triethylamine (TEA).

We observed a stronger selectivity for diisopropylamine transport than for hexylamine and triethylamine. We also observed by ^1H NMR spectroscopic analysis that the addition of diisopropylamine to neat $[\text{bmim}][\text{PF}_6]$ promotes a larger shift of the peaks for the 1-*n*-butyl-3-methylimidazolium cation than of those for triethylamine, which suggests that the high transport selectivity arises from the higher affinity of the secondary amine for $[\text{bmim}][\text{PF}_6]$. This affinity probably arises from the combination of the higher basicity of DIIPA than that of TEA and the steric hindrance of TEA on approach to the $[\text{bmim}]$ cation. Diffusivity does not play a major role in the selective transport of these amines because they have the same molecular weight and their different geometry and dipolar moment cannot explain such large differences in their selective transport through the RTIL supported liquid membrane.

As a result of this batch experiment, we turned our attention to the possibility of performing continuous separations. To illustrate the potential of this approach, we tested a

mixture of DIIPA (b.p. = 84°C) and TEA (b.p. = 89°C) as a separation case study of secondary and tertiary amines with similar boiling points. The cell presented in Figure 1 was used by circulating an equimolar mixture of DIIPA and TEA in diethyl ether in side A and fresh diethyl ether in side B. Figure 3 presents the observed transport selectivities at the

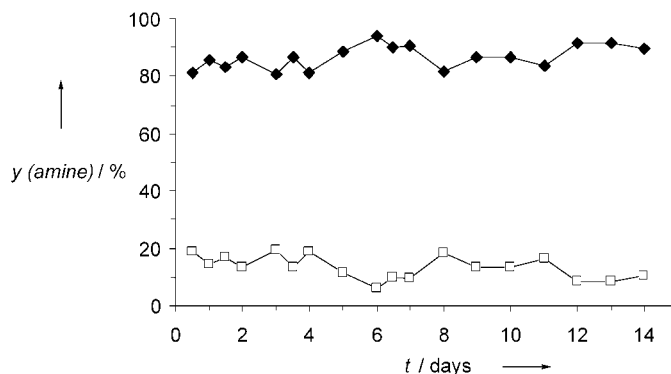


Figure 3. Relative percentage of each amine in the receiving stream obtained for eighteen collecting samples (12-h period), determined by GLC during 14 days of continuous operation. \blacklozenge diisopropylamine; \square triethylamine.

outlet of compartment B during 14 days of continuous operation. The observed DIIPA/TEA ratios in the collected samples were higher than 80:20 under optimized conditions, and a moderate decrease was only observed for the periods during which undesired variations of the flow rates occurred. Importantly, the transport selectivity did not decrease during the entire extended period of operation, which confirms the stable character of the supported liquid membrane system. The stability of the $[\text{bmim}][\text{PF}_6]$ -supported membrane suggests that longer continuous operation periods are feasible. The overall percentage of recovery (based on the 14 days of continuous operation) was 84.7% for DIIPA and 14.9% for TEA. Notably, the mass flux of DIIPA was 1070.6 g of DIIPA/(m^2 of membrane hour), which can be considered an excellent transport rate. Interestingly, the total amount of $[\text{bmim}][\text{PF}_6]$ used in the supported liquid membrane was only 202 g of $[\text{bmim}][\text{PF}_6]$ /(m^2 of membrane). As the solutes transported through the supported liquid membrane are continuously recovered in the receiving solution, the RTIL used is regenerated and may be effective for prolonged operation. To the best of our knowledge, there are no other supported liquid membranes that are able to separate these organic compounds. The system presented herein is particularly interesting because it involves the use of a supported liquid membrane with a high operating stability and an excellent selectivity for the recovery of the target compound.

The model system presented herein illustrates the potential for the continuous highly selective separation of mixtures of isomeric organic compounds that are structurally similar and have close boiling points by using the RTIL $[\text{bmim}][\text{PF}_6]$ in a supported liquid membrane. This separation process is feasible under simple technical conditions, and proved to be stable even during long periods of operation. This method

seems particularly appealing for large-scale operations and for different substrates; with the emergence of a considerable number of new RTILs,^[3, 11] it should be possible to design RTILs with high selectivity for specific substrates. The possibility of using nonpolar solvents with high boiling points or water instead of diethyl ether, and supported RTIL in hollow-fiber membranes will allow this technology to reinforce its environmentally benign character and become attractive for industrial application.

Experimental Section

For the batch studies, the cell indicated in Figure 1 was used without pumps. The ionic liquid 1-*n*-butyl-3-methylimidazolium hexafluorophosphate ([bmim][PF₆]) was immobilized in the porous structure of a polyvinylidene fluoride (PVDF) hydrophilic membrane (Gelman Sciences, FP Vericel, pore size 0.45 µm) by filtration in vacuo and placed in a metallic net (i.d. 1.65 cm) located between side A (*V* = 30 mL) and side B (*V* = 30 mL) of the cell. The amines (1:1:1 molar mixture) hexylamine (470 µL), DIIPA, (500 µL) and TEA (500 µL), and *n*-decane (400 µL; internal standard) in diethyl ether (30 mL) were added to side A of the cell. *n*-Decane (400 µL; internal standard) was added to diethyl ether (30 mL) in side B of the cell. The transport of amines to side B at room temperature was monitored by GLC by taking samples from side A and B of the cell at defined time intervals (15, 30, 60, 120, 240, 360 min). The recovery of each amine was determined by comparison of the areas of the peaks of each amine with those of *n*-decane and relative to the areas initially observed in side A.

For continuous operation conditions, the cell indicated in the Figure 1 was used, with each side of the cell connected to a piston pump (FMI lab pump, model QSY) to promote the circulation in each side. The RTIL [bmim][PF₆] was immobilized as indicated above. The amines (1:1 molar mixture) DIIPA (100 mL) and TEA (100 mL) in diethyl ether (5 L) were circulated with a flow rate of 1 mL/min in side A of the cell. Diethyl ether (5 L) was circulated with a flow rate of 1 mL min⁻¹ in side B of the cell. Both solutions were renewed every 2 days. The transport of each amine to side B was monitored by sequentially collecting samples from the outlet tube of side B every 12 h. During the 14 days of continuous operation, 23 samples were collected with a total volume of 20410 mL. The DIIPA/TEA ratio was determined for each sample by GLC. Eighteen samples (15460 mL) were fractionally distilled to afford a mixture of DIIPA/TEA (250 mL; 89.2:10.8, determined by GLC); ¹H and ¹³C NMR spectral data were identical to those of authentic samples. The distilled diethyl ether fraction and the remaining six samples contained a mixture of DIIPA/TEA (142.2 mL (81.6:18.4) and 105.7 mL (80.9:19.1), respectively, ratio determined by GLC analysis with *n*-decane as internal standard).

Received: January 25, 2002 [Z18583]

- [6] a) D. W. Armstrong, L. He, Y.-S. Liu, *Anal. Chem.* **1999**, *71*, 3873–3876; b) A. Heintz, D. V. Kulikov, S. P. Verevkin, *J. Chem. Eng. Data* **2001**, *46*, 1526–1529; c) R. D. Rogers, A. E. Visser, H. James, C. Koval, D. L. DuBoix, P. Scovazzo, R. D. Noble, *Abstract of Papers, 223rd ACS National Meeting, Orlando, USA, April 7–11, 2002*.
- [7] a) A. G. Fadeev, M. M. Meagher, *Chem. Commun.* **2001**, 295–296; b) T. Schäfer, C. M. Rodrigues, C. A. M. Afonso, J. G. Crespo, *Chem. Commun.* **2001**, 1622–1623.
- [8] a) J. G. Huddleston, H. D. Willauer, R. P. Swatloski, A. E. Visser, R. D. Rogers, *Chem. Commun.* **1998**, 1765–1766; b) S. G. Cull, J. D. Holbrey, V. Vargas-Mora, K. R. Seddon, G. J. Lye, *Biotechnol. and Bioeng.* **2000**, *69*, 227–233; c) A. E. Visser, R. P. Swatloski, W. M. Reichert, S. T. Griffin, R. D. Rogers, *Ind. Eng. Chem. Res.* **2000**, *39*, 3596–3604; d) A. E. Visser, R. P. Swatloski, W. M. Reichert, R. Mayton, S. Sheff, A. Wierzbicki, J. H. Davies, R. D. Rogers, *Chem. Commun.* **2001**, 135–136.
- [9] a) R. A. Brown, P. Pollet, E. McKoon, C. A. Eckert, C. L. Liotta, P. G. Jessop, *J. Am. Chem. Soc.* **2001**, *123*, 1254–1255; b) M. F. Sellin, P. B. Webb, D. J. Cole-Hamilton, *Chem. Commun.* **2001**, 781–782; c) L. A. Blanchard, J. F. Brennecke, *Ind. Eng. Chem. Res.* **2001**, *40*, 287–292; d) F. Liu, M. B. Abrams, R. T. Baker, W. Tumas, *Chem. Commun.* **2001**, 433–434; e) A. Bösmann, G. Franciò, E. Janssen, M. Solinas, W. Leitner, P. Wasserscheid, *Angew. Chem.* **2001**, *113*, 2769–2771; *Angew. Chem. Int. Ed.* **2001**, *40*, 2697–2699.
- [10] P. Bonhôte, A.-P. Dias, N. Papageorgiou, K. Kalyanasundaram, M. Grätzel, *Inorg. Chem.* **1996**, *35*, 1168–1178.
- [11] a) J. D. Holbrey, K. R. Seddon, *J. Chem. Soc. Dalton Trans.* **1999**, *13*, 2133–2139; b) A. S. Larsen, J. D. Holbrey, F. S. Tham, C. A. Reed, *J. Am. Chem. Soc.* **2000**, *122*, 7264–7272; c) J. G. Huddleston, A. E. Visser, W. M. Reichert, H. D. Willauer, G. A. Broker, R. D. Rogers, *Green Chem.* **2001**, *3*, 156–164; d) J. Pernak, A. Czepukowicz, R. Pozniak, *Ind. Eng. Chem. Res.* **2001**, *40*, 2379–2383.

Lewis Acid Controlled Regioselective 1,2 and 1,4 Reaction of α,β -Unsaturated Carbonyl Compounds with Ti^{IV} Enolates Derived from α -Diazo β -Keto Carbonyl Compounds**

Guisheng Deng, Xue Tian, Zhaohui Qu, and Jianbo Wang*

The addition of nucleophiles to α,β -unsaturated carbonyl compounds is a fundamental transformation in organic synthesis. Since there are two reaction sites in the α,β -unsaturated carbonyl functional group, this addition reaction can only be of practical synthetic utility in organic synthesis if one

- [1] J. G. Crespo, I. M. Coelho, R. M. C. Viegas in *Encyclopedia of Separation Processes*, Academic Press, San Diego, **2000**, pp. 3303–3311.
- [2] J. J. Pellegrino, R. D. Noble, *Trends Biotechnol.* **1990**, *8*, 216–225.
- [3] a) K. R. Seddon, *Kinet. Catal.* **1996**, *37*, 693–697; b) T. Welton, *Chem. Rev.* **1999**, *99*, 2071–2084; c) M. Freemantle, *Chem. Eng. News* **2001**, *January 1*, 21–25; d) J. Dupont, C. S. Consorti, J. Spencer, *J. Braz. Chem. Soc.* **2000**, *11*, 337–344; e) P. Wasserscheid, K. Wilhelm, *Angew. Chem.* **2000**, *112*, 3926–3945; *Angew. Chem. Int. Ed.* **2000**, *39*, 3772–3789; f) R. Sheldon, *Chem. Commun.* **2001**, 2399–2407; g) C. M. Gordon, *Appl. Catal., A* **2001**, *222*, 101–107; h) R. T. Carlin, J. Fuller, *Chem. Commun.* **1997**, 1345–1346.
- [4] L. A. Blanchard, D. Hancu, E. J. Beckman, J. F. Brennecke, *Nature* **1999**, *399*, 28–29.
- [5] a) R. M. Lau, F. van Rantwijk, K. R. Seddon, R. A. Sheldon, *Org. Lett.* **2000**, *2*, 4189–4191; b) S. H. Schöfer, N. Kaftzik, P. Wasserscheid, U. Kragl, *Chem. Commun.* **2001**, 425–426; c) K.-W. Kim, B. Song, M.-Y. Choi, M.-J. Kim, *Org. Lett.* **2001**, *3*, 1507–1509.

[*] Prof. J. Wang, G. Deng, X. Tian, Z. Qu
Key Laboratory of Bioorganic Chemistry
and Molecular Engineering of the Ministry of Education
Department of Chemical Biology, College of Chemistry
Peking University, Beijing 100871 (P. R. China)
Fax: (+86) 10-6275-1708
E-mail: wangjb@pku.edu.cn

[**] The project is generously supported by the Natural Science Foundation of China (Grant Nos. 29972002, 20172002) and Trans-Century Training Program Foundation for the Talents by the Ministry of Education of China.

Supporting information for this article is available on the WWW under <http://www.angewandte.org> or from the author.

can control the selectivity for the two possible regioisomers.^[1] There are several factors that control the regioselectivity (1,2 vs 1,4 addition). These include the attacking nucleophiles,^[2] solvent,^[3] temperature,^[4] steric bulk,^[5] and transition-metal additives.^[6, 7] In general, the softness or hardness of the nucleophiles is of primary importance. Hard nucleophiles, such as alkyl lithium compounds, give predominantly 1,2 addition, whereas soft nucleophiles, such as the anion of the activated methylene compounds, give primarily 1,4 addition products.^[8]

On the other hand, the complexation of Lewis acids with the carbonyl oxygen atom can dramatically affect the properties of the α,β -unsaturated carbonyl compounds.^[9] For example, both the reactivity and the selectivity of the Diels–Alder reaction of α,β -unsaturated carbonyl compounds with dienes could be greatly enhanced by Lewis acids.^[10] Lewis acids play an indispensable role in organic chemistry, especially in catalytic asymmetric synthesis. Herein we report the Lewis acid promoted nucleophilic addition of the TiCl_4 -derived enolate of β -keto α -diazo carbonyl compounds to α,β -unsaturated carbonyl compounds. We found that by choosing appropriate Lewis acids, it is possible to control the selectivity for either 1,2 or 1,4 addition.

The Ti enolate **1a** or **1b** was generated by treating the β -keto α -diazo carbonyl compounds with $\text{TiCl}_4/\text{Et}_3\text{N}$ in anhydrous CH_2Cl_2 at -78°C (Scheme 1).^[11] When the enolate **1a** reacts with enone **2a** at -78°C , a mixture of 1,2- and 1,4-addition products (60:40) was isolated in 70% yield (Table 1, entry 1). If the enone **2a** was stirred with another equivalent of TiCl_4 in CH_2Cl_2 before adding to the enolate **1a**, the 1,4-addition product was obtained as the major product (1,2/1,4 17:83) (Table 1, entry 4). If the enone **2a** was activated with SnCl_4 (1 equiv) instead of TiCl_4 , the selectivity for 1,4 addition was further enhanced (1,2/1,4 5:95; Table 1, entry 5). On the other hand, when the enone **2a** was activated with $\text{BF}_3 \cdot \text{OEt}_2$, the 1,2-addition product became predominant (1,2/1,4 83:17; Table 1, entry 2). The activation of enone with $\text{Ti}(\text{OiPr})_4$ further enhanced the selectivity for 1,2 addition (1,2/1,4 96:4; Table 1, entry 3). For Ti enolate **1b**, a similar enhancement of regioselectivity was observed (Table 1, entries 6–10).

When enone **2b** was employed as the substrate, the direct reaction with the Ti enolate **1a** gave equal amounts of 1,2- and 1,4-addition products (Table 1, entry 11). TiCl_4 activation of the enone significantly enhanced 1,4 addition (1,2/1,4 1:99;

Table 1. Regioselective nucleophilic addition of Ti enolate **1** with α,β -unsaturated carbonyl compounds **2**.

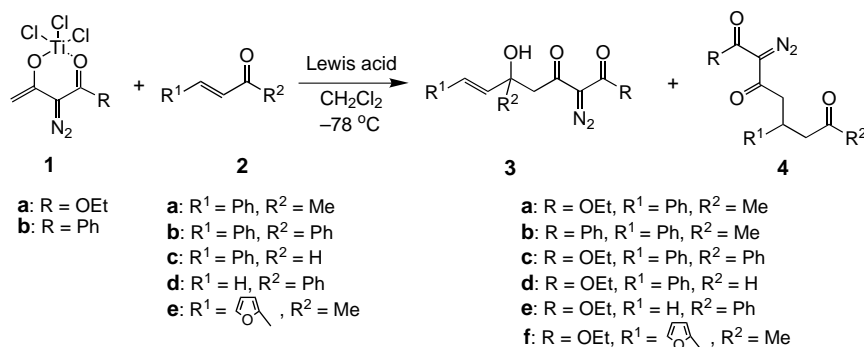
Entry	1	2	Lewis acid ^[a]	<i>t</i> [h]	3	4	3/4 ^[b]	Yield [%] ^[c]
1	a	a	none	6	a	a	60:40	70
2	a	a	$\text{BF}_3 \cdot \text{OEt}_2$	8	a	a	83:17	67
3	a	a	$\text{Ti}(\text{OiPr})_4$	8	a	a	96:4	78
4	a	a	TiCl_4	6	a	a	17:83	63
5	a	a	SnCl_4	10	a	a	5:95	50
6	b	a	none	8	b	b	50:50	42
7	b	a	$\text{BF}_3 \cdot \text{OEt}_2$	9	b	b	76:24	48
8	b	a	$\text{Ti}(\text{OiPr})_4$	8	b	b	94:6	60
9	b	a	TiCl_4	9	b	b	22:78	75
10	b	a	SnCl_4	8	b	b	0:100	58
11	a	b	none	9	c	c	50:50	71
12	a	b	$\text{BF}_3 \cdot \text{OEt}_2$	8.5	c	c	49:51	83
13	a	b	$\text{Ti}(\text{OiPr})_4$	8	c	c	76:24	90
14	a	b	TiCl_4	8	c	c	1:99	73
15	a	c	none	7	d	d	100:0	50
16	a	c	TiCl_4	5	d	d	100:0	71
17	a	d	none	8.5	e	e	40:60	73
18	a	d	$\text{Ti}(\text{OiPr})_4$	8.5	e	e	76:24	82
19	a	d	SnCl_4	8.5	e	e	0:100	76
20	a	e	none	8	f	f	71:29	78
21	a	e	$\text{Ti}(\text{OiPr})_4$	8	f	f	100:0	81
22	a	e	SnCl_4	8	f	f	0:100	54

[a] Lewis acid (1 equiv) was used to activate the substrate. [b] The product ratio was determined by ^1H NMR spectroscopic analysis (400 MHz) and was confirmed by separation by column chromatography. [c] Yield of isolated products.

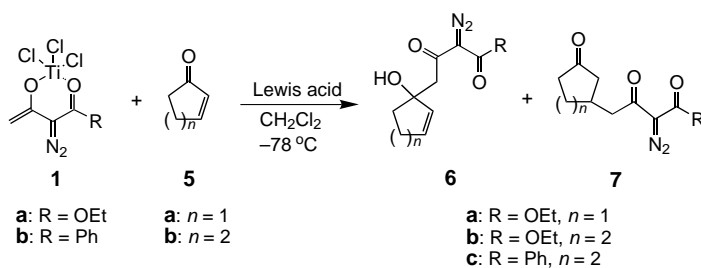
Table 1, entry 14), whereas $\text{BF}_3 \cdot \text{OEt}_2$ did not affect the selectivity for 1,2 addition (1,2/1,4 49:51; Table 1, entry 12). Evidently, the steric bulk of the phenyl group in enone **2b** overrides the activation of $\text{BF}_3 \cdot \text{OEt}_2$ for the carbonyl group.^[5a] However, activation by $\text{Ti}(\text{OiPr})_4$ can still enhance the selectivity for the sterically less favored 1,2 addition (1,2/1,4 76:24; Table 1, entry 13).

For enal **2c**, only the 1,2-addition product was isolated, even in the TiCl_4 -activated reaction (Table 1, entries 15, 16). The high reactivity of the aldehyde carbonyl group is the determining factor in controlling the regioselectivity in this case. On the other hand, for the enones **2d** and **2e**, similar control of diastereoselectivity as that for **2a** and **2b** was observed (Table 1, entries 17–22).

Regiocontrol by Lewis acids has also been observed for cyclic enones. Without the activation of the Lewis acid, the reaction of Ti enolate **1a** with cyclohexenone **5b** (Scheme 2) gave a mixture of 1,2- and 1,4-addition products in low selectivity (1,2/1,4 67:33; Table 2, entry 4). TiCl_4 activation gave almost only 1,4-addition product (1,2/1,4 1:99; Table 2, entry 7), whereas $\text{BF}_3 \cdot \text{OEt}_2$ activation slightly increases the amount of 1,2-addition product obtained (1,2/1,4 86:14; Table 2, entry 5). When the enone was activated with $\text{Ti}(\text{OiPr})_4$, the 1,2-addition product is greatly increased (1,2/1,4 99:1; Table 2, entry 6). For cyclopentenone **5a**, the reaction without Lewis acid activation gave a mixture of unidentified products (Table 1, entry 1). TiCl_4 activation gave the



Scheme 1. Lewis acid promoted nucleophilic addition of Ti enolate **1** with α,β -unsaturated carbonyl compounds **2**.



Scheme 2. Lewis acid promoted nucleophilic addition of Ti enolate **1** with cyclic enones **5**.

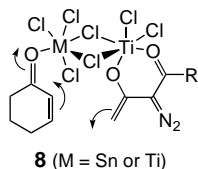
Table 2. Regioselective nucleophilic addition of Ti enolate **1** with cyclic enones **5**.

Entry	1	5	Lewis acid ^[a]	<i>t</i> [h]	6	7	6/7 ^[b]	Yield [%] ^[c]
1	a	a	none	8	a	a	—	— ^[d]
2	a	a	BF ₃ ·OEt ₂	6.5	a	a	—	— ^[d]
3	a	a	TiCl ₄	7	a	a	0:100	45
4	a	b	none	8	b	b	67:33	63
5	a	b	BF ₃ ·OEt ₂	8	b	b	86:14	40
6	a	b	Ti(O ^{<i>i</i>} Pr) ₄	8.5	b	b	99:1	68
7	a	b	TiCl ₄	7	b	b	1:99	52
8	b	b	none	8	c	c	70:30	51
9	b	b	BF ₃ ·OEt ₂	8.5	c	c	100:0	31 ^[e]
10	b	b	TiCl ₄	8.5	c	c	19:81	47
11	b	b	SnCl ₄	8	c	c	0:100	34 ^[e]

[a] Lewis acid (1 equiv) was used to activate the substrate. [b] The product ratio was determined by ¹H NMR spectroscopic analysis (400 MHz) and was confirmed by separation by column chromatography. [c] Yields of isolated products. [d] The reaction gave a complex mixture, 1,4-addition product could be isolated in low yield. [e] Considerable amounts of starting materials were recovered.

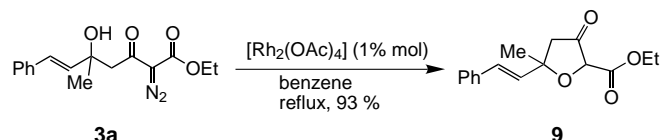
1,4-addition compound as the sole product (Table 1, entry 3). The 1,2-addition product could not be isolated when the reaction was activated with BF₃·OEt₂. This is believed to be a result of the low stability of the 1,2-addition product **6a**.

The Lewis acid controlled selectivity described above could be rationalized as follows. As the anion of the activated methylene compound, the Ti enolate **1** is considered to be a soft nucleophile.^[8b] From ab initio calculations it is known that the complexation of the Lewis acid with the oxygen atom of an α,β -unsaturated carbonyl compound increases its carbonyl coefficient of LUMO relative to that of the remote β -carbon atom,^[12] and hence the Lewis acid coordination should promote 1,2 addition. Therefore, BF₃·OEt₂ enhances the 1,2 selectivity. However, when enones are activated by TiCl₄ or SnCl₄,^[13] there is another factor that overrides the Lewis acid activation for 1,2 addition. It is known that TiCl₄ can form dimeric structures that involve bridging chlorine atoms.^[14, 15] Therefore we speculate that the complex **8** formed in the TiCl₄- or SnCl₄-activated reactions in which the two chlorine atoms serve as bridges for the two transition metals. Because of the steric proximity in this structure, 1,4 addition occurs much easier. Strong evidence to support this rationalization is that when Ti(O^{*i*}Pr)₄, which has no chlorine atoms for the bridging, is used as the



activator, 1,2 addition was again greatly enhanced (Table 1, entries 3, 8 13, 18, 21; Table 2, entry 6).

Since the nucleophilic addition products bear diazo functionality, both 1,2- and 1,4-addition products can be subjected to further synthetically useful transformations.^[16] For example, when **3a** was treated with [Rh₂(OAc)₄] (1 mol %) in benzene, highly efficient chemoselective intramolecular insertion into the O–H bond occurs to give tetrahydrofuran derivative **9** as a mixture of two diastereomeric isomers in excellent yield (Scheme 3).



Scheme 3. [Rh₂(OAc)₄]-mediated intramolecular O–H insertion.

In summary, we have demonstrated that both 1,2 and 1,4 selectivity of the nucleophilic addition could be controlled by Lewis acids. Similar control of selectivity may be possible for other types of nucleophiles. Investigations along this line are underway in our laboratory.

Experimental Section

Typical procedure: TiCl₄ (209 mg, 1.1 mmol) and Et₃N (111 mg, 1.1 mmol) were added dropwise to a solution of **1a** (156 mg, 1 mmol) in anhydrous CH₂Cl₂ (10 mL) at –78 °C. The dark-red mixture was stirred at –78 °C for 1 h. Ti(O^{*i*}Pr)₄ (284 mg, 1 mmol) and **2a** (146 mg, 1 mmol) in anhydrous CH₂Cl₂ (2 mL) were added to this mixture. The reaction mixture was stirred for another 8 h and then quenched with saturated aqueous NH₄Cl (5 mL). The organic layer was separated; upon workup, a crude product was obtained which was purified by flash chromatography to yield major product **3a** as an oil (224 mg) and minor product **4a** as a white solid (10 mg, m.p. 68–69 °C) in 78% total yield. Simultaneously, **1a** (13%) and **2a** (19%) were recovered.

Received: February 4, 2002 [Z18651]

- [1] For a review, see: P. Perlmutter, *Conjugate Addition Reactions in Organic Synthesis*, Pergamon Press, Oxford, **1992**.
- [2] a) D. A. Hunt, *Org. Prep. Proced. Int.* **1989**, 21, 707–749; b) W. C. Still, A. Mitra, *Tetrahedron Lett.* **1978**, 30, 2659–2662.
- [3] a) T. Cohen, W. D. Abraham, M. Myers, *J. Am. Chem. Soc.* **1987**, 109, 7923–7924; b) H. J. Reich, W. H. Sikorski, *J. Org. Chem.* **1999**, 64, 14–15; c) W. H. Sikorski, H. J. Reich, *J. Am. Chem. Soc.* **2001**, 123, 6527–6535.
- [4] a) A. G. Schultz, Y. K. Lee, *J. Org. Chem.* **1976**, 41, 4044–4045; b) P. C. Ostrowski, V. V. Kane, *Tetrahedron Lett.* **1977**, 3549–3552; c) K. Ogura, M. Yamashita, G.-I. Tsuchihashi, *Tetrahedron Lett.* **1978**, 1303–1306.
- [5] a) D. Seebach, R. Locher, *Angew. Chem.* **1979**, 91, 1024–1025; *Angew. Chem. Int. Ed. Engl.* **1979**, 18, 957–958; b) K. Maruoka, M. Ito, H. Yamamoto, *J. Am. Chem. Soc.* **1995**, 117, 9091–9092; c) J. Lucchetti, A. Krief, *J. Organomet. Chem.* **1980**, 194, C49–C52.
- [6] For reviews, see: a) G. H. Posner, *Org. React.* **1977**, 19, 1–113; b) B. H. Lipshutz, S. Sengupta, *Org. React.* **1992**, 41, 135–631.
- [7] J.-M. Lefour, A. Loupy, *Tetrahedron* **1978**, 34, 2597–2605.
- [8] For examples, see: a) E. M. Kaiser, C. L. Mao, C. F. Hauser, *J. Org. Chem.* **1970**, 35, 410–414; b) T. V. Rajan Babu, *J. Org. Chem.* **1984**, 49, 2083–2089.
- [9] For a comprehensive review, see: M. Santelli, J.-M. Pons, *Lewis Acids and Selectivity in Organic Synthesis*, CRC Press, Boca Raton, **1996**.
- [10] P. Yates, P. Eaton, *J. Am. Chem. Soc.* **1960**, 82, 4436–4437.

- [11] a) M. A. Calter, P. M. Sugathapala, C. Zhu, *Tetrahedron Lett.* **1997**, 38, 3837–3840; b) C. Zhu, M. A. Calter, *J. Org. Chem.* **1999**, 64, 1415–1419.
- [12] a) K. N. Houk, R. W. Strozier, *J. Am. Chem. Soc.* **1973**, 95, 4094–4096; b) A. Imamura, T. Hirano, *J. Am. Chem. Soc.* **1975**, 97, 4192–4198; c) A. Dargelos, D. Liotard, M. Chaillet, *Tetrahedron* **1972**, 28, 5595–5605; d) O. F. Guner, R. M. Ottenbrite, D. D. Shillady, P. V. Alston, *J. Org. Chem.* **1987**, 52, 391–394; e) R. J. Loncharich, T. R. Schwartz, K. N. Houk, *J. Am. Chem. Soc.* **1987**, 109, 14–23; f) P. Laszlo, M. Teston, *J. Am. Chem. Soc.* **1990**, 112, 8750–8754.
- [13] For a spectroscopic study on the complexation of TiCl_4 and SnCl_4 with enones, see: S. E. Denmark, N. G. Almstead, *Tetrahedron*, **1992**, 48, 5565–5578.
- [14] a) L. Brun, *Acta Crystallogr.* **1966**, 20, 739–749; b) I. W. Bassi, M. Calcaterra, R. Intrito, *J. Organomet. Chem.* **1977**, 127, 305–313.
- [15] S. W. Ng, C. L. Barnes, M. B. Hossain, D. van der Helm, J. J. Zukerman, V. G. Kumer Das, *J. Am. Chem. Soc.* **1982**, 104, 5359–5364.
- [16] For a comprehensive review on α -diazo carbonyl compounds, see: M. P. Doyle, M. A. McKervy, T. Ye, *Modern Catalytic Methods for Organic Synthesis with Diazo Compounds*, Wiley, New York, **1998**.

First Evidence of Fast S–H...S Proton Transfer in a Transition Metal Complex**

Gabriel Aullón, Mercè Capdevila, William Clegg, Pilar González-Duarte,* Agustí Lledós,* and Rubén Mas-Ballesté

In the quest to control noncovalent interactions, S–H...S hydrogen bonds are attracting great interest. Despite the prevalence of the thiol group in cysteine residues and the potential importance of S–H...S bridging bonds in biology, little is known about this interaction.^[1] Intermolecular S–H...S chains that play an organizing role in the solid state were found in X-ray structures of several compounds containing S–H groups.^[2] The S–H...S hydrogen bonds are typically very weak, but may become moderately strong in particular compounds. Resonance^[3] and charge^[4] assistances have been put forward as being responsible for strong intramolecular S–H...S bonds. The greater acidity of dithiols relative to their monothiol analogues has been attributed to enhanced stabilization of the thiolate anion by an intramolecular $\text{RS}^-\cdots\text{HSR}$ hydrogen bond.^[5] Evidence of S–H...S interactions in transition metal compounds are scarce,^[6] although the acidity of the SH group should be enhanced when the sulfur atom is coordinated to a transition

metal. Indeed, Sellmann et al. found strong intermolecular S–H...S bridges in the crystal structure of $[\text{Ru}(\text{SH}_2)(\text{PPh}_3)_3]^{+}$.^[6a] An influence of these bridges on the reactivity of the metal complexes has not been demonstrated, although intramolecular M–SH...hydride interactions have been proposed in the initial stage of the mechanism of hydride protonation.^[7] Here we show that a fast S–H...S proton exchange takes place in bimetallic platinum complexes with bridging SH^- and S^{2-} ligands.

Sulfide-bridged aggregates with the Pt_2S_2 core have a rich chemistry.^[8, 9] We proved that the reactivity of the Pt_2S_2 core is highly dependent on the nature of the terminal ligands.^[9, 10] We have now synthesized of the monoprotonated complexes $[\text{Pt}_2\{\text{Ph}_2\text{P}(\text{CH}_2)_n\text{PPh}_2\}_2(\mu\text{-S})(\mu\text{-SH})]\text{ClO}_4$ ($n=2$, dppe (**1**); $n=3$, dppp (**2**)) by adding HClO_4 to a solution of the corresponding $[\text{Pt}_2(\mu\text{-S})_2\text{P}(\text{P})_2]$ ($\text{P}=\text{dppe}$ or dppp) complex in benzene. The most remarkable spectroscopic feature of **1** and **2** is the equivalence of the four phosphorus nuclei at room temperature according to the ^{31}P NMR spectrum (Figure 1). The only analogous monoprotonated compound

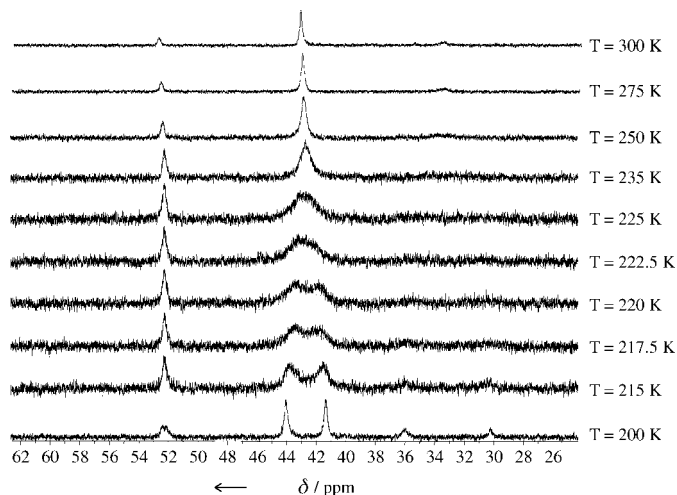


Figure 1. Variable-temperature $^{31}\text{P}\{^1\text{H}\}$ NMR spectra of **1**.

previously reported, namely, $[\text{Pt}_2(\mu\text{-S})(\mu\text{-SH})(\text{PPh}_3)_4]\text{PF}_6$, has two distinct environments about the P nuclei, as the SH group is *cis* to two phosphorus atoms and *trans* to the other two. Consequently, at room temperature, it shows two ^{31}P NMR signals with two distinct $^1J_{\text{Pt,P}}$ coupling constants.^[8b, 11] Surprisingly, each of the monoprotonated complexes **1** and **2** shows only one pseudotriplet with the following apparent spectroscopic parameters in $[\text{D}_6]\text{acetone}$: $\delta_{\text{P}} = 42.8$ ppm and $^1J_{\text{Pt,P}} = 3108$ Hz for **1**, and $\delta_{\text{P}} = -3.3$ ppm and $^1J_{\text{Pt,P}} = 2960$ Hz for **2**.

We optimized the geometry of the model compounds $[\text{Pt}_2\{\text{H}_2\text{P}(\text{CH}_2)_n\text{PPh}_2\}_2(\mu\text{-S})(\mu\text{-SH})]^+$ ($n=2$, dhpe (**1t**); $n=3$, dhpp (**2t**)) by B3LYP calculations.^[12] Two conformations with a hinged Pt_2S_2 skeleton were found as minima in both complexes; they differ in the *endo* (**e**) or *exo* (**x**) orientation of the thiol proton (see Figure 2). As expected, two different Pt–P and two different Pt–S distances were found in all cases (e.g., in **1t(x)** Pt–P(*trans*-S) 2.338, Pt–P(*trans*-SH) 2.279, Pt–S 2.389, Pt–SH 2.465 Å), and this reflects the different *trans* influences of the sulfide and thiol ligands. The *exo* form is slightly more stable than the *endo* form, although the *exo*/

[*] Prof. Dr. P. González-Duarte, Prof. Dr. A. Lledós, Dr. G. Aullón, Dr. M. Capdevila, Dipl.-Chem. R. Mas-Ballesté
Departament de Química
Universitat Autònoma de Barcelona
08193 Bellaterra, Barcelona (Spain)
Fax: (+34)935-812-920
E-mail: Pilar.Gonzalez.Duarte@uab.es, agusti@klignon.uab.es
Prof. Dr. W. Clegg
Department of Chemistry
University of Newcastle
Newcastle upon Tyne NE17RU (UK)

[**] Financial support is acknowledged from the Spanish Dirección General de Enseñanza Superior (DGES) under projects PB98-0916-CO2-01 and BQU2001-1976, and from EPSRC (UK).

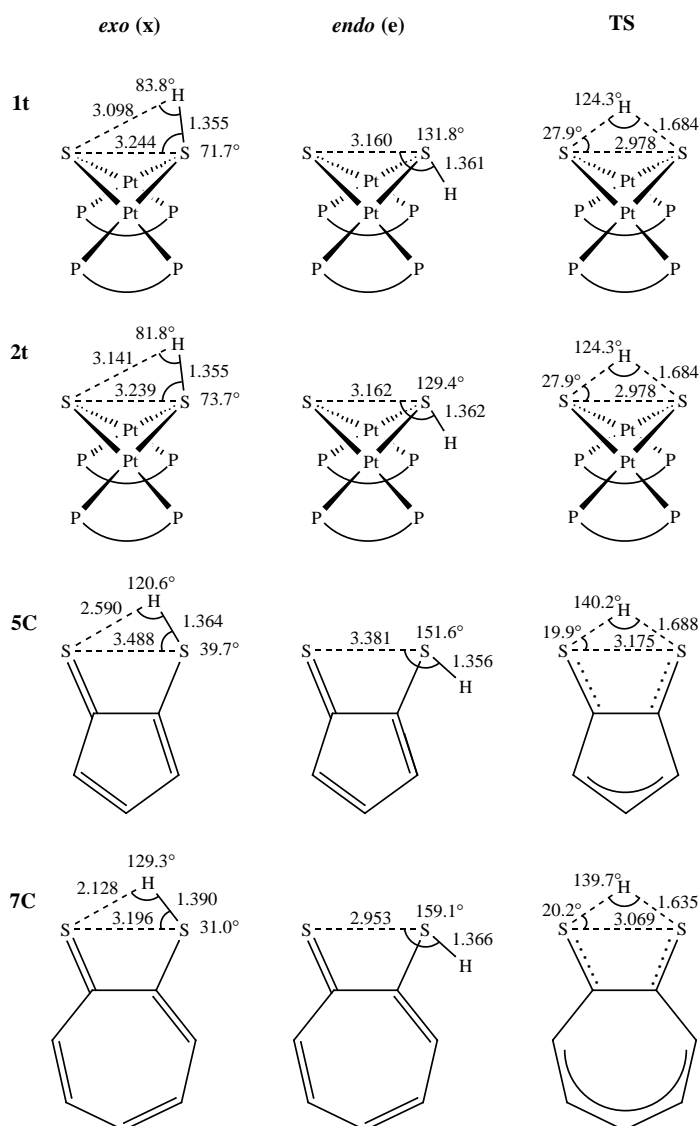


Figure 2. Optimized geometries of the *exo* and *endo* conformations and transition states for proton transfer in **1t**, **2t**, **5C**, and **7C** with bond lengths [Å] and angles [°].

endo interconversion, which takes place through ring inversion,^[13] is usually a very fast process. The S–H/S disposition in the *exo* conformations is compatible with the presence of a weak S–H...S hydrogen bond. Comparing the Pt–S–H angle in **1t(x)** (93.3°) with the Pt–S–C angle in the optimized geometry of the methylthiolate analogue (102.1°) reveals that the S–H proton is tilted towards the sulfide. The energy difference between the *exo* and *endo* forms (Table 1) can be taken as a rough estimate of the hydrogen-bond strength.

Table 1. B3LYP relative energies [kcal mol^{−1}] of the *exo* (x) and *endo* (e) conformations and the transition states (TS) for intramolecular proton transfer. In parentheses: MP2 values.

	Gas phase (ε = 1)			Acetone (ε = 20.7)		
	x	e	TS	x	e	TS
1t	0.0 (0.0)	0.9 (1.5)	19.7 (17.3)	0.0 (0.0)	−0.4 (−0.3)	19.5 (17.2)
2t	0.0 (0.0)	1.5 (2.3)	19.3 (16.1)	0.0 (0.0)	−0.2 (0.8)	18.0 (13.7)
5C	0.0	2.0	11.3	0.0	1.4	11.4
7C	0.0	2.2	2.3	0.0	1.0	1.6

Similar values (1–2 kcal mol^{−1}) have been reported for weak S–H...S hydrogen bonds.^[14]

The X-ray crystal structures^[15] of **1** and **2** show that the Pt₂(μ-S)(μ-SH) ring is nonplanar, with a dihedral angle between the two PtS₂ planes of 138.3° in **1** and 127.4° in **2** (Figure 3), and it is comparable to that in the singly proton-

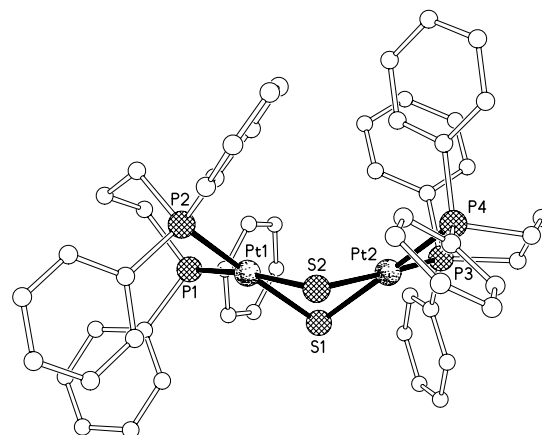


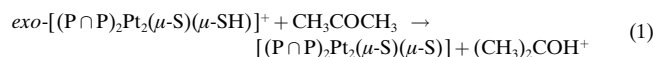
Figure 3. X-ray structure of **2**. Selected bond lengths [Å] and angles [°]: Pt1–S1 2.356(2), Pt1–S2 2.343(2), Pt2–S1 2.350(2), Pt2–S2 2.345(2); S1...S2 3.004, Pt1–S1–Pt2 86.92(7), Pt1–S2–Pt2 87.36(7). Selected bond lengths [Å] and angles [°] for **1**: Pt1–S1 2.374(3), Pt1–S2 2.339(3), Pt2–S1 2.365(3), Pt2–S2 2.343(3); S1...S2 3.057, Pt1–S1–Pt2 89.94(11), Pt1–S2–Pt2 91.37(10).

ated complex cation [Pt₂(PPh₃)₄(μ-S)(μ-SH)]⁺.^[11, 16] The H atom attached to S was not directly located in the structures of **1** and **2**, owing to the presence of heavy atoms and actual or possible disorder. Comparison of the Pt₂S₂ cores in **1** and **2** with those of their deprotonated precursors [Pt₂(μ-S)₂-(dppe)₂]^[9a] and [Pt₂(μ-S)₂(dppp)₂]^[10] shows that the S...S distance is shorter (by about 0.1 Å) and the dihedral angle smaller (by ca. 2° (**1**) and 7° (**2**)). However, these distortions do not allow a definite proposal for a unequivocal binding situation of the thiol proton in crystals of **1** or **2**. According to theoretical calculations both *endo* or *exo* conformations are possible, and thus weak interactions may determine the prevalence of one orientation over the other. In fact, an *endo* conformation for the thiol proton in **1** and **2** allows S–H...Ph hydrogen bonding.^[17] Regarding the acidity of the S–H group in **1** and **2**, NMR data allowed the corresponding pK_a values to be estimated. Both should be within the range 7–9 on the aqueous scale, as they are deprotonated by 4-aminopyridine (pK_a of the conjugated acid 9.11) but not by 2,4-lutidine (pK_a of the conjugated acid 6.99). This represents a decrease of ten pK_a units from the free SH[−] ligand (pK_a = 17–19).

Hydrogen bonds can be regarded as incipient proton-transfer reactions.^[1b] Thus, the equivalence of the phosphorus nuclei in **1** and **2** could be attributed to a fast SH...S proton transfer. To shed light on this process, variable-temperature NMR experiments were carried out (Figure 1). At low temperature, two distinct phosphorus environments were observed for **1** and **2** with the following parameters in [D₆]acetone: δ_{P(A)} = 44.1, δ_{P(B)} = 41.4 ppm, ¹J_{Pt,P(A)} = 2626, ¹J_{Pt,P(B)} = 3608 Hz for **1**, and δ_{P(A)} = −1.8, δ_{P(B)} = −4.9 ppm, ¹J_{Pt,P(A)} = 3401, ¹J_{Pt,P(B)} = 2408 Hz for **2**. Determination of the coalescence temperature allowed an estimation of the energy

barrier of the SH...S proton-transfer process. The values thus obtained are $T_c = 221$ K and $\Delta G^\ddagger = 10.7$ kcal mol⁻¹ for **1**, and $T_c = 240$ K and $\Delta G^\ddagger = 10.6$ kcal mol⁻¹ for **2**.

We also performed calculations on the intramolecular S-H...S proton-transfer process. The transition state was located and characterized for both complexes (**TS1** and **TS2**, respectively). Both TSs show a trigonal S-H-S arrangement, in which the partial rupture of the S-H bond is compensated by the partial formation of the new S-H bond (Figure 2). The moderate energy barriers found (Table 1) are consistent with the fast process observed on the NMR timescale. We carried out additional calculations to assess the validity of the theoretical values: 1) single-point MP2 calculations on the B3LYP optimized geometries (Table 1, values in parentheses); 2) inclusion of solvent effects by means of the PCM continuum model.^[18] The energy barriers are only slightly modified. Thus, theoretical calculations clearly show that intramolecular S-H...S proton transfer can occur in **1** and **2** with a low energy barrier. We also considered the possibility of an intermolecular solvent-assisted proton transfer, as defined in Equation (1). The values obtained for the activation energy of this reaction in acetone (32.2 kcal mol⁻¹ for **1t** and 32.0 kcal mol⁻¹ for **2t**, respectively) rule out this possibility.



To compare the S-H...S interaction in **1** and **2** with those in other compounds, in which stereochemical constraints place the S-H-S unit in a similar disposition, we performed calculations on dithiotropolone (**7C**) and the parent species with a five-membered ring **5C** (Figure 2, Table 1). The results obtained show that the structural and energetic parameters of the organic systems are similar to those of the platinum complexes, although the magnitude of the SH...S interaction decreases in the order **7C** > **5C** > **1** ≈ **2**.

In conclusion, the combined evidence from experimental and theoretical studies demonstrates the potential of a metal-coordinated thiol ligand to transfer its proton to a metal bound sulfide.

Experimental Section

1: HClO₄ (20 μL, 11.6 M) was added to a solution of [Pt₂(μ-S)₂(dppe)₂] (200 mg, 0.16 mmol) in benzene (50 mL). After 2 h, a pale yellow solid appeared. The solid product was collected by filtration, washed with benzene and water, and dried with diethyl ether. Yield: 146 mg (68 %). X-ray quality crystals of **1** were obtained by slow evaporation of a solution in methanol. ³¹P{¹H} NMR (162.1 MHz, [D₆]acetone, 295 K): δ_P(apparent) = 42.8 ppm, ¹J_{Pt,P}(apparent) = 3108 Hz. ESI-MS: *m/z*: 1251.

2: The same procedure as for **1** gave a yellow solid from the reaction of [Pt₂(μ-S)₂(dppp)₂] (200 mg) and of HClO₄ (20 μL, 11.6 M). Yield: 70 %. Recrystallization of **2** from methanol gave X-ray quality crystals. ³¹P{¹H} NMR (162.1 MHz, [D₆]acetone, 295 K): δ_P(apparent) = -3.3 ppm, ¹J_{Pt,P}(apparent) = 2960 Hz. ESI-MS: *m/z*: 1280.

Received: February 14, 2002 [Z18715]

- [1] a) G. R. Desiraju, T. Steiner, *The Weak Hydrogen Bond in Structural Chemistry and Biology*, Oxford University Press, New York, **1999**, pp. 258–263; b) T. Steiner, *Angew. Chem.* **2002**, *114*, 50; *Angew. Chem. Int. Ed.* **2002**, *41*, 48.

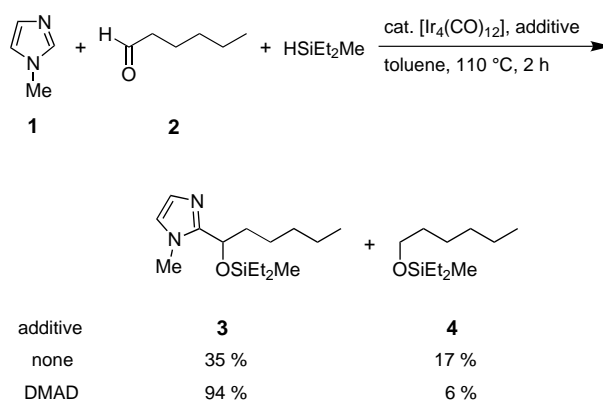
- [2] a) J. K. Cockroft, A. N. Fitch, *Z. Kristallogr.* **1990**, *193*, 1; b) C. H. Görbitz, B. Dalhus, *Acta Crystallogr. Sect. C* **1996**, *52*, 1756; c) P. R. Mallinson, D. D. MacNicol, K. L. McCormack, D. S. Yufit, J. H. Gall, R. K. Henderson, *Acta Crystallogr. Sect. C* **1997**, *53*, 90; d) T. Steiner, *Acta Crystallogr. C* **2000**, *56*, 876.
- [3] B. Krebs, G. Henkel, W. Stücker, *Z. Naturforsch. B* **1984**, *39*, 43.
- [4] P. M. Boorman, X. G. Gao, M. Parvez, *J. Chem. Soc. Chem. Commun.* **1992**, 1656.
- [5] J. M. Karty, Y. Wu, J. I. Brauman, *J. Am. Chem. Soc.* **2001**, *123*, 9800.
- [6] a) D. Sellmann, P. Lechner, F. Knoch, M. Moll, *J. Am. Chem. Soc.* **1992**, *114*, 922; b) R. J. Pleus, H. Waden, W. Saak, D. Haase, S. Pohl, *J. Chem. Soc. Dalton Trans.* **1999**, 2601.
- [7] a) D. Sellmann, J. Käppler, M. Moll, *J. Am. Chem. Soc.* **1993**, *115*, 1830; b) P. G. Jessop, R. H. Morris, *Inorg. Chem.* **1993**, *32*, 2236.
- [8] a) S.-W. A. Fong, T. S. A. Hor, *J. Chem. Soc. Dalton Trans.* **1999**, 639, and references therein; b) S.-W. A. Fong, W. T. Yap, J. J. Vittal, T. S. A. Hor, W. Henderson, A. G. Oliver, C. E. F. Rickard, *J. Chem. Soc. Dalton Trans.* **2001**, 1986.
- [9] a) M. Capdevila, Y. Carrasco, W. Clegg, R. A. Coxall, P. González-Duarte, A. Lledós, J. Sola, G. Ujaque, *Chem. Commun.* **1998**, 597; b) M. Capdevila, Y. Carrasco, W. Clegg, R. A. Coxall, P. González-Duarte, A. Lledós, J. A. Ramírez, *J. Chem. Soc. Dalton Trans.* **1999**, 3103.
- [10] R. Mas-Ballesté, M. Capdevila, P. A. Champkin, W. Clegg, R. A. Coxall, A. Lledós, C. Mégret, P. González-Duarte, *Inorg. Chem.* **2002**, *41*, 3218.
- [11] S.-W. A. Fong, J. J. Vittal, W. Henderson, T. S. A. Hor, A. G. Oliver, C. E. F. Rickard, *Chem. Commun.* **2001**, 421.
- [12] DFT calculations were carried out with the B3LYP functional. The structures were optimized, and transition states were checked by frequency analysis at the B3LYP level of theory. Single-point MP2 calculations were performed on the optimized B3LYP geometries. Effective core potentials and their related double-zeta basis set LANL2DZ were used for Pt, P, and S atoms, supplemented with polarization functions for the P and S atoms, whereas the 6-31G basis set was used for C and H atoms.
- [13] G. Aullón, G. Ujaque, A. Lledós, S. Alvarez, *Chem. Eur. J.* **1999**, *5*, 1391, and references therein.
- [14] a) J. E. Lowder, L. A. Kennedy, K. G. P. Sulzmann, S. S. Penner, *J. Quantum Spectr. Radiation Transf.* **1994**, *10*, 17; b) E. L. Woodbridge, T.-L. Tso, M. P. McGrath, W. J. Hehre, E. K. C. Lee, *J. Chem. Phys.* **1986**, *85*, 6991.
- [15] Crystal data for **1**: [C₅₂H₄₉P₄Pt₂S₂]ClO₄, *M*_r = 1351.5, monoclinic, space group *P*2₁, *a* = 9.5504(8), *b* = 14.9721(12), *c* = 17.6955(14) Å, β = 94.202(2)°, *V* = 2523.5(4) Å³, *Z* = 2, ρ_{calcd} = 1.779 g cm⁻³, μ = 5.84 mm⁻¹, *T* = 160 K, *R* = 0.056 (*F*² > 2σ), *R*_w = 0.152 (all *F*²) for 10719 data and 586 refined parameters. **2**: [C₅₄H₅₃P₄Pt₂S₂]ClO₄ · 2 CH₃OH, *M*_r = 1443.7, monoclinic, space group *P*2₁/*c*, *a* = 12.5409(8), *b* = 17.0421(10), *c* = 26.7036(16) Å, β = 98.817(2)°, *V* = 5639.7(6) Å³, *Z* = 4, ρ_{calcd} = 1.698 g cm⁻³, MoKα radiation (λ = 0.71073 Å, μ = 5.24 mm⁻¹), *T* = 160 K, *R* = 0.053 (*F*² > 2σ), *R*_w = 0.117 (all *F*²) for 13082 data and 641 refined parameters. CCDC-177519 (**1**) and CCDC 177518 (**2**) contain the supplementary crystallographic data for this paper. These data can be obtained free of charge via www.ccdc.cam.ac.uk/conts/retrieving.html (or from the Cambridge Crystallographic Data Centre, 12, Union Road, Cambridge CB21EZ, UK; fax: (+44) 1223-336-033; or deposit@ccdc.cam.ac.uk).
- [16] Note that the S²⁻ and SH⁻ bridging ligands in this complex are disordered and indistinguishable by crystallography, because they are symmetry-equivalent, although this is not explicitly stated in the publication.
- [17] a) M. S. Rozenberg, T. Nishio, T. Steiner, *New J. Chem.* **1999**, *23*, 585; b) To test the feasibility of S-H...Ph hydrogen bonding in the *endo* conformer, we took the reported crystal structure of **1** and **2** and located a hydrogen atom on one of the two bridging sulfur atoms with a S-H distance of 1.36 Å and *endo* orientation. Found S-H...C(phenyl ring) distances range between 2.8 and 3.0 Å, which, according to ref. [17a], are consistent with S-H...Ph hydrogen bonding.
- [18] a) Solvent effects were taken into account in polarized continuum model (PCM) calculations (acetone: ε = 20.70); b) J. Tomasi, M. Persico, *Chem. Rev.* **1994**, *94*, 2027.

[Ir₄(CO)₁₂]-Catalyzed Coupling Reaction of Imidazoles with Aldehydes in the Presence of a Hydrosilane to Give 2-Substituted Imidazoles**

Yoshiya Fukumoto, Katsutoshi Sawada, Motoyuki Hagihara, Naoto Chatani, and Shinji Murai*

Imidazole rings are components of a number of natural products and biologically active molecules. As a result, the development of methods for the alkylation of imidazole carbons is an important subject in organic synthesis.^[1] Generally, C2 of an imidazole ring can be alkylated by lithiation with strong bases at low temperature followed by treatment with electrophiles.^[1, 2] 1-Alkyl-2-trimethylsilylimidazoles react with electrophiles to give 2-substituted imidazoles in good yields, although a stoichiometric amount of *n*-butyllithium is required to prepare the 2-silylimidazoles.^[3] Thermal condensations with aldehydes^[4] or isocyanates^[5] have also been reported, but yields in the aldehyde reaction are dependent on the structure of substrates. Imidazolium ylides, which are generated by the reaction of 1-alkylimidazoles with acid halides in the presence of amines, have been proposed as the reactive intermediate in the pathway to 2-acylimidazoles.^[6] Quite recently, Hlasta reported that imidazolium ylides react with various electrophiles.^[7] It is known that transition-metal-catalyzed reactions are useful synthetic tools for selective C–C-bond formation.^[8] Cross-coupling reactions catalyzed by palladium complexes^[9] or copper salts^[10] were applied to introduce substituents at C2 of imidazoles. We have found that [Ru₃(CO)₁₂] is an efficient catalyst for direct carbonylation at a C–H bond in imidazole derivatives.^[11] Bergman, Ellman, and Tan demonstrated intramolecular cyclization of *N*- ω -alkenyl benzimidazole, which was proceeded by a RhCl(PPh₃)₃-catalyzed C–H/olefin coupling reaction.^[12] We report herein a unique new reaction for the derivatization of imidazoles. The new reaction enables direct coupling of 1-methylimidazole with aldehydes when [Ir₄(CO)₁₂] is used as the catalyst with a hydrosilane as a co-reactant.

The reaction of 1-methylimidazole (**1**; 1 mmol) with hexanal (**2**; 1 mmol) and diethylmethylsilane (2 mmol) in the presence of [Ir₄(CO)₁₂] (0.02 mmol) in toluene at 110 °C for 2 h gave 2-[1-(diethylmethylsiloxy)hexyl]-1-methyl-1*H*-imidazole (**3**) in 35% and the hydrosilylation product of hexanal **4** in 17% (Scheme 1). No reaction occurred in the absence of diethylmethylsilane. It occurred to us that the



Scheme 1. [Ir₄(CO)₁₂]-catalyzed reaction of 1-methylimidazole (**1**) with hexanal (**2**) with and without added DMAD.

addition of a hydrogen acceptor to the reaction system would improve the yield of **3**, since two hydrogen atoms (2-H of **1** and the hydrogen atom of H–SiR₃) were not found in the product on the formation of **3**. Among the hydrogen acceptors examined, it was found that diethyl acetylenedicarboxylate (DMAD) was the additive of choice; curiously, no hydrogenation products such as dimethyl fumarate or dimethyl succinate were detected. This result indicates that DMAD plays a role, not as a hydrogen acceptor, but rather as a ligand,^[13] although the details of the mechanism are not clear at present. Other transition-metal complexes including [Fe₃(CO)₁₂], [Ru₃(CO)₁₂], [Os₃(CO)₁₂], [Co₂(CO)₈], [Rh₄(CO)₁₂], [IrH(CO)(PPh₃)₃], [IrCl(cod)]₂ (cod = cycloocta-1,5-diene), [H₂IrCl₆], and [Ir(cod)]BF₄, had no catalytic activity.

The results of these reactions with some aldehydes are summarized in Table 1. All reactions were completed within 4 h and the products were isolated in good yields by bulb-to-bulb distillation. The reaction of pivaldehyde (**7**) required a higher reaction temperature to obtain **8** in good yield (Table 1, entry 3). Acetal (**11**) and ester (**13**) groups were also compatible in the present reaction (Table 1, entries 4, 5). The reaction of benzaldehyde (**15**) gave **16** in 76% yield as well as the silylated dimerization product, 1,2-bis(diethylmethylsiloxy)-1,2-diphenylethane, in 8% yield (Table 1, entry 7).^[14] Although the reaction of acetophenone resulted in the formation of the corresponding enol silyl ether, trifluoroacetophenone (**17**) afforded **18** (Table 1, entry 8) in 32% yield.

The reaction of *N*-propylisocyanate (**19**) with 1-methylimidazole and hydrosilane gave **20**, which might be formed by hydrolysis of the desired product during the work-up (Scheme 2). The reaction of 1-methylbenzimidazole (**21**) with hexanal required the further addition of DMAD and a longer reaction time (19 h) to give **22** (Scheme 3). Other heterocyclic compounds such as thiazole, oxazole, 1,2,4-triazole, and pyrimidine were also examined, but only hydrosilylation products of aldehydes were obtained in all cases.

A possible reaction mechanism is shown in Scheme 4. The addition of Ir–SiR₃ to the aldehyde, followed by carbonylation of the C–N double bond of the imidazole^[15] gives amidoiridium intermediate **A**. Successive β -hydride elimination of **A** gives the product and the Ir–H species. A very similar dehydrometallation reaction of iridium amide com-

[*] Prof. Dr. S. Murai, Dr. Y. Fukumoto, K. Sawada, M. Hagihara, Dr. N. Chatani

Department of Applied Chemistry
Faculty of Engineering, Osaka University
Suita, Osaka 565-0871 (Japan)
Fax: (+81) 6-6879-7396
E-mail: murai@chem.eng.osaka-u.ac.jp

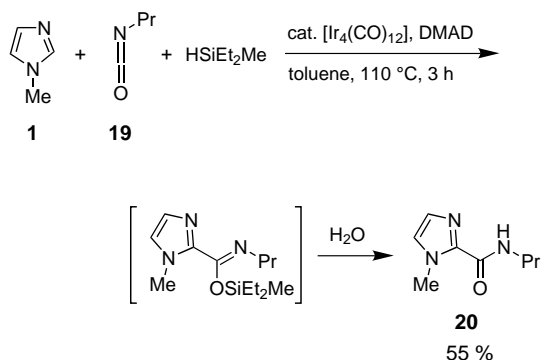
[**] This work was supported in part by a Grant-in-Aid for Scientific Research from the Ministry of Education, Culture, Sports, Science, and Technology, Japan. We also thank the Instrumental Analysis Center, Faculty of Engineering, Osaka University, for assistance in MS, HRMS, and elemental analyses.

Supporting information for this article is available on the WWW under <http://www.angewandte.org> or from the author.

Table 1. $[\text{Ir}_4(\text{CO})_{12}]$ -catalyzed coupling reaction of **1** with carbonyl compound in the presence of diethylmethylsilane.^[a]

Entry	Carbonyl Compounds	Product	<i>t</i> [h]	Yield [%] ^[b]
1			2	92
2			3	91
3			4	76 ^[c]
4			1	72
5			1	62
6			1	87
7			2	76 ^[d]
8			3	32

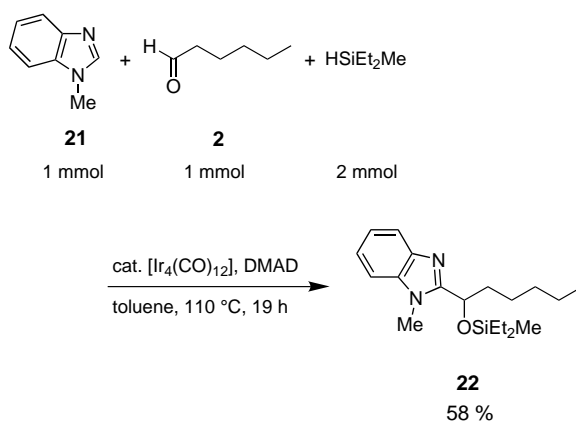
[a] Reaction conditions: 1-methylimidazole (1 mmol), carbonyl compound (1 mmol), diethylmethylsilane (2 mmol), $[\text{Ir}_4(\text{CO})_{12}]$ (0.02 mmol), DMAD (0.16 mmol), in toluene (5 mL) at 110 °C, unless otherwise noted. [b] Yields of isolated products. [c] $T = 135^\circ\text{C}$. [d] 1,2-Bis(diethylmethylsiloxy)-1,2-diphenylethane was also obtained in 8% yield.



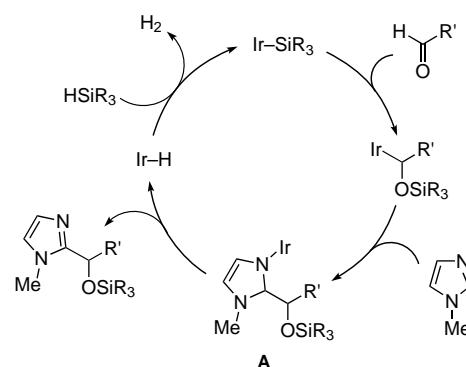
Scheme 2. $[\text{Ir}_4(\text{CO})_{12}]$ -catalyzed reaction of 1-methylimidazole (**1**) with *N*-propylisocyanate (**19**), with DMAD additive, to form **20**.

plexes has been observed directly.^[16] The regeneration of the initial catalyst species might take place by the reaction of the Ir–H species with H–SiR₃ to give Ir–SiR₃ and H₂.^[17]

In summary, $[\text{Ir}_4(\text{CO})_{12}]$ catalyzes the coupling reaction of imidazoles with aldehydes in the presence of a hydrosilane to



Scheme 3. $[\text{Ir}_4(\text{CO})_{12}]$ -catalyzed reaction of 1-methylbenzimidazole (**21**) with hexanal (**2**), with DMAD additive, to give **22**.



Scheme 4. Possible reaction mechanism.

give 2-alkyl imidazoles. Detailed mechanistic studies are currently underway in our laboratories.^[18]

Experimental Section

3: $[\text{Ir}_4(\text{CO})_{12}]$ (22 mg, 0.02 mmol), 1-methylimidazole (82 mg, 1 mmol), hexanal (100 mg, 1 mmol), diethylmethylsilane (204 mg, 2 mmol), DMAD (23 mg, 0.16 mmol), and toluene (5 mL) were mixed in a 10-mL flame-dried flask. The reaction mixture was heated at reflux for 2 h. After cooling to room temperature, the volatile components were removed in vacuo. Compound **3** was isolated by bulb-to-bulb distillation under reduced pressure. ¹H NMR (270 Hz, CDCl₃, TMS): $\delta = -0.05$ (s, 3H; CH₃Si), 0.51 (q, ³*J*(H,H) = 7.8 Hz, 4H; SiCH₂), 0.83 (t, ³*J*(H,H) = 7.8 Hz, 3H; SiCH₂CH₃), 0.86 (t, ³*J*(H,H) = 7.8 Hz, 6H; SiCH₂CH₃, CH₃), 1.27–1.50 (c, 6H; CH₂CH₂CH₂), 1.80 (m, 2H; CHCH₂), 3.74 (s, 3H; NCH₃), 4.88 (dd, ³*J*(H,H) = 6.2, 1.6 Hz, 1H; CH), 6.75 (d, ³*J*(H,H) = 1.1 Hz, 1H; =CH), 6.88 ppm (d, ³*J*(H,H) = 1.1 Hz, 1H; =CH); ¹³C NMR (68 Hz, CDCl₃, TMS): $\delta = -4.89$ (SiCH₃), 6.22 (SiCH₂), 6.33 (SiCH₂), 6.51 (SiCH₂CH₃), 6.54 (SiCH₂CH₃), 13.95 (CH₃), 22.50 (CH₂), 25.52 (CH₂), 31.48 (CH₂), 33.25 (NCH₃), 36.89 (CH₂), 70.51 (CH), 121.64 (=CH), 126.72 (=CH), 148.97 ppm (NCN); MS (70 eV): *m/z* (%): 282 ($[M^+]$, 8), 253 ($[M^+ - \text{Et}]$, 100); elemental analysis (%) calcd for C₁₅H₃₀N₂O_{Si}: C 63.78, H 10.70, N 9.92; found: C 63.53, H 10.96, N 10.19.

Received: March 1, 2002 [Z18810]

[1] For reviews on imidazole chemistry, see: a) M. R. Grimmett, *Adv. Heterocycl. Chem.* **1980**, 27, 241–326; b) M. R. Grimmett in *Comprehensive Heterocyclic Chemistry*, Vol. 4 (Eds.: A. R. Katritzky, C. W. Rees), Pergamon, Oxford, **1984**, pp. 345–498; c) M. R. Grimmett in

- Comprehensive Heterocyclic Chemistry II*, Vol. 3 (Eds.: A. R. Katritzky, C. W. Rees, E. F. V. Scriven), Pergamon, Oxford, **1996**, pp. 77–220.
- [2] a) B. Iddon, *Heterocycles* **1985**, 23, 417–443; b) B. Iddon, R. I. Ngochindo, *Heterocycles* **1994**, 38, 2487–2568; c) P. Merino, *Prog. Heterocycl. Chem.* **1999**, 11, 21–42.
- [3] F. H. Pinkerton, S. F. Themes, *J. Heterocycl. Chem.* **1972**, 9, 67–72.
- [4] A. M. Roe, *J. Chem. Soc.* **1963**, 2195–2200.
- [5] R. Gompper, E. Hoyer, H. Herlinger, *Chem. Ber.* **1959**, 92, 550–563.
- [6] E. Regel, K.-H. Büchel, *Liebigs Ann. Chem.* **1977**, 145–148.
- [7] D. J. Hlasta, *Org. Lett.* **2001**, 3, 157–159.
- [8] a) L. S. Hegedus, *Transition Metals in the Synthesis of Complex Organic Molecules*, University Science Books, Mill Valley, **1999**; b) J. Tsuji, *Transition Metal Reagents and Catalysts*, Wiley, Chichester, **2000**.
- [9] a) M. Kosugi, M. Koshiba, A. Atoh, H. Sano, T. Migita, *Bull. Chem. Soc. Jpn.* **1986**, 59, 677–679; b) T. Sakamoto, H. Nagata, Y. Kondo, M. Shiraiwa, H. Yamanaka, *Chem. Pharm. Bull.* **1987**, 35, 823–828; c) A. S. Bell, D. A. Roberts, K. S. Ruddock, *Tetrahedron Lett.* **1988**, 39, 5013–5016; d) D. A. Evans, T. Bach, *Angew. Chem.* **1993**, 105, 1414–1415; *Angew. Chem. Int. Ed. Engl.* **1993**, 32, 1326–1327; e) J. Ezquerro, C. Lamas, A. Pastor, J. L. García-Navío, J. J. Vaquero, *Tetrahedron* **1997**, 53, 12755–12764.
- [10] a) S. Pivsa-Art, T. Satoh, Y. Kawamura, M. Miura, M. Nomura, *Bull. Chem. Soc. Jpn.* **1998**, 71, 467–473; b) M. Ababri, F. Dehmel, P. Knochel, *Tetrahedron Lett.* **1999**, 40, 7449–7453.
- [11] a) T. Fukuyama, N. Chatani, J. Tatsumi, F. Kakiuchi, S. Murai, *J. Am. Chem. Soc.* **1998**, 120, 11 522–11 523; b) N. Chatani, T. Fukuyama, H. Tatamidani, F. Kakiuchi, S. Murai, *J. Org. Chem.* **2000**, 65, 4039–4047.
- [12] K. L. Tan, R. G. Bergman, J. A. Ellman, *J. Am. Chem. Soc.* **2001**, 123, 2685–2686.
- [13] It is well known that iridium complexes react with a variety of alkynes to form iridacyclopentadiene complexes; see: a) G. J. Leigh, R. L. Richards in *Comprehensive Organometallic Chemistry*, Vol. 5 (Eds.: G. Wilkinson, F. G. A. Stone, E. W. Abel), Pergamon, Oxford, **1982**, pp. 541–628; b) J. D. Atwood in *Comprehensive Organometallic Chemistry II*, Vol. 8 (Eds.: E. W. Abel, F. G. A. Stone, G. Wilkinson), Pergamon, Oxford, **1995**, pp. 303–417.
- [14] Examples of silylative dimerization of aromatic aldehydes catalyzed by transition-metal complexes: a) E. Frainnet, R. Bourhis, F. Simonin, F. Moulines, *J. Organomet. Chem.* **1976**, 105, 17–31; b) H. Shimada, J.-P. Qü, H. Matsuzaka, Y. Ishii, M. Hidai, *Chem. Lett.* **1995**, 671–672. We also have found that $[\text{Co}_2(\text{CO})_8]$ catalyzes the silylative dimerization of aromatic aldehydes: c) S. Murai, T. Kato, N. Sonoda, unpublished data.
- [15] Many examples of carbopalladation to C–O double bonds have been reported; see: I. P. Beletskaya, A. V. Cheprakov, *Chem. Rev.* **2000**, 100, 3009–3066.
- [16] J. F. Hartwig, *J. Am. Chem. Soc.* **1996**, 118, 7010–7011.
- [17] A similar reaction is known for the case of $[\text{Co}_2(\text{CO})_8]$; see: A. J. Chalk, J. F. Harrod, *J. Am. Chem. Soc.* **1967**, 89, 1640–1647.
- [18] A 1-methyl-3-(dimethylsilyl)imidazol-2-ylidene may be involved as a key intermediate in the present reaction; see: S. Solé, H. Gornitzka, O. Guerret, G. Bertrand, *J. Am. Chem. Soc.* **1998**, 120, 9100–9101.

[Lewis Acid]⁺[Co(CO)₄][−] Complexes: A Versatile Class of Catalysts for Carbonylative Ring Expansion of Epoxides and Aziridines**

Viswanath Mahadevan, Yutan D. Y. L. Getzler, and Geoffrey W. Coates*

Introduction of carbonyl functional groups by using transition-metal-catalyzed carbon monoxide (CO) insertion is a synthetically useful transformation.^[1–3] Application of this methodology, in conjunction with readily available epoxide and aziridine substrates provides facile access to β -lactones^[4] and β -lactams,^[5, 6] useful precursors for organic synthesis as well as for the synthesis of polymers such as poly(3-hydroxyalkanoates)^[7] and poly(β -peptides).^[8, 9] Few catalysts are known to perform ring-expansive CO insertion into epoxides to give β -lactones.^[10, 11, 12d] Likewise, a limited number of reagents^[13] and catalysts^[12, 14, 15] are known to carbonylate aziridines to yield β -lactams. Recently, regioselective epoxide and aziridine carbonylation was achieved using a catalyst system consisting of a mixture of [PPN]-[Co(CO)₄] and $\text{BF}_3 \cdot \text{Et}_2\text{O}$ (PPN = $\text{Ph}_3\text{P}=\text{N}=\text{PPh}_3$).^[12d] However, most of these catalysts require long reaction times, high temperatures, high catalyst loading, and/or external additives. There is continuing motivation for developing fast, single-component catalysts; ideally a single catalyst would efficiently carbonylate both epoxides and aziridines. Herein, we report a well-defined $[\text{Cp}_2\text{Ti}(\text{thf})_2][\text{Co}(\text{CO})_4]$ catalyst (**1**; Cp = C_5H_5),^[16] readily synthesized from commercially available $[\text{Cp}_2\text{Ti}(\text{CO})_2]$ and $[\text{Co}_2(\text{CO})_8]$, is efficient for carbonylation of both epoxide and aziridine substrates. During the course of this work we discovered that the discrete catalyst [(salph)Al(thf)₂][Co(CO)₄] (**2**),^[11, 17] is also active for regioselective aziridine carbonylation (Scheme 1).

The $[\text{Co}(\text{CO})_4]^-$ ion is the putative active species for CO insertion reactions that use $[\text{Co}_2(\text{CO})_8]$ as the catalyst.^[1, 11, 12a] Based on this postulate, a variety of [cation][Co(CO)₄] complexes^[18] were previously screened^[11] for CO insertion into propylene oxide. Complexes **1** and **2** are efficient catalysts for the carbonylation of a variety of both epoxides and aziridines.

Catalyst **1** (5 mol %) regioselectively carbonylates a variety of epoxides under mild conditions and in high yields. Propylene oxide is converted into β -butyrolactone in 95 % yield in 4 h at 60 °C; the carbonylation is highly regioselective producing exclusively the 4-methyloxetan-2-one isomer (Table 1, entry 1). Carbonylation of propylene oxide was not observed with other potential catalysts^[18, 19] under a variety of

[*] Prof. Dr. G. W. Coates, Dr. V. Mahadevan, Y. D. Y. L. Getzler
Department of Chemistry and Chemical Biology
Baker Laboratory, Cornell University
Ithaca, New York 14853-1301 (USA)
Fax: (+1) 607-255-4137
E-mail: gc39@cornell.edu

[**] G.W.C. gratefully acknowledges a Packard Foundation Fellowship in Science and Engineering, an Arnold and Mabel Beckman Foundation Young Investigator Award, and an NSF CAREER Award. V.M. was supported by the Cornell Center for Materials Research.

Supporting information for this article is available on the WWW under <http://www.angewandte.org> or from the author.

Table 1. Carbonylation of epoxides to β -lactones using **1**.^[a]

Entry	Substrate	Temp [°C]	Time [h]	Products	Yield [%] ^[b]
1		60	4		95
2		60	4		95 ^[c]
3		60	4		99
4		60	4		90
5		60	5		60
6		50	3		90
7		60	10		99
8		60	10		75

[a] 5 mol % catalyst **1** (0.2 M in DME), 6200 kPa (900 psi) CO, 1.92 mmol epoxide. [b] Yields determined by ¹H NMR spectroscopy. [c] >99% (*R*)- β -Butyrolactone.

conditions, which included changes in catalyst loading (2–10 mol %), temperature (50–100 °C), and reaction time (12–48 h). (*R*)-Propylene oxide is converted into (*R*)- β -butyrolactone in 95 % yield with >99 % retention of configuration (Table 1, entry 2), consistent with the high regioselectivity observed for CO insertion. Retention of stereochemistry allows the synthesis of enantiomerically enriched β -lactones from readily available chiral epoxides.^[20] Compound **1** also catalyzes the transformation of 1,2-epoxybutane to 4-ethyl-oxetan-2-one (Table 1, entry 3). Functional epoxides such as 1,2-epoxy-5-hexene (Table 1, entry 4) and epichlorohydrin (Table 1, entry 5) are carbonylated to the corresponding lactones. The hindered substrate isobutylene oxide reacts to generate a mixture of isomeric lactones in a 4:1 ratio with 90 % overall yield (Table 1, entry 6).

Catalyst **1** also carbonylates *cis*- and *trans*-2,3-epoxybutanes regioselectively to *trans*- and *cis*-lactones, respectively, in high yield and with inversion of configuration (Table 1, entries 7 and 8). The *cis*- and *trans*-lactone products were individually identified by comparing ¹³C NMR spectroscopic data with those reported,^[21, 22] as well as, by pyrolysis; thermal *syn* decarboxylation of the lactones generates alkenes with retention of stereochemistry.^[23] Comparison of the resulting alkenes with authentic *cis*- and *trans*-2-butene samples using ¹H NMR spectroscopy allowed identification of the parent lactones.^[24, 25]

Both **1** and **2** are capable of carbonylating aziridines to generate β -lactams, although they exhibit interesting differences in reactivity. Catalyst **1** carbonylates 1-benzyl-2-methyl aziridine in 90 % yield compared to 50 % obtained with **2** under similar conditions (Table 2, entry 1). However, in both cases, CO insertion occurs selectively at the least hindered ring C–N bond. Catalyst **1** also carbonylates 7-benzyl-7-azabicyclo[4.1.0]heptane in 80 % yield compared to <5 %

Table 2. Carbonylation of aziridines to β -lactams using **1** and **2**.^[a]

Entry	Substrate	Catalyst	Temp [°C]	Time [h]	Products	Yield [%] ^[b]
1		1	60	6		90
		2	60	6		50
2		1	80	18		80
		2	80	18		<5
3		1	90	6		35
		2	90	6		99
4		1	60	5		95

[a] 5 mol % catalyst (0.2 M in DME), 6200 kPa (900 psi) CO, 1.92 mmol aziridine; TBS = *tert*-butyldimethylsilyl, Ts = tosyl. [b] Yields determined by ¹H NMR spectroscopy.

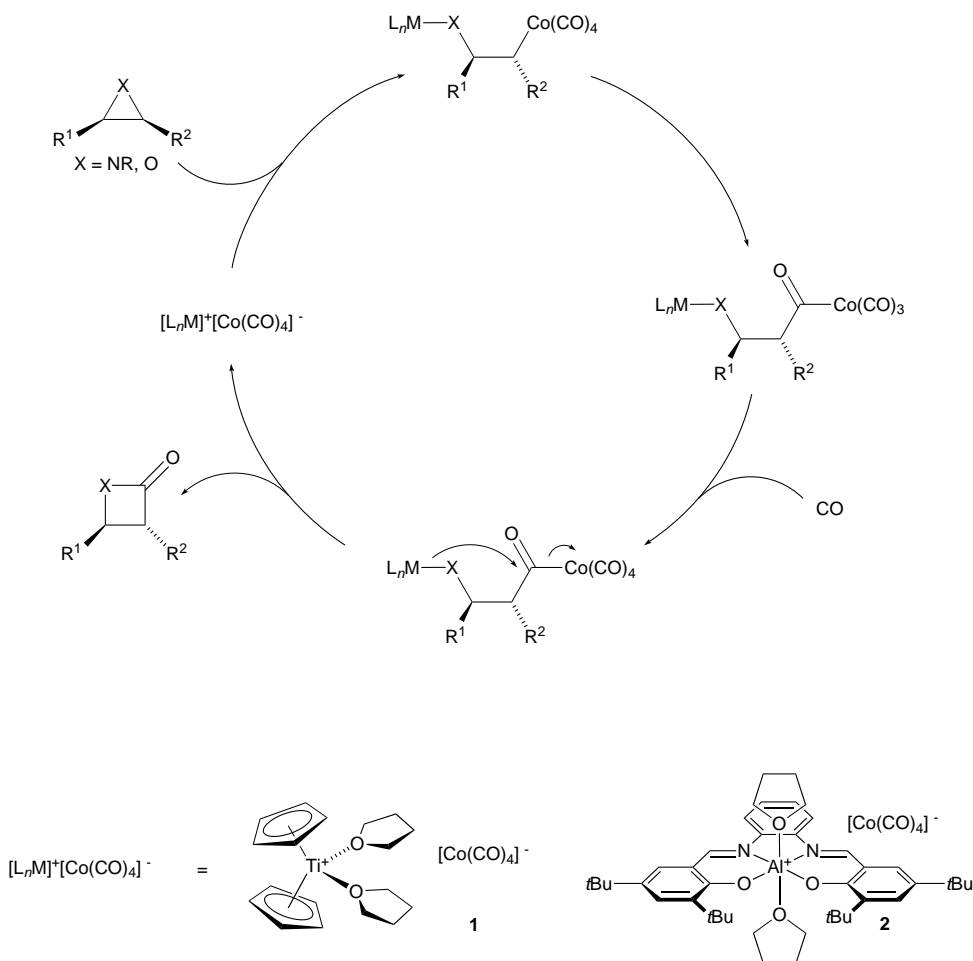
yield obtained with **2** (Table 2, entry 2). Both **1** and **2** show unprecedented activity in carbonylating the electron deficient 1-tosyl-2-methylaziridine substrate. However, **2** gives much higher lactam yields (99 %) than **1** (35 %) (Table 2, entry 3), which is important because of the availability of enantiomerically-pure *N*-tosyl aziridines.^[26, 27] Finally, **1** reacts with *cis*-1-benzyl-2-(*tert*-butyldimethylsilyloxymethyl)-3-methyl aziridine to predominantly yield the *trans*-lactone with high selectivity for CO insertion at the (Me)C–N bond of the aziridine (Table 2, entry 4). Relative to previously reported systems, **1** and **2** react faster, under milder conditions to generate lactams in higher yield and selectivity. However, the differences in reactivity between **1** and **2** are not understood at the current time.

We propose the carbonylations of both epoxides and aziridines proceed through a unifying mechanism involving a backside nucleophilic attack by the $[\text{Co}(\text{CO})_4]^-$ ion at the least-substituted carbon center (Scheme 1). The role of the cationic Lewis acid counterpart is to bind and activate the substrate.^[11] Insertion of CO followed by ring-closure results in lactone and lactam products, with inversion of configuration at the site of attack. Discrete catalysts such as **1** and **2** will allow the elucidation of the mechanism of CO insertion into these substrates.

In summary, the discrete catalysts $[\text{Cp}_2\text{Ti}(\text{thf})_2][\text{Co}(\text{CO})_4]$ (**1**) and $[(\text{salph})\text{Al}(\text{thf})_2][\text{Co}(\text{CO})_4]$ (**2**) are shown to efficient-

ly carbonylate a variety of epoxides and aziridines under mild conditions. Carbonylation of (*R*)-propylene oxide can be carried efficiently on a multigram scale. Between **1** and **2**, a variety of epoxides and aziridines are efficiently carbonylated in high yield and selectivity with intriguing differences in reactivity. Further, we propose the insertion of CO into both epoxides and aziridines proceeds through a similar mechanism, which generates β -lactone and β -lactam products with inversion at the site of nucleophilic attack.

Received: March 4, 2002 [Z18813]



Scheme 1. Proposed catalytic cycle for epoxide and aziridine carbonylation.

- [1] J. P. Collman, L. S. Hegedus, J. R. Norton, R. G. Finke, *Principles and Applications of Organotransition Metal Chemistry*, 2nd ed., University Science Books, Sausalito, **1987**.
- [2] R. F. Heck in *Organic Synthesis via Metal Carbonyls*, Vol. 1 (Eds.: I. Wender, P. Pino), Interscience Publishers, New York, **1968**, pp. 373–404.
- [3] L. S. Hegedus, *Transition Metals in the Synthesis of Complex Organic Molecules*, University Science Books, Mill Valley, **1994**.
- [4] H. W. Yang, D. Romo, *Tetrahedron* **1999**, 55, 6403–6434.
- [5] K. Khumtaveeporn, H. Alper, *Acc. Chem. Res.* **1995**, 28, 414–422.
- [6] P. A. Magriotis, *Angew. Chem.* **2001**, 113, 4507–4509; *Angew. Chem. Int. Ed.* **2001**, 40, 4377–4379.
- [7] H. M. Müller, D. Seebach, *Angew. Chem.* **1993**, 105, 483–509; *Angew. Chem. Int. Ed. Engl.* **1993**, 32, 477–502.
- [8] a) D. Seebach, M. Overhand, F. N. M. Kuhnle, B. Martinoni, L. Oberer, U. Hommel, H. Widmer, *Helv. Chim. Acta* **1996**, 79, 913–941; b) R. P. Cheng, S. H. Gellman, W. F. DeGrado, *Chem. Rev.* **2001**, 101, 3219–3232; c) J. J. Cheng, T. J. Deming, *J. Am. Chem. Soc.* **2001**, 123, 9457–9458.
- [9] For the direct copolymerization of CO with aziridines and epoxides, respectively, see: a) L. Jia, E. Ding, W. R. Anderson, *Chem. Commun.* **2001**, 1436–1437; b) M. Allmendinger, R. Eberhardt, G. Luinstra, B. Rieger, *J. Am. Chem. Soc.* **2002**, 124, 5646–5647. See also references [10], [11], and [12d] for prior reports of CO/epoxide copolymerization.
- [10] E. Drent, E. Kragtswijk (Shell Internationale Research B. V. Maatschappij, Neth.), EP 577206, **1994** [*Chem. Abstr.* **1994**, 120, 191517c].
- [11] Y. D. Y. L. Getzler, V. Mahadevan, E. Lobkovsky, G. W. Coates, *J. Am. Chem. Soc.* **2002**, 124, 1174–1175, and references therein.
- [12] For Co-catalyzed aziridine carbonylations, see: a) M. E. Piotti, H. Alper, *J. Am. Chem. Soc.* **1996**, 118, 111–116; b) P. Davoli, I. Moretti, F. Prati, H. Alper, *J. Org. Chem.* **1999**, 64, 518–521; c) P. Davoli, F. Prati, *Heterocycles* **2000**, 53, 2379–2389; d) J. T. Lee, P. J. Thomas, H. Alper, *J. Org. Chem.* **2001**, 66, 5424–5426.
- [13] a) W. Chamchaang, A. R. Pinhas, *Chem. Commun.* **1988**, 710–711; b) W. Chamchaang, A. R. Pinhas, *J. Org. Chem.* **1990**, 55, 2943–2950; c) S. V. Ley, B. Middleton, *Chem. Commun.* **1998**, 1995–1996.
- [14] For Rh-catalyzed aziridine carbonylations, see: a) H. Alper, F. Urso, D. J. H. Smith, *J. Am. Chem. Soc.* **1983**, 105, 6737–6738; D. Roberto,

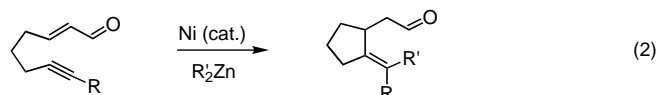
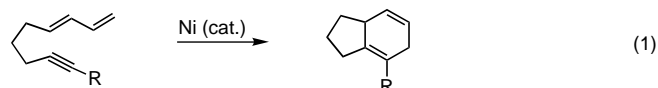
- H. Alper, *Organometallics* **1984**, *3*, 1767–1769; for enantiospecific carbonylation, see: b) S. Calet, F. Urso, H. Alper, *J. Am. Chem. Soc.* **1989**, *111*, 931–934.
- [15] For Pd-catalyzed aziridine carbonylations, see: a) H. Alper, N. Hamel, *Tetrahedron Lett.* **1987**, *28*, 3237–3240; b) G. W. Spears, K. Nakanishi, Y. Ohfuné, *Synlett* **1991**, 91–92; c) D. Tanner, P. Somfai, *Bioorg. Med. Chem. Lett.* **1993**, *3*, 2415–2418.
- [16] Compound **1** was first synthesized by Merola and co-workers, see: a) J. S. Merola, K. S. Campo, R. A. Gentile, *Inorg. Chem.* **1989**, *28*, 2950–2954; b) J. S. Merola, K. S. Campo, R. A. Gentile, M. A. Modrick, *Inorg. Chim. Acta* **1989**, *165*, 87–90.
- [17] $\text{salph} = N,N'$ -bis(3,5-di-*tert*-butylsalicylidene)phenylenediamine. Catalyst **2** is highly active for epoxide carbonylation (ref. [11]).
- [18] Complexes screened for activity included $\text{Na}[\text{Co}(\text{CO})_4]$, $[\text{Ph}_4\text{P}][\text{Co}(\text{CO})_4]$, $[\text{nBu}_4\text{N}][\text{Co}(\text{CO})_4]$, and $[\text{Cp}_2\text{Co}][\text{Co}(\text{CO})_4]$.
- [19] During the screening phase, $\text{Na}[\text{Co}(\text{CO})_4]$ (2 mol %, 16 h, 80 °C, 6900 kPa (1000 psi) CO, triglyme) reacted with propylene oxide to give a mixture of products, yielding mostly acetone (6 %) and poly(β -hydroxybutyrate) (40 %).
- [20] M. Tokunaga, J. F. Larrow, F. Kakiuchi, E. N. Jacobsen, *Science* **1997**, *277*, 936–938.
- [21] S. C. Casegreen, S. G. Davies, C. J. R. Hedgcock, *Synlett* **1991**, 779–780.
- [22] A. Griesbeck, D. Seebach, *Helv. Chim. Acta* **1987**, *70*, 1320–1325.
- [23] a) D. S. Noyce, E. H. Banitt, *J. Org. Chem.* **1966**, *31*, 4043–4047; b) W. Adam, J. Baeza, J. Liu, *J. Am. Chem. Soc.* **1972**, *94*, 2000–2006.
- [24] Alper and co-workers have reported the retention of stereochemistry in the carbonylation of 2,3-epoxybutanes (ref. [12d]), which is in variance with our results. As the result of a typographical error (personal communication, P. Dervan) in the literature upon which these assignments were based (ref. [25]), we propose that the $[\text{PPN}][\text{Co}(\text{CO})_4]/\text{BF}_3 \cdot \text{OEt}_2$ system in fact proceeds with inversion of stereochemistry, as well.
- [25] P. B. Dervan, C. R. Jones, *J. Org. Chem.* **1979**, *44*, 2116–2123.
- [26] H. M. I. Osborn, J. Sweeney, *Tetrahedron: Asymmetry* **1997**, *8*, 1693–1715.
- [27] D. Tanner, *Angew. Chem.* **1994**, *106*, 625–646; *Angew. Chem. Int. Ed. Engl.* **1994**, *33*, 599–619.

Remarkably High 1,5-Diastereoselectivity in a Nickel-Catalyzed Conjugate Addition of Me_2Zn and Carbonyl Compounds to 1, ω -Dienynes with Through-Space Coupling**

Akihiro Ezoe, Masanari Kimura,* Takahiro Inoue, Masahiko Mori, and Yoshinao Tamaru*

Carbon–carbon-bond formation is the most important and fundamental process in organic synthesis. In particular, the coupling reaction of unsaturated C–C bonds mediated by low-valent transition metals is a rapidly growing field and is now

an indispensable strategy in synthetic chemistry.^[1] Since the pioneering work of Wilke and co-workers,^[2] nickel complexes have been widely utilized as efficient catalysts for C–C-bond formations.^[3] Intramolecular variants such as the [4+2] cycloaddition reaction of 1, ω -dienynes [Eq. (1)],^[4] cyclization of 1, ω -bis(enones),^[5] ω -dienyl aldehydes,^[6] and ω -alkynyl enones [Eq. (2)]^[7] are all useful methods for the synthesis of rather complex cyclic molecules of physiological interest.^[8]



We report herein the four-component reaction of dimethylzinc, carbonyl compounds (aldehydes, ketones), and dienes and alkynes of 1, ω -dienylalkynes **1** in the presence of a catalytic amount of $[\text{Ni}(\text{acac})_2]$ (acac = acetylacetonato) at room temperature to provide alkylidene cyclopentanes **2a,b** ($\text{X} = \text{C}(\text{CO}_2\text{Et})_2$) and their heterocyclic analogues **2c–e** ($\text{X} = \text{O}$, NTs) in good yields and with excellent stereoselectivity (Table 1). This four-component reaction may be regarded as an extended version of the reactions portrayed in Equation (1) (a two-component coupling of a diene and an alkyne) and in Equation (2) (a three-component coupling of organozinc, alkyne, and enone).

The scope of the present reaction was examined with various 1, ω -dienynes **1a–e** (1.0 mmol) in the presence of a catalytic amount of $[\text{Ni}(\text{acac})_2]$ (0.1 mmol), an aldehyde or ketone (2.0 mmol), and dimethylzinc (2.4 mmol) in dry THF at room temperature under nitrogen. All the 1, ω -dienynes **1a–e** were so reactive that almost all the reactions were complete within 1 h at room temperature, irrespective of R^1 and X of **1** and of the carbonyl compounds (Table 1). The conjugate addition of $[\text{Me}_2\text{Zn}]$ and of the carbonyl compound to 1, ω -dienynes **1** occurs at the terminal positions of the alkyne and the diene moieties, respectively; the through-space interactions of the alkyne and diene groups ensure C–C coupling at the internal positions. Terminal alkyne **1a** provided **2a** in moderate yield (Table 1, entry 1), whereas internal alkynes **1b–e** general gave more satisfactory results (Table 1, entries 2–11). Especially rewarding here is that the 1, ω -dienynes tethered by a nitrogen (**1c**) or an oxygen (**1d,e**) reacted with similar ease and furnished pyrrolidine and tetrahydrofuran derivatives, respectively, in reasonable yields. Bulky substituents around the carbonyl group either retard the reaction (Table 1, entry 10) or cause a decrease in yield (Table 1, entry 11). The reaction displayed a remarkably high level of stereoselectivity (> 97 %, in most cases) between the cycloalkane methine and the OH-bearing carbon centers as well as excellent stereoselectivity (100 %) with respect to the exocyclic tri- and tetrasubstituted double bonds.^[9]

The structures of **2** were tentatively assigned by analogy with the structure of piperidine derivative **4**, which was

[*] Dr. M. Kimura, Prof. Dr. Y. Tamaru, A. Ezoe, T. Inoue, M. Mori
Department of Applied Chemistry
Faculty of Engineering, Nagasaki University
1-14 Bunkyo-machi, Nagasaki 852-8521 (Japan)
Fax: (+81)95-847-9008
E-mail: masanari@net.nagasaki-u.ac.jp, tamaru@net.nagasaki-u.ac.jp

[**] We thank Y. Ohhama (NMR Facility) for technical assistance. Financial support by the Ministry of Education, Culture, Sports, Science, and Technology, Japanese Government, is gratefully acknowledged.

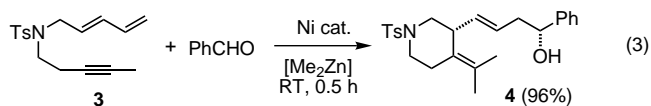
Supporting information for this article is available on the WWW under <http://www.angewandte.org> or from the author.

Table 1. Ni-catalyzed coupling reaction of 1, ω -dienynes, carbonyl compounds, and dimethylzinc.^[a]

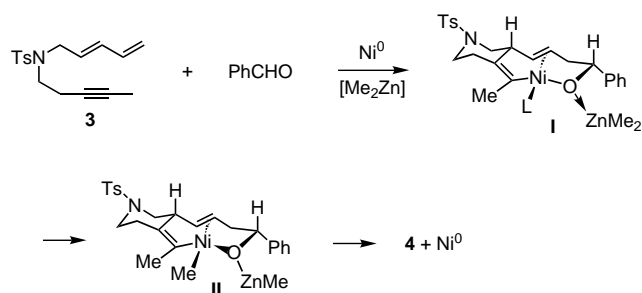
Entry	1	Carbonyl compound	<i>t</i> [h]	2	Yield [%] ^[b]	Ratio ^[c]
				$\text{X} \begin{array}{c} \text{CH=CH} \\ \text{C}\equiv\text{C-R}^1 \end{array} + \text{R}^2\text{CHO} \xrightarrow[\text{[Me}_2\text{Zn]}]{\text{Ni (cat.)}} \text{X} \begin{array}{c} \text{CH=CH} \\ \text{C=C(Me)-C}\equiv\text{C-R}^1 \end{array} \begin{array}{c} \text{R}^2 \\ \text{OH} \end{array}$		
1	a	PhCHO	1		45	11:1
2	b	PhCHO	1		63	7:1
3	c	PhCHO	1		67	> 30:1
4	d	PhCHO	0.5		71	> 30:1
5	e	PhCHO	1		61	7:1
6	b	PhCH ₂ CH ₂ CHO	1		89	> 30:1
7	b		1		64	> 30:1
8	c	PhCH ₂ CH ₂ CHO	1		64	> 30:1
9	c		1		71	> 30:1
10	c	<i>t</i> BuCHO	2		67	12:1
11	c		1		33	

[a] See Experimental Section for procedure. [b] Yield of isolated product. [c] The ratio of diastereomers was determined on the basis of the ^1H NMR spectra (400 MHz).

obtained as a single diastereomer in almost quantitative yield by reacting **3** and benzaldehyde under the standard conditions [Eq. (3)]; to our delight, a crystalline solid was formed which was suitable for X-ray crystallographic analysis.^[10]



A plausible reaction mechanism for the nickel(0)-catalyzed coupling reaction is shown in Scheme 1.^[11] Either a concerted or a stepwise mechanism could be involved in the oxidative cyclization of nickel(0) metal with aldehyde, alkyne, and diene to give rise to intermediate **I**, which would then undergo migration of a methyl group from zinc(II) to nickel(II) to afford a methylvinylnickel(II) intermediate **II**. The intermediate **II** undergoes reductive elimination to provide **4** and an active



Scheme 1. Plausible reaction mechanism for the Ni-catalyzed four-component coupling reaction.

nickel(0) species. It is premature to discuss the origin of 1,5-diastereoselectivity. This issue will be addressed in the near future with the help of quantum mechanics and additional experimental data. A scenario outlined in Scheme 1 also agrees well with the stereoselective formation of (*Z*)-**2a** and (*Z*)-**2e**, the structures of which were determined on the basis of NOE experiments.

The conditions applied to the present reaction is essentially the same as those developed in our laboratories^[12] for a three-component coupling reaction ($[\text{Me}_2\text{Zn}]$, 1,3-dienes, and carbonyl compounds) in which $[\text{Me}_2\text{Zn}]$ and the carbonyl compounds undergo conjugate addition to the 1,3-dienes in a 1,4-fashion and provide 3-hexenols; however, no such products were detected at all for all the reactions of **1** and **3** examined so far. This indicates that an alkyne is an excellent reaction partner.

In conclusion, we have developed a nickel-catalyzed conjugate addition reaction of [Me₂Zn] and carbonyl compounds to 1,ω-dienynes **1** and **3**, which afford cycloalkanes and their heterocyclic analogues **2** and **4**, respectively, in good yields. The products **2** and **4** are characterized by the stereodefined exocyclic tri- and tetrasubstituted double bonds (100% purity) and also by the remarkably high 1,5-diastereomeric purity (>97%, in most cases) with respect to C2 of cycloalkane rings and C4 of *trans*-4-hydroxy-1-butenyl side chains. Synthetic applications and further methodological studies, including a fully intermolecular version of the present four-component coupling reaction, that is, a coupling of four independent reaction partners, are in progress.

Experimental Section

2f (Table 1, entry 6): Dihydrocinnamaldehyde (268 mg, 2.0 mmol) and dimethylzinc (2.4 mL, 1M in hexane) were added successively to a homogeneous solution of $[\text{Ni}(\text{acac})_2]$ (25.6 mg, 0.1 mmol) and **1b** (278 mg, 1.0 mmol) in dry THF (5 mL). The reaction mixture was stirred at room temperature for 1 h under N_2 and then quenched by the addition of HCl (2 M, 20 mL). The mixture was extracted twice with ethyl acetate. The combined organic extract was washed with a saturated NaHCO_3 solution and a saturated NaCl solution and then dried (MgSO_4) and concentrated in vacuo. The residue was purified by column chromatography over silica gel (hexane/ethyl acetate 12:1) to give **2f** (380 mg, 89%). R_f = 0.56 (hexane/ethyl acetate 2:1); IR (neat): $\tilde{\nu}$ = 3480 (s), 2930 (s), 1732 (s), 1497 (m), 1252 (s), 1191 (s), 1062 (m), 972 (m), 700 (s) cm^{-1} ; ^1H NMR (400 MHz, CDCl_3 , TMS): δ = 1.23 (t, J = 7.1 Hz, 3H), 1.24 (t, J = 7.1 Hz, 3H), 1.58 (s, 3H), 1.66 (s, 3H), 1.76 (dt, J = 6.2, 8.4 Hz, 2H), 2.06 (dt, J = 13.7, 7.8 Hz, 1H), 2.11 (dd, J = 5.1, 13.2 Hz, 1H), 2.22 (dtm, J = 13.7, 5.5 Hz, 1H), 2.58 (dd, J = 8.4, 13.2 Hz, 1H), 2.68 (dt, J = 13.9, 8.4 Hz, 1H), 2.78 (br ddd, J = 6.2, 8.4, 13.9 Hz, 1H), 2.83 (br d, J = 15.3 Hz, 1H), 2.98 (br d, J = 15.3 Hz, 1H), 3.35

(br d, $J=5.1$ Hz, 1H), 3.60 (dddm, $J=5.5, 7.8, 8.4$ Hz, 1H), 4.16 (q, $J=7.1$ Hz, 2H), 4.17 (q, $J=7.1$ z, 2H), 5.30 (br ddd, $J=5.5, 7.8, 15.2$ Hz, 1H), 5.39 (br dd, $J=5.9, 15.2$ Hz, 1H), 7.16–7.32 ppm (m, 5H); ^{13}C NMR (100 MHz, CDCl_3 , TMS): $\delta=14.1, 20.9, 30.7, 35.3, 38.4, 40.5, 40.8, 44.1, 59.4, 70.2, 125.7, 125.8, 128.5, 133.1, 136.3, 140.3, 172.3$ ppm; elemental analysis calcd for $\text{C}_{26}\text{H}_{36}\text{O}_5$: C 72.87, H 8.47; found: C 72.94, H 8.29.

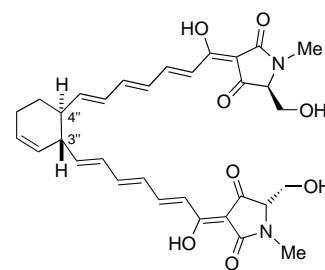
Received: March 15, 2002 [Z18903]

Total Synthesis of Polycephalin C and Determination of the Absolute Configurations at the 3'',4'' Ring Junction**

Deborah A. Longbottom, Angus J. Morrison, Darren J. Dixon, and Steven V. Ley*

Tetramic acids (2,4-pyrrolidinediones) are an important family of nitrogen-containing heterocycles, well known for their potent antibiotic, antiviral, antifungal, and cytotoxic activity.^[1] Many tetramic acid natural products are highly complex frameworks containing several stereogenic centers. It is this complexity, together with the fact that these targets have potential or known biological activity, which makes their synthesis a worthwhile and challenging goal for the organic chemist, particularly so when the natural product is in short supply from the natural source.

In 1998, Nowak and Steffan isolated polycephalin C (**1**) as a new member of this group of natural products from *Physarum polycephalum*.^[2] Polycephalin C (**1**) is a bis(trienoyltetramic acid), linked by an unusual asymmetric cyclohexene ring. The



polycephalin C (**1**)
showing unknown 3'',4'' absolute stereochemistry

tetramic acid unit of each terminus is derived from (*S*)-*N*-methyl serine and is linked by a fully conjugated *all-E*-triene chain to the cyclohexene ring. This unusual tetramic acid is thought to be one of several metabolites responsible for the yellow color of the wild-type plasmodia of *Physarum polycephalum*.^[2]

Although the structure elucidation had established that the relative stereochemistry at the 3'',4'' ring junction of the natural product was *trans*, the absolute configuration at these positions had not been determined.^[2] Therefore, intrigued by both the novel structure of this unusual polyenoyltetramic acid and the need to define the absolute stereochemistry at

- [1] J. Tsuji, *Transition Metal Reagents and Catalysts*, Wiley, Chichester, 2000.
- [2] a) G. Wilke, B. Bogdanovic, P. Hardt, P. Heimbach, W. Keim, M. Kröner, W. Oberkirch, K. Tanaka, D. Steinbrücke, E. Walter, H. Zimmermann, *Angew. Chem.* **1966**, 78, 157–172; *Angew. Chem. Int. Ed. Engl.* **1966**, 5, 151–164; b) R. Benn, N. Büssemeier, P. Holle, W. Jolly, R. Mynott, I. Tkatchenko, G. Wilke, *J. Organomet. Chem.* **1985**, 279, 63–86.
- [3] a) K. Tamao, K. Kobayashi, Y. Ito, *Synlett* **1992**, 539–546; b) E. Oblinger, J. Montgomery, *J. Am. Chem. Soc.* **1997**, 119, 9065–9066; c) M. Kimura, A. Ezoe, K. Shibata, Y. Tamaru, *J. Am. Chem. Soc.* **1998**, 120, 4033–4034; d) M. Kimura, H. Fujimatsu, A. Ezoe, K. Shibata, M. Shimizu, S. Matsumoto, Y. Tamaru, *Angew. Chem.* **1999**, 111, 410–413; *Angew. Chem. Int. Ed.* **1999**, 38, 397–399; e) Y. Tamaru, *Organomet. Chem.* **1999**, 576, 215–231; f) J. Montgomery, *Acc. Chem. Res.* **2000**, 33, 467–473; g) S. Ikeda, *Acc. Chem. Res.* **2000**, 33, 511–520; h) I. N. Houpi, J. Lee, *Tetrahedron* **2000**, 56, 817–846.
- [4] a) P. A. Wender, T. E. Jenkins, *J. Am. Chem. Soc.* **1989**, 111, 6432–6434; b) P. A. Wender, T. E. Smith, *J. Org. Chem.* **1995**, 60, 2962–2963; c) P. A. Wender, T. E. Smith, *J. Org. Chem.* **1996**, 61, 824–825; for rhodium-catalyzed reactions, see: d) L. McKinstry, T. Livinghouse, *Tetrahedron* **1994**, 50, 6145–6154; e) S.-J. Paik, S. U. Son, Y. K. Chung, *Org. Lett.* **1999**, 1, 2045–2047; f) B. Wang, P. Cao, X. Zhang, *Tetrahedron Lett.* **2000**, 41, 8041–8044; for palladium-catalyzed reactions, see: g) X. Xie, X. Lu, X. *Tetrahedron Lett.* **1999**, 40, 8415–8418.
- [5] A. V. Savchenko, J. Montgomery, *J. Org. Chem.* **1996**, 61, 1562–1563.
- [6] a) Y. Sato, M. Takimoto, M. Mori, *J. Am. Chem. Soc.* **2000**, 122, 1624–1634; b) K. Shibata, M. Kimura, M. Shimizu, Y. Tamaru, *Org. Lett.* **2001**, 3, 2181–2183.
- [7] a) J. Montgomery, E. Oblinger, A. V. Savchenko, *J. Am. Chem. Soc.* **1997**, 119, 4911–4920; b) J. Seo, H. M. P. Chui, M. J. Heeg, J. Montgomery, *J. Am. Chem. Soc.* **1999**, 121, 476–477; c) S. K. Chowdhury, K. K. D. Amarasinghe, M. J. Heeg, J. Montgomery, *J. Am. Chem. Soc.* **2000**, 122, 6775–6776.
- [8] a) X.-Q. Tang, J. Montgomery, *J. Am. Chem. Soc.* **1999**, 121, 6098–6099; b) M. V. Chevliakov, J. Montgomery, *J. Am. Chem. Soc.* **1999**, 121, 11139–11143; c) J. Seo, H. Fain, J. B. Blanc, J. Montgomery, *J. Org. Chem.* **1999**, 64, 6060–6065.
- [9] The two isomers of **2** are apparently as a result of the relative configuration of the 1,5-stereogenic centers and not that of exocyclic double bonds. For example, PCC oxidation of a 7:1 mixture of **2e** provided the corresponding ketone as a single isomer, which furnished a 1:1 mixture of **2e** upon reduction with NaBH_4 .
- [10] CCDC-178844 contains the supplementary crystallographic data for this paper. These data can be obtained free of charge via www.ccdc.cam.ac.uk/conts/retrieving.html (or from the Cambridge Crystallographic Data Centre, 12, Union Road, Cambridge CB21EZ, UK; fax: (+44) 1223-336-033; or deposit@ccdc.cam.ac.uk).
- [11] A similar reaction mechanism has been reported for a Ni-catalyzed alkylative carbocyclization of alkynyl enones [e.g., Eq. (2)] and for a Ni-catalyzed three-component coupling reaction of alkynes, aldehydes, and organozinc compounds: a) A. V. Savchenko, J. Montgomery, *J. Am. Chem. Soc.* **1996**, 118, 2099–2100; b) X. Q. Tang, J. Montgomery, *J. Org. Chem.* **1999**, 64, 9310–9313; c) K. K. D. Amarasinghe, S. K. Chowdhury, M. J. Heeg, J. Montgomery, *Organometallics* **2001**, 20, 370–372.
- [12] a) M. Kimura, S. Matsuo, K. Shibata, Y. Tamaru, *Angew. Chem.* **1999**, 111, 3586–3589; *Angew. Chem. Int. Ed.* **1999**, 38, 3386–3388; b) M. Kimura, K. Shibata, K. Koudahashi, Y. Tamaru, *Tetrahedron Lett.* **2000**, 41, 6789–6793; c) K. Shibata, M. Kimura, K. Kojima, S. Tanaka, Y. Tamaru, *J. Organomet. Chem.* **2001**, 624, 348–353.

[*] Prof. Dr. S. V. Ley, Dr. D. A. Longbottom, Dr. A. J. Morrison, Dr. D. J. Dixon
Department of Chemistry
University of Cambridge
Lensfield Road, Cambridge CB2 1EW (UK)
Fax: (+44) 1223-336-442
E-mail: svl1000@cam.ac.uk

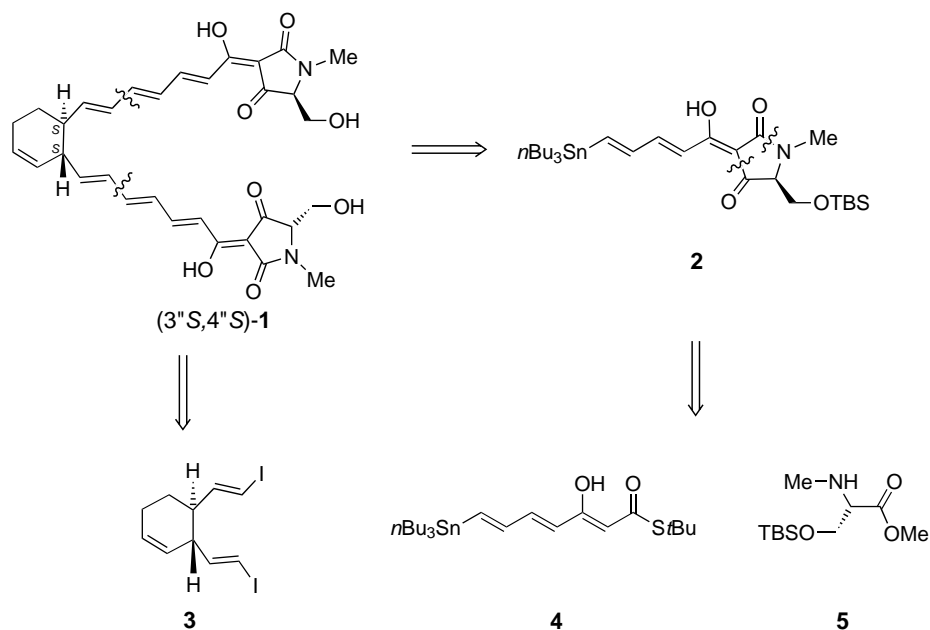
[**] We gratefully acknowledge financial support from the EPSRC (to D.J.D. and D.A.L.), AstraZeneca (to A.J.M.), and the Novartis Research Fellowship (to S.V.L.). The authors also thank Dr. B. Steffan (Thetis - Institut für biomolekulare Naturstoffforschung) for NMR and CD spectra of natural polycephalin C.

the 3'',4'' ring junction, we devised a synthesis route to the natural product.

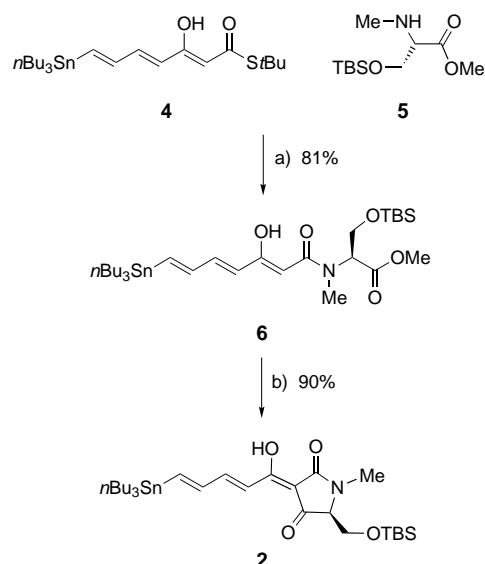
As the 3'',4'' ring junction configuration of polycephalin C (**1**) could be *R,R* or *S,S*, we arbitrarily selected the *S,S* isomer as the initial synthesis target. Analysis suggested a convergent approach, in which **1** is synthesized from two major fragments, the stannylated dienoyltetramic acid **2** and the bisiodovinyl intermediate **3** (Scheme 1). It was thought that **2** would be readily available from thioester **4** and amino ester **5**, fragments which had been devised and then used in the total synthesis of physarorubinic acid previously by our group.^[3] Double Stille coupling to connect bisiodide **3** and tetramic acid **2**,^[4] followed by TBS deprotection would then give polycephalin C (**1**) in a concise fashion. The synthesis of dienoyltetramic acid **2** is discussed first, followed by the synthesis of fragment **3** and the closing steps of the synthesis.

The two-step sequence which leads to the formation of dienoyltetramic acid **2** begins with an aminolysis reaction mediated by silver(I) trifluoroacetate (Scheme 2).^[5] In this particular case, it was found that an excess of triethylamine was crucial in preventing destannylation of the dienoylstannane **4**. Under these basic conditions, the silver-salt-mediated aminolysis reaction was complete after just 20 minutes at 0 °C and furnished the desired β -keto amide **6** in an excellent 81 % yield. Exposure of **6** to NaOMe in MeOH at 25 °C for two minutes then facilitated Lacey–Dieckmann cyclization which lead directly to dienoyltetramic acid **2** in a pleasing 90 % yield.^[6]

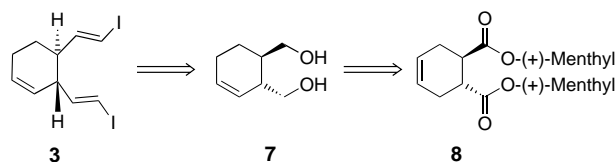
With the tetramic acid portion of polycephalin C in hand, attention was focussed on the synthesis of the bisiodovinyl fragment **3**. It was envisaged that, starting from key intermediate cyclohexene diol **7**, 1,4-dioxidation and an unprecedented double Takai reaction^[7] would provide the desired bisiodide **3** (Scheme 3). It was expected that diol **7** would be prepared from Diels–Alder adduct **8**; double-bond manipulation and exhaustive reduction would subsequently provide desired diol **7**.



Scheme 1. Synthetic plan for polycephalin C (**1**). TBS = *tert*-butyldimethylsilyl.



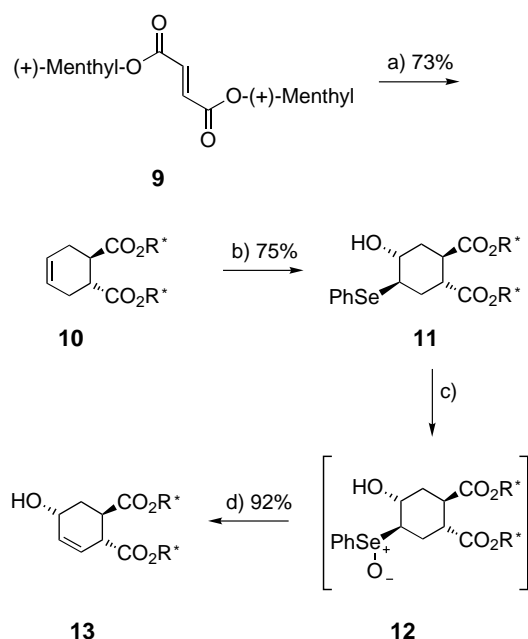
Scheme 2. Synthesis of dienoyltetramic acid **2**. a) $\text{CF}_3\text{CO}_2\text{Ag}$, NEt_3 , THF, 0 °C, 20 min; b) NaOMe, MeOH, 25 °C, 2 min.



Scheme 3. Synthetic plan for bisiodovinyl fragment **3**.

The asymmetric Diels–Alder reaction employed in this case combines the dienophile, dimethyl fumarate **9**, with 1,3-butadiene and is reported to occur with excellent diastereoselectivity.^[8] Indeed in this case, the low-temperature Lewis acid mediated reaction proceeded to afford exclusively the desired Diels–Alder adduct (*R,R*)-**10** (d.e. > 95 % by NMR) in a 73 % yield (Scheme 4).

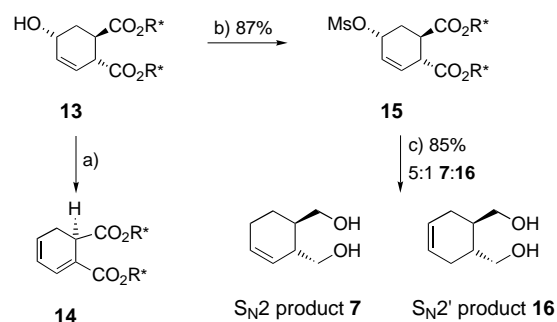
With the ring junction stereochemistry created in the Diels–Alder adduct **10**, double-bond transposition was then required. It was envisaged that overall addition of phenylselenenic acid and a subsequent oxidation–elimination sequence would effect the desired process. Overall addition of phenylselenenic acid to an alkene has been reported previously.^[9] In this case, phenylselenium bromide in MeCN/water (15:1) facilitated smooth addition across the double bond of Diels–Alder adduct **10** and provided analytically pure hydroxyselenide **11** as the only diastereomer. *m*-CPBA oxidation of the phenylselenium moiety in the addition product **11** produced hydroxyselenoxide **12**, which then underwent elimination in the pres-



Scheme 4. Synthesis of allylic alcohol **13**. a) Et_2AlCl , 1,3-butadiene, -60°C , 36 h; b) PhSeBr , $\text{MeCN}/\text{H}_2\text{O}$ (15:1), 50°C , 12 h; c) *m*-CPBA, CH_2Cl_2 , -30°C , 5 min; d) diisopropylamine, 50°C , 14 h. *m*-CPBA = *m*-chloroperoxybenzoic acid.

ence of diisopropylamine at 50°C to generate allylic alcohol **13** in an excellent 92 % yield (Scheme 4).

It was clear that the most efficient design of the synthesis would incorporate removal of the allylic hydroxy group with concomitant reduction of the (+)-menthyl esters. We believed that mesylation and subsequent exhaustive reduction would be effective. However, attempted mesylate formation at 0°C was found to give diene **14** as the main product of the reaction (Scheme 5), formed by elimination of the mesylate immediately after formation. To prevent this side reaction, mesylate

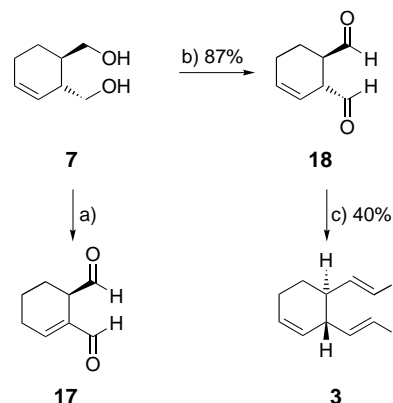


Scheme 5. Synthesis of diol **7**. a) MsCl , NEt_3 , CH_2Cl_2 , 0°C ; b) MsCl , NEt_3 , CH_2Cl_2 , $-78 \rightarrow -15^\circ\text{C}$; c) LiAlH_4 , THF, $-78^\circ\text{C} \rightarrow \text{RT}$.

formation was therefore carried out at lower temperature and pleasingly provided the desired allylic mesylate **15**, the structure of which has been confirmed by X-ray crystallography.^[10, 11] This was then used directly in the LiAlH_4 reduction of both esters and mesylate. The reduction led to an 85 % yield of a separable mixture of diols **7** (product of direct $\text{S}_{\text{N}}2$ attack) and **16** (product of $\text{S}_{\text{N}}2'$ attack) in a 5:1 ratio (Scheme 5), and provided a 71 % yield of the desired diol **7**. By

utilizing this synthetic sequence, gram quantities of diol **7** were accessed.

The 1,4-oxidation of diol **7** was then investigated and the Swern reaction selected as the optimum method.^[12] Unfortunately, initial attempts gave α,β -unsaturated dialdehyde **17** (Scheme 6); the double bond had moved into conjugation

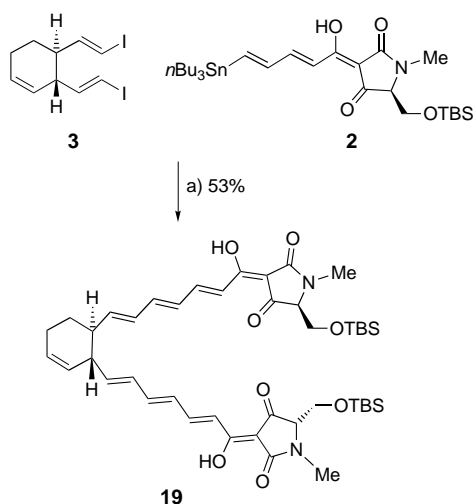


Scheme 6. Synthesis of bis-iodovinyl fragment **3**. a) $(\text{COCl})_2$, DMSO, CH_2Cl_2 , -78°C , 2 h; then NEt_3 , $-78 \rightarrow -10^\circ\text{C}$; b) $(\text{COCl})_2$, DMSO, CH_2Cl_2 , -78°C , 1.5 h; then $i\text{Pr}_2\text{NEt}$, $-78 \rightarrow -10^\circ\text{C}$; c) CrCl_2 , CHI_3 , THF, $0^\circ\text{C} \rightarrow \text{RT}$, 2 h.

with the proximal aldehyde as a result of the acidic nature of the allylic proton in the oxidation product **18**. However, this problem could be overcome by replacement of triethylamine with a more hindered base.^[13] Thus, Swern oxidation with diisopropylethylamine, followed by a cold acidic workup and washing with a pH 7 buffer solution provided the desired aldehyde **18** in high yield and purity (Scheme 6). The unstable nature of this compound meant that it was always freshly prepared for immediate use in the subsequent step, formation of the Stille coupling partner **3**.

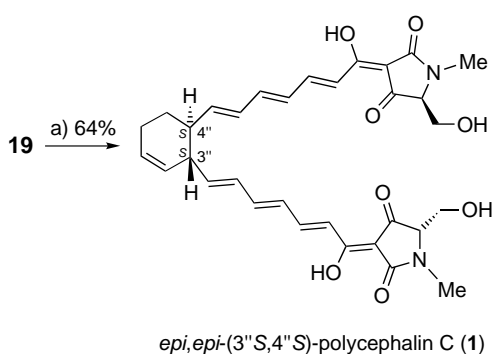
A double Takai olefination reaction^[7] was selected to ensure the required *E* double-bond geometry in bisiodide **3**. However, because of the nonpolar nature of **3**, it was impossible to separate it from the residual excess of iodoform employed in the Takai reaction. Therefore, to obtain pure material for the Stille coupling, it was not possible to use an excess of iodoform, a constraint which led to a slightly disappointing but acceptable 40 % yield considering the transformation which has been achieved (Scheme 6); the reaction was extremely selective for the desired product **3** (> 90 % bis-*trans* product by NMR) and hence the bisiodide **3** was formed from diol **7** in just two steps and overall 35 % yield (Scheme 6).

A number of catalysts were then screened to ascertain which would facilitate the desired double Stille coupling in the most efficient manner, the best of which proved to be $[\text{PdCl}_2(\text{CH}_3\text{CN})_2]$. Following optimization studies, the product **19** of the key double Stille coupling was successfully prepared in a good 53 % yield (Scheme 7); two key bonds are formed in this reaction and, considering the possible palladium-mediated side reactions, this was an extremely pleasing outcome.



Scheme 7. Stille coupling of fragments **2** and **3**. a) $[\text{PdCl}_2(\text{MeCN})_2]$ (15 mol %), DMF, RT, 1 h.

The final step of the synthesis, removal of the TBS ethers, was carried out with trifluoroacetic acid (TFA)/water (9:1) which facilitated smooth deprotection when added and immediately removed under reduced pressure (three times).^[3a] Because all side products and excess reagents are volatile, crude **1** was afforded directly (Scheme 8), as no reaction workup was necessary. Purification by reverse-phase HPLC then gave (3''*S*,4''*S*)-**1** in 64 % yield and overall 3.7 % yield from dimenthyl fumarate **9**.

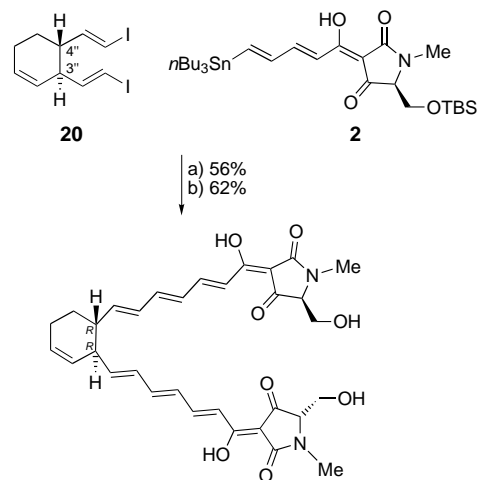


Scheme 8. Synthesis of *epi, epi*-(3''*S*,4''*S*)-polyccephalin C (**1**). a) TFA/H₂O (9:1) × 3, RT (64 %).

The spectroscopic data (¹H and ¹³C NMR, MS, IR) of this synthetic material compared well with that published in the literature and the coupling constants from the polyene chains indicated the *all-E* double-bond geometry. However, despite being of the correct sign, the optical rotation was found to differ from that given in the structure elucidation paper.^[2] The CD spectrum in the range from 300 to 450 nm was also different and from this it was concluded that the 3''*S*,4''*S*-configured compound was in fact *epi, epi*-(3''*S*, 4''*S*)-polyccephalin C (Scheme 8) and that the isolated natural product had the *R,R* configuration about the ring junction.

To prove that this was correct, the synthesis had to be repeated beginning with (–)-dimenthyl fumarate to create the opposite configuration at the 3'',4'' ring junction. Synthesis of

bis-iodovinyl fragment **20** proceeded uneventfully following the procedure outlined for **3**. Following Stille coupling with stannane **2**, deprotection gave polyccephalin C (**1**), with 3''*R*,4''*R* stereochemistry at the ring junction (Scheme 9).



polyccephalin C (**1**)
showing correct 3'',4''-(*R,R*) absolute stereochemistry

Scheme 9. Synthesis of (3''*R*,4''*R*)-polyccephalin C (**1**). a) $[\text{PdCl}_2(\text{MeCN})_2]$ (5 mol %), DMF, RT, 1 h; b) TFA/H₂O (9:1) × 3, RT.

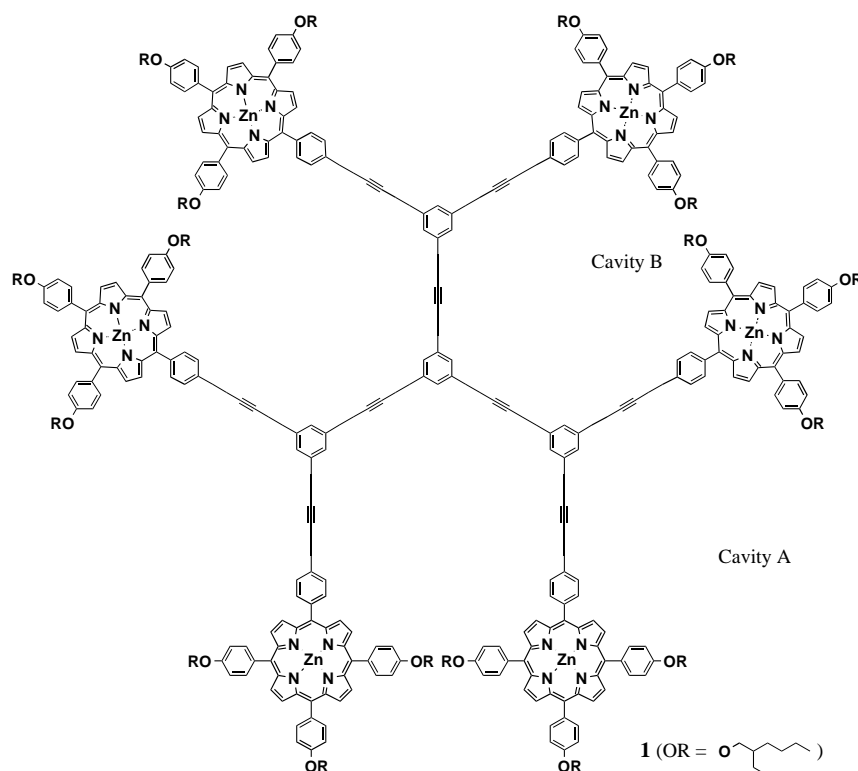
The spectroscopic data (¹H and ¹³C NMR, MS, IR) of this synthetic material were in excellent agreement with that published in the literature and the coupling constants from the polyene chains again proved that the *all-E* double-bond geometry was intact. In this case the optical rotation and the CD spectrum, crucial for confirmation of configuration, were also in excellent agreement with the published data.

Thus, the total synthesis of this unusual bistetramic acid, polyccephalin C (**1**), has been completed in a short and efficient fashion and the original challenge of defining the absolute configuration of the ring junction has been met. Through synthesis, we have been able to unambiguously assign the 3''*R*,4''*R* stereochemical configuration and thus complete the definition of the structure of this molecule.

Received: March 25, 2002 [Z18980]

- [1] B. J. L. Royle, *Chem. Rev.* **1995**, 95, 1981.
- [2] a) A. Nowak, B. Steffan, *Angew. Chem.* **1998**, 110, 3341; *Angew. Chem. Int. Ed.* **1998**, 37, 3139.
- [3] a) D. J. Dixon, S. V. Ley, D. A. Longbottom, *J. Chem. Soc. Perkin Trans. 1* **1999**, 2231; b) D. J. Dixon, S. V. Ley, T. Gratzka, P. Szolcsanyi, *J. Chem. Soc. Perkin Trans. 1* **1999**, 839.
- [4] a) T. N. Mitchell, *Synthesis* **1992**, 803; b) J. K. Stille, *Angew. Chem.* **1986**, 98, 504; *Angew. Chem. Int. Ed. Engl.* **1986**, 25, 508; c) J. K. Stille, B. L. Groh, *J. Am. Chem. Soc.* **1987**, 109, 813.
- [5] a) S. Masamune, S. Kamata, W. Schilling, *J. Am. Chem. Soc.* **1975**, 97, 3515; b) S. Masamune, Y. Hayase, W. Schilling, W. K. Chan, G. S. Bates, *J. Am. Chem. Soc.* **1977**, 99, 6756; c) S. V. Ley, P. R. Woodward, *Tetrahedron Lett.* **1987**, 28, 3019.
- [6] a) R. N. Lacey, *J. Chem. Soc.* **1954**, 850; b) J. Poncet, P. Jouin, B. Castro, L. Nicolas, M. Boutar, A. Gaudemer, *J. Chem. Soc. Perkin Trans. 1* **1990**, 611; c) S. V. Ley, S. C. Smith, P. R. Woodward, *Tetrahedron Lett.* **1988**, 29, 5829; d) S. V. Ley, S. C. Smith, P. R. Woodward, *Tetrahedron* **1992**, 48, 1145.

- [7] K. Takai, K. Nitta, K. Utimoto, *J. Am. Chem. Soc.* **1986**, *108*.
- [8] a) H. M. Walborsky, L. Barash, T. C. Davis, *J. Org. Chem.* **1961**, *26*, 4778; b) H. M. Walborsky, L. Barash, T. C. Davis, *Tetrahedron* **1963**, *19*, 2333; c) K. Furuta, I. Iwanga, H. Yamamoto, *Tetrahedron Lett.* **1986**, *27*, 4507.
- [9] a) M. A. Cooper, A. D. Ward, *Tetrahedron Lett.* **1995**, *36*, 2327; b) P. Ceccherelli, M. Curini, F. Epifano, M. C. Marcotullio, O. Rosati, *J. Org. Chem.* **1996**, *61*, 2882.
- [10] CCDC-181952 contains the supplementary crystallographic data for this paper. These data can be obtained free of charge via www.ccdc.cam.ac.uk/conts/retrieving.html (or from the Cambridge Crystallographic Data Centre, 12, Union Road, Cambridge CB2 1EZ, UK; fax: (+44) 1223-336-033; or deposit@ccdc.cam.ac.uk).
- [11] The authors thank Dr. J. E. Davies and Dr. A. D. Bond for X-ray analysis.
- [12] S. C. Howell, S. V. Ley, M. Mahon, *J. Chem. Soc. Chem. Commun.* **1981**, 507.
- [13] D. M. Walba, W. N. Thurmes, R. C. Haltiwanger, *J. Org. Chem.* **1988**, *53*, 1046.



A Dendritic Porphyrin Receptor for C₆₀ Which Features a Profound Positive Allosteric Effect

Masatsugu Ayabe, Atsushi Ikeda, Yohei Kubo, Masayuki Takeuchi, and Seiji Shinkai*

The developmental investigation of the novel application of dendrimers and dendritic compounds has been of recent concern.^[1] Dendrimers, as host molecules have attracted a great deal of attention because of their unique topology, well-defined structures, and unusual guest-binding behaviors compared to general polymers.^[2] As [60]fullerene (C₆₀) exhibits outstanding new chemical and physical properties, the molecular design of C₆₀ receptors is a growing research area.^[3] For the crystal state, several articles have shown that porphyrin derivatives cocrystallize with C₆₀ because of an attractive force between C₆₀ and a porphyrin-ring center.^[4] In organic solvents, Aida and co-workers^[5] and Reed and co-workers^[6] have shown that the porphyrin dimers have exceptionally high affinity for C₆₀. Herein, we describe a rigid star-shaped D₃-symmetric receptor **1**^[7] bearing six porphyrin

moieties linked with one another through phenylacetylene units. The dendritic receptor **1** has three rotational axes which affect the spatial arrangement of porphyrins (Figure 1), and the shape of the three clefts, each of which consists of two porphyrin planes. We have already demonstrated that the subunits for guest binding, which are rationally arranged around a rotational axis such as metal ion,^[8] C–C bond,^[9] or butadiynylene,^[10] work cooperatively to bind guest molecules in a nonlinear fashion (positive homotropic allostery). In addition, we have found that this effect is useful to bind guest molecules which are difficult to bind with a linear, 1:1 guest-binding fashion. As shown in Figure 1, when two porphyrins sandwich one C₆₀ molecule, the complexation site successively suppresses the rotational freedom of the remaining porphyrin “tweezers”. This “domino” effect is expected to be effective for the binding of three equivalents of C₆₀ in an allosteric manner to attain high C₆₀ affinity.

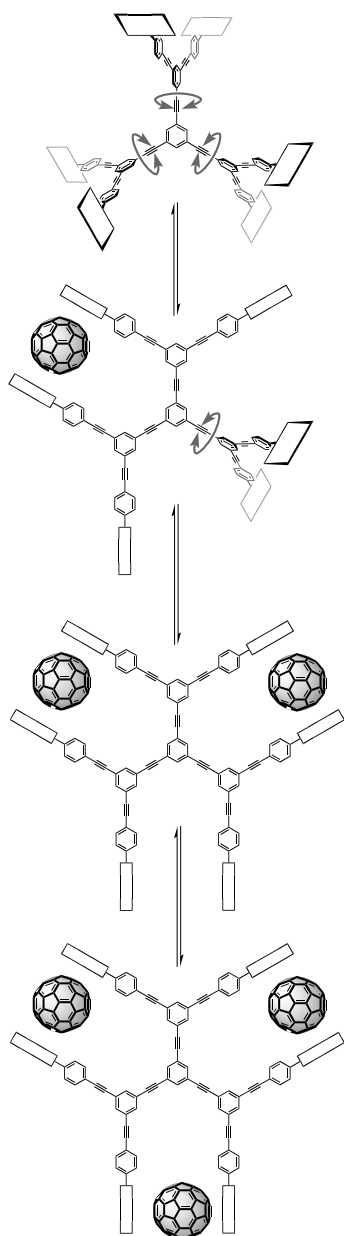
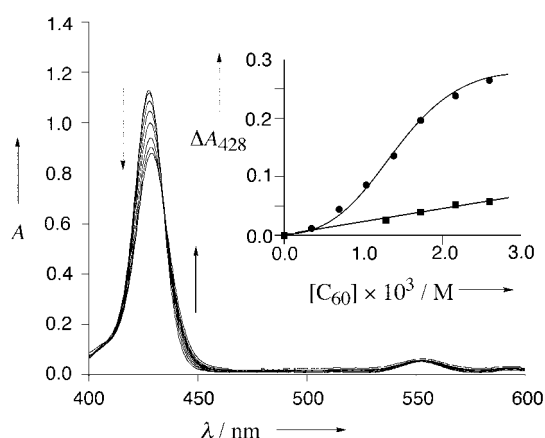
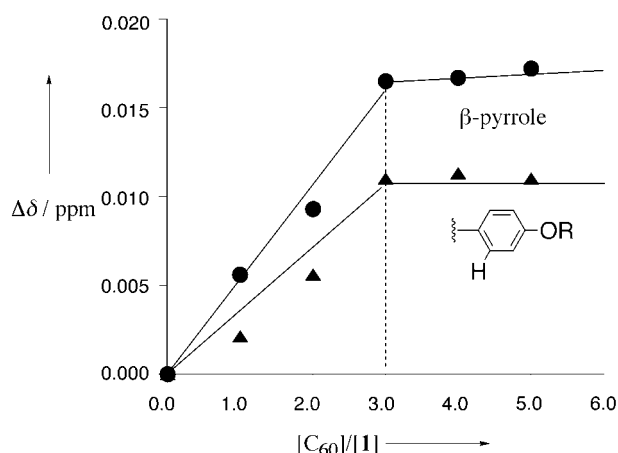
The formation of the **1**–C₆₀ complex in toluene was indicated by a change in the UV/Vis absorption spectra induced by successive addition of C₆₀ to **1** (Figure 2). The λ_{max} of the Soret band (428 nm) slightly shifts to longer wavelength (429 nm) with a tight isobestic point (435 nm in Soret band region). The spectral characteristics are coincident with those of recent findings for a few porphyrin–C₆₀ complexation systems.^[5, 6]

To estimate the stoichiometry between **1** and C₆₀, ¹H NMR spectra for [**1**]:[C₆₀] = 1:0–1:5 at 25 °C were measured in [D₈]toluene ([**1**] = 0.50 mM). The resonance signals of the *meso*-aryl protons and β-pyrrole protons shifted upfield on C₆₀ addition (see Supporting Information). As shown in Figure 3, a plot of Δδ versus [C₆₀]/[**1**] has a clear inflection point at [C₆₀]/[**1**] = 3.0. This value supports the view that the complex is

[*] Prof. S. Shinkai, M. Ayabe,^[+] Y. Kubo, Dr. M. Takeuchi
Department of Chemistry and Biochemistry
Graduate School of Engineering
Kyushu University
Fukuoka 812-8581 (Japan)
Fax: (+81) 92-642-3611
E-mail: seijitcm@mbox.nc.kyushu-u.ac.jp
Dr. A. Ikeda^[+]
Graduate School of Materials Science
Nara Institute of Science and Technology
8916-5 Takayama, Ikoma, Nara 630-0101 (Japan)

[+] PRESTO, Japan Science and Technology Corporation

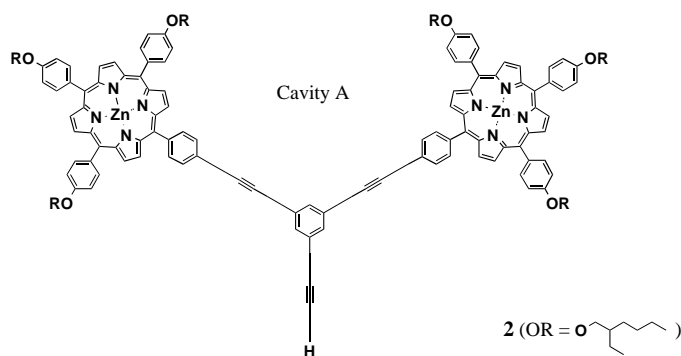
Supporting information for this article is available on the WWW under <http://www.angewandte.org> or from the author.


 Figure 1. Rotational axes of **1**.

 Figure 2. Absorption spectral change of **1** (5.3×10^{-6} M) in toluene at 25 °C: $[C_{60}] = 0 - 2.6 \times 10^{-3}$ M, 1 mm cell. Inset: plot of ΔA_{428} (●: **1**, ■: **2**) versus $[C_{60}]$. To normalize the porphyrin concentration, we set **[2]** to $3 \times [1]$.

 Figure 3. Plots of chemical-shift change versus $[C_{60}]/[1]$ where **[1]** was kept constant (0.5 mM); 400 MHz, $[D_8]$ toluene, 25 °C.

formed with a 1:3 **1**: C_{60} stoichiometry. These trends in the C_{60} -induced chemical-shift changes in the 1H NMR spectra are consistent with those of recent reports on porphyrin- C_{60} complexation systems.^[5, 6]

Very interestingly, a plot of the absorbance change at 428 nm (ΔA_{428}) versus $[C_{60}]$ featured a sigmoidal curve, which indicates that the binding of C_{60} to **1** occurs according to a well-defined cooperative phenomenon (inset of Figure 2).^[8a, b] This guest-binding profile was analyzed with the Hill equation: $\log(y/(1-y)) = n \log[\text{guest}] + \log K$, where K and n are the association constant and Hill coefficient, respectively, and $y = K/([C_{60}]^{-n} + K)$.^[11] From the slope and the intercept of the linear plot, we obtained $K = 1.4 \times 10^8 \text{ (M}^{-3}\text{)}$ for 1:3 **1**- C_{60} complex (correlation coefficient 0.995) and $n = 2.8$. The binding of the first C_{60} suppresses the rotation of two complexing porphyrin rings and consequently suppresses the rotation of two other neighboring porphyrin rings in same axes. The binding of the second C_{60} suppresses the rotation of residual two free porphyrin rings (Figure 1). Therefore, as the number of the bound guests increases, the loss of Gibbs free energy decreases. In fact, the results obtained by the analysis based on the Hill equation show that the K value is sufficiently large and the Hill coefficient is close to 3.0, which allows a highly cooperative binding of three C_{60} guests.

Compound **1** has two different kinds of porphyrin tweezers: one composed of two porphyrins in the same branch (cavity A in compound **1**) and the other composed of two porphyrins in the two adjacent branches (cavity B in compound **1**). To evaluate which cavity is acting as a real binding site in solution, we measured the UV/Vis absorption spectroscopy of model compound **2** bearing only cavity A. We confirmed that addition of C_{60} scarcely induces a spectral change in model compound **2**. From a plot of ΔA_{428} versus $[C_{60}]$, we estimated the K value to be lower than 10 M^{-1} . This result is consistent with examination of the computational models, which show that cavity A (distance between parallel-oriented porphyrins, 2.29 nm) is too large to sandwich C_{60} . Furthermore, if C_{60} were bound to cavity A, compound **1** should not exhibit the allosteric effect because the three phenylacetylene axes can rotate quite independently. On the other hand, the distance between parallel-oriented porphyrins in cavity B is



estimated to be 1.18 nm, which is comparable with the size of C_{60} (diameter, 1.00 nm).^[12] One can thus consider that cavity B is acting as a real binding site.

In conclusion, the present study demonstrated that the dendritic receptor **1** binds three C_{60} guests in the positive allosteric manner with high Hill coefficient of 2.8. With the aid of this effect, the K value is considerably enhanced. In addition, the findings have important implications because molecular recognition can be coupled with the control of various chemical and physical functions inherent to the porphyrin–fullerene interaction, such as solubilization of C_{60} in polar solvents, photochemical electron or energy transfer as a photosynthetic model, electrochemical redox reactions, etc.

Received: March 28, 2002

Revised: May 13, 2002 [Z19005]

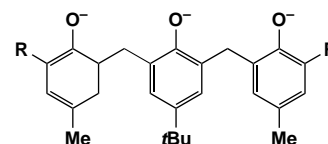
- [1] a) F. W. Zeng, S. C. Zimmerman, *Chem. Rev.* **1997**, 97, 1681; b) A. W. Bosman, H. M. Janssen, E. W. Meijer, *Chem. Rev.* **1999**, 99, 1665; c) S. K. Grayson, J. M. J. Fréchet, *Chem. Rev.* **2001**, 101, 3819.
- [2] a) J. F. G. A. Jansen, E. M. M. De Brabander-van den Berg, E. W. Meijer, *Science* **1994**, 266, 1226; b) G. Pistolis, A. Malliaris, D. Tsiourvas, C. M. Paleos, *Chem. Eur. J.* **1999**, 5, 1440; c) J. F. Nierengarten, L. Oswald, J. F. Eckert, J. F. Nicoud, N. Armaroli, *Tetrahedron Lett.* **1999**, 40, 568; d) M. Numata, A. Ikeda, C. Fukuhara, S. Shinkai, *Tetrahedron Lett.* **1999**, 40, 6945; e) J. F. Eckert, D. Byrne, J. F. Nicoud, L. Oswald, J. F. Nierengarten, M. Numata, A. Ikeda, S. Shinkai, N. Armaroli, *New J. Chem.* **2000**, 24, 749.
- [3] For example a) A. Ikeda, M. Yoshimura, H. Udzu, C. Fukuhara, S. Shinkai, *J. Am. Chem. Soc.* **1999**, 121, 4296; b) A. Ikeda, T. Hatano, S. Shinkai, T. Akiyama, S. Yamada, *J. Am. Chem. Soc.* **2001**, 123, 4855; c) T. Haino, M. Yanase, Y. Fukazawa, *Angew. Chem.* **1997**, 109, 288; *Angew. Chem. Int. Ed. Engl.* **1997**, 36, 259; d) J. Wang, C. D. Gutsche, *J. Am. Chem. Soc.* **1998**, 120, 12226; e) T. Anderson, K. Nilsson, M. Sundahl, G. Westman, O. Wennerström, *J. Chem. Soc. Chem. Commun.* **1992**, 604.
- [4] a) P. D. W. Boyd, M. C. Hodgson, C. E. F. Rickard, A. G. Oliver, L. Chaker, P. J. Brothers, R. D. Bolskar, F. S. Tham, C. A. Reed, *J. Am. Chem. Soc.* **1999**, 121, 10487; b) M. M. Olmstead, D. A. Costa, K. Maitra, B. C. Noll, S. L. Phillips, P. M. V. Calcar, A. L. Balch, *J. Am. Chem. Soc.* **1999**, 121, 7090.
- [5] a) K. Tashiro, T. Aida, J.-Y. Zheng, K. Kinbara, K. Saigo, S. Sakamoto, K. Yamaguchi, *J. Am. Chem. Soc.* **1999**, 121, 9477; b) T. Nishioka, K. Tashiro, T. Aida, J.-Y. Zheng, K. Kinbara, K. Saigo, S. Sakamoto, K. Yamaguchi, *Macromolecules* **2000**, 33, 9182; c) J.-Y. Zheng, K. Tashiro, Y. Hirabayashi, K. Kinbara, K. Saigo, T. Aida, S. Sakamoto, K. Yamaguchi, *Angew. Chem.* **2001**, 113, 1909; *Angew. Chem. Int. Ed.* **2001**, 40, 1858.
- [6] D. Sun, F. S. Tham, C. A. Reed, L. Chaker, M. Burgess, P. D. W. Boyd, *J. Am. Chem. Soc.* **2000**, 122, 10704.

- [7] a) O. Mongin, C. Papamicae, N. Hoyler, A. Gossauer, *J. Org. Chem.* **1998**, 63, 5568; b) P. Brodard, S. Matzinger, E. Vauthey, O. Mongin, C. Papamicae, A. Gossauer, *J. Phys. Chem. A* **1999**, 103, 5858.
- [8] For example, a) S. Shinkai, A. Sugasaki, M. Ikeda, M. Takeuchi, *Acc. Chem. Res.* **2001**, 34, 494; b) M. Takeuchi, A. Sugasaki, M. Ikeda, S. Shinkai, *Acc. Chem. Res.* **2001**, 34, 865; c) M. Takeuchi, T. Imada, S. Shinkai, *Angew. Chem.* **1998**, 110, 2242; *Angew. Chem. Int. Ed.* **1998**, 37, 2096; d) A. Sugasaki, M. Ikeda, M. Takeuchi, S. Shinkai, *Angew. Chem.* **2000**, 112, 3997; *Angew. Chem. Int. Ed.* **2000**, 39, 3839; e) A. Sugasaki, K. Sugiyasu, M. Ikeda, M. Takeuchi, S. Shinkai, *J. Am. Chem. Soc.* **2001**, 123, 10239.
- [9] M. Ikeda, S. Shinkai, A. Osuka, *Chem. Commun.* **2000**, 1043.
- [10] a) Y. Kubo, M. Ikeda, A. Sugasaki, M. Takeuchi, S. Shinkai, *Tetrahedron Lett.* **2001**, 42, 7435; Recently, Glass et al. demonstrated that ethynylene-linked trityl derivatives show cooperative silver-ion recognition: b) T. E. Glass, *J. Am. Chem. Soc.* **2000**, 122, 4522; c) J. Raker, T. E. Glass, *J. Org. Chem.* **2001**, 66, 6505.
- [11] a) B. Perlmutter-Hayman, *Acc. Chem. Res.* **1986**, 19, 90; b) K. A. Connors, *Binding Constants*, Wiley, New York, **1987**.
- [12] W. Kratschmer, L. D. Lamb, K. Fostiropoulos, D. R. Huffman, *Nature* **1990**, 347, 354.

Dinitrogen-Bond Cleavage in a Niobium Complex Supported by a Tridentate Aryloxy Ligand

Hiroyuki Kawaguchi* and Tsukasa Matsuo

The efficient activation of dinitrogen under mild conditions is a challenging topic in chemistry because of its important applications. Although dinitrogen complexes of almost transition metals have been prepared,^[1] there are few examples of well-characterized transition-metal compounds which are capable of cleaving the $N\equiv N$ bond.^[2] As part of studies aimed at developing new ancillary ligands to support reactive metal centers, we have found it attractive to employ linked aryloxy ligands ($R-L^{3-}$; $R = tBu$, Me; Scheme 1),^[3, 4, 5] to determine complex geometry and to limit ligand mobility. Furthermore, their steric size can be easily regulated by substituents at *ortho* positions of the outer aryloxides. We chose to investigate the chemistry of niobium complexes with the $R-L^{3-}$ ligands in dinitrogen activation. Herein we describe the reductive $N\equiv N$ -bond cleavage by the combination of $LiBH_4Et_3$ and a niobium complex supported by a tridentate aryloxy ligand.



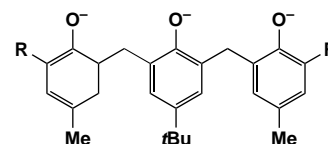
Scheme 1. Ligands, $R-L^{3-}$ ($R = tBu$, Me).

[*] Dr. H. Kawaguchi, Dr. T. Matsuo
Coordination Chemistry Laboratories
Institute for Molecular Science and CREST
Japan Science and Technology Corporation (JST)
Myodaiji, Okazaki, 444-8585 (Japan)
Fax: (+81)564-55-5245
E-mail: hkawa@ims.ac.jp

In conclusion, the present study demonstrated that the dendritic receptor **1** binds three C₆₀ guests in the positive allosteric manner with high Hill coefficient of 2.8. With the aid of this effect, the *K* value is considerably enhanced. In addition, the findings have important implications because molecular recognition can be coupled with the control of various chemical and physical functions inherent to the porphyrin–fullerene interaction, such as solubilization of C₆₀ in polar solvents, photochemical electron or energy transfer as a photosynthetic model, electrochemical redox reactions, etc.

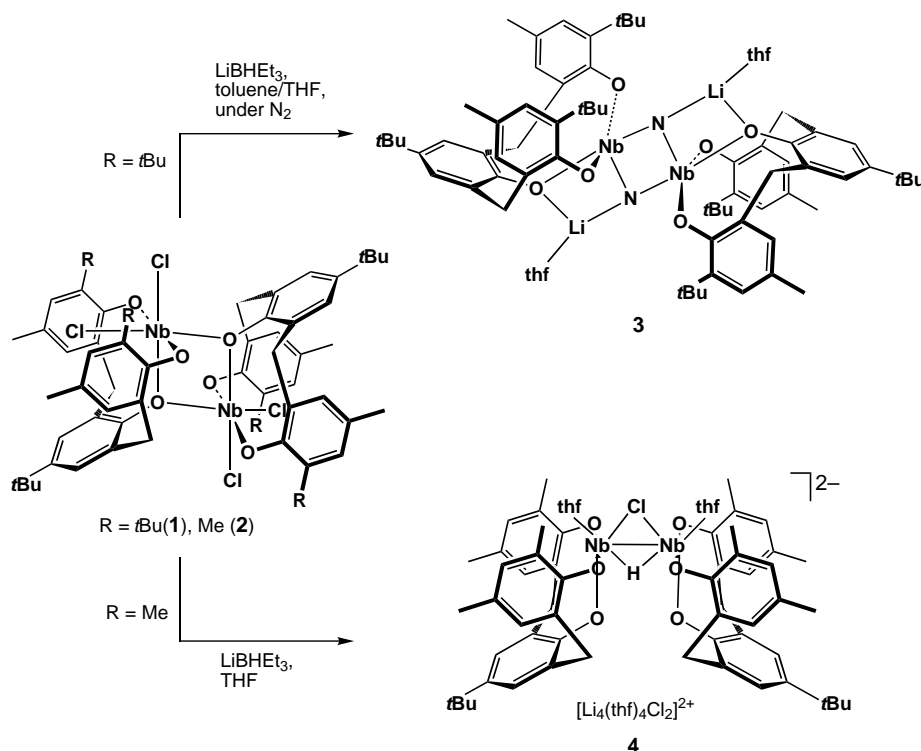
- [1] a) F. W. Zeng, S. C. Zimmerman, *Chem. Rev.* **1997**, 97, 1681; b) A. W. Bosman, H. M. Janssen, E. W. Meijer, *Chem. Rev.* **1999**, 99, 1665; c) S. K. Grayson, J. M. J. Fréchet, *Chem. Rev.* **2001**, 101, 3819.
- [2] a) J. F. G. A. Jansen, E. M. M. De Brabander-van den Berg, E. W. Meijer, *Science* **1994**, 266, 1226; b) G. Pistolis, A. Malliaris, D. Tsiourvas, C. M. Paleos, *Chem. Eur. J.* **1999**, 5, 1440; c) J. F. Nierengarten, L. Oswald, J. F. Eckert, J. F. Nicoud, N. Armaroli, *Tetrahedron Lett.* **1999**, 40, 568; d) M. Numata, A. Ikeda, C. Fukuhara, S. Shinkai, *Tetrahedron Lett.* **1999**, 40, 6945; e) J. F. Eckert, D. Byrne, J. F. Nicoud, L. Oswald, J. F. Nierengarten, M. Numata, A. Ikeda, S. Shinkai, N. Armaroli, *New J. Chem.* **2000**, 24, 749.
- [3] For example a) A. Ikeda, M. Yoshimura, H. Udzu, C. Fukuhara, S. Shinkai, *J. Am. Chem. Soc.* **1999**, 121, 4296; b) A. Ikeda, T. Hatano, S. Shinkai, T. Akiyama, S. Yamada, *J. Am. Chem. Soc.* **2001**, 123, 4855; c) T. Haino, M. Yanase, Y. Fukazawa, *Angew. Chem.* **1997**, 109, 288; *Angew. Chem. Int. Ed. Engl.* **1997**, 36, 259; d) J. Wang, C. D. Gutsche, *J. Am. Chem. Soc.* **1998**, 120, 12226; e) T. Anderson, K. Nilsson, M. Sundahl, G. Westman, O. Wennerström, *J. Chem. Soc. Chem. Commun.* **1992**, 604.
- [4] a) P. D. W. Boyd, M. C. Hodgson, C. E. F. Rickard, A. G. Oliver, L. Chaker, P. J. Brothers, R. D. Bolskar, F. S. Tham, C. A. Reed, *J. Am. Chem. Soc.* **1999**, 121, 10487; b) M. M. Olmstead, D. A. Costa, K. Maitra, B. C. Noll, S. L. Phillips, P. M. V. Calcar, A. L. Balch, *J. Am. Chem. Soc.* **1999**, 121, 7090.
- [5] a) K. Tashiro, T. Aida, J.-Y. Zheng, K. Kinbara, K. Saigo, S. Sakamoto, K. Yamaguchi, *J. Am. Chem. Soc.* **1999**, 121, 9477; b) T. Nishioka, K. Tashiro, T. Aida, J.-Y. Zheng, K. Kinbara, K. Saigo, S. Sakamoto, K. Yamaguchi, *Macromolecules* **2000**, 33, 9182; c) J.-Y. Zheng, K. Tashiro, Y. Hirabayashi, K. Kinbara, K. Saigo, T. Aida, S. Sakamoto, K. Yamaguchi, *Angew. Chem.* **2001**, 113, 1909; *Angew. Chem. Int. Ed.* **2001**, 40, 1858.
- [6] D. Sun, F. S. Tham, C. A. Reed, L. Chaker, M. Burgess, P. D. W. Boyd, *J. Am. Chem. Soc.* **2000**, 122, 10704.

The efficient activation of dinitrogen under mild conditions is a challenging topic in chemistry because of its important applications. Although dinitrogen complexes of almost transition metals have been prepared,^[1] there are few examples of well-characterized transition-metal compounds which are capable of cleaving the N≡N bond.^[2] As part of studies aimed at developing new ancillary ligands to support reactive metal centers, we have found it attractive to employ linked aryloxide ligands (R-L³⁻; R = *t*Bu, Me; Scheme 1),^[3, 4, 5] to determine complex geometry and to limit ligand mobility. Furthermore, their steric size can be easily regulated by substituents at *ortho* positions of the outer aryloxides. We chose to investigate the chemistry of niobium complexes with the R-L³⁻ ligands in dinitrogen activation. Herein we describe the reductive N≡N-bond cleavage by the combination of LiBHET₃ and a niobium complex supported by a tridentate aryloxide ligand.



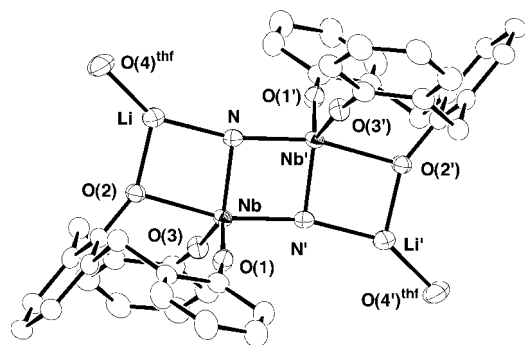
Scheme 1. Ligands, R-L³⁻ (R = *t*Bu, Me).

1433-7851/02/4115-2792 \$ 20.00+.50/0 *Angew. Chem. Int. Ed.* **2002**, *41*, No. 15

Scheme 2. Synthesis of **3** and **4**.

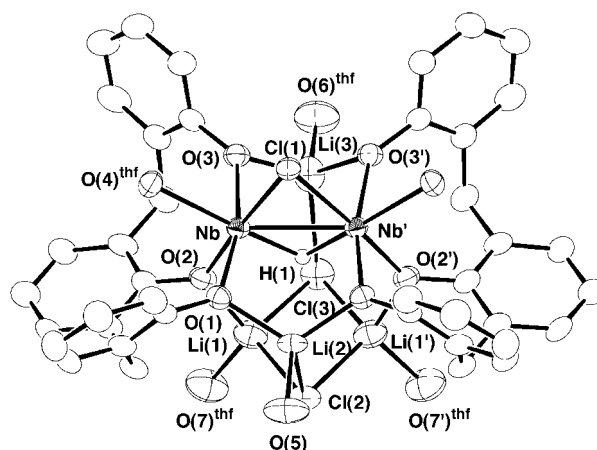
Addition of 6 equivalent of LiBHET_3 in THF to a toluene solution of $[\{\text{Nb}(\text{tBu-L})\text{Cl}_2\}_2]$ (**1**)^[6] at -78°C under N_2 gave a red solution. When the solution was stirred at room temperature, the solution gradually turned brown. After removal of an insoluble brown powder, $[\{\text{Nb}(\text{tBu-L})(\mu\text{-N})\text{Li}(\text{thf})_2\}_2]$ (**3**; Scheme 2) was isolated as yellow crystals in 41 % yield by the addition of hexane. On the other hand, the reaction carried out under argon resulted in an uncharacterized material. The combustion analysis and spectroscopic data of **3** is in agreement with the formula. The ^{15}N NMR spectrum of the isotopically enriched compound $[\{\text{Nb}(\text{tBu-L})(\mu\text{-}^{15}\text{N})\text{Li}(\text{thf})_2\}_2]$ (**3**- ^{15}N), analogously prepared under an atmosphere of $^{15}\text{N}_2$, displays a single resonance peak at $\delta = 312$ ppm in the ^{15}N NMR spectrum. This result unambiguously confirms that the bridging ligands of **3** originate from N_2 .

The X-ray diffraction analysis reveals that **3** is dimeric with two bridging nitrides (Figure 1).^[7] The tBu-L^{3-} ligands bind to

Figure 1. Molecular structure of **3**. Methyl and *tert*-butyl groups of tBu-L^{3-} ligands and the thf groups (except for the oxygen atom) have been omitted for clarity.

the niobium atoms in a facial manner. There are two lithium cations, each bridging the central aryloxide and the nitrogen atom. The trigonal-planar coordination around lithium centers is completed by thf. Each niobium atom in the centrosymmetric dimer is five-coordinate in a geometry that approximates a trigonal bipyramid, with the central aryloxide of tBu-L^{3-} and a bridging nitride unit occupying the apical sites. The bridging nitrides are arranged in an unsymmetrical fashion, with the axial Nb–N' bond of 1.935(3) Å being slightly longer than the equatorial Nb–N bond of 1.892(3) Å.^[2b, 2d, 8] Two nitrogen atoms are separated by 2.569(5) Å, indicative of the complete cleavage of the $\text{N}\equiv\text{N}$ bond. The short Nb...Nb separation of 2.837(4) Å is a result of the presence of two bridging nitride groups.

The use of Me-L^{3-} instead of tBu-L^{3-} ions introduced a significant modification in the reactivity pattern of niobium complexes. The analogous reaction of $[\{\text{Nb}(\text{Me-L})\text{Cl}_2\}_2]$ (**2**) with LiBHET_3 in THF gave $[\{\text{Nb}_2(\text{Me-L})_2(\mu\text{-H})(\mu\text{-Cl})(\text{thf})_2\}[\text{Li}_4(\text{thf})_4\text{Cl}_2]]$ (**4**; Scheme 2) as green crystals in 73 % yield. Compound **4** is diamagnetic, and its formulation was confirmed by spectroscopic data and X-ray analysis. Figure 2 presents the solid

Figure 2. Structure of **4**. Methyl and *tert*-butyl groups of Me-L^{3-} ligands and the thf groups (except for the oxygen atom) have been omitted for clarity.

state structure of **4**, where a crystallographically imposed mirror plane passes through the molecule.^[9] A striking feature of the structure is the presence of a $[\{\text{Nb}(\text{Me-L})(\text{thf})_2\}_2(\mu\text{-Cl})(\mu\text{-H})]^{2-}$ dimer, in which each Nb center possesses an octahedral geometry (if the Nb–Nb bond is ignored). The two Me-L^{3-} ligands are arranged in a *syn* configuration. The

dimeric $[\{\text{Nb}(\text{Me-L})(\text{thf})\}_2(\mu\text{-Cl})(\mu\text{-H})]^{2-}$ unit carries four lithium atoms coordinating at aryloxy units and two chlorine atoms bridging three lithium atoms. Taking account into the observed diamagnetism of **4**, the short Nb–Nb separation of 2.647(1) Å suggests the presence of the Nb–Nb double bond.^[10] Although determination of the position of the hydride ligand from X-ray data alone is difficult, the Fourier map yielded a residual peak on the side of the Nb–Nb vector, opposite that of the bridging Cl(1) atom, which could be assigned to the bridging hydride ligand (Nb–H(1) 1.80 Å).

The ^1H NMR spectrum of **4** in C_6D_6 is consistent with its solid-state structure. The resonance signal for the bridging hydride ligand is observed as a broad signal at $\delta = -1.1$ ppm. When **4** was dissolved into CDCl_3 , the signal at $\delta = -1.1$ ppm disappeared and the formation of **2** was indicated. While no terminal Nb–H stretching band was observed in the IR spectrum, the assignment of the bridging hydride ligand was impossible because of overlapping peaks. An attempt to prepare a dihydride-bridging dimer by the reaction of **4** with LiBHET_3 in THF was unsuccessful. The $\text{Nb}_2(\mu\text{-Cl})$ unit remained intact, and **4** was recovered from the reaction mixture.

In conclusion this work clearly shows that each R-L^{3-} ligand behaves in a very distinct manner with respect to dinitrogen activation and metal–metal interaction. In light of the isolation of **4**, the formation of **3** presumably proceeds via an $\text{Nb}^{\text{III}}(\mu\text{-H})_2\text{Nb}^{\text{III}}$ dimer. This intermediate could bind and cleave N_2 concomitant with the reductive elimination of H_2 to produce **3**, because the loss of H_2 to generate a dinitrogen complex is known.^[11] Further study to isolate such a species is currently underway.

Experimental Section

All manipulations were performed under N_2 using standard Schlenk techniques and dried, deoxygenated solvents.

3: A 100-mL flask was charged with **1** (1.10 g, 0.83 mmol), LiBHET_3 (1 M in THF; 5.0 mL, 5.0 mmol), and toluene (60 mL) at -78°C . Upon stirring the mixture at room temperature for 28 h, a brown solution was obtained. After centrifugation to remove insoluble material, the solution was layered with hexane to afford **3** as yellow crystals (0.57 g, 41%). ^1H NMR (500 MHz, $[\text{D}_8]\text{THF}$): $\delta = 1.40$ (s, 18H; $t\text{Bu}$), 1.43 (s, 36H; $t\text{Bu}$), 2.31 (s, 12H; Me), 4.62 (d, $J = 12.7$ Hz, 4H; CH_2), 5.54 (d, $J = 12.7$ Hz, 4H; CH_2), 6.84 (s, 4H; Ph), 6.86 (s, 4H; Ph), 7.00 ppm (s, 4H; Ph); ^{15}N NMR (50.55 MHz, $[\text{D}_8]\text{THF}$, CH_3NO_2 external standard): $\delta = 312$ ppm; elemental analysis calcd (%) for $\text{C}_{90}\text{H}_{118}\text{O}_8\text{N}_2\text{Li}_2\text{Nb}_2$: C 69.49, H 7.65, N 1.80; found: C 69.12, H 7.59, N 1.55.

4: A 100-mL flask was charged with **2** (0.94 g, 0.81 mmol), LiBHET_3 (1 M in THF; 4.9 mL, 4.9 mmol), and THF (50 mL) at -78°C . Upon stirring the mixture at room temperature for 32 h, a green solution was obtained. Concentration and subsequent cooling of the solution to -30°C gave **4** as green crystals (1.06 g, 73%). ^1H NMR (C_6D_6): $\delta = -1.1$ (br, 1H; Nb–H–Nb), 1.27 (s, 18H; $t\text{Bu}$), 1.3 (br, thf), 2.21 (s, 6H; Me), 2.93 (s, 6H; Me), 3.39 (d, $J = 12$ Hz, 4H; CH_2), 3.6 (br, thf), 5.73 (d, $J = 12$ Hz, 4H; CH_2), 6.83 (s, 4H; Ph), 7.09 (s, 4H; Ph), 7.19 ppm (s, 4H; Ph); elemental analysis calcd (%) for $\text{C}_{92}\text{H}_{135}\text{O}_{15}\text{Cl}_3\text{Li}_4\text{Nb}_2$: C 61.36, H 7.56; found: C 60.44, H 7.38.

Received: March 11, 2002
Revised: May 6, 2002 [Z18345]

- [1] a) M. D. Fryzuk, S. A. Johnson, *Coord. Chem. Rev.* **2000**, 200–202, 379–409; b) S. Gambarotta, *J. Organomet. Chem.* **1995**, 500, 117–126.

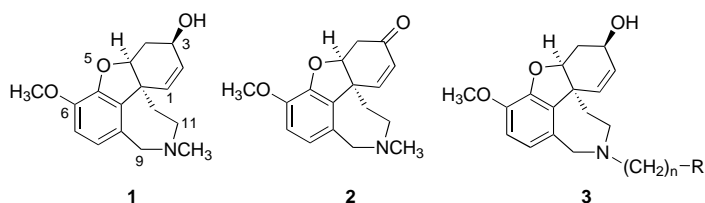
- [2] a) C. E. Laplaza, C. C. Cummins, *Science* **1995**, 268, 861–863; b) A. Zanotti-Gerosa, E. Solari, L. Giannini, C. Floriani, A. Chiesi-Villa, C. Rizzoli, *J. Am. Chem. Soc.* **1998**, 120, 437–438; c) G. K. B. Clentsmith, V. M. E. Bates, P. B. Hitchcock, F. G. N. Cloke, *J. Am. Chem. Soc.* **1999**, 121, 10444–10445; d) D. J. Mindiola, K. Meyer, J.-P. F. Cherry, T. A. Baker, C. C. Cummins, *Organometallics* **2000**, 19, 1622–1624; e) E. Solari, C. D. Silva, B. Iacono, J. Heschelbrouck, C. Rizzoli, R. Scopelitti, C. Floriani, *Angew. Chem.* **2001**, 113, 4025–4027; *Angew. Chem. Int. Ed.* **2001**, 40, 3907–3909; f) P. Berno, S. Gambarotta, *Angew. Chem.* **1995**, 107, 871; *Angew. Chem. Int. Ed. Engl.* **1995**, 34, 822–824.
- [3] T. Sone, Y. Ohba, H. Yamazaki, *Bull. Chem. Soc. Jpn.* **1989**, 62, 1111–1116.
- [4] Lithium complexes were recently reported; B. W. F. Gordon, M. J. Scott, *Inorg. Chim. Acta* **2000**, 297, 206–216.
- [5] T. Matsuo, H. Kawaguchi, *J. Chem. Soc. Dalton Trans.* **2002**, in press.
- [6] T. Matsuo, H. Kawaguchi, unpublished results.
- [7] a) Crystal data for **3**: $\text{C}_{76}\text{H}_{102}\text{N}_2\text{O}_8\text{Li}_2\text{Nb}_2 \cdot 2\text{C}_7\text{H}_8$ ($M_r = 1555.62$); crystal size $0.35 \times 0.20 \times 0.20$ mm, monoclinic, $P2_1/c$ (no. 14), $a = 12.984(1)$, $b = 18.647(2)$, $c = 17.567(2)$ Å, $\beta = 104.706(5)^\circ$, $V = 4113.7(7)$ Å³, $\rho_{\text{calcd}} = 1.256$ g cm⁻³, $Z = 2$, $\mu(\text{Mo}_{\text{K}\alpha}) = 3.34$ cm⁻¹, 32 459 measured, 9094 unique, 528 variables, GOF = 1.04, $R1 = 0.044$, $wR2 = 0.145$; b) Diffraction data of **3** and **4** were collected at -100°C on a Rigaku Mercury system equipped with a CCD detector ($\text{Mo}_{\text{K}\alpha}$ radiation, $\lambda = 0.71070$ Å; graphite-monochromated). The structures of **3** and **4** were solved by direct methods and refined by full-matrix least-squares on F^2 by using the CrystalStructure software package. All non-hydrogen atom were refined anisotropically, and hydrogen atoms were located at calculated positions. CCDC-175198 (**3**) and CCDC-175199 (**4**) contains the supplementary crystallographic data for this paper. These data can be obtained free of charge via www.ccdc.cam.ac.uk/conts/retrieving.html (or from the Cambridge Crystallographic Data Centre, 12, Union Road, Cambridge CB2 1EZ, UK; fax: (+44) 1223-336-033; or deposit@ccdc.cam.ac.uk).
- [8] M. G. Fickes, A. L. Odom, C. C. Cummins, *Chem. Commun.* **1997**, 1993–1994.
- [9] Crystal data for **4**: $\text{C}_{80}\text{H}_{111}\text{O}_{12}\text{Cl}_3\text{Li}_4\text{Nb}_2 \cdot 3\text{C}_4\text{H}_8\text{O}$ ($M_r = 1801.01$); crystal size $0.25 \times 0.10 \times 0.05$ mm, orthorhombic, $Pnma$ (no. 62), $a = 17.657(5)$, $b = 26.656(8)$, $c = 20.010(6)$ Å, $V = 9418(4)$ Å³, $\rho_{\text{calcd}} = 1.270$ g cm⁻³, $Z = 4$, $\mu(\text{Mo}_{\text{K}\alpha}) = 3.88$ cm⁻¹, 74 544 measured, 11 010 unique, 533 variables, GOF = 1.08, $R1 = 0.057$, $wR2 = 0.166$.^[7b] The $t\text{Bu}$ group and one of the thf molecules were disordered with 70/30 and 60/40 site occupancies, respectively.
- [10] a) A. Caselli, E. Solari, R. Scopelitti, C. Floriani, N. Re, C. Rizzoli, A. Chiesi-Villa, *J. Am. Chem. Soc.* **2000**, 122, 3652–3670; b) M. Tayebani, K. Feghali, S. Gambarotta, G. Yap, *Organometallics* **1998**, 17, 4282–4290; c) F. A. Cotton, R. A. Walton, *Multiple Bonds Between Metal Atoms*, 2nd ed., Oxford University Press, New York, **1993**.
- [11] a) M. D. Fryzuk, S. A. Johnson, B. O. Patrick, A. Albinati, S. A. Mason, T. F. Koetzle, *J. Am. Chem. Soc.* **2000**, 122, 3652–3670; b) C. Bianchini, A. Meli, Perruzini, F. Vizza, F. Zanolini, *Organometallics* **1989**, 8, 2080–2082; c) B. Chaudret, J. Devillers, R. Poilblanc, *Organometallics* **1985**, 4, 1727–1732.

An Efficient Enantioselective Synthesis of (–)-Galanthamine**

Barry M. Trost* and Weiping Tang

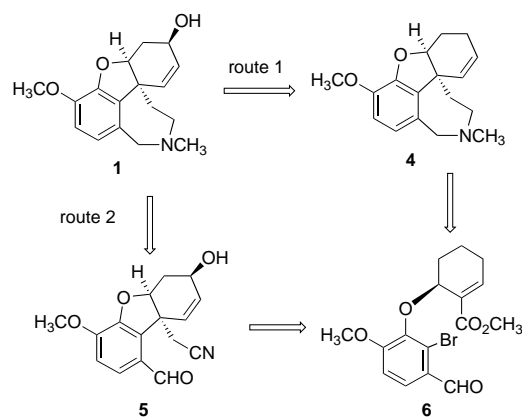
Galanthamine (**1**),^[1] the parent member of the galanthamine-type *Amaryllidaceae* alkaloids, is a centrally acting competitive and reversible inhibitor of acetylcholinesterase (Ache), which significantly enhances cognitive functions of patients suffering from Alzheimer's disease.^[2] It was first approved in Austria and most recently in the rest of Europe and in the United States for the treatment of Alzheimer's disease.

Because of the limited supplies and the high cost of its isolation from natural sources,^[3, 4] several syntheses have been reported which use biomimetic oxidative bisphenol coupling^[4, 5] to create the critical spiro quaternary carbon center of narwedine (**2**), which is converted into **1** by diastereoselective reduction.^[3] We^[6] disclosed the first enantioselective synthesis of (–)-**1** in 2000 in which a sequential palladium-catalyzed asymmetric allylic alkylation (AAA)^[7] and intramolecular Heck cyclization were used. At the same time, several other groups utilized similar Heck cyclizations to construct the quaternary carbon center of (±)-3-deoxygalanthamine^[8, 9] and (±)-**1**.^[10]



In the endeavor to search for more potent inhibitors of Ache, there is considerable interest in derivatives that are based on (–)-galanthamine as a lead structure,^[11, 12] since (–)-galanthamine is less toxic than other Ache inhibitors such as physostigmine and tacrine.^[11, 13, 14] Among them, galanthamine derivatives **3**^[14, 15] or their iminium salts, synthesized by selective N-demethylation followed by N-alkylation of galanthamine,^[16] were found to be more potent (up to 70-fold) than galanthamine in inhibiting Ache. To date, syntheses that employ the oxidative phenol coupling step have not been used for direct access to these derivatives.

Our previous approach to **1** relied on a direct allylic oxidation of deoxygalanthamine **4** (Scheme 1, route 1) based



Scheme 1. Retrosynthetic analysis of (–)-galanthamine (**1**).

on the success in the synthesis of the related *Amaryllidaceae* alkaloids. Attempts to directly oxidize **4** to **1** failed. Therefore, a four-step protocol was developed to introduce the C3 oxygen group stereoselectively. It appeared that the benzylic position is more labile towards oxidation than the allylic position.^[9]

We envisioned a second-generation strategy, which had two goals: 1) realization of an effective general strategy for this family of alkaloids by total synthesis of galanthamine, and 2) development of a flexible strategy to provide ready access to galanthamine analogues by simple modification of the synthetic scheme. Scheme 1 (route 2) illustrates the key feature of this new strategy, which envisions closing the hydrobenzazepine ring after the introduction of the C3 allylic hydroxy group. Direct allylic oxidation is proposed to set the C3 OH group for intermediate **5**, whose benzylic position was already at the oxidation state of an aldehyde.

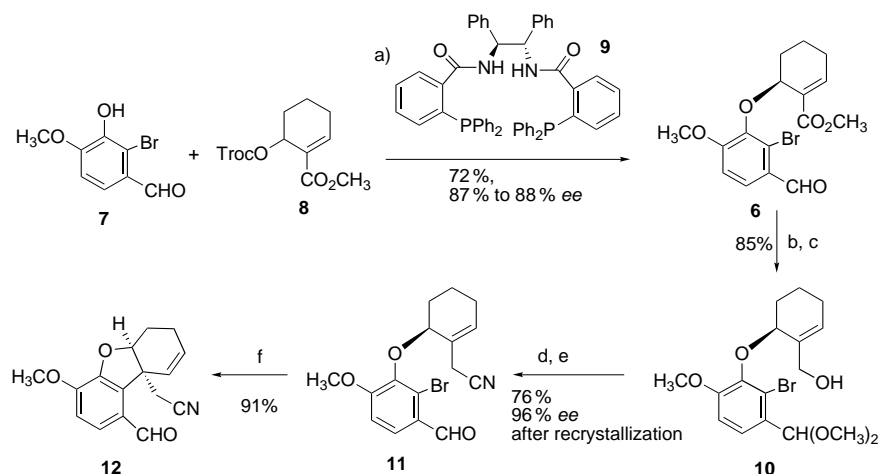
As in the first-generation synthesis, aryl ether **6**^[6] was prepared in good yield (72%) and with high enantiomeric excess (87% to 88% *ee*) by palladium-catalyzed reaction of 2-bromovanillin (**7**)^[17] with carbonate **8** (available in two steps from glutaraldehyde and the Emmons–Wadsworth–Horner reagent)^[18] in the presence of chiral ligand **9** (Scheme 2). All attempts to effect the intramolecular Heck reaction of aryl ether **6** failed in our previous synthesis, resulting primarily in ionized product phenol **7**. Early results^[19] suggested that the presence of electron-withdrawing substituents on the phenol ring favored the palladium-catalyzed ionization over the intramolecular Heck reaction. Therefore, in our earlier work **6** was reduced with DIBAL-H and the resulting diol was protected as the bis-silyl ether for the Heck reaction. Recent reports^[8, 9] showed that the Heck cyclization worked smoothly in similar systems in the presence of an aldehyde on the phenol ring. This observation suggested that the electron-withdrawing group on the olefin favored the ionization, whereas the electron-withdrawing group on the phenol ring facilitated oxidative addition of the palladium to both the C–O and C–Br bonds. We decided to keep the aldehyde functionality while removing the electron-withdrawing substituent on the olefin by homologation of the α,β -unsaturated ester to a β,γ -unsaturated nitrile.

To this end, aldehyde **6** was protected as its dimethylacetal by treatment with trimethyl orthoformate and catalytic

[*] Prof. B. M. Trost, W. Tang
Department of Chemistry, Stanford University
Stanford, CA 94305-5080 (USA)
Fax: (+1) 650-725-0259
E-mail: bmtrost@stanford.edu

[**] We thank the National Science Foundation and the National Institute of Health, General Medical Sciences (GM13598), for their generous support of our programs. Mass spectra were provided by the Mass Spectrometry Facility of the University of California, San Francisco, supported by the NIH Division of Research Resources.

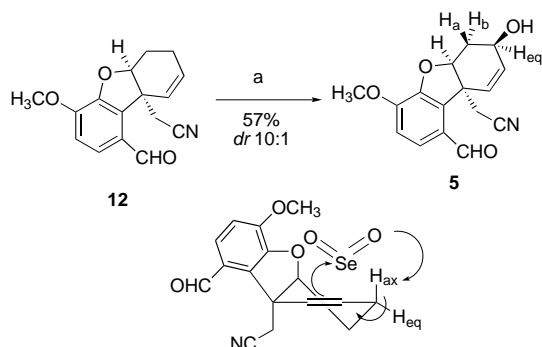
Supporting information for this article is available on the WWW under <http://www.angewandte.org> or from the author.



Scheme 2. Convergent synthesis of the carbon skeleton of galanthamine. a) 3% **9**, $[\eta^3\text{-C}_3\text{H}_5\text{PdCl}]_2$ (1%), Et_3N , CH_2Cl_2 , room temperature; b) TsOH (5%), $\text{CH}(\text{OMe})_3$, MeOH ; c) DIBAL-H /toluene, -78°C ; d) Ph_3P , acetonecyanohydrin, DIAD , Et_2O ; e) TsOH (20%), THF , H_2O ; f) $\text{Pd}(\text{OAc})_2$ (15%), dppp (15%), Ag_2CO_3 , PhCH_3 , 107°C , 24 h. Troc = 2,2,2-trichloroethoxycarbonyl, DIAD = diisopropyl azodicarboxylate, TsOH = *p*-toluenesulfonic acid, DIBAL-H = diisobutylaluminum hydride, dppp = bis(diphenylphosphanyl)propane.

p-toluenesulfonic acid. Selective reduction of the α,β -unsaturated ester with DIBAL-H at -78°C afforded allylic alcohol **10**. The β,γ -unsaturated nitrile **11** was prepared in 84% yield by using a modified Mitsunobu protocol^[20] followed by acid hydrolysis. The enantiomeric excess of **11** was improved to 96% *ee* by recrystallization from diethyl ether and petroleum ether with 90% mass recovery.

We examined the Heck reaction of the acetonitrile-substituted cyclohexene **11** (Scheme 2). The Heck product **12** was obtained in high yield (91%) by using a catalytic amount of dppp and $[\text{Pd}(\text{OAc})_2]$ in refluxing toluene in the presence of excess silver carbonate. Other solvent (DMF) or ligands (dppe , dppf) gave lower yields. Once we had established the core structure of the galanthamine, we turned our attention to the introduction of the C3 allylic hydroxy group. This can be realized by oxidation of the olefin to enone followed by known diastereoselective 1,2-reduction or more efficiently, direct oxidation to the allylic alcohol, which raises the question regarding the diastereoselectivity. Usually, the electrophile would approach the olefin from the less hindered convex face. We envisioned that SeO_2 would react with the olefin from the more hindered concave face through an ene mechanism^[21] (Scheme 3), because the axial proton H_{ax} is

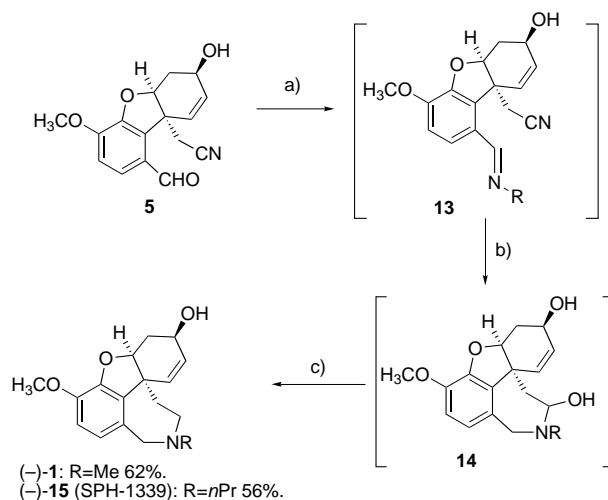


Scheme 3. Diastereoselective allylic oxidation. a) SeO_2 , NaH_2PO_4 , dioxane, 150°C 3 h, 64% based on recovered starting material.

perfectly aligned with the π system. Gratifyingly, treatment of olefin **12** with SeO_2 in dioxane at 150°C in the presence of NaH_2PO_4 and quartz sand in a sealed tube provided alcohol **5** in 57% yield (64% based on recovered starting material; *dr* 10:1) with 7% recovered starting material.^[22] Other additives, such as HCO_2H ,^[23] InCl_3 , YbCl_3 and Na_2HPO_4 , gave less of the desired product. Attempts to fully convert all the starting material by extending the reaction time or increasing the temperature resulted in more decomposition. Only trace amounts of product was found after 8 h when the reaction was carried out in refluxing dioxane (110°C). This represents the first successful allylic oxidation^[6, 9] of the galanthamine skeleton. The stereochemistry of **5** was tentatively assigned based on the coupling constants of $\text{H}_{\text{a}}/\text{H}_{\text{eq}}$ and $\text{H}_{\text{b}}/\text{H}_{\text{eq}}$ ($J < 5\text{ Hz}$). The

high diastereoselectivity reflects the stereoelectronic requirement for the ene reaction.

Allylic alcohol **5** together with its epimer (10:1) was then converted into the natural product in a one-pot process (Scheme 4). Aldehyde **5** was treated with methylamine in



Scheme 4. Completion of the synthesis by a one-pot procedure. a) RNH_2 , MeOH ; b) DIBAL-H (4 equiv), then aqueous NaH_2PO_4 ; c) NaCNBH_3 . $\text{R} = \text{Me}$: 62% of **1** and 6% of *epi*-**1**; $\text{R} = \text{nPr}$: 56% of **15**.

methanol solution. Excess methylamine and methanol was removed in vacuo. Concomitant reduction of the imine and nitrile by DIBAL-H followed by acid quenching presumably gave the seven-membered ring of hemiaminal **14**. The resulting solution was treated directly with sodium cyanoborohydride, and (–)-galanthamine (**1**) and *epi*-**1** were isolated in 62% and 6% yields, respectively. All spectral data (^1H NMR, ^{13}C NMR, IR) are identical to those of a sample of the natural product and to data from previous synthesis, $[\alpha]_{\text{D}} = -123.1$ ($c = 0.4$, EtOH), $\text{lit}^{[1]}$: $[\alpha]_{\text{D}} = -131.4$ ($c = 0.6$, EtOH), $\text{lit}^{[6]}$:

$[\alpha]_D = -112.8$ (88 % ee, $c = 0.5$, EtOH). SPH-1339 (**15**),^[15] a slightly more potent inhibitor of Ache than (–)-galanthamine **1**, was prepared in 56 % yield by this one-pot process, by using propylamine instead of methylamine.

This new synthesis of galanthamine (8 steps, 96 % ee, 14.8 % overall yield from **7** and **8**) is a significant improvement over and successfully addresses many of the shortcomings of the previous synthesis (14 steps, 88 % ee, 1.5 % overall yield). Furthermore, by exchanging methylamine for other alkyl amines in the last step various galanthamine derivatives are easily accessible, as demonstrated by the synthesis of **15**. This is the shortest and most efficient nonbiomimetic total synthesis of (–)-galanthamine to date. The sequential palladium-catalyzed AAA and intramolecular Heck reaction followed by a diastereoselective allylic oxidation provided the key intermediate **5** with all the functionality installed, except the hydrobenzazepine ring. The one-pot reductive cyclization represents a simple and efficient strategy to form the latter and to access many galanthamine analogues. All the stereochemistry emanates from the palladium-catalyzed AAA. This strategy should allow for entry into a variety of *Amaryllidaceae* alkaloids related to galanthamine.

Received: April 4, 2002 [Z19040]

- [1] For reviews see: O. Hoshino in *The Alkaloids*, Vol. 51 (Ed.: G. A. Cordell), Academic Press, New York, **1998**, pp. 323–424; S. F. Martin in *The Alkaloids*, Vol. 30 (Ed.: A. Brossi), Academic Press, New York, **1987**, pp. 251–376.
- [2] M. Weinstock, *CNS Drugs* **1999**, *12*, 307–323; U. Thatté, *Curr. Opin. Cent. Peripher. Nerv. Syst. Invest. Drugs* **1999**, *1*, 357–372; K. Unni, *CNS Drugs* **1998**, *10*, 447–460; A. Nordberg, A.-L. Svensson, *Drug Saf.* **1998**, *19*, 465–480; M. Rainer, *Drugs Today* **1997**, *33*, 273–279; H. A. M. Mücke, *Drugs Today* **1997**, *33*, 251–257.
- [3] W.-C. Shieh, J. A. Carlson, *J. Org. Chem.* **1994**, *59*, 5463–5465.
- [4] B. Küenburg, L. Czollner, J. Fröhlich, U. Jordis, *Org. Process Res. Dev.* **1999**, *3*, 425–431.
- [5] D. H. R. Barton, G. W. Kirby, *J. Chem. Soc.* **1962**, 806; T. Kametani, K. Yamaki, H. Yagi, K. Fukumoto, *J. Chem. Soc. D* **1969**, 425–426; T. Kametani, K. Yamaki, H. Yagi, K. Fukumoto, *J. Chem. Soc. C* **1969**, 2602–2605; T. Kametani, K. Yamaki, T. Terui, *J. Heterocycl. Chem.* **1973**, *10*, 35; K. Shimizu, K. Tomioka, S. Yamada, K. Koga, *Heterocycles* **1977**, *8*, 277–282; K. Shimizu, K. Tomioka, S. Yamada, K. Koga, *Chem. Pharm. Bull.* **1978**, *26*, 3765–3771; D. Krikorian, R. Vlahov, S. Parushev, M. Chinova, I. Vlahov, H. J. Schaefer, H. Duddeck, G. Snatzke, *Tetrahedron Lett.* **1984**, *25*, 2969–2972; R. Vlahov, D. Krikorian, G. Spassov, M. Chinova, I. Vlahov, S. Parushev, G. Snatzke, L. Ernst, K. Kieslich, W.-R. Abraham, W. S. Sheldrick, *Tetrahedron* **1989**, *45*, 3329–3345; J. Szweczyk, J. W. Wilson, A. H. Lewin, F. I. Carroll, *J. Heterocycl. Chem.* **1995**, *32*, 195–199; D. A. Chaplin, N. Fraser, P. D. Tiffin, *Tetrahedron Lett.* **1997**, 7931; L. Czollner, W. Frantsits, B. Küenburg, U. Hedenig, J. Fröhlich, U. Jordis, *Tetrahedron Lett.* **1998**, *39*, 2087–2088; Y. Kita, M. Arisawa, M. Gyoten, M. Nakajima, R. Hamada, H. Tohma, T. Takada, *J. Org. Chem.* **1998**, *63*, 6625–6633; D. Krikorian, V. Tarpanov, S. Parushev, P. Mechkarova, *Synth. Commun.* **2000**, *30*, 2833–2846; M. Node, S. Kodama, Y. Hamashima, T. Baba, N. Hamamichi, K. Nishide, *Angew. Chem.* **2001**, *113*, 3150–3152; *Angew. Chem. Int. Ed.* **2001**, *40*, 3060–3062.
- [6] B. M. Trost, F. D. Toste, *J. Am. Chem. Soc.* **2000**, *122*, 11262–11263.
- [7] B. M. Trost, F. D. Toste, *J. Am. Chem. Soc.* **1998**, *120*, 815–816; B. M. Trost, F. D. Toste, *J. Am. Chem. Soc.* **1998**, *120*, 9074–9075; B. M. Trost, F. D. Toste, *J. Am. Chem. Soc.* **1999**, *121*, 3543–3544; B. M. Trost, F. D. Toste, *J. Am. Chem. Soc.* **1999**, *121*, 4545–4554; B. M. Trost, H. C. Tsui, F. D. Toste, *J. Am. Chem. Soc.* **2000**, *122*, 3534–3535.
- [8] K. Pilger, B. Westermann, U. Flörke, G. Fels, *Synlett* **2000**, 1163–1165.
- [9] P. J. Parsons, M. D. Charles, D. M. Harvey, L. R. Sumoreeah, A. Shell, G. Spoors, A. L. Gill, S. Smith, *Tetrahedron Lett.* **2001**, *42*, 2209–2211.
- [10] C. Guillou, J.-L. Beunard, E. Gras, C. Thal, *Angew. Chem.* **2001**, *113*, 4881–4882; *Angew. Chem. Int. Ed.* **2001**, *40*, 4745–4746.
- [11] S. Y. Han, J. E. Sweeney, E. S. Bachman, E. J. Schweiger, G. Forloni, J. T. Coyle, B. M. Davis, M. M. Joullie, *Eur. J. Med. Chem.* **1992**, *27*, 673–687.
- [12] G. M. Bores, R. W. Kosley, Jr., *Drugs Future* **1996**, *21*, 621–635.
- [13] S. Y. Han, S. C. Mayer, E. J. Schweiger, B. M. Davis, M. M. Joullie, *Bioorg. Med. Chem. Lett.* **1991**, *1*, 579–580, and references therein.
- [14] A. Mary, D. Z. Renko, C. Guillou, C. Thal, *Bioorg. Med. Chem.* **1998**, *6*, 1835–1850; C. Guillou, A. Mary, D. Z. Renko, E. Gras, C. Thal, *Bioorg. Med. Chem. Lett.* **2000**, *10*, 637–639.
- [15] U. Jordis, J. Fröhlich, M. Treu, M. Hirsenschall, L. Czollner, B. Kälz, S. Welzig, PCT Int. Appl., WO 0174820, **2001**.
- [16] A. Mary, D. Z. Renko, C. Guillou, C. Thal, *Tetrahedron Lett.* **1997**, *38*, 5151–5152.
- [17] J. E. Toth, P. R. Hamann, P. L. Fuchs, *J. Org. Chem.* **1988**, *53*, 4694–4708.
- [18] H. Amri, M. Rambaud, J. Villieras, *Tetrahedron* **1990**, *46*, 3535–3546.
- [19] R. C. Larock, D. E. Stinn, *Tetrahedron Lett.* **1988**, *29*, 4687–4690.
- [20] B. K. Wilk, *Synth. Commun.* **1993**, *23*, 2481–2484; M. C. Aesa, G. Baán, L. Novák, C. Szántay, *Synth. Commun.* **1995**, *25*, 1545–1550.
- [21] K. C. Nicolaou, N. A. Petasis, *Selenium in Natural Products Synthesis*, CIS, Philadelphia, **1984**.
- [22] B. M. Trost, D. L. Van Vranken, *J. Am. Chem. Soc.* **1993**, *115*, 444–458.
- [23] K. Shibuya, *Synth. Commun.* **1994**, *24*, 2923–2941.

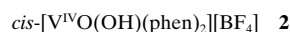
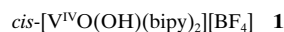
Monomeric Compounds Containing the *cis*-[V(=O)(OH)]⁺ Core

Evangelos J. Tolis, Manolis J. Manos, Anastasios J. Tasiopoulos, Catherine P. Raptopoulou, Aris Terzis, Michael P. Sigalas,* Yiannis Deligiannakis,* and Themistoklis A. Kabanos*

Monomeric metal compounds with terminal hydroxy ligands are important functional units in metalloproteins.^[1] Metal–OH (M–OH) units are proposed as the active species

- [*] Dr. T. A. Kabanos, Dr. E. J. Tolis, M. J. Manos, Dr. A. J. Tasiopoulos
Department of Chemistry
Section of Inorganic and Analytical Chemistry
University of Ioannina
45110 Ioannina (Greece)
Fax: (+30) 6510-44831
E-mail: tkampano@cc.uoi.gr
- Dr. Y. Deligiannakis
Department of Environmental and Natural Resources Management
Laboratory of Physical Chemistry
University of Ioannina
Seferi 2, 30100 Agrinio (Greece)
Fax: (+30) 6410-39576
E-mail: ideligia@cc.uoi.gr
- Dr. M. P. Sigalas
Department of Chemistry
Laboratory of Applied Quantum Chemistry
Aristotle University of Thessaloniki
54124 Thessaloniki (Greece)
Fax: (+30) 310-99-7739
E-mail: sigalas@chem.auth.gr
- Dr. C. P. Raptopoulou, Prof. A. Terzis
NRCPS Demokritos
Institute of Materials Science
15310 Agia Paraskevi Attikis (Greece)

in a wide variety of proteins and enzymes. The *cis*-[M(=O)(OH)]ⁿ⁺ center was identified in structurally characterized vanadium haloperoxidases^[2,3] and it has also been postulated as a key intermediate species in molybdoenzymes.^[4] At present, only a few examples of structurally characterized model mononuclear metal compounds with terminal hydroxy ligands are known.^[5] Furthermore, only the isolation of one model monomeric compound containing the *cis*-[M(=O)(OH)]ⁿ⁺ unit (but without structural characterization),^[6] has been reported. In almost all cases tripodal ligands with bulky substituents were used to isolate monomeric metal species containing terminal hydroxy ligands or the *cis*-[M(=O)(OH)]ⁿ⁺ fragment. Herein, we report the isolation, structural, and physicochemical^[7] characterization of the compounds **1** and **2**·H₂O which contain the *cis*-[V^{IV}O(OH)]⁺ structural unit supported by the bidentate ligands 2,2'-bipyridine (bipy) and 1,10-phenanthroline (phen). The electronic and magnetic properties of the complexes **1** and **2**·H₂O have been studied by continuous-wave electron paramagnetic resonance (c.w. EPR), electron spin echo envelope modulation (ESEEM) spectroscopy, and ab initio theoretical studies.



The mononuclear yellow-brown compound **1** was prepared by addition of AgBF₄ (5.6 mmol) to a stirred aqueous solution (~10 mL, pH ≈ 1) of [VOCl₂(thf)₂] (2.8 mmol). After removal of the AgCl, the filtrate was treated with bipy (5.6 mmol). Upon addition of bipy the blue color of the solution immediately changed to red, a yellow-brown precipitate was formed and the pH value of the solution changed to ≈ 4. Compound **2**·H₂O, the phen analogue of **1**, was synthesized in a similar fashion to **1**.

X-ray structural analysis of **1** (compound **2**·H₂O has a similar overall structure)^[8] revealed the presence of a discrete cation *cis*-[V^{IV}O(OH)(bipy)₂]⁺ (Figure 1) and a BF₄⁻ anion per molecule. The geometry of the complex cation is best described as a severely distorted octahedron with the vanadium center being displaced above the mean equatorial plane defined by three bipy nitrogen atoms and the hydroxy oxygen atom by 0.25 Å towards the oxo ligand. The notable structural feature of **1** is the presence of a hydroxy group in a position *cis* to the oxo ligand. The hydroxy group competes with the O²⁻ center for the same vacant d_{xz} vanadium orbital (see below) and this results in the substantial lengthening of the V=O bond (1.687(2) Å). The V=O bond in **1** lies well outside the range observed for oxovanadium(IV) complexes (≈1.56–1.63 Å).^[9] The two bipy ligands are unsymmetrically ligated to vanadium, with two long bonds (V–N4 2.247(3) Å and V–N2 2.175(3) Å) *trans* to the oxo and hydroxy ligands and two short bonds (V–N1 and N3, ≈2.114(3) Å) *trans* to each other. Bond valence sum calculation for O2 gives a value of 1.02, which is clearly indicative of monoprotonation for this oxygen atom.^[10] The O1–V–O2 angle, 106.8(2)°, of the *cis*-[V^{IV}O(OH)]⁺ core is almost identical to that observed for the closely related *cis*-[V^{VO}O₂(bipy)₂]⁺ ion (106.5(2)°) and very

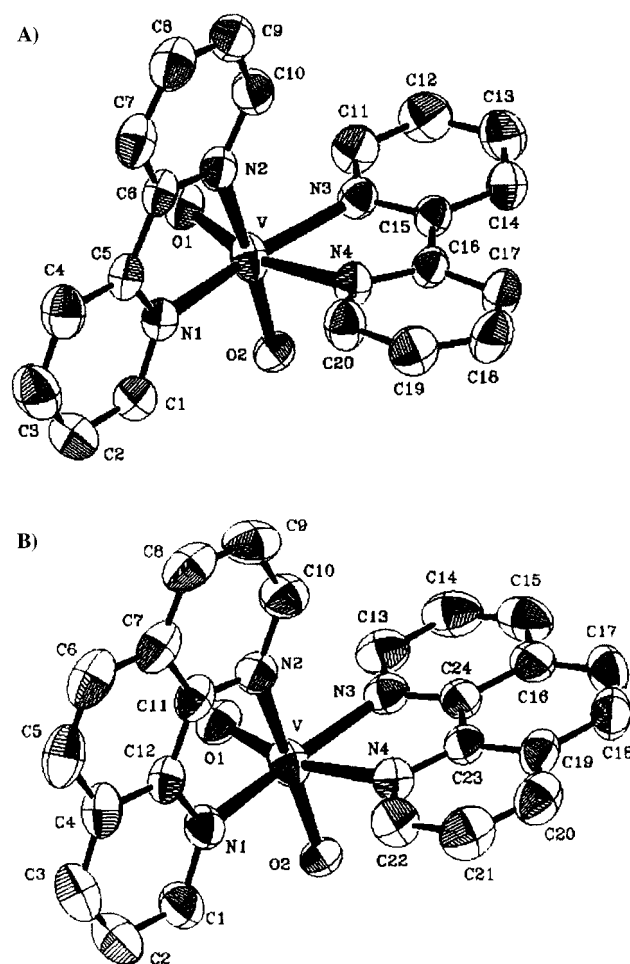


Figure 1. Molecular structures of the cations of **1** (A) and **2**·H₂O (B). Selected bond lengths [Å] and angles [°] for **1** [and **2**·H₂O in square brackets]: V–O1 1.687(2) [1.677(3)], V–O2 1.761(2) [1.778(2)], V–N1 2.115(3) [2.113(3)], V–N2 2.175(3) [2.173(3)], V–N3 2.111(3) [2.111(3)], V–N4 2.247(3) [2.246(3)]; O1–V–O2 106.8(12) [106.35(12)], O1–V–N3 93.10(12) [92.73(14)], O2–V–N3 92.20(10) [94.34(11)], O1–V–N1 100.05(11) [97.42(13)], O2–V–N1 90.13(11) [90.20(12)], N3–V–N1 165.44(11) [167.25(12)], O1–V–N2 89.56(11) [90.28(11)], O2–V–N2 160.27(11) [160.29(12)], N3–V–N2 98.88(10) [95.36(12)], N1–V–N2 75.17(11) [76.96(12)], O1–V–N4 161.75 (11) [163.74(12)], O2–V–N4 87.57(11) [86.11(12)], N3–V–N4 74.07(11) [75.61(12)], N1–V–N4 91.68(10) [92.85(12)], N2–V–N4 79.92(10) [79.76(11)].

close to other hexacoordinate mononuclear vanadium(V) compounds (hmv) containing the *cis*-[V^{VO}O₂]⁺ unit (~105°),^[9c] in which the two V=O bonds of the *cis*-[V^{VO}O₂]⁺ center do not differ by more than ~0.02 Å unless there are different donor atoms in positions *trans* to the oxo ligands. In hmv containing the *cis*-[V^{VO}O(OR)]²⁺ core the (O)–V–(OR) angles are ≈103° and the V^{VO}=O and V^{VO}–OR bonds are ≈1.60 and 1.74 Å, respectively.^[9c,f, 11, 12]

The frozen-solution EPR spectra for **1** and **2**·H₂O, recorded at 77 K, were characteristic of mononuclear V^{IV}O²⁺ complexes.^[13, 14] The ⁵¹V spin-Hamiltonian parameters, were derived from simulations of the EPR spectra and are the following: *g*_x = 1.981, *g*_y = 1.978, *g*_z = 1.944; *A*_x = 53, *A*_y = 64, *A*_z = 163 × 10⁻⁴ cm⁻¹ for **1** and **2**·H₂O as well. The *g* and *A* tensors for **1** and **2**·H₂O are identical and this can be interpreted as an indication of similar equatorial donor atoms

in both complexes.^[14] Information concerning the hyperfine coupling of the hydroxy proton was obtained by two-dimensional ESEEM^[15] spectroscopy (HYSCORE)^[16].

The HYSCORE spectra for **1** contain two characteristic sets of cross-peaks arising from the presence of $^{14}\text{N}(I=1)$ nuclei.^[17] One set consists of cross-peaks at frequencies $[\nu_\alpha, -\nu_\beta] = [3.4 \text{ MHz}, -7.1 \text{ MHz}]$ and $[\nu_\beta, -\nu_\alpha] = [7.1 \text{ MHz}, -3.4 \text{ MHz}]$ which can be assigned to an interacting $^{14}\text{N}(I=1)$ with $A_{\text{iso}} = [\nu_\beta - \nu_\alpha]/8\nu_1 = 4.6 \text{ MHz}$. The second pair of cross-peaks occur at frequencies $[\nu_\alpha, -\nu_\beta] = [4.7 \text{ MHz}, -8.8 \text{ MHz}]$ and $[\nu_\beta, -\nu_\alpha] = [8.8 \text{ MHz}, -4.7 \text{ MHz}]$ which corresponds to an interacting $^{14}\text{N}(I=1)$ with $A_{\text{iso}} = [\nu_\beta - \nu_\alpha]/8\nu_1 = 6.6 \text{ MHz}$. The two A_{iso} values, that is, 4.6 MHz and 6.6 MHz, correspond to two types of equatorially coordinated nitrogen atoms. Based on the crystal structure (Figure 1) we assign the $A_{\text{iso}}(^{14}\text{N}) = 4.6 \text{ MHz}$ to the two equivalent nitrogen atoms N1 and N3 oriented *trans* to each other. In the same context we assign the $A_{\text{iso}}(^{14}\text{N}) = 6.6 \text{ MHz}$ to the atom N2, *trans* to OH[−] group.

More interestingly the 2D HYSCORE spectrum of **1** (Figure 2) contains arc-shaped features centered at the proton Larmor frequency, that is, near 14.4 MHz, which correspond

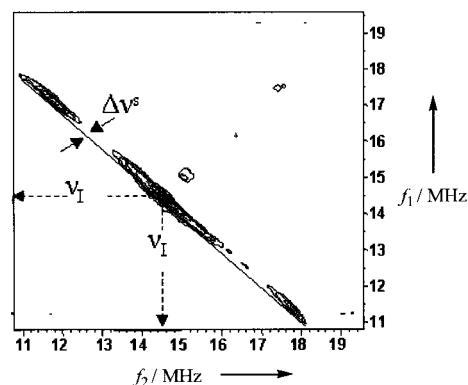


Figure 2. Contour plot of experimental frequency-domain main HYSCORE spectrum for the complex **1** in EtOH:H₂O (3:7) solution. $\Delta\nu^s$ is the maximum vertical shift from the antidiagonal at $(\nu_1, -\nu_1)$. Experimental conditions: $H = 3460$ Gauss, $\tau = 120$ ns, sample temperature 4 K. Time between successive pulse sets, 2 ms; microwave frequency, 9.64 GHz. The contour plots of HYSCORE frequency-domain spectrum were obtained after Fourier Transform in the magnitude mode, of 2D time-domain patterns containing 256×256 points with a step of 16 ns.

to a $^1\text{H}(I=1/2)$ coupled to the $\text{V}^{\text{IV}}\text{O}^{2+}$ electron spin. From the HYSCORE spectrum is deduced^[18] that the hyperfine coupling of this proton is characterized by $A_{\text{iso}} = 2.2 \text{ MHz}$ and strong anisotropy, that is, $T = 3.5 \text{ MHz}$. The size of this specific proton coupling falls between the hyperfine couplings reported for the two water protons in $[\text{V}^{\text{IV}}\text{O}(\text{H}_2\text{O})_5]^{2+}$ species.^[19] The anisotropic coupling of 3.5 MHz, when interpreted in the point-dipole model,^[17] implies a distance of 2.8 Å between the coupled proton and the metal spin. Overall the information from the HYSCORE data is consistent with a single ^1H nucleus located two bonds away from the metal, with the bond-pathway being mediated by an oxygen atom. Based on this, we assign this coupling to a hydroxy proton from the equatorial OH[−] moiety (*trans* to N2). Overall, the c.w. EPR and HYSCORE data provide conclusive evidence that the

complex **1** in solution has a planar donor set comprised of three nitrogen atoms plus one OH[−] group.

A DFT computational study of $[\text{V}^{\text{IV}}\text{O}(\text{OH})(\text{bipy})_2]^+$ has been carried out at the Becke3LYP computational level,^[20] using the effective core potential approximation of Hay and Wadt^[21] with a valence double- ζ basis set,^[22] and the calculations were performed using the Gaussian98 package.^[23] Full geometry optimizations starting from appropriate geometries were carried out without symmetry constraint and gave two minima, namely *cis*- $[\text{V}^{\text{IV}}\text{O}(\text{OH})(\text{bipy})_2]^+$ and *trans*- $[\text{V}^{\text{IV}}\text{O}(\text{OH})(\text{bipy})_2]^+$, both being real minima in the potential-energy surface of the molecule according to frequency calculations.

The *cis* isomer was calculated to be 10.9 kcal mol^{−1} more stable than the *trans* and its geometry agrees well with the experimental data. The two vanadium–oxygen bonds were calculated to be 1.690 and 1.780 Å for the oxo and hydroxy oxygen atoms, respectively. The V–N bond lengths are 2.195 and 2.254 Å for the nitrogen atoms N2 and N4 *trans* to OH[−] and O^{2−}, respectively, and 2.121 Å and 2.126 Å for N1 and N3. The optimization of the *trans* isomer gave a distorted structure, with the vanadium–oxygen bonds of 1.625 Å and 1.907 Å for the oxo and hydroxy oxygen atoms, respectively, and with a mean V–N bond lengths of 2.202 Å. A full discussion of the structural aspects of the calculated complexes will be published elsewhere.

Both the experimental and calculated bond lengths within the vanadium coordination sphere deserve some comments. Thus, whereas the elongation of the V–N2 bond by about 0.06 Å is nicely attributed to the *trans* influence of OH[−] group, the substantial elongation of the V=O bond by approximately 0.1 Å, compared to normal $\text{V}^{\text{IV}}=\text{O}$ bond lengths (mean $d(\text{V}^{\text{IV}}=\text{O})$ 1.60 Å), needs some attention. Possible intramolecular $\text{V}=\text{O} \cdots \text{H}-\text{O}=\text{V}$ hydrogen bond or intermolecular $\text{V}=\text{O} \cdots \text{H}-\text{O}-\text{V}$, $\text{V}=\text{O} \cdots \text{H}_2\text{O}$ or $\text{V}=\text{O} \cdots \text{O}=\text{V}$ interactions resulting in this elongation are excluded, because of the long calculated $\text{V}=\text{O} \cdots \text{H}$ distance (3.297 Å) and the absence of relevant short contacts in the crystal lattice of **1**. Such an elongation of the V=O bond has not been found in $[\text{V}^{\text{V}}\text{O}_2(\text{bipy})_2]^+$ (**3**;^[11] mean $d(\text{V}=\text{O}) \approx 1.626 \text{ Å}$) or in the closely related alkoxo compounds $[\text{V}^{\text{V}}\text{O}(\text{OC}_2\text{H}_5)_2\text{Cl}_2(\text{Hphca})]$ (**4**)^[12] (Hphca = *N*-(phenyl)pyridine-2-carboxamide), V=O 1.585 Å, V–OR 1.746 Å), both adopt the *cis* orientation of the O–V–O moiety. Both **3** and **4** are compounds of vanadium(v) whereas **1** is vanadium(iv). Thus, it seems that the excess positive charge on vanadium(v) in **3** and **4** lowers the d-block, makes the metal a better π acceptor, enforces the π interactions within the O–V–O moiety, and reduces the extent of V=O elongation. The V=O elongation in **1** has not been found in other $\text{V}^{\text{IV}}\text{O}^{2+}$ complexes. Thus, it can not be attributed only to the oxidation state of vanadium and still needs some explanation on the basis of electronic factors present in this particular case. According to our calculations this elongation could be explained as follows: The π -type donor orbitals of both the hydroxy (p_{OH}) and oxo oxygen atoms ($p_{=0}$) interact with the same vacant vanadium (d_{xz}) orbital. The d_{xz}/p_{OH} interaction destabilizes d_{xz} and increases the $d_{xz}/p_{=0}$ energy difference, which results in a decrease of the extent of the $d_{xz}/p_{=0}$ interaction and decrease of the double-

bond character of the $V^{IV}O^{2+}$ group. The shape of the occupied bonding molecular orbital resulting from this three-orbital/four-electron interaction, calculated at the DFT level, is shown in Figure 3. Finally, the weaker V=O bond results in a weaker *trans* influence of O^{2-} to the *trans* V–N bond, which is around 2.25 Å long, instead of its normal value of ~ 2.34 Å.

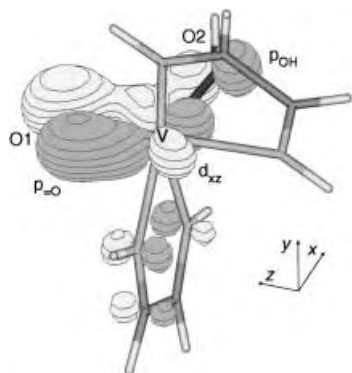


Figure 3. Shape of the occupied bonding molecular orbital resulting from the $p_{OH}/d_{xz}/p_{O}$ interaction, calculated at the DFT level. Only atoms the atomic orbitals of which participate in the molecular orbital are shown.

In conclusion, two monomeric oxovanadium(IV) compounds **1** and **2** · H₂O were isolated by treating $V^{IV}O^{2+}$ species with the bidentate ligands bipy or phen. These two compounds are the first examples of species containing the *cis*-[$V^{IV}O(OH)$]⁺ center to be structurally characterized. The presence of the hydroxy group *cis* to the O^{2-} center causes substantial changes in the bond lengths of these two compounds. The orbital interaction responsible for these changes can be explained by density functional computational studies. The continuous wave EPR and ESEEM parameters, obtained for **1** and **2** · H₂O provide spectroscopic signatures that enable the assignment of the *cis*-[$V^{IV}O(OH)$]⁺ center in vanadoproteins and $V^{IV}O^{2+}$ -substituted proteins.

Received: January 14, 2002
Revised: May 13, 2002 [Z18520]

- [1] a) W. N. Lipscomb, N. Sträter, *Chem. Rev.* **1996**, 96, 2375; b) B. A. Brennan, G. Alms, M. J. Nelson, L. T. Durney, R. C. Scarrow, *J. Am. Chem. Soc.* **1996**, 118, 9194; c) C. W. Hoganson, G. T. Babcock, *Science* **1997**, 277, 1953.
- [2] a) A. Messerschmidt, R. Wever, *Proc. Natl. Acad. Sci. USA* **1996**, 93, 392; b) M. Weyand, H.-J. Hecht, M. KeiB, M.-F. Liaud, H. Vilter, D. Schomburg, *J. Mol. Biol.* **1999**, 293, 595.
- [3] The existence of the *cis*-[$V^{IV}O(OH)$]⁺ center has been claimed in the reduced vanadium haloperoxidases and in solution after acidification of dioxovanadium(V) species as well as in a $V^{IV}O^{2+}$ dimeric compound. See for example: a) T. S. Smith, C. A. Root, J. W. Kampf, P. G. Rasmussen, V. L. Pecoraro, *J. Am. Chem. Soc.* **2000**, 122, 767; b) T. S. Smith II, R. Lobrutto, V. L. Pecoraro, *Coord. Chem. Rev.* **2002**, in press, and references therein; c) X. Li, M. S. Lah, V. L. Pecoraro, *Inorg. Chem.* **1988**, 27, 4657; d) G. J. Colpas, B. J. Hamstra, J. W. Kampf, V. L. Pecoraro, *Inorg. Chem.* **1994**, 33, 4669; e) M. Kosugi, S. Hikishi, M. Akita, Y. Moro-oka, *Inorg. Chem.* **1999**, 38, 2567.
- [4] a) H. J. Cohen, I. Fridovich, K. V. Rajagopalan, *J. Biol. Chem.* **1971**, 246, 374; b) M. W. W. Adams, L. E. Mortenson in *Molybdenum Enzymes* (Ed.: T. G. Spiro), Wiley, New York, **1985**, p. 519; c) A. V. Astashkin, M. L. Mader, A. Pacheco, J. H. Enemark, A. M. Raitsimirmir, *J. Am. Chem. Soc.* **2000**, 122, 9194.
- [5] C. E. MacBeth, B. S. Hammes, V. G. Young, Jr., A. S. Borovik, *Inorg. Chem.* **2001**, 40, 4733.
- [6] Z. Xiao, R. W. Gable, A. G. Wedd, C. G. Young, *J. Am. Chem. Soc.* **1996**, 118, 2912.
- [7] Elemental analysis (%) calcd for **1** (C₂₀H₁₇BF₄O₂N₄V): C 49.72, H 3.55, N 11.60, V 10.54; found: C 49.63, H 3.54, N 11.42, V 10.62; Elemental analysis (%) calcd for **2** · H₂O (C₂₄H₁₉BF₄O₃N₄V): C 52.49, H 3.49, N 10.21, V 9.28; found: C 52.39, H 3.58, N 10.03, V 9.50. Some characteristic IR bands for **1**: $\tilde{\nu}$ = 3582 [ν (O–H)], 1602 [ν (C=C=N)], 1053 [ν (B–F)], 970, 961 cm^{−1} [ν (V=O)]. Some characteristic IR bands for **2** · H₂O: $\tilde{\nu}$ = 3600 [ν (O–H)], 3452 [ν (O–H)] from H₂O], 1629 [ν (C=C=N)], 1062 [ν (B–F)], 968 cm^{−1} [ν (V=O)]. UV/Vis for **1** [CH₃CN, absorption, $\lambda/nm(\epsilon/dm^3\text{mol}^{-1}\text{cm}^{-1})$]: 744.0(23), 518(sh)(35), 304.2(21 553), 245.4(14 840), 194.4(43 240). UV/Vis for **2** · H₂O [CH₃CN, absorption, $\lambda/nm(\epsilon/dm^3\text{mol}^{-1}\text{cm}^{-1})$]: 742.5(23), 437(350), 292.5(sh)(14 750), 273.6(43 472), 226.8(47 083), 204.6(50 528). μ_{eff} (25 °C) for **1**: 1.75 μ_B , μ_{eff} (25 °C) for **2** · H₂O: 1.77 μ_B . Conductivity value for **1** (CH₃CN, C = 10^{−3} M, $\Lambda/\Omega^{-1}\text{mole}^{-1}\text{cm}^2$): 166. Conductivity value for **2** · H₂O (CH₃CN, C = 10^{−3} M, $\Lambda/\Omega^{-1}\text{mole}^{-1}\text{cm}^2$): 168.
- [8] Crystals of **1** and **2** · H₂O, suitable for X-ray analysis, were obtained by slow evaporation of a concentrated solution of **1** or **2** in CH₃CN:EtOH (1:1 v/v). Crystal data for **1**: [$V^{IV}O(OH)(bipy)_2$](BF₄):C₂₀H₁₇BF₄O₂N₄V, M_r = 483.13, space group $P\bar{1}$, a = 8.116(4), b = 9.490(5), c = 13.652(7) Å, V = 1023.0(9) Å³, Z = 2, ρ_{calcd} = 1.568 g cm^{−3}, T = 298 K. $R_1(\text{final})$ = 0.0598, wR_2 = 0.1687; crystal data for **2** · H₂O: [$V^{IV}O(OH)(phen)_2$](BF₄) · H₂O: C₂₀H₁₇BF₄O₂N₄V, M_r = 549.18, triclinic, space group $P\bar{1}$, a = 9.585(4), b = 15.911(8), c = 7.833(3) Å, V = 1166.2(9) Å³, Z = 2, ρ_{calcd} = 1.564 g cm^{−3}, T = 293(2) K. $R_1(\text{final})$ = 0.0657, wR_2 = 0.1940. CCDC 177 661 (**1**) and CCDC 177 662 (**2** · H₂O) contains the supplementary crystallographic data for this paper. These data can be obtained free of charge via www.ccdc.cam.ac.uk/conts/retrieving.html (or from the Cambridge Crystallographic Data Centre, 12, Union Road, Cambridge CB2 1EZ, UK; fax: (+44) 1223-336-033; or deposit@ccdc.cam.ac.uk).
- [9] a) D. Wang, M. Ebel, C. Schulzke, C. Grüning, S. K. S. Hazari, D. Rehder, *Eur. J. Inorg. Chem.* **2001**, 935; b) W. Priebsch, D. Rehder, *Inorg. Chem.* **1990**, 29, 3013; c) A. D. Keramidias, A. B. Papaioannou, A. Vlahos, T. A. Kabanos, G. Bonas, A. Makrigiannis, C. P. Raptopoulou, A. Terzis, *Inorg. Chem.* **1996**, 35, 357; d) E. J. Toliis, V. I. Teberikidis, C. P. Raptopoulou, A. Terzis, M. P. Sigalas, Y. Deligiannakis, T. A. Kabanos, *Chem. Eur. J.* **2001**, 7, 601; e) W. A. Nugent, J. M. Mayer, *Metal-Ligand Multiple Bonds*, Wiley, New York, **1988**; f) C. J. Carrano, M. Mohan, S. M. Holmes, R. Rosa, A. Butler, J. M. Charnock, C. D. Garner, *Inorg. Chem.* **1994**, 33, 646.
- [10] I. D. Brown in *Structure and Bonding in Crystals, Vol. II* (Eds.: M. O'Keefe, A. Navrotsky), Academic Press, New York, **1981**, p. 1.
- [11] S. G. Brand, N. Edelstein, C. J. Hawkins, G. Shalimoff, M. R. Snow, E. R. T. Tiekink, *Inorg. Chem.* **1990**, 29, 434.
- [12] K. D. Soulti, A. Troganis, A. Papaioannou, T. A. Kabanos, A. D. Keramidias, Y. G. Deligiannakis, C. R. Raptopoulou, A. Terzis, *Inorg. Chem.* **1998**, 37, 6785.
- [13] N. D. Chasteen in *Biological Magnetic Resonance, Vol. 3* (Eds.: L. Berliner, J. Reuben), Plenum, New York, **1981**, p. 53.
- [14] A. J. Tasiopoulos, A. N. Troganis, A. Evangelou, C. P. Raptopoulou, A. Terzis, Y. Deligiannakis, T. A. Kabanos, *Chem. Eur. J.* **1999**, 5, 910.
- [15] A. Schweiger, J. Jesche, *Principles of Pulsed Electron Paramagnetic Resonance*, Oxford University Press, Oxford, **2001**.
- [16] ESEEM is a pulsed EPR technique eminently suited for measuring weak magnetic interactions between the electron spin, that is, the $V^{IV}O^{2+}$ ion ($S = 1/2$) in the present case, and nearby nuclei, that is, the ligand atoms. The principles of ESEEM are thoroughly analyzed in the book of Schweiger and Jesche, ref. [15]. In the present case we rely on the application of HYSORE (Hyperfine Sublevel Correlation Spectroscopy ref. [17, 18] which is a 2D ESEEM technique based on the four-pulse [$\pi/2 - \tau - \pi - t_1 - \pi/2 - t_2 - \pi/2 - \tau - \text{echo}$] sequence. The applications of HYSORE to study the coordination environment of metal centers, including VO^{2+} complexes, have been reviewed by Deligiannakis et al. ref. [17].
- [17] The methodology of peak assignment in a HYSORE spectrum can be found in the following review article: Y. Deligiannakis, M. Louloudi, N. Hadjiladis, *Coord. Chem. Rev.* **2000**, 104, 1.

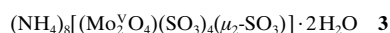
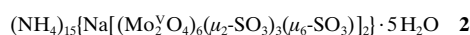
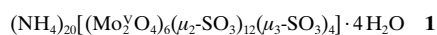
- [18] The proton hyperfine couplings have been estimated from Figure 2, based on the observed maximum shift $\Delta\nu^s$, according to the method of Pöppl and Kevan (A. Pöppl, L. Kevan, *J. Phys. Chem. B* **1996**, *100*, 3387). In Figure 2, $\Delta\nu^s$ is 0.3 MHz which based on the relationship $T = (\%)[8\Delta\nu^s\nu_i/(2)^{1/2}]^{1/2}$ gives a hyperfine anisotropy for this proton $T = 3.27$ MHz. Using this as starting value, we have calculated the proton isotropic hyperfine coupling based on numerical simulations. The final values are $A_{\text{iso}} = 2.2$ MHz, $T = 3.5$ MHz.
- [19] A. M. Tyryshkin, S. A. Dikanov, R. G. Evelo, A. J. Hoff, *J. Chem. Phys.* **1992**, *97*, 42.
- [20] a) D. Becke, *J. Chem. Phys.* **1993**, *98*, 5648; b) C. T. Lee, W. Yang, R. G. Parr, *Phys. Rev. B* **1988**, *37*, 785.
- [21] a) P. J. Hay, W. R. Wadt, *J. Chem. Phys.* **1985**, *82*, 270; b) W. R. Wadt, P. J. Hay, *J. Chem. Phys.* **1985**, *82*, 284; c) P. J. Hay, W. R. Wadt, *J. Chem. Phys.* **1985**, *82*, 299.
- [22] T. H. Dunning Jr., P. J. Hay in *Modern Theoretical Chemistry*, Vol. 3 (Ed.: H. F. Schaefer III), Plenum, New York, **1976**, p. 1.
- [23] Gaussian 98 (Revision A.7), M. J. Frisch, G. W. Trucks, H. B. Schlegel, G. E. Scuseria, M. A. Robb, J. R. Cheeseman, V. G. Zakrzewski, J. A. Montgomery, R. E. Stratmann, J. C. Burant, S. Dapprich, J. M. Millam, A. D. Daniels, K. N. Kudin, M. C. Strain, O. Farkas, J. Tomasi, V. Barone, M. Cossi, R. Cammi, B. Mennucci, C. Pomelli, C. Adamo, S. Clifford, J. Ochterski, G. A. Petersson, P. Y. Ayala, Q. Cui, K. Morokuma, D. K. Malick, A. D. Rabuck, K. Raghavachari, J. B. Foresman, J. Cioslowski, J. V. Ortiz, B. B. Stefanov, G. Liu, A. Liashenko, P. Piskorz, I. Komaromi, R. Gomperts, R. L. Martin, D. J. Fox, T. Keith, M. A. Al-Laham, C. Y. Peng, A. Nanayakkara, C. Gonzalez, M. Challacombe, P. M. W. Gill, B. G. Johnson, W. Chen, M. W. Wong, J. L. Andres, M. Head-Gordon, E. S. Replogle, J. A. Pople, Gaussian, Inc., Pittsburgh, PA, **1998**.

Polyoxomolybdenum(v) Sulfite Complexes: Synthesis, Structural, and Physical Studies**

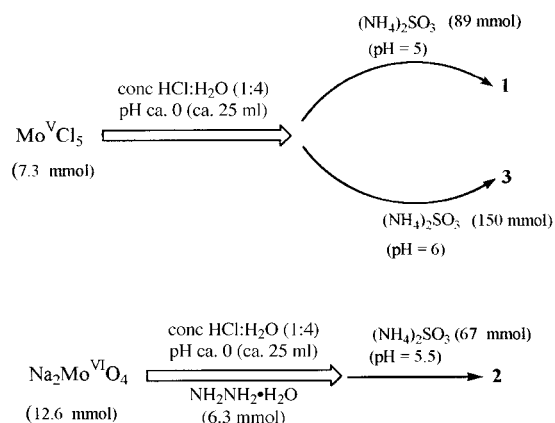
Manolis J. Manos, J. Derek Woollins, Alexandra M. Z. Slawin,* and Themistoklis A. Kabanos*

The contemporary interest in polyoxometalates reflects the ubiquitous nature of this family of inorganic networks, which exhibit a diverse compositional range and considerable structural versatility,^[1] as well as important magnetic,^[2] optical,^[1] and catalytic properties.^[1] A great deal of attention has been paid to heteropolyanions containing inorganic anionic ligands,^[3] mainly tetrahedral phosphate groups, be-

cause of the fascinating electronic and structural properties of polyoxomolybdenum and vanadium phosphates.^[4] Among these derivatized polyoxoanions, examples incorporating the pyramidal sulfite anion as the inorganic ligand are largely unknown, except for the molybdenum(vi) derivative $[\text{Mo}_5^{\text{VI}}\text{O}_{15}(\text{SO}_3)_2]^{4-}$.^[5] The lack of such complexes is surprising for two main reasons: first, metal–sulfite chemistry is very attractive in view of its potential for restricting the serious environmental problem of acid rain,^[6] and second, exploring the possibility of incorporating the pyramidal sulfite anion into frameworks, rather than the more frequently used tetrahedral phosphate groups, could result in unprecedented structural features and novel properties for these frameworks.^[7] Furthermore, molybdenum–sulfite chemistry is of great biological interest, since the enzyme sulfite oxidase, which is associated with the in vivo oxidation of SO_3^{2-} to SO_4^{2-} , contains a molybdenum atom at its active center.^[8] Herein, we describe the synthesis, structural, and physico-chemical characterization of the first polyoxomolybdenum(v) sulfite complexes **1–3**.



Complex **1** was prepared by treating $\text{Mo}^{\text{V}}\text{Cl}_5$ (7.3 mmol) in concentrated (37 %) $\text{HCl}:\text{H}_2\text{O}$ (1:4 v/v, pH approximately 0) with solid $(\text{NH}_4)_2\text{SO}_3$ (Scheme 1). Upon addition of



Scheme 1. The synthetic routes leading to the isolation of **1–3**.

$(\text{NH}_4)_2\text{SO}_3$ (89 mmol) the pH of the solution changed to approximately 5, and thus it is apparent that the SO_3^{2-} ion performs the dual role of raising the pH of the solution, as well as acting as a ligand. However, if the same reaction was performed with a larger quantity of $(\text{NH}_4)_2\text{SO}_3$ (150 mmol, final pH of the solution was approximately 6), complex **3** was isolated (Scheme 1). Reduction of $\text{Na}_2\text{Mo}^{\text{VI}}\text{O}_4$ dissolved in concentrated (37 %) $\text{HCl}:\text{H}_2\text{O}$ (pH approximately 0) with an excess of hydrazine, followed by addition of $(\text{NH}_4)_2\text{SO}_3$ (final pH of the solution was approximately 5.5) resulted in the formation of **2** (Scheme 1).

[*] Dr. T. A. Kabanos, M. J. Manos
Department of Chemistry
Section of Inorganic and Analytical Chemistry
University of Ioannina, 45110 Ioannina (Greece)
Fax: (+30)6510-44831
E-mail: tkampano@cc.uoi.gr
Dr. A. M. Z. Slawin, Prof. J. D. Woollins
Department of Chemistry
University of St. Andrews
St. Andrews, Fife KY16 9ST (UK)
Fax: (+44)1334-463-384
E-mail: jdw3@st-andrews.ac.uk

[**] We thank Assistant Professor S. Skoulika and Dr. T. Ozeki for helpful discussions as well as the Thermal Analyses Laboratory for performing the thermogravimetric analyses, and Mrs. Cate Statira for her subtle, nonetheless, useful contribution to the linguistic refinement of the text.

The X-ray structure of **1**^[9] exhibits a $[(\text{Mo}_2^{\text{V}}\text{O}_4)_6(\text{SO}_3)_{16}]^{20-}$ cluster **1a** (Figure 1 A), which contains 12 Mo^V centers within the main structural unit. Each molybdenum atom has octahedral coordination, and is bonded to a terminal oxo

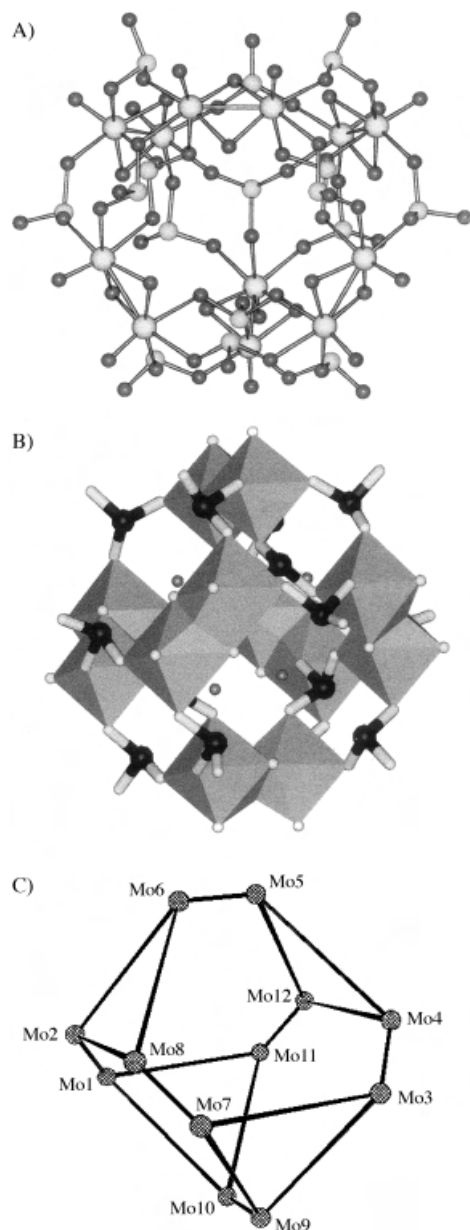


Figure 1. A) Ball-and-stick representation of the $[(\text{Mo}_2\text{O}_4)_6(\text{SO}_3)_{16}]^{20-}$ ion: Mo: gray, S: smaller gray balls, O: dark gray. Average bond lengths [Å]: Mo=O 1.69(1), Mo-O ($\mu_2\text{-O}^{2-}$) 1.944(9), Mo-O ($\mu_2\text{-SO}_3^{2-}$) 2.13(1), Mo-O ($\mu_3\text{-SO}_3^{2-}$) 2.20(1), Mo-Mo (single bond) 2.561(4), S-O (terminal) 1.49(1), S-O ($\mu_2\text{-SO}_3^{2-}$) 1.55(1), S-O ($\mu_3\text{-SO}_3^{2-}$) 1.537(9); B) polyhedral representation of the $[(\text{Mo}_2\text{O}_4)_6(\text{SO}_3)_{16}]^{20-}$ ion: S: black, O: white, N: gray; C) the arrangement of the twelve Mo^V atoms of the $[(\text{Mo}_2\text{O}_4)_6(\text{SO}_3)_{16}]^{20-}$ ion.

group, two $\mu_2\text{-O}^{2-}$ ions, and three sulfite (two $\mu_2\text{-}$ and one $\mu_3\text{-}$) oxygen atoms. The twelve Mo^V atoms form six binuclear units $[\text{Mo}_2^{\text{V}}\text{O}_4]^{2+}$ with a Mo–Mo separation of about 2.56 Å (single bond). The six $[\text{Mo}_2^{\text{V}}\text{O}_4]^{2+}$ moieties are connected to each other by twelve sulfite ligands. Twelve of which have a $\mu_2\text{-}$ (2L,2M) bonding mode, while the remaining four anions have

the novel $\mu_3\text{-}$ (3L,3M) mode of ligation (see below). The $\mu_2\text{-SO}_3^{2-}$ ions can be considered as “outer” groups, and each of these anions bridges two $\text{Mo}_2^{\text{V}}\text{O}_{10}$ units comprised of two edge-sharing $\text{Mo}^{\text{V}}\text{O}_6$ octahedra, while the four $\mu_3\text{-SO}_3^{2-}$ anions are the “inner” groups, and each of these anions are connected to three Mo_2O_{10} dimeric moieties (Figure 1 B).^[10] Four ammonium cations are located deep within the $[(\text{Mo}_2^{\text{V}}\text{O}_4)_6(\text{SO}_3)_{16}]^{20-}$ ion (Figure 1 B), and contribute to its stability. The arrangement of the molybdenum atoms in **1** is similar to an ϵ -Keggin isomer (Figure 1 C),^[1a, 11] except that **1** contains six separated $\{\text{Mo}_2\text{O}_{10}\}$ moieties (Figure 1 B). This arrangement is in contrast to ϵ -Keggin derivatives (and other Keggin forms), where the twelve MO_6 octahedra are arranged in four groups of three edge-shared octahedra, M_3O_{13} .

X-ray structural analysis of **2**^[9] revealed the presence of the discrete anion $[\text{Na}(\text{Mo}_2^{\text{V}}\text{O}_4)_3(\mu_2\text{-O})_3(\mu_2\text{-SO}_3)_3(\mu_6\text{-SO}_3)]^{15-}$ (**2a**; Figure 2 A), with ammonium cations and water of crystallization also present in the lattice. The anion **2a** consists of two identical hexanuclear polyoxomolybdenum sulfite anions $[(\text{Mo}_2^{\text{V}}\text{O}_4)_3(\mu_2\text{-O})_3(\mu_2\text{-SO}_3)_3(\mu_6\text{-SO}_3)]^{8-}$ (**2b**; Figure 2 B), linked by a sodium cation. The six molybdenum(v)

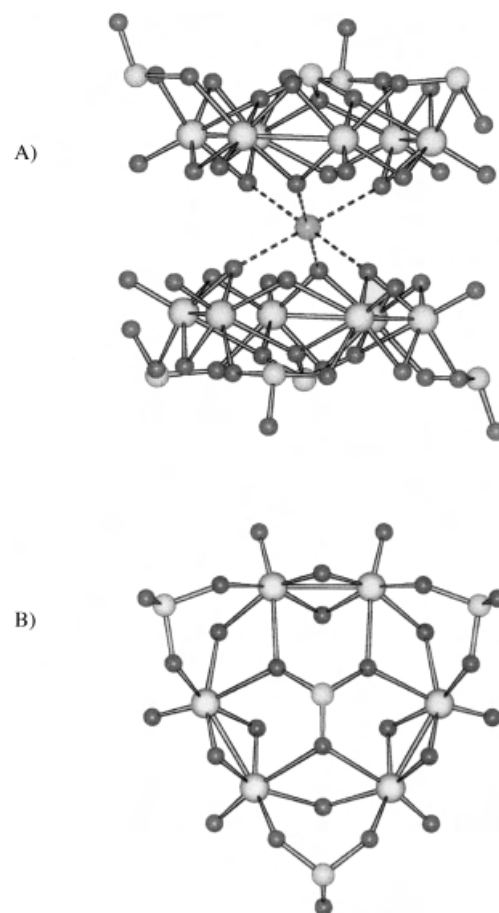


Figure 2. A) Representation of the $[\text{Na}(\text{Mo}_2\text{O}_4)_3(\text{O})_3(\text{SO}_3)_4]^{15-}$ dimer: Mo: light-gray, S: smaller light-gray balls, O: dark gray, Na: gray; B) ball-and-stick representation of **2b**: Mo: gray, S: smaller gray balls, O: dark gray. Average bond lengths [Å]: Mo=O 1.673(1), Mo-O ($\mu_2\text{-O}^{2-}$ of the $\{\text{Mo}_2\text{O}_4\}$ units) 1.944(8), Mo-O ($\mu_2\text{-O}^{2-}$ bridging $\{\text{Mo}_2\text{O}_4\}$ units) 2.11(1), Mo-O ($\mu_2\text{-SO}_3^{2-}$) 2.059(3), Mo-O ($\mu_6\text{-SO}_3^{2-}$) 2.36(2), Mo-Mo (single bond) 2.597(5), S-O (terminal) 1.48(1), S-O ($\mu_2\text{-SO}_3^{2-}$) 1.565(8), S-O ($\mu_6\text{-SO}_3^{2-}$) 1.528(2).

atoms are co-planar, and are arranged in a pseudo-hexagonal arrangement, in which alternating bonding and non-bonding contacts are evident. There are four sulfite groups in **2b**: three of these are on the periphery of the cluster and possess a terminal oxo group, while the unique central sulfite group provides three μ_2 -oxygen bridges, so as to join each pair of molybdenum(v) centers. There are three crystallographically independent molybdenum atoms in the asymmetric unit, (Figure 2B). Each atom has severely distorted octahedral geometry (ignoring the $\text{Mo}^{\text{V}}\text{--Mo}^{\text{V}}$ bond), being coordinated to three $\mu_2\text{-O}^{2-}$ ions, two sulfite (one μ_2 - and one μ_6 -) oxygen atoms, as well as an oxo group. The sulfite groups ($3\mu_2$ - and one μ_6 -) and the three “*syn*” $\mu_2\text{-O}^{2-}$ ions are located on one side, with the terminal oxo group and the six “*anti*” $\mu_2\text{-O}^{2-}$ ions found on the other side, such that the $[(\text{Mo}_2^{\text{V}}\text{O}_4)_3(\mu_2\text{-O})_3(\mu_2\text{-SO}_3)_3(\mu_6\text{-SO}_3)]^{8-}$ cluster takes the shape of an adorned crown. In the dimeric assembly **2a** (Figure 2A) a sodium cation is sandwiched between two identical **2b** anions. The two anions are staggered with respect to one another, so as to effect octahedral coordination of the sodium cation, which interacts with the six *anti*- $\mu_2\text{-O}^{2-}$ ions of the $[(\text{Mo}_2^{\text{V}}\text{O}_4)_3]^{2+}$ moieties. The anion **2b** is closely related to several molybdenum(v) oxometalates containing phosphate ligands^[4b, 12a–d] as well as sulfate/arsenite^[12e] and carbonate groups, for example **4**.^[12f]



All of these complexes, which are reminiscent of the “Anderson” species,^[1a] possess a Mo_6 -planar core with a central μ_6 and three peripheral μ_2 ligands as well as three additional hydroxy (in most cases) or oxo groups bridging the three $[(\text{Mo}_2^{\text{V}}\text{O}_4)_3]^{2+}$ moieties. In **2b**, these ligands are pyramidal SO_3^{2-} ions, whereas in the “Anderson”-like molybdenum(v) hexametalates so far reported, the equivalent ligands are generally tetrahedral (phosphates), or less frequently trigonal-planar anions (carbonates) or mixed tetrahedral-pyramidal building blocks (sulfate – arsenite anions).

A comparison of **1a**, **2b** and the ion $[(\text{Mo}_2^{\text{V}}\text{O}_4)_3(\text{OH})_3(\text{CO}_3)_4]^{5-}$ ^[12f] (**4a**) reveals that the same structural unit $[(\text{Mo}_2^{\text{V}}\text{O}_4)(\mu_2\text{-XO}_3)]$ ($\text{X} = \text{S}, \text{C}$) exists in all cases, where short $\text{Mo}^{\text{V}}\text{--Mo}^{\text{V}}$ separations ($\text{Mo}^{\text{V}}\text{--Mo}^{\text{V}}$ single bonds; **1a**: 2.561(4), **2b**: 2.597(5), **4a**: 2.5884(6) Å) alternating with longer $\text{Mo} \cdots \text{Mo}$ contacts (**1a**: 5.70(3), **2b**: 3.593(4), **4a**: 3.548(6) Å). This observation proves that the 4d electrons must be regarded as being localized in all $\{\text{Mo}_2^{\text{V}}\}$ pairs, a fact which corresponds to the diamagnetism and the red color of the cluster complexes **1**, **2**, and **4**.^[13]

As shown in Figure 3, the anion of **3** is a centrosymmetric dimer.^[9] Each molybdenum(v) atom is coordinated in a distorted octahedral geometry (ignoring the $\text{Mo}^{\text{V}}\text{--Mo}^{\text{V}}$ interaction) by two $\mu_2\text{-O}^{2-}$ ions, three sulfite (two terminal and one μ_2 -) oxygen atoms, and an oxo group. A comparison of **3**, which contains the *syn*- $\text{Mo}^{\text{V}}(\text{O})(\mu_2\text{-O})_2\text{Mo}^{\text{V}}(\text{O})$ core, with $[(\text{SO}_4)\text{Mo}^{\text{V}}(\text{O})(\mu_2\text{-S})_2\text{Mo}^{\text{V}}(\text{O})(\text{SO}_4)]^{2-}$,^[14] which contains the *syn*- $\text{Mo}^{\text{V}}(\text{O})(\mu_2\text{-S})_2\text{Mo}^{\text{V}}(\text{O})$ unit, reveals that the $\text{Mo}^{\text{V}}\text{--Mo}^{\text{V}}$ bond is approximately 2.60 Å for **3**, compared with 2.80 Å for the latter complex. In addition, the $\text{Mo-O}_b(\text{S}_b)\text{--Mo}$ ($b =$ bridging) bond angles are approximately 83.5 and 74.5°,

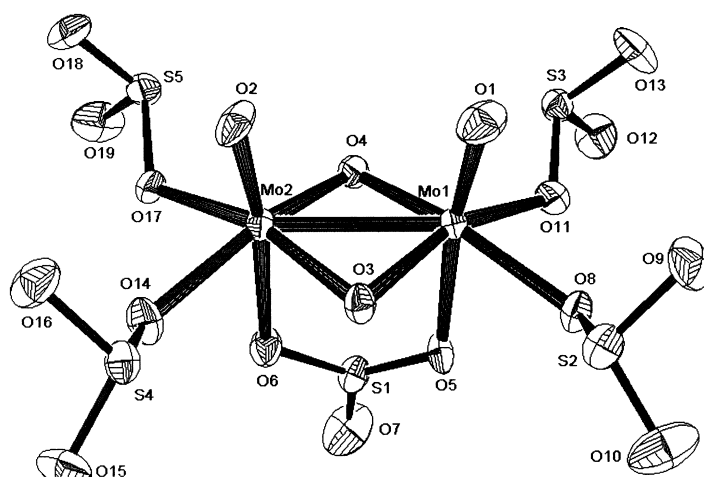
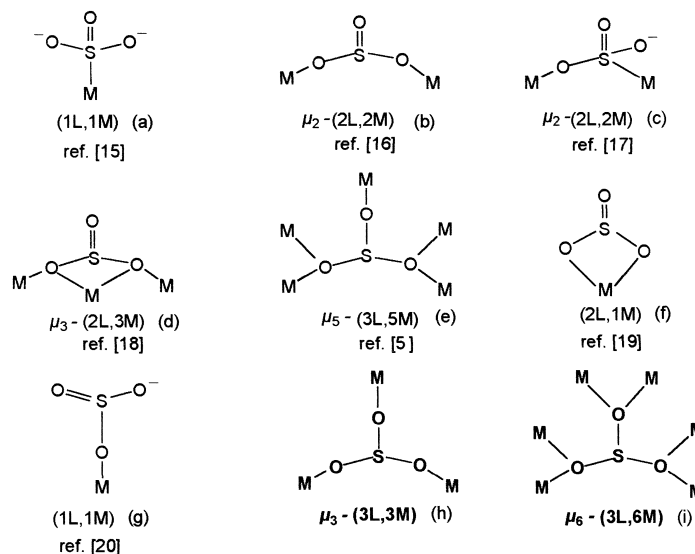


Figure 3. ORTEP plot of **3**. Displacement ellipsoids are plotted at the 50 % probability level. Average bond lengths [Å]: $\text{Mo}=\text{O}$ 1.686(5), Mo-O ($\mu_2\text{-O}^{2-}$) 1.940(9), Mo-O (terminal- SO_3^{2-}) 2.10(1), Mo-O ($\mu_2\text{-SO}_3^{2-}$) 2.27(1), Mo-Mo (single bond) 2.5872(18), S-O (terminal) 1.46(10), S-O ($\mu_2\text{-SO}_3^{2-}$) 1.57(2), S-O ($\mu_2\text{-SO}_3^{2-}$) 1.53(1).

respectively, while the $\text{O}_b(\text{S}_b)\text{--Mo-O}_b(\text{S}_b)$ bond angles are approximately 95° for **3** and 105° for the latter.

It is worth noting that the sulfite anion exhibits the bonding modes a–g, (Scheme 2) in the known metal complexes^[15–20] and the only polyoxometal sulfite complex.^[5] The two new



Scheme 2. The bonding modes (a–g) of SO_3^{2-} ions observed in metal complexes and the only polyoxometal sulfite complex, and the two new bonding modes (h and i) present in complexes **1** and **3**, respectively.

bonding modes h and i, observed in complexes **1** and **2**, are also shown in Scheme 2. Characteristic IR bands, solid- and solution-state UV/Vis spectra, as well as thermogravimetric analysis data for complexes **1–3** are reported in the Experimental Section.

In conclusion, the first polyoxomolybdenum(v) sulfite complexes **1–3** have been synthesized and structurally and physicochemically characterized. The modification of the

oxide microstructure by the incorporation of SO_3^{2-} groups is apparent in the structure of the dodecamer **1**, which exhibits a unique structural motif among polyoxomolybdenum(v) dodecamers (and polyoxometalates in general). Thus, the insertion of pyramidal SO_3^{2-} ions into polyoxometalate units can be effective for the assembly of frameworks with novel structural characteristics (and possibly new properties), as compared to established metal oxides containing tetrahedral phosphate ligands. Furthermore, the novel μ_3 -(3L,3M) and μ_6 -(3L,6M) coordination modes of the sulfite anion observed in **1** and **2**, respectively, reveal the great versatility of the sulfite group. Therefore, this seemingly pedestrian anion can be an excellent ligand not only in polyoxometalates, but in coordination complexes in general.

Experimental Section

1: Solid $(\text{NH}_4)_2\text{SO}_3$ (12.00 g, 89 mmol) was added in one portion to a light-red solution of MoCl_5 (2.00 g, 7.3 mmol, pH ~ 0) in concentrated (37%) $\text{HCl}:\text{H}_2\text{O}$ (1:4 v/v, 25 mL). After stirring the mixture for 5 min, the initially formed orange solid had redissolved, and a dark red (pH ~ 5) solution was obtained. The solution was kept in an open beaker for one day and then the precipitated red needles were filtered and dried in the air. Yield: 1.44 g (73% based on Mo). IR: $\tilde{\nu} = 1637$ [$\delta(\text{H}_2\text{O})$], 1401 [$\delta(\text{NH}_4^+)$], 1051 [$\nu(\text{SO}_3^{2-})$], 988 [$\nu(\text{Mo}=\text{O})$], 969 [$\nu(\text{Mo}=\text{O})$], 895 [$\nu(\text{SO}_3^{2-})$], 837 [$\nu(\text{SO}_3^{2-})$], 677 [$\nu(\text{SO}_3^{2-})$], 479 cm^{-1} [$\nu(\text{SO}_3^{2-})$]; UV/Vis (solid-state reflectance spectrum): $\lambda = 553$, 329 nm; UV/Vis (H_2O): λ/nm ($\epsilon/\text{dm}^3\text{mol}^{-1}\text{cm}^{-1}$) = 314 (30200); TGA: percentage weight loss (temperature ($^\circ\text{C}$)) = 5.17 (28.2), 32.53 (135.1), 9.52 (254.8), 4.66 (396); elemental analysis calcd (%) for $\text{H}_{88}\text{Mo}_{12}\text{N}_{20}\text{O}_{76}\text{S}_{16}$ (3249.14): H 2.73, N 8.62, S 15.79, Mo 35.43; found: H 2.85, N 8.50, S 15.90, Mo 35.65.

2: Hydrazine monohydrate (0.320 g, 6.3 mmol) was added to a stirred solution of $\text{Na}_2\text{Mo}^{\text{VI}}\text{O}_4 \cdot 2\text{H}_2\text{O}$ (3.00 g, 12.6 mmol, pH ~ 0) in concentrated (37%) $\text{HCl}:\text{H}_2\text{O}$ (1:4 v/v, 25 mL). The light-yellow color of the solution changed to dark-blue. Solid $(\text{NH}_4)_2\text{SO}_3$ (9.00 g, 67 mmol) was then added to the solution in one portion. Upon addition of $(\text{NH}_4)_2\text{SO}_3$ the dark-blue color of the solution became olive-green, and its pH value was ca. 5.5. The solution was kept in an open beaker for 2–3 days, after which time the precipitated red block-shaped crystals were filtered and dried in the air. Yield: 2.17 g (78% based on Mo). IR: $\tilde{\nu} = 1637$ [$\delta(\text{H}_2\text{O})$], 1408 [$\delta(\text{NH}_4^+)$], 1088 [$\nu(\text{SO}_3^{2-})$], 981 [$\nu(\text{Mo}=\text{O})$], 963 [$\nu(\text{Mo}=\text{O})$], 889 [$\nu(\text{SO}_3^{2-})$], 865 [$\nu(\text{SO}_3^{2-})$], 809 [$\nu(\text{SO}_3^{2-})$], 546 [$\nu(\text{SO}_3^{2-})$], 487 cm^{-1} [$\nu(\text{SO}_3^{2-})$]; UV/Vis (solid-state reflectance spectrum): $\lambda = 495$, 324, 251 nm; UV/Vis (H_2O) λ/nm ($\epsilon/\text{dm}^3\text{mol}^{-1}\text{cm}^{-1}$) = 470(sh) (310), 306 (16500), 208 (32200); TGA: percentage weight loss (temperature ($^\circ\text{C}$)) = 3.43 (69.4), 4.02 (128.2), 21.87 (236.4), 1.37 (374.3), 0.84 (397.0), 0.11 (579.1); elemental analysis calcd (%) for $\text{H}_{70}\text{Mo}_{12}\text{N}_{15}\text{NaO}_{59}\text{S}_8$ (2655.46): H 2.66, N 7.91, S 9.66, Mo 43.36; found: H 2.75, N 8.20, S 9.40, Mo 43.15.

3: This was synthesized in a similar fashion to **1**, except that the amount of $(\text{NH}_4)_2\text{SO}_3$ added to the MoCl_5 (2.00 g, 7.3 mmol) solution was 20.00 g (150 mmol) and the pH value of the resulting dark-red solution was ca. 6. The solution was filtered and red orthogonal crystals of **3** were formed by vapor diffusion of MeOH into the filtrate for one week. The crystals were filtered and dried in air. Yield: 1.20 g (39% based on Mo). IR: $\tilde{\nu} = 1403$ [$\delta(\text{NH}_4^+)$], 993 [$\nu(\text{SO}_3^{2-})$], 965 [$\nu(\text{Mo}=\text{O})$], 903 [$\nu(\text{SO}_3^{2-})$], 821 [$\nu(\text{SO}_3^{2-})$], 662 [$\nu(\text{SO}_3^{2-})$], 527 [$\nu(\text{SO}_3^{2-})$], 468 cm^{-1} [$\nu(\text{SO}_3^{2-})$]; UV/Vis (solid-state reflectance spectrum): $\lambda = 553$, 325 nm; UV/Vis (H_2O) λ/nm ($\epsilon/\text{dm}^3\text{mol}^{-1}\text{cm}^{-1}$) = 312 (4000); TGA: percentage weight loss (temperature ($^\circ\text{C}$)) = 67 (160), 1.36 (395.4); elemental analysis calcd (%) for $\text{H}_{36}\text{Mo}_2\text{N}_8\text{O}_{21}\text{S}_5$ (836.55): H 4.33, N 13.39, S 19.16, Mo 22.94; found: H 4.17, N 13.13, S 19.25, Mo 23.2.

Received: December 28, 2001
Revised: May 5, 2002 [Z18459]

- [1] a) M. T. Pope, *Heteropoly and Isopoly Oxometalates*, Springer, New York, **1983**; b) M. T. Pope, A. Müller, *Angew. Chem.* **1991**, *103*, 56; *Angew. Chem. Int. Ed. Engl.* **1991**, *30*, 34; c) *Polyoxometalates: From Platonic Solids to Anti-Retroviral Activity* (Eds.: M. T. Pope, A. Müller), Kluwer Academic Publishers, Dordrecht, **1994**; d) *Chem. Rev.* **1998**, *98*, 8 (guest editor: C. L. Hill).
- [2] J. M. Clemente-Juan, E. Coronado, *Coord. Chem. Rev.* **1999**, *193*, 361, and references therein.
- [3] A. Müller, F. Peters, M. T. Pope, D. Gatteschi, *Chem. Rev.* **1998**, *98*, 239, and references therein.
- [4] a) A. K. Cheetham, G. Férey, T. Loiseau, *Angew. Chem.* **1999**, *111*, 3466; *Angew. Chem. Int. Ed.* **1999**, *38*, 3268, and references therein; b) R. C. Haushalter, L. A. Mundi, *Chem. Mater.* **1992**, *4*, 31; c) C. du Peloux, A. Dolbecq, P. Mialane, J. Marrot, E. Riviere, F. Secheresse, *Angew. Chem.* **2001**, *113*, 2521; *Angew. Chem. Int. Ed.* **2001**, *40*, 2455.
- [5] K. Y. Matsumoto, M. Kato, Y. Sasaki, *Bull. Chem. Soc. Jpn.* **1976**, *49*, 106.
- [6] C. Brandt, R. van Eldik, *Chem. Rev.* **1995**, *95*, 119.
- [7] a) W. T. A. Harrison, M. L. F. Phillips, J. Stanchfield, T. M. Nenoff, *Angew. Chem.* **2000**, *112*, 3966; *Angew. Chem. Int. Ed.* **2000**, *39*, 3808; b) M. Shich, K. J. Martin, P. J. Squattrito, A. Clearfield, *Inorg. Chem.* **1990**, *29*, 958.
- [8] a) R. Hille, *Chem. Rev.* **1996**, *96*, 2757; b) J. L. Johnson in *Molybdenum and Molybdenum Containing Enzymes* (Ed.: M. P. Coughlan), Pergamon, Oxford, **1980**.
- [9] Crystal data for **1**: $(\text{NH}_4)_{20}[(\text{Mo}_2\text{O}_4)_6(\text{SO}_3)_{16}] \cdot 4\text{H}_2\text{O}$: $\text{H}_{88}\text{Mo}_{12}\text{N}_{20}\text{O}_{76}\text{S}_{16}$, $M_r = 3249.14$, monoclinic, space group $C2/c$, $a = 57.0591(3)$, $b = 15.6701(3)$, $c = 27.4303(5)$ Å, $\beta = 116.7510(10)$, $V = 21901.0(6)$ Å³, $Z = 8$, $\rho_{\text{calcd}} = 1.971$ g cm⁻³, $T = 293(2)$ K, $R_1(\text{final}) = 0.0490$, $wR_2 = 0.1260$. Crystal data for **2**: $(\text{NH}_4)_{15}[\text{Na}\{(\text{Mo}_2\text{O}_4)_3(\text{O})_2(\text{SO}_3)_4\}_2] \cdot 5\text{H}_2\text{O}$: $\text{H}_{70}\text{Mo}_{12}\text{N}_{15}\text{NaO}_{59}\text{S}_8$, $M_r = 2655.46$, monoclinic, space group $C2/m$, $a = 18.2657(8)$, $b = 14.5326(4)$, $c = 14.6891(7)$ Å, $\beta = 117.600(2)^\circ$, $V = 3455.5(2)$ Å³, $Z = 2$, $\rho_{\text{calcd}} = 2.552$ Mg cm⁻³, $T = 293(2)$ K, $R_1(\text{final}) = 0.0372$, $wR_2 = 0.0946$. The crystal was of poor quality. Crystal data for **3**: $(\text{NH}_4)_8[(\text{Mo}_2\text{O}_4)_3(\text{SO}_3)_5] \cdot 2\text{H}_2\text{O}$: $\text{H}_{36}\text{Mo}_2\text{N}_8\text{O}_{21}\text{S}_5$, $M_r = 836.55$, triclinic, space group $P\bar{1}$, $a = 8.8652(4)$, $b = 17.7368(8)$, $c = 19.2683(7)$ Å, $\alpha = 66.9160(10)$, $\beta = 88.167(2)$, $\gamma = 77.4370(10)^\circ$, $V = 2715.6(2)$ Å³, $Z = 4$, $\rho_{\text{calcd}} = 2.046$ g cm⁻³, $T = 293(2)$ K, $R_1(\text{final}) = 0.0372$, $wR_2 = 0.0946$. Further details on the crystal structure investigations may be obtained from the Fachinformationszentrum Karlsruhe, 76344 Eggenstein-Leopoldshafen, Germany (fax: (+49) 7247-808-666; e-mail: crysdata@fiz-karlsruhe.de), on quoting the depository numbers CSD-412299, CSD-412300, and CSD-412301.
- [10] Two examples of polyoxometalates that have inner and outer XO_3 groups are reported in the following papers: a) T. Ozeki, H. Ichida, Y. Sasaki, *Acta Crystallogr. Sect. C* **1987**, *43*, 1662; b) M. Leyrie, A. Teze, G. Herve, *Inorg. Chem.* **1985**, *24*, 1275–1277.
- [11] a) H. K. Chae, W. G. Klemperer, D. E. Pérez Loyo, *Inorg. Chem.* **1992**, *31*, 3187; b) I. Khan, A. Müller, S. Dillinger, H. Bögge, Q. Chen, J. Zubieta, *Angew. Chem.* **1993**, *105*, 1811; *Angew. Chem. Int. Ed. Engl.* **1993**, *32*, 1780; c) H. Ichida, K. Nagai, Y. Sasaki, M. T. Pope, *J. Am. Chem. Soc.* **1989**, *111*, 586; d) A. Müller, C. Beughalt, P. Kögerler, H. Bögge, S. Bud'ko, M. Luban, *Inorg. Chem.* **2000**, *39*, 5186.
- [12] a) G. Cao, R. C. Haushalter, K. G. Strohmaier, *Inorg. Chem.* **1993**, *32*, 127; b) L. M. Mundi, R. C. Haushalter, *Inorg. Chem.* **1992**, *31*, 3050; c) E. Cadot, A. Dolbecq, B. Salignac, F. Secheresse, *Chem. Eur. J.* **1999**, *5*, 2396; d) R. C. Haushalter, F. W. Lai, *Angew. Chem.* **1989**, *101*, 802; *Angew. Chem. Int. Ed. Engl.* **1989**, *28*, 743; e) C. Livage, E. Dumas, C. Marchal-Roch, G. Herve, *C. R. Acad. Sci. Ser. IIc* **2000**, *3*, 95; f) M. J. Manos, A. D. Keramidas, J. D. Woolins, A. M. Z. Slawin, T. A. Kabanos, *J. Chem. Soc. Dalton Trans.* **2001**, 3419.
- [13] A. Müller, S. Dillinger, E. Krickemeyer, H. Bögge, W. Plass, A. Stammler, R. C. Haushalter, *J. Naturforsch. B* **1997**, *52*, 1301.
- [14] C. G. Kim, D. Coucouvanis, *Inorg. Chem.* **1993**, *32*, 2232.
- [15] a) S. C. Gibney, G. Ferraud, M. Shang, *Inorg. Chem.* **1999**, *38*, 2898; b) V. C. Kinn, P. F. Kelly, C. Papadimitriou, A. M. Z. Slawin, D. J. Williams, J. D. Woolins, *J. Chem. Soc. Dalton Trans.* **1993**, 1805; c) S. Schmidt, F. W. Heineman, A. Grohmann, *Eur. J. Inorg. Chem.* **2000**, 1657.

- [16] a) P. T. Maragh, T. P. Dasgupta, D. J. Williams, *J. Chem. Soc. Dalton Trans.* **1995**, 1805; b) K. Wierhardt, S. Druke, P. Chaudhuri, U. Florke, H.-J. Haupt, B. Nuber, J. Weiss, *Z. Naturforsch. B* **1989**, *44*, 1093.
 [17] C. Fukahara, E. Asato, T. Shimoji, K. Katsura, M. Mori, K. Matsumoto, S. Ooi, *J. Chem. Soc. Dalton Trans.* **1987**, 1305.
 [18] M. Harvey, S. Baggio, R. Baggio, H. Pardo, *Acta Crystallogr. Sect. C* **1999**, *55*, 1278.
 [19] a) C. G. Kim, D. Coucouvanis, *Inorg. Chem.* **1993**, *32*, 1881; b) F. Cessoni, C. A. Chilardi, S. Middelini, S. Moneti, A. Orlandini, *J. Organomet. Chem.* **1987**, *323*, 5.
 [20] L. O. Larson, L. Niinisto, *Acta Chem. Scand.* **1973**, *27*, 859.

“Molecular Symmetry Breakers” Generating Metal-Oxide-Based Nanoobject Fragments as Synthons for Complex Structures: $[(\text{Mo}_{128}\text{Eu}_4\text{O}_{388}\text{H}_{10}(\text{H}_2\text{O})_{81})_2]^{20-}$, a Giant-Cluster Dimer**

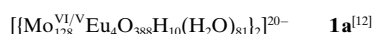
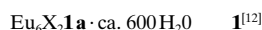
Leroy Cronin, Christian Beugholt, Erich Krickemeyer, Mark Schmidtman, Hartmut Bögge, Paul Kögerler, T. Kim K. Luong, and Achim Müller*

*Dedicated to Professor Karl Wieghardt
 on the occasion of his 60th birthday*

The synthesis and manipulation of a huge variety of nanoscaled species of similar chemical nature under one-pot reaction conditions requires access to a potential “dynamic library” of appropriate building blocks.^[1a] For instance, by exploiting a detailed knowledge of polyoxometalate chemistry, a variety of discrete clusters (see ref. [1b–g]) and related extended structures^[2] can be formed by the linking of well-defined metal–oxygen building blocks. These types of compounds have been shown to exhibit unusual topological as well as electronic properties and, furthermore, are interesting for materials science.^[3–5] A couple of years ago, we reported wheel-shaped mixed-valence molybdenum clusters of the type

$\{\text{Mo}_{154}\}$, $\{\text{Mo}_{176}\}$,^[1b, 6, 7] and $\{\text{Mo}_{248}\}$;^[1f] of these, the first two parent species—exhibiting nanometer-sized cavities and therefore presenting fascinating perspectives for a new type of host–guest chemistry—can now be obtained in high yields in facile syntheses.^[8] Herein, we describe for the first time a dimer of two giant clusters, that is, of structurally well-defined covalently linked nanoobjects with a rather high degree of complexity. The dimer contains two elliptical molybdenum oxide based units, linked together by two Eu–O–Mo bonds, each unit incorporates 128 $\text{Mo}^{\text{VI/V}}$ and 4 Eu^{III} centers and includes large fragments of the above-mentioned parent clusters. The interpretation would be that these dimers are formed by Eu^{III} centers acting as symmetry breakers which prevent the corresponding highly symmetrical parent-ring closure.^[1b, 6] *Of general importance is that in systems showing growth, potential (abundant) agents, such as Eu^{III} centers, can act as “symmetry breakers” which results in the generation of structural complexity.* In any case, it is important to realize that large nanoobject fragments can, in principle, be used as synthons. The ability to connect or assemble clusters in a predefined manner may allow the design of nanoscopic devices using the “bottom up” method (that is, generating large objects from small units).

While the “classical” reduction of an acidified aqueous molybdate solution leads to the blue, wheel-shaped tetra- and hexadecameric parent-cluster anions mentioned above,^[6] the generation of smaller species requires the presence of electrophiles, such as Pr^{III} ions which increase the curvature by replacing the larger electrophilic $\{\text{Mo}_2\}^{2+}$ -type building units (see below). In the presence of smaller Eu^{III} ions, even ring closure to the parent clusters does not take place, which allows the isolation of compound **1** containing a novel cluster collective. Compound **1** was characterized by single-crystal X-ray structure analysis^[9] (including bond valence sum (BVS) calculation to aid in the determination of the (formal) number of Mo^{V} centers and protonation sites),^[10] elemental analyses ((K), Eu, Mo; see details in ref. [12]), thermogravimetric analysis, redox titration (to aid in the determination of the (formal) number of Mo^{V} centers), IR, and EXAFS spectroscopy (Eu–L_{III} edge,^[11] with the option to distinguish in principle between the different Eu centers in the lattice and cluster sites) as well as magnetic susceptibility measurements with a SQUID magnetometer.



The crystal structure of **1** shows the dimeric unit **1a**, which comprises two linked nanosized clusters with 1202 non-hydrogen (including 264 metal) positions, of rather high structural complexity—regarding the versatility of different building blocks and protonation types—packed in a configuration that gives rise to channels incorporating Eu^{III} ions on the inner side of the cavities (Figure 1; see also ref. [12]). Compound **1a** can be geometrically related to fragments of the ring-shaped $\{\text{Mo}_{154}\} \equiv [\text{Mo}_{154}\text{O}_{462}\text{H}_{14}(\text{H}_2\text{O})_{70}]^{14-}$ (**2a**) parent-cluster archetype. The two cluster units of **1a** are elliptical with an outer and inner ring diameter of about 38

[*] Prof. Dr. A. Müller, Dr. L. Cronin, Dr. C. Beugholt, E. Krickemeyer, M. Schmidtman, Dr. H. Bögge, Dr. T. K. K. Luong
 Lehrstuhl für Anorganische Chemie I
 Fakultät für Chemie
 Universität Bielefeld
 Postfach 100131, 33501 Bielefeld (Germany)
 Fax: (+49) 521-106-6003
 E-mail: a.mueller@uni-bielefeld.de
 Dr. P. Kögerler
 Ames Laboratory
 Iowa State University, Ames, IA 50014 (USA)

[**] Contributions from Prof. Dr. A. Knöchel, Dr. A.-K. Meyer, M. Cichon, and T. Kinzel (Hamburg; EXAFS studies and elemental analyses) as well as A. Berkle (Bielefeld; analyses) are highly appreciated. L.C. (present address: School of Chemical Sciences, University of Birmingham, Edgbaston B15 2TT (UK)) gratefully acknowledges the Alexander von Humboldt Foundation for a fellowship. This work was supported by the Deutsche Forschungsgemeinschaft, the European Union (grant HPRN-CT-1999-00012), and the Fonds der Chemischen Industrie. The authors thank Dr. R. E. P. Winpenny, University of Manchester, for the provision of europium(III) chloride.

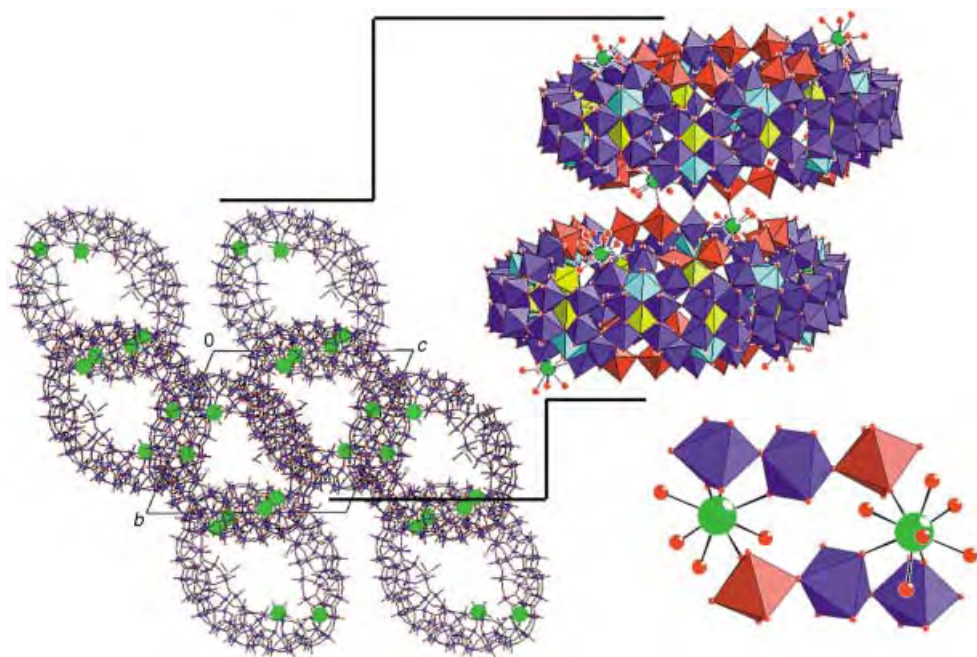


Figure 1. Left: a packing diagram of the cluster units of **1a** in ball-and-stick representation looking down the “cavities” (Eu^{III} ions in green). Right: a representation of **1a** with the molybdenum oxide based units displayed as polyhedra ($\{\text{Mo}_1\}$ yellow; $\{\text{Mo}_2\}$ red; $\{\text{Mo}_8\}$ blue with central pentagonal units in cyan; Eu^{III} coordination spheres in ball-and-stick representation). Bottom right: an expanded view of the Mo-O-Eu groups linking the two cluster rings.

and 20 Å, respectively, at their most elongated points, and with an outer and inner ring diameter of approximately 30 and 12 Å, respectively, at their most compressed points (Figure 1). There is only one type of Mo-O-Eu bond in the linking region as the midpoint between the two Mo-O-Eu links is an inversion center which generates the dimeric unit (Mo–O 1.71 Å; Eu–O 2.43 Å).

The giant ring-shaped “parent” clusters (see above) obtained from molybdenum blue solutions are based on the three different building blocks $\{\text{Mo}_1\}$, $\{\text{Mo}_2\}$, and $\{\text{Mo}_8\}$.^[1b, 6] These units are important for the related chemical versatility^[1b, 6] in that the clusters can be considered as a “nanostructured-landscape” allowing characteristic reactions at different well-defined positions.^[6] For instance some of the $\{\text{Mo}_2\}^{2+} \equiv \{\text{Mo}_2^{\text{VI}}\text{O}_5(\text{H}_2\text{O})_2\}^{2+}$ groups can be substituted by other electrophiles, such as Pr^{III} ions. If the related electrophile is (significantly) smaller in size than the $\{\text{Mo}_2\}^{2+}$ group, an increase of the curvature in the substitution region is observed. This effect can lead—as in the Pr^{III} case—to the formation of a smaller ring that exhibits an elliptical geometry^[15] but which still shows practically the same building units as the parent tetra- and hexadecameric rings. The remarkable feature in **1** is that this is no longer the case in presence of Eu^{III} ions as, besides larger basic fragments of **1a** corresponding to those of the parent ring, new structural features occur. This situation could be explained in that the presence of Eu^{III} ions, which have a smaller ionic radius than Pr^{III} ions, preventing ring closure to the parent ring type as the related dramatic increase of the curvature destabilizes the system.

The two ellipsoidal cluster entities of **1a** can be approximately described by the building-block scheme used for the

formation of the $\{\text{Mo}_{154}\}$ - and $\{\text{Mo}_{176}\}$ -type species, which comprise not only the building blocks $\{\text{Mo}_1\}$, $\{\text{Mo}_2\}$, and $\{\text{Mo}_8\}$, but also the additional “new” units of the $\{\text{Mo}_2^*\}$, $\{\text{Mo}_7\}$, and $\{\text{Mo}_9\}$ type ($\{\text{Mo}_2^*\} \equiv \{\text{Mo}_2^{\text{VI/V}}\text{O}_7(\text{H}_2\text{O})\}^{3-}$): the fragments are (formally) cut, as shown in Figure 2, from the $\{\text{Mo}_{154}\}$ -type giant wheel at four positions. The “cutting” process takes place between those polyhedra showing the least number of bonds. The large fragments obtained (Figure 2) have the composition $[\{\text{Mo}_1\}_6\{\text{Mo}_2\}_4\{\text{Mo}_8\}_2\{\text{Mo}_7\}_2\{\text{Mo}_9\}_2]$, that is, they include the two “new” $\{\text{Mo}_7\}$ and $\{\text{Mo}_9\}$ units which are formally generated by “cutting” asymmetrically two neighboring $\{\text{Mo}_8\}$ units at the above-mentioned positions to produce the two major parts of the new ellipsoidal ring. The complete ellipsoidal ring unit is formed when the two fragments are combined with two new $\{\text{Mo}_2^*\}$

units and four Eu^{III} ions (Figure 2).

An examination of the equatorial plane of one ring unit of **1a** reveals the same basic type of construction principle as described for the $\{\text{Mo}_{154}\}$ -type ring-shaped system **2a**, that is, the abundance of the typical $\{\text{Mo}_1\}$ units which are part of the $\{\text{Mo}_5\text{O}_6\}$ double-cubane-type compartments of the parent rings.^[1b, 6] In the present case, ten of the twelve abundant compartments possess one μ_3 -OH group,^[16] which is in contrast to **2a** in which they show a symmetrical distribution of the respective O-BVS values caused by a related disorder of the H atoms.^[16] The BVS of the Mo positions of the $\{\text{Mo}_5\text{O}_6\}$ -type double-cubanes show, in comparison to those in the parent cluster **2a** (with two delocalized Mo(4d) electrons per compartment), higher values for just two of those four Mo atoms (see above) which are positioned next to the two $\{\text{Mo}_2^*\}$ groups. As the latter show the correspondingly related lower Mo-BVS values, we have a situation that in these two special cases the two Mo(4d) electrons are delocalized over the two $\{\text{Mo}_2^*\}\{\text{Mo}_5\text{O}_6\}$ segments. The overall building-block scheme for **1a** can finally be presented as $[\{\text{Mo}_1\}_{12}\{\text{Mo}_2\}_8\{\text{Mo}_8\}_4\{\text{Mo}_7\}_4\{\text{Mo}_9\}_4\{\text{Mo}_2^*\}_2\text{Eu}_4]^{20-}$.

This “dimer” or “cluster collective” can be considered as the most complex discrete inorganic species structurally characterized to date while the results open new perspectives for nanochemistry. It seems possible to control the linking of certain types of polyoxometalate fragments, as in the present case in which the larger building units in **1a** can be considered as nanosynthons. The interesting related aspect is—formally speaking—that “molecular scissors” can be used to generate larger linkable nanoobject fragments. But the real interpretation is that the Eu^{III} centers subsequent to their coordination at the fragments prevent, as “symmetry breakers”, ring

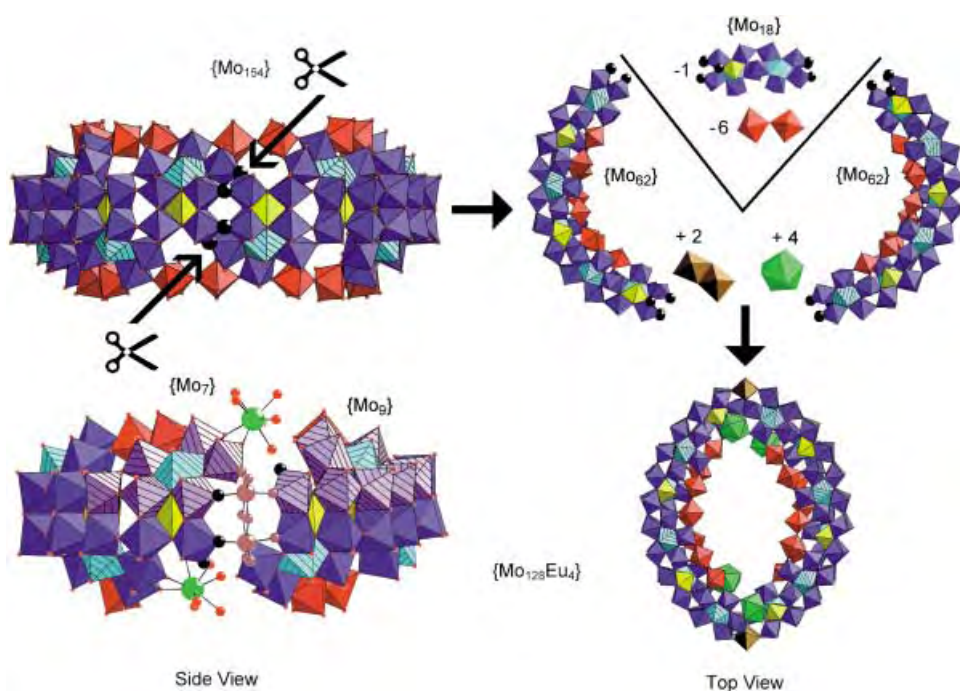


Figure 2. Demonstration of how an $\{\text{Mo}_{128}\text{Eu}_4\}$ ring of **1a** can formally be constructed from a parent $\{\text{Mo}_{154}\}$ -type cluster by a “cutting” process giving the two large important fragments. Top left: A side view of the $\{\text{Mo}_{154}\}$ ring, the cutting positions are marked as large black spheres; top right: those units which have to be removed from the $\{\text{Mo}_{154}\}$ ring and those which have to be added to the resulting two large fragments (left and right) to generate the $\{\text{Mo}_{128}\text{Eu}_4\}$ cluster; bottom: the $\{\text{Mo}_{128}\text{Eu}_4\}$ cluster from a side and top view (color code as in Figure 1) with the new $\{\text{Mo}_7^*\}$ units in brown which are shown in the side view together with the EuO_9 polyhedra in ball-and-stick representation; the MoO_6 octahedra of a selected $\{\text{Mo}_7\}$ and a $\{\text{Mo}_9\}$ group, respectively, as hatched violet polyhedra.

closure which would lead to the parent-cluster type. They cause even further symmetry breaking, thereby avoiding the direct action of translational symmetry operation after ring closure. Furthermore, by controlling the structure of a nano-object such as **1a**, it may be possible to control linking/assembly which may not only result in extended structures but also in well-defined collectives of nanoclusters, the formation of which is as yet an unsolved problem in chemistry. These types of nanocluster assemblies/collectives might be of importance for the development of electronic devices (cf. ref. [17]). Interestingly, it could also be demonstrated that it is possible to position open-shell metal centers with, for example, different electronic and magnetic characteristics, on the well-defined sites of the nanoobjects.

The present situation again supports our previous statement and arguments: Molybdenum oxide based building blocks in acidic solutions under reducing conditions show a type of flexibility allowing—as components of a dynamic library—a linking versatility with the option of generating an overwhelming variety of structures which seems to be a unique situation in inorganic chemistry (for further arguments see ref. [18]).

Experimental Section

1: A solution of $\text{EuCl}_3 \cdot 6\text{H}_2\text{O}$ (6.0 g, 16.4 mmol) in H_2O (500 mL) was quickly added under stirring to an aqueous solution of K_2MoO_4 (5.9 g, 24.8 mmol) in H_2O (500 mL). After stirring for 30 min the practically colorless precipitate was collected by filtration, washed with ice-cold H_2O , and dried at 120°C for 5 h (yield: 6.3 g; IR (KBr; $1700\text{--}500\text{ cm}^{-1}$): $\tilde{\nu} = 1630$

(m), 935 (m) , 858 (s) , 758 (s) , 700 cm^{-1} (m)).^[19]). To the solution of this precipitate (1.5 g), in a mixture of H_2O (15 mL) and 1M HCl (12.5 mL), an aqueous solution (1.5 mL) of $[\text{N}_2\text{H}_6]\text{Cl}_2$ (10 g L^{-1}) was added. The solution was heated (without stirring) in a 100-mL Erlenmeyer flask (wide necked; covered with a watch glass) in a preheated oil bath at $60\text{--}65^\circ\text{C}$ for 45 min. The resulting deep-blue solution was then taken from the oil bath, cooled to room temperature, and kept in a closed flask for 16 h. After a small amount of a colorless precipitation was removed by filtration the filtrate was kept in a closed 100-mL Erlenmeyer flask (closed with a rubber stopper) for two weeks. The deep-blue (longish) platelike crystals were collected by filtration, washed with ice-cold H_2O , and dried under inert atmosphere over CaCl_2 , yield: 0.48 g (39.4% based on Mo; for a detailed discussion of the analytical problem see ref. [12]). Characteristic IR bands (KBr; $1700\text{--}500\text{ cm}^{-1}$): $\tilde{\nu} = 1618\text{ (m)}$; $\delta\text{ (H}_2\text{O)}$, 990 (sh) , 968 (m) ; $\tilde{\nu}\text{ (Mo=O)}$, 905 (m) , 830 (m) , 740 (m-s) , 630 (s) , $561\text{ cm}^{-1}\text{ (s)}$.

The (corresponding) compound could be obtained, but not in pure form, using $\text{Na}_2\text{MoO}_4 \cdot 2\text{H}_2\text{O}$ as starting material.^[20]

Received: January 28, 2002 [Z 18588]

- [1] For general aspects and special references related to the type of chemistry see: a) J.-M. Lehn in *Essays in Contemporary Chemistry: From Molecular Structure towards Biology* (Eds.: G. Quinkert, M. V. Kisakürek), Wiley-VCH, Weinheim, **2001**, pp. 307–326; b) A. Müller, P. Kögerler, C. Kuhlmann, *Chem. Commun.* **1999**, 1347–1358; c) A. Müller, H. Reuter, S. Dillinger, *Angew. Chem.* **1995**, 107, 2505–2539; *Angew. Chem. Int. Ed. Engl.* **1995**, 34, 2328–2361; d) A. Müller, F. Peters, M. T. Pope, D. Gatteschi, *Chem. Rev.* **1998**, 98, 239–271; e) M. T. Pope, *Heteropoly and Isopoly Oxometalates*, Springer, Berlin, **1983**; f) A. Müller, S. Q. N. Shah, H. Bögge, M. Schmidtman, *Nature* **1999**, 397, 48–50; g) A. Müller, S. K. Das, E. Krickemeyer, C. Kuhlmann in *Inorg. Synth.*, Vol. 34 (Ed. J. Shapley), in press.
- [2] a) A. Müller, D. Fenske, P. Kögerler, *Curr. Opin. Solid State Mater. Sci.* **1999**, 4, 141–153; b) L. Cronin, P. Kögerler, A. Müller, *J. Solid State Chem.* **2000**, 152, 57–67; c) A. Müller, S. K. Das, E. Krickemeyer, P. Kögerler, H. Bögge, M. Schmidtman, *Solid State Sci.* **2000**, 2, 847–854.
- [3] E. Coronado, C. J. Gómez-García, *Chem. Rev.* **1998**, 98, 273–296.
- [4] T. Yamase, *Chem. Rev.* **1998**, 98, 307–325.
- [5] S. Polarz, B. Smarsly, C. Göltner, M. Antonietti, *Adv. Mater.* **2000**, 12, 1503–1507; S. Polarz, B. Smarsly, M. Antonietti, *ChemPhysChem* **2001**, 2, 457–461; D. G. Kurth, P. Lehmann, D. Volkmer, H. Cölfen, M. J. Koop, A. Müller, A. Du Chesne, *Chem. Eur. J.* **2000**, 6, 385–393; D. Volkmer, A. Du Chesne, D. G. Kurth, H. Schnablegger, P. Lehmann, M. J. Koop, A. Müller, *J. Am. Chem. Soc.* **2000**, 122, 1995–1998; D. G. Kurth, P. Lehmann, D. Volkmer, A. Müller, D. Schwahn, *J. Chem. Soc. Dalton Trans.* **2000**, 3989–3998; D. Kurth, D. Volkmer, M. Ruttorf, B. Richter, A. Müller, *Chem. Mater.* **2000**, 12, 2829–2831; F. Caruso, D. G. Kurth, D. Volkmer, M. J. Koop, A. Müller, *Langmuir* **1998**, 14, 3462–3465.
- [6] A. Müller, C. Serain, *Acc. Chem. Res.* **2000**, 33, 2–10.
- [7] A. Müller, P. Kögerler, H. Bögge, *Struct. Bond.* **2000**, 96, 203–236.
- [8] It required more than 200 years and many generations of chemists to obtain these compounds from molybdenum blue solutions, which contain the parent-ring clusters, in a facile synthesis (see ref. [1b, 6]).
- [9] Crystal data for **1**: $\text{H}_{1546}\text{Eu}_{14}\text{Mo}_{256}\text{O}_{1538}$, $M_r = 52854.45$, triclinic, space group $P\bar{1}$, $a = 31.935(2)$, $b = 32.869(2)$, $c = 37.400(2)$ Å, $\alpha = 111.292(1)$,

- $\beta = 97.542(1)^\circ$, $\gamma = 97.410(1)^\circ$, $V = 35592(3) \text{ \AA}^3$, $Z = 1$, $\rho = 2.466 \text{ g cm}^{-3}$, $\mu = 2.907 \text{ mm}^{-1}$, $F(000) = 25484$, crystal size $= 0.35 \times 0.20 \times 0.05 \text{ mm}^3$. Crystals of **1** were removed from the mother liquor and immediately cooled to 183(2) K on a Bruker AXS SMART diffractometer (three-circle goniometer with 1 K CCD detector, MoK_α radiation, graphite monochromator; sphere data collection in ω at 0.3° scan width in four runs with 606, 500, 606, and 500 frames ($\phi = 0, 88, 180$ and 268°) at a detector distance of 5.00 cm). A total of 371523 reflections ($0.66 < \theta < 27.05^\circ$) were collected of which 153584 reflections were unique ($R_{\text{int}} = 0.0511$). An empirical absorption correction using equivalent reflections was performed with the program SADABS. The structure was solved with the program SHELXS-97 and refined using SHELXL-93 to $R = 0.0559$ for 96134 reflections with $I > 2\sigma(I)$, $R = 0.1066$ for all reflections; max./min. residual electron density 3.680 and $-2.844 \text{ e \AA}^{-3}$. (SHELXS/L, SADABS from G. M. Sheldrick, University of Göttingen 1993/97; structure graphics with DIAMOND 2.1 from K. Brandenburg, Crystal Impact GbR, 2001.) Further details on the crystal structure investigation may be obtained from the Fachinformationszentrum Karlsruhe, 76344 Eggenstein-Leopoldshafen, Germany (fax: (+49) 7247-808-666; e-mail: crysdata@fiz-karlsruhe.de), on quoting the depository number CSD-411984.
- [10] I. D. Brown in *Structure and Bonding in Crystals, Vol. II* (Eds.: M. O'Keeffe, A. Navrotsky), Academic Press, New York, **1981**, pp. 1–30.
- [11] EXAFS measurements were performed at the beamline A1 at HASYLAB (Hamburg) on samples ground together with suprapure polyethylene and subsequently pressed into pellets with a thickness of 300 μm . Spectra were obtained in the transmission mode at the Eu-L_{III} edge covering the range from 6.75–8.00 keV. The magnitude of the Fourier transform of the EXAFS after background and phase correction shows a distinct and symmetric maximum at 243 pm which is clearly a result of almost only (!) one kind of oxygen coordination to the Eu absorber. A second coordination shell at about 350 pm is assigned to Eu...Mo separations.
- [12] Although the total number of molybdenum centers is certain, the (formal) number of Mo^V centers has a slight uncertainty, though the given number of 24 is the most reasonable one according to the comparison with previous related structures, that is, parts of the well known $\{\text{Mo}_{154}\}$ and $\{\text{Mo}_{176}\}$ clusters with respect to the related BVS values of comparable protonation sites and Mo_5O_6 -type building blocks.^[1b, 6] This assignment results in a charge of -20 per “dimer” **1a** by referring to the number of abundant protons and Mo^V centers (note: the related electron spins are paired here as in the reduced Keggin ions^[13]). Despite the nonmagnetic 7F_0 ground state, the Eu^{III} ions yield a temperature-dependent paramagnetism (TIP) since the weak spin-orbit splitting of the 7F term ($\lambda \approx 300 \text{ cm}^{-1}$) allows excited 7F_J states ($J = 1, 2, \dots$) to be thermally populated.^[14] As the relevant states are not significantly perturbed by ligand-field effects, the magnetism of a system containing N Eu^{III} positions corresponds very well to N times the free Eu^{III} ion contribution (typical $\chi_{\text{mol}}T$ value for an Eu^{III} ion at room temperature: $1.53 \text{ emu K mol}^{-1}$ ^[14b]). The observed paramagnetism of **1** ($\chi_{\text{mol}}T = 23.2 \text{ emu K mol}^{-1}$ at 290 K, corrected for diamagnetism and an estimated TIP value of the polyoxomolybdate ring) corresponds to $15(\pm 1)$ individual Eu^{III} centers per formula unit which is in agreement with the Eu analysis (calcd (%) for **1** with X = H: Eu 4.03; found: Eu 3.9). While eight of these are definitely constituents of the $\{\text{Mo}_{256}\}$ -type cluster dimer, the remaining six Eu^{III} cations per formula unit are strongly disordered in the crystal lattice and cannot be localized exactly. (The observed temperature dependence of $\chi_{\text{mol}}T$ for **1** also rules out the presence of Eu^{II} centers.) Thus, the resulting problem is to explain the charge difference between -20 (see above) and -18 corresponding to the presence of six Eu^{III} lattice cations. This might be a result of the (corresponding) presence of two alkali cations (found (%) ca. 0.07) or two H⁺ ions which is a more reasonable explanation (see formula). Based on the extremely small values of the potassium (and sodium) analyses this problem cannot be solved without doubt. Location of the water ligands was by comparison with previous structures while the related oxygen BVS indicate the presence of two “new type” water ligands per ring of **1a** on the building blocks adjacent to the new $\{\text{Mo}_2^*\}$ groups (see, Figure 2). The given crystal-water content corresponds to the maximum number with respect to the unit-cell volume according to our usual procedure (note: the rapid release of crystal water!).

- [13] M. T. Pope, A. Müller, *Angew. Chem.* **1991**, *103*, 56–70; *Angew. Chem. Int. Ed. Engl.* **1991**, *30*, 34–48.
- [14] a) O. Kahn, *Molecular Magnetism*, VCH, Weinheim, **1993**, p. 43; b) H. Lueken, *Magnetochemie*, Teubner, Stuttgart, **1999**, p. 38.
- [15] A. Müller, C. Beugholt, H. Bögge, M. Schmidtman, *Inorg. Chem.* **2000**, *39*, 3112–3113.
- [16] Investigating the O-BVS values of the equatorial $\mu_3\text{-O}$ atoms it turns out that, firstly, (exactly only) one atom per compartment is protonated and, secondly, moving from one equatorial bridging ligand ($\text{H}_2\text{O1}$) of the (“new”) $\{\text{Mo}_2^*\}$ unit to the corresponding other $\{\text{Mo}_2^*\}$ type bridging ($\text{H}_2\text{O2}$) ligand and passing six compartments of half a cluster ring, the sequence of protonated (p) and unprotonated (u) equatorial $\mu_3\text{-O}$ atoms is: $\text{H}_2\text{O1}$ u-p u-p u-p u-p u-u $\text{H}_2\text{O2}$. The alternating occupation of these positions is caused by the repulsive forces between the H atoms of adjacent compartments. That the above sequence is favored over the other possible sequence $\text{H}_2\text{O1}$ u-u p-u p-u p-u $\text{H}_2\text{O2}$ or to a 50:50 disordered situation as in the parent cluster type is caused by two Eu^{III} ions positioned close to the “u-u” compartment. Our present results support our earlier conclusion (correct formula): one $\mu_3\text{-OH}$ group per compartment.^[1b, 6]
- [17] U. Simon, G. Schön in *Handbook of Nanostructured Materials and Nanotechnology, Vol. 3* (Ed.: H. S. Nalwa), Academic Press, New York, **1999**, p. 131; G. Schön, U. Simon, *Colloid Polym. Sci.* **1995**, *273*, 101–217; G. Schön, U. Simon, *Colloid Polym. Sci.* **1995**, *273*, 202–218; G. L. Snider, A. O. Orlov, I. Amlani, X. Zuo, G. H. Bernstein, C. S. Lent, J. L. Merz, W. Porod, *J. Appl. Phys.* **1999**, *85*, 4283–4285.
- [18] A. Müller, E. Beckmann, H. Bögge, M. Schmidtman, A. Dress, *Angew. Chem.* **2002**, *114*, 1210–1215; *Angew. Chem. Int. Ed.* **2002**, *41*, 1162–1167.
- [19] The IR spectrum is practically identical to that of the related Pr^{III} molybdate educt used in ref. [15] and to that of a compound formulated there as $\text{Eu}_2\text{O}_3 \cdot 7\text{MoO}_3 \cdot n\text{H}_2\text{O}$ ($n = 6$ and 8) and obtained according to a preparation method given in the literature (*Gmelin Handbook of Inorganic Chemistry, Mo Suppl., Vol. B4*, Springer, Berlin, **1985**, p. 262 and *Chem. Abstr.* **1973**, *78*, 10950).
- [20] See C. Beugholt, *Dissertation*, Fakultät für Chemie, Universität Bielefeld, **2001**, with a preliminary formula.

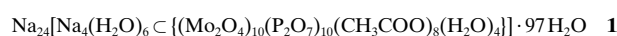
Mo^V/Pyrophosphate Polyoxometalate: An Inorganic Cryptate

Charlotte du Peloux, Pierre Mialane, Anne Dolbecq, Jérôme Marrot, and Francis Sécheresse*

Polyoxometalate chemistry continues to be a subject of great interest, since the wide and fascinating variety of structures and properties of these objects gives rise to numerous applications.^[1] Polyoxoanions containing phosphato groups constitute the largest class of heteropolyanions, with structures ranging from molecular complexes to extended frameworks.^[2] In contrast, very few polyoxometalate-containing polyphosphato groups have been structurally characterized. In 1994, Kortz and Pope reported the first X-ray structure of a polyoxomolybdate(vi) containing the pyrophosphato (P_2O_7)⁴⁻ ligand.^[3] Since then, only two other structures

[*] Prof. F. Sécheresse, C. du Peloux, Dr. P. Mialane, Dr. A. Dolbecq, Dr. J. Marrot
Institut Lavoisier, IREM, UMR 8637
Université de Versailles Saint-Quentin
45 Avenue des Etats-Unis, 78035 Versailles (France)
Fax: (+33) 1-39-25-43-81
E-mail: secheresse@chimie.uvsq.fr

have been reported.^[4] For these three compounds, the $(\text{P}_2\text{O}_7)^{4-}:\text{Mo}^{\text{VI}}$ ratio is between 1:6 and 1:18. The lack of information concerning this class of compound and the absence of Mo^{V} pyrophosphate complexes can be justified by the observations of Weil-Malherbe and Green.^[5] Indeed, they have shown that the hydrolysis of pyrophosphate into monophosphate is catalyzed in water by molybdenum. Moreover, this reaction is enhanced by Mo^{V} rather than by Mo^{VI} , and is optimal at pH 2 with a secondary maximum at pH 5.5. We are currently investigating the interaction between (poly)phosphate and Mo^{V} either under hydrothermal conditions^[6] or usual “bench” conditions. We have tried to determine a domain where the hydrolysis of pyrophosphate by Mo^{V} would be minimal. This work led us to the isolation and characterization of the first pyrophosphate/ Mo^{V} complex **1**, a highly charged and highly hydrated complex which comprises two nearly perpendicularly interconnected wheels, an unprecedented topology for an inorganic compound.



The synthesis has been performed in sodium acetate buffer. The success of this approach can be explained by considering that 1) the rate of hydrolysis of the $(\text{P}_2\text{O}_7)^{4-}$ ion must be lower at the pH of the acetate buffer and that 2) acetate can lead to the formation of the stable $[\text{Mo}_2\text{O}_4(\mu\text{-CH}_3\text{COO})]^+$ dimer,^[7] which possesses two free sites in *cis* positions on each Mo^{V} center. This arrangement must permit the formation of large rings in presence of bridging ligands. Compound **1** was synthesized by mixing sodium molybdate, pyrophosphate, and hydrazine and stirring the mixture for three hours. Then, the solution was allowed to crystallize at room temperature. The final yield is not affected if the Mo^{VI} species is first reduced by hydrazine before the addition of pyrophosphate, or if all the reagents are added simultaneously. This situation is evidence of the stability of pyrophosphate in this medium. Similar experiments have been performed in lithium, potassium, or cesium acetate buffer. The role of the alkaline cation seems crucial since compound **1** has not been obtained under these conditions.

Complex **1** is built up by two nonequivalent interconnected wheels (Figure 1). The largest wheel (noted $\{\text{Mo}_{12}\}$) is formed by twelve Mo^{V} centers (Figure 2a), and the smallest (noted $\{\text{Mo}_8\}$) contains eight Mo^{V} atoms (Figure 2b). All the

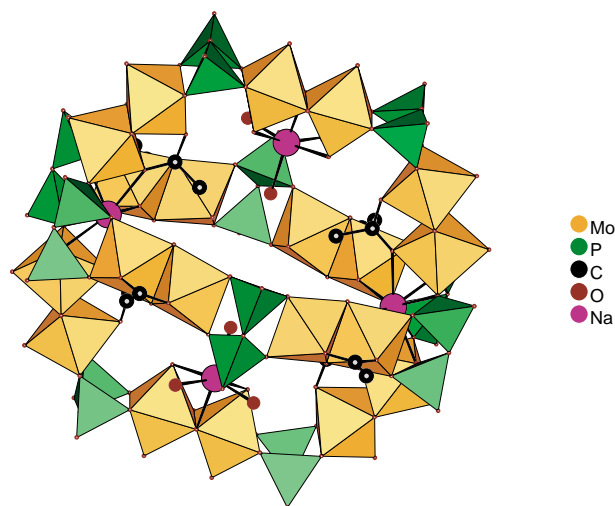


Figure 1. Polyhedral representation of **1**. Lengths range (average lengths) [Å]: Mo=O 1.659(7)–1.681(6) (1.668); Mo–O(Mo) 1.910(6)–1.937(6) (1.922); Mo–O(P) 2.055(8)–2.095(6) (2.076); Mo–O(C) 2.215(6)–2.331(6) (2.275); Mo–OH₂ 2.324(6)–2.328(6) (2.326); P=O 1.455(6)–1.487(6) (1.473); P–O(P) 1.578(8)–1.614(6) (1.605); P–O(Mo) 1.499(7)–1.520(6) (1.511); C–O 1.239(11)–1.262(10) (1.250); C–C 1.481(14)–1.498(13) (1.491).

molybdenum centers are in a distorted octahedral environment and have an Mo=O bond, that is, they contain a terminal oxygen atom. As usually observed,^[6, 7] the Mo^{V} atoms are arranged by pairs, forming the diamagnetic dinuclear unit $\{\text{Mo}_2(\mu\text{-O})_2\text{O}_2\}$, with an average Mo...Mo separation of 2.54 Å. These dimers are bridged by two types of pyrophosphate groups. Six pyrophosphate units connect two dimers, and four are bridging three dimers, ensuring the connection between the two wheels. These two wheels are nearly perpendicular (Figure 2c), with an angle of 92.8° (calculated considering the least-square planes defined by the metallic atoms). It follows that **1** can then be described as an inorganic cryptate of an overall D_{2d} symmetry. The coordination spheres of four of the six dimers of the $\{\text{Mo}_{12}\}$ entity is completed by a $\mu\text{-O}_2$ acetato anion, while those of the two remaining dimers are completed by water molecules (Figure 2a). The role of these exogenous ligands is crucial since it strongly influences the curvature of the dimers and thus the topology of the whole edifice. This effect can be emphasized by the distances between the axial ligands in a $\{\text{Mo}_2\text{O}_4(\text{H}_2\text{O})_2\}$ dimer ($d(\text{O}_t \cdots \text{O}_t) = 2.910(9)$ Å and $d(\text{O}_{\text{H}_2} \cdots \text{O}_{\text{H}_2}) = 3.144(9)$ Å) and in the $\{\text{Mo}_2\text{O}_4(\text{CH}_3\text{COO})_2\}$ dimers ($d(\text{O}_t \cdots \text{O}_t) = 3.172(9) -$

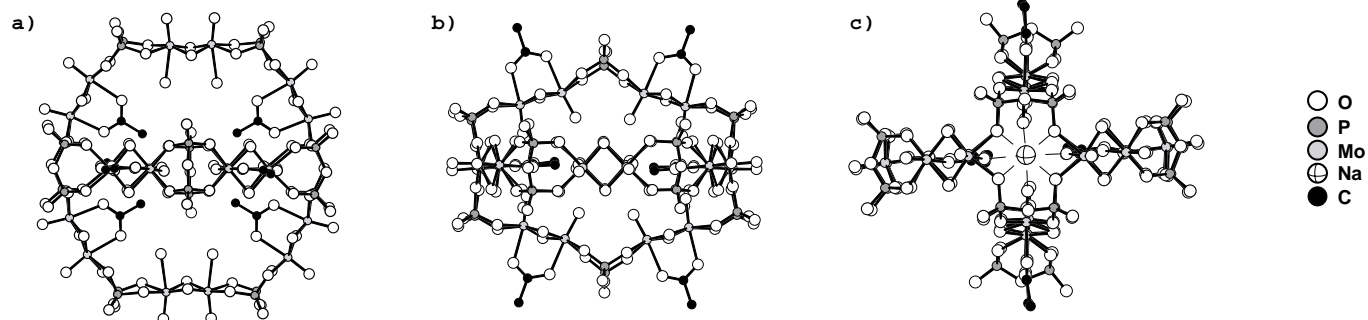


Figure 2. Ball-and-stick representations of **1** highlighting a) the $\{\text{Mo}_{12}\}$ ring and the inner acetate groups b) the $\{\text{Mo}_8\}$ ring and the outer acetate groups c) the near perpendicular arrangement of the $\{\text{Mo}_{12}\}$ and the $\{\text{Mo}_8\}$ planes.

3.254(10) Å and $d(\text{O}_{\text{OCH}_3} \cdots \text{O}_{\text{OCH}_3}) = 2.171(9) - 2.207(10)$ Å). In $\{\text{Mo}_{12}\}$, all the Mo=O groups are directed towards the outside of the cavity. The situation is different for the $\{\text{Mo}_8\}$ wheel, where each dimer is coordinated to an acetate anion, and the Mo=O groups are directed towards the inside of the cavity. Valence bond summations (VBS) have been applied on all the atoms.^[8] These calculations confirmed the oxidation state of molybdenum atoms and permitted us to conclude that all the pyrophosphato groups are fully deprotonated, which is consistent with the presence of the 28 sodium cations determined by elemental analysis. Four of these counterions have been found inside the cavity. Two are located at the intersections of the wheels, connecting four $\{\text{Mo}_2\text{O}_4(\text{CH}_3\text{COO})_2\}$ fragments through eight oxygen atoms ($d(\text{Na}-\text{O}) = 2.403(7) - 2.516(7)$ Å). These two tightly bound sodium cations must play a key role in the stability of the receptor which acts as a cryptand anion (Figure 1).^[9] Two additional alkaline cations have been found linked to the water molecules of the $\{\text{Mo}_2\text{O}_4(\text{H}_2\text{O})_2\}$ dimers, the remaining counterions being located outside the cage. Finally, a vacant site is available at the center of the polyanion.

The NMR spectrum of **1** at room temperature (Figure 3) exhibits three resonances located at $\delta_1 = 3.03$ ppm, $\delta_2 = 1.66$ ppm, and $\delta_3 = -0.64$ ppm with relative intensity of

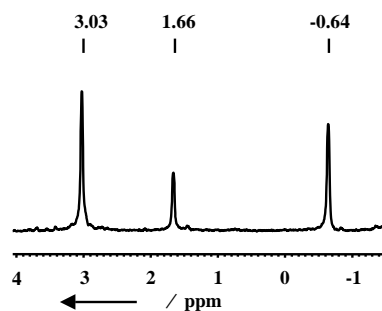


Figure 3. ^{31}P NMR spectrum of **1** in acetate buffer at room temperature.

2:1:2. This result is in agreement with the structure determined by X-ray diffraction. The spectrum of this solution remains unchanged over several weeks, which shows the high stability of **1** in this medium. The ^{31}P NMR spectrum has also been recorded in water and gives a complex pattern, which indicates decomposition of compound **1**. Among the large number of species observed, free phosphato groups and the well-known $[\text{P}_4\text{Mo}_6(\text{OH})_3\text{O}_{28}]^{9-}$ complex,^[6b, 10] which results from the hydrolysis of the polyphosphate moieties, have been identified. Indeed the pyrophosphate ligands in **1** are highly available to direct attack by the solvent compared to the only water-stable example of a Mo^{VI} -pyrophosphate compound, the Dawson-like $[(\text{P}_2\text{O}_7)\text{Mo}_{18}\text{O}_{54}]^{4-}$ ion, where the pyrophosphate group is encapsulated.^[3]

In conclusion, we have characterized the first Mo^{V} -pyrophosphate complex which possesses a unique double-wheel topology and a high $(\text{P}_2\text{O}_7)^{4-}:\text{Mo}^{\text{V}}$ ratio. This complex has been obtained in an acetate buffer medium. We are now investigating the possibility to insert a guest cation in the central cavity of **1**, and the behavior of Mo^{V} and pyrophosphate in various mono- and dicarboxylate buffers.

Experimental Section

$\text{Na}_2\text{MoO}_4 \cdot 2\text{H}_2\text{O}$ (10.33 mmol, 2.5 g) was dissolved in a 4 M sodium acetate/ acetic acid buffer (pH 4.67, 100 mL), to which $\text{N}_2\text{H}_4 \cdot \text{H}_2\text{O}$ (3.08 mmol, 150 μL) and $\text{Na}_4\text{P}_2\text{O}_7$ (5.6 mmol, 2.5 g) were added. The obtained green solution was stirred for 3 h and then allowed to stand at room temperature. Orange parallelepipedic crystals were collected by filtration after 3 days. Yield: 1.12 g (32 % based on Mo); elemental analysis (%) calcd for **1**: Mo 26.15, P 8.45, C 2.62, Na 8.78; found: Mo 26.86 P 8.23, C 2.86, Na 9.06. IR (KBr pellet): $\tilde{\nu} = 1638$ (s), 1549 (m), 1454 (w), 1424 (sh), 1203 (s), 1087 (s), 1036 (s), 969 (m), 748 (w), 678 (w), 581 (m), 522 (m), 483 cm^{-1} (m); UV/Vis (4 M sodium acetate/acetic acid buffer): $\lambda_{\text{max}}(\epsilon) = 301$ (104 700), 402 nm (1950), 465 (1000); ^{31}P NMR (121.5 MHz, 25 °C, H_3PO_4 85 %): $\delta = 3.03$, 1.66, -0.64 ppm.

Crystal data and structure refinement for **1**: an orange parallelepipedic crystal ($0.12 \times 0.10 \times 0.02$ mm) was analyzed with a Siemens SMART three-circle diffractometer equipped with a CCD bidimensional detector using $\text{MoK}\alpha$ monochromatized radiation ($\lambda = 0.71073$ Å). Monoclinic, space group $P2(1)/n$, $a = 20.8051(1)$, $b = 21.3293(1)$, $c = 22.6197(2)$ Å, $\beta = 94.270(1)^\circ$, $V = 10009.81(11)$ Å³, $Z = 2$, $\rho_{\text{calcd}} = 2.306$ g cm^{-3} , $\mu(\text{MoK}\alpha) = 1.567$ mm⁻¹, $F(000) = 6860$, 70 617 reflections measured, of which 26 891 were independent, 1377 refined parameters, $R = 0.0771$, $wR_2 = 0.1518$. Data reduction was performed with the SAINT software. The absorption correction was based on multiple and symmetry-equivalent reflections in the data set using the SADABS program based on the method of Blessing. The structure was solved by direct methods and refined by full-matrix least-squares using the SHELX-TL package. As crystal structure shows disorder in the range of water molecules and sodium cation, the exact formula and molecular weight have been established from thermogravimetry (TG) studies and the elemental analysis. The hydrogen atoms of the acetate groups were located and refined using a constrained "riding" model. CCDC-178291 (**1**) contains the supplementary crystallographic data for this paper. These data can be obtained free of charge via www.ccdc.cam.ac.uk/conts/retrieving.html (or from the Cambridge Crystallographic Data Centre, 12, Union Road, Cambridge CB2 1EZ, UK; fax: (+44) 1223-336-033; or deposit@ccdc.cam.ac.uk).

Received: February 4, 2002 [Z18647]

- [1] *Polyoxometalates: From Platonic Solid to Anti-Retroviral Activity* (Eds.: M. T. Pope, A. Müller), Kluwer Academic Publishers, Dordrecht, The Netherlands, **1994**.
- [2] a) A comprehensive review of the field of polyoxometalates has been given in *Chem. Rev.* **1998**, January/February, pp. 1-390; b) R. C. Haushalter, L. A. Mundi, *Chem. Mater.* **1992**, *4*, 31.
- [3] U. Kortz, M. T. Pope, *Inorg. Chem.* **1994**, *33*, 5643.
- [4] a) U. Kortz, *Inorg. Chem.* **2000**, *39*, 623; b) U. Kortz, *Inorg. Chem.* **2000**, *39*, 625.
- [5] H. Weil-Malherbe, R. H. Green, *Biochem. J.* **1951**, *49*, 286.
- [6] a) C. du Peloux, A. Dolbecq, P. Mialane, J. Marrot, E. Rivière, F. Sécheresse, *Angew. Chem.* **2001**, *113*, 2521; *Angew. Chem. Int. Ed.* **2001**, *40*, 2455; b) C. du Peloux, P. Mialane, A. Dolbecq, J. Marrot, E. Rivière, F. Sécheresse, *J. Mater. Chem.* **2001**, *11*, 3392.
- [7] a) A. Müller, C. Kuhlmann, H. Bögge, M. Schmidtman, M. Baumann, E. Krickmeyer, *Eur. J. Inorg. Chem.* **2001**, 2271; b) W. Yang, C. Lu, X. Lin, H. Zhuang, *Inorg. Chem.* **2002**, *41*, 452.
- [8] N. E. Brese, M. O'Keeffe, *Acta Crystallogr. Sect. B* **1991**, *47*, 192.
- [9] J.-M. Lehn, *Supramolecular Chemistry*, VCH, Weinheim, **1995**.
- [10] E. Cadot, A. Dolbecq, B. Salignac, F. Sécheresse, *Chem. Eur. J.* **1999**, *5*, 2396.

A Patterned TiO₂(Anatase)/TiO₂(Rutile) Bilayer-Type Photocatalyst: Effect of the Anatase/Rutile Junction on the Photocatalytic Activity

Tetsuro Kawahara, Yasuhiro Konishi, Hiroaki Tada,* Noboru Tohge, Junji Nishii, and Seishiro Ito

Semiconductor photocatalysts have recently attracted much interest because of their possible applicability to detoxification of environmental pollutants^[1] and solar-energy conversion.^[2] Among the photocatalysts, TiO₂ is believed to be the most promising presently known material because of its superior photoreactivity, nontoxicity, long-term stability, and low price. The photocatalytic activity of TiO₂ depends on various parameters, including crystallinity, impurities, surface area, and density of surface hydroxy groups; however, the most significant factor is its crystal form.^[3] TiO₂ is usually used as a photocatalyst in two crystal structures: rutile and anatase. Anatase generally has much higher activity than rutile.^[4] More interesting is the fact that the activity of P-25 (Degussa), which consists of anatase and rutile (4/1 w/w), exceeds that of pure anatase in several reaction systems.^[3b, 5] Indeed, P-25 has frequently been used as a benchmark for photocatalysts.

However, the origin of the high photocatalytic activity of P-25 remains unclear. Here we report on the fundamental mechanism and present a highly active photocatalyst film designed on the basis thereof. Thin films of photocatalysts not only serve as models of particulate systems but also aid in the development of their applications.^[1b]

Addition of 1-phenyl-1,3-butanedione (BzCH₂Ac) to a solution of Ti(OC₄H₉)₄ in methanol led to a red shift of the absorption peak for the π - π^* transition of BzCH₂Ac from 310 to 360 nm, owing to chelation of Ti⁴⁺. After hydrolysis, the resultant sol was used to form a gel film in which the chelate bonds were kept intact. Significant lower solubility of the gel film in alcohol was induced by photoexcitation of the π - π^* absorption band.^[6] Patterned (pat-) TiO₂ films were prepared by utilizing this phenomenon. The dimensions of the patterning are expressed by the width w of the stripes of the TiO₂ film and their spacing s . Figure 1 shows a 3D surface-structure photograph of a sample formed on quartz by using a photomask with slits of 0.2 mm in width. Regularly spaced,

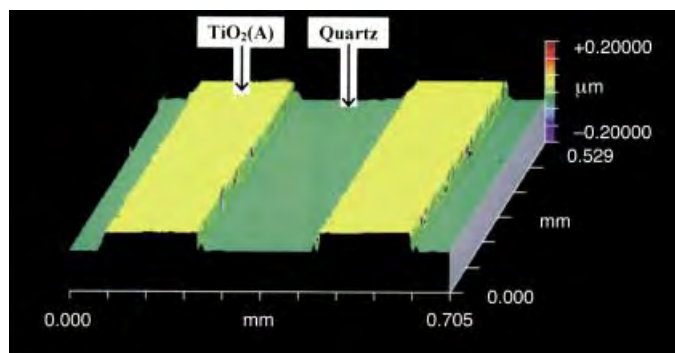


Figure 1. Three-dimensional surface-structure photograph of pat-TiO₂(A)/quartz ($w = s = 0.2$ mm).

0.2 mm wide stripes of TiO₂ film with a thickness of about 65 nm are present on the substrate with a spacing of 0.2 mm (TiO₂/quartz; $w = s = 0.2$ mm).

X-ray diffraction (XRD) patterns are shown in Figure 2 A for a sputter-deposited TiO₂ (sp-TiO₂) film (a) and a sol-gel TiO₂ (sg-TiO₂) film overlaid on the sp-TiO₂ film (b). In pattern (a), the diffraction peaks from the (110) and (211)

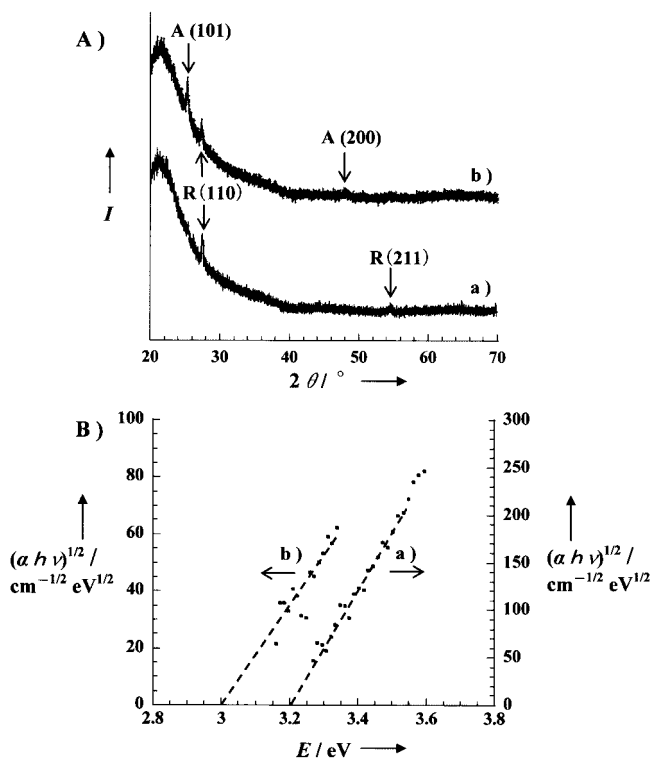


Figure 2. A) X-ray diffraction patterns of the sp-TiO₂ film (a) and the sg-TiO₂/sp-TiO₂ film (b). B) Plots of $(\alpha h\nu)^{1/2}$ vs photon energy for the sg-TiO₂ (a) and sp-TiO₂ (b) films.

planes of rutile are observed at $2\theta = 27.4$ and 54.3° , respectively. The peak intensity ratio $I(211)/I(110)$ is much smaller than that of randomly oriented rutile powder (ca. 0.6)^[7] and suggests that the sp-TiO₂ film has a preferred orientation towards the [001] and $\bar{1}10$ directions. In pattern (b), the diffraction peaks from the (101) and (200) planes of anatase appear at 25.3 and 48.0° , respectively, in addition to the rutile

[*] Prof. Dr. H. Tada
Molecular Engineering Institute
Kinki University
3-4-1, Kowakae, Higashi-Osaka, Osaka 577-8502 (Japan)
Fax: (+81)6-6721-3384
E-mail: h-tada@apsrv.apch.kindai.ac.jp
T. Kawahara
Nippon Sheet Glass Co. Ltd.
1-7, 2-Chome, Kaigan, Minato-Ku Tokyo, 105-8552 (Japan)
Y. Konishi, Prof. Dr. N. Tohge, Prof. Dr. S. Ito
Department of Applied Chemistry
Faculty of Science and Engineering
Kinki University
3-4-1, Kowakae, Higashi-Osaka, Osaka 577-8502 (Japan)
Dr. J. Nishii
National Institute of Advanced Industrial Science and Technology
Midorigaoka1-8-31, Ikeda, Osaka 563-8577 (Japan)

peaks. The broad intense background at $2\theta < 40^\circ$ in both patterns arises from the quartz substrate. Figure 2B shows the plots of $(ah\nu)^{1/2}$ versus photon energy $h\nu$ for the sg-TiO₂ (a) and sp-TiO₂ (b) films; α is the extinction coefficient. Extrapolation of each straight line provides the indirect band gaps E_g of 3.2 (a) and 3.0 eV (b), which are in agreement with the literature values for anatase and rutile, respectively.^[8] These results indicate that an anatase film was formed on a rutile film [TiO₂(A)/TiO₂(R)] by a two-step method consisting of sputter deposition and subsequent sol-gel processing.

Photocatalytic activities of various samples were evaluated in the gas-phase decomposition of CH₃CHO (Figure 3), which was used as a model for a harmful organic gas. This reaction is categorized as photocatalytic because both illumination

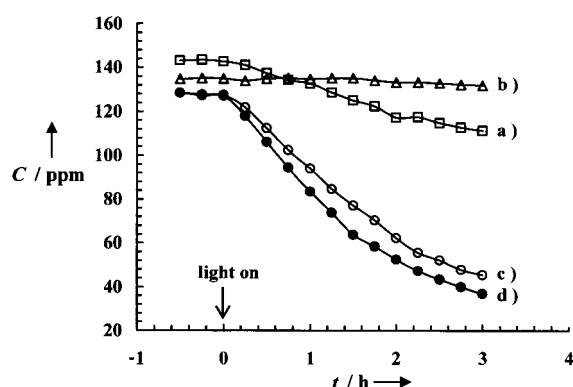


Figure 3. Time profiles of decomposition of CH₃CHO on illumination with TiO₂(A)/quartz (a), TiO₂(R)/quartz (b), pat-TiO₂(A)/TiO₂(R) ($w=s=1$ mm; c), and pat-TiO₂(A)/TiO₂(R) ($w=s=0.2$ mm; d).

($\lambda_{\text{ex}} > 300$ nm) and TiO₂ are needed for decomposition to occur and the turnover number is greater than 100 at $t = 3$ h.^[9] In all systems, the reaction followed a first-order rate law; Table 1 lists the apparent rate constants k . Evidently, anatase (a) exhibits higher activity than rutile (b) in this reaction. A significant increase in the activity with patterning is observed for pat-TiO₂(A)/TiO₂(R) ($w=s=1$ mm; c), in which the rutile covers the whole surface while the anatase is deposited in stripes that leave half of the rutile underlayer exposed. The k value (0.35 h^{-1}) is larger than the sum of values of 0.091 h^{-1} for samples (a) and (b), whereas no patterning effect was obtained for TiO₂(A)/quartz.

To identify the reduction sites of pat-TiO₂(A)/TiO₂(R), the photodeposition of Ag was carried out ($2\text{H}_2\text{O} + 4\text{Ag}^+ \rightarrow 4\text{Ag}^0 + \text{O}_2 + 4\text{H}^+$).^[10] Ag hardly deposited on the surface of sp-TiO₂(R). Since in the particulate system, rutile exhibits high activity in this reaction,^[11] this seems to indicate

sensitivity to the structure of the surface, that is, the developed (110) crystal plane of sp-TiO₂(R) is likely to be inactive. Figure 4a shows a SEM image of pat-TiO₂(A)/TiO₂(R) after Ag photodeposition. Particles are largely deposited on the

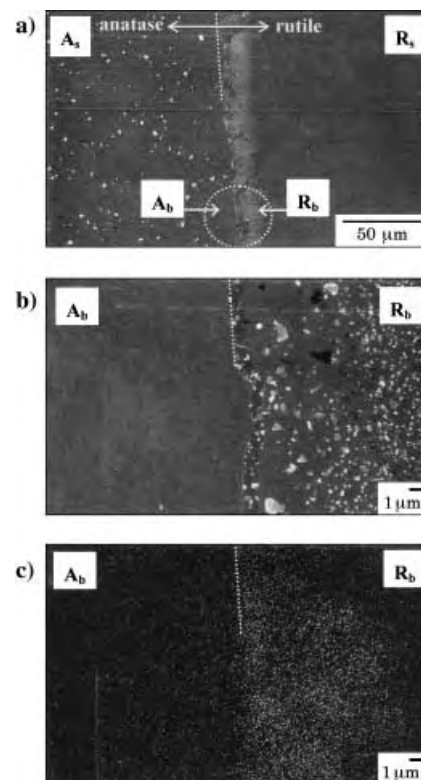


Figure 4. a) SEM image of pat-TiO₂(A)/TiO₂(R) ($w=s=1$ mm) after Ag photodeposition. b) SEM micrograph of the boundary region of the TiO₂(A) and TiO₂(R) films; c) X-ray image of Ag for the same region as B). Ag photodeposition was performed as follows: a TiO₂-film-coated sample was immersed in a 1.0×10^{-4} M aqueous solution of AgNO₃ (50 mL). After the solution had been purged with Ar for 15 min, photoirradiation was carried out with a high-pressure mercury arc at $30 \pm 0.1^\circ\text{C}$ ($I_{320-400} = 2.5 \text{ mW cm}^{-2}$) for 0.5 h.

sg-TiO₂(A) surface (A_s), while they are scarcely seen on the sp-TiO₂(R) surface (R_s). In contrast, this trend is entirely reversed near the anatase/rutile boundary, as shown in Figure 4b, which shows a magnification of the region circled in Figure 4a, that is, deposition occurs preferentially on the side of the sp-TiO₂(R) underlayer (R_b). Figure 4c shows an Ag X-ray image of the same region as that shown in Figure 4b, which identifies the deposits as Ag. This finding shows that some of the excited electrons are transferred from the conduction band (CB) of TiO₂(A) to that of TiO₂(R), and

Table 1. Photocatalytic activities for CH₃CHO oxidation.

Photocatalyst	Surface area (R/A)	Thickness (overlayer/underlayer)	width/spacing	k [h^{-1}]
nonpat-TiO ₂ (R)	4 cm ²	165 ± 5 nm	–	0.005
pat-TiO ₂ (A)/quartz	2 cm ²	70 ± 5 nm	0.2 mm/0.2 mm	0.086
pat-TiO ₂ (A)/TiO ₂ (R)	2 cm ² /2 cm ²	70 ± 5 nm/165 ± 5 nm	1 mm/1 mm	0.35
pat-TiO ₂ (A)/TiO ₂ (R)	2 cm ² /2 cm ²	65 ± 5 nm/165 ± 5 nm	0.2 mm/0.2 mm	0.43
pat-TiO ₂ (A)/SnO ₂ ^[a]	2 cm ² /2 cm ²	50 ± 5 nm/580 ± 80 nm	1 mm/1 mm	0.51
pat-TiO ₂ (A)/SnO ₂	2 cm ² /2 cm ²	45 ± 5 nm/580 ± 80 nm	0.2 mm/0.2 mm	0.53

[a] The conductivity of the SnO₂ film was $1.6 \times 10^3 \text{ S cm}^{-1}$.

the excess electrons give rise to Ag photodeposition on R_b . Another interesting fact is that the size of the Ag particles in R_b is much smaller than that in A_s , and the opposite is valid for their number density. The difference in the surface concentration of the excited electrons would affect the nucleation and growth processes of the Ag particles. The fact that the CB edge of $TiO_2(A)$ is about 0.2 eV higher than that of $TiO_2(R)$ is thought to facilitate interfacial electron transfer, and the energy barrier would suppress back electron transfer. Consequently, the holes left in the valence band of $TiO_2(A)$ efficiently oxidize organic substrates, while the electrons moving into $TiO_2(R)$ are consumed by the reduction of O_2 .^[12]

A closer inspection of Figure 4a indicates that Ag particles are deposited on the $TiO_2(R)$ surface within a distance of 10 μm from the boundary. The diffusion length L of electrons in solids is related to the mobility μ and the lifetime τ by the equation $L = (kT\mu\tau/e)^{1/2}$, where k is the Boltzmann constant. Calculations with the literature values of $\mu = 100 \text{ cm}^2 \text{ V}^{-1} \text{ s}^{-1}$ ^[13] and $\tau = 100 \text{ ns}$ ^[14] for TiO_2 gave an estimated L value of 5.1 μm , which is of the same order of magnitude as the width of Ag deposition. As shown in Figure 3d (see also Table 1), the activity increases by a factor of 1.23 on decreasing the patterning dimension from 1 to 0.2 mm. It is probable that the increase in the fraction of the $TiO_2(R)$ surface acting as reduction site results in effective attack of holes on CH_3CHO adsorbed on $TiO_2(A)$. The effect of the nanoscale junction between anatase and rutile in P-25 (ca. 10 nm)^[15] on its activity can be inferred along these lines. The activity of pat- $TiO_2(A)/SnO_2$, which exceeds that of pat- $TiO_2(A)/TiO_2(R)$, is almost independent of the patterning dimension (Table 1). The vectorial electron transfer from $TiO_2(A)$ to SnO_2 ^[16] and the long charge-separation distance of more than 100 μm ^[10] seem to be responsible for this.

This study has demonstrated that coupling of $TiO_2(A)$ and $TiO_2(R)$ in a bilayer form increases the photocatalytic activity for CH_3CHO oxidation relative to the individual components, and that reducing the patterning dimension to the charge-separation distance is of importance in increasing this activity. With regard to a model of P-25, its high photocatalytic activity is caused mainly by the increase in charge-separation efficiency resulting from interfacial electron transfer from $TiO_2(A)$ to $TiO_2(R)$.

Experimental Section

Patterned TiO_2 films: $BzCH_2Ac$ (40 mmol) was added to 40 mL of a 0.5 M solution of $Ti(OC_4H_9)_4$ in methanol. The solution was hydrolyzed and then used as a coating solution. Coating was carried out by dipping and withdrawing in ambient atmosphere. The dried gel films were irradiated with UV light through a photomask. An IR cut filter and a solution filter (0.40 M $CuSO_4 \cdot 5H_2O$ aq) were used to selectively pass light at around 350 nm. After the irradiated gel films had been leached out in ethanol, the resultant patterned gel films were heated in air at 773 K for 1 h.

Sputter deposition of TiO_2 films: TiO_2 thin films were deposited on quartz substrates by a conventional rf sputtering method. The sputtering target was prepared by sintering of rutile TiO_2 powder. Sputtering deposition was carried out under 1.33 Pa pressure of an O_2/Ar mixture at a growth rate of 10 nm min⁻¹. The thin film was annealed at 1073 K for 2 h in air.

Film characterization: The surface morphologies and cross sections of the TiO_2 films were observed by scanning electron microscopy (Hitachi S-700) and a 3D-imaging surface-structure analyzer (Zygo New View 100). The

film thickness was also determined with the surface-structure analyzer and a surface profilometer (Dektak³ Surface Profiler). XRD measurements were performed on a Rigaku Rotaflex RTP 300 RC.

Evaluation of photocatalytic activity: The photocatalytic activities of the samples for CH_3CHO oxidation were examined. A 508 ppm standard CH_3CHO gas was introduced into a reaction chamber (0.64 L), and diluted with air so that the initial concentration was controlled within the range 120 ± 10 ppm. After the adsorption equilibrium of CH_3CHO had been achieved in the dark, front-face irradiation ($I_{320-400} = 4.8 \text{ mW cm}^{-2}$) of the sample was started with a 300 W Xe lamp at room temperature. The concentration of CH_3CHO was determined as a function of illumination time by gas chromatography (Shimadzu GC-9A; f.i.d. column Shimadzu SHINCARBON A (3 mm $\phi \times 3$ m)). The carrier gas was N_2 (0.5 kg cm⁻²) at an injection temperature of 70 °C and a column temperature of 70 °C.

Received: November 22, 2001

Revised: April 19, 2002 [Z18264]

- [1] a) A. Mills, S. L. Hunte, *J. Photochem. Photobiol. A* **1997**, 108, 1; b) D. A. Tryk, A. Fujishima, K. Honda, *Electrochim. Acta* **2000**, 45, 2363.
- [2] B. O'Regan, M. Graetzel, *Nature* **1991**, 353, 737.
- [3] a) H. Tada, M. Tanaka, *Langmuir* **1997**, 13, 360; b) Z. Ding, G. Q. Lu, P. F. Greenfield, *J. Phys. Chem. B* **2000**, 104, 4815.
- [4] K. Tanaka, M. F. V. Capule, T. Hisanaga, *Chem. Phys. Lett.* **1991**, 29, 73.
- [5] a) H. Tahiri, N. Serpone, R. L. van Mao, *J. Photochem. Photobiol. A* **1996**, 93, 199; b) J. Jia, T. Ohno, Y. Masaki, M. Matsumura, *Chem. Lett.* **1999**, 963; c) R. Zhang, L. Gao, *Mater. Res. Bull.* **2001**, 36, 1957.
- [6] N. Tohge, K. Shinmou, T. Minami, *J. Sol-Gel Sci. Technol.* **1994**, 2, 581.
- [7] JCPDS card No. 211276.
- [8] H. Tang, K. Prasad, R. Sanjines, P. E. Schmid, F. Levy, *J. Appl. Phys.* **1994**, 75, 2042. Since the position of the valence band, which mainly consists of O_{2p} orbitals, is situated at +3.0 V (vs SHE), regardless of the crystal form, the difference in E_g between anatase and rutile is almost equal to that in the conduction band edge.
- [9] The turnover number was estimated by assuming that the active sites are the surface TiOH groups, whose density was reported to be about 5×10^{18} groups nm⁻²: H. P. Boehm, *Faraday Discuss. Chem. Soc.* **1971**, 52, 264.
- [10] H. Tada, A. Hattori, Y. Tokihisa, K. Imai, N. Tohge, S. Ito, *J. Phys. Chem. B* **2000**, 104, 4585.
- [11] S.-i. Nishimoto, B. Ohtani, H. Kajiwarra, T. Kagiya, *J. Chem. Soc. Faraday Trans. 1* **1983**, 79, 2685.
- [12] R. I. Bickley, *J. Catal.* **1973**, 31, 389.
- [13] M. Graetzel, *Energy Resources through Photochemistry and Catalysis* (Ed.: M. Graetzel), Academic Press, New York, **1983**.
- [14] R. Memming, *Semiconductor Electrochemistry*, Wiley-VCH, Weinheim, **2001**.
- [15] R. I. Bickley, T. Gonzalez-Carreno, J. S. Lees, L. Palmisano, R. J. D. Tilley, *J. Solid State Chem.* **1991**, 92, 178.
- [16] Flat-band potentials V_{fb} of the SnO_2 film and $TiO_2(A)$ film coated on soda-lime glass and Ti substrates were determined to be +0.07 and -0.34 V (vs SHE at pH 7.0 and 25 °C), respectively, from the intercepts of the Mott-Schottky plots. Direct evidence for the interfacial electron transfer is presented in ref. [10].

A Breathing Ionic Crystal Displaying Selective Binding of Small Alcohols and Nitriles: $K_3[Cr_3O(OOCH)_6(H_2O)_3][\alpha-SiW_{12}O_{40}] \cdot 16H_2O$ **

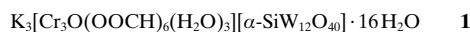
Sayaka Uchida, Masato Hashimoto, and Noritaka Mizuno*

The fabrication of nanostructured materials has produced a variety of materials with unique physical or chemical properties. Aluminosilicate zeolites and their inorganic analogues possess well-defined pores, which show shape-selective adsorption of molecules and are widely applied to adsorption, separation, and catalytic processes.^[1] Recently, “organic zeolites” based on organic or organometallic building blocks have been synthesized.^[2] These organic zeolites can be easily functionalized at the atomic/molecular level by the appropriate selection of the metals, ligands, or chemical bonds and show unique inclusion properties.^[2] For example, the compound Co-benzenetricarboxylate (Co-BTC) absorbs only aromatics but not acetonitrile or 1,2-dichloroethane^[2f] and the compound Zn-BTC absorbs only alcohols among various polar organic molecules.^[2i, 2k] As for the separation of alcohol molecules, the Ca-A zeolite^[3] adsorbs 1-butanol from a mixture of its isomers and the compound Zn-BTC^[2i] distinguishes alkyl alcohols from aromatic alcohols, although little is known of the separation of smaller alcohols ($< C_3$).

Polyoxometalates are discrete metal–oxygen cluster anions and have notable redox or acid–base properties.^[4] Some polyoxometalate compounds possess micropores in the crystal structure^[5, 6] or between the nanocrystallites.^[7] For example, Müller et al. synthesized a supramolecular molybdenum oxide cluster with cavities.^[6] Some polyoxometalate complexes contain acetonitrile or methanol as guests, but do not show reversible inclusion and removal.^[8] An acid-type polyoxometalate, $H_3PW_{12}O_{40}$, absorbs polar molecules in the

pseudoliquid phase, but the absorption is not selective because of the strong interaction of protons with absorbates.^[9] All these compounds do not show selective binding of polar organic molecules.

Herein we report the selective binding of small alcohols and nitriles smaller than C_3 by complex **1**, which is synthesized by the complexation of the Keggin-type $[\alpha-SiW_{12}O_{40}]^{4-}$ polyoxometalate ion with the large macro cation $[Cr_3O(OOCH)_6(H_2O)_3]^+$, and the separation of methanol from a mixture of alcohols.



The crystal structure of **1** (see Figure 1) shows polyoxometalates and macro cations lined up along the *c* axis to form a column and that three potassium ions balance the negative charge. The columns are hexagonally arranged to construct a

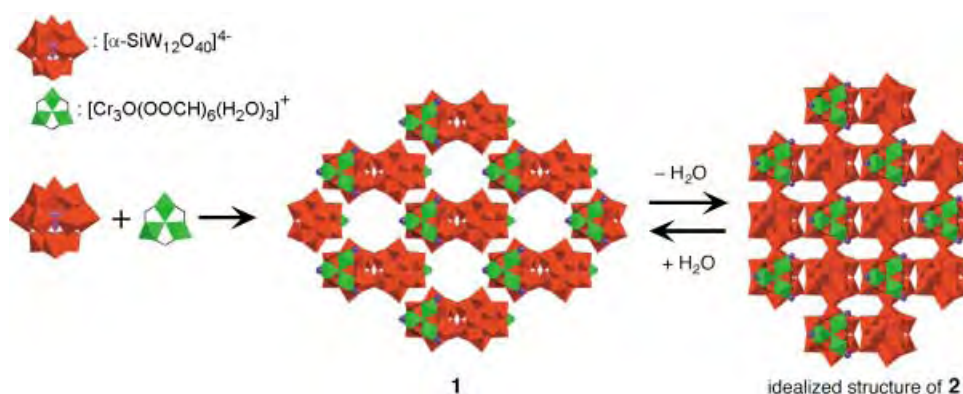


Figure 1. Synthesis and crystal structure of **1** and the ideal closest-packing model of **2**. The water of crystallization is omitted for the clarity; small blue spheres = K^+ ions.

straight channel with an opening of around 0.5×0.8 nm (36 % of the unit cell).^[10] The use of the macro cation with a large size (ca. 0.7 nm) and small charge (+1), which reduces the ion–ion interaction among the constituent ions, is essential to the formation of the channels. The water of crystallization is in the channels, and is weakly hydrogen bonded to ligand water molecules of the macro cations and oxygen atoms of the polyoxometalates. These water molecules were easily desorbed by the evacuation at 298 K (guest-free phase, **2**; Figure 1). The weight loss was 7.6 %, consistent with the removal of the water of crystallization. The BET surface area of **2** with N_2 adsorption was $2.0 \text{ m}^2 \text{ g}^{-1}$ and no micropores were observed.

Figure 2a and b show the powder X-ray diffraction patterns of **1** and **2**, respectively. Broad lines are observed in Figure 2b. This pattern is explained by a calculation with a closest-packing model of the columns, which is in accord with the low BET surface area and that no micropores were observed for **2**.^[11] Compound **2** absorbs water molecules upon exposure to saturated water vapor (ca. 3 kPa) at 298 K with the restoration of the powder X-ray diffraction pattern (Figure 2c). On the other hand, the binding of methanol by **2** changed the powder X-ray diffraction pattern (Figure 2d). No satisfactory fits were observed by changing the dimension of the channel in **1**. This occurrence is probably caused by the structure change

[*] Prof. Dr. N. Mizuno, Dr. S. Uchida
Department of Applied Chemistry, School of Engineering
The University of Tokyo
Bunkyo-ku, Tokyo 113-8656 (Japan)
Fax: (+81) 3-5841-7220
E-mail: tmizuno@mail.ecc.u-tokyo.ac.jp

Prof. Dr. M. Hashimoto
Department of Material Science and Chemistry
Wakayama University, Sakaedani, Wakayama 640-8510 (Japan)

[**] This work was supported in part by a Grant-in-Aid for Scientific Research from the Ministry of Education, Culture, Sports, Science, and Technology of Japan. Dr. K. Sugimoto of the Rigaku Corporation is acknowledged for the crystallographic analysis of $K_2[Cr_3O(OOCH)_6(H_2O)_{2.5}(CH_3OH)_{0.5}][\alpha-SiW_{12}O_{40}] \cdot 8CH_3OH$. S.U. acknowledges the Japan Society for the Promotion of Science for a Young Scientist Fellowship.

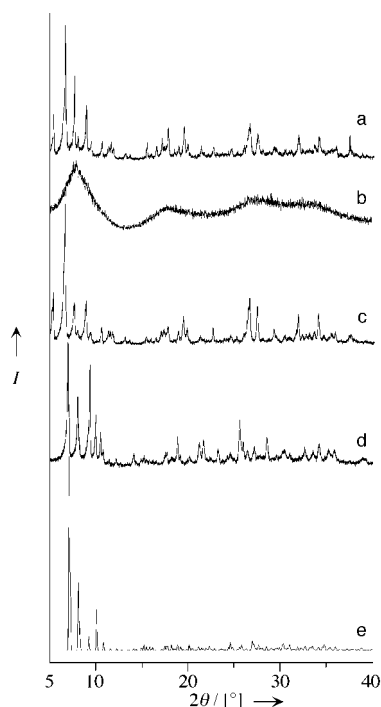


Figure 2. Observed powder X-ray diffraction patterns. a) **1**, b) **2**, c) rehydrated **2**, d) **2** after exposure to saturated methanol vapor for 5 min at 298 K, and e) calculated pattern for $\text{K}_3[\text{Cr}_3\text{O}(\text{OOCH})_6(\text{H}_2\text{O})_3][\alpha\text{-SiW}_{12}\text{O}_{40}] \cdot n\text{CH}_3\text{OH}$ based on that for $\text{K}_2[\text{Cr}_3\text{O}(\text{OOCH})_6(\text{H}_2\text{O})_{2.5}(\text{CH}_3\text{OH})_{0.5}]_2[\alpha\text{-SiW}_{12}\text{O}_{40}] \cdot n\text{CH}_3\text{OH}$.

with the methanol inclusion. Some organometallic complexes exhibit structure change upon the inclusion of guests, such as alcohols, amides, and nitriles, which have hydrogen-bonding nature.^[12] At present, the pattern in Figure 2d was only approximately reproduced by the calculation on the assumption that the occupancies of the $[\text{Cr}_3\text{O}(\text{OOCH})_6(\text{H}_2\text{O})]^{+}$ and K^{+} ions are fixed to 0.5 in the $[\text{Cr}_3\text{O}(\text{OOCH})_6(\text{H}_2\text{O})]^{+}$ sites of the known compound $\text{K}_2[\text{Cr}_3\text{O}(\text{OOCH})_6(\text{H}_2\text{O})_{2.5}(\text{CH}_3\text{OH})_{0.5}]_2[\alpha\text{-SiW}_{12}\text{O}_{40}] \cdot 8\text{CH}_3\text{OH}$ to give a theoretical pattern for $\text{K}_3[\text{Cr}_3\text{O}(\text{OOCH})_6(\text{H}_2\text{O})_3][\alpha\text{-SiW}_{12}\text{O}_{40}] \cdot n\text{CH}_3\text{OH}$ (Figure 2e).^[13] No changes in the IR and diffuse reflectance UV/Vis spectra were observed upon the repetitions (even after more than five) of the absorption–desorption cycles of either water or methanol, which shows the maintenance of the structures of the $[\alpha\text{-SiW}_{12}\text{O}_{40}]^{4-}$ and $[\text{Cr}_3\text{O}(\text{OOCH})_6(\text{H}_2\text{O})_3]^{+}$ ions in **1**.

Figure 3 shows the sorption isotherm of C_1 – C_4 alcohols. The amounts of the surface adsorption of alcohols calculated from the BET surface area was 0.24 – $0.40 \text{ cm}^3 \text{ g}^{-1}$ and was almost negligible. The amount of methanol increased with an increase in P/P_0 . The sorption amount reached $80 \text{ cm}^3 \text{ g}^{-1}$ (13 molecules per **2**) at $P/P_0 = 0.6$, which shows the sorption of methanol into the bulk material. On the other hand, the amount of ethanol sorption was less than that for the surface adsorption below $P/P_0 = 0.5$ and a sudden rise was observed around $P/P_0 = 0.6$. These unique adsorption phenomenon are explained by the structure change associated with the hydrogen-bond-regulated guest inclusion.^[14, 2k, 2q] Above $P/P_0 = 0.6$, ethanol molecules can diffuse into the bulk. 1-Propanol and 1-butanol were completely excluded. Figure 4 shows the

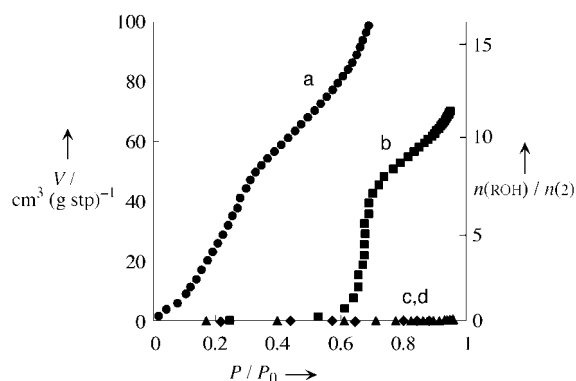


Figure 3. Sorption isotherm of alcohols at 298 K with **2** (0.1 g , $2.85 \times 10^{-2} \text{ mmol}$): a) methanol (\bullet , $P_0 = 15.6 \text{ kPa}$), b) ethanol (\blacksquare , $P_0 = 6.67 \text{ kPa}$), c) 1-propanol (\blacktriangle , $P_0 = 2.67 \text{ kPa}$), and d) 1-butanol (\blacklozenge , $P_0 = 1.35 \text{ kPa}$).

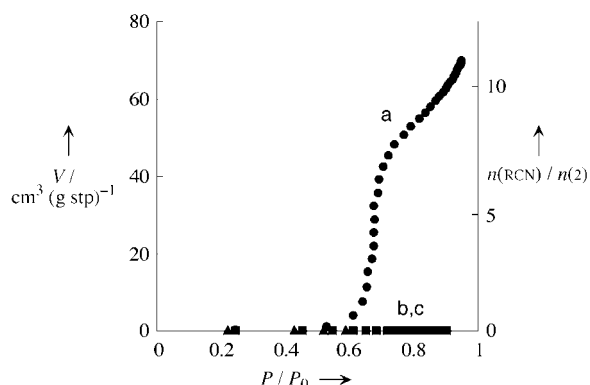


Figure 4. Sorption isotherm of nitriles at 298 K with **2** (0.1 g , $2.85 \times 10^{-2} \text{ mmol}$): a) acetonitrile (\bullet , $P_0 = 10.7 \text{ kPa}$), b) propionitrile (\blacksquare , $P_0 = 6.27 \text{ kPa}$), and c) butylnitrile (\blacktriangle , $P_0 = 2.67 \text{ kPa}$).

sorption isotherms of the nitriles. Acetonitrile showed a similar isotherm to that of ethanol while propionitrile and butylnitrile were excluded. The nonsaturation behavior at a high P/P_0 value is probably caused by the multilayer sorption on the surface.

The amounts of alcohols and nitriles absorbed decreased in the order of methanol > ethanol > 1-propanol \approx 1-butanol \approx 0 and acetonitrile > propionitrile \approx butylnitrile \approx 0. The same order was observed for the hydrophilicity. In addition, the more hydrophobic methane and nitrogen monoxide, the sizes of which are smaller than the C_1 – C_3 alcohols and nitriles, were excluded. Therefore, the sorption properties of **2** are chiefly associated with the hydrogen-bonding interaction between the polar molecules and oxygen atoms of $[\text{Cr}_3\text{O}(\text{OOCH})_6(\text{H}_2\text{O})_3]^{+}$ and $[\alpha\text{-SiW}_{12}\text{O}_{40}]^{4-}$.^[15]

Next, **2** was applied to the selective sorption from a mixture of alcohols. Figure 5 shows the separation of methanol from a mixture of C_1 – C_3 alcohols under dilute conditions (0.4 M of each alcohol in 1,2-dichloroethane). Methanol was selectively absorbed and the amount reached up to approximately 1.8 molecules per **2**, while ethanol and 1-propanol were excluded.^[16] Thus methanol could be separated from other C_1 – C_3 alcohols. Therefore, all the present results show the novel molecular sieving for small molecules.

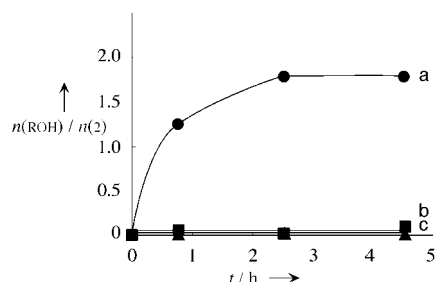


Figure 5. Selective binding of methanol in 1,2-dichloroethane at 298 K with **2** (0.74 g, 2.12×10^{-1} mmol): ● methanol (0.4 M), ■ ethanol (0.4 M), ▲ 1-propanol (0.4 M); conditions: 1,2-dichloroethane (16 mL), methanol: ethanol:1-propanol:1,2-dichloroethane = 1:30:30:900.

Experimental Section

1: $K_4[\alpha\text{-SiW}_{12}\text{O}_{40}] \cdot n\text{H}_2\text{O}$ (0.23 mmol) and $[\text{Cr}_3\text{O}(\text{OOCH})_6(\text{H}_2\text{O})_3](\text{OOCH}) \cdot n\text{H}_2\text{O}$ (0.27 mmol) were dissolved into dilute aqueous HNO_3 (pH 2, 30 mL). KCl (6.8 mmol) was added. The solution was filtered after 30 min and the filtrate was kept in air at room temperature for 1–2 days. Green crystals were isolated in about 50% yield. IR (KBr): 1634 and 1378 (vs, OCO), 981 (s, W=O), 929 (br, Si-O), 887 (m, W-O-W), 791 (br, W-O-W), 660 cm^{-1} (m, $\text{Cr}_3\text{-O}$). Elemental analysis (%) calcd for $\text{C}_6\text{H}_{44}\text{Cr}_3\text{K}_3\text{O}_{72}\text{SiW}_{12}$: C 1.91, H 1.01, Cr 4.13, K 3.09, Si 0.74, W 59.90; found: C 1.92, H 1.10, Cr 4.10, K 3.35, Si 0.80, W 59.91.

X-ray crystal determination of 1: X-ray intensity data were collected on a Rigaku AFC-5R diffractometer with graphite-monochromated $\text{MoK}\alpha$ radiation ($\lambda = 0.71069$ Å, 50 kV–150 mA). Lorentz polarization and empirical absorption correction based on ψ scan were carried out with TEXSAN. Tungsten and chromium atoms were located by direct methods and other non-hydrogen atoms were found by successive differential Fourier syntheses. Refinements were carried out by SHELX97. Monoclinic $C2/m$, $a = 27.258(4)$, $b = 15.764(6)$, $c = 17.285(4)$ Å, $\beta = 102.73(2)^\circ$, $V = 7245(3)$ Å³, $Z = 4$, $\rho_{\text{calcd}} = 3.396$ g cm^{-3} , $T = 293(2)$ K, 10885 unique reflections with $I > 2\sigma(I)$, $2.56 < \theta < 29.97$, 449 parameters, final R factors $R_1 = 0.059$; $wR_2 = 0.1446$. Only 12 out of 16 water molecules per **2** were located. CCDC 160502 (**1**) contains the supplementary crystallographic data for this paper. These data can be obtained free of charge via www.ccdc.cam.ac.uk/conts/retrieving.html (or from the Cambridge Crystallographic Data Centre, 12, Union Road, Cambridge CB21EZ, UK; fax: (+44) 1223-336-033; or deposit@ccdc.cam.ac.uk).

Powder X-ray diffraction measurements: All spectra were measured with a MXP3 diffractometer (Mac Science) using $\text{CuK}\alpha$ radiation ($\lambda = 1.54056$ Å, 30 kV–40 mA). The scanings were in the range of $2\theta = 2\text{--}40^\circ$ at a rate of $0.5^\circ \text{ min}^{-1}$.

Calculation of the powder X-ray diffraction pattern: Calculations were carried out by drawing the presumed structure with Crystal Maker (CrystalMaker Software) and displaying the pattern with Crystal Diffraction (CrystalMaker Software). The particle size (i.e. coherent length), which was translated to the half width of the reflection, was altered to give the best fit.

Sorption measurements: The sorption isotherms of **2** were measured with an automatic sorption apparatus Omnisorp 100CX (Coulter corporation). The uptake of alcohols by **2** was confirmed by the changes in the alcohol concentrations, which were detected by GC (Shimadzu GC-8A model with a Porapak QS column and a TCD detector). Methanol, ethanol, and 1-propanol (each 6.36 mmol) were added to 1,2-dichloroethane (ca. 16 mL 0.2 mmol) the anhydride (0.74 g, 2.12×10^{-1} mmol) was added to give a heterogeneous mixture.

Received: February 4, 2002

Revised: April 4, 2002 [Z18646]

- [1] a) S. M. Csicsery, *Pure Appl. Chem.* **1986**, 58, 841; b) J. M. Thomas, *Angew. Chem.* **1999**, 111, 3852; *Angew. Chem. Int. Ed.* **1999**, 38, 3588; c) S. M. Kuznicki, V. A. Bell, S. Nair, H. W. Hillhouse, R. M.

Jacobinas, C. M. Braunbarth, B. H. Toby, M. Tsapatsis, *Nature* **2001**, 412, 720; d) N. Guillou, Q. Gao, P. M. Forster, J. S. Chang, M. Nogués, S. E. Park, G. Férey, A. K. Cheetham, *Angew. Chem.* **2001**, 113, 2913; *Angew. Chem. Int. Ed.* **2001**, 40, 2831.

- [2] Recent reviews are a) S. Kitagawa, M. Kondo, *Bull. Chem. Soc. Jpn.* **1998**, 71, 1739; b) M. Eddaoudi, D. B. Moler, H. Li, B. Chen, T. M. Reineke, M. O'Keeffe, O. M. Yaghi, *Acc. Chem. Res.* **2001**, 34, 319; c) B. Moulton, M. J. Zaworotko, *Chem. Rev.* **2001**, 101, 1629; Recent reports are d) M. Fujita, Y. J. Kwon, S. Washizu, K. Ogura, *J. Am. Chem. Soc.* **1994**, 116, 1151; e) K. Endo, T. Sawaki, M. Koyanagi, K. Kobayashi, H. Masuda, Y. Aoyama, *J. Am. Chem. Soc.* **1995**, 117, 8341; f) O. M. Yaghi, G. Li, H. Li, *Nature* **1995**, 378, 703; g) M. Kondo, T. Yoshitomi, K. Seki, H. Matsuzaka, S. Kitagawa, *Angew. Chem.* **1997**, 109, 1844; *Angew. Chem. Int. Ed. Engl.* **1997**, 36, 1725; h) V. A. Russell, C. C. Evans, W. Li, M. D. Ward, *Science* **1997**, 276, 575; i) O. M. Yaghi, C. E. Davis, G. Li, H. Li, *J. Am. Chem. Soc.* **1997**, 119, 2861; j) C. J. Kepert, D. Hesk, P. D. Beer, M. J. Rosseinsky, *Angew. Chem.* **1998**, 110, 3335; *Angew. Chem. Int. Ed.* **1998**, 37, 3158; k) M. Eddaoudi, H. Li, O. M. Yaghi, *J. Am. Chem. Soc.* **2000**, 122, 1391; l) K. Biradha, Y. Hongo, M. Fujita, *Angew. Chem.* **2000**, 112, 4001; *Angew. Chem. Int. Ed.* **2000**, 39, 3843; m) J. S. Seo, D. Whang, H. Lee, S. I. Jun, J. Oh, Y. J. Jeon, K. Kim, *Nature* **2000**, 404, 982; n) A. J. Fletcher, E. J. Cussen, T. J. Prior, M. J. Rosseinsky, C. J. Kepert, K. M. Thomas, *J. Am. Chem. Soc.* **2001**, 123, 10001; o) K. S. Min, M. P. Suh, *Chem. Eur. J.* **2001**, 7, 303; p) O. R. Evans, H. L. Ngo, W. Lin, *J. Am. Chem. Soc.* **2001**, 123, 10395; q) R. Kitaura, K. Fujimoto, S. Noro, M. Kondo, S. Kitagawa, *Angew. Chem.* **2002**, 114, 141; *Angew. Chem. Int. Ed.* **2002**, 41, 133.
- [3] P. B. Weisz, V. J. Frilette, R. W. Maatman, E. B. Mower, *J. Catal.* **1962**, 1, 307.
- [4] a) M. T. Pope, A. Müller, *Angew. Chem.* **1991**, 103, 56; *Angew. Chem. Int. Ed. Engl.* **1991**, 30, 34; b) T. Okuhara, N. Mizuno, M. Misono, *Adv. Catal.* **1996**, 41, 113; c) Ed.: C. L. Hill, *Polyoxometalates*, Special Issue, *Chem. Rev.* **1998**, 98, 1; d) R. Neumann, *Prog. Inorg. Chem.* **1998**, 47, 317.
- [5] a) M. Hölscher, U. Englert, B. Zibrowius, W. F. Hölderich, *Angew. Chem.* **1994**, 106, 2552; *Angew. Chem. Int. Ed.* **1994**, 33, 2491; b) M. I. Khan, E. Yohannes, D. Powell, *Inorg. Chem.* **1999**, 38, 212; c) D. Hargman, P. J. Hargman, J. Zubieta, *Angew. Chem.* **1999**, 111, 3359; *Angew. Chem. Int. Ed.* **1999**, 38, 3165; d) J. H. Son, H. Choi, Y. U. Kwon, *J. Am. Chem. Soc.* **2000**, 122, 7432.
- [6] a) A. Müller, E. Krickemeyer, H. Bögge, M. Schmidtman, F. Peters, C. Menke, J. Meyer, *Angew. Chem.* **1997**, 109, 500; *Angew. Chem. Int. Ed. Engl.* **1997**, 36, 484; b) A. Müller, E. Krickemeyer, H. Bögge, M. Schmidtman, P. Kögerler, C. Rosu, E. Beckman, *Angew. Chem.* **2001**, 113, 4158; *Angew. Chem. Int. Ed.* **2001**, 40, 4034.
- [7] a) N. Mizuno, M. Misono, *Chem. Lett.* **1987**, 267; b) T. Okuhara, T. Nishimura, M. Misono, *Chem. Lett.* **1995**, 155; c) Y. Yoshinaga, K. Seki, T. Nakato, T. Okuhara, *Angew. Chem.* **1997**, 109, 2946; *Angew. Chem. Int. Ed.* **1997**, 36, 2833.
- [8] a) V. W. Day, W. G. Klemperer, O. M. Yaghi, *J. Am. Chem. Soc.* **1989**, 111, 5959; b) M. I. Khan, J. Zubieta, *Angew. Chem.* **1994**, 106, 784; *Angew. Chem. Int. Ed. Engl.* **1994**, 33, 760; c) Y. Hayashi, F. Müller, Y. Lin, S. M. Miller, O. P. Anderson, R. G. Finke, *J. Am. Chem. Soc.* **1997**, 119, 11401.
- [9] a) M. Misono, N. Mizuno, K. Katamura, A. Kasai, Y. Konishi, K. Sakata, T. Okuhara, Y. Yoneda, *Bull. Chem. Soc. Jpn.* **1982**, 55, 400; b) J. G. Highfield, J. B. Moffat, *J. Catal.* **1985**, 95, 108; c) J. G. Highfield, J. B. Moffat, *J. Catal.* **1986**, 98, 245; d) T. Okuhara, S. Tatemateu, K. W. Lee, M. Misono, *Bull. Chem. Soc. Jpn.* **1989**, 62, 717; e) J. B. Moffat, *Metal-Oxygen Clusters*, Kluwer Academic, New York, **2001**, chapt. 7.
- [10] The volume was estimated by considering ionic radii (Cr^{3+}) or van der Waals radii (other atoms) of the constituent atoms.
- [11] A similar closest packing to **2** was observed for the complex of Keggin-type polyoxometalate $[\text{CoW}_{12}\text{O}_{40}]^{6-}$ with $[\text{Cr}_3\text{O}(\text{OOCH})_6(\text{H}_2\text{O})_3]^+$ ions. The channel volume of this complex was 17% of the unit cell, which was comparable to the ideal closest packing model of **2** (20%). The details will be published elsewhere.
- [12] a) C. J. Kepert, T. J. Prior, M. J. Rosseinsky, *J. Am. Chem. Soc.* **2000**, 122, 5158; b) M. Edgar, R. Mitchell, A. M. Z. Slawin, P. Lightfoot, P. A. Wright, *Chem. Eur. J.* **2001**, 7, 5168.

- [13] $K_2[Cr_3O(OOCH)_6(H_2O)_{2.5}(CH_3OH)_{0.5}]_2[\alpha-SiW_{12}O_{40}] \cdot 8CH_3OH$ was crystallized from a methanol solution of **2**. Crystallographic data for $K_2[Cr_3O(OOCH)_6(H_2O)_{2.5}(CH_3OH)_{0.5}]_2[\alpha-SiW_{12}O_{40}] \cdot 8CH_3OH$: orthorhombic $Pna2_1$, $a = 24.796(6)$, $b = 15.406(3)$, $c = 22.042(5)$ Å, $Z = 4$, $R_1 = 0.0480$; $wR2 = 0.0480$.
- [14] D. Li, K. Kaneko, *Chem. Phys. Lett.* **2001**, 335, 50.
- [15] In the crystal structure of $K_2[Cr_3O(OOCH)_6(H_2O)_{2.5}(CH_3OH)_{0.5}]_2[\alpha-SiW_{12}O_{40}] \cdot 8CH_3OH$, methanol molecules are hydrogen bonded to the oxygen atoms of the bridging units of the macro cations.
- [16] The amount of methanol absorbed in Figure 5 seemed to be different from that in Figure 3a. This can be explained by the different equilibrium in the liquid–solid phase from that in the gas–solid phase.

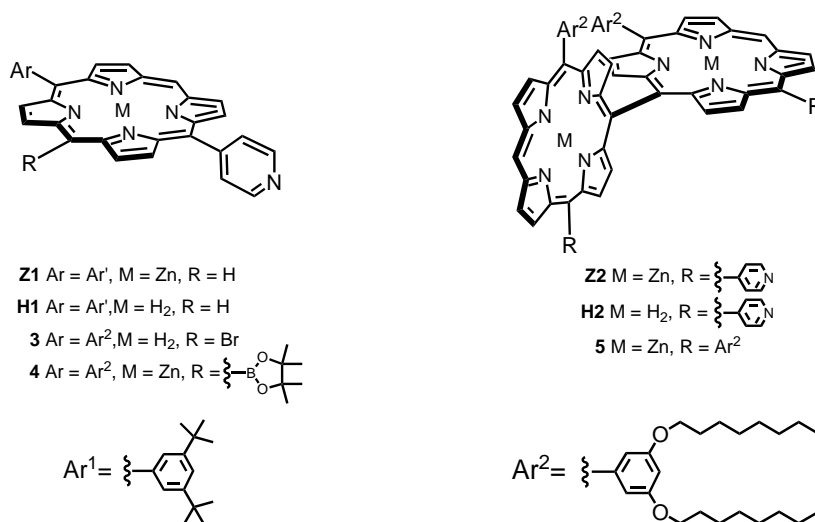
A Self-Assembled Porphyrin Box from *meso*–*meso*-Linked Bis[5-*p*-pyridyl-15-(3,5-di-octyloxyphenyl)porphyrinato zinc(II)]**

Akihiko Tsuda, Takeshi Nakamura, Shigeru Sakamoto, Kentaro Yamaguchi, and Atsuhiko Osuka*

Well-ordered architectures of self-assembling porphyrins^[1] have been attracting considerable interest in light of potential applications in material science,^[2] template-directed synthesis,^[3] reaction catalysis,^[4] and duplication of photosynthetic functions of light harvesting and charge separation.^[5] Among these, the coordination interaction between zinc porphyrin and pyridine groups have been often used to construct self-assembled porphyrin architectures both in infinite and discrete forms.^[1–6] Fleischer and Shachter have reported a linear infinite polymeric aggregate from 5-*p*-pyridyl-10,15,20-triphenylporphyrinato zinc(II),^[6] whereas Hunter and co-workers reported the formation of a cyclic tetramer from a zinc(II) porphyrin bearing a *p*-(iso-

nicotinamide)phenyl group^[7] and Imamura and co-workers reported a similar cyclic tetramer from 5-*p*-pyridyl-10,15,20-triaryl porphyrinato ruthenium(II),^[8] both without X-ray crystal structures. Herein, we report a self-assembling cyclic tetramer of 5-*p*-pyridyl-15-(3,5-di-*tert*-butylphenyl)porphyrinato zinc(II) (**Z1**) with its X-ray structure and a self-assembling box-shape tetramer of *meso*–*meso*-linked bis[5-*p*-pyridyl-15-(3,5-di-octyloxyphenyl)porphyrinato zinc(II)] (**Z2**; Scheme 1). In the latter case, a very stable supramolecular aggregate is constructed as a result of many cooperative interactions with simultaneous structural rigidification, as suggested by its unique absorption and fluorescence spectra.

5-*p*-Pyridyl-15-(3,5-di-*tert*-butylphenyl)porphyrin (**H1**) was prepared by condensation of 4-pyridinecarboxaldehyde and 3,5-di-*tert*-butylbenzaldehyde with 2,2'-dipyrrylmethane in 8% yield, and subsequent zinc insertion with $Zn(OAc)_2$



Scheme 1.

afforded **Z1** quantitatively. The ¹H NMR spectrum of **Z1** in CDCl₃ is concentration independent at >3 mM and exhibits large upfield shifts for the pyridyl protons at $\delta = 6.18$ and 2.17 ppm in comparison to those of **H1** at $\delta = 8.29$ and 7.81 ppm, which indicates the coordination of the pyridyl group to zinc(II) porphyrin. As judged from the chemical shifts of the pyridyl group, **Z1** forms a similar aggregate in C₆D₆ ($\delta = 5.94$ and 2.59 ppm) but exists in a monomeric form in [D₈]THF ($\delta = 8.97$ and 8.31 ppm). The latter result suggested the coordination of THF to the zinc center, thus preventing self-assembling. Vapor pressure osmometry (VPO) in CHCl₃ afforded average molecular weights of $2760 \pm 370 \text{ g mol}^{-1}$ for **Z1** and $550 \pm 20 \text{ g mol}^{-1}$ for **H1** in a range of $3.0\text{--}13.0 \times 10^{-3} \text{ M}$, which correspond to (**Z1**)₄ and monomeric **H1**, respectively. The absorption spectrum of **Z1** in CHCl₃ is concentration dependent in an range of roughly $10^{-6}\text{--}10^{-5} \text{ M}$ and shows the Q-band at 540 nm at $<10^{-6} \text{ M}$ and at 549 nm at $>\text{about } 10^{-5} \text{ M}$ (Figure 1), which correspond, respectively, to four-coordinate and five-coordinate zinc porphyrin units. A good fit for the observed sigmoidal curve is obtained by assuming porphyrin tetramer formation ((**Z1**)₄), which gives an association constant of $K_4 = 1.4 \times 10^{15} \text{ M}^{-3}$.^[9]

[*] Prof. A. Osuka, Dr. A. Tsuda, T. Nakamura
 Department of Chemistry
 Graduate School of Science
 Kyoto University
 Sakyo-ku, Kyoto 606-8502 (Japan)
 Fax: (+81) 75-753-3970
 E-mail: osuka@kuchem.kyoto-u.ac.jp
 Dr. S. Sakamoto, Prof. K. Yamaguchi
 Chemical Analysis Center
 Chiba University
 Yayoi-cho, Inage-ku, Chiba 263-8522 (Japan)

[**] This work was supported by Grant-in-Aids for Scientific Research from the Ministry of Education, Science, Sports and Culture of Japan and CREST (Core Research for Evolutional Science and Technology) of the Japan Science and Technology Corporation (JST). A.O. thanks the Toray Science Foundation. A.T. thanks the JSPS (Japan Society for the Promotion of Science) Research Fellowship for Young Scientists.

Supporting information for this article is available on the WWW under <http://www.angewandte.org> or from the author.

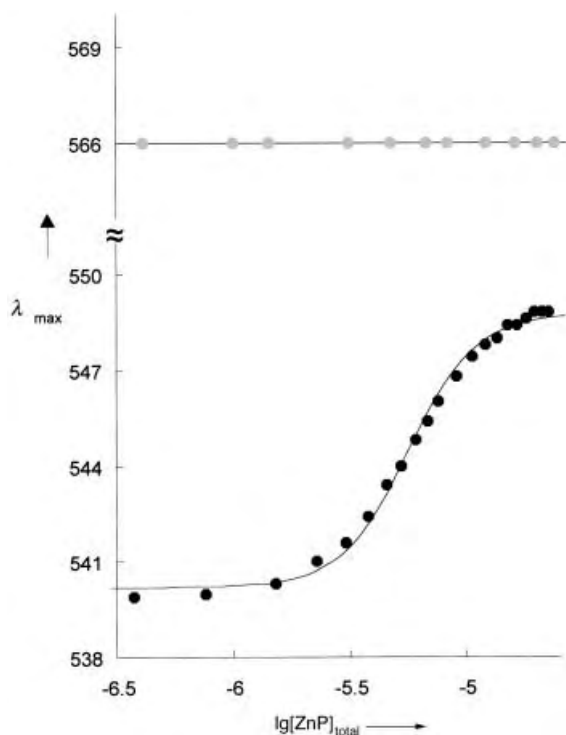


Figure 1. Concentration dependences (3.8×10^{-7} – 2.3×10^{-5} M) of Q-bands of **Z1** (●) and **Z2** (○) in CHCl_3 at 25°C . Solid line for **Z1** is the theoretical curve obtained by curve-fitting analysis for tetramer formation with $K_4 = 1.4 \times 10^{15} \text{ M}^{-3}$.

Slow diffusion of CH_3CN vapor into THF and benzene solutions of **Z1** gave two types of single crystals, which were both suitable for X-ray crystallography. In the crystal obtained from THF solution, **Z1** molecules coordinated by two THF molecules are arranged in a parallel manner without noticeable inter-porphyrin interaction (see Supporting Information), while in the crystal obtained from benzene solution, four **Z1** molecules form a square structure by the complementary coordination of the pyridyl groups to the zinc center (Figure 2).^[10] In this structure, the Zn–N bond lengths are



Figure 2. Molecular structure of self-assembled (**Z1**)₄ crystallized from benzene and CH_3CN . Hydrogen atoms and incorporated benzene molecules are omitted for clarity.

2.18 Å and 2.17 Å and the central zinc units displaced out of the porphyrin plane (C_{20}N_4) toward the axial pyridyl group by 0.44 and 0.42 Å. The dihedral angles between porphyrin mean planes are 89.1° and 90.9° . Both of the crystal structures are consistent with the behavior of the compounds in solution.

We examined the self-assembling behavior of *meso*–*meso*-linked zinc(II) diporphyrin **Z2** which has a unique perpendicular conformation. The silver(I)-promoted coupling reaction of **Z1** did not provide **Z2**, probably because of the presence of *meso*-pyridyl group.^[11] Instead, free-base diporphyrin **H2** (Scheme 1) was prepared by Suzuki-coupling^[12] of bromide **3** and boronic ester **4** in 40% yield, and was converted into (**Z2**)₄ quantitatively. The sharp resonance peaks in the ^1H NMR spectrum of (**Z2**)₄ in CDCl_3 excludes the formation of infinite polymeric aggregates (Figure 3). The pyridyl protons appear as split signals at $\delta = 6.59$ and 6.34 ppm, and $\delta = 2.88$ and 2.38 ppm, being shifted considerably upfield compared with those of **H2** at $\delta = 8.97$ and 8.19 ppm. Similarly the *ortho* protons in the 3,5-di-octyloxyphenyl group appear as split signals at $\delta = 7.32$ and 7.30 ppm, and the signals of the two octyloxy groups appear at different chemical shifts. These ^1H NMR data strongly suggest the formation of a self-assembled box-shape cyclic tetramer from **Z2** (Scheme 2, path a). A stable (**Z2**)₄ aggregate was inferred from the gel-permeation chromatography (GPC) HPLC with CHCl_3 as an eluent. Whereas the retention times of **H1** (18.4 min) and **Z1** (19.3 min) were found to be nearly the same, which suggests the dissociation of (**Z1**)₄ under the eluting dilute conditions, (**Z2**)₄ exhibited a sharp elution band with a distinctly shorter retention time (13.9 min) than that of **H2** (16.3 min), suggesting the preservation of the discrete (**Z2**)₄ aggregate. In THF, cold spray ionization mass spectrometry (CSI-MS)^[13] detected the parent ion of (**Z2**)₄ at 6258, which is exactly the position expected for (**Z2**)₄ (calcd M_r for $\text{C}_{376}\text{H}_{400}\text{N}_{40}\text{O}_{16}\text{Zn}_8 = 6258$; Figure 4). It is notable that an intense peak assigned to (**Z2**)₄ was practically the sole signal and peaks attributable to smaller fragments of monomer and dimer were scarcely detected, again suggesting a stable (**Z2**)₄ aggregate in solution.

The absorption spectrum of (**Z2**)₄ in CHCl_3 characteristically exhibits a split Soret band ($\lambda_{\text{max}} = 426$ and 433 nm) the splitting width of which is much less than that of the normal *meso*–*meso*-linked zinc(II) diporphyrins (e.g. the Soret band of **5**, (Scheme 2) coordinated to pyridine molecules, is split to give maxima at 423 and 457 nm), and a Q-band peak at about 566 nm similar to that of five-coordinate *meso*–*meso*-linked zinc(II) diporphyrin **5** (Figure 5a). These features are *entirely concentration independent* even at a very low concentrations of approximately 10^{-7} M (Figure 1), which indicates a large association constant, at least 10^{21} M^{-3} . Interestingly the fluorescence spectrum of (**Z2**)₄ in CHCl_3 clearly shows a vibrational structure ($\lambda_{\text{max}} = 613$ and 666 nm, Figure 5b), which also differs from those of the normal *meso*–*meso*-linked zinc(II) diporphyrins that show characteristic broader fluorescence emissions, as seen for **5** (Figure 5b). The addition of pyridine causes the dissociation of (**Z2**)₄ to monomeric **Z2**, which has been monitored by the changes to the usual split Soret band ($\lambda_{\text{max}} = 423$ and 457 nm) and broader fluorescence spectrum, both of which are quite similar to those of **5** in the presence of pyridine (Figure 5). In short, the electronic interaction within

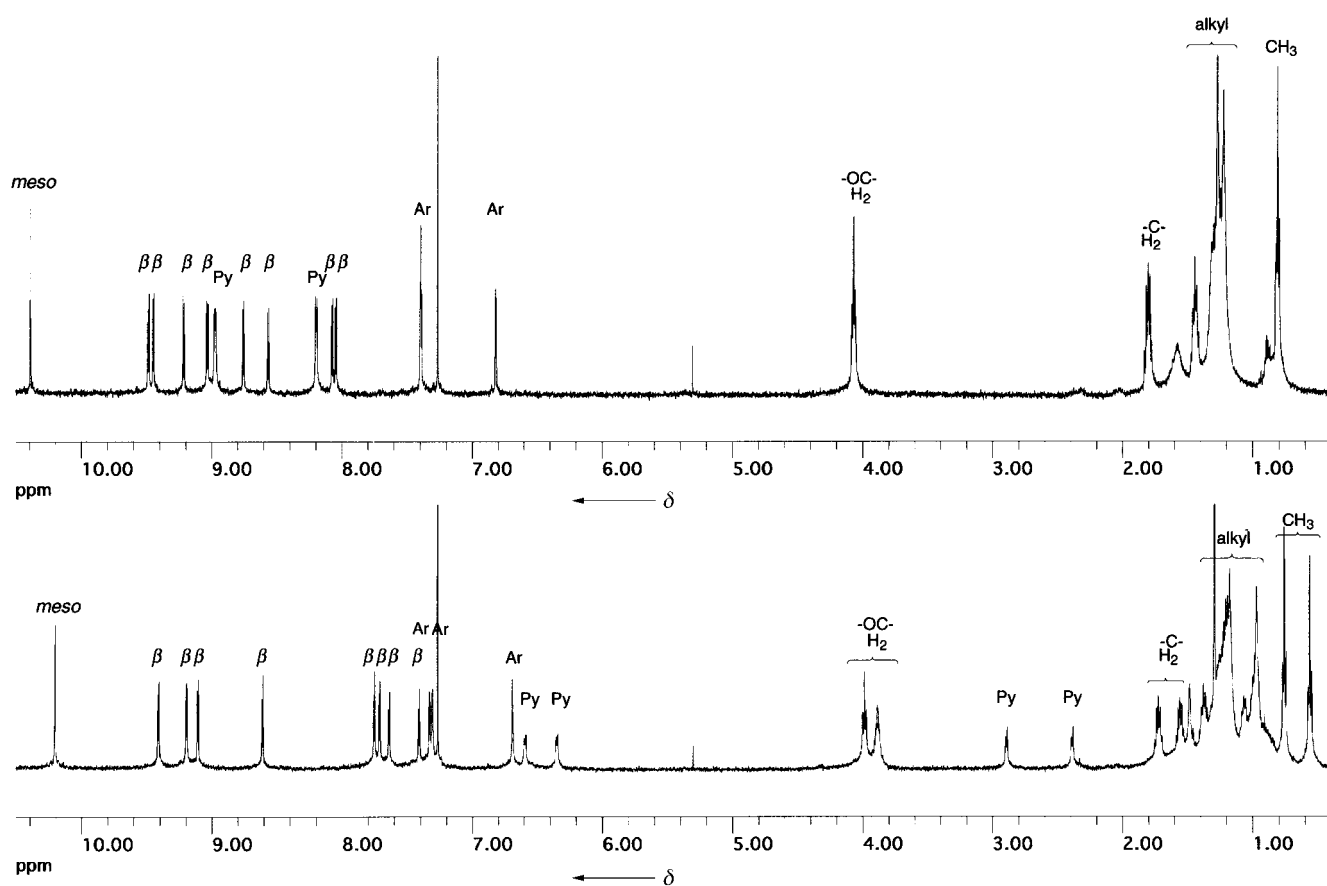
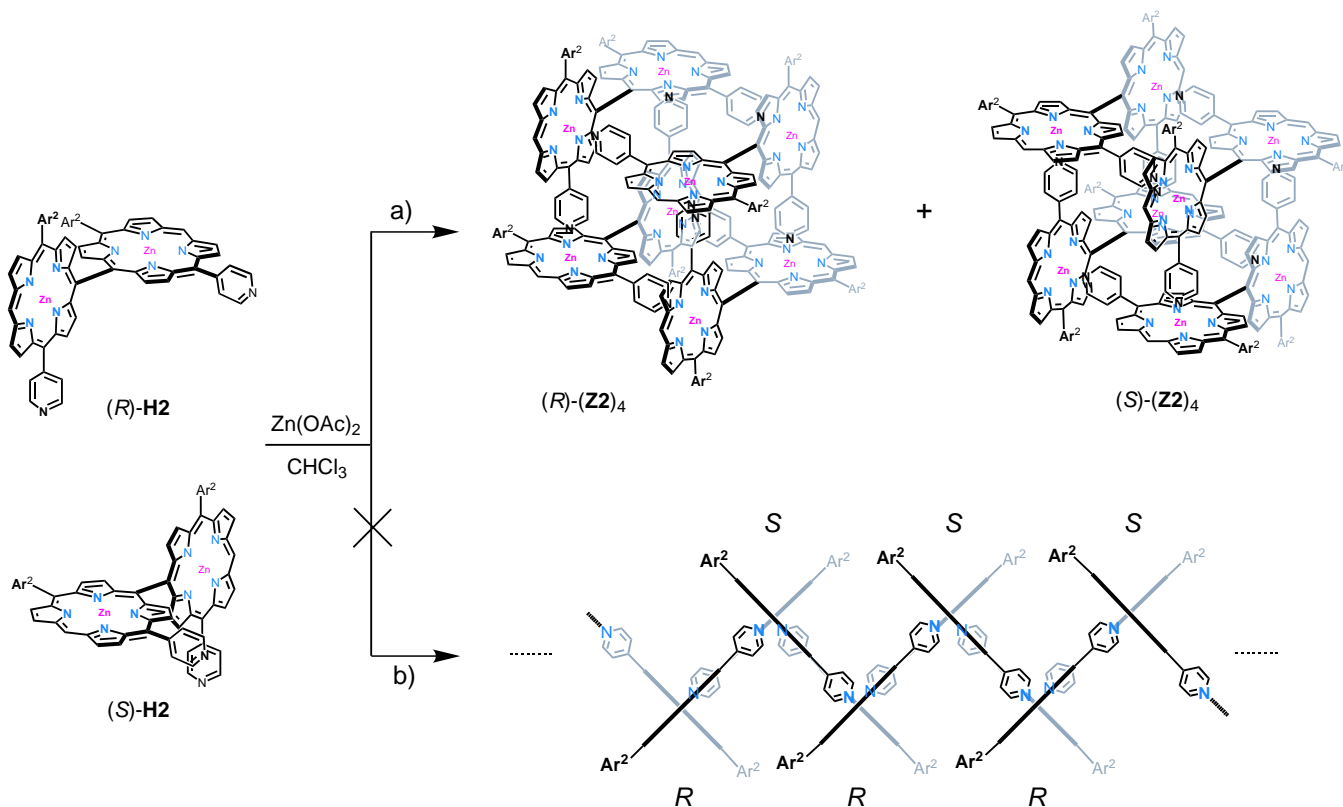


Figure 3. ^1H NMR spectra of **H2** (top) and **(Z2)₄** (bottom) in CDCl_3 , *meso*: porphyrin-*meso*, β : porphyrin- β , Ar: phenyl, Py: pyridyl protons.



Scheme 2.

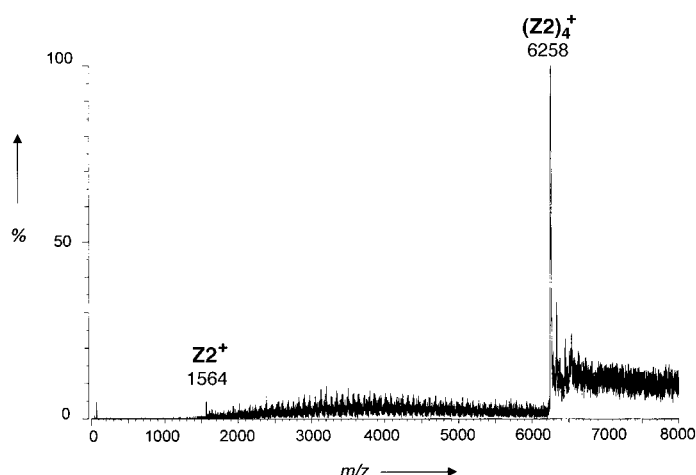


Figure 4. CSI-MS spectrum of $(\mathbf{Z2})_4$ in THF.

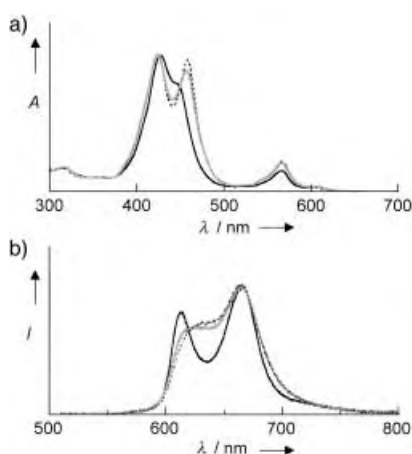


Figure 5. a) Absorption spectra of $(\mathbf{Z2})_4$ in CHCl_3 (—); $\mathbf{Z2}$ (from the dissociation of $(\mathbf{Z2})_4$) in CHCl_3 and pyridine (---); $\mathbf{5}$ in CHCl_3 and pyridine (----). b) Steady state fluorescence spectra of $(\mathbf{Z2})_4$ in CHCl_3 (—); $\mathbf{Z2}$ (from the dissociation of $(\mathbf{Z2})_4$) in CHCl_3 and pyridine (---); $\mathbf{5}$ in CHCl_3 and pyridine (----) for the excitation at 424 nm.

the *meso*–*meso*-linked diporphyrins is exceptionally small in $(\mathbf{Z2})_4$ in comparison to usual *meso*–*meso*-linked diporphyrins and is restored to the normal level upon the dissociation into monomeric $\mathbf{Z2}$. This may be rationalized in terms of the enhanced rigidification in the $(\mathbf{Z2})_4$ assembly, where the two porphyrins in a *meso*–*meso*-linked diporphyrin are forced to take a rigorously perpendicular orientation, thus minimizing the electronic interaction.^[14]

Given the strict perpendicular arrangement, $(\mathbf{Z2})_4$ defines a nanoscale box with a cavity of approximately $10 \times 10 \times 8 \text{ \AA}$. The association constant is difficult to determine but is at least 10^{25} M^{-3} in CHCl_3 as judged from the concentration independent (up to $1.6 \times 10^{-8} \text{ M}$) fluorescence spectrum. This result indicates a remarkable degree of cooperativity in the self-assembly process, given that the each interacting motif has the same association constant. Moreover, very high stability of the aggregate $(\mathbf{Z2})_4$ has been demonstrated by its preservation even in THF,^[15] in sharp contrast to $\mathbf{Z1}$.

Owing to the different *meso*-aryl substituents, $\mathbf{Z2}$ is chiral and hence two enantiomers, (*R*)- $\mathbf{Z2}$ and (*S*)- $\mathbf{Z2}$, are present in equal abundance in solution, since a free rotation around the

meso–*meso* linkage is severely prohibited.^[16] Among many possible aggregates, the sterically least demanding ones are a polymeric linear chain and a cyclic box-shaped tetramer as shown in Scheme 2. The former may be constructed by repetitive, alternate association of (*R*)- $\mathbf{Z2}$ and (*S*)- $\mathbf{Z2}$, while the latter is formed by *self-sorting association* of (*R*)- $\mathbf{Z2}$ and (*S*)- $\mathbf{Z2}$. The observed preferential formation of $(\mathbf{Z2})_4$ over the linear chain may be explained in terms of entropic as well as enthalpic advantages associated with a self-complementary cyclic array.

In summary, $\mathbf{Z1}$ forms a self-assembled cyclic tetramer both in solution and in the solid state only in the absence of coordinating molecules, while the *meso*–*meso* linked diporphyrin $\mathbf{Z2}$ forms a box-shape cyclic tetramer with an extraordinary large association constant, which is rather insensitive to coordinating molecules such as THF and alcohols. The latter aggregate compels the rigorous perpendicular orientation of the *meso*–*meso* linked diporphyrin, which may offer a new chance to examine the photophysical properties of the *meso*–*meso* linked diporphyrin with a precise perpendicular conformation.

Received: February 25, 2002
Revised: May 3, 2002 [Z18761]

- [1] Recent reviews: a) T. Imamura, K. Fukushima, *Cood. Chem. Rev.* **2000**, 198, 133; b) J. Wojaczynski, L. L. Grazynski, *Cood. Chem. Rev.* **2000**, 204, 113.
- [2] a) B. F. Abrahams, B. F. Hoskins, D. M. Michail, R. Robson, *Nature* **1994**, 369, 727; b) C. M. Drain, J.-M. Lehn, *J. Chem. Soc. Chem. Commun.* **1994**, 2313; c) P. Bhayappa, S. R. Wilson, K. S. Suslick, *J. Am. Chem. Soc.* **1997**, 119, 8492; d) P. J. Stang, J. Fan, B. Olenyuk, *Chem. Commun.* **1997**, 1453; e) R. K. Kumar, I. Goldberg, *Angew. Chem.* **1998**, 110, 3176; *Angew. Chem. Int. Ed.* **1998**, 37, 3027; f) K. Kobayashi, M. Koyanagi, K. Endo, H. Masuda, Y. Aoyama, *Chem. Eur. J.* **1998**, 4, 417; g) C. M. Drain, F. Nifatis, A. Vasenko, J. D. Batteas, *Angew. Chem.* **1998**, 110, 2478; *Angew. Chem. Int. Ed.* **1998**, 37, 2344; h) S. Knapp, J. Vasudevan, T. J. Emge, B. H. Arison, J. A. Potenza, H. J. Schugar, *Angew. Chem.* **1998**, 110, 2537; *Angew. Chem. Int. Ed.* **1998**, 37, 2368; i) C. V. K. Sharma, G. A. Broker, J. G. Huddleston, J. W. Baldwin, R. M. Metzger, R. D. Rogers, *J. Am. Chem. Soc.* **1999**, 121, 1137; j) C. Ikeda, N. Nagahara, E. Motegi, N. Yoshioka, H. Inoue, *Chem. Commun.* **1999**, 1759; k) D. Hagman, P. J. Hagman, J. Zubieta, *Angew. Chem.* **1999**, 111, 3359; *Angew. Chem. Int. Ed.* **1999**, 38, 3165; l) K. Ogawa, Y. Kobuke, *Angew. Chem.* **2000**, 112, 4236; *Angew. Chem. Int. Ed.* **2000**, 39, 4070; m) E. Iengo, B. Milani, E. Zangrando, S. Geremia, E. Alessio, *Angew. Chem.* **2000**, 112, 1138; *Angew. Chem. Int. Ed.* **2000**, 39, 1096; n) N. Fujita, K. Biradha, M. Fujita, S. Sakamoto, K. Yamaguchi, *Angew. Chem.* **2001**, 113, 1768; *Angew. Chem. Int. Ed.* **2001**, 40, 1718; o) G. A. Mines, B.-C. Tzeng, K. J. Stevenson, J. Li, J. T. Hupp, *Angew. Chem.* **2002**, 114, 162; *Angew. Chem. Int. Ed.* **2002**, 41, 154; p) A. Itasaka, M. Abe, T. Yoshimura, K. Tsuge, M. Suzuki, T. Imamura, Y. Sasaki, *Angew. Chem.* **2002**, 114, 481; *Angew. Chem. Int. Ed.* **2002**, 41, 463.
- [3] a) S. Anderson, H. L. Anderson, J. K. M. Sanders, *Acc. Chem. Res.* **1993**, 26, 469; b) J. Li, A. Ambrose, S. I. Yang, J. R. Diers, J. Seth, C. R. Wack, D. F. Bocian, D. Holten, J. S. Lindsey, *J. Am. Chem. Soc.* **1999**, 121, 8927.
- [4] M. L. Merlau, M. P. Mejia, S. T. Nguyen, J. T. Hupp, *Angew. Chem.* **2001**, 113, 4369; *Angew. Chem. Int. Ed.* **2001**, 40, 4239.
- [5] a) S. Anderson, H. L. Anderson, A. Bashall, M. McPartlin, J. K. M. Sanders, *Angew. Chem.* **1995**, 107, 1196; *Angew. Chem. Int. Ed.* **1995**, 34, 1096; b) A. K. Burrell, D. L. Officer, D. C. W. Reid, K. Y. Wild, *Angew. Chem.* **1998**, 110, 122; *Angew. Chem. Int. Ed.* **1998**, 37, 114; c) G. S. Wilson, H. L. Anderson, *Chem. Commun.* **1999**, 1539.
- [6] E. B. Fleischer, A. M. Shachter, *Inorg. Chem.* **1991**, 30, 3763.
- [7] X. Chi, A. J. Guerin, R. A. Haycock, C. A. Hunter, L. D. Sarson, *J. Chem. Soc. Chem. Commun.* **1995**, 2567.
- [8] K. Funatsu, A. Kimura, T. Imamura, Y. Sasaki, *Chem. Lett.* **1995**, 765.

- [9] M. Saunders, J. B. Hyne, *J. Chem. Phys.* **1958**, *29*, 1319.
- [10] This crystal structure was solved based on the two zinc(II) porphyrin molecules, and the tetrameric form was obtained by its expansion. This crystal also contains fourteen disordered benzene molecules per tetraporphyrin which fill large empty spaces. Crystal data for **Z1**: $C_{78}H_{70}Zn_2N_{10} \cdot 7C_6H_6$, $M_r = 1825$, crystal from C_6H_6/CH_3CN , crystal dimensions $0.35 \times 0.2 \times 0.2$ mm, space group monoclinic ($P2_1/n$), $a = 13.7485(2)$, $b = 18.3200(3)$, $c = 40.8739(7)$ Å, $\alpha = 90^\circ$, $\beta = 84.1947(3)^\circ$, $\gamma = 90^\circ$, $V = 10242.2(2)$ Å³, $Z = 8$, $\rho_{\text{calcd}} = 2.367$ g cm⁻³; $\mu_{\text{Mo}} = 10.44$ cm⁻¹; $\theta_{\text{max}} = 27.3^\circ$. For 63 126 reflections measured; $R_1 = 0.099$ for 9459 data [$I > 3\sigma(I)$], $wR_2 = 0.143$ for all measured data. The structures of all the compounds were solved by direct methods and refined by F^2 with all observed reflections. All non-hydrogen atoms without disordered *tert*-butyl group and incorporated solvent molecules were refined anisotropically, and hydrogen atoms were added to calculated positions. Programs used were structure determination by SIR92 and refinement by teXane for Windows. CCDC-173782 (**Z1**)₄ contains the supplementary crystallographic data for this paper. These data can be obtained free of charge via www.ccdc.cam.ac.uk/conts/retrieving.html (or from the Cambridge Crystallographic Data Centre, 12, Union Road, Cambridge CB21EZ, UK; fax: (+44) 1223-336-033; or deposit@ccdc.cam.ac.uk).
- [11] A. Nakano, H. Shimidzu, A. Osuka, *Tetrahedron Lett.* **1998**, *39*, 9489.
- [12] a) Y. Deng, C. K. Chang, D. G. Nocera, *Angew. Chem.* **2000**, *112*, 1108; *Angew. Chem. Int. Ed.* **2000**, *39*, 1066; b) N. Aratani, A. Osuka, *Org. Lett.* **2001**, *3*, 4213.
- [13] S. Sakamoto, M. Fujita, K. Kim, K. Yamaguchi, *Tetrahedron* **2000**, *56*, 955. CSI-MS spectrum measurement was performed with sector mass spectrometer (JMS-700, JEOL) equipped with the CSI source. Typical measurement conditions are as follows: (CSI-MS) acceleration voltage, 3.0 kV; needle voltage, 2.9 kV; orifice voltage, 197 V; resolution (10% valley definition), 1000; sample flow, 17 $\mu\text{L min}^{-1}$; solvent, dry THF; concentration, 10 mmol L⁻¹; spray temperature, 4 °C; ion-source temperature, 15 °C.
- [14] This consideration in turn suggests that apparently stronger electronic interactions in the normal *meso-meso*-linked diporphyrins result from the rotational flexibility around the *meso-meso* single bond.
- [15] Selected ¹H NMR signals of the pyridyl groups of (**Z2**)₄ in [D₈]THF; $\delta = 2.62, 3.11, 6.59$, and 6.86 ppm.
- [16] N. Yoshida, A. Osuka, *Tetrahedron Lett.* **2000**, *41*, 9287.

Crystal Engineering of a Nanoscale Kagomé Lattice**

Brian Moulton, Jianjiang Lu, Ranko Hajndl, Srikanth Hariharan, and Michael J. Zaworotko*

What would the properties of materials be if we could really arrange the atoms the way we want them? Although this question is scientifically and technologically topical, it is a

well-known excerpt from the Richard P. Feynman lecture “There’s Plenty of Room at the Bottom”.^[1] Recent advances in our understanding of supramolecular chemistry offer promise that Feynman’s dream will be realized since they have afforded design principles that have provided access to an array of new solid phases with specific and, in many cases, previously unknown molecular topologies. Indeed, as molecular scientists become ever more proficient at the supramolecular synthesis^[2] of new compositions and structures, the question that might now be posed is: “in what manner do we want to arrange the atoms?” In the context of magnetic materials, theorists have provided chemists with an array of target lattices,^[3] and synthetic chemists have developed new strategies for the generation of novel networks that contain magnetic components.^[4–7] Spin-frustrated lattices represent attractive targets that are exemplified by the antiferromagnetic Kagomé lattice.^[8] Herein we present the synthesis, crystal structure, and magnetic properties of, what is to our knowledge, the first example of a nanoscale Kagomé lattice.

The phase is sustained by paramagnetic dicopper(II) tetracarboxylate spin pairs (metal dimers) positioned at the vertices of a Kagomé lattice, and it exploits the concept of self-assembly of nanoscale secondary building units (nSBUs).^[9] It therefore offers a system where the effect of systematically substituting the molecular components can be evaluated. In this context, we compare the magnetic response of the Kagomé lattice arrangement with a system where identical secondary building units (SBUs)^[10] are arranged in a tetragonal 2D configuration, which is not expected to exhibit spin frustration.

We have recently demonstrated that regular molecular squares can self-assemble at their vertices to form square or triangular nSBUs, and that the use of an appropriate template and mild crystallization conditions facilitates the generation of a diverse range of discrete and infinite molecular architectures that are based upon these nSBUs.^[9, 11–13] The ubiquitous dimetal tetracarboxylates $[M_2L_2(O_2CR)_4]$ (L = coordinated ligand, M = transition metal) serve as ideal molecular squares in this context since they are synthetically accessible and, depending upon the metal, offer potential as catalysts^[14] or molecular magnets.^[15, 16] Figure 1 illustrates the two nSBUs that can be generated if the molecular squares are linked by 1,3-benzenedicarboxylate (bdc), that is, at 120° : a square nSBU (a cluster of four square SBUs) or a triangular nSBU (a cluster of three square SBUs). These nSBUs are known to self-assemble to form discrete nanoballs (sustained by both square and triangular nSBUs)^[12] or a tetragonal 2D lattice (sustained by square nSBUs only).^[9] It occurred to us that other supramolecular isomers are possible if triangular nSBUs alone are present: triangular or Kagomé 2D lattices (Figure 2). Few examples of molecular Kagomé lattices have been reported to date,^[17–19] and to our knowledge there have been no reports of a nanoscale lattice, despite the expectation of cooperative magnetic phenomena in such structures.

Slow diffusion of ethanolic copper(II) nitrate into a solution of bdc, pyridine (py), and an appropriate template (nitrobenzene, 1,2-dichlorobenzene, or naphthalene) in ethanol affords prismatic blue-green crystals of $[(Cu_2(py)_2(bdc)_2)_3]_n$ (**1**). The crystal structure of **1**^[20] (Figure 3) can be described as

[*] Prof. Dr. M. J. Zaworotko, B. Moulton, J. Lu
Department of Chemistry
University of South Florida
4202 E. Fowler Ave., SCA 400, Tampa, FL 33620 (USA)
Fax: (+1) 813-974-1733
E-mail: xtal@usf.edu
R. Hajndl, Prof. Dr. S. Hariharan
Department of Physics
University of South Florida
4202 E. Fowler Ave., PHY 114, Tampa, FL 33620 (USA)

[**] M.J.Z. gratefully acknowledges the financial support of the National Science Foundation (DMR-0101641). S.H. acknowledges support from a DARPA/AMRI subcontract (Grant No. MDA 972-97-1-0003).

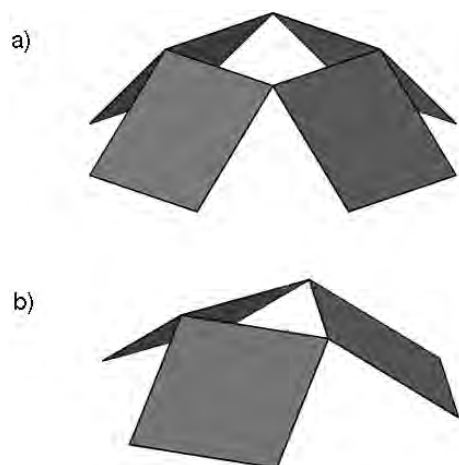


Figure 1. Illustrations of the square (a) and triangular (b) nSBUs that can be formed by linking the vertices of molecular squares.

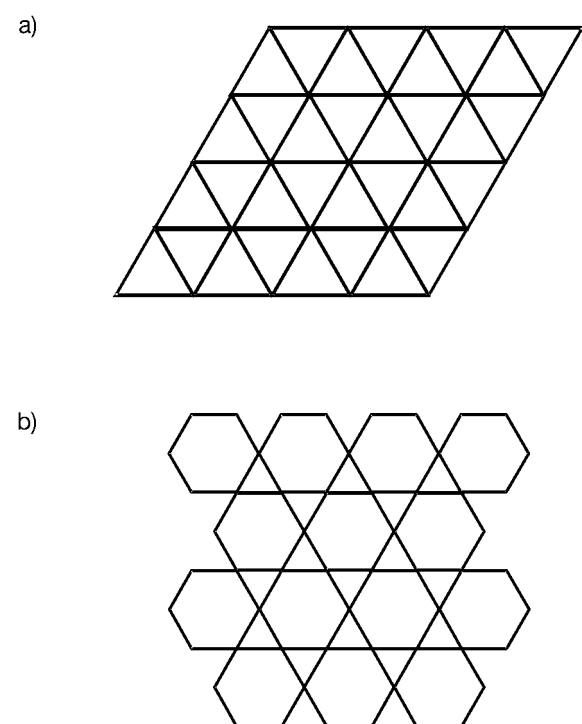


Figure 2. A schematic representation of triangular (a) and Kagomé (b) 2D lattices.

the result of self-assembly of bowl-shaped triangular nSBUs to yield a nanoscale Kagomé lattice. Cu_2 dimers are positioned at the lattice points and are bridged by the bdc ligands, thereby generating large hexagonal cavities within the layer. The bowl-shaped nSBU facilitates efficient packing when the bowls are eclipsed, which results in eclipsing of the hexagonal cavities (0.91 nm effective diameter) and in hexagonal channels of the same dimension. The layers are undulating because of the curvature imparted by the bdc moiety, and have an amplitude of 1.24 nm, with adjacent layers overlapping by approximately 20%. The apical positions of the Cu_2 dimers are occupied by coordinated pyridine ligands, and highly disordered solvent molecules occupy the hexagonal channels (approximately 28% by weight). Thermal analyses

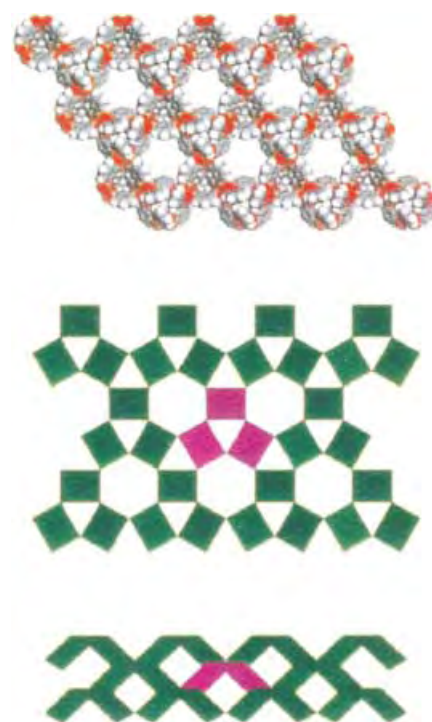


Figure 3. Space-filling and schematic representations of the arrangement of triangular nSBUs in the nanoscale Kagomé lattice structure exhibited by **1**.

(thermogravimetric analysis and differential scanning calorimetry) indicate that the solvent of crystallization and the pyridine ligands can be removed at approximately 200 °C, and that the desolvated lattice is thermally stable at temperatures in excess of 300 °C. The most intense peaks observed in the X-ray powder diffraction patterns from the bulk sample are consistent with those calculated from single-crystal diffraction data. A phase based on square nSBUs, $[((\text{py})_2\text{Cu}_2(\text{bdc})_2)_4]_n$ (**2**), can be obtained under different crystallization conditions.^[9]

The magnetic properties of **1** are featured in Figure 4. The temperature-dependent susceptibility (χ) at a constant field ($H = 0.1$ T) is shown in Figure 4a and the field-dependent magnetization at low temperature ($T = 5$ K) in Figure 4b. The graphs exhibit rich structure that can be associated with the combined intradimer and interdimer magnetic interactions. Cooperative magnetism in complexes based on Cu_2 dimers has been studied in the past and is known to predominantly exhibit antiferromagnetic coupling.^[21, 22]

The temperature-dependent χ shows a maximum just below 300 K and a minimum at around 60 K followed by an upturn at lower temperature. The data presented have been corrected for the diamagnetic contribution. The variation of χ with temperature is consistent with cooperative magnetic behavior observed in dimeric copper complexes. We have used a standard Bleaney–Bowers (BB) model^[23] to generate a fit to our experimental data, and this is also shown in Figure 4. The two main fit parameters are the intradimer (J) and interdimer (J') interaction terms. From our fit, we obtain values of $J = -350$ and $J' = -18 \text{ cm}^{-1}$. Our model also accounts for the presence of uncompensated moments that follow a Curie law.

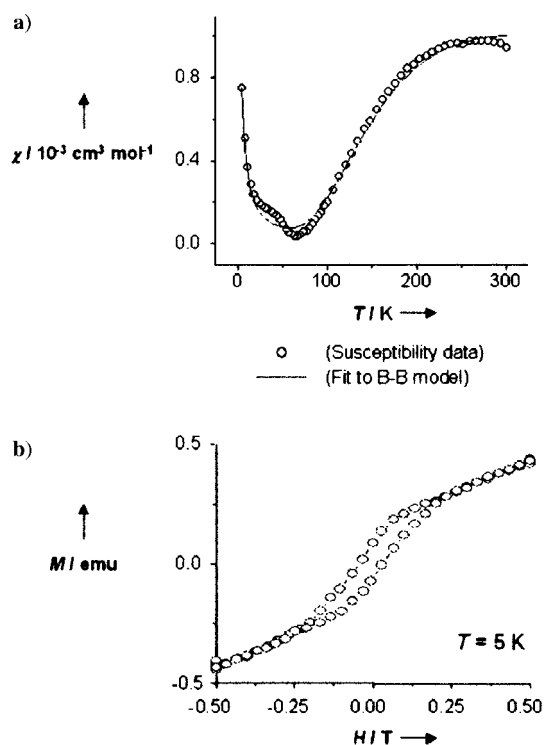


Figure 4. a) The temperature-dependent molar susceptibility (χ , per nSBU) of **1** at 0.1 T (data points) overlaid by a plot of the BB best-fit model (solid line): $J = -350 \text{ cm}^{-1}$ and $J' = -18 \text{ cm}^{-1}$; b) the field-dependent magnetization of **1** at $T = 5 \text{ K}$.

This phenomenon is responsible for the upturn in susceptibility at temperatures below 50 K.

A clue as to the nature of the geometrically frustrated antiferromagnetic state inherent in this compound is revealed on investigation of the field-dependent magnetization data, shown in Figure 4b. A well-defined hysteresis loop is observed which is indicative of ferromagnetic behavior. We have also confirmed the presence of hysteresis at 300 K. In a sense, we have demonstrated herein that it is possible to arrange nanoscale molecular objects (not atoms!) with precise control and achieve periodic magnetic nanostructures.^[24]

Within the context of the triangular Kagomé lattice, we can now attempt to understand the origin of the ferromagnetic-like response leading to magnetic hysteresis. The triangular lattice framework will result in disruption of perfect antiferromagnetic ordering by introducing spin frustration that leads to canted arrangement of spins. Of course, the term “spins” refers here to the moments of the individual dimers. Spin canting can lead to the appearance of effective weak ferromagnetic long-range order. It has also been pointed out that in low-dimensional systems such as semiconductor quantum dots and molecular magnets, electron correlation effects in an antiferromagnetic lattice can lead to flat-band ferromagnetism.^[25]

Phase **2** exhibits an alternative topology to **1**; the 2D square lattice that is shown in Figure 5. In this case, geometry considerations dictate that spin frustration is ruled out, which is reflected in the magnetic measurements shown in Figure 6. To keep our comparison direct and simple, we have plotted molar susceptibility and magnetization data using identical

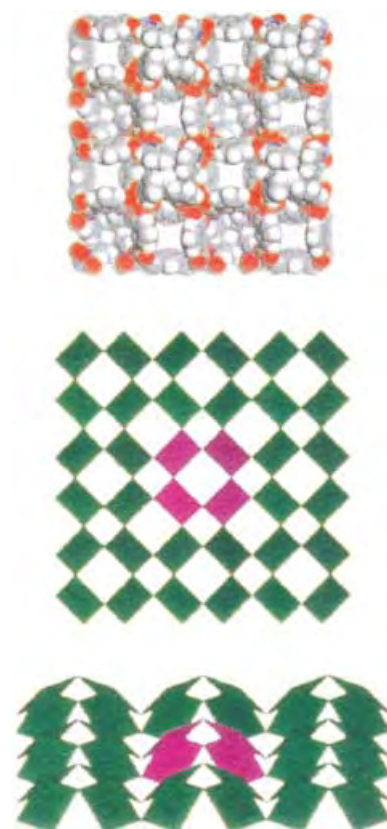


Figure 5. Space-filling and schematic representations of the arrangement of square nSBUs in the nanoscale square lattice structure exhibited by **2**.

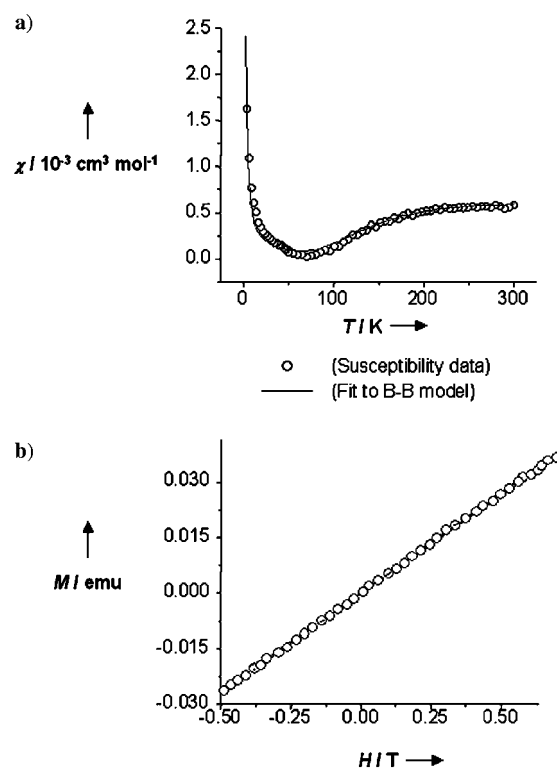


Figure 6. a) The temperature-dependent molar susceptibility (χ , per nSBU) of **2** at 0.1 T (data points) overlaid by a plot of the BB best-fit model (solid line): $J = -380 \text{ cm}^{-1}$ and $J' = -85 \text{ cm}^{-1}$; b) the field-dependent magnetization of **2** at $T = 5 \text{ K}$.

conditions to those described in Figure 4. These magnetic data are very similar to recent experimental results reported by other groups on complexes of Cu₂ dimers.^[26] Theoretical fit using the BB model to the temperature-dependent molar susceptibility data in this case yields fit parameters $J = -380 \text{ cm}^{-1}$ and $J' = -85 \text{ cm}^{-1}$. Clearly, the most striking feature is that the field-dependent magnetization does not display a hysteresis loop in this system, the straight line obtained being representative of a more traditional paramagnetic behavior.

Our results dramatically underscore the potential afforded by supramolecular chemistry for the design of molecular nanostructured assemblies with desirable physical properties, while emphasizing how the composition of a material is not the only feature one must consider when designing a phase that exhibits molecular magnetism. Future work will focus on the modularity of this system and on chemical modification of the components: substituting the metal; changing the coordinated ligand; substituting the bdc ligand; incorporation of different guest molecules. We expect a significant effect on magnetic properties as it has already been shown that simply varying the apical coordinated ligand has a measurable effect on the magnetism exhibited by the SBU used in our study.^[26]

Received: February 7, 2002 [Z18665]

- [1] R. Feynman, *Eng. Sci.* **1960**, 22–36.
- [2] B. Moulton, M. J. Zaworotko, *Chem. Rev.* **2001**, 101, 1629–1658.
- [3] E. Manousakis, *Rev. Mod. Phys.* **1991**, 63, 1–62.
- [4] K. R. Dunbar, *J. Solid State Chem.* **2001**, 159, 251–252.
- [5] E. Coronado, J. R. Galan-Mascaros, C. J. Gomez-Garcia, V. Laukhin, *Nature* **2000**, 408, 447–449.
- [6] S. R. Batten, B. F. Hoskins, B. Moubaraki, K. S. Murray, R. Robson, *Dalton Trans.* **1999**, 2977–2986.
- [7] S. S. Y. Chui, S. M. F. Lo, J. P. H. Charmant, A. G. Orpen, I. D. Williams, *Science* **1999**, 283, 1148–1150.
- [8] I. Syozi, *Prog. Theor. Phys.* **1951**, 6, 306–308.
- [9] S. A. Bourne, J. Lu, A. Mondal, B. Moulton, M. J. Zaworotko, *Angew. Chem.* **2001**, 113, 2111–2113; *Angew. Chem. Int. Ed.* **2001**, 40, 2169–2171.
- [10] D. W. Breck, *Zeolite Molecular Sieves: Structure, Chemistry and Use*, Wiley-Interscience, New York, **1974**.
- [11] J. Lu, A. Mondal, B. Moulton, M. J. Zaworotko, *Angew. Chem.* **2001**, 113, 2171–2174; *Angew. Chem. Int. Ed.* **2001**, 40, 2113–2116.
- [12] B. Moulton, J. Lu, A. Mondal, M. J. Zaworotko, *Chem. Commun.* **2001**, 863–864.
- [13] H. Abourahma, A. W. Coleman, B. Moulton, B. Rather, P. Shahgal-dian, M. J. Zaworotko, *Chem. Commun.* **2001**, 2380–2381.
- [14] D. E. Bergbreiter, M. Morvant, B. Chen, *Tetrahedron Lett.* **1991**, 32, 2731–2734.
- [15] O. Kahn, *Molecular Magnetism*, VCH, Weinheim, Germany, **1993**.
- [16] J. S. Miller, A. J. Epstein, *MRS Bull.* **2000**, 25, 21–28.
- [17] K. Awaga, T. Okuno, A. Yamaguchi, M. Hasegawa, T. Inabe, Y. Maruyama, N. Wada, *Phys. Rev. B* **1994**, 49, 3975–3981.
- [18] A. P. Ramirez, *J. Appl. Phys.* **1991**, 70, 5952–5955.
- [19] M. G. Townsend, G. Longworth, E. Roudaut, *Phys. Rev. B* **1986**, 33, 4919–4926.
- [20] Intensity data for **1** were collected at 173 K on a Bruker SMART-APEX diffractometer using MoK α radiation ($\lambda = 0.7107 \text{ \AA}$): Cu₆C_{123.08}H₅₄N_{9.37}O_{30.73}, 2536.69 g mol⁻¹, trigonal, space group *P*3c1, $a = b = 18.6523(11) \text{ \AA}$, $c = 19.8313(18) \text{ \AA}$, $V = 5975.1(7) \text{ \AA}^3$, $Z = 2$, $\rho_{\text{calcd}} = 1.410 \text{ g cm}^{-3}$, $\mu = 1.128 \text{ mm}^{-1}$, $F(000) = 2556$, $2\theta_{\text{max}} = 50.0^\circ$. Final residuals (for 265 parameters) were $R1 = 0.0491$ for 2112 reflections with $I > 2\sigma I$, and $R1 = 0.0764$, $wR2 = 0.1577$, $\text{GoF} = 0.985$ for all 3520 data. Residual electron density was 0.753 and $-0.574 \text{ e \AA}^{-3}$. Highly disordered solvent molecules in the hexagonal

channels were modeled as a group of variable-occupancy carbon atoms. CCDC-165791 contains the supplementary crystallographic data for this paper. These data can be obtained free of charge via www.ccdc.cam.ac.uk/conts/retrieving.html (or from the Cambridge Crystallographic Data Centre, 12, Union Road, Cambridge CB21EZ, UK; fax: (+44) 1223-336-033; or deposit@ccdc.cam.ac.uk).

- [21] R. W. Jotham, J. A. Marks, S. F. A. Kettle, *Dalton Trans.* **1972**, 428–438.
- [22] M. Kato, H. B. Jonassen, J. C. Fanning, *Chem. Rev.* **1964**, 64, 99–148.
- [23] B. Bleaney, K. D. Bowers, *Proc. R. Soc. London A* **1952**, 214, 451–465.
- [24] S. H. Sun, C. B. Murray, D. Weller, L. Folks, A. Moser, *Science* **2000**, 287, 1989–1992.
- [25] H. Tamura, K. Shiraishi, H. Takayanagi, *Phys. Status Solidi B* **2001**, 224, 723–725.
- [26] X. X. Zhang, S. S. Y. Chui, I. D. Williams, *J. Appl. Phys.* **2000**, 87, 6007–6009.

Substrate Distortion by a β -Mannanase: Snapshots of the Michaelis and Covalent-Intermediate Complexes Suggest a $B_{2,5}$ Conformation for the Transition State

Valérie M.-A. Ducros, David L. Zechel, Garib N. Murshudov, Harry J. Gilbert, Lóránd Szabó, Dominik Stoll, Stephen G. Withers, and Gideon J. Davies*

More than 6000 glycosidase sequences and related open reading frames are currently known. They have been classified into some 85 families based upon amino acid sequence similarities^[1] providing a rich context in which to explore variations in glycosidase mechanism. Experimental demonstration of pyranoside ring conformations along the reaction pathway may assist the design of transition state analogues both as therapeutic agents and mechanistic probes. Here we report the three-dimensional structures of the Michaelis complex and covalent glycosyl–enzyme intermediate for a family-26 β -mannanase, both of which display conformational features never previously seen on any glycosidase. When viewed in light of published work on mannosidase inhibition, this work suggests that the transition state for mannoside

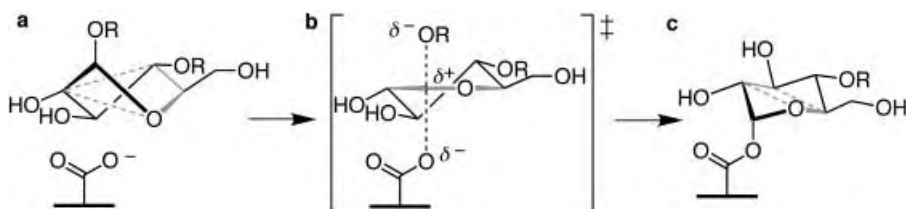
- [*] Prof. G. J. Davies, Dr. V. M.-A. Ducros, Dr. D. L. Zechel, Dr. G. N. Murshudov
Department of Chemistry
Structural Biology Laboratory
The University of York
Heslington, York, YO105DD (UK)
Fax: (+44) 1904-410-519
E-mail: davies@ysbl.york.ac.uk
Prof. H. J. Gilbert, Dr. L. Szabó
Department of Biological and Nutritional Sciences
The University of Newcastle upon Tyne
Newcastle upon Tyne, NE17RU (UK)
Dr. D. Stoll, Prof. S. G. Withers
Department of Chemistry
University of British Columbia
2036 Main Mall, Vancouver, BC, V6T1Z1 (Canada)

Supporting information for this article is available on the WWW under <http://www.angewandte.org> or from the author.

hydrolysis by family-26 enzymes adopts a $B_{2,5}$ boat conformation.

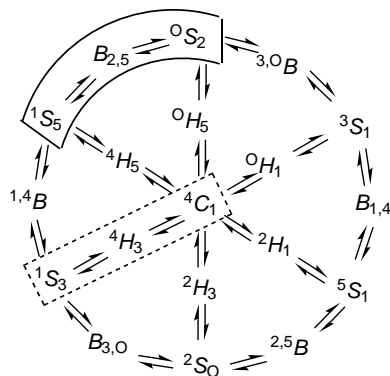
Catalysis by retaining β -glycosidases involves the formation (glycosylation) and subsequent hydrolysis (deglycosylation) of a covalent intermediate flanked by oxocarbenium-like transition states.^[2] Substrate distortion, first proposed for hen egg white lysozyme,^[3] has been unambiguously observed in the high-resolution crystal structures of Michaelis complexes for two structurally unrelated endoglucanases (from glycoside hydrolase families 5 and 7)^[4a,b] and a hexosaminidase (family 20).^[4c] For these enzymes, which work on *gluco*-configured substrates, the unhydrolyzed ligands adopt 1S_3 skew-boat pyranoside conformations (or a closely related 4E envelope) in the -1 subsite (Scheme 1 a) whilst the subsequent covalent intermediates have been observed as undistorted 4C_1 chairs (Scheme 1 c).^[5]

The corresponding transition state, deduced from kinetic isotope effects and inhibitor design, features considerable oxocarbenium character as the anomeric carbon becomes sp^2 hybridized. Such hybridization is best supported if C5, O5, C1, and C2 form a planar array at or near the transition state. The resulting conformation for the transition state is believed to



Scheme 1. Substrate conformations along the glycosylation step of family-5 and -7 retaining cellulases: a) Michaelis complex (1S_3), b) transition state (4H_3), c) covalent intermediate (4C_1). Planes containing four atoms within the pyranoside ring are indicated with gray solid and dashed lines.

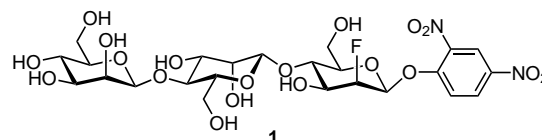
be the 4H_3 half chair (Scheme 1 b), close in conformational space to the 1S_3 skew-boat observed crystallographically.^[4] This implies a $^1S_3 \rightarrow ^4H_3 \rightarrow ^4C_1$ pseudorotational itinerary for the glycosylation step of the retaining mechanism (Scheme 2). Other glycoside conformations can, however, also place the C5, O5, C1, and C2 atoms within a plane, such as the 3H_4 half chair and both $^{2,5}B$ $B_{2,5}$ boats.^[6] Indeed, family-11 xylanases display a covalent xylobiosyl–enzyme intermediate in a $^{2,5}B$ boat conformation,^[7] suggesting that a similar conformation is



Scheme 2. Partial map of pyranoside ring interconversions (adapted from Stoddart^[23]) indicating the proposed cellulase (dashed line) and mannanase (solid line) glycosylation step pathways.

also adopted at the transition state for this class of enzymes, as had previously been suggested for yeast α -glucosidase on the basis of kinetic isotope effects.^[8]

Mannanase 26A (Man26A) from *Pseudomonas cellulosa* is a retaining *endo*- β -(1,4)-mannanase whose general acid–base catalyst and nucleophile have been identified as E212 and E320, respectively.^[9] The three-dimensional structure of the native enzyme has also been reported.^[10] A mechanism-based inactivator of mannanases, 2,4-dinitrophenyl 2-deoxy-2-fluoro- β -mannotrioxide (**1**),^[11] was used to probe the reaction coordinate of the enzyme. Incubation of wild-type Man26A with **1** failed to trap the covalent intermediate, which instead



slowly hydrolyzed as indicated by a steady-state release of dinitrophenolate over time. We followed the example of previous trapping studies^[5] and further slowed the deglycosylation step by eliminating base catalysis with the mutation E212A. Indeed, the intermediate was shown to accumulate on this mutant by ESI mass spectrometry (data not shown). Incubation of crystals of the E212A mutant with **1** for short times, however, resulted in the formation of a Michaelis complex of unhydrolyzed substrate,^[12] analogous to trapping of such species on other systems.^[4] The structure of the resultant Michaelis complex was determined by X-ray crystallography to 1.6 Å resolution. Unhydrolyzed **1** occupied subsites -3 to $+1$ with the DNP glycosidic linkage spanning the -1 and $+1$ subsites. While the -3 and -2 mannopyranoside rings are observed in normal 4C_1 chair conformations, the -1 mannopyranoside ring was clearly distorted from a 4C_1 chair to a 1S_3 skew boat, a conformation never before observed in a glycosidase active site (Figure 1 a, b).

As with the 1S_3 conformations observed previously for *gluco*-configured substrates, the 1S_3 conformation forces the scissile glycosidic bond into an axial position, consistent with stereoelectronic expectations, while simultaneously allowing unrestricted nucleophilic attack by E320 at the opposite face of the anomeric carbon. The remarkable feature of the 1S_3 conformation, however, is its subtle accommodation of both the C2 fluoro and C5 hydroxymethyl substituents of the mannopyranoside ring within favorable pseudo-equatorial positions (Scheme 3 a). The 1S_3 conformation achieves the same stability with *gluco*-configured substrates, which have the opposite configuration at C2. Thus in each case the conformation strikes an ideal balance of reactivity and conformational stability of the C2 and C5 substituents. It is noteworthy that isoquinuclidine **2** (Scheme 4), a potent β -mannosidase inhibitor, adopts a $^{1,4}B$ conformation that is

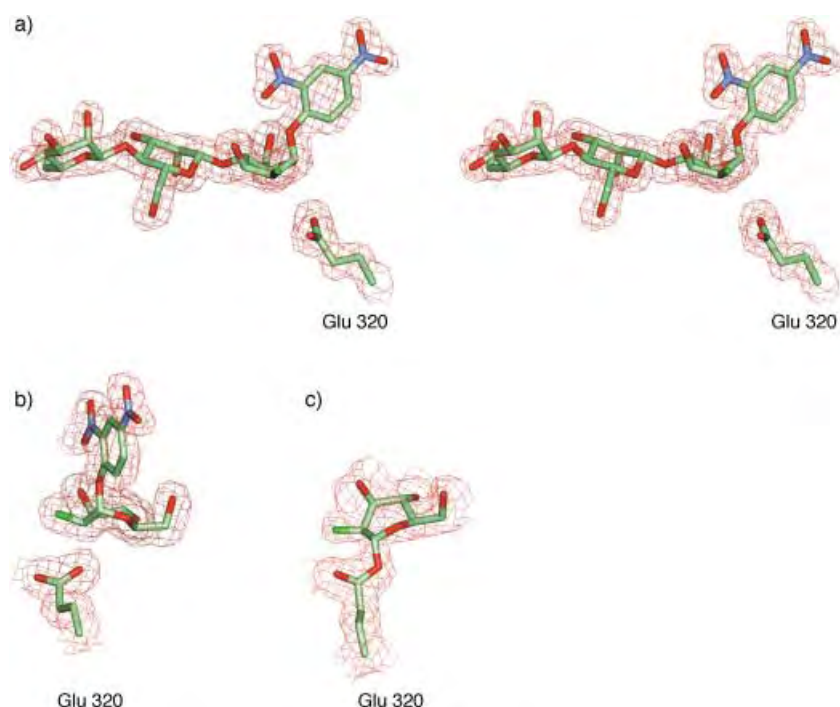
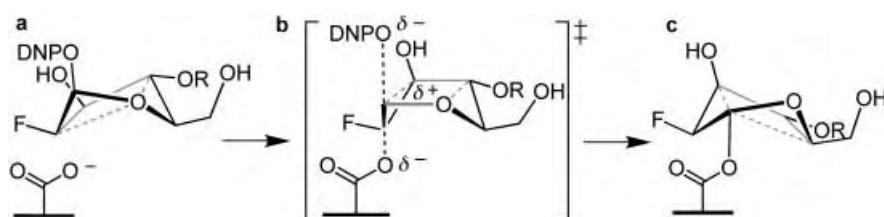
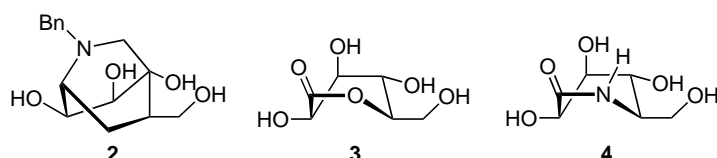


Figure 1. a) Crystal structure of the Man2A E121A complex with unhydrolyzed **1**, Michaelis complex side profile. The map is a maximum-likelihood-weighted $2F_{\text{obs}} - F_{\text{calc}}$ map contoured at 0.6 electrons \AA^{-3} and is shown in divergent (wall-eyed) stereo. b) Front profile of the Michaelis complex. c) Front profile of the covalent 2-fluoromannotriosyl-enzyme intermediate; only the trapped intermediate is shown (for clarity), although electron density reveals that some unhydrolyzed substrate remains with partial ($\sim 50\%$) occupancy.



Scheme 3. Substrate conformations along the glycosylation step of Man26A E121A. a) Michaelis complex (1S_5), b) transition state ($B_{2,5}$), c) covalent intermediate (0S_2). Gray lines indicate planes containing four atoms within the pyranoside ring.



Scheme 4. Observed conformations of mannosidase inhibitors: polyhydroxylated isoquinuclidine (**2**), D-manno-1,5-lactone (**3**), D-manno-1,5-lactam (**4**).

closely related to the high-energy 1S_5 conformation described here.^[13]

Pre-incubation of the acid–base mutant Man26A E121A with **1** prior to crystallization allowed partial^[14] accumulation of a 2-fluoromannotriosyl moiety covalently linked to the nucleophile E320. Intriguingly, the covalently linked –1 mannopyranoside ring was not observed in the expected 4C_1 chair but instead adopts a conformation close to the 0S_2 skew boat (Figure 1c, Scheme 3c).^[15] Together, the intermediate 0S_2 and Michaelis 1S_5 conformations flank the $B_{2,5}$ boat on the

pseudorotational itinerary (Scheme 2). This suggests that the transition state for formation of the mannotriosyl–enzyme intermediate features the $B_{2,5}$ conformation (Scheme 3b). The $B_{2,5}$ boat is also observed for the transition state analogs D-manno-1,5-lactone (**3**)^[16] and D-manno-1,5-lactam (**4**)^[17] both strong inhibitors of β -mannosidases (Scheme 4). In both cases, the conformation of these mannosyl oxocarbenium-ion mimics is dictated by the configuration at C2 as well as C5 (*gluco*-configured lactones and lactams instead assume 4H_3 half chairs),^[18] analogous to the $^{2,5}B$ transition state proposed for family-11 xylanases.^[7]

These unique substrate conformations appear to be favored by His211 and His143 interacting with the 2- and 3-hydroxyl groups, respectively, of the –1 sugar. Both residues have been shown to play significant roles in catalysis^[10] and may well be key determinants in mannanase substrate specificity. As noted above, the 1S_5 mannose and 1S_3 glucose conformations place the 2-hydroxyl group in similar equatorial positions. Indeed, both mannanases and cellulases from clan GH-A typically possess an Asn in an equivalent position to His211 of Man26A, to interact with the 2-hydroxyl group.^[19] In contrast, the 3-hydroxyl group is pseudoaxial in 1S_5 mannoses and pseudoequatorial in 1S_3 glucosides. Thus His143 is observed in a substantially different position relative to equivalent His residues in cellulases.^[4] The discrimination of *gluco*- versus *manno*-configured substrates appears to be transferred along the sugar ring from the 2-hydroxyl to the 3-hydroxyl group as a result of the

differing pyranoside ring conformations. Furthermore, the $B_{2,5}$ and 2S_0 conformations may actually permit close interaction between the pseudoequatorial 2-OH and the carbonyl oxygen of the nucleophile as observed for glucosidases acting on *gluco*-configured substrates.^[5d, 7c]

The assumption that all glycosidases react through the 4H_3 half-chair transition state is incorrect. Indeed, for a mannoside such a conformation results in *syn*-diaxial orientations for the 2-hydroxyl and the leaving group which may instead be alleviated through utilization of a transition state that places the 2-hydroxyl group pseudoequatorial. The 1S_5 and 2S_0 conformations for the Michaelis complex and intermediate, respectively, lie adjacent to the $B_{2,5}$ conformation which is also observed for known transition state analogs of β -mannosidases. Together these data lead us to suggest that the $B_{2,5}$ conformation may be adopted in the transition state for the hydrolysis of β -mannosides and that Man26A follows a reaction coordinate that is distinct from that of glucosidases, cellulases, and xylanases.

Experimental Section

The synthesis of **1** has been described previously.^[11] Details of the recombinant plasmid-encoding Man26A mutant E212A have been described,^[10] and the expression of the protein in *E. coli* and its subsequent purification were carried out as previously reported.^[9]

To obtain the Michaelis complex, a small quantity of powdered **1** was added to the mother liquor surrounding a single crystal of Man26A E212A^[10] and left for 5 min. The crystal was then transferred rapidly to a cryoprotectant stabilizing solution consisting of the crystal growth solution supplemented with 20% (v/v) glycerol prior to mounting in rayon fibre loops and freezing in a boiling nitrogen stream at 100 K. X-ray diffraction data, to 1.6 Å resolution, were collected at the Daresbury Synchrotron Radiation Source (SRS) on beamline PX14.2 using an ADSC (ADSC, Poway, CA, USA) Quad-4 charge-coupled device (CCD) as detector. Data were processed using the HKL suite of programs.^[20] The structure was isomorphous with the native structure described previously^[10] and was refined using REFMAC^[21] from the CCP4 suite.^[22]

Data for the covalent intermediate were obtained by first pre-incubating Man26A E212A with a stoichiometric quantity of **1** for 30 min at 293 K, prior to crystallization as described.^[10] Data were collected to a resolution of 1.65 Å on beamline ID14-2 of the European Synchrotron Radiation Facility, again at 100 K with an ADSC CCD as detector. The structure was refined as described above. Coordinates have been deposited with the Macromolecular Structures Database with accession codes 1gvy (Michaelis complex) and 1gw1 (covalent intermediate). Figure 1 was prepared using QUANTA (Accelrys Inc., San Diego, USA).

Received: March 7, 2002 [Z18846]

- [1] <http://afmb.cnrs-mrs.fr/~cazy/CAZY/>.
- [2] D. L. Zechel, S. G. Withers, *Acc. Chem. Res.* **2000**, 33, 11–18.
- [3] C. C. Blake, D. F. Koenig, G. A. Mair, A. C. North, D. C. Phillips, V. R. Sarma, *Nature* **1965**, 206, 757–761.
- [4] a) G. Sulzenbacher, H. Driguez, B. Henrissat, M. Schülein, G. J. Davies, *Biochemistry* **1996**, 35, 15280–15287; b) G. J. Davies, L. Mackenzie, A. Varrot, M. Dauter, A. M. Brzozowski, M. Schülein, S. G. Withers, *Biochemistry* **1998**, 37, 11707–11713; c) I. Tews, A. Perrakis, A. Oppenheim, Z. Dauter, K. S. Wilson, C. E. Vorgias, *Nat. Struct. Biol.* **1996**, 3, 638–648.
- [5] a) D. H. Juers, T. D. Heightman, A. Vasella, J. D. McCarter, L. Mackenzie, S. G. Withers, B. W. Matthews, *Biochemistry* **2001**, 40, 14781–14794; b) D. J. Vocadlo, G. J. Davies, R. Laine, S. G. Withers, *Nature* **2001**, 412, 835–838; c) W. P. Burmeister, S. Cottaz, P. Rollin, A. Vasella, B. Henrissat, *J. Biol. Chem.* **2000**, 275, 39385–39393; d) G. Sulzenbacher, L. F. Mackenzie, K. S. Wilson, S. G. Withers, C. Dupont, G. J. Davies, *Biochemistry* **1999**, 38, 4826–4833; e) V. Notenboom, C. Birsan, M. Nitz, D. R. Rose, R. A. J. Warren, S. G. Withers, *Nat. Struct. Biol.* **1998**, 5, 812–818; f) V. Notenboom, C. Birsan, R. A. J. Warren, S. G. Withers, D. R. Rose, *Biochemistry* **1998**, 37, 4751–4758; g) L. F. Mackenzie, G. Sulzenbacher, C. Divne, T. A. Jones, H. F. Woldike, M. Schülein, S. G. Withers, G. J. Davies, *Biochem. J.* **1998**, 335, 409–416.
- [6] L. Hosie, P. J. Marshall, M. L. Sinnott, *J. Chem. Soc. Perkin Trans. 2* **1984**, 1121–1131.
- [7] a) E. Sabini, K. S. Wilson, S. Danielsen, M. Schülein, G. J. Davies, *Acta Crystallogr. Sect. D* **2001**, 57, 1344–1347; b) E. Sabini, G. Sulzenbacher, M. Dauter, Z. Dauter, P. L. Jorgensen, M. Schülein, C. Dupont, G. J. Davies, K. S. Wilson, *Chem. Biol.* **1999**, 6, 483–492; c) G. Sidhu, S. G. Withers, N. T. Nguyen, L. P. McIntosh, L. Ziser, G. D. Brayer, *Biochemistry* **1999**, 38, 5346–5354.
- [8] L. Hosie, M. L. Sinnott, *Biochem. J.* **1985**, 226, 437–446.
- [9] D. N. Bolam, N. Hughes, R. Virden, J. H. Lakey, G. P. Hazelwood, B. Henrissat, K. L. Braithwaite, H. J. Gilbert, *Biochemistry* **1996**, 35, 16195–16204.
- [10] D. Hogg, E.-J. Woo, D. N. Bolam, V. A. McKie, H. J. Gilbert, R. W. Pickersgill, *J. Biol. Chem.* **2001**, 276, 31186–31192.
- [11] O. Nashiru, D. L. Zechel, D. Stoll, T. Mohammadzadeh, R. A. J. Warren, S. G. Withers, *Angew. Chem.* **2001**, 113, 431–434; *Angew. Chem. Int. Ed.* **2001**, 40, 417–420.
- [12] In the wild-type^[10] and Michaelis complexes described here a zinc ion binds to the nucleophile and the adjacent His211 and may mask the true interaction of His211 with the 2-substituent. Addition of 2 mM ZnCl₂ (as used in the crystallization conditions) to extensively dialyzed wild-type enzyme results in approximately 50% inhibition. It is unlikely that this zinc plays a catalytic function since upon partial trapping of the intermediate the zinc occupancy reduces by 50%, consistent with the occupancy of the trapped intermediate.^[14]
- [13] E. Lorthiois, M. Meyyappan, A. Vasella, *Chem. Commun.* **2000**, 1829–1830.
- [14] The structure reveals “double occupancy” of a covalent intermediate with the nonhydrolyzed substrate. The crystallographically determined occupancy of the covalent intermediate was approximately 0.5, with the remaining 0.5 accounted by unreacted **1**. This double occupancy is also reflected in two positions for His211 which interacts with 2-F in the intermediate.
- [15] The substitution of fluorine at the 2-position of mannose is unlikely to promote unusual ring conformations. For example, 2-deoxy-2-fluoro-β-mannosyl fluoride adopts a normal ⁴C₁ chair in solution (S. G. Withers, I. P. Street, *Can. J. Chem.* **1986**, 64, 232–236) and the anomeric equilibrium of 2-deoxy-2-fluoromannose is virtually identical to that of mannose (J. Adamson, A. B. Foster, L. D. Hall, R. N. Johnson, R. H. Heese, *Carbohydr. Res.* **1970**, 15, 351–359; L. Phillips, V. Wray, *J. Chem. Soc. B* **1971**, 1618–1624).
- [16] a) Z. Walaszek, D. Horton, I. Ekiel, *Carbohydr. Res.* **1982**, 106, 193–201; b) G. A. Levvy, S. M. Snaith, *Adv. Enzymol.* **1972**, 36, 151–181; c) G. A. Levvy, A. J. Hay, J. Conchie, *Biochem. J.* **1964**, 91, 378–384.
- [17] Y. Nishimura, H. Adachi, T. Satoh, E. Shitara, H. Nakamura, F. Kojima, T. Takeuchi, *J. Org. Chem.* **2000**, 65, 4871–4882.
- [18] It is remarkable that these B_{2,5} conformations are observed in both protic and aprotic solvents as well as in solution and crystalline states. See ref. [16, 17].
- [19] A number of related glycosidases form a clan, “GH-A”, of related structures. B. Henrissat, I. Callebaut, S. Fabrega, P. Lehn, J. P. Mornon, G. J. Davies, *Proc. Natl. Acad. Sci. USA* **1995**, 92, 7090–7094. Enzymes active on both *manno*- and *gluco*-configured substrates appear to share the same recognition elements, typically an invariant Asn or His, around the 2-OH position although family-1 β-mannosidases appear to use an Asp residue to interact with the 2-hydroxyl group which is implicated in mannoside specificity (See T. Kaper, H. H. van Heusden, B. van Loo, A. Vasella, J. van der Oost, W. M. de Vos, *Biochemistry* **2002**, 41, 4147–4155).
- [20] “Macromolecular Crystallography”: Z. Otwinowski, W. Minor, *Methods Enzymol.* **1997**, 276, 307–326.
- [21] G. N. Murshudov, A. A. Vagin, E. J. Dodson, *Acta Crystallogr. Sect. D* **1997**, 53, 240–255.
- [22] “Collaborative Computational Project Number 4”: *Acta Crystallogr. Sect. D* **1994**, 50, 760–763.
- [23] J. F. Stoddart, *Stereochemistry of Carbohydrates*, Wiley-Interscience, Toronto, **1971**.

The Consequences of Chirality in Crowded Arenes—Macromolecular Helicity, Hierarchical Ordering, and Directed Assembly**

Mark L. Bushey, Austin Hwang, Peter W. Stephens, and Colin Nuckolls*

Complex three-dimensional superstructures with useful properties^[1] can be created easily by reversibly assembling functionalized small molecules through hydrogen bonding and π overlap.^[2] Examples are **1a** and **1b** (Figure 1 a), which self-assemble through head-to-tail amide hydrogen bonds into arrays of stacked columns (Figure 1 b, c).^[3] In these molecules, the dodecyl ether substituents provide a liquidlike environment, while at the same time they force the amide groups out

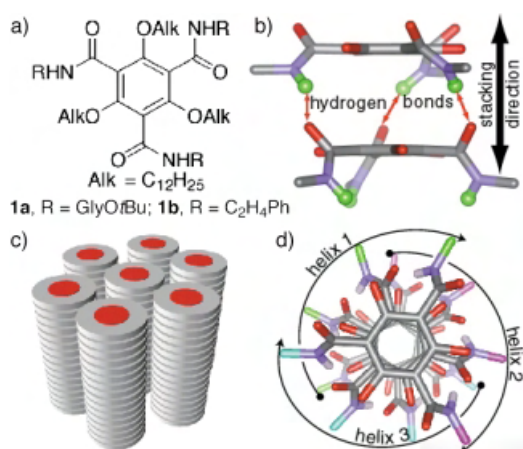


Figure 1. a) Crowded arenes; b) energy-minimized^[18] dimer displaying three intermolecular hydrogen bonds; c) hexagonal arrays; d) model of a tetramer showing three helices of hydrogen bonds surrounding the exterior of the column (methyl groups on the ether oxygen atoms were included in the models and removed to clarify the view).

[*] Prof. C. Nuckolls, M. L. Bushey, A. Hwang

Department of Chemistry
Columbia University
New York, NY 10027 (USA)
<http://nuckolls.chem.columbia.edu>
Fax: (+1) 212-932-1289
E-mail: cn37@columbia.edu

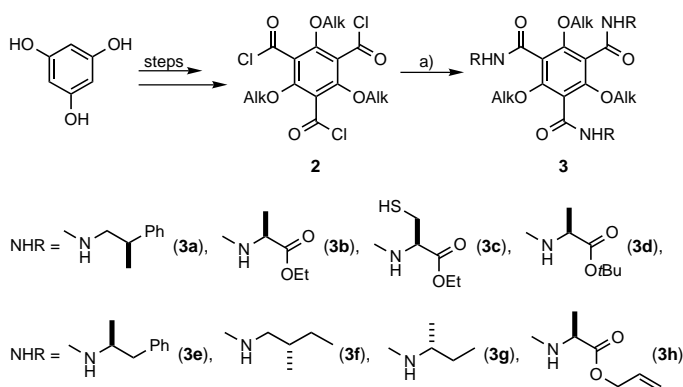
Prof. P. W. Stephens
Department of Physics and Astronomy
State University of New York at Stony Brook
Stony Brook, NY 11974 (USA)

[**] We are grateful to Dana Horoszowski and Dr. Gloria Proni for helpful discussions. We acknowledge financial support from the Chemical Sciences, Geosciences and Biosciences Division, Office of Basic Energy Sciences, US D.O.E. (DE-FG02-01ER15264) and US National Science Foundation, Nanoscale Exploratory Research Grant (DMR-01-02467). We utilized for a portion of this work the shared instrument facility supported by the MRSEC Program of the National Science Foundation (DMR-9809687). The Brookhaven National Laboratory NSLS is supported by the US D.O.E., Divisions of Chemical and Materials Sciences. The SUNY X3 beamline at the NSLS is supported by the Division of Basic Energy Sciences of the US D.O.E. (DE-FG02-86ER45231). A.H. thanks the National Science Foundation–REU Program.

Supporting information for this article is available on the WWW under <http://www.angewandte.org> or from the author.

of the plane of the central aromatic ring. As a consequence, the amide groups are oriented so to form intermolecular hydrogen bonds and therefore stacked structures.^[4, 5] Due to this mode of stacking the columns should have a macroscopic dipole moment parallel to the stacking direction (Figure 1 b).^[6] The study presented here details the macromolecular consequences of synthesizing molecules that are both chiral and liquid crystalline. Neat samples of these mesogens self-assemble into two-dimensional hexagonal arrays that can be directed with electric fields. In dilute solution circular dichroic (CD) spectroscopy shows that the molecules self-assemble into helical stacks. At higher concentrations, these stacks self-organize further into superhelical arrays characteristic of twisted nematic liquid crystals.

For our study we synthesized enantiopure **3a–h** in yields of 47–78 % by combining the versatile tris-acylchloride **2**, which can be made on a multigram scale from phloroglucinol,^[3] with optically active amines^[7] (Scheme 1). The calorimetric values



Scheme 1. a) RNH_2 , Et_3N , CH_2Cl_2 , 47–78 %. $\text{Alk} = \text{C}_{12}\text{H}_{25}$.^[8]

(DSC) for **3a–h**^[8] vary over a broad range, and many samples exhibit rich polymorphism.^[9] One compound, **3a**, emerged as unique from a screening with polarized-light microscopy because it forms a mesophase (191 to 233 °C) that is self-healing and birefringent (Figure 2 a).

It is the fluidity that distinguishes the mesophase of **3a** from all of the others. The synchrotron X-ray diffraction^[10] pattern from **3a** in a Lindemann capillary tube (Figure 2 b) shows an intense, low-angle peak ($d = 18.8 \text{ \AA}$) that is diagnostic of columnar assemblies^[11] and two higher-order reflections that allow the lattice to be indexed as two-dimensional hexagonal. In its wide-angle region, the diffractogram shows only a broad reflection ($d \approx 4.8 \text{ \AA}$) that in columnar liquid crystals has been attributed to the packing of fluid side chains.^[11] These values correlate well with the lattice parameters previously measured for the columnar, hexagonally ordered achiral **1b**.^[3]

Thin samples of **3a**, between ITO-coated glass slides spaced by 5 μm , show uniform birefringent domains that are uniaxial and negatively birefringent (Figure 3 a).^[12] The implication is that the long axes of the columns are parallel to the surface (the planar alignment).^[13] When 30 V is applied between the two electrodes while the material is again cooled into its mesophase, the films are optically isotropic. After removing of the polarizer micron-sized polygons are visible, each having

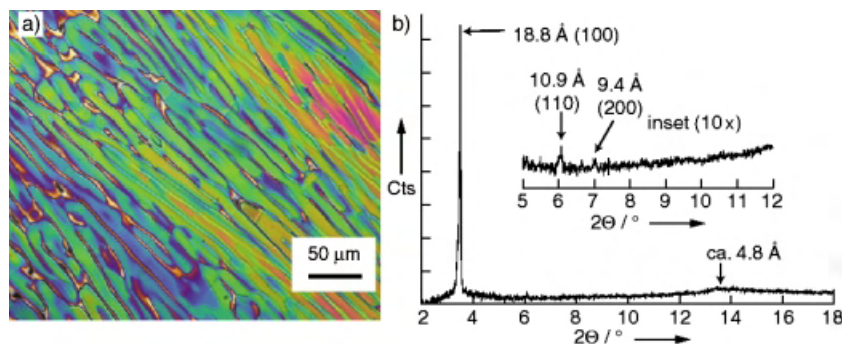


Figure 2. a) View between crossed polarizers at 210 °C as **3a** was cooled from the isotropic liquid. b) Synchrotron X-ray diffraction of **3a** at 220 °C as it was cooled from the isotropic liquid.

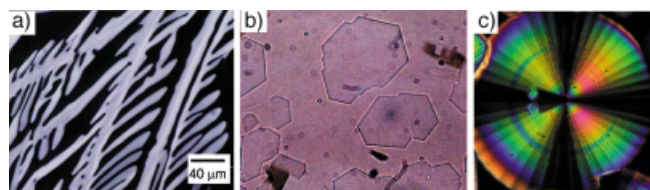


Figure 3. Light micrographs of samples of **3a** cooled to 200 °C from the isotropic liquid: a) optically active, between ITO electrodes separated by 5 μm, 0 V applied; b) optically active, between ITO electrodes separated by 5 μm, 30 V applied; c) racemic **3a** yielding spherulitic crystalline domains.

120° angles at their corners (Figure 3b), reflecting, in magnified form, the underlying hexagonal lattice symmetry.^[14] The implication is that the self-assembly into columns is directed perpendicular to the electrode surface by the applied electric field. When the film is again heated until it is an isotropic liquid and then cooled in the absence of an electric field, the planar alignment returns. Traditionally, discotics are highly viscous and they must be diluted until they are lyotropic nematics to be switched between planar and homeotropic alignments.^[15] What is unique about **3a** is that the entire two-dimensional lattice is directed by the electric field and is regularly arrayed over μm-sized length scales (Figure 3b). Molecular models indicate that polarity in the columns of **3a** results from the head-to-tail orientation of the amide side chains, as shown in Figure 1d, creating a macroscopic dipole moment parallel to the column axis.

Both racemic (\pm)-**3a**^[16] and a sample of **3a** that is a mixture of diastereomers [(dia)-**3a**]^[17] were prepared to test whether the chirality is involved in the liquid crystallinity and polarity of **3a**. The clearing points for pure **3a**, (\pm)-**3a**, and (dia)-**3a** were all within a few degrees indicating that the differences in their assemblies must be slight. The textures displayed by samples of (\pm)-**3a** (Figure 3c) and (dia)-**3a** as they are cooled from their isotropic states are those of spherulitic, crystalline materials. This is the same texture seen previously in the hexagonally ordered plastic crystals of **1b**, whose molecules lack the angular methyl groups.^[3] Neither (\pm)-**3a** nor (dia)-**3a** nor **1b** show an electrical response like that seen for optically active **3a**. The spherulitic textures persist even when up to 100 V is applied between the electrodes. Models, like the one in Figure 1d,^[18] constructed with the optically active side chains of **3a**, show that in the stacked molecules the phenyl groups in the side chains touch the methyl groups of their

nearest neighbors. These interactions provide a mechanism for the optically active side chains to stabilize the helicity of the columns. In the racemic or diastereomeric material, these contacts are absent.

CD spectroscopy^[19] was used to analyze the stacks because it has proven to be a sensitive reporter of helicity, through the coupling of transition dipoles, in polypeptides,^[20] other polymers,^[22–26] and discotic liquid crystals.^[6e, 21] Solutions of **3a** in hexane were not homogeneous but could be made so by dilution with ca. 15 % CH₂Cl₂. At these concentrations, the CD transitions of **3a**

show an exciton coupling between degenerate chromophores (a split CD, Figure 4b) indicative of helical order. As more CH₂Cl₂ is added (30 %), the aggregates dissociate and the transition dipoles no longer couple. Thus, only when the solvent is hydrocarbonlike do the molecules self-assemble through hydrogen bonds with their side chains close enough to interact with each other. Evidence that it is the contact between the methyl and phenyl groups that stabilizes the helices comes from studies with optically active **3f**, whose chirality arises only from the difference between a methyl and an ethyl group. It has no phenyl group in the side chains and its mesophase, shown in Figure 6a, looks like that of achiral **1a**.^[3]

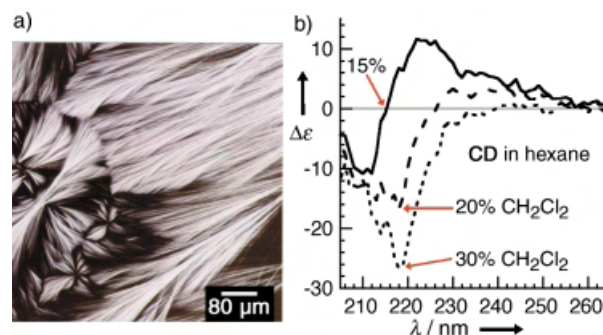


Figure 4. a) Polarized-light micrograph of fibrous **3a** grown from a hot dodecane solution; b) CD spectra of **3a** in hexane (7.5×10^{-4} M, path length = 100 μm).

If the aggregates of **3a** are helical and have a significant persistence length, they could display the common assembly motif of helically wound polymers that pack next to one another with defined twist angles.^[22–26] As this twist is propagated through the assembly, it gives rise to a superhelical structure (Figure 5c) like that of a twisted nematic liquid crystal. This type of liquid crystalline phase is uncommon in classic discotics possibly due to the low association in the stacking direction. Unfortunately, concentrated solutions of **3a** could not be tested for such a phase behavior because **3a** is insufficiently soluble in hydrocarbon solvents. (It forms the fibrous aggregates shown in Figure 4a.) However, **3a** is soluble up to 50 wt % in dodecane when it is mixed with **1a**! We presume this is because **1a** frustrates the ability of **3a** to crystallize from hydrocarbon solvent into fibers.

The CD spectra of dilute solutions of the **1a/3a** mixture are split, just like the spectra of **3a** discussed above. At high concentrations, the samples visibly reflect green light. Their CD spectra, an example of which is in Figure 5d, show intense

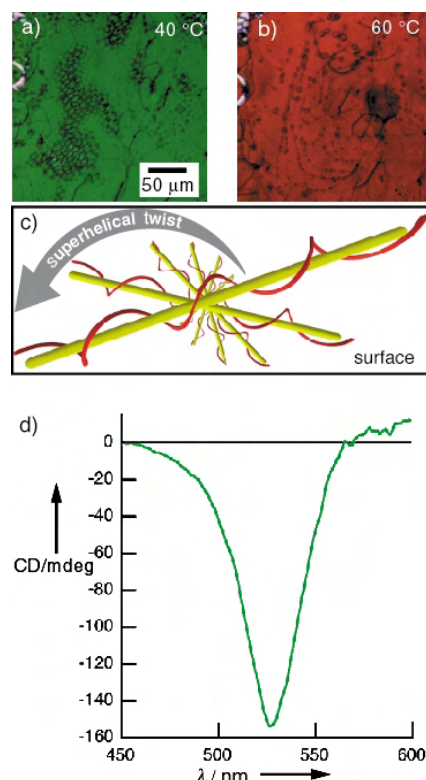


Figure 5. Studies on **3a/1a** (25% each by weight) solutions in dodecane. a) Polarized-light micrograph at 40 °C, b) at 60 °C; c) model of the superhelical arrangement of columns; d) CD spectrum at room temperature.

transitions at 525 nm,^[27] attributed to the selective reflection of circularly polarized light by the twisted nematic phase.^[28] The superhelical pitch expands when the temperature is raised, so the reflection is green at room temperature (Figure 5a) and red at 60 °C (Figure 5b). Concentrated **1a/3d** mixtures in dodecane display a “fingerprint” texture also characteristic of twisted nematic liquid crystals.^[29] Twisted nematic phases are rare for self-assembled columnar structures,^[21a] and the reason for their being seen in this study is that the hydrogen bonds working in concert with the chiral side chains enforce a regular helicity and a high association constant in the stacking direction. In essence, the aggregates in solution act as noncovalent polymers.^[28]

It is remarkable that just moving the methyl group in the amide side chain from the β position in **3a** to the α position in **3e** changes the morphologies drastically as shown in Figures 2a and 6b. In fact, with the exception of the extremely hindered **3d**, all the molecules with chiral centers adjacent to the nitrogen atom (**3b, c, e, g, h**) lead to μm -sized birefringent fibers as the materials are cooled from their isotropic liquid states. Like the fibers from other columnar systems,^[13] these too are uniaxial and negatively birefringent.^[12] X-ray diffraction shows these fibrous samples to consist of a two-dimensional hexagonal lattice of columns. Unlike the diffractogram

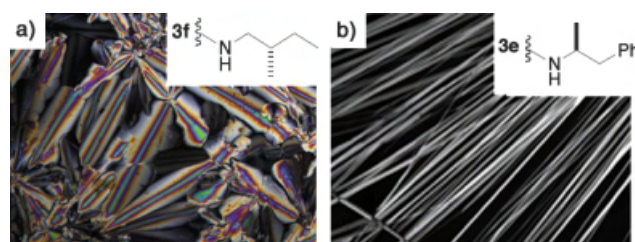


Figure 6. View between crossed polarizers as the samples were cooled from the isotropic liquid. a) **3f** at 197 °C; b) **3e** at 246 °C.

of the liquid crystalline phase of **3a**, the ones from the fibers of **3b, c, e, g, h** reveal larger lattice spacings and contain numerous, sharp higher-order reflections indicative of a crystalline phase with the columns running parallel to the fiber axis.^[13c, 30] These results show how seemingly minor variations in molecular structure can have drastic impacts on the resulting morphology and phase behavior.

In summary, we have shown that chiral side chains can be easily installed into the crowded nucleus of **1** and that they control the hierarchy of ordering in the stacks. First, the chiral centers in the side chains organize the columns into helices. These chiral columns further stack in concentrated solutions to create superhelical arrangements that reflect circularly polarized light at resonant wavelengths. In the neat samples the materials self-organize into hexagonally arranged fibers or liquid crystalline phases depending on where the chiral center is positioned. Some of these chiral phases are responsive to electric fields and their assembly can be directed from electrode surfaces. It is possible that these nanostructured columns may act as ferroelectric, piezoelectric, and other types of responsive materials.

Received: March 26, 2002 [Z18983]

- [1] a) G. M. Whitesides, J. P. Mathias, C. T. Seto, *Science* **1991**, 254, 1312–1319; b) J.-M. Lehn, *Supramolecular Chemistry*, VCH, Weinheim, **1995**; c) D. Philp, J. F. Stoddart, *Angew. Chem.* **1996**, 108, 1242–1286; *Angew. Chem. Int. Ed. Engl.* **1996**, 35, 1155–1196; d) M. Muthukumar, C. K. Ober, E. L. Thomas, *Science* **1997**, 277, 1225–1232.
- [2] Hydrogen bonds in liquid crystals: a) T. Kato in *Handbook of Liquid Crystals*, Vol. 2b (Eds.: D. Demus, J. W. Goodby, G. W. Gray, H. W. Spiess, V. Vill), Wiley-VCH, Weinheim, **1998**, pp. 969–979; b) A. H. Simmons, C. A. Michal, L. W. Jelinski, *Science* **1996**, 271, 84–87; c) C. M. Paleos, D. Tsiourvas, *Angew. Chem.* **1995**, 107, 1839–1855; *Angew. Chem. Int. Ed. Engl.* **1995**, 34, 1696–1711; d) V. V. Tsukruk, *Prog. Polym. Sci.* **1997**, 22, 247–311; e) C. Fouquey, J.-M. Lehn, A.-M. Levelut, *Adv. Mater.* **1990**, 2, 254–257; f) T. Gulik-Krzywicki, C. Fouquey, J.-M. Lehn, *Proc. Natl. Acad. Sci. USA* **1993**, 90, 163–167; g) R. K. Castellano, C. Nuckolls, S. H. Eichhorn, M. R. Wood, A. J. Lovinger, J. Rebek, Jr., *Angew. Chem.* **1999**, 111, 2764–2768; *Angew. Chem. Int. Ed.* **1999**, 38, 2603–2606.
- [3] M. L. Bushey, A. Hwang, P. W. Stephens, C. Nuckolls, *J. Am. Chem. Soc.* **2001**, 123, 8157–8158.
- [4] Leading references on discotic liquid crystals: a) D. Guillon, *Struct. Bonding* **1999**, 95, 41–82; b) S. Chandrasekhar, G. S. Ranganath, *Rep. Prog. Phys.* **1990**, 53, 57–84.
- [5] Amides used to organize discotic liquid crystals: a) C. M. Paleos, D. Tsiourvas, *Angew. Chem.* **1995**, 107, 1839–1855; *Angew. Chem. Int. Ed. Engl.* **1995**, 34, 1696–1711, and references therein; b) Y. Matsunaga, N. Miyajima, Y. Nakayasu, S. Sakai, M. Yonenaga, *Bull.*

- Chem. Soc. Jpn.* **1988**, *61*, 207–210; c) A. R. A. Palmans, J. A. J. M. Vekemans, H. Fischer, R. A. Hikmet, E. W. Meijer, *Chem. Eur. J.* **1997**, *3*, 300–307; d) M.-J. Brienne, J. Gabard, J.-M. Lehn, I. Stibor, *J. Chem. Soc. Chem. Commun.* **1989**, 1868; e) D. Goldmann, R. Dietel, D. Janietz, C. Schmidt, J. H. Wendorff, *Liq. Cryst.* **1998**, *24*, 407–411; f) G. Ungar, D. Abramic, V. Percec, J. A. Heck, *Liq. Cryst.* **1996**, *21*, 73–86; g) V. Percec, C.-H. Ahn, T. K. Bera, G. Ungar, D. J. P. Yearley, *Chem. Eur. J.* **1999**, *5*, 1070–1083; h) L. Brunsveld, H. Zhang, M. Glasbeek, J. A. J. M. Vekemans, E. W. Meijer, *J. Am. Chem. Soc.* **2000**, *122*, 6175–6182, and references therein; i) J. Malthête, A. M. Levelut, L. Liebert, *Adv. Mater.* **1992**, *4*, 37–41; j) D. Pucci, M. Veber, J. Malthête, *Liq. Cryst.* **1996**, *21*, 153–155.
- [6] Similar to the dipole moment that is generated in the following systems: a) vanadyl liquid crystals: D. Kilian, D. Knowby, M. A. Athanassopoulou, S. T. Trzaska, T. M. Swager, S. Wrobel, W. Haase, *Liq. Cryst.* **2000**, *27*, 509–521; b) pyramidal liquid crystals: H. Zimmermann, R. Poupko, Z. Luz, J. Billard, *Z. Naturforsch. A* **1985**, *40*, 149–160; c) J. Malthête, A. Collet, *J. Am. Chem. Soc.* **1987**, *109*, 7544–7545; d) helicene liquid crystals: C. Nuckolls, T. J. Katz, *J. Am. Chem. Soc.* **1998**, *120*, 9541–9544.
- [7] All of the amines were commercially available in nonracemic form with the exception of the one that yields **3d**. It was synthesized by a known procedure: D. A. Quagliato, P. M. Andrae, E. M. Matelan, *J. Org. Chem.* **2000**, *65*, 5037–5042.
- [8] Detailed synthetic procedures and differential scanning calorimetry (DSC) data are contained in the Supporting Information.
- [9] Their transition enthalpies vary between 1 and 40 kJ mol⁻¹. The low-temperature phases in samples that display several phase transitions are difficult to characterize because their powder X-ray diffractograms are extremely complex and their morphology is that of small grains.
- [10] Samples were loaded into 1 mm Lindemann capillary tubes that were rotated during data acquisition to eliminate any artifacts due to preferential alignment.
- [11] a) A. M. Levelut, *J. Chim. Phys. Phys.-Chim. Biol.* **1983**, *80*, 149–161; b) the citations in ref. [4].
- [12] N. H. Hartshorne, A. Stuart, *Crystals and the Polarising Light Microscope*, 3rd ed., Edward Arnold Ltd., London, **1960**, p. 290 ff.
- [13] Negatively birefringent discotics and discotic fibers: a) C. Vauchier, A. Zann, P. Le Barny, J. C. Dubois, J. Billard, *Mol. Cryst. Liq. Cryst.* **1981**, *66*, 423–433; b) A. J. Lovinger, C. Nuckolls, T. J. Katz, *J. Am. Chem. Soc.* **1998**, *120*, 264–268.
- [14] Hexagonal domains are an indicator of homeotropic alignment in discotics: a) C. Destrade, P. Foucher, H. Gasparoux, H. T. Nguyen, A. M. Levelut, J. Malthête, *Mol. Cryst. Liq. Cryst.* **1984**, *106*, 121–146; b) J. Billard, J. C. Dubois, H. T. Nguyen, A. Zann, *Nouv. J. Chim.* **1978**, *2*, 535–540; c) Y. Bouligand, *J. Phys.* **1980**, *41*, 1307–1315; d) S. D. Hudson, H. T. Jung, V. Percec, W.-D. Cho, G. Johansson, G. Ungar, V. S. K. Balagurusamy, *Science* **1997**, *278*, 449–452; e) V. Percec, G. Johansson, G. Ungar, J. Zhou, *J. Am. Chem. Soc.* **1996**, *118*, 9855–9866.
- [15] a) C. Nuckolls, R. Shao, W.-G. Jang, N. A. Clark, D. M. Walba, T. J. Katz, *Chem. Mater.* **2002**, *14*, 773–776; b) A. R. A. Palmans, J. A. J. M. Vekemans, R. A. Hikmet, H. Fischer, E. W. Meijer, *Adv. Mater.* **1998**, *10*, 873; c) N. Usol'tseva, G. Hauck, H. D. Koswig, K. Praefcke, B. Heinrich, *Liq. Cryst.* **1996**, *20*, 731; d) D. Krücker, P. Rudquist, S. T. Lagerwall, H. Sawade, G. Heppke, *Ferroelectrics* **2000**, *243*, 207.
- [16] Racemic mixtures were made by mixing equimolar amounts of the optically pure enantiomers.
- [17] A mixture of diastereomers was synthesized by using a racemic mixture of a chiral amine to react with the tris-acylchloride **2**.
- [18] Molecular modeling performed with MacroModel Version 7.0 (Amber*): F. Mohamadi, N. G. J. Richards, W. C. Guida, R. Liskamp, M. Lipton, C. Caufield, G. Chang, T. Hendrickson, W. C. Still, *J. Comput. Chem.* **1990**, *11*, 440–467.
- [19] N. Harada, K. Nakanishi, *Circular Dichroic Spectroscopy–Exciton Coupling in Organic Stereochemistry*, University Science Books, Mill Valley, CA, **1983**.
- [20] C. Branden, J. Tooze, *Introduction to Protein Structure*, 2nd ed, Garland Publishing, New York, NY, **1998**.
- [21] Similar to the enhancements seen with other chiral columnar aggregates: a) G. Gottarelli, E. Mezzina, G. P. Spada, F. Carsughi, G. Di Nicola, P. Mariani, A. Sabatucci, S. Bonazzi, *Helv. Chim. Acta* **1996**, *79*, 220, and references therein; b) A. R. A. Palmans, J. A. J. M. Vekemans, E. E. Havinga, E. W. Meijer, *Angew. Chem.* **1997**, *109*, 2763–2765; *Angew. Chem. Int. Ed. Engl.* **1997**, *36*, 2648; c) S. T. Trzaska, H.-F. Hsu, T. M. Swager, *J. Am. Chem. Soc.* **1999**, *121*, 4518–4519; d) C. F. van Nostrum, A. W. Bosman, G. H. Gelinck, P. G. Schouten, J. M. Warman, A. P. M. Kentgens, M. A. C. Devillers, A. Meijerink, S. J. Picken, U. Sohling, A.-J. Schouten, R. J. M. Nolte, *Chem. Eur. J.* **1995**, *1*, 171–182; e) H. Engelkamp, C. F. van Nostrum, R. J. M. Nolte, S. J. Picken, *Chem. Commun.* **1998**, *9*, 979–980.
- [22] A. A. Kornyshev, S. Leikin, *Phys. Rev. E* **2000**, *62*, 2576–2596, and references therein.
- [23] DNA and nucleic acid derivatives: a) F. Livolant, A. M. Levelut, J. Doucet, J. P. Benoit, *Nature* **1989**, *339*, 724; b) K. Merchant, R. L. Rill, *Biophys. J.* **1997**, *73*, 3154–3163; c) R. L. Rill, F. Livolant, H. C. Aldrich, M. W. Davidson, *Chromosoma* **1989**, *98*, 280–286; d) G. Gottarelli, G. Proni, G. P. Spada, S. Bonazzi, A. Garbesi, F. Ciuchi, P. Mariani, *Biopolymers* **1997**, *42*, 561–574; e) G. Proni, G. Gottarelli, P. Mariani, G. P. Spada, *Chem. Eur. J.* **2000**, *6*, 3249–3253.
- [24] In polypeptides: a) D. B. DuPré, E. T. Samulski in *Liquid Crystals—The Fourth State of Matter* (Ed.: F. Saeva), Dekker, New York, NY, **1979**; b) T. Hashimoto, S. Ebisu, N. Inaba, H. Kawai, *Polym. J.* **1981**, *13*, 701–713.
- [25] a) X. M. Dong, D. G. Gray, *Langmuir* **1997**, *13*, 3029–3034; b) T. Sato, J. Nakamura, A. Teramoto, M. M. Green, *Macromolecules* **1998**, *31*, 1398–1405.
- [26] T. Sato, Y. Sato, Y. Umemura, A. Teramoto, Y. Nagamura, J. Wagner, D. Weng, Y. Okamoto, K. Hatada, M. M. Green, *Macromolecules* **1993**, *26*, 4551–4559.
- [27] Although the CD spectra of all the rotations were very similar, the spectrum displayed in Figure 5d is an average of 24 rotations each through 15° to eliminate any artifacts from linear dichroism, a procedure similar to that of experiments with linear polymers and aggregates: a) A. Schoenhofer, H. G. Kuball, *Chem. Phys.* **1987**, *115*, 159–167; b) B. Norden, *Acta Chem. Scand.* **1972**, *26*, 1763–1776; c) M. J. B. Tunis-Schneider, M. F. Maestre, *J. Mol. Biol.* **1970**, *52*, 521–541; d) D. G. Cornell, *Colloid Interface Sci.* **1979**, *70*, 167–180; e) C. Nuckolls, T. J. Katz, T. Verbiest, S. Van Elshocht, H.-G. Kuball, S. Kieweswaller, A. J. Lovinger, A. Persoons, *J. Am. Chem. Soc.* **1998**, *120*, 8656–8660.
- [28] J. S. Moore, *Curr. Opin. Colloid Interface Sci.* **1999**, *4*, 108–116.
- [29] For selective reflection and fingerprint textures from twisted nematics see: H. Coles in *Handbook of Liquid Crystals*, Vol. 2b, (Eds.: D. Demus, J. W. Goodby, G. W. Gray, H. W. Spiess, V. Vill), Wiley-VCH, Weinheim, **1998**, pp. 335–409.
- [30] Similar to the orientation described in: a) M. R. Ghadiri, J. R. Granja, R. A. Milligan, D. E. McRee, N. Khazanovich, *Nature* **1993**, *366*, 324–327; b) H. Engelkamp, S. Middelbeek, R. J. M. Nolte, *Science* **1999**, *284*, 785–788; c) I. S. Choi, X. Li, E. E. Simanek, R. Akaba, G. M. Whitesides, *Chem. Mater.* **1999**, *11*, 684–690.

C₂-Symmetric Chiral Pentacyclic Guanidine: A Phase-Transfer Catalyst for the Asymmetric Alkylation of *tert*-Butyl Glycinate Schiff Base**

Tetsuya Kita, Angelina Georgieva, Yuichi Hashimoto, Tadashi Nakata, and Kazuo Nagasawa*

Phase-transfer catalysts (PTCs) have been recognized as useful reagents in synthetic organic chemistry. Since reactions that involved the use of PTCs have many advantages over homogeneous reactions, and PTCs are environmentally friendly as non-metal-containing organocatalysts, many efficient PTCs and related reaction systems have been explored.^[1] In particular, the development of enantioselective reactions that use effective chiral PTCs is an important and challenging issue in synthetic organic chemistry.^[2] Several chiral PTCs have been reported so far, most of which were developed from the cinchona alkaloid structure. The enantioselective alkylation of the *tert*-butyl glycinate benzophenone Schiff base **2** (Table 1) under biphasic conditions with *N*-benzylcinchonium salt catalyst was first reported in 1989 by O'Donnell et al.^[3] They improved the catalyst by using O-alkyl derivatives of the cinchona alkaloid,^[4] and recently, Corey et al.^[5] and Lygo et al.^[6] independently reported so-called third-generation catalysts in which a 9-anthracenyl-methyl group was introduced to mask the nitrogen face, thus inducing a high enantiomeric excess. In 1999, Maruoka and co-workers introduced a new PTC, a chiral C₂-symmetric ammonium salt with a binaphthyl structure, for alkylation of glycine derivative.^[7] This catalyst afforded a high enantiomeric excess of alkylated compounds under mild conditions (0 °C), with a short reaction time.

The guanidine group, which contributes to the stabilization of three-dimensional structures in proteins, is a superbase^[8] that forms stabilized complex salts with anionic compounds through parallel interactions, including hydrogen bonding. These features suggest that the guanidine-containing molecules can be used as new "reaction vessels". Indeed, several synthetic applications have been reported with guanidines and amidines as catalysts.^[9–13] In the course of our studies aimed at the development of new organocatalysts, we recently reported the novel C₂-symmetric chiral cyclic guanidine compounds **1a–c** as hetero Michael reaction catalysts (Figure 1).^[14] The structures of these catalysts **1a–c**

are based on the parent skeleton of the marine natural product ptilomycin A^[15] and related compounds,^[16] and were designed rationally to have a C₂-symmetric chiral reaction cavity around the substrate recognition/activation site (guanidine function). These catalysts **1a–c** effectively accelerated the hetero Michael reaction, depending on their cavity size,^[14] although no asymmetric inductions were observed. Since these results suggested the involvement of complex formation between guanidine salts **1a–c** and the substrate under these reaction conditions, possible applications of these new chiral catalysts **1a–c** in organic synthesis were intriguing. Herein, we wish to describe the first example of the enantioselective alkylation of the *tert*-butyl glycinate benzophenone Schiff base **2** in the presence of chiral pentacyclic guanidines **1a–c** as novel chiral PTCs.

The chiral pentacyclic guanidines **1a–c**, which have different cavity sizes around the central guanidine group, were prepared as described before.^[14, 17] Previous X-ray crystallographic analysis of **1a–c** (Figure 1) revealed that the **1a** and

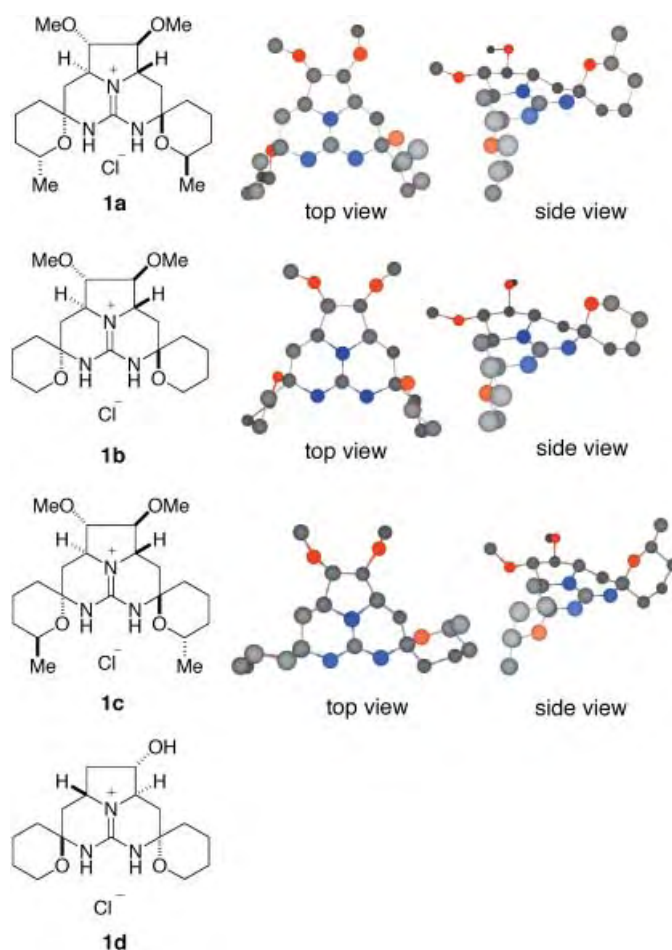


Figure 1. Novel guanidine-type PTCs and their X-ray structures.

1b have a closed-type cavity, whereas **1c** has an open-type cavity (top views).^[14] The spiro ether rings of **1a–c** and the methyl substituents on the spiro ether rings of **1a** and **1c** are directed vertically up and/or down with respect to the guanidine plane (side views).^[14] Thus, these catalysts are expected to show some asymmetric induction through steric

[*] Prof. Dr. K. Nagasawa, T. Kita, Prof. Dr. Y. Hashimoto
Institute of Molecular and Cellular Biosciences,
University of Tokyo

1-1-1 Yayoi, Bunkyo-ku, Tokyo 113-0032 (Japan)

Fax: (+81) 3-5841-8495

E-mail: nagasawa@iam.u-tokyo.ac.jp

Dr. A. Georgieva, Prof. Dr. T. Nakata

RIKEN (The Institute of Physical and Chemical Research)

2-1 Hirosawa, Wako, Saitama 351-0198 (Japan)

[**] We thank Toray Co., Ltd. for an Award in Synthetic Organic Chemistry, Japan and the Pharmacy Research Encouragement Foundation for their financial support. This research was also supported in part by a Grant-in-Aid for Encouragement of Young Scientists from the Ministry of Education, Culture, Sports, Science, and Technology of Japan.

hindrance at this cavity if the reaction proceeds at the substrate-activation site, that is, the guanidine moiety.

Firstly, alkylation of **2** with benzyl bromide (2 equiv) in the presence of a catalytic amount of **1a–d** was examined in an aqueous 1M KOH/dichloromethane (volume ratio 1:1) biphasic solution system at room temperature (Table 1). In the

Table 1. Alkylation of the Schiff base **2** with BnBr in the presence of PTC **1**.

2 $\xrightarrow[\text{BnBr (2 equiv.)}]{\text{1 (30 mol%)}} \text{CH}_2\text{Cl}_2\text{-KOH aq}$ **(R)-3a**

PTC	<i>T</i> [°C]	<i>t</i> [h]	Yield [%]	<i>ee</i> [%] ^[a]
1a	RT	140	90	81
1a	0	160	55	90
1b	0	140	64	13
1c	0	140	65	12
1d	0	140	50	7 (S)

[a] The enantiomeric excess of **3a** was determined by HPLC analysis of the alkylated imine with a chiral column (DAICEL Chiralcel OD) with hexane/2-propanol as the solvent. The absolute configuration was determined by comparison of the HPLC retention time and $[\alpha]_D$ value with the reported data of an authentic sample.^[5a]

presence of catalyst **1a** (10 mol %), the alkylation product **3a** was obtained in 70 % yield and 75 % *ee*, with the *R* isomer as the major component. An increase in the amount of catalyst **1a** to 30 mol % resulted in a higher yield (90 %) and *ee* value (81 % *ee*). A decrease in the temperature to 0 °C improved the asymmetric induction of (*R*)-**3a** to 90 % *ee*.^[18] The use of cesium hydroxide^[5a] or more concentrated aqueous KOH instead of 1M KOH solution caused decomposition of the catalysts. Alkylation reactions of **2** in the presence of the structurally related PTCs **1b–d**^[14] under the optimized conditions (30 mol % of **1** at 0 °C), were then examined, and the results are summarized in Table 1. The use of catalysts **1b** and **1c** led to the formation of (*R*)-**3a** with 13 % and 12 % *ee*, respectively. Catalyst **1d**, which has exactly the same type of cavity as **1b** but with the opposite stereochemical configurations around the guanidine moiety, led to the formation of (*S*)-**3a** with 7 % *ee*.

These observations indicate that the newly generated stereochemistry of the alkylated product **3a** is controlled by the configuration of the spiro ether rings of the pentacyclic guanidine core structure of the PTC **1** (**1b** versus **1d**). Furthermore, the substituent (methyl group) on the spiro ether rings of PTC **1** plays a critical role in effective asymmetric induction of (*R*)-**3a** (**1a** versus **1b**). As shown in Figure 2, the transition state of this alkylation reaction can be considered to arise as follows: the base form of the PTC **1a** or **1b**, generated from the corresponding guanidinium salt in aqueous potassium hydroxide, forms a complex with the *Z* enolate of **2** through ionic and hydrogen-bonding interactions, and the electrophile (benzyl bromide) approaches from the less hindered face (upper surface in this case) of this complex to give the alkylation product **3a**. Thus, (*R*)-**3a** was generated as the major alkylated product (Figure 2).^[19] The methyl groups on the spiro ether rings of **1a** are remarkably

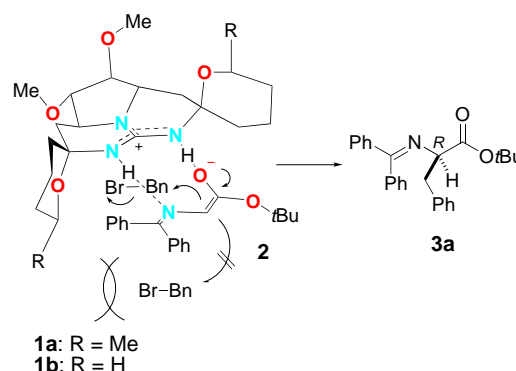


Figure 2. Alkylation mechanism of **2** with benzyl bromide in the presence of pentacyclic guanidine catalysts **1a** and **1b**.

effective as sterically hindering groups to control the electrophile approach, which results in a very high level of asymmetric induction. Moreover, the closed-type cavity of **1a** is also important for the high asymmetric induction of the alkylated product **3a** (**1a** versus **1c**). Thus, for high asymmetric induction in this alkylation reaction, both closed-type cavity structure and substituents at suitable positions on the spiro ether rings of the pentacyclic guanidine PTC **1** seem to be mandatory.

The results of the alkylation of **2** with various alkyl halides (5 equiv) in the presence of PTC **1a** are summarized in Table 2. In all cases examined, the alkylation products **3** were obtained with high enantiomeric excesses (76–90 % *ee*), which indicates the general applicability of this asymmetric reaction system. It should also be noted that these PTCs can be recovered easily in almost quantitative yield by the use of silica-gel column chromatography.

Table 2. Alkylation of the Schiff base **2** with electrophiles in the presence of PTC **1a**.

2 $\xrightarrow[\text{CH}_2\text{Cl}_2/\text{KOH (aq.)}]{\text{1a (30 mol%)}} \text{RX (5 equiv.), 0}^\circ\text{C}$ **(R)-3**

RX	<i>t</i> [h]	Product	Yield [%]	<i>ee</i> [%] ^[a]
MeI	145	3b	80	76
OctI	145	3c	83	80
	140	3d	61	81
	145	3e	85	81
	160	3f	72	79
	145	3g	84	81
	40	3h	80	82
	95	3i	81	90

[a] The enantiomeric excesses of **3** were determined by HPLC analysis of the alkylated imine with a chiral column (DAICEL Chiralcel OD) with hexane/2-propanol as the solvent. The absolute configurations were determined by comparison of the HPLC retention time and $[\alpha]_D$ value with the reported data of an authentic sample.^[5a, 20]

In conclusion, we have successfully employed the new type of chiral guanidine PTC **1** for the enantioselective alkylation reaction of the glycinate benzophenone Schiff base **2**, and high asymmetric induction was obtained in the case of **1a**. This catalyst can be modified easily by changing the stereochemistries and the positions of the substituents on the spiro ether rings to provide appropriate cavity sizes for other reaction substrates, and therefore should be applicable to the alkylation of other substrates or to other asymmetric reactions. Our studies into these reactions will be reported in due course.

Experimental Section

Typical procedure: A solution of the glycine imine **2** (0.03 mmol) in dichloromethane (0.15 mL) was treated sequentially with the guanidine catalyst **1** (0.01 mmol), alkylating agent (0.06 mmol), and an aqueous solution of potassium hydroxide (1M, 0.15 mL). The resulting mixture was stirred vigorously at 0 °C for 140 h. The aqueous layer was then extracted with dichloromethane (3 × 2 mL), and the combined organic layer was dried over MgSO₄ and concentrated under reduced pressure. The crude product was purified by column chromatography on silica gel (ethyl acetate/hexanes 1:12) to give **3**. The enantiomeric excess of **3** was determined by the use of chiral HPLC analysis (DAICEL CHIRALCEL OD-H, 0.46 cm (Ø) × 25 cm (L), *n*-hexane/2-propanol 100:1, flow rate = 0.5 mL min⁻¹).^[5a, 20]

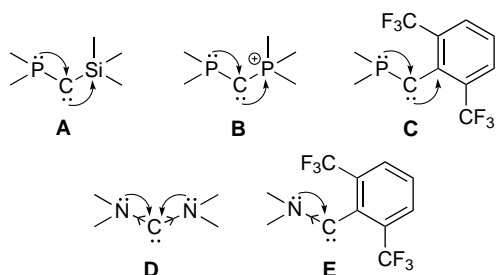
Received: March 14, 2002 [Z18894]

- [1] a) *Phase-Transfer Catalysis: Mechanisms and Syntheses* (Ed.: M. E. Halpern), American Chemical Society, Washington, DC, **1997**; b) *Handbook of Phase-Transfer Catalysis* (Ed.: Y. Sasson, R. Neumann), Chapman & Hall, London, **1997**; c) E. V. Dehmlow, S. S. Dehmlow, *Phase Transfer Catalysis*, 3rd ed., VCH, Weinheim, **1993**.
- [2] a) M. J. O'Donnell in *Catalytic Asymmetric Synthesis*, 2nd ed. (Ed.: I. Ojima), VCH, New York, **2000**, pp. 725–755; b) A. Nelson, *Angew. Chem.* **1999**, *111*, 1685–1687; *Angew. Chem. Int. Ed.* **1999**, *38*, 1583–1585; c) T. Shioiri in *Handbook of Phase Transfer Catalysis* (Ed.: Y. Sasson, R. Neumann), Chapman & Hall, London, **1997**, pp. 462–479; d) H.-U. Blaser, *Tetrahedron: Asymmetry* **1991**, *2*, 843–866.
- [3] M. J. O'Donnell, W. D. Bennett, *J. Am. Chem. Soc.* **1989**, *111*, 2353–2355.
- [4] M. J. O'Donnell, S. Wu, C. Hoffman, *Tetrahedron* **1994**, *50*, 4507–4518.
- [5] a) E. J. Corey, F. Xu, M. C. Noe, *J. Am. Chem. Soc.* **1997**, *119*, 12414–12415; b) E. J. Corey, M. C. Noe, F. Xu, *Tetrahedron Lett.* **1998**, *39*, 5347–5350; c) E. J. Corey, Y. Bo, J. Busch-Petersen, *J. Am. Chem. Soc.* **1998**, *120*, 13000–13001.
- [6] a) B. Lygo, P. G. Wainwright, *Tetrahedron Lett.* **1997**, *38*, 8595–8598; b) B. Lygo, J. Crosby, J. A. Peterson, *Tetrahedron Lett.* **1999**, *40*, 1385–1388; c) B. Lygo, *Tetrahedron Lett.* **1999**, *40*, 1389–1392.
- [7] T. Ooi, M. Kameda, K. Maruoka, *J. Am. Chem. Soc.* **1999**, *121*, 6519–6520.
- [8] M. Costa, G. P. Chiusoli, D. Taffurelli, G. Dalmonego, *J. Chem. Soc. Perkin Trans. 1* **1998**, 1541–1546.
- [9] a) V. Alcazar, J. R. Moran, J. Mendoza, *Tetrahedron Lett.* **1995**, *36*, 3941–3944; b) A. Howard-Jones, P. J. Murphy, D. A. Thomas, *J. Org. Chem.* **1999**, *64*, 1039–1041; c) D. Ma, K. Cheng, *Tetrahedron: Asymmetry* **1999**, *10*, 713–719; d) T. Ishikawa, Y. Araki, T. Kumamoto, H. Seki, K. Fukuda, T. Isobe, *Chem. Commun.* **2001**, 245–246.
- [10] a) T. Schuster, M. Bauch, D. Durner, M. W. Gobel, *Org. Lett.* **2000**, *2*, 179–181; b) T. Schuster, M. Kurz, M. W. Gobel, *J. Org. Chem.* **2000**, *65*, 1697–1701.
- [11] a) M. S. Iyer, K. M. Gigstad, N. D. Namdev, M. Lipton, *J. Am. Chem. Soc.* **1996**, *118*, 4910–4911; b) E. J. Corey, M. Grogan, *J. Org. Lett.* **1999**, *1*, 157–160.
- [12] R. Chinchilla, C. Najera, P. Sanchez-Agullo, *Tetrahedron: Asymmetry* **1994**, *5*, 1393–1402.
- [13] D. Simoni, M. Rossi, R. Rondanin, A. Mazzali, R. Baruchello, C. Malagutti, M. Roberti, R. B. Invidiata, *Org. Lett.* **2000**, *2*, 3765–3768.
- [14] K. Nagasawa, A. Georgieva, H. Takahashi, T. Nakata, *Tetrahedron* **2001**, *57*, 8959–8964.
- [15] Y. Kashman, S. Hirsh, O. J. McConnell, I. Ohtani, T. Kusumi, H. Kakisawa, *J. Am. Chem. Soc.* **1989**, *111*, 8925–8926.
- [16] a) E. A. Jares-Erijman, A. L. Ingrim, J. R. Carney, K. L. Rinehart, R. Sakai, *J. Org. Chem.* **1993**, *58*, 4805–4808; b) R. G. S. Berlinck, J. C. Braekman, D. Daloze, I. Bruno, R. Riccio, S. Ferri, S. Spampinato, E. Speroni, *J. Nat. Prod.* **1993**, *56*, 1007–1015.
- [17] K. Nagasawa, A. Georgieva, T. Nakata, *Tetrahedron* **2000**, *56*, 187–192.
- [18] The use of toluene instead of dichloromethane led to an increase in the enantiomeric excess of **3** to 95 %, although the chemical yield was 20 %, even after 160 h.
- [19] The asymmetric induction of the alkylation reaction with the cinchona-alkaloid-type or binaphthyl-type PTCs is explained by the complex with the *E* enolate of Schiff base **2**.^[5a,7] In our case, the *Z* enolate of **2** would be generated by forming the complex with the guanidine-type PTC **1** through the two parallel ionic and hydrogen-bonding attractions. The asymmetric alkylation results of **2** also support this hypothesis. More detailed investigations are currently underway in our laboratories.
- [20] T. Okino, Y. Takemoto, *Org. Lett.* **2001**, *3*, 1515–1517.

Stable Non-Push–Pull Phosphanylcarbenes: NMR Spectroscopic Characterization of a Methylcarbene**

Emmanuelle Despagne, Heinz Gornitzka, Alexander B. Rozhenko, Wolfgang W. Schoeller, Didier Bourissou, and Guy Bertrand*

Carbenes are compounds with a neutral dicoordinate carbon atom featuring either two singly occupied nonbonding orbitals (triplet state) or both a lone pair and an accessible vacant orbital (singlet state). The recent preparation of persistent triplet diarylcarbenes^[1] and isolation of singlet carbenes^[2] represent spectacular achievements. The former are potential building units for organic magnets,^[3] while the latter, when used as ligands for transition metal centers, afford complexes with enhanced catalytic activities.^[4] All of the stable singlet carbenes known to date possess bulky protecting groups and follow, to some extent, Pauling's predictions^[5] that the substituents should preserve the electroneutrality of the carbene center (Scheme 1). This situation is apparent for

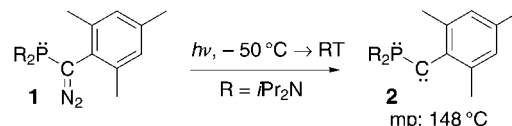


Scheme 1. Stable singlet carbenes **A**–**E**.

push–pull carbenes **A**–**C**,^[6–8] in which the carbene bears both a π -donating and a π -withdrawing substituent. Carbenes **D**^[9] have two π -donor substituents, and are sometimes referred to as push–push carbenes, but the amino groups also act as strong σ -electron-withdrawing substituents. Lastly, carbene **E**^[10] features a spectator substituent and an amino group, which is again both a π donor and σ attractor. Here we report the synthesis of stable and persistent carbenes featur-

ing a π - and σ -donor phosphanyl group and a spectator substituent, including a methyl group.

We first investigated the synthesis of a phosphanylcarbene featuring an electron-rich aryl group. The phosphanyl(mesityl)carbene (**2**) was generated by photolysis (254 nm, -50°C) of a tetrahydrofuran solution of the corresponding diazo compound **1** (Scheme 2). The ^{31}P and ^{13}C NMR chemical



Scheme 2. Synthesis of the phosphanyl(mesityl)carbene **2**.

shifts of **2** (^{31}P : $\delta = -23.5$ ppm; ^{13}C : $\delta = 151.1$ ppm) compare well with those observed for neutral push–pull phosphanylcarbenes **A** and **C**^[2a] (^{31}P : $\delta = -40$ to -20 ppm; ^{13}C : $\delta = 120$ to 150 ppm). The only noticeable difference is the magnitude of the coupling constant between the phosphorus atom and the carbene center, which is significantly smaller for **2** ($J_{\text{PC}} = 65$ Hz) than for **A** ($J_{\text{PC}} = 150$ – 200 Hz) and **C** ($J_{\text{PC}} = 271$ Hz). Although these data are difficult to rationalize (it is not possible to predict the influence of orbital, spin-dipolar, Fermi contact, nor higher order quantum mechanical contributions to the magnitude of the coupling constants), it is likely to indicate some peculiarity in the electronic structure of **2**.

Pale yellow crystals of **2** suitable for an X-ray diffraction study were obtained by cooling a saturated pentane solution to -80°C . The molecular structure of **2** is shown in Figure 1.^[11] As expected, because of the donation of the lone pair

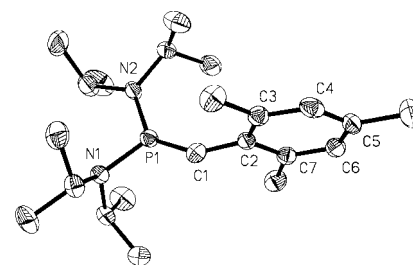


Figure 1. Thermal ellipsoid diagram (50% probability) of **2**. For clarity the hydrogen atoms are omitted. Selected bond lengths [Å] and angles [°]: P1–N1 1.678(2), P1–N2 1.661(2), P1–C1 1.564(3), C1–C2 1.438(3); N1–P1–C1 120.09(13), N2–P1–C1 134.24(13), N1–P1–N2 105.44(11), P1–C1–C2 148.7(2).

of electrons on the phosphorus atom into the vacant orbital of the carbene, the phosphorus atom is in a planar environment and the P1–C1 bond length is short (1.564(3) Å). The P1–C1–C2 angle ($148.7(2)^\circ$) is significantly smaller than in **C** ($162.1(3)^\circ$); the C1–C2 bond length (1.438(3) Å) is in the range typical for $\text{C}(\text{sp}^2)$ – $\text{C}(\text{sp}^2)$ single bonds, and is longer than that observed for the push–pull system **C** (1.390(4) Å). These results strongly suggest the absence of delocalization of the lone pair of electrons on the carbene into the aromatic ring. In other words, the carbene center interacts only with the phosphanyl group, while the mesityl substituent remains merely an electronic spectator.

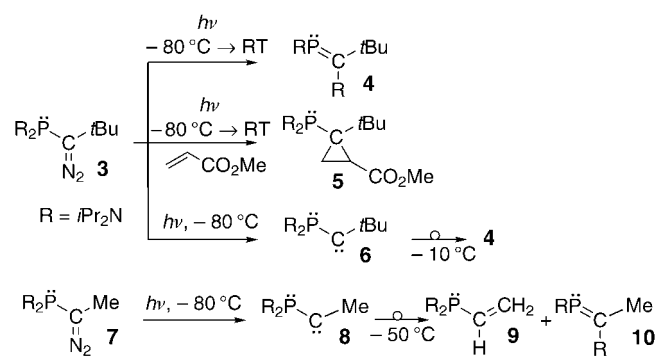
[*] Prof. G. Bertrand
UCR-CNRS Joint Research Chemistry Laboratory (UMR 2282)
Department of Chemistry
University of California, Riverside, CA 92521-0403 (USA)
Fax: (+1) 909-787-2725
E-mail: gbertran@mail.ucr.edu

Prof. G. Bertrand, E. Despagne, Dr. H. Gornitzka, Dr. D. Bourissou
Laboratoire d'Hétérochimie Fondamentale et
Appliquée du CNRS (UMR 5069)
Université Paul Sabatier
118, route de Narbonne, 31062 Toulouse Cedex 04 (France)

Dr. A. B. Rozhenko, Prof. W. W. Schoeller
Fakultät für Chemie der Universität Bielefeld
Postfach 10 01 31, 33615 Bielefeld (Germany)

[**] Financial support of this work by the Centre National de la Recherche Scientifique, the University Paul Sabatier (France), the University of California at Riverside, and the Deutsche Forschungsgemeinschaft is gratefully acknowledged.

Direct observation of singlet alkylcarbenes usually requires matrix-isolation conditions.^[12] Indirect observation and kinetic measurements in solution can be performed by laser-flash photolysis (LFP) using the pyridine ylide method.^[13] By incorporating the π -donating and σ -attracting methoxy substituent, Moss et al. were able to characterize the methoxy-(methyl)carbene MeOCMe by UV and IR spectroscopies, but only in a nitrogen matrix (at 10 K) or in solution, thanks to a nanosecond time-resolved LFP technique ($t_{1/2} < 2 \mu\text{s}$ at 20°C).^[14] The remarkable stability of carbene **2** both in the solid state (m.p. 148°C) and in solution (no degradation observed after several weeks at room temperature) prompted us to investigate the preparation of phosphanyl(alkyl)carbenes. Photolysis (254 nm, -80°C) of a toluene solution of the phosphanyl(*tert*-butyl)diazomethane **3**^[15] afforded the phosphalkene **4** in near quantitative yield upon warming to room temperature. Cyclopropane **5** was obtained in high yield when the low-temperature photolysis of **3** was performed in the presence of methyl acrylate (Scheme 3).^[16] These results



Scheme 3. Synthesis and reactivity of the phosphanyl(alkyl)carbenes **6** and **8**.

suggested the transient formation of the phosphanyl(*tert*-butyl)carbene **6**.^[17] This alkylcarbene could indeed be characterized spectroscopically by multinuclear NMR spectroscopy at low temperature (-50°C). The ^{31}P NMR chemical shift ($\delta = -36.4$ ppm) is in the expected range, while the ^{13}C NMR chemical shift ($\delta = 186.3$ ppm) is the highest reported for a phosphanylcarbene. The small coupling constant ($^1J_{\text{PC}} = 32$ Hz) is consistent with that observed for **2**.

Although the alkylcarbene **6** rearranges within a few minutes above -10°C to afford the 1,2-migration product **4**, it is still observable by ^{31}P NMR spectroscopy below -20°C . We thus decided to reduce the steric hindrance of the spectator alkyl group, and hence studied the photolysis of the phosphanyl(methyl)diazomethane (**7**)^[18] (254 nm, -85°C , toluene solution). A 1.6:1 mixture of derivatives **9**^[19] and **10**, which results from the 1,2-migration of a hydrogen atom and an amino group, respectively, was obtained on warming the solution to room temperature. The corresponding phosphanyl(methyl)carbene (**8**) was characterized spectroscopically at -85°C . The ^{31}P and ^{13}C NMR data for **8** (^{31}P : $\delta = -17.8$ ppm; ^{13}C : $\delta = 164.8$ ppm, $^1J_{\text{PC}} = 44$ Hz) are similar to those for **6**. Despite the poor steric protection and the potential to undergo 1,2-shifts,^[20, 21] the methylcarbene **8** could be ob-

served by ^{31}P NMR spectroscopy up to -50°C ($t_{1/2} \sim 10$ min at -50°C), where it quickly isomerizes.

The preparation of stable or persistent non-push–pull phosphanyl(aryl)- and phosphanyl(alkyl)carbenes demonstrates that a single substituent with even relatively weak π - and σ -donor effects allows for the spectroscopic characterization of singlet carbenes under standard laboratory conditions. Since the steric bulk of the spectator substituent can be decreased even to the size of a methyl group, these results open the way to a variety of new “observable” carbenes and consequently to new synthetic developments and applications in various fields.

Experimental Section

All reactions and manipulations were carried out under an atmosphere of dry argon, by using standard Schlenk techniques.

1: A solution of the lithium salt of hexamethyldisilazane ((Me_2Si)₂NLi·Et₂O; 0.27 g, 1.1 mmol) in diethyl ether (4 mL) was added to a solution of mesityldiazomethane^[22] (0.18 g, 1.1 mmol) in diethyl ether (3 mL) at -78°C . The reaction mixture was kept at this temperature for 1 h, before bis(diisopropylamino)chlorophosphane (0.29 g, 1.1 mmol) was added. After 30 min, the reaction mixture was allowed to warm to room temperature over a period of 1 h. After evaporation of the solvent under vacuum, the residue was extracted with pentane (20 mL) and filtered on neutral alumina. Orange crystals of **1** (0.2 g, 47%) were obtained by recrystallization from acetonitrile (10 mL) at -20°C : m.p. 120°C ; $^{31}\text{P}\{^1\text{H}\}$ NMR (CDCl_3): $\delta = 63.1$ ppm; IR (diethyl ether): $\tilde{\nu} = 2031$ cm^{-1} (CN_2); UV (toluene): $\lambda_{\text{max}} = 291$ nm.

2: A solution of **1** (100 mg, 0.26 mmol) in pentane (3 mL) was irradiated (254 nm) at -50°C for 6 h. Pale yellow crystals of **2** (33 mg, 35%) were obtained by cooling the reaction mixture to -80°C : m.p. 148°C ; $^{31}\text{P}\{^1\text{H}\}$ NMR (C_6D_6): $\delta = -23.5$ ppm; $^{13}\text{C}\{^1\text{H}\}$ NMR (C_6D_6): $\delta = 151.1$ ppm (d, $^1J_{\text{PC}} = 65$ Hz, $\text{C}_{\text{carbene}}$).

4: A solution of **3**^[15] (0.12 g, 0.37 mmol) in tetrahydrofuran (4 mL) was irradiated (254 nm) at -80°C for 4 h, and then warmed to room temperature. ^{31}P NMR spectroscopy indicated the quantitative formation of the corresponding phosphalkene **4**: $^{31}\text{P}\{^1\text{H}\}$ NMR (C_7D_8): $\delta = 268.5$ ppm; $^{13}\text{C}\{^1\text{H}\}$ NMR (C_7D_8): $\delta = 204.2$ (d, $^1J_{\text{PC}} = 69$ Hz, $\text{C}=\text{P}$), 44.5 (d, $^2J_{\text{PC}} = 5$ Hz, $\text{C}(\text{CH}_3)_3$), 31.2 ppm (s, $\text{C}(\text{CH}_3)_3$); elemental analysis calcd (%) for $\text{C}_{17}\text{H}_{37}\text{N}_2\text{P}$ (300.47): C 67.96, H 12.41, N 9.32; found: C 67.64, H 12.27, N 9.68.

5: A solution of **3**^[15] (0.12 g, 0.37 mmol) and methyl acrylate (0.16 g, 1.83 mmol) in tetrahydrofuran (4 mL) was irradiated (254 nm) at -80°C for 4 h, before warming to room temperature. After evaporation of the solvent and excess methyl acrylate, **5** was obtained as a yellow oil (0.1 g, 70%) by extraction with pentane (20 mL): $^{31}\text{P}\{^1\text{H}\}$ NMR (C_7D_8): $\delta = 71.8$ ppm; $^{13}\text{C}\{^1\text{H}\}$ NMR (C_7D_8): $\delta = 51.6$ (s, OCH_3), 30.1 (s, $\text{CH}(\text{ring})$), 19.2 ppm (s, $\text{CH}_2(\text{ring})$); elemental analysis calcd (%) for $\text{C}_{21}\text{H}_{43}\text{N}_2\text{O}_2\text{P}$ (386.56): C 65.25, H 11.21, N 7.25; found: C 64.88, H 11.07, N 7.51.

9 and **10:** A solution of **7**^[18] (0.14 g, 0.49 mmol) in toluene (2 mL) was irradiated (254 nm) at -80°C for 6 h, before warming to room temperature. ^{31}P NMR spectroscopy indicated the formation of vinylphosphane **9**^[19] and phosphalkene **10** as the major products (1.6:1). **10:** $^{31}\text{P}\{^1\text{H}\}$ NMR (C_7D_8): $\delta = 146.5$ ppm; $^{13}\text{C}\{^1\text{H}\}$ NMR (C_7D_8): $\delta = 203.7$ (d, $^1J_{\text{PC}} = 72$ Hz, $\text{C}=\text{P}$), 20.0 ppm (d, $^2J_{\text{PC}} = 4$ Hz, CCH_3).

Received: May 3, 2002 [Z19219]

- [1] a) H. Tomioka, *Acc. Chem. Res.* **1997**, *30*, 315; b) H. Tomioka in *Advances in Carbene Chemistry*, Vol. 2 (Ed.: U. H. Brinker), Jai, Stamford, **1998**, p. 175; c) H. Tomioka, E. Iwamoto, H. Itakura, K. Hirai, *Nature* **2001**, *412*, 626; d) H. Tomioka, T. Watanabe, M. Hattori, N. Nomura, K. Hirai, *J. Am. Chem. Soc.* **2002**, *124*, 474.

- [2] a) D. Bourissou, O. Guerret, F. P. Gabbaï, G. Bertrand, *Chem. Rev.* **2000**, *100*, 39; b) A. J. Arduengo III, *Acc. Chem. Res.* **1999**, *32*, 913.
- [3] a) H. Iwamura, N. Koga, *Acc. Chem. Res.* **1993**, *26*, 346; b) J. Veciana, H. Iwamura, *MRS Bull.* **2000**, *25*, 41.
- [4] a) W. A. Herrmann, C. Köcher, *Angew. Chem.* **1997**, *109*, 2256; *Angew. Chem. Int. Ed. Engl.* **1997**, *36*, 2162; b) W. A. Herrmann, T. Weskamp, V. P. W. Bohm, *Adv. Organomet. Chem.* **2001**, *48*, 1; c) W. A. Herrmann, *Angew. Chem.* **2002**, *114*, 1342; *Angew. Chem. Int. Ed.* **2002**, *41*, 1290.
- [5] L. Pauling, *J. Chem. Soc. Chem. Commun.* **1980**, 688.
- [6] A. Igau, H. Grützmacher, A. Baceiredo, G. Bertrand, *J. Am. Chem. Soc.* **1988**, *110*, 6463.
- [7] M. Soleilhavoup, A. Baceiredo, O. Treutler, R. Alrichs, M. Nieger, G. Bertrand, *J. Am. Chem. Soc.* **1992**, *114*, 10959.
- [8] C. Buron, H. Gornitzka, V. Romanenko, G. Bertrand, *Science* **2000**, *288*, 834.
- [9] a) A. J. Arduengo III, R. L. Harlow, M. Kline, *J. Am. Chem. Soc.* **1991**, *113*, 361; b) R. W. Alder, P. R. Allen, M. Murray, G. Orpen, *Angew. Chem.* **1996**, *108*, 1211; *Angew. Chem. Int. Ed. Engl.* **1996**, *35*, 1121; c) D. Enders, K. Breuer, G. Raabe, J. Runsink, J. H. Teles, J. P. Melder, K. Ebel, S. Brode, *Angew. Chem.* **1995**, *107*, 1119; *Angew. Chem. Int. Ed. Engl.* **1995**, *34*, 1021.
- [10] S. Solé, H. Gornitzka, W. W. Schoeller, D. Bourissou, G. Bertrand, *Science* **2001**, *292*, 1901.
- [11] Crystal data for **2**: $C_{22}H_{39}N_2P$, $M_r = 362.52$, monoclinic, space group $P2_1/n$, $a = 8.5825(7)$, $b = 18.3546(15)$, $c = 14.5145(12)$ Å, $\beta = 102.922(2)^\circ$, $V = 2228.5(3)$ Å³, $Z = 4$, $\rho_{\text{calc}} = 1.080$ Mg m⁻³, $F(000) = 800$, $\lambda = 0.71073$ Å, $\mu_{\text{MoK}\alpha} = 0.130$ mm⁻¹, crystal size $0.1 \times 0.1 \times 0.5$ mm³, $1.82^\circ \leq \theta \leq 23.25^\circ$, 9546 reflections (3195 independent, $R_{\text{int}} = 0.0689$), $T_{\text{min}} = 0.832369$, $T_{\text{max}} = 1.000000$, 237 parameters, $R1 [I > 2\sigma(I)] = 0.0425$, $wR2 [\text{all data}] = 0.0879$, largest electron density residue: 0.165 e Å⁻³. Data were collected at 193(2) K using an oil-coated shock-cooled crystal on a Bruker-AXS CCD 1000 diffractometer. Semi-empirical absorption corrections were employed.^[23] The structure was solved by direct methods (SHELXS-97),^[24] and refined using the least-squares method on F^2 .^[25] CCDC-184034 contains the supplementary crystallographic data for this paper. These data can be obtained free of charge via www.ccdc.cam.ac.uk/conts/retrieving.html (or from the Cambridge Crystallographic Data Centre, 12, Union Road, Cambridge CB21EZ, UK; fax: (+44) 1223-336-033; or deposit@ccdc.cam.ac.uk).
- [12] a) R. A. Moss in *Advances in Carbene Chemistry, Vol. 1* (Ed.: U. H. Brinker), Jai, Greenwich, **1994**, p. 59; b) U. H. Brinker, M. G. Rosenberg in *Advances in Carbene Chemistry, Vol. 2* (Ed.: U. H. Brinker), Jai, Stamford, **1998**, p. 29; c) M. S. Platz in *Advances in Carbene Chemistry, Vol. 2* (Ed.: U. H. Brinker), Jai, Stamford, **1998**, p. 133.
- [13] J. E. Jackson, M. S. Platz in *Advances in Carbene Chemistry, Vol. 1* (Ed.: U. H. Brinker), Jai, Greenwich, **1994** p. 89.
- [14] R. S. Sheridan, R. A. Moss, B. K. Wilk, S. Shen, M. Wlostowski, M. A. Kesselmayr, R. Subramanian, G. Kmiecik-Lawrynowicz, K. Krogh-Jespersen, *J. Am. Chem. Soc.* **1988**, *110*, 7563.
- [15] H. J. Nees, H. Keller, T. Facklam, A. Herrmann, J. Welsch, U. Bergsträsser, H. Heydt, M. Regitz, *J. Prakt. Chem.* **1993**, *335*, 589.
- [16] a) A. Igau, A. Baceiredo, G. Trinquier, G. Bertrand, *Angew. Chem.* **1989**, *101*, 617; *Angew. Chem. Int. Ed. Engl.* **1989**, *28*, 621; b) S. Goumri-Magnet, T. Kato, H. Gornitzka, A. Baceiredo, G. Bertrand, *J. Am. Chem. Soc.* **2000**, *122*, 4464; c) J. Krysiak, T. Kato, H. Gornitzka, A. Baceiredo, M. Mikolajczyk, G. Bertrand, *J. Org. Chem.* **2001**, *66*, 8240.
- [17] For recent theoretical investigations on phosphanylcarbenes, including **6**, see W. W. Schoeller, A. J. B. Rozhenko, A. Alijah, *J. Organomet. Chem.* **2001**, *617–618*, 435.
- [18] F. Castan, A. Baceiredo, D. Bigg, G. Bertrand, *J. Org. Chem.* **1991**, *56*, 1801.
- [19] R. B. King, P. M. Sundaram, *J. Org. Chem.* **1984**, *49*, 1784.
- [20] a) The activation energies for 1,2-hydrogen shifts^[21] are essentially zero for simple alkylcarbenes and significantly increase for heteroatom-substituted alkylcarbenes. Barriers of 11.5 and 24.5 kcal mol⁻¹ are predicted for the chloro- and methoxy(methyl)carbenes, respectively (J. D. Evanseck, K. N. Houk, *J. Phys. Chem.* **1990**, *94*, 5518). By comparison, activation energies for the H and NH₂ migration of the model carbene (H₂N)₂PCCH₃ were estimated to be 24.9 (H), 21.0 (NH₂ *trans* to CH₃) and 21.4 (NH₂ *cis* to CH₃) kcal mol⁻¹, respectively (at the MP2/6-31g* level of theory); b) Gaussian98 (Revision A.7), M. J. Frisch, G. W. Trucks, H. B. Schlegel, G. E. Scuseria, M. A. Robb, J. R. Cheeseman, V. G. Zakrzewski, J. A. Montgomery, R. E. Stratmann, J. C. Burant, S. Dapprich, J. M. Millam, A. D. Daniels, K. N. Kudin, M. C. Strain, O. Farkas, J. Tomasi, V. Barone, M. Cossi, R. Cammi, B. Mennucci, C. Pomelli, C. Adamo, S. Clifford, J. Ochterski, G. A. Petersson, P. Y. Ayala, Q. Cui, K. Morokuma, D. K. Malick, A. D. Rabuck, K. Raghavachari, J. B. Foresman, J. Cioslowski, J. V. Ortiz, B. B. Stefanov, G. Liu, A. Liashenko, P. Piskorz, I. Komaromi, R. Gomperts, R. L. Martin, D. J. Fox, T. Keith, M. A. Al-Laham, C. Y. Peng, A. Nanayakkara, C. Gonzalez, M. Challacombe, P. M. W. Gill, B. G. Johnson, W. Chen, M. W. Wong, J. L. Andres, M. Head-Gordon, E. S. Replogle, J. A. Pople, Gaussian, Inc., Pittsburgh, PA, **1998**.
- [21] R. Bonneau, M. T. H. Liu in *Advances in Carbene Chemistry, Vol. 2* (Ed.: U. H. Brinker), Jai, Stamford, **1998**, p. 1.
- [22] V. K. Aggarwal, J. G. Ford, S. Fonquerna, H. Adams, R. V. H. Jones, R. Fieldhouse, *J. Am. Chem. Soc.* **1998**, *120*, 8328.
- [23] SADABS, Program for data correction, Bruker-AXS.
- [24] G. M. Sheldrick, *Acta Crystallogr. Sect. A* **1990**, *46*, 467.
- [25] SHELXL-97, Program for Crystal Structure Refinement, G. M. Sheldrick, University of Göttingen (Germany), **1997**.

Stereoselective Pinacol-Type Rearrangement of 2,3-Epoxy Alcohols with Retention of Configuration Mediated by Bis(iodozincio)methane**

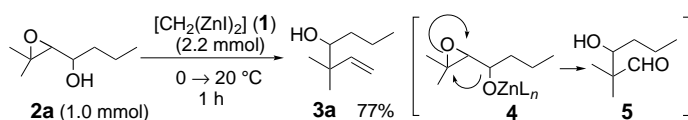
Seihiro Matsubara,* Hiromasa Yamamoto, and Koichiro Oshima

gem-Dizinc reagents that possess two nucleophilic sites on a carbon atom have been used for a variety of molecular transformations based on a repetition of C–C-bond formation on the same carbon atom.^[1] To understand and design these characteristic reactions, one should recognize that dimetallic reagents work not only as a double nucleophile but also as a double Lewis acid.^[2] The structure of *gem*-dizinc reagents allows them to act as double Lewis acids with substrates that contain heteroatoms at the 1,2- or 1,3-positions. In fact, we reported an example that emphasizes the importance of its double Lewis acidity through the nucleophilic reaction with 1,2-dicarbonyl compounds.^[3] Along this line, we treated 2,3-epoxy alcohols with bis(iodozincio)methane (**1**), anticipating a pinacol-type rearrangement.^[4, 5] The substrates are readily available in an enantiomerically enriched form by the Sharpless epoxidation.^[6]

Treatment of racemic **2a** (diastereomeric mixture, *erythrol threo* 84:16, 1.0 mmol) in THF (2.0 mL) with **1** (0.5 M in THF, 2.2 mmol) at 20 °C gave alkenol **3a** in 77% yield (Scheme 1).

[*] Prof. Dr. S. Matsubara, H. Yamamoto, Prof. Dr. K. Oshima
Department of Material Chemistry, Graduate School of Engineering
Kyoto University
Yoshida, Sakyo, Kyoto 606-8501 (Japan)
Fax: (+81) 75-753-4863
E-mail: matsubar@mc.kyoto-u.ac.jp

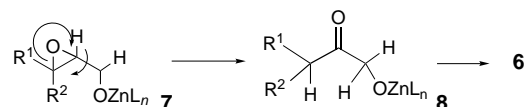
[**] This work was supported by a Grant-in-Aid from The Ministry of Education, Science, Sports, and Culture.



Scheme 1. Reaction of racemic **2a** with **1** to give alkenol **3a**.

The reaction was considered to proceed via aldehyde **5**, which was formed by a pinacol-type rearrangement (**4** to **5**), with subsequent methylenation of **5** to form **3a**.^[1a, 7] This type of rearrangement of silyl ethers of 2,3-epoxy alcohols was reported by Maruoka et al.,^[5a] who used the highly sterically hindered Lewis acid MABR (methylaluminum bis(4-bromo-2,6-di-*tert*-butylphenoxide)). Jung and Anderson also reported an example induced by $\text{BF}_3 \cdot \text{OEt}_2$.^[5b]

This *gem*-dizinc induced rearrangement/methylenation reaction was applied to other epoxy alcohols to study its limitation and generality. In Table 1, various types of substrates were examined in the reaction. In the reaction of primary alcohols, allylic alcohols **6** were formed as side products, which had not been observed in the reaction of **2a**. As shown in Scheme 2, alcohols **6** were assumed to be formed



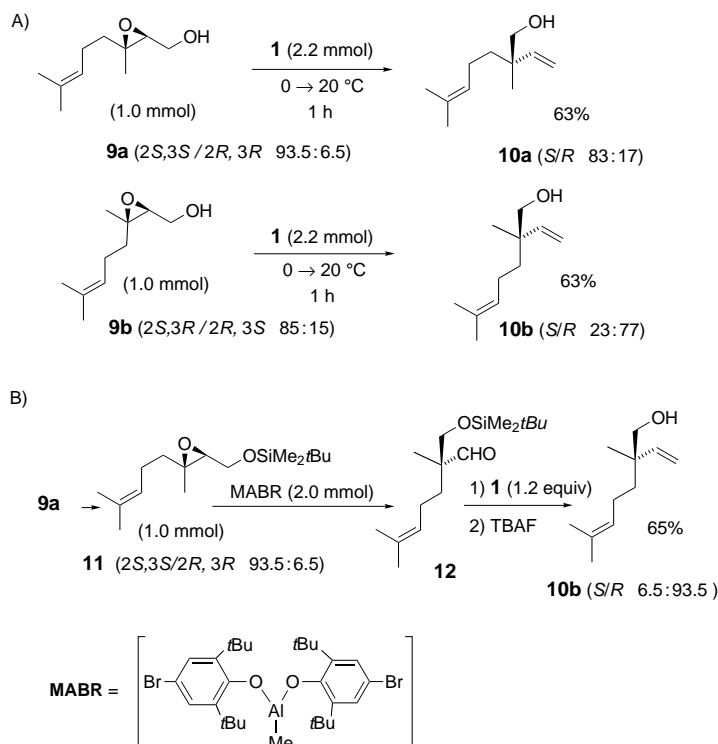
Scheme 2. Possible route for the formation of **6** as a side product.

by methylenation of α -alkoxy ketones **8**, which were formed through a hydride shift. Methylenation of α -alkoxy ketones **8** with **1** was shown to proceed smoothly.^[8] The ratio of **3** to **6** varied, depending on the substrate. A disubstituted *cis* epoxide yielded predominantly the hydride-shift-derived product **6** (Table 1, entry 4). The rearrangement did not occur in 2,3-epoxy alcohol substrates with substituents on C2 (Table 1, entries 8 and 9).

gem-Dizinc **1** reacts with 2,3-epoxy alcohols **2** to give zinc alkoxides (**4** and **7**) before the rearrangement reaction. The free hydroxy group in the substrate is indispensable for the reaction. Treatment of ether derivatives (methyl, trimethyl-

silyl, and dimethylphenylsilyl ethers) of 2,3-epoxygeraniol resulted in the quantitative recovery of the starting materials.

The wide availability of optically active epoxy alcohols by the Sharpless method prompted us to examine the possibility of chirality transfer in these reactions. This investigation led to the formation of quaternary asymmetric carbon centers.^[10] As shown in Scheme 3A, optically active epoxides were treated with bis(iodozincio)methane **1**. Alcohol **10a** was obtained in an optically active form from **9a**, although a slight decrease in enantiomeric purity was observed.^[11, 12] The highlight of the transformation is the absolute configuration of the product: the migrating group, $-\text{CH}_2\text{OH}$, attacks from the front side of



Scheme 3. Formation of alcohols **10** from 2,3-epoxy alcohols **9**. A) Treatment with bis(iodozincio)methane (**1**) results in retention of configuration. B) In contrast, treatment with MABR^[5a] gives inversion of configuration. TBAF = tetrabutylammonium fluoride.

Table 1. Treatment of 2,3-epoxy alcohol **2** with **1**.^[a,b]

Entry	R ¹	R ²	R ³	R ⁴	3	Yield [%]	6	Yield
1 ^[c]	Me	Me	H	Me	d	74	b	< 1 %
2	Me	Me	H	H	d	52	c	17
3	<i>n</i> Pr	H	H	H	d	23	d	35
4	H	<i>n</i> Pr	H	H	d	10	d	47
5	(Me) ₂ C=CH(CH ₂) ₂	Me	H	H	e	67	e	17
6	Me	(Me) ₂ C=CH(CH ₂) ₂	H	H	e	64	e	12
7	Ph	H	Me	H	f	30	f	< 1
8	Et	H	Me	<i>n</i> Bu	g	< 1 ^[d]	g	< 1
9	Me	Me	Me	H	h	< 1 ^[d]	h	< 1
10	Ph	H	H	H	i	75	i	7

[a] **1** (2.2 mmol) and **2** (1.0 mmol) were used. [b] Racemic substrate was used as the starting material. [c] The starting material was used as a mixture of diastereomers (*erythro/threo* 80:20). See also ref. [9]. [d] The starting epoxy alcohol was recovered quantitatively.

the C–O bond. This is an unusual retentive migration reaction.^[13, 14] Similarly, the alcohol **10b** (enantiomer of **10a**) was obtained from **9b** with a slight decrease in the enantiomeric purity. In this case, the rearrangement also proceeded with retention of the configuration at C3 of the 2,3-epoxy alcohol. In contrast, the rearrangement in the reported procedure^[5] proceeds with inversion of stereochemistry at C3: Silylation of **9a** provided **11**, which upon treatment with MABR gave **12**. Methylenation of **12** by **1** followed by desilylation with TBAF gave **10b** (Scheme 3 B).

In the case of the reaction of a phenyl-substituted substrate **13**, the rearrangement proceeded also with retention of configuration at C3 to give **14** (Scheme 4). The olefin **14** was hydrogenated to give **15** for comparison with an authentic sample^[15, 16] to confirm the absolute configuration. Even though the crucial stereogenic center is the benzylic position, only a slight decrease in the enantiomeric purity was observed.

The reaction pathway is not clear enough to rationalize the retention migration. One possible explanation is shown in Scheme 5: the dizinc compound coordinates 2,3-epoxy alco-

Purification by neutral silica-gel column chromatography (hexane/ethyl acetate 10:1) gave the corresponding product.

10a: Prepared from **9a** (87% *ee*) and **1**. $[\alpha]_D^{25} = -8.06 \pm 1.0$ (CHCl₃, *c* = 3.10). ¹H NMR spectroscopic analysis after conversion into the *S* Mosher ester showed that **10a** was obtained with 66% *ee*.

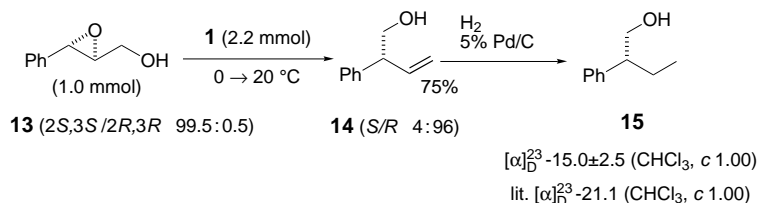
10b: Prepared from **12** and **1**. The aldehyde **12** was prepared from **9a** (87% *ee*) and MABR according to the reported procedure.^[5] ¹H NMR spectroscopic analysis after conversion into the *S* Mosher ester showed that **10b** was obtained with 87% *ee*. $[\alpha]_D^{25} = -8.96 \pm 1.0$ (CHCl₃, *c* = 3.10). Treatment of **9b** (70% *ee*) with **1** gave **10b** directly with 54% *ee*.

3i: ¹H NMR (CDCl₃, 23 °C, 300 MHz): δ = 7.4–7.3 (m, 2H), 7.3–7.2 (m, 3H), 6.02 (ddd, *J* = 17.1, 10.5, 7.8 Hz, 1H), 5.22 (ddd, *J* = 10.5, 1.5, 1.2 Hz, 1H), 5.19 (ddd, *J* = 17.1, 1.8, 1.2 Hz, 1H), 3.84 (dd, *J* = 10.8, 7.2 Hz, 1H), 3.82 (dd, *J* = 10.8, 7.2 Hz, 1H), 3.54 (dd, *J* = 7.2, 7.2 Hz, 1H), 1.60 ppm (bs, 1H); ¹³C NMR (CDCl₃, 23 °C, 75 MHz): δ = 141.4, 139.0, 129.5, 128.7, 127.7, 117.8, 66.8, 53.2 ppm.

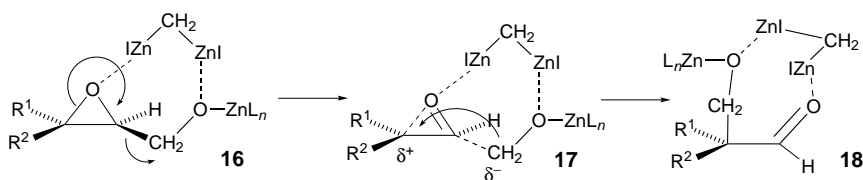
14: The enantiomeric purity (*R/S* 96:4) was determined by HPLC: Chiralcel-OD (Daicel), 2-propanol/hexane (1:9), 1.0 mL min⁻¹, *R* isomer: 5.93 min, *S* isomer: 7.43 min.

15: ¹H NMR (CDCl₃, 23 °C, 300 MHz): δ = 7.4–7.3 (m, 2H), 7.3–7.2 (m, 3H), 3.78 (dd, *J* = 10.8, 6.0 Hz, 1H), 3.73 (dd, *J* = 10.8, 7.8 Hz, 1H), 3.54 (dd, *J* = 7.2, 7.2 Hz, 1H), 2.71 (m, 1H), 1.8–1.5 (m, 2H), 1.25 (bs, 1H), 0.86 ppm (t, *J* = 7.5 Hz, 3H); $[\alpha]_D^{25} = -15.0 \pm 2.5$ (CHCl₃, *c* = 1.00), lit.^[16]: $[\alpha]_D^{25} = -21$ (CHCl₃, *c* = 1.00).

Received: May 6, 2002 [Z19228]



Scheme 4. Reaction of phenyl-substituted substrate **13** to give **14** with retention of configuration at C3.



Scheme 5. Possible mechanism for the dizinc-mediated reaction.

hol as a double Lewis acid (**16**), the Lewis acid induces isomerization into aldehyde, thus providing the negatively charged migrating group (**17**), and the migrating group is transferred to the positively charged carbon atom from the same side of the epoxide oxygen as dizinc coordinates to both oxygen atoms (**18**). The transformation indicate the important character of the dizinc species as a double Lewis acid. At the present stage, we have no evidence for the mechanism outlined in Scheme 5, and detailed investigations are currently underway.

Experimental Section

A solution of epoxy alcohol **2** (1.0 mmol) in THF (2 mL) was added dropwise to a THF solution of bis(iodozincio)methane (**1**, 0.5 M, 2.2 mmol, 4.4 mL) at 0 °C. The mixture was stirred for 1 h at room temperature, and then poured into aqueous HCl (1 M, 20 mL). The resulting mixture was extracted with diethyl ether. The combined ether solutions were washed successively with saturated NaHSO₃ and brine and dried over Na₂SO₄.

[1] a) S. Matsubara, K. Oshima, K. Utimoto, *J. Organomet. Chem.* **2001**, 617–618, 39; S. Matsubara, *J. Org. Synth. Soc. Jpn.* **2000**, 58, 118; b) P. Knochel, J.-F. Normant, *Tetrahedron Lett.* **1986**, 27, 4427; P. Knochel, J.-F. Normant, *Tetrahedron Lett.* **1986**, 27, 4431; c) I. Marek, J.-F. Normant, *Chem. Rev.* **1996**, 96, 3241; d) I. Marek, J.-F. Normant in *Organozinc Reagents. A Practical Approach* (Eds.: P. Knochel, P. Jones), Oxford University Press, Oxford, **1999**, p. 119.

[2] For examples of coordination of double Lewis acids to carbonyl compounds, see: J. D. Beckwith, M. Tschinkl, A. Picot, M. Tsunoda, R. Bachman, F. P. Gabbaï, *Organometallics* **2001**, 20, 3169; T. Ooi, M. Takahashi, K. Maruoka, *J. Am. Chem. Soc.* **1996**, 118, 11307; H. Adams, N. A. Bailey, J. T. Gauntlett, M. J. Winter, *J. Chem. Soc. Chem. Commun.* **1984**, 1360, and references therein.

[3] K. Ukai, K. Oshima, S. Matsubara, *J. Am. Chem. Soc.* **2000**, 122, 12047.

[4] For the transformation of 2,3-epoxy alcohols and their derivatives, see: C. H. Bahrens, K. B. Sharpless, *Aldrichimica Acta* **1983**, 16, 67.

[5] a) K. Maruoka, T. Ooi, S. Nagahara, H. Yamamoto, *Tetrahedron* **1991**, 47, 6983; b) M. E. Jung, K. L. Anderson, *Tetrahedron Lett.* **1997**, 38, 2605.

[6] T. Katsuki, K. B. Sharpless, *J. Am. Chem. Soc.* **1980**, 102, 5976; V. S. Martin, S. S. Woodward, T. Katsuki, Y. Yamada, M. Ikeda, K. B. Sharpless, *J. Am. Chem. Soc.* **1981**, 103, 6237.

[7] a) We also found that treatment of **2a** with bis(bromozincio)trimethylsilylmethane afforded the aldehyde **5**; b) the silyl-substituted dizinc species cannot react with the aldehydes without the addition of titanium salt: S. Matsubara, Y. Otake, T. Morikawa, K. Utimoto, *Synlett* **1998**, 1315.

[8] K. Ukai, D. Arioka, H. Yoshino, H. Fushimi, K. Oshima, K. Utimoto, S. Matsubara, *Synlett* **2001**, 513.

[9] Treatment of (2*S*,3*S*)-4-methyl-3,4-epoxypentan-2-ol (48% *ee*) with **1** afforded optically active 3,3-dimethyl-4-penten-2-ol (**11**) with 48% *ee*; the absolute configuration has not yet been determined.

[10] E. J. Corey, A. Guzman-Perez, *Angew. Chem.* **1998**, 110, 402; *Angew. Chem. Int. Ed.* **1998**, 37, 388.

[11] The enantiomeric purities of **10** and **11** were determined by ¹H NMR analysis after transformation into the corresponding Mosher esters.

- [12] The side product related to **6** was also formed, but the optical purity was not determined.
- [13] M. Shimazaki, H. Haram, K. Suzuki, G.-i. Tsuchihashi, *Tetrahedron Lett.* **1987**, 28, 5891; K. Suzuki, E. Katayama, G.-i. Tsuchihashi, *Tetrahedron Lett.* **1984**, 25, 1817.
- [14] Rearrangements of optically active vinyl epoxides mediated by Lewis acids give quaternary asymmetric carbon centers with inversion of the configuration: a) M. E. Jung, D. C. D'Amino, *J. Am. Chem. Soc.* **1995**, 117, 7379; b) for rearrangements that involve a sterically restricted cation center, see: S. A. Monti, S.-C. Chen, Y.-L. Yang, S.-S. Yuan, O. P. Bourgeois, *J. Org. Chem.* **1978**, 43, 4062.
- [15] The enantiomeric purity of **15** was determined by HPLC (Chiralcel-OJ, Daicel).
- [16] C. H. Senanayake, R. D. Larsen, T. J. Bill, J. Liu, E. G. Corley, P. J. Reider, *Synlett* **1994**, 199.



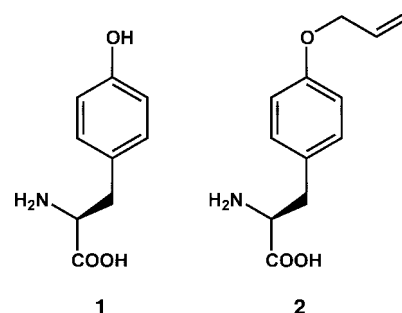
The Selective Incorporation of Alkenes into Proteins in *Escherichia coli***

Zhiwen Zhang,^[+] Lei Wang,^[+] Ansgar Brock, and Peter G. Schultz*

The addition of amino acids with novel functional groups to the genetic code of *Escherichia coli* should greatly enhance our ability to study protein structure and function, as well as generate proteins with novel properties. We recently showed that the unnatural amino acids *O*-methyl-L-tyrosine and L-3-(2-naphthyl)alanine can be site-specifically incorporated into proteins in *Escherichia coli* with high efficiency and fidelity.^[1,2] This result requires the addition of an orthogonal tRNA–codon pair and aminoacyl-tRNA synthetase to the translational machinery of the cell. The new synthetase (and only this synthetase) aminoacylates the orthogonal tRNA (and only this tRNA) with the unnatural amino acid only, which is inserted into proteins in response to the amber codon, TAG.^[3] We report here the site-specific incorporation

of *O*-allyl-L-tyrosine (**2**) into proteins in *E. coli*. The alkene functional group of this unnatural amino acid should provide new chemical methods for the selective modification of proteins.

Previously we generated an orthogonal tRNA–synthetase pair, mutRNA^{Tyr}_{CUA}–TyrRS, in *E. coli* by modifying the tRNA^{Tyr}–TyrRS pair of *Methanococcus jannaschii*.^[4,5] This mutRNA^{Tyr}_{CUA} is not aminoacylated by endogenous synthetases in *E. coli*, and functions well in translation. The TyrRS does not aminoacylate *E. coli* tRNAs,^[6] but aminoacylates the mutRNA^{Tyr}_{CUA} with tyrosine (**1**); the acylated mutRNA^{Tyr}_{CUA} inserts tyrosine in response to the amber nonsense codon. To change the substrate specificity of the TyrRS so that it aminoacylates the mutRNA^{Tyr}_{CUA} with **2** and not with any common amino acids, a mutant TyrRS library was generated



and selected. Based on an analysis of the crystal structure of the homologous TyrRS from *Bacillus stearothermophilus*,^[7] five residues (Tyr32, Glu107, Asp158, Ile159, and Leu162) in the active site of *M. jannaschii* TyrRS that are within 6.5 Å of the *para* position of the aryl ring of tyrosine were randomly mutated.^[1,8] This mutant library was first subjected to a positive selection based on the suppression of an amber codon introduced at a nonessential position (Asp112) in the chloramphenicol acetyl transferase (CAT) gene. Cells transformed with the mutant TyrRS libraries, the mutRNA^{Tyr}_{CUA} gene, and the amber mutant CAT gene were grown in minimal media containing 1 mM **2** and 70 µg mL⁻¹ chloramphenicol. The survivors must encode a mutant TyrRS that aminoacylates the mutRNA^{Tyr}_{CUA} with either **2** or endogenous amino acids. To remove mutant synthetases with specificities for endogenous amino acids, a negative selection was applied. Three amber codons were introduced at nonessential positions (Gln2, Asp44, Gly65) in the toxic barnase gene.^[9] Cells expressing the mutant synthetase from the positive selection, the mutRNA^{Tyr}_{CUA} gene, and the amber mutant barnase gene were grown in Luria–Bertani (LB) media in the absence of **2**. Cells encoding synthetases with specificities for any endogenous amino acids will produce barnase and die. Only those encoding a mutant synthetase with specificity for **2** can survive.

After three rounds of positive selection alternating with two rounds of negative selection, a clone was evolved whose survival in chloramphenicol was dependent on the presence of **2** when the selected mutant TyrRS gene (AL-TyrRS) was coexpressed with the Asp112amber CAT gene and the mutRNA^{Tyr}_{CUA} gene. Cells can survive in 120 µg mL⁻¹ chloram-

[*] Prof. P. G. Schultz
Department of Chemistry and
the Skaggs Institute for Chemical Biology
The Scripps Research Institute
10550 North Torrey Pines Road, La Jolla, CA 92037 (USA)
Fax: (+1) 858-784-9440
E-mail: schultz@scripps.edu

Dr. Z. Zhang
Department of Chemistry
The Scripps Research Institute
10550 North Torrey Pines Road, La Jolla, CA 92037 (USA)

L. Wang
Department of Chemistry
University of California at Berkeley
Berkeley, CA 94720 (USA)

Dr. A. Brock
Genomics Institute of the Novartis Research Foundation
10675 John Jay Hopkins Drive, San Diego, CA 92121 (USA)

[+] These authors contributed equally to this work.

[**] Support for this work was provided by the Department of Energy, Basic Energy Sciences Program, and the National Institutes of Health. We thank Dr. Steve Santoro for plasmid pREP(2) and Sheng Ding for helpful discussions. This is TSRI manuscript no. 14950-CH.

phenicol in the presence of **2**, and up to 10 $\mu\text{g mL}^{-1}$ chloramphenicol in the absence of **2**. For comparison, *E. coli* cells expressing the Asp112amber CAT gene and the mutRNA^{Tyr}_{CUA} gene survive in 4 $\mu\text{g mL}^{-1}$ chloramphenicol.^[5] This result suggests that the AL-TyrRS has higher activity for **2** than for natural amino acids. The evolved AL-TyrRS has the following mutations: Glu107 \rightarrow Ala107, Asp158 \rightarrow Cys158, and Ile159 \rightarrow Ala159. The residues Tyr32 and Leu162 remain unchanged. The mutations of Glu107 \rightarrow Ala107 and Ile159 \rightarrow Ala159 may enlarge the active site of the mutant synthetase to accommodate the allyl group. The exact roles of these mutations will be revealed by solving the crystal structure of AL-TyrRS, which is underway.

To confirm that the observed phenotype is caused by the site-specific incorporation of **2** by the mutRNA^{Tyr}_{CUA}–AL-TyrRS pair, a mutant Z domain^[10, 11] protein was produced and characterized. An amber codon was introduced at the seventh position in the gene encoding the Z domain. A His₆ tag was added to the C terminus of the Z domain to facilitate protein purification by Ni²⁺-affinity chromatography. As a positive control, the wild type *M. jannaschii* TyrRS was coexpressed with the mutRNA^{Tyr}_{CUA}, which resulted in the suppression of the amber codon with tyrosine and production of full-length Z-domain protein (Figure 1). When AL-TyrRS

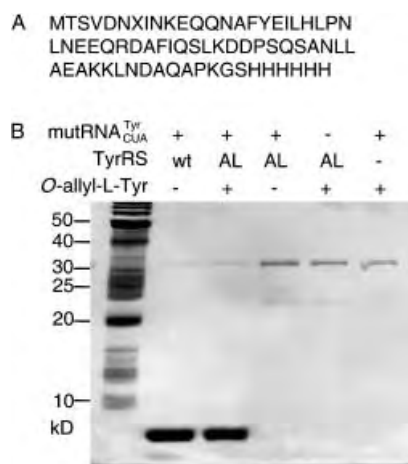


Figure 1. A) Amino acid sequence of the Z domain. X indicates the position for incorporation of **2** encoded by the amber nonsense codon; B) SDS-PAGE analysis of the accumulation of Z domain under different conditions. The far left lane is a molecular-weight marker. Expression conditions are noted at the top of each lane. Proteins were purified by Ni²⁺-affinity chromatography and the gel was silver-stained.^[12] AL-TyrRS = O-allyl-L-tyrosine-specific mutant synthetase; wt = wild type.

was expressed together with the mutRNA^{Tyr}_{CUA} in the presence of **2**, full-length Z domain was also obtained. In the absence of either the AL-TyrRS, the mutRNA^{Tyr}_{CUA}, or **2**, no full-length Z domain was observed. These results show that full-length mutant protein is produced only in the presence of the AL-TyrRS, the mutRNA^{Tyr}_{CUA}, and **2**. The yield of full-length mutant Z domain containing **2** is 5.6 mg L^{-1} in minimal media. For comparison, the yield of Z-domain is 9.2 mg L^{-1} when the mutRNA^{Tyr}_{CUA} and wild-type *M. jannaschii* TyrRS are coexpressed.

The mutant Z-domain protein expressed by the mutRNA^{Tyr}_{CUA}–AL-TyrRS was analyzed by electrospray ionization Fourier transform ion cyclotron resonance mass spectrometry (FT-ICR MS). The experimental monoisotopic mass of the intact protein was 7963.891 Da, which is within 1 ppm of the theoretical mass of 7963.889 Da. Another major signal corresponds to the protein without the first methionine moiety ($M_{\text{Experimental}} = 7832.861$ Da, $M_{\text{Theoretical}} = 7832.849$ Da). The signal-to-noise ratio of more than 1500 observed in the intact protein mass spectrum suggests a fidelity for the incorporation of **2** of better than 99.8%. This result clearly demonstrates the site-specific incorporation of **2** in response to the amber codon by the mutRNA^{Tyr}_{CUA}–AL-TyrRS, and that other endogenous *E. coli* synthetases do not utilize **2** as a substrate.

In summary, a useful nonnatural amino acid, O-allyl-L-tyrosine, has been site-specifically incorporated into proteins in vivo. The allyl group is versatile in organic transformations, including metathesis,^[13] Diels-Alder and 1,3-dipolar cycloaddition reactions.^[14] Olefin metathesis has been used successfully to cross-link amino acid derivatives^[15] and cyclize peptides.^[16, 17] Recent progress in developing water-soluble ruthenium catalysts^[18] should facilitate the application of this reaction to the modification of proteins containing alkene groups.^[19, 20] Moreover, the allyl side chain of this nonnatural amino acid may confer new physical properties on proteins as well.

Experimental Section

All chemicals were purchased from Aldrich. NMR spectroscopic data was recorded using a Bruker AMX 400. Mass spectra of small molecules were obtained from Scripps Center for Mass Spectrometry.

Synthesis of 2: O-allyl-L-tyrosine (**2**) was synthesized according to the published procedures^[21] with minor modifications. *N*-(*tert*-butoxycarbonyl)-L-tyrosine (2.95 g, 10 mmole) was dissolved in 80 mL of *N,N*-dimethylformamide (DMF). The solution was cooled to 5 °C and NaH (0.63 g, 26 mmole) was added. The reaction mixture was allowed to warm up to 10 °C and stirred for an additional 2 h. Allyl bromide (1.33 g, 11 mmole) was then added with stirring and the reaction mixture was warmed to room temperature and stirred for an additional 4 h. Water was added and the aqueous layer was extracted with ethyl acetate and CH₂Cl₂. The organic layer was dried over anhydrous MgSO₄. The organic solvent was removed to afford a white solid, which was then refluxed in 4 M HCl in 1,4-dioxane for 4 h. All solvent was evaporated to give the desired product as a white solid (1.9 g, 86 %); ¹H NMR (CD₃OD): δ = 3.12 (m, 2H), 4.13 (t, J = 5.1 Hz, 1H), 4.53 (d, J = 4.6 Hz, 2H), 5.37 (q, J = 17.4, 11.3, 10.6 Hz, 1H), 5.99 (m, 1H), 6.91 (d, J = 8.4 Hz, 2H), 7.12 ppm (d, J = 8.4 Hz, 2H);^[21] ¹³C NMR (CD₃OD): δ = 40.0, 69.5, 73.1, 115.8, 117.4, 130.5, 131.5, 135.6, 158.4, 177.5 ppm; m/z (ESI, MH⁺): 222.19.

Selection for AL-TyrRS: The positive selection based on the suppression of an amber codon in chloramphenicol acetyl transferase was carried out as described.^[1] For the negative selection, plasmid pLWJ17B3 was used to express the mutRNA^{Tyr}_{CUA} under the control of the *lpp* promoter and *rrnC* terminator, and the barnase gene with three amber codons at Gln2, Asp44, and Gly65 under arabinose induction. After positive selection, pBK plasmids encoding mutant TyrRS were isolated and transformed into *E. coli* DH10B competent cells harboring pLWJ17B3. Cells were grown in LB media containing 0.2 % arabinose, 50 $\mu\text{g mL}^{-1}$ kanamycin, and 35 $\mu\text{g mL}^{-1}$ chloramphenicol. After 8 h, cells were pelleted, and pBK plasmids were purified for further rounds of selection. After sequential positive, negative, positive, negative, then positive selection, the candidate pBK-ALRS encoding AL-TyrRS was identified and characterized using an in vivo chloramphenicol acetyl transferase assay.^[5]

Protein expression, purification, and characterization: Plasmid pLEIZ was used to express the Z-domain gene with an amber codon at the seventh position under the control of a bacteriophage T5 promoter and t_0 terminator, and the $\text{mutRNA}_{\text{CUA}}^{\text{Tyr}}$ gene under the control of the *lpp* promoter and *rrmC* terminator. The AL-TyrRS gene was encoded in plasmid pBK-ALRS under the control of the constitutive *E. coli* GlnRS promoter and terminator. *E. coli* DH10B cells cotransformed with pLEIZ and pBK-ALRS were grown in minimal media containing 1% glycerol and 0.3 mM leucine (GMML media) with $25 \mu\text{g mL}^{-1}$ kanamycin, $34 \mu\text{g mL}^{-1}$ of chloramphenicol, and 0.5 mM **2**. When cells reach an optical density (OD_{600}) value of 0.5, isopropyl- β -D-thiogalactopyranoside (IPTG; 1 mM) was added to induce protein expression. After 4 h, cells were pelleted and the protein was purified by Ni^{2+} -affinity chromatography according to the manufacturer's protocol under denaturing conditions (Quiagen, Valencia, CA). Proteins were then desalted by using a PD-10 column (Amersham Pharmacia, Piscataway, NJ) and eluted in water. The yield of protein was measured by Bradford assay (BCA kit, Biorad, Hercules, CA). Aliquots of protein were used for SDS-PAGE and mass spectroscopic analysis.

Received: April 19, 2002 [Z19118]

- [1] L. Wang, A. Brock, B. Herberich, P. G. Schultz, *Science* **2001**, 292, 498–500.
- [2] L. Wang, A. Brock, P. G. Schultz, *J. Am. Chem. Soc.* **2002**, 124, 1836–1837.
- [3] L. Wang, P. G. Schultz, *Chem. Commun.* **2002**, 1–11.
- [4] L. Wang, T. J. Magliery, D. R. Liu, P. G. Schultz, *J. Am. Chem. Soc.* **2000**, 122, 5010–5011.
- [5] L. Wang, P. G. Schultz, *Chem. Biol.* **2001**, 8, 883–890.
- [6] B. A. Steer, P. Schimmel, *J. Biol. Chem.* **1999**, 274, 35601–35606.
- [7] P. Brick, T. N. Bhat, D. M. Blow, *J. Mol. Biol.* **1989**, 208, 83–98.
- [8] A second mutant *M. jannaschii* TyrRS library was also constructed in such a way that six residues (Tyr32, Ala67, His70, Gln155, Asp158, Ala167) within 6.9 Å of the *meta* position of the tyrosine aryl ring were randomly mutated. This library was also subjected to the genetic selection, but failed to produce a mutant TyrRS which charges *O*-allyl-L-tyrosine.
- [9] D. R. Liu, P. G. Schultz, *Proc. Natl. Acad. Sci. USA* **1999**, 96, 4780–4785.
- [10] B. Nilsson, T. Moks, B. Jansson, L. Abrahamson, A. Elmlblad, E. Holmgren, C. Henrichson, T. A. Jones, M. Uhlen, *Protein Eng.* **1987**, 1, 107–113.
- [11] We have also successfully incorporated **2** into mouse dihydrofolate reductase (DHFR) with high fidelity (>99%).
- [12] The top two bands in Figure 1 with molecular weights of approximately 32 kD and 23 kD are *E. coli* proteins which bind to the Ni^{2+} column nonspecifically.
- [13] A. Fürstner, *Angew. Chem.* **2000**, 112, 3140–3172; *Angew. Chem. Int. Ed.* **2000**, 39, 3012–3043.
- [14] K. V. Gothelf, K. A. Jorgensen, *Chem. Rev.* **1998**, 98, 863–909.
- [15] S. C. G. Biagini, S. E. Gibson, S. P. Keen, *J. Chem. Soc. Perkin Trans. I* **1998**, 2485–2499.
- [16] J. F. Reichwein, C. Versluis, R. M. J. Liskamp, *J. Org. Chem.* **2000**, 65, 6187–6195.
- [17] H. E. Blackwell, J. D. Sadowsky, R. J. Howard, J. N. Sampson, J. A. Chao, W. E. Steinmetz, D. J. O'Leary, R. H. Grubbs, *J. Org. Chem.* **2001**, 66, 5291–5302.
- [18] D. M. Lynn, B. Mohr, R. H. Grubbs, L. M. Henling, M. W. Day, *J. Am. Chem. Soc.* **2000**, 122, 6601–6609.
- [19] J. C. M. van Hest, K. L. Kiick, D. A. Tirrell, *J. Am. Chem. Soc.* **2000**, 122, 1282–1288.
- [20] K. L. Kiick, J. C. M. van Hest, D. A. Tirrell, *Angew. Chem.* **2000**, 112, 2232–2236; *Angew. Chem. Int. Ed.* **2000**, 39, 2148–2152.
- [21] J. M. Fraile, J. I. Garcia, J. A. Mayoral, A. J. Royo, *Tetrahedron: Asymmetry*, **1996**, 7, 2263–2276.

Synthesis and Characterization of the Neutral “Digallene” $\text{Ar}^*\text{GaGaAr}^*$ and Its Reduction to $\text{Na}_2\text{Ar}^*\text{GaGaAr}^*$ ($\text{Ar}^* = 2,6\text{-Dipp}_2\text{C}_6\text{H}_3$, $\text{Dipp} = 2,6\text{-}i\text{Pr}_2\text{C}_6\text{H}_3$)**



Ned J. Hardman, Robert J. Wright, Andrew D. Phillips, and Philip P. Power*

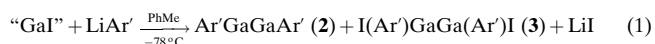
The publication of the remarkable gallium compound $\text{Na}_2\text{Ar}^*\text{GaGaAr}^*$ (**1**; $\text{Ar}^* = 2,6\text{-Trip}_2\text{C}_6\text{H}_3$, $\text{Trip} = 2,4,6\text{-}i\text{Pr}_3\text{C}_6\text{H}_2$) in 1997 resulted in much controversy owing to the claim that it contained a Ga–Ga triple bond.^[1] Initially, the triple bonding in this molecule was justified on the basis of a short Ga–Ga distance (2.319(3) Å) and the correspondence of the putative $[\text{Ar}^*\text{GaGaAr}^*]^{2-}$ ion to the neutral germanium species $\text{Ar}^*\text{GeGeAr}^*$ —a germanium–alkyne analogue. Although the existence of Ga–Ga triple bonding has received support from some calculations,^[2–6] others have questioned this view on the basis of 1) the *trans*-bent structure of the $\text{C}_{\text{ipso}}\text{GaGaC}_{\text{ipso}}$ array which indicates lone pair character at the gallium center,^[7–11] 2) the Na–aryl ring^[8] and Na–Ga interactions^[11] which shorten the Ga–Ga distance, and 3) the role of the *para*-*i*Pr groups on the flanking aryl rings which cause Ga–Ga–C angular distortions that can strengthen the Ga–Ga bond.^[11] Force constant calculations have also pointed to a relatively weak Ga–Ga interaction.^[12, 13] The publication of the cluster species $\text{K}_2\text{Ar}^*\text{Ga}_4\text{Ar}^*$, which contains a Ga_4 ring with no Ga–Ga triple bonding as part of an octahedral K_2Ga_4 core, has underlined the importance of the alkali metal for the stability of **1**.^[14] However, apart from this isolated report, all arguments regarding the Ga–Ga bonding in **1** have been grounded in calculations of various degrees of sophistication^[2–11] and the original experimentally determined structural parameters.^[1] In 1998 several experiments were suggested whose object was the elucidation of the important factors governing the nature of the Ga–Ga bond.^[15] Among these were the investigation of the effects of changing or removing the alkali metal ions and the isolation and characterization of the neutral “digallene” species $\text{Ar}^*\text{GaGaAr}^*$ which, should contain a Ga–Ga double bond if the assumption of triple bonding in **1** was correct. The former question has been partly answered through the synthesis of $\text{K}_2\text{Ar}^*\text{Ga}_4\text{Ar}^*$. However, no stable neutral Ga–Ga bonded dimers of the general formula RGaGaR (R = organic or related group) have yet been described. Calculations on a variety of model species, including HGaGaH ,^[10, 11, 16–19] MeGaGaMe ,^[9–11] and PhGaGaPh ,^[11] as well as IR spectroscopy of HGaGaH in a frozen matrix^[19, 20] point to weak Ga–Ga bonding. It is now shown that the compound $\text{Ar}^*\text{GaGaAr}^*$ (**2**; $\text{Ar}^* = 2,6\text{-Dipp}_2\text{C}_6\text{H}_3$, $\text{Dipp} = 2,6\text{-}i\text{Pr}_2\text{C}_6\text{H}_3$), can be isolated and characterized with

[*] Prof. P. P. Power, Dr. N. J. Hardman, R. J. Wright, Dr. A. D. Phillips
Department of Chemistry
University of California
One Shields Avenue, Davis, CA 95616 (USA)
Fax: (+1) 530-752-8995
E-mail: pppower@ucdavis.edu

[**] This work was supported by the National Science Foundation Grant No. 0094913.

use of a terphenyl substituent (Ar') that is closely related to the Ar* ligand employed in the synthesis of **1**.

Compound **2** was synthesized by the reaction of "GaI"^[21] with LiAr' in toluene in accordance with Equation (1).



Green crystals of **2** and yellow crystals of **3** were each isolated in about 25% yield from this reaction. The structure of **2** is illustrated in Figure 1 and consists of centrosymmetric

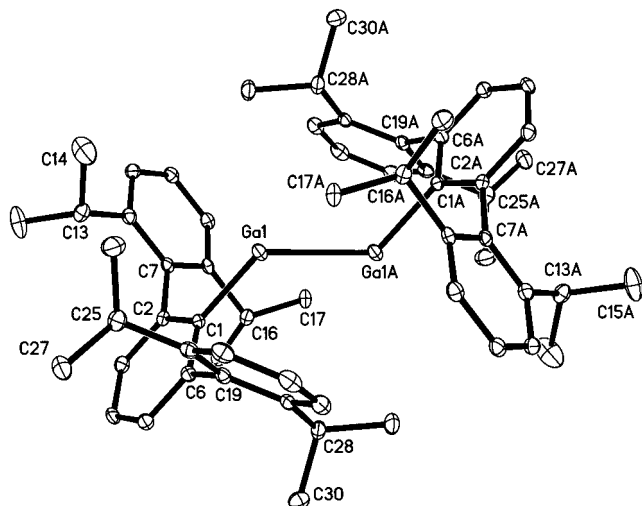


Figure 1. Structure of **2** (thermal ellipsoid plot; H atoms are not shown). Bond lengths [Å] and angles [°]: Ga1-Ga1A 2.6268(7), Ga1-C1 2.025(3), C1-C2 1.402(6), C1-C6 1.412(4); C1-Ga1-Ga1A 123.16(7), Ga1-C1-C2 122.6(2), Ga1-C1-C6 119.2(2), C1-C2-C6 118.2(3).

Ga-Ga-bonded dimers with a planar, *trans*-bent C1-Ga1-Ga1A-C1A core.^[22] The Ga-Ga and Ga-C distances are 2.6268(7) and 2.025(3) Å, respectively, and the Ga-Ga-C angle is 123.16(7)°. As is apparent from Figure 1, the plane of the central (C1) ring lies almost perpendicular (89.2°) to the C1-Ga1-Ga1A-C1A core and the flanking 2,6-*i*Pr₂C₆H₃ rings are almost perpendicular (89.8 and 85.7°) to the central ring. The structural parameters within the Ar' ligand are normal and there are only slight deviations from expected values. The Ga-Ga distance is about 0.1 Å longer than the upper end of the single bond length range (2.33–2.54 Å)^[23, 24] for digallanes and related compounds. It is also notably longer (by ca. 0.14 Å) than the Ga-Ga distance (2.493(2) Å) in **3**,^[22] which has similar steric loading. However, it lies within the range (2.57–2.71 Å) observed in the Ga-Ga-bonded tetrahedrane clusters (GaR)₄.^[25] These clusters are electron deficient with a formal Ga-Ga bond order of 2/3 and were found to dissociate in hydrocarbon solutions—a fact that was interpreted in terms of an equilibrium between monomers and tetramers. The tetramers are also known to dissociate to monomers in the vapor phase as shown by mass spectrometry and electron diffraction studies.^[29, 30] Similarly, compound **2** is partly dissociated to monomers in solution, and cryoscopic (cyclohexane) molecular weights that lie between those expected for monomers and dimers were observed at a concentration of 6 mmolal. It also sublimes readily at 150°C at a pressure of

0.05 mm Hg, suggesting a monomeric structure in the vapor phase. The structural and physical data for **2** thus point to species that has relatively weak Ga-Ga bonding and a bond order that is significantly less than unity.^[10]

The sodium derivative Na₂Ar'GaGaAr' (**4**) can be isolated as dark red crystals from the reduction of **2** or **3** with sodium metal in diethyl ether. This reaction establishes a direct connection between the neutral **2** and the doubly reduced **4**.

Compound **4**, the structure^[22] of which is illustrated in Figure 2, crystallizes as centrosymmetric molecules that

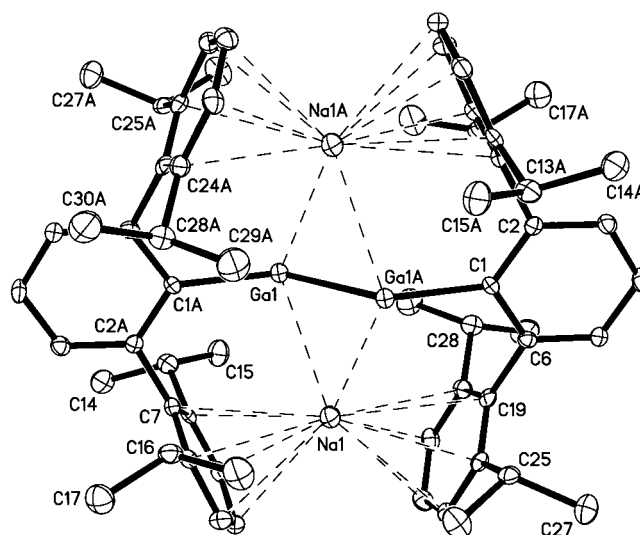


Figure 2. Structure of **4** (thermal ellipsoid plot; H atoms are not shown). Bond lengths [Å] and angles [°]: Ga1-Ga1A 2.347(1), Ga1-C1 2.059(5), Ga1-Na1 3.058(2), Ga1-Na1 3.101(2), Ga-Na 2.879(6)-3.051(5) (av 2.97(5)); Ga-Ga1A-C1 130.7(1), Na1-Ga1-Na1A 135.21(3).

feature a planar, *trans*-bent C1-Ga1-Ga1A-C1A core with sodium atoms that are complexed by Dipp rings and which almost symmetrically bridge the gallium atoms on each side of the C1-Ga1-Ga1A-C1A plane. The Ga-Ga and Ga-C distances are 2.347(1) and 2.059(5) Å, respectively, and the Ga-Ga-C angle is 130.7(1)°. The Ga-Na distances are 3.058(2) and 3.101(2) Å and the average Na-C(ring) distance is 2.97(5) Å. Most of these structural parameters are very similar to those previously reported for the structure of **1**,^[1, 14] for which the following values were determined: Ga-Ga 2.319(3), 2.324(1) Å; Ga-C(av) 2.044(16), 2.041(4) Å; Ga-Ga-C(av) 131.0(2.5), 130.7(1)°; Ga-Ga(av) 3.081(14), 3.084(19) Å; Na-C 3.04(2), 2.995(4) Å. The only parameter that shows a significant difference is the Ga-Ga distance, which in **4** is either 0.028^[1] or 0.021 Å^[14] longer than those reported for **1**. The Ga-Ga-C angle remains essentially unchanged so that, in this molecule at least, it does not correlate with the Ga-Ga distance as suggested by calculations on **1**. The reasons for the different Ga-Ga distances in **1** and **4** remain obscure. It should, however, be borne in mind that the Ga-Ga bond is weak and that changes in the aromatic substitution or molecular packing can affect the Ga-Ga bond length.

In summary the Ga-Ga bond in the "digallene" **2** is weak and the bond order is less than unity. Furthermore, the Ga-Ga bond order in the structurally uncharacterized Ar*-

substituted congener is likely to be lower than that in **2** owing to the greater steric crowding of the Ar* vis-a-vis the Ar' substituent.^[28–30] Numerous attempts^[30] to crystallize a species of the formula GaAr* have been unsuccessful. However, the experimental evidence suggests that this compound will be either a monomer like its indium congener InAr*^[29] or a weakly bonded dimer as suggested by calculations on model species such as PhGaGaPh.^[11] In either case, the results point to a bond order of between one and two in the original Na₂Ar*GaGaAr* species.

Experimental Section

All manipulations were carried out under anaerobic and anhydrous conditions.

2: A rapidly stirred slurry of “GaI” (1.49 g, 7.60 mmol) in toluene (20 mL),^[21] cooled to about –78 °C, was treated dropwise with a solution of (LiAr')₂ (3.07 g, 3.80 mmol) in toluene (40 mL) over about 1 h, after which time the mixture was allowed to come to room temperature over a period of 6 h. Stirring was discontinued and the suspension was allowed to settle. The dark green supernatant solution was filtered through Celite and concentrated to about 15 mL whereupon a yellow-orange precipitate formed. This was allowed to settle and the solution was separated by decantation. The yield of the orange-yellow solid, which is almost pure **3**, is 1.10 g (0.93 mmol, 24.4 %). The green supernatant liquid was stored in a freezer at about –20 °C for 12 h to afford a green crystalline solid. This was recrystallized from a minimum volume of warm hexane to afford the product **2** (0.90 g, 0.96 mmol; 25.3 %) as green crystals. M.p. 206–210 °C. Correct C,H analysis; ¹H NMR (C₆D₆, 400 MHz, 25 °C): δ = 1.07 (d, ³J_{H,H} = 6.6 Hz, 24H; CH(CH₃)₂), 1.09 (d, ³J_{H,H} = 6.6 Hz, 24H; CH(CH₃)₂), 2.98 (sept, ³J_{H,H} = 6.7 Hz, 8H; CH(CH₃)₂), 7.02 (d, ³J_{H,H} = 7.6 Hz, 8H; *m*-Dipp), 7.14, 7.19, 7.21 ppm (m, *p*-C₆H₃); ¹³C{¹H} NMR (100.6 MHz, C₆D₆, 25 °C): δ = 25.01 (CH(CH₃)₂), 25.37 (CH(CH₃)₂), 30.92 (CH(CH₃)₂), 123.03 (*p*-C₆H₃), 123.40 (*m*-Dipp), 128.20 (*m*-C₆H₃), 128.80 (*i*-Dipp), 138.87 (*o*-C₆H₃), 144.72 (*p*-Dipp), 147.16 (*o*-Dipp), 173.80 ppm (*i*-C₆H₃); UV/Vis (hexanes): λ_{max} (ε) = 350 (990), 437 nm (430 mol L^{–1} cm^{–1}). **3:** Yield: 1.08 g, 0.91 mmol; m.p. > 260 °C (decomp); ¹H NMR (400 MHz, C₆D₆, 25 °C): δ = 0.99 (d, ³J_{H,H} = 6.4 Hz, 24H; *o*-CH(CH₃)₂), 1.18 (d, ³J_{H,H} = 6.4 Hz, 24H; *o*-CH(CH₃)₂), 2.96 (sept, ³J_{H,H} = 6.4 Hz, 8H; *o*-CH(CH₃)₂), 7.11–7.15 (m, *m*-C₆H₃, *m*-, *p*-Dipp), 7.29 ppm (t, ³J_{H,H} = 7.6 Hz, 2H, *p*-C₆H₃); ¹³C{¹H} NMR (100.6 MHz, C₆D₆, 25 °C): δ = 25.43 (*o*-CH(CH₃)₂), 26.83 (*o*-CH(CH₃)₂), 31.23 (*o*-CH(CH₃)₂), 123.39 (*p*-C₆H₃), 124.58 (*m*-Dipp), 129.83 (*i*-Dipp), 130.60 (*m*-C₆H₃), 140.40 (*o*-C₆H₃), 145.36 (*p*-C₆H₃), 148.07 (*o*-Dipp), 152.12 ppm (*i*-C₆H₃).

4: A solution of **2** (1.02 g, 1.9 mmol) in diethyl ether (30 mL) was added to sodium metal (0.30 g, 13 mmol) and stirred for 4 h at 25 °C during which time the color changed from green to dark purple. The solution was separated from the excess sodium, concentrated, and cooled in a freezer at –20 °C for 30 h to afford **4** as dark red parallelepipeds. Yield: 0.37 g, 38 % M.p. 121–123 °C (decomp > 270 °C); ¹H NMR (400 MHz, C₆D₆, 25 °C): δ = 1.12 (d, ³J_{H,H} = 6.8 Hz, 24H; CH(CH₃)₂), 1.14 (d, ³J_{H,H} = 6.8 Hz, 24H; CH(CH₃)₂), 2.90 (sept, ³J_{H,H} = 6.8 Hz, 8H; CH(CH₃)₂), 7.10 (d, ³J_{H,H} = 8.0 Hz, 4H; *m*-C₆H₃), 7.18 (d, ³J_{H,H} = 8.0 Hz, 8H; *m*-Dipp), 7.21 (t, ³J_{H,H} = 8.0 Hz, 2H; *p*-C₆H₃), 7.31 ppm (t, ³J_{H,H} = 7.6 Hz, 4H; *p*-Dipp); ¹³C{¹H} NMR (150.6 MHz, C₆D₆, 25 °C): δ = 24.31 (CH(CH₃)₂), 24.43 (CH(CH₃)₂), 30.72 (CH(CH₃)₂), 122.82 (*p*-C₆H₃), 128.19 (*m*-Dipp), 128.37 (*m*-C₆H₃), 131.39 (*p*-Dipp), 139.65 (*o*-C₆H₃), 141.04 (*i*-Dipp), 146.82 (*o*-Dipp), 149.25 ppm (*i*-C₆H₃); UV/Vis (hexanes): λ_{max} (ε) = 342 (2700), 439 (1500), 528 nm (1200 mol L^{–1} cm^{–1}).

Received: April 5, 2002 [Z19048]

- [1] J. Su, X.-W. Li, C. Crittendon, G. H. Robinson, *J. Am. Chem. Soc.* **1997**, *119*, 5471.
- [2] K. W. Klinkhammer, *Angew. Chem. Int. Ed.* **1997**, *36*, 2320; *Angew. Chem.* **1997**, *109*, 2414.
- [3] Y. Xie, R. S. Grev, J. Cu, H. F. Schaefer, P. von R. Schleyer, J. Su, X.-W. Li, G. H. Robinson, *J. Am. Chem. Soc.* **1998**, *120*, 3773.
- [4] I. Bytheway, Z. Lin, *J. Am. Chem. Soc.* **1998**, *120*, 12 133.
- [5] Y. Xie, H. F. Schaefer, G. H. Robinson, *Chem. Phys. Lett.* **2000**, *317*, 174.
- [6] H. Grützmacher, T. F. Fässler, *Chem. Eur. J.* **2000**, *6*, 2317.
- [7] R. S. Simons, M. M. Olmstead, P. P. Power, *J. Am. Chem. Soc.* **1997**, *119*, 11 705.
- [8] F. A. Cotton, A. H. Cowley, X. Feng, *J. Am. Chem. Soc.* **1998**, *120*, 1795.
- [9] T. L. Allen, W. H. Fink, P. P. Power, *Dalton Trans.* **2000**, 407.
- [10] A. J. Bridgeman, L. R. Ireland, *Polyhedron* **2001**, *20*, 2841.
- [11] N. Takagi, M. W. Schmidt, S. Nagase, *Organometallics* **2001**, *20*, 1646.
- [12] J. Grunenberg, N. Goldberg, *J. Am. Chem. Soc.* **2000**, *122*, 6045.
- [13] R. Köppe, H. Schnöckel, *Z. Anorg. Allg. Chem.* **2000**, *626*, 1095.
- [14] B. Twamley, P. P. Power, *Angew. Chem.* **2000**, *112*, 3643; *Angew. Chem. Int. Ed.* **2000**, *39*, 3500.
- [15] P. P. Power, *J. Chem. Soc. Dalton Trans.* **1998**, 2939.
- [16] Z. Palagyi, H. F. Schaefer, *Chem. Phys. Lett.* **1993**, *203*, 195.
- [17] Z. Palagyi, R. S. Grev, H. F. Schaefer, *J. Am. Chem. Soc.* **1993**, *115*, 1936.
- [18] G. Treboux, J.-C. Barthelat, *J. Am. Chem. Soc.* **1993**, *115*, 4870.
- [19] H.-J. Himmel, L. Manceron, A. J. Downs, P. Pullumbi, *J. Am. Chem. Soc.* **2002**, *124*, 4448.
- [20] H.-J. Himmel, L. Manceron, A. J. Downs, P. Pullumbi, *Angew. Chem.* **2002**, *114*, 829; *Angew. Chem. Int. Ed.* **2002**, *41*, 796.
- [21] M. L. H. Green, P. Mountford, G. J. Smout, S. R. Speel, *Polyhedron* **1990**, *9*, 2763.
- [22] Crystallographic data for **2–4**: Recorded at 90 K with MoK_α (λ = 0.71073 Å) radiation: **2**: *a* = 9.1819(9), *b* = 12.7082(13), *c* = 13.0454(13) Å, *α* = 109.856(2), *β* = 98.329(2), *γ* = 110.940(2)°, triclinic, space group *P* $\bar{1}$, *Z* = 1, *R*1 = 0.0477 for 5131 (*I* > 2σ(*I*)) data; **3**: *a* = 17.059(9), *b* = 14.668(7), *c* = 22.259(16) Å, *β* = 101.88(4)°, monoclinic, space group *P*2₁/*c*, *Z* = 4, *R*1 = 0.0653 for 5732 (*I* > 2σ(*I*)) data; **4**: *a* = 11.487(3), *b* = 18.054(4), *c* = 13.413(4) Å, monoclinic, space group *P*2₁/*n*, *Z* = 2, *R*1 = 0.0498 for 2371 (*I* > 2σ(*I*)) data. CCDC-186153 (**2**), CCDC-186154 (**3**), CCDC-186155 (**4**) contain the supplementary crystallographic data for this paper. These data can be obtained free of charge via www.ccdc.cam.ac.uk/contents/retrieving.html (or from the Cambridge Crystallographic Data Centre, 12, Union Road, Cambridge CB2 1EZ, UK; fax: (+44) 1223-336-033; or deposit@ccdc.cam.ac.uk).
- [23] D. S. Brown, A. Decken, A. H. Cowley, *J. Am. Chem. Soc.* **1995**, *117*, 332.
- [24] W. Uhl, M. Layh, T. Hildenbrand, *J. Organomet. Chem.* **1989**, *364*, 289.
- [25] W. Uhl, *Rev. Inorg. Chem.* **1998**, *18*, 239.
- [26] A. Haaland, K.-G. Martinsen, H. V. Volden, D. Loos, H. Schnöckel, *Acta Chem. Scand.* **1994**, *48*, 172.
- [27] A. Haaland, H.-G. Martinsen, H. V. Volden, W. Kaim, E. Waldhör, W. Uhl, U. Schutz, *Organometallics* **1996**, *15*, 1146.
- [28] The greater steric crowding of Ar* in comparison to the Ar' group is borne out by the structures of InAr*, which is monomeric,^[29] and Ar'InInAr', which is dimeric.^[30]
- [29] S. T. Haubrich, P. P. Power, *J. Am. Chem. Soc.* **1998**, *120*, 2202.
- [30] R. J. Wright, A. D. Phillips, N. J. Handman, P. P. Power, *J. Am. Chem. Soc.* in press.